Concrete in the low carbon era

Jones, Rod; Newlands, Moray D; Halliday, Judith E; Csetenyi, Laszlo J; Zheng, Li; McCarthy, Michael

Publication date:
2012

Document Version
Publisher's PDF, also known as Version of record

Concrete in the Low Carbon Era

Edited by:
M Roderick Jones,
Moray D Newlands,
Judith E Halliday,
Laszlo J Csetenyi,
Li Zheng,
Michael J McCarthy and
Thomas D Dyer

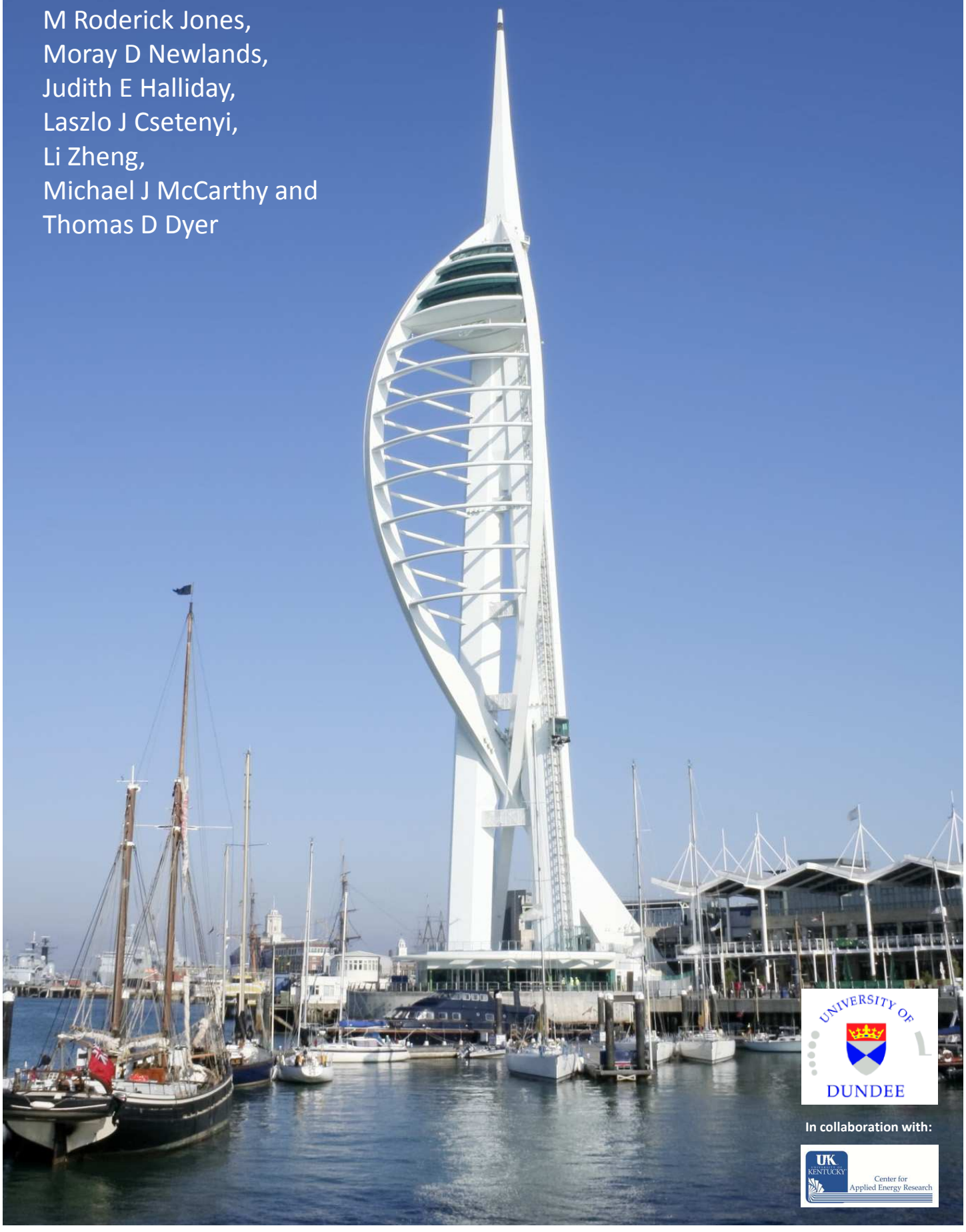

UNIVERSITY OF DUNDEE

In collaboration with:

UK KENTUCKY Center for Applied Energy Research

Concrete in the Low Carbon Era

Proceedings of the International Conference
held at the University of Dundee, Scotland, UK
on 9 - 11 July 2012

Edited by

M Roderick Jones
Director, Concrete Technology Unit
University of Dundee

Moray D Newlands
Lecturer, Concrete Technology Unit
University of Dundee

Judith E Halliday
Research/Teaching Fellow, Concrete Technology Unit
University of Dundee

Laszlo J Csetenyi
Research/Teaching Fellow, Concrete Technology Unit
University of Dundee

Li Zheng
Research/Teaching Fellow, Concrete Technology Unit
University of Dundee

Michael J McCarthy
Senior Lecturer, Concrete Technology Unit
University of Dundee

Thomas D Dyer
Lecturer, Concrete Technology Unit
University of Dundee

ABOUT THE EDITORS

Professor M Roderick Jones is the Director of the Concrete Technology Unit at the University of Dundee. A renowned practitioner in the field of concrete technology, he is a member of numerous national and international technical committees and has published extensively on many aspects of concrete technology, cement science and sustainable construction.

Dr Moray D Newlands is a Lecturer within the Concrete Technology Unit at the University of Dundee. His research focusses on balancing sustainability and durability performance in concrete construction, as well as the use of novel materials and the development of test methods for assessing concrete.

Dr Judith E Halliday is a Research/Teaching Fellow within the Concrete Technology Unit at the University of Dundee. She has been involved in numerous projects relating to sustainable and environmental issues of recycling materials in concrete construction. She has now shifted her focus on the awareness of the depletion of natural resources and the impact of their use in construction as a whole.

Dr Laszlo J Csetenyi is a Research/Teaching Fellow in the Concrete Technology Unit at the University of Dundee. His main areas of interest include cement and concrete science and technology with emphasis on waste stabilisation/solidification and practical use of these materials in construction.

Dr Li Zheng is a Research/Teaching Fellow within the Concrete Technology Unit at the University of Dundee. His current work is concerned with concrete durability, recycling aggregates, foamed concrete, fly ash recovery and beneficiation, cement hydration and temperature rise modelling and mix design/optimisation with novel cement combinations.

Dr Michael J McCarthy is a Senior Lecturer in the Concrete Technology Unit at the University of Dundee. He has carried out research in the field of concrete technology for the last 20 years. Much of his work has been concerned with the use of fly ash in various construction applications, deterioration of concrete in various exposure conditions and aspects of concrete construction technology. He has been involved in many projects and has published widely on his work.

Dr Thomas D Dyer is a Lecturer in the Concrete Technology Unit at the University of Dundee. His research has primarily involved investigation of interactions of by-products with cement. He is also involved in applying life-cycle assessment techniques to construction. Recently his work has extended to include imprinting of biomimetic microstructures in construction materials, and interactions of brownfield contaminants with fresh concrete.

Cover Photo: Spinnaker Tower, Portsmouth, courtesy of Dreamstime.com

Details of all publications from the University of Dundee - Concrete Technology Unit are available from:
http://www.dundee.ac.uk/media/dundeewebsite/ctu/documents/ctu_publications.pdf
Concrete Technology Unit, University of Dundee, Dundee, DD1 4HN, UK
Tel: 01382 384498, m.r.jones@dundee.ac.uk

Published by University of Dundee – Concrete Technology Unit, 2012

Requests to copy any part of this publication should be made to :
Concrete Technology Unit, University of Dundee, Dundee, DD1 4HN, UK
Tel: 01382 384498, m.r.jones@dundee.ac.uk

ISBN 978-0-9573263-0-9

INTRODUCTION

Concrete is used globally and the components are widely available. The activity of construction is also global and both advanced and developing countries aspire to improve living conditions and infrastructure that consumes large quantities of energy and materials continuously. A different attitude to concrete, manufacture and use needs to be developed if we are to address, if not redress, the consequences of in-action. Concrete in some form or another is responsible for our civilised well-being. However, its manufacture and use also require substantial energy use and carbon dioxide emissions and the consequences are global. We all have a duty of care to behave responsibly and the issues of profligacy with respect to these along with related wasteful and polluting activities need to be dealt with. To do this in a committed and balanced way requires both knowledge and experience.

Dundee, over the last three decades, has provided such fora during its conferences in the field of concrete and related materials and this conference will address the causes and solutions as far as concrete and other cementitious products are concerned. Within the themes of the event, the issues of production, use, design, longevity and sustainability will be addressed. In this regard we all have to find an acceptable balance if not a solution. There would seem to be little doubt that carbon-based economies and infrastructure-driven activities will have to increasingly address these.

The University of Dundee and, specifically, the Concrete Technology Unit (CTU) has played a dominant role in exchange of information and professional interaction between all involved in concrete whatever the disciplines. This conference will be equally relevant and informative. It is an opportunity to consolidate progress and to discuss options and experience.

The CTU organised this Conference to address these challenges, continuing its established series of events, namely, Concrete: Construction's Sustainable Option, 2008, Global Construction: Ultimate Concrete Opportunities in 2005, Challenges of Concrete Construction in 2002, Creating with Concrete in 1999, Concrete in the Service of Mankind in 1996, Economic and Durable Concrete Construction Through Excellence in 1993 and Protection of Concrete in 1990.

The event was organised in collaboration with the Centre for Applied Energy, University of Kentucky from the United States of America. Under the theme of Concrete in the Low Carbon Era, the Conference consisted of six Events: *(i) Low Carbon Design of Structures and Buildings, (ii) Efficient and Sustainable Use of Resources, (iii) Infrastructure and Transportation Construction and Resilience, (iv) Structural Health Monitoring and Life Extension, (v) Security and Geohazard Engineering, (vi) Renewable Energy.* In all, a total of 150 papers were presented from 50 countries.

The Opening Addresses were given by Professor Peter Downes, Principal and Vice-Chancellor of the University of Dundee, Mr Bob Duncan, Lord Provost, City of Dundee. The Conference was formally opened by Mr David Ball, CEO of the David Ball Group and the Conference Opening Paper was presented by Mr James Aldred, Associate Director, AECOM, Australia, and the Event Keynote Papers were presented by Dr Boudewijn Piscaer, Initiator and Consultant at SUSTCON EPV, Netherlands, Professor Tom Harrison, Private Consultant, France, Dr Eng Habib Zein Alabideen, Deputy Minister, Ministry of Municipal and Rural Affairs (MOMRA), The Kingdom of Saudi Arabia, Mr Gary Lee, Fyfe (Hong Kong) Limited, China, Professor P Sukontasukkul, King Mongkut's University of Technology North Bangkok, Thailand and the Closing Paper was presented by Professor Peter Hewlett, Visiting Professor, University of Dundee and Director of Research to the David Ball Group

The support of International Professional Institutions and Sponsoring Organisations was a major contribution to the success of the Conference. The work of the Conference was an immense undertaking and all of those involved are gratefully acknowledged, in particular, the Sponsors, members of the Organising Committee for managing the event from start to finish; members of the Scientific and Technical Committees for advising on the selection and reviewing of papers; the Authors and the Chairmen of Technical Sessions for their invaluable contributions to the proceedings.

Professor Rod Jones — Dundee
Chairman, Conference Organising Committee — July 2012

ORGANISING COMMITTEE

Professor M R Jones
Conference Chairman

Dr M D Newlands
Conference Secretary

Dr J E Halliday

Dr L J Csetenyi

Dr L Zheng

Dr M J McCarthy

Dr T D Dyer

Mr S R Scott
Conference Assistant

Professor P C Hewlett
University of Dundee and David Ball Group

Professor T A Harrison
University of Dundee and Private Consultant, France

Professor P Chana
Mineral Products Association, UK

SCIENTIFIC AND TECHNICAL COMMITTEE

Professor H Abdelgader
University of Tripoli, Libya

Dr S Al-Otaib
Kuwait Institute for Scientific Research, Kuwait

Professor N Banthia
The University of British Columbia, Canada

Dr P C Borges
CINVESTAV - Merida, Mexico

Dr S Caliskan
Saudi Aramco, Saudi Arabia

Professor M Changwen
Jiangsu Institute of Building Science, China

Professor D Damidot
Ecole des Mines de Douai, France

Professor R I Gilbert
University of New South Wales, Australia

Mr S Helland
Skanska Norge AS, Norway

Professor G Kaklauskas
Vilnius Gediminas Technical University, Lithuania

Dr E Kearsley
University of Pretoria, South Africa

Mr R Mangabhai
Mangabhai Consulting, UK

Professor B H Oh
Seoul National University, South Korea

Professor I Papayianni
Aristotle University of Thessaloniki, Greece

Dr A Princigallo
CTG - Italcementi Group, Italy

Professor S P Singh
Dr B R Amebedkar National Institute of Technology, Jalandhar, India

Professor M Sugiyama
Hokkai-Gauken University, Japan

Professor R Tepfers
Chalmers University of Technology, Sweden

Professor M Thomas
University of New Brunswick, Canada

Professor K van Breugel
Delft University of Technology, Netherlands

Professor S Wei
Southeast University, China

SPONSORING ORGANISATIONS

EXHIBITORS

BASF – The Chemical Company

Carbon War Room

Dundee and Angus Convention Bureau

Dundee City Council

Elkem Silicon Materials

Maney Publishing

Quantachrome UK Ltd

Scottish Precast Manufacturers Group

University of Kentucky Center for Applied Energy Research

UK Quality Ash Association

Zwick Testing Machines

SUPPORTING INSTITUTIONS

Association of Uruguayan Engineers

Concrete Society, UK

The Institute of Concrete Technology, UK

Mexican Institute of Cement and Concrete

National Telford Institute, UK

Singapore Concrete Institute

Slovak Chamber of Civil Engineers

Contents

Opening Paper

Removing Impediments to the More Sustainable Use of Concrete

J Aldred
AECOM, Australia

The concrete industry is keen to position itself as an integral part of the sustainable construction. Indeed, it is hard to think of sustainable development for the growing global population without thinking of concrete as the primary building material for structures and infrastructure. However, there are many impediments to the more sustainable use of concrete within projects. In fact, the contagion of excessive risk aversion and regulation sweeping the industry appears to be on a collision course with sustainably meeting the needs of the present. Sometimes even so-called “sustainable” requirements cobbled onto existing specifications may result in reduced sustainability. When asked to present the Opening Paper, I was informed that it generally sets the scene and provides a brief review of the state of the art and there is no boundary to what can be covered. I have taken this guideline seriously. This paper attempts to touch candidly on the issues facing the concrete industry in the low carbon era. As it is based on my experience and observations, it cannot help but be subjective to some extent. While I have tried to be balanced, I have also tried to avoid political correctness which so often interferes with appropriate debate about technical issues.

James has over 30 years experience in the concrete industry, working in in Australia, Asia, the Middle East, the United Kingdom and Canada. His background includes Research Scientist, Manager of the High Performance Concrete Research Group at the National University of Singapore, Technical Director and General Manager of an international building materials supplier and Technical Manager of Taywood Engineering. His responsibilities have included product development as well as technical support, training and market development, research on a range of building materials, preparation of specifications and durability plans as well as investigation of structures. James was also the Independent Verification and Testing Authority Manager for the Burj Khalifa with GHD in Dubai and currently is Associate Director in the Advanced Materials Group of AECOM based in Sydney. A Chartered Professional Engineer and a Fellow of the Institute of Engineers Australia, he is also a Fellow of the American Concrete Institute and the Institute of Concrete Technology as well as a LEED Accredited Professional

Keywords: Barriers, Concrete, Sustainability

INTRODUCTION

The concrete industry is keen to position itself as an integral part of the sustainable construction. Indeed, it is hard to think of sustainable development for the growing global population without thinking of concrete as the primary building material for structures and infrastructure. However, there are many impediments to the more sustainable use of concrete within projects. In fact, the contagion of excessive risk aversion and regulation sweeping the industry appears to be on a collision course with sustainably meeting the needs of the present. Sometimes even so-called "sustainable" requirements cobbled onto existing specifications may result in reduced sustainability.

When asked to present the Opening Paper, I was informed that it generally sets the scene and provides a brief review of the state of the art and there is no boundary to what can be covered. I have taken this guideline seriously. This paper attempts to touch candidly on the issues facing the concrete industry in the low carbon era. As it is based on my experience and observations, it cannot help but be subjective to some extent. While I have tried to be balanced, I have also tried to avoid political correctness which so often interferes with appropriate debate about technical issues.

ENVIRONMENTAL POLICY

In his speech at Harvard University in 1947, George C. Marshall said; "An essential part of any successful action …is an understanding on the part of the people … of the character of the problem and the remedies to be applied. Political passion and prejudice should have no part." The Marshall Plan was an inspired programme that became the foundation for the subsequent prosperity and freedom in Western Europe. As far as sustainability is concerned, the Montreal Protocol followed Marshall's recommended procedure and has been the most successful and important international collaboration.

Molina and Rowland [1] proposed that chlorofluorocarbons (CFC) would breakdown in the middle stratosphere and the resultant chlorine might cause the breakdown of large amounts of ozone. Other scientists had independently proposed that chlorine could breakdown ozone but none had recognized that the potential threat of CFCs in the stratosphere. The British Antarctic Survey published data on large losses in total ozone [2] which were confirmed by NASA satellite measurements. Within 4 years, the Montreal Protocol went into effect and has been extremely successful in phasing out ozone-depleting chemicals, primarily CFCs, and placing the ozone layer on the path to recovery.

The success of the Montreal Protocol is in stark contrast to the attempts to reduce carbon dioxide (CO_2) through the Kyoto Protocol and other efforts. Clearly there are important differences between CFCs and CO_2. CFCs were man-made chemicals with a limited number of manufacturers whereas carbon dioxide is an intrinsic part of life and a fundamental part of our current economy. However I would suggest that the crucial factor was that CFCs had a proven direct causal relationship to ozone depletion with demonstrable damage having already occurred. Scientists took the lead by proposing hypotheses which were confirmed by direct observation. This then galvanised the people and governments into effective and necessary action.

While Arrhenius [3] suggested that fossil fuel combustion may eventually result in enhanced global warming as far back as 1896, it was thought that human influences were insignificant compared to natural forces and that the oceans acted as such vast CO_2 sinks that there would be no net accumulation in the atmosphere. The decrease in global annual temperature from the 1940's to the 1970's in spite of significant increases in carbon dioxide shifted the focus to global cooling. Indeed, this was the main concern when I was at University in the late 1970's. The increase in global temperatures in the 1980's lead to modelling by Hansen [4] and others which suggested alarming temperature rise if the output of anthropogenic carbon dioxide were to continue unchecked. Their predictions were presented to the US Congress in 1988. In Great Britain, Margaret Thatcher also gave a speech on the dangers of global warming in the same year. By 1990, the Intergovernmental Panel on Climate Change (IPCC) had been established and issued its first report. The Kyoto Protocol was established in 1998 in an attempt to reduce greenhouse gas emissions to 1990 levels. However, the Kyoto Protocol and other attempts to control carbon dioxide emissions have had virtually no effect on carbon dioxide output. The current CO_2 level is virtually equivalent to Hansen's "business as usual" prediction in spite of billions of dollars spent to reduce emissions.

The general acceptance that anthropogenic global warming (AGW) is occurring has been underpinned by the repeated claims that there is a consensus within the scientific community. This has been a problem for two reasons. First, "the work of science has nothing whatever to do with consensus. Consensus is the business of politics. Science, on the contrary, requires only one investigator who happens to be right, which means that he or she has results that are verifiable by reference to the real world [5]." Secondly, there are a significant number of notable scientists who have made statements disagreeing with one or more of the principal conclusions of the IPCC and the so-called "mainstream" acceptance of AGW. There are highly credible scientists who question the accuracy of the IPCC and other climate models, the conclusion that CO_2 is the main cause of global warming and the assumption of negative consequences. A summary of the areas of concern is given by Prof. Bill Gray who is Emeritus Professor of Atmospheric Science at Colorado State University and head of the Tropical Meteorology Project at CSU's Department of Atmospheric Sciences [6]. He is a pioneer in the science of forecasting hurricanes and one of the world's leading experts on tropical storms. He has the appropriate credentials to give an informed opinion on the subject and Bill Gray is not alone. Obviously there is a significant degree of scepticism and frustration with the "mainstream" AGW position within the scientific community and it seems to be growing.

Hansen et al [4] predicted average temperature rises of approximately 0.35°C, 0.7°C and 0.8°C by 2010 for the Scenarios A, B and C respectively as shown in Figure 1. The actual average temperatures until 2012 are in shown in Figure 2. In spite of the carbon dioxide levels having risen at a rate similar to Scenario A (business as usual), the actual temperature rise has been less than Scenario C which is based on emissions not increasing beyond 2000. A more important point is the fact that there has been no apparent increase in global temperatures since the peak in 1998 or 14 years ago. Rather than reassess the original AGW hypothesis, CO_2 has morphed into the reason for extreme climate events or part of a complex, "wicked" system which cannot be expected to be fully understood. I fear that a continued lack of warming may not only discredit the AGW hypothesis but seriously undermine faith in the scientific community and governments. This could be a serious impediment to sustainability or future attempts to deal with important complex issues that require global cooperation.

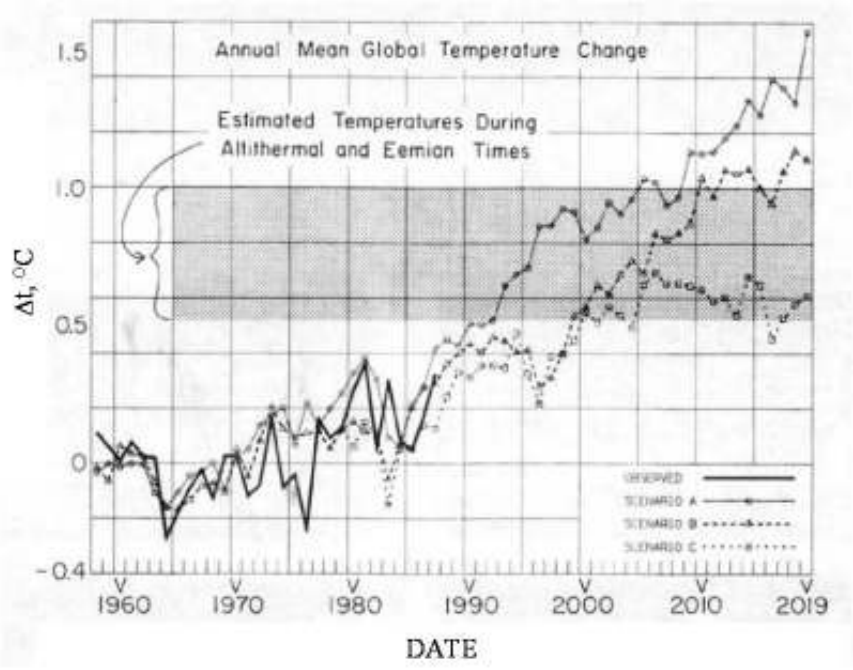

Figure 1 Data on annual mean global temperature based on observations to 1988 and predictions for emissions with no control "business as usual" (Scenario A), rate of growth controlled (Scenario B) and no increase beyond 2000 (Scenario C) [4]

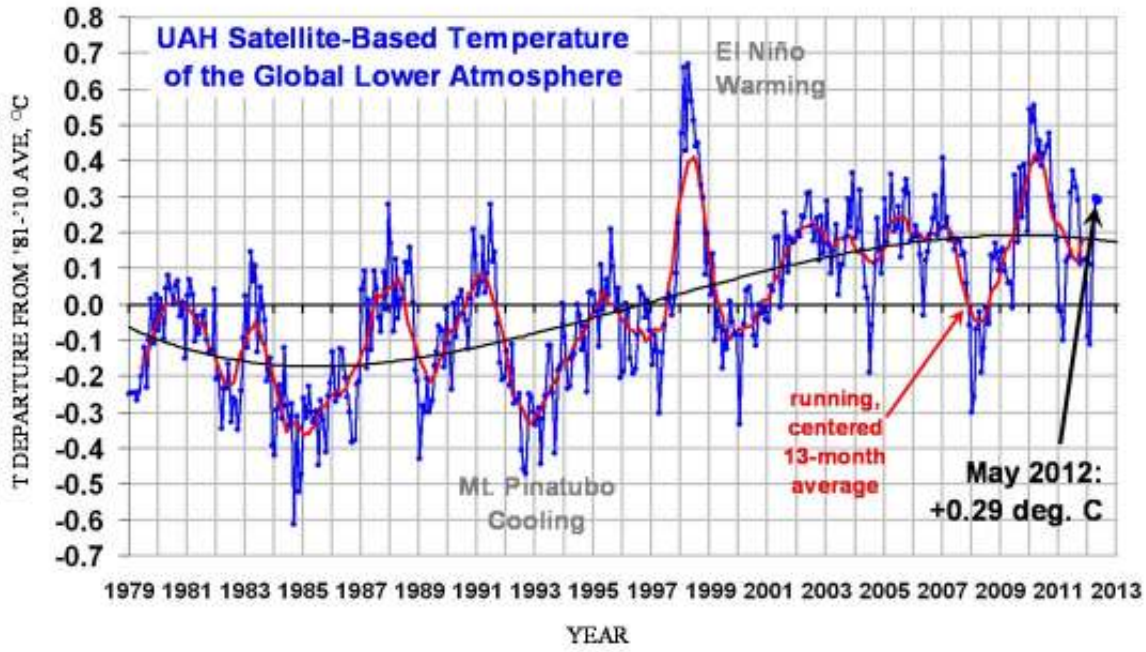

Figure 2 UAH monthly temperature anomalies from 1978 to 2012 [7]

AGW was an appropriate scientific hypothesis to investigate. The predictions by Hansen et al [4] and others regarding expected temperature rise provided an objective basis for its assessment. The problem arose with the rush to political action before confirmation of the hypothesis. Bypassing the normal scientific debate and assessment process prevented the development of a true understanding of the problem and exploration of possible remedies. As a result, the AGW discussions have been full of "political passion and prejudice" from the outset contrary to Marshall's recommendation.

I personally think that the AGW/CO_2 issue has now become a divisive impediment to the crucial sustainability issues of resource depletion and damage to the natural environment. At a recent meeting on adapting to the carbon tax in Australia which has come into force this month, I was told that the use of recycled aggregate was not a viable option as it had the same carbon footprint as virgin aggregate. This conference will be discussing increasing the efficiency of our built environment to minimise energy consumption, reducing the requirement for virgin resources, facilitating renewable energy and developing truly sustainable communities as well as the examples where the concrete industry is making considerable progress. If we were to achieve realistic targets in each of these areas, we would profoundly reduce fossil fuel consumption and CO_2 production without the need for carbon taxes and alike.

Living on a planet with seven billion people and limited resources, there is virtually universal agreement on the importance of resource depletion and damage to the natural environment, regardless of one's opinion on AGW. Refocusing attention back onto the primary sustainability goal of meeting the needs of the present without compromising the ability of future generations to meet their own needs would appear the best way to harness our collective efforts for optimum benefit.

RISK AVERSION

During a 2012 lecture in Sydney, Dr White [8] presented the different sea level rise scenarios as shown in Figure 3. The data available on water levels for La Jolla in California from 1924 is shown in the insert and in Figure 4. This establishes a linear rise of 2.07 $\pm$ 0.29 mm/year within 95% confidence levels which equates to a sea level rise of 0.18 – 0.24 metres or 0.6 – 0.8 feet over the 21st century. However, the Californian Coastal Conservancy estimate is 4.6 ft (1.4 m) or nearly six times the maximum expected from the historical data. The high estimate model by the US Army Corps of Engineers is 4.8 ft (1.46 m) and this model significantly over-estimates the sea level changes that have already. Globally sea level variations over centuries have fluctuated within a range of about 1.1 mm/year without any significant long-term trend [9-12]. Northwest European tide gauge records indicate little or no rise [13, 14, 9, 15]. Selected Pacific and Indian Ocean tide gauges give 1.4 mm/year [16]. Proposed global mean tide gauges give 1.45 mm/year with the actual rate for the last 40 years being only 1.2 mm/year [17].

Current development policies for coastal regions may be based on a vast acceleration of sea level rise that may never eventuate. California and most other economies around the world cannot afford to waste valuable resources on excessive over-design. This influences the concrete industry because concrete is a key component of many sea defences and coastal structures.

Engineers are placed in a difficult position; potentially over-design structures based on the highest predictions which may waste resources or design based on appropriate probabilistic engineering judgement and potentially face litigation and a plethora of expert witnesses if anything goes wrong, even if it had nothing to do with the sea level rise.

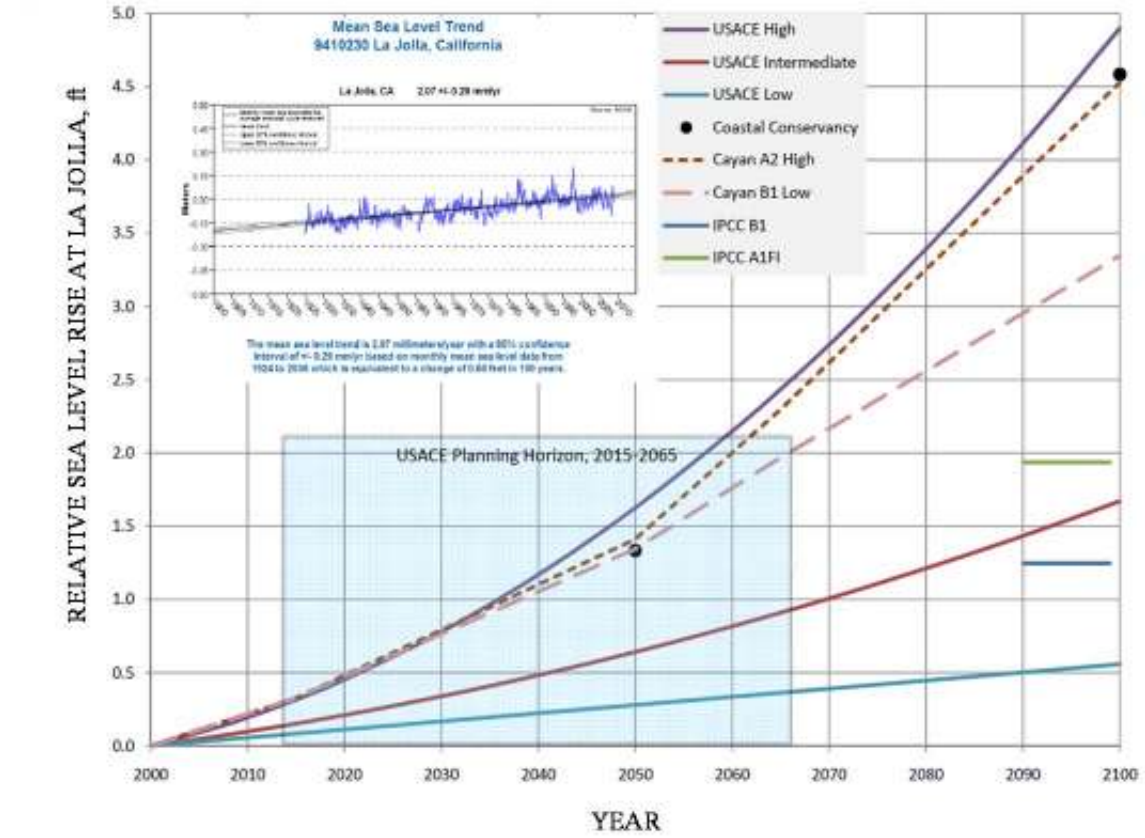

Figure 3 Comparison of sea level rise scenarios [8]

The actual rate of sea level rise is a vital consideration for the design of near shore or on shore concrete structures for the “Limpet” wave energy device has been operating since 2000 on an exposed cliff edge in the Orkney Islands in northern Scotland. Overestimating sea level rise reduces the commercial viability of this important source of renewable energy which is usually mounted on a concrete structure.

Problems with risk aversion also arise from limited data and engineers erring on the side of caution. Adjacent to a major project, there was a plan to extend a local waterway. It was suggested that this may raise the water table although it was deemed by one of the consultants involved to be a “50:50 call”. Even though the construction was underway, the consultants decided to increase the height of the pile caps over the massive site at significant time, cost and materials. If the announcement to extend the waterway had been delayed by a few months, the project would have been constructed based on the original design. The project would have had to deal with the effect of the waterway on the water table in the same way as the neighbouring structures which had been already completed and could not have made this “50:50 call”.

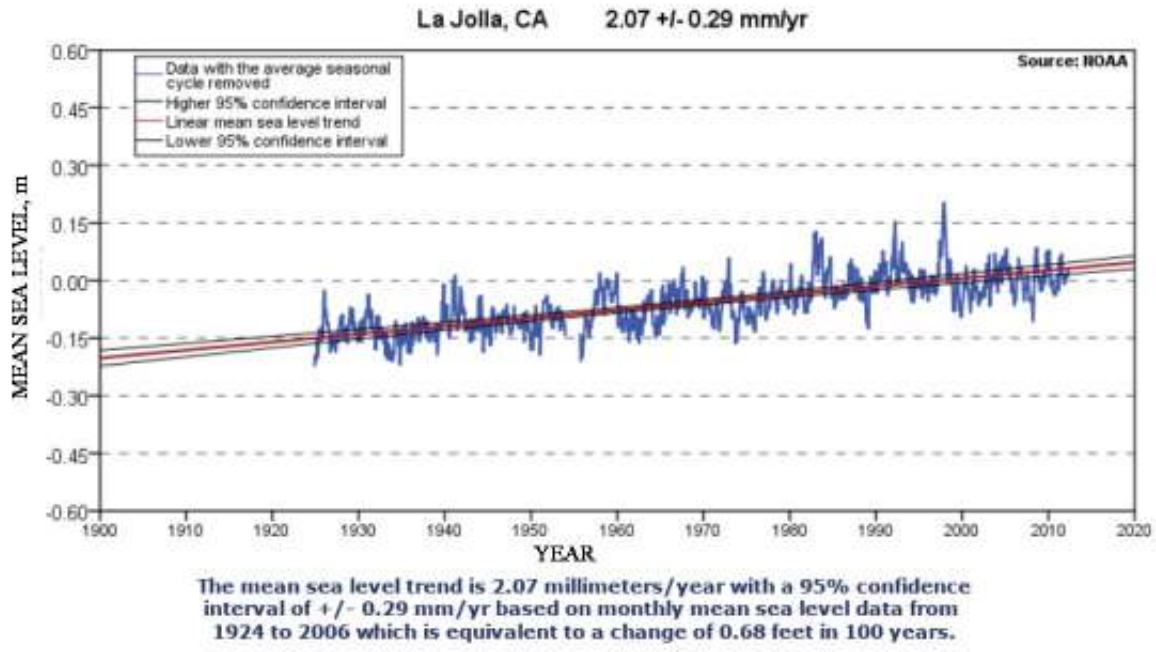

Figure 4 Historical mean sea level from 1924 to 2010 in California (http://tidesandcurrents.noaa.gov/sltrends/sltrends_station.shtml?stnid=9410230°)

Another major project had a number of engineering firms designing the different phases. The proposed reinforcement for the basement rafts varied by more than 300% despite each designer being given the same specification guidelines. One designer proposed massive perimeter restraint to limit predicted lateral movement and the others did not. How could there be such a range of different technical requirements to build essentially the same structural elements? One factor was the issue of calculating the limiting crack width. The highest reinforcement volume proposed was required to reduce the limiting crack width below the 0.2 mm nominated in the design brief on the basis that it would need to be a watertight structure when the waterproofing membrane eventually failed. Another important difference among the proposed designs was the expected stress caused by long-term shrinkage. The ACI guidance largely ignores shrinkage after one year on the basis that the rate of shrinkage will, in most structural sections, be sufficiently slow that creep would eliminate any shrinkage stress. BS EN 1992 [18] on the other hand, considers a completed piled raft as being exposed to end restraint and the reinforcement required to limit crack widths is significantly higher. End restraint was not even considered in BS 8007 [19]. I am not aware of significant problems with basements that were previously designed to that code.

BS EN 1992 [18] calculates long-term shrinkage based on the average shrinkage through the depth of the concrete section. In a raft slab, drying can only occur from the top surface with the bottom surface often encased in a membrane and surrounded by water. Gilbert et al measured the shrinkage profile through concrete that was sealed at the base as well as sealed and restrained at the base as in metal deck. They found a reduction in shrinkage of sections when evaporation was prevented from the base using a coating. However, when restrained and sealed, the base of the section exhibited no shrinkage as shown in Figure 5. A similar effect would be expected to occur within piled rafts with further reduced shrinkage at the base of the raft due to no evaporation from the bottom and restraint from distributed piles.

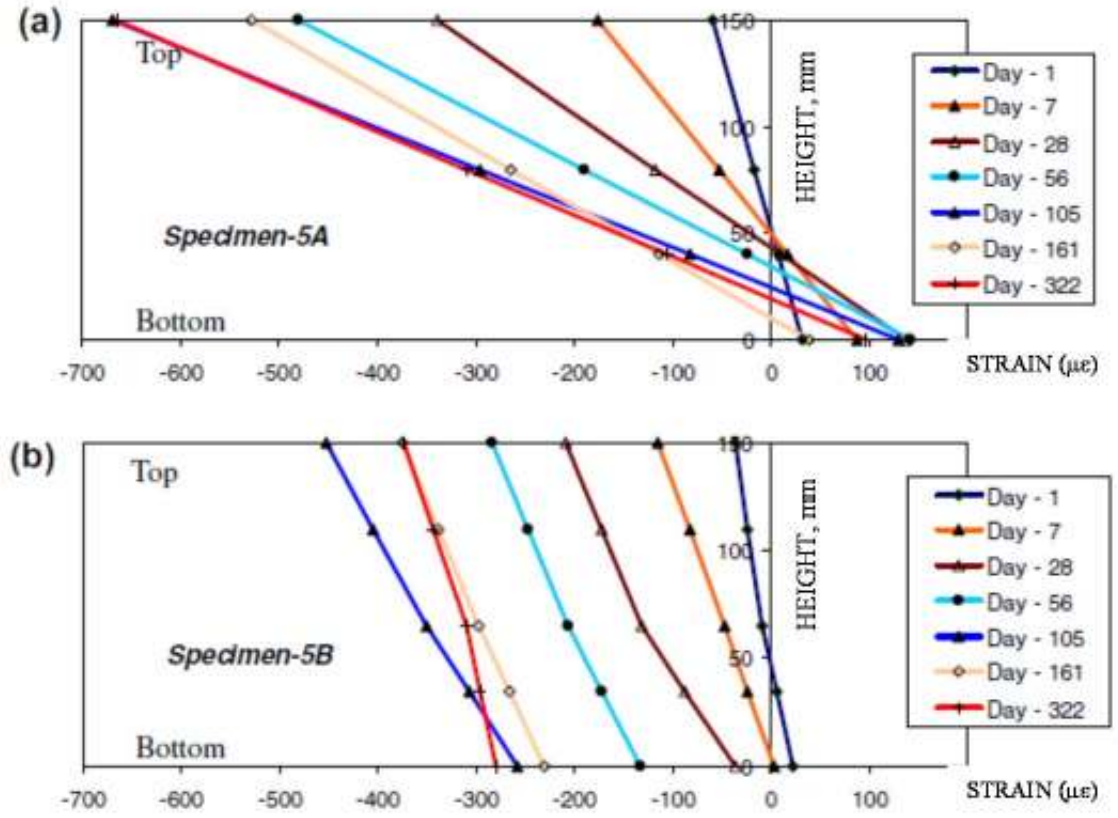

Figure 5 Shrinkage strains in concrete slabs that were sealed and restrained by metal deck (profile shown) (5A) and which sealed only on the base (5B).

Therefore the restrained drying shrinkage at the raft/pile interface may be much lower than anticipated from the average value calculated using CIRIA C660 [20]/BS EN 1992 [18] and the reinforcement requirement significantly reduced. It can be very easy for the Engineer to err on the side of caution and over-design. It provides a greater factor of safety and it is not his money!

In these types of situations, the important impediment to more sustainable use of concrete is the lack of in-situ monitoring of structures to verify the design assumptions and minimise any over-design in future. Advances in monitoring technology make it easier to acquire the required data. Accumulating more data on issues where over-design may be occurring would also provide a technical basis for more sustainable construction without exposing the Engineer to additional risk. This would progressively remove impediments the sustainable use of concrete. I would urge the concrete industry to collect and publish as much data as possible on the in-situ performance of concrete with appropriate cross references to initial compliance testing.

SPECIFICATIONS

Day [21] expressed the hope that the practice of specifying minimum cement contents and requiring mixes to be submitted and not subsequently varied would have finally died out by the publication of that edition of his book. However, these practices are still very much alive in 2012. Other prescriptive requirements of specifications, such as aggregate grading,

maximum supplementary cementitious replacement levels, placement temperatures, workability, etc. tend to stifle mix optimisation and are an impediment to sustainability. They also often lead to unintended detrimental effects of concrete performance.

Designers of concrete structures and infrastructure should specify the properties they have assumed in their design, including strength, movement and durability. However, few specifiers are also concrete technologists and many specifications are blend of sometimes contradictory prescriptive and performance requirements. The performance requirements often just added onto previous specifications.

Existing Codes accept that concrete strength follows a normally distribution and should be considered in terms of mean strength and standard deviation rather than an absolute limit. However, when cubes or cylinders are lower than specified strength, the Engineer often requires an investigation by coring rather by analysing the results to determine whether the low result constitutes a genuine downturn or an isolated statistical aberration. To avoid the inconvenience and cost of coring or other testing, producers may choose to overdesign their concrete mixes, significantly reducing the sustainability of the concrete. Unnecessary testing of in-situ concrete is an impediment to sustainability. Day [21] advocates a penalty system where concrete that is “contractually” deficient results in a nominal cost to the producer. Clearly where compliance testing suggests “structurally” deficient concrete, an appropriate investigation would be required.

There are two basic requirements of a concrete control system. One should provide an accurate assessment of quality and the other should facilitate intervention as quickly as possible to restore the required quality in the event of any downturn. Accordingly, the specification must ensure that mix design and quality control are controlled by the concrete producer. Any external party cannot require corrective action based on as little evidence as a properly motivated producer will require [21]. The large range of admixtures and supplementary cementitious materials now available makes external intervention even more difficult. A competent concrete producer has to conduct trials to establish which products, and which suppliers of materials, will best enable him to consistently produce the most economical compliant concrete for a particular project. He should be encouraged to do so by the specification. All parties to the project will benefit from a competent and motivated concrete supplier with consistent supply that complies with the specification requirements. Specifications for non-strength properties can be more complicated and this is often used as a justification for prescribing some mix features, sometimes significantly reducing the sustainability of the concrete or the ability of the supplier to innovate.

Premature deterioration of reinforced concrete is a global problem that costs billions of dollars annually. In severe environments, concrete structures have often failed to achieve their required service life without major maintenance which is unsustainable. As more specifications now require a minimum design life of 100 years for major projects and infrastructure, there is even more demand for appropriate specifications to ensure concrete durability. International codes provide prescriptive solutions to increase the required concrete quality and cover thickness to improve chloride resistance. The common practice to specify a minimum cementitious content to achieve “durability” is an impediment to sustainability. First, Buenfeld and Okundi [22] showed that, at a given w/cm ratio, the higher binder content actually increased chloride ion ingress in concrete. Similar results were found here at the University of Dundee by Dhir et al [23]. This is hardly surprising when transport processes occur primarily through the paste fraction of the concrete. Secondly, an unnecessarily high

cementitious content may lead to increased cracking due to thermal stresses and shrinkage which could reduce durability. Unnecessarily wasting cementitious materials also increases the environmental impact of the concrete. Another unintended consequence of minimum cementitious content requirements in specifications is that it creates a competitive disadvantage for the more competent concrete suppliers who have invested in effective quality control systems to be able to reduce variability and cementitious content.

One difficulty in specifying durability performance is the absence of a generally accepted comprehensive test at a reasonably early age. An increasing number of specifications require compliance testing of transport properties during construction in an attempt to improve the expected durability of reinforced concrete structures. However, the required performance for the different specified parameters to achieve the desired durability has often not been established. Unlike compressive strength, there is little information available on the expected variation in the results to calculate an appropriate characteristic value.

In the case of chloride induced corrosion, performance requirements may include diffusion, migration, resistivity or water transport measurements or combinations of these. The ASTM C1202 [24] test has been a commonly specified procedure in different parts of the world. This procedure is a measurement of saturated resistivity and has been correlated to chloride diffusion. While the standard includes a rough guideline for the interpretation of the coulomb values obtained, specifications can require more and more onerous performance limits which appear more related to risk aversion than technical performance. Faced with onerous absolute performance limits suppliers have tended to significantly overdesign their concrete mixtures to help ensure compliance which reduces sustainability and increases production cost with unknown benefit in terms of durability enhancement. The use of additional cementitious material to achieve certain performance limits at early ages may have a detrimental effect on fresh and hardened properties. The test result can have quite high variability so that individual results should not be specified as a rejection criterion for the sampled concrete, rather a characteristic value based on statistical analysis of results should be established.

Chloride diffusion is perhaps the most relevant test but it is expensive and time consuming to test and therefore not well suited for compliance testing. Chloride migration is a much faster and cheaper procedure which still measures chloride penetration. I would suggest that the best procedure would be to measure resistivity frequently and migration occasionally to confirm adequate performance based on service life predictions modelling using a characteristic value for assessment.

What is needed are more field data on the actual performance of concrete in aggressive environments related to its early age properties to provide a technical basis for performance requirements. There are good service life models which relate long-term field performance to early age properties but not all projects are going to conduct a detailed assessment of service life but simple/cheap compliance tests based on resistivity and desorptivity could easily be added to compressive strength to provide much more information on the concrete's potential durability. When tests are cheap and simple, accumulating statistical data is easy and producers would be encouraged to get to understand how to optimise their mixes rather than the current situation of sticking to a mix because it has a diffusion coefficient.

Specifications for temperature rise and differentials in massive pours require attention. A default peak temperature of 70°C is prudent as it would virtually eliminate the possible problem of delayed ettringite formation (DEF). While DEF is uncommon, it can cause

enormous damage. Many specifiers focus on the temperature differential within the concrete mass and a value of 20°C is often specified. However, in my experience which is primarily in temperate and tropical zones, most thermal cracking has been caused by external restraint of massive concrete elements by a rigid substrate during cooling. The attention on the differential temperature requirement in temperate conditions often leads to excessive insulation and increases both the peak temperature and the volume of concrete that reached high temperature. Therefore, to reduce a minor potential problem, the more likely problem is exacerbated.

Many specifications limit concrete placement temperature to 32°C or less. In hot countries, this usually means that premix companies need an ice plant and this has a high energy demand. For a four metre thick concrete raft in Kuwait, the batching plant did not have an ice plant or access to flake ice but needed to achieve the required peak temperature limit. I proposed the use of 55% fly ash replacement which achieved the required temperature limit as well as the other specified properties. In massive elements, very high replacement levels of fly ash and GGBS are extremely useful to limit temperature rise. The elevated temperature means that the in-situ maturity is high at relatively early ages so that acceptable strength and penetrability properties do not take long to develop. There are many situations where in-situ maturity monitoring can reduce unnecessary over-design of concrete mixes. An unnecessary impediment to sustainability and solving potentially serious thermal issues are the limits on supplementary cementing material replacement levels in many specifications. One does need to be cautious when using high replacement levels of fly ash in thin or suspended elements where the concrete could dry out and not develop the required properties. Well-meaning specifications which extend the compliance testing age for concrete specifically to enable high replacement levels without considering in-situ development of strength and other properties can be problematic.

There is a tendency to limit concrete workability in specifications based on the assumption that lower workability produces better concrete. While often true when added water was the only way to increase workability, it is certainly not true in the age of advanced admixtures. Poor workability can lead to honeycombing, slower construction and uncontrolled water addition after compliance sampling. Resultant defects can lead to costly repairs and even litigation. The problem of prescriptive specification of rheology can also occur with self-consolidating concrete (SCC) where over-zealous specifiers can require very high workability parameters which can lead to segregation. I would suggest that the specification should require that the contractor/premix company confirm that the rheology of the concrete is satisfactory for the proposed placement procedure and the mix developed complies with the performance parameters. This will reduce the amount of repairs and replacement necessary and encourage innovation.

Many specifications include limits on drying shrinkage according to a standard procedure such as ASTM C157 [25] or AS 1012.13 [26]. While this may seem prudent and would be expected to reduce cracking, it should be noted that most “shrinkage” cracking is due to plastic, thermal and autogenous shrinkage (in that order) not drying shrinkage. Drying shrinkage tests are conducted on well cured small specimens 75 mm x 75 mm (3” x 3”) in cross section dried at 50% relative humidity and therefore not representative of standard concrete elements exposed to drying in most environments. In-situ drying shrinkage is a slow process. Pour strips interfere with construction and do virtually nothing to accommodate drying shrinkage strains. Higher strength concrete with higher cementitious contents tends to exhibit lower shrinkage in these tests. However, such mixes may have greater movement due

to higher peak temperatures and more autogenous shrinkage which are not measured in the test. Creep helps to limit any long-term detrimental effects. The well meaning but poorly thought through use of a performance criterion may reduce both sustainability and concrete performance.

REGULATIONS

Standard concrete production in Australia has essentially been based on compressive strength performance for more than 20 years. The Australian system has resulted in good concrete producers, with well-equipped, suitably staffed and accredited laboratories, designing and controlling a range of mixes to meet the specified strength. Concrete producers prepare monthly reports on the mixes which are circulated to the purchasers. In the event of any marginally low result being predicted from early tests, the producer is required to inform the purchaser of the concrete in question. The better producers generally use a graphical and statistical control system on concrete and input materials data which helps identify any problem at an early stage.

The result of this system has been that typical concrete in Australia has a standard deviation of strength of between 2 – 3 MPa, well below most other countries. A lower standard deviation means a lower target mean strength and lower cementitious contents with reduced cost and environmental impact. Investment in quality control and quality testing was effectively incentivised.

The situation could not be more different for concrete from the same suppliers to various projects which must comply with prescriptive specification requirements, particularly when additional performance requirements have been added. Some State Authorities have prescriptive specification requirements to which performance requirements have been added such as chloride diffusion, sorptivity or volume of permeable voids. Mixture proportions and material suppliers have to be registered with the State authority. The considerable time and cost involved in obtaining registration is a disincentive to ongoing mix development and upgrading to more advanced admixtures and so on. The standard deviation of these registered mixes with minimum cementitious content and other requirements can be up to double that of the standard mixes which are controlled by the premix supplier to achieve a strength requirement only. When the variability in strength increases so does the variation in other properties.

An unexpected consequence of durability performance specification has been the submission of inappropriate concrete mixtures just because they had the necessary test data so that the producer did not have to conduct additional trial mixes and long or expensive testing. For a structural element with minimum thickness varying from 0.45 m to 1.8 m and a specified strength of 50 MPa, the premix company proposed a mix with cementitious content of 635 kg/m³ incorporating 25% fly ash. The mix was proposed because it was approved by the appropriate statutory body and the performance criteria had been met. We modelled the expected peak and differential temperatures using the proposed mix. The estimated peak temperature was 98°C and the differential was more than 60°C as seen in Figure 6. The mix may have achieved the required chloride diffusion but, if it had been used in this application, it would have resulted in severe cracking and significant delayed ettringite formation potential. In addition, the mix used over 200 kg/m³ more cementitious material than was necessary. In this situation, a performance requirement intended to improve durability and a

registration procedure intended to ensure compliance could have resulted in the use of a totally inappropriate concrete mixture with serious consequences in terms of premature deterioration and waste of resources. This was simply to avoid additional testing and paperwork caused by the specification and regulations.

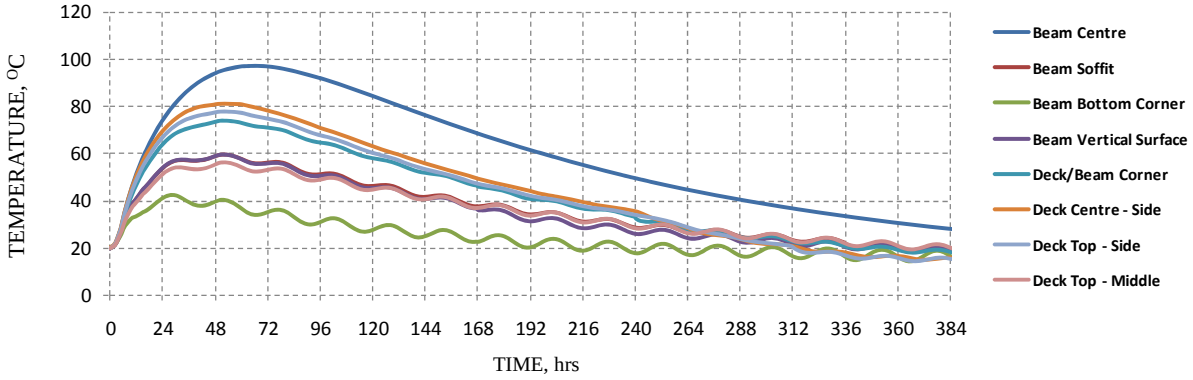

Figure 6 Results for Concrete Mix 635kg Binder, 25%FA. Temperature Profile at Locations of Interest with protected surfaces after formwork removal.

The Heart of Doha is an urban redevelopment in the historic centre of the city. It will transform the district into a network of sustainable interconnecting buildings, public squares, courtyards, and landscaped streets. I was involved in helping improve the sustainable use of concrete for the project which is targeting LEED™ Gold. Qatar had regulations preventing the establishment of a batching plant within the city. The “not in my backyard” rule. A comparison of the transport requirements for off-site compared with on-site concrete production of the estimated 1.25 million cubic metres showed a reduction of 55% in terms of truck-kilometers for on-site production. Other important sustainability benefits were the ability to reduce loads on road infrastructure, reduce rejection of non-compliant concrete and reduce disruption to city traffic. Based on these benefits, permission was given to have a site plant.

STANDARDS

Standards have necessarily been developed from the prevalent construction practices. Indeed, the time taken to develop standards means that they are often based on recent construction practices rather than current ones. This can be a serious impediment to the promotion and use of innovative materials and procedures. I was involved in preparing a state of the art report on a proprietary geopolymer concrete in Australia. While the standard is obviously based on Portland cement based concrete, the materials components of the AS 3600 for Concrete Structures are essentially performance based. The format of the report followed the engineering, durability and other significant properties listed in the Standard and compared the performance of the geopolymer concrete with the expected performance from a Portland cement based concrete. This approach has been quite successful in helping designers understand the performance properties of a novel material. This geopolymer concrete has now been used in a range of different applications.

Designers have requested independent verification of the use of the product to help mitigate any possible risks with using a non-traditional concrete. This has been an excellent system for introducing innovative sustainable concrete materials in actual structures rather than laboratory specimens to build confidence in the technology.

National Standards and Codes which are more prescriptive in nature and explicitly limit concrete to a Portland cement based binder are an impediment to non-Portland based binders being accepted in the industry.

CONSTRUCTION PRACTICES

Another impediment to the more sustainable use of concrete has been tradition construction practices which have covered concrete with marble, tiles, paster or paint. There is a different attitude to quality control of concrete when it is expected to have an off-form finish. I have seen repetitive defects where the first defect had been cosmetically patched rather than correct the placement method that produced the defect. This had huge cost implications. Self-consolidating concrete (SCC) can play an important role in improving the concrete quality and surface finish as well as saving Contractors significant cost on repairs. The fact that so many precasters now use SCC is testament to its advantage in reducing defects and repairs.
Properly constructed concrete using appropriate binder, pigments and formwork or grinding can provide an inexpensive, attractive and durable finish where the thermal mass of the concrete is directly in contact with the internal spaces for maximum benefit in terms of thermal attenuation. This can be augmented by the use of embedded water pipes within the concrete to efficiently control internal temperatures.

CONCLUSIONS

We can produce beautiful, off-form structures with minimal embodied energy and emissions where most of its components are locally available throughout the world. Such concrete structures require virtually no maintenance. They are fire resistant, flood resistant and hurricane proof in the event of severe weather with extremely low energy costs to maintain a comfortable living environment.

Engineers have always been uniquely placed to be able to do great things. It is probably one of the reasons that each of us entered the profession. Louis Pasteur once said; "Ce n'est pas la profession qui honore l'homme, c'est l'homme qui honor la profession", "It is not the profession that gives honour to a man, it is for the man to honour his profession". Let us bring honour to our profession by eliminating excessive over design, rationalising specifications to promote quality and innovation and improving construction practices.

Some are very cynical about sustainability because it can be more “spin” than substance and “spin” will not provide for the needs of humanity. Let us all work to remove the various impediments to the sustainable use of concrete so that this wonderful material can be used to its full potential in the service of mankind. My school motto was; “Esse quam videri”, “To be, rather than to seem to be” which is a great motto for anyone. I hope that the motto of the sustainability movement will become; “Ad faciendum quam videri”, “To do, rather than to seem to do”.

REFERENCES

1. MOLINA, M. J.AND ROWLAND, F. S. (1974). "Stratospheric sink for chlorofluoromethanes: Chlorine atom-catalysed destruction of ozone". Nature 249 (5460): 810.

2. FARMAN, J. C., GARDINER, B. G. AND SHANKLIN J. D (1985) "Large losses of total ozone in Antarctica reveal seasonal ClOx/NOx interaction" Nature 315, 207 – 210

3. ARRHENIUS, S. (1896) "On the Influence of Carbonic Acid in the Air upon the Temperature of the Ground" Philosophical Magazine and Journal of Science Series 5, Volume 41, pp 237-276.

4. HANSEN, J., FUNG, I., LACIS, A. RIND, D., LEBEDEFF, S., RUEDY, R., RUSSELL, G. AND STONE, P. (1988) "Global climate changes as forecast by Goddard Institute for Space Studies – Three dimensional model" J. of Geophysical Research, Vol. 93, No. D8, pp 9341-9364.

5. CRICHTON, M. (2003) "Aliens Cause Global Warming" Caltech Michelin Lecture

6. GRAY, W (2011) "On the highjacking of the American Meteorological Society" http://icecap.us/images/uploads/On_The_Hijacking_of_the_American_Meteorological_Society.pdf

7. SPENSER, R (2012) Latest global temperature anomaly. http://www.drroyspencer.com/latest-global-temperatures/

8. WHITE, K (2012) "Climate Change Adaptation for Water Resources: Moving from Science to Policy" Presentation to Engineers Australia 8-10 May.

9. MORNER, N.A. (2004) "Estimating future sea level changes". Global Planetary Change 40, pp49-54.

10. MORNER, N.A. (2005) "Sea level changes and crustal movements with special aspects on the eastern Mediterranean". Zeitschrift fur Geomorphologie 137 (Suppl.), pp91-102.

11. MORNER, N.A. (2008). Reply to Comment by Nerem et al. (2007) on "Estimating future sea level changes from past records" by Nils-Axel Morner (2004). Global Planetary Change 62, pp219-220.

12. MORNER, N.A. (2011) "Setting the Frames of Expected Future Sea Level Changes by Exploring Past Geological Sea Level Records" Evidence-Based Climate Science, Ed D. Easterbrook pp185-194, Elservier.

13. WOODWORTH, P., 1990. A search for accelerations in records of European mean sea level. International Journal of Climatology 10, pp129-143.

14. MORNER, N.A. (1996). "Sea level variability". Zeitschrift fur Geomorphogie N.F. 102 (Suppl.), pp223-232.

15. MORNER, N.A. (2010) “No alarming sea level rise. A great sea level humbug revealed”. 21st Century Science and Technology, 7e17. Winter 2010/11.

16. CHURCH, J.A., WHITE, N.J., HUNTER, J.R., 2007. Sea-level rise at tropical Pacific and Indian Ocean islands. Global Planetary Change 53, pp 155-168.

17. HOLGATE, S.J., 2007. On the decadal rates of sea level change during the twentieth century.Geophysical Research Letters 34.

18. BRITISH STANDARDS EN 1992 (2004), Design of concrete structures. General rules and rules of buildings, BSI London, UK

19. BRITISH STANDARDS 8007 (1987), Code of practice for design of concrete structures for retaining aqueous liquids, BSI, London, UK

20. CIRIA C660, Early-age thermal crack control in concrete, CIRIA, London, UK

21. DAY, K.W. (2006) Concrete mix design, quality control and specification. 3rd Edition. Taylor &Francis London

22. BUENFELD, N.R. AND OKUNDI, E. (1998) “Effect of cement content on transport in concrete.” Magazine of Concrete Research, Vol. 50, No. 4, 339-351

23. DHIR, R. K., MCCARTHY, M. J., ZHOU, S. AND TITTLE, P. A. J.(2004) “Role of cement content in specifications for concrete durability: cement type influences” Structures & Buildings Vol. 157 Issue SB2 pp 113-127

24. ASTM C1202, Rapid chloride permeability test, ASTM International, West Conshohocken, PA, USA

25. ASTM C157-8, Standard test method for length change of hardened hydraulic-cement mortar and concrete, ASTM International, West Conshohocken, PA, USA

26. AUSTRALIA STANDARDS (AS) 1012.13 (1993), Methods of testing concrete-Determination of the drying shrinkage of concrete for samples prepared in the field or in the laboratory, Standards Australia.

Theme 1 — Low Carbon Design of Structures and Buildings

Reducing CO_2 by Half in Concrete

B Piscaer
SUSTCON EPV, Netherlands

All aspects that influence the reduction of the CO_2 emissions in concrete will be mentioned briefly. Focus will however be presented on the production of the material itself in 2 main groups (i) Multiplication of "Best Practice" low clinker concrete, (ii) R & D effort towards the "State of the Art". "Best Practice" using several case studies from different geographical areas resulting in tailor made solutions will demonstrate the complexity of the subject. The interaction of all parties and academic disciplines in the ValueS Chain will be highlighted. Aspect will be dealt with such as (i) National and European regulation barriers to be resolved in order to facilitate the implementation of cross boarder Best Practice CO_2 reductions, especially in the applications of low carbon impact Supplementary Cementing Materials, (ii) human capacity development in concrete mix design such as particle size engineering and oxide engineering,(iii)supporting pillars such as developed in the European Eco-Innovation project SUSTCON EPV. The substantial CO_2 reductions from applying Best Practice will be calculated using real case stories. "R & D" will not only involve the large number of low CO_2 Non Portland Cement innovations that need to be put on the market. The demand to conduct "From Practice to Theory" R & D will be presented related with the need to bridge the gap between "Lab-Crete" and "Real-Crete". This will most likely result in more precise engineering of structures and lower the volume of concrete and rebar needed. On these efforts another figure as an objective for CO_2 reduction can be connected, justifying the ambition to half the CO_2 presently being emitted. Side effects from the ambition such as portraying concrete as an important high tech product thus attracting higher educated and motivated people will be mentioned. Finally the call will be made to improve the relation between the academic community, executive economy and policy makers.

Dr Boudewijn Piscaer is Initiator and Consultant at SUSTCON EPV, Netherlands. As an "Intrapeneur" within first German companies, he developed new markets in Europe, North America, the Caribbean and Asia. This was for high temperature resisting refractory brick. Through refractories he became familiar with the iron and steel, non ferrous metals, ceramic, glass, and especially the cement industry.

After a "Green concrete" workshop in Iceland in 1999 he combined his CO_2 reduction objectives with the application of practices from the refractory concrete. In May 2002 he organized a Green Concrete workshop and since then he presented numerous papers on Sustainable Concrete. In 2007 he discovered loopholes in the standards and a new verification methodology that could circumvent the barriers to innovations. In 2009 he initiated a European ECO-INNOVATION project proposal and united a Spanish - Dutch consortium for SUSTCON EPV (Sustainable Concrete - Environmental Performance Verified). Project previews November 2011 in Belgium and March 2012 in Madrid confirmed that substantial progress in civil concrete practice is now within reach. He consults the SUSTCON EPV project till November 2012.

Keywords: CO_2, Powder, Regulation, Sustain

INTRODUCTION

It is an honour to present this paper in a country that has probably the best Climate for Change in our profession. I have noticed that the UK seems to be up front with the subject that has been hardly on the agenda's of many other countries; a low carbon economy. Many specialized publishers on the topics of Ethics, Corporate Social Responsibility and Greening of the industry originate in the UK. Quoting Jo Confino from the Guardian on why the only real leadership being shown in addressing the numerous sustainability issues is from business;

"It's not that business has suddenly gone all gooey and philanthropic, but because they see in the hard data that unless they act now, there may not be a business left to run in the next 20 years or so".

Such hard data as the report by Eccles at al. of last November provided called "The Impact of a Corporate Culture of Sustainability on Corporate Behaviour" is more accessible here. It demonstrates the better financial yield for those who care about sustainability. The best proof however for the right Climate for Change is that the University of Dundee selected the topic of this conference and is helping the number 1 construction material and the number 2 in CO_2 product to act now.

We should realize that reducing by half the C from Ordinary Portland Cement use of > 3.3 Billion tons means that we can reduce far more then the airlines emit all together.

For many of us more important; the objective of reducing the environmental impact of concrete goes hand in hand in making it the most popular and attractive high tech sustainable construction material it has proven itself already 2000 years ago. This challenge will be a great opportunity for the educational and research institutes together with the industry in an overall drive to increase human capacity building.

My thanks go out to the European Commission/EACI that has recognized the importance of the sustainability of concrete by giving 2 Spanish and 2 Dutch consortium partners a hand in overcoming the barrier to realize Eco-Innovations in favor of the knowledge based economy in general and SME's in particular.

Personally I realized since 2002 WHAT had to be done, in 2007 I knew HOW and in 2009 with WHOM. Our project is on track.

The general task is to learn how to do more with less. For an industry that is built on "thinking and calculating in volume", the change to "thinking and acting in quality" does not come automatically. Yet the speaker has proof from refractory concrete that reduction can lead to adding more then one value.

HOLISTIC APPROACH

Reducing CO_2 and the linked reduction of raw materials has to be conducted on many fronts that mostly are intertwined. Energy that comes from non renewable sources is in production and transport of materials. The energy consumption of a ton of aggregates or OPC raw material can vary from 3kWh to 8kWh per ton. Energy use for making concrete varies between 2 kWh to as much as 20 kWh per m^3 of concrete. Transport takes yet another big

part of CO_2. While it is in the direct economical interest to reduce energy, we have to face the unavoidable problem; Portland clinker. As an average 1 T OPC = 1 T CO_2 and takes 1.6 T raw material (we send 600 kg up in the atmosphere). Modern clinker productions having "only" 824 kg and we may still further improve the process, but even if all energy comes from renewable source we ARE still calcining so we will never get under 600 kg CO_2/T of clinker. So how can we reduce the carbon footprint of concrete structures without compromising its sustainability? Unless we understand concrete better we cannot tell the engineers and architects how they should design.

Cement and/or Binders

Globally there is still great confusion on what cement is. Former Prime minister Yves Leterme called King Albert the cement of the Belgium Nation. Are we talking about Portland Cement/OPC or the binder listed in the prescriptive EN 197? So how can we prescribe Water Cement Ratio's and the linked Water Binder Ratio's when this is not clear? Here is the proof that the WCR and derived WBR have nothing to do with technology and all with market positions;

An SCC manufactured in a Dutch precast plant uses 180 kg Cem I 52.5R, 180 kg GGBS, 180 kg of GCC (Ground Calcium Carbonate). This mix has a binder ratio in the UK of 0.40, in the Netherlands 0.45, in France 0.66 in Germany, Spain and many other countries 0.92. If one would count the same 3 ingredients that are used for making "legal" EN 197 cements Cem II B LL and Cem III C, we all of a sudden have a Water Binder Ratio of 0.36.

This is a proof that we are still dealing with outdated regulations in conflict with several European principles that have little to do with technology.

And, this is the topic of our congress; this SCC has a carbon footprint on materials of 190 kg/m^3 replacing a vibration concrete with 370 kg/m^3.

I think we should thank the Water Cement Ratio and its national step sisters the Water Binder Ratio's for having done a nice job since the age that we made concrete from 3 shovels gravel, 2 sand and 1 cement and helped avoiding disasters by controlling somehow the water (in the plants). However, in the era of low carbon it does not have a place anymore and should finally retire for health reasons, ours.

From Practice to Theory

Using GCC to stabilize the mix we discovered all over the Netherlands early 2000 that nobody could make a C35 and 45 anymore. Using the nationalized EN 206 versions that prescribe the amount of prescriptive EN 197 cements they all increased concrete strength to C65 in 28 days, while having a demoulding strength after 14 h of > 20. The steel re-enforcement design is still not adapted to this, another area where serious CO2 is wasted in favor of a competing industry.

This SCC in question is more then well responding to the 6 basic intertwined criteria for concrete;

- Workability is ideal
- Strength, more than enough

- Durability is high due to low permeability
- Sustainability, both environmental plus social
- Aesthetics due to high powder content
- Cost AND too often still price.

So why did the rapid and high increase of strength happen using what was considered an inert material such as Ground Calcium Carbonate? In order to get the homogeneity and workability right for these SCC mixes Particle Size Engineering was also necessary for what was then considered the secret garden of some suppliers; looking at < 125 µ. So now we can say that there are 3, again intertwined, aspects for strength developments;

1. Mineralogical transformations, hydraulic and/or pozzolanic
2. Mechanical packing
3. Adhesion of all particles.

Another revealing pilot that was done in the framework of our European Eco-Innovation project SUSTCON EPV in 2011 was a water tight basement in the Netherlands (Figure 1).

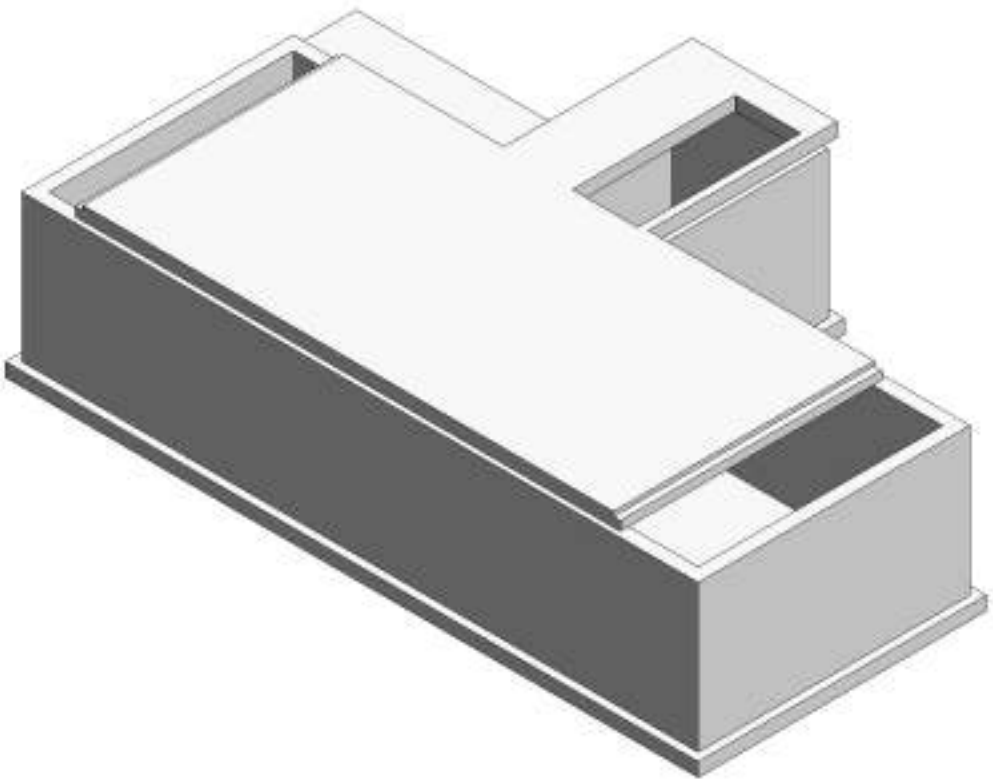

Figure 1 Water tight basement

Using only 68 kg CEM I 52.5 R, 140 kg of GGBS, 132 kg GCC a 28 normative strength of C38 of a very water tight mix without additional special admixtures was obtained. An estimated carbon footprint of < 80 kg/m3 for the most used concrete type the type C20/25 X III was reached instead of > 260 kg in many other countries. This pilot justifies the title of this presentation; we CAN reduce CO_2 in concrete by half if we let go of outdated regulations that are conflicting with European guidelines plus take our business seriously.

More and more engineers and contractors are abandoning 28 days strength as mandatory, so all powders can do what they should do for the tailor made concrete that is finally gaining its well deserved place in the market. Some concrete needs 8h, others 180 days strength etc. Why is Powder Coal Fly ash when mixed with CEM I up to 35% considered 100% a binder and when mixed by the concrete producer it only counts for 40%? Is this technology we need for our low carbon era concrete?

It is clear that present regulations are restricting the use of environmental friendly materials.

PLAN OF ACTION

Durability is NOT linked with strength, minimum "cement" or water binder ratio. There is however a relation with permeability when it comes to carbonation, chloride and acid resistance.

It would make sense to introduce the **Water Powder Ratio** as a guideline for concrete mix design only, not for standards. Powder being all materials < 125µm.

Looking at only the 2 above mixes that both used 165 liters of water plus good PCE admixtures, this would result in the Water Powder Ratio given in Table 1.

Table 1 Water powder ratio of the 2 mixes

	WCR (EN197)	WBR NL	WBR ES+DE+	W.POWDER R.
SCC prec. C56/65	0.92	0.45	0,92	0.29
RMC C20/25	2.43	0.78	2.43	0.48

Now there is an explanation of the too high strength and thus too high waste of CO_2 and resources. The waste of human resources I will address later.

As you know, all powders other than Portland cement have a low carbon footprint and most are called SCM (Supplementary Cementing Materials). Several of them are used in EN 197 type blended composite cements but their use by the concrete producers on an equivalent base is restricted by regulations. So I call in the first place for **Equal Rights concrete**. A producer should be allowed to use them in at least the same quantity as the cement producer does.

In the second place we should quickly integrate SCM's that are NOT recognized by the EN 197 such as Meta-Kaolin, Activated Paper Recycled Minerals, Reactive Rice Husk Silica etc. And in the third place the scientific and technology community should actively investigate Non Portland Cements.

Quality Control & Particle Size Engineered Ingredients

Yet the main ingredient for low carbon concrete, according to my friend Hugo Pettingell is consistency of the ingredients that will allow precise design of both structure and mix reducing waste due to usual over dimensioning of the mix to absorb variations.

Incoming QC should be done frequently also on powders by testing the water demand. If this is varying, you can check further by laser de-fraction. You can also have the material regularly checked like this by an outside source. Experience shows that the powder supplier will send the off materials to somebody who is not checking. In Germany the cement producer has two silo's for what is according to the standards the same CEM I 52.5R cement; one silo for the Germans who do not make SCC, one for the Dutch SCC market that demands higher quality.

Though adhesion of aggregates plays a definite role, this is not my field of expertise. A clear way of reducing the use of precious binders with relative high CO_2 due to production and transportation is good aggregate production that leaves very limited space for expensive binders. Also higher quality consistent supply deserves a premium.

By having CUSUM quality control as preached by the global concrete evangelist Ken Day will reduce waste by achieving smaller standard variations. The technique of remote testing of strength development will result in optimizing mix and reduce the use of Portland cement. The CONCREMOTE method applied introduced in the Netherlands is proof of such favorable outcome.

Sustainable Structural Design

Globally building and civil engineers are not sufficiently informed about sustainability aspects of concrete so how can we expect them to design sustainable structures properly? E.g. by doubling the strength of a concrete structure, one can reduce its volume by 25% which has in turn an effect on mostly urban transport. By redesigning the structures, as often demonstrated by Prof. Koji Sakai, materials can be used in a more intelligent way.

Yet another way of making concrete more sustainable and apply different raw materials is to design structures that do not need steel reinforcement. This will reduce the carbon footprint of the structure by means of eliminating steel already. 10% of worlds production of steel, that has also a high carbon footprint, goes into concrete. Steel free concrete can also make structures more durable, not having to worry about carbonation and chloride penetration. The writer realizes that it seems to take another step back but the most sustainable concrete structure, the Pantheon in Rome, has just proven that this approach makes sense.

There are production methods on the market that use CO_2 steam for curing concrete so permeability for uptake can be designed in the mix. Once such production method has solved the manufacturing process problems, it opens new perspectives for the concrete industry, provided the problem of steel reinforcement has been addressed in design. Possible CO_2 uptake figures on concrete in general are coming on to the market but have a high number of variables and are not presented here.

Regulations

As demonstrated above, the present prescriptive regulations do not make sense for a low carbon economy when the use of environmental friendlier materials is obstructed. Where would the automobile industry be if a minimum amount of steel would be imposed? With current and future fuel prices we would not drive far in our hummers and tanks on the average salary. Are there buildings in wood such as the Pantheon in Rome? So concrete can be a sustainable low carbon material. But do you think we would be allowed under present EN 197 and EN 206 to be build?

We need to move from outdated prescription regulations to credible performance criteria so we can upgrade the image of concrete as being high tech after all and attract better people plus be a very sustainable that means environmental friendly and social important product.

For this we developed in our Eco-Innovation project 6 pillars;

-The EN 206 5.2.5.3 Equivalent Concrete Performance Concept which is a loophole in a non harmonized standard that is in general in conflict with the Construction Product Directive/Regulation,

- A testing protocol that is based on a dynamic performance verification methodology instead of certification of static costly long lasting consensus based CEN/EOTA standardization that results in mediocre compromises,

- A Sustainability Index for Concrete, which is a Life Cycle SUSTAINABILITY Assessment,

- A Quality Brand Label called “Pantheon Performance” to counteract the FSC label

- A Science, Technology, Ethical Board of Advisors and Supervisors to prevent Green Washing, and the introduction of sound innovations,

- An insurance that will accompany the move from insuring Lab-Crete to Real-Crete and cover innovations.

WHAT WILL LOW CARBON CONCRETE MEAN FOR THE SUPPLIERS?

- The cement industry will become instead of a clinker distributer (“Clinkeristes”), sales engineers of high quality binders such as CEM I 62.5 RR and CEM III C22.5N, Cem IV, V and VI and propose their very stable reliable products for a premium. They will make more money with less clinker better used. They will approach customers with binders that are higher priced but cost less for the producer.

- Aggregate producers will sell as many different very precise consistent fractions with possibly good quality dust.

- Admixture producers will continue their work as sales engineers and get maybe involved in selling mineral admixtures as well.

- Concrete producers will attract better people who consider it more fun to supply changing tailor made concrete then following questionable regulations,

- On-site inspection of Real-Crete using new non destructive instruments for testing e.g. permeability will be new jobs taking away demolition jobs from the future.

- New institutes will rise that will accompany the producer with QC of incoming and outgoing materials, in mix optimization, according to the production and installation process.

- Companies such as the one that co-ordinates sustainability for the Olympics within the pyramid Owner, Specifiers, Producers, Contractors and Regulators, which will result in less waste will find more a place in the economy,

- Sustainability evaluation companies that know that Managing is Measuring will find a future.

- Vocational schools will turn out students with skills, proud to have their hands on a high tech material that is most used (and most abused).

- and, last but not least, Universities such as Dundee that will present students and industry a range of possibilities from Research that may be applied more, and students that realize that they can repeat what was done 2000 years ago, make concrete structures that will demonstrate that we can reduce carbon and add more then 1 value but 3 elements of Sustainability, People, Planet and Prosperity.

Amsterdam 18-5-2012

Shear Behaviour of Reinforced High Strength Concrete Beams Without Transverse Reinforcement

M Hamrat[1], M Chemrouk[2], S Amziane[3]
1 – University Hassiba Ben Bouali, Algeria
2 – University of Science and Technology Houari Boumediene, Algeria
3 – University Blaise Pascal, France

The paper describes a study in which sixteen reinforced concrete beams without transverse stirrups were tested to failure to investigate the influences of the shear-span/depth ratio, the longitudinal steel ratio and the compressive strength of concrete on the loaded behaviour of high strength concrete in shear. Crack development and propagation were studied through continuous monitoring of the shear cracking using digital video recording. The test results show that the shear capacity depends more on the shear-span/depth ratio and the longitudinal steel ratio and relatively less so on the compressive strength in the case of high strength concrete. Among the factors that contribute to the shear resistance of high strength concrete, the aggregate interlocking contribution is found to be less than in ordinary concrete due to the nature of inclined cracking, realatively straight and transgranular in this type of concrete instead of intergranular as in ordinary concrete. Using the test results, the applicability of the different modelling approaches used in the major design codes for the contribution of high stength concrete to the shear resistance is assessed and their use as design tools for high strength concrete beams without transverse reinforcement examined.

Dr M. Hamrat is a senior lecturer at University Hassiba Ben Bouali, Chlef, Algeria. His research work concerns the structural performances of concrete with particular attention on HPC, a topic on which he has co-authored several papers recently.

Dr M. Chemrouk is a Professor at University of Science and Technology Houari Boumediene, Algiers, Algeria. His research interests include concrete deep beams, the structural properties and performances of concrete materials and the behaviour of concrete structures in seismic regions. He has published and co-authored several papers related to these topics and won a Henry Adams Award.

Dr S. Amziane is a Professor at University Blaise Pascal, Clermont Ferrand, France; formerly a senior lecturer at University of Bretagn Sud, France. His research interests cover the performances of building materials with particular reference to concrete materials and the behaviour of structures of all types. He has recently published and co-authored several papers on these topics.

Keywords: Compressive, High strength concrete, Longitudinal steel ratio, Shear span, Shear strength, strength

INTRODUCTION

The shear behaviour of reinforced concrete elements, particularly those made of high strength concrete (HSC), is still a subject of interest in research despite the numerous experimental and theoretical work papers published on normal strength concrete (NSC). According to this literature, the compressive strength of concrete ($f_c^{'}$), the shear-span/depth ratio (a/d) and the longitudinal steel ratio (ρ) are thought to be the most important parameters affecting the shear resistance of normal strength concrete. Little is known, however, about the influence of these parameters for high strength concrete which has a number of advantages; its use in the construction industry is ever increasing in many regions of the world. This is due to its improved physico-mechanical properties such as the compressive strength, the stiffness and the long term durability and also to the economic gains which can be achieved with reductions in geometrical sections and gain in the architectural space to be exploited. Hence, technical, economic as well as aesthetic criteria point towards the choice of HSC instead of NSC.

In effect, with the advances in materials technology, particularly the development of superplaticisers and colour admixtures, concrete construction aesthetics are continuously improving through the use of high strength concrete.

On the other hand, HSC has proved to be a brittle material. Indeed, during the tests of this study, it was observed that cracking was sudden, transversing completely aggregate particles, as in Figure 1 below, producing relatively smooth fracture planes. The cracks do not go around the aggregate particles as is usually the case with NSC. Smooth fracture planes affect the concrete shear strength by reducing the contribution of the aggregate interlock between the fracture surfaces [1, 2, 3, 4].

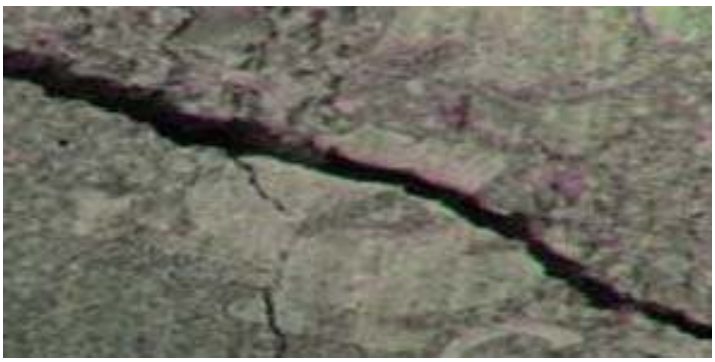

Figure 1 Typical inclined crack in HSC beams- transgranular

The rupture mechanism of a beam element without transverse reinforcement can be reasonably thought of as generating three internal contributing forces [5] to shear resistance (Figure 2). These consist of the contribution of concrete in the compression zone (V_c), the shear contribution due to aggregate interlock (V_a) and the shear contribution due to the dowel action of the longitudinal reinforcement (V_d).

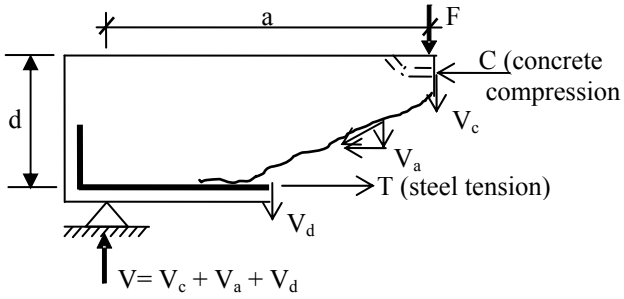

Figure 2 Internal shear forces in a beam without transverse reinforcement

The total shear resistance can be written as :

$$V = V_c + V_d + V_a \qquad \text{[Eq. 1]}$$

With an excessive opening of a diagonal crack, the components V_a and V_d become ineffective. Consequently, the component V_c carries all the acting shear. This leads to the collapse of the beam, initiated by crushing of concrete in compression [5]. The aggregate interlocking mechanism is a significant contributor to the shear capacity of beams and hence has a predominant influence on the ultimate load carrying capacity of beams failing in shear [6]. According to Talor [7], its contribution to the shear strength varies between 33% and 50% in ordinary concrete.

At higher concrete strengths, however, the aggregate interlocking does not seem to contribute greatly towards shear. This is supported by the smooth fracture planes and the straight cracks (Figure 1) which do not go around the aggregate particles but across them. Indeed, according to Mphonde [8], the contribution of the aggregate to the shear strength of high strength concrete is almost insignificant. Indeed, no aggregate interlocking was observed for the high strength concrete beams of the tests in this study and the shear capacity was not significantly increased even when compressive strengths had almost doubled, from 44.2 MPa to 85.5 MPa.

The state-of-the-art concerning shear in reinforced concrete reveals that there is no unifying rational theory explaining the interactions of the factors (V_c, V_d, V_a) which contribute to the shear resistance of this composite material. In this sense, the current major codes such as the American ACI-318, the British BS-8110, the Eurocode 2 and the French BAEL adopt empirical equations for the shear strength of concrete beams as functions of the longitudinal steel ratio, the shear-span/depth ratio, the concrete compressive strength and the sizes of the beam specimens (Table 1). Although most of these four major universal codes take into account the three parameters considered for investigation in the present work, the change from normal strength concrete (NSC) to high strength concrete (HSC) may induce changes in the way these parameters contribute to the shear capacity; the influence of these parameters may be different in the two types of concrete. Thus, the application of these equations to RC beams with higher compressive strengths ($f_c^{'} > 40$ MPa) needs to be carefully examined.

Table 1 Empirical equations for the shear strength used in the major design codes

CODES	EQUATION		COMMENTS
ACI-318 (American)	$V = \frac{1}{7}\left[\sqrt{f_c'} + 120\rho\frac{d}{a}\right].bd$		f_c' cylinder compressive strength of concrete, d effective depth of the section b width of the section
BS-8110 (British)	$V = \frac{0.79}{\gamma_m}\left(\frac{100A_s}{b_v d}\right)^{1/3}\left(\frac{400}{d}\right)^{1/4}\left(\frac{f_{cu}}{25}\right)^{1/3}.bd$	a/d ≥ 2	f_{cu} cube compressive strength of concrete, A_s section of the longitudinal steel γ_m safety factor for material $f_c' = 0{,}8\, f_{cu}$
	$V = \left(2\frac{d}{a}\right)\frac{0.79}{\gamma_m}\left(\frac{100A_s}{b_v d}\right)^{1/3}\left(\frac{400}{d}\right)^{1/4}\left(\frac{f_{cu}}{25}\right)^{1/3}.bd$	a/d < 2	
Eurocode-2 (European)	$V = \frac{0{,}0525}{\gamma_c}(f_c')^{2/3}(2{,}5d/a).(1{,}6-d).(1.2+40\rho)bd$	a/d < 2.5	ρ longitudinal steel ratio γ_c safety factor for concrete material a/d shear span /depth ratio
	$V = \frac{0{,}0525}{\gamma_c}(f_c')^{2/3}.(1{,}6-d).(1.2+40\rho)bd$	a/d ≥ 2.5	
BAEL (French)	$V = 0.3\, f_t K.b.d$		K= 1 (for shear through simple flexural loading) f_t tensile strength of concrete

TEST PROGRAMME

Test Specimens

Table 2 and Figure 3 show the details of the beam specimens which all had a constant width of 100 mm and a constant depth of 160 mm. The beams were tested under different shear-spans. A total of sixteen beams were constructed and loaded to failure under two-point loads. The beams were cast from of two types of concrete in terms of strength, using the ingredients given in Table 3. This has resulted in two groups of eight concrete beams of grades C40 and C80 as in Table 2. For each group, two longitudinal steel ratios were used (ρ_l =1.16 and 2.31 %) and four different shear-span/depth ratios were tested (a/d =1; 1.5; 2 and 3). The notation of the specimens (C40-1-1 or C80-3-2) is such that C40 and C80 designate normal strength concrete (NSC) and high strength concrete (HSC), respectively. The first number after the first hyphen gives the a/d ratio and the number after the second hyphen is the longitudinal steel percentage ($\rho = A_s/bd$).

Testing Instrumentation

The load was applied using a 250 kN servo-controlled hydraulic jack. One LVDT was attached to the bottom surface at midspan of the test specimen to measure the midspan displacement of the beam. Electrical strain gauges were attached to the surface of the longitudinal steel to record the bar strains. The strain gages were covered with silicone gel to prevent damage during and after casting. The applied load, the corresponding displacement and the strains were recorded automatically through a data logger.

A Video Gom-Aramis system was used to measure crack widths and to monitor the development of the diagonal cracking (Figure 4). The system follows the movements of some reference points indicated beforehand in each beam as the load increases. The analysis of the numerical image is carried out with the help of Gom-Aramis software which enables the strain fields to be evaluated over the whole zone studied. Moreover, this allows the detection of the initial crack opening with great precision.

Table 2 Details of test specimens and concrete strengths

	$f_c^{'}$ (MPa)	f_t (MPa)	d (mm)	a/d	LONGITUDINAL TENSILE STEEL	
					A_s (mm^2)	ρ (%)
C40-1-1			135	1	157	1.16
C40-1-2			133	1	308	2.31
C40-1.5-1			135	1.5	157	1.16
C40-1.5-2			133	1.5	308	2.31
C40-2-1			135	2	157	1.16
C40-2-2	44.2	3.37	133	2	308	2.31
C40-3-1			135	3	157	1.16
C40-3-2			133	3	308	2.31
C80-1-1			135	1	157	1.16
C80-1-2			133	1	308	2.31
C80-1.5-1			135	1.5	157	1.16
C80-1.5-2			133	1.5	308	2.31
C80-2-1			135	2	157	1.16
C80-2-2	85.5	4.50	133	2	308	2.31
C80-3-1			135	3	157	1.16
C80-3-2			133	3	308	2.31

Table 3. Ingredients of HSC (and NSC for comparison)

MATERIALS	UNITS	HSC	NSC
Cement type CEMI-52.5 N-CPJ	kg/m^3	425	275
Silica fume	-	42.5	-
Aggregate (3-10 mm)	kg/m^3	980	990
Sand (0-4 mm)	kg/m^3	700	740
Water	l	144	170
Filler (limestone)	kg/m^3	-	44
Superplasticiser (Chrysofluid Optima 206)	l	6.4	-
W/C	-	0.34	0.62

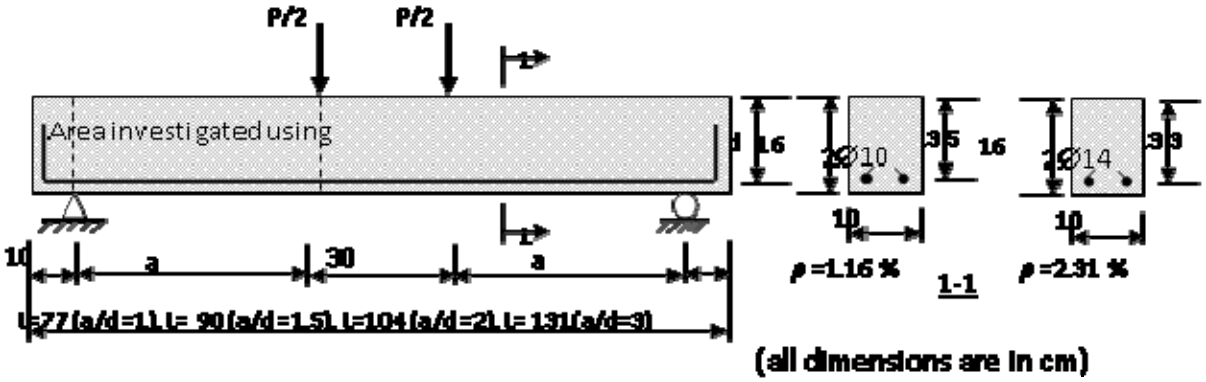

Figure 3 Geometry and reinforcement of beam

Figure 4 Experimental set-up of the test specimens and the video camera

TEST RESULTS AND DISCUSSION

Load-Deflection Response

The load-deflection behaviour consists of two stages (see Figure 5):

-The first stage corresponds to the elastic behaviour where no cracking exists in the tension zone of the concrete beam.

-The second stage starts with the appearance of flexural cracking in the central section of the beam which reduces in stiffness due to the cracking. At further increases of load, the existing cracks develop in length and new cracks would appear within the shear spans. One of the flexural cracks in the shear spans close to the supports would eventually depart from the vertical and bend diagonally towards the loading point. Alternatively, depending on the length of the shear span, a diagonal crack might develop independently within the shear span and extend towards the loading and support points. On further increase in load, concrete would crush in the compression zone near the loading point. Failure has always occurred during this second load-deflection behaviour stage (Figure5) since no confining lateral reinforcement was provided as expressed by the load-deflection curves.

In these tests, the load-versus-deflection response for RC beams seemed to be comparatively less dependent on the concrete compressive strength than on the longitudinal steel ratio and the shear-span/depth ratio as clearly seen in Table 4 and Figure 5.

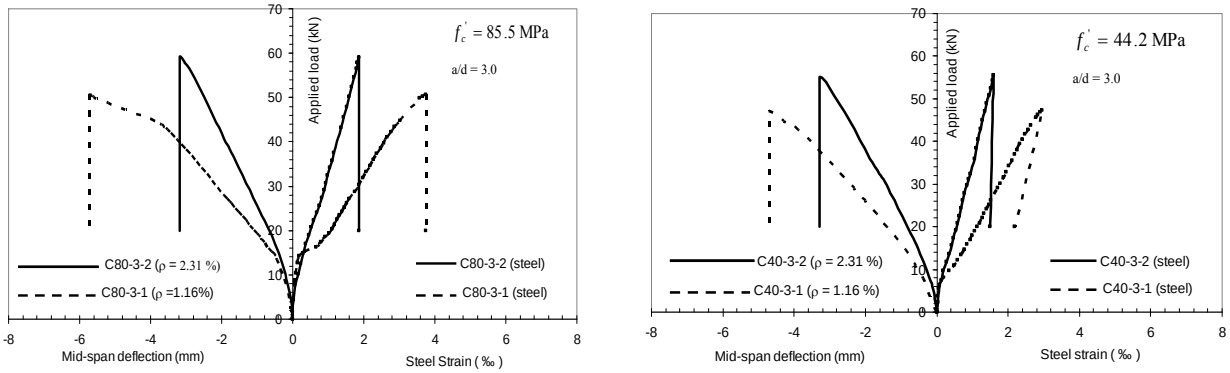

Figure 5 Typical Load –deflection and steel strain at mid-span for the beam specimens

Table 4 Test results of reinforced concrete beams

BEAMS	P_{fl}* (kN)	P_{cr} (kN)	P_u (kN)	P_u/P_{cr}	δ_u** (mm)	W*** (mm)	NUMBER AND TYPE OF CRACK (along the beam)
C40-1-1	25	133	187	1.45	2.84	0.46	1Diagonal shear + 4 flexural
C40-1-2	30	140	195	1.39	1.80	0.39	2Diagonal shear + 3 flexural
C40-1.5-1	22	96	129.4	1.35	3.04	0.53	2Diagonal shear + 5 flexural
C40-1.5-2	26	112	143.6	1.28	2.12	0.27	2Diagonal shear + 3 flexural
C40-2-1	17	67	85,1	1.27	3.77	0,81	1Diagonal shear+1 flexural shear+ 5flexural
C40-2-2	23	85	100.5	1.18	2.65	0.63	2Diagonal shear + 4 flexural
C40-3-1	11	44	47.3	1.07	4.70	1.10	4 Flexural shear + 6 flexural
C40-3-2	14	55	55	1.00	3.29	0.37	3 Flexural shear + 5 flexural
C80-1-1	31	132	210.9	1.60	3.04	0.51	2Diagonal shear+ 6 flexural
C80-1-2	55	152	224	1.47	1.65	0.22	1Diagonal shear + 5 flexural
C80-1.5-1	27	95	144.3	1.52	3.1	0.45	2Diagonal shear + 7 flexural
C80-1.5-2	34	109	158.3	1.45	1.97	0.39	1Diagonal shear + 5 flexural
C80-2-1	20	64	95.5	1.49	3.82	1.53	1 Diagonal shear + 6 flexural
C80-2-2	27	83	113.6	1.37	2.71	0.74	2Diagonal shear+2flexural shear+ 4 flexural
C80-3-1	15	40	50.7	1.27	5.72	1.20	7 Flexural shear + 9 flexural
C80-3-2	18	48.5	59	1.22	3.19	0.84	5 Flexural shear + 7 flexural

* Load at first flexural crack, ** Mid-span deflection corresponding to the ultimate load, *** Diagonal crack width.

Crack Development and Failure Modes

Typical crack propagation for the beams tested under the various shear span/depth ratios (a/d) is shown in Figure 6. Due to zooming restrictions of the recording equipment, the shear-span was monitored only at one end of beam and the crack pattern assumed to be symmetrical for both shear-spans.

The flexural cracks were the first to develop at the central part of the beams. They widened on subsequent loading but were never harmful enough to precipitate failure and tended to close up with the development of inclined and diagonal cracking in the shear span zone. Their formation, however, did reduce the stiffness of the beams. Such a reduction is clearly expressed by the flattening of the load-deflection curves of the test specimens (Figures 5&9).

For HSC beams, the first crack occurred vertically at a load level of 15% - 30% of ultimate. By comparison, those of NSC developed similar cracks at load levels of 13% - 25% of ultimate. In effect, HSC has a higher modulus of rupture than NSC which results in the delayed flexural cracking observed in these tests. However, the beams made of HSC showed more flexural cracking than those made of NSC (see Table 4). This might be explained by the better quality of the bond between concrete and steel in the case of HSC, resulting in the steel reinforcement restraining the crack opening better [9].

With further increase in load, new flexural cracks formed in the shear spans curving toward the loading area. The development of diagonal shear cracking which illustrate an inclined strut action, depended strongly on the a/d ratio:
-For small values of a/d ($a/d \leq 2$), the cracks develop diagonally within the shear span extending from the loading point to the support, clearly indicating an inclined strut.

-For larger values of a/d, the diagonal cracking, which is shorter, is rather the development of a flexural crack that bends towards the loading point without a clear inclined strut.

The slopes of the diagonal cracks were considerably different for the four a/d ratios. For beams with a/d =1, the diagonal crack was often unique and inclined at more than 45° to the longitudinal axis of the beam, whereas for a/d =3, the diagonal crack was more horizontal (about 38°) as in Figures 6 and 7. The same crack pattern was observed for both types of concrete as in Figure 6. A great difference, however, is noticed in the trajectories of the cracks which are straighter in beams made of HSC material. The cracks go right througth the aggregate particles and do not deviate around them, a cracking trajectory which is completely different from that observed in NSC beams. The diagonal crack width varied from 0.27 mm to 1.10 mm for beams made of ordinary concrete. Those in beams made of HSC were wider, ranging from 0.22 mm to 1.5 mm. This is probably due to the greater brittleness of the material, liberating more energy when cracking. In general, crack openings, cut right through the aggregate particles as observed (Figure 1).

All the beams failed in shear. Beams with shorter shear spans ($a/d \leq 2$) failed in shear-compression as in Figures 6&7. In this type of failure, the diagonal crack, which appears independently within the shear-span and not as a result of prior flexural cracks, extends towards the compression zone at the support or to the loading point resulting in crushing of the concrete at those locations. The crushing of concrete in the compression zone at the loading point occurs often in an explosive manner in HSC as a result of a sudden release of accumulated energy [9].

On the other hand, for beams having an a/d ratio equal to 3, the inclined crack resulting in failure develops from a flexural one within the shear-span and extends towards the support point (Figures 6&7). At subsequent loading, the diagonal crack widens to split the beam into two parts [9]. This type of failure is referred to as diagonal tension. At the lower end of the diagonal crack, a horizontal crack may develop along the longitudinal reinforcement, destroying the bond between concrete and the reinforcing steel. This failure mode is less explosive. Beams with a/d = 3 display more cracks during the loading. These cracks release the stored enegy gradually so that, at the ultimate state, the final amount of energy liberated is not as great as the cases with $a/d \leq 2$, and is therefore a less explosive failure [9, 10].

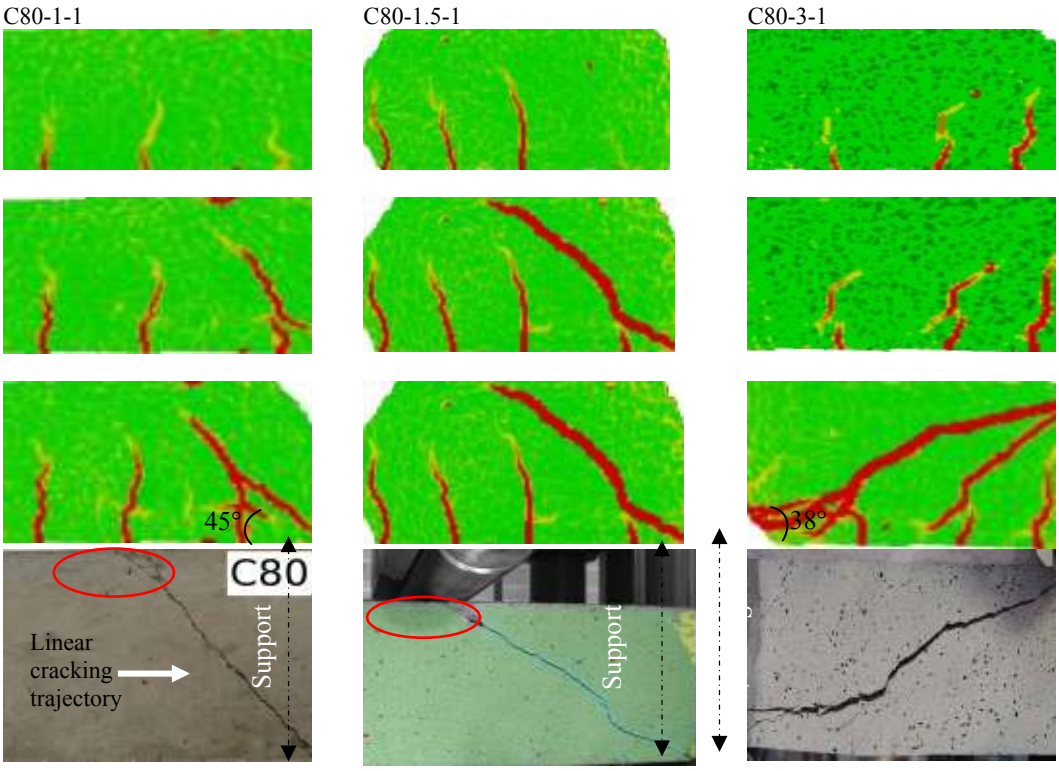

Figure 6 Typical crack development in HSC beams without stirrups

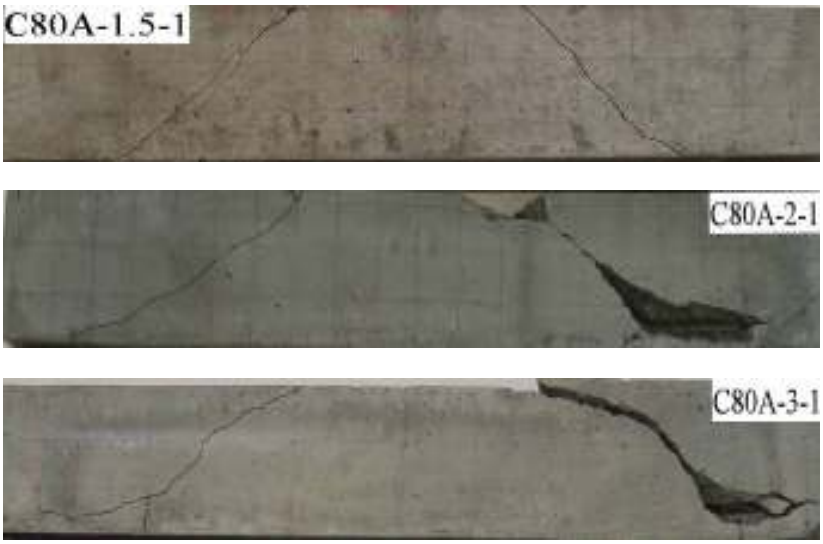

Figures 7 Typical Failure Modes of HSC beams without stirrups for a/d = 1.5; 2; 3

Effect of the Compressive Strength of Concrete

Figure 5 shows a typical load-defection response for the beams tested. When both a/d and ρ were constant as in (C80-1-1, C40-1-1) and in (C80-2-2, C40-2-2) the shear capacity increased by approximately 13% as the compressive strength increased from 44.2 MPa to

85.5 MPa (see Table 4). This could indeed be considered as only a small increase in relation to the almost doubling of the compressive strength of the concrete. Shear strength increases is, however, more related to the tensile strength improvement as clearly expressed in some codes such as the BAEL. Furthermore, previous work has shown that the tensile strength of concrete does not increase in proportion with the compressive strength [11, 12]. In this sense, the present test results show that, while the compressive strength almost doubled, the tensile strength increased by an average of only 30%. The second reason for the small increase in shear capacity is related to the aggregate interlock mechanism which is thought to be absent in HSC since the crack goes smoothly right through the aggregates particles and hence shear resistance contributed by aggregate interlocking is close to nil [9, 12]. The shear resistance in HSC is due mainly to the dowel action and to the compression zone; though the latter is not so deep in the case of higher compressive strengths. Indeed, the vertical flexural cracks were longer in beams made of HSC than in the case of NSC. This explains the relatively low increase of the shear capacity in high strength concrete even though the compressive strength of the material is increased considerably.

Effect of the Longitudinal Steel Ratio

An increase in the longitudinal steel ratio increases the ultimate shear capacity and reduces the deflection at mid-span as illustrated in Table 4 and Figure 5; an increase of 19 % was recorded between beam C80-2-1 and beam C80-2-2 as the steel percentage was increased from 1.16 to 2.31%. The increase is mainly due to the dowel action which improves with the amount of longitudinal steel crossing the cracks. The dowel contribution to the shear capacity is higher for high strength concrete beams since the bond between the dowel reinforcement and concrete is stronger [13, 14]. Moreover, the increase in the amount of longitudinal steel leads to an increase in the depth of the compression zone as shown in Figure 8 below leading to an improve in the shear strength, even though, not in proportion with the increase in the concrete strength.

The tests have also demonstrated that the beam specimens reinforced with ρ =2.31% exhibited less strains at ultimate in the longitudinal steel than those reinforced with ρ =1.16% (Figure 5). This is probably due to the fact that beams containing 1.16 % steel are more under-reinforced and hence exhibit more deformation than those with 2.31% steel; the balanced steel ratio for the present beams being 2.7%.

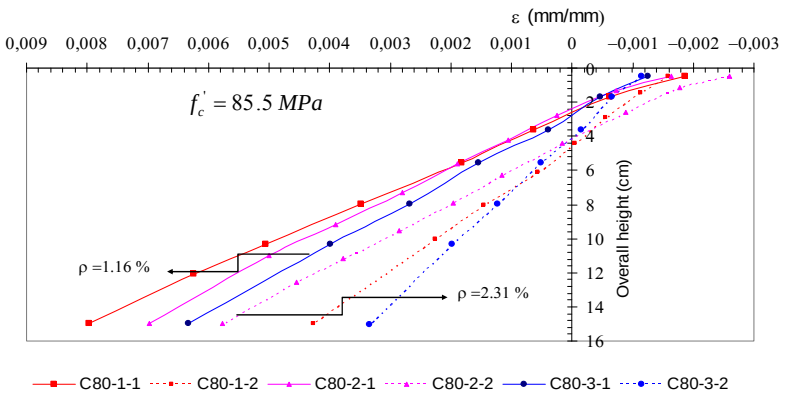

Figure 8 Evolution of the depth of the compression zone with the longitudinal steel ratio

Effect of the Shear-Span /Depth Ratio (a/d)

Figure 9 shows the mid-span deflections against the applied loads for HSC beams having a constant steel ratio of ρ = 1.16 % and varying a/d ratios. The load-deflection curves for beams with a/d = 1 are steeper than those with a/d of 1.5 and 2. The ultimate deflections of beams with a/d of 1.5 and 2 are greater than those when a/d = 1. Thus, the stiffness, as represented by the slope of the load-deflection curve, reduces as a/d increases. In the same manner, the ultimate load decreased as the a/d ratio increased. This is due to the strut and tie action (tied-arch action) effect which becomes greater as the a/d gets smaller. The ultimate loads for beams C80-1-1, C80-1.5-1, C80-2-1, and C80-3-1 were 210.9 kN, 144.3 kN, 95.5 kN, and 50.72 kN respectively; this trend being similar to that of NSC beams. The results for both types of concrete clearly reveal the decrease in the ultimate load as a/d increases.

Moreover, the mid-span deflection at ultimate load increased as the value of a/d increased, revealing the above pronounced flexural behaviour with greater a/d. For the smaller values of a/d, shear dominated the beam's behaviour and, hence, the deflection is smaller. Indeed, it is clearly known from the literature [15, 16] that for beams with a/d ≥ 2.5, flexure dominates the loading behaviour, resulting in a significant increase in deflection compared with beams having smaller values of a/d. It is to be noted that the maximum deflection for beams made of HSC (group C80) is 20% higher than for the corresponding beams made of NSC (group C40). This is thought to be mainly due to the better quality of the bonding between concrete and the reinforcing steel in the case of HSC, enabling a better transmission of internal stresses and strains from concrete to the reinforcing steel [9, 12].

The tests also demonstrated that the ratio P_u/P_{cr} (ultimate load / load causing diagonal cracking) decreased as a/d increased. This ratio, which represents the reserve of strength beyond diagonal cracking, was also seen to increase as the compressive strength increased from normal strength to high strength. In particular for a/d = 3, while no strength reserve was recorded for NSC beams, for HSC beams, the strength reserve was a little over 20% (table 4). This could be explained by the fact that the dowel effect is more important in HSC, helped by the better bond between the longitudinal steel and the surrounding concrete.

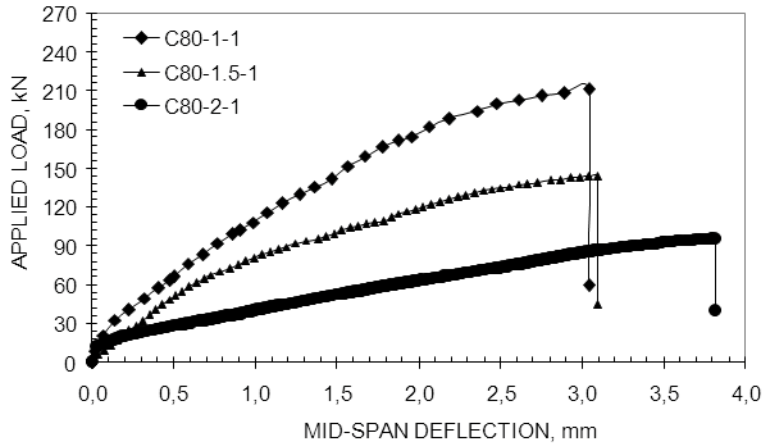

Figure 9 Load-deflection for HSC beams without stirrups tested under different a/d ratios

COMPARISON OF THE MEASURED SHEAR CAPACITY WITH THE PREDICTED ONE

Figure 10 shows the predicted shear capacity for beams without stirrups according to most of the main models in the literature such as ACI-318, BS-8110, BAEL, Eurocode-2. For comparison purposes, the measured shear capacities for the tested beams of this study are also shown. For ease of comparison, all the safety factors have been taken as equal to 1.0.

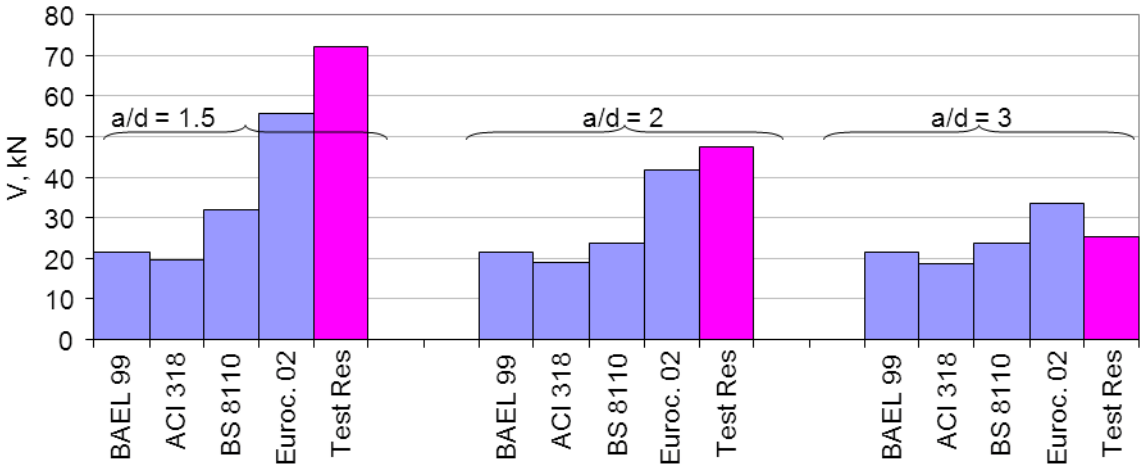

Figure 10 Shear capacity: Comparison of test results with the various predictions.

It can be seen from Figure 10 that for a/d=1.5, great differences exist between the different predictions and the experimental values. The values predicted by ACI-318, BAEL and, to a lesser extent, BS-8110, are excessively conservative. Those predicted by Eurocode-2 are better, though still relatively conservative. The difference between the experimental shear strengths and the predicted values reveals that most of the theoretical models, particularly ACI-318 and BAEL, do not take into account in a rational manner the increase in shear capacity of beams having shorter shear spans[9, 12]. Even the best predictions (those of Eurocode 2) do not adequately reflect the strut and tie action behaviour that is exhibited by beams with shorter shear-spans, a mechanism similar to that applying to deep beams. For HSC, Eurocode-2 seems to give better predictions, though this code may slightly overestimate the shear capacity of HSC beams having higher values a/d (3 and more) as illustrated in Figure 10.

In contrast, both the ACI-318 code and the BAEL code are excessively conservative. It is to be noted, however, that the results shows clearly that the four design models for shear capacity prediction are more conservative for NSC than they are for HSC, particularly in the case of Eurocode-2 [9, 12]. This latter design code should be considered with care, therefore, when used with high strength concrete, considering the catastrophic nature of shear failures in the case of HSC and the brittlness of this material.

For beams having a/d of 2 and more, the predictions improve for all the models, with the best correlation given by the Eurocode-2 procedure. In general, the prediction of the shear strength is better in the range of higher a/d values by comparison to that for smaller a/d values for the five models.

This is probably due to the influence of the strut-action behaviour which decreases in effect as a/d increases leading to a more pronounced beam-action behaviour. It is to be noted that the French code BAEL is the only one that does not explicitly take into account neither the main longitudinal steel ratio nor the a/d ratio. This explains why it is so conservative.

To sum up, it can be argued that the four shear design code provisions discussed in this paper seem to lead to a less safer design against shear forces for HSC than for NSC, though irrational for both type of concrete in the case of smaller a/d ratios. In effect, for beams with shorter shear-spans, the behaviour of the beam approaches that of a deep beam with more strength reserve beyond diagonal cracking. This strength reserve is related to the strut and tie action behaviour following the development of the diagonal crack. Such behaviour is clearly revealed by the crack patterns defining inclined compression struts within the shear spans and a tension tie region at the bottom where the cracks are uniformly distributed. In practical cases, this mechanism is present when the load is applied close to the support resulting in shorter shear-spans. None of the models being used take this mechanism into account explicitly.

CONCLUSIONS

The present study was aimed at evaluationg the contributions of a/d, ρ and $f_c^{'}$ on the global behaviour in shear for beams made HSC and compares this behaviour with that of NSC. Based on the experimental results obtained, the following conclusions are drawn.

1. Beams without stirrups, particularly those made of HSC, exhibit a brittle behaviour.

2. The shear strength is not greatly improved as the compressive strength of concrete is increased from normal strength to a higher stregth. A small increase is recorded for a concrete strength which had almost doubled.

3. An increase in the longitudinal steel ratio improves better the ultimate shear capacity and reduces the deflection at mid-span. A relatively higher increase in the shear capacity than that with the increase in the compression strength is recorded for a steel ratio which has doubled.

4. The ultimate load decreases as a/d increases. In the same manner, mid-span deflections at ultimate loads increase as the values of a/d increase, revealing the tendency for a pronounced flexural behaviour that is more associated with a beam-action as a/d increases. The tests also demonstrated that the ratio P_u/P_{cr} decreased as a/d increased. For a/d = 3, the ultimate load was effectively equal to the load at which diagonal cracking occured, without any strength reserve for beams made of NSC. For those made of HSC however, the ultimate load was greater than the diagonal cracking load. The effective dowel action of the longitudinal reinforcement in the case of HSC is thought to be making the positive difference.

5. The four major code provisions for shear in NSC are safe for use also in the case of HSC with the excepton that Eurocode-2 should be used with care as, in the case of HSC, it might have a tight safety margin against brittle shear failures.

6. The different models considered in this study do not accurately reflect the increase in the shear strength of beams with shorter shear spans (a/d = 1.5). For these types of beams, most of the design models are excessively conservative; the code predictions only seem to be more accurate as a/d increases beyond a value of 2.0. It seems that the guideline models for shear design given in the four codes considered above are better suited to NSC and HSC beams which exhibit a beam action behaviour.

REFERENCES

1. CARRASQUILLO, R. L., NILSON, A.H. AND SLATE, F.O. (1981). Properties of high strength concrete subject to short-term loads; ACI Journal, Proceedings, Vol. 78, No.3, 1981; pp. 171-178.

2. MARTINEZ, S., NILSON, A.H. AND SLATE, F.O. (1982). Short-Term Mechanical Properties of High Strength Light-Weight Concrete; Research Report N°.82-9, Departement of Structural Engineering, Cornell University, Itchaca, August 1982; 98 pp.

3. ELZANATY, A.H., NILSON, A.H. AND SLATE, F.O. (1986). Shear capacity of reinforced concrete beams using high-strength concrete; ACI Journal, Proceedings, Vol. 83, No. 2, 1986; pp 290-296.

4. COLLINS, M.P. AND KUCHMA, D. (1999). How safe are our large, slightly reinforced concrete beams, slabs, and footings ?; ACI Structural Journal, Vol. 96, No. 4, 1999; pp. 482-490.

5. TAYLOR, H.P.J. (1974). The fundamental behaviour of reinforced concrete beams in bending and shear; American Concrete Institute Special Publication, Vol. 42, SP42-03, 1974; pp. 43-78.

6. SARKAR, S., ADWAN, O. AND BOSE, B. (1999). Shear stress contributions and failure mechanisms of high strength reinforced concrete beams; Materials and Structures, Vol. 32, 1999; pp.112-116.

7. TAYLOR, H. P. J. (1970). Investigation of the forces carried across cracks reinforced concrete beams in shear by interlock of aggregate; Cement and Concrete Association, London, Technical Report, 42.447, 1970; 21 pp.

8. MPHONDE, A.G. (1988). Aggregate interlock in high strength reinforced concrete beams; Structural Engineering Group, Proceedingsof the Institution of Civil Engineers, Part 2, Vol. 85, No.3, 1988; pp.397-413.

9. HAMRAT, M., BOULEKBECHE, B., CHEMROUK, M. AND AMZIANE S. Shear behaviour of RC beams without stirrups made of normal strength and high strength concretes; Advances in Structural Engineering Journal, Vol. 13, No. 1, 2010; pp. 29-41.

10. BAZAN, Z. P. AND KAZEMI, M.T. (1991). Size effect on diagonal shear failure of beams without stirrups; ACI Structural Journal, Vol. 88, No. 3, 1991; pp. 268-276.

11. CHEMROUK, M. AND HAMRAT, M. (2002). High-strength concrete - Experimental Studies of the Material; Proceedings of the fifth international congress: Challenges of concrete construction; Edited by R.K. Dhir, P.C.Hewlett and L.J.Csetenyi, Titled: 'Innovation and Developments in Concrete Materials and Construction', Published by ThomasTelford Publishing, London, 2002; ISBN : 072773179 3, pp. 869-877.

12. HAMRAT, M. Comportement structural du béton à hautes performances (flexion et effort tranchant); Doctorate Thèse, University of Sciences and Technology Houari Boumediene, Algiers, 2010.

13. ABDELMADJID, H. AND MICHEL, L. Pull-out strength of bars embedded in high-strength concrete; Materials and Structures, Vol. 28, No.10, 1995; pp. 569-574.

14. MICHEL, L. (1996). Bonding and cracking of high-strength concrete; Journal of Laboratory of Bridges and Road, Special XIX, 1996; pp. 85-89.

15. PARK, R. AND PAULAY, T. Reinforced Concrete Structures, John Wiley and Sons, New York, 1975.

16. CHUNG, W. AND AHMAD, S.H. (1994). Model for shear critical high strength concrete beams; ACI Structural Journal, Vol. 91, No. 1, 1994; pp. 31-41.

The Optimum Conditions of Steam Heat Curing Cycles on Hydration of Fly Ash Cement for the Precast Industry

K Kagami, M Sato, Y Umemura
Nihon University, Japan

This paper reports the results of an investigation of effects steam heat-curing cycles on hydration of fly ash cement for the raising efficiency of precast concrete production. The steam heat-curing conditions for the investigation were varied by changing the preset curing time (time before steam curing), temperature rise rate, maximum temperature retention time, temperature drop rate. The Compression tests were conducted on mortars made using fly ash cement under steam heating-curing conditions. The hydrate composition was measured by thermogravimetric/differential thermal analyzer (TG-DTA), selective dissolution method and X-ray diffraction (XRD) Rietveld method to clarify the influence of steam heating-curing on fly ash cement hydration. The steam heat-curing of cement incorporating fly ash accelerates the pozzolanic reaction and results in considerable increase in the one-day compressive strength. The effect of temperature drop rate predominates over other factors of steam heat-curing condition. The optimum conditions of steam heat-curing cycles that shorten the length of the precast concrete manufacturing process within the investigated range appears to be a 4 hours consisting of a preset curing time 0.5 hour, temperature rise rate 30°C/h, maximum temperature and its retention time at 65°C for 2 hours, quick cooling.

Mr K Kagami is a second-year Doctoral Course student of Civil Engineering, Graduate School of College of Science and Technology, Nihon University, Japan.

Mr M Sato is a research assistant at the Department of Civil Engineering at College of Science and Technology, Nihon University, Japan. The main fields of research are the hydration reaction analysis of cement and admixture on ultra high strength concrete.

Professor Y Umemura is a Director of the Concrete Laboratory, the Department of Civil Engineering at College of Science and Technology, Nihon University, Japan. The main fields of research are the effect of organic and mineral admixtures on durability of concrete.

Keywords: Fly ash, Hydration, Precast concrete, Steam heat-curing, XRD/Rietveld

INTRODUCTION

In Japan, coal ash from coal fired power plants has reached an annual amount of 10 million tons and is still increasing every year [1]. The treatment of fly ash, accounting for a great percentage of coal ash, is posing a great problem that is difficult to solve. Despite the governmental effort to promote consumption, fly ash cement is not used effectively as a concrete admixture as in Europe. Nowadays, fly ash cement is also being used in precast concrete products (PCa products). In general, PCa products receive standard steam curing shown in Figure 1. To improve production efficiency and save energy, factories conduct daily two-cycle steam curing (accelerated steam curing) by shortening the total steam curing time as shown in Figure 1 [2]. The accelerated steam curing process is yet to be verified from the viewpoint of hydration. By this study, therefore, we clarified the influence of steam curing in the hydration of fly ash cement to extend the use of fly ash in PCa products. In particular, we verified that the accelerated steam curing of two cycles could ensure performance from the viewpoint of cement hydration. By cement hydration analysis, we investigated the influence of each steam curing process on the hydration of C_3S and C_2S, main components of cement, and the pozzolanic reaction of fly ash, and the amount of C-S-H generated.

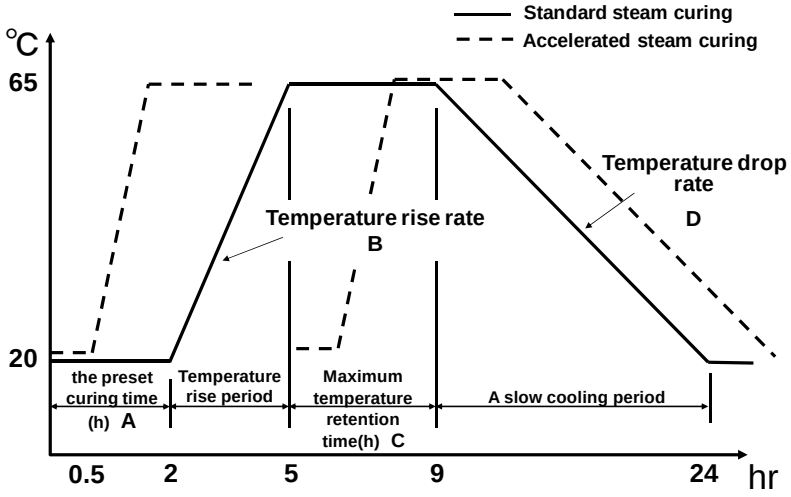

Figure 1 Steam curing program

EXPERIMENTAL DETAILS

Materials used and the mixture proportions of mortar. Table 1 show the materials used. The mixture proportions of mortar are shown in Table 2. The water-binder ratio (W/(C+FA)) was fixed at 50% and the amount of FA addition was set at 30 mass%.

Steam curing method

For the steam curing program in Figure 1, six patterns of preset curing time, temperature rise rate, maximum temperature retention time, and temperature drop rate were set as shown in Table 3 to compare and study compressive strength and hydration. For this study, the preset curing temperature was fixed at 20°C equal to room temperature, and the maximum temperature was fixed at 65°C. Then the preset curing time was set to 2 hours and 0.5 hour, the temperature rise rate to 15°C/h and 30°C/h, and the maximum temperature retention time

to 4 hours and 2 hours. The temperature drop rate was varied from 4.5°C/h for slow cooling to 45°C/h (based on actual measurement at the center of mortar) for quick cooling by exposing mortar of the maximum temperature to the room temperature environment (20°C). To verify daily two-cycle steam curing at factories, we also prepared the shortened program A05B30C2 from the total steam curing processes. Steam curing was followed by sealed curing in a thermostatic chamber of 20°C. To compare a case with no steam curing and one with steam curing, we conducted normal curing on cement sealed in a thermostatic chamber of 20°C immediately after mixing.

Table 1 Materials used

MATERIAL	SYMBOL	PROPERTY
Tap water	W	
Ordinary Portland cement	C	Specific gravity = 3.16 g/cm^3 Blaine fineness = 3260 cm^2/g
Fly ash	FA	Specific gravity = 2.21 g/cm^3 Blaine fineness = 4030 cm^2/g Ignition loss = 0.4 %
ISO standard sand	S	Standard surface-dry condition = 2.62 g/cm^3 Water absorption = 0.42 %

Table 2 Mix proportions of mortar

W/B %	S/B	UNIT WEIGHT, kg/m^3			
		W	B		S
			C	FA	
50	2.25	292	410	175	1316

Table 3 Steam curing programme

STEAM CURING PROGRAM	PRESET CURING TIME	TEMPERATURE RISE RATE	MAXIMUM TEMPERATURE RETENTION TIME	TEMPERATURE DROP RATE
	h	°C/h	h	°C/h
	A	B	C	D
A20B15C4D	2	15	4	4.5
A05B15C4D	0.5	15	4	4.5
A20B30C4D	2	30	4	4.5
A20B15C2D	2	15	2	4.5
A20B15C4	2	15	4	---
A05B30C2	0.5	30	2	---

Test method

The compressive strength test was performed according to JIS A 1108 "Method of test for compressive strength of concrete." For each steam curing pattern, mortar specimens of φ50×h100 mm were prepared using a can mold. After steam curing, the specimens were sealed in a thermostatic chamber with aluminium tape for sealed curing at 20°C until the compressive strength test age. The specimens were measured at the ages of 1, 3, 7, and 14 days.
For hydration analysis, hardened cement paste was cut with a diamond cutter into 2.5 mm cubes. The cubes were crushed and soaked in acetone for one day to stop hydration, and then stored in a drying furnace at 40°C for one day to evaporate the acetone and prepare the specimens. For the quantitative analysis of calcium hydroxide (CH), the specimens for hydration analysis were measured by thermogravimetric differential thermal analysis (TG-DTA) at the ages of 1, 3, 7, and 14 days.

The amount of un-reacted fly ash was measured by referring to a study by Aasaga et. al [3]. First of all, one gram of specimen for hydration analysis was put into 20 cc dilute hydrochloric acid (2mol/l) and agitated for 30 minutes for dissolution. Insoluble residue was dissolved by adding 30 cc of 5% sodium carbonate solution. The remaining solution was dried at 105°C and the amount of insoluble residue was measured. For this insoluble residue, the amount of bound water of hydrated product needs to be corrected by referring to a study by Kobayakawa et. al [4]. Therefore, the insoluble residue of the corrected amount of bound water is calculated by using Equation (2). For comparison, un-reacted materials of ordinary Portland cement partly replaced with fly ash at the weight ratio of 30% were dissolved and treated in the same way. From the difference between the insoluble residue of the corrected amount of bound water and the residue after treatment for comparison, the degree of FA hydration was calculated by using Equation (1).

$$B_d = (A_0 - A_d) / (A_0 / 100) \quad (1)$$

$$A_d = A_d' / (1 - IG_d / 100) \quad (2)$$

Where, B_d = The degree of FA hydration (%) of the specimen aged d days
A_0 = The insoluble residue (%) of mixed cement not hydrated
A_d = The insoluble residue (%) of the corrected amount of bound water
A_d' = The insoluble residue (%) of the specimen aged d days
IG_d = The ignition loss (%) of the specimen aged d days

Cement minerals and hydrate were quantified by XRD using the technique of Hoshino et al. For Rietveld analysis, TOPAS (Bruker AXS) was used. The cement ores and hydrates of alite (C_3S), belite (C_2S), interstitial materials (C_3A, C_4AF), gypsum dihydrate (Gyp), bassanite (Bas), calcium hydroxide (CH), ettringite (AFt) and mono-sulfate (AFm) and the internal standard substance of α-Al_2O_3 (10 mass%) were quantified simultaneously with each amorphous substance containing FA. To calculate the amount of C-S-H generated, the amorphous amount was calculated from the quantitative value of the internal standard α-Al_2O_3 as shown in Equation (1) and the un-reacted FA amount obtained by the selective dissolution method was subtracted. In this study, we assumed all hydrates generated to be C-S-H as Hoshino et al. did [5]. The amount was also replaced with the CH amount calculated by TG-DATA to determine phase composition by using the pore water (H) amount.

$$C\text{-}S\text{-}H = \left\{\frac{100}{A-R}\right\} \Big/ \left\{\frac{A\times(100-R)}{100}\right\} - S \quad (3)$$

Where,
C-S-H = Amount of C-S-H generated (mass%)
R = α-Al_2O_3 admixing ratio (mass%)
A = Quantitative value of α-Al_2O_3(mass%)
S = Un-reacted FA amount (mass%)

RESULTS AND DISCUSSION

Effects of Steam Curing on Compressive Strength

With A20B15C4D as the general steam curing program shown in Figure 1 for reference, Figure 2 compares the compressive strength in curing where the preset curing time, temperature rise rate, maximum temperature retention time, and temperature drop rate were varied and that in normal curing. In Figure 2-(A) where the preset curing time was shortened from 2 hours to 0.5 hour, the compressive strength at the initial age of 1 day became almost equal. At the age of 7 days and later, the compressive strength tended to become greater when the preset curing time was changed from 2 hours to 0.5 hour. The preset curing time from immediately after mixing until the temperature rise start time used to be set almost equal to the setting start time of the cement in use so that abnormal hardening would not occur. Accordingly, the preset curing time was set to 2 hours also in this study. Even when the preset curing time was shortened from 2 hours to 0.5 hour, however, the result of this test did not show any sign of hardening or effects on the compressive strength. In Figure 2-(B) where the temperature rise rate was changed from 15°C/h to 30°C/h, the compressive strength was almost equal between the ages of 1 day and 3 days. At the age of 7 days and later, however, the compressive strength was greater when the temperature rise rate was 30°C/h than when it was 15°C/h. In Figure 2-(C) where the maximum temperature retention time was changed from 4 hours to 2 hours, the compressive strength was almost equal from the age of 1 day until the age of 14 days. Even when the maximum temperature retention time was shortened from 4 hours to 2 hours, the compressive strength was not affected. In Figure 2-(D), compared with slow cooling at the temperature drop rate of 4.5°C/h, quick cooling from the maximum temperature to the room temperature (20°C) lowered the compressive strength by10% at the initial age of 1 day.

The compressive strength was about equal at the age of 3 days but greater at the age of 7 days and later. Since the temperature drop rate was changed from slow cooling to quick cooling, the compressive strength was lower at the age of 1 day. At the age of 3 days and later, however, the compressive strength was almost equal. Even when the temperature drop rate was changed from slow cooling to quick cooling, the compressive strength showed no effects at the reference shipping age of 14 days.

In Figure 2-(E), compared with the reference program A20B15C4D, the steam curing program A05B30C2 of totally shortened steam curing processes lowered the compressive strength by about 40% at the age of 1 day and about 20% at the age of 3 days but kept it almost equal at the age of 7 days and later.

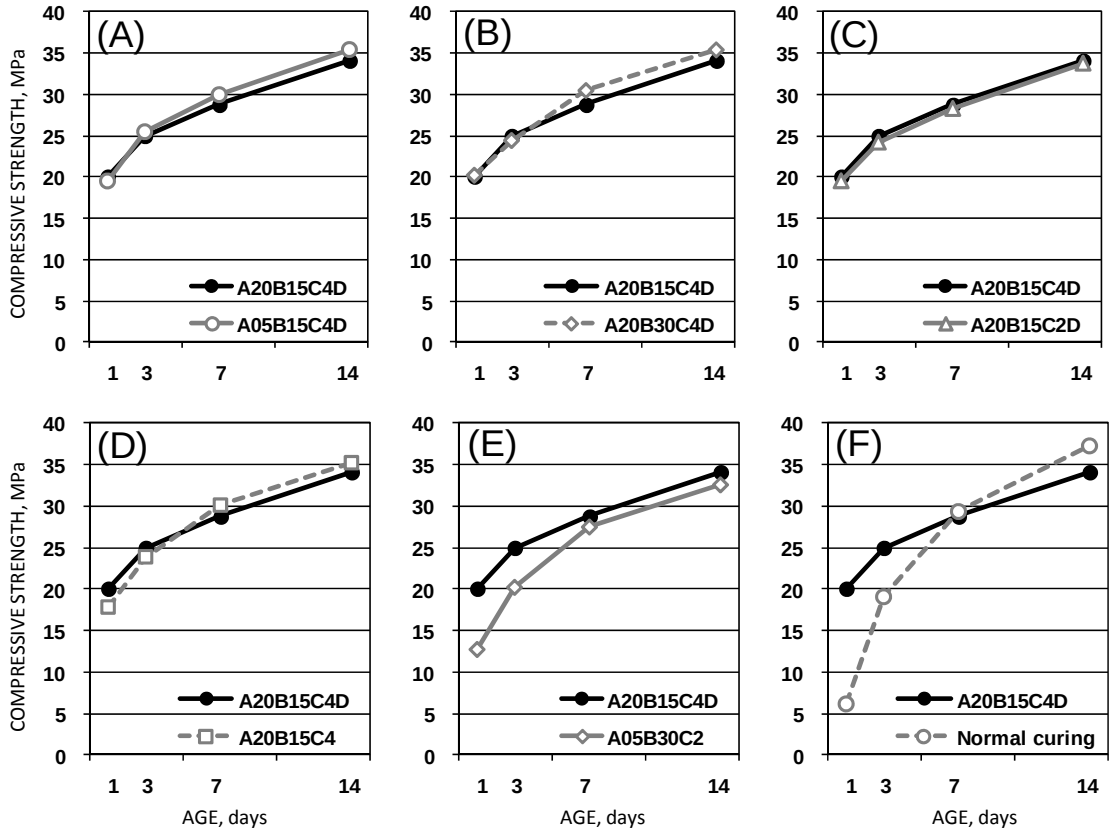

Figure 2 Effects of steam curing on compressive strength

In Figure 2-(F), normal curing without steam curing lowered the compressive strength by 70% or more at the age of 1 day, compared with the reference program A20B15C4D. Since the compressive strength increased remarkably, however, the decrease was about 20% at the age of 3 days, almost equal at the age of 7 days, and greater than the reference at the age of 14 days.

Compared with general daily one-cycle steam curing, daily two-cycle steam curing lowered the compressive strength at the age of 1 day for stripping necessary in terms of manufacturing efficiency. At the age of 14 days for shipping, however, the compressive strength became about equal to the reference. If the compressive strength at stripping is not affected, therefore, daily two-cycle steam curing will be possible.

Effects of Steam Curing on the Degree of C_3S Hydration

With A20B15C4D as the general steam curing program for reference, Figure 3 compares the degree of C_3S hydration in curing where the preset curing time, temperature rise rate, maximum temperature retention time, and temperature drop rate were varied and that in normal curing. In Figure 3-(A) where the preset curing time was shortened from 2 hours to 0.5 hour, the degree of C_3S hydration did not decrease. Even when the preset curing time was shortened, the degree of hydration was almost equal. In Figure 3-(B) where the temperature rise rate was changed from 15°C/h to 30°C/h, the degree of C_3S hydration at the age of 1 day was about equal to the reference. The degree of hydration tended to be higher at the ages of 3 days and 7 days and was almost equal at the age of 14 days. In Figure 3-(C) where the

maximum temperature retention time was changed from 4 hours to 2 hours, the degree of hydration became lower. At the age of 3 days an later, however, the degree of hydration was equal to or higher than that at 4 hours. In Figure 3-(D), compared with slow cooling at the temperature drop rate of 4.5°C/h, quick cooling from the maximum temperature to the room temperature (20°C) did not reduce the degree of C_3S hydration, but was about in degree to that of slow cooling. In Figure 3-(E), compared with the reference program A20B15C4D, the steam curing program A05B30C2 of totally shortened steam curing processes lowered the degree of C_3S hydration by about 15% at the age of 1 day and 5% or more at the age of 3 days. At the age of 7 days and later, the degree of C_3S hydration was about equal to that of the reference program. In Figure 3-(F), compared with the reference program A20B15C4D, normal curing lowered the degree of C_3S hydration to about 30% and 10% lower than the reference at the ages of 1 day and 3 days, respectively. At the age of 7 days and older, however, the degree of C_3S hydration was about equal to the reference.

The degree of C_3S hydration did not decrease even when preset curing time, temperature rise rate, maximum temperature retention time, and temperature drop rate were individually reduced. Compared with general steam curing, daily two-cycle steam curing of totally shortened steam curing processes lowered the degree of hydration greatly at the age of 1 day but showed about the same degree at the age of 7 days and later. Normal curing also showed similar tendency.

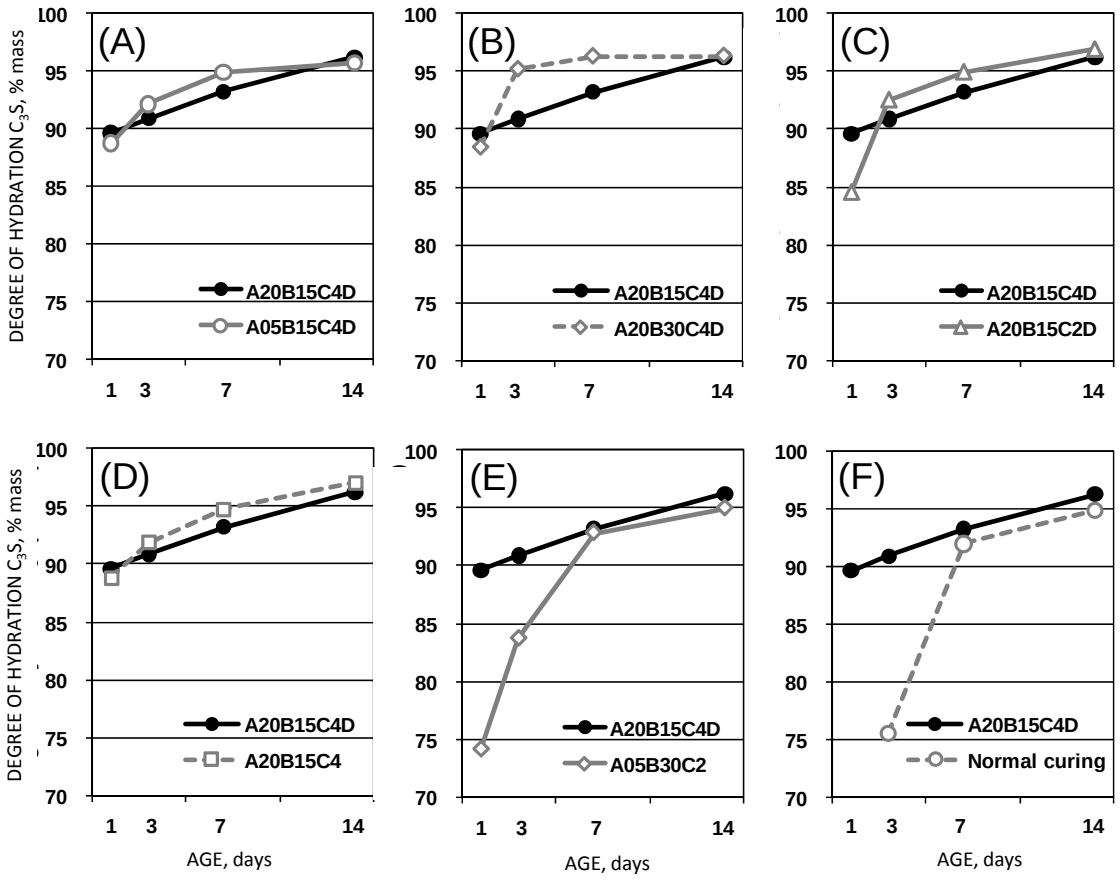

Figure 3 Effects of steam curing on of the degree of C_3S hydration

Effects of Steam Curing on the Degree of C_2S Hydration

With A20B15C4D as the general steam curing program for reference, Figure 4 compares the degree of C_2S hydration in curing where the preset curing time, temperature rise rate, maximum temperature retention time, and temperature drop rate were varied and that in normal curing. In Figure 4-(A), where the preset curing time was shortened from 2 hours to 0.5 hour, the degree of C_2S hydration became low at the initial age of 1 day but almost equal at the age of 3 days and later. In Figure 4-(B), where the temperature rise rate was changed from 15°C/h to 30°C/h, the degree of C_2S hydration was almost equal to that at 15°C/h at the ages of 1 day and 3 days but higher at the age of 7 days and later. In Figure 4-(C), where the maximum temperature retention time was changed from 4 hours to 2 hours, the degree of C_2S hydration was about equal to that by 4-hour retention at the ages of 1 day and 3 days but about 10% higher than the reference at the age of 7 days and about 5% higher also at the age of 14 days. In Figure 4-(D), compared with slow cooling at the temperature drop rate of 4.5°C/h, quick cooling from the maximum temperature to the room temperature (20°C) lowered the degree of C_2S hydration at the age of 1 day. However, hydration grew until about the age of 3 days and its degree was high at the ages of 7 days and 14 days. In Figure 4-(E), compared with the reference program A20B15C4D, the steam curing program A05B30C2 of totally shortened steam curing processes showed almost the same degree of C_2S hydration but the degree was higher by 10% or more at the age of 3 days and later. The degree of C_2S hydration was expected to be low due to short heating time but increased greatly. In Figure 4-(F), compared with the reference program A20B15C4D, normal curing showed a degree of C_2S hydration about equal at the ages of 3 days and 7 days and greater at the age of 7 days and later. Even when the preset curing time and temperature rise rate were individually reduced, the degree of C_2S hydration did not decrease. When the maximum temperature retention time and temperature drop rate were individually reduced, the degree increased at the age of 7 days and later. Not the general steam curing program A20B15C4D, but the daily two-cycle curing program A05B30C2 increased the degree of C_2S hydration greatly at the age of 3 days and later. Normal curing also showed a great increase at the age of 7 days and later.

Effects of Steam Curing on the Degree of Fly ash Hydration

With A20B15C4D as the general steam curing program for reference, Figure 5 compares the degree of FA hydration in curing where the preset curing time, temperature rise rate, maximum temperature retention time, and temperature drop rate were varied and that in normal curing. In Figure 5-(A) where the preset curing time was changed from 2 hours to 0.5 hour, the degree of FA hydration decreased, irrespective of age. Figure 5-(B) where the temperature rise rate was changed from 15°C/h to 30°C/h, the degree of FA hydration decreased at the age of 1 day but became equal at the age of 7 days and later. In Figure 5-(C) where the maximum temperature retention time was changed from 4 hours to 2 hours, the degree of FA hydration remained equal, irrespective of age. In Figure 5-(D), compared with slow cooling at the temperature drop rate of 4.5°C/h, quick cooling from the maximum temperature to the room temperature (20°C) lowered the degree of hydration at the age of 1 day and the degree also tended to decrease from the age of 3 days until the age of 14 days. In Figure 5-(E), compared with the reference program A20B15C4D, the steam curing program A05B30C2 of totally shortened steam curing processes showed a degree of FA hydration as low as about 10% at the age of 3 days. The degree of hydration increased then, but a degree of FA hydration as low as about 5% at the age of 14 days.

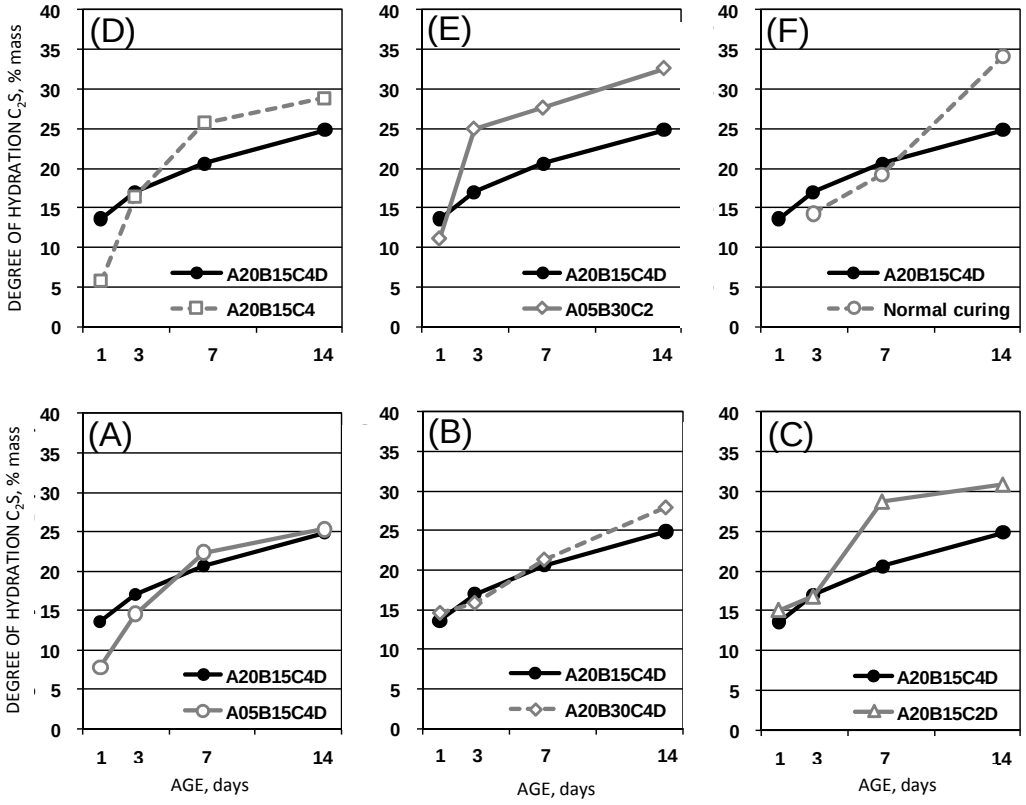

Figure 4 Effects of steam curing on of the degree of C_2S hydration

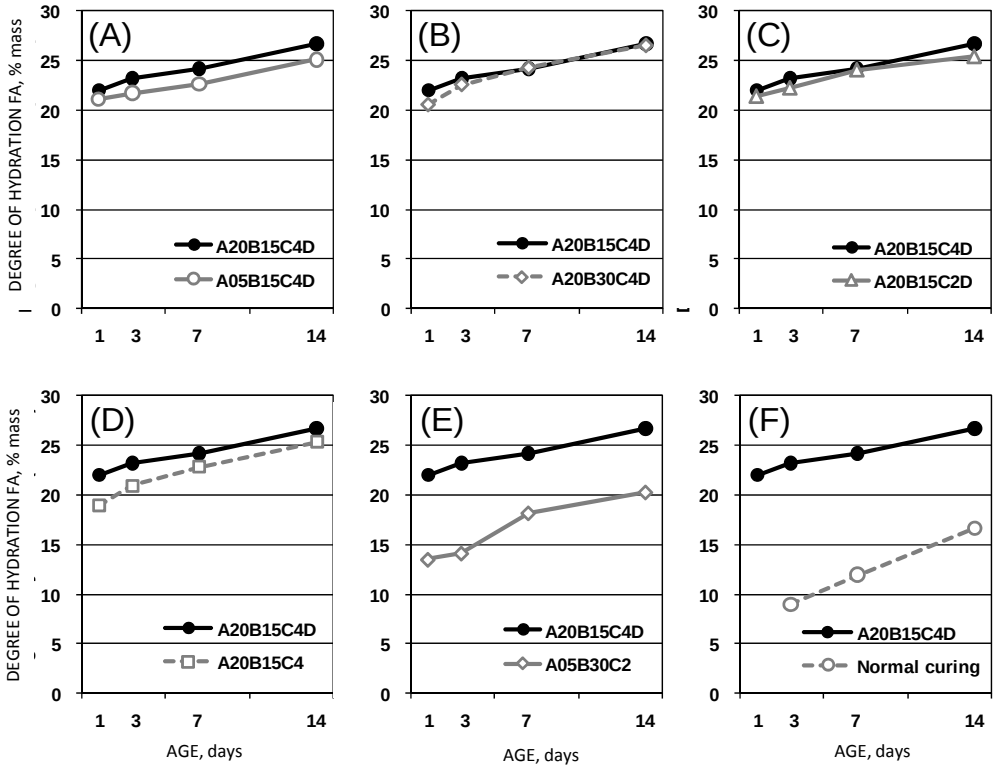

Figure 5 Effects of steam curing on of the degree of fly ash hydration

In Figure 5-(F), compared with the reference program A20B15C4D, normal curing showed a degree of FA hydration was not more than about 40% at the age of 3 days, 50% at the age of 7 days, and 60% at the age of 14 days. From the result, steam curing is expected to trigger pozzolanic reaction early.

Figure 6 shows the amounts of CH generated under different steam curing conditions that were measured by TG-DTA. Even when the preset curing time, temperature rise rate, and maximum temperature retention time were individually reduced, steam curing did not affect the amount of CH, compared with the reference program A20B15C4D. Quick cooling (A20B15C4) from maximum temperature to room temperature (20°C) generated more CH at the ages of 7 days and 14 days than slow cooling (A20B15C4D) at the temperature drop rate of 4.5°C/h. Compared with the reference program A20B15C4D, the steam curing program A05B30C2 of totally shortened steam curing processes showed the amount of CH as high as about 14% at the ages of 7 days and 14 days. Among the steam curing conditions, this pattern produced the greatest amount of CH. Compared with steam curing, normal curing generated less CH at the age of 1 day but more at the age of 3 days and later than the reference program A20B15C4D. Regarding the difference in the amount of CH, when the preset curing time, temperature rise rate, and maximum temperature retention time were individually reduced, the degree of FA hydration was equally high as 20% or more as the reference program A20B15C4D. Since the pozzolanic reaction was active and CH generated by C_3S and C_2S hydration was consumed, the amount of CH may not have increased despite aging. Compared with the reference program A20B15C4D, quick cooling at a high temperature drop rate and the steam curing program A05B30C2 of totally shortened steam curing processes showed a lower degree of FA hydration. Therefore, the pozzolanic reaction characteristic of FA was not active and the amount of CH generated by C_3S and C_2S hydration might have increased. Normal curing is also expected to show a similar tendency.

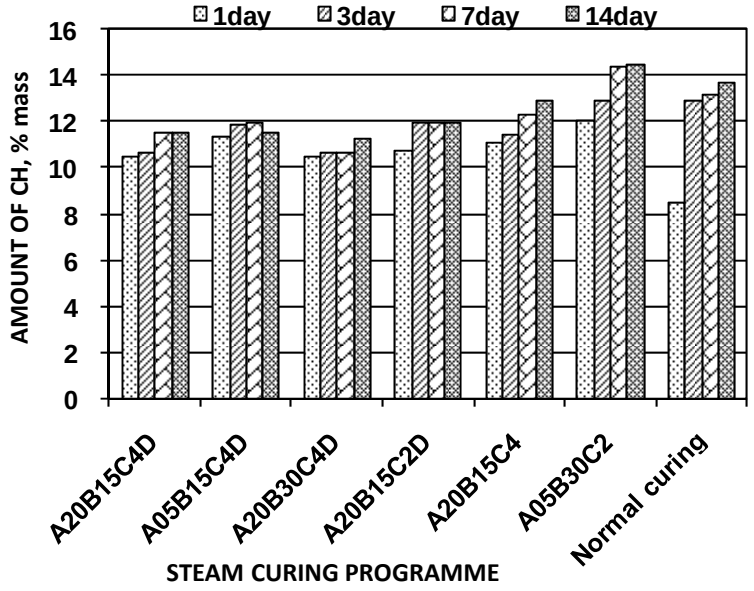

Figure 6 Effects of steam curing on amount of CH generated

Effects of Steam Curing on the Amount of C-S-H Generated

With A20B15C4D as the general steam curing program for reference, Figure 7 compares the amount if C-S-H generated in curing where the preset curing time, temperature rise rate, maximum temperature retention time, and temperature drop rate were varied and that in normal curing. In Figure 7-(A) where the preset curing time was changed from 2 hours to 0.5 hour, the amount of CH became small at the age of 1 day but about equal to the reference at the age of 3 days and later. In Figure 7-(B) where the temperature rise rate was changed from 15°C/h to 30°C/h, about the same amount of C-S-H was generated at the age of 1 day but a greater amount at the ages of 3 days and 7 days. At the age of 14 days, the same amount of C-S-H was generated. In Figure 7-(C) where the maximum temperature retention time was changed from 4 hours to 2 hours, the amount of C-S-H became smaller at the age of 1 day but about the same at the age of 3 days and later. In Figure 7-(D), compared with slow cooling at the temperature drop rate or 4.5°C/h, quick cooling from the maximum temperature to the room temperature (20°C) generated less C-S-H at the age of 1 day but about the same amount at the age of 3 days and later. In Figure 7-(E), compared with the reference program A20B15C4D, the steam curing program A05B30C2 of totally shortened steam curing processes generated much less C-S-H at the age of 1 day. Although the amount of C-S-H increased greatly at the age of 3 days and later, the amount of C-S-H generated was about 5% lower even at the age of 14 days. In Figure 7-(F), compared with the reference program A20B15C4D, normal curing lowered the amount of C-S-H by 10% or more at the age of 3 days. Because of a later increase, the amount of C-S-H generated was about 5% down at the age of 14 days.

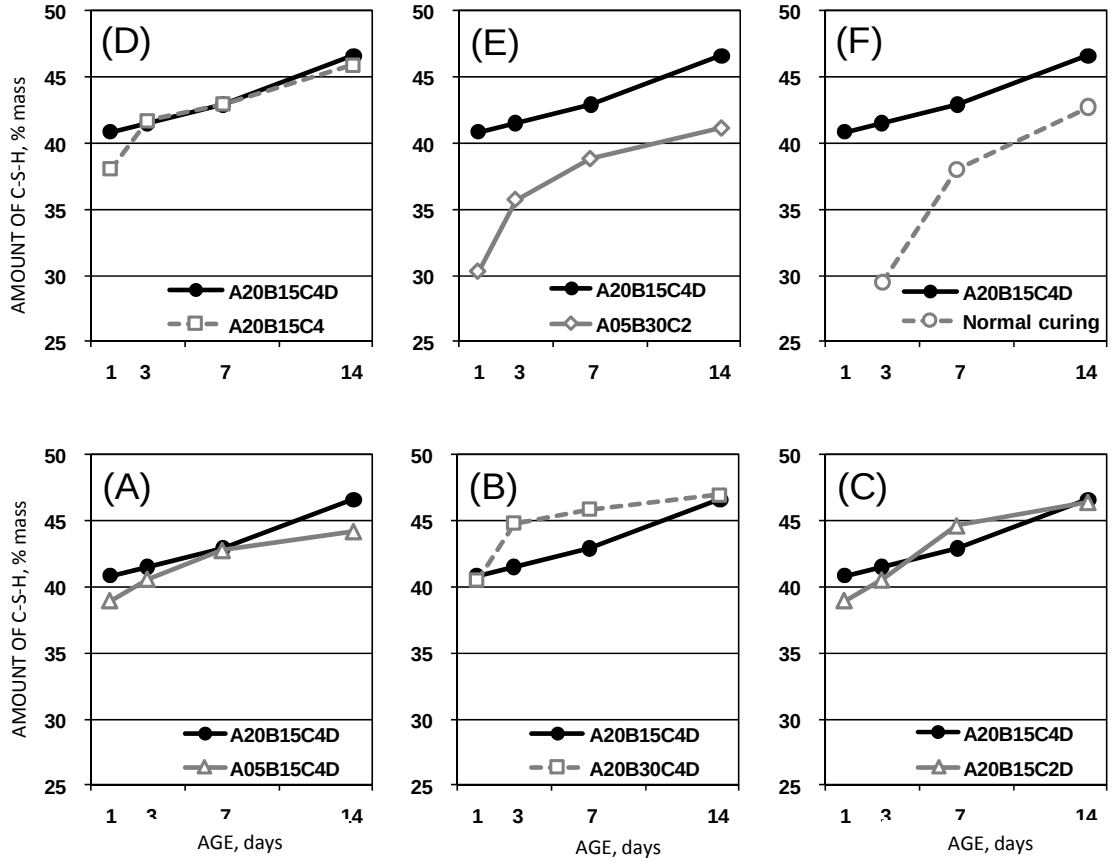

Figure 7 Effects of steam curing on amount of C-S-H generated

Judging from the results so far, the degrees of hydration of cement ingredients (C_3S, C_2S, and FA) may greatly affect the amount of C-S-H generated in the range up to the age of 14 days for PCa product shipping. Compared with the reference program A20B15C4D, the daily two-cycle steam curing program A05B30C2 generated less C-S-H at the ages of 7 days and 14 days, though the degree of C_3S hydration was equal. This may be attributable to the low degree of FA hydration.

CONCLUSIONS

The results of this experiment can be summarized as follows:

1. The compressive strength showed no decrease when the preset curing time, temperature rise rate, and maximum temperature retention time were individually reduced. Reducing the temperature drop rate made the compressive strength at stripping low at the age of 1 day. Daily two-cycle steam curing lowered the compressive strength at the ages of 1 day and 3 days but showed no influence at the age of 14 days for shipping.

2. The degree of C_3S hydration showed no decrease when the preset curing time, temperature rise rate, maximum temperature retention time, and temperature drop rate were individually reduced. Compared with steam curing, daily two-cycle steam curing of totally shortened steam curing processes made the degree of hydration very low at the ages of 1 day and 3 days but about equal at the age of 7 days and later.

3. The degree of C_2S hydration showed no decrease when the preset curing time and temperature rise rate were individually reduced. When the maximum temperature retention time and temperature drop rate were reduced, however, the degree increased greatly at the age of 7 days and later. Compared with general steam curing, daily two-cycle steam curing of totally shortened steam curing processes made the degree of C_2S hydration about equal at the age of 1 day but about 10% or more greater at the age of 3 days and later.

4. The degree of FA hydration showed no decrease when the preset curing time, temperature rise rate, maximum temperature retention time, and temperature drop rate were reduced individually. Compared with general steam curing, daily two-cycle steam curing of totally shortened steam curing processes greatly lowered the degree of hydration, irrespective of age.

5. The amount of C-S-H generated showed no decrease when the preset curing time, temperature rise rate, maximum temperature retention time, and temperature drop rate were individually reduced. The amount of C-S-H generated may greatly depend on the degrees of C_3S hydration and FA hydration.

REFERENCES

1. JAPAN COAL ENERGY CENTER. Status coal ash production (1994~2006) (in Japanese)

2. JAPAN CONCRETE INSTITUTE, Community Report of Design and Utilization of Precast Concrete Products, 2009, p 111 (in Japanese)

3. K, ASAGA. S, OHSAWA. G, UWANISHI. K, OHTA. M., DAIMON. Determination of Un-combined Quarts in Hydrothermal Reaction of Quartz and Portland Cement. Journal of the Ceramic Society of Japan, Vol.90, No.7, 1982, pp 397-400 (in Japanese)

4. M, KOBAYAKAWA. E, SAKAI. M, DAIMON. M, SATO. Influence of Pozzolanic Reaction of Fly Ash on Compressive Strength Development of Concrete. Journal of the Society of Inorganic Materials, Japan, 15(334), 2008, pp 137-145 (in Japanese)

5. S, HOSHINO. K, YAMADA. H, HIRAO. H, YAMASHITA. A Study on the Hydration Analysis by X-ray Diffraction/ Rietveld Method and the Mechanism of Strength Development of Cement Including Limestone Powder. Cement Science and Concrete Technology, No.60, 2006, pp 47-54. (in Japanese)

Effect of Water-Binder Ratio on Silicate Structures and Hydration of Silica Fume Cement

M Sato, Y Umemura, K Koizumi
Nihon University, Japan

The water-binder ratio of ultrahigh strength concrete is extremely low; therefore, the addition of low-heat Portland cement (LC), moderate-heat Portland cement (MC), and silica fume is indispensable in mixing. This research was conducted to elucidate the effects of the water-binder ratio (W/B) on the compressive strength and hydration properties concretes made with low-heat Portland cement and silica fume. The effects are discussed from the perspectives of cement hydration, investigated by powder X-ray diffraction using the Rietveld method; silica fume hydration, investigated by the selective dissolution method; and silicate-chain polymerization in calcium silicate hydrate (C-S-H), investigated by trimethylsilyl (TMS) derivatization method. When a water-binder ratio of 15% was used in the ultrahigh strength concrete, the reaction rate of SF and the amount of C-S-H generation were low, even though the compressive strength of this concrete was higher than that of concretes with water-binder ratios of 30% and 22%. The degree of polymerization of the silicate anion decreased with decreasing W/B. The addition of silica fume promoted polymerization.

M Sato is a research assistant at the Department of Civil Engineering at College of Science and Technology, Nihon University. The main fields of research are the hydration reaction analysis of cement and admixture on ultra high strength concrete.

Professor Y Umemura is a professor at the Department of Civil Engineering at College of Science and Technology, Nihon University. The main fields of research are the effect of organic and mineral admixtures on durability of concrete.

Dr K Koizumi is an assistant professor at the Department of Chemistry at College of Science and Technology, Nihon University. The main fields of research are the effect of silicate structures on hydration of cementitious materials, valuable reuse of industrial

wastes.

Keywords: C-S-H, Silica fume, Silicate anion, Ultra high strength concrete, Water-binder ratio

INTRODUCTION

Recently, construction using ultra-high strength concrete exceeding 120 N/mm^2 has been increasing. Important aspects of ultrahigh strength concrete are an extremely low water-binder ratio (W/B); the use of low-heat Portland cement (LC), which enables a lower water content; the addition of admixtures such as low-interstitial material cement (e.g., moderate-heat Portland cement (MC)); and the addition of silica fume (SF). Standards for concrete, however, have changed from a specification-based model to a performance-based model, and long-term performance assurance is now required for concrete structures. Accordingly, research on compressive strength, SF reaction rate and void structure [1] is being proactively conducted in relation to ultrahigh strength concrete with W/B = 20% or less, and much knowledge in this area has been accumulated. Although research results [2] on the reaction characteristics of SF and the reaction characteristics for the case that MC and SF are used together have been reported[3], information on the use of LC is limited. In addition, there are few reports where typical W/B levels for high-strength concrete and for ultrahigh strength concrete are simultaneously evaluated from the perspective of hydration. The strength development of SF concrete is evaluated by an activity index based on compressive strength in accordance with JIS A 6207; however, the experimental conditions are W/B = 50% without the use of a wetting agent, and thus the experimental conditions differ from the mixture conditions actually used. Accordingly, a method with W/B = 30% is now specified in JASS 5M-701:2005 “Quality standards for high-strength concrete cement” from the Architectural Institute of Japan as a new evaluation method. However, the activity index used as an evaluation standard until now is strongly focused on compressive strength, and evaluations from the perspective of hydration are not considered; hence, there is a low correlation between the strength development of ultrahigh strength concrete and this activity index.

The present research attempted to clarify the effects of W/B on the compressive strength development and hydration of LC and SF in cement where SF is mixed at 10 and 20 mass % into LC. In this research, mixtures with W/B = 30%, 22%, and 15% were used and the hydration properties were investigated from the perspectives of compressive strength; SF reaction rate, as measured by a selective dissolution method; cement reaction rate, as measured by powder X-ray diffraction (XRD) using the Rietveld method; C-S-H production; and degree of polymerization of C-S-H silica anion chains, as measured by trimethylsilyl (TMS) derivatization method.

EXPERIMENTAL SECTION

Materials used and mix proportions

The materials used were LC (ρ = 3.22 g/cm^3), SF (ρ = 2.20 g/cm^3), and ISO standard sand (S; ρ = 2.63 g/cm^3), with distilled water (W) used for mixing. A high-performance plasticizer for ultrahigh strength (an anion-base high molecular weight surface-active polymer (SP) with a polycarboxylic acid graft copolymer as the main component) was used as the superplasticizer, and a polyether-base foam inhibitor (DEF) was used as the antifoaming agent. Table 1 shows the physical properties and chemical compositions of the cement and silica fume, and Table 2 shows the mix proportions. The mix proportions were W/B = 30%, 22%, and 15%, and the SF amounts were 10 and 20 mass %. The paste mixture was made from a mortar mixture with the fine aggregate removed. Also, solid content was added as an outer rate for the SP. The mortar mixture was used for compressive strength testing and the paste mixture was used for analysis. A flow cone (JIS R 5201) was used, and the mortar flow rate was measured; SP was added to adjust the flow rate to 250 ± 20 mm. The air content was measured with a mortar air meter; the air content was adjusted to 3.0% or less by adding DEF. After adding water, mixing was performed for 5 min with a mortar mixer. After scraping the sides of the mixer and letting the mixture stand for 5 min, mixing was performed for 1 min. The mortar specimen was poured into a lightweight mould of φ50 mm × 100 mm. The upper surface of the mould was then covered with wrap and sealed with aluminium tape, and the specimen was seal-cured at 20 °C to a specified age. The paste specimen was poured into a 250 mL polyethylene bottle and set in a rotator for one day in order to prevent bleeding or separation. After removing the mould, the specimen at each age was cut with a diamond cutter and wrapped with aluminium tape. The paste sample used in the analysis was powdered to 0.15 mm or less with a hammer and planetary ball mill after removing the mould, stopping hydration with acetone, and drying at 40 °C. The powder was stored in a desiccator until measurement.

Table 1 Chemical composition of materials

MATERIALS	BRAIN SURFACE AREA, cm^2/g	BET SURFACE AREA, m^2/g	IG.LOSS %	CHEMICAL COMPOSITION, %							
				SiO_2	Al_2O_3	Fe_2O_3	CaO	MgO	SO_3	Na_2O	K_2O
LC	3470	-	1.04	21.80	4.49	2.90	63.90	1.84	2.26	0.20	0.38
SF	-	22	1.94	96.90	0.40	0.10	0.20	0.30	-	0.20	-

Table 2 Mix proportions

	W/B %	S/B %	QUANTITIY OF MATERIAL PER UNIT VOLUME kg/m 3				SP B mass%	DEF B mass%
			W	B		S		
				C	SF			
SF0-30	30	1.70	239	797	-	1354	0.65	0.03
SF10-30		1.74	234	701	78		1.20	0.03
SF20-30		1.78	229	610	152		1.70	0.03
SF0-22	22	1.00	236	1064	-	1064	1.05	0.07
SF10-22		1.03	230	932	104		1.30	0.05
SF20-22		1.05	223	808	202		1.80	0.06
SF10-15	15	0.40	240	1437	160	639	4.00	0.20
SF20-15		0.41	233	1240	310		4.00	0.25

Experimental method

Compressive strength measurement was based on JIS A 1108. The amount of calcium hydroxide (CH) and pore water (H) were measured by thermogravimetric differential thermal analysis (TG-DTA) using the paste specimen. The amount of CH and H were found from the endothermic peak and from the mass decrease near 400–450 °C, respectively. In XRD analysis, the measured value found by the Rietveld method is underestimated[3] due to amorphous material, and thus the CH amount from TG-DTA was used to determine the phase composition. This CH amount was also used in phase composition calculations for H. The amount of insoluble SF residue in SF10 and SF20 cement pastes was measured by selective dissolution[6] and the SF reaction rate was calculated from the amount of unreacted SF. The fixed quantities of cement minerals and hydrates were measured by XRD using a method developed by the authors[7]. Rietveld analysis was performed using TOPAS analysis software (Bruker AXS). α-Al_2O_3 (10 mass %) was taken as the fixed quantity with each of the cement minerals of alite (C_3S), belite (C_2S), pore substances (C_3A, C_4AF), gypsum dihydrate (Gyp), bassanite(Bas), calcium hydroxide (CH), ettringite (AFt), and the hydrate as internal standard materials, and the amorphous volumes including each mineral and the SF were measured simultaneously[8]. As shown in equation (1), the amount of C-S-H produced was found by determining the amount of amorphous material from the fixed quantity of the internal standard α-Al_2O_3 and subtracting the amount of unreacted SF measured by selective dissolution. In this research, C-S-H is assumed to be the only hydrate produced, in the same way as in previous research by the authors[7]. The determined C-S-H amount then replaced the CH amount measured by TG-DTA, and the phase composition was found from the H amount.

$$C-S-H=\left\{\frac{100}{A-R}\right\}\Big/\left\{\frac{A\times(100-R)}{100}\right\}-S \qquad (1)$$

Here, C-S-H is the amount of C-S-H produced (mass %), R is the α-Al_2O_3 mix ratio (mass %), A is the fixed α-Al_2O_3 amount (mass %), and S is the unreacted SF amount (mass %)

The silicate ion SiO_4^{4-} is a monomer with four O atoms arranged around a Si atom. When two of the monomers are linked, they share one O atom and form $Si_2O_7^{6-}$, a dimer. The silicate ions are present as monomers within the cement minerals C_3S and C_2S, but through a process of hydration and C-S-H formation, the silicate ions polymerize into a chain[9]. To ascertain the trend in the increasing silicate anion length (degree of polymerization) of the C-S-H with the progression of hydration, the silicate anion length distribution was measured by the TMS derivatization method. For this measurement, TMS derivation was performed on the paste specimen, the acquired TMS derivatives were analyzed by gas chromatography, and the component ratio of the silicate ions (the silicate anion length distribution) was measured from monomer to hexamer. The silicate anion length distribution can be found from the peak area from monomer to hexamer by gas chromatography and expressed as a molar fraction. In addition, although the silicate anion can be considered to correspond to the breakdown of silicate phase C_3S and C_2S and the silicate composition of the C-S-H, the mass ratio of the phase composition and the molar fraction of the silicate anion distribution cannot be simply compared. Furthermore, it is not possible to differentiate between the (unreacted) C_3S and C_2S derived silicate anions and the hydration of the cement minerals or the C-S-H derived silicate anion that has been formed by the pozzolanic reaction of SF.

Accordingly, Figure 1 shows an example of silicate anion length distribution measurement for SF10–30 measured by the TMS derivatization method. Based on previous research by the authors[7], the C_3S, C_2S, and C-S-H silicate amounts found by the Rietveld method are assumed to be almost proportional to the chain length (Si number), and the volume ratio was calculated by multiplying the chain length number (m = 1–6) by the molar fraction of silicate anion found by TMS derivatization, as shown in equation (2). As for the total C-S-H volume (Vn), the phase composition amounts of C_3S, C_2S, and C-S-H found by the Rietveld method were then calculated using the molecular weight, ignition weight, and density of an anhydrous base. In this way, the effect of the bound water in the sample after hydration is removed by using an anhydrous base in comparison with anhydrous cement.

$$F_{mn} = m \times M_{mn} \times V_n \qquad (2)$$

Here, F_{mn} (vol %) is the m-mer (m = 1–6) component ratio at material age n days, M_{mn} (mol %) is the m-mer (m = 1–6) molar fraction at material age n-days, and V_n (vol %) is the total silicate volume at material age n days.

The component ratio is small for silicate anions with length of 3 or more, and appropriately evaluating the progression of polymerization is difficult. Accordingly, the component ratio for the average degree of polymerization was found using equation (3) from the conventionally determined component ratio of dimer through to hexamer, and furthermore, the average degree of polymerization change ratio (R_n) of the average degree of polymerization component ratio (DP_n) at each material age in relation to the component ratio for the average degree of polymerization of the anhydrous cement prior to mixing (DP_0) was found from equation (4) and taken as the index of polymerization progression.

$$DP_n = \sum_{m=2}^{6} F_{mn} \tag{3}$$

Here, DP_n is the component ratio for the average degree of polymerization for dimers through to hexamers at material age n days.

$$R_n = DP_n / DP_0 \tag{4}$$

Here, R_n is the average degree of polymerization change ratio at material age n days. DP_0 is the component ratio for the average degree of polymerization for dimers through hexamers at material age 0 days, and DP_n is the component ratio for the average degree of polymerization for dimers to hexamers at material age n days. Measurements for each experiment were performed at material ages of 7, 28, and 91 days.

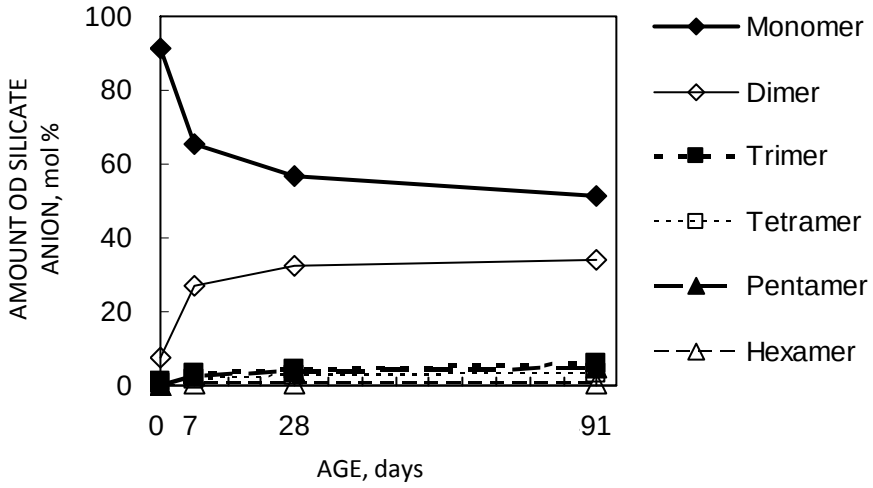

Figure 1 Measured amount of silicate anion in cement paste (SF10–30) by TMS derivatization

Table 3 Molecular weight and density of cement minerals and hydrates

CEMENT MINERALS AND HYDRATES	MOLECULAR WEIGHT, g/mol	IGNITION WEIGHT, g/mol	DENSITY (ANHYDRATE BASE) g/cm^3
C_3S	228.32	-	3.15 [10]
C_2S	172.24	-	3.26 [10]
C_3A	270.20	-	3.04 [10]
C_4AF	430.12	-	3.77 [10]
Gyp*	172.17	136.14	2.96 [11]
Bas*	145.15		
AFt*	1255.11	678.61	2.98 *
CH	74.09	56.08	3.35 [11]
C-S-H*	360.46	288.40	2.98 [12]
SF	-	-	2.20

*Gyp and Bas as anhydrite, AFt as C_3A and sum total of anhydrite, C-S-H as $C_3S_2H_4$, and Molecular weight, ignition weight and density assumed with anhydrite as C_3S_2 (rankinite)

TEST RESULTS AND DISCUSSION

Compressive Strength

Figure 2 shows the compressive strength test results. Concerning the effect of W/B on compressive strength, the strength difference for SF0 at W/B = 22% did not change in comparison to W/B = 30% from day 7 to day 91. For SF10 and SF20, the difference in strength as compared with W/B = 30% increased in along with advancement of material age from day 7 to day 91 for W/B = 22% and 15%. The strength increase for W/B = 15% was particularly striking for SF20. As shown in Figure 2, the effect of the SF addition amount was higher for all material ages in comparison with SF0 for W/B = 30%. For W/B = 22%, the effect of the SF addition amount was lower at material age 7 days, was almost equal at material age 28 days, and exceeded that of SF0 at material age 91 days. For W/B = 15%, both mixtures had the same difference in strength at material ages 7 and 28 days. At material age 91 days, the compressive strength of SF20 exceeded that of SF10. No significant difference due to SF addition was found in compressive strength between mixtures W/B = 30% and 22%.

Cement Hydration

Change in SF reaction rate with hydration

Figure 3 shows the SF reaction rate found by the selective dissolution method. The SF reaction rate displayed almost the same trend for W/B = 30% and 22%, increasing greatly at

material age 7 days and increasing slowly thereafter. For W/B = 15%, the SF reaction rate was 5–15 mass % at material age 7 days, and reached only approximately 25 mass % for SF10 and 20 mass % for SF20 at material age 91 days. The effect of W/B on SF reaction rate was the same for W/B = 30% and 22%, and the reaction rate was lower for W/B = 15%. As for the effect of the SF addition amount, reaction rate increased with increasing SF addition amount for W/B = 30% and 22%, and the reaction rate of SF20 exceeded that of SF10 with a maximum of approximately 30 mass % at material age 7 days and approximately 15 mass % at material age 91 days. Both mixtures exhibited the same trend for W/B = 15%. From the experimental results, the SF was found to react actively at W/B =30% and 22%, but much unreacted SF remained even at late material ages for W/B = 15%.

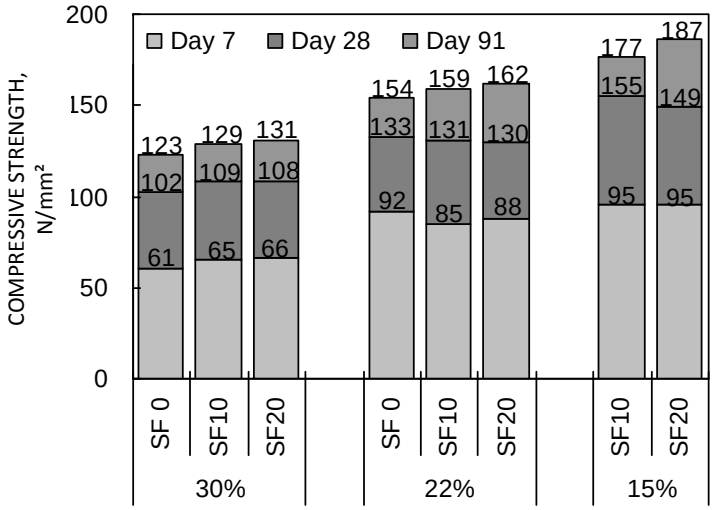

Figure 2 Compressive strength of mortar

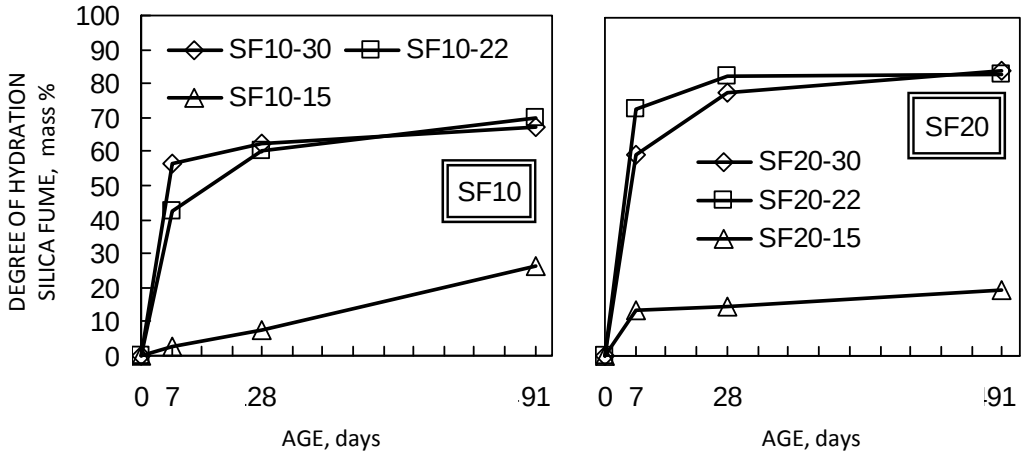

Figure 3 Measured hydration degree of silica fume in cement paste by selective dissolution method

Reaction of cement mineral with hydration

Figure 4 shows the phase constitution of each mixture acquired by XRD using the Rietveld method, Figure 5 shows the reaction rate of C_3S found from the phase composition, and Figure 6 shows the reaction rate of C_2S. The C_3S reaction rate at material age 7 days was approximately 90 mass % at W/B = 30% and 22% for SF0; approximately 80 mass % at W/B = 30%; approximately 75 mass % at W/B = 22%; and approximately 60 mass % at W/B = 15% for SF10. Fluctuations in reaction rate were small after 7 days, and the reaction rate became slow. Meanwhile, the reaction rate was approximately 80 mass % at W/B = 30% and 22% for SF20, and approximately 60 mass % at W/B = 15% for SF10. The effects of W/B were considered to have the same trend at W/B = 30% and 22%, and the hydration reaction readily occurred. The necessary water quantity for hydration was considered to be lacking at W/B = 15% and the reaction became slow. The effect of SF addition amount exhibited the same trend for W/B = 30% and 22%. Meanwhile, the reaction rate was almost identical for SF10 and SF20 at W/B = 15%. The reaction rate of C_2S was approximately 45 mass % up to a material age of 91 days for SF0, but was approximately 30–40 mass % for SF10 and SF20 at each W/B when SF was added. The effect of W/B is somewhat less when W/B is low, but this effect is considered to be small within the scope of these research results. Meanwhile, SF10 and SF20 had the same trend in the effect of SF addition, with the reaction rate of C_2S being approximately 10 mass % lower in comparison with SF0.

C-S-H production with hydration

Figure 7 shows the time course of C-S-H production. The effect of W/B exhibits the same tendency for SF0, SF10, and SF20, with C-S-H production reaching 50 mass % by a material age of 7 days at W/B = 30% and slowing thereafter. The result for W/B = 22% was somewhat lower in comparison with W/B = 30%, being approximately 45 mass % from material age 7 days to 91 days. Meanwhile, the C-S-H production for W/B = 15% became approximately 35 mass % by material age 7 days, and then slowed thereafter. This result is attributed to the water content having a large effect on the formation of C-S-H, and formation is considered to be delayed or the unchanged for W/B = 22% and 15% in comparison with W/B = 30% because the water content is less than the theoretical hydration water volume[13]. The effect of the SF addition amount had the same tendency irrespective of increases in the addition amount. Taking into account the reaction rate of SF and cement, the effect of SF and C_3S was considered to be large and the effect of C_2S was considered to be small for C-S-H production. However, in regard to the effect of C_2S, it is considered necessary to take into account data at material age beyond 91 days.

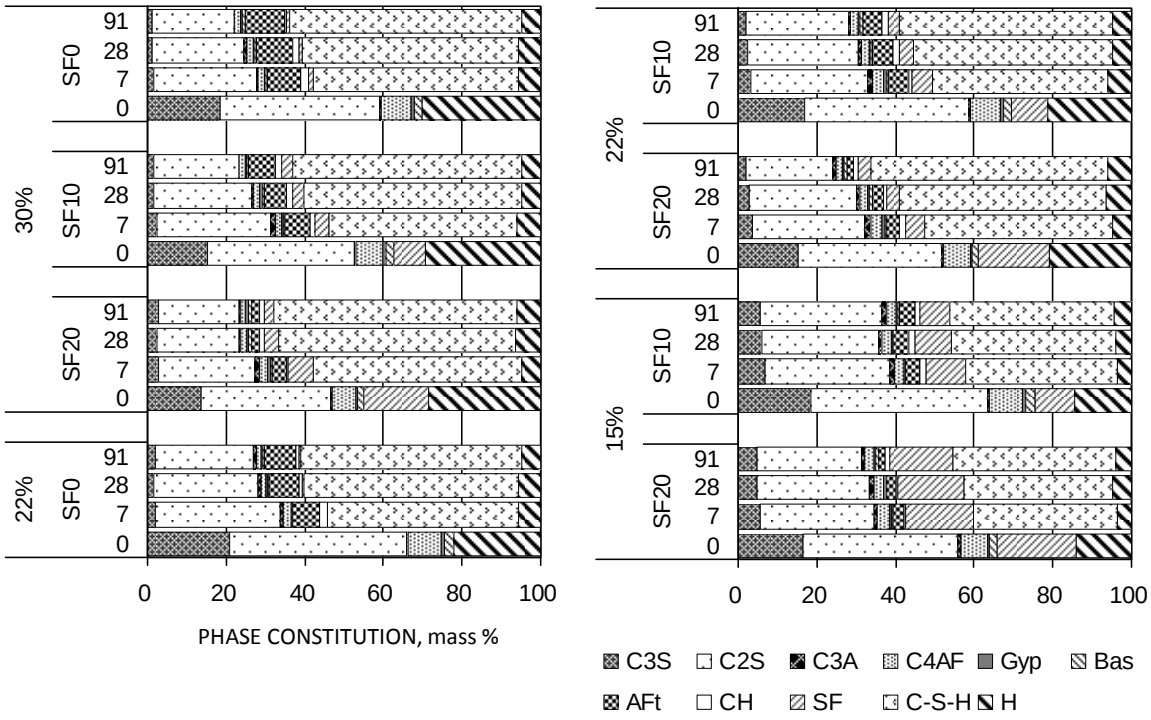

Figure 4 Phase composition of cement paste

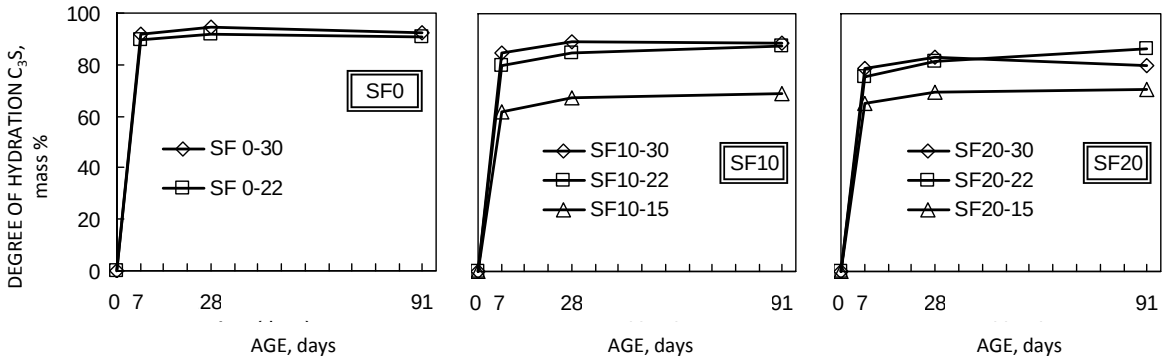

Figure 5 Measured hydration degree of C_3S by Rietveld method

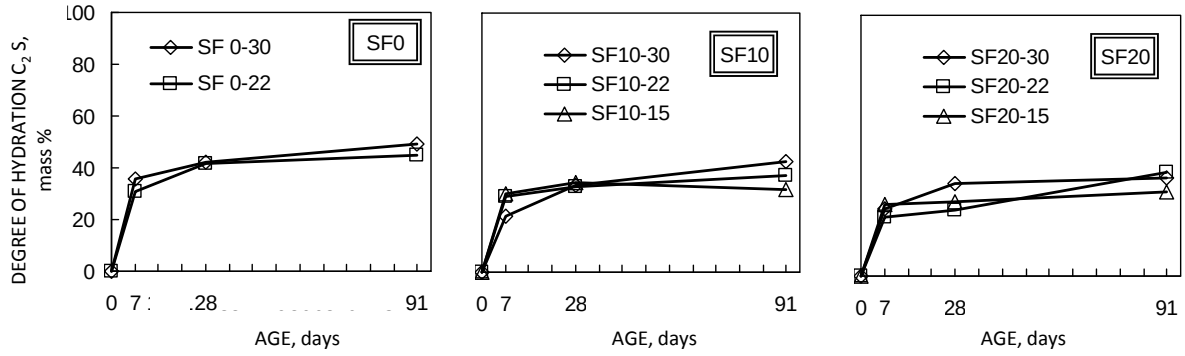

Figure 6 Measured hydration degree of C_2S by Rietveld method

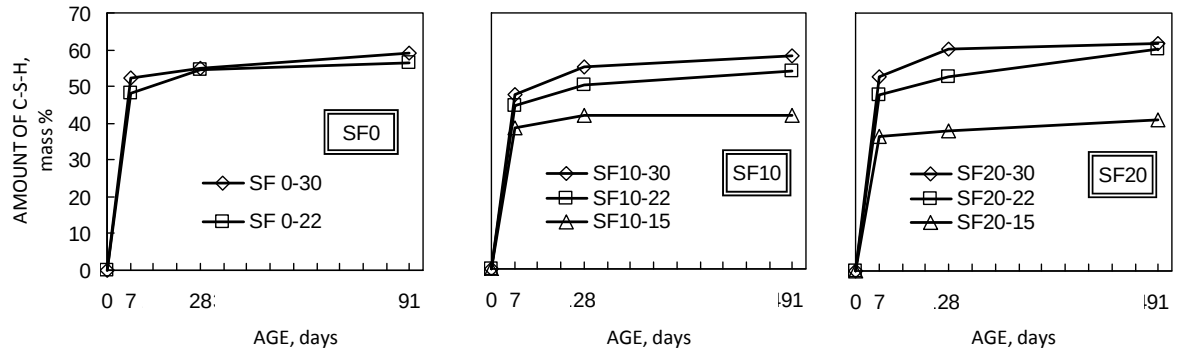

Figure 7 Measured C-S-H productions by Rietveld method

C-S-H silicate anion length analysis

Table 4 shows the analysis results for silicate anion length measured by the TMS derivatization method. Figure 8 shows a plot of the results in Table 4 and the results of having converted the mass ratios of C_3S, C_2S, and C-S-H silicate composition to a volume ratio by means of equation (2). Concerning the mixtures with added SF, the trend for the silicate phase could be understood well since the cement quantity when anhydrous is small, and the silicate phase provided and increased by the SF as C-S-H after adding water.

Figure 9 shows the average degree of polymerization change ratio for each mixture from dimer to hexamer found from equation (4). In previous research by the authors[7], the average degree of polymerization change ratio for SF10 and SF20 for a W/B = 22% mixture was found to be higher than that for SF0, and the polymerization of silicate anion was found to be promoted by SF addition. The present experiment showed the same results for W/B = 30% and 22%. The average degree of polymerization was higher for W/B = 30% compared with W/B = 22%, and silicate anion polymerization was more advanced. Furthermore, the average degree of polymerization for W/B = 15% was less than that for W/B = 22%. Concerning the effect of W/B, silicate anion polymerization decreased as W/B was lowered. As for the effect of SF addition, the average degree of polymerization was higher for W/B = 30% and 22%, as also found in past research[7], but a difference due to addition amount was not seen for W/B = 15%. Figure 10 shows the relation between C-S-H production analyzed by the Rietveld method and rate of average degree of polymerization change ratio. For W/B = 30% and 22% mixtures with added SF, C-S-H production increased in direct proportion to Rn, as also found in previous research[7]. Although polymerization advanced in the W/B = 15% mixture without added SF, formation of C-S-H was slow.

Accordingly, the results suggest that C-S-H was actively produced and silicate anion polymerized in mixtures with added SF at W/B = 30% and 22%, and C-S-H production was scarce with polymerization alone progressing at W/B = 15%.

Figure 11 shows the relationship between compressive strength and the average degree of polymerization change ratio. Arranging by W/B and the presence or absence of SF reveals a directly proportional correlation in the figure, but the approximate formula differs according to SF addition amount. Moreover, the amount of air pores has a stronger effect on compressive strength than does hydrate formation and silicate structure.

Table 4 Amount of silicate anion measured by TMS method

	AGE	AMOUNT OF SILICATE ANION, mol %					
	days	Monomer	Dimer	Trimer	Tetramer	Pentamer	Hexamer
SF0-30	0	89.54	8.47	1.36	0.44	0.15	0.04
	7	65.79	26.17	3.93	1.84	1.98	0.29
	28	55.92	34.45	3.53	2.16	3.58	0.36
	91	49.08	38.68	4.41	2.79	4.57	0.47
SF10-30	0	91.09	7.34	1.11	0.33	0.11	0.03
	7	65.23	26.97	3.26	1.73	2.52	0.29
	28	56.93	32.20	4.24	2.49	3.66	0.48
	91	51.10	34.05	5.80	3.37	4.92	0.76
SF20-30	0	90.80	7.87	0.98	0.27	0.07	0.02
	7	65.10	26.92	3.67	1.83	2.19	0.29
	28	57.20	30.41	5.35	3.08	3.33	0.63
	91	56.93	29.92	4.98	3.09	4.12	0.97
SF0-22	0	89.54	8.47	1.36	0.44	0.15	0.04
	7	75.22	19.56	2.50	1.14	1.41	0.18
	28	59.41	32.12	3.35	1.82	2.96	0.34
	91	53.36	35.36	4.99	2.49	3.37	0.44
SF10-22	0	91.09	7.34	1.11	0.33	0.11	0.03
	7	70.44	22.29	3.37	1.66	1.92	0.32
	28	63.58	28.99	2.74	1.53	2.86	0.30
	91	55.15	31.73	5.40	2.97	3.88	0.87
SF20-22	0	90.80	7.87	0.98	0.27	0.07	0.02
	7	71.49	20.66	3.36	1.86	2.22	0.41
	28	66.71	23.45	3.67	2.34	3.17	0.66
	91	57.60	27.99	5.91	3.67	3.56	1.27
SF10-15	0	91.09	7.34	1.11	0.33	0.11	0.03
	7	74.70	19.94	3.15	1.10	0.98	0.13
	28	77.24	17.82	2.87	1.09	0.84	0.14
	91	59.66	28.74	5.90	2.59	2.44	0.67
SF20-15	0	90.80	7.87	0.98	0.27	0.07	0.02
	7	72.81	20.72	3.44	1.43	1.38	0.23
	28	77.45	17.05	3.02	1.26	0.98	0.22
	91	61.54	27.02	5.57	2.64	2.39	0.83

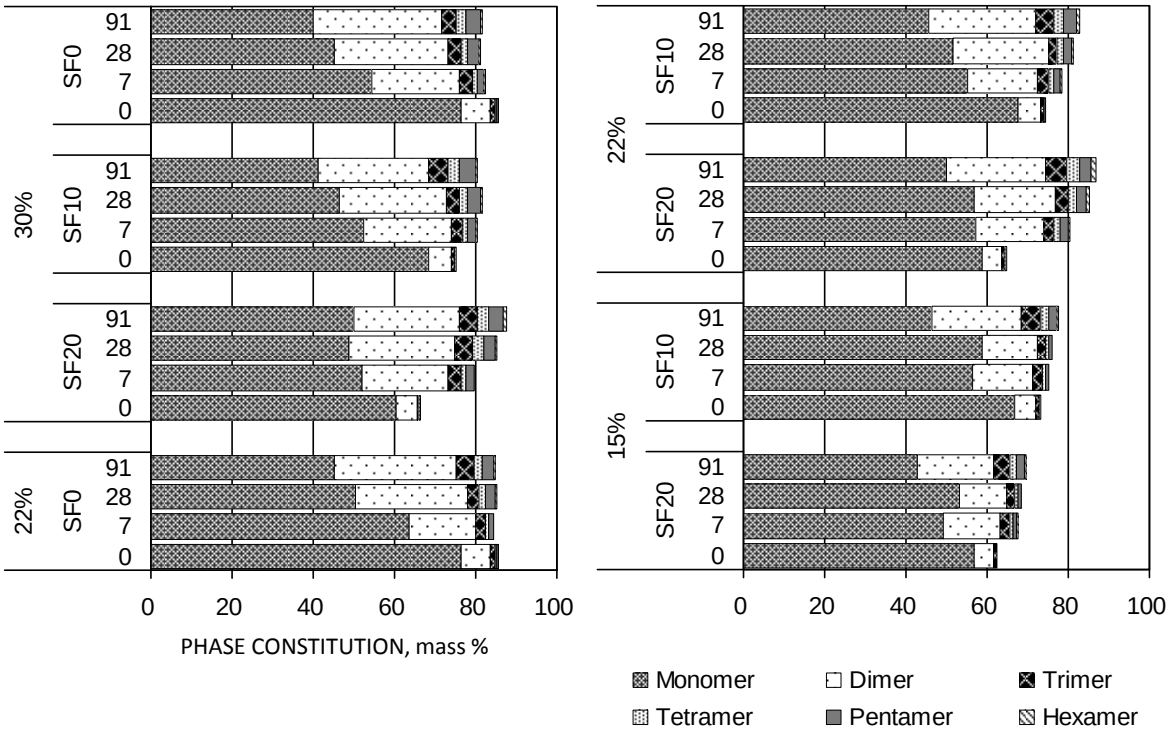

Figure 8 Composition ratio of silicate anion

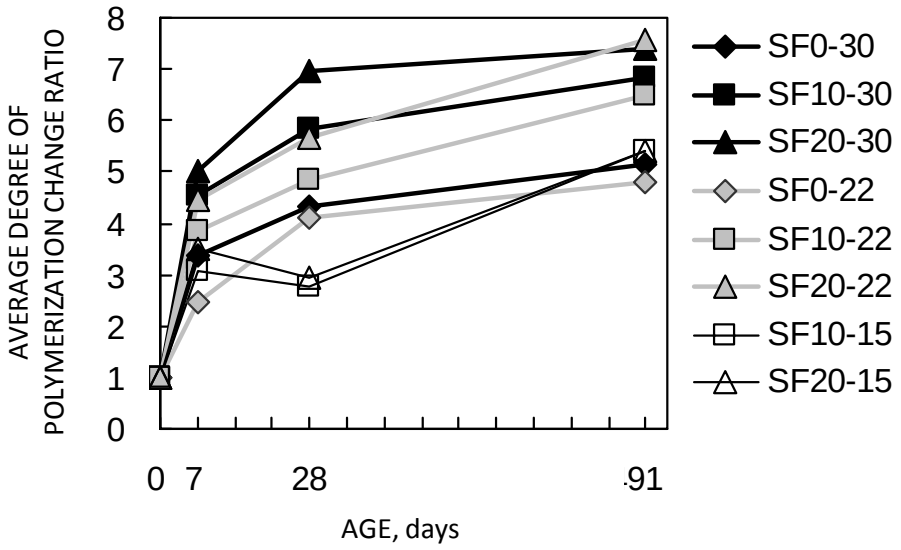

Figure 9 Average degree of polymerization change ratio versus material age

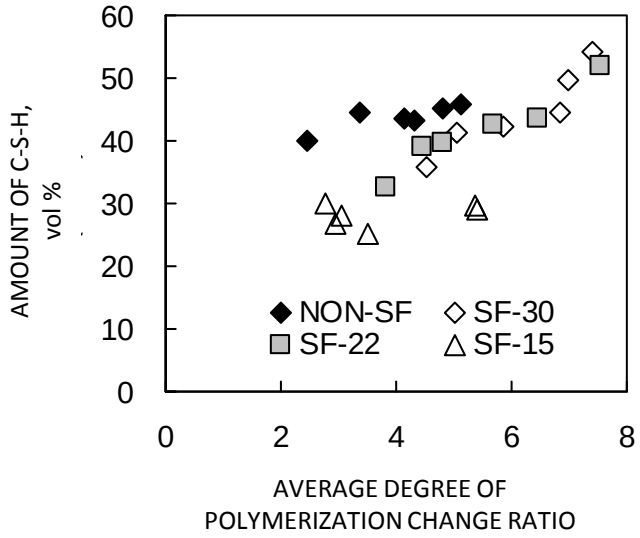

Figure 10 Relation between amount of C-S-H and average degree of polymerization change ratio

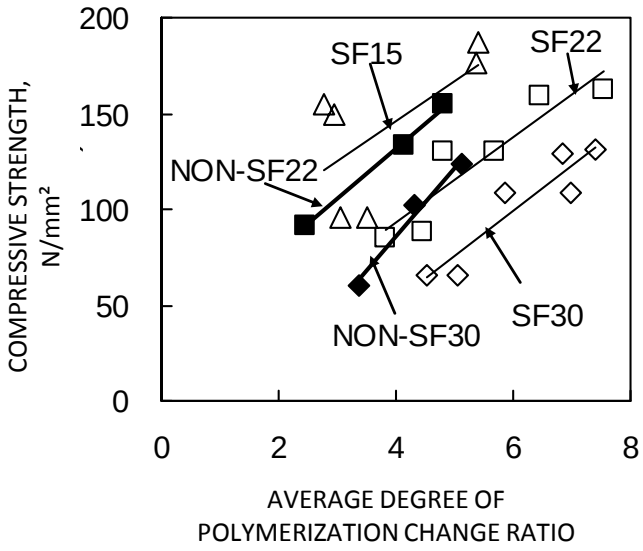

Figure 11 Relation between compressive strength and average degree of polymerization change ratio

CONCLUSIONS

The following knowledge was acquired when the effects of W/B on compressive strength, hydration, and silicate structure were investigated in concretes made with silica fume added to low-heat Portland cement.

The trend in compressive strength was found for W/B = 30% irrespective of the presence of SF, but the compressive strength at material age 91 days for WB = 22% and 15% was higher for mixtures with added SF than for those without.

Regarding the reaction rate of SF and C_3S, hydration was actively proceeded from material age 7 days for W/B = 30% and 22%, but the reaction did not proceed for W/B = 15%.

The effect of W/B or SF addition amount on the reaction rate of C_2S was slight, and no difference was observed.

C-S-H production was small for W/B = 15% irrespective of SF addition amount and was static after 28 days. The effect of W/B on C-S-H production decreased at lower W/B. Taking into account the reaction rate of SF and cement, the effect of SF and C_3S was considered to be large and the effect of C_2S was considered to be small for C-S-H production.

Silicate anion polymerization decreased as W/B was lowered. Addition of SF promoted production of C-S-H.

From the above results, a cement and silica fume reaction was actively performed for the W/B = 30% and 22% implemented in this research. Meanwhile, SF reaction, C-S-H production and polymerization of silicate anions was stalled for W/B = 15%, which corresponds to the water-binder ratio used in ultrahigh strength concrete. But the correlation between compressive strength and hydration ratio was low. It was considered that the effect on compressive strength of the hydrate framework and the void structure between cement and silica fume atoms was large.

REFERENCES

1. T SUGAMATA, S KOIZUMI, K HARADA, S OKAZAWA, Hydration effect cement-silica fume binder on the strength development of 150N/mm2 class concrete, Proceedings of the Japan Concrete Institute, vol.28 (1), 2006, pp 1193-1198.

2. K ONO, K ASAGA, M DAIMON, Hydration reaction of cement-silica fume, Japan Cement Association Cement technology annual report, 39, 1985, pp 41-44.

3. T NOZAKI, K YAMADA, K KONO,I MARUYAMA, Analysis by XRD / Rietveld of silica fume blended cement, Japan Cement Association, Review of the 63th general meeting, The Cement Association of Japan, 2009, pp 30-31.

4. ARCHITECTURAL INSTITUTE OF JAPAN, Japanese Architectural Standard Specification JASS 5 Reinforced Concrete Work, 2009, pp 716-719.

5. T YOSHIZAWA, Technological committee report, Point of JIS revision "Silica fume for concrete", Japan Silica Fume Technology Associate, Research symposium report, 2010, 1-1.

6. K ASAGA,S OHSAWA,G UWANISHI,K OHTA,M DAIMON : Determination of Uncombined Quartz in Hydrothermal Reaction of Quartz and Portland Cement, The Ceramic Society of Japan, Vol.90, 1982, pp 397-400.

7. M SATO,K KOIZUMI,Y UMEMURA, Hydration of hardened ultra high strength cement using silica fume and water-reducing agent, Cement Science and Concrete Technology, Vol.64, 2010, pp 442-449.

8. P STUTZMAN, S LEIGH, Phase Composition Analysis of the NIST Reference Clinker by Optical Microscopy and X-ray Powder Diffraction, NIST Technical Note 1441, 2002.

9. Y FUKAYA, N TSUYUKI, Gijyutsu-shoin, Cement concrete materials science, 2003, p57.

10. JAPAN CONCRETE INSTITUTE, Technical Committee on autogenous shrinkage on concrete, Committee report, 1996, p 15.

11. THE SOCIETY OF INORGANIC MATERIALS, JAPAN, Handbook of Cement, Gypsum and Lime, Gihodo Shuppan, 1995, pp 212-223.

12. S SABURI, I KUSACHI, C HENMI , A KAWAHARA, K HENMI and I KAWADA, Refinement of the structure of rankinite, MINERALOGICAL JOURAL, Vol. 8, No.4, 1976, pp 240-246.

13. JAPAN UNION OF CEMENT CONCRETE WATER COMMITTEE, Behaviour of water in cement and concrete, 1993, p 33.

An Experimental Study of Curing Temperatures on Workability Characteristics and Compressive Strength of Self-Compacting Geopolymer Concretes

M F Nuruddin, D Samuel, N Shafiq
Universiti Teknologi PETRONAS, Malaysia

The effects of self compacting geopolymer binder systems exposed to elevated temperature are examined. Self-compacting geopolymer concrete (SCGC) is an improved way of concreting operation that does not require compaction and is made by complete elimination of ordinary Portland cement content. SCGC were synthesized from low calcium fly ash, activated by combinations of sodium hydroxide and sodium silicate solutions, and by incorporation of superplasticizer for self compactability. The present study reports the details of experimental investigation on workability and compressive strength development of SCGC. The parameters studied were water to geopolymer solids ratio, curing duration and temperature. The water to geopolymer solids ratios were 0.31, 0.33, 0.35 and 0.39. The effects of water to geopolymer solids ratio on fresh properties such as filling ability, passing ability and resistance to segregation were evaluated. The fresh properties were measured using slump flow, V-funnel, L-Box and J-ring test methods. The essential workability requirements for self-compactability according to European Federation of National Associations Representing Producers and Applicators of Specialist Building Products for Concrete (EFNARC) were satisfied. This paper also reports the effects of curing durations and temperatures on compressive strength development. The curing durations were 24, 48, 72 and 96hrs and the curing temperatures were 60, 70, 80 and 90°C. Results showed that curing duration and temperature have a significant influence on compressive strength development. The optimum curing duration and temperature for improved performance of SCGC are also reported.

M F Nuruddin is a professor and the Dean for the Faculty of Engineering at Universiti Teknologi PETRONAS. He has 28 years of teaching, research, and consultancy experience and has published more than 200 technical papers at international and national levels. Professor Nuruddin has won numerous research awards at international innovation competition and exhibition. His current interest areas are in new binders, geopolymer concrete and carbon footprint reduction initiative. He is a registered professional engineer.

D Samuel is a research assistant at the Civil Engineering Department Universiti Teknologi PETRONAS. His work in geopolymer concrete under the supervision of Professor Nuruddin has granted him an MSc degree in 2012.

N Shafiq is an Associate Professor at the Civil Engineering Department Universiti Teknologi PETRONAS. He has many years of industrial exposures in the US and Singapore dealing with designs of tall building and airport. Currently his major research interest areas are in FRP, cement replacer, and ductile concrete. He has published more than 150 technical papers and won numerous research awards at international levels.

Keywords: Compressive strength, Fly ash, Geopolymer concrete, Self-compacting concrete, Water-to-geopolymer solids ratio

INTRODUCTION

The worldwide demand for concrete as a construction material is continuously increasing and the usage of cement globally is second to water. For the past many years, there were many concerns raised for the continuous increase of the use of cement because the manufacture of cement causes large amount of carbon dioxide (CO_2) emission and it also consumes significant amount of natural rock and minerals that deplete as the cement manufacture continues. Production of one ton of Portland cement (PC) liberates about one ton CO_2 to the atmosphere which constitutes 5% global CO_2 emission [1]. It is stated that the global production of PC contributes about 1.35 billion tons to greenhouse gas emissions annually [2, 3]. Due to the manufacture of PC, the CO_2 emission is likely to rise by about 50% from the current levels by the year 2020 [4]. Recently, to minimize the environmental impact as a result of cement production, a new type of binder produced from an alumino-silicate precursor activated in high alkali solution was proposed. This cementitious binder is known as geopolymer cement.

Huge efforts have been made to minimize the use of cement as a binder in concrete production. One of the pozzolanic materials that has been introduced in the construction industry is the fly ash (FA) [2, 5], which is a waste product from coal-fired electric and steam generating plants. Hardjito & Rangan [6] and Palomo et al. [7] developed a geopolymer concrete (GC) using the FA as the base material. Prior to the introduction of FA as a source material, metakaolin was used as the base material in many studies [8-10], however since last decade, much research has been done using FA because it contains high amount of alumina and silica contents. The work done on geopolymer technology shows a significant potential for its utilization in concrete industry, particularly low-calcium FA [6, 8, 11]. Consequently, the use of geopolymer as binder in concrete production not only resulted in reduction of CO_2 emission due to elimination of cement, but also utilizes the industrial by-products of alumino-silicate powders to produce environmental friendly construction material [1-4, 6-11].

The effective placement of concrete into formwork requires compaction efforts and also involves skilled labor. The process of compaction primarily aims to expel the entrapped air in fresh concrete and makes the aggregate particle to occupy a minimum volume so as to enhance the density of concrete [12, 13]**.** As the concrete is placed and compacted at the construction site, normal vibrating concrete that is made by usual construction practices, may fail to exhibit the required fresh and hardened properties. One solution to mitigate this problem is the utilization of self-compacting concrete (SCC) [14]. SCC transforms the concreting operation by complete elimination of vibration during compaction and allows the concrete to flow through sections with congested reinforcement under its own weight, filling the formwork with minimal bleeding and segregation. Such concrete needs a high slump flow [15] that can be achieved by adding superplasticizer to a concrete mix, controlling the mix proportion and limiting the maximum size of coarse aggregate. SCC was developed in Japan in the late 1980s because of shortage of skilled labor and emergence of heavily reinforced structure [13]. Xie et al. [16] and Khatib [17] studied the properties of SCC made with low calcium fly ash (Class F). They made experimental investigation on workability, structural and durability properties of self compacting concrete by replacing PC with fly ash up to 35% and 80% respectively. Results of investigation showed that SCC made with fly ash enhanced the workability and hardened properties. Adequate compaction of fresh concrete removes pockets of honeycombed material and is essential to achieve good

consolidation, uniform properties, better quality and durability [18], strong bond with reinforcement [19] and improved interface between the aggregate and hardened paste [20]. This paper presents the test results of behavior of SCGC in fresh and hardened states and the main objective of this paper was to investigate the effects of water-to-geopolymer solids ratio, curing time and temperature on workability and compressive strength of SCGC.

EXPERIMENTAL METHOD

Materials

In the experimental work, materials were selected according to the specifications of British Standards and EFNARC guidelines. Dry low-calcium fly ash obtained from thermo electric power station was used as a source material. American Standard Testing and Material (ASTM C618) classifies fly ash into Class F and C depending mainly on CaO content and the fly ash used in the research was Class F with chemical composition, as determined by X-Ray Florescence (XRF) analysis, given in Table 1. Coarse aggregate used in this research was crushed granite stone with maximum size of 14 mm (BS 812-103.2 1989). The specific gravity of coarse aggregate is 2.66 with SSD condition while the fine aggregate used is dry clean natural Malaysian sand with the fineness modulus of 2.76, maximum size of 5mm and a specific gravity of 2.61.

Table 1 Chemical composition of Low Calcium Fly Ash (LCFA) [25]

COMPOUNDS	MASS %	REQUIREMENT AS PER BS EN 450-1:2005
SiO_2	51.3	min. 25%
Al_2O_3	30.1	-
Fe_2O_3	4.57	-
SiO_2+ Al_2O_3+ Fe_2O_3	85.97	min. 70%
CaO	8.73	max. 10%
P_2O_5	1.6	-
SO_3	1.4	max. 3%
K_2O	1.56	-
TiO_2	0.698	-

Alkaline solution plays an important role in geopolymer synthesis for the dissolution of silica and alumina and for the catalysis of polymerization reaction [18]. In this experiment, a combination of sodium silicate and sodium hydroxide was chosen as the alkaline liquid. Na_2SiO_3 (Grade A53) used with a composition of 55.52% water, 29.75% SiO_2 and 14.73% Na_2O. NaOH (99% purity, in the form of pellets) was dissolved in distilled water to avoid the effect of unknown contaminants in the mixing water. The activator alkaline solution was prepared at least one hour prior to its use. The concentration of NaOH solution was 12M and in order to make 1 kg of solution, 361gm of water was added.

Super plasticizer (Sika Visco Crete-3430) was used to increase the workability to the extent required for self compactability of geopolymer concrete. The utilization of Viscosity Modifying Admixture (VMA) gives more possibilities of controlling segregation (stability) and homogeneity of the mix [21]. The amount of SP used was in accordance with European guideline [21]. The water used in the mix was tap water in accordance with B.S. EN 1008:1997.

Experimental Setup

The concrete mixing procedure consists of dry and wet mixings. The solids components of SCGC, i.e. the fly ash and the fine and coarse aggregates, were dry mixed in the pan mixer for about 2.5 minutes. The liquid part of the mixture, i.e. the sodium silicate solution, the sodium hydroxide solution, extra water and the super plasticizer, were premixed thoroughly and then added to the dry mixture. The wet mixing was done for 3 minutes. The chemical reaction between alkaline solution, super plasticizer and water took place and the reaction played an important role in giving the required workability for SCC and compressive strength of hardened concrete. The fresh SCGC had a flowing consistency and with high tendency of filling ability, passing ability and resistance to segregation. The fresh concrete was then filled in 100mmx100mmx100mm steel moulds and allowed to fill all the spaces of the moulds by its self weight (no need to vibrate for compaction). After casting, the specimens including the moulds were kept in an oven at different temperatures namely 60°C, 70°C, 80°C and 90°C over different curing duration of 24, 48, 72 and 96 hours. The ambient curing preceded by oven curing was adopted for this research to accelerate polymeric reaction at elevated temperature and to improve the compressive strength performance as claimed by [12]. The specimens were placed outside the room but protected from direct sunlight and rain. Later the specimens were demoulded and tested for direct compression in a digital 2000kN compression testing machine. The mix design proportion adopted in the research and details of these mixtures are shown in Table 2.

The ratio of sodium silicate to sodium hydroxide solution by mass was 2.5 for all mixture proportion. The mass ratio of fine aggregate to fly ash was 2.125 for all mixture. The water-to-geopolymer solid ratio was calculated by dividing the total mass of water with the total mass of geopolymer solids. The total mass of water in the mix was the sum of the mass of water in the sodium silicate solution, the mass of water in the sodium hydroxide solution and the mass of the extra water. The total mass of geopolymer solids was the sum of the mass of fly ash, the mass of sodium hydroxide solids and the mass of sodium silicate solids (mass of Na_2O and SiO_2 in sodium silicate solution). The concentration of sodium hydroxide solution was held constant at 12M and super plastisizer dosage of 7% by mass for all mix.

Test Procedure

A concrete mix can only be considered as SCC if the three characteristics for workability are satisfied. The three fresh concrete characteristics mandatory for SCC are filling ability, passing ability and resistance to segregation. Filling ability and passing ability can be measured by the test methods as shown in Table 3. Resistance to segregation can be assessed more or less in all the tests based on observation through visual stability. The European Guidelines [21], has proposed different test methods to characterize an SCC mix. Table 3 shows the test methods and properties of workability characteristics along with their recommended values given by EFNARC.

Table 2 Mix design proportions

MIX	FLY ASH	COARSE AGG	FINE AGG	NaOH	Na-Si	EXTRA WATER	W/G RATIO	L/F RATIO	SP	CURING	
										Time	Temp.
	kg/m^3	kg/m^3	kg/m^3	kg/m^3	kg/m^3	kg/m^3 (%)			kg/m^3 (%)	hr.	^0C
S_1	400	950	850	57	143	40 (10)	0.31	0.67	28 (7)	24	70
S_2	400	950	850	57	143	48 (12)	0.33	0.69	28 (7)	24	70
S_3	400	950	850	57	143	60 (15)	0.35	0.72	28 (7)	24	70
S_4	400	950	850	57	143	80 (20)	0.39	0.77	28 (7)	24	70
S_5	400	950	850	57	143	48 (12)	0.33	0.69	28 (7)	48	70
S_6	400	950	850	57	143	48 (12)	0.33	0.69	28 (7)	72	70
S_7	400	950	850	57	143	48 (12)	0.33	0.69	28 (7)	96	70
S_8	400	950	850	57	143	48 (12)	0.33	0.69	28 (7)	48	60
S_9	400	950	850	57	143	48 (12)	0.33	0.69	28 (7)	48	80
S_{10}	400	950	850	57	143	48 (12)	0.33	0.69	28 (7)	48	90

Table 3 Test methods, properties and recommended values as per EFNARC guidelines

NO.	METHODS	PROPERTIES OF WORKABILITY CHARACTERISTICS	ACCEPTANCE VALUES AS PER EFNARC GUIDE LINES	
			Minimum	Maximum
1	Slump flow by Abrams cone	Filling Ability	650mm	800mm
2	T_{50cm} Slump flow	Filling Ability	2s	5s
3	V-funnel	Filling Ability	6s	12s
4	L-Box (H2/H1, Ratio)	Passing Ability	0.8	1.0
5	J-Ring	Passing Ability	0mm	10mm

In this research, the mixes underwent slump flow, T-50, V-funnel, L-Box & J-Ring tests to ascertain their self-compacting capabilities. All those tests are in accordance with EFNARC

guidelines. The hardened compressive strength test was performed one day after curing period in accordance with BS EN 12390-3:2002 using 2000 KN Digital Compressive Testing Machine. A set of three cubes for each mix were tested for compressive strength measurement.

RESULT AND DISSCUSION

In this section, the experimental results of various fresh properties tested by slump flow test (slump flow diameter and T_{50cm}), J-ring test (J-ring Blocking step (B_J)); L-box test (ratio of heights at the two edges of L-box (H_2/H_1)); V-funnel test (time taken by concrete to flow through V-funnel after 10 s, T_{10S}); for various mix compositions are given in Table 4. The compressive strength results were also recorded at different ages. Workability is the main parameter that characterizes SCGC as superior workable in attaining self-consolidation and required hardened properties. All the workability tests were performed as per the European guidelines [21] for SCC. The compressive strength of the mix composition is also presented in Table 4.

Table 4 Workability and compressive strength test results

WORKABILITY TEST RESULTS									
Mix	Slump Flow	$T_{50\,cm}$ Slump Flow	V-funnel Flow time	L-Box (H_2/H_1)	J-Ring Blocking Step, B_J	Compressive Strength			
						1day	3day	7day	28day
	mm	sec	sec		mm	MPa	MPa	MPa	MPa
S1	630	6.5	12.5	0.82	12	53.4	54.33	55.08	56.29
S2	710	4	7	0.96	5	45.0	45.85	46.94	48.53
S3	770	3	6	1	3	37.7	37.90	38.56	39.78
S4	820	2.5	5.5	1	0	22.5	22.98	23.44	24.18
S5	710	4	7	0.96	5	51.0	51.98	52.26	53.80
S6	710	4	7	0.96	5	51.4	52.20	52.69	53.92
S7	710	4	7	0.96	5	51.6	52.33	52.72	53.99
S8	710	4	7	0.96	5	44.8	45.64	45.98	47.54
S9	710	4	7	0.96	5	48.5	49.22	49.80	50.77
S10	710	4	7	0.96	5	47.9	48.83	49.67	50.42
Acceptance criteria for SCC as per EFNARC [20]									
Min.	650	2	6	0.8	0				
Max.	800	5	12	1.0	10				

It was observed that Mix S_2 with lower water-to-geopolymer solids ratio of 0.33 showed highest compressive strength as compared to Mix S_3 and S_4 that have water-to-geopolymer solids ratio of 0.35 and 0.39 respectively. In contrary to OPC based concrete, water was required in GC to improve workability, but was expelled during curing at elevated temperature thus increasing the porosity of concrete. Water in the mix plays a vital role in synthesis and acts as a medium for dissolution, condensation and polymerization of Al and Si precursors into polymeric structures. Figure 1 shows that mix S_1 with water-to-geopolymer solids ratio of 0.31 exhibits good compressive strength of 56.52 MPa at 28 days of age as compared to all other mixes. But the mix

with water-to-geopolymer solids ratio of 0.31 failed to exhibit the required workability property for SCGC due to very low percentage of extra water (10% of fly ash) with only slump value of 630mm. The mix with relatively lower water-to-geopolymer solids ratio of 0.33, which exhibited the required workability for self-compactibility, showed highest compressive strength as compared to mixes that have water-to-geopolymer solids ratio of 0.35 and 0.39. As predicted, it was observed that an inverse relationship was obtained between water-to-geopolymer solids ratio and compressive strength i.e. as the water-to-geopolymer solids ratio increases, the compressive strength decreases.

The test results data given in Figure 1 demonstrate that the compressive strength of SCGC decreases as the water-to-geopolymer solids ratio by mass increases. This test trend is similar to the influence of water-to-cement ratio on the compressive strength of conventional Portland cement based concrete, although the mechanism of reaction involved in the synthesis of the binders of both these types of concretes are entirely different. During the curing process at elevated temperature, the water was expelled and evaporated from hardened concrete sample. Spaces that were formerly occupied by water remained as micropores within the concrete. These pores resulted a microcrack path which can lead to failure of concrete at lower stress level when exposed to compressive load, hence resulting in low compressive strength performance. It could be attributed to the fact that specimen with lower porosity would enhance the microstructure leading to a stronger and less porous hardened concrete. From this, it can be concluded that specimen with lower porosity yielded higher compressive strength.

Mixes S_2, S_5, S_6 and S_7 were prepared to study the influence of curing time on the compressive strength of SCGC. All the other test parameters were held constant while the curing time varied. The activator-to-fly ash ratio and water-to-geopolymer solids ratio were kept constant at 0.5 and 0.33 respectively. It was obtained that the compressive strength at 1 day after 48 hrs of curing was about 45 MPa. From Figure 2, it is observed that the longer curing time does not ensure higher compressive strength. As the curing duration increased there was a small increase in compressive strength of up to 96 hours. Figure 6 shows that Mix S_7 cured at 70^{o}C produced the highest compressive strength i.e. 53.99MPa.

There is no significant increase in the compressive strength for Mix S_5 as compared to Mix S_6. In normal GC as claimed by Mishra et al [22], it was evident that compressive strength increased with the increase in curing duration from 24 hrs to 48 hrs but no significant variation from 48 to 72 hrs. The results in this research indicated that GC cured at 70^{o}C longer than 48hrs resulted in a very small increase in the compressive strength. This was due to the fact that condensation polymerization had been duly completed and did not need further curing. This phenomenon is important for the construction industry as far as construction speed is concerned.

The influence of curing temperature on compressive strength development is demonstrated by the test result data shown in Figure 3. Mixes S_2, S_8, S_9 and S_{10} were prepared to study the effect of oven curing temperature on the compressive strength of SCGC. It was observed that the strength increased when the specimens were cured in oven for 48hrs up to 70^{o}C. Figure 3 showed that the specimen cured at temperature beyond 70^{o}C decreased the compressive strength of self-compacting geopolymer concrete. The extra water utilized for normal GC is usually ranges from 0

to 5%, but in this experimental work 12% extra water was added to attain higher workability or self-compactability.

The mechanism of reaction in GC is different from OPC based concrete as water is not involved in the geopolymeric reaction. The elevated temperature made the extra water (which is more than 12%) to be expelled from the hardened concrete sample during the curing process. Spaces that were previously occupied by water remained as micropores or nanopores. These pores resulted a microcrack path which can cause premature failure of concrete at lower stress level and hence decreased the compressive strength of samples cured at 80°C and 90°C. But van Jaarsveld et al., [23] suggested that small amounts of structural water need to be retained in order to reduce cracking and maintain structural integrity and stability in fly ash-based geopolymers.

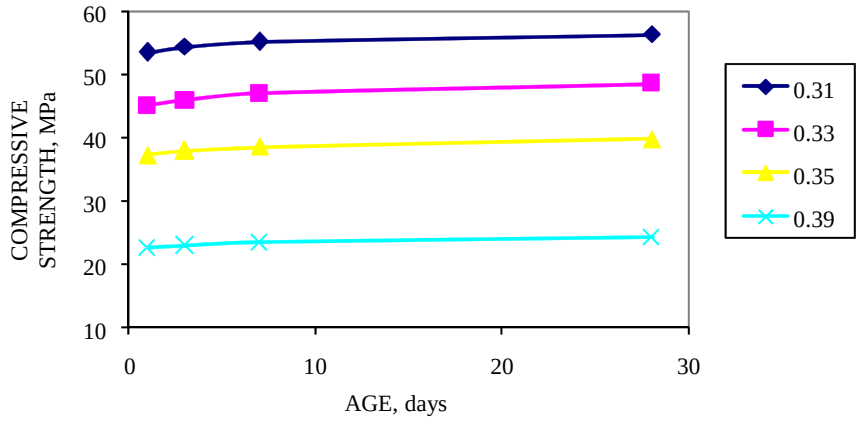

Figure 1 Effect of water to geopolymer solids on compressive strength

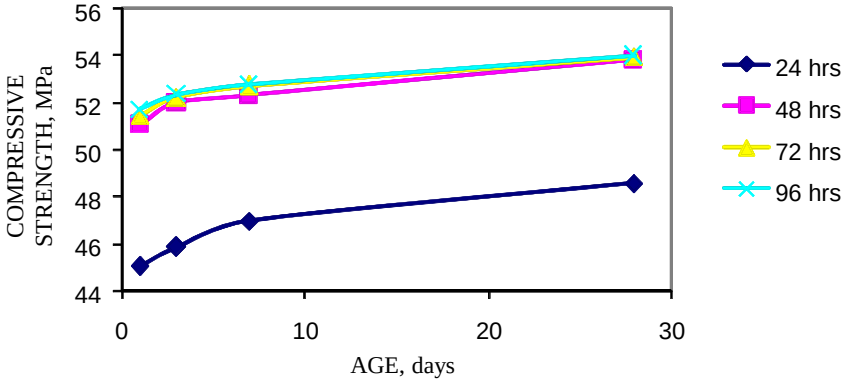

Figure 2 Compressive strength with different curing durations

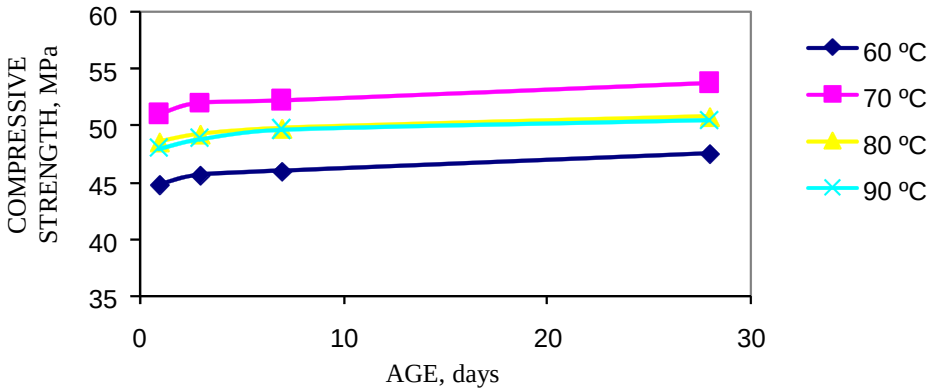

Figure 3 Compressive strength under different curing temperatures

CONCLUSIONS

Based on the test results, the following conclusions can be drawn:

1. Except for mix with water-to-geopolymer solids ratio of 0.31, all the other mixes had good filling and passing ability and the workability results were within the range of EFNARC limits of SCC. Concrete with water-to-geopolymer solids ratio of 0.33 exhibited the required workability and produced the highest compressive strength of 49.28 MPa at 28 days. The workability study showed that as the amount of water-to-geopolymer solids ratio increased, the workability of geopolymer concrete increased.

2. Longer curing time improved the geopolymerisation process resulting in higher compressive strength, as the curing time in the range of 24hrs to 96hrs increased. The compressive strength was highest when the specimens were cured for a period of 96 hours; however, the increase in strength after 48 hours was insignificant.

3. Higher curing temperature in the range of 60°C to 70°C produced higher compressive strength of SCGC, though, the strength decreased when the specimen cured further to 80°C and 90°C. Curing duration of 48hrs and temperature of 70^{o}C were found to be the best curing condition and produced the highest compressive strength.

ACKNOWLEDGEMENTS

The author would like to acknowledge the Universiti Technologi PETRONAS, Malaysia for providing the facilities and financial aid to accomplish the experimental work of this research and also the Ministry of Science Technology & Innovation Malaysia for the e-science grant.

REFERENCES

1. NURUDDIN, M.F., QUAZI, S., SHAFIQ N., AND KUSBIANTORO, A. (2010). Compressive strength & microstructure of polymeric concrete incorporating fly ash & silica Fume. Canadian Journal on Civil Engineering, 1(1), 15-18.

2. MALHOTRA, V.M. (2002) Introduction: Sustainable development & concrete technology",

3. HARDJITO, D., WALLAH, S. E., SUMAJOUW, D. M., AND RANGAN, B. V. (2004). Factors influencing the compressive strength of fly ash-based geopolymer concrete", Civil Engineering Dimension, 6(2), 88–93.

4. NAIK, T. R. (2005). Sustainability of cement and concrete industries. Proceedings of the International Conference Global Construction: Ultimate Concrete Opportunities, Dundee, Scotland, 141-150.

5. MEMON, A. F., NURUDDIN, M. F., AND SHAFIQ, N. (2011). Effect of Superplasticizer and NaOH Molarity on Workability, Compressive Strength and Microstructure Properties of Self-Compacting Geopolymer Concrete, International Journal of Civil and Environmental Engineering, 3(2), 72-78.

6. HARDJITO, D., AND RANGAN, B. V. (2005). Development and properties of low-calcium fly ash based geopolymer concrete. Research report GC 1, Faculty of Engineering Curtin University of Technology, Perth, Australia.

7. PALOMO, A., GRUTZEK, M. W., BLANCO, M. T., (1999). Alkali-activated fly ashes. A cement for the future. Cement and Concrete Research, 29(8), 1323-1329.

8. DAVIDOVITS, J. (1991). Geopolymers: Inorganic polymeric new materials. Journal of Thermal Analysis, 37(8), 1633–1656.

9. ROVNANIK, P. (2010). Effect of curing temperature on the development of hard structure of metakaolin-based geopolymer, Construction and Building Materials, 24(7), 1176–1183.

10. CASSAGNABÈRE, F., MOURET, M., ESCADEILLAS, G., BROILLIARD, P., AND BERTRAND, A. (2010). Metakaolin, a solution for the precast industry to limit the clinker content in concrete: Mechanical aspects, Construction and Building Materials, 24(7), 1109–1118.

11. RANGAN, B. V. (2008). Fly ash-based geopolymer concrete. Research Report GC-4, Faculty of Engineering, Curtin University of Technology, Perth, Australia.

12. NURUDDIN, M. F., SAMUEL, D, MEMON, A. F., AND SHAFIQ, N. (2011). Effect of Superplasticizer and NaOH Molarity on Workability, Compressive Strength and Microstructure Properties of Self-Compacting Geopolymer Concrete, International Journal of Civil and Environmental Engineering, 3(2), 122-129.

13. NEVILLE A. M. (2000). Properties of concrete. Prentice Hall. London.

14. OKAMURA, H., AND OUCHI, M. (2003). Self-compacting concrete. Journal of Advanced Concrete Technology, 1(1), 5 -15.

15. EFNARC. (2005). The European Guidelines for Self-Compacting Concrete: Specification, production and use.

16. XIE, Y., LIU, B., YIN, J., AND ZHOU, S. (2002). Optimum mix parameters of high-strength self-compacting concrete with ultrapulverized fly ash. Cement and Concrete Research, 32(3), 477-480.

17. KHATIB, J. M. (2008). Performance of self-compacting concrete containing fly ash. Construction and Building Materials, 22(9), 1963-1971.

18. OUCHI, M., NAKAMURA, S., OSTERSON, T., HALLBERG, S., AND LWIN, M. (2003). Applications of self-compacting concrete in japan, europe and the united states, ISHPC.

19. DEHN, F., HOLSCHEMACHER, K., AND WEIßE, D. (2000). Self-compacting concrete (scc) time development of the material properties and the bond behavior. LACER, no. 5.

20. AHMADI, M., ALIDOUST, O., SADRINEJAD, I., AND NAYERI, M. (2007). Development of mechanical properties of self compacting concrete contain rice husk ash. International Journal of Computer, Information, and Systems Science, and Engineering 1, no. 4.

21. EFNARC. (2002). Guidelines for Self-Compacting Concrete.

22. MISHRA, A., CHOUDHARY, D., JAIN, KUMAR, M., SHARDA, N., AND DUTT, D. (2008). Effect of concentration of alkaline liquid and curing time on strength and water absorption of geopolymer concrete. ARPN Journal of Engineering and Applied Sciences, 3(1), 14-18.

23. VAN JAARSVELD, J. G. S., VAN DEVENTER, J. S. J., AND LUKEY, G. C. (2002). The effect of composition and temperature on the properties of fly ash and Kaolinite-Based Geopolymers, chemical engineering Journal, 89(1-3), 63-73.

To Be Sustainable: Use High Performance Concrete!

R Lewis
Elkem Silicon Materials, UK

This may seem like a contradiction in terms, but if we consider the design capabilities – using supplementary cementing materials to reduce cement usage; recycled aggregates and concrete; higher strengths giving reduced volume; longer lifetimes with less repairs and fewer re-builds of significant structures – then using high performance concrete is very sustainable. The paper will look at the potential of HPC – placeability, high strengths, long term durability and review a series of reference projects where its use has meant considerable savings in natural resources – including overall cost savings. The focus of the paper is to get people thinking about the value of each cubic metre – and how that can be used – rather than the simple 'cost per cubic metre'. Examples include: High Rise Towers; Parking Structures; Industrial Floors and Sprayed Concrete usage.

Robert C. Lewis is the Technical Marketing Manager at Elkem Silicon Materials. He began his career in 1978, as a field technician, for Tarmac Topmix in the UK. After 8 years and two City and Guilds exams in Concrete Technology, he was the assistant to the two Area Technical Managers for the Southern Region. In 1986 he moved to Elkem, joining the technical services of concrete operations in the UK. Currently he provides technical support to Elkem Silicon Materials' international market, covering the European and Middle Eastern Regions – and other areas as necessary. He has written, co-authored and presented numerous papers on microsilica (silica fume) and its use in concrete – including a chapter in F.M.Lea's "The Chemistry of Cement and Concrete", and has been involved in many projects world-wide. He is an ad-hoc member of a number of British Standards committees as well as the UK expert on the CEN (European Standards) committee for Silica Fume. He works on several committees of the American Concrete Institute and is currently the Chair of Committee 234 – Silica Fume. He is a Member of the Institute of Concrete Technology, an International Member of the American Concrete Institute and, in 1999 was made a Fellow of the UK Concrete Society.

Keywords: Durability, High strength, Recycled aggregates, Silica fume, Supplementary cementitious materials

INTRODUCTION - CONCRETE AND THE WORLD

It is a simple fact that for every single person on this planet, there is one cubic metre of concrete produced each year. That is a lot of concrete – and, of course, concrete uses cement, aggregates and water. As an industry, we are under very close scrutiny as to how we make and use concrete and particularly how that affects our planetary resources and climate. Whether you agree with the 'Climate Change' lobby or not, we all have to try and use less of the natural resources we have, and control the use of energy and the production of CO_2. After all, this is the only planet we have and we cannot simply 'go next door' if we mess up this one!

So, firstly, we have cement – producing approximately 1 tonne of CO_2 for every tonne manufactured. That's going to mean 300 to 400 kg of CO_2 per cubic metre, from the cement alone. I think we can all agree that we need to do something about that. Secondly, there will be close to 2 tonnes of aggregates in each of those cubic metres we produce. That's normally natural resources, whether dredged, dug up or crushed from a mountain. We simply cannot keep using new aggregates all the time!

Then there is water. If we follow the Standards correctly we should use only fresh, drinkable water for our concrete. We are starting to see recycled water used at the plants, but it is still small beans. At roughly 150 litres per metre, the Burj Khalifa, one of the best sustainable designs most recently, will still have used over 50 million litres of water – and that's only what was in the concrete – no washing down, or other such uses.

Yet, even though these things are a part of the make up of the concrete, we cannot just stop using it – it is the world's greatest single construction material.

But we must be sensible in how we view our construction work – and the measures we take to be sustainable. To give an example, one of the first Platinum rated LEED projects on the East Coast of the USA is undergoing repair work after only 10 years – as the sustainable material used was not up to the performance required of it. If we're going to do this work – we must do it right – first time! So, what can we do? Let's take a look.

Cement and supplementary cementitious materials

At a conference in Scotland a few months back, the technical director of one of the world's largest cement companies said that he could not envisage the chemistry of Portland cement changing any further, to reduce the CO_2 component. The lowest potential they were looking at was about 750kg per tonne. Whilst that is a reduction of around 20 to 25%, it's still not good enough, environmentally speaking, and the comment made was that we must use more of the supplementary cementitious materials. This can easily be seen as vital, as global cement consumption is predicted to reach some 3.5 billion tonnes by the year 2020 (Ocean Shipping Consultants).

The industry has known about Ground Granulated Blastfurnace Slag (GGBS) and Fly Ash (FA) for much of the last century, and products such as microsilica / silica fume (SF) and metakaolin (MK) for the last 40 years. We know that we can use large quantities of GGBS to reduce the temperature of a fresh concrete and, that in long term development, we can get very durable concrete. The same can be said of FA, though the quantities used may be smaller. We know that SF and MK can be used to boost the slow rate of strength gain or

permeability reduction in the mixes using GGBS or FA. We know that SF is used to produce very high strengths and very impermeable concrete. We know that using these SCMs will significantly reduce the 'carbon footprint' of our concrete. Yet we still find it very difficult to get people to use these materials – it's much easier to use OPC… Here is a statement from the UK, made in January 2011:

A report from the Carbon Disclosure Project says a lack of ambition from companies in the energy, materials and utilities sector threatens government plans to cut emissions of greenhouse gases by 2020 (Daily Telegraph, p.B5). Luckily in the Middle East and in some other areas of the world, significant mix changes have been made and highly durable binary, ternary and quaternary blends of cementitious material have been used. Many large and significantly prestigious projects have worked at using the best material for the job – and have achieved great performance.

Example - Storebælt and Øresund Link Bridges, Denmark / Sweden

The Storebælt link in Denmark, and the follow-up bridge, the Øresund, from Denmark to Sweden. The Tsing Ma Bridge in Hong Kong and the East Sea Bridge in Shanghai, as well as the Burj Khalifa and similar towers, and many industrial applications for durability (Figure 1). Use of binary and ternary mixes with OPC, FA and SF. 100 years design life without major maintenance. Approximately 1million cubic metres in the Storebælt, some 2million in the Øresund, used triple blend mixes to achieve strength and durability.

Figure 1 The Øresund link and Burj Khalifa – two projects that have used binary and ternary blend concretes for rheology and durability

Aggregates

Obviously, there is only a finite amount of usable aggregate in the world – and therefore we should use it accordingly. There are, of course, many types of aggregate and they have different qualities and properties. How often do we sit down and think about what aggregates

we have and which we should use? How often have the best quality aggregates (Ras Al-Khaimah in the UAE, Granite in the UK) been used for C40 concrete – or less?

Example – Kinzua Dam, Pennsylvania

After only 7 years of use,high strength aggregates were imported to make high strength repair concrete for the Kinzua Dam in Pennsylvania. The repair lasted only 9 years. Local, weaker, aggregates encased in a silica fume concrete matrix have so far lasted over 25 years – and look to last four times as long again (Figure 2).

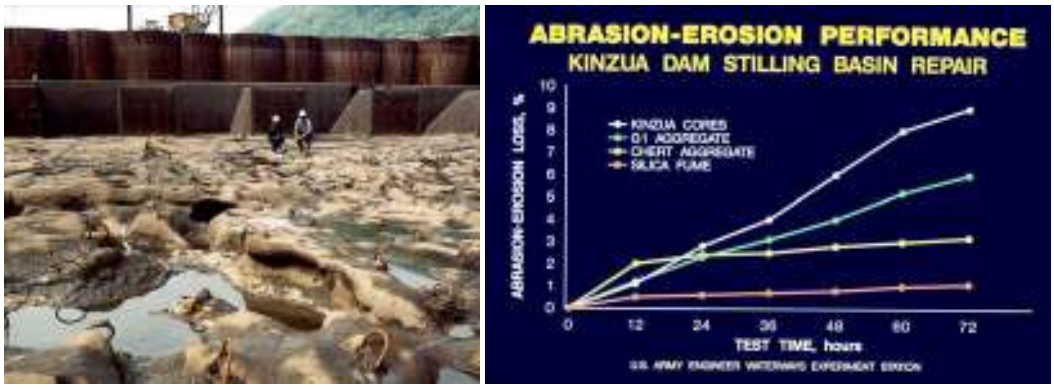

Figure 2 Kinzua Dam: The damage shown is in 1983, after only 9 years. The repair concrete using silica fume (lowest abrasion result in the USAEWES test) is not even being considered for replacement (2012).

Though only built in 1967, the stilling basin of the Kinzua Dam had worn so badly that it had to be replaced in 1974. The overlay slab – over 1m deep was cast using a high cement content OPC mix with specially imported high strength aggregates and steel fibres. By 1983 the swirling effect in the stilling basin – causing abrasion and erosion – had not only worn away the new concrete, but a further 30cm into the original concrete as well. The authorities requested the help of the US Army Corps of Engineers waterways section. They tested several concretes in their specialised equipment.

The results showed that a concrete made with local - normal strength - aggregates, but using silica fume to boost the bond and strength, resisted the abrasion erosion effects much better than the high strength material, made with the expensive imported aggregates. It was not strength, per se, that was needed, but bond within the matrix of the concrete. The basin floor was replaced, with over 1m depth of the silica fume concrete, in 1983. Inspection checks in 2008 (25 years on) noted that approximately 2% of wear, compared to the previous damage, had happened to the silica fume concrete. The potential is, therefore, for the Kinzua Dam to last well over a hundred years before the next repair - over 10 times the original concrete, or even the first repair.

Could we have used a lightweight aggregate instead of a normal weight for that low rise building – gaining insulation as well as reduced dead weight – and still achieving over C50? Many bridges in Norway have been built using lightweight sections enabling greater spans and less deadweight – and achieving 55MPa strengths.

Example - Kvisti Bridge and Norhordland Bridge in Norway

These bridges, shown in Figure 3, used a lightweight concrete mix designed around Liapor material and silica fume. The resulting concrete averaged 1900kg/m3 anda strength of over 55MPa. While only used for the central few hundred metres on the Kvisti Bridge, the majority of the concrete in the picture of the Norhordland bridge is lightweight. The tower and main anchor points are the only 'normalweight' concrete.

Figure 3 Kvisti Bridge has most of the central span cast in lightweight concrete, while the Norhordland Bridge floats across the fjord.

Could we have used recycled aggregates? This question will become greater and greater as we move through the next decade. In many parts of the world, recycled materials are being encouraged for use in concrete. At the moment this use is small – Standards allow some 15% recycled material. Research in the USA has shown that up to 50% recycled aggregates can be used, without affecting the performance of the concrete.

With the amount of building work going on in the Gulf Region – and the vast consumption of concrete – we have to think about using recycled aggregates and recycled concrete (as aggregate). With the effectiveness of SCMs, good bond can be achieved to recycled materials, so strength considerations for normal concretes up to C50 should not be a concern. For higher strengths, less recycled material would be used; for the ultra high strengths, C100 and above, there are high quality aggregates that can be used. Similar action will have to be taken in other high consumption areas of the world.

Using the strengths of concrete

We know we can produce C100, and upwards, in terms of compressive strength, but how often do we use that strength? If we know that we can achieve these levels, why are we not taking advantage of that in the design of the structure? Improved bond to rebar, or to fibres, within the concrete can give us more flexibility and allow more adventurous designs but, in the first instance, if we can utilise that high compressive strength, why not? The 'footprint' for a column – the strength over the area – can remain the same while the column size itself is decreased. You get the same support strength, but less volume in the column – and that means less volume of concrete used and more space within the structure, or around it.

Example – 331, South Wacker, Chicago, USA

311, South Wacker in Chicago used C80 + concrete for the first stages of the columns, and high performance, though lower strengths, for the remainder, as they went up the 70 storey building. This meant a saving of 3,000 tonnes of rebar and 7,650m3 of concrete (Figure 3). The skyscraper was designed around using the highest strength concrete that could be produced at the time. This was achieved by using a silica fume mix and the best admixtures available and working with the readymix supplier to trial the concretes. Thus the columns of the building were redesigned to use 12,000psi (83MPa) for the basement and the first 14 floors, then cutting down on the strength, but still using the SF in the mix to improve the pumpability. This enabled the use of one column size for the whole building, cutting down on formwork. It meant the use of only one pump to pump the concrete to the top. The faster rate of strength gain meant a faster turnaround on the construction. All this meant a quicker build, less cost and more space. The savings on the materials amounted to: 3,000 tonnes of rebar; 7,650 cubic metres of concrete = 3,000 tonnes of cement, 13,000 tonnes of aggregates and over 1 million litres of water.

Example – JJ Hospital Flyover, Mumbai, India

JJ Hospital Flyover in Mumbai, India. Where previously C30 and C40 concretes had been used, stepping it up to C75 meant a radical design change. Instead of triple columns at 10m distances, single columns at 34m distances were used – resulting in a considerable material saving over the 1.9km length of the flyover (Figure 4).

Figure 4 311 South Wacker Drive, Chicago (to the right of the Willis Tower) and The JJ Hospital Flyover in Mumbai. Both made significant savings through the use of high strength concrete.

With a long history of poor cement and aggregates giving low strength concrete – for example C40 was considered high / maximum strength - the use of a silica fume mix to make C75 was little short of a quantum leap in India. This strength allowed a radical step change in the design of the 1.9 km dual carriageway flyover. The high strength meant that the sections

for the road span could be thinner – and therefore lighter. This meant that the columns, now in C75 could be thinned down – and even better – only one column used every 34 m, as opposed to the 'normal' 3 columns at 10m intervals. With the construction being mainly precast, the build speed was much faster and the saving in volume was around 2,000 cubic metres for the columns alone. Not only was this volume saved, but the air space under the flyover was greatly improved, further reducing the pollution caused originally by slow moving traffic.

So why, when we know the concrete can be designed and supplied at these strengths, do we not use them and design – or redesign - our structures accordingly? Yes, we need to design for purpose, but we must look sensibly at that. There are designs for highway and airport pavement in the Gulf Region that are simply "cut and paste" from UK or US design codes. Why are specifications for airport runways, in areas that never see a temperature of less than 10^{o}C in the coldest nights of 'winter', calling for 7.5% air entrainment for freeze thaw protection?! Not only is this a waste of time, money and materials, it is quite pointless and can be avoided with a little thought.

Design the mix

The "cut and paste" effect can be seen in other areas as well, such as workability limits or use of plasticizers or superplasticizers. We should endeavour to make a project as easy as possible. The more straightforward it is the better it will be done. We can design superfluid SCCs now, that mean the labourers don't need to break their backs shovelling the concrete around – and then having to compact it. If it can be pumped, let's do that in preference to skipping it – it's faster and more efficient, and often has less impact on the formwork or steel.

When designing the concrete we can use software that can help us achieve the best particle packing for the mix. The better that is, the less cement we use to 'overcook' the mix – and the better the rheology of the mix – making it easier to use.

Design the mix to achieve the performance – at the right time. Many specifications are looking at long term results – 56 days and 90 days or more – for the strength or durability characteristics. Unfortunately, the concrete is already well into use at that time – unless it's a very long build up of precast units… But even so, is that concrete being cured at 20^{o}C in a humid environment for all of that time? If that concrete is in the ground, or up in the air as a column, is it getting cured as well as the labcrete, on which you base all the results? We know we can do great concrete with 70 or 80 or even 90% GGBS, or 40 or 50% FA, but they will take a little more looking after. We know that if we make a pure OPC with 10% or more SF, it might be difficult to handle. So we should use them in combination – designing to achieve the best results for the given situation. There are many precedents around the world – the examples are in this paper!

What about the cost?

Well, here we have it. The break point. Where everyone says, yes that would be nice, but we can't afford to do that. That may be true if you are looking at just the cost of the concrete per cubic metre, but why do you do that? Because that's the way it has always been done. That's an excuse, not a reason!

Nowadays, more than ever, with the environmental considerations that are being focussed on the construction industry, we must look at the total cost of our projects – cradle to grave. That means we have to take in all the construction costs, as well as the material costs, all the maintenance requirements and the service lifetime of the building / bridge / tunnel / industrial unit. This means that the cost per cubic metre for the concrete is now an unusable concept – we have to appreciate the value of the cubic metre in terms of the finished construction.

Example - Pune Expressway Tunnels, Mumbai, India

Shotcrete in the Mumbai – Pune Expressway Tunnels. The cost per cubic metre was much higher for the silica fume version of the shotcrete – in both wet and dry process works. But when the rebound volumes were taken into the calculation, and the speed of the work, and the greater coverage per work shift, the cost per finished metre of wall was much less than the concrete without the silica fume (Table 1).

The Konkan Railway Corporation did all the shotcreting on this project. They decided to use a silica fume based mix after trial work showed greatly reduced rebound of the shotcrete. In terms of the wet mix, the figures were a reduction from 25% to 10% and in dry, from 40% to 15%. Thus despite an average cost increase of 6.5%, the concrete on the wall worked out some 12% cheaper due to the reduction in waste. Environmentally friendly and less cost!

Table 1 Wet mix cost calculations for steel fibre shotcrete used in tunnel linings

MATERIAL	NO SILICA FUME			SILICA FUME		
	Quantity	Unit Cost	Cost/m³	Quantity	Unit Cost	Cost/m³
Cement	500	3	1500	460	3	1380
Silica Fume	-	-	-	22	30	660
Aggregate	1600	0.2	320	1600	0.2	320
Streel Fibres	50	60	3000	50	60	3000
Plasticizer	6	40	300	6	40	300
Accelerator	25	35	875	14	35	490
Total			5995			6150
Cost + Application			9000			9500
Cost + Rebound			12000@25%			10500@ 10%
Cost/m² @ 75mm layers			900			785

Example - Indianapolis International Airport Parking Garage, USA

A parking ‘house’, for 7,100 cars, built in 16 months. Designed using both Life 365 and LEED point criteria, the mix used was silica fume based. Keeping the concrete warm allowed for the post-tensioning to continue at 20 hours per pour, all through the construction. Redesign of the columns and slabs meant more space giving a light and safe atmosphere within the structure.

The mix design, using a percentage of recycled aggregates and supplementary cementitious materials, plus the improved speed of construction, gave overall savings of approximately **$3,000 per car space**.

That means an overall saving of **$21.3million**, making this project the best example of being sustainable, durable and very cost effective.

From the start conventional thinking was put to one side. They used the LEED system and Life 365 to design this unit and the concrete used. It enabled a continual turnaround of 20 hours between pouring concrete and post-tensioning. The strengths meant that beams and columns could be redesigned to give more space and the total project cost was considerably reduced (Figure 5).

Figure 5 Indianapolis International Airport Parking Garage

The use of high performance concrete enabled the design and construction of wide open, user friendly structure. There are not many car parks in the world where you will find that number of bays between the columns. So we must leave our “per cubic metre” mindset behind and look at the total value. There are many ways to reduce the costs in the whole project when we take all things into account:

Can we use a local aggregate – and put a high performance matrix around that?
Could we use a lightweight aggregate?
Can we use blended cement?
Can we pump it – use SCC?
Can we pump it further, vertically or horizontally?
Can we achieve the required strength / durability in a shorter time period?
Can we redesign the columns / floors / basements?
Can we make it last as long as possible – without any repairs/ maintenance?

And many other things we need to be thinking of when we are building for the future – not just the life of our buildings, but for the future of our natural resources for our children and grandchildren, and for the climate.

We know we can do this. We must use our knowledge – the concrete technology that we share – and do what we know we can do. Because in 50 years time, no-one is going to remember that you saved $10,000 on a project by using a cheaper concrete – but they’ll know

if that concrete is going to last another 100 years, or if they've had to replace it, at 50 times the original cost, and use up all those natural resources, all over again…

Example - Tsing Ma Bridge, Hong Kong

Use of two triple blends for this construction: approximately 200,000 cubic metres. OPC, FA and SF used for the support columns on the roadways and approaches. OPC, GGBS and SF used for the slipforming of the two towers, each 206m high. This latter mix was designed at 30% OPC, 65% GGBS and 5% SF. It had to be fluid enough to pump, yet rapid enough in setting to be used for slipforming, and cool enough to allow for the large sections that made up the towers. Without the SF this could not have been achieved. The triple blend mixes also improved the durability, giving very high chloride resistance – a significant part of the specification.

Example - East Sea Bridge, Shanghai

32.5 km of twin bridge across the Strait at Shanghai. Mainly built of standard cantilever low level sections, there were also four shipping channel high bridges of different heights and spans. This huge project was a 'first' of its complexity, with a very tight 'wish list' : Richter 7 durable; ASR resistance; chloride resistance; water resistance; carbonation resistance; highest wind / wave durable and such. The Shanghai Research Institute of Building Science made extensive investigations into bridge designs and concretes and came up with the use of two 'mineral cement' blends. MC l used a triple blend of OPC, GGBS and FA. MC ll used a quaternary blend – OPC, GGBS, FA and SF. While strengths were kept near the design target – C35 and C50 – the durability characteristics of the concretes – compared to pure OPC equivalents – were significantly enhanced. OPC content in the mixes was kept to less than 40%, helping to make this a very 'green' project. Using the pre-blended 'mineral cements' also simplified cementitious storage and production of concrete – improving construction times. The whole project took less than three years to build.

Example - Burj Khalifa

To build the best, you use the best – and this was no exception. The specification called for concretes ranging from C60 to C100, with low alkali, sulfate resistance, chloride resistance, water resistance and pumpable to record heights. A triple blend design specification – Moderate Sulfate Resisting Cement, FA and SF – allowed the production of a concrete that not only met, but exceeded, the strength and durability requirements:

- Water Penetration (BS EN 12390 - 8) <10mm actual = zero.
- Water Absorption (BS 1881:122) <1.5% actual = 0.70%
- RCPT (ASTM C1202) <1200 actual = 590
- Water Permeability (Din 1048) <5mm actual = zero

The pumping height achieved was over 601m – a world record –and this was using a high performance concrete with the above durability characteristics and containing 44% supplementary cementitious materials per cubic metre. High performance and high sustainability as well.

REFERENCES AND ACKNOWLEDGEMENTS

Unless cited within the text, all the examples are taken from case studies and personal notes on Elkem Silicon Materials supplied projects.

Additional data has been supplied by Per Fidjestøl, Elkem Silicon Materials, Norway and Tony Kojundic, of Elkem Silicon Materials, USA.

Experimental Creep Tests on Concrete Made with Montmorillonite Nano Particles

A Sprince, L Pakrastinsh, , A Korjakins
Riga Technical University, Latvia

The purpose of this research is to investigate and characterize the time-dependent behavior of new concrete compositions made with montmorillonite nano particles — and then comparing them with control specimens made from standard concrete. This paper presents experimental test results of the compression creep of the proposed concretes. Several concrete compositions with unconventional additives were designed and prepared. The tests were performed on both normal strength and high strength concretes. Specimens were tested in two extreme environments: in one case there was 100% humidity provided by protecting the specimens from desiccation, and in the other case specimens were air-dried and protected from any moisture. Concrete specimens were subject to load in a constant room temperature and with a constant level of moisture. The investigated properties include compression strength, modulus of elasticity, creep and creep coefficient.

Andina Sprince, Mg.sc.ing., Lecturer at RTU, Department of Structural Engineering. Acquired a Professional Master's degree in Civil Engineering, as well as a civil engineer's qualification at RTU, Department of Structural Engineering in 2009. Currently a 2nd year Phd student in the RTU Institute of Materials and Structures programme "Civil Engineering". Field of research: structural behavior of nano–modified concrete, long –term deformations.

Leonids Pakrastinsh, Dr.sc.ing., associate professor, Institute of Structural Engineering and Reconstruction, Riga Technical university, Head of Department of Structural Engineering, Convener of Technical Committee LVS/TC 30. Field of research: structural behavior of cementitious composites.

Aleksandrs Korjakins, Dr.sc.ing., professor, Institute of Materials and Structures, Riga Technical university, Head of Department of Building Materials and Units. Field of research: building materials and structures, ecological building materials, reuse of industrial waste.

Keywords: Compression strength, Creep, Creep coefficient, Modulus of elasticity, Montmorillonite nano particles

INTRODUCTION

The deformation characteristics of concrete are important in the design of sustainable structures. Concrete is an important structural material used in every country of the world. Moreover, the complexity of structures and their size have continued to increase, and this has resulted in a greater importance of their deformation characteristics and in more serious consequences of their behavior [1]. One type of strain that plays a major role in successful and continuous use of structures is creep – deformations that appear due to long-term loading of the structural element [2].

Formulation of creep and relaxation models has been ongoing from more than hundred years. In the case of concrete, elastic behaviour of concrete was taken for granted for a long time. However, in 1907 Hatt wrote an article on a test performed on reinforced concrete beams subjected to constant load. Hatt discovered that the deflection increased significantly with time [3].

Creep of concrete originates in the hardened cement paste that consists of a solid cement gel containing numerous capillary pores. The cement gel is made up of colloidal sheets of calcium silicate hydrates separated by spaces containing absorbed water. Creep is thought to be caused by several different and complex mechanisms not yet fully understood. Neville *et al* [1]. identified the mechanisms for creep. Recent research relates the creep response to the packaging density distributions of calcium-silicate-hydrates. At high stress levels, additional deformation occurs due to the breakdown of the bond between the cement paste and aggregate particles [1].

Therefore, designers and engineers need to know the creep properties of concrete and must be able to take them into account in the structure analysis. After all, the end product of an engineer's endeavours is a structure whose strength is adequate, but not wastefully excessive, whose durability is commensurate with the conditions of exposure, and whose serviceability ensures fitness for the purpose. Consideration of creep is a part of a rational approach to satisfying these criteria. Deformation characteristics of materials are an essential feature of their properties, and a vital element in the knowledge of their behaviour. After all, it is the subject that matters: creep is important if its deformation increases with time under a constant stress [1].

Nowadays nano-particles of clay minerals are used in production of polymeric nanocomposite in order to improve mechanical characteristics. Polymeric nanocomposites had been developed by Japan scientists in 1970 – 80th. In Latvia nanocomposites based on styrene-acrylate copolymer and organically modified with montmorillonite nano particles was prepared and investigated during recent 10 years [4].

Investigations on modifying concrete compositions by nano particles are carried out in present time in different countries. It is proved that nanosized silicium dioxide particles allow to achieve very dense microstructure and to improve performance characteristics of concrete [4]. Information about montmorillonite nano particles use as concrete nano-filler not found in literature. The aim of this study is to investigate influence of synthetized montmorillonite clay mineral nano-particles (MNP) on mechanical strength and creep behavior of concrete.

Used material is synthesized montmorillonite clay mineral named as Hydrated sodium calcium aluminum silicate, chemical formula $(Na,Ca)(Al,Mg)6(Si_40_{10})3(OH)6\text{-}nH_20$.

Montmorillonite mineral is a member of the smectite family. Montmorillonite crystal structure is 2:1, meaning that it has 2 tetrahedral layers of silicium dioxide sandwiching a central octahedral layer of aluminium oxide. Average density of montmorillonite clay mineral is 2.35 g/cm^3, specific surface 750 m^2/g. The particles are plate-shaped, average length 20-500 nm, Thickness of clay flakes about 1 nm, therefore clay may be classified as nano-admixture [5].

METHODS

One of the goals of the experiment was to find out whether the new concrete composition can be competitive and whether its physical and mechanical properties are equivalent to those of ordinary concrete. The object of this experimental study was ordinary and high strength concrete made with admixture of montmorillonite clay mineral nano particles (MNP) in amounts of 1per cent of the total cement volume. Other raw materials used for this study were natural coarse diabase aggregate, shingle, fine aggregate quartz sand and normal portland cement CEM I 42.5 N. Table 1 shows concrete mix composition [5].

Table 1 Concrete mix compositions [kg/m^3]

MIX DESIGNATION	HSC	HSC MNP	REFERENCE	MNP
Portlandcement CEM I 42.5 N	800	800	350	350
Diabaze 0/5 mm	640	320	-	-
Shingle 5/20	-	-	500	500
Shingle 2/12	-	-	500	500
Sand 0/2.5	640	320	750	750
Silicafume	120	120	80	80
MNP	-	8	-	3,5
Water	200	200	190	190
Superplasticizer	15	15	7	7
Water/ Cement ratio	0.25	0.25	0,54	0,54

Standard sample cubes 100x100x100 mm and prisms 40x40x160 mm were produced in order to investigate the mechanical characteristics of the material. Concrete mixtures were cast into oiled steel moulds and compacted at the vibrating table. After two days the moulds were removed. Standard hardening conditions (temperature +20 ± 1ºC, RH > 95%) were provided. After the hardening period, the samples were measured and tested in standard conditions. Their compression strength was determined in conformity with LVS EN 12390-3:2002.

At the beginning of the creep test, the specimens were 51; 57 and 63 days old. The tests were conducted in two extreme conditions. In one case no moisture exchange with the environment was permitted, which was ensured by protecting the specimens against desiccation, and in the other case drying was permitted under conventional conditions, by protecting the specimens against moisture [6]. In this paper shall be called these batches Reference (dry), Reference (moist), MNP (dry), MNP (moist), HSC MNP (dry) and HSC MNP (moist). In order to prevent humidity exchange between the specimen and the environment, the surface of the specimens was coated with two protective silicone layers. Before this sealing, four aluminium plates were centrally and symmetrically glued onto two sides of the test prism in order to provide a basis for the strain gauges. The distance between two plates was 50 mm. Two +/-

0.01 mm precision strain gauges were symmetrically connected to each specimen, and then the specimens were put into a creep lever test stand and loaded. Figure 1 shows the creep lever test stand. Specimens were kept in a dry atmosphere of controlled relative humidity in standard conditions: temperature 23 ± 1ºC and relative humidity 25 ± 3%.

Consider a point in a concrete specimen subjected to a constant, sustained compressive stress σ_{c0} applied at time τ_0 and equal to 30 per cent of the characteristic compressive strength of concrete for high strength concrete mixes specimens i.e. σ_{c0}= 0.3 f_c and 40 per cent for ordinary concrete mixes specimens, i.e. σ_{c0}= 0.4 f_c [6, 7]. Load was applied gradually in 4 steps and as quickly as possible.

They were kept under constant load for 90 days and for recoverable creep they were kept without load for 40 days.

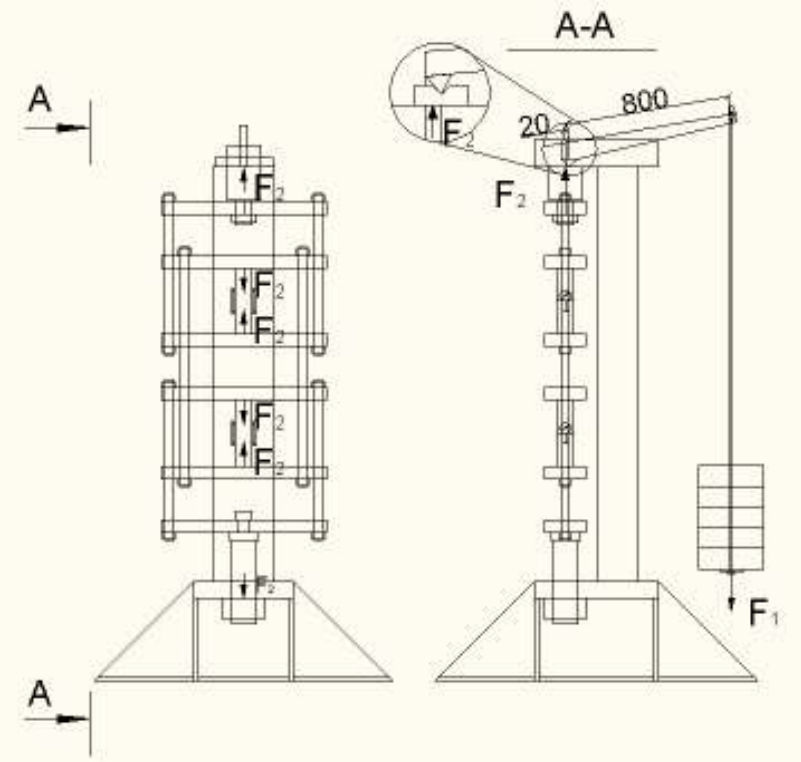

Figure 1 Specimens in the creep lever test stand

Equation 1 shows the instantaneous strain that occurs immediately upon application of the stress:

$$\varepsilon_{e(t)} = \sigma_c / E_c \tag{1}$$

where E_c is the elastic modulus at time τ_0

$\varepsilon_{e(t)}$ is the instantaneous strain

σ_c is the compressive stress

Equation 2 shows the creep strain $\varepsilon_{cc}(\infty, t_o)$ in time $t(\infty)$ subjected to a constant sustained compressive stress σ_c applied at age t_0:

$$\varepsilon_{cc}(\infty,t_o) = \varphi(\infty,t_o) \cdot \sigma_c / E_c \tag{2}$$

where $\varepsilon_{cc}(\infty,t_o)$ is the creep strain
$\varphi(\infty,t_o)$ is the creep coefficient

Equation 3 shows the capacity of concrete to creep is usually measured in terms of the creep coefficient $\varphi(\infty,t_o)$. In a concrete specimen subjected to a constant sustained compressive stress σ_c, first applied at age *t*, the creep coefficient at time *t* is the ratio of the creep strain to the instantaneous strain [2]:

$$\varphi(\infty,t_o) = \varepsilon_{cc}(\infty,t_o) / \varepsilon_{e(t)} \tag{3}$$

RESULTS

The tests to determine compression strength, modulus of elasticity and creep, creep coefficient were done on concrete samples in which montmorillonite nano particles (MNP) were used as admixture. Experimental work made it possible to compare the strength of reference concrete samples and samples containing MNP. Cubes' strength tests were carried out after 7; 37; 42 and 93 days of hardening in standard conditions. The various compression strengths of concrete specimens in different ages containing MNP as an aggregate were then compared to reference concrete specimens. Figure 2 shows that HSC MNP was 5% lower strength in the first 7 days, but on the 37th day the strength increased and was by about 4.8% larger than HSC, and on the 93rd day the strength of concrete with MNP was larger by about 3.5%.

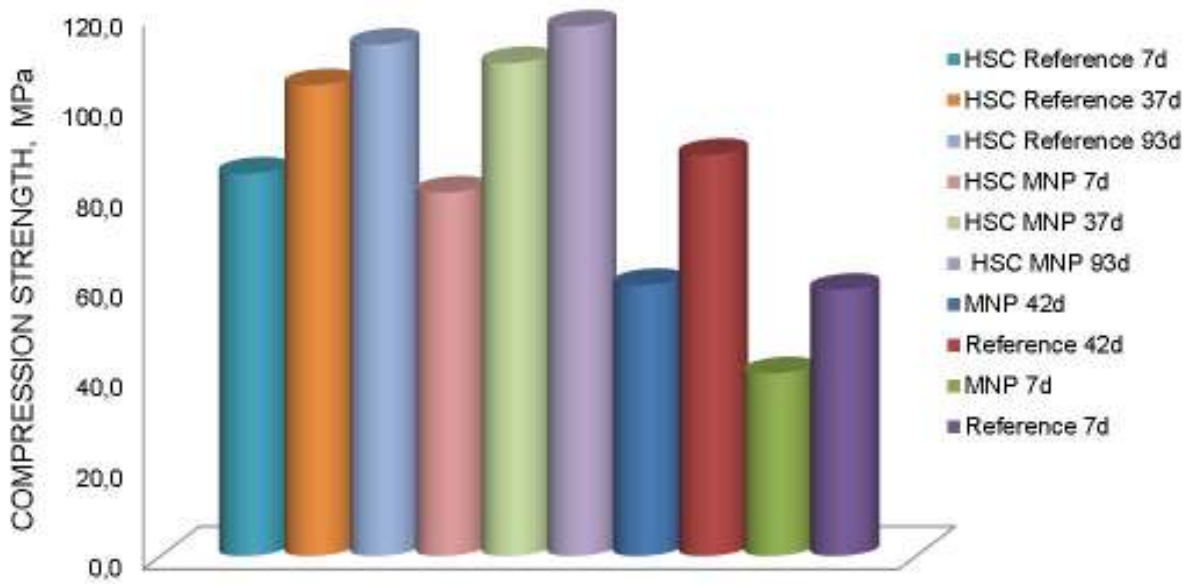

Figure 2 Concrete compression strength at 7; 37; 42 and 93 days, MPa

Ordinary concrete containing a MNP showed 31.4% lower strength in the first 7 days than reference concrete strength and on the 42nd day the strength was lower by about 32.4%.

High strength concrete mix containing montmorillonite nano particles perform good strength development during long-term hardening period. HSC MNP specimens showed a 45.8% increase of compression strength, while the HSC showed a 33.8% increase of compression strength on the same period. Ordinary concrete specimens with a MNP showed a 48.5% increase of compression strength, but the reference specimens showed a 50.8% increase of compression strength.

Figure 3 shows that the modulus of elasticity was determined by measuring the deformations on the sides of the specimens according to Hooke's law. For HSC at the age of 51 days the difference between specimens hardened in moist and dry conditions is approximately 1.9% but at the age of 63 days the difference is 16%. For HSC MNP this difference is approximately 17.4% and 11% respectively. The comparison of the modulus of elasticity of 51 days old HSC and HSC MNP specimens shows that the modulus of elasticity for specimens with montmorillonite nano particles is larger. For specimens hardened in moist conditions this difference is 34.5%, while for samples hardened in dry conditions it is 9%. However, the comparison of the modulus of elasticity of 63 days old HSC specimens and specimens containing MNP shows contrary results – the modulus of elasticity for HSC specimens is larger. For specimens hardened in moist conditions this difference is 43.5%, while for samples hardened in dry conditions it is 6.2%.

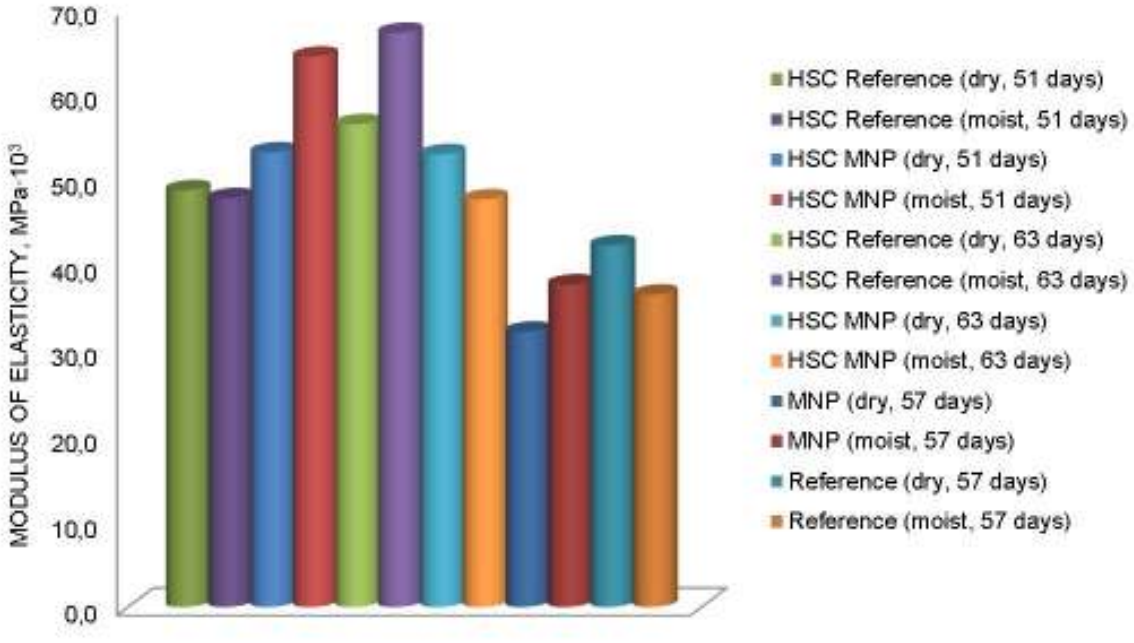

Figure 3 Modulus of elastisy of different concrete

Figure 3 shows that for reference concrete and for concrete specimens with MNP this difference between specimens hardened in moist and dry conditions are approximately 17% and 16% respectively. The comparison of the modulus of elasticity of reference concrete specimens and specimens with MNP shows that for specimens hardened in moist conditions this difference is 3.3%, while for specimens hardened in dry conditions it is 24%.

Figure 4 the stress-strain relation shows that the same tendency. The stresses are almost proportional to the strain, and therefore the stresses do not reach the point of microcracking.

In a loaded specimen that is in hygral equilibrium with the ambient medium (i.e. no drying), the time-dependent deformation caused by stress is known as *basic creep* [1]. Creep increases with time at a decreasing rate. In the period immediately after initial loading, creep develops rapidly, but with time the rate of increase slows considerably [2].

Figure 5 shows elastic strain plus linear basic creep and shrinkage as dependence of time. Under constant mechanical loading, the strain of HSC at the ages of 51 and 63 days increases significantly with the loading duration, the increase reaching 2.6 to 3.3 times the value of the instantaneous strain. At both ages, the strain increase of concrete specimens containing MNP reaches 2.6 to 4.8 times the value of the instantaneous strain.

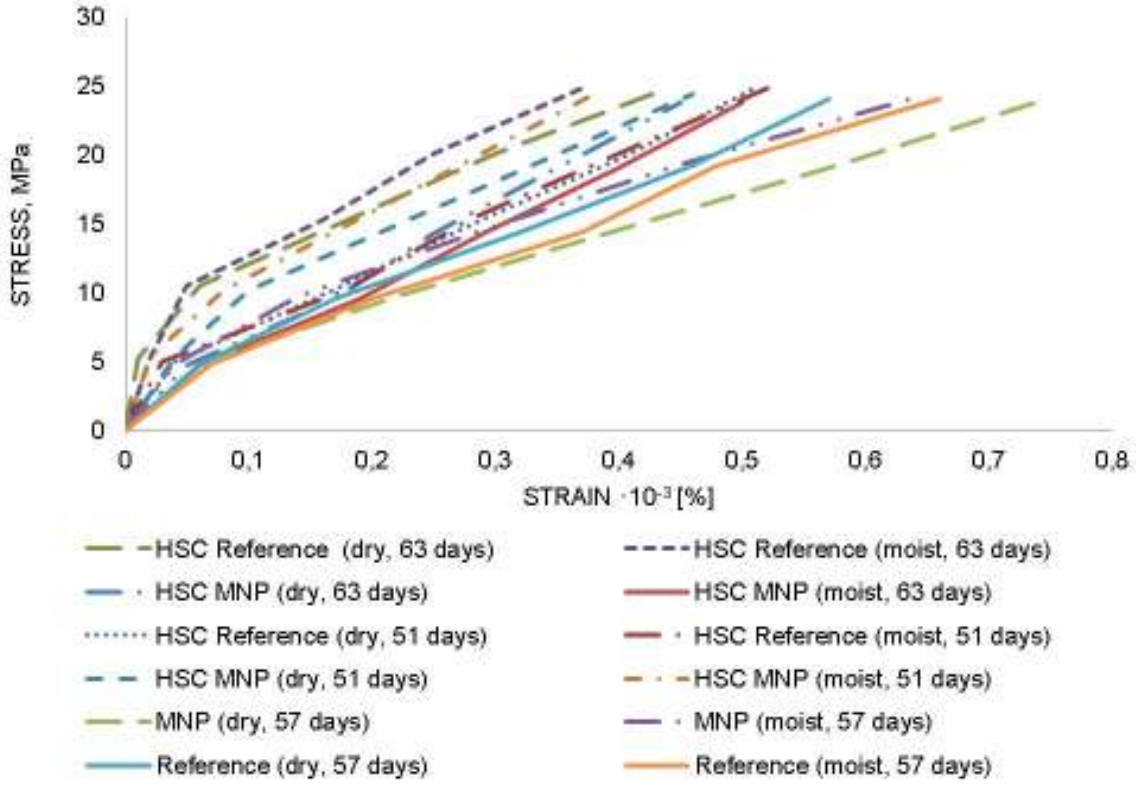

Figure 4 Relation between stress and strain

The smallest deformation was exhibited by HSC in moist conditions. The average difference between HSC specimens hardened for 51 days in moist and in dry conditions is approximately 23% and the smallest creep is for specimens in dry conditions, but for HSC specimens at the age of 63 days hardened in moist and in dry conditions the amount of

deformations is contrary – the creep is larger in dry-hardened specimens, and the average difference is approximately 30%. For 51 days old HSC MNP specimens this difference is approximately 46%, and for 63 days old specimens it is 28%. At both ages the larger deformation was exhibited by dry-hardened specimens. If we compare the average difference between the HSC specimens at 51 days and the HSC MNP ones of the same age, we can see that for specimens hardened in moist conditions this difference is 23%, and for specimens hardened in dry conditions it is 85%. In moist conditions the larger deformation is exhibited by HSC specimens, but in dry conditions it is contrary – the larger deformation is exhibited by HSC MNP specimens. In comparison with the 63 days old specimens, the difference is 38% and 24% respectively. In dry condition smaller deformation is shown by HSC specimens for both ages and in moist condition smaller deformation is by HSC containing MNP for both ages.

Figure 5 shows that under constant mechanical loading, the strain of reference concrete increases significantly, the increase reaching 3.15 to 3.61 times the value of the instantaneous strain, and for specimens containing MNP it reaches 2.88 to 4.32 times. The smallest creep is exhibited by reference concrete specimens in dry conditions. The average difference between basic creep of reference concrete specimens hardened in moist and in dry conditions is approximately 21%. For specimens containing MNP this difference is approximately 14.5%. By comparing the average difference between the reference concrete specimens and the MNP, it can be seen that for specimens hardened in moist conditions this difference is 12.8%, and for specimens hardened in dry conditions it is 22%.

Figure 5 shows recoverable and irrecoverable creep. Largest part of recoverable creep strain is instantaneous. At both ages for HSC the larger difference of irrecoverable creep strain was exhibited by moist-hardened specimens but for HSC MNP specimens it is contrary – the larger difference is exhibited by dry-hardened specimens. The creep coefficient increases with time at an ever-decreasing rate. The final creep coefficient is a useful measure of the creeping capacity of concrete.

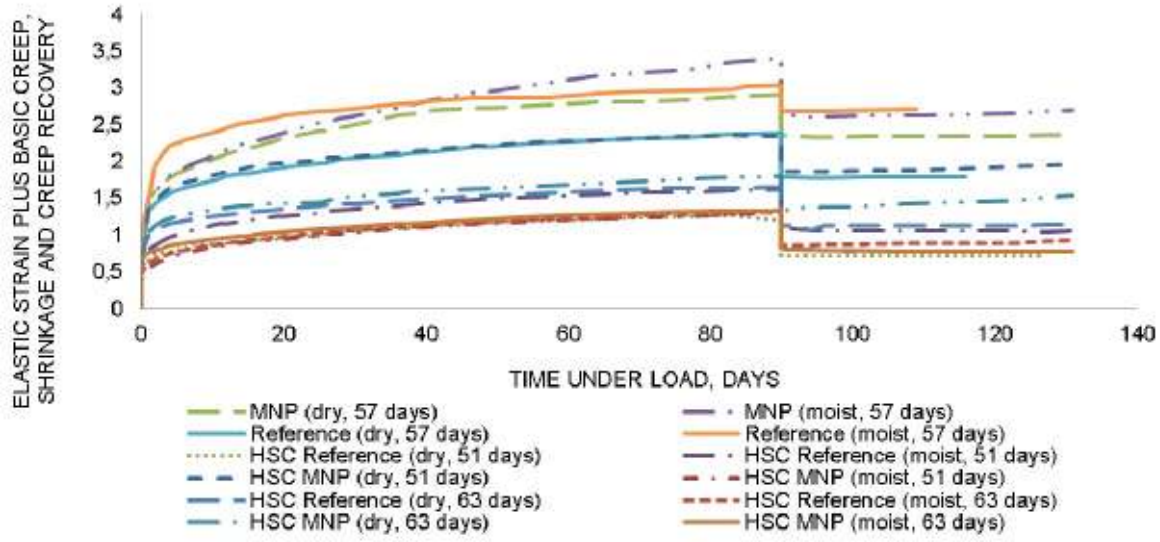

Figure 5 Elastic strain and long-term deformations of different kind concrete samples

Figure 6 shows the comparison of the creep coefficients of HSC and HSC MNP specimens at the age of 51 days. The creep coefficient for specimens in dry conditions with clay particles is larger but in moist conditions the creep coefficients are similar but at the age of 63 days the creep coefficients of dry-hardened specimens are similar, while in specimens cured in moist conditions the creep coefficient of concrete specimens containing MNP is smaller. The average difference between HSC specimens at the age of 51 days hardened in moist and in dry conditions is approximately 19%, but for HSC specimens at the age of 63 days hardened in moist and in dry conditions the coefficient is larger for dry specimens. The difference is approximately 5%. At both ages the larger coefficient is exhibited by moist-hardened specimens. For 51 days old MNP specimens this difference is approximately 50%, and for specimens at the age of 63 days it is 48%. At both ages the larger coefficient is exhibited by dry-cured specimens. If compare the average difference between 51 days old HSC specimens and the ones containing MNP than for samples hardened in moist conditions this difference is 10%, and for samples hardened in dry conditions it is 104%. In comparison with the 63 days old specimens, the difference is 29% and 11% respectively. Interesting that in moist conditions the larger coefficient is exhibited by HSC specimens, but in dry conditions the larger coefficient is shown by specimens containing MNP, but in moist conditions the smallest coefficient is exhibited by specimens containing MNP, but in dry conditions the smallest coefficient is shown by HSC specimens.

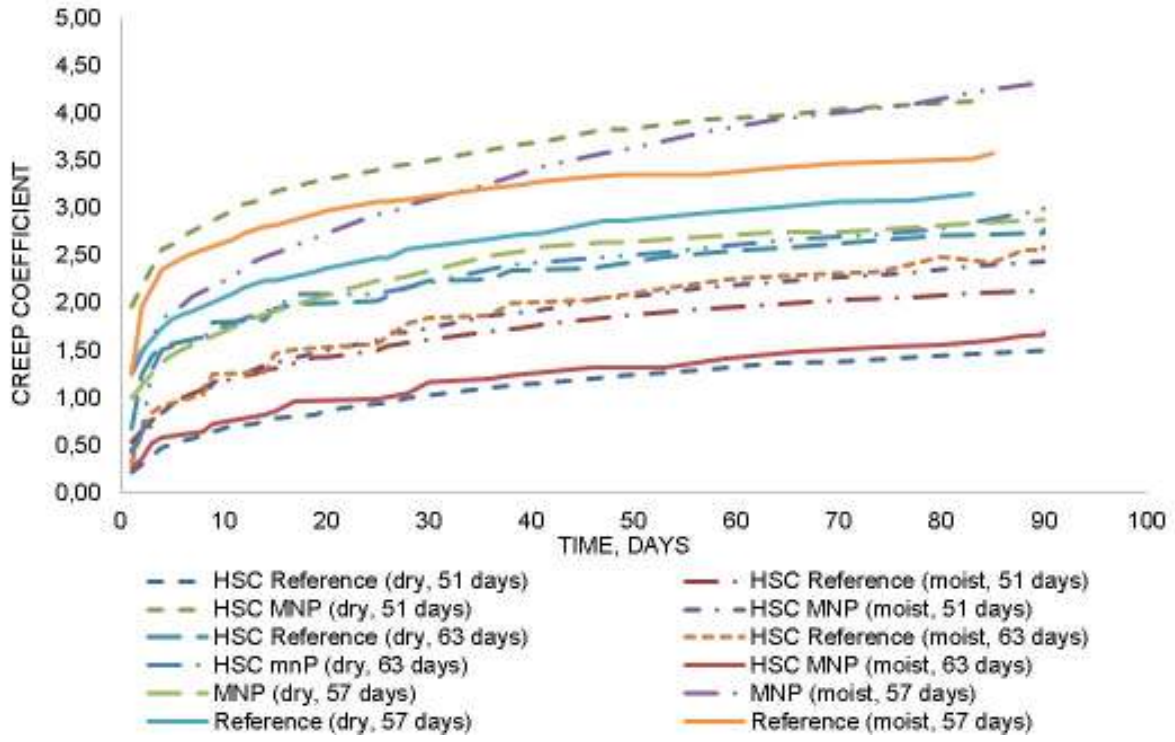

Figure 6 Creep coefficients of different kind concrete samples

The comparison of the creep coefficients of reference concrete specimens and MNP specimens shows that the creep coefficient of specimens containing clay particles and hardened in dry conditions is larger but in the moist conditions the creep coefficient is larger for reference concrete. The average difference between reference concrete specimens in moist and in dry conditions is approximately 10%, but for MNP specimens this difference is

approximately 27%. If we compare the average difference between reference concrete specimens and the ones containing MNP we can see that for specimens hardened in moist conditions this difference is 15.4%, and for specimens hardened in dry conditions it is 6.5%.

CONCLUSIONS

This experimental study proves that montmorillonite nano particles in small dosage (8 kg/m^3) don't have negative influence on mechanical and deformation characteristics of concrete. Some positive effects are established. Long-term deformation testing was carried out, and the modulus of elasticity and the compression strength of ordinary concrete and of concrete containing montmorillonite nano particles were determined.

High strength concrete mix containing montmorillonite nano particles perform long-term hardening effect. Compression strength of 93 days old high strength concrete specimens containing MNP was larger than that of HSC specimens. Ordinary reference concrete specimens and specimens containing MNP showed a similar increase of compression strength at both ages.

The modulus of elasticity in dry condition at all ages was larger for reference specimens, but in moist condition it was larger for concrete specimens containing MNP.

The smallest basic creep in dry conditions is for reference concrete specimens and in moist condition for concrete specimens containing MNP. Largest part of recoverable creep strain is instantaneous.

The final creep coefficient is a useful measure of the creep capacity of concrete. On the 90th day of testing, the value of the basic creep coefficient reaches 1.5 to 2.8 for HSC specimens and 1.7 to 4.1 for concrete specimens containing MNP. And for ordinary concrete the value of the basic creep coefficient reaches 3.1 to 3.6 and 2.8 to 4.3 for concrete specimens containing MNP. The results of this experiment can be used to predict creep deformations.

In the future, the physical and mechanical properties of new high-strength concrete containing montmorillonite nano particles as an alternative admixture should be investigated in a more detailed way. Possibilities to increase efficiency of montmorillonite nano particles must be regarded. Particle additional chemical treatment or thermal activation may be used in future research.

Obtained results indicate on quite high dispersion of experimental data. In order to decrease the dispersion of results, the number of specimens and tests should be increased.

ACKNOWLEDGEMENT

This work has been supported by the European Social Fund within the scope of the project “Support for the Implementation of Doctoral Studies at Riga Technical University”.

REFERENCES

1. NEVILLE A. M., DILGER W. H., BROOKS J. J. Creep of Plain and Structural Concrete, 1983, pp 1 - 13.

2. GILBERT R.I., RANZI G. Time-Dependent Behaviour of Concrete Structures, 2011, pp 1-9.

3. WESTMAN G. Concrete creep and thermal stresses, New creep models and their effects on stress development, Doctoral thesis, 1999, Department of civil and mining engineering, Division of structural engineering, Lulea University of Technology, Lulea, Sweden, p 7.

4. MAKSIMOVS R.D., GAIDUKOVS S., ZICANS J., KALNINS M., PLUME E., SPACEK V., SVIGLEROVA P. Nanocomposites based on styrene-acrylate copolymer and organically modified montmorillonite, 1. Mechanical properties. Mechanics of Composite Materials, Vol. 42, No3, 2006, pp 263-272.

5. SPRINCE A., PAKRASTINSH L., KORJAKINS A., SHAKHMENKO G. Effect of Montmorillonite Nano Admixture on Long-term Deformations of Concrete, Scientific Journal of Riga Technical University, Construction Science, Vol.12, pp 52 -53.

6. RILEM TC 107-CSP: Creep and shrinkage prediction models: principles of their formation. Measurement of time-dependent strains of concrete, Materials and Structure, Vol. 31, October 1998, p 509, 511.

7. ACI COMMITTEE 209, Report on factors affecting shrinkage and creep of hardened concrete (ACI 209.1R-05), American Concrete Institute, Farmington Hills, Michigan, 2005, p 10.

Environmental Aspects of Optimized Design of Concrete Structures

P Stepanek, I Lanikova, P Simunek, F Girgle, D Horak
Brno University of Technology, Czech Republic

The contribution describes some differences in results of practical design of a concrete structure. According to some standards for the design of concrete structures (e.g. EC2 and the original Czech standard CSN 73 1201-86) it is possible to design the structure by several methods. This paper documents the fact that even if a designed structure does not comply with the partial reliability factor method, according to EC2, it can satisfy to the reliability conditions according to the fully probabilistic approach when using the same materials, boundary conditions and the loading. The application of the fully probabilistic design approach and the verification of reliability enable the introduction of mass production with the option of control over the design procedure, and increasing quality. Individual input quantities, which are considered as random quantities with a given probability distribution (or statistical distribution parameters), can be gained by long-term monitoring and evaluation. To find the best possible design of a structure an optimising procedure (method) is appropriate to use. Economical and ecological aspects (acquisition costs, CO_2 and SO_2 emissions or embodied energy associated with concrete member production, respectively) are taken into account in objective function. The objective function has a significant influence on the obtained optimal result. Efficient design procedures can achieve not only cost savings during construction (materials and energy), erection, maintenance, disassembly and material recycling but also a more favourable environmental impact. A design example will be presented. From the example of prestressed spun concrete pole design by the partial factor method and simulation method (fully probabilistic approach according to the Eurocode) it is evident that an expert should apply a more precise (though unfortunately more complicated) design method and obtain "better" structure design.

Petr Stepanek, Prof., M.A., M.Sc, Ph.D., Head of the Department of Concrete Structures at BUT Brno. He coordinated 13 research projects and published more than 230 publications with specialisation in structural engineering, non-linear behaviour of structures, composite structures, optimization of constructions design, development of new materials and systems for building industry, programming systems for engineering tasks solution, repair, strengthening and reconstruction of constructions, identification of deterministic and stochastic systems.

Ivana Lanikova, M.Sc, Ph.D. was engaged in 5 research projects and published more than 44 publications with specialisation in optimisation of concrete structures design, integrated structure and material design, mathematical modelling of concrete structures.

Petr Simunek, M.Sc, Ph.D. cooperated on solution of 6 research projects and published more than 30 publications with specialisation in structural engineering, behaviour and design of concrete and masonry structures, management of structures risk and hazards.

Frantisek Girgle, M.Sc, Ph.D. cooperated on solution of 5 research projects and published more than 23 publications with specialisation in development of new materials and systems for building industry, composite structures, mathematical modelling of constructions and structures, design of structures.

David Horak, M.Sc, was engaged in 6 research projects and published more than 49 publications with specialisation in composite structures, development of new materials and systems for building industry (especially for load bearing structures), mathematical modelling of constructions and structures, non-linear behaviour of structures and systems.

Keywords: Concrete structures design, Environmental assessment, Optimization, Partial reliability factor, Probability based design

INTRODUCTION

The building industry is one of the largest consumers of material and energy resources and ranks among the largest producers of waste and harmful emissions. Therefore, it is useful to design a structure so that its environmental impact is minimal. To find the best possible design for a structure or member without a negative effect on the reliability system as a whole it is necessary to use a suitable optimisation method. Most of the standards enable the use of a variety of methods for the design of a particular structure. The obtained outcome of these methods depends on:

- the level of simplification of the calculation within a particular procedure,
- the quality of the input data,
- the expertise of the engineer, and the amount of time he/she has available to spend on the structural design.

The partial reliability factor method is presently mostly used for the design and review of a structure from the standpoint of ultimate states. This method is used especially for its simplicity and the ease of obtaining input data. The input data result from the used materials and loads (relating to the structure's function and its location). Characteristic input data values are given in relevant parts of the standards and drawing documentation. However, standard ČSN EN 1990 [1] alternatively also enables the application of probabilistic methods for the design and review of structures. Basic information is mentioned in ČSN EN 1990 and ISO 2394 [1, 2].

DESIGN METHODS

The design process includes a lot of uncertainties, especially:

- the randomness of physical quantities used in the design (as a natural characteristic of each quantity),
- statistical uncertainties during the description of a particular quantity caused by a lack of data,
- model uncertainties caused by inaccuracies in the calculation model in comparison with real structural behaviour,
- uncertainties caused by inaccuracies in the limit state definition, mistakes
- and human element deficiencies within the design procedure, execution, maintenance and usage of the structure, along with incomplete knowledge of real material and structural behaviour.

The partial reliability factor method

In the classic approach of evaluating the reliability of a structure using the partial reliability factor method, the first three above-mentioned groups of uncertainties are hidden within the partial reliability factors, which are determined separately both for the effects of load E and structural resistance R (Figure 1). During the application of this approach it is not necessary to know the particular "values" of the uncertainties. The reliability review is simplified within the observance of rules and recommendations but the real probabilistic base of the reliability review stays hidden.

The ultimate limit state (ULS) reliability condition is:

$$R_d \geq E_d \tag{1}$$

and for serviceability limit states (SLS)

$$C_d \geq E_d \tag{2}$$

where R_d is the design value of structural resistance (including the influence of partial reliability factors for materials and model uncertainty for ultimate state design), C_d is the design value of the relevant criterion of serviceability (including the influence of partial reliability factors for materials and model uncertainty for serviceability design) and E_d is the design value of the effect of loading (including the effect of partial reliability factors for load and model uncertainty for ultimate state design or for serviceability design).

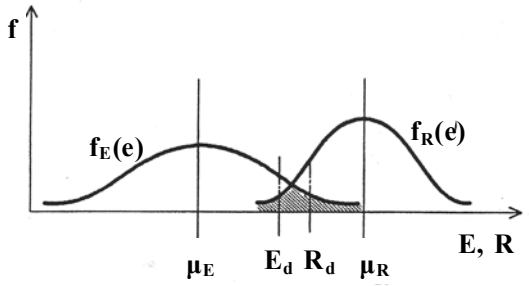

Figure 1 Random variables: R – structural resistance, E – effect of loading

The values of individual partial reliability factors depend upon the type of assessed limit state and the reliability category. These values are presented in [1] and in the appropriate EC standards and national appendixes.

The fully probabilistic approach

The probabilistic formulation procedure expressing structural reliability [4] considers the variable quantities entering the calculation to be random quantities whose uncertainties can be described by means of mathematical statistical methods. This approach requires either knowledge of the probability distribution of these quantities or at least knowledge of the distribution of the statistical parameters, and possibly the mutual statistical dependence or independence of individual quantities. The reliability condition is usually expressed with the help of failure function Z

$$Z = g(R, E) = R - E\,. \tag{3}$$

A value of $Z \geq 0$ means a failure-free state (reliability reserve); a value of $Z < 0$ means a structural failure.

The quantities E (effect of loading) and R (structural resistance) are random quantity functions that represent in principle the geometrical and material characteristics, load, and possibly the influences of other factors. The failure probability can be determined

$$p_f = P(R < E) = P(Z < 0) = \int_{Z<0} f_Z(z)dz \tag{4}$$

where $f_Z(z)$ is the density of the failure function distribution probability (Figure 2).

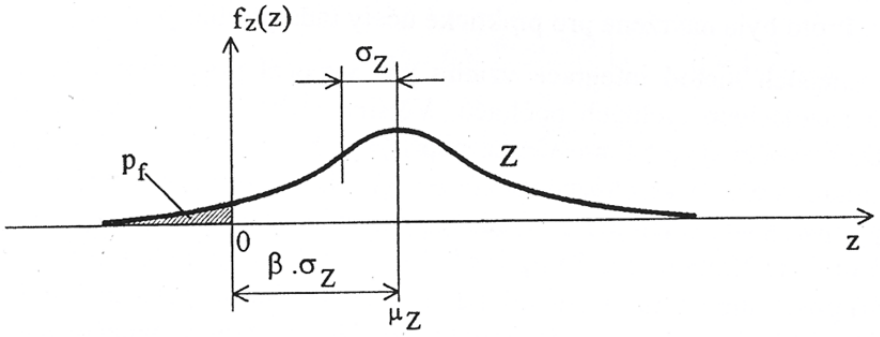

Figure 2 Failure function Z, failure probability p_f, reliability index β

The reliability condition is expressed as

$$p_f \leq p_0 \tag{5}$$

where p_0 is the target value of the structural failure probability.

If the failure function Z has normal distribution with the parameters μ_Z (mean value) and σ_Z (standard deviation), it is possible alternatively to use reliability index β as a reliability indicator according to the relation

$$\beta = \frac{\mu_z}{\sigma_z} \tag{6}$$

where it is valid that

$$p_f = P(Z \leq 0) = P(g \leq \mu_z - \beta\sigma_z) \tag{7}$$

The reliability condition is possible to express in the form

$$\beta > \beta_0 \tag{8}$$

where β_0 is the target value of the reliability index related to different design situations and the referential time for load- bearing members with a dependence on the reliability category given in [1] and [2].

Analytical representation of the failure function is only possible in simple cases, and thus its application is limited. The failure function $Z = g(R, E)$ generally depends on the number of random quantities, whose distributions do not always correspond to the normal distribution. The relations for determining the effect of loading E and resistance function R are often complicated and non-linear; therefore, numerical methods (simulation, semi-analytical) are used for failure probability calculation.

ILLUSTRATIVE EXAMPLE – A SPUN CONCRETE POLE

A pole made from spun concrete was designed. The geometry of the pole is displayed in Figure 3. The reinforcement of the pole is made of prestressed wire with a diameter of 6 mm (ØPN6), which is supplemented by 10 mm diameter B500B passive reinforcement (ØR10). The pre-stressing strands are situated along the entire pole and are bond-anchored both at the top and bottom of the pole. The passive reinforcement is designed in various lengths in order to contribute to the bearing capacity of the pole. The pole has an annular cross-section. The stress acting on the pole is given by the top horizontal force. The characteristic value of this force is V = 10 kN. It includes the tensions of cable lines and also climatic effects (such as wind and icing on overhead lines).

Restrictive conditions are formulated by the principles of standards [1] and [3] according to the reliability conditions of:

- ULS within normal force load (caused by prestressing) and the bending moment (caused by the top horizontal force V) in predefined discrete cross-sections along the pole depth,
- and SLS:
    - deflection of the pole head due to the top horizontal force V,
    - crack origin at 0.5V load
    - and crack widths for 1.0V load.

Design and assessment were carried out with software based on the algorithms determined and mentioned in [5]. This software was set up primarily for use in the partial factor method but then was modified for application in fully probabilistic design. The Monte Carlo simulation method was used to calculate the reliability, modified by the Latin Hypercube Sampling method (LHS). The statistical distributions of the material characteristics and some geometric characteristics were provided by the producer of the poles, while the uncertainties of the resistance model R and the calculation of the effect of loading E were taken from the recommendation in [6]. A description of the calculation is given in [7].

Pole design

The design was based on the assumption that the geometry of the pole is unchangeable (it is determined by the mold in which it is produced); only the thickness of the concrete, the number of prestressed strands and the passive reinforcement (number of bars, length of bars) were allowed to be changed. The wall thickness of the annular cross-section is not constant along the height of the pole; thickness at the bottom is denoted by t_d and at the top by t_h. Two pole wall thickness variants were considered: a pole with t_d = 70 mm and t_h = 60 mm (type T1), and a pole with 10 mm larger of annular cross-section thickness (type T2). The number and length of reinforcement bars was designed assuming the same amount of prestressing wire (again in two variants: 20ØPN6 (type P1) and 18ØPN6 (type P2)).

Poles designed using the partial safety factor method are denoted by PSF; PBD denotes those created via probability-based design. In all cases, the designed concrete reinforcement represents the minimum amount of reinforcement necessary to ensure compliance with all the reliability conditions stipulated by the used design method. An overview of some designed types of poles is shown in Table 1.

Reinforcing steel is designed in two lengths. Figure 4 shows the distribution of reinforcement along the pole length and in the cross-section (pole type T1P1-PBD).

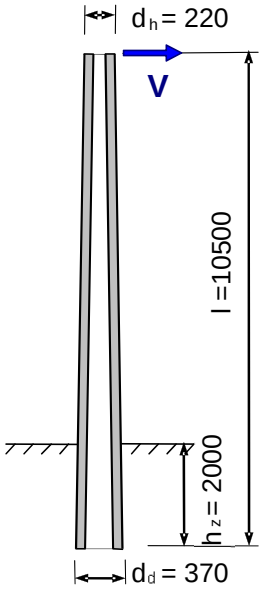

Figure 3 Geometry, loading and boundary conditions of the pole

Table 1 Types of designed poles

TYPES OF DESIGNED POLES				
type	t_d	t_h	prestressing wire	passive reinforcement
T1P1-PBD	70 mm	60 mm	20ØPN6	13ØR10
T1P2-PBD	70 mm	60 mm	18ØPN6	17ØR10
T2P1-PBD	80 mm	70 mm	20ØPN6	12ØR10
T1P1-PSF	70 mm	60 mm	20ØPN6	17ØR10
T1P2-PSF	70 mm	60 mm	18ØPN6	18ØR10
T2P1-PSF	80 mm	70 mm	20ØPN6	16ØR10

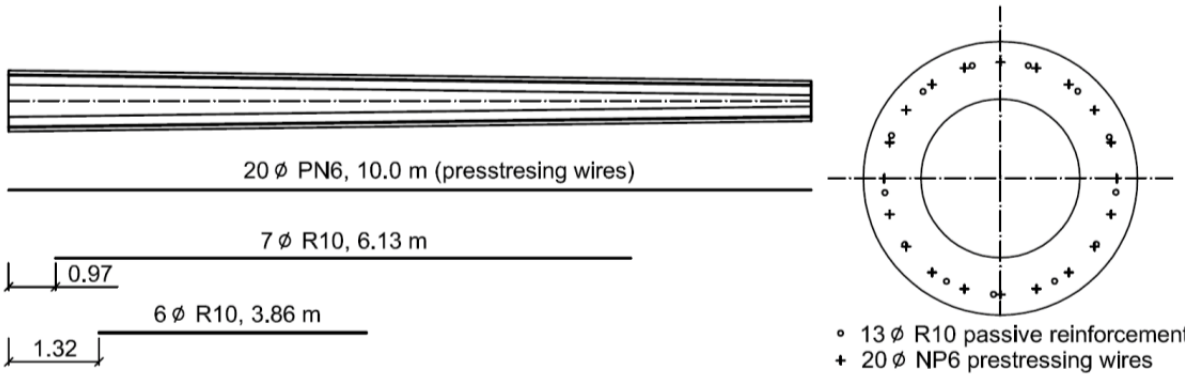

Figure 4 Scheme of the pole reinforcement (type T1P1-PBD)

Table 2 and 3 shows limit and resulting values which express the reliability of the designs in accordance with the used method; however, for comparison, the proposed pole types are assessed by both methods. The decisive criterion in most cases was the ULS reliability condition (loaded by bending moment and normal force), the SLS criteria were met with ease. Only for pole T1P2-PBD was the reliability condition of the crack origin the limiting criterion.

Table 2 Probability based design - ultimate and resulting values of the quantities under consideration

REVIEW VIA PROBABILITY - BASED APPROACH				
Quantity	ULS	SLS		
	M + N β	Deflection β	Crack origin p_f	Crack width p_f
Ultimate quantity	β_0 =3.8	β_0 =1.5	p_0 = 0.0668	p_0 = 0.0668
T1P1 PBD	3.85	4.02	0.0482	0.0261
T1P2 PBD	4.02	4.04	0.0668	0.0236
T2P1 PBD	3.80	3.95	0.0482	0.0386
T1P1 PSF	4.11	4.45	0.0482	0.0209
T1P2 PSF	4.08	4.06	0.0668	0.0209
T2P1 PSF	4.07	4.42	0.0505	0.0209

Table 3 Partial safety factor design - ultimate and resulting values of the quantities under consideration

REVIEW VIA PARTIAL SAFETY FACTOR METHOD				
Quantity	ULS	SLS		
	Load capacity V [kN]	Deflection f [mm]	Crack origin	Crack width w [mm]
Ultimate quantity	10	340.00	not allowed	0.150
T1P1 PBD	9.06	174.87	not expected	0.072
T1P2 PBD	9.76	180.17	not expected	0.078
T2P1 PBD	8.98	174.57	not expected	0.075
T1P1 PSF	10.03	166.20	not expected	0.061
T1P2 PSF	10.01	179.35	not expected	0.073
T2P1 PSF	10.01	165.17	not expected	0.063

Both of the methods provide the same level of reliability design, but the final designs are different. When using a probability-based method the designed amount of reinforcement is smaller than that designed according to the partial safety factor method (PBD poles fail in terms of the ULS according to the partial safety factor method; load capacity is lower than 10 kN).

Assessment of design quality

Although poles designed according to both methods show approximately the same reliability (within the used method), the various proposals differ both in wall thickness cross-section and in the amount of reinforcement and prestressing wires. To select the best proposal, it is necessary to determine the criterion by which to evaluate the design.

Factors that can be taken into account when assessing the suitability of a proposal are the economic and environmental aspects (acquisition cost, embodied energy and emissions of CO_2 and SO_2 caused during the production of concrete elements). The objective is to minimize all these aspects. The resulting multicriterial task should be solved using weighted sums. In the case that the individual terms of the objective function are expressed in different units the objective function could be normalized with reference values. The objective (target) function taking into account the following aspects relating to a single element (a pole) can be written as:

$$f(x) = \alpha_P \frac{P(x)}{{}^0P} + \alpha_{CO} \frac{CO_2(x)}{{}^0CO_2} + \alpha_{SO} \frac{SO_2(x)}{{}^0SO_2} + \alpha_E \frac{E(x)}{{}^0E} \quad (9)$$

where the used symbols mean:

P- acquisition costs

$$P = V_c U_p^c + m_s U_p^s + m_w U_p^w, \quad (10)$$

CO_2 – the amount of CO_2emissions

$$CO_2 = V_c U_{CO2}^c + m_s U_{CO2}^s + m_w U_{CO2}^w, \quad (11)$$

SO_2 – the amount of SO_2 emissions

$$SO_2 = V_c U_{SO2}^c + m_s U_{SO2}^s + m_w U_{SO2}^w \quad (12)$$

E– energy consumption

$$E = V_c U_E^c + m_s U_E^s + m_w U_E^w. \quad (13)$$

${}^0P$ (or ${}^0CO_2$, ${}^0SO_2$, ${}^0E$) stands for the reference values set by the problem designer for acquisition costs (or CO_2 emissions, SO_2 emissions, primary energy consumption); α_p (or α_{CO}, α_{SO}, α_E) represents weights in the objective function (9) for P (or CO_2 emissions, SO_2 emissions, energy respectively); V_c is concrete volume; m_s (m_w) is reinforcement weight (prestressing wires); U_p^c, U_p^s, U_p^w are the costs of concrete (or steel); U_E^c, U_E^s, U_E^w are the energy consumptions for a unit volume of concrete (or reinforcement and prestressing wire per 1kg); U_{CO2}^c is the embodied unit amount of CO_2 emissions from concrete production; U_{CO2}^s, U_{CO2}^w are the embodied unit amounts of CO_2 emissions from steel production; U_{SO2}^c is the embodied unit amount of SO_2 emissions from concrete production; and U_{SO2}^s, U_{SO2}^w are the embodied unit amounts of SO_2 emissions from steel production.

To evaluate the resulting design of poles according to the objective function (9) the unit cost and environmental impact values were considered with regard to data in Table 4 (which were obtained from publication [8]), and the weight coefficients in Table 5.

Table 4 Unit costs and environmental impacts [8]

ENVIRONMENTAL IMPACTS AND UNIT COSTS				
Material	Energy MJ/kg	CO_2emission $kgCO_2/kg$	SO_2 emission gSO_2/kg	Cost
Concrete C40/50	0.738	0.118	0.382	95.40 €/ m^3
Prestressing wire	31.895	2.776	16.325	1.20 €/kg
Reinforcement	27.311	2.505	15.519	0.97 €/kg

Table 5 Weight coefficient variants in the objective function

WEIGHT COEFFICIENTS				
Variants	α_P	α_{CO}	α_{SO}	α_E
Var1	1	0	0	0
Var2	0	1	0	0
Var3	0	0	1	0
Var4	0	0	0	1
Var5	0.125	0.125	0.125	0.5

Comparison of results– probability based design

A comparison of three types of pole designed using probability-based design can be found in the following graph in Figure 5. When evaluating the objective function, pole type T1P1-PBD is considered as a reference.

The graph clearly shows that the poles of type T1P1 and T2P1 are comparable in terms of objective function. The objective function value of pole T1P2 is higher than that of the other two. This is because the reliability given by the USL is higher (β = 4.02) than that of the other two as the crack origin reliability condition was limiting for the design of this pole.

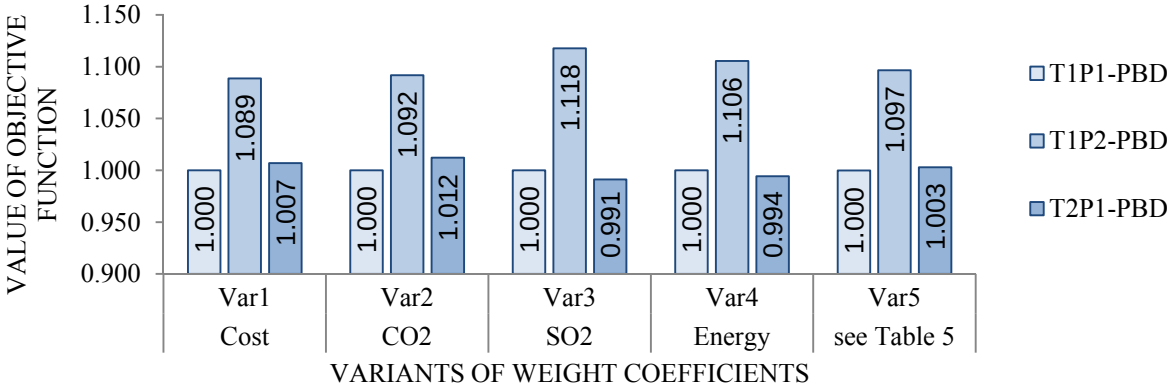

Figure 5 Comparison of pole designed via the probability-based method (reference pole type T1P1-PBD)

Comparison of results– partial safety factor method

The decisive criterion in the designs of the poles was in all cases fulfilment of the reliability conditions of the given USL; the poles have approximately the same load carrying capacity and therefore the reliability from the viewpoint of the ULS is the same for all of the three poles. It is clear from the graph in Figure 6 that the proposals are equivalent in terms of objective function evaluated for all weight coefficient variants; the maximum difference is 1.1% (relative to the reference pole, T1P1-PSF).

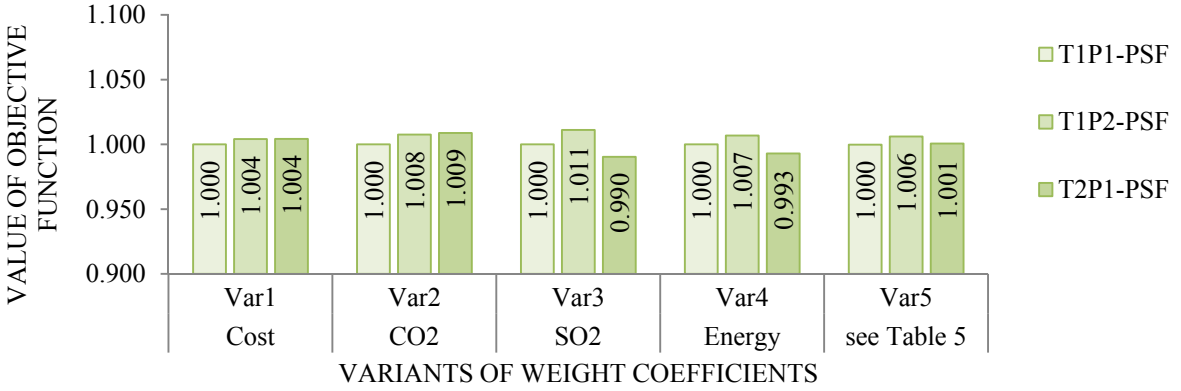

Figure 6 Comparison of pole designed via the partial factor method (reference pole type T1P1-PSF)

Comparison of both design method through the results

Designing of pole using the probability-based method provides a lower objective function value. In comparison with the best pole designed according to the partial safety factor method (pole type T1P1-PSF, which was considered as a reference pole), there is for example a difference in cost of up to 13.8%, and in CO_2 production of up to 14%, etc. (see Figure 7).

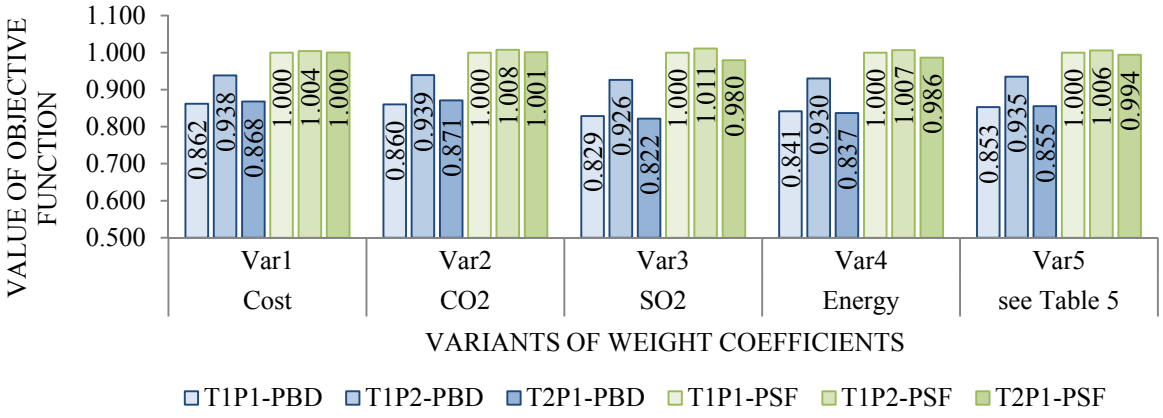

Figure 7 Comparison of poles designed using both methods (reference pole type T1P1-PSF)

CONCLUSIONS

Only economic and environmental aspects linked with the amount of individual materials that were used for pole production have been considered in assessing the suitability of the proposal. From this standpoint it can be stated that designing using the probability-based method is more economical and more environmentally friendly. However, fully probabilistic design requires, compared with the partial reliability factor method:

- knowledge of the definition of the distribution of input quantities, and of their characteristics,
- a calculating tool for re-design combined with statistical evaluation,
- the designer to possess sufficient professional knowledge.

The application of the fully probabilistic design approach and the verification of reliability enable the introduction of mass production with the option of control over the design procedure, and increases in quality. Individual input quantities, which are considered as random quantities with a given probability distribution (or statistical distribution parameters), can be gained by long-term monitoring and evaluation.

In the presented objective function it is also possible to take into account the following stages for a particular structure: the construction process, utilisation, and the end of its life cycle. Differences in the amount of used materials and particularly the different weights of the final products (and thus the handling and transportation of the products) may cause more significant differences in the objective function values than are shown in this paper. To find an optimal design, i.e. the best possible design that meets specified criteria, optimization methods should be used.

ACKNOWLEDGEMENTS

This research has been carried out with the support of the Czech Ministry of Education, Youth and Sports, project MSM0021630519 “Progressive reliable and durable load bearing structures” and of the Czech Ministry of Industry and Trade within the framework of research task FR-TI1/357 – “Concrete structures with non-metallic reinforcement with increased heat and aggressive environment resistibility”.

REFERENCES

1. ČSN EN 1990: 2004 Eurocode: Basic of structural design, ČNI 2004.

2. ISO 2394:1998 (E) General principles on reliability for structures.

3. ČSN EN 1992-1-1: 2006 Eurocode 2: Design of concrete structures – Part 1-1: General rules and rules for buildings, ČNI 2006.

4. LANÍKOVÁ, I., ŠTĚPÁNEK, P.: Optimised design of spun concrete poles -parametric studies, Proceedings of conference 14. Betonářské dny 2007, ČBS Servis, 2007, pp 421-426, (in Czech).

5. POPELA, P.: Numerical Techniques and Available Software, Chapter 8 in Part II. In J. Dupačová, J. Hurt, J. Štěpán: Stochastic Modeling in Economics and Finance. Applied Optimization. Dordrecht/Boston/London: Kluwer Academic Publishers, 2002. pp 206-227.

6. JCSS: Probability model code, http://www.jcss.ethz.ch

7. LANÍKOVÁ, I.; ŠTĚPÁNEK, P.; ŠIMŮNEK, P. Fully probabilistic design of concrete structures. In Mendel 2010, 16th International Conference on Soft Computing, Brno, Brno University of Technology, FSI. 2010. pp 426 - 433.

8. HÁJEK, P.; KYNČLOVÁ, M.; FIALA, C.: Life cycle assessments of concrete structures – a step towards environmental savings, Structural concrete, Journal of the fib, volume 12, Number 1, 20114, ISSN 1464-4177, pp 15-23.

Eco-friendly Concrete with Highly Reduced Cement Content

T Proske, S Hainer, H Garrecht, C-A Graubner
TU Darmstadt, Germany

The major environmental impact of concrete is caused by the CO_2-emission during the cement production. Recent studies at the TU Darmstadt revealed that the required CO_2-emissions can be reduced significantly in ordinary concrete with normal strength. The principles of the (U)HPC design were adapted for the development of these concretes. The use of superplasticizer and high reactive cements as well as the optimisation of the particle size distribution and the reduction of the water volume allows a significant reduction of the Portland cement clinker in the mixture. Essential is the addition of mineral fillers like limestone powder to provide an optimal paste volume. In addition the already practicable substitution of the cement clinker by secondary raw materials like fly ash or furnace slag is an appropriate opportunity but limited by the availability of these resources. For the practical application of the low carbon concretes, questions must be answered regarding the workability, the strength development, the design relevant mechanical properties as well as durability aspects like carbonation of the concrete.

At the TU Darmstadt different mixtures for ordinary reinforced concrete structures were developed. It was shown that concretes with cement contents lower than 125 kg/m³ were able to meet the usual required workability, strength (app. 40 MPa) and mechanical properties. The carbonation depth of concretes with app. 150 kg/m³ was equal or lower than the depth of the DIN-standard reference concretes for exterior structures. The ecological advantages were identified, using the environmental performance evaluation. A reduction up to 50% in environmental impact compared with the DIN-Standard reference concrete mixture and a reduction of more than 65% using blast furnace cement was calculated. The application in practice was verified conducting full-scale tests in a precast concrete plant. The special requirements on workability and early strength were fulfilled with a cement content of 150 kg/m³.

Dr.-Ing. Tilo Proske is an executive employee, Institut für Massivbau, TU Darmstadt, Germany with experience as a structural engineer in Prof. Dr.-Ing. Scholz und Partner, Munich. Previously Dr Proske studied at Bauhaus-Universität Weimar.

Dipl.-Ing. Stefan Hainer, is a scientific employee, Institut für Massivbau, TU Darmstadt, Germany.

Prof. Dr.-Ing. Harald Garrecht is Chair of Construction Materials, TU Darmstadt, Germany. Previously he was chair of Construction Materials and Building Physics, Karlsruhe University of Applied Science .

Prof. Dr.-Ing. Carl-Alexander Graubner, is chair of concrete structures, Technische Universität Darmstadt, with recognition as a supervising engineer for design of massive structures - 2001, Managing Director and Associate of engineering firm König Heunisch Planungsgesellschaft mbH, Frankfurt/M. Germany

Keywords: Carbon dioxide, Carbonation, Cement reduced concrete, Durability, Green concrete

INTRODUCTION

To ensure the competitiveness of concrete as a building material in the future, it is essential to improve the sustainability of concrete structures. Great potential for the reduction of the environmental impact and the consumption of scarce resources has been identified in the field of concrete construction, especially in the production of raw materials, concrete technology and structures [1] (see Figure 1). For concretes which are developed, produced and used in an environmentally friendly manner the term “Green Concrete” [2] or "ECO-Concrete" [3] is commonly used.

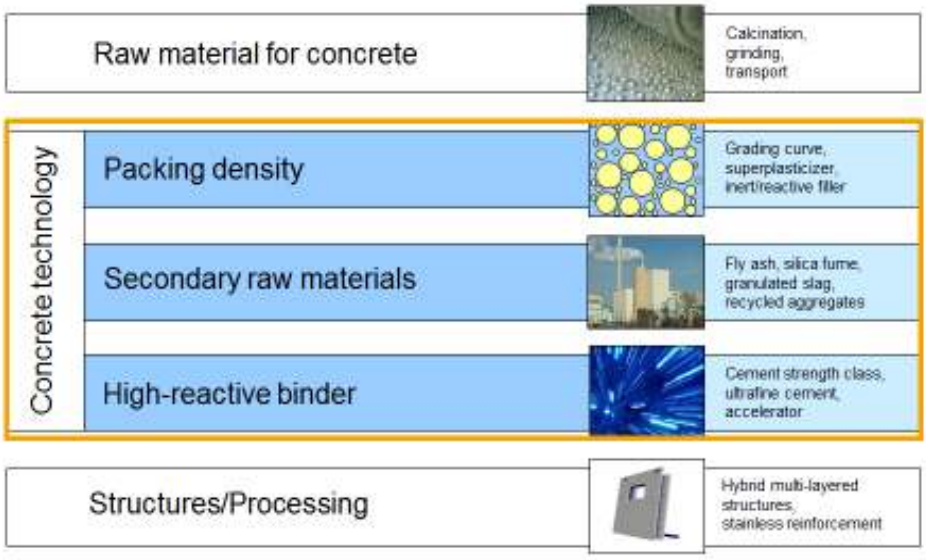

Figure 1 Opportunities for ecological optimisation in concrete construction [1]

The major environmental impact of concrete comes from the CO_2-emissions during cement production as a result of the calcination and grinding process including the decomposition of the calcium carbonate. Approximately five percent of the global anthropogenic CO2-emission is connected with the production of 3.3 billion tonnes of cement per year (2010) [4]. Therefore, the reduction of the cement-clinker content has positive effects on the environmental life cycle assessment of the concrete and can be achieved by the optimisation of the mixture design [5]. Some research work to reduce the Portland cement content in the concrete was already carried out [1-3, 5-10].

This paper presents the general procedure for the development of structural concrete with low environmental impact and normal compressive strength. This includes the stepwise development of the mix design. The results of performance tests on cement reduced concretes conducted in laboratory conditions are also presented. In addition, the advantages with regard to the environmental performance evaluation were verified. Finally, the application in the precast industry, as well as the technical advantages of the cement reduced "green" concretes, are presented.

PRINCIPLES FOR THE DEVELOPMENT OF LOW CARBON CONCRETE

Based on experimental results, a stepwise procedure for the development of low carbon concretes was developed. The first step is the selection of the cement. The environmental impact of the cement should be as low as possible and at the same time the strength performance relatively high. Composite and slag cements (CEM II and CEM III) with strength class 42.5 and 52.5 as well as Portland cement (CEM I) with strength class 52.5 are appropriate. However, the increased use of slag and slag cements as well as fly ash is limited in several countries by the availability of these materials and the requirements for the early concrete strength. For future application, along with modified low-water-concrete technology, the development of environmental friendly cements with higher limestone content is planned [11].

In the second step the volume of the cement and cementitious materials should be minimised. To achieve a significant reduction, the concrete technology for ordinary concretes was modified based on the principles of high performance concretes. Figure 2 shows, that the application of high performance superplasticizers increases the actual packing density of the solid powder particles (<0.125 mm). The optimisation of the particle size distribution also leads to a lower required water volume and a lower permeability. This allows the reduction of the water/powder-ratio in the mixture, still providing sufficient workability. Based on the decreased water, along with an increase in strength and durability, the reduction of the cement content is possible. The corresponding cement and water volume is substituted by environmentally friendly powders like limestone, fly ash or slag. Considering the availability of the reactive materials, inert materials like limestone should be preferred. However, investigations have shown a considerable contribution of optimised limestone powders to the strength development.

It has to be considered, that a certain paste volume is necessary to maintain the required workability. This implies that a minimisation of the paste content and hence an additional reduction of the cement content is based on an optimisation of the aggregate packing.

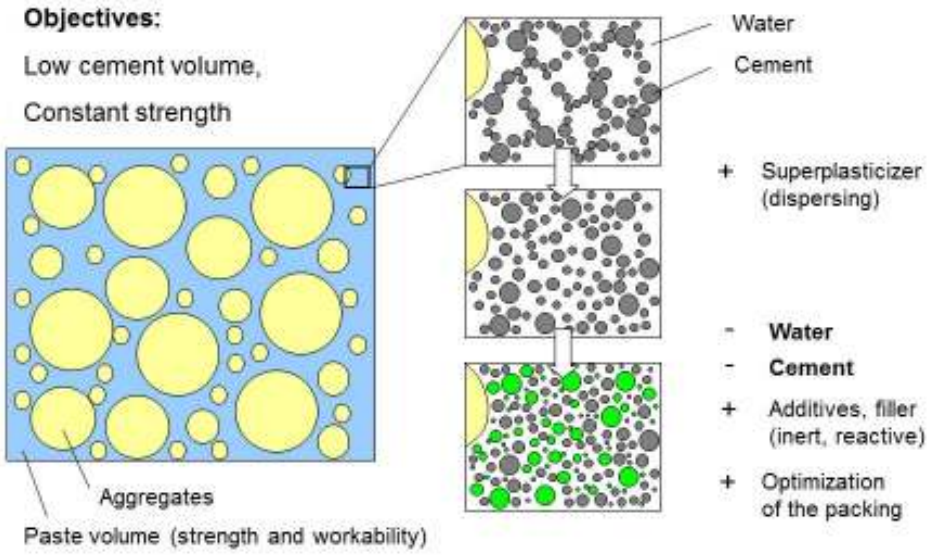

Figure 2 Evolution from the traditional mixture proportion to cement reduced green concrete [5]

The principles of the concrete development and the effects on the concrete strength, the water content and the workability are also presented qualitatively in Figure 3. The reduction of the clinker increases with the decrease of water and the contribution of cement and additives on the performance.

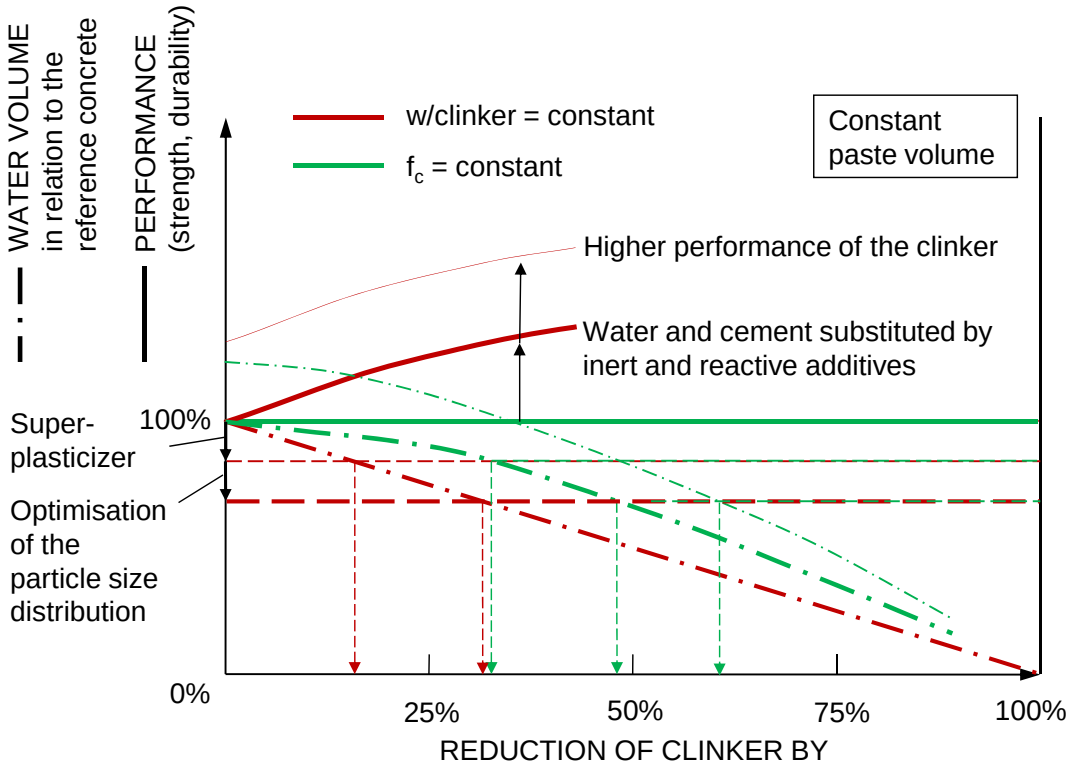

Figure 3 Reduction of the cement clinker in the concrete in relation to a conventional reference mixture

For the practical application of green concretes, questions must be answered with regard to the workability, the pumpability, the strength development and the durability. The expectation is that changes to the traditional mixtures should not diminish the material performance. If cement reduced concretes are used for exterior structures, the durability, including the performance against carbonation induced corrosion is of great importance [12].

CONCRETE MIX DEVELOPMENT

At the Technische Universität Darmstadt, intensive studies on the topic of “Green Concrete” were conducted as part of research projects in the field of Sustainable Concrete Structures. Different kinds of concretes with reduced cement content were developed especially for reinforced concrete structures. The initial investigations based on laboratory tests are described below.

A compressive strength of 10 N/mm² at an age of 24 h without heat treatment was targeted to enable the de-moulding. After 28 days a compressive strength of 38 N/mm² was desired to obtain concrete class C25/30. The cement reduced concretes must have sufficient workability

and a concrete surface without a large number of air voids. Therefore the slump flow value according to DIN EN 12350-05:2009-08 was chosen to be a = 550 mm. The cement reduced concretes are intended to be used for interior structures (exposure class XC1) as well as exterior structures (exposure classes XC4, XF1 and XA1). The German code DIN 1045-2:2008-08 defines the national requirements for concrete mix design depending on the exposure class. For the application in exterior structures (exposure class XC4, XF1 and XA1) the minimum cement content is 270 kg/m³ and for interior structures (XC1) 240 kg/m³. The water-cement ratio must not exceed 0.60 and 0.75 respectively. For the evaluation of the concrete performance, reference concretes based on the concrete mix design according to DIN 1045-2:2008-08 were included in the test program. The mix design for the reference concretes with a cement content of 240 kg/m³ and 270 kg/m³ is shown in Table 1.

Starting with the reference concrete, the cement content was reduced from 270 kg/m³ to 100 kg/m³ (see Table 2). The cement was gradually substituted by additives. At the same time, the water volume was reduced. The lowest value was 125 L/m³. To maintain sufficient workability the powder content (<0.125 mm) was increased up to 440 kg/m³ by the addition of fly ash und limestone powder. The concrete consistency was adjusted by changing the dosage of superplasticizer. A cement CEM I 52.5 R with high early strength, high strength class and a defined cement clinker content was usually used. In addition, a cement CEM I 32.5 R with a lower strength classification was included. Subsequently, the influence of a high performance CEM III/A 52.5 R (with reduced clinker content and an amount of slag up to 65%) was analysed. The limestone powder and fly ash additives were used in the ratios 0, 50, and 100% by volume. In an additional test series, the influence of the limestone powder fineness on the concrete properties was analysed (see Table 3). The Blaine value of the normal limestone was 3,100 cm²/g and of the fine limestone 16,000 cm²/g.

Table 1 Mix design of the reference concretes

		REFERENCE CONCRETES						
Mix design	Mass per m³ concrete	B270-CEM I 52,5 R-SFA10-w165-DIN	B270-CEM I 42,5 R-SFA10-w165-DIN	B270-CEM I 32,5 R-SFA10-w165-DIN	B240-CEM I 52,5 R-w180-DIN	B240-CEM I 42,5 R-w180-DIN	B240-CEM I 52,5 R-SFA160-w180	B240-CEM I 52,5 R-SFA160-w145
CEM I 52.5 R	kg	270			240		240	240
CEM I 42.5 R	kg		270					
CEM I 32.5 R	kg			270		240		
Fly Ash (EN 450)	kg	10	10	10			160	160
Limestone powder 1	kg							
Water	kg	162	162	162	180	180	179	142
Superplasticizer	kg	2.8	1.9	3.0		1.3	1.7	4.0
River sand 0-2 mm	kg	597	603	603	601	601	569	509
River gravel 2-8 mm	kg	446	446	446	444	444	394	446
River gravel 8-16 mm	kg	847	847	847	842	842	748	846
w/c	[-]	0.61	0.61	0.61	0.75	0.76	0.75	0.60
w/c_{eq}	[-]	0.60	0.60	0.60	0.75	0.76	0.66	0.53

Table 2 Mix design of the cement reduced concretes

		CEMENT REDUCED CONCRETES											
Mix design	Mass per m³ concrete	B200-CEM I 52,5 R-SFA160-w145	B175-CEM I 52,5 R-SFA160-w145	B150-CEM I 52,5 R-SFA250-w145	B150-CEM I 52,5 R-SFA125-KSM145-w145	B150-CEM I 52,5 R-KSM289-w145	B150-CEM I 52,5 R-SFA250-w125	B150-CEM I 52,5 R-KSM289-w125	B150-CEM III/A 52,5 R-SFA250-w145	B150-CEM III/A 52,5 R-SFA125-KSM145-w145	B150-CEM III/A 52,5 R-KSM289-w145	B125-CEM I 52,5 R-SFA275-w145	B100-CEM I 52,5 R-SFA300-w145
CEM I 52.5 R	kg	200	175	150	150	150	150	150				125	100
CEM III/A 52.5 R	kg								150	150	150		
Fly Ash (EN 450)	kg	200	225	250	125		250		250	125		275	301
Limestone powder 1	kg				145	289		289		145	289		
Water	kg	142	142	142	142	142	120	120	143	142	142	143	144
Superplasticizer	kg	4.1	3.9	3.1	4.0	5.1	6.9	6.5	2.4	3.3	4.5	3.1	1.9
River sand 0-2 mm	kg	515	519	523	524	524	542	542	523	524	524	528	534
River gravel 2-8 mm	kg	440	436	434	434	434	444	444	434	434	434	429	424
River gravel 8-16 mm	kg	834	828	823	823	823	843	843	823	823	823	814	804
w/c	[-]	0.73	0.83	0.96	0.97	0.97	0.84	0.83	0.96	0.97	0.97	1.16	1.45
w/c_{eq}	[-]	0.64	0.73	0.85	0.85	0.97	0.74	0.83	0.85	0.85	0.97	1.02	1.28

Table 3 Mix design of cement reduced concretes with different limestone fineness

	CEMENT REDUCED CONCRETES WITH DIFFERENT LIMESTONE							
Mix design	Mass per m³ concrete	B150-CEM I 52,5 R-KSM289/0-w145	B150-CEM I 52,5 R-KSM246/43-w145	B150-CEM I 52,5 R-KSM202/87-w145	B150-CEM I 52,5 R-KSM159/130-w145	B150-CEM I 52,5 R-KSM116/173-w145	B150-CEM I 52,5 R-KSM72/217-w145	B150-CEM I 52,5 R-KSM0/289-w145
CEM I 52.5 R [1)]	kg	150	150	150	150	150	150	150
Limestone powder 2 [2)]	kg	289	246	202	159	116	72	0
Limestone powder 3 [3)]	kg	0	43	87	130	173	217	289
Water	kg	142	142	142	142	142	142	142
Superplasticizer [1)]	kg	2.5	2.5	1.8	2.2	3.0	3.0	3.1
River sand 0-2 mm	kg	524	524	524	524	524	524	524
River gravel 2-8 mm	kg	434	434	434	434	434	434	434
River gravel 8-16 mm	kg	823	823	823	823	823	823	823
w/c	[-]	0.96	0.96	0.96	0.96	0.96	0.96	0.96

[1)] Different producer, [2)] normal finesses, [3)] high finesses

After mixing, the slump flow value of the concrete was determined, and the dosage of the superplasticizer was adjusted as necessary. Afterward, the specimens for the compressive strength (150 mm cubes) and the carbonation tests (prisms 100/100/500 mm) were produced. The samples were de-moulded after one day and the cubes stored according to DIN EN 12350-2:2009-08. The compressive strength was tested after 1, 3, 7, 28 and 91 days.

The progress of carbonation was analysed using the accelerated carbonation test (ACC-test method) according to [13]. The carbonation depth xc was determined at an age of 56 days. After de-moulding, the concrete specimens were stored 7 days in water with a temperature of T = 20°C. Subsequent to the water storage the specimens were placed in a climate chamber with (T = 20°C and RH = 65%). Afterwards the specimens were exposed for 28 days to an increased CO_2-concentration of 2% (T = 20°C and RH = 65%). At an age of 56 days the specimens were split and the carbonation depth was measured at the plane of rupture with an indicator solution (phenolphthalein). In addition to the ACC-test method, selected concretes were stored in a normal CO_2-concentration (T = 20°C and RH = 65%) for up to two years.

CONCRETE PROPERTIES

Workability and Strength Development

It was noted that the loss of compressive strength, corresponding to the cement reduction, can be compensated for by decreasing the water volume and by the addition of reactive powders like fly ash or higher strength cement (Figure 4). The requirements for slump flow and compactibility were also fulfilled. However, a higher demand of superplasticizer was necessary compared to the reference mixes. In addition, the plastic viscosity increased significantly with the loss of water. The optimum water volume was identified to be 145 L/m³.

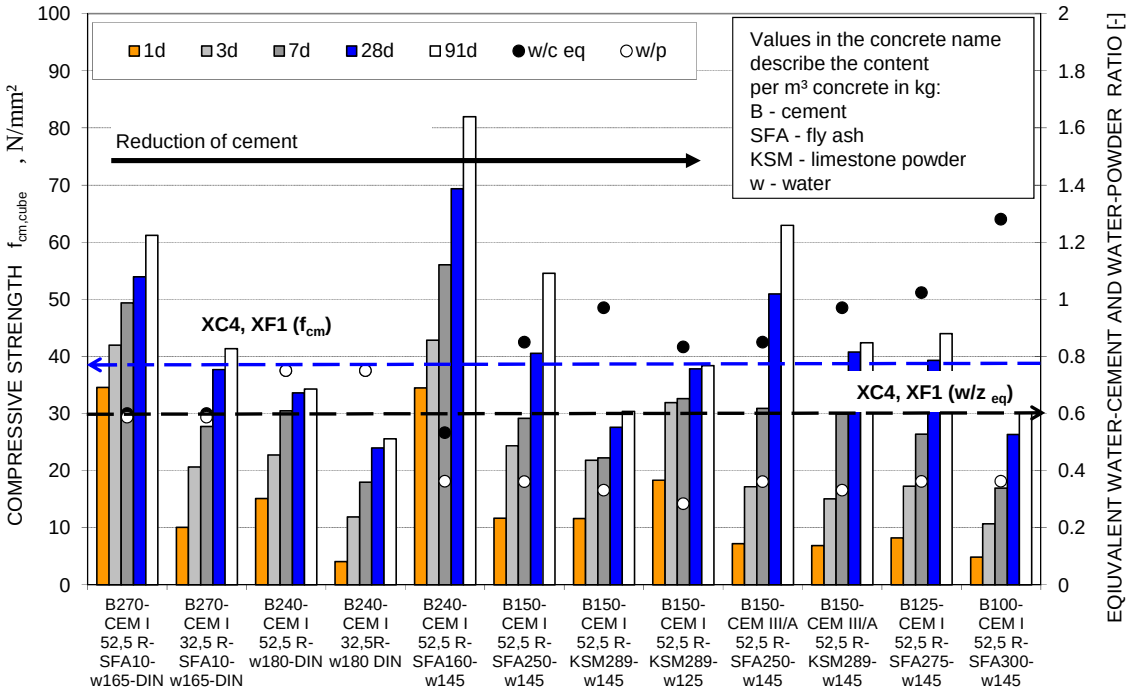

Figure 4 Strength development of selected concretes

Figure 4 shows that concretes with cement content lower than 150 kg/m³ were able to meet the defined strength requirements. Both the early strength and the 28-days-stregth were acceptable (see also Table 4). To enable further water reduction and hence an additional reduction of the cement content, a systematic optimization of the particle size distribution and packing density in the range of the particle sizes <0.125 mm was necessary.

Partial substitution of the ordinary limestone with fine limestone powder reduced the viscosity of the concrete considerably. Also the 28-day compressive strength increased from the reference value 32 N/mm² up to 46 N/mm² with fine limestone (Figure 5). It is assumed that the more homogeneous microstructure and the improved transition zone have positive effects.

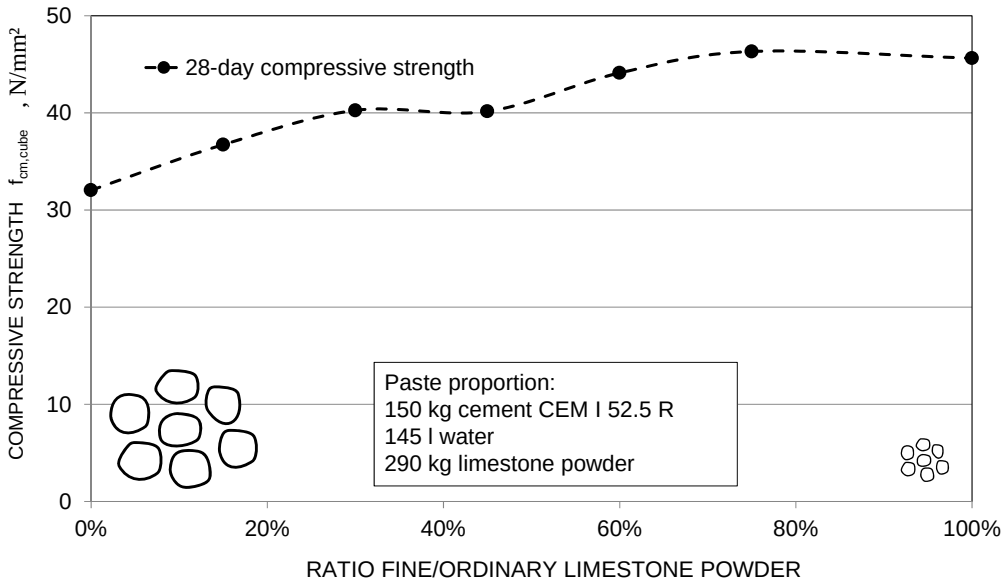

Figure 5 Influence of the limestone fineness on the compressive strength

Table 4 – Strength development and carbonation depth of the concretes

CONCRETE MIX	COMPRESSIVE STRENGTH					CARBONATION DEPTH
	$f_{cm,cube}$					x_c
	N/mm²					mm
	Concrete age					ACC-test
	1 d	3 d	7 d	28 d	91 d	28 d + 28 d, 2% CO_2, relative humidity 65%
B270-CEM I 52,5 R-SFA10-w165-DIN	34.6	42.0	49.4	53.9	61.2	2.88
B270-CEM I 42,5 R-SFA10-w165-DIN	15.9	30.1	38.5	40.8	52.3	2.84
B270-CEM I 32,5 R-SFA10-w165-DIN	10.1	20.6	27.7	37.7	41.4	5.99
B270-CEM I 32,5 R-SFA10-w165-DIN	10.0	21.1	30.0	31.7	37.8	5.21
B240-CEM I 52,5 R-w180-DIN	15.1	22.7	30.5	33.6	34.3	6.08
B240-CEM I 32,5R-w180 DIN	4.1	11.9	18.0	24.0	25.6	11.14
B240-CEM I 52,5 R-SFA160-w180	22.8	31.6	38.2	46.8	59.7	5.37
B240-CEM I 52,5 R-SFA160-w145	34.5	42.9	56.0	69.4	82.0	1.10
B200-CEM I 52,5 R-SFA200-w145	18.6	30.5	37.6	57.0	72.9	1.51 [1)]
B175-CEM I 52,5 R-SFA225-w145	21.3	32.6	38.5	55.0	66.5	2.75 [1)]
B150-CEM I 52,5 R-SFA250-w145	11.7	24.4	29.2	40.6	54.6	9.83
B150-CEM I 52,5 R-SFA125-KSM145-w145	15.0	25.6	30.7	38.8	52.9	9.37
B150-CEM I 52,5 R-KSM289-w145	11.6	21.8	22.2	27.6	30.4	12.25
B150-CEM I 52,5 R-SFA250-w125	14.3	28.4	32.2	55.3	69.6	2.06 [1)]
B150-CEM I 52,5 R-KSM289-w125	18.3	31.9	32.6	37.8	38.4	8.44
B150-CEM III/A 52,5 R-SFA250-w145	7.2	17.2	30.9	50.9	62.9	6.30
B150-CEM III/A 52,5 R-SFA125-KSM145-w145	6.2	18.1	29.7	45.4	50.0	6.97
B150-CEM III/A 52,5 R-KSM289-w145	6.9	15.0	29.9	40.8	42.4	7.41
B125-CEM I 52,5 R-SFA275-w145	8.2	17.3	26.4	39.3	44.0	14.17
B100-CEM I 52,5 R-SFA300-w145	4.8	10.7	16.9	26.3	31.9	20.95

[1)] Relative humidity 80%

Carbonation of the Concrete

Figure 6 shows the measured carbonation depth as a result of the ACC-test (see also Table 4). The concrete mix B270-CEM I 32.5 R-w165-DIN according to the German standard has a relatively high carbonation depth of approximately 6 mm. Compared to this the CEM I 52.5 R decreases the carbonation depth significantly.

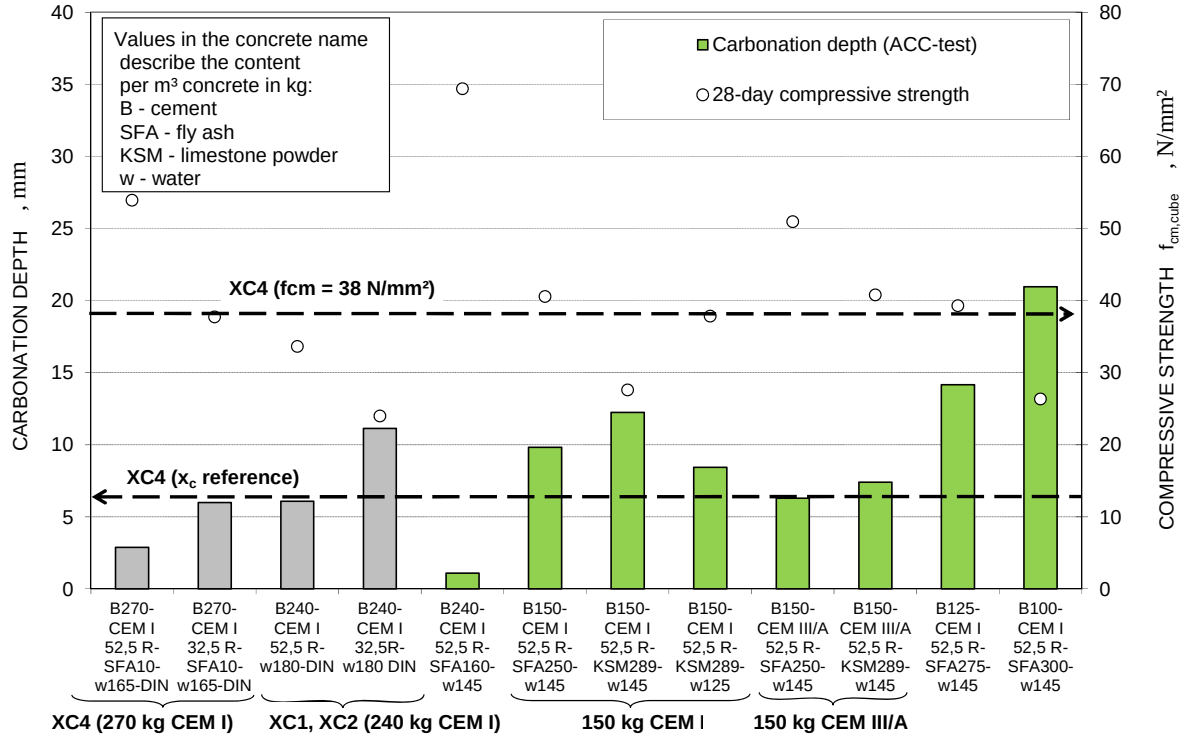

Figure 6 Carbonation depth of selected concretes

Compared with the carbonation depth of the concrete with CEM I 32.5 R, approximately the same value was measured for the concretes with only 150 kg/m³ blast-furnace cement CEM III/A 52.5 R. In contrast, the concrete mixes with 150 kg/m³ CEM I 52.5 R had a considerably higher carbonation depth than the reference concrete. However, requirements for exterior structures can be met by reducing the water content or by a slight increase in cement. The influence of the concrete additives on the carbonation was considerable. As expected, fly ash reduced the carbonation much more than limestone powder, notwithstanding the consumption of calcium hydroxide. A reduction of the cement content to 125 kg/m³ and 100 kg/m³ tends to yield values which are significantly higher than the carbonation depths of the reference concrete. These concretes are preferable for application in interior structures. An analytical model for the prediction of the carbonation depth based on an existing general model [13] is presented in [14]. This new model considers the specific mix proportion of the concrete. It shows especially the different contribution of the cement strength class, the water content and the additives on the carbonation resistance of the concrete.

Global Warming Potential

The optimisation of the clinker volume in the mixture composition leads to a significant reduction in environmental impact compared to the reference concrete mixtures. This improvement is specifically based on the use of fly ash and limestone-powder. The global warming potential (GWP) which considers the distinct effect of different greenhouse gases was reduced by more than 40% using CEM I 52.5R and more than 60% using CEM III/A 52.5R (see Figure 7). According to the environmental performance evaluation, other impact factors as well as the primary energy consumption are also reduced significantly [15]. However the improvement of the global warming potential is outstanding.

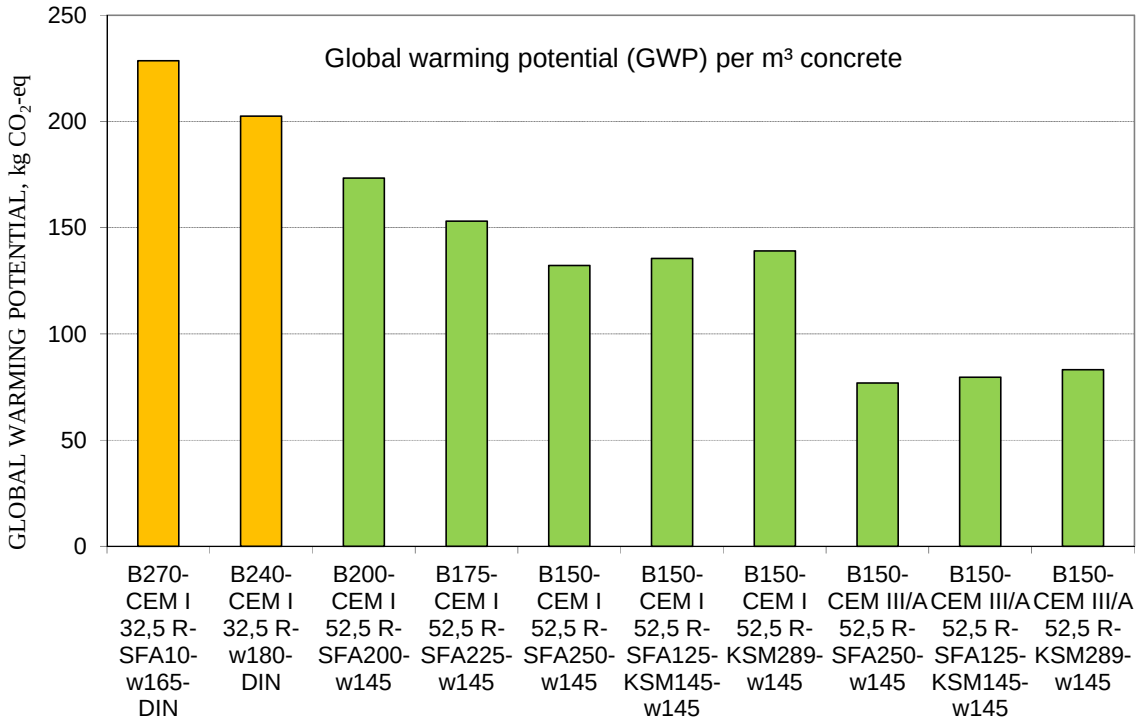

Figure 7 Global warming potential of selected cement reduced concretes (CML method, ökobau.dat 2010, without transport of the material)

TRANSFER IN PRACTICE

In cooperation with a producer of prefabricated concrete elements, the application of cement reduced concretes in practice was tested. The mixture development was focused on semi-finished concrete slabs and walls. At the construction site, the completion of the structural element is carried out with in-situ concrete. The processing as well as the field of application specifies the requirements for the fresh and hardened concrete properties. Concrete slabs are usually used for interior elements (XC1, C20/30), while concrete walls are used for both interior as well as exterior elements (XC4, XF1, C30/37 and C35/45). To meet the processing requirements a compressive strength of 7 N/mm² was targeted after 5 hours, including heat treatment with 50°C.

As a result of the mixture optimisation, the cement content (CEM I equivalent) for interior and exterior elements was decreased from 255 kg/m³ to 150 kg/m³ in ECO-Concrete1 and from 300 kg/m³ to 180 kg/m³ in ECO-Concrete3 respectively (see Figure 8). Hence the optimisation allowed a cement reduction of approximately 40%.

At the same time, the powder content was increased by 100 kg/m³. The cement content of the mixes developed is below the minimum accepted value according to DIN 1045-1:2008-08. This requires a building authority approval for the production of reinforced concrete elements.

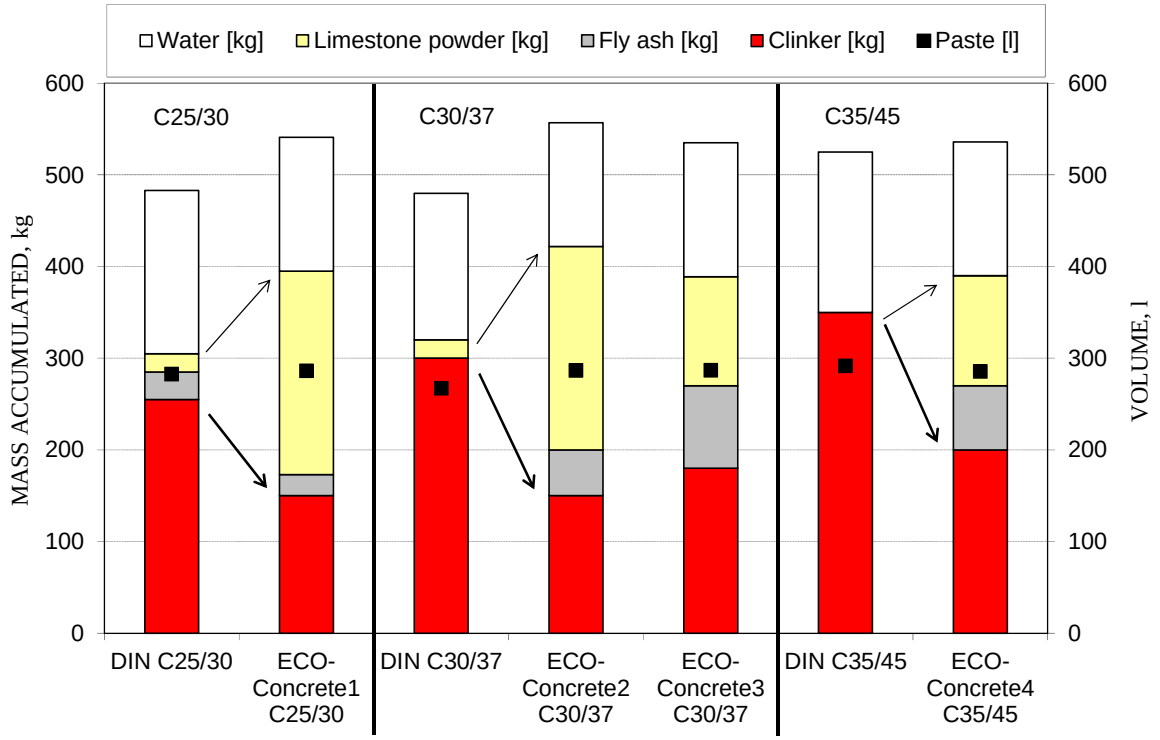

Figure 8 Paste proportion of the cement reduced concretes and the reference mixes

The performance of the laboratory tests was verified by producing the elements in a precast concrete plant and by full-scale tests. It was shown that an increased mixing time is necessary if the standard technology is used. The workability of the concretes during the processing time was sufficient. However, the quality and quantity of the materials must be controlled exactly. For example, the exact measurement of aggregate moisture is of importance. The high early strength allowed the integration of the new concretes in the normal production process. The texture of the concrete surface was very homogenous without unsightly air voids (see Figure 9).

Figure 9 Fabrication of semi-finished slabs with cement reduced ECO-Concrete1 (left), finished surface, view from the bottom (right)

Several mechanical properties of the cement reduced concretes were tested (Table 5). It must be noted, that the concrete specimens were produced with the maximum water content which is expected in the later fabrication process. The properties of the concretes developed are mostly equivalent to the conventional concretes and the normative standards. The increased modulus of elasticity, the low heat of hydration and the lower shrinkage can be considered as advantages resulting from the decreased water content (see Figure 10). In addition, ECO-Concrete3 fulfilled the requirements for exposure class XC4 (carbonation resistance) and XF1 (freeze-thaw resistance).

Table 5 Hardened concrete properties according to DIN EN 12390

HARDENED CONCRETE PROPERTIES AFTER 28 DAYS ACCORDING TO DIN EN 12390		DIN C25/30 (reference)	ECO - Concrete1 C25/30	ECO - Concrete2 C30/37	ECO - Concrete3 C30/37
Compressive strength $f_{cm,cube\ 150}$	N/mm²	30.0	35.9	40.8	49.1
Compressive strength $f_{cm,cyl\ 150}$	N/mm²	23.9	29.3	31.2	38.3
Splitting strength $f_{ctm,sp}$ cylinder 150/300 mm	N/mm²	2.63	3.14	3.56	3.81
Flexure strength $f_{ctm,fl}$ prisms 150/150/700 mm	N/mm²	4.61	4.48	5.38	4.86
Modulus of elasticity E_{cm} cylinder 150/300 mm $s_{max} = 0.333 f_{cm,cyl}$	N/mm²	23,557	30,277	34,095	38,819
Bond concrete/rebar $f_{bm,0,1mm}$ Pull-out test (RILEM), d_s = 10 mm, 0.1 mm displacement	N/mm²	6.4	6.0	7.6	15.1
Depth of penetration of water	cm	6.3	6.6	3.9	2.1

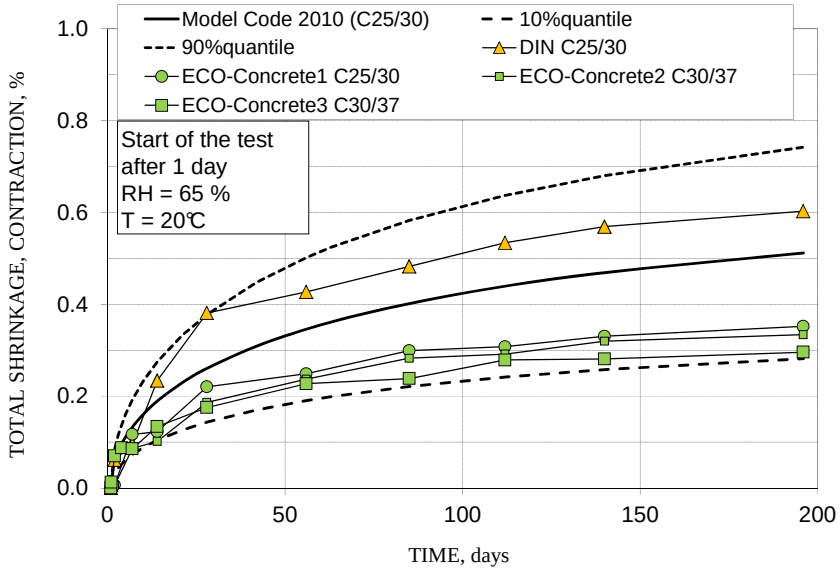

Figure 10 Time dependent shrinkage of the cement reduced and reference concretes compared to the approach of Model Code 2010

The environmental performance evaluation highlighted the advantages of the cement reduction for the construction of ordinary concrete structures with prefabricated elements. Figure 11 shows the global warming potential of reinforced concrete slabs produced with conventional concrete as well as ECO-Concrete. A decrease of the environmental impact by 50%, inclusive of the reinforcement and energy for the processing, is possible. However, cement reduced ECO-Concrete mixtures should be used for both the prefabricated and the in-situ concrete. For the production of the in-situ concrete, cement with low clinker content and moderate early strength (CEM III) is recommended.

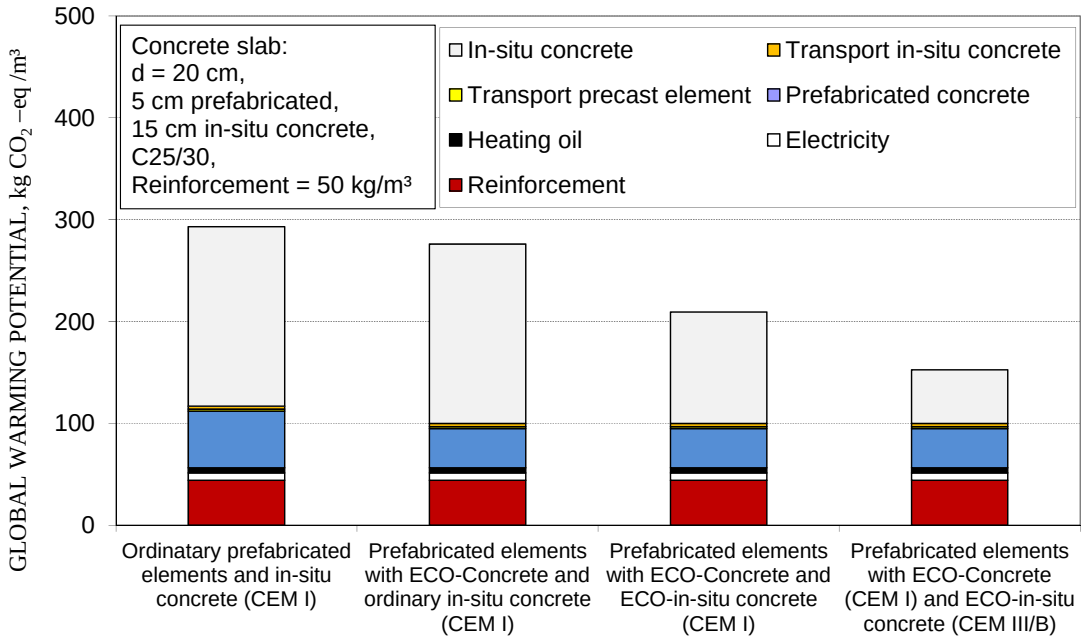

Figure 11 Global warming potential of the reinforced concrete slab with ECO-Concrete1 and cement reduced ready mix concrete containing CEM I or CEM III/B

The material costs for the cement reduced concretes are approximately the same compared to conventional ordinary concrete. Even a slight reduction is possible. However the costs are highly influenced by the price for the additives, especially for the limestone powder.

SUMMARY AND CONCLUSIONS

The presented studies revealed that the CO_2-emissions can be reduced significantly in structural concretes with normal strength. The use of superplasticizer and high reactive cements as well as the optimization of the particle size distribution and the reduction of the water volume allows a significant reduction of the Portland cement clinker in the mixture. Essential is the addition of mineral fillers like limestone powder to provide an optimal paste volume. In addition the already practicable substitution of the cement clinker by secondary raw materials like fly ash or furnace slag is an appropriate opportunity but limited by the availability of these resources.

It was shown that concretes with cement contents lower than 125 kg/m³ were able to meet the usual required workability, strength (app. 40 N/mm²) and mechanical properties. The carbonation depth of concretes with app. 150 kg/m³ was equal or lower than the depth of the

DIN-standard reference concretes for exterior structures. The ecological advantages were identified, using the environmental performance evaluation. A reduction up to 50% in environmental impact compared with the DIN-Standard reference concrete mixture and a reduction of more than 65% using blast furnace cement was calculated. The application in practice was verified conducting full-scale tests in a precast concrete plant. The special requirements on workability and early strength were fulfilled with a cement content of 150 kg/m³.

ACKNOWLEDGEMENTS

The authors are grateful for the financial support from the German Federal Ministry of Economics and Technology and the AiF Projekt GmbH. In addition, we would like to thank Beton Kemmler GmbH, Waibel KG, Mapei Betontechnik GmbH, BASF Construction Polymers GmbH, Dyckerhoff AG, HeidelbergCement AG and Lafarge Zement GmbH for their generous support.

REFERENCES

1. GRAUBNER, C.-A.; HOCK, C.; PROSKE, T.; SCHNEIDER, C.: Leadership through sustainability – New challenges for the concrete industry. In: The 11th annual international fib symposium. Concrete: 21st Century Superhero - Building a Sustainable Future, London, 22-24 June 2009. Lausanne, Fédération Internationale du Béton (fib), 2009, ISBN 978-1-904482-60-4.

2. NIELSEN, C. V.; GLAVIND, M.: Danish Experience with a Decade of Green Concrete. Journal of Advanced Concrete Technology, Vol. 5, No. 1, 2007, pp 3-12.

3. WALLEVIK, O. H.; MUELLER, F. V.; HJARTARSON, B.; KUBENS, S.: The green alternative of self-compacting concrete, Eco-SCC. In: Proceedings 17. Internationale Baustofftagung (ibausil), Bauhaus-Universität Weimar, 2009, pp 1-1105-1-1116.

4. U.S. GEOLOGICAL SURVEY, 2011, Mineral commodity summaries 2011: U.S. Geological Survey, 198 p, ISBN 978–1–4113–3083–2

5. GRAUBNER, C.-A.; PROSKE, T.; HAINER, S.: Low-Cement "Eco-Concretes" for the Production of Precast Elements (Zementreduzierte „Ökobetone“ für die Herstellung von Betonfertigteilen), In: Proceedings, 55. BetonTage, BFT International, 77. Jahrgang, 02/2011.

6. FENNIS, S.A.A.M.: Design of ecological concrete by particle packing optimisation. PhD Thesis, Delft University of Technology, Netherlands, Gildeprint, 2010, ISBN 978-94-6108-109-4.

7. FENNIS, S.A.A.M., WALRAVEN, J.C., NIJLAND, T.: Measuring the packing density to lower the cement content in concrete. In J.C. Walraven & D. Stoelhorst (Eds.); Tailor made concrete structures: new solutions for our society. London UK: Taylor & Francis Group, 2008, pp. 419-424.

8. DHIR, R.K., MCCARTHY, M.J. AND PAINE, K.A.: Engineering property and structural design relationships for new and developing concretes. Materials and Structures, Vol. 38 (275), 2005, pp. 1-9.

9. BILODEAU, A. AND MALHOTRA, V.M.: High-volume fly ash system: Concrete solution for sustainable development ACI Structural Journal, Vol. 97 (1), 2000, pp. 41-48.

10. HAIST, M.; MÜLLER, H.S.: Nachhaltiger Beton - Betontechnologie im Spannungsfeld zwischen Ökobilanz und Leistungsfähigkeit. In: Proceedings of the 9th Symposium Baustoffe und Bauwerkserhaltung, Nachhaltiger Beton, Werkstoff, Konstruktion und Nutzung, Karlsruhe, KIT Scientific Publishing, 2012, pp. 29-52.

11. GRAUBNER, C.-A.; GARRECHT, H.; PROSKE, T.: Innovative Betontechnologie - Voraussetzung für die Entwicklung umweltfreundlicher und ressourcenschonender Zemente. online-publication, www.oekobeton.de, 2010.

12. PROSKE, T.: Carbonatisierung von Beton mit reduziertem Zementgehalt. In: Proceedings 17. Internationale Baustofftagung (ibausil), Bauhaus-Universität Weimar, 2009, pp 2-0717-2-0722.

13. FIB BULLETIN 34: Model Code for Service Life Design, fib Task Group 5.6, International Federation for Structural Concrete (fib), February, 2006, 110 p.

14. HAINER, S.; PROSKE, T.; GRAUBNER, C.-A.: Carbonation of Cement Reduced Green Concrete. In: Proceedings of the International Congress on Durability of Concrete, ICDC, Trondheim, 18-21 June, 2012.

15. PROSKE, T.; VIDOVIC, N.; GRAUBNER, C.-A.: Carbonation of Cement Reduced Concretes. Darmstadt Concrete - Annual Journal on Concrete and Concrete Structures, Vol. 24, Darmstadt, 2009, ISSN 0931-1181.

Analysis of Compressive Strength in Two and Three Phase Systems of Alkali Activated Composites

Radhakrishna[1], G S Manjunath[2], P S Niranjan[3]
1 – R V College of Engineering, India
2 – Gogte Institute of Technology, India
3 – MVJ College of Engineering, India

Concrete and compressed mortar blocks were prepared using alkali activated binder adopting ambient and thermal curing r without the use of conventional cement. Since concrete has solid and fluid media, it forms the two phase system. Air content makes the compressed mortar blocks a three phase system. Both the forms of materials are useful in construction industry for specific purposes. In both the cases, strength data were generated changing various parameters. It was found that compaction characteristics of the mortar are marginally affected by fluid media. The compressive strength development in compressed blocks followed a specific pattern when the degree of saturation is maintained constant. Phenomenological models were developed separately for the compressed blocks and concrete. One of the models was validated by an independent set of experimental data by the authors and another researcher. The models developed would be helpful in re-proportioning the material for the required strength at a given age.

Dr. Radhakrishna obtained his Bachelor's Degree in Civil Engineering, M.Tech in Structural Engineering and PhD in Concrete Technology. Has has 22 years of teaching expereince in various subjetcs of civil Engineering. Currently, he is the Associate Professor and Dean at Department of Civil Engineering, R V College of Engineering, Bangalore. His areas of intrest include concrete technology with particualr referecne to alternative and sustainable building materials. Presently he is guiding three research scholars. He is serving as peer reviwer for three inernatinaol journals.

Prof.G. S. Manjunath obtained his Bachelor's Degree in Civil Engineering from Bangalore University (India) and Master's Degree in Structural Engineering from Karnatak University, Dharwad (India). He has been a Faculty in the Department of Civil Engineering, KLS Gogte Institute of Technology, Belgaum, Karnataka State, India for the past 26 years. His areas of interest are Concrete Technology, Geopolymer Technology, Structural Analysis, Design of RCC Structures etc. He has served as Special Officer at Visvesvaraya Technological University, Belgaum, India. He is persuing his doctoral programme under VTU, Belgaum.

Prof. P S Niranjan obtained his bachelor's Degree in Civil Engineeering. ME in Constiurction technology. He has 24 years of teching experience in various subjects. He is an active consultant. Currently he is heading the department of Civil Engineering at MVJ College of Engineering, Bangalore. He is persuing his doctoral programme under VTU, Belgaum. His areas of intrests include concrete technology with particualr reference to FaL-G composites.

Keywords: Air content, Alkali activated binder, Compressed block, Concrete, Phenomenological model

INTRODUCTION

Ordinary Portland Cement (OPC) based composites such as mortar, compressed mortar blocks and concrete are the most widely used construction materials in the world in view of their wide ranging performance attributes [1-2]. While the ever rising demand for such versatile construction materials is understandable, the undesirable issues related to environment and sustainable development associated with the ever increasing production of OPC have been well documented [3-4]. The requirement of huge quantity of raw materials and intense energy needs render the production of OPC unsustainable; the emission of green house gases on one-to-one basis into the atmosphere during its manufacture makes it environmentally unfriendly [5-6].

Therefore, conventional cement industry is under intense pressure to drastically cut down the consumption of conventional cement. Many industrial by-products/marginal materials have the potential to replace OPC partially/completely without compromising the performance properties. In this regard, Fly Ash (FA) and Ground Granulated Blast Furnace Slag (GGBFS), the by-products of thermal power and steel industries respectively and available world-wide in huge quantities, have been recognized not only as preferred supplementary cementitious materials (SCM) for producing blended cements partially replacing OPC, but also as major source/precursor materials for synthesizing altogether new novel binders alternative to OPC. Fly ash can replace the cement partially, bringing about improvement not only in mechanical performance but also the economical aspects of concrete [7-9].

The development of such binary/tertiary blended cements/high volume fly ash cements, incorporating many Pozzolonas and SCMs signify hardly any perceivable favourable impacts with regard to sustainability and environmental issues. Therefore, efforts are on to replace OPC *completely* by synthesizing *new binder* by the *alkali activation* of many industrial by-products/ marginal materials such as FA, GGBFS, silica fume, metakaolin, rice husk ash, red mud etc. which are rich in silica, alumina and Cao, adopting *Geopolymer Technology*, originally proposed by Joseph Davidovits [10] in 1978.

It is reported that fly ash can be activated using alkaline solution to produce inorganic polymeric binder, called *geopolymer*, a better preposition to completely replace conventional cement [11-13]. A study [14] by Feng-Qing Zhao et. al. reports the synthesis of ecological cementing material from GGBFS and class C fly ash with calcined gypsum as main activator ingredient. The elastic properties and strength behavior of structural members of fly ash based geopolymer concrete are found to be similar to that of Portland cement concrete [11].

Pull-Out tests [15] indicate that geopolymer concrete possesses satisfactory bond with reinforcing steel bars and conventional design process of reinforced structural components can be applied to GPC also. Geopolymers have been recognized to possess excellent fire resistance, acid resistance and stabilization/ solidification of heavy metals wastes [16-17]. These alkali activated cement composites have various advantages over conventional ordinary portland cement (OPC) composites, such as the use of marginal/waste materials, early strength development, excellent mechanical properties, denser structure, improved durability and other properties such as low shrinkage , low creep etc [18-21].

The methods of making these geopolymer composites are same as that of OPC composites except the binder component (source materials and alkaline fluid) used [22]. Sofi et. al. [23] concluded that key engineering properties of inorganic polymer concretes such as compressive strength, split tensile strength, flexural strength, static chord modulus of elasticity and poisson's ratio depend upon the mix design.

The study [24] on strength development, water absorption and water permeability of fly ash based geopolymer concrete with respect to water/binder ratio, aggregate/ binder ratio, aggregate grading, fluid/binder ratio indicate that good quality GPC can be produced with *appropriate parameterization and mix design.*

There are many methods for designing the Portland cement concrete mixes [25-26]. However, in case of geopolymer composites, too many parameters have complicated the process of mix design except Rangan [27]. He has proposed a method of proportioning heat cured geopolymer concrete requiring trial mix for adjusting strength and workability This investigation makes an attempt to analyze the compressive strength development in two and three phase systems of alkali activated composites (concrete and compressed mortar) and to develop phenomenological models for proportioning on lines similar to the one developed by Nagaraj and Zahida Banu [28] for Portland cement based composites.

Significance and Scope of the Research

The past research reported on alkali activated composites concentrate on the mechanical properties and durability aspects. But, there is no research reported on scientific methods of mix proportioning for making geopolymer composites to get the required strength at the given age. This paper attempts to address this issue.

The scope of the research is limited to the development of phenomenological models to re-proportion the materials both in two and three phase systems. The models have been validated with independent sets of experimental data. Further, the model for the two phase system has been validated with the data reported in the research papers by Rangan [27 and 29].

Materials and Methods

The properties of the source/binder materials used for the research are indicated in Tables 1a and 1b. The specific gravity and fineness modulus of the quarry dust (for fine aggregate) were found to be 2.6 and 2.62 respectively. The particle size distribution shows that more than 90% were finer than 1 mm size. The specific gravity and fineness modulus of river sand were 2.64 and 2.45 The specific gravity and fineness modulus of 20mm and down size course aggregate were found to be 2.68 and 6.10. Commercial grade sodium hydroxide flakes (minimum purity of 96%) and sodium silicate solution were used to prepare alkaline solution.

Table 1a Chemical Properties of the binders

BINDER	CHEMICAL COMPOSITION, %							
	Al_2O_3	Fe_2O_3	SiO_2	MgO	SO_3	Na_2O	Total Chlorides	CaO
Fly Ash	31.23	1.5	61.12	0.75	0.53	1.35	0.06	3.2
GGBFS	13.24	0.65	37.21	8.65	0.1	0.9	0.003	37.23
SilicaFume	0.06	0.03	97.20	1.10	0.2	0.1	0.02	0.5
Metakaolin	44.5	0.40	51.50	0.08	---	0.56	0.34	0.39

Table 1b Physical Properties of the binders

BINDER	SPECIFIC GRAVITY	% COARSER THAN 45 MICRONS	FINENESS, m^2/kg	LOSS ON IGNITION, %	LIME REACTIVITY, MPA IS:1727-1967[30]
Fly Ash	2.40	0.00	1134.1	0.9	7.23
GGBFS	2.50	10.45	370	0.3	---
Silica Fume	2.20	92.3	20600	0.89	---
Metakaolin	2.55	0.5	15000	0.68	---

Two and Three Phase Systems

The fresh geopolymer mortar having fluid-to-binder (f/b) ratio of less than 0.10 was very dry and was difficult to compact the material to get the block of required size and density. Further, the samples cracked immediately after casting without any cohesiveness. For f/b ratio in the range of 0.150 - 0.225, the mixture was more homogeneous with desired consistency. At this range of f/b ratio, the mortar was in *three-phase* system with solids, liquid and air content. This f/b range facilitated casting of the geopolymer mortar specimens with compaction effort and hence was selected to make compressed mortar blocks for further study. With f/b ratio of 0.25 and above, the mix attained full saturation resulting in a *two-phase* system with solids and liquid without any air content, making it almost impossible to cast blocks. But, the addition of coarse aggregate to this saturated mortar resulted in geopolymer concrete. Geopolymer concrete possesses good workability with f/b ratio in the range of 0.35–0.70. The resulting consistency would be adequate enough to cast geopolymer concrete specimens without any vibrations.

Geopolymer Mortar and Concrete

Geopolymer mortar was prepared using fly ash and/or GGBFS as binder and quarry dust or river sand as fine aggregate following the same procedure as for the OPC mortar. Alkaline solution used to mix the dry constituents was a mixture of sodium hydroxide and sodium silicate of 1:2 proportion. Standard Proctor test was conducted to find the maximum dry density and optimum fluid content required. The static compaction device was used to cast the compressed cylinders of 38mm diameter and 76 mm height. The specimens were thermally cured at 60^{o} C in oven for 24 hours. The samples were then removed from the oven and left in open air till the age of testing. Some of the samples were wrapped with aluminum foil to prevent the escape of moisture. Table 2 highlights the Mix proportion parameters and specimen designation for compressed blocks.

Table 2 Variables/Parameters for thermally cured geopolymer compressed blocks

SL NO	SERIES ID	FINE AGGREGATE	AGE, days	MOLARITY, M	W*/UW**
1	10M-Sand-W-7 Days	Sand	7	10	W
2	12M-Sand-W-3 Days	Sand	3	12	W
3	14M-Sand-W-1 Day	Sand	1	14	W
4	14M-QD-W-7 Days	QD	7	14	W
5	14M -QD-UW3 Days	QD	3	14	UW

M- Molarity, QD- Quarry dust, *W- Wrapped, **UW – Unwrapped

ACI method [31], currently used to manufacture OPC concrete, was adopted to proportion geopolymer concrete with fly ash, GGBFS, silica fume and metakaolin or their combinations as binders instead of OPC. Binder and fine aggregates were mixed in dry condition in a laboratory mixer. Later coarse aggregate was added and mixed again. Alkaline solution was then added and mixed till a homogeneous mix was obtained. The contents of fine and coarse aggregates were adjusted for various f/b ratios to get the slump between 100 and 110 mm. Geoplymer concrete having f/b ratio less than 0.35 was too harsh, while bleeding and segregation were observed at f/b ratios above 0.75.

The geopolymer mortar was prepared using the same binder and fine aggregate but without the coarse aggregate. 150 mm and 70.5 mm side cubes were used to cast concrete and mortar specimens respectively. The specimens were demoulded after hardening. Some of the cubes were transferred to the oven for thermal curing and some were kept in open air for ambient curing as indicated in Table 3. In all, 19 series were considered with different parameters. Geopolymer mortar and concrete specimens were tested for compression at the age of 1, 3, 7, 14, 28, 56 and 90 days as indicated. One typical mix proportion is shown in Table 4 for the series S19.

Table 3 Different parameters for the series.

SERIES ID	MORTAR/ CONCRETE	MOLARITY	FLUID CONTENT (KG/M^3)	FLY ASH, %	GGBFS, %	SILICA FUME %	META KAOLIN, %	CURING CONDITION
S1	Mortar	14	228	80	20	0	0	Ambient
S2	Concrete	14	207	100	0	0	0	Ambient
S3	Mortar	12	228	90	10	0	0	Ambient
S4	Concrete	14	228	80	20	0	0	Ambient
S5	Mortar	14	207	80	20	0	0	Thermal *
S6	Concrete	12	228	80	20	0	0	Ambient
S7	Mortar	12	228	80	20	0	0	Ambient
S8	Concrete	14	207	80	20	0	0	Ambient
S9	Mortar	14	207	80	20	0	0	Ambient
S10	Concrete	14	220	80	20	0	0	Thermal *
S11	Concrete	14	220	80	20	0	0	Ambient
S12	Concrete	14	220	100	0	0	0	Ambient
S13	Concrete	14	220	100	0	0	0	Thermal *
S14	Concrete	12	220	90	10	0	0	Ambient
S15	Concrete	14	220	90	0	0	10	Ambient
S16	Concrete	14	220	90	10	0	0	Ambient
S17	Concrete	14	220	90	0	10	0	Ambient
S18	Concrete	14	220	80	10	0	10	Ambient
S19	Concrete	14	220	80	10	10	0	Ambient

*Oven, 60^oC – 24 h.

Table 4 Mix proportions of Geopolymer Concrete of Series S19

CONSTITUENTS kg/m^3	f/b =0.35	f/b = 0.40	f/b = 0.45	f/b = 0.50	f/b = 0.55	f/b = 0.60	f/b = 0.65	f/b = 0.70
Fly ash	494.4	432.0	384.0	345.6	314.4	288.0	266.4	172.8
GGBFS	61.8	54.0	48.0	43.2	39.3	36.0	33.3	21.6
Silica fume	61.8	54.0	48.0	43.2	39.3	36.0	33.3	21.6
Fine aggregate	206	289	354	406	450	484	515	640
Coarse aggregate	912	912	912	912	912	912	912	912
14M Fluid	220	220	220	220	220	220	220	220
Fresh density	1956	1961	1966	1970	1975	1976	1980	1988

RESULTS AND DISCUSSION

Compaction characteristics of geopolymer mortar

To get the maximum dry density and optimum moisture content, Standard Proctor's compaction test was conducted on fresh geopolymer mortar. The fluid media used were water and alkaline solutions of different molarities. The variation of the dry density with f/b ratio is shown in Figure 1. Similar to the interaction of water with any particulate material, the dry density of geopolymer mortar increased initially and then decreased as f/b ratio is increased. At f/b ratio of 0.2, the mix attained maximum dry density for all the fluids. It can be seen that compaction characteristics were marginally affected by the fluid media.

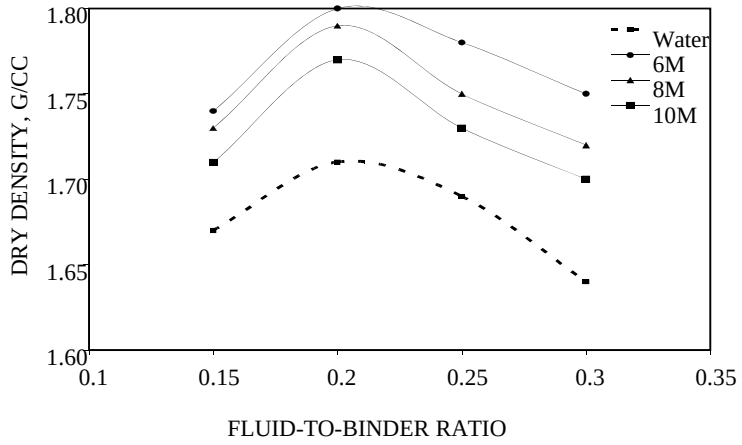

Figure 1 Variation of dry density of mortar blocks with water and alkaline fluid.

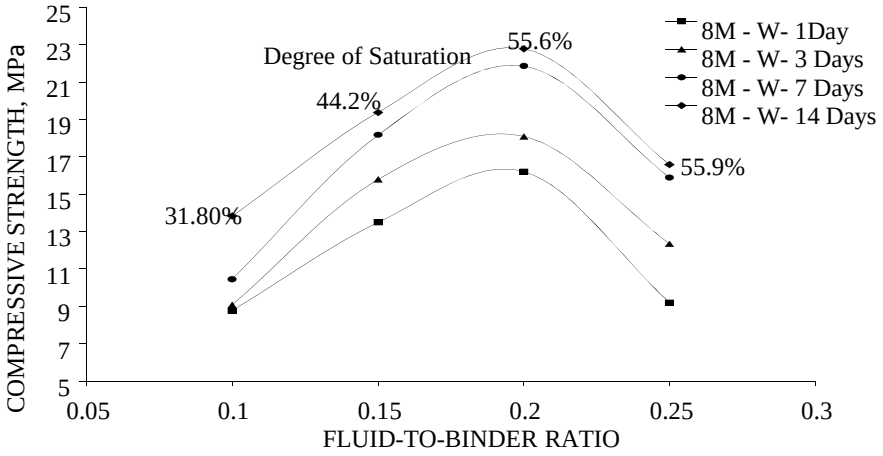

Figure 2 Compressive strength variation at constant density

After fixing the maximum dry density, the compressed blocks were prepared with different f/b ratios for molarity of 8 at a constant density of 1.79 g/cc. The unconfined compressive strength of the blocks was determined at the age of 1, 3, 7 and 14 days (Figure2). It was noticed that the strength increases with increase in f/b ratio from 0.10 to 0.20, and then decreases. This contradicts the trend of strength development according to Abrams' law.

In the case of cement concrete, strength decreases as the air content increases at saturated condition. In the case of partially saturated compressed blocks, wherein the material/matrix will be in three phase system - solids, liquid and air, the degrees of saturation at various dry density values were calculated to ascertain a similar possibility. Based on this concept, the degree of saturation was calculated, using the following basic relation of soil mechanics (Eqn. 1).

$$\gamma = \frac{\gamma_w G}{\left(1 + \frac{WG}{S_d}\right)} \quad \text{---------- Eqn. 1}$$

where, γ = Density in g/cc
γ_w = Density of water in g/cc
G = Specific gravity of the material
W = Water content in percent
S_d = Degree of saturation in percent

From Eqn. 1, it is observed that for the given density γ , as the water content (W) increases, the degree of saturation (S_d) and air content in the mortar increases. It can be seen from Figure2 that as f/b increases the degree of saturation (air content) gradually increases. It can also be seen that initially, as the f/b ratio increases from 0.10 to 0.20, strength increases (in contrary to Abrams' law). However, from f/b ratio 0.20 to 0.25 (i.e, at more or less same saturation level of 55.6 and 55.9 %), the strength drops down as per Abrams' law. This suggests that when degree of saturation is maintained constant, the effects of f/b ratio get truly reflected in the strength development as per Abrams' law. Hence the study of strength development of compressed blocks at constant degree of saturation was planned.

To maintain constant degree of saturation (specified constant air content) in the compacted state, adjustment of dry density would be essential by varying water content using Eqn. 1. If the water content (W) is known, the f/b ratio of the mortar can be calculated. This was carried out by pre-calculations as is done in gravimetric and volumetric calculations in particulate material such as soils. All the studies on compressed blocks are made at constant degree of saturation unless specified.

Strength variation at initial constant degree of saturation

From repeated trials, it was observed that it is possible to cast the compressed blocks at the degree of saturation of 44 percent without any practical difficulties. This degree of saturation was maintained constant for thermal cured blocks. In Figure 3 the strength variation is shown with f/b ratio at constant degree of saturation of 44 percent. The molarities of the alkaline activator solutions used were 6 and 8.

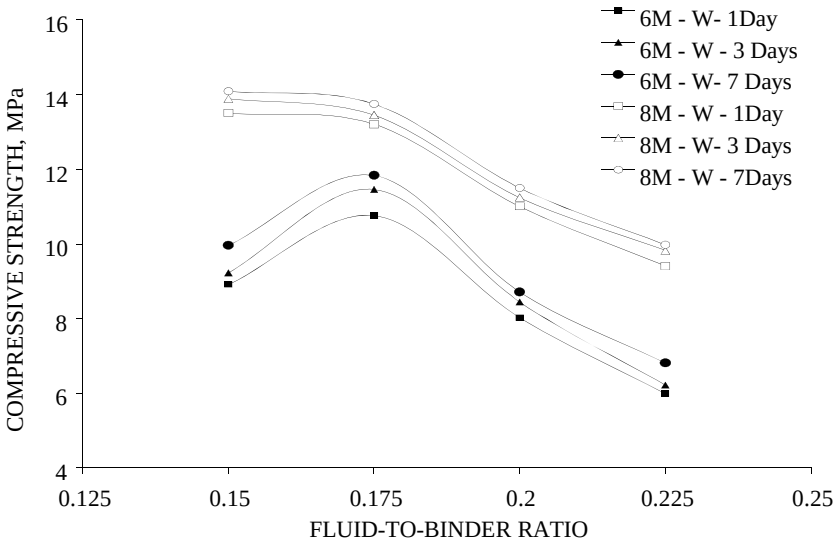

Figure 3 Compressive strength for the molarity of 6 and 8

The strength development particularly at low f/b ratio, despite the degree of saturation being constant, did not reflect the strength variation as expected according to Abrams' law. Owing to low molarity in low f/b ratio, the strength developed was less (Figure 3). This is also another factor which influences strength development. But distinctly, with alkaline solution of molarity 10 and above, at constant degree of saturation of 44%, the strength varies practically in tune with f/b ratios as shown in Figure 4. With increase in molarity, the concentration of alkaline salts was adequate enough to push the strength levels to be in tune with Abrams' law as expected. Alkaline fluid of molarity of 10 and beyond with constant degree of saturation could impart strength development in accordance with f/b ratios. Similar observations were made by Prinya *et. al.* [32] for geopolymer concrete.

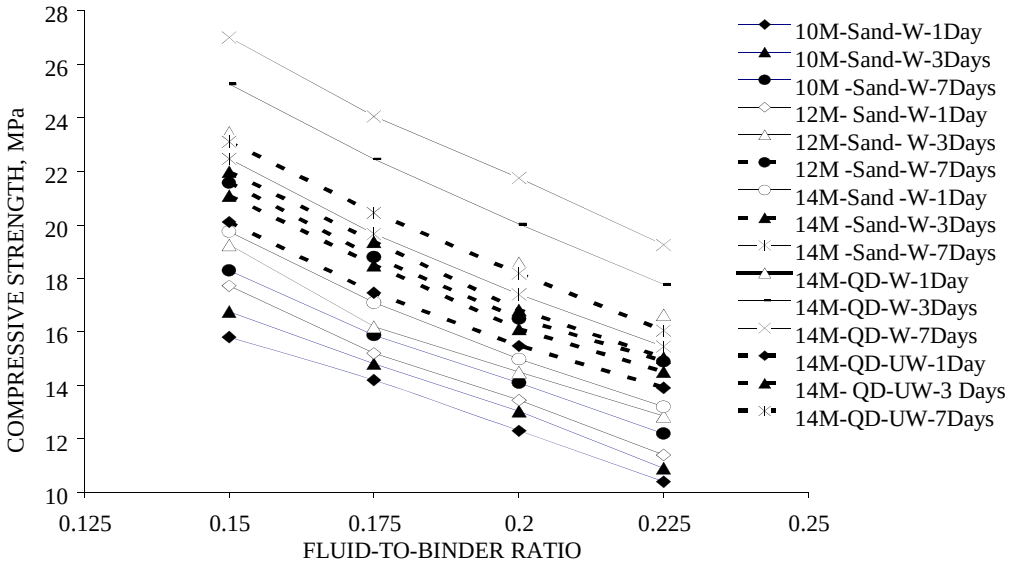

Figure 4 Compressive Strength variation with fluid-to-binder ratio

To summarize, the analysis of all test results of thermal cured fly ash-based geopolymer mortar blocks shows that strength development was influenced basically by f/b ratio. Degree of saturation was another influencing parameter in compressed blocks which has been maintained constant in all series of experiments. The trend remains the same in all the cases. This trend was the same in the case of cement compressed blocks as reported by Prasad *et. al*. [33].

Development of phenomenological model for blocks

A rational, rapid and simple method to arrive at the combination of ingredients to realize a specific strength at specified age is desirable. The variation of properties of materials necessitates recheck on the mix proportions with minimum test data and computations. In a wider context, the proposed method based on rational approach lends additional support and confidence to employ the same in practice.

It is interesting to note from the voluminous experimental data that at constant degree of saturation, f/b ratio alone determines the strength development with all other parameters remaining unchanged. Keeping this in mind, phenomenological model represented by the Eqn. 2 was developed for the given set of materials and parameters for thermally cured blocks, generalizing the compressive strength with reference to the strength at b/f of 5.0.

$$\left\{\frac{S}{S_{@\,b/f=5}}\right\} = 0.22\left\{\frac{b}{f}\right\} - 0.11 \quad \text{---------- Eqn. 2}$$

This model is shown graphically in Figure 5 having R^2 value of 0.94. The series considered for the development of the model is also indicated in the Figureure. The compressive strengths of thermally cured blocks can be predicted using Eqn. 2.

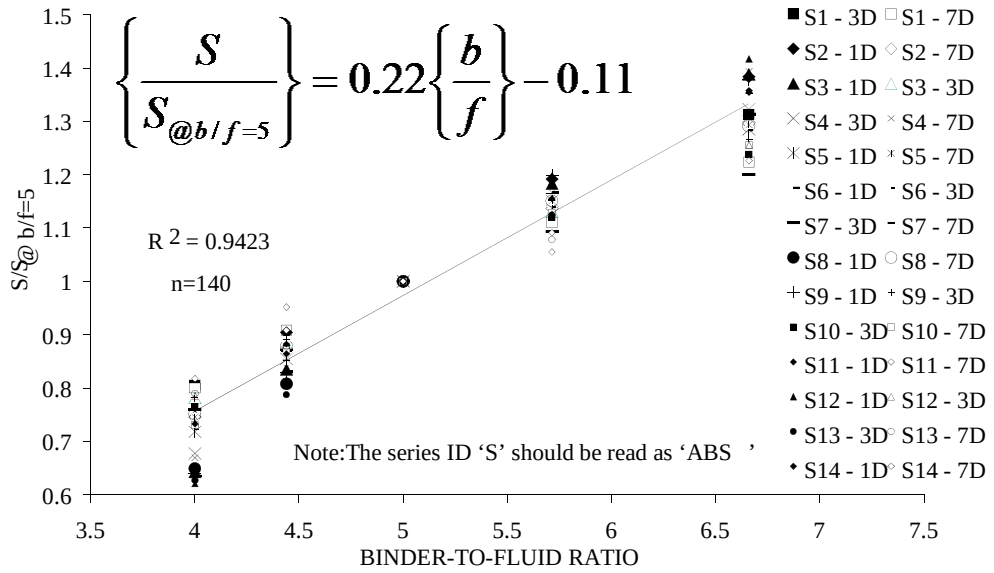

Figure 5 Graphical representation of the model (Eqn.2)

Validation of the proposed model for blocks

To use the phenomenological model represented by the Eqn.2 **,** for a given set of materials and conditions, the strength developed at a specified age for b/f ratio of 5.0 needs to be determined experimentally. Using this as an input parameter in the equation, the b/f ratio for any other desired/required strength can be calculated using the phenomenological model. All other variables like age, molarity, curing conditions should remain same except the b/f ratio. Using the calculated b/f ratio, all other ingredients in the mortar mix can be determined from the given set of materials and parameters used for developing the model. Hence, the mix proportions for the required strength can be arrived at. If anyone or in combination the ingredients of a set changes for the new set, the new input data is to be generated again to use the phenomenological model to obtain the corresponding binder-to-binder ratio to arrive at the appropriate mix proportions in order to meet the specific strength. This exercise is identified as 'Re-proportioning Method'.

It can be better illustrated as follows. In the Eqn.2, there are three variables – S, $S_{@b/f=5}$ and $\frac{b}{f}$. If the strength at f/b =5 ($S_{@b/f=5}$) is determined experimentally, for the given strength (S), binder-to-fluid ratio ($\frac{b}{f}$) can be determined mathematically. For any mix and a given set of materials, if b/f is known, all other ingredients can be found mathematically.

In order to validate the model, a series of experimental data with different conditions were considered. This independent set of data was not a part of data used in the formulation of phenomenological model. Binder-to-fluid ratio (b/f) was an independent parameter in each of the sets.

The other variables include molarity of solution, quarry dust as fine aggregate, age of samples 1, 3 and 7 days and lastly samples in wrapped and unwrapped condition. This exercise takes care of most of the parameters which are involved in practice. Within the same range of b/f ratio (i.e. 4.44 - 6.67), the strength developed in each set varies due to variation of other parameters. From each of these sets, the compressive strength at reference b/f ratio was taken into consideration in the denominator of the left-hand side of phenomenological model (Eqn.2). The strength developed at other f/b ratios is calculated and tabulated for comparison with experimental values as shown in Table 6. The values predicted using the developed model are found to be in close agreement with the experimental results, justifying the applicability of this model.

Table 6 Comparison of experimental and predicted compressive strengths

B/F RATIO	Series ID	ES* MPa	PS** MPa	ES/PS	B/F	SERIES ID	ES* MPa	PS** MPa	ES/PS
6.67	10M-Sand-W-7 Days	18.3	18.29	1.00	5.00	14M-Sand-W-1 Day	14.98	14.98	1.00
5.71	10M-Sand-W-7 Days	15.88	15.81	1.00	4.44	14M-Sand-W-1 Day	13.2	13.3	0.99
5.00	10M-Sand-W-7 Days	14.1	14.1	1.00	6.67	14M-QD-W-7 Days	27.01	28.2	0.96
4.44	10M-Sand-W-7 Days	12.2	12.52	0.97	5.71	14M-QD-W-7 Days	24.06	24.38	0.99
6.67	12M-Sand-W-3 Days	19.25	18.8	1.02	5.00	14M-QD-W-7 Days	21.75	21.75	1.00
5.71	12M-Sand-W-3 Days	16.19	16.25	1.00	4.44	14M-QD-W-7 Days	19.25	19.32	1.00
5.00	12M-Sand-W-3 Days	14.5	14.5	1.00	6.67	14M-QD-UW-3 Days	21.98	21.82	1.01
4.44	12M-Sand-W-3 Days	12.85	12.88	1.00	5.71	14M-QD-UW-3 Days	19.37	18.86	1.03
6.67	14M-Sand-W-1 Day	19.75	19.43	1.02	5.00	14M-QD-UW-3 Days	16.82	16.82	1.00
5.71	14M-Sand-W-1 Day	17.1	16.79	1.02	4.44	14M-QD-UW-3 Days	15.04	14.95	1.01

*ES – Experimental strength **PS – Predicted strength

Strength development in concrete

Geopolymer concrete cubes were prepared using different mix proportions. The parameters considered were:

- Molarity of alkaline activator: 12 and 14 M
- Fluid content: 207 and 227 kg/m^3
- Binder: Fly ash, GGBFS, Silica fume and Metakaolin.
- Curing Temperature: Ambient and 60° C
- Composite: concrete and constituent mortar

The range of strength for these series of composites is 1-60 MPa for different parameters. Depending on the requirement, parameters are to be selected to get the concrete of desired strength. It is to be noted that there are too many parameters which influence strength development. Proportioning becomes more and more complex as the number of parameters increase. One common phenomenon observed in Figure 6 is that strength development is sensitive to f/b ratio in all the cases. As this ratio increases, strength decreases with other parameters remaining the same. This pattern of strength development is the same as for cement concrete as per Abrams' law [34]. The strength decreases as the f/b ratio increases because of greater porosity with higher fluid content.
In case of geopolymer composites, when strength variation is plotted with binder-to-fluid ratio, it is linear (strength increases with increase in b/f ratio) in all the cases. Bolomey observed this kind of variation in the case of cement composites [35].

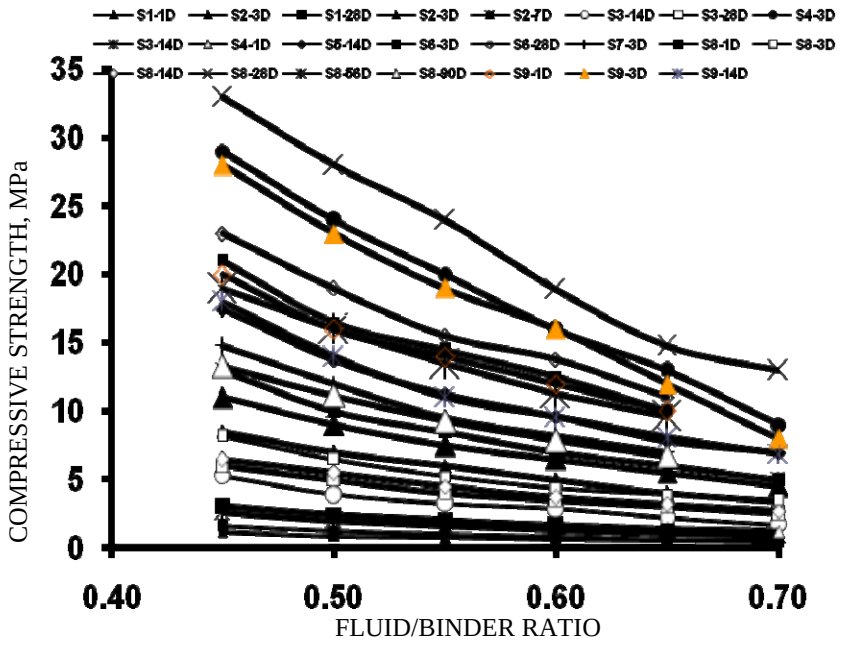

Figure 6 Variation of compressive strength verses f/b ratio (Abrams' Law)

Development of phenomenological model for concrete

Since the f/b ratio is a generic parameter for strength development with the age in geopolymers, it is an appropriate parameter to normalize the data to develop a model. Different f/b ratios within the range of 0.45 - 0.70, at different ages with similar reference strength data were considered. In this investigation, inverse of f/b ratio of 0.45, i.e., b/f ratio of 2.22 was considered as a reference for normalization. Again this chosen value of binder-to-fluid ratio is arbitrary, having no other significance. The generalization of the data with respect to the reference value of the strength at a binder-to-fluid ratio (b/f) of 2.22 ($S_{@b/f\ =\ 2.22}$) results in phenomenological model as given in Eqn. 3. The value of R^2 was found to be 0.96.

$$\left[\frac{S}{S_{@\,b/f=2.22}}\right] = 0.7708\left(\frac{b}{f}\right) - 0.7349 \text{ ---------- Eqn.3}$$

In the model (Eqn.3), shown graphically in Figure7, if the strength at binder-to-fluid ratio of 2.22 ($S_{@b/f\ =\ 2.22}$) is known, the strength at any binder-to-fluid ratio can be estimated as long as all other parameters, including age, are constant. The advantage of this model is that the input of single experimental data is sufficient to predict the strength at any other b/f ratio. This simple rational model avoids multiple trials. This is the major advantage in re-proportioning the geopolymer concrete.

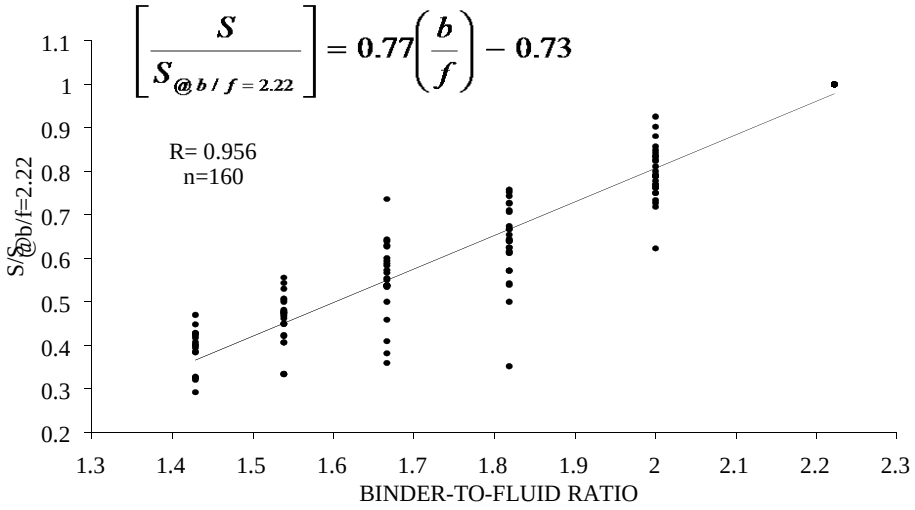

Figure 7 Graphical representation of the model (Eqn. 3).

Validation of the model for concrete

To use this model (Eqn. 3), for a given set of materials, the strength developed at a specified age for a binder-to-fluid ratio (b/f) of 2.22 (or f/b = 0.45) is to be determined. Using this as an input parameter in the equation, the binder-to-fluid ratio for any other desired strength can be calculated using the phenomenological model.

Using this calculated b/f ratio, all the ingredients of concrete can be calculated for the mix having f/b = 0.45 or b/f = 2.22. A separate series of experimental data was considered to examine the validity of the phenomenological model.

The data generated for the series S10–S19 was used exclusively for the validation apart from other series. From each of these sets, the compressive strength at reference b/f ratio was taken into consideration in the denominator of the left-hand side of the phenomenological equation. The strength predicted at other f/b ratios was calculated and tabulated for comparison with experimental values. A close match between the two (Figure 8) reinforces the applicability of the phenomenological model. With more data being generated the scope of this model can further be enhanced for still wider range of b/f ratio.

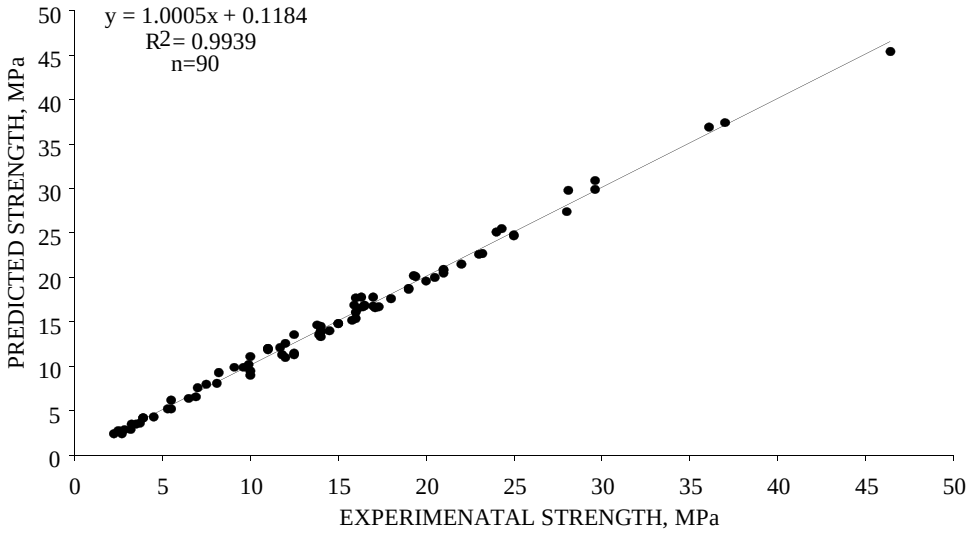

Figure 8 Comparison of experimental results and predicted strength using Eqn. 3

It is interesting to note that the model was used to predict the strength using the data generated by Rangan [11 and 12]. The predicted strength values were in line with the experimental values (Table 7). The maximum error was less than 6%. This reinforces the possibility of using this model for any geopolymer composites.

Table 7 Experimental [11 and 12] and predicted strength values

F/B	B /F	EXPERIMENTAL RESULTS(Rangan) MPa	PREDICTEDVALUES (Eqn.3) MPa	ERROR %
0.30	3.33	58.0	59.6	2.8
0.35	2.86	45.0	47.6	5.8
0.40	2.50	37.0	38.6	4.3
0.45	2.22	32.0	31.5	1.6

CONCLUSIONS

- Masonry blocks of considerable strength can be prepared using geopolymer mortar.
- Strength development in geopolymer mortar and concrete is in accordance with Abrams' law for the specified range of fluid-to-binder ratio and for a given air content represented by degree of saturation.
- The phenomenological models can be developed and used to re-proportion the mix required to cast the compressed blocks and concrete.
- The models were validated with independent sets of experimental data.
- The predicted compressive strength values show good agreement with the experimental results , reinforcing the possibility of using the models for the field applications.
- In case of geopolymer concrete, the phenomenological model developed by the authors was validated not only by a set of independent experimental data generated by the authors but also with the data reported by other researcher.

REFERENCES

1. JANNIE S.J. VAN DEVENTER, JOHN L. PROVIS, PETER DUXON, DAVID G. BRICE. (2010) "Chemical Research and Climate Change as Drivers in the Commercial Adoption of Alkali Activated Materials", Waste Biomass Valor, 1:145-155.

2. ELLIS GARTNER. (2004) "Industrially interesting approaches to 'low-CO_2' cements", Cement and Concrete Research 34, 1489-1498.

3. GAJANAN M. SABNIS, KENNETH DERUCHER, KRISTIN COOPER CARTER. (2009) "Concrete Construction and Sustainability", ICI Journal, 9-15.

4. ESTHER OBONYO, ELIE KAMSEU, UPHIE C.MELO AND CRISTINA LEONELLI. (2011) "Advancing the Use of Secondary inputs in Geopolymer Binders for Sustainable Cementitious Composites: A Review", Sustainability, 3, 410-423.

5. XIAOLU GUO, HUISHENG SHI, WARREN A. DICK. (2010) "Compressive strength and microstructural characteristics of class C fly ash geopolymer" , Cement and Concrete Composites, Vol.32, Issue 2, 142-147.

6. BUCHWALD, M. SCHULZ. (2005) "Alkali-activated binders by use of industrial by-products", Cement and Concrete Research 35, 968-973.

7. ZONGJIN LI, ZHU DING, YUNSHENG ZHANG. (2002) "Development of Sustainable Cementitious Materials", Proceedings of International Workshop on Sustainable Development and Concrete Technology, pp.55-76.

8. VENKATESH BABU.D.L., DIVYA MOHAN. (2005) "Study on Properties of Fly Ash Based Geopolymer Concrete - Concrete without Cement", Proceedings of International Congress on Fly Ash utilization, New Delhi, X 10.1 – 10.8, Dec 4-7, 2005.

9. LI HUI, XU DELONG. (2009) "The Future Resources for Eco-building Materials: II.Fly Ash and Coal waste", Journal of Wuhan University of technology-Mater. Sci. Ed., pp 667-672.

10. J. DAVIDOVITS. (1989) "Geopolymers and Geopolymeric Materials", Journal of Thermal Analysis, Vol. 35, 429-441.

11. HARDJITO.D. S. E. WALLAH, D. M. J. SUMAJOUW, B. V. RANGAN (2004) "On the development of fly ash based geopolymer concrete", ACI Material Journal 101, pp.467- 472.

12. HARADJITO, D., WALLAH, S.E., SUMAJIOUW, D.M.J, RANGAN, B.V., (2004) "Fly ash based Geopolymer concrete material for sustainable development", Invited Paper for Concrete World Conf. ACI India Chapter Mumbai.

13. HARADJITO, D., WALLAH, S.E., SUMAJIOUW, D.M.J and RANGAN, B.V., (2004) "Brief Review of development of Geopolymer concrete", Invited Paper, George Hoffman Sym. ACI Las Vegas, USA, 25th May 2004:1-10.

14. FENG-QING ZHAO, WEN NI, HUI-JUN WANG, HONG-JIE LIU. (2007) "Activated fly ash/slag blended cement", Resources, Conservation and Recycling, 52, 303-313.

15. RAJMANE N. P., NATARAJA M.C., LAKSHMANAN N., DATTATREYA J.K. (2011) "Pull-Out Tests for Strengths of Geopolymer Concretes", Proceedings of International Conference ICI-AMAS-2011, PEC, Puducherry, India, 350-358.

16. PETER DUXSON, JOHN L. PROVIS, GRANT C. LUKEY, J.S.J. VAN DEVENTER. (2007) "The role of inorganic polymer technology in the development of green concrete", Cement and Concrete Research 37, 1590-1597.

17. P. DUXSON, A.FERNANDEZ-JIMENEZ, J.L. PROVIS, G.C. LUKEY, A. PALOMO, J.S.J. VAN DEVENTER. (2007) "Geopolymer technology: the current state of the art", Journal of Material Sci., 42:2917-2933.

18. WALLAH, S.E., B. V. RANGAN. (2006) "Low-Calcium Fly Ash-Based Geopolymer Concrete: Long-Term Properties", Research Report GC 2 Faculty of Engineering, Curtin University of Technology, Perth, Australia.

19. XIUJIANG SONG. (2007) "Development and performance of Class F fly ash Based Geopolymer Concretes against Sulphuric acid attack", Ph.D Thesis, The university of New South Wales, Sydney, Australia.

20. BAKHAREV T. (2005) "Resistance of geopolymer materials to acid attack"., Cement and Concrete Research 35, pp.658–670.

21. BAKHAREV T. (2005) "Durability of geopolymer materials in sodium and magnesium sulfate solutions", Cement and Concrete Research 35, pp.1233– 1246.

22. RADHAKRISHNA. (2009) " Ph.D Thesis , "Development of Methods for Re-Proportioning of Fly Ash Based Composites", Visvesvaraya Technological University, Belgaum, INDIA

23. SOFI M., VAN DEVENTER J.S.J., MENDIS P.A., LUKEY, G.C. (2007) "Engineering properties of inorganic polymer concretes (IPCs)", Cement and Concrete Research 37, 251–257.

24. MONITA OLIVIA, HAMID R. NIKRAZ. (2011) "Strength and water permeability of fly ash geopolymer concrete", ARPN Journal of Engineering and Applied sciences, vol. 6, No. 7, 70-78.

25. NATARAJ M.C., DHANG N, GUPTA A.P. (1997) "Computer aided concrete mix proportioning", The Indian Concrete Journal, Vol. 71, No. 9, 487-492.

26. NATARAJ M.C., DHANG N and GUPTA A.P. (1999) "A simple equation for concrete mix design cures of IS 10262:1982", The Indian Concrete Journal, Vol. 73, No. 2, 111-115.

27. RANGAN B.V. (2008) "Fly Ash based Geopolymer Concrete", Research Report GC4, Curtin University of Technology, Perth, Australia.

28. NAGARAJ T.S., ZAHIDA BANU. (1996) "Generalization of Abram's Law", Cement and Concrete Research, Elsevier Science, 26(6):933-942.

29. VIJAYA RANGAN. (2008) "Mix design and production of fly ash based geopolymer concrete"., The Indian Concrete journal., 82(5):7-15.

30. IS:1727- 1967, "Methods of test for pozzolona materials (first revision-Jan.1999)

31. ACI COMMITTEE 211.1-91, (1994) "Standard practice for practice for selecting proportions for normal, heavy weight, and mass concrete", American Concrete Institute manual of concrete practice, part 1: Materials and General properties of concrete, pp38 (Detroit, Michigan, 1994).

32. PRINYA CHINDAPRASIRT, CHAI JATURAPITAKKUL, WICHIAN CHALEE , UBOLLUK RATTANASAK., (2009) "Comparative study on the characteristics of fly ash and bottom ash geopolymers", Waste Management, Vol. 29, Issue 2, February 2009, pp. 539-543.

33. NAGENDRA PRASAD.K., M.L. NARASIMHULU, T.S. NAGARAJ, J.M. NAIDU, SYED IFTHAKARUDDIN. (2005). “Strength Development in Compressed Cement Blocks – Analysis and Assessment” – Indian Concrete Institute Journal, 79(4), 4 pp49-54

34. ABRAMS D. “Design of concrete mixtures”. Bulletin No.1, 1918, Structural Materials Research Laboratory, Lewis Institute. Chicago, p20.

35. BOLOMEY, J. “Durecissenment des mortiers ets benton". Tech. Suisse Romande Nos. 16, 22 and 24. –2.4.1.,1927

Measuring the Albedo for Different Slag Contents and Surface Finishes of Concrete Slabs

A Sweeney[1], R P West[1], C O'Connor[2]
1 – Trinity College Dublin, Ireland
2 – Ecocem Materials, Ireland

This paper presents a review of ongoing research at Trinity College into measuring the effects of slag content and surface finish on concrete albedo, that is, the solar reflectance of concrete. There is a number of advantages to improving the albedo of surfaces which includes the reduced need for air conditioning thus reducing energy consumption, and mitigation of the urban heat island effect. The amount of light reflected back into the universe can be converted into an equivalent reduction in CO_2. The effect of the composition of concrete on the solar reflectance has been researched by others however this research is limited. The objective of this research is to quantify the improvement in albedo in concrete containing different quantities of ground granulated blast furnace slag (GGBS) (which is a cement lighter in colour) with different surface finishes. Four different percentages of GGBS and four different surface finishes representative of different applications of exposed horizontal concrete surfaces are investigated. A number of instruments is being evaluated over the course of the study as to their efficacy in measuring the albedo of the concrete samples, including a lux meter, albedometer, infrared camera and thermocouples. The surface moisture of the slabs (which affects their greyness) is being recorded using a moisture meter and the hours of sunshine using a sunshine duration sensor. Preliminary results of the lux meter, thermocouples and sunshine duration sensor indicate their sensitivity and reliability. It may be concluded that the surface finish has a measurable effect on the temperature of the specimens and that the specimens containing the higher percentages of GGBS recorded the lowest temperature increase under sunlight. It was also observed that direct sunshine is necessary to take light reflectance readings as the presence of cloud has a significant impact on the accuracy of the results.

Angharad Sweeney is a graduate of Trinity College Dublin in civil, structural and environmental engineering. She is currently a PhD researcher in TrinityHaus, the research centre for innovation and sustainability in construction. Her topic of research is the albedo effect on concrete.

R P West is an Associate Professor at The Department of Civil, Structural and Environmental Engineering at Trinity College Dublin and is currently Director of the Structural Laboratories and a former Head of Department. He is on the Examinations committee of the ICT and the Editorial Board of the Magazine of Concrete Research. His research interests lie in concrete durability and innovation and he has over 120 peer-reviewed publications

Ciara O'Connor is the Environmental Manager of Ecocem Materials; manufacturer of GGBS cement. She also manages EmissionZero, which advises Irish businesses on Carbon Reduction. Although from Dublin, Ciara has previously worked for the Carbon Trust in the UK, advising public sector organisations on strategic emissions reduction and legislative compliance issues. She is a graduate in Botany (BA) and Environmental Science (MSc) from Trinity College, Dublin

Keywords: GGBS, equivalent reduction in CO_2, heat island effect, solar reflectance, surface finish

INTRODUCTION

Solar reflectance, or albedo, is the ratio of the amount of light reflected from a surface to the amount of light incident on a surface [1]. Albedo is a dimensionless parameter and is measured on a scale from 0 to 1 and some typical values are given in Table 1. An albedo of 0 represents a black body that does not reflect any light and an albedo value of 1 represents a perfectly reflective surface.

A man-made surface such as asphalt absorbs more heat from the sun than, say, concrete as it has a low albedo value. Low albedo surfaces can contribute to the urban "heat island" effect as they raise the local ambient air temperature in urban areas [1]. By increasing the albedo of a paved surface, this keeps it cooler in the sun thereby reducing convection of heat from pavement to air. This decreases the ambient air temperature which decreases the demand for cooling energy and slows the formation of smog [2]. Other benefits include increased visibility at night time leading to reduced lighting by approximately 30% [3] and improved safety [4]. Increasing the albedo of urban surfaces can also improve the urban air quality and it also results in reflecting more of the incoming global solar radiation and countering to some extent the effects of global warming [5]. Concrete can be made more reflective by using suitable cement and aggregates [2]. Research conducted by Boriboonsomsin and Reza [1] has shown that high solar reflectance concrete using 70% ground granulated blast furnace slag (GGBS) as a cement replacement results in an albedo value approximately 70% higher than that of ordinary grey cement.

Table 1 Typical Albedo Values [6]

SURFACE	ALBEDO
Snow	0.90
Ice Caps	0.80-0.90
White Paint	0.80
GGBS Concrete (50%)	0.50
New Concrete(Traditional)	0.30-0.40
Aged Concrete(Traditional)	0.20-0.30
Aged Asphalt	0.10-0.15
Ocean	0.06-0.10
New Asphalt/Black paint	0.05

MATERIALS AND METHODOLOGY

Ground granulated blast furnace slag (ggbs)

Ground-granulated blast furnace slag (Figure 1) is a cement replacement which is significantly lighter in colour than ordinary Portland (CEMI) cement. It is a waste product from the blast furnace production of iron from ore. There are a number of benefits of the use of slag in concrete including but not limited to better paste aggregate bond, lower permeability, enhanced durability and reduced heat generation [1]. The use of this cement replacement in sufficiently high proportions results in a concrete that is lighter in colour, thus increasing its albedo.

Figure 1 GGBS and normal Portland cement [7]

The use of GGBS in construction can result in a project being awarded recognition in national standards such as LEED (Leadership in Energy and Environmental Design). This standard was developed by the United States Green Building Council which rates a building's environmental performance and credits are awarded for the improvement of albedo. The use of GGBS can have a positive outcome in a number of the credit categories as it has a higher albedo value and can help to reduce the heat island effect. Accordingly, up to 2 points can be awarded in the heat island category of the LEED assessment.

Initial research carried out by Boriboonsomsin and Reza [1] using 30, 60 and 70% GGBS replacement illustrated that a direct relationship exists between GGBS content and albedo. This relationship may be observed in Figure 2, where the albedo increases linearly with increasing GGBS content although the data is limited. Levinson and Akbari [2] examined the correlation between the albedo of smooth concrete and the albedo of cement. They manufactured a number of samples using grey Portland cement and white Portland cement. Of the 32 mixes which were manufactured, 24 of these were substandard and subsequently not included in the publication results. Of the 8 remaining samples, the four most reflective unexposed samples were constructed using white cement and had albedos ranging between 0.68 and 0.77. The four remaining samples which were the least reflective had results ranging between 0.44 and 0.52 and were made with grey cement.

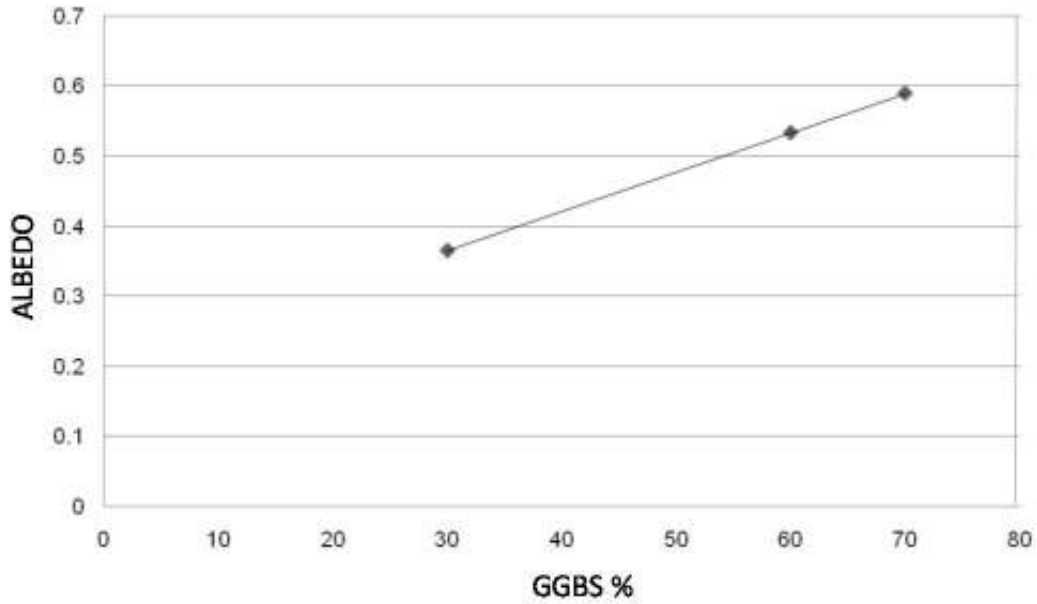

Figure 2 Relationship between albedo and GGBS content of concrete [1]

AGGREGATE TYPE

In the project reported in this paper, three different aggregate types were used in the manufacturing of the sample slabs; limestone, partially crushed limestone and sandstone. It is not believed that the aggregate type will significantly affect the surface albedo, however, it was included in the study to justify the elimination of this parameter to ensure consistency throughout all test samples. Each aggregate was taken from the same batch. The coarse aggregate was 20mm and 10mm in size and the moisture level of the sand was measured using the 'Speedy Test' in order to ensure that the same amount of water was present in each concrete mix.

METHODOLOGY

The primary focus of this paper is to examine the different mechanisms for measuring albedo. There are, however, a number of parameters which affect the albedo value, including the surface finish of the concrete, the level of cement replacement (GGBS in this case) and the aggregate type. For this reason, it was decided to manufacture a total of 96 concrete specimens (300mm square in surface area and 60mm deep), containing four different levels of GGBS, three different aggregate types and four different surface finishes. Two specimens of each type were manufactured for repeatability purposes. During the manufacturing process, the formwork was constructed with marine plywood to ensure a smooth surface finish and a small hole was drilled in one side to facilitate the inclusion of a thermocouple wire (20mm from the top surface) to record internal temperature at the centre of the slabs at a later stage.

The slabs were exposed to a strict and consistent curing regime for the first 24 hours before being placed on a rooftop within Trinity College Dublin in September 2010 (see Figure 3). There are a total of 6 boards, each one containing 16 slabs and a different aggregate type. As there are three aggregates used, each board has a duplicate. In the centre of the board, the thermocouple wires are protected from the elements in a box connected to a central data logger.

Figure 3 Layout of concrete slabs

Surface Finish

Research carried out by Bretz and Akbari [8] studied the long term performance of high albedo roof coatings. Their research did not look specifically at the effect of surface roughness on albedo however their roof coatings were categorized under smooth, medium

and rough substrates. They found that a rough substrate can result in a smaller surface albedo because of geometrical effects (multiple reflections) and because air borne particles can accumulate in depressions on the surface. Similarly research carried out by Taha and Sailor [9] measured the albedo of roofing materials and they concluded that for the same material or colour, a rough texture effectively decreases the albedo compared to that of a smooth texture. A rough texture increases the possibility that a reflected beam strikes the same surface again and is absorbed, therefore a rough surface will have a higher temperature than a smooth one.

Based on the existing limited research into the effect of surface roughness on solar reflection, surface roughness is investigated here: a total of four different surface finishes were chosen; two rough and two smooth finishes. These were achieved as follows:

Cast (smooth) – achieved by exposing the underside (cast face) of the slab
Screeded (semi-smooth) – using a steel float to seal the surface of the concrete
Brushed (semi-rough) – carried out by using a brush over the surface in one direction
Tamped (rough) – a piece of timber is used to tamp the surface resulting in an undulating surface

(a) (b) (c) (d)

Figure 4 Different surface finishes (a) Cast (b) Screeded (c) Tamped (d) Brushed

INSTRUMENTATION

The parameters being tested include the core temperature, measured using thermocouples, a greyness card to visually determine colour ageing of the concrete slabs, light reflectance using a light meter, and solar reflectance using an albedometer. Sunshine hours are also recorded using a sunshine duration sensor located on the rooftop parapet and moisture content on the surface is measured using a moisture meter.

Light Meter

A light meter is used to measure visible light reflection for both incident and reflected light off the surface. The device measures light in units of "lux" (lumens/m²) and the measurement of light reflected off a surface is an independent indication of the level of albedo. As visible light only accounts for 43% of the solar spectrum, this measurement does not determine the albedo directly. This can only be done using an albedometer which measures light across the entire frequency spectrum.

To measure the incident and reflected visible light, the light meter is used with a black box (Figure 5) which has been designed specifically to measure only the light reflected off the slab and eliminates any background light [10]. The box is placed on top of the slab and they are rotated in a horizontal plane so that the tunnel points towards the incoming light. Both the

slab and the box are then tilted in the vertical plane until there is no shadow cast on the surface of the slab, at which point the incoming rays are parallel to the sides of the tunnel. The incoming light is measured orthogonal to the ray at the slab surface and the reflected light is measured in the recess of the box.

Figure 5 Light meter and black box

Infrared Camera

A thermal image is a representation in colour of radiation differences in objects. Hotter objects appear brighter and this can be used to demonstrate differences in a material's temperature. An infrared thermal imaging camera (Figure 6) is being used to measure heat development of the slabs. As the slabs absorb sunlight, this is converted into heat and is reemitted as infrared radiation. Two parameters which are expected to be demonstrated as having an effect on the radiation observed are the GGBS content and surface finish however the dominating factor is yet to be established.

Figure 6 Thermal imaging camera

Thermocouples

The internal temperature of the slabs is being measured on a continuous basis using thermocouples which were placed in the slab 20mm from the top surface during the manufacturing process. They measure the increase in temperature inside the slab when the surface is exposed to natural sunlight and this is being used to indirectly evaluate the solar light absorption. A data logger is used to collect results every 10 minutes.

Albedometer and Sunshine Duration Sensor

The albedo of the concrete samples can be measured using an albedometer, as shown in Figure 8. The upper dome measures the incoming global radiation with a field view of 180° and the lower dome measures the reflected solar radiation with a field view of 170°. The instrument is required to be level when recording albedo and it has a spectral range from 285-2800nm i.e. it accounts for the infrared, visible and ultraviolet light. It is a very sensitive device and complies with ISO 9060. The output voltages of both domes are converted to irradiance in W/m² then the albedo is calculated. The instrument, normally used over large pavement areas, is currently being calibrated to enable it to measure the albedo over the smaller surface area of the concrete specimens (Figure 3).

The sunshine duration sensor (Figure 7) indicates whether or not there is sunshine at a particular time and also the direct irradiance or level of intensity which is measured in W/m². The instrument is pointed in the direction of the nearest pole and is rotated to the locations angle of latitude with an unobstructed horizon. This instrument is also set to record at 10 minute intervals in order to compare the sunshine intensity with the temperature changes in the slabs.

Figure 7 Albedometer (left) and sunshine duration sensor (right)

Moisture and Ageing

Research by Levinson and Akbari [2] found that wetting the surface of the concrete strongly depressed the albedos of the concretes by virtue of a darker surface colour, which pertained until their surfaces were dried. Therefore, as the slabs are exposed to the environment, the moisture level on the surface will change depending on weather conditions. The surface moisture is recorded using a moisture meter before taking readings of light reflectance as the moisture level may have an effect on the colour of the slab.

Similarly Levinson and Akbari [2] also found that on average weathered concrete is less reflective than unexposed concrete. As a result, a greyness scale was constructed in order to give an indication of the level of ageing of the slabs over time. The greyness scale (Figure 8) is compared with the surface of the slab and the percentage of greyness is recorded (white is equal to 0% and black to 100%). This is being recorded on a monthly basis to establish the effect of ageing due to exposure of the slabs with different surface finishes ageing differently.

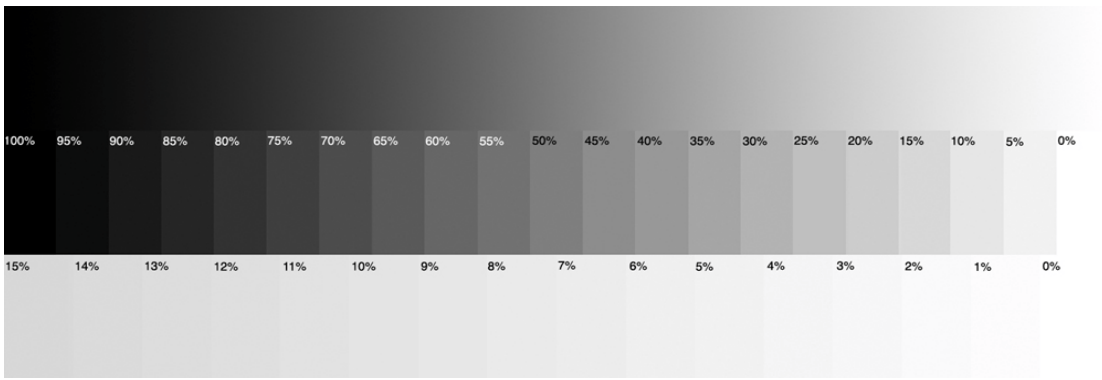

Figure 8 Greyness card [11]

RESULTS AND DISCUSSION

Thermocouples and sunshine duration

The effect of GGBS content on internal temperature

Figure 9 represents the temperature change for slabs with different GGBS contents (0, 30, 50 and 70%) for a cast surface finish during March 2011. The aggregate used in this case was partially crushed limestone. There is a discernable difference between the temperatures of the different slabs. The slab containing no GGBS is consistently the highest temperature, which is approximately 22°C in this case. This is followed by 30 and 50% GGBS slabs, with 70% reaching the lowest temperature of approximately 16°C. This indicates that the addition of GGBS reduces the internal temperature of the slabs (by approximately 6°C in this case) as the brighter slabs are reflecting the sunlight. In the more intense sunlight found in different regions of the world, this difference is likely to be considerably greater.

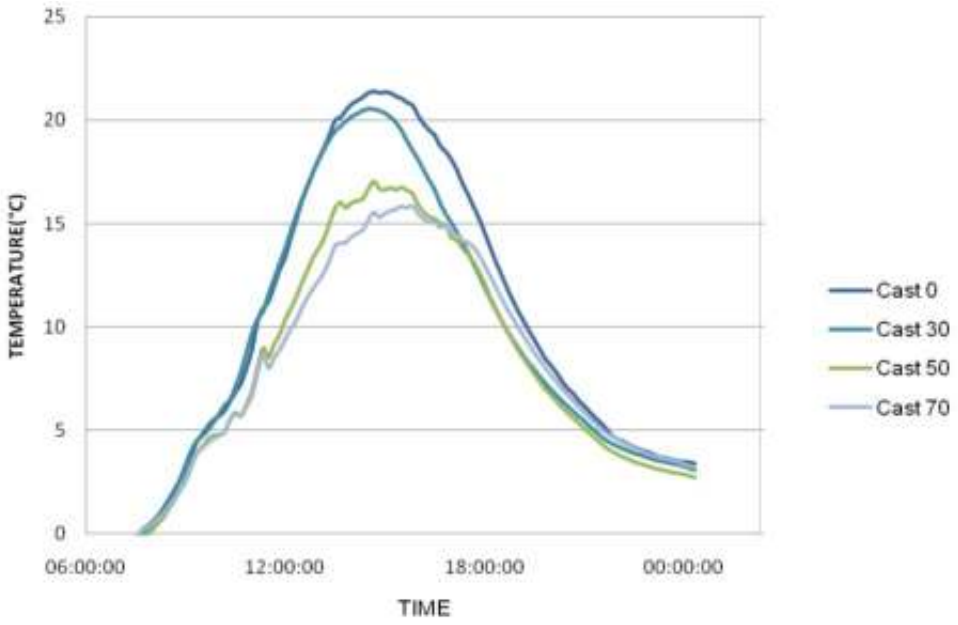

Figure 9 Time vs. Temperature – Cast Finish

The Effect of Surface Finish on Internal Temperature

Figure 10 illustrates results from thermocouple readings taken over four days during the month of July 2011 with the limestone aggregate. The graph represents four slabs containing no GGBS but with four different surface finishes. The corresponding sunshine data is also shown in Figure 10 indicating the intensity of sunshine, therefore, the peaks in temperature correspond to the peaks in this graph. The cast finish slab was the highest temperature followed by screeded, brushed and tamped slabs. This can be seen in particular on day 1 and 3. There is very little sunshine recorded on day 2, however, there is still a noticeable difference in the temperature. This could suggest that even on cloudy days, there is still an albedo benefit.

The smoother surface finishes (cast and screed) consistently reach the highest temperatures, with the rougher surfaces (brush and tamp) being lower in temperature which is unexpected based on literature review and the results of visible light reflectance. Due to the nature of the surface, it would appear that the rough surfaces are absorbing less light. Therefore the surface finish does have a discernible effect on the internal temperature of the slabs as there is approximately a 7°C difference between the cast finish and tamped finish slabs on day 1.

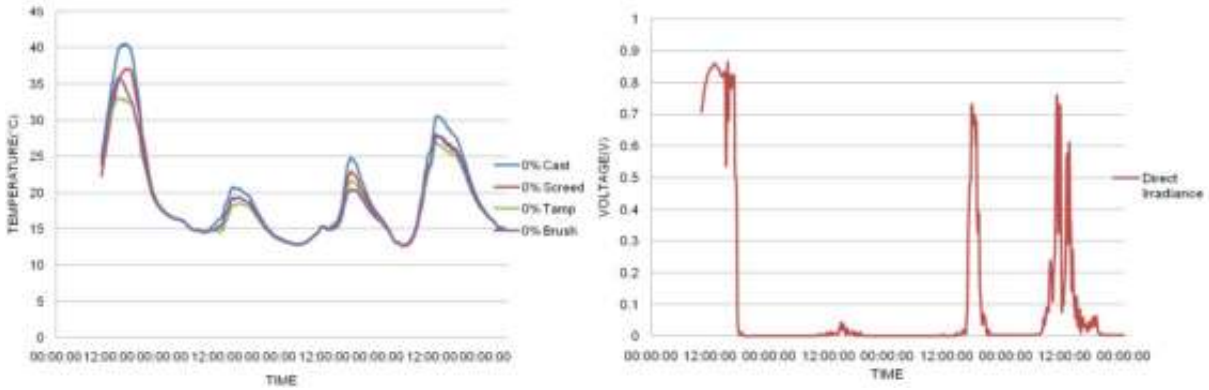

Figure 10 Time vs Temperature - 0% GGBS (left) and Corresponding Sunshine Data (right)

Figure 11 shows the temperature change for slabs with different GGBS contents but the same surface finish over the duration of one day during March 2011(as in Figure 9). The aggregate used in this case was limestone. Both 0 and 30% slabs reach their maximum temperature of approximately 19°C.

The slab containing 70% GGBS reached the lowest temperature of 14°C, with a difference in temperature between 0 and 70% slab of 5°C. As the brush finish is a rough finish, it is generally lower in temperature overall in comparison to the smooth cast finish in Figure 9. It can be concluded from these results that both the surface finish and the addition of GGBS have a significant influence on the temperature.

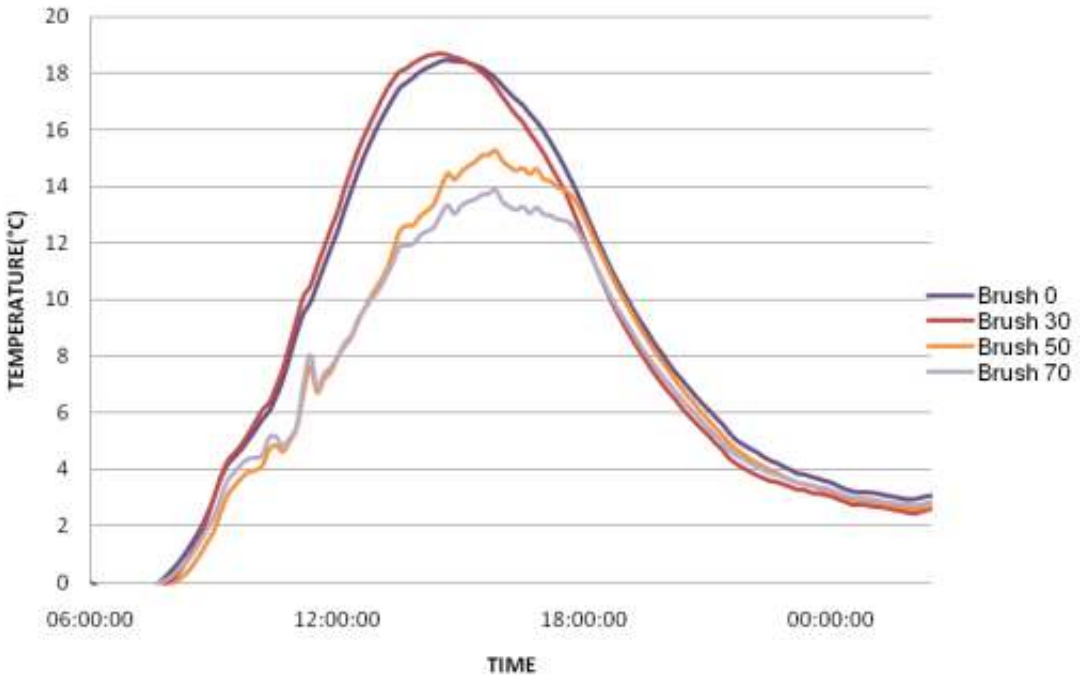

Figure 11 Time vs. Temperature - Brush Finish

LUX METER

A measure of visible light reflectance was taken for the slabs using a light meter and black box as described earlier. The set of results shown in Figure 12 were taken with an average incoming solar light reading of approximately 75,000 lumens (that is, in clear sunshine), as there is much less consistency in measurements when there is cloud present as the incoming lux is constantly changing. The readings were taken on July 27th 2011 and the aggregate is sandstone. There is a general increase in reflectance seen with the increase in GGBS content. The screed finish is the most reflective followed by the tamped finish. These two particular surface finishes look visibly brighter than the brush and cast finish. The cast finish is the least reflective which may be attributed to two main reasons; the surface looks darker in colour due to the finish and also the nature of the surface finish which results in it having a higher moisture content. The cast finish has open pores on the surface which absorb moisture in comparison to, say, the screeded finish which is a sealed surface finish. This is seen in the corresponding readings from the moisture meter where the cast finish has the highest moisture level of at least 4% in every case. Both the brush and screed finishes decrease in reflectance after 50% GGBS. The highest increase in reflectance is seen between 30 and 50% GGBS replacement.

Figure 13 illustrates thermocouple readings from one day in July 2011. In contrast to Figure 9, the lowest temperature in this result is the slab containing 50% GGBS as opposed to 70%. This is due to weathering of the slabs, in particular the 70% slab. This result coincides with the results of light reflectance in Figure 12 where both the brush and screed slabs decrease in light reflectance.

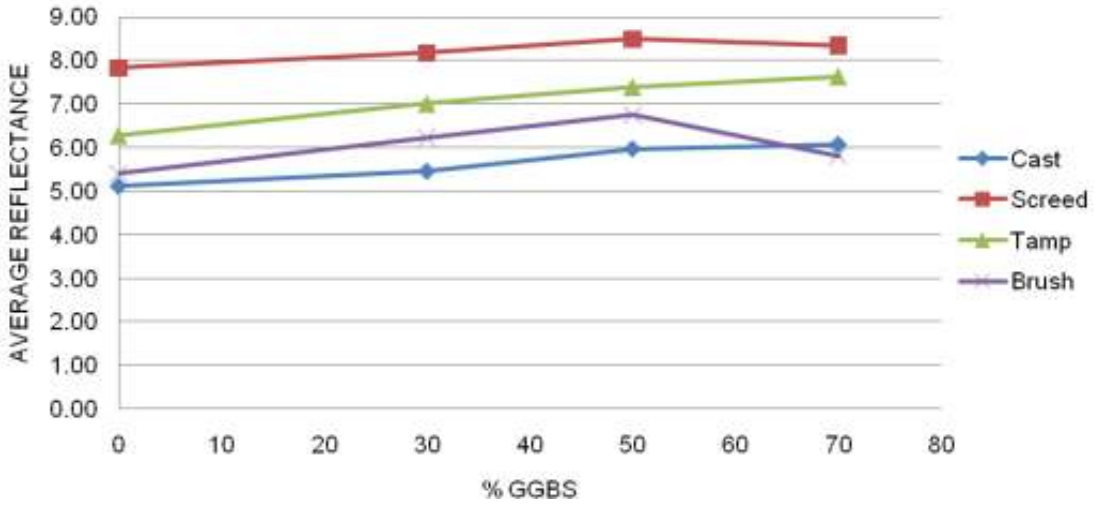

Figure 12 % GGBS vs. Average Reflectance

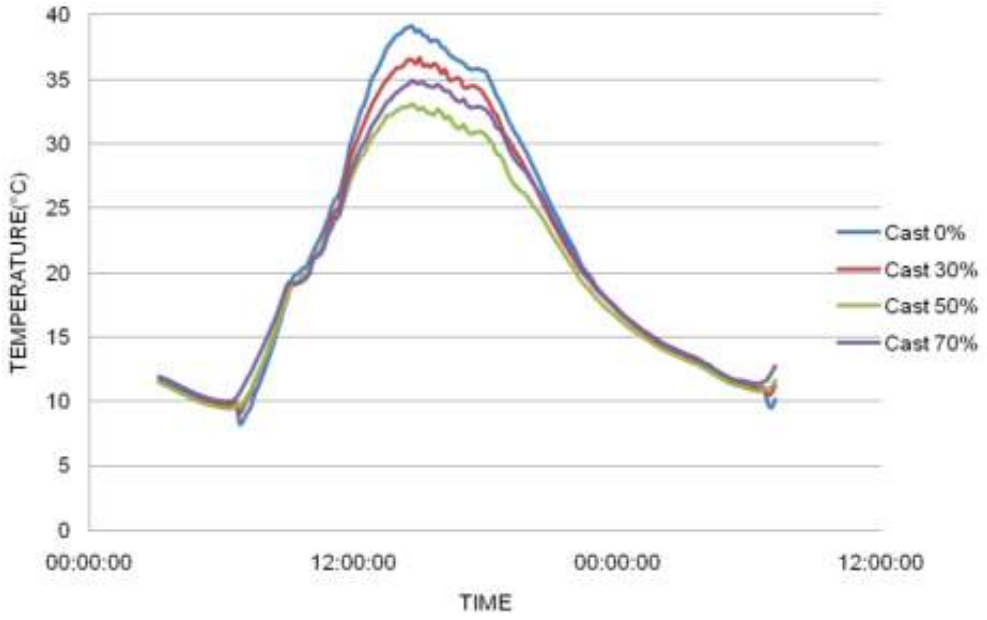

Figure 13 Time vs. Temperature - Cast Finish

INFRARED IMAGING

Figure 14 shows a sample set of results for slabs containing no GGBS (see Figure 4) with corresponding thermal images taken on the 27th July 2011. A summary of data is illustrated in Table 2. The results show that the cast finish reaches the highest surface temperature in all cases and the screed finish is the lowest, with tamp and brush finishes having similar temperatures. These results correspond with results of light reflectance and greyness. As the cast finish is darker in colour it is absorbing more radiation therefore reaching a higher temperature. The results also coincide with the thermocouple results for the cast finish only. The brighter screed finish is reflecting more of the sun's radiation thus experiencing a lower surface temperature. The tamped and brush finishes are similar in temperature. For the 70% cast and screed slabs, these recorded a higher temperature and this may be due to the visible ageing of these slabs.

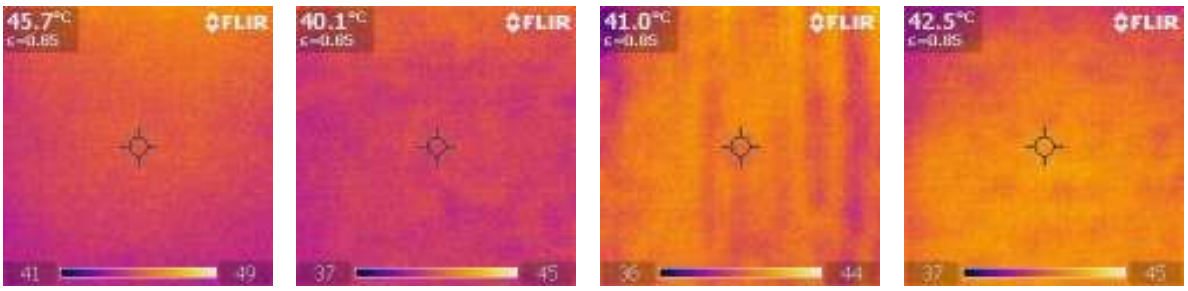

Figure 14 (a) (b) (c) (d)

Table 2 Thermal Imaging Average Temperatures

% GGBS	CAST	SCREED	TAMP	BRUSH
0	45.7	40.1	41.0	42.5
30	45.1	40.4	39.3	41.0
50	41.8	39.2	40.9	41.5
70	42.8	40.3	40.7	39.7

GREYNESS SCALE

The greyness scale was developed in order to visually assess the ageing of 'albedo' index over time and the value for greyness is calculated as (1 minus the % reading on the greyness card). Similar to the results of light reflectance, the greyness scale results (Table 3) show that the screed finish has the brightest colour and cast finish is the darkest, with the tamped and brush finish having a similar colour. This is a quick and very cost effective means of assessing the relative values of the albedo index.

Table 3 Greyness card results for brightness

	'ALBEDO'	INDEX		
% GGBS	Cast	Screed	Tamp	Brush
0	0.55	0.70	0.65	0.65
30	0.50	0.80	0.75	0.75
50	0.65	0.80	0.75	0.80
70	0.70	0.90	0.85	0.80

CONCLUSIONS

The main objective of this paper is to compare the various methods of measuring the albedo concrete slabs. A number of slabs were manufactured with four different levels of GGBS and four different surface finishes. These specimens have been placed on a rooftop and have been exposed to the environment since September 2010. The various methods of measurement include a light meter, thermal imaging camera, albedometer and thermocouples. A moisture meter is also being used to record the moisture of the slabs surface and a greyness card has been developed to give an indication of visible ageing of the slabs over time.

Based on the sample results, the light meter is an inexpensive and reliable instrument which gives a good indication of relative albedo value. It is used in conjunction with a black box which eliminates any background light. It does require that no clouds are present interrupting the direct sunlight when taking readings and is quite labour intensive. Similarly the thermocouples inside the concrete slabs are cheap, accurate and reliable and allow for remote full time monitoring of the slab's temperature to indirectly determine solar light absorption. These however need to be placed in the concrete at the time of production and there is the possibility that the connection within the concrete will fail resulting in no readout. This data is processed alongside the results from the sunshine duration sensor as they record at the same time and intervals. The sunshine data is reliable and also allows for full time monitoring.

The thermal imaging camera shows the infrared radiation emitted off the surface of the slab. Similar to the light meter, a high level of sunshine intensity is required in order to allow the slabs to heat up sufficiently so that there is a measurable difference between the temperatures of the different slabs. The thermal images can differentiate between the effects of the different levels of GGBS content and surface finishes as the temperature of the slab changes accordingly. The albedometer measures both the incoming and reflected solar radiation across all wavelengths and is a highly sensitive and expensive device. The concrete specimens are small in surface area and thus the device needs to be calibrated as it is generally used to measure larger surface areas. Research into the practicality of using this instrument is currently in progress.

Table 4 Methods of 'Albedo' Index Measurement

% GGBS	THERMOCOUPLE	LIGHTMETER	IR IMAGING	GREYNESS
0	Cast	Cast	Cast	Cast
	Screed	Brush	Brush	Brush
	Tamp	Tamp	Tamp	Tamp
	Brush	Screed	Screed	Screed
70	Cast	Brush	Cast	Cast
	Brush	Cast	Tamp	Brush
	Tamp	Tamp	Screed	Tamp
	Screed	Screed	Brush	Screed

Decreasing temperature/ Increasing reflectance ↓

Table 4 demonstrates a summary of results for the various different methods used to measure the 'relative' albedo. For the 0% slabs there is consistency in these results for three of the four methods used and for the 70% slabs the cast finish is almost always the highest temperature and screed the lowest, though early trends indicate different ageing behaviour. The fact that they are measuring different though related physical phenomena may go some way to explaining these discrepancies. In conclusion, based on results to date, of the various methods considered in which to measure the albedo value indirectly, the light meter and thermocouple wire are the most consistent, affordable and reliable.

Acknowledgements

The authors wish to gratefully acknowledge the support provided by Mr. John Newell and Mr. Peter Seymour of Ecocem Ireland in the execution of this work.

REFERENCES

1. BORIBOONSOMSIN, K. And REZA F., 'Mix Design and Benefit Evaluation of High Solar Reflectance Concrete for Pavements', Journal of the Transportation Research Board, No. 2011, Transportation Research Board of the National Academics, Washington D.C., 2007, pp. 11-20

2. LEVINSON, R. and AKBARI, H., 'Effects of Composition and Exposure on the Solar Reflectance of Portland Cement Concrete', Cement and Concrete Research, 32, 1679-1698, 2002

3. RILEY, R.C., 'The Cool Solution to Sustainable Pavements', Illinois Chapter 27.2, Illinois Ready Mixed Concrete Association, 2008

4. SCA, 'Slag Cement and the Environment' , Slag Cement in Concrete, Slag Cement Association, 2003

5. AKBARI, H., MENON, S. And ROSENFELD, A., Global cooling: increasing world wide urban albedos to offset CO2, Climate Change ,Vol. 95, Joint Issue 3-4, 2009

6. ACPA, 'Albedo: A Measure of Pavement Surface Reflectance', American Concrete Pavement Association, 2002

7. ECOCEM, 'GGBS and Reducing Global Warming – The Albedo Effect', www.worldcement.com , 2009

8. BRETZ, S. E. And AKBARI, H., Long–term performance of high albedo roof coatings, Elsevier Science S.A. , Lawrence Berkeley National Laboratory, 1997

9. TAHA, H., SAILOR, D. And AKBARI, H., 'High Albedo Materials for Reducing Building Cooling Energy Use', Energy and Environment Division, Lawrence Berkeley Laboratory, University of California, Berkeley, CA, 1992

10. SWEENEY, A., WEST, R. and O' CONNOR, C., 'Parameters affecting the albedo effect in concrete', Proceedings of BCRI 2010, Cork, 2010, pp. 513-520

11. Cobourg internet and Photography Images, www.cobourginternet.com, First accessed 9th June 2011

Study of Environmentally Friendly High-strength Concrete

Y Yoshida, K Yamamoto, H Jinnai, S Kuroiwa, K Tsujiya
Taisei Corporation, Japan

The spreading awareness of green issues in recent years has prompted us to develop environmentally friendly concrete: a high-strength concrete that contains high volume of by-products. Compressive strength tests were conducted using mortar and concrete specimens containing various by-products. As a result, compressive strength exceeded 100MPa even at the high cement replacement ratio of 70%. CO_2 emissions from the component materials of this environmentally friendly high-strength concrete were estimated to be 60% of the emissions for conventional high-strength concrete.

Yutaka Yoshida is a researcher in the Technology Centre of the Taisei Corporation, Japan. His reserch interests include high strength concrete, quality control of concrete, durability of concrete and environmentally friendly concrete.

K Yamamoto, H Jinnai,S Kuroiwa, K Tsujiya, are all researchers in the area of concrete durability and environmentally friendly construction in the in the Technology Centre of the Taisei Corporation, Japan.

Keywords: By-product, CO_2 emissions, Environmentally friendly, Estimation, High-strength concrete, Strength prediction model

INTRODUCTION

This study aims at development of environmentally friendly high-strength concrete with low CO_2 emissions per unit. And we tried to construct a basic framework for preparing environmentally friendly high-strength concrete; we present a method to approximately estimate the strength contribution of concrete containing multiple mineral admixtures and quantitatively discuss the preparation of environmentally friendly concrete having low CO_2 emissions per unit.

In recent years, the importance of environmentally friendly technology is increasing with the surge of environmental consciousness. Among environmental issues, the need to reduce CO_2 emissions is urgent. One method for reducing CO_2 emissions in construction is to reduce the CO_2 emissions from the production of construction materials. In the case of concrete, Portland cement has the largest CO_2 emissions per unit among concrete materials. And high-strength concrete which contains a lot of Portland cement have increasingly been put to practical use. For the reduction of CO_2 emissions of concrete, the use of fly ash and ground granulated blast furnace slag, industrial by-products, as supplementary cementitious materials (SCM) are known to be effective [1]. Therefore, we tried to replace Portland cement with a large quantity of by-products in mineral admixture.

On the other hand, when the replacement ratio of by-products against Portland cement is high in the mineral admixture, if by-products are used that do not contribute to the strength of concrete, the water-binder ratio must be kept low to maintain compressive strength. Then, the content of Portland cement should be increased in the concrete. All told, therefore, the influence of the type and replacement ratio of the mineral admixture on concrete strength is considered critical. Among the earlier studies on the strength contribution, Hwang et al.[2] and Wu et al.[3] proposed strength contribution coefficients for fly ash where the unit cement content and the specific surface area of fly ash were used as parameters. Regarding blast furnace slag, Sakai et al [4] recently discussed strength development considering the phase constitution of hardened cement. However, there have been few studies on the compressive strength of material in which the replacement ratio of multiple mineral admixtures is high. In particular, there have been few reports on material with a low water-binder ratio for the development of environmentally friendly concrete with resistance to carbonation, as we are interested in discussing.

EXPERIMENTS ON MORTAR

Materials

The first phase of this study is experiments on mortar. And the second phase is experiments on concrete. Tables 1 and 2 list the cement and mineral admixtures used in the mortar experiment. When cement is replaced by by-products such as fly ash in large quantities, early strength development is delayed, and thus ordinary Portland cement was chosen to ensure the early strength development. As the mineral admixtures, silica fume, fly ash, and ground granulated blast furnace slag were used, all of which are abundantly procurable by-products that are widely used in usual concrete. Further, andesite crushed sand (density in saturated surface-dry condition 2.61 g/cm^3) was used as fine aggregate, and a polycarboxylate-based superplasticizer was used in the admixture.

Table 1 Cement and mineral admixtures

SYMBOL	BINDER
P	Ordinary Portland cement (density 3.16 g/cm^3, specific surface area 3320 cm^2/g)
S	Silica fume (density 2.00 g/cm^3, specific surface area 200,600 cm^2/g)
F	Fly ash (density 2.22 g/cm^3, specific surface area 4,220 cm^2/g)
B	Ground granulated blast furnace slag (density 2.92 g/cm^3, specific surface area 2,980 cm^2/g)

Table 2 Characteristics of cement and mineral admixtures

SYMBOL	CO_2 PER UNIT	CaO Mass, %	Al_2O_3 mass %	SiO_2 mass %	R** μm
P	0.7666	63.28	5.65	20.61	16.99
S	0.0196*	0.38	1.07	92.60	0.87
F	0.0196	1.78	30.29	58.20	10.51
B	0.0265	42.65	14.00	34.02	22.59

CO_2 emissions per unit in t-CO_2/t [5]
*CO_2 emissions per unit of silica fume is replaced with that of fly ash
**Average size of 50% particles

Mortar mixtures

The mortar mixture was broadly classified into two groups. The combination of cement and by-products is shown according to the two experimental series summarized in Tables 3 and 4. In Series I, the mixture ratio between cement and by-products was kept the same in each water-binder ratio group to evaluate the relation between water-binder ratio and compressive strength. The replacement ratio of by-products was 10-30% in Series I.

In Series II, the water-binder ratio was held constant at 0.22 to evaluate the influence of the replacement ratio and combination of by-products, and we changed as parameters the replacement ratio and mixture ratio of by-products for each combination of by-products. The replacement ratio of by-products was 30-50% in Series II. Further, in both series, the unit contents of the binders of mortar and the fine aggregate were set by assuming high-strength content with unit water content of 155 kg/m^3, unit fine aggregate content of 865 kg/m^3, and air content of 2.0%.

Fabrication of specimens

We used a Hobart mixer to mix mortar. The addition rate of a superplasticizer was set depending on the water-binder ratio so that the flow value just after mixing would be over 200 mm without segregation. In the compressive strength test, we used cylinder speciments (Φ50 mm × 100 mm) with 7, 28, and 91 days (cured in water).

Table 3 Cement and by-products (Series I)

BINDER	MIXING RATIO (P:F:B:S)	CEMENT REPLACEMENT RATIO mass %	CO_2 EMISSIONS PER UNIT (t-CO_2/t)	MORTAR WATER-BINDER RATIO
P	10:0:0:0	0	0.7666	0.31, 0.26, 0.22, 0.19
S	9:0:0:1	10	0.6919	0.26, 0.22, 0.19
F	8:2:0:0	20	0.6172	
B	8:0:2:0		0.6186	
FB	8:1:1:0		0.6179	
FS	7:2:0:1	30	0.5425	
BS	7:0:2:1		0.5439	
FBS	7:1:1:1		0.5432	

Table 4 Cement and by-products (Series II)

BINDER	MIXING RATIO (P:F:B:S)	CEMENT REPLACEMENT RATIO mass %	CO_2 EMISSIONS PER UNIT (t-CO_2/t)	MORTAR WATER-BINDER RATIO
F	8:2:0:0, 7:3:0:0, 6:4:0:0	20-40	0.6172-0.4678	0.22
B	8:0:2:0, 7:0:3:0, 6:0:4:0	20-40	0.6186-0.4706	
FB	8:1:1:0, 7:2:1:0, 7:1.5:1.5:0, 7:1:2:0, 6:3:1:0, 6:2:2:0, 6:1:3:0	20-40	0.6179-0.4685	
FS	7:2:0:1, 6:3:0:1, 5:4:0:1, 6.5:3:0:0.5, 5.7:4:0:0.3	30-50	0.5425-0.3931	
BS	7:0:2:1, 6:0:3:1, 5:0:4:1	30-50	0.5439-0.3959	
FBS	7:1:1:1, 6:2:1:1, 6:1.5:1.5:1, 6:1:2:1, 5:3:1:1, 5:2:2:1, 5:1:3:1, 6.5:1.5:1.5:0.5, 5.7:2:2:0.3	30-50	0.5432-0.3938	

RESULTS ON MORTAR

Compressive strength test results

Figures 1 and 2 show the test results for compressive strength. In all of the by-products tested in this study, the compressive strength was always low at 7 days in comparison with the test samples made with ordinary Portland cement, and decreased as the replacement ratio was increased. In addition, the compressive strength of 100-150 MPa was obtained at 28 days.

In Series I, in which the replacement ratio of by-products was less than 30%, at and after 28 days regardless of water-binder ratio, the compressive strength was more than 90 percent of that of the test sample made with ordinary Portland cement, although there were minor differences between the mixtures.

In Series II, in which the water-binder ratio was fixed at 0.22 and the combination and replacement ratio of by-products were varied, the compressive strength of P:B:S=5:4:1, which was made with both ground granulated blast furnace slag and silica fume as mineral admixtures, was relatively large in the samples with a large replacement ratio, more exactly with the mixture ratio of 50%: P:F:S=5:4:1, P:F:B:S=5:3:1:1, P:F:B:S=5:2:2:1, P:F:B:S=5:1:3:1, and P:B:S=5:4:1. At and over 28 days, the compressive strength was more than 80% of that of the test sample made with ordinary Portland cement.

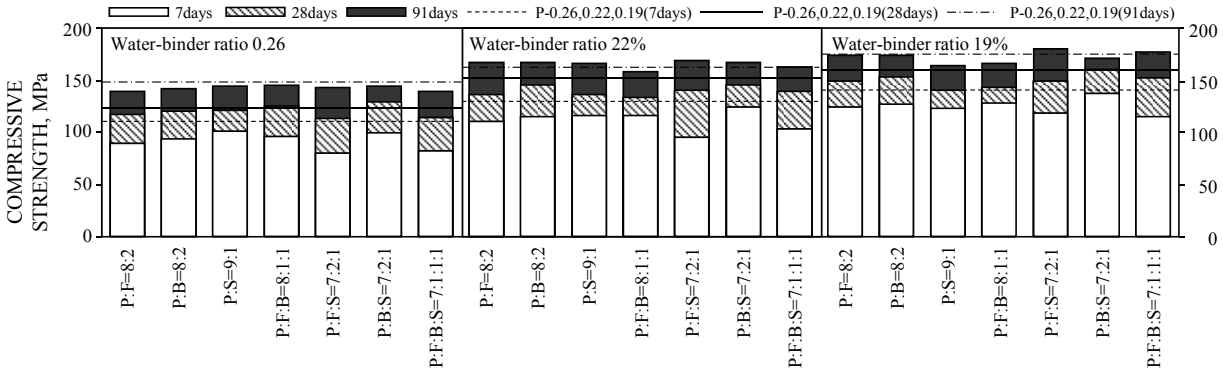

Figure 1 Compressive strength test results (Series I)

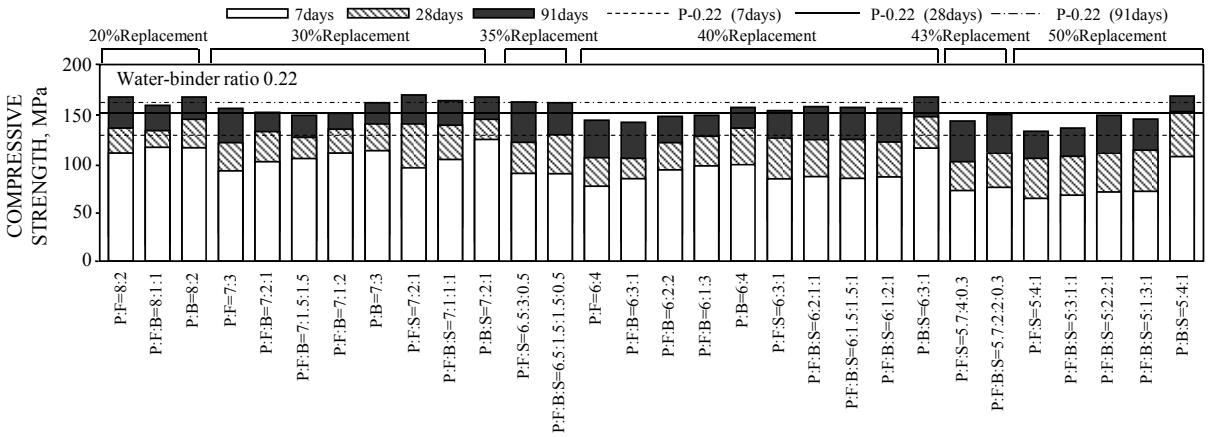

Figure 2 Compressive strength test results (Series II)

Figure 3 shows the relation between the strength contribution [6] of by-products and the unit cement content with age as a parameter. The strength contribution is obtained by using Eq. (1) to estimate the compressive strength using the strength contribution of fly ash given in the literature [6]. Overall, the strength contribution increased with age, but we did not find a clear relation between strength contribution and unit cement content at any age.

$$F_E=a(C+kE)/W+b \quad (1)$$

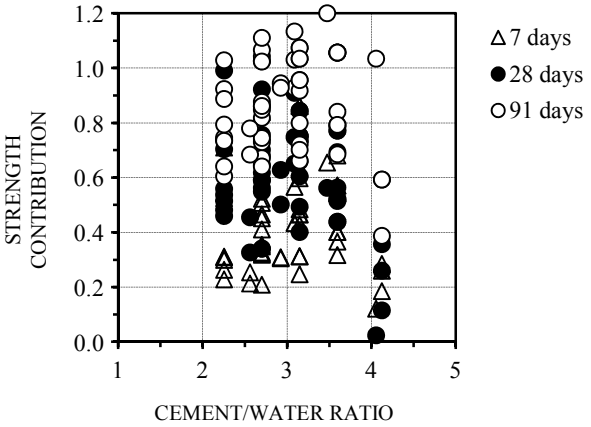

Figure 3 Relationship between cement-water ratio and strength contribution

Estimation of CO_2 emissions

On the basis of the experimental results, we calculated the amount of CO_2 emissions assuming a concrete mixture with unit water content of 155 kg/m^3, unit coarse aggregate content of 865 kg/m^3, and air content of 2.0%. The CO_2 emissions per unit are shown in Table 2. From the experimental results on mortar at 28 days, we show the results for the case of 30% replacement in Figure 4 and the case of 50% replacement in Figure 5, and the CO_2 emissions were compared with those of the concrete made with only portland cement. In addition, the strength of the concrete using only portland cement was controlled to the same levels of compressive strength.

On the vertical axis of the figures, the CO_2 emissions for each mixture are expressed as a percentage of the CO_2 emissions for the concrete made with only portland cement. As a result, it was shown that we could reduce CO_2 emissions almost 30% by replacing 30% of the Portland cement with by-products to the extent possible while retaining sufficient strength in Figure 4. On the other hand, in Figure 5, P:B:S=5:4:1 could reduce CO_2 emissions almost 50%, but P:F:S=5:4:1 couldn't reduce CO_2 emissions 50%. It was shown that the use of by-products in large quantities does not directly contribute to the reduction of CO_2 emissions.

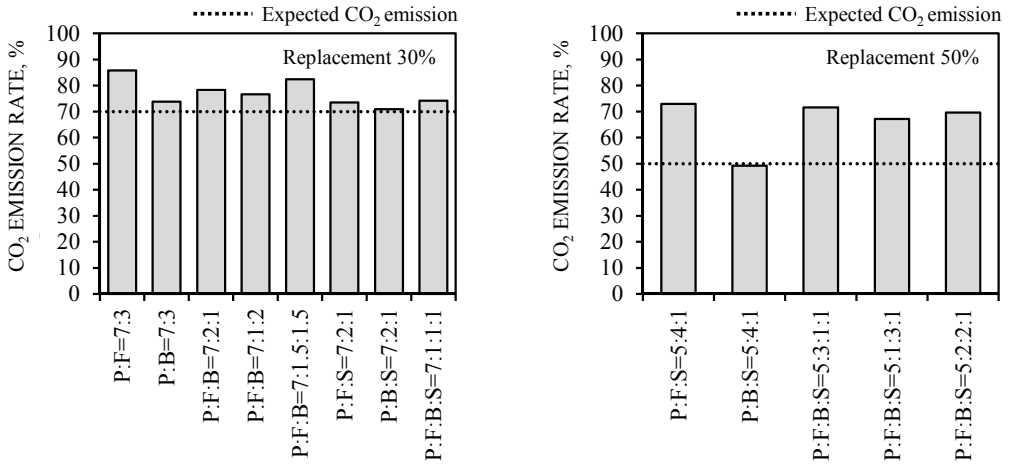

Figure 4 CO_2 emission rate

PROPOSAL OF STRENGTH PREDICTION MODEL

As discussed in the preceding section, we cannot greatly reduce CO_2 emissions simply by using by-products. We need to design better mixture to reduce CO_2 emissions while ensuring adequate compressive strength. To help design better mixture, we propose a simple compressive strength prediction model, assuming the use of multiple by-products, based on the results of tests on mortar.

Using Eq. (1) to estimate compressive strength using the strength contribution of fly ash in the reference [6], we attempted to extend the prediction model to include the use of multiple by-products. To be more precise, we performed multiple linear regression analysis with strength contribution as an objective variable and with unit cement content, the replacement ratio of by-products, the chemical composition, and the average grain size of by-products as explanatory variables. The solid-state properties of the materials are shown in Table 2. The proposed prediction model is given by Eqs. (2) and (3). The explanatory variables of Eq. (3) were chosen as follows. C and C/E were chosen by considering the influence of the ease of reactions occurred by cement reactant and by-products, by referring to the studies of Hwang et al[2] and Wu et al[3]. α was chosen by considering the influence of the reaction products of the chemical reaction with cement hydrate on the chemical composition, in reference to studies by Honda et al.[7] and Katayama et al.[8], and the concept of basicity defined in Japanese industrial standard. Although we also adopted CaO/SiO_2 and $(CaO+Al_2O_3)/SiO_2$ as explanatory variables, much better correlation was obtained by using $CaO/(SiO_2+Al_2O_3)$ as an explanatory variable. $1/R^2$ and $1/R$ were chosen by considering the influence of by-products on reactivity, by referring to studies by Hwang et al.[2], Wu et al.[3], and Li et al.[9]. In addition, although specific surface area was also examined as an explanatory variable, better correlation was obtained by using the reciprocal of particle radius.

$$F_E'=a(C+k'E)/W+b \quad (2)$$

$$k'=hC+j(C/E)+m\,\alpha+n(1/R^2)+p(1/R)+s \quad (3)$$

F_E, F_E' : Compressive strength (MPa)

a , b: Experimental coefficients

C: Unit cement content (kg/m^3)

k , k': Strength contribution

E: Unit by-product content (kg/m^3)

W: Unit water content (kg/m^3)

α: $CaO/(SiO_2+Al_2O_3)$ of binders

R: Average grain size of binders (μm)

h, j, m, n, p, s: Coefficients (See Table 5)

Table 5 Coefficients for proposed prediction model

AGE	*h*	*j*	*m*	*n*	*p*	*s*
7 days	-1.65×10^{-3}	-0.68×10^{-1}	1.09	-1.04×10^{3}	1.48×10^{2}	-0.52×10
28 days	-3.40×10^{-3}	-1.57×10^{-1}	1.79	-1.50×10^{3}	2.37×10^{2}	-0.87×10
91 days	-3.01×10^{-3}	-0.47×10^{-1}	1.56	-1.92×10^{3}	3.03×10^{2}	-1.07×10

Figures 9-11 (A) show the compressive strength as estimated by regression analysis with contribution ratio as the objective variable and with unit cement content as the explanatory variable, and substitution of the results into Eq. (1). The figures show that it is difficult to estimate the compressive strength assuming the use of multiple by-products at any age if the strength contribution is explained by unit cement content only. Figures 9-11 (B) show the relation between the estimation using the proposed model and the measured compressive strength. The figures show that at any age, the proposed model can estimate the compressive strength by considering not only unit cement content but also other factors.

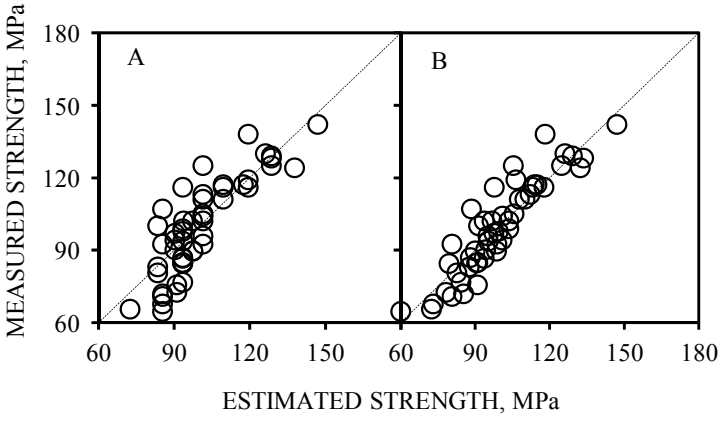

A. Estimation from cement-water ratio B. Estimation from proposed equation

Figure 9 Relation between estimated strength and measured strength (7 days)

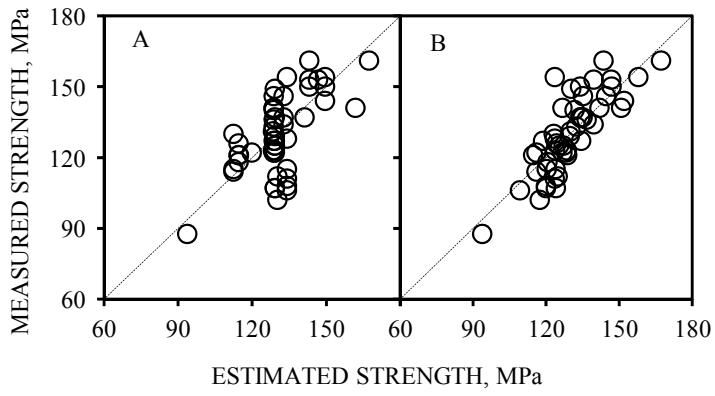

A. Estimation from cement-water ratio B. Estimation from proposed equation

Figure 10 Relation between estimated strength and measured strength (28 days)

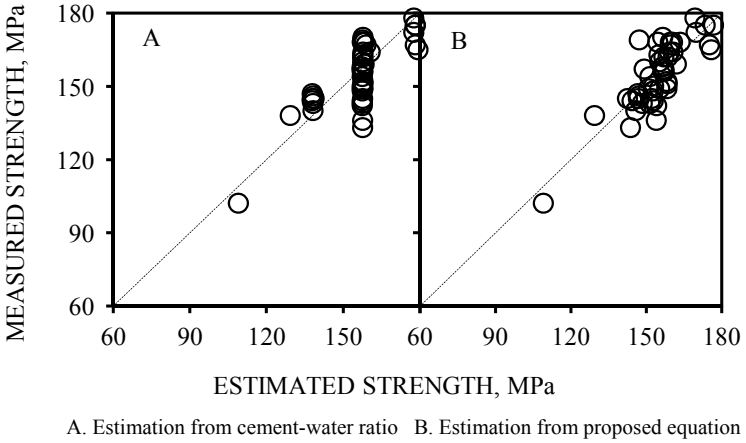

Figure 11 Relation between estimated strength and measured strength (91 days)

Then, under conditions where the water-binder ratio was 0.19, 0.22, and 0.26 and the cement replacement ratio was 30-70% (out of 30-70%, the replacement rate of silica fume was kept at 10% and the rest was fly ash and ground granulated blast furnace slag), the strength contribution at 28 days was calculated using the strength prediction model by changing the component ratio of fly ash and ground granulated blast furnace slag. The calculation results at 7, 28, and 91 days are show in Figures 12, 13, and 14, respectively. Note that, in the figures, the percentage ratio of ground granulated blast furnace slag in the by-product increases toward the left, and the ratio of fly ash increases toward the right.

The figures show that the strength contribution increases with age at any level of water-binder ratio. Further, if the by-product contains ground granulated blast furnace slag in great abundance, although the latent hydraulicity of ground granulated blast furnace slag moderately contributes to strength at 7 days, the strength contribution is less than 0.4 if the water-binder ratio is 0.19, 0.4-0.8 at 28 days and 0.6-0.8 at 91 days. It is shown that we can predict the situation where the strength of the concrete made with ground granulated blast furnace slag develops slowly at early ages.

On the other hand, in the mixtures abundantly containing fly ash, no contribution to strength is observed: the strength contribution is less than 0.1% at 7 days under the condition of water-binder ratio of 0.19. However, the strength contribution increases with age from 0.1-0.4 at 28 days to 0.3-0.5 at 91 days, and this result is thought to reflect the Pozzolanic reaction of fly ash. While the strength contribution ratio increases with the content of ground granulated blast furnace slag when the replacement ratio is 30-50%, the strength contribution reaches a peak at the mixture rate of around 60% between ground granulated blast furnace slag and fly ash at the replacement ratio of 60-70%.

As the replacement ratio increases, there tends to be a greater percentage of fly ash, of which the grain size is smaller than that of cement, and we can presume that the binder grain size shifts toward the optimum distribution and the chemical composition becomes better suited to chemical reaction. In the future, further study on the strength model will be necessary because the replacement ratio was investigated in this study only in the range of 30-50%.

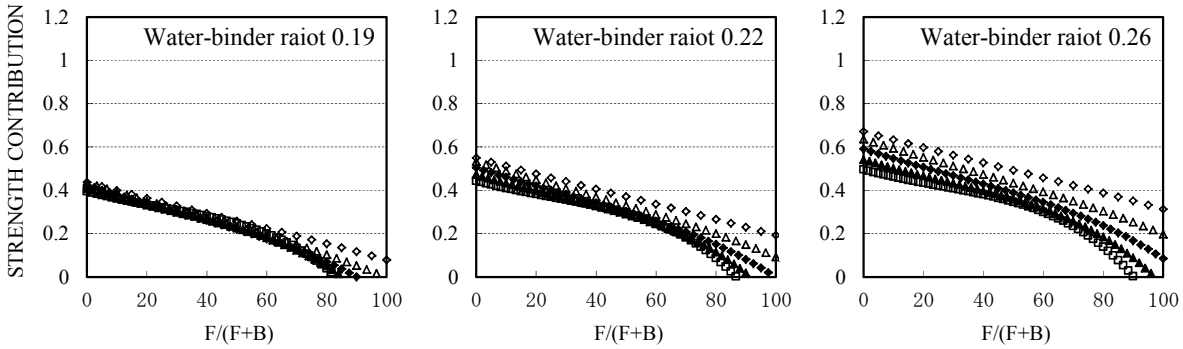

Figure 12 Relation between composition ratio (fly ash and granulated blast furnace slag) and strength contribution (7 days)

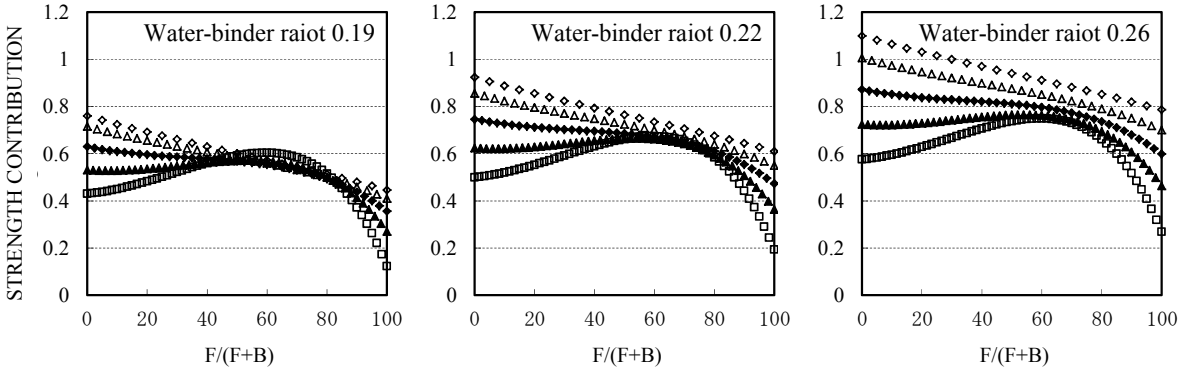

Figure 13 Relation between composition ratio (fly ash and granulated blast furnace slag) and strength contribution (28 days)

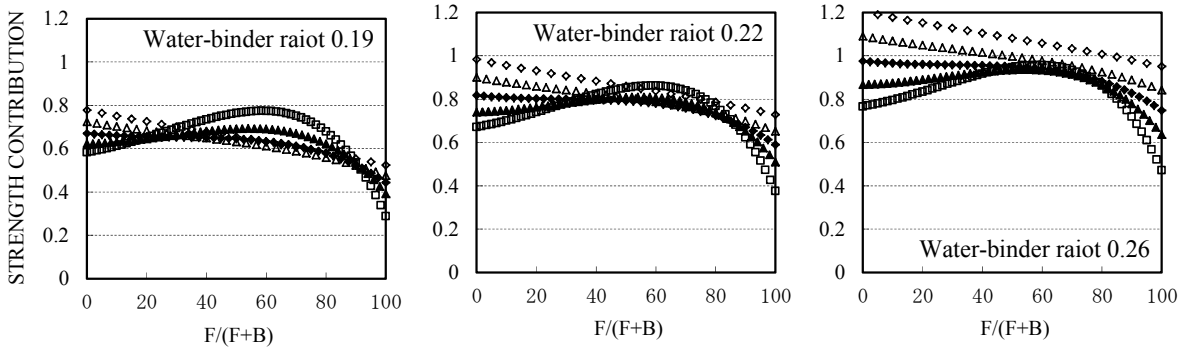

Figure 14 Relation between composition ratio (fly ash and granulated blast furnace slag) and strength contribution (91 days)

EXPERIMENTS ON CONCRETE

Experiments were conducted on concrete on the basis of the experiments on mortar and the calculation using the strength prediction model in Proposal of strength prediction model

Materials

Tables 6 and 7 shows the cement and mineral admixtures used in the experiments on concrete. Further, andesite crushed sand was used as fine aggregate (density in saturated surface-dry condition 2.62 g/cm^3; CO_2 emissions per unit weight 0.0037 t-CO_2/t), andesite crushed stone was used as coarse aggregate (density in saturated surface-dry condition 2.62 g/cm^3, CO_2 emissions per unit weight 0.0029 t-CO_2/t), and polycarboxylate-based superplasticizer was used in the admixture.

Table 6 Cement and mineral admixtures

SYMBOL	BINDER
P	Ordinary portland cement (density 3.16 g/cm^3, specific surface area 3280 cm^2/g)
S	Silica fume (density 2.20 g/cm^3, specific surface area 168,000 cm^2/g)
F	Fly ash (density 2.22 g/cm^3, specific surface area 3,830 cm^2/g)
B	Ground granulated blast furnace slag (density 2.92 g/cm^3, specific surface area 3,140 cm^2/g)

Table 7 Characteristics of cement and mineral admixtures

SYMBOL	CO_2 PER UNIT	CaO mass %	Al_2O_3 mass %	SiO_2 mass %	R** (μm)
P	0.7666	63.36	5.53	21.11	16.64
S	0.0196*	0.18	0.42	94.59	6.04
F	0.0196	1.26	31.00	58.00	9.67
B	0.0265	42.80	13.82	34.16	19.61

CO_2 emissions per unit in t-CO_2/t [5]
*CO_2 emissions per unit of silica fume is replaced with that of fly ash
**Average size of 50% particles

Mixture design

The basic concrete mixes are shown in Table 8. The unit amounts of binder and fine aggregate for the basic concrete mix were decided by assuming high-strength concrete with unit water content of 155 kg/m^3, unit coarse aggregate content of 865 kg/m^3, and air content of 2.0%. Three levels of water-binder ratio, namely, 0.20, 0.25, and 0.33, were chosen to cover the whole range to realize the compressive strength 100 MPa at the age of 28 days, based on the experiments on mortar (. Table 9 shows the combinations of cement and by-products. The replacement ratio of by-products was set to 50-70% from the fact that sufficient compressive strength was obtained at the replacement ratio of 50% in the experiments on mortar. Three combinations of by-products were adopted: fly ash and silica fume; fly ash with ground granulated blast furnace slag and silica fume in equal amounts; and ground granulated blast furnace slag and silica fume, referring to the calculation result regarding the strength contribution in the preceding section. Series P is consistent with the basic concrete mixture shown in Table 8. The fine aggregate content was controlled in the other series depending on the combination of by-products.

Table 8 Basic concrete mixture

WATER-BINDER RATIO	AIR CONTENT %	UNIT CONTENT, kg/m^3			
		Binder	Water	Fine aggregate*	Coarse aggregate
0.20	2.0	775	155	250	865
0.25	2.0	620	155	299	865
0.33	2.0	465	155	348	865

*Adjusted depending on the by-product content

Table 9 Characteristics of cement and mineral admixtures

SERIES	PERCENTAGE OF BINDER MASS, %				PERCENTAGE REPLACEMENT WITH BY-PRODUCTS, %	WATER-BINDER RATIO
	P	F	B	S		
P	100	0	0	0	0	0.20-0.33
FS	50	40	0	10	50	0.20-0.33
	40	50	0	10	60	0.20-0.33
	30	60	0	10	70	0.20-0.33
BS	50	0	40	10	50	0.20-0.33
	40	0	50	10	60	0.20-0.33
	30	0	60	10	70	0.20-0.33
FBS	50	20	20	10	50	0.20-0.33
	40	25	25	10	60	0.20-0.33
	30	30	30	10	70	0.20-0.33

Fabrication of specimens

We used a biaxial revolving-paddle mixer to prepare concrete. The additive rate of superplasticizer was controlled such that, after the mixing, the slump flow would be greater than 450 mm and segregation would not occur.

EXPERIMENTAL RESULTS FOR CONCRETE

Figure 11 shows the test result of the compressive strength of concrete. When the water-binder ratio was 0.20, the mixture ratios P:F:S=5:4:1, P:B:S=5:4:1, and P:B:S=4:5: 1 give compressive strength greater than 100 MPa at 28 days, indicating that high-strength concrete can be realized. Within the scope of our study, at 7 days, the compressive strength proved to be small at any water-binder ratio when cement was replaced with by-products in high percentages: the compressive strength was 40-50% for the Series P concrete when the water-binder ratio was 0.20, and the compressive strength was 25-50% for Series P concrete when the water-binder ratio was 0.33.

However, the compressive strength increased with age: at 91 days, compressive strength of 65-105% was obtained with the water-binder ratio 0.20, and compressive strength of 50-80% was obtained with the water-binder ratio 0.33. It is likely that the pozzolanic reaction of fly ash influences the strength more strongly as the age increases.

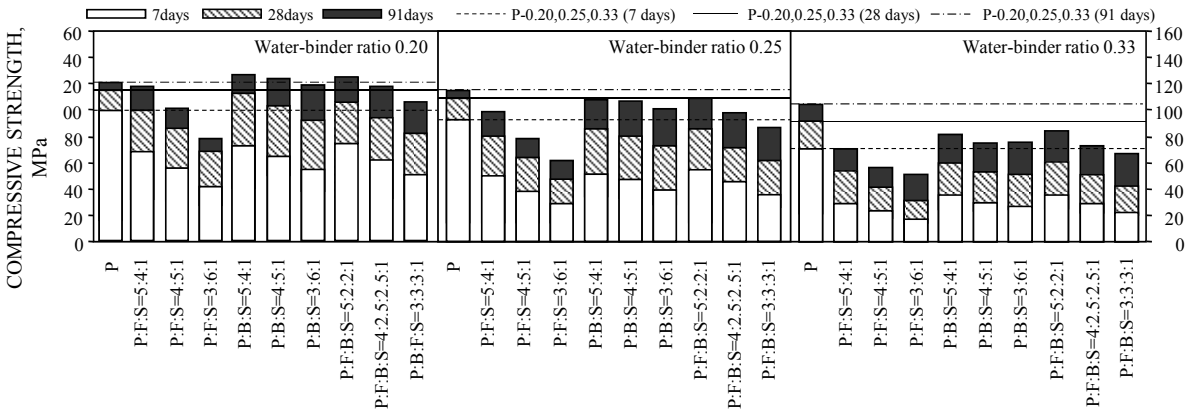

Figure 15 Test results on the compressive strength of concrete

ESTIMATION OF CO_2 EMISSIONS

We examined the CO_2 emissions by assuming and using concrete of 100 MPa, by referring to the result from the compressive strength test on concrete in Section 6 lists the mixtures fabricated. 100 MPa concrete mix is shown in Table 10. In Section 6, the series with higher compressive strength at the age of 28 days has a lower water-binder ratio; for example, abundant binder materials were used in FS-70 in which by-products were used in large quantities.

Table 10 100 MPa concrete mixture

SYMBOL	WATER-BINDER RATIO	UNIT CONTENT, kg/m³						
		Water	P	F	B	S	G	S
P	0.41	155	381	0	0	0	865	980
FS-50	0.24	155	322	258	0	64	865	649
FS-60	0.20	155	305	381	0	76	865	504
FS-70	0.15	155	306	612	0	102	865	200
BS-50	0.27	155	291	0	233	58	865	777
BS-60	0.26	155	243	0	304	61	865	750
BS-70	0.25	155	188	0	377	63	865	727
FBS-50	0.27	155	286	115	115	57	865	753
FBS-60	0.24	155	257	161	161	64	865	672
FBS-70	0.21	155	216	216	216	72	865	582

Comparing the series, the water-binder ratio decreased in the following order: BS series, FBS series, and FS series. Here too, the CO_2 emissions were compared with those of the concrete using only Portland cement just like in Estimation of CO_2 emissions. The result is shown in Figure 16. The figure clearly shows that the replacement ratio of by-products does not simply result in the reduction of CO_2 emissions. For example, comparing FS-50 and FS-60, we see a 10% increase in the replacement ratio, but only an approximately 5% reduction in CO_2.

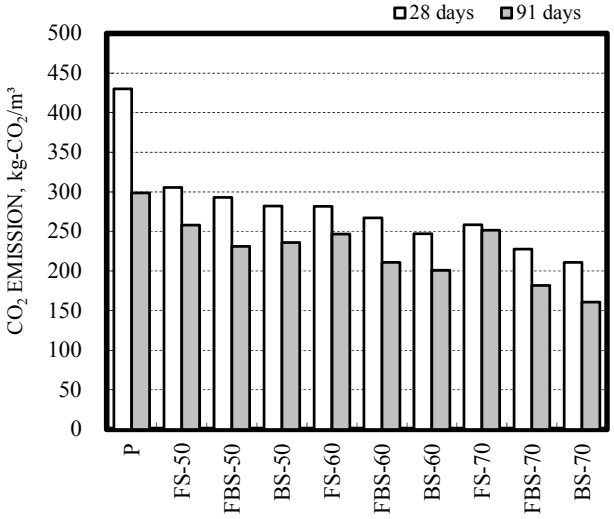

Figure 16 CO_2 emissions of 100 MPa concrete

Within the range of our test, BS-70 was the best in reducing CO_2 emissions, and the calculation showed that we could reduce around 40% of CO_2 emissions compared with the concrete using ordinary Portland cement only. Note that the calculation covers only the CO_2 emissions from the materials themselves, and it is further necessary to evaluate the CO_2 emissions from the transportation and production of materials used to produce concrete.

CONCLUSIONS

The main findings of this study are listed below.

1) The use of by-products in large quantities does not directly contribute to the reduction of CO_2 emissions.
2) We suggested a computation approach of the compressive strength of mortar by using a regression expression that uses the chemical composition and the mixing condition of the by-product as parameters.
3) In the calculation on high-strength concrete of 100 MPa, we showed that CO_2 emissions could be reduced by more than 40%.
4) In replacing cement, the combination of ground granulated blast furnace slag and silica fume is likely the best mixture for reducing CO_2 emissions.

On the basis of these findings, we will advance our study on environmentally friendly high-strength concrete by examining in detail the composition of the concrete mixtures in order to

improve the accuracy of the model for the compressive strength of concrete containing multiple by-products, and by testing the durability (e.g., resistance to carbonation and freeze-thaw resistance) of environmentally friendly high-strength concrete containing by-products in large quantities.

REFERENCES

1. V. M. MALHOTRA: Making Concrete "Greener" with Fly Ash – Supplementary cementing materials can reduce greenhouse gas emissions into the environment, Concrete international, pp.61-66, May, 1999.

2. HWANG KWANGRYUL, TAKAFUMI NOGUCHI, and FUMINORI TOMOZAWA, "Numerical prediction model for compressive strength development of concrete containing fly ash," Transactions of AIJ. Journal of Structural and Construction Engineering (519), pp. 1-6, May 1999

3. FURONG WU, YOSHIHIRO MASUDA, and SHIGEHARU NAKAMURA, "Strength efficiency of fly ash in high-strength concrete," Transactions of AIJ. Journal of Structural and Construction Engineering (587), pp. 1-6, Jan 2005

4. ETSUO SAKAI, HARUTAKE IMOTO, and MASAKI DAIMON, "Phase composition and strength development characteristics of the hardened cement body of Portland blast furnace slag cement pastes" Proceedings of the Japan Concrete Institute, Vol. 26, No. 1 , pp.135–140, 2004

5. JAPAN SOCIETY OF CIVIL ENGINEERS, Concrete Engineering Series 62, Assessment for environmental impact of concrete Part 2, 2004

6. ARCHITECTURAL INSTITUTE OF JAPAN, "Recommendations for production of concrete with fly ash," 2007

7. SATORU HONDA and HIROYUKI SHIIBA, "The effect of fly ash on the properties of concrete," Proceedings of the Japan Concrete Institute, Vol. 18, No. 1, pp. 351-356, 1996

8. KATAYAMA YUKIO, HIRONOBU NISHI, MAKOTO HIGAKI, TATSUMI OHTA, AKIRA NISHIDA, and TOYOHARU NAWA, "Quality control method of fly ash concrete and properties of the hardened concrete: part 4," Summaries of Technical Papers of Annual Meeting Architectural Institute of Japan (Tohoku), pp. 535-536, Aug. 2009

9. LI CHANGJIANG, AKIHIKO YODA, and TAKASHI YOKOMURO, "Effect of ground granulated blast-furnace slag on pore structure and compressive strength of hardened cement pastes," Transactions of AIJ. Journal of Structural and Construction Engineering (506), pp. 1-6, Apr. 1998

10. JIS A 6206: 2008, "Ground granulated blast furnace slag for concrete"

High Volume Slag Cement and Unwashed Crushed Rock Fine Limestone Aggregates to Produce Low Carbon Concrete for the Arabian Peninsula

A S Mohammod[1], K A Paine[2], P Walker[3]
1 – Xtramix Concrete Solutions, UAE
2 – University of Bath, UK
3 – BRE CICM, UK

Portland cement is the main contributor to the carbon footprint of concrete produced in the Arabian Peninsula. This study has considered a binder consisting solely of GGBS as an alternative to current cements in the production of structural grade concrete. Unwashed limestone crushed rock fine aggregate with a fines content of 10% by mass was also used in the concrete and compared with concrete made using aggregate that is currently acceptable by the local industry standards with only 5% fines content. The hardened and durability properties of concrete containing the GGBS cement and higher fines content have been found to be of an acceptable level. Implementation of the findings of this work to the production of concrete in the Arabian Peninsula will contribute greatly to a sustainable environment due to reduced use of Portland cement and elimination of the washing process for sand.

Abu Saleh Mohammod is a PhD student with the University of Bath and the Technical Manager, Xtramix Concrete Solutions, UAE. He has been working in the concrete and construction industry for last 20years. He has an MSc in concrete technology from the University of Dundee and a member of the Institute of Concrete Technology.

Dr Kevin Paine is a Senior Lecturer within the BRE Centre for Innovative Construction Materials at the University of Bath. Dr Paine specialises in the field of sustainable concrete technology and has carried out research in the use of low carbon cements, recycled and secondary aggregates and innovative concrete technologies.

Professor Pete Walker is Director of the BRE CICM. Professor Walker has gained extensive research experience in the field of structural masonry, timber engineering and sustainable building materials and technologies over the past 20 years in the UK, Australia and Zimbabwe.

Keywords: Compressive strength, Durability, GGBS, Portland cement, Unwashed sand

INTRODUCTION

The oil and gas industries in the Arabian Gulf region are driving economic growth by supporting a population boom and diversification into new business sectors. This rapid growth also means that the region is amongst the world's worst polluters per capita [1], although moves to address CO_2 in the region are developing at an extraordinary pace. Since the majority of construction within the Gulf region utilises concrete as the core building material it is imperative that CO_2 emissions related to its use are controlled [2] whilst the durability and quality of construction is maintained [3].

Since Portland cement is the most carbon emitting of the common cementitious materials, replacing it by a high volume supplementary cementitious material (SCM) such as ground granulated blast furnace slag (GGBS) is a practical approach and blastfurnace cements containing up to 70% by mass of GGBS are commonly used in Arabian Gulf concretes [4-5]. However, in previous work the lead author has studied the effect of high volume SCM including GGBS in self compacting concrete and found reasonable strength gain and durability properties for concrete containing GGBS as the sole cementitious material [6]. This research was carried out to further investigate whether the utilization of GGBS as the sole cementitious constituent was viable.

Furthermore, crushed limestone rock fines (CRF) are the main fine aggregate used in concrete in the Gulf region. Generally the CRF contains a high amount of fine particles passing 75μm (as high as 10% by mass). Local industry practice is to wash off the excessive fines to a maximum of 5%. Washing CRF is a very energy intensive process resulting in wastage of huge amount of water. Discarding of huge waste sludge due to removal of finer particles also creates another environmental impact. However, the finer limestone particles of 'Unwashed' CRF sand could be utilised as additional filler material, provided it does not consist of silt or clay, to aid particle packing and improve the strength parameters of high volume GGBS concretes should strength gain be a concern.

To determine the effect of GGBS cements and additional fines on the performance of concrete, two specific series of mix-designs using 'washed and unwashed' sands were designed and tested. Each series was comprised of two sets of mix-designs containing a control concrete with a blastfurance cement (70% GGBS/30% PC) and an alternative cement comprising solely of GGBS. A polycarboxylate based high range superplasticizer was used to meet the higher water demand of the extra fine particles. The superplasticizer chosen was also known to boost the hydration of GGBS. Each set contained three mixes with varied water to cement ratios of 0.40, 0.32 and 0.25. All together total 12 mixes were designed and tested for compressive strength (up to 56 days), water and chloride permeability, and resistance to sulfate attack.

A potential implementation of the outcome of this research will have a far-reaching effect on the environmental sustainability of the Arabian Peninsula. The industry will be able to save huge amount of resources in terms of energy, water, raw materials and money while enhancing the overall durability of structures.

METHODOLOGY

Experimental work consists of the following stages:

i. Characterization of the raw materials
ii. Design of concrete
iii. Testing and measurement of the properties of concrete

Constituents

The materials used throughout the test programme are given in Table 1 together with their respective sources, while Table 2 provides the composition and characteristics of the Portland cement and GGBS used in this work, as provided by the manufacturers.

Table 1 Concrete constituents used in this programme

	CONSTITUENT MATERIALS	SOURCE
	Cements	
1	Portland cement	National cement, Dubai
2	GGBS	Super cement, Abu Dhabi
	Aggregates	
3	20 mm crushed limestone aggregate	Ras Al Khaima, UAE
4	10 mm crushed limestone aggregate	Ras Al Khaima, UAE
5	5 mm crushed limestone aggregate	Ras Al Khaima, UAE
6	Dune sand	Al Ain, UAE
	Admixtures	
8	Polycarboxylate admixture	Chryso Fluid Optima 245 EMx
9	Retarding admixture	Sodamco Admix CR 152

Table 2 Properties of Portland cement and GGBS

PARAMETERS	% BY MASS	
	PORTLAND CEMENT	GGBS
LOI	2.9	0.34
SiO_2	21.67	34.5
Al_2O_3	6.41	13.8
Fe_2O_3	3.94	1.12
CaO	65.98	42.4
MgO	1.24	6.2
SO_3	2.68	0.24
Cl	0.01	0.008
Na_2O	-	0.24
K_2O	-	0.30
Total alkali (Na_2O+0.685 K_2O)	0.50	-
Fineness, m^2/kg	330	437
Soundness, Le Chatelier expansion, %	1.0	0.5
Initial setting time, Vicat test, min	160	205
Final setting time, min	255	310

The characteristics of the four aggregates used in this work, are given in Table 3. Crushed limestone aggregates were used as coarse aggregates, in two sizes 10/20mm and 5/10mm maximum size. All coarse aggregates have been tested for their strengths such as aggregate crushing values, geometrical properties such as grading, flakiness and elongation index test and their physical properties such as density, absorption and impurities such as clay lumps and friable particles.

Table 3 Aggregate characteristics

TEST DESIGNATION	TEST METHOD	RESULTS				
		10/20	5/10	0/5 WASHED	0/5 UNWASHED	DUNE
Particle Density (Oven Dry) Mg/m^3	BS 812: Part 2: 1995	2.80	2.80	2.79	2.73	2.61
Particle Density (SSD) Mg/m^3	BS 812: Part 2: 1995	2.81	2.81	2.81	2.79	2.63
Particle Density (Apparent) Mg/m^3	BS 812: Part 2: 1995	2.82	2.83	2.85	2.91	2.67
Water Absorption (%)	BS 812: Part 2: 1995	0.3	0.4	0.90	2.30	0.70
Clay Lumps & Friable Particles (%)	ASTM C 142 : 1997	0.3	0.4	0.30	0.50	>0.1
Flakiness Index (%)	BS 812: Sec. 105.1: 89	11.0	14.0	-	-	-
Elongation Index (%)	BS 812: Sec. 105.2: 89	17.0	12.0	-	-	-
Aggregate Crushing Value (%)	BS 812: Part 110:1990	19.0	18.0	-	-	-
Mean 10% Fine Value (kN)	BS 812: Part 111:1990	212	196	-	-	-
Material Finer than 75µ (%)	BS 812: Part 103:1985	0.5	1.0	3.8	9.3	0.1
Bulk Density (Compacted) Kg/m^3	BS 812: Part 2:1985	1599	1502	1763	1853	1531
Bulk Density (Un-compacted) Kg/m^3	BS 812: Part 2:1985	1465	1378	1603	1659	1448
Shell Content (%)	BS 812: Part 106:1985	-	-	0.20	0.10	>0.1

The main fine aggregates were CRF of limestone aggregate obtained from the same source as the coarse aggregates. For the purposes of the research the 0/5mm aggregates were either (i) washed or left (ii) unwashed. It is a common practice in the local industry to wash the limestone crushed rock fine aggregate to remove the finer particles below 75µm 'dust' to below 5% by mass. This is to satisfy local project specifications.

Fine aggregate with less than 5% dust is considered to be 'washed' sand and with approximately 10% dust has been termed as 'unwashed' sand in this work. Table 3 shows that the percentage of material finer than No. 200 sieve is 3.8% for washed and 9.8% for unwashed sand. This excess finer material in the unwashed sand mix is expected to contribute to the particle packing of the concrete and enhance its compressive strength properties.

The final aggregate used was dune sand, which is fine rounded natural sand in abundance in the desert dunes. It is used to aid achievement of finer particle sizes in the mix gradation. Dune sands are mostly single sized. The fine aggregates have been tested for grading, density, absorption and impurities including clay lumps, friable particles, and shell contents.

A high range water reducing admixture was used to assist the production of concrete mixes at w/c ratios less than 0.40 while maintaining a suitable consistence. The admixture used was a polycarboxylate based admixture that according to the manufacture includes a proprietary polymer to boost the hydration of high volume GGBS and fly ash concrete. Although the retention of slump was not a major requirement in this work, a retarding type admixture was used to maintain reasonable slump retention and achieve a level of consistence between mixes.

Table 4 Technical properties of admixtures

		SUPERPLASTICIZER	RETARDING ADMIXTURE
1	Nature	Liquid	Liquid
2	Colour	Brownish yellow	Light yellowish
3	Density	1.100 ± 0.020	1.103 - 1.108
4	pH	6 ± 2	
5	Cl^- ion content	Nil to EN 934 and BS 5075	Zero to BS 5075
6	Na_2O equiv	≤1.0 %	

Mix proportions

Four types of concrete were produced as shown in Table 5, with parameters varied to permit comparison of concretes made with either cement and both types of sand. Each concrete type was made at three water to cement ratios (w/c); of 0.25, 0.32 and 0.40, making 12 concretes in total. This permitted interpolation and comparison of concretes at different strengths and properties. The relative values of w/c were comparatively low as it was anticipated that concrete with 100% GGBS as cement would gain compressive strength at a slow rate. The use of low w/c should therefore give an acceptable level of compressive strength for structural application. The total cementitious content remains fixed at 400kg for all mixes.

Properties of Concrete

Beside fresh properties, among hardened properties compressive strength and durability properties of the concrete have been evaluated. Compressive strength at 7, 28 and 56 days were measured to understand the strength gain pattern of the mixes.

Water absorption of the concrete was measured in accordance with BS 1881-122, in which concrete was submerged in water for 30 minutes, and the increase in mass was measured in relation to the total mass of concrete. Water permeability was measured in accordance with BS EN 12390-8 in which concrete cubes were subjected to water pressure at 5 bar for 72 hours. The depth of water penetration was measured after splitting the cube into two halves along the same axis to the water penetration. The visible water profile was measured using a measuring scale.

Table 5 Mix designs

NO	REF	W/C	CEMENTITIOUS MATERIALS (kg/m^3)			AGGREGATES (kg/m^3)				WATER (kg/m^3)	ADMIXTURE (kg/m^3)	
			TOTAL	PC	GGBS	20 mm	10 mm	5 mm	DUNE SAND		SP	RETARDER
1	0.25/pc30ggbs70/w	0.25	400	120	280	647	438	678	303	100	7.0	1.0
2	0.32/pc30ggbs70/w	0.32	400	120	280	632	422	642	291	128	2.25	1.0
3	0.40/pc30ggbs70/w	0.40	400	120	280	633	384	614	269	160	2.15	0.85
4	0.25/pc0ggbs100/w	0.25	400	0	400	642	435	673	300	100	8.0	1.0
5	0.32/pc0ggbs100/w	0.32	400	0	400	638	418	638	280	128	5.0	1.0
6	0.40/pc0ggbs100/w	0.40	400	0	400	609	400	609	267	160	2.5	1.0
7	0.25/pc30ggbs70/u	0.25	400	120	280	647	438	673	303	100	9.0	1.0
8	0.32/pc30ggbs70/u	0.32	400	120	280	632	422	638	291	128	3.5	1.0
9	0.40/pc30ggbs70/u	0.40	400	120	280	633	384	609	269	160	2.0	0.5
10	0.25/pc0ggbs100/u	0.25	400	0	400	642	435	668	300	100	6.5	0.0
11	0.32/pc0ggbs100/u	0.32	400	0	400	638	418	633	280	128	2.5	0.0
12	0.40/pc0ggbs100/u	0.40	400	0	400	609	400	605	267	160	1.7	0.0

Rapid chloride permeability test (RCPT) was determined in accordance with ASTM C 1202. It is an indirect test, where an electric charge is measured in coulombs over a period of 6 hours. The charge is passed through a concrete disk test specimen whose two ends are immersed in sodium chloride and sodium hydroxide solutions, respectively. Although the variability and precision and bias between technicians and laboratories of this test is very high, RCPT was chosen since it is widely used and accepted in the Gulf Region, as a means of ensuring the resistance of concrete to chloride ingress. Consequently, the acceptance of new concretes without information pertaining to the RCPT permeability would be difficult.

The sulfate resistance of concrete was measured by a direct test of length change of 75mm x 75mm x 280mm concrete prisms immersed in Na_2SO_4 solution (50g/L). The test procedure was a modified method of ASTM C 1012–02, which uses mortar bars, to provide a more direct measurement of the performance of concrete rather than relying on mortar extracted from the concrete.

RESULTS AND DISCUSSION

Compressive Strength

As expected the compressive strength of the mixes containing 70% GGBS and 30% Portland cement are higher than those with 100% GGBS. Strength gain patterns followed the general norm in terms of lower w/c giving higher strength (Figure 1).The strength for 100% GGBS mixes as shown in Figure 1were low but still remarkable given that they did not contain Portland cement. The concrete at a w/c ratio of 0.25 produced a very reasonable strength profile starting with a 7 day compressive strength of 35.5 N/mm^{2}and 28 day compressive strength of 43.5 N/mm^2.However, the 7 day strength fell rapidly with increasing w/c ratio.

The strength pattern of the unwashed sand series was in general very similar to the washed sand series. However, the strength gain profiles for the 100% GGBS mixes appear to be almost linear up to 56days (Figure 2), suggesting the possibility of significant further development in strength after 56 days.

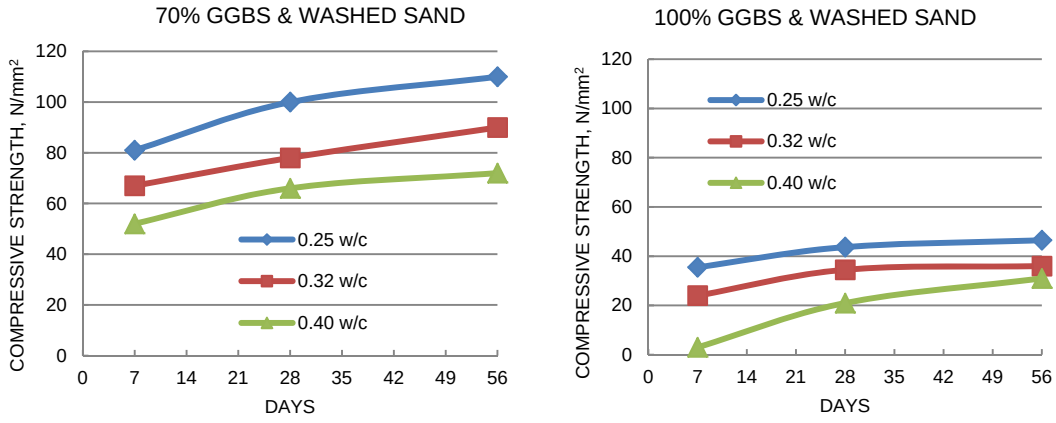

Figure 1 Effect of the GGBS content on the strength for washed sand mixes

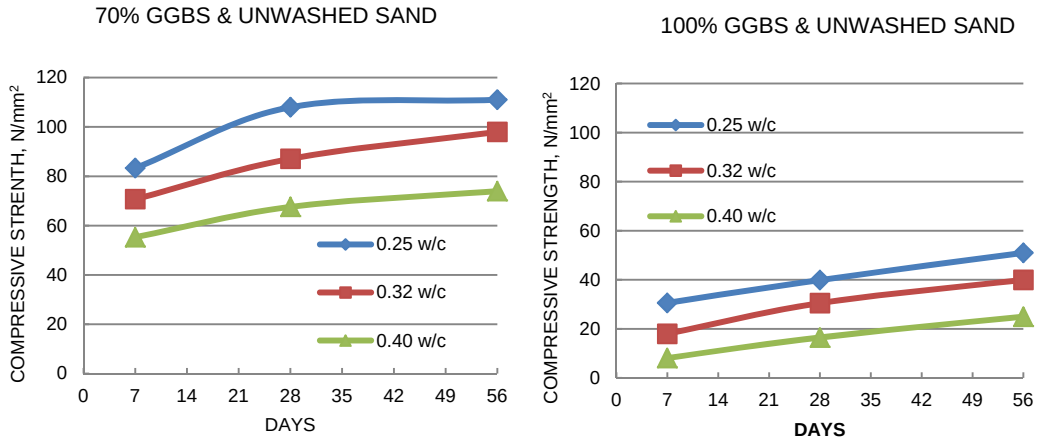

Figure 2 Effect of the GGBS content on the strength for unwashed sand mixes

Effect of Increased Fines

Figure 3 compares the compressive strengths of concrete with or without filler contribution for each w/c category. It is clear that the use of unwashed sand did not lead to concrete of significantly lower compressive strength than the use of washed sand, and it may be argued that the results show a general trend for higher compressive strength at a specific age when using unwashed sand; however further work in this area is required.

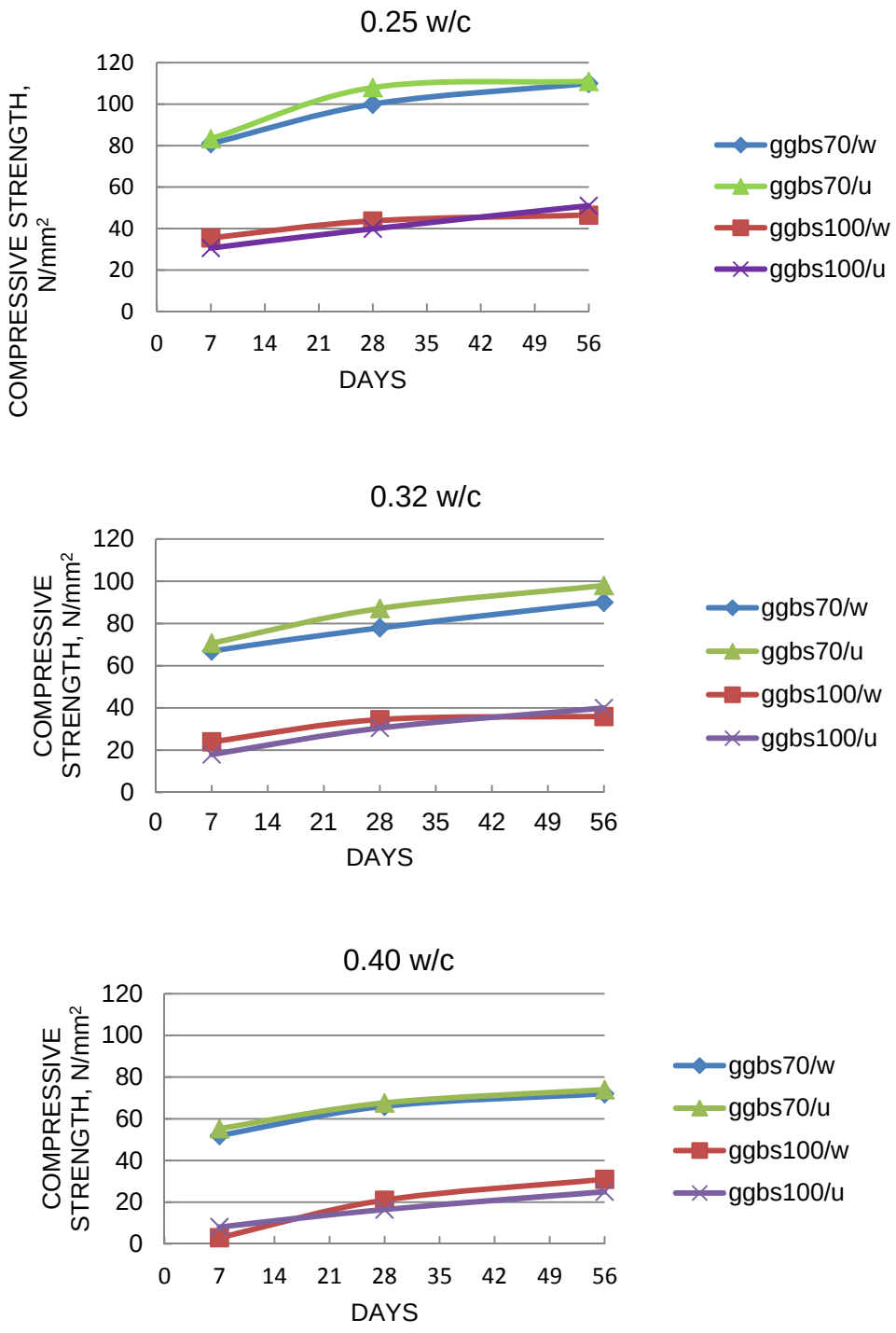

Figure 3 Effect of filler in the 'unwashed sand' in compressive strength gain

Durability

The results of RCPT, water absorption and water permeability tests are given in Table 6. In general the quality of the concrete was very high, reflecting the low w/c ratios used, the use of a minimum 70% GGBS, and the mix proportioning method used to create very dense low porosity concretes suitable for the Gulf environment.

Rapid chloride permeability

Guidelines for the severity of chloride penetration as given by ASTM C1202 are shown in Table 7. This categorizes chloride ion penetrability into five categories namely high, moderate, low, very low and negligible level in terms of the charge measured. According to these guidelines concrete having chloride permeability between 100-1000 coulombs will have very low chloride ion penetrability. Table 6 shows that the chloride permeability of all concretes tested in this work were within this range, and that there was no specific indication on the comparative performance of concrete in terms of RCPT test. This is perhaps due to the very high variation (42%) of results. Indeed this is acknowledged by the standard.

However, qualitatively it can be concluded that all concrete mixes achieved a degree of chloride ion resistivity which is very low irrespective of the content of GGBS or additional filler in the sand.

Table 6 Durability results

NO	REF	RAPID CHLORIDE PERMEABILITY	WATER ABSORPTION	WATER PERMEABILITY
		ASTM C1202	BS 1881-122	BS EN 12390-8
		COULOMB	%	mm
1	0.25/pc30ggbs70/w	380	0.8	0
2	0.32/pc30ggbs70/w	254	0.7	0
3	0.40/pc30ggbs70/w	306	1.6	0
4	0.25/pc0ggbs100/w	450	0.6	3
5	0.32/pc0ggbs100/w	535	0.6	3
6	0.40/pc0ggbs100/w	585	1.8	0
7	0.25/pc30ggbs70/u	475.2	0.7	0
8	0.32/pc30ggbs70/u	375.3	0.5	0
9	0.40/pc30ggbs70/u	342	0.7	0
10	0.25/pc0ggbs100/u	491.1	1.4	0
11	0.32/pc0ggbs100/u	508.4	1.8	0
12	0.40/pc0ggbs100/u	701.1	1.8	1

Table 7 Guidelines of the level of chloride ion permeability given by ASTM C1202

CHLORIDE PENETRABILITY BASED ON CHARGE PASSED ASTM C1202:1997	
CHARGE PASSED (COULOMBS)	CHLORIDE ION PENETRABILITY
>4000	High
2000 - 4000	Moderate
1000 - 2000	Low
100 - 1000	Very Low
<100	Negligible

Water permeability

All mixes except 4, 5 and 12 showed no penetration of water, proving that the concretes were robust. The maximum penetration of water measured was 3mm which can be considered negligible (Table 6). Results below 10mm are considered to be very good and the concrete can be considered to be water impermeable [7].

Water absorption

Likewise the water absorption results did not provide any quantitative conclusion on comparative performance of different mixes (Table 6). The results are all below 2%, which is considered to be acceptable [8].

Sulphate resistance

Results of sulfate diffusion tests are not presented as to date (after 14 months) all of the specimens have remained intact and have shown no evidence of sulfate attack. Again this demonstrates that the concretes are robust and durable.

CONCLUSIONS

The effect of 100% GGBS and the use of sand containing a higher fines content on the properties of concrete have been studied. It can be concluded that concrete with 100% GGBS can have sufficient strength for structural use, particularly at later ages. Furthermore, 7 day strengths of over 30 N/mm^2 can be achieved with low w/c ratios.

The effect of the extra fines in the concrete as a result of using unwashed sand may contribute to strength. The research provides some justification for using crushed limestone sand with a fines (that passing a 75μm sieve) as high as 10% by mass. Use of such sand would save huge amounts of water, which is currently being used to satisfy local requirement of maximum allowable limit of 5% by weight.

All mixes have demonstrated satisfactory level of performance with regard to durability and permeability.

It can be concluded that it is possible to use high volume slag concrete in some applications as a means of reducing the overall carbon footprint of concrete in the Gulf region. Furthermore, the sustainability of concrete produced in the Arabian Peninsula can be enhanced by stopping the practice of washing crushed rock limestone sand and by allowing the maximum fines content to be as high as 10% by mass.

REFERENCES

1. TOLBA, M.K., SAAB, N.W. (Eds) Arab Environment: Future Challenges. 2008 Report of the Arab Forum for Environment and Development. 2008

2. STANLEY, C. Sustainable concrete construction in the Middle East. 33rd Conference on Our World in Concrete and Structures, Singapore, 25-27 August 2008

3. SAMARAI, M.A., QUDAH, L. Durability and quality of construction: Challenges facing UAE. International Conference on the Role for Concrete in Global Development, Dundee, UK, 8-9 July 2008, pp15-26

4. WALKER, M. (Ed) Guide to the design of concrete structures in the Arabian Peninsula. The Concrete Society. CS163, 2008.
5. AL-RABIAH, A.R.A Performance of coated and uncoated slag cement concrete in the Arabian Gulf marine environment - A case study. Second International Conference on Engineering Materials, Vol II, pp 553-564, 2001

6. ABU SALEH, M., KEBEDE, M., YACOUB, N. 2009. Environmentally Sustainable Self Compacting Concrete – A Case Study. Grey matters and American Concrete Institute, The Second International Conference on Advances in Concrete Technology in the Middle East – Self-consolidating Concrete. Abu Dhabi, 8-10 December 2009. Abu Dhabi: Grey Matters and ACI

7. THRELFALL, T. Concrete construction for liquid retaining structures. In: Advanced Concrete Technology: Processes (Eds. Newman and Choo). Butterworth-Heinemann, 2003.

8. BUNGEY, J.H. The testing of concrete in structures (2nd Ed.). Chapman and Hall, 1989.

Benefits of Utilising Oil Drill Cuttings (ODC) as a Filler in PC and Ternary Cement Concrete

J O Ikotun[1], M D Newlands[2], L J Csetenyi[2], D O Olanrewaju[3]
1 – University of Witwatersrand, South Africa
2 – University of Dundee, UK
3 – Lagos State Polytechnics, Nigeria

This paper explores the benefits of utilizing oil drill cuttings as filler in Portland cement and ternary cement concretes. Hardened concrete properties such as compressive strength, permeation (water sorptivity and water penetration), rapid chloride permeability and carbonation were investigated. The study was conducted in two parts; 0, 5, 10 and 20% replacement of PC with oil drill cuttings (ODC) as filler and 10% ODC replacing ground granulated blast furnace slag (GGBS) and Fly Ash. All the mixes were designed with superplasticiser at fixed water/cement ratio of 0.5. Significant improvements were recorded for fresh properties for all the concretes. The influence of ODC on hardened properties of all the concretes was negligible. The investigation shows limitations and potentials in utilisation of oil drill cuttings as a cement replacement both in PC and ternary concrete.

Ikotun Jacob Olumuyiwa is a former student at Concrete Technology Unit, University of Dundee, Scotland, United Kingdom where he obtained MSc. in Concrete Engineering and Environmental Management. He is currently a doctoral Student at Civil and Environmental Engineering Department, University of the Witwatersrand, Johannesburg, South Africa and currently researching into service life modelling and durability assessment of reinforced concrete structure in Sub-Saharan Africa.

Moray Newlands is a Lecturer in the Concrete Technology Unit, University of Dundee. His research interests focus on utilising waste materials in concrete and added value applications in construction.

Laszlo Csetenyi is a research/teaching fellow at Concrete Technology Unit, University of Dundee. His main areas of interest include cement and concrete science and binder technology with emphasis on stabilisation and solidification processes as well as practical use of secondary materials in construction

Olanrewaju Deborah Olukemi obtained BSc in Building from Obafemi Awolowo University, Ile-Ife in 1997 and MSc in Construction Technology from University of Lagos, Nigeria in 2007. She is a lecturer at Building Technology Department, Lagos State Polytechnic, Nigeria.

Keywords: Concrete, Filler, Oil drill cuttings

INTRODUCTION

Oil drill cuttings are waste materials produced from drilling boreholes to subterranean oil and gas bearing formation during oil exploration activities [1, 2]. The cuttings contain a mixture of rock, drilling fluids and crude oil. The physical characteristics and mineralogical compositions of oil drill cuttings have been said to depend on the geological formations, drilling methods and drilling fluids and will influence the properties of concrete made with the material [1].

The disposal of these materials in major oil producing countries, like Nigeria, the UK, and the Gulf constitutes an environmental problem to marine life. More of these materials are being generated yearly. In the last 50 years statistics shows that, in UK, 16 million cubic meters of oil drill cuttings were generated [3]. This led to different methods of treatment e.g thermal desorption, stabilisation/solidification and mechanical separation to remove the hydrocarbon and heavy metals before sending to landfill.

However, drill cuttings have found some use in the construction industry and research has been conducted to examine their applications. Dhir et al [2], worked extensively on the physical and chemical composition of oil drill cuttings for its use as filler in bituminous mixtures. The compositions and the resulting mixtures with oil drill cuttings compared very well with bituminous mixtures with limestone. Moreover, the beneficial effect of minor addition in cement had been investigated upon to improve the rheological properties of concrete with consequential effect on the hardened and durability properties [4]. Moosberg-Brown et al [5] investigated the function of fillers in replacing cement at 10, 20, 30 and 40%, quartz sand were used, the result showed improvement in fresh and hardened properties of concrete at the optimum replacement. However, the use of quarry dust which similar in properties to oil drill cuttings as filler replacement has not been successful, there was reduction in 28 days compressive strength, but improvement in fresh properties was recorded [6].

In an attempt to create awareness in the use of oil drill cuttings in concrete, Ifeandi [7] used treated oil drill cutting to produce concrete interlocking bricks while Mohammed and Cheeseman [3] used the same to produce sandcrete blocks. The concrete bricks performed very well in strength, but the durability aspect was less successful. More research is still needed to see its wider application in concrete. If this is successful, there will be less demand on cement, and more durable concrete will be produced, thus promoting the sustainable development through the use of waste from the oil and gas industry.

This paper reports the result of laboratory study, investigating the benefits of utilising oil drill cuttings as filler in cement and ternary cement concrete for sustainable development. The research project is part of a research programme carried out at Concrete Technology Unit, University of Dundee. It investigates the fresh and hardened properties of concrete made using treated oil drill cuttings as filler replacement in cement and ternary cements.

EXPERIMENTAL PROGRAMME

The laboratory investigation was subdivided into two parts. In the first part, cement was replaced by oil drill cuttings at 0, 5, 10 and 20% (represented by mix codes M1, M2, M3 and M4) while the second part, ternary cements were replaced with 10% oil drill cuttings (represented as M5 (PC/GGBS), M6 (PC/ODC/GGBS), M7 (PC/PFA) and M8 (PC/ODC/PFA)). Concrete mixes were produced using these replacement levels. Fresh properties such as slump, compacting factor and plastic density were studied and compared. Also, hardened properties such as compressive strength, water penetration (to BS EN 933-10:2001) [8], rapid chloride permeability test (to ASTM C1202-97) [9] and accelerated carbonation test were carried out to see the beneficial effect of oil drill cuttings as filler in cement and ternary cement.

CONSTITUENT MATERIALS USED

Portland cement (CEM 1 52.5) conforming to BS EN 197- 1:2000 [10] and oil drill cuttings obtained from a location in the North Sea were used. Oil drill cuttings were pre treated using the rotomill method to remove heavy metals and hydrocarbon conforming to less than 1% content of hydrocarbon as limit requirement in BS EN 197-1:2000 [10] and to satisfy the size requirement of a filler material (<63 µm) in BS EN 933-10:2001 [8]. Ground granulated blast furnace slag and fly ash were also made use in the experiment. Three grades of aggregates were used in this investigation they were fine and coarse aggregate of size 4/10mm and 10/20mm of natural glacial gravel origin. All aggregates were air dried under laboratory conditions of 20±2°C, 55%±5% RH. The physical properties and grading curve of aggregates are shown in Figure 1. Superplasticiser of poly-carboxylic group was incorporated into all the mixes. Oil drill cuttings passing a 63µm sieve size was used as filler in cement and ternary cement.

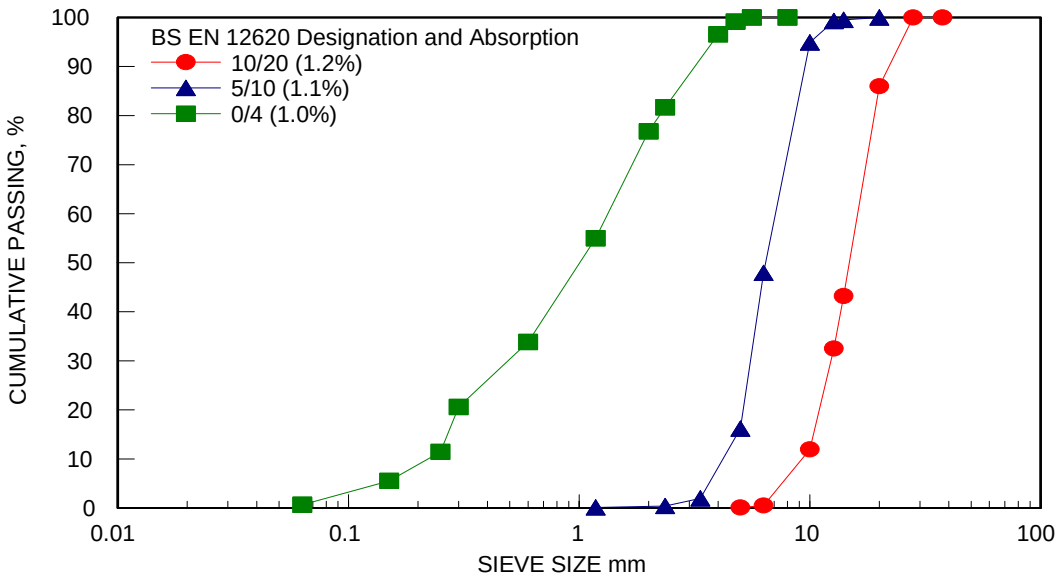

Figure 1 Grading of fine (0/4) and coarse (5/10, 10/20) aggregates and absorption values

Characterisation of Cements

The particle size distributions of the cements are shown in Figure 2. All the cements are well graded and within the limit of 70% passing 63µm as specified in BS EN 933-10:2001 [8] for fillers. However, Table 2 shows that ODC has the largest specific surface area (712 m²/kg) and the greatest fineness (749 m^2/kg) compared with other cements.

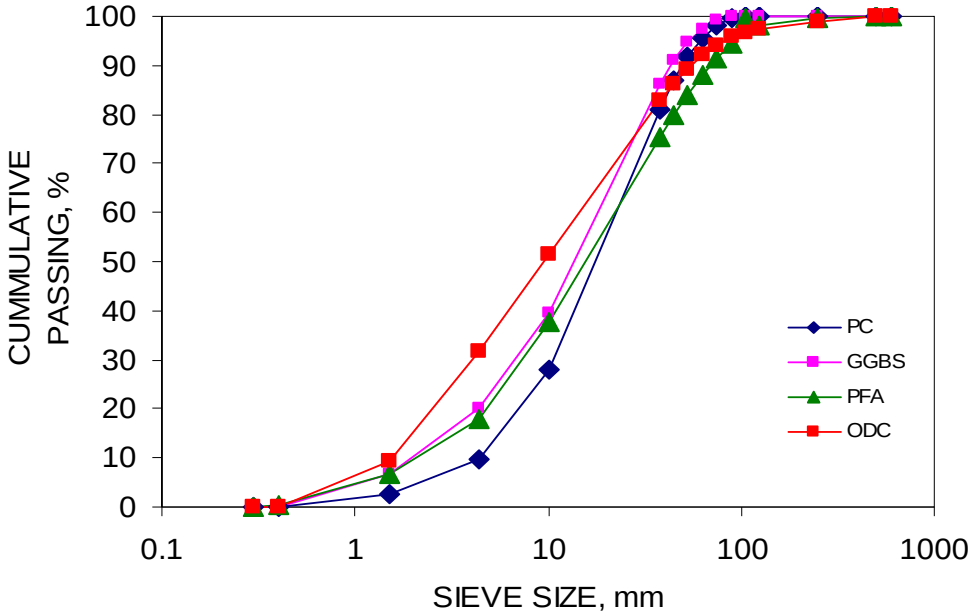

Figure 2 Grading curves of oil drill cuttings, PFA, GGBS, and PC

The chemical and mineralogical composition of the cements samples are presented in Table 1 The result shows the presence of large quantity of clay minerals, this makes oil drill cutting as silicate-based material. These minerals have been said to have high impact on fresh and hardened concrete properties, through increased water absorption tendency and reduced compressive strength as shown in compressive strength test [11].

Table 1 Mineralogical composition of ODC, determined by XRD

MINERALOGICAL NAME	CHEMICAL FORMULA	COMPOSITION %
Quartz	Silicon dioxide	16.10
Barite	$BaSO_4$	14.90
Calcite	$CaCO_3$	8.80
Halite	NaCl	5.80
Kaolinite	$Al_2Si_2O_5(OH)_4$	19.10
Muscovite	$KAl_2(Si_3Al)O_{10}(OH)_2$	3.50
siderite	$FeCO_3$	0.50
Corundum	Al_2O_3	0.00

Table 2 Physical and selected chemical properties of cements

CEMENT TYPES					
Physical properties		PC	GGBS	PFA	ODC
Apparent particle density		3.14	2.81	2.27	2.76
Loss on ignition %		1.40	0.31	5.00	8.40
Specific surface area, m^2/kg		251.00	409.00	535.00	712.00
Blaine fineness, m^2/kg		405.00	435.00	525.00	749.00
Oxide composition of cements					
Elements	Bulk oxide				
Ca	CaO	64.07	2.25	39.10	1.36
Si	SiO_2	20.15	24.60	37.03	72.10
Al	Al_2O_3	5.86	11.90	12.44	11.30
Fe	Fe_2O_3	2.27	7.80	0.57	4.37
Mg	MgO	2.24	0.72	6.77	1.88
Mn	MnO	0.05	0.06	0.52	0.08
Ti	TiO	0.27	0.82	0.68	0.68
K	K_2O	0.70	1.89	0.64	1.63
Na	NaO	0.37	0.58	0.49	2.08
P	P_2O_5	0.46	0.24	0.04	0.18
Cl	Cl	0.18	0.00	0.02	0.00
S	SO_3	2.58	0.65	1.07	0.05

Concrete mix proportions

Consistence was maintained at target slump of 100 to 120mm (BS 8500 slump class S3). The BRE digest 331 [12] method of mix design was employed for calculating the proportions of concrete materials. The detail of the mix proportions used in the experiment is shown in Table 3. Free water was kept constant at 165 l/m^3 for all the batches in all the concrete batches. Consistence was measured using slump as described in BS 1881: Part 102:1983 [13].

Table 3 Mix proportions of test concretes at water/cement ratio of 0.5

	MIX PROPORTIONS, kg/m^3									Slump, mm
	PC	GGBS	Fly Ash	ODC	Water	Aggregates			Super plasticizer	
						0/4	4/10	10/20		
M1	330	0	0	0	165	760	380	760	1.2	80
M2	314	0	0	17	165	760	380	760	1.2	90
M3	297	0	0	33	165	760	380	760	1.2	120
M4	264	0	0	66	165	760	380	760	1.2	80
M5	150	180	0	0	165	770	380	760	1.2	100
M6	150	162	0	18	165	770	380	760	1.2	100
M7	210	0	115	0	165	750	375	750	1.0	120
M8	210	0	103	12	165	750	375	750	1.0	110

RESULTS AND DISCUSSION

Influence of ODC on Consistence

The inclusion of ODC increased the superpasticiser dose by 29 and 42% to maintain the required workability in PC/ODC concretes. A similar effect was seen in PC/GGBS and PC/ODC/GGBS concretes which may be attributed to the combined effect of angular shape and large specific surface area of ODC and GGBS. Fly ash concretes exhibited a reduction of 33% in superplasticiser dose which may be due to its spherical shape. However, introduction of ODC improved the consistence of all concretes.

Compressive Strength Development

Compressive strength tests were conducted in accordance with BS EN 12390-3: 2009 [14] on all the cubes of the mix proportions at 1, 3, 7, 28 curing days, the results are shown in Figure 3. ODC concretes showed a reduction in compressive strength compared to the control PC concrete.

There were small reductions in strength at different replacement levels (5-15%). Similar results were seen for the ternary cement with GGBS and Fly Ash compared with the PC concrete. 10% ODC introduction shows a strength reduction of 21% in PC/ODC/GGBS compared with PC/GGBS, but PC/ODC/PFA maintained the same strength as PC/PFA concrete at 28 days. However, strength increases with age in all the concretes as shown in Figure 3. Furthermore, considering the result of concrete types, it is apparent that the increase in the ODC percentage reduces the strength at all ages this may be attributed to the presence of clay minerals which can inhibit hydration and formation of C-S-H gel in cement matrices [11].

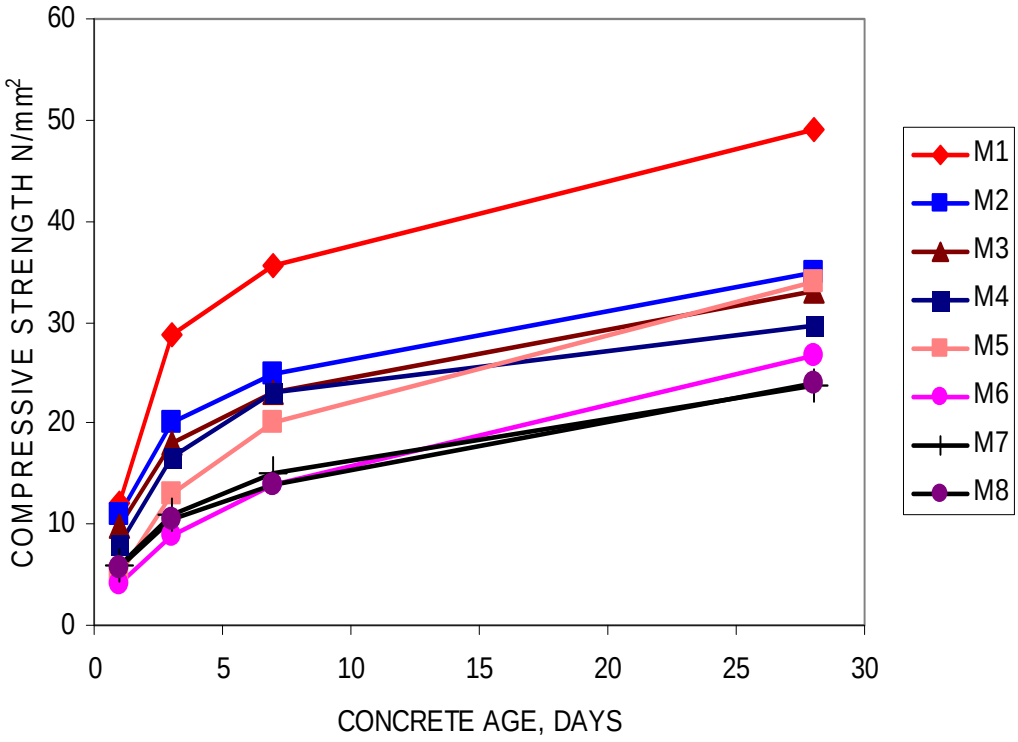

Figure 3 Compressive strength developments of concretes

Depth of Water Penetration

Water penetration tests were conducted on all the test cubes of the concrete batches after 28 days in accordance with BS 12390-8:2009 [15]. The results are shown in Figure 4. Water penetration depth increases with increasing percentages of ODC in the concrete. Similar results were also obtained for ternary cement concrete when replaced with 10% ODC. However, the increase in the water penetration depth could be as a result of presence of clay minerals in the ODC as revealed by the XRD analysis shown in Table 1. Clay minerals have the tendency for high water absorption capacity when exposed to water. Again, another factor that could have contributed to the increase in the water penetration depth of the concrete containing ODC is the decreasing concrete quality as a result of reduction in PC content.

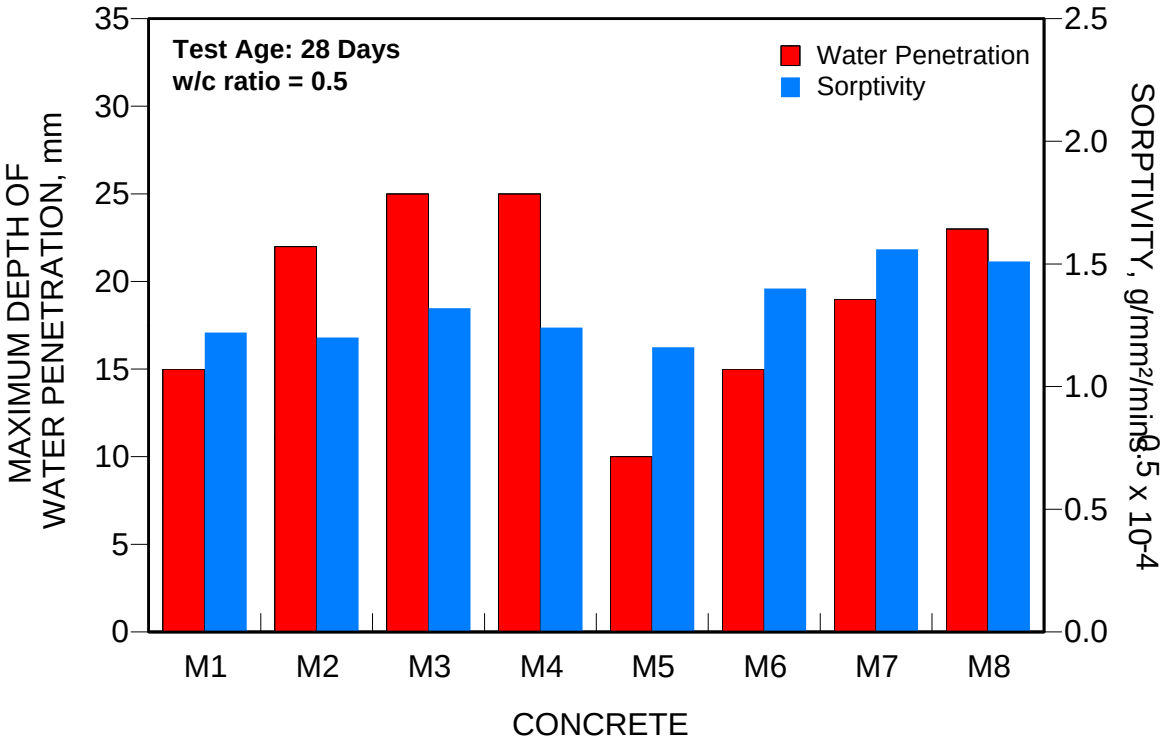

Figure 4 Comparison of maximum depth of water penetration and sorptivity at 28 days

Sorptivity

Sorptivity test was carried out in accordance with ASTM C 1585 [16] and the results are shown in Figure 4. It worth noting the change in behaviour of the concretes at different replacement levels with ODC. Portland cement content reduction in the concrete mix reduces the sorptivity and 10% replacement concrete has the highest sorptivity of 1.235 x 10^{-4}g/mm^2/min$^{0.5}$ while 5% replacement concrete gave the lowest sorptivity of 1.198 x 10^{-4}g/mm^2/min$^{0.5}$ compared to the control concrete. The increase in sorptivity can also be attributed to lower quality of the concrete as a result of PC replacement levels and possible presence of clay particles. However 5% replacement with ODC reduces sorptivity by 2%, which confirm the filler effect of oil drill cuttings in refinement of concrete pores for low permeability in concrete. Similar effect could be seen in PC/ODC/PFA concrete, where sorptivity was reduced by 3.2%. This shows that pore structure is more refined with ODC in PC/PFA concrete.

Rapid chloride permeability

The need to assess the potential movement of chlorides in a short period led to the development of rapid chloride permeability test. The test involves utilising voltage gradient to force chloride ions to migrate more rapidly through the pores of concrete. The samples were conditioned and test performed in accordance with ASTM C 1202 -97 [9]. The result is shown in Figure 5. The

result indicates high permeability in all the PC/ODC binary concrete samples with the control concrete having the highest value. However, there is negligible decrease at introduction of ODC. It could be seen that the control concrete at 100%PC has the highest total charge of 5843 coulombs while the GGBS and PFA are 2572 and 5272 coulombs respectively.

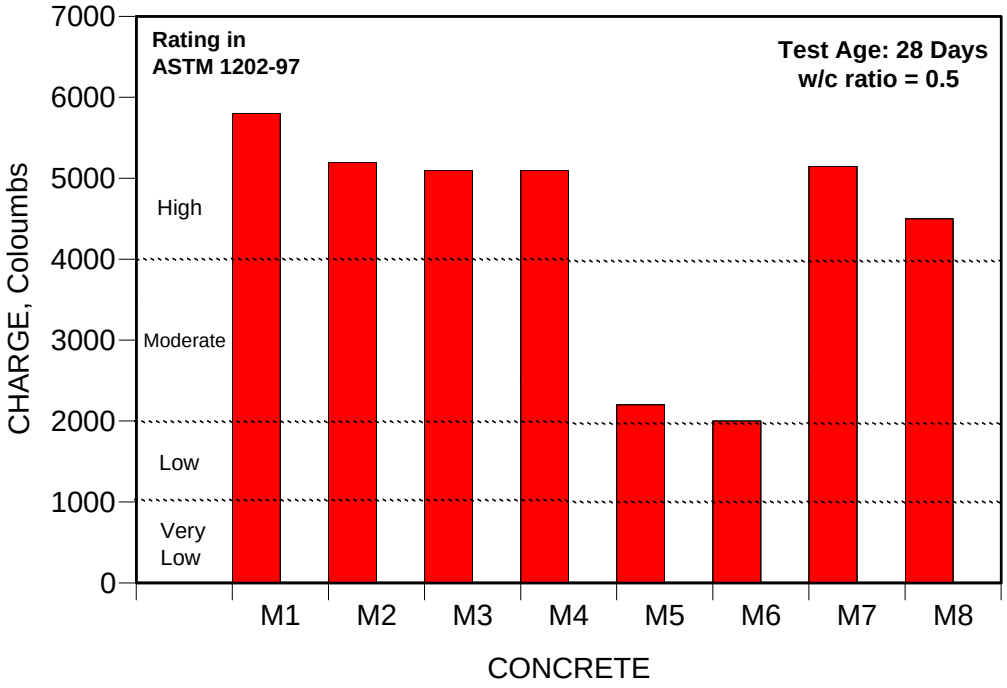

Figure 5 Average RCPT Charge at 28 days

It can be deduced that the control PC concrete may have lower resistance to chloride movement compared with the binary cement concretes. In addition, this shows the beneficial effect of GGBS and Fly Ash arising from the denser microstructure of hydrated cement paste. Although, the value is still relatively high in PC/Fly Ash concrete compare to PC/GGBS concrete, this may be due to the influence of the LOI of ODC and PFA as shown in Table 2. However, there is more than a 50% reduction with GGBS, and around 18% reduction with Fly Ash compared with the PC control concrete and a further replacement with 10% ODC reduces the chloride permeability by 8% and 10% respectively. However, one can rightly say that ODC acted as filler in this respect, it reduces the chloride permeability of all the concretes.

Accelerated carbonation

The result of accelerated carbonation test on concretes is shown in Figure 6. It can be observed that average carbonation depth increases along with increase in percentage replacement of PC with ODC and carbonation depth increases with exposure age. The increase in the carbonation depth can be attributed to lower quality of the concrete as a result of PC replacement level with ODC. Ternary cement concretes also behave in similar way. However, PC concrete shows no

carbonation at 7 and 14 days. It shows carbonation of 2.5 mm and 5.0 mm at 21 and 28 days respectively compare with other ternary cement concretes that have carbonation depth of more than 18mm at 28 days exposure period. This justified the assertion that the rate of carbonation is a function of cement content and concrete quality. However, one can observe that at 28 days, average carbonation depth of ternary cement concretes converges, this makes further research necessary.

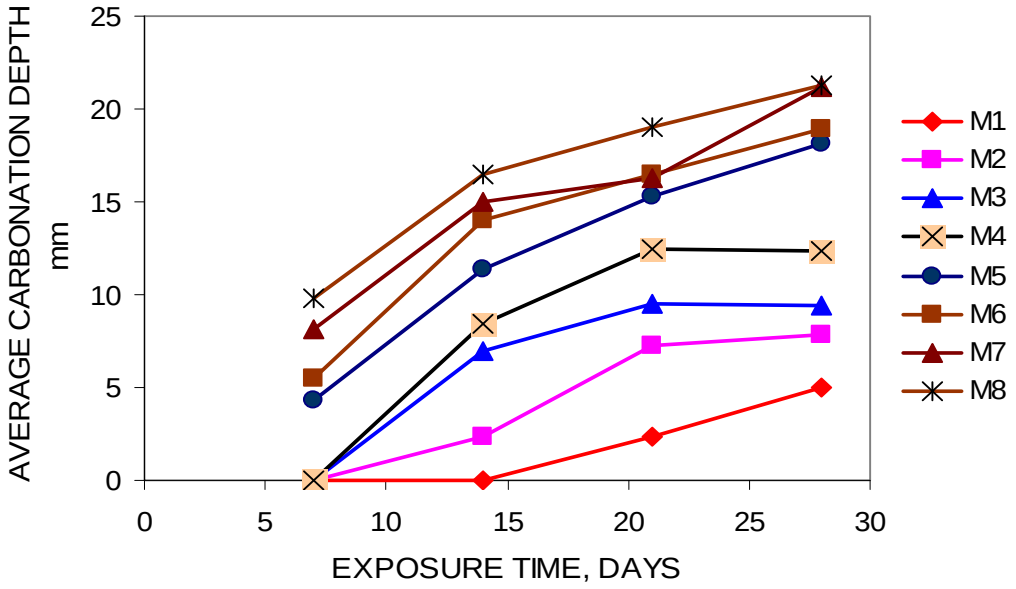

Figure 6 Average **c**arbonation depth and exposure time of concretes

CONCLUSIONS

This paper explores the benefits of utilizing oil drill cuttings as filler replacement in Portland and ternary cement concrete. Fresh properties such as workability and admixture demand were observed to see the beneficial influence of oil drill cuttings on concrete. Also, compressive strength, water permeation (sorptivity and water penetration), rapid chloride permeability and accelerated carbonation were among the hardened properties considered in this investigation. The investigation was in two parts, the first part studies the PC replacement with oil drill cuttings at 0, 5, 10 and 20% level. The second part investigates the role of oil drill cutting in replacing ternary cement at 10% level. All the mixes were designed using superplasticiser at fixed water cement ratio of 0.5. The results so far have yielded some benefits for its use in concrete. Improvements were recorded for fresh properties of ODC/PC binary and ternary cement concrete while the influence of it on hardened properties of concrete showed negligible benefits but importantly negligible negative effects. Thus, it is suggested that oil drill cuttings can be utilised in lower strength grade applications such foundation blinding, walling and concrete fill materials for affordable and sustainable housing solution in oil producing regions.

REFERENCES

1. AL-ANSARY, M.S., AL-TABBA, A. Stabilisation/solidification of synthetic petroleum drill cuttings. Journal of Hazardous Materials, Vol. 141, 2007, pp. 410-421.
2. DHIR, R.K., CSETENYI, L.J., DYER, T.D., SMITH, G.W. Cleaned oil-drill cuttings for use as filler in bituminous mixtures, Journal of Construction and Building Materials, Vol. 24, No. 3, 2010, pp. 322-325.
3. MOHAMMED, B., CHEESEMAN, C. Solidification/Stabilisation of treated oil drill cuttings in sandcrete construction products, Proceedings of Sustainable Management of Waste and Recycled Materials in Construction, 2009, WASCON, Lyon, France.
4. GUEMMADI, Z., RESHEIDAT, M., HOUARI, H., TOUMI, B. Optimal criteria of Algerian blended cement using limestone fines. Journal of Civil Engineering and Management, vol.14 No 4, pp. 299-275.
5. MOOSBERG-BUSTNESS, H., LAGERBLAD, B., FORSSBERG, E. The Function of Fillers in Concrete, Journal of materials and Structures, vol. 37, 2004, pp74-81
6. RAMANS, S.N., ZAIN, M.F.M., MAHMUD, H.B., TAN, K.S. Suitability of Quarry Dust as Partial Replacement Material for Sand in Concrete, Proceedings of the Seventh International Conference on Concrete Technology in Developing Countries, 2005, Kuala Lumpur, Malaysia.
7. IFEANDI, C.N. The treatment of drill cuttings using dispersion by chemical reaction (DCR), DPR Health, Safety & Environment (HSE) International conference on Oil and Gas Industry, 2005, Port Harcourt, Nigeria.
8. BS EN 933-10:2001 Tests for geometrical properties of aggregate. Assessment of fines
9. ASTM C 1202 – 97 Rapid Chloride Permeability Test
10. BSI.BS EN 197-1:2000. Cement composition, specification and conformity criteria for common cements.
11. JOSE, F.M., ISABEL, M.T., MARC, A.A. AND STEVEN, M.C. Detection of Aggregate clay coatings and impacts on concrete, ACI Materials Journal, 2010, pp387-395.
12. BRE Digest 331. Design of normal mixes
13. BSI BS 1881: part 102: 1986. Testing concrete – Method for determination of slump
14. BSI. BS EN 12390-3:2009. Testing Hardened Concrete - Compressive strength of Test.
15. BSI. BS EN 12390-8:2009. Testing Hardened Concrete. Depth of penetration of water under Pressure
16. ASTM C 1585: Concrete Permeability Testing – Part 2

Performance Evaluation of Two Types of Phase Change Materials in Cementitious Systems

S Manari[1], N Neithalath[2]
1 – Clarkson University, USA
2 – Arizona State University, USA

Increasing energy demand is one of the important 21st century challenges for the developing and the developed world. A significant portion of the energy used in commercial or residential buildings is spent on heating or cooling the interior space. Considerable energy savings can be realized if the heating and cooling loads in buildings can be controlled. One potential methodology to attain this objective is through the use of phase change materials (PCM) in building components. PCMs are latent heat thermal storage materials that store energy when subjected to temperatures in excess of their melting point by changing from the solid to the liquid state. The stored energy is released when the temperature drops below the melting point of the PCM. This study investigates the feasibility of using PCMs in cementitious systems to control the indoor thermal environment. Two different PCM incorporation methods – one using a microencapsulated powder, and another through impregnating porous aggregates with PCM – are evaluated. Differential scanning calorimetry (DSC) is used to understand the enthalpies associated with the pure PCM and the cement paste system incorporating the PCM. Semi-adiabatic calorimetry results are used to understand the influence of the PCM in altering the early age cement hydration reactions, which might beneficially influence early-age thermal cracking. Studies on small-scale slab systems to quantify the internal temperature reduction efficiency as a function of PCM type, dosage, and incorporation method is also reported.

Shilpa Manari is a Masters student in the Department of Civil Engineering at Clarkson University, Potsdam, NY. Her research interests are in thermally efficient concretes, characterization of the pore structure, and the beneficial effects of PCMs in concrete.

Dr. Narayanan Neithalath is an Associate Professor in the School of Sustainable Engineering and the Built Environment at Arizona State University, Tempe, AZ. His research interests are in the development and characterization of novel cementitious materials, performance evaluation and modeling of cementitious systems, computational materials science of concretes, and development of sustainable energy efficient concrete systems.

Keywords: Differential scanning calormetry, Enthalpy, Lightweight aggregate, Microencapsulation, Phase change materials

INTRODUCTION

Ever increasing energy demand is one of the most important challenges faced by the developing and the developed world in the 21st century. Nearly 40% of the total energy in the United States is utilised by commercial buildings, corporate offices, and residential complexes, and a significant portion of this is spent on heating or cooling and lighting the interior space. Today, 50% of fuels are used to heat or cool and to light buildings. There is a need for more energy conscious forms of heating or cooling and alternate source of energy. Recent research [1, 2] has shown that the latent heat energy storage systems can store large volumes of energy for thermal regulation of buildings. One potential methodology to attain this objective is through the use of phase change materials (PCMs) in building components. Phase change materials are latent heat storage materials which absorb and releases thermal energy as they undergo state transformations. A review on the mechanisms and classifications of PCMs has been provided by Pasupathy et al. [1] and Zalba et al. [2]. An extensive review on various types of PCMs, their applications and techniques for the measurement of thermophysical properties of PCMs is provided in Sharma and Sagara [3] and Sharma et al. [4]. PCM incorporated wallboards were reported to greatly reduce the energy cost of HVAC systems and reduce peak load energy consumption as they automatically absorb indoor redundant heat [5]. Entrop et al. [6] studied the use of phase change materials in concrete floors where the thermal energy from the sun is stored in the modified concrete to reduce the need of conventional heating during evening and nightfall. The preparation, characterization, performance and development of microencapsulated phase change materials was researched and reviewed in detail by Hawlader et al. [7] and Tyagi et al. [8]. Many detailed investigations on the preparation and performance of impregnated phase change materials were carried out [9-11]. Incorporation of PCM into fresh concrete was found to control or lower the peak temperature during cement hydration [12]. Addition of PCM to self-compacting concrete mixes showed an improvement in the thermal performance of concrete due to lower thermal conductivity and increased heat capacity [13].
The foregoing discussion demonstrates the beneficial impacts of using latent heat energy storage materials in building applications. While the incorporation of PCMs in gypsum wallboards have gained prominence, it is expected that the development of methodologies wherein the PCM is integrated as a part of the concrete material system will result in widespread implementation of energy efficient concretes. In this paper the influence of two types of PCMs – one a microencapsulated paraffin, and the second a glycol that is impregnated into the pores of lightweight aggregates, on the mechanical and thermal properties of cementitious systems are presented along with thermal performance studies of prototype chambers with PCM incorporated roof slabs.

EXPERIMENTAL PROGRAM

Materials

Type I/II ordinary Portland cement (OPC) conforming to ASTM C 150 was used to prepare cement pastes, mortar slabs and concretes for this study. Microencapsulated phase change material (MPCM) used in this study was Micronal DS 5008 X (manufactured by BASF) which is essentially a paraffin wax blend microencapsulated in an acrylic polymer. The MPCM has a phase change temperature in the range between 22 and 25°C. The melting enthalpy of this MPCM as reported is 110 kJ/kg.

Light weight aggregates (LWA) with a specific gravity of 1.4 was used to prepare impregnated phase change material (IPCM) by impregnating the LWA with polyethylene glycol (PEG 600). PEG 600 is reported to have a phase change temperature in the range between 16 and 22^{o}C and a melting enthalpy of 127 kJ/kg. The impregnation of the aggregates was carried out by first oven drying the LWA at 100^{o}C to remove all the evaporable water. The dried aggregates were then immersed in PEG 600 and wet vaccumed for 6 hours to ensure adequate de-aeration and then the residual vacuum was released to the atmosphere and the aggregates were left to soak in the sealant at atmospheric pressure for a period of 48 hours to facilitate penetration into the pores. After this, the aggregates were removed and the surfaces were cleaned off to remove the excess sealant (PEG 600).

Mixture Proportions and Specimen Preparation

All the cement pastes investigated in this study were made with a water-to-cement ratio (w/c) of 0.35. Cement pastes were made by replacing 0%, 3%, 5% and 10% of cement by mass with MPCM for semi-adiabatic calorimetric and differential scanning calorimetric (DSC) studies. The cement paste and the respective replacement material were mixed in a paste mixer for 2 minutes, after which water was added gradually and mixed for 3 minutes. The cement pastes with 0%, 5% and 10% replacement by mass of cement with MPCM were cast into 50 mm cube molds for compressive strength studies and was tested for strength after 1, 3, 7, 14 and 28 days of curing in a moist chamber (>98% RH).

Light weight aggregates impregnated with PEG 600 were crushed and preliminary studies were done using DSC to understand their phase change properties. Mortar mixtures with water-to-cement ratio of 0.40 were prepared by keeping the quantity of cement and LWA in the mixture constant (50% aggregate volume) and by varying the amount of PEG 600 by mass of light weight aggregates, by varying the duration of impregnation. In this study, mixtures with 0% and 5% IPCM by mass of cement was evaluated to determine the influence of IPCM on the compressive strength of the system. Semi-adiabatic calorimetric studies were conducted to evaluate the heat of hydration using mixtures with 0%, 13% and 15% of PEG 600 by mass of cement obtained by altering the duration of soaking of LWA after impregnation under vacuum.

For the evaluation of thermal performance of PCM incorporated slabs, mortar slabs with 50% sand volume and w/c of 0.40, having dimensions 10” x 6” x 3” (250 mm x 150 mm x 75 mm) were prepared with 0% and 10% replacement of cement by mass with MPCM. Slabs modified with IPCM were prepared similarly, where in 25% IPCM by mass of cement was incorporated into the slab by the impregnation of LWA constituting 50% aggregate volume of the constituent slab with PEG 600 for 48 hours.

Test methods

The compressive strengths of the cubes were determined at ages of 1, 3, 7, 14 and 28 days in accordance with ASTM C 109. The heat of hydration of the plain and modified cement pastes and concrete were determined from semi-adiabatic temperature measurements. Freshly mixed cement pastes were placed in a Styrofoam cup (355 cm^{3}) which was encased in a polystyrene chamber. The temperature development was recorded every 10 seconds over a period of 72 hours using J Type Thermocouples embedded into the specimens and connected to a 8 Channel Data Acquisition Module, interfaced with a personal computer.

This instrument was also used to record the temperature development during thermal performance studies of the mortar slabs. Differential scanning calorimetric (DSC) studies were carried out on the plain and modified cement pastes, and crushed impregnated LWA, to estimate the phase change temperature (°C) and enthalpy of the system (kJ/kg), i.e. the amount of latent heat that is stored or released when phase change occurs. The samples were crushed into a powder form for DSC analysis and the sample sizes ranged between 5.0 mg to 25.0 mg. The thermal cycles adopted had a heating rate of 5°C/min and ranged between -20°C to 40°C in a purified nitrogen atmosphere.

To understand the influence of the addition of PCMs on the thermal performance of building components, insulated chambers were made. The cubicles were constructed around 4 wooden posts connected by Styrofoam panels and held together by an adhesive tape. The mortar slab was placed on the top of the wooden supports. Foam insulation was used to seal all the joints. To simulate a 24 hour cycle of heating and cooling of the indoors through solar radiation, heat source (heat emitting 1200 W halogen work lights) was turned on for 12 hours to simulate the solar radiation during daylight and turned off for 12 hours to simulate the effect of nightfall. The experiments were run for 72 hours (3 day and night cycles) and the temperatures were recorded every 10 seconds using four J type thermocouples. One of the thermocouple was placed inside the cubicle, and another was placed outside to record the ambient temperature as shown in Figure 1. The remaining two thermocouples were attached to the mortar slab on its interior and exterior surfaces. Through this setup, temperature readings would represent the exterior surface of a concrete slab that is directly heated by the solar radiation, the outdoor temperature, the temperature on the interior surface of the slab which receives heat due to conduction through the concrete slab, and the indoor temperature.

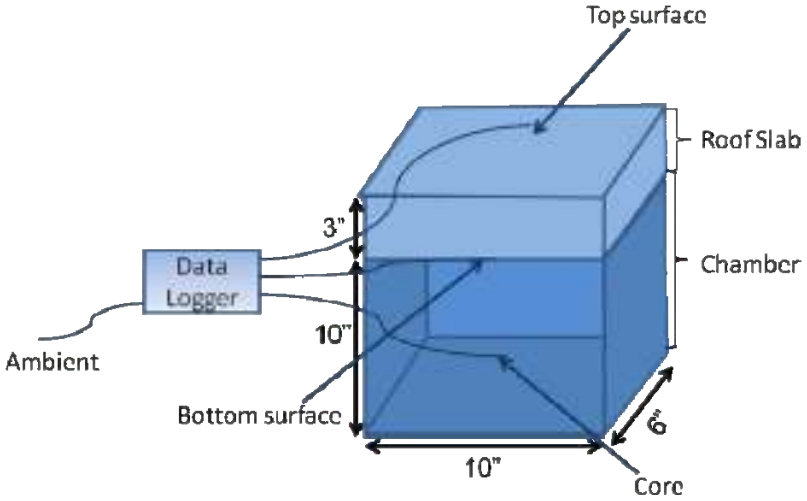

Figure 1 Schematic representation of temperature monitoring points of the cubicle

RESULTS AND DISCUSSION

Effect of Microencapsulated Phase Change Material (MPCM) in Cement Paste

Compressive strength and heat of hydration

Compressive strength development of plain cement pastes as well as those modified with 3% and 5% MPCM determined at 1, 3, 7, 14 and 28 days of hydration is shown in Figure 2. A decrease in strength with the increase in the amount of MPCM in the system at all ages was

observed. The major reason for this observation is the dilution in the system caused by the replacement of cement with a non-reactive material. Also, the elastic properties of the MPCM are very different from those of the cement pastes, with the MPCM being a few orders of magnitude more compliant than the cement paste in which it is incorporated.

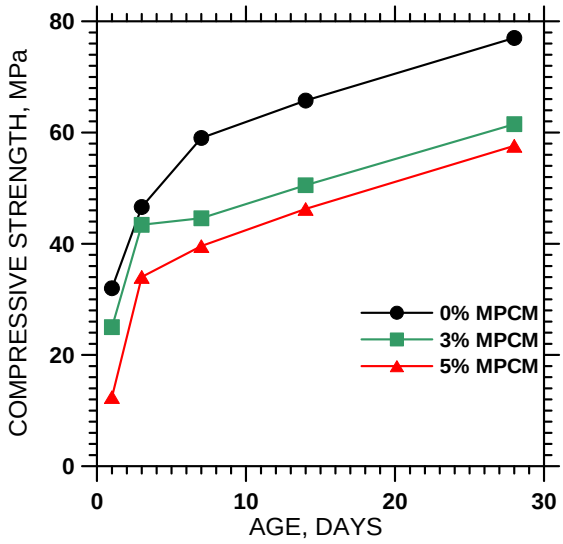

Figure 2 Compressive strength results of cement paste samples with varying amounts of MPCM by mass

At the age of 1 day, the strength of cement pastes containing 5% MPCM was lower by approximately 60% as compared to the plain cement pastes, while at the age of 28 days 5% MPCM modified cement paste showed about 25% lower strength than the plain cement paste. The breakage of the polymeric shell of the MPCM which being a hydrophobic paraffin blend could have released the paraffin into the matrix during specimen preparation, which in turn hinders the hydration process. This could be one of the reasons for the drastic decrease in the early age strength. Figure 3 shows the damaged microcapsules and paraffin possibly released into the cement paste.

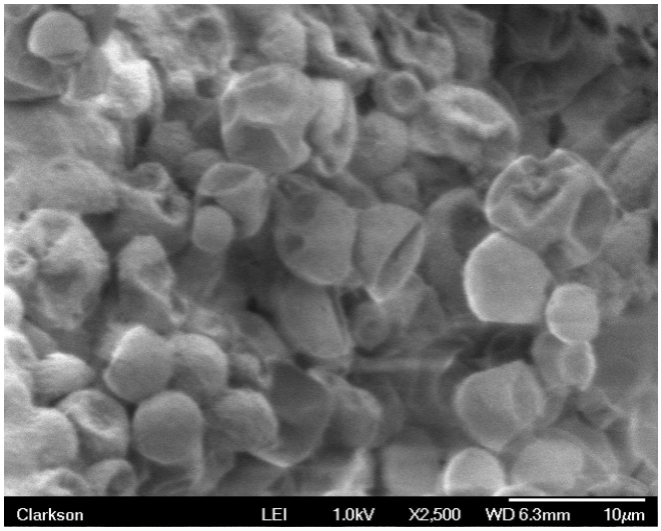

Figure 3 Micrograph of the damaged microcapsule and the paraffin released

The influence of MPCM on the heat of hydration of modified cement pastes were investigated by monitoring the temperature of the freshly prepared pastes containing 0%, 3%, 5% and 10% MPCM by mass of cement, using a semi-adiabatic setup for a duration of 72 hours and the recorded temperature curves are shown in Figures 4(a). Figure 4(b) shows the first 20 hours of temperature measurement to accurately discern the effect of PCM dosage.

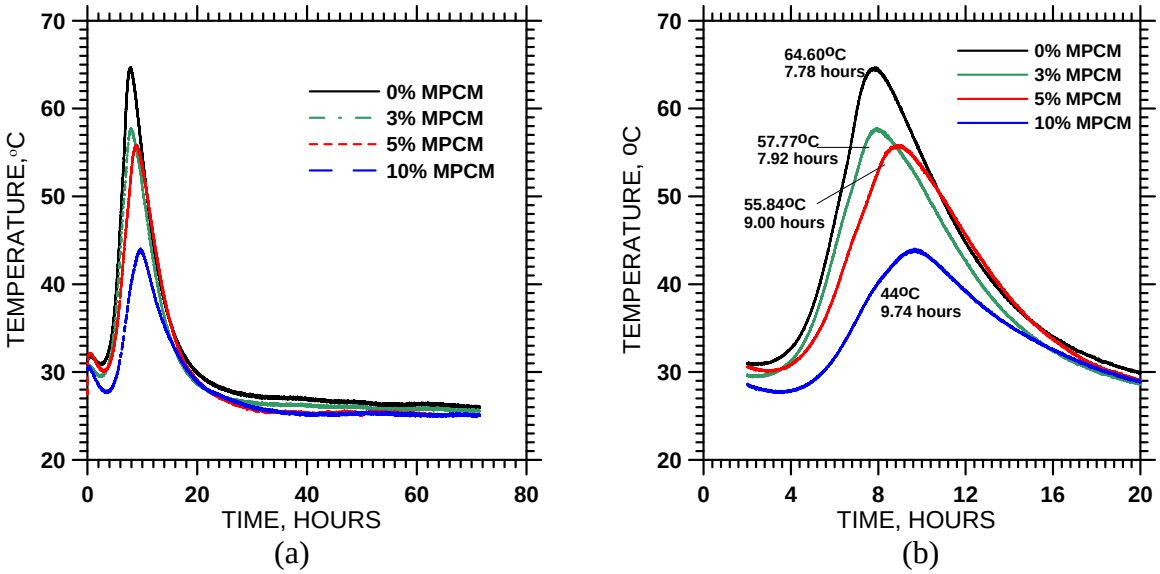

Figure 4 Semi-adiabatic temperature curves for (a) Plain pastes and pastes modified using MPCM and (b) Expanded area in range of the hydration peak.

A significant decrease in the peak reaction temperature from 64.6°C to 44°C was observed with increasing quantity of MPCM in the paste. Along with decrease in the area under the curve indicating reduction in the heat evolution, an increase in the content of MPCM which acts as a retarder, delayed the hydration of cement, i.e., the peak in these curves moves to the right, as reported in [12]. Figure 4(b) clearly shows this delay in the rate of hydration with increasing quantity of MPCM in the system. Plain cement paste reached its hydration peak in 7.78 hours while cement paste with 10% MPCM reached its peak temperature after 9.74 hours. It was also observed that even after 72 hours of hydration, the pastes with higher MPCM content showed slightly lower temperatures than the plain cement paste. The ability of MPCMs to reduce the heat generated in a hydrating cement paste as well as the rate of cool down could be beneficially used to control thermal stresses and cracking in mass concreting.

3.1.2 Influence of MPCM on the latent heat storage capacity of cement paste

The latent heat storage capacity and phase change temperature of plain and modified cement pastes were determined by differential scanning calorimetric (DSC) tests. The latent heat capacity was estimated from the total heat under the peaks of the solid-liquid transitions of paraffin in the system by numerical integration as reported in [11]. Figure 5(a) shows the phase change temperature range and heat flow per unit mass of the paste for plain and modified cement pastes. Figure 5(b) shows the peaks in the DSC curve at a higher magnification to clearly differentiate the changes in enthalpy facilitated by the addition of various amounts of MPCM. The increase in the latent heat storage capacity during melting was observed to increase with the increase in the quantity of PCM in the composite. An exothermic peak observed at about -18^{o}C could be attributed to the super-cooling of the water present in the paste matrix.

These composite mixtures showed relatively low peaks for latent heat capacity as compared to the pure MPCM powder (110 kJ/kg), as expected. Theoretical calculations showed that when 3% of MPCM was used in the cement paste, the expected enthalpy is 3.3 kJ/kg while only a maximum of 1.3 kJ/kg was obtained from the experimental studies shown in Figure 5(b). This shows that the MPCM is incapable of providing thermal storage to its full capacity when incorporated into a cement paste. This could be because of the breaking of the microcapsule during the mixing process (as shown in Figure 3), making them partly dysfunctional. The capsules could also crack due to the difference in the coefficients of thermal expansion between the PCM and the capsule [10]. Another factor is the low thermal conductivity of the MPCM which creates a high thermal resistance, hindering the transfer of heat to the interior surfaces of the matrix thereby isolating the melt process only near the heat source, i.e. phase change would occur only at the surface which is in immediate contact with the heat source as the heat will not get transferred to the interiors due to the thermal resistance.

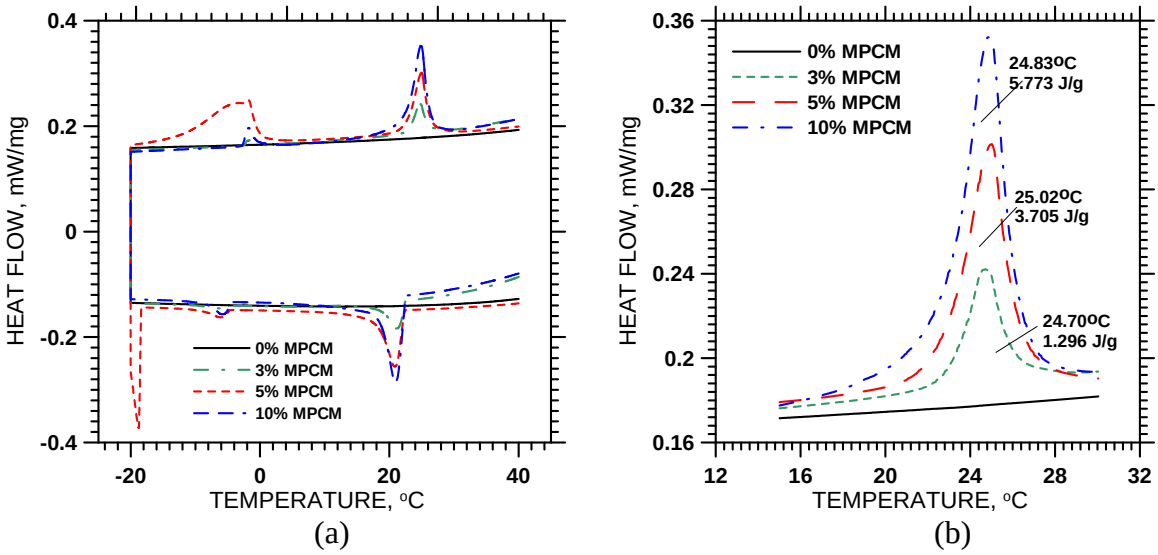

Figure 5 DSC heating and cooling scans showing (a) Heat flow in plain and MPCM modified cement pastes and (b) Expanded area in range of phase change to show the difference in enthalpies.

A general reduction in the latent heat storage capacity of the MPCM modified cement pastes with age was observed as shown in Figure 6. Although the MPCM is generally not influenced by the alkaline environment of concrete [14] a decrease of about 30% in the latent heat storage capacity of the modified pastes with age especially for the systems with higher MPCM content was observed. The reduction in enthalpy of the pastes containing higher amounts of MPCM could be due to the random cross-linking of the cement particles due to the dispersed PCM in the matrix, similar to the crossing linking of Epoxy-diamine resins [15]. Further investigation needs to be carried out to confirm this hypothesis.

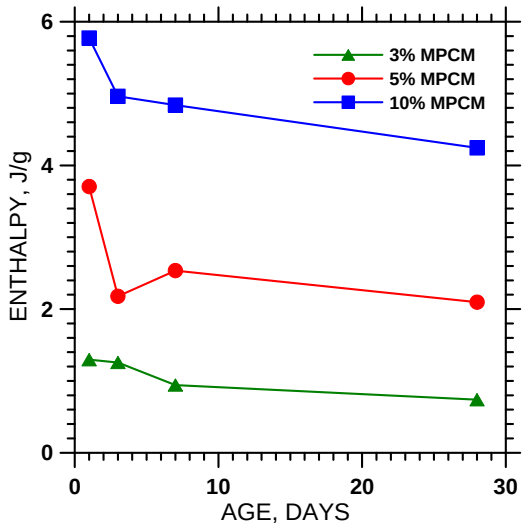

Figure 6 Reduction in enthalpy of the MPCM modified pastes with age

Effect of Impregnated Phase Change Material (IPCM) in Cement Paste

Compressive strength and heat of hydration

Compressive strength development of cement paste-light weight aggregate (LWA) composites with 0% and 5% IPCM by mass of cement determined at 1, 3, 7, 14 and 28 days of hydration is shown in Figure 7. A significant decrease in compressive strength with the incorporation of IPCM into the cement-LWA composite mix was observed.

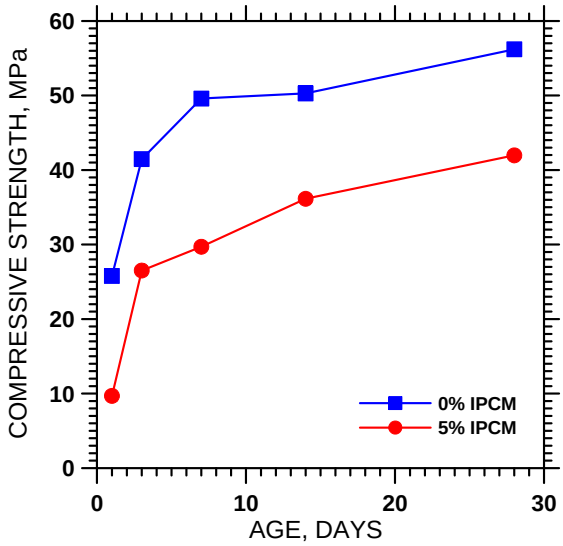

Figure 7 Compressive strength results of cement-LWA composites with 0% and 5% IPCM by mass of cement (PCM impergnated into LWA)

At the age of 1 day, a decrease of 60% in strength was observed while the least reduction of strength, 25% was observed at the age of 28 days. This strength reduction could be due to the binding of water with the PEG 600 molecules as they are water soluble, preventing the formation of complete hydration products.

The PEG 600 also could have leaked from the pores of impregnated LWA as shown in Figure 8, during the mixing process. This could be prevented by coating the impregnated LWA with a cement slurry so as to avoid the interaction of PEG 600 with the surrounding water.

To understand the effect of impregnated phase change material (IPCM) on the hydration process, semi-adiabatic calorimetric studies were carried out on mixtures consisting of cement and LWA with varying saturation levels of PEG 600. Three samples were tested with 0%, 13% and 15% PEG 600 by mass of cement and the results are given in Figure 9, which shows a significant decrease in the peak temperature when IPCM is incorporated. A prominent reduction in the rate of hydration and increased duration of dormant phase also can be observed by the shift of the hydration curves to the right with increasing amount of IPCM in the system.

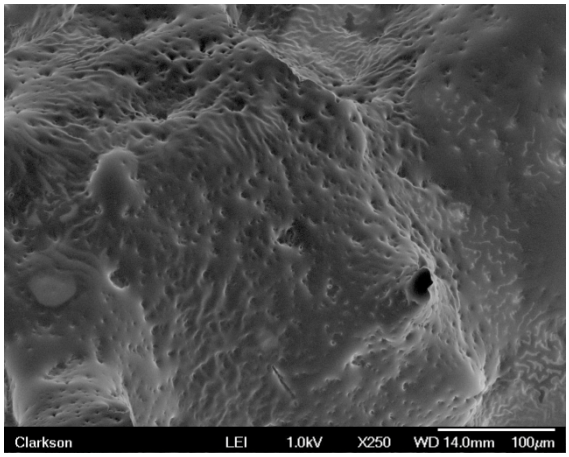

Figure 8 Micrograph of Impregnated LWA with PEG 600 on the surface

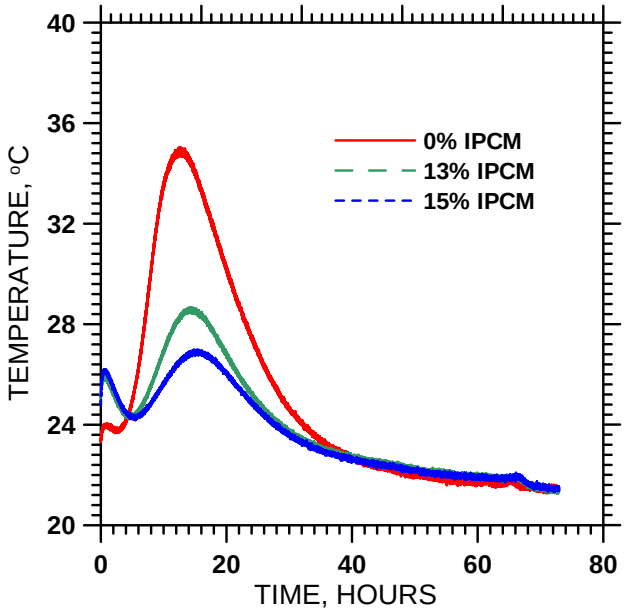

Figure 9 Semi-adiabatic temperature curves for cement pastes containing varying amounts of IPCM

The hydration peak temperature of the 0% IPCM mixture reaches about 35°C while the mixture with 15% IPCM is 8°C lower at 27°C. Also, the modified mixtures reached the hydration peak temperature 3 hours after that of the plain mixture. This is potentially beneficial in improving thermal cracking resistance of concretes. This enhanced efficiency can be observed in impregnated phase change materials as it prevents leakage of the PCM into the matrix and also the LWA enhances the thermal conductivity of the mixture [9].

Influence of IPCM on the latent heat storage capacity of cement paste

The latent heat capacities of plain LWA and LWA impregnated with 10% IPCM by mass were determined using DSC, to estimate the amount of heat storage it can provide when incorporated into a cementitious system as shown in Figure 10(a) and (b).

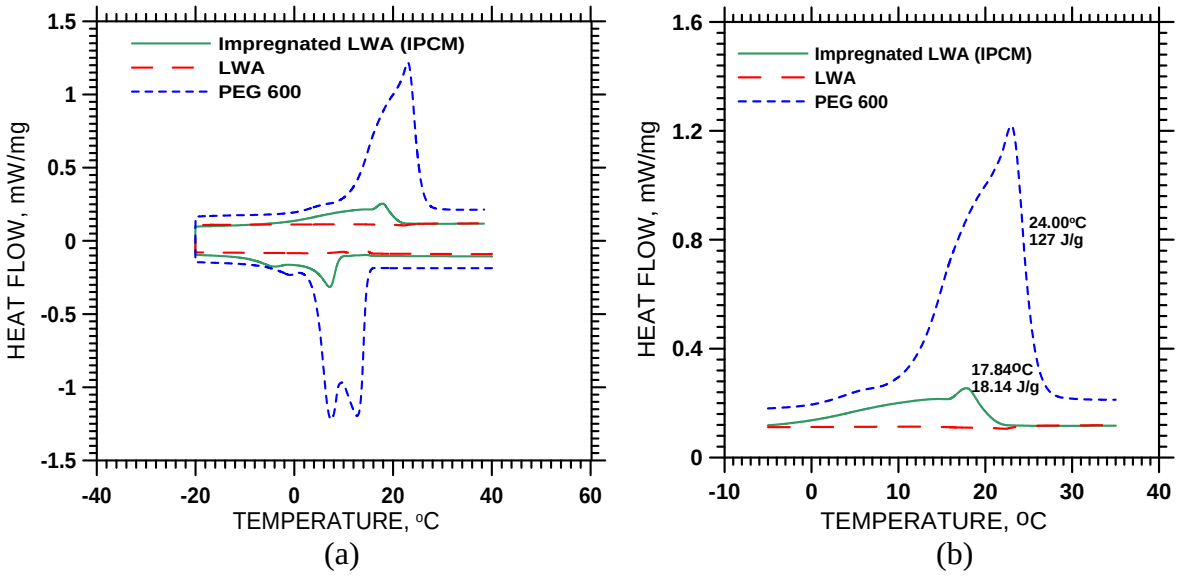

Figure 10 DSC heating and cooling scans showing (a) Heat flow in pure PEG 600, and in impregnated and non-impregnated LWA and (b) Expanded area in range of phase change to show the difference in enthalpies

Due to the effect of confinement of the PCM in the pores of the LWA, the DSC signals are broad and have a tail in the low temperature region, which is reported to increase in size inversely with the size of the pore. Due to this behaviour, the phase transition temperature is taken as the maximum value at the peak unlike the bulk material for which the phase transition temperature is taken as the onset of the transition peak in the DSC scan. The broadening could be due to the layer-by-layer melting of the confined PCM, which is similar to the pre-melting effects in the bulk PCM [16]. In confined pores, the increase in the volume of the PCMs during phase transition from solid to liquid would lead to an increase in the pressure within the confinement which in turn results in an increase in the melting temperature [17]. It can be seen that the phase change of bulk PEG 600 occurs at 12.36°C while that of PEG 600 confined in the pores of the LWA occurs at 17.84°C. An elevation of 4°C in the phase transition temperature can also be due to mild attractive interaction between the PCM and the pore surface [18]. PEG 600 experiences intra- and inter-molecular hydrogen bonding which leads to a reduction in the strength of interfacial interaction (attractive interactions) towards the pore walls/surfaces. [19].

Studies on PCM slabs

Thermal performances of plain mortar slabs as well as those modified with 10% MPCM and 25% IPCM were investigated during 72 hours day and night cycles and the thermal response of the these chambers is shown in Figures 11 (a), (b) and (c) respectively.

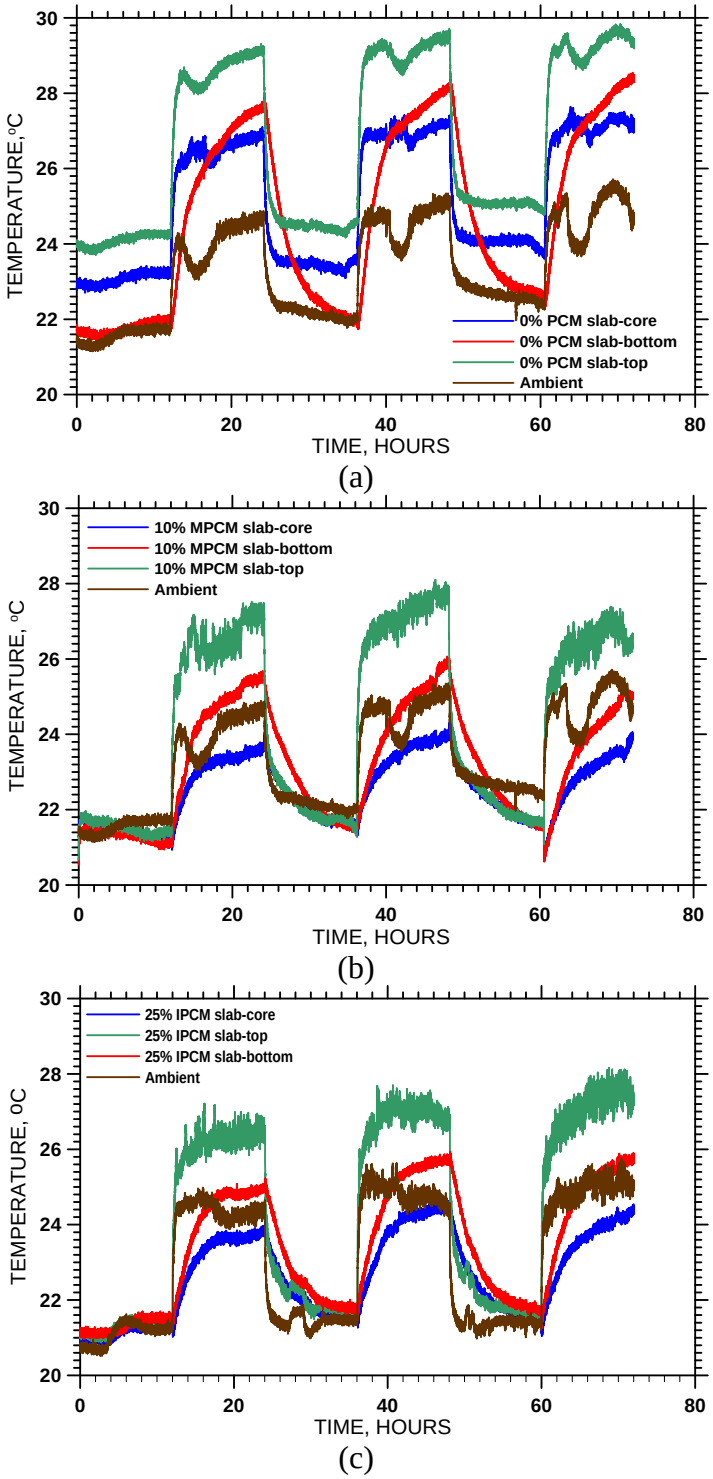

Figure 11 Temperature studies during 72 hours day and night cycles of (a) Plain mortar slab, (b) 10% MPCM modified slab and, (c) 25% IPCM modified slab

The temperature at the top surface of the plain mortar slab, as shown in Figure 11(a), recorded temperatures as high as 29.4^{o}C while the bottom surface of the mortar slab had a temperature of 28.1^{o}C and the chamber experienced a maximum core temperature of 27.4^{o}C. This shows that most of the heat from the source was transmitted through the slab into the interiors. While, the top surface of the 10% MPCM modified slab (Figure 11(b)) recorded a maximum temperature of 27.8^{o}C, the maximum temperature at the bottom surface was a recorded as 26^{o}C. This shows that there is nearly a 2^{o}C drop in the temperature of the inner surface of the slab with respect to the outer surface, which indicates that not all the heat from the exterior has passed through the slab to the inner surface and that certain quantity was absorbed by the PCM present within the slab [20]. Similarly, the slab modified with 25% IPCM, as shown in Figure 11(c) also showed a 2^{o}C decrease between the top and bottom surface of the roof slab. Also, the top surface of the modified slabs (Figures 11(b) and (c)) recorded lower temperatures when compared to plain mortar slab (Figure 11(a)), this could be due to the phase change activity of the PCM at the surface of the slab absorbing the heat from the source without increasing the temperature.

Significantly greater fluctuations of around 4^{o}C were observed between the maximum and minimum temperatures within the chamber having plain roof slab during the day and night cycles, when compared to the chambers with PCM modified roof slabs, having lesser than 3^{o}C variation. The raise in the indoor temperature or the core temperature of the chambers with PCMs is to a maximum of about 24.6^{o}C while the temperature of the outer surface of the slab facing the heat source goes up to about 27.8^{o}C. A relative decrease in the temperature between the top surface and bottom surface of plain LWA slab was observed, and this could be attributed to the air entrained within the pores of the LWA incorporated into the system.
The thermal response within the cubicle with plain and PCM modified slabs during the day and night cycle is given in Figure 12.

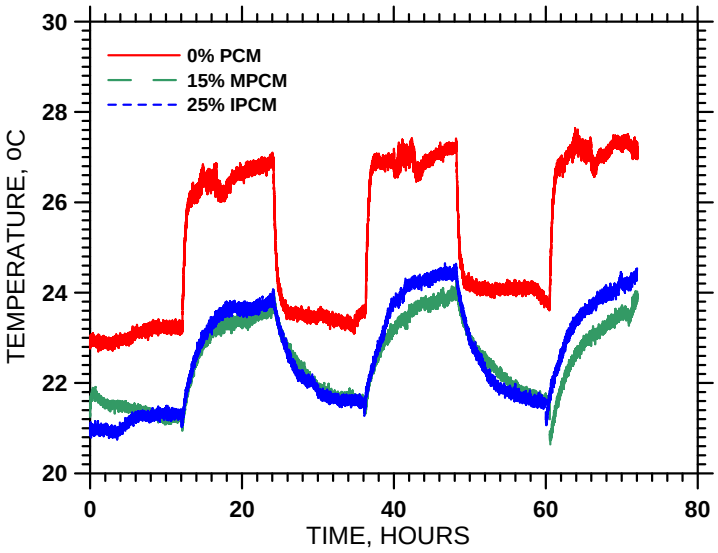

Figure 12 Indoor temperatures of the cubicle with plain and PCM modified mortar slabs during a 72 hour cycle

The observation from the 72 hours day and night cycle as seen in Figure 12, shows that the cubicle with both 10% MPCM and 25% IPCM modified roof slabs experiences thermal inertia when compared to the reference cubicle as there is a lag in the time taken to reach the temperature of the plain chamber. It can also be seen that the peak temperature of reference

chamber is about 27^{o}C while the chambers with MPCM and IPCM shows a maximum peak temperature to be about 24.2^{o}C and 24.6^{o}C respectively. The minimum temperature also differs by 3^{o}C; where the reference chamber has a minimum indoor temperature close to 23^{o}C while the chambers with PCM modified roof slabs shows temperatures as low as 20.5^{o}C. This reduction in temperature gradient within the cubicles with PCM modified roof slabs when compared to the reference cubicle core temperatures, provides a more thermally efficient and comfortable interior.

The core temperature of the chamber with roof slab modified with 10% MPCM by mass of cement was the lowest followed by roof slab containing 25% IPCM by mass of cement. Highest temperature was observed within the chamber consiting of plain mortar roof slab.

CONCLUSIONS

- The compressive strength of the mixtures decreased with the addition of PCMs at all ages. A strength reduction of 60% was observed at early ages while at 28 days the strength reduction reduced to 25%. Also reduction in the hydration peak temperatures and heat evolution was observed and both the PCMs retarded the hydration process which could be beneficially used to control thermal stresses and cracking in mass concreting.

- Presence of PCMs enhanced the latent heat storage capacity of the cement paste. 10% IPCM modified paste showed a higher heat storage capacity (18.14 kJ/kg) than cement paste with 10% MPCM by mass of cement which had a heat storage capacity (5.773 J/g). This can be attributed to the LWA used to impregnate PEG 600, enhancing the thermal conductivity of IPCM mixtures, as well as the effect of confinement of the PCM in pores of LWA.

- An increase in thermal efficiency and decrease in the core temperature of the insulated chamber was observed with the incorporation of PCM into the roof slabs. Reduction in the temperature fluctuations during day and night cycles were also observed. Modified slabs containing 10% MPCM by mass of cement was most efficient in maintaining and lowering the indoor core temperature.

REFERENCES

1. PASUPATHY, A, VELRAJ, R, SEENIRAJ, R V. Phase change material-based building architecture for thermal management in residential and commercial establishments, Renewable and Sustainable Energy Reviews, Vol. 12, 2008, pp 39-64.

2. ZALBA, B, MARÍN, J M, CABEZA, L F, MEHLING, H. Review on the thermal energy storage with phase change: materials, heat transfer analysis and applications, Applied Thermal Engineering, Vol. 23, 2003, pp 251-283.

3. SHARMA, S D, SAGARA, K. Latent heat storage materials and systems: A review, International Journal of Green Energy, Vol. 2, 2005, pp 1-56.

4. SHARMA, A, TYAGI, V V, CHEN, C R, BUDDHI, D. Review on thermal energy storage with phase change materials and applications, Renewable and Sustainable Energy Reviews, Vol.13, 2009, pp 318-345.

5. SHILEI, L, GOUHUI, F, NENG, Z, LI, D. Experimental study and evaluation of latent heat storage in phase change materials wallboards, Energy and Buildings, Vol. 39, 2007, pp 1088-1091.
6. ENTROP, A G, BROUWERS, H J H, REINDERS, A H M E. Experimental research on the use of micro-encapsulated phase change materials to store solar energy in concrete floors and to save energy in Dutch houses, Solar Energy, Vol. 85, 2011, pp 1007-1020.

7. HAWLADER, M N A, UDDIN, M S, KHIN, M M. Microencapsulated PCM thermal-energy storage system, Applied Energy, Vol. 74, 2003, pp 195-202.

8. TYAGI, V V, KAUSHIK, S C, TYAGI, S K, AKIYAMA, T. Development of phase change materials based microencapsulated technology for buildings: A review, Renewable and Sustainable Energy Reviews, Vol.15, 2011, pp 1373-1391.

9. ZHANG, D, ZHOU, J, WU, K, AND LI, Z. Granular phase changing composites for thermal energy storage, Solar Energy, Vol.78, 2005, pp 471-480.

10. NOMURA, T, OKINAKA, N, AKIYAMA, T. Impregnation of porous material with phase change material for thermal energy storage, Materials Chemistry and Physics, Vol. 115, 2009, pp 846-850.

11. ZHANG, Z, FANG, X. Study of paraffin/expanded graphite composite phase change thermal energy storage material, Energy Conversion and Management, Vol.47, 2006, pp 303-310.

12. BENTZ, D P, TURPIN, R. Potential applications of phase change materials in concrete technology, Cement and Concrete Composites, Vol. 29, 2007, pp 527-532.

13. HUNGER, M, ENTROP, A G, MANDILARAS, I, BROUWERS, H J H, FOUNTI, M. The behaviour of self-compacting concrete containing micro-encapsulated phase change materials, Cement and Concrete Composites, Vol. 31, 2009, pp 731-743.

14. HAWES, D W, FELDMAN, D. Absorption of phase change materials in concrete, Solar Energy Materials and Solar Cells, Vol. 27, 1992, pp 91-101.

15. MONTSERRAT, S, CORTES, P, CALVENTUS, Y, HUTCHINSON, J M. Effect of crosslink length on the enthalpy relaxation of fully cured epoxy – diamine resins, Journal of Polymer Science :Part B: Polymer Physics, Vol. 38, 2000, 456-468.

16. DOSSEH, G, XIA, Y, ALBA-SIMIONESCO, C. Cyclohexane and benzene confined in MCM-41 and SBA-15: Confinement effects on freezing and melting, Journal of Physical Chemistry B, Vol.107, 2003, pp 6445-6453.

17. ZHANG, D, WU, K, LI, Z. Tuning effect of porous media's structure on the phase change behaviour of organic phase change matters, Journal of Tongji University, Vol. 32, 2004, pp 1163-1167.

18. RADHAKRISHNAN, R, GUBBINS, K E. Free energy studies of freezing in slit pores: an order-parameter approach using Monte Carlo simulation, Molecular Physics, Vol. 96, 1999, pp 1249-1267.
19. MAHESHWARI, P., DUTTA, D., SHARMA, S.K., PUJARI, P.K., AND MAJUMDER, M., PAHARI,B., BANDYOPADHYAY, B., GHOSHRAY, K., GHOSHRAY, A., "Effect of interfacial hydrogen bonding on the freezing/melting behaviour of nanoconfined liquids," Journal of Physical Chemistry C, 114 (2010) 4966-4972

20. CABEZA, L F, CASTELLÓN, C, NOGUÉS, M, MEDRANO, M, LEPPERS, R, ZUBILLAGA, O. Use of microencapsulated PCM in concrete walls for energy saving, Energy and Building, Vol. 39, 2007, pp 113-119.

The Effect of Using GGBFS on Early-age Thermal Crack Control Reinforcement in Concrete

K Tang[1], G Beattie[2], S Millard[1]
1 – Xi'an Jiaotong-Liverpool University, China
2 – Arup, UK

As the biggest steel producing country, China accounted for half of the global steel production in 2009. As waste material in the steel manufacture process, over 160 million tonnes of blast furnace slag is generated in China every year. Of this total only 55% is recycled. The unwanted blast furnace slag would cover an area of 600 hectares annually if heaped 10 meters high. Blast furnace slag, ground to an appropriate fineness, can be used as a partial replacement cementitious material in concrete. In China, the major part of ground granulated blast furnace slag (GGBFS) however ends up in low-grade construction applications, including: (i)"Low heat" cementitious material in low-grade bulk concrete; (ii) Cementitious material in mortar. GGBFS has a slower reactivity than cement, which reduces the peak hydration temperature and as a result decreases the early age thermal loads experienced by concrete. The potential for using GGBFS in in-situ concrete slabs to minimise the use of more expensive supplementary thermal crack control reinforcement is being investigated at Xi'an Jiaotong-Liverpool University (XJTLU). The objective is to determine the 'optimum' GGBFS mix proportion which could result in the minimum level of crack control reinforcement.

Dr Kangkang Tang is a lecturer at Xi'an Jiaotong-Liverpool University. He has 4 year experience in China and 3 years in the UK in both design and construction, including new build and refurbishment. He got his PhD in the Department of Civil Engineering at the University of Liverpool and his research interests include cement replacement materials and the use of construction and demolition waste as aggregate in concrete.

Professor Steve Millard is Head of Department of Civil Engineering at Xi'an Jiatong Liverpool University in Suzhou, China. Previously he was a professor at the University of Liverpool, where he worked for 29 years. He has research interests in sustainable construction, in nondestructive testing of reinforced concrete structures, including corrosion assessment, and in blast and impact resistant concrete structures.

Dr Greg Beattie is an associate director at Arup (Liverpool) and he has 25 years' experience in the delivery of a wide range of engineering projects. He is an honorary fellow in the Department of Civil Engineering at the University of Liverpool and an industrial supervisor for a variety of research projects.

Keywords: GGBFS, Thermal crack control reinforcement, Thermal stresses

INTRODUCTION

Linear expansion and contraction always take place in concrete structures due to ambient temperature variations. Internal stresses will build up if these movements are restrained by columns or shear walls. This effect is more prominent in concrete at early ages, i.e. thermal hydration contraction and autogenous shrinkage will lead to tensile stresses which may cause deleterious cracks in concrete. There is therefore a maximum crack width requirement in reinforced concrete sections, specified by BS 8110 [1], Eurocode 2 [2] and GB50010-2002 [3]. Concrete early age thermal cracking can be prevented by leaving one metre wide construction gaps in slabs and beams when concrete is placed. These gaps will not be infilled until early age concrete hydration contraction has been completed on both sides. This provision however is often not cost effective because extra structural supports are required to enable stability on both sides of the gap during construction. Without careful consideration of the programme of construction, unacceptable deflections can occur due to inadequate temporary support or inadequate quality control, shown in Figure 1. Another effective method to limit concrete crack widths is to use supplementary crack control reinforcement. The latter has gained popularity in China when labour costs have become more significant in recent years.

Figure 1 A pour gap problem associated with quality control [6]

Concrete early age thermal contraction is caused by the heat development from cement hydration during early age setting. The early age heat development in concrete mixes containing GGBFS is slower than that of ordinary Portland cement mixes. The peak temperature in fresh GGBFS concrete is also lower and this will result in a reduced thermal

contraction. In China, however, the major part of GGBFS produced as a by-product of the steel industry ends up in low-grade applications such as cementitious material in mortar. This project, carried out in conjunction with ARUP, aims to promote an increased use of GGBFS in long-span concrete structures in China by minimising the use of more expensive crack control reinforcement. The research methodology is primarily based on a case study using Finite Element Analysis (FEA) software Oasys GSA [4]. The effects of temperature variations and of time-dependent concrete volume change, including creep and drying shrinkage, are applied as temperature differentials. Four mixes studied by Bamforth [5] have been chosen in this project to investigate the effect of temperature rises from cement early-age hydration. These mixes comprise:

- Mix M0: total binder content: 340kg/m3, CEM I 42.5N only, i.e. 0% GGBFS
- Mix M30: total binder content: 340kg/m3, 70% CEM I 42.5N and 30% GGBFS
- Mix M50: total binder content: 355kg/m3, 50% CEM I 42.5N and 50% GGBFS
- Mix M70: total binder content: 410kg/m3, 30% CEM I 42.5N and 70% GGBFS

Results from this previous study were used as input for the FEA modelling. It should be noted that a higher total binder content was required to achieve the designated concrete strength, C30/37, for 50% and 70% GGBFS.

CASE STUDY

A case study has been conducted of a typical commercial office accommodation block in Shanghai, shown Figure 2. This office block is 75m long and 37.5m wide. C30/37 concrete is used for the slabs at all floor levels. These slabs span a maximum of 7.5m, which provides good flexibility for service penetrations. Ground bearing slabs are used at the ground level. Thermal movements in the slab at upper levels are restrained along the longitudinal direction by concrete shear walls located on both ends. The office block was modelled using the above four mixes, i.e. M0, M30, M50 and M70, to investigate the potential crack mitigation effects of GGBFS on early-age thermal loading.

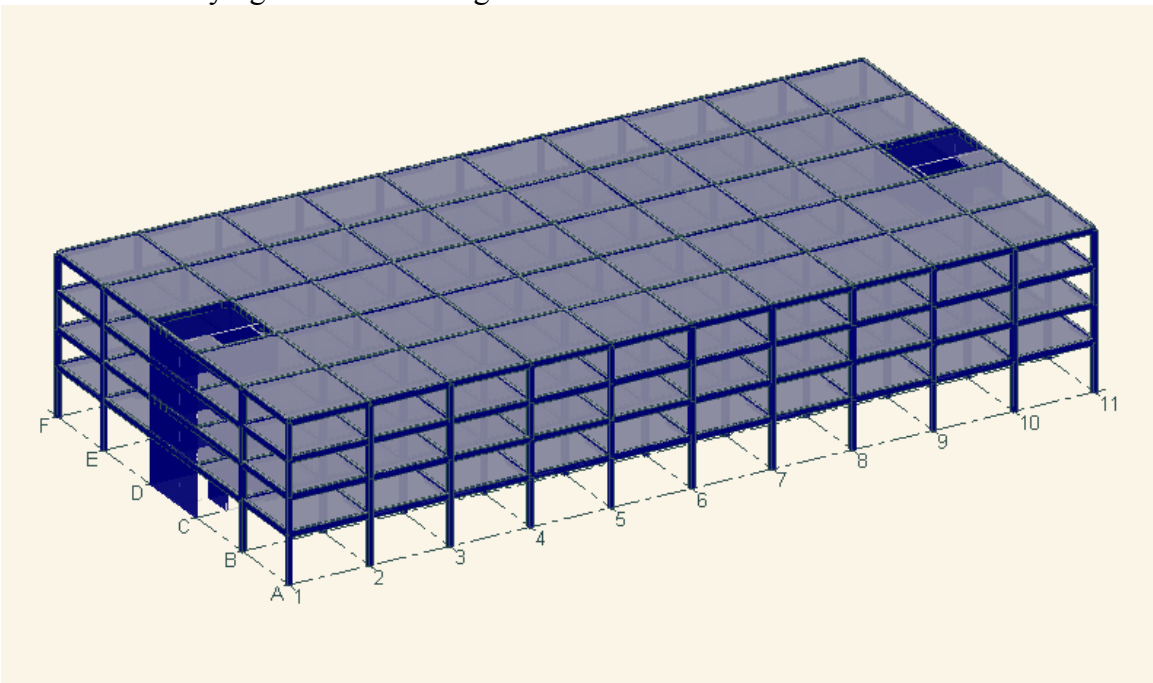

Figure 2 Office accommodation block model

The mechanical properties of C30/37 concrete from Eurocode 2 [2] are:

$f_{cm} = 38MPa$
$f_{ck} = 30MPa$
$f_{ctm} = 2.9MPa$
$E_{cm} = 33GPa$

Where:

f_{cm}: Mean value of compressive cylinder strength of concrete at 28 days
f_{ck}: Characteristic compressive cylinder strength of concrete at 28 days
f_{ctm}: Mean value of axial tensile strength of concrete at 28 days
E_{cm}: Secant modulus of elasticity of concrete at 28 days

The objective of this project is to determine the effect of using GGBFS as a cement replacement on the early-age thermal loading in concrete. Eurocode 2 [2] gives following equations to estimate the mechanical properties of concrete before 28 days:

$$f_{cm}(t) = exp\left\{s\left[1 - \left(\frac{28}{t}\right)^{0.5}\right]\right\} \times f_{cm}$$
$$f_{ctm}(t) = exp\left\{s\left[1 - \left(\frac{28}{t}\right)^{0.5}\right]\right\} \times f_{ctm}$$

$$E_{cm}(t) = \left[\frac{f_{cm}(t)}{f_{cm}}\right]^{0.3} E_{cm}$$
$$f_{ctk}(t) = 0.7 \times f_{ctm}(t)$$

Where:

t: Age of concrete in days
s: Coefficient dependent on the type of cement:
= 0.20 for CEM 42.5R, CEM 52.5N and CEM 52.5R
= 0.25 for CEM 32.5R, CEM 42.5N
= 0.38 for CEM 32.5N

$f_{cm}(t)$: Mean value of compressive cylinder strength of concrete at t days
$f_{ctm}(t)$: Mean value of axial tensile strength of concrete at t days
$E_{cm}(t)$: Secant modulus of elasticity of concrete at t days
$f_{ctk}(t)$: Characteristic axial tensile strength of concrete at t days

Concrete thermal loading has been modelled at the age of 3 days. The mechanical properties of C30/37 concrete at 3 days are estimated according to Eurocode 2 [2] too:

$$f_{cm}(3) = exp\left\{s\left[1 - \left(\frac{28}{t}\right)^{0.5}\right]\right\} \times f_{cm} = exp\left\{0.25\left[1 - \left(\frac{28}{3}\right)^{0.5}\right]\right\} \times 38 = 22.73MPa$$
$$f_{ctm}(3) = exp\left\{s\left[1 - \left(\frac{28}{t}\right)^{0.5}\right]\right\} \times f_{ctm} = exp\left\{0.25\left[1 - \left(\frac{28}{3}\right)^{0.5}\right]\right\} \times 2.9 = 1.73MPa$$
$$E_{cm}(3) = \left[\frac{f_{cm}(t)}{f_{cm}}\right]^{0.3} E_{cm} = \left[\frac{22.73}{38}\right]^{0.3} \times 33 = 28.28GPa$$
$$f_{ctk}(3) = 0.7 \times f_{ctm}(3) = 0.7 \times 1.73 = 1.21MPa$$

The linear coefficient of concrete thermal expansion is taken as 10×10^{-6}/°C according to Chinese code, GB50010-2002 [3]. In this project, 500MPa characteristic strength reinforcement [7] is used to resist both thermal actions in slabs.

CONCRETE EARLY-AGE TEMPERATURE DIFFERENTIALS

The short-term temperature difference T1 (°C) is defined as the difference between the peak temperature during the early age exothermic cement hydration reaction and the ambient temperature at the time of casting. The magnitude of T1 depends on the composition of the concrete mix, formwork materials and the ambient temperature. T1 for the above four mixes have been investigated by Bamforth [5]. These results were obtained from 225mm thick concrete specimens (slabs) cast against steel formwork. The concrete placing temperature was measured as 20°C. Test results showed the following short-term temperature differences:

- Mix M0: T1= 15°C
- Mix M30: T1= 12°C
- Mix M50: T1= 10°C
- Mix M70: T1= 9°C

A higher temperature difference, T1, is to be expected when the concrete placing temperature is higher than 20°C. The maximum allowable placing temperature recommended by ACI 305R, i.e. 38°C, is assumed to be appropriate in China and used in this case study investigation. Bamforth [5] proposed the following adjustments to T1 for a placing temperature of 38°C:

- Mix M0: Adjusted T1= 24°C
- Mix M30: Adjusted T1= 21°C
- Mix M50: Adjusted T1= 19°C
- Mix M70: Adjusted T1= 17°C

CONCRETE AUTOGENOUS SHRINKAGE

Autogenous shrinkage is a short-term effect caused by the hydration of the unhydrated cement. This shrinkage will become more significant with low water-cement ratio mixes. Eurocode 2 [2] gives following equation to predict the autogenous shrinkage strain.

$$\varepsilon_{ca}(t) = 2.5(f_{ck} - 10) \times [1 - \exp(-0.2 \times t^{0.5})] \times 10^{-6}$$

Where:

ε_{ca}: Autogenous shrinkage strain

Autogenous shrinkage occurs over a longer duration than early-age thermal contraction, although a large percentage takes place soon after casting, as shown in Figure 3.

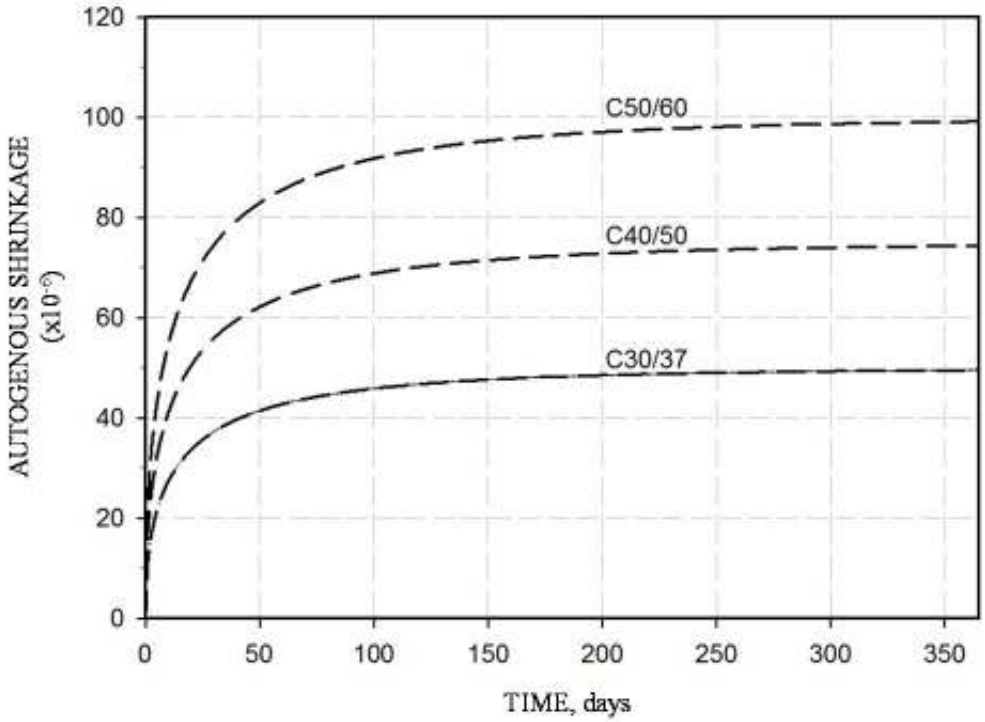

Figure 3 Autogenous shrinkage curves (reproduced from Eurocode 2 [2])

Autogenous shrinkage had been taken into considerations in GSA modelling by applying an equivalent temperature range, ΔT. The value for ΔT is calculated by dividing the autogenous shrinkage strain by the coefficient of thermal expansion, 10×10^{-6}/°C [2].

$$\Delta T = \varepsilon_{ca}(t) \div \alpha_C$$

Where:

α_C: Linear coefficient of concrete thermal expansions, taken as 10×10^{-6}/°C

THERMAL ANALYSIS

Concrete early age thermal contractions were investigated using GSA modelling. Concrete slabs and shear walls (Figure 4) were represented using a 2D element mesh comprising of flat shells which have the same 225mm thickness as the in-situ slabs. Cracking in concrete was modelled using an iterative analysis procedure [8]. The stiffness of highly stressed slab elements (maximum principal stress is greater than $f_{ctk}(3)$) was gradually reduced to enable the redistribution of residual thermal stresses after the development of concrete cracks. In this study, 4 different comparison analyses have been carried out using the same structural model:

- Analysis 1: Slabs with concrete made from “mix M0”. T1 has been considered in conjunction with ΔT;
- Analysis 2: A repeat analysis using “mix M30”;
- Analysis 3: A repeat analysis using “mix M50”;
- Analysis 4: A repeat analysis using “mix M70”.

Finite element analysis results from this study indicated that there is a high risk of formation of tensile cracks on Level 1 slabs. Tensile stresses exceeding 1.21MPa, i.e. $f_{ctk}(3)$, developed in a large region. Slab reinforcement designed based upon ultimate limit state combinations may yield in this highly stressed region and result in concrete cracks of excessive width. The magnitude of the concrete tensile stresses has been evaluated and supplementary crack control reinforcement was provided to prevent the yield of existing slab reinforcement, as shown in Figure 5. The amount of supplementary reinforcement was determined using the following equation. Reinforcement anchorage length has not been considered at this stage.

$$A_s = \frac{\sigma \times d \times 1000}{f_y}$$

Where:

As: Supplementary reinforcement (mm^2 per meter wide slab)
σ: Maximum principle stress in slabs (MPa)
d: Slab thickness (mm), 300mm in this case study
fy: Yield strength of supplementary reinforcement, 500MPa in this case study

The use of GGBFS reduces thermal stresses and the magnitude of thermal contractions (Figure 6). With up to 30% of the cement replaced by GGBFS, approximately 20% of the total supplementary thermal crack control reinforcement can be saved on Level 1 slabs. Over 40% of supplementary crack control reinforcement can be saved if 70% of the cement is replaced by GGBFS.

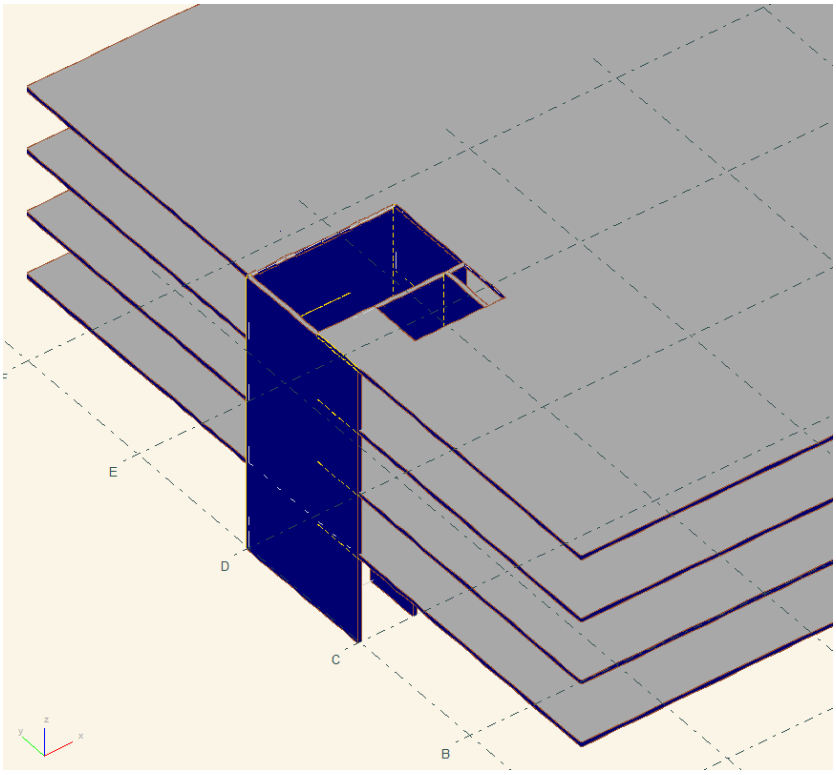

Figure 4 2D elements in GSA modelling

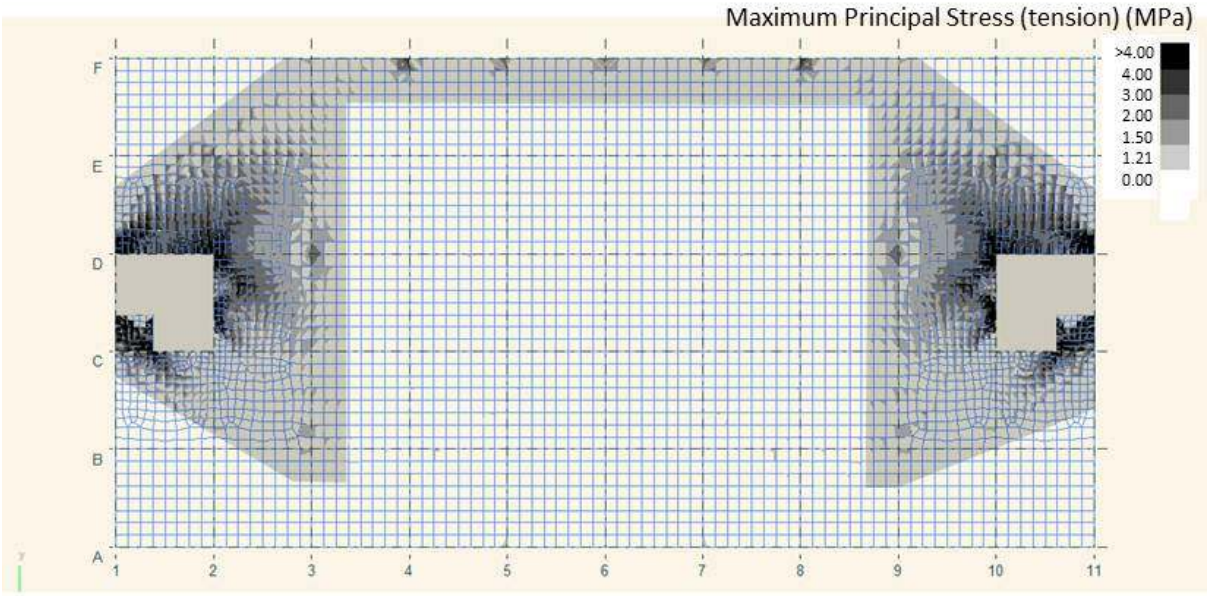

(1) Analysis 1 – Mix M0

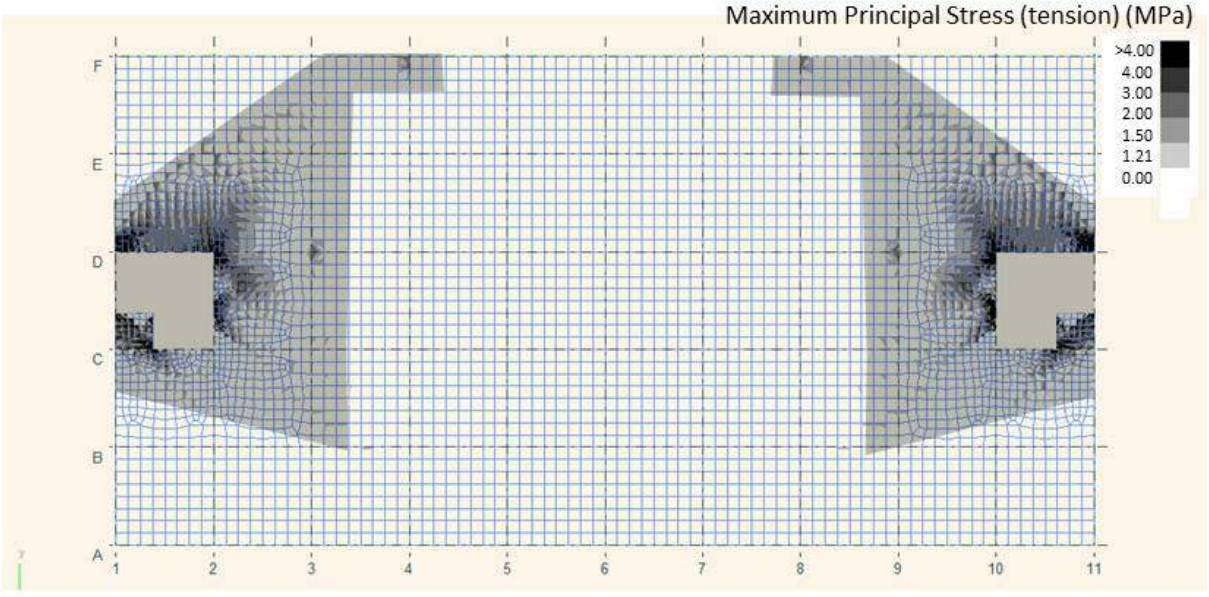

(2) Analysis 4 – Mix M70

Figure 5 Thermal stresses predicted by GSA analysis – crack control reinforcement required for highly stressed > $f_{ctk}(3)$ area presented in shadow

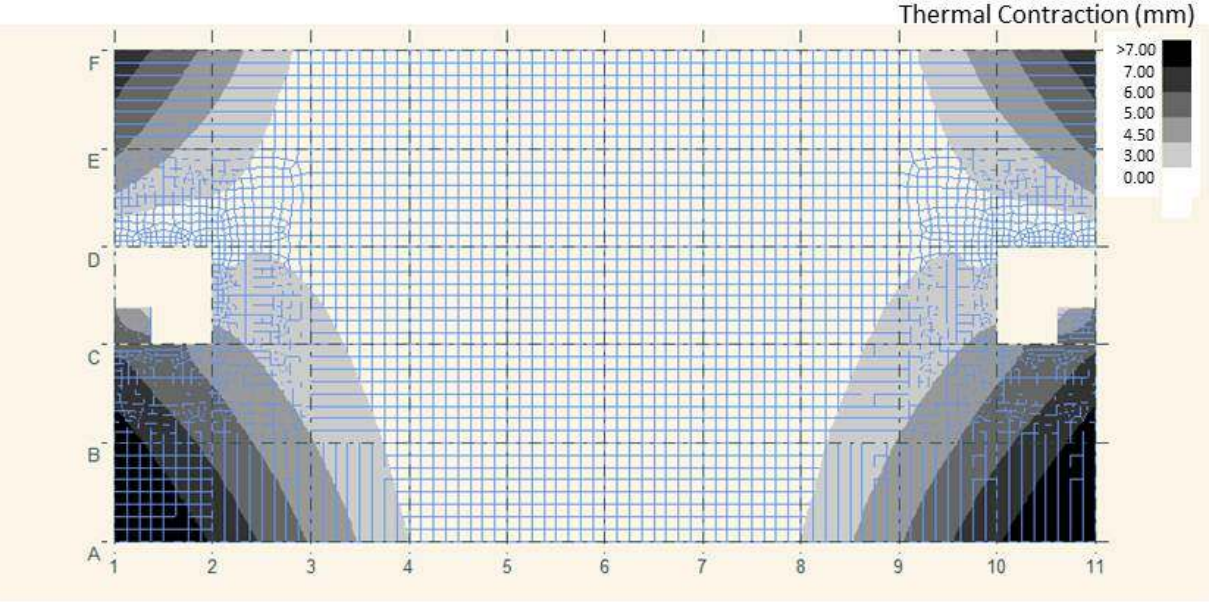

(1) Analysis 1 – Mix M0

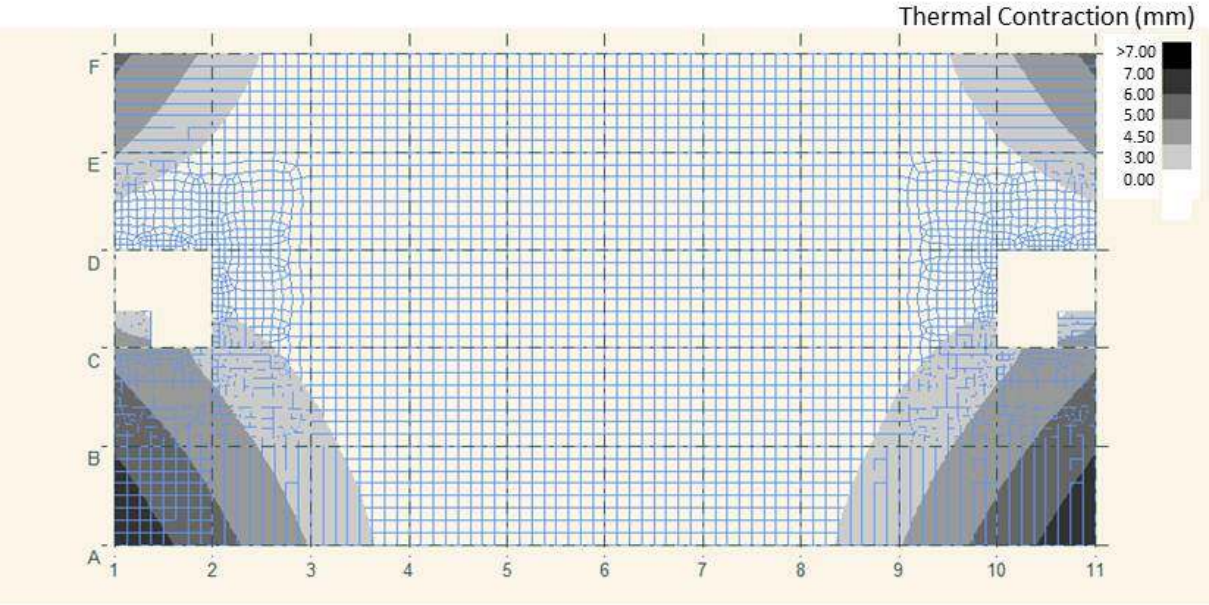

(2) Analysis 4 – Mix M70

Figure 6 Early age thermal contractions predicted by GSA analysis

CONCLUSIONS

FEA modelling based on GSA software can be used to predict movements and stresses in concrete structural elements for design purposes. The use of GGBFS in concrete slabs can significantly reduce the requirement for more expensive crack control reinforcement. With up to 70% of cement replaced by GGBFS, 40% of the supplementary crack control reinforcement can be saved in slabs based on a case study investigation.

REFERENCES

1. BSI BRITISH STANDARDS (1997) Structural Use of Concrete. BSI. ISBN 0 580 26208 1.

2. BSI BRITISH STANDARDS (2004) Eurocode 2: Design of Concrete Structures. BSI. ISBN 9780580617591.

3. PRC MINISTRY OF CONSTRUCTION (2002) Code for Design of Concrete Structures. PRC Ministry of Construction.

4. ARUP (2011) Oasys GSA 8.5. 8.5 ed. Oasys Limited.

5. BAMFORTH, P.B. (2007) CIRIA C660 Early-age Thermal Crack Control in Concrete. London. CIRIA ISBN 978-8-86107-660-2.

6. ZHENGZHOU ENGINEERING QA (2011) New Hope Project Block 1 Pour Gap Problem. Available from: http://www.zljd.com.cn/article_zldp.asp?zldp_id=44 [cited 1/12/2011].

7. BSI BRITISH STANDARDS (2009) Specification for Carbon Steel Bars for the Reinforcement of Concrete. BSI.

8. THE CONCRETE SOCIETY (2008) Movement, restraint and cracking in concrete structures. The Concrete Society. ISBN 978-1-904482-42-0.

Methods to Produce Low Carbon Two Stage Concrete

H S Abdelgader, A S El-baden
Tripoli University, Libya

During the last decades, the concrete industry has been widely developing in many ways such as the methods of pouring concrete in order to achieve high quality concrete and low cost. Some new concretes have been produced which are completely different from the conventional concrete in the method of mixing, pouring with no need for the normal compaction methods which require more labour, tools and higher cost. This paper presents two special types of concrete: Two-Stage Concrete and Rock Filled Concrete and demonstrates the advantages and special requirements for each of the two special types of concrete and their uses. The cost of Two-Stage concrete is less than the cost of normal concrete and there is no need for compaction or vibrating the concrete. Also, the risk of having aggregate segregation is completely avoided since the coarse aggregate is placed before adding the other remaining concrete constitutes. The use Rock Filled Concrete gives many advantages that related to quality, cost and environment. The RFC gives low heat of hydration because the use of its low cement content makes it more easier to ensure temperature control and allows continuous pouring of SCC and a reduce in the construction time

Hakim S. Abdelgader is Professor of Civil Engineering Department at Tripoli University, Tripoli, Libya. He received his MSc and Ph.D. degrees in 1990 and 1996 respectively from Gdańsk University of Technology, Gdańsk, Poland. The main focus of his professional activities is on research interests concrete technology and technology of concrete elements. Has devoted his international experience with concrete to improve construction in his native Libya through the use of two-stage concrete technology (Preplaced aggregate concrete), concrete mix design, self-compacting concrete, Concrete with recycled materials and concrete casing in fabric forms. He is a voting member of American Concrete Institute (ACI) Committees 221, 304, 444 and 555. and a reviewer and contributor to ACI, Elsevier and ASCE publications.

Ali S. El-baden Assistance Professor and a senior concrete technology researcher at the Department of Civil Engineering Faculty of Engineering Tripoli University,Libya. Interested field of researchers in concrte area includes; time dependent deformations ; utilization of pozzolanic materials ; industrial wastes and recycled materials in concrete industry ; using preplaced aggregate technology in concrete.

Keywords: Mass concrete construction, Rock filled concrete, Self-compacting concrete, Two-stage concrete

INTRODUCTION

During the last few decades, the concrete industry has been widely developing in many ways such as the methods of pouring concrete in order to achieve high quality concrete at a low cost. Some of these new concretes have been produced which are completely different from conventional concrete in the method of mixing, pouring with no need for the normal compaction methods which require more labour, tools and higher costs. This paper presents two special types of concrete; (i) Two-Stage Concrete and (ii) Rock Filled Concrete. In the Two-Stage Concrete or Pre-Placed Aggregate method, as the name implies, the coarse aggregate is laid first then the cement grout is poured by pumping tubes which are directed to the bottom of the formwork. The grout fills the voids between the aggregate particles. The Two-Stage Concrete differs from conventionally placed concrete in that it contains a higher percentage of coarse aggregate; consequently, the properties of the coarse aggregate appear to have a greater effect on the properties of the concrete. Rock Filled Concrete (RFC) which is a combination of consolidation Self Compacting Concrete (SCC) and large block or rock with the minimum size of 300mm. In general, RFC is produced by filling the working space with large-scale blocks of rock to form a rock-block mass first, and then, by either pumping SCC into the working space or pour it directly on to the surface of rock-block mass. The advantage and special requirements for each of the two special types of concrete and their uses are presented in this paper.

TWO-STAGE CONCRETE

Two-Stage concrete (TSC) is considered to be one of the modern techniques in the concreting industry. The two-stage concrete or pre-placed aggregate method, as the name implies, is produced by placing the coarse aggregate in the section to be cast then grouting the cavities (voids) of the coarse aggregate with a special mixture (grout) under pumping tubes extended to the bottom of the form, to fill the voids between aggregate particles as shown in Figure 1. The technology of concrete made in this two-stage method is quite different from the normal traditional concrete, not only in the method of placement but also in that it contains a higher proportion of stone aggregate; consequently, the properties of the coarse aggregate appear to have a greater effect on the properties of the concrete than on the cement mortar..

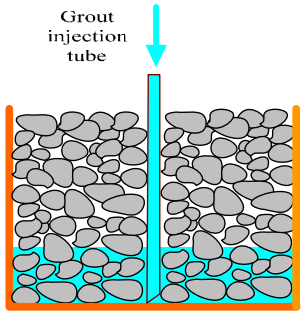

Figure 1: Two stage concrete

Properties of Coarse Aggregate

The choice of stone aggregate is of great importance in respect to the two-stage concrete method; the aggregate that is used in (TSC) should be washed, free of surface dust and other impurities. The void content of the aggregate should be as low as possible and is usually achieved when the coarse aggregate is graded uniformly from the smallest allowable particle size to the largest size [1]. It is typically 40 mm or larger; if aggregates smaller than 20 mm are used then the injected grout tends to bridge the interstices, thereby impeding grout flow. The mechanics of the two-stage concrete is depended on the mechanical properties of the coarse aggregate, because of the point-to-point contact of the coarse aggregate.

Properties of Grout

The grout that is used in (TSC) normally consists of ordinary Portland cement and well graded sand. The flow of the grout around the aggregate is essential, therefore some admixtures are normally recommended to improve the flow of the grout, improve penetrability, and control the potential for both shrinkage and bleeding.

Propagation of Mixture in Coarse Aggregate

The problem of flow and curve of mixture propagation in coarse aggregate is an important economic question. Mathematically the description of propagation is very difficult. The shape of the curve in Figure 2 depends on many factors such as: mixture density, intensity of mixing, hydraulic pressure, shape and size of grains and pores.

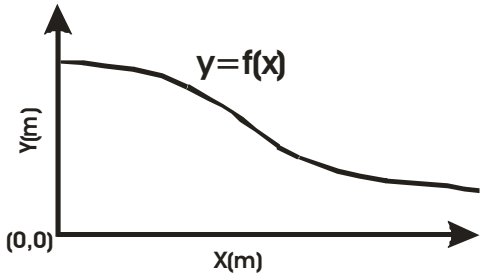

Figure 2 Propagation curve of mixture in stone

General empirical equation of propagation curve has been derived [2], and described in Equation1 as follows:

$$y = \frac{\alpha}{(\beta x^2 + 1)\sqrt{\frac{\gamma}{t} - \frac{1}{\beta} + 1}} \qquad (1)$$

Where: α = thickness of stone layer (m); β = (a×b×f) ; a = parameter dependent of mixture fluidity.; b = parameter dependent of stone : shape, size, kind of grain, surface , number and relation of fraction; f = Environment of construction; γ = (c×d×e); c=parameter dependent of efficiency of flushing pipe(m^3/min.); d=parameter dependent of perforation; e= parameter dependent on the kind of excavation bottom; t = time (min.); x = distance from flushing pipe(m); y = level of mixture mirror in stone (m).

Grouting Systems

The injection is achieved by pumping the grout through vertically mounted pipes which almost reach the bottom of the section to be cast. These pipes are rigid, normally 20 mm in diameter and placed at 1.5 m centers [1]. As the grout is pumped into the form the injection pipes are slowly raised. Injection of grout into small units can be achieved by pumping into the bottom of the form.

Advantages of Using TSC

The two-stage concrete completely differs from the normal concrete in the placement and implementation method. Some of the advantages of two-stage concrete are given as following:

Economics

The cost of two stage concrete is nearly 40% less than the cost of normal concrete. This is related to the reduction of cement content by some 30% with no need for compaction or vibrating [3]. In the case of using (TSC) method for underwater concreting, the cost of water-tight forms and dewatering may be eliminated and preparatory work can be done under water.

The Modulus of Elasticity

The modulus of elasticity of two stage concrete is slightly higher than that of conventional concrete because of point-to-point contact of the coarse aggregate and is mainly affected by the mechanical properties of stone aggregate. Extensive laboratory tests on the two-stage concrete using three different types of coarse aggregate (rounded, crushed, and mixed) and three different grout proportions (w/c = 0.45, 0.50, and 0.55; c/s = 1/1.5, 1/1, and 1/0.8) were performed to describe the concrete mechanical properties [4]. The results obtained and their statistical analysis enables formulation of the following comments. The linear part of the stress-strain curve may reach as much as 40–60% of the compressive strength of the specimens as shown in Figure 3.

The static modulus of elasticity (E_{TSC}) as a function of the compressive strength of the two-stage concrete (*fc)* is derived. See Equations 2a, 2b and 2c.

For rounded aggregate:

$$E_{TSC} = 28.7 + 0.080 \times f`_c \qquad (GPa) \qquad (2a)$$

For crushed aggregate:

$$E_{TSC} = 33.9 - 0.049 \times f`_c \qquad (GPa) \qquad (2b)$$

For mixed aggregate:

$$E_{TSC} = 34.9 - 0.090 \times f`_c \qquad (GPa) \qquad (2c)$$

The strength limit values in Eq. (2) are: $22\ MPa \leq f`_c \leq 32\ MPa$

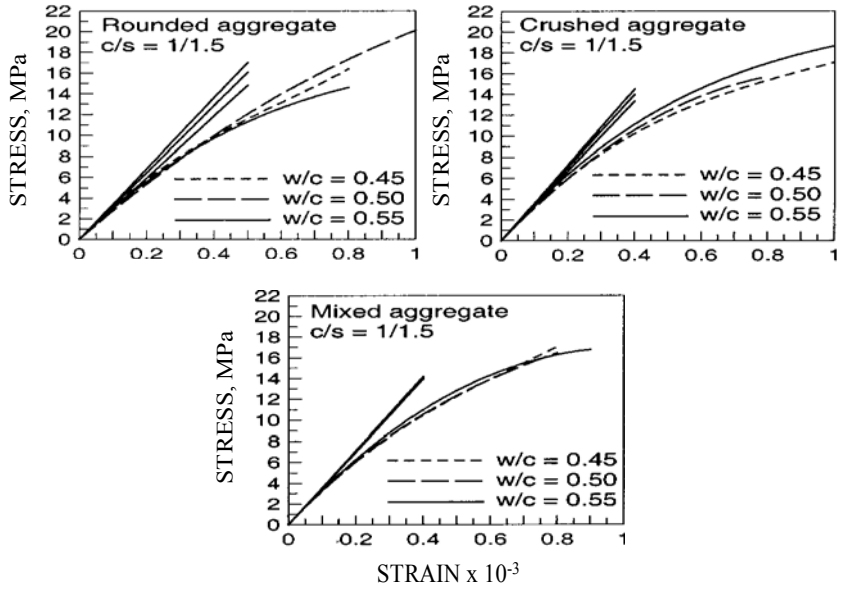

Figure 3 Graphical presentation of estimating two-stage concrete modulus of elasticity

The two-stage concrete static modulus of elasticity, for the examined types of aggregates and grout proportions, is mainly influenced by the mechanical characteristics of the aggregates—i.e., the compressive cylindrical strength, surface texture, and grading. The type of grout has a significant effect. The characteristic mechanical properties of the two-stage concrete can be explained by the specific stress distributions, which occur mainly through the particles of coarse aggregate (skeleton of the aggregate).

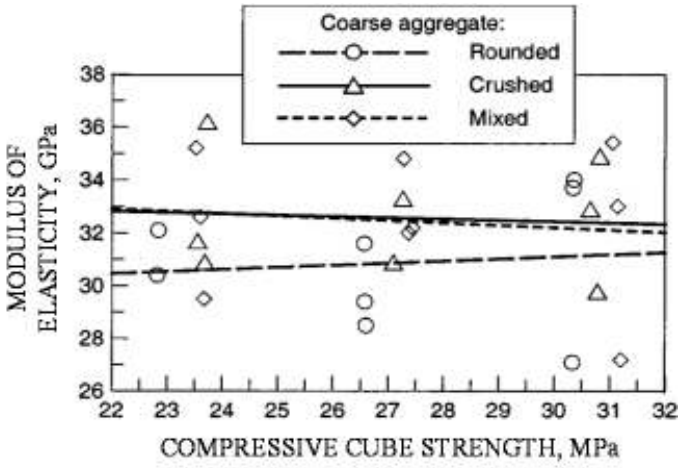

Figure 4 Relationships between modulus of elasticity and its compressive cube strength

Shrinkage

The drying shrinkage of two-stage concrete is about 50% lower than that of ordinary concrete, due to the contact between the large aggregate particles. This contact restrains the amount of shrinkage that can take place.

Segregation of the aggregate

The risk of having aggregate segregation is completely avoided in TSC since the coarse aggregate is placed before adding the other remaining concrete constitutes. In the case of using the two-stage concrete method for underwater concreting, the dense grout displaces upwards the water available between aggregate particles, producing a high aggregate/cement ratio concrete with point-to-point aggregate contact.

The Cold Joints

In the case of normal concrete, the cold joints should be executed in specific locations, but in the case of two-stage concrete these can be executed in any location, because the coarse aggregate pieces cross the joint, bond and shear , which in the majority of cases, will be adequate

Compressive and Tensile Strength of TSC

There is a good correlation between the compressive strength and tensile strength of (TSC). The compressive strength and the tensile strengths of (TSC) were investigated at 28 days for all grout proportions. On the basis of these results a relationship between tensile and compressive strength of TSC has been statistically derived. See Equation 3

$$F_t = (A) + (B) + fc` + (C) \times (fc`)^D \qquad (MPa) \qquad (3)$$

Where: $ft`$ is tensile strength and $fc`$ is compressive strength, A,B,C and D are regression coefficients shows Table 1 [5]. The measured tensile strength of TSC is in fact higher than that predicted by the ACI equation for conventional concrete. The greater mechanical interlocking among the particles could be responsible for this high tensile strength.

Table 1 Regression coefficients of equation (3)

TYPE OF GROUT	A	B	C	D	CORRELATION COEFFICIENT
Without admixture	-49.67	-0.44	38.63	0.150	0.724
Superplasticizer	39.97	0.36	-32.28	0.100	0.800
Expanding admixture	-4.30	-0.30	1.82	0.658	0.721
Combination of superplasticizer and expanding admixture	162.65	1.15	132.28	0.108	0.680

The uses of Two-Stage Concrete

TSC can be used for many applications just as:

- TSC is suitable for use in effecting repairs and making additions to concrete structures.
- Where placement by conventional methods is difficult (e.g., massive reinforcing steel)
- When low-volume change of the repair concrete is required to avoid cracking caused by excessive tensile stresses in the overlay concrete because of dry shrinkage and restraint provided by existing concrete.
- Where underwater placement is necessary because dewatering is difficult, expensive, or impractical and water conditions permit. In the case of using two-stage concrete method for underwater concreting, the water and air being displaced upward by the rising grout front. Injection is continued until a free washout of grout is emitted from the top of the pour and the voids between the aggregate is completely filed by the cement grout as shown in Figure 5.

Figure 5 Underwater concreting by using two stage concrete

ROCK-FILLED CONCRETE

Rock-filled concrete (RFC) is a new type of concrete for massive concrete construction works based on the technology of Self –Compacting Concrete (SCC). It is produced by pouring ready – mixed SCC into the voids of large blocks of rock with the minimum size 300 mm in the formwork. The SCC fills the void space between the blocks due to its good fluidity and segregation resistance, and thereafter the mix sets to form the RFC mass. Figure 6 shows, RFC is a combination of consolidated SCC and large blocks [6].

Figure 6 Rock-filled concrete

Self-compacting concrete (SCC) is defined as 'a concrete that is able to flow under its own weight and completely fill the formwork, while maintaining homogeneity even in the presence of congested reinforcement, and then consolidate without the need for vibrating compaction [7]. (SCC) has been used in various kind of practical structures all over the world. The immediate cause for the employment of SCC is summarized as follows:

- To shorten the construction period for large scale construction.
- To assure compaction in the confined zones of reinforcing bars where vibrating compaction is difficult or impossible.
- To eliminate noise or vibration due to compaction in concrete production.
- To assure durability with no initial defect of concrete or sure compaction.

However, in spite of these benefits, compared with conventional vibro-compacted concrete, SCC displays lower E-modulus, higher hydration heat and is also more costly in seeking to achieve the same compressive strength. Thus, SCC has still been used as a kind of special concrete rather than standard concrete in practical structures, especially in massive concrete in dam engineering. Yet scope exists to employ SCC in some degree, especially in light of the further challenge faced by dam engineering of the need to pay more attention to reducing costs and environmental impacts in future projects. To overcome challenges in the limitation of the use of SCC ,and to improve the economics and environmental performance of dam projects, Rock-filled concrete (RFC) was developed as a new type of concrete for structures, especially massive concrete structures such as dams Figure 7.

Figure 7 Self-compacting concrete

Advantages of Using (RFC)

There are many advantages for the employment of RFC in practical structures

1- Low heat of hydration because the use of low cement content which makes it more easier to ensure temperature control

2- Allowing continuous pouringing of SCC to reduce the construction time

3- No need for compaction by using SCC results in compaction being ensured independent of the quality of construction work

4- Simplifying the aggregate production and concrete mixing machinery contributing to cost reduction

5- Using the rock-block mass as skeleton of concrete results relatively little drying and shrinkage

6- Reducing noise as well as energy consumption contributes to lower emissions of the greenhouse gas (GHG) carbon dioxides and also sulphur dioxide.

Application of RFC

RFC has been put practical use in the following hydraulic projects:

Experimental Dam Construction

RFC was first used in a gravity dam in a reservoir project in Beijing. The 13.5 m high, 2,000 m^3 gravity dam was finished in 2005.

Auxiliary dam in Baoquan Pumped Storage Project

After successfully employed in experimental gravity dam RFC was applied in part of the auxiliary dam of the upper reservoir in Henan Baoquan pumped storage project.The dam was designed as a 50000 m3 , masonary construction , such as low construction with RFC to solve the problems in the practical masonary construction, such as low efficiency and low construction quality . It was finished in 2006 and the picture of the site during RFC construction is shown in Figure 8.

Figure 8 Auxiliary dam

Gully Backfill in Baoquan Pumped-Storage Project

After finishing the RFC construction on part of the auxiliary dam at Baoquan, most of the engineers involved, including those with the owners, designer and construction, understood more about the benefits of RFC and came to an agreement on using RFC instead of conventional vibro-compacted in the gully backfill project. The total volume of the backfill project was 130,000 m^3 ,and approximately 50,000 m^3 of them was constructed with RFC.

Caisson Backfill in Xiangjiaba Hydropower Project

RFC was also employed in the Caisson backfill in Xiangjiaba hydropower project, which would be the third largest hydropower station in China. Approximately 70,000 m^3 of RFC had been constructed in the Caisson backfill project and it was finished in the end of 2007 (see Figure 9).

Figure 9 Caisson

CONCLUSIONS

The cost of two stage concrete is almost 40% less than the cost of normal concrete. This is related to the reduction of cement content by 30% and there is no need for compaction or vibrating of concrete.

The risk of having aggregate segregation is completely avoided since the coarse aggregate is placed before adding the other remaining concrete constitutes.

Bond of two-stage concrete is excellent because the grout used to consolidate the pre-placed aggregate penetrates surface irregularities and pores to establish initial bond.

In the case of normal concrete, the cold joints should be executed in specific locations, but in the case of two-stage concrete can be executed in any location, this is because the strength of two-stage concrete depends specifically on the coarse aggregates itself.

The use of Rock Filled Concrete gives many advantages related to quality, cost and environment considerations.

The RFC gives low heat of hydration because the use of low cement content which makes it easier to ensure temperature control.

RFC Allows continuous pouring of SCC and reduce the construction time

In RFC method there is no need for compaction as using SCC results in compaction being ensured independent of the quality of construction work

Simplifying the aggregate production and concrete mixing machinery contributes to cost reduction

Using the rock-block mass as skeleton of concrete results relatively little drying and shrinkage

Reducing noise as well as energy consumption contributes to lower emissions of the greenhouse gas (GHG) carbon dioxides and also sulphur dioxide.

REFERENCES

1. ACI 304R-05. Guide for measuring, mixing, transporting, and placing concrete , American Concrete Institute,2005, 15 pp.

2. ABDELGADER, H S. How to design concrete produced by a two-stage concreting method. Cement and Concrete Research, 1999, Vol. 29, No.3, pp. 331-337.

3. ABDELGADER, H S. Polcrete economical mthod for dams, pProceeding of the MWA. International conference on dam engineering. 1995, Vol.1, pp.1-4, Kuala Lumpur, Malaysia, 1-2 August.

4. ABDELGADER, H S, GÓRSKI, J. Strain relations and modulus of elasticity of two-stage concrete. Journal of Materials in Civil Engineering ASCE, 2003, Vol. 15, No. 4, pp. 329-334.

5. ABDELGADER, H S, ELGALHUD, A A. Effect of grout proportions on strength of two-stage concrete. Structural Concrete. 2008, Vol.9, No.3, pp.163-170.

6. XUEHUI AN, MIANSONG HUANG, HU ZHOU AND FENG. Rock –filled concrete in China. Special report, 2009.

7. ACI 546.2R-98. Guide to Underwater Repair of Concrete: American Concrete Institute, 1998, 10 pp.

8. CONCRETE SOCIETY FEBRUARY. Self Compacting Concrete. Technical Report, 2008, No. 62 .

9. NEWMAN, J, SENG, B C. Advanced Concrete Technology. First Edition , 2003, pp.244-255.

Low Carbon Gound Floors for Housing: A Case Study

C Shaw
Independent Consultant, UK

The Paper describes the design and construction of the world's first fully integrated super insulated flexibly detailed hybrid reinforced concrete ground floor slabs for a housing development which incorporated 'underfloor heating' within the structural slab. This design provided a low cost low carbon floor which was constructed faster and easier than the previous slabs used for this type of development. The five house types were all designed using the same system. The first layer comprised super insulated carbon enriched units, which were laid on a sand blinded base of previously excavated material. The units each stand on integral legs, giving an air space under the main insulation, and interlock to give a thermal break within the thickness of the insulation. The next layer was the polythene damp proof membrane. New, specially designed soft formwork spacers were placed on the membrane and these hold a mix of flexibly detailed bar reinforcement combined with sheets of welded steel fabric reinforcement for economy. The underfloor heating pipes were fixed to the reinforcement in a specified pattern provided by the manufacturer to give individual heating control to each room on the ground floor of the house. The concrete was then poured and power floated to give the finished floor surface. The thermal mass of the concrete greatly enhances the storage capacity of the floor and reduces the thermal drift, giving a more comfortable environment. This design achieved a low cost low carbon floor.

Chris Shaw is a Chartered Civil Engineer and a Chartered Structural Engineer practising as a Consultant. He has more than 35 years experience in achieving the specified cover to the reinforcement in reinforced concrete structures, and devised the system for achieving this which was subsequently published as British Standard 7973 in 2001. He is now Chairman of the committee that prepared the Standard and gives advice, lectures, and training on the subject. He continues to carry out research and development on the products, their applications and innovative uses worldwide.

Keywords: Flexible detailing, Hybrid, Insulation, Low carbon, Spacers

INTRODUCTION

The increasing requirements of The Building Regulations in England and Wales, together with the rising cost of energy for both the construction and running costs of buildings, has resulted in more attention being given to the Carbon Cost and the Sustainability of new buildings. There is a need to reduce the number of 'goods miles' travelled for building materials as the transport is dependent on oil which continues to rise significantly in price. Progress is being made in the development and implementation of new types of construction. The paper describes one such development where a new system of ground floors for houses was built. It was the first in the world to be built using this system, and received approval from the United Kingdom National House Builders Council (NHBC). It was started in 2010 and completed in 2011.

BACKGROUND

The development comprised 12 houses of five different designs placed on a steeply sloping site. The sub-soil was chalk. The slope meant that the ground level around the houses varied considerably and suspended ground floor slabs were needed to comply with The Building Regulations.

The architectural drawings initially showed a pre-cast pre-stressed beam and block floor, with a void underneath, and a series of underfloor ventilators. On top of the beams and blocks there was a 20mm self levelling screed, and on this a polythene damp proof membrane (dpm). On the damp proof membrane there was 50mm of rigid insulation board, and on this another 50mm thickness of insulation with the heating pipes fixed in pre-formed grooves within the insulation. The top layer was a 50mm thick self levelling screed.

The foundations for the first few houses had already been cast when the Client was made aware of the Eco-slab insulation system and its advantages over the proposed floor construction. The insulation was changed to the Eco-slab system, and the structural design of the ground floor slabs commenced in conjunction with the guidance of the underfloor heating manufacturer.

The Eco-slab system has many advantages over the design of the originally proposed floor, especially in relation to its low cost and low carbon footprint.

- The pre-stressed beam and block floor requires a lot of energy in its manufacture and transportation, whereas the in-situ concrete for the floor is obtained locally;
- The pre-stressed beams require manual or mechanical handling, including lifting, whereas the concrete floor is placed in-situ;
- The ends of the steel pre-stressing wires of the pre-stressed beams are exposed and vulnerable to corrosion. This starts from the ends and progresses along the circumference of the pre-stressing wires cracking the concrete of the beam and reducing its shear capacity. The ends of the beams and the wires were traditionally coated with a black bituminous coating to protect them, but this practice has ceased in more recent years. Now the ends of the wires are exposed and can corrode in the presence of moisture. The in-situ concrete slab does not have this problem.

- It is well known that the actual size of a building varies from its design size due to tolerances and variability in its construction. The pre-stressed beams are ordered from the numerical size on the drawings, so they may not be of the correct length when placed on the walls below. If the walls are too close together the end of the beam will project into the cavity and locally reduce the thickness (and therefore effectiveness) of the thermal insulation, resulting in a 'cold bridge', which can result in condensation forming on the end of the beam causing corrosion of the pre-stressing wires. If the walls are slightly further apart than the designed dimension then the bearing of the end of the beam on the wall, which is usually only 100mm wide, can be significantly reduced and the masonry of the wall becomes overstressed and can ultimately fail in shear locally. The in-situ slab has none of these disadvantages and is formed to the actual size of the supporting walls below, thus ensuring a continuous bearing of the full width. As the support is continuous the bearing stress on the wall below is greatly reduced.
- The originally proposed system had a total of eight operations to complete the floor. The Eco-slab system had only five, giving a significant saving in the cost of labour, which is the most expensive part of the construction. The system used readily available site skills, and no special tools were needed to place the insulation.
- The Eco-slab system is much quicker to construct from start to finish and this has cost savings in both the programme time and the financing of the project.
- The originally proposed floor would be vulnerable to the weather for much longer than the Eco-slab system which, apart from the actual placing of the concrete, is independent of the weather conditions as it is an all 'dry' construction.
- The finishing screed of the proposed construction has a thickness of 50mm and a density of approximately 2,000kg/m^3. The Eco-slab system for this project had a typical concrete floor thickness of 200mm and a density of approximately 2,300kg/m^3. The thermal storage capacity of the Eco-slab floor is therefore greatly superior to that of the originally proposed design. This results in less thermal drift in the air temperature in the house, resulting in greater comfort and a better environment for the occupants.

THE INSULATION

The increasingly stringent thermal insulation requirements of The Building Regulations (as applied in England and Wales), together with the introduction of 'soft' permanent formwork had previously led to problems in ensuring that the formwork provided the steel reinforcement with the specified cover at all locations within the concrete. 'Soft' formwork is defined as either expanded polystyrene (EPS), (such as Eco-slab used for insulation purposes in low carbon construction), cellular plastic sheet (CPS), or plastic encapsulated welded steel fabric (PEWSF). Both CPS and PEWSF have no useful thermal insulation properties. 'Soft' formwork is usually used as permanent formwork. It is sometimes used for ground beams, ground bearing and suspended ground floor slabs, and foundations. In contrast 'hard' formwork is normally either plywood, timber or steel etc. and is usually temporary and removed after the concrete has set. Only expanded polystyrene provides both the formwork function and the thermal insulation. It is therefore a much more sustainable product than CPS or PEWSF, both of which use the increasingly expensive oil in their manufacture and do not have the thermal insulation benefits of expanded polystyrene.

Expanded polystyrene is a lightweight, totally inert foam material made by the polymerisation of styrene, and consists of approximately 98% air by volume. It is traditionally white in colour, and does not use the ozone depleting Chlorofluorocarbons (CFC's), Hydrochlorofluorocarbons (HCFC's) or Hydrofluorocarbons (HFC's) in its manufacture.

The insulation was formed with Eco-slab carbon enriched super insulation units. Carbon enriched expanded polystyrene is about 17% more thermally efficient than plain EPS of the same density. The carbon enrichment of the expanded polystyrene significantly increases its thermal insulation and this, together with the design of the units incorporating an air space beneath them, results in a 'super insulation'. The Eco-slab won the Shell Springboard 2010 Award for Innovation in Carbon Reduction, and has a Local Authority Building Control Type Approval Certificate. The Eco-slab units are made with up to 5% of recycled material and they can be recycled at the end of their life.

The insulation complies with BS EN 13163:2008, [1], and is manufactured under a Quality Management System to BS EN ISO 9001:2008, [2]. The polystyrene is of 100 grade (previously Heavy Duty (HD) grade).

The modular system consists of 1m square interlocking units with overlapping edges. Each unit sits on nine integral legs which create a void beneath the floor for services and ventilation. Testing at the United Kingdom Building Research Establishment (BRE) has shown the system to achieve a 'U' value of 0.19W/m^2K. If the density of the polystyrene is increased a 'U' value of 0.10W/m^2K can be achieved, and this gives scope for further development of the system as the thermal insulation requirements become more stringent over time. At the perimeter of the floor the insulation units sit on a continuous edge support made from the same polystyrene as the units, and this achieves a linear thermal transmittance of 0.016W/m^2K for the edge of the floor. This is several times better than that required by the current UK Building Regulations.

The modular units have a flat top surface for the placing of the 1200 gauge polythene damp proof membrane and to support the soft formwork spacers for the reinforcement. The units were easily cut to shape where necessary and the recessed top edges were filled with factory made infill strips of the same polystyrene which are supplied as part of the insulation units.

The units were placed on a sub-base formed by re-using inert excavated material from the foundations, and levelling this within the external walls. This provided support for the insulation units and at the same time reduced the quantity of excavated material that needed to be removed from the works and taken to the landfill site. This saved both on the transport cost and the landfill tax payment that would have been incurred, and reduced the carbon cost and footprint of the project. The re-used material did not need to be fully compacted as it ceased to be loadbearing once the concrete slab had been cast, resulting in further savings in time and cost. Figure 1 shows a typical example of the insulation units being placed.

Figure 1 Placing the insulation units

SOFT FORMWORK SPACER

Soft formwork spacers are relatively new to the construction market. They are intended for use with the types of 'soft' formwork previously mentioned, and were originally introduced in 2007 for use with expanded polystyrene insulation for ground beams and foundations where the cover to the reinforcement would normally be either 40mm or 50mm. Details of these spacers were published in an article in the August 2010 edition of Innovation and Research Focus [3]. The soft formwork spacer forms part of the ongoing development of spacers and chairs based on the previously published requirements [4, 5, 6, 7, 8]. This development was the first time that the Eco-slab insulation units had been used with an integrated reinforced concrete floor slab with the heating pipes cast within it.

The cover to the bottom reinforcement was selected at 25mm for economy and cost, but there was no 25mm soft formwork spacer made at that time. One was therefore quickly designed in a collaboration between the manufacturer of the Eco-slab, the manufacturer of the existing 40mm and 50mm cover soft formwork spacers, and the author, who has many years experience in the design and performance of spacers and chairs for concrete. The design was based on the previous experience with the first soft formwork spacers which were designed in 2007. Once the requirement was identified it took just 25 working days to achieve approval, having completed the design, prototyping and testing. Immediately upon receipt of approval the contractor ordered the spacers and production started. The first delivery of spacers, sufficient for the first few floor slabs, was made to the site within days.

The 25mm soft formwork spacer was tested to confirm compliance with British Standard 7973:2001 Part 1, [9], and the design drawings for the reinforcement included the requirement for them to be fixed in accordance with the requirements of British Standard 7973:2001 Part 2, [10].

FLEXIBLY DETAILED REINFORCEMENT

When reinforcement extends through a concrete member to each end the end cover becomes a critical factor in achieving durability. This situation is known as 'reinforcement between fixed faces (of the concrete)'. If the distance between the faces of the formwork is less than the designed dimension and the reinforcement is in one continuous length the specified cover will not be achieved and the durability of the reinforced concrete will be decreased. To overcome this problem it was decided many years ago that flexibly detailed reinforcement was the answer. For a slab this can be achieved by stopping alternate bars of the main reinforcement before the end bearing at one end. One of the problems with the reinforcement in slabs is that if straight bars (shape code 00 in British Standard 8666:2005 [11]) are used the permitted tolerance in Table 5 of British Standard 8666 is $\pm$ 25mm. If the bar is 25mm longer than the length specified in the bending schedule the end cover can be significantly reduced. If the specified length of the bar is reduced by 25mm to avoid this problem then the overlap at the bearing may be reduced to a minimal amount. There is also the ongoing problem of locating the bar with the correct end cover within the fixed faces of the formwork. This was solved by including the requirement of Clause 5.2 of British Standard 7973- 2:2001 [10] which specifies that the bar shall be fixed by locating it with the correct end cover and tying it from that end inward. The requirement for flexibly detailed reinforcement was also specifically included in The Standard Method of Detailing Reinforcement [12].

In this project four of the house types had simply supported floor slabs spanning between the side walls of the houses. The width of the slabs varied from 5,493mm to 6,041mm, and averaged 5,767.5mm. The slabs had 100mm bearing on the blockwork of the inner leaves of the external walls of the houses. The end cover to the reinforcement was specified as 40mm. The cover value therefore represented only 0.69% of the width of the slab. If a straight reinforcing bar had been used, without flexible detailing, then the end cover could have been reduced to 15mm by the +25mm tolerance on the length of the bar, a reduction in the cover to less than 38% of the specified value. In accordance with the flexible detailing requirement the main reinforcing bars were scheduled as shape code 11 to British Standard 8666:2005 [11], with a standard bend to Table 2 of British Standard 8666:2005 at one end, and the 'B' length reduced to give a greater end cover at the other (straight) end.

This flexible detailing of the reinforcing bars meant that tolerances in the setting out of the houses, the positions of the internal leaf of the walls, the formwork, and any out of square tolerances could all be accommodated within the layout of the reinforcement by locating the bent end of the bars with the correct cover and tying them from the bent ends inwards. The bent ends of the reinforcing bars were fitted with 40mm soft formwork spacers because the edge formwork was formed with rigid polyisocyanurate (PIR) foam insulation strips.

HYBRID REINFORCEMENT

Bar reinforcement was used for the main reinforcement because the span of the floor slabs was greater than the 4.8m length of standard sheets of welded steel fabric to British Standard 4483:2005 [13]. However, bar reinforcement takes longer to fix than sheets of fabric. The main bar reinforcement was therefore overlaid with a sheet of welded steel fabric with its main wires on the lower face and located between the main bar reinforcement. The area of main tensile reinforcement comprised the area of the bar reinforcement plus the area of the main wires of the fabric reinforcement, giving an economical solution. The combining of bar and fabric reinforcement in this way is called hybrid reinforcement. The distribution reinforcement for the slab was provided by the cross wires of the welded steel fabric. The reinforcement for the perimeter around the sheets of welded steel fabric was constructed with flexibly detailed individual reinforcing bars.

When using welded steel fabric there has been a problem where adjacent sheets are lapped together, and where the corners of four sheets are lapped there can be up to eight thicknesses of wires. This can move the wires up to, or sometimes above, the neutral axis of the slab. This problem is solved by butting the edges of the sheets together and using loose splice bars, tied to the wires of the fabric. In this way the wires of the fabric all remain in their correct planes.

Four types of house used a simply supported single span for the floor slabs, requiring only bottom reinforcement. The fifth type of house, which was the largest, required a partly two and partly three span slab which spanned from the front to the back of the house. This slab required both top and bottom reinforcement, and sheets of welded steel fabric were used for the top reinforcement. Normally the top reinforcement would have been supported from the bottom reinforcement by means of continuous steel wire chairs to British Standard 7973:2001 Parts 1 and 2.

However, in this project the central heating pipes were wired to the distribution reinforcement and there were no standard height continuous steel chairs available to give the correct cover to the top reinforcement. This was solved by using a hybrid comprising 500mm lengths of continuous cementitious spacers fixed to the distribution reinforcement of the slab at right angles to the main reinforcement, with lengths of goalpost type continuous steel wire chairs wired to the spacers at right angles. The top wires of the chairs supported the main wires of the top sheets of the welded steel fabric, giving the correct top cover.

All of the reinforcement was tied together in accordance with the requirements of British Standard 7973-2:2001, Clause 5. A combination of traditional 16 gauge black annealed soft iron tying wire and proprietary wire loop ties were used for the tying. Slash ties were used for tying both the reinforcement and the sheets of welded steel fabric together. Figure 2 shows a typical example of the reinforcement and heating pipe layout.

Figure 2 Typical example of the reinforcement and underfloor heating pipe layout

UNDERFLOOR HEATING

The underfloor heating was originally proposed to comprise a flexible pipework system placed in pre-formed grooves in 50mm thick insulation, with a 50mm thick self levelling screed laid on top of it. In the improved design the heating pipes were cast into the structural concrete floor slab. This is an established practice in mainland Europe for floors above ground level, but relatively new in the UK. Ground floors in Europe are often formed of ground bearing slabs with the heating pipes cast in the top part of the slab. The combination of all of the elements of this low carbon ground floor design is unique, and this site is the first to be constructed in this manner. The layout of the heating pipes was specially designed to ensure the integrity of the structural concrete floor slab.

The pipes were 16mm overall diameter and made principally from polybutylene (PB) which is more flexible than other materials commonly used for underfloor heating. The pipes have a 75 year design life and guarantee, and so they can be expected to last for at least the design life of the house. Each room on the ground floor had a separate heating circuit and the pipes were terminated at a manifold. Heat was provided from a gas boiler. The pipework complied with British Standard BS EN ISO 15876 Parts 1,2, 3 and 5 [14,15,16,17], and the system was designed to British Standard BS EN 1264 Parts 1 – 5, [18,19,20,21,22], under a Quality Management System to BS EN ISO 9001:2008 [2].

The pipes were fixed to the reinforcement in the bottom of the slabs with plastic cable ties. When complete, the pipes were pressurised to 2 bar and the pressure maintained and monitored until after the concreting had been completed.

CONCRETE AND FINISHING

The concrete mix was a standard RC25/30 N/mm^2 mix with Ordinary Portland Cement (CEM1), 250 kg/m3 minimum cement content, 0.65 water cement ratio, 70mm consistence target (previously known as the slump), and a 20mm maximum aggregate size, sourced locally to the site and delivered by ready mixed concrete lorry. The underfloor heating pipes were kept pressurised during the placing of the concrete and checked to ensure the pressure in them was being maintained. The concrete was vibrated with a vibrating poker, levelled off and then finished with a power float and cured with a sprayed curing membrane. The use of locally sourced concrete saved the carbon cost of producing and transporting pre-cast pre-stressed beams and blocks from the factory to the site. In the United Kingdom (UK) the pre-cast pre-stressed beams and blocks would be delivered from the factory which typically incurs a travel distance of 93 road miles (150 road kilometres) for a Heavy Goods Vehicle (HGV). In contrast the ready mixed concrete would typically be delivered from a local depot involving a distance of just 5 road miles (8 road kilometres) for the lorry to travel [23]. The pre-cast pre-stressed beams would normally require some form of mechanical handling to unload from the delivery lorry and place in position on the foundation walls. In contrast, the ready mixed concrete could be discharged directly into its final position in the slab, saving the cost of the mechanical handling.

COST COMPARISON

The five types of slab are each different due to the design of the various house types, and their resultant size, shape and thickness. The cost per square metre of floor slab therefore varies accordingly. The cost of slabs built using this system would also vary depending upon such factors as the number to be built on a site, and the site location within the UK or elsewhere. A cost comparison for the thickest slab, which was 225mm deep, was carried out using the national rates published in Spon's Architects and Builders Price Book [24]. The beam and block floor design cost £75.61/m^2 and the low cost floor slab design was £49.53/m^2, giving a considerable financial saving as well as a more sustainable and easily built floor. The savings in the energy used for space heating over the life of the house would be significantly more than the cost of the slab.

FURTHER DEVELOPMENTS

These houses were the first in the world to be built using this integrated low carbon system for the ground floor slabs. The slabs were designed and constructed to a very short timescale. As the first floor slabs were being constructed and their construction monitored it became clear that:-

1. The system worked in practice;
2. Now that it had been proven in practice there was considerable scope to develop the system further through the use of, for example, the partial replacement of primary aggregates with recycled aggregates, the use of pumped concrete, and the possible use of self levelling concrete.

There has now been time to consider these further enhancements to this system for low cost low carbon floor slabs on subsequent projects.

SUMMARY

The design and construction of this development project has shown that it is possible, practical and economical to construct low cost low carbon super insulated ground floors for houses. Savings in the carbon cost of the development have been made at many stages during both the design and construction phases, and these have produced an incremental saving in the financial cost and the carbon cost of the floors. In addition the better insulation provided by this design over the originally proposed design will give significant savings in the energy cost for heating the houses over their lifetime. At the end of their lives almost all of the components of the floors can be easily recycled with currently available technology.

CONCLUSIONS

The development and use of this integrated hybrid system for low cost low carbon ground floors is a major step forward in reducing the environmental impact of this element of construction. The savings accrue both from the energy saved in the actual construction process, and the thermal efficiency energy savings during the life of the houses.

The system has been proved to work in practice and should be adopted for new housing construction. There is potential to develop the system further, and to use it for other types of building applications.

ACKNOWLEDGEMENTS

The author would like to thank the following people for their assistance with this Paper.

Mr Roy Clifton and Mr Bernard Barker of Eco-slab, supplier of the insulation.
Mr John Stirley of Injection Plastics Limited, manufacturer of the spacers.
Mr Tony Crotaz of Siteright Construction Supplies Ltd, supplier of the reinforcement and concrete accessories.
Mr James Wilson of Wavin Underfloor Heating Division, manufacturer of the heating pipework.
Mr Terry White of EQ Builders Ltd for access to the site.
Mr Adam Marshall of Jablite Limited for technical information on the insulation.

REFERENCES

1. BRITISH STANDARDS INSTITUTION, British Standard BS EN 13163:2008, BSI, London, 2008, 52pp.

2. BRITISH STANDARDS INSTITUTION, British Standard BS EN ISO 9001:2008, BSI, London, 2000, 40pp.

3. THE INSTITUTION OF CIVIL ENGINEERS, Innovation and Research Focus, The Institution of Civil Engineers, London, 2010, 8pp.

4. ROBERTS, R F, Spacers for reinforcement, Cement & Concrete Association, Wexham Springs, 1981, 8pp.

5. CONCRETE SOCIETY, Spacers for reinforced concrete, Concrete Society, London, 1989, 30pp.

6. LANCASTER, R I, Spacers for reinforced concrete, 'Concrete' magazine, Vol. 23, November 1989, pp 27-28.

7. COMITE EURO-INTERNATIONAL DU BETON, Bulletin D'Information No. 201, Comité Euro-International Du Béton, Lausanne, 1990, pp 57-79.

8. SHAW, C B, Cover to Reinforcement – Getting it Right, Proceedings of the 6th International Congress on Concrete, 2005, 8pp.

9. BRITISH STANDARDS INSTITUTION, British Standard 7973-1, BSI, London, 2001, 18pp.

10. BRITISH STANDARDS INSTITUTION, British Standard 7973-2, BSI, London, 2001, 22pp.

11. BRITISH STANDARDS INSTITUTION, British Standard 8666, BSI, London, 2005, 32pp.

12. THE INSTITUTION OF STRUCTURAL ENGINEERS, Standard Method of Detailing Structural Concrete, The Institution of Structural Engineers, London, 2006, 188pp.

13. BRITISH STANDARDS INSTITUTION, British Standard 4483, BSI, London, 2005, 18pp.

14. BRITISH STANDARDS INSTITUTION, British Standard BS EN ISO 15876-1, BSI, London, 2003, 18pp.

15. BRITISH STANDARDS INSTITUTION, British Standard BS EN ISO 15876-2, BSI, London, 2003, 22pp.

16. BRITISH STANDARDS INSTITUTION, British Standard BS EN ISO 15876-3, BSI, London, 2003, 22pp.

17. BRITISH STANDARDS INSTITUTION, British Standard BS EN ISO 15876-5, BSI, London, 2003, 16pp.

18. BRITISH STANDARDS INSTITUTION, British Standard BS EN 1264-1, BSI, London, 1998, 12pp.

19. BRITISH STANDARDS INSTITUTION, British Standard BS EN 1264-2, BSI, London, 2008, 48pp.

20. BRITISH STANDARDS INSTITUTION, British Standard BS EN 1264-3, BSI, London, 2009, 22pp.

21. BRITISH STANDARDS INSTITUTION, British Standard BS EN 1264-4, BSI, London, 2009, 18pp.

22. BRITISH STANDARDS INSTITUTION, British Standard BS EN 1264-5, BSI, London, 2008, 16pp.

23. MPA-THE CONCRETE CENTRE, Concrete Credentials: Sustainability, The Concrete Centre, Camberley, 2010, 6pp.

24. DAVIS LANGDON, Spon's Architects and Builders Price Book 137th edition, Spon Press, Abingdon, 2012, 806pp.

Design of Concrete Bridges for Sustainability and Durability

J M Macia, S Mirza
McGill University, Canada

Sustainable and durable infrastructure facilities, including bridges, require optimum use of all resources during all phases of the project with savings in energy and water consumption. These involve planning, design, construction, maintenance, operations, repair and rehabilitation, and finally decommissioning and disposal of the debris at the end of its service life. Design of a sustainable and durable bridge structure requires consideration of a few feasible alternatives to develop an optimum option to fulfill all of the relevant limit states, with the most optimum life-cycle performance and the lowest life-cycle costs. The current national standards do not account for the anticipated increases in operating loads and the increasing deterioration of bridge structures over their service life. While these standards emphasize quality control in the choice of materials, design and construction, they do not provide guidance and scientific tools to design and maintain a bridge structure for durability over its service life, and include only prescriptive tools for preventing or minimizing some deterioration modes. This research program integrates sustainability and durability requirements in the design of a conventional bridge structure in a cold climate country, subjected to the various mechanical, natural and man-made loads and an aggressive environment, and considers the performance of the various materials and structural components over the design service life. The latest available models of the relevant deterioration modes have been incorporated in the life-cycle performance and design considerations. The basic procedure adopts a multiple protection strategy for all deterioration modes, resulting from the related aggressive actions, and integrates durability considerations with structural calculations for the final design and defines maintenance strategies and any needed supplementary protection techniques. The procedure is illustrated in a worked out design example, summarized in the paper.

Juan Manuel Macia obtained his title as Civil Engineer in 2003 at the National University of Colombia. He is currently finishing his Master of Engineering Program with emphasis in Structures and Construction Materials at McGill University. His professional experience has been related to Structural Design and Bridge Engineering.

Saeed Mirza is a professor of Civil Engineering and Applied Mechanics at McGill University. His specialty is structural engineering and rehabilitation of infrastructure, with special interest is the state of public structures like ports, bridges, roads and sewer systems. He has won awards for outstanding teaching and for contributions to the field of structural engineering. He joined the Department of Civil Engineering at McGill University in 1966 after working for a consulting engineer and the Public Works Department in Pakistan.

Keywords: Aggressive environment, Bridge design, Durability, Reinforced concrete, Sustainability

INTRODUCTION

Durability design aims to establish the performance of construction materials and the various bridge components and the overall bridge structure over its service life under all prevailing load and environmental conditions. The design procedure integrates different fields of engineering that concern the durability of a reinforced concrete structure, including construction materials, structural design, construction practices, durability and sustainability considerations, life-cycle costing, bridge management and maintenance strategies. It should be noted that durability can only be achieved through a holistic design approach.

Durability design of a structure incorporates multiple protection strategies against the different actions that may cause its deterioration over the service life. The key steps in designing for durability include: determination of the service life of the structure, analysis of the environmental effects, identification of the mechanisms of deterioration affecting the structure, selection of adequate models and evaluation of durability parameters, design and selection of good-quality construction materials, integration between durability parameters and structural calculations to define the final design, identification of supplementary protection measures, and definition of the required maintenance strategies. It is generally accepted that higher initial investments during the design and construction phases of a bridge project would normally require lower maintenance, repair and renovation costs over its service life.

THE DESIGN EXAMPLE

The proposed bridge structure crosses a river and connects an intermediate town with a major highway system. The town is located near the metropolitan region of Montreal, Quebec, Canada. This bridge is lifeline structure and part of an emergency system which must remain operational during and after a major catastrophe. The bridge will sustain traffic equivalent to 1000 daily trucks per lane. Figure 1 shows the elevation view of the bridge.

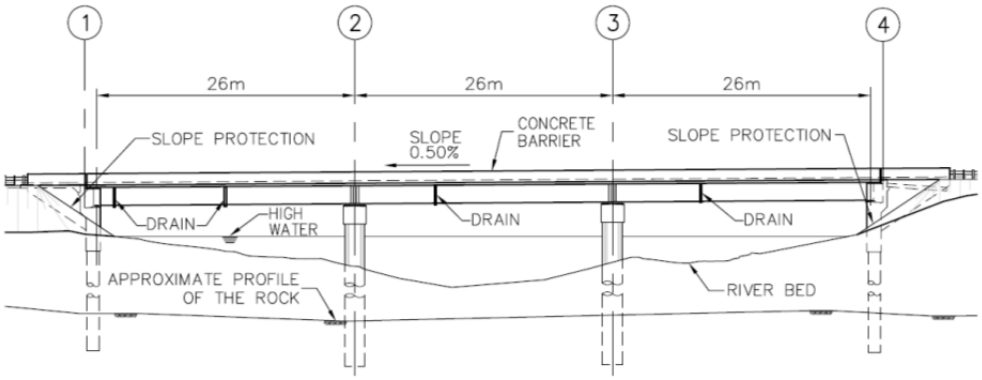

Figure 1 Bridge elevation

The total width of the bridge is 15.07m including four traffic lanes, two lanes in each direction, two shoulders of 1m each, and a concrete barrier placed on either side. The bridge has three equal spans of 26m each, with intermediate semi-continuous supports configured by the pier and bridge deck arrangements. The superstructure consists of two sets of seven simply-supported girders, arranged in three spans. The foundations are basically defined by two intermediate rigid-frame piers, and two cantilever abutments. These elements are supported by a series of circular caissons that transfer the loads to the bedrock.

DESIGN FOR SUSTAINABILITY AND DURABILITY

Sustainable Development

The concept of sustainability can be related to responsible and reasonable use of natural resources to provide important benefits to the society without compromising their supply for future generations. Sustainability in bridge design can be achieved by emphasizing conservation measures, use of renewable resources, waste reduction, recycling of used materials and structural elements, and complete environmental and economic assessments of the applied loads and the various macro- and micro-climates on the bridge structure, using valuable tools, such as life-cycle costs analysis and value engineering. This analysis involves not only the initial costs of design and construction, but also the future costs of maintenance, repair, rehabilitation, and decommissioning of the structure at the end of its service life. The design of a durable structure for sustainability requires advanced planning, thinking and rethinking and optimization of the design alternatives to identify the option with the most optimum performance and the lowest life-cycle costs [1].

The design for durability requires consideration of different mechanisms of deterioration that may be initiated by the environmental conditions (macroclimate and microclimates) present at the bridge. Bridge design for durability necessitates proper selection and design of the construction materials, the use of high quality construction practices, the identification and detailing of critical parts, the definition and implementation of an effective maintenance program and the monitoring of the performance of the structural components [2].

The different aspects related to sustainability and durability are not explained or introduced in the current national bridge design codes with a clear scientific and rational approach as used for structural analysis and design. The codes deal with these subjects by providing some prescriptive measures for durability of construction materials, including a minimum concrete cover thickness, type of reinforcement, chloride ion content, sulphate attack, and freezing and thawing cycles, among others. The current standards emphasize the need to employ high-quality concrete and steel. Additionally, a minimum service life of 75 years is normally required for bridge structures. However, the codes do not provide detailed guidance on how to attain this service life by ensuring adequate durability of a properly designed, constructed and maintained structure [3].

Durability Design Approach

The design procedure for bridge structures must established adequate durability, serviceability, safety, and general socio-economic and environmental benefits for the surrounding communities throughout its specified service life. During analysis and design stages, it is essential to consider the different load cases that may affect the structure during its service life, including not only the conventional mechanical actions, but also all possible environmental effects that may be developed globally and locally on the structure. Bridge design for durability can be implemented by integrating the results of traditional design for mechanical loads, and durability design parameters. The key steps that need to be considered in designing for durability of a reinforced concrete bridge are [3]:

1. Description and location of the bridge.
2. Definition of the service life of the structure.

3. Analysis of macroclimate and microclimates.
4. Identification of the controlling deterioration mechanisms.
5. Primary design and selection of materials.
6. Structural design integrated with durability considerations.
7. Analysis of the structural performance over service life of the structure.
8. Adjustment of the bridge characteristics to ensure the required service life.
9. Final design and detailing.
10. Description of supplementary protection measures.
11. Definition of maintenance strategies.

SERVICE LIFE OF THE STRUCTURE

Required Service Life

According to the Canadian Highway Bridge Design Code (CHBDC – May 2010) [4], the required target service life of a new structure must be 75 years. This minimum overall service life of the bridge of 75 years implies that the most critical elements of the structure, such as foundations (abutments and piers) and girders must perform satisfactorily over this time period and must fulfill all of the required limit states for the structure. Other components less critical to the integrity of the structure may have a shorter service life, with the need to replace them as part of the maintenance strategy. Some of these components may be the asphalt concrete pavement, waterproofing membranes, protective coatings for concrete and steel elements, expansion joints, bearings, barriers, drains, slope protection systems and others.

Durability Design Formulation

The service life of a structure is affected by the macro- and micro-environmental conditions that determine the type and severity of the degradation mechanisms of the materials that compose the different structural members of the bridge. Additionally, the quality of the construction materials and the degree of exposure of the different members to the aggressive conditions may vary significantly. Therefore, the performance and service life of this kind of structure should preferably be treated stochastically; this stochastic procedure takes into account the real nature of structural performance to produce a reliable structural design.

The various equations for load, resistance and service life are quite intricate, complicated further by the existence of the various deterioration modes. There is a need to define a lifetime safety factor for the bridge. The design service life is determined by multiplying the target service life by a lifetime safety factor [5].

$$t_d = \gamma_t t_g \tag{1}$$

where t_d = design service life, t_g = target service life, and γ_t = lifetime safety factor.

Determination of lifetime safety factor

The lifetime safety factor is the relationship between the mean service life obtained from a distribution of probable service life values of a structure, and the target service life that is required for the design of the project. The lifetime safety factor can be determined by a stochastic method, assuming a normally distributed degradation around a mean value, and a standard deviation of this degradation being proportional to the mean degradation. Following these assumptions, it is possible to obtain the following expression for the lifetime safety factor [5]:

$$\gamma_t = \left(\beta v_D + 1\right)^{1/n} \tag{2}$$

where γ_t = lifetime safety factor,
β = reliability index,
v_D = coefficient of variation of degradation, and
n = degradation rate exponent.

The CHBDC establishes that for the design of new bridges, its components must not fail suddenly, and abrupt collapse of the structure must be avoided. Accordingly, the lifetime target of the reliability index β can be defined as 3.75 for most bridge structures for the ultimate limit state (ULS). The Eurocode establishes for ULS two reliability indices of 3.8 and 3.1, which are associated with the probabilities of failure of 7.2×10^{-5} and 9.7×10^{-4}, respectively. Similarly, for the serviceability limit state (SLS), the Eurocode defines two reliability indices of 2.5 and 1.5, associated with the probabilities of failure of 6.2×10^{-3} and 6.7×10^{-2}, respectively. The degradation rate exponent n will affect the determination of the lifetime safety factor (Equation 2) in the following way: $n = 1$ represents a linear degradation, $n = 0.5$ represents a retarding degradation, and $n = 2$ represents an accelerating degradation.

Chloride-induced corrosion is perhaps the most critical deterioration mechanisms in most bridge structures in North-America where de-icing salts are usually employed for traction during the winters. Accordingly, the use of a degradation rate exponent of the order of 2 could closely represent the behaviour of a reinforced concrete element subjected to such aggressive environments. Considering that the various micro-climates can be developed in different bridge members, depending on the degree of exposure to certain environmental conditions, the extent of the deterioration mechanisms can be considered to be elevated. For this reason, high values of v_D can be adopted for the determination of the lifetime safety factor [3].

A reliability index of $\beta = 3.8$ is adopted for ULS, considering that any premature failure of the structure would represent serious consequences on the surrounding environment and to the local society. Accordingly, the ULS lifetime safety factor for this structure is selected as $\gamma_t = 2$. Consequently, the design service life for the ultimate limit state is $t_{d\ ULS} = 2 \times 75 = 150$ years. For the SLS, a reliability index of $\beta = 2.5$ is adopted, considering that any premature serviceability failure of the structure would represent serious consequences in the use of the structure. Accordingly, the lifetime safety factor results to be $\gamma_t = 1.73$. Consequently, the design service life for the serviceability limit state is $t_{d\ SLS} = 1.73 \times 75 = 130$ years [3].

DURABILITY PARAMETERS

Identification of Macro-climatic Conditions

The bridge project is situated in the southwest of the province of Quebec (Canada), near the city of Montreal, with a longitude of 73º 35’ west of the Greenwich meridian, and a latitude of 45º 30’ north of the Equator. The local environment is greatly influenced by the confluence of several climatic regions, generating a climate classified as humid continental, or hemiboreal. The range of monthly temperatures varies from -40ºC to 37ºC. This region receives an average of 1047mm of precipitation per year, around 87mm per month. There is an average annual precipitation of 218cm of snowfall, which occurs from November through March. The average annual relative humidity is 77.4%, and the average monthly relative humidity varies from 71% in May to 83% in September.

There exists an extreme possibility of accumulation of ice, generating important mechanical and environmental loads that must be considered. Additionally, due to the extreme cold temperatures during this period of the year, saturated soil can be subjected to freezing, up to a depth of about 2m. This factor must be considered in the design of the foundations, placing the foundation elements at an adequate depth to protect the footings, shafts, piles and pile-caps against the effects of freezing and thawing cycles [6, 7]. According to the CHBDC, an hourly mean wind pressure of 461Pa is calculated for analysis of wind loads on bridge structures located in the metropolitan area of Montreal with a return period of 150 years [4]. The bridge crosses a river, 75m in width and 6m in depth at its deepest point. During winters, the river does not freeze; however, it carries large ice blocks that can affect the foundations.

Identification of Micro-climatic Conditions

The macroclimate surrounding the bridge can create certain micro-climatic, or local conditions at different locations on the structure, depending on the degree of exposure to the specific environmental conditions. The different micro-climate zones that are identified for the bridge structure, as shown in Figure 2. The microclimates, exposure conditions and the mechanisms of deterioration that can occur in the different structural members are summarized in Table 1.

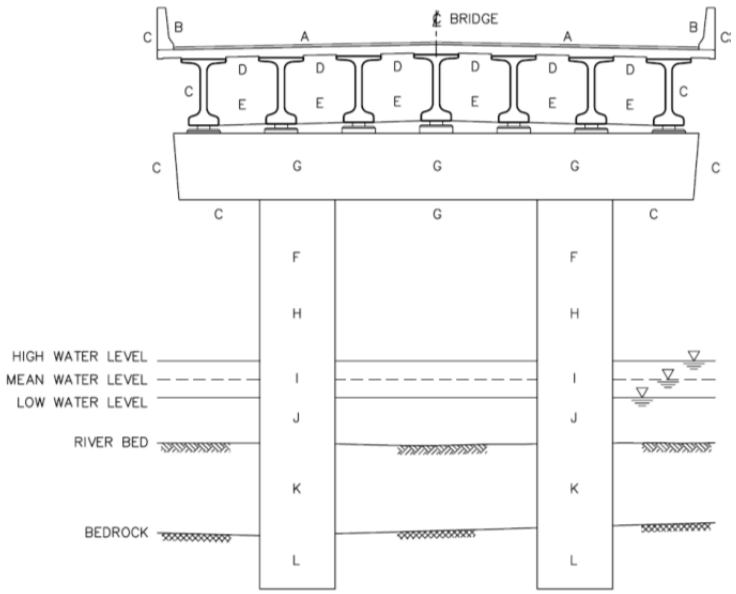

Figure 2 Microclimates at the bridge intermediate pier [3]

Table 1 Microclimates, exposure conditions and mechanisms of deterioration in different structural members of the bridge [3]

MICRO-CLIMATE	BRIDGE ELEMENT	EXPOSURE CONDITIONS	DETERIORATION MECHANISMS
A	Upper side of the deck slab	Rain and wind exposure; accumulation of de-icing salts; abrasive deterioration due to traffic; freezing and thawing cycles; exposure to CO_2; wetting and drying cycles; exposure to sunshine and daily temperature changes.	Frost attack; surface deterioration; carbonation and chloride-induced corrosion.
B	Interior face of the barrier	Rain and wind exposure; accumulation of de-icing salts; splashing of chloride solutions and water from traffic; freezing and thawing cycles; exposure to CO_2; wetting and drying cycles; exposure to sunshine and daily temperature changes.	Frost attack; surface deterioration; carbonation and chloride-induced corrosion.
C	Exterior face of the barrier; exterior girders; external faces of the piercap.	Exposure to rain; wind abrasion; accumulation of de-icing salts; wetting and drying cycles; freezing and thawing cycles; exposure to CO_2; rundown of water, or snowmelt carrying aggressive agents, especially de-icing salts; exposure to sunshine and daily temperature changes.	Frost attack; surface deterioration; carbonation and chloride-induced corrosion.
D	Lower face of the deck slab	Possible cracking and leakage of water carrying aggressive agents causing efflorescence; wetting and drying cycles; freezing and thawing cycles.	Frost attack; surface deterioration and chloride-induced corrosion.
E	Interior girders	Exposure to wind; wetting and drying cycles; freezing and thawing cycles.	Frost attack; surface deterioration and reinforcing steel corrosion.
F	Upper parts of the pier columns and abutments.	Exposure to rain and wind; wetting and drying cycles; freezing and thawing cycles.	Frost attack; surface deterioration and reinforcing steel corrosion.
G	Internal parts of the piercap; zone between the columns.	Exposure to wind; wetting and drying cycles; freezing and thawing cycles.	Frost attack; surface deterioration and reinforcing steel corrosion.
H	Middle part of the pier columns (spray zone).	Exposure to rain and wind; exposure to spray from the river; exposure to cyclical splashing; wetting and drying cycles.	Frost attack; surface deterioration and reinforcing steel corrosion.
I	Lower part of the pier columns at the transition zone between high tide and low tide.	Frequent wetting - drying and freezing - thawing cycles; exposure to rain and wind; ice abrasion and ice impact.	Frost attack; surface deterioration and reinforcing steel corrosion; abrasion of concrete by ice.
J	Lower part of the pier columns in the submerged zone.	Water and ice abrasion; ice impact; absence of air and free oxygen.	Surface deterioration; abrasion of concrete by ice.
K	Pier column foundations through the sedimentary deposits of the river bed.	Embedded zones into the sedimentary stratum; absence of air; no significant potential for chemical attack due to the interaction with aggressive soil deposits.	No major deterioration is expected.
L	Embedded zone of the pier columns into the bedrock.	Embedded zones into the bedrock; absence of air; no significant potential for chemical attack due to the interaction with aggressive soil deposits.	No major deterioration is expected.

Environmentally-induced mechanisms of deterioration

It is possible to identify the principal mechanisms of deterioration from the different possible modes of deterioration in a component, that may affect the integrity of the construction materials and hence, the load-carrying capacity of the structural member. These mechanisms of deterioration have to be analyzed with appropriate analytical deterioration-time models to evaluate the damage. While considerable research is in progress to develop these models, the models presented by Sarja and Vesikari (1996) [5], and by The International Federation for Structural Concrete (2010) [8] have been adopted in this research work; these can be updated using more accurate and up-to-date models as they become available. The mechanisms which were considered during the design for durability of the bridge are [3]:

1. Frost Attack: Caused by freezing and thawing cycles.
2. Abrasion of Concrete by Ice: From the permanent exposure to the flow of the river.
3. Abrasion of Concrete by Ice: From the permanent exposure to the flow of the river.
4. Surface Deterioration: Weathering caused by temperature and moisture fluctuations, leaching, accumulation of salts and efflorescence.
5. Corrosion of Reinforcement: Chloride- and carbonation-induced corrosion.

Minimum Requirements for Construction Materials

After an iterative process of analysis for the different modes of the deterioration [3], it is possible to identify the various rates of degradation of the different bridge elements, and then improve and adjust the design for the durability requirements for the construction materials, such as concrete cover, type of steel, concrete mixture design, and supplementary protective measures, with the purpose of attaining an appropriate optimum performance of the bridge during its required service life. Table 2 shows the different rates of the various mechanisms of deterioration of the bridge elements.

Table 2 Rates of deterioration, initiation time for corrosion and carbonation coefficients [3]

Mechanisms		RATES OF DETERIORATION, mm/year							
		Slab	Barriers	Pier caps	Columns	Abutments	Caissons	Girders	
								Edge	Interior
Frost attack		0.1953	0.2139	0.1307	0.1024	0.1500	0.0341	0.1193	0.0540
Abrasion of concrete by ice	Without loosening aggregates	-	-	-	2.3835	-	2.1792	-	-
	With loosening aggregates	-	-	-	22.3601	-	24.4564	-	-
Surface deterioration		0.4108	0.2884	0.0940	0.0476	0.2378	0.0048	0.1737	0.0135
Chloride-induced corrosion		0.031	0.024	0.019	0.002	0.021	0.002	0.024	0.002
		Corrosion initiation time, t_0 (years)							
		18	20	25	28	25	74	6	6
Carbonation-induced corrosion		Carbonation coefficient, K_c							
		0.92	1.01	1.17	2.36	1.18	1.18	0.90	2.01

Table 3 shows the minimum required concrete cover thicknesses for the various bridge elements that were calculated using the iterative improvement of the durability design parameters for the bridge. These values were different from the different prescriptive values of minimum concrete cover thickness described in the various codes used in Canada for the design of concrete structures. In one of the cases, the prescriptive value of concrete cover for the slab was lower than the minimum concrete cover thickness required to ensure an adequate durability and performance of this element. The manipulation of the construction materials during construction plays an important role on the final durability provisions of a concrete bridge. It is crucial to implement careful procedures during mixing, transporting, placing, finishing and curing the concrete. Similar care must also be exercised in handling the steel reinforcement, especially when galvanization or epoxy coatings are planned to be used.

Table 3 Concrete cover thicknesses for the analyzed members of the bridge

MINIMUM CONCRETE COVER THICKNESS, mm								
Concrete cover requirement	Reinforced Concrete						Prestressed Girders	
	Slab	Barriers	Piercap	Columns	Abutment	Caissons	Edge	Interior
CSA-S6-06	70	70	70	70	70	100	45	40
CSA A23.1	60	60	60	40	75	75	60	60
MTQ*	60	75	75	75	75	60	40	40
Required	73	56	34	44	50	20	37	33
Adopted	75	75	75	75	75	75	45	45

- Ministère de transport du Québec

STRUCTURAL DESIGN FOR DURABILITY

The structural design of the different bridge members was performed according to the guidelines and specifications provided by the CHBDC. The integration of the durability parameters with traditional structural design procedures necessitated the implementation of different models of analysis and design of the different bridge elements, based on their nature and design assumptions. Basically, these models incorporated the progress of a controlling degradation front towards the center of the section of the bridge element [9].

Prestressed Concrete Girder Design

The integration of the rates of deterioration that affect the girders cannot be made directly in the structural design formulation for these elements due to the complexity of the various parameters involved in the design of a prestressed concrete bridge girder. However, the input information for these parameters is influenced by the rates of deterioration at different time intervals, which enables establishing an iterative process that simulates the progressive deterioration of the bridge girder and the corresponding loss of load-carrying capacity and serviceability.

Figure 3 shows the progress of deterioration of the composite slab-girder section, represented as a grey-coloured zone that penetrates gradually into the girder and the slab with time, according to the rate of deterioration acting on the bridge deck.

The performance of the bridge girders during the design service life is summarized in Figures 4 to 6, for the different limit states considered for the design of these elements, such as ULS, SLS, and fatigue limit state (FLS).

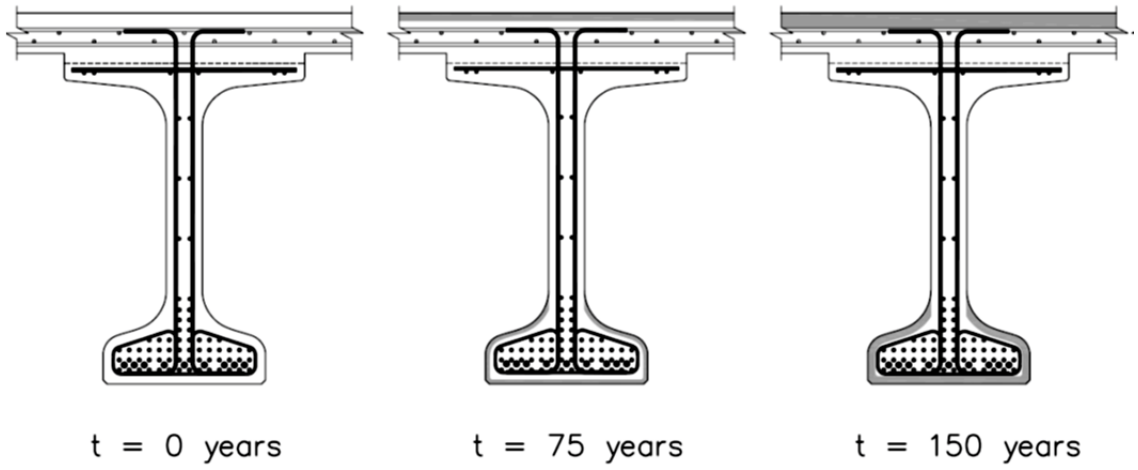

Figure 3 Degradation of the composite slab-girder section with time [3]

With time, the compressive and tensile stresses at the girder extreme fibres increase as a result of the loss of cross-sectional area of the composite slab-girder section. The tensile stresses increase at a higher rate than the compressive stresses during the service life. However, none of these internal stresses exceeded the maximum allowable levels, even after 150 years.

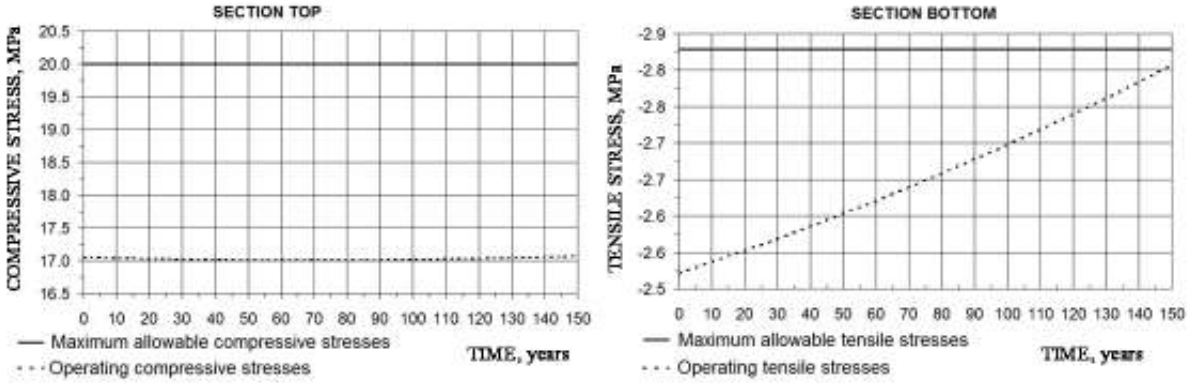

Figure 4 Internal stress levels of the composite section (ULS) [3]

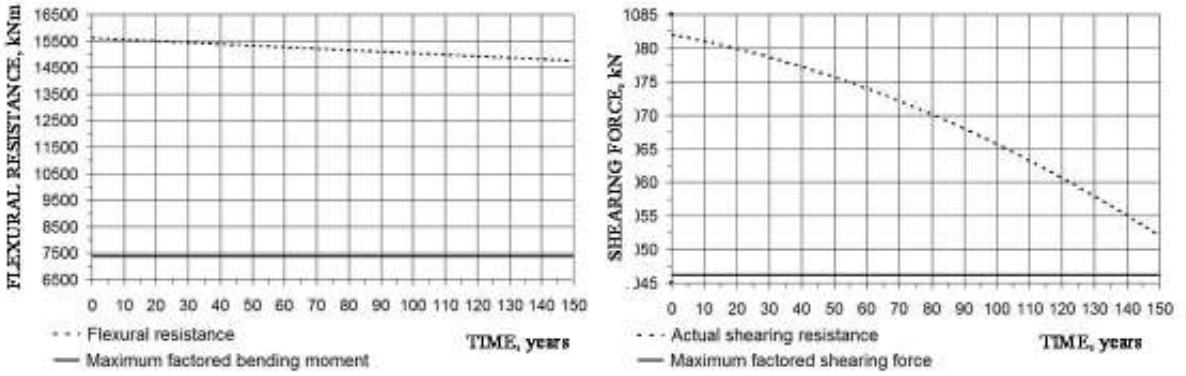

Figure 5 Flexural resistance and shearing resistance of the composite section (ULS) [3]

The loss of shearing resistance was more pronounced than the loss of flexural capacity (Figure 5). However, none of these ultimate limit states were attained by the composite section, even after 150 years. The increase of static deflection is represented by a second-degree curve, similar to the increments of the internal stresses in the composite section. The serviceability limit state of deflection is fulfilled throughout the service life of the bridge (Figure 6). The stress variation was within the maximum allowable strand stress range of 125MPa for fatigue considerations.

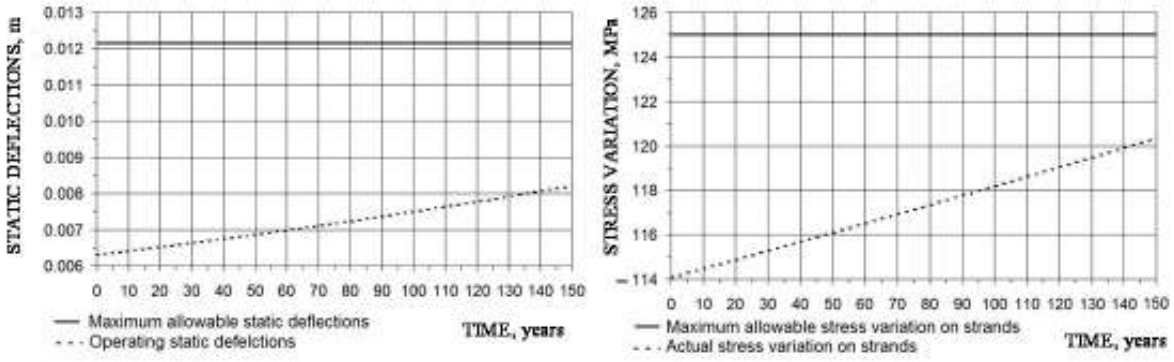

Figure 6 Static deflections (SLS) and prestressing steel stress variations (FLS) of the composite section [3]

As a general conclusion, the selection of the type of girder, as well as the careful design and selection of the construction materials for the deck elements produce a satisfactory performance of the composite slab-girder section during the design service life and beyond (150 years) for the different limit states considered in the design of the bridge superstructure for durability.

Deck Slab Design

Reinforced concrete elements, such as the bridge deck slabs, allow a more direct integration of the durability parameters into the structural design equations. Figure 7 presents the definition of a model that integrates all of these parameters, where b = width of the reinforced concrete section, h_0 = initial height of the section, d_0 = initial effective height of the section, c_{01} = initial concrete cover at the internal face of the section, c_{02} = initial concrete cover at the external face of the section, r_{c1} = depth of deterioration of concrete that takes place at the

internal face of the section, r_{c2} = depth of deterioration of concrete that takes place at the external face of the section, h_t = height of the section being affected by the rates of deterioration r_{c1} and r_{c2}, d_{t1} = effective height of the section being affected by the rate of deterioration r_{c1}, d_{t2} = effective height of the section being affected by the rate of deterioration r_{c2}, c_{t1} = concrete cover of the section affected by the rate of deterioration r_{c1}, c_{t2} = concrete cover of the section affected by the rate of deterioration r_{c2}, d_{b1} = initial diameter of the reinforcing bars near the internal face of the section, d_{b2} = initial diameter of the reinforcing bars near the external face of the section, d_{bt1} = diameter of the reinforcing bars affected by the rate of corrosion r_{s1}, d_{bt2} = diameter of the reinforcing bars affected by the rate of corrosion r_{s2}, r_{s1} = depth of corrosion of the reinforcing steel at the internal layer of reinforcement, and r_{s2} = depth of corrosion of the reinforcing steel at the external layer of reinforcement.

Figure 7(a) presents a reinforced concrete section to be analyzed per unit width (deck slab, barrier, beam, etc.), where the concrete cover on both sides are subjected to different mechanisms of deterioration. This will be the case of a bridge deck slab which is subjected to two microclimates with different rates of deterioration taking place on the two sides of the element. Figure 7(b) represents the situation where the concrete cover is completely deteriorated and then the reinforcing steel begins to corrode. The active corrosion process starts once the initiation period for corrosion is over, and then it continues according to relevant the rate of corrosion and other durability parameters. Figure 7(c) shows that corrosion first starts at the outermost exposed point of the reinforcing bar, and then it continues around the perimeter of the bar[i]. Figure 7 (d) shows that once corrosion on the rebar has occurred over the entire perimeter, corrosion will continue towards the inside of the rebar, reducing the cross section of the bar in proportion to the rate of corrosion.

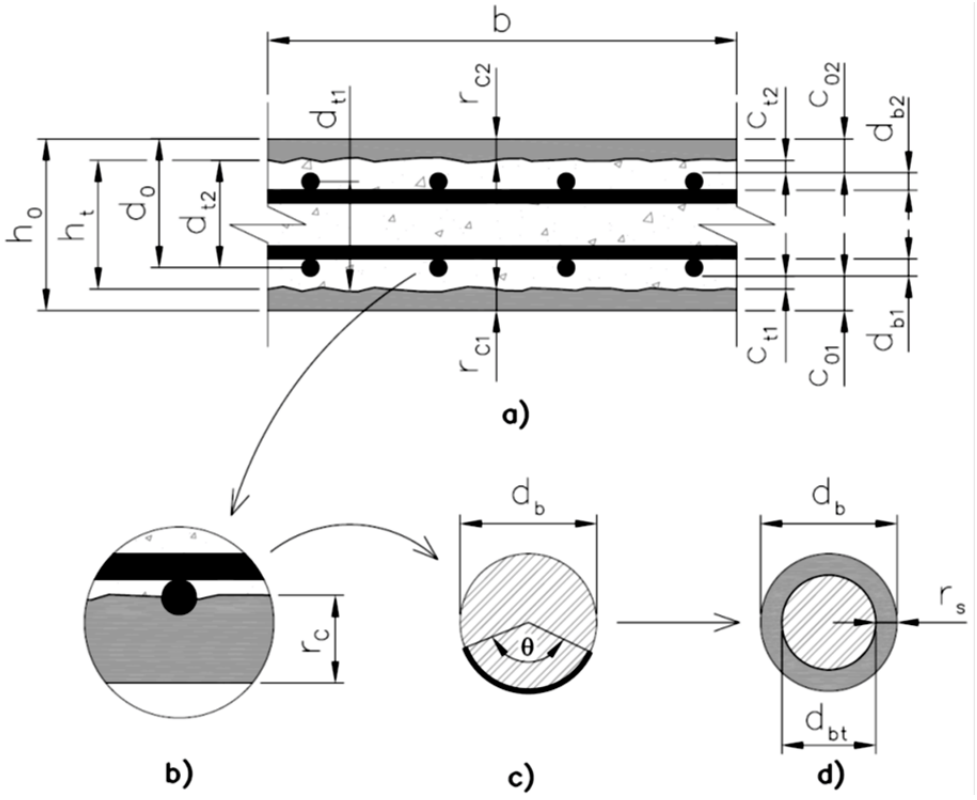

Figure 7 Reinforced concrete section parameters for the structural and durability design [3]

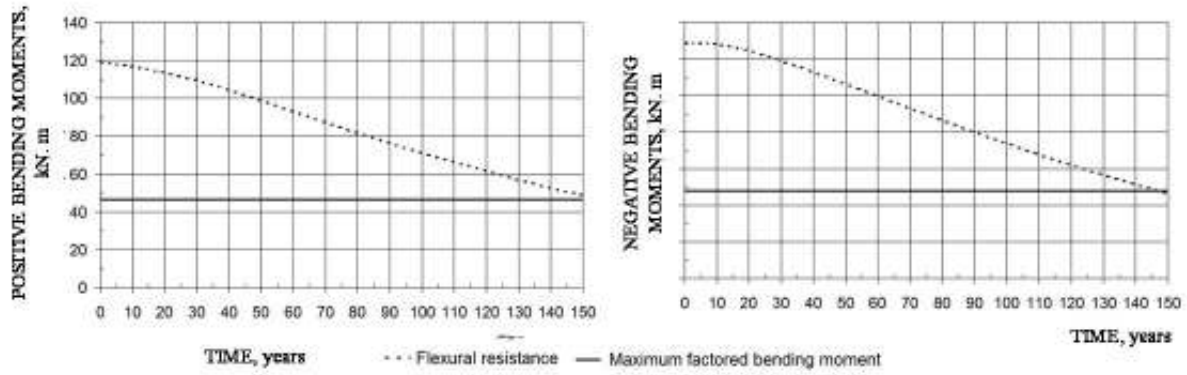

Figure 8 Positive and negative bending moments on the deck slab (ULS) [3]

Figure 8 shows the load-carrying capacity performance of the deck slab in terms of flexural capacity for positive and negative bending moments resulting from the loads applied to the different panels of the slabs. Figure 9 shows the performance of the cantilever overhang of the deck slab, showing the loss of flexural resistance in negative bending and an increase in the deflections at that portion of the slab.

It is evident that with proper reinforcement distribution, adequate selection of materials, and careful design of the concrete mixture, the slab presents an adequate performance throughout the service life of the bridge. For the ULS and SLS, both design service lives of 150 and 130 years were attained.

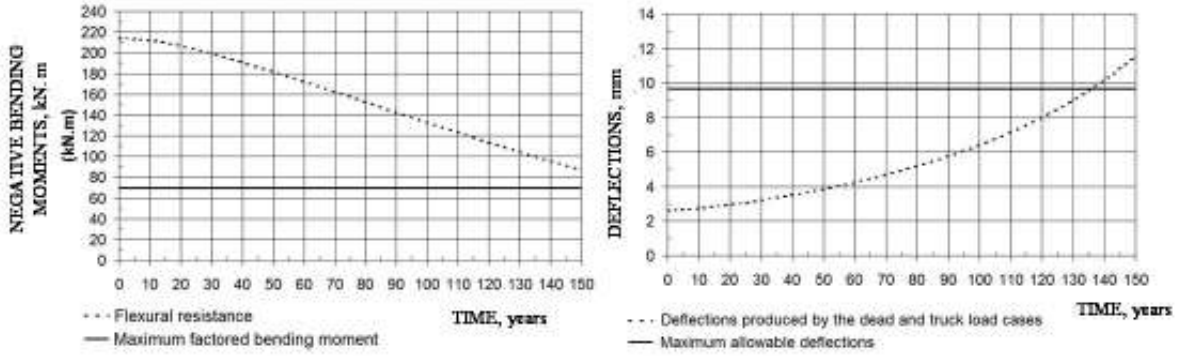

Figure 9 Flexural resistance (ULS) and deflections (SLS) of the cantilever overhang of the deck slab [3]

Pier Colum Design

The structural design for durability of pier columns was performed using an iterative analysis of the different column sections that are getting deteriorated by the various degradation mechanisms, and identifying their bearing capacity against the applied loads by using the interaction diagrams for flexural and axial loads for the different column sections.

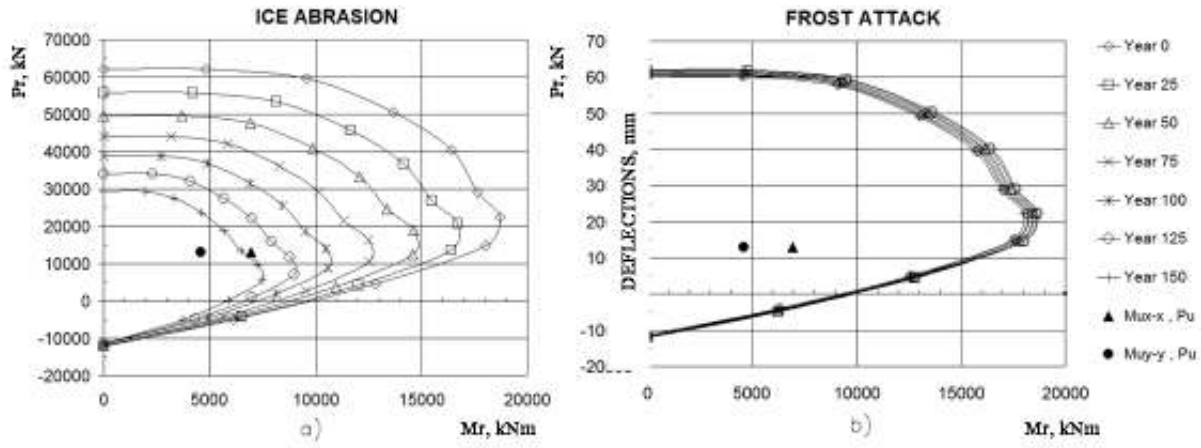

Figure 10 Interaction curves of the pier columns considering deterioration caused by abrasion by ice and frost attack [3]

The performance of the pier columns under the condition of flexural compression and deterioration mechanisms is analyzed initially for abrasion by ice as the controlling mechanism of deterioration. Figure 10 (a) shows, that the abrasion by ice on the pier columns produces a significant deterioration of the reinforced concrete section, up to the point of inducing failure of the column at the ULS after 145 years of service life.

The piers of a bridge play a critical role in the integrity of the bridge structure, and at the same time they are extremely difficult and costly to replace. Therefore, it is very important that these elements attain the required design service life of the bridge. For this reason, it is required to limit the aggressive action of ice abrasion on the pier column by implementing additional protective measures represented by the installation and construction of protective islands around the piers, made of protective rock layers placed and arranged to decrease the flow around the pier columns. Once these protective islands are installed, the controlling mechanism of deterioration acting on the pier columns is frost attack. Figure 10 (b) shows the performance of the pier column over the design service life, considering the effect of frost attack. It is evident that the performance of the pier column is satisfactory. At the end of the service life, there is enough column resistance against the ultimate flexural compression conditions developed in both principal directions of the columns.

SUPPLEMENTARY PROTECTION MEASURES

Following a multi-stage protection strategy, additional protective measures are implemented to reduce the impact of the deterioration mechanisms on the most vulnerable parts of the bridge, thereby extending its service life. There are some supplementary protection measures that are applicable to all reinforced concrete elements of the bridge. They are related to the high quality control standards during the production, handling, placing of the concrete, and adequate procedures for placing, compacting, vibrating and curing the concrete. However, there are some others which are more specific to the different bridge elements. These are:

1. Prestressed girders: The use of coatings, sealing treatments and/or membranes on the girder surfaces to prevent chloride penetration during the design service life, the use of regular steel for the passive reinforcement to reduce the electrochemical potential for corrosion of the prestressing strands, and the installation of parapet walls (tall

barriers) and cornices to minimize the splashing and rundown of water with de-icing salts to the external faces of the edge girders.

2. Bridge deck slab: The use of galvanized steel for the slab reinforcement, the installation of waterproofing coatings and membranes on top of the concrete slab, and the use of microfilament polypropylene fibres in the concrete mixture to control cracking, improve impact, shatter and abrasion resistance.
3. Pier columns: The use of galvanized steel for the column reinforcement, and the construction of protective islands around the piers to diminish the effects of abrasion by ice and to reduce the risk of any vessel collision.

MAINTENANCE STRATEGIES

The maintenance procedures must be addressed to ensure the attainment of the design service life for each bridge element, from the foundation to the superstructure. The maintenance strategies must consider different kinds of maintenance procedures to be performed on the bridge during its service life, including its maintainability, and the needed preventive and corrective maintenance. Figure 11 shows a scheme that brings the key aspects that need to be considered to define the maintenance strategies for the bridge.

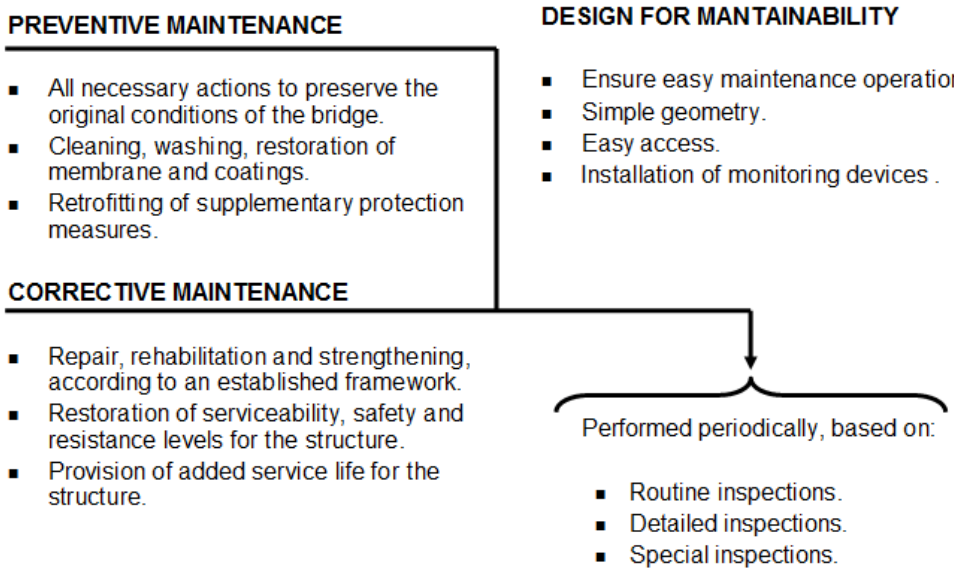

Figure 11 Key aspects of the maintenance strategies [3]

CONCLUSIONS

The following basic conclusions can be drawn from this research work:

- A complete structural design for durability is essential to ensure the attainment of the required service life.

- A holistic design approach is necessary to define an adequate design for durability.

- Different interdisciplinary studies need to be integrated within the holistic design approach.

- The feasibility of a bridge project must be based on its life-cycle performance and cost analysis, converting all future operation and maintenance costs into the present value.

- A thorough understanding of the macroclimatic and microclimatic conditions that surround the bridge is necessary to simulate the decline of the load-carrying capacity of the bridge, and to formulate the necessary supplementary protective measures.

- The integration between structural design and materials engineering is basic to define the time-dependant performance of the bridge structure.

- The structural design must be accompanied by a maintenance strategy for the owner and the operator to ensure satisfactory performance of the bridge throughout its service life and beyond.

REFERENCES

1. SOMMERVILLE, G., Engineering design and service life: a framework for the future. Prediction of Concrete Durability. Proceedings of STATS 21st Anniversary Conference. Edited by Glanville J. and Neville A. E & FN SPON. The London Geological Society. London, UK. November 1995.

2. BIJEN, J., Durability of Engineering Structures. Design, repair and maintenance. Woodhead Publishing Limited. CRC Press. Cambridge, England. 2003.

3. MACÍA, J. M., Design of Concrete Bridges for Sustainability and Durability. M. Eng Thesis. Department of Civil Engineering and Applied Mechanics. McGill University. Montréal, Canada. July 2011.

4. CANADIAN STANDARDS ASSOCIATION (CSA), Canadian Highway Bridge Design Code. CAN/CSA-S6-10. National Standard of Canada, Standards Council of Canada, November 2010.

5. SARJA, A, AND VESIKARI, E., Durability Design of Concrete Structures. Report of RILEM Technical Committee 130-CSL. RILEM (The International Union of Testing and Research Laboratories for Materials and Structures), Technical Research Centre of Finland. VTT Building Technology, Espoo, Finland. E & FN SPON. 1996.

6. ENVIRONMENT CANADA, Canadian Climate Normals 1971-2000. http://www.climate.weatheroffice.ec.gc.ca/climate_normals/index_e.html.

7. http://www.climatetemp.info/canada/montreal-quebec.html

8. FÉDÉRATION INTERNATIONALE DU BÉTON (FIB), COMITÉ EURO-INTERNATIONAL DU BÉTON (CEB), FÉDÉRATION INTERNATIONALE DE LA PRÉCONTRAINTE (FIP). Model Code 2010. First complete draft. Volume 2. April 2010.

9. ANDRADE, C., ALONSO, C., GONZALES, I.A., AND RODRIGUEZ, J., Remaining Service Life of Corroding Structures. Proceedings of the IABASE Symposium Durability of Structures. Lisbon. 1989.

10. JI, C., JEFREMCZUK, S., AND MIRZA, M. S., Design of Reinforced Concrete Elements for Durability Against Corrosion. 1st Canadian Conference on Effective Design of Structures, McMaster University, Hamilton, Ontario, Canada, July 10 – 13, 2005.

Rheological Measurement of Fresh Portland Cement Concrete Using Direct Shear Box Tests

S Girish[1], G S V Kumar[1], L Shobha[2], B S Santhosh[1]
1 – B.M.S College of Engineering, India
2 – Government of Karnataka, India

Generally the rheological properties of fresh concrete are described by the Bingham's parameters, namely yield stress and plastic viscosity. But, there is no concurrence in the measurement of rheological properties by various rheometers, besides, the stimulus provided to concrete during testing is dynamic. Systematic study of rheological properties using specially fabricated customised direct shear box is used for fresh Portland cement concrete in this study. The uniqueness of the procedure is that after finding the peak shear stress, the shear stress at zero normal stress and at zero displacement rate was found before finally finding the rheological properties. The important characteristics of the test are the very low shear rate applied on the specimen during testing which is similar to the condition experienced by the concrete in the field and also the static condition of the test. The water was varied from 160 to 190 l/m^3 and cement content from 300 to 450 kg/m^3. Different displacement rates (5 to 25 mm/min) and normal stresses (0.015 to 0.035 N/mm^2) were used. Total numbers of trials considered were 162. The rheological properties were obtained immediately after mixing and for few mixes after a lapse of 40 minutes and 60 minutes after through mixing. The results show that fabricated customised medium size direct shear box can be used as a new tool to find the relative values of yield stress and plastic viscosity of fresh concrete effectively as a static test with low shear rate and can be an alternative in place of rheometers with high shear rate. The values are higher as compared to the values obtained by other rheometers. However the trends are very similar to the studies using rheometers i.e., significant decrease in rheological properties as the paste content increases. Also thixotropic behaviour is clearly observer with elapsed of time.

Dr. S. Girish is Professor in the Department of Civil Engineering, B.M.S College of Engineering (BMSCE), Bangalore. He has worked on Self- compacting concrete for his doctoral work. He has published research papers in various National and International Journals and in Conferences. He was the recipient of Karnataka state academic award for the best project in the year 2009 and 2011. His research interests include Fly ash characterization, Self-compacting concrete, Bacterial concrete, Pervious concrete and Geopolymer concrete

Mr. Santhosh, B. S is pursuing his doctoral work on rheological properties of fresh concrete using direct shear box. Presently he is a Assistant Professor in the Department of Civil Engineering, JSS Academy of Technology Education, Bangalore. His areas of interest include SCC, Pervious concrete and Rehabilitation of Structures.

Mrs. Shobha.L, is at present working as Assistant Engineer, Irrigation Department, Government of Karnataka,Bangalore.She completed her Master's degree from SJCE in Industrial Structures. Her areas of interest include SCC, Rheology of fresh concrete, Pervious concrete and Rehabilitation of Structures.

Mr. Vinay Kumar is a Post graduate student in Construction Technology from B.M.S. College of Engineering, Bangalore. His research interest includes SCC, Rheological properties of fresh concrete and Green building and its implementation.

Keywords: Direct shear box, Plastic viscosity, Rheology, Rheometers, Yield stress

INTRODUCTION

Concrete is a complex material and its properties in the fresh state can have a large effect on hardened properties. Unfortunately, the technology to measure the properties of fresh concrete has not changed significantly in the last century. Fresh concrete property i.e. Workability is still measured using the slump test. In fact, concretes with the same slump may flow differently and have different workability. The reason two concretes with the same slump behave differently during placement is that, concrete flow cannot be defined by a single parameter [1]. Rheology is a study of deformation and flow of materials under loads. Workability of concrete mixture is closely related to the flow properties of the concrete and there is a need to develop methods based on a material science approach. Fluid rheology is a well established, widely used science that can be applied to the properties of fresh concrete. It can be said that fresh concrete is a concentrated suspension of aggregates in cement paste and the cement paste itself is a concentrated suspension of cement grains in water. To characterize and understand the fresh properties of concrete at least two physical properties, namely yield stress and plastic viscosity, need to be measured. Yield stress commonly occurs in multi phase fluids such as concentrated suspensions. The solid particles interact to form a flocculated, three-dimensional network structure that resists flow at sufficiently low stresses.

The yield stress is related to the force required to break down this structure and initiate flow. The concept of yield stress is readily seen in concrete slump test. Even though fresh concrete can be considered as a fluid, the characterization of its rheology is complicated by the fact that concrete is a complex heterogeneous material with time-dependent properties and wide range of particle sizes. Due to this complexity, no definite method for predicting the flow of concrete exists and measurements of the rheological parameters are not easily made. Therefore, the flow of a given concrete is usually measured at sites using one of the many empirical tests like slump test [2].

Flocculated systems such as cement pastes typically are thixotropic and exhibit a yield stress. Most researchers agree that the flow of concrete can be described reasonably well using a Bingham equation. This equation is a linear function of the shear stress (the concrete response) versus shear rate. Two parameters provided by the Bingham equation are the yield stress and the plastic viscosity. It describes a linear relationship between the stress acting to shear concrete (shear stress = τ) and the rate at which it is sheared (shear rate = γ) with viscosity (μ) being the slope in this relationship and the y intercept being the yield stress (τ_0) and the relation is as follows:

$$\tau = \tau_0 + \mu\gamma$$

The term yield stress and viscosity provides a more comprehensive description of fresh concrete than the conventional workability tools. Static measurement of yield stress measured when the material is initially at rest are typically higher than the measurements of yield stress obtained from dynamic measurements of the flow curves. Bingham flow model commonly assumes that if lower shear rates could be measured the flow curves would continue back and intercept shear stress axis [2]. Accurate data at low shear rates are needed to confirm that flow curves can truly be extrapolated to a zero shear rate. The accuracy of such low shear measurements is reduced by slip, fracture and expulsion of sample. The advent of modern controlled stress rheometers have allowed measurements to be made at significantly lower shear rates than previously possible. These rheometers show that at low shear rates viscosity is very high.

When the shearing is increased beyond a certain point, viscosity begins to decrease rapidly. It has been debated widely if a yield stress really exists or not, since in a given time all fluids will exhibit flow. But it is a term with practical significance. Static measurement of yield stress measured when the material is initially at rest are typically higher than the measurements of yield stress obtained from dynamic measurements of the flow curves.

Nguyen and Boger [3] state that yield stress is a model parameter but not a true material property. If it is assumed that yield stress is a relevant parameter to be measured, the actual measured value can vary significantly depending upon the test method used.

RHEOMETERS

Rheological properties can be measured in capillary tube viscometers or rotational rheometers. In concrete, rotational rheometers are used predominately in cases where the rheological parameters are to be determined in fundamental units while variations on capillary tube viscometers are used in limited cases. According to Hackley and Ferraris [4], rotational methods are generally better for concentrated suspensions, gels, and pastes despite the fact that capillary tube methods tend to be more precise in measuring viscosity. Rotational methods offer the advantage of being able to shear a sample continuously in order to achieve equilibrium and to monitor changes over time. Rheometers usually measure shear stress at varying shear rates. They are basically dynamic tests. By measuring a series of combinations of shear stress and shear rate, a flow curve can be determined.

Some of the concrete rheometers used are BML, BTRHEOM, CEMAGREF-IMG coaxial rheometer and IBB. While traditionally rheometers have been successfully used for fine particle suspensions, concrete presents unique challenges. Unlike traditional rheometers, concrete rheometers must deal with the large size of coarse aggregates, concrete segregation, and time dependence of flow properties. For instance, in order to achieve a linear flow gradient with coaxial cylinders rheometers, the difference between the inner and outer cylinder radii should be at least five times the maximum aggregate size. Rheometers constructed based on these particular requirements are generally too large to be practical. Indeed, many of the problems with rotational rheometers have yet to be overcome. Rotational rheometers are most typically used exclusively in the laboratory. Although some rotational rheometers have been designed to be sufficiently small and rugged for use on jobsites, the limited availability and high cost of these devices make them impractical for regular field use. There is also a problem of dead zone in co-axial cylinder rheometers. Dead zones are those where the material is static and does not flow.

The problem cannot be fully eliminated when the rotational speeds are low, particularly for concrete which exhibit significant yield stress. Methods to improve the accuracy of such rheometers are not always successful. In concrete, the presence of aggregates also influences the actual radius at which flow ceases and dead zones come into effect. Also, the range of shear rates applied in a rheometer for a given fluid should be similar to the shear rates present in an actual field conditions, but this does not happen in most rheometers. Not many studies seem to have been done to determine the actual shear rates in the field for different construction processes. A number of papers in the literature indicate that thixotropic and time dependent properties alter the values of yield stress and plastic viscosity and hence it is almost impossible to determine these parameters accurately in any dynamic rheometer. It is also known that it is inappropriate to test low slump concretes in concrete rotational

rheometers due to the high deborah number that indicates that the material is less of a fluid but nearer to a solid. The values of yield stress and plastic viscosity compiled by Ferraris et al. [5] from different rheometers, but measured on identical specimens, show that there is no agreement of the measured values among the different types of rheometers.

DIRECT SHEAR BOX

As reported by Newman [6], Herschel and Pisapia [7] and later L'Hermite and Tournon [8] studied the resistance of freshly mixed concrete in terms of shear stress. L'Hermite and his co-workers used direct shearing apparatus of the kind used for testing the strength of soils. The method chosen to follow indicates that they considered shearing stress in a freshly mixed concrete to be due to internal friction analogous to the friction between a solid body and a plane solid surface when that body is resting on the surface.

When they plotted the graphs between shear stress versus shear strain for various normal stresses, keeping the displacement rate constant, interestingly they found that shear stress increases linearly with the degree of distortion up to a maximum value, then decreases and finally levelling off. This was called as 'dilatancy' and the reason for this decrease in shear resistance was that after this stage, further distortion resulted in the formation of a sliding plane and the coarse particles originally interlocked take up positions with less resistance to movement. So, in a direct shear test apparatus, the shearing stress is created by imposing a movement of the lower half of the shear box while applying a static load to the load plunger and can be used to assess the cohesive strength of a fresh concrete mixture.

EXPERIMENTAL PROGRAMME

Materials

Ordinary Portland cement (C 53 grade), conforming to the requirements of Indian standard IS 12269-1987 (ASTM C 150-85A) was used. The specific gravity value and Blaine fineness were 3.15 and 265 m^2/kg. Natural river sand was used as fine aggregate and crushed angular granite stone as coarse aggregate. The bulk specific gravities of the coarse aggregate and fine aggregate were 2.68 and 2.67 g/cm^3 respectively and their absorption values were 0.35 and 2% respectively. The maximum size of the aggregate used was 20 mm.

Methodology

In this study, the cement content was varied from 300 to 450 kg/m^3 and water content from 160 to 190 l/m^3 covering practically the range used in the field covering a wide range of w/c ratio from 0.35 to 0.63. The mixture proportioning of concrete was based on absolute volume concept. Total of 162 trials consisting of three different strain rates of 5, 15, 25 mm/min, in combination with three different normal stresses of 0.015, 0.025, 0.035 N/mm^2, were used. The use of chemical admixture was avoided as it will influence and interfere in the test values. After through mixing of the fresh concrete in a pan mixer the rheological properties were determined and for few mixes after a lapse of 40 minutes and 60 minutes after mixing. The results immediately after mixing were considered as results at zero minutes. For each trial after through mixing the concrete was kept undisturbed till the required time of testing.

Medium Size Direct Shear Box

Based on the experience from the previous test results [9] obtained from using the smaller size direct shear box (60 mm × 60 mm × 25 mm) and the unique procedure adopted for obtaining rheological parameters for static loading condition, fabricated customized medium size direct shear box was used for testing fresh concrete in this study. The size of the sample was 150 mm cube and can be tested for coarse aggregate of maximum size 25 mm. The strain rate for shear load ranges from 1mm/min to 100 mm/min. The shear stress developed at such a faster rates is captured using servo-controlled data acquisition system. The loading unit has different normal stresses up to maximum of 30 N/mm². The normal loads are applied on the specimen through a pneumatic actuator and a stress regulator. Electronic data acquisition system comprises of micro controlled based signal conditional unit and a processing unit along with a Load cell of high sensitivity of 0.1 kN with a load measuring capacity of 50 kN. Data acquiring system can acquire and store the data at the rate of four consecutive readings per seconds. There are two specifically programmed softwares, namely, Tango and Direct Shear Multi cohesion version 1.0.1. Tango is used for acquiring the data and storing it to computer and the other is used to analyse the stored data (simple excel sheet can also do the job). Figure 1 shows the newly fabricated customized medium size direct shear box. The important characteristics of this test are the static condition of the test and very low shear rate applied on the specimen during testing which is similar to the condition experienced by the concrete in the field.

Figure 1 Medium size direct shear box

Procedure for the Determination of Rheological Properties

Extending the study of L'Hermite, the detailed procedure to determine the Bingham parameters at zero normal stress and zero displacement rate using fabricated customized medium sized Direct Shear Box was published for the first time by the authors elsewhere [10]. This section briefly illustrates the procedure once again for the benefit of the readers. The freshly mixed concrete (say Mix G) was placed in the direct shear box and a particular displacement rate (γ) and a normal stress was applied on the sample. The test was stopped when the shear load started to decrease (point of dilatancy) or when it became almost constant. The test was repeated for different normal stresses. One such plot for the mix (G) is shown in Figure 2. The plot of shear stress versus shear strain for displacement rate of 5 mm/min for normal stress of 0.015 N/mm² is shown in Figure 2 (a). From this relation the maximum shear stress (ζ') for the normal stress 0.015 N/mm² was found.

For the same normal stress, similar procedure was followed for the mix for finding the maximum shear stress with the displacement rates of 15 and 25 mm/min and the plots are shown in Figure 2 (b) and 2 (c). Similar plots of shear stress versus shear strain for the displacement rates of 5, 15 and 25 mm/min were obtained for other normal stresses 0.025 and 0.035 N/mm².

These plots are shown in Figures 2 (d) to 2 (i) and maximum shear stresses were obtained. Further, with the values of maximum shear stress for each displacement rate and the corresponding normal stresses, graphs are plotted and straight line fits were made (Figure 3). The line intersecting the y-axis (shear stress axis) gives the yield stress (ζ'_0) of concrete at zero normal stress for a particular displacement rate, as the direct shear box test cannot be carried out at a zero normal stress. Similar straight line fits were made for all displacement rates and yield stress at zero normal stresses were obtained.

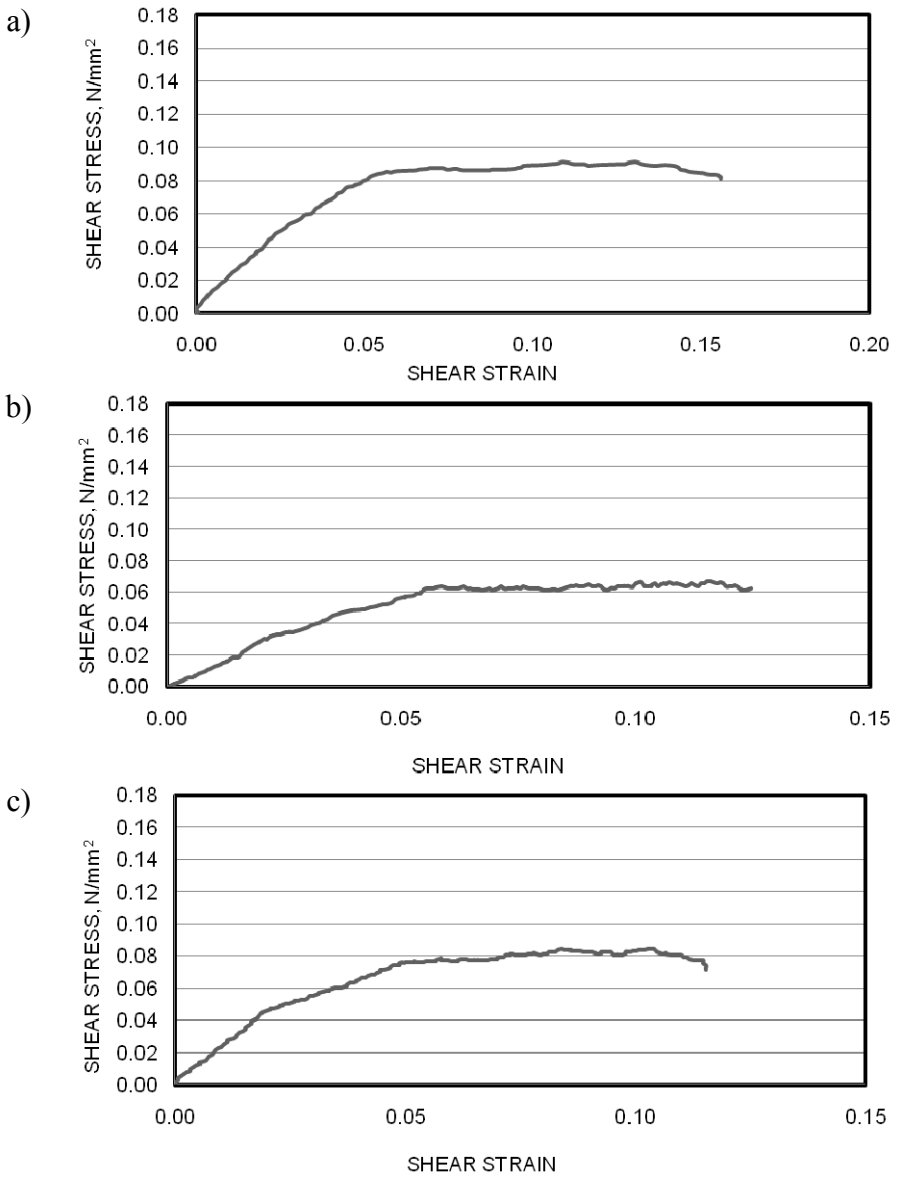

Figure 2(a, b, c) Shear stress versus shear strain curves for mix G at normal stress of 0.015 N/mm² and displacement rates of (a) 5 mm/min, (b) 15 mm/min and (c) 25 mm/min

d)

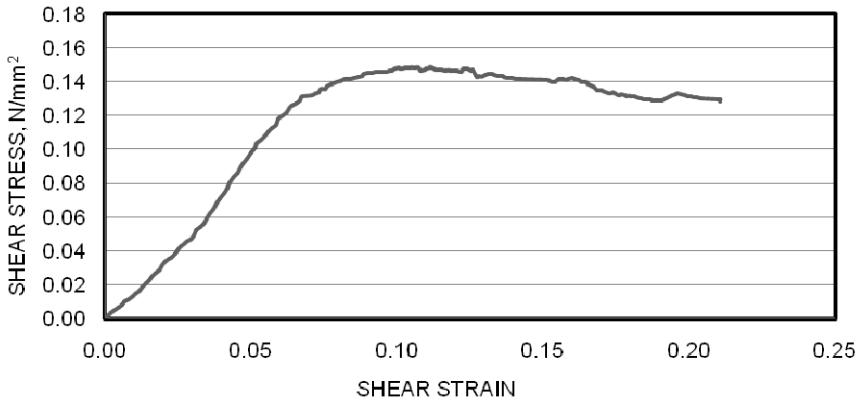

e)

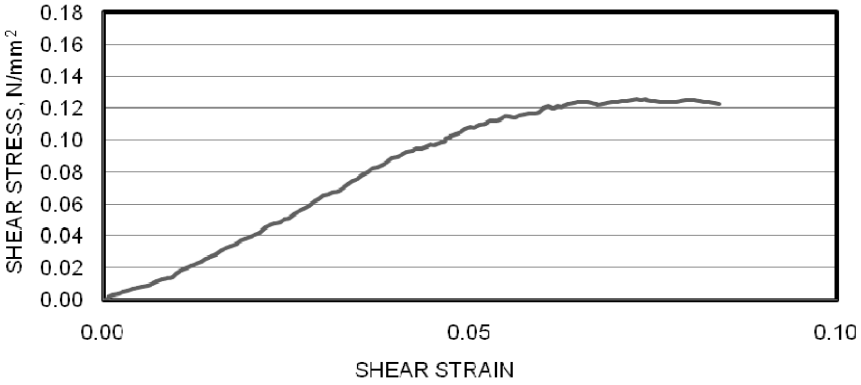

f)

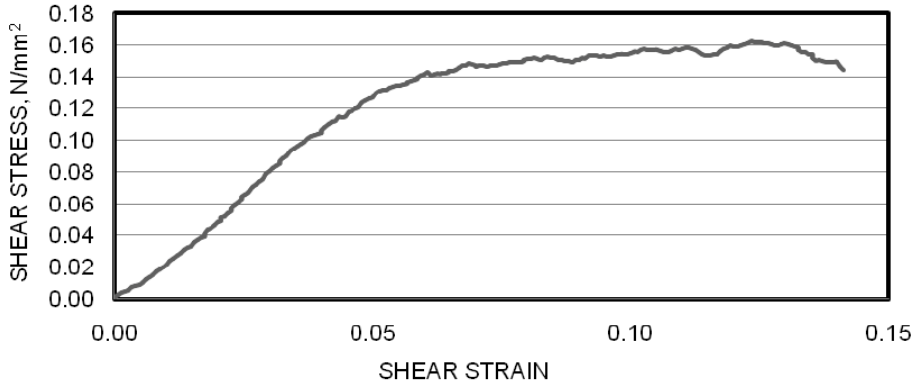

Figure 2(d, e, f) Shear stress versus shear strain curves for mix G at normal stress of 0.025 N/mm² and displacement rates of (d) 5 mm/min, (e) 15 mm/min and (f) 25 mm/min

g)

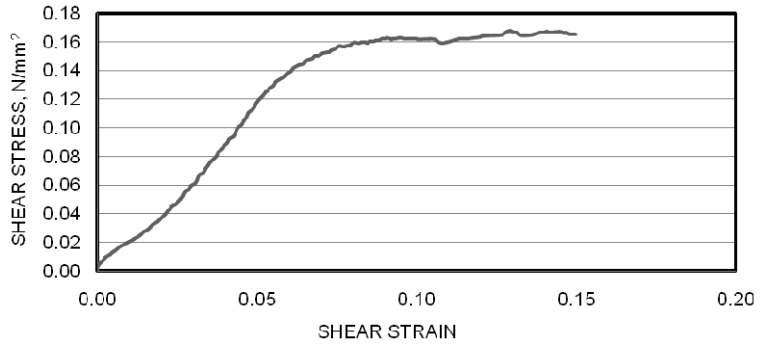

h)

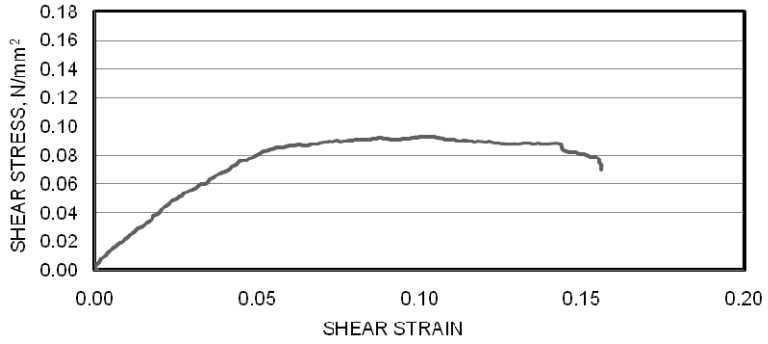

i)

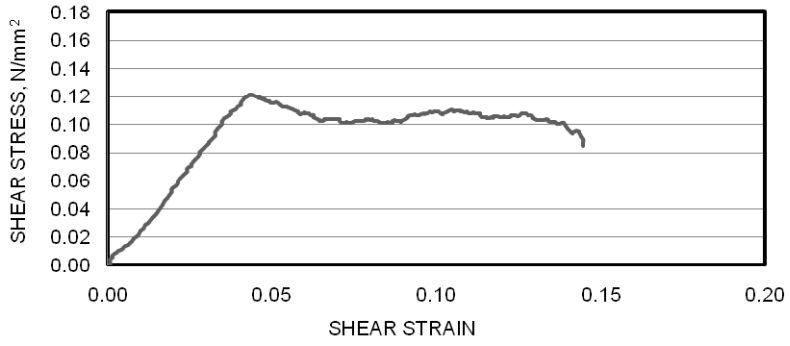

Figure 2(g, h, i) Shear stress versus shear strain curves for mix G at normal stress of 0.035 N/mm² and displacement rates of (g) 5 mm/min, (h) 15 mm/min and (i) 25 mm/min

a)

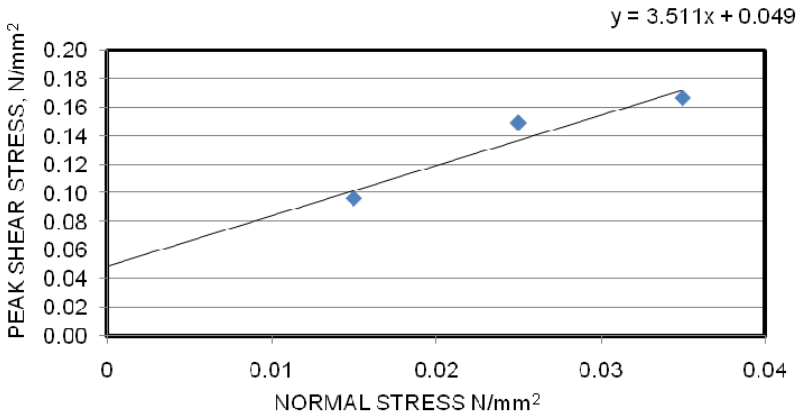

b)

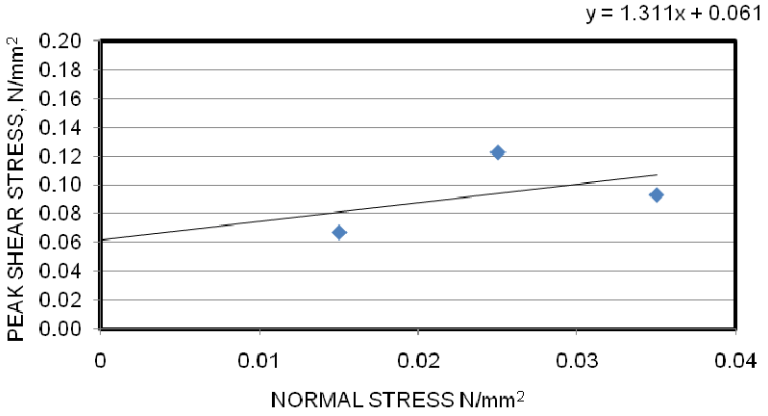

c)

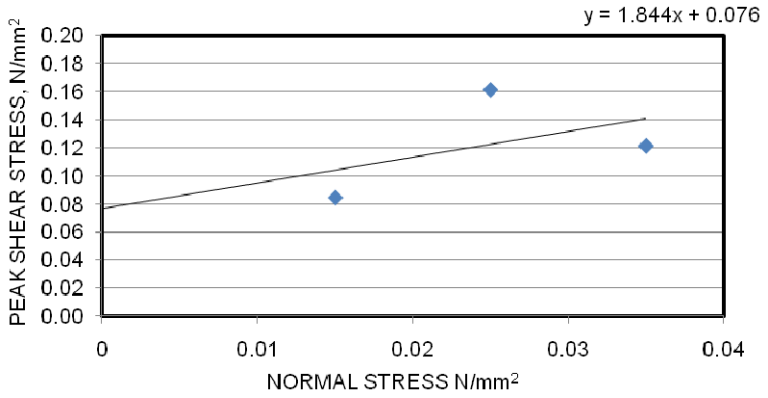

Figure 3 Peak shear stress versus normal stress for mix G at displacement rates of (a) 5 mm/min, (b) 15 mm/min and (c) 25 mm/min

Further, graph was plotted between displacement rates and the yield stress at zero normal stress obtained for different displacement rates (Figure 4). The intercept of the line on the y-axis (ζ'_0, shear stress axis) can be regarded as the relative yield stress (ζ_0) and the slope of this line as the relative plastic viscosity (μ) similar to Bingham parameters [11].

The uniqueness of this test method is that, the shear stress at zero normal stress and zero displacement was found before finally finding both the relative yield stress and the relative plastic viscosity. Other important characteristics of this test are the very low shear rate applied on the specimen during testing which is similar to the condition experienced by the concrete in the field and also the static condition of the test.

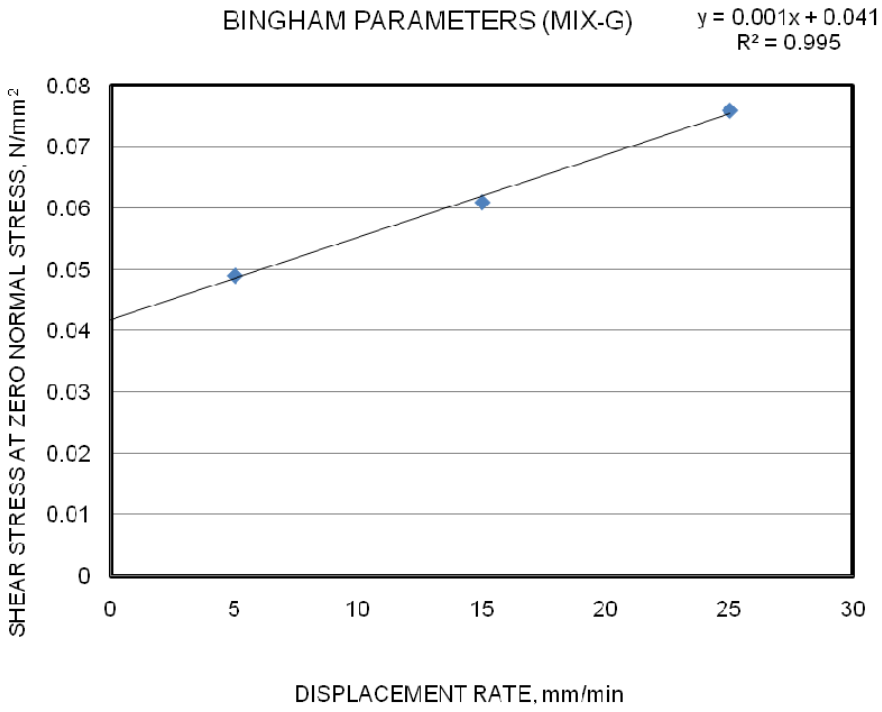

Figure 4 Shear stress at zero normal stress versus displacement rate for mix G

Rheological Properties with Elapsed Time

For the mixes with water content 175 l/m³ and for three different cement contents further tests were conducted at elapsed time of 40 minutes and at 60 minutes after thorough mixing, in addition to the tests conducted immediately after mixing of concrete. For each trial the concrete was kept without remixing till the required time of testing. The plots of shear stress versus shear strain for different elapsed time are shown in Figure 5 for the mix D. The same procedure enumerated in the previous section was followed for finding the rheological properties namely yield stress and plastic viscosity for elapsed time.

Figures 5 (a) to 5 (i) shows the plots of shear stress versus shear strain for different displacement rates and normal stresses. The plots are shown for the mix with cement content 300 kg/m³ and water 175 l/m³.

a)

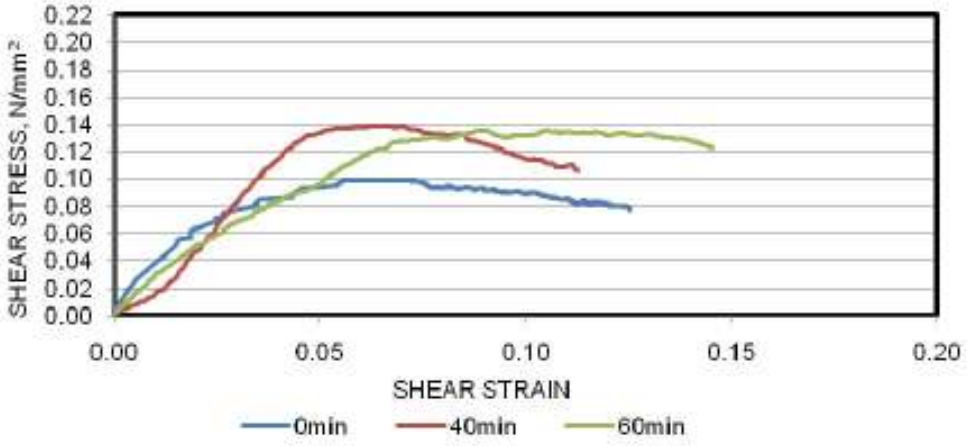

b)

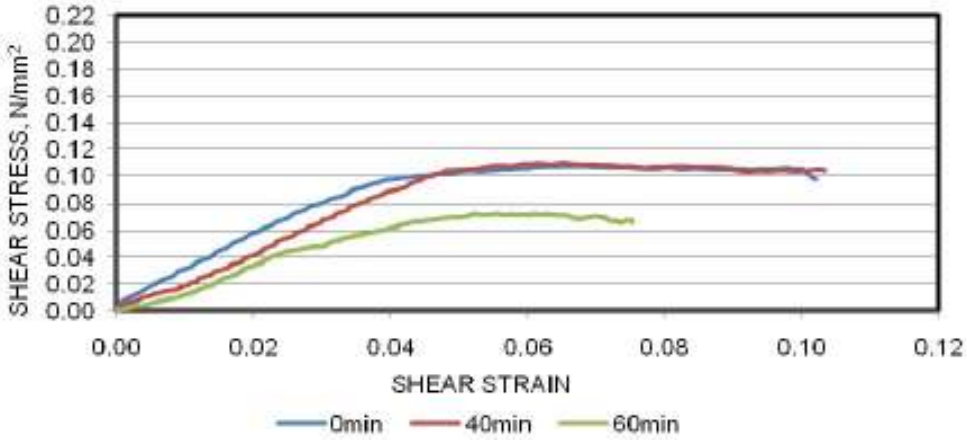

c)

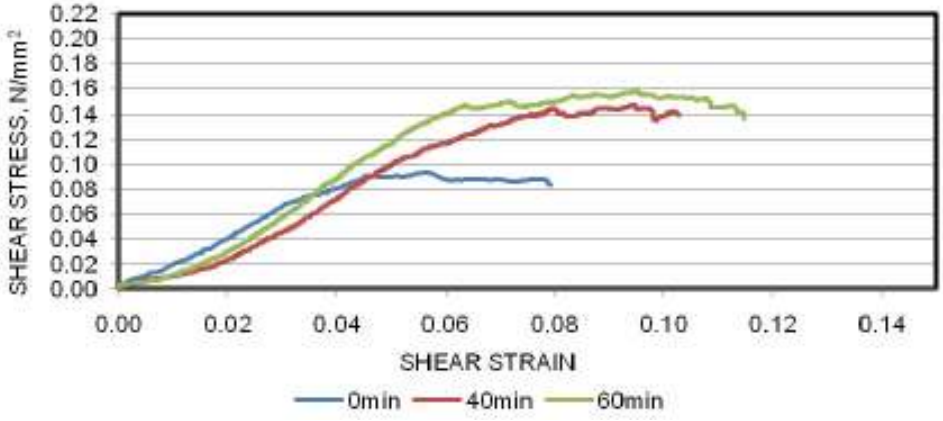

Figure 5(a, b, c) Shear stress versus shear strain curves for mix D at normal stress of 0.015 N/mm² and displacement rates of (a) 5 mm/min, (b) 15 mm/min and (c) 25 mm/min

a)

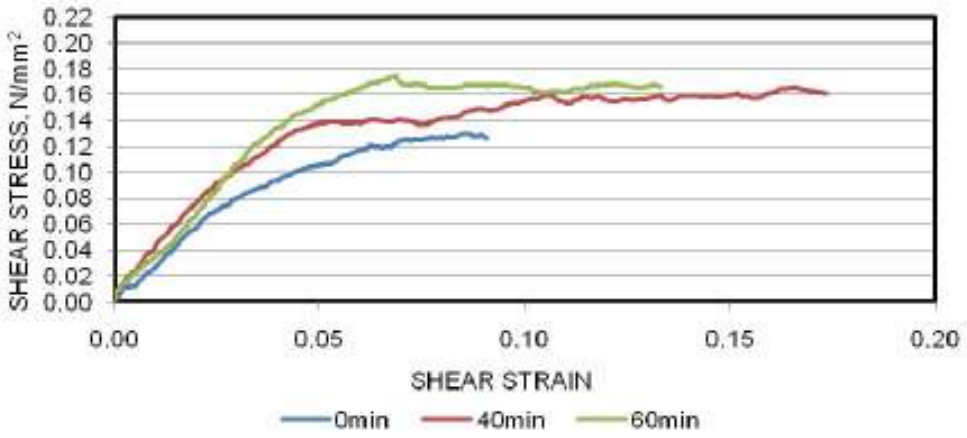

b)

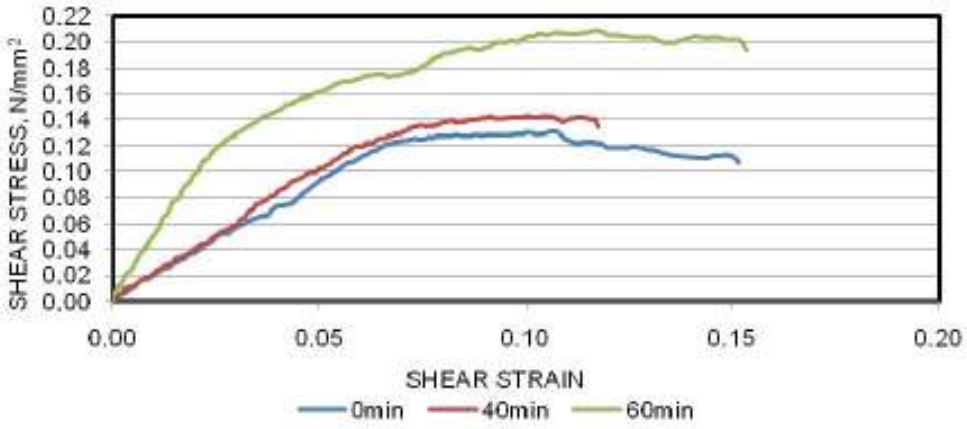

c)

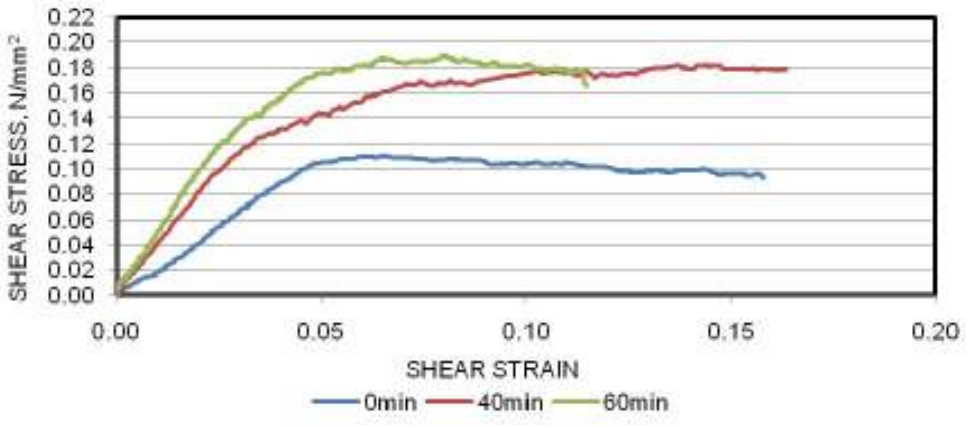

Figure 5(d, e, f) Shear stress versus shear strain curves for mix D at normal stress of 0.025 N/mm² and displacement rates of (a) 5 mm/min, (b) 15 mm/min and (c) 25 mm/min

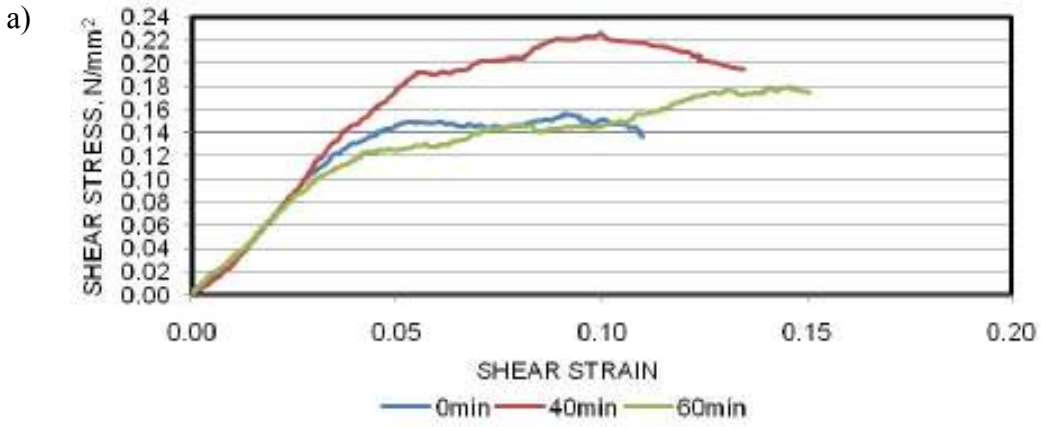

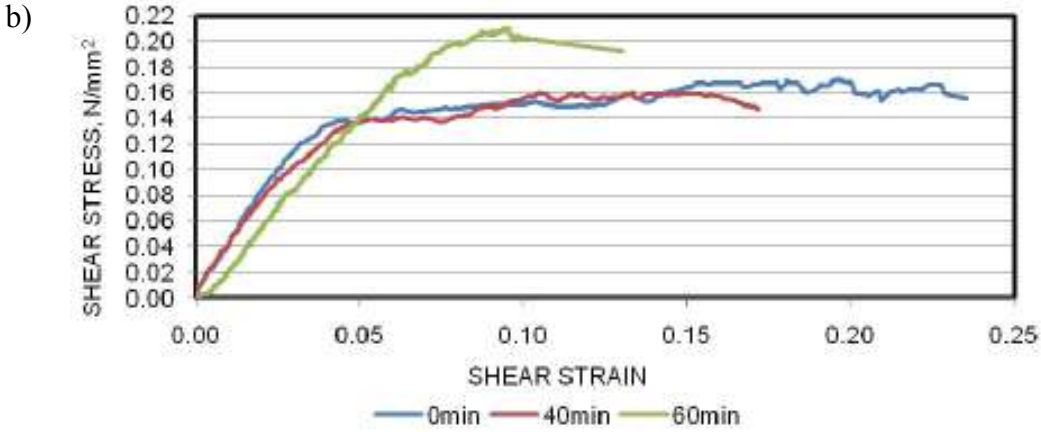

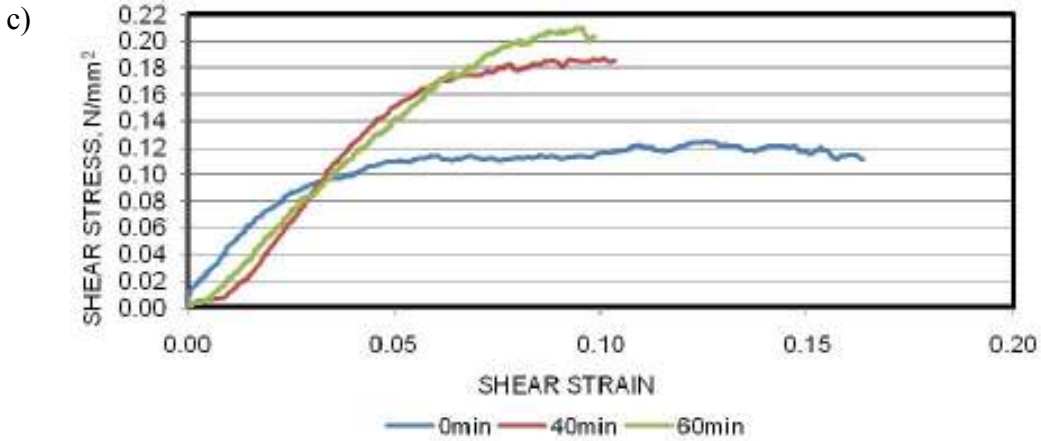

Figure 5(g, h, i) Shear stress versus shear strain curves for mix D at normal stress of 0.035 N/mm² and displacement rates of (a) 5 mm/min, (b) 15 mm/min and (c) 25 mm/min

RESULTS AND DISCUSSION

Table 1 shows the relative yield stress and relative plastic viscosity at zero minutes along with the mixture proportions of the mixes. From Table 1 it can be observed that in a given mix for the same water content as the cement content increased the relative yield stress of concrete decreased. For example for water content 175 l/m³ the relative yield stress decreased from 50995 Pa to 25497 Pa as the cement content increased from 300 to 450 kg/m³. This phenomenon is attributed to higher paste content (cement + water). As the cement content is increased for the same water content it results in higher volume of paste and better lubrication of the aggregate particles thereby reducing the inter-particle friction and also probably due to better coating of the paste on the aggregates. Also higher paste content means lower aggregate content and lower volume fraction of aggregates result in increased spacing between aggregates and thus lesser resistance to flow.

This is also true when the water content is increased for the same cement content. As such at lower paste content the interparticle friction dominates resulting in higher relative yield stress which is clearly brought out by the direct shear box test. Similarly, the relative plastic viscosity values are higher for the same water content with higher cement content as the mix becomes more cohesive.

An increase in the cement content at a constant water to cement ratio provides more paste to coat aggregates and to fill the spaces between the aggregates. Relative yield stress and relative plastic viscosity obtained in this study are higher than those reported in the literature using rheometers. This could be possibly due to particle interference or friction during shearing at low rates. In most rheometer experiments, initially the fresh concrete is sheared at high rate before the rheological tests and then the shear rate is reduced gradually in order to obtain the Bingham curve [2]. Such high shear rates are normally not encountered while placing of concrete. But the trends reported are similar to the results obtained using rheometers i.e. higher the paste content the lower the yield stress [5].

Table 1 Relative yield stress and relative plastic viscosity at zero minutes

MIX	CEMENT, kg/m³	WATER, l/m³	AGGREGATE, kg/m³		RELATIVE YIELD STRESS, Pa	RELATIVE PLASTIC VISCOSITY, MPa·s
			fine	coarse		
A	300	160	795	1184	80800	2.75
B	390		765	1139	75400	3.15
C	450		745	1108	44900	4.07
D	300	175	780	1160	50995	4.68
E	390		749	1115	30401	6.48
F	450		729	1085	25497	13.68
G	300	190	764	1136	40800	12.31
H	390		733	1091	26459	27.72
I	450		713	1060	23323	25.27

Table 2 Relative yield stress and relative plastic viscosity for elapsed time for mixes with water content 175 l/m³

MIX	CEMENT, kg/m³	WATER, l/m³	W/C	TIME	RELATIVE YIELD STRESS, Pa	RELATIVE PLASTIC VISCOSITY, MPa·s
D	300	175	0.58	0 min	50995	4.68
				40 min	54917	20.16
				60 min	56192	24.01
E	390		0.44	0 min	30401	6.48
				40 min	34323	18.72
				60 min	50995	23.76
F	450		0.38	0 min	25497	13.68
				40 min	27459	20.52
				60 min	58840	21.96

Table 2 shows the relative yield stress and relative plastic viscosity at elapsed time of 40 minutes and at 60 minutes after thorough mixing, in addition to the tests conducted immediately after mixing of concrete for the mixes with 175 l/m³. As can be seen from the Figure 5 the peak shear stress values are higher as the elapsed time is more, clearly bringing out the effect of structural built up. This clearly brings out the thixotropic and time dependent property of concrete and the degree of structural build up during the rest period as can be seen in the values of relative yield stress in Table 2. Similar behaviour was corroborated in case of relative plastic viscosity i.e. the plastic viscosity simply increases as the elapsed time increases.

CONCLUDING REMARKS

This experimental study has shown that specially fabricated customized medium size direct shear box can be used as a new tool for determining the rheological properties of fresh concrete. The uniqueness of the test is that the values arrived at, are by considering both the normal stress and displacement rate at zero values and the stimulus provided to the concrete is similar to the field practice. The procedure is simple and it follows the determination of intrinsic shear stress initially and then further relating this intrinsic shear stress at zero normal stress through interpolation to shear rate and finally through interpolation at zero displacement rate. The yield stress and plastic viscosity are named as relative values partly because the values so obtained are higher than those reported in literature as determined by high shear rate rheometers. For the same mix, as cement content increased there is a significant reduction in relative yield stress or plastic viscosity. This aspect may be useful in identifying the intrinsic changes in the mixes. The relative yield stress and plastic viscosity increases as the elapsed time increases and thixotropic behaviour is observed. The specially fabricated customized medium sized direct shear box can be used as a new tool to determine rheological properties effectively as a static test and can be an alternative in place of rheometers which use high shear rate.

REFERENCES

1 FERRARIS C AND BROWER L (eds.), Comparison of Concrete Rheometers: International Tests at MB (Cleveland OH, USA) October 2000, National Institute of Standards and Technology NISTIR 7154, September, 2001.

2 KOEHLER E P AND FOWLER D W, Development of a Portable rheometer for fresh Portland cement concrete, ICAR Report 105-3F, 2004.

3 NGUYEN Q D AND BOGER D V, Yield stress measurement for concentrated suspensions, Journal of Rheology, Vol. 27, No. 4, 1983, pp. 321-349.

4 HACKLEY V AND FERRARIS C F, The Use of Nomenclature in Dispersion Science and Technology, (Special Report 960-3), 2001, Gaithersburg, MD: National Institute of Standards and Technology.

5 FERRARIS C F AND BROWER L E, Comparison of concrete rheometers, Concrete International, Vol. 25, No. 8, 2003, pp. 41-47.

6 NEWMAN K, Concrete systems, In: Holliday L (ed.), Composite materials, Amsterdam, Elsevier Publishing Co. Ltd., 1966, pp. 335-452.

7. HERSHEL W H AND PISAPIA E A, Proceedings of American Concrete Institute, Vol. 32, 1936, pp. 641.

8. L'HERMITE R AND TOURNON G, Vibration of Fresh Concrete, Technical Publication No. 2, Centre d'Etudes et de Recherches de L'Industrie des Liants Hydraulique, Paris, 1948.

9 GIRISH S, INDUMATHI C, VENGALA J AND RANGANATH R V, Rheological Properties of Self-Compacting Concrete using Direct Shear Box, The Indian Concrete Journal, Vol. 83, No. 8, 2009, pp. 47-53.

10 GIRISH S AND SANTHOSH B S, A new methodology to study the rheological properties of fresh Portland cement concrete, International Journal of Earth Sciences and Engineering, Vol. 4, No. 6, SPL, 2011, pp. 797-800.

11 FERRARIS C F, Measurement of the rheological properties of high performance concrete: state of the art report, Journal of research of the national institute of standards and technology, Vol. 104, No. 5, 1999, pp. 461-478.

Durability Performance: Models & Test Methods

C A Clear
Mineral Products Association, UK

For reinforced concrete the environmental conditions that lead to corrosion of reinforcement, such as carbonation or chloride ingress, are recognized as well as those environmental conditions such as aggressive soil or freezing and thawing that lead to the deterioration of concrete itself. Although a complete understanding of all the deterioration mechanisms that affect concrete is some way off there are simplified models for some aspects of deterioration. The simplified models will only be useful where they can incorporate materials performance coefficients that can be obtained in a robust, repeatable and reproducible manner. For this reason it is important to continue to develop and standardize performance tests and models such that the results are both reliable and meaningful. At this time tests for chloride diffusivity, carbonation resistance and freeze thaw parameters have yet to be fully standardized at the European level, although European Technical Specifications are available and are being assessed. In some European Countries an equivalent performance concept has been adopted, a concept that formalizes testing of a proposed concrete to demonstrate performance of not less than a reference concrete of established durability. Formalised guidance for this concept at the European level is likely to be the most practical move towards performance based specification prior to the establishment of indicative performance criteria.

Chris A Clear BSc PhD CEng MICE FIMMM FICT is the Technical Director of the Mineral Products Association, UK and is a member of British and European Standardisation Committees concerned with concrete. Main subject areas of interest are concrete production, technology and all aspects of durability and performance.

Keywords: Carbonation, Chloride, Freeze-thaw, Standards, Testing

INTRODUCTION

As stated in the Standard itself consideration is being given to detailing a performance - related approach to the specification of durability in the European Standard for Concrete EN 206-1 [1]. Although some European member states have developed tests and criteria in which they are confident for use in their own country, the necessary Europe-wide consensus for the detailed requirements of performance based specifications is unlikely to be developed in the near future. This is unfortunate as 'sustainable development' is becoming a primary design consideration and the level of green-house gas emissions embodied in construction materials as well as during the in-use phase is already a requirement of an increasing number of buildings and infrastructure projects. Sustainable development should mean that all buildings and structures remain serviceable for their intended working life, preferably with a minimum level of maintenance or refurbishment. For this reason it is very important to have a comprehensive understanding of the likely deterioration processes and how the appropriate quality of material may be specified to provide the required durability.

Currently the UK has comprehensive guidance within the British Standard for Concrete BS 8500-1 [2] in terms of limiting values for intended working life of up to at least 50 or 100 years for concrete exposed to corrosion of reinforcement induced by carbonation or chloride ingress. The problem with the limiting value approach is that the values adopted may be accepted as safe, but there is no way of verifying if they are safe or overly-conservative. In previous years an overly-conservative specification for durable concrete may not have been of great concern as the cost of reinforced concrete construction was relatively inexpensive. The cost of concrete construction is increasing but there is also the added consideration of environmental impacts and social considerations. Environmental impacts and other sustainability aspects are of increasing significance, accepting it is currently difficult to make a technically sound comparison for either buildings [3], or structures such as bridges [4], as the metrics required have yet to be adequately defined.

To ensure that building and structures are not over-designed with respect to durability then it is necessary to develop a performance based specification, where the essential aspect is that the performance can be modelled and that the necessary materials coefficients can be identified and measured.

MODELLING DURABILITY

Exposure classes

There can be no single concrete durability model as the significant deterioration mechanisms will depend on the environment to which the concrete element or structure is exposed. According to European and British Concrete Standards there are five main classes of exposure, these are set out in Table 1.

Test methods

A requirement of any modelling process is the identification of relevant materials coefficients and the ability to measure them, preferably with a standard test method. Around the world there are many test methods pertaining to carbonation, chloride ingress, freeze-thaw and chemical attack. Unfortunately none of these have been developed into a European EN

standard but there are three test methods set out as CEN Technical Specifications. These are CEN/TS 12390-9 for freeze-thaw resistance - scaling [5], CEN/TS 12390-10 for relative carbonation resistance [6] and CEN/TS 12390-11 for the chloride resistance of concrete by unidirectional diffusion [7]. There is no European Technical Specification for testing concrete to measure its resistance to chemical attack. This is not because of a lack of interest rather than procedures have been established at National level where it would be near impossible to agree a test at European level that may result in significantly different guidance. For example, in the UK BRE Special Digest 1 [8] sets out comprehensive guidance on concrete in aggressive ground, but this is almost entirely based on BRE test procedures, experience largely from the UK, and for UK ground conditions. As this paper is limited to Europe wide developments it is only freeze-thaw, carbonation and chloride ingress that will be considered in greater detail.

Table 1 European concrete standard exposure classes

BROAD CLASS DESIGNATION AND DESCRIPTION		CLASS DESIGNATION AND DESCRIPTION	
XC	Corrosion induced by carbonation, where concrete containing reinforcement or embedded metal is exposed to air and moisture	XC1	Dry or permanently wet
		XC2	Wet, rarely dry
		XC3	Moderate humidity
		XC4	Cyclic wet and dry
XD	Corrosion induced by chlorides other than from sea water, where concrete containing reinforcement or other embedded metal is subject to contact with water containing chlorides, including de-icing salts, from sources other than sea water	XD1	Moderate humidity
		XD2	Wet, rarely dry
		XD3	Cyclic wet and dry
XS	Corrosion induced by chlorides from sea water, where concrete containing reinforcement or other embedded metal is subject to contact with water containing chlorides from sea water or air containing salt originating from sea water	XS1	Exposed to airborne salt but not in direct contact to sea water
		XS2	Permanently submerged
		XS3	Tidal, splash and spray zones
XF	Freeze-thaw attack, where concrete is exposed to significant attack from freeze-thaw cycles whilst wet	XF1	Moderate water saturation without de-icing agent
		XF2	Moderate water saturation with de-icing agent
		XF3	High water saturation without de-icing agent
		XF4	High water saturation with de-icing agent
XA	Chemical attack, where concrete is exposed to chemical attack	XA1	Slightly aggressive chemical environment
		XA2	Moderately aggressive chemical environment
		XA3	Highly aggressive chemical environment

Freeze-thaw resistance

For freeze-thaw resistance CEN/TS 12390-9 sets out one reference test method, the slab test, as well as a cube test and a capillary suction frost (CF/CDF) test. In all cases the sample preparation is the same with curing under polythene for the first day and then six days under water at 20 ± 2°C. Thereafter the test specimens are cured in a climate controlled room or chamber at 20 ± 2°C and an evaporation of 45 ± 14 g/(m² h) for 28, 20 or 21 days depending on the particular test. The evaporation rate is normally achieved with a wind velocity of ≤ 0.1 m/s and a relative humidity (RH) of 65 ± 5%. After this the specimens are either ponded or immersed with the fluid and left to stabilise for 3, 1 or 7 days prior to the freeze-thaw regime. For each test the freeze-thaw cycle is from -20°C to + 20°C, where the duration of one cycle is 24 hours for the slab and cube tests but only 12 hours for the CF/CDF test. The significant variations in test regime are summarized in Table 2 together with recommendations for limit values as discussed by Boos and Giergiczny [9] who tested a range of concretes containing various cement types using the CEN/TS 12390-9 suite of tests.

Table 2 CEN/TS 12390-9 Freeze thaw test methods

TEST, SPECIMENS SIZE AND SATURATION TECHNIQUE	TEST AGE	FLUID	FT CYCLES	CRITERIA	CLASS
Slab test: 150 x 150 x 50 sawn surface exposed to 3 mm deep pond of liquid	31 day min. 28 65%RH, 3 ponded	W			
		S	56 (24 h)	<1.0 kg/m²	
Cube method: 2 x 100 mm cubes, formed surfaces fully immersed in liquid	28 day min. 20 65%RH, 1 immersed	W	100 (24 h) 100 (24 h)	<10% <5%	XF1 XF3
		S	56 (24 h)	<5%	
Capillary suction frost test (CF/CDF Test): 150 x 150 x 70 mm PTFE formed surface immersed 5 mm deep in 10 mm reservoir of liquid	35 day min. 21 65%RH, 7 immersed	W (CF)	28 (12 h)	<1.0 kg/m²	
		S (CDF)	28 (12 h)	<1.5 kg/m²	
Notes: W = De-ionised water S = 97% tap water and 3% NaCl by mass					

Boos and Giergiczny note that the loss of up to 10% by mass of the cubes after 100 cycles of the cube test with de-ionised water is a concrete suitable for XF1 exposure, and at up to 5% by mass then XF3 exposure. This closes the circle in that there is a model, there is a test and there are limits that may directly pertain to an exposure class. Figure 1 show results from Romero et al [10] where two types of concrete were tested using the CEN/TS 12360-9 CDF test. The authors indicated that a scaling of less than 1.5 kg/m² after 28 (12 hour) freeze-thaw cycles is indicative of acceptable performance. As the density of concrete will be no more than 2500 kg/m³ then a material loss of 1.5 kg/m² is equivalent to an average erosion of 0.6 mm, which is the loss of some cement matrix and finer particles of sand.

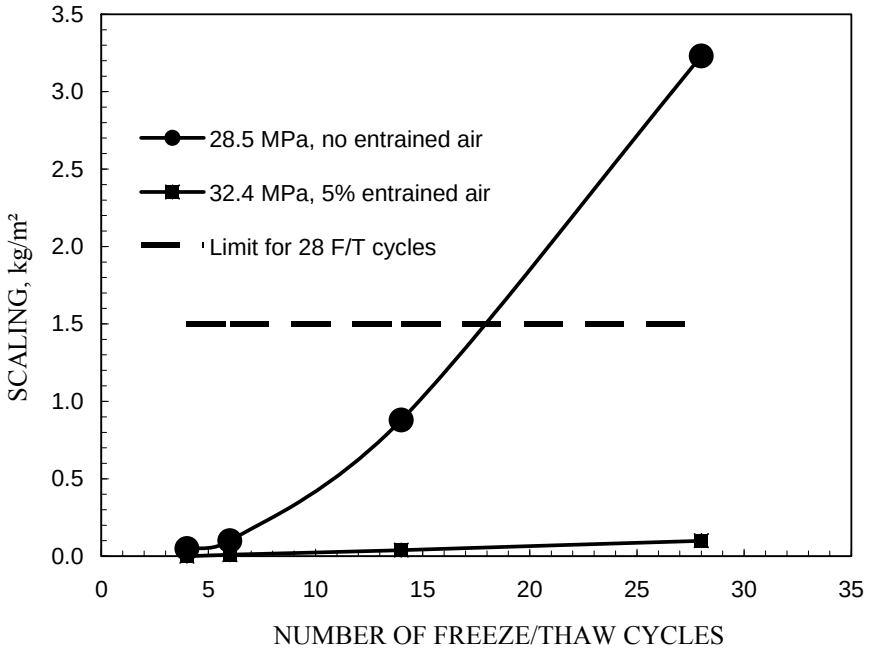

Figure 1 EN 12390-9 CDF performance of non- air entrained and air-entrained concrete

It is important to note that the CEN/TS 12390-9 tests are accelerated tests and that 28 freeze-thaw cycles in the test do not equate to real freeze-thaw cycles. In particular the test samples although cured for one week under water they are then exposed to three weeks curing at 65% RH. An exposure at 65% RH is about the optimum for carbonation and this may mean that concretes incorporating higher levels of ggbs or fly ash as part of the cement may not give test results that reflect their performance in real external environment where the ambient RH may be considerably higher. In addition for the CD/CDF test the samples are immersed in the fluid for seven days so they may be saturated before freezing, and then the temperature cycle goes from +20 to -20°C and back to +20°C in less than 12 hours.

Dransfield [11] summarized a record of freeze-thaw cycles over a six year period from covering the winters from 2006 to 2010 for a location close to a concrete specimen exposure site. This site is at an altitude of ~400 m and registered 182 freeze-thaw cycles defined as an air temperature drop to less than -1°C and then a rise to more than +1°C. The maximum recorded temperature drop over the five years was to -10°C, where it is important to note that the temperature of the test specimens would not have fallen as low as the air temperature. Dransfield did not quantitatively assess the level of attack on the exposure site specimens but did set out a visual ranking assessment after the specimens had been exposed to around 1100 air temperature freeze thaw cycles over nearly 12 years.

Figure 2 shows the NW corner of a nominal 30 MPa, non-air entrained, Portland cement concrete where the comparative assessment stated that this was one of the most severely attacked. Other specimens were either at a higher compressive strength or air-entrained.

Figure 2 Non air-entrained 30 MPa Portland cement concrete exposed for 12 years and around 1100 freeze thaw cycles as measured by air temperature

Interestingly it is a vertical face that exhibits more freeze thaw damage than the near-horizontal surface in the foreground. Current understanding of the freeze thaw mechanism is that a horizontal surface is more likely to become highly saturated and therefore more at risk of damage. It may be that at the particular location the combinations of air-frost and prevailing winds are more severe than ground-frost on a well drained albeit near horizontal surface.

Accepting that there is only a nominal similarity between the non-air entrained Portland cement concrete reported by Romero et al [10] and the field specimen shown in Figure 2 it is interesting to compare performance. The Romero et al concrete lost around 3 kg/m² of surface in 28 freeze-thaw cycles, equivalent to an average depth of 1.2 mm. The Figure 2 field specimen has probably not lost as much depth as this over most of the exposed surfaces, except as shown in the top corner closest to the viewer where damage is deeper as some of the coarse aggregate particle are partially exposed.

A conclusion of the comparison between the accelerated CEN/TS 12390-9 freeze thaw scaling test and the single field specimen is that there is no clear relationship. This does not mean that freeze-thaw testing is not useful because it is, for example the test and the performance limit of 1.5 kg/m² can differentiate between an air-entrained and non air-entrained concrete with respect to resisting damage by freezing and thawing.

Carbonation resistance

Carbonation is important with respect to durability as it reduces the alkaline environment of concrete from around a pH of 12 to below 9 where ferrous reinforcement is susceptible to corrosion provided there is sufficient moisture and air.

For the determination of the relative carbonation resistance of concrete CEN/TS 12390-10 sets out a method for comparing the carbonation resistance of one concrete with another concrete of the same 28 day reference strength, and where both concretes are cured in sealed polythene bags to an age where 50% of the reference strength is achieved. Once the 50% of the reference strength is achieved the specimens are exposed to one of two environmental conditions, A or B. Exposure A is a climate controlled chamber where temperature is maintained at 20±2°C, relative humidity 65±5% and carbon dioxide 0.035±0.005%. This

level of carbon dioxide is about the same as the natural atmospheric level but maintaining RH at around 65% means that carbonation is maximised. Exposure B is where the specimens are exposed to an external atmosphere but are protected from any precipitation. This container has an impermeable lid and Stevenson screen slats at the side to protect from driving rain but allow the free circulation of air. As the samples are kept dry the rate of carbonation under exposure B will be greater than most concrete exposed to the natural environment. As this test is reliant on curing each concrete until 50% of its reference strength is achieved then it is representative of very good curing. Using the data presented by Clear [11] a CEM I or CEM II/A type cements takes around 2 days moist curing at 20°C is required to attain 50% of the 28 day strength. Similarly for combinations of CEM I with 50 to 70% ggbs then around 4 days moist curing, and with 50% fly ash 5-6 days moist curing, are required. Carbonation depths are measured at 182, 273, 365, 547 and 730 days (±2%) for type A exposure. For exposure B measurements are at 365 and 730, and then as specified thereafter in days (±2%) Carbonation measurements are made by splitting the specimens and spraying with an indicator liquid that does not produce a colour change where the concrete is carbonated to a pH below around 9.

From the above summary of the CEN/TS 12390-10 test procedure it is evident that as the early curing is controlled to match the type of cement, and the exposure conditions are not representative of actual structures, then the results cannot be directly related to a service life performance. This is accepted as the declared aim of the full test is to show that one concrete may perform as well as another rather than for modelling quantitative performance.

With respect to the service life of a structure the depth of carbonation with time is only part of the information required to assess durability, as can be clearly seen in the traditional corrosion type model described by Somerville [12] and depicted in Figure 3. In this Figure the time taken for the carbonation front to progress from the surface of the concrete to the level of the reinforcement is called the initiation period. During this time there is no visible deterioration and hence damage = 0. Once carbonation is at the level of the reinforcement then it may start to corrode and a level of damage can be measured as the expansion caused by the formation of rust. The period of increasing damage is know as the propagation period as this is when crack will start to form above the reinforcement and may eventually lead to spalling. At some point the damage will reach a level that is unacceptable and this is the end of the service life, unless the damage is repaired.

Numerous studies have been carried on concrete carbonation where a recent study by Jones et al [13] is valuable in that it includes results from long term outside exposure for a wide range of materials. Figure 4 shows the carbonation depths of concrete for specimens externally exposed but protected from wind and rain, so in accordance with the CEN/TS 12390-10 type B requirements but the experiments were started prior to publication of the TS. The period of curing prior to exposure was recorded as up to one month sealed cure as the specimens were made around the UK and then transported to the various exposure sites. The two main exposure sites are Dundee in Scotland and Ringwood in the Southern counties of England. The range of materials include various aggregate and cementitious types where most mixes were made as plain concrete, with a water reducing admixture and a high range water reducing admixtures to achieve w/c ratios from 0.5 to 0.7. Figure 4 shows the relationship between carbonation depth measured at 5-6 years, and the 28 day cube strength.

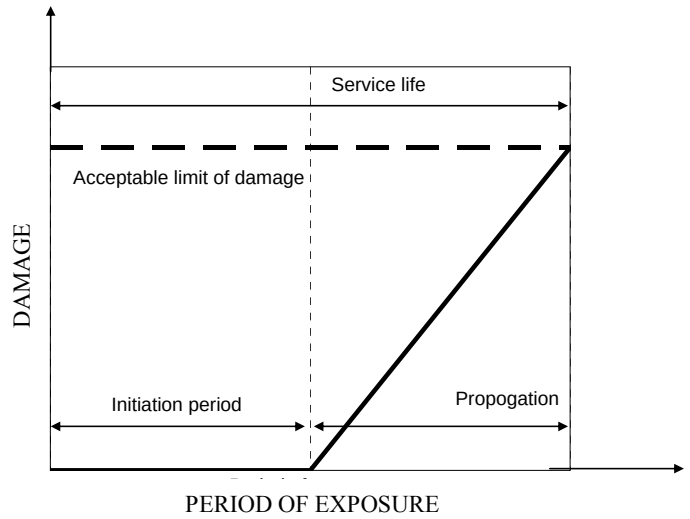

Figure 3 Traditional model for corrosion

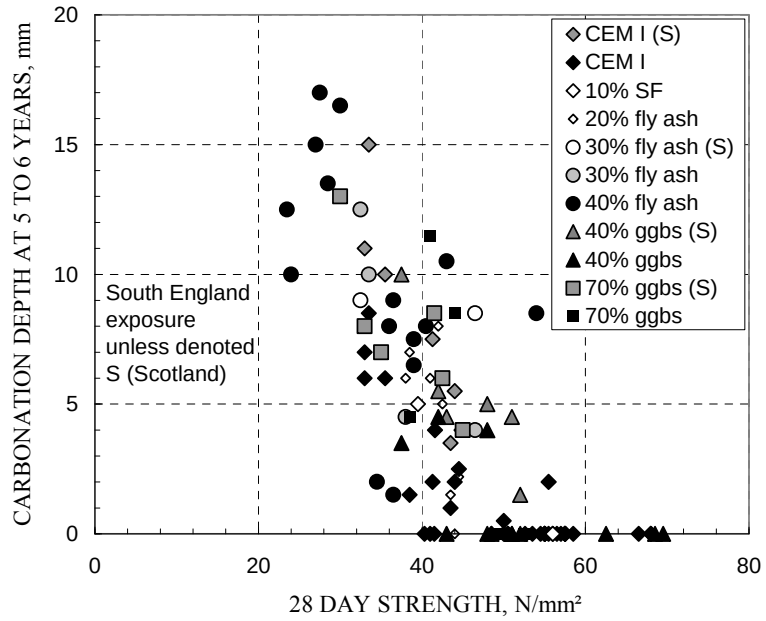

Figure 4 Relationship between carbonation depth and 28 day strength, after Jones et al [12]

From Figure 4 it is evident that there is a relationship between 28 day strength and depth of carbonation irrespective of cementitious material, accepting quite a high scatter of results. Even for the lower strength 25 MPa concrete the depth of corrosion is not much over 15 mm after five years. It is established that carbonation rate is not linear but decreases with time, where it is often quoted a being proportional to the square root of time. Jones et al confirm a similar relationship between the depth of carbonation and time as shown in equation:

$$x_c(t) = K \times t^{0.4}$$

Where x_c is the depth of carbonation at time t and where K is a constant.

A typical concrete strength for building is a C25/30 and from Figure 4 a 30 MPa concrete carbonates to a depth of 15 mm after more than 5 years. This indicates that K is 7.9 mm/$t^{0.4}$ and so after 50 years a carbonation depth of 38 mm may be expected.

At 38 mm means that the carbonation could have progressed through 30 mm of cover and almost enveloped a 10 mm diameter reinforcing bar.

However, carbonation is only the initiation part of corrosion, as shown in Figure 3 where it takes some time for damage to propagate. As well as simple carbonation Jones et al [12] also investigated the propagation period on pre-carbonated specimens containing reinforcing bars, where the specimens were exposed to an external unsheltered environment to ensure there was sufficient moisture for corrosion to progress at a measurable rate within a year or so. Based on these results they conclude that a minimum propagation period of 15 years is reasonable, and Mattila and Pentti [14] who considered a carbonation worse case of balcony façade elements suggest anything from 5 to 50 years.

So, the important observation is that although the carbonation resistance of concrete is important it is only part of the information required with respect to estimating the service life of a structure exposed to the atmosphere, even in a comparatively simple model.

Chloride ingress resistance

Within the alkaline environment of concrete a passive layer forms around any embedded ferrous reinforcement that protects it from corrosion. This passive layer breaks down if the concrete matrix carbonates or broken down by the ingress of chloride ions. As highway and marine structures will be exposed to the risk of chloride ingress then it is an important factor affecting their durability.

A method for the measurement of the chloride resistance of concrete by unidirectional diffusion is set out in CEN/TS 12390-11, where specimens are cured at 20±2°C under water for 28 days, conditioned and prepared for at least one day and then exposed for a minimum of 90 days to a chloride solution. The test is defined as non-steady state as the ingress of chloride into the sample is progressive, and there is also a likely to be a significant amount of continued cement hydration which will reduce the chloride diffusion coefficient over the 90 day test period. There are chloride diffusion tests where a thin sample of concrete is exposed to the diffusion of chloride from a defined high chloride concentration on one side of the sample to a low concentration on the other.

In this steady state test the diffusion coefficient is calculated once a stable diffusion rate is established, and as this is usually within hours or days then the effects of continued hydration can be regarded as insignificant. It is also important to note that in the standard non-steady state test the formed or trowelled surface is discarded and it is a cut or ground surface originally 10 mm within the specimen, which is exposed to chloride ingress.

Figure 5 shows a core or a cylindrical specimen but cube specimens are equally acceptable where the chloride ingress would normally be from a side face of the cube.

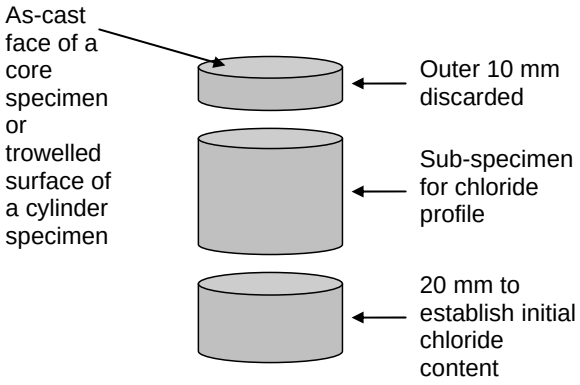

Figure 5 Specimen for determination of chloride diffusion coefficient

To determine the chloride diffusion coefficient at least 8 chloride content measurements are made from successive layers of the profile sub-specimen, where the measurements are expressed as percent chloride per mass of concrete. Guidance on the depth of each layer is provided in term of the w/c ratio and cement type. This is necessary as for low w/c ratio concrete, and/or concrete made with ggbs, fly ash or silica fume as part of the cement the chloride may not penetrate more than 10 to 20 mm. A typical chloride profile is shown in Figure 6 and the chloride diffusion coefficient is calculated by fitting a specified equation to the relevant points by means a non-linear regression analysis by least squares. In the example shown the actual measured surface chloride level, at an average 0.5 mm from the cut surface, is 0.96% and the 'zero point' chloride level 0.015%.

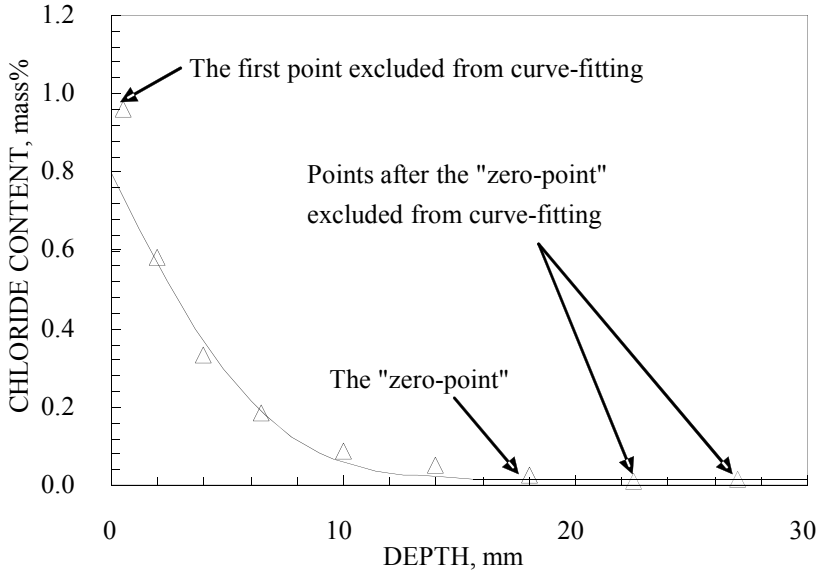

Figure 6 Specimen for determination of chloride diffusion coefficient

The curve fitted surface chloride C_s is 0.8% and the calculated non-steady state diffusion coefficient D_{nss} is 4.5 x 10^{-12} m²/s. As can be seen the determination of non-steady state diffusivity coefficient requires at least four months, and then preparation and analysis of numerous sub-samples as well as quite sophisticated calculations. Despite this it appears to be favoured for modelling the durability performance of reinforced concrete as described by what is a state-of-the-art report by Bamforth [15].

Measuring chloride diffusivity of concrete is essentially subjecting a specimen to XS2 exposure, which is permanently submerged, whereas in a real structure the most severe risk of corrosion is where the concrete is exposed in a tidal zone or subject to spray. This is one reason why chloride diffusivity can only be a partial indication as to the durability of reinforced concrete exposed to sea water, or chlorides other than seawater. In a similar manner to carbonation the progress of chloride to the reinforcement is only important for the initiation stage, and it is not clear how quickly damage is likely to propagate after chloride has reached the reinforcement. Bamforth points towards a minimum, or threshold, level of chloride before the rate of corrosion is significant and this threshold level may depend on the w/c ratio and type of cementitious material.

DISCUSSION AND CONCLUSIONS

The strength of the freeze-thaw scaling resistance test to CEN/TS 12390-9 is that the model of deterioration, the surface damage caused by a number of freeze/thaw cycles, appears to be similar to field conditions. Curing at 65% RH followed by saturation and then undergoing freeze-thaw under saturated conditions is a more severe test than that experienced in the field.

Measuring carbonation on exposure to a protected external environment or a 65% RH climate controlled environment to CEN/TS 12390-10 will also give a more severe degree of carbonation than field exposure. Results indicate that to get a measurable carbonation depth for 40 MPa concrete may take 5 years so this is a major drawback. Another weakness is that the test only gives result pertaining to the initiation period of corrosion, and a significant part of the useful service life may be during the propagation period where it may take some time for significant damage to develop. It is also noticeable that the optimum RH for carbonation is lower than the RH level at which corrosion of reinforcement is likely to occur at a significant rate.

Like carbonation resistance measuring the resistance to chloride ingress using the CEN/TS 2390-11 test only gives an indication of the initiation period under simulated permanently submerged conditions. In addition the test does not include the formed or trowelled surface of concrete where it is known that the cementitious content is likely to be high and hence enhance overall resistance to chloride ingress.

From this brief review of durability test methods it is noted that in each case the property being measured is only a part of the information required to model the service life of a concrete element or structure. It is also evident that the test conditions are generally more severe than those experienced by real structures. Having stated this it should be noted that useful and repeatable tests will always fall short of producing totally authentic materials coefficients often needed to enumerate durability models. This should not mean that durability testing is not carried out, just that when an Engineer or Designer requires a particular durability performance then he or she should be aware of the tests available and the limitations of the results produced.

Where an Engineer or Designer does not feel confident to specify a particular performance directly, then there is the option of specifying that the performance should not be less than that of a concrete where there is general acceptance of performance. This is the basis of procedure being developed by Harrison [15] where a candidate concrete may be proposed on

the basis that it can be demonstrated that it has a durability test performance of not less than that of a reference concrete. It is not difficult to envisage that if this procedure is only adopted for a minority of projects then it would not take long for the Engineer or Designer to establish direct performance values for the range of concretes they specify for particular applications.

ACKNOWLEDGEMENTS

The hard work and expertise of all the Research Team at the Dundee University Concrete Technology Unit over many years is gratefully acknowledged, particularly their contribution to the development of European standards for concrete test methods.

REFERENCES

1. EUROPEAN COMMITTEE FOR STANDARDIZATION (CEN) EN 206-1:2000 Concrete — Part 1: Specification, performance, production and conformity. p 69.

2. BRITISH STANDARDS INSTITUTION. BS 8500-1: 2006. Concrete — Complementary British Standard to BS EN 206-1 — Part 1: Method of specifying and guidance for the specifier. London. p 60.

3. BARRETT, N. Structural design benefits sustainability, The Structural Engineer. 1 May 2007, Arnold, pp 25-26.

4. COLLINGS, D. An environmental comparison of bridge forms. Proceedings of the Institution of Civil Engineering, Bridge Engineering. Volume 159. pp 163-168.

5. EUROPEAN COMMITTEE FOR STANDARDIZATION (CEN). CEN/TS 12390-9 Testing hardened concrete - Part 9: Freeze-thaw resistance - Scaling. p 24.

6. EUROPEAN COMMITTEE FOR STANDARDIZATION (CEN). CEN/TS 12390-10 Testing hardened concrete - Part 10: Determination of the relative carbonation resistance of concrete. p 21.

7. EUROPEAN COMMITTEE FOR STANDARDIZATION (CEN). CEN/TS 12390-11 Testing hardened concrete - Part 11: Determination of the chloride resistance of concrete, unidirectional diffusion. p 23.

8. BUILDING RESEARCH ESTABLISHMENT. BRE Special Digest 1:2005. Concrete in aggressive ground. Third Edition 2005. p 62.

9. BOOS, P and GIERGICZNY, Z. Testing the frost resistance of concrete with different cement types - experience from laboratory and practice. Architecture Civil Engineering Environment 2/2010. pp 41-51.

10. ROMERO, H L, CASATI, M J, GÁLVEZ, J C. NDT for concrete under accelerated freeze/thaw tests and surface scaling. fib Symposium. Prague 2011.

11. CLEAR, C A. Cement type/early age properties. Concrete Today. BRMCA supplement to Construction News. June 2011 pp 12-14.

12. JONES, M R, HARRISON, T A, KHANNA G, KANDASAMI, S. Research to extend the modelling and support for equivalent durability concept. Carbonation project - Phase 2 Final Report. Concrete Technology Unit, University of Dundee, May 2010. p 212.

13. SOMERVILLE, G. The design life of concrete structures. The Structural Engineer. February 1986, pp 60-71, and Discussion September 1986 pp 233-241.

14. MATTILA, J S, PENTTI, M J. Residual service-life of concrete façade structures with reinforcement in carbonated concrete in Nordic climate. Tailor Made Concrete Structures, editors Walraven & Stoelhorst. Taylor and Francis Group, London. pp 75-79.

15. BAMFORTH, P B. Enhancing reinforced concrete durability Guidance on selecting measures for minimising the risk of corrosion of reinforcement in concrete. Concrete Society Technical Report No. 61, 2004, p 208.

16. HARRISON, T A. Equivalent durability concept. Proceedings of Nordic Exposure Sites, Input to revision of EN 206-1. 12-14 November 2088, Hirtshals Denmark. pp 1-13.

Performance of Self-compacting Concretes Under Acid Environments

S V Rao[1], D Ramaseshu[1], P R Kumar[1], M V S Rao[2]
1 – National Institue of Technology, Warangal, India
2 – JNTU College of Engineering Hyderabad, India

The objectives of the work described in this paper were to compare the performance of Self Compacting Concrete (SCC) and vibrated Normal Concrete (NC) of M20, M30 and M70 grades immersed in acidic solutions. Self compacting concrete was developed using Nan-Su method of mix design and normal concrete was developed using IS method of mixed design. The cured self compacting concrete and normal concrete specimens of different grades viz. M20, M30 and M70 concrete were kept exposed to 2% and 5% solutions of both sulfuric acid and hydrochloric acids respectively upto 28 days. The response of the specimens to the solutions was evaluated through change in appearance, weight, compressive strength and solid diagonals. For determining the resistance of concrete specimens to aggressive environment such as acid attack, the durability factors such as Acid Strength Loss Factor (ASLF), Acid Attacking Factor (AAF), Acid Weight Loss Factor (AWLF) and Acid Durability Loss Factor (ADLF) were proposed in this investigation. In order to normalize the concentrations (normalities), Weighted Acid Durability Loss Factor (WADLF) was evaluated. It was noted from the durability studies there is almost all the cases the loss in durability is reduced with increase in grade of concrete. Further, a comparison of SCC and NC mixes has shown a good performance of SCC specimens as against NC specimens.

S Venkateswara Rao is an Assistant Professor in the Civil Engineering department of National Institue of Technology, Warangal, A.P, India.He received his PhD from Jawaharlal Nehru Technological University, Hyderabad, India. His research interest is in the field of self compacting concrete.

M V Seshagiri Rao, Professor, Dept. of Civil Engg., J N T U College of Engg., Hyderabad, A P, India. He has 23 years of teaching experience and published 80 papers in various journals and published one text book.

D Ramaseshu, Professor, Dept. of Civil Engg. NIT Warangal, A P, India. He has 20 years of teaching experience in the field of civil engineering.

P Rathish Kumar, Associate Professor, Dept. of Civil Engg. NIT Warangal, A P, India. He has 15 years of teaching experience in many aspects of civil engineering and is a peer reviewer for several journals.

Keywords: Acid durability factor, Normal concrete, Self-compacting concrete

INTRODUCTION

Self-compacting concrete (SCC) is defined as a concrete which can flow through and fill the gap in between the reinforcement and corners of the moulds without any need for external vibration. SCC compacts itself due to its self weight and de-aerates almost completely while flowing in the formwork. SCC can also be used in situations where it is difficult or impossible to use mechanical compaction for fresh concrete, such as underwater concreting, cast in-situ pile foundations, machine bases and columns or walls with congested reinforcement. The high flowability of SCC makes it possible to fill the formwork without vibration [1]. Since its inception, it has been widely used in large construction works or projects in Japan [2]. Recently, this concrete has gained wide use for different applications and structural configurations [3] across the world.

The functional requirements of a fresh SCC are different from those of a vibrated fresh Normal Concrete (NC). Filling of formwork with a liquid suspension requires workability performance like filling ability, passing ability and resistance against segregation [4]. Self compacting concrete can be produced by using standard cementing materials and additives [5]. It consists of mainly cement, coarse and fine aggregates, and filler, such as fly ash, Ground Granulated Blast furnace Slag (GGBS) and Rice Husk Ash, water, super plasticizer and viscosity modifying agent.

Although SCC is a very promising cementitious material, the actual application of SCC might be somewhat riskful due to lack of knowledge concerning its actual durability [6]**.** The degradation mechanisms of a cementitious material are greatly influenced by the permeability of the material for potentially aggressive media and there is an important interaction between ‘pore structure’,’ transport mechanism ‘and ‘degradation’. As the pore structure might be different for SCC in comparison with the traditional concrete, due to difference in the composition, some changes in durability behavior might occur. Acid attack, resistance to sulfate attack and resistance to chloride attack are some of the properties which determine the transport mechanism and chemical deterioration of the concrete [7].

From the literature available, it was noted that there are limited studies covering the durability issues on SCC though there is a lot of literature available on Normal Concrete (NC). Hence, it is felt that in the wake of SCC becoming an important material with numerous applications at present, there is a need to clearly bring out some of the durability based parameters which govern the mix design of SCC and the influence on strength and durability aspects of such a SCC. There is also a need to quantify the durability aspects of SCC.

EXPERIMENTAL PROGRAMME

The experimental programme consisted of casting and testing SCC specimens. Though basically Nan Su method of mix design [8] was adopted, several trials were made in producing SCC satisfying the EFNARC specifications [4]. A total of three grades of concrete are investigated viz. M20, M30 and M70 grades, representing ordinary, standard and high strength concrete respectively as per IS 456-2000 [9]. A total of 108 standard cubes of SCC, and 135 standard cubes of NC for acid attack study were cast and tested.

The properties of the constituent materials used in the present investigation are given in Table 1. The adequate dosage of Super Plasticizer (SP) was used in improving the flowability, self compacting ability and segregation resistance of fresh SCC for meeting the design requirements. Water content of the SP can be regarded as part of the mixing water. In the present work, SNF condensate (SP 430) was used as a water reducing admixture (Super Plasticizer). The dosage of SP was obtained based on trial and error to suit the requirements of EFNARC. Hydrochloric Acid of 35 – 38% LR with Specific gravity = 1.18 kg/lit and Sulphuric Acid of 98% LR – Merk. M = 98.08 g/mol with Specific gravity = 1.84 kg/lit with different concentrations viz. 2% and 5% was adopted in this study.

Table 1 Material property of ingredients used for SCC

CEMENT – OPC 53 GRADE		FLY ASH	
Specific gravity	3.10	Fineness	335 m^2/kg
Normal consistency	29.5%	Silicon Diaoxide (SiO_2)	62.94%
Coarse Aggregate		Lime reactivity	9.8 MPa
Specific gravity	2.65	Fine Aggregate	
Bulk density (kg/m^3)	1442	Specific gravity	2.5 5
Fineness modulus	7.16	Bulk density (kg/m^3)	1713
Super Plasticizer – Conplast SP 430		Fineness modulus	2.19
Specific gravity	1.22		

Mix proportioning

The mix design procedure adopted is as per Nan Su method [8]. The details of the mix proportion are shown in Table 2, while the fresh and hardened properties of the three grades of concrete are shown in Table 3.

Table 2 Mix proportions of SCC and NC

MIX	MIX PROPORTION	w/b	QUANTITIES, kg/m^3						
			Cement	Fly Ash	Fine Aggregate	Coarse Aggregate	S.P	VMA	Silica Fume
SCC M20	1: 1.4 2: 4.49:3.80:0.043	0.455	210	300.0	944.00	800.00	9.12	---	---
NC M20	1: 1.49:3.14	0.50	378	---	564.00	1188.00	---	---	---
SCC M30	1: 1.08: 3.47: 2.83:0.016	0.435	285	308.7	991.13	807.30	4.708	---	---
NC M30	1: 1.11: 2.51	0.42	456	---	508.00	1146.00	---	---	---
SCC M70	1:0.450:1.250:1.170:0.03	0.269	680	305.5	850.30	795.65	15.85	1.75	34.0
NC M70	1: 0.2: 0.875: 1.625:0.03	0.26	665	133.0	581.9	1080.7	19.95	---	39.9

Table 3 Fresh and hardened properties of M20, M30 and M70 grade SCC and NC

S. NO	GRADE OF CONCRETE	SLUMP FLOW VALUE	T_{50}	V-FUNNEL	V-Funnel AT_5 MINUTES	L-Box H_2/H_1	28 DAYS COMPRESSIVE STRENGTH MPa	
							SCC	NC
1.	M 20	660 mm	2.0 Sec	4.0 Sec	5 Sec	1.00	27.67	28.25
2.	M 30	695mm	4.2 Sec	4.0 Sec	7 Sec	0.98	49.75	41.00
3.	M 70	720 mm	4.0 Sec	6.0 Sec	6 Sec	1.00	79.30	79.20

DURABILITY TESTS ON SCC

In the present study acid attack of concrete under 2% and 5% hydrochloric and sulphuric acids were conducted.

Tests for Acid Attack on SCC

After 28 days of curing in water, each cube was tested for weight and compressive strength. The cured self compacting concrete and normal concrete specimens of different grades viz. M20, M30 and M70 concrete specimens were kept exposed to 2% and 5% solutions of both sulfuric acid and hydrochloric acids respectively. Cubes were continuously immersed in solution upto 28 days.

The response of the specimens to the solutions was evaluated through change in appearance, weight, compressive strength and dimensions of solid diagonals. Before testing, each specimen was removed from the baths, and brushed with a soft nylon brush and rinsed in tap water. This process removes loose surface material from the specimens. For determining the resistance of concrete specimens to aggressive environment such as acid attack, the durability factors [10] are proposed in this investigation, in lines of the philosophy of ASTM C 666 – 1997 [11].

Acid Strength Loss Factor (ASLF) is an indication of relative performance of concrete in strength, before and after immersion in a particular concentration of Acid. This also depends on the period of immersion of specimen. ASLF is mathematically calculated as:

$$ASLF = S_r \times (N/M) \quad (1)$$

Where:
S_r = Relative strength at N days, (%)
N = Number of days at which the durability factor is needed.
M = Number of days at which the exposure is to be terminated.

Acid Attacking Factor (AAF) is meant to determine indirectly the disruption of concrete near the corners of cube by way of measuring the change in the length of diagonal (referred as diagonal loss) in a typical concrete cube after immersion in acid for a certain period of time.

The extent of loss is determined by the formula:

AAF = (Loss of acid diagonal after immersion/ acid diagonal before immersion) x 100 (2)

Acid Weight Loss Factor (AWLF) is calculated by the percentage loss of weight of specimen immersing the cubes in various types and concentrations of acids for different immersion periods.

AWLF = (Loss of weight of the specimen after immersion/ Original weight of the specimen before immersion) x 100 (3)

DISCUSSION OF TEST RESULTS

The experimental studies on fresh and hardened properties of SCC were carried out. It was noted that the fresh properties were satisfied for all three grades of concrete. In all the three grades the compressive strength was satisfied.

From the detailed experimental studies on acid effect on SCC and NC specimens, it was noted that in most of the cases SCC specimens behaved well compared to NC specimens. To estimate the acid effect on SCC and NC, certain factors are determined as explained in the following paragraphs.

Acid Durability Loss Factor (ADLF) for SCC and NC

When the specimens were dipped in acid environment, the net loss in strength, physical change in the dimensions of the cube and weight loss were noted. All these can be summed up to get a unique factor typically depicting the various losses due to acid attack and is called as Acid Durability Loss Factor (ADLF) [10]. The different losses are individually quantified in terms of different factors.

Acid Strength Loss Factor (ASLF)

Acid Strength Loss Factor (ASLF) highlights the variation in the compressive strength of SCC and NC when dipped in different acidic environment viz. HCl, H_2SO_4 and for different concentrations. The ASLF is calculated as per equation (1). Figures 1, 2 and 3 shows the variation of ASLF in SCC and NC for 3, 7 and 28 days of immersion in acids.

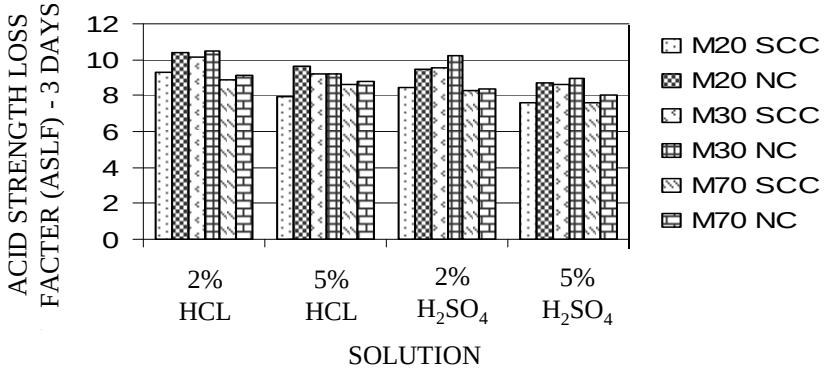

Figure1 Acid Strength Loss Factors for SCC and NC for 3 days of immersion

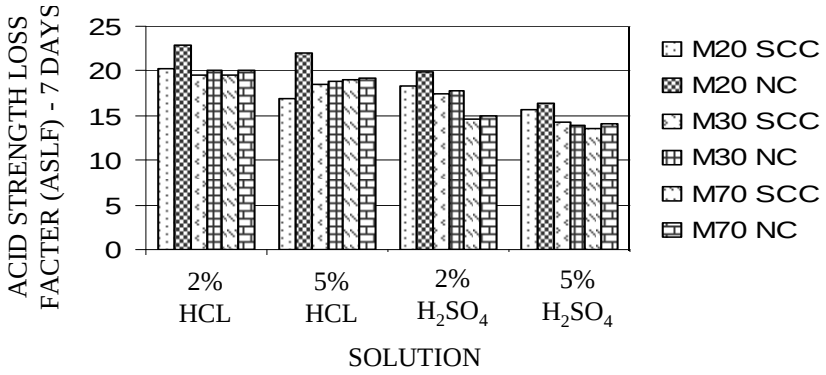

Figure 2 Acid Strength Loss Factors for SCC and NC for 7 days of immersion

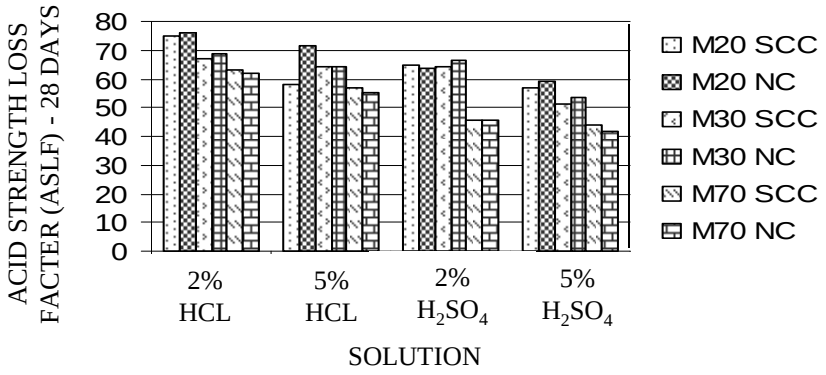

Figure 3 Acid Strength Loss Factors for SCC and NC for 28 days of immersion

Acid Attacking Factor (AAF)

Acid Attacking Factor (AAF) gives an idea of the disruption in the geometry of the specimen due to acidic environment. This is quantified by measuring the loss in diagonals of standard test specimen. The average loss in the diagonals was measured, for all the specimens immersed in acid at the end of 3, 7 and 28 days. Again a comparison for all the grades of concrete between SCC and NC revealed that SCC specimens behaved better than NC specimens. Figures.4, 5 and 6 shows the variation of AAF in SCC and NC for 3, 7 and 28 days of immersion in acids.

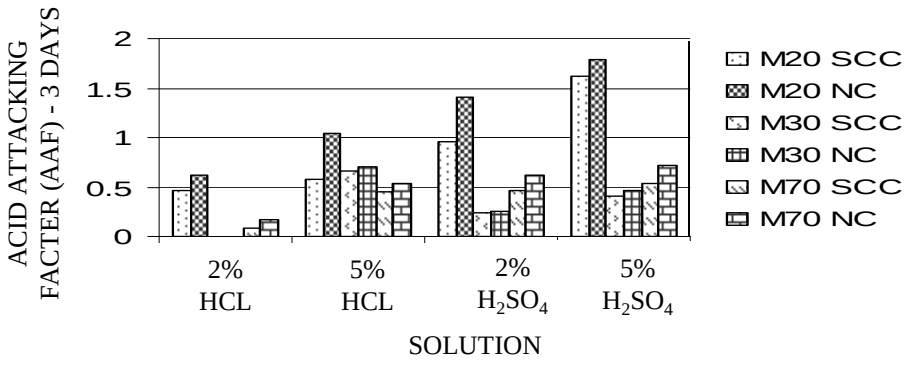

Figure 4 Acid Attacking Factors for SCC and NC at the 3 days of immersion

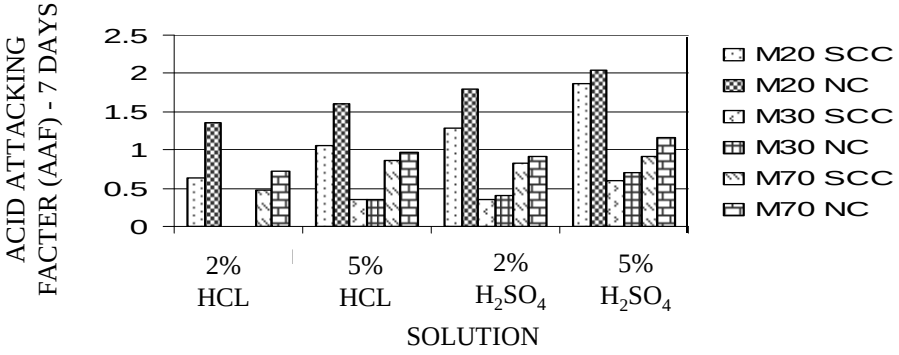

Figure 5 Acid Attacking Factors for SCC and NC at the 7 days of immersion

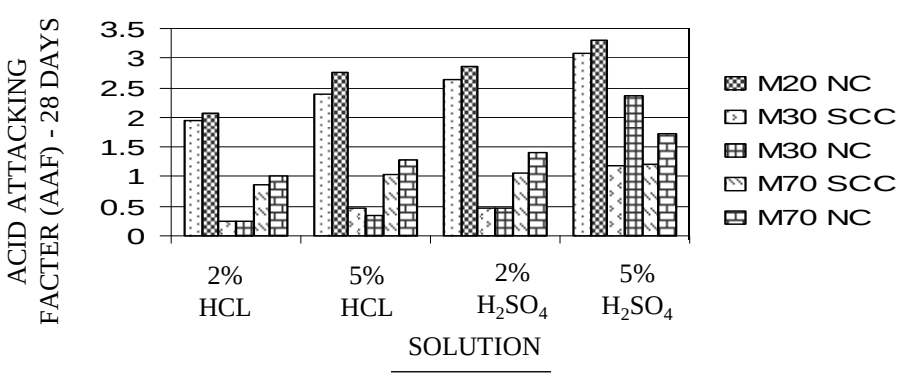

Figure 6 Acid Attacking Factors for SCC and NC at the 28 days of immersion

Acid Weight Loss Factor (AWLF)

Because of acidic environment, the pH of the concrete decreases, at the same time the cement and the mortar part in the interstices portion will be completely eaten away by the acid. This results in decrease in the weight of the specimen. It can be noted in general that the loss is more in case of 5% H_2SO_4 as compared to HCl. Figures. 7, 8 and 9 shows the variation of AWLF in SCC and NC for 3, 7 and 28 days of immersion in acids.

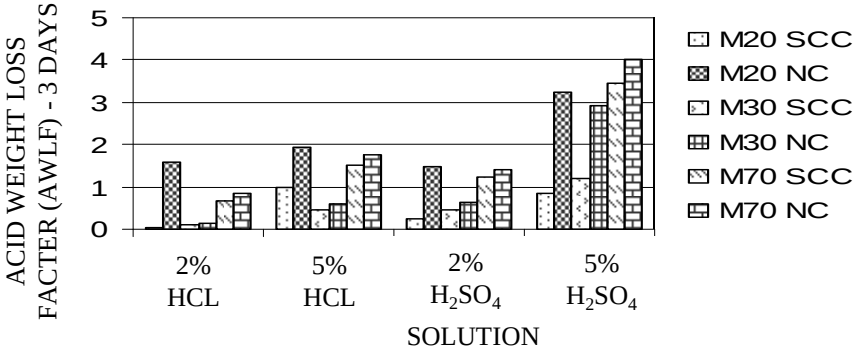

Figure 7 Acid Weight Loss Factors for SCC and NC for 3 days of immersion

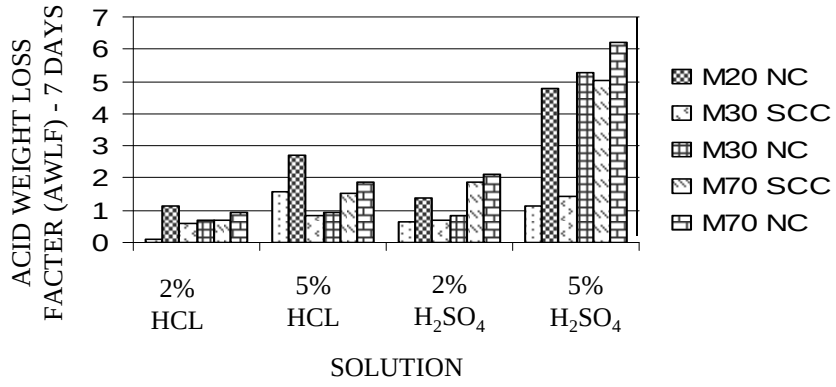

Figure8 Acid Weight Loss Factors for SCC and NC for 7 days of immersion

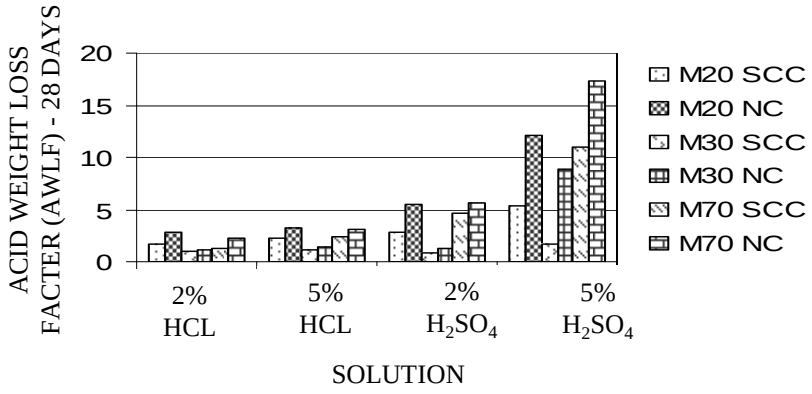

Figure 9 Acid Weight Loss Factors for SCC and NC for 28 days of immersion

Acid Durability Loss Factor (ADLF)

The above losses in strength, weight and geometry are summed up to obtain a durability factor called Acid Durability Loss Factor (ADLF). Figures 10, 11 and 12 shows the variation of ADLF in SCC and NC for 3, 7 and 28 days of immersion in acids. It can be noted that the losses are more in NC specimens compared to SCC specimens. Hence, it can be said at this stage that the SCC specimens are more durable compared to NC.

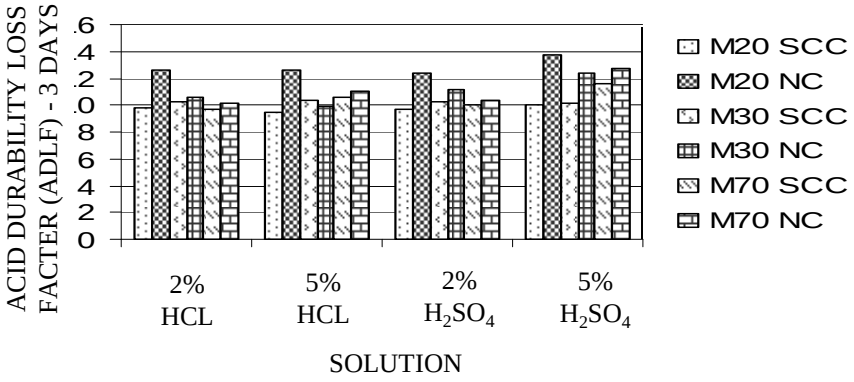

Figure 10 Acid Durability Loss Factors for SCC and NC at 3 days of immersion

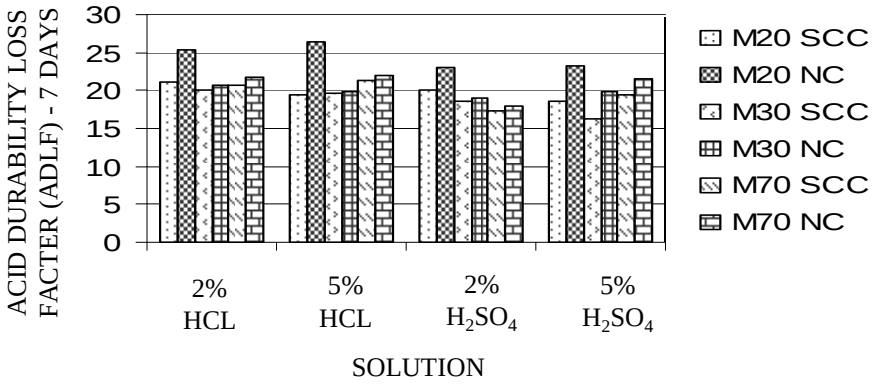

Figure 11 Acid Durability Loss Factors for SCC and NC at 7 days of immersion

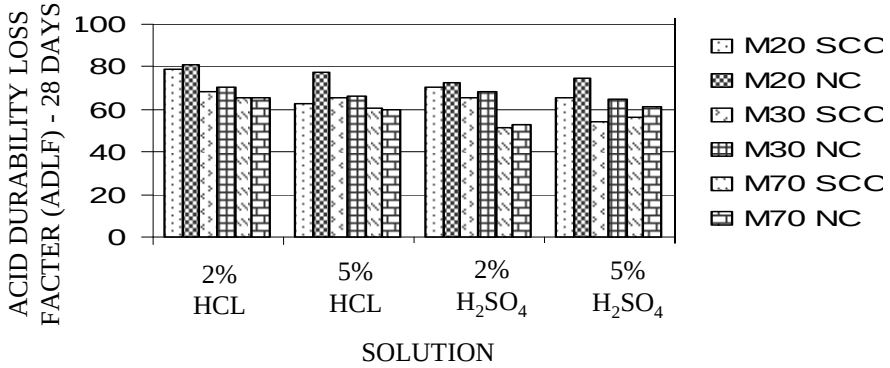

Figure 12 Acid Durability Loss Factors for SCC and NC at 28 days of immersion

In the present study as two types of acids (HCl and H_2SO_4) with two different concentrations (2% and 5%) are considered, in order to normalize the concentrations (normalities), Weighted Acid Durability Loss Factor (WADLF) was evaluated. After conducting a study of all the above with regard to various concentrations and type of acids, it is felt that a factor involving the concentration (normality) of acids can be involved to obtain a WADLF. WADLF values are shown in Tables. 4 and 5 for SCC and NC respectively.Figure.13 shows the plot of grade of concrete Vs WADLF.

Table 4 Weighted Acid Durability Loss Factor of SCC

SOLUTION	WEIGHTED ACID DURABILITY LOSS FACTOR (ADLF)					
	Normality	28 Days				
		SCC - M20		SCC - M30		SCC - M70
2% H Cl	0.23	78.68		68.21		65.49
5% H Cl	0.56	62.86	66.96	65.55	59.78	60.55
2% H_2SO_4	0.72	70.08		65.59		51.18
5% H_2SO_4	1.75	65.45		54.44		56.10

Table 5 Weighted Acid Durability Loss Factor of NC

SOLUTION	WEIGHTED ACID DURABILITY LOSS FACTOR (ADLF)					
	Normality	28 Days				
		NC – M20		NC - M30		NC - M70
2% H Cl	0.23	80.98		70.30		65.17
5% H Cl	0.56	77.42	74.93	66.25	66.06	59.82
2% H_2SO_4	0.72	72.29		68.34		52.64
5% H_2SO_4	1.75	74.41		64.51		60.95

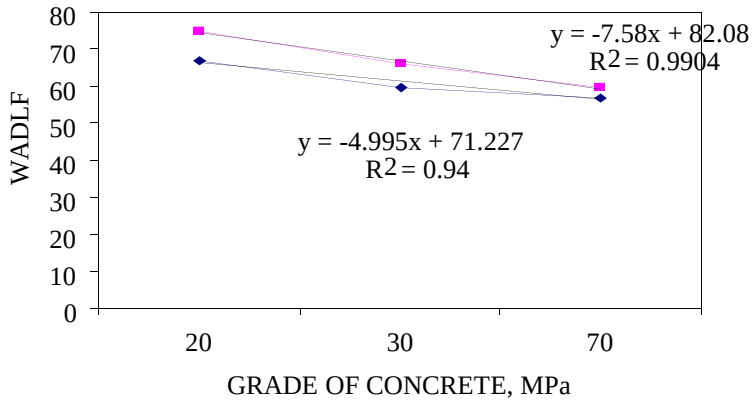

Figure 13 Graph between grade of concrete and weighted ADLF

From the above plot it can be concluded that with the increase in grade of concrete there is a decrease in weighted ADLF values, meaning, a better performance. A relationship between WADLF and grade of concrete was fitted for both SCC and NC.

WADLF = 0.712 – 0.049 x (grade of concrete) is for SCC (4)

WADLF = 0.821 – 0.076 x (grade of concrete) is for NC (5)

Figure 14 shows the visual condition of the samples after 28 days exposure in H_2SO_4 and HCl solutions.

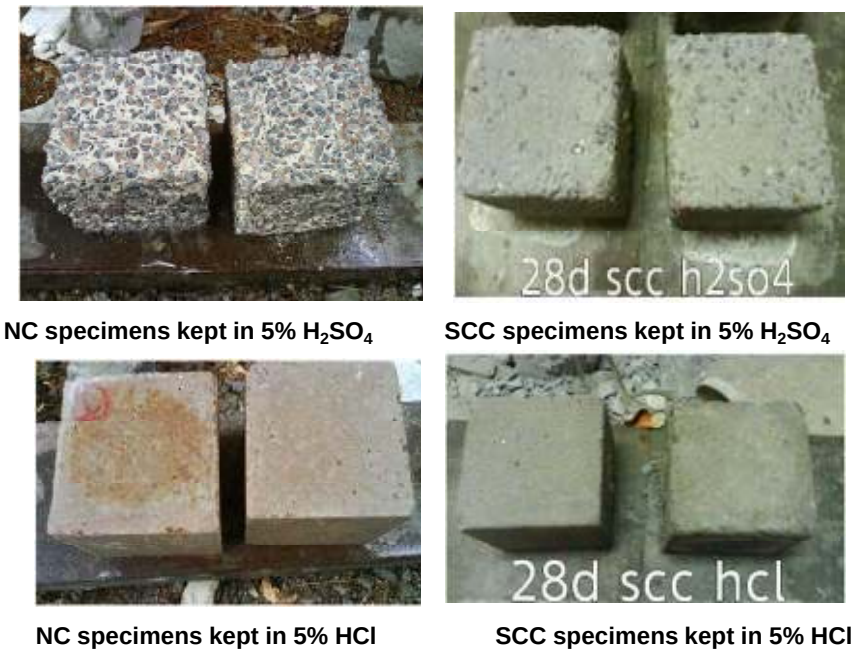

Figure 14 Visual condition of samples

It can be noted that the loss factor is high in NC as compared to SCC, meaning, a superior durability performance in case of SCC.

CONCLUSIONS

- With the increase in duration of curing the ASLF (Acid Strength Loss Factor) increased. This is true for both SCC and NC.
- With the increase in grade of concrete from M20 to M70 the ASLF value has considerably decreased which indicates that the loss is decreasing with increasing grade of concrete.
- The higher ASLF values in Normal Concrete indicated higher loss in NC specimens as compared to SCC specimens.
- With the increase in period of immersion of concrete in various types (HCl and H_2SO_4) and concentrations of acid, there is a considerable disruption of concrete near

the corners of the standard cube and such disruption in SCC is less as compared to NC, meaning, superior durability quality of SCC.

- The weight loss is however more in NC as compared to SCC. A comparison of all the above indicated a better performance in SCC as against NC specimens.
- The WADLF is more in case of NC and for lower grades, as against SCC mixes and high grade concretes. Hence, the SCC mixes were better than NC in all grades.

REFERENCES

1. KHAYAT K. H., GHEZAL A. AND HADRICHE M. S. "Factorial design models for proportioning self consolidating concrete". Materials and Structures/Mat6riaux et Constructions, November 1999, Vol. 32, pp 679-686.

2. OKAMURA HAJIME AND OUCHI MASAHIRO. "Self – Compacting Concrete". Journal of advanced concrete technology, 2003, Vol.1, No.1, pp 5 – 15.

3. BOUZOUBAA N, LACHEMI M. "Self-compacting concrete incorporating high volumes of class F fly ash: Preliminary results", Cement and Concrete Research, 2001, Vol. 31, No.3, pp 413-420.

4. EFNARC. "Specification and guidelines for self-compacting concrete", European Federation of Producers and Applicators of Specialist Products for Structures, May 2005.

5. DINAKAR P, BABU K.G, MANU SANTHANAM. "Durability properties of high volume fly ash self compacting concretes", Cement and Concrete Composites, November 2008,Volume 30, Issue 10, pp 880-886.

6. MD. SAFIUDDIN, WEST J.S., AND SOUDKI K.A. "Durability Performance of Self-consolidating Concrete". Journal of Applied Sciences Research, INSInet Publication 2008, Vol.4, No.12, pp1834-1840.

7. AL-TAMIMI A. K. AND SONEBI M. "Assessment of Self-Compacting Concrete Immersed in Acidic Solutions", ASCE- Journal materials in Civil Engineering, 2003, pp 354 – 357.

8. NAN SU, KUNG-CHUNG HSUB AND HIS-WEN CHAI. "A simple mix design method for self-compacting concrete". Cement and Concrete Research, 2001, Vol. 31, pp1799 – 1807.

9. IS: 456 – 2000 Code of practice for plain and reinforced concrete (fourth revision).

10. S. VENKATESWARA RAO "Experimental studies on the effect of size of aggregate and fines on the strength and durability properties of Self Compacting Concrete", PhD thesis of JNTUH, 2010.

11. ASTM C 666 – 1997 "Standard Test Method for Resistance of Concrete to Rapid Freezing and Thawing".

Special Additions in High Performance Concrete

A Principallo
CTG - Italcementi Group, Italy

Exploring the relationship between concrete mix proportions and performances is a fundamental step toward a full sustainability based assessment of structures. In this context, the present paper studies the effect of using addition in laboratory made high performance concrete. The study is focused on concrete mixes based on limestone cement including fly ash and finely ggbs as addition to concrete. It is shown that using specifically selected proportions of constituent materials may help saving clinker in high performance concrete by reducing its amount to typical contents available in ordinary concrete. Some limitations are also shown taking into account mechanical performances at young ages and durability related performances.

Professor Antonio Principallo, CTG - Italcementi Group, Italy, gained a degree in Chemical Engineering from the University of Pisa in 1999 and has presented several research papers published on cement based materials in journals and conference proceedings. In 2001, he spent 6 months at TU Delft University and gained his PhD in 2002 in Engineering of Materials from Polytechnic of Milan, Italy. He is currently manager or research projects at C.T.G. and is active in CEN and UNI standardisation committees CEN/TC104 (SC1, SC1/TG17, SC1/TG19); CEN/TC51 (WG6/AHG, WG12, WG12/TG1, WG12/TG5, WG14).

Keywords: Addition, Concrete, Durability, Modeling, Sustainability

INTRODUCTION

Understanding how concrete constituents affect durability is a fundamental step towards a thorough sustainability assessment of concrete structures [1].

Environmental issues and durability have to be comprehensively considered and, to this end, a feasible approach via the Environmental Product Declaration was recently made available as European Standard [2].

However, although reducing carbon footprint of a structure during its life cycle could be considered as an overarching goal, reducing concrete carbon footprint should be taken in account also in respect of durability-related performance. This subject is of uttermost relevance within Life Cycle Assessment [3] since the yearly impact brought about by the embodied carbon decreases as the service life lengthens [4].

Considering that concrete is often designed to fulfill durability requirements on the basis of provisions derived from well-tried experience [5], the beneficial effect of using additions into concrete may be overestimated if their intended use is solely aimed at reducing the carbon footprint.

On the contrary, above certain minimum clinker contents, saving clinker may be advantageous if concrete mixes are designed properly.

Finally, in order to evaluate correctly the effect of saving clinker to produce sustainable concrete, inputs to carbon footprint resulting from the need for more onerous maintenance or demolition/reconstruction operations should in principle be accounted for.

The present paper is mainly aimed at investigating the relationship between mix design and durability performance of concrete mixes containing special additions to contribute filling the gap between durability and sustainability assessment. Special attention was paid to concrete mixes including up to three different additions using activators.

Numerical modeling activities were also carried out focusing on studying concrete behavior at early ages since it can be considered as major hindrances to saving clinker.

MATERIALS AND METHODS

Concrete mixes were made containing different proportions of the following constituents:

- CEM II/A-LL 42.5 R, provided by Italcementi Group
- Ground granulated blast furnace slag (ggbs) with very high fineness:
    - ggbs@4000 – Blaine value: 4000 cm^2/g
    - ggbs@6000 – Blaine value: 6000 cm^2/g
- Siliceous fly ash (l.o.i. ~4%)
- Acrylic based superplasticizer
- Sandstone gravel with maximum aggregate size of 15 mm
- Activator: mixture of CaO, $CaSO_4$, Na_2SO_4

Concrete consistency class was kept constant (S5) by using similar paste volume (~385 l/m^3) and similar water/fines ratio (~0.35) while adjusting the superplasticizer content.

The following tests were made on concrete: slump flow and flow time [6]; compressive strength [7] using nominal 10x10x10 cm side cubes; hydraulic shrinkage [8].

Moreover, the following accelerated tests were also carried out to assess durability-related performance:

- freezing/thawing in the presence of de-icing salts [9]
- accelerated carbonation: 28-day-old specimens, previously cured at 100% RH and 20°C, were maintained for 70 days in a chamber at 55% RH, 20°C and 4% CO_2; afterwards the carbonation depth was detected according to [10].

Table 1 Plain additions and their binary mixes

CEMENT + ADDITION (c+a)				CONCRETE				SLUMP		COMPRESSIVE STRENGTH				SHRINKAGE			
%	%	%	kg/m^3	kg/m^3 (c)	% (c+a)	-	-	mm	s	MPa				µm/m			
CEM II/A-LL 42.5R	ggbs @ 4000	Fly ash	content	Cement (estimated clinker)	Superpl.	w/(c+a)	w/c	flow	time	2d	7d	28d	90d	7d	28d	60d	90d
100	-	-	533	533 (426)	1.5	0.35	0.36	460	9.5	51	62	71	78	233	570	562	602
80	20	-	531	425 (340)	1.0	0.35	0.45	560	2.5	43	58	71	76	293	519	561	600
75	25	-	531	398 (318)	1.0	0.35	0.48	610	3.1	42	59	71	82	293	508	542	569
70	30	-	531	371 (297)	0.8	0.35	0.51	600	2.9	38	55	71	77	303	514	549	573
70	-	20	525	420 (336)	1.5	0.34	0.44	630	3.4	46	60	72	85	308	494	584	622
75	-	25	527	395 (315)	1.2	0.33	0.45	570	3.9	40	54	65	78	314	496	598	629
70	-	30	526	368 (294)	1.5	0.33	0.48	730	2.4	41	56	71	92	220	368	451	472
70	15	15	528	370 (295)	1.2	0.34	0.50	680	2.9	40	60	74	85	280	428	491	518
70	10	20	530	371 (296)	1.3	0.33	0.49	670	3.8	39	58	75	85	296	462	534	562
70	20	10	531	372 (297)	1.0	0.34	0.50	600	3.6	39	58	74	81	329	484	502	578

EXPERIMENTAL

Table 1 shows both the composition and the main results of the mechanical and rheological tests performed on concrete mixes containing plain additions and their binary mixes.

Concrete based on CEM II/A-LL 42.5 R was taken as the reference. Mixes were prepared with the following content of additions (on binder basis):

- 20, 25 and 30% ggbs@4000 (mixes 20/0, 25/0 and 30/0 respectively)
- 20, 25 and 30% fly ash (mixes 0/20, 0/25 and 0/30 respectively)
- Binary mixes of ggbs@4000 and fly ash:
    - 15% ggbs@4000 + 15% fly ash (mix 15/15)
    - 10% ggbs@4000 + 20% fly ash (mix 10/20)
    - 20% ggbs@4000 + 10% fly ash (mix 20/10)

In particular, Table 1 shows test results concerning specially selected additions (low l.o.i. fly ash and ggbs with high fineness). The following remarks can made from Table 1:

- Over 100 kg/m^3 clinker was saved and the HPC behavior maintained.
- Losses in early compressive strength (at 2 days) were limited to about 10 MPa with respect to the reference concrete.
- Concrete rheology was improved by increasing slump-flow (~300 mm) and by reducing flow time (down to approximately one third) with limited superplasticizer content.
- The highest slump-flow (~730 mm) and the lowest flow time (~3s) were obtained using fly ash.
- The highest fly ash content (mix 0/30) led to the maximum reduction of hydraulic shrinkage (about 25% reduction at 90 days)

Table 2 Activated mixes

CEMENT + ADDITION (c+a)				CONCRETE					SLUMP		COMPRESSIVE STRENGTH				SHRINKAGE			
%	%	%	kg/m^3	kg/m^3 (c)	% (c)	% (c+a)	-	-	mm	s	MPa				µm/m			
CEM II/A-LL 42.5R	ggbs @ 4000	Fly ash	content	Cement (estimated clinker)	Activators	Superpl.	w/(c+a)	w/c	Flow	time	2d	7d	28d	90d	7d	28d	60d	90d
100	-	-	533	533 (426)	-	1.5	0.35	0.36	460	9.5	51	62	71	78	233	570	562	602
70	20	10	519	363 (291)	3%	1.0	0.35	0.51	500	NA	42	59	69	81	303	458	544	576
60	20	20	520	312 (249)	3%	1.0	0.34	0.58	560	4.7	36	56	67	77	261	496	500	521
50	50	-	518	259 (207)	3%	0.7	0.36	0.73	650	3.2	28	52	65	68	302	473	493	526
70	10	20	520	364 (291)	3%	1.2	0.34	0.50	650	2.8	38	57	71	80	320	491	561	592
60	10	30	513	308 (246)	3%	1.0	0.34	0.58	700	2.5	31	45	66	NA	250	432	502	526
50	10	40	514	257 (206)	3%	1.0	0.33	0.67	740	3.3	23	37	57	NA	217	408	462	480

Table 2 shows both the composition and the main results of the mechanical and rheological tests performed on concrete mixes containing activated binary mixes of additions.

Concrete based on CEM II/A-LL 42.5 R was taken as the reference. Mixes were prepared with the following content of additions (on binder basis):

- 50% ggbs@4000 (mix 50/0a)
- Binary mixes of ggbs and fly ash:
    - 20% ggbs@4000 + 10% fly ash (mix 20/10a)
    - 20% ggbs@4000 + 20% fly ash (mix 20/20a)
    - 10% ggbs@4000 + 20% fly ash (mix 10/20a)
    - 10% ggbs@4000 + 30% fly ash (mix 10/30a)
    - 10% ggbs@4000 + 40% fly ash (mix 10/40a)

Looking at Table 2, the following remarks can be made concerning the use of an activator in those concrete mixes containing mixes of traditional and specially selected additions:

- A generalized effect related to using an activator was hardly found, nevertheless by comparing mix 20/10 (Table 1) with 20/10a a slightly positive effect of the activator on early age compressive strength was apparent also considering the slightly lower clinker content and the slightly higher w/c ratio of mix 20/10a.
- Some 130 kg/m^3 clinker was saved and the HPC behaviour maintained.
- At increasing addition contents in excess of 30%, a reduction in strength was observed not only at early ages (down to about 50% reduction at 2 days) but also at later ages. Losses in early age (2d) compressive strength were up to about 20 MPa with respect to the reference concrete.
- Concrete rheology improved using additions with increasing slump-flow (~200 mm) and by reducing flow time (~down to one third) with limited superplasticizer content.
- A tendency to reduce hydraulic shrinkage was detected.

Table 3 shows compositions and main results of the mechanical and rheological characterization of concrete containing ternary mixes of additions.

Concrete based on CEM II/A-LL 42.5 R was taken as reference. Mixes were prepared with the following content of additions (on binder basis):

- 10% ggbs@4000 + 15% ggbs@6000 + 10% fly ash (mix 10-15/10a)
- 15% ggbs@6000 + 15% fly ash (mix 0-15/15)
- 10% ggbs@4000 + 10% ggbs@6000 + 10% fly ash (mix 10-10/10a)

The following remarks can be made from Table 3:

- Some 130 kg/m^3 clinker saving was possible complying with HPC behaviour
- Just in case of an overall content of addition limited to 30%:
    - Losses in early age compressive strength respect to the reference were held down (<10 MPa) at 2 days and they were not detectable at 7 days.
    - 7 days compressive strength reached the value obtained with the reference concrete in case of cumulative content up to 30%.
    - Concrete rheology improved with increasing slump-flow (~200 mm) and by reducing flow time (~down to one third) with limited superplasticizer content.
    - Shrinkage was to some extent decreased respect to the reference concrete.

Figure 1 shows available results from accelerated tests on freezing-thawing. It was noticed that disregarding a similar HPC mechanical behaviour, results from freezing-thawing tests were quite different one another. In particular:

Table 3 Ternary mixes

CEMENT + ADDITION (c+a)					CONCRETE							SLUMP		COMPRESSIVE STRENGTH			SHRINKAGE		
%	%	%	%	kg/m^3	kg/m^3 (c)	% (c)	% (c+a)					mm	s	MPa			µm/m		
CEM II/A-LL 42.5R	ggbs @ 4000	ggbs @ 6000	Fly ash	content	Cement (estimated clinker)	Activators	Superpl.	w/(c+a)	w/c	Flow	time	2d	7d	90d	7d	60d	90d		
100	-	-	-	533	533 (426)	-	1.5	0.35	0.36	460	9.5	51	62	78	233	562	602		
65	10	15	10	519	337 (270)	3%	8.8	0.35	0.55	460	NA	38	56	67	378	NA	647		
70	-	15	15	530	371 (297)	-	0.6	0.34	0.50	630	3.5	43	62	82	250	499	537		
70	10	10	10	520	364 (291)	3%	0.7	0.35	0.51	580	3.3	44	62	76	378	503	588		

- All the mixes have shown a higher scaled mass than the reference in presence of de-icing salts.
- Some concrete mixes (20/0, 25/0, 30/0, 0/20, 20/10a, 20/20a, 10-15/10a) showed very low scaling (< 0.2 kg/m^2).
- Some mixes (0/30, 10/20, 10/30a, 10/40a) showed a scaled mass higher than or very close to 1 kg/m^2.
- Using activator allowed keeping the mixes containing up to 30% fly ash within the limit value of 1 kg/m^3 whereas a general tendency of fly ash to increase scaled mass was noticed.

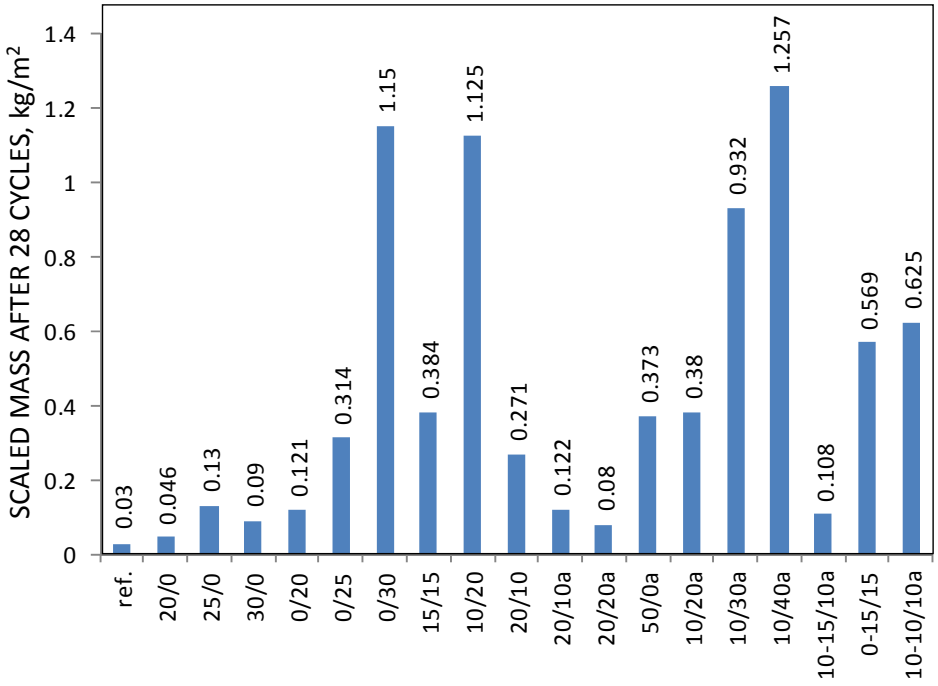

Figure 1 Scaled mass after 28 cycles in presence of de-icing salts

Table 4 shows the results from the accelerated carbonation test. It is possible to note that:

- The reference concrete as well as most of the concrete mixes containing binary mixes of additions have shown an undetectable depth of carbonation (< 0.5 mm).
- Depth of carbonation in some mixes (20/20, 10/20a, 20/20a) containing special additions was slightly detectable (~0.5 mm).
- Mix 10/40a showed greater carbonation depth.

Table 4 Accelerated carbonation test results

MIX	CARBONATION DEPTH, mm
(Reference concrete) 20/0; 25/0; 30/0; 0/20; 0/25; 0/30 15/15; 10/20; 20/10 20/10a; 50/0a	< 0.5
20/20; 10/20a; 20/20a	~0.5
10/30a	1.5
10/40a	5.5

MODELLING EARLY AGE MECHANICAL BEHAVIOUR

In order to study the effect of special activated additions on the early strength development of concrete mixes, the *r2d* parameter - called activity coefficient - was used according to the following equations:

$$R_{2d} = A \cdot e^{-B\left(\frac{w}{c}\right)^{eff}} \quad \text{(Abrams' law)} \qquad \text{Eq. 1}$$

$$\left(\frac{w}{c}\right)^{eff} \approx \frac{w \cdot (1 + ar)}{(c + r2d \cdot a)} \qquad \text{Eq. 2}$$

Where:

- R_{2d} is the compressive strength at 2 days [MPa]
- *ar* is the air content [-] estimated from the theoretical and measured density
- *c, a, w* are cement, addition and water content [kg/m^3]
- A≅227.5 and B≅-4.226 are two empirical constants

r2d is equal to 1 when the final concrete has the same 2-day compressive strength as the reference concrete in case the activated mixture of different additions is replaced by the same amount of CEM II/A-LL 42.5 R by weight. It is worth noting that such parameter must not be confused with k-value established in [5].

Figure 2 shows one possible R_{2d} vs. $(w/c)^{eff}$ relationship which can fit properly the whole dataset comprising all the investigated mixes.

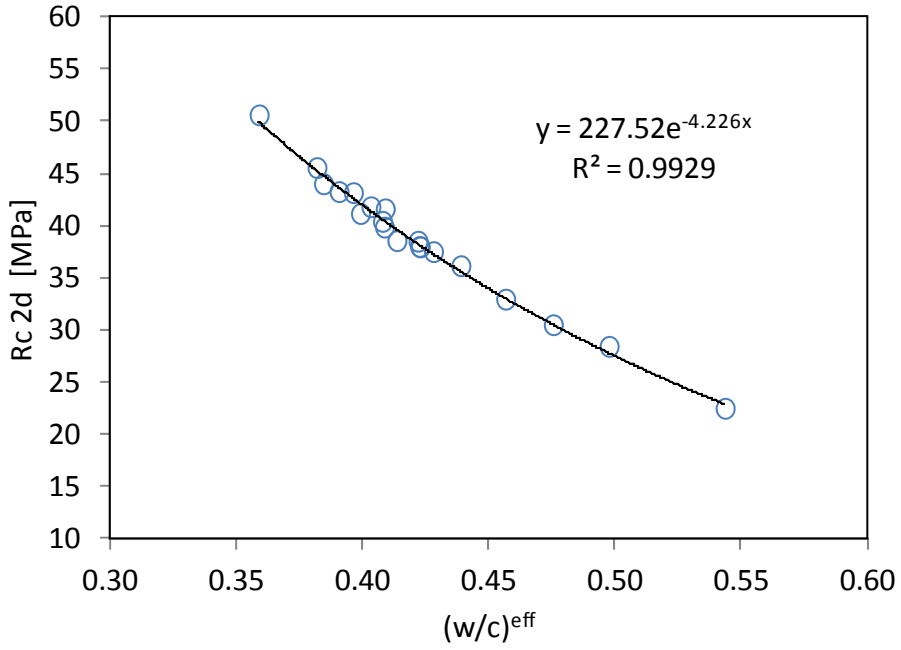

Figure 2 2-day compressive strength as a function of the effective w/c ratio.

r2d values from Figure 2 are shown in Table 5, divided in ranges per type of addition. In particular *r2d* was noticed to increase

- with decreasing cumulative content of additions
- with increasing ggbs fineness
- when using the activator

Table 5 Activity coefficient of special addition

SPECIAL ADDITION		CONTENT (cumulative)	r2d
Binary mixes	ggbs@4000	from 20 % to 30 %	= 0.50
	fly ash	from 20 % to 30 %	From 0.35 to 0.55
		< 30 %	From 0.40 to 0.50
Activated binary mixes	ggbs@4000 fly ash	< 30 %	From 0.35 to 0.60
		< 40 %	From 0.40 to 0.50
		< 50 %	From 0.25 to 0.45
	ggbs@6000 fly ash	< 30 %	~0.60
Activated ternary mixes	ggbs@4000 ggbs@6000 fly ash	< 30 %	0.80
		< 35 %	0.65

Finally a modelling exercise was carried out to parallel the impact of special additions to cracking risk. Since the dynamic phenomena occurring at micro-scale and having a strong impact on macro-scale have been disregarded, the present approach is far from exhaustive.

However a semi-empirical parameter, RCR, related to the risk of cracking occurring at 7 days, normalized to the reference concrete (RCR = 1) was calculated using Eq.3 and presented in Figure 3.

$$RCR = \frac{(\sigma - \sigma_R)}{(\sigma - \sigma_R)_{ref}} = f(\varepsilon, R_{ck}) \qquad \text{Eq. 3}$$

Tension stress (arising in case of restrained shrinkage), σ and tension strength, σ_R were estimated using Eq. 4 [11] taking the measured shrinkage (in non-restrained conditions), ε, and cubic compressive strength values (R_{ck}) as input values.

$$\sigma = \varepsilon \cdot E; \quad E = 22000 \cdot \left(\frac{f_{cm}}{10}\right)^{0,3}; \quad f_{cm} = f_{ck} + 8$$
$$\sigma_R = 0,7 \cdot f_{ctm}; \quad f_{ctm} = 0,30 \cdot f_{ck}{}^{2/3}; \quad f_{ck} = 0,83 \cdot R_{ck} \qquad \text{Eq. 4}$$

The physical meaning of such modeling exercise is to estimate using additions as clinker replacement, whether at short ages the negative contribute due to reduced strength development could be exceeded by the positive contribute due to the reduced shrinkage.

It was evidenced by RCR that in most the cases, by reducing clinker, a higher cracking risk (RCR >1) is expected. In more details:

- at 7 days RCR is in general between 1 and 2.
- at 28 days RCR is up to about 5; however a positive effect of using fly ash to reduce RCR was clearly noticed.

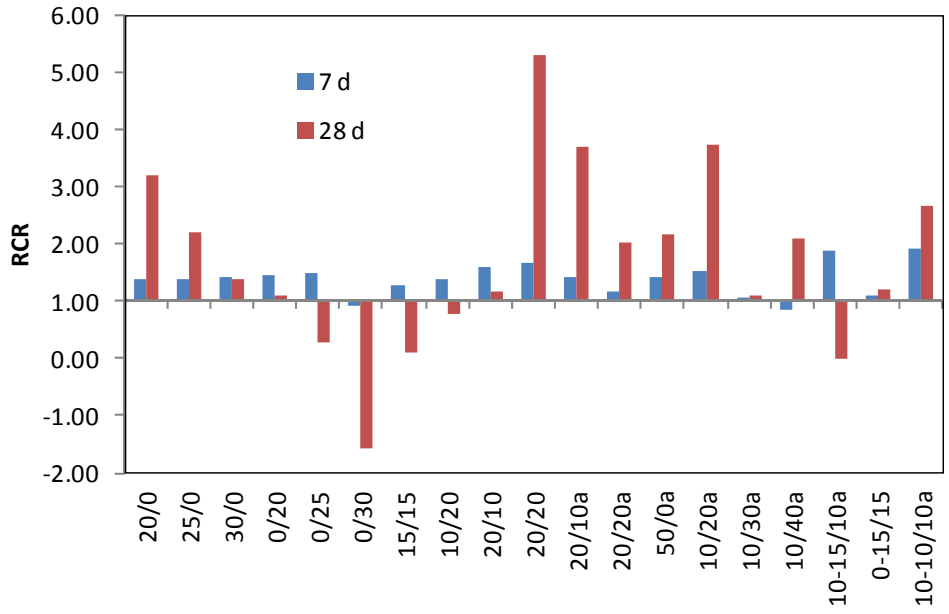

Figure 3 Relative sensitivity to cracking at 7 and 28 days.

CONCLUSIONS

The use of special additions could be a powerful tool to limit the carbon footprint of concrete mixtures although it might not help improve durability-related performance.

This paper shows how, using special additions, clinker savings in HPC have been possible reaching the carbon footprints typically detected in ordinary concrete.

However, since carbon footprint is not the only matter to be considered vis-à-vis sustainability, the impact of mix design variations on durability has to be carefully considered.

A general decrease in early strength was confirmed in HPC mixes using special additions. For this reason, a specific modelling activity was carried out to explore the mechanical behaviour at early ages more extensively.

REFERENCES

1. EN 15643-1 Sustainability of construction works - Sustainability assessment of buildings - Part 1: General framework

2. EN 15804 Sustainability of construction works - Environmental product declarations - Core rules for the product category of construction products

3. ISO 14040 Environmental management -- Life cycle assessment -- Principles and framework

4. EN 15978 Sustainability of construction works - Assessment of environmental performance of buildings - Calculation method

5. EN 206-1: Concrete - Part 1: Specification, performance, production and conformity

6. UNI 11041:2003 Prova sul calcestruzzo autocompattante fresco - Determinazione dello spandimento e del tempo di spandimento

7. EN 12390-3 Testing hardened concrete - Part 3: Compressive strength of test specimens

8. UNI 11307 Prova sul calcestruzzo indurito - Determinazione del ritiro

9. EN 1338 Concrete paving blocks - Requirements and test methods

10. UNI 9944 Corrosione e protezione dell'armatura del calcestruzzo. Determinazione della profondità di carbonatazione e del profilo di penetrazione degli ioni cloruro nel calcestruzzo.

11. D.M. 14 Jan 2008 – Ministero delle infrastrutture – Approvazione delle nuove norme tecniche per le costruzioni

Effect of Mineral Additives on Hydration Heat of Concrete Mixtures

G Skripkiunas, D Nagrockiene, G Girskas
Vilnius Gediminas Technical University, Lithuania

The investigation of Portland cement with different mineral additives used for the massive concrete structures are presented in the paper. The type of cement type and ambient temperature influence on the hydration heat of concrete mixture was determined. The laboratory experiments with different additives for cement were carry out: slag up to 20% (CEM II/A-S 42,5 N), limestone up to 20% (CEM II/A-LL 42,5 R), slag from 66 to 80 % (CEM III/B 32,5 N) and without mineral additives (CEM I 42,5 R). Also the industrial experiments with designed concrete mixtures and the modeling of concrete temperature during cement hydration where carried out. The investigation of concrete mixture temperature regime during a massive concrete structure construction and curing time were performed. Cement type and mineral additives influence on the hydration heat of concrete mixture was determined. The results suggests the hydration heat of concrete mixture is highest with cement without mineral additive (CEM I 42,5 R) and the lowest with cement with the maximum amount of slag (CEM III/B 32,5 N). Modeling of heat release from hardening concrete mixture derived the use of lower activity cement with a larger amount of slag (CEM III/B 32,5 N) stands higher than the heat content of the slag with Portland cement concrete with a smaller amount of slag (CEM II/AS 42,5 N) for requiring larger quantities of cement in concrete mixture. It was found that the used retarder has not a significant effect on hydration heat of concrete mixtures with slag cement. Concrete thermal regime modeling results and temperature measurements in a concrete structure has shown that the temperature in massive concrete structure with slag cement with up to 20% slag addition reaches 61 °C. The massive concrete structures with slag additives (CEM II/A-S 42,5) can be concreted without special cooling technology in average ambient temperature under 15 °C.

Gintautas Skripkiunas, is Associate Professor at the Department of Building Materials, Vilnius Gediminas Technical University, Lithuania

Dzigita Nagrockiene is Associate Professor at the Department of Building Materials, Vilnius Gediminas Technical University, Lithuania.

Giedrius Girskas is a PhD student at the Department of Building Materials, Vilnius Gediminas Technical University, Lithuania.

Keywords: Compressive strength, Density, Hydration heat, Portland cement, Slag

INTRODUCTION

Cement hydration is an exothermic reaction where large amount of heat is released. Portland cement hydration and curing is a complex process in which particles of various sizes hydrate at different speeds and mineral hydration processes overlap [1-3].

According to Taylor [4], cement hydration and liberation of heat during hydration process is caused by the following factors:

- Fineness and granulometric composition of cement particles;
- Water and cement ratio (W/C);
- Chemical composition of clinker;
- Grinding aids that improve clinker grinding efficiency and additives used to enhance the characteristics of cement paste and to substitute part of clinker, i.e. silicon dioxide dust, slag etc.

Paine, Dhir and Zheng [11] have conducted detailed experiments with ash and slag additives in concrete mixtures.

Taylor, Gallucci [4, 5] and other researchers distinguished three stages in cement hydration:

- Initial or preparatory: the formation of saturated solution of the product;
- Colloidal: direct hydration and formation of jelly products;
- Crystallization: further crystallization of colloidal particles into larger crystals.

Spontaneous dissolution of cement begins in the initial or preparatory phase, immediately after its contact with water. Small amounts of ettringite, calcium silicate hydrates (C-S-H) and calcium hydroxides (CH) are produced in the solid phase. This process lasts about 6 hours. In the second stage the formation of calcium silicate hydrate (C-S-H) continues. Calcium aluminate trisulphate hydrate, the so-called ettringite (Af_t), forms during the reaction of aluminium compounds in clinker with gypsum. The highest concentration of this hydrate is reached at the end of the second phase. This phase lasts from the 6^{th} until the 24^{th} hour. The processes that occur after 24 hours of hydration are called crystallization stage. In this stage Af_t compounds react with the remaining clinker minerals and form calcium aluminate monosulpahte (Af_m) hydrates. C-S-H and CH content and crystal size increase [3, 4].

Hydration of clinker minerals are exothermic reactions and therefore a certain amount of heat is released when cement is mixed with water. The biggest amount of heat is released during the hydration of C_3A and C_3S, whereas C_2S reaction with water liberates very little heat. Heat evolution is also more prominent in cements with greater glassy phase [4, 8, 9].

Heat liberation during cement curing has practical significance for concrete placing at low temperatures. On the other hand, big heat release has a negative impact in the manufacture of massive concrete structures. High temperature inside a massive structure and low temperature on the surface may cause the development of unfavourable stresses and cracking. Therefore, concrete placing in massive structures requires concrete mixtures that release little heat during curing (low-exothermic) – up to 165-190 J/g during three days and up to 210-330 J/g during seven days. Belite, slag and pozzolan cements are low-exothermic due to specific mineralogical composition or lower clinker content.

The rate of heat release during cement hydration is not steady – heat evolution is more rapid in the beginning and slows down in later stages. [10]

Set retarding additives are used to delay cement hydration and the rate of heat evolution. These additives have no or little effect on the curing rate of cement slurries. Retarders are used for concrete placing in high temperatures, for long-distance transportation of fresh concrete and for the manufacturing of massive structures. Retarders act as dispersing agents and produce the plasticizing effect, i.e. they enhance the workability of concrete and slow down the reactions thus enabling to maintain the characteristics of fresh concrete for a longer time compared to cement slurries without additives.

MATERIALS AND CONCRETE COMPOSITIONS

Concrete mixtures were designed from different types of cement, the characteristics of which are presented in Table 1 (all cements were produced in accordance with LST EN 197-1:2001 standard). Blastfurnace slag and limestone content in cements CEM II/A-S and CEM II/A-LL was 6 – 20% respectively; cement CEM III/B contained 66 – 80% of slag. Portland cement mixture CEM II/A-S 42.5 N (MA) released 20 % less heat during hydration compared to the regular type Portland cement CEM I. The hydration of cement mixture CEM II/A-LL 42.5 R (MA) released 16 % less heat and heat evolution rate in cement mixture CEM III/B 32.5 N-LH (SR) was 26 % lower.

Table 1 Different type of cement and their characteristics

CEMENT PROPERTIES	CEM I 42.5 R	CEM II/A-S 42.5 N (MA)	CEM II/A-LL 42.5 R (MA)	CEM III/B 32.5 N-LH (SR)
Compressive strength, MPa after 24 hours	-	-	-	-
Compressive strength, MPa after 2 days	28 ± 2	22 ± 3	29 ± 2	-
Compressive strength, MPa after 7 days	-	-	-	21 ± 3
Compressive strength, MPa after 28 days	54 ± 3	51 ± 3	52 ± 3	41 ± 3
Initial setting time, min	160	160	200	195
Final setting time, min	-	-	-	270
Soundness, mm	1.0	1.0	1.0	1.0
Water requirement, %	25.3	25.3	26.3	28.0
Residue on the 90 μm sieve, %	1.3	2.4	0.7	0.6
Specific surface area, (cm^2/g)	3700	3800	4400	4800
Loss on ignition, %	1.4	1.6	6.0	2.2
Insoluble residue, %	0.5	0.5	0.7	0.4
Sulphate content (as SO_3), %	2.8	2.60	2.63	2.54
Chloride content (Cl^-), %	0.005	0.007	0.001	0.014
Alkalinity (as Na_2O equivalent), %	< 0.8	< 0.8	< 0.8	< 1.2
Hydration heat, J/g	365	290	307	< 270

Sand and stone chippings were used as aggregates in concrete mixtures. Plasticizer *Muraplast FK-63-30* and retarder *Retard 310* were used as additives.

Cement mixtures of different composition were tested. Concrete mixtures presented in Table 2 differ by the addition of set retarding additive Retard 310 in phase II. Concrete mixtures were designed from different types of cement, aggregates, water and plasticizer.

Table 2 Concrete mixtures for laboratory testing

MATERIALS	CONCRETE MIXTURES (AMOUNTS OF MATERIALS IN kg PER 1 m^3 of CONCRETE MIXTURE)							
	I-I	I-II	I-III	I-IV	II-I	II-II	II-III	II-IV
CEM I 42.5 R	360	-	-	-	360		-	-
CEM II/A-S 42.5 N (MA)	-	360	-	-	-	360	-	-
CEM II/A-LL 42.5 R (MA)	-	-	360	-	-	-	360	-
CEM III/B 32.5 N- LH (SR)	-	-	-	360	-	-	-	360
Sand	931	931	931	931	931	931	931	931
Aggregate 5/11	476	476	476	476	476	476	476	476
Aggregate 11/16	529	529	529	529	529	529	529	529
Water	135	135	135	135	135	135	135	135
Plasticizer Muraplast FK-63.30	2.16	2.16	2.16	2.16	2.16	2.16	2.16	2.16
Set retarder Retard 310	-	-	-	-	1.08	1.08	1.08	1.08

Industrial testing was performed with concrete mixture presented in Table 3. The concrete was produced from cement CEM II/A-S 42.5 N, 0/4 fraction sand, 4/16 and 16/32 fractions stone chippings, water and plasticizer.

Table 3 Concrete mixture for industrial testing

MATERIALS	AMOUNTS OF MATERIALS IN kg PER 1 m^3 of CONCRETE MIXTURE
Cement CEM II/A-S 42,5 N	350
Sand 0/4	930
Stone chippings 4/16	605
Stone chippings 16/32	350
Water	165
Plasticizer Muraplast FK 63.30	1.925 (0.55 %)

TESTING METHODOLOGY

Characteristics of concrete mixtures used in the testing were determined according to the following standards: workability was tested according to LST EN 12350-2, density was tested according to LST EN 12390-7, and compressive strength after 7 and 28 days of curing was tested according to LST EN 12390-3. Hydration heat of concrete mixtures was tested according to the below-described method.

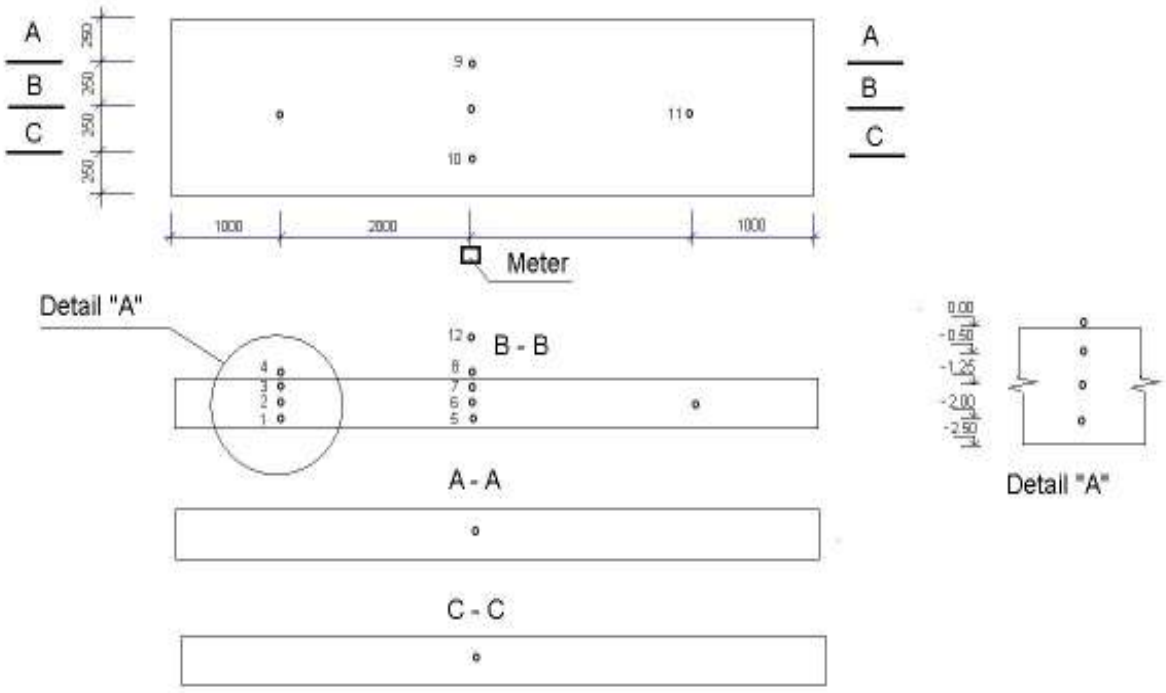

Figure 1 The layout of temperature sensors in a massive concrete structure

Exothermic reaction temperatures are determined in concrete mixtures where heat is released during curing and concrete specimen temperature increases. Exothermic reaction temperature taking procedure and basic requirements: the temperature of concrete components (water, cement aggregates and additives) must be (20 ± 1) °C; the testing must be done at room temperature (20 ± 1) °C; a concrete mixture specimen of 1.5 kg must be moulded in a demountable 100x100x100 mm formwork made of textolite. A glass tube with a T-type thermocouple shall be placed in the specimen during curing. After the concrete specimen is formed the textolite formwork shall be placed into a metal box and insulated with 50 mm thick polystyrene foam. The thermocouple shall be connected to a data transmitting device and to a PC. The temperature shall be measured and readings shall be recorded for 24 or 48 hours.

Concrete temperature in the structures was taken during industrial testing. The temperature was taken by 12 temperature sensors. The layout of temperature sensors in a massive concrete structure is presented in Figure 1.

MODELLING OF THERMAL REGIME IN CONCRETE

The thermal regime was modelled to forecast maximum temperatures in a massive concrete structure. The modelling was based on the assumption that all heat released during cement hydration is transferred to the concrete mixture, i.e. there is no heat exchange with the environment. Such assumption is possible only in the testing of massive structures with very small surface area protected from intensive transfer of heat to the environment. Significant loss of heat from the curing structure to the environment occurs after a longer setting time and the temperature in the structure starts falling. According to the research literature [7] data obtained from the practice of building massive concrete structures we may state that the temperature in the structure starts falling after 4 days (96 h) of curing and drops by 1 degree Kelvin per day.

The release of heat during cement hydration in one cubic meter of concrete mixture is calculated from the equation:

$$Q_h = q \cdot C, \text{ kJ} \tag{1}$$

where: Q_h is the amount of heat released during cement hydration in one cubic meter of concrete mixture, kJ;
q is cement hydration heat, kJ/kg;
C is cement content of concrete mixture, kg/m^3.

Hydration heat of different types of cement and the temperature changes are taken from the reference source [6].

Temperature change (increase) in concrete during hydration reaction is calculated from the equation:

$$\Delta T = \frac{Q_h}{C_0 \cdot \rho_b}, \text{ K} \tag{2}$$

where: C_0 is heat capacity of concrete mixture, kJ/(kg·K);
ρ_b is density of concrete mixture, kg/m^3 (assumed ρ_b = 2400 kg/m^3).

Heat capacity of concrete mixture and wet concrete is 1.05 kJ/(kg·K) [7].

Maximum temperature in concrete structure is calculated from the equation:

$$T = T_a + \Delta T, \quad \text{K (°C)} \tag{3}$$

where: T is maximum temperature in massive concrete structure, K (°C);
T_a is ambient temperature, K (°C).

Figures 2 and 3 illustrate the change in temperature due to the transfer of heat to the environment after 4 days of curing. The curves in Figure 2 represent the ambient temperature of 20°C and the curves in Figure 3 represent the ambient temperature of 15°C.

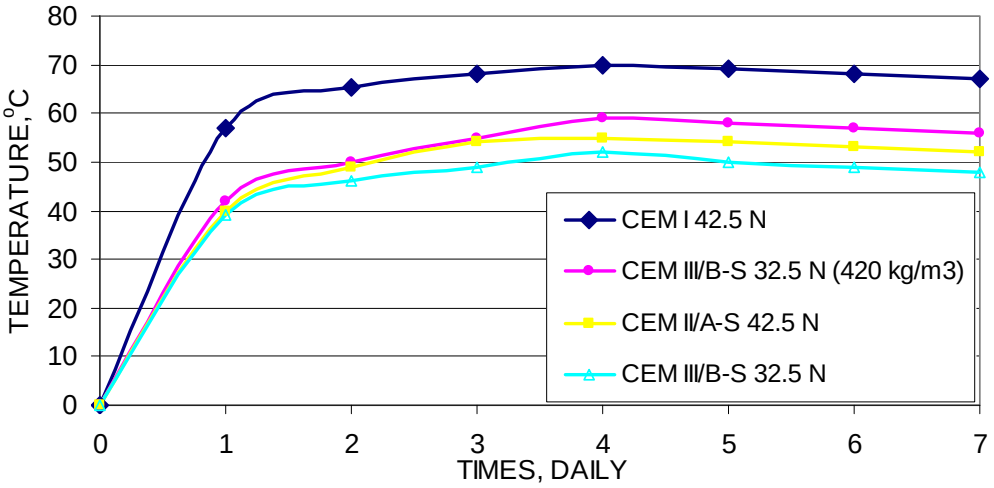

Figure 2 Temperature curves in a concrete structure taking into account the transfer of heat to the environment where the ambient temperature is 20°C

The biggest temperature rise in concrete and the greatest heat loss occurs during the first day of curing. Afterwards the transfer of heat slows down considerably and temperature rise in concrete is insignificant. The maximum temperature in concrete should be reached after 4 days of curing.

When the ambient temperature is 20°C (Figure 2) the maximum temperature is recorded in concrete made of Portland cement CEM I 42.5 N is 70°C. This temperature is rather high, therefore the said Portland cement is not recommended for placing concrete in massive structures.

Concrete made of slag cement CEM II/A-S 42.5 N reaches the temperature of 55°C, whereas concrete made of cement CEM III/B-S 32.5 N with higher slag content exceeds the maximum temperature indicated above. Thus we may confirm the conclusion that slag Portland cement CEM II/A-S 42.5 N suits the best for massive structures.

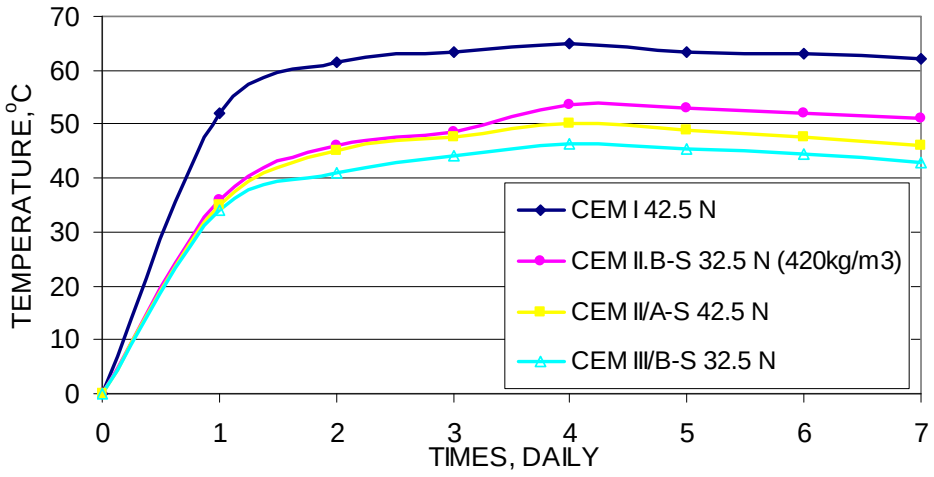

Figure 3 Temperature curves in a concrete structure taking into account the transfer of heat to the environment where the ambient temperature is 15°C

When the ambient temperature is 15°C (Figure 3) the temperature in concrete made of slag Portland cement CEM II/A-S 42.5 N is below 50 °C and the temperature in concrete made of Portland cement with higher slag content CEM III/B-S 32.5 N exceeds 50°C. Therefore slag Portland cement CEM II/A-S 42.5 N is recommended for placing concrete at the ambient temperature of 15°C. In this case the maximum temperature in the concrete mixture does not exceed 50°C, no significant temperature stresses occur and concrete can be placed without using any cooling technologies.

TEST RESULTS

The results of workability tests with concrete mixtures of different composition are presented in Table 4. According to the test results concrete mixture I-II had the lowest slump. CEM II/A-S 42,5 N (MA) type cement was used for this batch, and the slump of concrete mixture II-I was the lowest. Cement CEM I 42,5 R was used for this batch.

Table 4 Workability test results

CONCRETE MIXTURES	I-I	I-II	I-III	I-IV	II-I	II-II	II-III	II-IV
Slump, cm	25.0	15.0	20.0	25.0	2.5	11.0	17.0	17.5

The average values of densities of the tested concrete mixtures are presented in Figure 5. According to density test results in Figure 5 we may state that the highest density in the first and second stage of the test was obtained in concrete mixtures made of CEM I 42,5 R type cement, whereas concrete mixtures made of CEM III/B 32,5 N- LH (SR) type cement had the lowest density.

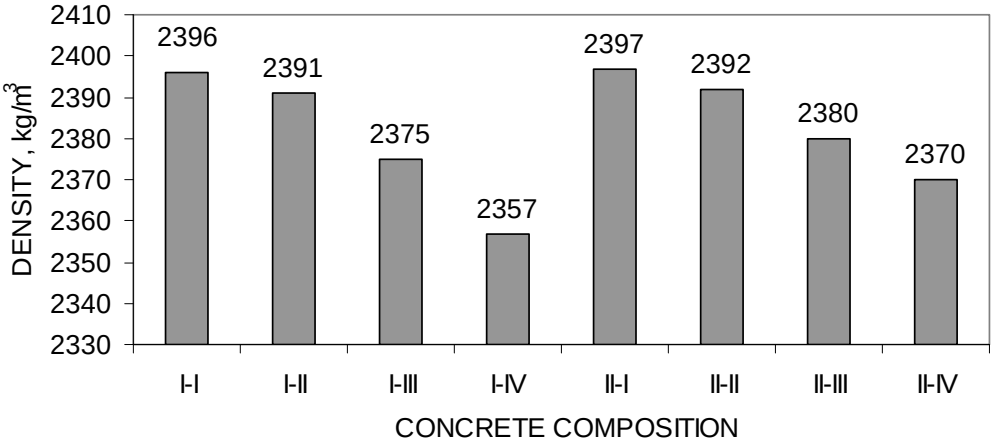

Figure 5 Concrete densities

Compressive strength was tested in specimens of both compositions after 7 and 28 days of curing. The test results are presented in Figures 6 and 7.

The test results (in the first testing phase) lead to the statement that the highest average compressive strength of 39.53 MPa after 7 days of curing is obtained in specimens of concrete mixture I-II made of CEM II/A-S 42,5 N (MA) type cement. The compressive strength class of this concrete was C 30/37. The highest average compressive strength of 43.80 MPa after 7 days of curing in the second testing phase was observed in specimens of concrete mixture II-I made of CEM I 42,5 R type cement.

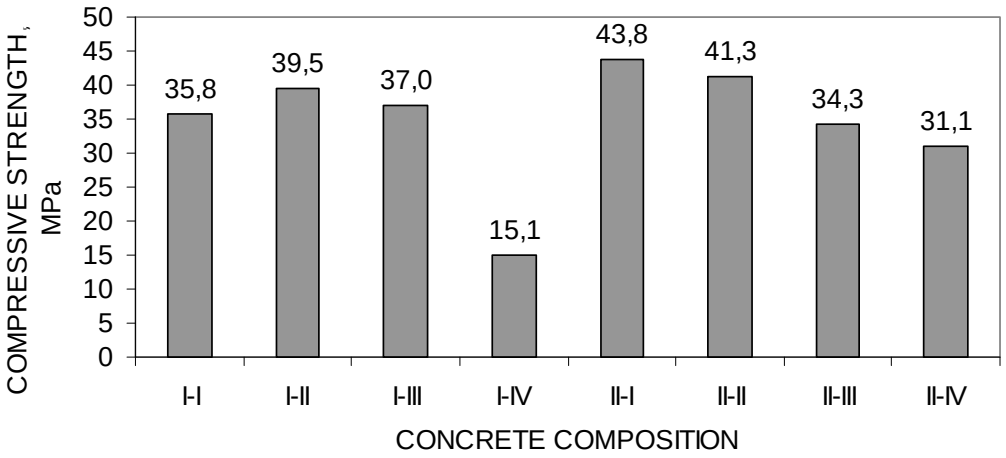

Figure 6 Average compressive strength after 7 days of curing

The testing of compressive strength after 28 days of curing revealed that specimens of concrete mixture I-II made of CEM II/A-S 42,5 N (MA) type cement had the highest compressive strength of 56.5 MPa. In the second testing phase the highest compressive strength of 50.5 MPa was observed in specimens of concrete mixture II-II made of CEM II/A-S 42,5 N (MA) type cement.

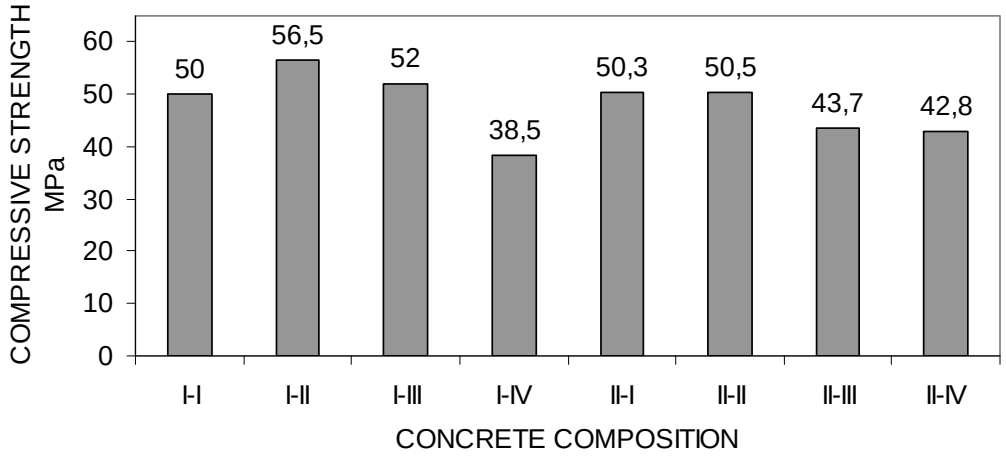

Figure 7 Average compressive strength after 28 days of curing

The curves of hydration heat in concrete mixtures are presented in Figures 8 and 9.

The data in Figure 8 show that the maximum temperature in all concrete compositions is obtained between the 18 and the 22 hour. The highest hydration heat is observed in concrete mixture I-I made of CEM I 42,5 R type cement with the plasticizer FK-63-30. The lowest hydration heat of 21.5°C was recorded in concrete mixture I-IV made of CEM III/B 32,5 N-LH (SR) type cement.

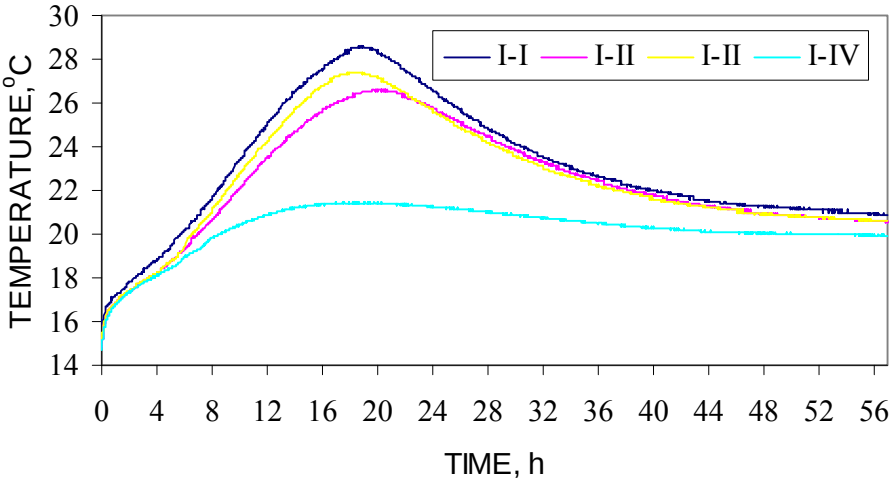

Figure 8 Curves of hydration heat in concrete mixtures (the first testing phase)

The curves of hydration heat obtained in the second testing phase (Figure 9) show that the highest hydration heat is released in concrete mixture II-I made of CEM I 42,5 R type cement when plasticizer Muroplast FK-63-30 and set retarder Retard 310 are added to the mix. It should be noted that set retarder Retard 310 has an effect on concrete mixture II-IV as well.

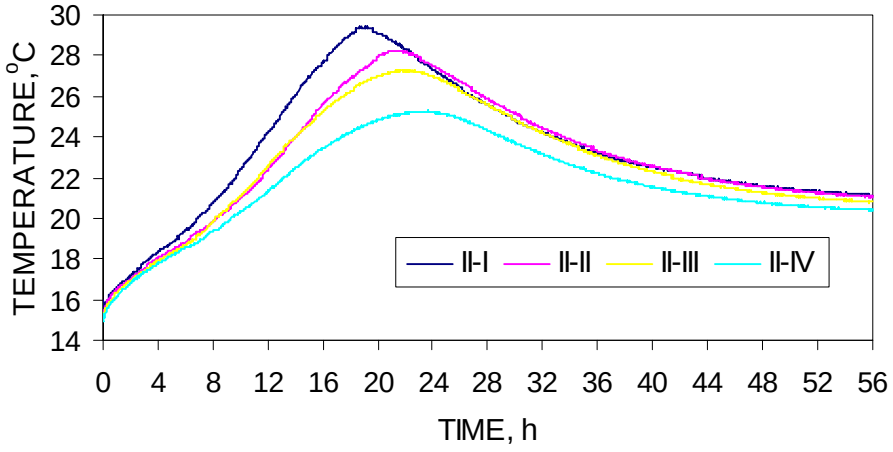

Figure 9 Curves of hydration heat in concrete mixtures (the second testing phase)

Concrete mixture II-I is the first to reach the maximum released temperature of 29.2 °C at the 19 hour. The lowest maximum temperature of 25.1 °C was observed in concrete mixture II-IV. This concrete mixture was also the last to reach its maximum temperature at the 25 hour.

The industrial testing of concrete mixtures included slump test, air content in the mix, density, as well as density and compressive strength after 3 days of curing. The testing results are presented in Table 5.

Table 5 Workability test results

PROPERTIES OF CONCRETE	RESULTS
Slump of fresh concrete, cm	17
Slump after 60 min, cm	18
Air content in the mixture, %	3.6
Density of fresh concrete, kg/m^3	2394
Density of concrete, kg/m^3	2338
Compressive strength after 3 days of curing, MPa	24.23

RESULTS OF TEMPERATURE TESTING IN CONCRETE STRUCTURES

The curves of temperatures in concrete structures are presented in Figures 10 (sensors 1, 2, 3, 4), 11 (sensors 5, 6, 7, 8) and 12 (sensors 9, 10, 11, 12). The temperature in concrete structures was taken every hour.

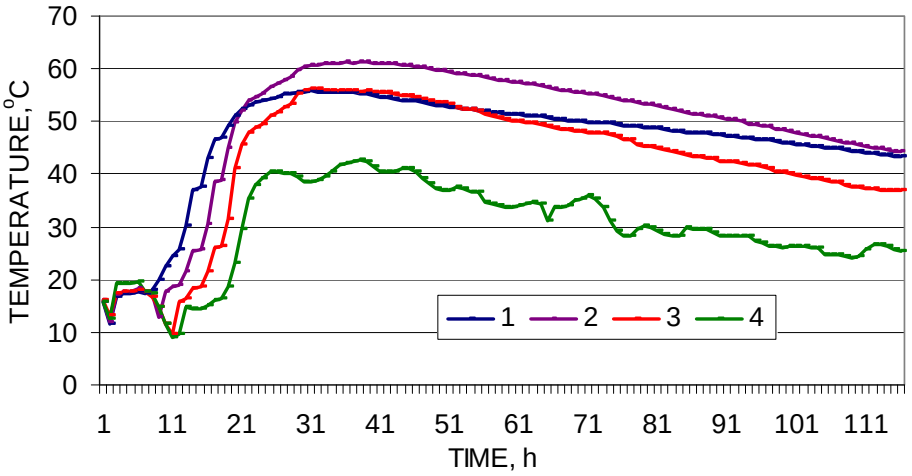

Figure 10 Temperatures of concrete in structures (sensors 1, 2, 3 and 4)

Figure 10 reveals that the highest temperatures of concrete were recorded by sensor 2 and the lowest temperatures were recorded by sensor 4. The highest recorded temperature was 60.9°C, whereas sensor 4 recorded the lowest temperature of 9.1°C.

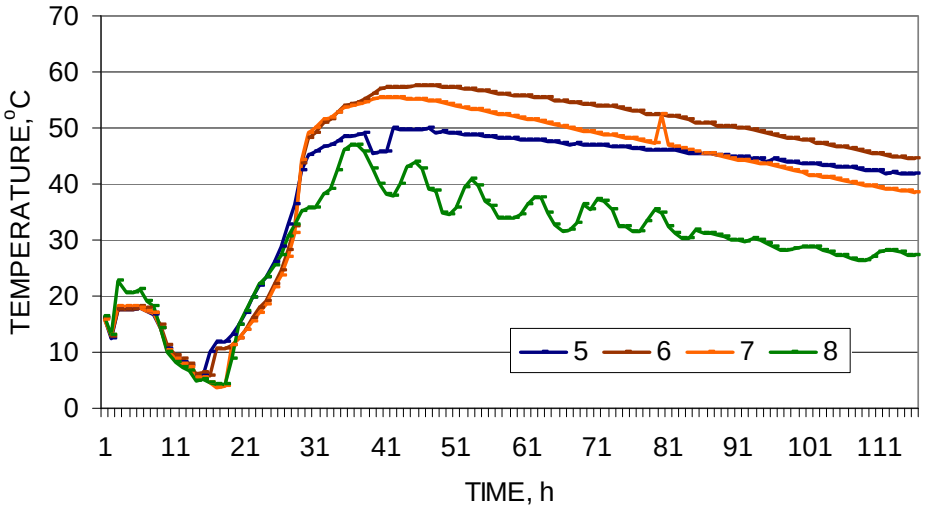

Figure 11 Temperatures of concrete in structures (sensors 5, 6, 7 and 8)

Figure 11 reveals that the highest temperatures of concrete were recorded by sensor 6 and the lowest temperatures were recorded by sensor 8. The highest recorded temperature was 57.5°C, whereas sensor 8 recorded the lowest temperature of 4.2°C.

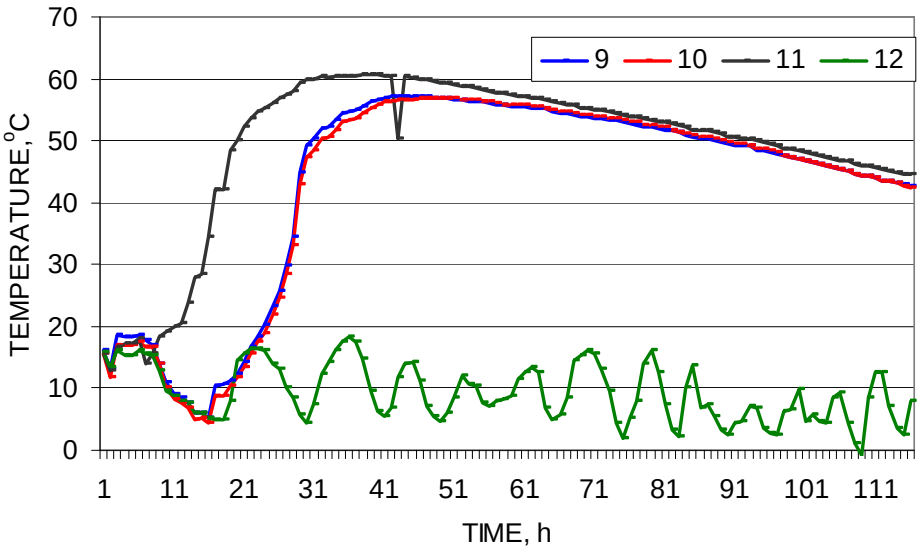

Figure 12 Temperatures of concrete in structures (sensors 9, 10, 11 and 12)

Figure 12 reveals that the highest temperatures of concrete were recorded by sensor 11 and the lowest temperatures were recorded by sensor 12. The highest recorded temperature was 60.6°C, whereas sensor 12 recorded the lowest temperature of -0.7°C.

The analysis of temperatures recorded by 12 sensors showed that the highest temperatures were recorded by sensor 2 showing the maximum temperature of 60.9°C and the lowest temperatures were recorded by sensor 12 showing the minimum temperature of -0.7°C.

CONCLUSIONS

1. The research into hydration heat of concrete mixtures have revealed that CEM I 42,5 R type cement released the highest hydration heat and CEM III/B 32,5 N-LH (SR) type cement released the lowest heat.

2. The testing showed that set retarder has no effect on the hydration heat in concrete mixtures, i.e. the addition of retarder does not reduce the hydration heat.

3. The results of thermal regime modelling revealed that concrete mixture made of slag Portland cement CEM II/A-S does not exceed the temperature of 55 °C, therefore slag Portland cement CEM II/A-S should be used for building massive concrete structures at the ambient temperature of 15°C.

REFERENCES

1. MARTUSEVIČIUS M, KAMINSKAS R, MITUZAS J A. Rišamųjų medžiagų cheminė technologija (Chemical Technology of Binding Materials), Kaunas, 2002, p 271 (in Lithuanian).
2. EISINAS A, BALTAKYS K. Portlandito kiekio hidratuotame portlandcementyje nustatymas vienalaikės terminės analizės metodu (Determination of portlandite content in hardened Portland cement paste by Simultaneous Thermal Analysis technique), Cheminė technologija, Vol. 50, No. 1, 2009, pp 18-23 (in Lithuanian).
3. LOTHENBACH B, WINNEFELD F, Thermodynamic modelling of the hydration of Portland cement, Cement and Concrete Research, ISSN 008-8846, Vol. 36, No. 2, 2006, pp 209-226.
4. TAYLOR H F W, Cement Chemistry, 2nd edition, Thomas Telford, London, ISBN 0727725920, Vol. 2, 1997, p 459.
5. GALLUCCI E, MATHUR P, SCRIVENER K, Microstructural development of early age hydration shells around cement grains. Cement and Conncrete Research, ISSN 0008-8846, Vol.40, No.1, 2010, pp 4-13.
6. BETON WEDLUG NORMY PN-EN 206-1, Komentarz, Pod kierunkiem L. Czarneckiego, Krakow: Polski Cement Sp. zo.o, 2004 (in Polish).
7. BATIANOVSKYJ E I, GOLUBEV N M, BABICKIJ V V, MARKOVSKIJ M F, Technologija i metody zimnevo monolitnovo i priobjektnovo betonirovanija, Minsk: Izdatelstvo ACB, 2009 (in Russian).
8. BENTZ D P, A Review of early-age properties of cement-based materials, Cement and Concrete Research, No. 38, 2008, pp. 196-204.
9. FUKUHARA M, GOTO S, ASAGA K,DAIMON M, KONDO R, Mechanisms and kinetics of C4AF hydration with gypsum, Cement and Concrete Research, No. 11, 1981, pp 407-414.
10. SKRIPKIUNAS G. Statybinių konglomeratų struktūra ir savybės (Construction conglomerate structure and properties), Kaunas: Vitae Litera, 2007, p 335 (in Lithuanian).
11. PAINE K A, DHIR R K, ZHENG L, Predicting early-age temperature of blended-cement concrete, Construction Materials, No. 159, 2006, pp 163-170.

Tests on Stub Columns of Concrete-filled CHS Sections

M Mimoune, F Z Mimoune
Constantine University, Algeria

The behaviour of stub columns of concrete-filled circular hollow sections (CHS) subjected to axial load was investigated experimentally. A total of 13 columns were studied. The main parameters varied in the tests are: length of columns, concrete resistance and loading mode. The main objectives of these tests were threefold: firstly to describe a series of tests on composite columns; and secondly, to analyze the influence of several parameters such as loading mode and length columns on the behaviour of circular stub concrete-filled. And finally, to compare the accuracy of the predictions by using Algerian code DTR-BC, European code EC4, AIJ Japan code and Chinese code. Experimental results indicate that the length columns and loading mode have significant influence on the compressive load and the ductility of steel tube. A disparity of results is obtained with the different design codes.

Dr M Mimoune is a Professor of steel and composite structures, Civil Engineering Department, Constantine University. Algeria.

Dr F Z Mimoune is a Professor of Steel Structures, Civil Engineering Department, Constantine University. Algeria.

Keywords: Axial loading, Composite columns, Design code, Ductility, Failure mode

INTRODUCTION

The composite columns are increasingly adopted in the construction because of their multiple benefits. Indeed, they offer excellent properties of resistance to the earthquake, ductility and large energy absorption capacity. Although the risk of a major earthquake in Algeria is large, this type of structure has not yet been adequately used, since it can offer advantages including the time of realization (No shuttering and steel reinforcements) is very short and opportunities for standardization, thus reducing the cost of construction. The generalization of this structural system in our country must go through a substantial research to master the process of construction and design methods and verification, knowing that the Algerian code of composite steel-concrete construction DTR-BC has only appeared in 2006. It is indisputable, that the combination of steel and concrete, significantly improves resistance regardless of the applied load. This has been proven by several researches in the world [1-6]. The tubular steel columns filled with concrete widely used in Europe, North America and Japan has proven their interest. Indeed, the concrete in the tube avoids buckling and the tubular steel provides confinement to concrete. It is also demonstrated that the confinement improves the strength [7-10] and concrete filled steel tubes have higher resistance than ordinary steel columns. The thickness of the tube, the concrete strength, the quality of steel, the slenderness of the column and the type of section, have also a significant influence on the strength of the composite section [11-13]. Columns made of metal profile totally encased in concrete offer another alternative for designers; they provided strength and very good resistance to fire. The objectives of this paper are double: Firstly, describing two series of tests on short composite columns and secondly, to compare the accuracy of prediction methods given by different codes, Algerian code [14], European code [15], Japanese code [16], and finally the Chinese code [17]. Three parameters have been studied: The method of loading the column (on the composite section, on the section of concrete or on the section of steel), the length of the column, the concrete strength and type of section.

EXPERIMENTAL PROGRAM

This experimental program is established to study the behaviour of the column sections made of circular tube filled with concrete. The tests were conducted on 13 tube columns filled with concrete and having a length of 300 mm and 600 mm. All columns were tested to destruction under axial loading, after being stored at ambient temperature inside the laboratory. The dimensions of the various sections and test results are given in Table 1. Table 2 summarizes the three mixtures studied. The tests were conducted on a universal machine with a capacity of 3000KN in the laboratory of Soil Mechanics and Structures at the University of Constantine Algeria. Figure 1 illustrates the way in which the load is applied to different sections of tube columns filled with concrete. The different configurations are chosen to distinguish the different phases of the columns behaviour with tubes and to make in evidence their ruins in every situation.

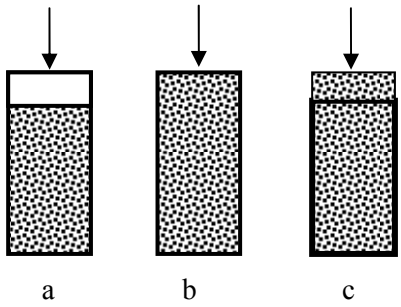

Figure 1 Axial loading of the columns. a: load applied on steel tube. b: load applied on composite section. c: load applied on concrete section.

Table 1 Characteristics of columns, and experimental results.

N°	Description	D(mm)	t (mm)	L (mm)	A_s (mm^2)	A_c (mm^2)	P_u (KN)	δ_y (mm)
1	S1	114	3	246	1045.6	9156	442.2	57.75
2	S2	114	3	300	1045.6	9156	462	63.0
3	S3	114	3	300	1045.6	9156	495	59.0
4	S4	114	3	300	1045.6	9156	429	56.5
5	S5	114	3	300	1045.6	9156	481.8	43.0
6	S6	114	3	300	1045.6	9156	554.4	151.0
7	S7	114	3	300	1045.6	9156	462	69.5
8	S8	114	3	600	1045.6	9156	415.8	53.25
9	S9	114	3	600	1045.6	9156	415.8	27.25
10	S10	114	3	600	1045.6	9156	488.4	21.5
11	S11	114	3	600	1045.6	9156	429	62.25
12	S12	114	3	600	1045.6	9156	415.8	59.5
13	S13	114	3	600	1045.6	9156	151.8	7.0

D : Diameter of tube ; t : tube thickness ; L: tube length; A_s: steel section; A_c: concrete section; P_u: experimental ultimate load; δ_y : ultimate axial shortening.

Table 2 Composition of the concrete tube filling

MIX	PROPORTIONS BY TO THE WEIGHT OF THE CEMENT			
	Cement	Sand	Gravel	Water
1	1.0	3.0	3.5	0.65
2	1.0	2.0	3.25	0.42
3	1.0	1.5	2.5	0.28

TEST RESULTS

The presentation of experimental results will be limited to those more directly related to the four configurations of the columns studied, the load-displacement curves expressed in terms of the shortening of columns, and the determination of failure modes depending on whether the load is applied to one or other of the constituents of the section.

The obtained results of the 13 columns under axial loading are given in table 1, and are translated into histograms in figures 2 and 3.

The overall analysis of the results shows that:

- The strength of the column is affected by the loading mode,
- The deformation capacity of the column depends on the type of material that receives the first applied load.
- When the load is directly applied on concrete, there is both a concrete crushing and sliding on the steel-concrete interface.
- The presence of voids in columns, lead to a failure mode with a total crushing of the tube, which seems quite different from that of steel tube alone because of the presence of concrete.
- The variation of the length of the column seems to have a significant impact particularly on the deformation capacity.
- The quality of concrete influences the bearing capacity of the columns especially those having a length of 300mm. However, the columns of 600mm length are not affected.
- The section type significantly affects the ultimate capacity and the failure mode.

Figures 2 and 3 which compare the different columns, made of circular tubes filled with concrete, show that the resistance follows certain logic as far as its increasing variation is concerned. The mixture 3 (Table 2) seems to give the best resistance in the case of columns of 300 mm, Figure 2. The same trend was recorded for the columns of 600 mm, but with a lesser degree.

In the case of columns S11 and S12, the trend is reversed probably because of a premature buckling observed during the tests, although a correct centring of the column in the machine. For columns made of profiled steel completely encased in concrete, it is clear that the length of the column goes in the opposite direction of the resistance. The concrete cover on the side of the soles of the profile seems not to play any role, since it cracks from the first loading and then detaches.

While the concrete lying between the flanges, continues to participate in the resistance until the profile begins to lose its stability by buckling effect. At this time, breaking the concrete cover is full of tight side and located at mid-height of the column for the compressed side.

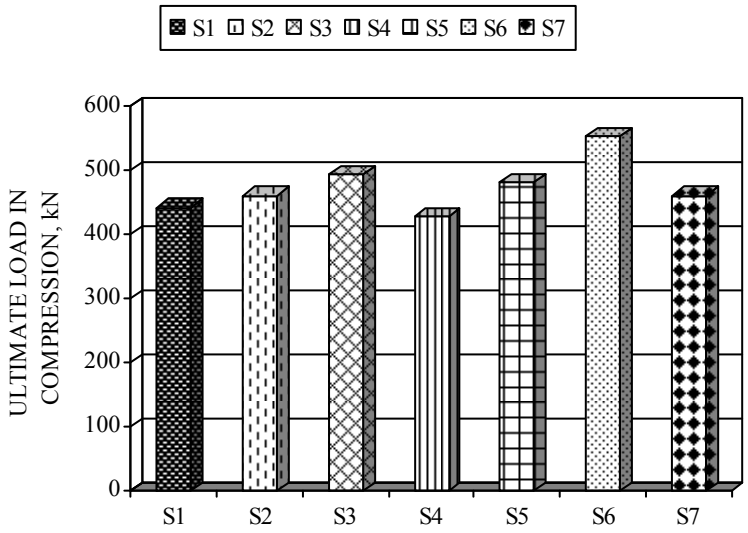

Figure 2 Ultimate compressive strength of columns. Length = 300 mm.

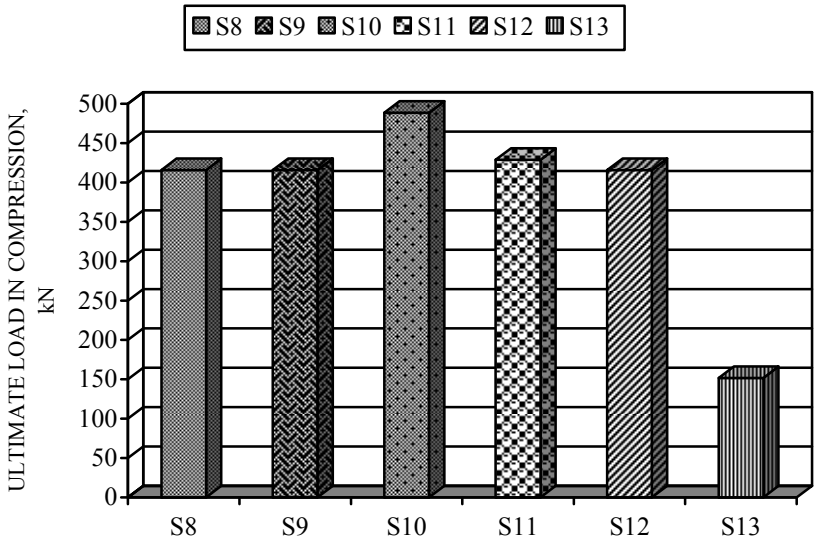

Figure 3 Ultimate compressive strength of columns. Length = 600 mm.

FAILURE MODES OBSERVED

The common observation between the various tube filled concrete columns is predominantly situated at the deformation of the steel tube, this is due to heavy compressions that tend to create wraps, Figure 4, whatever the mode of loading.

The observed failure modes can be classified into four categories, Ruin by crushing of the total unfilled portion of the tube, Shear failure and Shear failure and buckling.

Figure 4 Buckling of the tube wall

DISCUSSION OF TEST RESULTS AND COMMENTS

Loading on the Section of Steel Tube

We can say that the loading of the steel section alone does not give superior results for the axial capacity of the column, because the latter will be deformed strongly to form a bead of the first loading values. This state differs from that of a tube not filled with concrete, since the load reaches its ultimate value and then begins to decrease until a certain value of the composite action of the section is highlighted; Figure 5 illustrates perfectly this behaviour. Indeed, we can see three stages in the figures: The first corresponds almost to the total deformation of the tube, the second corresponds to stabilization and / or a decreasing load where the tube becomes almost flat, and the third corresponds to a load recovery reflecting the action of the composite section. It should be noted that the load continues to increase very slowly with large deformations of the column; this is obviously due to the ductility of the section and to the confinement of concrete provided by the steel tube.

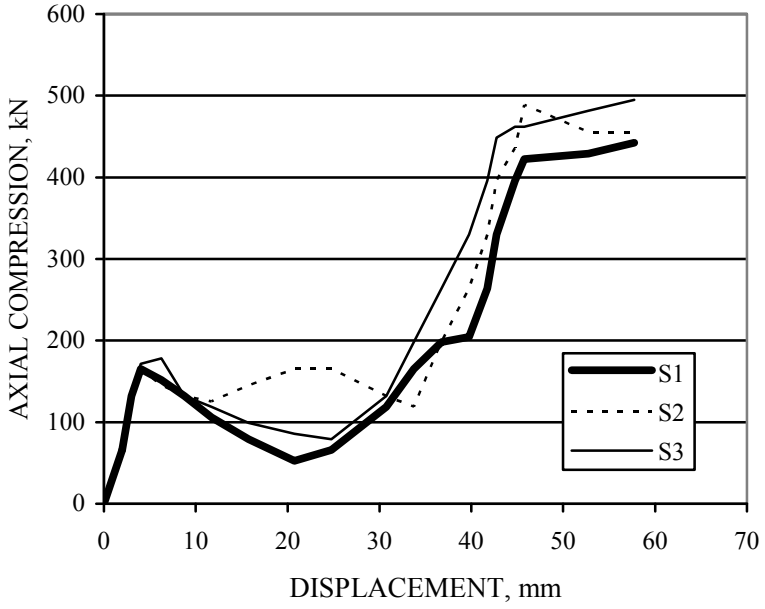

Figure 5 Compressive strength – Displacements

Loading on the Concrete Section

It was found that the section of concrete has suffered a crushing of the first load and then develops certain resistance as the compression stress increases, followed by a total settlement of this section. The curves of Figure 6 illustrates this behaviour which also goes through three stages: crushing and / or sliding of concrete loaded directly with a capacity of relatively low resistance, followed by an intermediate step that corresponds to a stabilization of the load with large displacements, the third stage corresponds to the composite action where the resistance capacity of the column increases greatly until collapse. The photos in figure 4 show clearly the deformation of the steel tube due to the action of concrete, which is similar to that of the shear concrete alone during a crushing test. The shear failure along an inclined line could occur if the thickness of the tube was sufficiently low. This has been proven by O'Shea and Bridge (1997) [1], Prion and Boehme (1993), and Johansson (2002) [3].

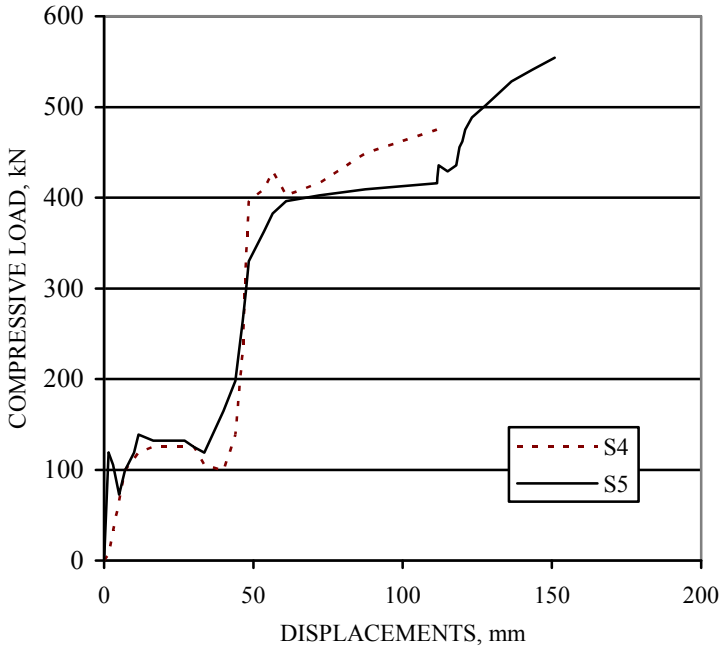

Figure 6 Compressive strength – Displacements

Loading on the Composite Section

The situation is totally different from the first two cases. Indeed, the application of the load is followed by a consequent increase in axial capacity of the column without significant deformations. The deformation mode occurs after a certain load value corresponding to the ultimate capacity in compression. Then the strength of the column falls rapidly accompanied by significant deformations of the tube wall which produces a series of beads. The stack of the latter favors the resumption of the resistance by acting as stiffeners, the load increases slowly producing more and more strain, Figure 7. The breaking of the column has not been reached.

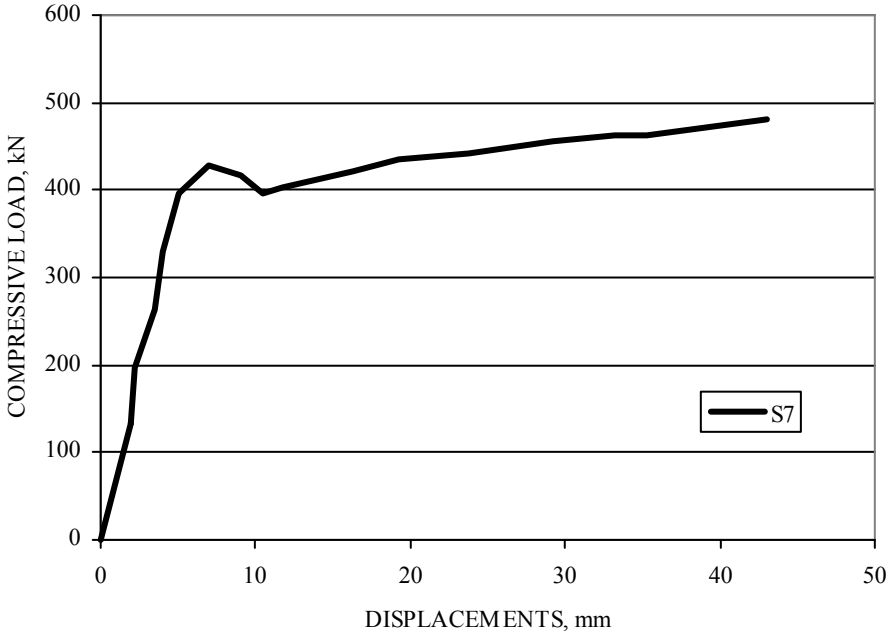

Figure 7 Compressive strength – Displacements

COMPARISON BETWEEN EXPERIMENTAL AND DESIGN CODES

The ultimate experimental strength in compression was compared with the axial strength of concrete filled tubes calculated by different codes, previously presented in Figures 8. The calculations were conducted with a safety factor equal to unity.

For columns of 300 mm length, all resistance values according to DTR (Algerian code) and EC4 (Eurocode) codes are lower than testing results; the average ratio P_{test}/P_{code} = 0.87 whatever the concrete strength used.

Contrarily, the two codes DL/T (Chinese code) and AIJ (Japanese code) provide a resistance slightly higher than those given by the tests; they are respectively about 1.04 and 1.02. These values are greater with normal concrete, reaching values of 31 to 39%, depending on the thickness of the steel tube. However, when we double the length of the column (L=600 mm), the strengths given by DL/T and AIJ codes also descend and become lower than those given by tests. The ratios P_{test}/P_{code} are respectively 0.94 and 0.93.

The differences obtained between the experimental values and forecast values are given much more to the principle on which each code is based. For others, (EC4, DL/T, AIJ), it is used either the combination of the calculation method of steel and concrete, or the superposition of the materials strengths constituting the composite section.

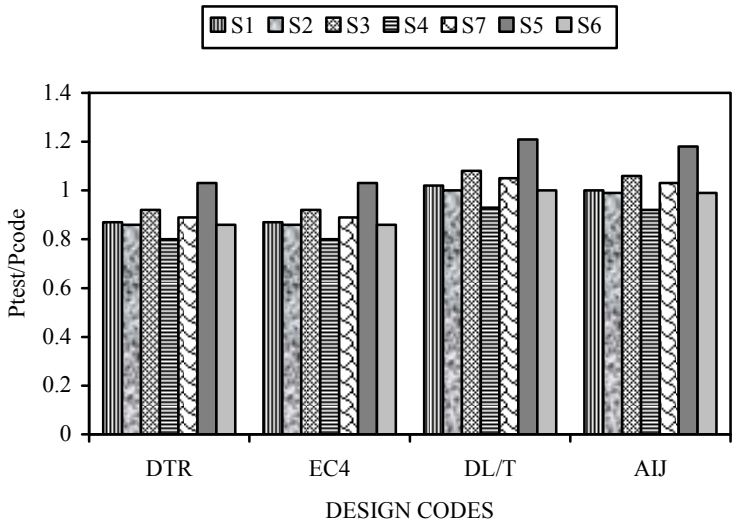

Figure 8 Comparison between tests and design codes. DTR: Algerian code. Eurocode EC4. Chinese code DL/T. Japanese code AIJ.

CONCLUSIONS

In this study, to evaluate tubular steel columns filled with concrete, 13 tests were performed. Four parameters were studied experimentally: The quality of concrete, the buckling length, the loading mode and the type of section. The results have shown that concrete quality did not have much impact on the overall behaviour of the columns. They have highlighted the influence of length on the failure mode of the columns. The loading mode has confirmed the interest of composite steel-concrete sections, since they give the best behaviour for axial loading. They also offer a wide safety reserve due to the consequent ductility of concrete confinement. The section type seems to influence significantly the axial capacity and failure mode. The comparison of tests with different codes, have shown some divergence which, according to the corresponding figures, we can observe an underestimation of the axial capacity in compression compared to DTR and EC4 codes, but DL/T and AIJ codes give results closer to those of tests.

REFERENCES

1. O'SHEA MD, BRIDGE RQ. Design of circular thin-walled concrete filled steel tubes. Journal of the Structural Engineering. ASCE 2000; 126(16):1295-303.

2. JOHANSSON M. The Efficiency of Passive Confinement in CFT Columns. Steel and Composite Structures, Vol. 2, No. 5, October 2002, Techno-Press, 379-396.

3. MOHANAD MURSI, BRIAN UY. Strength of slender concrete filled high strength steel box columns. Journal of Constructional Steel Research 60 (2004) 1825–1848.

4. GARDNER NJ, JAKOBSON ER. Structural behaviour of concrete-filled steel tubes. AI Journal 1967; 64(7):404-12.

5. SEONG-HUI LEE, BRIAN UY, SUN-HEE KIM, YOUNG-HWAN CHOI, SUNG-MO CHOI. Behavior of high-strength circular concrete-filled steel tubular (CFST) column under eccentric loading. Journal of Constructional Steel Research 67 (2011) 1–13.

6. MIMOUNE M. Design of steel-concrete composite columns subjected to axial compression. Fourth Saudi Technical Conference and Exhibition. STCEX 2006. Vol. 4. 2–6 January 2006. Riyadh – Saudi Arabia. Pp.482-487.

7. SHAKIR-KHALIL H, ZEGHICHE J. Experimental behaviour of concrete filled rolled rectangular hollow section columns. Struct. Eng. 1989; 67(19):346–53.

8. SHAKIR-KHALIL H, MOULI M. Further tests on concrete-filled rectangular hollow-section columns. Struct. Eng. 1990; 68(20):405–13.

9. HAN LH. The influence of concrete compaction on the strength of concrete filled steel tubes. Adv. Struct. Eng-An Int. J. 2000; 3(2):131–7.

10. HAN LH, ZHAO XL, TAO Z. Tests and mechanics model of concrete-filled SHS stub columns, columns and beam-columns. Steel & Composite Structure 2001a;1(1):51–74.

11. GHOSH RS. Strengthening of slender hollow steel columns by filling with concrete. Can. J. Civ. Eng. 1977; 4(2):127–33.

12. MANOJKUMAR V. CHTAWADAGI, MATTUR C. NRASIMHAN, S.M. KULKARNI. Axial capacity of rectangular concrete-filled steel tube columns – DOE approach. Construction and Building Materials 24 (2010) 585 – 595.

13. SHAMS M, SAADEGHVAZIRI MA. State of the art of concrete-filled steel tubular columns. ACI Struct. J. 1997; 94(5):558–71.

14. DTR-BC 2.34 Conception et dimensionnement des structures mixtes acier-béton. Ministère de l'habitat et de la construction. Algérie. 2006.

15. Eurocode 4, EN 1994-1-1 Eurocode 4 – Design of composite steel and concrete structures – Part 1-1: General rules and rules for buildings, 2005.

16. AIJ. Recommendations for design and construction of concrete filled steel tubular structures. Tokyo. Japan; 1997.

17. DL/T. Chinese design code for steel-concrete composite structures. In: DL/T 508561999. Beijing. China.

Contribution of precast concrete products to the good quality of indoor air

P Francisco, P Rougeau, F Jacquemot, C Badoz
Study and Research Centre for the French Concrete Industry, France

The aim of this study is to provide experimental results on regulated dangerous substances release and information on the release mechanisms of precast concrete products. The health and environmental aspects of construction products are closely considered by the European institutions driven by the consumers' requests. The Construction Products Directive includes in the third essential requirement "Hygiene, Health and the Environment" the obligation for a construction to be design and build in order to avoid emissions from hazardous substances. Different Member States have regulations and assessment procedures that are being harmonized by the European Standardization. It concerns harmonization of measurement and testing standards and assessment procedures. In addition, a suitable labeling based on these environmental indicators is supposed to be developed and addressed to the consumers to provide information and advice on construction product performance. All of these provisions will have to maintain a well balance between the consumers' need of information and the cost increase of construction products due to the extent of assessment procedures and. It is especially the case for products made with mineral raw materials that are used in concrete. Different precast concrete products for buildings were tested according to standardized test methods. The behavior of precast concrete products regarding their emission into indoor air is discussed including the type of environmental indicator declaration. These results may support the European institutions in the description of suitable environmental indicators and procedures for these products.

P. Francisco is a chemist with CERIB (Study and Research Centre for the French Concrete Industry) since 2004, chiefly leading research on the development of concretes with innovative qualities, and has specialized in concrete durability. He has recently defended his thesis on the time-dependant deformations of UHPFRC subject to heat treatment. In addition he manages the CERIB's international cooperation since 2009.

P Rougeau is an engineer for construction materials, doctorate (PhD) in the durability of concrete in storage facilities for radioactive waste. He has a 20 years experience in the domain of R&D concerning construction materials with hydraulic binders, environmental behaviour of concrete, new types of concrete (high and ultra-high performance concrete, self compacting concrete) as well as their durability (performance approach and probabilistic modelling). He is the Head of Materials and Concrete Technology Department and in charge of the CERIB studies in the field of concrete industry.

F Jacquemot is material engineer in CERIB and leads the Materials Section since 2012. His specialist areas of research are hydration of cementitious binders, durability of concrete, low environmental footprint concrete.

C Badoz is a chemist. She has worked in CERIB for 25 years particularly on the field of concrete chemistry and concrete durability. She has developed numerous test methods in partnership with other French or European laboratories. She has specialized in the behavior of concrete regarding its impact on drinking water and indoor air.

Keywords: Air quality, Performance, Precast concrete, Products

INTRODUCTION

The majority of the citizens are concern with the quality of indoor air spending more and more time in buildings (residences, workplaces, school, shopping centres etc.). A poor quality of indoor air can increase the number of serious health problems mainly due to high volatile organic compound (VOC) levels. VOCs can be emanated from a large number of sources: construction products, goods, combustion activities, individual and cleaning actions, etc.

The Construction Products Directive (CPD) includes in the third essential requirement "Hygiene, Health and the Environment" the obligation for a construction to be design and build in order to avoid emissions from hazardous substances. In order to implement these requirements, the European commission has published the M/366 mandate concerning the elaboration of horizontal standardised assessment methods for harmonised approaches as far as the dangerous substances are concerned within the framework of the CPD. Different Member States already have regulations or assessment procedures. Three protocols regarding emissions of dangerous substances from construction products into indoor air have been published: the ECA/IAQ (European Collaborative Action, Indoor Air Quality) protocol defined at European level in 1997, the AgBB (Ausschuß zur gesundheitlichen Bewertung von Bauprodukten – Committee of Health Evaluation of Construction Products) protocol in Germany in 2005 (last version published in 2008), and the AFSSET (Agence Française de Sécurité sanitaire de l'Environnement et du Travail – French Agency of Environment and Labour Health Safety) protocol in France in 2006 (last version published in 2009). The three protocols use the emission room described in ISO 16000-9 standard "Dosage of the emission of volatile organic compounds of construction products equipment devices. Emission test room method".

In the case of concrete products, several studies conducted in different European countries have shown that the release of dangerous substances into indoor air is very low because the constituents of concrete products are inert materials and because only very small quantities of organic chemical products are used to enhance the production. The organic chemical substances used in the composition are entrapped in the matrix and do not migrate to the surface. For those used at the concrete/mould interface as release agents for example, they can be present for a short period of time before disappearing within a few days after production.

The results presented in this paper come from tests carried out by a French third part laboratory according to the standardized test methods (ISO 16000 series) and performed on concrete products for buildings: concrete masonry units, floor plates and beams for floor systems. The concrete products were sampled from precast French concrete plants. The behaviour of the concrete products regarding their emission into indoor air is compared to the limits of the AFSSET and AgBB protocols and then with a French environmental labelling on volatile pollutant emission.

The radon emissions were not measured in this experimental campaign due to the lack of harmonized standards and because the natural release of radon from the ground is normally the dominant influence on radon and radioactivity levels in buildings due to locally effect of the soil.

EXPERIMENTAL PROGRAM

Specimen Sampling, Composition and Properties

The emission tests were carried out on concrete products sampled from precast French concrete plants according to the standard NF EN ISO 16000-11 (2006) "Indoor air — Part 11: Determination of the emission of volatile organic compounds from building products and furnishing — Sampling, storage of samples and preparation of test specimens" [1]. A concrete masonry unit was submitted entirely (see Figure 1a). For the floor plate and the beam for floor systems, two samples of 500 cm² (see Figure 1b) and a length of 50 cm (see Figure 1c) were respectively extract from the whole concrete products.

a)

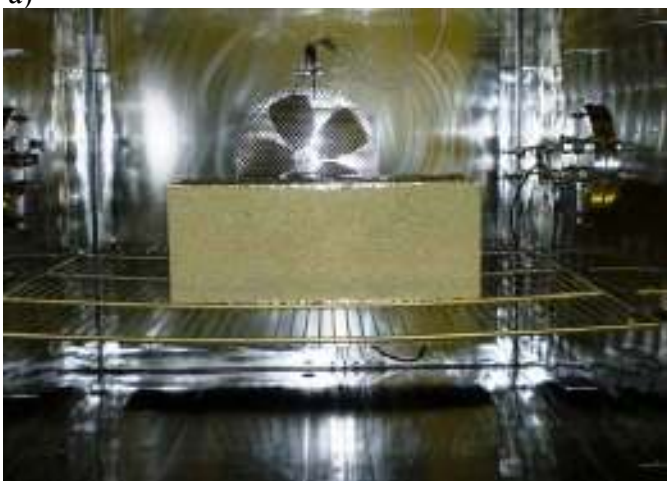

b)

c)

Figure 1 Specimens of concrete submitted to the emission test

The composition of the products is presented in Table 1. The origin of the constituents is different between the samples and the concrete formulas are commonly used for these construction products. The properties of the products are presented in Table 2. The properties are representative of those of these construction products.

Table 1 Product composition, kg/m³

CONSTITUANTS	CONCRETE MASONRY UNIT	FLOOR PLATE FOR FLOOR SYSTEMS	BEAM FOR FLOOR SYSTEMS
Cement	107 (CEM I 52.5 N)	218 (CEM I 52.5 R)	480 (CEM I 52.5 R)
Calcareous filler	76	0	0
Sand (siliceous-calcareous) (aggregate size)	670 (0/2)	827 (0/4)	230 (0/1)
	300 (2/4)		620 (0/4)
Coarse aggregate (aggregate size)	1000 (siliceous-calcareous) (4/8)	1165 (siliceous-calcareous) (4/14)	870 (calcareous) (4/6)
Admixture	0	1.57*	2.7**
Water/Cement ratio	***	0.64	0.39

* no dangerous substances declared in the safety data sheet
** residue of 2-octyl-4-isothiazoline-3-one declared in the safety data sheet
*** W/C not relevant for masonry unit

Table 2 Product properties

PROPERTIES	CONCRETE MASONRY UNIT	FLOOR PLATE FOR FLOOR SYSTEMS	BEAM FOR FLOOR SYSTEMS
Water absorption, %	*	5.7	4.4
Porosity, %	*	12.9	10.6
Strength class, MPa	B40	C25/30	B63
Age at test time, month	3	6	4

* data not available

Test Methods

The specimens were tested during 28 days in emission test chamber according to the NF EN ISO 16000-9 (2006) standard “Indoor air — Part 9: Determination of the emission of volatile organic compounds from building products and furnishing — Emission test chamber method” [2]. The emission test parameters are presented in Table 3. An area-specific airflow rate (q_{test} value) of 0.40 was chosen for all of the tests according to the informative annexe B of the NF EN ISO 16000-9 standard in order to simplify any further comparison. It corresponds to the worst case conditions: a wall surface of 24 m² and to an airflow rate of 8.71 $m^3 \cdot h^{-1}$ in a model room with a volume of 17.42 m³. Actually, a specific q_{test} value is defined for each part of the model room: walls, floors, ceilings, doors, sealants, etc. The smaller is the q_{test} value, the more severe is the test.

Table 3 Emission test parameters

EMISSION TEST PARAMETERS	CONCRETE MASONRY UNIT	FLOOR PLATE FOR FLOOR SYSTEMS	BEAM FOR FLOOR SYSTEMS
Temperature, °C	23 ± 2	23 ± 2	23 ± 2
Relative humidity, %	50 ± 5	50 ± 5	50 ± 5
A: specimen surface area exposed, m^2	0.224	0.248	0.197
V: chamber volume, m^3	1	0.0509	0.0509
L: loading factor, $m^2 \cdot m^{-3}$)	0.224	4.9	3.9
F: airflow rate, $m^3 \cdot h^{-1}$)	0.09	0.1	0.08
n: air exchange rate, h^{-1}	0.09	1.95	1.55
q_{test}: area-specific airflow rate, $m^3 \cdot m^{-2} \cdot h^{-1}$)	0.40	0.40	0.40
Link between test parameters: $q_{test} = n / L = n / (A/V) = (F / V) / (A / V) = F / A$			

The VOCs emission was measured according to the NF ISO 16000-6 (2005) standard "Indoor air — Part 6: Determination of volatile organic compounds in indoor and test chamber air by active sampling on Tenax TA® sorbent, thermal desorption and gas chromatography using MS/FID" [3] and the formaldehyde and aldehydes emission according to the NF ISO 16000-3 (2002) standard "Indoor air — Part 3: Determination of formaldehyde and other carbonyl compounds — Active sampling method" [4].

The measurements were performed before the test without specimens in the test chambers, and then after 3 and 28 days of specimen emission. For each of these three sampling times, two volumes were analysed and the average is calculated. The results for 3 and 28 days are corrected using the value measured before the test. They correspond to the concentrations $C_{x\text{-}test}$ in $\mu g \cdot m^{-3}$ of the VOCs taken into account in the AFSSET and AgBB protocols.

Calculation of exposure concentrations

The useful definitions of acronyms used for the assessment are listed in Table 4. The VOC concentrations ($C_{x\text{-}test}$) measured during the tests have to be normalized into specific emission rates ($q_{s\text{-}x}$) which are independent of the exposure scenarios. Then, an exposure scenario has to be chosen to calculate the exposure concentrations ($C_{x\text{-}scenario}$).

For this study, a mandatory French model room of 30 m^3 which the air exchange rate is fixed at 0.5 h^{-1} was selected. Once more, in order to simplify any further comparison, the equivalent area-specific airflow rate ($q_{scenario}$) corresponding to the worst case conditions (walls) was selected for the products tested. In consequence, $C_{x\text{-}scenario} = (C_{x\text{-}test} * q_{test}) / q_{scenario} = q_{s\text{-}x} / q_{scenario}$.

Table 4 Definitions used for assessment by AFSSET and AgBB protocols

ACRONYM	UNIT	DEFINITION
q_{test}	$m^3 \cdot m^{-2} \cdot h^{-1}$	Area-specific airflow rate used during the emission test
$C_{x\text{-}test}$	$\mu g \cdot m^{-3}$	Concentration measured during the test of an individual VOC or of a group of VOCs
$q_{s\text{-}x}$	$\mu g \cdot m^{-2} \cdot h^{-1}$	Specific emission rate per surface unit (independent of the exposure scenario) of an individual VOC or of a group of VOCs
$q_{scenario}$	$m^3 \cdot m^{-2} \cdot h^{-1}$	Area-specific airflow rate of the exposure scenario
$C_{x\text{-}scenario}$	$\mu g \cdot m^{-3}$	Exposure concentration of an individual VOC or of a group of VOCs according to the exposure scenario
$C_{i\text{-}scenario}$	$\mu g \cdot m^{-3}$	Exposure concentration of an individual VOC according to the exposure scenario
Σ [VOC]	$\mu g \cdot m^{-3}$	Sum of all VOCs in retention range C_6 to C_{16} according to the exposure scenario
Σ [SVOC]	$\mu g \cdot m^{-3}$	Sum of all semivolatile organic compounds in the retention range C_{16} to C_{22} according to the exposure scenario
C1, C2	-	Carcinogenic substance of EU categories 1 and 2
Σ [C1-C2]	$\mu g \cdot m^{-3}$	Sum of carcinogenic substance of EU categories 1 and 2 according to the exposure scenario
LCI_i	$\mu g \cdot m^{-3}$	Lowest concentration of interest of an individual VOC
R	-	Sum of ratios $C_{i\text{-}scenario}$ / LCI_i for all VOCs which $C_{i\text{-}scenario}$ exceeds 5 $\mu g.m^{-3}$
$C_{ni\text{-}scenario}$	$\mu g \cdot m^{-3}$	Exposure concentration of an individual VOC not identified or which do not have an LCI_i value
R_{ni}	$\mu g \cdot m^{-3}$	Sum exposure concentration $C_{ni\text{-}scenario}$ for all VOCs which $C_{ni\text{-}scenario}$ exceeds 5 $\mu g \cdot m^{-3}$

RESULTS AND DISCUSSION

The results of the exposure concentrations corresponding to a model room of 30 m³ which the air exchange rate is fixed at 0.5 h^{-1} are presented in Tables 5, 6 and 7. All the results conform to the AFSSET and AgBB protocols.

In addition, another comparison was made due to a new French regulation published on 25 March 2011 with details published on 13 May 2011 regarding a mandatory labelling of construction products installed indoors, floor and wall coverings, paints and lacquers. This regulation includes emission classes based on emission testing. The precast concrete products tested are not in the scope of this regulation. In consequence, the comparison presented in Table 8 is only informative. This regulation concern: walls, ceiling, floor coverings and coatings, panels for room partition and suspended ceiling, insulation products, doors and windows, all products used for the installation of the products listed above. The regulation does not cover untreated metal or glass, lockers, iron, screws etc. It specifies the ISO 16000 series standards for the testing methodology. The model room has a volume of 30 m³ and the air exchange rate is fixed at 0.5 h^{-1}. All the results conform to the CLASS A+.

Table 5 Exposure concentrations obtained for the concrete masonry unit

INDIVIDUAL COMPOUND DETECTED	OBTAINED VALUE, $\mu g \cdot m^{-3}$	
	3 days	28 days
Benzene (C1)	< 0.3	< 0.3
Trichloroethene (C2)	n.d.	n.d.
Toluene	< 5	1.0
Formaldehyde	< 10	4.3
Acetaldehyde	< 10	6.7
Butyraldehyde	< 10	3.0
Hexaldehyde	< 10	1.4

PARAMETERS	OBTAINED VALUE, $\mu g \cdot m^{-3}$		PROTOCOL LIMIT VALUE			
			3 days		28 days	
	3 days	28 days	AFSSET	AgBB	AFSSET	AgBB
Σ [VOC], $\mu g \cdot m^{-3}$	160.0	50.9	10000		10000	
Σ [SVOC], $\mu g \cdot m^{-3}$	-	8.8	-		-	100
Σ [C1-C2], $\mu g \cdot m^{-3}$	< 0.3	< 0.3	10		1	
R (without unit)	-	0.03	-		1	
28 day value for acetaldehyde > 5 $\mu g \cdot m^{-3}$		6.7	-		200	-
R_{ni}, $\mu g \cdot m^{-3}$	-	(1)	-		100	

n.d.: not detected

- : not considered by AFSSET or AgBB protocols

(1) no compound which do not have an LCI_i value exceeds 5 $\mu g \cdot m^{-3}$ at 28 days

Table 6 Exposure concentrations obtained for the floor plate for floor systems

INDIVIDUAL COMPOUND DETECTED	OBTAINED VALUE, $\mu g \cdot m^{-3}$	
	3 days	28 days
2-Methoxypropanol	14.8	6.0
Benzene (C1)	< 0.3	< 0.3
Trichloroethene (C2)	n.d.	n.d.
Toluene	2.0	< 0.3
Formaldehyde	0.4	< 0.3
Acetaldehyde	1.1	0.6
Propionaldehyde	3.3	< 0.3
Hexaldehyde	0.6	< 0.3

PARAMETERS	OBTAINED VALUE, $\mu g \cdot m^{-3}$		PROTOCOL LIMIT VALUE			
			3 days		28 days	
	3 days	28 days	AFSSET	AgBB	AFSSET	AgBB
Σ [VOC], $\mu g \cdot m^{-3}$	72.7	6.4	10000		10000	
Σ [SVOC], $\mu g \cdot m^{-3}$	-	19.3	-		-	100
Σ [C1-C2], $\mu g \cdot m^{-3}$	< 0.3	< 0.3	10		1	
R (without unit)	-	0.003	-		1	
28 day value for 2-Methoxypropanol > 5 $\mu g \cdot m^{-3}$		6.0	-		2000	-
R_{ni}, $\mu g \cdot m^{-3}$	-	(1)	-		100	

n.d.: not detected

- : not considered by AFSSET or AgBB protocols

(1) no compound which do not have an LCI_i value exceeds 5 $\mu g \cdot m^{-3}$ at 28 days

Table 7 Exposure concentrations obtained for the beam for floor systems

INDIVIDUAL COMPOUND DETECTED	OBTAINED VALUE, µg·m^{-3}	
	3 days	28 days
Benzene (C1)	< 0.3	< 0.3
Trichloroethene (C2)	n.d.	n.d.
Toluene	7.2	< 0.3
Pentadecane	4.8	1.6
Hexadecane	5.0	2.7
Formaldehyde	< 0.3	< 0.3
Acetaldehyde	1.6	0.4
Hexaldehyde	1.4	1.3

PARAMETERS	OBTAINED VALUE, µg·m^{-3}		PROTOCOL LIMIT VALUE			
			3 days		28 days	
	3 days	28 days	AFSSET	AgBB	AFSSET	AgBB
Σ [VOC], µg·m^{-3}	75.5	13.3	10000		10000	
Σ [SVOC], µg·m^{-3}	-	25.5	-		-	100
Σ [C1-C2], µg·m^{-3}	< 0.3	< 0.3	10		1	
R (without unit)	-	(2)	-		1	
R_{ni}, µg·m^{-3}	-	(1)	-		100	

n.d.: not detected

- : not considered by AFSSET or AgBB protocols

(1) no compound which do not have an LCI_i value exceeds 5 µg·m^{-3} at 28 days

(2) no compound which have an LCI_i value exceeds 5 µg·m^{-3} at 28 days

Table 8 Informative comparison between the results and a French mandatory labelling

COMPOUND	EXPOSURE CONCENTRATION AT 28 DAYS, µg·m^{-3}			LIMIT VALUE, µg·m^{-3}			
	Concrete masonry unit	Floor plate for floor systems	Beam for floor systems	Class			
				C	B	A	A+
Formaldehyde	4.3	< 1	< 1	> 120	< 120	< 60	< 10
Acetaldéhyde	6.7	< 1	< 1	> 400	< 400	< 300	< 200
Toluene	3.0	< 1	< 1	> 600	< 600	< 450	< 300
Tetrachloroethylene	< 1	< 1	< 1	> 500	< 500	< 350	< 250
Xylene	< 1	< 1	< 1	> 400	< 400	< 300	< 200
1,2,4-Trimethylbenzene	< 1	< 1	< 1	> 2000	< 2000	< 1500	< 1000
1,4-Dichlorobenzene	< 1	< 1	< 1	> 120	< 120	< 90	< 60
Ethylbenzene	< 1	< 1	< 1	> 1500	< 1500	< 1000	< 750
2-Butoxyethanol	< 1	< 1	< 1	> 2000	< 2000	< 1500	< 1000
Styrene	< 1	< 1	< 1	> 500	< 500	< 350	< 250
Σ [VOC]	50.9	6.4	13.3	> 2000	< 2000	< 1500	< 1000

CONCLUSIONS

The results obtained in this study confirm one more time the good behaviour of the precast concrete products regarding their emission into indoor air. For the concrete masonry unit, the floor plate and the beam tested, all the results conform to the AFSSET and AgBB protocols, and respect the threshold values for CLASS A+ of the new French. These results may support the European institutions in the description of suitable environmental indicators and procedures for these products.

REFERENCES

1. NF EN ISO 16000-11 standard, Indoor air — Part 11: Determination of the emission of volatile organic compounds from building products and furnishing — Sampling, storage of samples and preparation of test specimens, Afnor, 2006.

2. NF EN ISO 16000-9 standard, Indoor air — Part 9: Determination of the emission of volatile organic compounds from building products and furnishing — Emission test chamber method, Afnor, 2006.

3. NF ISO 16000-6 standard, Indoor air — Part 6: Determination of volatile organic compounds in indoor and test chamber air by active sampling on Tenax TA® sorbent, thermal desorption and gas chromatography using MS/FID, Afnor, 2005.

4. NF ISO 16000-3 standard, Indoor air — Part 3: Determination of formaldehyde and other carbonyl compounds — Active sampling method, Afnor, 2002.

Assessing the Potential for Product Stewardship for the UK Precast Concrete Industry

A A Aliyu[1], J Glass[1], A D F Price[1], H K Elhag[2]
1 – Loughborough University, UK
2 – British Precast Concrete Federation, UK

Sustainability and climate change have now become business imperatives to governments, businesses and all stakeholders in different sectors and industries. In the UK, the UK Government has shown strong commitment for sustainable construction over the years. The UK 'Strategy for Sustainable Construction' in 2008 has clearly underlined and shown areas that need the construction industry's attention which include: Climate change mitigation, Climate change adaptation, Materials, Water, Waste, Biodiversity and Materials. As part of a four year engineering doctorate research programme aimed at improving the sustainability of the UK precast concrete industry through Product Stewardship (PS), this paper explores the possibility of implementing the principles of PS in the UK precast concrete industry. Product stewardship (PS) helps all stakeholders within the lifecycle of a product to share, own or take (full or part) responsibility for reducing, mitigating or abating the environmental impacts of the product throughout its lifecycle. Governments, countries, corporate organisations and industries globally that manufacture different products, have recognised the importance of reducing the negative environmental and social impacts of products, goods and services through the development and implementation of PS programmes and initiatives. This research paper consists of an analysis of 2006 to 2010 key performance indicators of the UK precast concrete industry and findings from 12 industry interviews. Manufacturers' understanding of PS, its potential areas of operation and implementation were investigated. Potential gaps in the sustainability management of these companies were identified and possible PS options were assessed. The paper concludes with a discussion of whether there is any synergy between PS and existing industry initiatives on sustainable construction.

Abdullahi Adamu Aliyu is a Research Engineer, British Precast Concrete Federation/ Department of Civil and Building Engineering, Loughborough University, UK. Abdullahi Adamu Aliyu is principal researcher on joint collaborative research project to improve sustainability through product stewardship in the UK precast concrete industry. He has previously worked in the construction industry and the Liveable cities design and consultancy group, UK.

Dr Jacqueline Glass is a Senior Lecturer in Architecture and Sustainable Construction, AEDM Programme Director, Department of Civil and Building Engineering, Loughborough University, Loughborough, UK. Dr. Jacqueline Glass joined the Department of Civil and Building Engineering at Loughborough University in 2003. Her teaching and research interests include architectural design, decision making, process management, sustainability and concrete construction.

Prof Andrew D.F Price is Chair of Strategic Management in the Department of Civil and Building Engineering, Loughborough University. Prof. Price has over 30 years of design, construction and industry focused research experience. His current research interest includes; strategic management, sustainability and continuous performance improvement.

Dr Hafiz K. Elhag Product Association Manager, British Precast Concrete Federation, Leicester, UK. Dr. Hafiz K. Elhag is a Product Association Manager with British Precast. He previously worked as an architect with Danish consultants COWI at the Sultanate of Oman and has completed an MSc in Construction Management and a PhD on Lifecycle Assessment of Precast Concrete Flooring from The University of Reading and Loughborough University respectively.

Keywords: Corporate Sustainability, Environmental impacts, Low carbon, Product stewardship, Sustainable construction, research

INTRODUCTION

Precast concrete products are widely used in the UK construction industry and their advantages are numerous. The question of how to manufacture and produce precast concrete products with minimal or zero environmental impacts in modern day production and consumption cycles has been a major source of concern to both manufacturers, consumers and other stakeholders in recent years.

The UK precast concrete industry devised a sustainability programme (‘*More from less’*) in 2004, to measure and improve the environmental, social and economic credentials of precast concrete products. A sector sustainability strategy was developed and fully implemented [1] by 2008. Following the success of the ‘*More from less’* programme, British Precast Concrete Federation (BPCF) also known as British Precast in collaboration with Loughborough University decided to explore and understand the business and performance benefits of the concept of product stewardship (PS) in the precast concrete industry. PS is therefore being assessed for possible implementation through life-cycle thinking and shared responsibility by identifying and mitigating key environmental and social impacts of the industry [2]. Impacts within a product‘s life-cycle at different key stages result from: mineral or material extraction, design and development, production, transportation, use and end-of-life (cradle to cradle). A range of initiatives have been implemented through voluntary and regulatory frameworks to reduce these impacts in different industries (for example, the precast industry has been monitoring and measuring performance through the collation of Key Performance Indicators, or KPIs, since 2006).

Overarching this, the UK government, through different policy documents, has demonstrated the need for a more sustainable construction industry. The 2008 ‘Strategy for Sustainable Construction’ (SSC) highlighted several areas that need the construction industry‘s attention these include; Climate change mitigation and adaptation, Materials, Water, Waste, Biodiversity and Materials [3]. The strategy further provides clarity regarding the UK government‘s current and future policy frameworks and ways of achieving its aims. Climate change mitigation was recognised as one of the most important areas for addressing sustainable development and the UK government has revised the targets set to an 80% cut in greenhouse gas emissions by 2050 (based on 1990 baseline year) and 34% by 2020. Initially, government made a commitment of 60% cut in the Climate Change Act. Presently, all new homes and schools should be zero carbon or carbon neutral by the year 2016, public sector non-domestic buildings should be zero carbon or carbon neutral by 2018 and other non-domestic buildings should also be zero carbon or carbon neutral by 2019. All these targets form part of the UK‘s Low Carbon Transition Plan [3]. The government has also set a target of 50% reduction of construction, demolition and excavation waste sent to landfill by 2012 (based on 2008 levels). There is also regulatory pressure from the EU in the form of Construction Product Regulation (CPR) which comes into force on the 1st July, 2013 making it mandatory for construction products which fall under the CPR scope to be CE marked by declaring a product’s performance before they are being sold in the EU [4].

Other areas include developing a robust adaptation approach to climate change, conserving and enhancing biodiversity at all stages of development, using materials with least environmental and social impacts in construction and the reduction of per capita consumption of water in homes. The UK government through the principles of the SSC believes the construction industry can achieve sustainable construction.

Within the UK concrete industry, targets have been set by the industry to be identified as a leader in sustainable construction by 2012. The priorities for the industry are the same as those of the SSC and are powerful drivers for any sustainability initiative within the precast concrete industry.

This research paper explores the potential of PS for the UK precast concrete industry. Some of the key concepts enshrined in PS are already evident within the industry, including: responsible sourcing, waste and water minimisation and environmental management. However, the key challenge is to evolve a holistic and robust PS initiative that will link all sustainability management efforts within one PS framework. This paper outlines key performance indicator data, to establish the status of the industry and reflects on industry's current understanding of PS. It concludes with some specific recommendations for the development of a PS framework for the UK precast industry.

PRODUCT STEWARDSHIP

PS, as a subset of sustainability and sustainable development in the field of environmental management [5], requires all stakeholders to take some form of responsibility for example physical and/or financial responsibility for mitigating the life cycle environmental and social impacts throughout the supply chain [6], and from 'cradle to cradle', although it lacks a single unified definition. PS encourages business to become more responsible through proper ethical management and reducing costs and liabilities [7]. PS helps stakeholders within businesses, companies, organisations and multinational corporations to mitigate the environmental impacts associated with products throughout their entire life cycle. A conceptual understanding for the key components in PS is shown in Figure 1. A more detailed process tree is also shown in Figure 2.

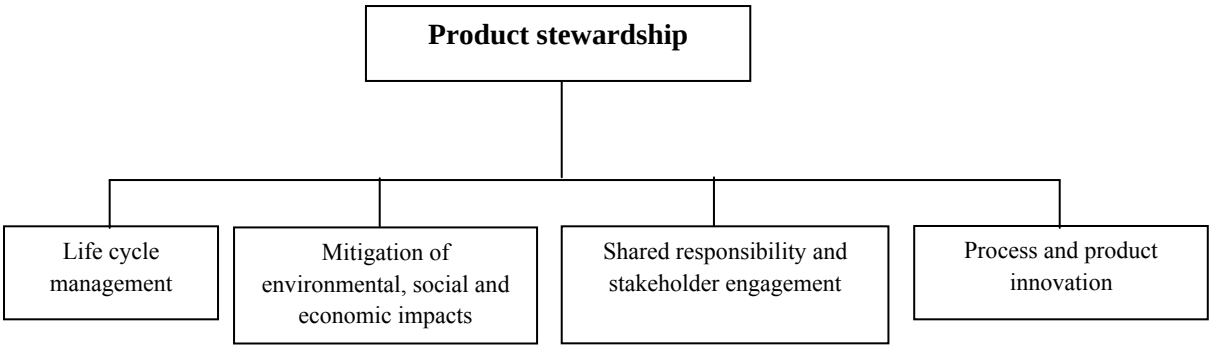

Figure 1 Key components of product stewardship

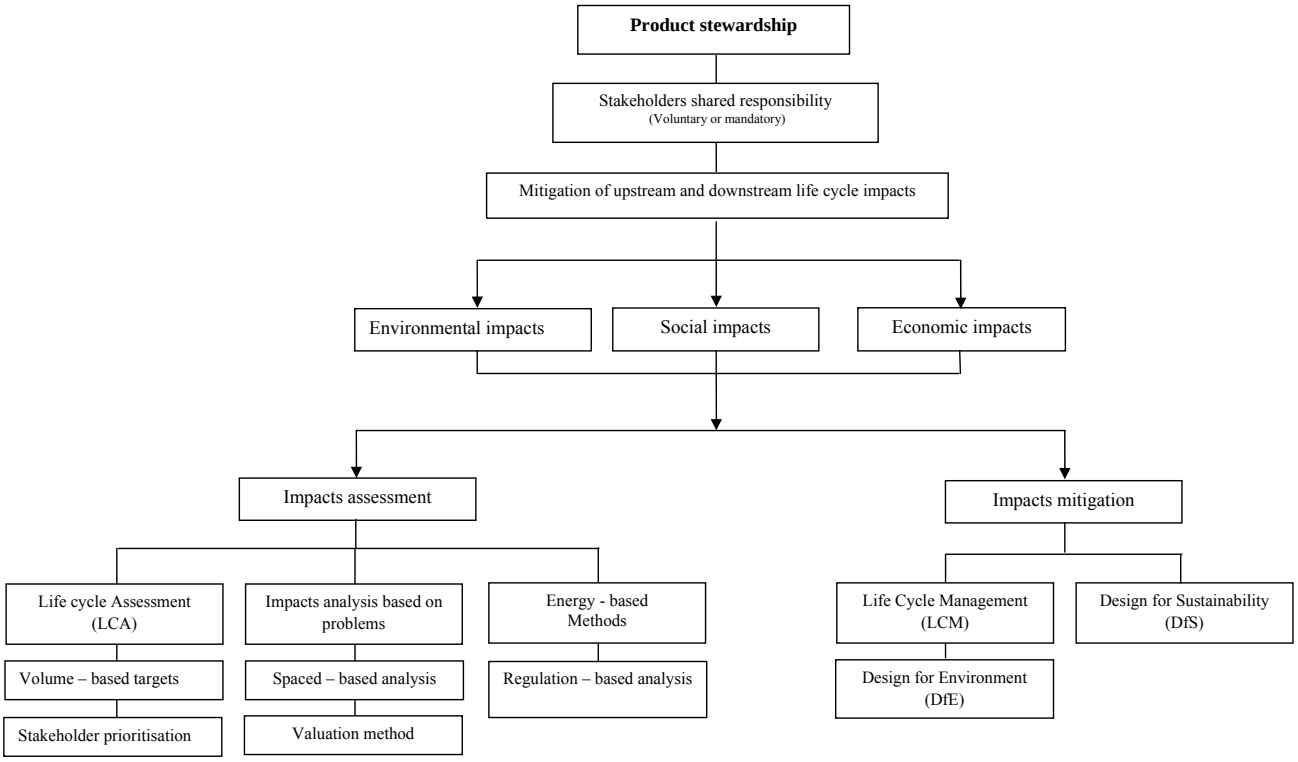

Figure 2 Product stewardship process tree from literature

Brady et.al [8] described PS as a key tool or management system to support sustainable development in industry, via the inclusion of environmental aspects such as; the use and consumption of resources and waste generated from raw material extraction and processing, production of the product, product use and final disposal of products. Properly implemented, PS offers the probability of revenue growth through product differentiation [9]. Indeed, since its early implementation in the 1970s [6], many industries, governments, multinational corporations and countries have developed and implemented PS schemes. A number of these are still in use for electric and electronic, chemical, packing and packaging, and car manufacturing. Further to this, a few product groups have successfully developed and implemented PS schemes, each of which has been implemented through voluntary or mandatory regulatory frameworks, agreed by stakeholders within the product's supply chain and lifecycle. The discourse revolves around two major aspects; responsibility and regulation, however its origin is generally attributed to three separate developments: The Responsible Care initiative by the Canadian and American chemical industry associations; the Extended Producer Responsibility (EPR) policies development around Europe; and the adaptation of PS as EPR in the US [10].

Subsequent to these developments, mandatory (legislated) and voluntary PS schemes[1] have been implemented at broadly five different strategic levels; globally, continental, national, industrial and at company level as shown in Figure 3.

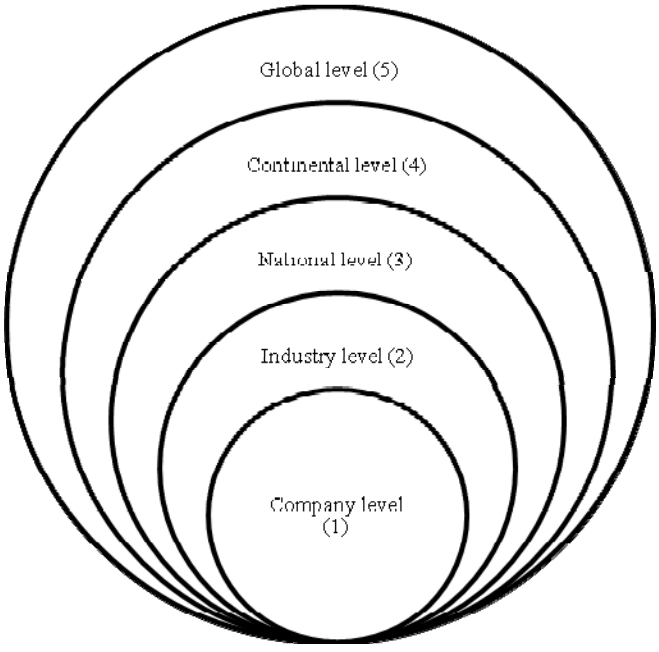

Figure 3 The strategic implementation of Product Stewardship

Level 1 (global level) is concerned with an overall implementation of the scheme throughout the world by an industry, a company or several national governments. For example the Responsible Care initiative - a voluntary global initiative of the Chemical industry has a

[1] A **Scheme** can be defined as a systematic plan or arrangement for achieving a particular object or effect [15], this term will be used throughout the paper to describe all PS initiatives, projects and schemes.

global outreach in 53 countries and applies to around 90% of global chemical production [11]. Level 2 and 3 (Continental and national levels), the OECD developed a voluntary guidance manual for national governments on EPR responsibilities and pollution control which has a predominant outreach in Europe. The Waste Electric and Electronic Equipment (WEEE) - Directive 2002/96/EC is a mandatory scheme within EU member countries has been implemented at four different levels; continental level; industry level; national level and at company levels (Level 2 - 5). Principally, PS is implemented by manufacturers and producers at company levels (Level 5) since companies have the greatest ability and responsibility [6] to make any modification or changes with regards to the environmental, health or social impacts of their products and services.

UK PRECAST INDUSTRY KEY PERFORMANCE INDICATORS (KPI)

Having reviewed the key components of PS, this section presents a snapshot of the UK precast concrete in the form of KPI data, collected from 2006-2010 from BPCF member companies (which account for around half of all precast production in the UK). KPI's are measures that focus on organisational performance that are key to both the current and future success of an organisation [12]. For the UK precast concrete industry, KPI are quantitative data that reflect the industry`s performance on: productivity, quality and satisfaction, resource use, health and safety, pollution, employment policies, respect for people, energy (including climate change), productivity, quality and satisfaction and emission [13], many of which are relevant to PS. The data provides both a mechanism for gauging the industry's performance over time, but also gives an overview of how social and environmental impacts are being managed. Here, we present a snapshot of the industry using a series of data Tables 1 - 11.

Table 1 Precast companies returning KPI data (2006 - 2010)

YEAR	NUMBER OF COMPANIES PROVIDING DATA	NUMBER OF PRODUCTION UNITS (Factories)	BPCF MEMBERS' REPORTED PRODUCTION (Tonnes)
2006	19	132	17,000,000
2007	25	122	19,900,000
2008	26	120	11,990,000
2009	27	135	9,300,000
2010	26	119	10,200,000

Table 2 Productivity levels

YEAR	NUMBER OF EMPLOYEES	TONNES OF CONCRETE PRODUCED PER EMPLOYEE
2006	8,309	1,648
2007	9,735	1,842
2008	8,681	1,427
2009	6,902	1,602
2010	6,732	1,516

Table 3 Quality management systems in place

YEAR	PRODUCTION COVERED BY ISO 9001 (TONNES)	PERCENTAGE OF BPCF MEMBERS REPORTED PRODUCTION
2006	14,000,000	81.5%
2007	14,300,000	80.0%
2008	10,100,000	84.5%
2009	8,200,000	87.7%
2010	9,500,000	93.1%

Table 4 Energy usage by fuel

YEAR	ENERGY USED PER TONNE OF CONCRETE PRODUCED (kWh/t)	PERCENTAGE BREAKDOWN BY FUEL SOURCE		
		Gas %	Electricity%	Gas oil or diesel%
2006	54.9	53	20	24
2007	52.9	54.5	20.7	24.8
2008	62.7	56.9	19.8	20.6
2009	67.9	47.9	16.4	35
2010	71.4	45	20.43	28.9

Table 5 Resource use – materials

YEAR	CEMENTITIOUS MATERIALS USED PER TONNE OF CONCRETE PRODUCED (/t)	AGGREGATE USED PER TONNE OF CONCRETE (/t)	PACKAGING MATERIALS USED PER TONNE OF CONCRETE PRODUCED (kg/t)
2006	0.140	0.754	3.0
2007	0.175	0.754	2.5
2008	0.130	0.832	4.89
2009	0.141	0.862	4.93
2010	0.141	0.800	4.94

Table 6 Resource use – water

YEAR	LITRES OF WATER USED PER TONNE OF CONCRETE PRODUCED (l/t)	PERCENTAGE BREAKDOWN BY SOURCE	
		Mains water	Licensed non-mains
2006	163	71	29
2007	156	70.4	29.6
2008	182.6	62	38
2009	146.7	79	21
2010	99.4	65	35

Table 7 Resource use – waste

YEAR	WASTE PER TONNE OF CONCRETE PRODUCED (kg/t)
2006	32
2007	41
2008	42.1
2009	43.7
2010	36

Table 8 Environmental management systems in place

YEAR	ISO 14000 SERIES OR EMAS (Production coverage in tonnes)	ISO 14000 SERIES OR EMAS (Percentage of production)
2006	12,900,000	75
2007	14,500,000	81
2008	10,100,000	85
2009	7,400,000	79.1
2010	9,220,000	90.3

Table 9 Average delivery distances

YEAR	AVERAGE ROAD DELIVERY PER TONNE (/t)	AVERAGE ROAD DISTANCE (MILES)
2006	27.4	108
2007	28	96
2008	18.6	122.37
2009	21.7	81.5
2010	21.8	123

Table 10 Health and Safety management systems in place

YEAR	PRODUCTION COVERED BY OHSAS 18001 HEALTH AND SAFETY (Tonnes)	PRODUCTION COVERED BY OHSAS 18001 HEALTH AND SAFETY (%)
2006	4,400,000	25
2007	4,800,000	26.7
2008	3,500,000	25.4
2009	2,700,000	39.1
2010	4,900,000	48.4

Table 11 Employment policies including training

YEAR	NUMBER OF EMPLOYEES	PERCENTAGE COVERED BY FORMAL TRAINING	AVERAGE HOURS OF TRAINING (hr/pa)
2006	8, 309	85%	12.6
2007	9,735	73%	14.1
2008	8, 681	94.1%	13.0
2009	6, 902	94.7%	7.3
2010	6, 732	98.5%	8.9

A Note on Environmental Incidences (EI)

In 2006, 14 environmental incidences were recorded, three in 2007 and one in 2008. No data was provided for 2009 and 2010. In terms of production, in 2006, this equates to one incident per 1.2 million tonnes of concrete produced. In 2007, one incident per 6 million tonnes of concrete produced which is a significant improvement compared to 2006. In 2008, again just one incident per 10 million tonnes of concrete produced was recorded.

A Note on Responsible Sourcing (RS)

Responsible sourcing of materials for precast concrete production is key to the achievement of PS within the industry. RS can be verified through an ethos of good supply chain management and PS [14]. In 2009, 39% of the industry's production (tonnes) was covered by BES 6001 certification and in 2010 this increased to 67.4% for the industry and a 65.29% of all production sites.

PRECAST MANUFACTURERS' ATTITUDES TOWARDS PRODUCT STEWARDSHIP

To gauge the industry's understanding on PS and its possible application within the industry, senior-level/executive staff from 12 members of the UK precast concrete industry were invited to take part in semi-structured interviews, an overview of which is provided in this section. The objectives were to: explore the feasibility and acceptability of PS implementation; obtain feedback on effective means and methods of developing consensus and facilitating progress; understand the current industry's perception and understanding of the term 'product stewardship', its importance, benefits, application within companies, areas of focus, operation and the possibility of part or whole scale future implementation of PS; and the most effective means of building consensus on PS in the UK precast concrete industry. A two-part interview schedule was developed to cover the aforementioned topics using a range of open and closed-ended questions.

Of the 12 respondents that took part in the survey, three were company directors; three Health Safety and Environment (HSE) Managers; two process managers, one head of sustainability, two environment leaders/ advisors, one process design manager and one precast design manager. The interviewees were sufficiently experienced and qualified to take part due to their experience and knowledge of sustainable construction and there was consistency observed in responses on completion of the 12 interviews, indicating sample validity. The 12

companies that took part in the survey account for approximately 55% of the UK precast industry's production (i.e. 5,433,912 tonnes), so can be said to be representative of the sector. Table 12 shows that a range of company sizes were targeted to ensure that the sample accounted for the viewpoints of large, medium and small businesses.

Table 12 Interview programme – participating companies by size

GROUPS	PRODUCTION CAPACITY (Tonnes)	NUMBER OF INTERVIEWEES
Group A (Small size)	$\leq$ 100, 000	5
Group B (Medium size)	$\geq$ 100, 000 to $\geq$ 500, 000	4
Group C (Large size)	$\geq$ 500,000 to $\geq$ 1, 000, 000	3

While there was a broadly consistent understanding of what PS might mean for precast concrete manufacturers, the company representatives appeared to have slightly different interpretations of PS, depending on their company's size and the individual's familiarity with key concepts such as RS and life-cycle management. Example definitions from each group are shown below:

Group A: *"Keep control on the main source ingredient which is concrete. That it is responsibly sourced."*

Group B: *"Everybody involved in the design, manufacture, installation and operation of a product has a responsibility somewhere along the chain .Taking responsibility by all key stakeholders for management of impacts".*

Group C: *"Encompassing full Life Cycle Assessment, Life Cycle Costing including use phase and responsibility taking at every bit of the building, building regulations, selling use, and end-of-life. It includes design for reusability, design for recycling, closing the loop, and cradle-to-cradle."*

All the companies thought PS was 'important', with one or two saying it was 'very important' and one suggesting that it would 'become more important'. The benefits were thought to centre on cost savings, efficiency savings and being seen to be 'doing the right thing'. The interviewees described a range of initiatives that they thought constituted important evidence of their participation in PS-type activities, such as 'a sustainability assessment framework' and 'Fairtrade' type ethical trading standards, but only a minority were actively participating in these. That said, there was extensive membership of established management system standards such as ISO 9001, ISO 14001 and OHSAS 18001 and the recently established RS certificate, BES 6001 [14]. While many spoke of the importance of a 'life-cycle attitude', it appeared that only the larger companies had obtained full life-cycle assessments for their products. Overall, the interviewees said that any PS scheme for the precast industry should integrate with existing practices and initiatives, and would probably be best managed through one of the key trade associations, like BPCF. They also suggested that any PS initiative by the industry should start voluntarily and later be made mandatory, and at least should take 1-2 years from before it comes into effect.

CONCLUSIONS

There is a clear case that a PS scheme could have potential to help the UK precast concrete industry further its sustainability activities, but the KPI data and evidence from industry leaders presented here suggests that companies are at different levels of understanding, participation and aspiration. The interviewees understood the basic premise of PS and recognised that it can offer benefits to their respective companies and potentially the industry in general. With a growing number of companies investing in life-cycle assessments of their products (in readiness for Type III EPDs), it is plausible that the first phase of a PS scheme would be to develop a life-cycle management strategy for the industry. In this way, the existing knowledge of manufacturers could be leveraged to gradually encompass other components of a fully-fledged PS scheme. That said, the interviewees urged caution owing to the difficult economic circumstances and highly competitive market that they currently face in the UK.

This paper has demonstrated the key sustainability performance of the UK precast concrete industry from 2006 – 2010. There are clear evidences to show the precast concrete industry's ability to capture and analyse state of the art data which can serve as a major step in helping towards present and future performance measurement, monitoring and improvements.

ACKNOWLEDGEMENTS

Special thanks goes to Loughborough University, British Precast Concrete Federation and to all member companies of the federation that have submitted data from 2006- 2010 and to all the individuals and companies that gave their time and helped in the research. Without all their support this research would not have been carried out.

REFERENCES

1. HOLTON I, GLASS J AND PRICE A. *Managing for sustainability: findings from four company case studies in the UK precast concrete industry.* Journal of Cleaner Production. Vol. 18, 2009, pp 152-160.

2. ALIYU A A, GLASS J, CLARKE, M A, ELHAG, H K, PRICE A D F, *The need for a product stewardship scheme to improve sustainability in the UK precast concrete industry*, Responsible Leadership. Proceedings of the Corporate Responsibility Research (CRR) Conference, University of Vaasa, Vaasa (Finland), Ed. Ketola T, 2009, pp 1-17.

3. DEPARTMENT FOR BUSINESS, ENTERPRISE AND REGULATORY REFORM. *Strategy for Sustainable Construction*. London: BERR; 2008.

4. EUROPEAN UNION. *The European Construction Sector.* [Online] available at: http://ec.europa.eu/enterprise/sectors/construction/index_en.htm [Accessed on: 11th August, 2011].

5. KREITH F, AND TCHOBANOGLOUS G. *Handbook of solid waste management*. McGraw - Hill Professional. 2002. Second ed. New York; London.

6. UNITED STATES ENVIRONMENTAL PROTECTION AGENCY. *What is Product Stewardship?* [Online] available at: http://www.epa.gov/epawaste/partnerships/stewardship/basic.htm. [Accessed on: 10th August, 2011].

7. JOHNEN B, FOSTER L AND THOMAS M. *Stewardship in the Agrochemical Industry. Zeneca Agrochemicals.* 2000. [Online] available at: http://www.rsc.org/delivery/_ArticleLinking/DisplayArticleForFree.cfm?doi=b006246o&JournalCo de=PO; [Accessed on: 13th July, 2009].

8. BRADY K, HENSON P, FAVA, J A. Sustainability, Eco -efficiency, Life cycle management, and Business Strategy. Environmental Quality Management. Vol. 8, No. 3, 1999, pp 33-41.

9. HART S L. *Capitalism at the crossroads: aligning business, earth, and humanity.* Wharton School Publishing, 2007. Upper Saddle River, New Jersey.

10. LEWIS, H. *Defining product stewardship and sustainability in the Australian packaging industry.* Environmental Science and Policy. Vol. 8, No. 1, 2005, pp 45-55.

11. RESPONSIBLE CARE. *Responsible Care Global Charter*. [Online] available online at: http://www.responsiblecare.org/page.asp?p=6341&l=1; [Accessed: 21st February, 2010].

12. PARMENTER, D. *Key performance indicators: developing, implementing, and using winning KPIs*. 2007. John Wiley and Sons, New Jersey. [Online] Available at: http://reader.eblib.com/. [Accessed on 13th July, 2011].

13. BRITISH PRECAST. *Sustainability Matters – Precast 2011 update edition.* [Online] accessed: 18th July, 2011. Available at: http://www.britishprecast.org/documents/BPCFSustainabilityMattersPRECAST2011updateMay2011.pdf.

14. ANDERSON J, SHIERS, D AND STEELE, K. *The Green Guide to specification.* 2009. Fourth edition. BRE, Oxford University and Wiley Blackwell, p 9.

15. SOANES C AND STEVENSON A. Concise Oxford English Dictionary. Eleventh edition. Oxford University Press, Oxford, 2009.

Shrinkage Induced Deformations of Composite Concrete Slabs with Profiled Steel Decking

I Gilbert, M A Bradford, Z-T Chang, A Gholamhoseini
University of New South Wales, Australia

Composite concrete floor slabs with profiled steel decking as permanent formwork are commonly used in the construction of floors in buildings. The steel decking supports the wet concrete of a cast in-situ reinforced or post-tensioned concrete slab and, after the concrete sets, acts as external reinforcement. Embossments on the profiled sheeting provide the necessary shear connection to ensure composite action between the concrete and the steel deck. Despite their common usage, relatively little research has been undertaken on the time-dependent in-service deformation of such slabs and little guidance is available to practising engineers for predicting deflection and axial shortening in design. The distribution of drying shrinkage through the thickness of a slab is known to be greatly affected by the impermeable steel deck at the slab soffit, but this has not yet been quantified. This paper presents the results of both experimental and analytical studies on the effects of drying shrinkage on the in-service deformation of composite concrete slabs with steel decking. Laboratory measurements of the distribution of shrinkage through the thickness of such slabs, together with their time-dependent deflection are presented and analytical procedures for modeling this behaviour are described. Design guidance for predicting time-dependent deformations is provided. The work has been supported by the Australian Research Council, Fielders Australia and Prestressed Concrete Design Consultants.

Dr Ian Gilbert is Emeritus Professor of Civil Engineering and Deputy Director of the UNSW Centre for Infrastructure Engineering and Safety in the School of Civil and Environmental Engineering at the University of New South Wales. He has published 4 books and over 300 papers in the fields of reinforced and prestressed concrete structures. He has been actively involved in the development of the Australian Standard for Concrete Structures (AS3600) for over 25 years.

Dr Mark Bradford is Scientia Professor of Civil Engineering and Research Director of the Centre for Infrastructure Engineering and Safety at the University of New South Wales. He is a Australian Laureate Fellow.

Dr Zhen-Tian Chang is a Research Associate in the Centre for Infrastructure Engineering and Safety at the University of New South Wales, Australia.

Mr Ali Gholamhoseini is a PhD student in the School of Civil and Environmental Engineering at the University of New South Wales, Australia.

Keywords: Composite slabs, Deflection, Serviceability, Shrinkage, Steel decking

INTRODUCTION

Composite one-way concrete floor slabs with profiled steel decking as permanent formwork are commonly used in the construction of floors in buildings (Figure 1). The steel decking supports the wet concrete of a cast in-situ reinforced or post-tensioned concrete slab and, after the concrete sets, acts as external reinforcement. Embossments on the profiled sheeting provide the necessary shear connection to ensure composite action (1) between the concrete and the steel deck (Figure 1b).

Despite their common usage, relatively little research has been reported on the in-service behaviour of such slabs and little guidance is available to practising engineers. In particular, the drying shrinkage profile through the slab thickness (which is known to be greatly affected by the impermeable steel deck at the slab soffit) and the restraint to shrinkage provided by the steel decking have yet to be quantified.

(a) Soffit of a one-way slab and beam floor system

(b) Decking prior to placing concrete

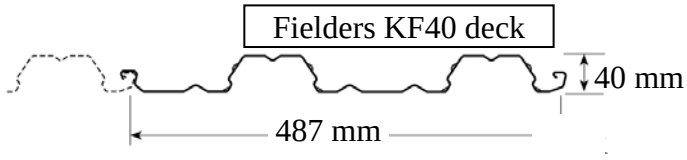

(c) Alternative steel decks showing embossments

Figure 1 Profiled steel decking for composite concrete slabs (Fielders Australia PL).

As a consequence, the techniques used to predict both the deflection and the on-set of cracking in conventionally reinforced concrete slabs are often applied inappropriately. Due to lack of guidance in the literature and in codes of practice, structural designers often specify the decking as sacrificial formwork, in lieu of expensive timber formwork and the associated falsework, and ignore the structural benefits afforded by the composite action. This will provide a conservative estimate of strength, but may well result in a significant under-estimation of deflection because of the shrinkage gradient and restraint provided by the deck.

In this paper, the results of a study of the effects of drying shrinkage on the in-service behaviour of composite concrete slabs are discussed. Laboratory measurements of drying shrinkage profiles through the thickness of composite slabs are presented. An analytical procedure is described to predict the time-dependent stresses and deformations of a composite slab when subjected to sustained service loads and drying shrinkage.

MEASURED SHRINKAGE PROFILES

The shrinkage strain distributions through the thickness of over 25 slab specimens have been measured at the University of New South Wales. At the time of writing this paper, the specimens had been drying for a period of 105 days. Three different and commonly used deck profiles manufactured by Fielders Australia Pty Ltd (one re-entrant profile, RF55, and two trapezoidal (or wave-form) profiles, KF40 and KF70), three different slab thicknesses and three different concrete mixes each with different final shrinkage strains were monitored. Each specimen was 1200 mm square in plan and was initially moist cured for between 7 and 21 days prior to the commencement of drying. For each combination of variables, two specimens (A and B) were constructed and monitored. The ‘A’ specimens were restrained, with the steel decking in place and providing restraint to drying. The ‘B’ specimens were unrestrained, with no decking in place during drying, and therefore no restraint to drying. The decking profile in the unrestrained specimens was created using polystyrene moulds fabricated to the same profile as the various decks and subsequently removed from the soffit prior to the commencement of drying. For each of these unrestrained specimens, the soffit was coated with an impermeable flexible sealant in an attempt to eliminate drying from that surface. The concrete side faces of all specimens were also sealed to ensure that drying only occurred from the top surface of each specimen.

For each specimen, concrete strains were measured using vibrating wire strain gauges embedded in the concrete at various depths through the thickness of the specimen, and a Demec gauge was used to measure concrete strains on the top and bottom surfaces of the slab. For the restrained slabs, with decking in place, strain gauges attached to the steel decking at various locations also record the steel strains that develop as a result of restraint. Figure 2 shows a typical unrestrained specimen with the soffit and side faces sealed. The specimens were mounted vertically as shown, to allow easy access to the top and bottom surfaces of the slab. The specimens were supported off round steel bars, to eliminate any restraint due to friction between the specimen and the laboratory floor, and located in a timber frame for stability.

Figure 3 shows the measured strain profiles in two 150 mm thick slab specimens with the KF40 waveform decking profile. Both the A and B specimens with and without restraint from the decking are shown (Figures 3a and 3b, respectively).

Figure 2 Typical type B shrinkage profile specimen

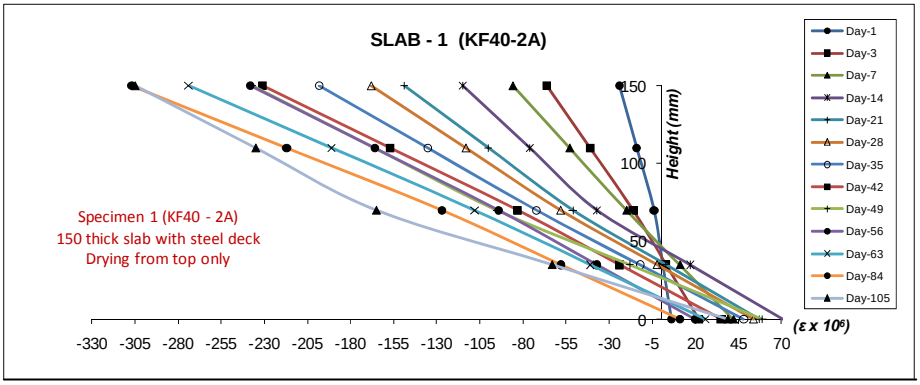

(a) Specimen - KF40-A – 150 mm thick slab with steel decking in place

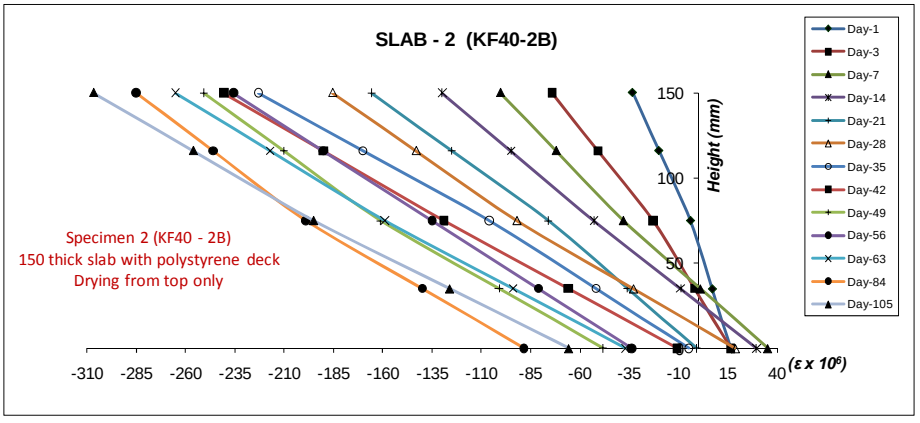

(b) Specimen KF40-B – 150 mm thick slab with no steel decking

Figure 3 Strain profiles through 150 mm thick slab – Fielders KF40 decking profile.

In Figure 3b, the strain being measured is the shrinkage strain with no restraint from the steel decking. Of course, the measured strain may include elastic and creep strains caused by eigenstresses that could develop if the actual shrinkage strain profile was non-linear. It appears that the sealing compound painted on the bottom surface of the specimens did not completely eliminate drying shrinkage, as significant strain was measured in the bottom

fibres after about 1 month of drying. While some of this measured strain may be due to autogenous shrinkage, it is more likely to be caused by drying as the bulk of the autogenous shrinkage tends to occur in the first two or three weeks after setting (and this was in the period of moist curing before drying commenced). The maximum shrinkage strain measured on the top surface of specimen B after 105 days of drying was -303×10^{-6}.

A comparison of the strain distributions in Figure 3a with those in Figure 3b shows that significant restraint was provided by the steel decking. For example, the bottom fibre strains in the 'A' specimen with restraint and in the 'B' specimen without restraint, after 105 days of drying were $+20\times10^{-6}$ (tensile) and -66×10^{-6} (compressive). The measured top fibre strain in specimen A after 105 days of drying was -307×10^{-6}.

Figure 4 shows the measured strain profiles in two 150 mm thick slab specimens with the deeper KF70 waveform decking profile. Both the A and B specimens with and without restraint from the decking are shown (Figures 4a and 4b, respectively). Clearly, the concrete mix used in these specimens was considerably wetter than that used for the KF40 specimens (see Figure 3). The top fibre strain in Figure 4b after 105 days of drying was -585×10^{-6}. The measure strain distributions through the thickness of the unrestrained specimens with this deeper deck profile were non-linear, as can be seen in Figure 4b.

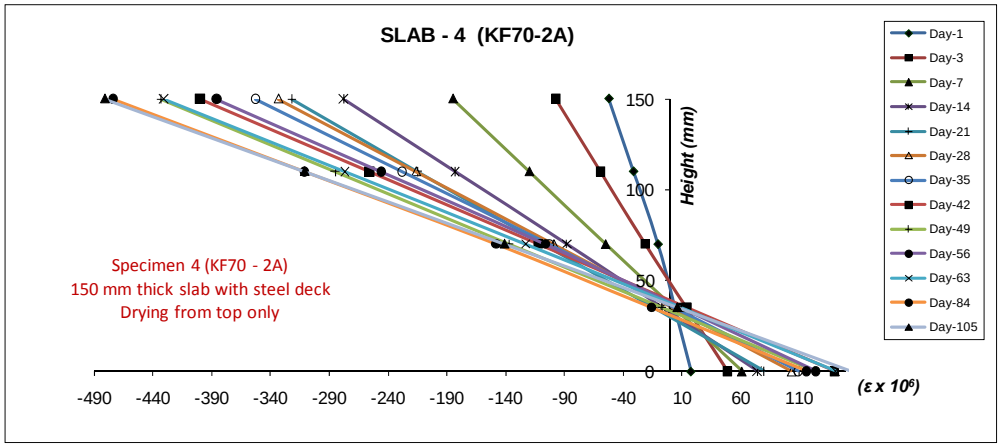

(a) Specimen – KF70-A – 150 mm thick slab with steel decking in place

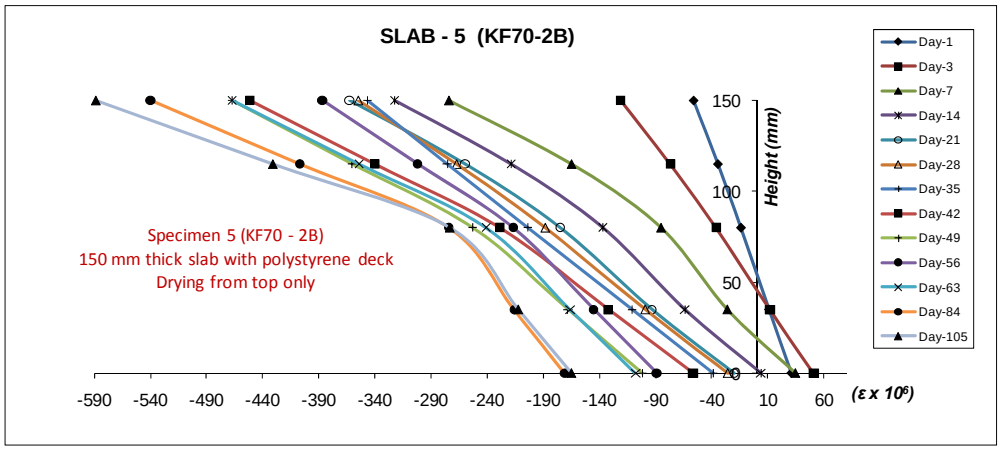

(b) Specimen KF70-B – 150 mm thick slab with no steel decking

Figure 4 Strain profiles through 150 mm thick slab – Fielders KF70 decking profile.

The strain profile changed direction at the top of the deck, i.e. at 70 mm above the soffit of the slab. This is thought to be due to the different drying conditions in the concrete above the deck to that in the troughs of the wave-form decking. In specimen A, with restraint provided by the steel decking, the strain distribution appears to be linear with no hint of the non-linear distribution evident in the unrestrained specimen. This observation was made in every set of specimens using the KF70 decking profile, irrespective of the slab thickness or concrete mix.

Significant strain was again measured in the bottom fibres of the unrestrained specimen after about 1 month of drying and this was typical of the results for all the unrestrained 150 mm thick slabs.

A comparison of the strain distributions in Figure 4a with those in Figure 4b shows that significant restraint was provided by the steel decking. For example, the bottom fibre strains in the 'A' specimen with restraint and in the 'B' specimen without restraint, after 105 days of drying were $+145\times10^{-6}$ (tensile) and -167×10^{-6} (compressive) and the top fibre strains in the 'A' and 'B' specimens at the same time were -480×10^{-6} and -585×10^{-6}. The relatively large tensile strains in the bottom fibres of the 'A' specimen indicate that cracking of the tensile concrete has almost certainly occurred.

CROSS-SECTIONAL ANALYSIS

For the calculation of the deflection of reinforced concrete slabs, the Australian Standard for Concrete Structures, AS3600-2009 [1], requires that the tensile stress induced by restraint to drying shrinkage of the concrete (σ_{cs}) be included in the estimation of the cracking moment and the flexural rigidity, as recommended in [2] and [3]. For slabs drying from the top and bottom surfaces, it is reasonable to assume that shrinkage is uniform through the depth of the slab and that the restraint is provided by the embedded reinforcement. Such an assumption is implicit in AS3600-2009. For composite slabs, however, restraint is provided by the deck (as well as any embedded reinforcement) through composite action [4], but the deck effectively prevents drying from the soffit of the slab and a shrinkage gradient is created through the slab depth. This shrinkage gradient has a significant impact on the long-term deflection and it also affects the tensile stresses induced by the restraint to shrinkage and hence affects the extent of cracking.

Surprisingly little research has been reported to determine the distribution of shrinkage strains in a composite slab and no guidance is provided in the literature for practising engineers. Frequently, the assumption of uniform shrinkage is made in structural design [5], but this is likely to be grossly inaccurate. A rigorous analytical procedure for the time-dependent analysis of composite concrete cross-sections with uniform shrinkage through the thickness of the concrete slab and with full interaction was presented by Gilbert and Ranzi [6] using the age-adjusted effective modulus method (see [7] and [8]). The method is extended here to calculate the effects of a non-uniform shrinkage gradient by layering the concrete cross-section, with the shrinkage strain in each concrete layer depending on its position within the cross-section.

A typical cross-section with m concrete layers is shown as shown in Figure 5. The thickness of the i-th concrete layer is t_i; the overall slab depth is D; $A_s(i)$ and $d_s(i)$ are the area and depth from the top surface to the centroid of the i-th layer of conventional reinforcement; d_{sd}

is the depth from the top concrete surface to the centroidal axis of the steel decking (with full interaction); and A_{sd} and I_{sd} are respectively, the cross-sectional area of the steel decking and the second moment of area of the steel decking about its centroidal axis.

In the subsequent cross-sectional analyses, the reference axis (the x-axis) is taken as the top surface of the concrete and the positive direction of the transverse y-axis is as shown in Figure 5. The following equations adopt the same notation as Gilbert and Ranzi [6] and the technique adopted for the analysis is an extension of the method fully-described in [6].

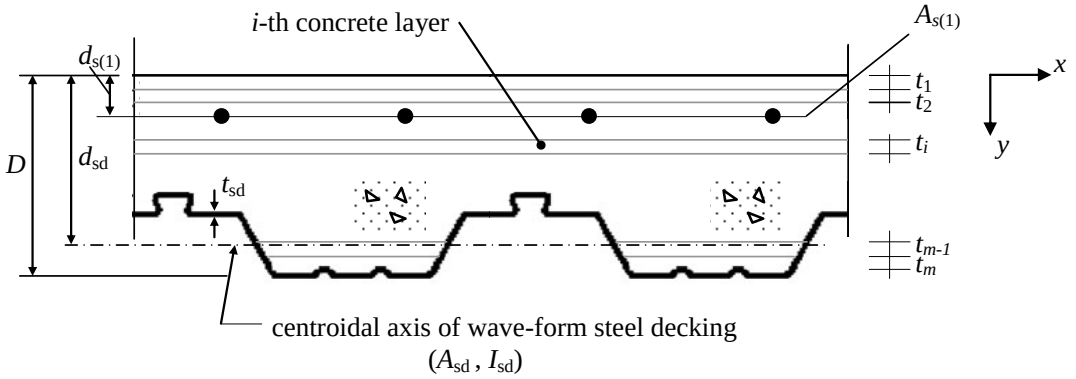

Figure 5 Typical slab cross-section with concrete subdivided into m layers.

Short-term Analysis

The instantaneous stress-strain relationships for each material (concrete, steel reinforcement and steel deck) at first loading (i.e. at time τ_0) are assumed to be linear-elastic:

$$\sigma_{c(i),0} = E_{c(i),0}\varepsilon_0 \;;\quad \sigma_{s(i),0} = E_{s(i)}\varepsilon_0 \;;\quad \sigma_{sd,0} = E_{sd}\varepsilon_0 \qquad (1a,b,c)$$

where $\varepsilon_0 = \varepsilon_{r,0} + y\kappa_0$ is the instantaneous strain at depth y below the top reference surface (the x-axis); $\varepsilon_{r,0}$ is the instantaneous strain at the top reference surface; κ_0 is the instantaneous curvature; and $E_{c(i)}$, $E_{s(i)}$ and E_{sd} are the elastic moduli of the concrete, steel reinforcement and steel deck, respectively. When the concrete stress exceeds the mean tensile strength of concrete (f_{tm}) cracking is deemed to have occurred and thereafter $E_{c(i)}$ is set to zero.

The internal actions carried by the i-th concrete layer (for inclusion in the equilibrium equations) can be expressed as:

$$N_{c(i),0} = \int_{A_{c(i)}} \sigma_{c(i),0}\,\mathrm{d}A = \int_{A_{c(i)}} E_{c(i),0}\left(\varepsilon_{r,0} + y\kappa_0\right)\mathrm{d}A = A_{c(i)}E_{c(i),0}\varepsilon_{r,0} + B_{c(i)}E_{c(i),0}\kappa_0 \qquad (2a)$$

$$M_{c(i),0} = \int_{A_{c(i)}} y\sigma_{c(i),0}\,\mathrm{d}A = \int_{A_{c(i)}} E_{c(i),0}y\left(\varepsilon_{r,0} + y\kappa_0\right)\mathrm{d}A = B_{c(i)}E_{c(i),0}\varepsilon_{r,0} + I_{c(i)}E_{c(i),0}\kappa_0 \qquad (2b)$$

where $N_{c(i),0}$ and $M_{c(i),0}$ are the axial force resisted by the i-th concrete layer and the moment of the axial force about the x-axis, respectively; and $A_{c(i)}$, $B_{c(i)}$ and $I_{c(i)}$ are the area of the i-th

concrete layer and the first and second moments of area of the i-th concrete layer about the x-axis, respectively. Similarly, the internal actions resisted by the i-th layer of conventional reinforcement and by the steel deck, respectively, are

$$N_{\mathrm{s(i),0}} = \left(A_{\mathrm{s(i)}}E_{\mathrm{s(i)}}\right)\varepsilon_{\mathrm{r},0} + \left(y_{\mathrm{s(i)}}A_{\mathrm{s(i)}}E_{\mathrm{s(i)}}\right)\kappa_0 \tag{3a}$$

$$M_{\mathrm{s(i),0}} = \left(y_{\mathrm{s(i)}}A_{\mathrm{s(i)}}E_{\mathrm{s(i)}}\right)\varepsilon_{\mathrm{r},0} + \left(y^2_{\mathrm{s(i)}}A_{\mathrm{s(i)}}E_{\mathrm{s(i)}}\right)\kappa_0 \tag{3b}$$

and

$$N_{\mathrm{sd},0} = \int_{A_{\mathrm{sd}}} E_{\mathrm{sd}}(\varepsilon_{\mathrm{r},0} + y\kappa_0)\mathrm{d}A = A_{\mathrm{sd}}E_{\mathrm{sd}}\varepsilon_{\mathrm{r},0} + B_{\mathrm{sd}}E_{\mathrm{sd}}\kappa_0 \tag{4a}$$

$$M_{\mathrm{sd},0} = \int_{A_{\mathrm{sd}}} yE_{\mathrm{sd}}(\varepsilon_{\mathrm{r},0} + y\kappa_0)\mathrm{d}A = B_{\mathrm{sd}}E_{\mathrm{sd}}\varepsilon_{\mathrm{r},0} + I_{\mathrm{sd}}E_{\mathrm{sd}}\kappa_0 \tag{4b}$$

The governing equilibrium equations for the entire cross-section are obtained by equating the sum of the internal stress resultants with the external actions on the cross-section ($N_{\mathrm{e},0}$ and $M_{\mathrm{e},0}$). That is

$$N_{\mathrm{e},0} = \sum_{\mathrm{i}=1}^{m_{\mathrm{c}}} N_{\mathrm{c(i),0}} + \sum_{\mathrm{i}=1}^{m_{\mathrm{s}}} N_{\mathrm{s(i),0}} + N_{\mathrm{sd},0} \quad \text{and} \quad M_{\mathrm{e},0} = \sum_{\mathrm{i}=1}^{m_{\mathrm{c}}} M_{\mathrm{c(i),0}} + \sum_{\mathrm{i}=1}^{m_{\mathrm{s}}} M_{\mathrm{s(i),0}} + M_{\mathrm{sd},0} \tag{5a,b}$$

and these can be written in compact form as

$$\mathbf{r}_{\mathrm{e},0} = \mathbf{D}_0\boldsymbol{\varepsilon}_0 \tag{6}$$

where

$$\mathbf{r}_{\mathrm{e},0} = \begin{bmatrix} N_{\mathrm{e},0} \\ M_{\mathrm{e},0} \end{bmatrix};\ \boldsymbol{\varepsilon}_0 = \begin{bmatrix} \varepsilon_{\mathrm{r},0} \\ \kappa_0 \end{bmatrix};\ \mathbf{D}_0 = \begin{bmatrix} R_{A,0} & R_{B,0} \\ R_{B,0} & R_{I,0} \end{bmatrix} \tag{7a,b,c}$$

and $\mathbf{D}_0$ is the matrix of cross-sectional rigidities in which

$$R_{A,0} = \sum_{i=1}^{m_{\mathrm{c}}} A_{\mathrm{c(i)}}E_{\mathrm{c(i),0}} + \sum_{i=1}^{m_{\mathrm{s}}} A_{\mathrm{s(i)}}E_{\mathrm{s(i)}} + A_{\mathrm{sd}}E_{\mathrm{sd}} = \sum_{\mathrm{i}=1}^{m_{\mathrm{c}}} A_{\mathrm{c(i)}}E_{\mathrm{c(i),0}} + R_{A,\mathrm{s}} + R_{A,\mathrm{sd}} \tag{8a}$$

$$R_{B,0} = \sum_{i=1}^{m_{\mathrm{c}}} B_{\mathrm{c(i)}}E_{\mathrm{c(i),0}} + \sum_{i=1}^{m_{\mathrm{s}}} y_{\mathrm{s(i)}}A_{\mathrm{s(i)}}E_{\mathrm{s(i)}} + B_{\mathrm{sd}}E_{\mathrm{sd}} = \sum_{\mathrm{i}=1}^{m_{\mathrm{c}}} B_{\mathrm{c(i)}}E_{\mathrm{c(i),0}} + R_{B,s} + R_{B,\mathrm{sd}} \tag{8b}$$

$$R_{I,0} = \sum_{\mathrm{i}=1}^{m_{\mathrm{c}}} I_{\mathrm{c(i)}}E_{\mathrm{c(i),0}} + \sum_{i=1}^{m_{\mathrm{s}}} y^2_{\mathrm{s(i)}}A_{\mathrm{s(i)}}E_{\mathrm{s(i)}} + I_{\mathrm{sd}}E_{\mathrm{sd}} = \sum_{\mathrm{i}=1}^{m_{\mathrm{c}}} I_{\mathrm{c(i)}}E_{\mathrm{c(i),0}} + R_{I,\mathrm{s}} + R_{I,\mathrm{sd}}\,. \tag{8c}$$

Solving Equations (6) gives

$$\boldsymbol{\varepsilon}_0 = \mathbf{D}_0^{-1}\,\mathbf{r}_{\mathrm{e},0} = \mathbf{F}_0\,\mathbf{r}_{\mathrm{e},0} \tag{9}$$

where

$$\mathbf{F}_0 = \frac{1}{R_{A,0}R_{I,0} - R_{B0}^2}\begin{bmatrix} R_{I,0} & -R_{B,0} \\ -R_{B,0} & R_{A,0} \end{bmatrix} \tag{10}$$

The stress distribution in each material is calculated from Eqs (1):

$$\sigma_{c(i),0} = E_{c(i),0}\varepsilon_0 = E_{c(i),0}[1 \;\; y]\;\boldsymbol{\varepsilon}_0; \quad \sigma_{s(i),0} = E_{s(i)}\varepsilon_0 = E_{s(i)}[1 \;\; y_{s(1)}]\;\boldsymbol{\varepsilon}_0 \text{; and} \tag{11a, b}$$

$$\sigma_{sd,0} = E_{sd}\;[1 \;\; y]\;\boldsymbol{\varepsilon}_0 \tag{11c}$$

Long-term Analysis

For the analysis of stresses and deformations on a composite cross-section at some time τ_k $(> \tau_0)$ after a period of sustained loading and/or shrinkage, the formulation of the age-adjusted effective modulus method (AEMM) outlined by Gilbert and Ranzi (2010) is used. The constitutive relationship for the i-th concrete layer at τ_k is expressed as:

$$\sigma_{c(i),k} = \overline{E}_{e(i),k}\left(\varepsilon_k - \varepsilon_{sh(i),k}\right) + \overline{F}_{e(i),0}\sigma_{c(i),0} \tag{12}$$

where $\varepsilon_{sh(i),k}$ is the shrinkage strain that develops in the i-th layer during the time interval τ_0 to τ_k; $\overline{E}_{e(i),k}$ is the age-adjusted effective modulus of the i-th concrete layer and $\overline{F}_{e(i),0}$ is an age-adjusted creep factor given by

$$\overline{E}_{e(i),k} = \frac{E_{c(i),0}}{1 + \chi_i(\tau_k,\tau_0)\,\varphi_i(\tau_k,\tau_0)} \text{ and } \overline{F}_{e(i),0} = \varphi_i(\tau_k,\tau_0)\frac{[\chi_i(\tau_k,\tau_0) - 1]}{[1 + \chi_i(\tau_k,\tau_0)\varphi_i(\tau_k,\tau_0)]} \tag{13a,b}$$

and $\varphi_i(\tau_k,\tau_0)$ is the creep coefficient for the concrete in the i-th layer associated with the time interval interval τ_0 to τ_k and $\chi_i(\tau_k,\tau_0)$ is the associated aging coefficient.

The contribution of the i-th concrete layer to the internal axial force and moment at τ_k can be determined as:

$$\begin{aligned} N_{c(i),k} &= \int_{A_{c(i)}} \sigma_{c(i),k}\,\mathrm{d}A = \int_{A_{c(i)}} \left[\overline{E}_{e(i),k}\left(\varepsilon_{r,k} + y\kappa_k - \varepsilon_{sh(i),k}\right) + \overline{F}_{e(i),0}\sigma_{c(i),0}\right]\mathrm{d}A \\ &= A_{c(i)}\overline{E}_{e(i),k}\varepsilon_{r,k} + B_{c(i)}\overline{E}_{e(i),k}\kappa_k - A_{c(i)}\overline{E}_{e(i),k}\varepsilon_{sh(i),k} + \overline{F}_{e(i),0}N_{c(i),0} \end{aligned} \tag{14a}$$

$$\begin{aligned} M_{c(i),k} &= \int_{A_{c(i)}} y\sigma_{c(i),k}\,\mathrm{d}A = \int_{A_{c(i)}} y\left[\overline{E}_{e(i),k}\left(\varepsilon_{r,k} + y\kappa_k - \varepsilon_{sh(i),k}\right) + \overline{F}_{e(i),0}\sigma_{c(i),0}\right]\mathrm{d}A \\ &= B_{c(i)}\overline{E}_{e(i),k}\varepsilon_{r,k} + I_{c(i)}\overline{E}_{e(i),k}\kappa_k - B_{c(i)}\overline{E}_{e(i),k}\varepsilon_{sh(i),k} + \overline{F}_{e(i),0}M_{c(i),0} \end{aligned} \tag{14b}$$

The equilibrium equations are therefore

$$\mathbf{r}_{e,k} = \mathbf{D}_k\boldsymbol{\varepsilon}_k + \mathbf{f}_{cr,k} - \mathbf{f}_{sh,k} \tag{15}$$

where

$$\mathbf{r}_{\mathrm{e,k}} = \begin{bmatrix} N_{\mathrm{e,k}} \\ M_{\mathrm{e,k}} \end{bmatrix} \; ; \quad \mathbf{D}_{\mathrm{k}} = \begin{bmatrix} R_{A,\mathrm{k}} & R_{B,\mathrm{k}} \\ R_{B,\mathrm{k}} & R_{I,\mathrm{k}} \end{bmatrix} \; ; \quad \boldsymbol{\varepsilon}_{\mathrm{k}} = \begin{bmatrix} \varepsilon_{\mathrm{r,k}} \\ \kappa_{\mathrm{k}} \end{bmatrix} \tag{16a,b,c}$$

and the time-dependent cross-sectional rigidities at τ_{k} are:

$$R_{A,\mathrm{k}} = \sum_{\mathrm{i}=1}^{m_{\mathrm{c}}} A_{\mathrm{c(i)}} \overline{E}_{\mathrm{e(i),k}} + R_{A,\mathrm{s}} + R_{A,\mathrm{sd}} \; ; \quad R_{B,\mathrm{k}} = \sum_{\mathrm{i}=1}^{m_{\mathrm{c}}} B_{\mathrm{c(i)}} \overline{E}_{\mathrm{e(i),k}} + R_{B,\mathrm{s}} + R_{B,\mathrm{sd}} \; ; \tag{17a,b}$$

$$R_{I,\mathrm{k}} = \sum_{\mathrm{i}=1}^{m_{\mathrm{c}}} I_{\mathrm{c(i)}} \overline{E}_{\mathrm{e(i),k}} + R_{I,\mathrm{s}} + R_{I,\mathrm{sd}} \tag{17c}$$

In Eq. 15, the effects of creep and shrinkage of the concrete elements are included within the vectors $\mathbf{f}_{\mathrm{cr,k}}$ and $\mathbf{f}_{\mathrm{sh,k}}$ given by

$$\mathbf{f}_{\mathrm{cr,k}} = \sum_{\mathrm{i}=1}^{m_{\mathrm{c}}} \overline{F}_{\mathrm{e(i),0}} \begin{bmatrix} N_{\mathrm{c(i),0}} \\ M_{\mathrm{c(i),0}} \end{bmatrix} = \sum_{\mathrm{i}=1}^{m_{\mathrm{c}}} \overline{F}_{\mathrm{e(i),0}} E_{\mathrm{c(i),0}} \begin{bmatrix} A_{\mathrm{c(i)}} \varepsilon_{\mathrm{r,0}} + B_{\mathrm{c(i)}} \kappa_0 \\ B_{\mathrm{c(i)}} \varepsilon_{\mathrm{r,0}} + I_{\mathrm{c(i)}} \kappa_0 \end{bmatrix} \tag{18a}$$

$$\mathbf{f}_{\mathrm{sh,k}} = \sum_{\mathrm{i}=1}^{m_{\mathrm{c}}} \begin{bmatrix} A_{\mathrm{c(i)}} \\ B_{\mathrm{c(i)}} \end{bmatrix} \overline{E}_{\mathrm{e(i),k}} \varepsilon_{\mathrm{sh(i),k}} \tag{18b}$$

Solving Eqs (15) gives the strain at time τ_{k} :

$$\boldsymbol{\varepsilon}_{\mathrm{k}} = \mathbf{D}_{\mathrm{k}}^{-1} \left(\mathbf{r}_{\mathrm{e,k}} - \mathbf{f}_{\mathrm{cr,k}} + \mathbf{f}_{\mathrm{sh,k}} \right) = \mathbf{F}_{\mathrm{k}} \left(\mathbf{r}_{\mathrm{e,k}} - \mathbf{f}_{\mathrm{cr,k}} + \mathbf{f}_{\mathrm{sh,k}} \right) \tag{19}$$

where

$$\mathbf{F}_{\mathrm{k}} = \frac{1}{R_{A,\mathrm{k}} R_{I,\mathrm{k}} - R_{B,\mathrm{k}}^2} \begin{bmatrix} R_{I,\mathrm{k}} & -R_{B,\mathrm{k}} \\ -R_{B,\mathrm{k}} & R_{A,\mathrm{k}} \end{bmatrix} \tag{20}$$

The stress distributions at time τ_{k} in each concrete element and in the reinforcement and deck are:

$$\sigma_{\mathrm{c(i),k}} = \overline{E}_{\mathrm{e(i),k}} \left(\varepsilon_{\mathrm{k}} - \varepsilon_{\mathrm{sh(i),k}} \right) + \overline{F}_{\mathrm{e(i),0}} \sigma_{\mathrm{c(i),0}} = \overline{E}_{\mathrm{e(i),k}} \left\{ \begin{bmatrix} 1 & y \end{bmatrix} \boldsymbol{\varepsilon}_{\mathrm{k}} - \varepsilon_{\mathrm{sh(i),k}} \right\} + \overline{F}_{\mathrm{e(i),0}} \sigma_{\mathrm{c(i),0}} \; ; \tag{21a}$$

$$\sigma_{\mathrm{s(i),k}} = E_{\mathrm{s(i)}} \varepsilon_{\mathrm{k}} = E_{\mathrm{s(i)}} \begin{bmatrix} 1 & y_{\mathrm{s(i)}} \end{bmatrix} \boldsymbol{\varepsilon}_{\mathrm{k}} \; ; \text{ and } \; \sigma_{\mathrm{sd,k}} = E_{\mathrm{sd}} \begin{bmatrix} 1 & y \end{bmatrix} \boldsymbol{\varepsilon}_{\mathrm{k}} \, . \tag{21b,c}$$

RESULTS OF ANALYSIS

Shrinkage-induced Stresses and Deformations on an Uncracked Section

Consider a 1 m wide strip of an unloaded and uncracked, simply-supported, composite, one-way slab spanning 4m and of overall depth D = 150 mm. The steel decking at the soffit of the slab is Fielders Australia's KF70 wave-form decking of thickness t_{sd} = 1.0mm. The dimensions of the cross-section of the slab strip are shown in Figure 6a, together with the assumed material properties. The stresses and deformations induced by four alternative shrinkage profiles are shown in Figures 6b to 6e and were determined using the analytical procedure described in the previous section, assuming full interaction between the concrete and the steel deck. In each analysis, the concrete was sub-divided into 10 layers of equal thickness.

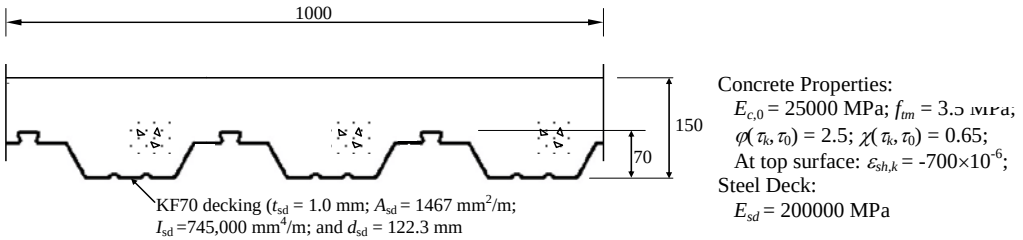

(a) Details of section and material properties

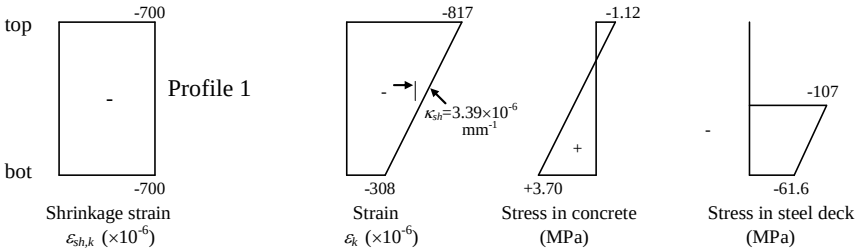

(b) Uniform shrinkage profile ($\varepsilon_{sh,k} = -700\times10^{-6}$ top and bottom)

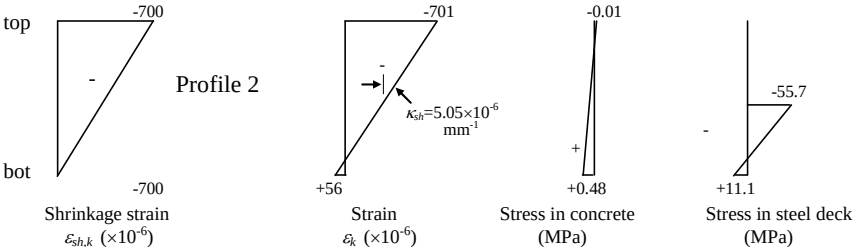

(c) Triangular shrinkage profile ($\varepsilon_{sh,k} = -700\times10^{-6}$ top and 0 bottom)

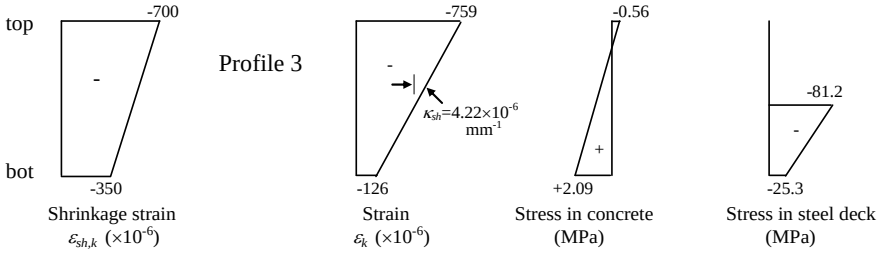

(d) Trapezoidal shrinkage profile ($\varepsilon_{sh,k} = -700\times10^{-6}$ top and -350×10^{-6} bottom)

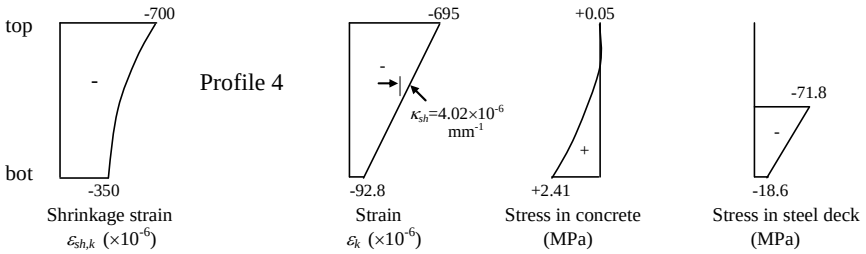

(e) Parabolic shrinkage profile ($\varepsilon_{sh,k} = -700\times10^{-6}$ top and -350×10^{-6} bottom)

Figure 6 Stresses and strains on an uncracked composite cross-section.

For composite slabs with steel decking at the soffit, the uniform shrinkage profile of Figure 6b (Profile 1) is unrealistic, but such a profile is frequently used in existing software packages for estimating the in-service behaviour of composite slabs. Profile 1 results in an overestimation of the tensile restraining force exerted on the concrete slab by the steel decking and hence the tensile stress in the bottom fibres of the concrete is overestimated. Indeed, the calculated tensile stress in the bottom fibre of the concrete is 3.70 MPa and this would probably cause cracking in an unloaded slab. However, Profile 1 results in an underestimation of the shrinkage induced curvature on the cross-section and hence an underestimation of the shrinkage-induced part of the time-dependent deflection.

The triangular shrinkage profile of Figure 6c (Profile 2) results in relatively little tension in the concrete. While such a profile results in a relatively small reduction in the cracking moment, it leads to the largest shrinkage-induced curvature of the four shrinkage profiles considered.

The two profiles that most accurately represent the measured shrinkage profile in a composite slab are Profiles 3 and 4. For both profiles, the restraint to shrinkage provided by the steel deck induces significant tension in the bottom fibres of the concrete and a significant reduction in the cracking moment with time. Both profiles also induce significant time-dependent curvature. For Profile 3, the shrinkage-induced curvature on the uncracked cross-section is $4.22\times10^{-6}\text{mm}^{-1}$ and, for a 4m span uncracked slab, this would results in a final shrinkage-induced deflection at mid-span of 8.4 mm (Span/476).

Shrinkage-induced Stresses and Deformations on an Cracked Section

If the one-way slab with cross-section shown in Figure 6a is subjected to a dead load of 4 kPa (which includes the self-weight of the slab) and a 3 kPa superimposed live load, the maximum in-service moment at mid-span is 14 kNm/m. Assuming the cross-section cracks when the tensile stress in the bottom fibre reaches 3.5 MPa, an instantaneous analysis of the cross-section indicates that, in the absence of any prior shrinkage, the cracking moment is 9.98 kNm/m.

On the cracked section, the depth to the neutral axis from the top surface of the slab is $43.1\,\text{mm}$ and the shrinkage induced stresses and deformations on the cracked section are calculated using the procedures of the previous section and are shown in Figure 7.

The trapezoidal shrinkage profile of Figure 6d has been assumed in these calculations. The shrinkage induced curvature on the cracked section at mid-span is $580\times10^{-6}\text{mm}^{-1}$ and, with the regions at each end of the span remaining uncracked, the shrinkage induced deflection at mid-span is 11.1 mm (Span/360).

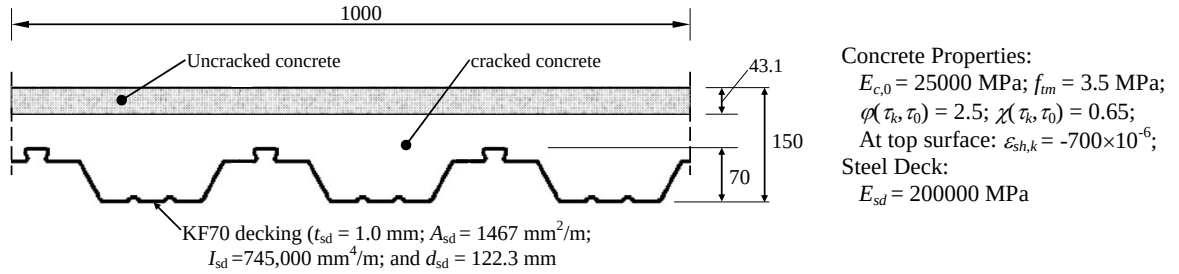

(a) Details of cracked composite slab cross-section and material properties

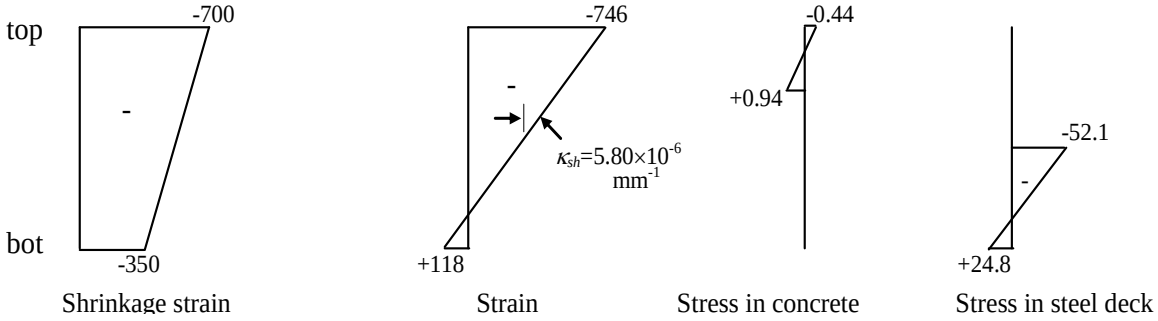

(b) Stresses and strains induced by a trapezoidal shrinkage profile

Figure 7 Stresses and deformations on a cracked composite cross-section.

CONCLUSIONS

In this paper, a procedure is presented for the instantaneous and time-dependent analyses of the in-service behaviour of composite concrete slabs with wave-form steel decking. The decking doubles as tensile reinforcement and permanent formwork. The effects of cracking, creep and the non-uniform shrinkage strain through the depth of the slab are accounted for using a mathematically tractable formulation of the age-adjusted effective modulus method, recently presented by Gilbert and Ranzi [6]. Laboratory measurements of drying shrinkage profiles through the thickness of a composite slab are also presented.

The shape of the shrinkage profile through the depth of the slab is shown to have a significant effect on the restraint offered by the steel deck and on the magnitude of the gradually developing shrinkage-induced tensile stresses near the bottom of the concrete section. The reduction of the cracking moment with time is readily quantified, as are the shrinkage-induced curvatures on the various cross-sections and the shrinkage-induced long-term deflection of the member.

ACKNOWLEDGEMENTS

The work has been undertaken with the financial support of the Australian Research Council, decking manufacturers Fielders Australia Pty Ltd and software developers Prestressed Concrete Design Consultants Pty Ltd. This support is gratefully acknowledged.

REFERENCES

1. STANDARDS AUSTRALIA, Australian Standard for Concrete Structures, AS3600-2009, Sydney, 2009.

2. GILBERT, R.I. Deflection Calculation for Reinforced Concrete Structures – Why We Sometimes Get It Wrong, ACI Structural Journal, Vol. 96, No. 6, 1999, pp 1027-1032.

3. GILBERT, R.I. Deflection by Simplified Calculation in AS3600-2001 – On the Determination of f_{cs}, Australian Journal of Structural Engineering, Vol. 5, No. 1, 2003, pp 61-71.

4. BRADFORD, M.A. Generic modelling of composite steel-concrete slabs subjected to shrinkage, creep and thermal strains including partial interaction, Engineering Structures, Vol. 3, No. 5, 2010, pp 1459-1465.

5. BROCK, G., RAPT Reinforced and Post-tensioned Structural Concrete Design Software, www.raptsoftware.com, 2008.

6. GILBERT, R.I. and RANZI, G., Time-dependent Behaviour of Concrete Structures, Spon Press, London, 2010, 426p.

7. DILGER, W. and NEVILLE, A.M., Method of Creep Analysis of Structural Members, American Concrete Institute, ACI SP 27-17, 1971, pp 349-379.

8. BAŽANT, Z.P., Prediction of Concrete Creep Effects using Age-Adjusted Effective Modulus Method“, ACI Journal, Vol. 69, April 1972, pp 212-217.

Cigarette Filter Material and Polypropylene Fibres in Concrete - Drying Shrinkage

A Richardson
Northumbria University, UK

Due to a reduction in demand for cigarette filter material (North East UK), significant quantities have arisen that have little commercial value. The filter manufacturers have been looking for another outlet for their product and polypropylene fibre replacement in concrete was considered. The purpose of adding Type 1 polypropylene fibres (BS-EN14889) to concrete is to control plastic shrinkage and reduce bleeding. A paired comparison test was carried out to examine concrete cured under extreme conditions of heat and air flow. This micro climate would cause uneven drying due to surface evaporation and internal stresses within the concrete matrix and as a consequence of this instigate drying shrinkage cracking. Type 1 micro polypropylene fibres have known properties to control drying cracking and the performance of concrete with polypropylene fibres was compared against plain concrete and concrete with cigarette filter material. The findings showed that when cigarette filter material and Type 1 polypropylene fibres were compared together their performance was very similar and showed less drying shrinkage cracks than plain concrete.

A E Richardson, MSc, FCIOB, MInstCES is a senior lecturer within the School of the Built Environment, University of Northumbria, UK (PhD in Civil Engineering – Newcastle University. His specialist areas are polypropylene fibres in concrete with regard to durability. He has extensive publications relating to fibre concrete, particularly with heat, spalling and curing, also freeze/thaw on very early life concrete and fully cured. In addition he is ex managing director of a family run SME with a history in construction since 1850.

Keywords: Cigarette filter, Curing, Elevated temperature, Polypropylene fibres

INTRODUCTION

Many product manufacturers are facing changes in demand due to changing behaviour in society. There is a reduction of smokers, coupled with cheap imported cigarettes, both legal and illegal that have driven product manufacturers to look at other uses for their products. This research is driven by such market forces.

Elevated temperatures during curing will cause an increased reaction between the cement particles and the moisture (water) within the concrete. This reaction will cause a double problem as there will now be a higher temperature within the concrete and also within the external environment of the concrete, thus leading to rapid reaction and dehydration of the mix. As dehydration starts, the damage to the long term durability of concrete also starts to manifest. Most notably in its failure to reduce pore sizes and bleed holes, which will inevitably facilitate the ingress of fluids. Polypropylene fibres and the manufacturing process are covered by BS-EN14889 and should not be exposed to temperatures above 140°C whilst curing, which may give cigarette filter material an advantage in terms of heat resistance.

Work by Dave and Desai [1] suggest that the incorporation of Type 1 polypropylene fibres (BS-EN14889) has a beneficial effect when concrete specimens are subject to heating and cooling cycles. They conclude that "it is observed that all fibre mixes have exhibited superior performance compared to control mixes" and a "definite improvement in thermal behaviour and cracking characteristics was observed" [1]. The inclusion of concrete with polypropylene fibres has acted as a benchmark to measure the performance of other concrete types. Type 1 micro fibres are mostly used in concrete to reduce shrinkage cracking. This research utilises two types of fibres - cigarette filter and Type 1 polypropylene fibres 20mm x 19 micron diameter to evaluate the relative performance of two fibre types compared to the performance of plain concrete.

MATERIALS AND PROPERTIES

Polypropylene Fibres

Polypropylene is a large molecule built up by a repetition of a small simple chemical unit until a polymer chain is formed. It is a relatively modern product and was not manufactured until 1957 [2] following innovative work by Staudinger (1920) and Flory (1937) both receiving the Nobel Prize for their work.

Polypropylene is a hydrocarbon containing only chemical elements, in consequence of that it is always referred to as hydrocarbon polymer. Hydrocarbon polymers are composed of common chemical structures and are produced entirely from carbon and hydrogen atom. Production of polypropylene fibres is an industrial based and controlled process, dependant upon the capability of thermoplastic raisins to melt at relatively low temperatures, then to be pressurized within the screw extruder and ejected in a filament form. The type of polypropylene fibres used in this research is Type 1, 20 mm long by 19 micron diameter

Properties of polypropylene fibre reinforced concrete

Polypropylene fibre reinforced concrete (PFRC) is considered to be an effective method to improve the shrinkage cracking, strength and toughness, durability and impact of concrete

materials. A considerable amount of research has been conducted to study the properties of the fibre reinforced concrete (FRC). Material properties of polypropylene fibre reinforced concrete (PFRC), depend strongly on fibre concentration and the form of the fibre reinforced [3]. Other major causes and effects of the properties of the fibre reinforcement is the bond strength of the polypropylene fibre with cement composite. The potential of the polypropylene fibre as concrete reinforcement also depends on the bond between fibre and matrix [3].

Cigarette Filter Fibre

Almost around 95% of cigarettes filters are made of cellulose acetate, a syntactic plastic like substance which is commonly used for photographic films and the remaining percentage are made from papers and rayon. A plasticizer, triacetin (glycerol triacetate), is applied to bond the fibres into a core [4].

The cellulose acetate fibres are white colour, and packed tightly together to form a filter and they look like cotton. Seeing the white faced cigarette filter with the naked eye and compression of the filter column with the fingers, would suggest that the filter is made of sponge like material. Nevertheless, opening of the cigarette filter by cutting it in lengthwise in razor shows that it consists of a fibrous mass. Teasing apart the fibre matrix would reveal more than 12,000 white fibres per cigarette filter. Microscopically these fibres are Y shaped [4] and the fibres as used in this test are shown in Figures 1 and 2.

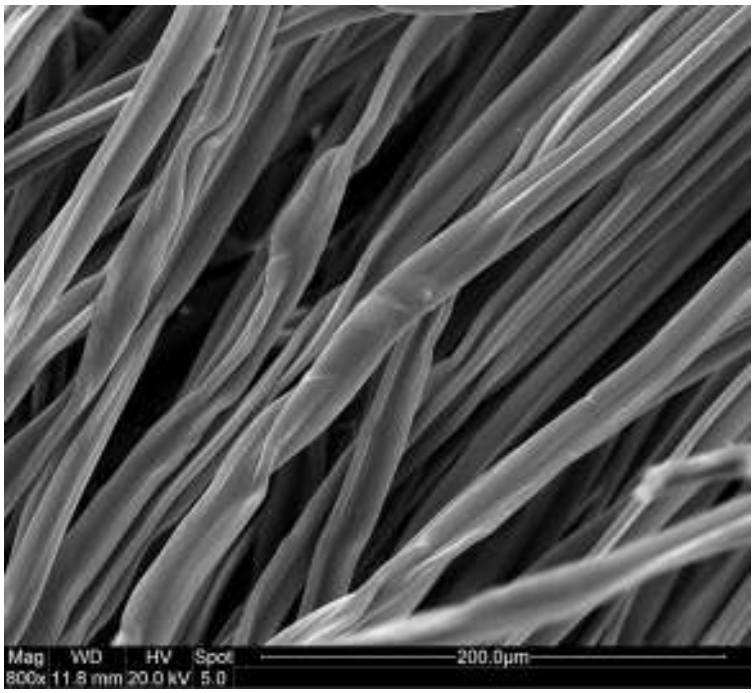

Figure 1 Cigarette filter fibre (800x magnification) – source Northumbria University laboratory

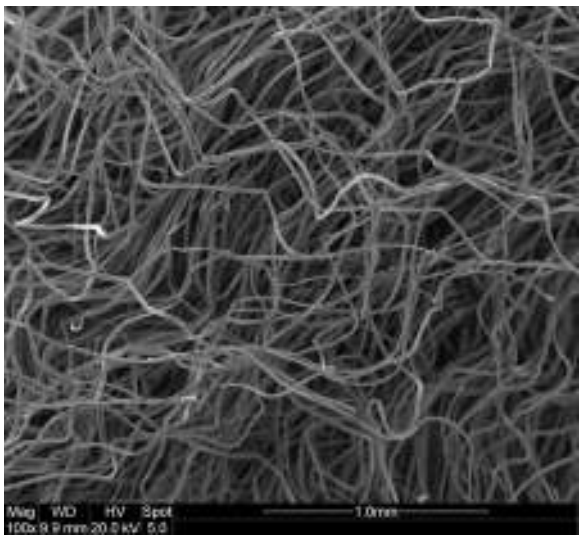

Figure 2 Cigarette filter fibre (100x magnification) – source Northumbria University laboratory.

The cigarette fibres were teased apart to separate the filter material prior to being added to the concrete mix to allow the individual stands to be coated and react with the cement paste. Fig 3 illustrates the Energy Dispersive Spectroscopy (EDS) image analysis of cigarette filter which shows the main chemical constituents as being carbon and oxygen.

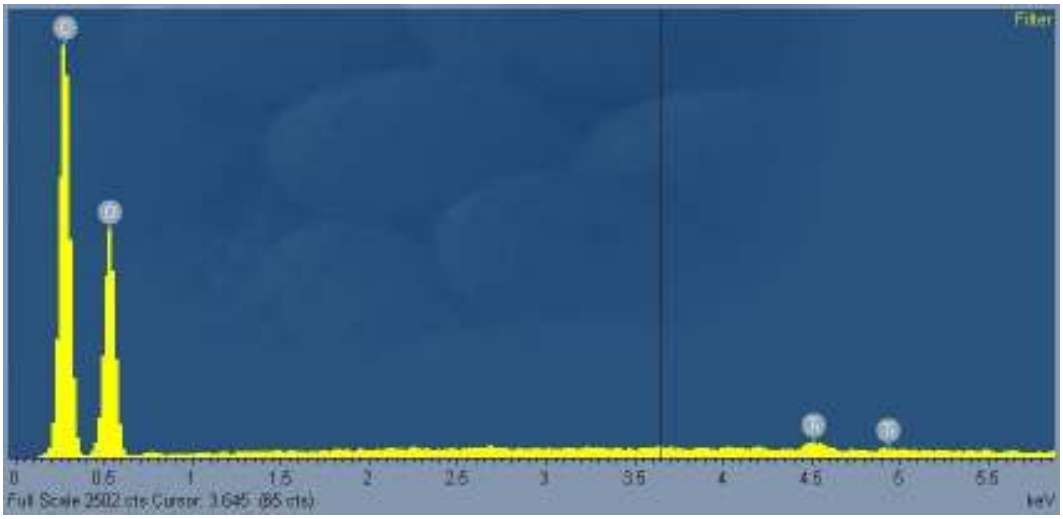

Figure 3 EDS Image of cigarette filter – source Northumbria University laboratory

Shrinkage Cracking

Shrinkage of concrete is the movement or strain due to thermal contraction or long term drying shrinkage. Some high strength concretes are prone to plastic shrinkage, which occurs in freshly placed concrete which has not set and it may result in significant cracking during the setting process. Since the bond between the plastic concrete and reinforcement has not developed, the reinforced material in the concrete would not be effective enough in

controlling such cracks [5]. Where there are different moisture contents between cover and heartcrete, tensile forces will develop and produce fine cracking of the concrete with a resultant reduction in surface durability and resistance to the elements". Non fibrous concrete usually cracks when the evaporation rate is greater than 0.0681 kg/m^2, polypropylene fibres reduce cracking in the range of 90 - 100% and reduce the water permeability between 34 - 75% [6] by interfering with the normal bleed channels and capillaries that are initially formed in the plastic state. According to Vondran and Webster, [7] "Fibres apparently have a log jamming effect on the pore structure that reduces the water flow", and this aspect is a consideration for further research to determine what fibre dosage and what fibre type have the best effect.

EXPERIMENTAL METHOD

In order to study the effect of the fibre on the concrete, three types of concrete were manufactured and tested for, surface cracking, and bleeding. The four cubes and two beams were cast and placed in front of a blown air heater. Whilst the beams and cubes were setting they were subjected to a hot air flow for 6 hours. The next day the concrete was checked for cracks with an optical microscope. The main aim of this experiment is to provide details of the early age surface shrinkage cracking.

Mix Design and Materials

A normal C40 concrete mix was chosen as it is a structural concrete that is widely used throughout the industry. The C40 design mix used is shown in Table 1.

Table 1 C40 Mix Design

MATERIAL	**QUANTITY kg /m^3**
Cement (CEM1- Ferrocrete)	403
Sand (0-4mm)	837
Aggregate (4-10mm) and (10-20mm)	336 and 621
Fibres 20 mm long (both)	2

The total of large aggregate within the mix was kept to a minimum to prevent aggregate segregation during the plastic phase. The water cement ratio was 0.45. Figure 4 illustrates the test program for this research.

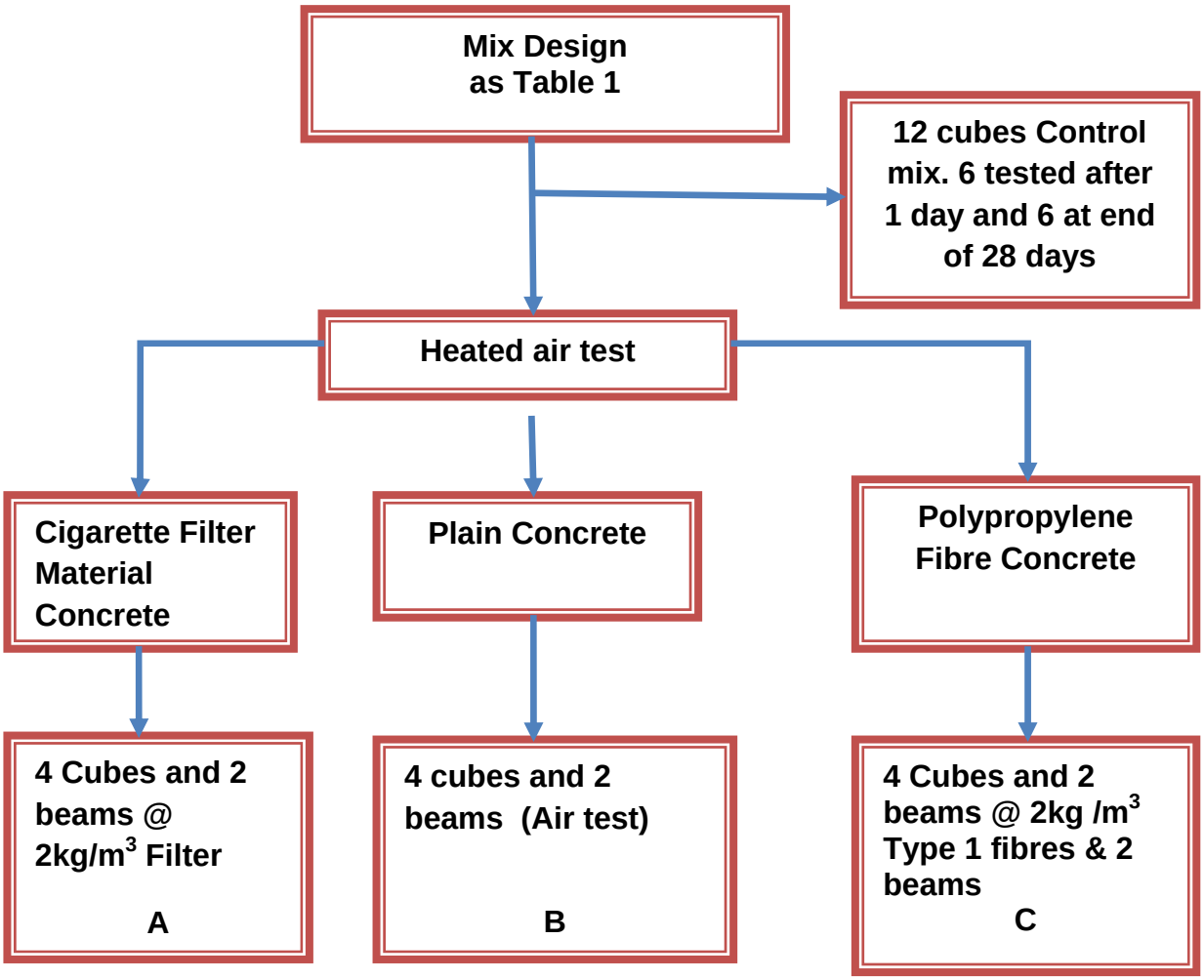

Figure 4 Test programme

Drying Shrinkage Test Method

The drying shrinkage test was conducted as described in Figure 5. Cast the beams and cubes and start heater once the slab is towelled and leave for 6 hours with the blown air heaters on. The heater was positioned 600 mm from the nearest cube. The next day the cracks were measured with an optical microscope (Surveying type). Compressive strengths were taken at 1 day and 28 days. Conclude as to the effect of fibres with regard to drying cracking compared to plain concrete.

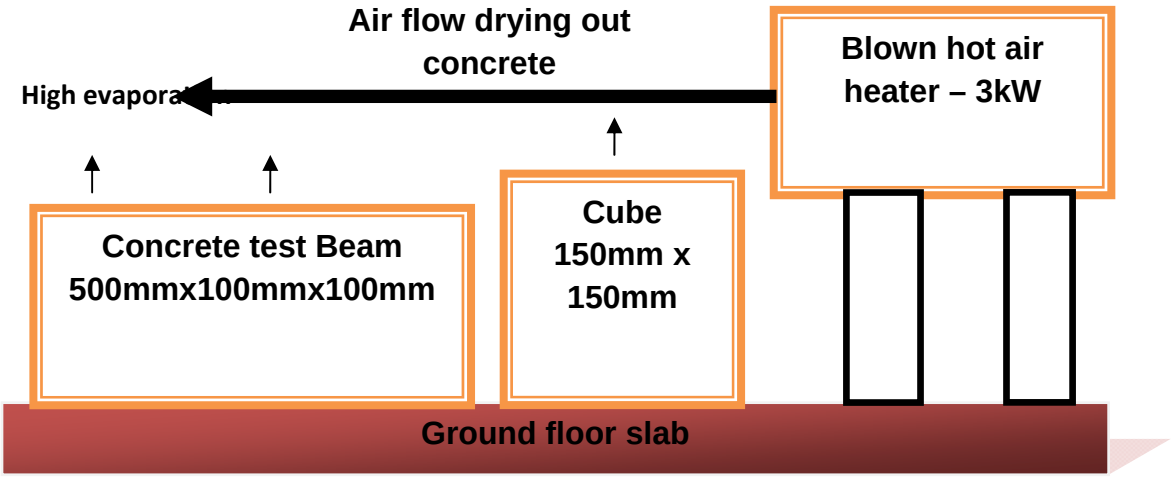

Figure 5 Test method for drying shrinkage

RESULTS

The slump for the plain concrete was 70mm whereas the fibre concrete produced a slump of 20 mm. The concrete test showed that there was not a great deal of shrinkage cracking on the surface of the concrete between 1 and 28 days. The cracking was not significant and the main reason for this was the low water cement ratio and saturated aggregates.

Fig 6 – Fig 8 shows the images of shrinkage cracking which was taken with a crack detection microscope (CDM). The greatest degree of shrinkage cracking was observed mainly on plain concrete with 15% more cracks being observable when compared to the fibre concrete. The cracking was of a greater width than the fibre concrete.

Shrinkage cracking which occurred was barely noticeable with the naked eye and it was only defined with crack detection microscope (CDM). This microscope is a high definition instrument which is operated with an adjustable light source. Measurement of the surface cracking was a superficial means of comparing data as no account was taken of crack area or depth, the frequency of the crack occurrence was the main characteristic measured.

Figure 6 Shrinkage cracking on cigarette filter concrete

Figure 7 Shrinkage cracking on polypropylene fibre concrete

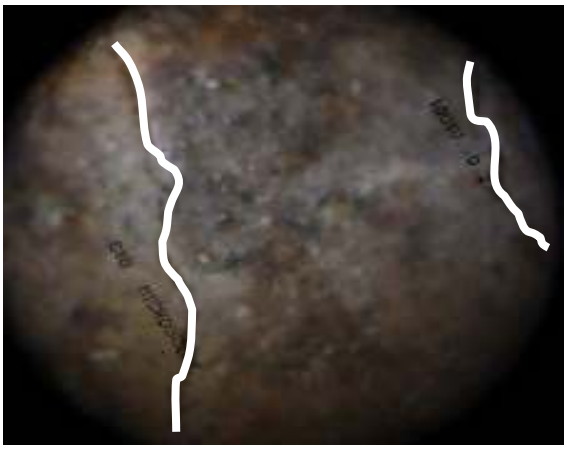

Figure 8 Shrinkage cracking occurrence on plain concrete

The compressive strength was determined at 1 day and 28 days using the control cubes and the respective strength was 6 N/mm^2 and 45 N/mm^2 which represents the early and part cured strength which was as the original design mix. The average compressive strength of the cubes subjected to the hot air flow was plain 35 N/mm^2, Type 1 polypropylene fibre 37 N/mm^2 and cigarette filter fibre 38 N/mm^2.The strength reduction compared to the control samples was 22% for plain concrete, 18% for polypropylene concrete and 16% for cigarette filter material. Given the variable nature of concrete it is not possible to say whether or not the fibres had a beneficial effect, however a 16 to 22 % strength loss shows that when concrete is subject to hot curing conditions with an air flow over the surface, measures must be taken in addition to fibre inclusion to ensure correct curing to enable the achievement the design strength.

CONCLUSIONS

The nature of the test was to impose severe curing/drying/setting conditions that should cause a great deal of distress to the concrete and the surface cracking created by these conditions was not found to be as great as expected. The inclusion of both polypropylene and cigarette filter fibres improved the drying shrinkage cracking performance of concrete. There was a 15% improvement in the fine drying shrinkage cracks with the use of fibres. The heat cured compressive strength results showed a strength reduction due to drying cracking that indicated internal cracking that cannot be seen. The identification of cracks only looked at the surface opening length. Depth, width and length should be quantified but this was beyond the scope of this preliminary study that may be used to inform a larger investigation. The test only considered one water cement ratio and one strength class and the concrete was batched very consistently which reduced the size and number of propagated cracks..

REFERENCES

1. DAVE U AND DESAI Y M, (2008), “Interaction between temperature and sulphate effects on polypropylene FRC”, Dundee Conference Proceedings, Harnessing Fibres for Concrete Construction, Ed Dhir R, Newlands M, McCarthy J and Paine K, UK pp 353 – 364
2. BILLMEYER, JR, FRED W, (1984), *Textbook of Polymer Science*, 3rd Edition, John Wiley and sons, UK, p 11
3. BROEN R, SHUKLA A, AND NATARAJAN R, (2002), “Fibre reinforcement of concrete structures”, *University of Rhode Island Transportation Center*, URITC PROJECT NO. 536101, USA
4. PAULY J L MEPANI A, LESSES J D, CUMMINGS K M, STRECK RJ. (2002). “Cigarettes with defective filters marketed for 40 years: what Philip Morris never told smokers”. *PMJ Journal. 11,* pp 84-86.
5. GILBERT R I, (2001), “Shrinkage, Cracking and Deflection-the Serviceability of Concrete Structures”, *Electronic Journal of Structural Engineering,* Vol. 1, No.1 pp 2-14
6. MATHER K & B, VONDRAN G, MEYER I A, (1987), *Concrete Durability, International Conference,* Volume 1, American Concrete Institute, USA, pp 21, 50-53, 63, 377-384, 820-821.
7. VONDRAN G AND WEBSTER, (1997), “The Relationship of polypropylene fibre reinforced concrete with regard to permeability”, *ACI*, USA.

Theme 2 — Efficient and Sustainable Use of Resources

Meeting the Challenge of Efficient and Sustainable Resource Use

T A Harrison
Private Consultant, France

As concrete is the most widely used construction material in the world, producing concrete from sustainable resources is essential. From a resource viewpoint the rock to make aggregates and the limestone and clay to make Portland cement are sustainable, but any fossil fuel used in their production is not sustainable nor is the use of GGBS or coal-based fly ash as they will depend upon the production of iron from iron ores and the burning of coal to produce power and the existing stockpile of fly ash. An environmental indicator is under development that measures the sustainability of the resources used over the lifecycle in terms of availability to future generations. Fossil fuel use has the biggest impact on this indicator for the material concrete and this in turn is dominated by the Portland cement clinker content of the concrete. However concrete with low PC clinker contents tend to have higher rates of carbonation. Optimization of performance can only be achieved if we develop the technical tools that allow durability to be specified by performance. Utilizing the thermal mass of concrete will save energy during the in-service phase of life and this can lead to significant savings over the lifecycle and therefore resource use must be considered over the full lifecycle.

Professor Thomas A Harrison is a Private Consultant in France, serving on numerous standards committees as well as a visiting industrial Professor to the Concrete Technology Unit, University of Dundee, UK

Keywords: Durability, Energy, Performance specification, Resource use, Sustainability

INTRODUCTION

The word ‘sustainability’ is the new buzz word and rightly so. However too often two of the pillars of sustainability (the social and economic pillars) are quickly forgotten and the focus is placed entirely on the environmental pillar of sustainability and on products. This is understandable as issues such as climate change, resource depletion and loss of bio-diversity are crucial issues for society to resolve. Such issues are also easier to understand and have a firm view upon. Compare this with trying to decide if it is better to use products that employ local people and use industries that pay taxes into the local economy, e.g. ready-mixed concrete, or better to create jobs in poorer countries to help raise their standard of living?

Fortunately the developments in Europe under CEN Technical Committee 350: Sustainable construction, are going in the right direction. It is developing in parallel standards for the three pillars of sustainability and focusing on sustainability over the life cycle. There are both technical and practical limits on what can be achieved at present. The technical limits include the lack of agreement on suitable indicators, e.g. bio-diversity, and the practical limits include the lack of agreement on combining all these indicators into a single value (as this is a subjective judgement, agreement is not going to be easy).

The development of more sustainable concrete construction cannot be at the cost of having structures that are not durable. The specification for durability is empirical and based on limiting values, e.g. maximum w/c ratio, and this provides a significant barrier to producing the most sustainable concrete. Such empirical specifications also create risks. For example a ‘green’ concrete with the binder comprising 40% fly ash and the coarse aggregate comprising 50% recycled concrete gave carbonation depth higher than ‘normal’ concretes and when the data are extrapolated, these concretes are not expected to achieve the intended service life [1]. Concrete with 40% fly ash and normal aggregates performed adequately.

RESOURCES USED ON CONSTRUCTION

The resources used in construction comprise materials, energy, water and land. Construction is the largest user of materials and fortunately many of these materials are common and will be available to future generations.

Energy is a serious issue. Burning fossil fuels is the main cause of climate change and the main impact in the University of Dundee’s resource indicator [2]. When used as fuel there is zero recycling potential. Bio-fuel is no answer due to the land requirements and in the developed world there is not too much scope for further hydroelectricity generation. In the future solar, tidal, wind and nuclear energy will have to replace fossil fuels, but the main drive has to be to reduce energy consumption. The role of concrete in reducing energy consumption is described later in this paper.

Water is also a key resource. The University of Dundee’s resource indicator includes water that is used in the product and process water that is not returned directly to the water system. For biotic resources water supplied directly by nature is not included but water used for irrigation is included. Over the lifecycle of a building, water used during the in-use phase is likely to dominate the water use and it can be argued that the designer has no real control over this use.

However given the system boundaries, Figure 1, water efficient appliances will show no benefit. For example, nearly all of the water used in a shower is returned to the system and the net water use is small regardless of how efficient are the showers. Water efficiency in the in-use phase of life is best addressed by requirements on the efficiency of appliances and by pricing.

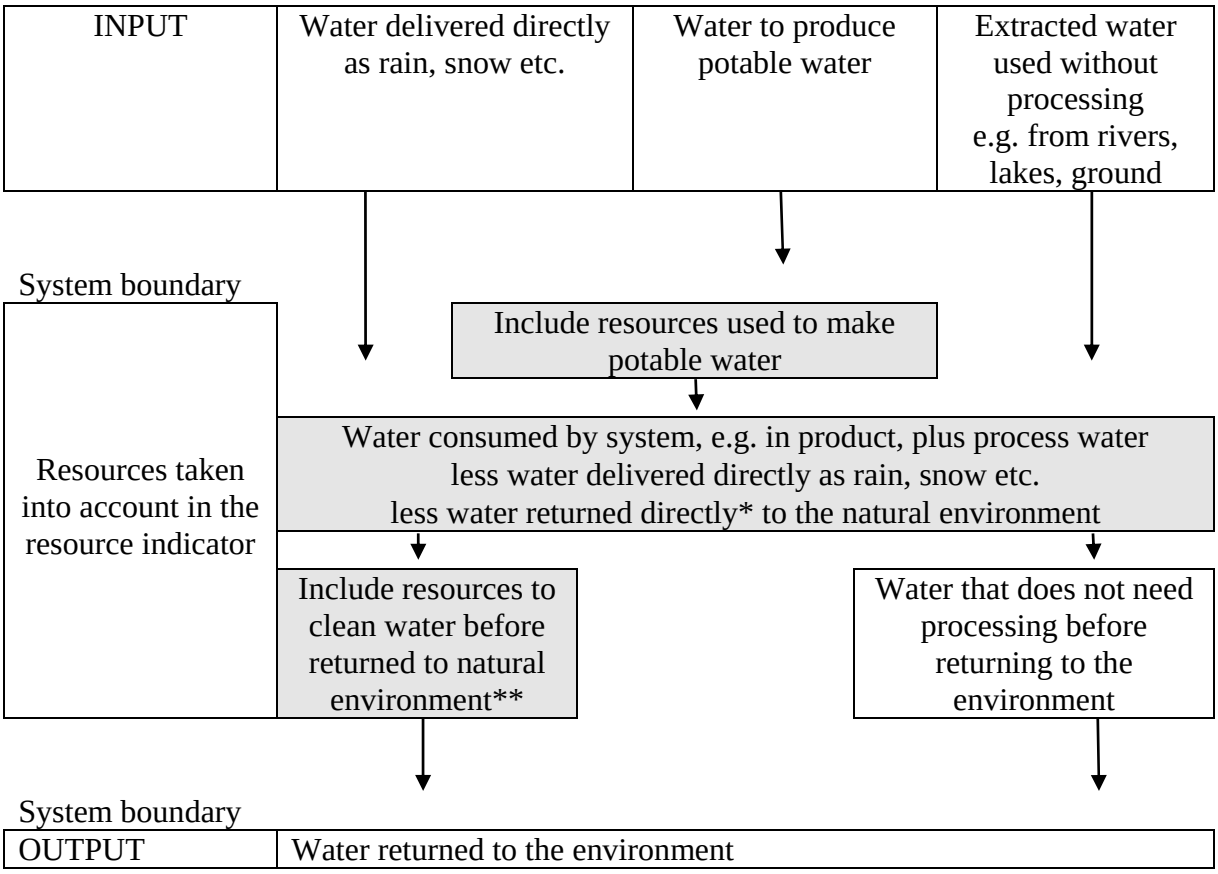

* This excludes water that is evaporated and water lost into the ground as the link to the local water cycle is tenuous.

** Excluding the resources needed to turn this returned water into potable water.

Figure 1 System boundaries for the resource, water [2]

Land use is often a resource that is overlooked when comparing solutions. Urban development is often on the best farmland. There is only 2.5 million square miles of tropical rainforest left and this is being depleted at a rate of 93000 square miles per year [3] mainly to provide bio-fuels, bio-feedstock for animals, mining and urban development. While a mine itself may take relatively little land, the land needed for access roads and land kept clear around power transmission lines can be substantial. According to the Friends of the Earth, Europe imports 350 million hectares of virtual land per year, i.e. this is the land used to provide the goods exported to Europe. The bulk of this land is used to provide food, clothing and animal feeds [4], but some is directly linked to products used in construction.

SUSTAINABLE STRUCTURES (BUILT WITH CONCRETE)

When taken into account during the design phase, the thermal mass of concrete can be utilised to reduce the energy required to cool or heat a building [5-7]. Put simply this is the fly wheel effect. If the mass of concrete is heated by the sun/air during the day, it will release this heat during the evening saving on heating costs. Alternatively cold air can be pumped through concrete during the night reducing the energy needed for air conditioning. Given the fact that the design life of buildings is in decades, the saving in energy can be significant when considered over the life cycle.

When designed and constructed correctly, concrete structures are durable. However there are limitations as to what concrete quality and cover to rebar can achieve and in special cases additional methods are required (e.g. stainless steel rebar, coatings and linings, cathodic protection, design for replacement).

The main cause of poor durability of reinforced concrete structures remains the lack of the specified cover. The concrete Eurocode [8] clearly shows that an allowance for fixing tolerances needs to be added to the minimum cover required for durability and structural purposes. Using the recommended tolerances, it is possible taking reasonable care to achieve the minimum covers. It is also possible to check the cover before placing the concrete. These simple measures can eliminate the main cause of corroding rebar in modern structures.

With rare exceptions, concrete and its reinforcement can be recycled at the end of the life of the structure. The concrete may be crushed to provide aggregates and the rebar recycled. Coarse recycled aggregates may be used in some concretes. If it is used in proportions not exceeding 30% of the coarse aggregate, there is no consequential increase in cement content [9]. Clean fine recycled concrete is also suitable for use in concrete. However fine recycled concrete aggregate that is contaminated with gypsum plaster is not suitable for use in concrete [10] due to the risk of delayed ettringite formation.

FREEING THE MATERIAL ‘CONCRETE’ TO MEET THE CHALLENGES OF A SUSTAINABLE WORLD

While the demands for more sustainable structures are increasing, the traditional roles of concrete in providing adequate strength, inherent fire resistance and durability must never be compromised. Strength is unlikely to be compromised as this is specified and measured directly. Fire resistance will remain a fundamental characteristic of concrete with normal materials. The challenge lies in developing tools to measure durability directly and systems to ensure that this determined performance is being continually produced.

Perhaps at the risk of being controversial, service-life design is not the answer for normal structures. The natural environment (rainfall and relative humidity) at the location of a structure does not produce a constant rate of carbonation or chloride penetration; these vary widely. For example the average carbonation depth is not the same on each the aspect (north facing etc.) of a structure [11] and within each aspect there will be local microclimates. It would be a brave designer who designs on anything but a realistic worst case environment. However service-life design has an essential role in setting the framework within which performance criteria apply and in the calibration of the performance criteria that are being developed.

There is often a misunderstanding that the limiting value specifications given in national standards, e.g. maximum w/c ratio, given in the national provisions give a constant performance. This is not the case, see Figure 2. All the sets of constituents with solid lines conform to the BS 8500-1:2002 [12] recommendations for limiting values of minimum cube strength of 40 N/mm², maximum w/c ratio of 0.55 and minimum cement content of 300 kg/m³. The non-solid bars are for sets of constituents where recommendations on limiting values were not given in BS 8500-1:2002 (see [13] for details). For example neither w/c ratio, cement content, compressive strength or in any combination of these parameters, gives a consistent carbonation depth [1, 13] when considered over the range of permitted constituent materials. It is assumed that the worse set of materials gives an adequate performance, but this may not be true where sustainability drives the constituent selection [1].

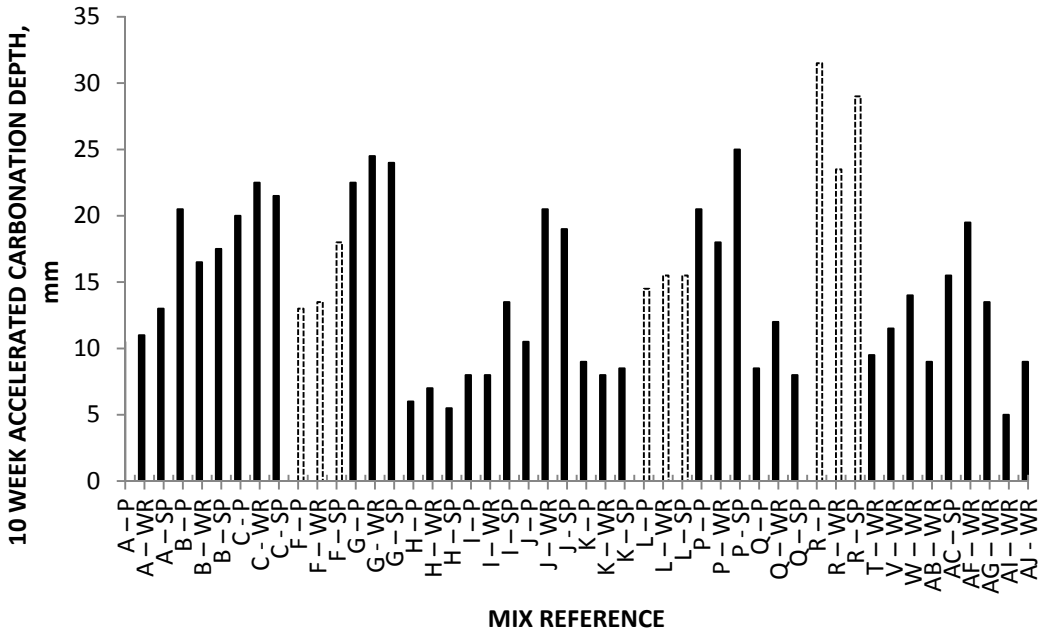

Figure 2 10 week accelerated carbonation depths (4±0.5% CO_2 55±5% RH, 20±2°C) for concretes satisfying 40 N/mm², 0.55, 300 kg/m³ [13]

Performance-related test methods have had a mixed history and a number of false starts. A few decades ago, permeability criteria were seen as the way in which durability could be ensured. Whilst these provided a measure of the inter-connected pore structure, they could lead to erroneous conclusions. For example with low permeability aggregates and a constant w/c ratio, as the cement content increases, the permeability increases and by implication, the durability decreases. However the durability does not change significantly with low water absorption aggregates [14] due to the fact that as the cement content increases the binding capacity increases and this offsets the increase in permeability. This generalisation is not true if the fines content (not necessarily cement) is insufficient to give a closed structure [14].

Performance-related tests for practical reasons have to be an acceleration of reality. Freeze-thaw tests use rapid extreme changes in temperature, carbonation tests increase the level of carbon dioxide and rapid chloride tests use an electric current to drive the ions. Even chloride diffusion tests at natural chloride concentrations only reflect the performance of the concrete at the age of testing. Over time the chloride resistance increases by a combination of hydration and surface skin effects [15].

Performance-related test methods take account of the actual concrete composition and factors not taken into account, or indirectly taken into account, by limiting value specifications, e.g. the effects of aggregate type, fines content and aggregate grading [13, 14]. Ranking of performance in accelerated tests is often similar to that obtained by long term testing, but the correlation between such test is often poor, see for example Figure 3. However specifying performance has the potential major advantage in that it frees the producer to design a more sustainable concrete while ensuring adequate durability.

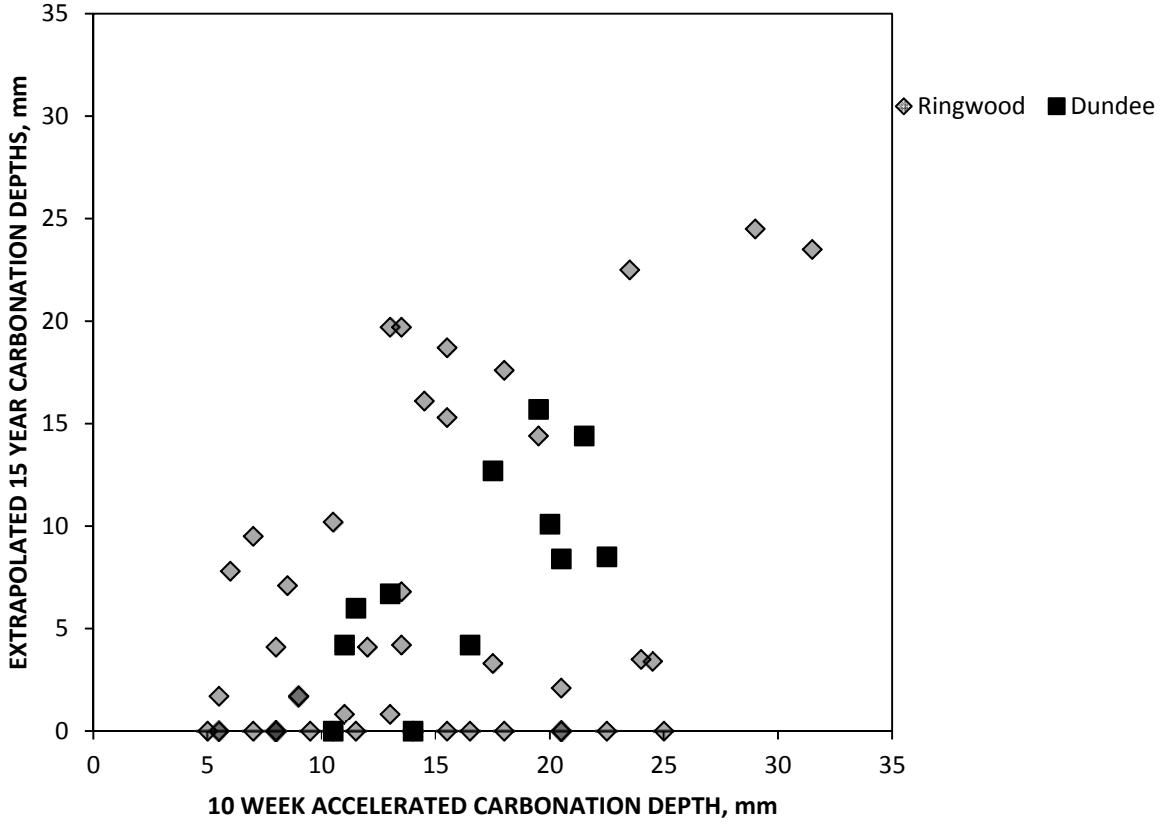

Figure 3 Comparison of 15 year normalised exposure site data with 10 week accelerated carbonation data (Exposure sites are at Ringwood and Dundee)

The author is the convenor of a European Task Group (CEN/TC104/SC1/TG17) that is attempting to produce a CEN Technical Report on the equivalent durability procedure. The equivalent durability procedure is an intermediate phase between limiting value specifications and a direct performance specification of durability. The concept is relatively simple. The performances achieved by concretes currently satisfying the local limiting value specifications are measured and from this range, a safe value of performance is selected. Any concrete that meets this safe value is regarded as having equivalent durability. Differences in ageing effects have to be taken into account and this is an area where there is no consensus at present. The concrete does not have to meet the local limiting value specification and once the mix is established, conformity is based on batching this or a safer mix. Changes to constituents from the same sources need to be controlled and one method for doing this is based on changes in strength. It was not possible to introduce this procedure into EN 206 [16] as it had been agreed that it would not be introduced until the associated test methods have

the status of a full European standards, i.e. they contain precision statements. There are also 'political' issues that slow progress. The cement and additions industries are reluctant to lose minimum cement/addition contents, the ready-mixed industry do not want a more complex procedure (life is very simple and almost risk free with limiting values) and contractors do not trust anything developed by material specialists. However there are people in all these industries who accept that the present largely empirical approach has to be replaced with a performance-based approach.

The differences between the equivalent durability procedure and a direct performance specification are in the values specified and in changing limiting values to a deemed-to-satisfy solution. This is best illustrated with an example. Table 1 gives the range of 10 week accelerated carbonation depths for a wide range of normal concretes [17].

The range of constituent materials included in the data set includes cement types of CEM I, CEM II (up to 30% fly ash, including conditioned fly ash, 10% silica fume and 15% metakaolin, 15% limestone), CEM III/A (up to 55% GGBS), a range of ternary cement concretes (with CEM I content as low as 50%), coarse aggregates with absorption values ranging from 0.7% to 3.6% (lightweight aggregates were not included), recycled concrete aggregates (up to 50%). Data from the extremes of composition, e.g. very low fines content, low fines to coarse ratio or high CEM I replacement with high absorption aggregates are not included.

Table 1 Range of depths of accelerated carbonation for 'normal' concretes used in the UK

10 WEEK ACCELERATED CARBONATION DEPTHS	W/C RATIO				
	0.45	0.50	0.55	0.60	0.65
Number of data	44	48	40	33	129
Maximum value, mm	12.7	17.5	16.5	25.0	36.5
Lowest value, mm	0.5	3.5	7.5	7.5	11.5
Average value (ACD10, av), mm	8.0	10.5	11.5	15.0	20.5
Standard deviation, mm	3.5	3.0	2.0	5.0	5.0
Coefficient of Variation, %	43	28	17	33	24

Great care needs to be taken when setting performance criteria. If the benchmark is successful performance in practice, the criteria should be based on the average concrete used in practice and not concrete just meeting the limiting values. Criteria that eliminate a large proportion of the concretes currently accepted and for which there is no evidence of inadequate performance will be unacceptable to industry.

Finding the right balance will not be easy. A slight worry without evidence that they do not perform adequately is that these performance criteria could be achieved with a CEM I concrete with relatively high w/c ratios. In Table 1 the lowest carbonation depths are with CEM I concretes. There is significant overlap in the ranges with a CEM I concrete at a w/c ratio of 0.65 performing better (11.5 mm) than a CEM I/30%FA/3.5%SF concrete at a w/c ratio of 0.45 (12.7 mm).

ACHIEVING MORE SUSTAINABLE CONCRETE

The largest negative contributors to the sustainability of concrete are the impacts on global warming and resource use. Figure 4 (based on [18]) shows the embodied carbon dioxide of constituents. This is not the same as the global warming potential as it does not, for example, include the energy used to mix the concrete. This energy use is unlikely to change significantly with different mix types and so it is not an option for the producer in the quest to produce more sustainable concrete.

Figure 4 shows that the main way of reducing the embodied carbon dioxide is to reduce the PC clinker content. The impacts of resource use are different [2], Figure 5. In this case it is the aggregates that dominate. While the weighting given to aggregates is the minimum value, the volumes are large and this is the reason why it is the major impact. This same minimum weighting is given to recycled aggregates.

The resources used to process and transport aggregates are the same regardless of whether they are primary or secondary materials and as the resources themselves have the same weighting, the lowest impact will depend upon the impacts of processing and transporting. The second largest resource impact comes from the Portland cement. While the volume used per cubic metre is not large, the short residual lives of the fossil fuels used to produce PC clinker and consequential high weighting push up the impact.

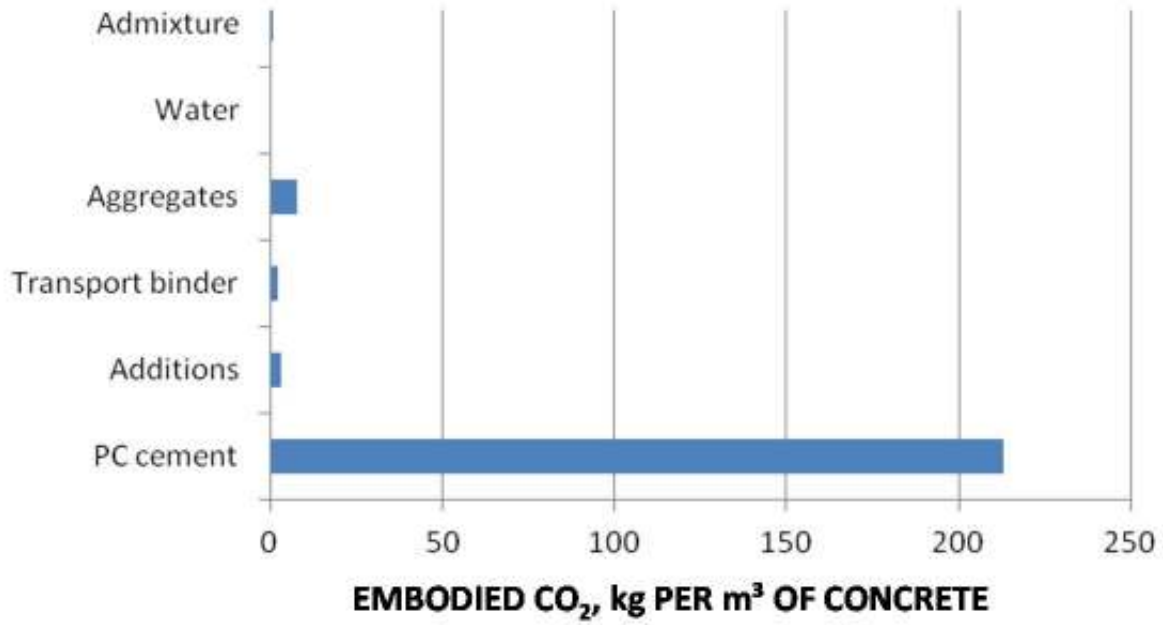

Figure 4 Embodied carbon dioxide per cubic metre of average UK concrete

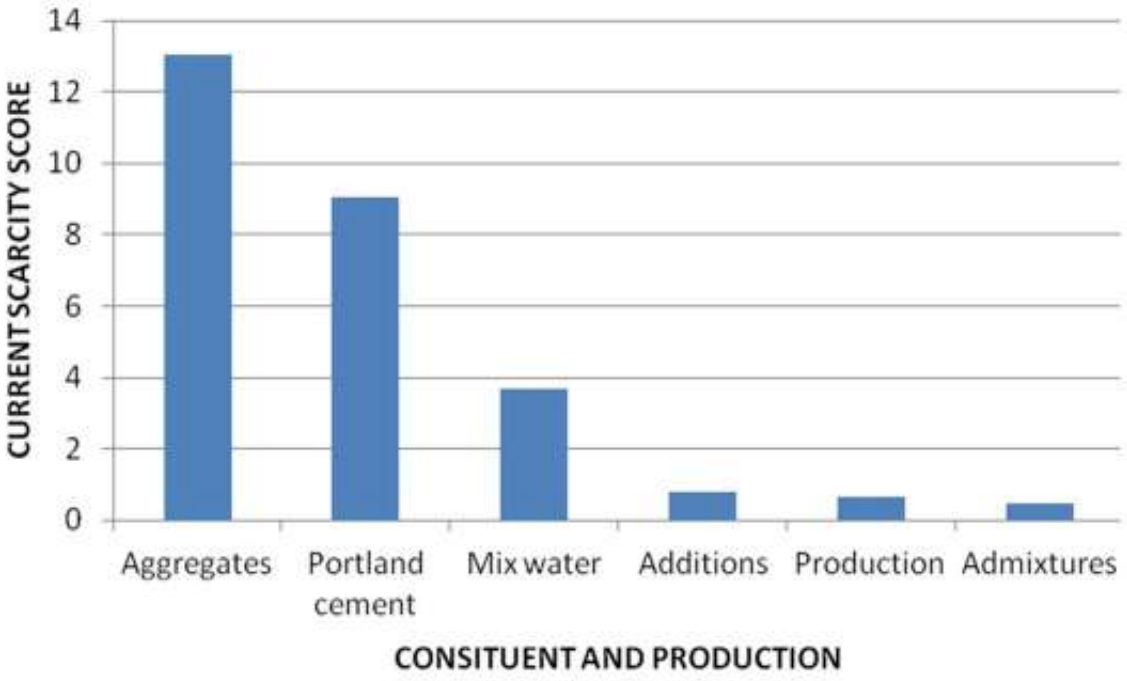

Figure 5 Resource use per cubic metre of concrete

The analysis above shows that if the sustainability of concrete is to be improved, reducing the Portland cement clinker content has to be the prime target. This may be achieved by the selection of cement type or by the use of additions. However the k-value concept in prEN 206 [16] requires significant increases in cement content when additions are used but not when the 'addition' is part of a cement. However prEN 206 also permits the use of performance concepts for additions and these should be used if the objective is to provide a more sustainable concrete.

A limiting value specification, maximum w/c ratio etc., may also be a limitation on achieving a more sustainable concrete. Specification of durability by performance must be the ultimate objective. Good progress is being made, but we have to proceed with caution and with incremental changes.

CONCLUSIONS

1. Current limiting values specification may not lead to adequately durable concretes.

2. Sustainability must be assessed over the life-cycle and include the environmental, social and economic pillars.

3. While construction is the largest user of minerals resources, many of these resources are available to future generations.

4. The thermal mass of concrete should be utilised to reduce the energy demand during the in-use phase of life of a building.

5. Concrete and rebar are recyclable at the end of their life in a structure.

6. Limiting value specifications do not lead to a consistent performance.

7. The natural environment is not a constant and even within a single structure, the ingress of aggressive species will vary widely. Consequently durability design has to be robust.

8. The standardization of performance-related test method is in progress, but there is still work to be done before criteria can be set with confidence.

9. The most effective way of improving the sustainability of concrete is to reduce the Portland cement clinker content, but this must not be at the cost of durability.

REFERENCES

1. HARRISON T, JONES R, KANDASAMI S AND KHANNA G, Effectiveness of the traditional parameters in specifying carbonation resistance, Magazine of Concrete Research, Vol. 64, No. 1, 2012.

2. HARRISON T, JONES R, DYER T AND HALIDAY J, A tool for reporting resource sustainability, http://www.snr-project.org/.

3. BAGHEERA, Tropical rain forests, http://www.bagheera.com/inthewild/. Accessed November 2011.

4. FRIENDS OF THE EARTH, measuring our resource use - A vital tool for creating a resource-efficient EU, April 2010.

5. PORTLAND CEMENT ASSOCIATION, Thermal mass, Concrete thinking for a Sustainable world, http://www.concretethinker.com/solutions/Thermal-Mass.aspx. Accessed 28 December 2011.

6. THE CONCRETE CENTRE, Thermal mass for housing - Concrete solutions for the changing climate, ISBN 1-904818-42-0, 2006, 25 p.

7. THE CONCRETE CENTRE, Thermal mass - A concrete solution for the changing climate, ISBN 1-904818-13-7, 2005, 25 p.

8. BRITISH STANDARDS INSTITUTION, Eurocode 2: Design of concrete structures – Part 1-1: General rules and rules for buildings, BS EN 1992-1-1:2004

9. DHIR R K, LIMBACHIYA M C AND LEELAWAT T, Recycled concrete aggregate for use in BS5328 designated mixes, DETR Research contract 39/3/327, January 1998.

10. DHIR R K, LIMBACHIYA M C AND BEGGS A, Resolving application issues with the use of recycled concrete aggregates, DETR Research contract 39/3/478 (CC1697), March 2001.

11. PARROTT L J, A review of carbonation in reinforced concrete, C&CA, July 1987.

12. BRITISH STANDARDS INSTITUTION, Concrete — Complementary British Standard to BS EN 206-1 — Part 1: method of specifying and guidance for the specifier, BS 8500 1:2002.

13. KANDASAMI S, HARRISON T A, JONES R AND KHANNA G, Benchmarking UK concretes using an accelerated carbonation test, Paper accepted for publication in the Magazine of Concrete Research, 2011.

14. DHIR R K, TITTLE P A J AND McCARTHY M J, Role of cement content in the specification for durability of concrete, BSI Research Contract 33/3/16 (CC 1629), May 2001.

15. HELLAND S, Ageing factor concept - Chloride Intrusion, Nordic Exposure Sites, Input to revision of EN206-1 Workshop proceeding from a Nordic miniseminar, Hirtshals, Denmark, November 2008, pp. 37-59. ISBN 978-82-8208-013-2.

16. BRITISH STANDARDS INSTITUTION, Concrete — Specification, performance, production and conformity, draft EN206 sent for public comment in the spring 2012.

17. HARRISON T A, JONES M R, NEWLANDS M D, KANDASAMI S AND KHANNA G, Experience of using the prTS12390-12 accelerated carbonation test to assess the relative performance of concrete, Paper accepted for publication in the Magazine of Concrete Research, 2011.

18. THE CONCRETE CENTRE, Embodied CO_2 of UK cement, additions and cementitious material, Fact Sheet 18, undated.

The Need for Technology Transfer for Revitalized Health Safety & Environment (RHSE) in Concrete Construction: A Case of the Great Man Made River in Libya

M S Tughar
Al Mergab University, Libya

The Libyan concrete construction in Water supply industry produces Million of tonnes of concrete products annually, worth an estimated cost which is roughly equivalent to the turnover of the cement and ready mix concrete industries in the country. After the wealth of experiences from concrete in Great Man Made River (GMMR) authors have developed Health Safety & Environment Management (HSEM) framework strategy and plan of action herein called as 'Revitalized' Health Safety and Environment (RHSE) to improve health safety and environment associated with concrete production, transportation, placement and compaction. The paper presents the interesting case study results to demonstrate that how new framework is capable of helping the new NTC authority in new Libya responsible for the Health Safety & Environment (HSE) management by putting an effective system, into managing health safety & environment impact and combat risks associated with climate change.

Dr. Muhieddin Saleh Tughar recently is an Associate Professor and Head of Department of Civil Engineering at Al Mergab University, Libya. He is a member of IABSE, International Association of Bridge and Structural Engineering. His area of interest is in concrete materials research, evaluation of existing structures, including investigation of structural problems, and in supervision on concrete repairs.

Keywords: Case study, Concrete products, Construction, HSEM-Revitalized Strategy, NTC of Libya, Water supply

INTRODUCTION

Rebuilding new Libya 2012 is a significant challenge for the Libyan National Transitional Council (LNTC). This is of interests to the decision makers, governmental sectors worldwide to participate in reconstruction of projects of Libyan which covers their immediate and urgent needs during the upcoming three years and this worth tens of billions US Dollars. The what so called costly Great Man-Made River (GMMR) done by the old regime in Libya as a case represents the most important international engineering project to bring water from aquifers beneath the Sahara and conveying it along a network of huge underground concrete pipes to the northern coastal belt to provide water to the country's 5.8 million people living in the inhabited fertile, coastal areas for municipal, industrial and agricultural use. The objective is to achieve self-sufficiency, food security and true independence, however practically none of this happened or achieved in time of the gone dictator-ship. It is only reported as an outcome of a triumph story against thirst and hunger.

It is a defeat against ignorance and backwardness (that’s propaganda for a person who claims engineered this project?!). Never the less, the fact is Libya has a complete "absence of permanent rivers or streams" – and it has "approximately twenty perennial lakes that are brackish or salty. The country bears the distinction of holding the world record for hottest recorded temperature (58°C) [10-14]. It has four major underground basins, viz. Kufra basin, the Sirt basin, the Morzuk basin and Hamad). Between 38,000 and 10,000 years ago the climate of North Africa was temperate, during which time there was considerable rainfall in Libya. The excess rainfall infiltrated into porous sandstone and was trapped between layers, forming reservoirs of underground fresh-water. The Libyan climate ranges between Mediterranean to arid and semi-arid. Rainfall ranges from 10 to 500 mm/y.

This GMMR mega construction project of Libya is planned way back in 1960 to serve as the largest water transport project ever undertaken and rightly described as the "eighth wonder of the world". It is a network of 1900 km long pipes (Figure 1) that supplies water from the Sahara Desert in Libya to the northern part.

It is the largest underground network of over 500,000 pre-stressed concrete pipes and aqueducts in the world. The pipes were required at rates of up to one per production line every 15 minutes; five production lines were needed, each 2.5 kilometers long and one kilometer wide. The manufacturing plants were designed and constructed by Price Brothers and were commissioned in 1986.

It consists of more than 1,300 wells, more than 500 m deep, and supplies 6,500,000 m^3 of fresh water per day to the cities of Tripoli, Benghazi, Sirte and others. The total cost of the huge project is over $25 billion (US). Brown & Root and Price Brothers gave the original design, and the primary contractor for the first phases was Dong Ah Consortium (a South Korean construction company) and present main contractor is Al Nahr Com. Among the Western firms that have been involved in the project are Franken Hal KSB Fluid Systems of Germany and Nippon Koei-Halcrow consortium.

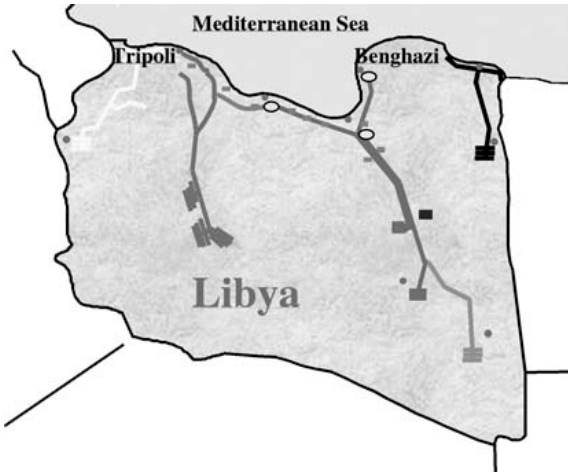

Figure 1 GMMR Concrete pipe line network

Each pipe of the river project is buried in a trench approximately seven meters deep, excavation of which requires the removal of some 100,000 cubic meters of material each working day. Excavation is carried out by large hydraulic excavators fitted with 7.6 cubic metre buckets. Once the trench has been prepared, prestressed concrete cylinder pipes 7.5 meters long (Figure 2) and weighing up to 80 tons are brought to the site using a fleet of some 128 specially designed transporters (Figure 3).

The concrete required for the GMMR project could construct a path to the moon! The prestressing wire needed could encircle the earth over 280 times. The transporters for the pipes would travel a total distance that reaches the sun and back!! It should be mentioned here for one reason or another that there is a running debate in the NTC of Libya about the economic visibility of GMMR multi-mega project and some silent views on the other alternatives for the country water supply were currently has been risen? [1-16].

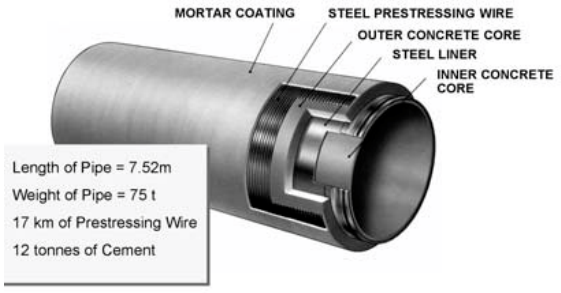

Figure 2 Cross section of pipe

Analysts say that the $25 billion groundwater extraction system is ten times cheaper than desalination, but according to University of Victoria researcher Stephen Lonergan, the aquifer — the largest in the world — could be depleted as soon as 60 years from now (this estimate stands in stark contrast to the like the rule of Libya's Fashionista Dictator & the gone Old Regime of Libya claim that supplies will last for 4,625 years)!

The Great Man-made River Project, which was only completed a few years ago, produces 6.5 million cubic meters of water per day, but the resource is not renewable?! [9].
Concrete is used because of:

- Good corrosion resistance
- Widespread availability
- High strength
- Good load supporting capacity.

In addition, concrete is a value-for-money bulk stiffness provider and for an extended design life, particularly where water exposure is concerned, this is a construction material which improves with age. However bearing in mind the disadvantages it requires careful installation to avoid cracking since it is heavy and susceptible to attack by H_2S and acids when pipes are not coated. It involved improved pipe manufacturing process that include incorporating styrene butadiene latex in sprayed mortar to increase consolidation and reduce absorption, and the pre-coating of pre-stressing wire with sodium nitrite-based corrosion inhibitor. It led to constantly reducing reject rates, savings on material costs and an improved final product.

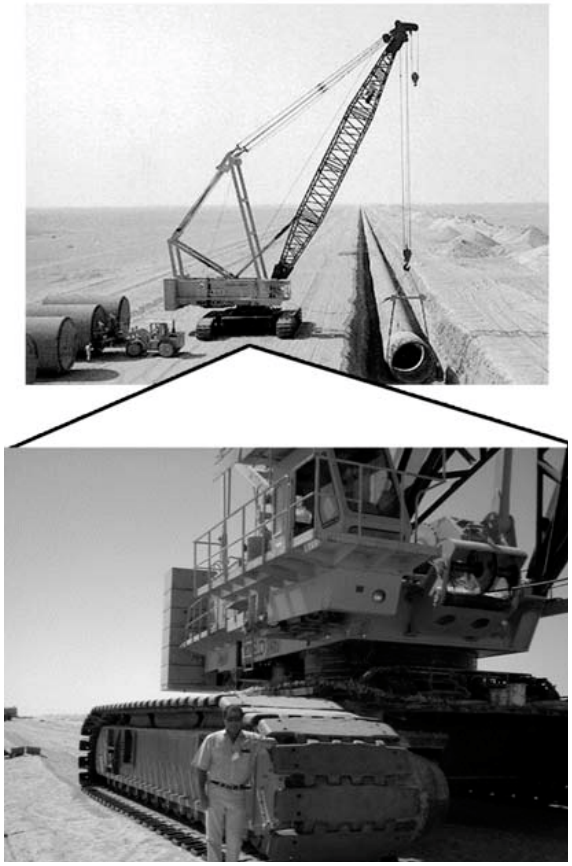

Figure 3 Pipe being lifted in to trench

The avoidance of sand-streaking (Figure 4) was achieved through more robust mix design with increased cohesion and lower slump but more importantly by educating and training site personnel.

Although the inner and outer concrete pipe walls were only 75 mm and 175 mm thick respectively, in situ temperature rises were significant. This was due to the inner pipe annulus being sealed by the top and bottom pallets to effectively provide insulation against heat loss. This became a problem when demoulding at night or in the cooler months. The effects were mitigated by:

- Depressing the initial concrete temperature by using ice
- Use of mist curing
- Use of thermocouples to monitor in situ, kiln and ambient temperatures
- Careful timing of kiln opening and demoulding.

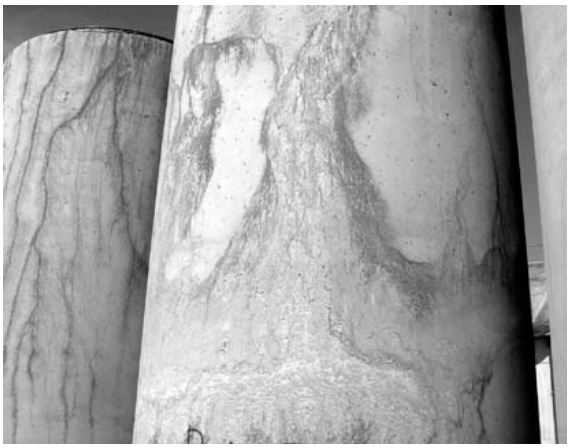

Figure 4 Sand streaked pipes

Occasionally, water spraying malfunctions would give localized rapid cooling leading to thermal cracking (Figure 5).

Management of health safety environment and economy due to energy and water saving for concrete construction are subject to maritime conditions unique to Libya that borders the sea and has 95% of hot and hostile desert area that poses a biggest challenge to concrete industry. This paper is aimed at assisting in HSE and economy by water and energy saving strategies for all those practicing professional including engineers concerned with the commissioning, design, construction or maintenance of concrete pipes for water supply and structures in or near the sea used for oil business in both MENA and Mediterranean countries. It also describes the nature of the marine environment and the effects of man-made concrete construction on the behavior of the sea. It deals with design of effective HSE and economy due to least water and energy requirements, the material properties of concrete and the design and specification of structures for coastal and desert environments.

The deterioration of concrete in coastal concrete pipes and structures is usually a result of lack of durability rather than overloading, so much of the paper is directed towards the production of durable concrete construction with least water and energy consumptions. Water supply related concrete pipes and structures management in coastal states predominantly deals with sustainable high performance of the pipe structures with HSE and economy resulting from least water and energy requirement. Sustainable concrete construction for water supply requires continuing commitment and action related to all matters pertaining to

health, safety, environmental protection and economy by all stakeholders at all levels of government, industry and the community. While there are regulations governing concrete pipe and related structure development, both the water supply and oil industry is being encouraged to adopt voluntary management procedures, such as using health safety environmental guidelines and economy with least water and energy requirement and codes of practice, rather than be strictly regulated. It is believed that self-regulatory techniques are likely to be more effective than statutory regulation in addressing specific environmental issues because they are flexible enough to adapt to changing circumstances. Also, the water supply and oil industry is more likely to take responsibility and ownership for any self-regulatory approach.

Figure 5 Thermal cracks

A number of market forces also encourage builders, developers and operators to make their venture sustainable requiring consideration of forces that include:

- increased consumer resistance to deteriorating structures and degraded environments
- evidence that sound health safety and environmental practices have long-term economic benefits with least water and energy requirement
- financial rewards and concessions for 'good' environmental practices
- fines for 'bad' environmental practices
- the likelihood of media exposure for 'bad' practice developments
- the growing demand for sensitive and innovative designs for developments in fragile environments.

Water supply and oil business development, that depends on the sustainable development of structures, can readily accept health safety least water and energy requirement, environmental, social and economic responsibility because such responsibility is vital to its

survival and growth. Like most economic activities, sustainable concrete structures use up materials and resources like water and energy and also creates waste products which have to be disposed of into the land, the air or the water, often creating pollution. As economic activity grows and expands, the readily available concrete structures, materials and resources get used up and the environment deteriorates as a result of the pollution.

It is also important to consider the social dimension of any development. Experience has shown that developments that do not involve consultation with local communities and special interest groups often result in costly and time-consuming litigation. This can lead to negative publicity and a community backlash against operations. So early and effective community consultation including consultation with Indigenous community groups, can not only decrease costs but also help to enhance community relationships and reduce the potential for least water and energy requirement and negative reactions to concrete construction.

REVITALIZING HEALTH SAFETY& ENVIRONMENT (RHSE)

Revitalizing health safety& environment (RHSE) is an initiative developed in new Libya to evolve an effective Health Safety and Environment (HSE) management strategy to improve health safety and environmental protection in all concrete construction works related to water supply and oil and gas sector in Libya. The initiative is in line with Libyan green and clean construction, green energy and economy presented elsewhere by one of the authors and good practices learnt from UK Safety Commission program launched on 7 June 2000 to target three elements: a set of improvement targets, a 10-point strategy and 44 action points to improve health and safety in concrete industry. This RHSE initiative is aimed at injecting new impetus into better health and safety in all construction related workplaces through:

- helping people at work to protect themselves and their business
- making work a better place to be
- helping stakeholders decide how to make their work safer and healthier.

The need to 'revitalize' health safety and environmental protection concerns in Libya has prompted the authors [1-16] to capitalize the experiences of Great Man Made River concrete construction and help planners, builders and decision makers to implement recently announced first green energy city with revitalized HSE in Libya. This Initiative is aimed at not only revitalized HSE but also developing low carbon concrete to supply the millions of cubic meters of concrete required to build the initial phases of Libyan green energy city expected to be the world's first carbon neutral, zero-waste city west of Tripoli a capital city in Libya. It will be powered by not only low carbon energy but also low carbon concrete as a core material used in the construction. This initiative for development of low embodied carbon concrete is essential to ensure the city achieves its ambitious sustainability targets. The initiative considers cement is as one of the main ingredients in concrete, and is the second most consumed commodity in the world after water. It examines how to manufacture and manage cement production in the country that is responsible for around five per cent of the world's carbon dioxide emissions according to the World Business Council of Sustainable Developments. It also considers measures to reduce the amount of cement used in the specially designed concrete mixes, which, therefore, reduce the embodied carbon by more than 30% while meeting all the durability criteria set by the new city developer.

A special scheme is under way to offset the remaining carbon embodied in the concrete required to build first Libyan green city. The goal is to creating a new product that will set a benchmark for sustainability with revitalized HSE not only in Libya but also in Middle East, Mediterranean Africa and world at large. This is in line with country declared policy to meet its international obligation under climate change convention, biodiversity convention and land degradation convention requiring developing a Low carbon concrete in the construction industry in general and water supply and oil sector in particular. This requires need to continue to explore and invest in new technologies that will help minimize the industry's impact on the environment. It would help in evolving much needed political will, practical steps and the partnership for a comprehensive research and development program to develop global standards for low CO_2 concrete with revitalized HSE for the advancement of sustainable concrete technologies. This would also include evolving strategy for its adoption of rigorous sustainability criteria for designing, producing, transporting and placing concrete on shore and offshore concrete structures and installation. This expertise is required in Libya for developing an integrated system in meeting the challenging requirements for producing concrete with the lowest possible carbon footprint and revitalized HSE [10, 15].

AN APPRAISAL OF HSE & ECONOMY MANAGEMENT FOR NEW LIBYA

Health safety and environmental protection concerns in new Libya is in response to experts warning of increased cases of workplace disasters not only globally but also in country where both local and international company employers are increasingly cutting spending on occupational safety and health in the wake of the global economic down turn and financial crisis. The cost cutting measures in this climate of economic slowdown as per International Labor Organization (ILO).has also left the human resources capital market reeling from layoffs employment caps to even considering slashing their occupational safety and health budgets to boost the impact of other strategies such as outsourcing, subcontracting, and increasing part-time. It is widely believed that this situation is likely to lead to more work-place accidents, diseases, fatalities and ill-health from unemployment, severely affecting social security, burdon of disease on health sector expenditures and productivity. As per one of case study observations construction industry firms are sitting on a time-bomb by cutting the occupational safety and health spending, which constitutes between 10-15 per cent of their budget. Accordingly to recent ILO sources related to occupational Safety and Health "The item is increasingly becoming a victim of cost cutting measures and this is worrying" The consequences could be seriously felt in the labor market in future. Recent meeting at Düsseldorf Germany, Kenya has reported hundreds of deaths at work places in last two years. This has activated the debate on compensations and safety. The country has set up an occupational health and safety fund wherein employer are asked to contribute as levy annually meant to reduce injuries and deaths at work place.

Revitalizing health safety and environment (RHSE) for concrete structures in Water Supply and Oil Sectors in new Libya should be based on an identified strategy and action points derived from experiences in UK & EU like:

1. Motivating Change to
    a. Promoting the business case
    b. Common Standards
    c. Involving Insurers
    d. Name and Shame

    e. Directors' responsibilities
2. Enforcement change by:
    a. Enforcing Compulsory Insurance
    b. Penalties
    c. Private prosecutions
    d. Directors' responsibilities
3. Leading by Example using:
    a. HSE checklist
    b. Annual reports
    c. High level HSE forum
    d. Signing up to the Clients' Charter
    e. Procurement lever
4. Changing World of Work by:
    a. Effective Guidance
    b. Review of incident reporting regulations
    c. Amendment to existing health safety rules and regulation
    d. Review HSE organizational structures
5. Occupational Health by:
    a. Better access
    b. New occupational health strategy
    c. Rehabilitation
    d. Right to work as partners
6. Education / Design it in:
    a. Protection for all workers
    b. Including HSE in the Curriculum
    c. Including HSE in higher education
7. Employee Involvement with:
    a. Training of Safety Reps
    b. Worker Representation
8. Engaging Small Business Firms by:
    a. Forging links with Small oil firms
    b. Better HSE representation
    c. Effective guidance
    d. Grant scheme
9. Regional Involvement by:
    a. Working with NTC Authorities
    b. Working with the Irrigation and water supply
    c. Reviewing regional structures
    d. Better HSE representation
10. Modernizing Organizations by:
    a. Equality
    b. Openness
    c. Accountability
    d. Sharing information.

Economy from Water & Energy Saving Strategy with least water and energy requirement for production of concrete that comes from three aspects like the governmental policy and social awareness, the pricing factor derived from the key enabling technology for renewable energy market during next 20 years is described and reported elsewhere by the author in extra bibliography [1-16]. The objective of ongoing need of this initiative is to present an overview

of the role of HSE & Economy. Criteria for selection of concrete as a material appropriate with HSE and economy requirement for coastal region are those logically depending upon position of material within the structure and on the changes which take place in the material properties during construction and after construction.

To address them comprehensively will require strong cooperation across the whole range of development partners. In addition we need technical assistance in relation to WTO agreement on technical barriers to trade (TBT) and application of sanitary and phyto sanitary measures (SPS).

AN OUTLINE OF CONCRETE CODE DEVELOPMENT PROCEDURES WITH ENHANCED HSE REQUIREMENT

An overview of the state of art on concrete code standard setting presented elsewhere by the authors shows that coastal states dealing water supply and export require concrete with least water and energy requirement to conform to the technical regulations that they apply to domestically produce ready mix concrete for performance, health safety environment and consumer protection. The scope of the work related standard setting work includes preparing [10]:

1. Specification for concrete in various geographical locations including the one for hot and humid hostile desert and marine environment
2. Handbook of quality control for concrete materials
3. Specification for materials both for normal and hostile hot and arid desert region and hot and humid marine environment
4. Recommended practice for various applications.

Appraisal further shows that most coastal states need technical assistance to:

- Overcome the problems they encounter in participating effectively in international standardization activities
- Meet effectively the technical requirements especially in their concrete prefabricated products export markets.

Build capacities for deriving full benefits from WTO agreements on TBT and SPS [10-16].

THE CASE STUDY IN NEW LIBYA- 2012

In order to identify the technical assistance needs of coastal states countries under a Libyan initiative framework a comprehensive study is underway as an extension of an on-going questionnaire survey the preliminary responses of the results of which have been already presented elsewhere in some of the international and regional conferences. Respondents from both coastal states having relatively more developed national institutions engaged in standardization conformity activities and those at widely different stages of development whose experiences at national levels in the area of standardization and conformity are at a nascent stage. It should be noted that the basis of selection is for analytical purposes only to assess broadly the technical assistance needs at widely different stages of development. The intention is not to be interpreted as involving and value judgment on the actual level of development in standardization activities in each of these countries.

Survey responses demonstrate an immediate need to resolve difficulties of most coastal states hindering the export of concrete product with enhanced HSE and economy leading to water and energy saving potential due to shortcomings in their standardization and conformity assessment structure. They do face HSE problems during concrete production, transportation, placement and compaction leading to 1. Injured while handling, lifting or carrying 2. Slipped, tripped or fell on the same level and 3. Hit by moving, flying or falling object. They do need assistance in tackling the main causes of occupational ill health leading to a. Musculoskeletal disorders (MSDs), b. Skin disease, e.g. Dermatitis and c. Respiratory disease, e.g. Occupational Asthma. Almost all the respondents strongly urge the need to address them comprehensively requires strong cooperation across the whole range of development partners. Keeping this in view Libyan initiative presented elsewhere [6-16], divides it into 3 levels - Common Level 1, Level 2 and Level 3. The Common Level 1 document provides the framework for and the basic principles underlying the code across the 3 Parts: Part 1-Design, Part 2-Materials and Construction and Part 3-Maintenance. The Level 2 documents specify the required performance and the ways and means for the structure to achieve such performances. It contains provisions that are common to all coastal states. The working Level 3 documents are to be prepared by each country that adopts the code by incorporating its own national coastal concrete engineering practices.

Currently the initiative in new Libya 2012 is for building configuration based software solutions and less software that is governed by the relatively rigid rules of code alone. This initiative further looks at the evaluation of the culture within the organization and the development of a program to create a positive health and safety culture in which the cultural norms are for safe and healthy working.

FINAL REMARKS AND RECOMMENDATIONS

This paper based on current story of GMMR in Libya is intended to be enlightening and presented to all who intend to become health safety and environmental protection leaders but also increase profitability by water and energy saving within an organization related to concrete production, transportation, placement and compaction especially for water supply industry. Paper has demonstrated the need of transfer of technology in the area of Revitalized Health Safety & Environment (RHSE) in the Concrete Construction. Development of an innovative Concrete code with enhanced RHSE and economy resulting from water and energy saving has a potential also in line with AU-EU / NEPAD supported APCI for producing concrete with the lowest possible carbon footprint and revitalized HSE.

To organize meetings and seminars on specific RHSE in construction aspects to exchange experiences, examine problems and solutions, promote co-operation between the national and international players, and identifying the future challenges defining common strategies be adopted by the country. It is recommended that a value chain approach to establish coastal states concrete code with RHSE and economy using water and energy saving potential to be adopted in line with the AU-EU & UNIDO current technical approaches.

REFERENCES

1. ATKINS LIMITED, Structural Integrity Management Framework for Fixed Jacket Structures. The Health and Safety Executive Research Report, RR684, HSE Books 2009.

2. FOOKES G P, STONER R J AND MACKINTOSH H J, The Libyan Great man-Made River Project: Concrete Technology of Prestressed Concrete Pipe Manufacture, Proc. of Institution Civil Engineering, Part 1, Vol. 4, 90, 1991, pp. 853-879.

3. AMAZO E, Development of Productive Capacities, UNIDO / NEPAD, Conference Presentation, Tunis, Tunisia, 26-28 Sept 2005.

4. BINDRA S P AND TUGHAR S M, Civil Engineering Education for Information Society — A Case Study, World Forum on Information Society, WFIS, Tunis, 2005.

5. ABULGASIM G E, KARA-ZAITRI C AND BINDRA S P, Revitalizing Health & Safety in the Concrete Construction in Oil & Gas Industry, Proc of 1st Int. SEMC, 2010, Cape Town, South Africa 2010.

6. NGAB A AND BINDRA S P, Towards Sustainable Concrete Technology in Africa, Proc. 1st International Conference on Recent Development in Structural Engineering, Mechanics and Computation, SEMC1, Cape Town, South Africa, 2001.

7. ROGERS A, GMMR Project, Libya, ICT 2005-2006.

8. TUGHAR M S M AND BINDRA S P, Management of Recreational Concrete Structures: Some Case Studies in Costal States, Proc of 2nd Int. Conf. on the Management of Coastal Recreational Resources, ICoDS, Oct 2006, Gozo, Malta, pp. 191-199.

9. PRESTON B, Colonel Qaddafi and the Great Man-made River, Journal of the Earth Institute, Columbia Water Center, Columbia University, 1 April 2011.

10. TUGHAR, M S M AND AWEDA A F, Code for Management and Rehabilitation of Coastal Concrete Structures, Proc. of 3rd International Conference on Concrete Solutions, Padua, Italy, CRC Press Balkema, 2009, pp. 315-323.

11. TUGHAR M S M, RIFAI A M, BINDRA S P AND YAHYA EDAAYF R M, Coastal Concrete Structures: Some Case Studies. Proc. of the 3rd Int. Conf. on Recent Development in Structural Engineering, Mechanics and Computation, SEMC3, Mill press Science Publishers, University of Cape Town, Cape Town, South Africa, 2007, 7-10 Sept, pp. 573-574.

12. TUGHAR M S M, YAHYA EDAAYF R M, BINDRA S P AND GOODA E A M, Management of Recreational Concrete Structures: Some Case Studies in Coastal States. Proc. of the 6th Alexandria Int. Conf. on Structural and Geotechnical Engineering, AICSGE6, Alexandria University, Alexandria, Egypt, 2007, 15-17 April, pp. MG45.

13. TUGHAR M S M et al., Salt-Induced Reinforcing Steel Corrosion in Concrete Structures. Proc. of the 8th Int. Conf. on Concrete Technology in Developing Countries, ICCTDC8, Hammamet, Tunisia, 2007, 8-9 Nov, pp. 57-66.

14. SRDJAN D V, Problems of Thermal Incompatibility of Concrete Components With Hot Climate, Proc. of 2nd Int. Conference on Concrete Technology in Developing Countries, ICCTDC2, Tripoli, Libya, 1986, 27-29 Oct, Vol. 1, pp. 1.100-1.110.

15. TASSIOS T P, Towards African Concrete Code, Proc of 8th Int. Conf. on Concrete Technology in Developing Countries, ICCTDC8, Hammamet, Tunisia, 2007, 8-9 Nov, pp. 416-423.

16. TUGHAR M S M, RIFAI A M; BINDRA S P, YAHYA EDAAYF R M AND HOKOMA R A, Management of Energy and Water savings for Concrete Structures in Coastal States, Proc. of 1st Int. Conference and Exhibition on Environmental Impact of Energy and Water Saving in Tourism, EIEWS1, International Energy Foundation, IEF-Publication, Tripoli, Libya, 30-31 May, 2007, pp. 148-160.

Assessment of Environmental Impact of the Addition of Photocatalytic Nanoparticles to Cementitious Materials

B Y Lee, A R Jayapalan, K E Kurtis
Georgia Institute of Technology, USA

Use of photocatalytic titanium dioxide (TiO_2) in cementitious materials is increasing due to its novel capabilities, including smog abatement, hydrophobicity/philicity, and self-cleaning. However, the contributions of TiO_2 nanoparticles to the overall environmental impacts of photocatalytic cementitious materials have not been thoroughly considered. That is, the balance between their potential beneficial long-term use and the environmental costs associated with their production should be considered. In the first part of this study, the potential influence of TiO_2 nanoparticles on early hydration kinetics of major components in portland cement are measured and these data compared with hydration models. Results, which showed nanoparticle acceleration of calcium silicate hydration, are used to assess whether cement fractions may be reduced when nanoparticles are included, while retaining similar concrete properties. The second part of this study examined the environmental impact of the photocatalytic cement, analyzed by SimaPro Life Cycle Assessment (LCA) software. The LCA study indicates that even though the introduction of nanoparticles increases the initial environmental impact of photocatalytic cement as compared to ordinary portland cement, the long term NOx binding capabilities of TiO_2-modified cements could result in a lower environmental impact. The contributions to sustainability can be further enhanced by reductions in cement fraction, based upon the results of the first part of this investigation.

Amal R. Jayapalan is a Graduate Student in the School of Civil and Environmental Engineering, Georgia Institute of Technology, Atlanta, GA. He received his B. Tech from the Indian Institute of Technology (IIT), Madras, India. His research interests include durability, microstructural characterization and sustainability of cement-based materials.

Bo Yeon Lee is a Ph.D. Candidate in the School of Civil and Environmental Engineering at Georgia Institute of Technology, Atlanta, GA, where she also received her MS. She received her BS in architectural engineering from Yonsei University, Korea. Her research interests include photocatalytic cements, modeling of cement hydration, and durability of cement-based materials.

Kimberly E. Kurtis, Ph.D., FACI, FACerS is Professor in the School of Civil and Environmental Engineering at Georgia Institute of Technology, Atlanta, GA. She is Chair of ACI Committee 236: Materials Science of Concrete and an Editorial Board member at Cement and Concrete Composites.

Keywords: Acceleration, Filler, Hydration rate, LCA, TiO_2

INTRODUCTION

Use of photocatalytic titanium dioxide (TiO_2) in cementitious materials is increasing due to its strong oxidizing capability. One of the major applications of photocatalytic cement-based materials is on the nitrogen oxides ($NO+NO_2=NOx$) oxidation. Nitrogen oxides are classified as one of the major air pollutants, mostly stemming from mobile sources such as cars, planes, and trains. NOx participates in the formation of photochemical smog and ozone (O_3), as well as threatening human health. Use of photoactive TiO_2 is considered one way of passively mitigating this problem. However, although this TiO_2-cement composite is effective in NOx oxidation, the effect of addition of these TiO_2 nanoparticles to cement substrate is relatively undocumented.

In this paper, the overall objective is to examine the global environmental impact of TiO_2-bearing cement-based materials. This is accomplished by first examining the influence of these chemically inert nanoparticles on cement hydration, to determine if cement factors may be reduced, reducing then the well-known environmental impact associated with cement. Commercially appropriate compositions are then analyzed and compared by life cycle assessment (LCA).

Prior work by these authors have shown that in alite (tricalcium silicate, C_3S) pastes where TiO_2 nanoparticles are added [1, 2], the early hydration is accelerated. The boundary nucleation (BN) model [3], which presumes surface nucleation and takes into account the cement and TiO_2 particle surface areas, provided a better fit to the hydration behavior than conventionally used Avrami model, which presumes heterogeneous nucleation in pore solution-filled space. Thus, the C_3S acceleration was ascribed the high surface area of the chemically inert nanoparticles of TiO_2. The work performed here will build upon the previous work by authors such that belite (dicalcium silicate, β-C_2S), the second major component of portland cement after alite, is examined. C_2S requires less energy to produce than C_3S but its use is limited due, in part, to its slower hydration rate [4]. Here, the hydration rate of C_2S in the presence of TiO_2 nanoparticles is measured and compared to two mathematical models, the BN model and the Avrami model.

Further, the potential global environmental impact of TiO_2-bearing cementitious materials is examined through a lifecycle analysis (LCA). While the NOx abatement capability of photocatalytic materials is a potential environmental benefit, a comprehensive investigation that includes all factors including embodied energy, embodied CO_2, transportation, cost, among other factors, is required to truly appreciate the impact of their usage on a commercial scale. In this study, SimaPro LCA software is used to perform a life cycle analysis on compositions of photocatalytic cementitious materials which are appropriate for field use.

EXPERIMENT AND MODELING

Materials

Pure belite (β-C_2S) powder was obtained from CTLGroup in Skokie, IL. C_2S powder was stabilized by boron trioxide (B_2O_3) and was ground to 100% passing No.325 sieve (45μm). Purity of C_2S was 100.00%, examined by quantitative X-ray diffraction under Cu-Kα radiation. Anatase TiO_2 that was used for this study was AMT-100 (Tayca Corp., Osaka, Japan), that is 93% pure, has average crystal size of 66nm, and pH of 7.0, as specified by the

manufacturer. Particle size distribution was measured by Zetasizer Nano (Malvern Instruments, UK) after ultrasonicating TiO_2-water-superplasticizer solution for 1 hour for better dispersion (Figure 1). Nitrogen BET surface area of the powders were determined by Micromeritics ASAP 2020 (Micromeritics, Norcross, GA) accelerated surface area and porosimetry analyzer. The BET surface area was measured to be 2.81 m^2/g and 611.54 m^2/g for C_2S and TiO_2 respectively.

Calorimetry and Hydration Modeling

For isothermal calorimetry, TiO_2 containing C_2S sample pastes were prepared at 0%, 5%, and 10% addition of TiO_2 by mass of C_2S with the addition of 2% calcium chloride ($CaCl_2$) in an attempt accelerate the reaction. $CaCl_2$ solution was first prepared, and TiO_2 powder was added to the solution and mixed for 1 min, then C_2S powder was added. Water-to-cement ratio (w/c) was constant at 0.50. The heat of hydration was measured by isothermal calorimetry (TAM AIR, TA instruments, New Castle, DE) at 20°C up to 90 days.

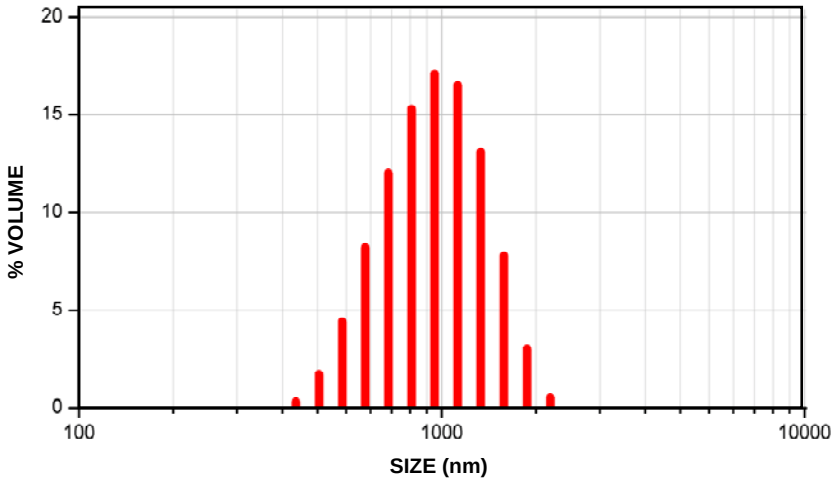

Figure 1 Particle size distribution of TiO_2 powder

The two models, Avrami model [5-7] and BN model [3], are applied to the experimental results. The model curves are fitted to the experimental data through an iterative process. Detailed model derivation and equations can be found from the previous work performed with pure C_3S powder [1].

LCA Methods

To examine the overall impact of the TiO_2-containing cement to the environment in comparison to ordinary portland cement, a life cycle assessment (LCA) was performed. This analysis is a technique that incorporates environmental impact of all the stages of a product from raw material through disposal or recycling. For this study, SimaPro software was used and the Eco-Indicator 99E [8] was selected as the calculation method for impact assessment. A generalized processing of TiO_2 based on data from manufacturer was considered for the material information in the analysis. Once the data for the different materials were input into the program, SimaPro conducted the life cycle impact analysis (LCA) that includes classification, characterization, normalization and weighting. In the classification step of

LCIA, SimaPro and Eco-Indicator 99E categorized the impacts of the materials into the following eleven impact categories based on ISO 14040 standard endpoints [9]: carcinogens, respiratory organics, respiratory inorganics, climate change, radiation, ozone layer, ecotoxicity, acidification/eutrophication, land use, minerals and fossil fuels. In this study, weighting factors for each of these eleven categories were selected based on Eco-Indicator 99 method [8]. Once the appropriate weights were applied by the program, a single indicator was generated and reported as "points," where one point is equivalent to one thousandth of the environmental load by an average European inhabitant. The final "single score" was used to compare the environmental impacts of the TiO_2-cement compared to ordinary portland cement. Also, further investigation was performed that takes into account the NOx oxidizing capability of TiO_2-cement. This offsets a part of the environmental impact of TiO_2-cement. The time required to offset the initial NOx emissions from material is calculated.

For this analysis, it was assumed that cement paste is replaced with 5% of TiO_2 by mass. Results were then compared to ordinary portland cement paste, where the cements were considered to be equivalent. The environmental impacts of both of the cases are discussed. Further, a case when additional "inert" filler is added is analyzed. This "inert" filler is assumed to have negligible life cycle cost, but is envisioned as having similar accelerating properties to the TiO_2 nanoparticles. As a result, inclusion of an additional filler material, with the TiO_2, could further contribute to reductions the life cycle cost of the entire photocatalytic cement, while retaining similar performance.

RESULTS AND DISCUSSION

Effect of TiO_2 Nanoparticles on Early Hydration

The rate of hydration per gram of dry C_2S is shown in Figure 2(a) for the first 90 days after mixing for each of the pastes examined. Corresponding cumulative heat data is presented in Figure 2(b). The effect of addition of chemically inert nanoparticles can be examined by comparing the C_2S samples containing 0%, 5%, and 10% TiO_2. From Figure 2(a), addition of nano-TiO_2 particles noticeably accelerated the hydration reaction. The 5% and 10% case clearly shows induction period at ~3 days, reaching rate peak at ~40 days. Comparing to 0% case where rate peak is observed at ~60 days, hydration of C_2S was accelerated by ~20 days with the addition of TiO_2 nanoparticles. This acceleratory effect of addition of chemically inert nano TiO_2 was also observed in authors' previous work performed with pure C_3S paste [1, 2]. On the other hand, not much difference is shown between 5% and 10% case. It could be that the rate of nuclei or hydration product formation is slow enough in the case of C_2S, that the added surface area of TiO_2 beyond the level of 5% does not have a noticeable effect on acceleration. Additional effects may be due to minor amount of sulfate ions on the TiO_2 stemming from its production; the sulfates at greater, but still minor, concentration at the higher dosage rates could interfere with the acceleration due to the additional surface area, as described in [10].

Cumulative heat of hydration plot in Figure 2(b) suggests that degree of hydration of TiO_2 containing C_2S pates surpass that of pure C_2S paste at about 20 days, and reaching 49% at 90 days as compared to 34% in case of pure C_2S paste. This is a 47% increase in degree of hydration. The degree of hydration was calculated by dividing the total heat of hydration at a given time by the enthalpy of reaction of C_2S (ΔH=45kJ/mol) [11]. Detailed description of C_2S hydration and Figure 2(a) and (b) can be found from elsewhere [10].

Overall, from these calorimetry data, it was found that method of isothermal calorimetry can be used to capture the hydration rate of C_2S, and TiO_2 nanoparticles accelerate the rate of C_2S hydration.

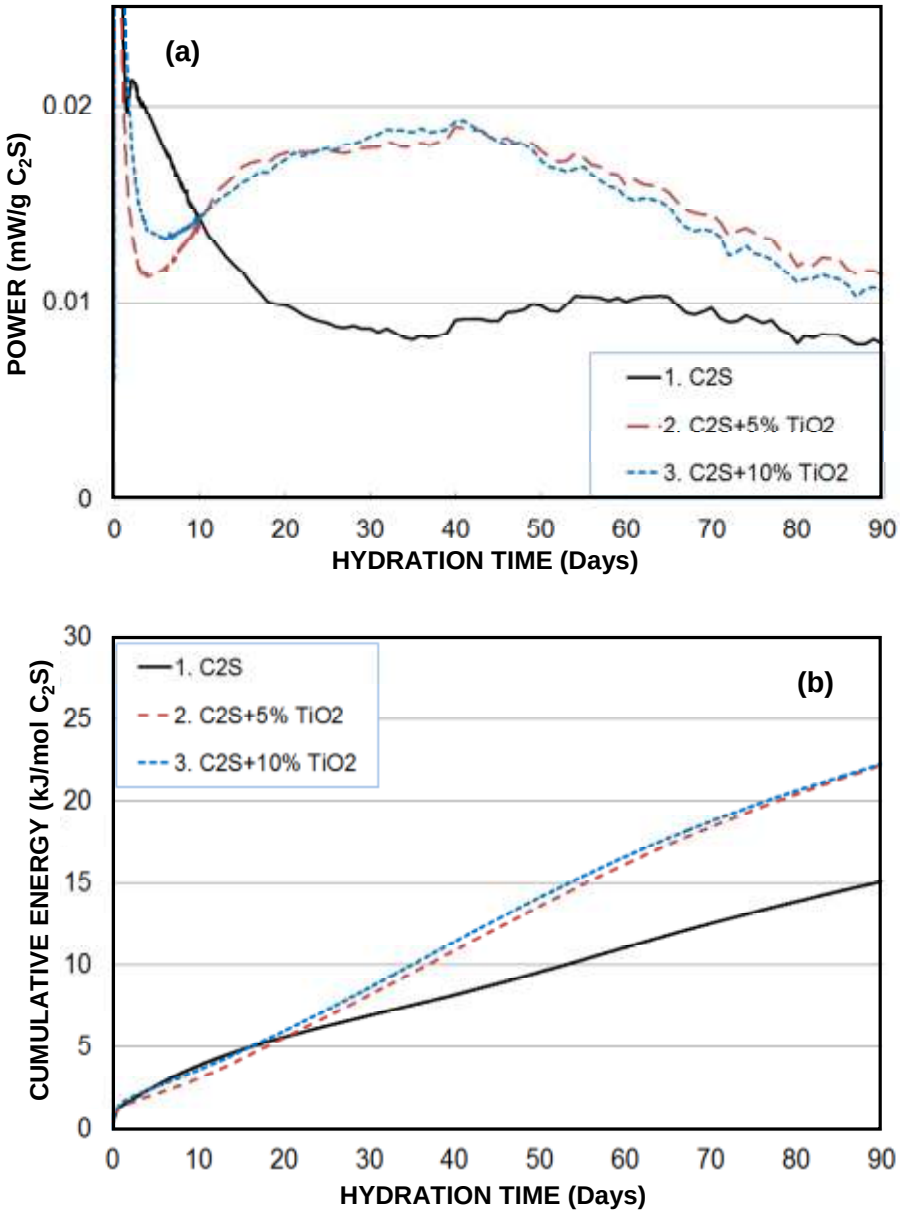

Figure 2 (a) Hydration rate of TiO_2-blended C_2S pastes
(b) Cumulative heat of hydration of TiO_2-C_2S pastes

Model Fits

The Avrami model and the BN model were fitted to the rate of hydration data for the C_2S pastes with 0%, 5%, and 10% TiO_2 addition. The initial rate peak that occurs immediately after mixing as a result of initial dissolution of C_2S was not considered for the model fit. Fitting was performed by manually adjusting model parameters: A, t_0, k_{avr}, and n were

adjusted in case of Avrami model, and A, t_0, G, I_B were adjusted in case of BN model. The O_V^B value for the BN model, which represents surface area of powder, was calculated by dividing the total surface area per gram of mixed powder by the volume occupied by the hydration products after complete hydration. The hydration volume of C_2S is 0.5694 cm^3/g C_2S and the volume of TiO_2 was incorporated based on the density of 4.23 g/cm^3. The increase in O_V^B as more TiO_2 is added represents the increasing surface area due to addition of nanoparticles. The values are presented in Table 1. Curve fitting was iteratively done until the model fit best approximates the experimental data. The finalized model fits are presented in Figures 3(a), 3(b), and 3(c), and the model parameters are presented in Table 1 and Table 2 for the Avrami model and the BN model, respectively.

In all the cases considered, the BN model approximates the experimental data better than the Avrami model, especially in the deceleration period. This is due to the unsymmetrical shape of the rate curve that could only be represented by the BN model. The Avrami model is capable of representing only a symmetrical bell shape while the BN model can present a skewed bell shape depending on the k_B/k_G ratio. As k_B/k_G ratio approaches zero, the shape gets symmetrical, and the model essentially is identical to the Avrami model. The k_B/k_G ratio also reflects the effect surface area, where nucleates are expected to form. In this study, the k_B/k_G ratio of C_2S hydration is determined to be around 1~2. Model fit parameters are summarized in Table 1 and Table 2 for the Avrami model and the BN model, respectively.

The t_0 parameter in both the Avrami model and the BN model shows a negative value, indicating that the curves are shifted to the left. This suggests that enough starting nucleates exist which accelerated the hydration reaction. There is no obvious trend in t_0 for the Avrami model, but for the BN model t_0 is decreasing (growing more negative) at higher nanoparticle dosage rates. That is, 450 hours of acceleration was observed for the 5% case in comparison to the 0% case, and additional 50 hours of acceleration was observed for the 10% case in comparison to the 5% case. This suggests that the additional surface area provided by the nanoparticles of TiO_2 accelerated the early C_2S reaction. The G parameter, which represents the linear growth rate of hydrated phases, is decreasing and the IB parameter, which represents nucleation rate per unit area of total surface area, is increasing as more TiO_2 nanoparticles are added. These suggest that hydration products are forming on a larger surface area, which is increased due to TiO_2 addition. This trend was also observed in case of C_3S paste [1, 2]. However, the order of magnitude is 2-3 times lower in case of C_2S paste, indicating slower hydration reaction is occurring, as expected.

The k_B/k_G ratio shows an increase from 0% case to 5% and 10% case; increase of 81% from 0% case to 5% case and 61% from 0% case to 10% case was observed. Interestingly, an 11% decrease in the k_B/k_G ratio was observed between 5% case and 10% case. The authors believe that this could be the result of “diminished returns” as stated previously [10], which resulted in the very similar curves despite the higher addition rate. Also, the sensitivity of the fitting parameters according to little changes in the shape, and unsmooth experimental data can be the reason for the drop k_B/k_G ratio. Nevertheless, the significant increase of the ratio after adding TiO_2 imply that the acceleration is due to the added surface area by TiO_2 nanoparticles, although other factors may also contribute the behavior observed. Certainly, additional research is needed to better understand the applicability of the BN model to belite hydration and the mechanism(s) of nanoparticle-derived acceleration.

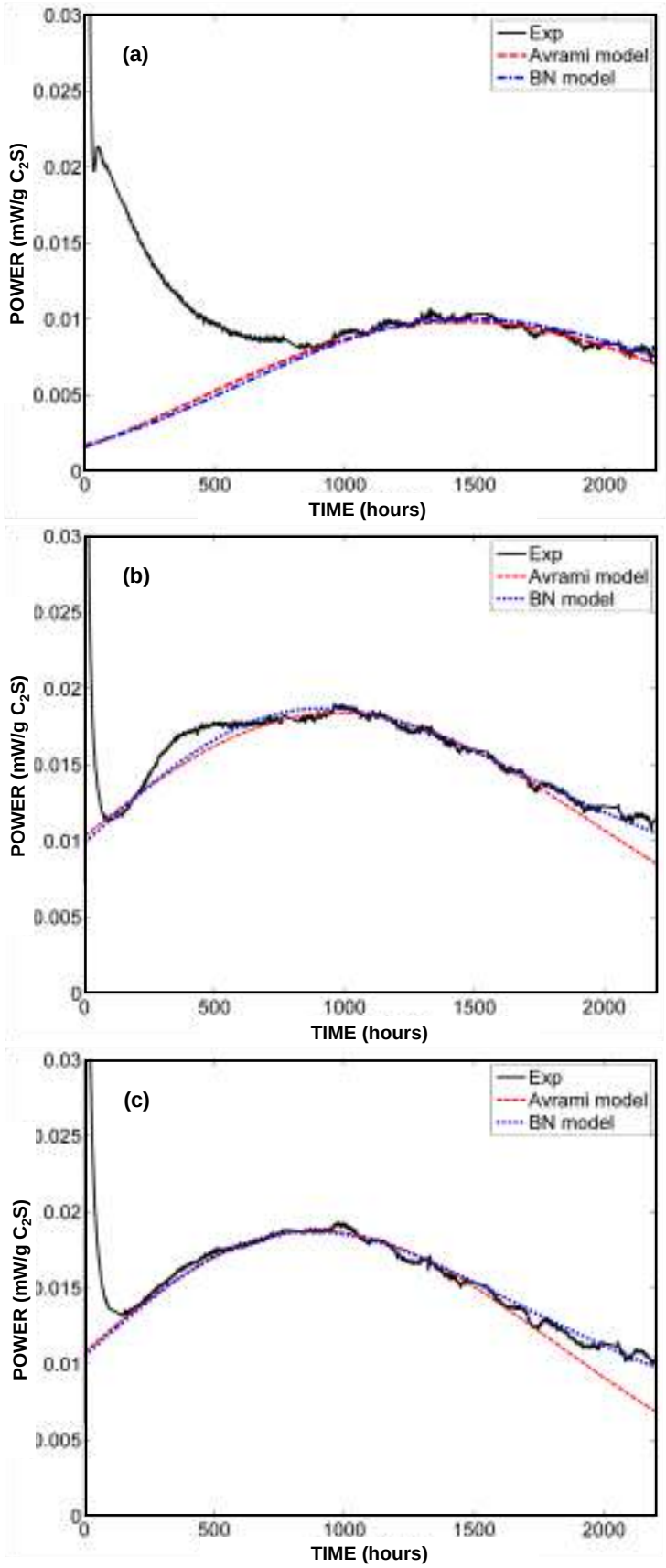

Figure 3 Rate of hydration: Experiment versus Avrami and BN models (a) 0% TiO_2, (b) 5% TiO_2, and (c) 10% TiO_2

Table 1 Fit parameters A, t_0, k_{avr} and n for Avrami model

TiO_2 (%)	A (kJ/mol)	t_0 (h)	k_{avr} (h^{-1})	n
0	21	-440	0.00045	2.6
5	42	-1050	0.00042	2.6
10	40	-950	0.00045	2.6

Table 2 Fit parameters O_v^B, A, t_0, k_B, k_G, and k_B/k_G for boundary nucleation model

TiO_2 (%)	O_v^B (μm^{-1})	A (kJ/mol)	t_0 (h)	G ($\mu m/h$)	I_B $(\mu m^{-2}h)^{-1}$	k_B ($h^{-1}*10^4$)	k_G ($h^{-1}*10^4$)	k_B/k_G
0	4.935	25	-1000	0.0000700	0.01	3.6070	3.4545	1.0441
5	57.443	60	-1450	0.0000033	8	3.5848	1.8956	1.8911
10	107.858	56	-1500	0.0000020	20	3.6245	2.1572	1.6802

Life Cycle Analysis

The life cycle analysis of ordinary portland cement, cement containing 5% of TiO_2, and cement containing 5% TiO_2 and an additional inert filler were performed using SimaPro. The results for 1000kg of each mixture are presented by a single point score as shown in Figure 4. Ordinary portland cement resulted a single point score of 22.14 points and TiO_2-modified cement resulted 40.47 points. This analysis considers only the materials production, including raw material acquisition and processing of the components used in the cement mixes. (Analysis of the TiO_2-modified cement with filler is described subsequently.) As the higher value designates greater detriment to the environment, the TiO_2-modified cement negatively impacts the environment 83% more than ordinary portland cement when only the material production is considered.

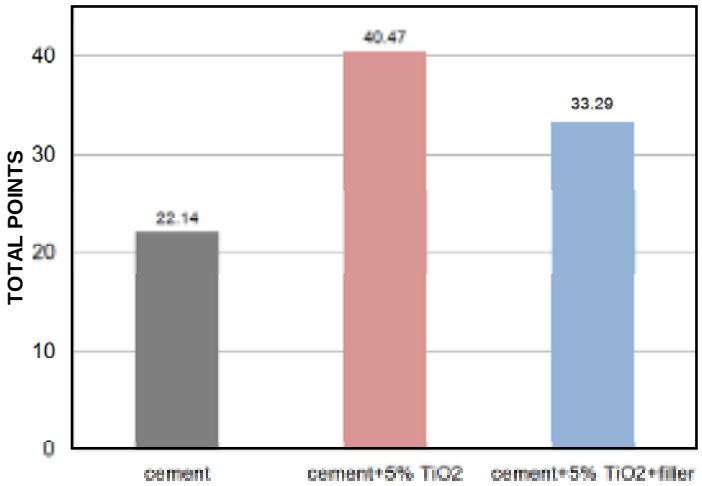

Figure 4 Single point LCA score for cement mix, TiO_2-blended cement mix and theoretical cement mix with TiO_2 and inert filler additives

Isothermal calorimetry has shown that 5% replacement of TiO_2 nanoparticles for cement increases the cumulative heat evolved by 21% at 48 hours of hydration (Figure 5), as compared to ordinary portland cement; similar results are also reported in [12]. This can directly be related to degree of hydration. This indicates that to some extent, cement can be replaced with other "inert" filler to achieve a similar degree of hydration as that of ordinary portland cement paste, thus decreasing cement content. Inert filler could be selected such that the life cycle cost of the filler be negligible compared to the cement or TiO_2, such as waste product or fine aggregate. If such "optimum" inert filler were added to TiO_2-blended cements to reach similar degrees of hydration as ordinary portland cement at 48 hours, the maximum replacement rate is calculated to be approximately 17%. For this mix (labeled cement+5% TiO_2+filler in Figure 4), the single point score according to LCA is 33.29 points. This is 50% higher than ordinary portland cement but results in 18% lower environmental impact than 5% TiO_2-cement due to the decreased cement content. Thus addition of inert (according to life cycle cost) filler decreases the total LCA single point score of the TiO_2-blended cement.

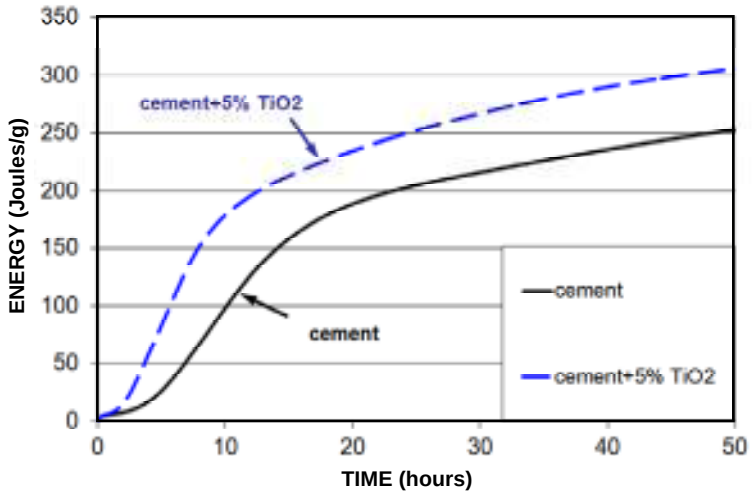

Figure 5 Cumulative heat of hydration of ordinary portland cement (OPC) mix and TiO_2-blended cement pastes

On the other hand, taking into account the photocatalytic NOx oxidizing effect of TiO_2-cement, a part of this impact – the initial NOx emissions - can be offset with time. Further analysis was performed based on the conditions in Atlanta, Georgia, USA to calculate the time required for the TiO_2-cement to offset the NOx from its production. Atlanta, USA with an average sunshine per day of 7.25 hours was selected because of the location where this research was conducted as well as its relevance to urban environmental conditions. The annual NO_2 concentration in Atlanta was reported 17.0 ppb in 2004 [13]. When 5% of TiO_2 was used as a replacement of cement by mass and 5mm thick layer is applied to a surface, 2.12 years are required to offset the initial NOx emissions by the TiO_2-modified cement. If the surface is frequently washed, as with rainfall, as is expected during the life of TiO_2-cement surfaces, the photocatalytic activity could be renewed and hence these surfaces should perform well throughout the life of the structure. The direct benefit of the use of this TiO_2-modified cement is reduction of pollutant gas (NOx) concentration and thereby positively impact the air quality and decrease of smog creation, especially in urban applications. Thus in the long term, TiO_2 modified cement could be beneficial to decrease the

initial higher environmental impact because of production and thereby resulting in a sustainable construction product.

CONCLUSIONS

Nanoparticles of TiO_2 were found to accelerate the rate of C_2S hydration and increase peak height with increasing percentage mixed with C_2S pastes. Similar acceleratory behavior with nanoparticle additions was noted from prior studies on C_3S and ordinary portland cement. The model fits for the C_2S hydration data indicated that these kinetics be described by the two models, with the BN model giving a better fit especially in the deceleration period than the Avrami model. Because the increased C_2S rate of hydration was not necessarily related to the k_B/k_G in the boundary nucleation model, other acceleratory mechanisms should be investigated to more fully understand the behavior.

The results from LCA show that initially the TiO_2-modified cement has higher environmental impact compared to ordinary portland cement. This can partly be ameliorated by adding up to 17% of inert filler without compromising the degree of hydration, due to the acceleratory effect of the nanoparticles on portland cement hydration. Also, it is likely that the negative environmental effect from production can be offset in the long term by the photocatalytic NOx oxidation of TiO_2, ultimately turning into more beneficial to the environment than ordinary portland cement.

ACKNOWLEDGMENT

This material is based upon work supported by the National Science Foundation under Grant No. CMMI-0825373. Any opinions, findings, and conclusions or recommendations expressed in this material are those of the authors and do not necessarily reflect the views of the National Science Foundation.

REFERENCES

1. LEE, B.Y. and KURTIS, K.E., Influence of TiO_2 Nanoparticles on Early C_3S Hydration, Journal of the American Ceramic Society, Vol. 93, No. 10, 2010, pp 3399-3405.

2. LEE, B.Y., THOMAS, J.J., TREAGER, M., AND KURTIS, K.E., Influence of TiO_2 Nanoparticles on Early C_3S Hydration, ACI Special publication, 267 SP, 2009, pp 35-44.

3. THOMAS, J.J., A New Approach to Modeling the Nucleation and Growth Kinetics of Tricalcium Silicate Hydration, Journal of the American Ceramic Society, Vol. 90, No. 10, 2007, pp 3282-3288.

4. GARTNER, E., Industrially Interesting Approaches to “Low-CO2” Cements, Cement and Concrete Research, Vol. 34, No. 9, 2004, pp 1489-1498.

5. AVRAMI, M., Kinetics of Phase Change 1 General Theory, Journal of Chemical Physics, Vol. 7, No. 12, 1939, pp 1103-1112.

6. AVRAMI, M., Kinetics of Phase Change 2 Transformation – Time Relations for Random Distribution of Nuclei, Journal of Chemical Physics, Vol. 8, No. 2, 1940, pp 212-224.

7. AVRAMI, M., Granulation, Phase Change, and Microstructure – Kinetics of Phase Change 3, Journal of Chemical Physics, Vol. 9, No. 2, 1941, pp 177-184.

8. HUNTZINGER, D.N. AND EATMON, T.D., A Life-cycle assessment of Portland Cement Manufacturing: Comparing the Traditional Process with Alternative Technologies, Journal of Cleaner Production, Vol.17, No.7, 2009, pp 668-675.

9. ISO, ISO 14040:2006-Environmental Management – Life Cycle Assessment – Principles and Framework, 2006.

10. LEE, B.Y. and KURTIS, K.E., Acceleratory effect of TiO_2 Nanoparticles on Belite Hydration, in review at Journal of the American Ceramic Society.

11. HEWLETT, P.C., Lea's Chemistry of Cement and Concrete, 4^{th} ed, 1998, Arnold.

12. JAYAPALAN, A.R., LEE, B.Y., FREDRICH, S.M., AND KURTIS, K.E., Influence of Additions of Anatase TiO_2 Nanoparticles on Early-Age Properties of Cement-Based Materials, Transportation Research Record: Journal of the Transportation Research Board, No.2141, 2010, pp 41-46.

13. Environmental Protection Division – Air Protection Branch, 2004 Ambient Air Surveillance Report, Georgia Department of Natural Resources, pp 97.

Observation of Fair-face Concrete Durability using Various Testing Methods

P Reiterman[1], K Kolář[1], O Holčapek[1], Z Kadlecová[2], J Adámek[2]
1 – Czech Technical University, Czech Republic
2 – Brno University of Technology, Czech Republic

An important parameter determining the durability of concrete is the quality of the surface layer, as it is directly exposed to the environment. In terms of durability properties, it is worth to monitor the parameters of the surface layers, particularly the transport processes. The paper presents the results of permeability measurements using methods Torrent Permeability Tester (TPT), Germanns Water permeation test (GWT) and the Initial Surface Absorbation Test (ISAT). These findings will serve to further optimization of the structure being created, thus ensuring its better aesthetic and functional characteristics.

Ing. Pavel Reiterman, Experimental centre, Fakulty of Civil Engineering, Czech Technical University in Prague, Prague, Czech Republic

doc. Ing. Karel Kolář, CSc., Experimental centre, Fakulty of Civil Engineering, Czech Technical University in Prague, Prague, Czech Republic

Ing. Ondřej Holčapek, Experimental centre, Fakulty of Civil Engineering, Czech Technical University in Prague, Prague, Czech Republic

Ing. Zlata Kadlecová, Institute of Building Testing, Faculty of Civil Engineering, Brno University of Technology, Brno, Czech Republic

prof. Ing. Jiří Adámek, CSc., Institute of Building Testing, Faculty of Civil Engineering, Brno University of Technology, Brno, Czech Republic

Keywords: Fair-face concrete, Permeability, Surface layer

INTRODUCTION

Owing to incidence of environment proceed many physiochemical changes in concrete surface layer. For fair-face concrete preparation are important changes noting by human eyes, and which decrease aesthetical parameters of material and surface quality. To material and consequently visual changes proceed mostly by action of surroundings and wage intensive interaction with component part of this material. Intensity of that proceeding depend of chemical and physical conditions such as concentration of proceeding medium, temperature, pressure, stream velocity, etc. Inception reasons may be divided into:

- physical influences (temperature and dampness changing, action of frost, UV radiation, corrosion of I. type co-called sulphurous water)
- chemical influences (acid rains, carbonation, corrosion processes of II. and III. type)
- physiochemical influences (action of water, de-icing salts, corrosion under load, etc.) [1]

All mentioned degradation processes closely cohere with quality of concrete surface layer and pore system of used concrete. Because surface layer is the most exposed part of whole structure, uniform distribution of tense in section does not happen. Stress is concentrated to the weakest part of material, along pores and cracks. That failure creates new access path to other aggressive media involved in gradual degradation of the material. It is very difficult process of physiochemical processes that is why we cannot separate them out, they proceed always currently. The most used magnitude for concrete durability evaluation is permeability. Very often is considered as a material characteristic, but in this simple experimental program we focused on influence of concrete "skin", because our previous research [1] has shown expressive effect of various modified surface layer.

EXPERIMENTAL PROGRAM

During the experimental program were measured to help introduced methods. An attempt was focused on comparing the effects of various surface agents for the fair-face concrete. The resulting surfaces were modified primarily through concrete. A reference concrete mixture was used, whose composition is shown in Table 1. Concrete mixtures were designed to achieve a soft consistency, which is commonly used in practice.

Table 1 Concrete mixtures composition

CONCRETE COMPONENT	MIXTURE			
	I	II	III	IV
	kg/m^3			
Cement CEM I 42,5 R Mokrá	350	394	400	400
sand 0-4mm, Dobříň	785	882	930	930
Aggregate: Crushed 4-8mm, Zbraslav	350	394	315	315
Crushed 8-16mm, Zbraslav	650	731	600	600
Plasticizer on carboxyl-ether base (Sika 1035)	0	0	3	2
Water	186	208	180	180

German Water Permeation Test (GWT)

Apparatus for determining permeability of surface layers of building materials, works by measuring the pressure of water flow velocity through the structure of the surface layer in time. From the time the surface water flow, selected water pressure and volume of hardened cement stone to the total volume of concrete is calculated from Darcy's law coefficient of concrete permeability. Of this magnitude is then determined by the permeability coefficient of internal k_i [m^2]. Its value depends on the difference between input and output flow pressure, its dynamic viscosity, density and gravitational acceleration. The value of internal permeability of surface layer is in many European countries standards considered essential evaluation criterion for assessing the durability of concrete construction. Eg. according to German standard DIN 1045 for concrete construction, durability of concretes considered those whose internal permeability surface layer is smaller than k_i 1.10^{-16} m^2.

The principle lies in the pressure chamber sealing ring on a test body, the cell is impregnated with water, sealed and turning the upper ring of the pressures from 0.25 to 2.5 bar. In the cell wall is built next to the micrometer gauge with a pin attached to the squeeze by screwing in the tank and maintains a constant pressure. The volume of water soaked for a defined period of the concrete is replaced by the volume telescopic pin. Once the pin is inserted into the entire volume of water and reduce the initial water pressure test ends. It is clear that pays direct correlation between the time required for the test and permeability test of concrete structures. In the test itself must make holes for a solid anchor fixation device to the surface of the sample. Testing apparatus is shown on Figure 1.

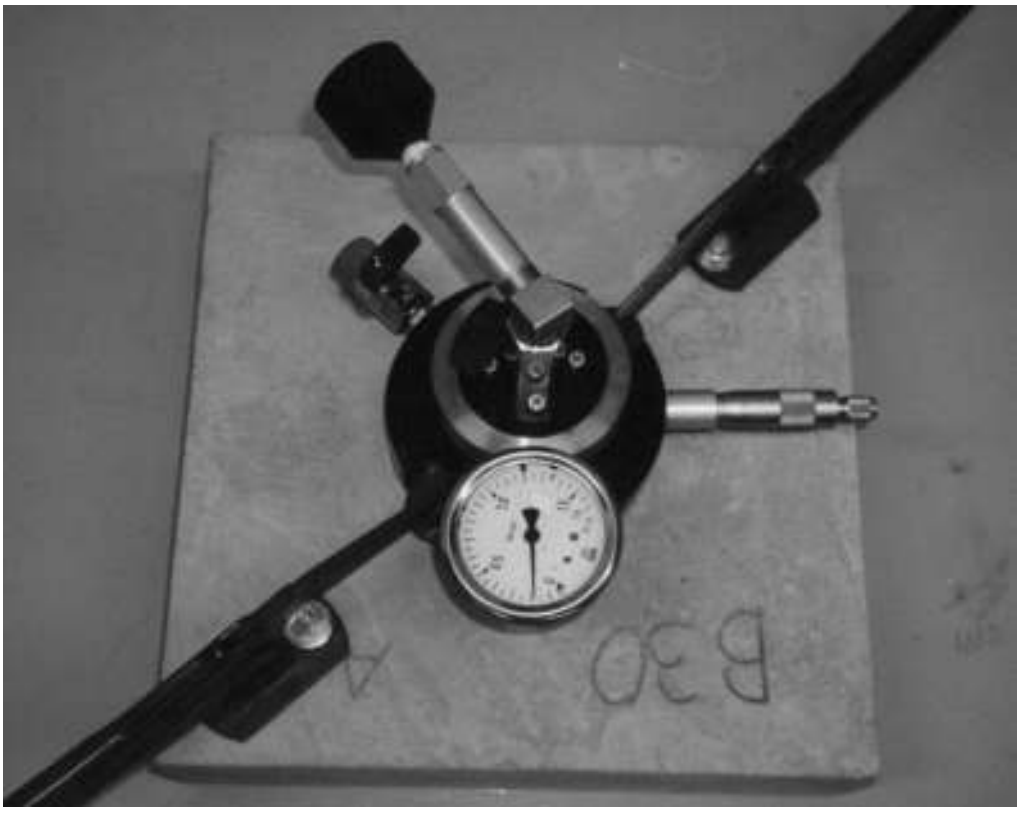

Figure 1 German Water permeation Test (GWT)

Torrent Permeability Tester (TPT)

Torrent Permeability Tester (TPT) was used for measuring. The apparatus works by creating a vacuum in the concrete derives vacuum pump and measuring the flow of fair from the surface layer of concrete over the bichamber cell by reducing the value of vacuum for specific value. From the measured time and changes in air pressure flowing into the middle chamber is calculated permeability coefficient k_T for air [2]. This is expressed in 10^{-12} m^2. Calculation flow of the medium pore structure of the inner cylinder chamber probe is a very complex process and is calculated by the Poiseuill's equation.

Torrent permeability tester (Figure 2) is a considerable advantage that the entire process of calculating the permeability coefficient k_T and depth of penetration vacuum happening in software. The instrument measures variation of the pressure and volume of air and automatically evaluates the display after the measurement readings can be deducted. The process of one measurement does not take more than 12 minutes, depending on the quality of concrete. A vacuum pump is used for creating a vacuum. This method has many advantages. Compared to other measuring instruments stands quite easy to handle. We do not need to make holes for measuring or dribbling anchors for fixation device. Lightweight for easy handling during the measurement. The test site does not need to be specially prepared or modified. We can perform tests in both laboratory and directly in situ. TPT is classified as a non destructive testing.

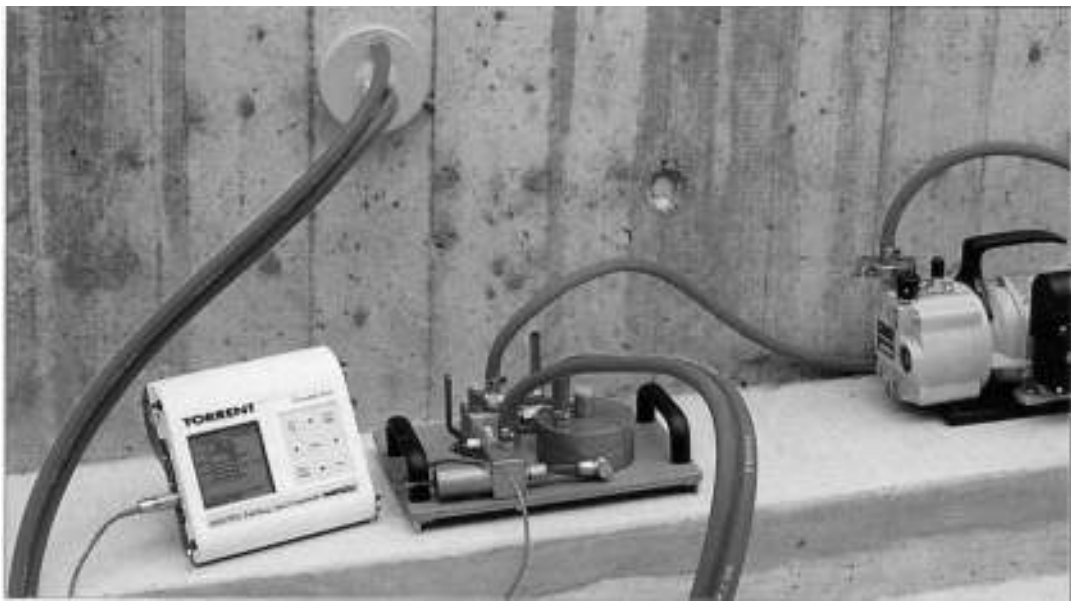

Figure 2 Torrent Permeability Tester (TPT)

Initial Surface Absorption Test (ISAT)

The test consists of the measurement of water flow into the test specimen through a known surface area. The contact area is defined by a plastic cell sealed onto the surface. Measurement of the volume flow is obtained by measurement of the length of flow along a capillary of known dimension. The cell is manufactured from clear acrylic to allow

observation of the water level and ensure the complete renewal of air. A clear reservoir is connected to the inlet of the cell. The outlet of the cell is connected to a capillary tube with an affixed scale. A valve is fitted to the inlet side to isolate the reservoir. The cell size is normally 100 mm diameter although for some specimens it is necessary to use a smaller cell. The British Standards require a contact area of not less than 5000 mm^2 (80mm diameter) which cannot always be achieved on a small sample.

Other Testing Methods

Introduced measuring methods were supplemented by other testing, their location on testing sample is shown on Figure 3. The most important factor is in this case surface moisture, which was measured by capacity hygroscope Kakaso, where is after calibration determine specific humidity. For the consideration of mechanical properties were used traditional testing methods as a Schmidt hammer and bond test. Location of provided tests is shown on following figure.

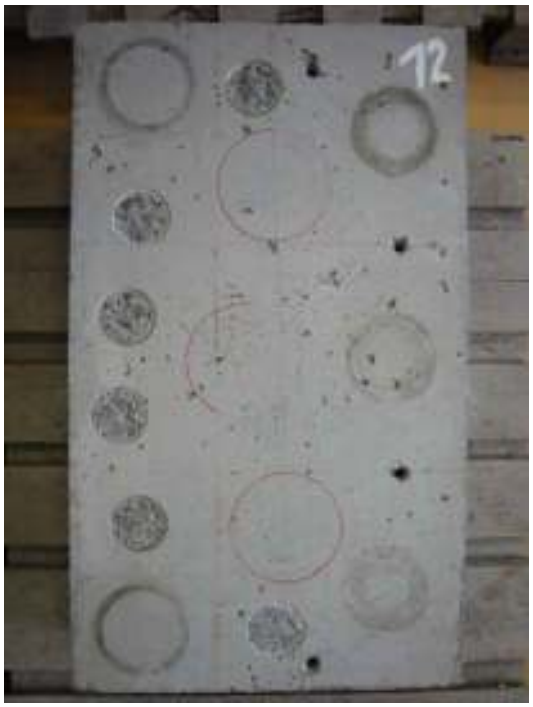

Figure 3 Location of provided measuring tests

DISCUSSION OF RESULTS

After measuring was gained number of various data describing quality of concrete surface layer. For testing were prepared block samples with base 400/100mm and height 700mm. Shape of this samples should present real production of fair-face concrete members. Average values of measured magnitudes by TPT and GWT are present on Table 2.

Table 2 General results of measuring by TPT and GWT

MIX.	TPT				GWT	
	Kakaso	Permeability coefficient $k_T.10^{-16}$	Translation of k_T on 3 % humidity	Surface quality	Permeability coefficient k_i	Durability
	%	m^2	m^2	1-5	m^2	yes/no
I	2,8	0,090	0,092	2 - good	$1{,}606.10^{-15}$	NO
II	2,5	0,434	0,265	3 - middle	$1{,}777.10^{-15}$	NO
III	4,0	0,021	0,039	2 - good	$2{,}272.10^{-15}$	NO
IV	3,2	0,015	0,013	2 - good	$2{,}277.10^{-15}$	NO

By the norm DIN 1045 parameter k_i (Table 3) can be used for durability evaluation. Surface layer is durable only in case of $k_i < 10^{-16} m^2$. Unfortunately did not reach durable concrete, it was caused by to high water/cement ratio, because all testing mixtures were designed to consistency S3 (180mm). Detailed values of measuring by ISAT are presented on Table 4.

Table 3 Classification of surface quality based on k_T

QUALITY OF CONCRETE COVER	INDEX	k_T (10^{-16} m^2)
Very poor	5	> 10
Poor	4	1,0 - 10
Middle	3	0,1 - 1,0
Good	2	0,01 - 0,1
Very good	1	< 0,01

Table 4 General results of measuring by ISAT and mechanical properties of surface layer

MIX.	ISAT							SCHMIDT HAMMER	BOND -TEST
	Kakaso	5 s	30 s	60 s	10 min	30 min	60 min		
	%	ml/m^2/s						MPa	MPa
I	2,6	1,08	0,98	0,91	0,27	0,16	0,12	39	3,1
II	2,4	1,56	1,46	1,32	0,23	0,15	0,11	34	2,2
III	4,0	0,24	0,16	0,13	0,09	0,05	0,03	39	3,2
IV	3,2	0,36	0,28	0,27	0,17	0,12	0,07	38	2,9

CONCLUSIONS

Measured durability parameters confirmed known relations in water content in pore system, surface humidity and changes incurred by different compaction through segregation of coarse aggregates [3]. Introduced testing methods are very different, because they are based on other physical principles and for permeability measuring they use other medium. In case of TPT we can gain interesting values for influence determination of aerial environments, where aggressive media are concentrated in air. On the other hand GWT brings worth data for moisture attack, which is often connected with penetration of many degradation reactants destroying the concrete micro-structure. Both methods are very hardly comparable, each of them characterizes other material property of concrete.

The results of experimental measurements show that the composition of concrete mixture significantly affects the properties of the surface concrete layer. An appropriate water-cement ratio is a key parameter for high surface layer quality of concrete. To test between similar, they have the same surface of the concrete surface moisture. Were therefore carried out comparative tests measuring [4] throughput and is currently testing and finishing calibration relationships that enable the conversion of the actual moisture to middle humidity of the concrete mass of 3 % thus allowing comparability of results in general.

ACKNOWLEDGEMENTS

The research work presented in this paper has been supported by the GAČR 103/09/H078.

REFERENCES

1. KEPPERT, M, VYTLAČILOVÁ, V, DVORSKÝ, T, REITERMAN, P, ČERNÝ, R. Vodotěsnost a permeabilita vysokohodnotného betonu, Stavební obzor, 2010, roč. 19, č. 5/2010, s. 145-148. ISSN 1210-4027.

2. ADÁMEK, J, JURÁNKOVÁ, A. Detection of Imperfection in Concrete Structure from Durability Viewpoint. XVI International Conference MCM - Mechanics of Composite Materials. Latvia. 2010. p. 20 - 25.

3. KADLECOVÁ, Z, ADÁMEK, J. Porovnání vodní a vzduchové propustnosti povrchových vrstev betonu. In XIV. Mezinárodní konference: Ekologie a nové stavební hmoty a výrobky (id 18292). VUSTAH. 2010. p. 364 - 367. ISBN 978-80-87397-02-2.

4. ADÁMEK, J, JURÁNKOVÁ, A, KUCHARCZYKOVÁ, B. Fibre Concrete And its Air Permeability, příspěvek na konferenci Proceedings of 5th International Conference Fibre Concrete 2009, ISBN 978-80-01-04381-3, CTU Prague, Praha, 2009.

Carbonation of Concrete: CO_2 Sequestration Potential vs Durability

P Woyciechowski
Warsaw University of Technology, Poland

The aim of the paper is to analyse the development of a theoretical model to predict the depth of carbonation in concrete. The experimentally determined model describes the depth of carbonation in function of exposure time, w/c ratio and early-age concrete curing conditions. It was assumed that the depth of carbonation as a function of the these variables is mathematically described by a hyperbolic function. According to such a model the carbonation process is self-terminating due to process of filling concrete pores with carbonation products in time. In the paper the results of tests of carbonation depth conducted in an environment with a natural concentration of CO_2 for concretes with various types of Portland cement were presented. Those results enabled the development of equations describing the relationship between depth and exposure time for each concrete. It is expected that the developed equations will provide a convenient tool for designing adequate thickness of concrete cover, sufficient to protect the reinforcement against corrosion.

Piotr Woyciechowski, Graduate at Faculty of Civil Engineering of Warsaw University of Technology (1990). Since 1991 a researcher at the Department of Building Materials Engineering at the Faculty of Civil Engineering of Warsaw University of Technology. Ph.D (1999). ACI member since 2000. Expert on building materials authorized by the Polish Society of Building Engineers.

Keywords: CO_2 sequestration, Carbonation, Modelling, Test methods

INTRODUCTION

The Portland cement based concrete absorbs carbon dioxide through carbonation process due to the reaction of alkaline calcium hydroxide and CO_2 from air. As a result calcium carbonate is produced inside concrete. The normal average concentration of CO_2 in atmospheric air is 380 ppm; however the higher values are recorded for industrialized areas. For example, concentration of CO_2 measured by the author in the Warsaw city center reached up to 430 ppm in the winter [1]. These values are seem high when consider the greenhouse effect. However, the carbonation process in such conditions is very slow (even slower than 1 mm per year in case of good quality concrete). Nevertheless, despite its low speed, the process is still very important from the viewpoint of durability of a reinforcement concrete. In humid conditions atmospheric CO_2 reacts with products of cement hydration (mainly with $Ca(OH)_2$) causing a decrease of concrete pH value and thus the neutralization of concrete cover which initiates a steel reinforcement corrosion [2]. In general – exposure to CO_2 reduces durability of reinforced concrete. For this reason, when designing reinforced concrete structures, the proper thickness of cover due to the need of protection against carbonation (XC environment classes according to EN 206-1) need to be determined. Minimal required values of cover thickness for each environment class (XC1-XC4) are given in Eurocode 2 – these values should provide the durability of the structure assumed by Eurocodes (e.g. for common building elements – minimum 50 years). At the same time concrete element can be considered as a material with certain potential for CO_2 sequestration. The calcium carbonate is a stable product of the carbonation reaction. The amount of CO_2 theoretically bound by concrete, depends on the cement content in concrete. The composition of cement or cement clinker can be calculated from the Steinour`s formula [3]. For a typical alite cement clinker, calculated value of "potential of CO_2 sequestration" is about 50-55% by weight of clinker [4]. Other investigations show that the actual mass of bound CO_2 does not exceed a quarter of this value [5].

Assuming that 1 kg of fully hydrated Portland cement is the source of about 0.3 kg of $Ca(OH)_2$ and typical level of hydration of cement in concrete does not exceed 93%, it can be calculated that each kilogram of Portland cement clinker is able to bind approximately 0.17 kg of CO_2. Contrary to that, the value of total CO_2 emissions from cement production is around 0.8 kg CO_2 per kg of Portland cement. Sequestration of CO_2 by Portland cement concrete could therefore improve the negative balance of the cement industry – the one of the major issuers of CO_2 emissions. Theoretically the emission value for Portland cement could be reduced during the life cycle (production – use, excluding, demolition) by 15-20% [4]. Of course the actual level of CO_2 sequestration is much lower, since only a part of the concrete surface of the structures is not protected against the carbonation process [6]. Furthermore, important factors are: rate of the process and its range (a carbonation depth). The concrete envelope around reinforcement is a safe CO_2 sequestration zone where a carbonation process does not reduce durability. As long as the carbonation front does not reach the reinforcement surface, corrosion is not initiated. Selecting the thickness of concrete cover that would prevent such risk during the exploitation time would be the optimal solution.

Selection of proper concrete cover thickness is a necessary condition for sustainable approach to the relationship: concrete ability of CO_2 sequestration – durability of reinforced concrete structure (Figure 1).

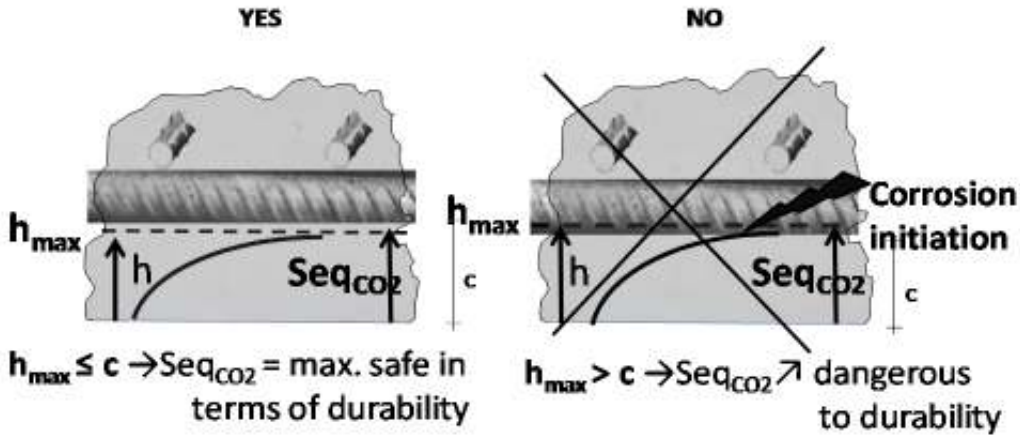

Figure 1 Illustration of a sustainable approach: the concrete cover thickness (c) and the depth of carbonation (h_{max})

A key issue for discussing sequestration potential of concrete is the answer to the question whether the carbonation progresses indefinitely or whether the process is by self-terminating nature and stops due to the densifying the concrete structure by the products of carbonation. Traditional approach to the matter is derived from Fick`s laws and shows carbonation progress as a continuous and infinite process that develops at a decreasing rate. It can be described by following model equation:

$$h = A + Bt^{0.5} \quad (1)$$

where h is a depth of carbonation, t is time of exposition, and A, B are material and technological constants. This particular model is referred to in all major publications in the field of carbonation [7 - 15]. Meanwhile, the author has published different variants of the model where main factors determining the carbonation (strength of concrete or class of strength, water-cement ratio, diffusion coefficient of CO_2 in concrete or the air permeability coefficient, capillaries and porosity, air humidity and ambient temperature) were taken into account [1, 16, 17, 18]. The earlier cited traditional models considered concrete as a material of constant internal structure, unchangeable in time. It should be highlight, that in case of concrete we are dealing with significant changes of structure related to exposure conditions. Carbonation process strongly affect those changes i.e. reducing porosity by filling pores with carbonation products, which on the other hand reduce diffusion of CO_2 [19, 20]. The fact that a significant reduction in porosity and simultaneously concrete structures sealing are a result of carbonation is documented in many publications, where values of 10-15% and even of 40% porosity reduction are given [8, 14, 15, 21]. Reported are also areas with no porosity in fully carbonated zones [22]. Taken into consideration above information it can be concluded that carbonation process may be considered as finite in time, limited to the period when the structure of concrete is still available for CO_2 penetration. The suggestion of a limited-time nature of carbonation has already been expressed by Fagerlund [23] in the form of hypotheses not confirmed by investigation.

The results of author's former research [16, 17, 18] confirmed that carbonation process can be considered as a process limited in time. However analysis of the results enabled author to claim, that that the finite carbonation depth in concrete, h, could be described according to following equation:

$$h = B + A \times t^{-0.5} \quad (2)$$

Moreover, the maximum depth of carbonation is limited by the asymptote described by equation:

$$\lim_{t\to\infty} h(t) = B \quad (3)$$

Above equations can be basis of designing the safe value of concrete cover thickness, also considered as an atmospheric CO_2 sequestration zone, that does not negatively influence the potential time of structure life.

EXPERIMENT DESCRIPTION

Research program assumed investigation of carbonation progress in time and statistical verification of hyperbolic modeling of carbonation as the approach proper in case of tested concretes. The study assumed variability of three material and technological characteristics (Table 1), two quantitative (water/cement ratio in range of 0.35 - 0.70 and initial water curing time: 2, 7 and 28 days) and one qualitative (type of cement: Portland cement CEM I 42.5R, fly ash cement CEM II/A-V 42.5 and blast furnace slag cement CEM III/A 42.5). The study major measurement was depth of carbonation change in time. In the framework of research program a number of tests showing the effects of carbonation (including the CO_2 diffusion coefficient, porosity, absorption, TGA and SEM microscopic observations) on concrete structure was performed. In addition, a routine identification of concrete properties was done (Table 1 presents the results for compressive strength and elastic modulus).

Carbonation tests were carried out for six years, in natural conditions, in the urban-industrial atmosphere of Warsaw. During the exposure the concentration of CO_2 was changing – the registered range was 290 (summer) - 430 (winter) ppm, which corresponded with a plants growth cycle. Concrete specimens of dimensions of 30 x 30 x 10 cm were exposed in unloaded state, under the influence of seasonal weather (sunshine, rain, snow).

Chemical test using thymol-phenolphtalein indicator [18] was the basic method of testing carbonation; the range of zone of pH ≥ 9,6 was treated as a depth of carbonation.

Compressive strength test was performed on cubes (150 mm), and the elastic modulus test – on the cylinders (150 x 300 mm), after 28 days of laboratory curing. Evaluation of the effects of carbonation on concrete microstructure was performed immediately prior to exposing the concrete to carbonation (the concrete age was 1-2 months) and then after 6 years of exposure. The measurements of CO_2 diffusion coefficient value were performed in chamber with constant high CO_2 concentration, in the fixed flow of carbon dioxide through 10 mm-thick specimen. The concrete porosity was determined using the experimental-computational method involving determining density (using pycnometer) and bulk density (with the use of paraffin) of irregularly shaped fragments taken from the subsurface zone of particular specimen.

Table 1 Concrete composition and basic properties

CONCRETE PROPERTIES		W/C RATIO					
		0.35	0.45	0.50	0.55	0.60	0.70
proportion for 1 m^3, kg	cement	510	460	435	410	385	335
	water	179	207	218	226	231	235
	aggregate	1740	1708	1700	1700	1708	1740
Concrete with CEM I 42.5R							
Compressive strength after 28 days, MPa		58.2	43.9	40.3	37.2	33.3	30.3
Elastic modulus, GPa		33.6	32.4	32.1	-	29.8	27.2
Concrete with CEM II/A-V 42,5R							
Compressive strength after 28 days, MPa		55.1	41.7	38.2	36.8	31.5	25.5
Elastic modulus, GPa		28.3	26.4	25.1	24.7	23.8	16.6
Concrete with CEM III A 42,5R							
Compressive strength after 28 days, MPa		44.4	34.2	27.3	27.7	24.2	18.1
Elastic modulus, GPa		25.3	24.1	21.9	22.7	-	-

RESULTS AND DISCUSSION

Investigation that lasted six years allowed to verify the mathematical model describing the carbonation process in time. The progressive densifying of concrete structure by products of carbonation leads to CO_2 diffusion blockage in concrete. In such case the traditional parabolic model $h(t^{0,5})$ [1, 16, 17,] should be replaced by hyperbolic model $h(t^{-0,5})$ limited by asymptote parallel to the axis of time, interpreted as the maximum carbonation depth which can be reached after the termination of the diffusion CO_2 in carbonated concrete.

Adequacy of proposed exponent of value -0.5 and the exponent of value 0.5 (traditional) was examined (Figure 2). The results of about 500 measurements obtained for three types of concrete in period of 6 years exposure (Table 2) were the basis of verification. Significantly higher values of coefficients of determination were obtained in case of $h(t^{-0,5})$ model. Exponent -0.5 was adopted as a basis of further discussion on the modeling of carbonation process according to equation (2). Hyperbolic models in the form (2) were determined for the studied combinations of cement type, W/C ratio, time of initial curing, t_{ec}. Table 3 shows very strong correlation of values obtained in the way of experiment and values calculated using mathematical model (correlation coefficient R, ranged from 0.81 to 0.99). Some of the results also revealed the concrete microstructure tendency to densification, as a result of carbonation (Table 4).

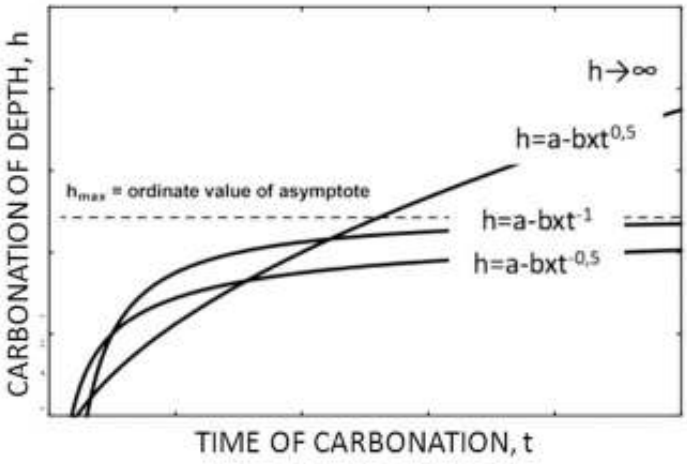

Figure 2 Different models of depth of carbonation progress in time (asymptote for model with -0.5 exponent),

Table 2 Depth of carbonation after 6 years of exposition in natural atmospheric conditions; t_{ec} – time of early curing in water

Type of cement	Time of carbonation, years	DEPTH OF CARBONATION IN mm, FOR CONCRETE WITH W/C:																	
		0.35			0.45			0.50			0.55			0.60			0.70		
		for t_{ec}, days			for t_{ec}, days			for t_{ec}, days			for t_{ec}, days			for t_{ec}, days			for t_{ec}, days		
		2	7	28	2	7	28	2	7	28	2	7	28	2	7	28	2	7	28
CEM I 42,5R	1	1.1	0.2	0.2	1.3	1.1	0.3	-	-	-	2.2	2.0	2.0	-	-	-	-	-	-
	2	-	-	-	-	-	-	2.2	1.7	1.7	-	-	-	3.9	3.7	3.2	6.7	5.0	3.4
	3	1.3	0.4	1.0	2.2	1.8	0.8	3.4	2.3	1.9	4.1	3.3	2.4	5.2	3.9	3.8	7.2	5.9	4.1
	4	1.7	1.5	1.5	2.5	1.9		3.7	2.5	2.1	4.1	3.7	2.7	5.3	4.0	3.9	7.4	6.0	4.3
	6	1.8	2.2	2.3	4.2	3.1	4.2	4.7	4.6	4.2	-	5.3	4.0	7.6	5.2	6.1	8.8	6.3	6.3
CEM II/A-V 42,5R	1	1.3	0.6	0.6	1.3	1.7	1.7	2.0	1.3	2.1	2.6	3.1	1.8	2.4	2.4	2.4	4.9	5.5	4.3
	2	1.4	0.9	0.7	1.8	2.2	1.3	2.3	2.9	2.6	3.3	3.0	2.3	4.2	2.7	4.5	8.6	6.1	6.3
	3	1.5	0.8	1.2	2.0	2.0	1.0	3.7	3.6	2.7	4.5	2.7	3.2	5.2	4.9	4.6	11.0	9.9	8.4
	5	1.8	1.2	1.1	2.0	1.4	1.1	4.4	4.3	2.9	4.5	3.7	-	6.5	-	-	15.6	14.3	12.8
CEM III A 42,5R	1	0.7	0.8	0.6	2.8	3.3	3.2	7.5	5.8	5.5	5.5	3.3	3.6	4.4	6.8	5.1	-	-	-
	2	0.6	0.8	0.7	4.3	4.5	3.2	7.3	7.1	7.5	6.4	6.9	4.9	6.4	9.8	5.9	9.7	11.0	7.8
	3	1.4	1.0	0.8	6.2	5.0	5.4	9.1	7.1	8.2	7.4	10.4	7.0	10.8	10.0	9.5	9.7	13.2	7.8
	5	1.7	1.5	0.8	6.1	4.1	5.0	9.6	7.8	8.2	6.8	9.8	6.1	11.0	11.9	10.3	15.4	13.1	12.8

Table 3 Maximal depth of carbonation (asymptote) for -0.5 exponent model

TYPE OF CEMENT	TIME OF EARLY CURING, DAYS	RESULT OF CARBONATION MODELING FOR CONCRETE WITH W/C:					
		0.35		0.5		0.7	
		A mm	R	A mm	R	A mm	R
CEM I 42,5 R	2	2.2	0.86	7.9	0.99	11.1	0.91
	7	2.9	0.81	7.6	0.89	8.1	0.96
	28	3.2	0.92	6.6	0.82	9.4	0.91
CEM II/ A-V 42,5R	2	2.1	0.89	6.1	0.91	22.5	0.97
	7	1.5	0.87	6.7	0.99	19.2	0.87
	28	1.6	0.86	3.6	0.99	17.7	0.92
CEM III 42,5R	2	2.4	0.82	11.1	0.82	24.3	0.87
	7	1.8	1.8	9.3	0.97	17.1	0.84
	28	1.0	1.0	10.9	0.96	20.6	0.87

A- asymptote ordinate, mm; R-regression coefficient

Table 4 Effects of carbonation on concrete microstructures

Type of cement	Time of early curing, days	DOCUMENTATION OF CARBONATION EFFECTS FOR CONCRETE WITH W/C RATIO:									
		0.35		0.50		0.55		0.60		0.70	
CEM I 42,5R	**P**	**Porosity , %, after 28 days of curing P_{28d} and after 6 years of carbonation P_{6y}**									
		P_{28d}	**P_{6y}**	**P_{28d}**	**P_{6y}**	**P_{28d}**	**P_{6y}**	**P_{28d}**	**P_{6y}**	**P_{28d}**	**P_{6y}**
	7	11.5	9.5	13.7	10.8	-	-	-	-	15.4	11.3
	D_{CO2}	**CO_2 diffusion coefficient, m^2/s, after 28 days of curing D_{28d} and after 6 years of carbonation D_{6y}**									
		D_{28d}	**D_{6y}**	**D_{28d}**	**D_{6y}**	**D_{28d}**	**D_{6y}**	**D_{28d}**	**D_{6y}**	**D_{28d}**	**D_{6y}**
	7	$2x10^{-8}$	$0.55x10^{-8}$	-	-	$5x10^{-8}$	$1.6x10^{-8}$	-	-	$10x10^{-8}$	$7x10^{-8}$
	TGA	**$CaCO_3$ and $Ca(OH)_2$ content , %, after 6 years of carbonation in surface zone 0-3mm (S) / internal zone ~25 mm (INT)**									
		$CaCO_3$ S/INT	**$Ca(OH)_2$ S/INT**	**$CaCO_3$ S/INT**	**$Ca(OH)_2$ S/INT**	**$CaCO_3$ S/INT**	**$Ca(OH)_2$ S/INT**	**$CaCO_3$ S/INT**	**$Ca(OH)_2$ S/INT**	**$CaCO_3$ S/INT**	**$Ca(OH)_2$ S/INT**
	7			13.0/8.4	0/4.1	-	-	13.9/9.8	0/4.5	15.0/9.1	0/2.5
	28	11.4/10.7	2.5/4.1	-	-	-	-	-	-	19.6/9.0	0/5.3
	N	**Water absorption, mass %, after 28 days of curing N_{28d} and after 6 years of carbonation N_{6y}**									
		N_{28d}	**N_{6y}**	**N_{28d}**	**N_{6y}**	**N_{28d}**	**N_{6y}**	**N_{28d}**	**N_{6y}**	**N_{28d}**	**N_{6y}**
	7	4.5	3.4	5.4	4.5	5.9	5.4	5.8	5.6	6.2	5.3
CEM II/A-V 42,5	7	3.7	3.2	4.3	4.0	4.4	4.0	4.3	3.4	4.5	3.4
	28	3.4	3.6	4.4	4.2	4.4	4.4	4.5	3.8	4.4	4.2
CEM III A 42,5	7	4.5	4.4	4.8	4.8	4.8	4.1	4.8	4.1	5.4	4.7
	28	3.9	4.0	4.2	4.2	4.2	4.2	4.8	4.4	5.1	4.6

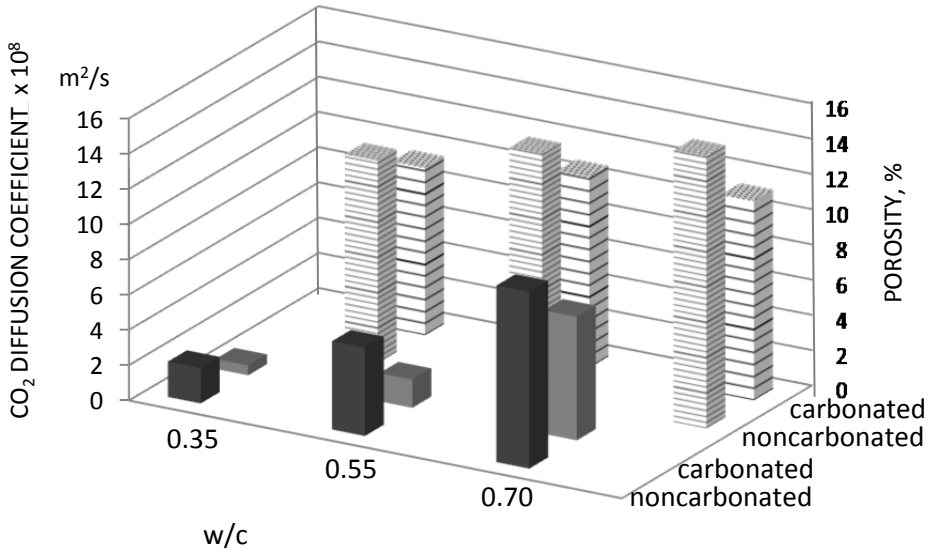

Figure 3 Changes in porosity (striped) and CO_2 diffusion (solid) due to 6 years of carbonation for concrete with different W/C ratio

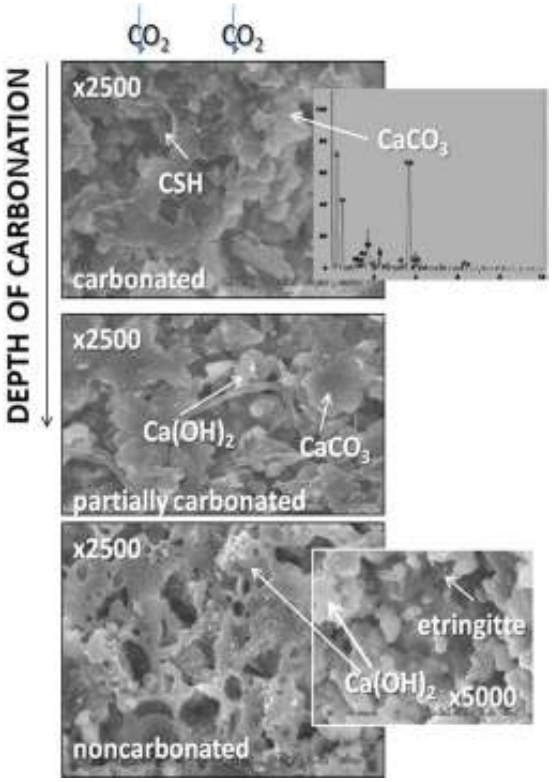

Figure 4 Changes in the microstructure as a result of the carbonation of concrete - concrete with CEM I, W/C = 0,5, t_{ec} = 7 days

A 20-25% decrease of porosity was measured after six years of carbonation (relationships P_{28d} and P_{6y} – Table 4). It was accompanied by an up to fourfold reduction in the CO_2

diffusion coefficient (D_{CO2}); this effect was stronger in case of concretes of lower W/C ratios (Figure 3). SEM images (Figure 4) clearly showed thickening of the structure by filling pores with calcium carbonate as a result of the carbonation progress. The high calcium carbonate content was identified using the XRD method. Traces of calcium hydroxide were seen on the carbonated surface of specimen and values of 4 - 5% $Ca(OH)_2$ content in its noncarbonated core. Relatively small changes of water absorption ability as a result of carbonation, especially at low W/C ratios, were observed. This effect was probably a consequence of the fact that the initial absorption tests were performed on regular cubic specimens while the tests conducted after six years of carbonation were performed on irregular pieces of concrete with fresh breaks; in the second case the open pores on the surface of breaks may have caused an overestimation of absorption results.

The determined asymptote value allowed to estimate the concrete potential of CO_2 sequestration (S_{CO2}) by 1 m^2 of carbonated surface. Assuming that:

h_{max}, m – maximal depth of carbonation
C, kg/m^3 – Portland cement content in concrete
s_{CO2}, kg/kg – potential of CO_2 sequestration by clinker
p_{cl}, kg/kg - clinker content in Portland cement,

potential of CO_2 sequestration by concrete – S_{CO2}, kg/m^2 can be calculated as follow:

$$S_{CO2} = h_{max} \cdot s_{CO2} \cdot C \cdot p_{cl} \quad (4)$$

Two examples based on the data from Table 3:

- C45/50 concrete with CEM I 42.5; t_{ec} = 2 days, W/C = 0,35
  S_{CO2} = 0.0022 m x 0.17 kg/kg x 510kg/m^3 x 0.95kg/kg = 0.18kg/m^2 – the maximal sequestration of CO_2 by 1 m^2 of Portland cement concrete surface,

- C20/25 concrete with CEM I 42,5, t_{ec}=2 days, W/C=0.7)
  S_{CO2} = 0,0094 m x 0.17 kg/kg x 335 kg/m^3 x 0.95 kg/kg = 0.51 kg/m^2 – the maximal sequestration of CO_2 by 1 m^2 of Portland cement concrete surface.

The results showed that the CO_2 sequestration potentials are due to the strength class of concrete; the S_{CO2} decreases with increasing of concrete strength. Unfortunately the value of the CO_2 sequestration potential of concrete is small compare to the CO_2 emission in Portland cement production.

CONCLUSIONS

The results and statistical analysis presented in this study provided compelling confirmation of the hypothesis describing a self-terminating nature of carbonation. The comparison of the results of the depth of carbonation and set of models for the tested range of concrete showed that:

- among the variables used in the study, the most essential influence on the carbonation process presented water/cement ratio – the higher W/C value, the greater depth of carbonation;

- the effect of cement type was visible at higher values of W/C ratio – in such cases the cement additives caused significant increase in the depth of carbonation; at low W/C ratio the effect was relatively small;
- time of the initial cure, t_{ec} affected the course of the carbonation but it was not a strong influence, greater susceptibility to carbonation showed shortly cured concrete; however the differences in depth of carbonation were not noticeable in case of concretes cured for 7 and 28 days.

It was demonstrated that decrease in porosity after 6 years of carbonation reached 20-25% and was accompanied by up to fourfold reduction of CO_2 diffusion coefficient. The effect was more intense at lower W/C ratios.

The conclusions on the multiannual course of carbonation have been drawn on the base of results of 5 - 6 years-long investigation. After such period of exposition in urban-industrial conditions the process is advanced in moderate extent – about 50% of calculated asymptote.

The time needed to verify correctness of models in more advanced way is much longer, at least 20 years, providing the process progress in at least 80% advance. The verification of the model can be also carried out in accelerated testing conditions. The higher level of CO_2 concentration, the higher degree of carbonation and the sufficient carbonation degree is obtained after only few months of testing. Predicted covariance of CO_2 concentration and time values due to the progress of carbonation is a subject of the author's ongoing research.

ACKNOWLEDGMENTS

This work has been done in the framework of project granted by Polish Ministry of Science and High Education – grant number N N506 257137. The author is thankful to Professor L.Czarnecki, Department of Building Materials Engineering at the Warsaw University of Technology for his valuable discussion and remarks.

REFERENCES

1. WIĘCŁAWSKI, R. Concrete carbonation in urban-industrial conditions, doctoral thesis, Warsaw University of Technology 2002, (in Polish).
2. CZARNECKI, L, EMMONS, P. Repair and protection of concrete, 2002, Polski Cement Sp. z o.o. (in Polish).
3. STEINOUR, H H. Some effects of carbon dioxide on mortars and concrete: a discussion, Journal of ACI, 1959, 30, pp905-907.
4. NAIK, T R, KUMAR, R. Global warming and cement-based materials, 2010, UWM Center for By-Products Utilization, Milwaukee, Wisconsin, USA.
5. MONKMAN, S, SHAO, Y. Assessing the carbonation behavior of cementitious materials. Journal of Materials in Civil Engineering, 37(2), 2006, pp302-310.
6. DIVSHOLI, B S, CAHYADI, J H. Concrete carbonation under wide range of conditions. VDM Verlag Dr. Muller, 2009, Saarbrucken, Deutschland.

7. CHANG, C F, CHEN, J W. The experimental investigation of concrete carbonation depth, Cement and Concrete Research, 36(9), 2006, pp1760-1767.
8. CURRIE, R J. Carbonation depths in structural-quality concrete: an assessment of evidence from investigation of structures and from other source, Building Research Establishment Report (UK), 1986.
9. MAEKAWA, K. Modeling of concrete performance hydration, microstructure formation and mass transport, 1991, E&FN SPON London, pp77-100.
10. PAPADAKIS, V, VAYENAS, C, FARDIS, M. Fundamental modeling and experimental investigation of concrete carbonation, ACI Material Journal 4(88), 1991, pp363-373.
11. SAETTA, A, VITALIANI, R. Experimental investigation and numerical modeling of carbonation process in reinforced concrete structures, Cement and Concrete Research 35, 2005, pp958-967.
12. ŚCIŚLEWSKI, Z. Ochrona konstrukcji żelbetowych, 1999, Arkady, Warszawa (in Polish)
13. UOMOTO, T, TAKADA Y. Factors affecting concrete carbonation rate, Durability Build. Mater. Components 6, 1993, pp1133-1141.
14. WANG, X-Y, LEE, H-S. A model for predicting the carbonation depth of concrete containing low-calcium fly ash, Construction and Building Materials 23, 2009, 725–733
15. WIECZOREK, G. Reinforcement corrosion initiated by chlorides or cover carbonation, 2002, Dolnośląskie Wydawnictwo Edukacyjne, Wrocław (in Polish).
16. CZARNECKI, L, WOYCIECHOWSKI, P. Model of concrete carbonation as limited process - experimental investigations of fluidal ash concrete, Proceedings of International Conference: Brittle Matrix Composites 9, Eds. A M Brandt, V.C. Li, I.H.Marshall, 2009, pp183-194.
17. CZARNECKI, L, WOYCIECHOWSKI, P. Model karbonatyzacji betonu z popiołem fluidalnym, Proceedings of 17 Theoretical Foundations of Civil Engineering, Polish-Ukrainian-Lithuanian Transactions, Eds. W.E.Szcześniak, A.Zbiciak, 2009, pp571-580.
18. CZARNECKI, L, WOYCIECHOWSKI, P. Metody oceny przebiegu karbonatyzacji betonu, Materiały Budowlane 2/2008 (in Polish) pp5-8.
19. PARROT, L J. Review of carbonation in reinforced concrete, 1987, Cement and Concrete Association, Wexham Springs, UK.
20. SANJUAN, M, ANDRADE, C, CHEYREZY, M. Concrete carbonation tests in natural and accelerated conditions, Adv. in Cem. Res. 15(4), 2003, pp171–180.
21. VILLAIN, G, PLATRET, G. Two experimental methods to determine carbonation profile in concrete ACI Material Journal, 103(4), 2006, pp265-271.
22. RIMMELE, G, BARLET-GOUEDARD, V, PORCHERIE, O, GOFFE, B, BRUNET, F. Heterogenous porosity distribution in Portland cement exposed to CO_2-rich fluids, Cement and Concrete Research 38, 2008, pp1038-1048.
23. FAGERLUND, G. Durability of concrete structures, 1997, Arkady (in Polish)

Development of a tool for measuring resource sustainability in construction materials and products

J E Halliday[1], T D Dyer[1], M R Jones[1], T A Harrison[2]
1 – University of Dundee, UK
2 – Private Consultant, France

This paper reports aspects of the development of an indicator for measuring the environmental impact of the use of resources in the manufacture of construction products. This was deemed necessary on the grounds that current established indicators of resource use placed insufficient emphasis on the relative scarcity of that resource. The proposed indicator discussed in this paper compiles the residual lives of all the resources which are employed in manufacturing a product and through the application of a characterisation system generates a current scarcity score (CSS) which is used as an indicator of resource sustainability with a higher score indicting lesser sustainability. Based on comparison against a set of criteria devised to select a characterisation system which best reflects the need for sustainability, along with the uncertainty of predicting future availability of relatively plentiful resources, a hyperbolic function has been selected.

Dr Judith E Halliday is a Research/Teaching Fellow within the Concrete Technology Unit at the University of Dundee. She has been involved in numerous projects relating to sustainable and environmental issues of recycling materials in concrete construction. She has now shifted her focus on the awareness of the depletion of natural resources and the impact of their use in construction as a whole.

Dr Thomas D Dyer is a Lecturer in the Concrete Technology Unit at the University of Dundee. His research has primarily involved investigation of interactions of by-products with cement. He is also involved in applying life-cycle assessment techniques to construction. Recently his work has extended to include imprinting of biomimetic microstructures in construction materials, and interactions of brownfield contaminants with fresh concrete.

Professor M Roderick Jones is the Director of the Concrete Technology Unit at the University of Dundee. A renowned practitioner in the field of concrete technology, he is a member of numerous national and international technical committees and has published extensively on many aspects of concrete technology, cement science and sustainable construction.

Professor Thomas A Harrison is a Private Consultant in France, serving on numerous British, European and ISO standards committees as well as a visiting industrial Professor to the Concrete Technology Unit, University of Dundee, UK

Keywords: Natural resources, Residual life, Scarcity score, Sustainability

INTRODUCTION

This paper reports aspects of the development of an indicator for measuring the environmental impact of the use of resources in the manufacture of construction products. This was deemed necessary on the grounds that current established indicators of resource use placed insufficient emphasis on the relative scarcity of that resource. It is important to address this aspect of resource availability on the grounds that such an indicator should present a measure of sustainability. Since sustainable development can be defined as "development that meets the needs of the present without compromising the ability of future generations to meet their own needs" [1] (World Commission on Environment and Development, 1987), it is essential that the extent to which the use of a resource compromises the availability of the resource to future generations should be reflected by the indicator. The new indicator discussed in this paper addresses the issue of resource scarcity through the concept of 'residual life'.

The residual life is defined as the quantity of a resource available divided by its rate of extraction. This gives the period of time before the quantity of resource is exhausted. The quantity which is used depends on what the residual life that is being calculated aims to indicate and the accuracy of data which is required. Quite often the 'mineral reserve' (the quantity of a resource which is known to be economically feasible for extraction) is used on the grounds that this is a value which is likely to have been estimated with some accuracy and can be used to give an indication of the 'guaranteed' life-time of a resource. However, in reality, there will be quantities of resource present on Earth which are currently unknown, or inaccessible under contemporary economic and technological restraints, but which could become more accessible in future. With this is mind, the indicator discussed in this paper utilises the 'mineral resource' as the quantity.

The mineral resource is defined as the amount of resource which is both demonstrated and for which reasonable prospects exist for eventual economic extraction. This quantity is, thus, more speculative than the reserve. However, it still cannot incorporate the prospect of future discoveries of deposits of that resource, and so residual lives derived from such a value are best viewed as being indicative of the magnitude of time before resource exhaustion.

The two most commonly encountered indicators of resource use are total material requirement (TMR) [2] and the abiotic depletion potential (ADP) [3]. TMR is wholly unsuitable for addressing the matter of resource scarcity, since it is simply the mass of raw materials used to produce a product. The ADP does address scarcity, in that its formula incorporates terms for resource quantity and rate of use. However, the form that its formula takes means that the residual life is not well represented.

The proposed indicator discussed in this paper compiles the residual lives of all the resources which are employed in manufacturing a product and through the application of a characterisation system generates a current scarcity score (CSS) which is used as an indicator of resource sustainability with a higher score indicting lesser sustainability.

This approach readily permits the incorporation of biotic resources and water as resources, and also allows the issue of products containing recycled materials to be easily addressed. However, these issues are not dealt with in this paper, which concentrates exclusively on the approach which has been taken to establishing the most appropriate means of converting residual life values into a CSS value.

IMPACT SCORE APPROACH

Before discussing the various approaches to obtaining a CSS value for a construction product, it is necessary to outline the procedural steps which are followed to arrive at that point. In brief, the steps are: compile and inventory of constituent resources; compile an inventory of energy resources; convert energy resources into volumes of resource; obtain residual lives for each constituent resource and calculate a CSS value for that resource; sum the CSS values to give an overall CSS for the product. The steps are described in more detail below.
The approach taken to calculating Impact Scores for products is outlined below.

1. A list of constituent resources required to manufacture a product was compiled from the literature or from information supplied by manufacturers.

2. The energy required to produce a given mass of product from the constituent resources is then determined from similar sources. This is broken down into the constituent energy sources shown in Table 1. Where electricity is included in this inventory, a European fuel mix is used to calculate the proportions of various energy sources used to generate the electricity. This is shown in Table 1. Where energy data is provided with electricity declared as 'delivered' electricity, a correction was applied to take into account the efficiencies of the different generation methods (also shown in Table 1).

   Because of the wide range of methods that can be used to generate electricity from biomass, an efficiency of 50% is assumed, which is likely to be an overestimate. However, the small contribution made by this source means that this assumption has a negligible influence on the calculation results. The contribution from the 'Other' sources of energy was discounted, since no detailed breakdown could be obtained, and because the vast majority was likely to be wind, solar and geothermal, and thus not contributing to the use of natural resources.

   Where required, data relating to energy for transportation is obtained for road freight from Roumegoux [4]. Data for air freight is from Kalivoda and Kudrna [5] and data for waterborne and rail transportation was from Rizet et al [6].

   Where the energy provided for the manufacture of the product did not include the production of the resources themselves, the energy requirement and breakdown of energy sources is also obtained for each resource and added to the energy inventory.

3. From the energy data, volumes of each of the energy resources are calculated using standard values of density and upper heating values. In the case of natural gas, the volume of a calorific equivalent of hard coal is used. Hard coal was selected on the grounds that it is similarly scarce in comparison to natural gas.

4. For each resource (including energy resources) two pieces of information are used to calculate their contribution to the product's CSS – the volume of resource used to make a given mass of product and the residual life of the resource.

   Once this information is available, characterisation is conducted by obtaining the CSS value appropriate to the residual life value obtained for each resource. During the initial development of the indicator, this was conducted in two ways to evaluate the implications of two different approaches. Firstly, a stepped system of characterisation values, as shown in Figure 1 and Table 2

Table 1 European fuel mix and electricity generation efficiencies

ENERGY SOURCE	PROPORTION OF EUROPEAN FUEL MIX FOR ELECTRICTY GENERATION, %[7]	EFFICIENCY, % [8, 9]
Hard coal	18.3	32
Brown coal	10.2	32
Crude oil	4.2	32
Natural gas	20.9	50
Biomass	1.0	50
Hydroelectricity	13.0	100
Nuclear	30.2	34
Other	2.2	-

. Using this approach, the CSS for an individual constituent resource was calculated using the equation

$$S_{NRi} = aw.V_{NRi}$$

where a = the allocation weighting for co-products applied in accordance with prEN15804;

w = the characterisation value selected from Table 1, based on the residual life of the resource, R_{NRi};

V_{NRi} = volume of resource R_i used to manufacture the product (m^3).

Secondly, a continuous characterization system was applied using the equation;

$$S_{NRi} = a.V_{NRi}.\left(206.9e^{-0.0047R_{NRi}} + 73.7e^{-0.0003R_{NRi}}\right)$$

where R_{NRi} = the residual life of the resource (years).

The curve formed by this equation is also plotted in Figure 1.

5. The overall score for a product was then obtained from the sum of all the individual resource scores:

$$CSS_P = \sum CSS_{NRi}$$

Evaluation of a number of different types of construction product identified issues with the two approaches to characterisation:

- the stepped system, whilst clearly easy to use, was potentially unfair where resources' residual lives were located close to the end of steps in the characterisation profile.

- the continuous system clearly avoided this problem, but created problems where large volumes of resources with long residual lives produced large scores, due to the continuous curve in Figure 1 having a relatively large value at high residual lives.

With these observations in mind, it was decided that a continuous characterisation system was most appropriate, but that modification and refinement of the characterisation function was likely to be necessary. This process is described in the following section.

Table 2 Stepped characterisation values

RESIDUAL LIFE (R_{NRi}), years	CLASSIFICATION	CHARACTERISATION VALUES PER UNIT VOLUME
≤ 200	Critical (with respect to future availability)	150
210 to 600	Concern (with respect to future availability)	75
610 to 1500	Short residual life	50
1600 to 5000	Medium residual life	20
≥ 5500	Long residual life	0

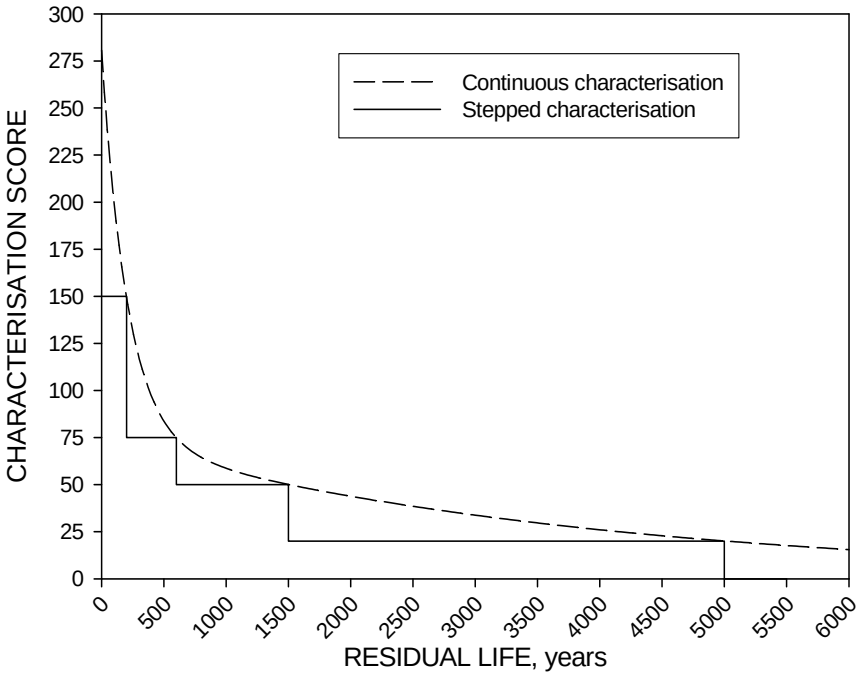

Figure 1 Stepped and continuous systems for characterisation.

MODIFICATION TO WEIGHTING SYSTEMS

From the outset it was proposed that the characterisation be the product of the volume and residual life with a maximum value of 5000 years. There are numerous systems that can be adopted and this paper looks at eight, namely; linear, negative linear, parabolic, circular, $\log_e$(residual life), $(\log_e(\text{residual life}))^2$, cubic spiral and hyperbolic. These can all be manipulated to give acceptable characterisation scores for any given residual life. All of these functions have been transposed to give higher weightings at shorter residual lives. Figure 2 shows the characterisation systems as a percentage of the score at a residual life of 100 years.

There is a characterisation value of zero beyond a residual life of 5000 years and all but one of the following systems adopts this benchmark. A negative linear system for characterisation values, given by the equation:

Characterisation Value = 5000 – residual life in years

A parabolic function ($y = ax^2$) is the simplest of the non-linear functions (it should be noted that the constant 'a' has been set at 10^{-4} to give values within the range 0–2500). The relationship for a circular curve is determined by ($y^2 + x^2 = 5000^2$). Figure 2 shows the characterisation values based on $\log_e$(residual life) and ($\log_e$(residual life))^2 as a percentage of the score at a residual life of 100 years.

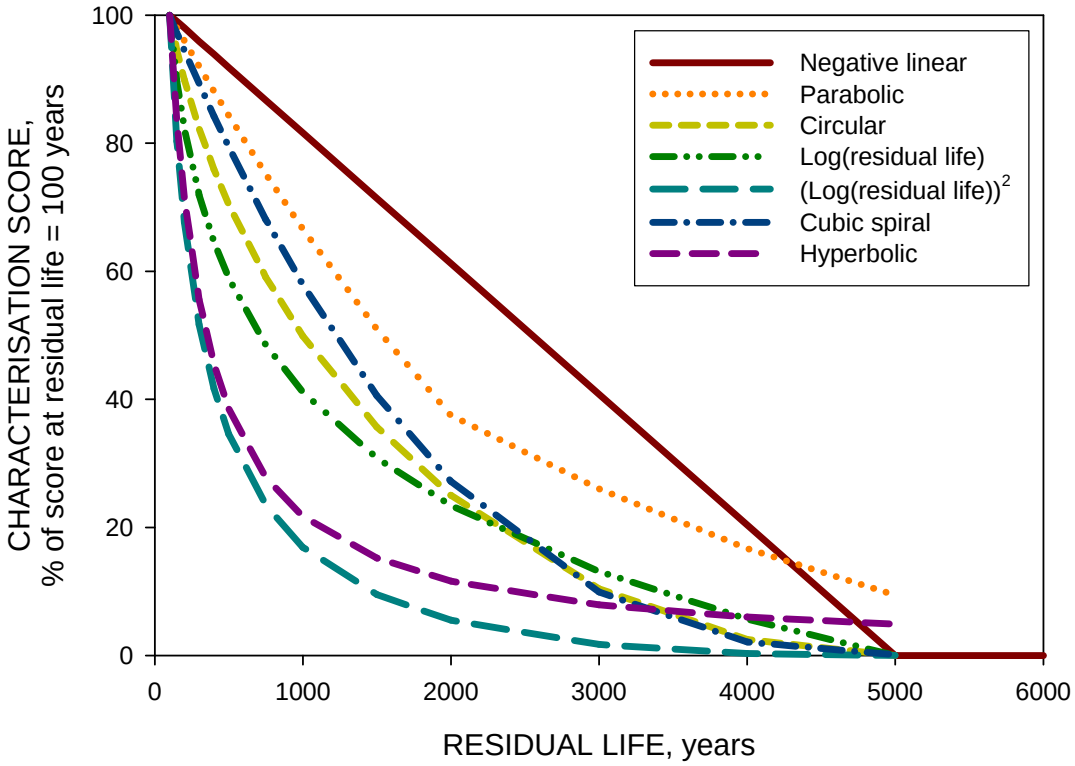

Figure 2 Characterisation system expressed as a percentage score at 100 years residual life

The $\log_e$ (residual life) and ($\log_e$ (residual life))² characterisation values give a rapid increase in weighting at short residual lives, but most of this occurs during residual lives of less than 100 years.

A characterisation values based on a cubic spiral are presented in Figure 2 with the curve being tangential to the x-axis at 5000 years. Also shown in Figure 2 is s hyperbolic function, which gives a symmetrical curve. The characterisation values are given by the equation:

Characterisation Value = ab/(b + residual life in years)

where; a = 500 and b = 150.

DISCUSSION

Before evaluating the different characterisation systems, a number of criteria were defined to allow the most appropriate system to be identified. These are outlined below.

1. There should be proportionally higher values for shorter residual lives to reflect the lesser sustainability of using such resources.

2. The majority of decline in score with residual life should occur within the 0 – 750 year range, since this is where it is argued the most concern for sustainability should be placed. However the decline should not occur over too short a timeframe.

3. Given the uncertainties with predicting very long residual lives, particularly with respect to patterns of use, the ideal characterisation system should have modest changes in value at long residual lives.

Outputs of the different systems in numerical form are provided in Table 3.

The linear characterisation system does not satisfy criteria 2 and 3, since the change in weighting is the same regardless of whether, for example, the residual life is changed from 200 to 100 years (halving the life) or from 5000 to 4900 years.

The parabolic characterisation system does not produce an ideal relationship, as the weighting for a residual life of 3000 years is about 20% of the maximum value and, therefore, does not satisfy the second and third criteria, which would be biased against resources with long residual lives. Similarly, the circular function gives relatively high characterisation value for longer residual lives.

The cubic spiral curve gives modest changes at long residual lives, but it is not sufficiently discriminating at the shorter, more critical, residual lives. The same is true for the $\log_e$ (residual life) curve. The ($\log_e$ (residual life))^2 curve is much more discriminating in the 0-750 year range and was a potential candidate for adoption. However, the hyperbolic curve was deemed to have a superior shape - characterisation values increase rapidly for residual lives of less than 850 years and change little at long residual lives, with their large uncertainty. Furthermore, at 5000 years the characterisation value is not zero. As agreed by CEN/BT WG206, the prime purpose of the resource indicator is a measure of availability to future generations and that other impacts of resource extraction and processing are covered by other indicators. It has also been suggested that there may be some small impacts not covered by these other indicators and so some positive weighting is appropriate regardless of the residual life.

Past history indicates that predictions of residual lives over a few hundred years are problematic, and so a hyperbolic function with a maximum residual life of 1000 years (giving a minimum weighting similar to that of the initial hyperbolic weighting) was derived and the curve generated is shown in Figure 3 (together with the initial hyperbolic curve). These characterisation systems will be referred to subsequently as hyperbolic 5000 and hyperbolic 1000.

Whichever characterisation system is selected there has to be some element of subjectivity to reflect the political desire to reduce consumption of resources with the shorter residual lives. If the objective is to discourage the use of resources with the shorter residual lives and to treat residual lives in the thousands of years with a high level of uncertainty, functions such as the hyperbolic, circular, $\log_e$ and $(\log_e)^2$ will satisfy these criteria. However, if it is accepted that the most concern is for those resources used in construction with residual lives less than, say, 750 years, and that the residual lives of all resources used in construction are likely to be proven in time as being at least 100 years, a wide range of weighting between these residual lives is necessary.

From Figure 2 and Table 3 this range between 100 and 750 years is 40.9%, 51.5%, 76.5%, 72.2% and 85% for the circular, $\log_e$ (residual life), $(\log_e(\text{residual life}))^2$, hyperbolic 5000 and hyperbolic 1000 functions respectively. The functions giving the largest percentage separation are the $(\log_e(\text{residual life}))^2$ and both the hyperbolic functions. In terms of the numerical difference in weighting, the hyperbolic 5000 function gives a range of 217 compared with 113 for the hyperbolic 1000 and 12 for the $(\log_e(\text{residual life}))^2$ function. When using the hyperbolic 5000 and hyperbolic 1000 weightings, the minimum characterisation for resources with residual lives greater than 5000 years or 1000 years is, respectively, 5% and 15% of the weighting at 100 years. This covers the impacts not taken into account by other indicators and this is reasonable in a system that has a comprehensive set of indicators.

Table 3 Comparison of characterisation systems; percentage of the value at a residual life of 100 years

RESIDUAL LIFE, years	CHARACTERISATION VALUE							
	Linear with negative slope	Parabolic	Circular	$\log_e$ (residual life)	$(\log_e$ (residual life))^2	Cubic spiral	Hyperbolic 5000 Year	Hyperbolic 1000 Year
40	101.2	102.5	109.1	123.4	152.3	103.4	131.6	210.1
60	100.8	101.6	105.6	113.1	127.8	102.2	119.0	153.7
80	100.4	100.8	102.6	105.7	111.7	101.1	108.7	121.2
100	100.0	100.0	100.0	100.0	100.0	100.0	100.0	100.0
150	99.0	98.0	94.5	89.6	80.3	97.2	83.3	69.6
200	98.0	96.0	89.9	82.3	67.7	94.5	71.4	53.4
300	95.9	92.0	82.3	71.9	51.7	89.3	55.6	36.4
400	93.9	88.1	75.9	64.6	41.7	84.2	45.5	27.6
500	91.8	84.3	70.4	58.9	34.6	79.4	38.5	22.3
750	86.7	75.2	59.1	48.5	23.5	68.1	27.8	15.0
1000	81.6	66.6	49.9	41.1	16.9	57.9	21.7	15.0
1500	71.4	51.0	35.7	30.8	9.5	40.6	15.2	15.0
2000	61.2	37.5	25.0	23.4	5.5	27.2	11.6	15.0
3000	40.8	26.0	10.4	13.1	1.7	9.9	7.9	15.0
4000	20.4	16.7	2.5	5.7	0.3	2.1	6.0	15.0
5000	0.0	9.4	0.0	0.0	0.0	0.1	4.9	15.0

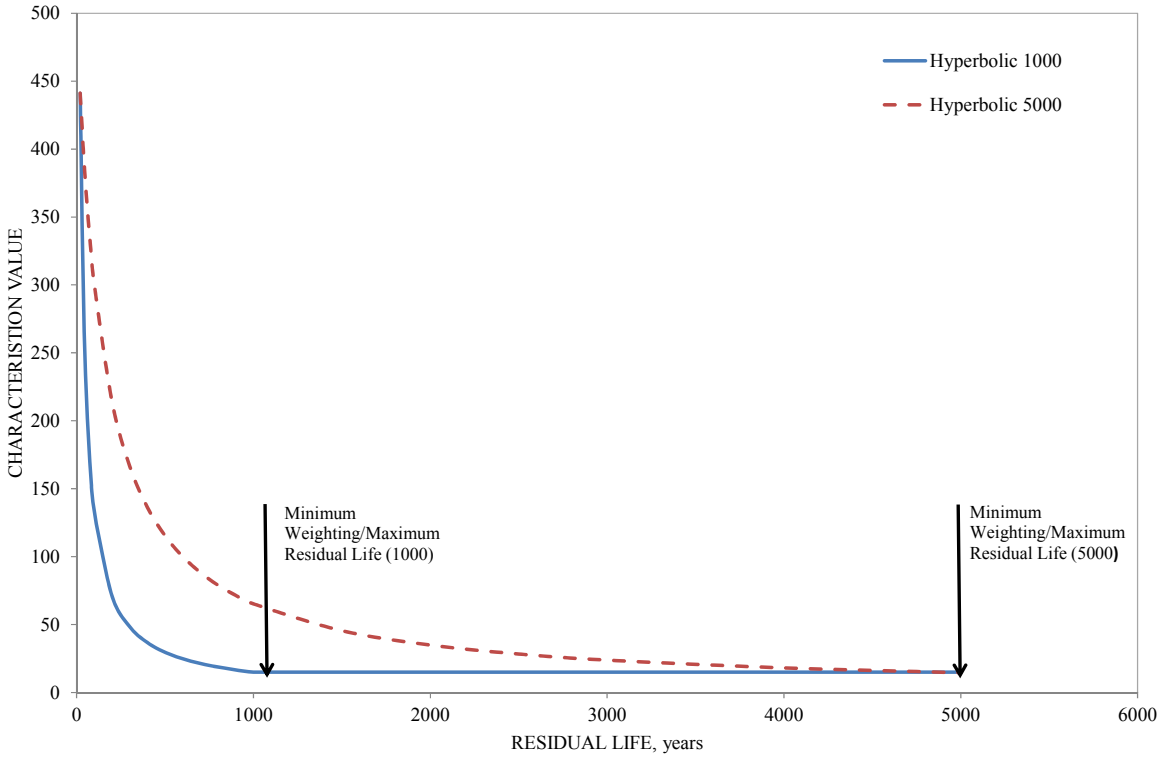

Figure 3 Characterisation values based on hyperbolic curves with 5000 year and 1000 year maximum residual life

Table 4 Mix proportions of reference concrete

CONSTITUENT	QUANTITY/m^3 (D)
Portland cement, kg	212
GGBS, kg	65
Fly ash, kg	19
Silica fume, kg	-
Limestone, kg	24
Recycled water, litres	50
Superplasticizer, litres	4
Natural sand, kg	389
Crushed rock sands, kg	166
Natural gravel, kg	567[C]
Crushed rock	647[C]
Recycled and secondary aggregate (8%), kg	106[C]

[A] (UK) Concrete Industry Sustainability Performance Report, 1st report [10]
[C] From UEPG 2009-2010 annual report [11]
[D] Market share estimated from MPA 2009 [12]

The effects of using hyperbolic curves with residual life ranges of up to 1000 and 5000 years were calculated for concrete (mix proportions given in Table 4), which is a product that contains a high proportion of resources with long residual lives. These impacts are shown in Table 5. In this example of a reference concrete that comprises the average quantities of constituents used in the UK, and not including water, the combined fossil fuels and the coarse aggregates have the higher impacts of 10.99 and 6.61 respectively.

When the hyperbolic 1000 characterisation model is applied, the ranking of the resources changes somewhat, with the impact of aggregates (10.63) being greater than that of fossil fuels (4.56). This is because the characterisation value for 100 years residual life using hyperbolic 1000 is lower (133) than that of the hyperbolic 5000 (300), and so those resources with shorter lives will have a lower impact value. Instinctively this does not seem a correct model even when the relative volumes are taken into account (0.709m^3 for aggregates and 0.048m^3 for fossil fuels). The hyperbolic 1000 function discriminates less between high volume / long residual life and low volume / short residual life resources that are used in the manufacture of a product. Considering:

- the curve shape;
- the characterisation value range between 100 years and 750 years;
- the uncertainty in estimates of long residual lives;
- the relative impact of high volume abundant resources v low volume scarce resources; it was proposed that a hyperbolic 5000 was adopted as the basis for the characterisation model and that all resources with residual lives ≥ 5000 years be given the same low characterisation value as obtained for a resource with a residual life of exactly 5000 years.

Table 5 Impact Scores for reference concrete using the hyperbolic characterisation models

RESOURCE[A)]	QUANTITY, m^3	RESIDUAL LIFE, years	IMPACT SCORE[B)]	
			Hyperbolic 5000	Hyperbolic 1000
Hard coal	0.014	90	4.40	2.04
Crude oil	0.014	100	4.15	1.84
Crushed rock	0.240	5500	3.49	3.60
Natural gravel	0.214	5500	3.12	3.21
Natural sand	0.150	5500	2.14	2.24
Limestone	0.127	5500	1.84	1.86
Natural gas[C)]	0.009	150	1.66	0.61
Crushed rock sand	0.061	5500	0.90	0.92
Brown coal	0.006	460	0.78	0.20
Recycled aggregate	0.044	5500	0.64	0.66
Clay	0.025	5500	0.36	0.37
GGBS[D)]	0.022	100	0.13	0.06
Gypsum	0.005	5500	0.07	0.07
Waste fuels	0.005	5500	0.07	0.07
Iron	0.000	100	0.06	0.03
Flyash	0.009	300	0.00	0.00
Total	1.183	-	23.81	21.32

[A)] System boundary is the gate of the concrete plant. [B)] Quantities per cubic metre.
[C)] Expressed as coal equivalent. [D)] 2% allocation of impacts of iron production.

CONCLUSIONS

This paper has examined possible options for characterising the residual lives of the resources which go into manufacturing a construction product, with concrete used as an example, such that a measure of environmental impact with regards to resource use is obtained. Based on comparison against a set of criteria devised to select a characterisation system which best reflects the need for sustainability, along with the uncertainty of predicting future availability of relatively plentiful resources, a hyperbolic function has been selected.

It should be stressed that the application of any sort of subjective function to achieve characterisation means that the resulting indicator is excluded for use in life-cycle assessment studies if they are to comply with BS EN ISO 14044 in its current form. However, there are potentially many other areas where such an indicator could be used including as an indicator within Construction Products Regulation BRCW7: 'Sustainable use of natural resources', CEN/TC350: 'Sustainable construction', or as a measure of resource efficiency decoupled from economic growth. The indicator was developed explicitly for construction products, but it could be applied more widely.

REFERENCES

1. WORLD COMMISSION ON ENVIRONMENT AND DEVELOPMENT, Our Common Future, Oxford University Press, Oxford, 1987

2. BUILDING RESEARCH ESTABLISHMENT, Methodology for Environmental Profiles of Construction Products: product category rules for Type III environmental product declaration of construction products, DRAFT, August 2007

3. VAN OERS L., DE KONING A., GUINÉE J.B., HUPPES G., Abiotic resource depletion in LCA: improving characterisation factors for abiotic resource depletion as recommended in the new Dutch LCA Handbook, Road and Hydraulic Engineering Institute of the Dutch Ministry of Transport, Public Works and Water Management, 2002

4. ROUMEGOUX, J-.P., Calcul des émissions unitaires de polluants des véhicules utilitaires, Science of The Total Environment, Vol.169, 1995, pp205-211

5. KALIVODA M.T. AND KUDRNA, M., Methodologies for estimating emissions from air traffic. Psia-Consult report n° 95.106, Perchtoldsdorf, Austria,1997

6. RIZET, C,. AND KEÏTA, B., Choix Logistiques des Enterprises et Consommation d'Energie, Institut National de Recherche sur les Transports et Leur Sécurité, Bron, France, 2002

7. EURACOAL, The Role of Coal for Power Generation in Europe 2005 (map), Euracoal, 2007, http://www.euracoal.org

8. BOYLE, G., EVERETT, B., AND RAMAGE, J., Energy Systems and Sustainability, Oxford University Press, Oxford, UK, 2003

9. RAMAGE, J., Energy - a Guidebook, Oxford University Press, Oxford, UK, 1997

10. THE CONCRETE CENTRE, The Concrete Industry Sustainability Performance Report - 1st Report, The Concrete Centre, Camberley, UK, 2009

11. UEPG EUROPEAN AGGREAGES ASSOCIATION, A Sustainable Industry for a Sustainable Europe, 2009-2010 annual report, Belgium, 2010

12. MINERAL PRODUCTS ASSOCIATION – Private Communication

The Influence of the Surface Area of Limestone on the Physical and Mechanical Behaviour of Ternary Cements

L Zeghichi[1], A Noui[2], A Lahmadi[1], L Belagraa[2]
1 – M'sila University, Algeria
2 – Bordj Bou Arreridj University, Algeria

During cement production, a significant amount of CO_2 released into the atmosphere, it is estimated that the production of each ton of clinker free about a ton of CO_2. The use of additions as constituents of cement reduces the amount of clinker, where CO_2 emissions are reduced. The combination of additions (2 or 3) with Portland cement can develop new types of binders (ternary or quaternary) with mechanical properties and durability superior to that of Portland cement alone. The objective of this work involves the study of the effects of the surface area of limestone on the physical and mechanical properties of ternary cements containing slag (SSB1=3500, SSB2= 5500, SSB3= 11000 cm^2/g). The amount of clinker is fixed at 65% ,that of lime stone varied from 5 to 30% by weight of cement ,the remain is constituted by slag. The results show that increasing the surface area of limestone with a favorable effect on the mechanical behavior of ternary cements.

Dr L Zeghichi is a Senior Lecturer in construction materials. In civil engineering at M'sila University (Algeria). She specializes in the use of benders and durability of concrete.

A Noui, is a Senior Lecturer in the department of civil engineering at Bordj Bou Arreridj University, his research interest deals with the ternary cement formulation.

A Lahmadi is a Senior Lecturer in the department of civil engineering, M'sila University.

L Belagraa, is a senior lecturer, civil engineering department, Laboratory of Materials and Electronic Systems [LMSE], Institute of Sciences and Technology, Bordj Bou Arreridj University, Algeria.

Keywords: Addition, Limestone, Setting time, Shrinkage, Slag, Specific area

INTRODUCTION

For environmental reasons and the shortage marked in the manufacturing of ordinary portland cement (OPC) and further to lower its cost, researchers have developed a binder in which are embedded natural resources such as limestone[1], industrial wastes like blast furnaces slag. Algerian cement companies incorporate into the production process these compounds to produce such type of cement with slag and limestone as additions in the cement manufactured [2]. It has been shown in several studies that the incorporation of additions mentioned above has several environmental and economical advantages, and sometimes even improving the mechanical properties of mortars containing these cements [2].

This research work studies the effect of adding limestone, and industrial waste (slag) on the mechanical strength of cements paste and mortars. In addition the setting time and shrinkage have been determined for this compound cement. For this we compared the behavior mixes containing different combinations of additions (10 to 25 % limestone), (10 to 25 % slag). The maximum amount of combined additions is 35 % - with fixed specific area of (3500cm²/g) for slag, and limestone addition having different SSA ranging from (3500-5500-11000 cm²/g).

MATERIALS AND EQUIPEMENT

Materials

Clinker (k)

The clinker used from cement plant of Ain Kebira company (Setif, region– East of Algeria), with a specific area of 3500 cm²/g and a Bulk density of 3.2 g/cm^3. The chemical and mineralogical composition of clinker is given in Tables 1 and 2 respectively.

Additions

Limestone (L)

Limestone is widely used as inert natural addition to cement. This property is granted for the hard limestone rock. It is considered that the soft rocks present difficulties during the grinding of clinker [3]. During the hydration of cement with mineral addition (e.g. limestone), the reaction of C_3A and C_4AF takes place and the complex compound $3CaO.\ CaCO_3.AL_2O_2.\ 11H_2O$ is formed. Based on this reaction, the increase of initial strength of cement with addition (lime) is explained; the setting time of cement extends according to the amount of limestone added [1]. The limestone used in this study is an inert natural addition of quarry of Ouled Eddouene, near Ain Kebira (region of Sétif). Its chemical composition is presented in Table 1.

Slag (S)

The slag is a byproduct of iron ore processing obtained from plant for steel manufacturing. To assess the quality of slag as active mineral additions for binders, we use several modules. First, there are two types of slag: Acid and basic slag [2]. Slag composition can vary within wide limits, depending on the nature of the ore. The slag used in this study is a waste of the factory iron Annaba (North-East Algeria). Its chemical composition is recorded in Table 1 [2].

Gypsum

Gypsum is a hydrated calcium sulfate with two molecules of water in its purest form. It has a laminated structure in which alternate a layer of water and two layers of calcium sulfate [4]. The gypsum used in this study is a natural addition delivered from the deposit of Djemila (East of Algeria) [5]. Its chemical composition is given in Table 1.

Table 1 chemical and mineralogical composition of materials.

	SiO_2	Al_2O_3	Fe_2O_3	CaO	MgO	SO_3	Na_2O	L.F	Σ
Clinker	21.42	4.58	4.96	63.73	1.43	0.72	0.24	2.94	100
Gypsum	3.8	0.5	0.1	22.5	0.58	32.84	/	39.09	99.41
Limestone	12.74	1.65	0.58	45.85	0.73	/	/	37.54	99.09
Slag	41.1	7.00	2.8	43.2	4.7	0.25	/	/	99.05
The mineralogical composition of clinker									
			C3S	C_2S	C_3A	C_4AF			
			58.11	17.03	3.75	15.09			

Sand

The sand used in the mortars is normalized sand, according to the French standard AFNOR NFP 15 -403 [6].

Water

The mixing water used for batching of cement pastes and mortars is a drinking water supplied by the network of public service, in the civil engineering laboratory.

EXPERIMENTAL PROGRAMME

Mix Design

To identify the benefits from the substitution of ternary additions in cements, we opted for making mixes of clinker, limestone and slag. In the mix limestone with three specific areas (SA = 3500, 5500 and 11000 cm²/g), clinker and slag with specific area fixed at 3500 cm ²/g were used. The sets of mortar obtained are related respectively to the proportions of the additions used in each mix.

It can be noted that the total percentage of (clinker + gypsum "62%+3%") is fixed to 65%. Each set includes three cubes (20×20×20) mm^3 of cement paste were used to assess compression strength [7]. Three prismatic specimens of dimensions (40×40×160) mm^3 for shrinkage tests were used. The different proportions for the five mix series are given in Table 2.

Table 2 Cement pastes and Mortars mixes combination.

Components			Mix 1		Mix 2		Mix 3		Mix 4		Mix 5	
Proportions (%)			S	L	S	L	S	L	S	L	S	L
			30%	5%	25%	10%	17,5%	17,5%	10%	25%	5%	30%
Specific Area / Mix	Slag (cm² /g)	Limestone (cm² /g)	1		2		3		4		5	
Group 01 (S1 L1)	3500	3500	M_1G_1*		M_2G_1		M_3G_1		M_4G_1		M_5G_1	
Group 02 (S1 L2)	3500	5500	M_1G_2		M_2G_2		M_3G_2		M_4G_2		M_5G_2	
Group 03 (S1 L3)	3500	11000	M_1G_3		M_2G_3		M_3G_3		M_4G_3		M_5G_3	

*M_iG_j refers to Mix i (i=1,…,5) and group j (j=1,2,3).

Batching and Curing of Specimens

The cement paste was prepared according to the following proportions: 3/4 cement and 1/4 water. The mortar specimens adopted the following proportions 1/4 cement, 3/4 sand and W/C = 0.26 according to the French standard (NF EN 196-3 standard) [8].

To characterize the mechanical resistance of cubes of cement pastes and shrinkage tests of mortars, prismatic specimens of dimensions (40×40×60) mm^3 were used. After 24 hours, specimens were demoulded and cured in the water until the time of testing for compressive strength. For shrinkage, specimens are air dried for 28 days till the due age of the test [7].

TESTS AND PROCEDURES

Physical Performance

Setting time

It is necessary to know the beginning and end of setting of cement pastes studied in order to assess the time available for proper placement of mortar and concrete which will then be made based on this type of cement [8].

Mechanical Performance

Flexural and compressive strength

The measurement of flexural strength is performed on IBERTEST machine equipped with a bending device by three points. The compressive strength, tests are performed according to

NF P 15403 standard. The half-prisms obtained after failure loading of the specimens were crushed using a press IBERTEST [6].

Shrinkage

This test has for object to define the shrinkage of five combinations of hydraulic binders obtained. Before each set of measurements, the instrument is calibrated with a metal rod of 160 mm in length and whose ends reproduce the face of the sides of the specimen [5].

RESULTS AND DISCUSSION

Consistence

The normal consistence is obtained for a W/C = 0.26 for mixes of reference cements (OPC, PCJS). For the mixtures studied, we note that the higher the percentage of the addition, the higher the amount of water needed to have a normal consistence.

Setting Time

The results of test of setting time for the different mixes are shown in Tables 3, 4 and 5.

The comparison of variation in the setting time of five sets of cement is presented in Figures 1, 2 and 3.

Table 3 The change in setting time as function of the additions proportions (Group 01).

		Reference Mortar			Mixes with Addition				
		OPC	REF-S	REF-L	M_1G_1	M_2G_1	M_3G_1	M_4G_1	M_5G_1
Consistance	W/C	0,26	0,26	0,26	0,26	0,26	0,26	0,26	0,26
Setting time	Initial (min)	255	290	190	267	255	240	237	232
	Final (min)	365	390	290	386	374	370	350	355

Table 4 The change in setting time according to the proportions of the additions (Group 02).

		M_1G_2	M_2G_2	M_3G_2	M_4G_2	M_5G_2
Consistance	W/C	0,26	0,26	0,26	0,26	0,26
Setting time	Initial (min)	200	209	215	222	228
	Final (min)	324	332	339	346	353

Table 5 The change in setting time according to the proportions of the additions (Group 03).

		M_1G_3	M_2G_3	M_3G_3	M_4G_3	M_5G_3
Consistance	W/C	0,26	0,26	0,27	0,27	0,27
Setting time	Initial (min)	237	225	212	206	200
	Final (min)	355	340	320	313	298

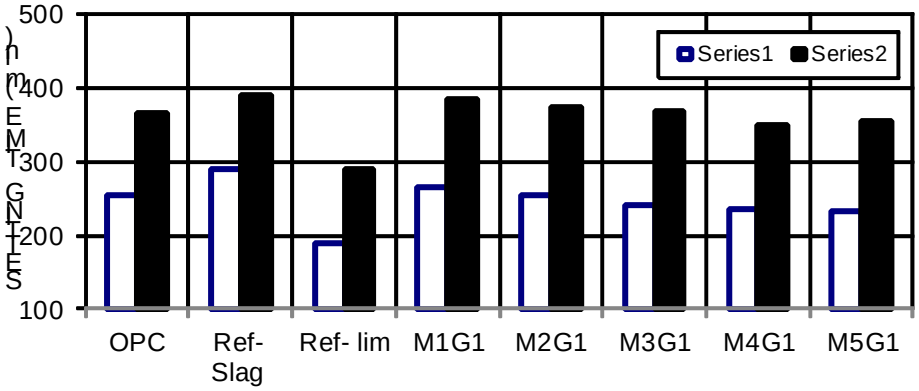

Figure 1 The change in setting time of studied mixtures (Group 01).

From the results obtained (Table 6 and plotted in Figure 1), it can be noted that the setting time increases with higher dosages of slag and limestone amounts, which can be explained by the low activity of additions, as the increase in surface area (3500, 5000, 11000 cm²/g) positively influences the time of setting so the amount of water used increases to obtain a cement with normal consistence.

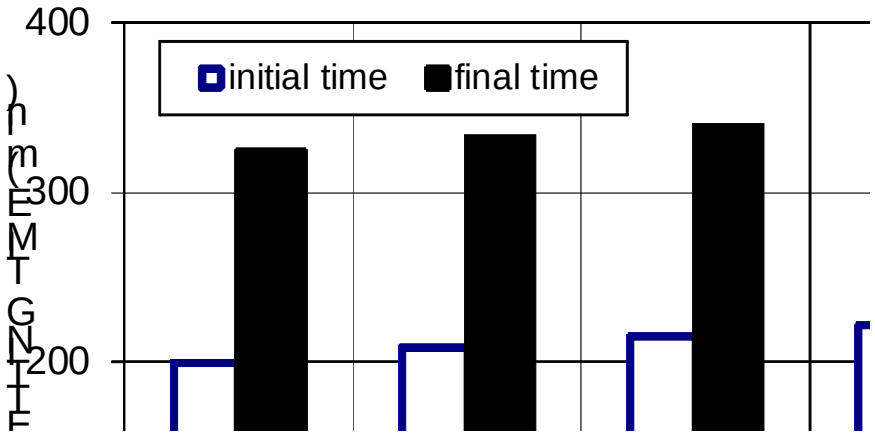

Figure 2 The change in setting time of studied mixtures (Group 02).

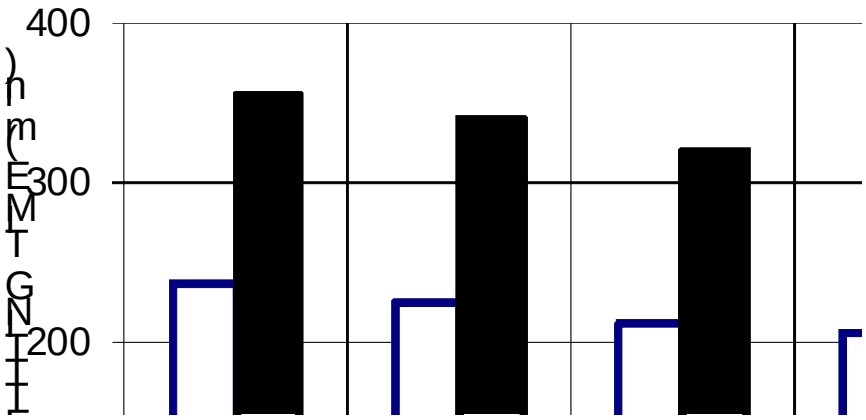

Figure 3 The change in setting time of studied mixtures (Group 03).

Flexural and Compressive Strength

The comparison of development in the mechanical strength of five sets of cement at 7, 14 and 28 days are shown in Figures 4, 5 and 6 respectively.

Table 6 The Compressive strength for Mixtures (Group 01)

	AGE	M_1G_1	M_2G_1	M_3G_1	M_4G_1	M_5G_1
Compressive strength (MPa)	7 days	15	18	20	22	25
	14 days	43	42	40	40	45
	28 days	55	50	48	45	43

Table 7 The Compressive strength for Mixtures (Group 02)

	AGE	M_1G_2	M_2G_2	M_3G_2	M_4G_2	M_5G_2
Compressive strength (MPa)	7 days	17	20	23	25	26
	14 days	34.5	36	37.5	40	41
	28 days	60	57	55	55	50

Table 8 The Compressive strength for Mixtures (Group 03)

	AGE	M_1G_3	M_2G_3	M_3G_3	M_4G_3	M_5G_3
Compressive strength (MPa)	7 days	25	29	33	35.5	37
	14 days	36	38	42	44	46
	28 days	58	55	40	53	55

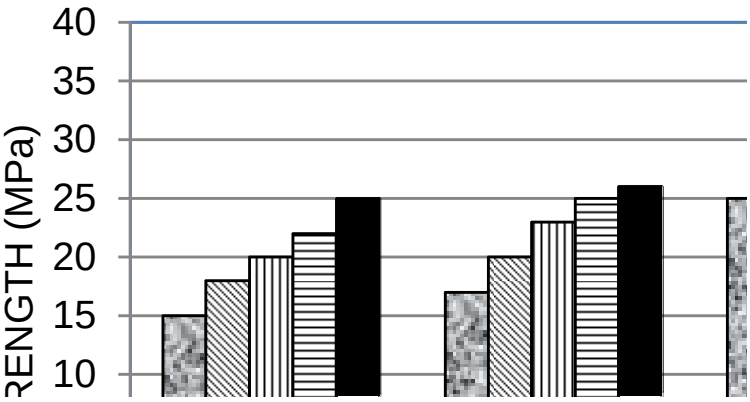

Figure 4 Variation of compressive strength for different mixtures at 7 days.

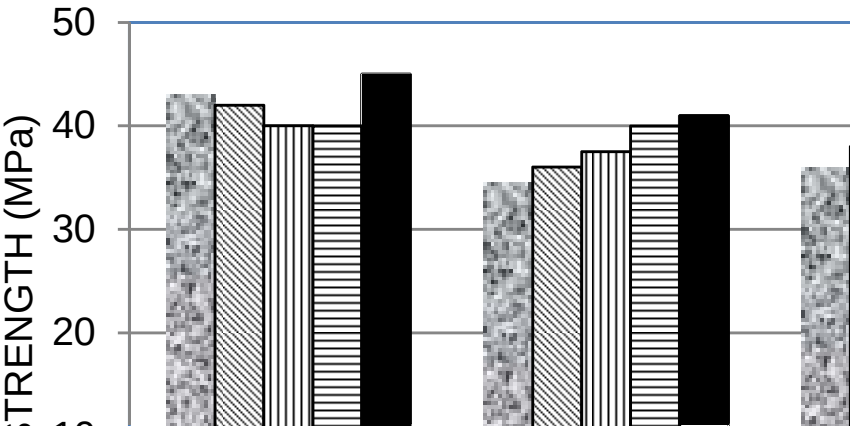

Figure 5 Variation of compressive strength for different mixtures at 14 days.

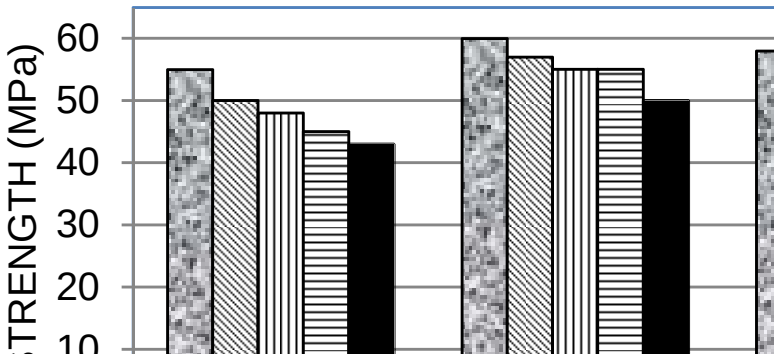

Figure 6 Variation of compressive strength for different mixtures at 28 days.

This clearly shows that at early age all the values of the compressive strength of the other four mixes remain below that of the fifth mix containing (30%) of limestone. This decrease is mainly attributed to the slow activity of added slag at early age and the quick response of added limestone at same age [4].

According to Figure 6, it can be seen that the composition of the mix (M5G3) containing 30% limestone gave a compressive strength comparable to that of the composition mix (M1G3) with 30 % of slag, since the surface area of the limestone has higher fineness of around 11000cm²/g. That clearly showed the influence of the surface area of limestone addition on its reactivity and then on the mechanical strength.

Regarding the evolution of the strength as a function of the fineness and the amount of additions at 28 days (Figure 6), it can be noticed that the strength value of the mix (M1G2) at this age had a significant increase compared overall the other mixes.

Shrinkage

According to the results obtained and presented in Table 9 and plotted in Figure 7, in accordance with NF P 15-433, which specifies the cements shrinkage "CPJ-CEM II", it says that all cements studied undergo low shrinkage of normal mortar specimens tested according to the standard above or below a 800 (μ/m) for the "CPJ-CEM II" class 32.5 and 1000 (μ/m) for Class 42.5 [6].

Based on the obtained results it can be noticed that:

The increase of the shrinkage is based on the hardening age (7, 14 and 28 days). This is due to the creation of a fine network of capillary pores within the cement hydrated paste. When these capillaries are saturated with water, consumption of water for hydration of cement causes drying; this results in the formation of meniscuses which produce attractive forces causing the shrinkage. The increase of the pores is due to the fact that the porosity of the mineral addition is higher than that of clinker.

The increase of the shrinkage also depends on the change in fineness of grinding. It is mainly due to the presence of a high capillary porosity. This causes the formation of a large amount of meniscuses and the kinetic of hydration becomes very fast within the hydrated cement paste (increased tensile forces that develop within the capillaries).

CONCLUSIONS

The results obtained in this study lead to the following conclusions to be drawn:

The setting time is much influenced by the degree of fineness of additions which is appeared to be advantageous for the decrease of both initial and final setting time of blended mixtures.

At early age, all values of the compressive strength of the four mixes remain lower compared to the fifth mix containing (30%) of limestone. The influence of the surface area of the addition on its reactivity and then on the mechanical strength is noticed.

This leads us to choose the optimal proportions which can be any set of the three groups studied as advantageous combinations except the last mix (M3G3) that contains 17.5% limestone and the same percentage of slag. Although the high specific surface area of limestone incorporated, no improvement was registered regarding the strength.

In general, the increase of shrinkage based on the age of hardening and assessed at 28 days is mainly depending on the degree of fineness of addition used.

Table 9 The change in the shrinkage of the mixtures studied.

	CURE MODE	OPC	REF. SLAG	REF. LIMESTONE	M_1G_1	M_2G_1	M_3G_1	M_4G_1	M_5G_1
Shrinkage (μ/m)	in air	555	547	600	555	547	600	590	630

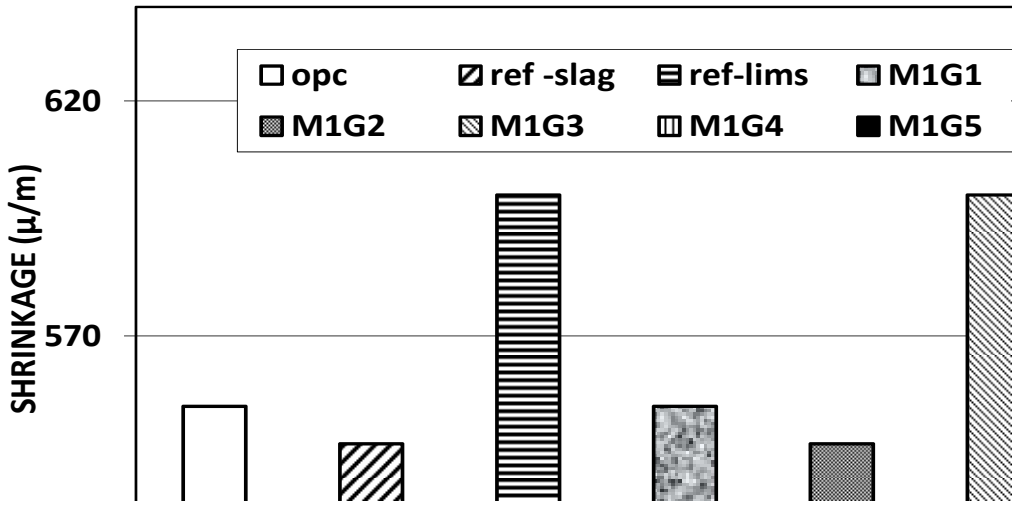

Figure 7 Shrinkage for different mixtures studied of mortars.

REFERENCES

1. CAID R, JAUBERTHIE R., BOUKHALED A., `effet de l'ajout calcaire sur la durabilité des bétons', Libanaise Science journal, Vol. 11, No 1, 2010. Pp91-103.

2. ZEGHICHI L, MEZGHICHE B., MERZOUGUI A, `la valorisation du laitier d'el hadjar dans la confection des ciments', Séminaire international de Géo-matériaux GEOMAT'02 , les 10-11 mars. Pp433437-608.

3. KERBOUCHE A, `influence des ajouts minéraux sur les résistances mécanique et la durabilité des mortiers', Mémoire de magister, ENSET Oran 2009,112pp.

4. ACHOURA D, LANOS Ch., JAUBERTHIE R. et REDJEL B. `influence d'une substitution partielle du ciment par du laitier de hauts fourneaux sur la résistance des mortiers en milieu acide', Journal de physiques IV France, EDP Science,(2002).

5. MANSOUR S, `Etude des propriétés des mortiers et bétons a base des ciments ternaires', Mémoire de magister, Université SAAD DAHLEB Blida 2003,143pp.

6. NF P ¨15-403, ' sable normal et mortier normal' AFNOR-Paris-1996-.

7. NA 442, Norme Algérienne' liants hydrauliques, ciment courants: composition, spécifications et critères de conformité' 30p, IANOR-Alger-2000.

8. NF EN 196-3, ' Méthodes d'essais des ciments: détermination du temps de prise et de la stabilité' AFNOR-Paris-1996-.

Effects of Curing Conditions on the Durability of Slag Concrete

A Bouikni[1], A Bali[2], R N Swamy[3], A Kasser[2], R Boutemeur[2]
1 – Institut du Génie Rural, Algeria
2 – Ecole Nationale Polytechnique, Algeria
3 – University of Sheffield, UK

Apart from reducing cost compared to plain Portland cement concrete, the benefits of inclusion of slag in concrete are essentially associated with the improvements it brings about to the quality and durability of concrete, and in particular, to energy savings resources conservation, and environment protection. The main objective of this study is to provide a method to get strength of 30 to 50 MPa at 28 days for a concrete having relatively high level of replacement of cement by slag of El hadjar steel factory [18] with low water binder ratio. Three curing conditions were analyzed: In air, in water and in air then water. The duration tests were: 1, 7, 28, 180 ,270, and 365 days. The method produced a slag concrete with strength comparable to ordinary Portland cement concrete from two days onwards. The compressive and flexural strength as well as elastic modulus of this concrete were highly affected by the curing conditions. High swelling strain at high slag replacement levels shows the need for longer wet curing for such concrete. The results also showed that even the condition of seven days water curing was inadequate for 50 percent replacement, and that prolonged exposure to a drying environment can have adverse effects on the long term durability of inadequately cured slag concrete.

A Bouikni is a Member of the laboratory of Geo-materials, Senior Lecturer at department of civil Engineering, Faculty of the Engineer, University of Blida with field of interests including concrete materials and concrete structures.

A Bali is Director of the Construction and Environment Laboratory, Professor at the Civil-Engineering department at the Polytechnique School of Algiers (E.N.P). His field of interests: Material including recycling, structural repairs and new materials.

R N Swamy is a Professor at the University of Sheffield, England. He has been involved in teaching, research and consultancy activities for over forty years. His research interests relate to construction technology with emphasis on concrete materials, concrete structures and their interactive performance in real environments.

A Kasser is a Member of the Laboratory of Materials Science and Engineering with research interests in bio-materials through powder metallurgies at the Polytechnique School of Algeries.

R Boutemeur is a Member of Construction and Environment Laboratory and a Lecturer at the Civil-Engineering department at the Polytechnique School of Algeries (E.N.P). His field of interest include materials, structure and construction.

Keywords: Blast furnace slag, Carbonation, Compressive strength, Concrete, Curing, Flexural strength, Modulus of elasticity, Shrinkage

INTRODUCTION

Today in the scientific literature, the use of slag concrete is widely studied through different publications. However, significant concrete projects around the world are still built with high strength structural cement concrete. Although, there is no much advancement in the use of structural slag concrete in Algeria, but there is certainly an outstanding potential for it in the future. Unfortunately, up to now, there still a great deal of confusion as to what is meant by slag concrete. The most important contribution of slag to concrete is its ability to reduce the heat involved during the exothermic reaction of cement and water. The truth is that this is only one of many positive attributes that the incorporation of slag in concrete can bring, not only to concrete as a material but also to the construction industry and society in term of energy and resource conservation and environmental protection [1, 2].

At the moment, there are no specific mixes proportioning methods designed for slag concrete. The material (i.e. slag) is used as a direct replacement of cement by weight, at proportions between 25 to 70 % by mass of the total cementitious content. Then current proportioning techniques for concrete made with Portland cement or blended cements slag are followed [1, 2, 15]. Generally, when slag fineness is of the same order of magnitude as Portland cement, the compressive strength of concrete containing slag is lower than that of a control concrete without slag, particularly at early ages and at replacement levels of 50 % and above [2, 3]. At low water-to binder- ratios, 28-days cube compressive strengths of 30 to 50 MPa have been obtained for such cements without much difficulty.

Because the hydration of slag in combination with Portland cement is generally a two- stages process, and because slag hydration tends to lag behind that of the Portland cement; components made of hydration slag concretes are likely to be more susceptible to poor or inadequate curing conditions than will concrete containing only Portland cement, as some early research has confirmed [4, 5, 11]. However, there are no systematic data about the effects of curing and strength on slag concrete in Algeria with high levels of cement replacements by slag.

Therefore, this paper is designed to establish the engineering properties of such concrete having high level of cement replacements by slag and adequate curing conditions with special reference to strength development, elastic modulus, shrinkage, swelling, porosity, microstructure and carbonation.

RESEARCH SIGNIFICANCE

The main focus of this paper is to emphasize and identify some of the engineering implications when 50 % by weight of Portland cement is replaced by slag supplied by El hadjar steel factory. The paper emphasizes the fact that adequate curing should be an essential specification when slag is incorporated in concrete. Prolonged drying of inadequately cured slag concrete can adversely influence its long-term durability, due to internal microcracking and loss of elastic modulus.

EXPERIMENTAL PROGRAM

The main objective of the research reported here was to establish the effect of curing environments that affect the durability of Portland cement concrete containing 50% cement replacement by mass with slag having higher specific surface than Portland cement. The primary objectives of the study are:

1. To develop mix proportions containing 50 % by mass of cement replacement with slag for 28-day cube compressive strength of about 30, 40 and 50 MPa under water curing
2. To produce mixtures with good workability, with slump in excess of 100 mm, and high-early-strength development comparable to all-Portland cement concrete and low water-to-binder ratio.
3. To establish the effects of a curing regime with age on a) compressive and flexural strength, b) elastic modulus, and c) shrinkage and swelling.

Materials

The Portland cement used in this work was supplied by the cement factory of Chlef [18]. It has a specific surface of 320 m²/ kg. The slag used was supplied as granules which were then milled by a ball mill down to a specific surface of 410m² /kg. The fine and coarse aggregates used in the mixtures were both unreactive - the former was natural river sand with a fineness modulus of 2.4, while the latter was natural river gravel consisting of a mixture of rounded angular material, with 10 mm maximum size. To achieve mixtures of high workability and low water-binder ratios, the mixtures used are: sika fluid, sulphonated melamine, formaldehyde high-range water reducer without chlorides in the form of an aqueous solution. The high-range water reducer was added at a rate of 1.8 % by weight of cement and slag.

Mix Proportioning

One concrete mixture having high workability and low water-binder ratios was used in the study. The mix proportions, by mass was 1:1.75:2.53:.43 (cement+slag: sand: aggregate: water) respectively. The mix proportions were arrived at after extensive tests reported earlier [17]. They were proportioned such that the slag concrete had similar cube (10 mm) compressive strengths as ordinary Portland cement concrete from 3 days onward. The concrete mixtures were designed to give compressive strengths of about 50MPa at 28 days (water curing). In practice, the actual strengths achieved were 23 to 28 MPa at 3 days, 35-40 MPa at 7 days and 55 to 60 MPa at 28 days [17]. The concretes were thus for structural application in aggressive environments, with durability as the main consideration.

Test Details

The workability of fresh concrete was determined by the conventional slump test. To determine the engineering properties of concrete, the following tests and sizes of specimens were used:

Compressive strength – 100- mm cubes.
Flexural strength, shrinkage, and swelling - 100 x 100 x 500-mm prisms.
Static modulus of elasticity -100 x 100 x 300-mm prism.

The curing regimes studied were:

1. Continuous water curing at 20 ± 2C and 100 ± 2% relative humidity (water, W).
2. Continuous uncontrolled internal environment (lab, L)
3. Seven days controlled water curing, followed by exposure to uncontrolled internal environment (7 W+ L).

The three curing conditions were chosen to reflect the relation between laboratory test and field practice. All test specimens were demolded after 24 hrs and then exposed to their respective curing regimes until test is over. Continuous exposure to the uncontrolled environment simulated the extreme case in the field where the formwork is removed very early, at about 24 hr, and no water curing takes place. The 7day water curing followed by the external exposure, reflects the normal practice of keeping in the formwork on for ages up to one week.

TEST RESULTS AND DISCUSSION

Workability

Trial mixture made without high range water reducer had low workability of 0 to 10 mm. Even with high-range water reducer, the control mixture had slumps of only 55 to 60 mm. All the other mixtures had slumps of 155 to 160 mm and were found to be cohesive and dense these are shown in Table 1 and 2. The water–to-binder ratio of the OPC-Slag concrete mixtures ranged from 0.32 to 0.62.

Table 1 Details of trial mixtures

TARGET STRENGTH	R30 MPa	R*30 MPa	R40 MPa	R*40 MPa	R50 MPa	R*50 MPa
Replacement, %	0	50	0	50	0	50
OPC, kg/m³	260	134	300	164	360	200
Slag, kg/m³	0	134	0	164	0	200
OPC + slag, kg/m³	260	268	300	328	360	400
Fine Aggregate, kg/m³	750	750	710	710	650	650
Coarse kg/m³	1100	1100	1068	1068	1011	1011
Total aggregate, kg/m³	1850	1850	1778	1778	1661	1661
Aggregate-cement ratio	6.90	6.90	5.42	5.42	4.15	4.15
Sand/total aggregate	40	40	40	40	39	39
Water/((cement & slag) ratio	0.62	0.55	0.50	0.42	0.55	0.32
Super plasticizer 1.8 % by weight of (cement & slag)	1.8	1.8	1.8	1.8	1.8	1.8
Slump, mm	55	155	60	>160	60	>160

Table 2 Results of compressive strength of selected trials mixtures

	COMPRESSIVE STRENGTH, MPa					
AGE, days	R30	R*30	R40	R*40	R50	R*50
1	9.3	12.3	12.9	15.4	15.6	19.0
3	14.8	13.4	26.7	22.4	27.8	25.2
7	25.1	24.1	33.3	27.8	40.2	37.2
28	35.6	32.2	46.5	45.1	54.3	51.3

*Mix R30 : 30 MPa with 50% slag replacement; W/C+S=0.55.
*Mix R*30: 30 MPa with control mixture.
*Mix R40: 40 MPa with a 50% slag replacement; W/C+S =0.42.
*Mix R*40: 40 MPa with control mixture...
*Mix R50: 50 MPa with 50% slag replacement; W/C+S = 0.35.
*Mix R*50: 50 MPa with control mixture;

Compressive Strength

The compressive strengths of the control and OPC-Slag concrete mixtures for the mix R30, R40, and R50 for ages from 1 to 28 days are shown in Table 2. The results show that all the mixtures were able to develop the required 28-day strength of 35 to 54 MPa. The results confirm that concrete containing a relatively coarse slag can be designed to give consistent 28-day strength results. Table 1 and 2 show that to obtain the required strength consistently, the total cementitious content (compared to the OPC control concrete) needs to be increased by about 10 % for 50 % cement replacement, in addition to the reduction in the water content. The magnitude of replacement shown in Table 1 is the same order as that reported by Swamy and Bouikni [7].

Under standard conditions, slag concrete mixes can be designed to have any required strength, and strengths of up to 50 MPa. Over the years, many researchers have reported comparative concrete behaviour studies between plain concrete and slag concretes. The latter type of concrete is based on partial replacement of cement by slag in the mix. This has resulted in conclusive reports that the inclusion of slag concrete brings lower concrete strengths and lower strength gains. The main reason for this is that the two concretes are compared on equal 28 day strength, as a typical age of judging the strength is 28 days. Then any comparison between the concretes should be made at equal strengths at that age.

Strength Development

Table3 shows strength developments of slag concrete and the rate of strength development of concrete respectively. Data from the table indicates that the mix designs are carried out with objective in mind, that rate of strength development of concrete containing 50% replacement of cement by slag can be ensured to be similar to that of normal concrete without slag. One of the reasons for the relatively high early strength found in this research can be attributed to the lower water to cementitious ratio of the mixes due to the combined inclusion of slag content and superplasticizer. The use of a super plasticizer effectively brought the cementitious particles closer together and this produced an increase in early strength [14].

The results in table 3 show that, the concrete cured 7 days in the water and then left in an uncontrolled internal environment exhibit the highest strength. About 1 to 4% over that of continuous water curing and between 11 and 28% over those continuously allowed drying in an uncontrolled internal environment. These data indicate that air curing preceded by water curing, even for a short period seems to have beneficial effects to strength development. These results are in accordance with Swamy and Bouikni [7].

Table 3 also shows that slag concrete specimens subjected to continuous air curing after demoulding failed to achieve their 28 day target strength. The 30, 40 and 50 MPa concretes were short of their required strength by 3 and 2% respectively.

Table 3 Compressive strength development of slag concrete

MIX N°.	AGE, Days	W/S+C	COMPRESSIVE STRENGTH, MPa		
			W	L	7w+L
R30	1	0.55	7.3	5.2	4.00
R40	1	0.42	12.8	11.9	12.1
R50	1	0.35	17.8	15.1	16.1
R30	7	0.55	22.4	23.1	22.9
R40	7	0.42	31.3	31.3	31.1
R50	7	0.35	37.8	37.7	39.1
R30	28	0.55	32.4	28.9	33.2
R40	28	0.42	42.5	38.7	44.3
R50	28	0.35	53.5	48.8	54.1
R30	180	0.55	51.8	33.9	35.6
R40	180	0.42	63.4	43.4	47.1
R50	180	0.35	75.5	55.3	66.0
R30	270	0.55	54.3	30.2	37.8
R40	270	0.42	69.5	41.2	55.4
R50	270	0.35	78.8	53.5	66.7
R30	365	0.55	57.8	31.5	35.2
R40	365	0.42	75.3	42.2	53.2
R50	365	0.35	82.5	54.1	66.5

*w= water curing; L= Lab curing; 7W +L = 7 day water curing + drying in internal environment

Effect of Curing Conditions

To establish the effect of curing conditions on the long term strength properties of high slag content concrete, compression tests were carried out for cures of up to 1 year. The results are shown in Table 3 and 4 and Figures 1 and 3.

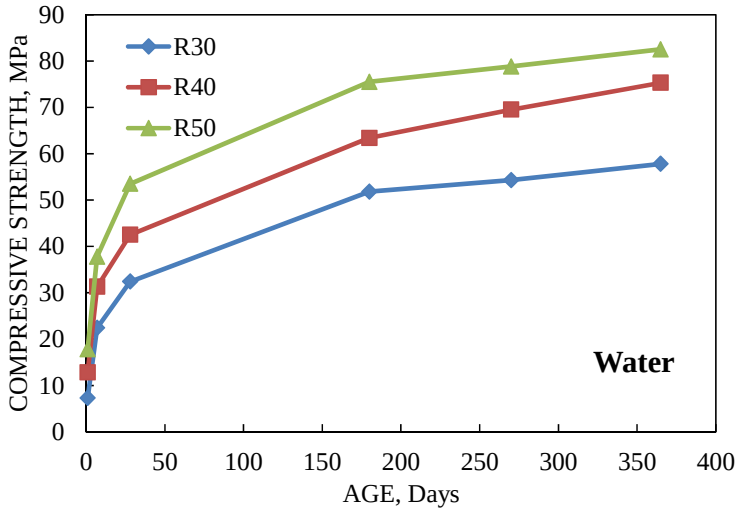

Figure 1 Compressive strength relationship with time (Water)

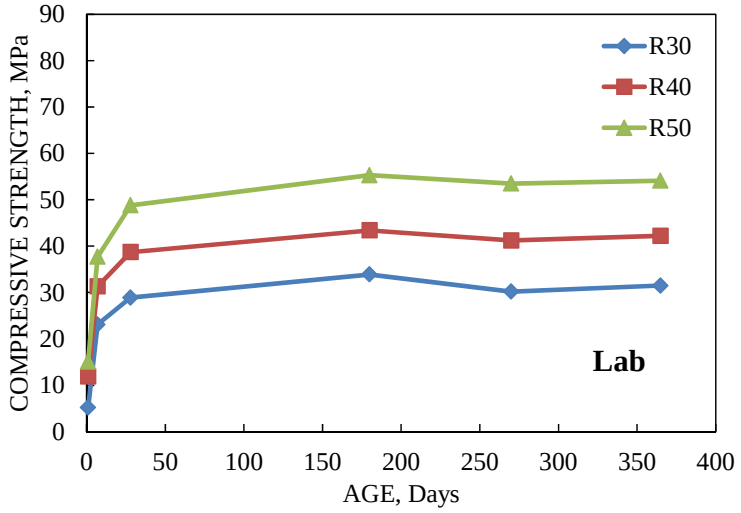

Figure 2 Compressive strength relationship with time (Lab curing)

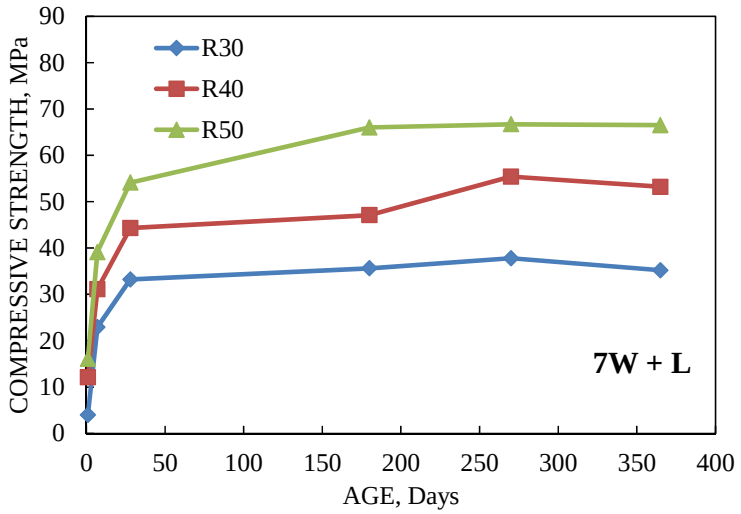

Figure 3 Compressive strength relationship with time (7W + L)

Table 3 shows the development of compressive strength with age for the 50 % replacement cured under the three curing conditions. The results confirm the previous data and showed that under continuous water curing (Figure 1), all the three concretes steadily developed strengths with age reaching their target strengths of 30, 40 and 50 MPa at 28 days. At 1 year, all three concrete registered an increase of about 78, 71, and 54 % over their 28-day strengths. The other two curing regimes also showed similar trend up to about 9 months, beyond which there was a gradual retrogression of strength. With no water curing and continuous exposure to ambient environment on demolding at 24 h (Figure 2), the three concretes failed to reach their target strength at 28 days, for which a fall in strength was observed between 9 months to 1 year. With 7 days wet curing followed by continuous drying (Figure 3), all three mixtures were again able to achieve their target strength at 1 year. Mixtures with and without 7 day water curing showed a retrogression of strength. Thus, from the data presented here, it appears that 50 % slag replacement may show some retrogression of strength with age when exposed to a drying environment.

Comparison with OPC Concrete

Although concretes made with blended cements should be considered in their own rights, it is inevitable that comparison will be made with concrete made from OPC alone. It would therefore be interesting to compare concretes with and without slag made under similar conditions. Under continuous wet curing conditions, data presented here in table3, and by others [6], Shows that slag concretes with excellent workability can be designed to have not only similar early age-strengths from 3 days onwards but also at later ages. Further, with continuous wet curing; the strength of present day Portland cements increases at ages of 28 days to a year. This increase is only of the order of 25, 20 and 18 % for the 25, 40 and 60 MPa, whereas with slag cement replacement, the strength increase is 109, 62 and 46 %.

When made under the same conditions, slag concrete shows real benefit, even when cured in dry conditions compared with ordinary Portland cement concrete. This can be seen by comparing (Tables 3 and 4), which presents some typical data for all OPC concrete with target cube strengths of 25, 40 and 60 MPa and exposed to continuous wet or dry curing after 24 hours [17]. OPC concrete virtually stops all hydration after 28 days in a drying environment, whereas slag concrete continues to hydrate. The data from Tables 3 and 4 indicated that for badly cured concrete in the “absence” of moisture, all OPC concrete will continue to lose its strength with age; whereas slag concrete is more likely to maintain its hydration process although at a very slow rate.

Flexural Strength

Flexural strength results of slag concrete cured in the three regimes for up to one year are shown in Table 5. Under continuous moist curing, maximum strength increase was observed at 9 months. The strength increase at this age as a percentage of the 28 days strength were in the order of 90, 45 and 47% for concrete strength of 20, 40 and 50 MPa. This behaviour is similar to that of the compressive strength when the concrete was subjected to continuous dry curing. The strength increase is only of the order of 14 to 44 %. The 50 % replacement concrete indicates a flexural strength loss after about one year. Obviously, the non-uniform drying affects compressive strength (Table 3) less than flexural strength and loss is likely to continue until moisture equilibrium is reached within the concrete.

Table 4 Strength developments of ordinary Portland cement Concrete [17]

REQUIRED STRENGTH, MPa	AGE, Days	COMPRESSIVE STRENGTH, MPa		PERCENTAGE OF 28-DAY STRENGTH	
		Fog	Dry	Fog	Dry
25	7	17.6	13.6	68	80
25	28	26.0	17.0	100	100
25	90	30.2	17.7	116	104
25	360	32.5	16.0	125	94
40	7	32.6	25.5	71	81
40	28	46.0	31.6	100	100
40	90	51.6	32.9	112	104
40	360	55.2	30.0	120	95
60	7	49.5	38.7	81	88
60	28	61.0	44.0	100	100
60	90	69.2	46.0	113	105
60	360	71.9	44.0	118	100

Table 5 Flexural Strength proprieties of high slag content concrete

MIX N°.	AGE, Days	FLEX. STRENGTH			% of 28 d STRENGTH, %		FLEX.ST. / COMP.ST. RATIO	
		Water, MPa	Lab, MPa	Lab/Water Ratio, %	Water	Lab	Water	Lab
R30	1	0.88	0.90	102	34	36	12.0	17.3
R40	1	1.80	2.10	117	39	54	14.1	9.2
R50	1	2.12	2.52	118	32	52	11.9	16.6
R30	7	1.90	1.80	105	73	70	8.5	7.8
R40	7	3.22	3.42	106	69	88	10.3	10.9
R50	7	5.92	4.25	72	90	76	15.7	11.3
R30	28	2.60	2.50	96	100	100	8.0	8.6
R40	28	4.66	3.90	84	100	100	11.0	10.1
R50	28	6.56	5.56	85	100	100	12.3	11.4
R30	180	4.65	3.01	65	176	123	9.0	8.9
R40	180	5.90	4.50	76	127	115	9.3	10.4
R50	180	7.2	6.14	84	110	109	9.5	11.1
R30	270	4.95	3.26	66	190	130	9.1	8.1
R40	270	6.70	5.70	85	144	146	9.6	9.7
R50	270	7.70	6.24	81	117	112	9.8	10.7
R30	365	4.80	3.66	74	185	143	8.3	11.4
R40	365	6.80	4.50	66	146	115	9.0	9.2
R50	365	7.72	5.70	76	117	103	9.3	10.8

Modulus of Elasticity

The values of the static modulus of elasticity at 28 days and one year are shown in Table 6. The results show that the highest values of elastic modulus are obtained under continuous wet curing; with age; are consistently higher than that of the dry cured specimens On the other hand air drying with no water curing produced significant reduction in elastic modulus of about 10 % for the 30 and 9 % for 50 MPa concretes but only 8 % for the 40 MPa concrete, when compared to moist cured specimens. A closer examination of the data in Table 7, however reveals that the development of the static modulus of elasticity resemble that of the compressive strength. For moist curing specimens, percentage increases with increasing age. This percentage increase of 1 year to that of 28 days static modulus is between 17-20 % was observed for the three concretes strengths, about one third of the corresponding compressive strength increase. Even for the air dried specimens, a modest reduction of between 8–26 % was observed. This confirms the finding of Swamy and Bouikni [7]; who found that the secant modulus of slag concrete containing a super plasticizer, decreases from 28 days to 180 days for dry specimens and similar losses have been reported in the literature [14].A closer examination of the data in Table 6 shows that for wet cured specimens, 80 – 83 % of the one year static modulus of elasticity developed within 28 days. So stronger concrete develops elastic modulus with faster rates. These results show that, except for the case of moist curing, compressive strength should not be used as a criterion of concrete quality after 28 days, since flexural strength and elastic modulus vary quite widely from compressive strength when insufficiently cured slag concrete begins to dry with time. For design purposes, the 28 days static modulus of dry cured specimen may be taken as the one year values.

Table 6 Static modulus of elasticity at 28 days and 1 year

MIX	TYPE OF CURING	COMPRESSIVE STRENGTH, MPa		MODULUS OF ELASTICITY, GPa		INCREASE OVER 28 DAYS, %		$\frac{E28}{E365}$, %
		28-day	1-Year	28-day	1-Year	Strength	Modulus	
R30	Water	32.4	57.8	30.1	37.8	78	26	80
R40	Water	42.5	75.3	33.5	40.5	77	21	83
R50	Water	53.5	82.5	35.6	42.7	57	20	83
R30	Lab	28.9	31.5	27.3	28.1	9	-1	-3
R40	Lab	38.7	48.7	30.7	29.7	26	-3	-5
R50	Lab	48.8	52.9	30.1	29.8	8	-1	-1

Shrinkage and Swelling

The shrinkage and swelling strain of slag concrete at various ages are shown in (Figures 4 to 6). It is well known that shrinkage increases with increasing water/cement ratio. From (Figures 4, 5 and 6), it can be seen that for the three concrete strength grades, the magnitude of shrinkage and swelling is the highest for the 30 MPa concrete (highest water/c+slag). For the structural concrete stored either in the laboratory or externally, it appears that the 50 MPa concrete show marginally higher shrinkage strain than the 40 MPa concrete. This observation cannot be explained by w/c+slag ratio alone.

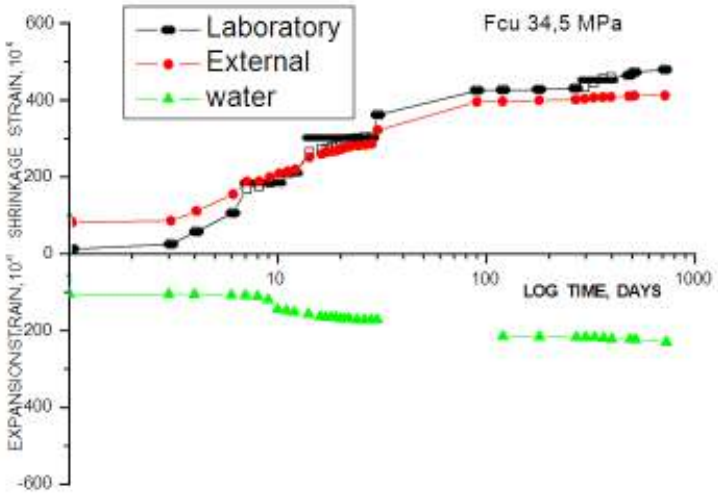

Figure 4 Shrinkage and expansion of 30 MPa concrete

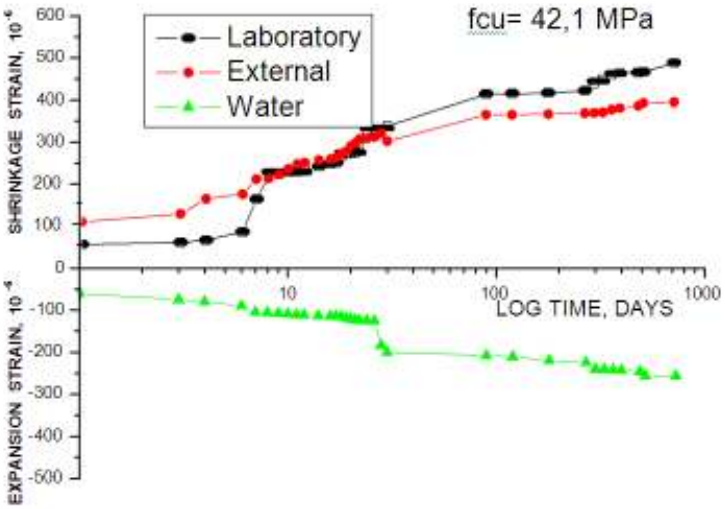

Figure 5 Shrinkage and expansion of 40 MPa concrete

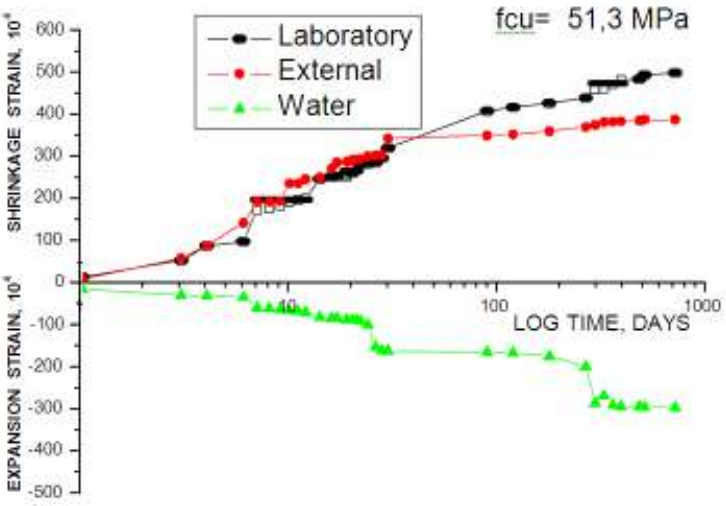

Figure 6 Shrinkage and swelling of 50 MPa concrete

The higher total cementitious content and lower aggregate content of the 50 MPa concrete may be the reason for this concrete to exhibit higher shrinkage than the 40 MPa concrete. However, the difference was not really significant, especially for specimens stored externally. The shrinkage results show that when specimens stored either in the laboratory or external environment, irrespective of the concrete strength, there is little difference in shrinkage. The difference in shrinkage was 3 % and 9 % for the former and latter curing regimes respectively. The two curing regimes also show that for a given concrete strength, the shrinkage of specimen cured externally (sheltered from rain and sun) was the lesser of the two. At 730 days, the shrinkage of these specimens was about 22 % less than that of the shrinkage of laboratory cured specimens. An explanation for this behaviour is that, for the specimens stored outside, moisture can be collected on the surfaces of the specimens during the wet season (higher humidity) and during this time, shrinkage remained constant and may even be reversed. Results in Fig (4, 5 and 6) show that, at the end of one year and a half, the specimens cured externally do not approach the values for the specimens stored inside the laboratory. The final measured shrinkage at (365 – 730) days varied between (393 – 505) micro strain, depending on the water/C+slag ratio and exposure condition. For given curing condition and age, the rate of shrinkage as a percentage of the measurement was remarkably constant regardless of the concrete strength. An interesting point to note is that, irrespective of the curing condition, 50 % of the 730 days shrinkage or swelling strain occurred within 14 days of exposure condition. The exception was the 50 MPa concrete under continuous moist condition which took about three month to attain this values. At three months, about 90 % and (75 – 80) % of the 730 days shrinkage and swelling strains respectively, had taken place. However, it can be argued that all the specimens were exposed to their respective curing regimes a day after casting and directly after demoulding. This type of exposure is indeed and extremely severe condition, one that is very unlikely to happen in practice. At early ages the concrete, has not fully matured, and combined with high temperatures (summer) experienced by the specimens, the high early shrinkage obtained from this investigation was expected. Although the concrete exhibited high shrinkage values early in its life, the final measured shrinkage of (393-505) micro strain are low. It is much lower than those cited in published literature [12, 13]. A possible explanation is the low water/composite ratio used in this investigation. At about (6-9) months, the shrinkage for all concretes and exposure conditions begins to stabilize. At 1 year, the shrinkage was almost stabilized. And the shrinkage values remained practically constant for the following 6 months to a year.

CONCLUSIONS

From the results presented in this paper, the following conclusions can be drawn.

1. Under water curing, there is a continuous increase in compressive strength with age.

2. Dry curing represents the worst curing condition for slag concrete.

3. Curing preceded by 7 days water curing is beneficial to the compressive strength development of high slag content concrete. Under this condition slag concrete exhibits the highest strength.

4. Concrete containing 50% slag and a super plasticizer is capable of developing compressive strength of 50MPa at 28 days and a strength of (20-35) Mpa at 3 days. The strength at 1 year of this concrete is in excess of 80 MPa.

5. The results of this paper indicate that continued exposure to drying environment of inadequately cured slag concrete can adversely affect its long-term durability.

6. Slag replacement can bring real benefits when no water curing occurs and the forms are removed within 1 day when compared with ordinary portland cement concrete under the same condition and targets. OPC concrete virtually stopped hydration after 28 days in drying environment, whereas slag concrete continued to hydrate.

REFERENCES

1. HIGGINS D. The historical development of GGBS, concrete, vol. 25, N6, Sept-Oct, 1991, pp. 07-19.

2. DOUGLAS, E. WILSON H. MALHOTRA VM. Production and Evaluation of a New Source of Granulated Blast-furnace Slag. In: Proceeding of the International workshop on granulated blast-furnace slag. Toronto, 1987. Ottawa: CANMET; 1987. p. 79-112.

3. WAINWIRIGHT PJ. The influence of slag cement on some of the properties of concrete related to thermal cracking. In: proceedings of the international workshop on granulated blast-furnace slag, Toronto, 1987. Ottawa; Canmet; 1987. p. 203-227.

4. MATHER, B, Laboratory test of Portland blast-furnace slag cements, ACI journal, proceedings V.54, N3, Sept. 1957. P.205-232.

5. ROY DM, IDORN GM. Hydration, Structure, and Properties of Blast Furnace Slag Cements, ACI Journal, Proceedings V. 79, No. 6, Nov-Dec. 1982. p.444-457

6. WAINWRIGHT PJ, TOLLOCZKO JJA. Early and Later Age Properties of temperature cycled Slag -OPC. Concrete. ACI Publication SP-91; 1986. p. 1293-1321.

7. SWAMY R.N, BOUIKNI A. Some Engineering Properties of Slag Concrete as Influenced by Mix Proportioning and Curing. ACI Mater J. 1990; 86(3); 210-20

8. BRITISH STANDARDS INSTITUTION (B.S.I), BS 4550: part 3, Method of Testing Cement., 1978.

9. ACI COMMITTEE 226 .Ground Granulated Blast Furnace Slag as a Cementituent in Concrete. (ACI 226.IR-87), Americain Concrete Institute, Detroit, 1987, 16p.

10. CANMET. Proceeding, International Workshop on Granulated Blast Furnace Slag; Toronto, 1987, Ottawa; p 553.

11. FULTON FS. The properties of Portland Cement Containing Milled Granulated Blast Furnace Slag. Monograph, Portland Cement Institute, Johannesburg, 1974, p. 4-46.

12. BRITISH STANDARDS INSTITUTION (B.S.I). The Structural Use of Concrete. (BS8110 Part2, 1985), British Standards Institute, Detroit, 1989, p. 453-475.

13. SWAMY RN, MAHMUD HB. Shrinkage and creep Behaviour of High Fly Ash Content Concrete, Fly Ash Silica Fume, Slag and Natural Pozzolans in Concrete, SP114, American Concrete Institute, Detroit, 1989, p. 453-475.

14. SWAMY RN. High Performance and Durability without Tears, Fourth international Concrete on Structural Failure, Durability and Retrofitting.

15. SWAMY RN. Cement replacement material, Editor R.N. Swamy, Surrey University Press, London, 1986, p 259.

16. MALHOTRA VM. Strength and durability Characteristics of Concrete Incorporating a pelletized Blast Furnace Slag, Fly Ash, Silica Fume, Slag and Other Mineral By-Products in Concrete, SP-79, American Concrete Institute, Detroit, 1984, p. 247-276.

17. HOGAN FJ. MEUSEL J W. Evaluation for Durability and Strength Development of agroundGranulated Blast Furnace Slag, Cement, Concrete, and Aggregates, V. 3, No 1, Summer 1981, p. 40-52.

18. Arcelor Mittal steel d'Annaba, Commune de Sidi Ammar, Annaba, Algeria.

19. BRITISH STANDARDS INSTITUTION. Methods of Testing Concrete, BS1881, London, 6 parts.

Effects of Calcined Clay as Low Carbon Cementing Materials on the Properties of Concrete

K-C Thienel, N Beuntner
University of the German Federal Army, Germany

Lias delta clay was calcined in a rotary kiln. It was ground leading to a surface area of 5700 m²/g and a mean particle diameter of 12,5 µm. The calcined clay was tested as a Type II addition in combination with different cements (CEM I, CEM II and CEM III) and two strength classes (32,5 and 42,5). In most tests calcined clay replaced 20 % of the cement. Additionally some tests went up to a replacement of 60 %. The parameters investigated were fresh concrete properties including bleeding, compressive strength of mortar samples and concrete cubes, depth of carbonation, chloride ingress, sulphate resistance and shrinkage. The addition of the calcined clay improves the stability of the fresh mortar and concrete. Bleeding is reduced significantly. Initial strength develops at a lower rate until seven days for most mixes containing calcined clay. Beyond this age mixes with a 20 % replacement exceed the strength of the companion pure cement mixes. This holds especially for mixes containing CEM II where in some cases even a replacement of 40 % leads to higher strength values at 28 days and beyond. A comparison was made of the non-renewable energy necessary to produce the calcined clay and the energy needed to produce the different types of cement. It reveals an ecological advantage for concrete containing a binder blend of cement and calcined clay. The possible advantage depends to a large extend on the k-value which can be considered for the calcined clay and the type of cement to be substituted. The tests prove a reasonable range for the k-value between 0,6 and 1,0.

Karl-Christian Thienel is professor and head of the Institute for Building Materials, University of the German Federal Army Munich, Germany. He received his diploma and Dr.-degree in civil engineering from TU Braunschweig. He was Alexander-von-Humboldt “Feodor-Lynen” stipendiary at ACBM, Northwestern University, Evanston, IL, and head of R&D at Liapor GmbH & Co. KG. He is chairman of CEN/TC 177 and member of CEN/TC 154 SC5. His research interests include lightweight concrete, lightweight aggregate, impact and micro cracking.

Nancy Beuntner is researcher at the Institute for Building Materials, University of the German Federal Army Munich, Germany. She studied civil engineering, especially technology of building materials at Bauhaus University Weimar, Germany. She worked from 2002-2008 as product manager and sales engineer at Rohrdorfer Baustoffgruppe, Germany.

Keywords: CO_2, Calcined clay, Strength, Type II addition, Workability

INTRODUCTION

Cement is a significant source of anthropogenic release of carbon dioxide. The CO_2 derives mainly from kiln fuel combustion, transport and distribution and decarbonating of limestone. The latter source is fairly constant. Thus one procedure to lower the release of carbon dioxide is reducing the clinker content of the cement by shifting the production from CEM I to CEM II or CEM III cements. Another approach is replacing cement partially in concrete mix design by Type II additions like fly ash, granulated blast furnace slag or silica fume. An alternative to these afore mentioned options provides the use of calcined clay either as reactive part of the cement [1] or as Type II addition in concrete [2].

Metakaolin is known as a very reactive calcined clay and has been in focus of many investigations [e.g. 3, 4, 5, 6, 11]. Its widespread use in concrete is prohibited mostly by its high price compared to other Type II additions. Suitable and less expensive clay qualities consist rather of a mixture of clay minerals, which range between the clays used in the ceramic industry and those required for the cement production [1] than of single type clay minerals. Thus it is worth taking a closer look at mixed clays.

The reactivity of any calcined clay depends on both its mineral composition and the calcination temperature [e.g. 1, 3 - 11]. In most cases these investigations used homogenous clay samples that were calcined at constant temperature and for a period of several hours. Furthermore these clays were ground prior to calcination ensuring a complete reaction to take place. If coarse crushed clay is fed into a rotary kiln it is exposed to varying temperatures on its journey through the kiln combined with temperature gradients due to the size of the chunks after crushing and in addition a varying degree of oxidation. This paper focuses on the impact of such calcined clay on various mortar and concrete properties and its inherent ecological potential.

MATERIALS AND METHODS

The calcined clay used was produced at the Liapor expanded clay plant in Pautzfeld, Bavaria, Germany. The source material originates from a Lias delta layer and is taken directly from the Liapor clay pit. Its chemical and mineral composition is given in Table 1. Coarse crushing is the only mechanical processing before feeding the raw clay into the rotary kiln. Maximum particle size of the raw clay is 100 mm. The clay passes the kiln within 35 minutes while being exposed to temperatures below 950 °C. After cooling the calcined clay is ground by means of a roller mill to its final grading. Figure 1 shows the particle size distribution of the calcined clay, which was obtained by laser granulometry. The mean particle diameter of the ground calcined clay is 12,5 µm, the diameter on cumulative 10 % is 5,3 µm and the diameter on cumulative 90 % is 21,4 µm. The resulting Blaine-surface area is 5700 m^2/g. Density was determined in a pycnometer to 2,57 g/cm^3.

Eight different cements coming from four different producers were included in the tests. They comprise the most common cements in the eastern part of Bavaria, Germany. The two CEM II/A-LL 32,5 R used come from different manufactures.

Two series of mortar tests were conducted. Composition of mortars and sample preparation and determination of strength were done according to EN 196-1 [12]. In both mortar series the replacement of cement by calcined clay was done on a mass by mass basis. Consistency was measured on a mortar flow table according to ASTM C230 [13]. In addition mortar was used to investigate sulphate resistance as described in [14].

Table 1 Chemical and mineral composition of Lias delta clay in its original condition

CHEMICAL COMPOSITION		MINERAL COMPOSTION	
SiO_2	55 ± 2	Quartz	21 ± 2
Al_2O_3	25 ± 2	Illite	42 ± 2
Fe_2O_3	7 ± 2	Kaolinite	15 ± 2
CaO	4 ± 1	Chlorite	10 ± 2
K_2O	3.6 ± 0.5	Feldspar	5 ± 1
MgO	2.2 ± 0.2	Calcite	3 ± 1
TiO_2	1.2 ± 0.1		
SO_3	0.4 ± 0.1		
P_2O_5	0.3 ± 0.1		
NaO_2	0.1 ± 0.1		
MnO	0.1 ± 0.1		

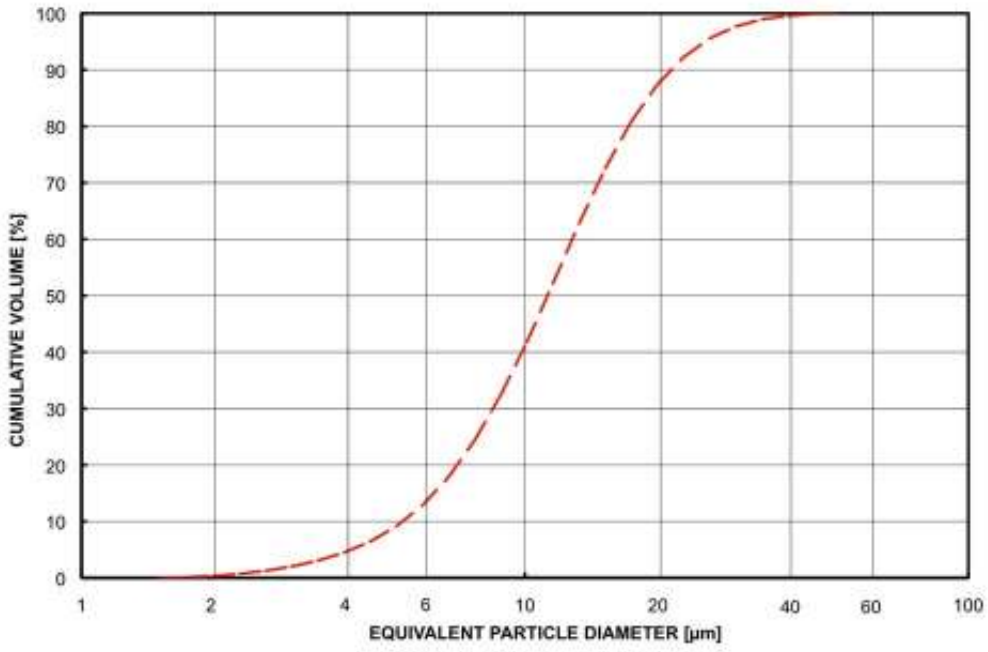

Figure 1 Particle size distribution of calcined clay by laser granulometry

The mortar tests were supplemented by concrete tests. The actual mix designs correspond "Concrete No 1a" (340 kg/m^3 CEM I 42,5R, w/c = 0,5) and "Concrete No 1b" (320 kg/m^3 CEM II/A-LL 32,5R, w/c = 0,6) [15]. The replacement rate was 20 % for "Concrete No 1a" and 25 % for the second one, which is identical to "Concrete No 2b" in [15]. The calcareous aggregate used originates from a local Munich pit and has a maximum size of 16 mm. Concrete compressive strength was tested on 15-cm-cubes. These tests should confirm the findings of the mortar tests. Additionally these concretes were taken to measure bleeding of

fresh concrete using the so call “bucket-test” [16] and shrinkage at 20/65 on 150/300 mm cylinders. Depth of carbonation was determined at 14, 28, 56, 90 and 181 days. After demoulding the concretes were immersed in water until an age of 7 days. Afterwards they were stored in normal climate 20/65 [17]. Dry drilling was used the measure the chloride ingress after immersion in 3 % sodium chloride solution for 90 days. The effect of the calcined clay up on sulphate resistance was investigated after storing flat mortar prisms (40/10/160 mm^3) at 8 °C in a 4,4 % sodium sulphate solution and subsequent drying [14].

TEST RESULTS AND DISCUSSION

Mortar Tests

The first mortar series (Table 2) compared the effect of a 20 % replacement of five different cements upon the development of compressive strength R_c and flexural strength R_f resp. The second series (Table 3) investigated the effect of different replacement ratios (20 %, 40 % and 60 %) on compressive strength R_c.

Table 2 Data of first mortar series

CEMENT TYPE		CEM I 42,5R		CEM II/A-LL 32,5R		CEM II/B-S 42,5N		CEM II/B-P 32,5N		CEM III/A 32,5 N - LH/NA	
Cement content	% by mass	100	80	100	80	100	80	100	80	100	80
Spread	cm	14,8	14,6	16,2	14,8	15,9	14,1	11,8	11,5	14,1	13,6
ρ_f	kg/dm^3	2,28	2,24	2,19	2,26	2,23	2,26	2,24	2,25	2,26	2,23
$R_{f,1d}$	MPa	2,4	1,9	2,6	2,1	-	-	2,8	1,9	1,6	1,3
$R_{f,7d}$	MPa	7,2	6,4	5,7	4,9	5,5	5,5	6,3	5,5	6,7	5,8
$R_{f,28d}$	MPa	8,1	8,5	6,8	7,5	7,7	8,4	6,6	7,4	8,4	8,2
$R_{f,56d}$	MPa	9,1	9,5	8,0	7,2	7,8	8,4	8,9	8,2	6,0	4,4
$R_{f,90d}$	MPa	10,8	8,6	9,6	9,2	8,2	8,8	9,6	9,4	8,3	5,5
$R_{f,180d}$	MPa	10,9	9,1	8,8	9,3	-	-	8,5	9,3	10,3	7,4
$R_{f,365d}$	MPa	7,9	8,0	7,5	7,9	-	-	7,4	8,0	8,8	6,5
$R_{c,1d}$	MPa	14	11	5	5	-	-	15	12	8	7
$R_{c,7d}$	MPa	51	43	37	34	34	37	42	35	37	32
$R_{c,28d}$	MPa	66	65	48	54	54	60	52	52	44	48
$R_{c,56d}$	MPa	80	79	60	67	62	67	68	65	60	54
$R_{c,90d}$	MPa	81	80	60	68	65	69	69	66	73	60
$R_{c,180d}$	MPa	80	80	59	69	-	-	68	66	74	63
$R_{c,365d}$	MPa	80	83	59	71	-	-	70	69	73	64

Table 3 Data of second mortar series

CEMENT TYPE		CEM II/A-LL 32,5R				CEM II/B-S 32,5R			CEM II/B-M (S-LL) 32,5R		
Cement content	% by mass	100	80	60	40	100	80	60	100	80	60
Spread	cm	17,3	16,7	14,5	12,9	17,5	15,7	14,2	17,0	14,9	14,1
ρ_f	kg/dm^3	2,23	2,28	2,26	2,23	2,24	2,23	2,21	2,23	2,28	2,27
$R_{c,7d}$	MPa	39	35	24	15	30	28	22	38	37	28
$R_{c,28d}$	MPa	49	50	48	36	41	50	44	48	54	49
$R_{c,56d}$	MPa	57	63	59	51	56	59	54	62	72	66
$R_{c,90d}$	MPa	66	75	75	63	58	70	63	57	72	66

Fresh Mortar and Concrete Properties

The addition of calcined changes already the fresh mortar properties. Workability of the three reference mortars differs hardly in the second test series (Table 3). An increasing content of calcined clay reduces the spread continuously. Differences between the three cements are significant at a replacement level of 20 %, but disappear at a level of 40 % replacement. Initial spread is smaller for the first mortar series. Again the replacement of 20 % cement by calcined clay reduced the spread (Table 2). The observed stiffening effect is due to a higher water demand of the calcined clay compared to the cements. Its stems mainly from the higher surface area provided by the calcined clay compared to the cements used. Consequently, the replacement of 20 % cement by calcined clay reduces bleeding of concrete significantly (Figure 2). A maximum value of 3 kg/m^3 is considered suitable for structural concrete. Below 2 kg/m^3 the concrete can be used for trafficked elements and below 1 kg/m^3 the mix is applicable for exposed concrete [16]. The improved water retention of mixes containing calcined clay is due to its higher water demand compared to the cements used. This effect may be attributed mainly to its higher surface area and partially to a different surface charge.

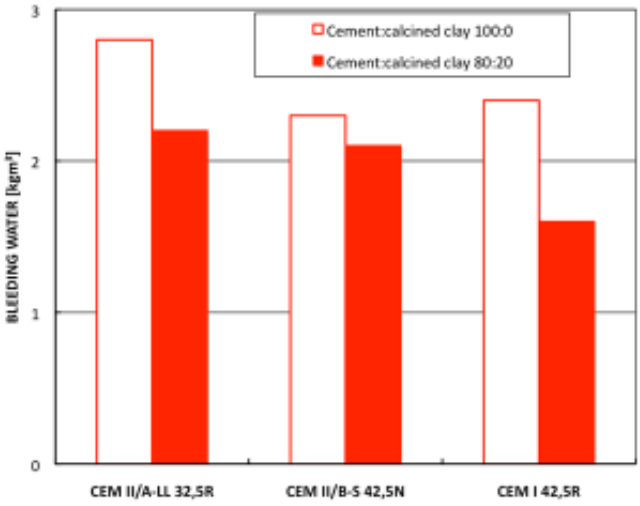

Figure 2 Effect of calcined clay content on bleeding of fresh concrete

Compressive Strength

The effect of a 20 % replacement on compressive strength was tested for all 8 cements. Results are given in Figure 3 as activity index. Thus strength measured with the mixes containing calcined clay can be compared directly with their references at each testing age. At the same time the potential can be evaluated of the combination of the calcined clay when used with different cement types. At a 20 % replacement level an activity index of 80 % stands for inert material while at 100 % the mixed binder can be denoted as efficient as the corresponding pure cement.

The activity index changes with mortar age. At one day the calcined clay acts mostly as inert material. A higher activity value at this age is rather due to the low strength of the reference mix (Table 2) and normal test scatter than a significant effect. At seven days differences between cement types show up. For CEM I, CEM II containing natural puzzolan and CEM III the effect of calcined clay becomes visible but is not very pronounced. On the other hand CEM II cements containing ground blast furnace slag approach or exceed the strength of the reference mixes at this age. The two CEM II/A-LL cements are in between the two other groups. At 28 days mortars containing 20 % calcined clay reach or exceed significantly the compressive strength of their corresponding references. CEM I and CEM II/B-P still represent the lower end while the others show no clear order. This does not change with increasing age except for CEM III/A. Its activity index decreases and levels off slightly above 80 %. This decline in due to a pronounced increase in compressive strength of the reference while the strength of the mix containing calcined clay remains constant (Table 2).

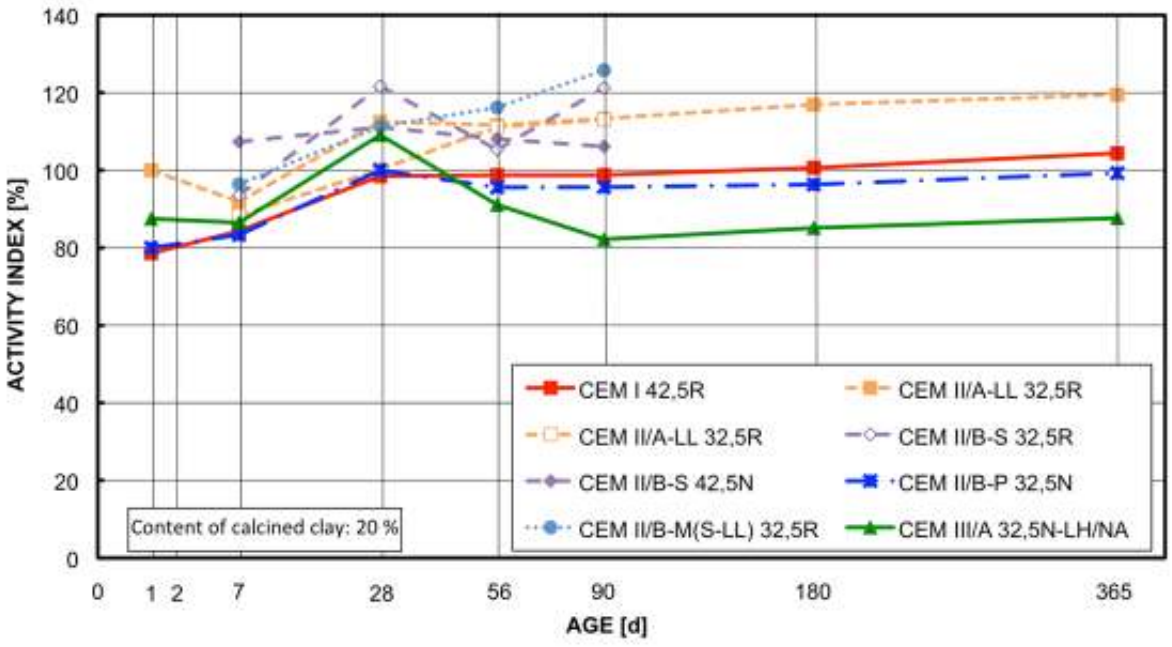

Figure 3 Development of the activity index based on compressive strength tests for a replacement of 20 % cement by calcined clay

Two strength classes (32,5 and 42,5) of CEM II/B-S were included in the tests. The results reveal that both strength classes benefit similarly from the addition of calcined clay.

A higher content of calcined clay does not change the basic observations (Figure 4). At 7 days the impact of the calcined clay is small for CEM II/A-LL and more pronounced for the two other cements. At 28 days and beyond all three combinations of cement and 40 % calcined clay reach or exceed the strength of their references.

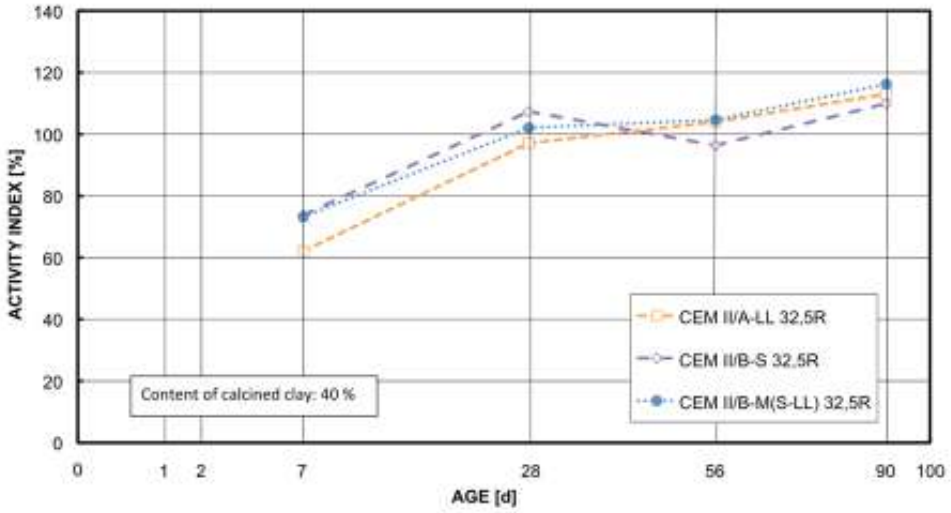

Figure 4 Development of the activity index based on compressive strength tests for a replacement of 40 % cement by calcined clay

Four cements were tested with a replacement of up to 60 % (Table 3). The activity index at an age of 28 days is given in Figure 5. It exhibits a most efficient replacement ratio in the range of 15 % to 25 %. Besides it proves that a one-by-one replacement of cement by calcined clay can be accomplished for the three CEM II cements up to a content of calcined clay of 40 % without jeopardizing strength.

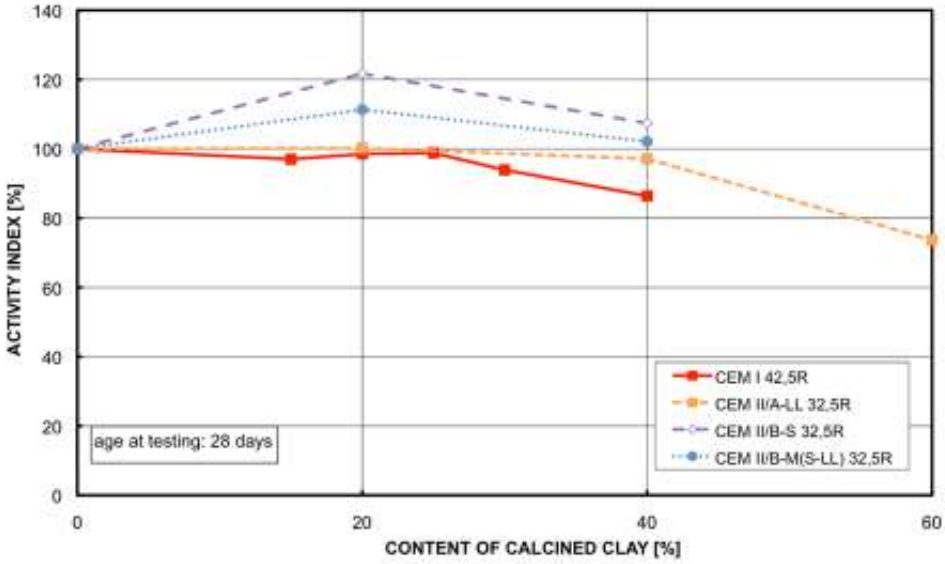

Figure 5 Effect of calcined clay content on the activity index at 28 days based on compressive strength tests

The general findings based on mortar tests are confirmed in concrete tests using two of the cements (Figure 6). At seven days no effect is visible yet. But, the impact of the calcined clay seems to be even more pronounced at 28 days and beyond.

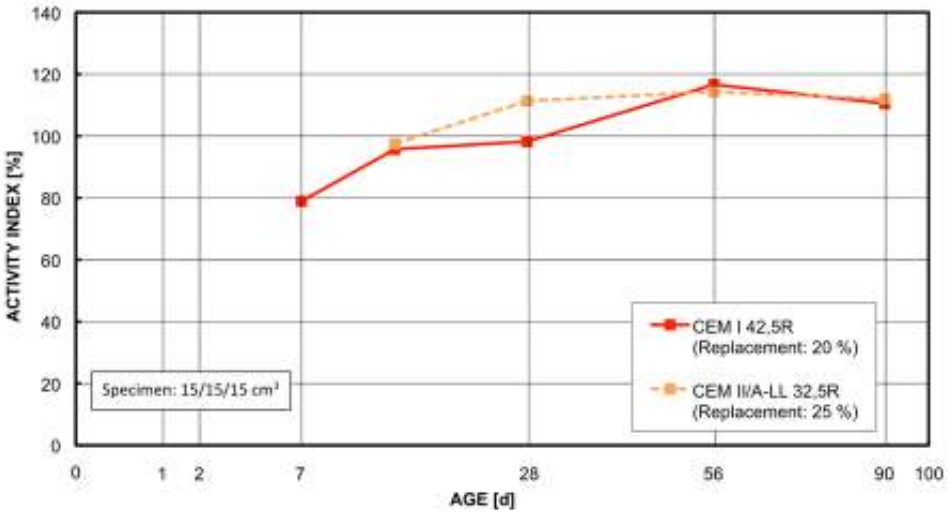

Figure 6 Development of the activity index of concrete based on compressive strength

The impact of the calcined clay on compressive strength can be attribute partially to its higher water demand. Thus less water is available for the cement. Secondly the calcined clay provides alkali soluble silicon and aluminium ions, which contribute to its puzzolanic reactivity and will form additional calcium silicate hydrate (CSH) and calcium aluminate hydrate (CAH) phases [6 - 11]. Obviously this process of releasing the ions is faster than the similar process that takes place when fly ash is used as Type II addition [18]. Due to the higher release rate calcined clay starts being effective as early as seven days.

Flexural Tensile Strength

The use of the calcined clay is less beneficial on the flexural tensile strength. Especially CEM I and CEM III seem to exhibit no or even an detrimental effect compared to the reference mixes (Figure 7). This effect visible on the activity index is more due to an increased flexural strength of the reference mixes rather than a strength reduction of the mixes containing calcined clay (see Table 2). The overall picture is similar to the one seen for the compressive strength results. The calcined clay is more effective in combination with CEM II than with CEM I or CEM III.

Shrinkage

The impact of calcined clay on shrinkage was tested on two concretes. A 20 % replacement of cement by calcined clay reduced slightly shrinkage in both cases beyond 90 days. Again the effect is more obvious in case of CEM II/A-LL 32,5R.

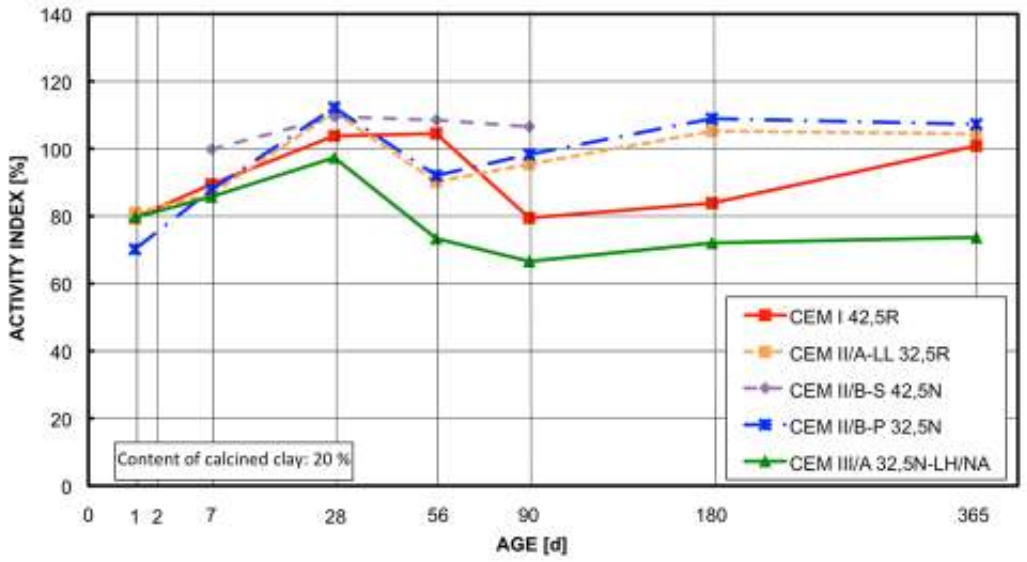

Figure 7 Development of the activity index based on flexural tensile strength tests for a replacement of 20 % cement by calcined clay

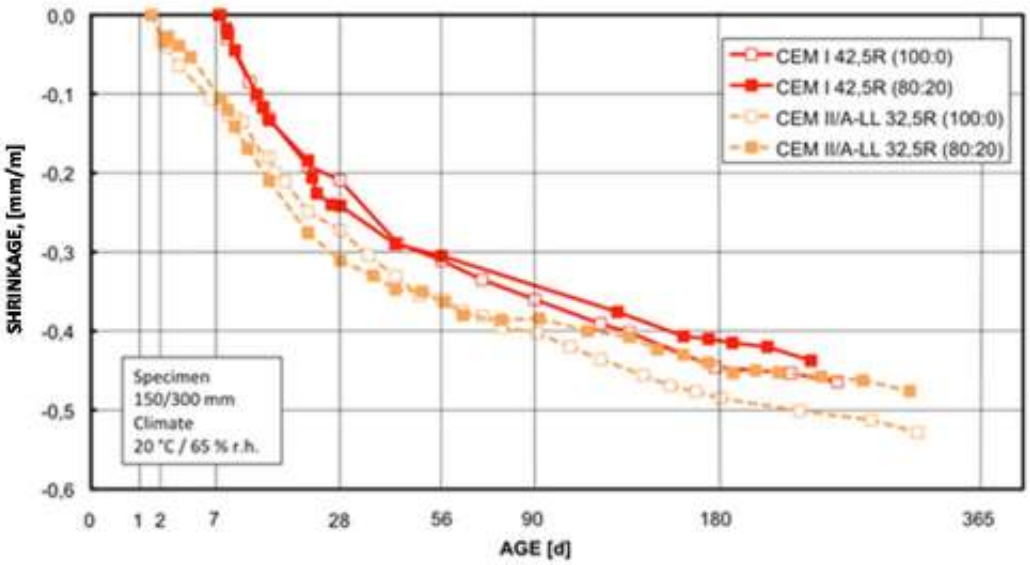

Figure 8 Shrinkage of concretes using cement only or a replacement of 20 % of these cements by calcined clay

Durability

Depth of carbonation tends to be slightly higher for concrete containing 25 % calcined clay (Figure 9). Considering the normal scatter of these measurements the difference is rather insignificant.

The ingress of chlorides was measured on concrete made with CEM I 42,5R. The concrete containing 20 % calcined clay exhibits hardly any difference compared to the reference concrete (Figure 10).

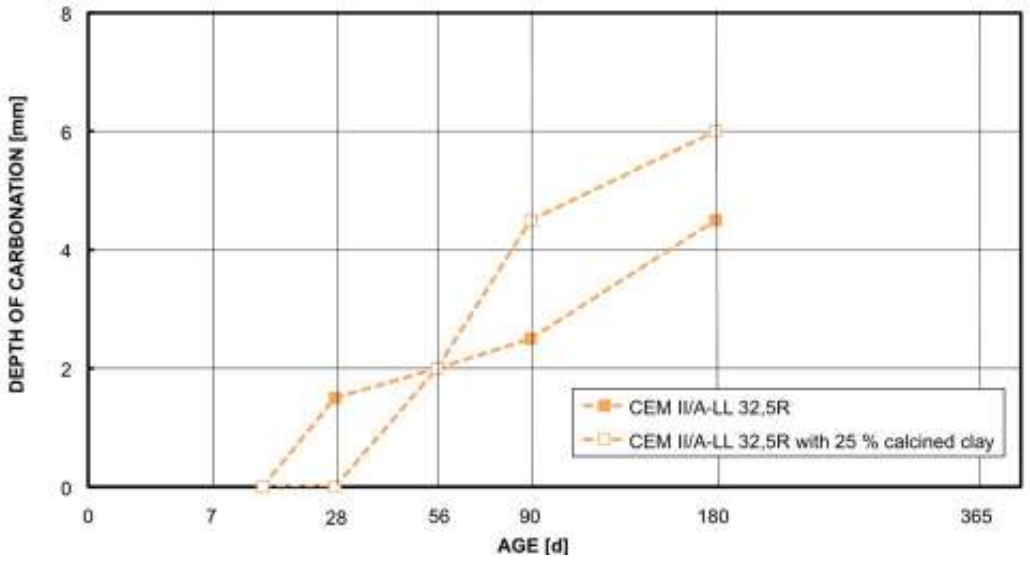

Figure 9 Depth of carbonation of concrete made with cement only or with a replacement of 25 % cement by calcined clay

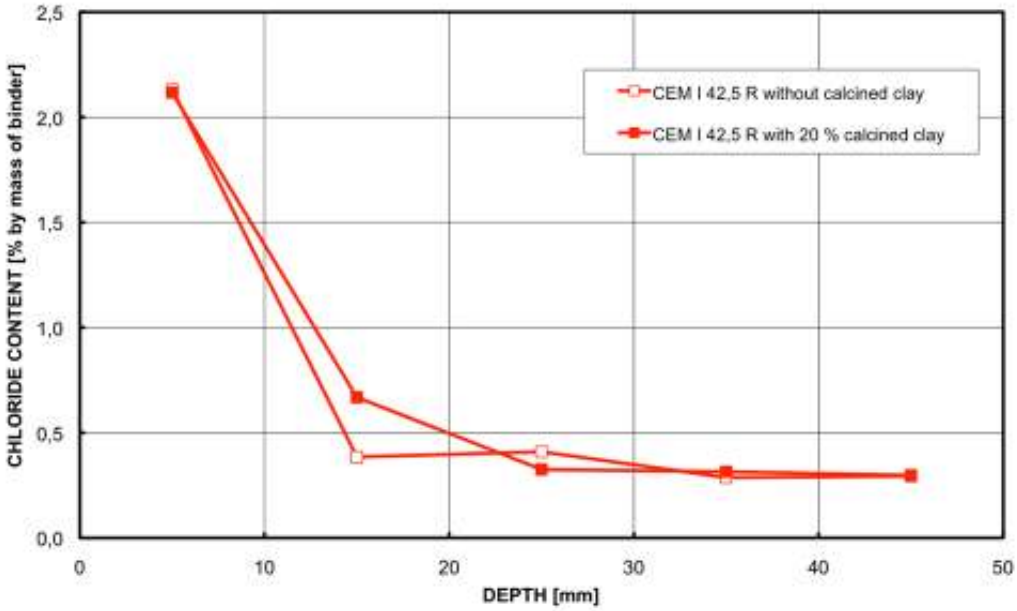

Figure 10 Chloride ingress in concrete made with cement only or with a replacement of 20 % cement by calcined clay

Length change due to sulphur attack increases at a slightly lower rate compared to the reference (Figure 11). Nevertheless the replacement of 20 % CEM I 42,5 R by calcined clay is not sufficient to limit the expansion to 0,5 mm/m at 56 days as required for a sulphate resistant binder [14].

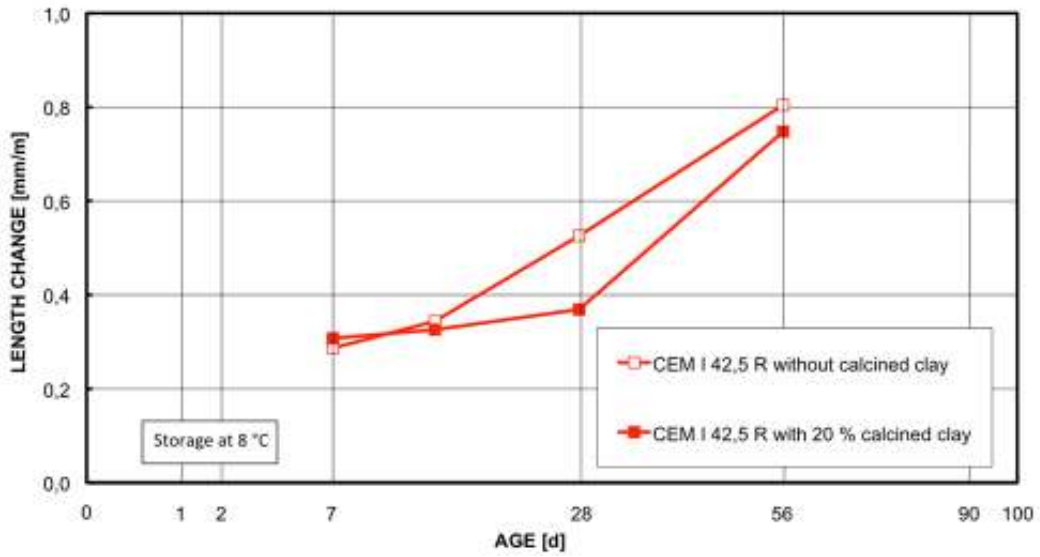

Figure 11 Length change due to sulphur attack of concrete made with cement only or with a replacement of 20 % cement by calcined clay

ECOLOGICAL ASPECTS

The production of calcined clay consumes less energy than the production of cement clinker. Information is given in Table 3 about the non-renewable primary energy needed for the different cement types and the calcined clay used. The overall average CO_2 release caused by clinker production in Germany adds up to 0,78 ton CO_2 per ton of Portland cement clinker [19]. Decarbonating the carbon content in the Lias delta clay yields 0,022 ton CO_2 per ton of calcined clay.

Table 3 Clinker content and non-renewable primary energy consumption of binders [20, 21, 22]

	CLINKER CONTENT [%]	NON-RENEWABLE PRIMARY ENERGY (MEAN VALUE) [MJ/t]
CEM I	95 - 100	4355
CEM II/B-M	65 - 79	3220
CEM III/A	35 - 64	2156
Calcined clay	-	1731

The possible quantity of non-renewable primary energy and CO_2 to be saved per m^3 of concrete due to replacing cement by calcined clay depends on the type of cement and the k-value considered for the calcined clay. The k-value approach considers a cementing equivalence value to Type II additions. Typical values for common Type II additions are 0,4 (fly ashes) [23], 0,6 (blast furnace slag) [24] and 1,0 (silica fume) [23]. Different k-values presuppose different quantities of calcined clay needed for replacing cement, which in turn

has a direct impact on the ecological balance. The result can be compared best, if a typical ready-mix concrete is taken as an example. A first estimate shall start with replacing 50 kg cement per m^3 of concrete. This quantity corresponds to the difference between the minimum cement content (320 kg/m^3) and the minimum cement content if Type II additions are considered (270 kg/m^3) [23]. Such concrete is suitable for exposure classes: XD2, XD3, XF2, XF3, XF4, XA2, XA3, XM2 und XM3 [23]. The production of a ready-mix concrete consumes typically 1350 MJ/m^3 to 1792 MJ/m^3 non-renewable primary energy and 0,124 to 0,243 t_{CO_2}/m^3 [15].

The comparison given in Table 4 highlights the saving potential with respect to non-renewable primary energy and CO_2 due to replacing cement by calcined clay. The quantities of calcined clay given in the heading of Table 4 are the replacements needed for 50 kg/m^3 of cement for the corresponding k-value. Even a low k-value of 0,4 will reduce the CO_2 emission by up to 14 %, but up to 12 % more energy will be required. Taking into account the full potential of the calcined clay used in this investigation a k-value of 1,0 is not far from being realistic. Thus a CO_2 reduction can be accomplished close to 15 % combined with savings in non-renewable primary energy of 6 to 8 %. This holds for a partial replacement of CEM I. Benefits will be smaller in case of CEM III.

Table 4 Possible savings per m^3 of concrete in non-renewable primary energy and CO_2 due to replacing cement by calcined clay

	K-VALUE: 0,4 (≙ 125 kg/m^3)		K-VALUE: 0,6 (≙ 80 kg/m^3)		K-VALUE: 1,0 (≙ 50 kg/m^3)	
	Energy [MJ/m^3]	CO_2 [t/m^3]	Energy [MJ/m^3]	CO_2 [t/m^3]	Energy [MJ/m^3]	CO_2 [t/m^3]
CEM I	- 49,8	0,035	46,6	0,036	110,8	0,037
CEM II/B-M	-106,5	0,025	-10,2	0,026	54,0	0,027
CEM III/A	-159,7	0,017	-63,4	0,018	0,8	0,018

CONCLUSIONS

Initial strength develops at a lower rate until seven days for most mixes containing calcined clay. At higher ages mixes with a 20 to 25 % replacement reach and exceed significantly the strength of the companion pure cement mixes. This holds especially for mixes containing CEM II where in some cases even a replacement of 40 % led to higher strength values beyond 28 days. The efficiency of the calcined clay as a Type II addition ranges in between granulated blast furnace slag and metakaolin. The inclusion of cement by calcined clay reduces consistency, bleeding and shrinkage. The effect on durability aspects is negligible. Besides the positive impact on strength the replacement of cement by calcined clay will yield ecological benefits. Considering a k-value close to 1,0 will help saving non-renewable primary energy and reduce the average CO_2 release of concretes utilizing this calcined clay as Type II addition.

ACKNOWLEDGEMENTS

The authors like to thank Liapor GmbH & Co. KG for the supply of the calcined clay.

REFERENCES

1. VEREIN DEUTSCHER ZEMENTWERKE E.V. (VDZ). Clay as pozzolanic main constituent of cement, VDZ-Activity Report 2007 – 2009, pp 51-52.

2. SCHRENK, J, WENDA, R. Improvement of the properties of cementitious systems. Application of clay powder containing metakaolin, BFT International, No. 4, 2006, pp 24-36.

3. JONES, R T. Metakaolin as a pozzolanic addition to concrete, Structure and Performance of Concrete, Eds. J Bensted and P Barnes, 2nd Edition, 2002, pp 372-397.

4. AMBROISE, J, MARTIN-CALLE, S, PERA, J. Pozzolanic behaviour of thermally activated kaolin. Fly Ash, Silica Fume, Slag and natural Puzzolans in Concrete, Ed. V M Malhotra, ACI SP132-40, 1992, pp 731-748.

5. WILD, S, KHATIB, J, M, JONES, A. Relative strength, pozzolanic activity and cement hydration in superplasticised metakaolin concrete. Cement and Concrete Research, Vol. 26, No. 10, 1996, pp 1537-1544.

6. HE, C, MAKOVICKY, E, OSBÆK, B. Thermal stability and pozzolanic activity of calcined kaolin. Applied Clay Science, Vol. 9, No. 3, 1994, pp 165–187.

7. HE, C, MAKOVICKY, E, OSBÆK, B. Thermal stability and pozzolanic activity of calcined Illite. Applied Clay Science, Vol. 9, No. 5, 1995, pp 337–354.

8. HE, C, MAKOVICKY, E, OSBÆK, B. Thermal stability and pozzolanic activity of sepiolite. Applied Clay Science, Vol. 10, 1996, pp 337–349.

9. HE, C, MAKOVICKY, E, OSBÆK, B. Thermal stability and pozzolanic activity of Na- and Ca-montmorillonite. Applied Clay Science, Vol. 10, 1996, pp 351–368.

10. HE, C, MAKOVICKY, E, OSBÆK, B. Thermal stability and pozzolanic activity of raw and calcined mixed-layer mica/smectite. Applied Clay Science, Vol. 17, 2000, pp 141–161.

11. FERNANDEZ, R, MARTRENA, F, SCRIVENER, K, L. The origin of the pozzolanic activity of calcined clay minerals: A comparison between kaolinite, illite and montmorillonite. Cement and Concrete Research, Vol 41, No. 1, 2011, pp 113-122.

12. EN 196-1. Methods of testing cement - Part 1. Determination of strength, 2005.

13. ASTM C230M – 08. Standard Specification for Flow Table for Use in Tests of Hydraulic Cement, 2008.

14. WITTEKIND, W. Sulfatbeständige Zemente und ihre Prüfung (in German) (Sulfate resistant cements and their testing). Zement-Kalk-Gips Vol. 13, No. 2, 1960, pp 565-572

15. European Organisation for Technical Approvals EOTA. CUAP Natural calcined pozzolana as Type II addition. 2005, p 17.

16. DEUTSCHER BETON- UND BAUTECHNIK-VEREIN E. V. Special testing methods for fresh concrete (in German), DBV-Merkblatt, 2007, p 24.

17. RILEM RECOMMENDATIONS. CPC-18 Measurement of hardened concrete carbonation depth, Materials and Structures, Vol. 21, No. 6, 1988, pp 453-455.

18. SYBERTZ, F. Beurteilung der Wirksamkeit von Steinkohlenflugaschen als Betonzusatzstoff (in German) Assessment of the Effectiveness of Coal Fly Ash as a Concrete Addition, Beuth Verlag, 1993, p 111.

19. MCKINSEY&COMPANY. Änderung der europäischen Richtlinie zum Emissionshandel: Auswirkungen auf die deutsche Zementindustrie (in German) (Changes in the European guideline for emission trading: Impact on the German cement industry), Düsseldorf, 2008, p 33.

20. DIN 197-1. Cement - Part 1. Composition, specifications and conformity criteria for common cements, 2004.

21. BUNDESVERBAND LEICHTBETONZUSCHLAG (BLZ). Ganzheitliche Bilanzierung von Blähton und Blähschiefer (in German) Holistic balance study of expanded clay and expanded shale (internal document), 1995.

22. EYERER, P, REINHARDT, H.-W. Ökologische Bilanzierung von Baustoffen und Gebäuden: Wege zur ganzheitlichen Bilanzierung (in German) (Ecological Balance study of building materials and buildings: Ways to holistic balancing). Birkhäuser, Berlin, 2000, p 233.

23. DIN 1045-2. Tragwerke aus Beton, Stahlbeton und Spannbeton – Teil 2: Beton – Festlegung, Eigenschaften, Herstellung und Konformität – Anwendungsregeln zu DIN EN 206-1 (in German) (Concrete, reinforced and prestressed concrete structures – Part 2: Concrete –Specification, properties, production and conformity – Application rules for DIN EN 206-1), 2008, p 62.

24. EHRENBERG, A. Hüttensandmehl als Betonzusatzstoff – Aktuelle Situation in Deutschland und Europa (in German) (Ground blast furnace slag as concrete addtion – Actual situation in Germany and Europe). Beton-Information No. 3/4, 2010, pp 48-63.

Study on Geopolymerization of Highlime Fly Ashes

I Papayianni, S Konopissi
Aristotle University of Thessaloniki, Greece

High calcium fly ashes (HCFAs) constitute more than half of the total fly ash production in Europe, but their exploitation is very low; about 20% of their output. This leads to the rejection of huge quantities of HCFAs without any benefit of their strength capacity. HCFAs usually consist of calcium aluminates and silicates and often free lime and sulfates. In this study, HCFA samples with 8.49% free lime and ≥25% silica content are treated with water (2 parts of HCFA : 1 part of water) containing 36% of a mixture of NaOH to Na_2SiO_3 (1:1). Such mixtures were placed in (40x40x160) mm specimens and were cured in three curing regimes: 1) 65°C for 2 days, 2) 40°C for 4 days and 3) 25°C for 7 days. After the curing some of the specimens were placed into climatic chamber (95% relative humidity) and the rest were left at indoor conditions (65% relative humidity). Mechanical and elastic properties and volume deformations of the pastes were tested at 7-d, 28-d and 90-d ages. Porosity measurements were also carried out at the same ages. A microstructure analysis was made by using X-ray diffractometry, DTA-TG methodology, FTIR spectroscopy and SEM microscopy, in order to determine the mechanisms to which the cementing properties are due. The alkali-activated fly ash pastes have developed 7-d compressive strength, from 22 to 32 MPa, 28-d from 22 to 35 MPa and 90-d strength from 33 to 46 MPa. This is considered very encouraging for alkali-activation process. Volume stability measurements also have completed the study regarding the deformation of geopolymerized HCFA.

I Papayianni is currently Professor and Director of the Laboratory of Building Materials at the Civil Engineering Dept. of the Aristotle University of Thessaloniki, Greece. She is a member of ACI and RILEM Committees and the scientific responsible of many National and European Research Projects. Her specialist research fields include concrete technology, supplementary materials and repair materials.

S Konopisi is a Chemist MSc and a PhD candidate at the Laboratory of Building Materials at the Civil Engineering Dept. of the Aristotle University of Thessaloniki, Greece. She has participated in several research projects on concrete chemistry and on conservation and restoration of monuments. Her specialist areas of research include geopolymerization and construction material characterization.

Keywords: Alkaline activator, Geopolymerization, High calcium fly ash (HCFA), Mechanical strength

INTRODUCTION

As known, geopolymers are inorganic polymeric materials developed by J. Davidovits in 1970s. These materials can polycondense just like organic polymers, at temperatures lower than 100 °C. Geopolymerization involves the chemical reaction of alumino-silicate oxides with alkali polysilicates yielding polymeric Si – O – Al bonds [1]. The mechanisms proposed for the geopolymerization includes the following four stages that proceed in parallel and thus, it is impossible to be distinguished [2-4]: (i) dissolution of Si and Al from the solid alumino-silicate materials in the strongly alkaline aqueous solution, (ii) formation of oligomers species (geopolymers precursors) consisting of polymeric bonds of Si – O – Si and/or Si – O – Al type, (iii) polycondensation of the oligomers to form a three-dimensional alumino-silicate framework (geopolymeric framework) and (iv) bonding of the unreacted solid particles and filler materials into the geopolymeric framework and hardening of the whole system into a final solid polymeric structure.

Davidovits [5, 6] described the alkali activation process with the following general formula:

$$Mn[-(Si\text{-}O2)z\text{-}Al\text{-}O]n \cdot wH_2O \quad (1)$$

Where M is the alkaline element, - indicates the presence of a bond, z is 1, 2 or 3, and n is the degree of polymerization.

According to this, another form of cementitious material using silicon and aluminum activated in a high alkali solution was developed [7]. This material is usually based on fly ash as a source material and is termed geopolymer or alkali-activated fly ash cement [8, 9]. The mortar and concrete made from this geopolymer present similar strength and appearance to conventional Portland cement [10]. Fly ash is a solid waste product created by the combustion of coal. Its appearance is light to dark-gray powder and has very find granulometry [11, 12]. Fly ashes are distinguished between Class F - low calcium and Class C - high calcium (called HCFAs) according to ASTM C618 [13]. HCFAs consist of calcium aluminates and calcium silicates, therefore, present both pozzolanic and cementitious properties [14]. Fly ashes Class C, especially from the combustion of lignite coal, usually contain more than 10% CaO, high amounts of alkalies, are low in silica and alumina, but usually contain large amounts of sulfates mostly in the form of sodium sulfate. The crystalline minerals found in fly ashes Class C, are quartz, tricalcium aluminate ($3CaO \cdot Al_2O_3$), calcium aluminosulfate ($4CaO \cdot 3Al_2O_3 \cdot SO_3$), anhydrite ($CaSO_4$), free CaO, periclase (free MgO), and alkali sulfates. Additional, except quartz and periclase, all the crystalline minerals are reactive and this also explains why the HCFAs are more reactive from low-calcium fly ashes [15]. In this paper, a high calcium fly ash (HCFA) from Amyntaio area (AMN) in North Greece was examined.

EXPERIMENTAL WORK

Materials

Lignite fly ash, from the Power Station of Public Power Corporation in the north of Greece, named AMN was used as raw material. Sodium hydroxide, NaOH in pellets form 99.5% purity, water glass (sodium silicate neutral solution: 8.9% Na_2O, 28.7% SiO_2, 62.4% H_2O and d=1.365) and tap water were also used for the synthesis of paste specimens for

geopolymerization. Sodium hydroxide pellet was dissolved in distilled water to prepare NaOH solution 10M. The alkaline activator- liquid phase- used was a mixture of sodium hydroxide and sodium silicate solution with NaOH : Na_2SiO_3 weight ratio 1:1.

The chemical composition of fly ash determined by Atomic Absorption Spectrometry, AAS, analysis and according to EN 451-1 [16] is given in Table 1:

Table 1 Chemical composition of fly ash AMN (% wt)

CHARACTERISTICS	HCFA
Chemical composition (% by mass)	
Na_2O	1.13
K_2O	0.89
CaO	32.46
MgO	2.90
$Fe2O_3$	7.23
$Al2O_3$	11.12
SiO_2	35.40
Loss of ignition	1.30
SO_3	7.16
CaO_{free}	8.49
Si_2O/ Al_2O_3	3.18
Fineness	
Retained on 45 μm sieve	33.7
Apparent specific density	2.508

Preparation of Geopolymer Paste Specimens

Sodium hydroxide first was mixed with sodium silicate solution and tap water in order to prepare the liquid phase (18% NaOH solution, 18% Na2SiO3 solution and 64% water). For making geopolymer paste, fly ash (solid phase, S) and alkaline activator (liquid phase, L) were mixed in proportion 2:1 together in a mixer according to EN 196-1 [17] to produce homogeneous pastes.

The fresh mixtures were placed into metallic moulds in order to prepare (40x40x160) mm specimens and were cured in an oven in three curing regimes: a) 65 °C for 2 days, b) 40 °C for 4 days and c) 25 °C for 7 days. After the curing, the specimens were removed from the moulds. Half of the specimens were placed into climatic chamber (95 %RH) and the rest of them were left at indoor conditions (65 %RH).

Table 2 Fresh HCFA mixtures

COMPOSITION CONSTITUENTS			
	HCFA	Water	Alkalies
Mass, kg	1	0.32	0.18
Mass, %	66.7	21.4	12
Composition Characteristics			
Liquid/Solid Ratio		Vicat plug penetration (mm)	
0.5		6	

Analysis and Tests

Samples from the above specimens were examined, in order to determine the mechanisms due to which the cementing properties have been developed. For this purpose the following methodologies and tests were used:

- Determination of mechanical strengths, flexural and compressive at ages 7-d, 28-d and 90-d. Tests were performed in digital testing machines according to EN 196-1.The reported mechanical strength is the average value of three specimen crushing values.
- The method RILEM CPC 11.3, by using n-heptane as absorbed liquid, for open porosity.
- Ultrasonic sonometer measurement for calculation of the dynamic modulus of elasticity.
- The volume deformations were monitored by using extensometers.
- Mineralogical analysis of crystal phases with X-Ray Diffraction (XRD). The X-ray diffractograms of powdered samples were obtained with a Philips PW 1840 diffractometer using Cu Ka radiation with 2θ ranges from 2° to 70°.
- Analysis of crystal phases and microstructure (crystal lattice, form and size of crystals) and elemental composition by scanning electron microscope – SEM/EDX (model JOEL JSM 840A).
- Phase transformations through the absorptions of characteristic bands were identified by FTIR spectroscopy. The FTIR spectra diagrams were carried out by using a spectrometer (model Nicolet 6700) in the wave number range from 400 to 4000cm-1 and KBr pellet technique. Specimens were prepared by mixing 1mg of sample in 300mg of KBr.
- Control of the rate of dehydration and decomposition of the derived products by the thermogravimetric method (DTA-TG) model TA Instruments SDT 2960 using nitrogen.

RESULTS AND DISCUSSION

Mechanical Strengths, Open Porosity, Modulus of Elasticity and Volume Deformation

Mechanical strengths, modulus of elasticity, open porosity and volume deformation are presented in Tables 3 and 4.

Table 3 Mechanical strengths of hardened HCFA pastes

	COMPRESSIVE STRENGTH (fc), MPa			FLEXURAL STRENGTH (fb), MPa			fb/fc		
Age, days	7	28	90	7	28	90	7	28	90
RH 95%									
Curing at 25°C	32.75	33.50	46.04	4.22	4.76	5.32	0.13	0.14	0.12
Curing at 40°C	23.15	35.06	40.15	2.29	5.18	4.64	0.10	0.15	0.12
Curing at 65°C	22.80	32.75	40.14	5.24	5.16	5.22	0.23	0.16	0.13
RH 65%									
Curing at 25°C	29.69	21.10	35.03	1.26	0.87	1.63	0.04	0.04	0.05
Curing at 40°C	28.30	33.98	35.94	1.21	1.02	1.65	0.04	0.03	0.05
Curing at 65°C	18.85	18.87	33.61	1.89	1.90	1.69	0.10	0.10	0.05

Table 4 Characteristics of hardened HCFA pastes

	OPEN POROSITY, %			ELASTICITY MODULUS (E), GPa		
Age, days	7	28	90	7	28	90
RH 95%						
Curing at 25°C	8.19	5.58	2.71	14.4	16.4	17.9
Curing at 40°C	1.93	1.37	2.56	14.2	16.00	15.0
Curing at 65°C	6.52	5.58	3.46	17.4	17.1	18.7
RH 65%						
Curing at 25°C	14.73	13.63	10.91	14.0	12.6	12.9
Curing at 40°C	10.44	24.50	10.86	14.7	13.5	12.0
Curing at 65°C	14.27	12.56	14.18	14.7	14.5	14.1

For comparison reasons strength values of HCFA pastes of similar W/HCFA ratios without alkaline activator are given in Table 5. The histograms of strength development of alkali activated HCFA pastes are shown in Figures 1 and 2. It should be noted that some abnormalities in the results such as lower value of 28-d strength compared to that of 7-d is due to the intensive cracking of the specific specimen.

Table 5 Mechanical strengths of HCFA pastes without geopolymerization

HCFA pastes	COMPRESSIVE STRENGTH (fc), MPa			FLEXURAL STRENGTH (fb), MPa		
Age, days	7	28	90	7	28	90
	16.07	16.22	18.88	3.15	3.49	2.49

Ratio W/HCFA=0.44, W=water. Normal consistency pastes (EN 196-3:1994).

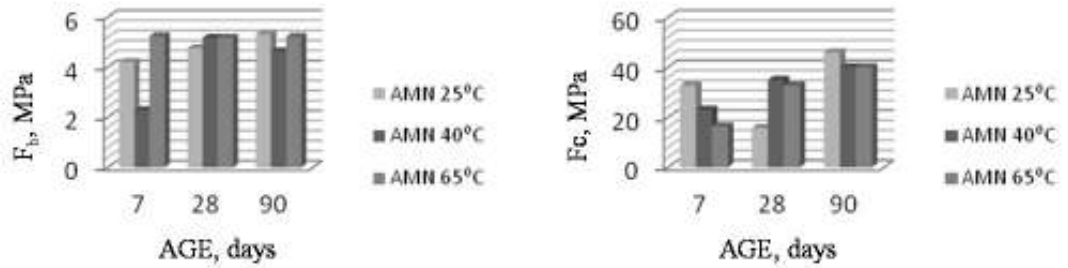

Figure 1 Flexural and Compressive strength of AMN 95% RH.

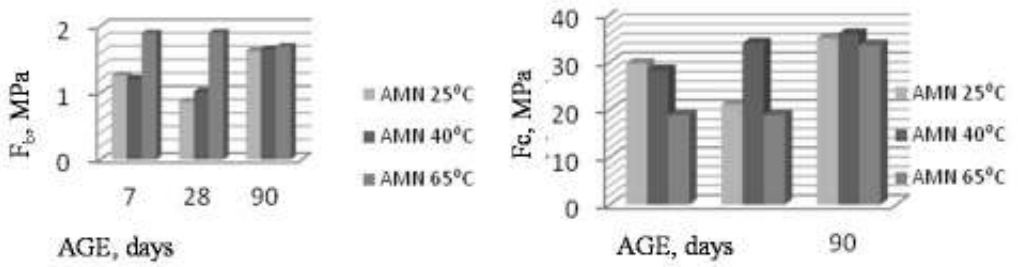

Figure 2 Flexural and Compressive strength of AMN 65% RH

Table 6 Volume deformation (DV %) of HCFA

	DV,% (RH 95%)	DV,% (RH 65%)
AMN 25 °C	1.16	3.15
AMN 40 °C	1.28	2.17
AMN 65 °C	2.28	2.28

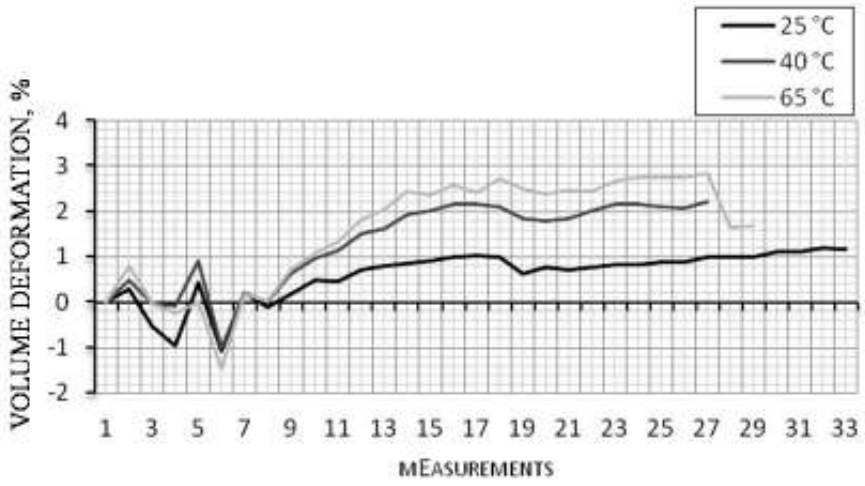

Figure 3 Measurements of % Volume deformation of HCFA pastes at 95% RH curing in 25, 40 and 65 °C

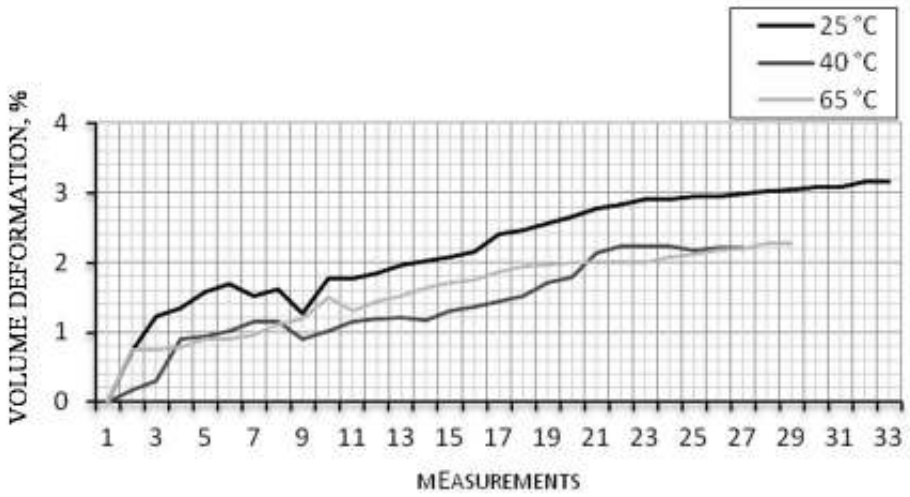

Figure 4 Measurements of % Volume deformation of HCFA pastes at 65% RH curing in 25, 40 and 65 °C

Mineralogical Analysis by XRD

Results of XRD of fly ash (AMN) and geopolymer pastes AMN 40 °C in 65% RH and 95% RH for the samples of 28 days shown in Figures 5, 6 and 7.

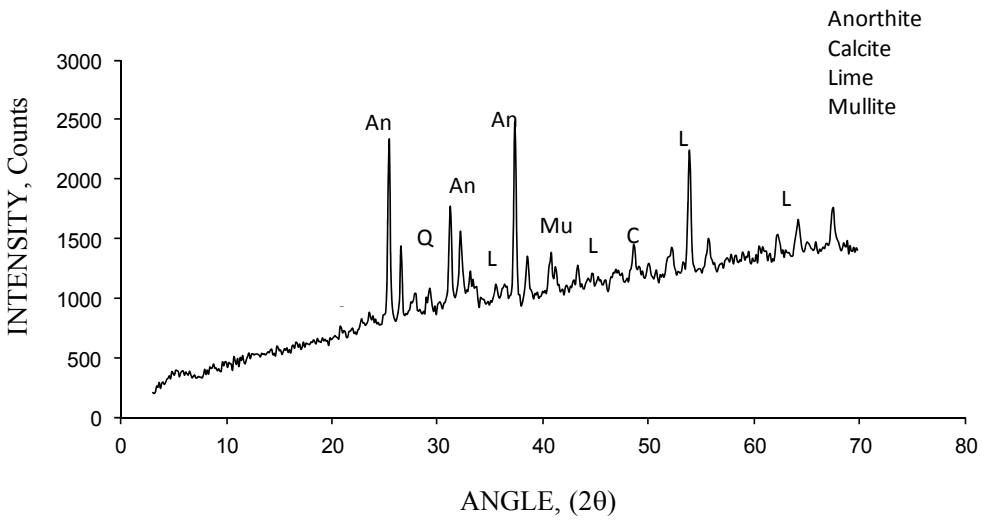

Figure 5 XRD diagram for raw HCFA

The raw fly ash is constituted of quartz, anhydrite, lime and some minor crystalline phases such as calcite, hematite, mullite, portlandite, and gypsum. The hump registered between 2θ=20°-30°.

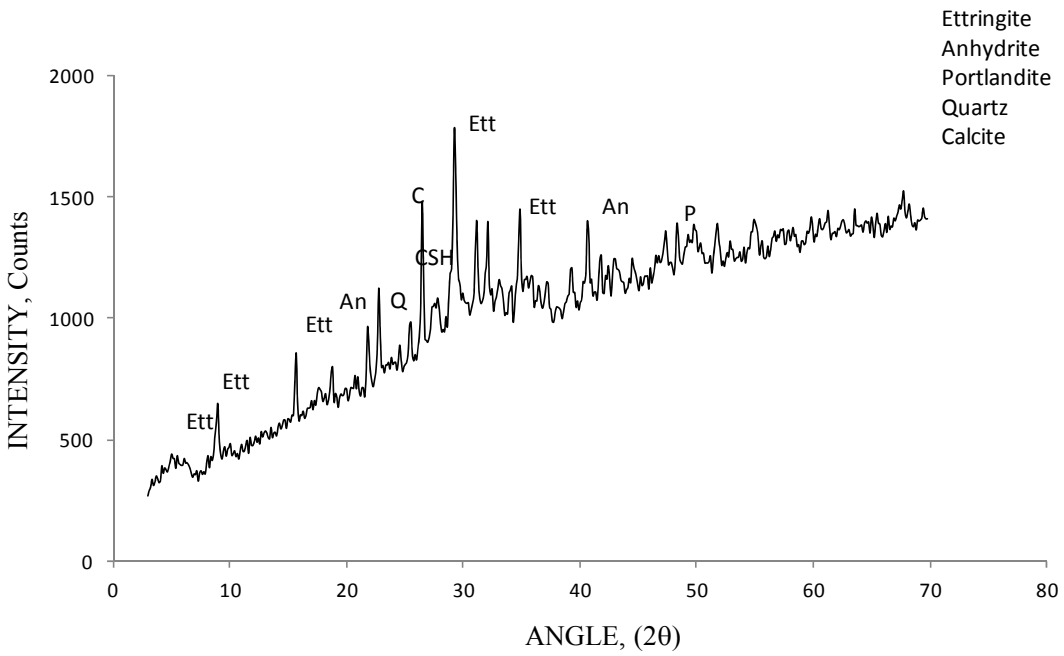

Figure 6 XRD diagram for HCFA paste geopolymerized in 40 °C, at 95%RH, at 28-d age

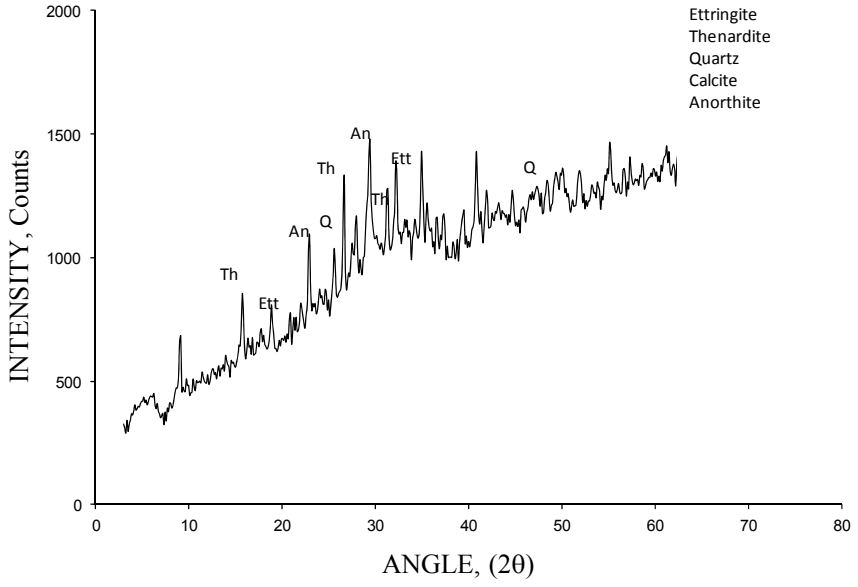

Figure 7 XRD diagram for HCFA paste geopolymerized in 40 °C, at 65%RH, at 28-d age

In all of the geopolymer pastes, micro-crystallized calcium-silicate, calcium-aluminate stable complex compounds were present. These compounds react with water to form hydrate products (all expressed as C-S-H) in gel form [18]. Formation of these compounds provides rapid hardening and strength and they have studied in most of XRD diagrams. The hump, in the XRD diagrams appears slightly shifted toward higher values between 2θ=25°-35°.

Additionally, in all of the geopolymers were detected ettringite because of the high sulfates level in the raw fly ash and some new crystalline phases (zeolites) such as herschelite ($NaAlSi_2O_6 \cdot 3H_2O$) [19]. The formation of all these products were registered between $2\theta=5°$-15°.This formation also affects the compressive strength of geopolymers.

Microstructure and Elemental Analysis by SEM/EDX

According to Figure 8, the raw fly ash AMN was composed by compact spheres of different size with an almost regular smooth texture which are included into the matrix with loose cohesion.

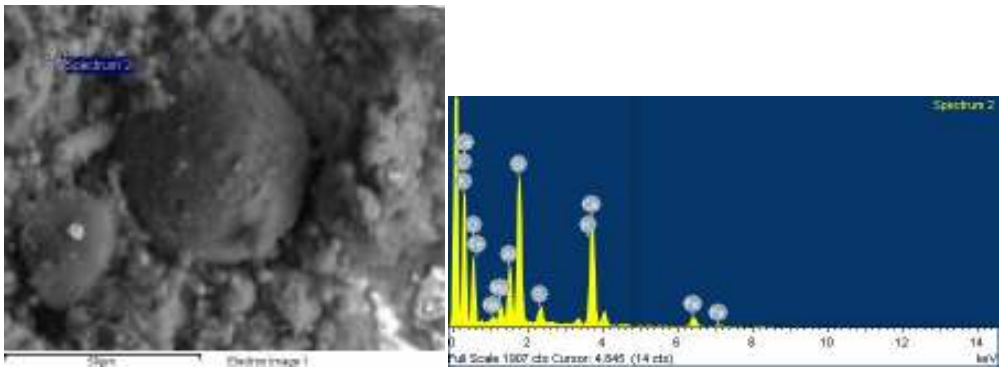

Figure 8 SEM/EDX analysis for raw HCFA

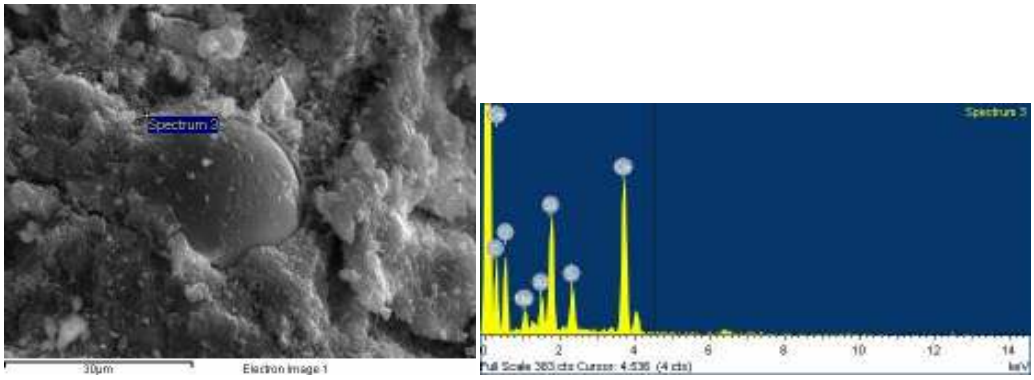

Figure 9 SEM/EDX analysis for HCFA paste geopolymerized in 40 °C, at 65%RH, at 28-d age

In Figure 9 is shown the reaction between the geopolymerized fly ash grain and the paste. The EDX diagram indicates the composition of the products in the contact zone. For geopolymer product was observed that together with the unreacted spheres and around of these there exists the amorphous alumino-silicate gel.

Figure 10a shows the morphology of fly ash grains and the surface reaction due to the chemical attack. Figure10b indicates the assimilation of the grains by the paste. Figure 11 depicts crystal growth in a compact structure. The EDX diagram shows the composition of the needle-like crystals, which could be attributed to ettringite.

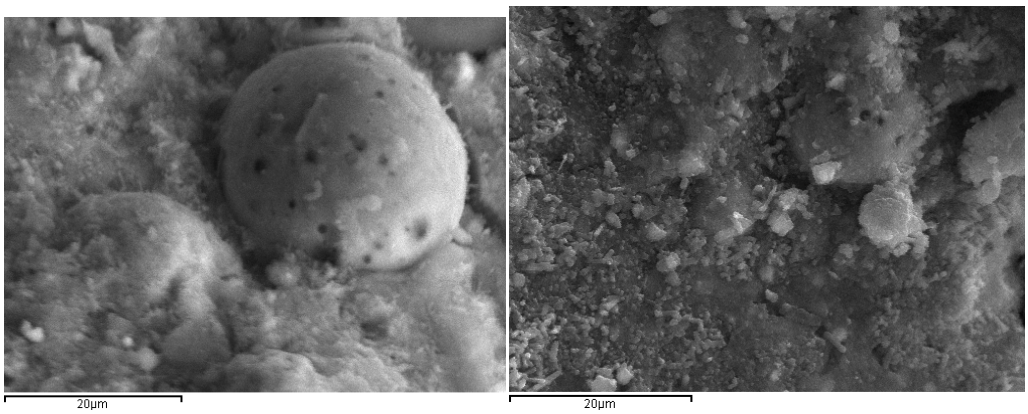

Figures 10a-10b SEM analysis for HCFA paste geopolymerized in 40 °C, at 65%RH, at 90-d age.

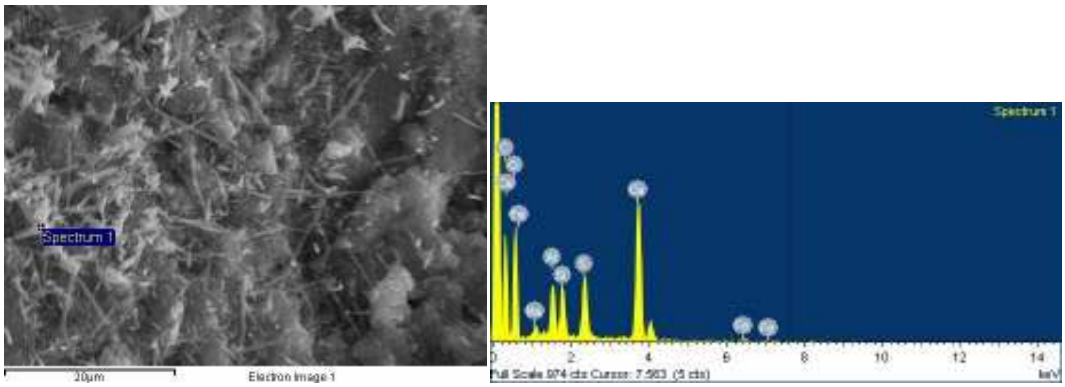

Figure 11 SEM/EDX analysis for HCFA paste geopolymerized in 40 °C, at 95%RH, at 28-d age.

Phase Transformations by FTIR

FTIR spectrum of raw fly ash (AMN) and geopolymer pastes AMN 40°C in 65% RH and 95% RH for the samples of 28 days shown in Figures 12, 13 and 14. Significant broad bands were observed at 3450-3400 cm-1 and 1650-1600 cm-1 for O-H stretching and O-H bending vibrations of bound water molecules.

The fly ash FTIR spectrum shows one broad component at 1113 cm-1 ascribed to Si-O or Al-O stretching vibrations and another located at 462 cm-1 ascribed to O-Si-O bending modes. In the FTIR spectra of geopolymers the main absorption bands were at 1111, 1107, 972, 971, cm-1.The band Si-O at 1113 cm-1 of the raw fly ash becomes sharper and shifts towards lower frequencies in geopolymers indicating the formation of amorphous alumino-silicate gel. On the other hand, the reaction of geopolymerization of fly ash hardly affects the bending band O-Si-O at 462 cm-1 (457, 459 cm-1 in geopolymers) indicating that the quartz is almost inert in the alkaline activators [20].

Finally, the bands appearing at 611 and 605 cm-1 in the spectrum of geopolymers products have been associated with the presence of zeolites [20].

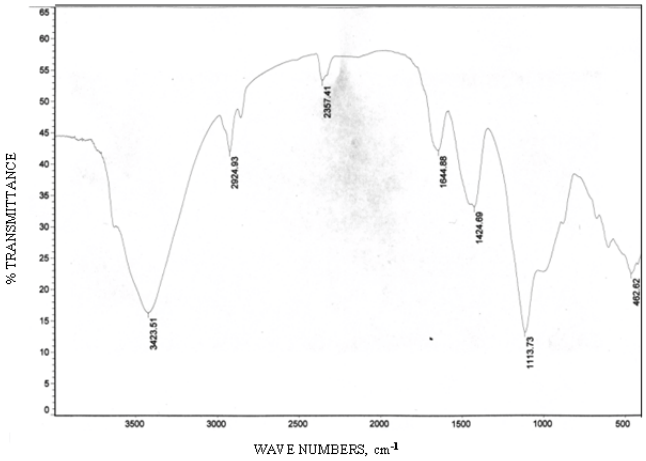

Figure 12 FTIR spectrum of raw HCFA

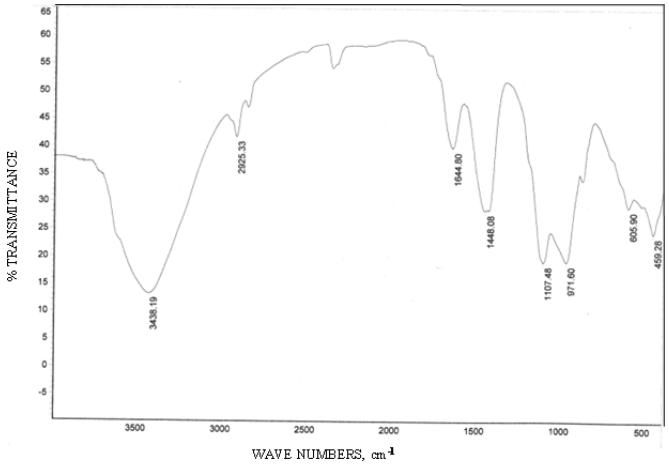

Figure 13 FTIR spectrum of raw HCFA paste geopolymerized in 40 ^{0}C, at 95%RH, at 28-d age

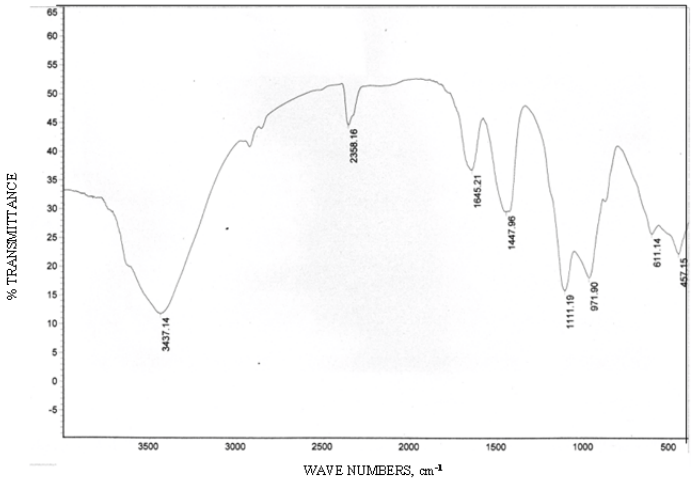

Figure14 FTIR spectrum of raw HCFA paste geopolymerized in 40 °C, at 65%RH, at 28-d age

Analysis of HCFA Paste by DTA-TG

From the thermogravimetric diagrams DTA-TG it seems that the loss of free water at 110 °C occurs with low rate in the samples AMN40 at the 95% RH than the one in 65% RH, at the early ages of 7 days. This dehydration is due to the water evaporation from the pores resulting in porosity change [21]. The lower the water evaporation the higher the compressive strength as it is indicated by the experimental results in the samples cured at 95% RH. In conclusion, the water is an essential part of the geopolymeric structure. The optimum quantities of water as well as the curing period of the samples are important parameters for the geopolymers to obtain the maximum strengths.

The loss of weight of the samples from 110 °C until 550 °C represents the loss of hydroxyls OH- in the form of bound water from geopolymeric gel [22]. As is known, when calcium hydroxide, $Ca(OH)_2$,is added to a reactive aluminum-silicate material (e.g. fly ash), a mechanism with specific kinetics occurs [23]. This pozzolanic reaction forms stable complex compounds, such as calcium-silicate, C_2S, and calcium-aluminate, CA. When these compounds come into contact with water, they rapidly react to form hydrate products C-S-H and C-A-H (in gel form) according to the following reaction:

$$C_2S + CA + H_2O \rightarrow C\text{-}S\text{-}H + C\text{-}A\text{-}H$$

In Figures 15a and 15b is marked lack of $Ca(OH)_2$ decomposition between 400 and 480 °C, which enforces the above mechanism.

Additionally, the loss of weight at 650-750 °C represents the loss of carbonate ions in the form of carbon dioxide, CO_2, from molecules such as calcium carbonate, $CaCO_3$, due to the carbonation process. Above that temperature the weight is stabilized as no crystallization phases are taken place. The reaction of carbonation is:

$$Ca(OH)_2 + CO_2 + H_2O \rightarrow CaCO_2 + 2H_2O$$

The process depends on humidity and temperature conditions. The carbonation rate does not seem to be affected by the geopolymerization of fly ash in different curing regimes.

CONCLUSIONS

High calcium fly ash (HCFA) with a ratio SiO2/Al2O3 around 3 has been alkali-activated. HCFA pastes develop significant strength after curing at temperatures 25 °C for 7 days, 40 °C for 4 days and 65 °C for 2 days. In particular, at 25 °C the compressive strength ranges from 22 to 46 MPa for the period from 7 to 90 days. At curing 40 °C the corresponding strength fluctuates from 23 to 40 MPa while at 65 °C the strength increases from 22 to 40 MPa.

Compared to the strength level of HCFA paste without alkaline activation (Table 5) it is obvious that geopolymerization contributes to strength increase from 50 up to 100% of 7-d and 90-d strength respectively.

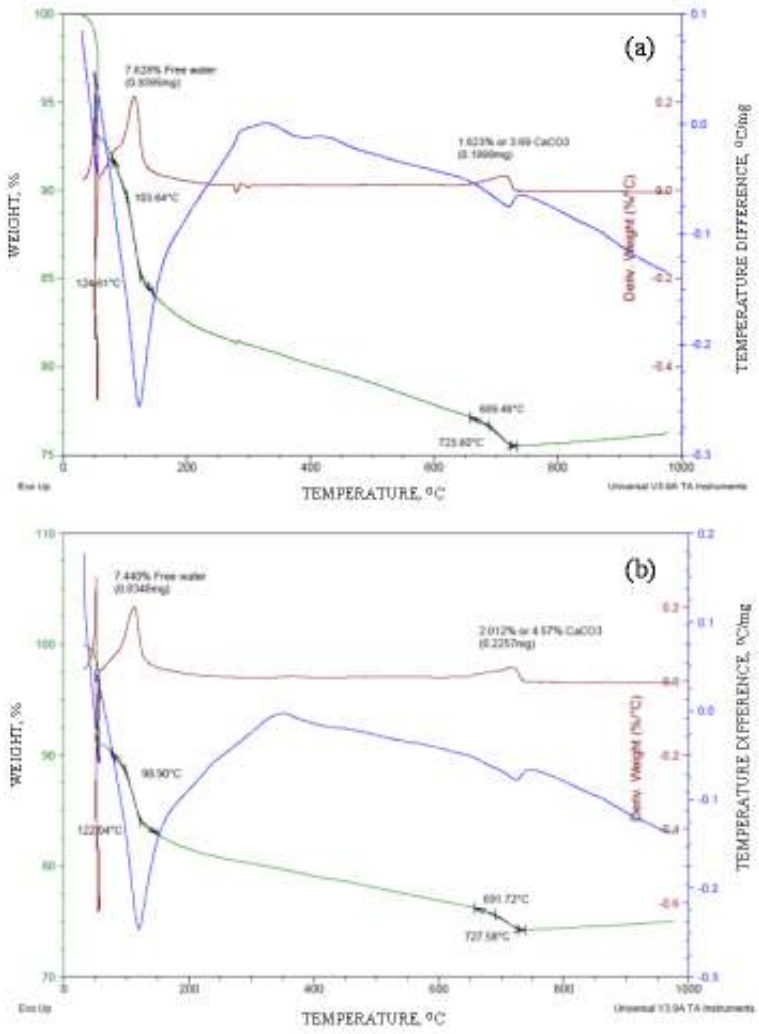

Figures 15 Thermogravimetric diagrams DTA-TG for HCFA paste geopolymerized in 40 °C, at (a) 65% RH and (b) 95% RH, at 7-d age

Furthermore, curing at 95% RH after treatment with alkaline activator helps in developing higher strength levels especially flexural ones, in comparison with those at in 65% RH. Therefore, the fb/fc ratios at 95% RH curing regime are higher than those at 65% RH. In addition, volume deformations are lower at 95% RH compared to those at 65% RH (Table 6).

A first investigation of the mechanisms showed that hydration products due to the self-cementing character of HCFA are in parallel formed apart from alumino-silicate (Si – O – Si, Si – O – Al) oligopolymers. Therefore, calcium silicate and calcium aluminate hydrates as well as ettringite are detected by XRD and SEM-EDX while the main absorptions of Si – O, Al – O are determined by FTIR spectrum.

Furthermore, DTA-TG analysis of HCFA geopolymerized hydrates indicated that there is not noticeable $Ca(OH)_2$ inside the mass. This implies that $Ca(OH)_2$ has been bound in C-S-H compounds at 95% RH curing or even in $CaCO_3$ at 65% RH curing.

REFERENCES

1. DAVIDOVITS, J. Inorganic polymeric new materials, Journal of Thermal Analysis, Vol. 37, 1991, pp 1633-1656.

2. XU, H, VAN DEVENTER, J S J. The geopolymerization of alumino-silicate minerals, Int. J. Miner. Process., Vol. 59, 2000, pp 247-266.

3. SWANEPOEL, J C, STRYDOM, C A. Utilization of fly ash in a geopolymeric material. Appl. Geochem., Vol. 17, 2002, pp 1143-1148.

4. VAN JAARSVELD, J G S, VAN DEVENTER, J S J, LUKEY, G G. The effect of composition and temperature on the properties of the fly ash -and kaolinite- based geopolymers, Chem.Eng. J., Vol. 89, 2002, pp 63-73.

5. DAVIDOVITS, J. Mineral polymers and methods of making them, USA patent 4, 349, 386, 1982.

6. DAVIDOVITS, J. Early high strength mineral polymer, USA patent 4, 509, 985, 1985.

7. DAVIDOVITS, J. Chemistry of geopolymeric systems, terminology. Geopolymer ’99 Int. Conf., France, 1999, pp 9-40.

8. PALOMO, A, GRUTZECK, M W, BLANCO, M T. Alkali-activated fly ashes, a cement for the future, Cem Concr Res, Vol. 29, No. 8, 1999, pp 1323-1329.

9. FERNANDEZ-JIMENEZ, A, PALOMO, A, CRIADO, M. Microstructure development of alkali-activated fly ash cement: a descriptive model, Cem Concr Res, Vol. 35, 2005, pp 1204-1209.

10. CHINDAPRASIRT, P, CHAREERAT, T, SIRIVIVATNANON, V. Workability and strength of coarse high calcium fly ash geopolymer, Cement and Concrete Composites, Vol. 29, 2007, pp 224-229.

11. COLLINS, R J, CIESIELSKI, S K. Utilization of waste materials in civil engineering construction, New York: ASCE; 1992.

12. HAUSMANN, M R. Engineering principles of ground modification. Singapore: McGraw-Hill; 1990.

13. ASTM C618. Standard specification for coal fly ash and raw or calcined natural pozzolan for use in concrete. American society for testing and materials. West Conshohocken, PA, USA: ASTM International; 2003.

14. SENOL, A, BIN-SHAFIQUE, M D S, EDIL, T B, BENSON, C H. Use of class C fly ash for stabilization of soft subgrade, ACE proceedings, 2002, p 96372.

15. MALHOTRA, V M, MEHTA, P K. High-Performance, High-Volume Fly Ash Concrete: Materials, Mixture Proportioning, Properties, Construction Practice, and Case Histories, Marquardt Printing Ltd., Ottawa,Canada, 2002, pp 14-17.

16. EN 451-1, 2003. Title Identifier, Method of testing fly ash. Determination of free calcium oxide content.

17. EN 196-1. 2005, Methods of testing cement – Part 1: Determination of strength.

18. BROWN, P W, CLIFTON, J R. Mechanisms of deterioration in cement-based materials and lime mortars, Durability of Building Materials, Vol. 5, 1998, pp 409-420.

19. FERNANDEZ-JIMENEZ, A, PALOMO, A. Composition and microstructure of alkali activated fly ash binder: Effect of the activator, Cement and Concrete Research, Vol. 35, 2005, pp 1984-1992.

20. MOZGAWA, W, SITARZ, M, ROKITA, M. Spectroscxopic studies of different aluminosilicate structures, J. Mol. Struct, Vol. 511-512, 1999, pp 251-257.

21. KONG, D L Y, SANJAYAN, J G. Damage behavior of geopolymer composites exposed to elevated temperatures, Cement and Concrete Composites, Vol. 30, No. 10, 2008, pp 986-991.

22. SUBAER, VAN RIESSEN, A. Thermo-mechanical and microstructural characterisation of sodium-poly(sialate-siloxo) (Na-PSS) geopolymers, J Mater Sci, Vol. 42, No. 9, 2007, pp 3117-3123.

23. BROWN, P W, CLIFTON, J R. Mechanisms of deterioration in cement-based materials and lime mortars, Durability of Building Materials, Vol. 5, 1998, pp 409-414.

Low-carbon Calcium Sulphoaluminate Cements Synthesized from Industrial Wastes and By-products

A Telesca, M Marroccoli, M L Pace, G L Valenti
University of Basilicata, Italy

Compared to Portland cements, calcium sulphoaluminate (CSA) cements are energy saving and low-CO_2 hydraulic binders, due to the decrease of synthesis temperature and kiln thermal input associated with the reduced limestone requirement and carbon dioxide generation. Further enhancements in terms of environmentally friendly features can be achieved if some industrial wastes are used as partial or total substitutes for the natural materials (limestone, bauxite, gypsum) involved in the CSA cement manufacture. This paper deals with a laboratory investigation of synthetic CSA clinkers generated in an electric oven at 1150°, 1200°, 1250° and 1300°C from raw mixtures containing (i) bottom ash derived from the fluidized bed combustion (FBC) of coal (essentially a source of non-carbonated lime and calcium sulphate) and (ii) anodization mud (AM) or alumina powder (AP), Al_2O_3 rich by-products originated by the production of anodized aluminium elements and the secondary aluminium manufacture, respectively. Six bauxite-free ternary blends, containing 10-35% limestone plus 0-31% natural gypsum or 0-40% FBC bottom ash plus 0-69% AM or 0-50% AP, and four binary blends, consisting only of 37-60% FBC bottom ash and 52-63% AM or 40-45% AP, were explored. They were generally more suitable than a reference mixture composed by 42% bauxite, 33% gypsum and 25% limestone. XRD analysis showed a complete conversion of reactants and a very good selectivity towards the main CSA cement component.

A. Telesca is Researcher in Materials Science and Technology at the Department of Environmental Engineering and Physics at the University of Basilicata, Italy. His main research interests are the development of special cements and the utilization of industrial by-products as sources of raw materials.

M. Marroccoli is Professor of Materials Technology and Applied Chemistry at the Department of Environmental Engineering and Physics, University of Basilicata, Italy. Her scientific activity deals with cement technology and utilization of industrial wastes in civil engineering works and building materials industry.

M. L. Pace is PhD in Environmental Engineering at the University of Basilicata, Italy. Her research activity concerns calcium sulphoaluminate cements and their synthesis, hydration and manufacture from industrial by-products.

G. L. Valenti is Professor of Industrial Wastes and Sustainable Development at the Department of Environmental Engineering and Physics, University of Basilicata, Italy. He is mainly engaged in researches devoted to both development of special cements and utilization of industrial wastes in civil engineering works and building materials industry.

Keywords: Alumina powder, Anodization mud, Calcium sulphoaluminate cements, Fluidized bed combustion ash, Sustainable development, Waste utilization

INTRODUCTION

Calcium sulphoaluminate (CSA) cements contain $C_4A_3\bar{S}$ as main component together with calcium sulphates and dicalcium silicate; they may include also tetracalcium iron aluminate (C_4AF), calcium sulphosilicate ($C_5S_2\bar{S}$), calcium aluminates (C_3A, CA, $C_{12}A_7$), calcium silicoaluminates (C_2AS, CAS_2), perovskite (CT), spinel (MA), periclase (M) and other unreacted oxides [1-11].

Upon hydration, calcium sulphates (under hydrated and/or anhydrous form, added and belonging to CSA clinker) react with $C_4A_3\bar{S}$ and generate ettringite ($C_6A\bar{S}_3H_{32}$) which, depending on the conditions of its formation [3, 4, 8, 12-27], controls various technical properties of CSA cements (shrinkage compensation, self-stressing behaviour, rapid hardening associated with dimensional stability). C_2S can add strength and durability at medium and long ages, while C_4AF and calcium aluminates may contribute to the ettringite formation; on the other hand, $C_5S_2\bar{S}$, C_2AS, CAS_2 and other minor phases display a poor hydraulic activity. The distribution of the secondary components of CSA cement is mainly influenced by the synthesis temperature as well as the nature and proportioning of raw materials [3, 6, 11]

As far as the manufacturing process is concerned, CSA-based binders show noticeable environmentally friendly characteristics [28-30]. Compared to ordinary Portland cements, they need a lower synthesis temperature and a reduced limestone requirement inasmuch as $C_4A_3\bar{S}$ forms at about 1200°-1350°C and the specific CaO requirement (referred to unit mass of compound) for its synthesis is 0.368 against 0.736, 0.657, 0.624 and 0.460 necessary for the formation of C_3S, C_2S, C_3A and C_4AF, respectively; hence, a strong decrease of kiln thermal input and CO_2 emission, both dependent to a considerable extent on limestone calcination, can be achieved: the specific carbon dioxide generation, in terms of CO_2/pure cement compound mass ratio, is 0.216 for $C_4A_3\bar{S}$ against 0.578, 0.511, 0.489 and 0.362 for C_3S, C_2S, C_3A and C_4AF, respectively [31].

Another environmentally friendly feature related to the production of CSA cement is represented by the greater usability of industrial by-products, generally difficult to utilize in the field of ordinary cement and concrete, as substitutes for limestone, bauxite and gypsum in the CSA clinker-generating raw mix [32-38]. An example is given by fluidized bed combustion (FBC) waste containing CaO, SiO_2, Al_2O_3 and SO_3 as major oxides and consisting of exhausted sulphur sorbent and coal ash [36-38]. Two separate streams, FBC fly- and FBC bottom-ash are generally available; the latter is particularly interesting because (i) it is a non-carbonated source of lime and (ii) its high CaO and SO_3 concentration can allow substantial savings of limestone and gypsum. Al_2O_3-rich industrial wastes, such as anodization mud and alumina powder, respectively generated during the production of anodized aluminium elements and the secondary aluminium manufacture, both able to replace an expensive natural material like bauxite [11], are also worthy of consideration.

In this paper six bauxite-free ternary blends, containing 10-35% limestone plus 0-31% natural gypsum or 0-40% FBC bottom ash plus 0-69% anodization mud or 0-50% alumina powder, and four binary blends (without limestone, bauxite and gypsum) consisting only of 37-60% FBC bottom ash and 52-63% anodization mud or 40-45% alumina powder, were explored as CSA clinker-generating raw mixtures. A reference mix composed by 42% bauxite, 33%

gypsum and 25% limestone was also investigated. All the raw mixtures were synthesized in a laboratory electric oven at temperatures ranging from 1150° to 1300°C and then submitted to X-ray diffraction analysis in order to assess their ability to convert the reactants into useful CSA cement components.

EXPERIMENTAL

The chemical composition of the materials used in this investigation was evaluated through X-ray fluorescence analysis using a BRUKER Explorer S4 apparatus. It is listed in Table 1, where the symbols L, B and G indicate limestone, bauxite and gypsum, respectively, and the symbols FBC, AM and AP indicate bottom ash from fluidized bed coal combustion, anodization mud and alumina powder, respectively.

FBC has a relatively low l.o.i. value and contains small amounts of silica, alumina and iron oxides: it is essentially a mixture of calcium sulphate and calcium oxide. Compared to bauxite, AM has a similar l.o.i. value, is much higher in sulphate and lime as well as lower in alumina and silica, whereas AP has higher Al_2O_3, SiO_2 and MgO contents, and a much lower l.o.i. value.

Table 1 Chemical composition of natural materials and industrial wastes, mass %

	L	B	G	FBC	AM	AP
CaO	54.70	1.69	10.20	53.59	15.40	2.10
SO_3	-	0.03	63.53	36.81	12.70	0.20
Al_2O_3	-	55.22	-	0.81	41.40	63.60
SiO_2	-	6.48	-	1.80	2.60	11.30
MgO	0.30	-	-	0.35	1.20	6.70
TiO_2	-	2.34	-	0.07	-	-
Fe_2O_3	-	6.25	-	1.03	0.70	1.60
l.o.i.*	42.61	27.68	23.70	5.63	25.70	8.20
Total	97.61	99.69	97.43	100.09	99.70	93.70

*loss on ignition at 950°C

The CSA clinker-generating raw mixes were heated in a laboratory electric oven for 2 hours at 1150°, 1200°, 1250° and 1300°C, then submitted to X-ray diffraction (XRD) analysis with the purpose of evaluating both conversion and selectivity of the reacting systems. A PHILIPHS PW1710 diffractometer, operating between 5 and 60° 2θ (Cu kα radiation), was used.

RESULTS AND DISCUSSION

Proportioning of Raw Mixtures

Eleven mixtures, numbered from 0 to 10, whose composition is shown in Table 2, were investigated. Mixture 0, used as a reference term, was based only on natural materials. Mixtures 1 and 2 contained L, G and AM or AP, respectively. Mixtures from 3 to 6 included L and FBC: for Mixtures 3-4 and 5-6, the third component was AM and AP, respectively. Mixtures from 7 to 10 were binary blends consisting of FBC and AM (No.7-8) or AP (No. 9-10).

The proportioning of all the mixtures was made by assuming that (i) reacted lime was preferably combined in $C_4A_3\bar{S}$, (ii) reacted SO_3 and Al_2O_3, on the one hand, and SiO_2, on the other, gave only

Table 2 Composition of raw mixtures, mass %

MIX NO.	0	1	2	3	4	5	6	7	8	9	10
L	25.2	24.1	34.9	16.0	10.0	22.0	10.0	-	-	-	
B	42.1	-	-	-	-	-	-	-	-	-	
G	32.5	14.9	30.9	-	-	-	-	-	-	-	
FBC	-	-	-	19.0	21.0	39.0	40.0	48.0	37.0	60.0	55.0
AM	-	61.0	-	65.0	69.0	-	-	52.0	63.0	-	-
AP	-	-	34.2	-	-	39.0	50.0	-	-	40.0	45.0

$C_4A_3\bar{S}$ and C_2S, respectively, and (iii) solid solution effects were absent. In order to avoid the decomposition of calcium sulphoaluminate, the sulphur content was twice the stoichiometric amount required by its formation.

From the comparison of Mixtures 1 and 2 with Mixture 0, it is interesting to observe that both AM and AP can enable a total replacement of bauxite; however with AM the requirement of gypsum is reduced, whereas with AP that of limestone increases. By comparing Mixtures 3-4 with Mixture 1 and Mixtures 5-6 with Mixture 2, it can be noted that the use of FBC promotes a decrease of limestone concentration which is even more limited if, in order to enhance the $C_4A_3\bar{S}$ formation at the expense of that of C_2S, the AM or AP concentration is further increased (Mixtures 4 and 6).

Within Mixtures 7-10 limestone (as well as bauxite and gypsum) is absent. Similarly to ternary blends 4 and 6, Mixtures 8 and 10 (with a higher AM or AP concentration) are potentially able to produce more $C_4A_3\bar{S}$ at the expense of C_2S, as confirmed by Table 3 where the potential concentration values of $C_4A_3\bar{S}$, C_2S and $C\bar{S}$ are reported for the CSA synthetic clinkers generated by all the mixtures.

Table 3 Potential concentration of $C_4A_3\overline{S}$, C_2S and $C\overline{S}$ in the burning products of Mixtures 0-10, mass %

MIX NO.	0	1	2	3	4	5	6	7	8	9	10
$C_4A_3\overline{S}$	66.58	72.20	59.40	70.70	74.70	59.10	71.60	52.86	64.06	55.41	62.32
C_2S	11.23	9.50	19.60	7.70	-	17.30	-	8.10	-	5.16	-
$C\overline{S}$	14.85	15.70	12.50	18.70	19.70	15.70	12.20	37.01	30.75	27.97	22.82

Characterization of CSA Synthetic Clinkers

The conversion of reactants was generally complete at all the investigated temperatures. Some traces of (i) silica for Mixture 0 burnt at 1150 and 1200°C, (ii) alumina for Mixtures 6, 7, 9 and 10 heated at the lowest temperature, and (iii) lime for Mixture 7 at 1150° and 1200°C were detected in their XRD patterns.

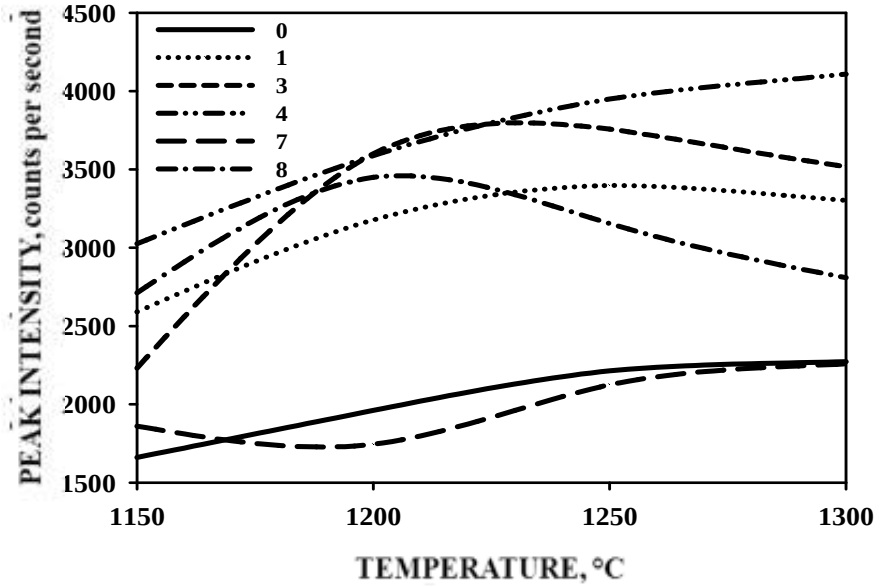

Figure 1 XRD intensity of $C_4A_3\overline{S}$ main peak for the burning products of the mixtures containing anodization mud *vs.* synthesis temperature
(Mixture 0 is the reference mix based on natural materials)

In terms of selectivity towards $C_4A_3\overline{S}$, the best results were more frequently obtained at 1250°C and, in some cases, at 1200° or 1300°C (optimum temperature for the reference mixture), according to the following sequence:

M4>M3>M8>M1>M2>M5>M10>M9>M0>M7>M6.

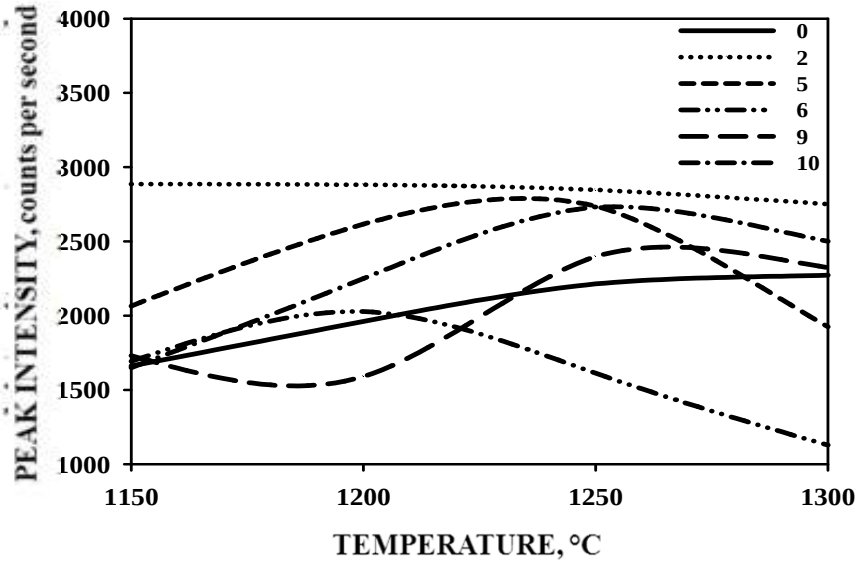

Figure2 XRD intensity of $C_4A_3\overline{S}$ main peak for the burning products of the mixtures containing alumina powder *vs.* synthesis temperature
(Mixture 0 is the reference mix based on natural materials)

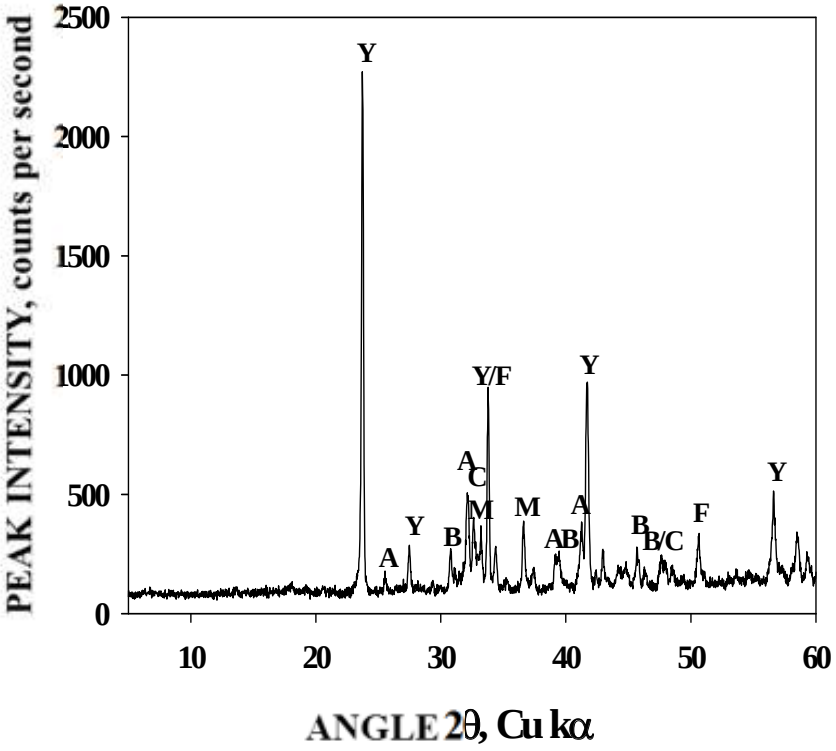

Figure 3 XRD pattern of mixture O at 1300°C:
Y= $C_4A_3\overline{S}$, A= $C\overline{S}$, B=C_2S, C=C_3A,F=C_4AF, M=$C_{12}A_7$

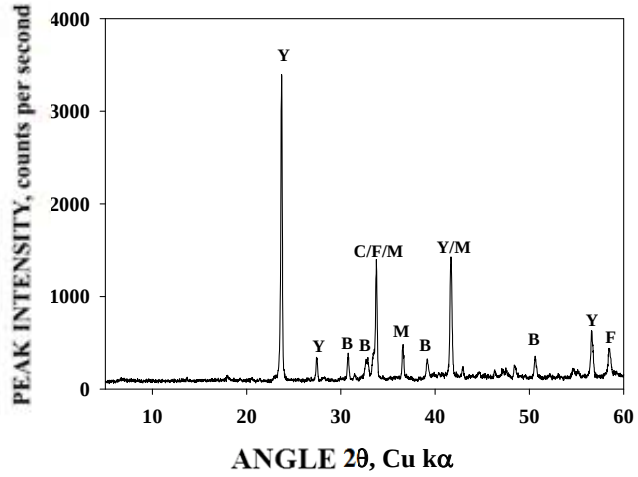

Figure 4 XRD pattern of mixture 1 at 1250°C: Y=$C_4A_3\overline{S}$, B=C_2S,C=C_3A,F=C_4AF, M=$C_{12}A_7$

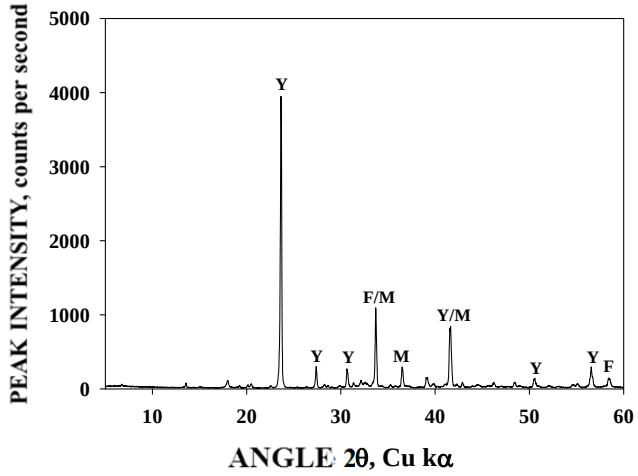

Figure 5 XRD pattern of mixture 4 at 1250°C: Y=$C_4A_3\overline{S}$, F=C_4AF, M=$C_{12}A_7$

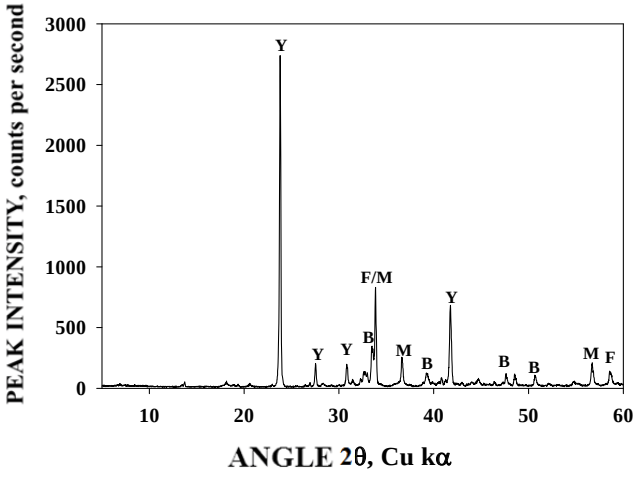

Figure 6 XRD pattern of mixture 5 at 1250°C: Y=$C_4A_3\overline{S}$, B=C_2S, F=C_4AF, M=$C_{12}A_7$

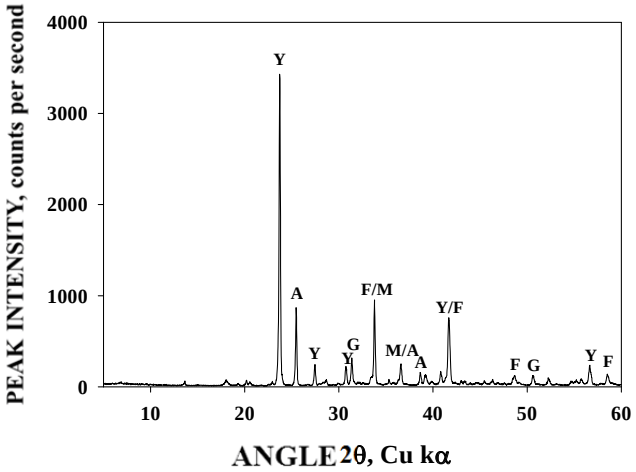

Figure 7 XRD pattern of mixture 8 at 1200°C:
Y=$C_4A_3\overline{S}$, A=$C\overline{S}$, F=C_4AF, M=$C_{12}A_7$, G=C_2AS

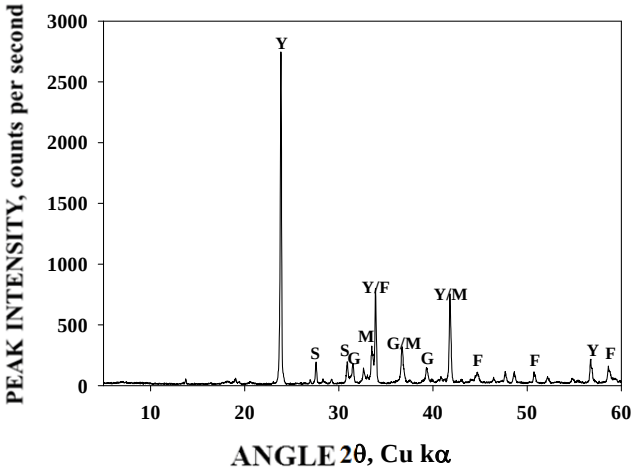

Figure 8 XRD pattern of mixture 10 at 1250°C:
Y=$C_4A_3\overline{S}$, F=C_4AF, M=$C_{12}A_7$, G=C_2AS, S=$C_5S_2\overline{S}$

Figures 1 and 2 show the XRD intensity of the main $C_4A_3\overline{S}$ peak as a function of the synthesis temperature for the mixtures containing AM and AP, respectively. Figures 3-8 illustrate the XRD patterns of Mixtures 0, 1, 4, 5, 8 and 10 heated at the optimum synthesis temperatures.

Within CSA cement commercial formulations C_2S and $C\overline{S}$ are generally the most important secondary constituents. Some difficulties were encountered in the synthesis of the investigated CSA clinker-generating raw mixtures as far as the formation of dicalcium silicate is concerned. Compared to $C_4A_3\overline{S}$, C_2S was produced with a greater difficulty. Dicalcium silicate was absent in the heated mixtures conceived without it but, with regard to the systems which should contain it, the pertinent XRD peaks at each synthesis temperature were observed only for Mixtures 0, 1, 2 and 5. Difficulties were also encountered in the preservation of $C\overline{S}$ against its thermal decomposition: at 1250° and 1300°C, its XRD signals

were often weak or absent and only for Mixtures 0, 2, 7 and 8 the XRD peaks related to $C\bar{S}$ were observed at all the investigated temperatures. With reference to the other minor phases, the following components, in order of importance, were detected: $C_{12}A_7$, C_4AF, C_2AS, C_3A, $C_5S_2\bar{S}$.

CONCLUSIONS

The carbon dioxide emission related to Portland cement manufacture derives from both fossil fuel combustion and limestone calcination. Calcium sulphoaluminate (CSA) - based hydraulic binders have interesting engineering properties and are low-CO_2 cements inasmuch as reduced synthesis temperature and limestone requirement are involved in their production. Industrial by-products, generally unsuitable for applications in the field of ordinary cement and concrete, can be conveniently used as raw materials for CSA cement manufacture. Non-carbonated CaO sources, able to further reduce limestone requirement and CO_2 generation, are worthy of consideration. In this regard, fluidized bed combustion (FBC) waste and, in particular, its heavier fraction (bottom ash), basically consisting of a mixture of lime and anhydrous calcium sulphate, is quite interesting allowing also to save natural gypsum.

Through a XRD investigation on CSA synthetic clinkers obtained in a laboratory electric oven at temperatures ranging from 1150° to 1300°C, it has been found that (i) ternary blends, containing a reduced limestone amount plus natural gypsum or FBC bottom ash plus anodization mud or alumina powder (Al_2O_3-rich industrial by-products, both used as substitutes for bauxite), and (ii) binary blends, composed only by FBC bottom ash and anodization mud or alumina powder, are suitable CSA clinker-generating raw mixtures. In practice, reactants were fully converted and a high selectivity towards the main CSA cement component ($C_4A_3\bar{S}$) was achieved, particularly at 1250°C. C_2S and $C\bar{S}$ are usually the most important CSA cement secondary constituents: some difficulties were encountered in the synthesis of the former and in the preservation of the latter against thermal decomposition, especially at the higher burning temperatures.

REFERENCES

1. DENG, J, WEN-MIN, G, MUZHEN, S, XIU-YING, L. Sulfoaluminate cement series, Proc. 7th Int. Congr. Chem. Cem., Paris. Vol. IV, 1980. pp 381-386.

2. MEHTA, P K. Investigations on energy-saving cements. World Cement Technology. Vol. 11, 1980. pp 166-177.

3. KURDOWSKI, W, GEORGE, C M, SORRENTINO, F P. Special cements, Proc. 8th Int. Congr. Chem. Cem., Rio de Janeiro. Vol. I, 1986. pp 292-318.
4. MUDBHATKAL, G A, PARMESWARAN, P S, HEBLE, A S, PAI, B V B, CHATTERJEE, A K. Non-alitic cement from calcium sulphoaluminate clinker-Optimisation for high-strength and low-temperature application, Proc. 8th Int. Congr. Chem. Cem., Rio de Janeiro. Vol. IV. 1986. pp 364-370.

5. VALENTI, G L, SANTORO, L, GAROFANO, R. High-temperature synthesis of

calcium sulphoaluminate from phosphogypsum, Thermochimica Acta. Vol. 113, 1987. pp 269-275.

6. MUZHEN, W, KURDOWSKI, W, SORRENTINO, F P. Developments in non-Portland-cements, Proc. 9th Int. Congr. Chem. Cem., New Delhi. Vol. I, 1992. pp 317-354.

7. YANMOU, W, MUZHEN, S. The third series cement in China, Proc. 3rd Int. Symp. Cem. and Concr., Shanghai. Vol. 3, 1993. pp 116-121.

8. MUZHEN, S, YANMOU, W, ZHANG, L, DEDONG, L. Preliminary study on the durability of sulfo/ferro-aluminate cements", Proc. 10th Int. Congr. Chem. Cem., Goteborg. Vol. IV, 1997. Paper 4iv029.

9. KOUZNETSOVA, T V. Development of special cements, Proc. 10th Int. Congr. Chem. Cem., Goteborg. Vol. 1, 1997. Paper 1i001.

10. TANGBO, S, YAN, Y. Recent progress in special cements in China, Proc. 11th Int. Congr. Chem. Cem., Durban. Vol. 4, 2003. pp 2028-2032.

11. TELESCA, A, MARROCCOLI, M, PACE, M L, VALENTI, G L. Calcium Sulfoaluminate Cements Obtained from Bauxite-Free Raw Mixes, Proc. 13th Int. Congr. Chem. Cem., Madrid, 2011. Paper 151.

12. MEHTA, P K. Mechanism of expansion associated with ettringite formation, Cement & Concrete Research. Vol. 3, 1973. pp 1-6.

13. WANG, L, GLASSER, F P. Hydration of calcium sulphoaluminate cements, Advances in Cement Research. Vol. 8, 1996. pp 127-134.

14. ZHANG, L, GLASSER, F P. New concretes based on calcium sulphoaluminate cements, Modern Concrete Materials. 1999. pp 261-274.

15. GLASSER, F P, ZHANG, L. High-performance cement matrices based on calcium sulphoaluminate-belite compositions, Cement & Concrete Research. Vol. 31, 1999. pp 1881-1886.

16. GLASSER, F P. Advances in sulphoaluminate cements, Proc. 5th Int. Symp. Cem. & Concr., Shanghai. Vol. 1, 2002. pp 14-24.

17. BERNARDO, G, TELESCA, A, VALENTI, G L. A porosimetric study of calcium sulfoaluminate cement pastes cured at early ages, Cement & Concrete Research. Vol. 36**,** 2006. pp 1042-1047.

18. MARROCCOLI, M, NOBILI, M, TELESCA, A, VALENTI, G L. Early hydration of calcium sulfoaluminate-based cements for structural applications, Proc. 1st Int. Conf. Sust. Constr. Mat. and Tech., Coventry, 2007. pp 389-395.

19. BERNARDO, G, BUZZI, L, CANONICO, F, PARIS, M, TELESCA, A, VALENTI, G L. Microstructural Investigations on Hydrated High-Performance Cements Based on

Calcium Sulfoaluminate, Proc. 12th Int. Congr. Chem. Cem., Montreal, 2007. Paper W3 11.4.

20. BUZZI, L, CANONICO, F, TELESCA, A, VALENTI, G L. High-performance and low-CO_2 cements based on calcium sulphoaluminate, Zement Kalk Gips International. Vol. 5, 2010. pp 39-45.

21. GASTALDI D, CANONICO F, CAPELLI L, BIANCHI M, PACE M L, TELESCA A, VALENTI G L. Hydraulic Behaviour of Calcium Sulfoaluminate Cement alone and in Mixture with Portland Cement, Proc. 13th Int. Congr. Chem. Cem., Madrid, 2011. Paper 153.

22. MARCHI M, COSTA, U. Influence of the Calcium Sulphate and W/C Ratio on the Hydration of Calcium Sulfoaluminate Cement, Proc. 13th Int. Congr. Chem. Cem., Madrid, 2011. Paper 191.

23. ARANDA, M A G, CUBEROS, A J M, CUESTA, A, ALVAREZ-PINAZO, G, DE LA TORRE, A G, SCHOLLBACH, K, POLLMANN, H. Hydrating Behaviour of Activated Belite Sulfoaluminate Cements, Proc. 12th Int. Congr. Chem. Cem., Madrid, 2011. Paper 197.

24. PELLETIER-CHAIGNAT, L, WINNEFELD, F, LOTHENBACH, B, LE SAOUT, G, MULLER, C J, FAMY, C. Hydration mechanism of Portland cement-calcium sulphoaluminate clinker-calcium sulphate binders: characterization of the X-ray amorphous hydrate assemblage, Proc. 12th Int. Congr. Chem. Cem., Madrid, 2011. Paper 155.

25. WINNEFELD F, BEN HAHA M, LOTHENBACH B. Hydration mechanism of calcium sulphoaluminate cements assessed by scanning electron microscopy and thermodynamic modeling, Proc. 13th Int. Congr. Chem. Cem., Madrid, 2011. Paper 192.

26. JUENGER, M, CHEN, I. Composition-Property Relationships in Calcium Sulfoaluminate Cements, Proc. 13th Int. Congr. Chem. Cem., Madrid, 2011. Paper 154.

27. BUZZI, L, CANONICO, F, SCHAFFEL, P. Investigation on High-Performance Concrete based on Calcium Sulfoaluminate cement, Proc. 12th Int. Congr. Chem. Cem., Madrid, 2011. Paper 152.

28. Marroccoli, M, Montagnaro, F, Nobili, M, Telesca, A, Valenti, G L. Synthesis, hydration properties and environmentally friendly features of calcium sulfoaluminate cements. Proc. 12th Int. Congr. Chem. Cem., Montreal, 2007. Paper W3 11.2.

29. DAMTOFT, J S, LUKASIK, J, HERFORT, D, SORRENTINO, D, GARTNER, E M. Sustainable development and climate change initiatives, Cement & Concrete Research. 2008, Vol. 38. pp 115-127.

30. MARROCCOLI, M, MONTAGNARO F, TELESCA, A, VALENTI G L. Environmental Implications of the Manufacture of Calcium Sulfoaluminate-based Cements, Proc. 2nd Int. Conf. Sust. Constr. Mat and Tech., Ancona (Italy), 2010. Paper 162

31. GARTNER, E. Industrially interesting approaches to ''low-CO_2'' cements, Cement & Concrete Research, 2004. Vol. 34. pp 1489-1498.

32. SAHU, S, MAJLING, J. Preparation of sulphoaluminate belite cement from fly ash, Cement & Concrete Research, 1994. Vol 24. pp 1065–1072.

33. BELZ, G, BERETKA, J, MARROCCOLI, M, SANTORO, L, SHERMAN, N, VALENTI, G L Use of fly ash, blast furnace slag and chemical gypsum for the synthesis of calcium sulphoaluminate based cements, 5th CANMET/ACI Int. Conf. on fly ash, silica fume, slag and natural pozzolans in concrete, Milwaukee, 1995. pp 513-536.

34. IKEDA, K, FUKUDA, K, SHIMA, H. Calcium sulphoaluminate cements prepared from low-alumina waterworks slime, Proc. 10th Int. Congr. Chem. Cem., Goteborg. Vol. IV, 1997. Paper 1i025.

35. ARJUNAN, P, SILSBEE, M R, DELLA ROY, M. Sulfoaluminate-belite cement from low-calcium fly ash and sulphur-rich and other industrial by-products, Cement & Concrete Research, 1999. Vol. 29. pp 1305–1311.

36. BERNARDO, G, MARROCCOLI, M, MONTAGNARO, F, VALENTI, G L. Use of fluidized bed combustion wastes for the synthesis of low energy cements. Proc. 11th Int. Congr. Chem. Cem., Durban, 2003. pp 1227-1236.

37. MARROCCOLI, M, NOBILI, M, TELESCA, A, VALENTI, G L. Use of wastes generated within coal-fired power stations for the synthesis of calcium sulphoaluminate cements, Proc. 7th Int. Conf. – Concrete: construction's sustainable option – role for concrete in global development, Dundee (UK). 2008. pp 299-310.

38. MARROCCOLI, M, MONTAGNARO, F, PACE, M L, TELESCA, A, VALENTI, G L. Use of fluidized bed combustion ash and other industrial wastes as raw materials for the manufacture of calcium sulphoaluminate cements, Proc. 20th Int. Conf. Fluid. Bed Comb., Xi'an (China), 2009. pp 1072-1077.

Effect of a New Type of CaO Expansive Agent on the Leaching of Calcium Hydroxide from High Performance Concrete

J Liu, F Guo, Q Tian, S Zhang
Jiangsu Bote New Materials Co. Ltd, China

The hydration products of a new type of CaO expansive agent is calcium hydroxide whose solubility is relatively high, and it is necessary to determine concrete performance change due to calcium leaching when CaO expansive agent is mixed in concrete. An electrochemical acceleration test was used on the research of leaching of calcium hydroxide from high performance concrete. Tests were carried out using various amount of CaO expansive agent and water binder ratio. Experimental results showed that the quantity of dissolved Ca^{2+} of concrete mixed with 2% CaO is minimum, 94.5% of reference specimens at 42d; when the amount of CaO expansive agent is higher than 2%, the quantity of dissolved Ca^{2+} of concrete is higher than that of reference specimens. The quantity of dissolved Ca^{2+} of concrete decreased with water binder ratio; the quantity of dissolved Ca^{2+} of concrete with 4% CaO is higher than that of reference specimens when water binder ratio is 0.30,0.35,0.40 and 0.45. The shrinkage of mortar mixed with 2%CaO expansive agent was observed much lower than that of mortar without CaO expansive agent.

Jiaping Liu is currently leader of Jiangsu Bote New Materials Co.,Ltd.. Nanjing, China. He has led several research projects on concretes, and his specialist areas of research are deformation and durability of high performance concrete.

Fei Guo is currently an engineer of Jiangsu Bote New Materials Co.,Ltd.. Nanjing, China. His specialist areas of research are application of shrinkage-compensating concrete and self-compacting concrete.

Shouzhi Zhang is currently an engineer of Jiangsu Bote New Materials Co.,Ltd.. Nanjing, China. His specialist areas of research are the preparation of expensive agent and deformation of shrinkage-compensating concrete.

Qian Tian is currently Professor of Jiangsu Bote New Materials Co.,Ltd.. Nanjing, China. She has led several research projects on concretes, and his specialist areas of research are deformation of high performance concrete.

Keywords: Electrochemical acceleration test, Expansive agent, Leaching, Shrinkage

INTRODUCTION

Early cracks of concrete became a worldwide problem which troubled civil engineers, many researchers found that the existence of cracks in concrete significantly modifies the transfer properties of the material, and thus seriously endanger the integrity, service life, and aesthetics of the buildings [1, 2].

To build expansion in concrete within a safe rage has been proved to be an effective way to improve the shrinkage cracking problems of concrete. Expansive agent has been widely used in Chinese engineering to produce shrinkage compensating concrete. The swelling of the gel state expansive ingredients by water adsorption and the crystallization pressure can build effective expansion at the early age of hydration and compensate the shrinkage of concrete [3]. The quality of expansive agent will determine the performance of shrinkage compensating concrete. In China a new type of CaO expansive agent is considered to be the current of expansive agent, by reason of its outstanding advantages, such as faster expanding rate, bigger expansion, fewer water requirement and etc. 20% of hydration product of cement is calcium hydroxide whose solubility is relatively high, calcium hydroxide will gradually dissolves in water under hydraulic pressure. It usually happens in Hydraulic concrete, and may destroy the construction. Hydration product of a new type of CaO expansive agent is calcium hydroxide, the amount of calcium hydroxide will rise when we use CaO expansive agent in concrete, so it is necessary to determine concrete performance change due to leaching of calcium hydroxide when CaO expansive agent is mixed in concrete.

EXPERIMENTAL

Materials

Binders: Type II Portland cement with 52.5 grade from Nanjing Jiangnan cement plant was used. Class I fly ash specified came from Nanjing Thermo Electrical Plant. A ground granulated blast furnace slag (GGBS) with Blaine fineness of 439 m^2/kg was used here. The chemical and physical properties of the binders are shown in Table 1.

Table 1 chemical composition and physical properties of the cementitious materials

NAME (symbol)	CHEMICAL COMPOSITION, weight-%							DENSITY kg/m^3	SPECIFIC AREA m^2/kg
	SiO_2	Al_2O_3	CaO	MgO	Fe_2O_3	SO_3	LOI		
Cement(C)	19.89	4.29	64.21	1.55	3.94	3.25	2.31	3180	300
Fly ash (FA)	56.20	33.10	1.62	0.55	4.59	0.96	2.49	2200	/
Slag(GGBS）	36.50	20.31	31.49	5.31	1.54	2.51	3.0	2800	439

Superplasticizer: Poly-naphthalene sulfonates Superplasticizer(JM-B) was used. It came from

Jiangsu Bote New Materials Co., Ltd.

Coarse Aggregate: 5-25mm continuous graded crushed basalt. Its density was 2700 kg/m^3.

Fine Aggregate: River sand with fineness modulus of 2.65 and density of 2650 kg/m^3.

Expansive Agents: The expansive agent used is a new type of CaO expansive agent (named MC), which was newly developed in Jiangsu Bote New Materials Co.Ltd.

Mix Proportions

The mix proportions of the concretes are shown in Table 2.

Table 2 Mix proportions of the concretes

NAME (symbol)	WATER TO BINDER RATIO	CONCRETE MIX PROPORTION, kg/m^3						
		C	Fa	GGBS	Sand	Coarse aggregate	water	JM-B
W45ref	0.45	231	84	105	724	1087	189	0.76
W40ref	0.40	231	84	105	733	1099	168	1.26
W35ref	0.35	231	84	105	741	1112	147	2.30
W30ref	0.30	231	84	105	750	1124	126	3.12

Test Methods

Hiroshi Saito described an electrochemical acceleration test method for leaching degradation [4,5]. The method can accelerate cement hydrate dissolution by increasing Ca^{2+} ion moving speed in the pore water by applying a constant potential gradient across a specimen in contact with water. With this method, the method, the ions moving are not the same as under natural condition, but similar deterioration conditions are obtained. Other researchers [6] have used the method.

Electrochemical acceleration test was used on the research of leaching of calcium hydroxide from high performance concrete. To exclude any temperature influence, the tests were carried out in an air-conditioned room at 20±2°C. Figure 1 shows the experimental apparatus used in the test the size of which is 400*300*200mm. 703 silica gel was used to airproof the contact part of specimen and experimental apparatus, and the experimental apparatus was divided into two parts each of which contains 4L ion-exchanged water. The solutions of the two parts were replaced once a week.

Figure 1 Experimental apparatus

RESULTS AND DISCUSSION

Quantity of Dissolved Ca^{2+} of Concrete Mixed with Various Amount of CaO Expansive Agent

Calcium leaching will lead to an increase in porosity. Figure 2 shows the specimen under saturated condition, the surface is compact. Figure 3 shows the specimen under electrochemical acceleration test condition, after 28days we can see the sand and no hydration product of cementitious materials.

Also calcium leaching modifies mechanical and transport properties of the material [7]. V.H. Nguyen observed that there is strong coupling between the calcium leaching and mechanical behaviour, as quantity of dissolved Ca^{2+} grows, a loss of stiffness and of strength are observed [8].

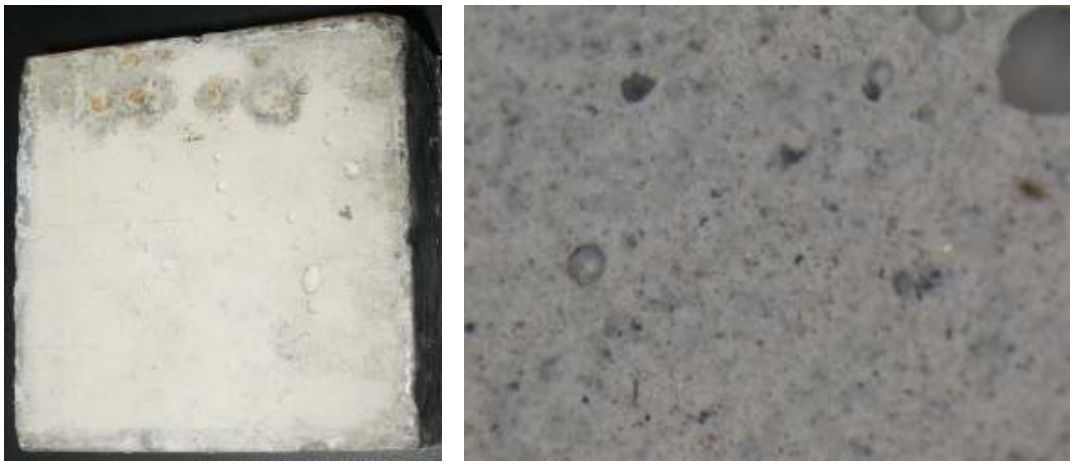

Figure 2 Specimen under saturated condition

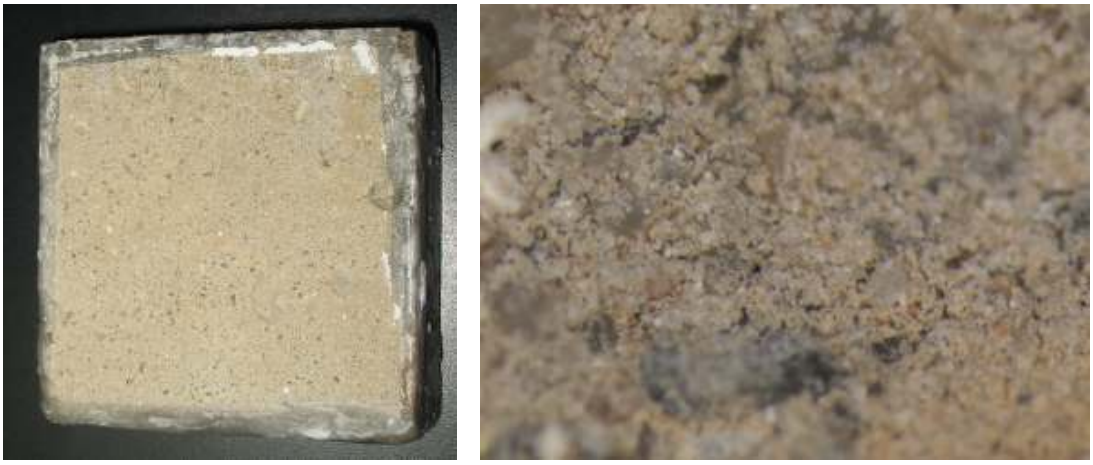

Figure 3 Specimen under electrochemical acceleration test condition

Figure 4 shows the quantity of dissolved Ca^{2+} of concrete mixed with various amount of CaO expansive agent. Water binder ratio of the concrete is 0.40. Y-axis is the ratio of the quantity of dissolved Ca^{2+} of concrete mixed with various amount of CaO expansive agent (N) and W40ref (N_0). In the test, only the quantity of dissolved Ca^{2+} of concrete mixed with 2% CaO expansive agent is smaller than that of W40ref, 94.5% of W40ref at 42 days. Incorporation of 2%CaO expansive agent can reduce calcium leaching of concrete. When the amount of CaO expansive agent mixed is higher than 2%, the quantity of dissolved Ca^{2+} of concrete increases with the amount of CaO expansive agent, and the quantity of dissolved Ca^{2+} of concrete is higher than that of W40ref.

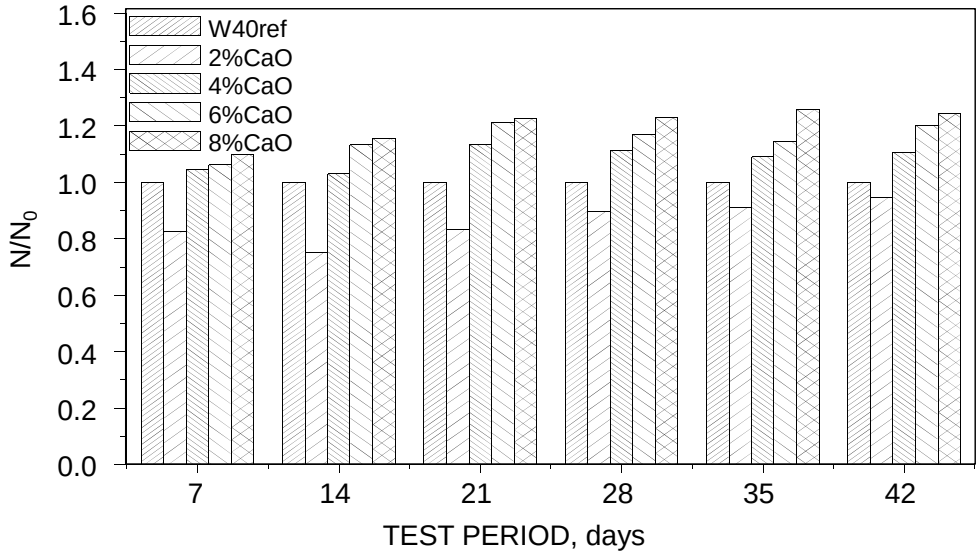

Figure 4 Quantity of dissolved Ca^{2+}

The quantity of dissolved Ca^{2+} of concrete is not only related to the amount of Ca^{2+} in

concrete, but also related to the permeability of concrete. ASTM test method C1202 was used to test the permeability of concrete. Figure 5 is test result of concrete mixed with various amount of CaO expansive agent. Charge passed of concrete mixed with 2% CaO expansive agent is smaller than that of W40ref, and charge passed of concrete mixed with higher than 2% CaO expansive agent is bigger than that of W40ref. Improvement of permeability of concrete mixed with 2% CaO expansive agent results in smaller quantity of dissolved Ca^{2+} although its amount of Ca^{2+} in concrete is higher.

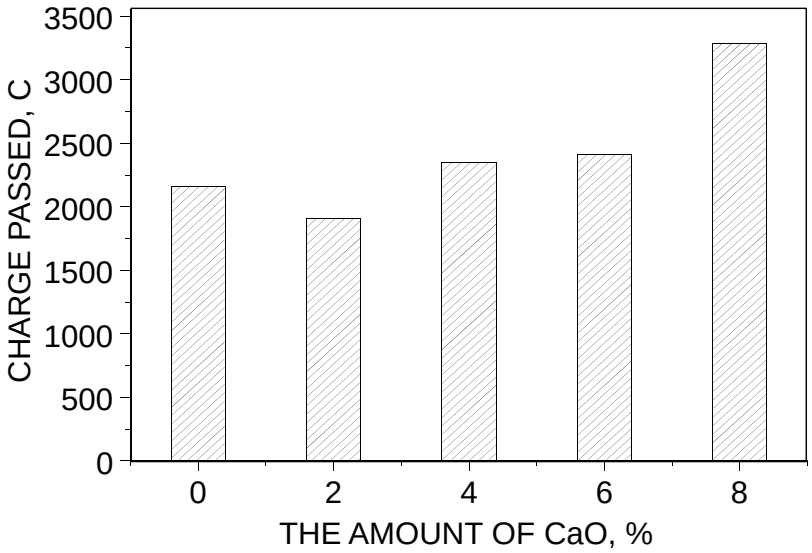

Figure 5 Charge passed of concrete

Quantity of Dissolved Ca^{2+} of Concrete with Various Water Binder Ratio

The influence of water binder ratio on the quantity of dissolved Ca^{2+} of concrete was examined at 28 days, water binder ratio of concrete is 0.45, 0.40, 0.35 and 0.30. Figure 6 shows the quantity of dissolved Ca^{2+} of concrete with various water binder ratio. Y-axis is the ratio of the quantity of dissolved Ca^{2+} of concrete with various water binder ratio and W45ref (N_0). The quantity of dissolved Ca^{2+} of concrete decreased with water binder ratio. The quantity of dissolved Ca^{2+} of W30ref is smallest, only 81.69% of W45ref at 28 days. Because permeability of concrete with lower water binder ratio is lower.

Figure 7 shows the quantity of dissolved Ca^{2+} of concrete mixed with 4% CaO expansive agent and without CaO expansive agent. We can see that for each water binder ratio the quantity of dissolved Ca^{2+} of concrete with 4%CaO expansive agent is higher than that of concrete without CaO expansive agent. Incorporation of 4% CaO expansive agent is disadvantageous to calcium leaching of concrete. The amount of CaO expansive agent should not be higher than 4% when we used.

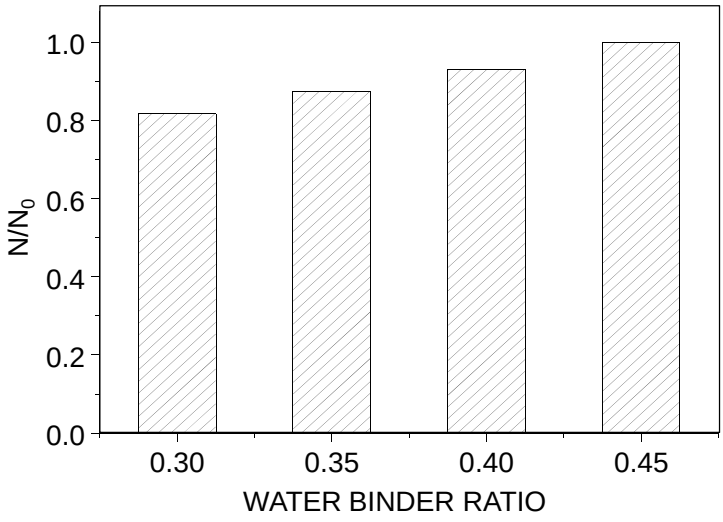

Figure 6 The quantity of dissolved Ca^{2+} of concrete with various water binder ratio

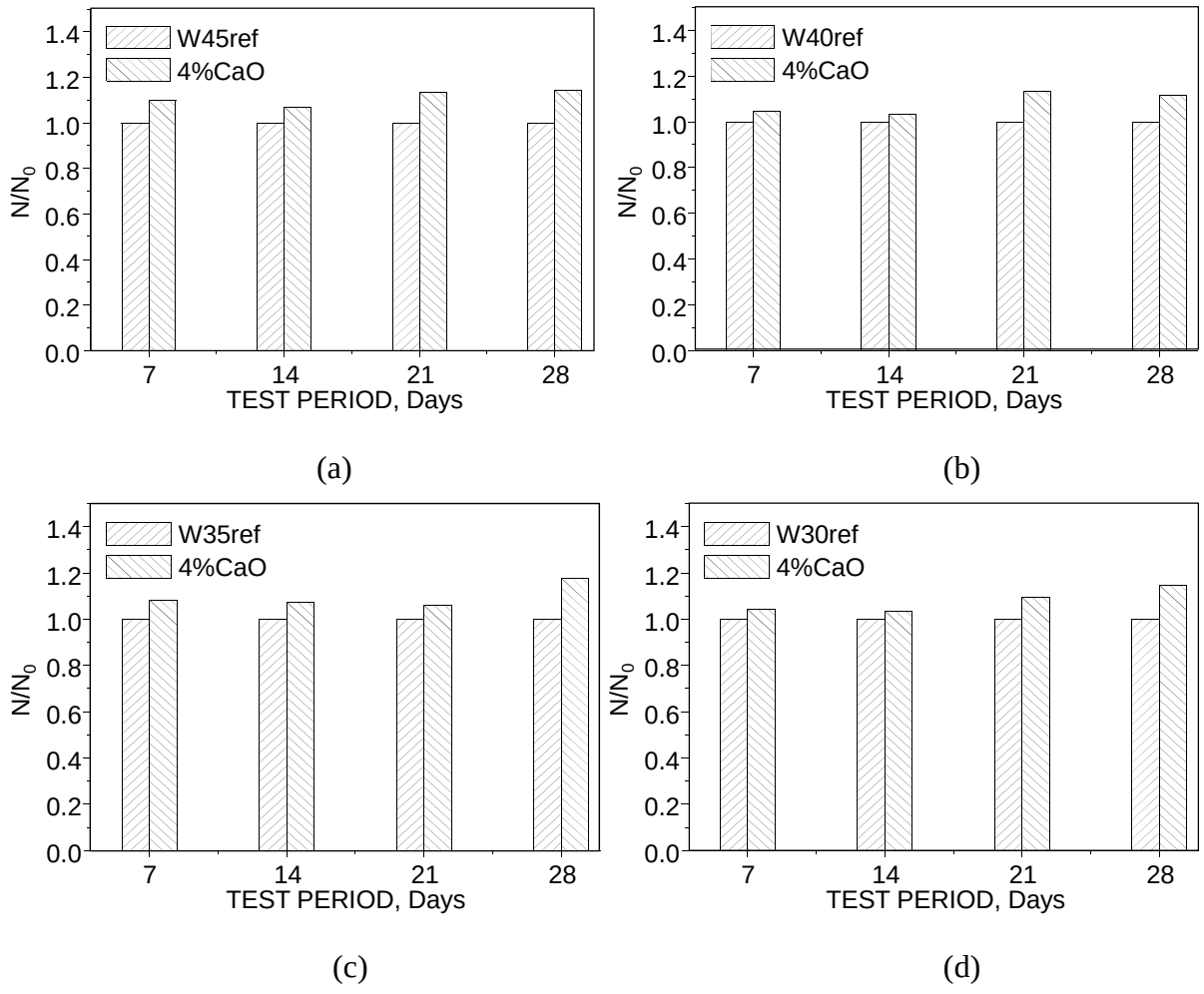

Figure 7 Quantity of dissolved Ca^{2+}

Deformation Behaviour of Mortar after Leaching

Deformation behavior of mortar after leaching was tested. The mortars whose water binder ratio is 0.40 are mixed without CaO expansive agent and with 2% CaO expansive agent. Figure 8 shows the deformation behaviour of the mortar after leaching. The shrinkage of mortar mixed with 2%CaO expansive agent was observed much lower than that of mortar without CaO expansive agent, because the quantity of dissolved Ca^{2+} of mortar mixed with 2% CaO is lower than the mortar mixed without CaO expansive agent.

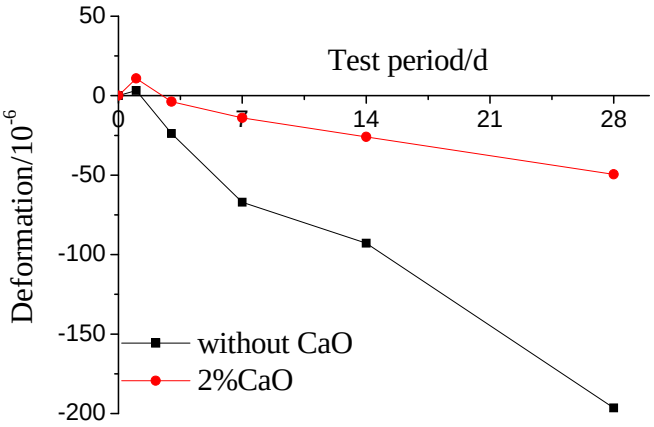

Figure 8 Deformation behavior of mortars

CONCLUSIONS

The purpose of the experimental study presented in this paper is to investigate influences of a new type of CaO expansive agent on the leaching behavior of concrete. Based on the information provided in this paper, the following conclusions can be drawn:

- The quantity of dissolved Ca^{2+} of concrete mixed with 2% CaO is minimum, 94.5% of reference specimens at 42d; when the amount of CaO expansive agent is higer than 2%, the quantity of dissolved Ca^{2+} of concrete is higher than reference specimens.
- The quantity of dissolved Ca^{2+} of concrete decreased with water binder ratio. The quantity of dissolved Ca^{2+} of W30ref is smallest, only 81.69% of W45ref.The amount of CaO expansive agent should not be higher than 4% when we used.
- The shrinkage of mortar mixed with 2%CaO expansive agent was observed much lower than that of mortar without CaO expansive agent.

Experimental results indicated that although the amount of calcium hydroxide will rise when we use CaO expansive agent in concrete, but calcium leaching of concrete will not get worse if we use it at a proper dosage.

ACKNOWLEDGEMENTS

The study of this work is financially supported by National Basic Research Program of China (973 program) (Grant No.2010CB735801), National Natural Science Foundation of China Grant No. 50808094 and Grant No. 50978126 and Jiangsu Provincial National Natural Science Foundation Grant No. BK2008508.

REFERENCES

1. RICHARD W. BURROWS, The visible and invisible cracking of concrete. ACI Monograph. 1998, No. 11, American Concrete Institute, Farmington Hills, Michigan.

2. GERARD B, BREYSSE D, Ammouche A, Houdusse O, et al. Cracking and Permeability of Concrete Under Tension. Material and Structure, 1996, 29: 141-151.

3. NAGATAKI S.，GOMI H., Expansive Admixtures (Mainly Ettringite). Cem. Concr. Res., 20(1998) 163-170.

4. H. SAITO, S. NAKANE, Comparison between diffusion test and electrochemical acceleration test for leaching degradation of cement hydration products. ACI Mater J 96 (2) (1999) 208~211.

5. HIROSHI SAITO, AKIRA DEGUCHI, Leaching tests on different mortars using accelerated electrochemical method. Cem. Concr. Res.,30(2000)1815-1825.

6. P. FAUCON, B. GERARD, J.F. JACQUINOT, J. MARCH, Water attack of cement paste: Towards an improved accelerated test? Adv Cem Res 10 (2)(1998) 67±73.

7. I. YURTDAS, S.Y. XIE, N. BURLION, J.F. SHAO, J. SAINT-MARC, A. Garnier, Influence of chemical degradation on mechanical behavior of a petroleum cement paste. Cem. Concr. Res., 41(2011) 412-421.

8. V.H. NGUYEN, H. COLINA, J.-M. TORRENTI, C. BOULAY, B. NEDJAR, Chemo-mechanical coupling behaviour of leached concrete part I: experimental results, Nucl. Eng.Des. 237 (2007) 2083–2089.

The Engineering Properties of Alkali Activated Fly Ash Mortar

Y Ma, G Ye
Delft University of Technology, Netherlands

The development of alkali activated materials has obtained increasing interest during the last decade, due to the great potential in building materials and low CO_2 emission. In order to utilize alkali activated materials in engineering applications, an evaluation of its engineering properties is essential. In this study, the engineering properties of alkali activated fly ash mortar, including setting time, mechanical strength and drying shrinkage, were studied with different amount of sodium silicate solutions. In addition, the microstructure and the interfacial transition zone (ITZ) between the paste and aggregates were examined by environmental scanning electron microscopy (ESEM). The result presents the compressive strength of around 50 MPa could be obtained after 7 days curing at 40°C of alkali activated fly ash mortar, with similar setting time and workability as Portland cement. The drying shrinkage were greatly influenced by the activating solutions (SiO2 and Na_2O content). Furthermore, the alkali activated fly ash mortar has a dense microstructure; no apparent ITZ could be identified near the aggregates.

Y Ma is an PhD candidate in Microlab, section of Materials and Environment

Faculty of Civil Engineering and Geosciences, Delft University of Technology. Her PhD research topic is ”study on alkali activated fly ash as an environmental friendly alternative to Portland cement”.

G Ye is an associate professor in Microlab, section of Materials and Environment Faculty of Civil Engineering and Geosciences, Delft University of Technology, the Netherlands. His research interests include ”Supplementary Cementitious Materials”, ”concrete material properties at early ages”,”hydration and microstructure, numerical simulation and durability of concrete”.

Keywords: Alkali activated fly ash mortar, Drying shrinkage, Engineering properties, Microstructure

INTRODUCTION

Alkali activated materials (AAM) are mainly produced by mixing industrial waste materials, e.g. fly ash and blast furnace slag with alkali silicate solutions. They are also referred to as geopolymers [1] or inorganic polymers [2]. The reaction product is a three-dimensional aluminosilicate gel [3], which is completely different from the calcium-silica-hydrates (CSH) in cement-based materials, but possesses comparable mechanical property. Additionally, alkali activated materials are reported to outperform the cement-based materials with respect to CO_2 emission (very low CO_2 footprint) [4], compressive strength [5], as well as chemical resistance [6, 7] and fire resistance[8]. As a consequence, alkali activated materials are gaining substantial attention during the last decade.

Fly ash is generally regarded as a good source material for AAM, since it is the residue from burning coal in the power plant and with the main composition of silica and alumina. A significant amount of literatures on the reaction mechanism of alkali activated fly ash (AAF) have been reported [9, 10]. Some of the studies investigated the reaction factors related to the dosage of the mixture [11, 12] and curing conditions [13] on the alkali activated fly ash, while others reported the microstructure of AAF [14]. However, the published research on the engineering properties of AAF is limited, except for a few studies [5, 15, 16]. In order to utilize alkali activated materials in engineering applications, an evaluation of its engineering properties is essential.

Therefore, in the present work, the engineering properties of alkali activated fly ash mortar, including setting time, mechanical strength and drying shrinkage, were studied with different amount of sodium silicate solutions. In addition, the microstructure and the interfacial transition zone (ITZ) between the paste and aggregates were examined by environmental scanning electron microscopy (ESEM).

MATERIALS AND EXPERIMENTS

Materials

The Class F fly ash (according to ASTM classification) obtained in The Netherlands and standard siliceous sand were used to produce alkali activated fly ash mortar. The chemical compositions of hereby used fly ash and cement (CEM I) were determined by X-ray fluorescence (XRF) spectrometer, as shown in Table 1. The alkaline solutions were prepared by mixing sodium hydroxide (analytical grade, >98% purity) with sodium silicate solution (Na_2O: 8.25 wt. %, SiO_2: 27.5 wt. %) and demi-water. Three AAF mixtures were used in this study. Table 2 presents the detailed mix proportion of activating solutions.

Table 1 Compositions of Fly Ash and cement (wt. %)

OXIDES	SiO_2	Al_2O_3	Fe_2O_3	CaO	MgO	K_2O	Na_2O	TiO_2	P_2O_5	SO_3
Fly Ash	48.36	31.36	4.44	7.14	1.35	1.64	0.72	1.24	1.9	1.18
Cement	19.5	5.6	2.3	63.3	1.1	0.9	0.3	--	--	2.7

Sample Preparation and Testing Methods

The sand/binder mass ratio used in the AAF mortars was 2:1 and the water/binder mass ratio was 0.35(including water in water glass). After the fly ash and sand were mixed in a mixer for 2 minutes, the prepared activating solution was added and mixed for a further 5 minutes. The mixture was then poured into the 40 × 40 × 160 mm^3 moulds, vibrated for 1 minute to remove the entrapped air from the mixture. Afterwards, all samples were sealed with plastic film and first cured in an oven at 40°C for 7 days; followed by curing at 20 °C (relative humidity > 98%) until the age of testing. Samples submitted to ESEM observation were crushed by a hammer into small pieces in the range of 1-2 cm^3. The reaction was stopped by immersing samples in liquid nitrogen and then the samples were kept in freeze-dryer until the weight change was within 0.1%.

Table 2 Composition in alkali solutions (mol) mixing with 1 kg fly ash

SAMPLE	SiO_2, mol	Na_2O, mol	H_2O, kg
1 -1.0	1.0	1.0	0.35
1 -1.5	1.0	1.5	0.35
1.5–1.5	1.5	1.5	0.35

Setting time： Setting time (initial setting time) was measured according to the standard (NEN-EN 196-3:2005).

Mechanical properties: Standard bending strength test was measured on 40 × 40 × 160 mm^3 prisms and standard compressive strength test was carried out on 40 × 40 mm^2 cubes. There were at least 3 replicates for each group.

ESEM observation: A Philips-XL30-Environmental Scanning Electron Microscope was used to obtain the micrographs of fly ash-based geopolymers. Backs scattered electron (BSE) detector was used to acquire the images. Before the observation, the samples were first subjected to epoxy impregnation and further grinded and polished. The acceleration voltage was 20 KV and the water vapor pressure at 1.0 Torr. The magnification of the images was 500× and the corresponding physical size of the region was 248 μm in length and 188 μm in width.

Drying shrinkage: The specimens of AAF for shrinkage test were demoulded after 40 °C curing for 7 days. Afterwards, the 40 x 40 x 160 mm^3specimens were stored in the laboratory at 20 °C with a relative humidity approximately 50%. The initial length measurement was measured at 20 minutes after demoulding. After that, measurements were carried out twice a day in the first 2 weeks and then 3 times a week. For comparison, the drying shrinkage of Portland cement mortar with w/c = 0.5 and sand/binder mass ratio 3:1 was also measured. The specimens of cement mortar for shrinkage test were demolded after 7 days sealed cured at 20 °C; then the specimens were cured at the same 50% relative humidity room as AAF mortar. The initial length measurement of cement mortar was recorded immediately after demolding, since there is no temperature difference for the specimens.

RESULTS AND DISCUSSION

Setting Time

The setting time of three AAF mixtures is shown in Table 3. It's apparent from the table that when the alkali content increased from 1.0 to 1.5 mol (with respect to 1 kg fly ash), setting time extended from 3 hours to more than 8 hours; while with the same increase of silica content, the setting time decreased to around 5 hours. The setting time of AAF was assumed related to the amount of dissolved silica and alumina from fly ash particles for the geopolymerization. With longer setting time, more reactive silica and alumina dissolved from the fly ash, which was thought beneficial to the strength development.

Table 3 Setting time of alkali activated fly ash

SAMPLE (SiO_2-Na_2O)	1 - 1.0	1 - 1.5	1.5 – 1.5
Setting time	3 h	8 h 47 min	5 h 13 min

Compressive and Flexural Strength

Figure 1 presents the compressive and flexural strength of AAF at the curing age of 7, 28 and 91 days. After 7 days sealed cured at 40 °C, AAF mortar showed an optimal compressive strength of 49 MPa with the SiO_2-Na_2O ratio of 1.5-1.5 (sample 1.5-1.5), which is generally higher than conventional cement mortar with w/c of 0.5. Additionally, the compressive strength continued to increase with time, though more slowly than the first 7 days. With more silica and alkali content, sample was observed to exhibit substantial improvement in compressive strength as shown in Figure 1 (a). The addition of alkali (sodium oxide) in the AAF system was believed to enhance the further dissolution of fly ash particles, ready for the next steps of reaction (geopolymerisation) [12]. Thus a higher compressive strength was obtained with higher reaction degree. The reaction was retarded with an addition of silica in the activator [17], while the soluble silica improved the microstructure by reacted with the dissolved alumina into aluminosilicate gel, resulting in a higher compressive strength.

The flexural strength of AAF was obtained from three point bending test. As apparent from Figure 1 (b), sample 1-1.5 presented the highest flexural strength at all the curing age, followed by sample 1.5-1.5 and 1-1.0. The trend of flexural strength of AAF was found different from compressive strength when the activator composition varied. It was mentioned that the added alkali enhanced the reaction, while silica prohibit the further dissolution of fly ash, thus sample 1-1.5 was expected to have the highest reaction degree. It was assumed that the flexural strength of AAF mortar was more related to the extent of reaction than the compressive strength. The higher reaction degree of AAF led to a higher flexural strength.

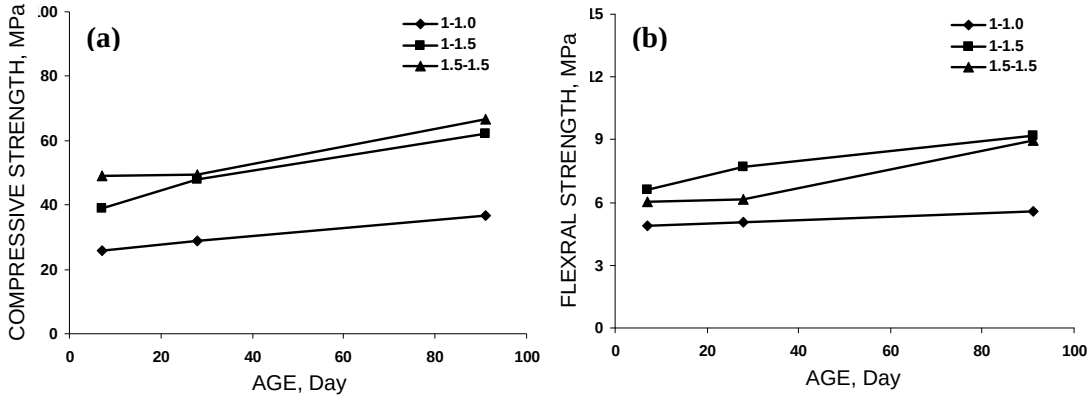

Figure 1 The compressive strength and flexural strength of AAF mortar with time

Drying Shrinkage of AAF

The drying shrinkage of AAF was relatively small compared to ordinary Portland cement as reported by some authors [5] . This is true for AAF cured at high temperature, which is similar to the low shrinkage of high temperature-cured Portland cement. It was reported by Hardjito et. al [15] that the drying shrinkage of AAF is considerably large at low or room curing temperature. In the present study, the drying shrinkage measurement was carried out after 7 days curing at 40 °C. The drying shrinkage of AAF with different activating solution content is shown in Figure 2. It was observed that the shrinkage of AAF mortar was significantly affected by the silica and sodium oxide content: sample with more silica and alkali content (1.5-1.5) of AAF mortars exhibited a higher extent of drying shrinkage of the strain around 1000×10^{-6} after 70 days. Compared to OPC mortar (w/c=0.5), the drying shrinkage of sample 1-1.0 and 1-1.5 was smaller, while it was larger for sample 1.5-1.5. Similar results were also reported by Ridtirud et. al [18].

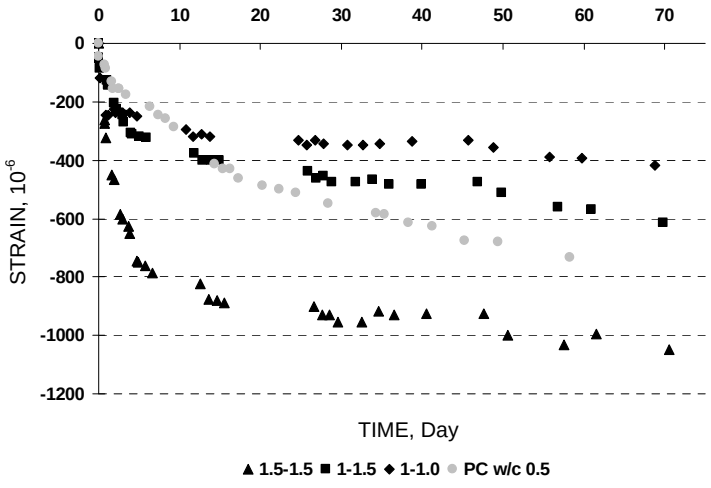

Figure 2 Drying shrinkage of AAF mortar and OPC w/c of 0.5 with time

The weight change of the shrinkage specimens due to loss of moisture from the sample, expressed as percent weight change of the total specimen weight is shown in Figure 3. For all AAF mortars, more weight loss of water were observe compared to OPC mortar. It was believed that not like the water in cement-based materials, which reacts with the cement, most of the water in AAF is existed as free water. Thus more free water in AAF mortar is ready to escape from the matrix than in OPC mortar under drying condition.

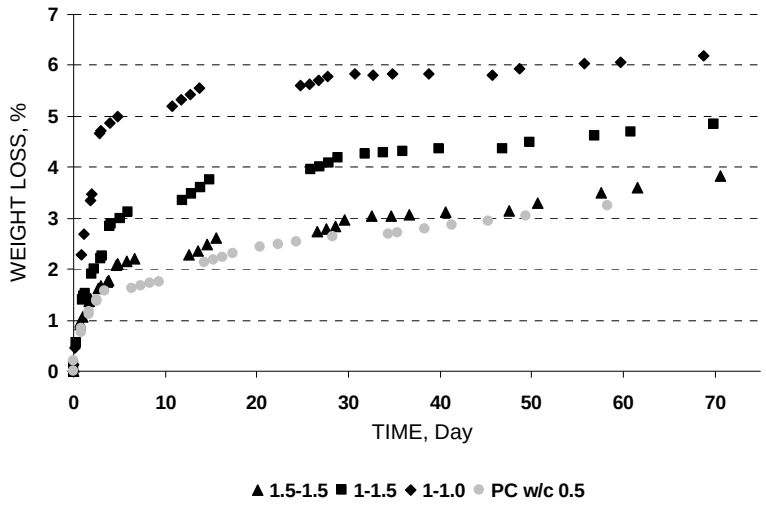

Figure 3 Water loss with time of AAF mortar and OPC w/c of 0.5

It was also interesting to note that for AAF mortars, specimen with the highest drying shrinkage (Figure 2, 1.5-1.5) presented the lowest water loss, while specimen with the least drying shrinkage (Figure 2, 1-1.0) exhibited the highest weight loss in Figure 3. This phenomenon was very different than in cement-based materials, in which the drying shrinkage magnitude is in consistent with the weight loss of water from the materials. It was assumed that the pore size distribution had a significant effect in determining the drying shrinkage of AAF [19]. From the previous study of the pore structure of AAF paste[20], sample 1.5-1.5 presented a finer pore size distribution than sample 1-1.5, followed by sample 1-1.0. Meanwhile, given that most of the water in AAF was free water, the free water of AAF was expected to stay in a smaller pore in sample 1.5-1.5 than 1-1.0. According to the drying shrinkage model proposed by Shimomura and Maekawa [21, 22], specimen with smaller average pore radius would have larger the capillary tensile forces, hence higher shrinkage.

The Microstructure of AAF Mortar

Figure 4 displayed the BSE images of AAF mortar and OPC mortar at 7 days. When fly ash was in contact with alkali silicate solutions, soluble silicate and aluminate species dissolved from the fly ash particles, reacting into alunimosilicated gels. These gels connected the remained fly ash and sands into a homogeneous matrix as shown in Figure 4.

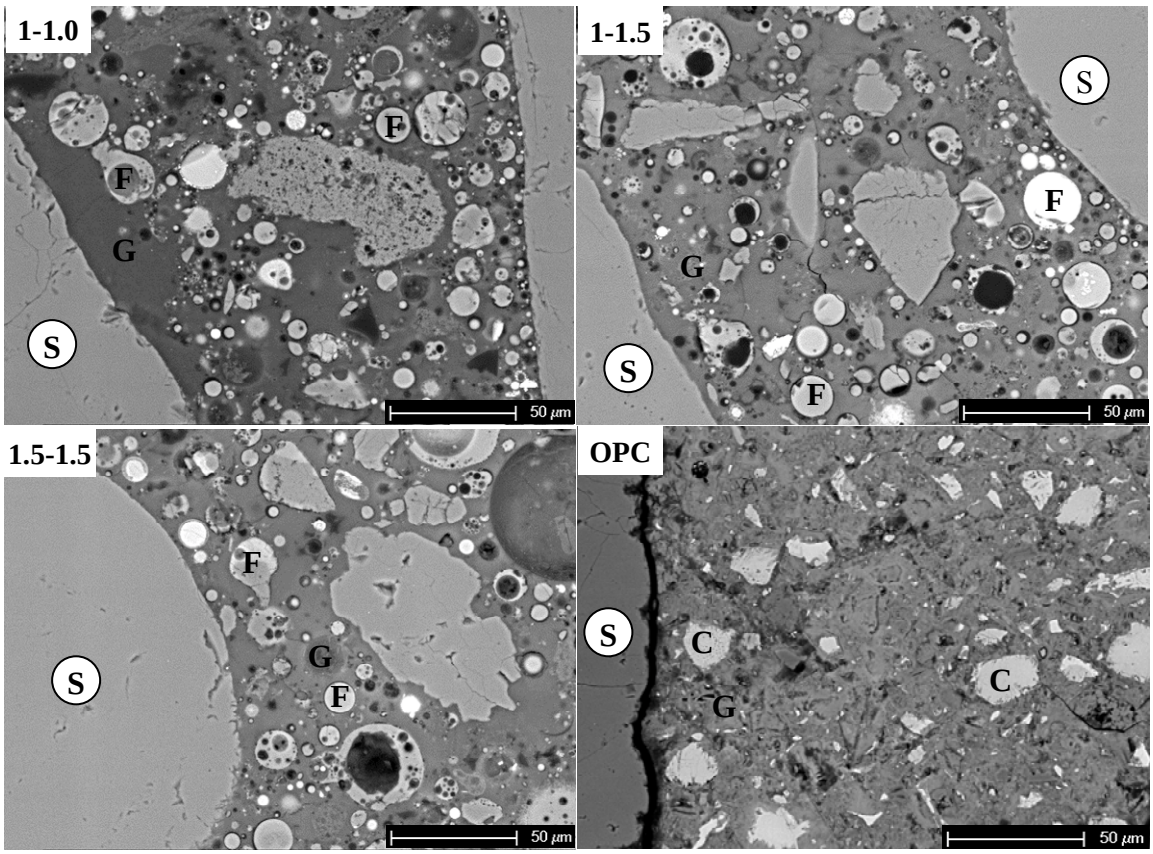

Figure 4 The BSE image of AAF mortar and OPC mortar at the curing age of 7 days. S= Sand, G= gels (reaction products), F = fly ash particles, C = cement particles.

Compared the microstructures of AAF mortar to the OPC mortar in Figure 4, the interfacial transition zone (ITZ) between the reaction products and aggregates were observed very different. An obvious porous transition zone between the sand and paste was obvious with a thickness of 4-7 μm. In OPC concrete, the thickness of the ITZ was reported ranging from 50 to 100 μm [23]. The ITZ of OPC, typically consisting of a high concentration of calcium hydroxide and low calcium silicate hydrate concentration with high porosity [24], is regarded as the weakest region within a mortar or concrete structure. However, in the AAF mortars presented in this study, no clear interface could be identified between the sand grains and the AAF binders (Figure 4). The interfacial area appeared to be very dense and uniform. This finding was in agreement with other observations on alkali activated materials [25]. No ITZ in AAF mortar may indicate that AAF mortar is expected to outperform OPC mortar in many important properties, such as permeability and durability.

CONCLUSIONS

In this study, the engineering properties of alkali activated fly ash mortar were investigated. It was found that an increase of silica and sodium oxide content both resulted in longer setting time and higher compressive strength of AAF mortars. Sample with the highest flexural strength was regarded related to the highest extent of reaction (1-1.5). With more silica and alkali content of AAF mortar (1.5-1.5), sample exhibited a higher extent of drying shrinkage but with lower weight loss from water, which was assumed related to the finer pore size

distribution. Unlike OPC mortar, no clear interface could be observed between the sand gain and AAF binders, indicating AAF mortar may have better durability than OPC mortar.

REFERENCES

1. DAVIDOVITS, J Chemistry of geopolymeric systems, terminology. Geopolymere, Vol. 99, No., 1999, pp 9-39.

2. DUXSON, P, PROVIS, J L, LUKEY, G C AND VAN DEVENTER, J S J The role of inorganic polymer technology in the development of 'green concrete'. Cement and Concrete Research, Vol. 37, No. 12, 2007, pp 1590-1597.

3. DUXSON, P, PROVIS, J L, LUKEY, G C, SEPAROVIC, F AND VAN DEVENTER, J S J Si-29 NMR study of structural ordering in aluminosilicate geopolymer gels. Langmuir, Vol. 21, No. 7, 2005, pp 3028-3036.

4. DAVIDOVITS, J Geopolymers and geopolymeric materials. Journal of Thermal Analysis and Calorimetry, Vol. 35, No. 2, 1989, pp 429-441.

5. FERNANDEZ-JIMENEZ, A M, PALOMO, A AND LOPEZ-HOMBRADOS, C Engineering properties of alkali-activated fly ash concrete. Aci Materials Journal, Vol. 103, No. 2, 2006, pp 106-112.

6. FERNÁNDEZ-JIMÉNEZ, A, GARCIA-LODEIRO, I AND PALOMO, A Durability of alkali-activated fly ash cementitious materials. Journal of Materials Science, Vol. 42, No. 9, 2007, pp 3055-3065.

7. OLIVIA, M AND NIKRAZ, H Durability of Low Calcium Fly Ash Geopolymer Concrete in Chloride Solution. Proceedings of the 6th Asian Symposium on Polymers in Concrete, No., 2009, pp 153-161.

8. TEMUUJIN, J, MINJIGMAA, A, RICKARD, W, LEE, M, WILLIAMS, I AND VAN RIESSEN, A Fly ash based geopolymer thin coatings on metal substrates and its thermal evaluation. Journal of Hazardous Materials, Vol. 180, No. 1-3, 2010, pp 748-752.

9. PROVIS, J L AND VAN DEVENTER, J S J Geopolymerisation kinetics. 2. Reaction kinetic modelling. Chemical Engineering Science, Vol. 62, No. 9, 2007, pp 2318-2329.

10. REES, C A, PROVIS, J L, LUKEY, G C AND VAN DEVENTER, J S J In situ ATR-FTIR study of the early stages of fly ash geopolymer gel formation. Langmuir, Vol. 23, No. 17, 2007, pp 9076-9082.

11. CRIADO, M, FERNANDEZ-JIMENEZ, A AND PALOMO, A Alkali activation of fly ash: Effect of the SiO2/Na2O ratio Part I: FTIR study. Microporous and Mesoporous Materials, Vol. 106, No. 1-3, 2007, pp 180-191.

12. FERNÁNDEZ-JIMÉNEZ, A AND PALOMO, A Composition and microstructure of alkali activated fly ash binder: Effect of the activator. Cement and Concrete Research, Vol. 35, No. 10, 2005, pp 1984-1992.

13. CRIADO, M, FERNANDEZ-JIMENEZ, A AND PALOMO, A Alkali activation of fly ash. Part III: Effect of curing conditions on reaction and its graphical description. Fuel, Vol. 89, No. 11, 2010, pp 3185-3192.

14. LLOYD, R R, PROVIS, J L AND VAN DEVENTER, J S J Pore solution composition and alkali diffusion in inorganic polymer cement. Cement and Concrete Research, Vol. 40, No. 9, 2010, pp 1386-1392.

15. HARDJITO, D, WALLAH, S E, SUMAJOUW, D M J AND RANGAN, B V On the development of fly ash-based geopolymer concrete. Aci Materials Journal, Vol. 101, No. 6, 2004, pp 467-472.

16. SOFI, M, VAN DEVENTER, J, MENDIS, P AND LUKEY, G Engineering properties of inorganic polymer concretes (IPCs). Cement and Concrete Research, Vol. 37, No. 2, 2007, pp 251-257.

17. CRIADO, M, FERNANDEZ-JIMENEZ, A, DE LA TORRE, A G, ARANDA, M A G AND PALOMO, A An XRD study of the effect of the SiO2/Na2O ratio on the alkali activation of fly ash. Cement and Concrete Research, Vol. 37, No. 5, 2007, pp 671-679.

18. RIDTIRUD, C, CHINDAPRASIRT, P AND PIMRAKSA, K Factors affecting the shrinkage of fly ash geopolymers. International Journal of Minerals, Metallurgy, and Materials, Vol. 18, No. 1, 2011, pp 100-104.

19. FERRARIS, C AND WITTMANN, F H Shrinkage mechanisms of hardened cement paste. Cement and Concrete Research, Vol. 17, No. 3, 1987, pp 453-464.

20. MA, Y, YE, G AND VAN BREUGEL, K. Effect of Alkaline Activating Solutions on Fly ash-based Geopolymers The Seventh International Symposium on Cement & Concrete and the 11th International Conference on Advance in Concrete Technology and Sustainable Development, Jinan, China, 2009.

21. SHIMOMURA, T AND MAEKAWA, K, Micromechanical model for drying shrinkage of concrete based on the distribution function of porosity. in 5th International RILEM Symposium on Creep and Shrinkage of Concrete, Barcelona, Spain, E & FN Spon, London, (1993), CHAPMAN & HALL, 133-139.

22. SHIMOMURA, T AND MAEKAWA, K Analysis of the drying shrinkage behaviour of concrete using a micromechanical model based on the micropore structure of concrete*. Magazine of Concrete Research, Vol. 49, No. 181, 1997, pp 303-322.

23. WEI, S, MANDEL, J A AND SAID, S, Study of the interface strength in steel fiber-reinforced cement-based composites. in, (1986), ACI.

24. BRETON, D, CARLES-GIBERGUES, A, Ballivy, G and Grandet, J Contribution to the formation mechanism of the transition zone between rock-cement paste. Cement and Concrete Research, Vol. 23, No. 2, 1993, pp 335-346.

25. SHI, C AND XIE, P Interface between cement paste and quartz sand in alkali-activated slag mortars. Cement and Concrete Research, Vol. 28, No. 6, 1998, pp 887-896.

Interfacial Bond between Reinforcing Fibres and CSA Cements: An Examination of its Influence on Fibre Pullout Characteristics

R B Jewell, K C Mahboub, T L Robl
University of Kentucky, USA

This paper presents the results of an experimental investigation on the influence of the interfacial bond of reinforcing fibres embedded in a calcium sulfoaluminate (CSA) matrix on the fibre pullout energy. Bonding at the fibre-matrix interface plays an important role in controlling the mechanical performance of cementitious composites. In particular, composites formed from sulfate-based systems (CSA) as opposed to the silicate systems found in Portland cement. To examine the fibre-matrix bonding within the CSA and Portland cement system various types of fibres were selected, including polyvinyl-alcohol (PVA), polypropylene, and copper-coated steel. The fibres were embedded in three different matrices, two sulfate-based including one commercially available CSA cement and a CSA fabricated from coal-combustion byproducts. The thirds matrix was a silicate-based OPC. In this study, the results of the single-fibre pullout test was coupled with scanning electron microscopy to examine the interfacial bond between the fibre and CSA matrix for evidence of debonding and possible reaction products.

Robert B Jewell, Research Scientist for the Center for Applied Energy Research at the University of Kentucky, currently conducting research into the application of coal combustion by-products in the formulation low energy cement and concrete.

Kamyar C Mahboub, Dr. Mahboub has been working on mechanistic characterization of construction materials. He has also worked on pavement design, analysis, construction, and management. In addition in his journal publications, he has published two chapters in a popular civil engineering textbook: chapters on Superpave, and Pavement Management, “Pavement Analysis and Design”, with Professor Y.H. Huang. Dr. Mahboub received his BSCE from The University of Texas at Austin in 1982, and MSCE and Ph.D. from Texas A&M University in 1985 and 1988, respectively. He is the Lawson Professor of Civil Engineering at University of Kentucky, an ASCE Fellow, and a registered professional engineer (PE) in Kentucky.

Thomas L Robl, Associate Director of the Center for Applied Energy Research at the University of Kentucky, currently conducting research into the application of coal combustion by-products in the formulation low energy cement and concrete.

Keywords: CSA Cement, Low-energy cement, Single-fibre pullout

INTRODUCTION

The primary reason behind the addition of fibres to cementitious matrices is to delay and contain cracking [1]. While it is generally believed that the inclusion of fibres enhances the pre-cracking behaviour of cement composites by increasing its cracking strength, the effect of fibre addition becomes dramatic only after cracking [1, 2]. The reason for this is the fibres bridge the cracked parts of the matrix, thus delaying the sudden global failure of the composite [2]. Therefore, in the post-cracking stage the behaviour of fibres is governed by their interfacial bond stress response as being subjected to pull-out loads [1].

Fibre-reinforced composites (FRC) resist tensile forces through a composite action, whereby part of the tensile force is resisted by the matrix, while the balance is taken by the fibres [1]. The transmission of forces between the fibre and the matrix is achieved through bond defined as the shearing stress at the interface between the fibre and the surrounding matrix [1]. It is generally agreed that the fibre contribution to increasing the toughness of the composite is primarily dictated by the mechanisms of fibre pullout [1]. The term toughness, or fracture toughness, refers to the work dissipated, or the total energy absorbed prior to complete failure; or the critical potential energy release rate of a composite specimen with a unit mJ [3].

Fibre pull-out tests are often used to study the fibre-matrix bond behaviour in fibre reinforced cement composites. The pull-out test is also important by itself as it simulates the fibre bridging-pull-out mechanism during the fracture process of FRC. In relating the pull-out test results with the fibre-matrix bond characteristics, numerous models have been developed and many of them have been reviewed. Uniform shear bond strength between the fibre and the matrix is often assumed in FRC models and the bond strength from pull-out tests is frequently reported in terms of the average value over the embedded fibre surface area.

The cement-fibre interfacial bond results from some combination of mechanical interlocking of cement hydration products with the fibre surface and chemical reaction between fibre and cement paste within the interstitial transition zone [3, 4]. In fibre reinforced composite materials, the principal factor governing load transfer from the matrix to the fibre is the shear strength of the interfacial bond between the two components. Fractured specimens of fibre-reinforced concrete shows that failure takes place primarily due to fibre pullout or debonding. Generally fibre pullout rather than rupture confers a larger ductility to the fibre reinforced composites [2, 5]. Ideally composites will exhibit strain-hardening behaviour achieved through multiple cracking of the reinforced matrix. Unlike plain concrete, a fibre-reinforced concrete specimen does not break immediately after initiation of the first crack. This has the effect of increasing the work of fracture, or toughness.

The length and volume of fibres present in a concrete mix are critical in controlling the flexural strength and toughness of the hardened concrete, including the prevention of crack propagation. Generally, the composite will carry increasing loads after the first cracking of the matrix if the pull-out resistance of the fibres at the first crack is greater than the load at first cracking. Within the cracked section, the matrix does not resist any tension and the fibres carry the entire load taken by the composite. With an increasing load on the composite, the fibres will tend to transfer the additional stress to the matrix through bond stresses. If these bond stresses do not exceed the bond strength, then there may be additional cracking in the matrix. This process of multiple cracking will continue until either fibres fail of the accumulated local debonding will lead to fibre pullout [6, 7].

The principal phases of CSA clinker are $C_4A_3\acute{S}$ (also called Klein's compound or yeelimite and where $\acute{S}$ = sulfate), C_2S (or belite), and C_4AF (or brownmillerite) [8]. Other phases such as calcium aluminates (e.g. $C_{12}A_7$ or $C_{11}A_7CaF_2$) are also sometimes present. Unlike Portland cement which gains its strength from the hydration of the calcium silicates, alite (C_3S) and belite (C_2S), C_SA cement gains it from the hydration of Klein's compound with calcium sulfate (such as gypsum $C\acute{S}H_2$ or anhydrite $C\acute{S}$) to form ettringite via these reactions [9]:

$$C_4A_3\acute{S} + 2C\acute{S}H_2 + 34H \rightarrow C_6A\acute{S}_3H_{32} + 2AH_3$$

$$C_4A_3\acute{S} + 2C\acute{S} + 38H \rightarrow C_6A\acute{S}_3H_{32} + 2AH_3$$

These reactions are relatively fast, and are nearly complete within 1 month. When sulfate anion is depleted, ettringite $C_6A\acute{S}_3H_{32}$ (AFt phase) is converted to monosulfate $C_4A\acute{S}H_{12}$ (AFm phase or "mono" phase) which reduces the strength of the cement [10].

Some hydration studies have already been done on the influence of gypsum, calcium sulfate hemihydrate (referred to as "hemihydrate") and anhydrite on the hydration of CSA clinker containing C_2S and $C_4A_3\acute{S}$ as main phases. According to Majling et al. [11], active anhydrite (depending on the heating temperature and mechanochemical activation) is necessary for the high rate of initial strength development. Furthermore, Sahu et al. [12] found that ettringite formation depends on the calcium sulfate used. With hemihydrate or gypsum, ettringite formation is very intensive and can cover the aluminate phases, which retards their hydration. Conversely with anhydrite, there is no "supersaturation" and the hydration continues.

RESEARCH SIGNIFICANCE

The bond between the fibre and matrix is important, if the fibres have a weak bond with the matrix they can slip out at low loads and do not contribute to preventing the propagation of cracks. However, if the bond is too strong then the fibres will rupture before they can contribute to the post-crack strength of the matrix material. Therefore this paper presents the development of the CSA-fibre interfacial bond characteristics in the context of material design under the guidance of micro-mechanical tools. Specifically this study illustrates how the fibre/matrix interface is enhanced by the use of sulfate-based cements when compared to silicate-based systems; providing some guidance in properly selecting a combination of fibre and matrix that provides efficient bond strength.

EXPERIMENTAL PROGRAM

The single-fibre pullout test was conducted to investigate the maximum interfacial bond strength and corresponding pullout energy. The major parameter investigated here is the effect of sulfate-based hydration products ability to bond to various fibre types over silicate-based hydration products.

Materials

Three types of cements were investigated; ordinary Portland cement, a commercially available CSA cement, and a CSA cement fabricated from coal combustion byproducts (CCBs), at the University of Kentucky Center for Applied Energy Research (CAER), referred to in this study as CSAB#4. Polypropylene (PP) fibre, from Propex Inc. as-well-as Polyvinyl

Alcohol (PVA) produced by Nycon and Type-1 copper-coated steel fibres (Nycon-SF®) from Kuraray Company will be used in the tests (Table 2). The purpose of using a hybrid fibre cement system is to utilize the best properties of individual fibres in an effort to maximize desired composite properties [13].

Fabrication of CSAB Cement from CCBs

Mixtures of FBC spent bed material, PCC fly ash; bauxite and limestone were interground for clinkering. The clinker tests were conducted from 1000oC to 1250oC and included compositions in the stability fields of Klein's compound and belite. Mineral composition of the products was determined by X-ray diffraction. The first cement formulation was calculated using Bogue equations that were modified for phases in CSAB clinker; this formulation is termed "CSAB#1". The phases assumed to be present were Klein's compound, belite, ferrite (C4AF), calcium sulfate, and a minor amount of lime (<0.5%). However, it was found that the normative equations could not be used to optimize the CSAB compositions, probably because of the formation of minor amounts of other phases such as gehlenite, and the simplistic assumption that the aluminum:iron ratio in the ferrite phase = 1. Therefore, adjustments were made to the formulations to meet several objectives: 1) minimize the proportion of limestone used and thus the free lime formed (CaO), 2) maximize the proportions of by-products (i.e. CFBC and PCC ash), and 3) produce a cement that will approach the performance of the commercial CSAB cement. The adjustments were made by analyzing each clinker using XRD until the desired composition was achieved resulting in the synthesis of formulations termed "CSAB#2" and "CSAB#4". Figure 1 shows the XRD profiles of the laboratory synthesized clinkers compared to three commercial CSAB cements: a CSAB manufactured in China, Commercial CSAB #1, and Commercial CSAB #2. The chemical mineral composition of these cements, in addition to Portland cement, is provided in Table 1. The Gilbert FBC material is a potential source of CaO and SO_3 and thus was used as a partial substitute for gypsum and limestone in the laboratory CSAB raw materials.

Table 1 CSAB cement composition from XRF analysis.

CEMENT	CEMENT COMPOSITION, %							
	SiO_2	Al_2O_3	Fe_2O_3	CaO	MgO	Na_2O	K_2O	SO_3
OPC	20.5	5.4	2.6	63.9	2.1	0.61	0.21	3.0
CSAB from China	11.12	26.94	1.76	44.99	3.18	0.04	0.19	12.23
Commercial CSAB 1	5.89	20.48	2.53	42.29	0.78	0.1	0.15	25.71
Commercial CSAB 2	14.92	16.12	1.32	48.91	1.63	0.24	0.49	15.46
CSAB#2	16.90	16.95	2.39	47.10	2.25	0.15	0.68	13.52
CSAB#4	8.21	24.30	2.59	40.02	1.32	0.14	0.62	22.30

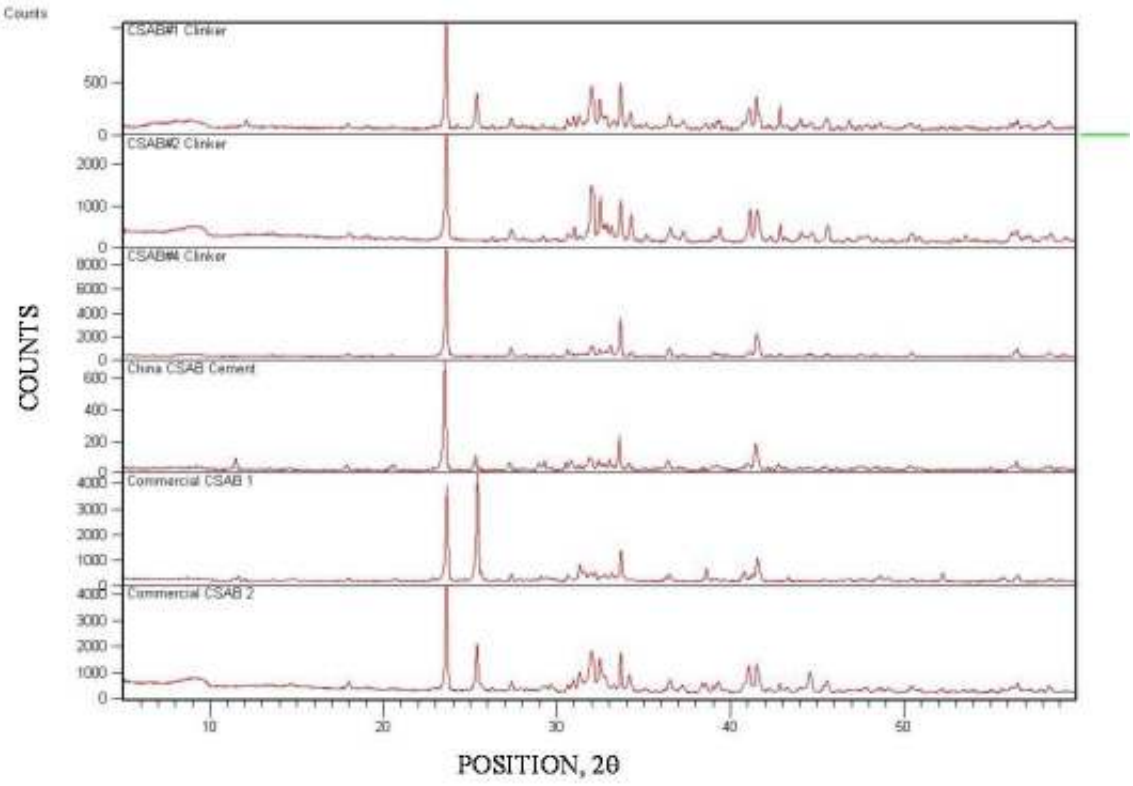

Figure 1 XRD profiles of the laboratory synthesized clinkers compared to the commercially available CSAB cements. K = Klein's Compound; An = anhydrite; B = belite (C2S).

The optimum firing temperature for the FBC material based CSAB cement was chosen to be 1250°C. At this temperature the maximum amount of Klein's compound and belite was formed with minimal quantities of silicosulfate, an unreactive phase. Table 2 provides a list of phases present in the cement formulations.

Table 2 Comparison of clinker phases

PHASE	COMPOSITION	OPC	CHINA CSAB	CSAB#4
C_4A_3S`	Ca4Al6O12SO4	—	√	√
C_2S	Ca2SiO4	√	√	√
C_4AF	Ca2(Al,Fe+3)2O5	√	—	—
CS`	CaSO4	√	√	—
C	CaO	—	—	—
C_2AS	Ca2Al2.22Si.78O6.79(OH).22	—	—	—

Single-Fibre Pullout Test Setup and Fibre-Matrix Interface Property

The pullout tests were conducted on an Instron 600DX universal testing machine with the specimen configuration shown in Figure 2. A 2 kN load cell was used to measure the pullout load of the fibres with a displacement rate of 0.02 mm/s. The displacement shown on the pullout curve in Figure 3 was measured as the crosshead movement. Fibre-free length was kept at a maximum of 1 mm to reduce the effects of fibre elongation. The fibres were embedded 6 mm into a paste plug, which was held in place with a screw-type grip that was secured into the 2 kN (450 lbf) load cell. The fibre-free end was glued to a plastic-anchor plate and then secured in the jaws of the upper grip as seen in Figure 2.

Figure 2 Instrument and specimen configuration for the single-fibre pullout test

Preparation of Test Specimens - Fibre Pull-Out Test

The test specimens were embedded in a paste plug with an 8-mm diameter and 25-mm length (Figure 3). The shortest fibre was 12 mm in length; therefore a depth of 6mm was selected to maximize the available fibre/matrix bond surface to allow for a quantitative comparison. A depth gauge was used to ensure the fibres were embedded to 6 mm and perpendicularly aligned to the mould surface.

Figure 3 Fibre pullout specimen preparation: (Left) Fibres embedded in matrix mould; (Right) Fibre glued to anchor plate

EXPERIMENTAL RESULTS AND DISCUSSION

Crack-interface interactions

Composites made with brittle fibres, such as steel, and brittle matrices, i.e. CSA cement, can exhibit high fracture toughness when failure occurs preferentially along the interface before fibres fracture. Most of the important toughening mechanisms are a direct result of the interface-related shear failure which gives rise to an improved energy absorption capability with a sustained crack growth stability through crack surface bridging and crack tip blunting [4].

Many fracture toughness theories of composite materials have been developed mainly for those with unidirectional fibres. Kim and Mai [4] emphasized the various origins of fracture toughness in composites may be characterized by considering the sequence of microscopic fracture events that lead to crack propagation macroscopically under monotonic increasing loads, such as the single-fibre pullout test. The cracks in a cement matrix can propagate along the fibre-matrix, referred to as longitudinal cracking; or transversely through the fibre and matrix, referred to as transverse cracking. The longitudinal cracking relies heavily on the physical and chemical adhesion between the fibre and matrix; with an additional bond component related to frictional stresses [14]. The prevalent type of cracking depends on the properties of the interface relative to the fibre and matrix [4]. According to Kim and Mai [4], when a crack present in the matrix approaches an isolated fibre, the following failure mechanisms may be expected to take place: 1) fibre-matrix interface debonding; 2) post-debonding friction; 3) fibre fracture; 4) stress redistribution and 5) fibre pullout.

Single fibre pull-out test

Tests were performed using single fibres to compare the pullout (direct tension) resistance and energies consumed during debonding and pullout of the PVA, PE and steel fibres. The results of the single-fibre pullout test indicated increased peak load and energy consumption values for CSA-based cements then results obtained with an ordinary Portland cement. The load-position curves were very different between the three fibre types.

PVA fibre

A typical single PVA fibre pullout curve is shown in Figure 4. The breaking of the chemical bond is evident in the first significant load drop. The second increase in load with fibre pullout has resulted from a slip hardening affect; this behaviour is achieved through multiple cracking of the reinforced matrix [15]. However, as the matrix continues to hydrate and chemically bonds to the fibre surface fibre failure is experienced more often as seen in Figure 5. This type of failure occurs when the fibre-matrix bond is greater than the load capacity of the fibre, thus the fibre ruptures in the fibre-free zone or debonded region of the fibre.

PVA fibres are hydrophilic and have the ability to chemically bond to the surrounding matrix along the interface boundary [15-17]. The hydrogen bond is formed by the available hydroxyl-groups on the PVA fibre. The chemical bond creates a cohesive fracture (matrix phase adheres to the fibre) when the fibre is pulled from the matrix [18].

Another possibility for the increased bond with PVA fibres is attributed to the PVA fibre providing nucleation sites for the crystallization of hydrated cement phases [19-21].

The use of PVA fibres has caused the mechanism of failure to change. The strong bond between the fibre and matrix has caused the failure site to move from the fibre surface to the more porous matrix region. The porous region is most likely more brittle by comparison with the ductile interfacial layer with steel fibres [17].

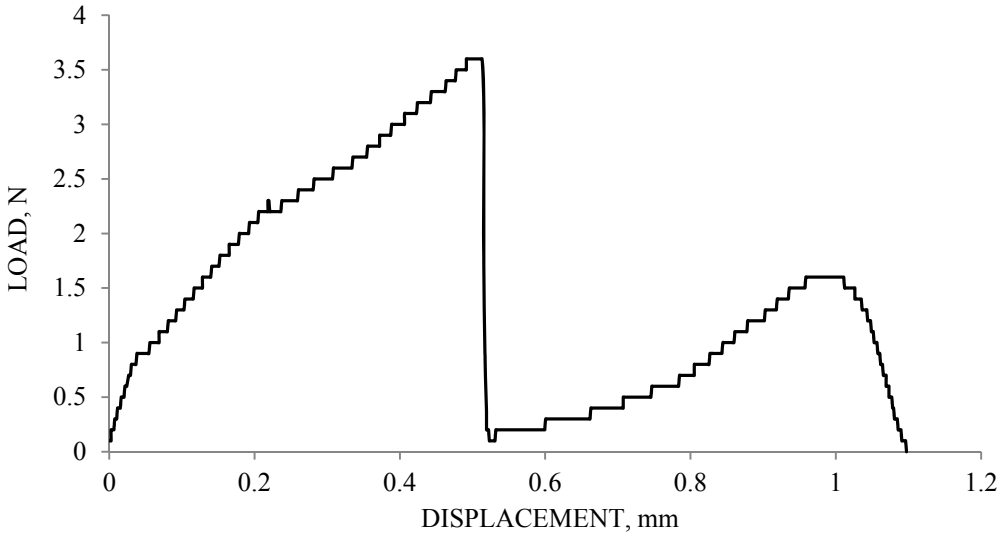

Figure 4 Typical pullout behaviour of a PVA fibre from a cementitious matrix

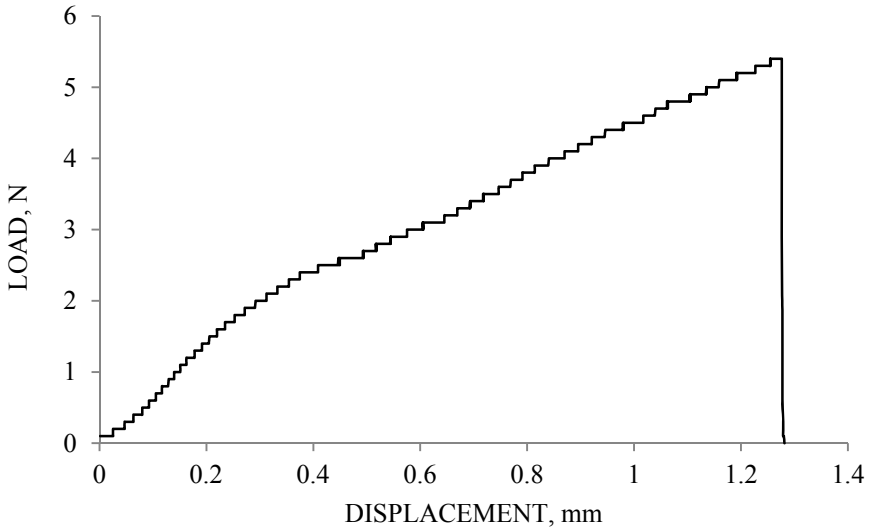

Figure 5 Fibre pullout curve demonstrating fibre failure

Fibre surfaces were observed with a scanning electron microscope (Hitachi S-4800) to determine mechanical-bond characteristics that can be related to the data collected from the fibre pullout test (Figure 6).

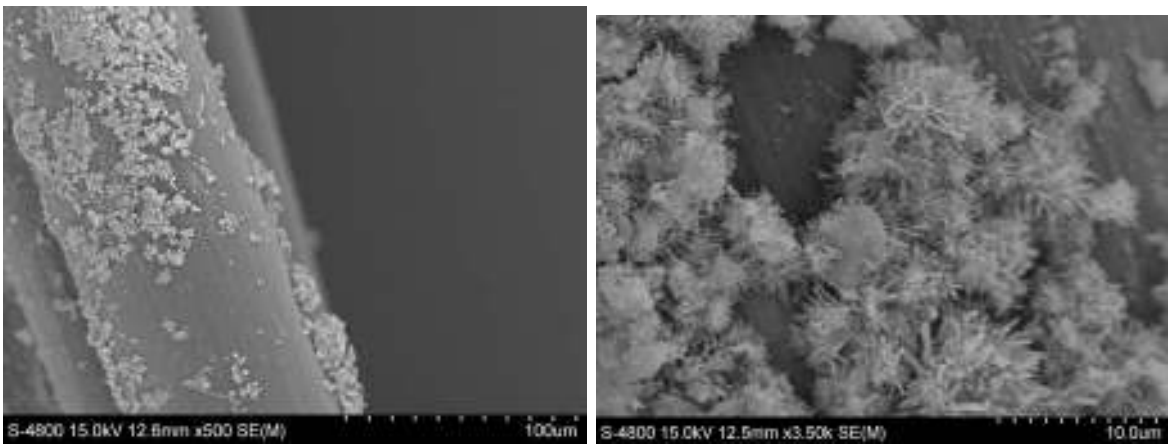

Figure 6 Clusters of ettringite crystals adhered to a single PVA fibre; Left: 500x magnification; Right: 3500x magnification.

Polypropylene fibre

A typical single polypropylene-fibre pullout curve is shown in Figure 7. The curve shows a broad curve with a large area value below the curve, demonstrating the PP fibre's ability to increase the toughness of the composite. The PP fibre does not chemically bond to the surrounding matrix, they are hydrophobic and non-polar; therefore fractures from the matrix in an adhesive (no matrix phase residue on the fibre) manner [3, 18]. The surface morphology of the PP fibre allows for surface irregularities ideal for matrix bonding; in addition to the potential for increased frictional loading, during fibre pullout, due to the valley-and-ridges found on fibre surface (Figure 8).

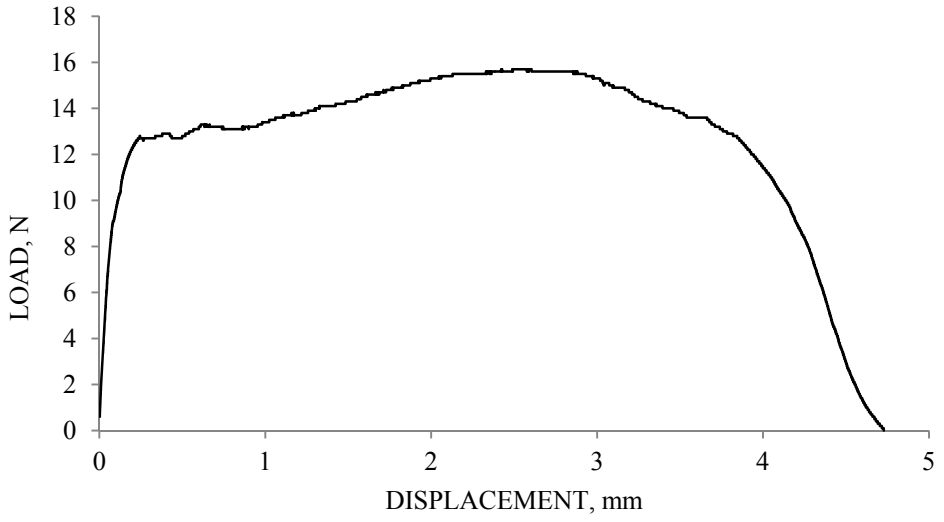

Figure 7 Typical pullout behaviour of a PP fibre from a cementitious matrix.

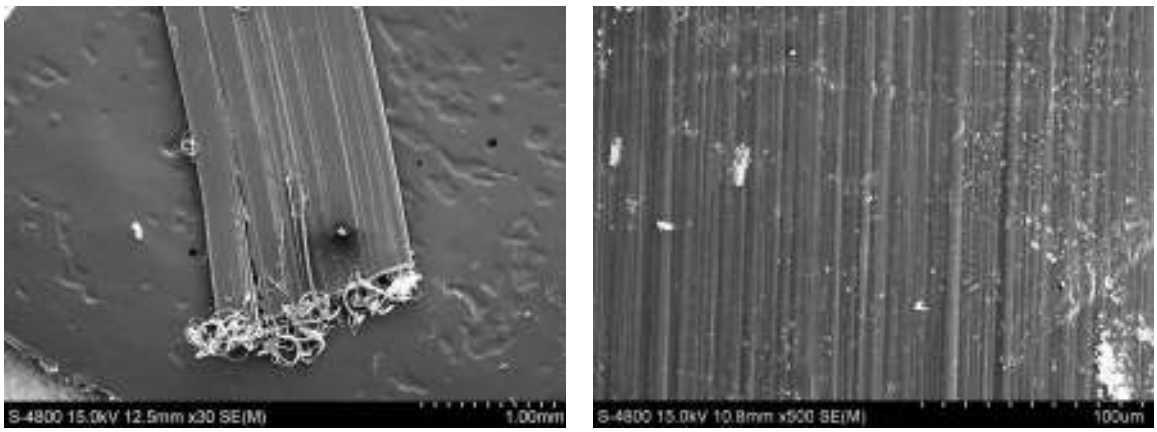

Figure 8 (Left) Polypropylene fibre after the single-fibre pullout test. (right) Surface of polypropylene fibre displaying valleys and ridges increasing available surface area for bonding.

Copper-Coated Steel fibre

A typical single steel fibre pullout curve is shown in Figure 9. High peak loads, relative to the PVA and PP fibres are characteristic along with a shallow-sloping slip hardening curve; providing a large energy consumption value for the area beneath the curve. The steel fibres are coated in copper for corrosion resistance as stated by the manufacturer's product specifications. An SEM analysis of the fibre surface after the pullout test revealed the copper coating provided a preferential bonding surface for hydration products (Figure 10). The high values for peak loading with the steel fibres are attributed to the copper coating. The hydration products likely have formed a complex with the copper in the surface (as well as copper ions in solution), to form a strong bond [17]. This bond allowed the interfacial layer of the matrix to remain bonded to the fibre during pullout.

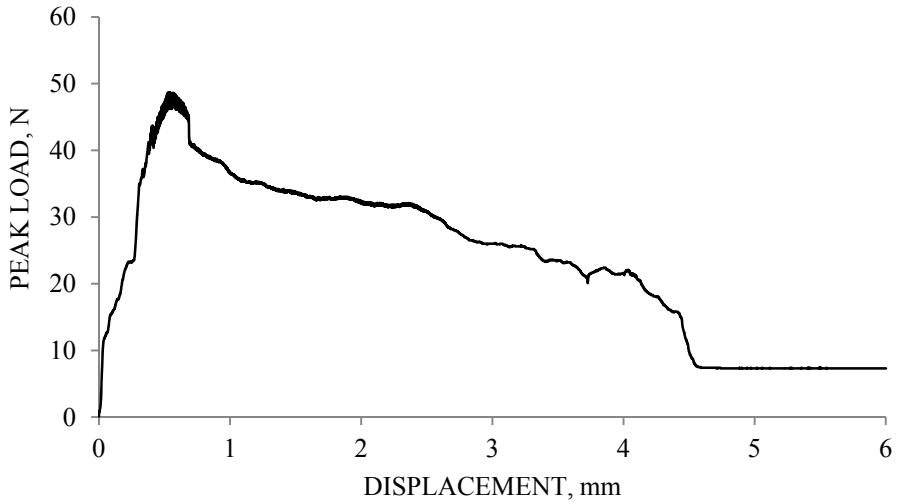

Figure 9 Typical pullout behaviour of a brass-coated steel fibre from a cementitious matrix

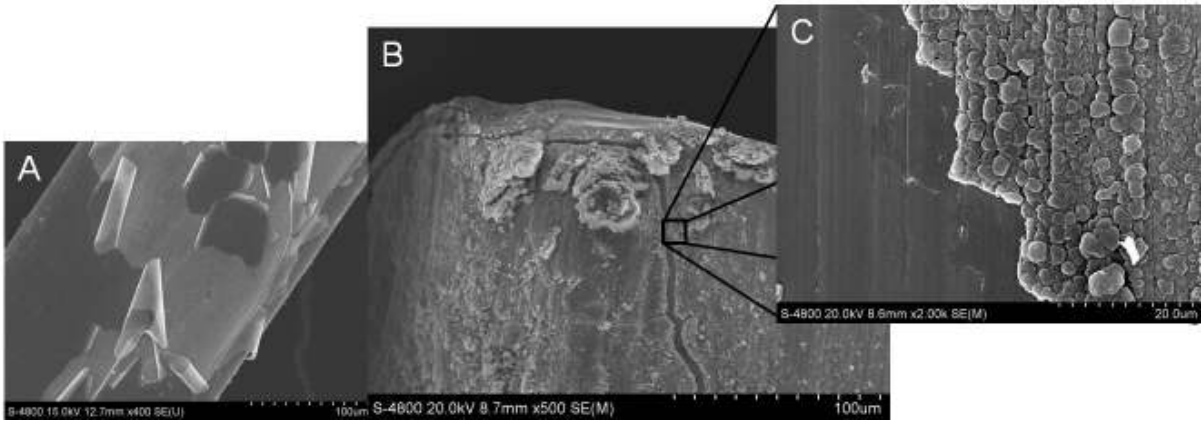

Figure 10 SEM images of a copper-coated steel fibre with hydration products bonded to coating surface: (A) Copper coating peeling from surface of steel fibre (400x magnification); (B) Fibre end with crack in copper coating (500x mag); (C) Zoomed image (2000x mag) with defined boundary between copper coating and steel surface

Ordinary Portland cement

The copper-coated steel fibres obtained the highest overall bonding strength from 7 to 56 days of curing, as represented by the peak-load values in Figure 11; with similar trending toughness values, Figure 12. However the polypropylene fibres exhibited greater bond strength at one day of curing and the highest toughness values at 1 and 7 days of curing. PVA fibres achieved a maximum peak load of 4.0 N at 56 days of curing; and a maximum energy consumption of 8.5 mJ at 28-days.

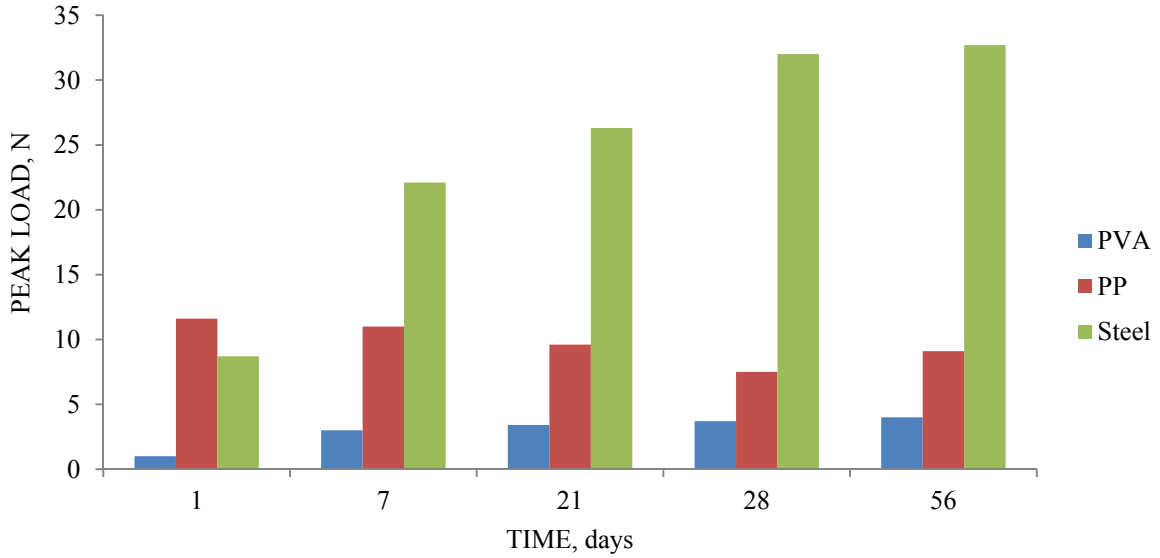

Figure 11 Comparison of peak load development over time between PVA, PE and steel fibres

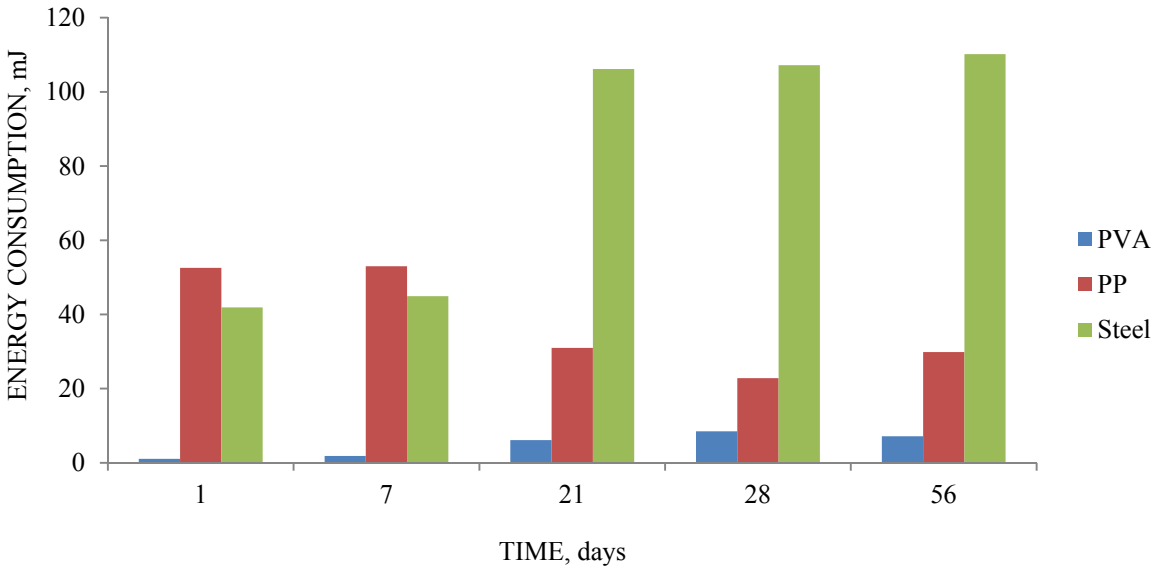

Figure 12 Comparison of energy consumption development over time between PVA, PE and steel fibres

The SEM images in Figure 13 indicate that the fibres were completely pulled from the matrix since there was no indication of fibre failure at its end. As the images show there are particles attached to the fibres which indicate the presence of bonding between the fibre and matrix; as compared to the surface of the fibre before they were embedded in the matrix. The strands of PP fibre that appear to have been peeled from the main fibre body play a large roll to the large energy consumption values exhibited by this type of fibre. In addition to the fibre-matrix bond, which appears minimal when compared to the matrix remnants bonded to the PVA and steel fibres, as the strands of PP are peeled away they add to the energy consumption by majorly enhancing the frictional stresses during loading; which along with the plastic nature of the PP fibre catastrophic failure of the fibre is never witnessed, instead a broad stress-strain curve is produced. The CSH grains form a fibrous, or fibrillar, morphology within the hardened paste [22, 23]. These grains help form the interfacial bond between the fibre and surrounding matrix. However they are thin and do not form an extremely dense structure as seen within the ettringite crystal structure.

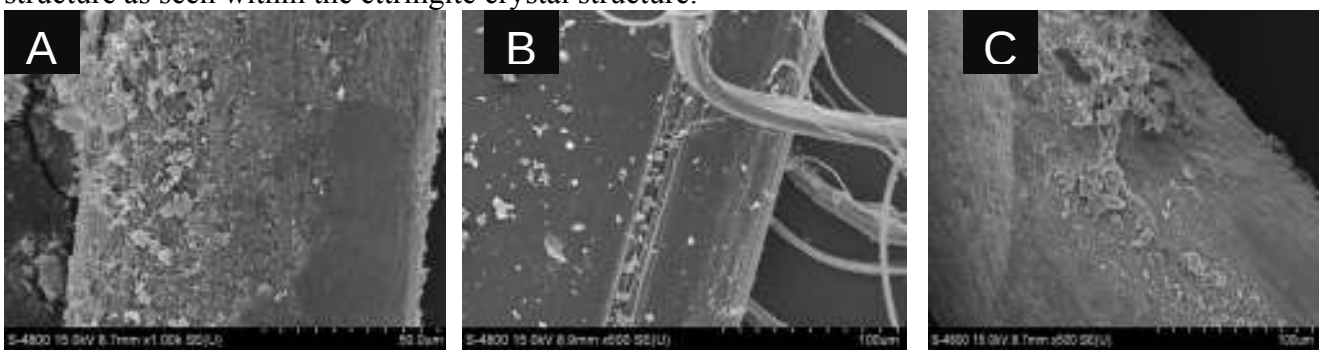

Figure 13 SEM images of fibres pulled from the OPC matrix: (A) PVA (1000x magnification); (B) PP (500x mag); (C) Steel (500x mag)

Commercial CSAB cement

As previously mentioned, the main hydration product of CSA is ettringite, which precipitates together with amorphous Al(OH)3 until the available calcium sulfate is consumed after around 1 – 2 days of hydration. Afterwards, monosulfate is formed. However the microstructure of the CSA cement is denser than the Portland cement even after 16 hours of hydration [24]. The dense structure and acicular nature of the ettringite crystals aids in the increased bond strength development (Figure 14). Whereas, the hydration products of Portland cement form layers on the fibre surface of C-S-H gel and CH crystals; a minor amount of a phase of or near the composition of ettringite also forms during early hydration stages [25].

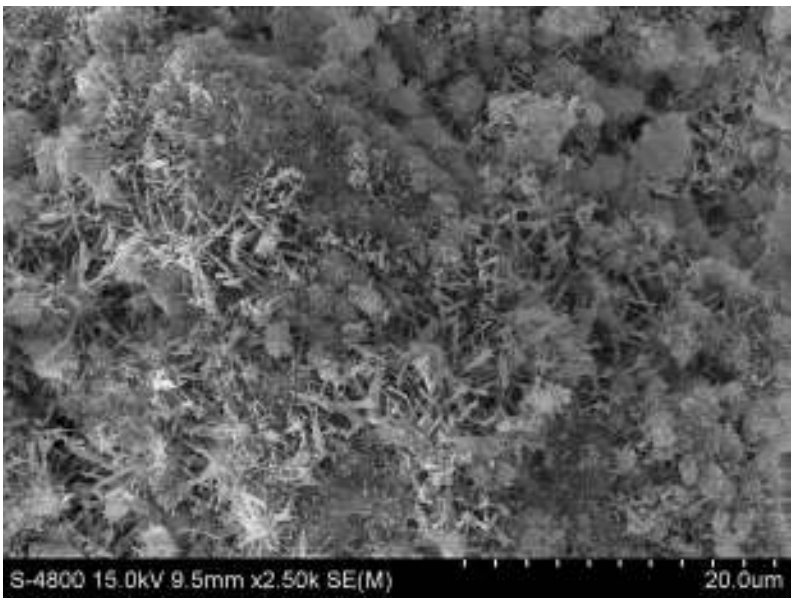

Figure 14 SEM image of the matrix morphology for the commercial CSAB cement (2500x magnification)

The copper-coated steel fibres obtained the highest overall bonding strength from 3 hours to 56 days of curing, as represented by the peak-load values in Figure 15; with similar trending energy consumption values (Figure 16). The polypropylene fibres exhibited an increasing peak load from 3 hours to 56 days with a maximum load of 15.5 N attained at 28 days of curing.

The PVA fibres achieved a maximum peak load of 5.5 N at 28 days of curing; and a maximum energy consumption of 8.19 mJ after only 6 hours of curing. The decrease in energy consumption values may be attributed to a decrease in ductility with increasing hydration of Klein's Compound to form ettringite. The rapid-setting nature of CSA cement allowed for the quantification of the fibre-matrix bond strength at 3 and 6 hours of curing.

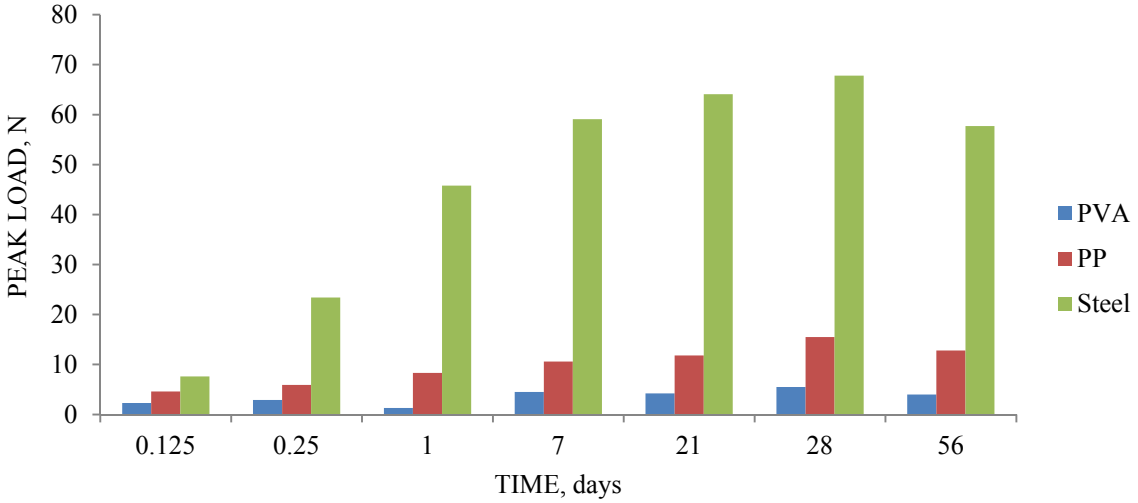

Figure 15 Comparison of peak load development over time between PVA, PP and steel fibres

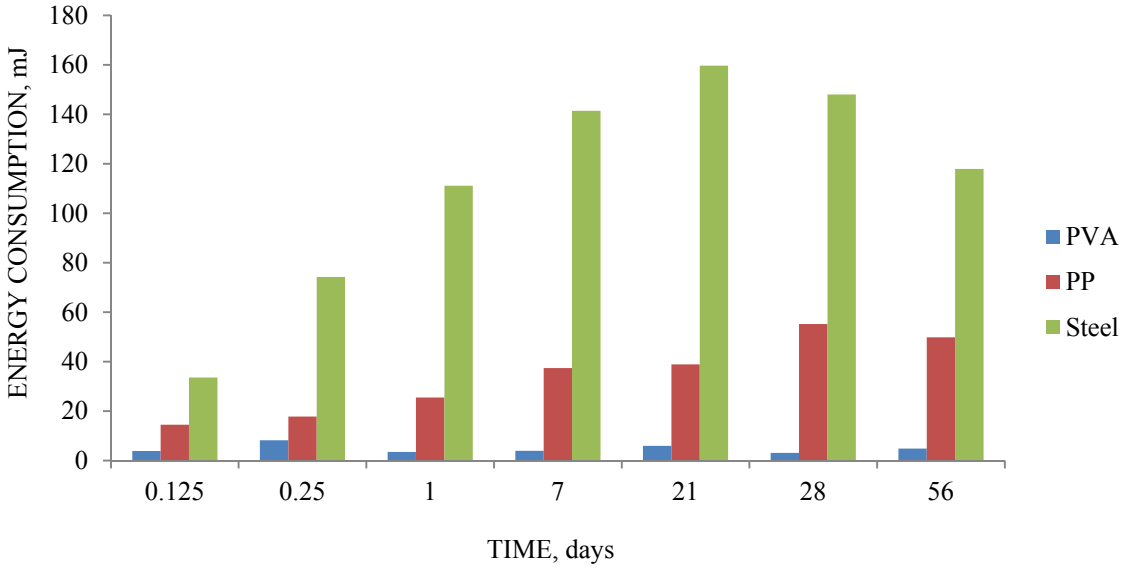

Figure 16 Comparison of energy consumption development over time between PVA, PP and steel fibres

The SEM images in Figure 17 provide a qualitative comparison of the fibre-matrix bond that occurs during hydration of the cement matrix. From left to right, the PVA fibre demonstrates some surface deformation due to the interfacial bonding with the CSA matrix; the PP fibre shows less deformation than the OPC and CAER CSAB cement with an increased percentage of the surface coated with hydrated phases from the matrix; the steel fibre demonstrated large areas of bonding with the CSA matrix.

In Figure 17C the boundary between the copper coating and the bare-steel fibre can be seen; the copper coating in the lower half of the image is completed covered with hydrated phases from the matrix.

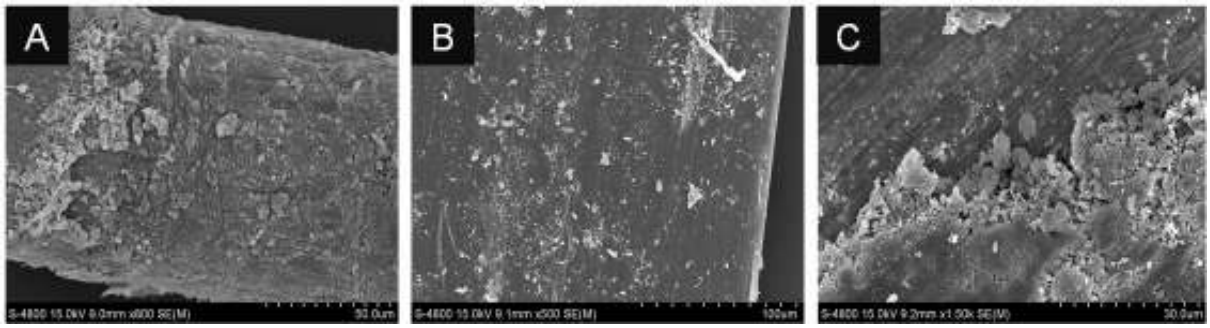

Figure 17 SEM images of fibres pulled from the Commercial CSAB matrix: (A) PVA (800x magnification); (B) PP (500x mag); (C) Steel (1500x mag)

CAER CSAB cement

The CAER CSAB cement is rich in Klein's compound, which in the presence of FGD-gypsum hydrates rapidly to form ettringite. The CAER CSAB cement differs from the commercially available CSA cement in that the ettringite crystals formed are longer and more slender; allowing for a tighter-interwoven network of crystals (Figure 18). This explains the increased bonding strengths seen in Figure 19 and Figure 20 as compared to those of the commercial CSAB cement in Figure 15 and Figure 16. The steel fibres exhibited higher peaked loads as compared to the PP and PVA fibres.

As previously mentioned, the increased load values may be attributed to the copper-coating and which has enhanced the bonding of the steel fibre with the cement matrix. The SEM images in Figure 21 demonstrate the increased fibre/matrix bond that can be visually noted. From left to right, the PVA fibre shows a high level of deformity when compared to its original form; the PP fibre shows a minor degree of deformity with voids and impressions filled with the hydrated phases of the matrix; the steel fibre was displayed greater than 90% coverage of matrix material bonded to the surface, or copper layer.

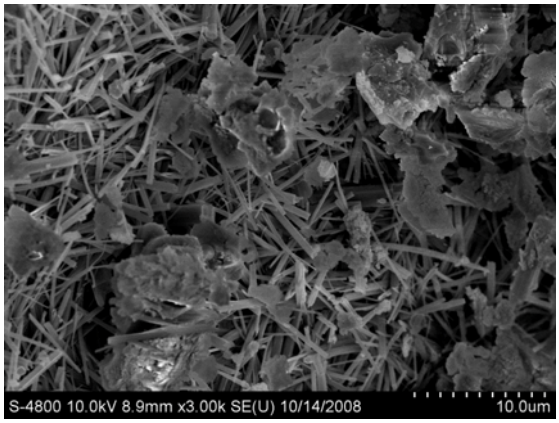

Figure 18 SEM image of the CAER CSAB cement demonstrating the long needle-like ettringite crystals (3000x magnification)

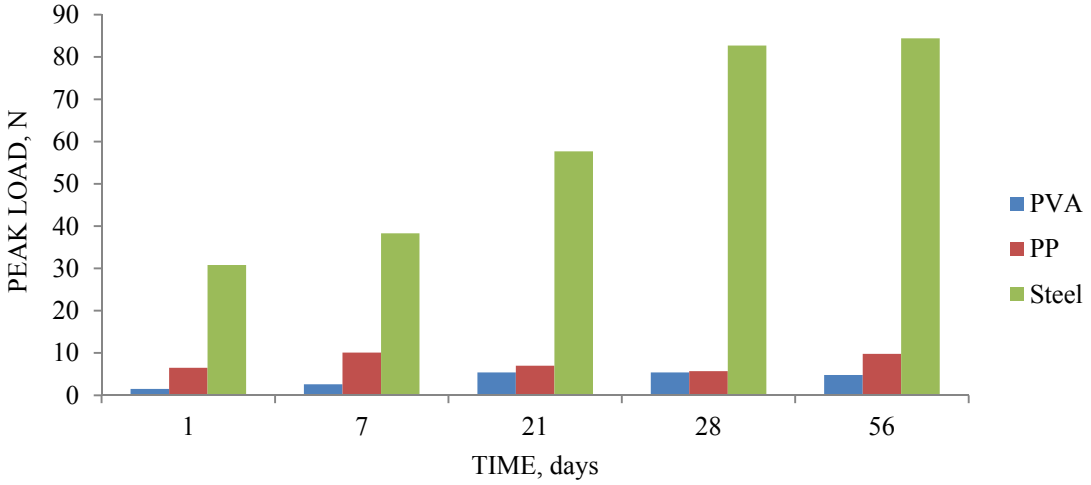

Figure 19 Comparison of peak load development, over time, between PVA, PE and steel fibres

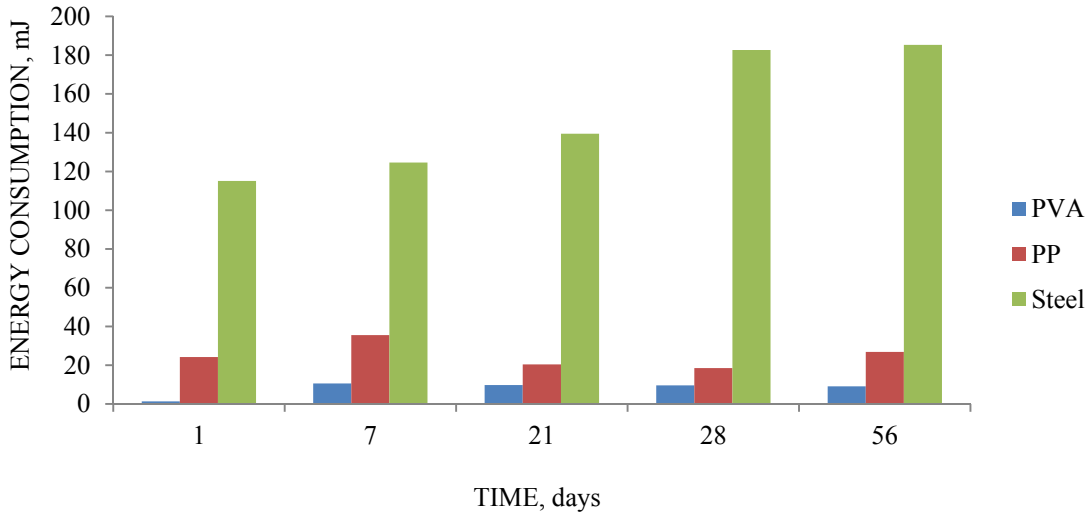

Figure 20 Comparison of energy consumption development over time between PVA, PE and steel fibres

Figure 21 SEM images of fibres pulled from the CAER CSAB matrix: (A) PVA (500x magnification); (B) PP (600x mag); (C) Steel (500x mag)

CONCLUSIONS

In this paper, the interfacial parameters of three fibre types and three different types of cement were examined. The interfacial parameters were analyzed by utilizing the single-fibre pullout test to quantify peak load and energy consumption; SEM analysis was used to qualitatively compare the physical bonding characteristics of the fibres and matrix.

An important factor contributing to the bond strength between fibre and matrix was the ability to transfer interfacial stress from fibre to matrix. The more rigid-dense structure provided by the ettringite crystal structure yielded higher peak loads and larger energy consumption (toughness) values. While the thin-fibrous structure of the CSH in the OPC matrix provided good bonding values though lacked the strength and dense-structure found with ettringite in the CSA matrixes. This allowed for large values for maximum peak loads but small values for toughness as the thin structure of the CSH phases were unable to resist the shear stresses from debonding.

The peak load exhibited by the copper-coated steel fibres in the OPC matrix yielded values nearly of the load obtained with the CSA matrix due to the more dense-acicular ettringite crystal formation along the interfacial boundary. However the energy consumption values were greater for the OPC matrix, this was due to the more porous, less rigid, nature of the CSH crystals which provided some ductility to the interfacial boundary between the fibre and matrix. The more ductile boundary provided a medium for the transfer of load stresses from the fibre to the matrix. The denser ettringite structure of the CSA matrix created a brittle region that fractured when the peak stress was attained and fibre pullout followed.

The peak load and energy consumption values for the copper-coated steel fibres demonstrated similar trending values. After 28 days the peak load was the highest for the CAER CSAB cement followed by the Commercial CSAB cement and then the OPC cement; this relationship remained the same for energy consumption. The PVA fibres differed after 28 days with the highest peak load was achieved with the Commercial CSAB and the CAER CSAB cement followed by the OPC cement. However the CAER CSAB cement had the highest energy consumption values, followed by the OPC cement and then the Commercial CSAB cement. The PP fibres attained the highest peak load values with the Commercial CSAB cement followed by the OPC cement and then the CAER CSAB cement. The energy consumption values showed the same relationship.

In summary, the CAER CSAB cement, fabricated from CCBs, demonstrated optimum bonding characteristics with both the copper-coated steel fibres and the PVA fibres; optimum define by maximum peak load and energy consumption values. However the PP fibres demonstrated optimum bonding with the Commercial CSAB cement.

ACKNOWLEDGMENTS

I would like to thank my advising committee for their support and guidance throughout my graduate career. Also I'd like to thank my wife Meghan and twin sons Elliott and Isaac for supporting me on my journey to reach for a major milestone in my life.

REFERENCES

1. NAAMAN, A.E., et al., Fiber Pullout and Bond Slip. I: Analytical Study. Journal of Structural Engineering, 1991. 117(9): p. 2769-2790.

2. LIN, Z. AND V.C. LI, Crack bridging in fiber reinforced cementitious composites with slip-hardening interfaces. Journal of the Mechanics and Physics of Solids, 1997. 45(5): p. 763-787.

3. BROWN, R., SHUKLA, A. AND NATARAJAN, K.R., Fiber Reinforcement of Concrete Structures, Technical Report No. URITC FY99-02, 2002, University of Rhode Island, Dept. of Chemical Engineering: Kingston, RI. p. 51.

4. KIM, J. AND MAI, Y., Engineered Interfaces in Fiber Reinforced Composites. 1998, New York: Elsevier. 401.

5. LI, V.C. AND STANG, H., Interface property characterization and strengthening mechanisms in fiber reinforced cement based composites. Advanced Cement Based Materials, 1997. 6(1): p. 1-20.

6. MEHTA, P.K. AND MONTEIRO, P.J.M., Concrete, Microstructure, Properties and Materials. 3rd ed. 2006: McGraw-Hill, USA. 659 p.

7. SHAH, S.P., Do Fibers Increase the Tensile Strength of Cement-Based Matrixes? American Concrete Institute Materials Journal, 1991. 88(6): p. 595-602.

8. ARJUNAN, P., SILSBEE, M.R. AND DELLA, M.R., Sulfoaluminate-belite cement from low-calcium fly ash and sulfur-rich and other industrial by-products. Cement and Concrete Research, 1999. 29(8): p. 1305-1311.

9. MARROCCOLI, M., et al., Early Hydration of Calcium Sulfoaluminate-Based Cements for Structural Applications, ed. Chun, et al. 2007, London: Taylor & Francis Group.

10. IKEDA, K. Cements along the join C_4A_3S-C_2S. in International Congress on the Chemistry of Cement. 1980.

11. MAJLING, J., et al., The influence of anhydrite activity upon the hydration of calcium sulphoaluminate cement clinker. Thermochimica Acta, 1985. 92: p. 349-352.

12. SAHU, S., et al., Hydration behaviour of sulphoaluminate belite cement in the presence op various calcium sulphates. Thermochimica Acta, 1991. 175(1): p. 45-52.

13. ZHENG, Z. AND FELDMAN, D., Synthetic fibre-reinforced concrete. Progress in Polymer Science, 1995. 20(2): p. 185-210.

14. NAJM, H., et al., Effects of poly(vinyl alcohol) on fiber cement interfaces. Part I: Bond stress-slip response. Advanced Cement Based Materials, 1994. 1(3): p. 115-121.

15. REDON, C., et al., Measuring and Modifying Interface Properties of PVA Fibers in ECC Matrix. Journal of Materials in Civil Engineering, 2001. 13(6): p. 399-406.

16. BETTERMAN, L.R., OUYANG, C. AND SHAH, S.P., Fiber-matrix interaction in microfiber-reinforced mortar. Advanced Cement Based Materials, 1995. 2(2): p. 53-61.

17. CHU, T.J., et al., Effects of poly(vinyl alcohol) on fiber cement interfaces. Part II: Microstructures. Advanced Cement Based Materials, 1994. 1(3): p. 122-130.

18. HERTZBERG, R.W., Deformation and Fracture Mechanics of Engineering Materials. 4th ed. 1996, Canada: John Wiley & Sons, Inc. 786.

19. Naebe, M., et al., Electrospun single-walled carbon nanotube/polyvinyl alcohol composite nanofibers: structure-property relationships. Nanotechnology, 2008. 19(30): p. 305702.

20. BIN, Y., et al., Morphology and mechanical and electrical properties of oriented PVA-VGCF and PVA-MWNT composites. Polymer, 2006. 47(4): p. 1308-1317.

21. CADEK, M., et al., Morphological and mechanical properties of carbon-nanotube-reinforced semicrystalline and amorphous polymer composites. Applied Physics Letters, 2002. 81(27): p. 5123-5125.

22. NEVILLE, A.M., Properties of Concrete. Fourth ed. 1995, Singapore: Pearson Education Ltd. 844.

23. RICHARDSON, I.G., The nature of C-S-H in hardened cements. Cement and Concrete Research, 1999. 29(8): p. 1131-1147.

24. WINNEFELD, F. AND LOTHENBACH, B., Hydration of calcium sulfoaluminate cements -- Experimental findings and thermodynamic modelling. Cement and Concrete Research, 2009. In Press, Corrected Proof.

25. TAYLOR, H.F.W., Cement Chemistry. 2nd ed. 1997, London: Thomas Telford.

The Effect of Titanium Dioxide on the Structure and Reactivity of Ferrite

T Duvallet[1], T L Robl[1], F P Glasser[2]
1 – University of Kentucky, USA
2 – University of Aberdeen, UK

Minor constituents can have a major impact on the structure and reactivity of Portland cement and Calcium Sulfoaluminate cement. An important example of this is the effect of titanium dioxide on the reactivity of the ferrite phase, the end member of which is brownmillerite. The effect of TiO_2 on ferrite reactivity was investigated by forming the pure end member from reagent grade materials and adding in TiO_2 at the dosages 0%, 0.5% 1.6% 2.6% and 3.6% by weight. The powders were mixed and pressed into pellets, preheated to 800 °C and then fired at 1350 °C for 30 minutes. The brownmillerite was milled for 1 hour and characterized by X-ray diffraction, energy-dispersive X-ray spectroscopy, isothermal calorimeter and thermogravimetric analysis. The addition of TiO_2 was expressed in the principle XRD peak with values of TiO_2 greater than 1.6% shifting it to higher d-spacing. For TiO_2 greater than 1.6% the hydration and subsequent set time was found to be retarded, from only a few minutes for the materials with no TiO_2 to approximately 5 to 6 hours. The addition of very low levels of TiO_2 (0.5%) appeared to slightly increase the set time of the brownmillerite over the pure end member. The rate of strength development of mortar cubes also varied significantly with the higher TiO_2 samples (i.e. 2.6 and 3.6%) having lower one-day strengths but much higher (by up to twice) at 7 and 28 days. It was demonstrated that the behavior of brownmillerite as a cementitious material was greatly affected by relatively small dosages of TiO_2 indicating the importance of even low levels of minor components in the Portland cement and Calcium Sulfoaluminate cement.

Tristana Duvallet, University of Kentucky, Center for Applied Energy Research, 2540 Research Park Drive, Lexington, Kentucky, 40511, USA.Ms. Duvallet is PhD Candidate in Materials Science and Engineering at the University of Kentucky,and received her Diploma of Engineer in Material Sciences from ESIREM, Dijon, France in 2008. She is currently investigating calcium aluminate cement systems.

Dr. Thomas L. Robl, University of Kentucky, Center for Applied Energy Research, 2540 Research Park Drive, Lexington, Kentucky, 40511, USA. Dr. Robl is an Associate Director of the Center for Applied Energy Research of the University of Kentucky. He is currently conducting research into the application of coal combustion and other industrial by products into low energy cement systems.

Professor Fred P. Glasser, Chemistry Department, University of Aberdeen, Aberdeen, UK. Dr. Glasser holds the position Professor Emeritus at Aberdeen University. He is currently active in investigations of CSA and other low energy cement systems. Professor Glasser is preeminent among the experts in cement chemistry.

Keywords: Brownmillerite, Ferrite, Reactivity, Titanium dioxide

INTRODUCTION

The use of industrial by-products in the fabrication of Portland cement and Calcium Sulfoaluminate cement contributes to their sustainability. Using waste materials reduces cost and can also reduce CO_2-emissions by lowering the amounts of limestone used in the raw mix. Examples of by-products can include red mud from bauxite processing, slag and coal combustion fly ash. [1, 2, 3, 4, 5] However minor elements as impurities in the by-products, and materials as well, can affect the chemical and physical properties of the cements and their performance. Several studies have been completed on the subject of incorporating impurities (alkali oxides, fluoride or transition metal oxide) into the cements [6].

This study focuses on the effect of titanium dioxide on the reactivity of the ferrite the end member of which is also called brownmillerite, nominally C_4AF. This is an important phase in Portland cement, as well as in calcium sulfoferroaluminate cement (CSFA). Other research on this topic include that of Miller [7] who found that titanium has insignificant effect on the manufacturing of the cement when titanium dioxide (TiO_2) is introduced at a low concentration levels. Kakali [8] found that the addition of titanium dioxide of 2% by weight in the raw materials of ordinary Portland cement does not show any significant increase in the rate of hydration. In fact, the addition of TiO_2 slightly retards the hydration process during the first 2 days. But after 28 days its effect on the hydration rate becomes negligible. Teoreanu [9] observed that the mechanical properties of cement, such as compressive strength, where TiO_2 was incorporated were better than without TiO_2. Titanium dioxide (around 1%) can also reduce the melting temperature of clinker by about 50-100°C [10, 12]. Teoreanu [9], Knofel [11, 12], Marinho [13] and Hornain [14], found that after cooling to ambient temperature, titanium dioxide is preferentially partitioned into the ferrite phase.

Marinho and Glasser [13] studied the effect of titanium dioxide in a concentration range from 1 to 10% on the crystal structure of the ferrite phase by XRD and electron diffraction. They regarded the structure as distorted perovskite and concluded that Fe^{3+} was substituted by Ti^{4+}, charge being balanced by incorporation of additional oxygen atoms. From 1 to 9 % of Ti contents, the C_4AF structure is disordered with respect to the random distribution of oxygen. But at higher Ti content, more than 9%, a different stacking arrangement appears, the formula of which is given as $Ca_5(Fe_{4-x}Al_x)TiO_{13}$.

The hydration of ferrite phase with addition of gypsum was studied by Collepardi [15], who determined that the hydration of the ferrite phase is retarded by gypsum which was attributed to ettringite coating unreacted C_4AF grains. They also observed the conversion of ettringite to monosulfate (AFm) following depletion of gypsum. Fukuhara [16] also observed the retardation of C_4AF hydration by the presence of gypsum. The most realistic hydration reaction was the following:

$$C_4AF + 4CaSO_4.2H_2O + \frac{35}{3}H_2O \rightarrow \frac{4}{3}C_3(A_{0.75}F_{0.25}).3CS.H_{31} + \frac{2}{3}FH_3$$

Emanuelson [17] and Meller [18] confirmed the previous results. Ferrite hydration without gypsum produces first AFm phases, $C_2(A,F)H_8$ and $C_4(A,F)H_{19}$, followed by hydrogarnet. With addition of gypsum, AFt is the first phase formed followed by AFm phases due to the conversion of ettringite to AFm due to lack of SO_4^{2-} ions and then followed by the hydrogarnet phase.

Our research is focused on the effect on TiO_2 at low levels, i.e. 0% to 4% on the properties of the ferrite phase. Hydration analyses, calorimetric analyses, TGA, EDS and XRD analyses and mortar strength testing were performed to determine the influence of the TiO_2 on the C_4AF.

EXPERIMENTS

The raw materials used are reagent grade hydrated lime $Ca(OH)_2$, aluminum hydroxide $Al(OH)_3$, iron oxide Fe_2O_3 and titanium dioxide TiO_2.

In order to study the effect of the titanium dioxide on C_4AF, different amounts of TiO_2 were introduced in the raw mix of C_4AF before firing. The formula used to make the solid solutions is: $C_4A_{1-x}F_{1-x}T_{4x}$ [13] (which may also be written as $Ca_4Al_{2-2x}Fe_{2-2x}Ti_{4x}O_{10+2x}$), with x equal to 0, 0.1, 0.3, 0.5 and 0.7 (Table 1). This stoichiometry results in samples that have 0% (BT-0), 0.52%, (BT-0.5), 1.57% (BT-1.6), 2.61% (BT-2.6), and 3.65% (BT-3.6) of TiO_2 by weight.

The raw mix was formed into pellets to provide more intimate contact among the oxide and improve reactivity. The pellets were then fired in an electric tube furnace, preheated at 800°C for 30 minutes and then fired at 1350°C for 30 minutes. The fired pellets were quickly removed from the furnace at the maximum temperature and rapidly air quenched. Other attempts have been made using firing temperatures below 1350°C, but were unfavourable as too much free lime persisted in the final product.

Table 1 Weight percentage of compounds into each sample

	BT-0 C_4AF	BT-0.5 $C_4A_{0.99}F_{0.99}T_{0.04}$	BT-1.5 $C_4A_{0.97}F_{0.97}T_{0.12}$	BT-2.6 $C_4A_{0.95}F_{0.95}T_{0.20}$	BT-3.6 $C_4A_{0.93}F_{0.93}T_{0.28}$
$Ca(OH)_2$	48.42	48.42	48.41	48.41	48.40
$Al(OH)_3$	25.49	25.23	24.72	24.20	23.69
Fe_2O_3	26.09	25.83	25.30	24.78	24.26
TiO_2	0	0.52	1.57	2.61	3.65

The samples were crushed and ground in a ball mill for one hour. Each sample of ferrite was then analysed for particle size, surface area and particle density as presented in Table 2. The skeletal density was measured by helium pycnometer AutoPycnometer 1320 (Micromeritics). Surface area was measured with the Blaine apparatus. The particle size distribution was determined by a particle size analyser Mastersizer 2000 (Malvern).

Calorimetric analyses were performed on a TAM Air calorimeter at 23°C for 300 hours. Hydration tests were conducted over a period of 28 days for BT-0, BT-0.5 and BT-3.6 only. The mix was composed of 10 g of total cement and 4.5 g of distilled water (water/cement ratio of 0.45). The mix was blended in a plastic vessel. The vessel containing a wet towel to keep a relative humidity of 100% was tightly closed. The hydration was stopped at different

times: 3-hour, 1-day, 4-day, 7-day and 28-day, by washing with acetone twice and drying for 1 hour in an oven at 50°C. The samples were stored in desiccators prior to TGA and XRD analyses.

Table 2 Density, surface area and particle size for each BT

	SKELETAL DENSITY BY HELIUM PYCNOMETER ($g.cm^{-3}$)	SURFACE AREA BLAINE ($m^2.kg^{-1}$)	PARTICLE SIZE BY LASER ANALYSIS d(0.5) (μm)
BT-0	3.852	255.77	10.733
BT-0.5	3.907	273.82	10.481
BT-1.5	3.878	201.89	8.739
BT-2.6	3.904	187.68	10.853
BT-3.6	3.858	191.66	10.176

The TGA instrument used is a TA Instruments SDT Q600 and the analyses were performed from 50 to 1000°C with a ramp of 20°C/min in a continuous flow of nitrogen gas.

XRD analyses were performed on each sample of the various batches after firing to verify the obtained phases. The XRD equipment is a Philips X'Pert diffractometer operating at 45 kV and 40 mA with Cu K-α radiation. The samples were ground by hand in a ceramic mortar and pestle, dry mounted in aluminum holders, and scanned from 8 to 60° - 2θ.

The samples with TiO_2 addition were subjected to EDS analysis to verify that the TiO_2 was fully integrated into the structure and that brownmillerite was the only phase. The composition determined from this analysis was close to the calculated compositional stoichiometry of the TiO_2 contaminated brownmillerite within the limits of accuracy of the method as shown in Table 3.

Table 3 Atomic percentages of titanium in BT-0.5, BT-1.6, BT-2.6 and BT-3.6 by EDS

At. % of Ti	BT-0.5	BT-1.5	BT-2.6	BT-3.6
Ideally	0.22	0.67	1.10	1.55
EDS	0.25	0.50	1.16	1.62

Mortar strength testing followed a modification of ASTM C109. The mix consisted of 500 g brownmillerite, 1375 g sand and 225 g DI water (water to cement ratio of 0.45). The very rapid set of BT-0 and BT-0.5 did not allow flow tests to be conducted. Also because of the rapid set and limitations on the materials available, smaller batches were employed, making one or two cubes at a time rather than the conventional 6. The cubes were tested in duplicate after 1, 7 and 28 days for compressive strength.

RESULTS AND DISCUSSIONS

Effect of Ti on the Brownmillerite Structure

All the samples were found to be generally similar by XRD. They all showed that the ferrite phase C_4AF to be the major component present. There are several "brownmillerites" listed in the ICDD files, 01-070-2765, with Mg and Si impurities, $Ca_2Al_{0.95}Fe_{0.95}Mg_{0.05}Si_{0.05}O_5$; was very close to that of BT-0, the end member material of this study. The Al-Fe brownmillerite without any mentioned impurities, 01-071-0667 was further to the left.

The addition of TiO_2 resulted in broadening and flattening of the X-ray diffraction peaks and also shifting them to lower 2 theta. Figure 1 presents the X-ray data from 33 to 35° 2Φ showing the range of this effect on the 141 reflection, for BT-0 and BT-3.6. It is found that the X-ray patterns for BT-0 and BT-0.5 are similar as are BT-2.6 and BT-3.6, with BT-1.6 intermediate between the two. The 141 peak also shifted to lower values with the shifts to larger d-spacing was the most pronounced for the BT-2.6 and BT-3.6 samples. The lowest level of TiO_2 addition, BT-0.5, had little effect. The addition of TiO_2 seems to cause a transformation of the lattice structure of the brownmillerite.

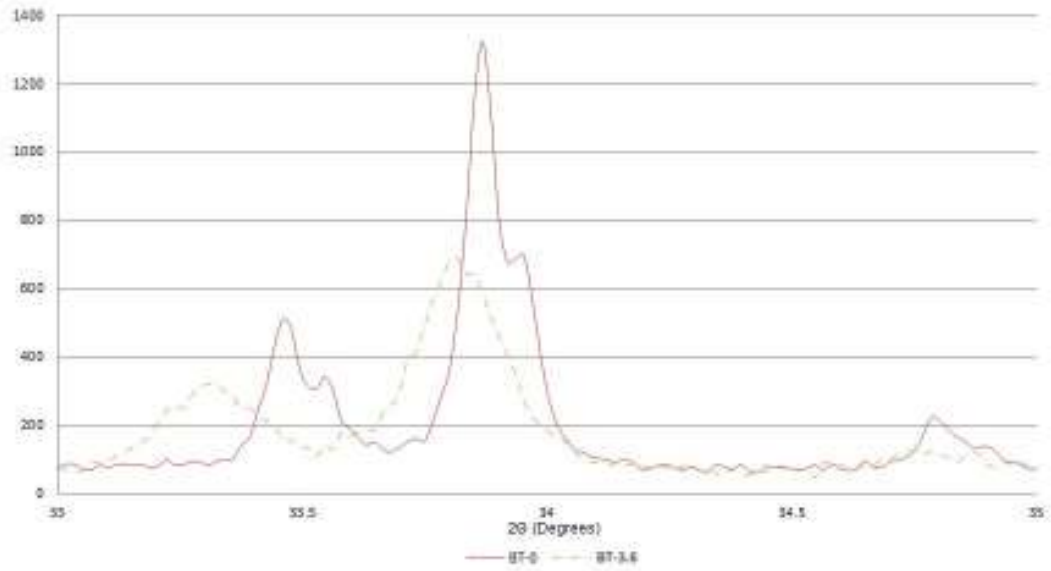

Figure 1 X-ray diffraction for 141 peak for BT-0 and BT-3.6

Effect of Ti on Brownmillerite Reactivity

Isothermal calorimeter was used to track the exothermic reaction of the brownmillerite to hydrogarnet hydration reaction over a period of 300 hours. The most significant differences among the samples were in the first few hours. The samples BT-0 and BT-0.5 present similar curves (Figures 2 and 3), except that BT-0.5 has a slightly faster hydration reaction than BT-0 by about 15 minutes. BT-1.6 shows the initiation of hydration peak at around 30 minutes. BT-2.6 and BT-3.6 have delayed hydration which initiates at about 5 hours.

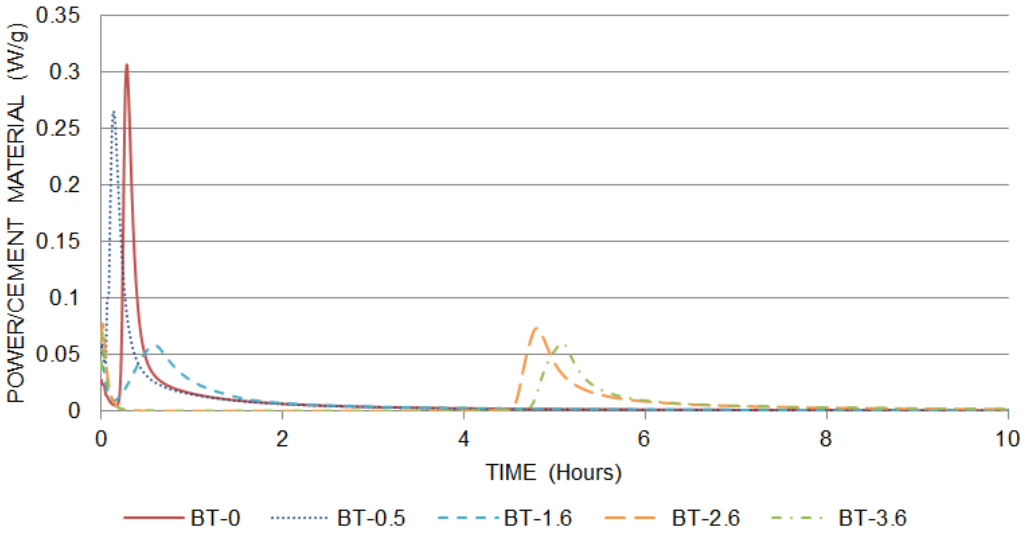

Figure 2 Hydration reaction followed by isothermal calorimeter - Power/Cement Material

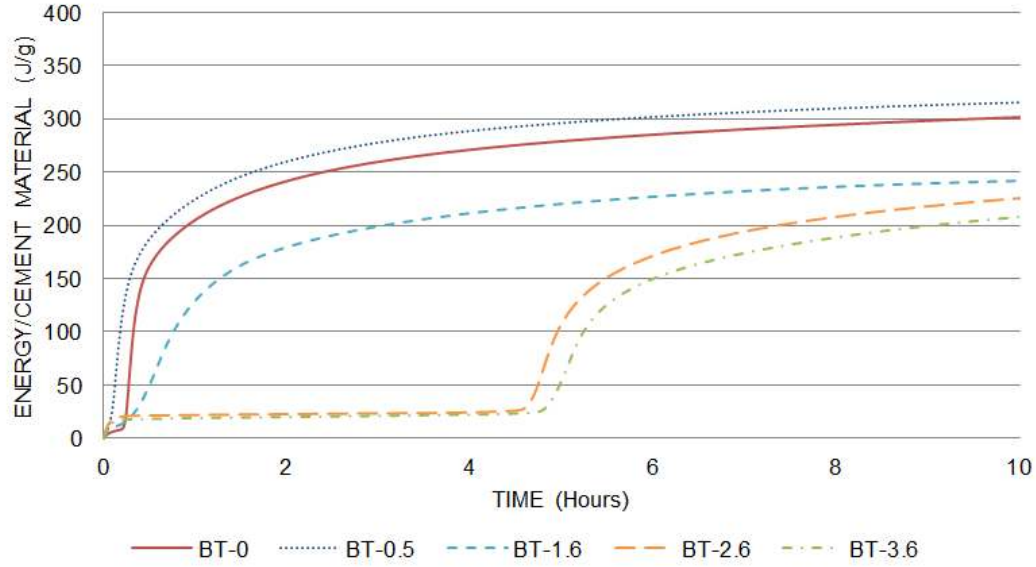

Figure 3 Hydration reaction followed by isothermal calorimeter - Energy/Cement Material

The peak of the first derivative of the isothermal energy curve is related very closely to set time. The end member BT-0 sets very quickly, within a few minutes of hydration. The addition of 0.5% of TiO_2 seems to accelerate the hydration reaction by a few minutes, while more than 1.5% of TiO_2 retards the hydration reaction by about 5 hours.

The delay in hydrogarnet formation was confirmed by both XRD and TGA. After 3 hours of hydration, BT-0 and BT-0.5 show both peaks of C_4AF and hydrogarnet and BT-3.6 shows only peaks for C_4AF. This is also evident in the TGA traces (Figure 4) where the weight loss from the hydrogarnet at 300 °C is missing from BT-3.6 at approximately 4 hours, but present in BT-0 and BT-0.5. After 1 day and until 28 day, all samples show X-ray reflections of C_4AF and hydrogarnet, but the diffraction peaks for the hydrogarnet are less sharp for BT-3.6 at day 1 (Figure 5). Also, at 28 days BT-3.6 shows traces of calcium monocarboaluminate ($3CaO.Al_2O_3.CaCO_3.11H_2O$ or $C_4A\acute{C}H_{11}$) (Figure 6).

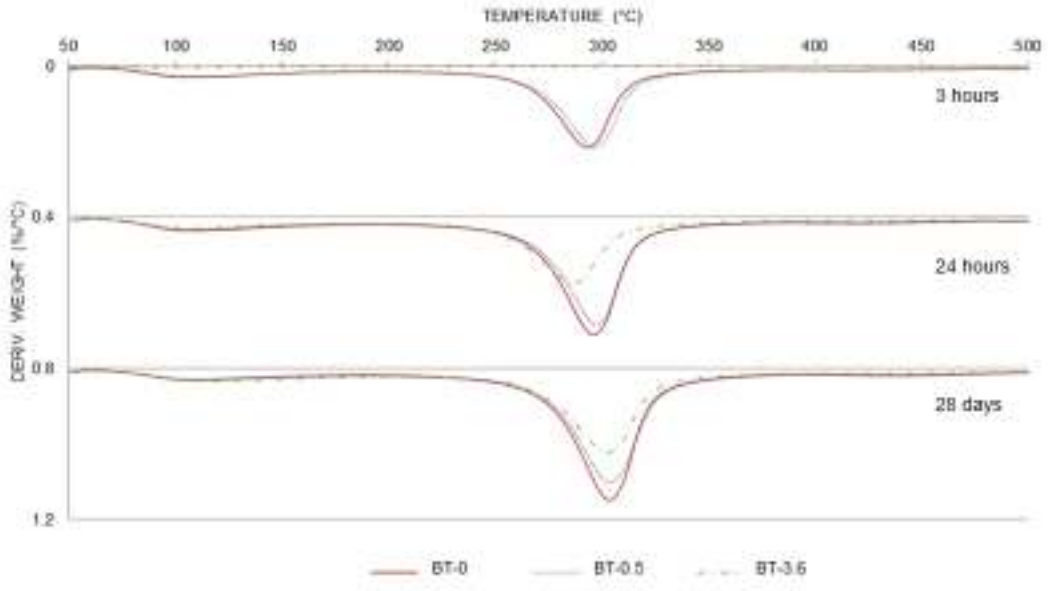

Figure 4 TGA results from hydration of BT-0, BT-0.5 and BT-3.6

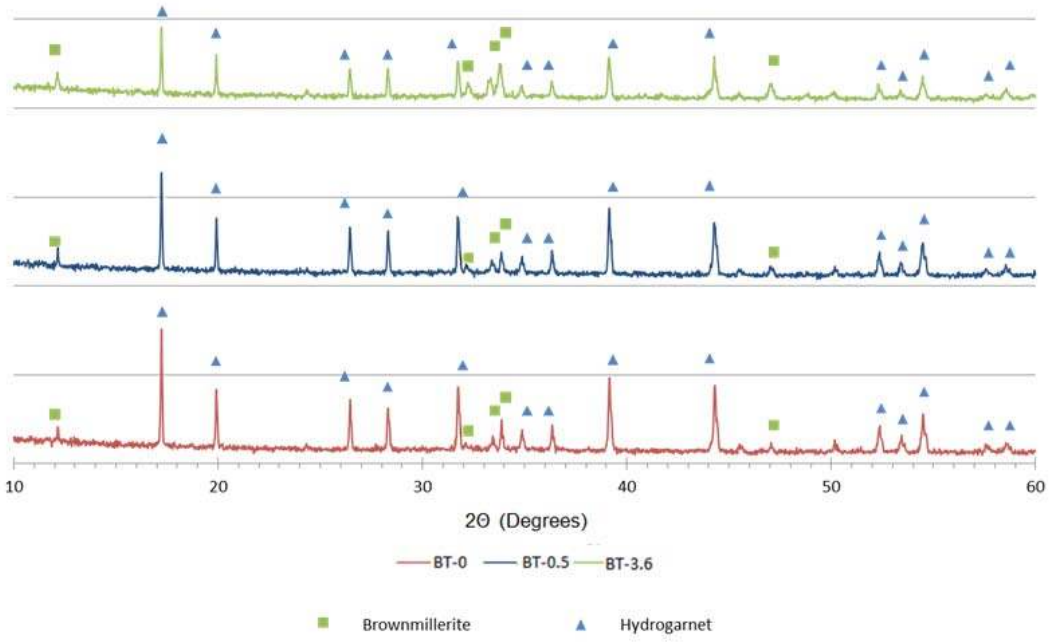

Figure 5 XRD results for BT-0, BT-0.5 and BT-3.6 after 1-day hydration at room temperature

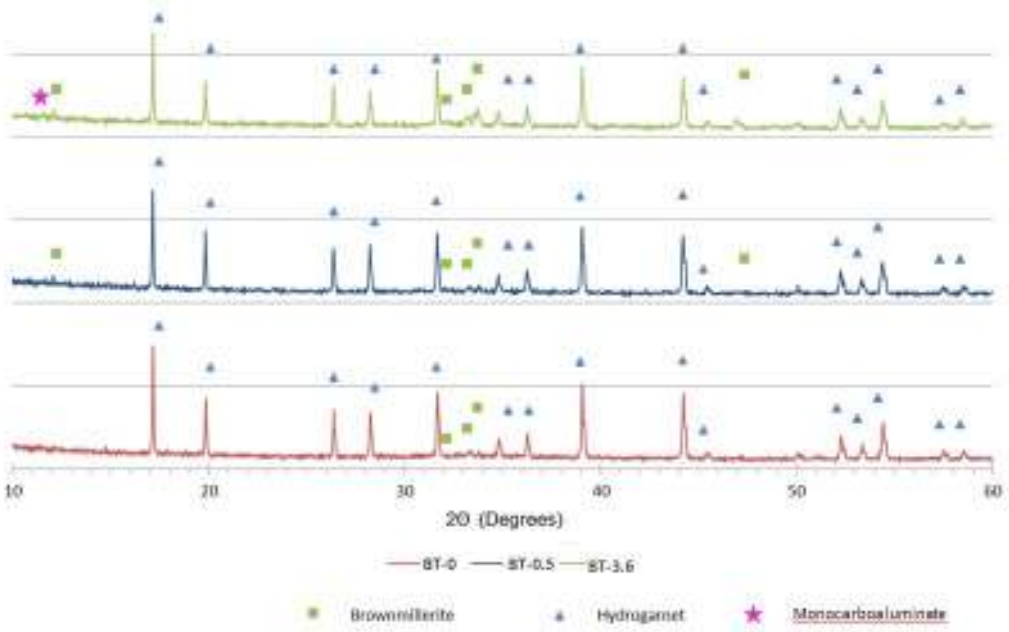

Figure 6 XRD results for BT-0, BT-0.5 and BT-3.6
after 28-day hydration at room temperature

The mortar strength data is presented in Figure 7 for 1, 7 and 28 days. The low TiO_2 samples, BT-0 and BT-0.5 were found to produce the highest mortar strengths at day 1, 7.6 and 7.8 MPa respectively versus 2.3, 5.5 and 4.9 MPa for BT-1.6, BT- 2.6 and BT-3.6. However by day 28 the high TiO_2 samples had reversed this trend, with BT-2.6 and BT-3.6 having almost doubled the strength of the pure end member.

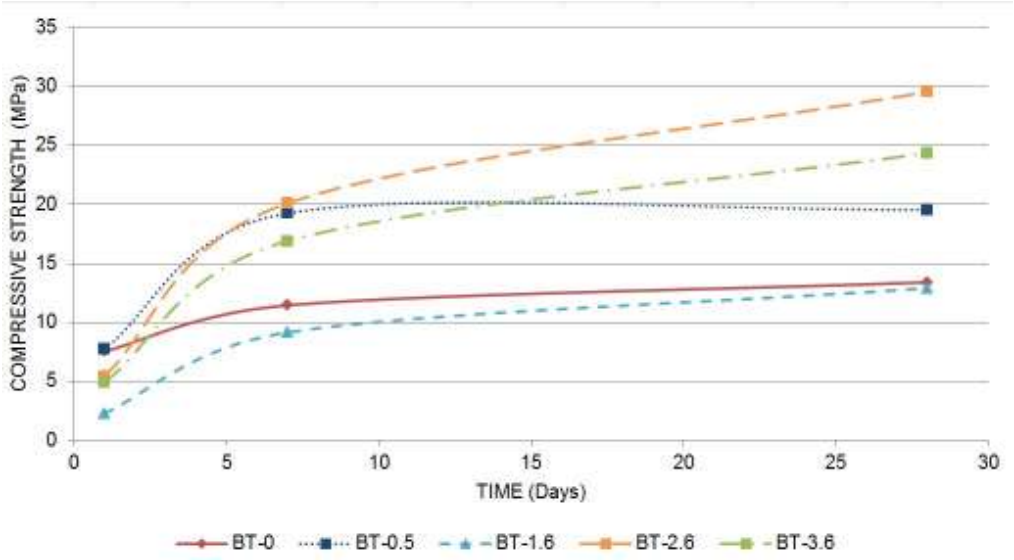

Figure 7: Compressive Strength of each BT after 1, 7 and 28 days of curing

DISCUSSION AND CONCLUSION

The effect of even small quantities of TiO_2 on the reactivity of brownmillerite was found to be measurable. At the lowest levels, 0.52%, little change was noted in the x-ray pattern but the sample actually hydrated faster, and produced ultimately higher strengths that the Ti-free material. Additions of TiO_2 at higher levels, 2.6% and 3.6%, produced notable shifts in the X-ray of the ferrite, and the 141 peak was shifted to higher d-spacing. Both of these materials behaved in a similar fashion and displayed with a delayed set time, but had the highest long term mortar strengths. The intermediate sample, with 1.6% TiO_2 was somewhat enigmatic having the lowest long term strength.

The reactivity reported here is an intrinsic reactivity: the sample is wet and sufficient solid dissolves to increase the pH to its saturation value, close to 12. Thus the reaction is self-initiating and self-accelerating as the pH increases. On the other hand, when ferrite occurs in a polyphase cement, pH change in the course of hydration is controlled in part by other phases and, moreover, the nature of the phases formed is affected by sulfate: the measured reaction is extrinsic. For present purposes, to demonstrate the role of Ti in reactivity, intrinsic reaction is the least complex to interpret. But for application to commercial or complex polyphase cements, it is also important to measure the extrinsic reaction. This is, however, more difficult to interpret as it is conditional, in the sense that numerical values depend on the exact proportions of the reactive components.

In summary, the structure and behavior of brownmillerite as a cementitious material was greatly affected by relatively small dosages of TiO_2, indicating the importance of even low levels of minor components in the Portland cement and in Calcium Sulfoaluminate cement.

ACKNOWLEDGEMENTS

The authors wish to thank Dr. Y. Zhou and Dr. K. Henke for their help during this project.

REFERENCES

1. DUVALLET, T, RATHBONE, R, HENKE, K, JEWELL, R. Low-Energy, Low CO_2-Emitting Cements Produced from Coal Combustion By-Products and Red Mud, World of Coal Ash Conference, 2009, Lexington, Kentucky.

2. ARJUNAN, P, SILSBEE, M R, ROY, D M. Sulfoaluminate-belite cement from low-calcium fly ash and sulfur-rich and other industrial by-products, Cement and Concrete Research, Vol. 29, 1999, pp 1305-1311.

3. BERNARDO, G, MARROCOLI, M, MONTAGNARO, F, VALENTI, G L. Use of Fluidized Bed Combustion Ash as Raw Feed in the Manufacture of Calcium Sulfoaluminate Cements, 8th CANMET/ACI International Conference on Fly Ash, Silica Fume, Slag, and Natural Pozzolans in Concrete, May 23-29, 2004, Las Vegas.

4. SINGH, M, UPADHAYAY, S N, PRASAD, P M. Preparation of iron rich cements using red mud, Cement and Concrete Research, Vol. 27, No. 7, 1997, pp 1037-1046.

5. GARTNER, E. Industrially interesting approaches to "Low-CO_2" cements, Cement and Concrete Research, 34, 2004, pp 1489-1498.

6. BHATTY, J I. Role of Minor Elements in Cement Manufacture and Use, Research and Development Bulletin RD109T, Portland Cement Association, Skokie, Illinois, U.S.A., 1995.

7. MILLER, F M. Minor elements in cement clinker, Cement Chemists Seminar, Paper No. 16, Portland Cemetn Association, Lincolnwood, Illinois, February 23-25, 1976, 24 pp.

8. KAKALI, G, TSIVILIS, S, TSIALTAS, A. Hydration of Ordinary Portland Cement made from raw mix containing transition element oxides, Cement and Concrete research, Vol. 28, No. 3, 1998, pp. 335-340.

9. TEOREANU, I, MUNTEAN, M, BALASOIU, H, Addition of titanium dioxide to Portland cement clinkers, Il Cemento, 4, 1987.

10. TIMASHEV, V V. The kinetics of clinker formation: the structure and composition of clinker and its phases, 7th International Congress of Chemistry of Cement, Paris, France, Vol. 1, 1980, pp I-3/1-I-3/20.

11. KNOFEL, D. The incorporation of TiO_2 into the phases of portland cement clinker, Zement Kalk Gips, Vol. 32, No.1, 1979, pp. 35-40.

12. KNOFEL, D. Modifying some properties of Portland cement clinker and Portland cement by means of TiO_2, ZKG, No.4/77, 1977, pp 191-196.

13. MARINHO, M B, GLASSER, F P. Polymorphism and phase changes in the ferrite phase of cements induced by titanium substitution, Cement and Concrete Research, Vol. 14, 1984, pp 360-368.

14. HORNAIN, H. The distribution of transition elements and their influences on some properties of clinker and cement, Revue de Materiaux de Construction et de Travaux Publics, No. 671-672, 1971, pp 203-218.

15. COLLEPARDI, M, MONOSI, S, MORICONI, G. Tetracalcium aluminoferrite hydration in the presence of lime and gypsum, Cement and Concrete Research, Vol. 9, 1979, pp 431-437.

16. FUKUHARA, M, GOTO, S, ASAGA, K, DAIMON, M, KONDO, R. Mechanisms and kinetics of C_4AF hydration with gypsum, Cement and Concrete Reasearch, Vol.11, 1981, pp 407-414.

17. EMANUELSON, A, HENDERSON, E, HANSEN, S. Hydration of ferrite Ca_2AlFeO_5 in the presence of sulphates and bases, Cement and Concrete Research, Vol. 26, No. 11, 1996, pp 1689-1694.

18. MELLER, N, HALL, C, JUPE, A C, COLSTON, S L, JACQUES, S D M, BARNES, P, PHIPPS, J. The paste hydration of Brownmillerite with and without gypsum: a time resolved synchrotron diffraction study at 30, 70, 100 and 150°C, Journal of Materials Chemistry, 14, 2004, pp 428 – 435.

Sustainable Low Carbon Foamed Concrete

K Ozlutas, A Yerramala, K S Rao, M R Jones
University of Dundee, UK

Universally increased concern for sustainability, reduced carbon dioxide emissions and responsible use of resources has made governments and authorities upgrade related standards and regulations. There is no doubt, the sustainability strategies agreed and the regulations set by the authorities have a vital effect on restructuring construction industry practices. Being the most widely used construction material and therefore the most resource demanding material, concrete needs to be designed and produced responsibly. So the concrete industry has shown an 18% reduction in CO_2 emissions through the use of recycled materials and alternative fuels compared to 1990 baselines only until 2010. As the rest of the concrete industry, foamed concrete also contributes to sustainable construction effectively. Research has shown that recycled and secondary aggregate (RSA) materials can effectively replace primary aggregates or high carbon materials in foamed concrete either fully or partially, whilst maintaining the performance properties. Despite a number of risky factors such as high heterogeneity and water absorption capacity of the RSA materials used in foamed concrete, the key advantage arising from the use of these materials is their 0-3 mm particle sizes, which is not a suitable range for use in normal weight concrete. Furthermore, the study concluded that, foamed concrete can easily be recycled and used in the production of new foamed concrete.

Kezban Ozlutas is a PhD student University of Dundee.

Amarnath Yerramala is a former PhD student in University of Dundee.

Kharidu Srinivasa Rao is a former PhD student in University of Dundee.

M Roderick Jones is a Professor of Civil Engineering in University of Dundee.

Keywords: Embodied carbon dioxide, Foamed concrete, RSA materials, Sustainability

INTRODUCTION

Universally increased concern for sustainability, reduced carbon dioxide emissions and responsible use of resources has made governments and authorities upgrade related standards and regulations. Like many other industries, construction industry, one of the largest users of resources, has shown ambitious progress with an increasing demand of both public and private sectors to improve their sustainable construction skills and practices. There is no doubt, the sustainability strategies agreed and the regulations set by the authorities have a vital effect on restructuring the construction industry's practices.

As recently stated in the European Commission Construction Products Regulation, construction works need to be designed, built and demolished whilst maintaining sustainable use of natural resources. Accordingly, construction works need to be durable, the raw and secondary materials used need to be environmentally compatible and the materials and demolition wastes of construction works need to be recyclable [2].

Being the most widely used construction material and therefore the most resource demanding material, concrete needs to be designed and produced responsibly. It was reported that compared to 1990 baseline levels, UK concrete industry has shown an 18% reduction in CO_2 emissions through the use of recycled materials and alternative fuels and will exceed the target set in the UK Government Sustainable Construction Strategy for 2012. However, it should be emphasized that, the concrete industry is not only responsible for the production of low carbon concrete using responsibly sourced materials, but also for the operational and end-of-life performance of concrete. This is vital in order to minimise the CO_2 emissions, and maximize the energy efficiency of the built environment as well as minimising the waste formation [8].

Similar to the actions practised for traditional concrete products, foamed concrete is also designed, produced and specified with performance properties such that, it contributes to sustainable construction and reductions in CO_2 emissions during its production, as well as its operational and end-of-life performances.

Given its unique characteristics, foamed concrete naturally contributes to sustainable construction and reduction in CO_2 emissions. Its high air content leads to a reduction in constituent materials, flexibility in design allows for production of lower density foamed concretes further reducing the material requirement and even an elimination of the fine aggregate content. Moreover, partial or full replacement of constituent materials with recycled and secondary aggregate (RSA) materials contributes to responsible material sourcing as well as waste management. Performance properties of foamed concrete such as excellent thermal insulation and good durability [3, 4] provide additional contributions to sustainability during its operational life. Finally, when it comes to the end of its life, the potential for recycling foamed concrete minimises the demolition wastes without requiring high energy inputs for processing, given its low bonding energy [5].

Use of RSA Materials and the Effects on the Performance of Foamed Concrete

Primary aggregates, one of the main constituents of concrete, has a considerably high negative impact on the environment, therefore, minimising the use of primary aggregates by substituting them with recycled and secondary aggregates is vital [9]. Forming 28% of the UK aggregates market in 2010, recycled and secondary materials have increased their

popularity [10]. A wide range of RSA materials exist which can be effectively used in normal weight concrete to replace primary aggregates. However, the silt/sand sized RSA materials are problematic due to their high water absorption and particle shapes, hence they are not suitable for using in normal weight concrete [6, 11].

Increased use of recycled and secondary aggregates that are either wastes or by-products of various processes, has also brought a new aspect to foamed concrete production improving its sustainability. According to a recent study conducted in University of Dundee [6,12], RSA materials can successfully replace primary aggregates in foamed concrete either partially or fully. Unlike normal weight concrete, RSA materials used in foamed concrete are in the range of silt/sand aggregate size, which have mean particle sizes of 0-3 mm (see Figure 1).

Figure 1 Range of RSA grades

Considering the limitations when specifying RSA materials for the production of foamed concrete, it should be emphasized that the heterogeneity of the RSA materials needs to be analysed carefully [6]. Additionally, it is also important to consider the transportation distance of the RSA materials.

Incorporation of RSA materials in concrete leads to reduced eCO_2 levels of up to 15% compared to primary aggregates if the site of origin and use is same. However, if the transportation distance of RSA materials to site of use is over 15 km, eCO_2 levels are up to 14% higher than in the case where primary aggregates are used [7]. Therefore, special care should be taken regarding the material properties and heterogeneity as well as the transportation distance before specifying the use of RSA materials.

In addition to its contribution to sustainable and reduced carbon construction through its production and service life performance, foamed concrete maintains its manner even at the end of its service life, producing no waste. When it reaches its end-of-life, foamed concrete can easily be removed and recycled without requiring high energy inputs for excavating and processing [5, 12].

EXPERIMENTAL DETAILS

First Approach: Incorporation of RSA Materials in Foamed Concrete

Foamed concretes with plastic densities ranging from 600 to 1600 kg/m³ were covered, with the main focus on 1000 kg/m³ density. Cement contents of 300 and 400 kg/m³ were used for all the mixes except from 1600 kg/m³ density mix, for which only 400 kg/m³ cement content was used. Water/cement ratio of 0.5 was used for all mixes except from 1000 kg/m³ density CR mixes. Natural sand was replaced with RSA materials at rates of 50 and 100 %. CFA and crumb rubber were not applicable for 600 kg/m³ density mix. Foamed concrete produced with natural sand and Portland cement was used as reference.

A range of RSA materials sourced from across the UK was tested for particle size distribution, density and water absorption. The effects of RSA materials on the performance of foamed concrete were evaluated in terms of consistence, seal-cured cube strength, durability and thermal conductivity. Each of RSA materials used to replace primary aggregates in foamed concrete and their mean particle sizes are outlined in Table 1. Table 2 shows the physical properties of the materials used.

Table 1 Types, sources and mean particle sizes of RSA materials [6]

TYPE	DENOTED	MEAN PARTICLE SIZE, mm	SOURCE
Demolition fines	DF	0.8	Construction demolition and excavation waste
Incinerator bottom ash	IBA	2.5	Municipal solid waste incineration
Glass fines	GF	0.5	Building flat glasses
Foundry sand	FS	0.18	Sand used in the metal casting industry
China Clay sand	CCS	0.6	Fines from China Clay waste
Conditioned fly ash	CFA	0.02	Coal combustion (water addition for conditioning)
Crumb rubber	CR	1.0	Shredded truck tyres

Table 2 Physical properties of RSA materials used in foamed concrete [6]

	NATURAL SAND	DF	IBA	GF	FS	CCS	CFA	CR
Particle density in SSD state, g/cm³	2.63	2.18	1.95	2.36	2.08	2.61	2.04	1.07
Water absorption, % by mass	0.50	8.83	10.97	0.01	6.03	0.58	†	0.75

† Not applicable

Recycling potential of foamed concrete

Recycling potential of foamed concrete was assessed using RSA foamed concrete demolition wastes. Demolished foamed concrete was broken with a hammer and crushed in a ball mill to the size of material 95-100% passing through the 4.75 mm sieve.

The tests were carried out with 1000 kg/m³ density mixes in order to assess the use of recycled foamed concrete in the production of new foamed concrete. Evaluated properties of foamed concrete produced with recycled foamed concrete aggregates were plastic density, slump spread and seal-cured cube strength [12].

Second Approach: Embodied Carbon Dioxide (eCO_2)

As a second approach, embodied CO_2 of foamed concretes arising from the production were calculated using the eCO_2 figures for the constituent materials given in [7] and the mix design method given in [4]. ECO_2 arising from the transportation of materials was not included in the calculations. Foamed concretes produced with densities ranging from 200 to 1600 kg/m³, 300 kg/m³ cement content and water/cement ratio of 0.5 were evaluated. ECO_2 calculations were performed on both 100% Portland cement and 70% Portland cement, 30% coarse fly ash (conforming to BS EN 12620 [1]) mixes.

RESULTS AND DISCUSSIONS

Incorporation of RSA Materials in Foamed Concrete

- Flow characteristics of RSA foamed concretes were comparable with sand foamed concrete except for foamed concrete containing 100% CR and 300 kg/m^3 cement content, as a result of the low particle density of crumb rubber. Above 1000 kg/m^3, slump flow was reduced. This is thought to occur as a result of the reduced foam/paste phase offsetting the effect of increased self-weight (see Figure 2).

- Cube strengths of RSA foamed concretes were similar to sand foamed concretes. The material density of RSA materials is an important factor affecting strength. Given RSA materials with low density and water absorption resulted in higher strengths at all ages compared to the high density and water absorption materials.

- Although variations occur with changing RSA type and percent level replacement, drying shrinkage strain of RSA foamed concretes were generally higher. Although it is difficult to compare, RSA foamed concretes showed similar resistance to sulfate attack. Results for drying shrinkage and resistance to sulfate attack suggested further work is required.

- In terms of indicative thermal conductivity, RSA foamed concretes performed similar to sand foamed concrete, suggesting that thermal conductivity is more dependent upon the density of foamed concrete Thermal conductivities obtained for the range of foamed concrete densities tested were found to be between 0.1 and 0.7 W/mK (see Figure 3).

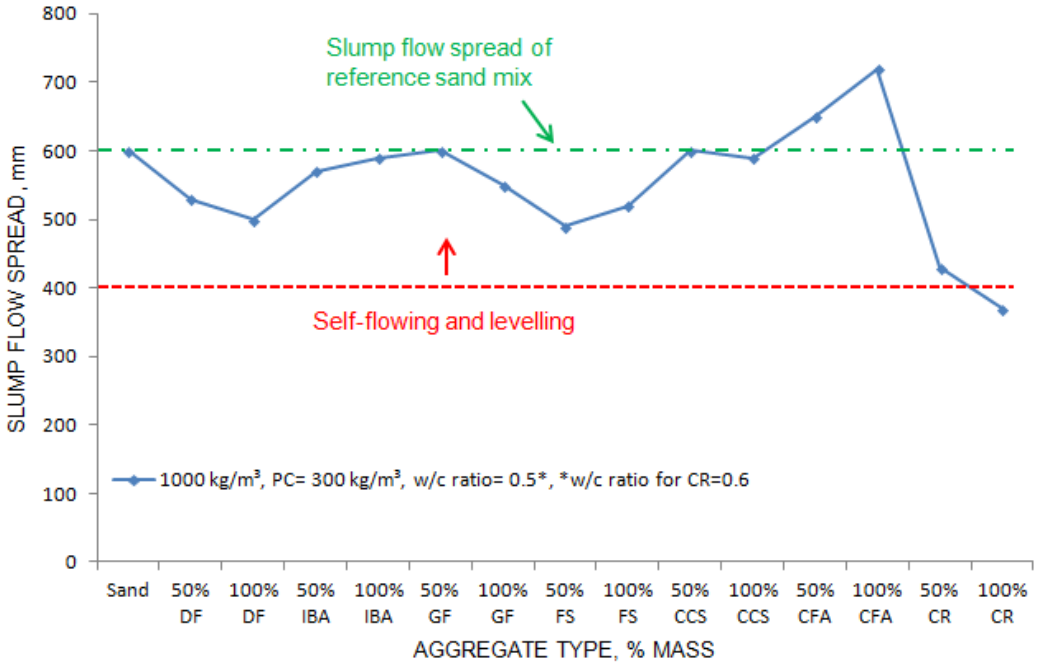

Figure 2 Relationship between aggregate type and slump flow [6]

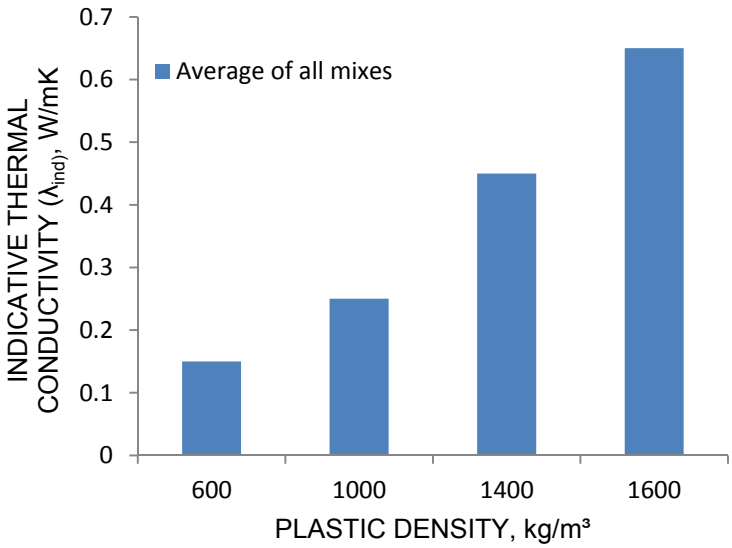

Figure 3 Effect of plastic density on indicative thermal conductivity of foamed concrete [6]

Recycling Potential of Foamed Concrete

- Increased number of crushing cycles improved the performance properties of foamed concrete produced with recycled foamed concrete aggregates (see Table 3).

- Possibly, the improved consistence resulted from the additional water added to cover the high water absorption capacities of the recycled foamed concrete aggregates. At the time when the consistence was measured the additional water may not have been fully absorbed, resulting in higher consistence.

- It is thought, the increased strengths may have resulted from the hydration of un-hydrated cement particles existing in the recycled foamed concrete aggregates.

Table 3 Effect of the number of recycles on the performance of foamed concrete [5,12]

NUMBER OF CRUSH/RECYCLE	FOAMED CONCRETE PROPERTIES			
	Plastic density (kg/m^3)	Slump spread (mm)	Cube strength (MPa) 7-days	28-days
0	1035	520	0.5	0.6
1	985	700	0.6	1.3
2	1020	700	1.1	1.7
3	1010	700	1.5	2.9
4	990	710	1.6	3.2
5	1015	705	1.7	3.5
6	1030	710	1.7	3.9

Embodied carbon dioxide (eCO_2)

- Partial replacement of PC with 30% FA reduced the eCO_2 by approximately 30% (see Figure 4).

- Designed plastic density, therefore, the cement content is the governing factor for the eCO_2. Reducing the density from 1600 to 200 kg/m^3 reduced the eCO_2 by around 57% which is 160 kg of CO_2 per 1 m^3 of foamed concrete (see Figure 4).

- Including the eCO_2 arising from the transportation of the materials may greatly change these eCO_2 levels calculated.

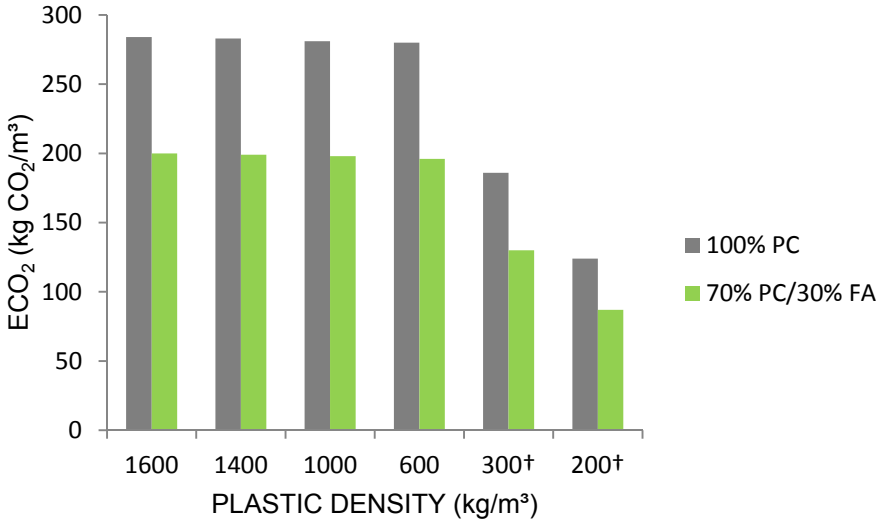

† Cement contents are 200 and 133 kg/m³ respectively, no aggregates used

Figure 4 Effect of partial replacement of PC with fly ash on eCO_2 of foamed concrete

CONCLUSIONS

- RSA materials can effectively be used in foamed concrete without adversely affecting the performance properties.
- The properties of RSA materials have a significant effect on the performance of foamed concrete. Therefore, careful assessment of material properties is vital.
- Similar to the reference foamed concrete, RSA foamed concretes were found to increase the energy efficiency of the built environment, possessing very good thermal insulation properties. Therefore, it is concluded that thermal conductivity is more dependent on the plastic density of foamed concrete.
- Foamed concrete demolitions can easily be processed and recycled to be used as recycled aggregates, resulting in zero waste at the end of its life cycle.
- Through careful specification of foamed concrete, reductions up to 57% in eCO_2 can be achieved per 1 m^3 of foamed concrete.
- Calculated eCO_2 figures suggested that, by specifying low density foamed concretes, where applicable, eCO_2 can be reduced significantly.

REFERENCES

1. BSI, BS EN 12620: Aggregates for concrete. BSI, London, UK, 2002.

2. HARRISON T, JONES R, DYER T, HALLIDAY J, A tool for measuring resource sustainability. University of Dundee, Scotland, 2012.

3. JONES M R, AND GIANNAKOU A, Thermally insulating foundations and ground slabs using highly-foamed concrete. ASTM Special Technical Publication 2004, pp.100-112.

4. JONES M R, AND MCCARTHY A, Preliminary views on the potential of foamed concrete as a structural material. Magazine of Concrete Research, 2005, 57(1), pp. 21-31.

5. JONES M R, ANSELL T, ALDRIDGE D, Foamed concrete for sustainable construction. Concrete, 43(5), pp. 16-18, 2009.

6. JONES M R, ZHENG L, YERRAMALA A AND RAO K S, Use of recycled and secondary aggregates in foamed concretes. Magazine of Concrete Research, ICE, 2012.

7. THE CONCRETE CENTRE, Specifying sustainable concrete. Mineral Products Association, 2011.

8. THE CONCRETE CENTRE, This is Sustainability. Mineral Products Association, 2011.

9. WRAP (Waste and Resources Action Programme), The sustainable use of resources for the production of aggregates in England. The Waste and Resources Action Programme, Oxon, UK, 2006.

10. WRAP (Waste and Resources Action Programme), Business Plan 2011-2015. WRAP, 2011.

11. RAO, K S, Development of concrete materials with no or minimal primary aggregate content. Degree of Doctor of Philosophy Thesis, University of Dundee, Scotland, 2008.

12. YERRAMALA A, Development and characteristics of foamed concrete containing fine recycled and secondary aggregate. Degree of Doctor of Philosophy Thesis, University of Dundee, Scotland, 2008.

Secondary Aluminas - A Sustainable, Low Cost Source of Alumina for Clinker Production

H Epstein
Independent Consultant / RVA, France

Portland clinker contains calcium aluminate minerals such as C_3A and C_4AF. Alumina is a crucial ingredient of cement raw materials to form these minerals when burning the cement clinker. RVA, a French chemical reprocessing company, produces a high alumina material from the recycling of aluminium salt slags. These slags arise during melting operations from secondary aluminium refining operations. The slag is a hazardous waste the landfilling of which is prohibited in Europe. Plants such as RVA receive the slag from aluminium refiners and recover useful products from it. One of RVA's outputs is the alumina material, generically referred to as a secondary alumina but known more widely under its trade name, Valoxy. As a result of its chemical, mineral and physical properties, Valoxy has proven to be an effective alumina source in cement production. Potential benefits to the cement producer include: improved burnability of the clinker; improved sintering; reduced residence time; and improved lime saturation factor and silica ratios. Valoxy is sustainable since it derives from an industrial process and not from virgin ore. It also offers potential savings in operating costs through reduced fuel consumption and lower communition energy. Recognising the technical, economic and environmental benefits, many of Europe's leading cement producers have incorporated Valoxy into their kiln feed.

Howard Epstein graduated with a degree in chemistry from the University of Manchester, UK and then went on to complete an MBA at the London Business School. He began his professional career as an applications technologist for ICI Organics before being appointed European marketing manager with a subsidiary of Sigma Chemicals, St. Louis. In 1994 Howard joined Bernhard Metals, at that time the leading secondary aluminium smelter in the UK. He was subsequently appointed Managing Director of Bernhard Metals Group of which RVA was an associate company. Since 2006 he has been working independently as a consultant to the chemical and related industries. This work includes a long-standing consultancy relationship with RVA.

Keywords: Alumina, Cement, Clinker, Minerals, Recycling

INTRODUCTION

In recent years non-energy raw material markets have seen major shifts in supply and demand patterns combined with short-term shocks. This commercial environment motivated the EU to launch a Raw Material Strategy ensuring the continued availability of essential inputs for European industry [1].

The present situation has highlighted the need for "home-grown" alternatives to globally traded minerals. In particular, recycling as a source of value-added secondary materials, is becoming increasingly important. RVA, a company in north eastern France, produces three secondary material streams, one metallic and two mineral–based. One of the outputs is a secondary alumina known as Valoxy. Valoxy is well established as a low cost, sustainable source of alumina for the cement industry. Using Valoxy as the alumina source for clinker formation can offer process benefits to the cement producer as well as reducing raw material and operating costs. Furthermore, since Valoxy is derived from an established recycling process, price and availability are predictable - a sharp contrast to the vagaries of virgin material extracted from nature.

AN ESSENTIAL ENVIRONMENTAL SERVICE

RVA provides a critical environmental service to the aluminium smelters of Western Europe. In the aluminium refining process, scrap is melted in rotary or reverbatory furnaces under a bath of molten salt which floats on the metal surface. The salt is typically a eutectic or near-eutectic mixture of sodium and potassium chlorides containing low levels of fluorides (cryolite). Molten metallic aluminium and its salt cover are successively tapped from the rotary drum surface. The last salt mix tapped from the furnace contains residual aluminium metal (around 5%) and various metal oxides, mainly aluminium oxide. This mixture solidifies in pans to become what is termed "salt slag."

The molten salt layer performs two main functions:

1. Salt coats the metallic aluminium in the melt phase hence minimizing oxidation losses.
2. Fluoride in the salt facilitates break-down of prior oxide layers on the surface of the scrap and thence promotes improved separation between the aluminium and non-metallic contaminants.

At the end of the melt cycle the salt layer is tapped off and, on cooling, solidifies into a salt slag. This salt slag is a hazardous waste which must be disposed of under controlled conditions. Historically, in Europe, aluminium salt slag was landfilled. More recently, a combination of tighter environmental regulation and high landfill costs has terminated this practice. Instead, aluminium salt slag is recycled in dedicated plants such as RVA.

Reprocessing is recognised across the EU as the best practicable environmental option for salt slags. By contrast, the United States has yet unequivocally to mandate the processing salt slags. As a consequence landfilling of salt slags is still widespread.

The interesting feature from a European perspective is that, with appropriate re-processing, salt slag is actually a source of essential raw materials. Thus, RVA is playing its part to mitigate the supply pressures worrying the EU.

FROM WASTE TO VALUABLE RAW MATERIALS

Three material streams are reclaimed from salt slag in the RVA process.

- Aluminium oxide-based material known as Valoxy. Valoxy comprises around 70% alumina by weight and is offered as an effective, sustainable, low cost source of alumina for cement clinker production.
- Aluminium metal in the form of granules. This is returned to the refiners where it is melted as part of a scrap mix.
- A salt mixture comprising NaCl, KCl and CaF_2. This material is also returned to the refiners for re-use as the salt layer in the aluminium melting cycle.

All three streams are therefore returned to productive use in a double loop recycling process (Figure 1).

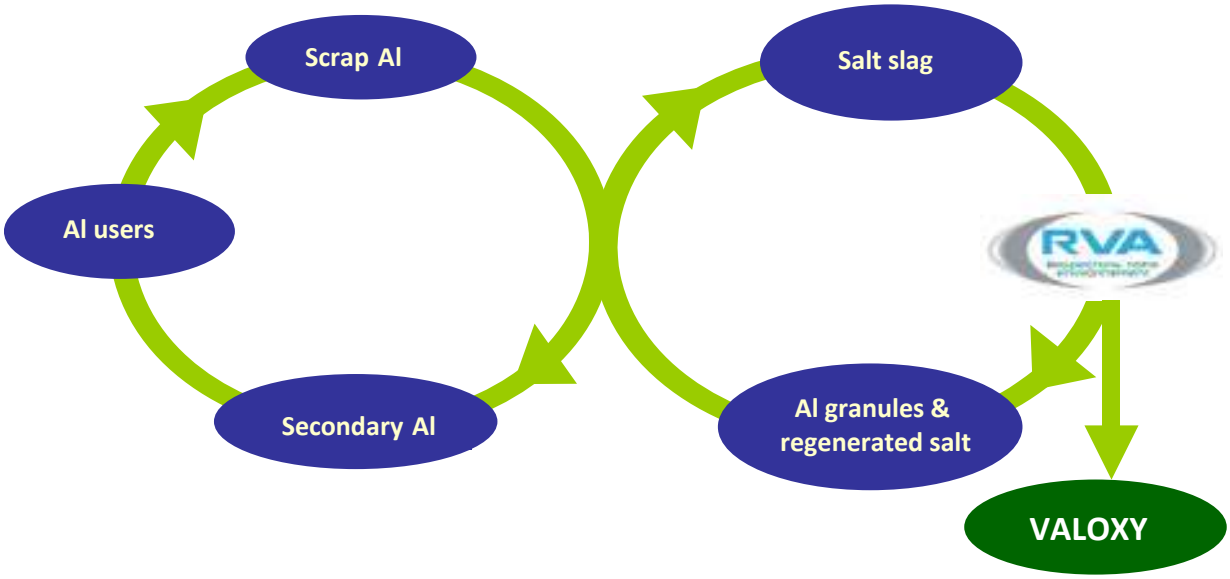

Figure 1 Material flows from salt slag to value-added raw materials

ALUMINIUM SALT SLAGS: ESTIMATE OF GLOBAL VOLUMES

Since secondary aluminium production is largely dependent on molten salt, global arisings of salt slag closely follow output from that industry. Between 300-800 kg of salt slag are produced for every tonne of secondary aluminium alloy. In 2010 worldwide secondary aluminium production stood at around 12 million tonnes. Taking an average figure of 550 kg slag/tonne aluminium, salt slag arisings may be estimated at 6.6 million tonnes worldwide (Figure 2). The distribution of salt slags around the world follows the distribution of secondary aluminium production. This means around a 1.3 million tonnes of slag are generated annually in Europe, 1.8 million tonnes in the US and China, now the dominant player, currently generating an estimated 2.4 million tonnes of salt slag p.a.

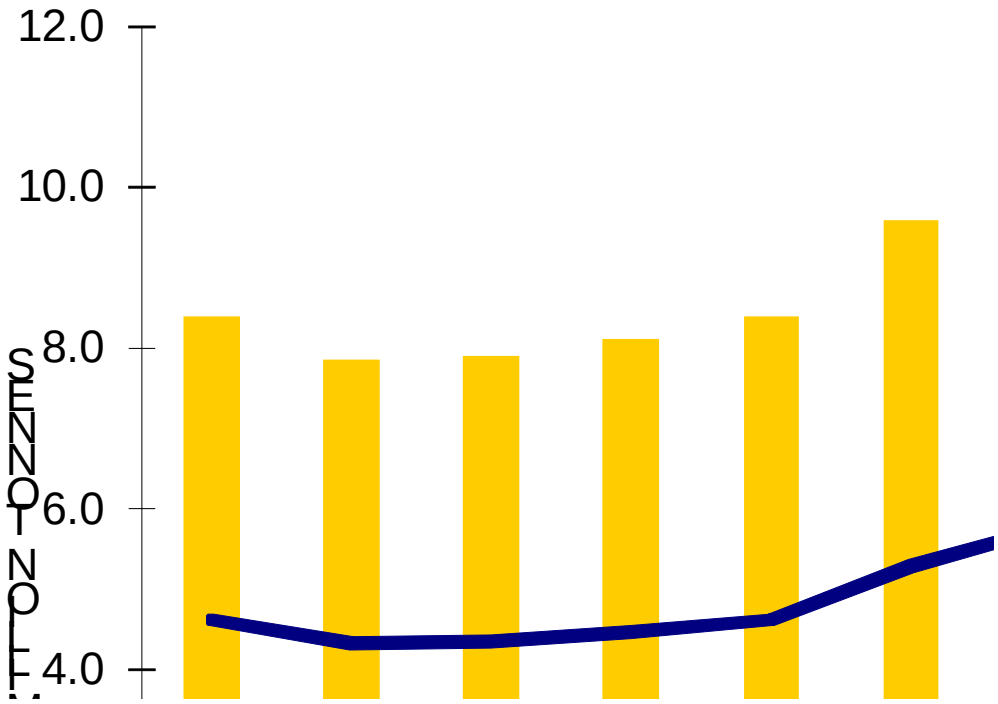

Figure 2 World arisings of salt slag - a function of secondary aluminium production

THE GLOBAL POTENTIAL FOR SECONDARY ALUMINAS

Around 40% of salt slag by weight is the original salt mix used in the melting process. A further 5% is aluminium metal in granular form. The balance is the oxide material from which RVA's secondary alumina, Valoxy, is derived.

On average, the production of one tonne of aluminium alloy generates around 550 kg of salt slag which in turn can be used to produce 300 kg of secondary alumina such as Valoxy. The global potential output of secondary aluminas can therefore be estimated at around 3.6 million tonnes per annum. However, this material is not immediately available worldwide. The production of secondary aluminas, such as RVA's Valoxy, unlike primary materials, is driven by two factors:

- a regulatory environment that prohibits landfilling of salt slags and mandates their reprocessing into useful products
- product and market development of secondary aluminas which enables their inherent economic value to be maximized

Prohibition of landfilling salt slags is very much advanced in Europe allowing companies such as RVA to offer a critical service using their slag reclamation technology.

As environmental regulations tighten in the US and also China, new slag recycling plants are likely to come on stream bringing with them a new secondary source of bauxite/alumina-type material. Utilizing the chemical and physical properties of secondary aluminas will make them ever more attractive economically also.

Furthermore, the cost of producing those 3.6 million tonnes of bauxite/alumina by conventional means is orders of magnitude greater than the production cost of secondary alternatives such as Valoxy.

THE RVA RECYCLING PROCESS

The RVA process comprises four main stages (Figure 3).

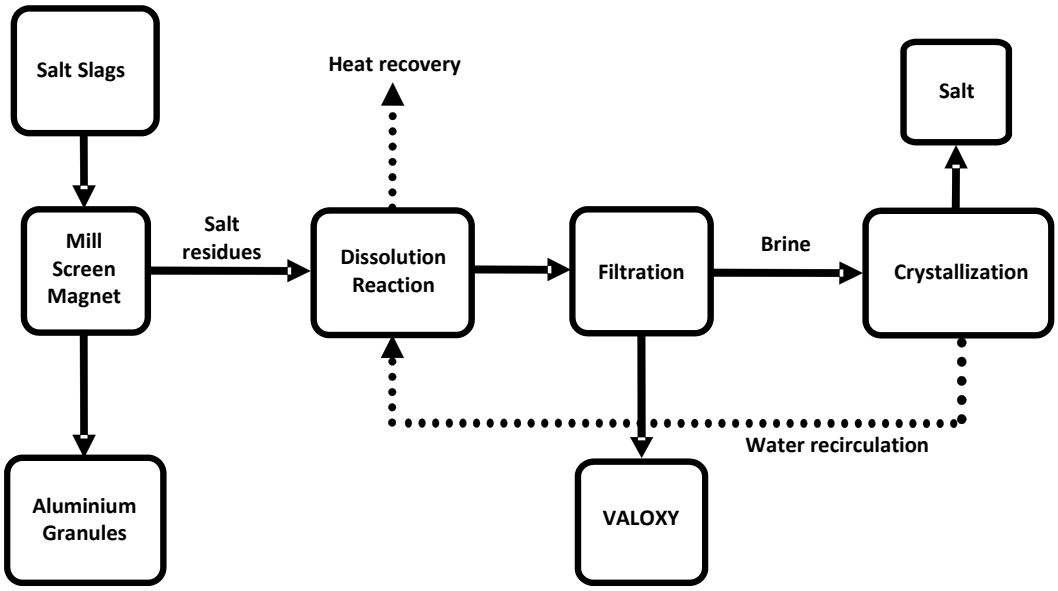

Figure 3 RVA process flow chart showing three main outputs: aluminium granules, salt and Valoxy

Firstly, salt slag is milled with optional recirculation to liberate aluminium by eddy current separator and iron by magnet.

As in many aspects of production, milling demands a compromise between two conflicting parameters: if the slag is milled too fine, valuable aluminium particles are lost as dust; conversely if the milling is too coarse more slag is left adhering to the granule. This ultimately means less efficient dissolution/reaction (see next stage below) and more free aluminium in the Valoxy – the latter limiting Valoxy's application options. Fine particulate from the mill plant is removed by the de-duster.

Next, the remaining salty material is introduced to a dissolution section where it is mixed with water (recovered later in the process). The ensuing slurry is pumped into pressurized reaction vessels where it is agitated as the reaction temperature rises. Gaseous reactants are produced including hydrogen, methane and ammonia. These are incinerated and exhausted from the stack. Energy from the waste gases is recovered for other parts of the process. RVA recently commissioned an additional reactor vessel. The new reactor greatly upgrades the destruction of precursors to noxious gases within the slag. This is particularly important with respect to ammonia emissions: hydrolysis of residual nitrides in the slag can cause the formation of ammonia on contact with moisture.

The residual from the reaction phase is conveyed to a belt filter. Brine and water are sucked out under vacuum, leaving the solid residue, Valoxy. Clean water and the water removed in the dissolution stage are used to wash the solids.

Finally, the effluent brine continues to the three stage crystallization section. Three vessels operate in series stepping down temperature and pressure in succession. This enables NaCl and KCl to be crystallized out of solution, initially separately and then in combination, under optimal conditions to bring the salt mixture to the required specification. An in-line decanter increases the concentration of solids in the slurry and facilitating higher salt recovery. The final mixture salt is conveyed to storage bays for onward shipment back to the secondary aluminium refiners. Water recovered from the crystallizers is recirculated back to the dissolution section.

A proprietary computerized control system monitors the whole process to ensure that key variables remain within pre-defined limits and outputs meet stringent specifications.

RVA‘s slag recycling process is a closed-loop system making minimal demands on the environment: there is no solid waste; water used for washing is recirculated; gaseous emissions are incinerated to harmless residues and ammonia gas is neutralised by dedicated scrubbers.

VALOXY® - A SECONDARY ALUMINA

From a cement point of view, the most interesting of the three outputs at RVA is Valoxy, an effective low cost source of alumina for clinker production.

Chemically, the alumina content of Valoxy is typically around 70%. The balance is silica, magnesia and other oxides (Table 1).

Table 1 Valoxy - Typical chemical analysis (dry weight)

COMPONENT	TYPICAL CONTENT
Al_2O_3	70%
MgO	10%
SiO_2	6-8%
CaO	2%
Na_2O/K_2O	2.3%
F^-	0.4%
Cl^-	0.5%

A typical mineralogical analysis of Valoxy (Table 2) shows that alumina is present in several forms including $Al(OH)_3$ [Gibbsite], AlO(OH) [Boehmite] and $MgAl_2O_4$ [Spinel].

Table 2 Valoxy - Typical Mineralogical Analysis

PHASE	FORMULA	AVERAGE (%)
Spinel	$MgAl_2O_4$	33.0
Boehmite	AlOOH	24.7
Corundum	Al_2O_3	14.9
Glass	$AlMg_3Na_4Si_{38}O_{50}$	8.1
Nordstrandite	$Al(OH)_3$	4.7
Bayerite	$Al(OH)_3$	4.6
Quartz	SiO_2	1.5
Fluorite	CaF_2	1.4
Goethite	FeOOH	1.1
Diaspore	AlOOH	1.0
Periclase	MgO	1.0
Halite	NaCl	0.8
Aluminium	Al	0.8
Calcite	$CaCO_3$	0.7
Gypsum	$CaSO_4$	0.7
Magnetite	Fe_3O_4	0.5
Silicon	Si metal	0.3

Particle size distribution of Valoxy indicates that most grains fall within the silty region namely, 2.5-62.5µm (Table 3).

Table 3 Valoxy - Typical particle size distribution

FRACTION (%)	AVERAGE (%)
>500 µm	11.6
100-500 µm	28.1
40-100 µm	12.4
< 40 µm	47.9
Total	100.0

VALOXY – APPLICATION IN CLINKER PRODUCTION

As well as low price and stable supply, Valoxy offers cement producers technical benefits. Valoxy has proven to be a valuable additive in clinker manufacture. Hundreds of thousands of tonnes of Valoxy have been used by the European cement industry to introduce alumina into the clinker burning process of the cement kiln.

Portland clinker contains calcium aluminate minerals such as C_3A and C_4AF. Alumina is a crucial ingredient of cement raw materials to form these minerals when burning the cement clinker. Valoxy is well suited as the alumina source in clinker production for the following reasons:

- Valoxy consists of natural high alumina minerals such Gibbsite, Boehmite and Spinel.
- Valoxy contains approximately 70% alumina that is available for clinker mineral formation. Besides the alumina fraction, other non-volatile components present in Valoxy are incorporated into the clinker.
- Due to its minor constituent, fluorspar, Valoxy can boost the formation of clinker minerals such as C_3S, C_3A and $11CaO.7Al_2O_3.CaF_2$. Valoxy, therefore favourably affects the lime saturation and silica ratio. As a result, Valoxy can improve the burnability of the clinker as well as the early setting strength development of the cement. This improvement to the sintering process leads to fuel savings during kiln operation.
- Valoxy has a fineness similar to cement raw meal. Therefore, it consumes less communition energy than lumpy alumina raw materials.
- Valoxy is available as a bulk ware.

When used as the alumina source in the kiln, Valoxy is added in the range 1-3% of the total raw meal input, depending on the other raw materials used at the time.

VALOXY – SOUND ECONOMICS AND GOOD FOR THE ENVIRONMENT

Why does a secondary alumina material such as Valoxy make commercial sense for the cement producer? Most industrial businesses try to avoid shocks. Valoxy derives from an established industrial process. It is not subject to the vagaries of extraction from natural sources and the variability associated with a global commodity. As a result supply is predictable. Though influenced by the supply/demand balance for bauxite and alumina, pricing for secondary alumina is driven predominantly by the economics of salt slag processing. This enables long–term pricing structures at levels which are very attractive compared to bauxite and alumina. Based on the chemistry and initial applications data, there is the potential for downstream savings in operating cost. These of course need to be confirmed in process-specific evaluation by potential users. Weight for weight, the alumina content of Valoxy costs a fraction of alumina from conventional sources.

Finally, from an environmental point of view, Valoxy is a sustainable material: every tonne of bauxite substituted by Valoxy is a tonne less that has to be dug out of the ground. Valoxy is classified by the French environmental authorities as non-hazardous. The material may therefore be freely traded across the EU and beyond.

ABOUT RVA

RVA's origins go back to 1989 when the company began with a simple dross milling operation. Today RVA treats over 80,000 tonnes of salt slag per annum. It is the only slag treatment plant in France and one of only two salt slag re-processors in western Europe. The company is located in the picturesque village of Les Islettes, 200 km east of Paris and only 100 km from the German border. RVA is therefore well placed to service and supply customers across western Europe.

The provision of salt slag treatment is likely to remain concentrated in western Europe and new processors are not currently expected to emerge. The economics of slag recycling are largely driven by transportation costs. Markets are therefore fairly regionalized with minimal competition between industry players.

By providing a critical environmental service and supplying useful secondary products, RVA is playing its part in securing Europe's raw material supply line. That should mean smiles all round in Brussels. What is more, bauxite supply solutions may come full circle from discovery of natural bauxite in one French village (Les Baux-de-Provence in 1821) to production of synthetic bauxite in another (Les Islettes in 2011).

REFERENCES

1. Communication from the Commission to the European Parliament, the Council, the European Economic and Social Committee and the Committee of the Regions tackling the Challenges in Commodity Markets and on Raw Materials, February 2011.

Howard Epstein is consultant to RVA on the Valoxy project. For more details on Valoxy and RVA please email: hepstein@013net.net

Geopolymer Concrete with Recycled Concrete Aggregate

B Galvin, N Lloyd
Curtin University, Australia

Geopolymer concrete replaces cement based binder with a binder which contains no Portland cement. One type of geopolymer binder is that which contains fly-ash activated by an alkaline solution of sodium silicate and sodium hydroxide. Utilising recycled concrete waste from construction and demolition sites, that would otherwise be disposed of into landfill, as a source of aggregate offers a potential environmental and economic benefit. The term recycled concrete aggregate (RCA) is used to define aggregate produced from crushed demolition and construction waste. Research has been conducted into both recycled concrete aggregate (RCA) and geopolymer concrete; however there was limited published data on using RCA in geopolymer at the time of this research. This paper reports on the outcomes of the research into the mechanical properties of geopolymer concrete with recycled concrete aggregate as partial replacement of the natural coarse aggregate which indicate the potential of incorporating RCA in geopolymer concrete mixtures.

Benjamin Galvin was an undergraduate student at the time of this research; he graduated with honors from Curtin University in 2011.

Natalie Lloyd is a senior lecturer at Curtin University; her research interests include geopolymer concrete and sustainable structural materials, durability and structural behaviour of concrete and composites.

Keywords: Compressive strength, Construction waste, Fly ash, Geopolymer, Recycled concrete aggregate

INTRODUCTION

Global warming and climate change are increasingly important issues, with many governments looking at different ways to reduce greenhouse gas emissions to help fulfil their obligations under the Kyoto Protocol [1]. Carbon dioxide is one of the most detrimental greenhouse gases with 65 percent of global warming caused by carbon dioxide [2]. Portland cement contributes significantly to greenhouse gas emissions with total emissions due to cement production estimated to be about 1.35 billion tons annually [3]. Cement production results in approximately 0.8-1 tonne of carbon dioxide per tonne of cement [4], equating to approximately 3 percent of global total greenhouse emissions [1]. One option to reduce cement utilization is to use geopolymer concrete.

Development of Geopolymer

The development of geopolymer concrete is attributed to Davidovits [5] who, in 1978, first proposed that a geopolymer matrix could replace cement as the binder in concrete. Davidovits' theory was that an alkaline solution could be added to an aluminium-silicon rich source material to produce cement-like binder and termed this a 'geopolymer' binder. Fly ash is the most widely used source material for geopolymer concrete in Australia because of its availability and suitable composition, being a low calcium content fly ash with low loss of ignition. However, other materials that are high in silicon and aluminium can be used including rice husk ash, blast furnace slag, metakaolin and natural Al-Si minerals. Fly ash is a by-product of the coal industry. and its use in Portland cement concrete is well documented [6]. In Australia alone 14 million tons of fly ash was produced in 2008 [7]. However, less than 30% is used in a beneficial way despite increased utilisation for some applications [7]. The alkaline solution, used to activate the fly ash or other source material, is generally a combination of sodium hydroxide and sodium silicate or potassium hydroxide and potassium silicate. The silicates result in a reaction which is very rapid and significantly faster than that caused by the hydroxides [8]. Therefore a combination of the two is used to provide a matrix which is both workable, strong and sets fairly rapidly.

Properties of Geopolymer

The compressive and tensile strength of fly ash based geopolymer concrete has been shown to be comparable to General Portland (GP) concrete of up to 65 MPa (9500 psi) [9]. The strength is mainly dependent on the following parameters: alkaline liquid-to-fly ash ratio by mass, water-to-geopolymer solids ratio by mass, the wet-mixing time, the heat-curing temperature, and the heat-curing time are selected as parameters [10]. The fly ash used in this research typically has a loss of ignition of around 1.6% and calcium oxide content of less than 2% by mass [11]. Geopolymer concrete has also demonstrated very little shrinkage and creep, excellent resistance to sulphate attack and good acid resistance [11].

Recycled Concrete Aggregate (RCA)

Construction and demolition waste contributes up to 40 percent of all waste generated worldwide. The majority of recycled aggregate that is used in Australia is recycled concrete aggregate (RCA) produced form construction and demolition waste, as it is the most suitable replacement of natural coarse aggregate. Fine recycled aggregates are also used to replace natural sand however this isn't as prominent [12]. Utilising recycled aggregate can result in around 60 percent less waste and 50 percent less mineral depletion per cubic metre of

concrete produced [13]. The strength of ordinary Portland cement concrete utilising recycled aggregate depends largely on the percentage of recycled aggregate used. The larger the percentage of RCA, the weaker the concrete becomes in both compressive and tensile strength. Recycled concrete aggregate Portland cement based concrete also suffers from high water absorption and thus up to 160% higher shrinkage and creep concrete made with natural aggregates [14].

RESEARCH PROGRAMME

Materials and Mixture Design

The basic mixture design used for the non RCA geopolymer mixture was developed based on the geopolymer mix designs formulated at Curtin University in previous research [9]. The other mixtures were derived from this with different percentages of the natural aggregate replaced with the RCA. Only the 20 mm (3/4 in.) natural aggregate was replaced in order to maintain a relatively continuous grading of the combined aggregates; however the percentage replacement was determined as a percentage of the total mass of coarse aggregates, either 20%, 30% or 40%. This produced the mixture designs outlined in Table 1.

The moisture content was assessed for samples of the aggregates brought to surface saturated dry condition (SSD) by soaking, draining and drying the aggregates on trays in the laboratory. Once the SSD moisture content was determined for each aggregate type (0.8% for coarse aggregate and 2.5% for fine aggregates), the water content of the aggregates at the time of mixing was adjusted to SSD moisture content by adding water to the aggregates before the addition of fly ash or chemicals. This water added to achieve SSD of the aggregates is in addition to the water noted in the mixture details of Table 1.

The RCA was nominal 20 mm (3/4 in.) aggregate containing granite, quartz and crushed concrete, approximately 1/3 of which contained steel fibres. There were small quantities of plaster and masonry contaminants. The aggregate did not comply with AS 2758.1 limits for a 20 mm (3/4 in.) aggregate with only 25% of the aggregate retained on the 20 mm (3/4 in.) sieve (AS 2758.1 limit 85-100%). The fineness modulus of the graded aggregates for all mixtures was approximately 5.0 which had previously been found to be suitable for geopolymer mixtures.

Casting and Curing Regime

The method described in AS1012.8.1 [15] was used as the basis for casting. The geopolymer cylinders were cured in a steam curing room for 18 hours at 60°C (140 ^{o}F), a curing regime found to be effective in previous research conducted at Curtin University.

Data logging of the temperature via K type thermocouple wires within the steam room chamber found the temperature varied between 50-65 °C (120-150 °F) and temperature within the geopolymer specimens was 40 – 50 °C (100-120 °F) within a few hours; consistent with other curing regimes at Curtin University [16].

Table 1 Mix details

CONSTITUENT	MIX PROPORTIONS, kg/m^3 (lb/ft^3)			
	R0	R20	R30	R40
20 mm (3/4 in.)	554 (35)	306 (19)	18 (1)	57 (4)
10 mm (3/8 in.)	227 (14)	227 (14)	227 (14)	227 (14)
7 mm (1/4 in.)	462 (29)	462 (29)	462 (29)	462 (29)
RCA	0	249 (15)	373 (23)	497 (31)
Sand	554 (35)	554 (35)	554 (35)	554 (35)
Flyash	408 (25)	408 (25)	408 (25)	408 (25)
Sodium Silicate (55.9% solids)	103 (6.4)	103 (6.4)	103 (6.4)	103 (6.4)
Sodium Hydroxide (8M)	41 (2.5)	41 (2.5)	41 (2.5)	41 (2.5)
Water litres	20 (1.2)	20 (1.2)	20 (1.2)	20 (1.2)
Total Mass	2350 (145)	2350 (145)	2350 (145)	2350 (145)
Slump, mm (in.)	250 (10)	220 (9)	200 (8)	220 (9)

RESULTS AND DISCUSSION

Compressive Strength

Three compression cylinders were tested at 1 day, 7 days, 28 days and 91 days after casting in accordance with AS1012.9 [17]. The compressive strength was 25 to 33 MPa (3600 to 4800 psi) at 28 days and the ratio of day 1 to day 28 mean compressive strength was around 70%. These strengths are suitable for many applications and correspond to a characteristic strength of approximately 25 to 30 MPa (3600 to 4400 psi).

The addition of the RCA to the geopolymer concrete did not result in an increase in the standard deviation of the compressive strengths thus showing that the batches had adequate consistency compared with the non RCA batch despite the compositional variability of the RCA. As shown in Table 2, the 28 day mean compressive strengths of all batches containing RCA were less than the R0 batch; however the strength decrease of the R20 and R30 batches were statistically insignificant. The decrease in strength is expressed by the average ratio of the relative compressive strengths in Table 2 (the ratio is calculated as the ratio of the compressive strengths for each age compared with the corresponding R0 compressive strengths e.g. for R20 the ratio was, at day 28, equal to 29/33 = 0.88).

The reduction is similar to what has been observed with GP concrete containing RCA and falls within a range of strength reduction (less than 10%) for the R20 and R30 mixtures observed in OPC mixtures with similar proportions of RCA. However, a more severe reduction (of the order of 20% for the mean compressive strengths) is shown in the R40 mixture which is greater than that indicated by other research on GP cement concrete with RCA [18]. This suggests that the proportion of RCA should be limited to 30 percent due to strength considerations. However, the mix design can be adapted to produce geopolymer concrete with a similar compressive strength to the R0 batch. This can be achieved by adjusting the water-to-geopolymer solids ratio by mass in a manner analogous to adjusting the water to cement ratio in conventional concrete.

Table 2 Mechanical Properties data

PROPERTY	MIXTURE DESIGNATION			
	R0	R20	R30	R40
Day 1 Compressive Strength (f_{cm1}), MPa	23±2 (3300 ±300)	20±2 (2900 ±300)	20±2 (2900 ±300)	17±1 (2500 ±150)
Day 7 Compressive Strength (f_{cm1}), MPa	26±1 (3800 ±150)	26±1 (3800 ±150)	24±2 (3500 ±300)	22±2 (3200 ±300)
Day 28 Compressive Strength (f_{cm1}), MPa	33±2 (4800 ±300)	29±2 (4200 ±300)	29±1 (4200 ±150)	25±2 (3600 ±300)
Day 91 Compressive Strength (f_{cm1}), MPa	36±3 (5200 ±400)	34±0.5 (4900 ±100)	34±1 (4900 ±150)	30±1 (4400 ±150)
Relative (to R0) compressive strength (average for all days 1, 7, 28 and 91)	1	0.93	0.91	0.80
Day 1 Indirect Tensile Strength ($f_{ct.sp1}$), MPa	2.2±0.1 (320 ±15)	2.1±0.4 (300 ±50)	2.1±0.2 (300 ±30)	1.6±0.1 (230 ±15)
Day 28 Indirect Tensile Strength ($f_{ct.sp1}$), MPa	2.7±0.1 (390 ±15)	2.6±0.3 (380 ±50)	2.8±0.5 (400 ±75)	2.5±0.3 (360 ±45)
Day 91 Indirect Tensile Strength ($f_{ct.sp1}$), MPa	2.9±0.2 (420 ±30)	2.9±0.5 (420 ±75)	3.7±0.2 (530 ±30)	3.2±0.2 (460 ±30)
Ratio $f_{ct}/\sqrt{f_{cm}}$ at Day 28	0.42	0.36	0.47	0.41
Ratio f_{cm1}/ f_{cm28}	0.70	0.70	0.70	0.68
Measured Density, kg/m^3 (lb/ft^3)	2370±35 (148±2)	2350±30 (147±2)	2360±30 (147±2)	2340±20 (146±1)

Indirect Tensile Strength

The tensile cylinders were tested using the Brazilian indirect tensile method. Tensile tests were conducted on 2 cylinders at 1 day, 28 days and 91 days in accordance with AS1012.10 [19]. The tensile cylinder tests produced the tensile strengths illustrated in Table 2. The general observation is that the indirect tensile strength was approximately 15% greater than the predicted value using A.S. 3600- 2009 where f_{ct} =0.9 $f_{ct.sp}$ or in the absence of such data may be estimated as $0.36\sqrt{f_{cm}}$. This is consistent with other geopolymer concrete mixtures with a variety of compositions and curing conditions [16]. The ratio of f_{ct} to $\sqrt{f_{cm}}$ for the geopolymer mixtures was 0.41 at 28 days, 15% greater than 0.36.

CONCLUDING REMARKS

Geopolymer concrete can be produced with fly ash and alkaline solutions utilising conventional concrete mixing and casting procedures. Steam curing at relatively moderate temperatures of 60 ^{o}C (140 ^{o}F) overnight (16 hours) result in geopolymer concrete which exhibits mid-range compressive strengths of the order of 32 MPa (4600 psi) and increased tensile strength compared with GP concrete of the same compressive strength. The observed compressive strength decrease in geopolymer concrete mixtures with the partial replacement of natural coarse aggregate with RCA is similar to that observed in comparable GP cement based concrete with RCA. This demonstrates that strengths for nominal grade 32 MPa (4600

psi) concrete can be developed by geopolymer concrete containing up to 30 percent RCA with no change to the mix design and higher strengths may be able to be produced with minor changes to the mix design, analogous to adjusting the water to cement ratio, by adjusting the water to geopolymer solids ratio. The compressive strength results of the RCA geopolymer batches presented low standard deviations, which demonstrate that the RCA may not affect the quality and consistency of the mix in terms of compressive strength and further research is currently underway at Curtin to assess this impact in both geopolymer and GP cement base concretes with RCA.

REFERENCES

1. REHAN, R and NEHDI, M "Carbon dioxide emissions and climate change: policy implications for the cement industry," Environmental Science & Policy, vol. 8, pp. 105-114, 2005.

2. MCCAFFREY, R "Climate Change and the Cement Industry," Global Cement and Lime Magazine, pp. 15-19, 2002.

3. MALHOTRA,V M "Introduction: Sustainable Development and Concrete Technology," ACI Concrete International, vol. 24, p. 22, 2002.

4. WBCSD, "Cement Sustainability Initiative: Recycling Concrete," World Business Council for Sustainable Development, Geneva, Switzerland9/5/10 2009.

5. DAVIDOVITS, J "Geopolymers - Inorganic polymeric new materials," Journal of Thermal Analysis, vol. 37, pp. 1633-1656, August 1991

6. ACI COMMITTEE 232, Use of Fly Ash in Concrete. Farmington Hills, Michigan, USA: American Concrete Institute, 2004.

7. ADAA, "Annual Membership Survey Results," Ash Development Association of Australia 2008.

8. PALOMO, A; GRUTZECK, M W; BLANCO, M T "Alkali-activated fly ashes: A cement for the future," Cement and Concrete Research,1999, 29(8) pp. 1323-1329.

9. HARDJITO, D AND B. V. RANGAN, "Development and Properties of Low-Calcium Fly Ash-Based Geopolymer Concrete," Curtin University of Technology, Perth, Australia 2005.

10. RANGAN B. V., "Fly Ash Based Geopolymer Concrete," Curtin University of Technology, Perth, Australia 2008.

11. WALLAH, S E AND RANGAN, B. V., "Low-Calcium Fly Ash-Based Geopolymer Concrete: Long Term Properties," Curtin University of Technology, Perth, Australia2006.

12. CEMENT CONCRETE & AGGREGATES AUSTRALIA, "Use of Recycled Aggregates in Construction," CCAA2008.

13. MARINKOVIC, S. RADONJANIN, V., MALESEV, M. AND IGNJATOVIC, I. (2010) , "Comparative environmental assessment of natural and recycled aggregate concrete," Waste Management, 30(11), 2255-2264

14. KATZ, A "Properties of concrete made with recycled aggregate from partially hydrated old concrete," Cement and Concrete Research, vol. 33, pp. 703-711, 2003.

15. STANDARDS AUSTRALIA, "Methods of testing concrete - Method of making and curing concrete - Compression and indirect tensile test specimens," ed: AS1012.8.1, 2000.

16. LLOYD N A AND RANGAN B V "Geopolymer Concrete with Fly Ash", in Zachar, J. and Claisse, P. and Naik, T. and Ganjian, G. (ed), Second International Conference on Sustainable Construction Materials and Technologies volume 3, pp. 1493-1504. Ancona, Italy: UWM Center for By-Products Utilization. " Spain,2010

17. STANDARDS AUSTRALIA, "Methods of testing concrete - Determination of the compressive strength of concrete specimens," ed: AS1012.9, 1999.

18. LI, X (2008) "Recycling and reuse of waste concrete in China: Part I. Material behaviour of recycled aggregate concrete," Resources, Conservation and Recycling, 53, 36-44,.

19. STANDARDS AUSTRALIA, "Methods of testing concrete - Determination of indirect tensile strength of concrete cylinders (Brasil or splitting test)," ed: AS1012.10, 2000.

Strength and Durability of High Calcium Fly Ash in High Volume Fly Ash Concrete (HVFAC)

G M Ganesh, A S Santhi, S B Murugan
VIT University Vellore, India

The performance of cement with high volume fly ash is superior to normal Portland cement in almost all aspects; there are also significant environmental benefits, i.e. the production of one tonne of Portland cement results in the release of about one tonne of CO_2 into the atmosphere. Thus, if expensive cement can be conserved by replacing around 50% of fly ash, it can make significant contributions to the green house gas emissions and reduction in the manufacturing cost. In addition to this, fly ash reduces the rise in temperature in the concrete, at the same time increasing the compressive strength and durability properties. Further using the high calcium fly ash variety in the concrete, is more reactive than low-calcium (ASTM Class F) fly ash because it contains most of the calcium in the form of reactive crystalline compounds, such as C_3A, CS, and C_4A_3S; also there is evidence that the principal constituent (i.e., non-crystalline phase) contains enough calcium ions to enhance the reactivity of the aluminosilicate glass. Hence it is decided to use the high Calcium Class C fly ash in the HVFAC with a constant binder content of 360kg/m^3. This paper reports the results from experimental studies on the compressive strength, rise in temperature and durability studies of the concrete containing the high calcium class C fly ash replaced with various proportions (20%, 40%, 60% and control) of cement.

Dr G Mohan Ganesh is Professor, Programme Manager & Division Leader, Structural and Geotechnical Engineering Division, School of mechanical and building Sciences, VIT University, Vellore. He has led three research projects on High volume fly ash concrete. His research interests include Steel Structures, Flyash Concrete, Steel – Concrete Composite structures, Artificial Neural Network (ANN), and Genetic Algorithms (GA).

Dr A S Santhi is Professor and Assistant Director in centre for Structural Engineering, Structural and Geotechnical Engineering Division, Director, School of mechanical and building Sciences, VIT University, Vellore. She has led three research projects on High volume fly ash concrete. Her research interests include Creep and Shrinkage Properties in RCC Structures, Flyash Concrete.

S B Murugan has completed M.Tech (Structural Engineering) at VIT University nad pursuing PhD. At VIT University in the area of High volume fly ash concrete. He did his under graduate studies in Civil Engineering.

Keywords: CO_2, Durability, High calcium, High volume fly ash

INTRODUCTION

Fly ash is a residue produced from the thermal power stations after burning Coal / Lignite as a fuel. It is collected by using the electrostatic precipitator in the power plants. Fly ash is very fine in nature, and disposed as a waste in dry or wet state at nearby areas. In India, the available quantity has already exceeded 130 million tons, and its generation is likely to cross 170 million tonne in the year (2011-2012). The estimated utilization of fly ash is 46% in the annual production [1]. Remaining fly ash is disposed in the nearby area of the thermal power stations in wet or dry state. The sizes of the fly ash are very smaller in nature, land, water and air pollution are occurring. Heavy toxic metals like Ni, Cd, Sb, As, Cr, Pb are present in the fly ash which are cause for the diseases like respiratory problem, lungs cancer, skin cancer and etc. [2]. Hence there is a need to utilize higher volume of fly ash in the various fields like agriculture and construction industries. The major problem in the fly ash concrete is its less early age strength. Increase the fly ash content in the concrete increases the setting time [3]. The concrete which contains higher volume of fly ash attains higher compressive strength at 90 days. The permeability of concrete decreases due to curing [4]. This study aims to investigate the effect of the use of high volume high calcium fly ash as partial replacement of ordinary Portland cement in various percentages on concrete properties. The mechanical and durability characteristics of concrete were studied and the details are given in this paper.

MATERIALS USED

Cement

Ordinary Portland cement 53 Grade [5] was used for this experimental work. The properties are given in Table 1.

Table 1 Properties of Cement

PROPERTY	
Fineness, m^2/kg	291.70
Normal Consistency	33%
Setting Time, mins	
Initial	75
Final	350
Soundness	
Le - Chatelier Expansion, mm	1.125
Autoclave Expansion, %*	0.0505
Specific gravity of cement	3.12

Fly Ash

Fly ash was obtained from the Neyveli Lignite Corporation (NLC) thermal power station, India. Specific gravity of fly ash was found in the laboratory as 2.46. The chemical compositions are given in Table 2.

Table 2 Chemical compositions of fly ash

CHARACTERISTICS	%
Silica (as $Si0_2$), *Min*	57.65
Calcium Oxide (Lime Content) as CaO	11.64
Alumina (as Al_20_3)	15.29
Iron oxide (as Fe_2O_3)	6.10
Magnesia (as MgO), *Max*	0.37
Sulphuric Anhydride (as $S0_3$), *Max*	1.82
Total Loss on ignition, *Max*	2.86
Total Chlorides (as Cl)	0.02
Sodium Oxide (as Na_2O)	0.44
Potassium Oxide (as K_2O)	0.04
Total alkalies (as Na_2O)	0.47
Silicon dioxide ($Si0_2$) + Aluminium oxide (Al_20_3) + Iron oxide (Fe_2O_3) in % by mass, *Min*	79.04

Aggregates

Naturally available river sand was used as the fine aggregate for this experimental study. The specific gravity and fineness modulus of the river sand was 2.56 and 2.55 respectively. Crushed stone aggregates obtained from the local quarry were used as coarse aggregate. The specific gravity and fineness modulus of coarse aggregate is 2.6 and 7 respectively [6].

Chemical admixture

Polycarboxylic ether based superplasticizer was used in this study, to satisfy the water demand in concrete due to high volume of fly ash and to increase the workability of concrete. As per ASTM C494-C494M-10a [7], this SP comes under the Type F admixture. The pH value is 7 and the color is light brown. The specific gravity of SP is 1.09 and solid content is 35 % of its weight.

Reagents

As per the ASTM C1202-10 [8], 3.0% of Sodium Chloride was diluted in the distilled water and 0.3 N Sodium Hydroxide solution was prepared and the test was conducted for all the samples.

MIXTURE PROPORTIONS OF CONCRETE

The constant binder content of 450kg/m^3 with water – binder ratio of 0.35 was used for all the mixtures [9]. The control mix is designated as C 0. The last numerical term ‘0’ is replaced with either ‘2’ or ‘4’ or ‘6’; which denotes the 20% or 40% or 60% replacement of the fly ash in the binder content. The amount of materials used for 1m^3 is shown in Table 3.

Table 3 Mixture proportion of concrete for $1m^3$

MIXTURE CODE	CEMENT, kg	FINE AGGREGATE, kg	COARSE AGGREGATE, kg	WATER, l	FLY ASH, kg	CHEMICAL* ADMIXTURE, %
C 0	450	717	1075.5	157.5	-	0.2
C 20	360	717	1075.5	157.5	90	0.3
C 40	270	717	1075.5	157.5	180	0.4
C 60	180	717	1075.5	157.5	270	0.8

*Chemical admixture was used 0.2-0.8% by weight of binder (cement + fly ash)

Specimen casting and testing

Cubes of size 100mm x 100mm x 100 mm and cylinder of 100 mm Ø dia. with 50mm thickness were used to make the specimens for compressive strength and permeability test respectively. All the cast specimens were demoulded after 24 hours and kept for the continuous curing in the water.

Compressive strength test

As per the Indian standard, BIS 516-1959 [10] tests was conducted to find the compressive strength of cubes at 1, 7, 28 and 90 days on the high volume fly ash concrete and all the values are given in Fig. 2.

Rapid Chloride Permeability Test (RCPT)

The resistance of the concretes to the penetration of chloride ions was determined by the method prescribed in ASTM C 1202 [8]. This test consists of monitoring the amount of electrical current which passes through a 100mm diameter x 50mm thick concrete disc, when a potential difference of 60 V DC is maintained across the specimen for a period of 6 hours. Chloride ions are forced to migrate out of a sodium chloride (NaCl) solution subjected to a negative charge, through the concrete, into a sodium hydroxide (NaOH) solution maintained at a positive potential. The experimental arrangement is shown in Figure 1.

Figure 1 Multi-cell RCPT Apparatus with specimens

The total charge passed, in coulombs, has been found to be related to the resistance of the specimen to chloride ion penetration. It is generally agreed that for low-permeability concretes, the value of the charge in coulombs passed through the specimens should not exceed 1000. The limiting values are given in Table 4 as per ASTM C 1202. Therefore the tests for resistance to chloride-ion penetration were carried out on 100mm x 50mm discs. For all mixes, Chloride Ion Penetrability (based on charge passed) values are given in the Fig. 3.

Rise in temperature

The rise in temperature was found by placing the fresh concrete in the wooden box surrounded with thermocol sheet of size 0.5m x 0.5m x 0.5m. Two thermometers were inserted in the concrete to measure the temperature. The temperature values were noted at 30 minutes intervals, upto 24 hours. The average value of the two thermometers is given in the Table 5.

RESULT AND DISCUSSION

Compressive Strength

The compressive strength of the different mixtures of high volume fly ash concrete is shown in Figure 2. In this, the one day strength of control mix (C 0) is high (32.1 N/mm^2). By replacing cement with 20% fly ash (C 20), the compressive strength reduced from 32.1 N/mm^2 to 28.6 N/mm^2. Further by increasing the fly ash in concrete for C 40 and C 60 mix, the one day strength reduced considerably.

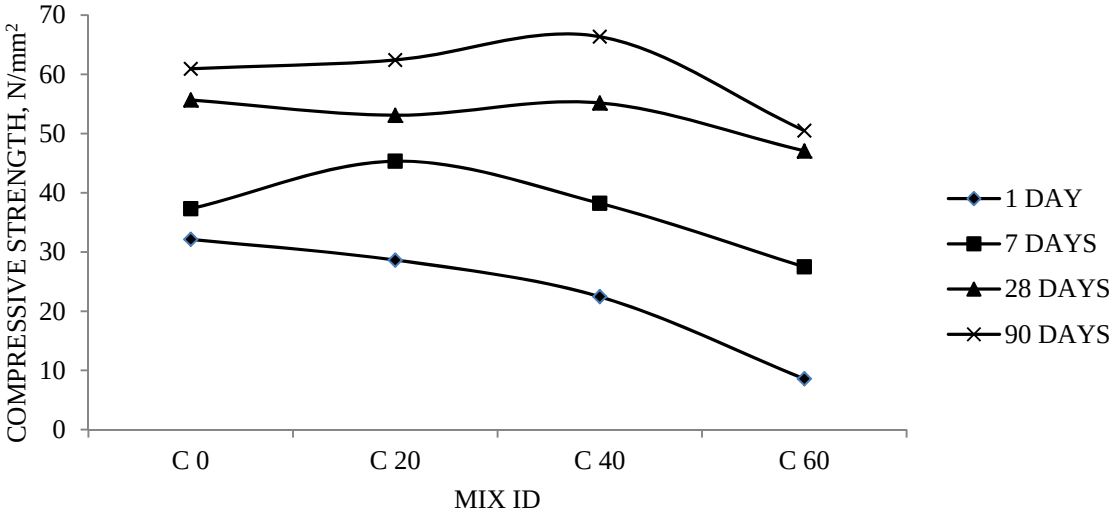

Figure 2 Compressive Strength of the High Volume Fly Ash Concrete Mixtures

At 7 days, the concrete with 20% fly ash (C 20) attains more strength (45.3 N/mm^2) than the control mix (37.3 N/mm^2). The C 40 mix also attained the strength which is equivalent to control mix concrete. For C 60 mix, the compressive strength increased drastically from 8.58 N/mm^2 (one day strength) to 27.5 N/mm^2. This shows the pozzolanic reaction has taken place in the fly ash concrete mixtures [11]. The same trend is also observed at 28 days and 90 days.

Rapid chloride permeability test

For all mixtures, Chloride Ion Penetrability (based on charge passed) values are given in the Figure 3. In this, the charge in coulombs, a measure of the resistance of the concrete to the penetration of chloride ions is very high at seven day and all the values are reduced after 28 days curing which is within the limit as per ASTM C1202. Further all these RCPT values are reduced at 90 days. The presence of fly ash (FA) leads to the maximum resistance to the passage of the Chloride Ions and hence these values are very low as compared to the control mix. This may be due to increased degree of hydration and refinement of microstructure. The decrease in the permeability with time in the high volume fly ash concretes is due to the change in the pore structure of the hydrated cementitious system (presence of fly ash).

Table 4 ASTM C 1202 limit values

CHARGE PASSED, coulombs	Chloride permeability
>4000	High
2000 – 4000	Moderate
1000 – 2000	Low
100 – 1000	Very low
< 100	Negligible

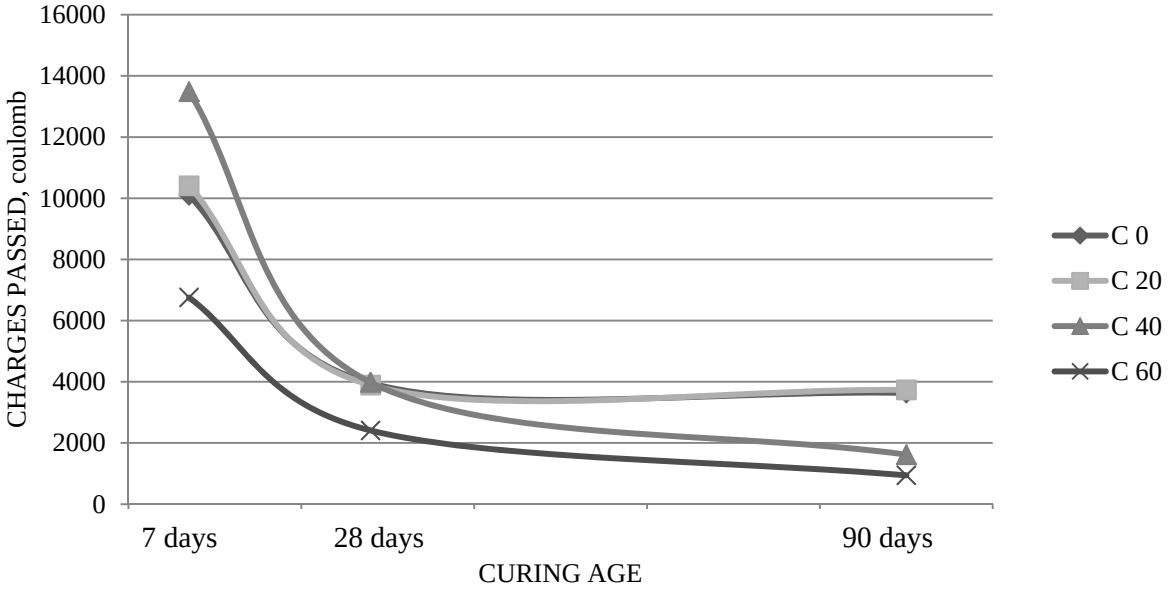

Figure 3 Chloride Permeability of the Concretes Containing Fly Ash

Rise in temperature

The results show that the temperature of the control mix for the cement content of 450kg/m^3 reached the highest value of 52^o C. But the partial replacement of 53 Grade cement by fly ash reduced the rise in temperature of the concrete drastically, i.e. 28 ^{o} C – 38^o C. Hence high volume class C fly ash can be used for the mass concrete works which can reduce the rise in temperature and thus reduce shrinkage cracks.

Table 5 Rise in temperature for binder content 450kg/m^3

MIX ID	TEMPERATURE, ^oC
C 0	52
C 20	38
C 40	34
C 60	28

CONCLUSIONS

From the experimental results, the following conclusions were made;

- Using the binder content as 450kg/m^3, the concrete with 20% fly ash (C 20) attains more strength (45.3 N/mm^2) than the control mix (37.3 N/mm^2) at 7 days. The C 40 mix also attained the strength which is equivalent to control mix concrete and the strength of the mix C 60 is comparable. The same trend is also observed at 28 days and 90 days.

- The resistance of the HVFA concrete to the penetration of chloride ions is very high at seven day and all the values are reduced either at 28 days or 90 days curing. The presence of fly ash in the high volume fly ash concrete leads to the maximum resistance to the passage of the Chloride Ions and hence these values are very low as compared to the control mix.

- The partial replacement of 53 Grade cement by fly ash in the concrete reduced the rise in temperature of the concrete drastically.

Hence high calcium fly ash in high volume fly ash (C 60) can be used for the mass concrete works which can reduce the rise in temperature without compromising both strength and durability. The mix C 20 and C 40 can be used in all the concrete works.

ACKNOWLEDGEMENTS

The authors convey their sincere thanks to the fly ash mission, Department of Science and Technology, Government of India, India, for sanctioning this research project and providing financial support for further experimental work.

REFERENCES

1. CHATTERJEE ANJAN, K., Indian Fly Ashes, Their Characteristics, and Potential for Mechano-Chemical Activation for Enhanced Usability, Second International Conference on Sustainable Construction Materials and Technologies.

2. SENAPATI MANAS, R, Fly ash From Thermal Power Plants – Waste Management and Overview, Current Science, 100, Vol. 12, 25, 2011.

3. DURÁN-HERRERA, A., JUÁREZ,C.A., VALDEZ, P. AND BENTZ,D.P., Evaluation of Sustainable High-Volume Fly Ash Concretes, Cement & Concrete Composites, 33, 2011, 39 –45.

4. UYSAL M AND AKYUNCU V, Durability Performance of Concrete Incorporating Class F and Class C fly ashes, Construction and Building Materials, 34, 2012, 170–178.

5. IS 112269-1987, Indian Standard Specification for 53 Grade Ordinary Portland Cement, reaffirmed in 2004, Bureau of Indian standards, New Delhi.

6. IS: 383-1970, Indian Standard Specification for Coarse and Fine Aggregates from Natural Sources for Concrete, reaffirmed in 1997, Bureau of Indian standards, New Delhi.

7. ASTM STANDARD C494/C494M – 10a. Standard Specification for Chemical Admixtures for Concrete, American Society for Testing and Materials (ASTM), West Conshohocken, PA19428-2959, USA.

8. ASTM Standard C1202-10. Standard Test Method for Electrical Indication of Concrete's Ability to Resist Chloride Ion Penetration, American Society for Testing and Materials (ASTM), West Conshohocken, PA19428-2959, USA.

9. IS: 10262-1982, Indian Standard Recommended Guidelines for Concrete Mix Design, reaffirmed in 2004, Bureau of Indian standards, New Delhi.

10. BUREAU OF INDIAN STANDARDS, BIS 516-1959. Methods of Tests for Strength of Concrete.

11. MCCARTHY, M.J. AND DHIR, R.K., Development of High Volume Fly Ash Cements for Use in Concrete Construction, Fuel, 84, 2005, 1423–1432.

Study of the Effect of Sulfate Resistant Cement on the Mechanical Strength of a Recycled Concrete Aggregate Containing Marble Fillers

L Belagraa[1], A Bouzid[1], M Beddar[2], S Tabet[2]
1 – Bordj Bou Arreridj University, Algeria
2 – M'sila University, Algeria

The needs of the construction sector are still increasing for concrete. However the shortage of natural resources of aggregate could be a problem for the concrete industry, in addition to the negative impact on the environment due to the demolition wastes. In the last decade a major interest has developed for the reuse of recycled aggregates that presents more than 70 % of the concrete volume. These should fulfill the requirements of lower cost and better quality, in order to establish its role in the concrete. The aim of this study is to assess the effect of sulfate resistant cement combined with the local admixtures on the mechanical behaviour of recycled aggregate concrete (RAC). Physical and mechanical properties of RAC were investigated including the density, water absorption, water reduction and the resistance. The non destructive test methods (pulse-velocity, rebound hammer) were used to determine the concrete strength. The results obtained were compared to crushed aggregate concrete (CAC) using the normal compressive testing machine test method. Thus, the convenience of indirect tests in the case of a recycled agregate concrete were demonstrated.

Larbi Belagraa is Senior lecturer, civil engineering department, Laboratory of Materials and Electronic Systems [LMSE], Institute of sciences and Technology, Bordj Bou Arreridj University center, Algeria.

Miloud Beddar is a Lecturer in the Department of Civil Engineering, M'sila University, Algeria.

Souad Tabet is a Post graduate student in the Department of Civil Engineering, M'sila university, Algeria.

Abderrazak Bouzid is a Lecturer and Head of Materials and Processes Team, Laboratory of Materials and Electronic Systems [LMSE], Institute of sciences and Technology, Bordj Bou Arreridj University Centre, Algeria.

Keywords: Demolition waste, Fillers, Mechanical strength, Non-destructive tests, Recycled concrete aggregate, Sulfate resistant cement

INTRODUCTION

Concrete is still the mostly used material by the construction industry and the highway construction sector. The industry need in this field for such a material has increased over the years. The conservation of natural resources and preserving the environment have lead the specialists in the civil engineering domain to focus their efforts on the management of wastes resulting from demolition [1].

The reuse of recycled aggregate that comes from construction waste presents a major interest for users and researchers of concrete as it occupies 70% of concrete. The study herein concerns an investigation of the properties of recycled aggregate concrete (RAC) incorporating marble filler waste based on sulfate resistant cement thus to formulate a much more durable concrete.

It can be noted that the concrete proved to be less durable than it was thought and is now showing signs of deterioration due to its exposure to chemical attack from environment sources or internal composition. Further to the climate change that may alternate the physical and mechanical properties of the concrete matrix by reducing the alkalinity medium. This is due to carbonation effects or chloride penetration, sulfate attack and alkali silica reaction. The deterioration of concrete and mortars caused by these factors influences its performance and limits the service life of the concrete structures [2]. In fact the humidity level of the environment could be enhancing factor of the deterioration process [3]. To overcome this handicap some types of cements are used mainly to formulate concrete in the aggressive environment. These cements — the sulfate resistant type — is mostly used in foundation soils containing sulfate with high risk on the behaviour of reinforced concrete elements [4, 5].

The experimental programme here in has the objective of studying the effect of additions of marble waste filler on the behaviour of Recycled Aggregate Concrete (RAC) based on sulfate resistant cement (SRC). The effect of these factors on the mechanical strength (Rc) was assessed. Dosages of 0, 5, 8 and 10% by weight of cement of marble filler were maintained for the experimental program.

The non-destructive test methods were carried out to evaluate this hardened property and to see if methods such as rebound hammer and ultrasonic techniques can be conveniently adapted in this case. Other physical properties like the density were studied. The third aim of this research study is to see the performance of recycled aggregate concrete with sulfate resistant cement combined with this mineral addition in comparison with conventional concrete based on ordinary crushed aggregate (CAC) and without filler additions.

TEST PROCEDURES

The objective of the testing programme was to achieve a recycled aggregate concrete having the performance of a normal concrete with crushed stone aggregate. Recycled concrete specimens were cast using different percentages of addition (0, 5, 8 and 10%). The ordinary concrete was prepared with similar aggregate size (8/16 and 16/25) and without marble waste fillers. Tests of the specimens at different ages 3, 7, 14 and 28 days using a compressive testing machine and non-destructive methods were used to evaluate the mechanical response of concrete. In all mixes a constant workability of 50 mm was maintained using the slump test method [6].

Materials and Equipment

Sand

The sand used in this study was a clean siliceous and fine sand of fraction 0/5 mm from Boussaada region. Its characteristics are reported in Table 1 and the grading curve is shown in Figure 1 [7].

Gravel

Ordinary gravel was obtained from crushed limestone rock and delivered from the quarry of COSIDER El Euch region (Bordj Bou Arreridj). The gravel fraction used in this study was 8/16, 16/25 in proportions of 40 and 60% respectively. The characteristics are shown in Table 1 and the grading curve in Figure 1 [8].

Recycled aggregate

Pieces of old concrete specimens were crushed using a steel hammer provided by the civil engineering laboratory. The size of the particles maintained for this investigation was 8/16 an 16/25 at a percentage of 40% and 60%. The characteristics of the recycled aggregate are reported in Table 2 and Figure 2 [8].

Table 1 Some characteristics of the sand and ordinary crushed aggregates used in the tests

MATERIAL	DENSITY, kg/l	BULK DENSITY / SPECIFIC WEIGHT, kg/l	COMPACTNESS / POROSITY, %	E_{sp}, %
Sand	2.57	1.48/1.64	36.18/63.82 42.41/57.59	84.99
Gravel				
Gca 8/16	2.50	1.34	53.89/46.16	
Gca 16/25	2.59	1.35	52.07/47.93	

Table 2 Some characteristics of the recycled aggregate

MATERIAL	DENSITY, kg/l	BULK DENSITY / SPECIFIC WEIGHT, kg/l	COMPACTNESS, %	POROSITY, %
Recycled Aggregate				
Gra 8/16	2.514	1.13	44.80	55.21
Gra 16/25	2.451	1.20	48.60	51.40

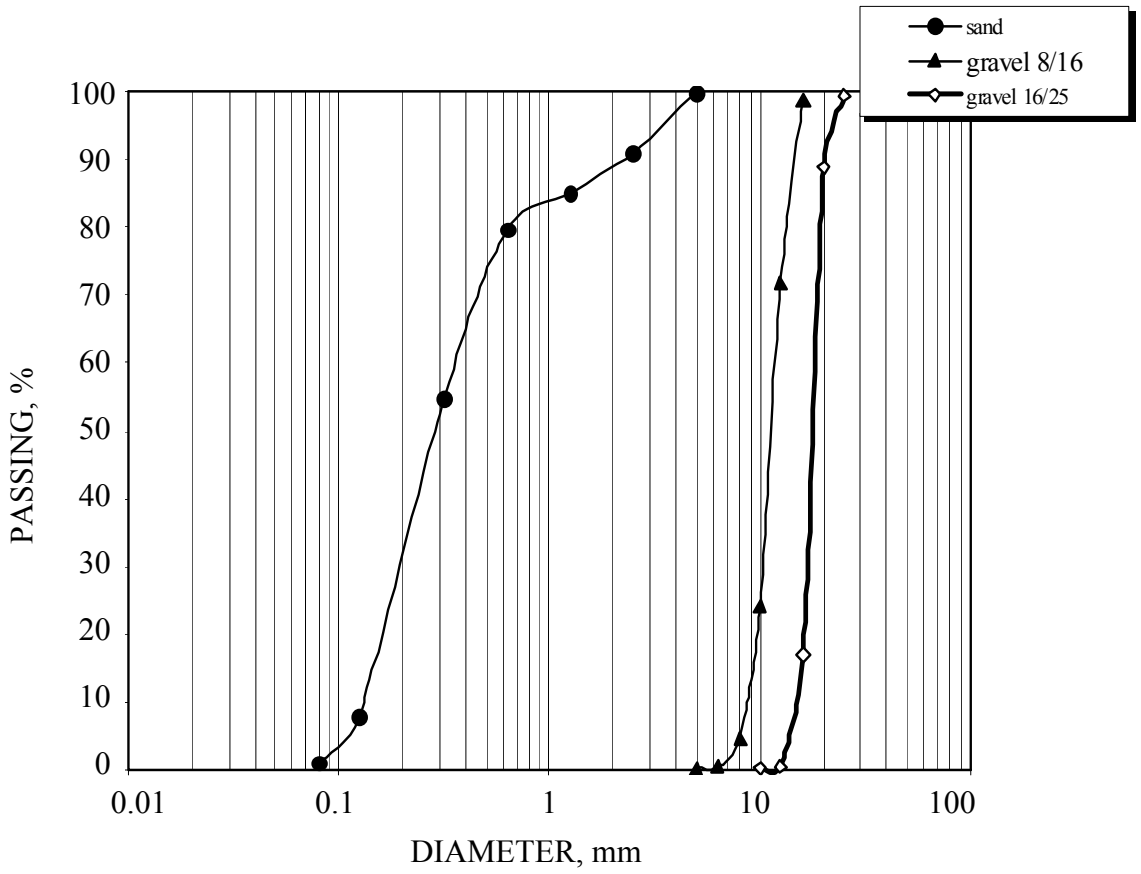

Figure 1 Grain size distribution of the sand and crushed aggregate (ca)

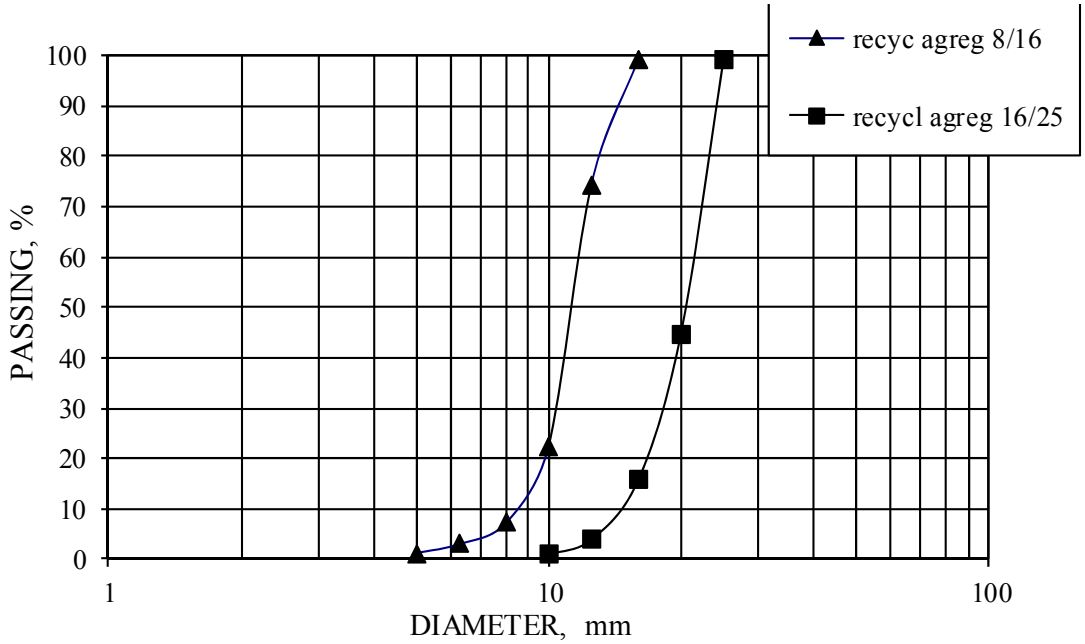

Figure 2 Grain size distribution of recycled aggregate (ra)

Cement

The cement used was type CEM I 42.5 delivered from Algerian Cement Company and widely used in the construction sector in Algeria for sulfate attack purposes. Its specific weight is about 3.08 g/cm³ and fineness of around 3593 g/cm². The chemical and mineralogical compositions are reported in Table 3 [5].

Table 3 Chemical and mineralogical compositions of cement

Chemical composition

CONSTITUENTS	CaO	SiO_2	Al_2O_3	Fe_2O_3	Na_2O	K_2O	MgO	SO_3
%	63.70	21.66	4.09	4.54	0.03	0.51	1.53	1.90

NB: LOI = 0.85%

Mineralogical composition

CONSTITUENTS	C_3S ($3CaOSiO_2$)	C_2S ($2CaOSiO_2$))	C_3A ($3CaOAl_2O_3$)	C_4AF ($4CaOAl_2O_3Fe_2O_3$)
%	55.18	20.78	3.17	13.83

NB: with the condition [$2xC_3A+C4AF< 20$]

Addition

The marble filler was collected from local marble factories in the region. It is a white powder having a bulk density of 1.036 kg/l, the specific area is around 3850 g/cm². The chemical composition of the fillers is shown in Table 4.

Table 4 Chemical composition of marble filler addition

CONSTITUENTS	CaO	SiO_2	Al_2O_3	Fe_2O_3	Na_2O	K_2O	MgO	SO_3
%	55.3	1.47	0.35	0.147	0.12	0.04	0.01	0.01

NB: LOI = 42.56%

Water

A tap water from the civil engineering laboratory was used for concrete batching.

Concrete mix

The concrete mix proportions used were for a Grade 350 mix, determined by the absolute volume method [9].

- Cement 351 kg/m³
- Sand 778 kg/ m³
- Gravel 8/16 391 kg/m³ (40%)
  16/25 587 kg/m³ (60%)
- Water (total) 187.5 litre (this quantity takes into account the degree of aggregate absorption).

TESTING

Workability

The method used to assess the workability for both ordinary and recycled concrete was the slump test method. A workability of about 50 mm was maintained for all mixes [6].

Compressive Strength

Compression tests were carried out on cubic specimens (100 mm × 100 mm × 100 mm). Tests were done using the hydraulic press model "STRASSENTEST FHF". The specimens were centred on the tray of the press and a continuous load was applied. The ultimate compression load for each concrete cube was recorded at 28 days age [10].

Rebound Hammer Test

The specimens were placed in the centre of the hydraulic machine press, a continuous load was applied and maintained within a range of 10 to 20 kN. The rebound hammer test was carried out on five different points spaced at 2 cm intervals on both faces of the cubic specimens [11].

The final result from the test was calculated using the following equation:

$$Rs = {}_{i=1}\sum^{n} S/n \tag{1}$$

where

n – Number of tests carried out on both faces of the cube.
S – The recorded value of rebound hammer.

Ultrasonic Method

The pulse velocity test was carried out on the two opposite sides of the specimens (100x100x100) mm^3 using direct transmission [12]. The transit time t in μs was recorded and the velocity V is measured as:

$$V=d/t \tag{2}$$

V – Velocity in km/s.
d – The distance between the two transducers.
t – The transit time in μs.

ANALYSIS OF RESULTS

Presentation of Results

In this study the concrete mixes have been prepared according to the method of absolute volume [9]. Filler additions of 0, 5, 8 and 10% were chosen. The cubic specimens (100 mm × 100 mm × 100 mm) were cast and cured in water to be tested at ages of 3, 7, 14 and 28 days.

Prismatic specimens measuring (100 mm × 100 mm × 400 mm) were prepared in similar conditions to evaluate the flexural strength. Specimens measuring 100 mm × 100 mm × 100 mm with different dosages for all the concrete mixes were tested using the compressive testing machine. In addition, the non-destructive tests (ultrasonic and rebound hammer) were carried out prior to the compression test.

The value of compressive strength Rc is compared to the combined values of ultrasonic (V) method and the rebound hammer reading (S). The strength R_{us} is then assessed according to the formula of Feret [9];

$$R_{us}=[S/n_o+n_1 \cdot S-n_2 \cdot V]^2 \quad (3)$$

$n_0 = 3.64$ S – Rebound hammer reading;
$n_1 = 0.023$ R_{us} – Ultrasonic-rebound hammer resistance;
$n_2 = 0.56$ V – Velocity.

Table 5 Results of flexural strength and density for Recycled Aggregate Concrete (RAC) and crushed aggregate concrete (CAC) at 28 days age

FILLERS, %		BULK DENSITY (ρ), kg/m³	FAILURE LOAD (F), kN	FLEXURAL STRENGTH (Rt), N/mm²
B_C*	0	2500	8.15	5.02
Br_0**	0	2353	8.30	5.02
Br_5	5	2410	9.94	6.08
Br_8	8	2410	10.51	6.44
Br_{10}	10	2380	9.15	5.61

Bc* Normal Crushed Aggregate Concrete (CAC).
Br** Recycled Aggregate Concrete (RAC).

Table 6 Results of mechanical strength and density for Crushed Aggregate Concrete (CAC) and Recycled Aggregate Concrete (RAC)

AGE	MIX	FILLERS		BULK VELOCITY V km/s	STRENGTH		
		%	Density ρ kg/m³		Reb-hammer S/R_s N/mm²	Reb-Ultrason R_{us} N/mm²	Compressive strength Rc, N/mm²
3	B_C*	0	2350	-	20.77/14.50	14.50	24.76
	Br_0**	0	2250	-	22.00/17.00	17.00	22.00
	Br_5	5	2350	-	22.33/18.60	18.60	27.08
	Br_8	8	2340	-	21.77/16.50	16.50	27.73
	Br_{10}	10	2340	-	21.33/16.00	16.00	19.80
7	B_C*	0	2403	4.26	28.55/27.00	22.32	33.65
	Br_0**	0	2352	4.22	25.66/22.20	18.90	25.60
	Br_5	5	2350	4.30	24.99/21.80	19.09	30.62
	Br_8	8	2300	4.98	21.33/16.00	12.54	28.73
	Br_{10}	10	2300	4.14	22.22/15.00	14.70	25.71

Bc* Normal Crushed Aggregate Concrete (CAC).
Br** Recycled Aggregate Concrete (RAC).

Table 6 Results of mechanical strength and density for Crushed Aggregate Concrete (CAC) and Recycled Aggregate Concrete (RAC), cont'd

AGE	MIX	FILLERS	BULK VELOCITY	STRENGTH		
		Density ρ	V	Reb-hammer S/R_s	Reb-Ultrason R_{us}	Compressive strength
		%	km/s	N/mm²	N/mm²	Rc, N/mm²
14	B_C*	0	2370	4.32	28.08/26.20	22.63	40.13
	Br_0**	0	2350	4.28	24.77/21.00	28.60	27.35
	Br_5	5	2330	4.25	31.53/32.00	25.20	40.56
	Br_8	8	2320	4.06	31.13/31.80	22.35	40.45
	Br_{10}	10	2320	4.15	31.60/32.20	23.92	34.55
28	B_C*	0	2400	4.45	31.86/32.00	28.76	48.15
	Br_0**	0	2330	4.44	35.86/39.00	32.86	45.13
	Br_5	5	2350	4.44	31.00/37.00	27.55	42.28
	Br_8	8	2320	4.15	33.20/34.20	25.53	42.00
	Br_{10}	10	2350	4.13	33.00/34.00	25.02	37.60

Bc* Normal Crushed Aggregate Concrete (CAC).
Br** Recycled Aggregate Concrete (RAC).

RESULTS AND DISCUSSION

Compressive Strength

According to Figure 3 and Table 6, the behaviour of recycled aggregate concrete (Br) and normal crushed aggregate concrete (Bc) show the same trend of strength development for all dosages of marble fillers at 3, 7, 14 and 28 days. However for a dosage of 5%, the recycled concrete gives a compressive strength compared to normal concrete with crushed stone aggregate. For additions contents 8% and 10% the recycled concrete showed lower values of resistance in comparison with reference concrete (Bc) with values of (37.60, 42.00; and 48.15 N/mm²) respectively. Thus, performances of recycled aggregate concrete (Br) similar to ordinary concrete can be achieved by the incorporation of marble fillers addition at optimal percentages around 5% as reported by researchers in previous work [13].

Ultrasonic Tests

Figure 4 illustrates that whatever the type of aggregate used, strength development is similar for normal concrete and recycled aggregate mixes. Furthermore, the values of strength of ordinary concrete are nearly the same the results given for Br mixes. The contribution of marble filler to increasing strength is much marked according to the results obtained for the dosage of 5% where the same as the results of those of normal concrete (Bc). Other researchers have concluded that the use of ordinary cement OPC with marble fillers proved to give good resistance at an optimal dosage of 5% relatively to conventional concrete [13]. Whereas the 0 percentage for Br mix showed good resistance reaching the value of 32 MPa at 28 days of age in comparison with conventional ordinary concrete.

Rebound Hammer Results

Although the rebound hammer test results are affected by many factors, such as the mix characteristics (cement type, content and the aggregate type) or the member characteristics (mass, density, surface type, age, curing type and surface carbonation) [14], only the main factor of aggregate type is considered in this study. The rebound hammer test results in Figure 5 and Table 5 show that it is much difficult to assess the strength at early age of concrete. The 0% fillers addition showed a slight increase in strength for (Br) all over other combinations and normal concrete at 28 days age.

The recycled aggregate concrete (RAC) proved to give greater results compared to normal concrete (CAC) in general but this is not confirmed by the compressive machine test which is more reliable in strength assessment compared to the non destructive method of rebound hammer that can be reflecting the resistance of concrete element surface only. Only the 5% dosage of marble filler incorporated presented better performances at 28 days age overall of the mixes tested.

Flexural Strength

The results in Table 5 and presented in Figure 6 show that the addition has no significant effect on the behaviour of recycled aggregate compared to the reference concrete. The dosages of 0 and 10% gave similar values and the slight increase in the strength regarding bending action that can be noticed for the 5 and 8% addition. Thus no clear conclusion regarding the influence of this parameter of fillers dosage on the mechanical response under flexural loading can be drawn.

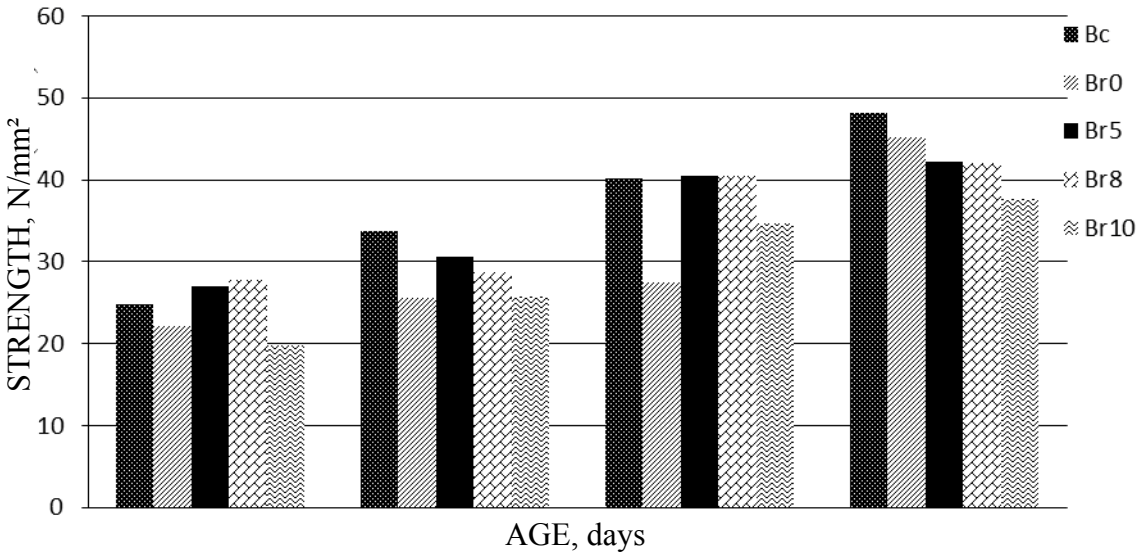

Figure 3 The compressive strength development (Rc) as a function of concrete age for recycled and normal concrete

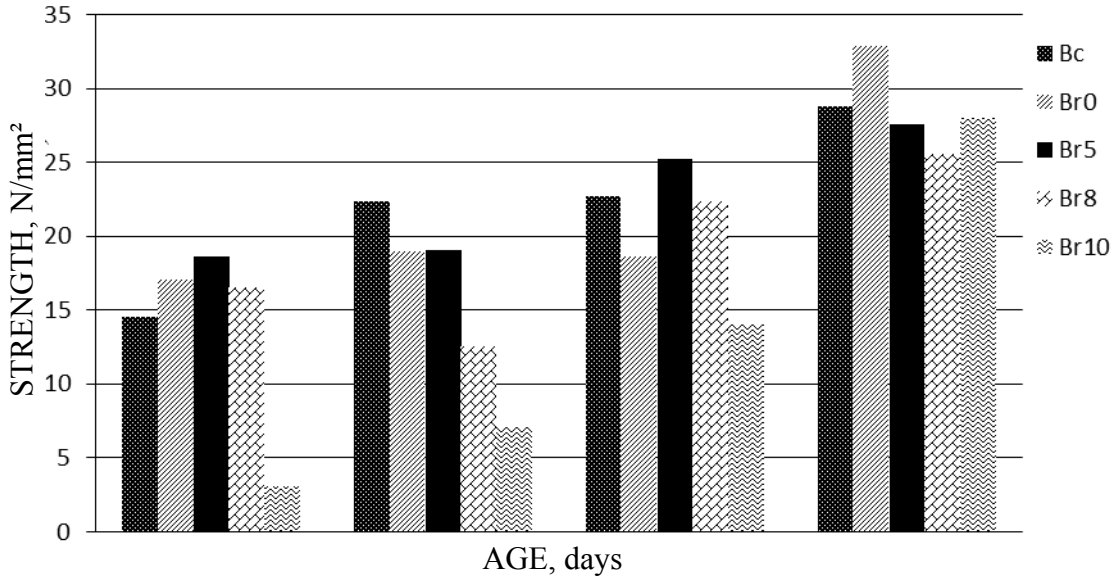

Figure 4 The combined strength development (Rus) as a function of concrete age for recycled and normal concrete

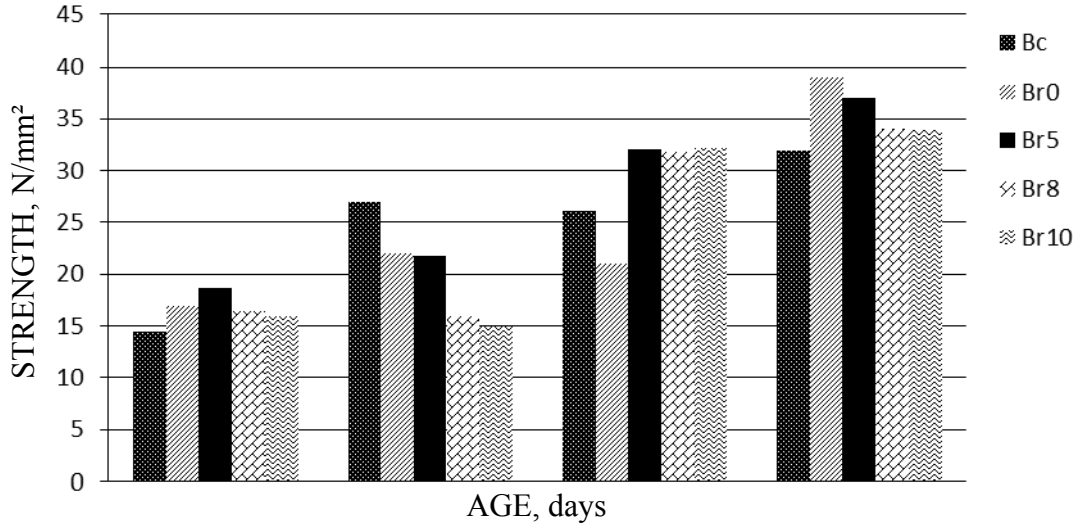

Figure 5 The strength (Rs) of rebound hammer as a function of concrete age for recycled and normal concrete

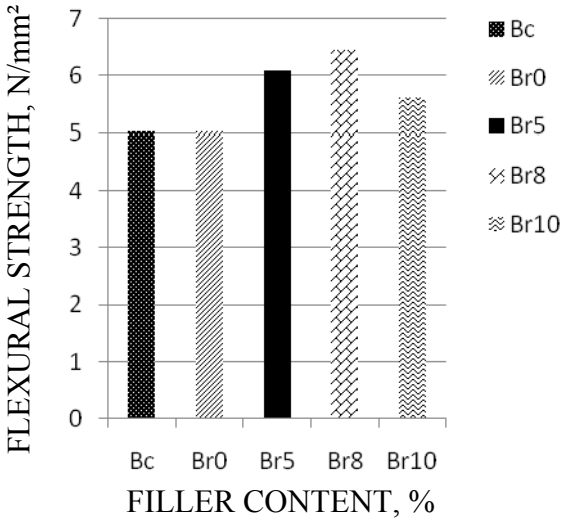

Figure 6 The flexural strength (Rt) at 28 days of age for recycled and normal concrete

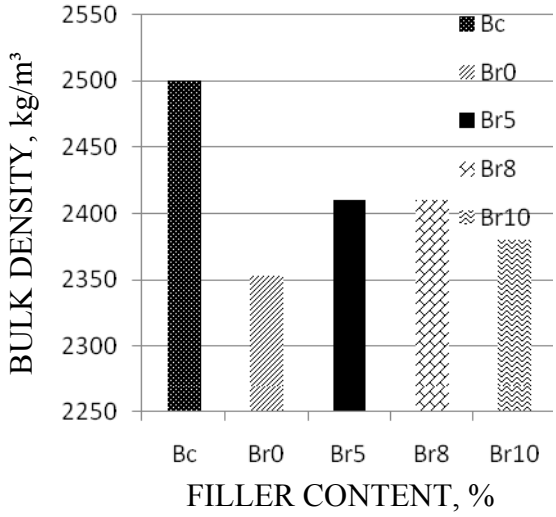

Figure 7 The bulk density for recycled at 28 days of age for recycled and normal concrete

Density

Figure 7 shows that the bulk density of normal concrete mix (Bc) marked a slight increase in hardened specimens compared to recycled concrete aggregate mixes (Br). This may be related to the heavy density of the crushed aggregate type; where the degree of compactness is greater with less porosity in the contrary to the recycled old concrete aggregate. This is more evident for dosages of 0, 8, and 10% of marble filler addition where the effect of aggregate type can be appreciated. For the mix without addition Br0, the density of recycled aggregate showed a reduction of its value to be 2353 kg/m³ compared to normal concrete with 2500 kg/m³ determined for the prismatic specimens tested at the age of 28 days.

CONCLUSIONS

In the light of this study and the interpretation of these results, the following is concluded:

1- The compressive strength development is similar for both recycled aggregate concrete (RAC) and crushed aggregate concrete (CAC).
2- The recycled aggregate concrete shows the same performance compared to normal concrete at the optimal addition of 5%.
3- The density of crushed aggregate concrete presents higher values than recycled aggregate concrete. This is attributed to the type of recycled aggregate being less compact and so less dense.
4- Non-destructive tests can be used to assess the strength of RAC, but a correction coefficient is required to obtain a similar value to the compressive strength given by the compression machine test.
5- The incorporation of a combination of sulfate resistant cement and marble filler in recycled concrete design compared to normal concrete without addition is a promising venture for economic purposes where the substitution of an amount of cement by this addition of fillers could be beneficial.

REFERENCES

1. HANSEN T C, Recycling of Demolished Concrete and Masonry, RILEM report 37, DRC, Chapman and Hall, 2nd edition, 1996.

2. BELAGRAA L, The adhesion of polymer mortars to concrete and steel, M Sc (Eng.) Thesis, Liverpool University, 1989.

3. VAN DEN BOCH V D, Performance of mortars specimens in chemical and accelerated marine exposure", Performance of Concrete in Marine Environment, SP-65, American Concrete Institute, 1980, Detroit, pp. 487-507.

4. BS 110 Concrete exposed to sulfate attack, Table 6.1

5. NA 443 Ciment pour travaux dans les milieux fortement agressifs NF P 15-319:1995 08/11/2000

6. NA 431, Normes Algériennes, Détermination de la consistance- essai d'affaissement, 29/11/1989

7. NA 456, Normes Algériennes, Détermination de la propreté du sable, équivalent de sable à 10% de fines, 29/11/1989.

8. NA 255, Essais pour déterminer les caractéristiques mécaniques et physiques des granulats - Détermination de la masse volumique réelle et du coefficient d'absorption d'eau, EN 1097-6:2001 P 18-650-6 26/11/2005

9. DREUX G AND FESTA J, Nouveau guide du béton, édition Eyrolles, 1995.

10. NA 427, Bétons — Détermination de la résistance à la compression des éprouvettes ISO 4012:1978 29/11/1989.

11. NA 2786, Mesure de la dureté de surface par rebondissement à l'aide d'un scléromètre, EN 12504-2:2003 30/06/1992.

12. NA 5027, Béton — Auscultation sonique — Mesure du temps de propagation d'ondes soniques dans le béton, NF P 18-418:1989 30/11/1992.

13. MESSADI N, Effet des fillers de marbre sur le béton à base d'agrégats recyclés, PFE, Département de Génie civil, Université de M'sila, Algérie, 2003.

14. BUNGEY, T.H, Testing of concrete structures, Surrey University Press, 1982.

An Experimental Plan Method to Formulate a Resin Concrete

M Beddar[1], Z Boudaoud[2], M A Chikouche[2], H S M'hammed[1]
1 – M'silia University, Algeria
2 – Ouem Elbouaghi University, Algeria

Abstract— This work is an experimental approach based on the method of experimental plans to determine a specific formulation of a resin concrete. In this study, an unsaturated polyester resin (thermosetting resin) was used with two types of mineral fillers (dune sand and crushed sand), and with the addition of a marble powder to ensure the continuity of the particle size mixing granular. The lack of the methods for developing this kind of composite materials, had led us to perform an initial experimental approach to define the experimental field, that is to say determine the mass proportions of the various compounds of mixture of our study. In the second approach, we have established and implemented fully experimental plans with three factors namely: (factor 1: sand, factor 2: resin, factor 3: marble powder). Test results being the density of polymer concrete and the mechanical resistances. Finally, multi-parameters regression allowed us to determine predictive mathematical models for the different responses of the study. Tests results showed that at three days we got a tensile strength of about 16 MPa with a resin concrete density of 1.9 g/cm^3 . This shows the advantages of this material.

M. Beddar is an associated professor in civil and hydraulic engineering department, Faculty of Technology, M'sila University, Algeria. His is the director of materials and mechanical structures Laboratory. His research interests are fibers reinforced concrete , behavior of concrete under extremes conditions and valorization of solid waste in civil engineering materials. His member of several national and international scientific associations.

Z.Boudaoud is an associated professor in civil engineering department, Faculty of Technology, Ouem elbouaghi University, Algeria. His research interests structural analysis of concrete., and valorization of waste in cimentious materials.

M. A.Chikouche is a lecturer in civil and hydraulic engineering department, Faculty of Technology, M'sila University, Algeria. His is member in the materials and mechanical structures Laboratory. His research interests are study of the durability of civil engineering materials. .

H.S.M'hammedi is an engineer of civil engineering department. Graduted from M'sila University , she is now doing a research about the use of rubber waste in the concrete made from local materials.

Keywords: Experimental plans method, Index terms concrete, Mechanical resistance, Polyester resin

INTRODUCTION

Resin or polymer concrete is relatively new high performance material that has significantly progressed in the last 30 years. It is generally produced from a liquid resin mixed with coarse and fine inorganic aggregates such as gravel or crushed stone and sand. It is usually used in severe conditions in industrial and public buildings as well as transportation and hydraulic structures [1, 2].

Comparatively to the Portland cement concrete, resin concrete has high mechanical strength, good durability and in general greater resistance to the chemical products and corrosive agents [3]. It has also very low water absorption property and high freeze-throw stability.

The resins used to obtain a resin concrete are generally polymers based on four types of monomers or systems: methyl methacrylate, polyester prepolymer-styrene, epoxide prepolymer hardener and fiarfurolic alcohol [4, 5]. The use of polymer resins in concrete as a binding material has shown that the strength and failure modes of the produced concrete are mainly influenced by curing method, temperature and strain rate.
The resin binders are usually two components systems: one containing the resin (base) and the other a hardener (in the case of epoxy resins) or an accelerator (in the case of polyester resins) that reacts with the resin to form the binding material [6,7]. The performance of resin concrete depends on the binder properties, type of filler and aggregates, curing temperature and components dosage.

The use of resin concrete has not limited on repair of structural elements, as it was, but it extended to be used with efficiency in precast components for buildings, bridges panels, hazardous waste containers, machine bases, and in various utility and transportation components [8 , 9].

The resin preferred in this study is an unsaturated isophatalic polyester resin because of its low cost. The concrete made from this kind of resin is hard; rigid, and has high mechanical strength, but there is the risk of cracking with thick block moulding due to the internal stresses related to shrinkage of resin [10].

The purpose of this study was to find the least amount of resin that be used to achieve acceptable strength and the cost effective in the same time. Following this step, the method of experimental plans to determine a specific formulation of a resin concrete was used.

MATERIALS AND SPECIMENS PREPARATION

Used Materials

Sand: Two types of sand were used to prepare test specimens.

Dune sand: this is a clean, siliceous and fine sand of fraction 0/5 taken from BOUSAADA region. It was free of asphalt, dirt, and other organic materials. Its characteristics are regrouped in table 1.

Quarry sand: This type of local well-graded sand is obtained by crushing of the limestone rock from the quarry of COSIDER situated in EL-EUCH region (B.B.A). Its physical proprieties were shown in Table 1.

Table 1 Physical properties of dune and quarry sand used in this study

CHARACTERISTICS	DUNE SAND	QUARRY SAND
Relative density	2,60	2,48
Bulk density in loose state, kg/m³	1,703	1,640
Bulk density in compact state, kg/m³	1,603	1,50
Porosity in compact state, %	32,61	34,4
Porosity in loose state, %	38,35	40
Compactness	64,8	70,55
Sand equivalent Visual/piston	80,8/78,7	///

Resin

The resin used in this study is unsaturated orthophthalic polyester, with blue color and a relative density of 1.25. It is polymerized in cold by the addition of a catalyst. This unsaturated polyester orthophthalic was used as matrix. The initial styrene content is about 39 % by weight, methyl ethyl ketone peroxide (about 1.5 % by weight was added as catalyst, the accelerator is the cobalt octoate (environ 0.2 % by weight) [11].

Marble powder

It is a very fine powder, one of its main constituent is $CaCO_3$. Its granularity is varied between 30 to 40 μm and its relative density equals to 2.71 g/cm^3. The chemical composition of the powder is given in table 2.

Table 2 Chemical composition of marble powder

BULK OXIDE, % by mass							
SiO_2	CaO	Al_2O_3	Fe_2O_3	MgO	SO_3	K_2O	Na_2O
1.47	55.3	0.35	0.14	0.01	0.01	0.04	0.12

Table 3 Different proportions of used materials

PROPORTIONS, gr		
Ps (sand)	Pr (resin)	Pm (marble)
500	88.23	0
	125	0
	166.67	0
	214.28	0
500	92.30	14.28
	133.33	33.33
	181.81	45.45
	240	60
500	96.77	48.38
	142.85	71.43
	200	100
	272	136.36

Specimens Preparation.

- **Preliminary phase** : First, due to the lack of methods to formulate a resin concrete, the objective of the first phase was the research for a resin concrete which should be homogenous easy to be implemented. For this, the amount of sand was fixed while the two other parameters namely the resin and marble powder are variable.

- **Resin content**: The content of the resin used in this study varies between 15 and 30 % by weight in comparison with the other constituents. The ration in weight between the marble powder (P_m), and the unsaturated polyester resin (P_r) varies between 0 and 50 %. The different proportion of the materials used are regrouped in table 3 according to the fraction below :

$$\begin{cases} \dfrac{P_R}{P_S + P_R + P_M} = 15 - 20 - 25 - 30\ \% \quad \text{……. (1)} \\ \dfrac{P_M}{P_R} = 0 - 25 - 50\ \% \quad \text{……. ……...(2)} \end{cases}$$

PRESENTATION OF THE OBTAINED RESULTS

Mixes based on the materials mentioned above were mixed according to the table 3 and cast in 40 × 40 × 160 mm prisms [12]. They were prepared by mixing the polyester resin and hardener and, then adding the considered charges (dune and quarry sand, polyester resin and marble powder). These preliminary tests have revealed us some remarks with respect to the density, compressive and tensile strength.

Bulk Density

As shown in figure 1**,** the bulk density **of** the tested specimens decreases with increasing the content of resin by weight. This diminution is due to the main characteristics of the unsaturated polyester resin which is the lightness. The bulk density is varied between 1.79 and 2.01 g/cm^3.

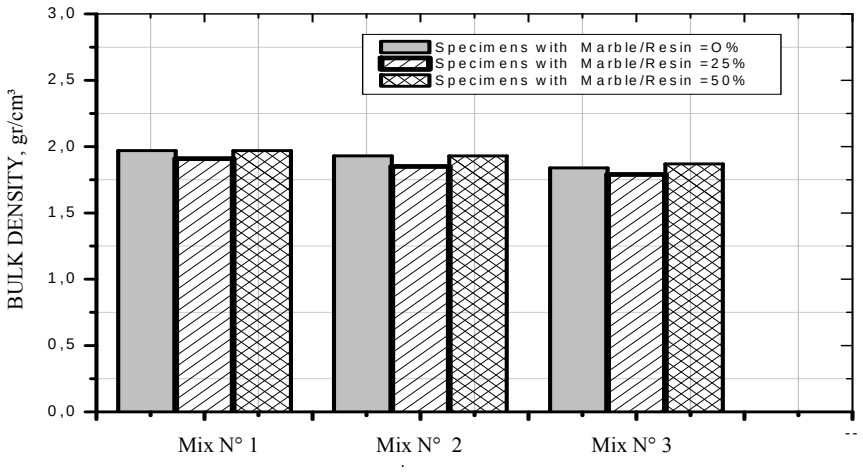

Figure 1 Variation of bulk density in function of Marble/Resin ratio

Tensile Strength

Specimens were tested in indirect tension after 28 days of curing at room temperature. The results obtained have been reported in figure 2.

Test results show that at 15% by weight of the resin which means the lowest content of this study, the tensile strength is very low. This can be explained by the fact that resin has not wrapped all the grains of sand to create a union between the grains so that they are detached from each other. However, at 20 % by weight the resin, curve is already at the maximum which means a good cohesion between the different constituents of the material

Compressive Strength

The results obtained after testing all the specimens under compressive load are shown in figure 3. The increase in the amount of resin increases the compressive strength as it is shown in the figure 3. This can be explained by the fact that the used resin provides to the mixture its characteristic strength. A strength of 90 MPa can be seen in these results with an amount of 30% by weight of resin

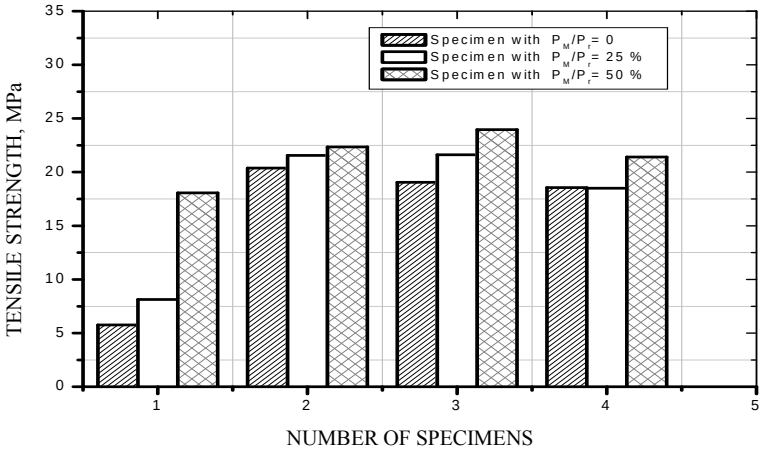

Figure 2 Variation of R_{t28} in function of Marble/Resin ratio

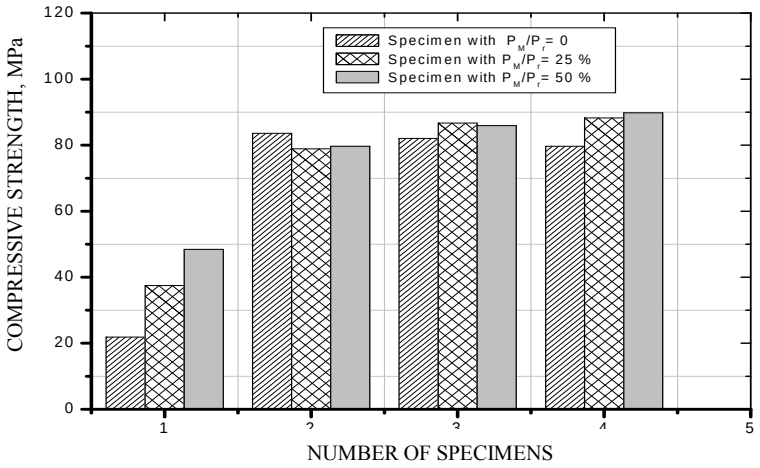

Figure 3 Variation of R_{c28} in function to Marble/Resin ratio

EXPERIMENTAL PLANS

We have opted for the technology of the experimental plans because, in comparison with a classical approach, we shall have a good quality of results, and a predictive capacity of trial results due to the mathematical modelling which allows by this method. This modeling allows the calculation of the value and the sign of the influential factors which maximize or minimize the system response [13, 14,15]. This method also allows:

- The knowledge of the parameters effects, and the deduction of influential parameters,
- The possibility of assessing the correlations effects between parameters,
- If experimental field is known enough, this technology can allow the reduction of some tests in this study.

The Three Factors of Study

Having performed preliminary study, we deducted the levels of the different factors of this study. The three factors are at two levels (Table 4 and 5), which give us for a full factorial plan, eight tries to be accomplished.

Table 4 Different factors and levels of the experimental plan method

SAND (S)		UNSATURATED POLYESTER RESIN (R)		MARBLE POWDER (M)	
Level (-1)	Level (+1)	level (-1)	Level (+1)	Level (-1)	Level (+1)
Dune sand	Quarry sand	20%	30%	0%	30%

Table 5 Test Matrix

NUMBER OF EXPERIENCE	S	R	M
1	-1	-1	-1
2	+1	-1	-1
3	-1	+1	-1
4	+1	+1	-1
5	-1	-1	+1
6	+1	-1	+1
7	-1	+1	+1
8	+1	+1	+1

This kind of plan allows the determination of all factors effect of this study and their respective significance in the response. It allows the writing of a complete mathematical model as follows:

$$Y= A_0 + A_1S+A_2R+A_3\ M + A_{12}S.R+A_{23}\ R.\ M + A_{13}S.\ M + A_{123}S.R.M \ldots.\text{Eq. (3)}$$

MATRICES AND RESPONSES OF DIFFERENT FACTORS

Bulk Density

The different measurements of the bulk density of the plan and the effects of the different factors are given in Table 6.

Table 6 The matrix of the effects and the measurements of the bulk density (g/cm³)

TEST	AVERAGE	M	R	S	R. M	S.R	S. M	R.S. M	B.D
1	1	-1	-1	-1	1	1	1	-1	1,87
2	1	-1	-1	1	1	-1	-1	1	1,79
3	1	-1	1	-1	-1	-1	1	1	1,95
4	1	-1	1	1	-1	1	-1	-1	2,14
5	1	1	-1	-1	-1	1	-1	1	1,83
6	1	1	-1	1	-1	-1	1	-1	1,82
7	1	1	1	-1	1	-1	-1	-1	1,87
8	1	1	1	1	1	1	1	1	1,91
Effect	A0	A3	A2	A1	A23	A12	A13	A123	1,93
	1,8975	0,0175	0,0700	0,040	0,400	-0,0300	-0,0100	-0.0275	

Range of bulk density which is [1.79, 2.14] enables us to say that the made concrete belongs to the lightweight category of building materials. With the reading of the results of the multi-parametric regression, it appears clearly that:

- The quarry sand, the presence of marble powder and a strong percentage of resin increase the density;
- The interaction between the resin (up to 30%) and marble powder is very significant.

Tensile Strength

It is noted that the resin and the marble powder play a major role. To obtain a high tensile strength, the mixture of the dune sand with marble powder (continuous granularity) and 20 % by weight of resin will give this result. Table 7 will give the matrix of tensile strength effects of different tests

Table 7 Matrix of tensile strength effects of different tests

TEST	AVERAGE	M	R	S	R.M	S.R	S. M	R.S. M	f_t
1	1	-1	-1	-1	1	1	1	-1	11,93
2	1	-1	-1	1	1	-1	-1	1	21,43
3	1	-1	1	-1	-1	-1	1	1	16,94
4	1	-1	1	1	-1	1	-1	-1	17,15
5	1	1	-1	-1	-1	1	-1	1	10,48
6	1	1	-1	1	-1	-1	1	-1	16,73
7	1	1	1	-1	1	-1	-1	-1	16,52
8	1	1	1	1	1	1	1	1	16,75
Effect	A0	A3	A2	A1	A23	A12	A13	A123	17,69
	15,99	2,02	0,85	-0,87	-1,91	0,45	-0,40	0,41	

Compressive Strength

All the factors effects are significant in the compressive strength model and even certain interactions. It is noticed also that the factors have the same effects on the compressive strength as on the tensile strength. Table 8 will give the matrix of the compressive strength effects of different tests.

Table 8 Matrix of the compressive strength effects of different tests

TEST	AVERAGE	M	R	S	R. M	S.R	S. M	R.S. M	f_c
1	1	-1	-1	-1	1	1	1	-1	46,88
2	1	-1	-1	1	1	-1	-1	1	62,03
3	1	-1	1	-1	-1	-1	1	1	61,72
4	1	-1	1	1	-1	1	-1	-1	71,09
5	1	1	-1	-1	-1	1	-1	1	39,06
6	1	1	-1	1	-1	-1	1	-1	59,69
7	1	1	1	-1	1	-1	-1	-1	57,03
8	1	1	1	1	1	1	1	1	55,47
Effect	A0	A3	A2	A1	A23	A12	A13	A123	58,59
	56,62	5,45	4,71	-3,81	-3,50	-1,72	-0,68	-2,05	

EFFECT OF FACTORS VARIATION

Effect of Factors Variation on Bulk Density

It is observed that for all the test specimens, as soon as there is an increase in the percentages by weight of the resin, the test specimen becomes lighter as it is clearly shown by the experimental plan, and the interval of this density which ranges between 1,79 and 2,14 enables us to say that the made concrete belongs to the light category. All the results are reported in Table 9 and Figure 4.

Table 9 Response of different factors on the bulk density

MATERIAL	FACTOR	BULK DENSITY, g/cm³
Sand (Factor 1)	-1	1.9150
	0	1.8975
	1	1.8800
Resin (Factor 2)	-1	1.9675
	0	1.8975
	1	1.8275
Marble powder (Factor 3)	-1	1.8575
	0	1.8975
	1	1.9375

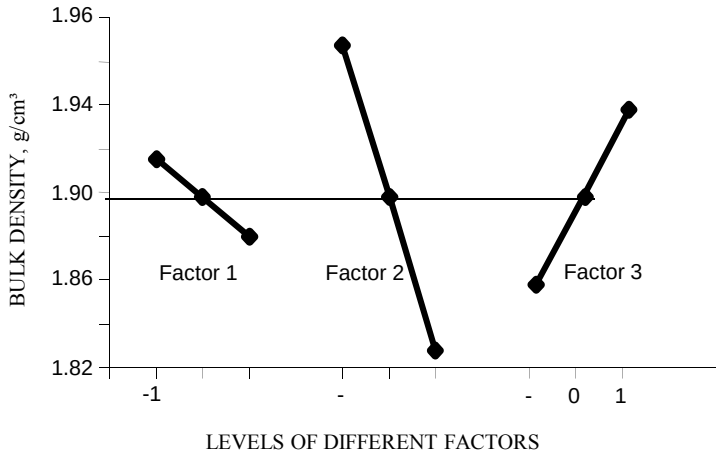

Figure 4 Response of different factors on the bulk density

Effect of Factors Variation on the Tensile Strength

It is noticed that the quarry sand offers a poor strength while the dune sand of makes it higher. Figure 5 and Table 10 shows the response of different factors for tensile strength.

Table 10 Responses of different factors for tensile strength

MATERIAL	FACTOR	TENSILE STRENGTH, MPa
Sand (Factor 1)	-1	18.0180
	0	15.9939
	1	13.9698
Resin (Factor 2)	-1	16.8422
	0	15.9939
	1	15.1457
Marble powder (Factor 3)	-1	15.1223
	0	15.9939
	1	16.8656

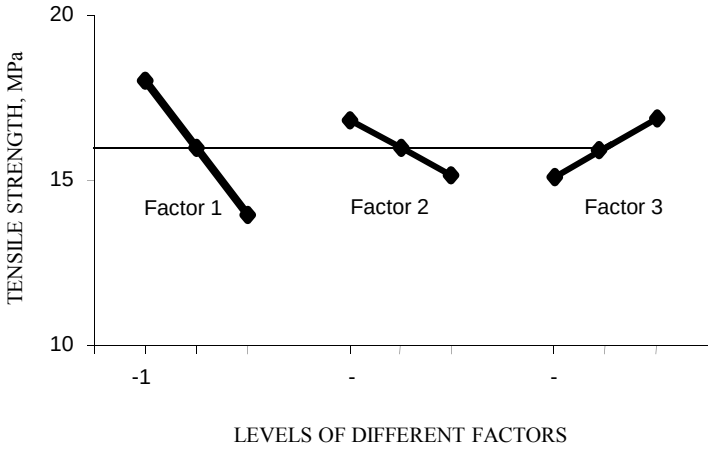

Figure 5 Responses of different factors for tensile strength

The resin must be estimated with precision because a great quantity of resin can disrupt the strength and make it lower, while a continuous granularity gives an output higher. This high strength can be offered by the marble powder.

Effect of Factors Variation on the compressive Strength

Compressive strength results are reported in table 10 in which, it is clearly shown that dune sand gives a better performance than quarry sand, and the resin is a determinant factor to obtain a high compressive strength. Table 11 shows the effect of level of different factors on compressive strength. All results are shown in Table 11 and illustrated in Figure 6.

Table 11 Effect of level of different factors on compressive strength

MATERIAL	FACTOR	COMPRESSIVE STRENGTH, MPa
Sand (Factor 1)	-1	62.07
	0	56.62125
	1	51.1725
Resin (Factor 2)	-1	61.3275
	0	56.62125
	1	51.915
Marble powder (Factor 3)	-1	52.8125
	0	56.62125
	1	60.43

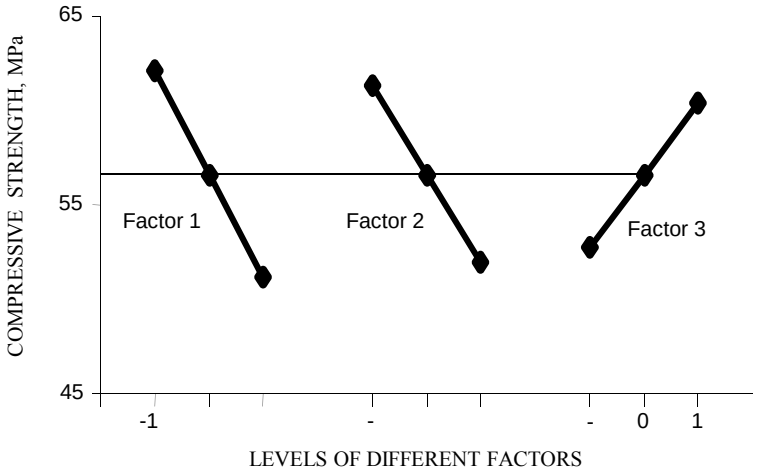

Figure 6 Response of different factors on compressive strength

CONCLUSIONS

This experimental study concerning the unsaturated resin concrete has as principal objective which is to formulate a resin concrete by using the experimental plans as a method to get the optimal proportions of different constituents.

Experiments were planned and executed according to the factorial design technique using three variables at two levels.

The results obtained showed that the experimental plans method is a feasible method to formulate this special concrete.

This study shown also that the resin concrete using an unsaturated polyester resin and local materials is a very feasible material for building applications and public works. Even its use is very specific and limited to repair works, the addition of dune sans and marble powder improves the mechanical properties and reduced the cost of the composite.

In general, on the basis on the test results, the following conclusions can be made.

- This kind of concrete is lightweight; its bulk density is around 1.89 g/cm^3.
- The tensile strength is tripled compared to the strength of traditional concrete even with aggregates of higher dimension.
- The compressive strength reaches a more substantial numbers of high performance concrete.
- A mixture of sand dune and a content of 20% by weight of the resin provide the best experimental responses.
- The continuity of the mixture in this type of concrete is preferred to get high performance.

REFERENCES

1. Y.OHAMA . Concrete-polymer Composite: The Past, Present and Future" Key Engineering Materials, Scientific.net,Vol 466, 2011,pp.1-14.
2. L.K. AGGARWAL, AND AL. Properties of polymer modified mortars using epoxy and acrylic emulsions. Construction and Building Materials, 2007, Vol 21,No .2 pp. 379-383.
3. WAHBY, W. S. Fifty years history of polymer in concrete in Review, AC International, Publication-SP 214-2, 2003, pp.13-14
4. W. J. BYING , AND AL .Mechanical properties of nano-MMT reinforced polymer composite and polymer concrete, Construction and Building Materials, Elsevier, Vol 22, 2002, pp. 14-20.
5. N. AHN . Effects of diacrylate monomers on the bond strength of polymer concrete to wet substrates. Journal of Applied Polymer Science, WILLEY, Vol 90,2003, pp. 991-1000.
6. A. BLAGA AND J.J. BEAUDOIN. Polymer Modified Concrete, Division of Building Research, National Research Council Canada, Canadian Building Digest 241, Ottawa, 1985.
7. K. S. REBEIZ . Precast of polymer concrete using unsaturated polyester resin based on recycled PET waste . Construction and Building Materials, Elsevier, Vol 10, N° 3, 1996, pp. 215-250.

8. M. C. S. RIBEIRO , AND AL .Bending Characteristics of Resin Concretes , Materials Research , Vol 06, N° 2, 2003, pp. 247-254.

9. H. ABDELFATTAH , M. ELHAWARY .Flexural behavior pf polymer concrete)," Construction and Building Materials, Elsevier, Vol 13, 1999, pp. 253-262.

10. M. ROKBI AND AL .Behaviour in rupture and Mechanical characteristics of polyester-glass fibre composites, M.Sc thesis,M'sila University , 2001.

11. J. BARON, J.P. OLLIVIER .Concretes : data bases of mix design. 3rd edition, , Paris, Eyrolls edition, 1996, pp 410-470.

12. RILEMPC2, TECHNICAL COMITTEE TC-113. Method of making polymer concrete and mortar specimens. Symposium on Properties and Test Methods for Concrete - Polymer Composites,Ostende, 1995, pp.129–132.

13. HARRIS AND SABNIS. Structural Modeling and Experimental Techniques. CRC Press 1999.

14. BAILEY, R.A. (2008). Design of Comparative Experiments. Cambridge University Press. ISBN 978-0-521-68357-9. Pre-publication chapters are available on-line.

15. BOX, G. E., HUNTER,W.G., HUNTER, J.S., HUNTER,W.G., .Statistics for Experimenters: Design, Innovation, and Discovery", 2nd Edition, Wiley, 2005, ISBN 0471718130

Influence of Recycled Aggregate in SCC Properties

K M de Vasconcelos Moreira, A E B Cabral
Federal University of Ceará (UFC), Brazil

Self-compacting concrete (SCC) has emerged from the need to produce structures heavily armed or with complex geometry in which the use of vibration results in problems. On the other hand, construction and demolition wastes (CDW) are a great problem in many countries. In Brazil, as in many parts of the world, CDW are already crushed and sieved, been transforming in recycled aggregates (RA). Once RA has different properties than natural aggregates, its use in concrete modifies concrete's properties. The aim of this article is study the replacement of natural coarse aggregate in 10%, 20% and 30% of volume by recycled coarse aggregate in SCC production. The water/cement ratio was fixed in 0.35. The influence of RA in SCC fresh conditions was verified using L box, V funnel, J ring and slump flow tests. Specimens were casted to measure compressive strength, modulus of elasticity, voids content, water absorption and specific density of SCC with RA. The results show the self-compacting properties do not decrease with the increase of RA replacement. SCC hardened properties still reach values that allow it to be used in current applications.

K M de Vasconcelos Moreira, Federal University of Ceará (UFC), Brazil. Civil Engineer, Masters Student in Structures and Civil Construction Post Graduation Program (PEC).

A E B Cabral, Federal University of Ceará (UFC), Brazil. PhD in Environmental Sciences, Professor of Structures and Civil Construction Post Graduation Program (PEC).

Keywords: Construction and demolition waste, Fresh testing, Hardened testing, Recycled aggregate, Self-compacting concrete

INTRODUCTION

Self-Compacting Concrete (SCC) is designated as a special concrete because it has the ability to mold to the shape of the structures without the aid of vibrating equipment once it uses just gravity force. This feature allows its use mainly in structures with high content of rebars and complex geometries.

To obtain a high quality, SCC has to reach some essential properties as: fluidity higher than conventional concrete to fill forms corners; cohesion enough to promote the smooth flow of concrete through the armor and resistance to segregation to prevent the formation of stone nests in concrete.

The use of SCC in Brazil is not yet all spread, primarily because there is not an accepted dosage method although Gomes and Barros [1] list nine Brazilian and international dosage methods specific to SCC. Secondly because there is not knowledge by the Brazilian constructors about the SCC performance in a real structures and they are afraid to swap to a new concrete technology. Just in 2010 the Brazilian Standard Association published a Standard NBR 15823 [2] that establish the requirements for classification, control and acceptance of SCC in the fresh conditions. This Standard also prescribes necessary tests to check the properties of SCC.

The Brazilian federal law n° 12305 [3] established the National Solid Waste Political. By this law, builders become now responsible for the waste generated in their activities and should draw up an Integrated Management Plan for Construction and Demolition Wastes for each contract. In this plan, it should be provided how many wastes will be generated and what will be doing with it. Recycling is stimulated once in some public contracts the use of recycled aggregate (RA) is obligatory.

In Brazil, the use of RA in paving work is already consolidated. Brazilian Standart NBR 15115 [4] establishes the criteria for execution of reinforcement layers of subgrade, subbase and base floors, as well as primary coating layer with RA. However, its use in structural concrete is not yet allowed. Researches should be done to convince Brazilian Standard Association members that RA is also applicable to concrete.

Join these two great areas, concrete technology and sustainability in civil construction, the objective of this paper is to analyze SCC with RA. Natural aggregates were replaced by RA in volume and fresh and hard concrete properties were analyzed.

MATERIALS AND METHOD RESEARCH

Materials

Portland cement type CPII-Z-32-RS, commonly used in Brazil, specific gravity of 3.0, was used. The fine material used was limestone fillers whose chemical composition was determined by X-ray fluorescence (Table 1). This material has specific gravity of 2.68, according to NBR NM 23 [5], and D10%, D50% and D90% of 1.194 μm, 5.555μm and 62.511μm, respectively, according test particle size by laser Mastersizer 2000 E.

Table 1 X-ray fluorescence of fine material

OXIDE	Al_2O_3	SiO_2	P_2O_5	K_2O	CaO	Fe_2O_3	SrO
Concentration, %	0,54	0,81	0,66	0,12	97,63	0,19	0,05

The fine aggregate used was washed quartz sand from river bed. Natural middle and coarse aggregates were crushed granite. The recycled coarse aggregate was obtained from concrete rubble that was crushed and screened until obtain the same maximum particle size of natural coarse aggregate. The physical indices of all aggregates are in Table 2 and the size distribution curves are shown in Figure 1.

Table 2 Physical characteristics of aggregates

Physical Indices	MATERIAL				Test Procedure
	Fine Aggregate	Natural Middle Aggregate	Natural Coarse Aggregate	Recycled Coarse Aggregate	
Maximum particle size, mm	2.40	9.50	19.00	19.00	NBR NM 248 [7]
Fineness modulus	2.52	5.72	6.74	6.81	NBR NM 248 [7]
Specific gravity	2.54	2.46	2.74	2.35	NBR NM 52 [8] - fine NBR NM 53 [9] - coarse
Bulk density, g/cm³	1.25	1.35	1.48	1.30	NBR NM 45 [10]
Compressed bulk density, g/cm³	1.37	1.46	1.59	1.40	NBR NM 45 [10]
Absorption, %	1.05	0.48	0.17	3.92	NBR NM 30 [11] - fine NBR NM 53 [9] - coarse
Content of filler material, %	1.16	0.31	0.19	0.64	NBR NM 46 [12]

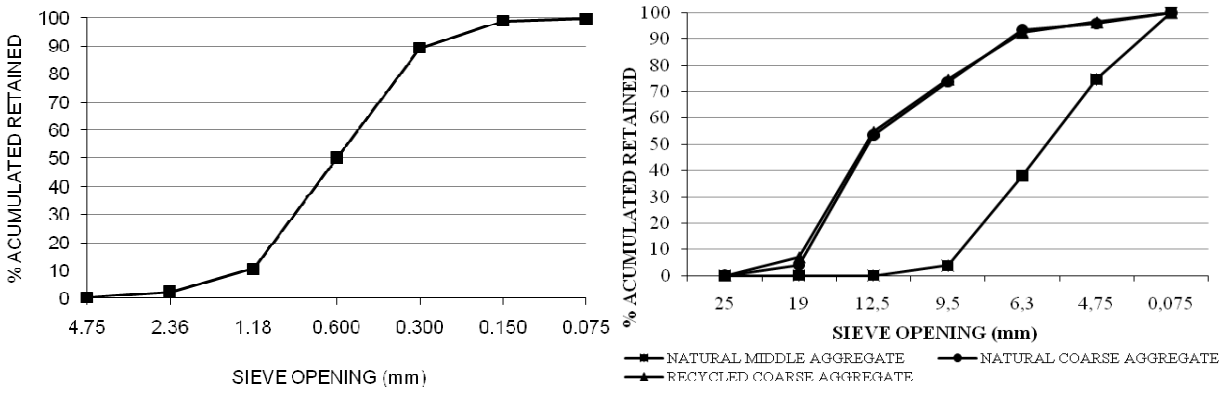

(a) (b)

Figure 1 Particle size distribution (a) of fine aggregate, (b) of middle aggregate and natural and recycled coarse aggregates.

The additive was a third generation superplasticizer based on polycarboxylic ether with 30% of solids and the water comes from public water supply system.

Research Method

The production of SCC was based on a methodology proposed by Gomes [13] that is performed by separated study of self-compacting mortar and the granular skeleton which is made by all aggregates.

Initially the granular skeleton was determined, which is defined as the proportion of materials that propitiates the less voids content. To determine this proportion, aggregates were packaged two by two in order of decreasing size and the compressed bulk density and the voids content of the aggregates mixtures were determined. Thus, coarse aggregate was packaged with middle aggregate, resulting in mixture 1. This mixture was packaged with fine aggregate resulting in the mixture 2.

Figure 2 shows the results of granular packaging of mixing 1 and 2. The voids content of mixture 1 was 39.53% for a granular skeleton composed by 60% of coarse aggregate and 40% of middle aggregate. Mixture 2 has 29.87% of voids content and it was composed by 50% of fine aggregate and 20% of middle aggregate and 30% coarse aggregate.

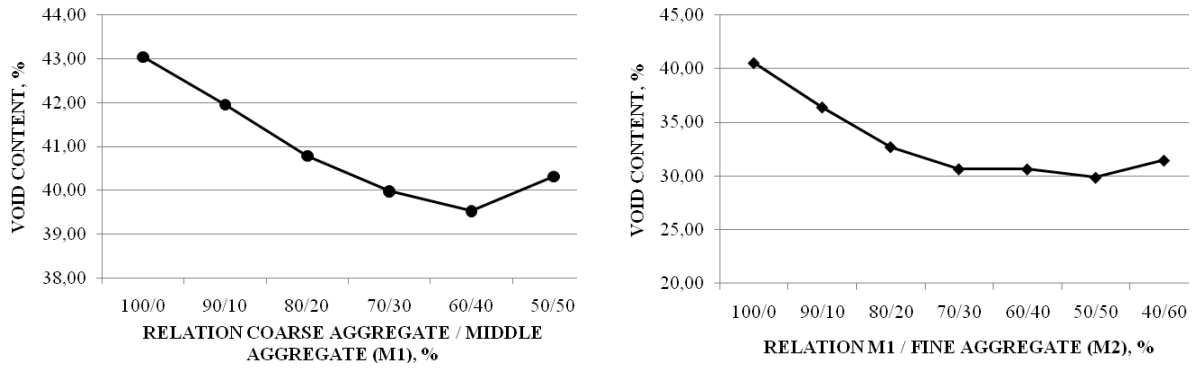

(a) (b)

Figure 2 Voids content behavior of granular skeleton (a) of mixture 1; (b) of a mixture 2.

Separately, the study of self-compacting mortar was carried out by testing solid superplasticizer/binder ratio (sp/b) through Marsh cone test (figure 3-a) and consistency table truncated cone (figure 3-b). The water/cement ratio (w/c) and the filler/cement ratio (f/c) were fixed at 0.35 and 0.4, respectively.

The Marsh cone test was used to measure the maximum content of superplasticizer that can be used in the mixture (saturation point). From this value, there is no increase in the mortar fluidity and superior contents of superplasticizer may cause segregation.

(a) (b)

Figure 3 (a) Marsh cone; (b) consistency table truncated cone.

The test consists in adding 1 liter of mortar in the cone and measure the time (t) that the mortar needs to flow and fill a 500 ml beaker. Thus, the amount of cement, fine material, sand and water was fixed. The superplasticizer was added in levels of 0.45%, 0.50%, 0.55% and 0.60%. A graph log (t) versus sp/b was plotter as in Figure 4. Gomes [13] comments that the optimum percentage of additive corresponds to an interior angle in the curve that is equal to 140° ± 10°. For this experiment the sp/b ratio of 0.50% represents the saturation point.

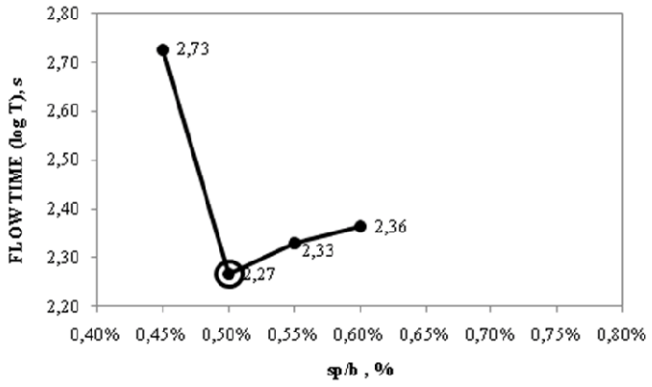

Figure 4 Marsh cone curve detailing the saturation point of the superplasticizer

After the determination of the saturation point of the mixture, the consistency table truncated cone was used to analyze the mixture flowability. The test consists in put the truncated cone on a smooth glass plate, fill it with mortar and quickly raise it. After the mortar stop flow, the diameter should be measured by two perpendicular lines. The average diameter should be between 200mm and 300mm, as Gomes [13] recommend.

The average diameter obtained by the mixture in this test was 290mm obeying the required range as can be seeing in Figure 5-a. It was also possible to see that was no segregation in the mortar (Figure 5-b), indicating that the ratio f/c of 0.40 was adequate for SCC production.

To obtain the final proportion for all materials the volume of paste in the concrete was fixed in 40%, according to Gomes [13]. The obtained SCC mix was 1:0.4:1.62:0.65:0.97:0.35 (cement: fine material: fine aggregate: middle aggregate: coarse aggregate: w/c ratio).

Four types of concretes were produced naming then SCC_Ref, SCC10%, SCC20% and SCC30% for a self-compacting concrete without recycled aggregate and self-compacting concrete with replacement of 10%, 20% and 30%, respectively, of natural coarse aggregate by recycled coarse aggregate, in volume.

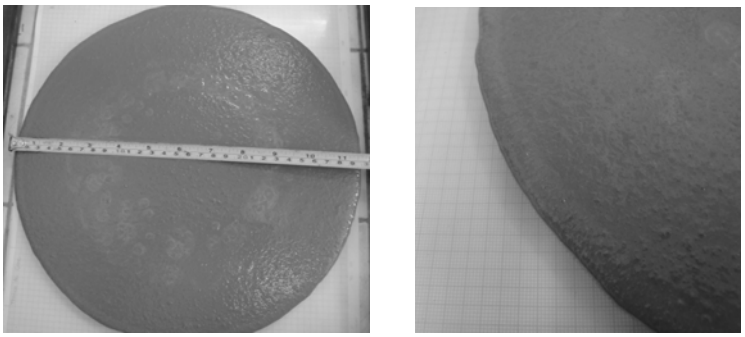

(a) (b)

Figure 5 Testing with truncated cone showing (a) the final spread and (b) non-segregation of the mortar

SCC were produced employing an inclined axis mixer with a capacity of 120 liters. All materials were weighed on a calibrated scale and placed in the mixer in the same order (aggregates and a half content of water, cement and limestone fillers, remaining water and additive). For SCC with recycled aggregates, an additional water was used due to the high water absorption of recycled aggregates. This additional water was calculated from the content of recycled aggregate in the mixtures and its absorption. This water was incorporated to the mixing water.

For all SCC, slump flow, flow time for Abrams cone, J ring, L box and V funnel tests were performed in fresh state, according to the proceedings of NBR 15823 [2]. Cylindrical specimens (10cm x 20cm) were casted according to NBR 5738 [14] and cured until 28 days age. Compressive strength (NBR 5739 [15]), water absorption, voids content and specific gravity (NBR 9778 [16]) were determined for all concretes.

RESULTS AND DISCUSSION

SCC Fresh Conditions

Table 3 presents fresh concrete results for each mixture and its variation in percentage to the referential SCC properties. The Brazilian Standard NBR 15823 [2] brings limits to each fresh property test according to concrete application. Thus, reference SCC was produced aiming to be used for current applications, like concrete walls, beams and columns. As can be seen in Table 3, for the slump flow test the replacement of natural coarse aggregate by recycled coarse aggregate virtually did not had influence. This behavior is coherent with results found by Kou and Poon [17] and Ridzuan et al. [18].

However, RA has some influence for the other SCC fresh properties. L box and J ring had reductions when RA was inserted in concrete mixtures presenting mean reductions around 6% and 43%, respectively. Flow time and V funnel tests presented an undefined behavior once they reduced their values for 10% of replacement, increased for 20% and decreased

again for 30%. In a general, the replacement of natural coarse aggregates by recycled aggregates did not cause relevant changes in fresh properties of SCC although SCC20% behaved more distinct from the others, showing cohesion and segregation resistance.

Table 3 Fresh property results of SCC

TESTS	SCC_Ref	SCC10%		SCC20%		SCC30%	
		Obtained results	Percentage variation to SCC_Ref	Obtained results	Percentage variation to SCC_Ref	Obtained results	Percentage variation to SCC_Ref
Slump flow (mm)	751	757	+ 0.80%	750	- 0.1%	750	- 0.1%
Flow time (s)	5.27	4.94	- 6.3%	7.59	+ 44.0%	5.75	+ 9.1%
V funnel (s)	17.25	15.28	- 11.4%	25.63	+ 48.6%	16.46	- 4.6%
L box*	0.93	0.93	0.0%	0.87	- 6.5%	0.88	- 5.4%
J ring (mm)	46.00	27.50	- 40.2%	25.50	- 44.6%	25.00	- 45.7%

*adimensional

Compressive Strength

Figure 6 presents the results obtained for compressive strength at 28 and 56 age days. The introduction of 10%, 20% and 30% of RA in the SCC mixtures resulted in an increase of 15%, 36% and 35% in compressive strength at 28 age days, respectively. As can be seen in Figure 6, the behavior of compressive strength at 56 age days was similar to 28 age days, increasing it in 12%, 22% and 24%, respectively. This indicates that the presence of recycled aggregates did not jeopardize this mechanical property, probably due to the great involvement of recycled aggregates by the new mortar, improving the interfacial transition zone (ITZ). This behavior is coherent with results found by Kou and Poon [17] and Ridzuan et al. [18] in SCC with recycled aggregates.

Modulus of Elasticity

Figure 7 shows test results for modulus of elasticity for SCC specimens at 28 days of age. As can be noted, only the replacement of 20% of natural coarse aggregate by recycled coarse aggregate had a considerable influence in this property, with an improvement of 8%. For 10% and 30% of replacement, the increase/decrease in this property was less than 1%. This behavior is coherent with results of Etxeberria et al. [19] but with non self-compacting concrete, once the module of elasticity for concretes with 25% replacement of natural coarse aggregate by recycled aggregate decreases only 3.8%.

Water Absorption

Generally concrete made with recycled aggregates are characterized by a high percentage of meso and macro pores, thus suggesting a greater porosity and water absorption than those prepared with natural aggregates [20].

According to Gómez-Sobéron [21], the distribution of pores in concrete with replacement of natural aggregate by recycled is modified, being most sensitive for high levels of replacement.

Figure 8 shows test results for water absorption by immersion performed at 28 days of age for all SCC. For concrete with 10% of RA the water absorption decreases 17% comparing to reference concrete's absorption. It increases 29% and 36% with an introduction of 20% and 30% of RA in concrete, respectively.

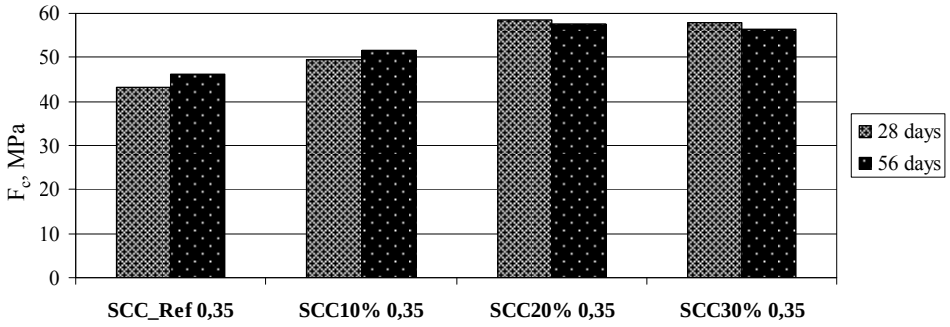

Figure 6 Results for compressive strength test at 28 and 56 age days

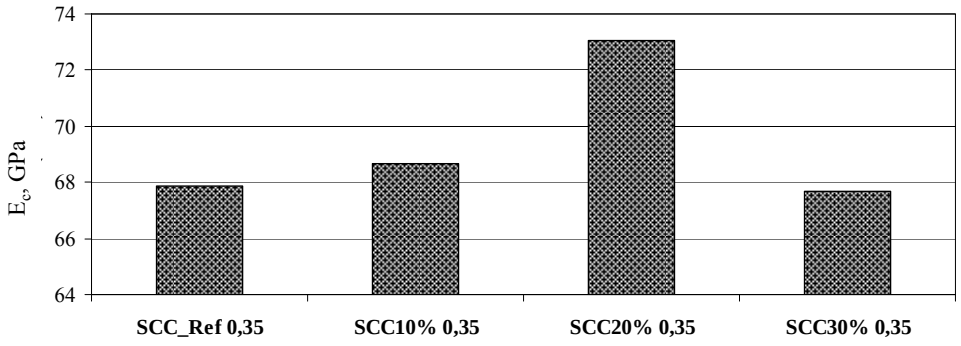

Figure 7 Results for modulus of elasticity test at 28 age days

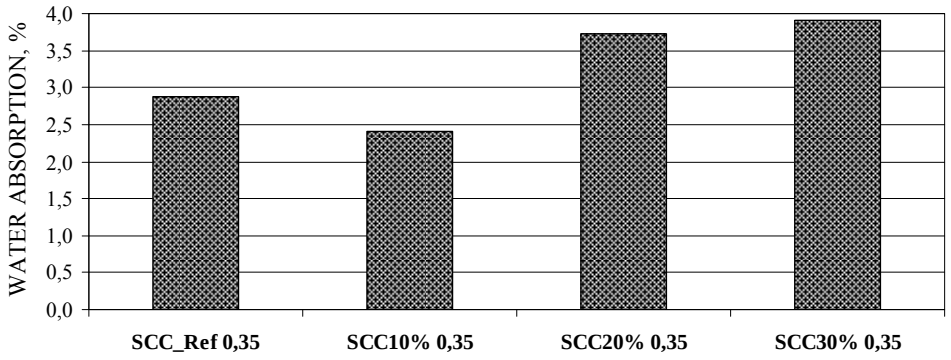

Figure 8 Results of water absorption test at 28 days

It is believed that there was a failure when SCC10% water absorption test was carried out, once its result was lower than SCC_Ref absorption. The expectation was that the higher the recycled aggregate content, the higher the water absorption, once recycled aggregate have more porous than natural aggregate. The aggregate's water absorption test results shown in table 2 reveal that the recycled coarse aggregate's water absorption is 23 times the natural coarse aggregate's water absorption. This high content of porous serves as path for water intake into the concrete, that explain the higher concrete's water absorption for high content of recycled aggregates.

Void Content

Figure 9 shows voids index test results for SCC carried out at 28 days of age. As occurs to water absorption, void content of SCC20% and SCC30% are 28% and 32% higher, respectively, than the reference SCC's void content. Although, for SCC10%, void content was 17% lower than to SCC_Ref.

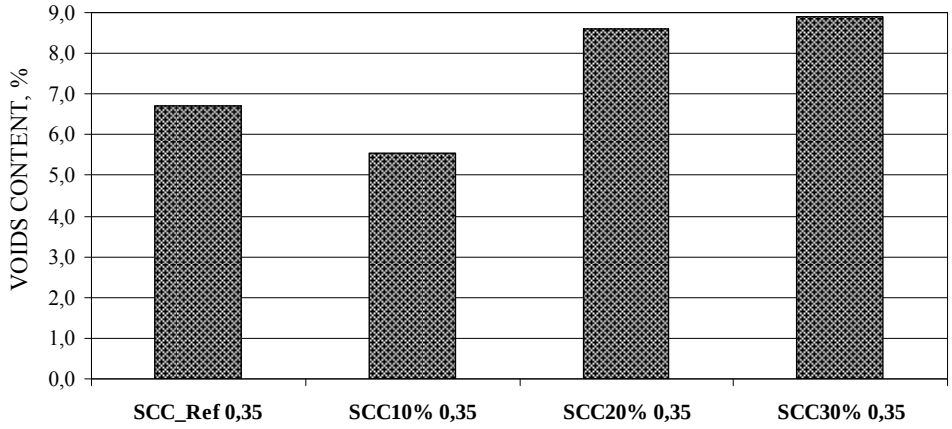

Figure 9 Results of void content test at 28 age days

As the procedure of void content test is the same procedure used to water absorption test, Brazilian Standard NBR 9778, it is believed that there was a failure when SCC10% void content test was carried out, resulting in a void content lower to SCC10% than to SCC_Ref. Analyzing SCC20% and SCC30% void content results it is possible to deduce that the presence of recycled aggregate has a negative influence in concrete's void content, increasing it. Excepting the SCC 10% result, this behavior in coherent with Rizvi et al. [22], once their concrete containing 15% had void content very similar to that of the control mix. Samples that contained 30% of recycled aggregate or greater had a significant increase in void content.

Specific Gravity

Figure 10 shows specific gravity of SCC at 28 days of age. As can be seen, recycled aggregate virtually has no influence in this concrete's property, once the maximum decrease/increase was 2.2% for 10% of recycled aggregate and this value is in the error range intrinsic to the test. This behavior is coherent with Etxeberria et al. [19] results in non SCC with 25% recycled aggregate once its specific density was less than 1% lower than conventional concrete specific density.

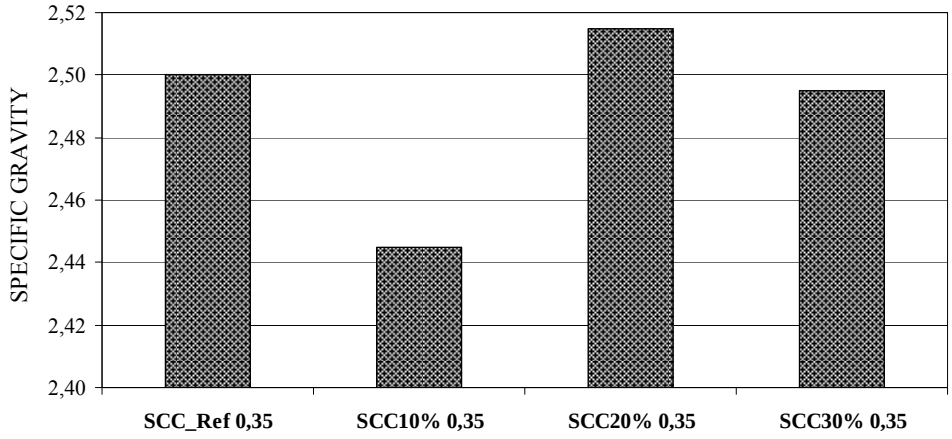

Figure 10 Results of specific gravity test at 28 age days

FINAL CONSIDERATIONS AND CONCLUSIONS

According to test results obtained from concretes with a content of coarse recycled aggregate, it may be concluded that the replacement of natural aggregate by recycled aggregate did not cause relevant changes in concrete's fresh properties, allowing then to use in current applications, like concrete walls, beams and columns.

For hard properties, recycled aggregate introduced irrelevant changes in SCC. Compressive strength and modulus of elasticity had satisfactory results, indicating that recycled coarse aggregates can replace natural aggregate up to 30%. However, water absorption and void content of SCC increased by the presence of recycled aggregate in the concrete. This behavior occurs due to the high porosity of recycled aggregates that make SCC with more porous and voids. Recycled aggregate has no influence in SCC specific density.

ACKNOWLEDGEMENTS

Authors thank to the Brazilian National Council for Scientific and Technological Development (CNPq) and to the Structures and Civil Construction Materials Research Group of Federal University of Ceará (GPMATE/UFC).

REFERENCES

1. GOMES, P. C. C.; BARROS, A. R. Dosage methods for self-compacting concrete. São Paulo: PINI, 2009.

2. BRAZILIAN STANDARD ASSOCIATION (ABNT). NBR 15823: Self-compacting concrete (Parts 1 to 6). Rio de Janeiro, 2010.

3. NATIONAL POLITICS OF SOLID WASTES (PNRS). Federal Law Nº 12305. 02 ago 2010.

4. BRAZILIAN STANDARD ASSOCIATION (ABNT). NBR 15115. Recycled aggregates of construction and demolition wastes – Construction of pavement layers – Procedures. Rio de Janeiro, 2004.

5. BRAZILIAN STANDARD ASSOCIATION (ABNT). NBR NM 23: Portland cement and other powder materials: specific density determination. Rio de Janeiro, 2001.

6. BRAZILIAN STANDARD ASSOCIATION (ABNT). NBR 15115: Recycled aggregates of construction and demolition wastes – Construction of pavement layers - Procedures. Rio de Janeiro, 2004.

7. BRAZILIAN STANDARD ASSOCIATION (ABNT). NBR NM 248: Aggregates: determination of particle size distribution. Rio de Janeiro, 2003.

8. BRAZILIAN STANDARD ASSOCIATION (ABNT). NBR NM 52: Fine aggregate: determination of specific gravity and bulk density. Rio de Janeiro, 2003.

9. BRAZILIAN STANDARD ASSOCIATION (ABNT). NBR NM 53: Coarse aggregate: determination of specific gravity, bulk density and water absorption. Rio de Janeiro, 2003.

10. BRAZILIAN STANDARD ASSOCIATION (ABNT). NBR NM 45: Aggregates: determination of bulk density and volume of voids. Rio de Janeiro, 2006.

11. BRAZILIAN STANDARD ASSOCIATION (ABNT). NBR NM 30: Fine aggregate: determination of water absorption. Rio de Janeiro, 2001.

12. BRAZILIAN STANDARD ASSOCIATION (ABNT). NBR NM 46: Aggregates - Determination of material finer than 75μm sieve by washing. Rio de Janeiro, 2003.

13. GOMES, P. C. C. Optimization and characterization of high-strength self-compacting concrete. Universitat Politécnica de Catalunya. (Thesis), Escola Técnica Superior d'Enginyers de Camins, Canals i Ports de Barcelona. Barcelona, 2002.

14. BRAZILIAN STANDARD ASSOCIATION (ABNT). NBR 5738: Concrete: procedure of molding and curing of concrete test specimens. Rio de Janeiro, 2007.

15. BRAZILIAN STANDARD ASSOCIATION (ABNT). NBR 5739: Concrete: compression test of cylindrical specimens – Method of test. Rio de Janeiro, 2007.

16. BRAZILIAN STANDARD ASSOCIATION (ABNT). NBR 9778: Hardened mortar and concrete - Determination of absorption, voids and specific gravity. Rio de Janeiro, 2006.

17. KOU, S. C., POON, C. S. Properties of self-compacting concrete prepared with coarse and fine recycled concrete aggregates. Cement & Concrete Composites, 31, p. 622–627, 2009.

18. RIDZUAN, A. R. M., FAUZI, M. A. M., KASSIM, A. The evaluation of self consolidating concrete incorporating crushed concrete waste aggregate. In: 3rd International Symposium & Exhibition in Sustainable Energy & Environment, Melaka, Malaysia. 2011.

19. ETXEBERRIA, M.; VÁZQUEZ, E.; MARÍ, A.; BARRA, M. Influence of amount of recycled coarse aggregates and production process on properties of recycled aggregate concrete. Cement and Concrete Research, 37, p. 735–742, 2007.

20. SANI, D.; MORICONI, G.; FAVA, G. CORINALDESI, V. Leaching and mechanical behavior of concrete manufactured with recycled aggregates. Waste Management, Vol. 25, p. 177-182, 2005.

21. GÓMEZ-SOBERÓN, J. M. V. Porosity of recycled concrete with substitution of recycled concrete aggregate: na experimental study. Cement and Concrete Research, Vol. 32, p. 1301-1311, 2002.

22. RIZVI, R.; TIGHE, S.; HENDERSON, V.; NORRIS, J. Evaluating the Use of Recycled Concrete Aggregate in Pervious Concrete Pavement. Transportation Research Record: Journal of the Transportation Research Board. Vol. 2164, 2010.

The Use of Concrete Filler as a Mineral Admixture in Concrete

V Bilek
ZPSV a.s., Czech Republic

One of the most important challenges of present time concrete science is how to reduce Portland cement production and limit its use. One reason for this is a need for CO_2 emission reduction and another a need for a saving of natural resources (limestone, energy). The present paper deals with some results achieved by a replacement of natural ground limestone with ground recycled concrete. Two different concretes were used as the source of concrete filler. Both of them were ground to three specific surfaces. A limestone of similar specific surfaces was used too. Mortars were mixed with a blend of Portland cement, fly ash and concrete filler or limestone filler. The compressive strengths at the age of 24 hours and 28 days are presented in the paper. The results prove that mortars with fly ash and concrete filler show a similar workability; worse early-age strengths and better 28-day strengths than those with fly ash and limestone

Vlastimil Bilek is a Research Engineer at the ZPSV a.s., He received his MS and PhD from Brno University of Technology. His research interests include alkali activated materials, concretes with mineral admixtures and durability of concrete. He is involved in the organisation of Non-Traditional Cement and Concrete Conferences in Brno, Czech Republic (2002, 2005, 2008 and 2011).

Keywords: Concrete filler, Fly ash, Limestone, Synergy, Ternary binders

INTRODUCTION

Concrete production is increasing and it will continue to increase in the years to come. That is why alternative binders are being searched for. The substitution of a part of cement by mineral admixture can save an amount of cement, but this is often accompanied by a decrease of (early) strength and other mechanical properties. Some results have been published about ternary binders – for example, mixtures of PC, ground blast-furnace granulated slag and fine limestone. An optimum composition of these materials can enhance early strength.

Some interesting results with ternary blends have been published in literature. For example, Irassar *et al.* [1, 2] tried to combine the positive properties of ground granulate blast furnace slag and ground limestone and depress their negative properties. Limestone filler improves the early strength of concrete while slag improves the later strength. Sometimes, the results were unexpected – mortars containing ternary blend reached higher strengths than mortars with binary blends. This phenomenon can be called a synergic effect. They present two reasons for explaining this. The first is the effect of limestone on the hydration C_3A. In accordance to [3], during hydration of C_3A in the presence of limestone, carboaluminates are formed and the ettringite – monosulfoaluminate transformation is delayed or impeded.

The second reason is the fact that small limestone particles constitute nucleation sites of calcium hydroxide crystals at early ages accelerating the hydration, especially C_3S.

A similar explanation is also given by Kadri *et.al*. [4]. They emphasize the role of submicroscopic particles of limestone which serve as precipitation nuclei of hydration products. They, similarly to [1-3] point out a higher content of portlandite in hydrated paste from cement with limestone filler. Also Bilek [5, 6] studied the strengths of ternary blends with limestone filler and blast furnace slag and limestone filler and fly ash, and also some other compositions of ternary blends. Although the effect of its use is rather beneficial, limestone represents a natural non-renewable material which should rather be replaced by some waste material. But is there a material similar to limestone. It can potentially be old concrete.

As concrete is the most widely used construction material around the world, large volumes of old recycled concrete can be obtained from demolished structures. As the volumes of produced concrete increase, also the volumes of demolished structures increase. Recycled concrete can be used as a replacement of aggregates in new concrete of lower class, but fraction under 4 mm are usually not used for concrete production – they contain a high portion of hardened cement paste which increases absorption capacity and worsens the workability of concrete. Besides, fractions under 4 mm contain a high content of fine particles, which may cause some problems, too. On the other hand, however, all of these properties make the “fine” recycled concrete suitable to be used as a replacement of limestone. Old concrete is usually carbonated – part of concrete is $CaCO_3$ – and also aggregates can come from limestone. This indicates certain similarity between old concrete and limestone. Some experiments with concrete filler as a mineral admixture have already been performed, see [7, 8].

MATERIALS AND EXPERIMENTAL PROCEDURE

Fly ash met requirements of EN 450 “Fly ash for concrete production“. The composition of the fly ash is shown in Table 1. The activity index of the fly ash exceeds 85%.

Limestones which differ by a specific surface were also used, for properties see Table 1 and 2. These limestones are usually used in concrete production – especially in Self-Compacting Concrete production – as inactive mineral admixtures.

Concrete filler was obtained by the crushing of two types of concrete. Filler S arose from 1-year old cubes of SCC – 440 kg CEM I 42.5R, 150 kg limestone, water / (cement + limestone) ratio was 0.32, aggregates / paste volume ratio was 1.32. This concrete was ground in a ball mill to three different specific surfaces – see Table 2. Concrete filler P arose from cubes from control tests of concrete sleepers. The age of the cubes was 1 year, the concrete contained 365 kg CEM I 52.5N, water/cement ratio was 0.31, aggregate / paste volume ratio was 3.26. This concrete was ground in a ball mill to specific surfaces 241, 341 and 487 m²/kg. Portland cement CEM I 42.5 R (see EN 197) was also used, see Table 1 and 2.

Table 1 Chemical composition of compounds

	CaO	SiO_2	Al_2O_3	Fe_2O_3	MgO	K_2O	Na_2O	TiO_2	SO_3
Fly ash	3.6	49.7	24.9	14.7	1.15	1.9	0.6	1.4	1.3
Limestone 7,8,9	97.0	1.5	0.7	0.3	0.9	-	-	-	0.05
CEM I 42.5 R	61.7	22.5	5.2	3.6	1.0	1.0	0.14	-	3.2

Table 2 Properties of compounds

	SPECIFIC SURFACE, m^2/kg	POZZOLLANA ACTIVITY*, g CaO/g	COMPRESSIVE STRENGTH, MPa		
			1 day	7 days	28 days
Fly ash	468	222	-	-	-
Limestone 7	248		-	-	-
Limestone 8	360	33	-	-	-
Limestone 9	458		-	-	-
Concrete filler S 250	259		-	-	-
Concrete filler S 350	380	56	-	-	-
Concrete filler S 450	501		-	-	-
Concrete filler P 250	241		-	-	-
Concrete filler P 350	341	19	-	-	-
Concrete filler P 450	487		-	-	-
CEM I 42.5 R	382	-	13.0	47.7	54.4

* Chapelle test

Mortars were prepared using drinking water and three sands of narrow fractions (standard sands). The composition of mortars was based on the composition of standard mortars in accordance to EN 196-1. This composition is also prescribed for the evaluation of the activity index of fly ash (EN 450). For this purpose, the substitution of 25% of cement by fly ash is prescribed. The 28-days´ strength of this mortar must represent a minimum 75% of comparative mortar from cement only. Except for the mortar with fly ash, the mortar with a replacement of 25% of cement with mixture of fly ash or limestone also mortars with a replacement of 25 % of cement by blends of grounded limestone (L) or fly ash and concrete filler (CF) were prepared – for the composition of the mortars see Table 3.

All mortars were mixed in a laboratory mixer. The workability of mixtures was measured by means of the minicone flow method (truncated cone bottom base 100 mm, upper base 70 mm, height 60 mm). In this test, a cone is filled with mortar. The mortar cone is shaken 15 times in the jolting table and the cone flow is measured in two perpendicular directions; the result is the average value of these values.

Table 3 Composition of mortars (all masses are in grams)

	COMPA-RATIVE	25% FA	18.7 FA + 6.3 L	12.5 FA + 12.5 L	6.3 FA +18.7 L	25% L
Cement	450	338	338	338	338	338
Fly ash	0	112	84	56	28	112
L or CF	0	0	28	56	84	0
Drinking water	225	225	225	225	225	225
Sand 1	450	450	450	450	450	450
Sand 2	450	450	450	450	450	450
Sand 3	450	450	450	450	450	450

Three beams were made from each mix, 6 beams for each mortar composition. The beams were demoulded at the age of 24 hours. After demoulding, 2 beams were tested and another 4 beams were stored in water at a temperature of 20°C (in saturated solution of $Ca(OH)_2$) for tests at the age of 7 and 28 days. Bending strengths and compressive strengths were measured in accordance to EN 196-1.

RESULTS AND DISCUSSION

The workability of the mortar with fly ash or mortar with fly ash and a small amount of the second admixture was better than that of the other ones (see Figure 1). This was expected as grains of fly ash are usually spherical and enhance workability.

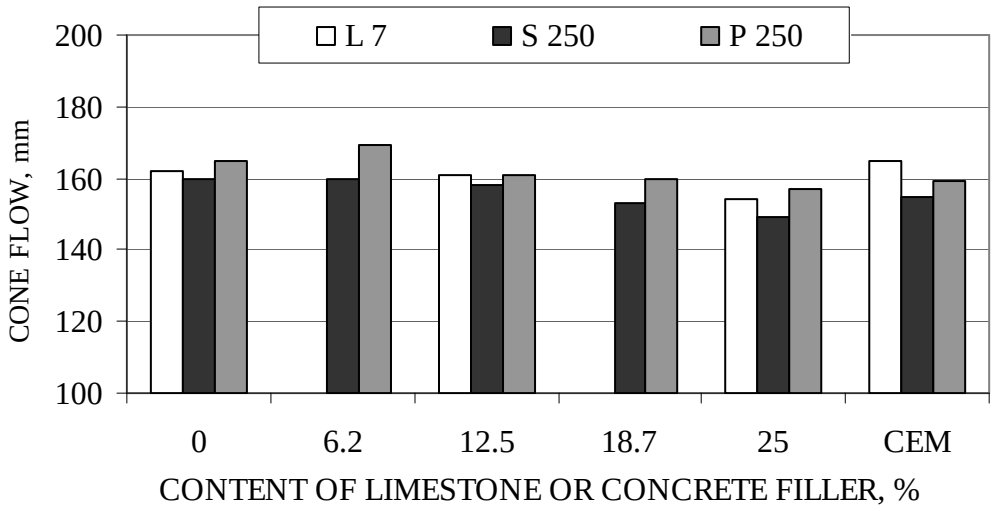

Figure1 Workability of mortars with replacement of cement by mix of fly ash (supplement up to 25%) and limestone or concrete filler with specific surface cca 250 m²/kg

The activity indices for relatively coarse admixtures show a beneficial effect of limestone on early compressive strength (see Figure 2). The strength of mortar with 12.5% of limestone and 12.5% of concrete filler is the best – higher than the other two. This agrees with the discussion presented in introduction. The early strengths of mortars with concrete fillers are lower (lower activity indices) and they reach nearly the same value for all ratios of fly ash /concrete filler. At the age of 28 days the situation is different. The mortars with the highest content of concrete filler show the highest strengths. This might have been a consequence of unhydrated cement grains in concrete filler.

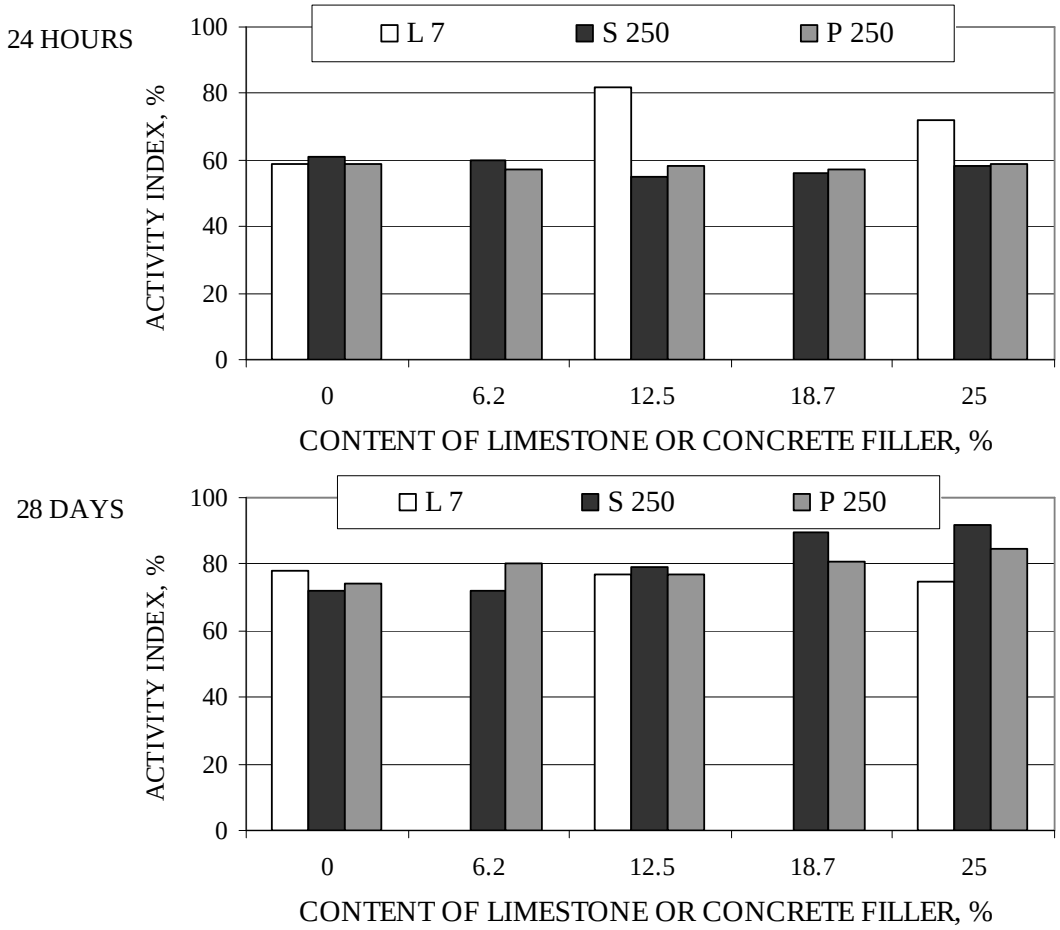

Figure 2 Indices of activity of ternary blends composed from fly ash and limestone or concrete fillers with specific surfaces of approximately 250 m²/kg

Workability of mortars with admixtures with specific surfaces of approximately 350 m²/kg is shown in Figure 3. In the case of mortar with fly ash and P 350 (grey columns), the ternary blend has the best workability. In all cases the workability of mortars with optimum amount of admixtures is better than that of mortar with cement only.

Indices of activity of mortars with limestone and concrete fillers with specific surfaces of approximately 350 m²/kg - Figure 4 - are similar as in the previous case. Again – the ternary binder with limestone shows the best early strength – nearly as good as the mixture with ordinary Portland cement only. The early strengths of mortars with concrete filler instead of limestone show substantially lower strengths without a dependence on the ratio between fly ash and concrete filler. At the age of 28 days mortars with concrete filler show the same or even better indices of activity than mortars with limestone.

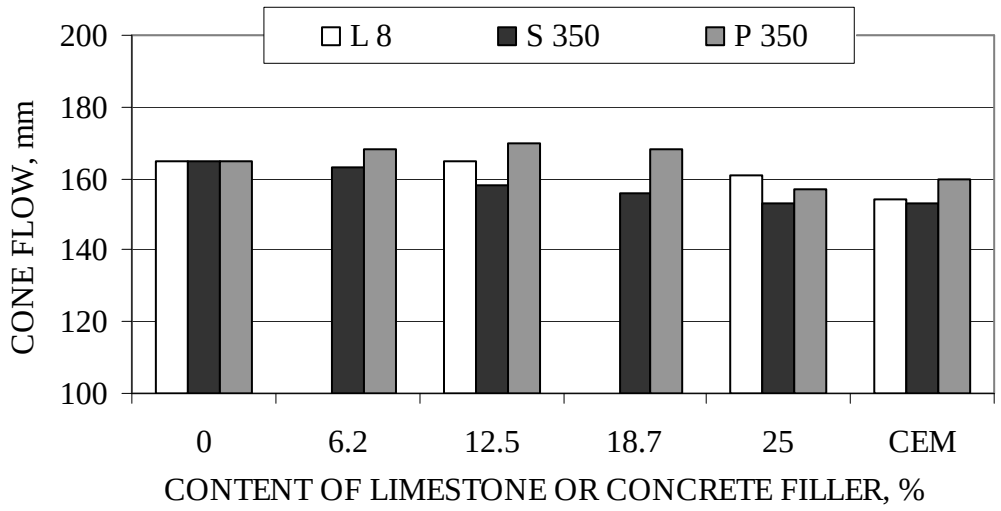

Figure 3 Workability of mortars with replacement of cement by mix of fly ash and limestone or concrete filler with a specific surface of approximately 350 m²/kg

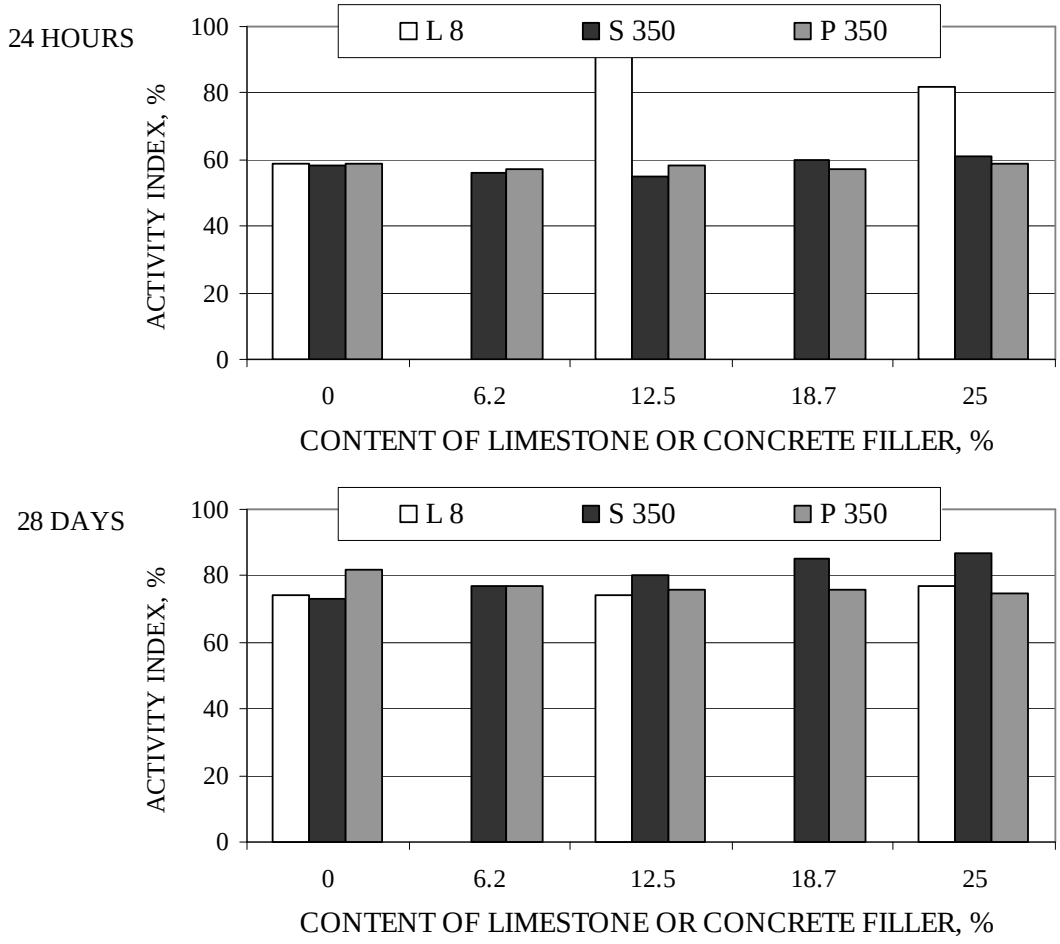

Figure 4 Indices of activity of ternary blends composed from fly ash and limestone or concrete fillers with specific surfaces of approximately 350 m²/kg

For the most fine admixtures – specific surface approximately 450 m²/kg - the workability of mortars with fly ash are better then the other ones – see Figure 5. Also the workability of mixture with limestone is a bit better than that with concrete filler.

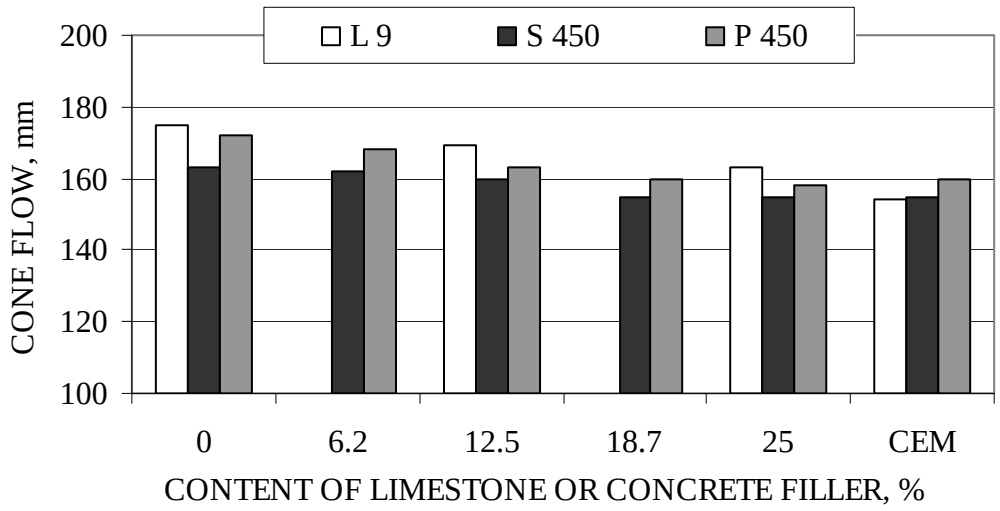

Figure 5 Workability of mortars with replacement of cement by mix of fly ash and limestone or concrete filler with a specific surface of approximately 450 m²/kg

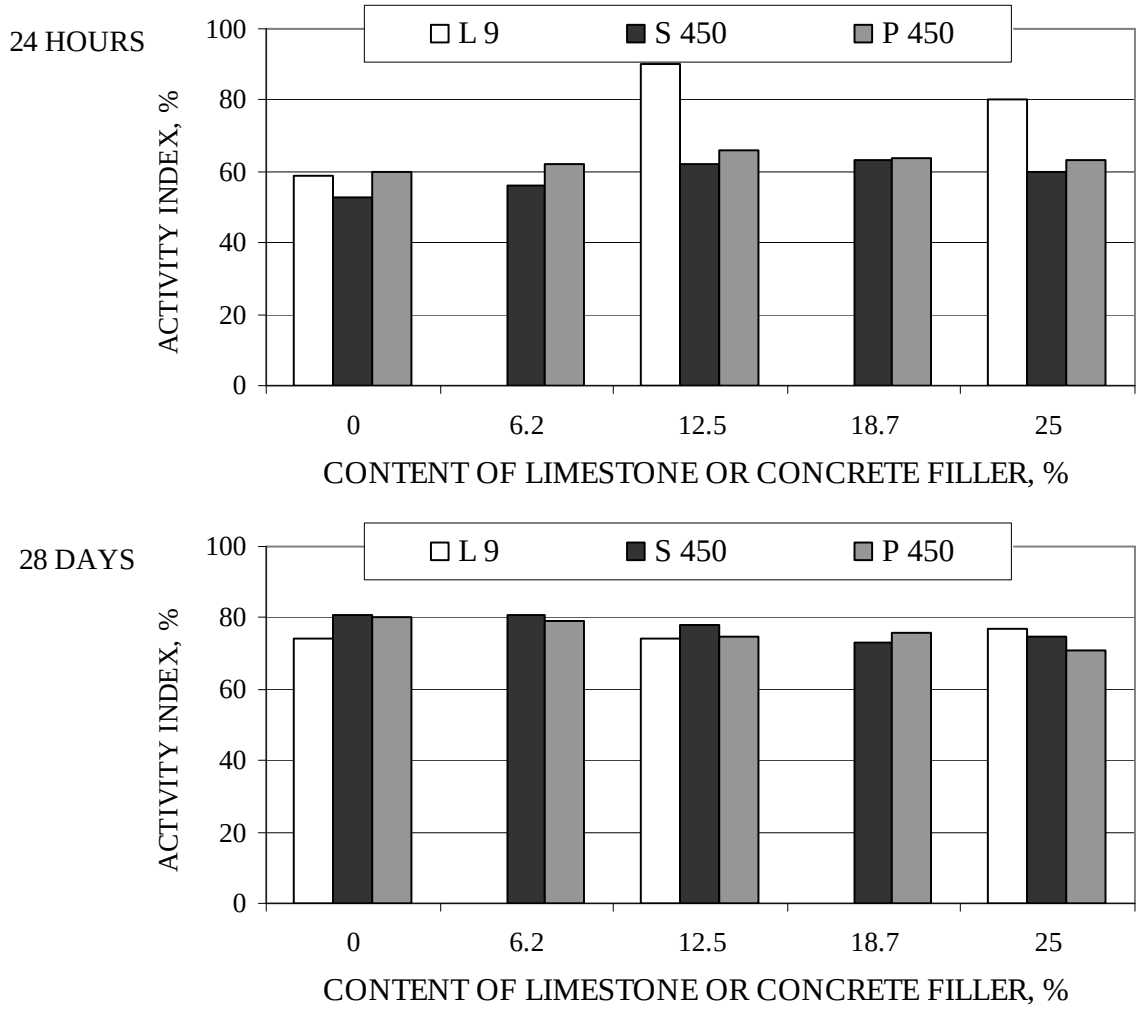

Figure 6 Indices of activity of ternary blends composed from fly ash and limestone or concrete fillers with specific surfaces of approximately 450 m²/kg

As Figure 6 shows, in the case of the most fine limestone and concrete fillers the indices of activity of mortars with limestone are again much higher in comparison with mortars with concrete fillers. Limestone shows a synergic effect again – the strength of ternary binder is the best. But concrete fillers also show some poor synergy in this case. Ternary binders show slightly better indices of activity. At the age of 28 days the indices lie between 70 and 80%; the values for mortars with concrete filler are usually higher.

CONCLUSIONS

It clearly follows from the presented results that concrete filler is a quite good choice when considering a substitution of natural limestone with waste material. Early strengths of mortars with concrete fillers are lower than those with limestone, but 28-day strengths are often higher for concrete filler. Also the workability of ternary blends with concrete filler is fairly good – comparable with that of mortar with limestone fillers.

The synergic effect (better early strength of ternary blend) is noticeable for finely ground concrete filler (450 m^2/kg in our case) and a dependence on the composition of the concrete was not observed. The presented results should awake an interest in these waste materials.

ACKNOWLEDGEMENTS

This work was financially supported by the Ministry of Industry and Business of Czech Republic, project FR TI 1/004.

REFERENCES

1. CARRASCO M F, MENÉNDEZ G, BONAVETTI V AND IRASSAR E F, Strength development of ternary blended cement with limestone filler and blast furnace slag, Cement and Concrete Composites Vol. 25, 2003, pp. 61-67.

2. CARRASCO M F, MENÉNDEZ G, BONAVETTI V AND IRASSAR E F, Strength optimization of tailor-made cement with limestone filler and blast furnace slag, Cement and Concrete Research, Vol. 35, 2005, pp. 1324-1331.

3. KAKALI G, TSIVILIS S, AGGELI E AND BATTI M, Hydration products of C_3A, C_3S and Portland cement in the presence of $CaCO_3$, Cement and Concrete Research, Vol. 30, 2000, pp. 1073-1077.

4. KADRI E H, AGGOUN S AND DE SCHUTTER G, Combined effect of chemical nature and fineness of mineral powders on Portland cement hydration, Materials and Structures, Vol. 43, 2010, pp. 665-673.

5. BILEK V, Ternary binders development and some properties, Proc. of Int. Conference Dostizenia i problemy materialovedenija i modernizacii stroitelnoj industrii, edited by R. Rakhimov, Kazan University Publishing, Kazan, Russia, 2004, pp. 190-194, (in Russian).

6. GHRICI M, KENAI S AND SAID-MANSOUR M, Mechanical properties and durability of mortar and concrete containing natural pozzolana and limestone blended cements, Cement and Concrete Composites, Vol. 29, 2007, pp. 542-549.

7. CORINALDESI V, ORLANDI G AND MORICONI G, Self-Compacting Concrete incorporated recycled aggregate, Proc. of Conf. Innovations and Developments in Concrete Materials and Constructions, Eds. R K Dhir, P C Hewlett, L J Csetenyi, Dundee (Scotland), 2002, pp. 455-463.

8. COLLEPARDI M, The New Concrete, ENCO s.r.l., 2006, 400 p.

Fibre Reinforced Aerated Cement with Composite-based Rubber Tyre Particles

A Benazzouk[1], O Douzane[1], T Langlet[1], M Merzoud[2]
1 – University of Picardie Jules Verne, France
2 – University of Badji Mokhtar, Algeria

The large demand on building material industry has resulted from the increasing population, leading to a chronic shortage of building materials. The engineers have been challenged to convert the industrial wastes to useful building and construction materials. Accumulation of unmanaged wastes is one of significant environmental concerns, especially in developing countries. Recycling of such wastes as building materials appears to be viable solution to both pollution problem and economical design of buildings. In recent years, considerable research has been conducted on the utilisation of waste like fly ash, silica fume, blast furnace slag, lightweight crushed bricks, pozolanic materials, lightweight expanded clay aggregates, and foam polystyrene in civil engineering materials. Each of these wastes has provided a specific effect on the properties of fresh and hardened cement based materials. The two main potential fields in which recycled waste materials have been successfully used are the transportation and construction industries. One of the new and popular products in this sense is modified cementitious composites with scrap tyre rubber. The accumulation of rubber can be considered non-decaying materials that disturb the surrounding environment make the disposition of tyres a relevant problem to be solved. However, a positive method for disposing of this non-decaying material, such as reuse in concrete mixes, would have a beneficial effect like lower density, increased toughness and ductility, higher impact resistance, and more efficient heat and sound insulation. The use of recycled tyre rubber in Portland cement concrete mixtures also helps alleviate disposal problems and address the growing public concern about the need to preserve natural sand and aggregates. The work presented herein focuses on the feasibility of aerated cement composite, containing rubber tyre particles, and reinforced with polymer fibres. The composite consists of mortar incorporating rubber particles and polymer fibres as replacement to the sand. The replacement levels were 0 (control specimen), 25, 50, 75, and 100% by volume. An experimental test program was conducted mainly to investigate some of the fresh and hardened properties thought to be significant in relation to composite performances. The test properties were consistency, air content, dry unit weight, and compressive and flexural strengths measured at 28 days.

Dr A Benazzouk is a lecturer in Civil Engineering at the University of Picardie Jules Verne, Amiens. His research interests the durability and physico-mechanical behaviour of cement composite based on natural and local materials.

Dr Douzane O., Is a lecturer in Civil Engineering, University of Picardie Jules Verne, Amiens. His major center of interest is thermal and mechanical behaviour of building materials.

Pr Langlet T., Is a professor in Civil Engineering, University of Picardie Jules Verne, Amiens. His major center of interest is thermal and mechanical behaviour of building materials.

Dr M Merzoud is a Lecturer in Civil Engineering Department at the University of Badji Mokhtar, Annaba, Algeria. His research interests the behavior of masonry structures, the use of natural local materials in composites.

Keywords: Aerated cement composite, Fresh and hardened properties, Polymer fibres, Rubber tyre particles

INTRODUCTION

Hazardous waste materials are being generated and accumulated in vast quantities causing an increasing threat to the environment. In the construction sector, the operation and recycling of wastes are increasingly considered. They are many lightweight composites that contain recycled materials, including waste glass [1], fly ash [2], kraft pulps from sisal and banana waste [3], steel slag [4], lightweight crushed bricks, lightweight expanded clay aggregates [5], foam polystyrene and its wastes [6]. Therefore, the development of composite construction materials using these wastes will be an interesting alternative that would solve simultaneously energy and environment concerns.

The accumulation of rubber wastes can be considered non-decaying materials that disturb the surrounding environment. Landfill disposal which is the most prevailing method will be drastically reduced, due to the recent introduction of European Union directives that include significant restrictions on this practice in favour of alternatives oriented toward materials and energy recovery. The reuse of rubber wastes to serve as a building material, in aggregate form, provides a significant market potential for waste recycling that have proven to be effective in protecting our environment and conserving natural resources.

Several research programs have been conducted on waste tyre modified Portland cement concrete [7–13]. Results have revealed the influence of rubber aggregate type on the material mechanical properties. A study of this composite has also demonstrated the importance of rubber particle type with respect to the hydraulic transport properties of the composite when coming into contact with water [14]. Unfortunately, not much attention has been paid to use the waste tyres in Portland cement aerated concrete mixtures, particularly for cellular concrete applications use such as load-bearing wall materials. Limited work was done by researchers to investigate the potential use of rubber tires in conventional concrete mixtures.

The work presented herein focuses on the feasibility of using rubber waste as aggregates in cement composite, to develop usable materials in cellular concrete applications. Cellular concretes are materials belonging to the lightweight concrete classification, in which air voids are artificially entrapped in the matrix by means of either chemicals (metallic powders such as Al, Zn and H_2O_2), mechanical agents (foaming agents) or aerating agents. The aim behind their use is to significantly reduce material density. Through appropriate production methods, aerated concrete featuring a wide range of densities (300–1800 kg/m³) may be obtained, in comparison with 2300 kg/m³ for traditional concrete. The key advantage of aerated concrete is its light weight, which can yield mechanical characteristics that comply with the specifications issued for building applications. The material also provides a high degree of thermal insulation due to their porous structure [15-17]. Depending upon their physico-mechanical characteristics, these materials can be used as a suitable material for insulated load bearing walls. In addition, aerated concrete are primarily recommended to improve the freeze-thaw resistance [18]: air-voids act as empty chambers in the matrix to allow for both freezing and migrating water to enter, thereby relieving hydraulic pressure and preventing damage to the concrete. By appropriate method of production, aerated concrete with a wide range of densities can be obtained thereby offering flexibility in manufacturing products for specific applications (structural, partition and insulation grades). Therefore, to promote the use of cementitious building, materials reinforced with rubber additives could be a way to achieve a more sustainable construction.

The main objective of this study was to evaluate the suitability of rubber wastes, in aggregates form, as a raw material to manufacture aerated cement composite. The material, containing different amounts of rubber additives was aerated by artificially entrapping air-voids, by means a proteinic air-entraining agent. The rubber additives have been used as partial replacement of sand in mixture at different levels: 0% (Aerated Control Mortar), 25%, 50%, 75%, and 100% (ACC) by volume. Some of fresh and hardened properties thought to be significant in relation to composite performances such as consistency, air-entrainment, hardened and plastic density, compressive and flexural strengths were examined.

MATERIALS AND EXPERIMENTAL TESTING

Materials

Rubber additives used in this research were obtained from mechanical shredding of waste automobile tires. This waste comprises rubber particles finer than 1 mm in size and contains approximately 30% of polypropylene fibres as well by volume. The bulk density of rubber additives is 180 kg/m³. For aerating composite, proteinic air-entraining agent "Vepro 95 BHF" in the powder form was used. The cement used in this study was ordinary Portland cement (PC) CPJ CEM II 32.5 produced according to Standard NF P15-301 [19]. The sand was siliceous type with a size smaller than 1 mm.

Both cement and water were initially mixed in a planetary mixer. To avoid balling of rubber and fibre additives, polymer materials were pre-mixed with sand and then were uniformly dispersed with slow increment throughout the cement binder. The fresh composite was mixed in a laboratory mixer for a total time of 3 min. Total mixing water added had been adjusted so as to achieve the same workability (as measured by flow test) of that of control mortar mixture proportions of 1:3:0.6 by weight of cement, sand, and water respectively. The rubber additives were added to mortar mixture as a partial replacement of sand at four levels up until obtaining a uniform mixture, the required amount of proteinic air-entraining agent, as 1% by weight of cement, was added and the mixture was mixed for another 1 min. The resultant material was first characterized in its fresh state. For measurements of hardened composite, prismatic specimens of 40 mm × 40 mm × 160 mm in size were prepared and subjected to moist curing for 28 days at 20 ± 2°C and 98% relative humidity. The composite mixes are shown in Table 1.

Table 1 Composite mixes

COMPOSITE TYPE	RUBBER, %	CEMENT, kg/m³	SAND, kg/m³	RUBBER, kg/m³	WATER, kg/m³
AMC (ACC0)	0	450	1,350.0	0.0	270.0
ACC25	25	450	1,012.0	40.5	283.5
ACC50	50	450	675.0	81.0	306.0
ACC75	75	450	337.5	121.5	333.0
ACC100	100	450	0.0	162.5	355.5

AMC (ACC0): Aerated Mortar Control (without rubber) ; ACC: Aerated Cement Composite

Experimental Testing

The properties tested on the fresh sample included consistency and air-entrainment. The consistency of aerated mix has been determined by measuring the flow % using a standard flow cone [20]. After filling the cone with the mixture, the cone is lifted and average flow is measured without raising and dropping of the flow table as it may affect entrained-air bubbles in the mix. The fresh density of mix was measured by filling a standard container of known volume. Air-entrainment was measured using pressure method according to Standards NF P 18-353 [21]. The properties tested on hardened composites included density, as determined by means of geometrical measurement and weighing. The compressive and flexural tests were carried out in accordance with Standard EN 196-1 [22], using a universal testing machine. The rates of loading of compressive and flexural specimens were 45 and 3 kN/min, respectively. Three replications were used for each properties tested.

EXPERIMENTAL RESULTS AND DISCUSSION

Properties of Fresh Composite

Consistency

In order to study the relative flow behaviour, the flow of mixes after the addition of air-entraining agent is compared in Figure 1. It is clear from this figure that the flow decreases as the rubber additive content was raised. This reduction can be attributed to the higher level of inter-particle friction that occurs between the rubber aggregate and the other mix constituents (owing to the surface texture of the rubber particles) as well as the overall reduction in the plastic density of mix. These findings are in general agreement with several other studies [23-25] but the magnitude of reduction depends upon the size of rubber and replacement percentage. The reduction in flow after the addition of aerating agent is a maximum at lower densities of the mix. A possible reason for this is that, at lower densities there will be more air-bubbles in comparison to paste and the adhesion between the bubbles and solid particles in the mixture increase the stiffness of the paste.

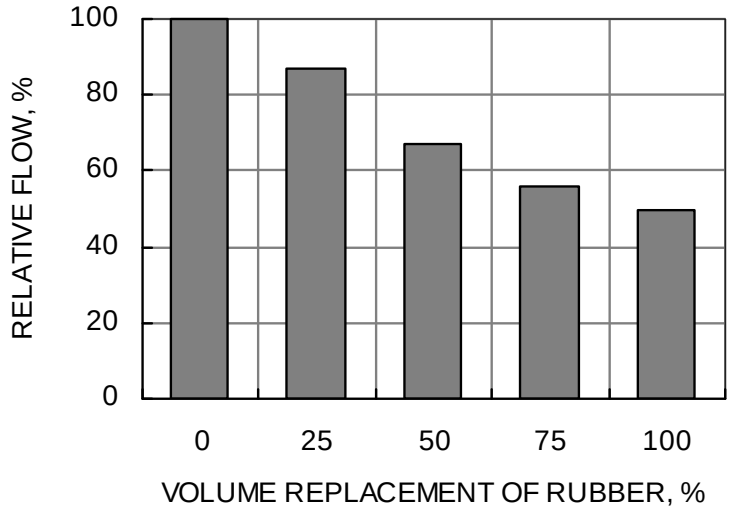

Figure 1 Flow characteristics of aerated cement composites

Air-entrainment

The results of air-entrainment measurements of the composite, with respect rubber replacement, are displayed in Figure 2. It clearly indicates that the addition of rubber increases the level of air-entrainment. For rubber volume varied from 0 to 100% replacement, air-entrainment of fresh material increases from 15% to 41.6%. The higher air content in mixtures is may be due to the capability of rubber particles to entrap air at their rough surface due to their non-polar nature. Similar observations were also made by several authors [12-14]. Reviewing paste literature on air-entrainment revealed that it is clearly an extremely complex process, which is affected by many factors, including the mixing process, material mixture proportioning, fine and coarse aggregates, water amount, dosage and properties of air-entraining agent and a range of other parameters [26]. In addition, when mixing the ingredients, protein additive acts as foaming agent and an air-entraining promoter, due probably to its chemical composition and emulsion properties. It should be noted that aerated composite gives rise to a foamed specimen. Figure 3 shows the distribution of air bubbles in hardened composite with 100% rubber replacement, compared to AMC sample without rubber.

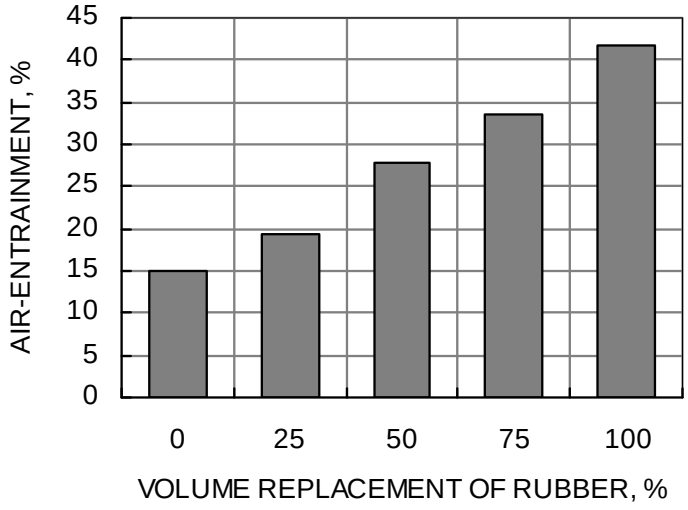

Figure 2 Air-entrainment vs. rubber volume

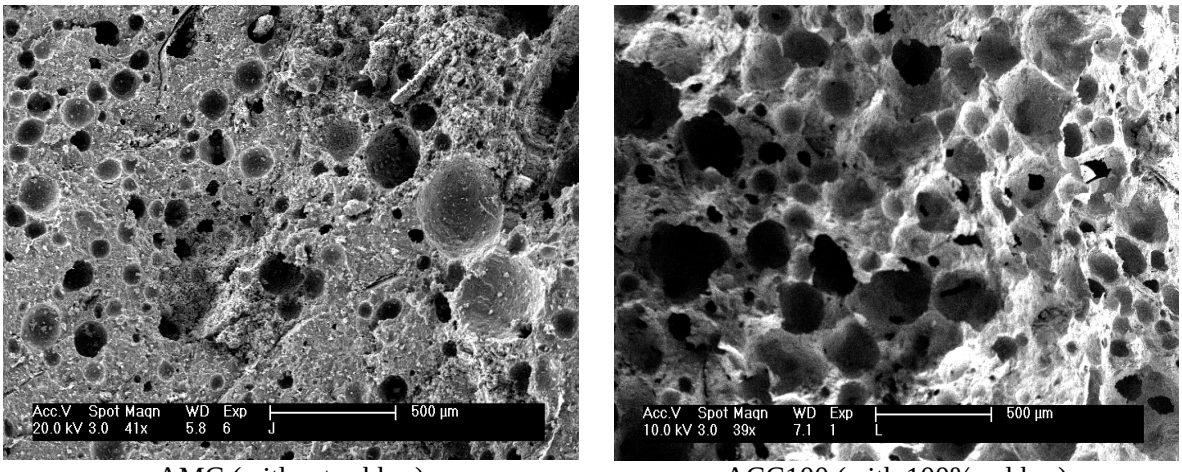

AMC (without rubber) ACC100 (with 100% rubber)

Figure 3 SEM micrographs of air-voids distribution in the composites (magnification ×35)

Properties of Hardened Composites

Dry density of composites

The variation in hardened dry density of composite vs. rubber volume is shown in Figure 4a. Value decreases from 1,480 kg/m³, for AMC without rubber to 800 kg/m³ for ACC sample containing 100% rubber replacement. These values correspond to reduction of up to 46%. The decrease in density is due to the physical properties of rubber, since it has lower density than sand materials. In addition, air-entrapped in the matrix contributes to lightening the material. However, it should be noted that the decrease in density, derived by aerating sample, is regular regardless of rubber volume ratio and stems from the stability of the entrained air bubbles. However, air-bubbles in fresh material are inherently unstable [27]. Previous works have indicated that have three fundamental physical mechanisms may lead to the collapse of air-bubbles: (1) diffusion of air from a small bubble (higher internal pressure) to a larger one (lower internal pressure), (2) bubble coalescence due to capillary flow leading to rupture of the interface between the dispersed air and the surrounding matrix, and (3) rapid hydrodynamic drainage of mix water between bubbles leading to rapid collapse. In addition, if specimen setting is severely retarded, lack of small air bubbles may be expected. In this study, no measurements of air-entrainment in hardened specimen were carried out. The stability of air-bubbles was indirectly evaluated through the relationship between dry density and plastic density of sample. Figure 4b shows a linear variation which indicates that entrained air-bubbles are stable. No reduction of the sample volume was observed when the material setting occurs.

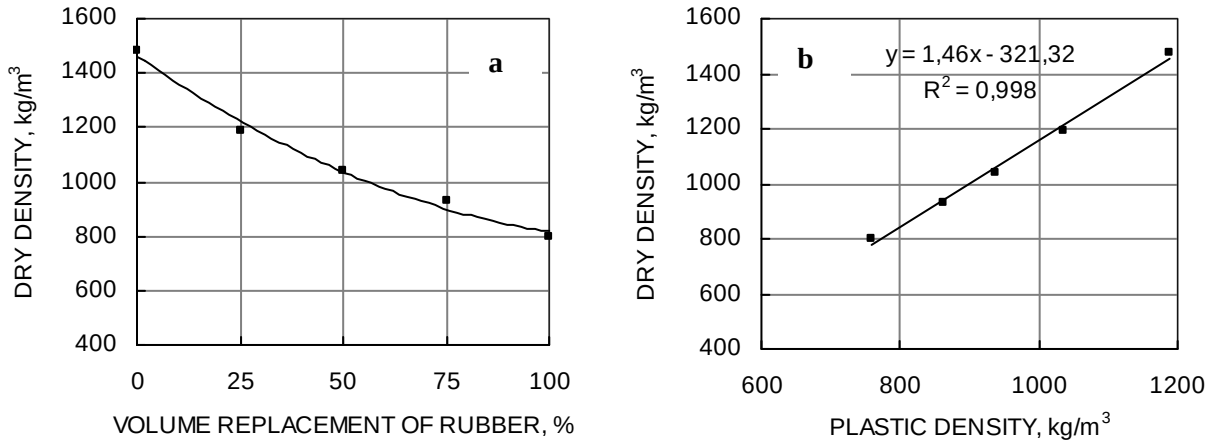

Figure 4: (a) Lightening of composite vs. rubber replacement;
(b) Relationship between dry density and plastic density of composite

Mechanical strength of composites

Results of compressive strength vs. rubber volume are shown in Figure 5a. Value decreases from 9.5 MPa for AMC to 3.5 MPa, for ACC with 100% rubber replacement. The reduction is approximately of 63%. The decrease in compressive strength is attributed to the physical properties of rubber particles since they are less stiff than the surrounding cement paste. The low strength of rubber may be the limiting factor affecting the composite mechanical properties that leads to interfacial bond defects between particles and matrix. Under loading, cracks are initiated around the particles and accelerate the failure in the matrix. It is assumed that mechanical strength of composite is opposite to its density. In addition, the decrease in

compressive strength is related to porous structure of sample. The more the air-voids ratio, the lighter the specimen, and the lower its mechanical strength. Therefore, it is convenient to establish a function to investigate the influence of aerating cement composite on its mechanical properties that describe the balance between density and strength, as required in related codes. The performances of ACC samples have been investigated by evaluating CLPA factor (compressive strength loss per air-entrainment) as defined by proportioning compressive strength loss between aerated and non-aerated composite to air-entrainment, as expressed by Eq. 1 [27].

$$CLPA(\%) = \frac{(\sigma_{CC} - \sigma_{ACC})/\sigma_{CC}}{A_{ACC}} \quad (1)$$

Where, σ_{CC} and σ_{ACC} are the compressive strengths of CC (non-aerated composite) and ACC samples, respectively. and A_{ACC} is the correspondent air-entrainment of ACC sample for a given rubber volume replacement.

The variation of 28-day CLPA factor vs. air-entrainment of ACC is shown in Figure 5b. It is shown that the value decreases from 4.57 % for AMC to 1.44 % for ACC with 100% rubber replacement. However, although increasing in air-entrainment with rubber addition, the CLPA significantly decreases. It should be observed that this CLPA is lower than that for conventional aerated concrete, which has the value typically in the range of approximately 4% to 6% [27]. These results highlight the effect of the proteinic air-entraining agent on the cement matrix/rubber interaction system, as regards the mechanical strength of the composite. Similar results were obtained by several authors [28] on the properties of aerated concrete produced by means of saponin air-entraining agent: for air-entrainment of 7%, the aerated concrete displayed a higher compressive strength than a traditional concrete with 2% of air-entrainment.

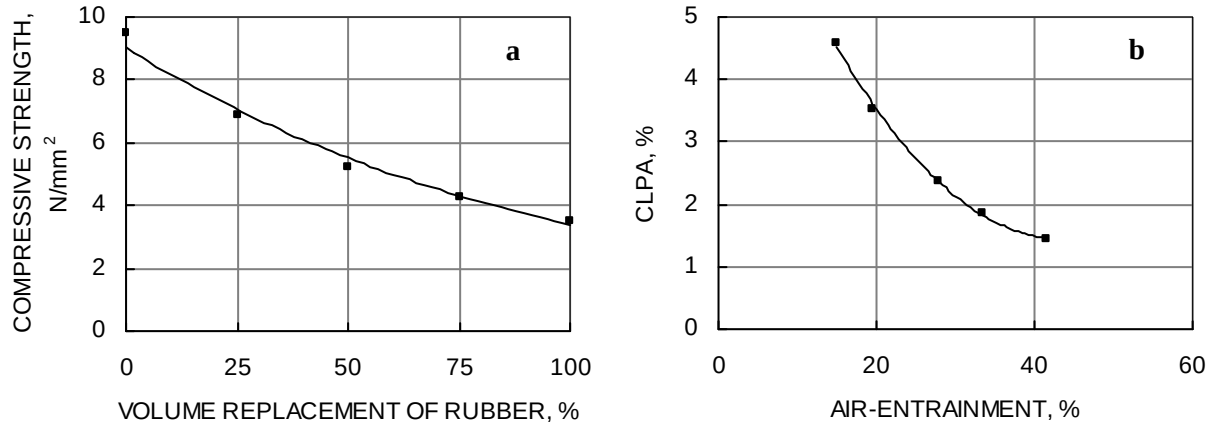

Figure 5 Compressive strength of composite vs. rubber replacement

The variation in 28-days flexural strength with different rubber replacement is shown in Figure 6. A reduction in the flexural strength of the composite is observed. Value decreases from 3.5 MPa, for AMC, to 2 MPa for ACC containing 100% rubber additives. It corresponds to reduction of up to approximately 43%. This finding suggests that both mechanical properties of rubber and sample's porous structure decrease the mechanical strengths of composite. Results also indicated that for a given rubber replacement, the decrease in flexural strength is lower than that in compressive strength, probably due to the

dilution effect of fibres. It is generally considered that, the tension effect of the fibres occurs during the diffuse micro-cracking phase of ‘‘bending’’ the active micro-cracks and then in delaying the onset of their appearance, which serves to improve material strength and durability. This effect is more substantial as the percentage of fibres increases [29].

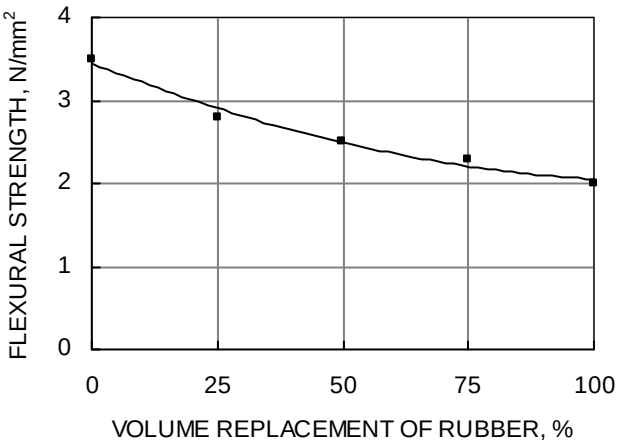

Figure 6 Compressive strength of composite vs. rubber replacement

Figure 7 shows optical micrograph of the composite containing 100% rubber additives. In terms of bonding, the rough surface of particles favours greater contact between rubber and cement matrix. The particles appear well covered by cement matrix. We can also observe good adherence of the synthetic fibres in the cement matrix that may result in a lower decreases in flexural strengths.

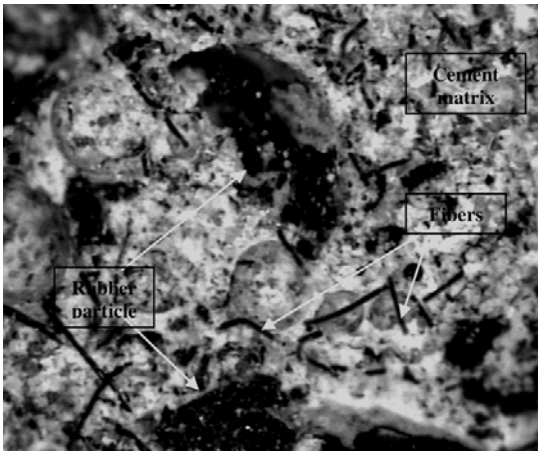

Figure 7 Optical micrograph of ACC 100,
with greater bond of rubber additives (magnification ×75)

CONCLUSIONS

A test program was carried out to develop information about properties of aerated cement composite containing rubber additives. The test results of this study indicate that there is great potential for the utilization of rubber waste in cement mixes, to produce lightweight construction materials usable in cellular concrete applications such as load-bearing wall materials. Results tests performed on fresh composite have shown that the replacement of

sand with rubber decreases consistency of composite and provide low density of mixes due to higher degree of air-entrained. According to physical and mechanical tests, the composite containing rubber additive reached a dry density of about 800 kg/m³ with a compressive strength of 3.5 MPa. The reduction in flexural strength is lower than that in compressive strength. Although the strength was reduced, the composite satisfies the basic requirement for load-bearing wall.

This research highlighted the effect of adding rubber wastes in attaining substantial properties of aerated composite and allows considering a broad range of applications in the field of cellular concrete. In spite of the positive implications of the test results, more research is required to evaluate the durability of the composite.

REFERENCES

1. DUMAN V, MLADENOVIC A AND SUPUT J S, Lightweight aggregate based on waste glass and its alkali-silica reactivity. Cem. Concr. Res., Vol. 32, 2002, pp. 223-326.
2. KEARSLEY E P AND WAINWRIGHT P J, The effect of high fly ash content on the compressive strength of foamed concrete. Cem. Concr. Res., Vol. 31, 2001, pp. 105-112.
3. SAVASTANO J R H, WARDEN P G AND COUTS R S P, Brazilian waste fibres as reinforcement for cement-based composite. Cem. Concr. Comp., Vol. 22, No. 5, 2000, pp. 379-384.
4. YUE Y L, LI G Z, XU X S AND ZHAO Z J, Properties and microstructures of plan-fiber-reinforced cement-based composites. Cem. Concr. Res., Vol. 30, No. 5, 2000, pp. 1983-1986.
5. MALEK K, BATAYNEH I M AND ASI I, Promoting the use of crumb rubber concrete in developing countries. Waste Manag., Vol. 28, 2008, pp. 2171-2176.
6. LAUKAITIS A, ZURAUSKAS R AND KERIENE J, The effect of foam polystyrene granules on cement composite properties. Cem. Concr. Comp., Vol. 27, 2005, pp. 41-47.
7. BIGNOZZI M C AND SANDROLINI F, Tyre rubber waste recycling in self-compacting concrete. Cem. Concr. Res., Vol. 36, No. 4, 2006, pp. 735-739.
8. CHIU C T, Use of ground tire rubber in asphalt pavements: field trial and evaluation in Taiwan. Reso. Conser. Recy., Vol. 52, No. 3, 2008, pp. 522-532.
9. ESTEVEZ M, Use of coupling agents to stabilize asphalt-rubber-gravel composite to improve its mechanical properties. J. of Clean. Prod., Vol. 17, No. 15, 2009, pp. 1359-1362.
10. GANJIAN E, KHORAMI M AND MAGHSOUDI A A, Scrap-tyre-rubber replacement for aggregate and filler in concrete. Const. and Build. Mat., Vol. 23, No. 5, 2009, pp. 1828-1836.
11. GUNEYISI E, GESOGLU M AND OZTURAN T, Properties of rubberized concretes containing silica fume. Cem. Concr. Res., Vol. 34, No. 12, 2004, pp. 2309-2317.

12. HERNÁNDEZ-OLIVARES F, BARLUENGA G, BOLLATI M AND WITOSZEK B, Static and dynamic behaviour of recycled tyre rubber-filled concrete. Cem. Concr. Res., Vol. 32, No. 10, 2002, pp. 1587-1596.
13. BENAZZOUK A, DOUZANE O AND MEZREB K, Thermal conductivity of cement composites containing rubber waste particles: Experimental study and modelling. Const. and Buil. Mat., Vol. 22, No. 4, 2008, pp. 573-579.
14. BENAZZOUK A, DOUZANE O, LANGLET T, MEZREB K AND ROUCOULT J M, Physico-mechanical properties and water absorption of cement composite containing shredded rubber wastes. Cem. Concr. Comp., Vol. 29, 2007, pp. 732-740.
15. NARAYANAN N AND RAMAMURTHY K, Structure and properties of aerated concrete: a review. Cem. Concr. Comp., Vol. 22, 2000, pp. 321-329.
16. KEARSLEY E P AND WAINWRIGHT P J, Ash content for optimum strength of foamed concrete. Cem. Concr. Res., Vol. 32, 2002, pp. 241-246.
17. KEARSLEY E P AND WAINWRIGHT P J, The effect of porosity on the strength of foamed concrete. Cem. Concr. Res., Vol. 32, 2002, pp. 233-239.
18. TIKALSKY P J, POSPISIL J AND MACDONALD W, A method for assessment of the freeze-thaw resistance of preformed foam cellular concrete. Cem. Concr. Res., Vol. 34, No. 5, 2004, pp. 889–893.
19. AFNOR, Liants hydrauliques, ciments courants–composition, spécification et critères de conformité, 1994.
20. ASTM, Specification for flow table for use in tests of hydraulic cement, ASTM C 230-98, Philadelphia. 1998.
21. AFNOR, Adjuvants pour bétons, mortiers et coulis - Mesure du pourcentage d'air occlus dans un béton frais à l'aéromètre à béton. 1985.
22. AFNOR, Méthodes d’essai des ciments, Partie I: Détermination des résistances mécaniques, 1995.
23. CAIRNS R, KEW H Y AND KENNY M J, The use of recycled rubber tyres in concrete construction. The University of Strathclyde, Glasgow; 2004.
24. ZHENG L, SHARON H X AND YUAN Y. Experimental investigation on dynamic properties of rubberized concrete. Constr. Build. Mater., Vol. 22, No. 5, 2008, pp. 939-947.
25. MEHMET G AND GUNEYISI E, Strength development and chloride penetration in rubberized concretes with and without silica fume. Mater. Struct., Vol. 40, 2007, pp. 953–964.
26. DU L AND FOLLIARD K J, Mechanism of air entrainment in concrete. Cem. Concr. Res., Vol. 35, 2005, pp. 1436–1471.
27. MEYERS D, Surfaces, interfaces and colloids: Principales and applications. 2nd ed.Wiley-VCH, 1999, New York.
28. YANG Q, ZHU P, WU X AND HUANG S, Properties of concrete with a new type of saponin air-entraining agent. Cem. Concr. Res., Vol. 30, 2002, pp. 1313-1317.
29. BECHER P, Dictionary of colloid and surface science. New York: Marcel Dekker, 1990, Inc. 323 p.

Reducing Sulphates in Crushed Concrete: Improving the Building Material Properties of Recycled Concrete Aggregates

K Weimann[1], A Müller[2], E Linß[3], T Schulz[3], B Adamczyk[1]
1 – Federal Institute for Materials Research and Testing (BAM), Germany
2 – IFF Weimar e. V., Germany
3 – Bauhaus-University of Weimar, Germany

The material properties of recycled concrete aggregates (RCA) are correlated to the sorting accuracy of the former demolition waste. Impurities like wood, clay bricks or gypsum can lead to inferior building material properties. Harmful substances like heavy metals or organic pollutants should be minimised as well. Hence the non-concrete materials have to be separated from the concrete material stream. This can be done during the demolition process by using selective dismantling techniques. Alternatively a variety sorting and classifying techniques to purify the crushed concrete can be utilized.

A research project, funded by the Federal Ministry for the Environment, Nature Conservation and Nuclear Safety, investigated the possibilities of gaining recycled concrete aggregates of a high quality for the reuse in the production of concrete. The work focuses especially on how gypsum respectively sulphates in the crushed concrete can be reduced. Sulphates can impair the setting behaviour of concrete and also damage set concrete by causing expansion. Therefore the content of sulphates in RCA is restricted by guidelines and standards in Germany. Generally, gypsum in construction waste originates from interior fittings like gypsum walls, floor screeds, plaster boards and also plaster. Most of these materials can be reconstructed using selective dismantling techniques. This can be achieved either by manual labour or by using mechanical equipment e.g. to remove floor screeds by milling. Depending on the specific deconstruction site it can be more effective and/or more environmentally compatible to remove sulphates by treating the crushed concrete. Applicable treatments for sulphate reduction include dry processes like manual sorting of gypsum wall blocks as well as wet treatments e.g. jigging. In addition this research project an environmental performance evaluation was undertaken to assess different techniques for reducing sulphates in recycled concrete aggregates.

Dr. Karin Weimann, scientist for the Federal Institute for Materials Research and Testing (BAM) in Germany, Division 4.4, Thermochemical Substance Separation

Prof. Dr. Anette Müller, senior scientist at IFF Weimar e. V., Germany

Dr. Elske Linß, Tabea Schulz are scientists at the Faculty of Civil Engineering, Bauhaus-University of Weimar, Germany

Dr. Burkart Adamczyk, scientist for the Federal Institute for Materials Research and Testing (BAM) in Germany, Division 4.4, Thermochemical Substance Separation

Keywords: Building material properties, Environmental performance evaluation, Gypsum, Recycled concrete aggregates, Sulphates

INTRODUCTION

The importance of reusing waste materials in order to conserve natural resources increased significantly in the last decades. Approximately 50% of domestic and industrial waste in Europe is generated by the construction industry, on average about 500 kg of construction and demolition (C&D) waste per capita annually. Furthermore, decreasing resources of natural aggregates and also the limited areas for deposits have lead to an increased awareness for the need to recycle and for the importance of environmental conservation. Accordingly, the recycling of C&D waste has become more important [1].

The use of recycled building materials as secondary resources for new buildings reflects the commitment to sustainable development in the construction industry. By conserving primary raw materials today they will be available much longer in the future. Effective conservation of natural resources will also decrease land consumption by landfilling. Depending on the techniques used to recover recyclables, energy consumption and thereby emissions can be also be decreased.

In general recycling strategies aim to reuse materials in closed loops (i.e. material recycled as or nearly as the same product as the original) and to utilize as much of the contents of the material as possible [2]. An example for the recycling of C&D waste on a high level and a closed-loop recycling is the reuse of crushed concrete as recycled concrete aggregates (RCA) [3].

In Germany about 200 million tons of mineral building wastes are generated annually. The highest percentage, approximately 56% in 2008, consists of excavated soil and stones. C&D waste (30.3%) and road construction waste (7.1%) are the remaining main fractions and add up to the basic material for recycled concrete aggregates. Separately registered C&D waste based on gypsum was about 0.3% of the total amount of mineral building wastes (see Table 1). The composition of mineral building wastes in Germany in 2008 is shown in Figure 1 [4].

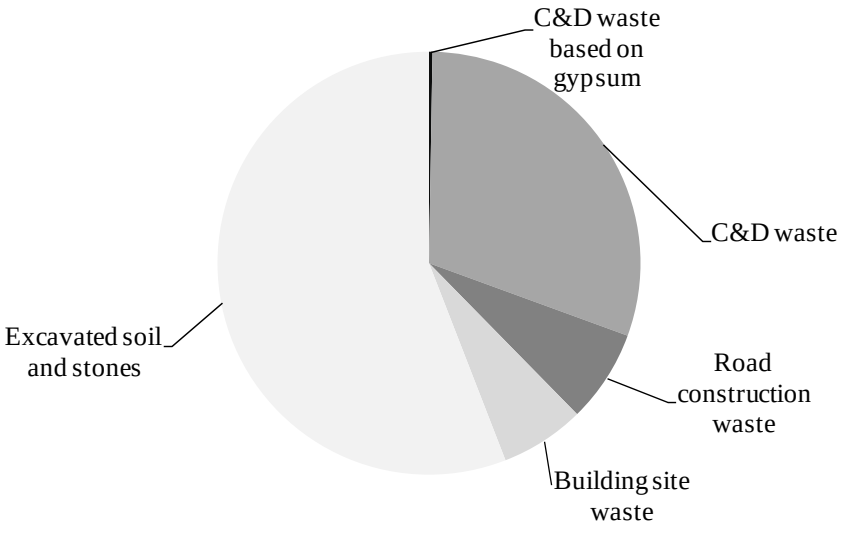

Figure 1 Composition of mineral building waste, data from 2008 [4]

The mass ratio of mineral building wastes (with and without excavated soil and stones) is shown in Table 1. Approximately 85% of that material consists of road construction rubble and construction and demolition waste, about 0.6% is construction and demolition waste based on gypsum.

Table 1 Composition of mineral building waste in Germany, year 2008

	Building mineral waste		Building mineral waste without excavated soil	
	m t	%	m t	%
C&D waste	58.2	30.3	58.2	68.7
Road construction waste	13.6	7.1	13.6	16.1
C&D waste based on gypsum	0.5	0.3	0.5	0.6
Building site waste	12.4	6.4	12.4	14.6
Excavated soil and stones	107.3	55.9	-	-
Total amount	192.0	100.0	84.7	100.0

The reuse of C&D waste and especially the production of recycled concrete aggregates (RCA) depend on the sorting accuracy of the demolition waste. The feasibility of using crushed concrete as a substitute for natural aggregates (up to a certain percentage) in the concrete production has been proven in several studies [5-9]. Impurities can lead to inferior building material properties. On the one hand, harmful substances like heavy metals or organic pollutants can damage the health of living beings and the environment. On the other hand, non-concrete materials like wood or clay bricks can impair e.g. the strength of concrete made with RCA. Accordingly, the purity of concrete from dismantling or demolition sites is of great importance and the non-concrete materials have to be separated from the concrete material stream.

The content of sulfates in C&D waste in general and also in concrete rubble became an increasing problem in the last years and technical standards and guidelines restrict sulfates in original substances and also in eluates. Sulfates in C&D waste usually origin from construction elements that are made of gypsum. Because of its importance, the C&D waste based on gypsum has been statistically registered in a separate waste category in Germany since 2004 (see Table 1).

SULFATES IN RECYCLED CONCRETE AGGREGATES

Although gypsum is an established building material, due to the possible emission of sulfates it is categorised as an impurity in construction and demolition waste. Sulfates can impair the setting behaviour of concrete and also damage hardened concrete. In addition there has been some controversy if sulfates in RCA can also affect the quality of ground water and subsequently other receiving water courses. The content of sulfates is, therefore, limited in technical regulations and standards for recycled building materials [10-12].

The impairment of the building material properties of mortar and concrete by sulfates is usually a consequence of the formation of damaging mineral phases. The generation of ettringite in building materials has been investigated for several decades and is still the subject of intensive research [13-15]. This mineral phase can be formed during an interaction between sulfates, reactive alumina and tricalcium silicates in the presence of water. The damaging effects of ettringite phases in concrete are mainly crack formation and deterioration of the surface. These damages are caused by an increase of volume up to eight times of the original volume and also less density [13].

Another mineral phase, thaumasite, also results from a reaction of sulfates with other substances in water. At temperatures below 15°C thaumasite is formed in a chemical reaction between tricalcium silicate, sulfate and carbonate. This mineral phase also has a higher volume than the initial phases, but the main damaging effect results from a loss of strength of the hardened cement paste matrix – up to the dissolution of the micro structure [16]. The formation of both mineral phases can affect the building material properties of mortar and concrete and accordingly endanger the stability of constructions.

Furthermore, the content of sulfates in the eluates of recycled building materials is limited because of environmental considerations. This is based on the property of gypsum to dissociate in water and to elute sulfates. Rainfall or contact with ground water can lead to an elution of sulfates from building materials. Accordingly, the sulfates can affect the quality of ground water and subsequently other receiving water courses. Some scientists suspect that the elution of sulfates in ground water may lead to an increase of salinity. However, large amounts of gypsum are still used for the improvement of soil in agriculture.

Usually gypsum originates from interior fittings like gypsum walls, floor screeds, plaster boards and also plaster. It has good building material properties for interior purposes and relatively low production costs. Hence the amount of produced gypsum and gypsum building elements increased disproportionately to the amount of manufactured concrete and clay bricks in the last decades (Figure 2). The comparatively high gypsum production has led to an accumulation of gypsum in buildings and consequently also in existing and future construction and demolition waste [13].

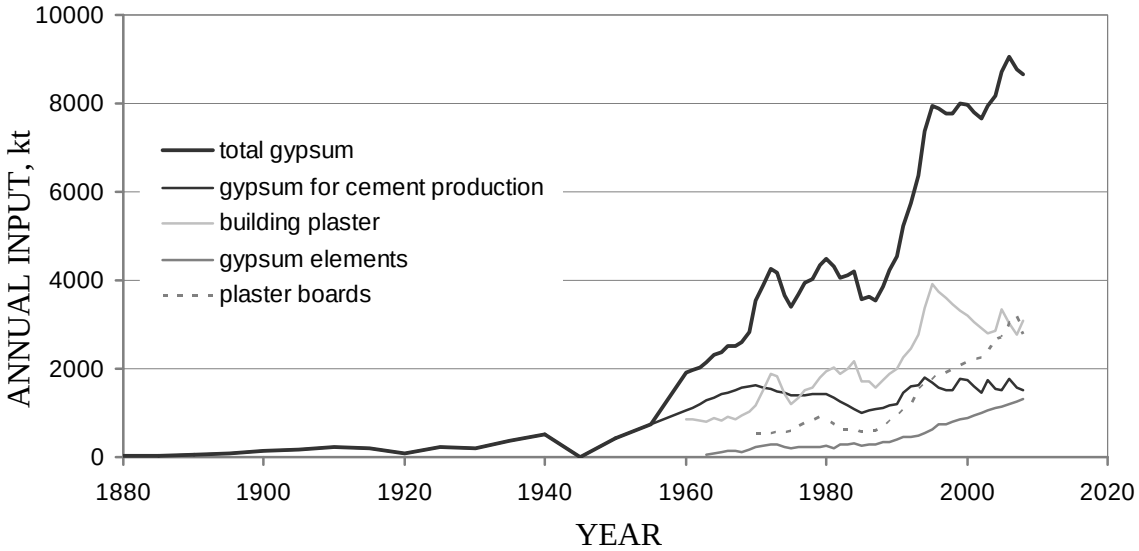

Figure 2 Annual consumption of gypsum in Germany [17]

It can be assumed that the low percentage of construction and demolition waste based on gypsum (0.6%) in the year 2008 represents only a small part of the gypsum which has been used for interioir fittings in the last decades. The increase of gypsum production will have to result in an increase of gypsum in construction and demolition waste in the future and the content of sulfates in RCA will become a serious problem.

If the average lifetime of interior fittings that contain gypsum and the production volume is taken into account, future levels of gypsum in construction and demolition waste can be estimated [17]. Although the production of different types of plaster boards like ceiling elements or single-sheet walls had the highest increase in the last decades, the amount of products that are made of building plaster will dominate for the foreseeable future (Figure 3). Building plaster is mainly used for gypsum plaster and floor screeds (anhydrite floor as well as plaster floor). Accordingly, during deconstruction and demolition activities specific attention should be paid to these materials.

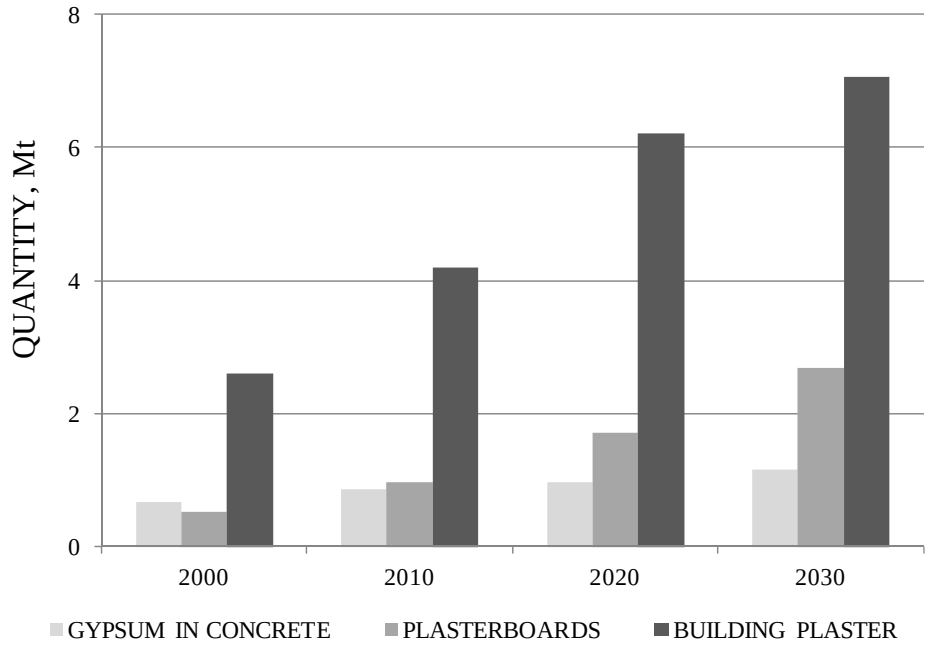

Figure 3 Prognosis for the discharge of gypsum during the deconstruction of buildings

STRATEGIES TO REDUCE THE CONTENT OF SULFATES IN RECYCLED CONCRETE AGGREGATES

In order to reduce the content of sulfates in RCA, it is necessary to remove gypsum building materials from the concrete material stream. This can be done during the demolition process by using techniques for selective dismantling. Alternatively, a variety of sorting and classifying techniques to purify the crushed concrete can be utilized.

The best strategy for a demolition project is always dependant on the respective circumstances. The strategy should be developed by an expert planner or an appropriate consultant. First an inventory and/or a measurement of the installed gypsum building materials has to be made. Then an applicable procedure for the selective dismantling or

demolition can be worked out. In this context not only aspects of gaining mono-material fractions but also technical regulations with respect to statics as well as occupational health and safety issues have to be considered. The economic feasabilty of the strategy can, of course, also not be neglected. A relatively short distance to an appropriate plant for C&D waste recycling should be taken into account as well. It is important that the different materials, especially gypsum residues, are handled separately including storage and transport.

After the concept for minimising sulfates in the upcoming RCA is finalised, a subsequent call for tenders should be prepared. An expert company, which has the know-how and the equipment for the special treatment of different building material fractions, should be assigned with the demolition respectively selective dismantling work.

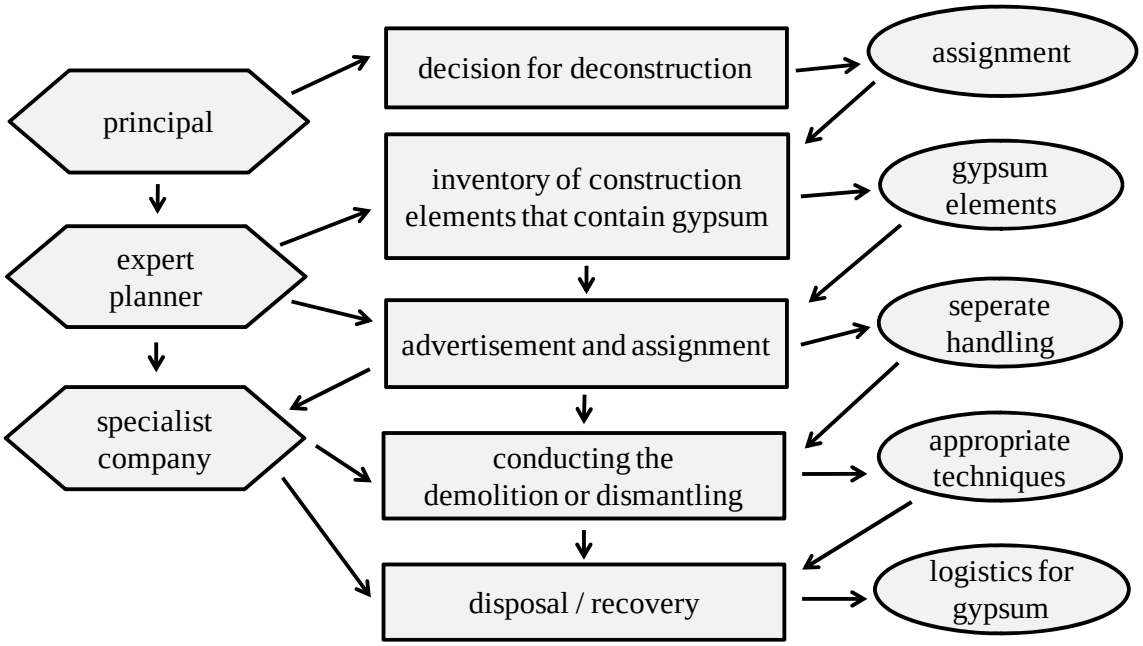

Figure 4 Scheme of the main actors and main actions

Selective Dismantling

Depending on the circumstances of the demolition project (configuration of the building, space available, disposition of staff and equipment, etc.) the preferred way to decrease the content of sulfates in C&D waste is the selective removal of gypsum building materials and construction elements. Most of those materials can be dismantled either by manual labour or by using mechanical equipment. A distinction has to be made between the various types of gypsum building materials.

Different types of gypsum plates and walls, e.g. gypsum plasterboards or ceiling elements, are used as interior fittings in buildings. These prefabricated building elements can usually be dismantled manually or by using tools without difficulties. If tools have to be used, care must be taken to ensure health and safety protection at the workplace (e.g. caulking hammers with reduced noise and recoil).

The selective dismantling of floating floor screeds usually can be conducted without difficulties as well. After using techniques to pry the floor open, the gypsum floor fragments can be gathered for further processing. For health and safety reasons this work should be done by machines – depending on the static of the building.

The removal of bonded gypsum screeds is comparatively time consuming and expensive. The bond between the gypsum floor and the concrete ground is intensive and accordingly difficult to loosen. The floor screeds can be pried open by caulking hammers - but this procedure is much more tedious and difficult than rebuilding floating floor screeds. Bonded gypsum screeds can also be removed by using special milling machines. Whenever possible, the dismantling work on bonded gypsum screeds should be done by machines.

It is very difficult – and sometimes even impossible, to remove gypsum plaster on walls or ceilings either by manually or by machines. The good adhesion properties of gypsum plasters result in a strong bond between plaster and the wall or ceilings. Additionally, the hygroscopic properties of gypsum can cause smudging while trying to mill the plaster. Hence selective dismantling techniques are not very suitable to remove gypsum plaster.

If gypsum building materials can be deconstructed by using techniques for selective dismantling, it is necessary to handle the residues separately. If the gypsum can't be separated during the deconstruction process the following treatment of the gained C&D waste should be conducted and supervised carefully.

Treatment of Construction and Demolition Waste

The treatment of CDW occurs in mobile or stationary processing plants. Depending on the configuration of the plant the processing usually proceeds in three or four steps. The three main process steps are as follows:

Crushing

The crushing of the material is an essential step in the treatment of C&D waste. Not only the reduction of the grain sizes of the old concrete is the goal of the crushing, this is also important for the liberation of the main components of concrete. During this process step the bond between the grains of natural aggregates and the cement matrix is broken at several points. The different resistance against comminution of gypsum, cement paste and natural grains results in different particle sizes. This leads to an enrichment of cement paste and especially gypsum in the fine fractions. Regarding the reduction of the gypsum in the RCA, it can be necessary to have a two-stage crushing process.

Sieving

The sieving of the crushed concrete is important for the generation of fractions with defined upper and lower particle sizes. With regard to the content of sulfates in RCA, it is important to separate the fine fraction which has a higher percentage of gypsum from the RCA.

Sorting

The separation of different building materials can be conducted using sorting techniques. To reduce the content of sulfates in RCA dry sorting processes can be used as well as wet processing. Regarding the sulfate reduction, manual sorting of e.g. gypsum wall blocks before the crushing process is a routine step in many processing plants.

The sorting of gypsum from RCA can also be achieved by a wet treatment using density separation in a jig. In a jig, pulsating water causes the particles to float in the water. Particles of different density but of the same grain size stratify within the material flow: heavy grains sink and lighter particles rise to an upper zone. The resulting layers of heavy and light materials can be discharged separately as a heavy fraction and a light fraction.

Other influencing factors are grain shape and grain size. Flat particles, that are undesired in concrete or mortar production, sink slower, hence spherical grains accumulate in the heavy fraction. The sinking of grains is also affected by the grain size, smaller grains – like gypsum particles – sink more slowly and enrich in the upper zone together with light material. Therefore, the heavy fraction produced from crushed concrete by jigging is of higher building material properties.

Tests for the reduction of gypsum using a density separation have been conducted with different materials: crushed concrete from railway sleepers, crushed bricks, selectively demolished gypsum building materials and also practical mixtures [18, 19]. A side-air-pulsed jigging machine with a throughput of 50 t/h was used for the test runs. The test results showed a clear improvement of the building material properties of the processed crushed concrete. The higher quality of the produced RCA was mainly caused by a significant reduction of the gypsum content and other fine constituents and also an increase in bulk density.

ENVIRONMENTAL EVALUATION

Besides technical feasibility, for a recycling process and the resulting materials the environmental compatibility plays a significant role. Therefore, selective dismantling steps and also the treatment of C&D waste have been assessed by an environmental performance evaluation for the deconstruction of three different types of concrete buildings: a one-family dwelling, a multiple dwelling unit and an industrial building. The results were compared to those of the evaluation of the deconstruction of the three building types by using conventional demolition methods. Thus, six different model scenarios were evaluated.

The basis for the environmental evaluation was an estimation of the process flows for the model scenarios. The data for the process flows were taken from manufacturers' data for building machines and tools and also from the life cycle inventory (LCI) database ecoinvent data v2.2 [20]. The parameters for the evaluation were greenhouse gases (CO_2 and CO_2-equivalents), acidification (SO_2 –equivalents), ozone precursor substances (primary pollutants are nitrogen oxides (NO_x) and volatile organic compounds (VOC)) and land consumption (guide parameters in m²). The calculation of material flows and energy consumption was carried out with a special software for ecobalance and lifecycle analysis [21, 22].

The results showed that the use of selective dismantling techniques is usually connected with a higher consumption of energy and higher environmental impacts than the use of conventional procedures for the demolition of a building. In contrast, the efforts for processing the construction and demolition waste to get high quality RCA and also the efforts for depositing residues of not selectively gained C&D waste were, as a rule, higher than for material that origins from selective dismantling procedures.

The main environmental impacts in all scenarios were energy consumption and the associated emissions (green house effect). Selective dismantling procedures and also multistage treatment of C&D waste lead to higher energy consumption and, therefore, higher expenses during the process, but result finally in lower environmental costs. These benefits can be attributed to good sorting accuracy and, thereby, less land consumption and also less energy consumption by avoiding landfilling deposits and energy required for the machines depositing the residues.

Figure 5 shows the results for the environmental effects climate change and land consumption for the production of one ton RCA made of the C&D waste gained from the deconstruction of a multiple dwelling unit.

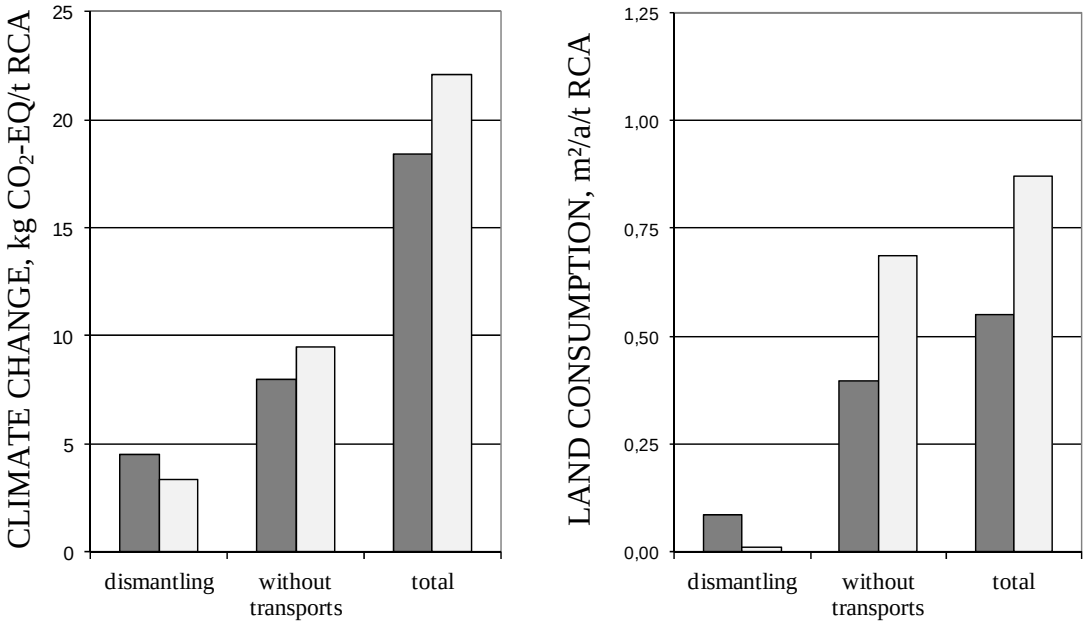

Figure 5 Comparison of climate change and land consumption impacts between selective (dark) and conventional dismantling (light) of a multiple dwelling unit

The results of the environmental evaluation also clearly showed that transport distances have a strong influence on the environmental (and other) costs. Therefore, it is important to take into account the specific circumstances of every demolition project.

CONCLUSIONS

In this study, possibilities to reduce the content of sulfates in recycled concrete were investigated. The main conclusions can be summarized as follows:

- Two strategies to eliminate sulfates by using different techniques of selective dismantling and the subsequent treatment of the crushed material were investigated. Both strategies can be effective and goal-orientated.

- Sulfates in RCA origin from gypsum in building elements. During deconstruction processes, the content of sulfates respectively gypsum can be decreased by using techniques for selective dismantling to remove gypsum containing building materials.

- Several gypsum building materials like plasterboards, dry walls or floating floor screeds can be deconstructed manually or by using tools without difficulties. Bonded gypsum screeds and plaster are usually quite difficult to remove during the deconstruction process.

- The reduction of sulfates in RCA can also be achieved by mechanical processing of the C&D waste. This can be done by manual sorting of gypsum elements and also by two-stage crushing processes and the subsequent enrichment and removal of sulfates in the fine fractions. An innovative way to reduce sulfates in RCA is by wet treatment in a jigging process.

- The environmental evaluation of six model scenarios for gaining RCA by the deconstruction of concrete buildings and the subsequent C&D treatment showed that steps for the reduction of sulfates usually have an environmental impact which must be considered. Due to the fact that a large quantity of environmental impacts can result from material transports it is obvious that every project must be assessed individually.

- The procedural methods during the demolition of concrete buildings and the treatment of crushed concrete should be coordinated in order to minimize the environmental impacts. Because of the multitude of influencing parameters such as transport distances, composition of the building and accordingly the C&D waste, projects need to be individually planned and implemented.

ACKNOWLEDGEMENTS

Sincere thanks go to the Federal Ministry for the Environment, Nature Conservation and Nuclear Safety and the Federal Environment agency Germany for funding the research for reducing gypsum in C&D waste in the project no. Ufoplan 3709 33 317. Furthermore we thank the European Union for funding our work on wet treatment of crushed concrete fines in the LIFE Environment program (Demonstration project LIFE00 ENV/D/000319).

REFERENCES

1. SYMONDS GROUP LTD, Construction and demolition waste management practices and their economic impacts. European Commission, Final Report, London, 1999, 104 p.

2. THORMARK C, Conservation of energy and natural resources by recycling building waste, Resources Conservation & Recycling, Vol. 33, No. 2, 2001, pp. 113-130.

3. WEIL M AND JESKE U, Ökologische Positionsbestimmung von Beton mit rezyklierten Gesteinskörnungen, Recycling 2005, Weimar, Bauhaus-Universität Weimar (Publisher), Conference Proceedings Vol. 1, 2005, 15 pp.

4. ARBEITSGEMEINSCHAFT KREISLAUFWIRTSCHAFT BAU (KWB), Mineralische Bauabfälle Monitoring 2008, Berlin, 2011, 9 p.

5. HANSEN T C AND NARUD H, Strength of Recycled Concrete Made from Crushed Concrete Coarse Aggregate, Concrete International, Vol. 5, No. 1, 1983, pp. 79-83.

6. NAELEN A AND RÜHL M, Consistency aspects in the production of concrete using aggregates from recycled demolition material, Darmstadt Concrete, Vol. 12, 1997, pp. 199-205.

7. CHEN H-J, YEN T AND CHEN K-H, Use of building rubbles as recycled aggregates, Cement and Concrete Research, Vol. 33, 2003, pp. 125-132.

8. KATZ A, Properties of concrete made with recycled aggregate from partially hydrated old concrete, Cement and Concrete Research, Vol. 33, 2003, pp. 703-711.

9. JACOBS F AND HOFFMANN C, Erkenntnisse zu Recyclingbeton, Baustoff Recycling + Deponietechnik (BR), Vol. 24, No. 2, 2008, pp. 48-50.

10. DEUTSCHER AUSSCHUSS FÜR STAHLBETON, DAfStb-Richtlinie "Beton nach DIN EN 206-1 und DIN 1045-2 mit rezyklierten Gesteinskörnungen nach DIN EN 12620". Richtlinie, Deutscher Ausschuss für Stahlbeton, 2010.

11. DIN-DEUTSCHES INSTITUT FÜR NORMUNG E.V., DIN EN 12620:2002+A1:2008: Gesteinskörnungen für Beton Beuth Verlag, 2008.

12. ERSATZBAUSTOFFV, Verordnung zur Festlegung von Anforderungen für das Einbringen und das Einleiten von Stoffen in das Grundwasser, an den Einbau von Ersatzbaustoffen und für die Verwendung von Boden und bodenähnlichem Material, Verordnung, 2011.

13. MÜLLER A, SCHNELLERT T AND KEHR K, Gypsum under control, AT Mineral processing, Vol. 51, No. 6, 2010, pp. 34-43.

14. ODLER I AND COLÁN-SUBAUSTE J, Investigations on cement expansion associated with ettringite formation, Cement and Concrete Research, Vol. 29, 1999, pp. 731-735.

15. VAN AARDT J H P AND VISSER S, Thaumasite formation: A cause of deterioration of Portland cement and related substances in the presence of sulphates, Cement and Concrete Research, Vol. 5, No. 3, 1975, pp. 225-232.

16. DAFSTB, Positionspapier des Deutschen Ausschuss für Stahlbeton: "Sulfatangriff auf Beton - Stellungnahme des DAfStb". Deutscher Ausschuss für Stahlbeton, Berlin, 2003.

17. MÜLLER A, LINß E AND SCHULZ T, Vom Störstoff zum Rohstoff, Recycling Magazin, No. 09, 2011, pp. 26-31.

18. MÜLLER A, SCHNELLERT T AND KEHR K, Gypsum reduced - Gypsum constituents in recycled concrete - origin, effects and removal by jigging, part 2, AT Technical Solutions, Vol. 51, Nos. 7/8, 2010, pp. 54-69.

19. MÜLLER A AND WEIMANN K, Leistungsfähigkeit der Setztechnik, Baustoff Recycling + Deponietechnik (BR), Vol. 26, No. 2, 2010, pp. 20-27.

20. ECOINVENT CENTRE, Database ecoinvent data v2.2 - life cycle inventory (LCI) data, St. Gallen, Switzerland 2011.

21. IFU, Umberto. ifu - Institut für Umweltinformatik Hamburg GmbH, Internet, 2004.

22. WEIL M, JESKE U AND SCHEBEK L, Beton mit und ohne rezyklierten Zuschlag im mineralischen Baustoffstrom, Wasser- und Geotechnologie, Vol. 1, No. 2, 2002, pp. 93-105.

CO_2 Sequestration by Means of High Energy Milled Asbestos-cement Containing Waste

L De Stefano[1], G Accardo[1], F Colangelo[2], C Ferone[1], R Cioffi[1]
1 – University of Naples, Italy
2 – Univesity of Basilicata, Italy

High Energy Milling (HEM) is a brand new technology able to destroy, at microscopic level, the fibres present in the asbestos containing materials (ACM), thus causing their complete inertisation. The obtained materials are powders with fine granulometry that can be re-used in different fields. In this work, we present some experimental results on the recycling of inertised ACM in building applications and suggest another innovative application in the field of CO_2 chemical sequestration.

Luca De Stefano graduated cum laude in Physics at University of Naples ”Federico II” and is currently a Researcher at the Italian National Council of Research

Grazia Accardo graduated cum laude in Industrial Chemistry at University of Naples ”Federico II” and is currently undertaking a PhD at the University Parthenope of Naples, Italy.

Francesco Colangelo graduated cum laude in Civil Engineering at the University of Basilicata and is currently an Assistant Professor at the University of Naples Parthenope, Italy.

Claudio Ferone graduated cum laude in Chemical Engineering at the University of Naples ”Federico II” and is currently an Assistant Professor at the University of Naples Parthenope, Italy.

Raffaele Cioffi graduated cum laude in Chemical Engineering at the University of Naples ”Federico II” and is currently a Full Professor at the University of Naples Parthenope, Italy.

Keywords: Asbestos, CO_2, CO_2 sequestration, High energy milling

INTRODUCTION

HEM is a mechanical process that results in deformations, fractures and local welding of powder particles caused by highly energetic collisions between grinding media (rings, rolls, balls, hammers) and the material. The mechanical transfer of high energy levels into the powders may determine the destruction of crystalline lattice [1] and a great increase of specific surface [2]. HEM is born in ores industry to obtain fine powders and is very used for mechanical alloying too: scale production of copper and bronze flakes is known [3]. Recently, HEM has been applied to a large category of environmental problems, most of them concerning organic pollutants: destruction of DDT in presence of Calcium oxide [4], dehalogenation of chlorobenzenes over Calcium hydride [5], detoxification of PCBs polluted soils mixed with NaH and $NaBH_4$ [6]. Finally, starting from studies about amorphisation of aluminosilicate during micronization process [7], the HEM mechanochemical process has been applied to pure asbestos and to ACM [8]. We have already presented some results about the re-utilisation of inertised ACM in building construction but, in that case, we have considered ACM treated by thermal processes, such as vitrification and glass-ceramic sintering [9].

In this work, we report a careful experimental study about the potential uses of an inert powder produced from HEM process applied to some insulator ACM coming from renovation operations. In fact, we have investigated the pozzolanic activity of inert powder in systems containing calcium hydroxide up to 40 % w/w and we have compared it with that of a tuff in similar systems.

After the HEM treatment of ACM, the inert powder has crystalline and morphological structure completely changed but its chemical composition (magnesium silicate) remain unchanged [10]. So that it can be supposed its use in "mineral sequestration of CO_2". Shortly, mineral sequestration involves the reaction of CO_2 with mineral silicates to form geologically stable carbonates: the resulting carbonates are thermodynamically stable solids, so that mineral carbonation reduces the CO_2 concentration in the atmosphere via permanent disposal of CO_2. Normally the mineral carbonation occurs according to the following equations, regarding the carbonation of forsterite and serpentine [11], respectively:

$$Mg_2SiO_4 + 2\ CO_2 \rightarrow 2\ MgCO_3 + SiO_2 + 95\ kJ/mole$$
$$Mg_3Si_2O_5\ (OH)_4 + 3\ CO_2 \rightarrow 3\ MgCO_3 + 2\ SiO_2 + 2\ H_2O + 64\ kJ/mole$$

This possible application has been investigated following the formation of solid carbonates, such as aragonite, through reactions between atmospheric CO_2 and sludge of inert powder. This process assure a permanent fixation of CO_2 that can be economically viable, especially if mineral silicates are not extracted ones but inertised ACM.

MATERIALS AND METHODS

Some ACM, coming from demolition of insulation system, containing Amosite, Chrysotile and calcium carbonate, have been finely grinding in a ring mill (FRITSCH, model Pulverisette 9, rotational speed 750/1000 rpm, energy consumption 0.6 kW, ring total mass 3637 g, volume capacity 350 ml) for different time intervals: 8, 24, 64, 90, 150 and 270 minutes. At each time, a sample has been kept to be analysed. The analysis performed were: X ray powder diffraction (on a Philips PW3020 X'Pert automatic diffractometer, Cu Kα

radiation at 40 kV and 45 mA, Bragg-Brentano configuration θ - 2θ□ 0.2 mm receiving slit, 0.04 rad Soller slit, 1/2° divergence slit and 15 mm beam mask) and FT-IR (Pelkin-Elmer) to control the crystalline order and the disappearance of principal analytical peaks of Chrysotile; TG and DSC (Netzsch Instrument) to evaluate new phases formation; BET in N_2 (Quantachrome Corporation) to verify the specific area; laser scattering (Malvern Instruments SB.0C) for granulometry assessment and SEM-EDS (JEOL JSM 6310) to get morphology information.

Once we have verified that the milled materials were asbestos-free, we have checked its properties in buildings application and its ability in sequestration of CO_2 atmospheric.

To check the properties of the inert powder in buildings application some samples have been prepared by mixing hydroxide of calcium or with inert powder or with tuff dust in the ratio 40/60 w/w. These mixtures were hydrated at 25°C and 100% RH, kept in a closed environment and circumscribed for avoiding the carbonation of the calcium hydroxide. The water/solid ratio was equal to 0.5. The hydration time ranged between 1 and 28 days.

To investigate the ability of the inert powder to seize CO_2 atmospheric, the samples have been prepared by mixing the material with deprived water of CO_2 (previously boiled). The water/inert powder ratio equal to 0.5. These last samples have been submitted to carbonation treatments at 25°C for times ranging from 1 to 28 day. Particularly the carbonation treatments were conducted in two ways: in a closed-system condition, with respect to CO_2, where pCO_2 constantly decreased in the time, due to the carbonation itself, and in an open-system where wet CO_2 was fed continually. After the treatments of carbonation or hydration at 25 °C, the hardened samples were ground and analysed by means of X-ray diffraction and thermal differential analysis to check variation of mineralogical composition and the formation of new phase. The samples were also characterised morphologically by means of scanning electron microscopy (SEM).

RESULTS AND DISCUSSION

Preparation of inert powder by HEM

In Figure 1 one of the most brilliant proof of fibres destruction is shown: increasing the milling time corresponds to a continuos reduction of principal peaks intensities of Chrysotile (at 12.1° (2θ) and 24.5° (2θ), respectively), which are directly related to the abundance of the crystalline phase. After 270 minutes (green line in Figure 1) no crystalline asbestos phase can be revealed. The same effect can be detected in FT-IR: the analytical absorption band (3690 cm^{-1}) of Chrysotile disappears after HEM process. In Table 1 are reported the correspondent results obtained in BET: samples specific area first increases, reaches a maximum, then decreases. This is well confirmed by SEM analysis too: fibres dimensions rapidly decrease with increasing milling time up to some tenth of microns, then the amorphous powders begin to aggregate more and more.

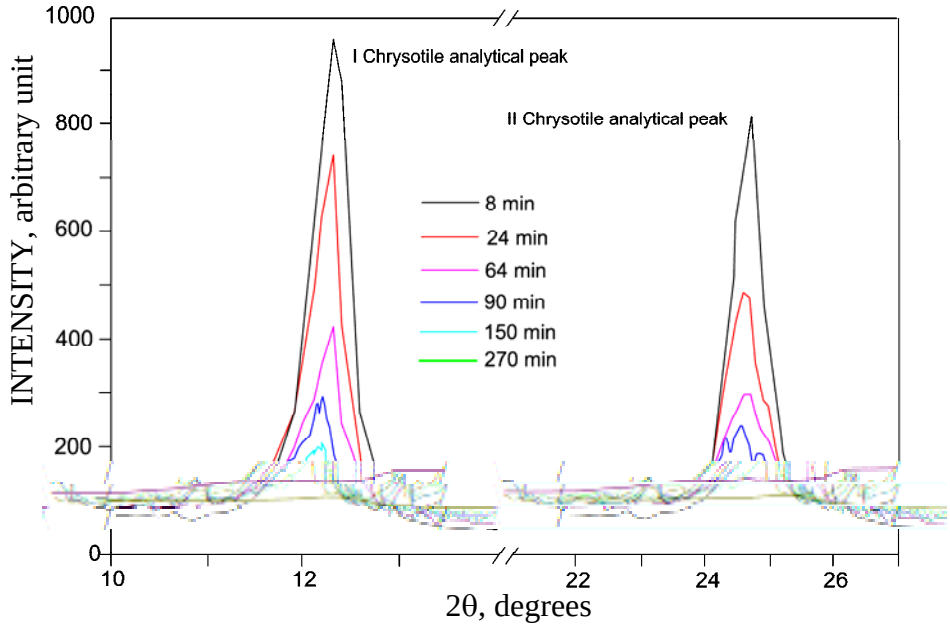

Figure 1 Diffraction analysis of ACM HEM treated

Table 1 Specific Area for different milling times

MILLING TIME, min	SPECIFIC AREA, m^2/g
8	21.35
24	24.37
64	18.96
90	16.23
270	12.34

Laser scattering results are coherent with SEM-EDS and BET indications: in Table 2 are reported the undersize diameters for 0.9, 0.1 and 0.5 percentiles. In the first milling interval (8-24 min) the average size of fibres strongly decreases then some kind of agglomeration process starts.

Table 2 Undersize diameters for 0.9, 0.1 and 0.5 percentiles

MILLING TIME, min	∅ 0.9 per., μm	∅ 0.1 per., μm	∅ 0.5 per., μm
8	170.36	8.02	37.78
24	36.43	2.97	10.39
64	55.95	2.54	11.84
90	82.26	3.70	17.46

Application of inert powder in sequestration CO_2

All the systems, submitted to carbonation treatments previously described, have shown ability to CO_2 atmospheric sequestration due to the formation carbonate solids as Aragonite. This compost is a crystalline solid polymorph of $CaCO_3$ and it is less thermodynamically stable than Calcite. In all case evidence was found that, independently from the conditions of carbonation, Aragonite is quickly produced and it already reaches maximum abundance after 3 days of curing. Figure 2 shows the result of the X-ray diffraction analysis carried out on the sample cured for 3 days in the system where wet CO_2 was fed continually.

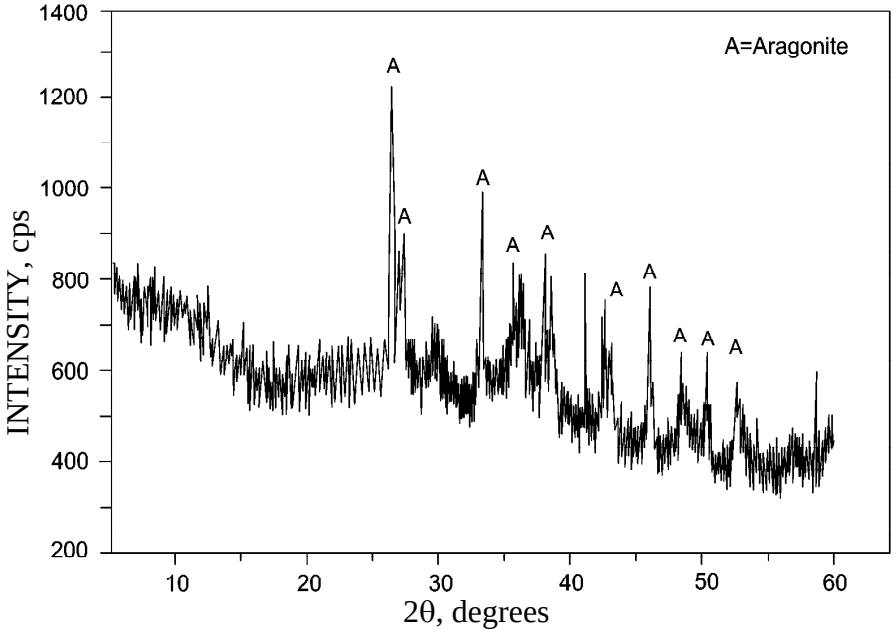

Figure 2 Diffraction analysis of system submitted in treatment of carbonation

To explain this experimental result it is necessary to start from the consideration that in natural process CO_2 sequestration is performed by the high-pH waters of the OH-Ca type, which are typically related to ultramafic rocks, variably affected by serpentinization [12]. In our systems it is probable that high pH values of water mixed to inert powder are due either to some hydrolysis reaction either to the low pCO_2 resulting from the treatment of carbonation in condition of closed-system with respect to CO_2. Water, due to its high pH values, adsorbs atmospheric CO_2 and, according to the following reaction: $CO_2+2OH^-=CO_3^{2-}+H_2O$, it is saturated by carbonate ions, which are quickly precipitated in solid carbonates.

The formation of Aragonite, rather than Calcite, is encouraged either by condition of water, highly supersaturated with carbonate ions, which can no longer dissolve aragonite, either by the presence of Mg ions that represent some nucleuses of crystallisation [10]. The condition of supersaturation is affected, at temperature of 25°C, by water/inert powder ratio. It seems probable that for a water/inert powder ratio equal to 0.5 both the treatments of carbonation assure the conditions either of supersaturation either of pH values of water that support the formation of aragonite.

Recycling of inert powder in binder applications

All the mixtures containing hydroxide of calcium-inert powder, submitted to the hydrothermal treatments, have shown ability to harden, due to the formation of an amorphous phase gel-type acting as binder among the particles originally present in the mixtures.

Evidence was found by X-ray diffraction and thermal analysis (results are not shown here for brevity) that the amount of calcium hydroxide is reduced continually with curing time and this is not referable to an increase of the calcium carbonate (Calcite). Furthermore, by thermal analysis, there is evidence that an endothermic effect at 95°C constantly increases with curing time. This is related to dehydration of a product of reaction between inert powder, calcium hydroxide and water similar to calcium silicate hydrate (C-S-H): main cement hydration product. Figure 3 shows typical results of thermal analysis in terms of DTA curves for the samples containing respectively calcium hydroxide/inert powder and calcium hydroxide/tuff dust cured 28 days.

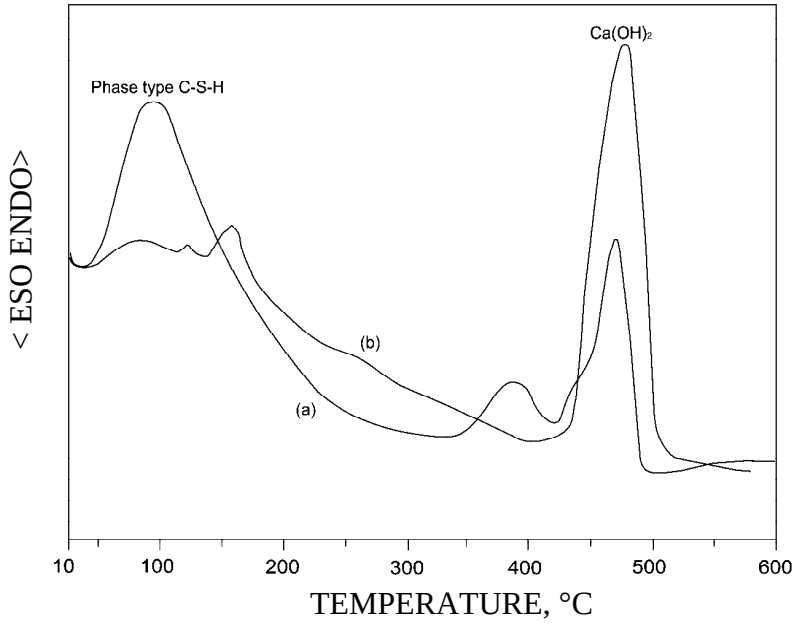

Figure 3 Results of DTA carried out on samples (a) system calcium hydroxide/inert powder (b) system calcium hydroxide/tuff dust after 28 days in hydrothermaln treatment

The system containing inert powder shows, rather than that containing tuff dust, a great tendency to consume calcium hydroxide and to produce phase type C-S-H agent as binder. This would confirm an elevated pozzolanic reactivity of the silicate phases present in inert powder.

The DTA trace for the sample containing inert powder also shows the presence of two endothermic effects at 380°C and at 430°C of uncertain origin. These effects are probably related to dehydration of binding neo-formed phases type afwillite ($Ca_3H_2Si_2O_8$ $2H_2O$).

Morphologically the system containing inert powder is characterised by an homogeneous structure gel-type that englobes particles originally present in the mixtures, as it can be seen in Figure 4 where a micrographs of sample cured for 28 days in hydrothermal treatment is shown.

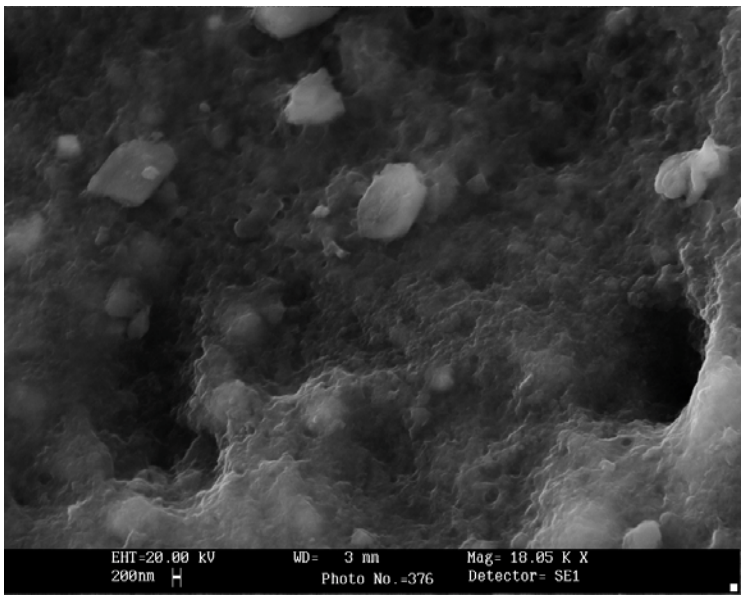

Figure 4 SEM micrograph of sample system calcium hydroxide/inert powder after 28 days in hydrothermal treatment

CONCLUSIONS

In this work we have studied the effects of HEM treatment on ACM by means of several experimental techniques: XRD, FT-IR, TG/DTA, SEM-EDS, BET, LASER scattering. We have checked that after less than five hours of grinding, there is no evidence of asbestos crystalline structure. The starting ACM is converted in an inert, partially amorphous, very reactive material. Subsequently we have verified that this material can be recovered with success both as agent of pozzolanic activity and as agent to mineralise the emissions of CO_2. In this last case, further studies are necessary to provide the understanding of reaction mechanism and to facilitate the engineering of carbonation processes for carbon dioxide sequestration.

ACKNOWLEDGEMENTS

The authors thank Mr. G. Ferrara for the collaboration offered in the elaboration of the experimental data.

REFERENCES

1. SANDVIK K L, KLEIV R A AND HAUG T A, *Mechanically activated minerals as a sink for CO_2,* Advanced Powder Technology, Vol. 22, No. 3, 2011, pp. 416–421.

2. FABIAN M, SHOPSKA M, PANEVA D, KADINOV G, KOSTOVA N, TURIANICOVÁ E, BRIANCIN J, MITOV I, KLEIV R A AND BALÁZ P, *The influence of attrition milling on carbon dioxide sequestration on magnesium–iron silicate,* Minerals Engineering, Vol. 23, 2010, pp. 616-620.

3. ZOZ H, ERNST D, MIZUTANI T AND OKOUCHI H S, *CM100s, semi-continuously Mechanical Alloying in a production scale using Cycle Operation-Part I*, Metall, Vol. 51, No. 10, 1997, pp. 568-572.

4. HALL A K, HARROWFIELD J M, HART R J, MCCORMICK P G, *Mechanochemical reaction of DDT with calcium oxide,* Environmental science and technology, Vol. 30, No. 12, 1996, pp. 3401-3407.

5. LOISELLE S, BRANCA M, MULAS G AND COCCO G, *Selective Mechanochemical Dehalogenation of Chlorobenzenes over Calcium Hydrides*, Environmental science and technology, Vol. 31, No. 1, 1997, pp. 261-265.

6. DE STEFANO L, CARAMUSCIO P, PASTORE T AND TORTORELLA C, *Un trattamento innovativo per i terreni contaminati da policlorobifenili*, Siti Contaminati, No. 1, 2000, pp. 26-29.

7. MILOSEVIC S, TOMASEVIC-CANOVIC M, DIMITRIJEVIC R, PETROV M AND DJURICIC M, *Amorphization of aluminosilicate mineral during micronization process*, American Ceramic Society Bulletin, Vol. 71, No. 5, 1992, pp. 771-775.

8. PLESCIA P, MACCARI D, MARRUZZO G, PAGLIETTI F AND LOPEZ S, *La tecnologia meccanochimica per il trattamento dei Rifiuti di Amianto,* Atti del Convegno RICICLA 99; Rimini 17-20 settembre, 1999.

9. CIOFFI R, DE STEFANO L, PALUMBO M, PLESCIA P AND QUATTRONI G, *Re-use of inertized asbestos containing materials in building construction*, Proceedings of the 2nd National Congress Valorization and Recycling of Industrial Wastes, 127-133, L'Aquila 5-8 Luglio 1999.

10. O'CONNOR W K, DAHLIN D C, RUSH G E, DAHLIN C L AND COLLINS W K, *Carbon dioxide sequestration by direct mineral carbonation: process mineralogy of feed and products*, Minerals and Metallurgical Processing, Vol. 19, No. 2, 2002, pp. 95–101.

11. SEIFRITZ W, *CO_2 disposal by means of silicates*, Nature, Vol. 345, 1990, pp. 486.

12. RICCIONI M R, BROCK P W G AND SCHREIBER B C, *Evidence for early aragonite in paleo-lacustrine sediments*, Journal of Sedimentary Research, Vol. 66, 1996, pp. 1003-1010.

A Study on Bond Strength of Self-compacting Concrete Made using Recycled Aggregates

D R Seshu
National Institute of Technology, Warangal, India

Reutilization of construction and demolition waste as a new construction material is becoming a primary objective for sustainable construction activities. Many waste materials have proved to be successfully utilized in the manufacturing of normal and high performance concretes. However, the utilization of Recycled Aggregates can minimize environmental impact and slowdown the huge consumption of natural resources used for concrete applications. Further in recent years, self-compacting concrete (SCC) has gained wide use for placement in congested reinforced concrete structures with difficult casting conditions. For such applications, the fresh concrete must possess high fluidity and good cohesiveness. This paper presents the experimental investigation on the bond behavior of Recycled Self Compacting concrete. A comparison of bond behavior and bond strengths in concrete grades M20 and M40 Normal and self compacting concretes with different percent replacement of recycled aggregates. The results indicated that the Self compacting concrete bond performance is better compared to normal concrete.

D Rama Seshu is currently working as Professor of Civil Engineering, National Institute of Technology, Warangal, India.

Keywords: Bond strength, Recycled aggregates, Self-compacting concrete

INTRODUCTION

In recent years, self-compacting concrete (SCC) has gained wide use for placement in congested reinforced concrete structures with difficult casting conditions. For such applications, the fresh concrete must possess high fluidity and good cohesiveness. The use of fine materials such as fly ash can ensure the required concrete properties. Self-compacting concrete (SCC) is considered as a concrete which can be placed and compacted under its self-weight with little or no vibration effort, and which is at the same time, cohesive enough to be handled without segregation or bleeding. It is used to facilitate and ensure proper filling and good structural performance of restricted areas and heavily reinforced structural members.

Reutilisation of construction and demolition waste as a new construction material is becoming a primary objective for sustainable construction activities. Many waste materials have proved to be successfully utilized in the manufacturing of normal and high performance concretes. However, the utilization of recycled aggregates can minimize environmental impact and slowdown the huge consumption of natural resources used for concrete applications. Further the use of fibres enhances the performance of concrete such as crack control, deflection hardening, strain hardening, and high energy absorption.

During the past three decades, number of works pertaining to experimental and analytical methods for evaluating the bond characteristics between concrete of various grades and steel reinforcement has been carried. There is a lot of experimental data available on various grades of concretes with natural aggregates relating bond behaviour. But there has been very few works done dealing with experimental and analytical investigations of the relation of bond characteristics in concretes made of recycled concrete aggregate. Further, very little work has been reported in literature on bond studies in self compacting concretes made of recycled aggregate**.**

PRESENT INVESTIGATION

The proposed investigation aims to investigate the bond strength of self-compacting concrete using aggregates from demolished structures. The experimental program was designed to study the comparison of bond behaviour and bond strengths in concrete grades M20, M40 Normal and self compacting concretes and variations of % replacement of recycled aggregate concrete.

The program consisted of casting and testing a total number of 36 specimens of cylinders with 16 mm ∅ Tor steel bars and 36 cubes of 150 mm × 150 mm × 150 mm size, were casted in 3 batches. Of these 36 cylinders 9 cylinders for M20 normal concrete and 9 cylinders for M20 self compacting concrete and in the remaining 18 cylinders 9 specimens of M40 grade normal concrete and 9 No. of M40 self compacting specimens, and their corresponding 36 cubes for compressive strength. Of these 9 cylinders from each type of mix which consists of 3 groups of mixes with 0%, 50%, 100% recycled aggregate replacements respectively for 28 days strength. The details of the specimen's cast are shown in Table.1.

Table 1 Details of specimens cast

DESIGNATION OF SPECIMEN	GRADE OF CONCRETE	TYPE OF CONCRETE	% REPLACEMENT OF RCA	NUMBER OF CYLINDERS CAST (pull-out test) ∅150 mm × 300 mm
AN-0	M20	Normal	0	3
AN-50			50	3
AN-100			100	3
AS-0	M20	SCC	0	3
AS-50			50	3
AS-100			100	3
BN-0	M40	Normal	0	3
BN-50			50	3
BN-100			100	3
BS-0	M40	SCC	0	3
BS-50			50	3
BS-100			100	3

MATERIALS USED

Cement used in the investigation was 53 Grade Ordinary Portland cement confirming to IS: 12269. The fine aggregate conforming to Zone-2 according to IS: 383 were used. Crushed granite and recycled concrete aggregate was used as coarse aggregate. From the data of the sieve analysis and the grading curve shown in Figure 1, it was noticed that the grading of the natural and recycled aggregates was more or less same with a slightly coarser grading observed in the case of recycled aggregate. The variation in the fineness modulus with replacement of recycled aggregate is shown in Figure 2.

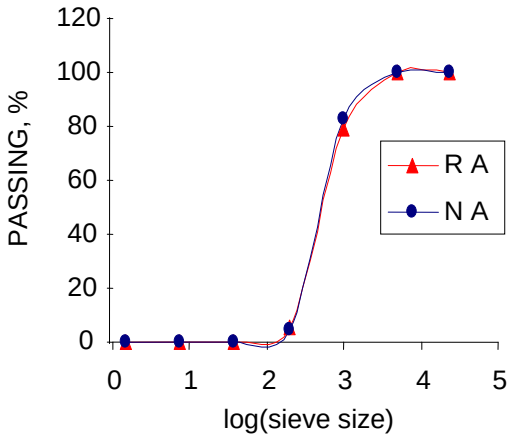

Figure 1 Percentage passing vs. logarithm of sieve size

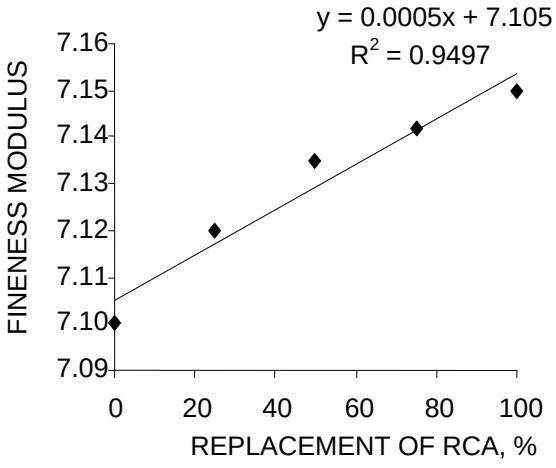

Figure 2 Fineness modulus vs. recycled aggregate content

The various properties of natural aggregate with replacement of a part by recycled aggregate varying from 0-100% in steps of 25% is given Table 2.

Table 2 Properties of natural and recycled aggregate concretes

PROPERTIES	AGGREGATE				
	100% Natural	25% Recycled	50% Recycled	75% Recycled	100% Recycled
Bulk density, g/cm³	1.46	1.44	1.39	1.35	1.28
Void content, %	44.26	44.95	45.21	46.18	48.26
Void ratio	0.79	0.82	0.825	0.85	0.93
Specific gravity, g/cm³	2.78	2.72	2.68	2.61	2.55
Fineness modulus	7.10	7.12	7.135	7.142	7.15
Water absorption	1.00	2.10	3.52	4.85	5.68
Flakiness index	3.56	3.82	4.06	4.31	4.6
Elongation index	7.13	7.43	7.75	8.05	8.4
Agg. impact value	32.20	33.15	33.68	34.15	34.48
Agg. crushing value	22.77	23.00	24.21	27.08	28.16
IAPST	18.10	18.72	19.29	19.79	20.41
Angularity number	10.31	11.35	12.09	13.30	13.99

The mix proportion for M20 & M40 grade of normal and self compacting concrete (SCC) used are given in Table 3. The fly ash was incorporated in the above mix proportion by replacing 20% of cement. Water reducing admixtures are added into mixes on requirement till the desired properties as shown in Table 4 are exhibited by them.

Table 3 Material proportions

DESIGNATION	TYPE	CEMENT	AGGREGATE		WATER CEMENT RATIO
			FINE	COARSE	
M20	NC	1	2.28	2.61	0.53
	SCC	1	2.45	1.96	0.53
M40	NC	1	1.46	1.89	0.36
	SCC	1	1.96	1.73	0.43

Table 4 Basic properties of self-compacting concrete

METHOD	UNIT	% REPLACEMENT OF CA WITH RCA			% REPLACEMENT OF CA WITH RCA			EFNARC SPECIFI-CATION
		0% RCA	50% RCA	100% RCA	0% RCA	50% RCA	100% RCA	
Slump flow (Abrams cone)	mm	725	718	715	710	695	680	650-800
T50 cm slump flow	s	4.73	4.5	4.00	4.73	4.5	4.00	2-5
V-funnel	s	4.71	4.55	4.78	5.79	6.43	6.89	up to 12
V-funnel at T5 minutes	s	1	1.25	1.6	2	2.3	2.5	0-3
J-ring	mm	8	10	12	7	10	11	0-10
U-box	mm	22	25	42	23	27	43	0-30

CASTING OF SPECIMENS

The cylindrical specimens were cast with the steel rebar in perfect vertical position with help of fasteners at the top end of mould in order to avoid secondary stresses in the bar. The steel bars were rust free and perfectly straight. The bond length to be used in the specimens for each grade has been calculated using the following formula as per IS: 456.

$$Ld = \Phi \times fst/4\ \tau bd$$

Where Φ = nominal diameter of the bar,
fst = allowable tensile stress in the steel bar and
τbd = design bond stress.

The values of design bond stress have been taken from IS: 456 for each corresponding grade of concrete mix. The allowable tensile stress value has been taken as the 60% of average designated yield stress of the bar. The preliminary bond lengths have been taken as 300 mm for M20 normal and self compacting concretes and 150 mm for M40 normal and self compacting concretes for the convenience of casting. Deformed steel bars of 16 mm diameter and with calculated bar length have been put in the cylindrical specimens, while casting for use in pull out tests and fastened properly so as to keep the bars perfectly straight and concentric in the moulds during casting. The embedded length has been controlled carefully such that the calculated amount of length will only get inserted in the specimen at casting time. The general details of bar length have been shown below in the Figures 3 and 4. A grip length of 100 mm for fixing, and lower platen coverage of 350 mm, 250 mm free length for extensometer provision has been considered as the projected bar length excluding embedded length for all the specimens. An embedded length of 150 mm for M40 grade concretes and 300 mm for M20 grade concretes has been adopted. The cylindrical specimens cast were arranged in the universal tensile test machine (UTM) of 100 ton capacity.

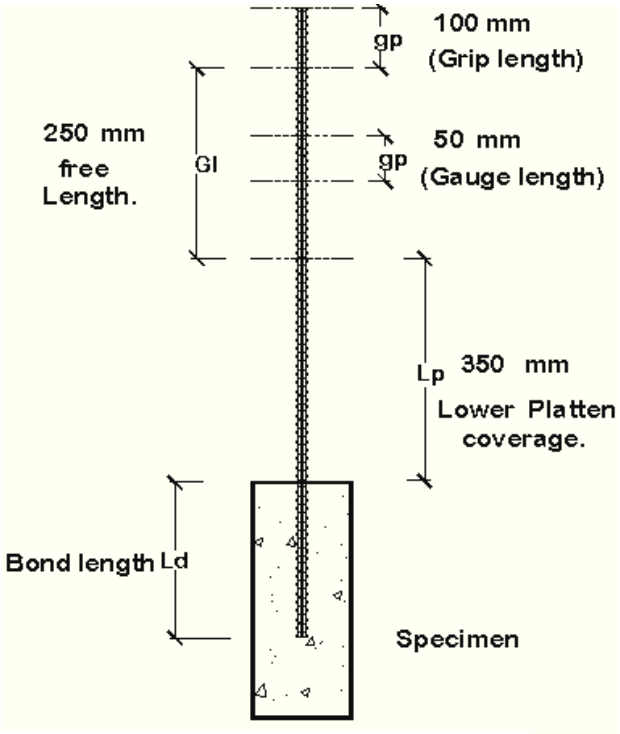

Figure 3 General details of free bar in the specimens

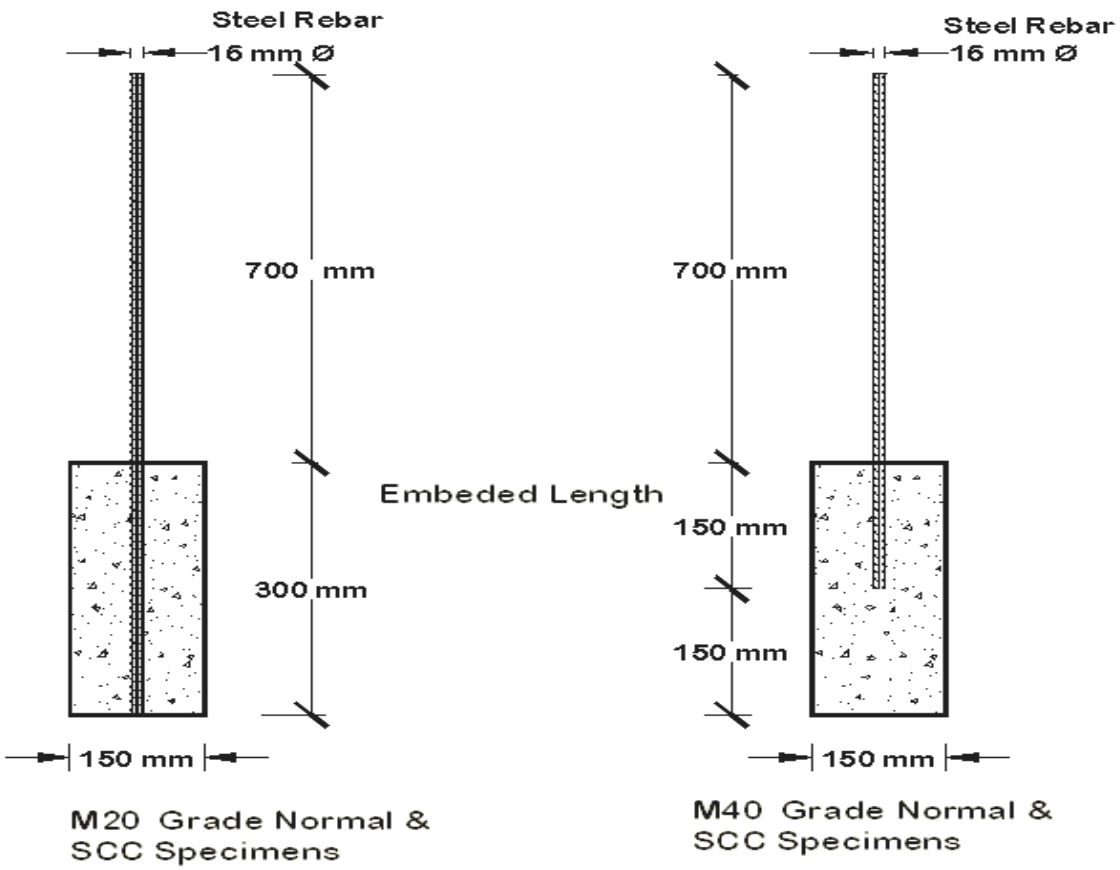

Figure 4 Details of bar profile and embedded length for the four types of grades

TESTING

The arrangement of the test setup has been shown in Figure 5. An idea of load transfer mechanism has been given in the Figure 6. The cylinder with rebar in its vertical position has been inserted carefully through the gap with grips loosened in the bottom adjustable platen. And the inserted bar was tightened at the top grips to hold the specimen firmly. A 20 mm thick iron plate with 20 mm wide slit was arranged over the specimen to avoid it from penetrating into the large opening provided above it for accommodating grips as the pullout load increases in the lower adjustable platen.

The adjustable platen was lift up and down to set the specimen exactly in position for testing. An extensometer meter with gauge length of 50 mm and 0.002 mm precision was arranged at the middle of the rod in the open portion to measure the elongation of the bar with load. A dial gauge with 0.01 mm precision has been set at the top of the main arm as shown in the Figure 5 to read total movement including extension and slip in the bar and specimen respectively.

Test setup in long view Test set in close view

Figure 5 Details of the test setup for pull-out test

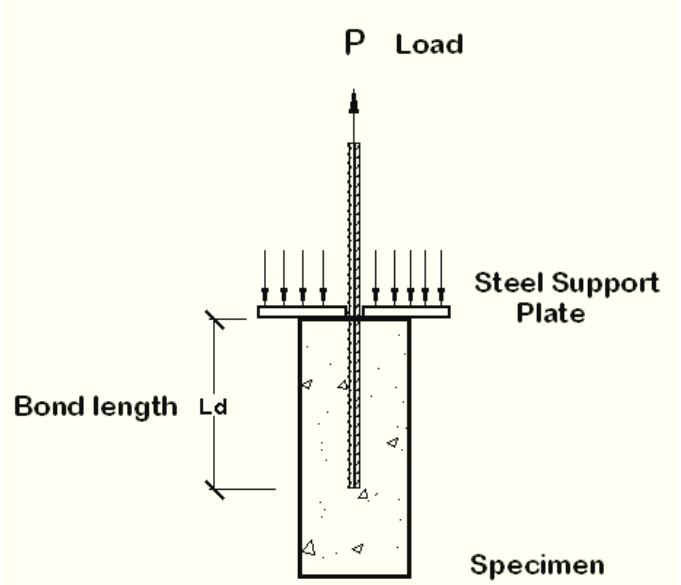

Figure 6 Development of load transfer mechanism on the specimen

A protecting box was arranged under the specimen to avoid sudden fall after failure. Extensometer and dial gauge readings have been taken for every load increment with an interval of 0.4 tonne. Under different loading levels, the relative displacement between the steel rebar and the concrete, that is the slippage value at the free end of the rebar, can be computed by the displacement difference between the two dial gauges. With application of load on the specimen the static mechanical energy (load) will be transferred to the specimen through the bar. In this process some amount of energy will be absorbed by the bar itself resulting in the elongation of the bar. The reading obtained from the dial gauge at the top arm

of the UTM is the combined effect of elongation of free bar and as well as the slip produced in the specimen. The extensometer arranged to the bar will take the effect of elongation till the specimen ultimately fails in slip which is initiated by formation of micro cracks on the surface of specimen at top end and leading to giant fracture. The total movement of the setup can be assumed as Δa and elongation of bar taken as Δe from which slip in the specimen for a given embedded length of the bar is given by

$$\text{Slip } \Delta s = \Delta a - \Delta e$$

Where Δe = Total elongation of bar measured
Δa = Total movement between the cross heads of the frame

DISCUSSION OF TEST RESULTS

Effect of percentage replacement of RCA on Ultimate Bond stress

Table 5.shows the result of tested specimens for Bond stress for different replacement of RCA (0%, 50%, 100%) in natural aggregate for M20 & M40 grade concretes. From Table 5 it is evident that with the increase in replacement of recycled aggregate concrete in natural aggregate (NA), there is general decrease in bond stress. It may be noted from Table 5 that the percentages decrease in bond stress is increasing with increase in replacement of recycled concrete aggregate in natural aggregate. This is true for both M20 & M40 grade normal and self compacting concrete. For both 50% and 100% replacement, percentage decrease is less for M40 grade concrete as compared to M20 grade concrete. It may be observed that the % decrease of bond stress is more for higher grade concrete.

Table 5 Average ultimate bond stress for normal and self compacting specimens

SPECIMEN	AN-0	AN-50	AN-100	BN-0	BN-50	BN-100
AVERAGE BOND STRESS, τu, N/mm²	8.07	8.00	7.31	10.54	9.28	8.33
SPECIMEN	AS-0	AS-50	AS-100	BS-0	BS-50	BS-100
AVERAGE BOND STRESS, τu, N/mm²	8.35	7.89	7.03	13.06	11.76	10.02

Effect on Fracture Energy with percentage replacement of RCA

Table: 6 shows specimen designation with amount of average fracture energy for different replacement of RCA (0%, 50%, and 100%) in natural aggregate for M20 & M40 grade concretes. From Table.6 it is evident that with the increase in replacement of recycled aggregate concrete in natural aggregate (NA), there is general decrease in fracture energy. It may be noted from Table 6 that the percentages decrease in fracture energy is increasing with increase in replacement of recycled concrete aggregate in natural aggregate. This is true for both M20 & M40 grade concrete. Further for both 50% and 100% replacement, % decrease is less for M40 grade concrete as compared to M20 grade concrete. Also it is observed that the average fracture energy in M20 Normal grade is been decreasing with increase in the % replacement of RCA.

Table 6 Average fracture energy

SPECIMEN	AN-0	AN-50	AN-100	BN-0	BN-50	BN-100
AVERAGE FRACTURE ENERGY, N/mm	58.80	51.50	23.00	30.21	23.34	13.31
SPECIMEN	AS-0	AS-50	AS-100	BS-0	BS-50	BS-100
AVERAGE FRACTURE ENERGY, N/mm	30.60	11.03	7.62	53.90	31.70	24.64

It is been observed from the Table 6 that the fracture energy is decreasing with increase in the grade of concrete. But in the case of self compacting concrete the fracture energy has increased increasing with the increase in the grade of concrete even for same RCA replacements in natural aggregate.

Effect on Ultimate Slip with percentage replacement of RCA

From Table 7 it is observed that the average ultimate slip in both M20 and M40 grade concretes is been decreasing with increase in the % replacement of RCA. Similar behaviour is observed for SCC also. The average bond stress versus slip curves are shown in Figure 7.

Table 7 Average ultimate slip and bond stress

SPECIMEN	AN-0	AN-50	AN-100	BN-0	BN-50	BN-100
AVERAGE BOND STRESS, N/mm²	8.07	8.00	7.31	10.54	9.28	8.33
AVERAGE ULTIMATE SLIP, mm	66.27	57.20	40.04	23.40	8.67	6.51
SPECIMEN	AS-0	AS-50	AS-100	BS-0	BS-50	BS-100
AVERAGE BOND STRESS, N/mm²	8.35	7.89	7.03	13.06	11.76	10.02
AVERAGE ULTIMATE SLIP, mm	42.48	26.06	9.07	39.26	29.38	11.84

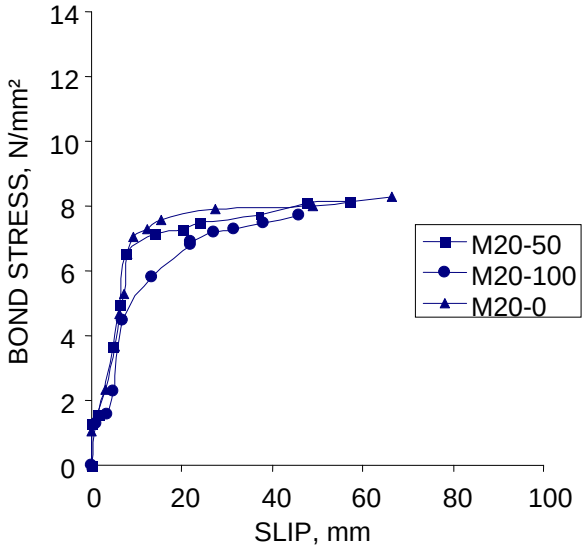

Figure 7.1 Average bond stress versus slip curves in M20 normal concrete

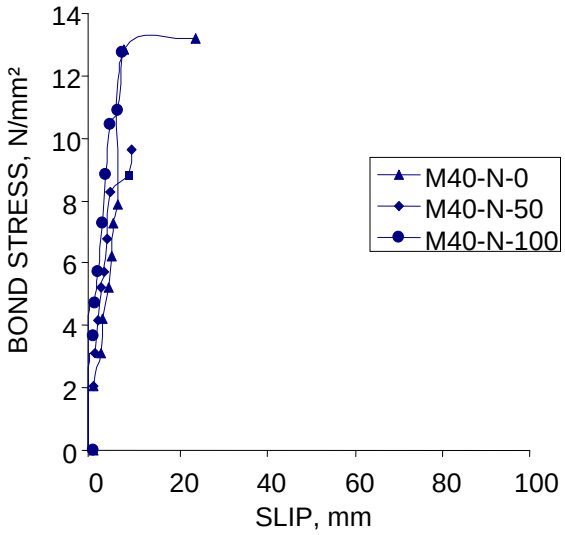

Figure 7.2 Average bond stress versus slip curves in M40 normal concrete

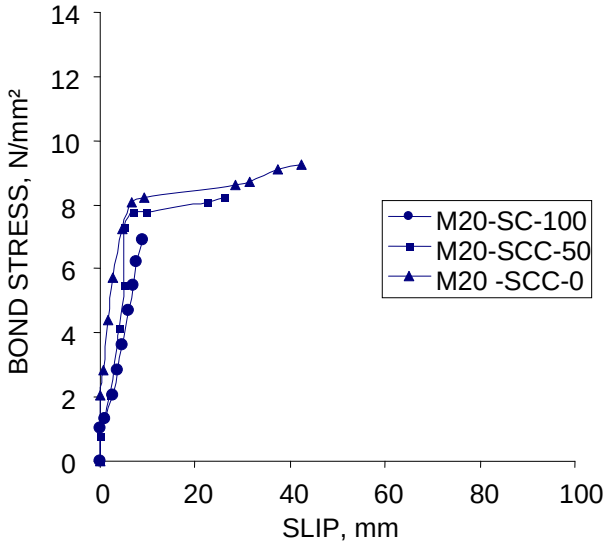

Figure 7.3 Average bond stress versus slip curves in M20 self compacting concrete

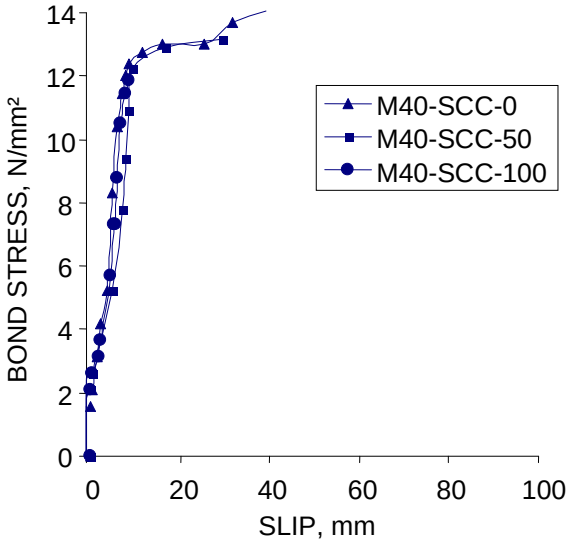

Figure 7.4 Average bond stress versus slip curves in M40 self compacting concrete

Figure 7 Average bond stress versus slip curves

CONCLUSIONS

From the detailed experimental results and analysis in the following conclusions can be drawn.

1. There is a decrease in the compressive strength with increase in the percentage of recycled aggregate in natural aggregate. This is true for both M20 and M40 grades of concrete.
2. The percentage decrease in compressive strength with percentage replacement of recycled aggregate in natural aggregate, is low in the case of self compacting concrete as compared to vibrated concrete (normal concrete) for identical grades. The target mean strength could easily be achieved even at 100% replacement of recycled aggregate in natural aggregate.
3. In case of M20 grade concrete the bond stress is more or less remained constant up to 50% replacements of recycled aggregate in natural aggregate. While for higher level replacements the bond stress decrease is considerable. The percentage decrease with a replacement of 50% & 100% is 10% and 20% respectively in vibrated concrete. While it is 15% and 20% in self compacting concrete.
4. There is a decrease in the slip value with percentage replacement of recycled aggregate concrete in natural concrete. This is true for both M20 and M40 vibrated and self compacting concrete. The decrease in average ultimate slip with increase in replacement exhibit brittle behaviour in both grade of concrete. Further in self compacting concrete the slip is less for identical percentage replacement of recycled aggregate in natural aggregate both for M20 and M40 grade concretes exhibiting brittleness of SCC.
5. The fracture energy decreases with increase in the percentage of recycled aggregate in natural aggregate and the decrease is around 12% in M20 and 20% in M40 in 50% RCA replacements. For 100% replacements the decrease in fracture energy is more than 50%. This is true in case of M20 and M40 grade normal and self compacting concretes.

ACKNOWLEDGEMENTS

The Author acknowledges the support of Mr. V. Saradhi a graduate student and colleague faculty.

REFERENCES

1. NIXON P J, Recycled concrete as an aggregate for concrete – a review, Materials and Structures, Vol. 11, No. 65, 1978, pp. 371–380.

2. HANSEN T C, Recycled aggregate and recycled aggregate concrete, second state-of-the-art report, developments from 1945–1985, Materials and Structures, Vol. 19, No. 111, 1986, pp. 201–246.

3. HANSEN T C, Recycling of demolished concrete and masonry. London, E&FN SPON, 1992.

4. ACI COMMITTEE 555. Removal and reuse of hardened concrete. ACI Mater Jl, Vol. 99, No. 3, 2002, pp. 300–325.

5. XIAO J, LI J AND ZHANG C H, Mechanical properties of recycled aggregate concrete under uniaxial loading. Cem Concr Res, Vol. 35, No. 6, 2005, pp. 1187-1194.

6. ACI COMMITTEE 408. Bond stress-the state of the art. ACI J, Vol. 63, No. 11, 1966, pp. 1161-1190.

7. ACI COMMITTEE 408. Opportunities in bond research. ACI J, Vol. 67, No. 11, 1970, pp. 857–867.

8. ACI COMMITTEE 408. State of the art report: Bond under cyclic loads. ACI Mater J, Vol. 88, No. 6, 1992, pp. 669–673 [abstr].

9. MUKAI T AND KIKUCHI M, Fundamental study on bond properties between recycled aggregate concrete and steel bars. Cement Association of Japan, 32nd review.

10. EDWARDS A D AND YANNOPOULOS P J, Local bond–stress to slip relationships for hot rolled deformed bars and mild steel plain bars. ACI J, Vol. 76, No. 5, 1979, pp. 405-419.

11. POON C S, SHUI Z H AND LAM L, Effect of microstructure of ITZ on compressive strength of concrete prepared with recycled aggregates, Constr Build Mater, Vol. 18, No. 6, 2004, pp. 461–468.

12. HARAJI M H, Development/splice strength of reinforcing bars embedded in plain and fiber reinforced concrete. ACI Struct J, Vol. 91, No. 5, 1994, pp. 511–520.

RILEM recommendation. Specification for concrete with recycled aggregates. Materials and Structures, Vol. 27, 1994, 173 p.

Concrete with Fluorescent Waste Glass Suspension

P Kara, A Korjakins
Riga Technical University, Latvia

The accumulation of non-recyclable waste glass in the plants without being used represents two major problems: a solid waste disposal and a negative impact to the environment. Borosilicate glass (DRL) and leaden silicate glass (LB) remaining after fluorescence lamp utilization is the waste which is not possible to recycle by traditional methods due to specific chemical composition. It causes a problem for glass disposal because glass is not biodegradable and landfill is not the best environment friendly solution for it. Using fluorescent waste glass as micro filler which partially substitute cement in concrete is a good way to solve these problems. In present study was investigated: the possibility to increase the fineness of fluorescent waste glass powder as micro filler by its additional grinding in water environment with water/glass (160/90 and 125/125) weight proportions and influence on concrete's compressive strength by incorporating waste glass powder suspension into the mix. Fourteen different concrete mixes with additionally ground DRL and LB waste glass powders and powder suspensions were prepared. The particle grading of waste glass suspension was determined by Laser diffraction method. The best obtained particle size was in range from 0,6 μm to 11 μm with average grain size 5 μm. The concrete specimens were tested at the age of 7, 28, 56, 84 and 112 days. The most prospective results were obtained using additionally 30 & 90 minutes DRL ground glass powder and DRL glass suspensions made within 90 minutes, especially DRL suspension with water/glass weight proportion 160/90 shown the highest result at the age of 112 days of 83,7 MPa. However, LB waste glass mixes showed lower results in comparison to control mix, there were observed improvements for mixes with additional grinding for 90 minutes of glass powder with compressive strength result of 66 MPa at the age of 112 days and suspension LB suspension with water/glass weight proportion 125/125 with compressive strength of 68,1 MPa.

P Kara is currently Scientific researcher at Professor Group of Building Materials and Products, Institute of Materials and Structures, Riga Technical University, Member of LVS STK 30 Eurocode Sub-Committee. The main fields of research are building materials and structures reuse of industrial wastes and by-products, concrete technology.

A Korjakins is currently Professor and Chair of Professor Group of Building Materials and Products, Institute of Materials and Structures, Riga Technical University. The main fields of research are building materials and structures, ecological building materials, reuse of industrial waste.

Keywords: Compressive strength, Fineness, Fluorescent waste glass powder, Micro filler, Waste glass suspension

INTRODUCTION

The accumulation of non-recyclable waste glass in the plants without being used represents two major problems: a solid waste disposal and a negative impact to the environment. Borosilicate glass and leaden silicate glass remaining after fluorescence lamp utilization is the waste which is not possible to recycle by traditional methods due to specific chemical composition. It causes a problem for glass disposal because glass is not biodegradable and landfill is not the best environment friendly solution for it.

Using fluorescent waste glass as micro filler which partially substitute cement in concrete is a good way to solve these problems and is up to date task in concrete technology. Micro filler is one of the most expensive mix component, it cost may make up a half part from cement cost. Micro filler replacement by waste products gives possibility to achieve economical effect and to solve environmental protection task simultaneously. Glass waste application as a micro filler in concrete (partial replacement of sand, of cement) was investigated by many researchers in previous years [1-15].

The main component of glass is silicate oxide SiO_2 in amorphous state. A coarse crushed glass used as concrete aggregate can cause the alkali-silicate reactions (ASR) in hard concrete resulting in harmful expansion in interface between cement and glass surface [11-12]. The ground glass particles (<75 μm) are initiating pozzolanic reactions without harmful expansion deformations [13]. Waste glass can be used in concrete not only as a coarse or fine aggregate but also as a powder with nanosized silicium dioxide particles forming a very dense microstructure and improving concrete properties. The coarse and fine aggregates can trigger ASR in concrete whereas glass powder can suppress tendency to ASR and produce the effect similar to that of supplementary cementitious materials such as pozzolan [14].

Additionally ground glass demonstrates properties of active micro filler which performs long-term hardening effect [10]. In papers of other researchers [1-15] if waste glass was ground it was ground in dry environment in order to achieve fineness. In present study was investigated the possibility to increase the fineness of borosilicate (DRL) and leaden silicate (LB) waste glass powder as micro filler by its additional grinding in water environment and influence on concrete's compressive strength by incorporating waste glass powder suspension into the mix.

MATERIALS AND METHODS USED

Local Industrial By-Products

The industrial by-products used in this study are borosilicate (DRL) and leaden silicate (LB) waste glass powders obtained from fluorescent lamp chippings. Lamp recycling process includes lamp classification, glass separation, cleaning from harmful components, crushing into chippings and grinding. The chemical analysis of waste glass powders was determined in conformity with LVS EN 196-21 methodology and the results are summarized in Table 1.

Table 1 DRL and LB waste glass powders chemical composition

COMPONENTS	DRL CONTENT % by mass	LB CONTENT % by mass	TOLERANCE ± %
SiO_2	74.20	69.07	0.5
PbO	0	20.02	0.5
B_2O_3	16.63	0	0.5
Al_2O_3	1.65	1.03	0.3
Fe_2O_3	0.16	0.19	0.05
CaO	2.09	1.39	0.2
MgO	0	0	0.2
Na_2O	3.82	8.02	0.1
K_2O	0.93	1.17	0.1
Total	99.48	99.72	-

Fluorescent lamp chippings were ground to the Blaine specific surface of 2310 cm²/g for DRL and of 2360cm²/g for LB. In order to improve fineness, waste glass powders were additionally ground for 30 and 90 minutes in laboratory planetary ball mill Retsch PM400 (with rotation speed 300 min^{-1}).

Mix Compositions

Ordinary Portland cement CEM I 42.5N from "Kunda Nordic" (Estonia) was applied as binding agent. Natural local washed gravel (2-12 mm) and natural sand (0-1 and 0.3-2.5 mm) were applied as rough/fine aggregates. Proportions between aggregates were calculated in order to obtain the best grading curve of aggregate, taking into account optimum range curves in conformity with DIN 1045. Cement was substituted with fluorescent waste glass at level of 20%. The aggregates and water amount were kept constant. Concrete mixes were designed without plasticizing agent.

Control concrete mix and fourteen different concrete mixes with glass powders and glass powder suspensions were mixed in a power-driven rotary mixer with a moving bottom (but with no blades or paddles). Most of mixes were made with capacity of 10.3 liters. The mix compositions are summarized in Table 2.

Table 2 Concrete mix compositions, kg/m³

MATERIALS	CONTROL MIX	DRL & LB GLASS POWDER / GLASS SUSPENSION MIXES
Portland cement CEM I 42.5 N	410	330
Gravel 2/12 mm	1000	1000
Sand 0.3/2.5 mm	650	650
Sand 0/1 mm	120	120
Glass powder (20%)	---	80
Water	200	200
Water/cement ratio	0.49	0.49

At first part of experiments, DRL and LB glass powders with total volume of material of 250 g in each of 4 containers were additionally ground for 30 and 90 minutes and obtained activated powders were used for concrete mixes preparation. At second part of experiments, DRL and LB glass powders with total volume of material of 250 grams in each of 4 containers were additionally ground for 30 and 90 minutes in water environment with water/glass (160/90 and 125/125) weight proportions in order to obtain waste glass suspension which lately was incorporated into the concrete mixes. The particle grading of waste glass suspensions was determined by method of laser diffraction analysis and the results are shown in Table 3.

The dry components were weighed and mixed for a one minute in drum mixer, 50% from designed water or glass suspension content was added during next 1 minute. Remaining water, glass suspension has been added into the mix during mixing. As soon as the mixing finished, Abram slump test was carried out for each mix in accordance with LVS EN 12350-2:2009 "Testing fresh concrete – Part 2: Slump test" in order to test the workability of mixes. Water dosage was selected to provide cone slump in range of 80…150 mm (cone slump classes S2, S3).

Specimens were cast in 100 mm × 100 mm × 100 mm plastic or steel moulds, which conform to standard LVS EN 12390-1:2009 "Testing hardened concrete – Part 1: Shape, dimensions and other requirements for specimens and moulds". The moulds were cleaned and lightly coated with form oil before the casting procedure. Concrete was compacted on a vibrating table. After that the specimens were covered with polyethylene pellicle and left to set for 24 hours. Then they were removed from moulds and cured in water (with temperature +20±2°C) for 7 days and in curing chamber (with air temperature +20±2°C and relative humidity ≥95%) for other 21 days or until testing, thus conforming to LVS EN 12390-2:2009 "Testing hardened concrete – Part 2: Making and curing specimens for strength tests".

To evaluate hardened concrete properties compressive strength test was carried out. Before the test, the specimens were dried in an oven for 20 min in 50ºC temperature. The testing was done according to LVS EN 12390-3:2009 "Testing hardened concrete – Part 3: Compressive strength of test specimens". Compression testing machine with the accuracy of ±1% was used; the rate of loading was 0.65 MPa/s. Compressive strength for: (i) mixes with DRL and LB powders/suspensions with grinding time up to 30 minutes was conducted up to 84 days, (ii) for control mix and DRL and LB powders/suspensions with grinding time up to 90 minutes was conducted up to 112 days. Three specimens per mix for each age were prepared and the mean compressive strength value was calculated.

EXPERIMENTAL RESULTS AND DISCUSSIONS

Cement Substitution with Waste Ground Glass Powders and Waste Glass Suspensions

The aim of the experiments was to clarify the influence on the concrete properties of fluorescent waste glass powder and glass powder suspension applied as Portland cement partial substitution. Waste glass suspensions are shown in Figures 1 and 2. As it possible to see the colour of DRL suspension is darker than the colour of LB suspension. During experiment it was observed that sedimentation of glass powder suspensions (sDRL30, sLB30) ground up to 30 minutes occurs much faster than of suspensions (sDRL90, sLB90) which were ground up to 90 minutes. Also it was observed that sedimentation of sDRL30,

sLB30 harden very fast forming hard glass layer already after 12 hours. Suspensions should be incorporated into the concrete mix straight ahead after grinding. The forming of glass layers also can be described by waste glass chemical composition and special conditions appeared during the grinding process (high temperature and pressure) in laboratory mill's moulds during grinding process. As to sDRL90, sLB90 suspensions sedimentation process occurred but after 12 hours did not harden and could be applicable even after 30 days when the suspension was shaken well before the use.

Figure 1 DRL glass suspension

Figure 2 LB glass suspension

Particle grading was obtained by laser diffraction method, the results for volume diameters d_{v10}, d_{v50} and d_{v90} are shown in Table 3. According to [10] grading composition analysis showed that rough ground material contains wide particle size in range from 2 μm up to 70 μm with average grain size 26.3 μm. Grading analysis indicated on considerable increase in fine particle content after powder additional grinding average grain size. Present grading composition analysis of waste glass suspensions showed that particle size of additionally ground glass suspension for 90 minutes was in range from 2 μm up to 31 μm with average grain size 10 μm. In order to see how will influence additional grinding on particle size range, there was made experiment with increased time up to 4 hours of grinding for DRL160/90 and LB 160/90 and it gave possibility to obtained particle size in range from 0.6 μm up to 11 μm with average grain size 5 μm.

Table 3 Waste glass suspension particle grading

GLASS SUSPENSIONS	VOLUME DIAMETER, μm		
	d_{V10}	d_{V50}	d_{V90}
LB 160/90/30	3.147	9.488	26.958
LB 160/90/90	2.931	2.932	30.023
LB 125/125/30	3.149	8.780	20.116
LB 125/125/90	3.108	9.307	30.882
DRL 125/125/30	3.099	10.249	29.612
DRL 125/125/90	2.029	5.586	14.435
DRL 160/90/30	3.054	9.738	23.846
DRL 160/90/90	2.605	8.266	30.616
LB 160/90/240	0.79	4.26	10.17
DRL 160/90/240	0.60	3.87	10.32

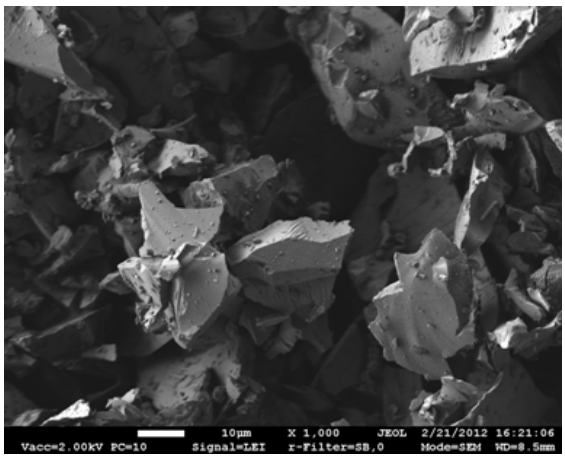

Figure 3 SEM micrograph of DRL powder

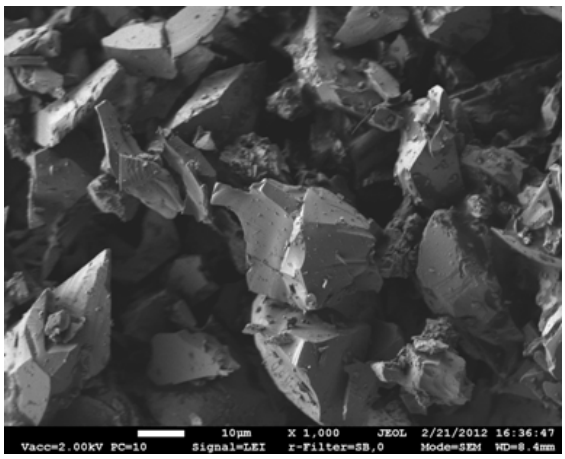

Figure 4 SEM micrograph of LB powder

SEM micrographs are shown in Figures 3 and 4 for DRL powder (Blaine specific surface of 2310 cm²/g) and LB powder (Blaine specific surface of 2360cm²/g). SEM analysis showed nanoparticles in LB waste glass suspension with grain size of 500 nm.

The determined results of compressive strength of concrete mixes conducted up to the age of 84 and 112 days, density and cone slump test results are summarized in Tables 4 and 5.

Table 4 Comparison of determined results for control mix and waste glass powder mixes

	CONTROL MIX	GLASS POWDER DRL			GLASS POWDER LB		
Grinding time, minutes	----	0	30	90	0	30	90
Cone slump, mm	135	40	42	60	40	48	85
Density, kg/m³	2361	2308	2335	2336	2328	2321	2364
Compressive strength, MPa							
7 days	45.8	35.7	44.8	45.4	35.3	36.0	39.3
28 days	57.3	46.2	60.2	59.4	43.4	46.2	50.4
56 days	66.3	51.1	66.5	68.5	48.3	54.9	59.4
84 days	71.6	55.5	67.5	70.4	51.2	56.8	65.3
112 days	72.1	----*	----*	72.0	----*	----*	66.0

Table 5 Comparison of determined results for control mix and waste glass suspension mixes

	CONTROL MIX	GLASS POWDER SUSPENSION (160/90)				GLASS POWDER SUSPENSION (125/125)			
		DRL	LB	DRL	LB	DRL	LB	DRL	LB
Grinding time, minutes	---	30	30	90	90	30	30	90	90
Cone slump, mm	135	20	30	105	75	30	20	90	105
Density, kg/m³	2361	2318	2307	2350	2330	2305	2329	2345	2315
Compressive strength, MPa									
7 days	45.8	38.8	33.7	43.5	33.4	38.2	34.8	48.1	37.9
28 days	57.3	50.2	43.0	66.3	48.1	50.2	47.0	63.2	47.9
56 days	66.3	57.1	49.6	76.8	54.7	54.9	50.1	72.8	59.2
84 days	71.6	59.2	52.3	82.5	53.4	62.5	55.8	73.0	64.2
112 days	72.1	----*	----*	83.7	58.8	----*	----*	76.8	68.1

* ---- the compressive strength test was not carried out.

It was observed that the concrete mixes containing ground fluorescent waste glass have more viscous consistency in comparison with control concrete mix. Also the results of cone slump tests are lower in values in comparison to control mix. It is evident from the slump test data shown in Tables 4 and 5 that LB waste glass powder contributed to workability of concrete more than DRL waste glass powder did. Addition of plasticizing agent into the mixes [16] with waste glass powders ground for 30 minutes showed the opposite results for slump test, DRL waste glass powder contributed to workability of concrete more than LB waste glass powder did. In present research the differences of slump test can be explained by DRL and LB particle size and shape, chemical composition. As it can be observed the grinding time of waste glass powders/suspensions influenced a lot on workability. The results from Table 4 show that, there is slightly difference in results for the slumps of mixes with waste glass powder grinding times for 0 and 30 minutes and 1.5..2 times greater results for the slumps of mixes with waste glass powder grinding time for 90 minutes. If to compare waste glass suspension mix slumps, it is possible to observe that: (i) DRL125/125/30 contributed to workability better than DRL160/90/30 but at the same time LB160/90/30 contributed to workability better than LB125/125/30, (ii) DRL160/90/90 contributed to workability better than DRL125/125/90 but LB125/125/90 contributed to workability better than LB160/90/90. Therefore, for better slump results for waste glass suspensions, which are close to control mix slump result, can be DRL160/90/90 and LB125/125/90 with the value of 105 mm (S2).

Glass powder increased concrete mix setting time. DRL glass powder had accelerating effect on setting time. Concrete mixes containing all types of glass powder very quickly (during first 40 min) were losing workability. Negligible effect of glass grinding on density of all mixes (mostly within 1%) was observed.

Experimental results indicate decrease of the compressive strength of concrete at the age of 7, 28 and 56 days for substitution with DRL waste glass and at all ages for LB waste glass. Figure 5 shows that concrete with 20% DRL waste glass substitution have higher overall results in comparison with 20% LB waste glass substitution on Figure 6.

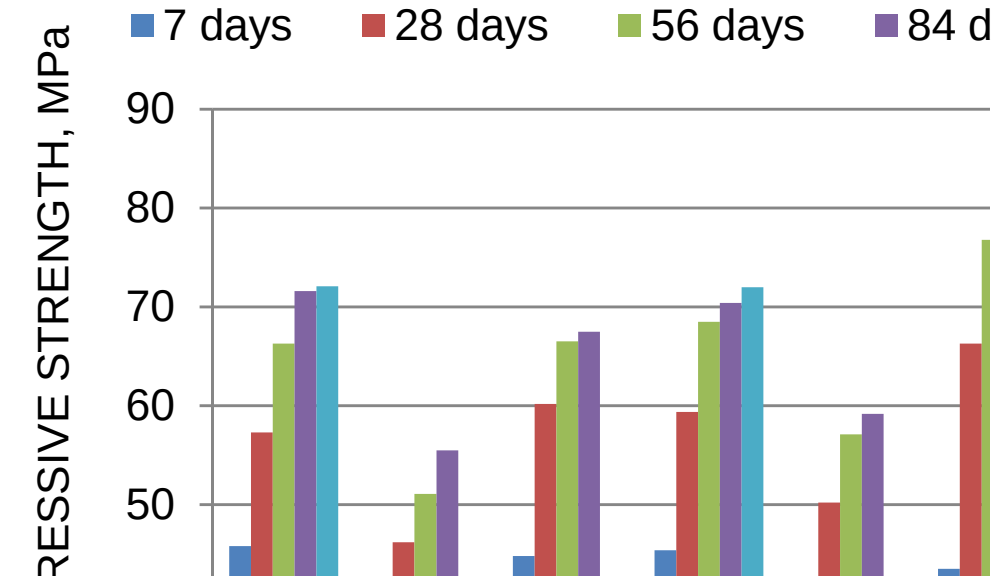

Figure 5 Influence of DRL waste glass powder/suspension grinding time and curing time on the concrete compressive strength. sDRL1 (sDRL160/90/30), sDRL2 (sDRL160/90/90), sDRL3 (sDRL125/125/30), sDRL4 (sDRL125/125/90)

Investigation showed that early strength levels of mixes with DRL waste glass powder/suspension substitution are lower at the age of 7 days in comparison with control concrete mix, but this is expected, as the strength improvements from pozzolanic reactions are mostly seen at later ages, in this case – at 56 days and especially at 112 days, when the differences are much smaller than at the early stages. In case of the use of additionally ground waste glass powder increase in compressive strength was observed after 28 days hardening.

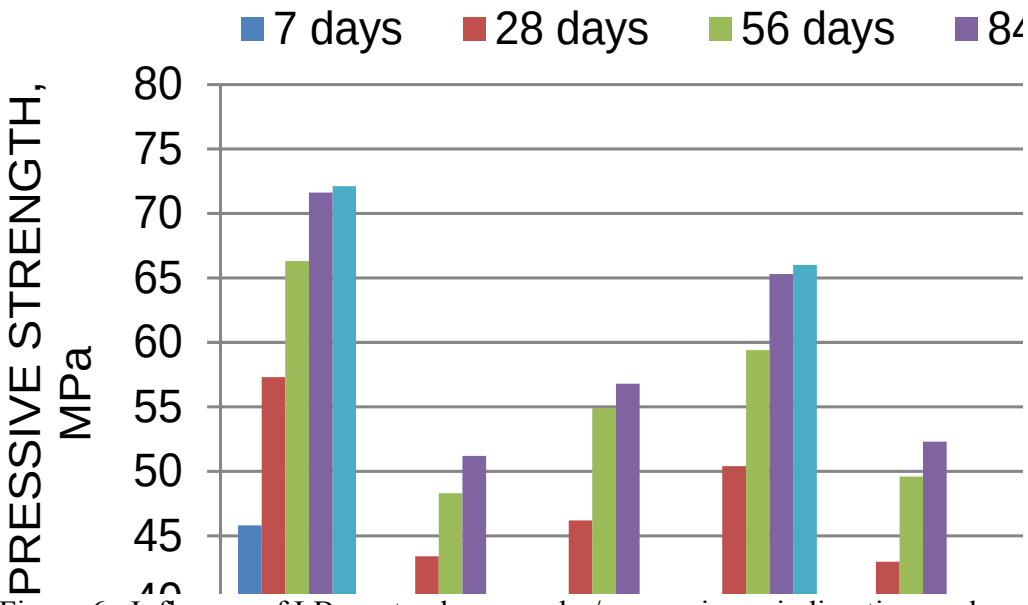

Figure 6 Influence of LB waste glass powder/suspension grinding time and curing time on the concrete compressive strength. sLB1 (sLB160/90/30), sLB2 (sLB160/90/90), sLB3 (sLB125/125/30), sLB4 (sLB125/125/90)

This effect may be explained by activating of pozzolanic reactions caused by glass additional grinding and increasing of specific surface. The most prospective results were obtained using additionally 30 and 90 minutes DRL ground glass powder and DRL glass suspensions made within 90 minutes, especially sDRL160/90/90 shown the highest result at the age of 112 days of 83.7 MPa. However, LB waste glass mixes showed lower results in comparison to control mix, there were observed improvements for mixes with additional grinding for 90 minutes of glass powder with compressive strength result of 66 MPa at the age of 112 days and suspension sLB125/125/90 with compressive strength of 68.1 MPa. The differences between strength results for DRL waste glass are within 4.4% - 9% and for LB waste glass are within 4.1%-7.3%. Experimental results indicate that it is possible to achieve environmentally friendly concrete compositions with low cement content utilizing non-recyclable fluorescent waste glass. Durability and physical properties of concrete containing glass powder/suspension must be investigated in the future in a more detailed way. Careful evaluation of hygienic and ecological aspects of using lamp glass recycling products as concrete micro-filler must be also carried out.

CONCLUSIONS

The aim of the experiments was to clarify the influence on the concrete properties of fluorescent waste glass powder and glass powder suspension applied as Portland cement partial substitution. During fluorescent waste glass grinding in water finer particles were obtained in comparison to dry grinding. Present grading composition analysis of waste glass suspensions showed that particle size of additionally ground glass suspension for 90 minutes was in range from 2 μm up to 31 μm with average grain size 10 μm. It improved concrete mix workability and compressive strength. The properties of fresh concrete mix and properties of hardened concrete considerably depend on finesse of DRL & LB glass powder/suspension. Additionally ground fluorescent waste glass powder/suspension accelerates setting time. Lose of mix workability (during first 40 minutes) took place for all types of concrete mixes with fluorescent waste glass powder/suspension. Cement substitution with additionally ground DRL waste glass powder/suspension reduces compressive strength in 7 days and demonstrates considerable strength gain after 28 days keeping them equal to control mix on 56^{th} and 84^{th} days. Experimental results indicated decrease of the compressive strength of concrete at all ages for LB waste glass powder/suspension and increase of the compressive strength at later ages which was close to control mix one. Cement substitution with additionally ground DRL 160/90/90 glass suspension reduced compressive strength at the age of 7 days and gained higher value for 13% in comparison to control mix on 28^{th} day, keeping higher values on 56^{th}, 84^{th} and 112^{th} days. The test results showed that DRL glass suspension itself has pozzolanic characteristics and using it as a mineral admixture in concrete, had an effect on workability, improved considerably mechanical properties of concrete at later ages. Using waste glass as a construction material is a good way to help the environment through grinding and using it as a partial replacement of cement by weight in concrete.

ACKNOWLEDGEMENTS

The authors would like to thank the Vilnius Gediminas Technical University Thermoinsulation Scientific Institute for providing access to their laboratory. The financial support of the ERAF project Nr. 2010/0286/2DP/2.1.1.1.0/10/APIA/VIAA/033 „High efficiency nanoconcretes” is acknowledged.

REFERENCES

1. SIDDIQUE R, Waste materials and by-products in Concrete, Springer, 2008, 413 p.
2. SHAO Y, LEFORT T, MORAS S AND RODRIGUEZ D, Studies on concrete containing ground waste glass, Cement and Concrete Research, Vol. 30, 2000, pp. 91-100.
3. MEYER C AND BAXTER S, Use of recycled glass and fly ash for precast concrete, Rep. NYSERDA98-18(4292-IABR-IA-96) to New York State Energy Research and Development Authority, Dept. of Civil Engineering and Mechanical Engineering, Columbia University, New York, 1998.
4. POLLERY C, CRAMER S M AND DE LA CRUZ R V, Potential for using waste glass in Portland cement concrete, J Mater, Civil Eng, Vol. 10, No. 4, 1998, pp. 210-209.
5. BYARS E A, MORALES-HERNANDEZ B AND ZHU H Y, Waste glasses as concrete aggregate and pozzolan, Concrete, Vol. 38, No. 1, 2004, pp. 41-44.
6. TOPCU I B AND CANBAZ M, Properties of concrete containing waste glass, Cem Conc Res, Vol. 34, 2004, pp. 267-274.
7. MALHOTRA V M AND MEHTA P K, Pozzolanic and cementitious materials, Advances in concrete technology. New York: Gordon and Breach Publishers; 1996.
8. FEDERICO L M AND CHIDIAC S E, Waste glass as a supplementary cementitious material in concrete – Critical review of treatment methods, Cem. Conc. Comp., Vol. 31, 2009, pp. 606-610.
9. POON C S, Management of construction and demolition waste, Waste Management, Vol. 27, No. 2, 2007, pp. 159-160.
10. SHAKHMENKO G, KORJAKINS A AND BUMANIS G, Concrete with microfiller obtained from recycled lamp glass, Proceedings of the 10th international Conference Modern building materials, structures and techniques, Vilnius Lithuania, 19-21 May, 2010, pp. 280-284.
11. SHAYAN A AND XU A, Performance of glass pozzolanic material in concrete: A field trial on concrete slabs, Cement and Concrete Research, Vol. 36, 2006, pp. 457-468.
12. SHAYAN A, Value-added utilisation of waste glass in concrete, Proceedings of IABSE symposium, Melbourne, 2002.
13. SCHWARZ N AND NEITHALATH N, Influence of a fine glass powder on cement hydration: Comparison to fly ash and modeling the degree of hydration, Cement and Concrete Research, Vol. 38, 2008, pp. 429-436.
14. KARAMBERY A AND MOUTSATSOU A, Participation of colored glass cullet in cementitious materials, Cement, Concrete, Composites, Vol. 27, No. 2, 2005, pp. 391-327.
15. SOBOLEV K, TURKER P, SOBOLEVA S AND ISCIOGLU G, Utilization of waste glass in ECO-cement: strength properties and microstructural observations, Waste management, Vol. 27, 2007, pp. 971-976.
16. KARA P, KORJAKINS A AND KOVALENKO K, The Usage of Fluorescent Waste Glass Powder in Concrete, Scientific Journal of Riga Technical University Construction Science, 2012 (in press)

Feasibility of Using Spent Printer Toner as a Colouring Additive in Concrete

K Moock[1], L J Csetenyi[2], M D Newlands[2], L Zheng[2]
1 – Moock Environmental Solutions Ltd, UK
2 – University of Dundee, UK

The growing demand for quality print-outs, wider availability and more economical operation of laser printers also means that more toner cartridges are made and recycled world-wide. However the toner powder removed from spent cartridges is not suitable for printers anymore and currently sent to landfill. Toner does not mix with water either and therefore cannot be used directly to colour concrete. The paper reports the development of a patented, multi-component, surfactant-based admixture, which makes toner powder compatible with concrete. Properties of such coloured concrete are investigated as a function of toner levels, including strength and permeability (ingress of water at atmospheric conditions and under pressure). Beyond its decorative values, toner coloured concrete also shows improved water tightness resulting in enhanced durability.

K Moock is Managing Director of Moock Environmental Solution Ltd, which is part of Easdale Environmental Development Ltd.

L J Csetenyi is a Research/Teaching Fellow in the Concrete Technology Unit, University of Dundee. His main areas of interest include cement and concrete science and technology with emphasis on waste stabilisation/solidification and practical use of these materials in construction.

M D Newlands is a Lecturer in the Concrete Technology Unit, Division of Civil Engineering, at the University of Dundee, UK. His research interests lie in concrete durability, sustainability and the development of test methods.

L Zheng is a Research Fellow in the Concrete Technology Unit in the Division of Civil Engineering, at the University of Dundee, UK. His research focuses mainly on Recycling of waste materials, concrete durability, mix optimisation, cement hydration and modelling.

Keywords: Colour, Concrete, Pigment, Toner

INTRODUCTION

The increasing demand for producing quality documents results in using a large amount of office consumables, including toner cartridges, world-wide. Recycling, as required by law [1] is usually well-organised and efficient, but the toner powder removed from spent cartridges is degraded, hence not suitable for the use in printers any more. It is a very fine material, does not mix with water and therefore cannot be used as it is to colour concrete, which is an aqueous medium. Handling of toner powder poses a dust hazard and so far the only disposal option has been landfilling in closed containers.

OBJECTIVES OF THE RESEARCH

In order to remove toner powder from landfilling and find a use in construction industry products, dominantly in concrete, solutions of the following problems were aimed at:

1. Characterise toner and find compatible interfacing material(s) between toner and fresh concrete, which also serve(s) as dispersing agent.
2. Eliminate dust hazard by developing a means of transforming the powder to a more manageable form, e.g. slurry or paste, for ease of handling and precise proportioning.
3. Assess main engineering properties of the obtained coloured concrete.

The miscibility problem has been recently solved by developing a suitable multi-component admixture at the University of Dundee. The new admixture is now patented and utilises surfactants interfacing toner particles and the aqueous system of fresh concrete. In practice, toner is first turned into a homogeneous slurry, paste or damp non-dusting powder, which is then mixed with the rest of concrete constituents.

PROPERTIES OF TONER

Toner particles are polymer based beads containing small pigment seeds. Due to the very narrow tolerances dictated by the operation of laser printers, toner particles are practically of uniform size (8-10 µm in diameter). This is illustrated in Figures 1 and 2 showing particle size distribution and morphology of the material. A Malvern Mastersizer2000 analyser and a Philips XL-30 scanning electron microscope were used.

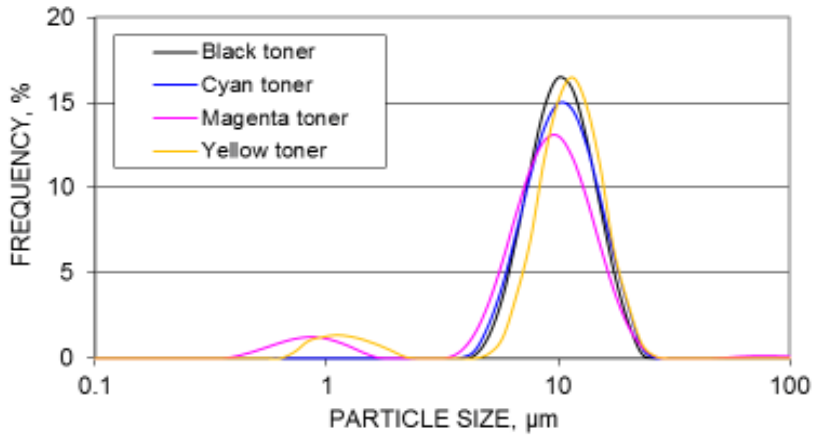

Figure 1 Particle size distribution of toners

Scanning electron microscopic images revealed that black toner has spherical particles, whereas cyan, magenta and yellow toner particles are slightly angular, which is in line with the different 'flowing' characteristic observed for the dry materials (Figure 2).

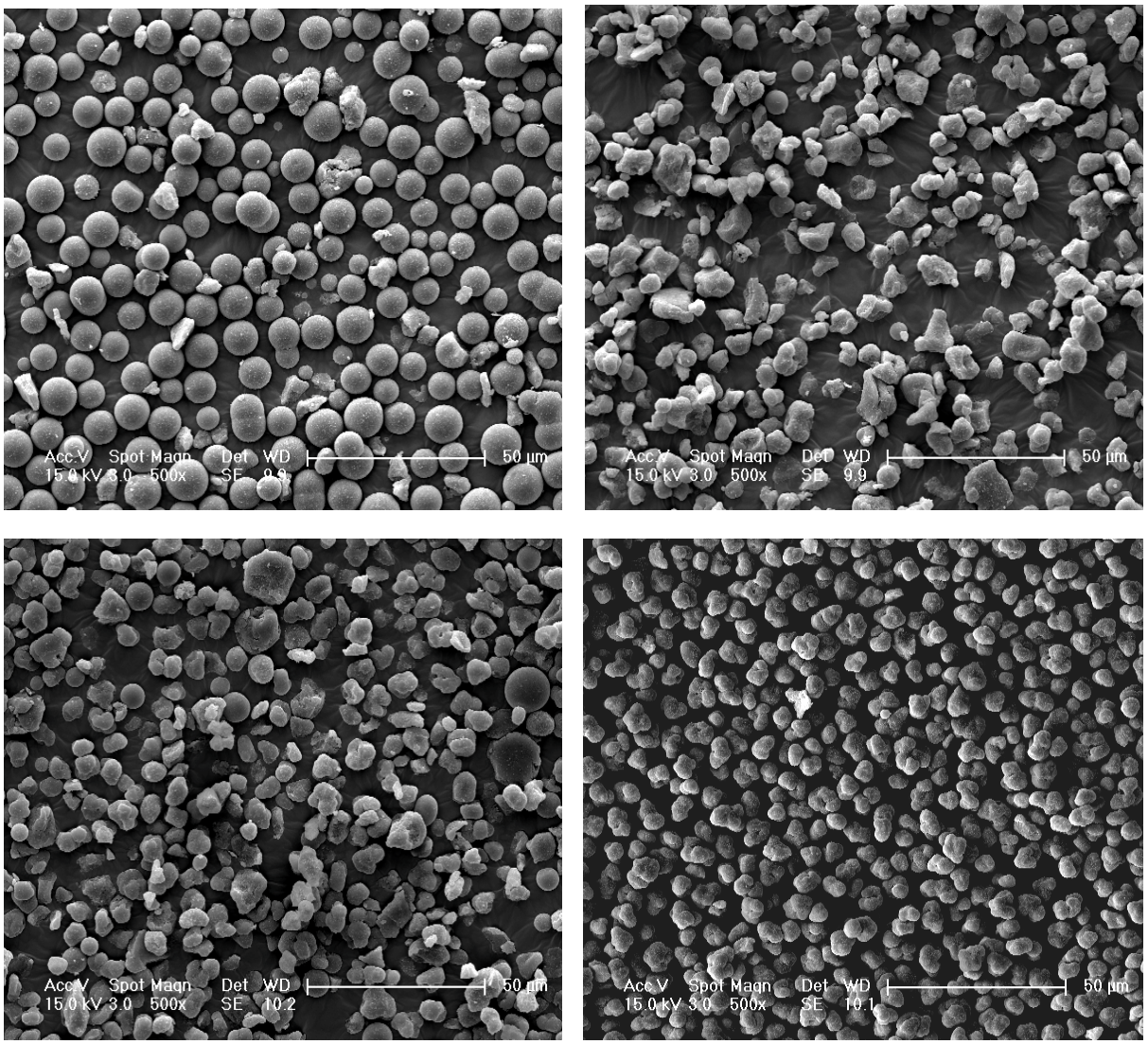

Figure 2 Scanning electron microscopic images of toners (magnification ×500) black (top left), cyan (top right), magenta (bottom left), yellow (bottom right)

MIXING CONCRETE WITH TONER

Toner powder arises in four colours: black (majority by quantity), magenta, cyan and yellow. These basic colours can be mixed at any proportion to obtain other colours or a particular tint, especially if white cement is used for colour accuracy. Given the small particle size of toner, a certain pore blocking / water repellent effect is also anticipated, entailing increased durability to concrete.

In the scope of the current paper, experimental work with cyan toner is shown. Concrete samples were made in a drum mixer with 0 (reference) 15, and 30% toner powder contents (Table 1). Local aggregates and sand used were in saturated surface dry condition. Toner was used as slurry in half the mixing water, with admixture applied at 0.2% (m/m) of toner.

Table 1 Concrete mix design

TONER, %	WATER, kg/m³	CEM I, kg/m³	TONER, kg/m³	SAND, kg/m³	GRAVEL, kg/m³		W/(C+T)	S/A	T/(C+T)
					10 mm	20 mm			
0	175	350	0.0	610	375	750	0.50	0.35	0.00
15	175	297.5	52.5	600	370	735	0.50	0.35	0.15
30	175	245	105.0	600	370	735	0.50	0.35	0.30

Figure 3 Mixing concrete coloured with cyan toner

RESULTS AND DISCUSSION

The investigated properties of concrete included i) compressive strength at 7 and 28 days [2], ii) water penetration at 28 days [3], iii) Initial Surface Absorption at 28 days [4], and iv) capillary absorption at 28 days [5]. The test results obtained are given in Table 2.

Table 2 Concrete test results with different quantities of toner

Toner content, %	PROPERTIES							
	Slump, mm	Compressive strength, N/mm^2		Water penetration under pressure, mm	ISAT, ml/(m^2·s)			Capillary absorption mg/mm^2
		7 days	28 days		10 min	30 min	60 min	
0	15	37.9	46.5	18	0.38	0.25	0.17	0.44
15	25	28.7	35.4	20	0.33	0.15	0.11	0.34
30	45	17.9	21.3	22	0.23	0.10	0.09	0.22

Compressive Strength

Increasing level of toner at the expense of Portland cement in concrete resulted in decreased strength, but not as much as the percentage of cement replacement, indicating some net strength improvement. With suitable modifications of the mix design, compressive strengths similar to that of control concrete is anticipated to be achieved with some savings of cement, due to pore blocking effect of toner particles.

Water Absorption

Initial surface absorption and capillary absorption tests reveal that ingression of moisture in toner concrete reduced at atmospheric pressure, which is attributed to water repellent and pore blocking properties of toner. The slight increase of water penetration under pressure shows the detrimental effect of lack of cement, similarly to compressive strength results.

CONCLUSIONS

During the experimental work it was established that for successful inclusion i.e. homogenous dispersion of spent or reject printer toner powder in concrete, the toner has to be first mixed with the specialty admixture and then added to the rest of the concrete constituents.

Increasing toner powder content improves water repellent properties of concrete. Given that toner was used to replace cement, the compressive strength results obtained were lower at increasing toner contents, but not proportional to the level of replacement. This indicates that pore blocking effect of toner particles may have resulted in improved packing and equivalent strength concrete may potentially be able to achieve at somewhat reduced cement contents.

Aesthetic values and environmental credentials of toner coloured concrete, diverting waste from landfill to high added value utilisation are clearly recognized additional benefits.

ACKNOWLEDGEMENTS

This study has been supported by funding received from the Scottish Funding Council. Laboratory work by Zsófia Kolozsi (IAESTE student at the time of the experiments, now post-graduate student at the University of Guildford, UK) is gratefully acknowledged.

REFERENCES

1. Directive 2002/96/EC of The European Parliament and of The Council, on waste electrical and electronic equipment (WEEE), Annex II, (2003) pp. 24-38

2. BS EN 12390-3:2009 Testing hardened concrete — Part 3: Compressive strength of test specimens, BSI, London, UK

3. BS EN 12390-8:2009 Testing hardened concrete — Part 8: Depth of penetration of water under pressure, BSI, London, UK

4. BS 1881-208:1996 Testing concrete — Part 208: Recommendations for the determination of the initial surface absorption of concrete, BSI, London, UK

5. BS 1217: 2008 Cast stone — Specification, BSI, London, UK

Comparative Study of Self-compacting Concrete with Manufactured and Dune Sand

L Zeghichi, Z Benghazi, L Baali
University of M'sila, Algeria

Sand is an inert element which essential in the composition of concrete; its use ensures granular continuity between the cement and gravel for better cohesion of concrete. This paper presents the results of a study that investigated the influence of sand quality on the properties of fresh and hardened self-compacting concrete SCC. The dune sands are very fine materials characterized by a high intergranular porosity, high surface area and low fineness modulus; on the other hand crushed (manufactured) sand has a high rate into thin, irregular shapes which are influencing the workability of Concrete. The amount of dune sand varies from (0% 50%, to 100%) by weight of fine aggregates. The results show that the rheological properties favor the use of dune sands; however the mechanical properties support the use of crushed sand.

Dr Leila Zeghichi is a senior lecturer in construction materials. In civil engineering at the Faculty of Technology, Department of Civil Engineering, University of M'sila (Algeria). She specializes in the use of binders and durability of concrete.

Mr Zied Benghazi is a PhD student at the Faculty of Technology, Department of Civil Engineering, University of M'sila (Algeria). He specializes in binders and concrete technology.

Mr Laïd Baali is an assistant professor at the Faculty of Technology, Department of Civil Engineering, University of M'sila (Algeria).). He specializes in binders and durability of concrete.

Keywords: Crushed sand, Dune sand, Mechanical properties, Segregation resistance, Self-compacting concrete

INTRODUCTION

A self-compacting concrete (SCC) is a concrete that flows and sets up in the most complex and scrapped forms under the effect of its own weight. It is important to note that the material should not undergo any form of segregation and should have qualities similar to those of conventional vibrated concrete [1, 2].

Aggregates are very important components of ordinary and self-compacted concretes (Figure 1). It's well known that they affect both fresh and hardened concrete properties. Concrete flowability depends on the properties of cement paste, the amount and gradation of aggregates. The lowest the surface area and voids are, the best the flowability is [3].

The sand is the key component to insure the granular continuity between the coarse aggregates (the gravel) and powders (cement and fillers). Crushed sands often require more water than round sands (obtained from dunes or rivers) to reach an aimed workability [4]. However, the round sands are characterized by a high intergranular porosity, which affect the aggregates packing and needs more powder to fill the voids and may increase the coast of SCC. The effect of round sand on mechanical properties of SCC is to be investigated.

The effect of crushed and round sands on the SCC is discussed here for both rheological and mechanical properties. The round sand used in this work is dune sand.

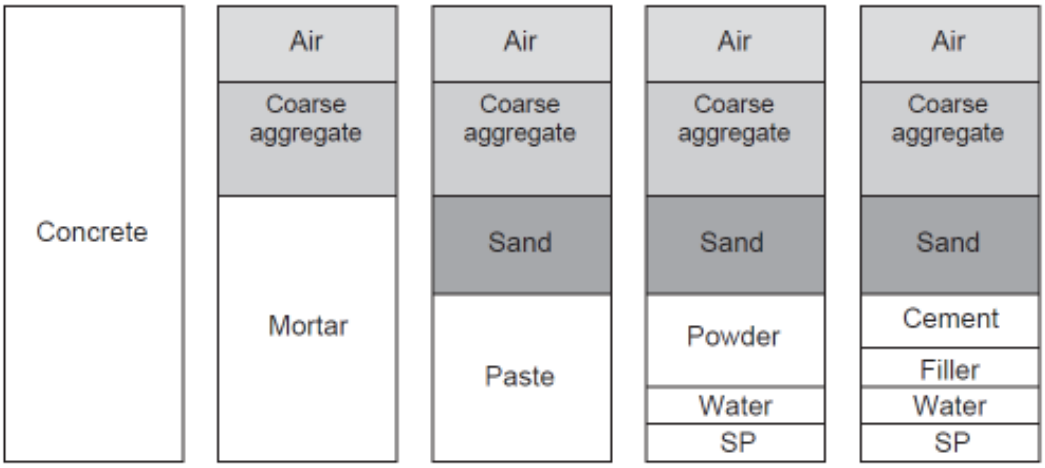

Figure 1 Schematic composition of SCC [5]

MATERIALS AND METHODS

The physical properties and the chemical composition of the material used are given in Tables 1 and 2, respectively. According to the particles size distribution (Figure 2) we can see that the dune sand used in this work is fine (with a fineness modulus Mf = 1.85 < 2.2) and not entirely suitable to be used in concrete if we are looking for a good strength. For the crushed sand: Mf = 2.1, which may be considered as acceptable sand.

Table 1 Physical properties of materials used

MATERIAL	TYPE	ρ, kg/m³	BLAINE, cm²/g
Cement	CEM II/A 42.5	3100	4000
Filler 1	Limestone powder	2660	1600
Filler 2	Granular slag powder	2940	3200
Dune sand	Boussaada sand 0-3	2540	/
Crushed sand	COSIDER quarry sand 0-3	2530	/
Crushed Gravel 1	COSIDER quarry gravel 3-8	2560	/
Crushed Gravel 2	COSIDER quarry gravel 8-16	2550	/
Superplasticizer (liquid)	MEDAFLOW 30 (GRANITEX)	1070	/

Table 2 Chemical composition of materials used

MATERIAL	SiO_2	Al_2O_3	CaO	Fe_2O_3	MgO	SO_3	Na_2O	Cl^-
Cement	20.70	4.75	62.92	3.75	1.90	1.98	0.09	0.005
Filler 1	10.81	0.31	47.51	0.76	0.21	/	/	/
Filler 2	40.80	5.20	43.01	0.53	6.40	0.80	0.01	0.007
Dune sand	86.95	1.92	6.33	0.09	0.53	0.44	/	/
Crushed sand	40.65	8.87	40.56	3.25	3.65	0.79	0.01	/
Crushed gravel	40.65	8.87	40.56	3.25	3.65	0.79	0.01	/

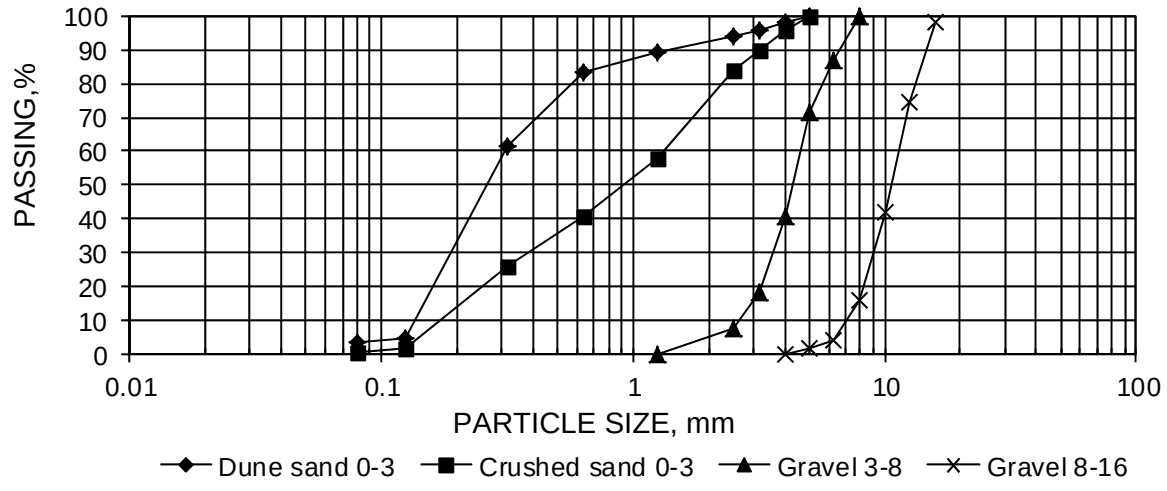

Figure 2 Particles size distribution of used aggregates

According to the recommendations of The European Guidelines for Self Compacting Concrete [6]: five mixtures were prepared as a function of the nature and proportion of sand used, as well as the nature of filler used (Table 3).

With: Powder/Water = 0.40 and Superplasticizer/Powder = 1.2%.

The mix composition of mixtures used is given in Table 4.

The experiments made on fresh concrete are:

- The passing ability (three bars L-box test);
- The flowability (slump-flow test using Abrams cone);
- The segregation resistance (sieve segregation resistance test).

All the experiments were done according to The European Guidelines for Self Compacting Concrete [6], based on the EN standards.

Table 3 Mix design for the experimental work

FACTORS	SCC 1	SCC 2	SCC 3	SCC 4	SCC 5
Dune sand	100%	100%	50%	50%	0%
Crushed sand	0%	0%	50%	50%	100%
Filler 1	0%	100%	0%	100%	0%
Filler 2	100%	0%	100%	0%	100%

Compressive strength is measured for hardened concrete at 14, 28 and 45 days, using cubic specimens (100 mm × 100 mm × 100 mm). While tensile strength is measured at 28 days, by the Brazilian test on cylindrical specimens (∅160 mm, height 320 mm).

All specimens have been poured and conserved in moulds for 24 hours, after that they have been removed from moulds and immersed in water basin at a temperature of 20 ± 2°C, until the time of test.

Table 4 Mix composition of mixtures used

COMPONENT [kg/m³]	SCC 1	SCC 2	SCC 3	SCC 4	SCC 5
Cement	400	400	400	400	400
Filler 1	/	100	/	100	/
Filler 2	100	/	100	/	100
Dune sand	850	850	425	425	/
Crushed sand	/	/	425	425	850
Crushed Gravel 1	425	425	425	425	425
Crushed Gravel 2	425	425	425	425	425
Water	200	200	200	200	200

Superplasticizer (liquid)	6	6	6	6	6

EXPERIMENTAL RESULTS ON FRESH CONCRETE

Passing Ability

Experiments show that mixtures 1 and 2 (with 100% of dune sand) give a high passing ratio, which means a good flowability of the SCC (Figure 3). In the case of mixtures with 50% dune sand / 50% crushed sand: SCC3 give higher passing ratio. These results are to be due to the round shape of dune sand particles as well as fineness of the filler used (SCC 1 and 3).

The fine dune sand used (Mf < 2.2) gives more flowability to the concrete. In the case of SCC 5 (with 100% of crushed sand) the flowing ability is very low, because of both the angular shape of crushed sand and the low fineness of the filler used (limestone powder).

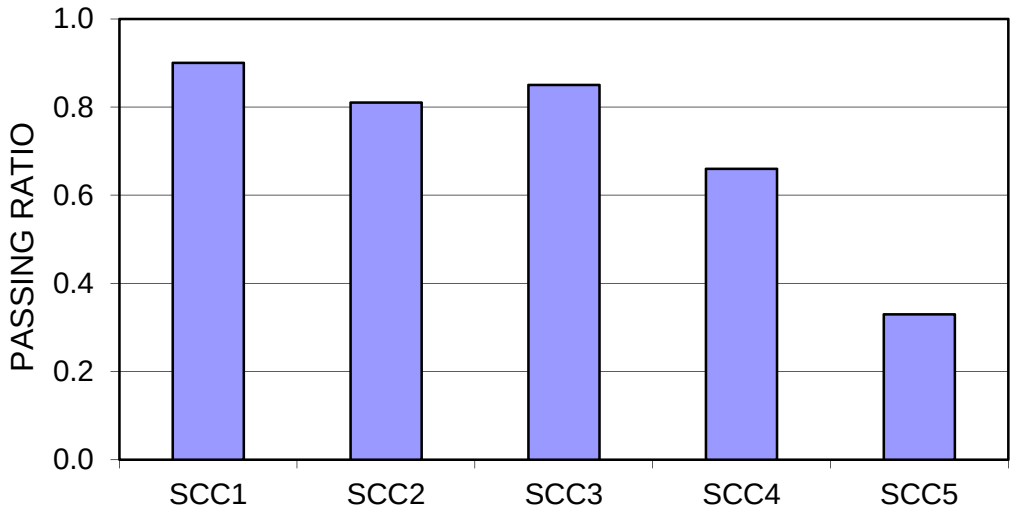

Figure 3 Passing ratio for the different SCC mixtures using 3 bar L-box test

As mentioned above, the use of a 3 bars L-box means that the passing ability class of the three first mixtures is PA2. Which means that they have the ability to flow through structures with a gap of 60 to 80 mm, (e.g. civil engineering structures) [6].

Flowability

According to the results shown in Figure 4: only SCC 5 gives a low slump-flow. This may be to the same reasons mentioned above for which it gives low passing ratio. We can classify the slump flow of the other mixtures as following [6]:

SF2 (660 – 750 mm) for SCC 2: Suitable for many normal applications.

SF3 (760 – 850 mm) for SCC 1, 3 and 4: Suitable for vertical applications in very congested structures, structures with complex shape, or for filling under formwork.

These good results were obtained with a low amount of superplasticizer (1.2%), while the ulterior studies showed that a high percentage is required to have a high fluidity [7, 8]. This

means that the high fluidity of the studied mixtures is due to the presence of round particles of dune sand.

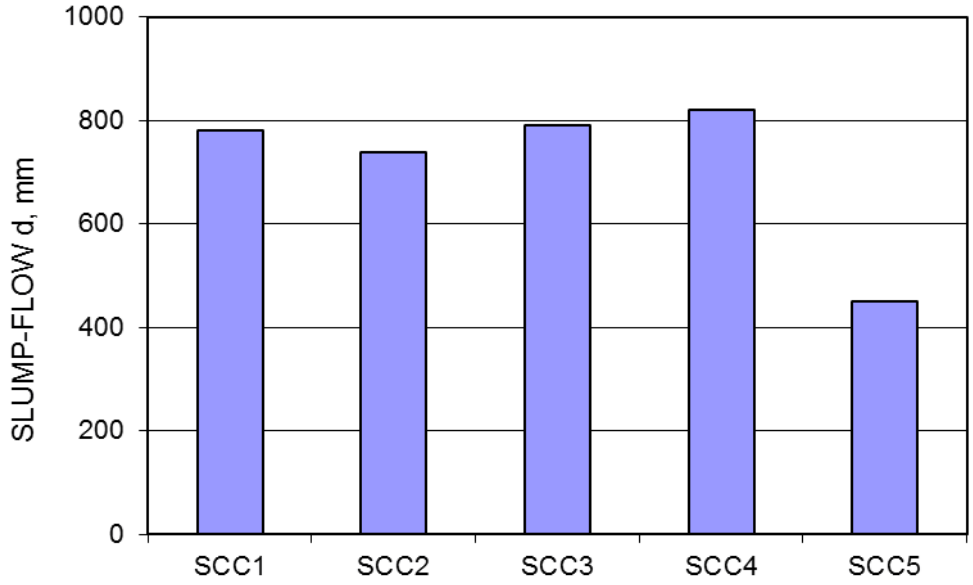

Figure 4 Slump-flow for the different mixtures prepared

Segregation Resistance

All the mixtures prepared in this work show very high segregation resistance (Figure 5). The segregation class of the prepared mixtures is SR2 < 15% [6]. The SCC 5 shows no segregation risks, for the same reasons of particles shape of crushed sand and the low fineness of the limestone powder used.

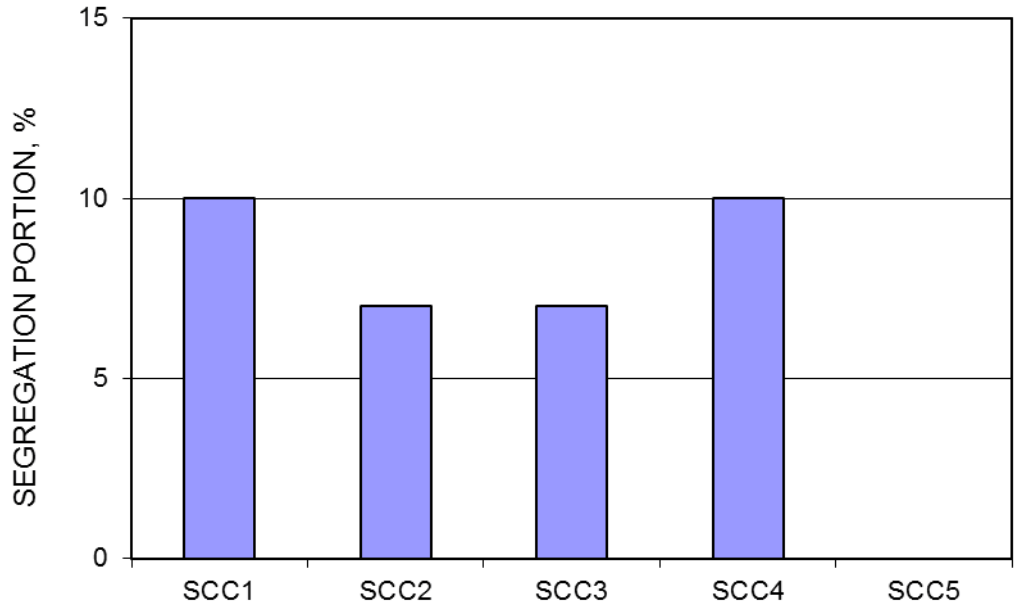

Figure 5 Segregation proportion for the different mixtures prepared

EXPERIMENTAL RESULTS ON HARDNED CONCRETE

Compressive Strength (f_c)

The compressive strength tests show that mixtures with 100% of dune sand give less strength than those with a partial substitution with crushed sand (50% - 50%), which give a normal compressive strength (at 28 days) higher than 45 MPa (Figure 6).

The SCC 5 (100% of crushed sand) gives a normal compressive strength near to SCC 1 (100% of dune sand), which has the same filler used (granular slag powder).

The mixtures with granular slag powder as filler developed compressive strength quicker despite the nature of the sand used. This is because of the hydraulic nature of granular slag powder and its good fineness, forming additional C-S-H and increasing the concrete's strength [9].

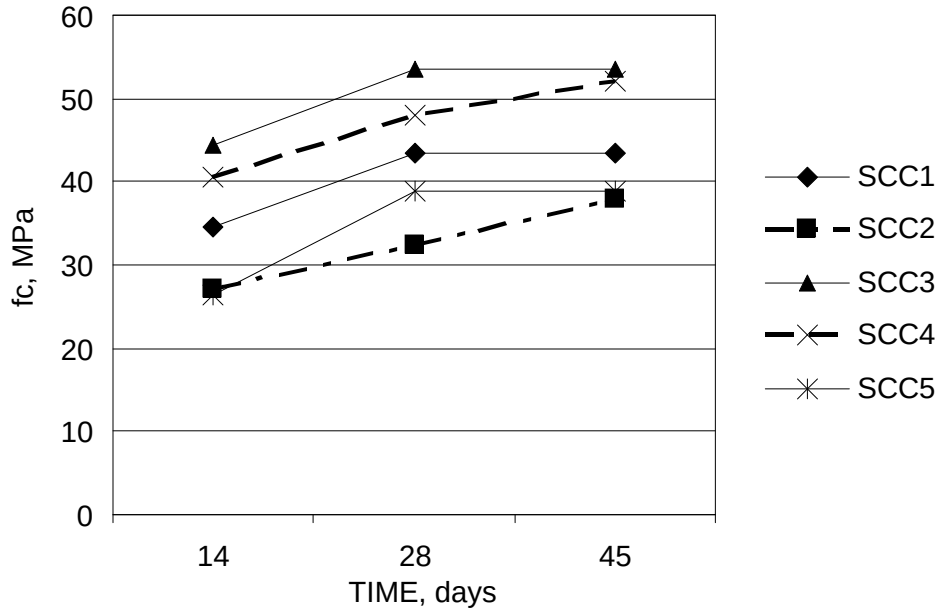

Figure 6 Compressive strength for the different mixtures

The low compressive strength developed by the mixtures with limestone powder at 28 days is due to the low fineness of the latter, which slows down the kinetic of hydration. Also the limestone is a semi-inert addition in comparison with granular slag.

At 45 days the compressive strength of the mixtures with limestone powder reaches about 90% of those with granular slag powder.

Tensile Strength (f_t)

The tensile strength measured at 28 days for the different mixtures prepared (Figure 7) are proportional to the compressive strength at the same age, in exception of the SCC 5, which shows better results than in compressive strength tests.

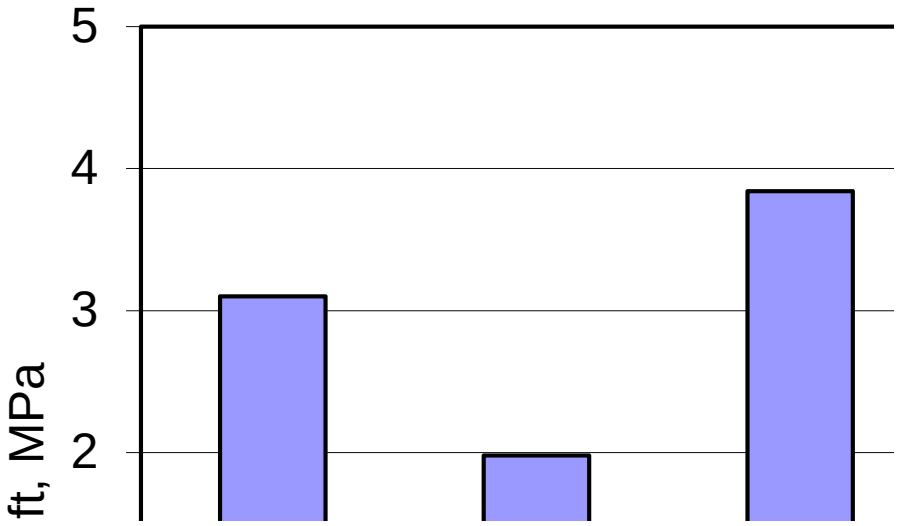

Figure 7 Tensile strength for the different mixtures at 28 days

In fact the three last mixtures with partial or total substitution of dune sand with crushed sand, despite the nature of addition. This means that the angular shape of crushed sand gives better adherence, packing and compatibility with the crushed coarse gravel.

CONCLUSIONS

This paper has focused on the physical effects of both dune (round) sand and crushed sand on the SCC.

Dune sand gives less viscosity and then better flowability to the SCC, due to its round shape which reduces the intergranular friction between sand particles themselves and between sand and gravel. Spheres move easier than angular shape particles [10].

This makes the particles interactions more hydrodynamic. In the other hand, crushed sand gives less flowability to the SCC, due to the high intergranular friction between the different particles > 0.125 mm [11]. Crushed sand needs more water to give the aimed workability; but also the nature of this sand (limestone) makes absorbs some amount of mixing water. This is to be discussed in further works.

Contrary to the rheological properties of fresh SCC, it has been shown that crushed sand has better contribution to the strength development, especially in the case of tensile strength. Dune sand needs more past to cover its fine particles.

In both fresh and hardened SCC properties, the association of dune and crushed sands gives better results than mixtures with only one kind of sand. Dune sand alone gives high slump-flow, but not as high as in case of mixtures with both kinds of sands. This is due to the fine particles of dune sand which reduce the concrete workability [10].

A higher fineness of limestone powder used as filler in this work could give better results for both fresh and hardened SCC and will give more clear answers concerning the effects of both dune and crushed sands.

ACKNOWLEDGEMENTS

The authors would like to thank all persons who insured the good running of experiments in the laboratory of construction materials, University of M'sila, Algeria.

REFERENCES

1. YE G, LIU X, DE SCHUTTER G, POPPE A-M AND TAERWE L, Influence of limestone powder used as filler in SCC on hydration and microstructure of cement pastes, Cement & Concrete Composites, Vol. 29, 2007, pp. 94–102.

2. GÜNEYISI E AND GESOĞLU M, Properties of self-compacting mortars with binary and ternary cementitious blends of fly ash and metakaolin, Materials and Structures, Vol. 41, 2008, pp. 1519–1531.

3. HU J AND WANG K, Effects of Size and Uncompacted Voids of Aggregate on Mortar Flow Ability, Journal of Advanced Concrete Technology, Vol. 5, No. 1, February 2007, pp. 75-85.

4. GEIKER M, BRANDL R M, THRANE L N AND NIELSEN L F, On the effect of coarse aggregate fraction and shape on the rheological properties of self-compacted concrete, Cement, Concrete, and Aggregate, Vol. 24, No. 1, 2002, pp. 3-6.

5. BROUWERS H J AND RADIX H H J, Self-Compacting Concrete: Theoretical and experimental study, Cement and Concrete Research, Vol. 35, 2005, pp. 2116-2136.

6. THE SELF-COMPACTING CONCRETE EUROPEAN PROJECT GROUPE. The European Guidelines for Self Compacting Concrete – Specification, Production and Use, May 2005, 63 p.

7. AUDENAERT K, BOEL V AND SCHUTTER G D, Carbonation of Self Compacting Concrete, Proceeding of the 6th International Symposium on High Strength/High Performance Concrete, Leipzig, June 2002, pp. 835-862.

8. OKAMURA H AND OUCHI M, Self-Compacting Concrete, Journal of Advanced Concrete Technology, Vol. 1, No. 1, 2003, pp. 5-15.

9. BENGHAZI Z, L'effet des additions minérales sur les propriétés du ciment au laitier activé, Magister thesis (in French), 2008, Department of Civil Engineering, University of M'sila, Algeria, 110 p.

10. AL-HARITHY A S, ABDEL HALIM M, TAHA R AND AL-JABRI K S, The properties of concrete made with fine dune sand, Construction and Building Materials, Vol. 21, 2007, pp. 1803-1808.

11. YAMMINE J, CHAOUCHE M, GUERINET M, MORANVILLE M AND ROUSSEL N, From ordinary rheology concrete to self-compacting concrete: A transition between frictional and hydrodynamic interactions, Cement and Concrete Research, Vol. 38, 2008, pp. 890-896.

Influence of the Variety of Superplasticizer on the Properties of Blastfurnace Slag Concrete

A Laichaoui, R Kettab, A Bali
Polytechnic National School (ENP), Algeria

High performance cementitious materials have been developed with the use of polymer additives (superplasticizers). Superplasticizers can produce high workability of concrete and high strength, but they may produce undesirable effects on setting and hardening of concrete if used in large amounts in mixes. In this work the parameters involved are superplasticizer content and optimal percentage of mineral addition. The experimental study has been carried out using two different families of superplasticizers (Polycarboxylates and Poly-Melamine Sulfonate) and blastfurnace slag as a mineral addition. This investigation aims also to valorize an industrial waste (slag) and to incorporate it into the concrete formulations at high proportions, without altering the rheological properties of grouts and concretes with the presence of superplasticizers. The results obtained show that the type of superplasticizer used has a great influence on the variation of rheological parameters - plastic viscosity and shear stress – of grouts. Moreover, the optimum percentage of mineral addition (slag) is strongly related to the type of superplasticizer and cement.

Ahmed Laichaoui is a Lecturer and PhD student in civil engineering department at the Polytechnic National School (ENP), Algeria. His field of interest includes materials, structures, repair and cementitious materials

Ratiba Mitiche-Kettab is a lecturer in Civil Engineering and a researcher in the construction and environment laboratory of the Polytechnic National School (ENP) in Algiers. His research interests focus on the mechanical behaviour of concrete, the performance of roads and building materials, dune sand concrete, and the use of local materials and reuse of materials.

A Bali, Professor in Civil Engineering Department, is the Director of the Construction & Environment laboratory, his field of interest covers the materials, recycling of industrial and demolition wastes, structures reparing, new sustainable materials, valorisation of local materials.

Keywords: Cement grouts, Concrete properties, Slag, Superplasticizer, Viscosity

INTRODUCTION

Engineers seek to obtain concretes with high performances without neglecting the rheology of the material, in the fresh state, which is a very significant technological parameter.

Concrete is a composite material in which the aggregates (gravel and sand) are bound by a hydrated cement paste. The quantity of water necessary for the reactions of hydration represents approximately 25 % by weight of cement. However, an additional quantity of water (at least double) is necessary in order to obtain a satisfactory workability of the freshly-mixed concrete during placing. The water excess will evaporate in the long term, leaving voids in concrete.

In a Portland cement paste with water/cement ratio of 0.5, total porosity represents between 25 and 30 % of the volume and the size of the pores vary from a nanometre to a few millimetres [1, 2]. Porosity in the material greatly decreases its mechanical resistance and durability. Concrete is therefore a porous composite material, whose performances vary according to its capillary porosity and thus to the water excess necessary to the workability of the fresh concrete. Concrete production which was once based on a simple ternary association: cement, water and aggregates, has gradually become more complicated so that a current concrete actually contains five components: cement, water, aggregates, additions and additives.

The need for improving concrete's performance, and reducing the quantity of mix water to decrease porosity, requires the use of new materials such as the superplasticizers. Added in small quantities (usually from 0.5 to 2 % of the mass of cement), these admixtures make it possible to reduce considerably (30 % and more) the quantity of water necessary to obtain satisfactory rheological properties for a good placement of the concrete [3].

In this study, two types of superplasticizers of different chemical nature - polycarboxylate (Pcx**)** and poly-melamine sulphonate (PMS**)**-have been chosen. To align the materials with the principles of sustainable construction, a mineral addition (slag), which is an industrial waste, has been incorporated, with various percentages as a substitution of a part of cement.

The Pcx and PMS point of saturation with cement CPJ (corresponding to CEM II: Portland cement with addition) has been determined, as well as the optimal slag percentage which gives the best rheological characteristics in grouts. For mortars, the optimal percentage of the mineral addition is considered, with the aim of checking the capacity to relocate the results obtained for grouts with mortars; measurements of the density, spreading and time of flow have been carried out.

CHARACTERIZATION OF CEMENT, SLAG AND SUPERPLASTICIZERS

Chemical analyses and leach testing had shown that slag coming from waste dumps presented no significant environmental concerns with regards to use in various applications in construction [4].

Tests for the determination of the chemical composition were carried out according to the standard, NF EN 196-4. The results are given in Table 1.

Table 1 Chemical composition of the CPJ and slag

OXIDES	CPJ, %	SLAG, %
CaO	59.24	45
SiO_2	18.99	34
Fe_2O_3	4.2	2.5
Al_2O_3	5.78	12.4
MgO	3.9	8.6
MnO	0.09	0.29
SO_3	1.74	0.097

The superplasticizers were organic polyelectrolytes, belonging to the polymeric dispersing agent category of compounds. In this investigation, two types of superplasticizers, the polycarboxilates (Pcx) and Poly-melamine Sulfonate (PMS**)** have been used. Their chemical formulas are illustrated on Figure 1.

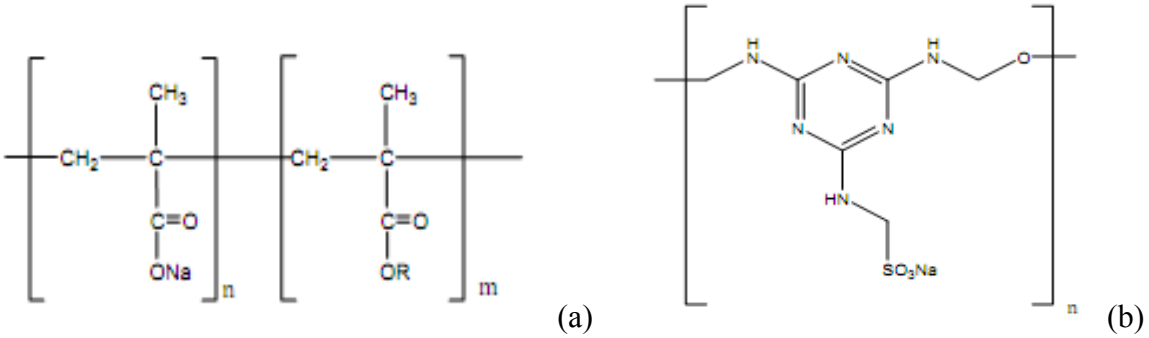

Figure 1 (a) Pcx, (b) PMS

EXPERIMENTAL STUDY

Cement Grout

Rheological measurements were carried out using a viscometer with rotary cylinders in permanent mode (HAAKE - Viscotester VT550 with the device of measurement SV DIN). It was connected to a cryostat controlled by a computer, which maintained the temperature of the sample of the experiment to 20°C. The acquisition of the data by computer generated curves of flow (shear stress) and of viscosity for a given rate of shear.

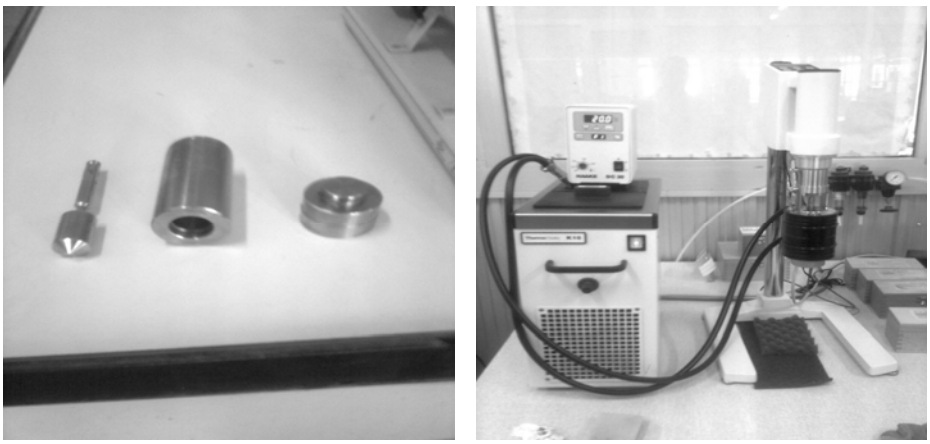

Figure 2 Device SV DIN and viscometer VT550 used

The principle consists of shearing the suspension between a surface at rest and a mobile surface. The fluid to be analyzed is placed between two coaxial cylinders. The laminar movements of shearing are obtained by communicating to one cylinder (interior cylinder) a uniform rotational movement, the other cylinder remaining motionless (Figure 2).

Mixes studied

The description of the studied proportioning and mixtures is as follows:

- CPJ a grout of CPJ without superplasticizer or mineral addition
- CPJ+ X% Pcx a grout of CPJ + X% of Polycarboxylates
- CPJ+ X% PMS a grout of CPJ + X% of PMS
- CPJ+1% Pcx+ y% Slag a grout of CPJ + 1% of Polycarboxylates + y% of slag
- CPJ+1.2% PMS+ y% Slag a grout of CPJ + 1.2% of PMS + y% of slag

W/C Ratio used in the presence of the superplasticizers is 0.35

Mortars

The density of mortars was determined by weighing a mould of known volume (4×4×16 cm³) before and after filling with mortar. Spreading was measured using the vibrating table and workability was measured with the mortar maniabilimeter LCL [5] where the time of flow of a fresh mortar subjected to vibrations was measured.

Mixes studied

Mortar 0 was made according to standard, NF EN196-1 [6] and contained (by weight) one part of cement and three parts of standardized sand and half of one part of water. Mortar 1 was of the same composition as mortar 0 with a w/c ratio of 0.35 with 1% of Pcx. Mortar 2 was of the same formulation as mortar 0 with a w/c ratio of 0.35 and 1.2% of PMS. For the other mortars the percentage by mass of slag used in the formulations of grouts was that which gave the best rheological performances. Thus, mixes with Pcx contents 40, 45 and 50%, and 25, 30 and 35% for PMS were retained.

RESULTS AND DISCUSSIONS

Cement Grout

The first part of the tests consists of the determination of the optimal percentage of the superplasticizers in cement grouts yielding the best rheological characteristics.

It should be noted that, according to Figures 3 and 4, that for three cement grouts (CPJ alone, CPJ + Pcx and CPJ + PMS) the rheological behaviour is Bingham-like for the fluids with CPJ alone and CPJ + Pcx, and Newtonian for the fluid CPJ + PMS.

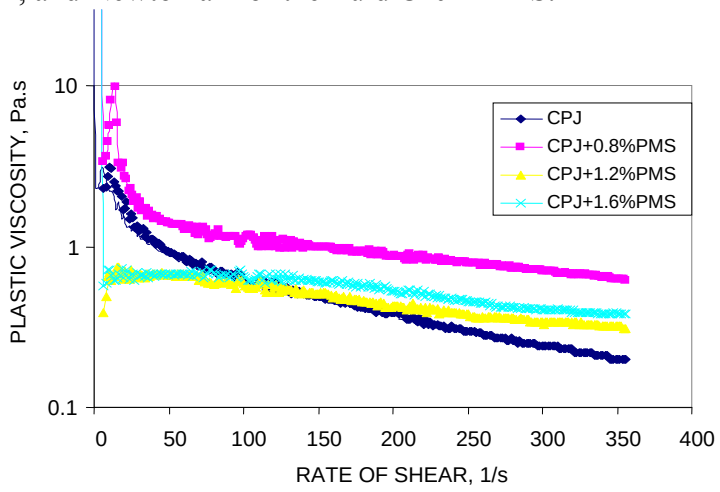

Figure 3 Plastic viscosity according to the rate of shear for a CPJ without and with various percentages of PMS with w/c = 0.35

It should also be noted that the polycarboxylate has a dispersing action more effective than that of the PMS, and this is influenced by the capacity of adsorption of the polycarboxylate on the anhydrous phases and cement hydrates [7].

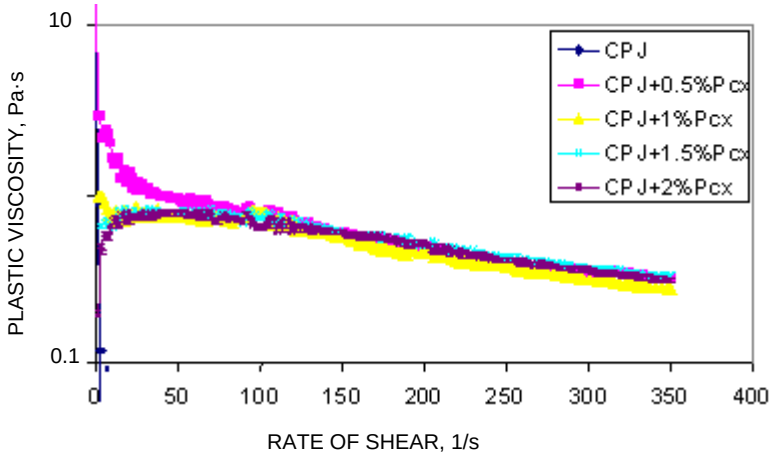

Figure 4 Plastic viscosity according to the rate of shear for a CPJ without and with various percentages of Polycarboxylate with W/C = 0.35

The curves of Figures 3 and 4 indicate the points of saturation for the two organic additions used. It is 1 % for the polycarboxylate (Pcx) and 1.2 % for the PMS.

Figures 5 and 6 allow the determination of the maximum percentage of cement which can be substituted by slag, whilst preserving the rheological properties of cement grouts.

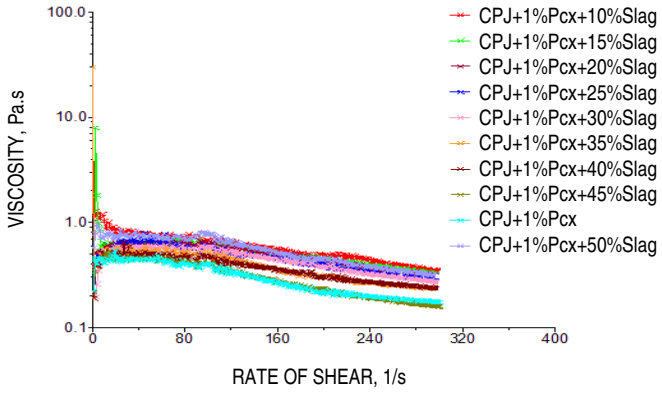

Figure 5 Plastic viscosity according to the rate of shear for a CPJ with 1% of Pcx and various percentages of slag (with W/C = 0.35)

The percentages of slag which can be used without changing the rheological properties of the grouts are 45% by weight of cement for the polycarboxylate and 30% for the PMS.

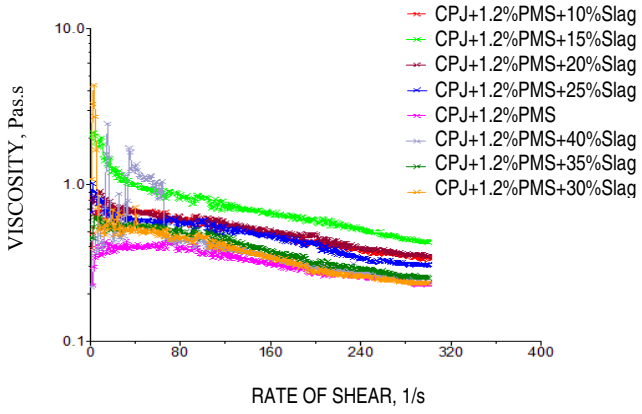

Figure 6 Plastic viscosity according to the rate of shear for a CPJ with 1.2% of PMS and various percentages of slag (with w/c = 0.35)

The rheological behaviour is Newtonian in the presence of slag and polycarboxylate and Bingham-like in the presence of PMS and slag.

Mortar

Figure 7 illustrates the variation of the density according to slag content as a substitute of cement.

It can be seen in Figure 7 that the density decreases with the substitution of cement by slag. This is explained by the fact that the mineral addition has a density lower than that of cement.

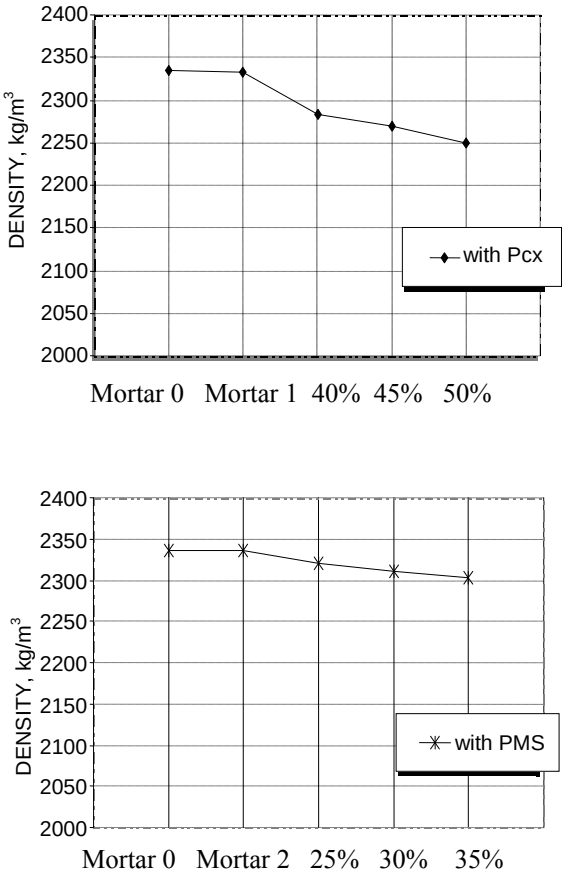

Figure 7 Variation of the density according to slag content

Figures 8 and 9 show the rheological characteristics of the mortar for various superplasticizers and percentages of slag.

The results given in Figures 8 and 9 show that spreading decreases for the PMS mortars, when the percentage in slag increases, whereas spreading for Pcx mortars increases with the percentage of substitution. These tendencies would be due to the fact that Pcx is more fluidising in the presence of slag than the PMS.

Moreover, the time of flow increases with slag content where PMS is used and decreases when Pcx is present.

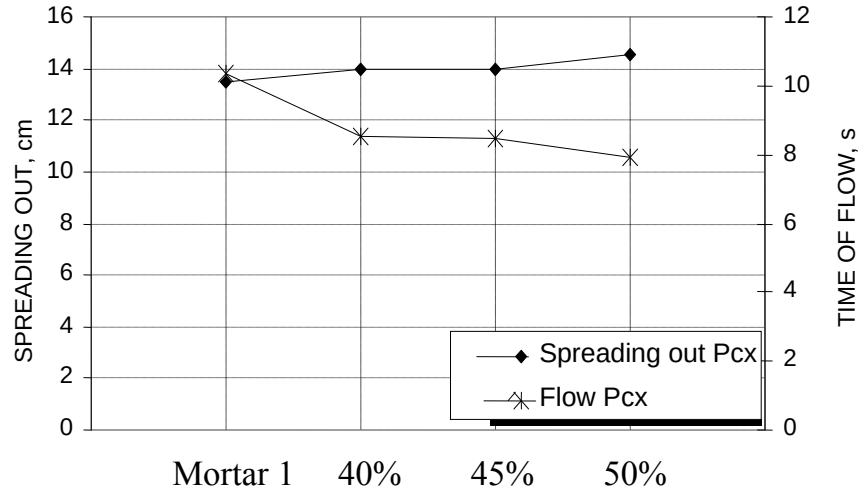

Figure 8 Variation of the spreading and the time of flow for mortars containing slag with 1% of Pcx

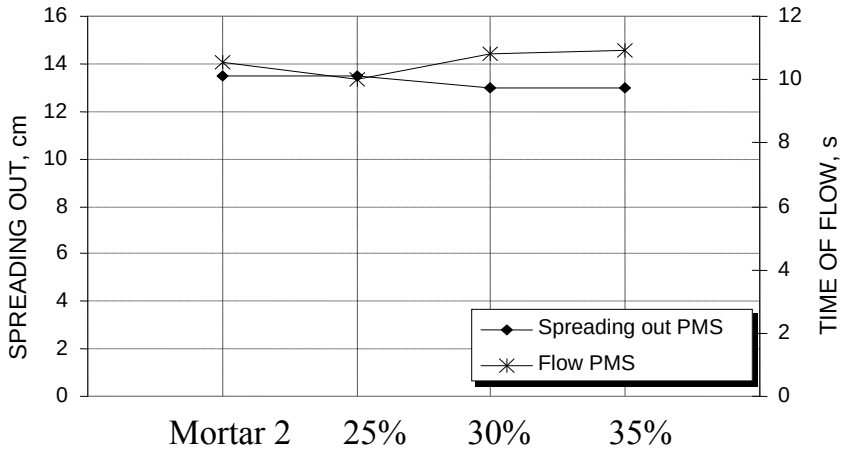

Figure 9 Variation of the spreading and the time of flow for mortars with slag with 1.2% of PMS

CONCLUSIONS

The results obtained highlight the dispersing effect of the superplasticizers. Indeed, the w/c ratio of 0.5 (without additives) could be lowered to 0.35 (with additives) while keeping comparable rheological properties. It is clear that by decreasing mixing water while preserving good rheological characteristics of cement grout (which means adequate workability of fresh concrete) we obtain a concrete of good mechanical characteristics because it will be less porous and thus more compact, and more durable.

The results show that superplasticizers based on polycarboxylates have more significant fluidising and dispersing effects than those based on poly-melamine sulphonate.

The highly fluidising properties of Polycarboxylates are very useful for making high performance concretes.

The obtained results show that cement can be substituted by slag at very significant quantities, 45 % by weight of cement with the polycarboxylates and 30 % with the PMS; this substitution has been made without losing much in terms of rheological properties.

Incorporating slag in the formulations of grouts and concretes, leads to the valorisation of an industrial waste. With a high percentage of replacement the environmental benefit is potentially considerable.

REFERENCES

1. MORANVILLE-REGOURD M, Microstucture des Bétons à Hautes Performances, Presses de l'École Nationale des Ponts et Chaussées, 1992, Paris, France.

2. LAICHAOUI A, KETTAB R AND BALI A. Influence de la nature du superplastifiant sur la rhéologie des coulis de ciment au laitier, Actes de la 29ème Rencontre de l'AUGC, Tlemcen, Algérie, Mai 2011, pp. 158-167.

3. BANFILL P F G, The rheology of fresh cement and concrete − a review, 11th International Cement Chemistry Congress, Durban, May 2003.

4. AMINI A, Influence des superplastifiants sur la rhéologie des bétons et mortiers, Master thesis, 2010, ENP, Algiers, Algeria.

5. NF P 15-437; liants hydrauliques, temps d'écoulement d'un mortier frais soumis à des vibrations, Juin 1987 AFNOR.

6. NF EN196-1, Méthodes d'essais des ciments Partie1: détermination des résistances mécaniques, Avril 2006, AFNOR.

7. UCHIKAWA H, Hydration of cement and structure formation and properties of cement paste in the presence of organic admixture, Importance of recent microstructural development in cement and concrete, Sherbrooke, Canada, 2004.

Rapid Pozzolanic Reactions with Silicate Solutions

K Koizumi, N Tsuyuki
Nihon University, Japan

Hardened specimens of measurable compressive strength were made from mixtures of calcium hydroxide (CH) and aqueous silicate solutions through rapid pozzolanic reaction. The hydration products were assumed to be non-crystalline as there were no new crystalline phases detected by X-ray diffraction. Indeed, calcium silicate hydrates (C-S-H) have been synthesized as confirmed by the trimethylsilylation (TMS) method. However, the distribution of the various types of silicate anions in the C-S-H generated by mixing CH and water glass were different from C-S-H as cement hydration product. In addition, the pozzolanic reaction of CH with water glass was found to be very rapid, as assessed by analysing the structure of silicate anions. This technique can be widely used to appraise the potential of calcium containing construction wastes for utilisation.

Dr K Koizumi is an assistant professor at the Department of Chemistry at College of Science and Technology, Nihon University. The main fields of research are the effect of silicate structures on hydration of cementitious materials, valuable reuse of industrial wastes.

Professor N Tsuyuki is Director of the inorganic chemistry laboratory at the Department of Chemistry at College of Science and Technology, Nihon University. His main research interests include the hydration control of cement, the permeable paving with variety of wastes based on inorganic technique.

Keywords: Calcium silicate hydrate (C-S-H), EPMA, Pozzolanic reaction, Silicate solution, Trimethylsililation

INTRODUCTION

Use of pozzolanic reaction can be traced back to the ages before Christ, when soils were treated and mud hardened for construction purposes. In essence, this is a reaction of siliceous materials and lime in the presence of water. The hardening normally takes a long time, often several days, depending on the reaction conditions.

The pozzolanic reaction has been studied mostly in terms of reactivity of various siliceous materials such as zeolite rock [1], cohesive soil in a stabilizing cement-lime system [2], metakaolin-cement system [3], silica of different crystallinity calcium hydroxide system [4] and fly ash – calcium hydroxide system [5]. These studies have contributed to the understanding of the pozzolanic reaction mechanisms using special techniques such as NMR [3], while controlling the pozzolanic reactions has never been discussed. This study proposes a new method capable of accelerating the pozzolanic reaction and obtaining hardened products in a short time, with examples of powdered calcium hydroxide and calcium carbonate.

Cement is well known as a high-strength material owing to the hydration reactions. The strength development can be attributed to the formation of calcium aluminate and calcium silicate hydrates. However, powdered calcium hydroxide or calcium carbonate cannot be hardened when mixed with water, but with silicate solutions, a quick reaction can be expected. This study focuses on the reaction as a widely applicable industrial technology in the field of hydraulic materials.

Colloidal silica is a well-known silicate solution. It is produced from sodium silicate that can be obtained by dissolving silicon dioxide with sodium hydrate. Hydrochloric acid is then added to the sodium silicate to produce a silicate solution with a small quantity of chloride ion. The viscosity of such produced silicate solution is quite high, which is not suitable as mixing water for powdered materials.

Calcium silicate hydrate is generally produced through the reactions of calcium compounds and silane solutions with organic carbons such as tetramethoxysilane and tetraethoxysilane. In this study, we were able to produce a silicate solution with a viscosity as low as that of water and without organic carbons using electrolysis of sodium silicate. The silicate solution was then applied to powdered calcium hydroxide and calcium carbonate for a rapid pozzolanic reaction. The obtained hardened specimens are discussed in terms of their properties and hydration mechanisms.

EXPERIMENTS

Materials Used

Calcium hydroxide and calcium carbonate used in this experiment were of the highest quality reagents. A new apparatus capable of electrolysing sodium silicate solution and removing sodium ions was introduced (Commercial name: SIONT). The pH value of the resulting silicate solution could be controlled according to the silicon content. In this experiment, two types of silicate solutions were produced: an acidic one (A) and an alkaline one (B).

Test Methods

Properties of the silicate solutions

Properties of the silicate solutions (A) and (B) varied according to the silicon content and trace sodium concentration. The concentrations of silicon and sodium were determined with molybdenum blue spectrometry and Inductively Coupled Plasma Atomic Emission Spectroscopy (ICP-AES), respectively. Properties of the silicate solutions are shown in Table 1.

Table 1 Properties of silicate solution

	A	B
pH	3.29	9.40
Viscosity at 25°C, mPa·s	2.00	2.00
SiO_2 concentration, mg/l	11000	20000
Na concentration, mg/l	24	690

Preparation of hardened specimens

Powdered calcium hydroxide and calcium carbonate were mixed with the alkaline silicate solution (B) at a solution/powder ratio of 1.0. Figures 1 and 2 show photographs of the hardened specimens taken at the age of three days. The hardened specimens were cured under a room temperature of 20°C and compressive strength was determined at ages of 3, 7, 28, 90 and 180 days. No chemical admixture for concrete was used in this experiment.

Hydration heat liberation rates

A high-precision conduction-type calorimeter was used to determine the hydration-heat liberation rate for a specimen of 2 g of powdered calcium hydroxide treated with the alkaline silicate solution (B). The solution/powder ratio was 2.5, but for comparison, a specimen with a water/powder ratio of 2.5 was also prepared.

Hydration products

The hardened specimens were crushed and subjected to X-ray diffraction analysis (XRD: Bruker AXS, D8-Focus). Scanning Electron Microscope (SEM) was used to observe the fractured surfaces of the hardened specimen. Electron Probe Micro Analyser (EPMA) was also used to map silicon and calcium on the surface.

Amount of dissolved calcium

Determination of dissolved calcium in the silicate solution (B) was carried out using a silicate solution of 100 ml with 2 g of calcium hydroxide or calcium carbonate dispersed in it. Changes in the dissolved calcium were determined with ICP-AES as CaO in mg/l.

Structure of silicate anions in the hardened specimen

The hardened specimens of powdered calcium hydroxide and calcium carbonate were subjected to trimethylsilylation (TMS). The trimethylsilylation agents were trimethylchlorosilane (TMCS) and hexamethyldisiloxane. Derivatisation of TMS was performed referring to the works of Nakamura and Suginohara [6] and Ohkusu et al. [7, 8]. The resulting TMS derivatives were analysed with a gas chromatograph (Shimazu CC-14B) and the composition ratios of silicate anions, from monomer to hexamer, were determined. Quantification of each component was made with the peak-area ratio of the chart from the gas chromatograph.

RESULTS AND DISCUSSION

Preparation of Hardened Specimens

Hardened calcium hydroxide and calcium carbonate, both treated with silicate solution (B) at a solution/powder ratio of 1.0 were prepared and cured for 3 days, as shown in Figures 1 and 2, respectively. Compressive strengths of the hardened specimens are shown in Table 2. Because of their low strength, the manufactured hardened specimens are not suitable for structural use, while higher strength may be expected when used with other hydraulic materials that may induce pozzolanic reactions faster.

Bulk densities of the hardened specimen, determined at a temperature of 20°C, are shown in Table 3 and tended to be low. Strength development was also generally low. However, the starting powdered materials, which would never harden in normal situation, did harden and the compressive strength of the powdered calcium carbonate developed as high as 0.8 N/mm² at the age of 3 months. This strength development may be attributed to a quick pozzolanic reaction. Pozzolanic reactions generally occur in a long term while it can be significantly accelerated due to the silicate solution used. Strength development was observed when powdered calcium carbonate reacted with the alkaline silicate solution (B) while no development was observed when treated with the silicate solution (A).

Figure 1 Hardened specimen of calcium hydroxide

Figure 2 Hardened specimen of calcium carbonate

Table 2 Compressive strength of hardened specimen made with silicate solution (B)

	7 DAYS	28 DAYS	90 DAYS	180 DAYS
Calcium hydroxide	0.19	0.27	0.41	1.10
Calcium carbonate	0.20	0.21	0.80	N/A

Table 3 Bulk density of hardened specimen, $\times 10^3$ kg/m^3

	3 DAYS	4 DAYS	5 DAYS	6 DAYS	7 DAYS
Calcium hydroxide	0.95	0.66	0.67	0.67	0.68
Calcium carbonate	1.45	1.34	1.34	1.33	1.34

Hydration Products

Hydration products of the hardened calcium hydroxide powder and calcium carbonate reacted with the alkaline silicate solution (B) at ages from 1 to 28 days were subjected to XRD analysis after crushing. The results are shown in Figures 3 and 4, respectively. Except for calcium hydroxide and its carbonated products, no other crystalline phases were observed hence the hydration products of the hardened specimens are likely to be amorphous. Scanning electron micrographs of the calcium hydroxide based hardened specimen at the age of 28 days are shown in Figure 5 and an EPMA-mapping of Ca and Si distributions at a narrow area is shown in Figure 6. It is shown that SiO_2 can be found intensively at areas where CaO is distributed.

Hydration Heat Liberation Rates

Hydration heat liberation rates of powdered calcium hydroxide in contact with two grams of water and with alkaline silicate solution (B) are shown in Figure 7. It was confirmed that the first heat liberation peak can be attributed to the heat of dissolution and the second peak, observed 6 hours after mixing and only when the alkaline silicate solution was used, can be attributed to the reaction of calcium hydroxide and silicate.

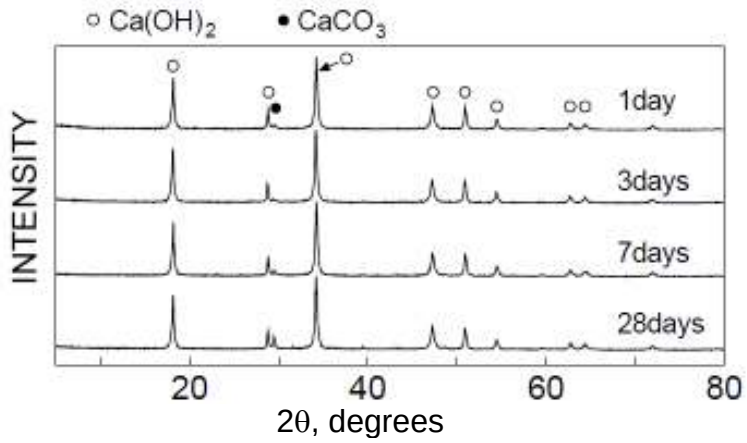

Figure 3 XRD patterns (CuKα) of calcium hydroxide hardened specimen treated with alkaline silicate solution

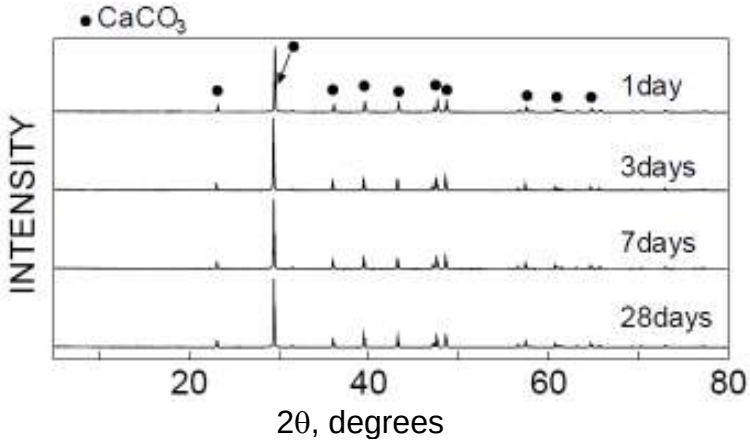

Figure 4 XRD patterns (CuKα) of calcium carbonate hardened specimen treated with alkaline silicate solution

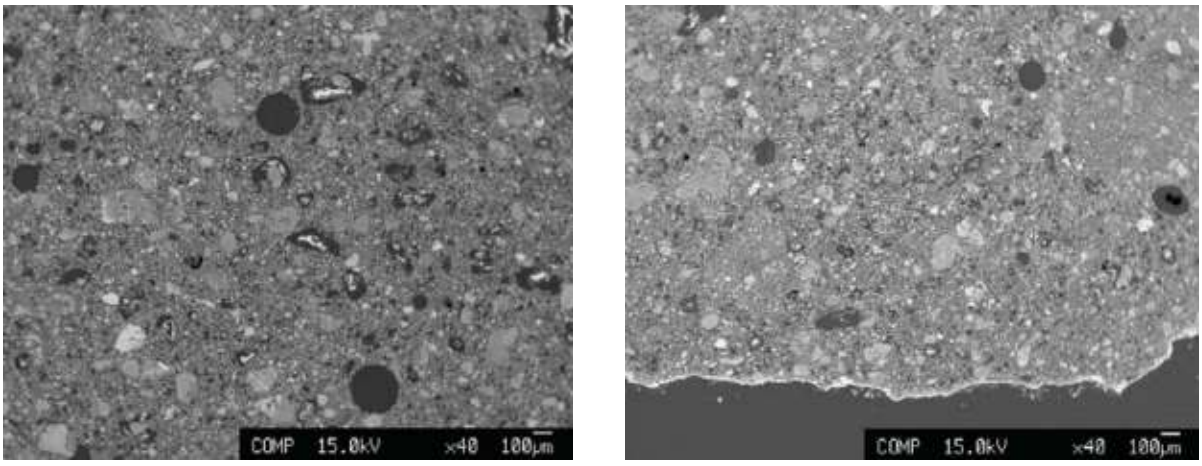

Figure 5 SEM of hardened specimen treated with alkaline silicate solution [Left: calcium hydroxide, Right: calcium carbonate]

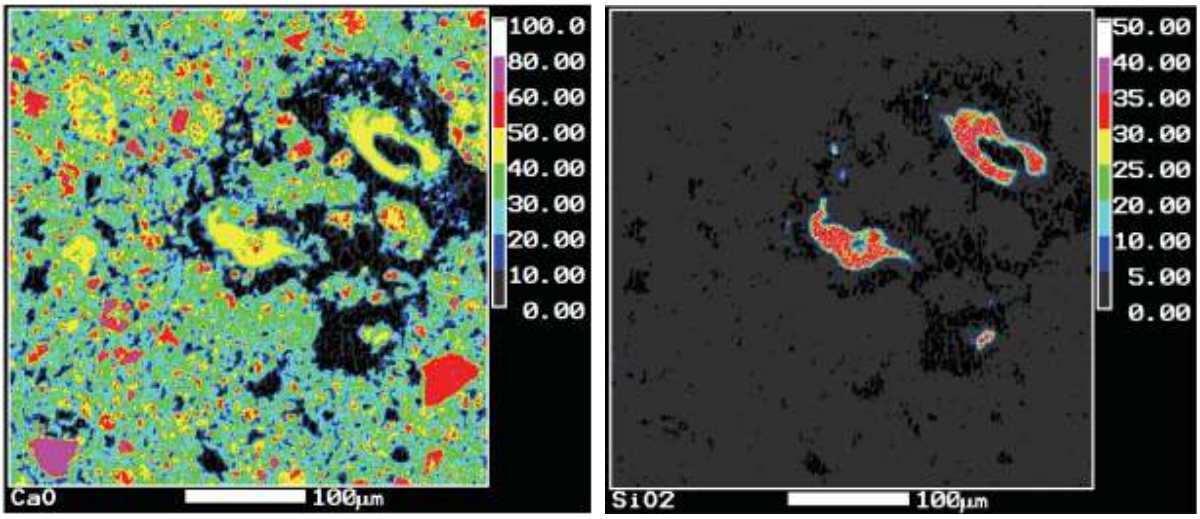

Figure 6 EPMA mapping of CaO and SiO_2 in the hardened specimen treated with alkaline silicate solution

Dissolved Calcium Content

Solubility of calcium when calcium hydroxide or calcium carbonate is dispersed in the alkaline silicate solution (B) is represented as CaO mg/l of the solution and is shown in Figure 8. The residual Si concentration is also represented as SiO_2 mg/l of the solution and is shown in Figure 9. The solubility of calcium hydroxide in water is 1200 mg (CaO) per litre and the CaO can be rapidly consumed in the silicate solution (B). However, as seen in Figure 8, CaO concentration again increased at 5 hours after mixing and subsequently exhibited a tendency to decrease with time. The cause of this change is unknown, but most likely to be attributed to the formation of amorphous products of the $CaO\text{-}SiO_2\text{-}H_2O$ system, associated with a subsequent change in the morphology of the hydration products.

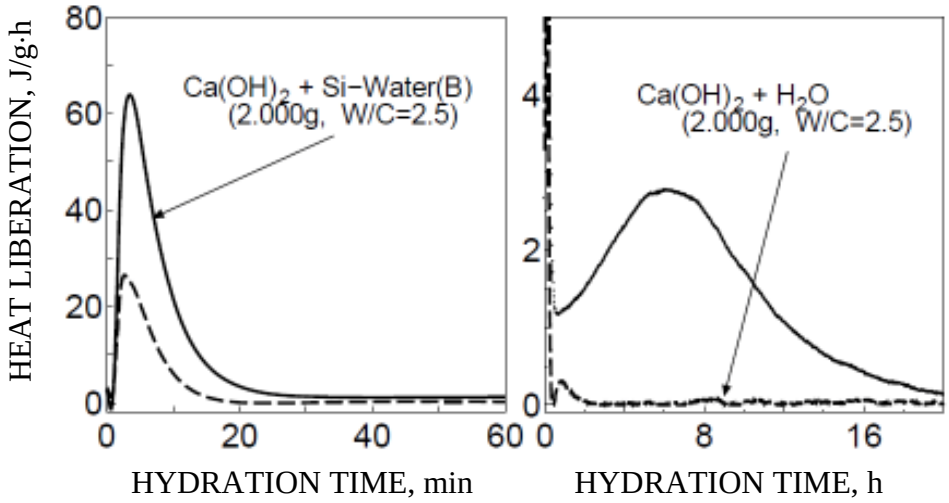

Figure 7 Heat liberation rates of calcium hydroxide treated with alkaline silicate solution or pure water

The solubility of calcium carbonate in water is quite low and may be considered negligible. However, when dispersed in the silicate solution, it dissolves 100 to 150 mg (CaO) per litre and finally converged to 50 mg CaO per litre. The difference is due to the CaO consumption originated from the formation of hydration products of the $CaO\text{-}SiO_2\text{-}H_2O$ system.

Consumption of SiO_2 in the solution with calcium hydroxide is, on the other hand, considerable as seen in Figure 9 implying the development of rapid hydration reactions while that with calcium carbonate is slow probably due to the formation of hydration products of the $CaO\text{-}SiO_2\text{-}H_2O$ system.

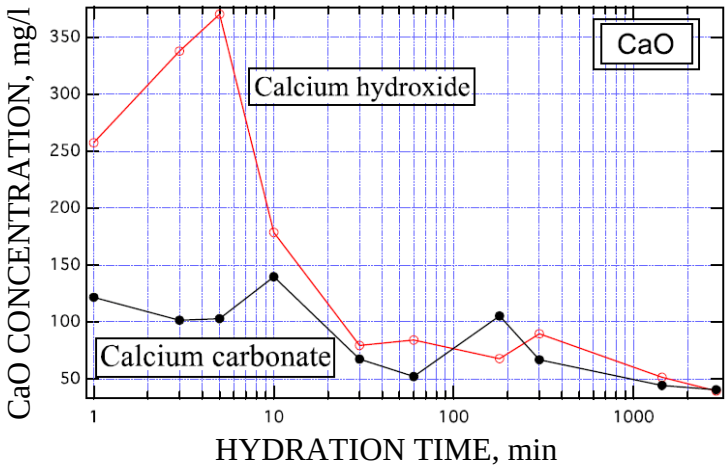

Figure 8 Solubility of calcium hydroxide or calcium carbonate in alkaline silicate solution with reaction time

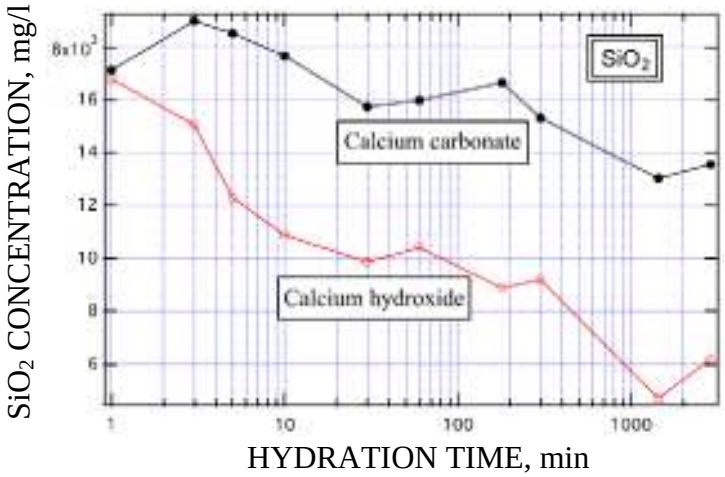

Figure 9 Changes in solubility of silicate dioxide dispersed in calcium hydroxide or calcium carbonate in alkaline silicate solution

Structure of Silicate Anion

Because the hydration products based both on calcium hydroxide and calcium carbonate were found to be amorphous, the reason of the hardening has to be attributed to any calcium silicate hydrates where the morphology of -Si-O- needs to be investigated. Hence the composition ratios of the silicate anions were determined with TMS and the results are shown in Figure 10.

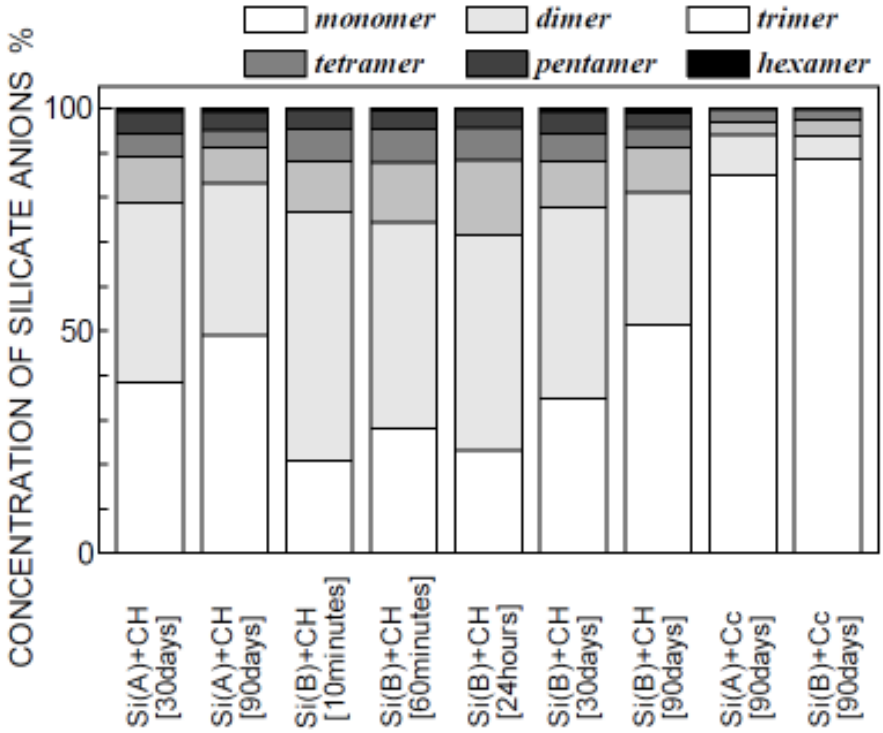

Figure 10 Polymer ratio of silicate anion in hardened specimen treated with alkaline silicate solution vs. hydration time

It was confirmed that the most dominant silicate anion was dimer at 10 minutes after mixing among other silicate anions of monomer and trimer. This implies a morphology of silicate anion present as H_4SiO_4 (monomer), $H_6Si_2O_7$ (dimer) and $H_8Si_3O_{10}$ (trimer). Among silicate anions in the hardened specimen, monomer and dimer may make chemical bonds between Ca^{2+} while the contribution of trimer and pentamer, though detected in the analysis, may be negligible judging by their composition ratios. The composition ratio of dimer, dominated immediately after mixing, decreased with time and at the same time monomer became dominant. This may be attributed to the decomposition of dimer due to carbonation and resulting transitions to monomer as seen in the XRD pattern of Figure 4. Compared with hydration of ordinary Portland cement [9], where monomer is dominant at early stages, the changes in morphology of silicate anions in this study is obviously different [10]. This may lead to a conclusion that a rapid pozzolanic reaction could develop in the silicate solution.

CONCLUSIONS

(1) Solubility of silicon dioxide in water is quite low while a new electrolysis apparatus made it possible to have a silicate solution with a silicon dioxide concentration of 20 g/l.

(2) Calcium hydroxide can react with the silicate solution and form a calcium hydroxide hardened specimen as a result of a rapid pozzolanic reaction.

(3) Products of the pozzolanic reaction were amorphous.

(4) The pozzolanic reaction is a solution reaction and CaO concentration in the solution decreased rapidly immediately after dispersing calcium hydroxide in silicate solution (B). CaO in calcium carbonate was also soluble in the same manner.

(5) Concentration of SiO_2 in the calcium hydroxide solution decreased rapidly while more slowly in the calcium carbonate solution.

(6) The structure of the silicate anion was studied with the TMS method. Dimer was dominant at early stages of the reaction while it may have decomposed later, due to carbonation, which resulted in the formation of monomers. This is quite different from the early-stage behaviour of ordinary Portland cement.

ACKNOWLEDGEMENTS

This research was partially supported by KAKENHI (23560555), Grant-in-Aid for Scientific Research (C), 2011.

REFERENCES

1. MARTÍNEZ-RAMÍREZ S, BLANCO-VARELA M T, EREÑA I AND GENER M, Pozzolanic reactivity of zeolitic rocks from two different Cuban deposits: Characterization of reaction products, Applied Clay Science, Vol. 32, 2006, pp. 40-52.
2. PRUSINSKI J R AND BHATTACHARJA S, Effectiveness of Portland cement and lime in stabilizing clay soils, Transportation Research Record, 1652, Portland Cement Association, Skokie, Illinois, 1999, pp. 1-13.
3. SHA W AND PEREIRA G B, Differential calorimetry study of ordinary Portland cement paste containing metakaolin and theoretical approach of metakaolin activity, Cement and Concrete Composites, Vol. 23, 2001, pp. 455-461.
4. BALTAKYS K, JAUBERTHIE R, SIAUCIUNAS R AND KAMINSKAS R, Influence of modification of SiO_2 on the formation of calcium silicate hydrate, Materials Science - Poland, Vol. 25, 2007, pp. 663-670.
5. BIERNACKI J J, WILLIAMS P J AND STUTZMAN P E, Kinetics of reaction of calcium hydroxide and fly ash, ACI Materials Journal, Vol. 98, 2001, pp. 340-349.
6. NAKAMURA R AND SUGINOHARA Y, Improved trimethylsilylation to analyse silicate anions, Journal of Japan Institute of Metal, Vol. 44, 1980, pp. 352-358 (in Japanese).
7. OHKUSU H, MASUDA J, WAKITA M AND SUGINOHARA Y, Fundamental study of silicate anions by modified TMS method, Journal of Japan Institute of Metal, Vol. 45, 1981, pp. 915-922 (in Japanese).
8. OHKUSU H, TAKESHITA S, MIZOGUCHI S AND SUGINOHARA Y, Morphology of silicate anions in lead silicate compound by modified TMS method, Journal of Japan Institute of Metal, Vol. 47, 1983, pp. 956-963 (in Japanese).
9. KOIZUMI K, UMEMURA Y AND TSUYUKI N, Effect of chemical admixtures on silicate structure of hydrated Portland cement, Cement Science and Concrete Technology, No. 60, 2006, pp. 25-31 (in Japanese).
10. DUNSTER A M, PARSONAGE J R AND VIDGEON E A, Silicate Anion Analysis in Portland Cement Paste, Materials Science and Technology, Vol. 5, 1989, pp. 708-713.

Manufactured Sand for a Low Carbon Era

M Pilegis, D Gardner, B Lark
Cardiff University, UK

In 2000 the Welsh Assembly acknowledged the need to find a sustainable use for the growing stock piles of crusher fines in Wales, and commissioned research into their use as a replacement for natural sand in concrete. This study concluded that crusher fines were not a suitable replacement for natural sand in concrete due to their inconsistent grading and a lack of particles in the 0.3 to 1 mm range. New methods of manufacturing sand are now available, which can more accurately control the sand particle size, shape and gradation, including particles in the usually deficient range. Therefore a study has been launched to investigate the suitability of this manufactured sand for use in concrete applications. Concrete that incorporates sand manufactured from quarry waste is a major development in achieving a sustainable construction material. However, the characteristics of manufactured fine aggregates are different to those of natural sands and their effects on the performance of concrete are not fully understood. The most common issues associated with manufactured sands are poor shape, gradation, and the quantity and quality of filler material. To investigate the effects of these and other parameters a test programme has been undertaken. Laboratory tests have been used to evaluate the mineralogical and physical characteristics of a range of quarry waste sands. This paper describes the methodology of this study, presents the results to date and discusses the significance of the findings in the context of manufactured sand for a low carbon era. These results show that it is viable to produce workable concretes of satisfactory strength in which the natural sand has been completely replaced by manufactured sand.

Martins Pilegis graduated Cardiff University with a 1st class BEng degree in Civil Engineering in 2010. Currently he is a research student at the Cardiff School of Engineering, Cardiff University.

Dr Diane Gardner graduated from Cardiff with a 1st class MEng degree in Civil Engineering in 2002. Following this she undertook a PhD in experimental and numerical studies of the permeability of concrete. She obtained PhD in 2005 and joined Hyder Consulting UK Ltd, and spent 3 years working in their bridge/civil structures team. She took up her present academic post in January 2009 and her primary research interests are in experimental testing of sustainable cementitious materials.

Professor Bob Lark is a Chartered Engineer with over 30 years of varied Civil Engineering experience. He has been an academic at Cardiff University for 15 years and during this time has undertaken research on the design and behaviour of concrete and steel structures, bridge monitoring and assessment, and the development of life cycle analysis and asset management techniques. He has solely and jointly generated research income in excess of £1M. He has supervised 10 successful PhDs and is currently jointly supervising a further 4 PhD students and a Research Associate. He has over 60 publications in international journals and refereed conferences since 1996.

Keywords: Concrete, Manufactured sand, Sand replacement, Strength, Workability

INTRODUCTION

As natural resources of concrete aggregates are being depleted or a resistance to the usage of dredged sand due to environmental concerns is met, an alternative source of fine aggregate has to be found. One such source is crushed rock material from stone quarries. However, the material produced differs in characteristics from natural sands. The major differences are shape and texture, grading and amount of fine filler. These characteristics can detrimentally affect concrete, therefore manufactured fine aggregates are only reluctantly accepted within the industry [1].

The manufactured fine aggregate (MFA) shape is typically highly angular, elongated or flaky. This characteristic greatly influences the fresh and therefore hardened properties of concrete. MFA shape depends on the parent rock and to large extent on the crushing method [2], [3].
Typical particle size distribution of MFA or "quarry dust" rarely conforms to the requirements of national standards. These types of aggregate can produce "harsh" mixes with bleeding problems if it is washed and screened to fall within the prescribed limits [1]. This is mainly due to an excess of fine particles passing the 63 micron sieve and a deficiency of particles in the size range 0.3mm to 1mm. Thus manufactured sands are commonly used in blends with fine natural sands to overcome these shortcomings and minimise the negative effects on fresh and hardened concrete properties.

An alternative to washing and blending is reprocessing the quarry fines by employing another crusher to refine the particle shape and size distribution. Furthermore, if the classification process of the product employs a dry instead of a wet system then environmental benefits can be gained.

In 2000 the Welsh Assembly acknowledged the need to find a sustainable use for the growing stock piles of crusher fines in Wales, and commissioned research into their use as a replacement for natural sand in concrete [1]. This study concluded that crusher fines were not a suitable replacement for natural sand in concrete due to their inconsistent grading and a lack of particles in the 0.3 to 1 mm range. New methods of manufacturing sand are now available which can more accurately control the sand particle size, shape and gradation including particles in the usually deficient range. Therefore this study has been launched to investigate the suitability of this manufactured sand for use in concrete applications in Wales and the UK as a 100% replacement for natural sand.

In this study the first two manufactured sands of different mineralogy were considered. The resulting consistency and compressive strength of concrete when these sands were used as 100% replacement for natural sand are presented.

MANUFACTURING PROCESS

The manufactured sand used in this study was produced using a plant for which a simplified setup is shown in Figure 1. The feed material for manufacturing sand is usually a 0/8 mm crusher dust with a water content less than 1.5%. It is fed to a vertical shaft impact (VSI) crusher and afterwards separated using an air screen. Oversize and some coarser particles are re-circulated, while the required particle sizes are delivered as a product and most of the dust is fed to a "skimmer".

The “skimmer” separates coarser particles as well as some filler from the dust. The separated particles are added into the final product increasing the yield, allowing control of the fines content as well as providing the usually deficient 0.3 to 1 mm particles in the manufactured sand.

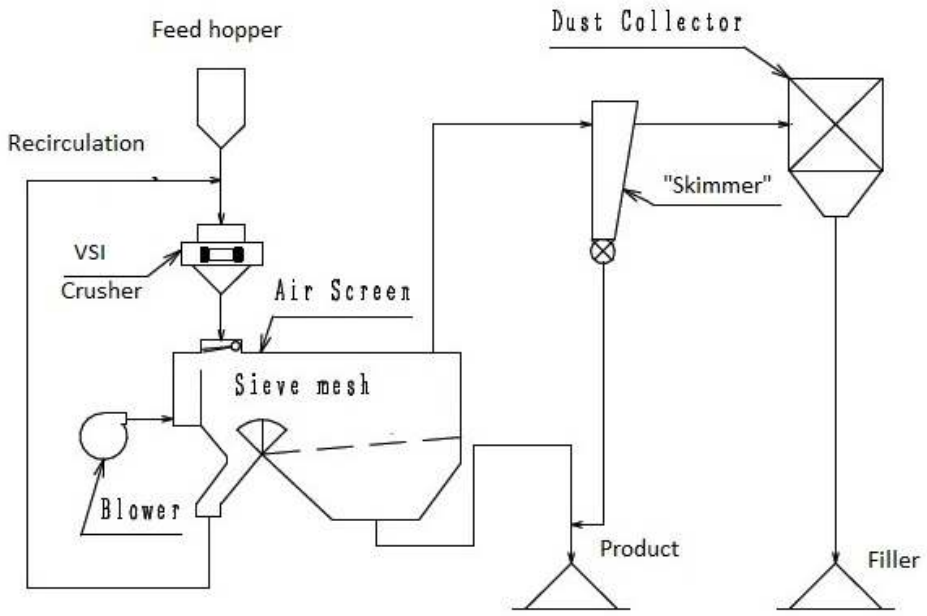

Figure 1 Simplified diagram of manufacturing process

For the project at least four sand gradations were produced from each crusher dust. The sands slightly differ with particle size distributions as shown in Tables 2 to 4.

MATERIALS

Cement

The cement used was CEM I 52.5 N conforming to EN 197-1.

Coarse Aggregate

The coarse aggregate used was crushed limestone 4/20mm and its particle size distribution is shown in Table 4.

Fine Aggregate

The manufactured sand was processed from 0/8 mm crusher dusts taken from two quarries located in UK. One quarry produces basalt whereas the other produces granite aggregate. Properties of the 0/4mm parts of the crusher dusts are included in Tables 1 to 3 for comparison purposes. In all tables and figures the basalt crusher dust is denoted as B-FEED and the granite as G-FEED.

From the crusher dusts four basalt sands and five granite sands with different particle size distributions were produced. Basalt sands are denoted by letter B in the tables and figures whereas granite sands are denoted by letter G. Following the letter B or G indicating the

quarry, the sands are further denoted with a letters A to D, E (E for granite sand) depending on the sub 63 micron particle content. For example, B-A is a basalt sand with the least fines content, whereas B-D is a basalt sand with the highest fines content. Particle size distributions are shown in Tables 2 and 3.

Table 1 Fine aggregate test results

SAMPLE	MBV, g of MB solution per kg of sand	RMBV, g of MB solution per kg of sand	SE	NZFC VOIDS, %	NZFC FLOW TIME, sec	WA_{24}, %	ρ_{ssd}, Mg/m^3	ρ_{rd}, Mg/m^3	ρ_a, Mg/m^3
G-FEED	0.77	0.94	50	42.4	29.1	0.58	2.64	2.62	2.66
G-A	0.39	0.42	80	45.2	25.3				
G-B	0.40	0.50	74	44.6	24.4				
G-C	0.47	0.71	71	43.7	23.9	0.58	2.63	2.61	2.65
G-D	0.50	0.88	70	43.6	23.4				
G-E	0.63	0.90	69	42.7	23.9				
B-FEED	5.36	6.16	48	45.7	36.7	1.92	2.89	2.83	3.00
B-A	2.10	2.3	73	45.8	25.7				
B-B	2.29	2.54	61	44.5	23.2	1.67	2.91	2.87	3.01
B-C	2.64	2.97	60	43.7	22.5				
B-D	2.90	3.75	58	43.7	22.3				

* BS EN 1097-6 test was carried out only for manufactured sands with the lowest fines content as the sub-63 micron particles are washed out of the sample prior to testing.
** WA_{24} - water absorption
***ρ_{ssd} – particle density on saturated surface dry basis
****ρ_{rd} - particle density on oven dry basis
*****ρ_a- apparent particle density

The fine aggregate used in the study was characterized using the following standard tests:

- Methylene blue test (MBV) according to BS EN 933-9 on 0/2mm fraction
- Sand equivalent test (SE) according to BS EN 933-8 on 0/2mm fraction
- Particle size distribution according to BS EN 933-1
- Particle density and water absorption according to BS EN 1097-6.

MBV and SE tests are intended to assess if there are potentially deleterious fines e.g. clays in the fine aggregate which could adversely affect the fresh and hardened properties of the concrete.

Table 2 Aggregate particle size distribution

SAMPLE	B-FEED	B-A	B-B	B-C	B-D
SIEVE SIZE mm	PERCENT PASSING BY MASS				
8	100.0	100.0	100.0	100.0	100.0
6.3	100.0	100.0	100.0	100.0	100.0
4	94.0	100.0	100.0	100.0	100.0
2.8	86.0	99.0	99.2	99.3	99.3
2	73.0	88.0	90.3	91.0	91.4
1	54.0	56.0	64.2	66.4	67.7
0.5	41.0	34.0	44.9	48.7	50.8
0.25	29.0	16.0	27.1	32.2	34.7
0.125	20.0	4.0	10.9	15.9	18.8
0.063	13.0	1.0	2.9	5.1	7.4

Table 3 Aggregate particle size distribution continued

SAMPLE	G-FEED	G-A	G-B	G-C	G-D	G-E
SIEVE SIZE mm	PERCENT PASSING BY MASS					
8	100.0	100.0	100.0	100.0	100.0	100.0
6.3	99.0	100.0	100.0	100.0	100.0	100.0
4	87.0	100.0	100.0	100.0	100.0	100.0
2.8	77.0	99.0	99.1	99.2	99.2	99.2
2	66.0	90.0	90.8	91.8	92.1	92.3
1	49.0	63.0	65.7	69.4	70.2	71.1
0.5	35.0	39.0	43.2	48.9	50.6	51.9
0.25	24.0	17.0	21.9	29.1	31.4	33.3
0.125	16.0	4.0	7.5	13.0	15.6	17.8
0.063	10.0	2.0	2.8	5.1	6.5	9.0

In addition to the above tests the following fine aggregate tests were also used:

- New Zealand Flow cone (NZFC) according to NZS 3111-1986
- Rapid Methylene blue test (RMBV) developed by Grace on the 0/2mm fraction of the sands.

The NZFC test evaluates sand flow and the un-compacted voids ratio. A fixed volume of sand is passed through a cone and collected in a container of known volume whilst measuring the flow time. Using the density of the sand particles allows the un-compacted voids ratio to be calculated. The test result is affected by the grading of the sample, by the particle shape and by the surface texture of the particles. The flow of the material is mostly affected by the shape and surface texture of the particles while the voids result is mostly influenced by grading and shape [4]. Although the British European Standards EN 933-6 and BS EN 1097-6 evaluate the flow time and un-compacted voids, they do not provide the opportunity to do that simultaneously.

The NZFC is a rapid test that does not require sophisticated equipment and experienced operator as opposed to visual shape and texture estimation techniques. The results are plotted on the diagram shown in Figure 2 with reference to a standard envelope adopted by the New Zealand authorities, therefore, the NZFC test was adopted in the study.

The RMBV test evaluates the same properties as the BS EN 933-9 MBV test, however, using a different approach. The British European standard procedure determines the absorption of methylene blue dye by consecutively adding a drop of the dye and checking for the test's endpoint. The endpoint of the test is determined by dropping a small amount of the suspension on a filter paper until a light blue halo around a central deposit is observed and this endpoint is often open to interpretation.

The RMBV test eliminates this problem as well as reducing the testing time. The test portion is mixed with a methylene blue solution of known concentration, shaken for a fixed time and an aliquot of the suspension is filtered. Afterwards a known volume of the filtrate is diluted with a set amount of water and a pre-calibrated colorimeter is used to estimate the concentration of the solution. This allows direct estimation of the absorbed amount of methylene blue solution eliminating possible errors due to human judgement. The RMBV test was used in this study to compare the results obtained by the two methods and evaluate the feasibility of the new method.

Table 4 Aggregate particle size distribution continued

SAMPLE	COARSE AGGREGATE
SIEVE SIZE mm	PERCENT PASSING BY MASS
40	100
31.5	100
20	95
16	68
14	58
10	36
6.3	16
4	6
2	5
0.063	2

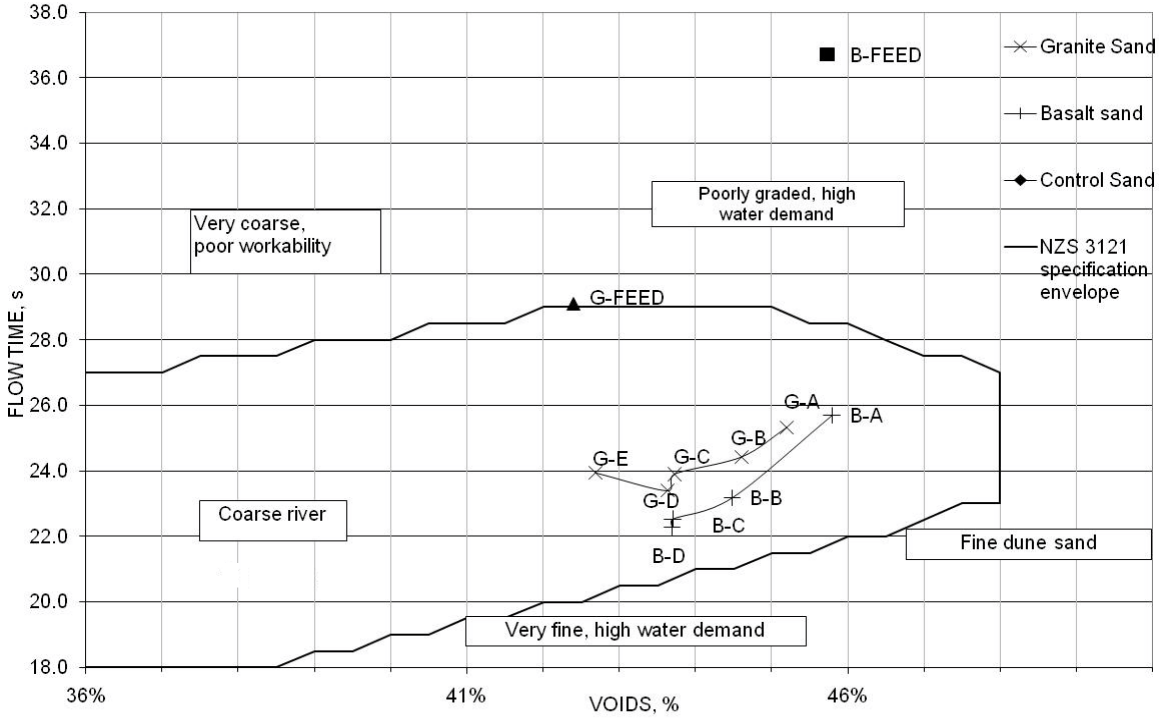

Figure 2 New Zealand Flow Cone results and specification envelope

CONCRETE MIXTURES

For each quarry a trial mix using 100% manufactured sand with a fines content of 2.8% (G-B or B-B) was made adjusting the water content to reach a slump of 80mm. Other mixes of that quarry material were made using the established w/c ratio

The absorption capacity and water content of fine and coarse aggregates were taken into consideration and the mixture's water content was adjusted accordingly to maintain the w/c ratio and mixture proportions, as presented in Table 5.

Fresh Concrete Tests

Fresh concrete was tested for slump according to BS EN 12350-2:2009, plastic density and air entrapment. The results of these tests are presented in Table 6.

Hardened Concrete Tests

Hardened concrete was tested for compressive strength at 1, 7 and 28 days according to BS EN 12390-3:2009, for flexural strength at 28 days according to BS EN 12390-5:2009. The concrete specimens were de-moulded 16 to 20 hours after casting and placed in water tanks at a constant temperature of 20°C until the test age was reached. Results of these tests are presented in Table 6.

Table 5 Concrete mixture proportions at SSD conditions

MIX	CEM kg/m^3	CA kg/m^3	FA kg/m^3	WATER kg/m^3	W/C	FA/ CA	FINES CONTENT % of FA
G-A	350	1040	753	202	0.58	0.42	2.0
G-B	350	1040	753	202	0.58	0.42	2.8
G-C	350	1040	753	202	0.58	0.42	5.1
G-D	350	1040	753	202	0.58	0.42	6.5
G-E	350	1040	753	202	0.58	0.42	9.0
B-A	350	1040	753	234	0.67	0.42	1.0
B-B	350	1040	753	234	0.67	0.42	2.9
B-C	350	1040	753	234	0.67	0.42	5.1
B-D	350	1040	753	234	0.67	0.42	7.4

*FA – fine aggregate, CA – coarse aggregate

RESULTS AND DISCUSSION

In this section fresh and hardened concrete properties are presented and discussed with reference to the fine aggregate properties shown in Tables 1-4 and Figure 2.

Fine Aggregate Test Results

One objective of the project was to compare the RMBV test with the MBV standard test. It can be seen in Figure 3 that the test results obtained using both methods exhibit a very good linear correlation with R^2 = 0.99 suggesting that both test methods evaluate the same property, although providing different numerical values. This suggests that the RMBV test could be used as an alternative test to the standard MBV test.

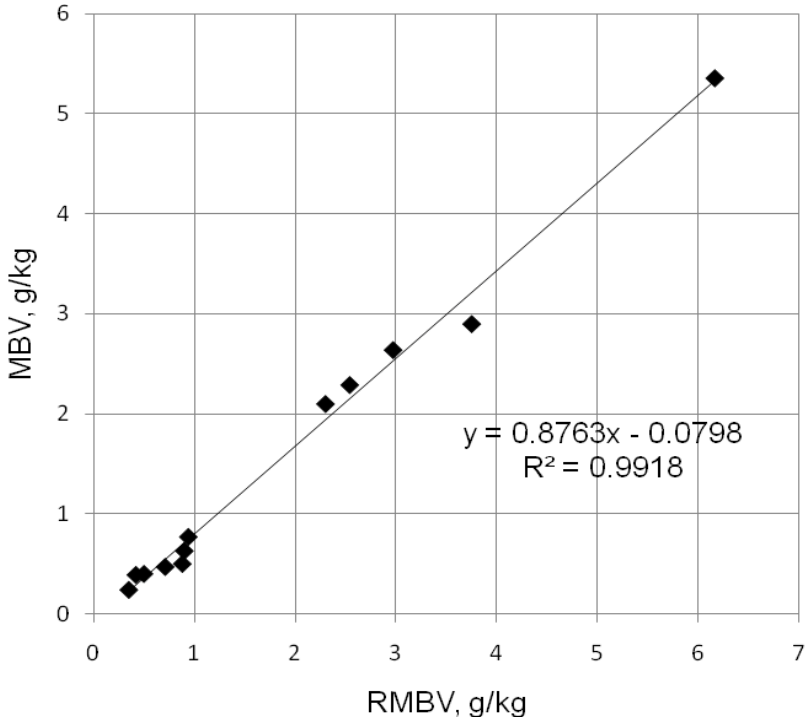

Figure 3 Correlation between RMBV and MBV values for all samples

Table 1 shows that there are differences between the feed material for each quarry and the resulting manufactured sands. B-FEED basalt quarry dust has a high MBV of 5.36 g/kg (RMBV 6.16 g/kg) whereas the highest fines basalt manufactured sand B-D possesses an MBV of 2.90 g/kg (RMBV 3.75 g/kg). A similar trend can be seen with the granite manufactured sands. The G-FEED MBV is 0.77 g/kg whereas the highest fines granite sand G-E MBV is 0.63 g/kg. It can be concluded that during the processing a proportion of clay sized particles (<2 micron) has been removed from the material as part of the filler component lowering the MBV value of the sand.

From Table 1 it can be seen that the sand equivalent (SE) values have increased for the processed quarry dusts. The SE values are the highest for manufactured sands with the least fines and gradually decrease with increasing fines content. A similar inverse trend to that was observed in the MBV values that can be attributed to the removal of clay sized particles during the manufacturing process.

The SE values for granite sands are in range from 80 to 69; for basalt sands they are lower - from 70 to 58. Similarly to the MBV values this suggests that the basalt sands contain some deleterious fines or clays which may adversely affect the water demand of concrete mixtures.

Figure 2 shows the results from NZFC. The processed manufactured sands lie within the New Zealand specification envelope whereas the feed material from both quarries does not conform to the specification. It suggests that the G-FEED and B-FEED are poorly shaped and graded.

The flow time has been greatly reduced for the manufactured sands; at least 4 seconds for granite sands and 11 seconds for basalt sands. This suggests that the particle shape has been modified and after processing it is less angular and flaky. The voids content of the G-FEED is 42.4% whereas for the manufactured sands it ranges from 45.2% for the least fines sand to 42.7% for the highest fines sand G-E, whereas the voids content of the B-FEED is 45.7% and it is decreasing for manufactured sands with more fines. Visual inspection suggests that the basalt crusher dust particles are mostly angular and flaky whereas the manufactured sand particles are mostly rounded without sharp edges. Similarly granite crusher dust particles are highly angular and flaky, however the manufactured sands are mostly cubical with sharp edges but without flaky particles.

These observations suggest that angular and flaky particles result in a higher voids content and flow rate. Similarly, cubical particles with sharp edges increase the voids content, but to a lesser extent than flaky ones. Rounded particles result in the lowest voids content and flow rates. Increased fines contents lower the voids content and generally improve the flow rate.

Workability

To achieve the desired 80 mm slump the granite sand (G-B) required a water / cement ratio of 0.58. This was lower than that of the basalt sand (B-B) (w/c ratio 0.67) because of the lower MBV of the latter. In both cases viable concrete mixes resulted.

Figure 4 shows the slump versus the amount of fines for the granite and basalt mixtures. The general trend is that the higher the amount of fines, the lower the slump of the concrete.

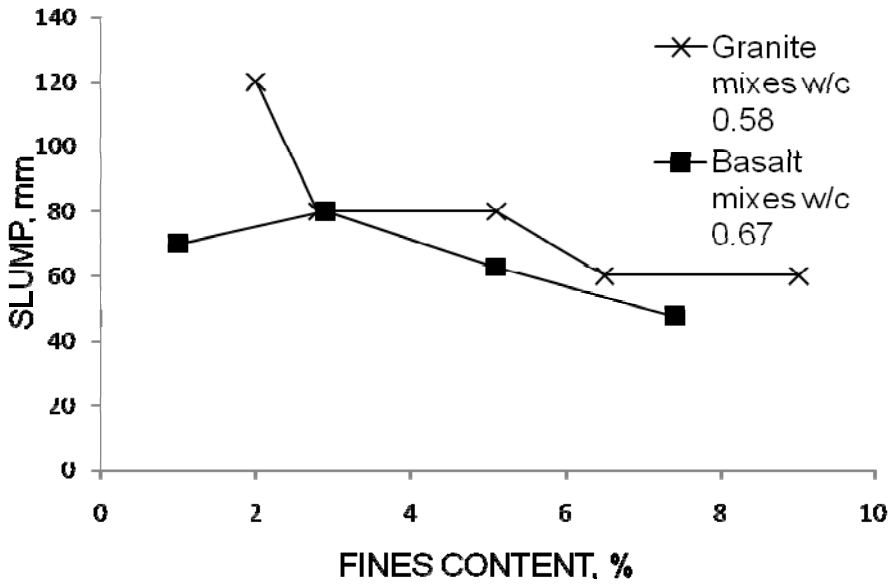

Figure 4 Variation of slump with fines content

However, it has to be noted that the manufactured sand mixtures with the lowest fines content were observed to be hard to work and finish even though the slump was still between 70 and 120 mm. Mixtures with higher fines contents such as B-B, B-C and G-B, G-C, G-D were easier to finish and work even with lower slump values. However, the B-D and G-E mixtures were very cohesive due to the amount of fines.

Hardened Concrete Properties

Table 6 shows the compressive and flexural strengths of the concrete mixes that were tested. The compressive strength of the basalt mixes were in the range 41.7 N/mm^2 for the B-A mix to 45.6 N/mm^2 for the B-D mix. Similarly the compressive strength of granite sand mixes were in the range 48.1 N/mm^2 for the G-E mix to 52.3 N/mm^2 for the G-D mix.

An increase in fines content of the manufactured sands did not show any correlation with the compressive strengths at 28 days. This suggests that there are no negative effects of a higher fines content on the compressive strength for the given mix compositions and the range of fines content investigated in this study.

The 28 day flexural strength for all mixes is in the range 5.3 to 6.1 N/mm^2 and seems to follow the trend of compressive strength, with higher compressive strengths corresponding to higher flexural strengths.

CONCLUSIONS

These results show that it is feasible to produce workable concretes with satisfactory 28 day compressive and flexural strengths using manufactured sand. Additionally, while great care is required to ensure that the mix design used is appropriate for the type and properties of the feed material, these results have also demonstrated that it is possible to completely replace natural sand in concrete.

Table 6 Fresh and hardened concrete properties

MIX	SLUMP mm	AIR %	FRESH DENSITY kg/m^3	COMPRESSIVE STRENGTH, N/mm^2			FLEXURAL STRENGTH, N/mm^2
				1 day	7 day	28 day	28 day
G-A	120	0.45	2393	17.6	43.5	52.2	5.6
G-B	80	1.6	2375	17.0	40.2	49.9	5.6
G-C	80	0.9	2378	17.9	40.4	50.1	6.0
G-D	60	0.65	2393	19.3	42.2	52.3	5.8
G-E	60	0.78	2393	16.6	40.6	48.1	5.4
B-A	70	0.5	2430	11.8	30.4	41.7	5.3
B-B	80	0.5	2423	12.9	31.3	43.7	5.5
B-C	62.5	0.45	2434	13.0	33.1	42.7	5.4
B-D	47.5	0.65	2410	13.2	35.2	45.6	5.6

The fine aggregate test results showed that the processing of crusher dusts improved the shape and grading as well as having removed some deleterious clay sized particles as indicated by the MBV and SE tests. The test results also suggest that the RMBV test could be used as an alternative to the standard MBV test in order to rapidly assess the presence of potentially deleterious fines.

It is important to assess the presence of harmful fines in the fine aggregates as it can dramatically affect the water demand for the same workability, as shown by the basalt sands in comparison to the granite sands.

The next phase of this ongoing study will investigate the performance of other manufactured sands, in particular from Welsh quarries to address the needs of the Welsh Assembly Government, and manufactured sand concrete mixes containing admixtures to enhance their workability and general applicability regardless of the source. The results of these further studies will be published in due course

ACKNOWLEDGEMENTS

The authors would like to acknowledge the financial and technical support of the Aggregate Levy Fund for Wales project consortium including Kayasand, Kemco, Grace Construction Products, Cemex and Aggregate Industries.

REFERENCES

1 HARRISON, D J, WILSON, D, HENNEY, P J, HUDSON, J M. Crushed Rock Sand In South Wales, A Reconnaissance Survey. British Geological Survey Technical Report No. WF/00/0. 2000.

2 AHN, N, FOWLER, D W. An Experimental Study On The Guidelines For Using Higher Contents Of Aggregate Microfines In Portland Cement Concrete. International Centre For Aggregate Research. Research report No. ICAR 102-1F, 2001.

3 MANNING, D. Exploitation and Use of Quarry Fines, Mineral Solutions Ltd. Technical Report No. 087/MIST2/DACM/01, 2004.

4 CEMENT CONCRETE & AGGREGATES AUSTRALIA. Manufactured Sand National test methods and specification values. Research report, 2007, pp 17-18

Carbon Dioxide Capturing Ability of Cementitious Building Finishing Materials

Y Kitsutaka[1], K Yoshida[2]
1 – Tokyo Metropolitan University, Japan
2 – Asahikasei Homes Company, Japan

In this study, we focused on the carbon dioxide capturing ability of cementitious materials for the use of the building wall finishing. Carbon dioxide capturing tests were performed for various finishing materials by using the 10-litre Tedlar bag filled with 20% concentration carbon dioxide gas and with a finishing material. Reduction of the concentration of carbon dioxide gas in the Tedlar bag was measured by the carbon dioxide detector tube. Finishing materials such as Japanese plaster, diatomite, autoclaved aerated concrete, moisture control finishing, mortar, tile were used for the carbon dioxide capturing test. It was found that the materials including the chemical element of calcium have high carbon dioxide capturing ability.

Y Kitsutaka is a Professor in the Department of Architecture and Building Science at Tokyo Metropolitan University, Japan, Eng. Dr. from Tokyo Institute of Technology in 1986, aesthetics of building finishes, durability of building materials, new concrete material, fracture mechanics of structural materials, the 2001 paper prize of Architectural Institute of Japan.

K. Yoshida is an engineer with Asahikasei Homes Company, Japan.

Keywords: Capturing ability, Carbon dioxide, Finishing materials, Greenhouse gases

INTRODUCTION

Technical development has been in progress in various spheres to reduce carbon dioxide, a greenhouse gas. Building technology with low CO_2 emission has been attracting attention in the architectural field as well. A variety of interior materials adsorbing air pollutants such as VOC (volatile organic compounds) have recently been developed. These include materials having a specific surface increased by numerous micropores to increase physical adsorption and those containing reactive elements to induce chemical adsorption. The development of interior materials that capture CO_2 in the air by similar principles will contribute to reduction of greenhouse gases.

In this study, carbon dioxide capturing tests were performed for various finishing materials by using the tedla bag filled with carbon dioxide gas and the ability of the concentration of carbon dioxide gas for various finishing materials was discussed.

OUTLINE OF EXPERIMENT

In this study, Japanese plaster, diatomite, autoclaved aerated concrete, and moisture-conditioning finishing, which absorb VOCs including formaldehyde, were used as test specimens, while mortar and tile were used representing general building finishing materials. Table 1 gives the properties of test materials. Specimens shaped as shown in Figure 1 were kept in a thermo-hygrostatic chamber at 20°C and 60% RH for one week or more.

Table 1 Properties of test materials

TEST MATERIAL	SIGN	PROPERTY
Japanese plaster	JP	Slaked lime, $Ca(OH)_2$
Diatomaceous earth	DM	Diatomite, SiO_2
AAC	AAC	Autoclaved lightweight aerated concrete
Moisture conditioning finishing	MC	Particle of AAC
Mortar	MO	Normal Portland cement, sand
Tile	TL	Porcelain tile

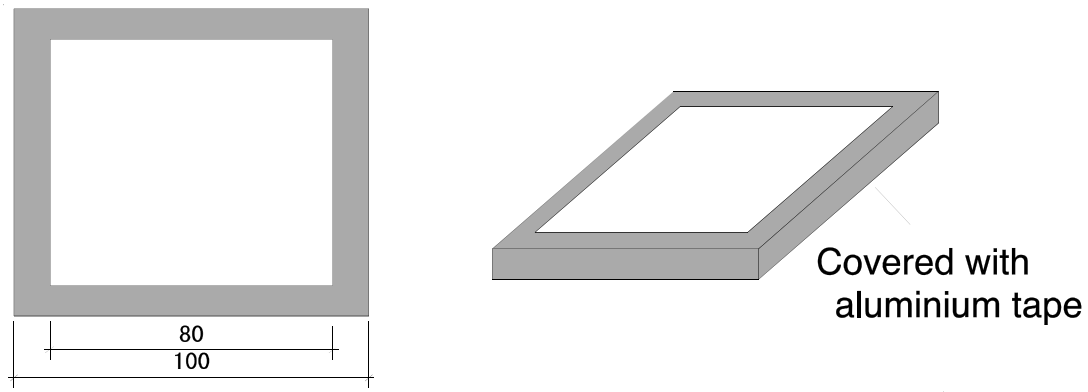

Figure 1 Specimen

All sides and ends except the surface to be exposed were then covered with aluminium tape to prevent contact with the air. The margins of the exposure surface were also covered with aluminium tape to leave an effective absorption area of 80 by 80 mm. Specimens with different thicknesses (5, 10, and 20 mm) were prepared as given in Table 2, while keeping the exposed surface area constant, to examine the effect of depth on CO_2 reduction. As for Japanese plaster, three levels of water-binder ratios (W/B) at the time of mixing (0.5, 1.0, and 2.0) were selected to investigate their effect. Two specimens were fabricated for each set of conditions.

Table 2 Thickness of test materials

TEST MATERIAL	5 mm	10 mm	20 mm
Japanese plaster	○	○	○
Diatomaceous earth	○	○	○
AAC	—	○	○
Moisture conditioning finishing	○	—	—
Mortar	—	○	—
Tile	—	○	—

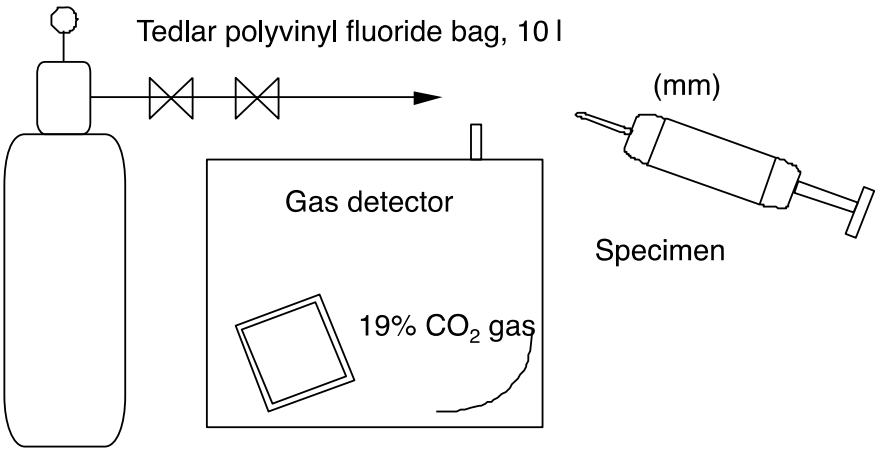

Figure 2 Test set up

Table 3 Test conditions

ITEM	CONDITION
Container	Tedlar polyvinyl fluoride bag, 10 l
Measuring period	0, 1, 3, 6, 12, 24 hours, 3, 7, 14 days
Specimen size	100 mm × 100 mm × 5, 10, 20 mm
Capturing area	6400 mm² (80 mm × 80 mm)
Environment	20°C, 60% RH
Gas	19% Carbon dioxide

As shown in Figure 2, each specimen was placed in a 10-liter Tedlar polyvinyl fluoride bag, which was sealed and left to stand in a thermo-hygrostatic room at 20°C and 60% RH for 24 hours. These bags were then filled with a gas controlled to contain 19% CO_2. The CO_2 concentration in each bag was measured at regular time intervals using a gas detector tube with a measurement range of 1 to 20%. Table 3 gives the test conditions. The weight of each specimen was also measured at the end of the tests. Note that blank tests were conducted as well to confirm the bag's absorptivity and sealing performance.

RESULTS AND DISCUSSION

Figure 3 shows the changes in the CO_2 concentration in tedlar bags over time under different test conditions. This graph shows the changes up to 24 hours from the beginning, during which the differences were most significant. Measurement was continued up to 14 days or when the CO_2 concentration decreased to nearly zero.

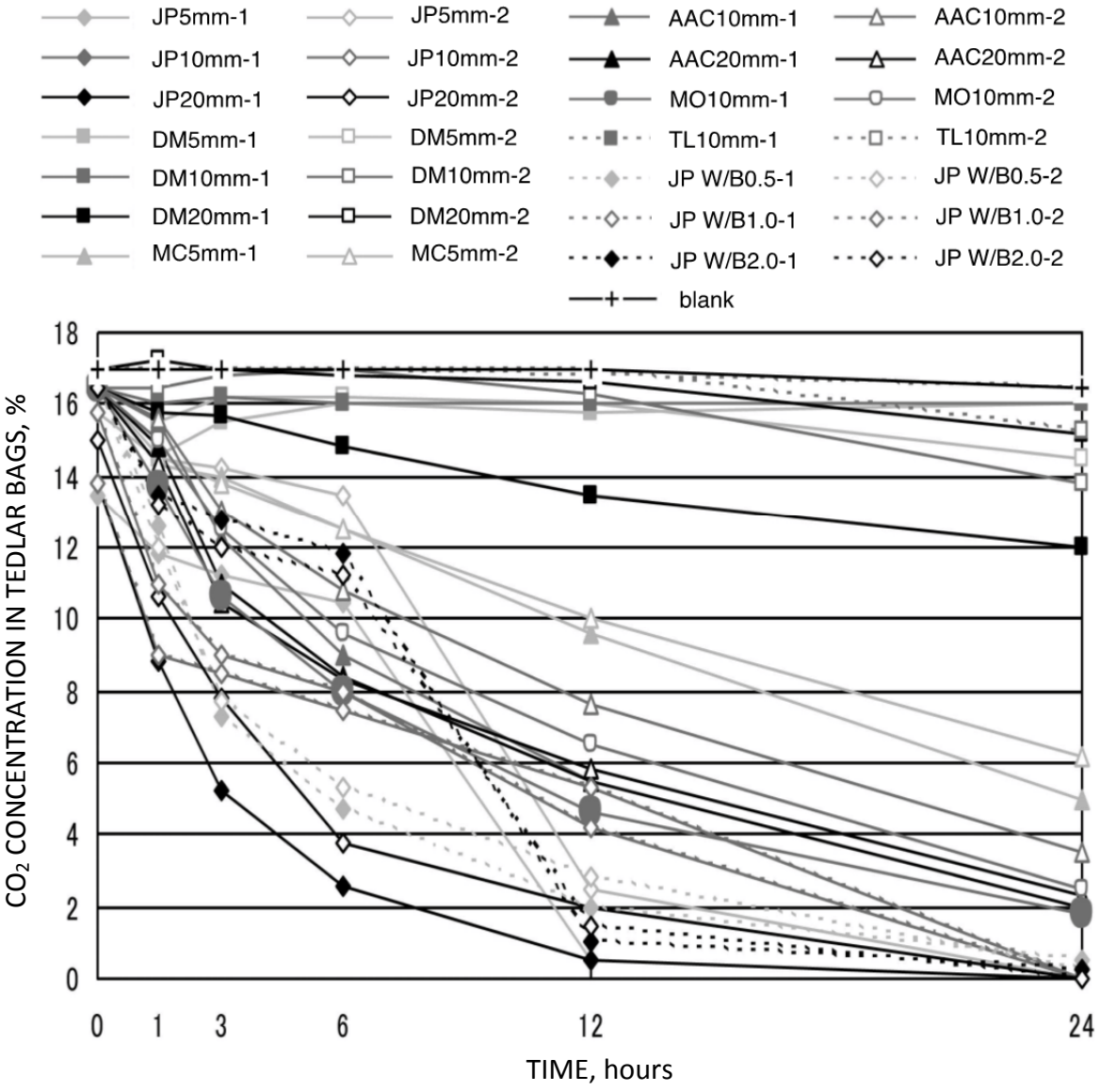

Figure 3 CO_2 concentration in tedlar bags over time

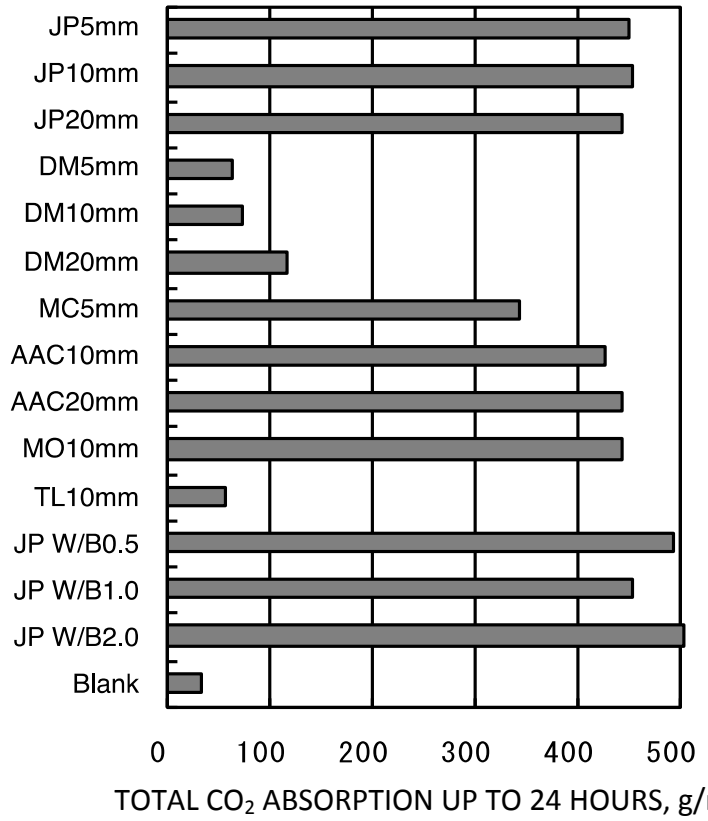

Figure 4 CO_2 absorption calculated from the CO_2 loss in tedlar bag

Figure 4 shows the estimated total CO_2 absorption of each specimen up to 24 hours calculated from the average CO_2 loss in each bag. Figures 3 and 4 reveal that the CO_2-capturing performance of Japanese plaster (JP), moisture-conditioning finishing (MC), autoclaved aerated concrete (ALA) and mortar is high. As expressed by the chemical formula for Japanese plaster $Ca(OH)_2 + CO_2 = CaCO_3 + H_2O$, quicklime reacts with CO_2, forming calcium carbonate and water. Waterdrops were actually observed in tedlar bags for Japanese plaster at the time of concentration measurement, suggesting its reaction with a significant amount of CO_2. Though mortar reacts similarly to Japanese plaster, the reaction rate is slower. Also, the main ingredient of autoclaved aerated concrete and moisture-conditioning finishing is calcium silicate, and CO_2 capture by materials containing calcium silicate has been confirmed in past studies. It is therefore inferred that the calcium component reacts with CO_2 gas1). Meanwhile, diatomite (DM), which shows high VOC absorption rates according to the literature2), showed low CO_2 absorption. The CO_2 concentration with tile (TL) was nearly the same as that in the blank tests, showing little absorptivity of tile. In regard to thickness, a thicker specimen of diatomite (DM) demonstrated higher absorptivity, showing significant differences in CO_2 absorption. A higher water-binder ratio of Japanese plaster (JP) led to a higher absorption performance up to 12 hours.

Figure 6 shows the relationship between the measured weight loss at the end of testing of specimens that showed high absorptivity and their CO_2 absorption calculated from Figure 5 and converted to weight. Both are found to agree well. It can therefore be said that the mass increased by an amount equal to the amount of CO_2 absorption. These calculations are based on the assumption that 1 mol = 22.4 litres, C = 12, and O = 16, and thus 44 g of CO_2 is contained per 22.4 litres.

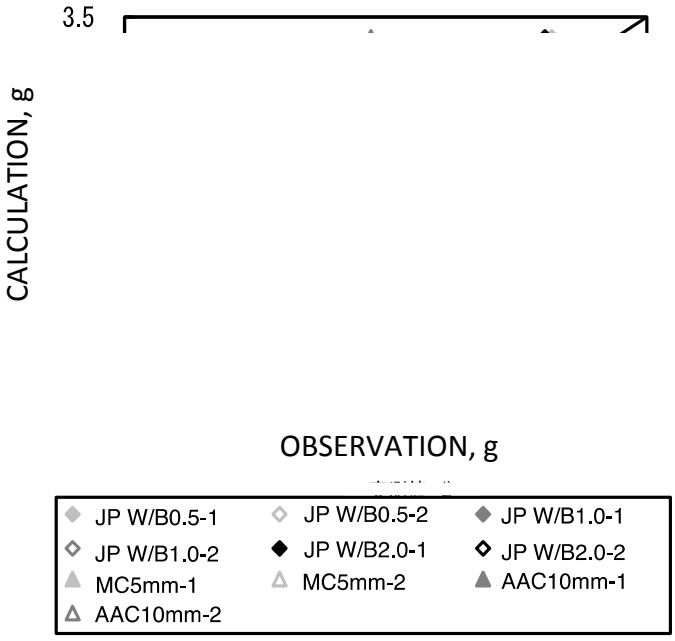

Figure 6 Relationship between the measured and the calculated weight loss

CONCLUSIONS

Conclusions obtained from this study are as follows,

1. The differences of CO_2 absorption for specimens were most significant up to 24 hours from the beginning.
2. CO_2-capturing performance of Japanese plaster, moisture-conditioning finishing, autoclaved aerated concrete and mortar becomes high.
3. The materials including the chemical element of calcium have high carbon dioxide capturing ability.

ACKNOWLEDGEMENTS

We thank ALC (Autoclaved Light-weight Concrete) society in Japan for giving us materials and cooperation during our research.

REFERENCES

1. TSUTSUMI J, Carbon dioxide absorption performance by mineral coating materials, Summaries of technical papers of Annual Meeting Architectural Institute of Japan, D-1, 2008.9, pp. 1175-1176.

2. KURUMA S, KITSUTAKA Y AND TAMURA M, Study on Reducing Effect of Indoor Air Pollutant by Building Interior Finishing Materials, Summaries of technical papers of Annual Meeting Architectural Institute of Japan, A-1, 2005.9, pp. 933-934.

Possible Use of Iron- and Steelmaking Slag as Replacements for Cement

D Adolfsson[1], L Andreas[2], F Engström[2], B Björkman[2]
1 – SSAB EMEA, Sweden
2 – Luleå University of Technology, Sweden

Steelmaking slags have mainly been used as aggregates in road construction, while only 1 % was used in cement production in Europe 2004. There are at least two good arguments to why the utilization of steelmaking slags should be increased in cement production, i.e. to decrease CO_2 emissions and to conserve natural resources which thereby reduce the amount of slags sent to landfill. In addition to a general evaluation of the possibility to use slags as replacement for cement or as a raw material in production of cement, some examples will be given. Results provided in this study show that the level of CO_2 emissions can be reduced by about 30-35 % in comparison to ordinary Portland cement production (OPC) when a major fraction of steelmaking slags are used as raw material for production of slow hardening sulphoaluminate belite cement (SAB). The formation of calcium aluminate hydrates in ladle furnace slag (LFS) results in high early strength which is why LFS is considered to be used as binder supplement for OPC in for instance metallurgical briquettes. Another application is the use of LFS in barrier constructions, as for example the liner layer in a landfill top cover. An ongoing field-study in the community of Hagfors, Sweden, shows that LFS in combination with electric arc furnace slag (EAF) can fulfill the technical and environmental requirements for a cover of a municipal solid waste landfill.

Dr D Adolfsson is a researcher with SSAB EMEA, Oxelösund, Sweden.

Dr Lale Andreas is an Assistant Professor in Waste Science and Technology at Luleå University of Technology, Sweden.

Dr F Engström is a Lecturer and Professor B Björkman is a Professor, in process metallurgy at Luleå University of Technology, Sweden.

Keywords: Binder additive, Cement replacement, Liner material, SAB cement, Steelmaking slag

INTRODUCTION

Ordinary Portland cement (OPC) is one of the most common construction materials in the world and is based on raw materials that are rather cheap, i.e. mainly limestone and clay. There is, however, still an important challenge in reducing the levels of carbon dioxide emissions as well as to conserve natural resources by for instance finding alternative replacement materials. Important alternatives have been the usage of fly ashes and steelmaking slags, but steelmaking slags and/or fly-ashes cannot fully replace the use of limestone due to the limitation of volumes that can be provided as well as the properties of the final clinker. It is still, however, worthwhile considering the use of by-products in applications where the high quality and standard performance of already existing commercial cements are not needed which would help reducing both the amount of CO_2 emissions and the exploitation of natural resources. Steelmaking slags have mainly been used as aggregates in roads [1], but have also been found to be appropriate in cement applications either in blends with commercial binders like OPC or as part of the raw material [2-8]. Table 1 lists the major crystalline phases found in three types of commercial cements [9-13] whereas Table 2 summaries typical phases in different steelmaking slags.

Table 1 Typical compositions of commercial cements [9-13]

CAC		OPC		SAB	
Mineral	Wt-%	Mineral	Wt-%	Mineral	Wt-%
CA	60-70	C_3S	55-65	$C_4A_3\overline{S}$	10-55
C_2S	minor	C_2S	15-25	C_2S	10-60
$C_{12}A_7$	2-5	C_3A	8-14	$C\overline{S}$	0-25
C_4AF	10-20	C_4AF	8-12	C_4AF	0-40
F	minor			C	0-25
CT	minor				
C_2AS-C_2MS_2	minor				

Tricalcium silicate (C_3S) in OPC contributes to the short-term strength by forming calcium silicate hydrates (C-S-H), whereas dicalcium silicate (C_2S) is important for the long-term strength via the formation of similar C-S-H-gels as formed by C_3S. The main minerals found in sulfoaluminate belite cement (SAB) which is based on limestone, bauxite and gypsum calcined at about 1300-1350°C [14], refers to the phase assemblage $C\text{-}S\text{-}A\text{-}\overline{S}$ [9]. The principal phases in the final clinker may vary according to Table 1. High amount of sulfoaluminate ($C_4A_3\overline{S}$) gives high early strength to the cement, and is also considered to provide good corrosion resistance and controllable expansion [15]. C_2S reacts slowly and contributes to the long term strength like in OPC. Calcium aluminate cements (CAC) are highly reactive yielding significant early strength to the material by forming calcium aluminate hydrates, i.e. CAH_{10}, C_2AH_8, CAH_{13} and C_3AH_6 [13]. Monocalcium aluminate (CA) is the main crystalline phase present [11], but there may also exist few percentages of other minerals, e.g. $C_{12}A_7$, C_2S, C_2AS as well as C_4AF depending on the raw materials that are used [13].

On closer examination of steelmaking slags it appears that there are similarities between these compositions and the commercial cements. The most important difference is the amount of short-term strength giving phases. Silicate-based slag compositions like the slags from the AOD-, BOF- and EAF-processes typically contain significant amounts of dicalcium

silicate but lacks in the presence of tricalcium silicate, sulfoaluminate and monocalcium aluminate. Table 2 gives the most common phases present in these slags as well as in the ladle furnace slag (LFS). Depending on the steel produced and the operational practice the relative amount of these phases will vary in some extent. The present paper therefore intends to highlight the advantage of steelmaking slags and discuss how the previously mentioned similarities can be used with favour in different applications.

Table 2 Abundant phases typically seen in steelmaking slags

AOD	BOF	EAF	LFS
		α'-C_2S	α'-C_2S
β-C_2S	β-C_2S	β-C_2S	β-C_2S
γ-C_2S		γ-C_2S	γ-C_2S
C_3MS_2		C_3MS_2	
CaO	CaO		CaO
MgO	MgO	MgO	MgO
C_2AS-C_2MS_2		C_2AS-C_2MS_2	
CaF_2			
			C_3A
	C_2F	C_2F	C_2F
	f	f	f
			$C_{12}A_7$

THE POSSIBLE USE OF STEELMAKING SLAGS

Sulfoaluminate Belite Cement (SAB)

The advantage of SAB cement is basically that the lime saturation factor can be reduced [16], and that the firing temperature can be lowered by about 100-150°C [17] as sulfoaluminate is formed at a lower temperature than tricalcium silicate is formed. Steelmaking slag in contrast to limestone is an already "burned material" and therefore the energy demand can be expected to decrease. The range of applications, however, may be limited for cement that is based on a high fraction of steelmaking slags, but there are reasons to believe that the considered type of cement is appropriate in applications like, landfill construction, soil stabilisation or stabilisation of industrial by-products where the high performance of commercial cement may not be needed.

Dicalcium silicate is one of the principal phases in slow hardening SAB cement, as in many of the steelmaking slags. To reduce both CO_2-emissions and the use of natural resources an attempt to combine several types of steelmaking slags for the production of slow hardening SAB cement was presented by Adolfsson et al. [18]. Four slag mixtures were examined, of which Mix a and Mix B, seen in Figures 1a-b [18-19] will be further discussed in this section. The interesting difference between these mixtures was that Mix A contained a much higher fraction of AOD slag than Mix B which in contrast to Mix A also included EAF slag from ordinary steel production, as well as a higher amount of LFS [18-19].

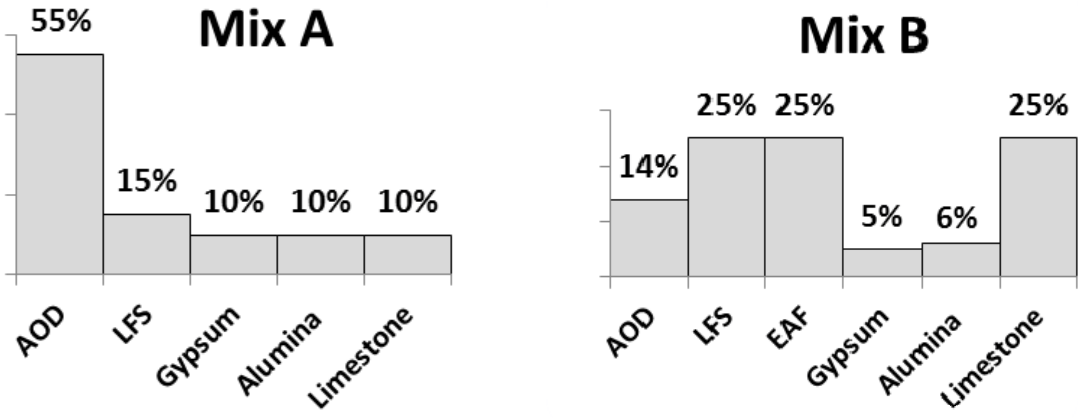

Figure 1a-b Wt-% fractions of constituents in Mix A and Mix B according to data given in the studies by Adolfsson et al. [18-19]

The mixtures given in Figures 1a-b were fired at 1200°C for approximately 30 minutes and then quenched in water. Changes in weight as well as endo- and exothermic reactions upon heating were also analysed with a TG/DTA instrument that was equipped with a quadruple mass spectrometer [18]. At about 700-800°C, decomposition of calcium carbonate ($CaCO_3$), was noted and determined to 4.2 wt-% for Mix A and 9.4 wt-% for Mix B [18]. Results suggesting levels in the range of 4 and 9 wt-% in carbon dioxide emissions and not the approximately 45 wt-% typically seen for raw mixtures that are based on limestone and clay is an important argument to why steelmaking slags should be further considered as a possible resource, at least in applications that do not require a cement with the high quality and standard performance of commercial cements like OPC. After quenching, it was concluded that sulfoaluminate, and bredigite, i.e. the Mg-analogue of α'-C_2S, were the most abundant phases formed in Mix A, whereas Mix B revealed strong peaks of larnite (β-C_2S), brownmillerite (C_4AF) as well as free periclase (MgO) instead of bredigite, according to the characterisation with powder x-ray diffraction [18].

Compressive strength tests suggested performance similar to slow hardening SAB compositions, as illustrated in Figure 2. After 2 days hydration with the addition of 5% gypsum Mix A reached 4.2 MPa and Mix B 7.5 MPa, and after a total of 28 days Mix A measured 8.5 MPa and Mix B 13.5 MPa [19]. One explanation for the difference was according to authors that Mix B was finer in size with the same grinding conditions which partly could be due to a higher content of metal particles in Mix A [19]. The difference could however, also be due to bredigite being more difficult to grind. Another important aspect considering the reactivity could be the slow hydration of bredigite in Mix A in parallel to a more reactive ferrite phase in Mix B which was calculated to 39 wt-% based on modified Bogue calculations [18-19].

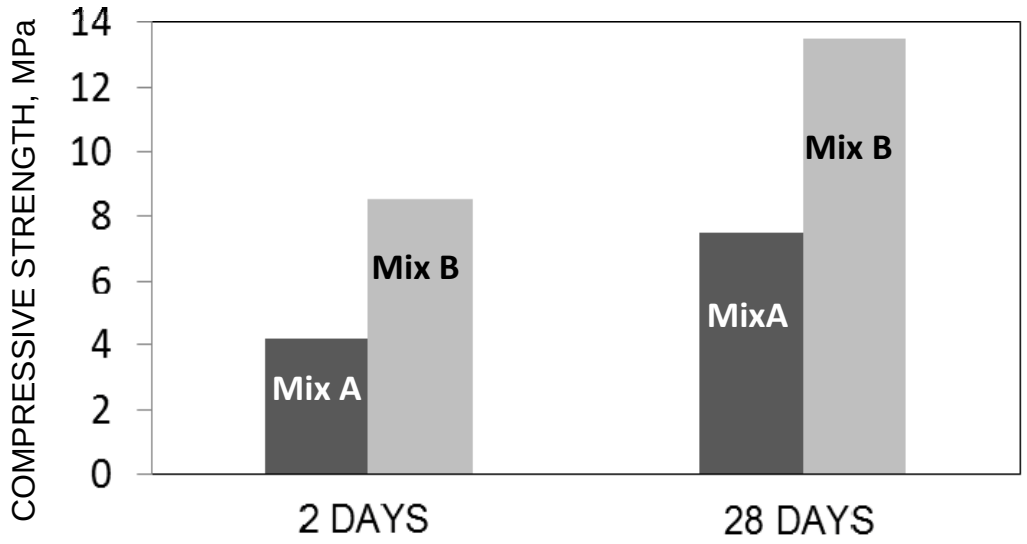

Figure 2 Compressive strength of Mix A and Mix B
based on data given in the study by Adolfsson et al. [19]

Ladle Furnace Slag (LFS)

The composition of LFS, as described in Table 2, suggests promising hydration properties. In a recent publication [20], this potential was further demonstrated and it was suggested that the use of LFS in for instance metallurgical briquettes as binder supplement can save costs for both binder and landfill [20], also discussed in [21]. An important compositional difference between that ladle furnace slag and the composition given in Table 2 was that a significant amount was represented by pleochroite or Q-phase ($C_{20}A_{13}M_3S_3$) which is an Mg-analogue of pleochroite.

Rietveld analysis of this slag suggested Q-phase to be present at about 21 wt-%. It was also given that calcium aluminates in this slag, mayenite and tricalcium aluminate were present in the order of approximately 12 and 9 wt-% respectively [20]. Although the amount of pleochroite was noted as a major crystalline phase it was concluded that the influence of calcium aluminates is more relevant during the early hours of hydration due to very strong peaks of calcium aluminate hydrates, specifically C_2AH_8, $C_2AH_{7.5}$ and C_4AH_{19} at 20, 25 and 30°C, whereas $C_2AH_{7.5}$ was the dominating phase according to [21] at 15°C.

Compressive strength tests measured 33.1 MPa after 2 days hydration but only 21.9 MPa after 28 days. The decline in strength was explained as conversion of metastable hydrates to the thermodynamically stable C_3AH_6 and therefore a further evidence that the properties of calcium aluminates present in LFS in principle decides the strength development, at least up to 28 days, meaning that Q-phase being the major crystalline phase should be avoided if possible [20].

These results therefore lead us to the conclusion that calcium aluminates, and perhaps mayenite in particular deserves closer examination with regard to its rate of hydration.

Hydration Properties of Mayenite

Experimental procedure

Figure 3 below shows the particle size distributions of a mayenite, $C_{12}A_7$ that has been synthesised at three different temperatures, namely 1400°C, 1380°C and 1350°C. Analytical grades of $CaCO_3$ and Al_2O_3 were blended stoichiometrically, and then fired at the respective temperatures for 24 hours, which was followed by slow cooling. The purity of mayenite was confirmed with x-ray powder diffraction (XRD), which indicated traces of CA in samples $C_{12}A_7$ (1400°C) and $C_{12}A_7$ (1380°C) and traces of CA and C_3A in sample $C_{12}A_7$ (1350°C). The particle size distribution was characterised with a Malvern optical sizing unit and the BET surface was determined as well.

The hydration properties were investigated with a thermal activity monitor (TAM) instrument, by Cementa Research AB, Sweden. Duplicate samples were run with a w/c-ratio that was set to 0.5 and 1.0. The analysis was conducted at T = 20°C, and the experiment was run for 24 hours.

Results

There are according to Figure 3 differences in the size distribution. At 63 µm, $C_{12}A_7$ (1400°C) = 93 wt-% passage, $C_{12}A_7$ (1380°C) = 98 wt-% passage and $C_{12}A_7$ (1350°C) = 96 wt-% passage. At 32 µm, $C_{12}A_7$ (1400°C) = 81 wt-% passage, $C_{12}A_7$ (1380°C) = 87 wt-% passage and $C_{12}A_7$ (1350°C) = 79 wt-% passage. At 5 µm, $C_{12}A_7$ (1400°C) and $C_{12}A_7$ (1380°C) are equal with both having a 38-wt-% passage. Between 4.5 µm and until 0.7 µm $C_{12}A_7$ (1400°C) is finer in size. In addition to the distributions given in Figure 3, the BET-surface was determined to $C_{12}A_7$ (1400°C) = 1.32 m^2/g, $C_{12}A_7$ (1380°C) = 4.64 m^2/g, and $C_{12}A_7$ (1350°C) = 3.47 m^2/g.

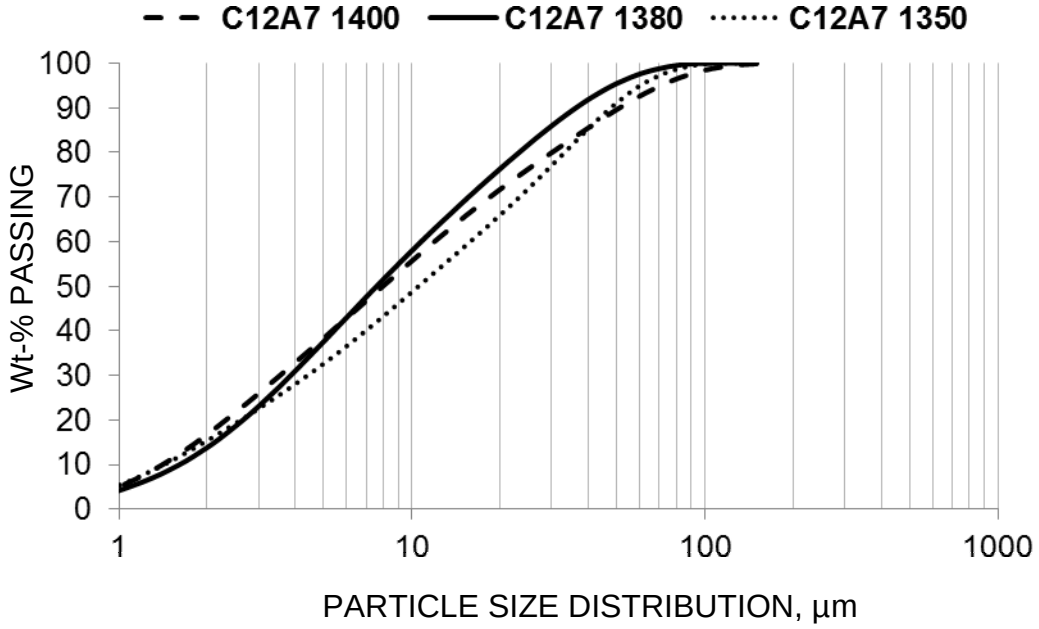

Figure 3 Particle size distributions of mayenite samples

In Figures 4a-d, the heat of hydration is given for two w/c-ratios, i.e. w/c = 0.5 and w/c = 1.0. The first very exothermic peak in Figure 4a refers to the dissolution and ions going into solution. There may also exist formation of semi-crystalline hydrates of C_2AH_8 at this stage, which has been reported for calcium aluminate cements [12]. At a w/c = 0.5 it can be seen that $C_{12}A_7$ (1350°C) levels off earlier than $C_{12}A_7$ (1400°C) and $C_{12}A_7$ (1380°C), but heat evolution remains for a longer period of time noticed as a steady drop, whereas sample $C_{12}A_7$ (1400°C) has a clear second peak after approximately 5 hours which could not be observed for $C_{12}A_7$ (1380°C) which continuously levels off after the first initial peak. In Figure 4b, the same result is presented as accumulated heat in J/g. Most heat evolved is overall clearly obtained for $C_{12}A_7$ (1400°C). That result was not expected considering the particle size distribution and the BET-surface.

Similar conclusions can be made for results given in Figures 4c-d. A difference being that the second peak of $C_{12}A_7$ (1400°C) is obtained earlier than for w/c = 0.5. The steady drop of $C_{12}A_7$ (1350°C) discussed in Figure 4a, is now seen as a major second peak in Figure 4c (w/c = 1.0). $C_{12}A_7$ (1380°C) looks very similar, even with an increased water content, but there does exist a declining plateau in Figure 4c that could not be designated at a w/c = 0.5. Figure 4d, show that more mayenite is dissolved with an increased water content as could be expected, but also that $C_{12}A_7$ (1400°C) is clearly more reactive than $C_{12}A_7$ (1380°C) and $C_{12}A_7$ (1350°C) despite the difference seen in measured BET surface.

The results seen in Figures 4a-d suggest that the formation temperature of mayenite at 1400°C is preferable in terms of reactivity. It could, however, be expected that a lower temperature provides for a more rough surface and, thereby, a higher reactivity, but a potentially higher fraction of cavities and unevennesses at the surface could not, however, explain the differences observed based on the given results. At this stage of the evaluation, the difference in reactivity is assumed to be due to a higher degree of crystallinity at 1400°C than at 1380°C and 1350°C. The influence of crystallinity on the reactivity of mayenite has been reported in a similar study [22].

The importance of considering the conditions of formation, like burning temperature, cooling rate, presence of impurities etc. has also been a subject concerning the reactivity of C_2S [16], which in terms of impurities was realized in for instance the previously discussed data dealing with the formation of bredigite. The substitution of Ca by Mg in the formation of bredigite ($Ca_{1.7}Mg_{0.3}SiO_4$), which may form either from α'-C_2S or merwinite (C_3MS_2) [23], clearly retarded the hydration properties of Mix A in comparison to those experienced of Mix B [18-19]. The slow reactivity of bredigite was also pointed out in a study by Moseley et al. [23]. Conditions of formation also seem to be important for the ferrite phase. This phase is reported to be more reactive in SAB cements than in OPC, and a suggested explanation for it, is that the formation occurs at a lower firing temperature [16]. The formation conditions have thus an important role, which also should be considered for slags that are to be used as cement replacement.

Future work is therefore suggested to involve hydration properties of pure slag minerals as function of particle size and temperature as well as the influence of formation conditions. The characterisation would also need to include microscopy and SEM-analyses for the comparison of surface roughness relating to parameters such as different firing temperatures as was carried out for mayenite. The role of impurities can be expected to be significant when using steelmaking slags in cement applications.

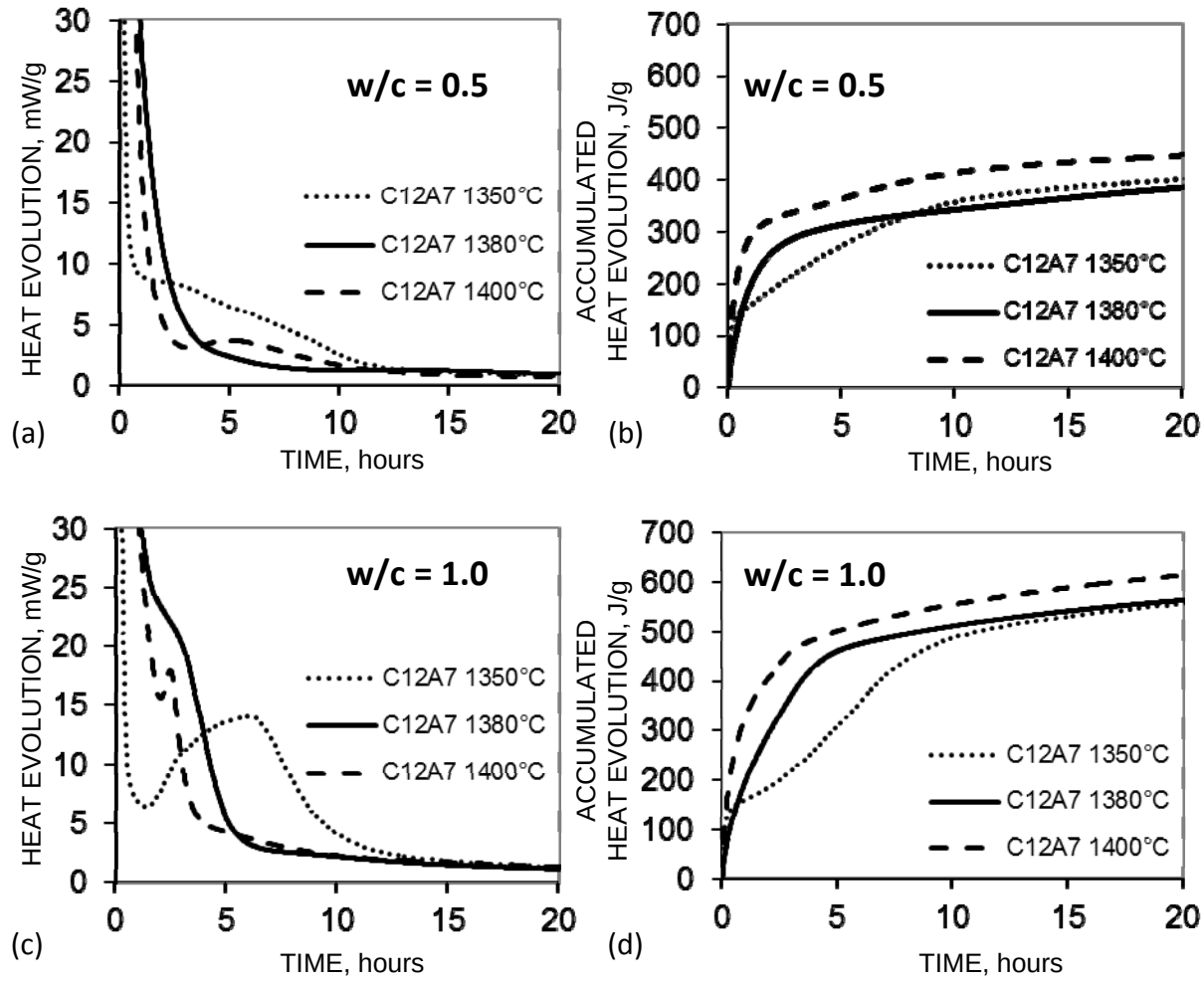

Figure 4a-d Heat evolution of mayenite fractions at w/c = 0.5 and w/c = 1.0

The Use of Steelmaking Slags as Liner Layer in a Landfill Top Cover

The hydraulic properties of steelmaking slags can be beneficially used in low permeable barrier layers such as the liner layer in a landfill top cover. A final landfill cover construction is a system of layers that all contribute to achieve the desired function. The legal requirement in Sweden is directed towards the maximum amount of leachate generated: < 5 and < 50 l $(m^2 \cdot a)^{-1}$ for landfill class 1 and 2, respectively [24]. To meet these demands, a layer of low permeability is needed to reduce leachate generation and gaseous emissions. Using steel slags can be a sustainable option as one recycles industrial by-products and thereby reduces the use of virgin materials, reduces transports and, in some cases, also avoids landfilling advantageous construction materials.

Combinations of electric-arc furnace (EAF) slag and ladle furnace slag from high-alloyed steelmaking were tested as liner material in the cover of a municipal waste landfill in Hagfors, Sweden. The slag mixtures were developed during several pre-studies [25-26]. The lab tests included chemical and mineralogical material characterization (elemental analysis; leaching tests, X-ray diffraction and IR-techniques), grain size distribution, curing properties, compaction properties, hydraulic conductivity and compressive strength. For the assessment of the future development of both function and emissions, the long-term behaviour was investigated using a designed ageing experiment [27].

Three test areas were constructed on the landfill. The used slags were crushed, sieved and mixed according to the developed recipes, and mixed with water (9-11% of the dry weight). A mixture of 50% EAF slag and 50% ladle furnace slag was tested as liner material in the first test area. Area 2 and 3 were built using less ladle furnace slag and coarser fractions of EAF slag. Used amount of slag then being more in accordance with the produced amount of slag. Laboratory tests had given satisfactory results also for these recipes.

The liner was installed and compacted in three layers. Laboratory tests had shown that both the hydraulic conductivity and the compaction properties of the liner material were strongly affected by the time between water addition and compaction. Hence, the material was compacted as soon as dispersed on the construction area. Directly after the construction the liner was covered with drainage, protection and vegetation layer.

The construction of the steel slag liner posed no problems, even though some additional work regarding the up-scaling was necessary. The crushing, sieving, mixing of steel slags, water addition as well as the construction technique was improved during the construction of the second test area. The stability of the whole cover construction being up to 3 m high and constructed at a slope (inclination about 1:8) was good. Even though, relatively large amounts of rainfall occurred in some years, no erosion or other instabilities were observed.

The test areas were monitored for 3-6 years until now with focus on the permeability (amount of water that percolates through the liner) and the leaching properties (quality of the water that percolated through the liner). The amount of leachate collected below the liner corresponded to 41, 77 and 75 $l/m^2 \cdot$year for area 1, 2 and 3, respectively, with a decreasing trend for area 2 and 3. In comparison to the legal limit of 50 $l/m^2 \cdot$year, so far, only area 1 with a liner consisting of 50% EAF slag and 50% ladle furnace slag meets the requirement. However, not only the liner is responsible for the infiltration of water into the landfill, but all layers, as well as the design of the area (slope and drain system) will affect the leachate generation. As the soils used for protection layers in area 2 and 3 were highly permeable in comparison to the material used in area 1, the amount of rainwater that could be retained in the protection layer for later evaporation was less in area 2 and 3 compared to area 1. Hence, the hydraulic load on the liner surface was higher in area 2 and 3, which is a contributing factor to the higher amounts of leachate.

DISCUSSION

The world faces the challenge of reducing CO_2 emissions as well as the need to conserve natural resources. This is an important reason to why it is needed to start considering alternatives when it comes to recycling possibilities of by-products like steelmaking slags. Steelmaking slags are challenging materials to work with due to the significant variety of oxides, but the present paper and others have shown examples of application where these materials could be useful. Use of steelmaking slags is not necessarily a question of optimisation depending on the considered application. Examples shown in this paper tell us that slags have the potential to be used both as part of a raw material for cement production, e.g. SAB cement or as a binder in cover liner or binder supplement without any specific refining. The potential and extent of its use can of course be increased if steel producers reconsider type of slag formers as well as the distribution of slag formers without necessarily affecting the steel production itself. An improved slag composition is therefore likely to provide for a better flexibility, i.e. a wider range of application. A key factor, however, is that

a slag which is destined to become a cement product also must be treated accordingly, i.e. the slag handling methodology seen today needs to be improved considering watering and weathering of the slag at the slag yard, [20-21] otherwise there is little point in reconsidering the "slag production".

The fact that silicate-based slags are rich in for instance C_2S tells us that we need to find areas where such a composition could be of interest and optimise the slag thereafter. Slags from the AOD, EAF and BOF converter are, therefore, suggested to have C_2S as a main compositional target phase, yellow area in Figure 5 [29]. Stabilisation of dicalcium silicate to β-C_2S can be accomplished in case the slag, for instance, is rapidly cooled with water [18, 28] whereas any C_3S (green area Figure 5 [29]) that is formed in parallel to β-C_2S positively affects the rate of hydration in terms of activation. A slag that is rich in β-C_2S reacts very slowly, but the benefits are, that it can be used either as binder supplement internally at the steel work or as raw material for cement production which contributes well to the flexibility for the steel producer in terms of having several options available. There is however, a need for activation as far as the material is considered to be used as binder supplement or substitute due to slow reactivity in the short-term. An increase in the rate of hydration can be obtained with dopants or admixtures (high-belite blended cement). Dopants, however, are considered more costly and complicated from a practical point of view and, therefore, the addition of an admixture like OPC or perhaps ladle furnace slag seems like a more attractive alternative.

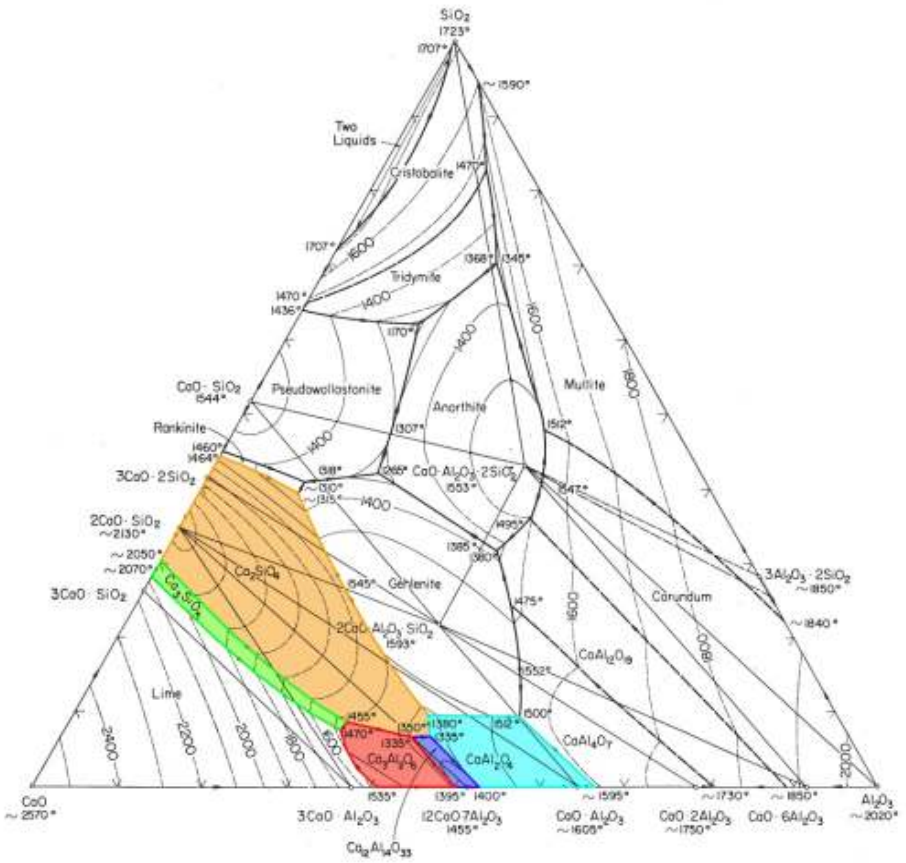

Figure 5 Phase assemblage $CaO-Al_2O_3-SiO_2$ with highlighted phase areas of advantageous minerals in the solidified steel slag [29]. Reprinted with permission of The American Ceramic Society, www.ceramics.org. All rights reserved

Ladle furnace slag can also much like the other mentioned silicate-based slag compositions be optimised towards a belite cement-type of composition, but the high content of alumina that also is characteristic for these slags suggests that LFS also could be considered optimised on the content of calcium aluminates, e.g. $C_{12}A_7$ (lilac in Figure 5 [29]) and C_3A (red area in Figure 5 [29]). A high early strength that follows with the formation of calcium aluminate hydrates can be very useful from a binder point of view in metallurgical briquettes which further could lead to a minimisation of the ordinary Portland cement that is presently used, and subsequently, a decrease in LFS sent to landfill.

The target area of dicalcium silicate in silicate-based slag compositions and/or calcium aluminates in ladle furnace slag also includes a minimisation of MgO. It has for instance been addressed [20-21] that the content of MgO which may come from either the refractory of the converter or slag formers added during steel production enables formation of solid solutions like pleochroite/Q-phase, akermanite as well as bredigite which adversely affect the hydration properties of the slag and, therefore, needs to be avoided. Another mineral that is commonly seen in ladle furnace slags is gehlenite. Gehlenite, C_2AS, is also known to be weakly or non-hydraulic [11], and therefore also needs to be avoided in the solidified slag.

The understanding of individual minerals that are present is a very important parameter to consider and the reason to why thermodynamic calculations on the solidification of steelmaking slags in combination with additional investigations based on pure slag minerals warrants more attention than seen so far. The solubility of pure slag minerals can further help explaining the overall leaching behaviour that in many ways are unclear due to the complexity that is created by simultaneous interaction of several minerals which cannot be distinguished in those slags that have been tested. Information on the solubility of pure slag minerals can therefore help us to a better understanding of the overall mechanism experienced in the actual slags which is needed in the aspect of appropriate applications.

In summary, it can be concluded that there are possible applications for steelmaking slags and that their specific properties refer to the hydration behaviour of each mineral that is present. The possibility of keeping several options available (binder substitute and raw material for cement) means that the flexibility can be maintained from both a steel and slag production point of view. An increase in the utilisation of by-products does not solve the overall challenge in reducing CO_2 emissions and the exploitation of natural resources, but it could contribute in a positive way.

CONCLUSIONS

Steelmaking slags can be used in cement applications and barrier constructions in a greater extent than seen so far considering the given examples in this paper. The final slag composition is dependent on the slag formers used and can be controlled thereafter. The cooling rate on solidification is another way of controlling the final mineralogy, as well as a minimisation of free MgO in order to avoid formation of weakly hydraulic phases such as pleochroite/Q-phase and akermanite. For this reason, the slag composition is suggested to be directed towards a belite-cement type of composition as far as possible from a metallurgical point of view since a high belite content is believed to provide for a better flexibility for the steel producer.

Ladle furnace slag should also be considered optimised on the content of calcium aluminates e.g. mayenite, as the formation of calcium aluminate hydrates contributes to a high early strength that can be used with favour in an application like metallurgical briquettes. The use of steelmaking slag in the construction of a landfill cover liner has been tested at a municipal landfill in Sweden. A compacted mixture of 50% EAF slag and 50% ladle furnace slag was able to meet the Swedish limit for leachate generation of 50 litres per square meter and year for non-hazardous waste landfills.

ACKNOWLEDGEMENTS

The authors would like to thank SSAB Merox, SSAB EMEA, Uddeholm AB, the Swedish Governmental Agency for Innovation Systems (VINNOVA), Hagfors municipality, Jernkontoret - The Swedish Steel Producers' Association (TO55 - Steel production residues) as well as the Centre of Advanced Mining and Metallurgy (CAMM) at Luleå University of Technology for financial support and commitment during various parts of this work.

REFERENCES

1. MOTZ H AND GEISELER J, *Products of steel slags an opportunity to save natural resources*, Waste Management, Vol. 21, 2001, pp. 285-293.

2. MONTGOMERY D G AND WANG G, *Preliminary laboratory study of steel slag for blended cement manufacture*, Materials Forum, Vol. 15, 1999, pp. 374-382.

3. MONSHI A AND ASGARANI M K, *Producing Portland cement from iron and steel slags and limestone*, Cement and Concrete Research, Vol. 29, 1999, pp. 1373-1377.

4. MUHMOOD L, VITTA S AND VENKATESWARAN D, *Cementitious and pozzolanic behavior of electric arc furnace steel slags*, Cement and Concrete Research, Vol. 39, 2009, pp. 102-109.

5. LI D, FU X, WU X AND TANG M, *Durability study of steel slag cement*, Cement and Concrete Research, Vol. 27, 1997, pp. 983-987.

6. DUDA A, *Hydraulic Reactions of LD Steelwork Slags*, Cement and Concrete Research, Vol. 19, 1989, pp. 793-801.

7. MURPHY J N, MEADCROFT T R AND BARR P V, *Enhancement of the cementitious properties of steelmaking slag*, Canadian Metallurgical Quarterly, Vol. 36, 1997, pp. 315-331.

8. IONESCU D, MEADCROFT T R AND BARR P V, *Hydration Potential of High Iron Level Glasses: Criteria for the Recycling of Steel Slag as a Portland Cement Additive*, ICSTI/Ironmaking conference proceedings, 1998, pp. 1245-1254.

9. ODLER I, Cements containing calcium sulfoaluminate. *Special Inorganic Cements*, E&FN Spon, London & New York, 2000, 1st ed. Chapter 4, pp. 69-87.

10. BENSTED J AND BARNES P (eds.), *Structure and Performance of Cements.* E & FN Spon, London & New York, 2002, 2nd ed, Chapter 1, pp. 1-24.

11. ODLER I, Calcium aluminate cement. *Special Inorganic Cements*, E&FN Spon, London & New York, 2000, 1st ed. Chapter 10, pp. 173-201.

12. TAYLOR H F W, Calcium aluminate, expansive and other cements. In *Cement Chemistry*, 2nd ed. Thomas Telford Publishing, London, 1997, Chapter 10, pp. 295-321.

13. BENSTED J AND BARNES P (eds.), *Structure and Performance of Cements.* E & FN Spon, London & New York, 2002, 2nd ed, Chapter 4, pp. 114-138.

14. GLASSER F P AND ZHANG L, *High-performance cement matrices based on calcium sulphoaluminate-belite compositions*, Cement and Concrete Research, Vol. 31, 2001, pp. 1881-1886.

15. ZHANG L, SU M AND WANG Y, *Development of the use of sulfo- and ferroaluminate cements in China*, Advances in Cement Research, Vol. 11, 1999, pp. 15-21.

16. SHARP J H, LAWRENCE C D AND YANG R, *Calcium sulphoaluminate cements – low-energy cements, special cements or what?*, Advances in Cement Research, Vol. 11, 1999, pp. 3-13.

17. QUILLIN K, *Performance of belite-sulphoaluminate cements*, Cement and Concrete Research, Vol. 31, 2001, pp. 1341-1349.

18. ADOLFSSON D, MENAD N, VIGGH E AND BJÖRKMAN B, *Steelmaking slags as raw material for sulphoaluminate belite cement*, Advances in Cement Research, Vol. 19, 2007, pp. 147-156.

19. ADOLFSSON D, MENAD N, VIGGH E AND BJÖRKMAN B, *Hydraulic properties of sulphoaluminate belite cement based on steelmaking slags*, Advances in Cement Research, Vol. 19, 2007, pp. 133-138.

20. ADOLFSSON D, ROBINSON R, ENGSTRÖM F AND BJÖRKMAN B, *Influence of mineralogy on the hydraulic properties of ladle slag*, Cement and Concrete Research, Vol. 41, 2011, pp. 865-871.

21. ADOLFSSON D, ENGSTRÖM F, ROBINSON R AND BJÖRKMAN B, *Cementitious phases in ladle slag*, Steel research international, Vol. 82, 2011, pp. 398-403.

22. YOU K-S, AHN J-W, LEE K-H AND GOTO S, *Effects of crystallinity and silica content on the hydration kinetics of* $12CaO{\cdot}7\,Al_2O_3$, Cement and Concrete Composites, Vol. 28, 2006, pp. 119-123.

23. MOSELEY D AND GLASSER F P, *Properties and composition of bredigite-structured phases*, Journal of material science, Vol. 17, 1982, pp. 2736-2740.

24. FS (2001) Ordinance on the landfilling of waste (Förordning (2001:512) om deponering av avfall), Swedish statute book (SFS, Svensk författningssamling) No: 2001:512 (in Swedish), Miljödepartementet (Ministry of the Environment), Stockholm, Sweden http://www.notisum.se/ rnp/sls/lag/20010512.htm

25. ANDREAS L, HERRMANN I, LIDSTROM-LARSSON M AND LAGERKVIST A, *Physical properties of steel slag to be reused in a landfill cover*, Tenth International Waste Management and Landfill Symposium, S. Margherita di Pula, Cagliari, Italy; 3-7 October, 2005.

26. HERRMANN I, ANDREAS L, DIENER S AND LIND L, *Steel slag used in landfill cover liners: laboratory and field tests*, Waste Management & Research, Vol. 28, 2010, pp. 1114-1121.

27. DIENER S, ANDREAS L, HERRMANN I, ECKE H AND LAGERKVIST A, *Accelerated carbonation of steel slags in a landfill cover construction*, Waste Management, Vol. 30, 2010, pp. 132-139.

28. ENGSTRÖM F, ADOLFSSON D, YANG Q, SAMUELSSON C AND BJÖRKMAN B, *Crystallization of some Steelmaking Slags*, Steel research international, Vol. 81, 2010, pp. 362-371.

29. OSBORN E F AND MUAN A, revised and redrawn, *Phase Equilibrium Diagrams of Oxide Systems*, American Ceramic Society and the Edward Orton, Jr., Ceramic Foundation, 1960, 219 p.

Use of Double Punching Test (Barcelona test) for Quality Control of Fibre Reinforced Concretes

S Carmona[1], A Aguado[2], C Molins[2]
1 – Universidad Tecnica Federico Santa Maria, Chile
2 – Universitat Politècnica de Catalunya, Spain

Traditionally, flexural testing is used to characterize the strength and post – peak behavior of fiber – reinforced concretes (FRC). Nevertheless, these tests results exhibit a high dispersion, and therefore invalidate their use as tests for the systematic control of FRCs in works. Also, they have the disadvantage of being complex tests, which require heavy specimens and highly qualified staff. With the aim to solve these problems, an indirect tensile test based on double punching test set up, called the Barcelona test, has been proposed to control tensile behavior of FRC. This test requires smaller specimens, with a high specific surface of fracture, allowing obtain values representative of strength and toughness of materials, with considerably less dispersion than other experimental methodologies, and was recently standardized in Spain. This paper presents the results of an experimental program, which validate the use of Barcelona test as a suitable methodology to systematic characterization FRC in works.

S Carmona is currently Professor of Concrete Technology at the Universidad Tecnica Federico Santa Maria, Valparaiso, Chile. He has led several researches on concrete, and also submitted several papers about fibre reinfoced concrete, high performance concrete, and sulphur concrete.

A Aguado is Full Professor of Concrete Technology, and Concrete Structures of the Department of Construction Engineering at Universitat Politècnica de Catalunya, Barcelona, Spain. He carries out many researches on high performance concrete, fibre reinforced concretes, and structures for dams and tunnels.

C Molins is Associated Professor of the Department of Construction Engineering at Universitat Politècnica de Catalunya, Barcelona, Spain. His research interest are design and analysis of the behavior of reinforced and prestressed concrete, design and analysis of precast elements for tunnels.

Keywords: Barcelona test, Fibre reinforced concrete, Toughness

INTRODUCTION

The advantages of reinforcing concrete with fibres are widely known and have been deeply studied [1, 2], and widely applied in the fields of pavements and sprayed concrete in slopes or tunnel linings. However, fibre reinforced concrete (FRC) is currently being used in other applications, especially in precast members [3, 4] and segmental linings in tunnel projects [5-7].

Along with the development of these applications, many European standards have incorporated fibres as a structural reinforcing material, for example, Germany [8], Italy [9] and Spain [10]; and more recently, FRC has also been included in the latest version of the Model Code of CEB – FIP [11].

In FRC, toughness and ability to absorb energy has been recognized as one of the most important benefits of incorporating fibres, improving the performance before the fracture, impact and fatigue [12]. Ideally, FRCs toughness should be quantified through direct tensile test. However, this test is very difficult to perform, then the use of bending test is recommended to determine FRC toughness, which, besides being simple, represents the load conditions of many FRC applications.

Currently, there are many standards to evaluate and quantify the effect of fibres in concrete, such as ASTM C 1018 [13], ASTM C – 1609 [14], NBN B 15 – 238 [15], JSCE SF – 4 [16], UNE 83 – 510 [17], UNI 11 039 [18], among others. However, as shown in Table 1, each of these standards or recommendations has a particular experimental procedures which include different specimen shapes and sizes, testing layouts and do not define a single common parameter to characterize FRC toughness.

One of the most extended tests, widely accepted is the three point bending test on notched beams, proposed by RILEM TC – 162 [19], currently European standard EN – 14 651 [20], which is also the selected test in the Model Code of CEB – FIP [11]. This method is simple and it is controlled by crack mouths opening displacement (CMOD), which ensures stable crack propagation, even for plain concrete. The curve load – CMOD or load – deflection obtained through this test can be used to calculate the stress – strain or stress – crack width relationships and, thus, evaluating the fibres effect on concrete.

However, these tests are aimed to characterize FRC properties and are difficult to apply for the systematic quality control of the FRC in works. In addition, this kind of tests need relatively heavy specimens, their experimental procedures are relatively complex and their results show significant scatter due to be directly related with the specific number of fibres on cracked section.

Table 1 Main tests used to characterize properties of FRC

MAIN TESTS USED TO CHARACTERIZE PROPERTIES OF FRC			
Standard	Test Set up	Specimen dimension, mm×mm×mm	Main parameters to characterize FRC
ASTM C – 1018	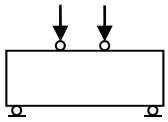	100 × 100 × 350	First crack strength Toughness index
ASTM C – 1609			Residual strength Toughness
NBN 15 – 238		150 × 150 × 600	Energy absorbed Equivalent flexural strength
UNE 83 – 510 – 89		d/b < 1.5; l = 3d	Energy adsorbed
JCI SF4 l_f <40 mm		d = b = 100 mm l = 3d +80 mm	Energy absorbed Equivalent flexural strength
JCI SF4 l_f >40 mm		d = b = 150 mm l = 3d +80 mm	
RILEM 162 – TDF	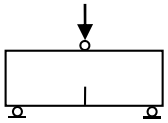	150 × 150 × 550	Flexural strength Residual load
EN – 14651			

In this way, double punching test or Barcelona test proposed by Molins *et al*. [21], has proved to be very suitable for the control of FRC at works [21-23] and has been standardized in Spain by AENOR as UNE 83 515 [24]. This standard establishes the test procedure and toughness and residual strength calculation, using the diagram load (*P*) – Total Circumferential Opening Displacement (TCOD) of the specimen.

The BCN test has several advantages over other standard procedures to characterize the toughness of FRC, among these, the use of relatively small specimens with high fracture surface, which can be moulded (cylinders of 150 mm × 150 mm), cut from standard cylinders of 150 mm × 300 mm or from extracted cores of hardened concrete, and can be tested using conventional testing machines, which are normally available in laboratories of quality control of materials [25].

This paper shows the results of an experimental program carried out to measure toughness of three steel fibre reinforced concretes by means of Barcelona test.

BARCELEONA TEST

The BCN test is an indirect tensile test, in which a cylindrical specimen of FRC is subject to compression load by means of two cylindrical steel punches placed at the centre of upper and lower faces, respectively, as shown in Figure 1. The cylinder has a diameter (2b) equal to its height (2h), this is a slenderness of 2b/2h = 1. The punches have a diameter (2a) equal to 0.25 of the specimen diameter. The punch thickness has to be >30 mm to ensure a uniform transmission of load to the cylinder. In order to obtain the P - TCOD diagram during test, the applied load (P) and the TCOD at half height of specimen were recorded continuously.

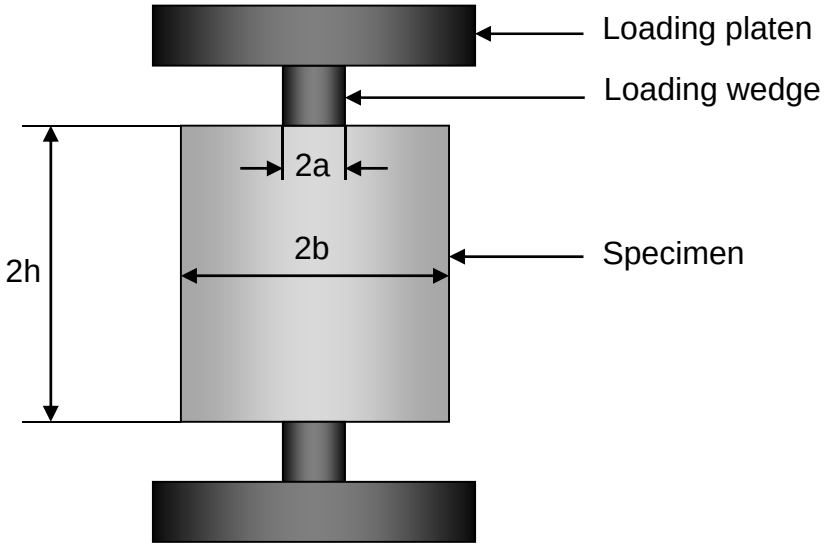

Figure 1 Geometry of the layout of Barcelona test

During the test, the applied load produces a conical volume under triaxial compression just beneath the punches, increasing the cylinder diameter and producing tensile stresses perpendicular to the radial planes of the specimen. Due to these axisymmetrical tensile stresses, when they exceed the tensile strength of concrete, several cracks perpendicular to the tensile stresses propagate throughout the specimen. Then, the compression cone penetrates into the cylinder, increasing the specimen radius and producing two or more cracks. Then, in the final state of the specimen can be seen two aligned cracks or three cracks arranged approximately 120° apart, or four cracks perpendicular.

When specimen cracks, the circumferential dilatation corresponds to the total cracks opening displacement (TCOD) and toughness of FRC can be calculated as:

$$E(TCOD) = \int_0^{TCOD} P(TCOD)\ d(TCOD) \quad (1)$$

Where E (TCOD) is the energy to a certain TCOD value, which is directly related to the toughness determined by means of flexural test following the Belgian standard NBN B 15 – 238 [21].

EXPERIMENTAL PROGRAM

To validate the BCN test, several experimental programs have been developed at the Universitat Politècnica de Catalunya and at the Universidad Técnica Federico Santa María de Valparaíso (Chile). The results of a particular experimental program developed on three FRC with different fibre contents is presented.

Studied Materials

All the concretes studied were designed to be poured by pumping and their mix proportions by weight are: cement : sand : gravel as 1:2.89:0.88. To increase the workability of the FRCs, a admixture (SikaViscocrete 5940®) was added at a ratio of 4.5% with respect to cement weight to obtain the expected workability. The complete mix proportions are shown in Table 2. Fibres incorporated in the concrete were collated hooked ends steel fibres from Arcelor Mittal He 55/35, with a length of 35 mm, a diameter of 0.55 mm; a tensile strength of 1200 MPa and maximum elongation of 5%.

Table 2 Mixes details of tested FRCs

MATERIALS	MIX COMPOSITIONS OF TESTED FRCS, kg/ m^3		
	SFRC – 25	SFRC – 50	SFRC – 75
Cement I 52.5 R	450	450	450
Gravel 5/10	395	395	395
Sand 0/5	1300	1300	1300
Superfluidifying admixture	4.5	4.5	4.5
Water	175	195	205
Fibre	25	50	75

The concretes were prepared at the laboratory of PROMSA Co. in Barcelona, using a conventional paddle mixer of 250 litres capacity. For the BCN tests, the specimens of SFRC – 25 and SFRC – 50 concretes were cast in cylindrical moulds with a diameter of 150 mm and a height of 150 mm; and for SFRC - 75, standard cylinders with a diameter of 150 mm and a height of 300 mm were cast and cut in two halves before testing. In addition, six standard cylindrical specimens were cast for each mix to determine the compressive strength. All specimens were unmoulded after 24 hours and kept in a fog room.

Table 3 shows the results obtained with different properties of the concretes, both in fresh and in hardened states. These results show that in the case of the concretes with a higher content of fibres, it was necessary to increase the water/cement ratio in order to reach an adequate workability. This fact, in addition with the high porosity due to the high fibre content, produced a decrease in compressive strength.

Table 3 Studied FRCs properties

PROPERTY	SFRC – 25	SFRC – 50	SFRC – 75
Water/cement ratio	0.44	0.43	0.46
Consistency, cm	11	12	17
Occluded air, %	4.5	4.2	5.2
Density fresh, kg/m^3	2,328	2,325	2,310
Compressive strength, f_c, MPa	50.9	51.2	43.9
(CV, %)	(2.97)	(3.02)	(0.95)
Volumetric substitution, %	0.32	0.64	0.95

Tests and results

A total of 30 BCN tests were carried out using a conventional hydraulic Ibertest MEH 3000 W system of 3 MN capacity. The stroke displacement was used as control parameter and was increased at a constant rate of 0.5 mm/min. The circumferential dilatation was measured by means of an MTS extensometer, model 632.12F– 20, fixed to the ends of a chain and placed at half the height of the specimen, as can be seen in Figure 2. The test data were recorded by a Hewlett Packard, model 34970A, data acquisition system at a frequency of two data per second.

Figure 2 BCN test set up used

Figure 6 shows a sample of the final state of the specimens tested. It can be observed that they present from 2 to 4 main radial cracks on loading faces, which usually extend along the whole height of the cylinder, frequently accompanied by secondary cracks which do not open completely. The number of cracks which appeared at half the height of the specimen, over the perimeter where the *TCOD* is measured, was 4 in 67% of the specimens and 3 in the other 33%. Figure 4 shows *P - TCOD* diagrams obtained in the BCN tests. In these diagrams the *TCOD* is close to zero until the maximum load is reached and increases when cracking of specimen occurs. In the post- cracking regime, the material exhibits a softening, governed by the fibre content.

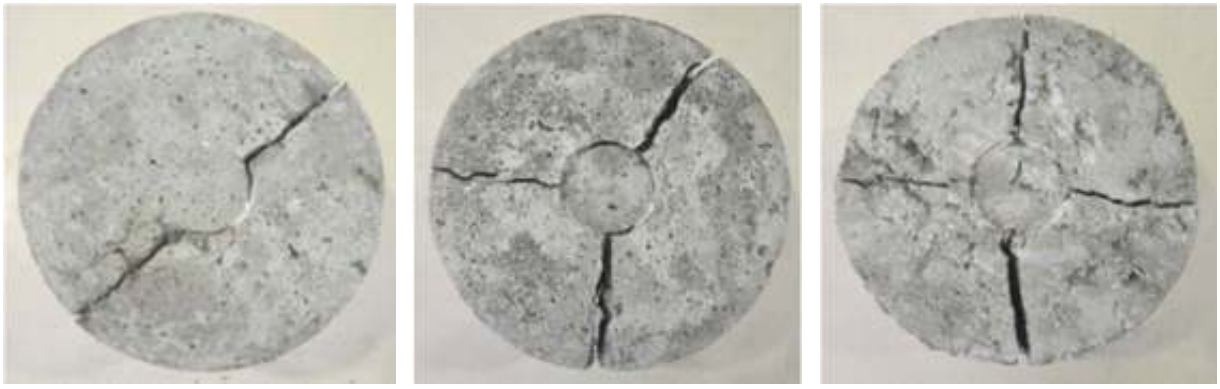

Figure 3 Final specimens state with typical cracks patterns

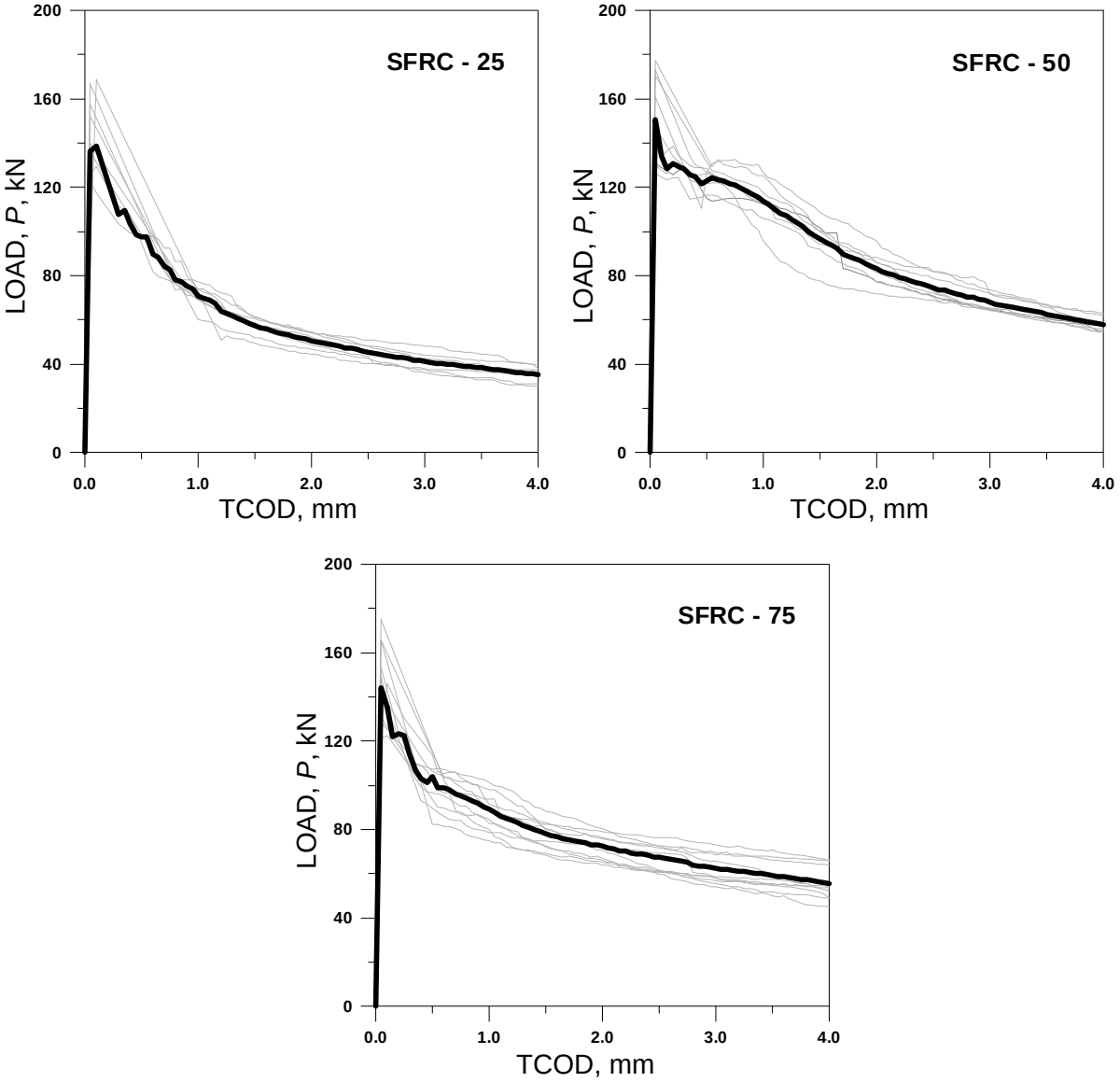

Figure 4 The *P* - *TCOD* curves obtained in BCN tests with studied FRCs

Toughness of FRCs by means of standard UNE 83.515

The energy (*E*) dissipated during the load process was calculated by following the procedure for BCN test given by the standard UNE 83.515 (2010), using post-peak branch of *P – TCOD* curve obtained in each test using equation (1). The average *P – TCOD* and *E – TCOD* curves of tested concretes are shown in Figure 5, and mean values of dissipated energy along with its coefficient of variation (CV) can be found in Table 4.

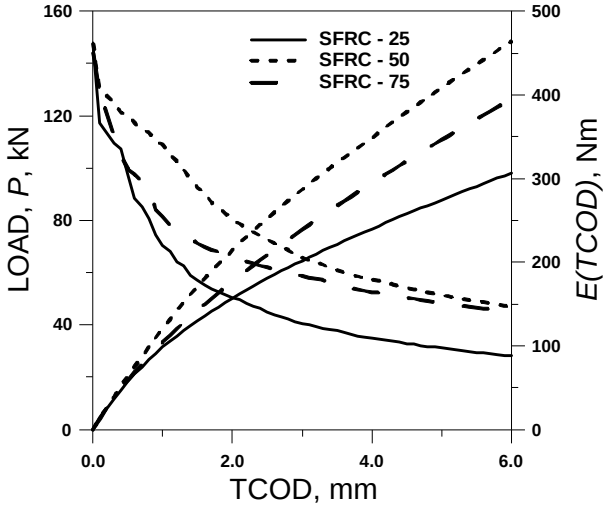

Figure 5 Post cracking response of FRC and energy determined by BCN test

Table 4 Energy of FRCs, *E*(*TCOD*), N × m

ENERGY OF FRCS, *E*(*TCOD*), N × m					
Concrete	Fibre content, kg/m³	*TCOD*, mm			
		2.0	2.5	4.0	6.0
SFRC - 25	25	158.90 (3.43)	184.16 (3.62)	241.81 (4.78)	306.37 (4.92)
SFRC - 50	50	216.08 (7.89)	254.60 (6.96)	350.63 (6.23)	463.88 (6.15)
SFRC - 75	75	174.49 (14.22)	205.61 (13.61)	292.98 (14.35)	394.81 (14.65)

CV, Coefficient of variation, %

The results show that, by means of the BCN test, it is possible to evaluate the effect on energy due to the increase of fibres content in the concrete. The decrease in the energy observed in SFRC – 75 is related with higher porosity of this kind of concrete, which is also reflected in a lower compressive strength, as can be seen in Table 5.

With respect to the scatter of the results, evaluated by means of coefficient of variation, it can be observed that, with the only exception of SFRC – 75 for the reasons previously discussed, it is lower than 10% and in no case does exceed 15%.

CONCLUSIONS

By means of the BCN test, the toughness of different FRCs has been evaluated, obtaining values for the coefficient of variation always lower than 15%. As the amount of fibres increases, so does the dispersion of the results. This increase could be due to the higher heterogeneity produced by the high fibre content in the mass of concrete, and the consequent reduction of workability.

ACKNOWLEDGEMENTS

The research works introduced in this paper were possible thanks to the research projects "Theoretical bases and experimental development of a Double-Punching test for the control of steel fibre reinforced concrete (C59/2006)", funded by the Ministry of Public Works, and HATCONS, funded by FCCSA. The authors wish to thank the PROMSA company from Barcelona for their collaboration (they produced the concretes studied), and are especially grateful to Domenic Masó. The authors also wish to acknowledge the collaboration of R. Sainz, an undergraduate student from the UTFSM of Chile. S. Carmona's stay in Barcelona during the development of this research was funded by the Fundación Carolina from Spain and the Universidad Técnica Federico Santa María Technical of Valparaíso, Chile.

REFERENCES

1. ACI, Report on fibre reinforced concrete, Reported by ACI Committee 544, Farmington Hills, MI, USA, 2008, 66 p.

2. FERRARA L AND MEDA A, Relationships between fibre distribution, workability and the mechanical properties of SFRC applied to precast roof elements, Materials and Structures, Vol. 39, 2006, pp. 411-420.

3. CHIAIA B, FANTILLI A AND VALLINI P, Evaluation of minimum reinforcement ratio in FRC members and application to tunnel linings, Materials and Structures, Vol. 40, 2007, pp. 593-604.

4. KASPER T, EDVARDSEN C, WITTNEBEN G AND NEUMANN D, Lining design for the district heating tunnel in Copenhagen with steel fibre reinforced concrete segments Tunnelling and Underground Space Technology, Vol. 23, 2008, pp. 574-587.

5. MORA F, AGUADO A AND MOLINS C, Distribución y orientación de fibras en dovelas aplicando el ensayo Barcelona, Hormigón, Vol. 931, 2009, pp. 28-37.

6. CHIAIA B, FANTILLI A AND VALLINI P, Combining Fibre – reinforced Concrete with Traditional Reinforcement in Tunnel Linings, Engineering Structures Vol. 3, 2009, pp. 1600-1606.

7. CARATELLI A, MEDA A, RINALDI Z AND ROMUALDI P, Structural behaviour of precast tunnel segments in fibre reinforced concrete, Tunnelling and Underground Space Technology, Vol. 26, 2011, pp. 284-291.

8. DBV, Guide to Good Practice Steel Fibre Concrete, Edited by German Society for Concrete and Construction Technology, Berlin, Germany, 2001, 77 pp.

9. CNR DT 204 Guide for the Design and Construction of Fibre – Reinforced Concrete Structures, Rome, Italy, 2006, 55 p.

10. EHE (2008), Instrucción de Hormigón Estructural, Madrid, Spain, 2008, 304 p.

11. CEB-FIP, Model Code – First Complete Draft, Vol. 1, FIB Bulletin, Vol. 55, 2010, 318 p.

12. GOPALARATNAM V AND GETTU R, On the Characterization of Flexural Toughness in Fibre Reinforced Concretes, Cement & Concrete Composites, Vol. 17, 1995, pp. 239-254.

13. ASTM INTERNATIONAL, C 1018 Standard Test Method for Flexural Toughness and First – Crack Strength of Fibre – Reinforced Concrete (Using Beam with Third – Point Loading), ASTM Annual Book of Standards, Vol. 04.02, 2002, pp. 546-553.

14. ASTM INTERNATIONAL, C 1609 Standard Test Method for Flexural Performance of Fibre – Reinforced Concrete (Using Beam with Third-Point Loading), 2010, 9 p.

15. NBN B 15 238, Test on Fibre Reinforced Concrete Bending Test on Prismatic Simples, Norme Belge, Institut Belge de Normalisation, Brussels, Belgium, 1992, 9 p.

16. JSCE, Method of Test for Flexural Strength and flexural Toughness of Fibre Reinforced concrete, JCI Standard SF - 4, Japan Society of Civil Engineers, Tokyo, Japan, 1984. pp. 45-51.

17. AENOR, UNE 83-510 Hormigones con fibras. Determinación del índice de tenacidad y resistencia a primera fisura, Madrid, Spain, 2004, 6 p.

18. UNICEMENTO, UNI 11039-1, Calcestruzzo rinforzato con fibre di acciaio - Definizioni, classificazione e designazione - Steel fibrereinforced concrete - Definitions, classification and designation, Rome, Italy, 2003, 7 p.

19. RILEM, TC 162 TDF Test and Design Methods for Steel Fibre Reinforced Concrete: Bending Test, Materials and Structures, Vol. 35, 2002, pp. 579-582.

20. CEN, EN 14651: Test method for metallic fibered concrete - Measuring the flexural tensile strength (limit of proportionality (LOP), residual), European Committee for Standardization, Brussels, Belgium, 2005, 20 p.

21. MOLINS C, AGUADO A AND SALUDES S, Double Punch Test to Control the Tensile Properties of FRC (Barcelona Test), Materials and Structures, Vol. 42, 2009, pp. 415-425.

22. MOLINS C, AGUADO A AND MARÍ A, Quality control test for SFRC to be used in precast segments, Tunnelling and Underground Space Technology, Vol. 21, 2006, pp. 423-424.

23. CARMONA S, AGUADO A, MOLINS C AND CABRERA M, Control de la tenacidad de los hormigones reforzados con fibras usando el ensayo de doble punzonamiento (ensayo Barcelona), Revista Ingeniería de Construcción, Vol. 24, 2009, pp. 119-140.

24. AENOR, UNE 83-515 Hormigones con fibras. Determinación de la resistencia a fisuración, tenacidad y resistencia residual a tracción. Método Barcelona, Madrid, Spain, 2010, 7 p.

25. CARMONA S, AGUADO A AND MOLINS C, Generalization of the Barcelona test for toughness control of FRC, Materials and Structures, accepted 2011. DOI 10.1617/s11527-011-9816-8.

Properties of Mortar Reinforced with Jute Fibres

S Menadi[1], A Benazzouk[2], T Langlet[2], O Douzane[1], M Merzoud[1], M F Habita[1]
1 – University of Badji Mokhtar, Algeria
2 – University of Picardie Jules Verne, France

Efficient utilization of natural resources is very important from the perspective of sustainability. The importance of recycling and promotion of biomass is expected to constitute a major share of the future total use of renewable energy sources in many countries. Agriculture wastes were generally used for fertiliser and fuel for energy production, but little work has been carried out to develop utilisation of these wastes in the production of building materials. Cement composite manufactured with lignocellulosic materials from different sources will have some variation in properties related to their various chemical components. The materials inhibit cement setting and reduce mechanical strengths development due to the amount of alkalis and dissolved component extracts. However, the viability of the use of lignocellulosic materials in cement depends on the appropriate chemical treatment that can be used to preventing components hindering cement harden. The main objective of this study was to investigate the potential utilisation of jute fibres as reinforcement additives in cement mortar, within the scope of providing an alternative solution to an environmental problem. The jute fibres were used as partial replacement of sand at different levels: 0% (control mortar), 0.5%, 1%, 1.5% and 2% by weight. The average length of jute fibres was less than 1 cm. The chemical compatibility of jute fibres to cement was evaluated using hydration test. The results have shown that the corresponding inhibitory effect classifies the mixture as being of ”low inhibition”. An additional experimental test program was conducted mainly to investigate the properties of fresh and hardened composite, including consistency, air-entrainment, unit weight, compressive and flexural strengths.

S Menadi, is a PhD student at the University of Badji Mokhtar, Annaba, Algeria. She is currently finalizing thesis at the « Laboratoire des Technologies Innovantes », University of Picardie, Jules Verne, Amiens, France.

Dr Benazzouk A., is a lecturer in Civil Engineering at the University of Picardie Jules Verne, Amiens. His research interests the durability and physico-mechanical behaviour of cement composite based on natural and local materials.

Dr O Douzane, is a lecturer in Civil Engineering, University of Picardie Jules Verne, Amiens. His major center of interest is thermal and mechanical behaviour of building materials.

Pr T Langlet, is a professor in Civil Engineering, University of Picardie Jules Verne, Amiens. His major center of interest is thermal and mechanical behaviour of building materials.

Pr M F Habita, Professor in civil engineering department at the University of Badji Mokhtar, Annaba Algeria. Member of civil Engineering laboratory of Annaba University. His research interests concrete behaviour and masonry structures.

Dr M Merzoud, Senior Lecturer in Civil Engineering Department at the University of Badji Mokhtar, Annaba, Algeria. Member of Civil Engineering laboratory of Annaba University. His research interests the behavior of masonry structures, the use of natural local materials in composites, structures with reinforced concrete.

Keywords: Hydration test, Inhibitory effect, Jute fibres, Mechanical properties, Reinforced cement mortar

INTRODUCTION

Wastes from different sources are causing environmental problems associated with their storage and their rising quantities. In the construction sector, the operation and recycling of agricultural and industrial wastes are increasingly considered [1-4]. The needs to conserve traditional building materials that are facing depletion have obliged engineers to look for alternative materials. However, the use of renewable raw material derived from agricultural products has been the subject of extensive research. Various types of agriculture wastes (flax, hemp, coir, jute, palm etc.), after being processed, have been used as particles and/or fibres replacement of sand and aggregates in concrete and mortars [5-7]. The application of these elements is interesting as regards the recycling of the wastes, since these are easily available and renewable low-cost raw materials, and has advantage for economy and environment. Presently these wastes are either burnt or and filled. These approaches cause various environmental problems like air pollution, emission of green house gases and occupation of useful land. The increasing charges of landfill are further aggravating the problem. Moreover, these methods of disposal are certainly wastage of a primary resource.

The composites containing renewable sources display lower density and have several potential applications such as acoustic and thermal insulation, fire resistance cladding etc. Other natural fibres have also been considered, including hemp [5], rice husks [6], and flax by-products [7]. Results have indicated that the mortar mixes containing these admixtures are already used for insulating or coating applications. Although the result from these researches on insulation properties of the materials are satisfying, brut from the point of view of the durability, the main disadvantage is their sensitivity to the water absorption and dimensional instability in service in the presence of change in relative humidity [8]. To enhance the performances of vegetable particles-mortar composite, several approaches have been studied including particles impregnation with blocking agent and water repellent agent, sealing of the matrix pores system, reduction of the matrix alkalinity, and combination of particles impregnation and matrix modification [9]. Composite manufactured with vegetable materials from different sources will have some variations in properties related to the chemical constituents and physical properties of the lignocellulosic materials. They are composed of lignin and cellulosic compounds as main chemical constituents. The lignocellulosic material to cement compatibility is a still problem to cement composite development. The materials inhibit cement setting and reduce mechanical strengths development. Thus, the bonding of lignocellulosic material with cement is limited. As described in previous works, the lignocellulosic materials to cement compatibility generally decreases as the extractives content increases [10, 11]. This chemical incompatibility can be attributed to the amount of alkalis and dissolved material extracts that inhibit the adhesiveness and hardening of the composite. These extractives are generally composed of terpenes, fatty acids, cellulose, hemicellulose, lignin, sugars available…etc. Inhibition of cement occurs when the calcium silicate hydrate nucleation sites on the originally positively charged surfaces are poisoned by the main inhibiter such as sugar-acid anions and lignin [12]. The viability of the use of lignocellulosic materials in cement paste depends on the appropriate chemical treatment of the materials. To minimize detrimental effects of cement hydration, the effects of various chemical treatments of lignocellulosic materials have been studied [13, 14]. The results have shown that it is possible to control negative effects of lignocellulosic materials-cement interaction. Enhanced of some mechanical properties of the cement composite has been reported by modifying the chemical constituents of the particles [15]. Therefore, to promote the use of cementitious building materials reinforced with vegetable fibres could be a way to achieve a more sustainable construction. This paper deals with the subject of natural fibres

reinforced cementitious materials by examining the feasibility of the composite based-jute fibres. The main objective of this study was to investigate the potential utilisation of jute fibres as reinforcement additives of cement mortar, within the scope of providing an alternative solution of steel and synthetic fibres reinforcement. The jute fibres were used as partial replacement of sand at different levels: 0% (control mortar), 0.5%, 1%, 1.5%, and 2% by weight. The inhibitory effect that corresponds to the chemical compatibility between jute fibres and cement was evaluated using hydration test. An additional experimental test program was conducted mainly to investigate the properties of fresh and hardened composite, including consistency, air-entrainment, unit weight, and compressive and flexural strengths.

MATERIALS AND EXPERIMENTAL TESTING

Jute is the cheapest vegetable fibre procured from the bast or skin of the plant's stem and the second most important after cotton, in terms of usage, global consumption, production, and availability. It is one of the most versatile natural fibres that have been used in raw materials for packaging, textiles, non-textile, construction, and agricultural sectors. It helps to make best quality industrial yarn, fabric, net, and sacks.

The fibres used in this study are derived from burlap served as bags of packing for food and agricultural products, converted into fibres with a maximum length of 10 mm, and 35 kg/m^3 in bulk density. The shape of jute fibres is shown in Figure 1.

Figure 1 Shape of jute fibres

The physical and chemical properties of vegetable fibres vary considerably with their source and storage conditions. Vegetable fibres are natural material with a cellular structure. Different proportions of cellulose, hemicellulose and lignin constitute the different layers. Cellulose is a polymer containing glucose units and hemicellulose is a polymer made of various polysaccharides. As for lignin, it is an amorphous and heterogeneous mixture of aromatic polymers and phenyl propane monomers. The properties of natural jute fibres are shown in Table 1 [16].

Table 1 Properties of natural jute fibres [16]

Length, mm	128 -1525
Diameter, mm	2-3.5
Tensile strength, N/mm^2	29-312
Elongation, %	19
Hemicellulose, %	22.7
Cellulose,%	33.4
Lignin,%	28

Constituent materials for cement composite mixes included a Type II CPJ 32.5 Portland cement according to Standard NF P 15-301 [17] requirements, natural hydraulic lime NHL5 meeting Standard EN 459 [18], and natural sand with 5 mm maximum size. Jute fibres were added as a partial replacement of sand at five levels: 0% (control mortar), 0.5%, 1%, 1.5%, and 2% by weight.

Both cement and lime were initially mixed in a planetary mixer. The total mixing water, containing 1.5% of plasticizer by weight of cement, added were adjusted for all composites in order to achieve the same workability (as measured by flow test) of control mortar mixture proportions of 0.7:0.3:3:0.5 by weight of cement, hydraulic lime, sand, and water respectively [19]. To avoid balling of fibres, the vegetable materials were pre-mixed with sand and then were uniformly dispersed with slow increment throughout the cement and lime binder. The cement composite materials were allowed to mix for three minutes. All the specimens were well compacted on a vibrating table and moist-cured for 28 days at 20±2°C and 98% relative humidity. The material was first characterized in its fresh state. For measurements of the hardened properties, prism samples of 40 mm × 40 mm × 160 mm in size were prepared. Five mix composites based on cement, lime, sand and jute fibres were designated. For all mixes, the binder is composed by 70% of cement and 30% of hydraulic lime. The ratio of (sand+fibres)/binder is 3. The composite mixes are shown in Table 2.

Table 2 Composite mixes

MATERIAL	CFM0	CFM0.5	CFM1	CFM1.5	CFM2
Cement, kg/m^3	344.3	315.0	300.0	280.2	258.2
Lime, kg/m^3	147.6	35.0	128.6	120.0	110.7
Sand, kg/m^3	1475.4	1343.2	1272.8	1182.0	1084.4
Fibres, kg/m^3	0	6.7	12.9	18.0	22.1
Water, kg/m^3	245.9	315.0	321.4	360.0	424.2
Plasticizer, %	1.5	1.5	1.5	1.5	1.5
Entrapped air, %	3.5	3.6	3.5	3.5	3.5
Fresh density, kg/m^3	2221	2122	2043	1966	1905

The hydration test was conducted under the methodology described in the literature [20]. The test was carried out in order to classify fibres-cement compatibility. The term compatibility refers to the degree of cement setting after mixing with water and with a given fibre additives. Generally, if the chemical process of cement hardening is undisturbed by the presence of jute fibres, it is considered that cement and fibres are compatible. On the other hand, if cement hardening is impaired by the presence of fibre additives, then cement and jute fibres are referred as incompatible. The test was performed with the addition of fibres ranged

from 0% (control sample contained neat binder) to 3% by weight of cement, to the 400 g of cement and lime mixture. Based on experiment reported in previous work [13], the amount of water added was 0.3 ml per gram of cement and additional 2.26 ml per gram of jute fibres. Immediately after mixing, the sample was placed in a with-mouth insulated flask with a thermocouple wire and then covered with Styrofoam for insulation purposes. The flask was sealed with wrapping tape. The temperature rise of the mixture was recorded with a data acquisition system and plotted against the time. The time to attain maximum temperature was considered to be the required final setting time of the mixture. All experiments were undertaken in a controlled room at 21°C and three replications were run for each amount of jute fibres. However, the results have been compared to that obtained with fibres derived from the bark of the natural plant. The experimental set-up is shown in Figure 2a. The inhibitory effect of fibre additives was quantified by using inhibitory index parameter I (%) that was calculated using Eq. 1 [11].

$$I = 100.\left(\frac{T - T'}{T}\right)\left(\frac{t' - t}{t}\right)\left(\frac{S - S'}{S}\right) \tag{1}$$

Where T and T' (°C) are the maximum hydration temperatures of neat cement and the mixture, respectively; t and t' (h) are the correspondent times to reach maximum hydration temperature; and S and S' (°C/h) are the maximum slopes of neat cement and the mixture, respectively. The effect of the inhibited cement setting was classified according to Table 3 [11]. However, the smaller the I-value the higher the compatibility between cement and particle additives. Typical hydration curves are shown in Figure 2b.

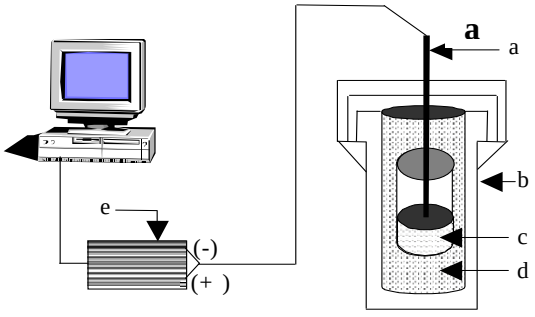

(a) Thermocouple wire, (b) Dewar flask, (c) sample mixture, (d) Vermiculite, (e) Thermometer with data acquisition.

Figure 2a Experimental set-up for hydration test

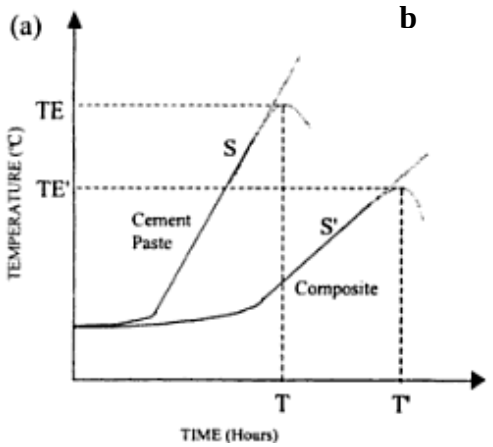

Figure 2b Schematic representation of typical hydration curve

Table 3 Inhibitory index used to classify the compatibility level [11]

INHIBITORY INDEX I (%)	GRADE
I < 10	Low inhibition
I = 10 - 50	Moderate inhibition
I = 50 - 100	High inhibition
I > 100	Extreme inhibition

The setting time measurements of the fresh composite were conducted using the Vicat apparatus according to the Standard NFP 15-431 [21]. The air content of the fresh composite was measured using the pressure method according to the Standard NFP 18-353 [22]. The properties tested on the hardened composite included dry unit weight, as determined by means geometrical measurement and weighing.

The compressive and flexural tests were carried out in accordance with Standard EN 196-1 [23], using a universal testing machine. The rates of loading of compressive and flexural specimens were 45 and 3 kN/min, respectively. Three replications were used for each properties tested.

EXPERIMENTAL RESULTS AND DISCUSSION

Hydration Test

The variation of hydration temperature vs. time for composite containing different amounts of jute fibres is shown in Figure 3. The correspondent parameter-values of hydration tests are listed in Table 4. The ideal material mixture should provide higher maximum temperature and maximum slope of the curve and lower hydration time to achieve the maximum temperature. The mixture containing fibres jute was associated with approximately the same maximum temperature achieved as compared to the control binder (0% of jute fibres). The hydration rate varied from 1.18°C/h, for control binder, to 0.64°C/h for composite containing 3% of fibres.

The correspondent initial setting time varied from 5 h to 8 h. The results clearly indicated that the low inhibitory index-value of 0.08% to 1.02% classifies the mixture as being of "low inhibition". These results suggest that the fibrous additives don’t exert a certain inhibitory influence on the cement setting and make them suitable for cement composite development.

When fibres derived from the bark of the natural plant (composite 3%a) were used, results showed a reduction in maximum temperature attained with increasing time to achieve the maximum temperature, as compared to the control binder. The correspondent inhibitory index-value of 23.92% classifies the mixture as being of "moderate inhibition". The lower hydration process shows the interactive effect of fibres on rate of hydration in mixtures, with correspondent initial setting time of 16 h.

This inhibitory effect can be attributed to the amount of alkalis and dissolved material extracts that severely delay the hydration process. Inhibition of cement occurs when the calcium silicate hydrate nucleation sites, on the originally positively charged surfaces, are poisoned by the sugar-acid anions and lignin component [24].

However, the main inhibiters of cement hydration are sugars and lignin whose act as set retarder [25]. The chemical treatment made evident to be necessary in order to minimise detrimental effects of cement-cellulosic materials interactions.

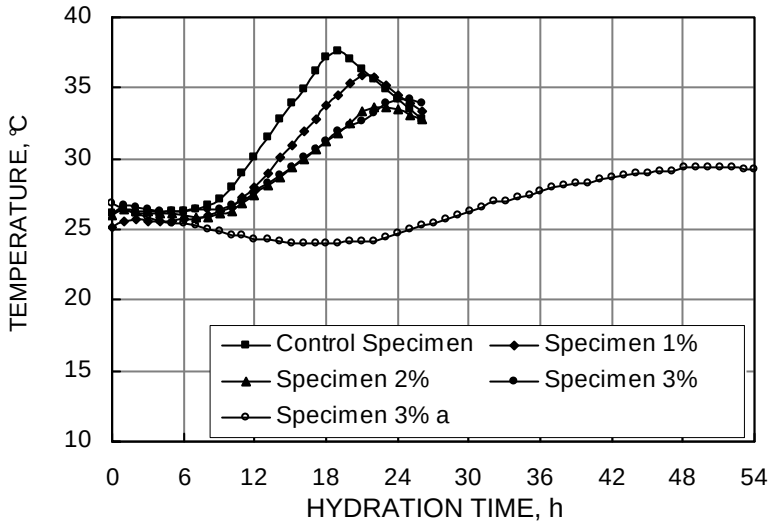

Figure 3 Hydration temperature vs. time of composites

Table 4 Average values of hydration-test results

JUTE FIBRES, %	MAX. SLOPE, °C/h	INITIAL SETTING TIME, h	MAX. TEMPERATURE, °C	MAX. SETTING TIME, h	INHIBITORY INDEX VALUE, %
0	1.18	5	37.5	19.1	-
1	0.97	6	35.8	21.1	0.08
2	0.67	7	33.7	22.0	0.67
3	0.64	8	34.3	24.1	1.02
3a	0.32	16	29.4	48.0	23.92

a: Jute fibres derived from the natural plan (fibres without washing).

Physico-Mechanical Properties of the Composites

Dry unit weight

The effect of change in jute fibres content on dry unit weight of hardened composite is shown in Figure 4. Dry unit weight-value decreases from 2080 kg/m^3 for control mortar to 1820 kg/m^3 for composite containing 2% of fibre additives. These values correspond to reduction of up to 12.5%. The decrease in unit weight is due to the physical properties of fibre, since it has lower density than natural sand. In addition, the variation in dry unit weigh of the composite is related to the entrapped air voids, in the matrix, that contribute to lightening the material. As shown in Table 1, the value of air-entrainment measurement of all fresh composites is of 3.5%. The reduction in unit weight is very attractive particularly in both building renovation works and the design of lightweight structural elements.

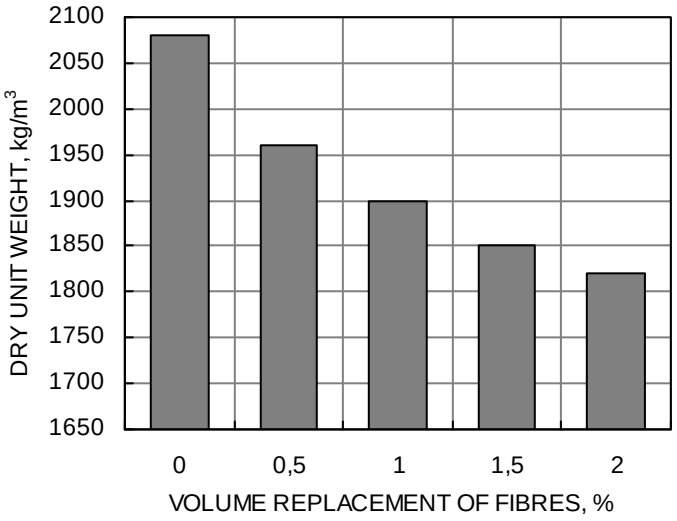

Figure 4 Dry unit weight-values of composite vs. volume fibres

Compressive strength

Results of compressive strength vs. jute fibre amount at different curing times are given in Figure 5a. Values indicated that the development of mechanical properties of the composites has not been affected. At 3-days curing time, the part of compressive strength developed for mortar control and composite containing 2% of fibres, compared to 28-days values, is 54.6% and 51%, respectively. Composite manufactured with lignocellulosic materials from different sources will have some variation in properties related to the chemical constituents and physical properties of the lignocellulosic materials. The particles inhibit cement setting and reduce mechanical strengths development. The material surface is probably the most likely place to find the inhibitory effects to hydration taking place, which interfere in the cement hydration process, and hence, in the formation of the essential products that contribute to the strength development of the composite. This result is consistent with that obtained bellow, which indicated that jute fibre additions don't exert inhibition on cement hydration.

The effect of fibre additives on 28-days compressive strength of composites is shown in Figure 5b. Results indicated that the increase of fibre amount serves to decrease compressive strength. The corresponding values varied from 26 N/mm^2, for control mortar, to 10 N/mm^2 for composite containing 2% fibres, which corresponds to loss of up to 61.5%. The decrease in compressive strengths is attributed to the physical properties of the fibres, since they are less stiff than the surrounding cement paste. Under loading, cracks are initiated around the particles, which accelerate the failure in the matrix. The decrease is also explained by the interfacial bond defects between fibres and matrix.

Figure 6 shows a plot of compressive strength vs. dry unit weight of the composite. It is evident that a decrease in unit weight ρ (kg/m^3) induces a reduction of compressive strength σ (N/mm^2). The following relationship has been proposed: $\sigma = 0.0198e^{0.0035\rho}$ (yielding a correlation coefficient of $R^2 = 0.978$. The variation obtained is similar to that reported in previous work conducted on lightweight wood-concretes [26]. The reduction in compressive strength of the composite is due to the fact that increasing fibre additives yields a low density of specimen. In fact, if the fibres are stiff, their packing become difficult at high amount and voids are introduced into the product).

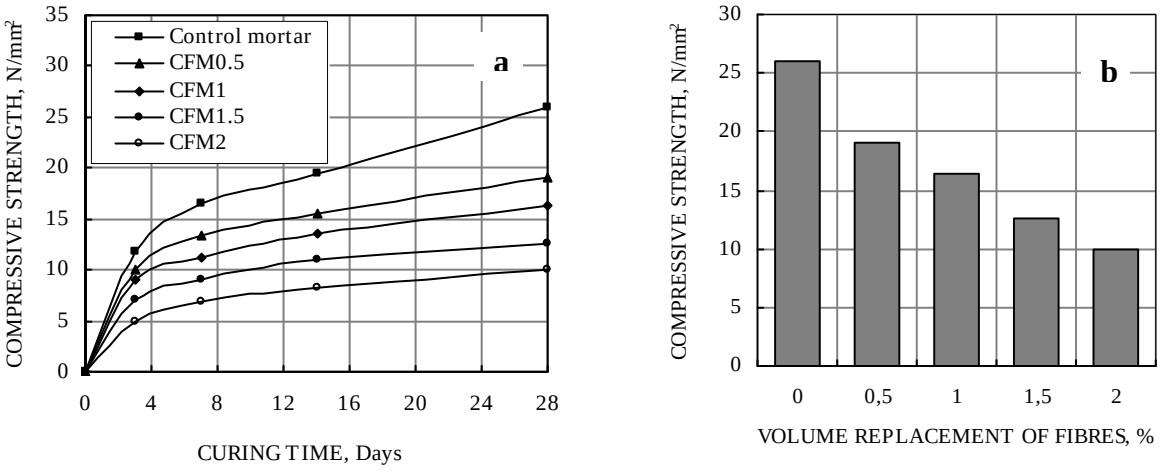

Figure 5 Compressive strength of the composites

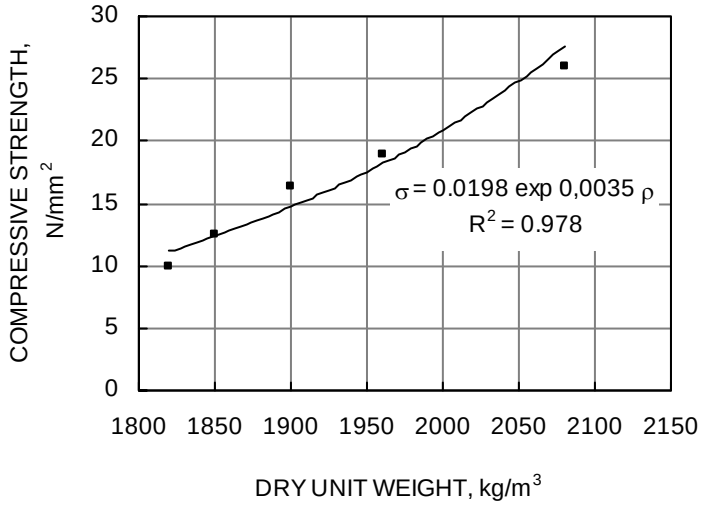

Figure 6 Compressive strength / dry unit weight relationship

Flexural strength

The variation in 28-days flexural strength with jute fibre amount is shown in Figure 7. A reduction in the flexural strength of the composite is observed. Value decreases from 5 N/mm² to 2.6 N/mm², as the fibre additives varied from 0% (control mortar) to 2%. It corresponds to reduction of up to 48.7%. The flexural strength reduction observed is due to both mechanical properties of fibres and porous structure effect.

Results also indicated that for 2% of fibre amount, the decrease in flexural strength is lower than that in compressive strength. The lower reduction in flexural strength is probably related to the dilution effect of fibres on the high deflection under loading of the composites.

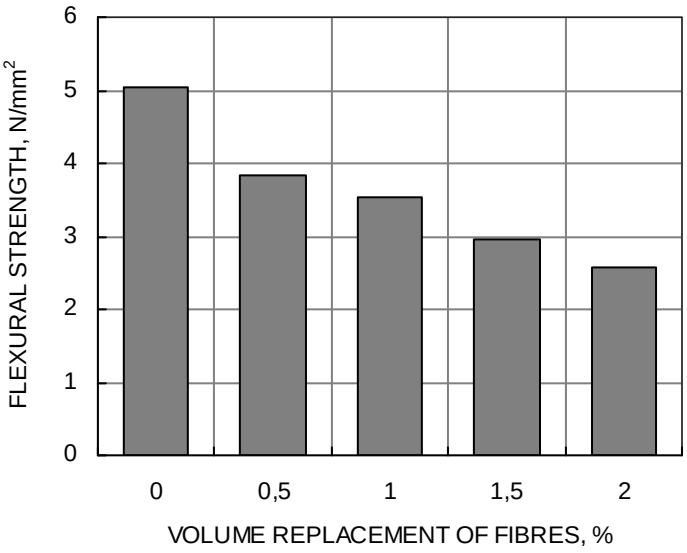

Figure 7 Flexural strength of the composites

CONCLUSION

This work explores the possibility of the use of jute fibres in the cement matrix as the reinforcing materials. The study of the compatibility between cement and these fibres, by measuring the appropriate inhibitory index, has shown that the materials produced a low inhibition index on the cement setting, making them viable candidates for panel manufacturing. Test-Results of mechanical properties of the composites have shown that fibre additives reduced compressive and flexural strength. The quality of the composites was directly related to the interfacial bond defects between fibres and matrix. Despite the reduction in the mechanical properties, the composite containing jute fibres, the results showed that it is possible to produce acceptable panels with these fibres.

The application in civil construction of cement composite based-jute fibres appears to be feasible considering the results obtained from analysis of its properties. This study contributes toward the program of vegetable residue recycling and pollution reduction, since this material is biodegradable. To conclude, the studies on the thermal properties and durability have started and display encouraging results.

REFERENCES

1. AAMR-DAYA E, LANGLET T, BENAZZOUK A AND QUENEUDEC M, Feasibility study of lightweight cement composite containing flax by-product particles: Physico-mechanical properties. Cement and Concrete Composites, Vol. 30, 2008, pp. 957–963.

2. BENAZZOUK A, DOUZANE O AND MEZREB K M, Physico-mechanical properties of aerated cement composites containing shredded rubber waste. Cement and Concrete Composites, Vol. 28, 2006, pp. 650–657.

3. MERZOUD M AND HABITA M F, Elaboration de composite cimentaire à base de Diss Ampelodesma Mauritanica. Afrique Science, Vol. 4, No. 2, 2008, pp. 236-242.

4. MIR A, ZITOUNI R, COLOMBET F AND BEZZAZI B, Studie of Mechanical and thermomechanical properties of jute/epoxy Composite Laminate. Journal of reinforced plastics and composites. October 2009. ISSN 0731-6844 Edition Sage.

5. SAVASTANO Jr H, WARDEN P G AND COUTTS R S P, Microstructure and mechanical properties of waste fibre–cement composites. Cement and Concrete Composites, Vol. 27, 2005, pp. 583–592.

6. BOGHOSSIAN E, LEON D AND WEGNER R, Use of flax fibres to reduce plastic shrinkage cracking in concrete. Cement and Concrete Composites, Vol. 30, 2008, pp. 929-937.

7. KRIKER A, DEBICKI G, BALI A, KHENFER M M AND CHABANNET M, Mechanical properties of date palm fibres and concrete reinforced with date palm fibres in hot-dry climate. Cement & Concrete Composites, Vol. 27, 2005, pp. 554–564.

8. ELSAID A, DAWOOD M, SERACINO R AND BOBKO C, Mechanical properties of kenaf fiber reinforced concrete. Construction and Building Materials, Vol. 25, 2011, pp. 1991–2001.

9. MOSLEMI A A AND LIM Y T, Compatibility of southern hardwoods with Portland cement. Forest Prod J., Vol. 34, Nos. 4/7, 1984, pp. 22-26.

10. HOFSTRAND A D, MOSLEMI A A AND GARCIA J F, Curing characteristics of wood particules from mine northern rocky mountain species mixed with Portland cement. Forest Prod. J.; Vol. 34, No. 2, 1984, pp. 57-61.

11. HACHEMI M, MOSLEMI A A AND CAMPBEL A G, A new technique to classify the compatibility of wood with cement. Wood Sci. Technol., Vol. 24, No. 4, 1990, pp. 345-54.

12. SEMPLE K E, CUNNINGHAM R B AND EVANS P D, The suitability of five Western Australian mallee eucalypt species for wood-cement composites. Int. Jour of Industr. Crops and products, Vol. 16, 2002, pp. 89-100.

13. BLANKENHORN R P, BLANKENHORN B D, SILSBEE M R AND DICOLA M, Effect of fiber surface treatment on mechanical properties of wood-fiber cement composite. Cement & Concrete Research, Vol. 31, 2001, pp. 1049-1055.

14. OKINO E, DE SOUZA M R, SANTANA M A E, ALVES M V, DE SOUZA M E AND TEIXEIRA D E, Cement bonded wood particle board with a mixture of eucalypt and rubberwood. Cement concrete Composite, Vol. 26, 2004, pp. 729-34.

15. MOSLEMI A A, GARCIA J F AND HOFSTRAND A D, Effect of various treatment and addition on wood Portland cement water systems. Wood fibbers Sciences, Vol. 15, No. 2, 1983, pp. 64-76.

16. RAMAKRISHNA G AND SUNDARARAJAN T, Studies on the durability of natural fibres and the effect of corroded fibres on the strength of mortar. Cement and Concrete Composites, Vol. 27, 2005, pp. 575–582.

17. AFNOR, Liants hydrauliques, ciments courants–composition, spécification et critères de conformité, 1994.

18. EUROPEAN STANDARD EN 459-1. Building lime: part 1. Definition, specification and conformity criteria, 2001.

19. AFNOR. Bétons. Mesure du temps d'écoulement des bétons et des mortiers aux maniabilimètres; 1988.

20. HOFSTRAND A D, GARCIA J F AND MOSLEMI A A, Effect of various treatments and additives on wood-Portland cement water-systems. Wood Fibers Sciences, Vol. 2, No. 15, 1983, pp. 163-175.

21. AFNOR, Liants hydrauliques - Technique des essais - Détermination du temps de prise sur mortier normal, 1994.

22. AFNOR. Adjuvants pour bétons, mortiers et coulis-Mesure du pourcentage d'air occlus dans un béton frais à l'aéromètre à béton, 1985.

23. AFNOR, Méthodes d'essai des ciments, Partie I: Détermination des résistances mécaniques, 1995.

24. PEHANICH J L, BLANKENHORN P R AND SISBEE M R, Wood fiber surface treatment level effects on selected mechanical properties of wood fiber-cement composites. Cement & Concrete Research, Vol. 34, 2004, pp. 59-65.

25. MARIUS E, OVIDIU M AND MARCEL M, Influence of the wood waste characteristics and its chemical treatment on the composites properties, NOCMAT/3 Vietnam International Conference, 2002, pp. 245-249.

26. PIMIENTA P, CHANDELLIER J, RUBAUD M, DUTRUEL F AND NICOLE H, Etude de faisabilité des procédés de construction à base de béton de bois. Cahier du CSTB, Janvier-Février, No. 2703, 1994, 45 p.

Glass Fibre Reinforced Concrete as a Material for Large Hanging Ceiling Designs in Underground Station Restorations

N Shangina, A Kharitonov
Saint Petersburg State University, Russia

The fabrication of hanging ceiling designs for underground's platform hall by hand spray-up method is a new direction of the use glass fiber reinforced concrete. There is the demand of decisions some technological and constructive problems for ensuring required level of working and decorative features at the restoration of history ceiling to Avtovo station in Saint-Petersburg. The motivation of the background technical decisions that are adopted at the restoration and referring both to material and design as a whole has been presented in the article.

N Shangina Ph.D., is a University Professor of Communications, University of St. Petersburg and CEO "Ajio-Proekt", Russia.

A Kharitonov Ph.D., is a Professor of Architecture and Construction at the University, St. Petersburg and Deputy CEO "AjioProekt", Russia.

Keywords: Glass fibre reinforced concrete, Historic structures, Restoration

INTRODUCTION

A new generation of concrete – High-Performance concrete and High-Strength concrete – became possible due to the achievement of low values of the water-cement ratio on the basis of application with modern effective plasticizing additives (hypersofteners). There are high operational characteristics of similar concretes (compression strength 60-130 MPa), nevertheless, this can be improved significantly regarding the increase of strength on a bend (in 4-5 times), that opens all-new scopes of cement systems. In this paper special attention is given to the technology of fibrous concrete and glass fibrous concrete, in particular [1].

ADVANTAGES OF GLASS FIBROUS CONCRETE IN RECONSTRUCTIONS

The combination of the low water-cement attitude, high-modulus alkali-durable the glass fibre, that is oriented in a matrix in one plane due to the application of advanced technology (spray-up method), as well as a variety of the chemical and mineral additives acting upon castability of a mixture and raising the durability of concrete, is the reception way of glass fibrous concrete (GFRC) with new levels of its properties. The ratio of tensile strength and compression strength reaches 0.8 (for not the reinforced material, this size does not exceed 0.2). Thus this concrete keeps to a category high-strength; it possesses high impact strength, as well as frost resistance and water resistance. We have become used to associate a similar combination of characteristics with materials of quite a different nature, for example, metal or polymeric compositions. However GFRC, because of durability and the quality-price ratio, has the great advantage. Besides, the compatibility of glass fibrous concrete with mineral building materials makes its very attractive, and in some cases irreplaceable for restorative works.

Using a hand spray-up method gives GFRC extremely high technological properties at the formation of products of any form, relief and texture of a surface. The basic diagram of hand spray-up method is shown on Figure 1.

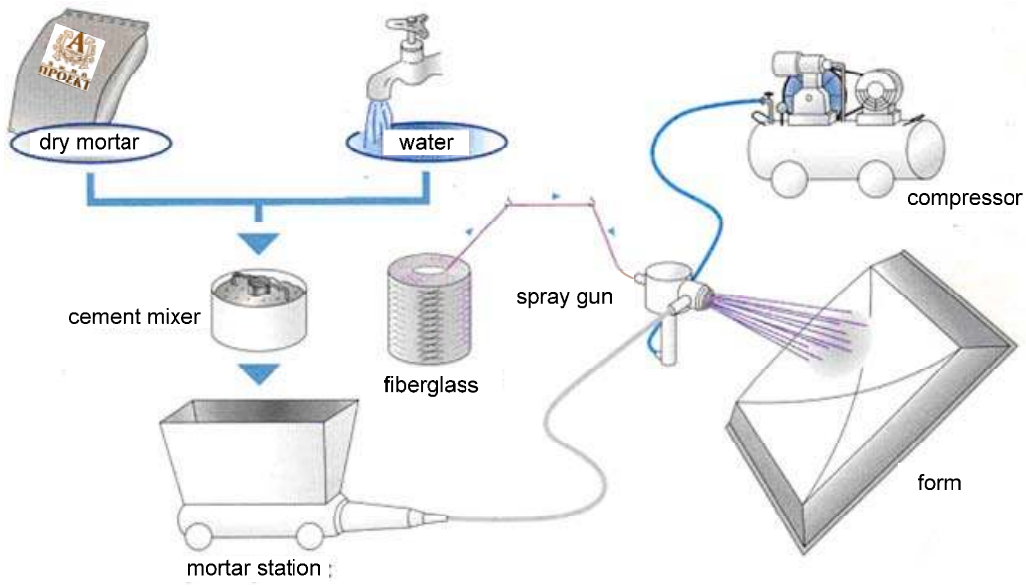

Figure 1 The basic technological diagram of the GFRC production

Its light weight also gives an advantage to glass fibre reinforced concrete: high tension strength allows us to make thin-walled designs (in thickness of 12-25 mm) without steel reinforcing. Besides the possibilities of installation is important that under any weather conditions (considering there is frequently an "abnormal" weather phenomena); the guaranteed level of strength characteristics of elements it is comprised of are provided in stationary conditions.

INVESTIGATION OF THE EFFECT ON THE PROPERTIES OF GFRC

The most important questions in technology glass fibre reinforced concrete are the optimum length of a fibre, its durability in the cement stone, and shrinkage.

In Figure 2 and 3 are graphs of the experimental data [2] reflecting the dependence between the strength parameters GFRC, expense of fibre (in percentage of weight) and its lengths are presented. The sand, cement and fibre glass mixed in a laboratory bowl mix to a homogeneous consistency.

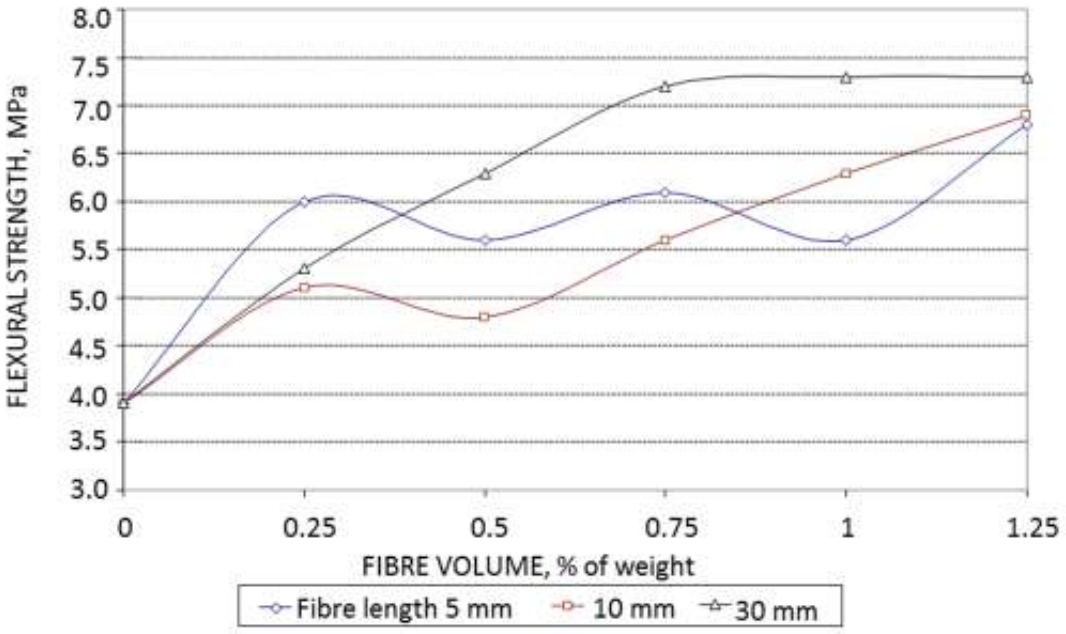

Figure 2 The influence of the fibre percentage and its lengths on flexural strength

As shown in the data, the increase in degree of reinforcement is connected with the growth of compression and tensile strength. But introducing a fibre by manually does not allow to reach the volume of dispersive reinforcing over 1.25%. Applying a spray-up method the amount of a fibre can be increase up to 5% from the weight of a mixture.

Structures with a fibre length of 5 mm are characterized by heterogeneity of properties. Use of a fibre with a length of 30 mm is not rational when the degree of reinforcing more than 0.75% (there is no growth of tensile strength). Thus, the 10 mm fibre is best. At this length (10 mm) it is kept castability of the mixture that also important and allows to shape the surface of a product with a very complex form.

Other important problem that is required to take into account for products from GFRC, is shrinkage. The high cement content in the matrix of glass fibre reinforced concrete is capable of giving significant shrinkage deformations.

Shrinkage cracks develop in the direction of preferred orientation of the fibres due to insufficient of the fibres amount that perpendicular to the direction of the crack growth. Although the introduction of glass fibre in cement matrix did not significantly reduce the dry shrinkage, but dispersed reinforcement reduces the risk of spread of shrinkage cracks.

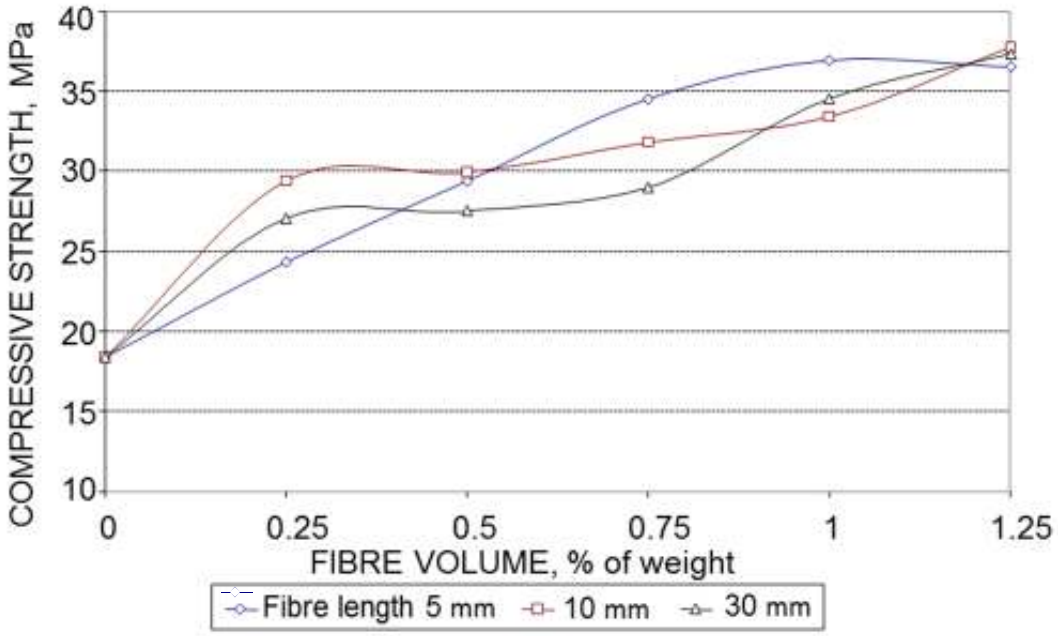

Figure 3 The influence of the fibre percentage and its lengths on compression strength

Traditional formulations of the GFRC matrix suggests of cement-sand ratio equal to 1:1. Increase in the proportion of sand leads to a deterioration of the rheological properties of the mortar and, accordingly, "conformability", reducing the strength characteristics of concrete. However, the decline in the share of cement in concrete is a priority for improving economic and technical efficiency of GFRC.

The durability of a fibre in a concrete structure is defined in alkali resistance, therefore for dispersed reinforcing it is necessary to use fibre glass on the basis of zirconium.

An additional measure to increase of stability of fibre glass is the use of the active mineral additive that connects the lime and lowers the alkalinity environments. Apart from the above mentioned the additives raising the corrosion stability of the matrix component of the GFRC.

The system's approach of considering aforesaid aspects for the design of structures and the adjustment of technological process of manufacture's GFRC, has allowed us to create a material that meets high operational requirements (Table 1).

Figure 4 shows the data on the shrinkage of the matrix of normal, the modified matrix (dry mixture produced by AjioProekt) and GFRC (produced by AjioProekt).

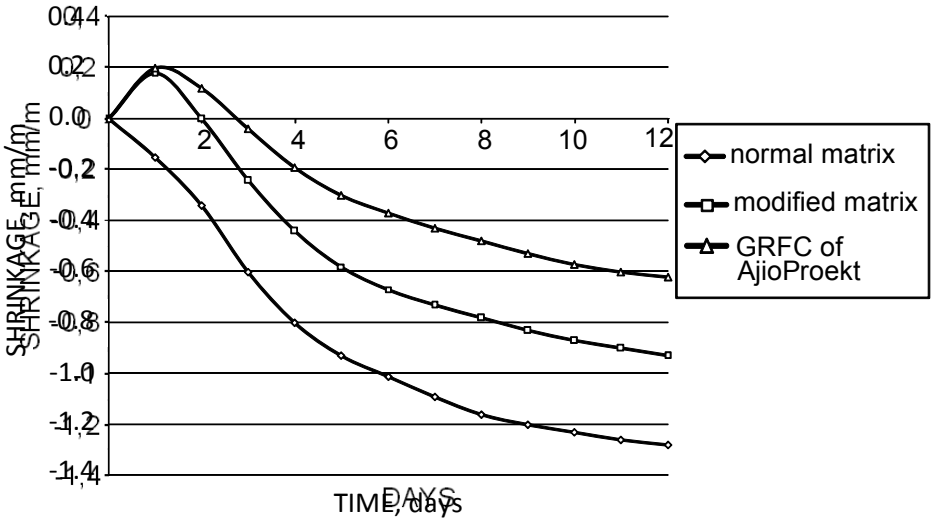

Figure 4 Dry shrinkage of GFRC

Table 1 Basic characteristics of GFRC

CHARACTERISTIC	VALUE
Density	1900-2200 kg/m³
Impact strength	2.0 kg·mm/mm²
Compression strength	Not less than 55 MPa
Flexural strength	Not less than 40 MPa
Modulus of elasticity	2.0-2.5 GPa
Tensile strength	7.8 MPa
Lengthening at destruction	0.8%
Factor of temperature expansion	$9 \cdot 10^{-6}$/°C
Heat conductivity	0.65 W/(m·K)
Water resistance	1.2 MPa
Frost resistance	Not less than F300

In Figure 5 the comparison of a matrix and GFRC strength is given.

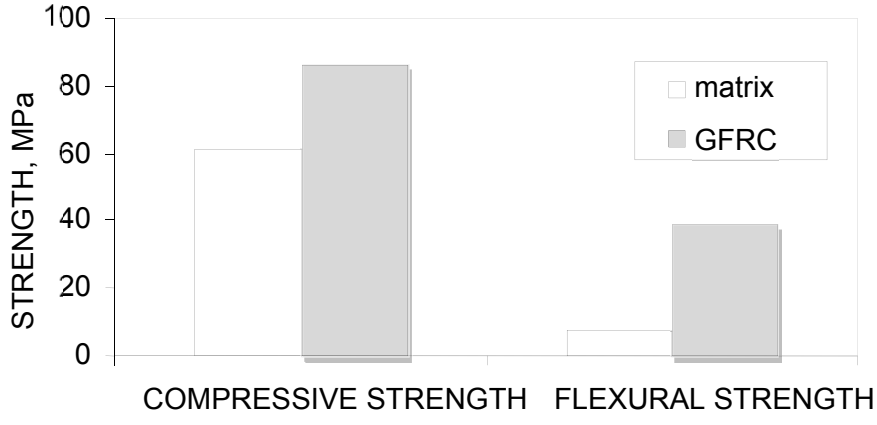

Figure 5 Strength of matrix and GRF concrete

When we receive GFRC it is used as white CEM I, quartz-feldspar sand, a complex mixture of chemical and mineral additives. As a fibre, the alkaline glass fibre containing 10-15% alkaline oxide is applied. The string of fibre glass in diameters of 10-20 microns is collected in bundle and reeled up on a reel. This degree of reinforcing makes a 3% difference in the weight of a mixture.

For manufacturing glass fibrous concrete the special process equipment is used to manage the installation with a spray-gun (Figure 6).

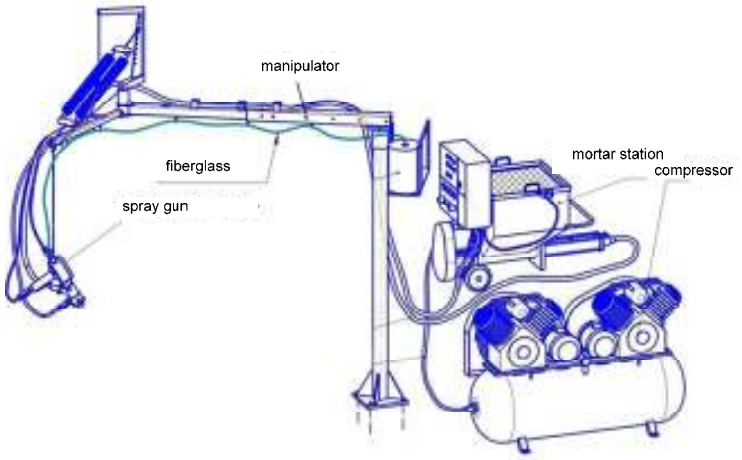

Figure 6 The general view of installation with the manipulator

PRACTICAL EXPERIENCE

The given technology has a practical use of restoration the false ceiling of a platform hall of the Saint-Petersburg underground station (Avtovo). The historical false ceiling is decorated with many modelled elements. The basis of its composition is made with decorative caissons and is structured on the surface of the station's ceiling. Between the decorative caissons under the longitudinal and cross-sectioning beams of a covering, the flat inserts are placed, decorated by garlands from leaves and wreaths in angular zones. The ornamental motive of the decorative caissons is represented by repeating stylized natural forms (sheet stocking, sockets), and dividing decorative corbel. In angular zones of decorative caissons, triangular plaster drafts can be found (Figure 7).

During long-term operations under dynamic loads and leakage, as well as being in view of the insufficient reliability of fastening a major part of the decorative elements of the ceiling has collapsed (Figure 8). For this reason, demanded restorative works and maintenance of the operational reliability of an object during a prolonged period of time. A mandatory operating condition was created from the existing architectural shape of the station. In addition, restoration work should to be carried out without interruption of the station.

Given these requirements, has been developed a draft providing for the implementation of the ceiling's designs (decorative panels and caissons) of GFRC. The thin-walled suspended elements – caisson or flat panel – are being made in polyurethane forms from glass fibrous concrete by spray-up method with integration a metal skeleton of stainless steel, that providing spatial rigidity of panels during installation and operation (Figure 9). The size of a caisson is 4800 mm × 4800 mm, depth of 350 mm.

Figure 7 Interior station Avtovo

Figure 8 The platform hall of station with the dismantled designs and false ceiling

Figure 9 Design of a false ceiling of platform hall from GFRC

To achieve glass fibrous concrete critical strength, the skeleton of the panel is mounted by turnbuckles to overhead to beams. Technological process of manufacturing the panel includes three consecutive stages of the spray procedure.

In the first stage splashing with the objective of creating a smooth obverse surface on the panel as the first layer of the structure without glass fibre is used. This mixture is applied via a spray gun in thicknesses of 2-3 mm.

In the second stage, splashing up is also applied by means of spray gun. The basic constructional layer made of the glass fibrous concrete is applied and has a thickness of 5-10 mm. The thickness of a stacked layer by manufacturers is supervised by tracer. Sprayed plaster base of the glass fibrous concrete is made continuously on all parts of the panel. After applying a layer of GFRC, its needs to thorough seal by special rollers to remove air and ensuring a monolithic material of the panel (the first and second layers).

In the third stage we connect wet-made panels from the glass fibrous concrete with a spatial skeleton, thus making splashing. No less than 36 hours later properly moisture solidification of the overhead designs can be mounted on a seat. At this time it is achieved no less than 70% of the branded strength of concrete.

CONCLUSIONS

Thus, using glass fibrous concrete by manufacturing larger pendant is a whole new way to use the product. Good qualities of this material are: low weight, high strength on a bend, and high dynamic strength.

Distinctive features of company "AjioProject" glass fibrous concrete produces various purposes is the systems scientific approach, mentioning both the design structure of concrete, and its constructive elements. Thusly we consider the operating conditions, the technological parameters, and the required level of properties and economic feasibility.

REFERENCES

1. RABINOVICH F N, Composite on the basis of the reinforced concrete. Questions of the theory and design, technology, a structure, Moscow: ACB, 2004, 560 p.

2. GABIDULLIN M G, BAGMANOV R T AND SHANGARAEV A YA, Research on the influence of characteristics glass fibre on physicomechanical properties of the glass fibrous concrete, XV Academic readings RAACS – Materials of the international scientific and technical conference "Achievements and problems of materiology and modernization of the building industry ", Kazan, 2010, KSACU, pp. 268-273.

3. HO C Y AND LEE Y C, Effects of humidity on the deformation of GFRC composite material, The Arabian Journal for Science and Engineering, Vol. 34, No. 1C, 2009, pp. 73-79.

The Influence of Polypropylene Fibres on Early Autogenous Shrinkage of Fibre Reinforced High Performance Concrete

B Bandelj, D Saje, B M Saje, J Šušteršič, J Lopatič, F Saje
University of Ljubljana, Slovenia

Polypropylene fibres have been widely used in concrete to improve its engineering properties. Many researchers have studied the mechanical properties of fibre reinforced concrete, but less data are available on its rheological properties, especially for high-strength concrete at early ages. In the proposed paper the experimental results of the early autogenous shrinkage of high performance polypropylene fibre reinforced concrete with the volume content of polypropylene fibres between 0.25% and 0.75% are presented and analysed. In order to compare the autogenous shrinkage of polypropylene fibre reinforced concrete with that of a comparable concrete without fibres, also the shrinkage of comparable plain concrete was measured. The test results show that early autogenous composite shrinkage decreases with the increase of the amount of polypropylene fibres in the composite.

Branko Bandelj, Ph.D., is Design Engineer in Primorje, Slovenia. His main research activity is fibre reinforced concrete.

Drago Saje, Ph.D., is Assistant professor at the Faculty of Civil and Geodetic Engineering, University of Ljubljana. His main research activities are the mechanical and rheological properties of high performance concrete and the design of concrete and timber structures.

Barbara Mihaela Saje, M.Sc.. Her research activities mainly concern the design and safety of concrete structures, mechanical and rheological properties of ordinary and high-performance concrete at normal and elevated temperatures, nonlinear analysis of reinforced concrete structures, as well as fire resistance of concrete structures.

Jakob Šušteršič, Ph.D., is Director of Institute for Research in Materials and Applications Ljubljana, Slovenia. His main activities are associated with fibre reinforced concrete, polymer modified concrete, high performance concrete and other special concrete.

Jože Lopatič, Ph.D., is Assistant professor at the Faculty of Civil and Geodetic Engineering, University of Ljubljana. He is a Head of the Chair of Concrete and timber Structures. His main research interests include the modelling of nonlinear creep and shrinkage of concrete, design and nonlinear time-dependent analysis of reinforced concrete structures, as well as field testing of structures.

Franc Saje, Ph.D., is Associate professor at the Faculty of Civil and Geodetic Engineering, University of Ljubljana. His research activities mainly concern the design, safety and reliability of concrete and timber structures, mechanical properties of concrete at normal and elevated temperature, nonlinear analysis of reinforced concrete structures, as well as fire resistance of concrete and timber structures

Keywords: Autogenous shrinkage, High-performance concrete, Polypropylene fibre, Silica fume, Water-binder ratio

INTRODUCTION

High performance concretes are frequently used in construction practice, not only because of their high-strength qualities, but also because of their higher resistance to other external influences. Fibre reinforcement made of steel or other artificial fibres affects ductility, the width of cracks, and the rheological characteristics of composites [1-3]. To ensure high performance in concretes, the water-to-binder ratio in such concretes is relatively low, so that superplasticizers need to be added in order to ensure an appropriate level of workability. Since the amount of free water in a fresh, high performance concrete is, with respect to the amount of cement, so small that it is insufficient for the process of hydration to take place fully, part of the water in the fine pores is consumed during the chemical process, thus giving rise to negative pressures or tensile forces acting on the pore walls. This results in a reduction of the volume of the relatively soft concrete which has not yet hardened, which corresponds to the physical phenomenon known as the autogenous shrinkage of concrete. In high performance concretes, unlike concretes of normal strength, autogenous shrinkage represents a significant part of the total shrinkage [4, 5].

In their research into the effect of the geometry of polypropylene fibres on the cracking of concrete due to plastic shrinkage, Banthia and Gupta [6] found that polypropylene fibre reinforcement was very effective in limiting this kind of cracking in concrete. They suggest that polypropylene fibres generally result in a favourable decrease in the width and number of cracks. Thinner fibres are, according to them, more effective than thicker ones, and longer fibres are in turn more effective than shorter ones. Kovler et al. [7] stated that the presence of polypropylene fibres results in a considerable decrease in the plastic shrinkage of fibre reinforced concrete. With regard to the total shrinkage of fibre reinforced concrete, they stated that the effect of polypropylene fibre reinforcement is virtually insignificant up to a volumetric content of 0.2%. According to their findings, crack width can be reduced by as much as 50% by increasing the volumetric content of polypropylene fibres.

Myers et al. [8], however, were of the opinion that, when added to concrete, polypropylene fibres exert a very small influence on shrinkage. Contrary to the findings of the above-cited researchers, Swamy and Stavrides [9] found that the drying shrinkage of polypropylene fibre reinforced concrete was about 20% less than that of concrete without added fibres. Zollo [10] and Zollo et al. [11] have argued that, in the case of an appropriate quantity of added polypropylene fibres, the drying shrinkage of concrete can be reduced by as much as 75%. Bayasi and Zeng, who investigated the influence of reinforcing fibres on the compressive strength of fibre reinforced normal strength concrete [12], found that concrete compressive strength increased by 15% when reinforced with 1.27 cm long polypropylene fibres with a volumetric content of 0.1%, and by 19% in the case of a volumetric content of 0.3%, whereas at a volumetric content of 0.50% it decreased by 2.5% in comparison with concrete having no reinforcing fibres. Aly et al., who studied the effect of polypropylene fibres on the shrinkage and cracking of normal strength concrete [13], concluded that the shrinkage of test specimens made of fibre reinforced concrete containing 0.50% by volume of polypropylene fibres increased by 15% after they were cured for 1 day and then exposed to a temperature of 23°C and a relative humidity of 50%, and by 22% after they had been cured for 7 days, when compared to the shrinkage of concrete containing no polypropylene fibres. At the same time, however, they stated that their results were in disagreement with those of several other authors. They justified their results with the increased porosity of fibre reinforced concrete as compared to the porosity of concrete having no fibres, and with the accelerated decrease of moisture in fibre reinforced concrete.

Within the framework of this work, the influence of various volumetric contents of dry and previously moistened polypropylene fibres on the early autogenous shrinkage of polypropylene fibre reinforced high performance concrete was studied.

EXPERIMENTAL

For all fibre contents, the effect of polypropylene fibres on the shrinkage of fibre reinforced concrete at a water-to-binder ratio of fresh concrete mixtures of 0.36 was investigated. Measurements of the shrinkage of the composites on prism test specimens were performed. For estimation of the concrete or composite compressive strength, cube-shaped test specimens were used. For each individual volume content (0.25%, 0.50% and 0.75%) of dry and moistened polypropylene fibres, 3 test prisms measuring 10 cm × 10 cm × 40 cm, and three 15 cm cube specimens, were prepared. All the test specimens were, during the experimental investigations, stored in a climatic chamber at constant relative humidity of 70 ± 3% and a temperature of 22 ± 3°C.

Preparation of the Test Specimens

The fibre reinforced concrete test specimens were prepared from washed crushed limestone aggregate with a maximum nominal grain size of 16 mm, and the addition of fine silica sand. The cement used was CEM II / A-S 42.5 R. To assure appropriate workability [14] at a relatively low water-to-binder ratio, which amounted to 0.36, a naphthalene type superplasticizer was used, which was, according to its chemical composition, a sulfonated naphthalene-formaldehyde condensate. Properties of the used polypropylene fibres are presented in Table 1.

Table 1 Properties of the used polypropylene fibres

DENSITY, g/cm³	LENGTH, mm	CROSS-SECTION, μm	TENSILE STRENGTH, MPa	MODULUS OF ELASTICITY, MPa
0.91	12	35 × (250-600)	340-500	8500-12500

The test specimens were made from six different mixtures of fibre reinforced high performance concrete, and one mixture of a comparable concrete without fibres. Mixture M1 contained no polypropylene fibres, whereas mixtures M2, M3 and M4 contained 0.25%, 0.50% and 0.75% by volume of dry polypropylene fibres, and mixtures M5, M6 and M7 contained the same amounts of previously moistened polypropylene fibres.

The total content of the binder in each of the mixtures was 400 kg per m^3 of the composite, 90% of which was cement (360 kg/m^3) and 10% silica fume (40 kg/m^3). The water-to-binder ratio of mixtures M1 to M7 was 0.36. The compositions and properties of the fresh and hardened comparable concrete without fibres, and the fibre reinforced concrete mixtures, are given in Table 2.

Table 2 Mix proportions of the composites

MIXTURE	M1	M2	M3	M4	M5	M6	M7
Fine aggregate 0-4 mm, kg/m³	1133	1135	1130	1126	1134	1130	1126
Coarse aggregate 4-16 mm, kg/m³	755	756	753	750	755	753	750
Polypropylene fibres	-	dry	dry	dry	moist	moist	moist
Fibres, % by volume	-	0.25	0.50	0.75	0.25	0.50	0.75
Water-to-binder ratio	0.36	0.36	0.36	0.36	0.36	0.36	0.36
Mixing water, kg/m³	144.0	144.0	144.0	144.0	144.0	144.0	144.0
Naphthalene based superplasticizer, % by weight of binder	2.05	2.05	2.05	2.05	2.05	2.05	2.05

Preparation of the Moistened Polypropylene Fibres

For mixtures M5, M6 and M7, polypropylene fibres which had been previously immersed for 24 hours in water were used. After soaking, the fibres were drained and wrung manually, so that no surface water was visible on them. The water content of the fibres was determined by weighing them before and after soaking, and the amount of water retained by individual fibres was also verified by the thermo-gravimetric method. The previously moistened polypropylene fibres served as an inner store of water within the cement paste [15]. The surface of the polypropylene fibres used was furrowed, and the fibres were surrounded by tiny fibrils, which enable the retention of water on the fibre surface. As well, water can also be retained within the existing fibre furrows, which are partly filled with fine particles of predominantly calcium composition, and partly with water accumulated in the voids. It is thought that water is retained not only between the fibrils and in the furrows of individual fibres, but also in the 3-dimensional pores which are formed between the individual fibres in the bunches of fibres [15]. Data on the water content retained by the soaked fibres are presented in Table 3.

Table 3 Water content in the moistened polypropylene fibres

MIX.	FIBRE CONTENT, %	DRY FIBRE MASS, g	MOISTENED FIBRE MASS, g	MASS OF WATER IN FIBRES, g	MASS CONTENT OF WATER IN THE MOISTENED FIBRES, %
M5	0.25	82	256	174	68
M6	0.50	164	482	318	66
M7	0.75	246	930	684	74

Test methods

The compressive strength of the composites was measured on 28 days old 15 cm cube specimens by using an electro-mechanical testing machine of capacity 5000 kN. The autogenous shrinkage of fibre reinforced concrete was measured on the test specimens which were sealed in impermeable polyethylene foil in order to prevent them drying out. Computer-controlled measurements of the autogenous shrinkage of the sealed test specimens were performed in accordance with the provisions of the corresponding Japanese standard [16], by means of an electronic displacement transducer. A teflon sheet was inserted between the test specimen and the base in order to reduce the friction between two surfaces. The temperature in the middle of the specimen was measured by means of a thermocouple.

RESULTS AND ANALYSIS OF THE EKSPERIMENTAL INVESTIGATIONS

Properties of the Fresh and Hardened Composites

The results of the laboratory investigations of the fresh and hardened composites with a normal quantity of mixing water and different contents of dry or previously moistened polypropylene fibres (Table 4) show that the flow of the fresh composites and the compressive strengths of the hardened composites are, in the case of using previously moistened polypropylene fibres (composites M5, M6, M7) practically the same as in the case of using dry fibres (composites M2, M3, M4).

Table 4 Properties of the fresh and hardened composites

MIXTURE	M1	M2	M3	M4	M5	M6	M7
Flow, cm	55	35	33	41	33.5	34.5	38
Density, kg/m³	2436	2409	2459	2383	2413	2382	2339
Density – st. dev. kg/m³	9	27	35	15	34	17	9
$f_{cm,28days}$, MPa	69.0	74.3	76.5	78.2	74.1	76.3	78.1
$f_{cm,28days}$ – st. dev., MPa	1.1	1.6	4.7	5.1	1.7	2.6	3.2

Measurement of Early Autogenous Shrinkage of the Composites

The measured variations over time of the length of test specimens consist of variations due to the shrinkage of the concrete, and variations due to changes in the temperature of the specimen. The temperatures in the middle of the test specimens, and the changes in specimen length, were measured simultaneously. The variations over time of specimen shrinkage were determined from the differences between the development over time of the measured deformations, and the temperature dilatation of the test specimens due to variations in temperature. The variations over time of the test specimen length due to temperature variations in the period of rapid setting of the cement were determined analytically from the coefficient of thermal expansion of the concrete, and the measured variations over time of the temperature. Thus a value of $\alpha_{T,f} = 1.48 \cdot 10^{-5}$, determined by separate measurements [17], was taken for the coefficient of thermal expansion of the fresh concrete, and a value of $\alpha_T = 1.0 \cdot 10^{-5}$ [16], obtained from the literature, was assumed for the coefficient of thermal expansion of the hardened concrete.

The concrete was considered fresh until its temperature began to rise significantly. In order to determine intermediate values of the coefficient of thermal expansion in the period of rapid hardening of the concrete until 24 hours after its casting, linear interpolation between the values for fresh concrete and hardened concrete were used. Figure 1 shows the mean values of the temperature and the total deformations measured on the three test specimens of mixture M1, during the first 24 hours after casting. The lower curve shown in Figure 1 also shows the time dependence of the autogenous shrinkage of concrete, determined from the mean values of the differences between the total deformations measured on the three specimens, and their calculated deformations due to the increase in temperature.

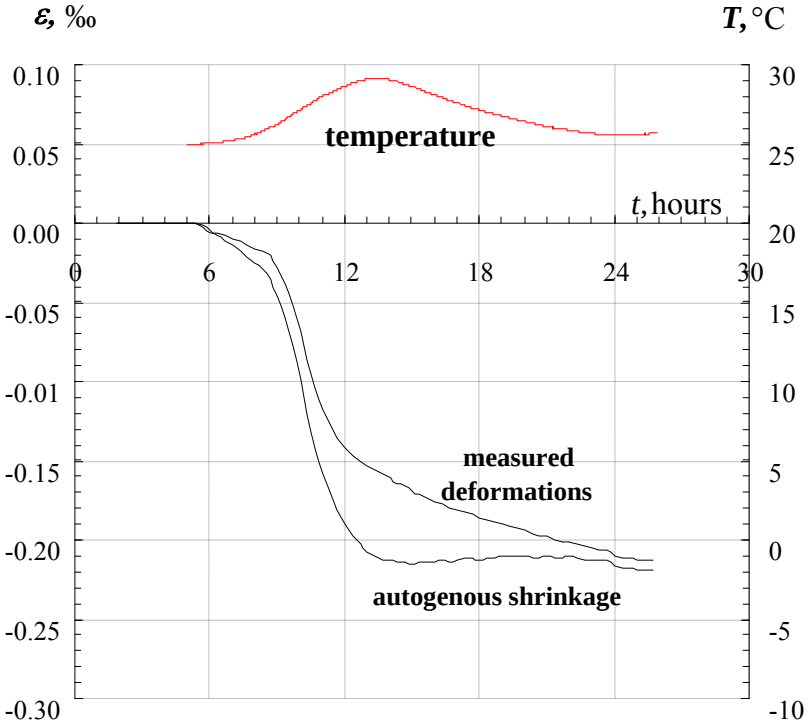

Figure. 1 Measured deformations and autogenous shrinkage of the comparable concrete M1

Early Autogenous Shrinkage of the Composites

The development over time of the temperature and autogenous shrinkage of the investigated test specimens of fibre reinforced high performance concrete, over the first 24 hours, is shown in Figures 2, 3, 4 and 5. The shrinkage of the composite was determined as the difference between the measured and temperature-related deformations of the test specimens.

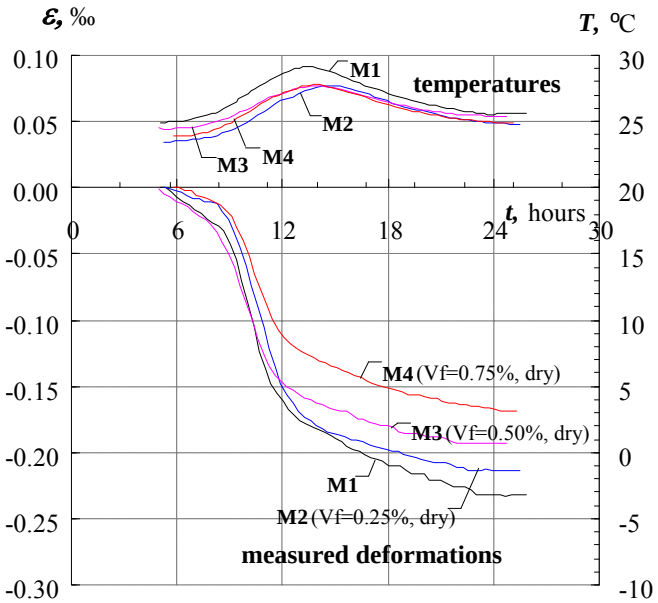

Figure 2 The measured deformations of the composites containing dry polypropylene fibres, during the first 24 hours

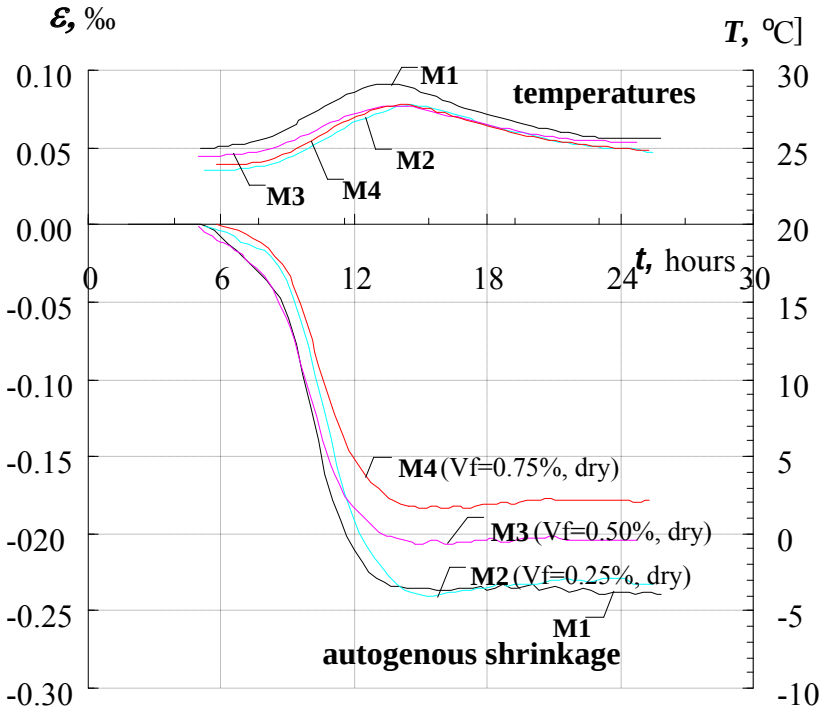

Figure 3 The autogenous shrinkage of the composites containing dry polypropylene fibres, during the first 24 hours

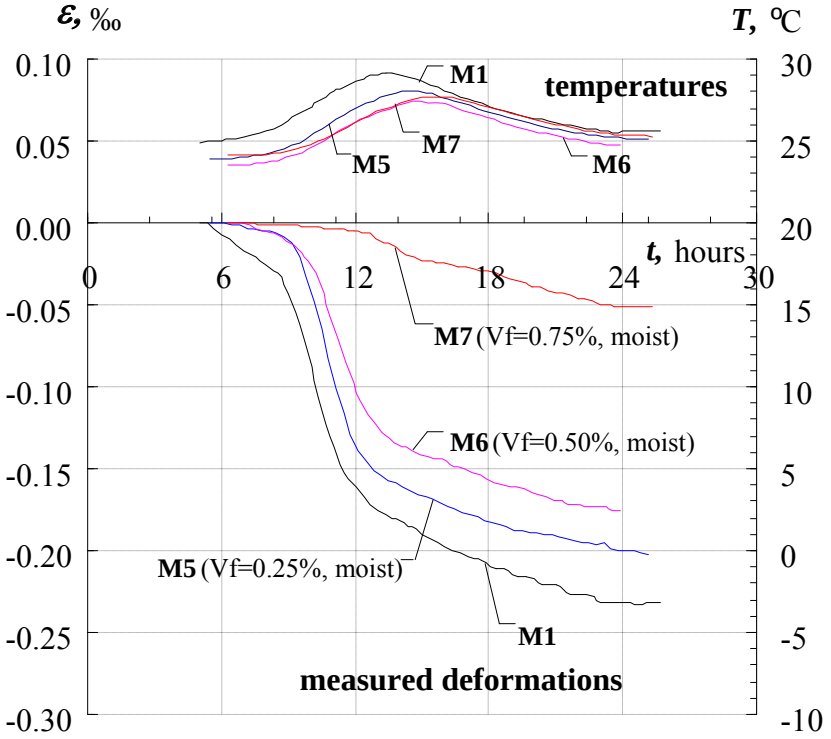

Figure 4 The measured deformations of the composites containing moistened polypropylene fibres, during the first 24 hours

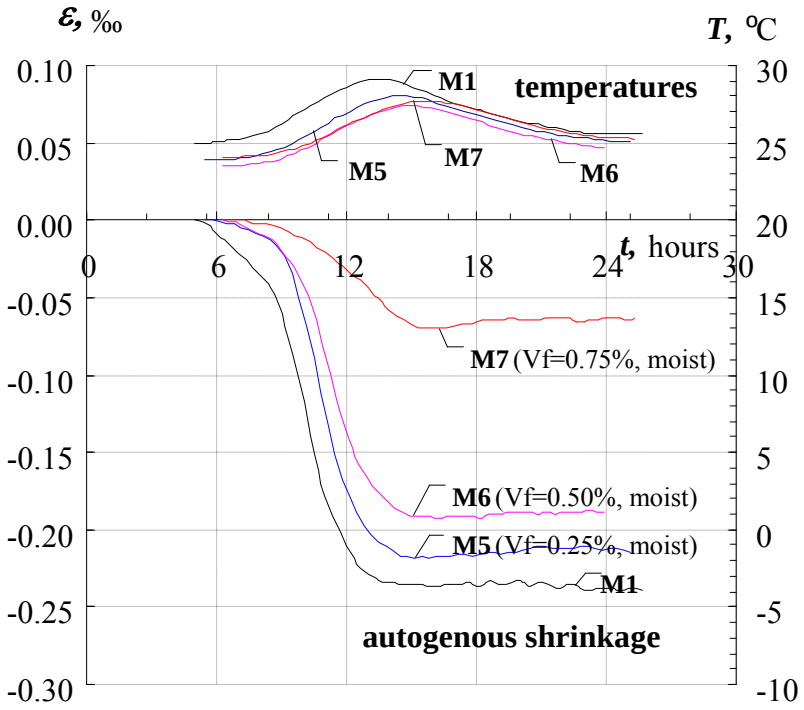

Figure 5 The autogenous shrinkage of the composites, containing moistened polypropylene fibres, during the first 24 hours

Figure 2 shows the total shrinkage, over the first 24 hours, of the high performance concrete containing various volumetric contents of polypropylene fibres. All of the fresh concrete and composite mixtures M1, M2, M3 and M4 had the same water-to-binder ratio of 0.36. The amount of aggregate in the composite mixtures M2, M3 and M4, containing dry polypropylene fibres, was reduced by the respective volumetric amounts of the added fibres.

Figure 3 shows the variation over time of the test specimen temperature, and the time development of autogenous shrinkage, of the fibre reinforced high performance concrete containing various volumetric contents of added polypropylene fibres, over the first 24 hours after the casting of the specimens. The effect of thermal expansion/contraction due to changes in the specimen temperature during the period of rapid setting of the cement has already been implicitly considered in this case. It is evident from the presentation of the experimental results that the shrinkage of fibre reinforced concrete decreases with an increasing content of polypropylene fibres.

The shrinkage of high performance concrete without fibres is about the same as the shrinkage of high performance concrete with a fibre content of 0.25% by volume. The shrinkage of the test specimens prepared from the high performance concrete mixture M4, which contained 0.75% by volume of polypropylene fibres, is about 25% less than the shrinkage of the comparable concrete without fibres, and 10% less than the shrinkage of the specimens of mixture M3, which contained 0.50% by volume of polypropylene fibres.

Figure 4 shows the measured deformations of the fibre reinforced high performance concrete test specimens containing 0%, 0.25%, 0.50% and 0.75% by volume of previously moistened polypropylene fibres. It is clear from the presented results that the shrinkage of fibre

reinforced concrete decreases with an increased volumetric content of polypropylene fibres. Thus, the lowest shrinkage occurred in the case of mixture M7, which contained 0.75% of polypropylene fibres.

The previously moistened polypropylene fibres in mixtures M5, M6 and M7 acted as an internal water reservoir in the cement paste. In this way, water is properly spatially distributed throughout the whole volume of the composite, and its content is also higher than in the case of the comparable mixture without any added moistened polypropylene fibres. This results in lower capillary forces in the relatively fresh fibre reinforced concrete, and thus lower autogenous shrinkage during the first 24 hours after casting, compared to the shrinkage of the comparable concrete without fibres – mixture M1.

It is clear from the presentation of the results (Figure 5) that shrinkage decreases with an increase in the volumetric content of polypropylene fibre. The autogenous shrinkage of the test specimens based on concrete mixture M6, which contained 0.50% of moistened polypropylene fibres, is approximately 25% less than the shrinkage of the comparable concrete without fibres, and 15% less than the shrinkage of the test specimens based on mixture M5, which contained 0.25% of moistened polypropylene fibres. The shrinkage of the test specimens based on mixture M7, with a polypropylene fibre content of 0.75% by volume, is 73% less than the shrinkage of the comparable concrete without fibres.

Discussion of the Experimental Results

From the measured deformations (Figure 2) and the autogenous shrinkage (Figure 3) of the dry polypropylene fibre reinforced high performance concrete, it is clear that the deformations, and, respectively, autogenous shrinkage of the composites decrease in about the same proportion as the fibre content increases. On the basis of the measured results it can be concluded that polypropylene fibres restrain the autogenous shrinkage of composites to a certain degree, from the very beginning of the hardening process. The strength of the bond between the fibres and the cement paste increases with the simultaneous increase in the stiffness of the cement paste during the composite hardening. For this reason, the shrinkage restraint of the cement paste by means of the fibres increases over time, so that the differences in autogenous shrinkage among the composites with various contents of fibres increase over time, too.

The differences in the measured deformations and autogenous shrinkage between the comparable concrete without fibres and the composite with a volumetric fibre content of 0.25% are about equal to the differences in the measured deformations and autogenous shrinkage between the composite with a fibre content of 0.25% and the composite with a fibre content of 0.50% (Figures 4 and 5). It therefore follows that the mutual differences in the measured deformations and autogenous shrinkage are approximately proportional to the fibre content. The measured deformations and, respectively, autogenous shrinkage of the composite with a fibre content of 0.75% are, however, essentially less than those of the composite with a fibre content of 0.50%.

Two physical effects have a favourable effect on the decrease of the autogenous shrinkage of the high performance composite with previously moistened polypropylene fibres. The influence of dry or moistened polypropylene fibres through the fibre stiffness on the restraining of the autogenous shrinkage of the composite is approximately the same. In the

case of using of previously moistened polypropylene fibres, as a consequence of the water reserves retained by the fibres an additional reduction in the autogenous shrinkage of the composite, compared to the composite containing dry fibres, was observed.

CONCLUSIONS

The early autogenous shrinkage of high performance concrete reinforced by polypropylene fibres is lower than that of the comparable high performance concrete without fibres. The reduction in shrinkage depends primarily on the volumetric content of the fibres used, and on their previous moistening.

Depending on the fibre content and previous moistening of the polypropylene fibres, the autogenous shrinkage of the composite within the first 24 hours is 5% to 78% less, than the shrinkage of the comparable concrete without fibres, respectively.

The autogenous shrinkage of high performance fibre reinforced concrete containing previously moistened polypropylene fibres is lower than that of a comparable fibre reinforced concrete containing non-previously moistened fibres, whereas the 28-day compressive strength and the flow of fresh composite are approximately the same.

ACKNOWLEDGEMENTS

The investigation described in this paper was partly financed by the European Union, from the European Social Fund.

REFERENCES

1. BALAGURU P N AND SHAH S P, Fiber-Reinforced Cement Composites. McGraw-Hill, Inc., New York, 1992.

2. BENTUR A AND MINDESS S, Fiber Reinforced Cementitious Composites. Taylor and Francis, London and New York, 2007, 601 p.

3. BANDELJ B, SAJE D, ŠUŠTERŠIČ J, LOPATIČ J AND SAJE F, Free shrinkage of high performance steel fibre reinforced concrete. Journal of Testing and Evaluation, Vol. 39, No. 2, 2011, pp. 166-176.

4. BARR B AND EL-BADEN A, Shrinkage of normal and high strength fibre reinforced concrete. Proceedings of the Institution of Civil Engineers, Structures & Buildings, London, Vol. 156, No. 1, 2003, pp. 15-25.

5. SAJE D, LOPATIČ J AND SAJE F, The Influence of Concrete Ingredients on Shrinkage of High Performance Concrete. Journal of the Mechanical Behavior of Materials, Vol. 14, Nos. 2/3, 2003, pp. 173-182.

6. BANTHIA N AND GUPTA R, Influence of polypropylene fibre geometry on plastic shrinkage cracking in concrete. Cement and Concrete Research, Vol. 36, No. 7, 2006, pp. 1263-1267.

7. KOVLER K, SIKULER J AND BENTUR A, Free and restrained shrinkage of fibre reinforced concrete with low polypropylene fibre content at early age. Fourth RILEM International Symposium on Fibre Reinforced Cement and Concrete, RILEM, Sheffield, 1992, pp. 91-101.

8. MYERS D, KANG T H K AND RAMSEYER C, Early-Age Properties of Polymer Fibre-Reinforced Concrete. International Journal of Concrete Structures and Materials, Vol. 2, No. 1, 2008, pp. 9-14.

9. SWAMY R N AND STAVRIDES H, Influence of Fibre Reinforcement on Restrained Shrinkage and Cracking. ACI journal, Vol. 76, No. 1, 1979, pp. 443-460.

10. ZOLLO R F, Collated fibrillated polypropylene fibres in FRC. Fibre reinforced concrete –international symposium 81, American Concrete Institute, Detroit, Vol. 81, 1984, pp. 397-409.

11. ZOLLO R F, ILTER J A AND BOUCHACOURT G B, Plastic and drying shrinkage in concrete containing collated fibrillated polypropylene fibres. 3rd Int. Symp. on Developments in Fibre Reinforced Cement and Concrete RILEM Symposium FRC, Vol. 86, No. 1, 1986, RILEM Technical Committee 49-TFR, Cachan, France.
12. BAYASI Z AND ZENG J, Properties of polypropylene fibre reinforced concrete. ACI Material Journal, Vol. 90, No. 6, 1993, pp. 605-610.

13. ALY T, SANJAYAN J G AND COLLINS F, Effect of polypropylene fibres on shrinkage and cracking of concretes. Materials and Structures, Vol. 41, No. 10, 2008, pp. 1741-1753.

14. EN 206. CONCRETE - Specification, performance, production and conformity. CEN, Brussels, Belgium, 2000.

15. SAJE D, BANDELJ B, ŠUŠTERŠIČ J, LOPATIČ J AND SAJE F, Shrinkage of polypropylene fibre reinforced high performance concrete. ASCE Journal of Materials in Civil Engineering, Vol. 23, No. 7, 2011, pp. 941-952.

16. TAZAWA E, Autogenous shrinkage of concrete, E&FN Spon, London, 1999, 411 p.

17. SAJE D, Compressive strength and shrinkage of high strength concrete. Ph.D. thesis, 2001, University of Ljubljana, Ljubljana, Slovenia (in Slovenian).

Repair of Pre-loaded RC Columns Using External CFRP Sheets and Embedded Longitudinal Steel Reinforcement

A Morsy, M El-Tony
Alexandria University, Egypt

This paper presents results of an experimental investigation on the behavior of axially preloaded short circular columns that have been repaired with carbon fiber-reinforced polymer (CFRP) wrap. A total of six R.C. columns have been subjected to compression load up to three different loading levels (unloaded column "0% of ultimate load", loaded until cracking load "85% of the ultimate load", and loaded till failure 100% of ultimate load) then all the loaded column confined using CFRP wrap and subjected again to compression loading. Also a unique method has been presented in this paper for those three repaired columns using four reinforcing steel bars were embedded as near surface mounted with epoxy in grooves through the concrete cover then covered by the CFRP wrap, those additional longitudinal reinforcement could consider as replacement of any corroded existing reinforcement.

Dr. Alaa Morsy has ten years of experience in Structural engineering, practice and research. During this period he teaches more than 15 courses for under-graduate students He has a strong background in Design of Reinforced Concrete & Metallic Structures, Use Advanced Composite Materials (FRP) in Repair and Strengthening of R.C., Heat Transfer and fire Protection, and Use Finite Elements Soft wares in Modelling.

M. El-Tony is a Structural Engineering Department within the Faculty of Engineering, Alexandria University, Egypt.

Keywords: CFRP, Confinement, Preloading, Strengthening, Wrapping

INTROUDUCTION

Carbon fibre-reinforced polymer (CFRP) jackets have been extensively used to improve the performance of columns in terms of strength and ductility by providing adequate lateral confining pressure to the column. This confining pressure places the concrete in a tri-axial state of stress, altering the load-deformation characteristics of the concrete and enable concrete to sustain both higher axial load and ultimate axial strain [1, 2]. In case of a circular cross-section, the jacket exerts a uniform confining pressure resulting in a uniform tri-axial stress field. However in a non-circular cross section, the confinement results in a complex non-uniform tri-axial stress field, which generally results in a lower level of performance in comparison to circular cross sections [3].

Several studies have been conducted to investigate the axial behavior of concrete columns confined with CFRP jackets [-13]. These studies have all indicated that CFRP jackets enhance the compressive strength and axial strain of confined concrete. Thus far, the main thrusts of research involving CFRP-jacketed columns aimed at characterize the behavior of columns with circular cross sections [4-8]. The results of such research have wide applicability, particularly with regard to circular bridge piers. However, the vast majority of all columns in buildings are square or rectangular columns. Therefore, their strengthening and rehabilitation need to be given attention to preserve the integrity of building infrastructure.

Another method for strengthening RC members with FRP is the Near surface mounting (NSM) technique, where grooves are cut in the concrete cover and FRP rods or thin plates referred to as strips are installed inside these grooves and bonded using an epoxy adhesive. These techniques were widely used specially in shear or flexural strengthening of beams [13-17].

The authors therefore suggest similar technique for strengthening RC columns, where grooves are cut through the column concrete cover and then steel bars are embedded in the grooves using grout or epoxy adhesive then the columns wrapped using CFRP sheets. This technique has the same advantage as the NSM technique in beams; in addition the embedment of the steel external reinforcement bars inside the columns will improve the carrying loading capacity of the column and compensate any corroded internal longitudinal reinforcement. The presence of the reinforcement inside the column may also improve ductility of the columns. On the other hand, few researches deal with the confining effect of preloaded columns with different percentage of loading capacities of the ultimate load [18], and the efficiency of CFRP wrapping in column repairing. The details and results of a pilot test program that was undertaken to examine the feasibility of this technique and the effect of repairing preloaded columns are presented in the following sections

RESEARCH SIGNIFICANCE

The research aim to study two main parameters, first; the pre-loading effect on the efficiency of the CFRP wrapping in enhancing the R.C. column axial load capacity, then three columns specimens were tested under different loading level (0%, 85%, 100% of the ultimate failure column load) which indicate the control column without loading, the column load until the first cracks appear, and the totally failed column respectively.

Second; the research investigates a unique method for strengthening using additional four longitudinal steel bars embedded in the concrete cover grooves similar to near-surface mounted method then covering it using wrapping by CFRP sheets.

EXPERIMENTAL DETAILS

Six specimens were tested in this program; all columns have been wrapped with one layer of CFRP sheets. Three specimens were tested without embedded longitudinal steel reinforcement and the other three specimens with the embedded longitudinal steel reinforcement. All the specimens tested under the three different loading levels. The following is a description of the specimens and the materials used.

Description of the columns

Six molds made of 6 mm PVC were constructed and used for casting the specimens vertically. Specimens were cast immediately after mixing in the moulds, and then compacted with the help of vibrating table. All specimens were exposed to identical curing conditions. The columns have circular cross section with 160 mm diameter and of total height 1000mm. Four steel bars of 8 mm diameter were used as longitudinal reinforcement, the transverse reinforcement were at spacing 120 mm with 6 mm diameter. While the top and bottom of the column having extra stirrups at spacing 50 mm to prevent failure due to stress concentration at both ends of column. Figure 1 shows the Longitudinal and cross section reinforcement detail of the experimental columns. The concrete cover was kept constant at 20 mm in all RC columns. As an attempt to prevent the occurrence of premature failure at the ends, the column ends were also capped with external steel cap of 4 mm thickness as shown in Fig. 2. This configuration forced general failure to occur within the test region. Also the steel cap served to stabilize the column during testing.

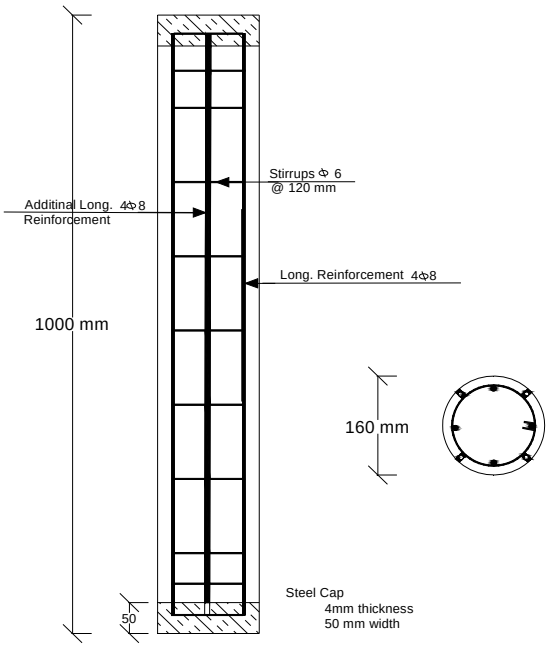

Figure 1 Longitudinal and cross section detail of the experimental columns

Figure 2 Confined column with steel capping before loading

Strengthening Process

Preparation of the concrete substrate and application of CFRP materials were carried out in accordance with the guidelines for application to concrete that was provided by the material manufacturers. The surfaces of all columns to be wrapped are ground using mechanical metallic brush (grinding) to remove any dust or grease from concrete surface and to open the pore structure to make the epoxy primer penetrate through the concrete and ensure strong bond between the concrete and CFRP sheets. The prepared concrete surface is coated with a layer of epoxy-based primer using a short nap roller. CFRP sheet is then placed on concrete surface and pressed normally to the concrete surface using roller brush to remove air pockets from beneath the fibre sheets. A 100-mm overlap is necessary to provide sufficient anchorage in order to achieve the full tensile strength of the fibre sheet and prevent slip between layers. In all cases, the principal fibres were oriented perpendicular to the column axis.

Instrumentation and Load Application

Before assembling the reinforcing cages, electrical resistance strain gages were installed to measure the strain in both longitudinal embedded bars and lateral strain gauge on the CFRP at the mid height of the column and they were oriented in vertical and lateral directions to monitor the axial and lateral strains, respectively. In addition to the dial gauge to measure the vertical deformability of the column. Universal compression testing with 3000 kN capacity were used for testing. The loads were applied in small increments and the strains were recorded at a 50 kN-interval. The load control mode was followed throughout the program. Tests were conducted at the material laboratory of the structural engineering department in Alexandria University, Figure 3 shows the test setup and instrumentation of the tested column

Figure 3 Test Setup and column instrumentation

Test Specimens and Preparation

Six identical column constructed as mentioned in the previous section were tested in this program. All columns have been strengthened using one layer or CFRP. The specimens divide into two groups according to the presence of embedded near surface mounted longitudinal reinforcement. The first group consists of three specimens were not reinforced using external near surface mounted steel bars, "Control C1" was a control specimen strengthened and testing without any preloading, the second specimen "C2" strengthened after loaded up to 80% of the ultimate load which correspond to the visual of first crack in the column, the third specimen "C3" strengthened after loaded up to failure load and repairing the column in the crushing part at the top of column using concrete with admixture for bonding the old concrete with the new repairing concrete after removing the loose concrete the spalled area was repaired using a fast-set non-shrink mortar as shown in Figure 4.

The second group consists of three specimens reinforced using four external near surface mounted steel bars of diameter 8mm and steel grade of yielding strength 240 MPa and ultimate strength 360 MPa, the external reinforcement embedded inside groove in the column concrete cover and cover by cementitious grout material, as shown in Figure 5, the forth column "C4" was a strengthened and testing without any preloading, the fifth specimen "C5" strengthened after loaded up to 80% of the ultimate load which correspond to the visual of first crack in the column, the six specimen "C6" strengthened after loaded up to failure load and repairing the column in the crushing part. Table 1 provides a summary of the details of the specimens used in this program.

Figure 4 Repairing the top part of the loaded column (C3) before strengthening

Figure 5 Failure and first crack loads and embedding the external reinforcement into the column concrete cover

Table 1 Specimen specifications

SPECIMEN	SPECIFICATION
C1	Strengthened R.C. column with FRP, without internally embedded steel reinforcement and un-loaded
C2	Strengthened R.C. column with FRP, without internally embedded steel reinforcement and loaded till 80% failure load
C3	Strengthened R.C. column with FRP, without internally embedded steel reinforcement and loaded till full failure load after curing and repairing the crushed part
C4	Strengthened R.C. column with FRP, with internally embedded steel reinforcement and un-loaded
C5	Strengthened R.C. column with FRP, with internally embedded steel reinforcement and loaded till 80% failure load
C6	Strengthened R.C. column with FRP, with internally embedded steel reinforcement and loaded till full failure load after curing and repairing the crushed part

Material Properties

The concrete used in these tests had strength of 30 MPa based on testing 150 mm cubes. The steel bars used for the longitudinal and stirrups reinforcement had nominal yield strength of 240 MPa respectively. Sikawrap 230 CFRP sheets manufactured by SIKA chemical company were used for column strengthening with 0.131 mm thickness. The mechanical properties of the used CFRP laminate and its epoxy are shown in Table 2.

Table 2 Mechanical properties for CFRP laminate and adhesive

MATERIAL	PROPERTY			
	Ultimate Tensile Strength, MPa	Ultimate Strain	Elastic Modulus, MPa	Density
CFRP laminate	4300	1.8%	238,000	1.76 g/cm3
Adhesive	30	---	4,500	1.31 kg/l

RESULTS AND DISSCUSSION

The test results of the six columns are listed in Table 3 that includes the ultimate load and the ultimate strain in CFRP sheets. Other collected data at various load stages is represented graphically. Observed crack patterns and mode of failure are discussed for each column.

Overall Behavior and Failure Modes

The failure of the columns in all cases was brittle an early noise due to concrete cracking was noticeable related to the micro cracking of concrete core was evident when the applied load approached 60 ton, This level may be corresponding to the unconfined strength of the column, indicating the start of stress transfer from the dilated concrete to the CFRP wrap.

Prior to the failure, cracking noises were frequently heard. The failure was gradual, ending with a sudden and explosive noise.

The failure of the wrap initiated away from the overlap region at mid-height of the specimen and progressed to the top and bottom of the specimen. The sudden and explosive nature of the failure indicates the release of extraordinary amount of energy as a result of the uniform confining stress provided by the wrap. Inspection of the broken samples showed good contact between the wrap and the concrete indicating that no de-bonding took place at any stage throughout the loading process, and test was terminated due to the rupture of CFRP sheets. Figure 6 shows failure mode for all columns.

Table 3 Failure and first crack loads

SPECIMEN NO	PROPERTY			
	Failure load, ton	FRP Ultimate strain	% increase/decrease over un-loaded specimens	% increase / decrease over the specimen without external reinforcement
C1	102	0.0039	----	----
C2	108	0.0052	+ 5.8%	----
C3	60	0.0012	- 41.1%	----
C4	100	0.0004	----	-2.0%
C5	105	0.007	+ 5.0%	-2.7%
C6	80	0.0008	- 20%	33.3%

Comparing the failure loads for the tested columns as shown in Figure 7, it can be found that there are very slight effect for preloading columns up to the cracking load (80% of the ultimate load) compared to the unloaded columns either the columns with or without embedded steel reinforcement. However this preloading level put a slight positive effect on the capacity of confined columns, these phenomena is clearly shown also in both columns with or without external embedded reinforcement.

On the other hand preloading the column up to failure load decrease its carrying loading capacity compared to the unloaded column by 41.1% and 20% for the columns without embedded steel reinforcement and with embedded steel reinforcement respectively, in spite of this decrease in the loading capacity the column keep the same capacity of the unconfined column without any strengthening, that is means that the totally failed/crushed column then repaired using one layer of CFRP sheets can attain its initial capacity before strengthening.

Moreover the presence of embedded steel reinforcement could help in increasing the carrying loading capacity of the columns especially in the totally loaded column before repairing with CFRP sheets. Also it is clearly shown that there no effect of presence embedded steel reinforcement in the unloaded columns or the columns loaded by 80% of the ultimate load, this may be related to the weak bond between the embedded steel reinforcement and the concrete. While it gives significant effect in the loaded columns up to failure over the same columns without embedded steel reinforcement by 33.3%

Figure 6 Failure modes for all columns

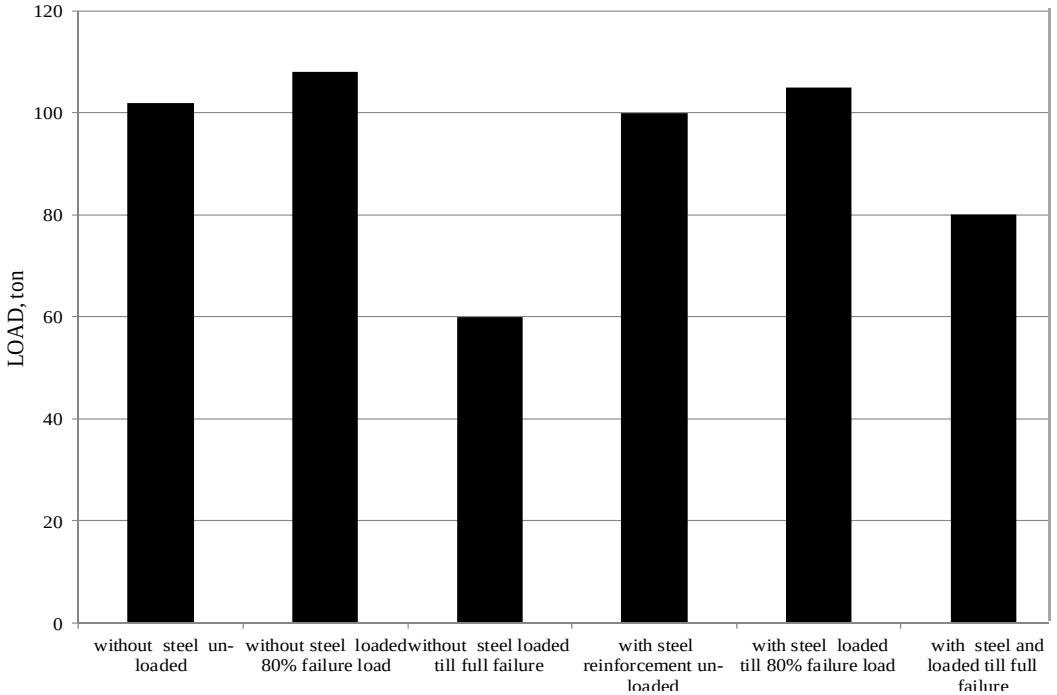

Figure 7 Ultimate loads for all tested columns

Load-Deflection and Load-Strain Relationships

The columns were tested using a load control universal testing machine. The transverse strain in CFRP sheets and the longitudinal strain in external near surface mounted steel bars were recorded using electrical strain gauges. The loads were applied continuously and recorded, along with the dial gauge and strain gauges readings using digital strain indicator. Application of the loads and the recording process continued until complete failure of the column occurred. The load versus transverse strain in CFRP sheets behavior of all the six tested specimens are shown in Figure 8.

It is clearly shown that the three columns (C1, C2, and C5) attain a large transverse strain up to 0.004, 0.005 and 0.007 mm/mm respectively compared to the other three columns (C3, C4 and C6) which indicate very low transverse strain 0.0012, 0.0004 and 0.0008 respectively. This implies that failure initiated at a location away from the location of strain gage, as all the strain gauge located at the mid height of the column while in specimens C3, C4, and C6 the failure occur at the upper third of the column height.

It should be reported herein that the maximum measured transverse strain in CFRP was found in column C5 was approximately 0.007 mm/mm, which corresponded to 38.8 % only of the reported ultimate strain of CFRP, that's confirmed that the rupture of CFRP away from the position of the strain gauge.

Also it is clearly shown that when comparing the stiffness for all columns, both preloaded columns up to failure exert lower stiffness than the unloaded column or preloaded up to 80% of the failure load; this may be related to the repairing process for those columns decrease the stiffness for the columns.

Also it can be stated obviously the column C1 has the largest stiffness as it is unloaded before testing compared to the loaded columns C2, and C3, and to ensure this behavior also the column C4 having large stiffness compared to C5, and C6. This indicates that the pre-loading the columns decrease the stiffness of the columns either having embedded steel reinforcement or without embedded steel reinforcement

Comparing the effect of embedded steel reinforcement the behavior of the two columns C2 and C5, which has the same preloading load (80%) and the same failure zone (mid-height) while C2 without embedded steel reinforcement and C5 with embedded steel reinforcement. It can be concluded that presence of embedded steel reinforcement lower the stiffness of the column and increase its ductility.

Comparing the strain in longitudinal embedded steel reinforcement with the unloaded specimen, C4 with the loaded specimen up to 80% of failure load C5, it clearly shown that the preloading effect decreased the strain in the longitudinal embedded steel reinforcement.

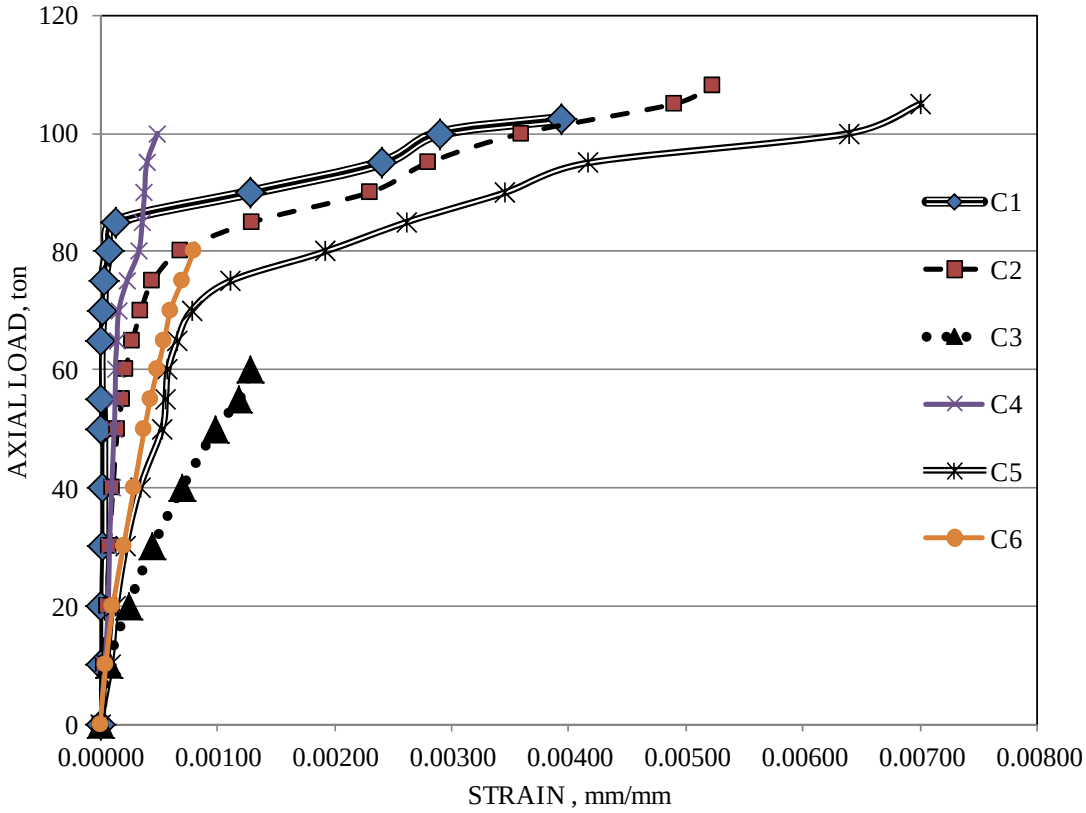

Figure 8 Load vs transverse strain in CFRP sheets for all specimens

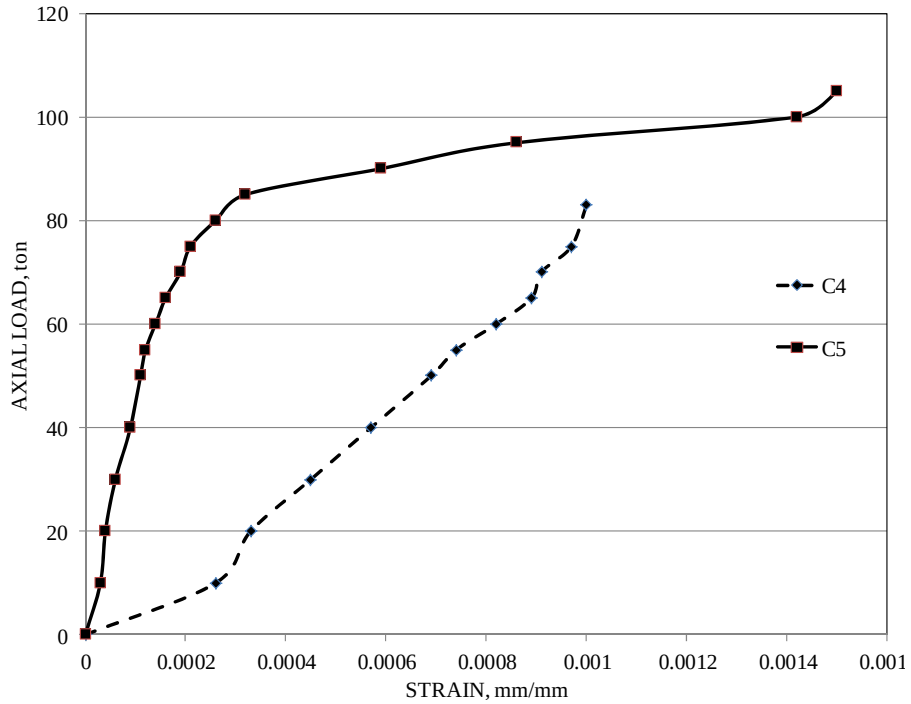

Figure 9 Load vs. longitudinal strain in external steel bars for specimen C4 and C5

CONCLUSIONS

This paper has presented the results of an experimental program investigating the effect of preloading on the confinement effect of columns repaired by CFRP sheets and also the effect of adding additional external steel reinforcement as near surface mounted in the behavior of repaired preloaded specimens. Based on the experimental results, and observations, the following conclusions can be stated:

- There is a very slight effect for preloading strengthened columns up to the cracking load (80% of the ultimate load) compared to the unloaded strengthened columns either the columns with or without embedded steel reinforcement.
- Preloading the column up to failure load decrease its carrying loading capacity compared to the unloaded column by 41.1% and 20% for the columns without embedded steel reinforcement and with embedded steel reinforcement respectively.
- The totally loaded column up to failure can attain its initial capacity without strengthening by repairing the spalled concrete parts it then wrapping it by one layer of CFRP.
- The presence of embedded steel reinforcement could help in increasing the carrying loading capacity of the columns especially in the totally loaded column before repairing with CFRP sheets.
- The pre-loading the columns decrease the stiffness of the columns either having embedded steel reinforcement or without embedded steel reinforcement
- The positions of both CFRP strain gauge and the CFRP failure zone have large effect for the value of transverse strain, as failure zone initiated at a location away from the location of strain gage.
- Presence of embedded steel reinforcement lowers the stiffness of the columns and increases its ductility.

REFRENCES

1. CHIRS COLE AND ABDELDELIL BELARABI, “FRP Jacketed Reinforced Concrete Columns,” Center For Infra Structure Engineering Studies, Department of Civil Engineering, University of Missouri-Rolla, May 2001
2. AZADEH PARVIN AND WEI WANG, “Behavior Of FRP Jacketed Concrete Columns Under Eccentric Loading,” Journal of Composites for construction, ASCE, Vol 5, No.8, August 2001, pp.146-152.
3. AMIR MIRMIRAN AND MOHSEN SHAHAWY, “Behavior of Concrete Columns Confined By Fibre Composites,” Journal of Structural Engineering, ASCE, Vol. 123,No. 5, May 1997, pp.583-590.
4. KALED SALEH, “New Aspects In Strengthening R.C. Columns With FRP” Proceeding of Structural Composites For Infrastructure Applications Conference, Aswan, Egypt, 2002.

5. ABDELHADY HOSNY,HAMDY SHAHIN,AMR ABDELRAHMAN AND TAMER EL-AFANDY, " Uni-axial Tests on Rectangular Columns Strengthened With CFRP " Proceeding of Structural Composites For Infrastructure Applications Conference, Aswan, Egypt, 2002.

6. HATEM GITH AND HANAN ANWAR, "Confinement Effect of Continuous GFRP wrapping On the Behavior of R.C. Columns" Proceeding of Structural Composites For Infrastructure Applications Conference, Aswan, Egypt, 2002.

7. SAID M.ALLAM AND TAREK I.EBEIDO, "Efficiency of CFRP Wrapping on R.C. Columns under Concentric and Eccentric Loading," Alexandria Engineering Journal, Vol.41, 2002, No.3, 449-512

8. YUNG C. WANG AND JOSE I. RESTREPO, " Investigation of concentrically loaded reinforced concrete columns confined with Glass Fibre Reinforced Polymers jackets," ACI Structural Journal, May –June 2001, pp 337-385

9. OMAR CHAALLAL , MOHASEN SHAHAWY AND MUNZER HASSAN , " Performance of Axially Loaded Short Rectangular Columns Strengthened With Carbon Fibre-Reinforced Polymer Wrapping , "Journal of Composites for construction, ASCE, Vol 7,No.3, August 2003, pp.200-208.

10. PIERRE ROCHETTE AND PIERRE LABOSSIERE, " Axial Testing Of Rectangle Column Models Confined With Composites, "Journal of Composites for construction, ASCE, Vol 4,No.3, August 2000, pp.129-136.

11. ACI COMMITTEE 318, "Building Code Requirements for Reinforced Concrete (ACI 318-02)," American Concrete Institute, Farmington Hills, Michigan, 2002.

12. SAATCIOGLU, M., AND YALCIN, C., "External Prestrssing Concrete Columns for Improved Seismic Shear Resistance," ASCE Journal of Structural Engineering, Vol. 129, No. 8, 2003.

13. ALAA MORSY.ET AL, "Behavior of axially loaded columns strengthened with carbon fibre reinforced polymers," Fifth Alexandria international conference for structural and geotechnical engineering , December 2003.

14. RIZZO, A AND DE LORENZIS, L. 2009. Behavior and capacity of RC beams strengthened in shear with NSM FRP reinforcement. Construction and Building Materials 23: 1555-1567.

15. DE LORENZIS L AND TENG J.G. 2007. Near-surface mounted FRP reinforcement: an emerging technique for structural strengthening. Composites: Part B. 38(2):119–143.

16. DE LORENZIS L, NANNI A. 2001. Shear strengthening of reinforced concrete beams with NSM fibre-reinforced polymer rods. ACI Structural Journal. 98(1):60–68.

17. DIAS, S.J.E. AND BARROS, J.A.O. 2010. Performance of reinforced concrete T beams strengthened in shear with NSM CFRP laminates. Engineering Structures. 32: 373-384.

18. ZHENG HE, et al "Seismic performance of preloaded R.C. columns confined with CFRP materials" 16th International Conference on Composite Structures, FEUP, Porto, 2011

Compressive Strength and Microstructure of Autoclaved Aerated Concrete Produced with Partial Replacement of Cement by Bottom Ash and Fly Ash

W Wongkeo, P Thongsanitgarn, K Pimraksa, A Chaipanich
Chiang Mai University, Thailand

This research investigated the use of coal bottom ash and fly ash from Mae Moh power plant, Lampang, Thailand, as Portland cement replacement to produce autoclaved aerated concrete. Portland cement, sand, bottom ash, fly ash, aluminium powder (added at 0.2 percent by weight) and calcium hydroxide were used. Compressive strength and physical properties tests were then carried out after the concrete were autoclaved for 6 hours and left in air for 7 days. The results show that the compressive strength and unit weight increased while the permeable of void decreased when bottom ash and fly ash was used. Therefore, both bottom and fly ashes can be seen to have the benefit in enhancing the strength of aerated concrete (11.5 MPa for 30% bottom ash concrete and 11.0 MPa for 30% fly ash concrete) when compared to the results of the control Portland cement concrete (9.5 MPa). This is due to the tobermorite ($C_5S_6H_5$) formation as shown by scanning electron micrographs which gives a denser microstructure than α-C2SH phase formed in Portland cement mix.

Watcharapong Wongkeo is a Post Graduate Student (Ph.D.) at the Department of Physics and Materials, Faculty of Science, Chiang Mai University.

Pailyn Thongsanitgarn is a Post Graduate Student (Ph.D.) at the Department of Physics and Materials, Faculty of Science, Chiang Mai University.

Kedsarin Pimraksa is an Assistant Professor at Department of Industrial chemistry, Faculty of Science, Chiang Mai University.

Arnon Chaipanich is an Assistant Professor at Department of Physics and Materials, Faculty of Science, Chiang Mai University. His research interests include waste and by-products, cement replacement, concrete technology and advanced cement-based materials.

Keywords: Autoclaved concrete, Bottom ash, Compressive strength, Fly ash, SEM

INTRODUCTION

Concrete has been widely used as a construction material, commonly made by mixing Portland cement as a binder with sand, crushed rock and water. In the cement industry, a lot of energy is used in the burning process and this causes pollution in the form of carbon dioxide emissions which is known to directly cause global warming. Thus, the reduction of cement would save energy and reduce the environmental pollution. Nowadays, pozzolanic materials such as fly ash, blast furnace slag, silica fume and rice husk ash were used in blended cement especially fly ash (FA) which is widely used in cement replacement for concrete construction [1-6]. It is well known that the used of FA can improve workability and durability of concrete [7, 8].

Bottom ash (BA) is a by-product of thermoelectric power plants as well as FA. It is consisted of chemical composition similar to FA. However, the utilization of BA in the substitution of Portland cement is limited due to its high particle size (similar to that of natural sand) and porous particle, compared to FA. Thus, BA is mostly used as a partial sand replacement of concrete production and as a substitution of fine aggregates in lightweight concrete [9-11]. Kurama et al. [12] investigated the use of BA as an aggregate to produce aerated concrete. It is reported that the unit weight and compressive strength of autoclaved aerated concrete (AAC) decreased with increased BA content and the highest compressive strength of 2.78 MPa can be found. However, BA can be used to replace part of cement by reducing the particle size. Cheriaf et al. [13] studied the pozzolanic properties of BA by varying the time of grinding. It was found that the pozzolanic activity of BA increased with increased time of grinding and strength can be improved. Therefore, the utilization of BA as cement replacement can reduce cement usage while giving similar compressive strength.

In recent years, lightweight concrete (LWC) has been widely used in building construction due to its low density, low thermal conductivity, low shrinkage and high heat resistance. Aerated concrete is a type of lightweight concrete produced by creating gas bubbles in a cement slurry which when it sets leaves a sponge-like cellular structure [14]. Generally, aerated concrete is made from quartz-rich sand, lime, cement and aluminium powder as pore-forming agent. Mostly, these concrete was cured by autoclave under saturated steam pressure, termed ‘autoclaved aerated concrete (AAC)’ [12]. The aluminium powder reacts with calcium hydroxide to form hydrogen gas in the making of aerated concrete, as follows in Eq. (1) [14].

$$2Al + 3Ca(OH)2 + 6H2O \rightarrow 3CaO.Al2O3.6H2O + H2 \quad (1)$$

Autoclaved and the term autoclaving are synonymous with high-pressure steam curing. The most important improvement are product ready for use within 24 h (the strength is generally equivalent to 28 days under ambient curing), less shrinkage and lower moisture content after curing. High-pressure steam curing can only be used for precast concrete products. It can be used to advantage in the manufacture of specialty products, such as lightweight cellular concrete and calcium silicate (sand-lime) bricks [15]. Under the conditions of high temperature and pressure, the chemistry of hydration is changed. The α-C2SH phase is formed which cause an increase in porosity and reduction in strength. However, in the presence of reactive silica, tobermorite (C5S6H5) phase is formed on continued heating [16].

Pozzolanic materials such as fly ash or natural pozzolans are the important source of reactive silica. From previous studies, fly ash can be used as the source of reactive silica. Jing et al.

[17] found that the addition of fly ash 10–20 mass% was favorable to tobermorite formation on hydrothermal process. Yazici et al. [18] studied the use of fly ash and ground granulated blast furnace slag as an alternative silica source in reactive powder concrete. It is found that fly ash (FA) can be used as an alternative silica source to replace part of cement and it revealed the tobermorite formation after the samples were autoclaved.

Many researches studied physical properties of lightweight aggregate concrete produced from lightweight aggregate material such as pumice, expanded perlite and fly ash [19-23]. Little is known on the effect of BA as cement replacement using autoclaved curing method. Thus, the compressive strength of lightweight concrete made from bottom ash was investigated. BA and FA (in order to give comparison) were used to replace part of Portland cement at 10%, 20% and 30% by weight, respectively. All specimens were cured by autoclave under high-pressure stream curing. Compressive strength and physical properties tests were then carried out.

MATERIALS AND METHODS

Materials

Portland cement type 1, river sand and calcium hydroxide ($Ca(OH)_2$) were used in this study. Fly ash (FA) and bottom ash (BA) was obtained from Mae Moh Power Plant, Lampang, Thailand and aluminium powder (93% of purity) was supplied by HiMedia Laboratories Pvt. Ltd, India. The chemical composition of materials used in this research is given in Table 1. For FA and BA, the sum of SiO_2, Al_2O_3 and Fe_2O_3 are seen to be 70.21 and 81.97 %, respectively. Figure 1 shows XRD pattern of fly ash and bottom ash which consisted mainly of amorphous glassy phase with some crystalline phases. In addition, bottom ash can be seen to be irregular shape compared to spherical shape of fly ash as shown in Figure 2. The sieve size of fine aggregate is shown in Figure 3 with the maximum size at 4.75 mm.

Table 1 Chemical composition of materials used in this research

OXIDE	PORTLAND CEMENT (%)	FLY ASH (%)	BOTTOM ASH (%)	CALCIUM HYDROXIDE (%)
SiO_2	20.85	39.50	44.56	1.34
Al_2O_3	4.98	16.04	22.48	1.03
CaO	64.3	10.46	10.54	66.83
Fe2O3	3.52	14.67	14.93	0.89
MgO	1.53	9.26	2.54	3.27
Na_2O	0.12	3.76	0.77	0.57
K_2O	0.59	1.55	1.76	0.07
P_2O_5	-	0.26	0.19	0.15
TiO_2	-	0.21	0.46	0.07
MnO_2	-	0.27	0.12	0.17
SO_3	2.71	1.87	0.65	4.20
Loss on ignition	1.40	2.15	1.00	21.41

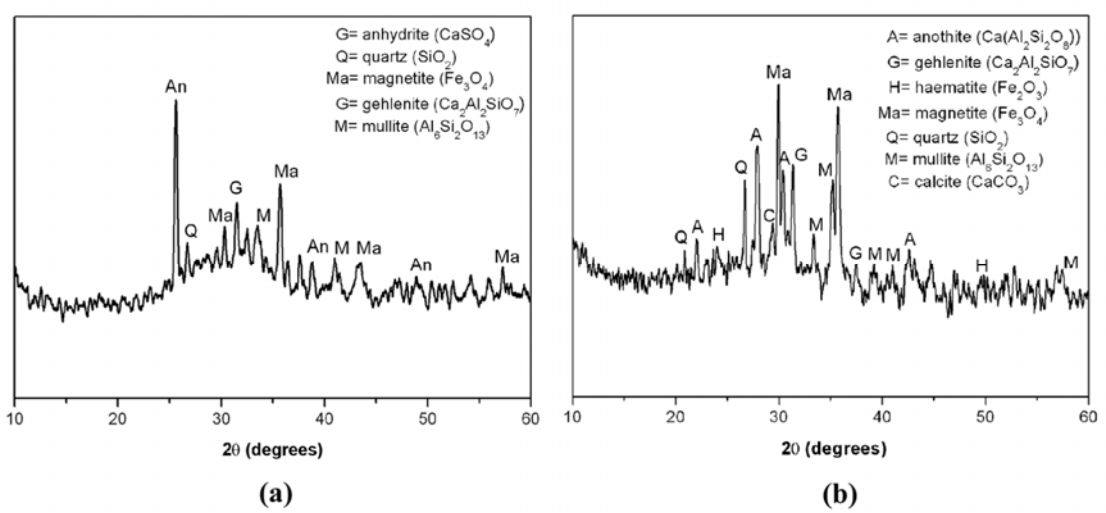

Figure 1 XRD pattern (a) Fly ash and (b) Bottom ash

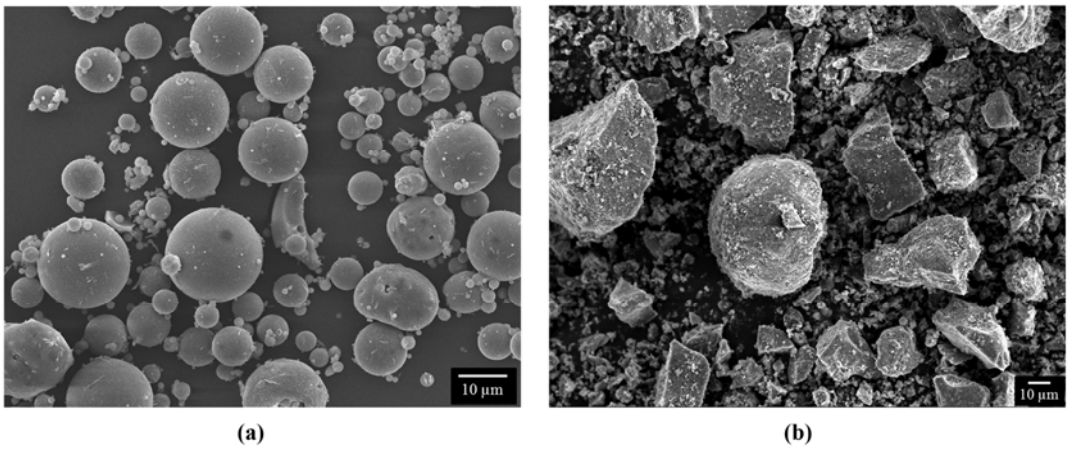

Figure 2 Scanning Electron Micrograph (a) Fly ash and (b) Bottom ash

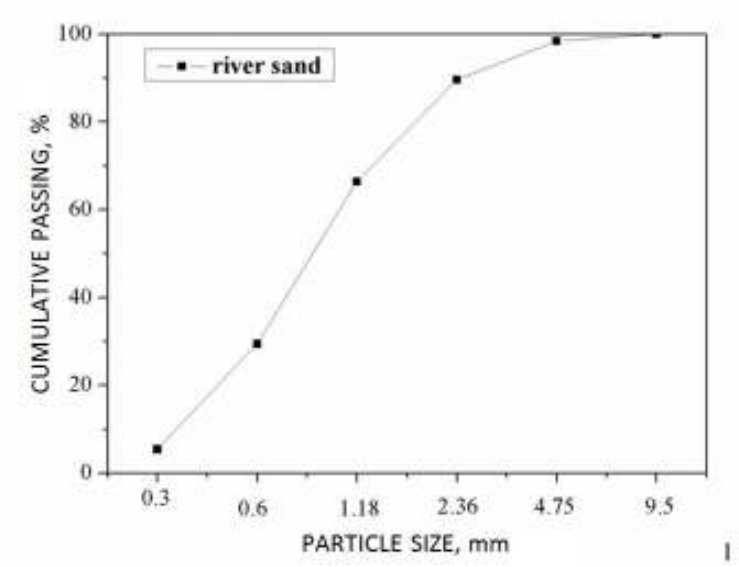

Figure 3 Sieve size distribution of fine aggregate used in the investigation

Mix Proportions

In this research, cement/sand/calcium hydroxide ratio (C: S: CH ratio) of 55: 40: 5 percent by weight at water to solid ratio (w/s ratio) of 0.29 was used in this design. FA and BA were used to replace Portland cement at 10%, 20% and 30% by weight and aluminium powder was added at 0.2% by weight of solid, respectively. The mix proportions of this research are given in Table 2.

Table 2 Mix proportion of FLWC and BLWC at PC:S:CH = 55:40:5

MATERIALS	MIX DESIGN						
	PC	10FA	20FA	30FA	10BA	20BA	30BA
Portland cement (kg/m^3)	853	768	682	597	768	682	597
Fly ash (kg/m^3)	-	85	171	256	-	-	-
Bottom ash (kg/m^3)	-	-	-	-	85	171	256
Sand (kg/m3)	620	620	620	620	620	620	620
Calcium hydroxide (kg/m^3)	78	78	78	78	78	78	78
Aluminium powder, 0.2% (kg/m^3)	3.08	3.08	3.08	3.08	3.08	3.08	3.08
Water, w/s = 0.29 (kg/m^3)	449	449	449	449	449	449	449
Ca/Si ratio[a]	3.36	2.85	2.41	1.79	2.78	2.32	1.70

[a] Calculated from percentage of chemical composition

Preparation of Specimens

BA was ground by ball mill for 6 hr (average size of 10 μm). The mixtures were mixed in a rotary mixer. After that, the mixtures were casted into cubic moulds (50x50x50 mm), compacted using a vibrating table and then kept at room temperature for 24 h. The specimens were then demoulded and were exposed to autoclave curing for 6 hr at the temperature of 126°C and pressure of 20 psi. Thereafter, the specimens were cured in air for a further 7 days. At 7 days, three samples per mix were investigated for compressive strength in accordance to ASTM C495-99a. In addition, three specimens were also tested for unit weight in accordance with the standard of ASTM C138-92.

RESULTS AND DISCUSSION

Compressive Strength

The compressive strength results of fly ash lightweight concrete (FLWC) and bottom ash lightweight concrete (BLWC) are indicated as shown in Figure 4. The compressive strength increased with increased FA and BA replacement of Portland cement. The increased compressive strength of FLWC and BLWC was resulted from the presence of tobermorite phases. In the autoclaved process, tobermorite has larger volume of the solid phase and therefore a reduction in porosity than α-C2SH phase when compared with LWC without FA and BA content that resulted to the increase in compressive strength. It is found that the Ca/Si ratio is decreased with increased FA and BA as cement replacement. The lower Ca/Si ratio would result to tobermorite (C5S6H5) formation but not lower than 0.8 [24]. The highest

compressive strength of 11.61 MPa was obtained from 30BA mixture and the increasing was 22.6% when compared with PC control (PC mixture). Kurama et al. [12] examined the use of coal bottom ash (BA) as an aggregate to produce aerated concrete using the water to solid ratio (w/s ratio) between 0.6 and 0.75 and with addition of 0.5 % aluminium powder. The specimens were cured at 12 atm and 180-200 °C for 8 and 18 hr. The highest compressive strength of 2.78 MPa was obtained from BAC-50 (50%BA) mixture and the increasing was 9.45% when compared with reference specimen at 18 hr curing time.

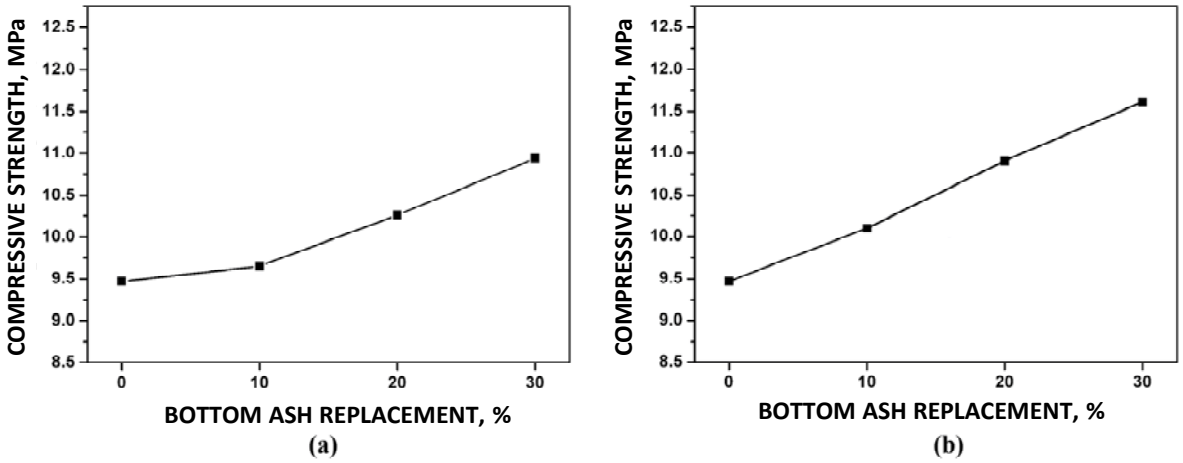

Figure 4 Compressive strength results at (a) FLWC and (b) BLWC

Physical Properties

Figure 5 shows the unit weight (bulk density) of FLWC and BLWC specimens related to FA and BA replacement. It can be seen that unit weight of LWC had slightly increased with increased FA and BA contents but not more than 1600 kg/m^3. Unit weight of LWC increased due to denser microstructure of FA and BA mixes benefited from the presence of tobermorite phases. Unit weight results agree with those of compressive strength results where the compressive strength had increased with increased BA contents. It is clear that unit weight has a direct relationship with compared compressive strength. In this study, the highest compressive strength and unit weight were 11.61 MPa and 1556 kg/m3, respectively. Similar strength and unit weight results were found by Topcu and Uygunoglu [21] whom investigated the properties of autoclaved lightweight aggregate concrete using pumice as an aggregate and found strength of ≈11 MPa at similar unit weight of 1500 kg/m3 when cured in autoclave for 6 hr.

The volume of permeable voids of FLWC and BLWC are shown in Figure 6. The volume of permeable voids is an important property of concrete as it affects the transport mechanisms through the concrete such as ingress of aggressive liquids and gases [25]. It is found that the volume of permeable voids decreased with increased FA and BA content. This agrees with the unit weight results where the voids decreased as the unit weight increased.

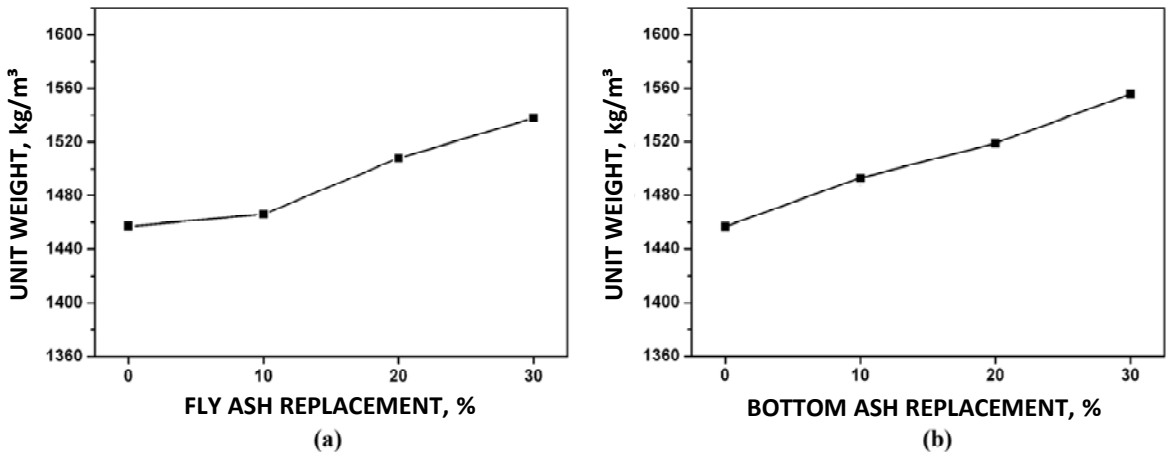

Figure 5 Unit weight results at (a) FLWC and (b) BLWC

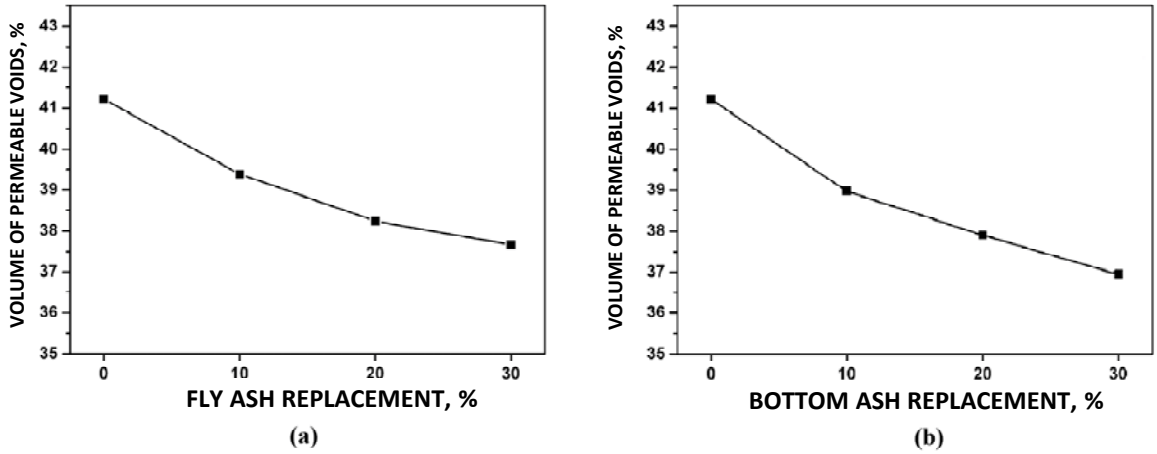

Figure 6 Volume of permeable voids results at (a) FLWC and (b) BLWC

Table 4 Summary of the compressive strength and physical properties results as relative percentage to autoclaved Portland cement control concrete

MIX	COMPRESSIVE STRENGTH (MPa)	RELATIVE COMPRESSIVE STRENGTH (%)	UNIT WEIGHT (kg/m^3)	RELATIVE UNIT WEIGHT (%)	VOLUME OF PERMEABLE VOIDS (%)	RELATIVE VOLUME OF PERMEABLE VOIDS (%)
PC	9.47	100.00	1457	100.00	41.22	100.00
10FA	9.65	101.90	1466	100.62	39.39	95.56
20FA	10.26	108.34	1508	103.50	38.24	92.77
30FA	10.94	115.52	1538	105.56	37.66	91.36
10BA	10.10	106.65	1493	102.47	38.97	94.54
20BA	10.91	115.20	1519	104.26	37.90	91.94
30BA	11.61	122.60	1556	106.79	36.94	89.62

SEM OBSERVATION

The SEM micrographs of LWC at PC: S: CH ratio of 55:40:5 with and without BA as a cement replacement can be seen in Figure 7. The micrograph (Figure 7 (a)) shows the fibrous-like C-S-H phase for LWC without BA as replacement part of cement (PC control) while the lath-like tobermorite and plate-like tobermorite phases show in LWC with BA as

replacement part of cement (Figure7 (b), (c) and (d)). From SEM micrographs, it can be seen that the tobermorite phases (both of lath-like and plate-like formation) give denser microstructure than fibrous-like C-S-H phase. The tobermorite phase was formed when the temperature of curing method has above 100 °C and Ca/Si ratio has ranged between 0.8 – 1.5 [24]. Normally, Ca/Si of LWC (PC control) has above 2.0 while LWC with BA as replacement part of cement (10, 20 and 30BA) has Ca/Si ratio below 2.0 due to the increasing of reactive silica (obtained from BA) which suitable for tobermorite formation . When cured in high temperature (100-150 °C), the α-C2SH was formed at PC control mixture while the tobermorite phase was formed at 10, 20 and 30%BA mixture. The α-C2SH phase has smaller volume of the solid phase and therefore an increase in porosity when compared to the tobermorite phase. As a consequent, denser microstructure due to the presence of tobermorite structure would lead to higher compressive strength.

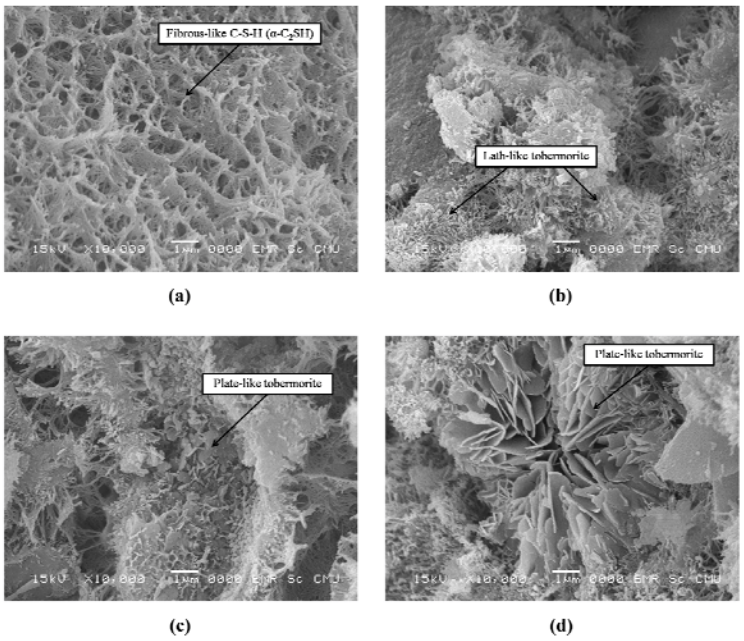

Figure 7 SEM micrograph of all BLWC (a) PC control (b) 10BA (c) 20BA and (d) 30BA

CONCLUSIONS

This research work investigated the production of lightweight concrete (LWC) using FA and BA as cement replacement materials by the autoclaved aerated concrete method. It was found that, the compressive strength and unit weight increased while the volume of permeable voids decreased with increased FA and BA replacement level part of Portland cement. SEM micrographs shows the tobermorite (C5S6H5) phase in BA concrete (BLWC) while α-C2SH phase was found in the LWC without BA content.

Tobermorite phase especially plate-like tobermorite indicated denser microstructure than α-C2SH phase. According to these test results, FA and BA can be used as a reactive silica source in autoclaved LWC which would result in a denser microstructure than pure Portland cement mix.

ACKNOWLEDGEMENTS

The authors are would like to thank National Research University, the Office of the Higher Education Commission (Commission on Higher Education), Thailand for financial support. The Graduate School, Chiang Mai University is also acknowledged.

REFERENCES

1. MAHLOTRA, V M, MEHTA, P K. Pozzolanic and cementitious materials, 1996, Gordon and Breach Science Publishers SA, p 7.

2. RAVINA, D, MEHTA, P K. Properties of fresh concrete containing large amount of fly ash, Cement and Concrete Research, Vol. 16, 1986, pp 227–238.

3. MEHTA, P K. Effect of fly ash composition on sulfate resistance of cement, Journal of the American Concrete Institute, Vol. 83, 1986, pp 994-1000.

4. BLANCO, F, GARCIA, M P, AYALA, J, MAYORAL, G, GARCIA, M A. The effect of mechanically and chemically activated fly ashes on mortar properties, Fuel, Vol. 85, 2006, pp 2018–2026.

5. MCCARTHY, M J, DHIR, R K. Development of high volume fly ash cements for use in concrete construction, Fuel, Vol. 84, 2005, pp 1423–1432.

6. RUKZON, S, CHINDAPRASIRT, P. Use of disposed waste ash from landfills to replace Portland cement, Waste Management and Research, Vol. 27, 2009, pp 588-594.

7. PAPAYIANNI, I, ANASTASIOU, E. Production of high-strength concrete using high volume of industrial by-products, Construction and Building Materials, Vol. 24, 2010, pp 1412–1417.

8. TORKITTIKUL, P, CHAIPANICH, A. Utilization of ceramic waste as fine aggregate within Portland cement and fly ash concretes, Cement and Concrete Composites, Vol. 32, 2010, pp 440–449.

9. NISNEVICH, M, SIROTIN, G, SCHLESINGER, T, ESHEL, Y. Radiological safety aspects of utilizing coal ashes for production of lightweight concrete, Fuel, Vol. 87, 2008, pp 1610–1616.

10. OZKAN, O, YUKSEL, I, MURATOGLU, O. Strength properties of concrete incorporating coal bottom ash and granulated blast furnace slag, Waste Management, Vol. 27, 2007, pp 161-167.

11. YUKSEL, I, BILIR, T, OZKAN, O. Durability of concrete incorporating non-ground blast furnace slag and bottom ash as fine aggregate, Building and Environment, Vol. 42, 2007, pp 2651-2659.

12. KURAMA, H, TOPCU, I B, KARAKURT, C. Properties of the Autoclaved Aerated Concrete Production from Coal Bottom Ash, Journal of Materials Processing Technology, Vol. 209, 2009, pp 767-773.

13. CHERIAF, M, ROCHA, J C, PERA, J. Pozzolanic properties of pulverized coal combustion bottom ash. Cement and Concrete Research, Vol. 29, 1999, pp 1387–1391.

14. SHORT, A, KINNIBURGH, W. Lightweight Concrete, 1963, C.R. Books Limited, p.3-5.

15. MINDESS, S, YOUNG, J F, DARWIN, D. Concrete, 2003, Pearson Education, Inc, USA. p 298.

16. YAZICI, H. The effect of curing conditions on compressive strength of ultra high strength concrete with high volume mineral admixtures, Building and Environment, Vol. 42, 2007, pp 2083-2089.

17. JING, Z, JIN, F, HASHIDA, T, YAMASAKI, N, ISHIDA, E H. Influence of additions of coal fly ash and quartz on hydrothermal solidification of blast furnace slag, Cement and Concrete Research, Vol. 38, 2008, pp 976–982.

18. YAZICI, H, YIGITER, H, KARABULUT, A S, BARADAN, B. Utilization of fly ash and ground granulated blast furnace slag as an alternative silica source in reactive powder concrete, Fuel, Vol. 87, 2008, pp 2401-2407.

19. UYSAL, H, DEMIRBOGA, R, SAHIN, R, GUL, R. The effects of different cement dosages, slumps, and pumice aggregate ratio on the thermal conductivity and density of concrete, Cement and Concrete Research, Vol. 34, 2004, pp 845-848.

20. GUNDUZ, L. The effects of pumice aggregate/cement ratios on the low-strength concrete properties, Construction and Building Materials, Vol. 22, 2008, pp 721-728.

21. TOPCU, I B, UYGUNOGLU, T. Properties of autoclaved lightweight aggregate concrete, Building and Environment, Vol. 42, 2007, pp 4108-4116.

22. BYUNG-WAN, J, SEUNG-LOOK, P, JONG-BIN, P. Properties of concrete made with alkali-activated fly ash lightweight aggregate (AFLA), Cement and Concrete Composites, Vol. 29, 2007, pp 128-135.

23. GESOGLU, M, OZTURAN, T, GUNEYISI, E. Effect of cold-bonded fly ash aggregate properties on the shrinkage cracking of lightweight concretes, Cement and Concrete Composites, Vol. 28, 2006, pp 598-605.

24. MELLER, N, KYRITSIS, K, HALL, C. The mineralogy of the CaO–Al2O3–SiO2–H2O (CASH) hydroceramic system from 200 to 350 °C, Cement and Concrete Research, Vol. 39, 2009, pp 45–53.

25. TEO, D C L, MANNAN, M A, KURIAN, V J. Durability of lightweight OPS concrete under different curing conditions, Material and Structure, Vol. 43, 2010, pp 1-13

Utilising Fly Ash and Fine Tailings in Foamed Insulation Building Materials

W She, Y S Zhang, W H Zhang
Southeast University, China

This paper describes an extensive laboratory-based investigation into the use of fly ash and fine tailings in one type of insulation materials of building materials-foamed concrete. Foamed concrete with apparent density from 500 to 1000 kg/m^3, compressive strength from 1 to 14.5 MPa and thermal conductivity from 0.06 to 0.145 W/(m°C) were prepared when a large volume of cement(up to 60 wt.%) have been replaced with fly ash and fine tailings. The rheologic, mechanical and heat preservation properties were investigated for the foamed concrete.The results shows that using fly ash and fine tailings can significantly enhance the rheologic property of fresh foamed concrete. In addition, up to 60% of the cement could be replaced without obvious reductions in long-term strength and thermal conductivity in relative higher density(1000kg/m^3). By using fly ash or fine tailings as fine aggregate in foamed concrete, the high volume utilization of these industrial waste becomes possible, thus providing a means of economic and safe disposal of these waste residues.

She Wei is a PhD student in Jiangsu Key laboratory for Construction Materials, Southeast University, Nanjing, China. His research interests include foamed insulation materials of building.

Zhang Yunsheng is a professor in Jiangsu Key laboratory for Construction Materials, Southeast University, Nanjing, China. He received his PhD in Structure Engineering from Southeast University in 2004. His research interests include microstructure formation process of cementitious materials, high performance concrete made with fly ash or slag, durability and service life prediction of high performance concrete.

Zhang Wenhua is a PhD student in Jiangsu Key laboratory for Construction Materials, Southeast University, Nanjing, China. His research interests include ultra-high performance cementitious materials.

Keywords: Compressive strength, Fine tailings, Fly ash, Foamed concrete, Thermal conductivity

INTRODUCTION

Foamed concrete is a novel type of lightweight insulation material consisting of Portland cement paste or cement filler matrix (mortar), in which a homogeneous air-void or pore structure are created by introducing air suitable foaming agent [1-2]. Foamed concrete can be designed to have any density within the range of 400-1600kg/m^3,which possesses self-compacting, light weight, low strength (e.g. between 1 and 10 MPa) [3-4] and excellent thermal insulation properties, suitable for application to partition, insulation and filling grades. There have been renewed interest in its potential for large scale utilization of wastes such as fly ash, incinerator bottom ash , recycled glass and foundry sand [3,5]. Both fly ash and tailing are two types of industrial by-products and main source of solid contamination in china. A immense amounts of fly ash and tailings were generated every year. These wastes occupied many fields of plantation and caused environment pollution. Against these background issues, this paper addresses the potential of using fly ash and fine tailings as a cement replacement in building wall insulation materials and how this affected the rheological, strength development and thermal conductivity properties. Not only does this allow fly ash and fine tailings to be used, it reduces the dependence on primary aggregate resources and helps develops a more sustainable approach to foamed concrete.

EXPERIMENTAL PROGRAMME

Raw Materials

The constituent materials used to produce foamed concrete were comprised of (1) Portland cement (PC) with 28 days of compressive strength of 64.5MPa; (2) Fly ash (FA) with the median particle size of 35um, The scanning electron micrograph of the fly ash (Figure 1) shows both many spherical particles and some irregular-shaped grains. (3) Fine iron ore tailings (FT) with the median particle size of 249um (4) Polycarboxylic type of superplasticizer (SP) with water reducing ratio of 35% or greater and (5) Foam produced by mixing an organic foaming agent and water (dilution ratio 1:20 by weight) in an foam generator to a apparent density of 55kg/m^3.

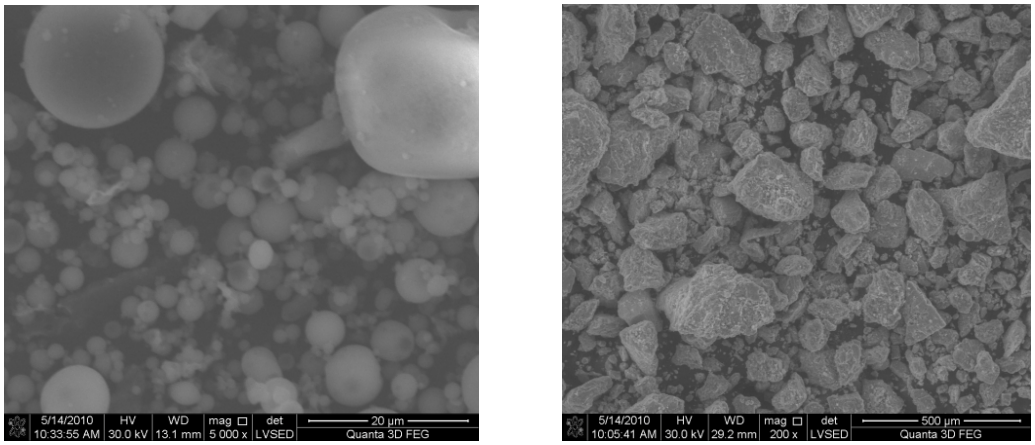

Figure 1 Micrograph of fly ash particles (left) and fine iron tailings (right).

The properties of cement, fly ash and fine tailings used in this study are presented in Table 1 and corresponding size distribution is shown in Figure 2.

Table 1 Chemical composition and physical properties of raw materials

OXIDES	PORTLAND CEMENT, %	FLY ASH, %	FINE TAILINGS, %
CaO	64.8	6.09	11.75
SiO_2	21	49.96	46.66
Al_2O_3	6.16	34.02	17.02
Fe_2O_3	4.01	4.52	7.11
Na_2O	0.1	0.66	5.15
K_2O	0.4	0.98	1.19
MgO	1.94	1.17	3.81
SO_3	1	0.62	1.03
Blaine surface area, m^2/kg	350	360	32
Relative density	3.15	2.4	2.7

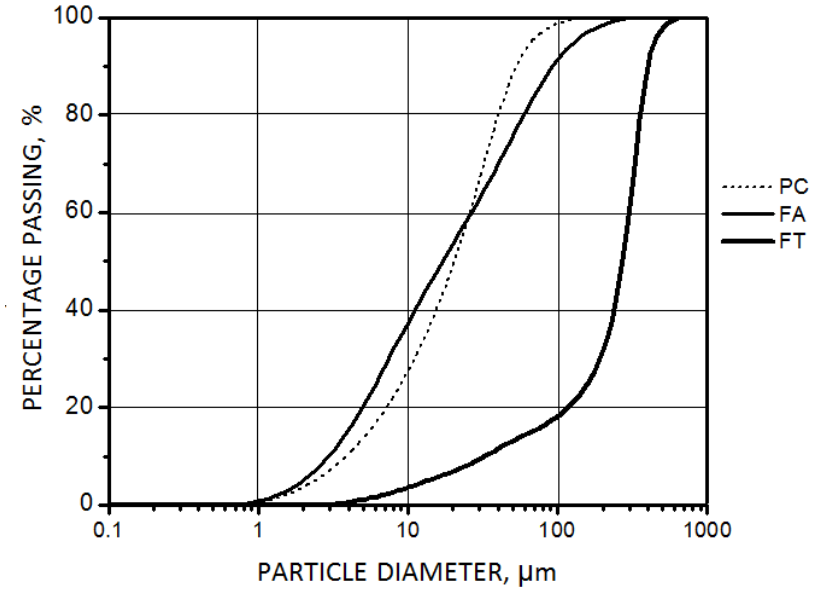

Figure 2 Particle size distribution of raw materials

Mix Proportions

The mix proportion of foamed concretes, which are summarized in Table 2, were calculated by solid-volume calculation [3]. Fourteen mixtures were prepared and the water/solid (w/s) ratio is weight ratio.

The fly ash and fine tailings are taken as fine aggregates as a replacement of cement. 20%, 40% and 60% of Portland cement is replaced by fly ash and fine tailings respectively. The

first two mixtures contained only cement. Mixture numbers 3 to 8 contained the fly ash while mixture 9 to 14 contained fine tailings.

Table 2 Composition of foamed concrete mixtures

NO.	TARGET DENSITY kg/m^3	REPLACEMENT, %	W/S	COMPOSITION OF MIXTURE, /m^3)				
				PC, kg	Aggregates, kg	Water, kg	Foam, l	SP, kg
1	500	0	0.3	385	-	115	761	3.85
2	1000	0	0.3	769	-	231	521	7.7
3/9	500	20%	0.3	308	77	115	754/759	3.85
4/10	500	40%	0.3	231	154	115	746/748	3.85
5/11	500	60%	0.3	154	231	115	739/743	3.85
6/12	1000	20%	0.3	615	154	231	507/511	7.7
7/13	1000	40%	0.3	461	308	231	492/496	7.7
8/14	1000	60%	0.3	308	461	231	478/483	7.7

Specimen Preparation

The Portland cement and fine aggregates are first dry-mixed for 1 min, then the water and superplasticizer are put into the premixed powders and mixed for 3 min. Finally, the preformed foam are added to the above mix and mixed for 3 min until there was no physical sign of the foam on the surface and the foam was uniformly distributed in the mix. The plastic density of the mix is then measured and values within ±50 kg/m^3 is accepted. If the density was higher, additional foam is added incrementally until target value is achieved, followed by further mixing. Mixes with densities lower than the range of acceptable values were rejected and repeated. After mixing, the foamed concrete paste is cast into polythene moulds and then covered with plastic film to prevent evaporating. Finally, the specimens are stored for 24h, then removed from the moulds, and cured in standard curing condition (20^{o}C,100%RH) until testing.

Testing Methods

Consistence

The consistency of the mix after adding foam was determined by measuring the slump flow using a standard flow cone [6]. After filling the cone with the mixture, the cone is lifted and average flow of the concrete is measured without rising and dropping of the flow table as it may lead to separation of bubbles from the mix.

Compressive strength

Compressive strength was measured according to ASTM C495 on 100mm cube specimens

following 7, 28 and 90 days curing. The strength recorded are average of three cubes (with the difference between the average and the individual values limited to less than 10%).

Thermal conductivity

Specimen preparation and measurement of thermal conductivity were all carried out according to ASTM C177, Standard Test Method for Steady-State Heat Flux Measurements and Thermal Transmission Properties by means of the Guarded Hot-Plate Apparatus.

RESULTS AND DISCUSSION

Consistence

In order to study the flow behaviour, the slump flow spread of mixes after the addition of foam is compared in Figure 3. It is interesting to note that (i) the flow increases steeply with an increase in design density. (ii) For a given density, the flow increases with an increase in cement replacement ratio, especially in the mix with fly ash. A possible reason for these are that, at lower densities there will be more foam which lead to the reduced self-weight and the adhesion between the bubbles and solid particles in the mixture increase the stiffness of the paste.

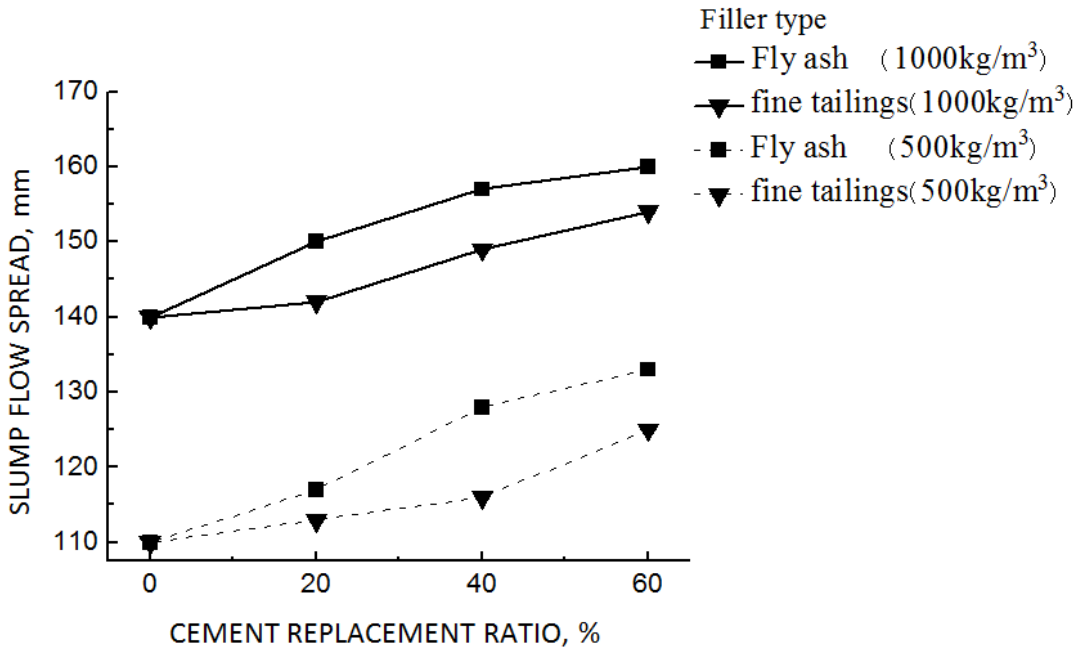

Figure 3 Effect of cement replacement ratio and filler type on slump flow spread

For a given density, for one thing, the flow value is relatively higher for fly ash mixes as it contains a smaller volume of foam due to its low specific gravity compared to fine tailings, for the other, the enhanced consistence of the fly ash compared to fine tailings is likely to be

due to the "ball-bearing effect" of FA particles (Figure 4)due to their spherical morphology[7] , improved packing of the solid phase and absorption of mix water on to the FA particles reducing inter-particle friction[8]. As regards the latter, an increase in the mix water will reduce the yield stress value of concrete [9], and , in turn, improve spread.

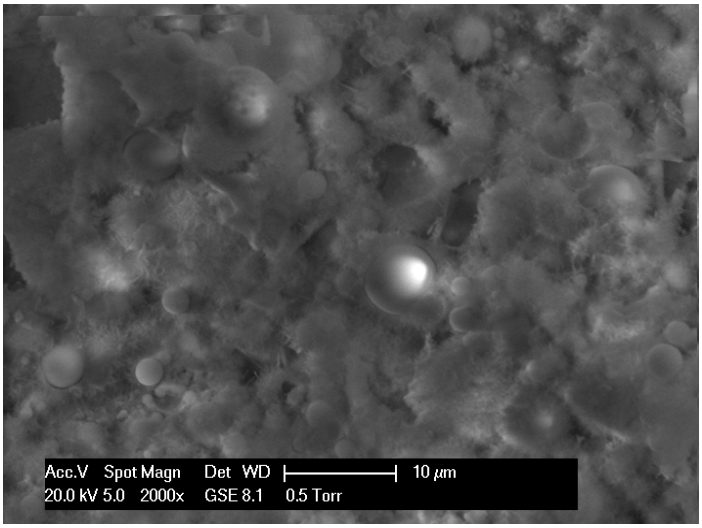

Figure 4 "Ball-bearing effect"of FA particles

Compressive Strength

The compressive strengths of foamed concrete mixtures with different fine aggregates contents and densities of 1000 and 500kg/m^3 are shown as function of time in Figures.5 and 6, respectively. The left graph in each of these Figures is for mixtures containing fly ash while the right graph is for mixtures containing fine tailings.

From Figure 5 it can be seen that the compressive strengths have an obvious increase for foamed concrete when curing age increases from 7 days to 28 days, the further prolonging of curing age shows a relatively little strength gain. For example, the compressive strength of 1000kg/m^3 mixtures with 20% fly ash are 2.7,10.5 and 14.4 MPa at age of 7, 28 and 90 days, respectively. There is a 7.8 MPa strength gain when curing age increases from 7 days to 28 days, while only 3.9 MPa gain from 28 days to 90 days. Thus, 28 days of curing ages is enough to achieve most of the ultimate strength from the viewpoint of time and energy saving. The type of fine aggregates used (fly ash or fine tailings) seems to have some effects on the strength of these foamed concrete. In the same replacing ratio, the compressive strength of the mixtures containing fly ash is higher than that for mixtures containing fine tailings. This was the result of the microaggregate effect [10] and pozzolanic reaction of fine fly ash . The small and spherical fly ash particles filled the microvoids and increased the density.

Besides, it should be pointed out that the fly ash used in this study has a high fraction of reactive oxides (Al_2O_3+SiO_2+Fe_2O_3 =88.5%), which means that it has high reactivity with the further prolonging of curing age. The smaller particle size of fly ash with higher surface area and glassy phase content also improved the pozzolanic reaction [11].

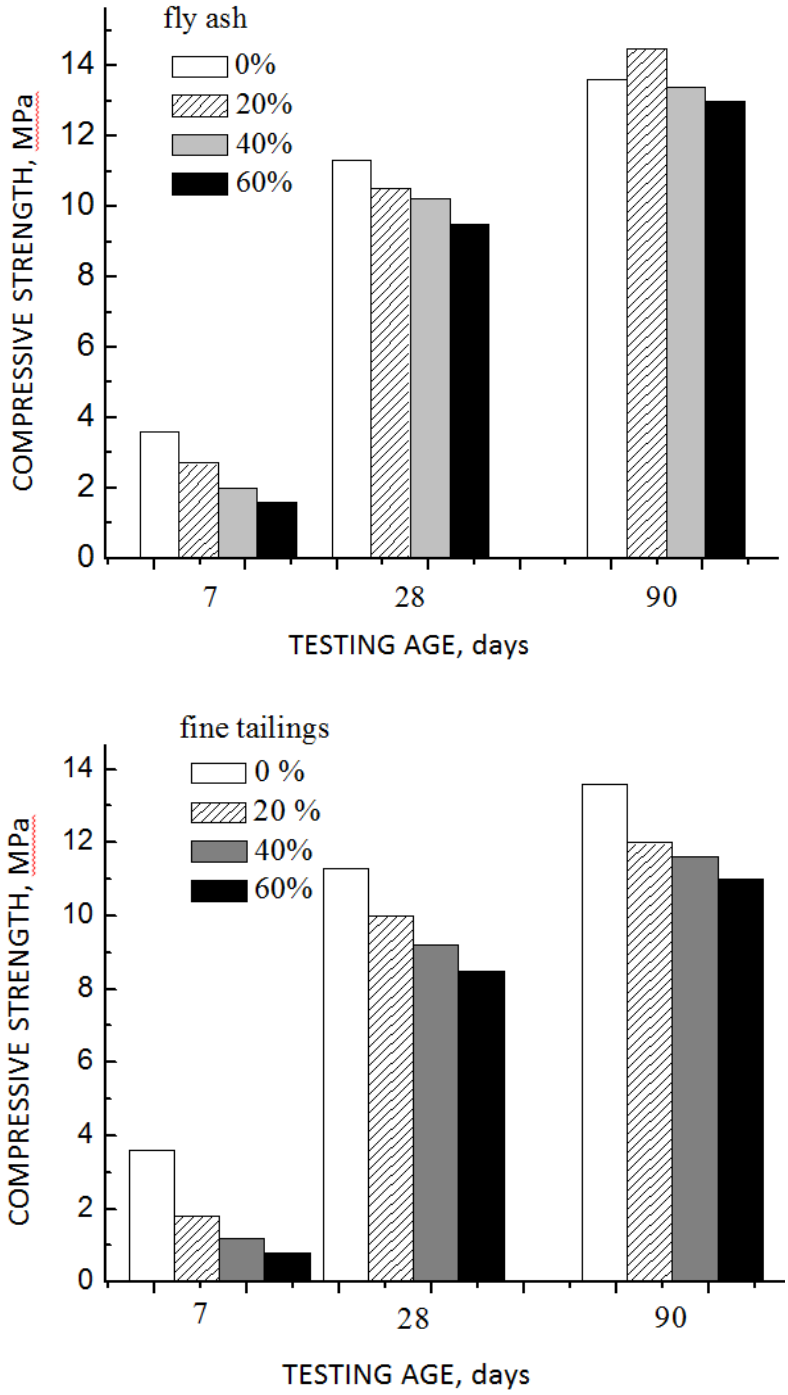

Figure 5 Compressive strength of 1000kg/m^3 mixtures as a function of time

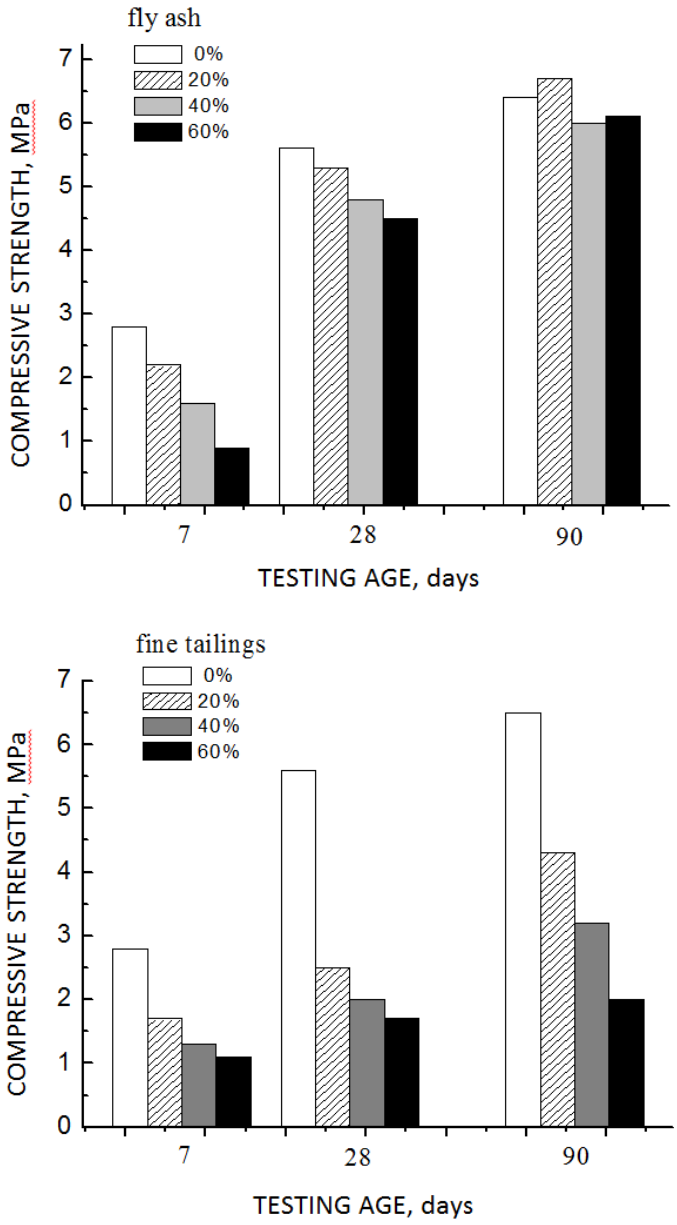

Figure 6 Compressive strength of 500kg/m^3 mixtures as a function of time

From Figure 6 it can be seen that after 90 days, the compressive strengths of 500 kg/m^3 mixtures with fly ash varies from 6 to 6.7 MPa, indicating a similar trend in long-term strength gain to that observed for the 1000 kg/m3 mixtures containing fly ash(see Figure 4). It is interesting to note that, unlike those mixtures with higher casting densities, the compressive strength of mixtures containing fine tailings are significantly lower than those of the mixtures containing fly ash. The contribution to the long-term gain in strength of fine tailings seems to be reduced at low density. Similar behaviour was observed when fly ash was replaced by unclassified fly ash[5].

By comparing Figure 5 and Figure 6, we can see that the compressive strengths of foamed concrete decreased sharply with the decrease of density. This result can be derived qualitatively from Figure 7, with increasing the volume of foam to decrease the objet density,

the porosity and average diameter of the air voids increases. Furthermore, the quantity of irregularly formed pores increases considerably. The smaller the diaeter of the pores, the more regularly they are formed. Higher porosity、larger pore size and irregular pore property decrease the compressive strength of foamed concrete.

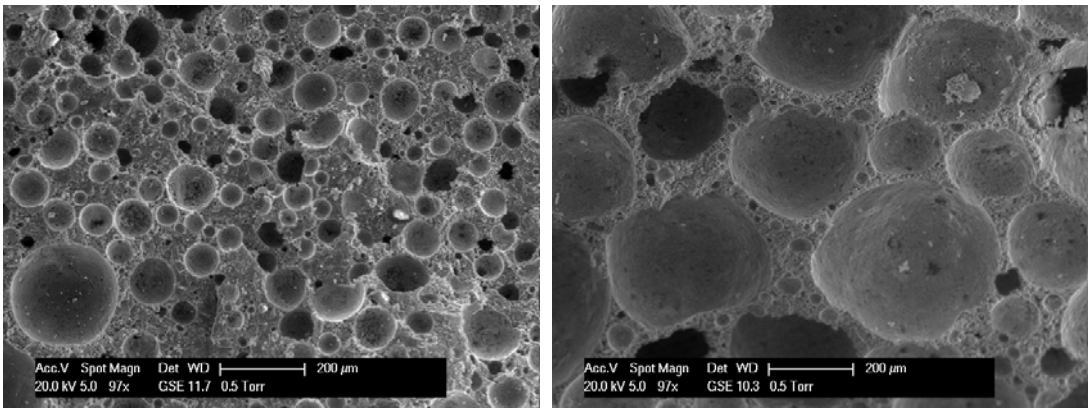

Figure 7 Microstructure of two foam concretes (40% FA); left: 1000 kg/m^3 mixture; right: 500 kg/m^3 mixture.

Thermal Conductivity

Foamed concrete has excellent thermal insulating properties due to its cellular microstructure, the thermal conductivity of foamed concrete with different filler type and cement replacement ratio is compared in Figure 8. It is interesting to note that (i) the thermal conductivity of foamed concrete decreased sharply with the decrease of density. For example, the thermal conductivity varies from 0.13 to 0.145 W/(m°C) when its density is 1000kg/m³ , and the thermal conductivity drop to the values from 0.06 to 0.09 W/(m°C) when its density decreases to as low as 500kg/m³.

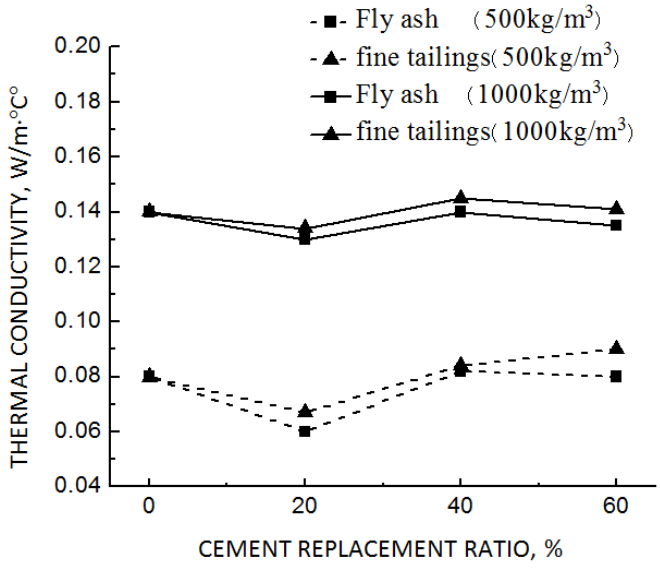

Figure 8 Effect of cement replacement ratio and filler type on thermal conductivity

Whereas the thermal conductivity of normal concrete is as high as 1.70 W/(m°C) which is about 12 to 28 times of that of foamed concrete prepared in this paper. Therefore, reducing the density of foamed concrete is an effective way to reduce its thermal conductivity, hence enhance the foamed concrete characteristic of thermal insulation. The thermal conductivity of the mixtures containing fly ash is slightly lower than that for mixtures containing fine tailings. this can probably also be attributed to the finer particle size compared to fine tailings, resulting in a greater "interface" area, which is known to provide a more effective thermal barrier[12].

CONCLUSIONS

The conclusions drawn from this study and summarized below are applicable to the characteristics of the materials used and the range of parameters investigated: (i) the flow behaviour mainly depends on the foam volume and as the foamed volume decreases (i.e., increase in design density) the flow increases. For a given density, an increase in filler content of the mix result in increased flow values and the foamed concrete with fly ash showed relatively higher flow values; (ii) in relative higher density (1000 kg/m^3), replacing high proportions of cement with fine aggregates (fly ash or fine tailings) does not significantly affect the long-term compressive strength of well cured foamed concrete and the foamed concrete with fly ash showed relatively higher strength values. (iii) the thermal conductivity of foamed concrete decreases with its density. Foamed concrete with the thermal conductivity of 0.06-0.09 W/(m°C) and 0.13-0.145 W/(m°C) in the casting density 500kg/m^3 and 1000 kg/m^3 can be prepared by utilizing large amount of industrial waste(i.e., fly ash or fine tailings).

ACKNOWLEDGEMENTS

The authors gratefully acknowledge the financial support from key projects in the national science & technology pillar program during the eleventh five-year plan period (2006BAJ04A10), Program for New Century Excellent Talents in University and 973 Program (2009CB623200).

REFERENCES

1. RAMAMURTHY, K, NAMBIAR, E K K, RANJANI,G I S. A classification of studies on properties of foam concrete. Cement and Concrete Composites, Vol.31,2009,388-396.

2. ABDULKADIR KAN, RAMAZAN DEMIRBOGA. A novel material for lightweight concrete production. Cement and Concrete Composites, Vol.31, 2009, pp 489-495.

3. JONES, M R, A. McCARTHY M. J . Utilising unprocessed low-lime coal fly ash in

foamed concrete, Fuel, Vol.84, 2005, pp 1398-1409.

4. PHAIBOON P, MALLIKA P. Reuse of thermosetting plastic waste for lightweight concrete. Waste Management, Vol.28, 2008, pp 1581-1588.

5. KEARSLEY, E P, WAINWRIGHT, P J. The effect of high fly ash content on the compressive strength of foamed concrete, Cement and Concrete Research, Vol.31, 2001, pp 105-112.

6. ASTM.(1998). “Specification for flow table for use in tests of hydraulic cement.” ASTM C230, ASTM, Philadelphia.

7. AGULLÓ L, TORALLES-CARBONARI B, GETTU R, AGUADO A. Fluidity of cement pastes with mineral admixtures and superplasticizer- a study based on the Marsh cone test. Mater Struct , Vol.32,1999, pp 79-85.

8. GIANNAKOU, A, JONES, M R. Potential of foamed concrete to enhance the thermal performance of low-rise dwellings. Innovations and developments in concrete materials and construction. Proceedings of the international congress challenges of concrete construction, University of Dundee, Scotland, 5-11 September 2002, London, Thomas Telford.2002, pp 33-44.

9. MARRS, D L, BARTOS PJM. Development and testing of self-compacting low strength slurries for SIFCON. Proceedings of the international RILEM conference ‘production methods and workability of concrete ’, London: E＆FN Spoon: 1996:199-208.
10. AIQIN W, CHENGZHI Z, WEI S. Fly ash effects Ⅲ. The microaggregate effect of fly ash. Cement and Concrete Research, Vol.34, 2004, pp2061-2066.

11. NAIK T R, RAMME B W. Low-strength concrete and controlled low-strength material (CLSM) produced with class F fly ash. In: Adaska WS, editor. Controlled low-strength materials, ACI SP-150. American Concrete Institute.1994, pp 1-13.

12. XU Y, CHUNG D.D.L. Effect of sand addition on the specific heat and thermal conductivity of cement. Cement and Concrete Research, Vol.30, 2000, pp 59-61.

Effect of Steel and Polypropylene Fibres on the Performance of Self-compacting Concrete (SCC) Incorporating Calcareous Fly Ash

I Papayianni, E Anastasiou, M Papachristoforou
Aristotle University of Thessaloniki, Greece

Calcareous fly ashes often increase the water demand of concrete mixtures, which is problematic in the case of SCC where the balance between fluidity robustness of the mixture and added water is very sensitive. However, by adjusting the dosages of superplasticizer and viscosity modifying agent, it was achieved to replace 30% and 50% by mass of the Portland cement in SCC mixtures with this fly ash, without modifying the water to cementitious ratio. Furthermore, in an effort to eliminate shrinkage deformations of the SCC mixtures, which typically have a high value of cementitious matrix to aggregate ratio, steel and polypropylene fibers were added at two different percentages, 0.4% and 0.7% by volume, for each type of fiber. The influence of fiber addition on the properties of fresh SCC and the mechanical and elastic characteristics of the hardened fiber-reinforced SCC at 28-d age were measured. In addition, the toughness of fiber-reinforced SCC with and without calcareous fly ash was studied by plotting flexural strength – deflection diagrams and using relevant standards. Shrinkage deformations were measured after demoulding and placing into a climatic chamber with 60% RH. It seems that the addition of fibers at the above-mentioned percentages does not influence the fluidity and robustness of the mixture significantly. By adding fibers in the SCC, strength of the same or higher level than that of the plain SCC mixtures is developed. Furthermore, fiber-reinforced SCC shows increased toughness and reduced shrinkage deformations.

I Papayianni is currently Professor and Director of the Laboratory of Building Materials at the Civil Engineering Dept. of the Aristotle University of Thessaloniki, Greece. She is a member of ACI and RILEM Committees and the scientific responsible of many National and European Research Projects. Her specialist research fields include concrete technology, supplementary materials and repair materials.

E Anastasiou is a Researcher at the Laboratory of Building Materials at the Civil Engineering Dept. of the Aristotle University of Thessaloniki, Greece. He has participated in several research projects and published several articles on concrete technology. His specialist areas of research include industrial by-products utilization in concrete, supplementary cementing materials and fiber-reinforced concrete.

M Papachristoforou is a Civil Engineer and a PhD candidate at the Laboratory of Building Materials at the Civil Engineering Dept. of the Aristotle University of Thessaloniki, Greece. He has participated in several research projects on concrete and his specialist areas of research include industrial by-products utilization in concrete, fiber-reinforced concrete and radiation shielding concrete.

Keywords: Drying shrinkage, Fibre reinforced self-compacting concrete, Fracture toughness, High calcium fly ash

INTRODUCTION

Self-Compacting Concrete (SCC) is a recently developed concrete which requires specific design in terms of fines content (< 0.125 mm) and fine to coarse aggregate ratio. In order to achieve adequate flow, passing ability and self-consolidation, the mixture proportioning has to be carried out very carefully and admixtures such as viscosity modifying agents (VMA) may be added apart from superplasticizers. While fresh concrete slump or expansion is usually adequate to assess the consistency of ordinary concrete, the robustness of SCC mixtures needs to be determined in terms of fluidity, passing ability and segregation resistance. Regarding the sensitivity of fresh SCC properties to changes in the constituent materials, several methodologies are proposed in the literature [1, 2]. Based on relevant guidelines and regulations, some limits for the constituents of SCC are suggested, as well as methods of assessing fresh SCC mixtures [3, 4].

Since the SCC production process is rapidly evolving in the construction market, supplementary concrete-making materials, such as mineral admixtures and fines, as well as new materials and new methods are continuously tested for their suitability in SCC [5, 6]. Along these lines, fibre-reinforced self-compacting concrete (FRSCC) is also under development in order to optimize such mixtures for the benefit of performance and economy [7-10]. The present report deals with the use of high volume of high calcium fly ash (HCFA) in the production of FRSCC. Greek HCFA is a by-product of the lignite-fired power stations and has been used successfully in concrete production over the past decades, but research regarding its use in SCC and, furthermore, in FRSCC is very limited [11]. This could be attributed to the fact that the use of HCFA in concrete often increases water demand and therefore decreases fluidity in SCC mixtures making them more difficult to achieve self-compactability. The use of suitable admixtures (superplasticizer and VMA), however, has proven to be sufficient in order to overcome the increased water demand and allows HCFA to have a positive effect on the robustness of SCC mixtures by improving segregation resistance [12] and reducing early shrinkage deformations [11].

The aim of this study is to develop a high performance FRSCC by using large volume of HCFA (30% and 50% wt. of the total binder) and with different fibre types (steel and polypropylene) used at different percentages (0.40% and 0.70% by volume of the total mixture). The different parameters studied will allow determining the maximum possible cement substitution and the optimum type and percentage of fibres.

In order to assess the quality of the different FRSCC mixtures, a series of laboratory mixtures was prepared tested for their fresh and hardened properties. The robustness of the fresh FRSCC mixtures was measured by recording flowability, slump-flow viscosity, passing ability and segregation resistance, while the characteristics of the hardened FRSCC test mixtures were assessed by measuring compressive and flexural strength, elastic moduli and drying shrinkage. Furthermore, since fibre reinforcement enhances the energy absorbing ability of concrete [13, 14] fracture toughness measurements were also carried out according to relevant EN [15] and ASTM Standards [16].

EXPERIMENTAL SETUP

Materials Selection and Concrete Mix Design

The binders used in the test mixtures were ordinary Portland cement type CEM I 42.5 N and unprocessed HCFA. In order to increase the content of fines, limestone filler was also added. Some characteristics of the fines used in the test mixtures are shown in Table 1. Following trial mixtures and based on previous experience, the amount of cement replacement with HCFA was decided to be 30% and 50%, while the total binder content was 400 kg/m^3. In order to improve fresh concrete fluidity and robustness, 160 kg/m^3 of limestone filler was also added, reaching a total of 560 kg/m^3 of fines (< 125 μm). The aggregate used in all mixtures was crushed limestone with a maximum size of 16 mm and the aggregate gradation curve was optimized by combining three aggregate fractions (0-4 mm, 4-8 mm, 8-16 mm). The water to binder ratio was selected equal to 0.50, aiming at a 28-day compressive strength of 35-40 MPa.

Table 1 Characteristics of the fine material used for FRSCC test mixtures

MATERIAL CONSTITUENTS, %	CEM I42.5N	HCFA	LIMESTONE FILLER
SiO_2		29.4	3.8
CaO	66.84	41.7	51.3
Al_2O_3	2.40	6.69	1.0
Fe_2O_3	8.11	5.26	0.4
SO_3		3.85	-
MgO	3.91	7.30	1.2
CaO free		10.6	-
K_2O	1.08	0.80	-
Na_2O	0.57	0.38	-
L.O.I.	1.91	8.46	41
Insoluble residue	0.80	9.93	
Fineness, R45 retained, %	1.50	19.0	
Apparent specific density kg/dm^3	3.14	2.55	2.71
EN 450-1 pozzolanicity index with cement at 28-days, %	-	85	-

The fluidity and robustness of the fresh FRSCC mixtures was also controlled with the use of chemical admixtures. The workability loss either from the substitution of cement with HCFA or from the use of fibre was compensated for with increased superplasticizer dosage. A polycarboxylate-based superplasticizer and a viscosity modifying agent (VMA) were used at varying percentages in order to achieve the required workability and segregation resistance limits. The superplasticizer was usually added at rates of 1-2% wt. of the total binder, while VMA was used at rates of up to 1% wt. of the total of fines.

Two types of fibres were selected to be used in the test mixtures; hooked-end steel fibres with 30 mm length and 0.75 mm width, and wave-profiled polypropylene fibres with 50 mm length and 0.75 mm width. Both fibre types were used at percentages of 0.40% and 0.70% by volume. The percentage, type and shape of fibre addition were selected based on aggregate size, specimen dimensions (minimum dimension of 150 mm) and previous experience from laboratory mixtures.

The use of different cement replacement percentages, fibre types and percentages resulted in 15 different test mixtures as described in Table 2. Table 3 shows the proportioning of the test concrete mixtures.

Table 2 Characteristics of test FRSCC mixtures

CONSTITUENTS kg/m^3	REFERENCE MIXTURES					30% HCFA MIXTURES					50% HCFA MIXTURES				
Mixture No.	1.1	1.2	1.3	1.4	1.5	2.1	2.2	2.3	2.4	2.5	3.1	3.2	3.3	3.4	3.5
Total binder content kg/m^3	400	400	400	400	400	400	400	400	400	400	400	400	400	400	400
w/b ratio	0.50	0.50	0.50	0.50	0.50	0.50	0.50	0.50	0.50	0.50	0.50	0.50	0.50	0.50	0.50
HCFA cement replacement	-	-	-	-	-	30%	30%	30%	30%	30%	50%	50%	50%	50%	50%
Steel fibres % by total volume	-	0.40	0.70	-	-	-	0.40	0.70	-	-	-	0.40	0.70	-	-
Polypropylene fibres % by total volume	-	-	-	0.40	0.70	-	-	-	0.40	0.70	-	-	-	0.40	0.70

Table 3 Proportioning of test FRSCC mixtures

CONSTITUENTS kg/m^3	REFERENCE MIXTURES					30% HCFA MIXTURES					50% HCFA MIXTURES				
Mixture No.	1.1	1.2	1.3	1.4	1.5	2.1	2.2	2.3	2.4	2.5	3.1	3.2	3.3	3.4	3.5
CEM I42.5 N	400	400	400	400	400	280	280	280	280	280	200	200	200	200	200
HCFA	-	-	-	-	-	120	120	120	120	120	200	200	200	200	200
Water	200	200	200	200	200	200	200	200	200	200	200	200	200	200	200
Fine aggregate	765	765	765	765	765	750	750	750	750	750	740	740	740	740	740
Coarse aggregate	825	825	825	825	825	809	809	809	809	809	798	798	798	798	798
Limestone filler	160	160	160	160	160	160	160	160	160	160	160	160	160	160	160
Superplasticizer	5.6	5.6	5.6	5.6	5.6	6.0	6.0	6.0	6.0	6.0	8.0	8.0	8.0	8.0	8.0
VMA	4.8	4.8	4.8	4.8	4.8	4.5	4.5	4.5	4.5	4.5	5.6	5.6	5.6	5.6	5.6
Steel fibres (SF)	-	31.5	55	-	-	-	31.5	55	-	-	-	31.5	55	-	-
Polypropylene fibres (PF)	-	-	-	3.6	6.3	-	-	-	3.6	6.3	-	-	-	3.6	6.3

The European Guidelines for Self Compacting Concrete (EFNARC) recommend indicative constituent limits in order to achieve SCC mixtures, which consider powder, paste, water and aggregate contents as well as water to powder ratio. Regarding the test FRSCC mixtures in the present report, all fall within the constituent limits of the guidelines, as it can be seen in Table 4.

Cement replacement with HCFA, however, increases total paste volume and reduces the water to powder ratio. This is due to the fact that cement replacement with HCFA is calculated by weight and therefore due to the lower density of HCFA compared to cement there is a larger paste volume in the mixture, which results in a lower coarse aggregate content and a decreased water to powder ratio. Although the change in coarse aggregate content is not significant and is not expected to affect the overall consistency of the mixture, the lower water to powder ratio could reduce the fluidity of the fresh FRSCC. Since increasing water and, thus, altering the water to binder ratio and the ultimate strength of the concrete was not desired, it was decided to keep the lower water to binder ratio and use different chemical admixtures dosages to account for the loss in workability.

The inclusion of fibres is expected to alter the fluidity and passing ability of the test mixtures, while current standards do not include this effect in the concrete mix design. The fibre types used have different surface texture and, therefore, could have diverse effect on fresh FRSCC consistency. In order to identify the effect of both HCFA use and different fibre type inclusion in FRSCC, fresh concrete properties tests have been carried out regarding the measurement of fluidity, slump-flow viscosity, passing ability and segregation resistance.

Table 4 SFRCC fresh concrete properties

CONSTITUENT	REFERENCE MIXTURES	30% HCFA MIXTURES	50% HCFA MIXTURES	TYPICAL RANGE [3]
Powder, kg/m^3	560	560	560	380-600
Paste, lt/m^3	329	340	348	300-380
Water, kg/m^3	200	200	200	150-210
Coarse aggregate, kg/m^3	825	809	798	750-1000
Fine aggregate, % of total	48	48	48	48-55
Water/powder ratio by Volume	0.92	0.88	0.85	0.85-1.10

RESULTS

Fresh Concrete Properties

The slump-flow test was used to assess fresh FRSCC flowability, while T500, which is the time required for the fresh concrete to reach a diameter of 500 mm during the slump-flow test and serves an indication of viscosity, was also recorded in the same test. Passing ability was measured using the L-box test, although no bars were used in front of the L-box gate due to the blocking effect of fibres. The bars in the L-box test have either 41 mm or 59 mm gaps and since the fibres used were up to 50 mm long, the required bar distance would be greater than 100 mm in order to prevent blocking [17]. Segregation was measured by the segregation resistance sieve test which calculates the percentage of the fresh mixture passing from a No.4 sieve after being left to consolidate. The results of the fresh concrete testing are shown in Table 5. The minimum target values for each test are based on guideline recommendations.

Despite the increased use of superplasticizer and the modification in the VMA content in order to optimize fresh mixtures, it is clear that the use of HCFA reduces flow of fresh concrete, while T500 time, on the other hand, is increased, showing that the use of HCFA can improve the viscosity of fresh SCC mixtures. Both effects, however, occur within the limits of the target values and do not alter fresh concrete robustness significantly. Also, no significant change is observed regarding passing ability, as measured by the L-box test. It should also be noted that, although HCFA, used with suitable amount of superplasticizer and VMA, seems to contribute towards more viscous mixtures (increased flow time and reduced flowability), segregation might still occur, especially if the amount of water and chemical admixtures used is not optimum.

Table 5 SFRCC fresh concrete properties

MIXTURE	SLUMP-FLOW mm	T500 s	L-BOX H2/H1	SEGREGATION %
1.1	660	2.3	0.90	8.6
1.2	620	2.6	0.85	7.6
1.3	605	3.2	0.84	8.8
1.4	585	2.7	0.85	5.2
1.5	595	3.1	0.83	5.8
2.1	625	3.5	0.90	6.2
2.2	620	3.2	0.88	5.5
2.3	615	3.6	0.83	5.0
2.4	630	2.9	0.89	5.4
2.5	595	3.9	0.81	5.2
3.1	600	4.5	0.90	9.7
3.2	640	3.7	0.88	8.7
3.3	625	3.7	0.81	7.0
3.4	625	4.6	0.86	8.2
3.5	615	3.9	0.80	8.0
Target value	> 550	> 2	> 0.80	< 15%

Regarding the use of fibres, the results in Table 5 show that their use reduces the passing ability of fresh mixtures. When increased amount of fibre is used (0.7% instead of 0.4%), passing ability decreases further while a decrease in flow and is also observed. On the other hand, fibre reinforcement had little in viscosity and segregation resistance of the mixtures. Steel and polypropylene fibres affect the fresh FRSCC properties in a similar way and despite the reduction in passing ability, robust FRSCC mixtures can easily be produced with fibre content of up to 0.7% and cement replacement with HCFA of up to 50% wt.

Following mixing and fresh concrete testing, specimens were cast from all the test mixtures. The specimens cast were 150 x 150 x 150 mm cubes used for compressive strength testing, 150 x 300 mm cylinders used for the determination of split tensile strength and elastic modulus, 150 x 150 x 700 mm prisms used for fracture toughness measurements and 100 x 100 x 1000 mm prisms used for the measurement of drying shrinkage.

All the specimens were cured at 20°C and 95% RH until testing except for the prisms used for the determination of drying shrinkage which were stored at 20°C and 50% RH, in order to simulate drying conditions.

HARDENED CONCRETE PROPERTIES

Unit weight, compressive and split tensile strength, flexural strength and elastic modulus were determined at 28 days for all test mixtures. The results are shown in Table 6 and are obtained as a mean of three specimens for all tests and as a mean of six specimens for compressive strength testing.

Table 6 Mechanical properties of FRSCC mixtures tested

	REFERENCE MIXTURES					30% HCFA MIXTURES					50% HCFA MIXTURES				
Mixture No.	1.1	1.2	1.3	1.4	1.5	2.1	2.2	2.3	2.4	2.5	3.1	3.2	3.3	3.4	3.5
Fibre content	0%	0.4%	0.7%	0.4%	0.7%	0%	0.4%	0.7%	0.4%	0.7%	0%	0.4%	0.7%	0.4%	0.7%
Fibre type	-	SF	SF	PF	PF	-	SF	SF	PF	PF	-	SF	SF	PF	PF
28-d unit weight kg/m^3	2320	2301	2344	2304	2335	2314	2329	2370	2281	2296	2258	2257	2287	2199	2246
28-d cubic compressive strength, MPa	42.1	40.0	42.1	38.1	39.1	39.5	39.9	39.1	37.6	36.7	32.4	32.6	34.2	31.2	32.7
28-d split tensile strength, MPa	2.92	3.04	3.40	3.10	3.08	2.65	3.24	3.49	3.34	3.59	2.87	3.34	3.82	3.16	3.20
28-d flexural strength, MPa	5.36	5.67	6.68	4.61	5.19	5.06	5.30	4.98	5.15	5.98	4.57	4.36	5.44	3.62	4.66
28-d elastic modulus, GPa	31.8	30.6	32.4	29.2	29.3	28.2	27.8	27.5	27.2	26.9	25.7	26.0	26.2	25.0	25.4

The 28-day compressive strength is reduced slightly with increased cement replacement with HCFA (5-10% with 30% replacement and 10-20% with 50% replacement) which is expected due to slower rate of the pozzolanic reaction compared to cement hydration. Ultimate strength, however, is expected to increase further for the mixtures of HCFA and reach the strength levels of the reference mixtures. The same pattern applies for all the other mechanical properties measured including the elastic modulus. Unit weight also slightly decreases with increasing use of HCFA due to the lower density of fly ash compared to cement.

Fibre addition does not seem to affect the mechanical properties of mixtures considerably. Compressive strength and elastic modulus are slightly reduced in FRSCC mixtures with lower unit weight than the reference mixtures (mixtures 2.4 and 2.5 compared to 2.1), mainly due to the reduced compaction achieved. On the other hand, mixtures with increased unit weight show also slightly higher mechanical properties compared to the reference mixtures (mixture 1.3 compared to 1.1 and 2.2 compared to 2.1) due to improved fibre-paste bonding achieved. Furthermore, fibre addition generally increases split tensile strength and may also increase ultimate flexural strength. Depending on fibre content, type and compaction achieved, the ultimate strength of FRSCC under bending load can be equal to the first crack strength of concrete or may be increased considerably due to fibre bonding. Figure 1 shows a typical stress-strain diagram of a FRSCC beam tested in flexure.

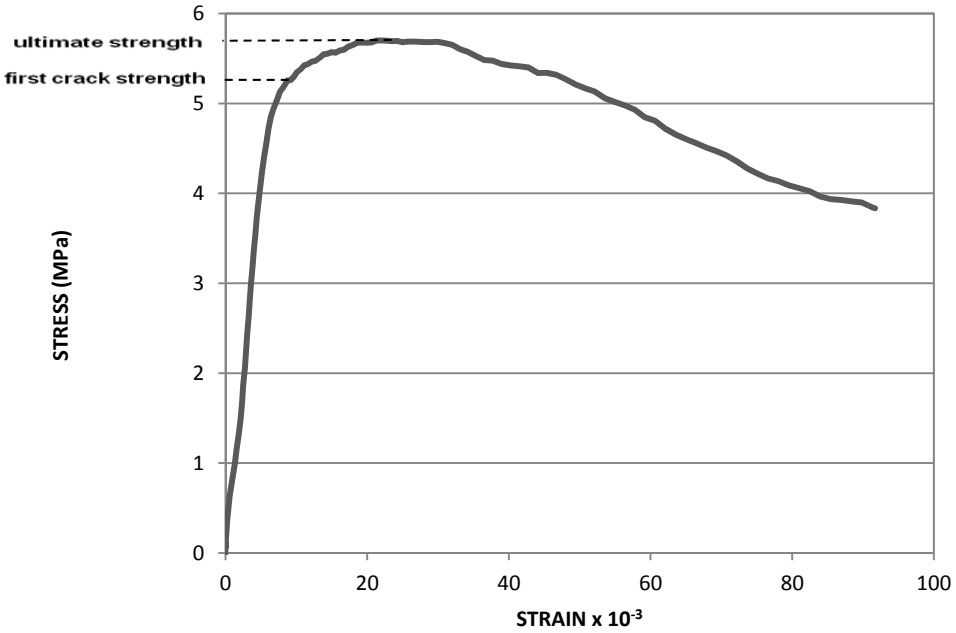

Figure 1 Stress-strain diagram of FRSCC under flexure

In order to assess the effect of fibre addition in SCC, fracture toughness measurements were carried out according to the European Standard EN 14651 [15] and also according to ASTM C1018-95 [16]. Notched 150x150x700 mm specimens were used in flexural bending tests, while crack mouth opening displacement (CMOD) was measured by using a clip gage. Load-CMOD curves were plotted for each specimen and were used to calculate the limit of proportionality (LOP) as described in EN 14651, as well as the toughness indices I5, I10 and I20 as described in ASTM C1018-95. The results are shown in Table 7.

LOP values show similar values for steel fibres (SF) and polypropylene fibres (PF). An increase in the LOP value is observed when the percentage of the fibre addition is increased from 0.4% to 0.7% by volume. Regarding the toughness index values, I5 is similar for all mixtures, ranging from 3.70 to 4.48. When higher deflections are examined, as in I10 and especially in I20, it can be seen that increased fibre percentage contributes to higher toughness for both types of fibres and also that steel fibres increase fracture toughness more than polypropylene fibres, probably due to their increased strength and anchoring potential.

Table 7 Fracture toughness properties of FRSCC mixtures tested

	REFERENCE MIXTURES				30% HCFA MIXTURES				50% HCFA MIXTURES			
Mixture No.	1.2	1.3	1.4	1.5	2.2	2.3	2.4	2.5	3.2	3.3	3.4	3.5
Fibre content	0.4%	0.7%	0.4%	0.7%	0.4%	0.7%	0.4%	0.7%	0.4%	0.7%	0.4%	0.7%
Fibre type	SF	SF	PF	PF	SF	SF	PF	PF	SF	SF	PF	PF
LOP, MPa	3.74	4.44	3.73	4.00	3.68	4.22	3.83	4.11	4.14	4.34	3.76	4.48
I5	4.51	4.74	4.47	4.69	4.09	3.91	4.02	4.36	3.89	3.96	3.70	4.34
I10	9.33	9.41	8.40	8.68	8.06	7.96	7.77	8.48	7.38	7.57	6.11	8.15
I20	18.3	19.9	15.2	16.9	16.8	18.7	14.1	16.4	15.8	17.4	11.6	15.5

The drying shrinkage was measured in 10 x 10 x 1000 mm specimens, which were stored in a controlled environment chamber, at 20°C and 50% RH, immediately after demoulding. Both fibre types did not alter the drying shrinkage of concrete significantly. Steel fibre addition showed a small reduction in drying shrinkage of HCFA FRSCC mixtures, as it can be seen in Figure 2, but the result is not statistically significant. On the other hand, HCFA seemed to have a more pronounced effect on drying shrinkage. Figure 3 shows reduced drying shrinkage for FRSCC with increased content of HCFA. Overall, fibre addition and different fibre types show little effect on drying shrinkage, while HCFA seems to reduce shrinkage, although this effect would be more evident in concrete with higher paste volume.

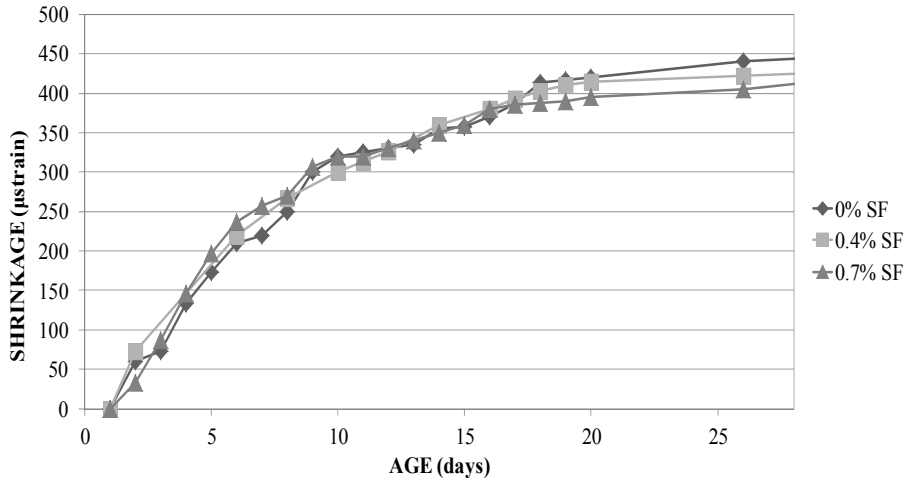

Figure 2 Drying shrinkage of FRSCC mixtures with different steel fibre (SF) content and 30% HCFA

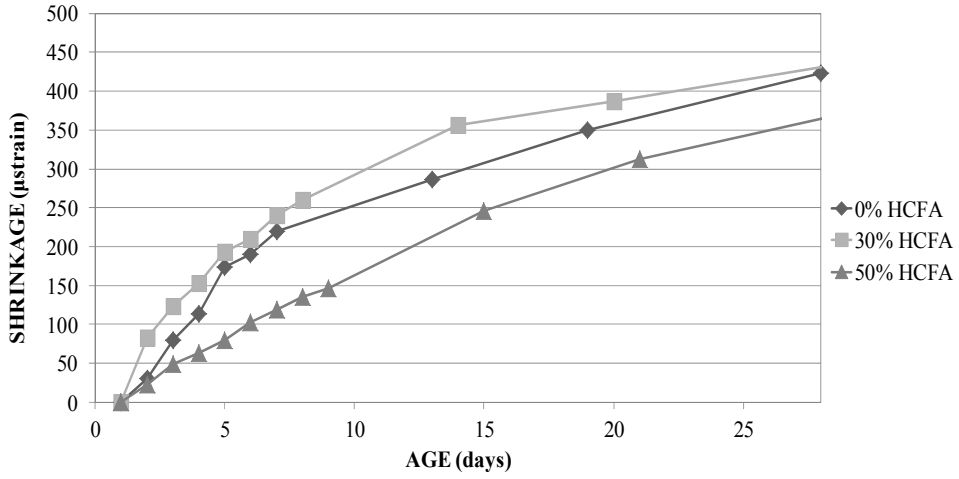

Figure 3 Drying shrinkage of FRSCC mixtures with 0.4% polypropylene fibres

CONCLUSIONS

Regarding the different mixtures tested, it seems that by replacing up to 50% wt. of the total binder volume with HCFA in FRSCC mixtures with 400 kg/m^3 of total binder, robust FRSCC can be produced easily, simply by adjusting the rate and type of chemical

admixtures used (superplasticizer and VMA). Also, robust FRSCC mixtures were achieved with the addition of steel and polypropylene fibres at volumes of up to 0.7% by volume. The fresh concrete properties showed reduced flowability and flow rate with increased HCFA percentage, while passing ability and segregation resistance were not affected. Increased fibre addition percentage, on the other hand, had an effect mostly on passing ability and flowability of fresh concrete, while flow rate and segregation resistance were not affected. Overall, the changes in fresh SCC due to HCFA and fibre addition are relatively small and, with the use of proper chemical admixtures, fall within the required limits of the standards.

Regarding hardened concrete properties, early age mechanical properties of high HCFA volume FRSCC seem to decrease, as all HCFA concretes do, due to the slow rate of the pozzolanic reaction. The use of HCFA as 30% and 50% of the binder in 400 kg/m^3 total binder FRSCC mixtures, however, produces sufficient 28-day compressive strengths of up to 39.9 MPa and 34.2 MPa, respectively, compared to 42.1 MPa of the reference mixtures. Also, HCFA seems to have a positive effect on drying shrinkage, which would be more pronounced in mixtures with higher paste content.

Fibre reinforcement does not seem to affect significantly mechanical properties and drying shrinkage, although in some cases ultimate flexural strength due to fibre anchoring. The effect of fibre addition in SCC is determined by measuring fracture toughness, where toughness indices show that concretes with different fibre types and percentages behave in a similar way in low deformations, but in higher deformations it can be seen that by using steel instead of polypropylene fibres and increased fibre reinforcement percentage, increased fracture toughness is achieved.

REFERENCES

1. SU, N, HSU, K C, CHAI, H W. A simple mix design method for self-compacting concrete, Cement and Concrete Research, Vol. 31, 2001, pp 1799-1807.

2. KHAYAT, K H. Workability, Testing, and Performance of Self-Consolidating Concrete, ACI Materials Journal, Vol. 96, No. 3, 1999, pp 346-353.

3. EFNARC. Specification and guidelines for self-compacting concrete, 2002, EFNARC, UK.

4. NUNES, S, FIGUEIRAS, H, MILHEIRO OLIVEIRA, P, SOUSA COUTINHO, J, FIGUEIRAS, J. A methodology to assess robustness of SCC mixtures, Cement and Concrete Research, Vol. 36, 2006, pp 2115-2122.

5. YE, G, LIU, X, DE SCHUTTER G, POPPE, A-M, TAERWE, L. Influence of limestone powder used as filler in SCC on hydration and microstructure of cement pastes, Cement and Concrete Composites, Vol. 29, 2007, pp 94-102.

6. KHAYAT, K H, ROUSSEL, Y. Testing and performance of fibre-reinforced, self-consolidating concrete, Materials and Structures, Vol. 33, 2000, pp 391-397.

7. GRÜNEWALD, S, WALRAVEN, J C. Parameter-study on the influence of steel fibres and coarse aggregate content on the fresh properties of self-compacting concrete, Cement and Concrete Research, Vol. 31, 2001, pp 1793-1798.

8. FORGERON, D, OMER, A. Flow Characteristics of Macro-Synthetic Fibre-Reinforced Self-Consolidating Concrete, ACI SP 274, 2010, pp 1-14.

9. SONG, P S, HWANG, S. Mechanical properties of high-strength steel fibre-reinforced concrete, Construction and Building Materials, Vol. 18, 2004, pp 669-673.

10. FERRARA, L, PARK, Y D, SHAH, S P. A method for mix-design of fibre-reinforced self-compacting concrete, Cement and Concrete Research, Vol. 37, 2007, pp 957-971.

11. PAPAYIANNI, I, ANASTASIOU, E. Development of Self Compacting Concrete (SCC) by using High Volume of Calcareous Fly Ash, Proceedings of the 2011 World of Coal Ash (WOCA) Conference – May 9-12, 2011 in Denver, USA (available at http://www.flyash.info).

12. KHATIB, J M. Performance of self-compacting concrete containing fly ash, Construction and Building Materials, Vol. 22, 2008, pp 1963-1971.

13. TAYLOR, M, LYDON, F D, BARR, B I G. Toughness Measurements on Steel Fibre-reinforced High Strength Concrete, Cement and Concrete Composites, Vol. 19, 1997, pp 329-340.

14. JENG, F, LIN, M-L, YUAN, S-C. Performance of toughness indices for steel fibre reinforced shotcrete, Tunnelling and Underground Space Technology, Vol. 17, 2002, pp 69-82.

15. EN 14651. Test method for metallic fibreed concrete - Measuring the flexural tensile strength (limit of proportionality (LOP), residual), CEN, 2005.

16. ASTM C 1018. Standard Test Method for Flexural Toughness and First-Crack Strength of Fibre-Reinforced Concrete (Using Beam With Third-Point Loading), ASTM, 1997.

17. GRÜNEWALD, S, WALRAVEN, J C. Maximum Fibre Content and Passing Ability of Self-Consolidated Fibre-Reinforced Concrete, ACI SP 274, 2010, pp 15-30.

Thermal Activation Effect on Fly Ash Based Geopolymer Concrete

S Mandal[1], S Pal[2]
1 – Jadavpur University, India
2 – Larsen & Toubro Ltd, India

It is now well accepted that new binders are needed to replace Portland cement (OPC) to enhance the environmental and durability performance. The development of alkali-activated binders seems to be a greener alternative to OPC. The present study on geopolymer concrete has been made on low calcium fly ash with alkali activators as main binder along with Conventional river sand and 12 mm down coarse aggregates. The alkali activator fluid consists of commercial grade sodium silicate (Na_2SiO_3) pellets and sodium hydroxide (NaOH) solution. The thermal activation for geopolymer concrete in its initial stage is needed for early strength gain and thus its effect on the strength of at different ages of 3, 7, 28 days has been reported. Thermal activation was done in two distinct methods- (1) By keeping the geopolymer concrete specimens (without mould) in a microwave oven for a smaller duration (30, 45 and 60 minutes) after 3 days of casting and (2) By keeping in a hot air oven at temperatures of 600°C, 750°C and 900°C for a longer duration (48 hours) just after casting along with steel moulds. It is concluded that the compressive strength of geopolymer concrete increases with the increase of heat energy in both form cases.

Professor S Mandal, Civil Engineering Department , Jadavpur University , Kolkata -700032 , India

Mr S Pal, Research & Development, Larsen & Toubro Ltd., Powai, Mumbai-400072, India

Keywords: Alkali activation, Fluid to fly ash, Fly ash, Hot air oven, Microwave oven

INTRODUCTION

The urge to reduce emissions of carbon dioxide (1 tonne of OPC generates almost 1 tonne of CO_2) and the fact that OPC structures, which have been built a few decades ago, are already facing disintegration problems points out the handicaps of OPC binders.[1] In fact, the number of premature cases of OPC structures disintegration is overwhelming. On the other hand, the disposal of fly ash, a coal burnt by-product is an environmental issue. As a useful mineral admixture, fly ash has been widely utilized in concrete replacing OPC partially all over the world [2,3,4].

So far, research works carried out on alkali-activated binders show that this binder is likely to have enormous potential to become an alternative to Portland cement. The present research has been dealt with the activation of Indian fly ash (conforming to Class F as per ASTM) by sodium hydroxide (NaOH) and sodium silicate (Na_2SiO_3) solution, both are of commercial grade. The thermal activation on the geopolymer concrete at an early stage has an important role in the improvement of its compressive strength gain[5,6,7]. In general, thermal activation is made by hot air oven to increase the rate of polymerization to achieve an acceptable strength within a reasonable time. Thus the mixture may be used as pre-cast products for practical purpose. It is reported that strength of such concrete increases with the increase of activation temperature and also the duration [9,10,11]. However, thermal activation in the form of microwave heating for a very short period on geopolymer has not been reported so far.

The main aim of the paper is to establish and envisage into two different form of thermal activation for the evaluation of gain in compressive strength of geopolymers. The power consumed (in terms of heat energy) for attaining the required compressive strength of geopolymers can also help to calculate the cost of electricity needed for making such concrete. The implementation of such an activation is done mainly to study the energy consumption for practical use of this material and to compare the results with normal hot air oven activation of the same mix.

EXPERIMENTAL PROGRAM

Materials

Low calcium (ASTM Class F) fly ash has been used in the study. The main source of the fly ash is power plant at Farakka of National Thermal Power Corporation, at Murshidabad, West Bengal. The properties of fly ash and the grain size distribution are presented in Table-1(a) and 1(b). Locally available sand and 12 mm down aggregates were used as fine and coarse aggregates respectively. A mixture of NaOH and Na_2SiO_3 was used as alkali activator. The sodium hydroxide used is of commercial grade in pellet forms with 99% purity and white in colour. Liquid sodium silicate is also a commercial grade having 45% solid content and specific gravity of 1.53 g/cc. It is light grey in colour and highly viscous. The details of Na_2SiO_3 and NaOH of the activator compounds are shown in Table-2(a) and 2(b).

Table –1(a) Properties of fly ash

SL. NO	CONSTITUENTS	% COMPOSITION
1.	Silica (as SiO_2)	64.97
2.	Alumina (as Al_2O_3)	26.64
3.	Ferric Oxide (as Fe_2O_3)	5.69
4.	Calcium Oxide (as CaO)	0.33
5.	Magnesium Oxide (as MgO)	0.08
6.	Sodium (as Na_2O)	0.046
7.	Potassium (as K_2O)	0.023
8.	Sulphur (as SO_4)	0.33
9.	Moisture	0.13
10.	Loss On Ignition (excluding moisture)	1.03

Table 1(b) Size Distribution

SIZE	PERCENTAGE
> 500 micron	NIL
300-500 micron	0.05
212-300 micron	0.62
150-212 micron	5.41
<150 micron	93.93

Table 2(a) Test Results Of Sodium Silicate

SL. NO.	CONSTITUENTS	% COMPOSITION
1.	Na_2O	11.47
2.	SiO_2	29.93
3.	Solids	45.57
4.	Water	54.25

Table 2(b) Physical Property Of Activator Compound

CHEMICAL	NATURE	PURITY & GRADE	COLOUR	COST/KG
NaOH Pellets	Solid	99% Purity	White	Rs.38
Na_2SiO_3	Liquid	45% solid and commercial grade	Greyish	Rs.18

During the preparation of activator liquid of a particular concentration, the effect of impurity in NaOH and the solid content of Na_2SiO_3 solution have been taken care off.

Mixture Proportion

The ratio of (fly ash : sand : coarse aggregate) for the mix proportions of geopolymer concrete was fixed at 1 : 1.644 : 2.466 (by weight) by several trials . Fluid to fly ash ratio (by weight) was fixed at 0.35. The concentration of NaOH solution was taken as 8M. The ratio of Na_2SiO_3 and NaOH was fixed at 1.75 (by weight). The proportionate amount of NaOH was mixed with potable water to obtain the above concentration.

Concrete Specimens

At first, sand and coarse aggregates were mixed at dry condition and then fly ash was added and mixed properly in a mixture machine as usual. The appropriate amount of activator fluid was added to it and mixed thoroughly. Cube specimens of 100 mm x 100 mm x 100 mm size were cast and well compacted. The mould size of 100 mm was taken to maintain the better control of the study for 12 mm down coarse aggregates. Average compressive strength of six samples are reported of each data .

Thermal Activation

For normal hot air oven activation, the concrete specimens (after 30 minutes of casting) with moulds were inserted in a hot air oven.. The moulds were thermally activated at different temperatures of 25^0C (room temperature), 60^0C, 75^0C and 90^0C, for a fixed period of 48 hours. The period 48 hours are fixed based on trials and previous research [11]. The specimens were then demoulded and kept at room temperature till testing.

In case of microwave thermal activation, the activation process starts on the concrete cubes only (without mould) after 3 days of casting. It was decided from several trials that a minimum three days time is required to remove the specimen from the cube moulds. The concrete specimens were then subjected to thermal activation in the microwave with respect to different electrical power (320 Watts, 480 Watts and 640 Watts) and different duration (30 min, 45 min and 60 min). The ranges were fixed by trials. The specimens are tested at the age of 3, 7 and 28 days..

RESULTS AND DISCUSSIONS

The fresh geopolymer concrete mixture was greyish in colour and very cohesive. As expected the mixture becomes more workable with the increase of fluid to fly ash ratio [11,12] . It was concluded that the maximum strength was obtained for 48 hrs of thermal activation for the present mix [11] . The results show that with the increase of temperature of hot air oven, the geo-polymeric reaction is accelerated which resulted in higher compressive strength of geo-polymer concrete specimens assuming all other test variables remaining constant. It may be observed from Table -3 and Figure 1 that the compressive strength gain is more pronounced up to a temperature of 75^0C and become almost flat beyond activation temperature of 75^0C at all ages. The strength of concrete at 75^0C is almost 96% of strength at 90^0C at all ages. Therefore, for the present mixture the activation temperature of 75^0C may be treated as optimum for a period of 48 hours. It is also noted that the gain in strength is not so high at 3 or 7 days at ambient temperature compared to hot air activation (Ref Fig. 1). It seems that the heating of the samples has an important role in early strength gain.

Table 3 Effect of temperature of hot air oven on strength

NO.	HOT AIR OVEN TEMP, ^{0}C (48hrs)	COMPRESSIVE CUBE STRENGTH, MPa		
		3 Days	7 Days	28 Days
C1	At room Temp. (25^0C)	3.50 (17.07%)	5.50(23.66%)	20.10(81.6%)
C2	60^0C	16.75(81.71%)	19.62(84.40%)	22.25(87.25%)
C3	75^0C	19.88(96.95%)	22.75(97.85%)	24.63(96.57%)
C4	90^0C	20.50	23.25	25.50

Note : ( ) value indicates the percentage Compressive Strength corresponding to 90^0C.

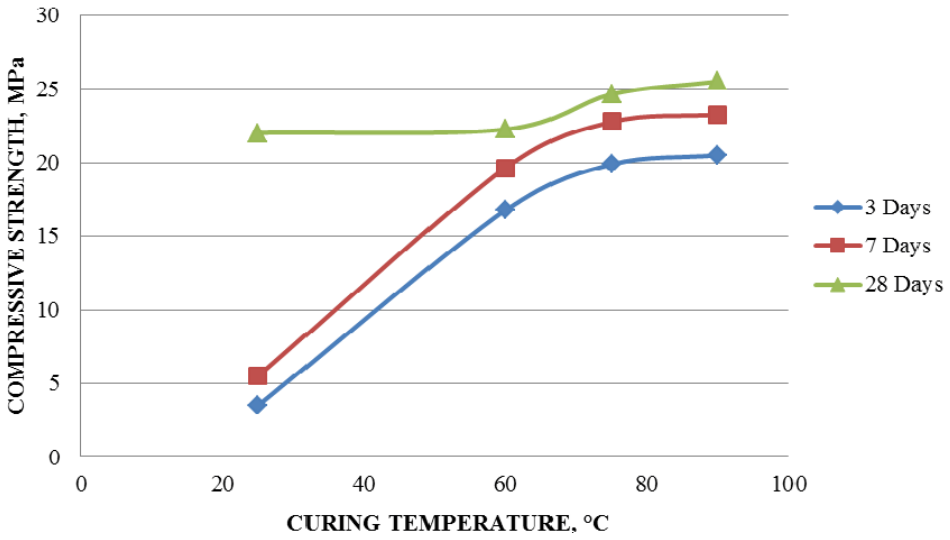

Figure 1 Effect of thermal activation temperature on strength of geopolymer concrete in hot air oven

Unlike hot air oven, the whole sample is heated uniformly in the micro-oven heating process. It is observed that with the increase of electrical energy (Watt-hour), Table 4 the compressive strength of geopolymer concrete also increases. The maximum rate of gain of strength occurred at the energy of 480 Watt-hour, which may be treated as the optimum energy level. Cubes activated above 800 Watts for duration above 30 minutes showed signs of cracking and thus not tested. Increase in strength of geopolymer concrete specimens show that there may be an increased amount of geo-polymerisation due to more energy injected during the thermal activation process. The colour of the concrete surface after micro-oven thermal activation becomes more whitish compared to hot air oven activation. It is obvious that the microwave heating shows higher strength compared to hot air oven activation within a very short period having same mixture proportion. However, a more detailed study is needed to obtain cost effectiveness of microwave thermal activation.

Table 4 Effect of energy (watt-hour) on the strength of geopolymer

Sample No.	Power, Watts	Duration, hrs	Energy, Watt-Hour	COMPRESSIVE CUBE STRENGTH, MPa		
				3 Days	7 Days	28 Days
C5	320	0.5	160	20.00	29.38	30.38
C6	480	0.5	240	33.25	36.38	40.00
C7	640	0.5	320	36.75	40.13	42.38
C8	480	0.75	360	43.00	45.00	46.25
C9	480	1.0	480	44.25	45.00	45.13

CONCLUSIONS

Based on the present experimental investigation it can be concluded that increased rate of polymerization reaction takes place in microwave oven than in normal hot air oven thermal activation. Uniform heating from all surfaces of the geopolymer concrete specimens during microwave oven heating is also an important aspect in the gain of compressive strength. Overheating in microwave for a longer period has a negative effect on the strength of geopolymer concrete.

ACKNOWLEDGEMENTS

The financial assistance to this experimental study received from All India council of Technical Education, New Delhi, India and their R&D grant and file no 8023/BOR/RID/RPS-64/2007-08 dated 24.06.08 is gratefully acknowledged.

REFERENCES

1. FERNANDO P.T, JOAO C.G, SAID J. Alkali-activated binders: A review Part 1. Historical background, terminology, reaction mechanisms and hydration products Construction and Building Materials, 2008, no. 22, pp. 1305–1314.

2. MEHETA, P.K, Durability of concrete: Fifty years of Progress ACI SP 126 Edited by V.M Malhotra 1991, pp. 1-32

3. MALHOTRA. V.M., High performance high volume fly ash concrete, American Concrete Institute Concrete International, 2002, No.-24, Vol. 7, pp.1-5.

4. 4. TARUN, R. N. High strength concrete containing large quantities of fly ash, ACI material Journal, 1989, pp.111-116.

5. HARDJITO D., WALLAH S.E., SUMAJOUW D.M.J AND V. RANGAN, Fly ash-based geopolymer concrete, Australian. Journal of Structural. Engineering. 2005, No-6, pp. 1–9.

6. HARDJITO D AND B.V. RANGAN. B.V. Development and properties of low-calcium flyash-based geopolymer concrete, Research Report GC, Faculty of Engineering, Curtin University of Technology, Perth, Australia, 2005, pp.1-103.

7. MATTHEW R AND BRIAN O'C Chemical optimisation of the compressive strength of luminosilicate geopolymers synthesized by sodium silicate activation of metakaolinite, Journal of material Chemistry, 2003, No 13, pp.1161–1165.

8. IS 650 : 1991 Specification for standard sand for testing of cement , Bureau of Indian Standard.

9. NGUYEN V.C, TRUNG B.D, DANG. Recent Research Geopolymer Concrete, 3rd ACF International Conference, ACF/VCA 2008.

10. HARJITO D, WALLAH S.E, SUMAJOUW M.J AND RANGAN B.V. Factors influencing the compressive strength of fly ash based Geopolymer Concrete. Civil Engineering Dimension. Vol. 6, No. 2, 88-93. Sept. 2004.

11. 11. MANDAL, S. AND PAL S., The Effect of Concentration of Alkali Activator Solution on Fly Ash Based Geo-polymer Concrete Proceedings of the International Conference on Advanced Material and Building Construction at VIT , Tamilnadu 2009 .

12. MANDAL S.AND MAJUMDER , D "Study on the Alkali Activated Fly Ash Mortar" The Open Civil Engineering Journal, 2009, vol 3, pp 98-101

Valuation of the Residual Obtained from the Burning of Rice Husk for Use in Concrete

G R de Sensale, C Romay, F Cost
Universidad de la República, Uruguay

In Uruguay rice production has had a dramatic increase over the past ten years, becoming the most important crop since 2001. Rice production generates large volumes of residual rice husk, fact that leads to serious accumulation issues. Rice is a plant that contains a high amount of sílica, mainly in its husk. When burnt, large quantities of ash are obtained (each ton of paddy produces aprox. 40kg of ash). A large amount of rice husk is used for the production of electricity in cogeneration systems, and as fuel in the rice milling process. In these processes the rice husk ash (RHA) obtained has different characteristics from those produced under controlled conditions: presents high-carbon content and a part of silica in crystalline state. The RHA has about 90% silica. The morphology of the silica is very dependant on the burning conditions; if it is not amorphous (crystalline), it can harm the human organism. Therefore, this paper presents the development of a pretreatment of the rice husk with HCl for the purpose of obtaining amorphous rice husk ash, and a methodology to obtain an amorphous pozzolanic mineral admixture (PRHA) for concrete from the ashes as well. Microstructure and the influence of the milling time on the pozzolanic activity index of the ash obtained are studied. Also, a part of the cement in concretes was substituted by the PRHA in order to study its influence in the compressive strength, elastic modulus, air permeability, chloride ion penetration and shrinkage. The results obtained with the PRHA are compared with those obtained without rice husk ash, proving the viability of its use in concrete when replacing part of the cement.

Dr G R de Sensale is a Full Professor in the Instituto de la Construcción and the Instituto de Ensayo de Materiales of the Faculty of Architecture and Engineering of the Universidad de la República, Montevideo, Uruguay. She has been working in the field of concrete with rice-husk ash since 1997. She is also active as a consulant to government and industry.

M Sc C Romay is an Assistant at the Instituto de la Construcción and the Instituto de Ensayo de Materiales of the Faculty of Architecture and Engineering of the Universidad de la República, Montevideo, Uruguay.

Keywords: Concrete properties, Rice-husk ash, Waste utilization

INTRODUCTION

The annual world production of husked rice is, according to economic forecasts (OCDE-FAO 2008), near the 660 million tons. Forecasts for the 2008-2017 period indicate a strong growth for the rice production in almost every region of the world.

Through elaboration, the initially husked rice is transformed following these stages: 1) pre-washing ; 2) peeling: rice husk is obtained (20% in rice weight); 3) refining: white rice and mill run (residue with commercial value) are obtained ; 4) glazing; 5) parabolizing (optional). As a result of the second stage, taking into consideration the values of rice production, it can be inferred that the production of rice generates important volumes of residual rice husk per year. No attractive commercial alternatives are known for this husk, due to the fact that it does not have any nutritional value and, because of its constitution, it is too resistant to the natural degradation, creating serious accumulation issues. For these reasons, the husk is usually burnt in order to reduce its volume and/or take advantage of its calorific power. Each ton of paddy produces approximately 40kg of rice husk ash (RHA).

Generally this burning is not effectively controlled, reason why the ashes obtained here has characteristics different from those of the ones produced under controlled conditions, high carbon content and a part of silica in crystalline state [1]; for example, in Uruguay, in the best possible conditions, have 60% of crystalline silica [2]. It cannot be said enough that the crystalline silica can cause silicosis, among other adverse effects [3].

The stated problems have been studied in papers from different researchers, which have proved that, through acid pre-treatment of the rice husk, its impurities (sodium and potassium) can be eliminated [4-6], collaborating in the obtention of amorphous silica when the husk is burnt. Some authors like Sugita [7, 8], also point that, through a pre-treatment in HCl, the rice husk ashes' pozzolanic activity is stabilized and improved, and also the ashes' sensitivity to the burning process in relation to the time of exposition to the high temperature. Never the less, there's no literature available providing major details in relation to the variables that influence the pre-treatment (concentration of the solution or exposition time).

Taking into consideration the production perspective on the rice field, as well as the mentioned background, the importance of solving the environmental issues that come as consequence of the rice husk ash and promoting ways of using this seemingly useless residual seems self-explanatory. This is why, in Uruguay, studies concerning pre-treatments of the rice husk are being made, in order to help eliminating the negative effects of the rice husk ash (RHA) obtained nowadays due to the high percentages of crystalline silica. These mentioned studies are being done at the Universidad de la República, as a project financed by the Instituto Nacional de Investigación Agropecuaria (INIA) as a part of the Fondo de Promoción de Tecnología Agropecuaria (FPTA); the project is named INIA FPTA 285 "Valuation of the Residual Obtained From the Burning of Rice Husk". This paper presents the results obtained in the project INIA-FPTA 285 in the optimization of the ash left from its burn (in order to obtain an amorphous pozzolanic mineral admixture, which will be referred to as PRHA) and the viability of its use in concrete when replacing part of the cement. The results obtained are compared with reference values without the mineral admixture

EXPERIMENTAL PROGRAM

The following materials where used: regular rice husk, RHA obtained from husk pre-treated with hydrochloric acid; natural, RHA obtained from regular rice husk (with no pre-treatment done); residual RHA (obtained from drying and parabolizing rice grains); Portland cement type I; as fine aggregate local natural sand with a maximum nominal size of 4.75mm, fineness modulus of 2.92 and specific gravity of 2.62; as coarse aggregate, crushed granite with a maximum nominal size of 12.5 mm, and specific gravity of 2.65; as water , from the local water supply system.

The regular rice husk used was obtained through a representative sampling of different national rice mills from the most common varieties of rice cultivated in our country ("Paso 144", "Tacuarí" and "Olimar"). With all of them, very similar results were obtained, reason why this paper will only present results from the variety "Paso 144", which is the most cultivated in Uruguay. For the pre-treatment of the rice husk, hydrochloric acid solutions (HCl) were used [7, 8], being needed to study its influence in the following variables: concentration of the HCl solution, exposition time and effect of the mechanical agitation of the rice husk in the solution. Concerning the concentration of HCl, the effects of concentrations of 0.35N, 1N and 1.75N were studied. The exposition times to the solution varied from 1 to 24 hours. The mechanical agitation of the HCl solution during the required time for the pre-treatment was also analyzed by using a batch reactor with speeds of 50 rpm and 200 rpm during times that varied from 20 to 40 minutes.

All the samples pre-treated on HCl solution were washed until the water after the washing showed pH values identical to the ones before the immersion of the samples, dried in a lab stove until the weight became constant, and then burn in the laboratory. The burning conditions applied to obtain the RHA simulated the ones from the industrial-scale boiler that nowadays turn the husk into ashes to take advantage of its calorific power. Then, the obtained RHAs were analyzed through X-ray diffractions (XRD) in order to identify crystalline peaks and enable the choice of the pre-treatment to be used to study their applications as amorphous mineral admixture for cement and concretes. The chemical composition of the ash obtained from the pre-treated husk and loss on ignition was determined; in this stage, the residual RHA (RRHA) obtained from the burning of non-pre-treated regular husk from the only company that nowadays uses rice husk as fuel (to generate steam for the parboilization of rice) was also studied, in order to establish their differences.

For the optimization of the ash for its use as pozzolanic admixture, the obtained ash was milled in a grinding mill for times from 1 to 5 hours, studying intervals of 30 minutes. The optimal milling time will be the one to show the highest pozzolanic activity index (AI). This is why the pozzolanicity of the milled ashes was evaluated during different times through resistance-to-compression of mortars, elaborated with the reference cement, and also with 10% (in weight) of rice husk ash instead of cement, according to ASTM C1240-05. In order to be considered as a pozzolanic ash, the quotient between compression tension of the specimens without and with ash had to be higher than 0.75. With the ash milled during the optimal time obtained (PRHA), studies to determine whether the requirements for pozzolanic materials (UNIT 1047) and the viability of its use for the elaboration of conventional concrete were done; with this in mind, concretes with 10% PRHA were done. In concretes resistance to compression, elastic modulus, shrinkage, air permeability, and chloride penetration ions were studied.

RESULTS AND DISCUSSION

Concerning the Pre-treatment for the Obtention of Amorphous Rice Husk Ash

According to the study of variables concerning the pre-treatment in HCl, it can be seen that:

- the increment in concentration of the HCl solution from 1N to 1,75 N and the reduction from 1N to 0,35 N, even with longer exposition times, do not report significant changes concerning the mineralogical composition of the obtained rice husk ash. This can be seen in Figure 1.

- in relation to the exposition time to the HCl solution, although times from 1 to 24 hours were studied. It can be seen that, as time increases, the ashes' crystalline peaks decrease, increasing their condition of amorphous. However, this effect does not translate to long periods of exposition according to the observations done at exposition times of 24 hours, which did not show substantive improvements, as shown in Figure 1(a).

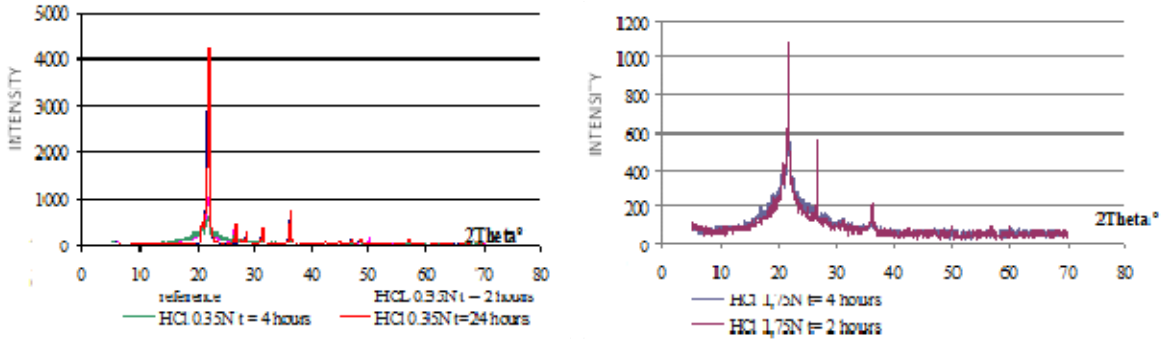

(a) (b)

Figure 1 DRX of samples subjected to HCl pre-treatment (a) 0.35N; (b) 1.75N

- in relation to the effects of mechanical agitation of the HCl solution, by increasing the agitation speed, amorphous ashes can be obtained, although these results are not quite significant.

- Through XRD analysis, the pre-treatment to be done to the husk in HCl 1N solution during an hour without mechanical agitation was defined. Figure 2 shows SEM of pre-treated and non-pre-treated rice husk, where it can be seen that the pre-treatment produces cuts in the husk. Figure 3 shows SEM and RHA EDX obtained from those husks in equal conditions of temperature and exposition time. It is clearly seen that the pre-treatment done leads to fibre breaks, increments of the silica percentages and lower potassium percentages of the RHA, as pointed by different authors in relation to pre-treatments in acid applied to the rice husk (Della y Hotza, 2006; Tzong-Horng Liou, 2004) .

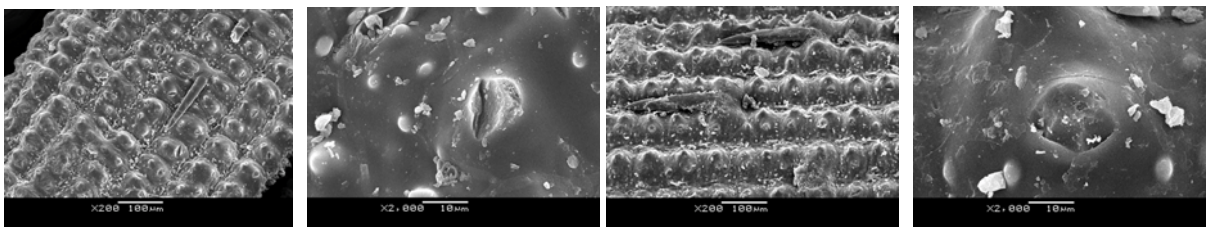

(a) **(b)**

Figure 2 RHA SEM : (a) pre-treated 1hour in HCl 1N ; (b) natural

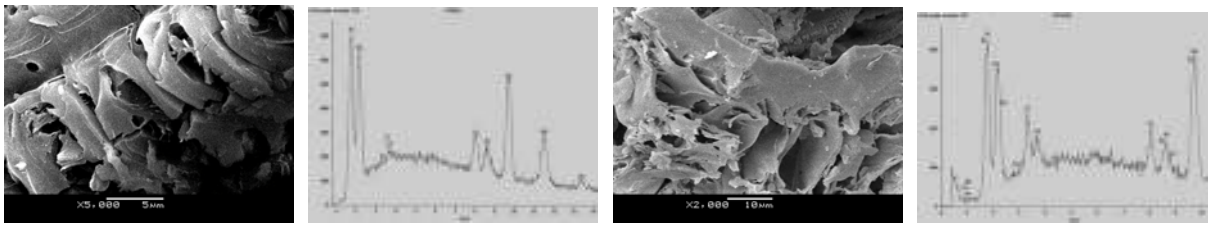

(a) **(b)**

Figure 3 RHA SEM and EDX obtained from rice husk :
(a) pre-treated 1 hour in HCl 1N ; (b) natural

Concerning the Obtention of Amorphous Pozzolanic Mineral Admixture

Rice husk was subjected to pre-treatment with the previously described process in 1 N HCl solution during one hour; then, it was washed (in order to delete the trails of acid), preheated for 24 hours at 100 ^{o}C and, finally, burnt at 700 ^{o}C for one hour. Figure 4 shows the XRD of the obtained RHA, where the absence of crystalline peaks is observed. Then, the pre-treated RHA was characterized and optimized through milling in order to obtain the amorphous pozzolanic mineral admixture.

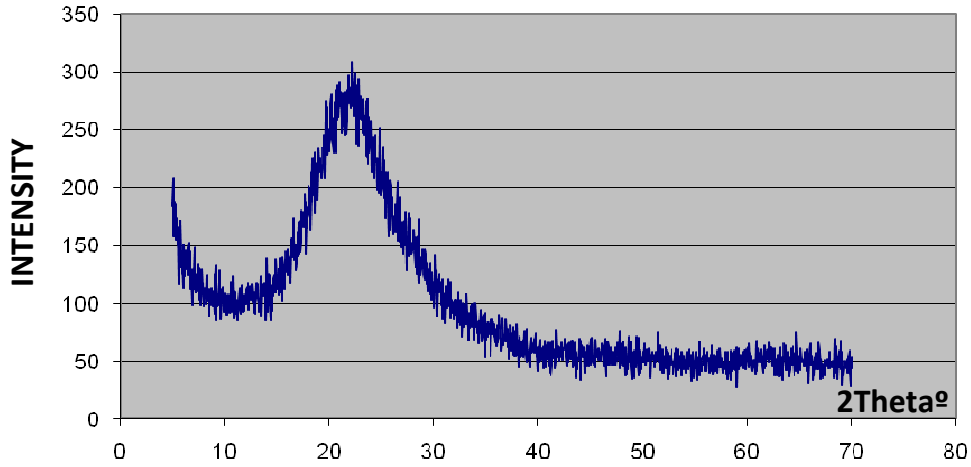

Figure 4 DRX of the RHA obtained with pre-treated rice husk in HCl 1N for 1 hour.

Table 1 shows the chemical composition of the natural and pre-treated RHA obtained at 700ºC for an hour (named NRHA and PRHA, respectively), which is compared with the Uruguayan residual RHA (RRHA). It can be seen that the residual ashes' percentage of sílica is lower, and the loss of ignition is higher than the ones from the lab-obtained RHA.

Table 2 shows the pozzolanic activity index (AI) reached with milling times from 1h30min to 5 hs. From the obtained results, it can be verified that the optimal milling (for the available mill) is reached with a time of 3h30min, time that leads to the highest AI value. The correspondent medium particle size is of 8.225 micrometres. According to Mehta [9], sizes around the 8 micrometres are recommended for the use of RHA as a mineral admixture.

Table 1 Chemical Composition (%) of the of different RHA obtained at 700 ^{O}C during one hour, and of the residual RHA named RRHA

NAME	SiO_2	Al_2O_3	Fe_2O_3	CaO	MgO	MnO	Na_2O	K_2O	SO_3	LOI
PRHA	95.16	0.05	0.05	0.22	0.21	-	0.05	0.76	-	3.5
NRHA	92.86	0.09	0.30	0.64	0.46	-	0.1	3.15	-	2.4
RRHA	87.2	0.15	0.16	0.55	0.35	-	1.12	3.6	0.32	6.55

Table 2 Pozzolanic activity index of the PRHA at different milling times (ASTM C1240)

MILLING TIME	1h30m	2h	2h30m	3h	3h30m	4h	4h30m	5h
AI (%)	72.91	78.95	84.44	89.26	118.91	77.19	116.06	105.32

Table 3 shows the physical and chemical characteristics of the RHA obtained from rice husk pre-treated in 1N HCl solution for 1 hour and milled for 3h30min (PRHA), comparing them to the requirements for pozzolanic materials demanded by norm (UNIT 1047). The viability of its use as pozzolanic mineral amorphous admixture for cements and concretes is seen.

Table 3 Characteristics of the PRHA optimized in comparison to the norm requirement (%)

Name	AI	SiO_2	Al_2O_3	Fe_2O_3	CaO	MgO	MnO	Na_2O	K_2O	SO_3	LOI
PRHA	118.91	95.16	0.05	0.05	0.22	0.21	-	0.05	0.76	-	3.5
UNIT 1047	>75	$SiO_2+Al_2O_3+Fe_2O_3$ >34						Alkalis in Na_2O < 1.5		< 4	< 6

Results Obtained in Concretes

For study the effects of the PRHA in concrete the water/cementitious material ratio used was 0.50, the replacement of cement by PRHA was made by mass. Table 4 shows the mixture proportions of the materials used, in weight. The use of PRHA decreases the slump in comparison with the reference concrete (without PRHA)

Table 4 Mix proportions of concrete

W/ (c+RHA)	PRHA %	CEMENT kg/m^3	RHA kg/m^3	FINE AGG. kg/m^3	COARSE AGG kg/m^3	SUPER-PLAST. %	SLUMP cm
0.50	0	400	-	721	1003	-	15
	10	360	40	721	1003	-	12

Tables 5 and 6, Figures 5 and 6, shows the results obtained by the replacement of 10% cement by PRHA.

Table 5 corresponds to the resistance to compression, elastic modulus (Ec) and chloride resistance according to the ASTM C1202 of concretes. Higher compressive strength results are obtained without the use of the PRHA. The values of modulus of elasticity at 28 days of age show that the reference concrete is less deformable than the concrete with the addition, but the difference between them is approximately 10% (equal to the percentage of cement replaced). Chloride penetration was determined in concretes obtaining the values of electric current, Q (Coulomb) and its classification according to ASTM C 1202, as indicated in Table 5. Concretes with and without PRHA, have low permeability to chloride ions.

Table 5 Results obtained in concretes with and without PRHA

	COMPRESSIVE STRENGTH (MPa)				Ec (GPa)	CHLORIDE RESISTANCE (Coulombs)	
	14 days	28 days	56 days	91 days	28 days	56 days	ASTM C1202
Reference	28.87	32.03	34.27	43.3	41.23	1550	Low
10% PRHA	24.25	25.4	30.27	38.6	36.23	1569	Low

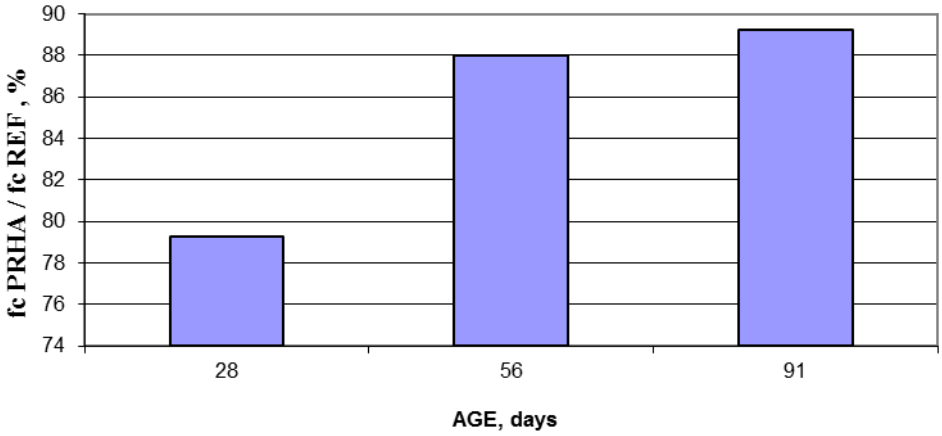

Figure 5 Relative compressive strength (fc PRHA concrete / fc reference concrete)

As shown in Figure 5 the older ages tendency shows an increase favourable in resistance of the concrete with PRHA in relation to the reference concrete, since the differences between

them are reduced; according the literature [2, 10], the reaction to pozzolans is slow, fact that should be taken into account in the norms by demanding higher test times when used as supplementary cementitious materials.

The air permeability, evaluated by the Torrent method, at different ages by the coefficient Kt (10^{-16} m^2), the electrical resistivity value ρ (kΩ cm), and concrete quality are given in Table 6. The air permeability values are consistent with the values of compressive strength obtained for both concretes (class classified as good and normal to the age of 28, 56 and 91 days).

Table 6 Air Permeability: coefficient Kt (10^{-16} m^2), electrical resistivity ρ (kΩ cm) and concrete quality, according Swiss Standard SIA 262/1:2003.

AIR PERM.	28 DAYS			56 DAYS			91 DAYS		
	Kt	ρ	Concrete quality	Kt	ρ	Concrete quality	kt	ρ	Concrete quality
Reference	0.053	14		0.109			0.178		
	0.011	11		0.013			0.034		
	0.09	16	Good	0.022	s/d	Good	0.024	s/d	Good
10 % PRHA	0.534	15		0.762			0.148		
	1.149	21		0.945			0.258		
	0.499	18	Normal	0.810	s/d	Normal	0.176	s/d	Normal

The shrinkage calculated by the percentage change in length of the specimens, at ages up to 91 days are presented in Figure 6; the incorporation of PRHA reduces the shrinkage of concrete, which is very beneficial since it involves less crack with corresponding benefits to the durability of concrete with respect to entry of aggressive agents (water, salts, etc..).

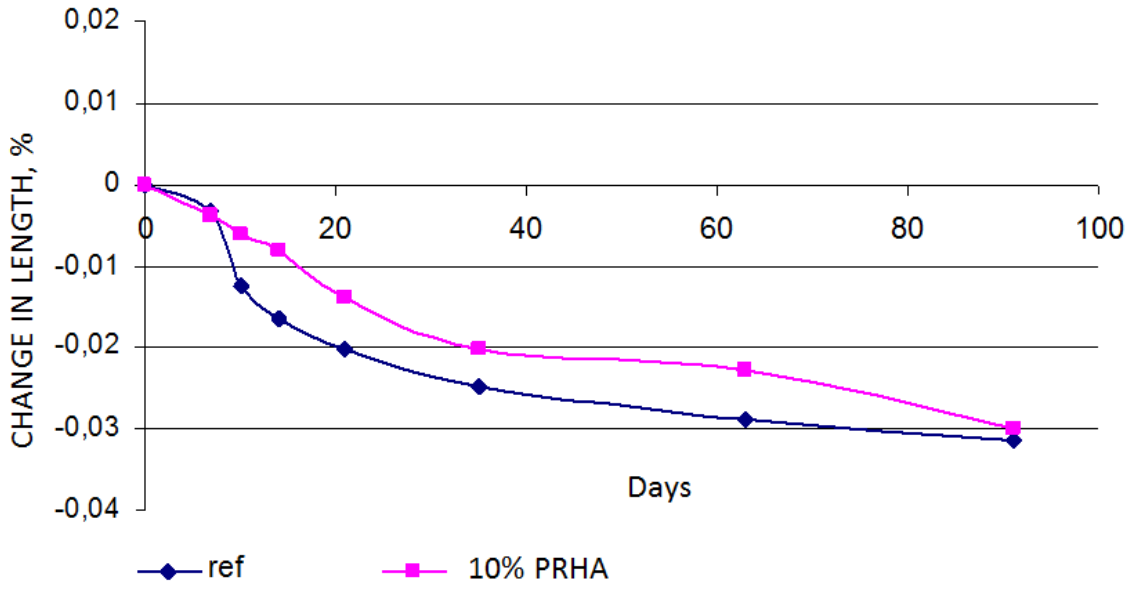

Figure 6 Shrinkage in concretes with and without PRHA

CONCLUDING REMARKS

The results obtained in this research lead to the conclusion that, by pre-treating the rice husk in 1N HCl solution for one hour, it is possible to obtain rice husk ash with high percentages of amorphous silica. This pre-treatment increases the silica percentage and lowers the potassium percentage in the rice husk ash obtained. By comparing the characteristics of the ash obtained with the normative values, the viability of its use as pozzolanic material is proven.

The studies done by milling the rice husk ash allowed the obtention of activity index values much better than the ones pointed as requirements for pozzolanic materials (UNIT NM 1047) and, by finding the substitution percentage with the highest pozzolanic activity index, an amorphous mineral pozzolanic admixture was developed (PRHA), increasing the value of the residual obtained by burning the rice husk.

In concretes with 10% substitution of cement by PRHA, the viability of its use in relation to the studied properties (compressive strength, elastic modulus, chloride ion resistance, air permeability and shrinkage) was proven.

Summarizing, this paper promises a bright future for the use of the developed PRHA in concrete. In the studied properties, the possibility of obtaining performances with less use of cement is shown, reducing by this means the environmental damage that the CO_2 emissions and the use of fossil fuels for the clinker production cause. Therefore, after the conclusion of the INIA FPTA 285 project, this research will help solve, in a not-so-distant future, two critical issues: the one of the final disposal of the rice husk ash, and the one that involves its danger on the human health (due that the developed pre-treatment leads to RHA with no crystalline peaks).

ACKNOWLEDGEMENTS

The author acknowledges the support provided for the INIA and CSIC-UDELAR, Uruguay. The author is grateful to Hormigones Artigas S.A. and Arroz Uruguayo S.A. for their help.

REFERENCES

1. CHAGAS CORDEIRO G. et al. Use of ultrafine rice husk ash with high-carbon content as pozzolan in high performance concrete. Materials and Structures, Vol. 42, pp.983-992, 2009.

2. RODRIGUEZ DE SENSALE G. Strength development of concrete with rice-husk ash. Cement and concrete composites, Vol. 28, No. 2, pp.158-160, 2006.

3. LEGRAND A.P. The surface properties of silicas. John Wiley & Sons, 470p., 1998

4. DELLA V.P. et al. Rice husk ash as an alternate source for active silica production Materials Letters 57, pp. 818-821, 2002

5. DELLA V.P., HOTZA D. Estudo comparativo entre sílica obtida por lixívia ácida da casca de arroz e Sílica obtida por tratamento térmico da cinza de casca de arroz. Quim. Nova, Vol. 29, No. 6, 1175-1179, 2006.

6. TZONG-HORNG L. Evolution of chemistry and morphology during the carbonization and combustion of rice husk. Carbon, Vol. 42, 785–794, 2004.

7. FENG, Q. et al. Study of thermal decomposition process of raw and hydrochloric acid treated rice husk. Rev. Hachinohe Institute of technology, pp.67-74, 2003.

8. FENG Q. et al. Study on the pozzolanic properties of rice husk ash by hydrochloric acid pre-treatment. Cement and Concrete Research , Vol. 34, pp. 521–526, 2004.

9. MEHTA PK. Highly durable cement products containing siliceous ashes. USA Patent 5,3467,548, 1994.

10. MEHTA PK., MONTEIRO PJM. Concrete: Microstructure, Properties and Materials, Mc Graw Hill, Third Edition, 2006.

11. ORGANIZATION FOR ECONOMIC CO-OPERATION AND DEVELOPMENT – FOOD AND AGRICULTURE ORGANIZATION OF THE UNITED NATIONS, OECD/FAO. Agriculture Outlook: 2008 to 2017, 73p, 2008.

12. RILEM. Detection of potential alkali-reactivity in concrete- Outline guide to the use of RILEM methods in assessments of alkali-reactivity potential. Materials and Structures, Vol. 36, pp. 472– 479, 2003.

Influence of Circulating Fluidized Bed Combustion (CFBC) Fly Ash on the Properties of Cement Pastes

H Cam[1], N Neithalath[2]
1 – Clarkson University, USA
2 – Arizona State University, USA

Circulating fluidized bed combustion (CFBC) technology is one of the most promising clean coal technologies. With increasing emphasis on lowering greenhouse gas emissions, CFBC boilers are widely adopted by thermal power plants in an effort to reduce NOx and SOx emissions. This paper provides the details of a systematic study tailored to understand the influence of a CFBC fly ash (high in CaO, SO_3, and LOI) as a partial cement replacement material, on the hydration behavior, and fresh and hardened properties of cement pastes. The influence of CFBC fly ash on air entrainment efficiency in cement pastes is evaluated in detail using modified foam index tests.

Hieu Cam was a Masters student in the Department of Civil Engineering at Clarkson University, Potsdam, NY. His research interests are in alternate cement replacement materials for concrete and their property evaluation.

Dr. Narayanan Neithalath is an Associate Professor in the School of Sustainable Engineering and the Built Environment at Arizona State University, Tempe, AZ. His research interests are in the development and characterization of novel cementitious materials, performance evaluation and modeling of cementitious systems, computational materials science of concretes, and development of sustainable energy efficient concrete systems.

Keywords: CFBC fly ash, Calcium hydroxide content, Compressive strength, Foam Index test, Hydration

INTRODUCTION

Circulating fluidized bed combustion (CFBC) technology is one of the most promising clean coal technologies. With increasing emphasis on lowering greenhouse gas emissions, CFBC boilers are widely adopted by thermal power plants in an effort to reduce NO_x and SO_x emissions [1]. CFBC boilers can use several co-firing materials as fuel, and even low-grade fuels high in ash and sulfur contents that cannot be used in pulverized coal combustion (PCC) plant can be used in CFBC plants [2]. CaO liberated from the decomposition of limestone captures SO_x and produces $CaSO_4$ which contributes to the high sulfate content of CFBC fly ash [3]. Large amounts of CFBC ash (both fly ash and bottom ash) are being generated each year from CFBC power plants all over the world, but with limited uses due to the large quantity of sulfates and carbon present in the material. Large amounts of unburned carbon have been recognized to have adverse effects on the efficiency of air entraining agents (AEA) used in concrete [4-9].

ASTM C 618 specifies limits of 5% and 6% respectively for the SO_3 content and loss on ignition (LOI) of Class F and C fly ashes. CFBC fly ashes exceed these limits, with SO_3 content and LOI close to 20% in some cases, thus making their use in concrete subject to current standards impossible. A few studies have evaluated means of utilizing CFBC ashes in pavement construction [10] and in conductive low strength concretes [11]. Utilizing CFBC fly ash in cement based materials, previously seen as harmful due to the presence of large amount of sulfates, free lime and carbon, are currently being carefully examined [12-15]. Some studies have shown that cement paste or concrete systems containing high calcium, high sulfate fly ash as a partial cement replacement material exhibit satisfactory strength development [12, 16, 17].

This paper provides the details of a systematic study tailored to understand the influence of a CFBC fly ash (high in CaO, SO_3, and LOI) as a partial cement replacement material, on the hydration behavior, and fresh and hardened properties of cement pastes. The influence of CFBC fly ash on air entrainment efficiency in cement pastes is evaluated in detail using modified foam index tests. Detailed analysis of cement hydration is carried out using non-evaporable water contents and calcium hydroxide contents in the plain and modified pastes.

EXPERIMENTAL PROGRAM

Materials

Table 1 shows the chemical composition and physical properties of Type I Ordinary Portland Cement (OPC), and CFBC fly ash used in this study. The chemical composition of the CFBC fly ash used in this study falls within the range of values reported for such fly ashes. When compared to typical fly ashes used in concrete, CFBC fly ash has higher Fe_2O_3 and SO_3 contents as well as a much higher LOI. The higher LOI can be attributed to the higher amount of unburned carbon in CFBC fly ash, and the higher SO_3 to the high-sulfate coke. The CFBC fly ash also has a higher CaO content when compared to a typical Class F fly ash, attributable to the limestone added as a sorbent. The CFBC fly ash is slightly coarser than the Type I OPC used in this study, but has a comparable particle size distribution to a typical Class F fly ash as shown in Figure 1.

Table 1 Chemical composition and physical characteristics of cement and CFBC fly ash

CHEMICAL COMPOSITION / PHYSICAL PROPERTY	TYPE I OPC	CFBC FLY ASH
	Weight %	
Silicon dioxide	20.2	24.1
Aluminum oxide	4.70	9.93
Iron oxide	3.00	11.9
Calcium oxide	61.9	24.4
Magnesium oxide	2.60	0.94
Sodium oxide	0.19	0.58
Potassium oxide	0.82	1.32
Sulfur trioxide	3.90	17.0
Loss on Ignition (LOI)	1.90	14.7
Fineness (% passing, Sieve Size)	97.4 (45 µm)	85 (45 µm)

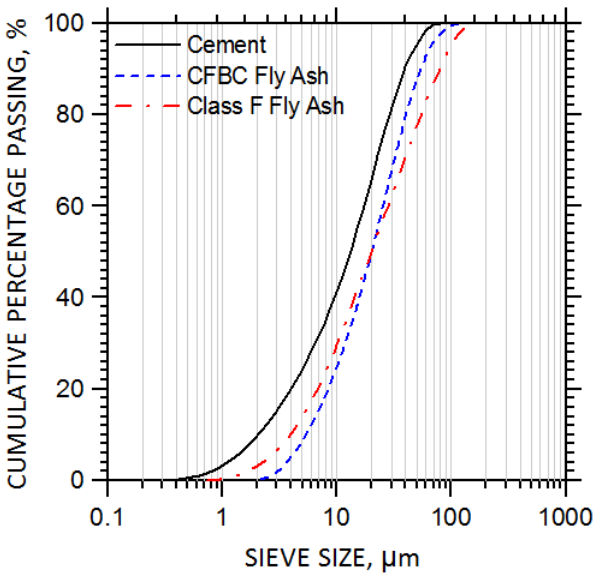

Figure 1 Particle size distribution curves of cement, CFBC fly ash, and Class F fly ash

XRD patterns of OPC and CFBC fly ash are shown in Figure 2. The positions and relative intensities of the peaks corresponding to these constituents are very similar to that of a CFBC fly ash reported in [15]. In this figure, the XRD pattern of a typical Class F fly ash also is shown in order to compare the relative magnitudes of the diffuse bands corresponding to the glassy phase.

For Class F fly ash, this band peaks at a 2θ of about 23°. Even though a slight glass hump is noticeable for the CFBC fly ash, it is not as distinct as in the case of the Class F fly ash. This could be because of the relatively lower combustion temperatures reached in the CFBC process (800-900°C) as opposed to higher temperatures in pulverized coal combustion (PCC) process (1300-1700°C). However, it has been reported that these temperatures are sufficient to dehydroxylate the clay minerals such as kaolinite and illite in the coal and make them pozzolanic to some extent.

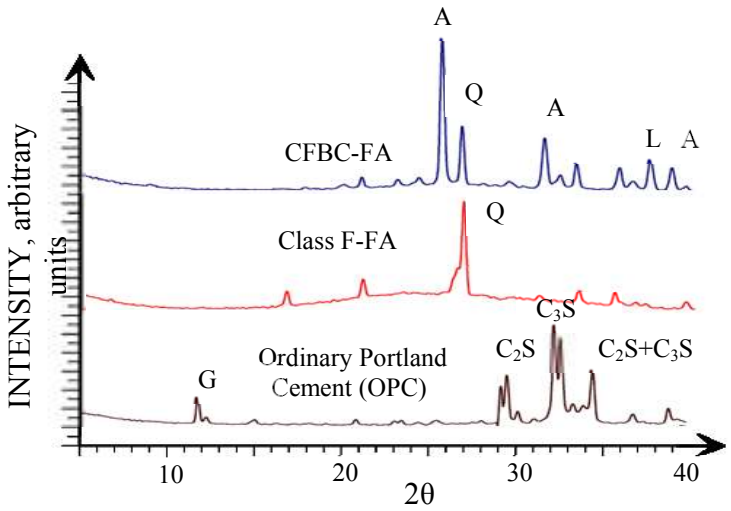

Figure 2 X-ray diffraction patterns of CFBC fly ash, Class F fly ash and ordinary Portland cement. (A: Anhydrite, Q: Quartz, L: Free Lime; C_3S: Tricalcium silicate, C_2S: Dicalcium silicate)

Figure 3 shows the morphology of the CFBC fly ash used in this study. The CFBC fly ash particles are less spherical as compared to commonly used Class C or F fly ashes. This has implications in the workability of cement pastes containing CFBC fly ash, as well as its capability in entraining and maintaining requisite amount of air voids that are necessary for freeze-thaw resistance of concretes, which are discussed in detail in this paper.

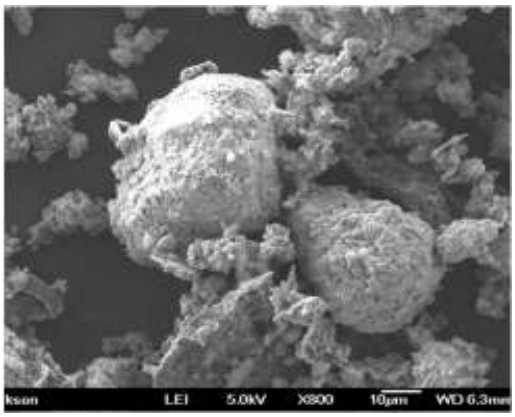

Figure 3 Morphology of CFBC fly ash.

Test Methods

Determination of cement paste workability using flow values

The flow values of Type I OPC paste and CFBC fly ash modified pastes were determined in accordance with ASTM C 1437 specifications. Flow values of a typical Class F fly ash were also measured so as to obtain an indication of the influence of particle shape on flow. The flow values of CFBC fly ash modified pastes were determined using a water-to-cementing materials ratio (w/cm) of 0.42, whereas a w/cm of 0.32 was used for the Class F fly ash modified pastes. The particle shape of CFBC fly ashes as well as the porous nature of carbon particles in this fly ash results in a higher water demand for CFBC fly ash modified pastes to produce measurable flow values.

Modified foam index test

Modified foam index test [8] was carried out to determine the influence of CFBC fly ash as a partial cement replacement material on the air entrainment in cement pastes. 10 g of cement and 25 ml of water were mixed in a 90 mm diameter glass jar. The jar was sealed and shaken vigorously for 15 seconds. The diluted air entraining agent (AEA) solution (AEA to water ratio of 1:9) was added to this mixture gradually (2 drops at a time). The jar was shaken again vigorously for another 15 seconds. The process was repeated until the surface of the cement-water mixture was covered completely with foam. The test was repeated with 10% or 20% of CFBC fly ash by mass as a cement replacement material. In order to evaluate the stability of the foam with time, the jar was shaken vigorously for 15 seconds every 60 minutes. If the surface of the cement-water mixture became discontinuous during any of these hourly agitations, additional AEA solution was added to the mixture to maintain a continuous foam layer on the top. This process was repeated up to 8 hours.

Non-evaporable water contents

Thin strips of pastes (150 mm x 50 mm x 10 mm) were cast and cured in saturated limewater. After 1, 3, 7, 14, 28, 56, and 90 days of hydration, about 5 – 7 g of the paste was ground into a powder and soaked in acetone to prevent further hydration. After removing from acetone and drying in air, the specimens were placed in an oven at 105 ± 5^{o} C for 24 hours to allow all loosely bound water to evaporate. The initial mass (m_{105}) of the specimen was determined, and the specimen was placed in a furnace at 1050 ± 10^{o} C for 3 hours. The final mass (m_{1050}) was determined after removing it from the furnace and allowing it to return to ambient conditions in a dry environment.

The non-evaporable water content (w_n) is calculated as:

$$w_n = \frac{m_{105} - m_{1050}}{m_{1050}} - \sum (LOI_{cm} * m_{cm}) \quad (1)$$

where LOI_{cm} is the loss on ignition of the cementing materials (dry cement or CFBC fly ash), and m_{cm} is the mass fraction of the respective cementing material in the paste.

Thermogravimetric analysis (TGA) of pastes

TGA on plain and modified cement pastes was conducted using a Perkin-Elmer TGA system at 14, 28, 56, and 90 days of hydration. 30-40 mg of pulverized sample was heated from 50^{o} C to 1050^{o} C in both inert (Nitrogen) and oxidizing (air) environments at gas flow rates of 45 ml/min. The reasons for using both of these conditions are explained in a later section. The percentage of mass remaining as a function of temperature was recorded.

RESULTS AND ANALYSIS

Influence of CFBC Fly Ash on Flow and Air Entrainment Characteristics of Pastes

The flow values of the plain and modified pastes were determined in accordance with ASTM C 1437, as described in Section 2.2.1. The normalized flow values (flow values of modified pastes divided by that of plain paste of the same w/cm) of CFBC fly ash modified pastes and Class F fly ash modified pastes are shown in Figure 4. The flow of CFBC fly ash modified pastes decreases with increasing amount of CFBC fly ash in the pastes. The influence of particle shape and texture (rounded and smooth for Class F fly ash, or for that matter Class C fly ash also, as against non-spherical and rough for CFBC fly ash) on paste workability is obvious from this figure. Another factor that contributes to a reduction in flow values of the CFBC fly ash modified pastes is the porous nature of carbon particles that result in water absorption by these particles.

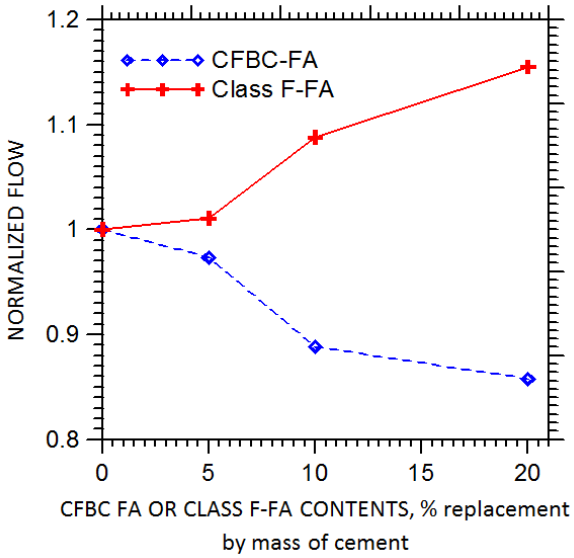

Figure 4 Normalized flow values of modified cement pastes.

Modified foam index test was carried out on the chosen binder combinations as explained in Section 2.2.2, and the results are shown in Figure 5. Contrary to the conventional foam index test where the AEA dosage is obtained only initially, this test continues up to 8 hours after the initial addition of AEA, to allow equilibration.

It has been reported that a longer time is needed for the AEA to enter into the less accessible pores of the carbon particles and thus to attain equilibrium [4], and thus the conventional foam index test might not provide accurate indications of the AEA requirement.

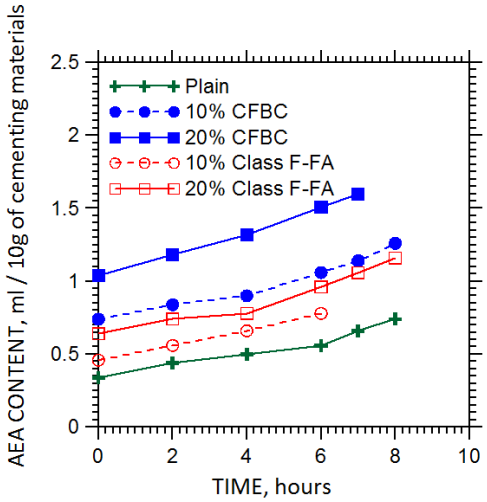

Figure 5 AEA dosage requirements of plain and modified pastes to achieve foam stability, as a function of time.

AEA requirements for CFBC fly ash (higher LOI) modified pastes are contrasted with those of Class F fly ash (lower LOI) modified pastes in Figure 5. It is seen from this figure that the initial AEA requirement of the plain paste is lower than that of the modified pastes. Increasing amounts of cement replacement by CFBC fly ash or Class F fly ash is found to require higher initial AEA dosage to achieve a continuous foam layer on the surface. The required dosage of AEA is higher for CFBC fly ash modified pastes as compared to Class F fly ash modified pastes for the same cement replacement level. This is attributed to the higher carbon content in CFBC fly ash and the porous nature of carbon particles [5]. The higher AEA requirement for Class F fly ash modified pastes as compared to the plain paste could be due to the slightly higher carbon content of Class F fly ash than the cement and the lower alkalinity of the Class F fly ash modified pastes. Even when the replacement material has a higher carbon content, the effects of carbon on air entrainment is minimized if the paste has a higher alkalinity.

It can also be noticed from Figure 5 that all the pastes required additional dosages of AEA at later times in order to achieve a surface with a stable foam layer. The mixture with 20% replacement of cement by CFBC fly ash shows the highest AEA requirement at all times than the other mixtures. This could be because of the gradual intake of AEA into the micropores of the carbon particles [5, 9]. A portion of the increased AEA requirement for all the mixtures could also be attributed to the loss of foam as a result of agitating the jar every hour. The modified foam index values provide an indication of the AEA requirement as a function of time, and thus could be related to the air loss occuring as a result of transporting the concretes.

Compressive Strengths of Plain and CFBC Fly ash Modified Cement Pastes

Compressive strengths of cement pastes modified with either 5%, 10%, or 20% CFBC fly ash were determined at 1, 3, 5, 7, 14, 28, and 90 days of hydration. Companion OPC pastes were also tested for comparison. A w/cm of 0.42 was used for all the cement pastes. Figure 6 shows the compressive strength development of CFBC fly ash modified pastes. The average compressive strength values of three 50 mm size cubes are reported here.

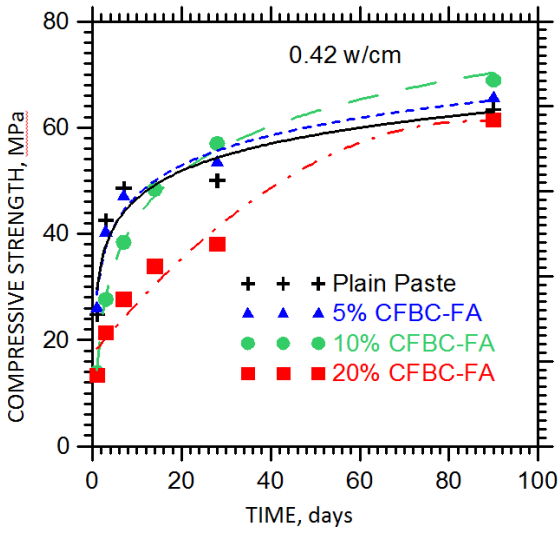

Figure 6 Compressive strength development of plain and CFBC fly ash modified cement pastes

It can be seen from this figure that the compressive strengths of modified pastes decrease with increase in the amount of CFBC fly ash in the pastes, at early ages. This is because of an overall dilution effect where the cement replacement material is not as effective as the cement it replaced, in early age strength development. The replacement of cement by CFBC fly ash of up to about 10% by mass does not cause appreciable property loss. Replacement of 20% of the cement by CFBC fly ash results in appreciable strength loss at all ages up to about 60 days. The higher amount of CaO in CFBC fly ash might be considered to be influential in strength development of CFBC fly ash modified cement pastes because of self-cementitious properties of a high-calcium cement replacement material.

One of the main factors that can contribute to the strength of CFBC fly ash modified cement pastes is the amount of ettringite formed in these mixtures. Satisfactory strength development of concretes or cement pastes incorporating fly ashes high in sulfates and calcium has been attributed to the formation of ettringite [12, 16, 17]. The strength enhancement in CFBC fly ash modified pastes after 28 days is significant, especially at higher replacement levels. The strength increase could be attributed to some pozzolanic reaction of CFBC fly ash with the calcium hydroxide (CH) formed from cement hydration to produce additional C-S-H gel. Later age ettringite formation also could be partly responsible for the strength enhancement of CFBC fly ash modified pastes.

Non-Evaporable Water (w_n) and Calcium Hydroxide (CH) Contents

Non-evaporable water contents

Figure 7 shows the non-evaporable water content values (w_n) of plain and CFBC fly ash modified cement pastes until 90 days of hydration. It can be seen from these figures that the modified pastes have lower w_n values than the plain paste at all ages of hydration. Larger amounts of anhydrite or hemihydrate present in CFBC fly ash can hydrate to form gypsum, thus leaving less water for cement hydration and consequently lowering the w_n.

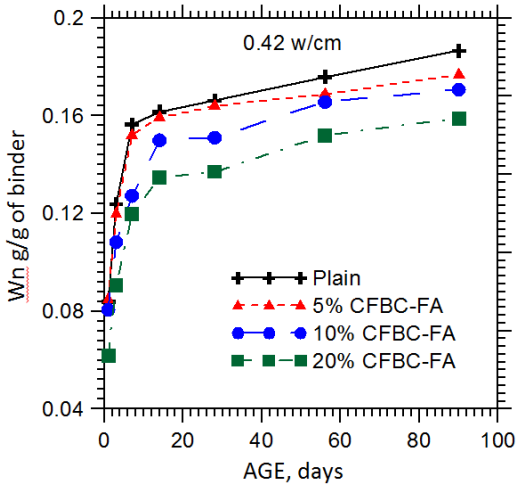

Figure 7 Non-evaporable water contents, of plain and CFBC fly ash modified pastes at several ages of hydration

Calcium hydroxide contents

The calcium hydroxide (CH) contents were obtained from the thermal analysis data obtained by heating in an inert environment as described in the previous section. The mass loss between 400°C to 470°C in a thermal analysis curve is attributed to CH decomposition. The CH contents of CFBC fly ash modified pastes at hydration ages of 14, 28, 56, and 90 days are presented in Figure 8(a). It can be seen that CH contents of plain paste increases steadily until 90 days even though the increase is more marked at early ages.

For the pastes with 10% or 20% cement replacement by CFBC fly ash, CH increases up to 28 days, and a reduction is observed thereafter. The pozzolanic reaction in CFBC fly ash modified pastes could be responsible for the consumption of some of the CH after 28 days. The lower levels of CH present in CFBC fly ash modified pastes could also be due to consumption of CH for ettringite formation [13]. The 20% CFBC fly ash modified paste shows lower CH contents than the plain and 10% CFBC fly ash modified paste.

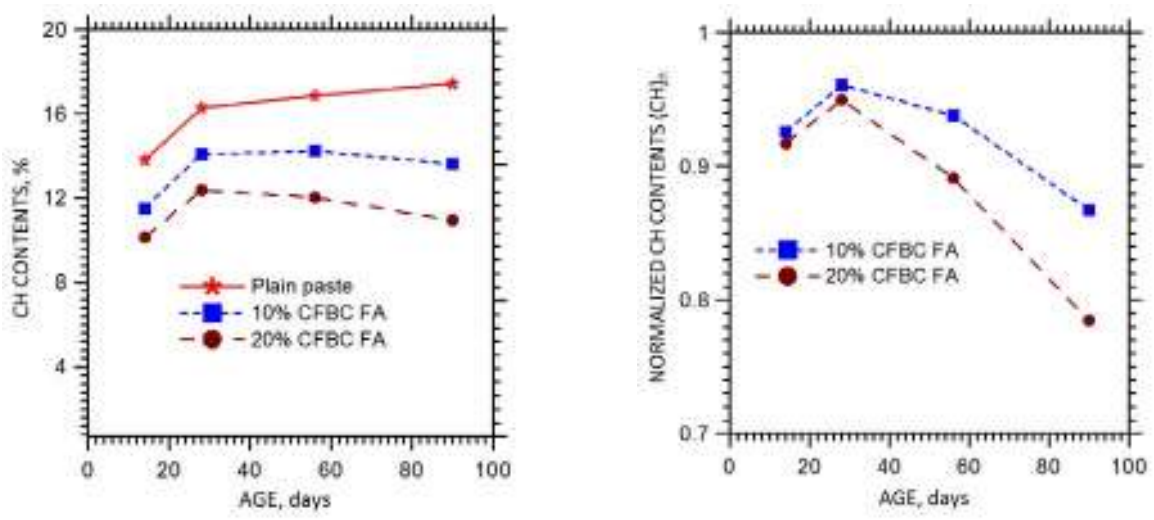

(a) (b)

Figure 8 (a) CH contents, and (b) normalized CH contents of plain and modified pastes as a function of curing time

The CH contents of plain cement pastes are typically used to measure the progress of hydration. However, in cement pastes with supplementary cementing materials, the CH contents may be: (i) lower because of the lower cement contents and/or the pozzolanic reaction that consumes CH, or (ii) higher because of the enhancement in cement hydration in the presence of the supplementary cementing material. Hence, a normalized CH content $(CH)_n$ has been used to compare the CH contents of plain pastes and modified pastes [18]. $(CH)_n$ is calculated as shown below.

$$(CH)_n = \frac{(CH)_{ModifiedPastes}}{(CH)_{Plain} * m_c} \quad (2)$$

where $(CH)_{Modified\ Paste}$ is the CH content in the CFBC fly ash modified pastes, $(CH)_{plain}$ is the CH content in the plain paste, and m_c is the mass fraction of cement in the paste. Values of $(CH)_n$ greater than 1.0 indicate that the CH contents in the modified pastes are higher than those in plain cement pastes having a similar cement content, attributable to the enhancement in cement hydration because of the presence of the replacement material. $(CH)_n$ values lower than 1.0 might indicate either the retarding effect of the cement replacement material at the given age, or pozzolanic reaction which results in reduction of CH. In CFBC fly ash modified pastes or cement pastes containing large amounts of sulfate, consumption of CH for ettringite formation can further reduce the value of $(CH)_n$.

Figure 8(b) shows the $(CH)_n$ values of CFBC fly ash modified pastes at various ages of hydration. It can be seen that the $(CH)_n$ values of all the modified pastes are consistently less than 1.0 and generally decreases after 28 days of hydration. It is anticipated that, for CFBC fly ash modified pastes, the reduction in $(CH)_n$ is likely due to a combination of pozzolanic reaction and the consumption of CH for ettringite formation. The relative magnitudes of these are not attempted to be quantified here.

A Brief Quantification of Ettringite Formation in these Systems

In a system containing significant amounts of sulfates, large amounts of ettringite will be formed. Figures 9 (a) and (b) show scanning electron micrographs of 20% CFBC fly ash modified pastes after 14 and 90 days of hydration. Large amounts of ettringite are observed in both these micrographs. CH also could be consumed for ettringite formation, as observed from the drop in CH contents of the modified pastes after 28 days of hydration. The consequences of ettringite formation such as expansion and cracking is a valid concern in CFBC fly ash modified concretes and should be addressed. Figures 9 (a) and (b) also show marked variations in the morphology of ettringite crystals. Fine acicular ettringite crystals, largely present on particle surfaces as seen in these figures, are possibly a result of topochemical reaction (on the surface of the aluminates), while coarser and prismatic crystals are preferred in through-solution reaction. Ettringite formation in the bulk solution or in the spaces left behind by CH could also be a result of the finer ettringite crystals dissociating into the pore solution and recrystallizing as relatively coarser crystals in order to ensure thermodynamic stability.

XRD was used to identify the phases and carry out a relative quantification of ettringite that is formed when cement pastes containing CFBC fly ash hydrates. XRD was conducted after 1, 3, 7, 14, and 90 days of hydration for plain paste and the CFBC fly ash modified pastes containing either 10% or 20% of cement replacement. Figures 10 (a) and (b) show typical XRD patterns of these pastes after 14 and 90 days of hydration respectively. Figure 10 shows that, at both early and later ages of hydration, the ettringite peaks (corresponding to 0.973 nm and 0.561 nm) become stronger as more cement is replaced with CFBC fly ash. Also, the ettringite peaks for the CFBC fly ash modified pastes are higher after 90 days of hydration as compared to 14 days indicating the formation of increased amounts of ettringite with hydration. The area under the ettringite peaks in the XRD is used to infer the relative amounts of ettringite formed at various ages of hydration. In plain pastes, ettringite content increases from 1 to 3 days of hydration.

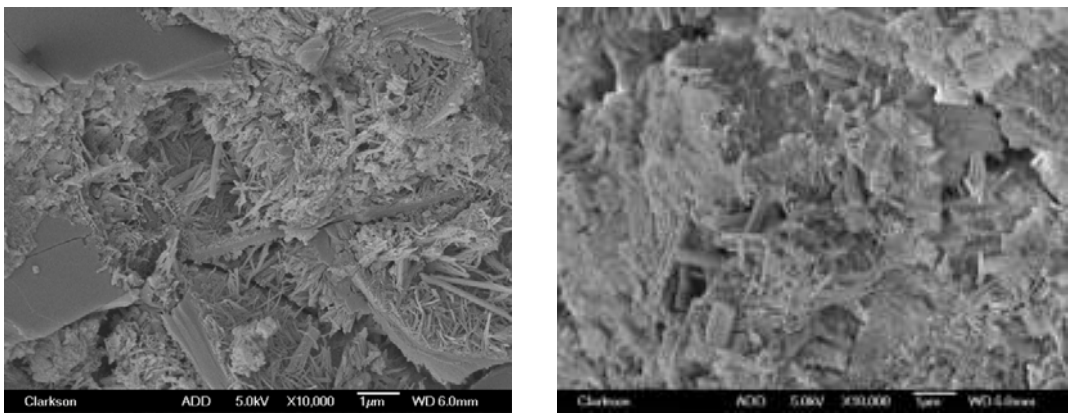

(a) (b)

Figure 9 Micrographs of 20% CFBC fly ash modified pastes at (a) 14 days, and (b) 90 days of hydration

Figure 10(c) shows the estimated amounts of ettringite from semi-quantitative XRD. The sulfates are released into the pore solution faster than the aluminates, and hence the higher SO_3 to Al_2O_3 ratio could be postulated as the reason for the increased formation of ettringite until 3 days. As

more aluminates continue to be released, if there are enough sulfates available, more ettringite will form resulting in an increase in the amount of ettringite from 1 to 3 days in the plain paste. However, after three days of hydration, little free sulfates are likely to remain to react with aluminates. The ettringite dissolves by releasing some of its sulfates to form monosulfate, thus resulting in a reduction in the amount of ettringite in the paste. For the CFBC fly ash modified pastes, the amount of ettringite increases continuously up to 90 days of hydration. In this case, there are excessive sulfates available to form additional amounts of ettringite as more aluminates are available, resulting in a continuous increase in the amount of ettringite in such pastes.

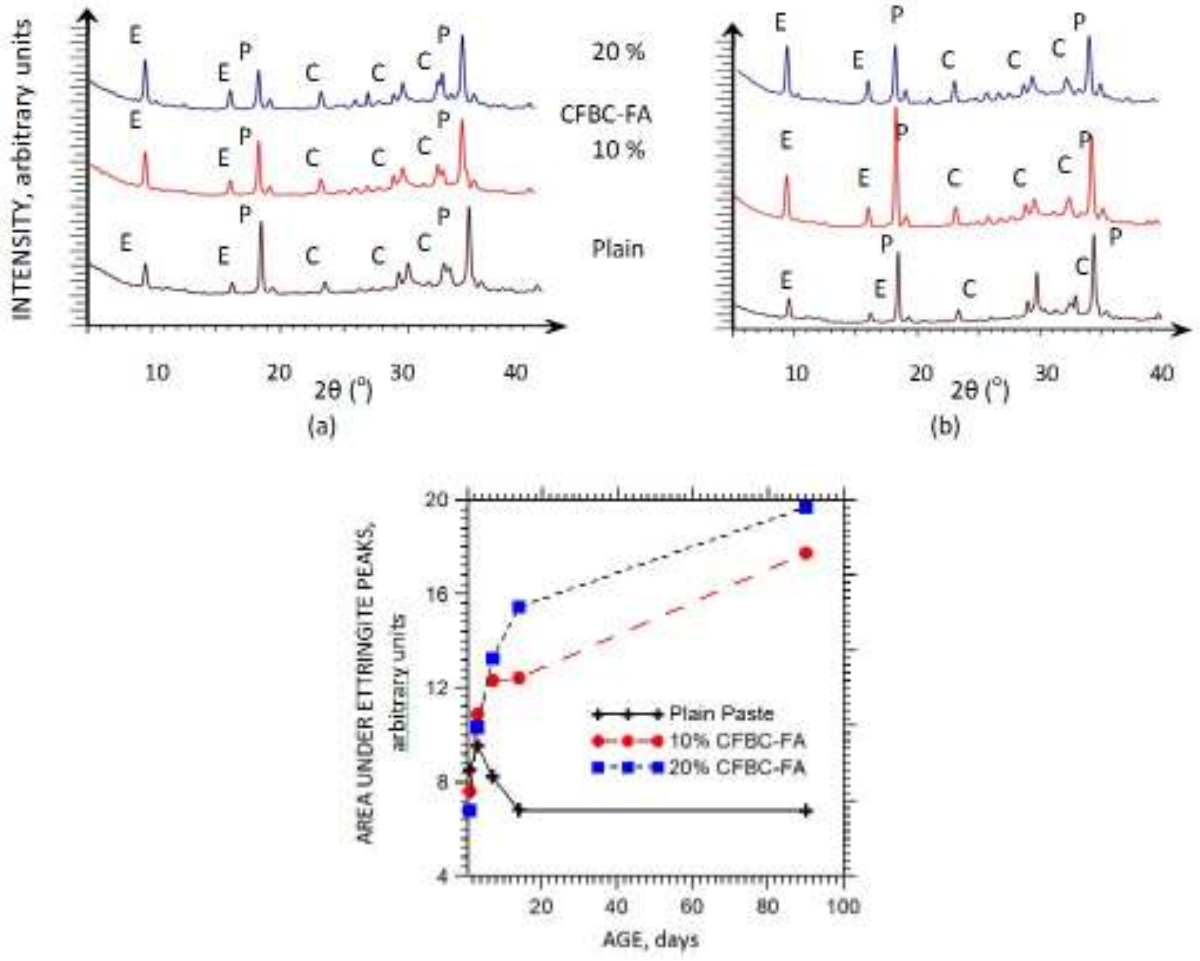

Figure 10 (a) and (b) XRD patterns of plain paste, 10%, and 20% CFBC fly ash modified pastes at 14 and 90 days respectively (E-Ettringite, C-Calcite ($CaCO_3$), P-Portlandite (CH)), (c) Estimated amounts of ettringite for plain, 10% and 20% CFBC fly ash modified pastes up to 90 days of curing.

CONCLUSIONS

This study has investigated the effects of CFBC fly ash as a partial cement replacement material on the fresh and hardened properties of cement pastes. The studies show that CFBC fly ash can be used as a partial cement replacement material in concretes, when the performance of the material is better known. Some aspects relating to the formation of the hydration products and their morphology and composition also needs to be considered (accounting for the formation of large amounts of ettringite in these systems). This aspect is briefly mentioned towards the end of this paper.

The following conclusions are arrived at based on detailed experimental studies.

1. The use of CFBC fly ash as a partial cement replacement decreased the workability of the pastes, attributable to the particle shape of CFBC fly ash as well as the porous nature of carbon particles that absorb water. The modified foam index test used to ascertain the AEA requirement pointed to the increased AEA dosage required to maintain foam stability with increasing amounts of CFBC fly ash in the paste.

2. Up to 10% cement replacement by CFBC fly ash, no appreciable early age compressive strength reduction was observed, while the effect of dilution was evident as shown by reduced compressive strengths at 20% cement replacement level by CFBC fly ash. The modified pastes were found to have lower non-evaporable water contents (w_n) as compared to the plain paste.

3. CH contents in CFBC fly ash modified pastes increased until 28 days and showed a slight decrease afterwards. The pozzolanic reaction of the CFBC fly ash coupled with the consumption of CH for ettringite formation resulted in this observation. Ettringite formation has been confirmed using micrographs and quantified using semi-quantitiative XRD.

REFERENCES

1. P. BASU, Combustion of coal in circulating fluidized-bed boilers: A review, Chem Eng Sci, Vol. 54, No. 22, 1999, pp 5547-5557.

2. J.CHEN, X. LU, Progress of petroleum coke combusting in circulating fluidized bed boilers - A review and future perspectives, Resources, Conservation & Recycling, Vol. 49, 2007, pp 203-216.

3. F.H. Li, J.P. ZHAI, X.R. FU, G.H. SHENG, Characterization of fly ashes from circulating fluidized bed combustion (CFBC) boilers cofiring coal and petroleum coke, Energy Fuels, Vol. 20, No. 4, 2006, pp. 1411-1417.

4. I. KULAOTS, A. HSU, R.H. HURT, E.M. SUUBERG, Adsorption of surfactants on unburned carbon in fly ash and development of a standardized foam index test, Cem Concr Res, Vol. 33, No. 12, 2003, pp 2091-2099.

5. K.H. PEDERSEN, A.D. JENSEN, M.S. SKJOTH-RASMUSSEN, K. DAM-JOHANSEN, A review of the interference of carbon containing fly ash with air entrainment in concrete, Prog in Ener and Comb Sci, Vol. 34, No. 2, 2008, pp 135-154.

6. R.L. HILL, S.L. SARKAR, R.F. RATHBONE, J.C. HOWER, An examination of fly ash carbon and its interactions with air entraining agent, Cem Concr Res, Vol. 27, No. 2, 1997, pp 193-204.

7. Y.M. GAO, H.S. SHIM, R.H. HURT, and E. M. SUUBERG, Effects of carbon on air entrainment in fly ash concrete: The role of soot and carbon black, Energy & Fuels, Vol. 11, 1997,pp 457-462.

8. E. FREEMAN, Y.M. GAO, R.H. HURT, E.M. SUUBERG, Interactions of carbon-containing fly ash with commercial air-entraining admixtures for concrete, Fuel, Vol. 76, No. 8, 1997, pp 761-765.

9. J. P. BALTRUS, R.B. LACOUNT, Measurement of adsorption of air-entraining admixture on fly ash in concrete and cement, Cem Concr Res, Vo.l 31, No. 5, 2001, pp 819-824.

10. N. M. JACKSON, S. SCHULTZ, P. SANDER, L. SCHOPP, Beneficial use of CFB ash in pavement construction applications, Fuel, Vol. 88, No. 2009, pp 1210–1215.

11. T. R. NAIK, R.N. KRAUS, B.W. RAMME, Y.M. CHUN, R. KUMAR, High-carbon fly ash in manufacturing conductive CLSM and concrete, ASCE J of Mat in Civ Eng, Vol. 18, No. 6, 2006, pp 743-746.

12. G. SHENG, J. ZHAI, Q. LI, F. LI, Utilization of fly ash coming from a CFBC boiler co-firing coal and petroleum coke in Portland cement, Fuel, Vol. 86, No. 16, 2007, pp 2625-2631.

13. G. SHENG, Q. LI, J. ZHAI, F. LI, Self-cementitious properties of fly ashes from CFBC boilers co-firing coal and high-sulphur petroleum coke, Cem Concr Res, Vol. 37, No. 6, 2007, pp 871-876.

14. M.A. GLINICKI, M. ZIELINSKI, The influence of CFBC fly ash addition on phase composition of air-entrained concrete, Bull. Pol. Ac.: Tech., Vol. 56, No. 1, 2008, pp 45–52.

15. X. FU, Q. LI, J. ZHAI, G. SHENG, F. LI, The physical-chemical characterization of mechanically-treated CFBC fly ash, Cem Concr Com, Vol, 30, No. 3, 2008, pp 220-226.

16. Y. ZHANG, W. SUN, L SHANG, Mechanical properties of high performance concrete made with high calcium high sulfate fly ash, Cem Concr Res, Vol. 27, No. 7, 1997, pp 1093-1098.

17. T. SEBOK, J. SIMONIK, K. KULISEK, The compressive strength of samples containing fly ash with high content of calcium sulfate and calcium oxide, Cem Concr Res, Vol. 31, No. 7, 2001, pp 1101-1107.

18. N. NEITHALATH, J.PERSUN, A.HOSSAIN, Hydration in high-performance cementitious systems containing vitreous calcium aluminosilicate or silica fume, Cem Concr Res, Vol. 39, No. 6, 2009, pp. 473-481

Maximizing the Use of PFA in the Production of Sustainable Structural Materials

S Adu-Amankwah[1], J M Khatib[1], L K A Sear[2], D Searle[1]
1 – University of Wolverhampton, UK
2 – UK Quality Ash Association, UK

Despite concrete having universal acceptance, approximately one tonne of CO_2 is emitted per tonne of Portland cement produced. Notwithstanding the promotion and increasing acceptance of high volume fly ash concrete (HVFAC), over 80% of PFA generated in the UK has yet to find acceptance as a cement supplement due to non-compliance to the fineness and or loss on ignition (LOI) criteria set out in EN 450. Alkali activation of higher LOI ashes reveals compressive strength inadequacy for structural application. It is believed that, like the interaction with air entrainment admixtures, unburned carbons might have a role in rendering the alkalis less effective in dissolving adequate alumino-silicate species. Fly ash with and without 20% Portland cement (OPC) in the feed material was treated with sodium silicate with 0.41 silica modulus and setting time, compressive strength and LOI assessed on activated samples. It is observed that, 20% Portland cement (OPC) in the feed material resulted in improved compressive strength compared to that which had only fly ash after curing at room temperature. Loss on ignition tests on the alkali-activated samples however revealed 3.8% mass loss compared to 9% on the un-activated PFA.

Samuel Adu-Amankwah is a researcher at the University of Wolverhampton. His research is on Maximizing the use of Fly Ash in the Production of Sustainable Construction Materials. His research actitivities include low carbon cementitious materials and correlating composition cementitious materials to performance.

Dr. Jamal M. Khatib is a Principal Lecturer at the University of Wolverhampton. Jamal is currently involved in a number of research projects on sustainable construction materials.

Dr. David Searle is a Senior Lecturer at the University. His research interests include sustainable construction materials and environmental engineering.

Dr. Lindon K.A. Sear is the Technical Director of the UK Quality Ash Association.

Keywords: Alkali-activation, Alumino-silicate, Fly ash, LOI, Portland cement

INTRODUCTION

Notwithstanding the universal usage of concrete as a construction material, the high carbon footprint associated with Portland cement clinker which affords concrete its superior properties makes it imperative to intensify the search for sustainable alternatives. The high CO_2 footprint emanates from both the intensive energy required for the process together with the decomposition of limestone into quicklime. Models for sustainable construction materials converge that, substitution of Portland cement clinker presents the single most important alternative to significantly minimize the CO_2 emissions from the construction industry [19]. The search for alternatives binders fall into two broad streams. These are partial replacement with supplementary cementitious materials and chemically or mechanically activating only pozzolanic materials. Literature is however scarce on the composite action of alkali-activated pozzolans and Portland cement clinker.

Although EN 197-1 permits binary to quaternary composite binders with replacement levels up to 95% supplementary materials, replacement levels for most applications are limited to class CEM II with 35% substitution of Portland cement clinker with fly ash and 50% in the case of slag. The latter is however not available in large quantities, especially in the bagged cement market [21]. EN 450 however limits acceptable fly ashes to those simultaneously satisfying fineness (retention on 45µm sieve not exceeding 40%) and loss on ignition (LOI) (not exceeding 7% for common use) criteria. Fly ashes deviating from the aforementioned criteria are reported to compromise on mechanical properties [20] and durability particularly absorption of air entrainment admixtures [11] which are purposely incorporated to enhance freeze and thaw resistance of concrete. Like many European countries, approximately 80% of the hundreds of tonnes of pulverized coal fly ash generated in the UK has yet to find entry into cement production, the reason being among others, low early age mechanical properties, freeze and thaw-resistance, discolored concrete and to a greater extent non-conformance to EN 450. They are thus disposed off in landfills. Potential leaching of the heavy metal content of fly ashes [4] however poses a hazard to the environment thus underscoring the need to put the material to a more sustainable use.

The inferior mechanical and durability properties associated with fly ashes with high loss on ignition (LOI) contents compared to those reported elsewhere could be related to factors including the mineralogy hence reactivity and to some extent physical absorption of activating species by the unburned carbons in the ash. It has been demonstrated that [23], amorphous rather than the crystalline assemblages undergo transformation during alkali-activation. Although interrelationships between LOI and the resulting geopolymer properties have not critically investigated, literature review indicates that most alumino-silicate source materials for alkali-activated binders have LOIs barely exceeding 4% [7]. The hindrance to compressive strength development in geopolymers has recently been reported by Lee *et al.* [16] who employed froth flotation technique to remove unburned carbons. The cost of ash beneficiation notwithstanding, their chemical and physical footprint on the resulting ash may not always be advantageous. For example Hamley *et al.* [12] suggested that, hydrogen peroxides (H_2O_2) under supercritical conditions have the potential to convert unburned carbons into carbonates which may be ridden off as gaseous matter.

However, Thomas and Jeffery [22] reported pronounced induction period and overall delayed hydration rate in the presence of hydrogen peroxide compared to using standard water (H_2O). This implies that, traces of hydrogen peroxide would also have to be driven off following the beneficiation.

In a previous study [1] it was observed that, activating high LOI fly ash with sodium silicate solution with silica modulus of 0.41 resulted in quick setting binders with superior early age properties. However, the high early age strength did not significantly improve as the specimen matured. It was therefore deduced that, the alkalis needed to ensure further reaction with the aluminosilicate species were depleted. The objective of the current study is thus to exploit the additional alkali provided by hydrating clinker in supplementing the alkalinity during hydration of alkali activated high LOI fly ashes. Significance of the study lies in the development of low clinker binders for structural applications.

EXPERIMENTAL DETAILS

Materials

Unconditioned Run of Station pulverized fuel ash (RoS- PFA) obtained directly from electrostatic precipitating hubs from a UK Power station was used in this study. The oxide composition obtained through x-ray fluorescence analysis is shown in Table 1. It is observed that the PFA for the study falls within the F Class of fly ashes according ASTM 618 and siliceous according to EN450. Portland cement throughout the study was a general purpose (CEM I) cement. In the alkali activated – Portland cement composite system, total powder consisted of 20% OPC with 80% PFA and liquid to powder ratio of 0.45. The control mix consisted of 65% OPC and 35% PFA (CEM II/B-V). The fineness and LOI of the latter however conformed to EN 450.

Activators were sodium silicate solution and 98% purity sodium hydroxide pellets (reagent grade). Sodium silicate solution comprised of 8.5±0.3% Na_2O and SiO_2 27.8±0.5% (silica modulus of 3.27±0.05). The viscosity and specific gravity was 70-120 MPa.s and 1.364 – 1.385 respectively. 15M concentration of NaOH prepared in the laboratory by dissolving the appropriate mass in warm water at temperature exceeding 40^0C, was used to adjust the silica modulus to 0.41. The resulting solution was sealed and stored for 24 hours. Potential carbonation of pellets was minimized by reducing the air exposure duration.

Tests and preparation of specimen

Materials were weight-batched and hand mixed. Fly ash was first weighed into the mixing pan and the activating solution added. Small batches were mixed at a time to ensure thorough mixing and casting was completed within 5 minutes. Specimens were cast in 50 x 50mm moulds and left overnight before de-molding. All specimens were then wrapped in polythene bags and then stored at 20^0C and 65% RH and tested at 3 and 7 days.

Setting time was monitored using the Vicat apparatus and the outlined procedure in EN196-3. In all cases, setting was monitored under saturated conditions. Compression tests were carried out on an automatic testing system in accordance with EN196. Loss on ignition (LOI) was determined after 7 days of hydration and the test method followed the recommendations from EN 196-2 with an ignition time of 60 minutes at an ignition temperature of 950^0C after preheating samples to 105^0C.

Table 1 Chemical analysis of Fly Ash

Oxide	SiO_2	Al_2O_3	Fe_2O	CaO	MgO	Na_2O	K_2O	TiO_2	SO_2	LOI	SiO_2/Na_2O
%	51.42	24.33	13.10	4.06	2.16	0.85	2.45	1.15	0.52	9.0*	2.11

*Determined on separate sample other than that for XRF

RESULTS AND DISCUSSION

Effect of Composite System on Setting Time

Setting times of alkali activated binders and CEM II/B-V which contains 35% PFA are summarized in table 2. Figure 1 also shows the setting profile of alkali activated composite binders with and without 20% ordinary Portland cement. The profile reporting is adopted to decipher differences in the reaction kinetics from a microstructure (setting) evolution view point. To compete with Portland cement, the developed binder should attain initial and final setting within reasonable time. This is relevant to allow for mixing, placing and attainment of adequate hardening for form striking. Although EN 197-1 defines limits for the setting of common cements (as standard EN 197-1 in table 1), different applications have different setting requirements making it relevant in exploring alternatives to the commonly known high alumina or rapid setting binders. It is observed from Table 2 that, alkali activated mixes with or without Portland cement addition sets quicker than CEMII/B-V. This class of composite binders however deviates from the duration for initial setting required for normal strength binders as in EN 197-1. They constitute quick setting binders on the basis of the 5 minutes minimum and 30 minutes maximum initial and final setting criteria respectively [3, 10].

Table 2 Initial and final setting times of composite binders

BINDER	INITIAL SET, mins	FINAL SET, mins
PFA + Activator	7	23
PFA+20%OPC+Activator	5	40
35%PFA + 65%OPC	300	470
Standard (EN 197-1	≥ 60	

By comparing the alkali activated composites to the system which contains no external alkali silicates other than those in the dry PFA and OPC, it is deduced that both the alkali and silicate species are of significance with regards to setting. This observation is consistent with previous findings [8]. The alkalis on one hand increase the pH hence raise the heat of reaction while the silicates which have high buffer intensity at higher pH initially to maintain alkalinity hence enhanced dissolution and subsequent polymerization [5] which characterizes network formation hence microstructure formation. The high pH afforded by the alkali concentration within the hydrating medium [17] enhances hydrolysis of the alumina and silicate species [6]. Contrary to the silicate species releasing heat to shorten the peak hydration time [15] and thus accelerated hardening, it can be deduced from the setting profiles shown in figure 1 that, the alkali concentration plays a significant role on setting. Additional alkali from the 20% OPC slightly speeds initial setting. The delay in final setting in the composite system containing Portland cement could be traced onto the hydration products formed, that is the sodium silico-aluminate hydrates (N-A-S-H) forming faster than the corresponding calcium silicate hydrate (C-S-H) [9]. It can thus be concluded that, in alkali activated systems, initial setting is dependent on the pH of the hydrating matrix whereas later stage microstructure formation is controlled by the hydrating products.

Effect of composite binder compressive strength

Figure 2 shows compressive strength of the composite binders under investigation after 3 and 7 days curing at room temperature. Specimens were stored in sealed plastic bags to minimize the risk of carbonation. It should however be noted that the PFA used in formulating the 65% OPC and 35% PFA (CEM II/B-V) binder satisfied the requirements of EN 450. The fineness of the Run-of-Station PFA for this study was reported in our previous paper [1]. It was found that approximately 48% of the PFA was retained on the 45µm sieve compared to the maximum of 40% retention limit.

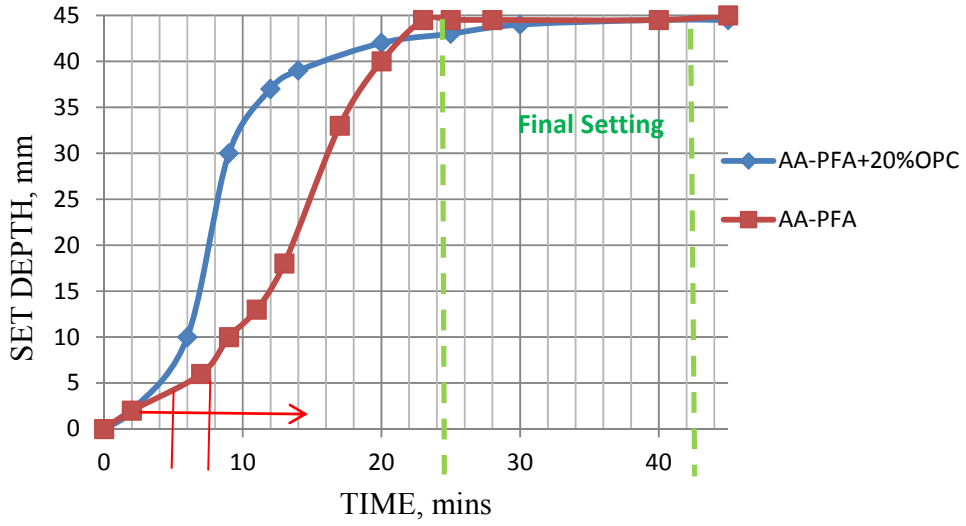

Figure 1 Setting profile of alkali-activated composite binders

It is observed from Figure 2 that, irrespective of the age of testing, the compressive strength was higher for the CEM II/B-V compared to the alkali-activated systems. From the chemistry view point, the three systems may all be described as alkali activated systems except that in CEM II/B-V, the alkali is supplied by the quicklime (CaO) which is the major oxide in Portland cement. On the other hand, PFA is predominated by silico-aluminates. Due to the superior ionic charge (valency) of calcium (oxide) in OPC compared to the externally supplied sodium (hydroxide), the former dissociates to provide relatively higher alkalinity. This may culminate into more stable and stronger network of C-S-H which characterizes later age properties. It is also understood that, the mineralogy of the silico-aluminate influences the reactivity, hence mechanical properties with William and van Riessen [23] suggesting that during alkali-activation only the amorphous phases in the silico-aluminate material undergo reaction. Although not reported in this paper, potential differences in the amorphous and unburned carbon content of the EN 450 conformant PFA and the RoS-PFA may be responsible for the differences in the compressive strength. Furthermore, the 20% OPC, in addition to supplementing alkalis in the system contribute greatly to the compressive strength development.

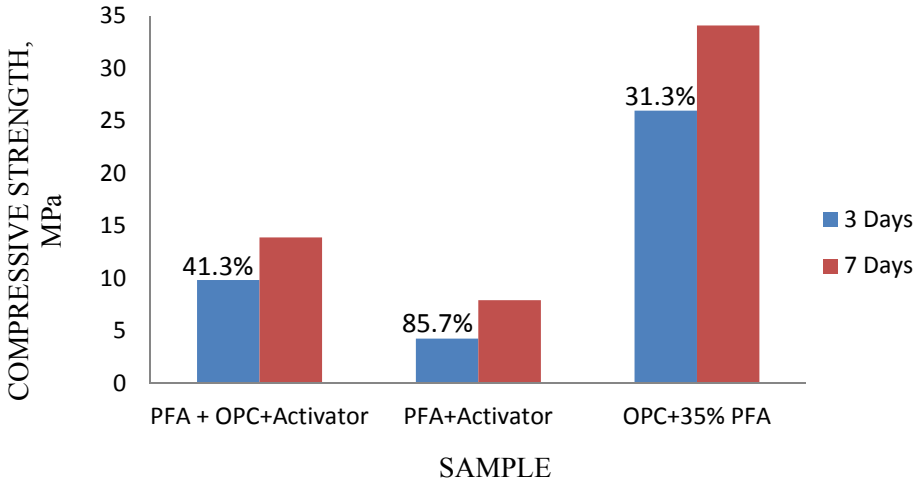

Figure 2 Compressive strengths of composite binders (% = gain in strength from 3 – 7 days)

Of further interest is the difference in the rate of strength increase between the 3rd and 7th day. Although of lower magnitude, the rate of compressive strength gain was found to be higher in the alkali activated systems compared to OPC. For example, the strength gain from the 3rd to 7th day for PFA + Activator only was over 85% as against 31.3% for CEMII/B-V. The following deductions may thus be made; formation of sodium-alumino-silicate hydrates (N-A-S-H) occurs at a faster rate compared to C-S-H in the case of OPC, the load bearing capability of N-A-S-H appears to be lower than the CSH. These assertions are substantiated by the alkali-activated – OPC blend.

Post activation loss on ignition (LOI)

PFAs with high unburned carbon contents are disadvantageous for reasons including concrete segregation and discoloring, inferior mechanical and deleterious effects on the durability of concretes containing them especially under freeze and thaw conditions. Disposal of such ashes

however is not cost-free, coupled with hazard posed to the environment while beneficiation methods such as re-combustion, separation and supercritical techniques among others come at comparatively higher cost. These methods further modify the properties of the resulting materials differently with detailed information on the modifications not fully documented yet.

Figure 3 compares the loss on ignition for un-activated PFA and hydrated alkali-activated binders formulated from the same PFA. Although often criticized for its accuracy, quantification of the unburned carbon content from the mass loss following an ignition at 950^0C for an hour, the method is still deemed satisfactory for the purpose. In the case of Portland cement-PFA composite alkali-activation, the sulfate content was determined on separate samples which have not been subjected to ignition according to EN 196-2 and the LOI corrected for sulfates.

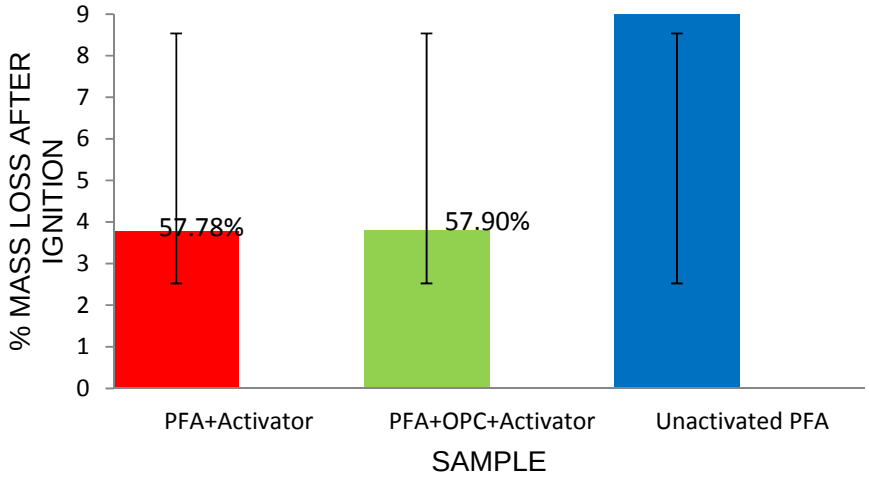

Figure 3 Loss on Ignition for un-activated and alkali-activated PFA (% reduction in LOI)

It is observed that alkali-activated fly ashes experience lower mass loss following ignition. Whereas the un-activated fly ash experienced 9% mass loss when tested to the aforementioned conditions, alkali activated samples with or without Portland cement in the powder recorded 3.8% mass loss. This represent approximately 58% lower LOI compared to the original fly ash. However, no significant difference was observed in the composite sample which contained 20% general purpose cement. The 58% reduction in LOI compares very well with the reduction in LOI reported from supercritical beneficiation [12]. The resultant 3.8% loss on ignition also brings the initially unsatisfactory PFA within the acceptable 7.0% limit required for incorporation into concrete. The mechanisms for reduction in unburned carbon content due to alkali-treatment and the role of additional alkali for subsequent reaction are of interest and are discussed below.

Mechanisms for LOI reduction following alkali treatment

To postulate the potential interaction(s) between unburned carbon particles and alkalis, the morphology and reactivity of unburned carbons are worth attention. Morphologically, unburned carbons in fly ashes exist as aggregated particles with recognizable macroporous vesicular

structure. Since the solid carbons are discrete and not encapsulated by inorganic particles [14] the mechanisms guiding the reaction of the inorganic species could not be said to engineer their transformation. Structurally, unburned carbons in fly ashes may be classed as inertinite, isotropic or anisotropic with the former denoting unreacted coal particles during combustion. It is imperative to note that unburned carbons may however contain volatile organic substances [2] which may interact chemically with other species during alkali activation.

The chemical interaction between air entrainment admixtures and unburned carbons is not fully understood but it is generally thought that the polarity, surface chemistry and oxygen functional groups have significant influence on the adsorption characteristics of unburned carbons. Hill *et al.* [13] postulated from their analysis of the organic fraction of unburned carbon that, adsorption was pronounced in predominantly isotropic carbon fly ash and apparently increased with oxygen content in the unburned carbon. Maroto-Valer *et al.* [18] however obtained inconclusive results on the presence and structure of the carbon-oxygen groups in isotropic carbons using FTIR. There is therefore insufficient knowledge of the existing bonds based on which chemical reactions could be inferred. The potential presence of hetero-atoms including oxygen and sulfur even in isotropic or anisotropic carbons which are deemed to have undergone extensive reaction during combustion could explain the interaction between alkali activators and unburned carbons. Probable reaction between alkalis and acidic hetero-atoms may lead to pH reduction which would impact on the dissolution of species and subsequently culminating into inferior mechanical properties.

The 3.8% mass loss following combustion of alkali-activated samples as against 9% on the un-activated fly ash suggests that, approximately 58% of unburned substances in fly ash which would otherwise be associated with carbons determinable from the conventional LOI test method are transformed during alkali-activation. It is believed that, for example fly ashes predominated by particles which have been shielded during combustion may contain inorganic species which would react during geopolymerization. The potential mechanism governing such reaction may be physical absorption of alkalis by the unburned membranes which would eventually reach the engulfed alumino-silicates. However, ruptured carbon membranes are still recorded as mass loss based on the LOI test method with no recognition for the substances entrained. Since such alumino-silicates may still be associated with volatile substances, which may interact with alkalis possibly resulting in species which are not decomposable during the LOI test temperature regions. It is however worth stressing that further analysis of the activated products and the ignited samples is necessary to confirm the above.

Although no significant difference was observed in the percentage mass loss following ignition, the effect of the additional alkali can be deduced from the difference in the compressive strength of the hydrated samples. It is observed from figure 2 that, even the three day compressive strength of the Portland cement-PFA alkali-activated composite is greater than the 7 day strength of the binder without Portland cement. The trend may be attributed to the additional alkali supplied by the major calcium phases in Portland cement. However, the alkali-activated system without Portland cement experienced the highest rate of strength development between the 3rd and 7th day.

The rate of strength gain was lowest for CEM II/B-V. The reason for the reduction in strength gain when 20% OPC is present in the alkali-activated binder remains uncertain at this stage. By inference from the magnitude of compressive strength, it may be attributed to greater portion of the reactive species in the feed materials initially undergoing conversion such that the remnant unreacted species after the third day do not produce large high strength magnitude.

CONCLUSIONS

The effect of alkali activation on the unburned carbon content in fly ashes has been examined in this paper. Irrespective of the presence or otherwise of OPC in the feed material, approximately 58% lowering of loss on ignition was observed. The mechanism for the conversion of unburned carbons is postulated to involve physico-chemical interactions between coal particles which have not been completely combusted and the highly polarized concentrated sodium hydroxide NaOH in the activating solution. The presence of 20% OPC in the activating solution resulted in superior mechanical properties compared to that which had only PFA. This strength however fell short of the compressive strength for CEM II/B-V whose fineness and LOI conformed to the criteria for PFAs for concrete production.

The effect of varying the OPC content which would provide a major step in optimizing the constituents has however yet to be explored. Further mineralogical characterization would also be useful in broadening understanding of the mechanism for the alkali-unburned carbon interaction.

REFERENCES

1. ADU-AMANKWAH, S., KHATIB, J.M., SEAR, L.K.A., AND SEARLE, D. (2011) Sustainable Construction Materials from Pulverized Fuel Ashes: Fresh State Properties. In: AZIZ, Z., SUTRISNA, M., EGBU, C., ARIF, M. & UNDERWOOD, J., eds. 10th International Postgraduate Research Confrence, 2011 Salford University, Salford, UK, pp. 685-695

2. ALONSO, M.J.G., BORREGO, A.G., ALVAREZ, D., AND MENEDEZ. R. A reactivity study of chars obtained at different temperatures in relation to their petrographic characteristics, Fuel Process Technology, Vol. 69, 2001, pp. 257–272

3. DAVIS, A. C. (1943) Portland Cement. London, UK, Concrete Publications Ltd.

4. DUTTA, B.K., KHANRA, S., AND MALLICK, D. Leaching of Elements from Coal Fly Ash: Assessment of its Potential for Use in Filling Abandoned Coal Mines, Fuel, vol. 88(7), 2009, pp. 1314-1323

5. DUXSON, P., FERNANDEZ-JIMENEZ, A., PROVIS, J.L., LUKEY, G.C., PALOMO, A., AND VAN DEVENTER, J.S.J. Geopolymer Technology: the current state of the art, Materials Science, Vol 42 No. 9, 2007, pp. 2917-2933

6. FERNÁNDEZ-JIMÉNEZ, A., PALOMO, A. SOBRADOS, I., SANZ, J. The role played by the reactive alumina content in the alkaline activation of fly ashes, Microporous and Mesoporous Materials, Vol 91 No. 1-3, 2006, pp. 111-119

7. FERNANDEZ-JIMENEZ, A. AND PALOMO, A. Composition and microstructure of alkali activated fly ash binder: Effect of the activator, Cement and Concrete Research 35, 2005, pp. 1984-1992

8. FERNANDEZ-JIMENEZ, A. AND PUERTAS, F. Effect of Activator Mix on the Hydration and Strength Bahaviour of Alkali-Activated Slag Cements, Advanced Cement Research, Vol 15, No. 3, 2003, pp. 129 – 136

9. FERNÁNDEZ-JIMÉNEZ, A. AND PUERTAS, F. Setting of Alkali-Activated Slag Cement. Influence of Activator Nature, Advanced Cement Research, Vol 13 No. 3, 2001, pp. 115 – 121

10. GANI, M. S. J. (1997) Cement and Concrete. London, UK, Chapman & Hall

11. GAO, Y.M., SHIM, H., HURT, R.H., AND SUUBERG, E. Effects of Carbon on Air Entrainment in Fly Ash Concrete: The Role of Soot and Carbon Black, Energy Fuels, Vol. 11 No. 2, 1997, pp. 457-462

12. HAMLEY P., LESTER, E., THOMPSON, A., CLOKE, M., AND POLIAKOFF, M. The Removal of Carbon from Flay Ash Using Supercritical Water Oxidation. International Ash Utilization Symposium, Centre for Applied Energy Research, University of Kentucky, 2001, paper No. 85

13. HILL, R.L., SARKAR, S.L., RATHBON, R.F., AND HOWER, J.C. An Examination of Fly Ash Carbon and its Interactions with Air Entraining Agent. Cement and Concrete Research, Vol. 2, 2001, pp. 193-204

14. HURT, R., SUUBERG, E., AND GAO, Y.M. The Passivation of Carbon for Improvement of Air Entrainment in Fly Ash Concrete. Conference on Unburned Carbonon Utility Fly Ash, 2000

15. KRIZAN, D., AND ZIVANOVIC, B. Effects of Dosage and Modulus of Water Glass on Early Hydration of Alkali-Slag Cements. Cement and Concrete Research, Vol. 32 No. 8, 2002, pp. 1181-1188

16. LEE, S., SEO, M.D., KIM, Y.J., PARK, H.H., KIM, T.K., HWANG, Y., AND CHO, S.B. Unburned Caron Removal Effect on Compressive Strength Development in a Honey-comb Briquette Ash-Based Geopolymer. Intern. Journal Of Mineral Processing, Vol. 97 No.1-4, 2010, pp. 20-25

17. LODEIRO, I. G., FERNÁNDEZ-JIMÉNEZ, A., PALOMO, A., AND MACPHEE, D.E. Effect on Fresh C-S-H gels of the Simultaneous Addition of Alkali and Aluminate. Cement and Concrete Research, Vol 40 No.1, 2010, 27 – 32

18. MAROTO-VALER, M.M., TAULBEE, D.N., AND HOWER, J.C. Chracterisation of Differing Forms of Unburned Carbon Present in Fly Ash Separated by Density Gradient Centrifugation. Fuel, Vol. 80 No.6, 2001, pp. 795-800

19. MEHTA, P. K. Sustainable Cements and Concrete for the Climate Change Era - A Review. 2nd International Conference on Sustainable Construction Materials and Technology, Ancona, Italy, 2010

20. MCCARTHY, M.J. AND DHIR, R.K. Towards Maximizing the Use of Fly Ash as a Binder. Fuel, Vol. 78 No. 2, 1999, pp.121-132

21. SEAR, L.K.A. (2011) Private Communication

22. THOMAS, J.J., AND JENNINGS, H.M. The Effect of D_2O and Mixing on the Early Hydration Kinetics of Tricalcium Silicate. Chem. Mater. Vol. 11, 1999, pp. 1907 – 1914

23. WILLIAMS, R. P. AND VAN RIESSEN, A. Determination of the reactive component of fly ashes for geopolymer production using XRF and XRD. Fuel, Vol 89 No. 12,2010, pp. 3683-3692

Towards the Development of Carbon Dioxide Neutral Renewable Cement (BioCement)

H M Jonkers, N N Carr
Delft University of Technology, Netherlands

Concrete is currently the most extensively used construction material and the global consumption of concrete increases every year. As an essential component in concrete, cement consumption also increases annually. Global cement production grew from 594 Mt in 1970 to 2770 Mt in 2007. Cement production is extremely energy-intensive and accounts for about 2% of the global primary energy consumption, or up to 5% of the total global industrial energy consumption. Between the large quantities produced and the huge energy consumption, cement is responsible for significant amounts of CO_2 being released into the atmosphere. The production of cement contributes to CO_2 emissions through two sources: the decomposition of limestone and the combustion of fossil fuel. The CO_2 emissions resulting from conversion of limestone into calcium oxide are fairly constant and equate to approximately 540 kg CO_2 per tonne of clinker produced. Since multiple factors are involved (such as the thermal efficiency of the kilns), the CO_2 emissions resulting from the combustion of fossil fuels fluctuate. In 2006 the global average gross CO_2 emissions per tonne of clinker was 866 kg. This value accounts for 5-8% of total human atmospheric CO_2 emissions. Recently many steps have been taken to combat CO_2 emissions in the cement industry including improving energy efficiency of the kilns, replacing fossil fuel with renewable energy sources and substituting part of Portland cement with other cementitious materials. While these actions have made progress in reducing CO_2 emissions they still do not provide a completely sustainable solution.

HM Jonkers is senior scientific researcher at the Sustainability unit of the Materials and Envionment group of the Delft University of Technology, The Netherlands. He is leading scientists of several currently running research projects on the development of bio-based civil engineering materials.

NN Carr is PhD student at the Sustainability unit of the Materials and Envionment group of the Delft University of Technology, The Netherlands. Her specialist area of research is application of biomass derived ashes as cement replacement.

Keywords: Biocement, Carbon dioxide, Cement, Neutral, Renewable

INTRODUCTION

Concrete is currently the most extensively used construction material and the global consumption of concrete increases every year. As an essential component in concrete, cement consumption also increases annually. Global cement production grew from 594 Mt in 1970 to 2770 Mt in 2007 [1] [2]. Cement production is extremely energy-intensive and accounts for about 2% of the global primary energy consumption, or up to 5% of the total global industrial energy consumption [3]. Between the large quantities produced and the huge energy consumption, cement is responsible for significant amounts of CO_2 being released into the atmosphere. The production of cement contributes to CO_2 emissions through two sources: the decomposition of limestone and the combustion of fossil fuel. The CO_2 emissions resulting from conversion of limestone into calcium oxide are fairly constant and equate to approximately 540 kg CO_2 per tonne of clinker produced. Since multiple factors are involved (such as the thermal efficiency of the kilns), the CO_2 emissions resulting from the combustion of fossil fuels fluctuate. In 2006 the global average gross CO_2 emissions per tonne of clinker was 866 kg [4]. This value accounts for 5-8% of total human atmospheric CO_2 emissions [5]. Recently many steps have been taken to combat CO_2 emissions in the cement industry including improving energy efficiency of the kilns, replacing fossil fuel with renewable energy sources and substituting part of Portland cement with other cementitious materials [4]. While these actions have made progress in reducing CO_2 emissions they still do not provide a completely sustainable solution.

CONCEPT

The aim of this project is to produce a binding material capable of replacing original Portland cement. This binder will have a reduced impact on the environment specifically regarding the release of CO_2 into the atmosphere and the drain on limited resources. The objective is divided into two initial tasks:

1. Obtain a material comprised of hydraulic minerals from the ashes produced in the combustion of a blend of sustainable biomasses and/or waste-products.
2. Adapt the raw materials and the sintering process so that the combustion of biomasses and/or waste-products can be conducted in a way that also generates energy (i.e. using a fluidized bed combustor instead of a rotary kiln).

Through the combination of the above-mentioned tasks a CO_2 neutral binder capable of replacing original Portland cement should theoretically be produced. The project will be conducted in a way that will develop a scientific basis for techniques to produce sustainable cement, or bio-cement.

CO_2 NEUTRALITY

By replacing the traditional raw materials used in the production of Portland cement (limestone and clay) with biomass and waste products a bio-cement will be created that does not further deplete limited resources. Since biomass is renewable source of raw materials and energy, there is no concern over depleting limited supplies. Landscape mutilation resulting from the mining of limestone will also be avoided. Furthermore the burning of biomass and the resulting decomposition of $CaCO_3$ into CaO does not contribute new CO_2 into the

atmosphere, unlike the combustion of fossil fuels or the decomposition of limestone which release carbon that has been stored for millions of years. By replanting harvested biomass the emitted CO_2 will be absorbed and returned for a new growth cycle. This cyclical process ensures that no "new" CO_2 will be released into the atmosphere [6]. Since firing of the biomass will be done in conjunction with energy production, the ashes, or bio-cement, can be viewed as a by-product. In this regard all the energy invested in harvesting, processing and preparing the biomass will be associated with energy production and not bio-cement production. The utilization of the ashes also provides a solution to the disposal of the waste which would otherwise contribute to landfilling. The utilization of biomass, particularly those stemming from landscaping and agricultural residues, provides a solution for their disposal as well.

RAW MATERIALS

The initial task is to identify biomasses and waste-products apt to replace traditional raw materials used in the production of Portland cement. Since the raw mix will also be required to produce energy upon combustion it is also necessary that the biomass conforms to the requirements of fuel used in energy production. Often these two objectives are at odds with each other. A biomass rich in a desirable element may not always be the most suitable for energy conversion and conversely a fuel that combusts well and provides a large amount of energy may have no validity as kiln feed. With these two objectives in mind raw materials need to be chosen that accommodate one need without adversely effecting on the other.

REQUIREMENTS FOR CLINKER

Any materials may be used to produce Portland cement so long as they will give the proper chemical composition after burning [7]. The clinker minerals found in Portland cement, which we are attempting to replicate, are C_3S, C_2S, C_2A and C_4AF. The cementing action of Portland cement is derived largely from the chemical reaction between the clinker minerals C_3S and C_2S with water. Due to its favorable hydration characteristics, primary importance is placed upon C_3S and, to a lesser extend, C_2S. In order to form the clinker minerals C_3S and C_2S we need to obtain both calcium and silica from the biomass both of which need to be present is suitable quantities, proportions and forms [8]. In traditional cement the calcium is provided in the form of calcium carbonate obtained from limestone chalk marl or even seashells. The silica comes from clays and shales.

Generally mineralizers are also incorporated to facilitate the formation of calcium silicates at reduced temperatures. The standard mineralizers are aluminum oxide and iron oxide coming from bauxite and iron ore. In addition to calcium, silicon, aluminum, and iron trace amounts of minor elements (such as sodium, potassium, magnesium, and titanium) often enter into the crystal structures of the clinker minerals [9]. However raw materials with contain excessive amounts of sodium or potassium oxide are considered to be undesirable. These compounds are capable of reactions which can ultimately result in degradation of the concrete. Other oxides such as manganese oxide and phosphorus pentoxide are less common but should also be avoided because they can create problems during burning and degrade the overall quality of the cement produced [7].

REQUIREMENTS FOR ENERGY PRODUCTION

Selecting the best-suited biomass or fuel for energy production depends on a variety of factors all of which relate to the composition of the biomass. Biomass fuels are generally divided into 4 different primary classes: (1) wood and woody materials, (2) herbaceous and other annual growth materials, (3) agricultural by-products and residues, and (4) refuse-derived fuels (RDF) and waste or non-recyclable papers often mixed with plastics [10]. The structural compositions of hemicellulose, cellulose, and lignin, as well as the concentration and composition of inorganic materials account for the distinctions among the first three classes. The calorific value or the heating value is the measure of the energy content of a fuel and is a decisive factor in selecting an appropriate biomass. The heating values for common fuels are generally known but they can also be broadly predicted through characteristics of the biomass such as the ash concentration, the carbon concentration, and the amount of cellulose vs. lignin. Among biomasses a decrease in ash concentrations corresponds to an increase in the heating value.

Higher heating values are also associated with higher carbon contents. Since heating value correlates to the amount of oxygen required for complete combustion, lignin has a higher heating value than cellulose due to its lower degree of oxidation. When selecting a biomass it is critical to choose a fuel with a high enough calorific value to in order to achieve a sufficient net energy. The moisture content of a particular fuel is a limiting factor in biomass combustion due to large amount of energy necessary to evaporate the water which can severely affect the heating value. Generally, self-supporting combustion proceeds up to a moisture content of 65%, otherwise more energy is necessary to satisfy evaporation than that which is liberated during combustion. Biomass with larger hydrogen to carbon ratios (and similarly but lesser so oxygen to carbon ratios) are known to lose a larger portion of fuel during the pyrolysis stage of combustion [10]. With that in mind it is important to select biomasses with low ratios. Nevertheless biomasses still lose a significant portion of their mass in comparison to coal. The quantity of certain elements (such as Si, K, Na, S, Cl, P, Ca, Mg, Fe) should be reduced or when possible eliminated due to their involvement in reactions which lead to ash fouling and slagging. As their principal ash-forming constituents, herbaceous fuels contain silicon and potassium. The presence of silicon is necessary in the formation of clinker minerals but the combination of the two can present potentials ash deposition problems.

The alkali and the silica can react to form alkali silicates which will soften or melt at temperatures below 700˚C. While we cannot reduce the concentration of silicon beneath the minimum amount necessary to form suitable quantities of C_3S and C_2S, we can attempt to limit the presence of alkalis (which correlates well to cement requirements). Alkalis will also react with sulphur to form compounds that damage the combustor heat transfer surfaces. Potassium is the alkali to be most cautious of since it is the dominant source of alkalis in most biomass fuels. While all biomasses are subject to fouling behaviour the rate at which fouling can transpire is dependent upon the composition of the biomass and can be predicted with the alkali index. By comparing the quantity of alkali oxide in the fuel to the unit of fuel energy one can analyse a biomass' propensity to foul. The lower the ratio the less likely a particular biomass will foul. While the alkali index does not completely predict fouling behaviour it acts as a suitable guide to aid in the selection of biomass and thus reduces the risk.

COMBINATION OF REQUIREMENTS

Finding a biomass rich in CaO or at least in the quantities necessary to form C_3S can be problematic. While most biomasses contain significant quantities of Ca, even those used in energy production, the values pale in comparison to that of limestone. With this in mind our proposal is to form the bulk of the raw feed on woody biomass from maintenance of parks and roads. This fuel is already used in the biomass power plant in Cuijk (The Netherlands) for which the 80 MW bubbling fluidized bed combustor has been adapted. From this power plant we have received samples and the ash was found to contain 21,9 M-% Ca (and 12,5 M.-% Si). While significantly below the necessary requirement it is particularly high for a locally available biomass. One option to boost the CaO in the raw feed is to incorporate egg shells which are a by-product of food industry. Egg shells have limited potential in the production of energy but they are extremely rich in CaO (95%) and small quantities can make a significant impact on the overall CaO concentration. Another solution is to incorporate waste products from pulp and paper mills, particularly lime mud and green liquor dregs. While these materials are rich in Ca one must be cautious of the moisture content. Finding a biomass rich in silica is less problematic than it is for calcium. In fact there has been ample research conducted using the ashes of plant residues (such as rice husks and sugar cane bagasse) as secondary cementing materials due to their rich concentrations of SiO_2 and their ability to act as a pozzolanic admixture [11] [12]. While these plants are very common in tropical regions, they are not typically grown in northwestern Europe. There are however non-tropical plants currently grown as energy crops which still have a significant concentration of silica, for example Miscanthus and switch grass [13] [14]. The goal is to combine the various biomasses to get a raw mix with 65% CaO, 22% SiO_2, 6% Al_2O_3 and 3% Fe_2O_3. Based on these concentrations we should theoretically be able to create clinker so long as we achieve the necessary sintering temperature.

FIRING

Once a raw mix design is finalized it will be fired in a standard kiln and the resulting ash will be analyzed to determine the chemical and mineralogical composition. The raw feed will then be optimized until the desired clinker minerals are achieved and present in the ideal quantities. Subsequently the best raw feed mixes will be fed into the fluidized bed combustor. The resulting ashes will be analyzed and compared to those produced in the kiln. At this point both the firing method and the raw mix will be further adapted to optimize the resulting bio-cement. The concept of using a fluidized bed to manufacture Portland cement is not new. In 1962 Pyzel became the first person to use a fluidized bed for the sintering stage in cement production. Heertjes continued that work into the 70’s using a sprouting bed. He reported that the manufacture of clinker in a sprouting bed is a promising process [15]. Although, over the subsequent years, research regarding this form of production seems to have been abandoned as rotary kilns have been further optimized to be increasingly more energy efficient. Nevertheless the possibility of producing cement in a fluidized bed exists and over the last few decades the technology of fluidized beds has also advanced. One major concern which arises when replacing a rotary kiln with a fluidized bed combustor is the disparity in firing temperature. It is standard practice in energy production to utilize a combustion temperature in the range of 500-900˚C. Of course in the production of clinker it is necessary to achieve a much higher temperature in order to reach the sintering point. Even with the incorporation of mineralizers it will be difficult to fire at temperatures lower than 1450 ˚C and still get sufficient quantities of C_3S.

PRODUCT DEVELOPMENT

Once the raw feed mix and firing method are optimized a variety of bio-cements for various applications will be produced at the laboratory scale. The goal is to develop a series of bio-cement-based products with characteristics and performance similar to currently available products. From these bio-cements the sustainability and durability will be tested and then compared to what is presently available on the market. A life cycle analysis will be performed on the bio-cements to verify the improved sustainability in comparison to original Portland cement. At this point any potential up-scaling issues will be addressed and the bio-cements' ability to replace original Portland cement in the short and long term will be ascertained.

CONCLUSIONS

The goal of this paper is to present the project 'Towards the development of CO_2 neutral cement'. At this time the project is in its initial and still largely theoretical stage, and aims for utilizing various biomasses as the raw materials to develop a cementitious binder, or bio-cement. The bio-cement will be produced concurrently with the production of energy, making this binder CO_2 neutral. After the bio-cement is produced on the laboratory scale its sustainability will be quantified and a series of products will be developed.

ACKNOWLEDGEMENTS

We would like to acknowledge Technology foundation STW for financial support of this project STW 11338 'Towards the development of carbon dioxide neutral renewable cement'.

REFERENCES

1. TAYLOR, M., C. TAM, AND D. GIELEN, Energy efficiency and CO2 emissions from the global cement industry. Korea, 2006. 50(2.2): p. 61.7.

2. OSS, H.G.v., US Geological Survey (USGS) Cement - 2007. 2009.

3. WORRELL, E., et al., Carbon dioxide emissions from the global cement industry. Annual Review of Energy and the Environment, 2001. 26: p. 303-329.

4. INITIATIVE, C.S., Cement industry energy and CO2 performance: getting the numbers right. 2009, Geneva: World Business Council for Sustainable Development.

5. SCRIVENER, K.L. AND R.J. KIRKPATRICK, Innovation in use and research on cementitious material. Cement and Concrete Research, 2008. 38(2): p. 128-136.

6. MCKENDRY, P., Energy production from biomass (part 1): overview of biomass. Bioresource Technology, 2002. 83(1): p. 37-46.

7. BOGUE, R.H., The Chemistry of Portland Cement. 2nd ed. 1955, New York: Reinhold Publishing Corporation.

8. MEHTA, P.K. AND MONTEIRO, P.J.M., Concrete: microstructure, properties and materials. 2006: McGraw-Hill.

9. HEWLETT, P.C., Lea's chemistry of cement and concrete. 2004: A Butterworth-Heinemann Title.

10. JENKINS, B.M., et al., Combustion properties of biomass. Fuel Processing Technology, 1998. 54(1–3): p. 17-46.

11. MEHTA, P.K. AND K.J. FOLLIARD, Rice husk ash - A unique supplementary cementing material: Durability aspects. Advances in Concrete Technology, 1995. 154: p. 531-541.

12. CORDEIRO, G.C., et al., Pozzolanic activity and filler effect of sugar cane bagasse ash in Portland cement and lime mortars. Cement and Concrete Composites, 2008. 30(5): p. 410-418.

13. HEATON, E.A., et al., Chapter 3 - Miscanthus: A Promising Biomass Crop, in Advances in Botanical Research, K. Jean-Claude and D. Michel, Editors. 2010, Academic Press. p. 75-137.

14. WOLI, K.P., et al., Evaluating silicon concentrations in biofuel feedstock crops Miscanthus and switchgrass. Biomass and Bioenergy, 2011. 35(7): p. 2807-2813.

15. HEERTJES, P.M., DE NIE, L.H., AND VERLOOP, J., The manufacture of Portland cement clinker in a spouting bed. Powder Technology, 1971. 4(5): p. 269-274.

Characterisation of Alkali Activated Co-fired Fly Ash Geopolymers

C R Shearer[1], J L Provis[2], S A Bernal[2], K E Kurtis[1]
1 – Georgia Institute of Technology, USA
2 – University of Melbourne, Australia

Alkali-activation of waste and industrial by-products is a growing technology for the production of sustainable alternative binders for the substitution of portland cement. One of the main precursors used in the production of alkali-activated geopolymer binders is fly ash obtained from the combustion of coal. The need to reduce CO_2 emissions associated with coal combustion has promoted the development of processes involving the combined combustion of coal with other organic materials, generating a by-product referred to as 'co-fired fly ash'. The chemical composition and physical properties of co-fired fly ash can be comparable to those identified in coal fly ash, rendering it a potentially suitable option for geopolymer production, for application in the construction field as a less CO_2-intensive material. However, these ashes differ from standard fly ashes because they contain biomass ash, which has been shown to change phosphate, alkali, magnesium, and reactive silica levels in addition to altering the morphology of the resulting ash product. In this study two ashes—one commercially available coal ash and one co-fired ash produced by burning coal with wood chips—are activated with alkali silicate and hydroxide solutions, to evaluate the feasibility of using co-fired ash in the production of geopolymer binders. X-ray diffraction shows that using this co-fired ash, the formation of zeolitic phases including chabazite-Na ($NaAlSi_2O_6 \bullet 3H_2O$) and faujasite ($Na_2Al_2Si_4O_{12} \bullet 8H_2O$) is favoured within an otherwise X-ray amorphous binder. Infrared spectroscopy reveals that this co-fired ash is more polymerised after alkali-activation compared to the coal ash. This paper elucidates some fundamental properties of these materials—a necessary endeavour before utilisation in future low-carbon infrastructure, and in understanding the future of geopolymer technology as the U.S., Europe and other regions move increasingly to biomass co-firing (rather than pure coal) as a fuel source for electricity generation.

Christopher R. Shearer is a Ph.D. student in the School of Civil and Environmental Engineering at Georgia Institute of Technology. His current research is on the characterisation and potential reuses of biomass and co-fired fly ash in concrete, geopolymers and fired bricks. He holds a B.S. in Civil Engineering from Ohio Northern University and a M.S. in Civil Engineering from Georgia Institute of Technology.

Susan A. Bernal holds a Bachelors degree and a Doctorate in Materials Engineering from Universidad del Valle, Colombia, and she is currently a Research Fellow in the Geopolymers and Minerals Processing Group at the University of Melbourne, Australia. She specialises in valorisation of waste and industrial by-products through alkaline activation, and the assessment and understanding of the durability properties of these materials. Her current work is developed in collaboration with the industrial partner Zeobond Pty Ltd, which focuses on the development, commercialisation and manufacturing of geopolymer technology.

John L. Provis is currently a Senior Research Fellow and leader of the Geopolymer and Minerals Processing Group in the Department of Chemical and Biomolecular Engineering, the University of Melbourne, Australia. He will commence a Professorial position in the Department of Materials Science and Engineering, University of Sheffield, UK, in June 2012. He holds BE(Hons) (2002), BSc (2002) and PhD (2006) degrees from the University of Melbourne, and is Secretary of RILEM TC 224-AAM.

Kimberly E. Kurtis, Ph.D., FACI, FACerS is Professor in the School of Civil and Environmental Engineering at Georgia Institute of Technology, Atlanta, GA. She is Chair of ACI Committee 236: Materials Science of Concrete and an Editorial Board member at Cement and Concrete Composites.

Keywords: Biomass, FTIR, Fly ash, Geopolymer, X-ray Diffraction

INTRODUCTION

The search for green energy solutions has resulted in the use of biomass fuels as a partial replacement of coal during combustion. This process can be considered a sustainable energy source when the consumption of the biomass is less than its rate of growth [1]. Furthermore, co-firing biomass for power generation can be CO_2-neutral when the amount of CO_2 released into the atmosphere is less than or equal to the amount of CO_2 plants take in during their lifetime [2]. The by-product of this process, known as co-fired fly ash, is not addressed in the U.S. standard for fly ash use in concrete ASTM C 618 [3], but studies have begun to examine its impact on concrete properties [4-9]. Conversely, the European standard for fly ash in concrete (EN450-1) [10] does permit the use of co-fired fly ash, although with additional restrictions. However, there has been little research to find other pathways to utilise this emerging waste stream.

One growing technology that beneficially reuses waste and industrial by-products is to generate sustainable alternative binders through alkali-activation. Since coal fly ash is one of the predominant precursors in alkali-activated geopolymer production, this research examines whether co-fired fly ash—which can have comparable chemical compositions and physical properties to coal fly ash—can be successfully geopolymerised. Aluminosilicate geopolymeric gels have a Si-O-Al framework where the silicon and aluminium cations are tetrahedrally coordinated and linked by oxygen bridges, creating a net negative charge that is neutralised through the addition of alkali cations [11]. These binders have broad applications in the construction field as a cost-effective and durable alternative to portland cement. Furthermore, the absence of a high temperature calcination step during geopolymer synthesis significantly reduces its embodied CO_2, by estimates of up to 80% compared to Portland cement concrete [12], although it is necessary to consider the CO_2 emissions in the production of the activator in conducting such calculations.

In this study, two ashes—one coal ash and one co-fired ash produced by burning coal with wood chips—are activated with alkali silicate and hydroxide solutions to evaluate the feasibility of fabricating co-fired fly ash geopolymers. Since co-firing can result in a reduced glassy phase and higher phosphate, alkali, and magnesium levels compared to coal ash [10,13], developing a viable mix design can present challenges. Previous investigations have successfully geopolymerised ashes with co-combusted fuels including petroleum coke [14] and rice husk and bark [15, 16], but no research has been conducted on wood co-fired ashes. Research must be performed on alkali-activation of these ash types because the structure and composition of biomass sources can vary significantly. In this study, analytical techniques including X-ray diffraction and infrared spectroscopy are used to identify reaction products after activation, and to investigate the evolution of the molecular structure of the different raw fly ash samples as they are transformed into a gel product.

This research, which aims to determine some of the fundamental properties of this new material, is a necessary endeavour before its utilisation in future low-carbon infrastructure, and is important for understanding the future of geopolymer technology as the U.S., Europe, and other regions move increasingly to biomass co-firing (rather than pure coal) as a fuel source for electricity generation.

EXPERIMENTAL PROGRAM

Materials

One ash sample produced by pure coal combustion and one ash sample derived from a biomass co-firing process with coal serve as the raw materials in this study. The coal fly ash is a commercially available ash from Southern Company's Plant Bowen in Cartersville, GA produced by burning Central Appalachian bituminous coal. The co-fired fly ash was acquired from Southern Company's E.C. Gaston Electric Generating in Wilsonville, AL. This sample is the by-product of a co-combustion process that combined eastern bituminous coal with 1/2 in. mean diameter pine wood chips containing no limbs and minimal bark. The wood chips replaced 4% of the coal by weight and generated 1.14% of the total energy. The wood chips and coal were mixed on a belt and pulverised together prior to combustion.

A chemical analysis was performed on both fly ash samples by X-ray fluorescence on a Philips PW-2400 XRF instrument. Fused beads of each sample were created through digestion in Li-borate at >1020°C. Loss on ignition (LOI) was determined gravimetrically using a LECO TGA 601. Samples were held to a constant weight at 107°C to determine free moisture content, and then weighed before and after ignition at 950°C to determine LOI, which is a measure of the unburned carbon content in the ash. Results for both are presented in Table 1. Both unprocessed ash samples were also sputtered with gold for analysis with a LEO 1530 Thermally-Assisted Field Emission Scanning Electron Microscope (SEM). Operating conditions were set at an accelerating voltage of 8 kV and varying magnifications under high vacuum. SEM images of both ashes can be seen in Figure 1.

Table 1 Composition of ash samples (mass % as oxide)

TYPE	SiO_2	Al_2O_3	Fe_2O_3	CaO	MgO	Na_2O	K_2O	Na_2O_{eq}	P_2O_5	Other	LOI
Coal	55.28	27.21	7.98	1.26	1.23	0.47	3.02	2.46	0.19	1.61	1.39
Co-Fired	42.84	26.21	13.87	4.01	1.25	0.52	2.08	1.89	0.65	1.88	5.47

The silica content of the coal ash is nearly 30% higher than in the co-fired ash, but alumina contents are similar for both. Calcium levels in the co-fired ash are more than three times that of the coal ash; however, both ashes are still classified as Class F (or low-calcium ashes) under ASTM C 618 [3], as both ashes satisfy the requirement for Class F ashes by having a primary oxide content (the summation of SiO_2, Al_2O_3 and Fe_2O_3) greater than 70%. The distribution of these primary oxides is quite different for each ash, with the iron content of the co-fired ash nearly double that of the coal ash. The co-fired sample has a much higher unburned carbon content (as measured by LOI) compared to the coal ash sample. Still, both samples fall below the maximum LOI limit of 6% specified in ASTM C 618. Pure coal combustion produces a much higher ash content (~10%) compared to pure biomass combustion (~1%) depending on its composition [2]. This fact, coupled with the low biomass fuel percentage used to produce this ash, suggests that the differences observed between these ash compositions (especially with regard to the silica content) are more a function of production variables (e.g., pulverisation process, oxygen levels, furnace temperature, etc.) and the raw coal properties rather than the biomass properties.

Nevertheless, the biomass addition does impact some of the ash characteristics. Previous research conducted by some of the authors [7, 8] on a larger distribution of coal and co-fired

samples with varying physical and chemical characteristics determined that co-firing can increase phosphate levels in the ash. Other investigations [17] have found that co-firing can also increase alkali levels depending on the biomass source, which for the purpose of geopolymer manufacture could actually prove beneficial through increasing the available alkalis in the system. However, biomass inclusion was not found to impact the alkali content of the co-fired ash in this study. Co-combustion in the Southern U.S. typically occurs in older, smaller plants, which tend to be less efficient at burning fuel, resulting in by-product materials with greater unburned carbon levels as seen with the co-fired ash in this study. However, coal ashes produced at these older plants with the same coal and similar processing conditions can actually have higher carbon contents than their companion co-fired ashes, suggesting that biomass replacement of coal at these low quantities does not strongly impact the ash carbon content.

The SEM image in Figure 1a shows the spherical glassy particles that are characteristic of coal fly ash. The large particle in the centre of the image is likely a plerosphere filled with much smaller particles, some presumably being cenospheres. A fibrous wood particle can be clearly seen in the image of the co-fired ash (Figure 1b) surrounded by glassy spheres and carbon. These images demonstrate that co-firing can alter the morphology of the ash, with some of the wood retaining its original structure even after combustion. The coal ash, with a mean particle size of 16.2 μm, is finer than the co-fired ash, which has a mean particle size of 26.9 μm measured through dry-dispersion laser analysis. The coarser nature of the co-fired ash can partly be attributed to its higher carbon content (amorphous carbon particles tend to be large) and also the presence of these woody structures.

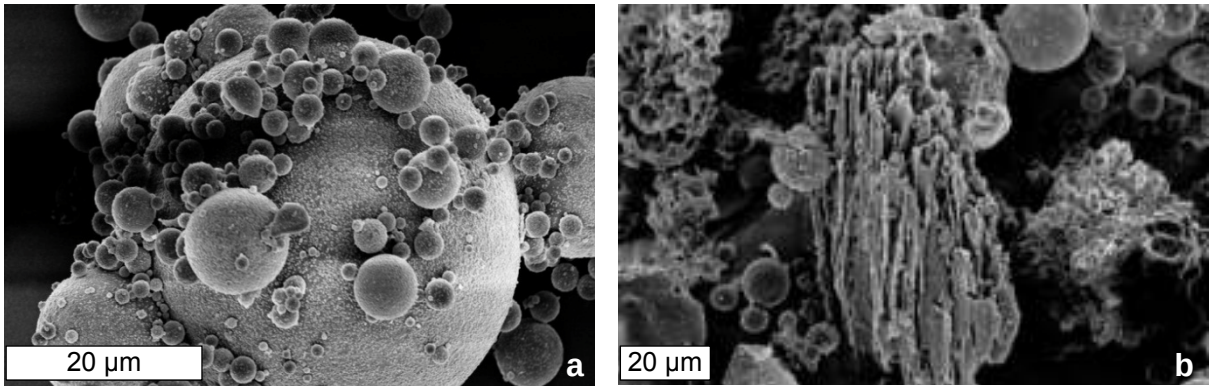

Figure 1 SEM images showing morphology of (a) coal ash and (b) co-fired ash

Paste Synthesis

Geopolymer pastes were prepared by mixing both fly ash samples with two sodium-containing activating solutions: one with a composition of $Na_2O{\cdot}11H_2O$ and the other $Na_2O{\cdot}2SiO_2{\cdot}11H_2O$. Thus the modulus of solution (Ms = molar ratio SiO_2/Na_2O) is 2 for the silicate-containing activator and 0 for the hydroxide activator. A constant activator content of 7% Na_2O by mass of fly ash was used for all mixes. The co-fired ash pastes had less workability due to the coarser particles and higher carbon content, so required a higher water/fly ash ratio (0.4) compared to the coal ash (0.25) to develop similar workability. Specimens were cast in cylindrical moulds and cured at 40°C before analytical testing was conducted.

Analytical Techniques

X-ray powder diffraction was performed on both raw ashes and pulverised samples of each geopolymer paste after 28 days of curing. Diffractograms were recorded under Cu-Kα radiation from 3-70° 2θ in 0.02° 2θ increments with a count time of 4 s per step, using a Bruker D8 ADVANCE diffractometer. Fourier transform infrared (FTIR) spectrometry was conducted on all samples after 7-days of curing using the KBr pellet technique with a Bruker TENSOR instrument, scanning from 1300 to 400 cm^{-1} with a resolution of 2 cm^{-1}.

RESULTS AND DISCUSSION

X-Ray Diffraction

The raw coal ash (Figure 2a) contains primarily an X-ray amorphous phase with a small quantity of the following crystalline components: quartz (SiO_2) (Powder Diffraction File (PDF) card 01-083-0539), mullite ($Al_6Si_2O_{13}$) (PDF# 00-015-0776), and iron oxides. Multiple iron oxide phases with overlapping peaks were observed in this diffractogram so it is difficult to specifically identify them. However, the iron content in the coal ash is mostly a ferrite spinel (with substitution of other elements onto both the Fe^{2+} and Fe^{3+} sites as previously observed [18]) but also may include magnetite. The major phase in the co-fired ash (Figure 2b) is also X-ray amorphous with similar crystalline phases to the coal ash: quartz (PDF# 01-075-8321), mullite (PDF# 00-015-0776), a ferrite spinel phase, and possibly maghemite. The higher iron content of the co-fired ash is evident in the intensified peaks for these phases.

X-ray diffraction studies of pure pine wood ash samples have revealed that calcite ($CaCO_3$), fairchildite ($K_2Ca(CO_3)_2$), and calcium hydroxide ($Ca(OH)_2$) are its primary crystalline components [19]. However, no calcium-containing crystalline phases were detected in this co-fired ash even though pine wood was used in the co-firing process. The small quantity of the pine wood ash in the overall co-fired ash matrix—which mostly contains coal ash—likely masks these peaks, or it is possible that the calcium is present in amorphous phases. One previous study [9] determined that pure wood ash does not have a visible amorphous hump on its XRD pattern, which could be evidence that it has an insignificant glassy phase. Both ashes in this report, however, do have an amorphous hump at around 15-35° 2θ. The co-fired ash used in this investigation appears to have a slightly smaller amorphous component compared to the coal ash, but this is likely a consequence of its lower silica content.

After activation with alkaline solutions this amorphous hump appears to become broader, extending from 15-40° 2θ and intensifying over the 25-35° 2θ range for both ashes. This shift indicates that gel product has been formed and its composition is primarily amorphous aluminosilicate [20]. For the ashes activated with the hydroxide solution this intensification was not observed, suggesting that a less polymerised matrix was formed. No other observable crystalline phases were formed in either ash after activation with the silicate solutions. Thus there are no crystalline sodium-containing phases in these pastes, which indicates that these alkali ions have either been incorporated into the amorphous phase or are still available in the pore solution. An increase in soluble silica has been shown to slow zeolite formation [21], which could explain the absence of zeolites observed here.

However, the sodium hydroxide solution when reacted with the co-fired ash did form zeolitic phases including chabazite-Na ($NaAlSi_2O_6 \cdot 3H_2O$) (PDF# 00-019-1178) and faujasite

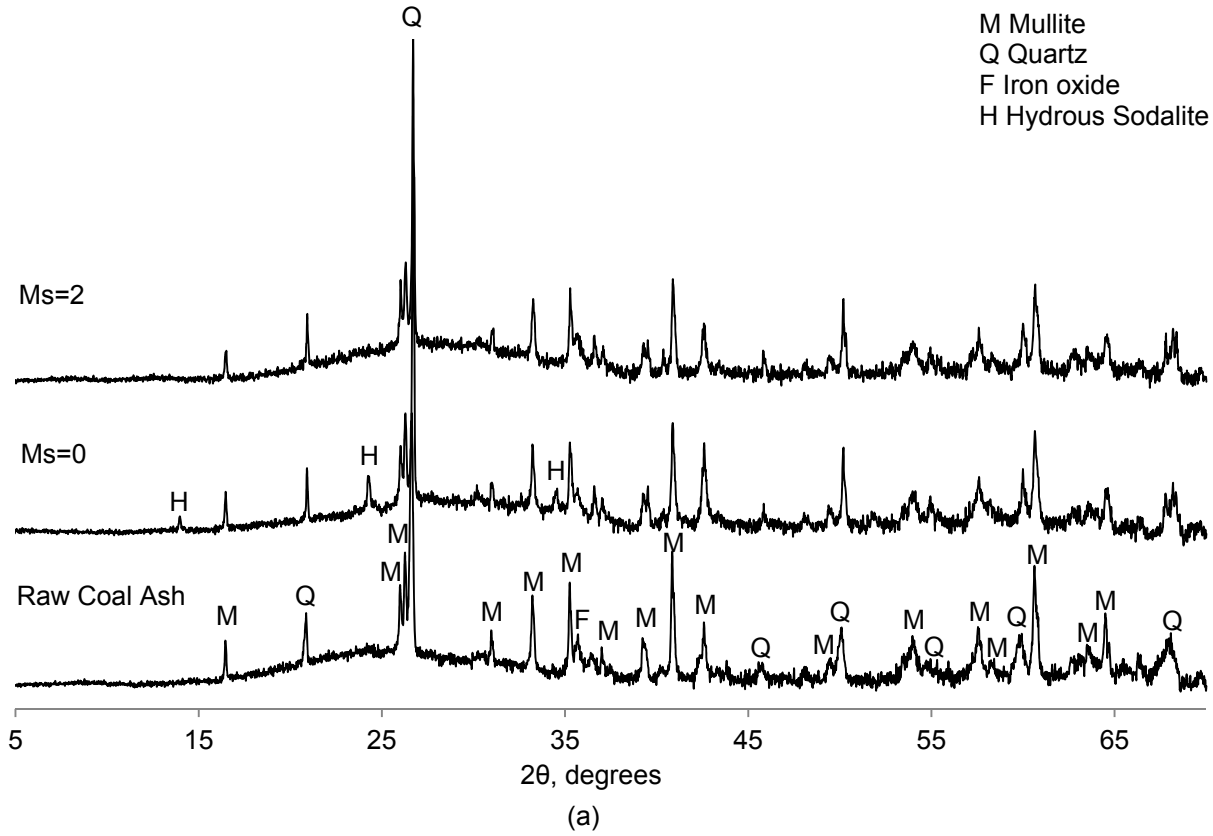

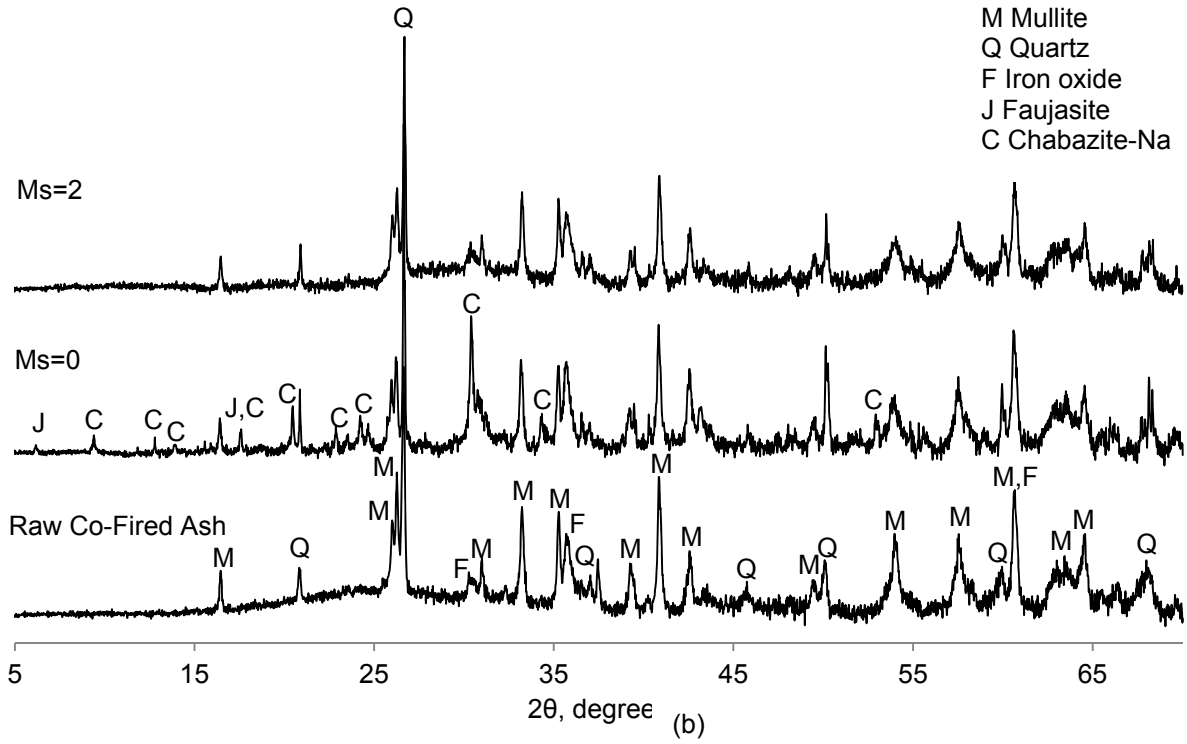

Figure 2 X-ray diffraction patterns of (a) coal ash sodium-activated pastes and (b) co-fired ash sodium-activated pastes

($Na_2Al_2Si_4O_{12}\cdot 8H_2O$) (PDF# 00-039-1380). The crystallization of chabazite-Na and faujasite after alkali-activation of an aluminosilicate fly ash is consistent with previous literature [22,23]. The same solution also formed new zeolitic phases when mixed with the coal ash. Hydrous sodalite ($Na_6[AlSiO_4]_6\cdot 4H_2O$) was identified at these new peaks. These crystalline phases demonstrate that zeolite formation is favoured in these systems, with less alkalis being incorporated into the amorphous framework.

Infrared Spectroscopy

Infrared spectroscopic results are reported in Figure 3 for both raw ashes and for polymers formed after activation with two different alkali solutions. The primary peaks of interest for this study are linked to the bending and stretching modes of the main T-O bonds, where T is either Si or Al in tetrahedral coordination [24]. The raw coal ash and co-fired ash exhibit wide and intense peaks at 1068 cm^{-1} and 1070 cm^{-1}, respectively, associated with the asymmetric stretching of the T-O bonds. Alkali-activation of both ashes shifts this peak to a lower wavenumber. This shift shows that there has been incorporation of Al and/or substitution of the alkali metal oxide into the network. The result is a depolymerisation of the original tetrahedral silicate and/or aluminosilicate framework of the fly ash and the subsequent polymerisation of a new aluminosilicate geopolymer gel. Previous research [20, 25] has found that the T-O-Si asymmetric stretching vibration of the TO_4 tetrahedra that form the glassy content of fly ash shifts to a lower energy after alkali-activation due to its lower molecular vibration force constant, which is a result of Al substitution in the matrix and higher concentrations of non-bridging oxygen atoms.

The different shifts in this peak for each gel compared to its original ash reflect the varying chemistry of the activating solutions and their impact on the formation of reaction products. The hydroxide solution reduces the wavenumber associated with this main asymmetric stretching peak most notably for both ashes, to ~1000 cm^{-1}. Generally, this reduction can be attributed to the lower Si/Al ratio of these systems at this age. The silicate activator produces a matrix that is more highly polymerised and Si-rich, as indicated by a higher wavenumber in this region (1015 cm^{-1} for the coal ash and 1021 cm^{-1} for the co-fired ash). At early ages an increase in available soluble silica can significantly impact the reaction kinetics and hydration products of these gels. An Al-rich gel is initially formed after activation of fly ash, before being replaced with a more Si-rich gel at later ages [23, 25]. This secondary, more highly polymerized gel is the primary strength-providing phase [20]. An increase in soluble silica content accelerates the formation of this secondary condensed gel because it promotes the development of higher Si/Al gels [21]. The results of this study with regard to the addition of silicate in the activating solution support these earlier findings for both ash types.

The ash composition also impacts the position of this main asymmetric stretching band. Activation of the co-fired ash results in a smaller shift towards lower wavenumbers compared to the coal ash for the silicate solutions. However, it is not clear from the data whether this can be attributed to the inclusion of biomass particles in the ash. Because the ashes were produced from two different coal sources and under different conditions, their silica and calcium contents are considerably different as previously mentioned. It may be that the higher silica content of the coal ash was more readily available to be corroded by the activating solutions, thus resulting in a more depolymerised matrix at this age. Furthermore, the co-fired ash has a higher alkaline earth metal content (i.e., Mg^{2+} and Ca^{2+}), which can increase the strength of the alkali-activated product by acting as a network modifier [26].

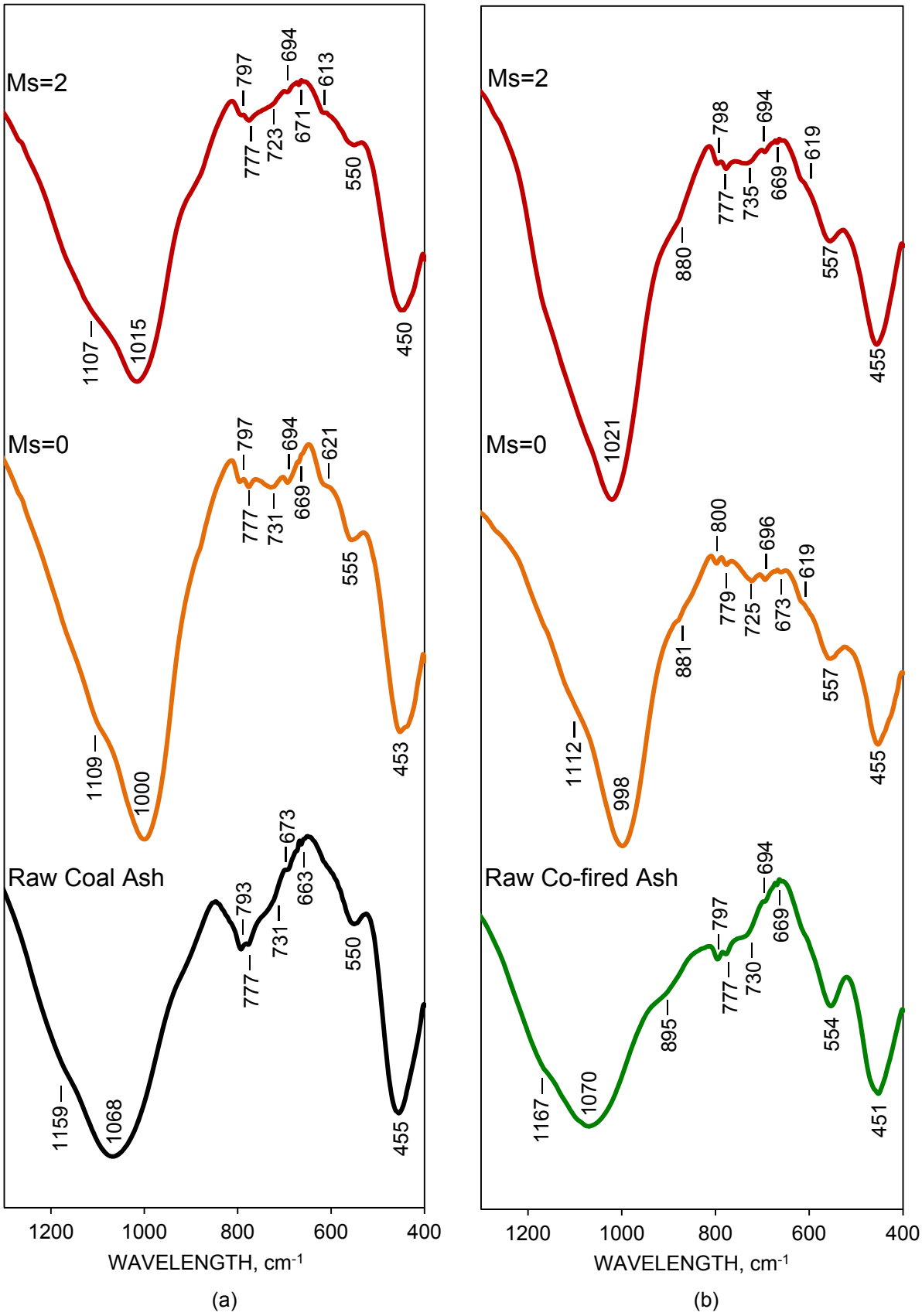

Figure 3 Fourier transform infrared spectra of (a) the coal ash and its activated pastes and (b) the co-fired ash and its activated pastes

The inclusion of these earth metals into the gel network could have impacted this main peak. Lastly, the higher carbon content of the co-fired ash may adsorb some of the alkalis in solution and inhibit the breakdown of the glassy phase necessary for re-polymerisation.

The shoulders visible at 1159 cm^{-1} and 1167 cm^{-1} on the raw coal ash and co-fired ash, respectively, represent the asymmetric Si-O-Si stretching vibration. After alkali-activation this band disappears and a new band is formed in the range of 1107-1109 cm^{-1} for the coal ash and 1112 cm^{-1} for the co-fired ash (note that it was not detected for the silicate-activated sample). The multiple overlapping signals in this wavenumber region make it difficult to identify the exact causes for this shift, but it is likely a combination of the depolymerisation of the original glass framework and incorporation of Al. The shoulder at 895 cm^{-1} in the raw co-fired ash is attributable to the asymmetric stretch of AlO_4^- tetrahedra [27]. The vibration energy of this band decreases after activation as illustrated by its shift to 878-881 cm^{-1}.

Quartz bands were detected as a doublet at 793 and 777 cm^{-1}, and peaks at 690 cm^{-1} and 455 cm^{-1} for the coal ash, and as a doublet at 797 and 777 cm^{-1}, and peaks at 694 cm^{-1} and 451 cm^{-1} for the co-fired ash [28]. Activation of the ash does not significantly alter this α-quartz phase and thus these values do not strongly shift. However, the intensity of the doublet band in the coal ash is reduced, indicating a potential change in its structure or quantity after activation for this ash. The bands at 451 and 455 cm^{-1} are also associated with the internal deformation vibrations of the T-O bonds also known as the in-plane bending mode [29]. The small peak at 669 cm^{-1} observed in the co-fired ash as well as two of the activated pastes from both ash types is identifiable as the symmetrical stretching vibration of either Si-O-Si or Al-O-Si bands [30].

A wide band representing mullite is seen at 550 cm^{-1} and 554 cm^{-1} in the coal and co-fired ash, respectively [28]. After activation this spectral shoulder does not appreciably shift horizontally, but its vertical intensity is reduced for all mixes. The coal ash gels exhibit more reduction in this shoulder than the co-fired ash gels. Additionally, the silicate activating solution reduces this shoulder intensity more than the hydroxide activation solutions for the coal ash. It is possible that this could be the result of a dilution effect and that by adding the activator the mullite is now a lower percentage of the total sample mass. However, it is more likely that this reduction signals an attack on a glassy mullite-like phase [20]. This supports the earlier finding that the activating solutions are more effective in destroying the amorphous content in the coal ash compared to the co-fired ash, with silicate solutions performing best. The much higher silica content and presumably higher glassy content of the coal ash could partly explain this phenomenon.

New infrared vibration modes known as psuedo-lattice bands were also observed after activation in the region between 800 and 600 cm^{-1}. Previous literature [21,31] identifies these new bands as external ring vibrations composed of different numbers of units, which may form either two- or three-dimensional structures. These secondary building units (SBUs) form cyclic structures around the AlO_4^- and SiO_4 tetrahedra. The vibrations associated with lattice rings are not observed here because they only appear below 400 cm^{-1} (see Figure 3). One pseudo-lattice band is formed in the spectra at 731-723 cm^{-1} in the activated coal ash and at 735-725 cm^{-1} in the activated co-fired ash. This band is very pronounced for the hydroxide-activated matrices as it may be linked with the Al-rich zeolites previously identified by XRD [32]. Another band is formed in the spectra at 621-613 cm^{-1} in the activated coal ash and at 619-615 cm^{-1} in the activated co-fired ash. These vibrations represent the formation of six-membered rings with structures similar to α and β-cristobalite [31].

CONCLUSIONS

Co-fired fly ash derived from coal and wood co-combustion was successfully used as a precursor for geopolymerisation using sodium activating solutions for the first time. A standard coal fly ash was also alkali-activated for comparison. XRD results indicate both ashes are primarily composed of a vitreous, amorphous phase consisting of Si and Al intermixed with a small amount of crystalline phases including quartz, mullite, and iron oxides. No zeolites were formed after activation of both ashes using sodium silicate. However, the coal ash formed hydrous sodalite while the co-fired ash favoured the formation of chabazite-Na and faujasite after activation with a sodium hydroxide solution. Infrared spectra reveal that there has been incorporation of Al and/or substitution of the Na into the network after activation of both ashes. The activating solutions are more effective in depolymerising the glassy content of the coal ash compared to the co-fired ash, presumably due to the higher silica content of the coal ash. However, co-firing in this sample did not likely impact the silica content of this ash—it is more a result of differing raw coal compositions. Co-firing did, however, elevate the phosphate content of the ash, but this had no discernible impact on gel formation. Furthermore, the angular morphology of the wood particles within the co-fired ash and its higher unburned carbon content increased water demand. However, these issues can be alleviated with a proper mix design in order to develop viable binders using this emerging waste stream.

ACKNOWLEDGEMENTS

This research is supported in part by the Department of Energy Office of Science Graduate Fellowship Program (DOE SCGF), made possible in part by the American Recovery and Reinvestment Act of 2009, administered by ORISE-ORAU under contract no. DE-AC05-06OR23100. The research is also based on the work supported by the National Science Foundation under Award No. 1107736 and by the Australian Academy of Science. We would like to thank Dr. Laura Gordon, Suhandy Winata, Nortey Yeboah, and Mitchell Napolitano for their help with this research. The participation of JLP and SAB was supported by the Australian Research Council, including partial funding through the Particulate Fluids Processing Centre.

REFERENCES

1. BAXTER, L. Biomass-coal co-combustion: opportunity for affordable renewable energy, Fuel, Vol. 84, 2005, pp 1295-1302.

2. MACIEJEWSKA, A, VERINGA, H, SANDERS, J, PETEVES, S D. Co-firing of biomass with coal: Constraints and role of biomass pre-treatment, DG-JRC Institute for Energy. <http://ie.jrc.ec.europa.eu/publications/scientific_publications/2006/EUR22461EN.pdf.> 2006.

3. AMERICAN SOCIETY FOR TESTING AND MATERIALS. Standard Specification for Fly Ash and Raw or Calcined Natural Pozzolan for Use in Concrete, ASTM C 618, West Conshohocken, PA, 2008.

4. WANG, S, BAXTER, L. Comprehensive study of biomass fly ash in concrete: Strength, microscopy, kinetics, and durability, Fuel, Vol. 88, 2007, pp 1165-1170.

5. RAJAMMA, R, BALL R J, TARELHO, L A C, ALLEN, G C, LABRINCHA, J A, FERREIRA, V M. Characterisation and use of biomass fly ash in cement-based materials, Journal of Hazardous Materials, Vol. 172, 2009, pp 1049-1060.

6. JOHNSON, A, CATALAN, L J J, KINRADE, S D. Characterization and evaluation of fly-ash from co-combustion of lignite and wood pellets for use as cement admixture, Fuel, Vol. 89, 2010, pp 3042-3050.

7. SHEARER, C R, YEBOAH, N, KURTIS, K E, BURNS, S E. Investigation of biomass co-fired fly ash properties: Characterization and concrete durability performance, Proceedings of the Second International Conference on Sustainable Construction Materials and Technologies, Eds. J Zachar, P Claisse, T R Naik and E Ganjian, Ancona, Italy, 2010, pp 1719-1729.

8. SHEARER, C R, YEBOAH, N, BURNS, S E, KURTIS, K E. Evaluation of biomass fired and co-fired fly ash for alkali-silica reaction mitigation in concrete, paper accepted for Proceedings of 14th International Conference on Alkali-Aggregate Reaction, Austin, TX, 2012.

9. SHEARER, C R, YEBOAH, N, KURTIS, K E, BURNS, S E. The early age behavior of biomass fired and co-fired fly ash in concrete, Proceedings of World of Coal Ash, Denver, CO, 2011.

10. EUROPEAN STANDARD. Fly ash for concrete - Part 1: Definition, specifications and conformity criteria, EN-450, Brussels, Belgium, 2005.

11. DUXSON, P, FERNÁNDEZ-JIMÉNEZ, A, PROVIS, J L, LUKEY, G C, PALOMO, A., VAN DEVENTER, J S J. Geopolymer technology: the current state of the art, Journal of Materials Science, Vol. 42, 2007, pp 2917-2933.

12. DUXSON, P, PROVIS, J L, LUKEY, G C, VAN DEVENTER, J S J. The role of inorganic polymer technology in the development of 'green concrete', Cement and Concrete Research, Vol. 37, 2007, pp 1590-1597.

13. FONT, O, MORENO, N, QUEROL, X. IZQUIERDO, M, ÁLVAREZ, E, DIEZ, S, ELVIRA, J, ANTENUCCI, D, NUGTEREN, H, PLANA, F, LÓPEZ, A, COCA, P, PEÑA, F G. X-ray powder diffraction-based method for the determination of the glass content and mineralogy of coal (co)-combustion fly ashes, Fuel, Vol. 89, 2010, pp 2971-2976.

14. ÁLVAREZ-AYUSO, E, QUEROL, X, PLANA, F, ALASTUEY, A, MORENO, N, IZQUIERDO, M, FONT, O, MORENO, T, DIEZ, S, VÁZQUEZ, E, BARRA, M. Environmental, physical and structural characterisation of geopolymer matrixes synthesised from coal (co-)combustion fly ashes, Journal of Hazardous Materials, Vol. 154, 2008, pp 175-183.

15. SONGPIRIYAKIJ , S, KUBPRASIT, T, JATURAPITAKKUL, C, CHINDAPRASIRT, P. Compressive strength and degree of reaction of biomass- and fly ash-based Geopolymer, Construction and Building Materials, Vol. 24, 2010, pp 236–240.

16. NAZARI, A, BAGHERI, A, RIAHI, S. Properties of geopolymer with seeded fly ash and rice husk bark ash, Materials Science and Engineering A, Vol. 528, 2011, pp 7395–7401.

17. DEMIRBAS, A. Sustainable cofiring of biomass with coal. Energy Conversion and Management, Vol. 44, 2003, pp 1465-1479.

18. PROVIS, J L, ROSE, V, BERNAL, S A, VAN DEVENTER, J S J. High-resolution nanoprobe X-ray fluorescence characterization of heterogeneous calcium and heavy metal distributions in alkali-activated fly ash, Langmuir, Vol. 25, 2009, pp 11897–11904.

19. MISRA, M K, RAGLAND, K W, BAKER, A J. Wood ash composition as a function of furnace temperature. Biomass and Bioenergy, Vol. 4, 1993, pp 103-116.

20. LEE, W K W, VAN DEVENTER, J S J. Use of infrared spectroscopy to study geopolymerization of heterogeneous amorphous aluminosilicates, Langmuir, Vol. 19, 2003, pp 8726-8734.

21. CRIADO, M, FERNÁNDEZ-JIMÉNEZ, A, PALOMO, A. Alkali activation of fly ash: Effect of the SiO_2/Na_2O ratio Part I: FTIR study, Microporous and Mesoporous Materials, Vol. 106, 2007, pp 180-191.

22. HAJIMOHAMMADI, A, PROVIS, J L, VAN DEVENTER, J S J, Time-resolved and spatially-resolved infrared spectroscopic observation of seeded nucleation controlling geopolymer gel formation, Journal of Colloid and Interface Science, Vol. 357, 2011, pp 384-392.

23. FERNÁNDEZ-JIMÉNEZ, A, PALOMO, A. Mid-infrared spectroscopic studies of alkali-activated fly ash structure, Microporous and Mesoporous Materials, Vol. 86, 2005, pp 207-214.

24. VAN JAARSVELD, J G S, VAN DEVENTER, J S J. Effect of alkali metal activator on the properties of fly ash-based geopolymers, Industrial & Engineering Chemistry Research, Vol. 38, 1999, pp 3932-3941.

25. REES, C A, PROVIS, J L, LUKEY, G C, VAN DEVENTER, J S J. In Situ ATR-FTIR study of the early stages of fly ash geopolymer gel formation, Langmuir, Vol. 23, 2007, pp 9076-9082.

26. DUXSON, P, PROVIS, J L. Designing precursors for geopolymer cements, Journal of the American Ceramic Society, Vol. 91, 2008, pp 3864-3869.

27. BERNAL, S A, MEJIA DE GUTIERREZ, R, PROVIS, J L, ROSE, V. Effect of silicate modulus and metakaolin incorporation on the carbonation of alkali silicate-activated slags, Cement and Concrete Research, Vol. 40, 2010, pp 898-907.

28. GADSDEN, J A. Infrared Spectra of Minerals and Related Inorganic Compounds, 1975, Butterworths, pp 45-47.

29. RAHIER, H, SIMONS, W, VAN MELE, B. Low-temperature synthesized aluminosilicate glasses: Part III Influence of the composition of the silicate solution on production, structure and properties, Journal of Materials Science, Vol. 32, 1997, pp 2237-2247.

30. YU, P, KIRKPATRICK, R J, POE, P, MCMILLAN, P F, CONG, X. Structure of calcium silicate hydrate (C-S-H): Near-, mid-, and far-infrared spectroscopy, Journal of the American Ceramic Society, Vol. 82, 1999, pp 742-48.

31. SITARZ, M, HANDKE, M, MOZGAWA, W. Identification of silicooxygen rings in SiO_2 based on IR spectra, Spectrochimica Acta Part A, Vol. 56, 2000, pp 1819-1823.

32. FERNÁNDEZ-JIMÉNEZ, A, MACPHEE, D E, LACHOWSKI, E E, PALOMO, A. Immobilization of cesium in alkaline activated fly ash matrix. Journal of Nuclear Materials, Vol. 346, 2005, pp 185-193.

Experimental Study on the Partial Replacement of Cement by Fly Ash on Self-compacting Concrete

K Nagamani, B Mahalingam
Anna University, India

This paper presents the results of an experimental investigation of fly ash based Self Compacting concrete (SCC). The results of fresh and hardened properties including rapid chloride ion permeability realized fly ash as partial replacement by replacing cement via 30%,40% and 50% in a binder content (Cement + fly ash) of 500kg. The fresh and hardened properties are influenced by all mixture factors: the compressive strength, modulus of rupture and split tensile strength decreases marginally with the increase of fly ash and reduces chloride ion permeability. The Produced SCC with water reducing admixture and without adding viscosity modifying agent both in terms of flow performance and early strength, of quality comparable or better than conventional concrete.

Dr K Nagamani graduated (B.E(Hons)Civil Engineering)in 1983 from University of Madras, Master's M.Tech(Ocean Engineering)1985 and Ph.D(Offshore structures) 1991 from Indian Institute of Technology, Madras,India. At present Professor in Civil Engineering,Division of Structural Engineering,College of Engineering, Anna University, Chennai, India

B Mahalingam graduated B.E. Civil Engineering 1987 from Bangalore University,Bangalore and M.E.(Structural Engineering)1994 from Annamalai University, Chidambaram, Tamil Nadu,India.

Keywords: Fly ash, Fresh properties, Hardened properties, Permeability, Self-compacting concrete

INTRODUCTION

One of the most outstanding advances in concrete technology during the last two decades is represented by Self-Compacting Concrete (SCC). SCC concept was introduced in to scientific world in Japan in 1986 by Professor Hajime Okamura from Tokyo University [1]. This new concrete was the result of a research on the achievement of durable concrete structures in independent of quality of construction work, since the SCC can be compacted itself in to every corner of a formwork, purely by means of its own weight without the need for vibrating compaction. SCC mix demand greater cement paste content, as well as larger quantity of fine materials than the conventional concrete [2]. As an additional component of the SCC, the fine materials are powders with large specific surface, which has measurable impact on the rheological properties of fresh concrete [3-7]. The fine materials used are lime stone powder, fly ash, blast furnace slag and silica flume etc., SCC have limitations: higher material costs (not only for the admixtures itself, but also for the increased quality control testing for concrete and aggregates). Use of fly ash and blast furnace slag reduces the dosages of super plasticizer in self-compacting concrete needed to obtain similar slump/flow compared to concrete made with portland cement only [8]. Fly ash is an industrial derivative from coal industries. Fly ash is one of the most widely used additions in concrete because of the benefits of heat reduction and pozzolanic activities thus have been exclusively investigated for many years [9-13]. Investigations have been made on SCC incorporating more than 50% fly ash [14-20]. In India, the estimated quantities of annual fly ash reach about 225 million tones by 2017. As Per 2005 statistical data, with the available technology only 45 million tones was utilized annually. These materials pose problems of disposal and health hazards if not utilized properly [21]. To reduce the disposal and pollution problems emanating from these Industrial wastes, it is most essential to develop profitable building material from them. Keeping this in view, investigations were undertaken to produce fly ash based SCC by blending various ratios of cement with fly ash. In this paper, the experimental results made for fly ash based SCC are presented.

MATERIALS

For the experimental researches of fly ash based SCC, the following materials were used: cement, processed fly ash, coarse aggregate, fine aggregate, super plasticizer and water. Ordinary Portland cement of 53 grade was used and found to be conforming to IS: 12269-1987[22]. Coarse Aggregate of size of 12.5 mm of granite from a local source with the specific gravity 2.61 and fineness modulus 6.1 was used. Two types of fine aggregate with fineness modulus 3.1 and 2.38 are combined in the ratio 30:70 to have a fineness modulus of 2.57[23]. This was made to increase fine material content into SCC. Super plasticizer of type Sulphonated Naphthalene Formaldehyde (SNF) condensate, a viable super plasticizer conforming to ASTM-C-494 Type A and F as well as satisfying IS: 9103-1979 was used because it contributes to the homogeneous flow [24]. Processed fly ash was used as a cement replacement material. The maximum retention of processed fly ash on 45 microns (fineness residue retained on 325 mesh sieve) IS sieve (wet sieving) is limited to 34% alone was used in this study. The chemical properties of Cement and fly ash are as shown in Table 1 [25-26]. By processing of fly ash, the unburnt carbon was considerably reduced. The particle size distribution analysis of fly ash is shown in Table 2. It was inferred that the fly ash particles are of Diameter at 10 %: 2.22 µm, Diameter at 50 %: 14.13 µm,

Diameter at 90 %: 79.84 µm and the Mean diameter: 28.88 µm. Potable water available in the laboratory was used for mixing concrete and curing the specimens as well.

Table 1 Chemical composition of cement and fly ash

S.NO	CHEMICAL COMPOSITION		RESULT OBTAINED FOR CEMENT	RESULT OBTAINED FOR FLYASH
1	Silica	(SiO_2)	20.69	95.67(SiO_2+ Al_2O_3+ Fe_2O_3)
2	Alumina	(Al_2O_3)	6.56	
3	Iron Oxide	(Fe_2O_3)	4.23	
4	Calcium Oxide	(CaO)	62.52	-
5	Magnesium Oxide	(MgO)	1.77	1.86
6	Sodium Oxide	(Na_2O)	0.36	1.12
7	Potassium Oxide	(K_2O)	0.42	0.05
8	Sulphuric anhydride	(SO_3)	2.18	0.68
9	Loss on Ignition	(LOI)	1.27	0.62

Table 2 Particle size distribution of fly ash

X:DIAMETER/ µm	25	37	45	63	75	90	150	212
Q3:cumulative value (%)	61.42	71.37	75.94	83.99	88.43	92.85	92.66	100

DETAILS OF EXPERIMENTAL STUDY

Three types of compositions were studied in the experimental program:

There were three mixtures for Self Compacting Concrete. In each mix, the binder (cement + fly ash) content maintained as 500 Kg/m^3, the ratio of coarse aggregate to total aggregate was maintained as 0.54 and the free water added to the mix was fixed as 195 liters/m^3. Processed fly ash as partial replacement by replacing cement via 30%, 40% and 50%. The water to cementitious material ratio fixed as 0.39. The absolute volume method of mix design was followed and the dosage of the super plasticizer alone changed for each mix depending upon the requirement to satisfy the guideline of European Federation dedicated to specialist construction chemicals and concrete systems (EFNARC 2005) in the fresh state of concrete [27-29].

The mixtures are given in Table 3. The ingredients are mixed in a laboratory drum type mixer for about 15 minutes. These mixtures are obtained by trial process and by proper selection of aggregate grading curve. The test methods viz., slump flow spread, V funnel flow, L-Box test and U- Box test are as shown in Figure 1 were used to characterize the workability properties of SCC for the final acceptance of the SCC mixture proportions. After these tests, if the mix satisfies the required SCC properties, specimens were cast in steel moulds without any compaction or vibration. Test specimens were of 150 mm x 150 mm x 150 mm cubes for

evaluating compressive strength, 150Ø x 300 mm cylinders for evaluating cylindrical compressive strength and split tensile strength, 150 mm x 150 mm x 700 mm prismatic specimens for evaluating flexural strength and 100 Ø x 50 mm cylinders for Rapid Chloride Permeability Test (RCPT). Depending on their final setting, de-molding of the specimens was carried out after 18 hours and above. Visual inspection of hardened samples revealed that the surface characteristics of SCC mixtures were excellent and the concrete had flown and compacted without segregation.

Table 3 Composition of SCC mixtures per m^3 of concrete

COMPOSITION	DESIGNATION OF SCC MIX		
	M1	M2	M3
Cement (Kg)	350	300	250
Fly ash (Kg)	150	200	250
Free water (litres)	195	195	195
Coarse Aggregate (Kg)	862	850	839
River Sand Coarse (Kg)	220	217	214
River Sand Fine (Kg)	511	507	500
Total Water (litres)	208	208	208
Superplasticizer (litres)	2.5	2.25	2.00


Flow spread of SCC


L – box test


V- funnel flow test


U- box test


Cube mould with SCC


Beam mould with SCC

Figure 1 SCC in moulds

Then these specimens are marked and placed immediately in the curing water tank at room temperature (25^{o}C approximately) upto 28 days and then air curing was followed for the remaining periods. These hardened specimens were tested as per IS: 516 – 1969 [30]. RCPT test was conducted as per ASTM C1202 – 94.

The amount of current passing through the concrete specimens, an indication of chloride permeability, is monitored during the 6 hours of test duration [31]. All the testing was conducted in room temperature and it has been completed on three samples along with the average values of the same reported.

RESULTS AND DISCUSSIONS

Workability

Before casting of fly ash based SCC specimens, workability measurements like slump flow spread, V- funnel test, L- Box test and U- Box test are carried out. The fresh concrete properties are given in Table 4. As it is evident, the basic requirements of high flow ability, filling ability and segregation resistance are as specified by guidelines on SCC by EFNARC and it satisfies all the required rheological and self-compatibility [27-29]. The workability values are maintained by adding suitable quantities of super plasticizers. On the basis of the experimental study it was concluded that addition of fly ash in concrete gives a reduction in bleeding and blow holes as stated earlier [32]. A reduction in bleeding improves surface integrity of concrete, improves its homogeneity and reduces the probability of cracks occurring where there is some restraint to settlement. The dosage of super plasticizer considerably reduced with the higher replacement levels of fly ash to maintain the same filling ability as shown in Table 3, which is in line with other research [15]. The values of loss on ignition is less than 1.0 % , particles of the unburnt carbon absorbs very less quantity of the super plasticizer and hence more super plasticizer remains available for reduction in water demand imparting good flow ability in SCC in the absence of viscosity modifying agent. The super plasticizer dosage decreased with an increase in fly ash content, which leads to the increased viscosity. To achieve the same range of filling ability, the required super plasticizer dosage decreased. The reason could be that fly ash acts as a lubricant material; it does not react with super plasticizers and produce a repulsive force and the super plasticizer may react only on the cement [33]. As a result, the larger amount of fly ash contained, the less super plasticizer needed. The optimized SCC has no bleeding, was highly cohesive and has excellent self-compatibility properties.

Table 4 Fresh state properties of SCC mixtures

WORKABLITY CHARACTERISTICS	DESIGNATION OF SCC MIX			EFNARC REQUIREMENTS
	M1	M2	M3	
Slump Flow Spread(mm)	630	660	600	600-800 mm
V funnel V_0 Sec	4.3	4.0	2.8	6 to 12 secs
V funnel V_5 Sec	4.5	4.8	3.0	0 to +3 secs
L Box ratio	0.76	0.79	0.80	0.8 to 1.0
U Box Difference in mm	5	20	11	0 to 30 mm

Due to the presence of a large content of fly ash, the microstructure of the SCC mixtures would be more dense and homogeneous and the transition zone near the aggregate would be almost absent. These factors contribute to an increase in stiffness. A visual stability index rating of zero was indicated [34].

Mechanical characteristics

The following mechanical characteristics (Compressive strength, modulus of rupture, and split tensile strength) of fly ash based SCC were determined. All the mechanical properties namely, compressive strength, split tensile strength and flexural tensile strength compare favorably with conventional concrete mixtures [38]. Compressive strength results are presented in Table 5 and Table 6.

Table 5 Compressive strength (cube specimens) of SCC mixtures (N/mm^2)

AGE OF CONCRETE	DESIGNATION OF SCC MIX		
	M1	M2	M3
3 days	14.00	17.00	10.00
7 days	28.00	20.00	23.00
28 days	45.00	45.00	37.00
56 days	53.00	54.00	46.00
91 days	57.00	56.00	51.00

Table 6 Compressive strength (cylindrical specimens) of SCC mixtures (N/mm^2)

AGE OF CONCRETE	DESIGNATION OF SCC MIX		
	M1	M2	M3
28 days	36.00	36.00	31.00
56 days	42.00	44.00	37.00
91 days	46.00	45.00	41.50

Table 7 Split tensile strength (cylindrical specimens) of SCC mixtures (N/mm^2)

AGE OF CONCRETE	DESIGNATION OF SCC MIX		
	M1	M2	M3
28 days	3.50	3.00	2.00
56 days	4.00	3.50	3.00
91 days	5.00	4.00	3.50

The influence of fly ash on strength was more significant at higher contents. In addition, most data are with in the range for SCC [35]. For all the distinct mixtures the ratio of cylindrical compressive strength to cube compressive strength was worked out to be 0.807. The compressive strength of concrete was increased even after 28 days due to pozzolanic activity of the fly ash used. The results of Split tensile strength, Modulus of rupture, Rapid chloride permeability values are presented in Table 7, Table 8 and Table 9 respectively. Tensile strength is one of the

most important fundamental properties of concrete. An accurate prediction of tensile strength of concrete will help in mitigating cracking problems which improves the shear strength and minimizes the failure of concrete in tension [36]. There is some higher split tensile strength reported [37].

Table 8 Modulus of rupture of SCC mixtures (N/mm ^{2})

AGE OF CONCRETE	DESIGNATION OF SCC MIX		
	M1	M2	M3
28 days	5.00	5.00	4.50
56 days	5.50	5.50	5.00
91 days	6.00	6.00	5.00

Table 9 Rapid chloride ion permeability test values of SCC mixtures (Coulombs)

AGE OF CONCRETE	DESIGNATION OF SCC MIX		
	M1	M2	M3
28 days	3187	2737	1654
56 days	1432	1835	1054
91 days	848	1040	855

The minimum value of modulus of rupture for all the mixtures is 11% of 28 days of corresponding cube compressive strength. The minimum percentage of development in compressive strength was about 18% with respect to 28 days compressive strength. Higher replacement levels led to a reduction in the compressive strength and split tensile strength. Higher the replacement levels of fly ash, the higher the reduction in compressive strength. The reduction is higher at early ages and decreases at later age.

Chloride diffusion was assessed using rapid chloride permeability test because of speed with which the test results can be completed. This test is therefore recommended for pre-qualifying mixtures and not for job-site testing and acceptance. The processed fly ash based SCC improves the concrete resistance to very low chloride ingress at 91 days of age of concrete. It can be concluded that all the three fly ash based SCC mixtures have performed well in aggressive chloride environment. Fly ash based SCC considered in this study is comparatively more durable as compared to conventional ordinary Portland cement concrete with fly ash [38]. This is due to fact that the fly ash is finer than the cement and it therefore fill the voids leading to lower porosity. Fly ash dilates the voids between cement particles. At the higher replacement ratio the voids between the fly ash particles lead to higher porosity. Clearly the longer the curing time, the finer the pore structure and the less interconnection between the capillary pores and in particular, the porous paste/aggregate interface zone formed at early ages is densified by continuous curing in water [9]. It is worth re-emphasizing that the permeability of HVFA SCC is greatly influenced by curing.

Earlier, at 28 days of curing researchers investigated the chloride permeability (RCPT) of SCC with that of normal concrete at 28 days. They observed that the (RCPT) values of SCC specimens were in the range of 1100-1500 coulombs as compared to the average 4000 coulombs of the normal concrete specimens. They further stated that this high resistance of SCC might be due to the high filler materials and low w/p ratio in producing SCC gives a concrete a denser microstructure than conventional concrete with a high w/p ratio [39]. The present study results are very much similar to the results obtained by the above researchers.

Chloride diffusivity is measured in terms of penetration depth and so would be expected to be more sensitive to changes in the state of sample at the time of testing, instead of the total pore volume and size. The significant reduction of chloride diffusivity due to the incorporation of fly ash may be partly explained by this mechanism since the spherical fly ash particles could improve the particle packing density both in the matrix and in the interfacial zone. Poor dispersion of fine powders in some SCC was also suggested as a possible cause of high chloride diffusivity [40]. This test method does not measure concrete permeability. What it does measure is concrete resistivity. It has been shown that there is a fair correlation between concrete resistivity and concrete permeability.

Other factors that may have contributed to the difference in chloride diffusivity of the various SCC may include: the relative magnitude of chloride diffusivity of the aggregates, the paste and the interfacial area; the enhanced water retain ability of the fresh SCC mixtures; and possibly the chemical and physical binding of chloride ions by filler particles and the cement hydration products. So this test is sensitive to permeability and absorption measurements to the moisture content of concrete and it may not represent the true permeability (or potential permeability) for concrete that contains supplementary cementitious materials or chemical admixtures which is the limitation of this test. When dealing with real durability problems, such as the corrosion of reinforcement in concrete structures, different transport mechanisms and their interactions and relative importance, as well as reactions between the transport media and cement matrix have to be considered. More research is clearly required in this aspect. In conclusion, fly ash based SCC developed in this study not only posses the required fresh properties but also develops adequate mechanical and chloride ion penetrability characteristics that can be used as a structural concrete. Out of other mixtures studied, M2 mix is more stable.

CONCLUSIONS

1. Fly ash can replace significant part of the necessary filler when used in to a Self Compacting Concrete. Fly ash has emerged as a preferred material due to its various associated advantages in SCC.

2. The experimental researches concerning the fly ash based SCC had the principal objectives such as the decreasing the cement dosage, better flowability, durability and maintaining the mechanical characteristics by using the fly ash fine filler.

3. Processing of fly ash will make it more effective in improving the performance of SCC, but this is supported by the test results obtained for three replacement levels on a binder content of 500 kg .

4. This SCC can be used for realizing structural elements such as beams, columns, foundation beams etc.

5. With the increase of content of fly ash in the SCC reduced the cost of the composite, super plasticizer dosage and help the concrete to behave as a cohesive mass in fresh state.

6. This holistic approach aims to spread the benefits of fly ash based SCC as widely as possible and assists decision making at local, regional and international levels.

REFERENCES

1. OZAWA K, MAEKAWA K, OKAMURA H. Development of the High performance concrete, Proc JSI, 1989;11(1):699-704.

2. KHAYAT KH, HU C, MONTY H. Stability of self-consolidating concrete, advantages, and potential applications, First international RILEM symposium SCC. Eds. In: Wallevik O, NieLon I, Stockholm: RILEM Publications, 1999, p. 134–42.

3. ZHANG XIONG, HAN JIHONG. The effect of ultra-fine admixture on the rheological property of cement past, Cement and Concrete Research, Vol. 30,No.5, 2000,pp 827–30.

4. GEIKER METTE R, BRANDL MARI, THRANE LARS N, BAGER DIRCH H, OLAFUR WALLEVIK. The effect of measuring procedure on the apparent rheological properties of self-compacting concrete, Cement and Concrete Research, Vol. 32, No.1, 2002, pp 1791–5.

5. D'ALOIA SCHWARTZENTRUBER L, LEROY R, CORDIN J. Rheological behaviour of fresh cement pastes formulated from a Self Compacting Concrete (SCC), Cement and Concrete Research, Vol. 36, 2006, pp 1203–13.

6. SU N, HSU KC, CHAI HW. A simple mix design method for self-compacting concrete, Cement and Concrete Research, Vol. 31, No. 12, 2001, pp 1799–807.

7. NUNES S, FIGUEIRAS H, MILHEIRO OLIVEIRA P, COUTINHO JS, FIGUEIRAS J. A methodology to assess robustness of SCC mixtures, Cement and Concrete Research, Vol. 36, No. 12, 2006, pp 2115–22.

8. YAHIA, A., TANIMURA, M., SHIMBABUKURO, A., AND SHIMOYAMA Y. 'Effect of rheological parameter on self-compatibility of concrete containing various mineral admixtures', Proceeding of the First RILEM International symposium on Self-Compacting concrete, Stockholm, Eds. In: A.Skarendahl, O.Petersson, September 1999.

9. MARSH B. High-volume fly ash concrete. Concrete (London), Vol. 37, No.4, 2003, pp 54–5.

10. BILODEAU A, MALHOTRA VM. High-volume fly ash system: concrete solution for sustainable development. ACI Materials Journal, Vol. 97, No. 1, 2000, pp 41–8.

11. MALHOTRA VM. High-performance high-volume fly ash concrete. An environmentally friendly solution to the infrastructure needs of developing countries, Concrete International, Vol.24, No.7, 2002, pp 30–4.

12. SEAR LKA. 'Should you be using more pfa?' In 6th International Congress – Global Construction – Ultimate Concrete Opportunities, In Eds. Dhir RK, Harrison TA, Moray DN, 5–7 July 2005. University of Dundee: Thomas Telford Publishing, Thomas Telford Ltd., pp. 693–700.

13. ZHANG MH. Microstructure, crack propagation, and mechanical properties of cement pastes containing high volumes of fly ashes, Cement and Concrete Research, Vol. 25, No. 6, 1995, pp. 1165–78.

14. ATIS CD. High-volume fly ash concrete with high strength and low drying shrinkage, Journal of Materials in Civil Engineering, Vol. 15, No.2, 2003, pp 153–6.

15. BOUZOUBAA N, LACHEMI M. Self-compacting concrete incorporating high volumes of class F fly ash: preliminary results, Cement and Concrete Research, Vol. 31 No. 3, 2001, pp 413-20.

16. CHRISTENSEN BJ, ONG FS. The performance of high-volume fly ash self consolidating concrete (SCC), In: Editor Shan SP, USA: A Hanley Wood Publication, Special Publication, 2005, pp 139-44.

17. DIETZ J. Preliminary examinations for the production of self-compacting concrete using lignite fly ash, Materials Journal, Vol. 5, LACER 2000, pp 125–30.

18. LACHEMI M, HOSSAIN KMA, PATEL R, SHEHATA M, BOUZOUBAA N. Influence of paste/ mortar rheology on the flow characteristics of high-volume fly ash self consolidating concrete. Magazine of Concrete Research, Vol.59, No. 7, 2007, pp 517–28.

19. NEHDI ML, PARDHAN M, KOSHOWSKI S. Durability of self-consolidating concrete incorporating high-volume replacement composite cement, Cement and Concrete Research, Vol. 34, No.11, 2004, pp 2103–12.

20. XIE Y, LIU B, YIN J, ZHOU S. Optimum mix parameters of high-strength self compacting concrete with ultra pulverized fly ash, Cement Concrete Research, Vol. 32, No. 3, 2002, pp 477–80.

21. VIMALKUMAR, MUKESH MATHUR, SHASHANK SHEKHAR SINHA, SAGAR DHATRAK. 'Fly Ash: an Environment Savior', Fly Ash Utilization Programme (FAUP), 2005, TIFAC, DST, New Delhi.

22. IS: 12269-1987 Specification for Grade 53 Ordinary Portland Cement, Bureau of Indian Standards, New Delhi, India

23. IS: 383-1970 Specifications for Coarse and Fine aggregate from natural source for concrete, Bureau of Indian Standards, New Delhi, India.

24. IS: 9103-1979 Specifications for Admixtures for concrete, Bureau of Indian Standards, New Delhi, India.

25. IS: 3812(Part- I)-2003 Specifications for fly ash, Bureau of Indian Standards, New Delhi, India.

26. Standard Specification for Fly Ash and Raw or Calcined Natural Pozzolana for Use as Mineral Admixture in Portland Cement Concrete (ASTM C618-92a) Annual Book of ASTM Standards Vol.04.02, 1994.

27. EFNARC. Specifications and guidelines for self-compacting concrete, February 2002. Available from: www.efnarc.org.

28. BIBM, CEMBUREAU, ERMCO, EFCA, EFNARC. The European guidelines for self-compacting concrete specification, production and use, 2005.

29. BRITE-EURAM PROJECT NO. BE96-3801/Contract BRPR-CT96-0366, 1998

30. IS: 516-1959 Methods for test for strength of concrete, Bureau of Indian Standards", New Delhi, India.

31. Standard Test Method for Electrical Indication of Concrete's Ability to Resist Chloride Ion Penetration (ASTM C1202) Annual Book of ASTM Standards 1997, pp 639-643.

32. OUCHI M, NAKAMURA S, OSTERSON T, HELLBERG S, LWIN M. Applications of self compacting concrete in Japan. Europe and the United States, ISHPC, 2003, pp 1– 20.

33. WATTANALAMLERD C, OUCHI M. Flowability of fresh mortar in self-compacting concrete using fly ash. In: Editors Yu Z, Shi C, Khayat KH, Xie Y, Paris: RILEM Publication SARL, 2005, pp. 261–70.

34. PRECAST/PRESTRESSED CONCRETE INSTITUTE TR-6-03, Interim Guidelines for the use of Self-Consolidating concrete in Precast/Pre stressed Concrete Institute Member Plants Interim SCC Guidelines, FAST Team 2003, pp A1-30

35. MIAO LIU. Self-compating concrete with different levels of pulverized fuel ash, Construction and Build Materials, Vol. 24, 2010, pp 1245-1252.

36. SUKUMAR B, NAGAMANI K, SRINIVASA RR. Evaluation of strength at early ages of self-compacting concrete with high volume fly ash, Construction and Building Materials, Vol. 22, No. 7, 2008, pp 1394–401.

37. HOLSCHEMACHER K, KLUG Y. A database for the evaluation of hardened properties of SCC, Vol. 7, LACER 2002, pp 124–34.

38. DONALD BURDEN. The Durability of Concrete Containing High Levels of Fly Ash, Masters of Science in Engineering thesis, The University Of New Brunswick, PCA R&D Serial No. 2989, 2006, pp 1- 110.

39. RAGHAVAN K.P., SIVARAMA SARMA B. AND CHATTOPADHYAY D. Creep, Shrinkage and Chloride Permeability Properties of Self Consolidating Concrete, Conference Proc. First North American Conference on the Design and Use of Self Consolidating Concrete, November 12-13 2002, Center for Advanced Cement based Materials, pp. 341-348.

40. L. TANG, A. ANDALEN, J.O. JOHANSSON, S. HJELM. Chloride diffusivity of self-compacting concrete, In Eds: A °. Skarendahl, O¨. Petersson, Proc. 1st Int. RILEM Symposium on Self-Compacting Concrete, RILEM Publications s.a.r.l., France, 1999, pp. 187– 198.

Ammonia in PFA and Cementitious Products Manufacture

L K A Sear[1], J Guest[2]
1 – UK Quality Ash Association, UK
2 – Hanson Building Products, UK

In order to reduce NOx emissions, increase precipitator efficiency from coal fired power stations and to ensure compliance with the EU Large Combustion Plant Directive,ammonia will need to be injected in the furnace gases of many UK coal fired power stations. While ammonia does not have any detrimental effects on the performance of concrete, concerns have been expressed about the Health & Safety aspects of possible contamination of Pulverised Fuel Ash (PFA)/fly ash. Ammonia injection is used to convert NOx gases to nitrogen when the furnaces gases pass over Selective Catalytic Reduction (SCR) units. Ammonia may also be injected into the furnace gases to enhance the efficiency of electrostatic precipitators by increasing the ionising efficiency. Excess ammonia not converted within the SCR may thereby be found within the PFA. This ammonia will be released when used in concrete and aircrete block manufacture, due to the high pH of these products. However, this raises a number of issues such as the measurement of ammonia in PFA. With there being no recognised test method and the existence of a considerable number of techniques, what is an acceptable level of ammonia contamination and what are the possible short and long term effects on these products? This paper will review the issues associated with the use of ammonium injection, measurement of ammonia in PFA, the possible effects on concrete and aircrete block properties, experience from mainland Europe and its use in the UK. In addition it will look at the techniques for post processing PFA to remove ammonia.

Dr Lindon K A Sear, joined the newly formed UK Quality Ash Association in 1977 and has been working for the last 14 years promoting the interests of coal-fired power station operators as the UKQAA Technical Director. Lindon attends 20 different British and European Standard Committees and sub-committees and a number of research projects steering committees on behalf of the UKQAA.

Miss Jodie Guest, is Product Development Manager for Hanson Building Products, where she has worked for 9 years. Jodie provides product and process development expertise and technical support for a range of building products, particularly Thermalite autoclaved aerated blocks, which contain up to 80% PFA. Jodie also represents Hanson on the UKQAA technical commitee.

Keywords: Aircrete, Ammonia, Fly ash, Pulverised fuel ash, Selective catalytic reduction

INTRODUCTION

The ever demanding environmental legislation within the EU requires that coal fired power stations reduce further their emissions to levels previously thought impractical. Nitric and nitrogen oxides (NO_x) have been seen as being a particular problem being associated with acid rain, smog and human health issues. Though low NO_x burners have been fitted to all UK coal fired power stations over the last 10 years, EU regulations such as the Large Combustion Plant Directive (LCPD) [1] require further reductions in emissions, or the power stations will be forced to close down. These limits will only be achieved by the fitting of gas treatment units, such as selective catalytic reduction.

SELECTIVE CATALYTIC REDUCTION (SCR)

These low levels of NO_x emissions can only be achieved by the injection of ammonia into the furnace gas stream, which is then passed over a SCR unit. This converts any NO_x to ammonium compounds, oxygen and nitrogen. One additional beneficial effect of ammonia in the furnace gas stream is it aids the ionisation of the PFA particles within the electrostatic precipitators, thus improving their efficiency in removing the ash from the gas stream. This is generally used where low sulphur coals are routinely being burned, such as anthracite.

The formulas for the chemical conversion within the SCR are as follows:

$$4NO + 4NH_3 + O_2 = 4N_2 + 6H_2O \quad \text{and} \quad 6NO_2 + 8NH_3 = 7N_2 + 12H_2O$$

There are many places the SCR unit can be placed in the gas stream, between the furnace and the precips (high dust) being the most common, though after the precipitators (low dust/tail end) and even after FGD equipment (low temperature). As the SCR's work only at higher temperatures, 320 – 400°C, the low dust and low temperature positions require the gases to be re-heated, hence why they are least common. In theory the above reactions don't need a catalyst but the natural reaction rate makes SCR necessary in order to prevent high levels of ammonia being required.

Ammonium injection does have some drawbacks, in that it may not be fully converted to stable compounds within the SCR for one or more of the following reasons;

- if the levels of injected ammonia are higher than is necessary to convert the NO_x being produced into nitrogen and oxygen within the SCR, or;
- the gas temperatures passing over the SCR are too low reducing conversion efficiency, or;
- SCR efficiency is somehow impaired, e.g. gas flow issues, SCR needs cleaning or replacing, arsenic poisoning, calcium sulfate masking, etc [2].

The result is the excess ammonia is deposited on the fly ash particles as various ammonium salts, so called ammonia slip. This can also have detrimental effects elsewhere within the boiler, such as the formation of ammonium compounds on the various surfaces and lead to an ammonium chloride plume being emitted from the stack.

The efficiency of SCR is sensitive to load factor, for example a lower gas stream velocity leads to greater contact time with the SCR and more efficient removal. The ammonia input is controlled by monitoring the NO_x output. Urea can be used as an alternative to ammonia, which works exactly the same. Ammonia on demand plants are being used in some power stations.

The catalyst in an SCR will last ~2 to 3 years and to ensure efficiency, the gas streams must be flow modelled to prevent erosion problems and ensure efficient working of the system. They should be tuned to ensure the ammonia concentration is consistent across the whole area of the catalyst and cleaning devices may be used on the catalyst in order to reduce ammonia slip. Another issue with SCR is that SO_2 is turned into SO_3 in the catalyst (it doubles the output approximately) which can lead to a sulphuric acid plume, e.g. a brown tinge to the station exhaust plume, with enamel plates being used in colder parts of the furnace to prevent acid corrosion. Ammonia slip also affects the air heater efficiency. Ideally the plates should be cleaned twice a year using 400bar pressure – but this takes 1 week to do! Hence controlling ammonia slip to <2ppm (~equivalent <100ppm in the fly ash) is important not only for the fly ash but to maintain air heater efficiency.

An alternative is selective non-catalytic reduction (SNCR) which is less complex and less expensive but also less efficient than SCR. Again ammonia is injected into the furnace to convert NO_x to N, but it requires sufficient reaction time in the furnace, through mixing and a temperature of 760 to 1,093°C to be effective. As a result higher levels of NO_x and a greater risk of ammonia slip are to be expected.

Where ammonia is simply being used to improve precipitator efficiency, the injection levels can be considerably higher than would be used for SCR purposes rendering the ash useless in many applications unless treated in some manner.

It is believed that up to 80% of ammonia slip is adsorbed on the fly ash with the majority of the ammonia existing as ammonia salts, ammonium sulfate and bisulfate. In addition some ammonia will be chemically absorbed onto the residual carbon surfaces. There is a degree of ash particle size dependency and there is more ammonia slip found in finer ash particles.

The adsorption capacity of fly ash has been found to be a minimum of 350mg/kg (NH_3) at 350°C, i.e. at about the operating temperature of an SCR unit. At lower temperatures (<120°C) moisture will increase the adsorption of ammonia further. However, the adsorption capacities of fly ash differ with coal source and firing conditions and the differences are not clearly understood.

Immediately ammoniated fly ash is mixed with water and a strong alkali medium, such as in concrete or aircrete block manufacture, the ammonia is released as a gas. It is this reaction that the commercially available ammonia removal units rely on. If the ash is simply mixed with water only, then the gaseous ammonia may be released very slowly, depending on the inherent chemistry/alkalinity of the fly ash. With high concentrations in the fly ash detectable levels of ammonia may be released over a period of days [3]. The rate of emission will reduce relatively quickly. The ammonia released is directly proportional to the ammonia content of the fly ash and the quantity of fly ash and/or fly ash based aggregates being used.

Gaseous ammonia is not pleasant and at high concentrations can cause health problems, however, there is no evidence it causes any significant deleterious effect on cementitious based products, e.g. blocks and concrete – it is primarily a Health and Safety issue.

Health and Safety Issues

Ammonia is a colourless alkaline gas which is readily soluble in water. Its solubility in water can cauterise respiratory tracts resulting in death at concentrations of 5,000ppm by volume (ppmv). It is an inhalation hazard but NOT a skin absorption hazard, though it begins to affect skin moisture at 10,000 ppmv, at significantly higher levels than at which respiratory failure will occur.

The exposure limits [4] for TWA (Time Weighted Average) exposure is 25ppmv (18mg/m^3), STEL (Short Term Exposure Limit) of 35ppmv (25mg/m3) and IDLH (Immediate Danger to Life & Health) of 300ppmv. At concentrations of around 50ppmv and above, ammonia will cause irritation to the eyes and respiratory tract. Of course ammonia is the basis for smelling salts, used to revive the semi-conscious, but the exposures are relatively small, with the Odour Detection limit for humans being about 3ppmv. In relation to other odorous gasses, the human nose is particularly sensitive to ammonia.

Measurement of Ammonia in fly ash

As ammonia has potential to causes health problems and is a pungent material, the measurement of the ammonia content of fly ash would seem to be an important and critical test to carry out. It was therefore with some surprise when researching this area that numerous different methods of measuring ammonia exist, with varying repeatability of which no standardised method has ever been established as such.

There are many ways to detect ammonia. High concentrations are easy to detect because the gas has a very penetrating odour. To quantify the ammonia concentration or determine lower concentrations of ammonia, the human nose fails. However, on many occasions, the ammonia concentration has to be known, even at ultra-low concentrations of less than parts per billion in air by volume (ppbv).

Test methods

There are numerous methods of testing ammonia, ranging from direct wet chemistry through to Radar and Infra-Red Spectrometry. It is difficult to resolve which of these methods are best suited for use in the fly ash industry and which ones are sufficiently accurate as manufacturers claims seem to vary wildly. Rathbone & Majors [5] reviewed various techniques for fly ash, mortar and concrete in 2003.

Since then more potential methods have appeared as technology becomes ever more advanced. The following section attempts to summarise the various techniques that could be employed.

Measurement of Ammonia Gas

These methods are suitable for ambient monitoring of NH_3 gas, e.g. for health and safety monitoring. Alternatively, they could be used for measuring ammonia in ash, for example by heating or mixing the ash in alkaline solution and testing the gases evolved.

Optical absorption spectroscopy

Optical absorption spectroscopy is used in the most sensitive and selective ammonia detectors when looking for ambient ammonia. Systems with a detection limit of 1 ppb, that do a full measurement in 1 second, have been reported. Such systems basically use a laser and a spectrograph. They are very expensive and attempts at miniaturisation result in reduced sensitivity. They may use visible, ultra violet or infrared light to carry out the analysis, with infrared seeming to be the preferred.

Fourier transform infrared spectroscopy (FTIR) is a type of spectroscopy where all the light passing through the gas is analysed by creating interference patterns which are analysed mathematically using a computer and the Fourier Transform. This is opposed to only analysing the wavelength(s) required by using a monochromatic light source to filter out other frequencies. FTIR has basically taken over from other forms of spectroscopy.

Differential optical absorption spectroscopy (DOAS)

This is a method to determine concentrations of trace gases by measuring their specific narrow band absorption structures in the UV and visible spectral region.

Tuneable diode laser absorption spectroscopy (TDLAS)

By scanning across a very narrow bandwidth in the IR region where no cross interferences occur, the absorption of the IR source by the targeted gas is proportional to the target gas concentration.

Photo-acoustic IR spectrometer (PAS)

This technique is a variant on the above and uses the fact that gases will absorb differently IR radiation which can be detected by sensitive microphones within a relatively small devise. The accuracy of ppb or ~0.5ppm is claimed, however, as would be expected these devices are prone to extraneous noise affecting them.

Radar detection

For ammonia in vapours, radar detectors have been used as the Guided Radar signals are attenuated as the density of vapour increases. Radar detection is best for use in high pressure systems.

Gas sensors

Various types are in existence which all have benefits and drawbacks;

- **Metal Oxide Gas Sensors:** The ammonia sensors that have been manufactured in the largest quantities are without doubt metal-oxide gas sensors, mostly based on $C_{2-x}T_xO_3$+z for measuring ammonia. They work by absorbing and de-absorbing the gas by cycling the temperature of the sensor and the changes in electrical conductivity are measured to determine the ammonia concentration. They are accurate to ~5ppm.

- **Catalytic Bead Ammonia Sensors:** Also known as Wheatstone Bridge LEL sensors. Ammonia sensitive field effect transistors are called GASFET (Gallium Arsenide Field Effect Transistor or Gas Sensitive Field Effect Transistor – depending which site you read). They use a palladium gate material and have a detection limit of 1 ppm. They have also been combined with polymers, see below. However, they are also sensitive to methane gas and at high concentrations their life may be limited to minutes or hours.

- **Conducting polymer gas detectors:** A polymer is used which reacts with the ammonia. First, there is an irreversible reaction between ammonia and the polymer and, secondly, ammonia can reversibly reduce the oxidized form of polypyrrole. The reduction of the polymer film causes a change in the conductivity of the material, making it a suitable material for resistometric or amperometric ammonia detection. However, these polymers cannot be easily regenerated. The lower detection limit of gas sensors based polymers is about 1 ppm.

- **Photo Ionisation Potential (PID):** Ammonia has an ionisation potential of 10.18eV and therefore measured using a PID. They can measure up to 10,000 ppm. A PID is not specific to ammonia and will measure other compounds.

Measurement of Ammonia in Solution

Many proposed test methods are based on environmental tests for NH_3 in soil or water. The ammonia is brought into solution by washing or distillation, and then the quantity can be determined by a range of wet chemical or instrumental methods.

In aqueous solution, ammonia exists in equilibrium between the molecular and ionised forms, with the degree of dissociation depending on the temperature and pH:

$$NH_3 + H_2O = NH_4^+ + OH^-$$

Some methods can selectively test for one form or the other, whilst other methods detect both forms. The units that results are reported in also vary between test methods and laboratories. Results may be reported as ammonia (NH_3), ammonium ion concentration (NH_4^+) or ammoniacal nitrogen (NH_3-N). Ammoniacal nitrogen (also called ammonia nitrogen) is the sum of both molecular and ionised forms of ammonia, expressed in terms of the nitrogen content.

Wet chemistry methods

These types of methods are those usually preferred in European standards as they are describable and can be carried out generally using normal chemical apparatus. Nesslerisation would probably be considered the defacto method to use to calibrate/verify all the other methods of measuring ammonia. However, it has never been established by any validation testing to our knowledge. It is these chemical methods that also form the basis of the many test strips available, though with a considerable reduction in accuracy.

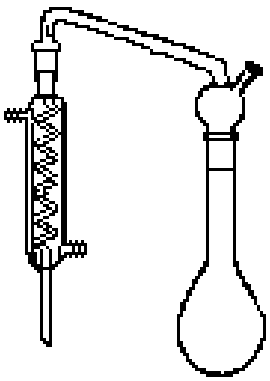

Figure 1 Kjeldahl digestion flask

Nesslerisation (EPA 350.2): This is a classic chemical distillation method for the determination of ammonia-nitrogen and is the preferred method of choice by the USA EPA. There are three possible analytical methods, colorimetric (0.05 to 1.0mg NH_3-N/l), titrimetric (1 to 25mg/l) and an electrode method (0.05 to 1400mg/l).

Basically the method requires adding sodium hydroxide to the material being tested, driving off the ammonia, this is then distilled off into boric acid and the ammonium salt in solution is measured. The conversion to ammonium salt is carried out in a Kjeldahl digestion flask as shown in Figure 1. The level of ammonia is measured colorimetrically using the Nessler reagent.

The Nessler reagent consists of potassium tetraiodomercurate(II) in a dilute alkaline solution, normally sodium hydroxide. This reagent is toxic and potentially fatal on skin contact, inhalation or by ingestion [6]. It should not be released into drains or similar as it’s very toxic to aquatic life.

Berthelot reagent (EPA 350.1): This method is the same as the Nesslerisation method, except Berthelot reagent is used colorimetrically. Berthelot reagent is where alkaline phenol and hypochlorite reacts with ammonia to form indophenol blue, the colour depth being measured using colorimetrically.

Other reagents: Various other reagents based on obtaining the blue indophenol blue, for example by using chloramine-T instead hypochlorite or by adding buffering solutions. Another alternative is sodium nitroprusside with hypochlorite and phenol, again producing the indophenol blue colouring.

Ammonium Ion Selective Electrodes (ISE)

These are used to measure ammonia content in solution, such as in the AiRRMonia system. The theory of operation is the ammonia electrode uses a hydrophobic gas-permeable membrane to separate the sample solution from the electrode filling solution. In any given sample the partial pressure of ammonia will be proportional to its concentration. Dissolved NH_3 is gaseous and passes through the hydrophobic membrane of the ammonia ISE. The pH change of the electrolyte solution on the other side of the membrane caused by the diffused gas is sensed by the inner body of the ammonia electrode—a pH electrode. The pH change is relative to the amount of dissolved NH_3 present and can be measured with a pH or Ion meter capable of mV readings or, better yet, direct ion concentration. These devices need to be calibrated and can be difficult to get right. They are reported as being accurate to 1ppm, though the electrodes only last ~1 year.

Spectrophotometric ammonia detection

This process is basically using a chemical that changes colour in contact with ammonia. These may be in the form of pH papers on strips (Figure 2) or more complex miniaturised measuring devices. Various reagents can be used such as fluorometric or indophenol blue, which are used to detect ammonia in fish tanks. They are generally claimed to be accurate to ~<6 to 50ppm and supplied for differing ranges of concentrations.

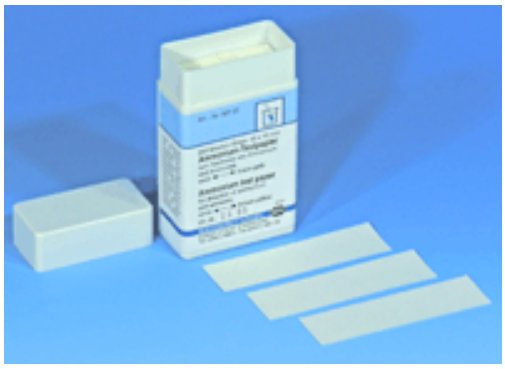

Figure 2 Typical ammonia strips

The reagents used are;

- **Nessler reagent:** This is the best known technique, as described above but the reagent is highly toxic.
- **Berthelot reaction:** Another common reagent and similar alternatives. This can be altered to suit the material being tested, as described above.

Ion Chromatography

This is used to detect ammonium ions, by passing the solution through a column that will absorb ions at different rates depending on their charge. The ions passing out of the column can be detected by a variety of techniques such as electrochemical or spectrophotometric methods. Ion chromatography has the advantage of being able to differentiate between different forms of nitrogen species in solution.

Standards for Ammonia Testing

There are no performance standards against which NH_3 monitors can be certified, and there are no adopted methodologies for the certification of continuous NH_3 monitoring. While comparisons have been made between these methods based on the literature, few comparisons of accuracy and repeatability/reproducibility have been carried out to our knowledge. ISO standards contain differing methods for differing materials, and even water quality methods allow a range of differing test procedures [7].

As part of a trial programme to assess the effects of ammonia on aircrete block manufacture, some comparisons in test methods were carried out. Table 1 shows the results of testing a range of ash samples using three different methods, all results are expressed as mg/kg NH_3. This clearly shows the differences associated with the different methods.

Table 1 Ammonia concentrations from differing test methods

		CONTROL ASH 1	CONTROL ASH 2	SCR ASH 1	SCR ASH 2	SCR ASH 3
RESULT	METHOD	mg/kg NH^3				
Water soluble ammonia	UV-visible light spectroscopy[1]	<1.21	<1.21	9.68	24.8	26.6
Water soluble ammonia	Ion chromatography[2]	0.98	0.19	26.3	33.3	30.3
Total ammonia	Steam distillation & titration[3]	5.07	2.25	32.8	40.5	41.2

Notes

1. An extract using a water solid ratio of 1:1 is taken from the sample; the ammonia is then reacted with hypochlorite ions by alkaline hydrolysis in the presence of sodium nitroprusside to form indophenol blue, as modified version of the Berthelot reaction. The absorbance of this compound is then measured spectro-photometrically with a UV/Vis spectrophotometer and related to the ammonia concentration in the sample by means of a calibration curve.
2. Ammonia extracted using 10:1 water:solid ratio to BS EN12457-2 [8] with the water extract being distilled with steam, see BS 6068-2 & ISO 5664, and then analysed by Ion Chromatography calibrated for ammonium ions in solution based on BS EN ISO 14911 [9].
3. Extracted after alkalization of the ash with sodium hydroxide and then using steam distillation and then analysed by Ion Chromatography as in 2 above.

Clearly there is a need for a defacto test method by which the other techniques could be assessed. The wet chemical Nessler method would seem to be the strongest candidate, but drawback is the toxicity of the Nessler reagent. The Berthelot reaction would seem to be the next serious contender but with a somewhat reduced accuracy.

The gas sensors and light spectroscopy methods claim good accuracies, but no independent evidence has been found that supports the various manufactures claims. The simpler methods involving indicator papers and similar all appear to suffer with a considerable reduction in sensitivity in comparison with wet chemistry techniques, although these could be useful as a rapid qualitative or semi-quantitative test.

Limiting values for ammonia in fly ash

Differing limits for ammonia in fly ash are quoted throughout the EU. For example, the NH_3 limit in the Netherlands the requirement is for the average <75mg/kg with an absolute limit of 100mg/kg, absolute limits of 200mg/kg in Germany and Denmark and 100mg/kg in Spain apply. In general terms selective catalytic reduction (SCR) efficiency is about ~88% in removing the ammonia and the resulting content in the PFA is limited typically ranges from 10 to 100ppm. NH_3 removal rate is 99.7% efficient. However, there still can be enough to cause problems in the fly ash. NH_4HSO_4 can form if the catalyst is run at too low a temperature. This accounts for about 20% of the NO_x removal.

It is clear from all sources that ammonia in fly ash of >200mg/kg as NH_3 will cause odour problems with in concrete production in confined spaces and preferably it should be limited to <100mg/kg, where no effects would normally be noticed. However, for power station operational reasons, ammonia slip should be minimised and kept to <2ppmv, which equates to ~100kg/kg in the fly ash.

Effects on the manufacture of aircrete blocks

Primarily the problems with using ash containing excessive levels of ammonia are identical whether it is normal concrete or aircrete blocks being produced. The issue is that when a caustic alkali material, such as lime or cement, comes into contact with ammoniated fly ash in the presence of water, ammonia is released as a gas. The classic reaction of lime with ammonium salts would be;

$$2NH_4Cl + CaO = 2NH_3 + CaCl_2 + H_2O$$

For the SO_3 formed in the SCR and combined with ammonia, when this combination comes into contact with an alkali, e.g. cement or lime, a similar reaction takes place;

$$2NH_4HSO_4 + Ca(OH)_2 = 2NH_3 + CaSO_4 + 2H_2O$$

It is clear that ammonium salts are chemically weakly bound and in the presence of a stronger alkali the ammonium salt is easily decomposed releasing it as a gas. It is these basic reactions that are employed in the commercial ammonia removal plants.

Aircrete blocks are produced by casting a slurry of fly ash, cement, quicklime, calcium sulphate and aluminium powder in to a large open-topped mould. The mix is left to rise and set in a warm chamber, before being cut into blocks and cured in an autoclave.

As aircrete block manufacture uses greater quantities of fly ash than traditional concrete manufacture, up to 80% of the material content may be fly ash, there is the potential for a significant release of ammonia in the manufacture of these blocks.

Hanson Building Products have undertaken a series of laboratory and factory trials using SCR fly ashes to manufacture Thermalite® aircrete blocks. The aim was to determine what effect such ash would have on the manufacturing process and products, and what an acceptable ammonia limit may be.

When small-scale aircrete mixes were prepared in the laboratory using SCR fly ash with a high ammonia level (~340 mg/kg NH_3), a peak reading of 80ppmv airborne NH_3 was detected above a freshly cast mix. This is well above the exposure limits and at a level likely to cause rapid irritation to the eyes and respiratory tract. This clearly shows the potential health and safety risk from ammonia contaminated raw materials.

A series of factory trials were conducted using SCR fly ash with a low ammonia level (~40 mg/kg NH_3), using around 100 tonnes of ash in total. This ash was not found to have any detrimental effects on the manufacturing process, for example the setting time of the product. Airborne ammonia levels were monitored around the manufacturing plant during the trials, but nothing significant was detected. Blocks made with this SCR fly ash passed all of the relevant product standard tests. The compressive strength, density, thermal conductivity and drying shrinkage results were comparable to those for blocks made using a non-SCR fly ash.

The laboratory results shown in Table 3 indicate that even high levels of ammonia in fly ash are removed from aircrete by the final stage of the manufacturing process, where the blocks are cured in a high-pressure steam autoclave. Therefore there would be no risk to end users of an aircrete product made using ammoniated fly ash.

Table 2 Ammonia found in aircrete

Control fly ash	1.2
Aircrete made with control fly ash	3.0
Non-SCR fly ash	342
Aircrete made with SCR fly ash	1.8

Therefore, the use of SCR fly ash for the manufacture of aircrete does not appear to have any detrimental effect on the finished product, or present any risk to the end user. However, it could cause a significant health and safety risk in the manufacturing plant unless carefully monitored and controlled. The limits of 100-200 mg/kg ammonia suggested in some EU countries could be unacceptable for the UK aircrete market. Further work is required to determine a maximum NH_3 limit, based on an appropriate and practicable test method.

Effects on the manufacture of concrete

The Danish Technological Institute produced a series of reports on the effects of ammoniated fly ash on concrete, emissions rate, etc. They concluded that fly ash with up to 200mg/kg as NH_3

will not cause concentrations of ammonia hazardous to health in well ventilated rooms and the ammonia will have evaporated to such an extent after a few months as to not cause indoor climate problems.

Rathbone and Robl [10] demonstrated that ammonia is lost from mortars at a higher rate for higher water-cement ratios, with a rapid rate of emission for the first 24 hours, followed by a much slower rate thereafter. This is similar to what was observed for aqueous solutions of ammonia. The total emissions were directly proportional to the initial concentrations and ventilating the samples increased the rate of ammonia from the mortars. They concluded that for concretes containing 20% fly ash of cement, ammonia levels in fly ash could be as high as 240 to 375 mg/kg as NH_3 for the full range of common concrete mixes. They also concluded that 15% of the ammonia was lost after 40 minutes of mixing the concrete. Approximately 50% of the ammonia in a concrete slab had dissipated after 1 month, but air concentrations in the air were below 1-2 ppm after several days of curing. The problems with ammoniated ash concrete are most likely to occur within 3 to 5 hours of placing, e.g. during the placement and finishing processes.

Removing ammonia from fly ash

Bittner et al [11] describes one possible method of removal of ammonia using the STI patented process. This uses lime and water as reactants to liberate the ammonia from the ash by mixing and thereafter drying. With the correct proportioning of lime and water the considerable majority of the ammonia is released within 2 to 3 minutes, making this process an effective solution to ammoniated ash.

The STI system operated by Lafarge, has proven particularly effective at the Aberthaw power station, where ammonia injection is used to improve precipitator efficiently only i.e. has no SCR unit. This results in relatively high NH_3 levels, often above 200mg/kg in the fly ash. After processing very low levels of NH_3 remain in the fly ash, making it suitable for use in cement and concrete manufacture.

Other methods of removing ammonia seem to rely on heat treatment such as fluidised bed to drive off the ammonia or adding compounds to mortar or concrete to supress the ammonia release. Heat treatment methods are usually associated with carbon burn out techniques [12] of fly ash and can remove ammonia down to <5ppm. To the knowledge of the authors no other ammonia specific systems than the STI ammonium removal system are in use world-wide.

CONCLUSIONS

In order to define acceptable limit values for ammonia in fly ash, it is clear that industry agreed test method is needed, thereby making compliance and sensible comparisons possible. At this stage it has proven impossible to obtain a consensus as to which method is considered the most appropriate for fly ash. Liaison throughout the European ash producer’s industry trade association and users of fly ash will continue until an appropriate method is agreed.

REFERENCES

1. DIRECTIVE 2001/80/EC OF THE EUROPEAN PARLIAMENT AND OF THE COUNCIL of 23 October 2001 on the limitation of emissions of certain pollutants into the air from large combustion plants, EU Commission 2001.

   United Kingdom National Emission Reduction Plan for implementation of the revised Large Combustion Plants Directive (2001/80/EC), February 2006, UPDATE No. 6, 14 July 2011. See http://www.defra.gov.uk/environment/quality/industrial/eu-international/lcpd/ for details.

2. BRENDEL G F, BONETTI JE, RATHBONE R F & FREY JNR. R N Investigation of ammonia adsorption of fly ash due to installation of selective catalytic reduction systems, DOE Award No. DE-FC26-98FT40028, GAI Consultants, Center for Applied Energy Research and Air/Compliance Consultants Inc. for US Dept. of Energy, November 2000.

3. BODKER J, Ammonia in fly ash – Instructions for concrete manufacturers, Danish Technological Institute, 27 September 2006.

   BODKER J, Ammonia in fly ash – Determination of the emission rate, Danish Technological Institute, 30 June 2006.

   BODKER J, Ammonia in fly ash – Determination of equilibrium, Danish Technological Institute, 21 April 2006.

4. Control of Substances Hazardous to Health Regulations, reference list EH40 table 1, Health and Safety Executive, UK, October 2007.

5. RATHBONE R F, MAJORS R K, Techniques for measuring ammonia in fly ash, mortar and concrete, International Ash Symposium, University of Kentucky, 2003.

6. See http://chemexper.otavachemicals.com/chemicals/supplier/cas/7783-33-7.html for Health and Safety information. Accessed 29 Nov 2011. CAS registry Number 7783-33-7

7. BS 6068-2.7:1984, ISO 5664-1984 Water quality. Physical, chemical and biochemical methods. Determination of ammonium: distillation and titration method

   BS 6068-2.10:1984, ISO 6778-1984 Water quality. Physical, chemical and biochemical methods. Determination of ammonium: potentiometric method

   BS 6068-2.11:1984, ISO 7150-1:1984 Water quality. Physical, chemical and biochemical methods. Determination of ammonium: manual spectrometric method

8. BS EN 12457-1:2002. Characterisation of waste. Leaching. Compliance test for leaching of granular waste materials and sludges. One stage batch test at a liquid to solid ratio of 2

l/kg for materials with high solid content and with particle size below 4 mm (without or with size reduction)

9. BS EN ISO 14911:1999. Water quality. Determination of dissolved Li$u+, Na.

10. RATHBONE R F, ROBL T L, Study of the Effects of Post-Combustion Ammonia Injection on Fly Ash Quality: Characterization of Ammonia Release from Concrete and Mortars Containing Fly Ash as a Pozzolanic Admixture, University of Kentucky Center for Applied Energy research, Kentucky, DE-FC26-00NT40908, 2003.

11. BITTNER J, GASIOROWSKI S & HRACH F, Removing ammonia from fly ash, International Ash Utilisation Symposium, Kentucky, 2001, See http://www.flyash.info

12. GIAMPA V W, Ammonia removal from fly ash by carbon burn-out, International Ash Utilisation Symposium, Kentucky, 2003, See http://www.flyash.info

Low-carbon Concrete Using Local Industrial By-products

G Shakhmenko, A Korjakins, P Kara, G Bumanis
Riga Technical University, Latvia

Micro fillers are important components in concrete mix in modern concrete technology. It improves workability of concrete mix, allows to achieve cement economy and to provide special performance of hardened concrete characteristics. The most effective micro fillers have pozzolanic action. Natural pozzolanic admixtures are not available in the most of countries (for example, in Latvia), but commercial products (such as silica fume) are quite expensive. Possibilities for use of local industrial by-products are discussed in this study. One revised direction is recycled bore silicate glass powder obtained from fluorescent lamp utilization. Based on practical experiments it is proved that roughly ground glass powder affects as passive micro-filler, but additionally ground one demonstrates properties of active micro filler which performs long-term hardening effect. Up to 20% of cement may be replaced by specially prepared glass material, providing the same mechanical strength of concrete and improving durability factor. Other revised direction is concrete sawing waste remaining in pre cast concrete plants. Sawing sludge paste contains 70% water and 30% dust concrete particles. Experimental results indicate that it is possible to find the optimum dosage of sludge, which ensures the required performance characteristics of concrete. The results of research help to select the most effective way to utilize concrete sawing waste, with due account of economical and ecological aspects. Questions of energetic effectiveness of concrete containing recycled micro fillers are discussed, taking into account cement partial replacing by waste material and environmental benefit based on waste rational application. It is proved that recycled micro fillers may be regarded as an instrument for reducing cement content and minimizing carbon dioxide emission.

G Shakhmenko is currently Docent at Professor Group of Building Materials and Products, Institute of Materials and Structures, Riga Technical University. The main fields of research are building materials and structures, reuse of industrial waste, concrete micro structural behaviour, concrete fracture, concrete technology.

A Korjakins is currently Professor and Chair of Professor Group of Building Materials and Products, Institute of Materials and Structures, Riga Technical University. The main fields of research are building materials and structures, ecological building materials, reuse of industrial waste.

P Kara is currently Scientific researcher at Professor Group of Building Materials and Products, Institute of Materials and Structures, Riga Technical University, Member of LVS STK 30 Eurocode Sub-Committee. The main fields of research are building materials and structures reuse of industrial wastes and by-products, concrete technology.

G Bumanid has recently obtained his Bachelor degree and prepares for Master studies at Professor Group of Building Materials and Products, Institute of Materials and Structures, Riga Technical University. The main fields of research are building materials and structures.

Keywords: Concrete sawing sludge, Ground glass, Micro filler

INTRODUCTION

Nowadays is important to provide material re-circulation, effectively using the non-renewable natural products and minimizing the emission of carbon dioxide into the atmosphere [1]. Micro fillers play a significant role in the creation of concrete structures, as they provide and improve the particle packing in the binder's matrix, the stability of concrete mixture and homogeneity. Micro filler research and composition optimization issue becomes particularly topical in the last 10 years, when the world started actively to use the concrete with advanced properties. Industrial development in any country is one of the most important indicators of economic growth. Consequently, industrially manufactured products and raw materials increase in volume also increases the production of waste and by-products volumes. World Wildlife Fund's experts estimated to prevent the continuation of global warming, so CO_2 emissions into the atmosphere must be reduced by 80% and other greenhouse gas emissions - by 50% in developed countries by 2050 [2]. Energy consumption after 2006 year data on cement production accounts for about two-thirds of the total amount of energy is spent on non-metallic mineral products. The Cement Technology Roadmap [3] declares that production of cement clinker is responsible for 7-8% of CO_2 emissions. While the CO_2 emission volume of cement industry consists of 0.65 to 0.92 tones of CO_2 per tone of cement [3]. Cement production efficiency improvement is one of the ways to reduce carbon dioxide emissions and save natural resources. Appropriate use of cement in construction is just as topical as the issue of the production process to increase efficiency, because it is directly linked not only with raw materials and fuel (natural resource) economy, but also the construction cost reduction. Replacement part of cement by effective micro fillers is the most effective solution. Different micro fillers commercially used in concrete mix production can be divided as passive (such as dolomite, limestone powder) and active having pozzolanic action. The most effective admixture with high pozzolanic action is silica fume. Silica fume is a by-product obtained from production of silicon and ferrosilicon alloys. Silica fume allows improve strength and durability of concrete, it makes concrete more resistant to corrosion and more impermeable. Commercially available silica fume is quite expensive material (the price of silica fume is about 500 EUR per ton, or about 6 times more expansive than cement). Investigations for reuse of industrial by-product in order to obtain effective cement replacing micro filler are important direction of research nowadays. Micro-filler replacement by waste products gives possibility to achieve effect of economy and to solve environmental protection task simultaneously.

The aim of this study is to propose alternative micro fillers obtained from local industrial by-products (sawing sludge and glass powder), investigate possibility to replace part of cement by these micro fillers and estimate ecological effectiveness of elaborated mixes.

USED MATERIALS AND METHODS

Local industrial by-products

The first used industrial by-product in this study is bore silicate glass powder (GP) obtained from fluorescent lamp utilization. Lamp recycling process includes lamp classification, glass separation, cleaning from harmful components and grinding. Preliminary results of chemical analysis indicate presence of following oxides: SiO_2 (74.3 %), B_2O_3 (16.6 %), Al_2O_3 (1.65 %), CaO (2.09 %), Na_2O (3.82%), K_2O (0.93 %), Fe_2O_3 (0.16 %). Glass powder has grain size smaller than 0,1..0,2 mm. In order to improve reactivity, glass powder additionally was ground in laboratory planetary ball mill machine (with rotation speed 300 min^{-1}).

The second used industrial by-product is sawing waste from precast concrete production plant which remains after sawing of hardened concrete elements using diamond tool in water environment (Figure 1).

Figure 1 Moulding and sawing process of precast reinforced concrete floor slabs

Investigated concrete sawing sludge (SL) contains 70% of water and 30% of dry small concrete particles. Concrete sawing sludge (SL) contains water suspension of hydrated cement paste particles and aggregate particles. The large part of dry sludge particle (95%) is smaller than 0.063 mm. Bulk density of sludge paste is 1240 kg/m^3 and dry particle density is 2650 kg/m^3. Chemical composition depends on concrete used (any harmful substances do not present). The average amount of produced waste is about 0.5-1% of the total amount of pre-cast concrete. Sludge utilization is a problem in the pre-cast concrete plant.

Traditional micro filler such as silica fume (SF) and dolomite powder (D) were also used as reference materials. Particle size distribution of observed disperse materials was determined by laser diffraction analysis method. Grading curves of used micro fillers are summarized in Figure 2. The finest material is silica fume (particle size below 1 μm). Dolomite powder and glass powder contain particles sizes in range 10 … 100 μm, slightly coarser than cement, while sawing sludge is slightly finer than cement (Figure 2). Additionally (60 minutes) ground glass powder (GGP) is characterized by wide range of particle size from 0.1 up to 10 μm and considerable amount of fine particles < 1 μm (almost 50%). Grading curve of GGP is situated between curves of cement and silica fume.

Normal type Portland cement (CEM I 42.5 N) was used as binding agent, natural washed gravel and sand in optimum proportion were used as aggregate.

Concrete components were batched and then mixed in the laboratory drum mixer during 4 minutes. Standard testing sample 100 ×100 × 100 mm cubes were produced. Two days later the samples were dismantled. Standard curing conditions (temperature 20±2^{o}C, RH > 95±5%) were provided during the process of concrete hardening. Compressive strength of hardened concrete samples was determined at the age of 7 and 28-days. Compression testing machine with the accuracy of ±1% was used, the rate of loading was 0.7 MPa/s (according to LVS EN 12390-3:2002 standard).

Workability for Ordinary Concrete was determined with Abrams Cone slump test method and for Self Compacting Concrete workability was determined by cone flow method. Water absorption value was computed taking into account the saturated surface-dry mass of sample.

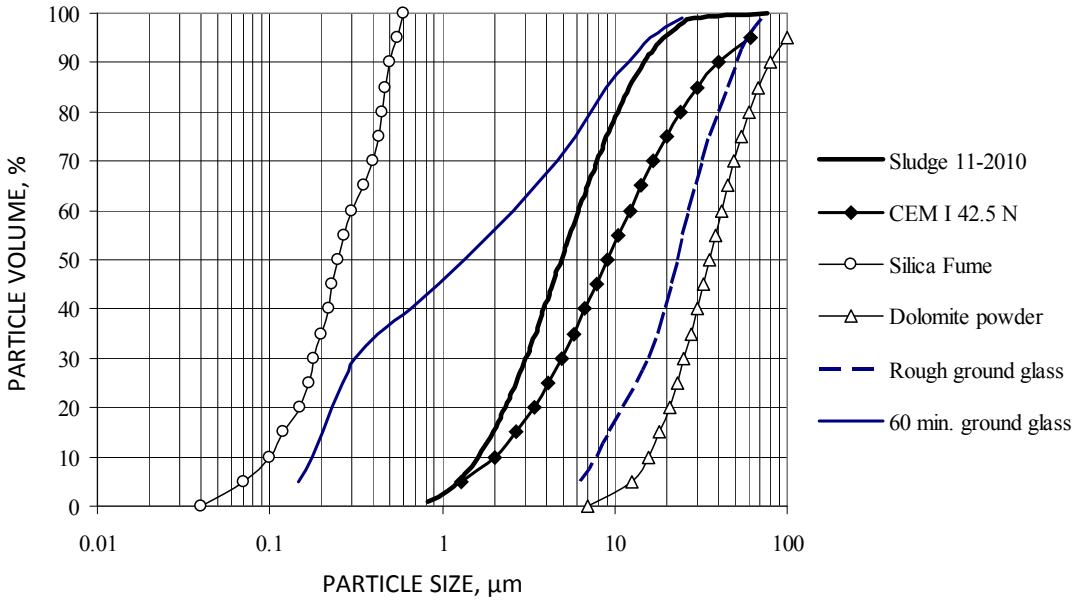

Figure 2 Grading curves of micro filler used in concrete mixes

EXPERIMENTAL RESULTS AND DISCUSSIONS

Comparing of concrete mixes with different micro fillers

The first experimental part provides preparation, testing and comparing of pilot concrete mixes containing different micro fillers with the same amount of 80 kg/m^3 of micro filler in each mix without any plasticizing agents. Sawing waste (SL) was added to the concrete mixes in the initial paste form. This way is more acceptable from the practical point of view because it allowed avoiding additional drying and grinding of the material prior to use. Mixes based on standard dolomite powder (D) and silica fume (SF) were selected as reference compositions. Mix composition (CC) containing additional corresponding amount of cement (+80 kg/m^3) as micro filler also was prepared. Water dosage was selected in order to provide approximately constant workability (cone slump in the range of 80 - 110 mm) of concrete mixtures. Experimental results showed that mix with concrete saw sludge suspension used as micro filler required more total water amount to achieve designed consistency. Mix with silica fume (SF) also required more water resulting higher value of water cement ratio (Tab. 1). Compressive strength results are summarized and compared in Figure 3. Mixes containing standard dolomite powder (D), sawing sludge (SL) and rough glass powder (GP) indicate the same results (28 day strength 30 – 34 MPa) with the least result 29.9 MPa for mix containing sludge. The best strength characteristics showed mixes based on silica fume (SF) and additionally ground glass powder (GGP). These two mixes demonstrate the highest gain of strength, comparing 7 and 28 days results (36 and 61 % accordingly). This effect can be explained by pozzolanic reactions between Portland cement and fine graded particles of pozzolans. Particle grading composition was improved, resulting dense packing of cement matrix.

Mix containing additional amount of cement as micro filler (CC), showed the highest 7 days result (38.3 MPa), and 28 days strength result only 43.5 MPa, the gain of strength was only 14%. This fact shows small effect of applying high amount of cement. The best way is to add micro fillers in optimal proportion taking into account its grading and pozzolanic activity. Initial test results showed that rough ground glass (GP) and sawing sludge (SL) act as passive micro filler, at the same time ground glass powder can be regarded as an active admixture having pozzolanic action.

Table 1 Concrete mix compositions containing different micro fillers

	CC	D	SF	GP	GGP	SL
Portland cement CEM I 42.5 N			330			
Gravel 2/12 mm			1000			
Sand 0.3/2.5 mm			650			
Sand 0/1 mm			120			
Additional cement	80					
Dolomite powder		80				
Silica Fume			80			
Glass powder GP				80		
Ground glass powder GGP (60 min)					80	
Sludge (dry)						80
Water	200	200	271	214	214	214
Water/ Cement ratio	0.61	0.61	0.82	0.65	0.65	0.75
Cone slump, mm	100	100	80	110	110	80
Cone slump class	S3	S3	S2	S3	S3	S2

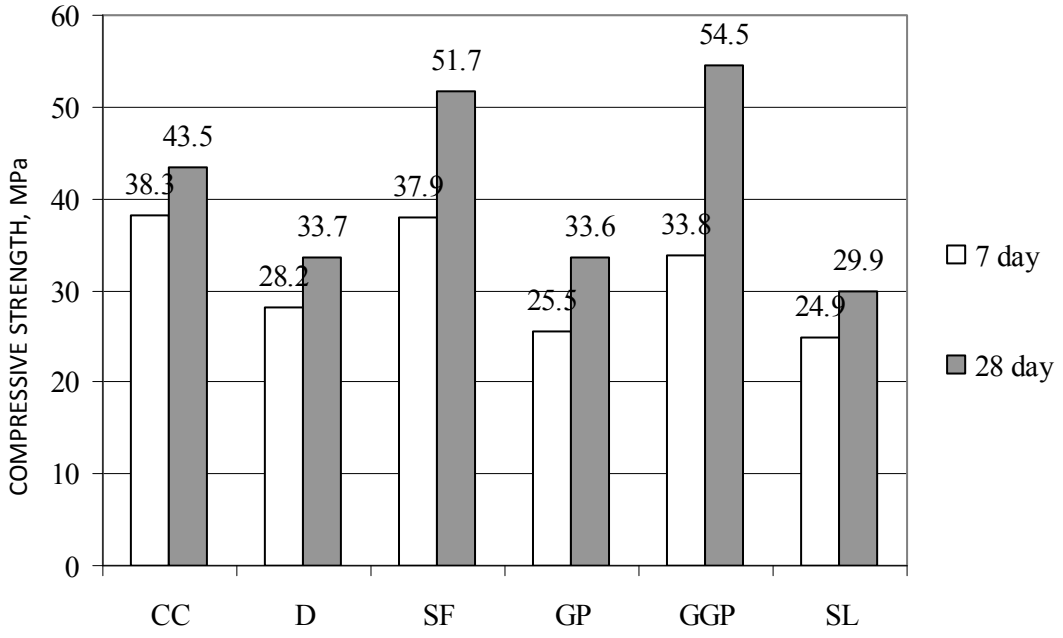

Figure 3 The results of compressive strength

Saw sludge as a filler by replacement of sand in small amount

The first series of experiments showed that sludge can be applied as micro filler, but high dosage of sludge (80 kg/m^3) cause decrease in strength due to high water absorption capacity. The second experimental part provided preparation of mixes with replacement of sand with sludge as micro filler in amount up to 5 %. The basic mix proportions and obtained results of compressive strength are summarized in Table 2. It was observed, that concrete mixes containing sawing sludge in moderate amount have more plastic and homogeneous consistency comparing to reference mix without sludge. Experimental results indicated that small dosage of sludge had not significant affect to the concrete strength and water absorption capacity of hardened concrete. The best compression strength result 41.5 MPa was obtained with replacing of 1.5 % sand by sludge (11 % strength gain compared to reference mix). The sludge positive effect in this case can be explained by improved grading composition of concrete mix.

Table 2 Concrete mix compositions and properties of hardened concrete

PERCENT OF SLUDGE:	0	1.5	2.5	5
Portland cement CEM I 42.5 N			350	
Gravel 10/20 mm			520	
Gravel 2/10 mm			520	
Sand 0/4 mm	730	719	712	694
Sludge (wet / calculated in dry)	-	36 / 10.8	61 / 18.3	122 / 36.6
Water (added + sludge water)	215	215	220	225
Water / cement ratio	0.61	0.61	0.63	0.64
Cone slump, mm	190	190	160	155
Characteristics of concrete mix:	Little segregation	Quite homo-geneous	Plastic and homogeneous	Plastic and homogeneous
Compressive strength, MPa:				
2 Days	20.8	21	19.9	20
7 Days	29.5	31.4	29.4	29
28 Days	37.3	41.5	36.0	36.7
Water absorption (28 day), %	2.05	2.05	2.08	2.15

Cement replacing by ground glass

The aim of third part of experiments was to clarify the effect of glass powder applied as partial replacing material of Portland cement. Two types of glass materials were used: rough bore silicate glass powder (GP) obtained from lamp recycling plant and additionally (60 min) ground glass powder (GGP). The mix compositions are summarized in Table 3. In the case of rough ground glass powder (GP) it was observed the trend of strength reduction in proportion to the quantity of replaced cement (Figure 4). The analysis of the 28 days compressive strength showed the strength reduction by 59 % in case of 50 % cement replacement and 26 % in case of 20 % replacement by weight. The most prospective results were obtained using additionally 60 minutes ground glass powder (GGP). Half of cement replaced by glass showed reduction of strength by 23 %, but 20 % replacement showed almost the same compressive strength as reference mix.

Analyzing the environmental impact of obtained concrete mix compositions it is important to calculate ecological and economical characteristics of materials [3]. One of the important characteristic of modern building material is energy consumption related to unit of material. Cement and fine grounded materials are the most energy demanding components in concrete mix, while fine and coarse have negligible impact comparing to cement. Energy consumption for cement production from different literature sources varies in range of 3 - 5 MJ/kg depending on technology, the value of 3.9 GJ/t (3.9 MJ/kg) was taken for the present study [4]. More difficult task was to estimate grinding energy for micro filler components. Actually, grinding energy largely depends on fineness of ground material. Additional increase in specific surface requires more energy consumption for grinding process. In accordance with [7] grinding energy of cement clinker is close to 0.14 MJ/kg. The fineness of cement particles is average 10 μm, rough ground glass powder (GP) has the similar value of fineness (particle average dimensions 10 – 20 μm in accordance to grading curve in Figure 1). The grinding energy of traditional micro fillers (dolomite, limestone) also may be assumed as 0.14 MJ/kg (value of 0.2 was accepted for future calculations).

Table 3 Cement replacement by ground glass powder (GGP): mix composition and environmental impact

		CEMENT, % REPLACED BY GLASS					
	Price, EUR/t	0	10	20	30	40	50
Portland cement CEM I 42.5 N	78	350	315	280	245	210	175
Gravel 10/20 mm	15			520			
Gravel 2/10 mm	15			490			
Sand 0/4 mm	9			730			
CO_2, kg/m^3		263	236	210	184	158	131
Rough glass powder (GP)	0	0	35	70	105	140	175
Water		200	200	200	200	200	200
Water-Cement ratio		0.57	0.63	0.71	0.82	0.95	1.14
Concrete density, kg/m^3		2334	2349	2331	2336	2324	2317
Concrete components price, EUR/m^3		49	46	44	41	38	35
Energy consumption, GJ/m^3		1.37	1.24	1.11	0.98	0.85	0.72
Energy consumption, MJ/MPa m^3		32.9	34.4	35.9	35.7	39.5	42.7
Additionally ground glass powder (GGP)	25	0	35	70	105	140	175
Water		200	200	200	200	200	200
Water-Cement ratio		0.57	0.63	0.71	0.82	0.95	1.14
Concrete density, kg/m^3		2355	2333	2337	2342	2313	2299
Concrete components price, EUR/m^3		49	47	45	43	42	40
Energy consumption, GJ/m^3		1.37	1.37	1.37	1.38	1.38	1.38
Energy consumption, MJ/MPa m^3		32.9	34.5	34.3	35.9	38.3	43.2

To achieve glass micro-filler with finer particle size distribution energy consumption increases considerably. For example, preparing the samples of 1 kg of glass powder was ground during 60 minutes in the laboratory planetary ball mill machine having electrical power of 1.5 kW, thereby actual energy consumption was 1.5 kWh/kg, or 5.4 MJ/kg. This value is 1.4 times more than thermal energy consumption for1 kg of cement clinker. It may be assumed that efficiency factor of large industrial mill should be higher due smaller relative loss of energy (value of 4.0 was accepted for future calculations). The information about grinding energy for rock material is not sufficient. One of the articles [9] presents the following data about grinding energy depending on final fineness of material: 100 μm requires 0.01 MJ/kg, 10 μm – 0.3 MJ/kg, but 1 μm requires 10 MJ/kg.

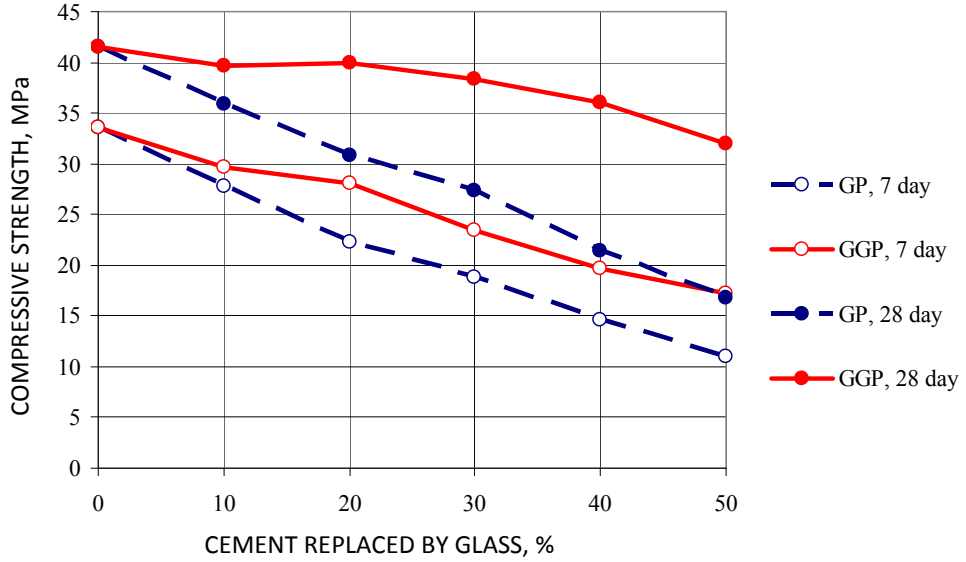

Figure 4 The results of compressive strength

These data corresponds to real laboratory value. It must be emphasized, that more fine grinding (< 100 nm) requires much more energy (up to 100 MJ/kg). This fact must be taken into account selecting technology of utilization of industrial waste.

Table 3 presents values of energy consumption E (GJ) related to 1 m^3 of concrete. The following formula was used for calculation:

$$E = C \cdot 3.9 + GP \cdot 0.2$$

where: C – Portland cement amount, kg/m^3;
3.9 – Thermal energy consumption per 1 kg of cement;
GP – rough glass powder content in 1 m^3;
0.2 – grinding energy of rough glass powder.

The mix containing additionally ground glass was calculated using this formula:

$$E = C \cdot 3.9 + GGP \cdot 4.0$$

where: GGP – additionally (60 min.) ground glass powder content in 1 m^3;
4.0 – grinding energy of 1 hour additionally ground glass powder.

When part of cement is replaced, energy consumption is reduced in the case of rough ground glass and energy consumption remains the same value in the case of additionally ground glass. Carbon dioxide direct emission decreasing proportionally to amount of replaced cement.

It is established that cement replacement is associated with strength decreasing, in this respect parameter of specific energy consumption related to 1 MPa of compressive strength and $1m^3$ of concrete is used. The corresponding parameter of specific carbon dioxide consumption also was calculated. It is found small increasing of specific energy consumption both in the case of rough ground as well as additionally ground glass powder. Specific carbon dioxide consumption increases in the case of rough ground glass and decrease in the case of additionally ground glass (Table 3).

Cement partial replacing by additionally ground glass is very environmentally beneficial. Comparing price factor for different concrete components, it can be concluded that mix containing 20% of GGP is the most effective economically (price is decreased by 8%), 28 days strength is the same as the reference mix and carbon dioxide direct emission is decreased by 20%.

Self-Compacting concrete mixes

Conception of Self compacting concrete was worked out in the 1990^{th} by professors H. Okamura and K. Ozava from Tokyo University [8]. The basic specific components of SCC concrete are superplaticizer and significant amount of micro filler powder as mix stabilizing agent. Traditional Self Compacting concrete contains considerable amount of paste (up to 35-45 % by volume) and corresponding high amount of cement (more than 380 kg) and micro-filler (>150 kg). The conception of ecologically friendly or "Green" Self Compacting concrete has been developed nowadays [10].

At present study SCC mixes are prepared with low cement and micro-filler to reduce the amount of energy consumption and CO_2 emission. The compromise between flowability and cement minimum paste content must be found when "Green" SCC composition is designed. Three SCC pilot mix compositions were made using micro fillers from dolomite, silica fume and additionally ground glass. Mix design and testing results are summarized in Table 4.

The mix containing silica fume and ground glass powder performed the best specific carbon dioxide consumption (3.5 and 3.9 kg / MPa m^3 correspondingly). The mix based on silica fume (SCC-SF) is the most expansive and mechanically strong. The mix containing ground glass powder performed the best relation between price and strength, the drawback of this composition is decreased in flowability (only 540 mm). It must be pointed that mix containing additionally ground glass have accelerated setting time, so it must be considered in future research.

Table 4 Mix compositions and properties of Self compacting concrete

MIX COMPOSITION	EUR:	SCC-D	SCC-SF	SCC-GGP
Portland cement I CEM 42.5 N	100	300	300	300
Gravel 2/16 mm	15	1035	1035	1035
Sand 0/4 mm	9	837	837	837
Super plasticizer	1.5	3	3	3
Water		185	185	185
Dolomite powder	25	30		
Silica fume	500		30	
Glass powder	25			30
Cone flow, mm		825	725	540
Compressive strength, MPa				
7 Day		39.1	53.8	43.8
28 Day		47.4	65.0	57.3
Price, EUR/m^3		53.8	68.1	53.8
CO_2, kg/m^3		225	225	225
CO_2, kg/MPa m^3		4.7	3.5	3.9

CONCLUSIONS

It is possible to use concrete sawing sludge as micro filler in concrete. Sludge improves mix workability. It is clarified that high dosage of sludge (80 kg/m^3 recalculated in dry) decrease compressive strength due to higher water cement ratio. Small dosage (up to 30 kg/m^3 as sand replacement) improves workability and does not effect significantly on compressive strength. There is tendency of concrete strength to decrease with partial replacement of cement with ground lamp bore silicate glass. But if to replace cement partially with extra ground glass (60 min) it is possible to achieve similar strength with cement economy up to 20-30%. Obtained results demonstrate pozzolanic activity of ground glass powder (GGP) and it could be considered to replace silica fume by GGP. Ecological effect is related to CO_2 emission and industrial waste reduction. When effectiveness of mix composition is estimated the parameters of specific energy consumption and specific carbon dioxide consumption related to 1 MPa of compressive strength are used. It allows evaluating produced mix compositions more objectively taking into account ecological impact and actual strength value. When micro filler reactivity by additional grinding up to 1 μm is evaluated it is important to take into account that high energy consumption is required, which can be higher than needed for cement production. However, additional grinding significantly improves the properties of concrete, cement savings are achieved.

ACKNOWLEDGEMENTS

The financial support of the ERAF project Nr. 2010/0286/2DP/2.1.1.1.0/10/APIA/VIAA/033 “High efficiency nanoconcretes” is acknowledged.

REFERENCES

1. DIRECTIVE ON AMBIENT AIR QUALITY AND CLEANER AIR FOR EUROPE 2008/50/EC.

2. CEMEX, CEMEX invests in preservation of the environment and decreases emissions, press release 17 June 2009 http://www.cemex.lv

3. CEMENT TECHNOLOGY ROADMAP, Carbon Emissions Reductions up to 2050, 2010.

4. HENDRIKS C,A, WORELL E, DE JAGER D, BLOK K AND RIEMER P, Emission reduction of greenhouse gases from the cement industry, 2004.

5. TAYLOR M, TAM C, GIELEN D, Energy Efficiency and CO2 Emissions from the Global Cement Industry, Energy Technology Policy Division International Energy Agency, 2006.

6. DONZA H, CABRERA O, IRASSAR E, F, High-strength concrete with different fine aggregate, Cement and Concrete Research, 32, 2002, p. 1755–1761

7. Technology, energy efficiency and environmental externalities in the cement industry, Asian Institute of Technology, 1997.

8. OKAMURA, H, OZAWA, K, Mix design for self-compacting concrete, Concrete library of JSCE, 25, 1995, p. 107 – 120.

9. КРАСНОВ А, А, Влияние на процесс сверхтонкого помола энергозагруженности мельницы РВМ, Новые технологии и инжиниринг, 2011, http://www.ntds.ru

10. HUSKEN, G, BROUWERS, H, Eco-SCC: From Theory to Practical Application, Proceedings of the 1st International Conference on Sustainable Construction Materials: Design, Performance and Application (SusCoM2010), 10-12 August 2010, Wuhan, p. 720-732.

Concrete Mixes Made with Limestone Powder, Metakaolin and Light Fill: The Indian Scenario

S P Singh, B Bhardwaj
Dr B R Ambedkar National Institute of Technology Jalandhar, India

The paper reports the influence of the composition of ordinary Portland Cement (PC) and locally available materials in India such as lime stone powder (LS), metakaolin (MK) and light fill (LF) binders on the compressive strength and water permeation characteristics of concrete. Concrete mixes covering two different total cement replacement levels i.e. 20 and 35% for concrete with various LS/MK and LS/LF proportions and cured in water up to three months have been investigated. To investigate the water permeation characteristics, tests such as sorptivity and initial surface absorption have been conducted on concrete specimens. The changes in compressive strength, sorptivity and initial surface absorption with curing age at different cement replacement levels are compared with those of control concrete.

Surinder Pal Singh, is a Professor of Civil Engineering at Dr B R Ambedkar National Institute of Technology Jalandhar, India. He obtained Ph.D. from University of Roorkee in 1999 and has worked as a Commonwealth Research Fellow at the Concrete Technology Unit of the University of Dundee from October 2006 to March 2007. His research interests are fatigue behaviour of concrete composites and recycling of materials in concrete.

Bavita Bhardwaj, is a post graduate student in the Department of Civil Engineering of Dr B R Ambedkar National Institute of Technology, Jalandhar, India.

Keywords: Compressive strength, Initial surface absorption, Sorptivity, Water permeation

INTRODUCTION

Concrete is the most extensively used construction material in the world and is only second to water as the most heavily consumed substance. This is largely due the abundance of raw materials for cement manufacture, low relative cost and versatility and adaptability of concrete in forming various structural shapes. The deterioration of concrete usually involves movement of water from the surrounding environment to the concrete which leads to physical and chemical reactions resulting is irreversible damage. Thus the permeation properties, rather than mechanical properties, are the important factors for concrete durability. In order to minimize the water permeation of concrete to reduce the ingress of water containing sulphates and chlorides, blends of materials have been employed. The use of materials such as fly ash (FA), lime stone powder (LS), metakaolin (MK) and light fill (LF) in concrete has received considerable interest in the recent years.

Metakaolin consists of clay calcined at high temperatures 650–800°C, resulting in a high fineness material with pozzolanic properties [1]. Metakaolin enhances the strength and durability of concrete through three primary actions which are the filler effect, the acceleration of ordinary Portland Cement (PC) hydration and the pozzolanic reaction with calcium hydroxide (CH). Wild et al. [2] found that the filler effect is immediate, the acceleration of PC hydration has its major impact within the first 24 hours and the maximum effect of pozzolanic reaction occurs between 7 and 14 days. Metakaolin accelerates hydration reaction of cement which results in high heat of hydration compared to conventional concrete [3]. It was found that the optimum replacement level of PC by MK to give maximum long term strength is about 20% by weight. A 10% replacement of cement with MK reduced the CH content in concrete by 70%, and a 20% replacement reduced it to almost zero after 28 days [4]. However, the amount of MK required for complete elimination of CH depends on a number of factors such as purity of MK, Portland cement composition, water/binder ratio and curing conditions [5]. Metakaolin concrete exhibited significantly lower chloride permeability, gas permeability and sorptivity [6]. Addition of MK has been found to decrease the average pore diameter of concrete paste and increase total pore volume due to which presence of MK is found greatly beneficial in reducing the water absorption by capillary action [7]. Increase in MK content in concrete improves chemical resistance [8] and has been found to lower the carbonation depth [9] and increases the sulphate resistance of concrete [10]. With regard to inhibition effect on chloride diffusion and sulphate attack, optimum MK content was found to be between 10% and 15% [11].

Increasing MK content from 5 to 15%, has been found to decrease the initial surface absorption, and there found to be a decrease in the sorptivity till 10% metakaolin replacement. Whereas higher MK replacements of 15% were not found helpful in improving inner core durability, even though it has been found helpful in improving surface durability characteristics [12]. Up to 15% replacement of MK in PC has been found to improve the mechanical properties of concrete. It was concluded that corrosion of carbon steel improved by the addition of MK up to 15% [13]. Metakaolin was found as a very efficient strength enhancing addition with showing increase in tensile strength, peak strain, bend strength, compressive strength and higher long term strength with small changes in tensile elastic modulus [14].

Limestone powder (LS) does not participate in the chemical reaction of cement. However, it acts as an accelerator during early cement hydration [15]. It acts as filler in concrete and accelerates the hydration reaction of alite and aluminate at early ages which lowers setting

time of concrete [16]. Its filling effect could make the paste matrix and the interfacial transition zone between matrix and aggregate denser, which would improve the performance of concrete [17]. Up to 20% replacement of cement by LS was found to improve the workability of SCC with 7 day and 28 day compressive strength was also found to improve. Further addition reduced the strength. All the hardened properties like cylinder compressive strength, split tensile strength, flexural strength and modulus of elasticity improved with the addition of LS [18]. Whereas LS more than 15% of cement weight had negative effect on the mechanical properties of concrete [19]. Increasing LS content beyond 15% of the cement content had adverse effect on many properties of concrete such as permeation and concrete durability performance and strength performance [20].

RESEARCH SIGNIFICANCE

To investigate the benefits of mineral admixtures as partial replacement of PC in concrete is a subject of interest to many researchers all over the world and mineral admixtures have been observed to improve the strength and durability properties of concrete. Economic and environmental advantages by reducing CO_2 emissions are well known. From the study of literature it is concluded that extensive literature is available on the strength and durability properties of metakaolin but literature on properties of LS is not sufficient.

However, both supplementary materials have certain shortfalls. Addition of LS to PC causes an increase of hydration at early ages including a high early strength, but it can reduce the later strength due to dilution effect. On the other hand, MK contributes to hydration after improving the strength at medium and later ages. Hence, ternary blended concrete (PC-LS-MK) with better performance could be produced.

A locally made industrial by-product light fill (LF) is also used in the present investigation. There was no investigation yet found in the literature on the use of LF as cement replacement in concrete. So, this could also be used in concrete to know its effect on the properties of concrete is proposed to be studied in this investigation.

EXPERIMENTAL PROGRAMME

The concrete mix proportions used for casting the test specimens is shown in Table 1. Ordinary Portland Cement (PC) 43 Grade, crushed stone coarse aggregates (maximum size 12.5 mm) and river sand was used as fine aggregates. The materials used conformed to relevant Indian Standard specifications.

Table 1 Mix proportions

WATER/CEMENT RATIO	SAND/CEMENT RATIO	COARSE AGGREGATE/CEMENT RATIO
0.45	1.52	1.88

Locally available materials such as LS, MK and LF were used as partial cement replacement. Some chemical and physical properties of the materials used are shown in Table 2.

Table 2 Chemical composition and some physical properties of PC, LS, MK and LF

COMPOSITION	PC	LS	MK	LF
Chemical compositions, %				
SiO_2	20.10	< 1	52.1	85-90
Al_2O_3	6.80	< 1	41.0	5-6
Fe_2O_3	4.30	< 1	4.32	
$CaCO_3$	-	85-97	-	-
CaO	61.30	48-54	0.39	-
MgO	2.60	-	-	-
SO_2	1.30	-	-	-
Loss of Ignition, %	1.20	42.50	< 1	5-6
Physical properties				
Specific gravity	3.15	2.18	2.60	-

Concrete mixes with binary and ternary blends of PC, LS, MK and LF were prepared with water/binder ratio as shown in Table 1. Different binder combinations are given in Table 3. Mixes were compared with control mix of 100% PC for strength development and permeation properties. Initial Surface Absorption Test (ISAT) as per BS 1881-208 (1996) [21] and Capillary Suction test as per ASTM standard C 1585-04 [22] were conducted to test permeation properties of concretes. Cube specimens of size 150 mm x 150 mm x 150 mm were used for ISAT, whereas cylinder specimens with 100mm diameter and 50mm depth sliced from 200 mm long cylinders were used for Capillary Suction Test and cubes of size 100 mm x 100 mm x 100 mm were used for obtaining compressive strength of the various mixes. Tests for ISAT and Capillary Suction were conducted at the age of 28, 60 and 90 days, whereas, compressive strengths at the age of 7, 28, 60 and 90 days were determined.

Specimens were tested on 200T capacity Universal Testing Machine (UTM) for compressive strength. The compressive strength values were determined from the average of three specimens. For water permeation tests, specimens were conditioned prior to testing. Specimens were kept in oven for drying at (105 ± 5)°C until constant mass was achieved, i.e. not more than 0.1% weight changed over after 24 hours drying period. After that the specimens were placed in the dessicator to cool down. The temperature in the cabinet was allowed to fall to within 2°C of that of the room. Specimens were kept in the cabinet until testing.

For ISAT, after conditioning specimens were tested at three different periods i.e. after 10, 30 and 60 min of contact with water on two opposite faces of the cube placed under the water head of 200mm. Specimens used for Capillary Suction test were coated with paraffin wax on circumferential surfaces and with tightly attached plastic sheet on the top surface to allow uniaxial (i.e. one dimensional) diffusion of water through the uncoated surface. From this test the initial rate of water absorption was obtained as the slope of the line that is the best fit to I plotted against the square root of time ($Sec^{1/2}$) using linear regression analysis of the plot. For the regression analysis, all the points from 1 minute to 6 hours were used, excluding points

for times after the plot shows a clear change of slope. A typical plot of cumulative water absorption against the square root of time for concrete mix with 65%PC+25%LS+10%MK cured at 28 days is shown in Figure-1. Similar plots were obtained for all concrete mixes at all curing ages. The results clearly show the influence of curing time on the sorptivity of the concrete. For all the specimens tested, this duration of time produced linear relationships which gave correlation coefficients greater than 0.993.

Table 3 Binder proportions in concrete mixes

MIX NO.	BINDER PROPORTIONS, %			
	PC	LS	MK	LF
Mix-1	100	-	-	-
Mix-2	80	20	-	-
Mix-3	80	15	5	-
Mix-4	80	10	10	-
Mix-5	80	15	-	5
Mix-6	80	10	-	10
Mix-7	65	35	-	-
Mix-8	65	30	5	-
Mix-9	65	25	10	-
Mix-10	65	30	-	5
Mix-11	65	25	-	10

RESULTS AND DISCUSSIONS

Compressive Strength Results

The variation in compressive strength of the concretes measured at 7, 28, 60 and 90 days is shown in Table 4. Moreover Figure 2 shows the normalized compressive strengths of the concretes with respect to the control concrete. It was observed that the control concrete had 7-, 28-, 60- and 90-day compressive strength of approximately 18.85, 31, 39.25 and 47.55 MPa, respectively. Replacing PC with LS within binary blends, however, reduced the compressive strengths as shown in Table 4.

Even though the use of LS decreased the compressive strength, the ternary use of LS and MK mostly improved the compressive strength of the concretes at all ages. The highest strengths of as high as 50.60 MPa were observed at 90 days and at 10% MK content. Mixes with 5% MK content mostly showed strengths comparable to control concrete mix at all ages. Whereas, at 10% MK content, the compressive strength is increased by 16% and 6% at 28 and 90 day curing age, respectively. At 35% PC replacement, 5% MK addition showed more

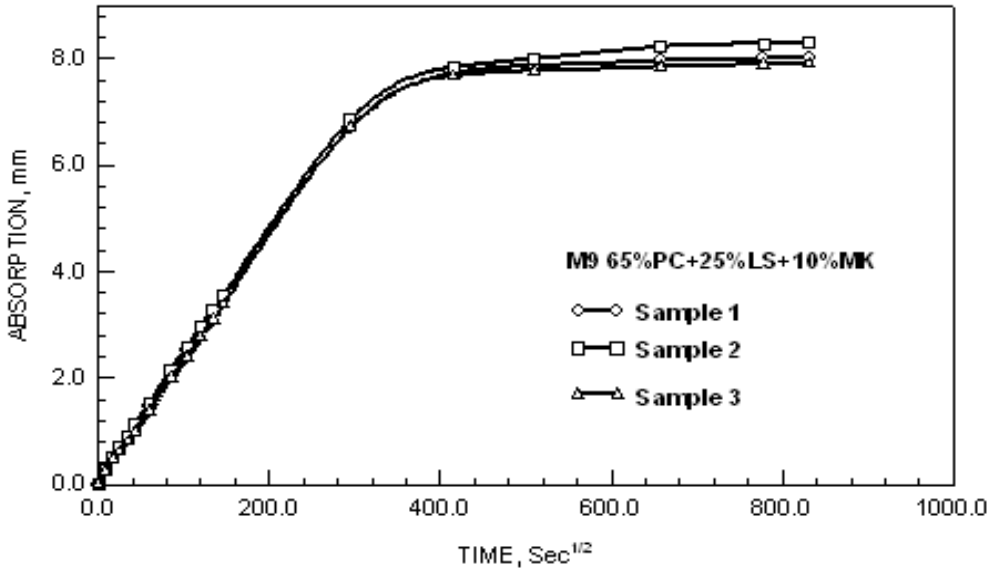

Figure 1 Cumulative absorption of water with test time for concrete mix with 65%PC+25%LS+10%MK at 28 days of curing

or less the same 7 day compressive strength, but at later ages of curing, the compressive strength was found to be 14%, 11% and 9% less than control concrete mix. Whereas, 10% MK addition showed marginal increase in compressive strength at later ages.

Similarly, the combined use of LS and LF shows a higher compressive strength than those containing binary blends of LS especially at 10% addition of LF. However, mixes with 10% LF showed strength comparable to control concrete mix.

It was observed that concretes with PC replacement by 20% performed better than concretes with 35% replacement. Replacement of PC by LS within binary blends decreased the compressive strength. Decrease in strength with increase in LS content may be as a result of clinker dilution effect. Even though the use of LS decreased the compressive strength, the ternary use of LS and MK improved the compressive strength of the concretes. Even the ternary use of LS and LF too showed good or comparable strength as compared to control concrete mix up to 60 day of curing age, but at 90 days, the compressive strength was found to be less than that of control concrete mix.

Initial Surface Absorption Results

This test provides data for assessing the uniaxial water penetration characteristics of a concrete surface. As mentioned, the absorption was measured at 3 different periods i.e. 10, 30 and 60 minutes. Table 5 shows the ISAT values (10 min) of different concrete mixes at different curing ages. Figure 3 also demonstrates the normalized ISAT values (10 min) of the concretes with respect to the control concrete mix at different curing ages. As shown in Table 5 and Figure 3, the absorption values varied with the mixes and decreased with increase in period and curing age.

Table 4 Compressive strength results of all mixes at different curing ages

MIX NO.	DESCRIPTION	COMPRESSIVE STRENGTH, MPa			
		7D	28D	60D	90D
1	100%PC (Control Mix)	18.85	31.00	39.25	47.55
2	80% PC+20% LS	20.25	26.95	32.70	42.40
3	80% PC +15% LS+ 5% MK	22.60	33.15	43.65	48.25
4	80% PC+10% LS+10% MK	24.85	35.95	45.35	50.60
5	80% PC+15% LS+ 5% LF	21.85	34.60	40.80	41.80
6	80% PC+10% LS+10% LF	23.95	35.75	44.10	45.20
7	65% PC+35% LS	18.95	23.25	32.30	41.35
8	65% PC+30% LS+5% MK	19.20	26.60	35.00	43.40
9	65% PC+25% LS+10% MK	21.10	31.80	41.40	48.80
10	65% PC+30% LS+5% LF	22.40	29.40	38.65	43.35
11	65% PC+25% LS+10% LF	23.60	30.75	40.65	46.55

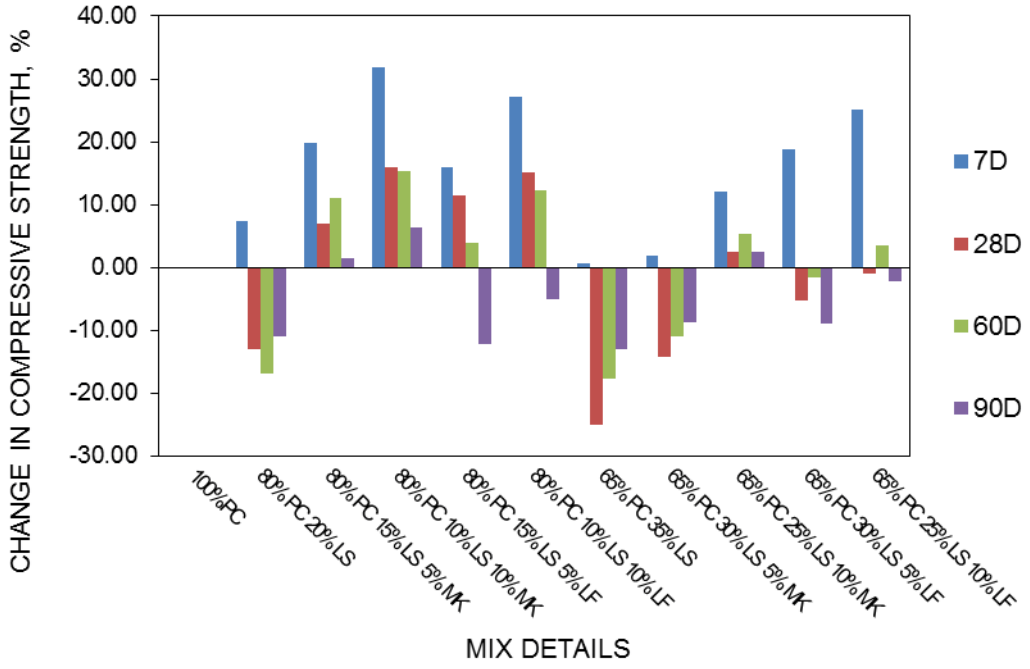

Figure 2 Normalized compressive strengths of concrete mixes w.r.t. control mix at 7 day curing age

Table 5 Initial surface absorption (10 min) values of mixes at different curing ages

MIX NO.	DESCRIPTION	INITIAL SURFACE ABSORPTION, ml/(m^2.sec)		
		28D	60D	90D
		10 min	10 min	10 min
1	100%PC (Control Mix)	0.641	0.260	0.114
2	80% PC+20% LS	0.616	0.406	0.398
3	80% PC +15% LS+ 5% MK	0.622	0.460	0.343
4	80% PC+10% LS+10% MK	0.494	0.443	0.315
5	80% PC+15% LS+ 5% LF	0.546	0.405	0.141
6	80% PC+10% LS+10% LF	0.462	0.259	0.102
7	65% PC+35% LS	0.627	0.612	0.578
8	65% PC+30% LS+5% MK	0.690	0.560	0.380
9	65% PC+25% LS+10% MK	0.597	0.555	0.360
10	65% PC+30% LS+5% LF	0.606	0.464	0.375
11	65% PC+25% LS+10% LF	0.533	0.444	0.273

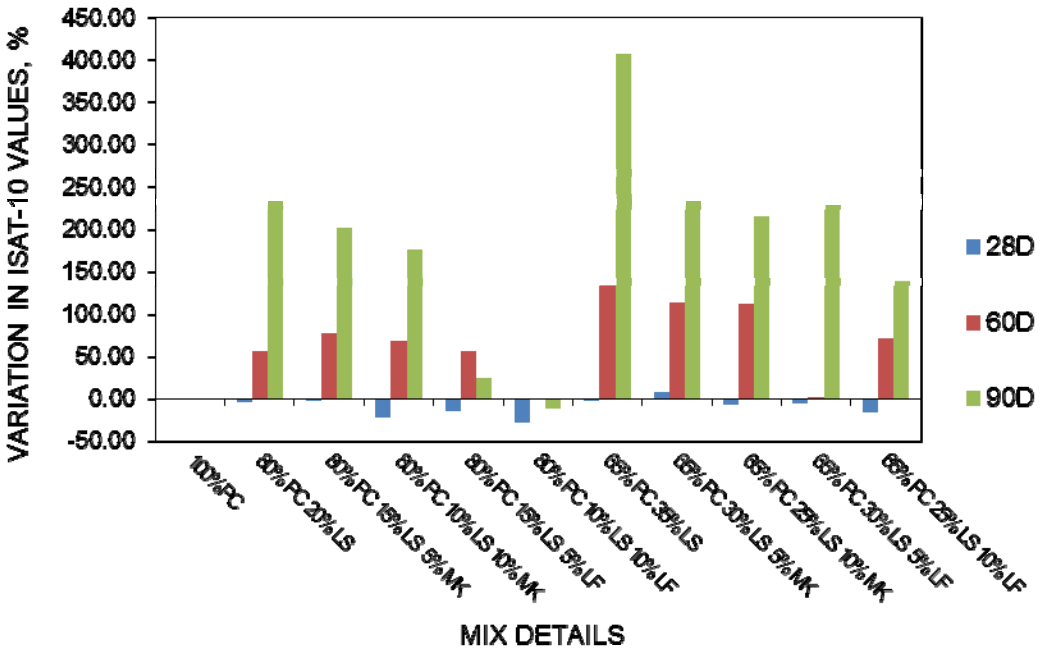

Figure 3 Normalized ISAT-10 values of concrete mixes w.r.t. control mix at different curing ages

The lowest values of ISAT-10 i.e. 0.462, 0.259 and 0.102 ml/(m^2.Sec) at curing period of 28, 60 and 90 days are observed for a concrete mix containing 80%PC+10%LS+10%LF, whereas, the highest value of ISAT-10 is observed as 0.690 ml/(m^2.Sec) at 28 days of curing for a concrete mix containing 65%PC+30%LS+5%MK. At 60 and 90 days of curing, the highest values of ISAT-10 are recorded as 0.612 and 0.578 ml/(m^2.Sec), respectively for concrete mix containing 65%PC+35%LS. Further, the ISAT-10 values for control mix i.e. 100%PC, are 0.641, 0.260 and 0.114 ml/(m^2.Sec) at 28, 60 and 90 days of curing, respectively.

Concrete mixes with 20% PC replacement showed lower absorption values than concrete mixes with 35% PC replacement. With increase in curing age, the effect of LS on absorption was noticeable. At 60 days of curing, the absorption value of mix with 20% and 35% LS were 56% and 135% more than control concrete mix, but at 90 days of curing it was found about 233% and 407% more than control concrete mix, respectively. Similarly, within ternary blends, the mixes with 20% LS showed lower absorption values than mixes with 35% LS. Further, concrete mixes with LF in ternary blends showed lower absorption values than mixes with MK. The use of LF appeared to be the most effective in reduction of water absorption, especially as the effect was increased with increasing LF content.

Capillary Suction Results

Uptake of water by unsaturated, hardened concrete may be characterised by the sorptivity. Table 6 shows the variation in average initial rate of absorption (IRA) values i.e. sorptivity of different concrete mixes at different curing ages, whereas, Fig.-4 shows normalized variation in average IRA values with curing age w.r.t. control mix. The rate of absorption was found to decrease with the curing age. It was observed that concrete mix with 80%PC+10%LS+10%LF showed lowest IRA value followed by mix with 80%PC+10%LS+10% MK, whereas mix with 65%PC+35%LS showed highest IRA values than all mixes at all curing ages. The lowest values of IRA i.e. 0.0168, 0.0156 and 0.0154 mm/($Sec^{1/2}$) at curing period of 28, 60 and 90 days respectively are observed for a concrete mix containing 80%PC+10%LS+10%LF, whereas, the highest values of IRA are observed as 0.0270, 0.0260 and 0.0255 mm/($Sec^{1/2}$) at 28, 60 and 90 days of curing respectively for a concrete mix containing 65%PC+35%LS. Further, the IRA values for control mix i.e. 100%PC, are 0.0199 mm/($Sec^{1/2}$) at 28, 60 and 90 days of curing.

It was found that replacing PC with LS within binary blends increased the rate of absorption by concretes. MK addition, within the ternary blends, decreased the IRA values of different concrete mixes. The mixes with 10%MK replacement showed lower IRA values. At 90 days curing, the mix with 80%PC+10%LS+10%MK showed IRA about 20% less than control concrete mix. Whereas, in all MK mixes with 35%PC replacement, IRA was found to be more than that of control mix. Concrete mixes with LF showed lowest IRA values. It was observed that LF replacement as ternary blend decreased the average IRA value of the mixes. At 20% PC replacement level, mix with 10% LF addition showed IRA value 23% less than control mix at 90 days of curing. Whereas, at 35% PC replacement level, the decrease in IRA of mix with 10% LF was found to be 14% less than control mix at curing age of 90 days.

In general, replacement of LS as binary blend increased the average IRA value than control mix, whereas, LS with MK and LF as ternary blends have been found to lower the values of IRA.

Table 6 Variation in initial rate of absorption values of different mixes

MIX NO.	DESCRIPTION	AVERAGE IRA, mm/sec$^{1/2}$		
		28D	60D	90D
1	100%PC (Control Mix)	0.0199	0.0199	0.0199
2	80% PC+20% LS	0.0227	0.0226	0.0224
3	80% PC +15% LS+ 5% MK	0.0197	0.0193	0.0192
4	80% PC+10% LS+10% MK	0.0170	0.0163	0.0160
5	80% PC+15% LS+ 5% LF	0.0189	0.0182	0.0179
6	80% PC+10% LS+10% LF	0.0168	0.0156	0.0154
7	65% PC+35% LS	0.0270	0.0260	0.0255
8	65% PC+30% LS+5% MK	0.0242	0.0241	0.0240
9	65% PC+25% LS+10% MK	0.0234	0.0234	0.0234
10	65% PC+30% LS+5% LF	0.0223	0.0188	0.0187
11	65% PC+25% LS+10% LF	0.0188	0.0175	0.0174

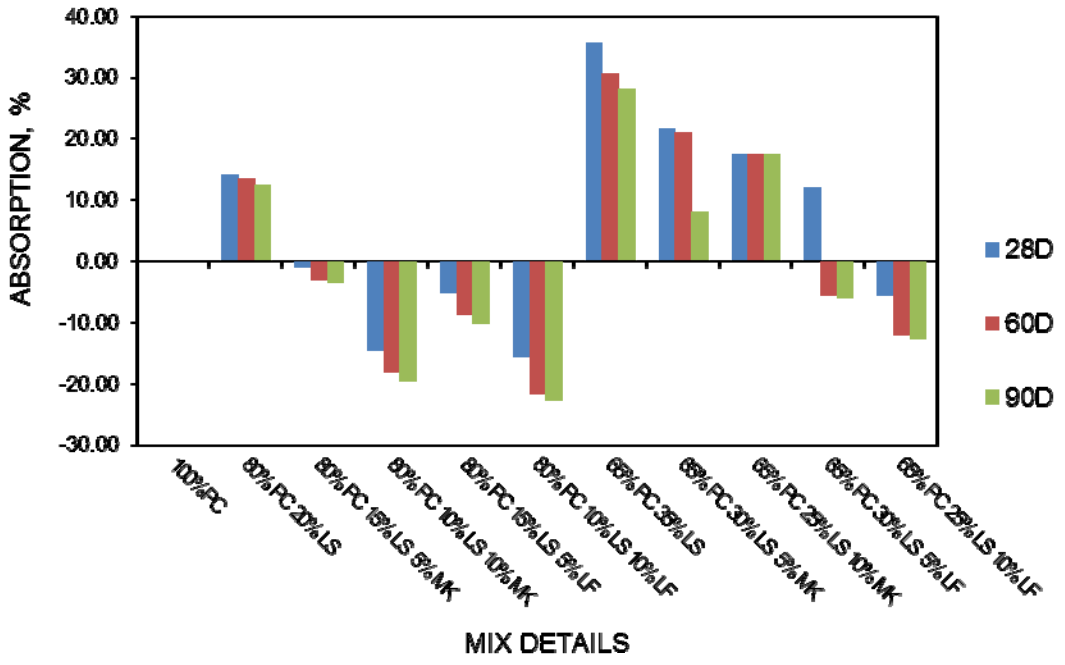

Figure 4 Normalized variation in average IRA values of different concrete mixes

CONCLUSIONS

It has been showed that replacing PC with LS partially within the binary blends, showed comparable strengths after 7-days of curing, however, the compressive strength reduced at further ages of curing, this may be due to dilution effect. Addition of MK within ternary blends increased the compressive strength with significant increase in 7-day strength. The addition of 10% MK showed better compressive strength than 5% MK. Mix with 80%PC+10%LS+10%MK gave the maximum compressive strength than all concrete mixes at all ages of curing. Light fill addition within ternary blends showed good initial strength but with increase in age and LS content, the strength was decreased. The addition of 10% LF showed better compressive strength than 5% LF. ISAT-10 values increased with increase in LS content. While it showed comparable results at 28-day of curing, but at later ages, there was increase in water absorption. Addition of MK within ternary blends, lowered the initial surface absorption at all ages but these mixes showed more absorption than control mix. Light fill addition within ternary blends decreased the initial surface absorption. 10% LF addition showed lower ISAT-10 values than 5% LF. Concrete mix with 80%PC+10%LS+10%LF showed the lowest initial surface absorption as 11% less than control concrete mix at 90 days of curing. Sorptivity of concrete increased with increase in LS content. The IRA values decreased with MK addition and it decreased with increase in curing period. The addition of LF reduced the IRA value and further decrease was observed with increase in curing age. The mix 80%PC+10%LS+10%LF showed the lowest IRA values followed by mix 80%PC+10%LS+10%MK. From the results, it can be concluded that concrete mix containing 80%PC+10%LS+10%LF can be adjudged as the most appropriate concrete mix for compressive strength, initial surface absorption and capillary suction taken together.

REFERENCES

1. JEAN, P. Metakaolin and calcined clays – guest editorial. Cement and Concrete Composites.Vol. 23(6), 2001.

2. WILD, S, KHATIB, J M, JONES, A. Relative strength, pozzolanic activity and cement hydration in superplasticized metakaolin concrete. Cement and Concrete Research. Vol. 10, 26 (10), 1996. pp 1537-1544.

3. FRIASA, M, SÁNCHEZ, M I, DE ROJASA, CABRERA, J. The effect that the pozzolanic reaction of metakaolin has on the heat evolution in metakaolin-cement mortars. Cement and Concrete Research. Vol. 30(2), 2000. pp 209–216.

4. KOSTUCH JA, WALTER GV, JONES T R. High performance concretes containing metakaolin – A review. In: Proceedings of the International Conference – Concrete 2000, Dundee. Vol. 2, 2000. pp. 1799–811.

5. ORIEL M, PERA J. Pozzolanic activity of metakaolin under microwave treatment. Cem Concr Res Vol. 25(2), 1995. pp 265–70.

6. BADOGIANNIS, E, TSIVILIS, S. Exploitation of poor Greek kaolins: Durability of metakaolin concrete. Cement and Concrete Composites. Vol. 31, 2009. pp 128-133.

7. KHATIB, J M, CLAY, R M. Absorption characteristics of metakaolin concrete. Cement and Concrete Research. Vol. 34 (1), 2004. pp 19–29.

8. ROY, D M, ARJUNAN, P, SILSBEE, M R. Effect of silica fume, metakaolin, and low-calcium fly ash on chemical resistance of concrete. Cement and Concrete Research. 31, 2001. pp 1809–1813.

9. BAI, J, WILD, S, SABIR, B B. Sorptivity and strength of air-cured and water-cured PC–PFA–MK concrete and the influence of binder composition on carbonation depth. Cement and Concrete Research. Vol. 32, 2002. pp 1813–1821.

10. NAMBIL, M, AL-AKHRAS. Durability of metakaolin concrete to sulfate attack. Cement and Concrete Research. Vol. 36 (9), 2006. pp 1727–1734.

11. COURARD, L, DARIMONT, A, SCHOUTERDEN, M, FERAUCHE, F, WILLEM, X, DEGEIMBRE, R. Durability of mortars modified with metakaolin. Cement and Concrete Research. Vol. 33, 2003. pp 1473–1479

12. SIDDIQUE, R, KAUR, A. Effect of metakaolin on the near surface characteristics of concrete. Materials and Structures, Vol. 44, 2011. pp 77–88.

13. PARANDE, A K, BABU, B R, KARTHIK, M A, D KUMAAR K K, PALANISWAMY N. Study on strength and corrosion performance for steel embedded in metakaolin blended concrete mortar. Construction and Building Materials. Vol. 22, 2008. pp 127–134.

14. QIAN, X, LI, Z. The relationships between stress and strain for high-performance concrete with metakaolin. Cement and Concrete Research. Vol. 31, 2001. pp 1607–1611.

15. YE, G, LIU, X, DE SCHUTTER, G, POPPE, A M, TAERWE, L. Influence of limestone powder used as filler in SCC on hydration and microstructure of cement pastes. Cement and Concrete Composites. Vol. 29,2007. pp 94–102.

16. MOON, H Y, JUNG, H S, KIM, J P. Diffusion of Chloride Ions in Limestone Powder Concrete. Journal of the Korea Concrete Institute. Vol. 16 (6), 2004. pp 859-865.

17. SHUHUA, L, PEIYU, Y. Effect of limestone powder on microstructure of concrete. Journal of Wuhan University of Technology- Material Science Edition. Vol. 25(2), 2010. pp 328-331.

18. SURABHI, C S, SOMAN, M, SYAM PRAKASH V. Influence of limestone powder on properties of self-compacting concrete. 10th National Conference on Technological Trends (NCTT09), November, 2009. pp 6-7.

19. AHMED, A H H, ABDURRAHMAN, R B, MOHAMMED, Z A. Influence of Limestone Powder as Partial Replacement of Cement on Concrete and the Effect of High Temperature on It. http://alrafidain.engineering-coll-mosul.com/files/2010/no5/E/A-4-3-2010.pdf ,2009

20. DHIR, R K, LIMBACHIYA, M C, MCCARTHY, M J, CHAIPANICH, A. Evaluation of Portland limestone cements for use in concrete construction. Materials and Structures. Vol. 40, 2007. pp 459–473.

21. BS 1881-208. Recommendations for the determination of the initial surface absorption of concrete. 1996

22. ASTM C 1585. Standard test method for measurement of rate of absorption of water by hydraulic-cement concretes. 2004

Properties and Performance of Alkali Activated Fly Ash and Hydrated Lime Concrete

K Abora[1], K A Paine[1], K Quillin[2], A M Dunster[2]
1 – University of Bath, UK
2 – Building Research Establishment, UK

There is still limited knowledge on the properties and performance of concrete produced using alkali activated technology. Most research has been based on either alkali activation of fly ash or ground granulated blastfurnace slag (GGBS). However, an extensive review and experimental trials has identified that the production of an alkali activated concrete with a combination of fly ash and GGBS provides further advantages in terms of setting and hardening at ambient temperature and 28 days concrete cube strength of 30 N/mm^2 can be achieved. The long-term viability of alkali activated concrete has, however been questioned due to possible limited availability of certain raw materials. This research was undertaken to investigate a promising alternative combination using fly ash and hydrated lime and assesses the impact of this formulation on strength, consistence and embodied CO_2 when compared to a combination of fly ash and ggbs. The experimental results obtained demonstrate that 5% of hydrated lime by mass of total binder could be substituted for 10% of GGBS without adversely affecting the consistence and strength of the concrete. However, it was identified that at higher hydrated lime to fly ash ratios (>5%), consistence reduced and there was also a risk of flash setting. Furthermore the results indicated that although the amount of hydrated lime used with fly ash was less than the quantity of GGBS required to give equivalent strength performance of 35 N/mm^2 at 28 days, the climate change of the concrete (kg CO_2 eq) was 8% higher with the concrete, made with hydrated lime.

Kofi Abora is a PhD student at the BRE CICM, University of Bath. His current research is on alkali activated systems with the focus on performance and durability especially the effect of alkali silica reaction on alkali activated concrete.

Kevin Paine is a Senior Lecturer in civil engineering at the BRE CICM at the University of Bath. He carries out research on low carbon and sustainable forms of concrete construction, with current focus on geopolymers, nanoparticles and the use of bacteria and mineral-precursors.

Keith Quillin is an Associate Director in BRE's Building Technology Group. He manages research and consultancy on low carbon cements, integration of assisted living measures in the built environment and the application of wireless technologies.

Andrew Dunster is a Principal Consultant in BRE's Building Technology Group. He manages research and consultancy on recycled aggregates, low carbon cements and the application of industrial by-products and wastes in construction products.

Keywords: Alkali activation, Fly ash, Ground granulated blastfurnace slag, Hydrated lime, Performance, Properties

INTRODUCTION

Concrete plays a vital role in infrastructural development and there are many benefits associated with its use. However, its production and use also has a significant detrimental impact on the environment, because the primary constituent, Portland cement (PC), produces a considerable quantity of CO_2 during manufacture: due to emissions arising from the intensive energy required to generate temperatures in excess of 1400°C in the kiln and because of calcination of the calcium carbonate. Data from The Concrete Centre [11] estimates that on average 0.93 tonnes of CO_2 are generated for every tonne of Portland cement produced.

The demand for PC is likely to increase by 28% to over four and a half billion tonnes per annum by 2050 (Figure 1). Alkali activated technology which utilises locally available waste materials and industrial by-products are considered to have an important role in reducing the environmental impact associated with the concrete industry.

Investigations on alkali activated technology date back to the 1940's [1], however there is still limited data on the properties and performance of concrete produced using alkali activated technology. Most research has been based on either alkali activation of fly ash or GGBS. However extensive review and trials has identified that the production of an alkali activated concrete with a combination of fly ash and GGBS provides further advantages in terms of setting and hardening at ambient temperature [2] that still produce 28 days concrete strengths of 30 N/mm^2 and over.

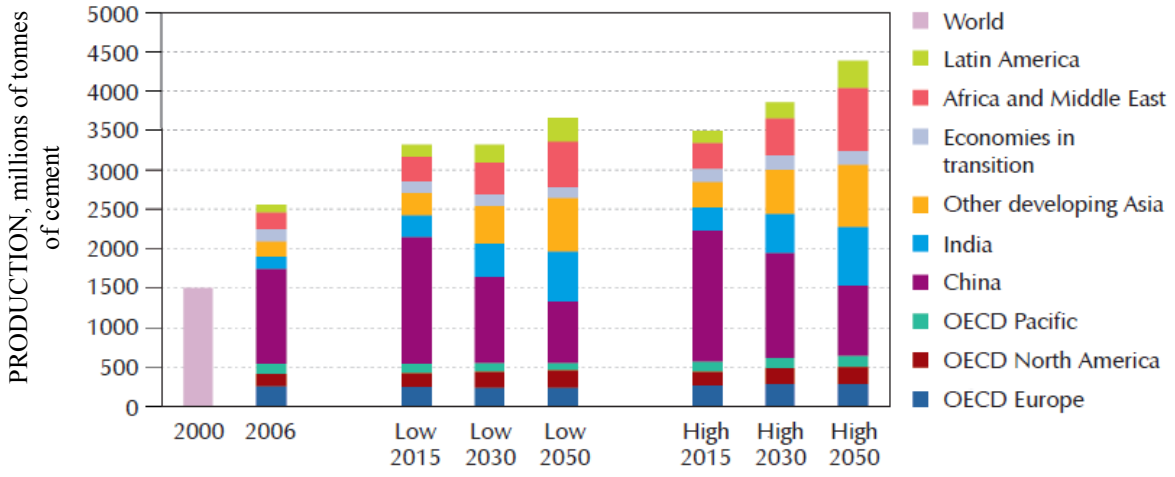

Figure 1 Predicted growth in global cement demand [8]

Fly ash is a common artificial pozzolan that is generated as a result of electrostatic precipitation of exhaust fumes from the coal fired power plants [3]. In the UK, fly ash may be classified as class F, according to ASTM C 618, due its low CaO content. Although such fly ash can be used in alkali activated concrete due to its reactivity with sodium silicate, investigation by Abora et al. [2] identified that it requires thermal curing to induce the hardening process for it to gain reasonable strength within a 24 hour period. Fernandez-Jimenez and Palomo [4] also noted in their characterization of fly ash that the reactive silica was quite important and therefore the percentage of reactive silica within the fly ash should be known. This is because the reactive silica is responsible for reacting with the alumina and the alkalis in generating a concrete with good cementitious properties.

GGBS is widely used as an addition to PC, however its pozzolanic and binding properties in alkaline media make it suitable for use in alkali activated concrete [5]. The use of GGBS in addition to fly ash provides an added advantage to the production of alkali activated concrete. This is due to the fact that the addition of GGBS to fly ash enables the hardening process to occur within a twenty four hours period without any thermal curing [2]. This provides a reasonable strength development within the early stages of manufacturing that is similar to that achievable with Portland cement.

The long-term viability of using GGBS in alkali activated concrete for this purpose has however been questioned. This is due to the fact that as demand for low carbon cement using GGBS as an addition increases, the global production of GGBS is not meeting the demand required for addition in PC concrete and secondly it is not readily available worldwide as steel production contracts in some countries.

To mitigate against the above problem, alternative binders suitable for GGBS substitution (and that can exhibit similar performance in alkali activated systems), need to be identified. One such binder is hydrated lime (produced from limestone, a naturally occurring mineral which is widely available around the world).

Hydrated lime is formed as an exothermic reaction and it involves exposing quicklime (CaO) to moist air or treated with water [6]. The CaO is derived when the principal component, calcium carbonate ($CaCO_3$) is exposed to high temperatures usually within the region of 800^{o}C and above. The final stage is then formation of the hydrated lime as it hydrates. Hydrated lime is often referred to as slaked lime.

The source materials used in the production of alkali activated concrete (fly ash, GGBS and hydrated lime) are activated with a high pH alkali metal solution, which breaks down the Si-O chemical bonds in the glassy phases of the material. The activator is then consumed within the reaction [7]. The chemistry is dependent on the composition of the source material and the type of activator used.

MATERIALS AND EXPERIMENT

Materials

The chemical composition of the fly ash, GGBS and hydrated lime used are given in Table 1. The fly ash used conformed to BS EN 450 and consist of spherical glassy particles of SiO_2, Al_2O_3, Fe_2O_3 and CaO. As can be identified from Table 1, the summation of Si_2O, Al_2O_3 and Fe_2O_3 was greater than 70% by mass indicating a class F type fly ash [3]. The GGBS used conformed to BS 6699.

Soluble sodium silicate (often referred to as waterglass) was used as the activator. Waterglass is a colourless and odourless alkaline liquid which contains three main components namely, silica (the primary component), soda and water. The alkaline activator used for this work contained 19% by mass of SiO_2 and 15% by mass of Na_2O.

Table 1 Chemical composition of binders

BINDERS	FLY ASH	GGBS	HYDRATED LIME
Source	Ash Resources	Civil & Marine	Castle Cement
Silicon Dioxide (SiO_2), %	44.0	35.3	1.10
Aluminium Oxide (Al_2O_3), %	24.6	11.3	0.60
Ferric Oxide (Fe_2O_3), %	11.7	0.20	0.20
Calcium Oxide (CaO), %	5.49	40.0	73.0
Magnesium Oxide (MgO), %	2.12	10.3	1.10
Sulfur Trioxide (SO_3), %	0.19	4.00	-
Sodium Oxide (Na_2O), %	1.07	0.30	-
Potassium Oxide (K_2O), %	2.43	0.40	-

Experimental Work

Alkali activated concrete was made using five different combination of binders for the study of determining a suitable mix design, three of which were then used to assess compressive strength. The five combinations were:

- Fly ash (80% by mass) and hydrated lime (20% by mass) [consistence only]
- Fly ash (90% by mass) and GGBS (10% by mass)
- Fly ash (95% by mass) and hydrated lime (5% by mass)
- Fly ash (97.5% by mass) and hydrated lime (2.5% by mass)
- Fly ash (100% by mass) [consistence only]

In all concretes the liquid activator to binder ratio was set at 1:0.66 by mass.

Each mix was made in a pan mixer. The dry aggregates and the binders were mixed for a few seconds to ensure all the materials were mixed thoroughly. The activator was then added and mixing continued for three and a half minutes. The concrete was then compacted into 100 mm cube moulds. During casting, all of the specimens were compacted by vibration.

The samples were subjected to a standard curing regime involving 24 hours in moulds under damped Hessian. After demoulding, the specimens were wrapped in polythene to prevent moisture loss during the initial curing. The sealed samples were then stored in a controlled room maintained at 20°C until the test date.

100 mm cubes specimens were crushed to determine the effect of varying the binder composition on compressive strength development. The strength test was prepared in accordance with BS EN 12390-3:2009 and was carried out at various date intervals up to 1 year. Each strength test conducted on a particular date was performed on two duplicate concrete cubes to allow for validation of the results.

The suitability of the mix was determined by visual observation of the consistency of the concrete after three minutes and hardening of the concrete after twenty four hours. Values

ranging from zero to two were assigned to the observations made, for the consistency (W), a value of two was indicative of a good consistency whilst a value of zero was assigned to poor consistency. Concrete which hardened within a 24 hour period was assigned a hardening value (H) of two and concrete that did not harden within 24 hours was assigned a value of one. The final scoring to determine the suitability of the mixes was the multiplication of the W and H values.

RESULTS AND DISCUSSION

Effect of Binder Ratio on Strength Development

The compressive strengths for the alkali activated concretes and their evolution with time are shown in Figure 2. Compressive strengths of more than 30 N/mm^2 were achieved at 28 days, with larger compressive strengths obtained at later ages.

The effect of substituting GGBS with hydrated lime on the compressive strength development is shown in Figure 2. Although the mass of hydrated lime (five per cent) used is half that used for the GGBS mix, both mixes gained similar strength development over time.

Figure 2 indicates that the concrete made with hydrated lime gained a higher initial strength development up to the twenty eight days. After twenty eight days, the concrete with GGBS gained higher strength than the hydrated lime concrete until both exhibited similar strength at one year.

In the studies, same mix composition with various proportions of hydrated lime was evaluated to determine strength development. As expected, the mix with the lower proportion (two and a half percent by mass of hydrated lime) had a lower strength development than the mix with five percent of hydrated lime.

It was also identified that using at least two and a half percent of hydrated lime provided a reasonable strength development reaching 22.5 N/mm^2 at twenty eight days compared to the 35 N/mm^2 for the mix with five percent of hydrated lime (Figure 2).

Studying the influence of different ratios of hydrated lime to fly ash on strength and hardening, it was observed that the addition of the hydrated lime initiated the hardening of the concrete within a twenty four hours period and secondly it was also identified that the strength value increased as the percentage of hydrated lime was increased. This is related to the fact that calcium rich binders are easier to be activated than the fly ash which had a very low quantity of calcium (Table 1).

The similar strength development achieved by the alkali activated concrete with five percent hydrated lime to the alkali activated concrete with ten percent GGBS can be explained by the level of calcium contributed by the hydrated lime which was equivalent to that found in the fly ash/GGBS concrete.

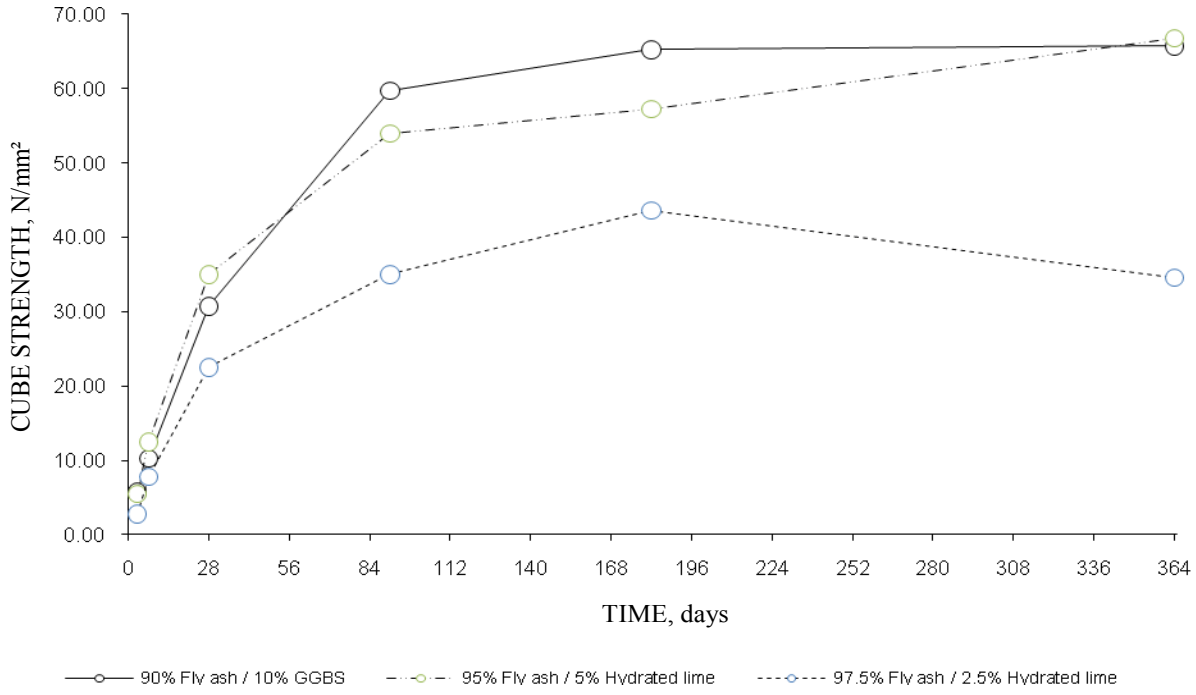

Figure 2 Substitution of GGBS with hydrated lime: strength development

Effect of Binder Composition on Suitability of Mix Design

Unlike PC concrete, the consistence of alkali activated concrete is prone to rapid changes over a short period of time and this can be critically dependent on the mix proportions used. The consistence is dependent on the concentration of the activator as well as the composition of the binders.

Following on from previous work by Abora et al. [2], it was identified that the hardening process of alkali activated fly ash alone (of type class F) within a twenty four hours period required thermal curing. To provide a solution to the problem of long setting time, a calcium rich binder (in the context of this paper, hydrated lime) was introduced to investigate its effect on consistence

It was observed that the suitability of the mix design decreases as the ratio of hydrated lime to fly ash increased (Figure 3). As indicated in Figure 3, the suitability score for the concrete mix with 80% fly ash and 20% hydrated lime was scored zero, this was due to the fact that there was a case of rapid setting and hardening within the three minutes period, making the concrete difficult to place within the moulds and thus unsuitable as a mix.

Embodied CO_2 of Alkali-Activated Concrete

There is limited knowledge on the environmental impacts of alkaline ash binder production. The general principles of assessing these properties have been investigated by Weil et al. [9]. In their review they noted that potential reduction of CO_2 emissions varied from a moderate 20% up to 80% [10]. The study focused on comparing the alkali activated fly ash/GGBS and alkali activated fly ash/hydrated lime at similar compressive strength.

The impact of the two binder types on climate change potential (kg CO_2 eq), was analyzed using the BRE environmental profiles methodology to identify and assess the environmental effects associated with concrete mix designs over their life cycle.

The aim of the life cycle assessment was to investigate the impact of:

- the extraction and processing of the raw materials
- the production of the concrete mix,
- transportation to site
- and its use

The functional unit used in the study was the production of a tonne of alkali activated concrete with two different binder types. The proportion of the raw material used as the underlying data is presented in the Figure 4 and Figure 5. For the fly ash/GGBS mix (Figure 4), the activator made up 12% by mass of the mix, 2% by mass for the GGBS and 17% by mass for the fly ash. For the fly ash/Hydrated lime mix (Figure 5), the activator made up 13% by mass of the mix, 1% by mass for the hydrated lime and 18% by mass for the fly ash. The results shown in Figure 6 indicates that the climate change impact of the fly ash/hydrated lime mix was 8% higher than the fly ash/GGBS concrete mix, although the proportion of hydrated lime used within the concrete mix was half the proportion of GGBS used.

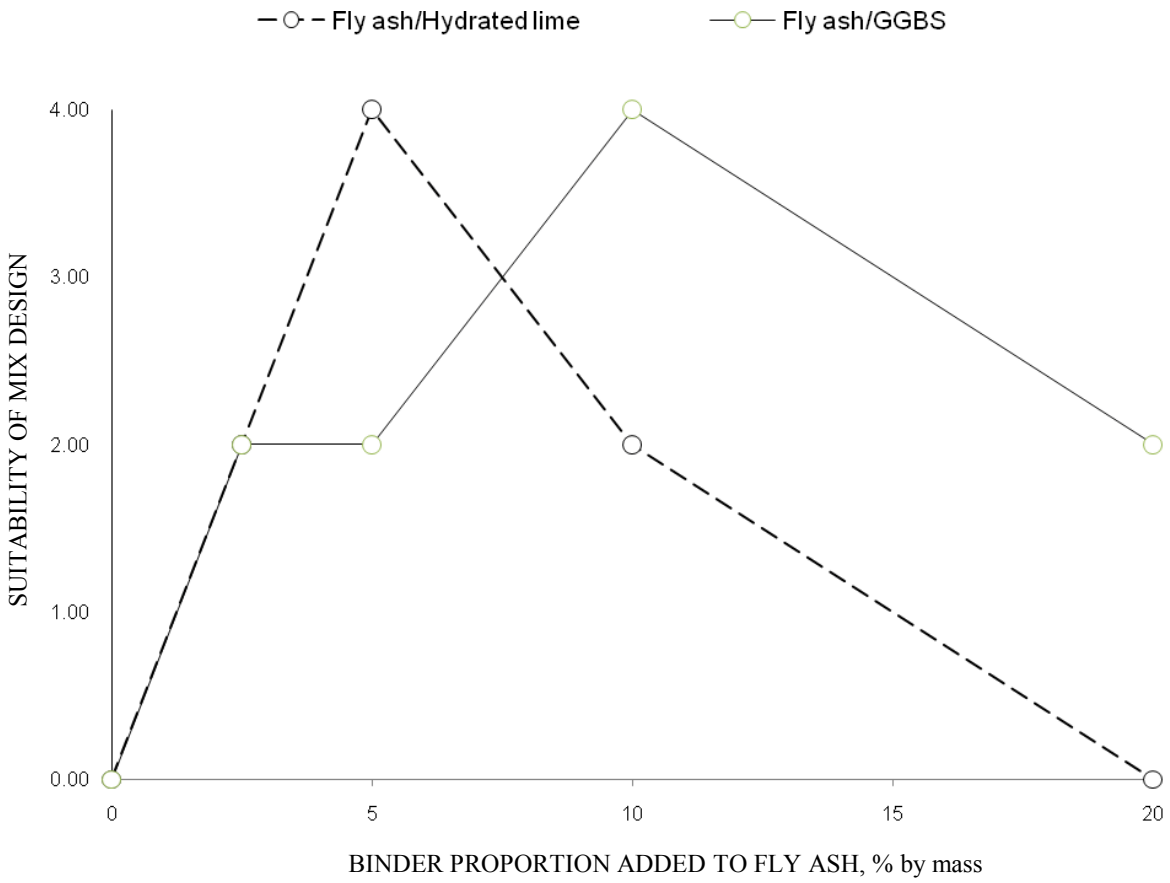

Figure 3 Suitability of alkali activated concrete mix design

The analysis also indicated that the major contributor to the climate change impact was that of the activator which contributed about 66% of the total environmental impact on the alkali activated concrete mix (Figure 7). This was mainly due to the significant electricity, heat and water used in the manufacture of the activator. Based on the findings, the application of the activator and the hydrated lime should be kept to a minimum to minimize the climate change impact of the alkali activated concrete

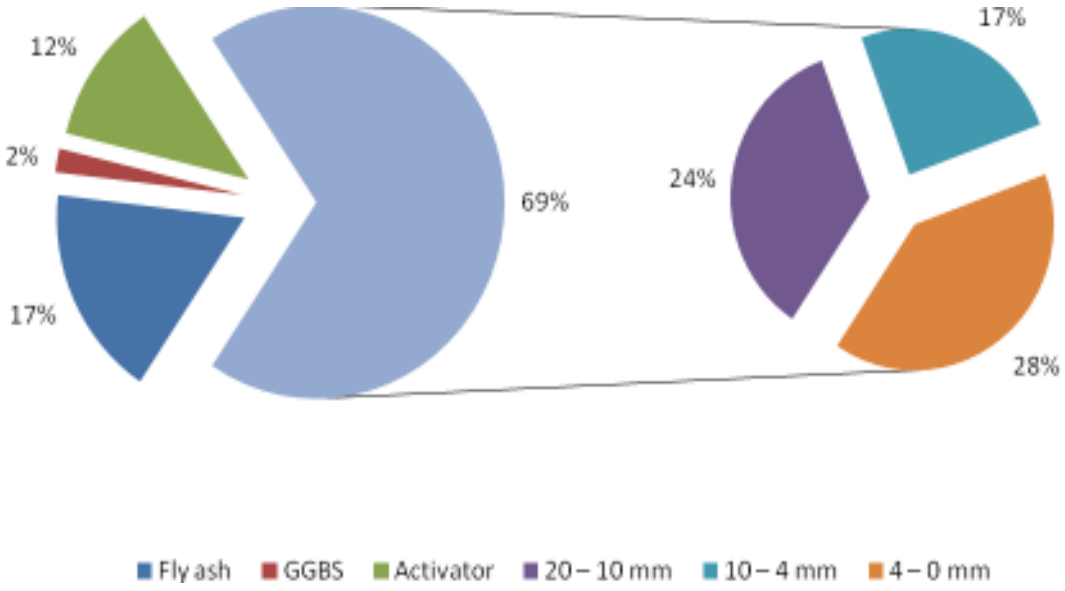

Figure 4 Proportion of raw materials in alkali activated fly ash/GGBS concrete (% by mass)

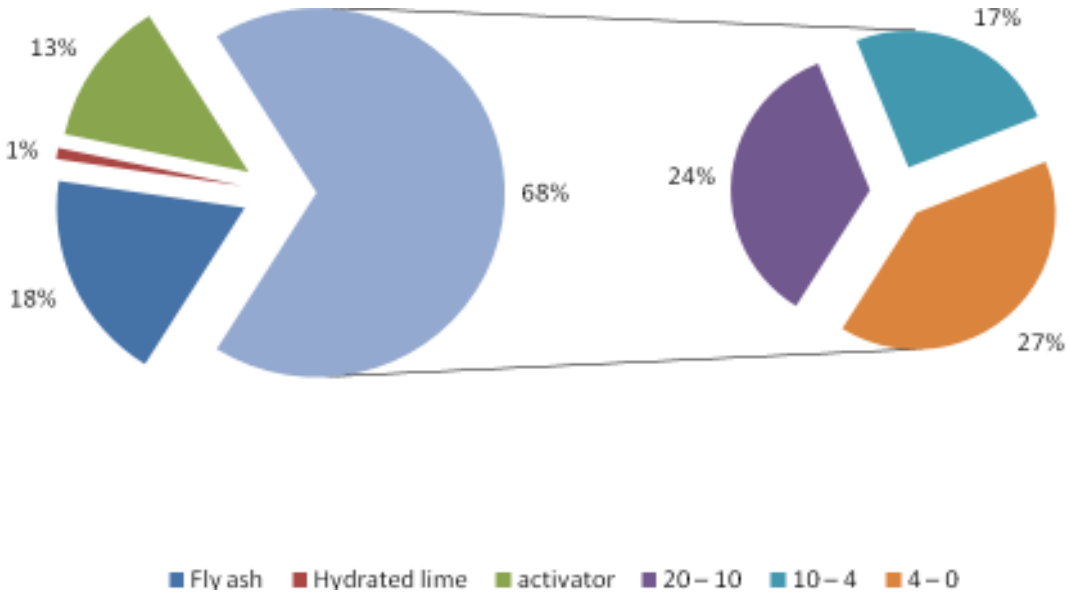

Figure 5 Proportion of raw materials in alkali activated fly ash/hydrated lime concrete (% by mass)

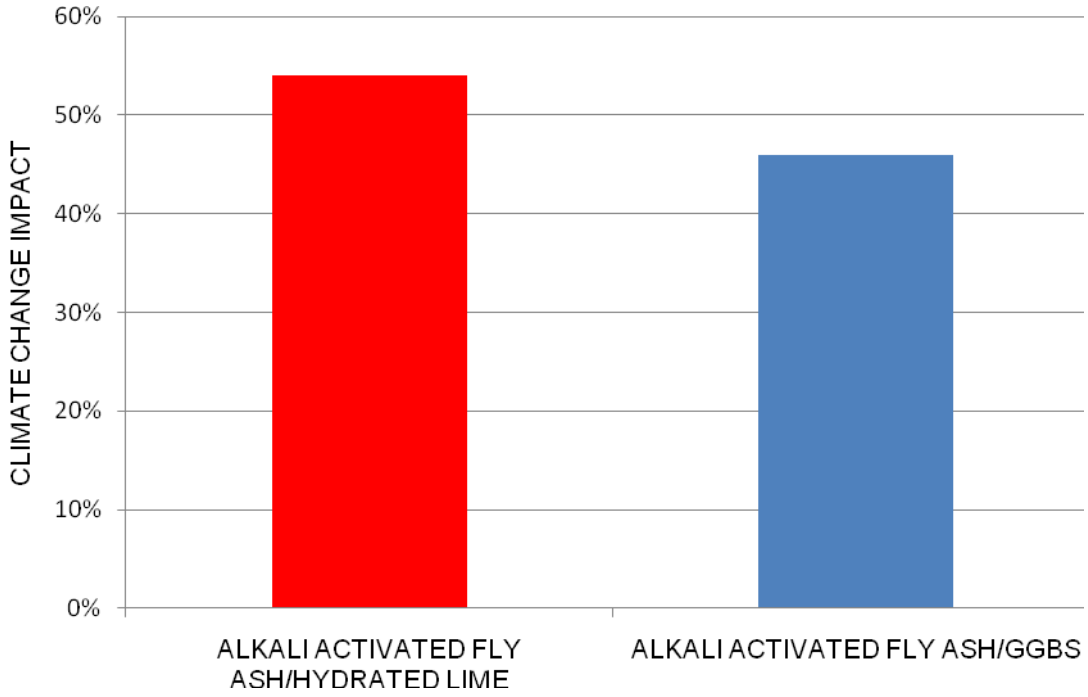

Figure 6 Comparison of alkali activated concrete climate change impact

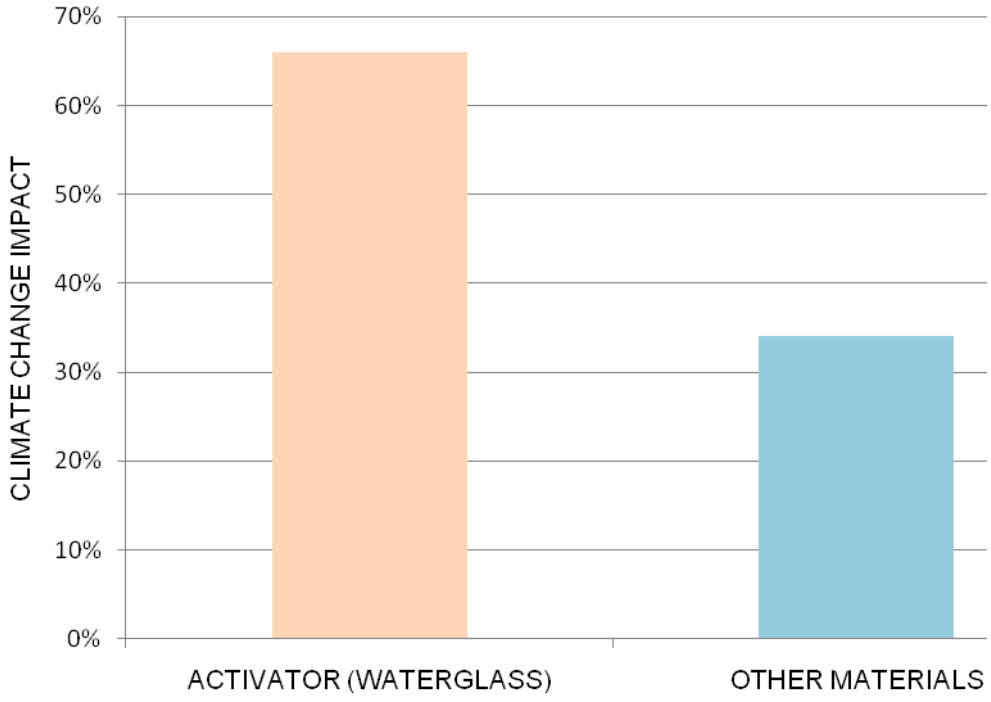

Figure 7 Climate change impact of raw materials in alkali activated concrete

CONCLUSIONS

The laboratory work described has demonstrated that when the composition of the binder is varied (in this instance the mixture of components in the binder) there is an effect on the consistency and compressive strength of the concrete. There is also an effect on the embodied CO_2 of the alkali activated concrete. The properties and performance of the alkali activated concrete are dependent on the type of binder used. The following observations were made during the investigations:

- The results identified from the research indicates that the addition of hydrated lime to fly ash provides sufficient calcium ions within the alkali activated concrete to lead to higher strength and quicker hardening of the concrete within 24 hrs at ambient temperatures (compared with fly ash as the sole binder).
- The development of compressive strength is dependent on the proportion of hydrated lime used. The higher the proportion of hydrated lime to fly ash, the higher the compressive strength. This indicates that the strength of the concrete is influenced by the variation in the binder composition.
- The consistence of the alkali activated concrete increased with the decrease in the proportion of the hydrated lime used. It was also identified that higher proportion of hydrated lime to the fly ash could lead to flash setting.
- GGBS could be substituted with hydrated lime and added in proportion to fly ash to produce an alkali activated concrete with similar properties and performance to alkali activated fly ash/GGBS concrete.
- Five percent of hydrated lime substituted for ten percent of GGBS in the alkali activated concrete provided similar compressive strength at 28 days ranging between 30 and 35 N/mm^2.
- The climate change impact on alkali activated fly ash/GGBS was 46% as compared to 54% for the alkali activated fly ash/hydrated lime concrete.
- The activator contributed the most to the overall climate change impact.

In summary although the concretes made with the alkali activated fly ash and five percent of hydrated lime had a similar range of compressive strength to the alkali activated fly ash and ten percent of GGBS, the impact on climate change was higher for the alkali activated fly ash/hydrated lime. The impact was identified to be 8% higher than the alkali activated fly ash/GGBS concrete.

REFERENCES

1. ROY D. M., 1998. Alkali-activated cements, opportunities and challenges. Cement and concrete research, 29(1999), pp.249-254

2. ABORA K., QUILLIN K., PAINE K. A. AND DUNSTER A., 2009. Effect of mix design on consistence and setting time of alkali activated concrete. Proceedings of the 11th International Conference on Non-conventional Materials and Technologies, 2009, Bath, UK.

3. SHI C., KRIVENKO P. V AND ROY D., 2006. Cementing components. In SHI C., KRIVENKO P. V AND ROY D. Alkali-activated cements and concrete. Oxon: Taylor & Francis Ltd, pp.30-63.

4. FERNÁNDEZ-JIMÉNEZ A. AND PALOMO A., 2003. Characterisation of fly ash: Potential reactivity as alkaline cements. Fuel, 18(2003), pp2259-2265.

5. ATIŞ C. D., BILIM C., ÇELIK Ö AND KARAHAN O., 2009. Influence of activator on the strength and dry shrinkage of alkali-activated slag mortar. Construction and building materials, 23(2009), pp.548 – 555.

6. HERATH J. W., 1992. Lime industry in Sri Lanka. In Hill N., Holmes S and Mather D. editor. Lime and other alternative cements. London : Intermediate Technology Publications Ltd, pp.56-64.

7. QUILLIN K, 2007. Calcium sulfoaluminate cements. CO_2 reduction, concrete properties and applications. Bracknell: IHS BRE Press.

8. DUNSTER A., ABORA K. AND QUILLIN K, 2010. Alkaline ash binders: Reduced environmental impacts of precast concrete products. Garston: IHS BRE Press (IP 9/10).

9. WEIL M., DOMBROWSKI K. AND BUCHWALD A. Life-cycle analysis of geopolymers, 2009. In Provis J. L and van Deventer J. S. J editor. Geopolymers: Structure, processing, properties and industrial applications. Cambridge : Woodhead Publising Limited, pp. 194-210

10. PRICE W., 2009. Cementitious materials for the twenty-first century. Proceedings of ICE, 162(2009), pp.64-69.

11. THE CONCRETE CENTRE, 2011. Specifying sustainable concrete. URL: http://www.concretecentre.com

Influence of Silica Fume on the Properties of Self-compacting Concretes

S Al-Sanusi
Benghazi University, Libya

A self-compacting concrete is the one that can be placed in the form and can go through obstructions by its own weight and without the need of vibration. Since its first development in Japan in 1988, has gained wider acceptance in Japan, Europe and USA due to its inherent distinct advantages. Although there are visible signs of its gradual acceptance in the North Africa through its limited use in construction, Libya has yet to explore the feasibility and applicability of SCC in new construction. The contributing factors to this reluctance appear to be lack of any supportive evidence of its suitability with local aggregates and the harsh environmental conditions. The primary aim of this study is to explore the feasibility of using SCC made with local aggregates of Eastern Province of Libya by examining its basic properties characteristics. This research consists of: Development of a suitable mix for SCC such as the effect of water to cement ratio, limestone and silica fume that would satisfy the requirements of the plastic state; Casting of concrete samples and testing them for compressive strength and unit weight. Local aggregates, cement, admixtures and industrial waste materials were used in this research.

Dr S K Alsanusi BSc, MSC., obtained his PhD from the School of Engineering, University of Pittsburgh, Pittsburgh, Pennsylvania, USA. He is currently a teaching staff member at the University of Benghazi, Libya, in the area of structural analysis and soil mechanics, research areas such as self compacting concrete, light weight concrete, fracture mechanics, soil structure interaction, and elastic-plastic-fracture of weak tension materials.

Keywords: Admixtures, Limestone, Self-compacting concrete, Silica fume

INTRODUCTION

Development of self- compacting concrete (SCC) is a desirable achievement in the construction industry in order to overcome problems associated with cast-in-place concrete. Self-compacting concrete is not affected by the skills of workers, the shape and amount of reinforcing bars or arrangement of a structure, and due to its high –fluidity and resistance to segregation it can be pumped longer distances [1]. The concept of self-compacting concrete was proposed in 1986 [2], but the prototype was first developed in 1988 in Japan [3]. Self-compacting concrete was developed at that time to improve the durability of concrete structures. Self-compacting concrete is cast so that no additional inner or outer vibration is necessary for the compaction. It flows like "honey" and has a very smooth surface level after placing. With regard to its composition, self-compacting concrete consists of the same components as conventionally vibrated concrete, which are cement, aggregates, and water, with the addition of chemical and mineral admixtures in different proportions. Usually, the chemical admixtures used are high-range water reducer (super plasticizers) and viscosity-modifying agents. Mineral admixtures are used as an extra fine material, besides cement, and in some cases, they replace cement. Self-compacting concrete, in principle, is not a new. Special applications such as underwater concreting have always required concrete which, could be placed without need for compaction [1]. In such circumstances vibration was simply impossible. Early self-compacting concretes relied on very high contents of cement paste and, once super plasticizers became available, they were added in the concrete mixes. The mixes require specialized and well –controlled placing methods in order to avoid segregation, and the high contents of cement paste made them prone to shrinkage. The overall costs were very high and application remained very limited. In the early 1990's there was only a limited public knowledge about SCC, mainly in the Japanese language. Simultaneously with the Japanese developments in the SCC area, research and development continued in mix-design and placing of underwater concrete where new admixtures were producing SCC mixes with performance matching that of the Japanese SCC concrete. The motive for development of self-compacting concrete was the problem on durability of concrete structures that arose around 1983 in Japan .Due to a gradual reduction in the number of skilled workers in Japan's construction industry , a similar reduction in the quality of construction work took place .As a result of this fact, one solution for the achievement of durable concrete structures independent of the quality of construction work was the employment of self-compacting concrete, which could be compacted into every corner of a formwork , purely by means of its own weight. Studies to develop self-compacting concrete, including a fundamental study on the workability of concrete, were carried out [3] at the University of Tokyo. The main reasons for the employment of self-compacting concrete one to shorten construction period , second to assure compaction in the structure; especially in confined zones where vibrating compaction is difficult, third to eliminate noise due to vibration. A mix proportioning system for SCC was proposed [3]. In this system, the coarse aggregate and fine aggregate contents are fixed and self-compactibility is to be achieved by adjusting the water /powder ratio and super plasticizer dosage. The coarse aggregate content in concrete is generally fixed at 50 percent of the total solid volume, the fine aggregate content is fixed at 40 percent of the mortar volume and the water /powder ratio is assumed to be 0.9-1.0 by volume depending on the properties of the powder and the super plasticizer dosage. The required water /powder ratio is determined by conducting a number of trials. One of the limitations of SCC is that there is no established mix design procedure yet.

This paper describes a procedure specifically developed to achieve self-compacting concrete. In addition, the test results for acceptance characteristics for self-compacting concrete such as slump flow, J-ring, V-funnel, U-box and L-Box are presented. Further, the strength characteristics in terms of compressive strength for 7-days and 28-days are also presented.

MATERIALS IMPLEMENTED

- Cement All types of cement are suitable for SCC. For all mixes in this research, an Ordinary Portland Cement Type I meeting (ASTM 150) manufactured by Libyan cement company was used in concrete mixes. Its Chemical composition and physical properties are as given in Table 1.
- Limestone was used as filler (in the range of 0 to 50% of the mass of powder. Limestone was supplied from Libyan plants. Chemical composition and physical properties of Limestone are given in the Table 1..
- Aggregates Locally available natural sand with 4.75 mm maximum size was used as fine aggregate, having physical properties as shown in Table 2. Crushed stone with 19 mm maximum size having physical properties as shown in Table 3. Both fine aggregate and coarse aggregate conformed to BS and ASTM Standard Specifications.
- Admixtures A visco-crete 5400 based super-plasticizer complying with ASTM C- 494, Type G and F was used.
- Silica-fume also known as condensed silica fume or micro-silica (ACI 116R), is very fine, non-crystalline silica produced in electric arc furnaces. Chemical properties of Silica-fume are given in the Table 1

Table 1 Chemical properties of lime stone and silica fume

.NO	COMPOUNDS NAME	COMPOUNDS	PERCENT BY WEIGHT, %		
			Cement	Lime stone	Silica fume
1	Calcium Oxide	CaO	62.70	52.35	0.17
2	Silicon Dioxide	SiO_2	20.60	0.45	95
3	Aluminum Oxide	AL_2O_3	4.90	0.33	0.35
4	Magnesium Oxide	MgO	3.10	1.05	0.09
5	Sulphur Trioxide	SO_3	2.80	0.04	0.42
6	Ferric Oxide	Fe_2O_3	2.70	0.14	0.2
7	Potassium Oxide	K2O	0.8	0.02	0.51
8	Sodium Oxide	Na2O	0.23	0.06	-
9	Loss on ignition		-	45.15	-
	Specific Gravity		3.15	2.71	2.25

Table 2 Fine aggregate properties

PROPERTY	TEST	VALUE
Specific gravity	ASTM C128	2.58
Absorption capacity	ASTM C128	0.4%
Fineness Modulus	ASTM C 33	2.72

Table 3 Coarse aggregate properties

PROPERTY	TEST PROCEDURE	VALUE
Specific gravity	ASTM C 127	2.56
Water Absorption	ASTM C 127	2.15%
Bulk Density	ASTM C 29 / 29M	1419..45
Angularity Number	BS 812 : Part 1	6.1
Impact Value	BS 812 : Part 3	24.13%
Crushing Value	BS 812 : Part 3	29.3 %

TEST METHODS

Self- Compacting Concrete is characterized by filling ability, passing ability and resistance to segregation. Many different methods have been developed to characterize the properties of SCC. No single method has been found until date, which characterizes all the relevant workability aspects, and hence, each mix has been tested by more than one test method for the different workability parameters. Typical acceptance criteria for SCC with a maximum aggregate size of up to 20 mm are presented in Table 4.

Table 4 Acceptance criteria for SCC [5].

METHOD	UNIT	VALUES RANGE	
		minimum	maximum
Slump flow by Abram's cone	mm	650	800
T50cm Slump flow	second	2	5
J-ring	mm	0	10
V-funnel	second	6	12
Time increase V-funnel at T5 min	second	0	+3
L-box (h2.h1)	-	0.8	1.0
U-box (h2-h1)	mm	0	30

MIXING PROCEDURE

All concrete batches were prepared in rotating drum mixer. First, the aggregates are introduced and then one-half of the mixing water was added and rotated for approximate two minutes. Next, the cement, most manufacturers recommend at least 5 minutes mixing upon final introduction of admixtures. Once, the mix was determined to have sufficient visual attributes of SCC, the rheological tests were performed in quick succession. Typically, the order of testing employed was as follows:

- U-box (height of concrete in each compartment)
- V-funnel (time to empty).
- L-Box (T20, T40 and heights at 20 and 40cm).
- Flow Test.
- Density (Unit weight).
- Ring test.
- Air Determination (using pressure meter).
- Casting of Specimens

After the flow test was conducted, concrete's visual stability index (VSI) was determined. Criteria used for VSI rating is described in Table 5.

Table 5 Visual stability index rating criteria

VISUAL STABILITY INDEX RANGES FROM 0 TO 3	
VSI	criteria
0	No evidence of segregation in slump flow patty, mixer drum or wheelbarrow
1	No mortar halo in slump flow patty, but some bleeding on the surface of concrete mix drum or wheel barrow
2	A slight mortar halo (<3/8in (10mm)) in slump patty and noticeable layer of mortar on the surface of resting concrete in mixer
3	Clearly segregating by evidence of large mortar halo(>3/8in (10mm)) and a thick layer of mortar and bleed water in the surface of resting concrete

EXPERIMENTAL PROGRAM

Nine trial mixes were prepared by varying the silica fume content and water to powder ratio. Three levels of the silica fume: 3, 6, 9% by mass of powder, three levels of water to powder ratio: 0.3, 0.34, 0.37, and super-plasticizer (1.15% by mass of powder) were used for preparing and testing nine trial mixes. For each trial mix, a constant Powder Content: 550 (kg/m^3). Lime stone 40% by mass of powder and a constant fine to total aggregate ratio: 0.525 (by mass) of concrete were taken. Proportions of the trial mixes, determined using the ACI method, are presented in Table 6

Table 6 Experimental tests to study effect of silica fume.

RATIOS OF SAND, AGGREGATE, LIME, AND WATER									
sand to total aggregate ratio	0.525								
Powder content	550 kg/m^3								
Lime stone	40 %								
Water to powder ratio (w/p)	0.3			0.34			0.37		
Silica fume (SF)	3%	6%	9%	3%	6%	9%	3%	6%	9%

Table 7 Workability and compressive strength results

RATIOS OF WATER TO POWDER AND WORKABILITY MEASURMENTS											
mix		air %	γ kg/m^3	slump flow (mm)	T50 sec	U box	I box	V funnel (sec)	J ring (mm)	VSI	f_{cu} (MPa)
w/p	SF										
0.34	3%	4	2298	530	2	0.76	0.78	11	510	1	36.84
	6%	2	2285	660	3	0.9	0.87	5	510	1	47.63
	9%	4.5	2315	550	3	0.95	0.87	8	520	2	46.18
0.37	3%	4	2303	500	2	1	0.93	10	530	1	33.21
	6%	6	2303	600	1	1	0.83	8	530	1	36.40
	9%	5	2347	870	3	1	0.68	10	532	2	35.89

RESULTS AND DISCUSSION

Mixes were prepared and test performed according to procedures described earlier. Table 7 provides the details of the rheological properties observed for concrete mixes with silica fumes. Fig.ure 1 below show the effect of silica fume on various rheological and harden concrete properties. From the rheological point of view, a silica fume content of 6% should be recommended.

The 28-day strength chart is very intriguing. The compressive strength of SCC mix prepared showed a distinct U-shape curve with respect to w/p ratio. This could be perhaps explained by the fact that at higher w/p ratio, the concrete is more workable and assumes a denser configuration. This phenomenon needs to be further studied

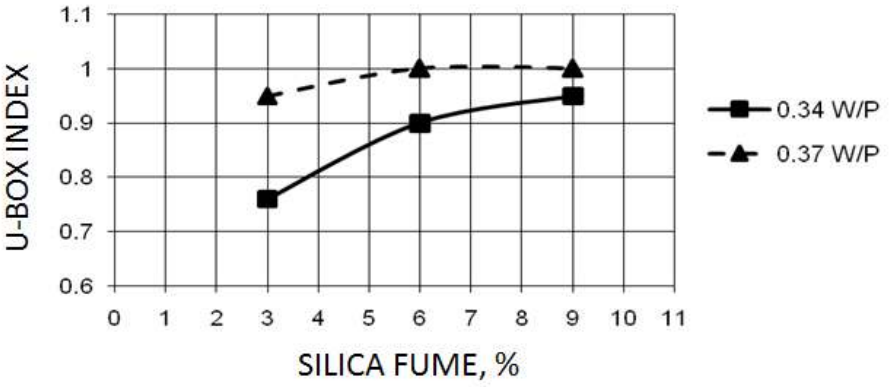

Figure 1 Effect of silica fume on U-Box index

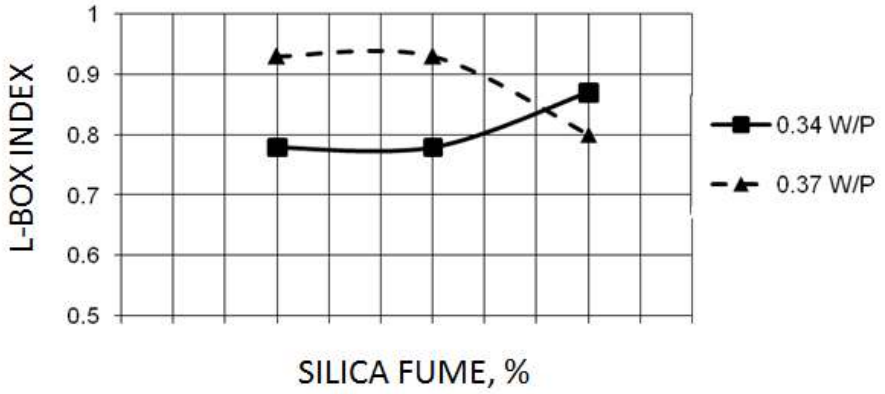

Figure 2 Effect of silica fume on L-Box index

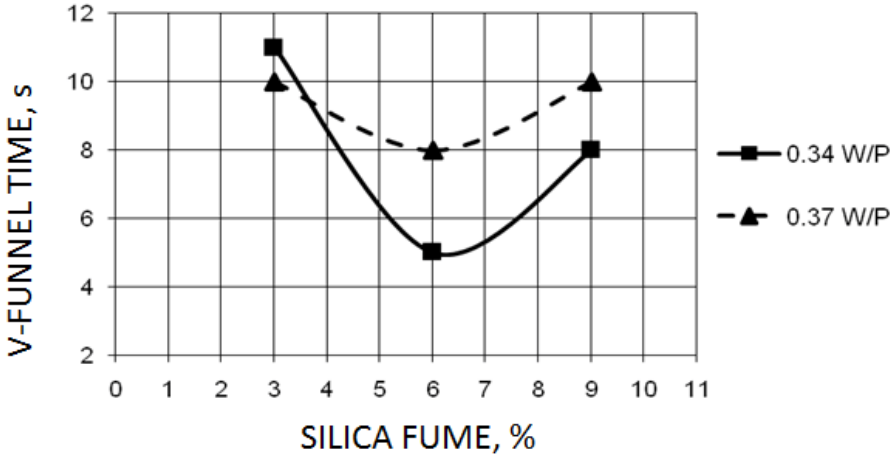

Figure 3 Effect of silica fume on V-Funnel Index

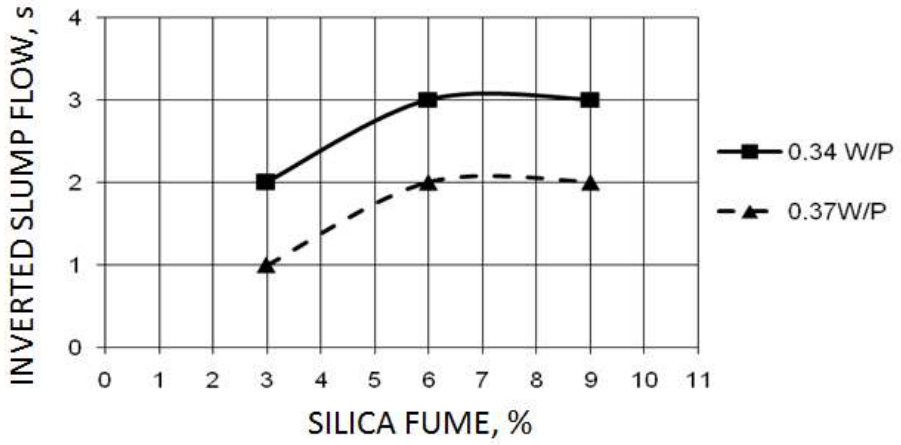

Figure 4 Effect of silica fume on inverted slump flow

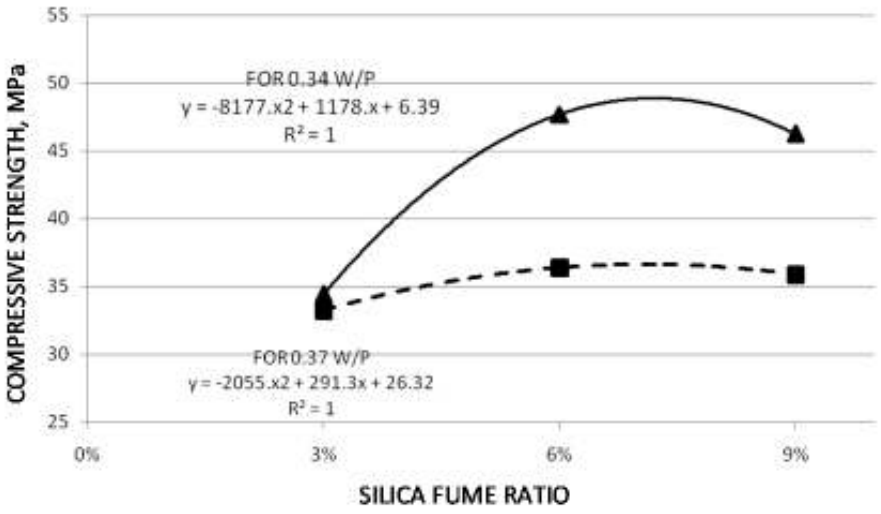

Figure 5 Relationship between compressive strength of concrete and silica fume ratio

CONCLUSIONS

1. Silica fume is a viable secondary mineral material. It leads to higher than usual modulus value and from the mixes studied, it is suggested that no more than 6% silica be replaced by mass.

2. Rheological tests chosen and performed were sufficient to ascertain whether the mix will have all the attributes of SCC or not, i.e., the fresh concrete test used were sufficient to measure the filling ability and passing ability.

3. It is recommended that, at the minimum, Slump test, U-Box and L-box should be performed for the laboratory verification tests.

REFERENCES

1. BARTOS, J. M., “Measurement of Key Properties of Fresh Self-compacting Concrete”, CEN/PNR Workshop, Paris, 2000.

2. OKAMURA, H., "Self-Compacting High-Performance Concrete", Concrete International, pp. 50-54, 1997.

3. OZAWA, K., MAEKAWA, K., KUNISHIMA, M., AND H. OKAMURA, "Development of High Performance Concrete Based on the Durability Design of Concrete Structures", Proceedings of the Second East-Asia and Pacific Conference on Structural Engineering and Construction (EASEC-2), Vol. 1, pp. 445-450, January 1989.

4. FERRARIS, C. F., BROWER, L., DACZKO J., OZYLDIRIM, C., “Workability of Self-Compacting Concrete”, Journal of Research of NIST, Vol. 104, No. 5, pp.461-478, 1999.

5. EFNARC, “Specifications and Guidelines for Self-Compacting Concrete”, EFNARC, UK (www.efnarc.org), pp. 1-32, February 2002.

Development of Concrete Mixes with the Addition of Crushed Tyres

A Benítez, M Polzinetti, J Agnello
National Institute of Concrete Technology (INTI), Argentina

The ecological problem of final disposal of used tyres has led to several technological developments in many countries. Concrete has been found to be an interesting way to recycle tyres chips. In Argentina there are two options in this respect: the crushing and classification of the metallic, textile and rubber compounds and the crushing without classification. The present paper deals with the second alternative regarding the important investment that a classification process implies. The mixes studied consisted in 0 %, 5 %, 7,5 %, 10 % and 12,5 % of aggregate replacement and two different water:cement relation. The compressive cylindrical strength was determined to calculate the decrease against the reference mix. The objective was to find the optimum percentage that causes the less significant reduction so the equation cost:benefit becomes convenient. The workability of the mixes were assessed with the Vebe consistometer (ASTM C 1170) as the mixes become dry with the tyre chips aggregates. Air content and density was also measured. Testing carried out to date has lead to select a percentage of replacement that can achieve the minimum required characteristics. Ongoing work will investigate the feasibility of producing rubberised concrete block with the required strength on a commercial basis and investigate the potential for enhanced thermal capacity and sound insulation. The ability to produce cost effective rubberised concrete products for industry depends on overcoming some of the practical production difficulties. The development of practicable concrete products with tyre chips is under research at the Center of Construction of the National Institute of Industrial Technology. In addition to meeting recycling and sustainability objectives, the aim is to produce a material with enhanced properties in specific applications. The use in pervious concrete also shows a great potential for success at present.

Alejandra Benítez, Civil Engineer, Postgraduate studies in Advanced Concrete Technology, Advanced Concrete Technology Diploma (UK), Member of the Institute of Concrete Technology (ICT-UK), Head of the Concrete Technology Area of the Construction Center at the National Institute of Industrial Technology (INTI), Postgraduate and graduate teacher at the Buenos Aires University (UBA), Technical Auditor for the Argentinian Accreditation Organism (OAA), Auditor in Construction Materials Certification, applied technological developments on innovative concretes and mortars.

Matías Polzinetti,Civil Engineer, Engineer Assistant at the Concrete Technology Area of the Construction Center at the National Institute of Concrete Technology (INTI), Auditor for Construction Materials Certification, Development of concrete and mortar mixes, Assistant Teacher at the Buenos Aires University (UBA).

Julio Agnello, Civil Engineer Student, Techinician at the Concrete Technology Area of the Construction Center at the National Institute of Concrete Technology (INTI), Development of concrete and mortar mixes, Auditor for Construction Materials Certification.

Keywords: Aggregate replacement, Compressive strength, Density, Rubber chips, Workability

INTRODUCTION

The disposal of waste tyres is not major waste management problem in Argentina yet. It is estimated that not more than 5 to 7 million car and truck tyres (aprox. 100.000 t a 120.000 t) are being discarded annually although this number is set to increase, in line with the growth in road traffic and car ownership. At present, it is estimated that 58 % of the waste tyre generation is concentrated in Buenos Aires surrounding area, with 8 % in the North West region, 8 % in the West, 18 % in the North East and 8 % in the South. As there are not environmental policies regarding tyres yet, the final disposal of them is under study.

The separation of waste is encouraged and some provinces have started to transport them to collection points. There is a government interest to identify alternative solutions for this problem. These options have to promote recycling instead of disposal and energy recovery. In that direction INTI has been leading a number of actions tending to unify effort from the different involved actors. Two projects of law have already been presented and brochures for the diffusion of recycling procedures have been developed in different communities.

When considering the different possibilities, the usage of waste tyres in civil engineering is currently inexistent. This is due to the lack of high and constant volume waste, the difficulty in obtaining the classified chips and the proposal of useful applications and products involving recycled tyres. A major use in energy recovery is as a fuel source for cement kilns but it is not a widespread practice for our cement manufacturing industry because of long transport distances.

Innovative alternatives to cope with the tyre disposal problem is therefore a challenge to our country. There is still another drawback to the possibility of using this type of waste because the appropriate equipment to obtain the chips and separate the components is extremely expensive yet and there is just one plant which belongs to a private company.

Some attention has been given to the potential use of rubber as concrete aggregate in concrete for pavements repair or in pervious concrete but it is still in the research stage. There may be a limited market for concrete products containing rubber aggregate but studies may show the environmental solution could be feasible. This study investigates the optimum percentage of rubber chips in concrete mixes in order to establish on going lines of work.

OBJECTIVES

The overall aim of the project is to investigate the feasibility of incorporating rubber tyre chips as a replacement for natural mineral aggregates in concrete. The specific objectives of the project are as follows:

1. To use rubber chips without separating the constituents of the tyre
2. To establish the density and grading of the rubber aggregate
3. To establish a family of concrete mixes with different percentages of replacement
4. To evaluate the optimum percentage compatible with an acceptable reduction of mechanical properties
5. To evaluate compressive strength in dry mixes for concrete blocks

SCOPE OF WORK

The programme of work developed may be described as follows:

- -Characterisation of constituents
- -Grading and density determinations of the rubber chips
- -Mix design and measurement of properties of fresh rubberised concrete: workability, density and air content
- -Assessment of properties of hardened rubberised concrete: Compressive strength.
- -Assessment of a dry mix for concrete blocks
- -Applications of rubberised concrete for further research

The first potential application of rubberised concrete is the production of concrete blocks incorporating rubber aggregate with the aim of demonstrating that they can meet industry requirements for strength, conductivity and weight. The second possibility is the study of pervious concrete which is under development.

DESCRIPTION OF CONSTITUENTS

Rubber Aggregate

Rubber aggregates are obtained by reducing scrap tyres to smaller sizes using two general processing technologies: direct mechanical crushing and/or a mechanical grinding which includes a separating process of the nylon, steel and rubber constituents. This method consists of using a variety of grinding techniques to mechanically break down the rubber into small particle sizes ranging from several centimeters to fractions of a centimeter. The steel in the tyres is magnetically separated during the various stages of granulation, and sieve shakers separate the nylon fibres in the tyre. Although this is a very effective process because it permits a recycling of the steel and fibres, there is just one plant in our country[1,2,3].

As a result of this, the objective of the present work was to use the material as it is obtained from a second technology available which consists of a simple crushing and a subsequent size classification.

A local plant provided the chips in different sizes in order to study the factibility for the use of the chips in concrete mixes. The gradings determined can be seen in Table 1. Two different types of intermediate sizes were used. Figures 1 to 3 show the different characteristics of the rubber aggregates.

The density of the rubber aggregates was determined by immersing the samples in alcohol and determining the volume displacement. The results are included in Table 1.

The variations between specific gravity found in the bibliography and the obtained values can be due to varying rubber quality, the quantity of textile and steel fibres and/or experimental errors [1]

Table 1 Grading of rubber aggregates

SIEVE SIZE, mm	INTERMEDIATE RA1	INTERMEDIATE RA2	FINE RA
	Cumulative Amount Retained, %		
25,4	0,0	0,0	0,0
19,5	0,0	0,0	0,0
13,2	0,0	0,0	0,0
9,5	0,0	0,0	0,0
4,75	73,8	77,7	37,7
2,36	94,8	92,7	71,5
1,18	95,9	95,8	77,9
0,600	97,9	97,2	88,0
0,300	98,9	98,6	93,4
0,150	99,8	99,5	98,3
Fineness Modulus	5,6	5,6	4,7
Nominal Maximum Size	9,5	9,5	9,5
Density, g/cm^3	1,575	---	1,198

The finer fraction of the RA was not considered to be used in the present mixes because they showed high absorption due to the high specific surface and the textile fibres.

The intermediate fraction was selected in the first approach in order to find an optimum % of replacement.

Figure 1 Intermediate RA1

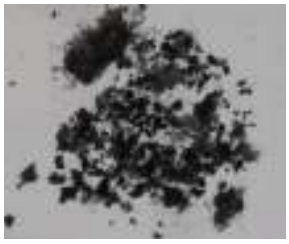

Figure 2 Intermediate RA2

Figure 3 Fine RA

Ordinary Aggregates

The natural coarse aggregate used was a crushed granite identified “6-20”. The Nominal Maximum Size was 25,4 mm and is the most usual size used in Argentina.

The fine aggregate consisted was a combination of a fine natural river sand and a crushed granitic sand originated in the granite crushing process. The gradings, fineness modulus, absorption and density are included in Table 2. Figures 4 to 6 illustrate the aggregates.

Table 2 Grading of natural aggregates

SIEVE SIZE, mm	NATURAL AGGREGATES		
	CCAgg 6-20	NRSand	CGSand
	Cumulative amount retained, %		
25.4	3,1	0,0	0,0
19,5	34,8	0,0	0,0
13,2	53,9	0,0	0,0
9,5	64,3	0,0	0,7
4,75	94,9	0,0	12,1
2,36	99,7	0,0	45,5
1,18	99,7	1,0	69,8
0,600	99,7	6,9	84,1
0,300	99,7	58,7	92,0
0,150	99,7	98,0	96,3
< 0,150	99,9	100,0	100,0
Fineness Modulus	7,5	1,6	4,0
Nominal Maximum Size	25,4	---	---
Density g/cm^3	2,63	2,63	2,64
Absorption %	1,90	0,03	0,40

References: CCAgg 6-20: Crushed Coarse Granitic Aggregate-Nominal Maximum Size 25,4 mm, NRSand: Natural River Sand, CGSand: Crushed Granitic Sand

Figure 4 Crushed Coarse Granitic Aggregate

Figure 5 Natural River Sand

Figure 6 Crushed Granitic Sand

Total Aggregate Grading Analysed

The partial replacement of ordinary aggregate by rubber was calculated in volume and then it was converted to weight using the specific gravity measured. Table 3 includes the proportions of aggregates used for the mixes studied.

Table 3 Proportions of aggregates used (%Agg/% Total Agg)

MIX	CCAGG 6-20	NRSAND	CGSAND	RA
Control M1	0,53	0,28	0,19	0,00
Control M2	0,48	0,28	0,24	0,00
M1 y M2 (5)	0,46	0,27	0,23	0,05
M1 y M2 (7,5)	0,44	0,26	0,22	0,075
M1 y M2 (10)	0,43	0,25	0,22	0,10
M1 y M2 (12,5)	0,42	0,25	0,21	0,125

Figure 7 shows the grading of the combination of the aggregates used for 10 % of replacement. It can be seen that the combination meets the requirements of the grading limits stated by IRAM National Standards [4].

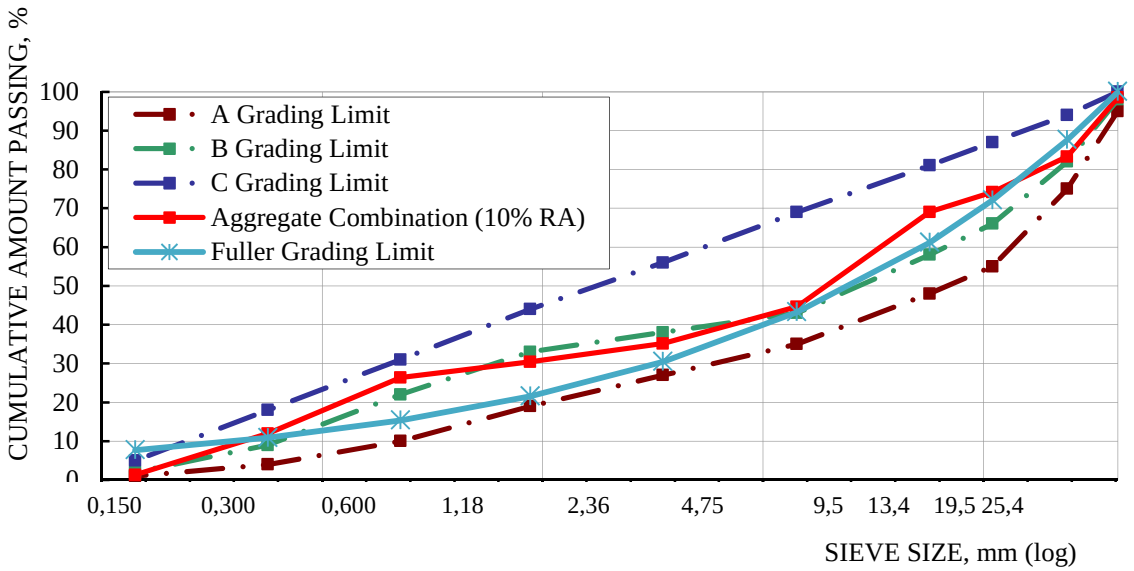

Figure 7 Grading curves for 10 % of rubber aggregate replacement

Cement

Ordinary Portland Cement CPN50(ARI)(*) was used in concrete mixes in the present investigation because it is suitable when it is required high strength at early ages. The main characteristics of the cement used are included in Table 4.

The use of “PFA” originated for a recently constructed thermal power station is under consideration as the volume of this by-product is high and it would represent both a cost and environmental benefit. Although the PFA was analysed and it meets the requirements for this kind of additions, the development of trial mixes using this supplementary cementing material is the objective of another stage of the present project.

Table 4 Characterisation of cement

PHYSICAL AND MECHANICAL PROPERTIES CPN50(ARI)(*) [5]	
Density, g/cm^3	3,12
Specific surface (Blaine Method), m^2/kg	445
Compressive strength, MPa	
1 day	19,2
2 days	34,6
3 days	39,9
7 days	50,5
28 days	60,5

(*) CPN: Ordinary Portland Cement; 50: compressive strength in MPa; ARI: Early High Strength equivalent to CEM I 52,5 according to EN 197-1.

Admixtures

A superplasticiser admixture of high range water reducing was used in an average dosage of 0,5 % of the mass of cement[6]. This admixture was used to get better workability considering that the addition of the rubber aggregates decreases slump. This product is typically used for precast units and presents a limited effect in time which is not a problem in a controlled process.

Mix Design

Selection of the optimum rubber aggregate replacement

Mix design for the present objective was based on a fixed cement content, two different water/cement ratios and constant aggregate volume proportion. Table 5 and 6 show the quantities of the constituents used for the mixes studied for one cubic metre of concrete. A 0% replacement of rubber aggregate was considered as control mix. The total volume of aggregate was replaced by the 5; 7,5; 10 and 12,5 % of RA and the relative proportions of the ordinary aggregates were maintained for both w/c ratios according to Table 3.

Table 5 Mix proportions for the designed mixes M1 w:c = 0,45

MATERIAL PROPORTIONS, kg/m^3	M1	M1(5)	M1(7,5)	M1(10)	M1(12,5)
Cement (OPC)	330	330	330	330	330
Water	148,5	148,5	148,5	148,5	148,5
CCAgg 6-20	937,7	890	866,6	843,2	819,7
NRSand	494,2	469,1	456,8	444,4	432,1
CGSand	464,1	440,5	428,9	417,3	405,7
RA1	0,0	57,4	86,1	114,8	143,5
Dosage SP %	0,5	0,8	0,8	0,8	0,8

Table 6 Mix proportions for the designed mixes M2 w:c = 0,55

MATERIAL PROPORTIONS, kg/m³	M1	M1(5)	M1(7,5)	M1(10)	M1(12,5)
Cement (OPC)	330	330	330	330	330
Water	181,5	181,5	181,5	181,5	181,5
CCAgg 6-20	896,2	851,4	829,0	806,6	784,2
NRSand	472,4	448,8	436,9	425,1	413,3
CGSand	443,6	421,4	410,3	399,2	388,1
RA1	0,0	54,9	82,4	109,8	137,3
Dosage SP %	0,36	0,36	0,36	0,36	0,36

Mix preparation

All mixtures were mixed in a conventional blade-type mixer with 24 rpm, optimum capacity 150-250 dm^3. Mixing procedures were the same for all of the concrete mixes. The natural aggregates with 30 % of mixing water were loaded in the first place and they were mixed in order to wet them. After that the rubber aggregate was introduced and thoroughly mixed. Then the cement and the rest of the mixing water with part of the admixture were added, mixing them during 3 min. Finally all the superplasticiser was incorporated with an additional mixing time of 2 min to produce a uniform mix. Figures 8 to 10 show the aspect of the mix in the different stages.

Figure 8 Mixing of the RA with the natural aggregates

Figure 9 Addition of cement

Figure 10 Aspect of the mix

Standard cylinders (100 mm diameter x 200 mm height) specimens were prepared for compressive strength. Moulds were filled with fresh concrete in two layers and compacted with the standard 16 mm diameter rod. The casting of the specimens for measuring thermal conductivity had to be compacted by means of a mechanical vibrator. Immediately after casting, the specimens were covered with a polythene sheet to prevent water evaporation. The specimens were then demoulded 24 hours later and cured in a water tank at a constant temperature of 23˚C in accordance with ASTM C 39.

Properties of Rubberised Concrete

Workability

As it was expected it was observed a decrease in slump with increased rubber aggregate content by total aggregate volume. Angular, irregular shapes and the presence of steel fibres contributed to reduce fluidity of the mixes as well.

The use of a superplasticiser contributed to achieve an acceptable workability. In order to measure a representative parameter both slump and Vebe time were determined when the method were applicable. Table 7 and 8 includes the results of the tests mentioned.

The appearance of the finished surfaces was similar to that of ordinary concrete and surface finishing was not problematic.

In general, the rubberised concrete batches showed acceptable performance in terms of ease of handling, placement and finishing.

Concrete density

The replacement of natural aggregates with rubber aggregates reduced the density of the concrete. This reduction is due to the lower unit weight of rubber aggregate compared to ordinary aggregate. The values determined can be seen in Table 7 and 8.

Air content

When rubber aggregate was added to the concrete, the air content showed no significant change as it can be observed in Table 7 and Table 8.

Table 7 Properties measured in fresh state M1 w:c = 0,45

PROPERTY	M1	M1(5)	M1(7,5)	M1(10)	M1(12,5)
Slump, cm	16,5	5,5	1,0	0,5	0,0
Vebe time, s	---	---	10,2	12,9	21,0
Air content, %	3,4	1,8	2,4	2,9	2,0
Unit weight, kg/m^3	2404	2361	2328	2368	2296
Workability	Good	Acceptable	Acceptable	Acceptable	Acceptable
Appearance	Good	Acceptable	Acceptable	Acceptable	Acceptable

Table 8 Properties measured in fresh state M2 w:c = 0,55

Determination	M2	M2(5)	M2(7,5)	M2(10)	M2 (12,5)
Slump, cm	19,0	14,5	10,0	6,5	2,0
Vebe time, s	---	---	---	---	---
Air content, %	2,1	2,7	3,8	3,6	2,9
Unit weight, kg/m^3	2340	2268	2240	2252	2255
Workability	Excellent	Very Good	Good	Acceptable	Acceptable
Appearance	Excellent	Very Good	Good	Acceptable	Acceptable

Mechanical properties

This study focused on compressive strength in relation to the quantity of rubber included in the concrete. Some preliminary studies have also been carried out to investigate thermal conductivity. The tests are still under development. For the compressive strength tests the specimens used were cylinders according to ASTM C 39.

The present development has demonstrated that the addition of rubber aggregate into the concrete mixture produces a reduction in the mechanical strength. It was found that the reduction in concrete strength increased with increasing the rubber aggregate volume content.

The sets of specimens were tested for each water/cement ratio covered the control mix with 0% and 5; 7,5; 10 and 12,5 % of total aggregate volume RA replacement.

Figure 11 shows the compressive strength evolution from 7 to 28 days for the different % of RA replacement for both water/cement ratios mixes and Figure 12 represents the compressive strength reduction.

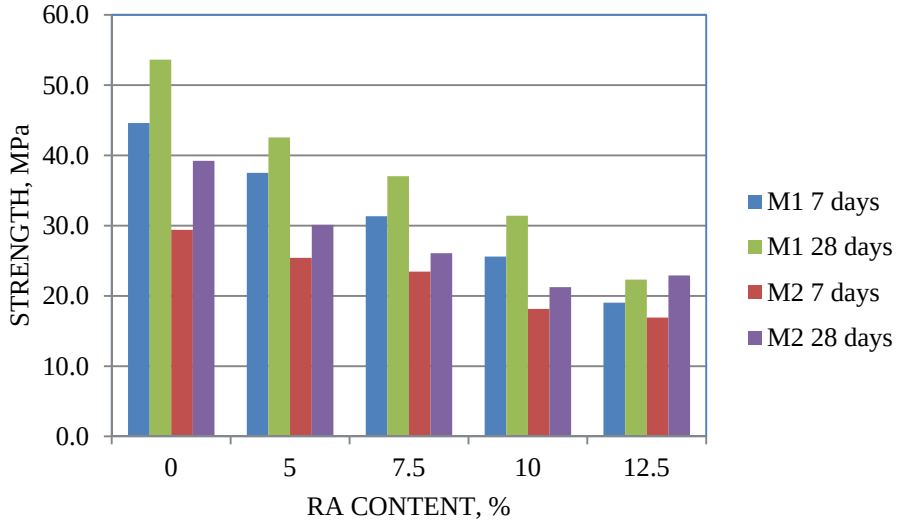

Figure 11 Compressive Strength vs rubber aggregate content

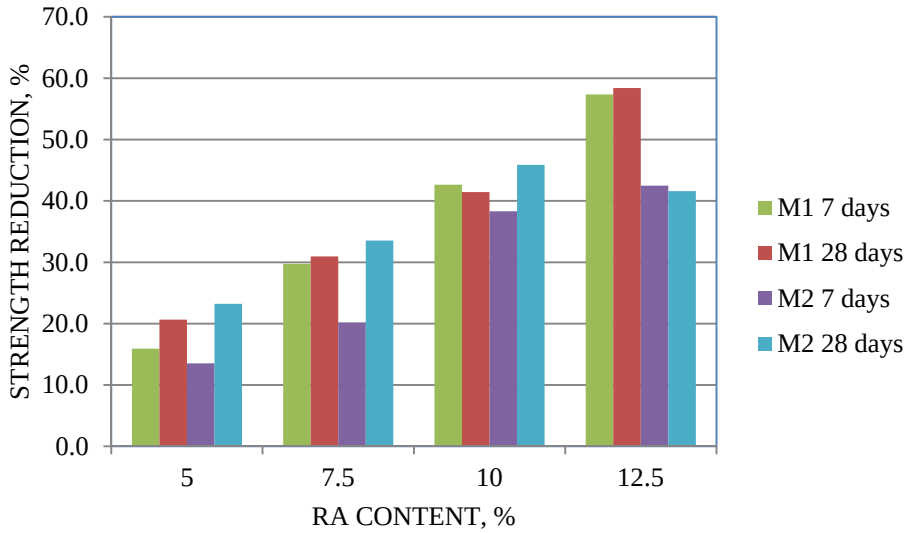

Figure 12 Strength reduction vs rubber aggregate content

Type of failure

The failure was found to be more ductile than conventional concrete. This was assessed by means of the splitting tensile test according to ASTM C 496. This may be due to the fiber constituents of the rubber aggregate.

Figure 13 shows that the presence of rubber aggregate plus the nylon fibers tend to hold the sample fragments together at failure [1]. Test results are not included because studies are still under development.

Figure 13 Type of failure

Dry Mixes for Concrete Blocks

In this case a 15 % percentage of intermediate rubber aggregate was chosen. Table 9 includes the mix proportions. The sequence of addition of materials was in the first place the sand and the rubber chips with half content of total water at low rate of mixing speed during 1,5 min and in the second place the cement and the rest of the water at high rate of mixing speed for 2 min.

The compaction applied was initially with a vibrating table and then by applying 5 and 10 MPa compression. The demoulding was immediate and moist curing was applied. The compressive strength results were not satisfactory due to the difficulty in reproducing in the lab the manufacturing process of concrete masonry units. To go on with this part of the project it is necessary to encourage private precast industries to make trial units.

Table 9 Mix proportions for dry mixes

MATERIALS	MIX PROPORTION, kg/m³
Cement (OPC)	300
Water	120
CGSand	1328,9
RA1	243,1
Dosage SP %	1,2

CONCLUSIONS

- The overall objective of the project was to investigate the feasibility of incorporating rubber tyre chips as a replacement for natural mineral aggregates in concrete. The work undertaken includes the design of rubberised concrete mixes, the evaluation of the fresh and mechanical properties of rubberised concrete and the investigation of the feasibility of concrete products incorporating rubber aggregate. The following are the main conclusions assessed.
- The replacement of aggregates by rubber caused a decrease in workability but due to the use of a superplasticizer the fresh rubberised concrete mixes did not show difficulties in terms of finishing, casting and compaction.

- The air content showed no significant variation in the present studies.

- The density showed a reduction with the increase of RA content.

- The compressive strength test results showed that the use of rubber aggregate in concrete mixes produces a significant reduction in concrete compressive strength which grows with increasing rubber aggregate content. However, if the amount of rubber in the concrete is limited, a normal strength concrete can still be produced with potential uses in non structural applications. This confirmed the results presented in previous investigations included as references [1].

- At this stage a 10 % of replacement was selected to go on studying thermal conductivity improvement.

- It has to be considered that the characteristic of the rubber particles are not constant due to the crushing process and they were used without separating the different constituents.

- The improvement in the type of failure may be interesting to consider in the development of the optimized mixes. This confirms the results obtained in studies used as references [1].

- The dry mixes studied did not show a satisfactory compressive strength due to the difficulty in reproducing in laboratory the necessary compaction energy of precast masonry blocks.

FURTHER RESEARCH

The following are the main guidelines for further research which are under development.

- -Measurement of thermal conductivity: the improvement of this parameter will lead to a cost analysis in order to take advantage of recycled concrete in low cost housing projects
- -Pervious concrete: to use it in parking lots and urban pavements and prevent deterioration from accumulation of water on the surface
- -Measurement of flexural strength with deformation control in order to establish the influence of the fibers present in the rubber aggregates.

ACKNOWLEDGEMENTS

The authors gratefully acknowledge Lic. Liliana Rehak from the Center of Development and Research in Rubber of INTI for the advice and the data provided. The authors also thank REGOMAX for supplying the rubber chips used in the study, Cementos Avellaneda S.A. for the supply of the cement and Grace Construction Products for the supply of the superplasticiser (WR Grace Adva Flex DI 1).

REFERENCES

1. CAIRNS, R, KEW, H Y, KENNY, M J. The Use of Recycled Rubber Tyres in Concrete Construction. Final Report. October 2004. The Onyx Environmental Trust. The University of Strathclyde in Glasgow.

2. KISHORE, K, MATERIALS ENGINEER, ROORKEE. Concrete Aggregates From Discarded Tyre Rubber. Posted in Concrete Engineering, Project Reports, Research Papers.

3. EL DIEB, AS, ABDEL-WAHAB, MM, ABDEL-HAMEED, ME. Concrete using rubber tyre particles as Aggregate. Egyptian army Corps of engineers. Proceedings of the International Symposium Organised by the Concrete Technology Unit, University of Dundee and Held at the University of Dundee, UK on 19-20 March 2001. Edited by RAVINDRA K. DHIR, MUKESH C. LIMBACHIYA, KEVIN A. PAINE.

4. STANDARD IRAM 1627:1997. AGGREGATES. AGGREGATE GRADINGS FOR CONCRETE.

5. STARDARD IRAM 50000. Cements for general use. IRAM 50001:2010. Cements. Special Properties.

6. SPIRATOS, N., PAGÉ, M., MAILVAGANAM, N., MALHOTRA, V.M., JOLICOEUR, C. superplasticizers for concrete. Fundamentals, Technology and Practice. 2003 by Supplementary Cementing Materials for Sustainable Developments Inc., Ottawa, Canada, K1Y2B3.

Gigaton Analysis of the Cement Industry: The Case for Adoption of Proven Technologies

A Gupta[1], M Cullinen[2]
1 – Harvest Power, USA
2 – Carbon War Room, USA

The cement industry is one of the most carbon-intensive industries due in large part to the thermal energy required to produce clinker, the key component of cement. The world produced 3 billion metric tons of cement in 2009, emitting more than 2.4 gigatons (Gt) of CO_2 into the atmosphere. The industry predicts global cement production is projected to grow to 5.9 billion tons by 2020 amounting to annual CO_2 emissions from the production of cement to more than 4.8 Gt. China alone is expected to produce an extra 4 billion metric tons of cement annually by 2020. At a price of roughly $100 per metric ton, the profit margin for the industry is around 33 percent. The total size of the global cement market is more than $250 billion. Aggressive pursuit of proven carbon intensity reduction measures has the potential to reduce emissions from cement production by 0.9 Gt annually before 2020.The largest potential source of reductions with proven technology isthe accelerated use of alternative fuel (370 Mt), followed by clinker substitution with alternative materials (300 Mt), thermal energy efficiency improvements (140 Mt), and electricity efficiency improvements (90 Mt). Switching from coal to biomass for firing cement kilns requires an initial investment of $6.5 million for a 1 million metric ton capacity plant, and would yield savings of $3.8 million per year. Lowering the clinker content of cement requires additional capital expenditures of $13 million for a 1 million metric ton capacity plant for storage and handling, Using blast slag and fly ash to create a 50 percent blend would yield $11.8 million in savings annually, just from the reduced cost of clinker alone.

Carbon War Room explores the barriers preventing the implementation of these low-carbon pathways and generates market-based solutions for overcoming these impediments.

A Gupta is currently a Project Developer at Harvest Power, a leader in processing organic wastes across North America. He Holds an S.M. from the Massachusetts Institute of Technology, and a B.S./B.A. from University of California - Berkeley in Civil Engineering and Economics.

M Cullinen is currently Senior Associate for Research and Intelligence at Carbon War Room, a global non-profit focused on profitable solutions for reducing CO_2 emissions. He holds an M.A. from New York University, and a B.A. from Indiana University - Bloomington.

Keywords: Economic analysis, Efficiency, Greenhouse gas emissions, Low-carbon

INTRODUCTION

Potential for Gigaton Scale Reduction of CO_2 in Cement Industry

The cement industry is one of the most carbon-intensive industries due in large part to the thermal energy required to produce clinker, the key component of cement. The world produced 3 billion metric tons of cement in 2009, emitting more than 2.4 gigatons (Gt) of CO_2 into the atmosphere. The industry predicts global cement production is projected to grow to 5.9 billion tons by 2020 amounting to annual $C0_2e$ emissions from the production of cement to more than 4.8 Gt. China alone is expected to produce an extra 4 billion metric tons of cement annually by 2020. At a price of roughly $100 per metric ton, the profit margin for the industry is around 33 percent [1,2]. The total size of the global cement market is more than $250 billion.[1]

Aggressive pursuit of proven carbon intensity reduction measures has the potential to reduce emissions by 0.9 Gt to 3.4 Gt annually before 2020. Upgrades to existing cement plants and the construction of new buildings using efficient technologies translates to at least a 0.9 Gt emissions savings.

The largest potential source of reductions with proven technology is the accelerated use of alternative fuel (370 Mt), followed by clinker substitution with alternative materials (300 Mt), thermal energy efficiency improvements (140 Mt), and electricity efficiency improvements (90 Mt).

Emerging technologies have the potential to further reduce emissions significantly. Since calcination is the primary source of emission in the cement industry, the most promising technologies going forward are binders that are adequate alternatives to clinker. These include alkali-activated, magnesia, and sulfo-aluminate cements. Another promising class of technologies—those with the potential to sequester CO_2 from flue gas and process it to produce building materials—is fast emerging, but is unlikely to scale within the time frame of interest. The potential for scaling traditional methods of carbon capture and storage (CCS) is remote, owing to high estimated capital costs for using such technology - $592.9 billion according to the IEA BLUE scenario, with little expected return without a price on carbon.[3]

Investment Opportunity

Reaching a gigaton-scale reduction in CO_2 emissions from the production of cement will require a capital investment of $175 billion, of which increasing thermal efficiency is the most capital intensive ($149 billion) and also the least cost effective. With an investment of $10 billion for alternative fuels, $17 billion for clinker reduction, and $.6 billion for electricity efficiency ($27.6 billion), there is an opportunity to reduce emissions by 760 Gt of CO_2 annually while also generating significant returns with short payback periods.

Switching from coal to biomass for firing cement kilns requires an initial investment of $6.5 million for a 1 million metric ton capacity plant, and would yield savings of $3.8 million per year.

Lowering the clinker content of cement requires additional capital expenditures of $13 million for a 1 million metric ton capacity plant for storage and handling, Using blast shag and fly ash to create a 50% blend would yield $11.8 million in savings annually, just from the

reduced cost of clinker alone. The savings derived from a reduced thermal energy requirement (producing blended cement requires less heat and thus less fuel) would significantly add to the savings. A 25% blend would yield $5.7 in annual savings.

Upgrading to state-of-the-art equipment with an energy efficiency of 89 kWh/t production requires an initial investment of $660,000 per 1 million metric ton capacity plant, and would yield annual savings of $1.19 million.

Market Barriers

Due to high capital expenditure requirements, most cement plants are highly leveraged. As a result, cement manufacturers encounter difficulties accessing capital for investment in efficiency improvements to reduce emissions. A million metric ton capacity plant has an average lifespan of 50 years and costs about $250 million to construct, equivalent to approximately three years of production. Efficiency improvement efforts usually entail large capital costs. For instance, upgrading to pre-heaters and pre-calciners costs about $90 million for a million metric ton capacity plant, and waste heat cogeneration usually accounts for 15 percent of the total investment of cement enterprises.

Globally, 18 major cement producers, including the top five cement producing companies—Lafarge (France), Holcim (Switzerland), Heidelberg (Germany), CEMEX (Mexico), and Italcementi (Italy)—together account for a mere 30 percent of the total cement production on the planet. In China, the top 10 producers account for only 23 percent of total cement production in the country. The situation is similar in India, with the top five producers accounting for approximately 46 percent of their market. Thus, it is difficult for any one actor to have unilateral impact by altering production habits. Cement producers are in a competitive market dominated by price and cannot compromise on quality. As a result, the industry is risk averse and reluctant to invest in unproven technology.

Calcination of limestone to produce clinker contributes to about 50 percent of CO_2 emissions from cement manufacturing. Thus, two important levers for decreasing emissions are reducing the clinker content of cement and finding alternative ways of producing clinker. However, each measure has an impact on one or more of the desired characteristics of cement such as strength, durability, malleability, and price. Alternative cements therefore end up being used in most cases for niche applications, though certain types of blended cements are being used as direct replacements for OPC.

Because cement is used for the construction of structures that we trust with our lives, the industry faces stringent regulations to uphold the highest standards for safety. In addition to such regulations on cement manufacturers, large purchasers of cement (such as Departments of Transportation) impose their own restrictions in the form of procurement standards, which are often even more stringent. Such restrictions often become embedded in the system and create barriers against positive change, particularly those that are prescriptive rather than performance-based.

EMISSIONS FROM CEMENT PRODUCTION

The production of one metric ton of cement creates an average of 820 kg of CO_2 emissions. Collectively, the production of 3 billion metric tons of cement in 2009 accounted for 5 percent of total global anthropogenic CO_2 emissions.

Table 1 Carbon emissions from cement manufacture

CARBON EMISSIONS BY PRODUCTION PHASE		
Production Phase	kg $CO_2/t_{clinker}$	kg CO_2/t_{cement}
Calcination	510	403
Fuel	353	318
Electricity	-	100
Total	-	800

Clinker, the main ingredient in cement, is made by heating limestone along with clay, sand, and small amounts of bauxite and iron ore at temperatures as high as 1,450˚C in a kiln. Current processes require an average of 3.9 gigajoules per metric ton of clinker ($GJ/t_{clinker}$). Coal and petcoke are the most common fuels used for cement production, accounting for about 90 percent of the derived thermal energy.

Table 2 Thermal energy & carbon intensity of fuel sources

COMMON AND POTENTIAL FUEL SOURCES		
Fuel Source	Derived Energy - 2010	kg CO_2/t_{cement}
Coal	90%	374.4
Petcoke	*incl. above.*	393.9
Natural Gas	5%	211.38
Fossil Based Alternatives	3%	273
Carbon-Neutral Fuels	2%	-

Electrical energy is used in the rotary kiln and for grinding and mixing raw materials as well as finished cement. The average amount of electricity used at a cement plant is 111 kWh/t_{cement} and the average concentration of emissions from the power sector is 0.9 kg/kWh.[3] Thus, the average CO_2 emissions from electricity consumption are 100 kg of CO_2/t_{cement}.

At the current average clinker-cement ratio of 79 percent, the total CO_2 emissions resulting from cement manufacturing are 820 kg of $CO_2/t_{cement.}$

Industry Growth

Global cement production grew by 6.5 percent between 2004 and 2009, with growth rates in China and India higher than 11 and 8 percent respectively. The Chinese cement industry grew at an annual rate of 12.2 percent between 1970 and 1995 and higher than 9.5 percent per year consistently for all but one of the last ten years.[4,5] The Chinese growth rate used in this report is based on the seemingly realistic projections made by 8.4 percent per year between

2010 and 2015, and 7.8 percent per year between 2015 and 2020.[5] Similarly, the Indian cement industry has been growing at higher than 8 pecent per year and is expected to grow at 8 percent per year for the next decade.[6] The third largest cement producing country in the world, the US, shrunk at -6.2 percent per year between 2004 and 2009, but is projected to recover and grow at more than 4 percent per year till 2020.[2] The cement industry in the rest of the world grew at an average 2.1 percent per year between 2004 and 2009, and is projected to grow at the same rate going forward to 2020.

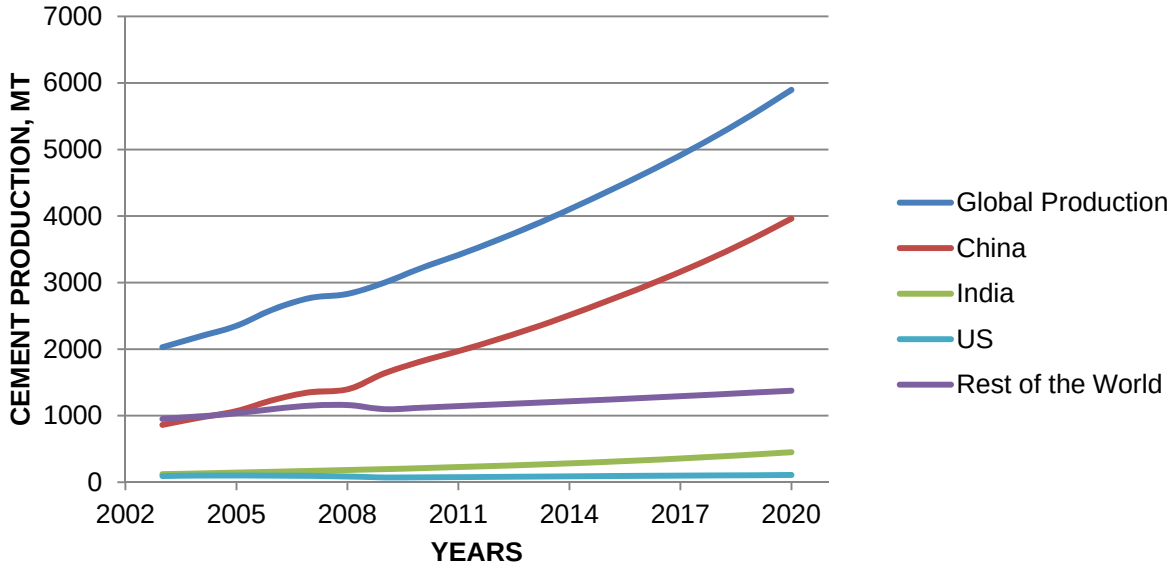

Figure 1 World cement production 2003-2020

Under these assumptions, cement production is expected to almost double from the 2009 level to 5.9 billion metric tons in 2020 – an average annual growth rate of 6.24 percent. China, with the highest production share (currently 54 percent) and one of the highest growth rates alone will account for 80 percent of this growth with production reaching 3.96 Gt in 2020.

Notably, this industry growth projection is largely different from growth projections made by the WBCSD (1.25 percent per year between 2000 and 2050 to 4.4 Gt in the high growth scenario and merely 0.84 percent to 3.69 Gt in the low growth scenario), McKinsey (3.20 percent between 2005 and 2030 to 5.2 Gt), and WWF/Lafarge (1.49 percent per year to 5.5 Gt by 2050). Our projections seem most realistic given the explosive historic and expected growth rates in China and India, and the high and accelerating global rate of growth since 1970.

CONFRONTING GLOBAL GHG EMISSIONS IN THE CEMENT INDUSTRY

By aggressively pursuing implementation of proven technologies, the cement industry can reduce emissions by an estimated 900 Mt annually by 2020. The largest potential source of reductions with proven technology is the accelerated use of alternative fuel (370 Mt), followed by clinker substitution with alternative materials (300 Mt), thermal energy efficiency improvements (140 Mt), and electricity efficiency improvements (90 Mt).

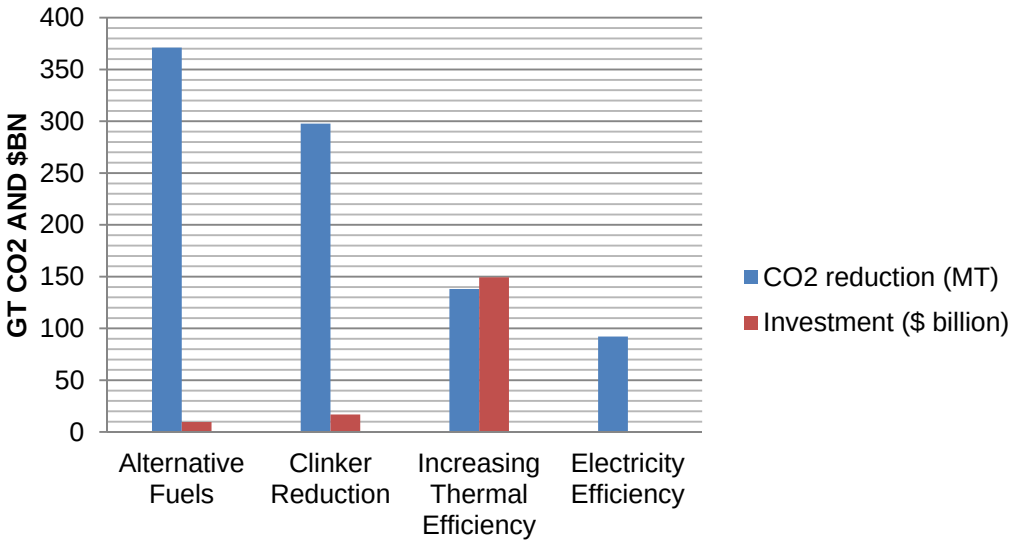

Figure 2 The path to gigaton scale reduction

High Efficiency Kilns

Switching from wet kilns to state-of-the-art dry kilns could result in savings as high as 3.8 GJ/$t_{clinker}$. If coal or petcoke is the fuel of choice at the plant, these energy savings translate to 380 kg of CO_2 emissions reduction per metric ton.

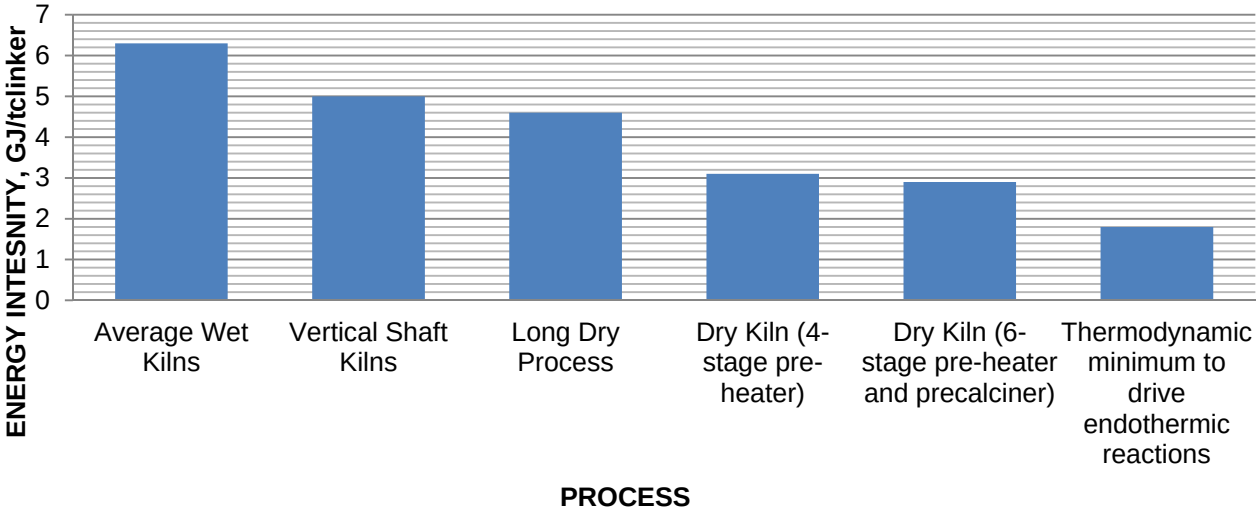

Figure 3 Energy intensity of cement production processes

The efficiency of the average cement plant today is roughly 3.9 GJ/$t_{clinker}$.[3] Thermal efficiency will likely improve at an annual rate similar to that achieved between 1994 and 2003 to 3.62 GJ/$t_{clinker}$ in 2020, meaning that 51 percent of all new plants are predicted to have an efficiency of 2.9 GJ/$t_{clinker}$.[7] To reach gigaton-scale CO_2 reductions, all new plants built between 2011 and 2020 (3321 Mt of capacity) must be state-of-the-art, resulting in an average thermal efficiency of 3.3 GJ/$t_{clinker}$ by 2020.

In comparison, the top five percent of cement plants today operate at a thermal energy intensity of 2.9 GJ/t_{cement}. The target for the 2020 efficiency scenario is achievable, especially with China's mandate to demolish all vertical shaft kilns by 2020 and replace them with state of the art technology.[8] China has already replaced 260 Mt of vertical shaft kilns since 2006 and is on course to replace the entire remaining stock (approximately 30 percent) with state-of-the-art technology by 2020.[9]

Clinker Replacements

Blended cements consist of a mixture of Ordinary Portland Cement (OPC) and replacement material, which can be naturally derived or the product of silica-rich waste material that reacts with calcium hydroxide to form calcium silicate hydrate. Popular pozzolans used today include fly ash, slag, and silica fume. Ground limestone and recycled concrete can also be blended in small quantities as filler material with clinker. "The economic benefits of using natural pozzolans could save contractors up to 25% per bag of cement."[10]

Blended cements have a lower heat of hydration, improved workability and higher resistance to chemical effects associated with alkali-aggregate reactions. Portland cement can be replaced with pozzolans today, for example using standard ASTM C 1157 in the US or EN 197 in Europe. Blended cements already have a 68 percent market share in India, 52 percent in Europe, and 40 percent in China, but only 4 percent in the United States. Though blended cements are allowed in most jurisdictions to contain up to 35 percent fly ash or up to 70 percent blast furnace slag, much smaller percentages are actually mixed in with OPC.[11] The addition of replacement materials entails no process emissions and greatly reduces the thermal energy required for production.

Also noteworthy, adding 5 percent limestone and 5 percent recycled concrete as filler material will yield an ambitious but viable blend of cement (50 percent clinker, 45 percent supplementary cementing materials, and 5 percent gypsum). China and India have already set aggressive targets for decreasing the clinker content of cement produced domestically from 65 percent down to 49 percent by 2020 in China, and from 75 percent down to 52 percent by 2030 in India.

Emissions from calcinations will account for more than 2.2 Gt of emissions annually by 2020 in the business as usual (BAU) scenario. By reducing the clinker-cement ratio from 74 percent to 64 percent by 2020 in the BAU scenario, the industry can save 298 Mt of CO_2 emissions per year from the reduction of calcination alone.

In order to reach gigaton scale, the industry would have to utilize 85 percent of available fly ash, slag, and natural pozzolanic material in the manufacturing process by 2020, along-with substitution of 5 percent clinker each by limestone and recycled concrete filler.

Since the replacement of 1 metric ton of clinker results in the reduction of 0.51 metric tons of CO_2 emissions, the total abatement potential from the reduction of calcination is 298 Mt CO_2.

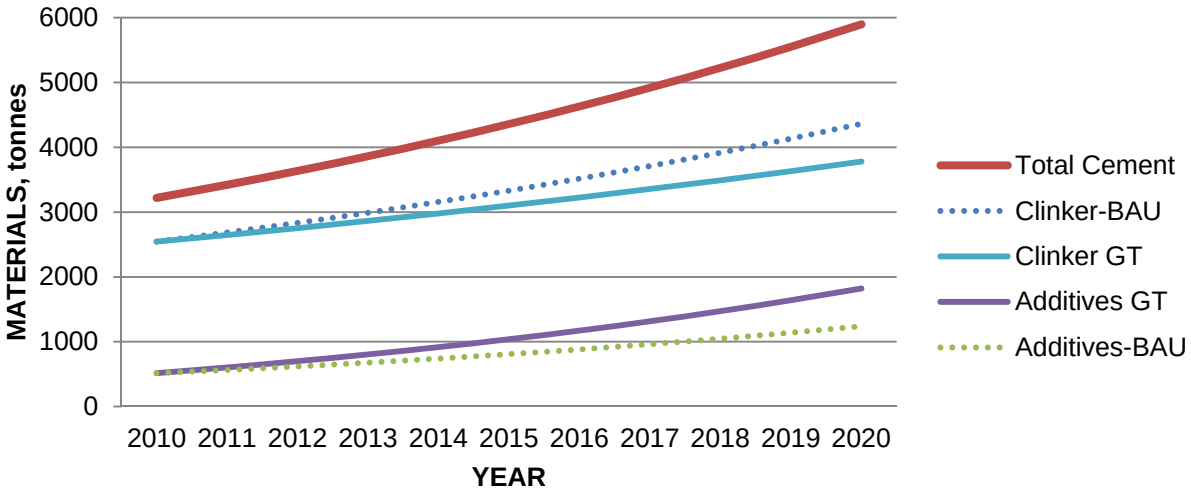

Figure 4 Potential blended cement production 2010–2020

Table 3 Potential Changes in Cement Composition

CHANGES NEED TO REACH GIGATON SCALE			
Material	2020 BAU (Mt/%)	2020 Gt (Mt/%)	Availability (Mt/%)
Clinker	4364 (74%)	3780 (64%)	-
Gypsum	295 (5%)	295 (5%)	-
Alternatives-Total	1238 (21%)	1822 (31%)	-
Fly Ash	619	765	900
Slag	124	213	250
Pozzolan	186	255	300
Limestone	186	295	-
Recycled	124	295	3500

Electrical Energy

Processing blended cements requires an additional 8.9 kWh/$t_{cement,}$ mainly due to an increased grinding requirement.[12] Since the total additional quantity of blended cement produced in the gigaton scenario is 1.3 billion metric tons and the carbon intensity of electricity is 0.9 kg/kWh, the total additional emissions amount to 10.4 Mt CO_2.

The reduction potential is substantial: a study of European cement plants found that the 90th percentile kilns consume roughly 130 kWh/t_{cement} while the 10 percent best in class kilns consume just 89 kWh/t_{cement}.[13] The global average is close to 111 kWh/t_{cement}.

The 2020 efficiency scenario envisages reduction of the electricity intensity of cement plants from 106 kWh/t_{cement} in the BAU scenario to the current state of the art 89 kWh/t_{cement} on average.[3] This would yield an emissions reduction of 92 Mt of CO_2 at a total additional capital cost of $0.61 billion.

Alternative Fuels

Moving toward a cleaner fuel mix has the greatest potential to reduce CO_2 emissions in the industry. The predominant fuels used in the cement industry today are also the most polluting. The two biggest cement manufacturers—China and India—each depend almost entirely on coal. It is possible to derive 100 percent of thermal energy from alternative fuels sources, including various types of waste.

Waste materials such as used tires can also be used to fire kilns and can result in significant emission reductions. The use of waste materials has lower carbon intensity than coal or petcoke, and cement kilns are more efficient than incinerators that would otherwise be used to dispose of these wastes. Another advantage is that the process does not generate residues because the ashes are incorporated into the clinker mixture.

Other alternative fuels include agricultural and forestry biomass as well as waste materials including biodegradable municipal waste, animal waste, paper waste, animal meat, and bone meal.

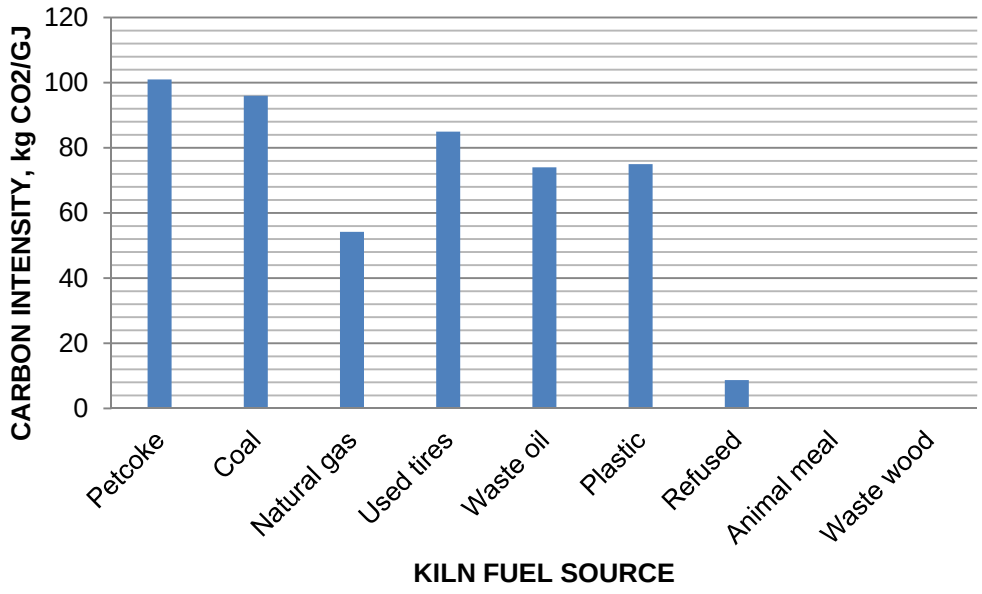

Figure 5 Intensity of emissions for various fuels

In order to reach a gigaton-scale reduction in CO_2 emissions, cement manufacturers worldwide would have to use a mix of fuels to fire their kilns that consist of 40 percent less coal and petcoke, which will reduce the amount of CO_2 emitted per GJ of thermal energy produced from the current average of 92.3 to 67.6.

Table 4 Potential changes in cement kiln fuel sources

POTENTIAL SCALE-UP SCENARIO			
Fuel Source	2010	2020 BAU	2020 Efficiency
Coal/Petcoke	90%	75%	50%
Natural Gas	5%	15%	15%
Fossil – Waste	2%	5%	15%
Non-Fossil	3%	5%	20%
kg CO_2/GJ	92.3	85.1	67.6%

At 2.55 GJ/t_{cement}, the estimated thermal energy requirement given the use of high efficiency kilns and an aggressive blend, the total heating value requirement from non-fossil alternative fuels to reach gigaton scale by 2020 is 3 billion GJ. At an average energy content of 10 GJ/t, the total requirement of non-fossil alternative fuels in the global cement industry in 2020 amounts to 301 Mt. Meeting this feedstock requirement does not present a challenge: The total energy value of unused forest biomass residues in ten provinces in 2006 in China alone was 1.6 billion GJ.[14] At 10 GJ/t, the 1500 Mt of collected municipal solid waste globally accounts for another 15 billion GJ of thermal energy.[15]

Table 5 Alternative Fuel Requirements

POTENTIAL SCALE-UP SCENARIO					
Fuel Source	Energy Content (GJ/t)	Unit	2010 Usage	2020 BAU	2020 Efficiency
Coal/Petcoke	3021	MT	332	449	251
Natural Gas	5322	BCM	14	71	59
Fossil – Waste	4023	MT	6	22	56
Non-Fossil	1024	MT	33	90	301

INVESTMENT REQUIREMENTS

In order to achieve an annual reduction of 900 Mt of CO_2 representing a 19 percent reduction in emissions, $176 billion in capital expenditures is required over 10 years.

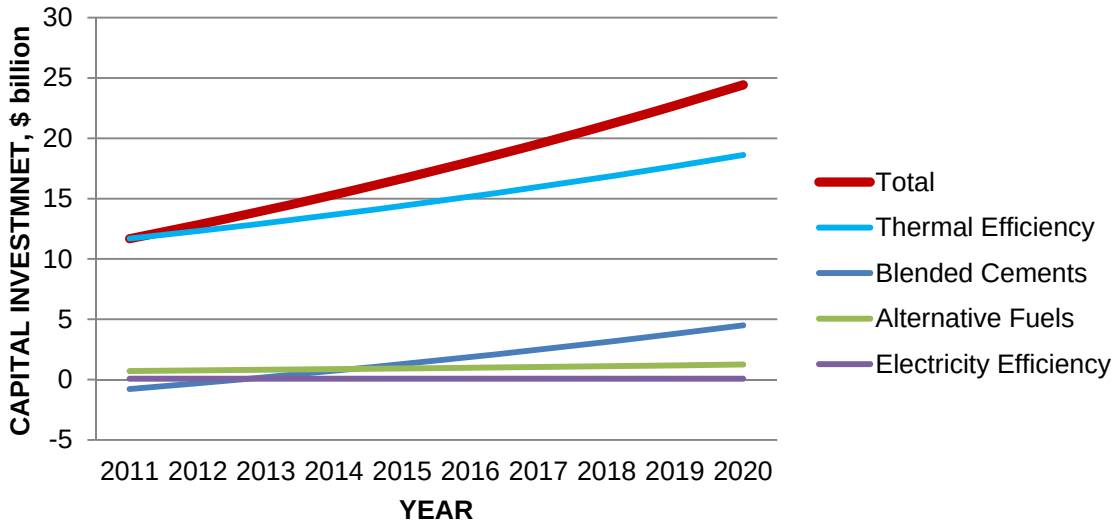

Figure 6 Total capital investment required 2010-2020

Thermal Efficiency and Fuel Substitution

Upgrading to pre-heaters and pre-calciners saves between 0.9 and 2.8 GJ/$t_{clinker}$ and costs around $91 million for a one million metric ton capacity plant. Switching from coal and petcoke to natural gas and alternative fuel plants costs $6.5 million per million metric ton capacity. To achieve the business as usual (BAU) target of 3.62 GJ/$t_{clinker}$, 51 percent of new plants (1680 Mt) need to incorporate the highest thermal efficiency technology. To meet the fuel substitution targets, cement plants representing 884 Mt of production capacity will need to burn natural gas and plants representing 295 Mt each need to burn fossil waste and carbon-neutral fuels.

In order to reach gigaton scale, 100 percent of the new plants (3552 million metric tons of capacity) must utilize the highest thermal efficiency technology, resulting in an overall thermal intensity of 3.34 GJ/$t_{clinker}$. To meet the fuel substitution targets, plants producing a combined annual total of 884 Mt of cement, need to burn natural gas and fossil-waste, and plants producing a combined total of 1179 Mt need to burn carbon-neutral fuels. The additional capital investment required is $159 billion by 2020, as outlined in the Table 6.

Table 6 Capital Investment for Thermal Efficiency and Fuel Substitution

INVESTMENT (2010-2020 $BN)			
Item	BAU	GT	Additional
Subtotal - Efficiency	153	302	149.3
Natural Gas	4.7	4.7	-
Fossil Waste	1.5	5.3	3.8
Carbon Neutral Fuels	1.3	7.0	5.7
Subtotal – Fuel Substitution	7.5	17.1	9.6
Total	160	319	159

Rate of Return

The capital cost to upgrade the pre-heaters and pre-calciners in a 1 million ton cement plant is $91 million dollars. These upgrades yield energy savings of .9-2.8 GJ/$t_{clinker}$. At an average cost of $141.90 per ton of coal, the savings derived from such an upgrade would be $2,128,500-$6,622,000 annually for a million ton capacity plant producing cement with a 50% clinker content, and $4,044,150-$12,581,800 annually for a plant producing OPC. As a result, the internal rate of return varies widely, and is only positive within a 10-year timeframe (6%) in the highest possible efficiency scenario (2.6 GJ savings) for plants producing OPC.

The average price per metric ton of biomass alternative fuels is $32.50.[7] Given the rising price of coal ($141.90 per metric ton in Jan. 2011), switching to non-fossil alternative fuels to fire cement plant kilns, particularly biomass, is increasingly attractive.[16] With an average energy content of 10 GJ/t, savings from using biomass as a replacement for coal in a 1 million metric ton capacity plant, at an average energy requirement target of 2.55 GJ/t_{cement} would be approximately $3.8 million per annum. Switching from coal to alternative fuel requires an additional investment of $6.5 million per million metric ton capacity plant, therefore switching from coal to biomass will begin yielding savings after a year and a half. For a plant with a 50-year life span, the total savings could amount to $184 million.

As the price of coal is variable, as is the price of biomass each plant must conduct an individual analysis of the potential savings from switching fuel sources. Other factors such as transportation may add additional costs as well.

Blended Cement

Storage and handling of alternative materials requires between $10 and $16 million per million metric ton of cement production capacity [17]. A weighted average of $13 million has been used for this analysis.

Table 7 Capital Investment for Cement Capacity

INVESTMENT (2010-2020 $BN)			
Type	BAU	Gt	Additional
OPC	371	47	-324
Blended	483	824	341
Total	854	871	17

Based on the regular composition of Ordinary Portland Cement (OPC) (approximately 95 percent clinker and 5 percent gypsum) and the aggressive blend (50 percent clinker), 53 percent of cement will remain as OPC by 2020 in the BAU scenario. In the efficiency scenario, this number changes to 31 percent in order to achieve an average clinker-cement ratio of 64 percent.

Thus, the production capacity of blended cement in the gigaton scenario grows by 3130 Mt, and that of OPC cement by 190 Mt, between 2010 and 2020. In the BAU scenario, the corresponding numbers are 1840 Mt and 1480 Mt. The total additional capital investment required for the gigaton scenario calculates to $17 billion. Operational cost savings will depend on price of clinker substitutes and reductions in fuel use.

Rate of Return

Lowering the clinker content of cement has the potential to generate large cost savings for cement plant operators with very short payback periods for initial capital expenditure for new handling and storage equipment.

The average price of clinker in China is $55.00 per metric ton, including shipping costs.[18] Substitutes for clinker, cost substantially less: $30 per metric ton for fly ash and $5 per metric ton for blast furnace slag.[19,20]

Processing blended cements requires an additional 8.9 Kwh/$t_{cement,}$ raising the costs for operating a 1 million metric ton plant by $623,000 per year.[21] Even with this additional cost, switching to a mix of these clinker alternatives can save $11.8 million for a 50 percent blend and $5.6 million for a 25 percent blend annually for a 1 million metric ton plant.

Factoring in the high capital cost for new handling and storage facilities that cost on average $13 million for a 1 million ton capacity plant, the internal rate of return would be 90 percent for the 50 percent blend and 41 percent for the 25 percent blend, and that doesn't even include the savings generated from the reduced cost of fuel derived from the reduced thermal energy requirement achieved by reducing clinker content.

Electrical Energy

The capital investment required for these efficiency measures ranges between $0.20 metric ton of CO_2 emissions reduction (efficient motors) and almost $12 per metric ton of CO_2 emissions reduction (raw meal blending systems).[5] The weighted average of these electricity efficiency improvement measures amounts to $6.60 per metric ton of CO_2 emissions reduction. Thus, the total additional capital investment required to reduce 92 Mt of emissions between the BAU and the Gt scenarios is $0.61 billion.

Rate of Return

By reducing the amount of electricity necessary to produce cements from 106 kWh/t in the BAU scenario to the current state-of-the-art 89 kWh/t_{cement} production equipment, cement manufacturers can save $1.19 million per annum.

The capital expenditure required for upgrading to state-of-the-art equipment with an efficiency of 89 kWh/t is $660,000 per 1 Mt capacity plant, yielding an internal rate of return of 198%. The payback period will vary for individual plants based on the kWh cost in a given location.

BARRIERS TO IMPLEMENTATION

Key Barriers for Blended Cement

The potential for future applications of blended cements depend upon the industry's attitude, availability of blending materials, regulatory standards, and legislative requirements. In addition, there remain technical issues that need to be addressed.

OPC has proven to be a reliable and high-performing material and its raw materials are cheap and easy to produce in large quantities. This has led to a lack of innovative drive in the cement industry and limits the uptake of alternative materials. Leadership by large procurement agencies and enhanced visibility of structures such as the Freedom Tower in New York (50 percent fly ash) and the De Young Museum in San Francisco (50 percent fly ash) using high percentages of alternative materials have helped to raise awareness about the potential for these materials, however much more must be done to increase its adoption.

The composition of OPC and blended cements is very different, resulting in several variations in performance. For instance, OPC generally has higher 7-day strength than blended cements, even though the ultimate strength of blended cements is often higher than OPC. The lower initial strength can reduce the speed of construction and thus negatively affect the economics of a project.[22] There are also concerns about using waste materials in cement since industrial wastes can contain high and variable levels of toxic metals.

Development of innovative blends that closely mimic the properties of OPC would greatly accelerate adoption. A leading player for blended cements is Taiheyo Cement Corporation in Japan, which manufactures Eco-cements by using traditional pozzolans and pozzolans created by treating the ash from incinerating a wide variety of industrial and municipal waste sources. There is both a limitation and large uncertainty surrounding the availability and cost of alternative materials such as fly ash and granulated blast furnace slag. The estimated global quantities of fly ash, slag, and natural pozzolans were around 500, 200, and 300 million metric tons respectively in 2006, compared to global cement production in excess of 2 billion metric tons.[3] In addition to limits on gross volumes, regional and local availability of such materials varies. This is a critical challenge, since transportation costs often make the use of blending materials prohibitively expensive.

Regulations and procurement standards have historically been prescriptive, specifying floors and ceilings for various cement constituents, rather than setting standards based off of performance. While some countries have introduced performance-based standards, the main actors in the cement industry are reluctant to prescribe or adopt them owing to lack of information and incentives. For instance, of all the State Departments of Transportation in the United States, only two allow for the use of performance-based standards. These departments argue that there was a lack on incentive for the cement industry to shift away from the tried and tested prescriptions.

Other types of regulation can also limit the use of alternative materials. For instance, the U.S. Environmental Protection Agency is considering a new policy of treating coal combustion products (such as fly ash) as hazardous wastes under Subtitle C of the Resource Conservation and Recovery Act. Industry experts believe that this 'hazardous' designation would create a stigma resulting in rejection of fly ash by the market place."[23]

Challenges Reaching Thermal Energy Efficiency and Fuel Replacement Goals

The greatest barriers to the adoption of energy efficient kilns are the large investment requirements, and the large costs of production disruption. Reducing the GJ/t_{cement} usage on a level necessary to reach gigaton scale would require an investment of $150 billion. In addition, even if this investment is attainable, the implementation of energy efficient kilns will require alternative fuels, which poses a problem in production schedules. Acquiring alternative fuels and preparing them for use can be a logistically difficult task given the varying legislative and environmental barriers in different countries.

Some countries make heavy use of alternative fuels to meet a majority of their needs. For instance, the Netherlands cement industry derives approximately 83 percent of its thermal energy needs from alternative fuels. However, various barriers prevent alternative fuels from being the fuel of choice globally.

Pre-treatment is often required to ensure uniform composition and optimal combustion, which may increase thermal energy consumption. There are other technical issues, such as the control of chlorine and heavy metals that require special handling, transportation equipment, and storage facilities.

Reusable biomass is more readily available in an agricultural belt and municipal waste is found near urban centers. Moreover, consistency of quality is a major challenge. Co-location of industries may help relieve this problem.

There is varying legislative support and enforcement related to co-processing, land filling, and incineration within and across countries. Classification and control at the source point of the waste favors the use of municipal solid waste in the cement production system, but the waste streams in critical countries such as China and India are mixed and lack classification and control. Moreover, the waste collection networks in these countries are inadequate.

There is also a poor public understanding and acceptance of the incineration of municipal solid waste and other waste materials that are thought to be toxic but in fact do not release any pollutants.

Alternative fuel costs are likely to increase as competition with alternative end-use producers (biogas, biofuels, energy generation in other industries) continues to increase their demand for feedstock.

FUTURE SOLUTIONS

While it is clear that the use of high efficiency kilns, the use of alternative fuels, and clinker substitutions can reduce CO_2 emissions from the cement industry on a gigaton scale, there are other solutions that should receive consideration and funding for further development.

Solar Power for Thermal Energy

The use of solar thermal energy in the cement industry should be strongly encouraged in countries with good solar radiation. Heat generated by solar concentrators can be used for preheating the air supply for the plant, preheating the raw mill, or generating additional heat

to increase the electricity output of waste heat recovery units during daytime. As the uptake of cements based on alternative chemistry increases, solar thermal technology will become even more important due to the lower kiln temperatures (700°C–800°C) required.

As highlighted in the gigaton scenario, the biggest opportunity for emissions reduction in the cement industry is from the use of carbon-neutral fuels. In order to fully capture this potential, the cement industry needs to be assured of a consistent supply of biomass and the biomass industry of a consistent source of revenue.

The concepts of co-location of industries and collection and characterization of wastes have a heavy dependence on urban planning.

Carbon Capture and Storage

Though carbon capture and sequestration is a potentially game changing technology, only 10 percent of current plants can be linked to CCS. Other researchers have also dismissed the prospects of any traditional CCS technology (oxyfuel, chemical/physical absorption, membrane processes, sorbent processes, etc.) taking off in the cement industry, citing cost as the largest barrier [24].

The argument against CCS in the cement industry rests on both the concentration of emissions in electricity generation from coal and on the guaranteed rate of return based on expenses in the power industry. Current estimates for the cost of CCS in cement plants are around $50 to $100 per metric ton of CO_2, which would double the price of cement.

However, alternative approaches to CCS could be commercialized in the cement sector by 2020 given adequate support. At least four such approaches are gaining attention and investment.

One of the most promising processes is Calera, which has received a $20 million investment from the U.S. Department of Energy as well as investments from Khosla Ventures and Peabody Coal. Though initially producing only aggregate substitutes, Calera proposes to eventually produce alternatives to clinker. The process involves bringing seawater, brackish water, or brine into contact with the waste heat in power station flue gas where CO_2 is absorbed, resulting in bicarbonate minerals. After turning CO_2 into bicarbonate, the process involves a second step of electrochemistry to turn bicarbonate into carbonate, which is the substitute building material. Calera reports that a 20 to 50 percent replacement of Portland cement has been tested against ASTM C 1157 concrete specifications [25,26].

Calera states that it has achieved greater than 90 percent CO_2 capture at its pilot plant and makes a conservative estimate of 70 percent capture for commercial scale plants. It projects that for a 2 Mt cement plant, it will capture 1.1 million metric tons of CO_2 per annum and increase building material production to 2.4 Mt. The total capital expenditure will be between $180 and $220 million ($90–$110 million/Mt capacity). The cost of CO_2 capture will be between $50 and $60 per metric ton of CO_2. The company is confident that it can make money if it can sell the building materials that it produces for a price of $25 per metric ton [27].

The technology is still in development and several more pilot plants have to be built to assess various parts of the process and suitability to a number of conditions, including those where a natural source of electrolytes is not available. Issues relating to the disposal of hydrochloric acid, a byproduct of the electrochemical process, also need to be addressed.

ACKNOWLEDGEMENTS

The authors would like to thank colleagues Alisdair Pettigrew of Blue Communications and Justin Fishkin of Carbon War Room for their input. In addition, the authors would like to acknowledge Jorgen Clausen of DK Group for helpful comments on the Executive Summary. More than 70 industry experts were consulted in preparation of the Full Report.

Research and production of this report was generously supported by the Gigaton Throwdown Initiative. Additional information can be found at **www.gigatonthrowdown.org.**

REFERENCES

1. SNAP MAGAZINE. ENR Cost Reports: Concrete & Lumber." February-March, 2010.

2. IBISWORLD. Cement Manufacturing in the US: U.S. Industry Report, 2010.

3. WORLD BUSINESS COUNCIL FOR SUSTAINABLE DEVELOPMENT (WBCSD), Cement Technology Roadmap: Carbon Emission Reductions Up To 2050, OECD/IEA and WBCSD, Geneva, 2009.

4. HENDRIKS, C.A. ET AL. Emission Reduction of Greenhouse Gases from the Cement Industry, Paper presented at the Greenhouse Gas Control Technologies Conference, IEA Greenhouse Gas R&D Programme, 2004.

5. TSINGHUA UNIVERSITY OF CHINA. Assisting Developing Country Climate Negotiators through Analysis and Dialogue: Report of Energy Saving and CO2 Emission Reduction Analysis in China Cement Industry, Center for Clean Air Policy, 2008.

6. CONFEDERATION OF INDIAN INDUSTRY. Low Carbon Roadmap for Indian Cement Industry, CII-Sohrabji Green Business Center, Hyderabad, 2010.

7. INTERNATIONAL ENERGY AGENCY (IEA). Tracking Industrial Energy Efficiency and CO2 Emissions, OECD/IEA, Paris, 2007.

8. MCKINSEY & CO. Pathways to a Low-Carbon Economy: Version 2 of the Global Greenhouse Gas Abatement Cost Curve, 2009.

9. TONGBO, S. A brief on China Cement Status: Towards A Sustainable Industry, Paper presented at the IEA-BEE Internation Workshop on Industrial Energy Efficiency, New Delhi, January 27-28.

10. HARRIS, R.A, EATMON, T.D, & SEIFERT, C.W.A. Natural Pozzolans for Sustainable Development: Mapping Poverty in the Philippines, proceedings of the 25th Annual ESRI International User Conference, July 25-29, San Diego, CA, 2005.

11. BHUSHAN, C. Challenge of the New Balance, New Delhi: Center for Science and Environment, 2010.

12. HASANBEIGI, A, MENKE, C, THERDYOTHIN, A. Technical and Cost Assessment of Energy Efficiency Improvement and Greenhouse Gas Emission Reduction Potentials in Thai Cement Industry, Energy Efficiency, Springer, Netherlands, 2010.

13. WORLD BUSINESS COUNCIL FOR SUSTAINABLE DEVELOPMENT (WBCSD). Cement Industry Energy and CO2 Performance: Getting the Numbers Right, Cement Sustainability Initiative, Geneva, 2006.

14. MURRAY, A, PRICE, L. Use of Alternative Fuels in Cement Manufacture: Analysis of Fuel Characteristics and Feasibility for Use in the Chinese Cement Sector, Berkeley, LBNL 525E, 2008.

15. HOLCIM. The GTZ-Holcim Strategic Alliance on Co-processing Waste Material in Cement Production, GTZ, Holcim and FHNW PPP, Coprocem, 2009.

16. INTERNATIONAL MONETARY FUND (IMF). Primary Commodity Prices.

17. EUROPEAN CEMENT RESEARCH ACADEMY (ECRA). Development of State of the Art-Techniques in Cement Manufacturing: Trying to Look Ahead, CSI/ECRA-Technology Papers, ECRA/WBCSD, Duesseldorf, 2009.

18. FIJI TIMES. Fiji Cement Prices Dawn - Fiji Times, Today's Concrete Technology, 2010.

19. AMERICAN COAL ASH ASSOCIATION (ACAA). Frequently Asked Questions, 2011.

20. CLIMATE TECH WIKI. Blast Furnace Slag Granulation, 2010.

21. ENERGY INFORMATION ADMINISTRATION (EIA). Average Retail Price of Electricity to Ultimate Customers by End-Use Sector, by State, 2010.

22. WU XUEQUAN, W, HONG, Z, XINKAI, H, HUSEN, L. Study on Steel Slag and Fly Ash Composite Portland Cement, Concrete and Cement Research vol. 29, pp. 1103-1106, 1999.

23. ADAMS, T H. Is Coal Combustion Product Recycling an Endangered Industry? American Coal Ash Association. House Small Business Subcommittee on Rural Development, Entrepreneurship and Trade, Washington, D.C., 2010.

24. VDZ RESEARCH INSTITUTE OF THE CEMENT INDUSTRY & PENTA ENGINEERING CORP. Carbon Dioxide Control Technology Review, Portland Cement Association, Skokie, 2010.

25. CONSTANTZ, B. CEO of Calera Corporation, and Consulting Professor at Stanford University: Testimony before the United States Senate Subcommittee on Energy and Water Development, a committee within Senate Appropriations, May 6, 2009.

26. DAMTOFT, J S, LUKASIK, J, HERTFORT, D, SORRENTINO, D, GARTNER, E M. Sustainable Development and Climate Change Initiatives, Cement and Concrete Research 38:2, 115-127, 2008.

27. CALERA. Notes on Sustainability and Potential Market, 2010.

Theme 3 — Infrastructure and Transportation Construction and Resilience

Quality Control of Concrete in Mecca Mega Projects

H Z Alabideen
Ministry of Municipal and Rural Affairs (MOMRA), The Kingdom of Saudi Arabia

Many consulting engineers consider it adequate to evaluate concrete quality through merely obtaining the mean of compressive test samples routinely collected by concrete supplier or the project contractor. However, from our long experience and exhaustive testing programs of Mega Projects, we found that these simple procedures are no guarantee for the quality and consistency desired in concrete production. The paper summarizes results obtained from a comprehensive and detailed program designed to monitor quality of ready-mix concrete in mega projects which took more than ten years to construct and 10 Million cubic meters of concrete to build. The concrete specified 28 day strength ranged between 30 to 80 MPa. One hundred thousand compression samples were tested and their results analyzed by statistical evaluation using different international standards. The research showed the importance of monitoring by a neutral external quality control agency to control quality by unscheduled surprise visits; this is carried out in parallel with the routine self monitoring conducted by supplier/contractor or his consultant. The differences in test results between self and neutral agency monitoring were large at the beginning of the construction ; however, with implementing the external monitoring program it became smaller at the end. This is in agreement with experiences of some European companies using similar procedures. The study also showed that statistical evaluation of test results makes it possible to better assess the consistence of concrete production and consequently the concrete quality by obtaining a measure for the scatter of the results. This is in agreement with European standards EN 206-1 and DIN 1045-2 as well as the American standard ACI 214R-02. The results revealed the need to adopt acceptance criteria for ACI 318 consistent with the requirements of ACI 214R-02 and EN 206-1. This is very important for countries that rely on ACI in developing their national concrete codes such as the Saudi Building Code SBC 304.

Dr Habib Zein Alabideen, obtained his B.Sc. and Ph.D. degrees from German Universities Hannover in 1970 and University of Aachen in 1975 respectively. He represents his country in several international committees. He wrote five books in material, design and construction management, he is also the author of numerous scientific papers. He supervised the construction of many project in the development of Holy sites in Makkah with budgets up to 1.8 Billion US Dollars totaling 6 Billion US $ in 15 years.

Keywords: Monitoring production, Quality control, Statistical evaluation, Strength, Testing

INTRODUCTION

The Kingdom of Saudi Arabia (KSA) constructed many projects [1] to develop the infrastructure and services to solve problems that existed in the Al Mashaer Al Muqaddasa (Holy Sites) in order to accommodate the ever increasing number of pilgrims and provide comfort and safety for the guests of God. Some of the prominent examples of these projects is the new Jamarat structure, Fire Proof Tents, Storm and Torrents Drainage systems, Dams Projects in Mena and Muzdalifah , elevated Mashaer train (the Southern Line), only to name a few (Figure 1). Cost of these projects is around 6 Billion US Dollars.

Figure 1 General Views of Four Mega Projects in Makkah AlMukarrama(Mecca) , KSA

These projects were constructed during the last fifteen years and all were finished within budget and on time; the projects or stages of projects must be finished between six and a maximum of eleven months which is the available period between two yearly seasons of pilgrimage. These projects have witnessed exceptionally high standards of quality control monitoring. Ready mix concrete for CIP as well as precast was monitored in two levels; self monitoring by contractor and supervising consultant (internal) and externally through, inspection -surprise- visits, by the Laboratories Central Directorate for Development of Projects (CDDP), in the ministry of Municipal and Rural Affairs (MOMRA) in KSA.

Table 1 gives cost of three of these projects all were directed towards the comfort, safety and security of the some (3.5 – 4.0) million pilgrims who perform the Hajj (pilgrimage) every year.

Table 1 Cost of some Mega Projects in Mecca Holy Site

PROJECT	SAUDI RIYALS, MILLIONS	$ U.S., MILLIONS
New Jamarat Structure	4200	1200
Storm Rain and Torrents Drainage	900	255
Elevated Railway (Southern Line)	6650	1800

The paper deals with details and results related only to the New Jamarat Structure program for monitoring the quality of Ready-Mix Concrete.

NEW JAMARAT STRUCTURE

This structure is one of the Pioneering Mega projects from size point of view as well as methods of construction and technologies utilized. It is located in Mena valley east of the centre of the Holy City Mecca [2, 3]. In its first tier it comprises a basement, ground floor and four above ground floors. Foundations and columns were designed to carry in total eight stories above ground. Figure 2 shows a general view of the structure after completion of first tier. The length of the structure is 550 m without approach ramps with more than 100 m maximum width and 50 m high for the four above ground floors . Material used totaled 1.75 million cubic meters of concrete, 400.000 tons of High tensile steel and 22.500 tons of pre-stressing cables 15.7 mm diam.

Figure 2 General view of the New Jamarat Structure after completion of first tier

Concrete Types and Production

Several mixes were used for cast in- situ (CIP) concrete ranging 30-80 MPa . Precast pre-stressed concrete grades of 35-60 MPa were used. Concrete grades refer to f'_c specified by ACI-318 [4] as the 28 day compressive strength of a standard cylinder 150 mm diameter and 300 mm high tested according to ASTM standard C 39 [5]. Concrete CIP was supplied from a factory (Plant) 4-6 km East of Jamarat structure (Plant A). Production for Precast/pre-stressed was carried out in a Factory in the town of Bahra half way between Mecca and Jeddah cities (Plant B). For the purposes of this paper only results of Plant A are shown

Similar results were obtained from Plant B. Concrete mix design was carried out by plants to satisfy the strength required.

CONCRETE QUALITY MONITORING

Self Monitoring by Contractor / Supervising Consultant

Compressive strength samples were extracted in site from the truck (6 cylinders from each truck) as per ACI 318 [4] for 7 and 28 day testing. The test result is considered as the average compressive strength of these samples. Table 2 shows one page of such report [6] which includes test results for a CIP self compacting concrete (SCC) grade 60 MPa at 7 and 28 day compressive strength. Fig 3 shows a quality chart [7,8] for the same concrete which is produced by plant A. Table 2 and Fig 3. indicate that ACI requirements for this concrete grade are achieved.

Table 2 Plant A – March 2009, 60MPa (SCC)

SAMPLE ID	SAMPLING DATE	FLOW, mm	TEST DATE	7 DAYS				
				Weight, g	Density, kg/m³	Load, kN	Strength, MPa	Mean, MPa
SCC60-3520	09-02-2009	700	16-02-09	13650	2503	946	52.9	53.2
				13900	2549	957	53.5	
				13710	2514	955	53.4	
SSC60-3521	10-02-2009	580	17-02-09	13500	2476	1039	58.1	57.3
				13530	2481	1016	56.8	
				13500	2476	1022	57.1	
SCC60-3522	10-02-2009	580	17-02-09	13480	2472	1050	58.7	57.7
				13840	2538	1027	57.4	
				13660	2505	1022	57.1	
				28 DAYS				
			09-03-09	13710	2514	1233	68.9	69.3 (60)
				13650	2503	1247	69.7	
				13770	2525	1240	69.3	
			10-03-09	13500	2476	1202	67.2	67.1 (60)
				13530	2481	1184	66.2	
				13570	2489	1215	67.9	
			10-3-09	13890	2547	1347	75.3	72.1 (60
				13730	2518	1229	68.7	
				13790	2529	1292	72.2	

Required mean 28 day strength in brackets

External Monitoring by Ministry

This independent monitoring is performed through unannounced (surprise) inspection visits to the site or to the pre-cast factory. This was carried out at the rate of 10 -15 surprise visits each year for each of the five stages of the project that lasted 5 years in construction. Visits were designed by the supervisor of external monitoring. Each visit lasted several days to 2 weeks. Samples were taken once or several times during one visit. Consideration was observed that the samples are representing well the casting conditions (time of day, temperatures, days of the week, months etc.) , the ordered amounts of concrete (large or small) and of course for the different grades of concrete (35, 40, 50, 60 and 80 MPa).

Samples handling , curing , and testing were done according to ASTM- C31 [9] and ASTM C39 [5]. Results were documented for each visit [10] and a report after evaluation of the results were written at the end of program.

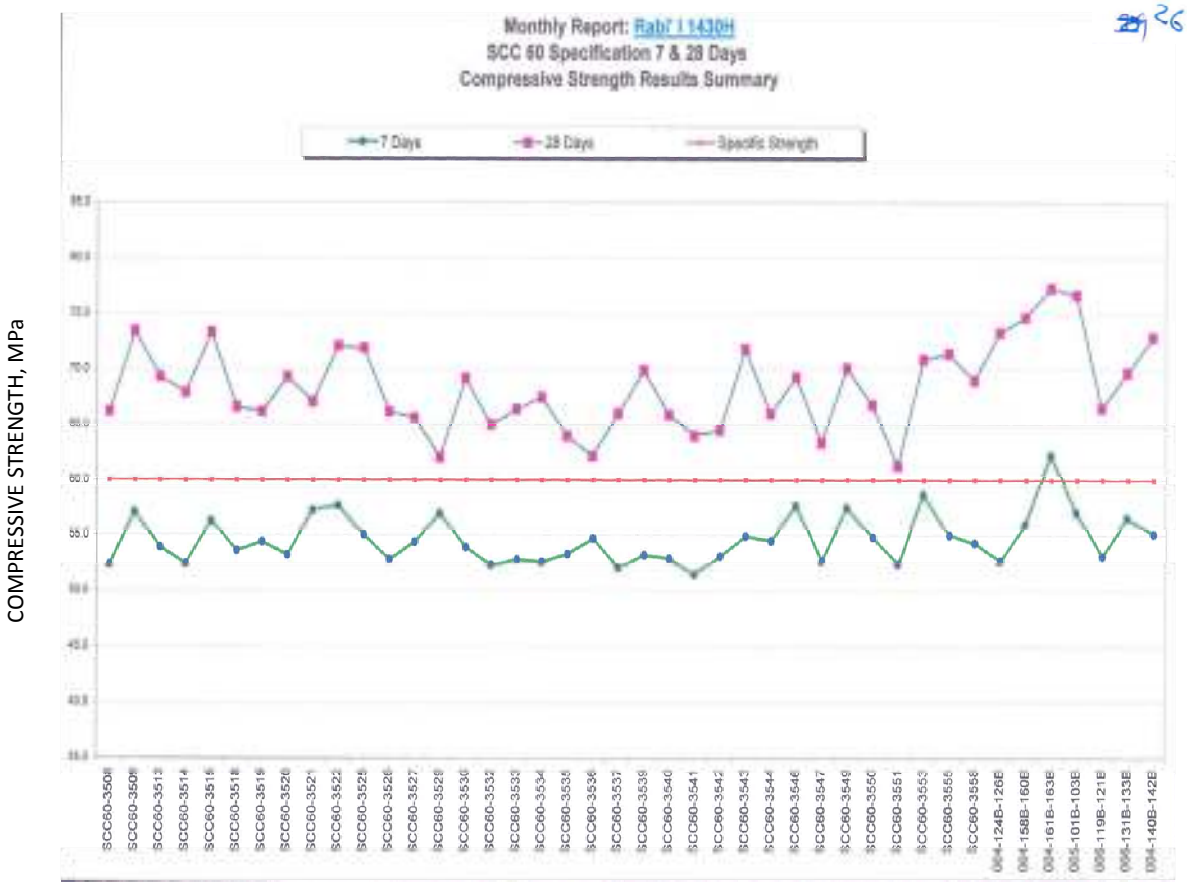

Figure 3 Total number of samples extracted from concrete production

FIVE – YEAR MONITORING PROGRAM FOR JAMARAT STRUCTURE

Number of Samples

Nearly fifty thousand samples were taken during the five – year monitoring program to be tested for compression strength at 28 days. This enabled the monitoring agency to have continuous , accurate as well as realistic data for concrete production. Tables 3 shows number of samples for each production plant A & B ; this includes both self – and external – monitoring programs.

Test Results Analysis

The ministry experts responsible for this external monitoring studied the test results of self monitoring [6] as well as the external monitoring results [10] from the aforementioned surprise visits. It is not looked at merely as obtaining the arithmetic average X_{mean} to determine acceptance or otherwise [7, 11]. A more comprehensive approach was adopted to evaluate all grades of concrete used on the project. Statistics principles were applied to determine variance in compressive strength, dispersion of results by obtaining the standard

deviation S, coefficient of variation V and characteristic strength f_{ck}. It was assumed that samples were random samples from the original population which has the same constituents, curing conditions and age. Therefore, the samples represent the population and are valid to apply statistics principles on the results.

Table 3 Total number of Samples Extracted from Conc. Production

TOTAL NUMBER OF SAMPLES EXTRACTED FROM CONC. PRODUCTION OF PLANT A (CIP)			
Concrete Class	Self Monitoring Contractor &consultant	External Monitoring MOMRA	Total number of samples (cylinders)
C 30 to C 80	26788	2237	29025
TOTAL NUMBER OF SAMPLES EXTRACTED FROM CONC. PRODUCTION OF PLANT B (PRECAST)			
C 30 to C 60	20076	571	20647
	Overall Total		49672

The importance of using statistical measures can be best illustrated by the normal distribution graphs depicted in Figure 4. The two curves in the figure represent two groups (populations) of results with the same mean. The narrow and higher curve represents a group that has its values close to the mean reflecting a less dispersion of values (low standard deviation). On the contrary, the wider (flatter) curve has individual values with more dispersion from its mean (high standard deviation value).

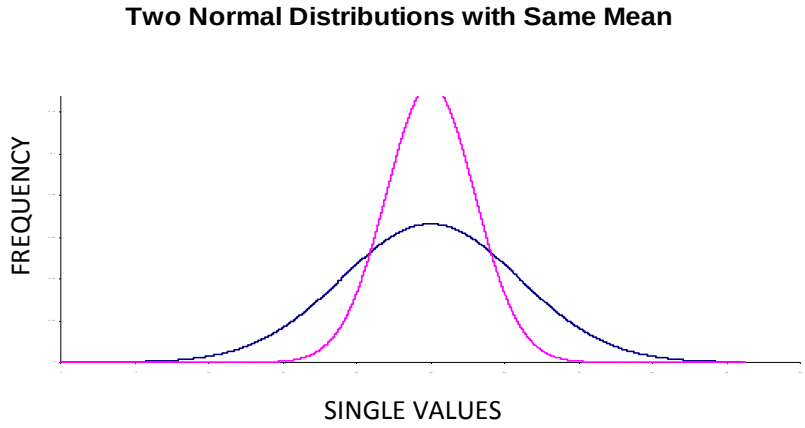

Figure 4 Two Normal Distribution with same mean

The Effect of External Monitoring on Development of Results

Analysis was carried out on different levels; namely the individual visit for each concrete grade and for each plant (A & B). The analysis was also conducted at the level of all surprise visits, the monthly reports from contractor/ consultant and for each stage (year) of project construction duration of 5 years (2005-2009).

Equations 1 to 3 indicate arithmetic average X_{mean}, standard deviation S, and coefficient of variation V.

$X_{mean}=(1/n)\ .\ _{i=1}\sum^{n}.\ X_I$ .....…… (1)

$V=S^2=[1/(n-1)].\ _{i=1}\sum^{n}(X_i - X_{mean})^2$…… (2)

$S=\sqrt{V}$.....……. (3)

Table 4 to Table 7 show calculated statistical values for the years 2005, 2007 and 2008/2009 at the beginning, middle and end of monitoring program application.

Table 4 Statistical Evaluation of Test Samples , Year 2005 Plant "A"

TYPE	INTERNAL MONITORING CONTRACTOR & CONSULTANT					EXTERNAL MONITORING MOMRA				
	n	X_{mean} MPa	S MPa	V= S/ X_{mean}.100	consistence of production	n	X_{mean} MPa	S MPa	V= S/ X_{mean}.100	consistence of production
C 30	341	36.0	2.88	8	V. good	…	…	…		
C 35	1181	44.56	2.73	6.12	Excel.	407	40.0	4.68	11.7	Good/ Fair
C 50	380	66.19	2.74	4.14	Excel.	…	…	…		

Table 5 : Statistical Evaluation of Test Samples , Year 2007 Plant "A"

TYPE	INTERNAL MONITORING CONTRACTOR & CONSULTANT					EXTERNAL MONITORING MOMRA				
	n	X_{mean} MPa	S MPa	V= S/ X_{mean}.100	consistence of production	n	X_{mean} MPa	S MPa	V= S/ X_{mean}.100	consistence of production
C 35	363	47.88	3.06	6.4	Excel.	15	43.18	3.03	7.02	Excel.
C 40	804	55.47	2.80	5.05	Excel.	81	54.66	4.97	9.1	V. good/ Good
C 50	804	62.79	3.75	5.96	Excel.	39	56.38	5.1	9.4	Good
C 60	1299	73.26	3.77	5.14	Excel.	84	64.49	6.78	10.5	Good
C60 SCC	2730	74.12	3.98	5.37	Excel.	123	66.44	7.38	11.11	Fair
C 80	358	87.41	4.96	5.7	Excel.	…	…	…	…	

The careful study and analysis of Tables 4 to 7 reveal the following observations:

- Table 4 of the program of the year 2005, at the beginning indicates coefficient of variation (V) of 4 – 8 (v. good to excellent) calculated from self-monitoring results, whereas the V calculated from external monitoring is 11.7 (fair) or just pass, this gives doubt about the accuracy and more significant, the transparency of self-monitoring. With reference to Figure 4, the small unrealistic values of standard deviation (1.5 -2) are a proof of results manipulation by self-monitoring to show a rosy picture. In earlier research

by the author (12 , 13) this fact was demonstrated without a doubt for the production of ready-mix concrete factories in Riyadh, the Capital city of K.S.A.

- Table 5 of the year 2007 for concretes grades 35 to 80 MPa indicates more consistent values V calculated from self-monitoring classified excellent which agrees with external monitoring classification of (Good to Excellent). The self-monitoring standard deviation from 3 – 5 is more realistic now than it was at the beginning (below 3.0). This somewhat indicates that the program had a positive effect on the care taken by concrete producers which is a positive development.

- Table 6, the only Table that depicts test results of grade 60 concrete (Plant B). The production of all precast elements were all finished 08/2008. An observation that cannot be ignored without a comment is the following: The overall arithmetic mean of internal monitoring of 2008 was less than 2007 and also less than results of external monitoring. This was attributed by the author to the fact that many internal monitoring samples (results of 2 months) have failed the acceptance criterion. This situation was resolved by taking concrete cores from the corresponding precast members and proved adequate to be used in the structure.

- Table 7 of the year 2009 shows calculated coefficient of Variation V of self-monitoring which indicate Very Good to Excellent classifications and standard deviation settled at 4 – 5 MPa. These results coincide with external monitoring. All show improvement to 2007 values. Self-monitoring values of mean have also become closer to those calculated by the ministry.

Table 6 Statistical Evaluation of Test Samples , Year 2008 Plant "B"

TYPE	INTERNAL MONITORING CONTRACTOR & CONSULTANT					EXTERNAL MONITORING MOMRA				
	n	X_{mean} MPa	S MPa	$V = S/X_{mean}.100$	consistence of production	n	X_{mean} MPa	S MPa	$V = S/X_{mean}.100$	consistence of production
C 60 Segments	4638	66.82	2.91	4.36	Excel.	116	68.63	6.71	9.78	Good
C 60 T-beams	1811	66.45	2.79	4.3	Excel.	63	69.98	7.27	10.30	Good

Table 7 Statistical Evaluation of Test Samples , Year 2009 Plant "A"

TYPE	INTERNAL MONITORING CONTRACTOR & CONSULTANT					EXTERNAL MONITORING MOMRA				
	n	X_{mean} MPa	S MPa	V= S/ X_{mean}.100	consistence of production	n	X_{mean} MPa	S MPa	V= S/ X_{mean}.100	consistence of production
C 35	188	43.12	3.91	9.07	V. good	…	…	…	…	
C 40	297	48.1	3.99	8.29	V. good	…	…	…	…	
C 50	287	59.24	4.49	7.58	V. good	54	57.64	3.36	5.83	Excel.
C 60	179	64.96	2.67	4.11	Excel.	…..	…..	…..	…..	
C60 SCC	649	68.57	3.81	5.55	Excel.	78	71.39	6.25	8.75	V. good
C 80	90	91.71	5.00	5.45	Excel.	132	106.62	8.89	8.34	V. good

QUALITY CONTROL AND ACCEPTANCE OF CONCRETE IN EUROPEAN / AMERICAN AND SAUDI STANDARDS

Nominal Strength

This is known in the European Specification EN 206 [14, 15] as the characteristic strength f_{ck} which is defined as the 5% fractile value for which it is allowed to have 5% of test results below this value.

$f_{ck}=f_{cm}-1{,}645*\sigma$ (4),

where:
σ is the standard deviation,
f_{cm} is the average of all samples.

This indicates that for a concrete grade 60 MPa, the arithmetic mean of all extracted samples should be about 70 MPa.
In the American ACI 318 [4] & Saudi SBC 304 [16]the nominal strength is defined as the specified strength f'_c used in structural design of members when concrete mix is designed by the concrete supplier. It should be considered that average of test results should not be less than f'_c. In other words: target mean strength for design of concrete mix shall be greater than f'_c.

Production Monitoring

EN 206 : European Criteria and Rules

Concrete produced is considered to achieve conformity with specified nominal strength if extracted samples during concrete production in the plant met the following [12 , 13, 15]:

- normal strength concrete (f_{ck}, cylinder ≤ 50 MPa)
- the mean f_{cm} of "n" samples ≥ f_{ck} + 4 MPa
- each single value $f_{ci} \geq f_{ck} - 4$ MPa

(n ≤ 35 tests) …….. (5-a)

- the mean f_{cm} of "n" samples ≥ f_{ck} + 1.48 σ , where σ ≥ 3 N/mm^2
- each single value $f_{ci} \geq f_{ck} - 4$ MPa

(n > 35 tests) ……...(5-b)

- high strength concrete (f_{ck}, cylinder ≥ 55 MPa)
- the mean f_{cm} of "n" samples ≥ f_{ck} + 5 MPa
- each single value $f_{ci} \geq f_{ck} - 5$ MPa

(n ≤ 35 tests) ……(5-c)

- the mean fcm of "n" samples ≥ fck + 1.48 σ , where σ ≥ 5 N/mm^2
- each single value $f_{ci} \geq 0.90 * f_{ck}$

(n > 35 tests) ……(5-d)

Acceptance Criteria of Concrete on the Site in European Standard EN 206

Compressive strength samples are extracted for each concrete grade used on site. Test results are considered acceptable if they meet the following requirements [17]:

- normal strength concrete (f_{ck}, cylinder ≤ 50 MPa)

(n ≤ 6);

- the mean $f_{cm} \geq f_{ck}$ + 2 MPa and
- the single value $f_{c\,i} \geq f_{ck} - 4$ MPa

……(6-a)

(6 < n < 35);

- the mean $f_{cm} \geq f_{ck} + (1{,}645 - 2{,}58/\sqrt{(n)}) * \sigma$; where σ = 4 MPa
- the single value $f_{c\,i} \geq f_{ck} - 4$ MPa

……(6-b)

(n ≥ 35);

- the mean $f_{cm} \geq f_{ck} + (1{,}645 - 2{,}58/\sqrt{(n)}) * \sigma$; where σ ≥ 3 MPa
- the single value $f_{c\,i} \geq f_{c\,k} - 4$ MPa

…….(6-c)

- high strength concrete ($f_{ck,\ cylinder} \geq 50$ MPa)

(n ≤ 6);

- the mean $f_{cm} \geq f_{ck}$ + 2 MPa and
- the single value $f_{c\,i} \geq 0.90 * f_{ck}$ ……..

(6-d)

(6 < n < 35);

- the mean $f_{cm} \geq f_{ck} + (1{,}645 - 2{,}58/\sqrt{(n)}) * \sigma$; where σ = 4 MPa
- the single value $f_{c\,i} \geq 0.90 * f_{ck}$ ……..

(6-e)

(n ≥ 3);

- The mean $f_{cm} \geq f_{c\,k} + (1{,}645 - 2{,}58/\sqrt{(n)}) * \sigma$; where σ ≥ 5 MPa
- the single value $f_{c\,i} \geq 0.90 * f_{c\,k}$ ……

(6-f)

Criteria for Strength Requirements in American Standard ACI 214

The minimum average of required compression strength is determined from the following equation (7):

$$f'_{cr} = f'_c + z\,s \qquad \text{.....(7-a)}$$

where Z is a statistical coefficient assuming that test results follow the Natural Distribution Curve (Gausian – Bellshape curve) . Relationships between compressive strength mean and the specified compressive strength (f'_c) depends on acceptance criteria which are usually specified for a particular project .

Criterion (1) : The arithmetic mean of three consecutive test samples (moving arithmetic mean) must be equal to or exceed specified strength f'_c . This criterion is adopted by ACI-318. Value of statistical coefficient Z in Eq. 7-a is taken as 2.33 from Table 4-3 of ACI 214. This is equivalent to having 1% of the number of tested samples not meeting the required criterion which leads to Eq. 7-b and 7-c that give, the minimum value of compressive strength average :

$$f'_{cr} = f'_c + (2.33)\,s / \sqrt{3} \qquad \text{.....(7-b)}$$
$$f'_{cr} = f'_c + (1.34)\,s \qquad \text{.....(7-c)}$$

Criterion (2): Compressive strength of any individual test (average of two samples) shall not be less than f'_c by more than a specified value. This value is taken by ACI-318 as 3.5 MPa where $f'_c \leq 35$ MPa and shall not be more than $0.10\,f'_c$ where $f'_c > 35$ MPa . This gives the minimum of compressive strength with only 1% of samples failing the requirement as :

$$f'_{cr} = (f'_c - 3.5) + z\,s \quad , f'_c \leq 35 \text{ MPa} \qquad \text{.....(7-d)}$$
$$f'_{cr} = 0.90 * f'_c + z\,s \quad , f'_c > 35 \qquad \text{.....(7-e)}$$

Acceptance of Concrete on the Site , in ACI 318 & SBC 304

Test samples are extracted for compression tests, from site, for each concrete grade. The strength of an individual class of concrete shall be considered acceptable if the following two conditions are satisfied [4,16]:

- Each arithmetic mean of 3 tests (one test is average of two samples) is not less than f'_c
- Each individual test (av. of two samples) shall fulfill:

  Individual Test $\geq f'_c - 3.5$,for $f'_c \leq 35$ MPa .....(8.a)

  Individual test $\geq 0.90 * f'_c$,for $f'_c > 35$ MPa ..... (8.b)

Total Evaluation of Concrete

All results obtained from both self (internal) – and independent (external)- monitoring of concrete quality were subject to statistical assessment. International standards [4 , 17] for total evaluation of concrete were applied.

The study and evaluation were carried out for each inspection surprise visit, for each concrete grade and for each factory (A and B). Tables 8-A & 8-B show examples for documenting

such studies in a short-format. The Table depicts the total statistical evaluation of results from samples extracted during the year 2008 in accordance with the European specification EN 206 [14 , 15 ,17] and the American ACI 318 [4]for concrete grade 60 MPa produced in plant (A). Comparing standard deviation of Table 8-A (self monitoring) and table 8-B (internal monitoring), we can observe that the first gives small standard deviation which indicates a rosier picture of the production; whereas the standard deviation of Table 8-B (external monitoring) gives higher standard deviations which indicates a realistic situation.

Table 9 shows summary of total evaluation of the year 2008 . It is obvious that the self monitoring that gave stable standard deviation with a small values 1.5 – 3.0 and coefficient of variation of 5 – 7 compared whereas the external monitoring obtained unstable values of 3 – 6 for standard deviation and coefficient of variation up to 12. This is an indication of manipulations by the self monitoring agency which was proved by obtaining more realistic values in their reports as the program progressed.

Application was also conducted at the level of overall results of surprise visits and the monthly reports submitted by the contractor / consultant for each year (stage) of construction. Tables 10-12 show the total evaluation of both self- and independent- monitoring by extracted samples during whole construction period 2005-2009 for concrete grades 50 to 80 of plant (A) CIP.. The careful study and analysis of results for concrete Grades 35 to 80 MPa produced in plant A reveals the following observations:

- Average strength of n samples (f_{cm}) obtained from self monitoring results (C 35 to C 60) satisfy min. required value calculated according to EN 206 acceptance criteria . It is observed that f_{cm} values were very big in beginning of monitoring program, but tend to be smaller & more realistic at end, while still satisfying the EN 206 acceptance criteria. Average strength of n samples (f_{cm}) obtained from self monitoring results for C 80 did not always satisfy EN 206 acceptance criteria, best results were achieved during year 2009.

- Average strength of n samples (f_{cm}) obtained from external monitoring results (C 35 , C 40) satisfy min. required value calculated according to EN 206 acceptance criteria . Average strength of n samples (f_{cm}) obtained from external monitoring results for (C 50 – C 80) did not always satisfy EN 206 acceptance criteria, best results were achieved during years 2008, 2009.

- The min. value of the average strength according to EN 206 acceptance criteria of external monitoring get smaller with time passing, which means improvement of consistence of production of concrete.

- The min. value of the average strength according to EN 206 acceptance criteria of internal monitoring is stable for each concrete grade for project duration. This may be attributed to the fact that the European standard assumes a minimum value for the standard deviation not permitted to the calculated one on the basis of test results to go below it. However, all values of standard deviation in contractor's results do not meet this condition; therefore it was necessary to adjust these values accordingly.

Table 8 A Evaluation of Grade 60 MPa Concrete(SCC) in accordance with European EN 206 and American ACI 318, **External Monitoring, 2008**

Number of samples **n**		3	9	30	36	21	45	24	27	27	33	9	30	57	27
Failed samples		3	7	1	2	0	0	3	3	4	2	0	0	0	0
Average strength (f_{cm}) of **n** samples MPa		52.87	56.6	66.71	71	69.1	72.4	64.75	64.5	62.06	68	67.46	70.85	72.64	72.76
Standard deviation S MPa		6.37	4.58	3.7	6.26	4.88	3.69	3.84	3.99	3.94	5.58	1.22	3.11	2.86	3.28
Coefficient of variation V%		12.06	8.09	5.55	8.82	7.06	5.1	5.94	6.19	6.35	8.21	1.8	4.39	3.94	4.51
min. MPa		46.2	50.6	58.1	52.4	61	62.2	55.42	55.5	50.68	47.8	66.04	62.78	66.08	66.48
max. Mpa		58.9	63.7	75.4	84.8	77.7	79.4	70.8	74.5	68.17	76.1	69.5	75.34	78.31	77.39
Range R MPa		12.7	13.1	17.3	32.4	16.7	17.2	15.38	19	17.49	28.3	3.46	12.56	12.23	10.91
ACI 318	Mean value criteria moving average ≥ **$f'_c \geq 60$**	Insufficient number of samples	60 x	60 √	60 √	60 √	60 √	60 √	60 √	60 √	60 √	60 √	60 √	60 √	60 √
	Single value criteria ≥ **$0.9\ f'_c \geq 54$**	Insufficient number of samples	54 x	54 √	54 √	54 √	54 √	54 √	54 √	54 √	54 √	54 √	54 √	54 √	54 √
EN 206	Mean value criteria f_{cm} (3^{rd} raw) ≥ values in this raw	62 x	63.14 x	64.7 √	67.6 √	64.34 √	66.3 √	64.50 √	64.6 x	64.59 x	65.58 √	63.14 √	64.7 √	66.52 √	64.59 √
	Single value criteria Values in 6^{th} raw ≥ **$0.9\ f_{ck} \geq 54$**	54 x	54 x	54 √	54 √	54 √	54 √	54 √	54 √	54 x	54 x	54 √	54 √	54 √	54 √
	Visit date	3.6	8.6 to 9.6	21.6 to 23.6	30.6 to 2.7	5.7 to 7.7	12.7 to 15.7	20.7 to 23.7	26.7 to 29.7	16.8 to 19.8	30.8 to 1.9	14.9 to 16.9	18.10 to 19.10	25.10 to 28.10	to 11.11
		Jun-08				Jul-08				Aug-08		Spt. 08	October 08		Nov. 08
		Summer										Autumn / Winter			

√ = fulfilled , x = not fulfilled

Table 8 B Total Evaluation of Grade 60MPa Concrete (SCC) in accordance with European EN 206 and American ACI, Internal monitoring-2008

Number of samples n		117	261	422	702	720	570	672	423	246	753
Failed samples		0	2	4	5	14	10	10	8	4	7
Average strength (f_{cm}) of n samples MPa		72.61	70.76	69.46	67.61	67	67.1	66.14	66.2	66.43	67.9
Standard deviation S MPa		2.24	3.88	3.87	3.15	3.52	3.77	2.96	3.08	3.52	3.39
Coefficient of variation V %		3.09	5.48	5.5	4.66	5.26	5.62	4.47	4.65	5.3	4.99
min. MPa		66.7	58.7	57.2	56.5	57.7	57.4	57.1	57	57.1	57.9
max. Mpa		78	77.6	78.7	77	77.9	78.2	76.4	76.4	75.2	79.4
Range R MPa		11.8	18.9	21.5	20.5	20.2	20.8	19.3	19.4	18.1	21.5
ACI 318	Mean value criteria moving average $\geq f'_c \geq 60$	60 √	60 √	60 √	60 √	60 √	60 √	60 √	60 √	60 √	60 √
	Single value criteria $\geq 0.9 f'_c$	54 √	54 √	54 √	54 √	54 √	54 √	54 √	54 √	54 √	54 √
EN 206	Mean value criteria f_{cm} (3rd raw) ≥ values in this raw	67.4 √	67.4 √	67.4 √	67.4 √	67.4 x	67.4 x	67.4 x	67.4 x	67.4 x	67.4 √
	Single value criteria Values in 6th raw ≥ 0.9 f_{ck}	54 √	54 √	54 √	54 √	54 √	54 √	54 √	54 √	54 √	54 √
	Monthly Reports	1	2	3	4	5	6	7	8	9	10
		10.01 to 05.02	06.02 to 06.03	08.03 to 03.04	04.04 to 04.05	05.05 to 05.06	06.06 to 04.07	05.07 to 03.08	04.08 to 31.08	02.09 to 01.10	02.10 to 17.11
comments							Ministry Visits (14 visits)				

√ = fulfilled , x = not fulfilled

Table 9 Summary of total evaluation of the year 2008

COMPARISON ELEMENT	EXTERNAL - MONITORING	SELF (INTERNAL) - MONITORING
Arithmetic Mean f_{cm}	Unstable considering all visits	Stable in all reports especially before implementation of external monitoring
Standard Deviation S	Unstable 3-6 MPa	Stable 1.5 - 3 MPa
Coefficient of Variation, V	Variable from highest value 12 (poor) first visit, for all subsequent visits (4-5) (Very Good to Excel.)	Stable 5-7 MPa Indicating excellent consistence productio (manipulation)
Acceptance Criteria of Stren Results in European EN 206	Conc. Strength did not meet acceptance	Concrete always satisfied acceptance criter
Acceptance Criteria of Strength Results in American ACI 318	Concrete does not always satisfies acceptar criterion "Eqs.8" which depends on f'_c not on σ	Concrete always satisfies acceptance criteri "Eqs.8" which depends on f'_c not σ

Table 10 Total evaluation of 50 MPa grade CIP concrete in accordance with EN 206 – Self and independent monitoring for 5 years Plant "A"

C 50	MONITORING								
	Internal	Internal	External	Internal	External	Internal	External	Internal	External
Number of samples n	380	1305	84	804	39	1620	201	287	54
Average strength of n samples (f_{cm}) MPa	66.19 √	61.64 √	61.03 x	62.79 √	56.38 x	57.8 √	55.42 x	59.24 √	57.64 √
S MPa	2.74	3.95	8.18	3.75	5.1	3.27	4.49	4.49	3.36
V= $S/X_{mean}.100$	4.14	6.4	13.41	5.96	9.04	5.66	8.11	7.58	5.83
Max. MPa	72.9	78	78.5	76	65.5	70.5	67.7	72.4	64.61
Min. MPa	58	50.2	32.8	52.5	41.3	47.7	40.5	50.1	50.6
EN 206 Mean value criteria $f_{cm} \geq f_{ck} + 1.48\ \sigma$ MPa	54.4	55.85	62.10	55.5	57.55	54.84	56.51	56.65	54.97
year	2005	2006		2007		2008		2009	

Table 11 Total Evaluation of (60 MPa grade SCC) CIP concrete in accordance with EN 206 – Self and independent monitoring for 5 years Plant "A"

C 60 SCC	MONITORING							
	Internal	External	Internal	External	Internal	External	Internal	External
Number of samples n	1503	315	2730	123	4886	378	649	78
Average strength of n samples (f_{cm}) MPa	72.71 √	67.29 x	74.12 √	66.44 x	67.57 √	68.8 √	68.57 √	71.39 √
S MPa	4.48	9.69	3.98	7.38	3.44	5.8	3.81	6.25
V= $S/X_{mean}.100$	6.17	14.41	5.37	11.11	5.08	8.43	5.55	8.75
Max. MPa	86.9	96.0	92.9	82.1	79.4	84.8	81.9	84.07
Min. MPa	60.3	44.6	53.8	45.3	56.5	46.2	60.2	44.04
EN 206 Mean value criteria $f_{cm} \geq f_{ck} + 1.48\ \sigma$ MPa	67.4	74.34	67.4	70.93	67.4	68.58	67.4	69.25
year	2006		2007		2008		2009	

√ = fcm in 2nd raw fulfill values in 7th raw
x = fcm in 2nd raw does not fulfill values in 7th raw

Table 12 Total Evaluation of 80 MPa grade CIP Concrete in accordance with EN 206 – Self and independent monitoring for 5 years Plant "A"

C 80	MONITORING				
	Internal	Internal	Internal	Internal	External
Number of samples n	294	358	589	90	132
Average strength of n samples (f_{cm}) MPa	86.57 x	87.41 √	84.24 x	91.71 √	106.6 √
S MPa	4.1	4.96	1.99	5.0	8.89
V= $S/X_{mean}.100$	4.74	5.7	2.36	5.45	8.34
Max. MPa	98.5	101.5	94.6	100.8	129.2
Min. MPa	80.1	76.4	80	79.9	86.18
EN 206 Mean value criteria $f_{cm} \geq f_{ck} + 1.48\ \sigma$ MPa	87.4	87.4	87.4	87.4	93.15
year	2006	2007	2008	2009	

√ = $\mathbf{f_{cm}}$ in 2nd raw fulfill values in 7th raw
x = $\mathbf{f_{cm}}$ in 2nd raw does not fulfill values 7th raw

CONCLUSIONS AND RECOMMENDATIONS

The study revealed the importance of external Quality Control by a neutral agency. It proves that it is not sufficient to rely on internal – monitoring (self monitoring) of concrete quality performed by the contractor/supervising consultant. The difference between results obtained from self monitoring and those from external agency monitoring was large at the beginning of the program. As a result of the continuous application of the external monitoring program throughout the construction stages of a mega project that took 5 years to build, the differences between results became smaller. The paper recommends that it is necessary to apply external monitoring programs with unannounced (surprise) visits for all projects. The number of visits shall be proportional to the project size. The study also shows that statistical evaluation of tests enables to assess the results consistence and conformity in a better and more correct manner than depending only on the average (or mean) without correlating to statistical measures. This approach conforms to requirements of EN 206 [12, 13, 15] and ACI 214 [7]. The paper indicates the need to adopt acceptance criterion for ACI 318 in accordance with those adopted in ACI 214 or EN 206. this is of utmost importance in countries which have no external quality assurance and rely on ACI specifications and standards in their national building codes such is the case in the Kingdom of Saudi Arabia Code and its concrete section SBC 304 [16]. In order to be more realistic it is advisable to consider local conditions in developing countries such as KSA & Gulf Countries in order to adapt Equations in EN 206 and ACI 214 and similar British codes. Studies may be conducted by a committee of experts from these countries to find the right values for standard deviation & coefficient of variation and number of samples that can be adopted in the local codes with a high level of certainty. Due to the success of the external monitoring in improving concrete quality it was decided to apply the procedures in all subsequent projects of Al Mashaer Holy sites.

REFRENCES

1. ZEIN ALABIDEEN, H. M. , " Some of the Activities of Ministry of Municipal & Rural Affairs in Planning, Construction and Operation of Mega Projects in Mecca", Building Technology Magazine issued by Ministry of Municipal & Rural Affairs , Vol. 22, 2011.

2. ZEIN ALABIDEEN, H. M. , " The Development of Multistory Jamarat Bridge and Surrounding Area, a unique structure for the safety of Pilgrims", International Congress, University of Dundee, Scotland, 2005.

3. ZEIN ALABIDEEN, H. M. , " Post-Tensioned Precast Segments for Multistory Jamarat Bridge in Holy Makkah, a unique structure for the safety of Pilgrims", International Congress, University of Dundee, Scotland, 2008.

4. ACI 318- 08 : Building Code Requirements for Structural Concrete and commentary, American Concrete Institute, 2008.

5. Compressive Strength 7 & 28 days test results, Contractor/ Supervising Consultant Material Monthly Reports (from 2005 to 2010), new Jamarat structure.

6. Compressive Strength 7 & 28 days test results, Contractor/ Supervising Consultant Material Monthly Reports (from 2005 to 2010), new Jamarat structure.

7. ACI 214R-02, Evaluation of Strength Test Results of Concrete, , reported by ACI committee 214.

8. ASTM MNL7 : Manual 7 on Presentation Data and Control Chart Analysis, 6th Edition.

9. ASTM C31/C31M: Standard Practice for Making and Curing Concrete Test Specimens in the Field, American Society for Testing and Materials, 2010.

10. THE CENTRAL DIRECTORATE FOR THE DEVELOPMENT OF PROJECTS (CDDP), Test Results of compression strength samples extracted from Bridge Project in Mecca, Central Laboratories, Ministry of Municipal and Rural Affairs (MOMRA), Riyadh, The Kingdom of Saudi Arabia, 2005 to 2011 Files.

11. ZEIN ALABIDEEN, H. M., "Safety Assessment of Concrete Structures" , 2nd edition, Riyadh 1992.

12. ZEIN ALABIDEEN, H. M., "Status of Quality Control on Ready Mixed Concrete in K.S.A." AR-10-033, King Abdul Aziz City for Science and Technology (KACST), K.S.A.,1992

13. ZEIN ALABIDEEN, H. M., "Quality Control System for Ready Mixed Concrete & Technical Specifications for its Production", ARP-19-022, King Abdul Aziz City for Science and Technology (KACST), K.S.A., 2004.

14. EN 206-1: Concrete, Part 1: Specification, Performance, production and Conformity, 2000.

15. DIN EN 206-1; Beton, Teil 1:Festlegung,Eigenschaften, Herstellung und konformitaet, 2001.

16. SBC 304: Concrete Structures, "Structural Requirements - The Saudi Building Code" , National Committee of Saudi Building Code, Ministry of Municipal and Rural Affairs Riyadh, KSA, www.sbc.gov.sa.

17. "BETON – Herstellung nach Norm: Arbeitshilfe fuer Ausbildung, Planung und Baupraxis", Chapter 11, Verlag Bau+Technik, 2006.

Reliable Production of Air Entrained Concrete with Sustainable Slag Cements

V Feldrappe, A Ehrenberg
FEhS-Institut – Building Materials Institute, Germany

Worldwide approximately 300 Mt per annum of blast furnace slag is produced. Today about 70 % is already granulated. Granulated blast furnace slag (GGBS) is commonly used as a cement main constituent or as a concrete addition for more than 100 years. While long time only technical and economical advantages of GGBS were centred, its positive effect on the carbon footprint of building materials like concrete becomes nowadays also an increasing importance since ecological aspects are of growing interest. Although many experiences of GGBS use and examples of durable concrete constructions exist, national concrete standards still restrict (e.g. Germany) its use for concrete applications in a freeze-thaw and de-icing salt exposure (XF4). The positive effect of a sufficient micro pore structure by the use of air entraining agents (AEA) is well known since the nineteen-thirties. But a sufficient formation is influenced by several parameters. However AEA's on the basis of natural substances are considered as robust in their use. But several practical experiences have shown that an unerringly production of a sufficient micro pore structure is not always possible with synthetic AEA's, for which reason the use of slag cement is often refused for such exposures. The article will present the results of a large research program, which dealt with the questions – whether the slag cement can be used for freeze-thaw and de-icing salt resistant concrete at all and which impacts are causal and important. From the results it could be clearly shown that the production of freeze-thaw and de-icing salt resistant concrete is possible with slag cements if some basics are considered. How-ever, it also appeared that the unerring production of air entrained concrete can be problematic even under the stable lab conditions, especially if plasticizer is used in addition. Effects and impacts of these interactions will be discussed in more detail and conclusions will be drawn. The results might be support to extend the ecological, economical and sustainable worthwhile utilization of GGBS in concretes exposed to severe conditions. Based on the technical data the CO_2-balance of XF4-concretes made with Portland cements and slag cements is presented.

Dr.-Ing. Volkert Feldrappe is Head of Cement Laboratory at FEhS-Institut – Building Materials Institute, Duisburg. Previously he had studied civil engineering at Technical University Braunschweig and was a Research Engineer at the Research Institute of the German Cement Association, Düsseldorf. He was recently a Quality Engineer at European Technical Centre of Lafarge Cement, Vienna.

Dr.-Ing. Andreas Ehrenberg, studied Mineral Engineering at Technical University RWTH Aachen and completed his PhD in Material Science and cat Technical University Clausthal. Since 1992 he has been Head of Building Materials Department at FEhS-Institut – Building Materials Institute, Duisburg.

Keywords: Air entrained concrete, De-icing salt resistance, Durability, Ecological footprint, Freeze-thaw, Slag cement

INTRODUCTION

The importance of ecological aspects continuously rises in the construction industry during the last decades. Besides, concrete is probably the most important construction material in the world. Therefore it is a task and a challenge to improve its ecological footprint. The main concrete constituent with the highest impact on the Global Warming Potential (GWP) is the cement, because it is originated from an energy intensive and de-calcining process. The GWP, however, differs depending on the cement type. For instance it is significantly lower for slag cement than for Portland cement because of its lower clinker content [1, 2]. Consequently a proper cement constituent selection can be an important improvement lever. But its definitely existing ecological potential for concrete can only be used if the concrete performance is still ensured.

Meanwhile it is undisputed that concrete performance is characterised not only by strength development but also by durability [3]. In the end of the 1930ies, first, but rather accidental experience had showed the positive impact of artificial air pores in concrete concerning the freeze-thaw and de-icing salt resistance. Frost damages could be significantly reduced due to a target oriented production of concretes with air entraining agents (AEA). If the created artificial air pores are small enough and available in a sufficient amount and distance, they act as expansion space of the freezing water and interrupt the capillary porosity effectively [4, 5, 6]. The formation of an adequate micro air pore system depends on several parameters like concrete raw materials, concrete recipe, production or environmental conditions. Mainly Portland cement is used for concrete in freeze-thaw and de-icing salt exposure in Germany, although a lot of positive experiences exist in the application of slag cement concretes in severe conditions. Recent practical experiences, however, have shown that an unerringly production of an artificial micro pore system is not always possible even with Portland cement especially if synthetic AEAs are used.

An extensive research program was carried out at the FEhS-Institute, in order to extend the knowledge for concretes made with slag cement and synthetic AEAs in a freeze-thaw exposure. The result has shown that CEM III/A cements can be unrestricted used for air entrained concretes if some basic principles concerning concrete production and curing are considered. The ecological footprint of concrete used in a freeze-thaw exposure can, therefore, be improved if slag cements are used instead of Portland cements.

PRINCIPLES OF ARTIFICIAL AIR VOID FORMATION

During concrete mixing molecules of AEA are dissolved in the mixing water. Furthermore air will be entrained by the mixing. This air is fixed in small pores by the dissolved AEA molecules and is stabilized in concrete by the adsorption of the hydrophilic part of the AEA molecule at the cement grain surface. However, especially in the younger past, practical experiences have shown that concretes with too high air content were delivered to the construction side although it was in the right order after mixing at the RMX plant.

These observations can be explained as follows: Some AEA molecules remain unsolved in the mixing water during initial mixing at RMX plant. These molecules can be activated if a new energy is taken to the concrete (e.g. by moving the RMX truck drum or during vibrating). As a result additional inserted air can be stabilized and increases the air content of the fresh concrete [7].

This behaviour is characterized as additional activating potential of the AEA. It is problematic especially if the air content significantly increases, e.g. during transportation to the construction side in a RMX truck. Consequently the required compressive strength cannot be achieved anymore.

Objective and volume of the investigations

The research program was focused on three objectives. The main one, about which is only reported in the article, dealt with the interactions between AEAs with other concrete admixtures, especially with plasticizers. Basically attention was paid on the use of slag cements (CEM III/A), which sometimes showed already some specific features, when they were used in combination with AEAs also on natural basis. Nevertheless the scientific investigation of the reasons was not considered as so essential so far, because of the effective operation of air entrained concretes in general. The other two objectives, which are only mentioned here, dealt with special questions concerning the curing impact during construction of washed-out concrete roads and with the use of ground granulated blast furnace slag according to DIN EN 15167 as concrete addition. The final report about the whole research project was already published [8, 9].

ENVIRONMENTAL IMPACTS

Concrete is probably the most important building material of the world. The production of its binder, cement, is increasing and reached about 3.040 Mt in 2009. The cement production is energy-intensive [10] and causes 5-8 % of the worldwide CO_2-emissions [2]. The CO_2-emissions and the emissions of other green house gases are combined in the GWP as CO_2-equivalent. It is one important factor of the ecological footprint.

It is well known, that slag cements have as well technical as ecological advantages. For example the GWP (primary energy content and CO_2-emissions during cement production) is much lower compared to Portland cement [2, 11, 12]. According to [1] slag cement with approx. 50 % slag has only about 55 % CO_2-emissions compared to Portland cement as it is presented in

Figure 1.

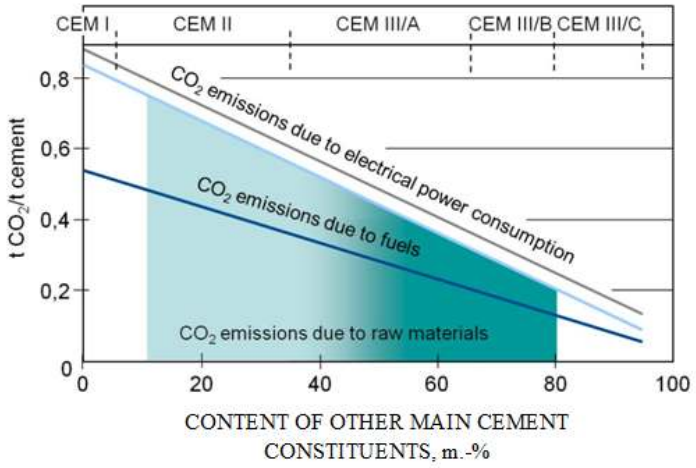

Figure 1 CO_2-emissions during cement manufacturing [1]

Because cement is the concrete constituent with the highest ecological impact on concrete [10, 13] it is evident that concretes made with slag cements have a significant lower GWP, too. Already in 1995 the U.S. Environmental Protection Agency published a guideline recommending among others the use of concretes containing ground granulated blast furnace slag [14].

EXPERIMENTAL PROCEDURE

Basic materials

Three different commercial slag cements were used. According to Table 1 the chemical and physical properties of the used cements – two CEM III/A 42,5 N cements of two different cement manufactures (A & B) and one CEM II/A-S 42,5 of cement manufacture A – are presented.

Table 1 Chemical and physical properties of the considered cements

Cement CEM		II/A-S 42,5 R	III/A 42,5 N	
Producer		A	A	B
property	unit			
SO_3	M.-%	2,90	3,22	2,08
SiO_2		22,4	26,6	27,2
Al_2O_3		6,63	8,47	7,13
Fe_2O_3		1,90	1,50	1,53
CaO		60,4	53,7	55,7
K_2O		0,59	0,92	0,75
Na_2O		<0,10	0,25	0,24
Na_2O_{eq}		0,73	0,86	0,73
Slag content	M.-%	19,5	66,5	63,1
Density	g/cm³	3,10	3,01	3,02
Specific surface (Blaine)	cm²/g	3570	4280	3980
Grain size d’	µm	21,2	16,5	18,1

distribution	n	-	1,080	1,104	1,112
Water demand		M.-%	32,5	30,5	28,0
Initial setting		h:min	3:55	3:35	3:45
Compressive strength	2 d	N/mm²	25,5	21,4	21,6
	28 d		56,2	57,9	59,4

Different fractions of gravel and sand were used from a producer at the lower Rhine area. The maximum aggregate grain size was 16 cm and 32 cm respectively depending on the concrete recipes (compare section “Concrete composition”). The proportions of the fractions, however, were calculated in both cases in order to achieve a grading curve of the aggregate mix in the middle between the standardized curves “A” and “B” according to German concrete standard DIN 1045-2. All coarse aggregates fulfilled the requirements of category F_2 for the freezing resistance and the category MS_{18} for the freeze-thaw and de-icing salt resistance according to DIN EN 12620.

Two AEAs on synthetic (producer C & D) and one on natural basis (producer E) were chosen as admixture for the investigations. Furthermore a plasticizer with "classical" active agent (Lignin-, Melamin-, or Naphthalinsulfonate) and one on the basis of Polycarboxylatether (PCE) were considered from each admixture producer for testing the interactions between AEAs and plasticizers. All admixtures were according to DIN EN 934-2. Effectiveness tests with the air entraining agents exist for all plasticizers and were provided by the relevant admixture producers.

Concrete composition, manufacturing and storage

The findings should be gained on practical concrete recipes for typical applications and not on rather theoretical “limiting” compositions according to German concrete standard DIN 1045-2. The recipes which are used in the program are common for bridge cappings. An air content of 5.5 Vol.-% was always targeted in fresh concrete 45 minutes after water addition. To investigate the impact of different concrete consistency the concretes were applied with and without plasticizers in order to meet the consistency classes F3/F4 and F2 of DIN EN 206-1 respectively. The used concrete recipes are listed in Table 2.

Table 2 Requirements and recipes of concretes for the two considered applications

APPLICATION		BRIDGE CAPPING	
RECIPE NO.		1	2
Require-ments	Strength class	C25/30	C25/30
	Air content after 45’	5,5 Vol.-%	5,5 Vol.-%
	Consistency after 45’	F2	F3/F4
	Exposure class	XF4	XF4
Compo-sition	Cement	340 kg/m³	340 kg/m³
	w/c ratio	0,48	0,48
	Aggregate grading curve	A16/B16	A16/B16

Admixtures	AEA	AEA + Plast.

In a first step the aggregates were slightly wetted in the mixer. After 5 minutes they were shortly mixed with the cement. The AEA were dosed with the required mixing water within 15 seconds. When plasticizer was used, it was added approximately 60 seconds after water dosage. In general the mixing time was 2 minutes when the mixing water was added. In some cases the mixing time had to be prolonged in order to guarantee a proper pulping of the AEA.

The test specimens were always casted 45 minutes after water dosage. All specimens were compacted on a vibrating table and stored 1 day in moulds, 6 days under water and afterwards until testing in laboratory climate at 20 °C and 65 % RH according to the German national annex of DIN EN 12390-2.

Testing methods

For all concretes the air content and the consistency were measured after 10 and 45 minutes after water addition according to DIN EN 12350-7 and 5. The concrete was always shortly remixed for 30 seconds before the air content was measured. The compressive strength according to DIN EN 12390-3 was specified at an age of 2, 7, 28 and 91 days.
The additional activating potential of the AEA was characterized as difference of the air contents of fresh concrete after 10 and 45 minutes in the laboratory. A positive value, which means an air content increase, indicates a clear additional activating potential of this specific AEA.

The freeze-thaw and de-icing salt attack was simulated with the CDF test method according to DIN CEN/TS 12390-9. As decision criteria the cumulative scaling from the testing surface within 28 freeze-thaw cycles (ftc) is taken. But up to now no limiting values are fixed in the valid German standards and guidelines. An acceptance criterion of 1500 g/m² was only defined by the Federal Waterways Engineering and Research Institute (BAW) for the special scope of waterway constructions [15]. Even this criterion is only valid for specific area of waterway constructions it is meanwhile frequently adopted also for the general construction area.

Interpreting the results especially in respect to the acceptance criterion is difficult. The reasons are on the one hand the criterion of 1500 g/m², which represents a scaling depth of only less than 1 mm on average. On the other hand concretes, especially those made with slag cements, may show scalings which are significantly higher than the acceptance criterion even if concretes with these recipes have demonstrated a high freeze-thaw and de-icing salt resistance in constructions for decades. The observed mismatch between lab test and practical behaviour can be explained by the defined unfavourable storage conditions for such concretes made with slag cements or other cements with a lower early strength development [16, 17].

The carbonation of the concrete surface due to CO_2 attack was measured on concrete beams with phenolphthalein test. Specimens were stored in laboratory climate at 20 °C and 65 % RH and in practical environment, outside under a roof. The measurements took place in regular intervals over a period of 12 months.

RESULTS

Properties of fresh and hardened concrete

If the required air content of 5.5 Vol.-% after 45 minutes was met, normally also the required strength class C25/30 was achieved. But the compressive strength significantly dropped down, if the air content exceeded values clearly above 6.0 Vol.-% after 45 minutes as it is shown in Figure 2. Despite of careful pilot tests, this happened for concretes made with CEM III/A 42.5 N of both producers when standard mixing procedure was used.

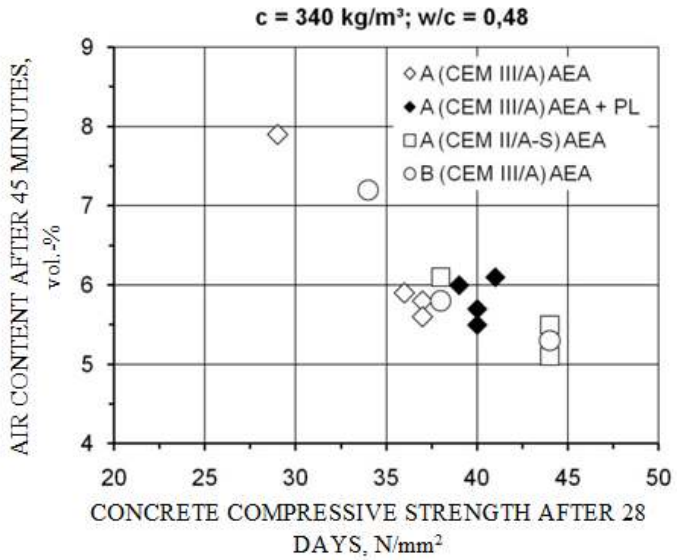

Figure 2 Impact of air content of fresh concrete after 45 minutes on the 28 days compressive strength

Impact of AEA on concretes with slag cements

As expected more AEA on natural basis was needed than those on synthetic basis in order to achieve the required air content of the fresh concrete 45 minutes after water adding. The reason is that the solubility of AEAs on natural basis is harder than those of synthetic basis. As a result fewer molecules are available to stabilise the inserted air.

Figure 3 shows the additional activating potential of the three different AEAs measured as the difference of the fresh air content after 10 and 45 minutes after water addition. The tests were made on concretes with all three different cements, which were used within these investigations.

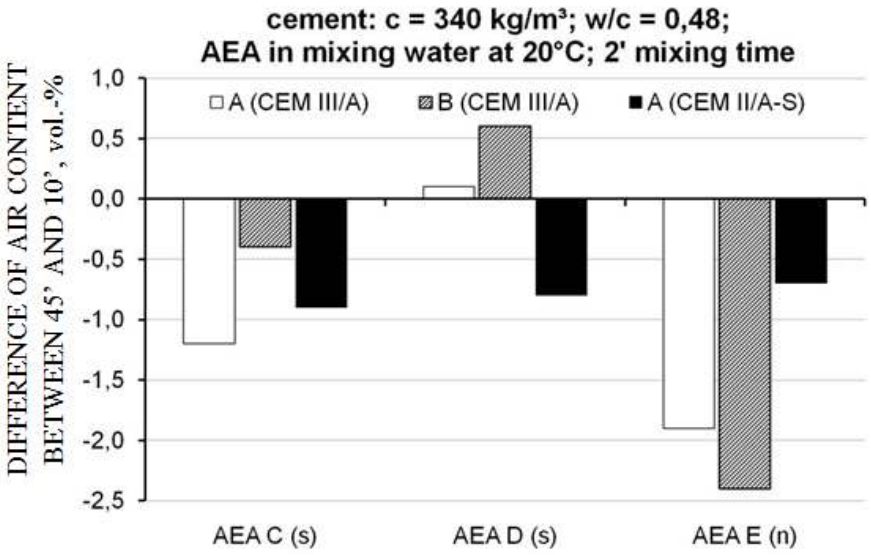

Figure 3 Additional activating potential of the AEAs

AEAs on natural basis were properly solved within a mixing time of two minutes for all cements (types and manufactures). This behaviour reflexes the known experiences on construction sides. In contradiction the fresh air content increased 45 minutes after water addition for concretes made out of CEM III/A and synthetic AEA of producer D (Figure 3: AEA D (s)). The mixing time of two minutes was not sufficient in that case to dissolve the AEA properly. This AEA had a distinctive additional activating potential. It has to be considered during concrete production.

A sufficient artificial air pore systems was formed in all concretes independent of the type of AEA. The requirements concerning the micro air content ≥ 1,8 Vol.-% and the air void spacing factor ≤ 0,20 mm were definitely fulfilled. The scaling after 28 FTC was always below the acceptance criteria of ≤ 1.500 g/m², which is defined by BAW [15], if the concretes fulfilled the requirements concerning composition, pore structure and strength (C25/30). This relation is illustrated in Figure 4. Type of cement and slag content of cements did not impact the freeze-thaw and de-icing salt resistance of the tested concretes.

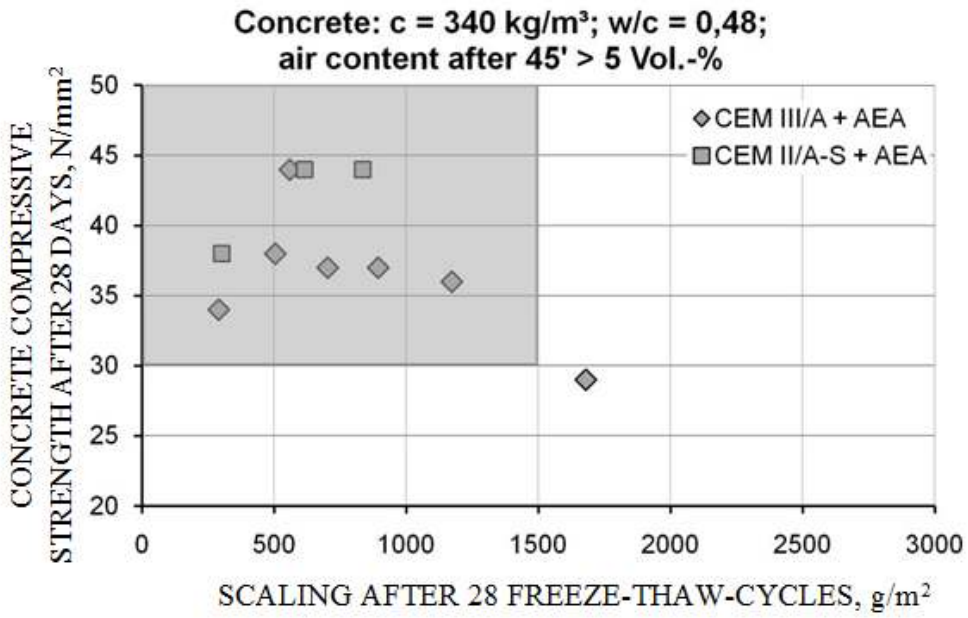

Figure 4 Effect between concrete strength and scaling acc. to CDF-test after 28 FTC

Impact of interactions between AEAs and plasticizers on concretes with slag cements

If plasticizer was used in addition, generally less AEA was needed, because artificial air voids can be inserted and stabilized much easier when the concrete consistency is smoother. However the difference between AEAs on natural and on synthetic basis, which were described in section before, remained same.

Furthermore some undesirable interactions occurred between AEAs and plasticizers.

Figure 5 shows the additional activating potential of the three AEAs in combination with different plasticizers as showcase for the concretes made with CEM III/A of producer A.

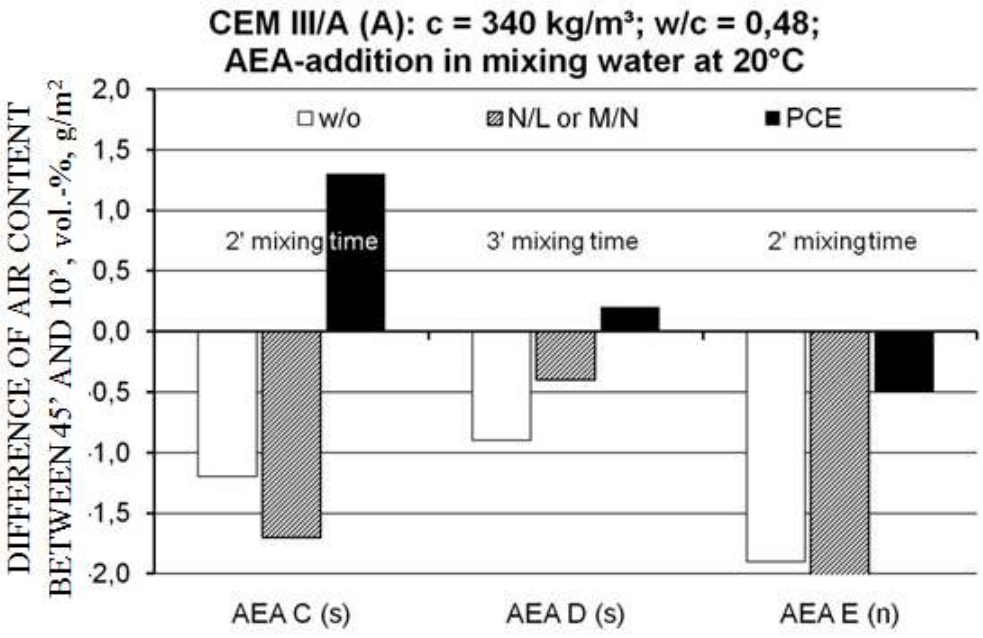

Figure 5 Impact of type of plasticizer on the additional activating potential of the AEAs

In relation to the concretes without plasticizers the additional activating potential rose once more if plasticizers were used. This impact is tending higher with an increasing slag content of the cement. Generally slag cements behave more sensitive than Portland or Portland slag cements in this regard. This fact is probably reasonable because admixtures adsorb rather on Portland cement clinker surfaces than on slag surfaces [18]. Consequently a higher admixture content is, therefore, available in relation to the Portland cement clinker. Beside of this effect the interactions were also more pronounced if synthetic AEAs were used in combination with PCEs as plasticizers.

The additional activating potential could be significantly reduced if the initial mixing time was prolonged. Due to the increased initial energy input the AEAs could dissolved better. A mixing time up to four minutes was necessary for the synthetic AEA of producer D. This extension of mixing time would probably be shorter in practical application because the energy input is more intensive for modern mixers in RMX plants than for a laboratory mixer. Anyway these results clearly indicate the need to develop admixtures specifically for cements with several main constituents and to customise the properties like surface structure and charge of the admixture ingredients accordingly.

If the concretes had the required fresh air content 45 minutes after water addition, the required specimens were manufactured. A sufficient pore structure was formed in all cases which fulfilled the requirements concerning micro air content $\geq$ 1.8 Vol.-% and spacing factor $\leq$ 0.20 mm. Also the strength requirement of strength class C25/30 was always met. Nevertheless the amount of scaled material, determined within 28 FTC with the CDF-test, exceeded the acceptance criteria [15] significantly in some extent as it is exemplified in

Figure 6 for the concretes made with CEM III/A of producer A.

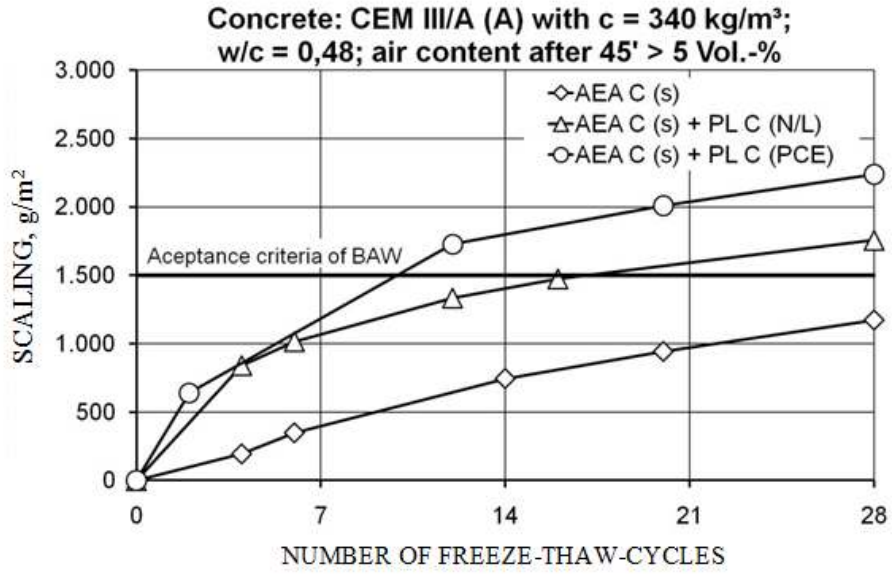

Figure 6 Scaling behaviour of the concrete made with CEM III/A of producer A and AEAs and plasticizers of producers C

Compared to the concrete made only with AEA, an increased initial scaling is clearly visible in

Figure 6 for those concretes which contained plasticizers in addition. The ongoing scaling behaviour, however, was for both types of concrete (concrete with AEA and with AEA + plasticizer) similar. Consequently the concretes with plasticizers in addition would have a scaling after 28 FTW in a similar order than those made without plasticizers if the initial scaling would not be accounted.

An increased initial scaling during testing the freeze-thaw and de-icing salt resistance of concretes with slag cements is often reported in the literature [16, 19]. It is unquestioned that the reasons are in the curing conditions (20 °C and 65 % RH) which are defined in DIN CEN/TS 12390-9. These conditions are unfavorable especially for concretes with slag cements. The slower reacting slag cements have a lower degree of hydration due to these dry curing conditions. As a result often the porosity of the surface layer of lab-scale concretes is increased. This layer can carbonate much easier and spalls during the first freeze-thaw cycles. However, within the investigation an increased carbonation of the surface layer could not be identified as reason of the severe initial scaling. The results showed a similar carbonation behavior for all concretes without significant differences. But the surface layer of concretes with AEA and plasticizer in addition had a higher capillary porosity. Furthermore the distribution of micro air pores tended to be more heterogeneous in this layer. It has to be investigated in more detail whether the occurrence of such air void clusters is significant. But both aspects might be reasons for the increased initial scaling behavior of the lab test.

CO_2 BALANCE OF THE CONCRETES

The Global Warming Potential (GWP), expressed as CO_2-equivalent, of a concrete is influenced as well by the GWP of its main constituents as by manufacturing and transportation.
Calculations made by different authors clearly indicate that the predominant factor on the GWP of RMX concrete is the cement [e.g. 8, 13, 20, 21]. According to the different authors the portion varies between 90 and 96 %.

The German Cement Association has calculated the positive impact of the exchange of Portland cement clinker with slag on the CO_2-emission during cement production [1]. Consequently the GWP of a CEM III/A cement with approx. 50 % slag is reduced by ca. 45 % compared to pure Portland cement as it is illustrated in

Figure 1.

Based on the numbers given in [1] and [21] the CO_2-equivalent of the concrete composition considered in the research project were calculated. The calculations were made on the one hand for a Portland cement which is the most common used cement for such applications in Germany and on the other hand for the CEM III/A cements used in the investigations. The slag content was approx. 50 %. The results are listed in Table 3. The CO_2-equivalent of the slag cement concrete is considerably reduced by approx. 43 % compared to the Portland cement concrete as it is clearly depict in

Figure 7.

Table 3 Global Warming Potential measured as CO_2-equivalent for the concrete recipe used in the investigations depending on the used cement type acc. to [21]

CONCRETE CONSTITUENT			CO_2-EQUIVALENT FOR CONCRETE MADE WITH	
Name	Content	CO_2-equivalent	Portland cement	slag cement
	kg/m³	kg/t	kg/m³	kg/m³
Cement OPC / SC	340	746 / 411	254	140
AEA	1.75	1470	3	3
Sand	650	3	2	2
Gravel	1200	5	6	6
Concrete			265	151

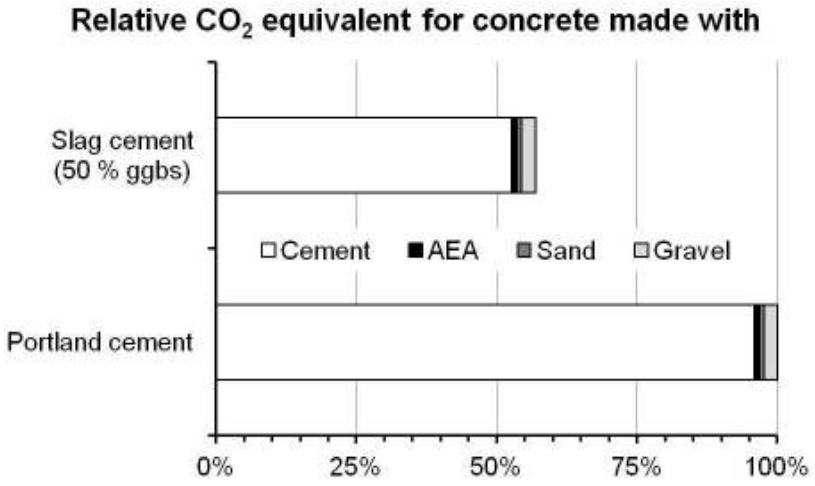

Figure 7 Comparison of CO_2-equivalent of the concretes recipe used in the research program depending on the cement type

It is quite clear that the calculated ecological footprint depends partly on the calculation methods. For example the allocation principle of energy demands, emissions, etc. (input/output flows) to main products (e.g. steel) and by-products (e.g. granulated blast furnace slag) influences the result. Up to now in most cases only those factors are allocated to the slag which are generated during the granulation process and later. In future EN 15804 [22] has to be considered. Based on this standard an allocation shall be done based on relative economic values of main and by-products. Due to the high difference between steel and slag prices no significant change of the ecological footprint of granulated blast furnace slag has to be expected.

This reduction potential can be made more obvious by an example. In Germany approx. 150 km highway were built in 2010 with about 500.000 m³ of mainly Portland cement concrete. If CEM III/A had been used instead of Portland cement, approx. 60.000 t CO_2-equivalent could have been saved only for the new highway constructions. This small example clearly indicates which potential RMX concrete has to contribute to sustainable constructions.

CONCLUSIONS

All in all concrete with a high freeze-thaw and de-icing salt resistance can be produced with slag cements! A precondition is a proper handling from production to curing even if it might be slightly different compared to Portland cement concretes. It has to be stated there is no “single solution” available to avoid any problems with air entrained concrete, especially if plasticizer is used in addition. But based also on these presented investigations recommendations can be given to reduce the risk concerning the occurrence of such problems.

Always all concrete raw materials should be very carefully selected and tested concerning their compatibility. In this respect a special attention has to be given to the additional activating potential of the AEA. AEA based on natural materials are much more robust than the synthetic ones especially if plasticizer has to be used in addition. Synthetic AEAs are very effective in air pore formation but may have a more significant additional activating potential.

In particular synthetic AEAs in combination with PCEs as plasticizer need a special diligence.

Concrete need a sufficient mixing energy so that the AEA can be dissolved properly. Therefore the mixing time should be aligned accordingly on order to take the additional activating agent into account.

The additional activating potential should be taken into account by aligning the initial mixing time accordingly. As a result a later increase of fresh air content can be avoided which is always accompanied by an unwanted strength decrease (compare Figure 2). Furthermore the chosen and pre-tested mixing order should be consequently maintained. It turned out to be helpful to add the AEA a specific time before adding the plasticizer.

Since decades slag cements have shown that durable concrete structures can be achieved, especially in aggressive exposures. Beside technical they show also ecological advantages. The use of slag cements in concrete applications supports the efforts to increase the sustainability of concrete constructions. It is a constitution to “green building”. Even if the cement part on the CO_2-emissions with regard to the complete life cycle of a concrete structure is only small, the total number, which has to be allocated to the cement and concrete production, is, however, not negligible. The global warming potential of slag cements with 50 % GGBS is approximately 43 % lower than those of pure Portland cement.

As it was shown 60.000 t CO_2-equivalent would have been reduced if a slag cement with 50 % GGBS had been used instead of Portland cement for the new constructed highways 2010 in Germany. This huge number for only one application should be an appeal to all involved parties started from planer via authorities, cement and concrete producers to construction companies to leave ancient traditions and to open up for innovative and sustainable constructions.

ACNOWLEDGEMENTS

The results presented within the article and prepared at the FEhS-Institute were gathered in the frame of an extensive research project [7]. The IGF-project No. 15326 of the steel institute (VDEh) was financially supported by the AiF within the budget of the Federal Ministry of Economics and Technology (BMWi) through the programme to promote joint industrial research and development (IGF).

REFERENCES

1. CEM II- und CEM III/A-Zemente im Betonbau – Nachhaltige Lösungen für das Bauen mit Beton, Ed.: Verein Deutscher Zementwerke e.V., Düsseldorf, 2008

2. EHRENBERG, A.: CO2-emissions and energy consumption of granulated blastfurnace slag, Proceedings 3rd European Slag Conference, Keyworth, 02.-04.10.2002, Euroslag Publication No. 2, 2003, pp. 151-166

3. MEHTA, P. K.: Durability - Critical issues for the future, Concrete International 19 (1997) No. 7, pp. 27-33

4. WALZ, K., HARTMANN, E.: Eigenschaften und Wirkung luftporenbildender Zusatzmittel für Beton, DAfStb-Schriftenreihe Heft 123, 1956

5. BONZEL, J.: Beton mit hohem Frost- und Tausalzwiderstand, Beton 15 (1965) No. 11, pp. 469-515

6. POWERS, T.C.: Void spacing as a basis for producing air-entrained concrete, Portland Cement Association Research Department Bulletin 49 (1954)

7. EICKSCHEN, E.: Reactivation potential of air-entraining concrete admixtures, Cement International (2011) No. 5, pp. 76-81 and No. 6, pp. 66-77

8. EHRENBERG, A.: Zusammenwirken von Luftporenbildnern und Fließmitteln in hüttensandhaltigen Betonen und ihr Einfluss auf den Frost- und Frost-Tausalz-Widerstand, final report of the AiF research program 15326 N, 2010

9. FELDRAPPE, V.; EHRENBERG, A.: Luftporenbeton mit hüttensandhaltigen Zementen, Report des FEhS-Instituts 17 (2010), No. 2, pp. 13-17

10. ROBERTS, F.: Energy consumption in the production of materials, Metals and Materials (1974) No. 3, pp. 167-173

11. HAYNES, D. J., CONNELL, M. D.: GGBS an environmental cement, Proceedings International Conference on Concrete for Environment Enhancement and Protection, Dundee, 24.-26.06.1996, pp.331-342

12. HENDRIKS, C. A. et al.: Emission reduction of greenhouse gases from the cement industry, IEA GHG papers presented at the Conference on Greenhouse Gas Control Technologies GHGT-4, Interlaken, 30.08.-02.09.1998

13. VARES, S., HÄKKINEN, T.: Environmental burdens of concrete and concrete products, Nordic Concrete Research Publication (1998) No. 21, pp. 130-143

14. U.S. ENVIRONMENTAL PROTECTION AGENCY: Comprehensive guideline for procurement of products containing recovered materials, 40 CFR Part 247, 1995

15. MERKBLATT: Frostprüfung von Beton (BAW-Merkblatt "Frostprüfung"), Bundesanstalt für Wasserbau Karlsruhe, Hamburg, Ilmenau, Dezember 2004

16. LANG, E.: Einfluss unterschiedlicher Karbonatphasen auf den Frost-Tausalzwiderstand – Labor und Praxisverhalten, Beton-Informationen 43 (2003), No. 3, pp. 39-59

17. LANG, E.: Freeze-thaw resistance of blast furnace cements: Laboratory test and long term experience, Proceedings of the International Conference on Challenges of Concrete Construction, Dundee, 09.09.-11.09.2002

18. RICKERT, J.: Zeta-Potential und Rheologie von Zementleimen – Einfluss von Fließmittel sowie Hüttensand und Kalkstein, Beton 60 (2010) No. 7+8, pp. 315 - 320 and No. 9, pp. 363-365

19. LUDWIG, M.: Zur Rolle der Phasenumwandlungen bei der Frost- und Frost-Tausalz-Belastung von Beton, Selbstverlag, Weimar, 1996

20. DRINKGERN, G.: Energy content of the concrete and concrete building components, Betonwerk + Fertigteil – Technik 56 (1983) No. 9, pp. 588-591 and No. 10, pp. 638-642

21. GRAUBNER, C.-A.; PROSKE, T.; HAINER, S.: Zementreduzierte "Ökobetone" für die Herstellung von Betonfertigteilen, In: Proceedings, 55. BetonTage, BFT International 77 (2011), No. 2

22. E DIN EN 18804 Sustainability of construction works – Environmental product declarations — Product category rules, May 2005

Effect of Entrained Air Voids on Salt Scaling Resistance of Concretes Containing Composite Cements

A A Ramezanianpour, M J Nadushan, M Peydayesh
Amirkabir University of Technology, Iran

Salt scaling is a major damage problem for concrete and concrete pavements, so the phenomenon has been the subject of an extensive research effort in the world. Replacement of cement with SCMs in the production of concrete not only improves the mechanical properties and durability of concrete but also decreases the amount of consumed cement in construction projects. In order to reduce energy consumption, CO_2 emission and increase production, cement plants produce composite cements, comprised of supplementary cementitious materials such as natural pozzolan, limestone and other SCMs. Effects of composite cement and air void on de-icer scaling resistance of concrete were investigated in this research work. Specimens with modified Portland cement (type II) and composite cement with and without air void were investigated. Mechanical properties such as compressive strength, tensile strength, and abrasion resistance were measured. Specimens were tested for freeze–thaw de-icer salt scaling resistance in accordance with ASTM C672 Standard test method. Visual examination according to ASTM C 672 and the mass of scaled material in salt scaling for every five cycles of freeze–thaw were assessed. It has been shown that the use of de-icing salt on concrete surface causes gradual deterioration from the surface into the inner section. This study shows that surface strength of concrete plays an important role in salt scaling resistance. Entrained air bubbles in the concrete reduce bleeding and will result in increased surface resistance. Therefore, entrained air bubbles improve concrete salt scaling resistance. The performance of type II Portland cement mixtures was better than that for composite cement mixtures when no air entraining admixture was used. The mixtures containing composite cement with entrained air bubbles showed the best performance in salt scaling test.

A A Ramezanianpour, M J Nadushan, M Peydayesh are Professor and students at the Concrete Technology and Durability Research center (CTDRc), Amirkabir University of Technology, Tehran, Iran.

Keywords: Composite cement, Entrained air, Freeze-thaw cycle, Salt scaling

INTRODUCTION

Concrete is a material used in many civil engineering projects. As a result of its beauty, strength and durability, concrete is used in most Types of construction, including buildings, bridges, airports and road pavements. Concrete exposed to several damage issues that result in high maintenance costs. For example, repair of the concrete infrastructure in the United States costs nearly $50 billion annually [1].

Replacement of cement with supplementary cementitious materials (SCMs) in the production of concrete reduces energy consumption and greenhouse gas emissions and improves the mechanical properties and durability of concrete.

In cold climates, deicing salts (NaCl, $CaCl_2$) are usually used on roadways. When a salt is applied and the concrete surface is exposed to freeze-thaw cycles, progressive scaling of the surface layer of concrete can occur [2]. It was demonstrated that the maximum rate of damage occurs when the concentration of salt is moderate, namely about ~3 % by mass [3]. It is clear that many factors such as water to cement ratio, air entrainment, cement content, replacement of cement with SCMs and the maturity of concrete have influences on the scaling of concrete in freezing conditions [3].

Salt scaling alone will not lead to the destruction of a structure. This damage results in accelerated ingress of aggressive chemical species, such as chloride ions, and the tendency for a high degree of saturation. Entrance of chloride ions makes the concrete susceptible to corrosion of the reinforcing steel [4-6, 10], while the increase in the degree of saturation results in strength loss from internal frost action [7-10]. These phenomena decrease the service life of concrete.

Valenza and Scherer [10] made a review study of salt scaling. The glue-spall mechanism was proposed as the primary cause of salt scaling. When a solution freezes on a concrete surface a composite material forms. As the composite temperature is reduced below the melting point of the solution, the ice layer tends to contract 5 times as much as the underlying concrete. According to the glue-spall theory, the damage results from cracking of the ice on the surface of concrete, when the thermal expansion mismatch stress exceeds the strength of the ice. It was previously shown that cracks in the ice layer are expected to penetrate the underlying cementitious binder, and subsequently propagate in a path that is parallel to the composite interface, which results in the removal of a scallop- shaped fragment [10].

The air content was shown to have a dramatic effect on scaling. Air-entrained mortars contract upon freezing, while non-air entrained mortars expand [11]. The contraction of the mortar caused by air entrainment offsets the thermal expansion mismatch sufficiently to prevent cracking.

In this study the performance of concrete made with modified Type II and composite Portland cements with and without air entrainment with respect to salt scaling was examined. Another objective was to investigate effects of compressive strength, tensile strength, abrasion resistance and water penetration on salt scaling.

EXPERIMENTAL PROGRAM

Materials and Mix Proportions

Modified Type II and composite Portland cements were used in the concrete mixes. The composite Portland cement consisted of 80% clinker and 18% natural pozzolan (volcanic ash, Tuff) and limestone. The remainder was gypsum. The clinker, natural pozzolan and limestone had been ground simultaneously. The chemical and physical characteristics of modified Type II and composite Portland cements are shown in Table 1 and Table 2 respectively. Tuff and limestone make clinker easier to mill. The specific surface of composite Portland cement is greater than that of Type II Portland cement. Therefore, the replacement of cement with SCMs reduces the cost of cement production, energy consumption and pollution caused by cement production.

Table 1 Chemical characteristics of cementitious materials

CHEMICAL COMPONENTS	CEMENTITIOUS MATERIAL	
	Modified Type II Portland cement	Composite Portland cement
Calcium Oxide (CaO), %	62.4	59.23
Silicon Dioxide (SiO_2) , %	21.07	24.47
Magnesium Oxide (MgO) , %	2.89	2.13
Aluminum Oxide (Al_2O_3), %	4.99	5.54
Ferric Oxide (Fe_2O_3) , %	3.64	3.28
Sulphate Oxide (SO_3) , %	2.31	1.67
Potassium Oxide (K_2O) , %	0.65	0.8
LOI, %	2.02	6.2
Mineralogical composition, %		
C_3S	49.41	-
C_2S	22.83	-
C_3A	7.07	-
C_4AF	11.08	-

Table 2 Physical characteristics of cementitious materials

PHYSICAL PROPERTIES		CEMENTITIOUS MATERIALS	
		Modified Type II Portland cement	Composite Portland cement
Blaine, cm^2/g		3078	3240
Specific gravity, g/cm^3		3.13	2.99
Initial setting time, min		135	140
Final setting time, min		187	195
Compressive strength, MPa	3 days	21.7	19.6
	7 days	31.4	28.7
	28 days	40.4	37.0

For all mix designs, the coarse aggregate was crushed calcareous stone with a maximum size of 19 mm and the fine aggregate was a natural sand. The coarse aggregates had a specific gravity and water absorption of 2560 kg/m^3 and 1.75% respectively, the fine aggregate had a water absorption value of 2.3% and a specific gravity of 2570 kg/m^3. The grading of the aggregates according to the Iranian standard grading curves is presented in Figure 1. Potable water was used for casting and curing all concrete specimens. A high range water reducing (HRWR) admixture based on modified polycarboxyl-ether, with a specific gravity of 1.1 was employed to achieve the desired workability in all concrete mixes.

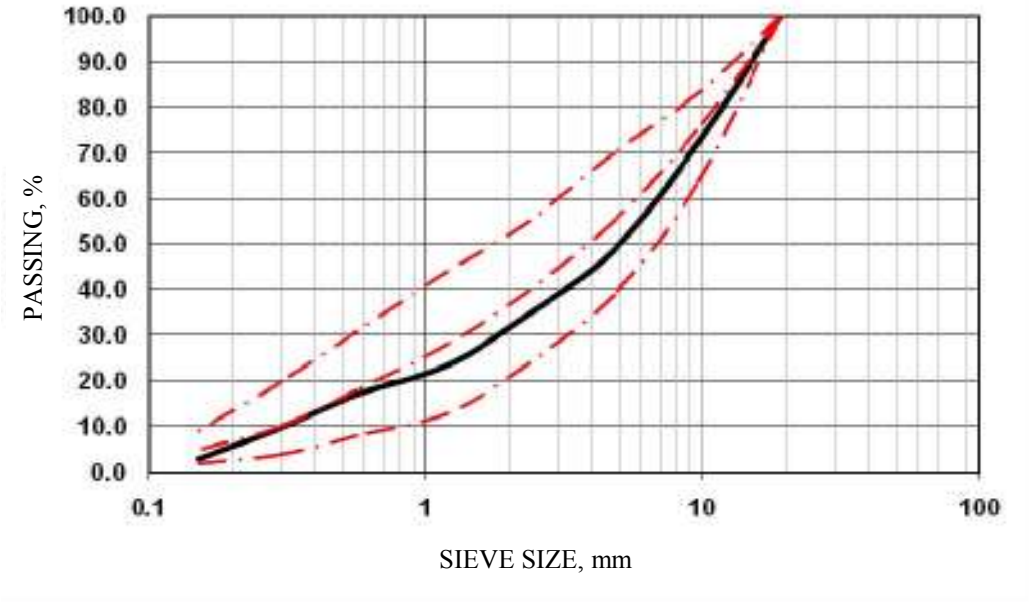

Figure 1 The grading of the aggregate

A synthetic detergent air-entraining agent (Microair by BASF) was employed to achieve the desired air content. The dosage range of this air-entraining agent is 0.06 to 0.2 percent of the cement content by weight. According to ACI 2012r-01 the recommended values of air content in concrete with 19 mm nominal maximum aggregate size exposed to severe exposure conditions of freezing and thawing (concrete pavement, bridge decks, water tanks etc) is 6%.

A total of 4 concrete mixes were made. The mix proportions for concrete specimens are summarized in Table 3. The concrete mixes were prepared with a constant total binder (cement + SCMs) content of 375 kg/m^3. The designed air content in the mixes was 6 ± 1%, except for the reference non-air-entrained mix. Standard testing procedures were applied for determination of mix consistency using the slump test, the mix density and the air void content using a pressure method (ASTM C231). Slumps were kept constant at 70 ± 20 mm. To achieve the target slump and air content the required amount of chemical admixtures was established experimentally. Concrete test specimens were compacted by external vibration and kept protected after casting to avoid water evaporation. After 24 hour they were de-molded and cured in lime-saturated water at 23 ± 2°C to prevent possible leaching of $Ca(OH)_2$ from these specimens.

Table 3 Mix proportions of concrete

MIX	MIX PROPORTION								
	Cement Type	w/c	Cement	Water	Agg	Air content	Air-entraining agent	SP	Slump
			kg/m³			%	% of binder		mm
A-40-0	Modified Cement	0.4	375	150	1806	0	-	0.2	70 ± 20
B-40-0	Composite Cement	0.4	375	150	1806	0	-	0.2	70 ± 20
A-37-6	Modified Cement	0.37	375	139	1721	6	0.135	0.3	70 ± 20
B-37-6	Composite Cement	0.37	375	139	1721	6	0.135	0.3	70 ± 20

Testing Procedure and Specimen Preparation

Concrete cubes of 100×100×100 mm dimension were cast for compressive strength. They were tested after 7, 28, 90 and 180 days of water curing. Tensile strength was determined on 150×300 mm cylinders using the ASTM C 496 splitting test at 7, 28, 90 and 180 days. Abrasion resistance was established according to ASTM C779-00, which consists of measuring the depth of wear made by three steel disks in conjunction with abrasive grit on 300×300×95 mm samples at ages of 7, 28, 90 and 180 days. The abrasive grit consists of 250μ silicon carbide particles. Readings were taken every thirty minutes for 60 minutes. The water penetration test, which is most commonly used to evaluate the permeability of concrete, is that described in BS EN 12390-8:2000. The maximum depth of water penetration in specimens was recorded at the ages of 7, 28, 90 and 180 days.

Salt scaling resistance of concrete was investigated according to the ASTM C672 standard procedure [12], based on determination of concrete resistance to repeated freezing and thawing (F/T) in contact with 4% calcium chloride ($CaCl_2$) solution. Special specimens (300 × 200 × 75 mm) were used for this test (Figure 2). The specimens had been removed from moist storage at an age of 14 days and were subsequently stored in air for a further 14 days at 23±2 °C and 45 to 55 % relative humidity. The total number of freeze–thaw cycles was 50. Both visual examination according to ASTM C 672 and the mass of scaled material in salt scaling for every five cycles of freeze–thaw were considered. The best way to quantify the degree of scaling is to collect and measure the mass of scaled-off material. This quantity is reported as the ratio of mass loss to the area of the test surface (kg/m^2). As a criterion for concrete road pavements, it is common to assume the limit of allowable mass of scaled material of about 1.5 kg/m^2 after 50 cycles.

Figure 2 Laboratory scaling specimen with Styrofoam dike applied

RESULTS AND DISCUSSIONS

The compressive strengths of concrete specimens are presented in Figure 3. As expected, the compressive strength of all concrete specimens increases with the period of curing. In general, the concrete specimens containing Type II Portland cement had higher compressive strength at various ages and up to 180 days when compared with the concrete specimens containing composite Portland cement.

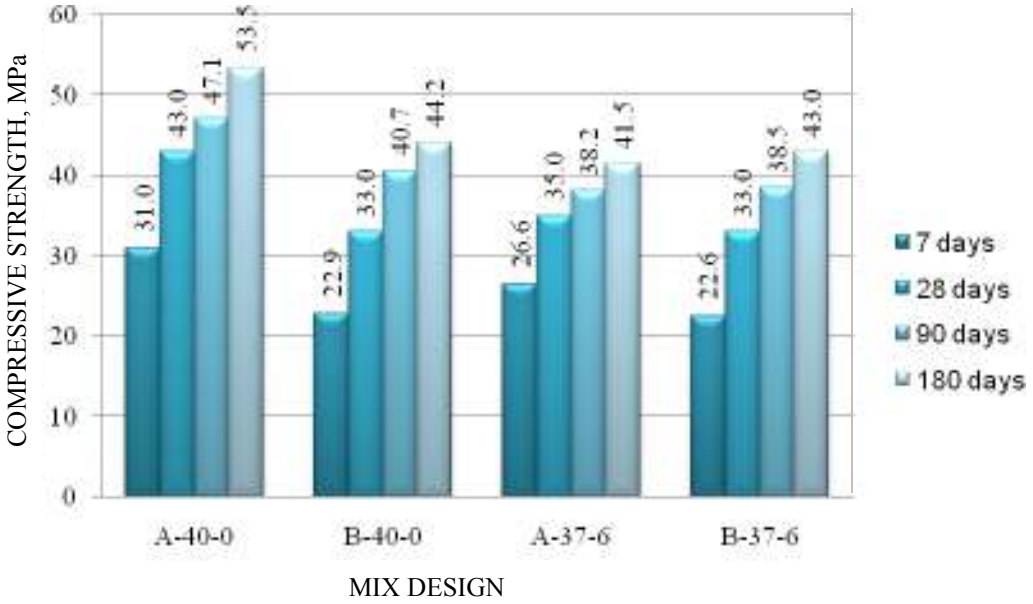

Figure 3 Compressive strength at various ages

The reduction in compressive strength could be related to the degree of hydration, which is lower for composite Portland cement concrete than for Type II Portland cement at all ages. The reduction in degree of hydration of concrete specimens containing composite Portland cement is explained as the result of a clinker dilution effect. The dilution effect is a consequence of replacing a part of cement by the same quantity of tuff and limestone. In composite Portland cements, the filler effect and heterogeneous nucleation can compensate the dilution effect. As seen in Figure 3 entrained air caused a reduction in compressive strength at various ages and up to 180 days. Entrained air bubbles have a smaller effect on the compressive strength of concrete samples containing composite cement and this is an advantage of such materials.

Figure 4 shows the tensile strength of concrete specimens at various ages and up to 180 days. Generally, due to the filler effect at early ages and the pozzolanic reaction of tuff with $Ca(OH)_2$ at later ages, the concretes containing composite Portland cement provide comparable tensile strengths to concretes containing Type II Portland cement. Re-crystallization of $CaCO_3$ by the reaction of limestone and $Ca(OH)_2$ has little contribution to increasing the tensile strength. The abrasion resistance data (depth of wear at 60 min) are shown in Figure 5. The abrasion resistance of concrete is markedly influence by factors such as aggregate properties and content, concrete strength, mix proportions, the use of supplementary cementitious materials, fiber additions, curing conditions and surface finish. Experimental results indicated that concrete containing composite Portland cement had better abrasion resistance than either modified Portland cement concrete. Several researchers have reported that the addition of limestone reduces bleeding [13] and will result in increased surface strength and abrasion resistance.

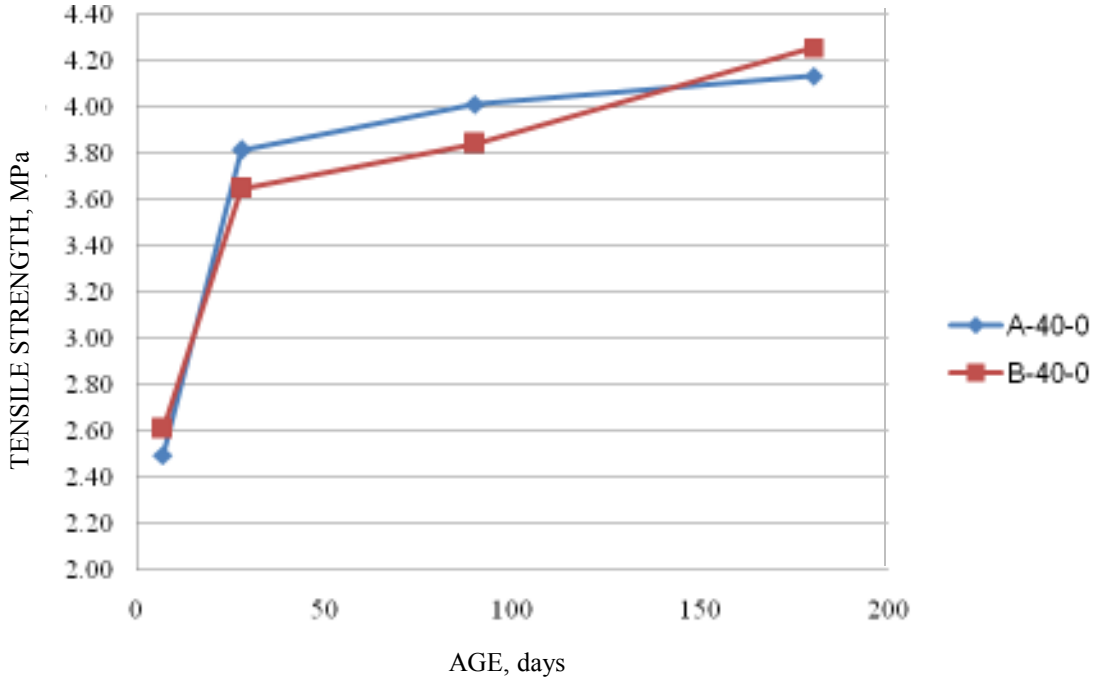

Figure 4 Tensile strength at various ages

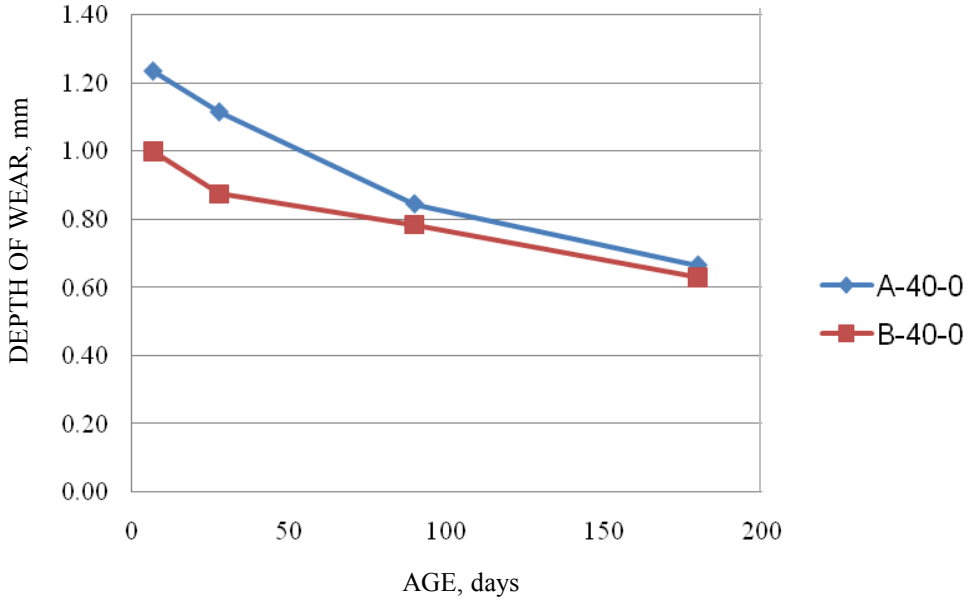

Figure 5 The depth of wear at various ages

Figure 6 summarizes the results of the water penetration depths in all concrete mixes. It is observed that for air-entrained and non-air-entrained concrete mixes, the water penetration depth increases with replacing a part of the Portland cement by the same mass of tuff and limestone. These issues are related to the dilution effect. At various ages and up to 180 days, the maximum depth of water penetration is for the B-40-0 mix and the minimum is for the A-37-6 mix. Due to the filler effect, there is no significant difference between the water penetration depth of specimens containing Type II Portland cement and composite Portland cement at the early age of hydration.

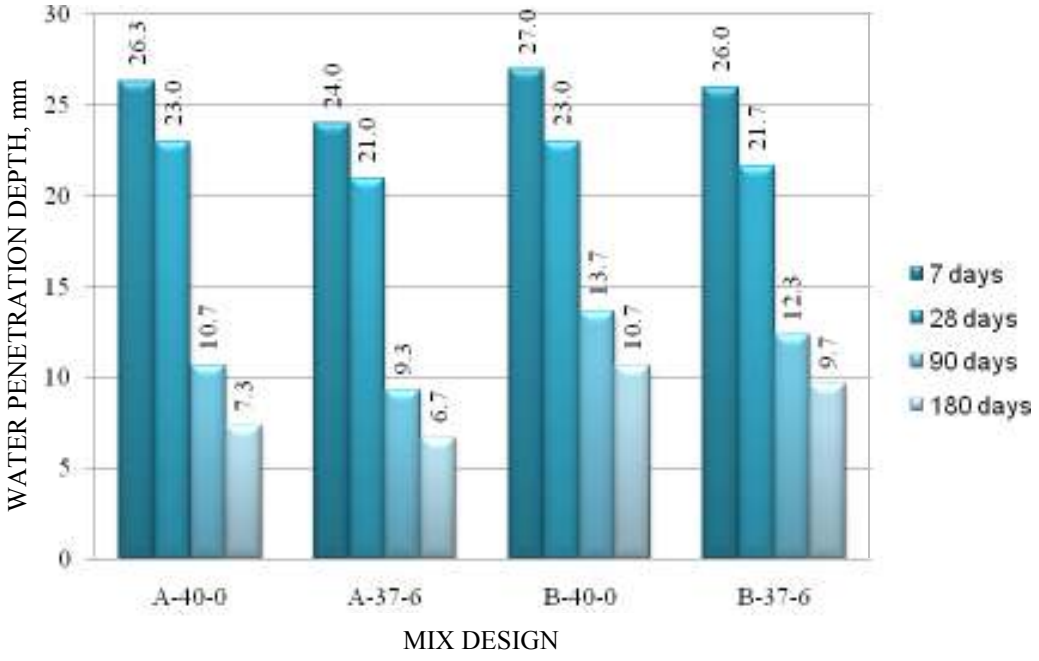

Figure 6 The water penetration depth (mm) at various ages

Water transportation in cementitious materials depends on capillary porosity, its connectivity and the pore structure (tortuosity and constriction or disconnection); these parameters are directly related to the progress of cement hydration.

The results indicate that air-entrained concrete generally has lower depths of water penetration than non-air-entrained concrete (Figure 6). Cavities and air voids form regularly, uniformly and discretely in air-entrained concrete. Therefore an entrained air system causes a reduction in water penetration depth.

The specimens under freeze-thaw salt scaling were inspected by visual examination according to ASTM C672- 98 [12]. Based on this standard, the criteria for visual inspection are; 0 (no scaling), 1 (very slight scaling), 2 (slight to moderate scaling), 3 (moderate scaling), 4 (moderate to severe scaling) and 5 (severe scaling). Rating of the measured scaling for every five cycles of freeze–thaw is reported in Table 4. As shown in this table, the highest rate of the scaling was observed in non-air-entrained concrete specimens containing composite Portland cement while the air-entrained concrete specimens containing composite Portland cement had the highest resistance to scaling.

Table 4 Results of visual examination according to ASTM C 672-98

MIX CODE	SAMPLE NUMBER	VISUAL EXAMINATION									
		Number of cycles									
		5	10	15	20	25	30	35	40	45	50
A-40-0	1	1	2	2	2	2	2	2	2	2	3
	2	2	3	3	3	3	3	3	3	3	3
A-37-6	1	2	2	2	2	2	3	3	3	3	3
	2	2	2	2	2	2	2	2	2	2	2
B-40-0	1	2	3	3	3	3	3	3	3	4	4
	2	2	3	3	3	3	3	3	3	4	4
B-37-6	1	2	2	2	2	2	2	2	2	2	2
	2	1	2	2	2	2	2	2	2	2	2

The mass of scaled material in salt scaling for every five cycles of freeze–thaw are presented in Figure 7. It is clearly seen that the results of visual examination is consistent with the mass of scaled material. It can be found in Figure 7 shows that the non-air-entrained concretes containing Type II Portland cement performed significantly better than the non-air-entrained concretes containing composite Portland cement. It is possibly the case that tuff and limestone fills the cavities and pores in hardened concrete, thus reducing the presence of voids which would otherwise reduce ice expansion. The air content has a significant impact on salt scaling. Figure 7 shows that the air-entrained concretes performed significantly better than the non-air-entrained ones. Entrained air could be beneficial to salt scaling resistance in three ways: (1) entrained air bubbles reduce bleeding [3, 14]; (2) the formation of ice in the air voids draws pore fluid from the surrounding matrix, which compresses the porous body [15] and (3) entrained air system caused a reduction in solution penetration depth in concrete.

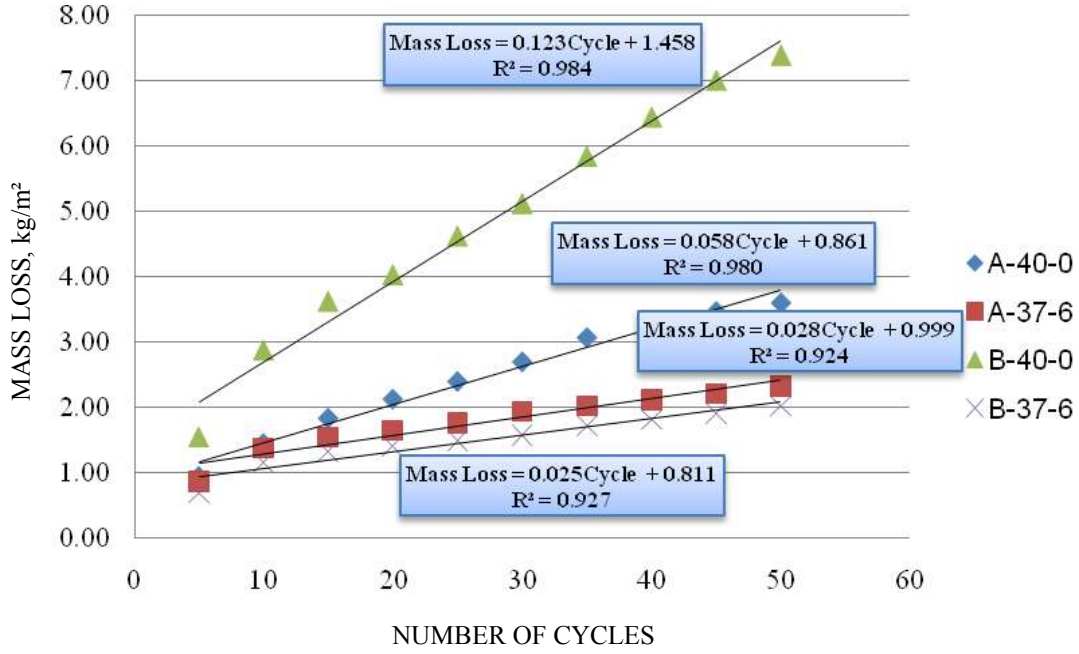

Figure 7 The mass of scaled-off particles versus number of cycles for all mix designs

Air bubbles reduce bleeding by adhering to cement particles, making the particles buoyant [3]. Entrained air bubbles improve the resistance to salt scaling because of this, limiting reduction in strength at the concrete surface. Powers and Helmuth [15] showed that air-entrained concrete contracts, because ice nucleates in the voids and draws liquid from the surrounding pores. The contractions of air-entrained concrete offsets the thermal expansion mismatch resulting from glue spall sufficiently to prevent cracking.

Entrained air bubbles can improve salt scaling resistance due to reducing solution penetration (Figure 6), because cavities and air voids form regularly, uniformly and discretely in the air-entrained concrete. The amount of ice formation decreases in the air-entrained concrete as a function of permeability reduction. The reduced amount of ice formation results in lower salt scaling.

The most important parameter affecting the scaling resistance of concrete is air-entrainment [16]. It was shown that the concrete containing composite Portland cement had better tensile and surface strength and abrasion resistance than either modified Portland cement concrete. For this reason the air-entrained concretes containing composite Portland cement performed better than those air-entrained concretes containing modified Portland cement in scaling test (Figure 7). In other words, the reduction in mass loss for specimens containing composite Portland cement is probably because of the higher surface strength in the presence of air voids. Therefore in the presence of air voids, surface strength plays a crucial role in improving salt scaling resistance of concrete. Mechanisms related to internal crystallization for salt scaling have been proposed [10]. Also several mechanisms have been proposed that focus on the role of salts (thermal shock, precipitation and growth of salt and salt concentration in the pore solution). None of these mechanisms adequately account for all of

the characteristics of salt scaling [10]. A purely physical mechanism known as glue spalling adequately accounts for all the characteristics of salt scaling damage.

As can be seen in Figure 7, a very clear linear relationship between mass loss and number of cycles is evident for all concrete mixes. The results in Table 5 reveal that the mass of scaled material varies during the initial freeze/thaw cycles due to bleeding and finishing effects. Glue spalling analyses indicate that the depth of crack penetration depend on the mechanical properties of the concrete. Therefore, due to the fact that the mechanical properties of the concrete do not vary significantly in the surface, each freezing cycle result in a relatively constant amount of damage (See Table 5).

Table 5 The amount of scaling particles from the unit area, kg/m^2

Number of cycle	MASS OF SCALED-OFF PARTICLES FROM UNIT AREA, kg/m²			
	Mix			
	A-40-0	A-37-6	B-40-0	B-37-6
0-5	0.93	0.85	1.54	0.68
5-10	0.50	0.52	1.33	0.46
10-15	0.39	0.17	0.74	0.17
15-20	0.29	0.11	0.41	0.08
20-25	0.27	0.11	0.59	0.09
25-30	0.30	0.18	0.50	0.08
30-35	0.37	0.08	0.72	0.15
35-40	0.22	0.10	0.60	0.09
40-45	0.18	0.09	0.56	0.10
45-50	0.13	0.12	0.39	0.11
Mean (20th-50th cycle)	0.25	0.11	0.54	0.10
Variance (20th-50th cycle)	0.007	0.001	0.014	0.001

CONCLUSIONS

From the results obtained in this investigation, the following conclusions are drawn:

- The compressive strength of concrete reduces and the water penetration depth increases with replacing a part of cement by the same quantity of tuff and limestone. These issues are related to the dilution effect.

- Experimental results indicate that concrete containing composite Portland cement had better abrasion resistance than modified Portland cement concrete.

- Entrained air caused a reduction in compressive strength at various ages for all concrete mixes. Entrained air bubbles have smaller effect on the compressive strength of concrete samples containing a composite cement. Air-entrained concrete generally, permits water penetration to a lesser depth than non-air-entrained concrete.
- The results of visual examination are consistent with the mass of scaled material in the salt scaling test. It is confirmed that entrained air can improve salt scaling resistance of concrete considerably. The surface strength of concrete plays an important role in salt scaling. Entrained air bubbles reduce bleeding and therefore display less loss in strength at the surface. Also, the air-entrained mixes displayed a reduction in solution penetration depth in concrete.

- The most effective parameter, after air-entraining use is surface strength.

- Results indicate that air-entrained concrete specimens containing composite Portland cement had the highest resistance to scaling. The non-air-entrained concretes containing Type II Portland cement performed significantly better than the non-air-entrained concretes containing composite Portland cement.

- The glue spall mechanism was proposed as the primary cause of salt scaling. Each freeze- thaw cycle result in a relatively constant amount of salt scaling damage. This reveals that the purely physical mechanism known as glue-spall accounts for salt scaling damage.

REFERENCES

1. NATIONAL RESEARCH COUNCIL, Nonconventional Concrete Technologies: Renewal of the Highway Infrastructure, NMAB-48, National Academy Press, Washington, DC, 1997.

2. SAHMARAN M., LI V C., De-icing salt scaling resistance of mechanically loaded engineered cementitious composites, Cement and Concrete Research 37, 2007, pp. 1035–1046.

3. VALENZA J J., SCHERER G W., A review of salt scaling: I. Phenomenology, Cement and Concrete Research 37, 2007, pp. 1007–1021.

4. ALONSO C., ANDRADE C., CASTELLOTE M., CASTRO P., Chloride threshold values to depassivate reinforcing bars embedded in a standardized OPC mortar, Cem. Concr. Res. 30, 2000, pp. 1047–1055.

5. HIME W G., The corrosion of steel — random thoughts and wishful thinking, Concr. Int., 1993, pp. 54–57.

6. BECKETT D., Influence of carbonation and chlorides on concrete durability, Concrete, Feb. 1983, pp. 16–18.

7. FAGERLUND G., The international cooperative test of the critical degree of saturation method of assessing the freeze/thaw resistance of concrete, Mater. Constr. 10 (58), 1977, pp. 230–251.

8. SCHERER G W., Crystalization in pores, Cem. Concr. Res. 29, 1999, pp. 1347–1358.

9. SCHERER G W., VALENZA J J., Mechanisms of frost damage, in: J. Skalny, F. Young (Eds.), Materials Science of Concrete, vol. VII, American Ceramic Society, 2005, pp. 209–246.

10. VALENZA J J., SCHERER G W., A review of salt scaling: II. Mechanisms, Cement and Concrete Research 37, 2007, 1022–1034

11. SUN Z., SCHERER G W., Effect of air voids on salt scaling and internal freezing, Cement and Concrete Research 40, 2010, pp. 260–270

12. American Society for Testing and Materials, Standard test method for scaling resistance of concrete surfaces exposed to deicing chemicals, ASTM Standard C672, 1992.

13. TSIVILIS S., CHANIOTAKIS E., KAKALI G., BATIS G., An analysis of the properties of Portland limestone cements and concrete, Cement Concrete Comp, 2002;24:371–8.

14. MARCHAND J., PIGEON M., BOISVERT J., ISABELLE H L., HOUDUSSE O., Deicer salt scaling resistance of roller compacted concrete pavements containing fly ash and silica fume, in: V.M. Malhotra (Ed.), ACI Special Publication SP-132, 1992, pp. 151–178.

15. POWERS T C., HELMUTH R A., Theory of volume changes in hardened Portland-cement paste during freezing, Proc. Highw. Res. Board 32, 1953, pp. 285–297.

16. AHIN R., Tasdemir M A., GUL R., CELIK C., Determination of the optimum conditions for de-icing salt scaling resistance of concrete by visual examination and surface scaling, Construction and Building Materials, 2009

An Experimental Study for Shrinkage Cracking Resistance of BFS Blended Cement Concrete Subjected to Different Ambient Temperature

T Kanda[1], A Shintani[1], H Momose[1], K Imamoto[2], A Ogawa[3]
1 – Kajima Technical Research Institute, Japan
2 – Tokyo University of Science, Japan
3 – Takenaka Corporation, Japan

Applying cement blended with blast-furnace slag fine powder is an important option to achieve low carbon emission due to concrete materials in construction. However, concrete with this blended cement (BFS concrete, hereafter) has been believed vulnerable to shrinkage cracking and traditionally avoided to use in building construction except underground structural elements in Japan. To extend BFS concrete usage in building construction necessitates to quantitatively evaluate this concrete's shrinkage cracking resistance. Scope of this study is to experimentally reveal shrinkage resistance of BFS concrete, in which effects of ambient temperature are emphasized. In experiments, restraint shrinkage cracking tests were conducted with BFS concrete subjected to three levels of ambient temperatures, 10, 20, 30 °C in comparison with normal concrete. We adopted cracking age in the restraint shrinkage cracking tests as a performance index showing cracking resistance. As a result, it was demonstrated that cracking ages in BFS concrete were heavily influenced by ambient temperature, while this is not the case for normal concrete. Furthermore, free shrinkage strain in BFS concrete is larger with higher ambient temperature. These trends resulted that BFS concrete's cracking resistance is much lower than normal concrete at 30 °C while the former is better than the latter at 10 °C. This interesting result appears due to i)increased autogenous shrinkage in BFS concrete in higher temperature, ii)lower cracking strength in BFS concrete than normal concrete, and iii)comparable elastic modulus between the both types of concrete.

T. Kanda, A. Shintani, and H. Momose are research eingineers in Kajima Technical Research Institute, Tokyo Japan. Their specialized technical areas are: shrinkage, creep, restraint cracking in concrete. Their recent interest is most in application of low carbon concrete with large volume of mineral admixtures.

K. Imamoto is an associate professor at Department of Architecture, Tokyo University of Science, Tokyo, Japan. He is an active member of AIJ, JSCE, JCI, ACI, and RILEM. He has led many research projects and his research interests are: microstructure and its relation to creep and shrinkage, control of shrinkage induced cracking, non-destructive test for penetrability of concrete cover, durability design, and recycling/reuse of building materials.

A. Ogawa is a former graduate student at Tokyo University of Science and currently an employee of Takenaka corporation. Her research interests are: microstructure and its relation to creep and shrinkage, and control of shrinkage induced cracking.

Keywords: Autogenous shrinkage, Blast furnace slag, Cracking, Creep, Drying shrinkage

INTRODUCTION

Application of blast-furnace slag fine powder blended cement is an important option to achieve low carbon emission from concrete materials in construction. However, concrete using such blended cement (BFS concrete, hereafter) has been believed to be vulnerable to shrinkage cracking and traditionally avoided for use in building construction except for underground structural elements in Japan. To extend the use of BFS concrete in building construction, it is necessary to quantitatively evaluate the shrinkage cracking resistance of BFS concrete.

BSF concrete with relatively low water to binder ratio (w/b) has been broadly investigated in terms of autogenous shrinkage in the literatures. It is generally known that higher BFS content leads to a larger autogenous shrinkage ([1]). Furthermore, temperature increase due to hydration heat at early age causes an increase in larger autogenous shrinkage [2]. Hence massive concrete elements with BFS concrete or even thin element with low w/b BFS concrete are prone to early age cracking.

However, relatively long term restraint shrinkage cracking behavior due to autogenous plus drying shrinkage has not been sufficiently clarified for BSF concrete with normal strength level when applied to thin building element such as floor slabs and walls. While few restrained cracking test data were published under limited testing conditions in literatures [3, 4], accumulated technical knowledge for this problem is insufficient to accomplish the shrinkage controlling design in the construction practice.

Based on the above background, the ultimate goal of this research is to establish shrinkage cracking controlling design for BFS concrete building construction. Toward this goal, the scope of this study is to experimentally reveal shrinkage cracking resistance of BFS concrete with particular attention to effects of ambient temperature. In experiments, restraint shrinkage cracking tests were conducted with BFS concrete subjected to three ambient temperatures, 10, 20, 30°C in comparison with the normal concrete. We adopted cracking age in the restraint shrinkage cracking tests as a performance index representing cracking resistance. As a result, it was demonstrated that shrinkage cracking resistance in BFS concrete were heavily influenced by ambient temperature unlike the normal concrete. Mechanisms in these phenomena were also discussed in terms of shrinkage and creep.

EXPERIMENTAL DESIGN

Experiments Overview

Restrained shrinkage cracking experiment and creep experiment were performed. Experimental parameters and their variations are shown in Table 1. Combinations of the parameters are shown in Table 2 and 3. BFS concrete and concrete with the ordinary portland cement (hereafter referred to as the normal concrete) were used for the restrained shrinkage cracking experiment. To imitate the shrinkage cracking of slabs or walls under construction conditions in different seasons, the curing temperatures were varied in 10°C, 20°C and 30°C. Above two types of concrete were also subjected to the creep experiment while the ambient temperature was 20°C and the loading ages and curing moisture conditions after loading were varied. Larger creep strain heavily promotes shrinkage cracking resistance when induced shrinkage strain is same. Hence creep experimental results simultaneously obtained with shrinkage cracking experiments are expected to help us to understand tendency in cracking resistance results.

Table 1 Test parameters and variation

Experiment	Experimental parameters	Variations
Restrained shrinkage cracking experiment	Concrete type	Normal concrete, BFS concrete
	Ambient temperature	10 °C 20 °C 30 °C
Creep experiment	Concrete type	Normal concrete, BFS concrete
	Loading age	7 day 28 day
	Curing condition after	Sealed curing, Air curing

Table 2 Combination of the test parameters in restrained shrinkage cracking experiment

Specimen	Experimental parameters	
	Concrete type	*Ambient temperature
N10	Normal concrete	10 °C (RH40%)
N20	Normal concrete	20 °C (RH60%)
N30	Normal concrete	30 °C (RH60%)
B10	BFS concrete	10 °C (RH40%)
B20	BFS concrete	20 °C (RH60%)
B30	BFS concrete	30 °C (RH60%)

* Numbers in parenthesizes show ambient relative humidity.

Table 3 Combination of the test parameters in creep experiment

Specimen	Experimental parameters		
	Concrete type	Loading age (day)	*Curing condition
N7S	Normal concrete	7	Sealed
N7A	Normal concrete	7	Air
N28S	Normal concrete	28	Sealed
N28A	Normal concrete	28	Air
B7S	BFS concrete	7	Sealed
B7A	BFS concrete	7	Air
B28S	BFS concrete	28	Sealed
B28A	BFS concrete	28	Air

* Ambient air condition in curing room: 20°C/RH60%

Materials, Mix Design, Mixing and Placing Method

Materials used and their mix proportions are shown in Table 4 and 5. Portland cement was the only binder for the normal concrete while for BFS concrete, ground blast-furnace slag fine powder substituting 42 percent of portland cement was used as an alternative to the

blast-furnace slag mix cement type B specified in JIS R 5201, which is very popular in Japanese construction market. Quality of the blast-furnace slag fine powder is shown in Table 6.

The targeted slump and air content were 18±2.5cm and 4.5±1.5% respectively common to the normal concrete and the BSF concrete. Mixing was performed with a biaxial forced mixer. Coarse aggregate, sand and cement was mixed without water for the first 15 seconds and, after introducing water and admixture, all the constituents were mixed for 120 seconds at a room temperature of 20°C, and placed in the molds set in chambers with different temperatures

Table 4 Materials of concrete

Material	Type	Characteristics	Satisfying standard in
Cement	Normal portland cement	Density 3.16g/cm^3	JIS R 5210
BFS	-	Density 2.86g/cm^3	JIS A 6206
Fine aggregate	Crashed sand	Density in saturated surface-dry condition: 2.64g/cm^3 Percentage of water absorption: 1.10% Fineness modulus: 2.74	JIS A 5005
Corse aggregate	Crashed gravel 1	Density in saturated surface-dry condition: 2.66g/cm^3 Percentage of water absorption: 0.55% Fineness modulus: 7.0	JIS A 5005
	Crashed gravel 2	Density in saturated surface-dry condition: 2.66g/cm^3 Percentage of water absorption: 0.62% Fineness modulus: 6.14	JIS A 5005
Chemical	Super plasticizer	Polycarboxylic acid type	JIS A 6204

Table 5 Mix proportions

Concrete type	water to binder ratio (%)	sand-aggregate ratio (%)	Unit weight (kg/m3)					
			water	cement	BFS	Fine aggregate	Corse aggregate 1	Corse aggregate 2
BFS concrete	50	46.3	175	203	147	813	437	512
Normal concrete	50	46.7	175	350	0	825	437	512

Testing Items and Methods

Restrained cracking experiment

Testing items and methods of the restrained shrinkage cracking experiments are shown in Table 7. The restrained shrinkage cracking test and free shrinkage test were performed on the basis of the literature [5]. Specimen for the restrained cracking test is shown in Figure 1. The restrained shrinkage stress over the concrete section due to autogenous and drying shrinkage was measured with a strain gauge adhered at the center of the restraining steel bar and calculated with the equation (1).

$$\sigma_i^r = -\frac{\varepsilon_i^s \cdot E_s \cdot A_{rs}}{A_{rc}} \tag{1}$$

Table 6 Properties of BFS powder

Items		Characteristics	Requirement in JIS A 6206
Density	(g/cm^3)	2.86	≧ 2.8
Specific surface area	(cm^2/g)	4170	≧ 3000
Reactivity index	(%)	70 at 7day age 93 at 28 day age 115 at 91 day age	≧ 55 at 7 day age ≧ 75at 28 day age ≧ 95 at 91 day age
Relative flow value	(%)	99	≧ 95
Content of magnesium oxide	(%)	5.66	≦ 10.0
Content of sulfur trioxide	(%)	2.03	≦ 4.0
Ignition loss	(%)	0.93	≦ 3.0
Content of chloride ion	(%)	0.004	≦ 0.02
Basicity		1.84	≧ 1.6

where σ_i^r is restrained shrinkage stress at a time i (N/mm^2), ε_i^s is the strain of steel bar at a time i, E_s is elastic modulus of restraining steel bar (N/mm^2), A_{rs} is cross-sectional area of the restraining steel bar (mm^2) and A_{rc} is the cross-sectional area of concrete specimen at the center of the test area (mm^2).

Table 7 Items of experiments

Experiment	Testing items	Specimen size (mm)	Testing method
Restrained shrinkage cracking experiment	Fresh tests (slump, air content, concrete temperature, unit weight)	-	Japanese Industrial Standard
	Compressive and splitting tensile tests	f100x200	
	Restrained shrinkage cracking test	100x100x1100	JCI method
	Free shrinkage test	100x100x400	
Creep experiment	Creep test	f100x200	JIS A 1157
	Free shrinkage test	f100x200	-

The restraining steel bar with a diameter of 32mm was threaded equivalent to M33 screw over the embedment length of 400mm in each end in Figure 1. Specimen for the free shrinkage test was 100x100x400mm in size and an embed-type strain gauge was set at the center. To measure autogenous shrinkage, low modulus gauge capable of measuring deformation at vary early stage of hydration, autogenous shrinkage, was selected.

All the specimens were subjected to sealed curing without unmolding in a chamber with a temperature of 20°C and a relative humidity of 60% till the age of 7 days. After unmolding, specimen was sealed with aluminum foil leaving only two sides of the specimen opened for drying. For restrained shrinkage cracking test and free shrinkage test, 2 specimens are respectively prepared in each testing condition.

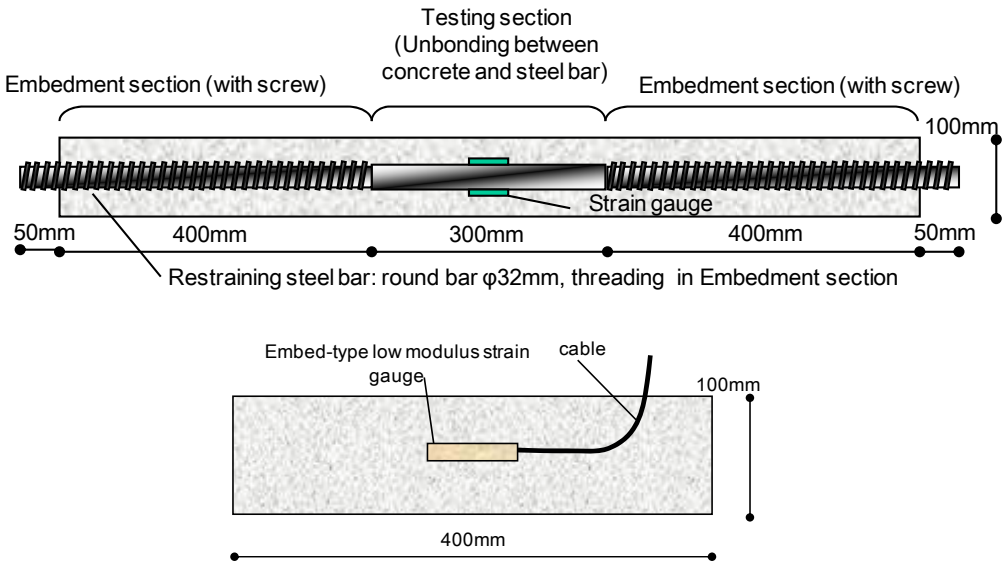

Figure 1 Specimen for the restrained shrinkage cracking experiment, upper: restrained cracking test specimen, lower: free shrinkage test specimen

Mechanical properties such as compressive strength, elastic modulus and split tensile strength were tested at material ages of 3, 7 and 28 days. Curing condition of the specimens subjected to the mechanical tests were the same as that of the restrained cracking test; sealed curing till the age of 7 days and subsequent air curing. As a control, specimens cured under water of 20°C were prepared and tested at the age of 28 days.

Creep experiment

As shown in Table 1, test parameters were loading age (7 and 28 days) and curing condition after loading (air curing and sealed curing), whose combinations are shown in Table 3. Testing items are listed in Table 7. Creep test was based on the Japanese Industrial Standard JIS A 1157 which required two cylindrical specimens with a diameter of 100mm and the height of 200mm subjected to compressive loading at a temperature of 20°C. Loading was controlled to be one third of the compressive strength of the specimen at the loading age. Deformation during the test was measured with a mould gauge embedded at the center of the specimen. Along with the creep test, two control specimens were prepared for the respective creep test, and free shrinkage was measured and subtracted from the apparent creep strain data to obtain the creep strains.

RESULTS

Restrained Cracking Experiment

Properties of concrete at fresh state are shown in Table 8. Workability of all the mixes after mixing was generally favorable and specimen was placed and formed without problems. Results of the mechanical tests are compiled in Table 9 and the developments of mechanical properties are shown in Figures 2, 3 and 4. It is seen in Table 9 that compressive strength and split tensile strength of BFS concrete are at maximum 20% smaller than that of the normal concrete when compared at the same material age, while the reduction in elastic modulus was slight compared to that of the strengths.

Changes in free shrinkage strain of BFS and the normal concrete are shown in Figure 5. The free shrinkage strains of the normal concrete at the age of 80 days were nearly equal regardless of the ambient temperatures while that of B30 of BFS concrete showed more than 100μ larger strain than that of others as a result of an significant increase in shrinkage strain at early stages up to material age of 30 days.

Results of the restrained shrinkage cracking tests are compiled in Table 10 and the developments of restrained shrinkage stresses are shown in Figures 6. As shown in Figure 6, development of the restrained shrinkage stress in BFS concrete was largely depending on temperature while the normal concrete was less sensitive to temperature. In Table 10, i) retrained shrinkage stress at drying initiation is larger, and ii) cracking age is earlier in BFS concrete at 20 and 30°C than in normal concrete.

Table 8 Fresh properties

Specimen	Fresh property			
	Slump (cm)	Air content (%)	Concrete temperature (^{o}C)	Unit weight (kg/L)
B30	19.0	4.6	20.3	2.30
B20	19.0	4.7	20.2	2.29
B10	19.0	4.3	20.5	2.30
N30	19.5	4.9	20.6	2.29
N20	19.5	5.1	20.8	2.28
N10	18.0	4.9	20.9	2.29

Table 9 Mechanical properties

Specimen	Identical curing condition to restraint shrinkage test specimen (sealing 7day, and drying thereafter)									Water curing at 20 ^{o}C	
	Compressive strength (N/mm^2)			Elastic modulus (×10^{3}N/mm^2)			Splitting tensile strength (N/mm^2)			Comp. strength (N/mm^2)	Elastic modulus (×10^{3}N/mm^2)
	3 day	7 day	28 day	3 day	7 day	28 day	3 day	7 day	28 day	28 day	28 day
B30	21.4	34.1	41.9	22.1	27.8	28.5	2.09	2.92	3.70	-	-
B20	15.4	26.4	40.4	20.5	23.7	28.2	1.64	2.31	3.51	43.6	29.8
B10	8.7	20.3	37.5	15.6	22.6	28.4	0.98	1.93	3.53	-	-
N30	29.0	38.1	48.6	26.0	29.6	30.6	2.83	2.99	4.39	-	-
N20	24.8	36.1	47.8	22.9	30.4	29.7	2.62	3.04	4.32	48.3	31.6
N10	17.3	33.9	44.8	21.0	26.0	29.6	1.80	2.67	3.66	-	-

Table 10 Results of restrained shrinkage cracking experiment

Specimen	Restrained shrinkage tensile stress at dying initiation (N/mm^2)		Cracking age (days)		Cracking strength (N/mm^2)	
B30	0.59 0.60	0.60	21.2 17.2	19.2	2.46 2.22	2.34
B20	0.45 0.45	0.45	37.6 31.9	34.7	2.80 2.87	2.83
B10	0.27 0.23	0.25	57.9 38.2	48.0	2.90 2.56	2.73
N30	0.32 0.39	0.36	40.8 32.8	36.8	2.66 2.51	2.58
N20	0.34 0.37	0.35	42.8 41.2	42.0	3.00 2.99	3.00
N10	0.32 0.33	0.33	56.1 30.9	43.5	3.06 2.32	2.69

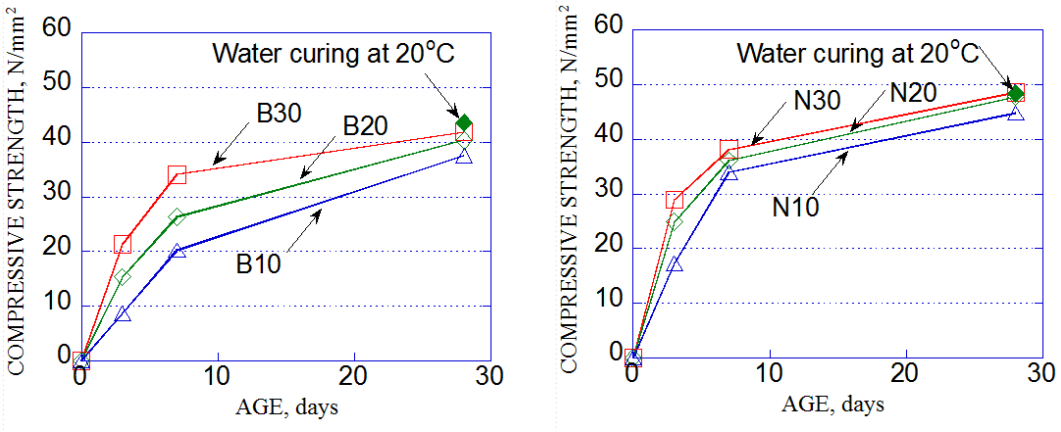

(a) BFS concrete (b) Normal concrete

Figure 2 Compressive strength test results

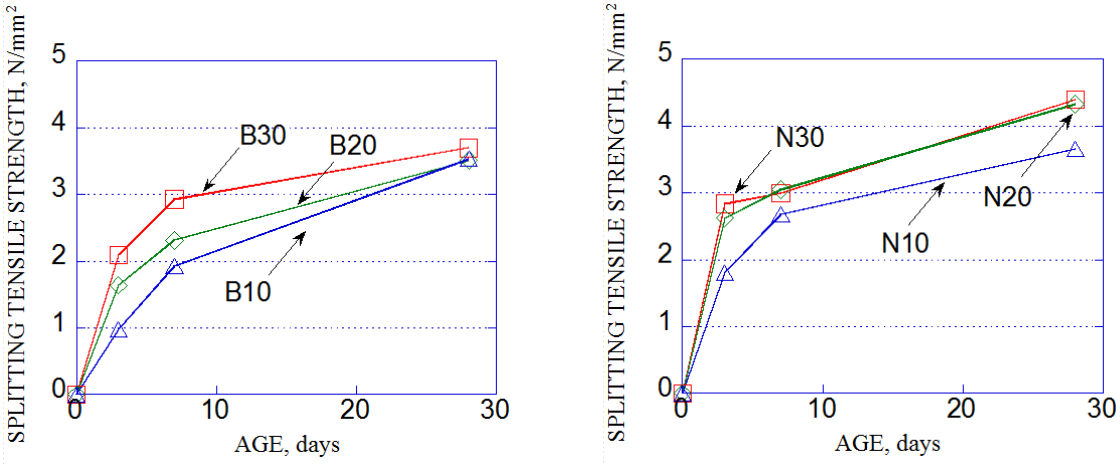

(a) BFS concrete (b) Normal concrete

Figure 3 Splitting tensile strength test results

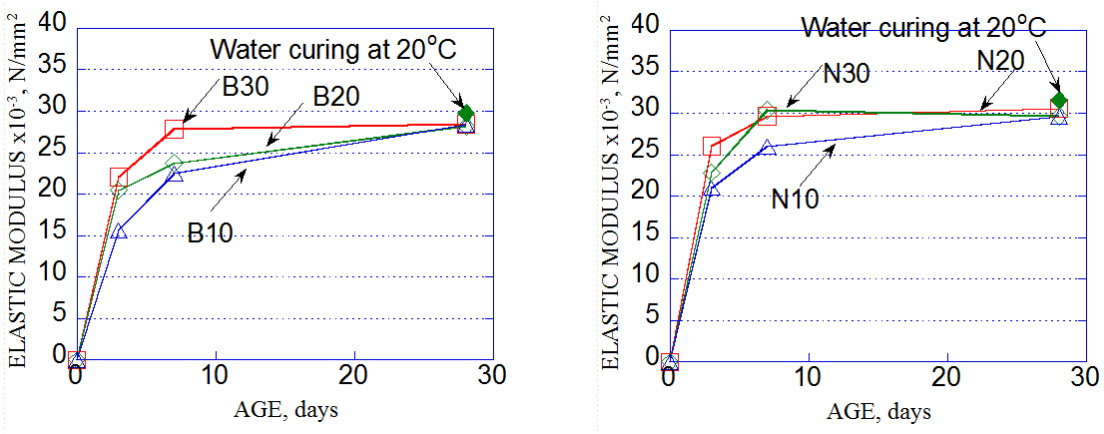

(a) BFS concrete (b) Normal concrete

Figure 4 Elastic modulus test results

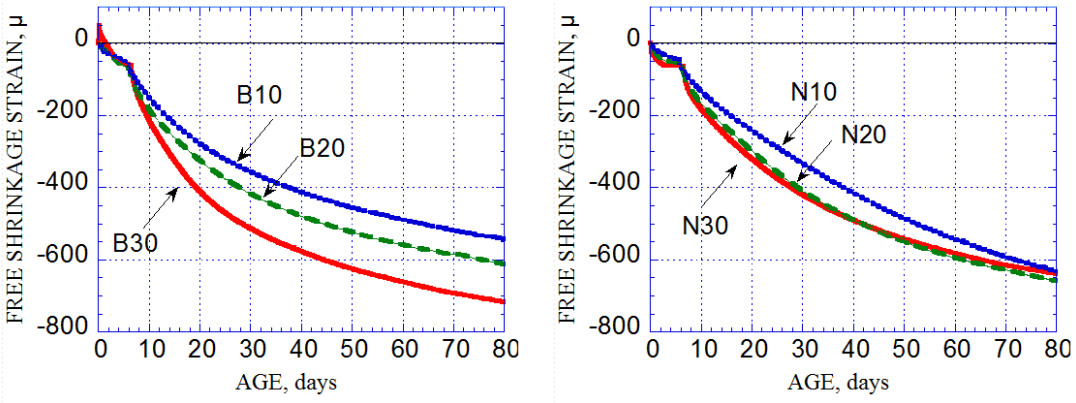

(a) BFS concrete (b) Normal concrete

Figure 5 Free shrinkage test result examples

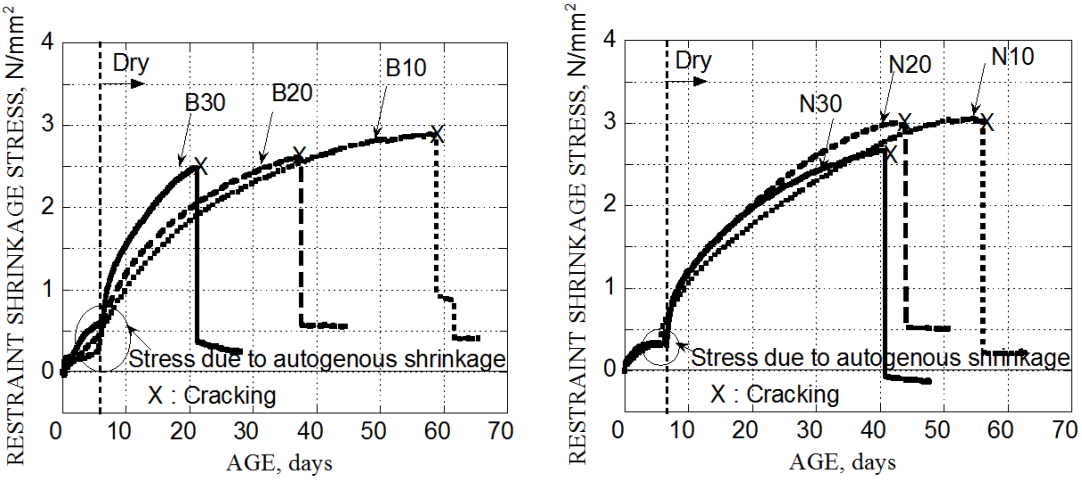

(a) BFS concrete (b) Normal concrete

Figure 6 Restrained cracking test result examples

Creep Experiment

Results of the creep experiment are shown in Figure 7. The specific creep strain, creep strain per unit applied compressive stress, increased with time and the increasing rate became smaller. Specimens with a loading age of 7 days showed larger specific creep strain than those of 28 days. Furthermore, BFS concrete showed smaller specific creep strain than that of the normal concrete.

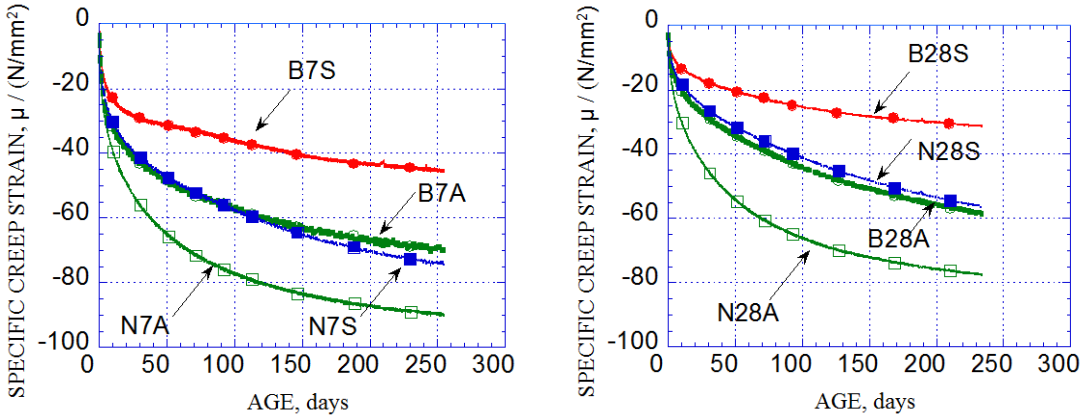

(a) 7 day loading age (b) 28 day loading age

Figure 7 Creep test results

DISCUSSION

Effects of Concrete Type

Effects of concrete type and ambient temperature on the cracking age are shown in Figure 8. As shown in Figure 8, cracking age of BFS concrete was earlier than that of the normal concrete and hence the cracking resistance of BFS concrete is lower than that of the normal concrete when ambient temperature is higher than 20 ^{o}C. The sources for this phenomenon are discussed below.

Primary reason for BFS concretes' low crack resistance at higher temperature appears larger free shrinkage as shown Figure 5. This is likely due to considerable autogenous shrinkage which drives the development of restrained shrinkage stress than that of the normal concrete. This is particularly prominent in B30 specimen that was subjected to high temperatures.

Secondly, the cracking strength that can resist to cracking was much lower in BFS concrete than normal concrete. Cracking strength represents restrained shrinkage stress at cracking age in restrained shrinkage cracking tests. This is demonstrated in Figure 9a, where splitting tensile strength of BFS concrete is 20% lower than normal concrete. In Figure 9, horizontal axis represents maturity according to CEB-FIP 90[6], and compressive and tensile strength are accurately reproduced as a function of maturity both in BFS and normal concretes. Figure 10 shows relative cracking strength, which is defined as ratio of cracking strength to splitting tensile strength at cracking age. The relative cracking strength was reported around 0.7 in general while large scatter was observed[7]. Values in Figure 10 are similar to this reported result independent of concrete type. Summarizing results in Figures 9 and 10, it is found that cracking strength of BFS is smaller than normal concrete.

Thirdly, Yong's modulus of BFS concrete is almost same as normal concrete while lower Elastic modulus is important to moderate developing restrained shrinkage stress in BFS concrete as demonstrated by Aly and Sanjayan[4]. In the current study, Smaller particle size in BFS used (Table 6) and higher ambient temperature likely promote hydration of BFS and cause comparable elastic modulus in BFS concrete with normal concrete as shown in Figure 11. Finally, the creep coefficient was smaller in BFS concrete and the restrained stress relaxation by creep may be more difficult than in the normal concrete [4]. This is implied in Figure 12, where creep coefficient profile with increasing loading duration is depicted. Creep coefficient in Figure 12 is defined as creep strain relative to elastic strain assuming elastic modulus at 28 day age, following CEB-FIP 90[6]. Creep coefficient in Figure 12 is smaller in BFS concrete than normal concrete independent to loading age or curing condition.

Effects of Ambient Temperature

The cracking resistance of BFS concrete was largely influenced by the ambient temperature as shown in Figure 8 and evidently tended to be decreased as the temperature increases while the temperature dependency of the normal concrete was small. Cracking age in Figure 8 is represented by average values of two specimens.

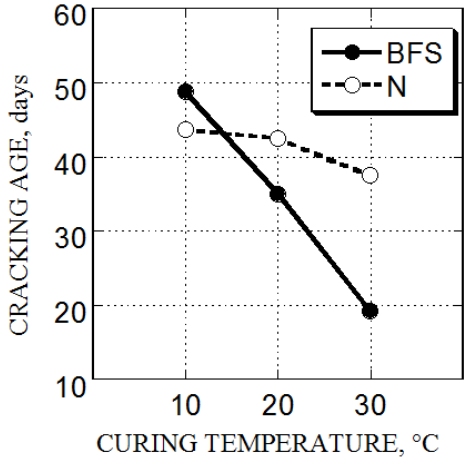

Figure 8 Effects of concrete type and ambient temperature on the cracking age

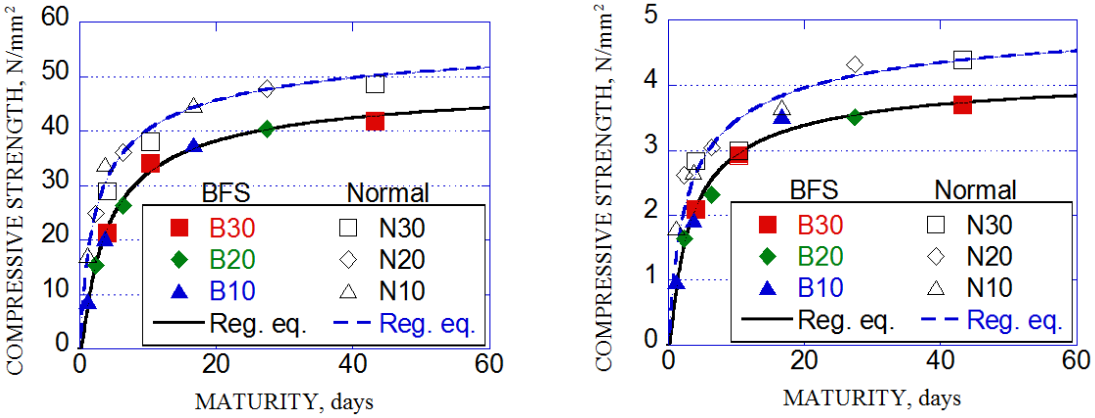

(a) Compressive strength (b) Splitting tensile strength

Figure 9 Development of compressive and splitting tensile strength with maturity

This tendency is shown in Figure 5 where free shrinkage of BFS concrete increases with an increase in temperature while that of the normal concrete is less sensitive to the temperature. Because the temperature dependency of autogeneous shrinkage of BFS concrete was already pointed out in the literature [2], high ambient temperature could be a cause of large autogenous shrinkage and lead to significant degrading the cracking resistance.

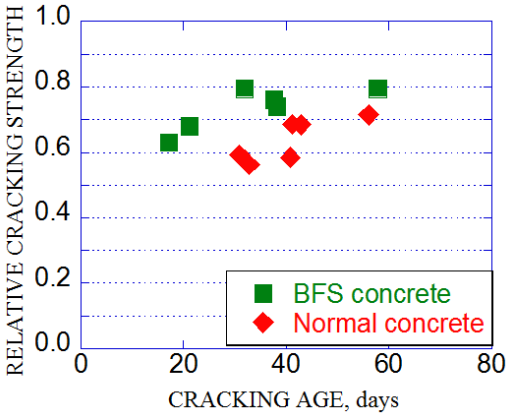

Figure 10 Relative cracking strength independent of concrete types and cracking age

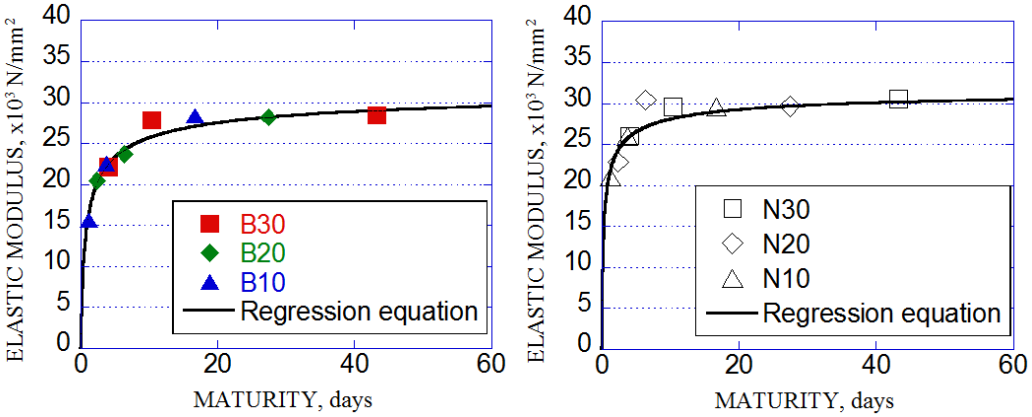

(a) BFS concrete (b) Normal concrete

Figure 11 Development of Elastic modulus with maturity

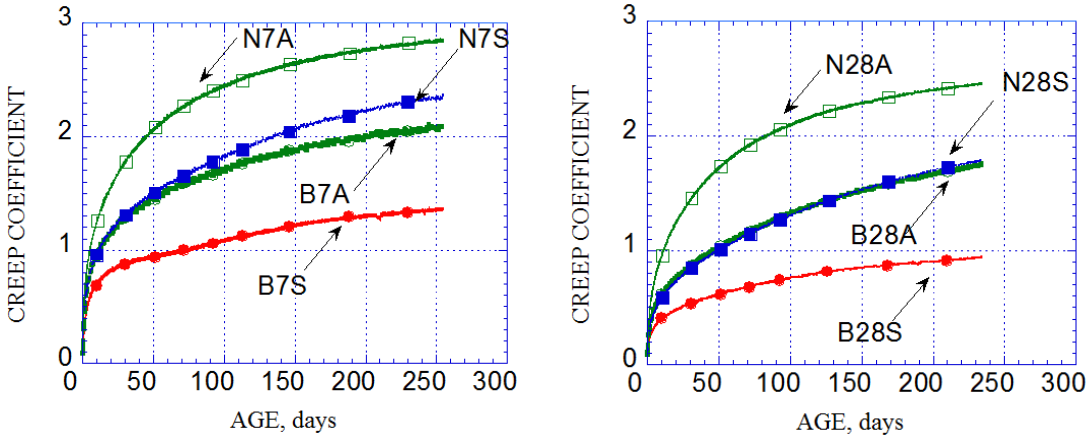

(a) 7 day loading age (b) 28 day loading age

Figure 12 Development of creep coefficient

CONCLUDING REMARKS

The major findings of this study are as follows.

1. Shrinkage cracking resistance of BFS concrete tended to be lower than that of the normal concrete and may be particularly decreased at high ambient temperatures.
2. Unlike BFS concrete, the shrinkage cracking resistance of the normal concrete was less sensitive to the ambient temperature.
3. Specific creep strain and creep coefficient of BFS concrete were lower than those of the normal concrete at 20°C making the relaxation of restrained shrinkage stress more difficult.
4. Larger free shrinkage (particularly at high temperatures), smaller creep deformation and low cracking strength were a cause of lower shrinkage cracking resistance of BFS concrete than that of the normal concrete.

AKNOWLEDGEMENTS

Part of this work was supported by Japan Society for the Promotion of Science, through research grant 5301-23360252-0002 to Kajima Technical Research Institute and Tokyo University of Science.

REFERENCES

1. SARIC-CORIC, M., AÏTCIN, P-C. Influence of curing conditions on shrinkage of blended cements containing various amounts of slag, ACI Materials Journal, Vol. 100, No.6, 2003, pp.477-483,

2. PANE, I, HANSEN, W. Investigation on key properties controlling early-age stress development of blended cement concrete, Cement and Concrete Research, Vol.38, No.11, 2008, pp.1325-1335.

3. PANE, I, HANSEN, W. Predictions and verifications of early-age stress development in hydrating blended cement concrete, Cement and Concrete Research, Vol.38, No.11, 2008, pp.1315-1324.

4. ALY, T, SANJAYAN, J,G. Factors contributing to early age shrinkage cracking of slag concrete, Materials and Structures, vol. 41, 2008, pp.633-642.

5. JAPAN CONCRETE INSTITUTE: JCI-TC083A Technical Committee on Reduction of Shrinkage Cracks and Durability Enhancement from Viewpoints of Mineral Admixtures, Technical Committee Reports, 2010. (http://www.jci-net.or.jp/j/publish/etc/guide_0069.html)

6. Comite Euro-International Du Beton: CEB-FIP Model Code 1990, Thomas Telford, 1991

7. JAPAN ARCHITECTURAL INSTITUTE Recommendations for Practice of Crack Control in Reinforced Concrete Buildings, 2006 (in Japanese)

Study on Capacity of Reinforced Concrete Beams With Chloride Induced Damage

K Matsuda[1], M Yokota[1], K Yonezawa[2], M Matsushima[3]
1 – Shikoku Research Institute Inc, Japan
2 – Shikoku Electric Power Co Inc, Japan
3 – Kagawa University, Japan

It is very important for infrastructures to be maintained appropriately and utilized effectively over the long term in the low carbon era. Reinforced concrete structures received severe chloride induced damage has been observed in the coastal area of Japan. Quantitative comprehension of load-bearing capacity of deteriorated reinforced concrete members received chloride induced damage is required for appropriate maintenance. Chloride ions from sea penetrate into concrete and they reach the reinforcement. When the content of chloride ions close to reinforcement exceed the threshold, corrosion of reinforcement starts. After that, crack occurs on the concrete surface due to the pressure of expanded corrosion products. The load-bearing capacity of member depends on the ammount of corrosion of reinforcements. Corrosion induced crack on concrete surface is apparent, but ammount of corrosion of reinforcements in concrete is uncertain in the case of in-service real structure. Loading experiments were carried out. Specimens of reinforced concrete beams were prepared for the experiments. In order to be imitated real damaged structures, they were made of fresh concrete added sodium chloride, and exposed to cyclic dry and wet environment. Based on the results of experiments, the relationship between ammount of corrosion of reinforcements, corrosion induced crack width and load-bearing capacity of reinforced concrete members was researched. And the characteristics of capacity deterioration with the progress of corrosion was estimated.

Mr. Kousaku Matsuda is a senior research engineer at Shikoku Research Institute Inc., Takamatsu, Japan. He received his Master's Degree of Engineering from Kobe University in 1979. His research interests is the application of deterioration model to member received chloride induced damage. He is member of the AIJ and JCI.

Dr. Masaru Yokota is a senior research engineer at Shikoku Research Institute Inc., Takamatsu, Japan. He received his Doctor's Degree of Engineering from The University of Tokushima in 1995. His research interests include the deterioration of RC structures and the inspection model of corroded steel bar received the severe environments. He is member of the JSCE and JCI.

Mr. Kazuhiro Yonezawa is an engineer at Shikoku Electric Power Co.,Inc., Takamatsu, Japan. He received his Bachelor's Degree of Engineering from The University of Tokushima in 2003. His research interests is upgrading of maintenance of RC structures in thermal power station. He is member of JSCE and JCI.

Dr. Manabu Matsushima is a professor of Kagawa University, Takamatsu, Japan. He received his Doctor's Degree of Engineering from Tokyo Denki University in 1994. His research interest is the application of reliability theory to concrete members in RC structures. He is member of the JSCE, AIJ and JCI.

Keywords: Corrosion of reinforcement, Corrosion-induced crack, Cross-sectional loss, Load-bearing capacity, Loading experiment

INTRODUCTION

It is very important for infrastructures to be maintained appropriately and utilized effectively over the long term in the low carbon era [1]. Reinforced concrete structures received severe chloride induced damage has been observed in the coastal area of Japan [2]. Chloride ions from sea penetrate into concrete and they reach the reinforcement. When the content of chloride ions close to reinforcement exceeds the threshold, corrosion of reinforcement starts. After that, corrosion crack occurs due to the pressure of expanded corrosion products.

Quantitative comprehension of load-bearing capacity of deteriorated reinforced concrete structures received chloride induced damage is very important for appropriate maintenance. Two factors are required for accurate estimate of load-bearing capacity of structures by ordinary visual inspection. One is estimating amount of corrosion of steel reinforcement in concrete by means of the degree of cracking on concrete surface, and the other is clarifying the relationship between amount of corrosion of reinforcement and load-bearing capacity of member.

For the solution of these problems, electrolytic corrosion has been frequently carried out in previous experimental studies. But it has been said that the configurations of corroded reinforcements in the case of electrolytic corrosion are different from those in real structures. And reinforcements used in previous specimens were usually thin one which have 13mm diameter or less.

Thus loading experiments by means of specimens, which corrosion environment and size of reinforcements are similar to real structures, have been carried out. Based on the results of the experiments, the relationships between cross-sectional loss of reinforcement, corrosion crack width and load-bearing capacity of reinforced concrete members were researched. This paper aims to represent the achievement of the research.

SPECIMENS

Two kinds of specimens were prepared for experiments in order to be considered the corrosion induced cracking mode as shown in Figure 1. The shape and bar scheduling of specimens are shown in Figure 2. Type-A is imagined as the mode of vertical cracking along longitudinal reinforcements. Type-B is imagined as the mode of horizontal cracking between longitudinal reinforcements. The specimens were made of fresh concrete added sodium chloride containing 5kg/m^3 chloride ions in order to be accelerated the corrosion.

The specimens had been exposed to the cyclic drying and wetting environment by 3.5 days in water tank for about 30-70 weeks, which is in the atmosphere at 15℃ and in sea water at 70℃. When the corrosion induced crack occurred on the whole area of bottom surface, the specimen was stopped being immersed in sea water in order to be prevented corrosion products flowing out of crack. After that the specimen had been exposed to wet environment in the atmosphere.

The crack width which occurred along reinforcements on the corner of bottom surface of specimens was measured at 10cm intervals. The measured value which covers 85% of crack width distribution was defined as the characteristic value of each specimen as shown in Figure 3.

(a) Vertical Cracking along Reinforcements (b) Horizontal Cracking between Reinforcements

Figure 1 Cracking mode

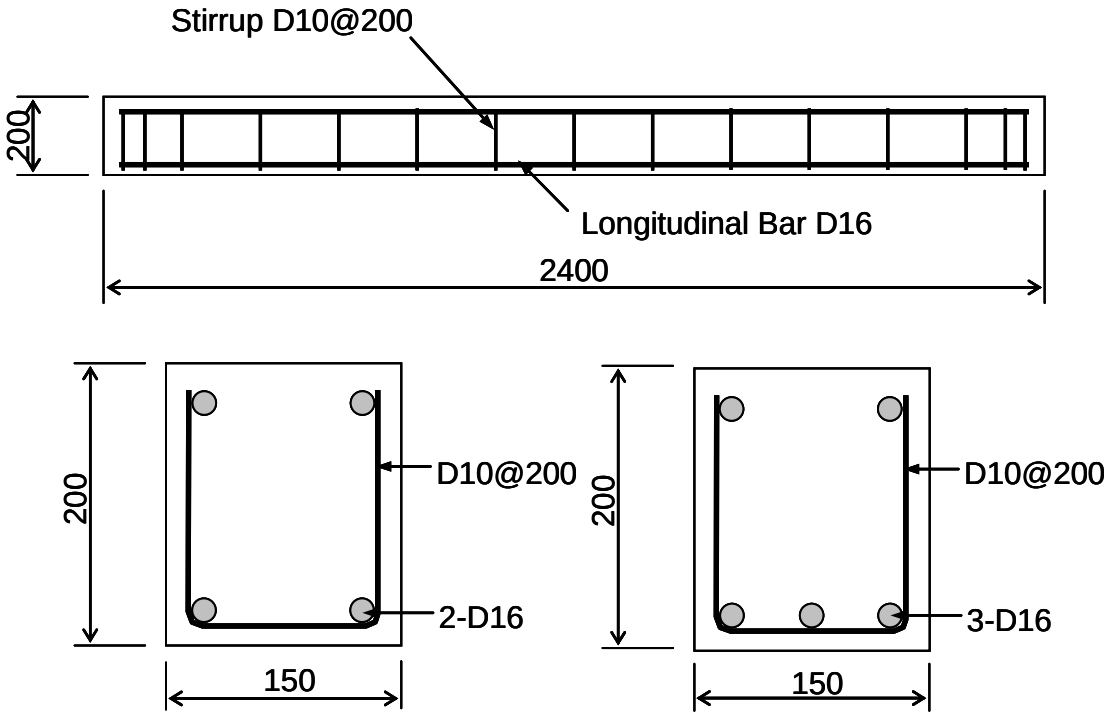

Figure 2 Specimen

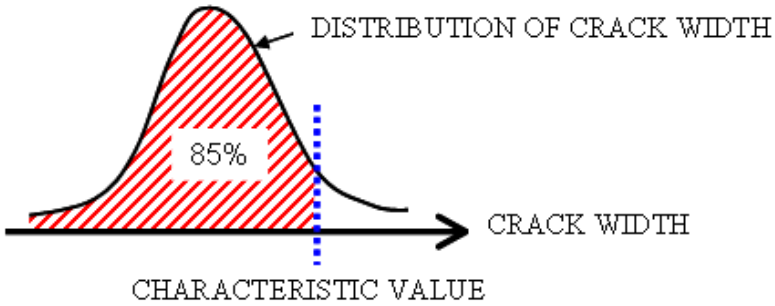

Figure 3 Definition of characteristic value of crack width

EXPERIMENTAL METHOD

The specimens were loaded symmetrically at two points of the centre by loading actuator as shown in Figure 4. Loading was controlled by displacement of the actuator. The displacement of specimen was measured at the centre of them.

Steel reinforcements of each specimen were chipped out after the loading experiment, and they were sampled by 14cm in length from unyielding area as shown in Figure 5. Then they were immersed in 10% solution of diammonium hydrogen citrate at 40°C, and corrosion products were removed from corroded reinforcements. Mass of the each reinforcement after the removal was measured, and amount of corrosion per unit surface area and cross-sectional loss were obtained.

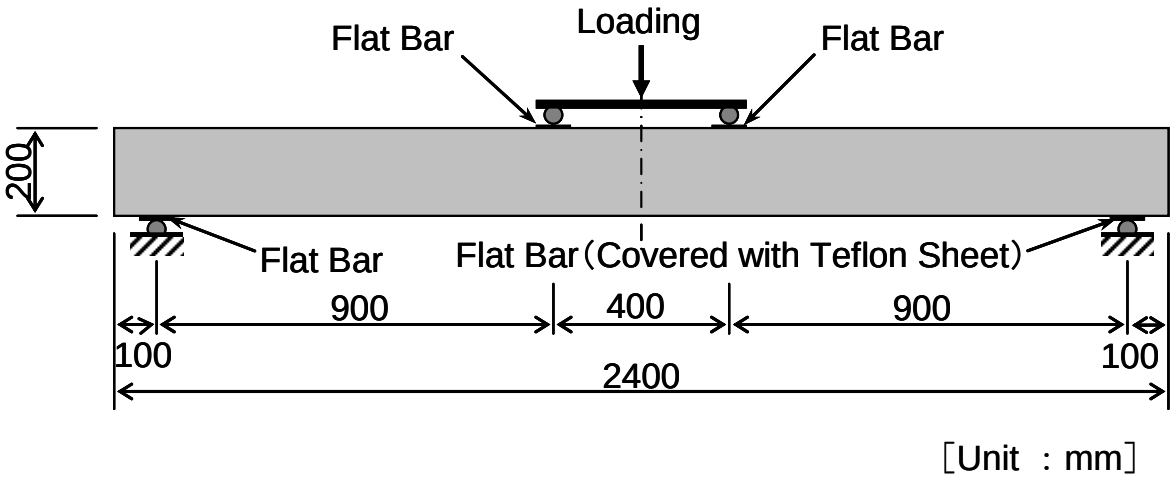

Figure 4 Experimental method

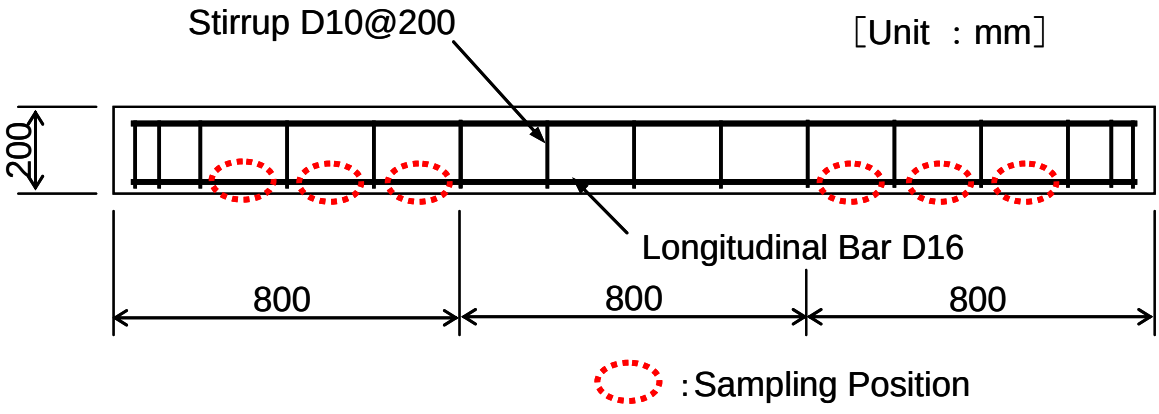

Figure 5 Sampling position of corroded reinforcements

RESULTS OF EXPERIMENTS AND DISCUSSION

Results of Loading Experiments

Whole results of loading experiments are shown in Figure 6.
Non-linear behaviour appears strongly before the yielding of reinforcement because of corrosion cracks in corroded specimens. Therefore, it is assumed that the yield strength of each specimen is determined at the point of maximum curvature of load-displacement relationship. In addition, we regarded the point of compression failure on upper surface as ultimate state of each specimen. Figure 6 shows the load-displacement relationships of the specimens to the ultimate state.

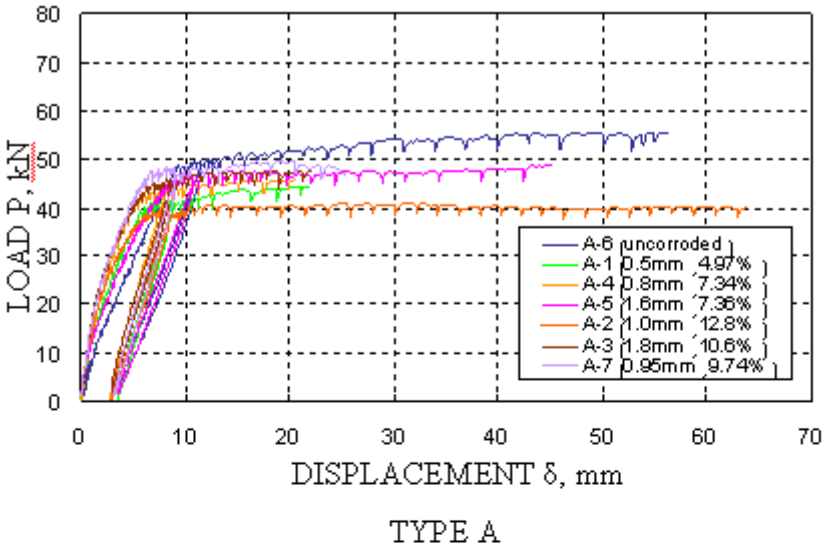

TYPE A

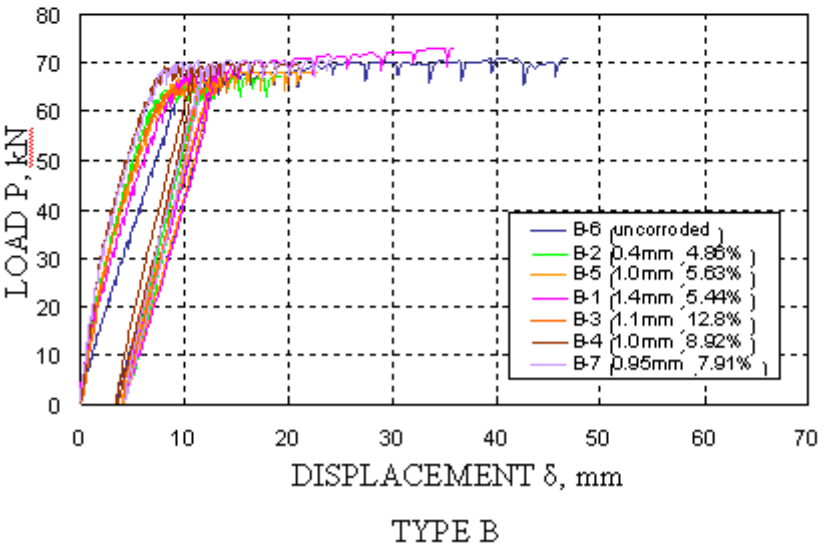

TYPE B

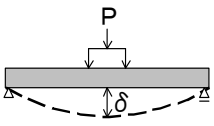

Figure 6 Load-displacement relationships

Relationship between Amount of Corrosion of Reinforcements and Crack Width

Relationships between the cross-sectional loss of reinforcements and the characteristic value of crack width of specimen are shown in Figure 7. In specimens Type-B (3 longitudinal reinforcing bars), the cracks appeared along the central reinforcement did not almost expand because they were restrained by cracks occurred along the both sides. And the corrosion boundary condition of the central reinforcements is different from that of the both sides' reinforcements. Therefore the data of amount of corrosion obtained from central reinforcement are not included in Figure 7.

The relationship between the cross-sectional loss of each corroded reinforcement and the characteristic value of crack width of each specimen become clearer by being divided into two groups as shown in Figure 7. Two groups correspond to the elapsed time of dry and wet environment to which the specimens had been exposed at an early age; one is comparatively long period and the other is short period. Crack width of the former reaches the ceiling at around 1mm, while that of the latter reached nearly 2mm and does not show the sign of ceiling yet. The relationships of the two groups between amount of corrosion of reinforcements per unit surface area and the characteristic value of crack width are shown in Figure 8 respectively. Straight lines in the figure indicate the approximations.

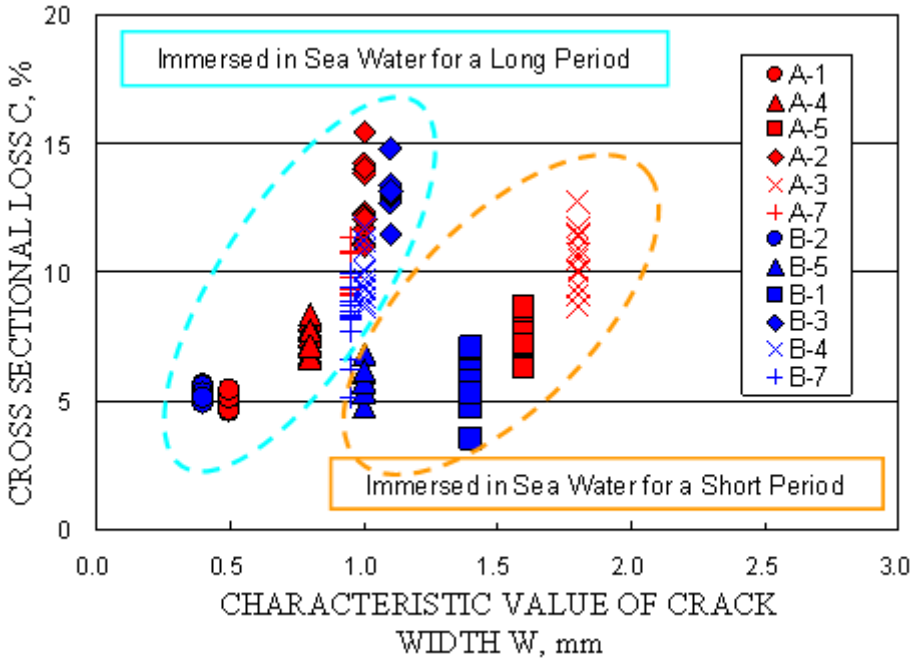

Figure 7 Relationships between cross-sectional loss and crack width

Progress of crack width of each specimen is shown in Figure 9 in order to be described the cause divided into two groups. It is found that the expanding rate of crack width of the group immersed in sea water for a short period was extremely faster than that of the group immersed for a long period.

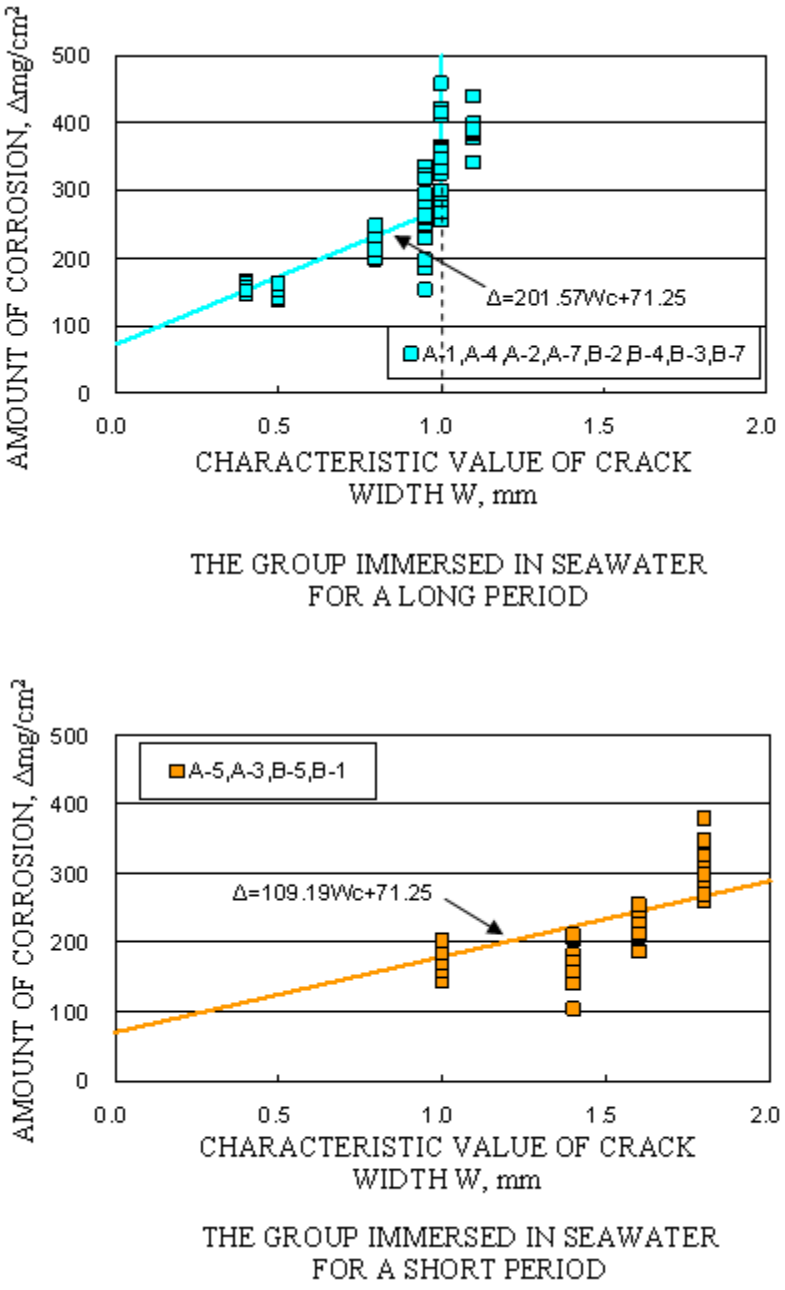

Figure 8 Relationships between amount of corrosion and crack width (Difference of two groups)

The specimens of the former group were taken out of the tank at the age of 30-40 weeks, and those of the latter group were at the age of 60-70 weeks. Figure 8 and Figure 9 show that there are two cases of the progress of corrosion induced crack width for the same amount of corrosion. We interpret this result as the difference of flowability of corrosion products. The corrosion products had considerably contributed to expanding of crack width in the former group because of their low flowability. However, they hadn't much contributed in the latter group because of their high flowability. Applied to real structures built in coastal area, the former group corresponds to permanent splash zone, and the latter corresponds to tidal zone, respectively. Amount of corrosion of reinforcements in concrete can be estimated by using the two groups described above.

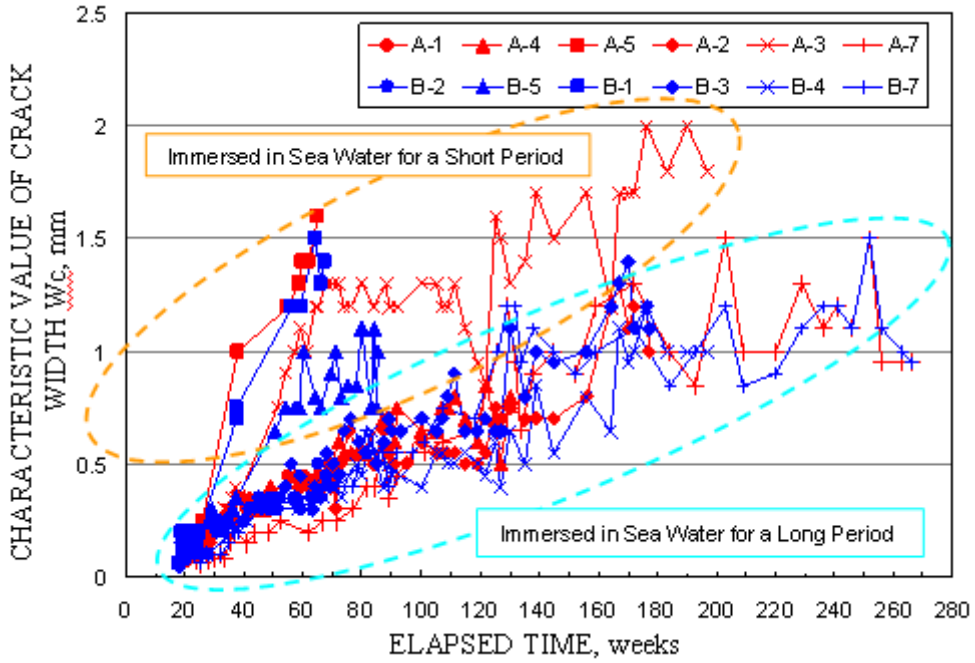

Figure 9 Progress of crack width of each specimen

Relationship between Load-bearing Capacity of Member and Amount of Corrosion of Reinforcements

The relationship between yield strength of the specimen and cross-sectional loss of the reinforcements is shown in Figure 10. The relationship between maximum strength and cross-sectional loss is shown in Figure 11, as well. Vertical axis in each figure indicates the ratio of corroded specimens' strength to uncorroded one. Calculated values based on theoretical formula are adopted as the standard that is uncorroded specimens' strength. The solid lines in these figures show the regression formulas. The dotted lines in these figures show the theoretical formulas which assume that amount of corrosion distributes uniformly.

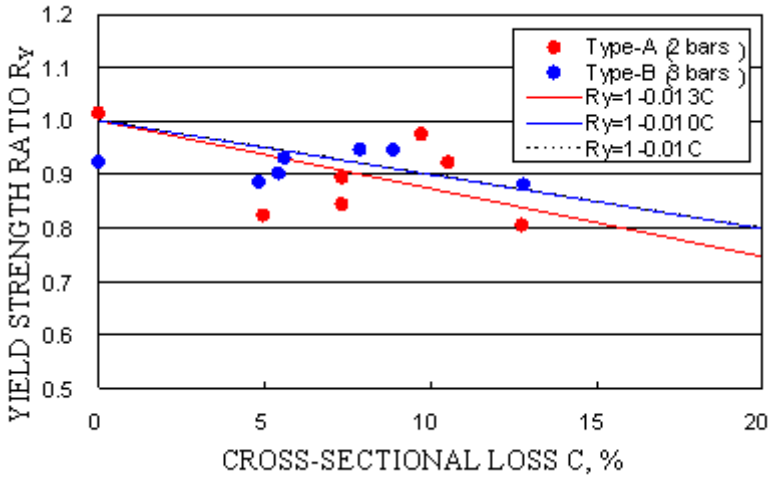

Figure 10 Relationship between yield strength and cross-sectional loss

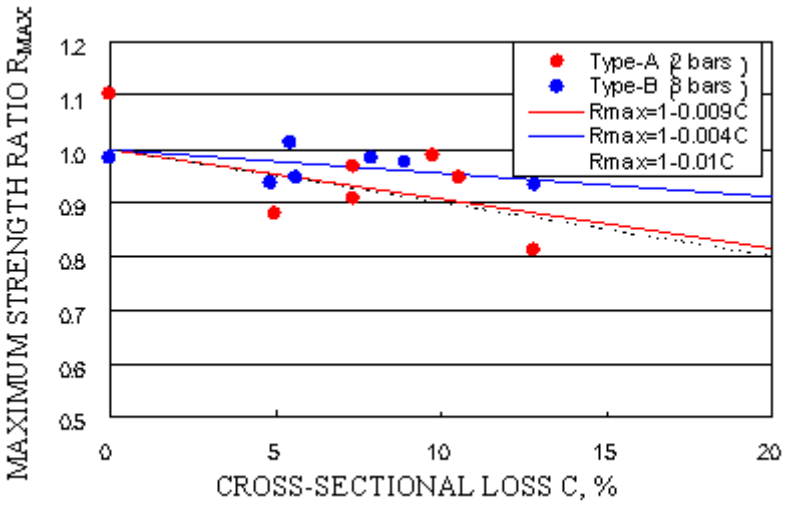

Figure 11 Relationship between maximum strength and cross-sectional loss

The declining rate of yield strength of Type-B (3 longitudinal reinforcing bars) with the cross-sectional loss of reinforcements is obviously lower than that of Type-A (2 longitudinal reinforcing bars) in Figure 10. The declining rate of maximum strength of Type-B is also obviously lower in Figure 11. Figure 12 shows the cause of these results conceptually. Bending strength of beam specimen depends on minimum of Aj (where, Aj: total cross-sectional area of reinforcements at section j in central four partitions of specimen divided by stirrups).

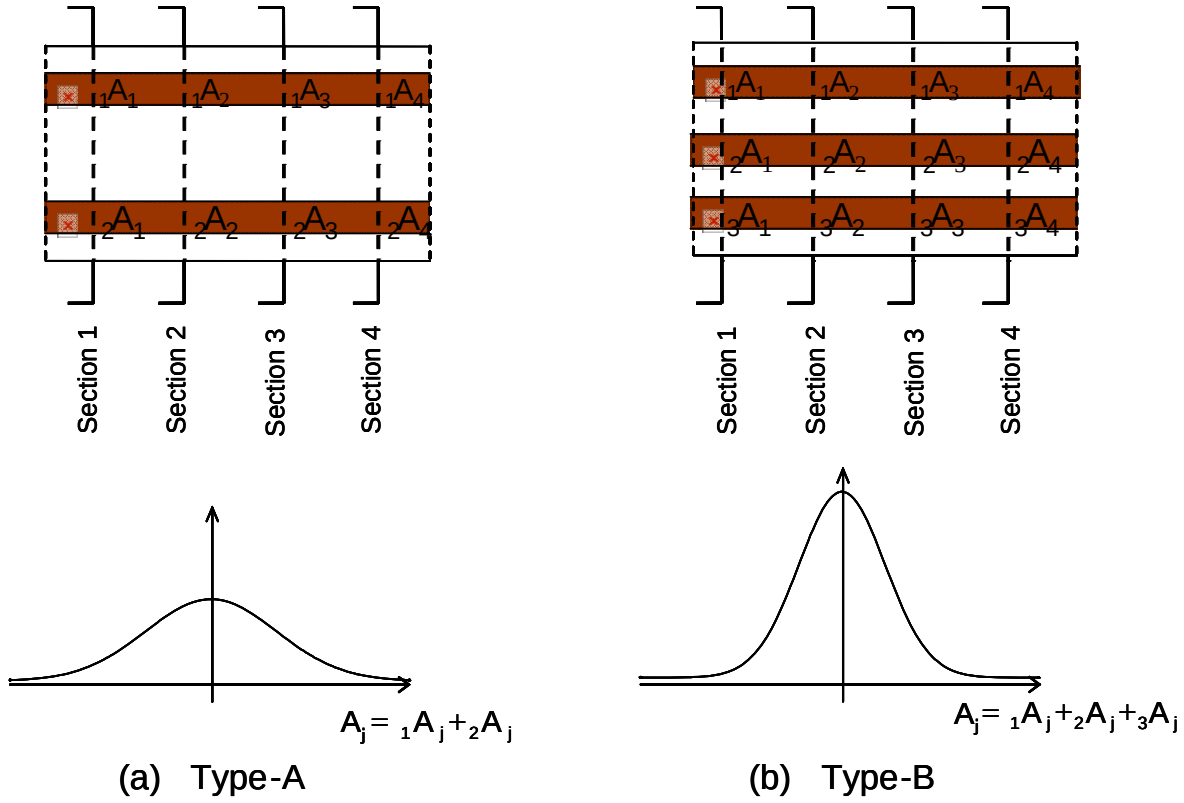

Figure 12 Comparison of the variation of total cross-sectional area between Type-A and Type-B

Even if the variations of corrosion amount of each reinforcement in both Type-A and Type-B are equivalent, the variation of total cross-sectional area in Type-B (3 bars) is smaller than that in Type-A (2 bars) because of law of large numbers. Therefore, the loss of minimum total cross-sectional area in Type-B is also smaller. That's why the declining rate of strength of Type-B with the cross-sectional loss of reinforcements is lower than that of Type-A.

The second point to be discussed is comparing the declining rate of yield strength and that of maximum strength with the cross-sectional loss of reinforcements. The latter is lower than the former in both Type-A and Type-B. In order to be discussed this reason on mechanical characteristics of corroded reinforcements, tensile tests of reinforcements of which the amount of corrosion was measured were carried out as shown in Figure 13.

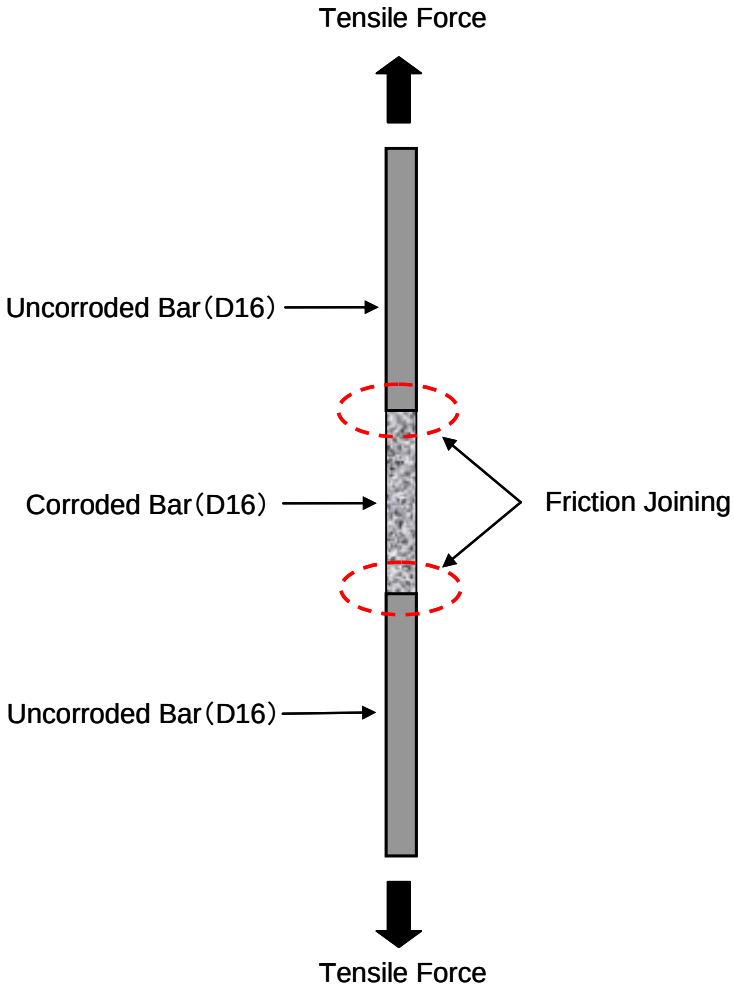

Figure 13 Tensile test method of corroded reinforcement

Test pieces were made by joining new reinforcing bars at both ends of corroded bar. Friction joining method was adopted for the joints. The pieces were pulled by universal testing machine and fractured at the corroded reinforcement. Tensile force at yielding and maximum force before the fracture were divided by nominal cross-sectional area (198.6mm2) of deformed bar D16, respectively. Then apparent yield stress and tensile strength of the corroded reinforcements were obtained. Yield stress ratio and Tensile strength ratio to those of uncorroded one were calculated by using the apparent yield stress and tensile strength. The relationship between the yield stress ratio and the cross-sectional loss is shown in

Figure 14. And the relationship between the tensile strength ratio and the cross-sectional loss is shown in Figure 15. The solid lines in these figures show the regression formulas. The dotted lines in these figures show the theoretical formulas which assume that the amount of corrosion on the surface of reinforcements distributes uniformly. The declining rate of the yield stress and the tensile strength with the cross-sectional loss are higher than theoretical formulas because of the influence of pitting corrosion. And the declining rate of the tensile strength is lower than that of the yield stress.

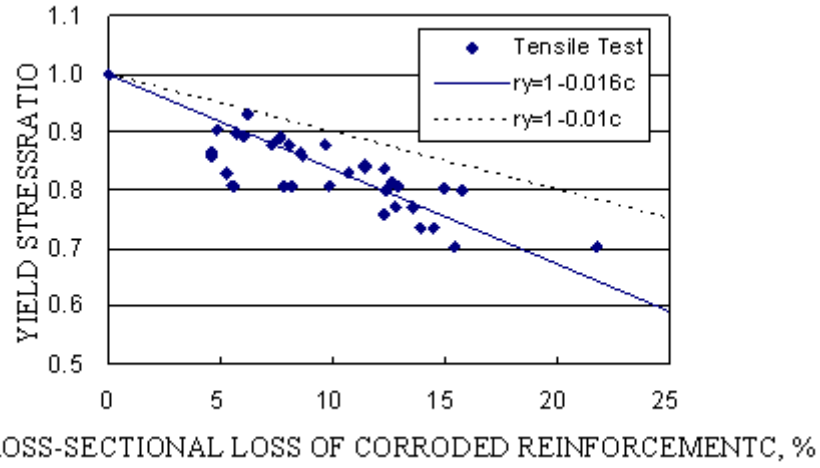

Figure 14 Relationships between yield stress of corroded reinforcement and cross-sectional loss

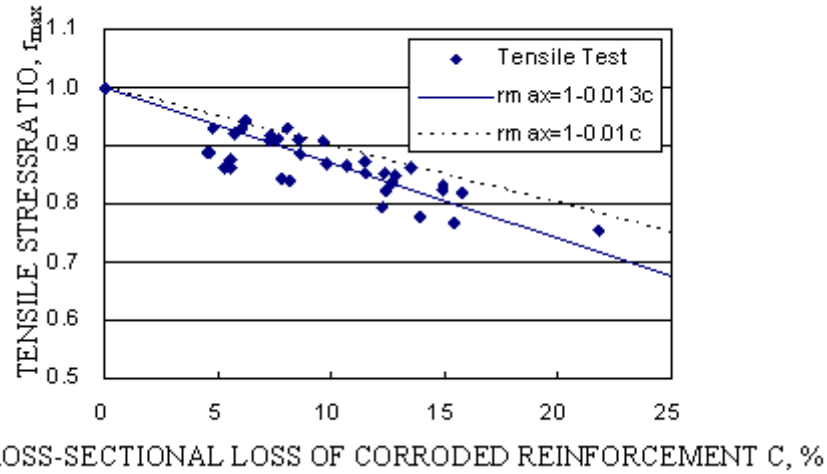

Figure 15 Relationships between tensile strength of corroded reinforcement and cross-sectional loss

This cause is regarded as a thing by the following mechanism. First yielding of corroded reinforcements occurs at the most weak section where cross-sectional area is minimum because of pitting corrosion. After that the most weak section enters the strain hardening domain and the stiffness of the section increases. Then new yielding occurs at another weak section. The range of yielding spreads along the reinforcement and the stress is redistributed one by one until the fracture through this process. As a result, the declining rate of tensile strength affected by stress redistribution is lower than that of yield stress which depends on

only minimum cross-sectional area. Although reinforcements in beam specimens did not fracture, it is conceivable that the declining rate of maximum strength of specimens affected by stress redistribution described above is lower than that of yield strength.

CONCLUSIONS

Loading experiments of beam specimens were carried out. The specimens of two types were exposed to cyclic dry and wet environment in order to be imitated real structures received chloride induced damage. Based on the results of experiments, we researched the relationships between cross-sectional loss, corrosion induced crack width and load-bearing capacity of reinforced concrete members. The findings that have been obtained are as follows.

1. The relationships between cross-sectional loss of corroded reinforcements and characteristic value of crack width of specimens could be divided into two groups because of the different flowability of corrosion products. Applied this result to real structures, one corresponds to permanent splash zone, and the other corresponds to tidal zone.

2. Amount of corrosion of reinforcements in concrete can be estimated using the two groups described above.

3. The declining rates of yield strength and maximum strength of specimens Type-B (3 longitudinal bars) with the cross-sectional loss of reinforcements are lower than that of Type-A (2 longitudinal bars). This cause is that the variation of total cross-sectional area of the specimens which have more reinforcements is smaller than that of the specimens which have fewer reinforcements.

4. The declining rate of the maximum strength of specimen with the cross-sectional loss of reinforcements is lower than that of yield strength. It is conceivable that the mechanical characteristics of corroded reinforcements affect this result.

REFERENCES

1. YANEV, B. Bridge Management, John Wiley & Sons, INC., 2007.

2. YOKOTA, H., KATO, E., IWANAMI, M. Chloride-induced corrosion of reinforcement and its effect on performance of structures, International Conference on Durability of Concrete Structures, 26-27 November, 2008, Hangzhou, China, pp 223-229.

Fundamental Research on the Freeze-thaw Resistance of Concrete with Post-added Drying-shrinkage Reducing Agent

M Sugiyama
Hokkai-Gakuen University, Japan

The weakness of concrete with drying-shrinkage reducing agent is poor freeze-thaw resistance. Drying-shrinkage reducing agent that improves this weakness has been recently developed, and requires that the agent be added to the concrete at a later stage. This study compared the freeze-thaw resistance of concrete with post-added drying-shrinkage reducing agent against concrete with existing drying-shrinkage reducing agent. The results showed that the recently developed drying-shrinkage reducing agent was effective for improving freeze-thaw resistance.

Masashi Sugiyama is the professor of the Hokkai-Gakuen University, Department of Building Construction & Materials Engineering in Sapporo city, Japan. He received his doctorate in engineering from Hokkaido University in 1981. His doctoral dissertation was « The effect of concrete in structure of the drying on physical property ». His specialty is research into technologies which improve the durability of concrete. He received prize for research into super-high durable concrete from Japan Concrete Institute in 1988, and for research into curing concrete using new heating sheet from the Hokkaido branch of Architectural Institute of Japan in 2010.

Keywords: Drying shrinkage, Drying shrinkage reducing agent, Freeze-thaw resistance

INTRODUCTION

Drying-shrinkage reducing agents are outstanding mixing agents that are capable of reducing the drying-shrinkage of concrete in a precise manner, and have been in use since the end of 1980s [1-4]. Yet damage due to freezing resistance was generally observed to increase in concrete with drying-shrinkage reducing agent. We had long been waiting for a drying-shrinkage reducing agent to be developed that has minimal damage due to freezing resistance. Recently in Japan, certain drying-shrinkage reducing agents with improved freezing resistance properties have been commercialized.

This paper first outlines the performance of conventional shrinkage reducing agents, and then reports on the results of tests on freeze-thaw resistance properties of recently developed drying-shrinkage reducing agents.

OVERVIEW OF EXISTING DRYING-SHRINKAGE REDUCING AGENTS

Outline of tests

Materials and mixture proportions

Three types of concrete shrinkage reducing agents were used, with admixtures created based on water-insoluble glycol ether (A), water-soluble low grade alcohol (B), and water-soluble polyether (C) as the main constituents. Table 1 shows the physical properties of these three drying-shrinkage reducing agents.

The cement used was ordinary Portland cement (JIS standard, specific gravity 3.16), the coarse aggregate was crushed stone (specific gravity 2.66, the maximum aggregate size 20mm), and the fine aggregate was river sand (specific gravity 2.63, fineness modulus 2.73). In concrete with shrinkage reducing agent A, no other admixture was used. In contrast, concrete with shrinkage reducing agents B and C also included an air entraining water-reducing agent (with lignosulfonate as the main constituent) based on recommendations listed by shrinkage reducing agent manufactures.

Table 1 Physical properties of drying-shrinkage reducing agents

AGENT	MAIN CONSITUENTS	APPEARANCE	SPECIFIC GRAVITY	SOLUBILITY
A	Polyglycol	Light yellow liquid	1.04	Poor solubility
B	Low grade alcohol	Colorless liquid	1.01	Dissolves easily
C	Polyether	Colorless liquid	1.02	Dissolves easily

Length change test

The size of concrete specimens was 10 x 10 x 40 cm. Specimens were cured underwater at 20ºC for one week, and then left standing in 20 ºC air and 60% humidity. Measurements of change in length were conducted using a comparator.

Freeze-thaw test

Freeze-thaw tests were conducted in accordance with ASTM C 666 - Procedure A. Assessments of test results were conducted based on the relative dynamic modulus of elasticity.

TEST RESULTS AND DISCUSSION

Compressive strength

Figure 1 shows a part of test results of compressive strength. The compressive strength of concrete with drying-shrinkage reducing agent decreased slightly as the amount of agent was increased, however, no adverse effects were observed from a practical standpoint. Similar results were achieved with all drying-shrinkage reducing agents.

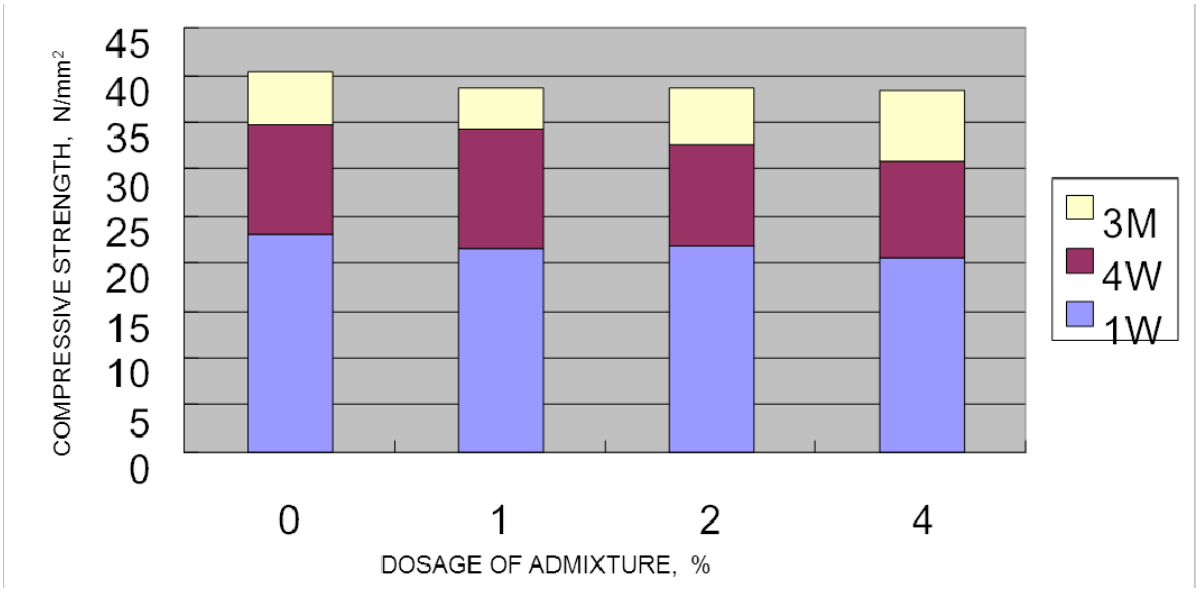

Figure 1 Compressive strength (w/c 60%, sl 18cm)

Length change

Figure 2 shows the results of drying-shrinkage conditions of an 8 cm slump of concrete obtained by adding 1%, 2%, and 4% of drying-shrinkage reducing agent A. Figure 3 shows the results of an 18 cm slump of concrete. With both the 8 cm and 18 cm slumps, the change in length decreased as the amount of shrinkage reducing agent was increased.

Figure 4 shows the results of drying-shrinkage conditions of concrete with 4% of glycol ether derivative (A), low grade alcohol derivative (B), and polyether derivative (C) added. Similar results were achieved with all drying-shrinkage reducing agents. While there are many papers outlining the drying-shrinkage reducing mechanism of organic drying-shrinkage reducing agents, these results are believed to be due to the effects of shrinking based on the capillary tube tension theory, where the drying-shrinkage agent worked to decrease the surface tension of the water.

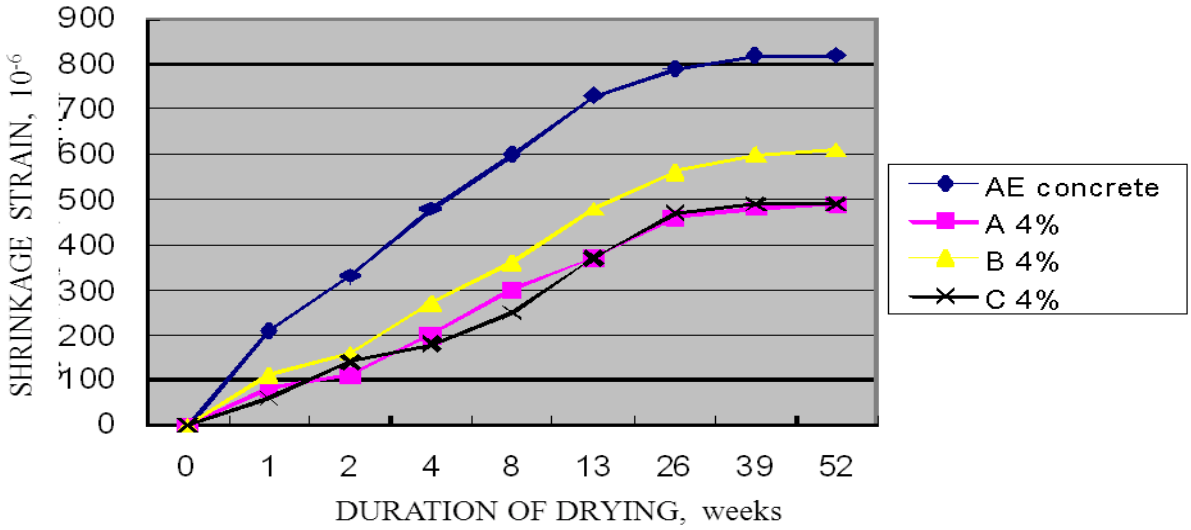

Figure 2 Drying shrinkage at 8cm slump at admixture A

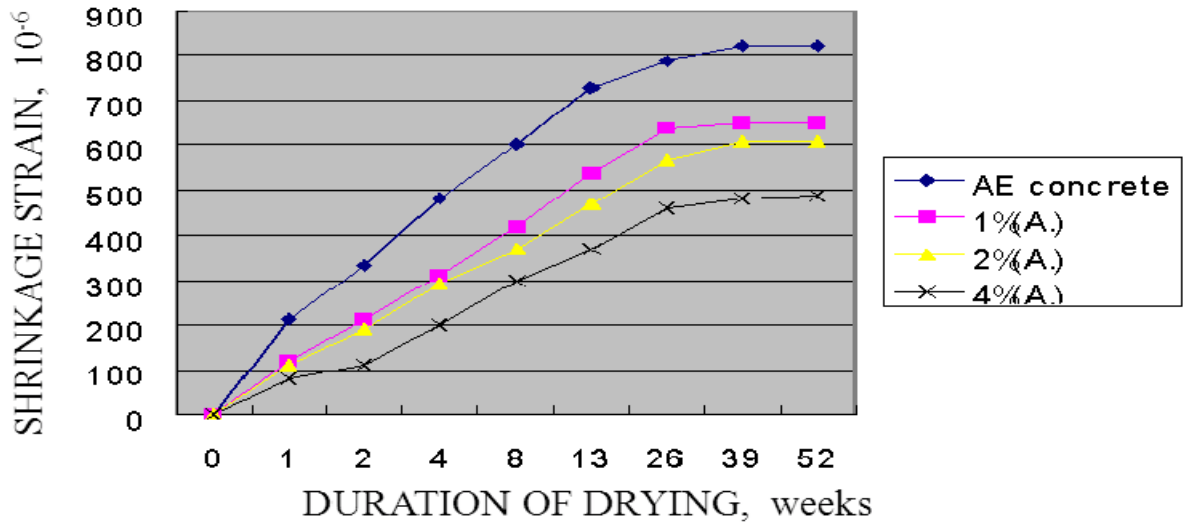

Figure 3 Drying shrinkage at 8cm slump at admixture A

Freeze-thaw action

Figure 5 and Figure 6 shows the results of freeze-thaw tests of concrete with shrinkage reducing agent A. Figure 5 shows the results where tests were conducted immediately after the concrete had cured underwater for two weeks, while Figure 6 shows the results where tests were conducted on specimens left to dry for one week in 20 ºC air and 60% humidity. Although the air content of concrete with shrinkage reducing agent A was approximately 1%, improvements were observed on freeze-thaw action by allowing the concrete to dry slightly.

Figure 7 shows the results of freeze-thaw tests of concrete with low grade alcohol ether shrinkage reducing agent (B) that had dried for two days, four days and seven days respectively. Although the air content was about 5% in these tests, the concrete deteriorated in short cycles despite the drying. As outlined above, the freeze-thaw performance of concrete with drying-shrinkage reducing agent remained unstable.

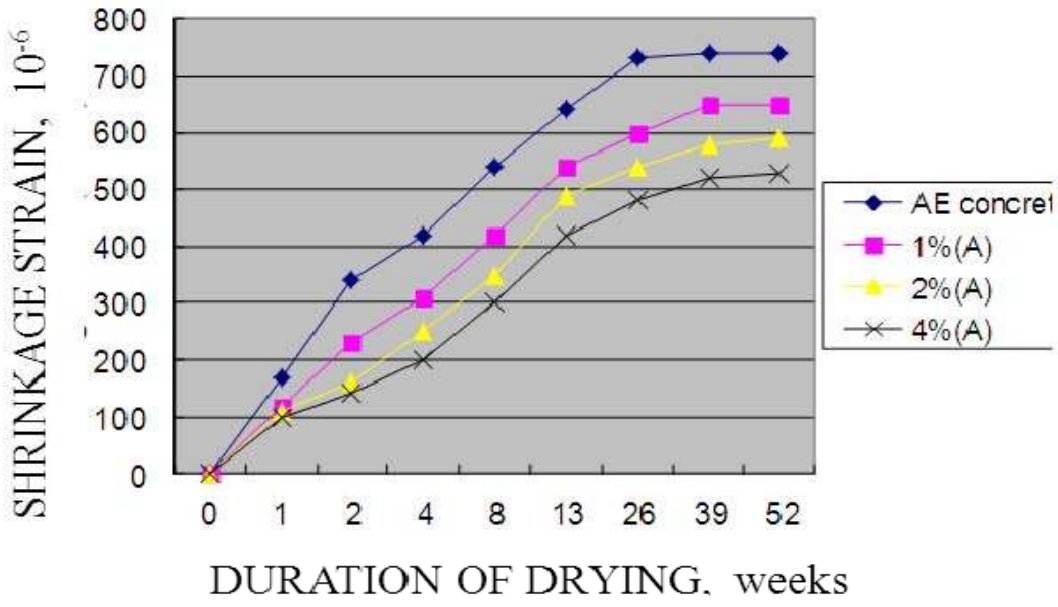

Figure 4 Drying shrinkage at commercial admixture

Summary of past research

The compressive strength of concrete with drying-shrinkage reducing agent was slightly lower than concrete without added agent, however no adverse effects were observed. Drying-shrinkage of concrete with shrinkage reducing agents decreased as the amount of agent increased. The freeze-thaw resistance of concrete with drying-shrinkage reducing agent A displayed sufficient resistant under conditions with slightly dry concrete, however deterioration was observed under wet conditions. Concrete with drying-shrinkage reducing agent B deteriorated even when it was slightly dry. The freeze-thaw performance of concrete with drying-shrinkage reducing agent remained unstable.

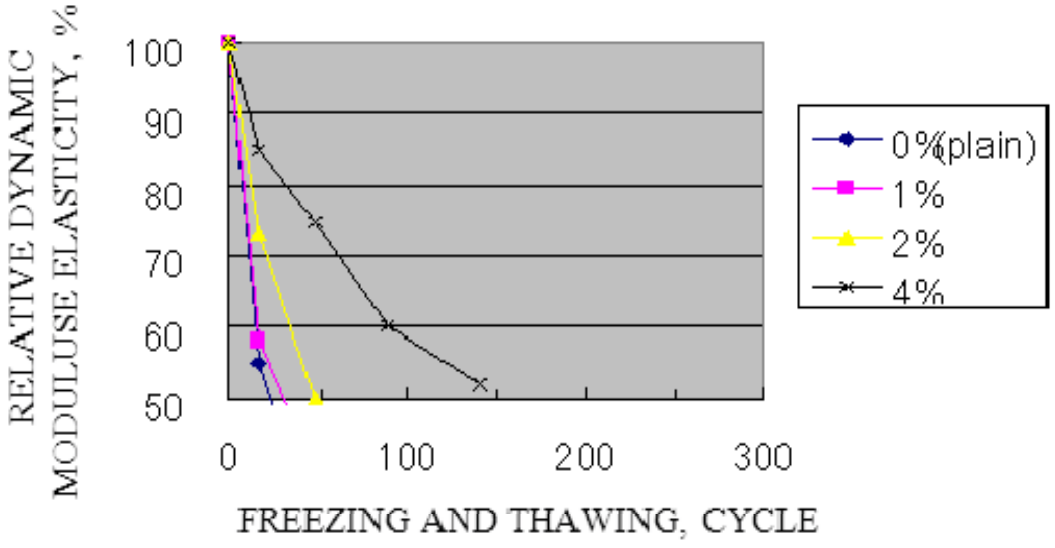

Figure 5 Freezing and thawing durability with admixture A (0 day drying)

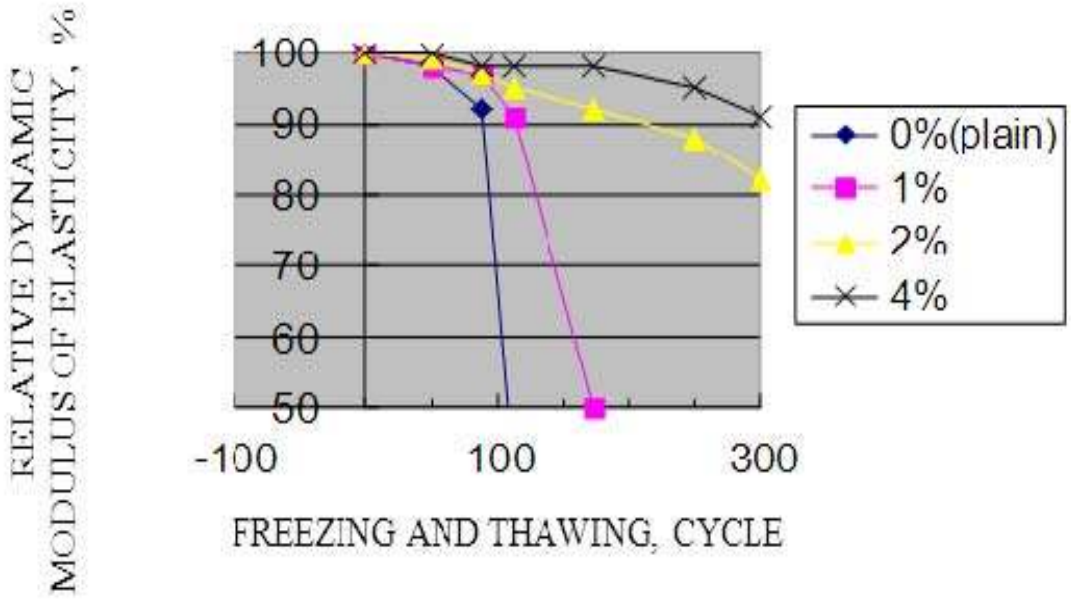

Figure 6 Freezing and thawing durability with admixture A (7 day drying)

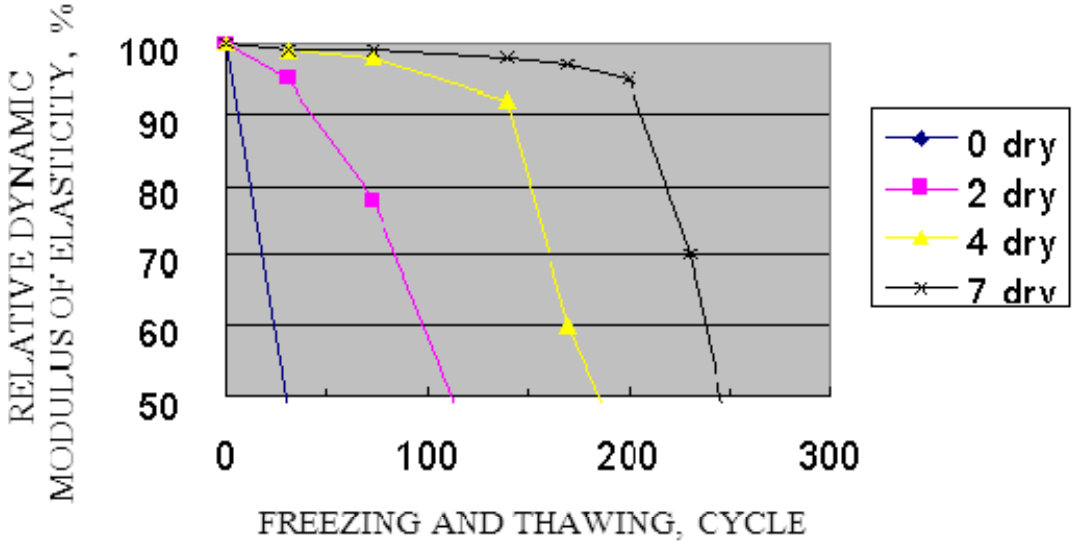

Figure 7 Freezing and thawing durability with admixture B (0-7 day drying)

FREEZING-THAWING-RESISTANCE NATURE BY CONTRACTION REDUCTION AGENT DEVELOPED RECENTLY

Purposes

The directions of the contraction reduction agent (S) developed recently recommend post-addition. Then, the amount of addition verifies the freezing-thawing-resistance nature by post-addition also including one third and the case where it is few. Moreover, the air bubbles of drying-shrinkage (10x10x40cm) and hardening concrete and intensity also carry out comparison examination.

Table 1 Overview of tests

NO	TYPE	AMOUNT OF SHRINKAGE REDUCING AGENT	ITEMS TESTED
1	Base AE water-reduced concrete	—	Freezing, shrinkage, strength, air bubbles
2	Concrete with post-added shrinkage reducing agent S	2 kg/m^3 (1/3 of recommended)	Freezing, shrinkage, strength, air bubbles
3	Concrete with post-added shrinkage reducing agent S	6 kg/m^3 (standard)	Freezing, shrinkage, strength, air bubbles
4	Concrete with post-added shrinkage reducing agent H	6 kg/m^3 (standard)	Freezing, shrinkage, strength, air bubbles

* Main constituent of shrinkage reducing agent S: hydrocarbon compound and glycol ether derivative, density 0.9 to 0.95, light yellow liquid
Main constituent of shrinkage reducing agent H: polyether derivative, density 0.950 to 1.050, light yellow liquid

EXPERIMENT METHOD

Freeze dissolution examination

The underwater freeze underwater dissolving method of JIS A 1148 (freeze dissolution test method of concrete) is followed. Care of health considers it as four weeks of 20-degree-C underwater curing, and starts an examination to four weeks of material ages. Freeze 2hr+ dissolution 2hr, 4 hr/cycle, 6 cycle/day. Although it is usually up to 200 cycles or 300 cycles, since this time clarifies a comparison difference, an examination cycle is performed up to 600 cycle.

Drying-shrinkage examination

An embedding distortion gauge is used and it applies to JIS A 1129 (length change measuring method of concrete) correspondingly. Basis length shall be after one week of 20-degree-C underwater curing (one week of material ages). Continuous measurement of the measurement is carried out by an interval.

Compressive strength examination

JIS A 1108 (compressive strength test method) is followed. Care of health considers it as 20-degree-C underwater curing, and is examined to four weeks of material ages

Air bubble characteristic of hardening concrete

The cellular interval coefficient by the linear traversing method is measured.

Post-addition of a contraction reduction agent

Supply necessary quantity (weight) after measurement from the unit capacity mass measurement result of fresh concrete, feed the concrete of predetermined quantity (45l.) into an inclination type mixer for this with a bucket, back-add and mix a mixture agent for 1

minute. It kneads and mixes and the back examines the quality (a slump, an air content, unit capacity mass) of fresh concrete. A target air content is made into 4.5%, and when there is much air, an antifoaming agent adjusts.

Concrete

Concrete is ready mixed concrete (24-18-20N).

EXPERIMENTAL RESULTS AND CONCLUSIONS

The result of the freezing and thawing test

An underwater freeze underwater dissolution test result is shown in Figure 1 and Figure 2. Elegance (H) is falling (the relative dynamic elastic coefficient of Figure 1) to less than 100 cycles conventionally, and this tendency is the same as that of the result seen conventionally. When the amount of standard addition of the contraction reduction agent (S) developed recently was back-added, the improvement effect of freezing-thawing-resistance nature was accepted. Contraction reduction agent S and the amount of standard addition was (contraction reduction agent S.1 / 3 quantity of the relative dynamic elastic coefficient in 300 cycles of base concrete) about 70% about 80% about 90%.

Table 2 Concrete mix proportions, kg/m^3

W/C	CEMENT	WATER	FINE (1)	FINE (2)	COARSE (1)	COARSE (2)	ADMIXTURE
55.0%	313	172	526	338	470	480	3.13

Fine (1): sand, Fine (2): sand, Coarse (1): crushed stone, Coarse (2): crushed stone, Admixture: standard AE water reducing agent

Table 3 Properties of fresh concrete

MIX	SLUMP, cm	AIR CONTENT, %	TEMPERATURE, ºC
Base	19.0	5.0	28.5
Shrinkage reducing agent S (1/3 amount)	17.5	5.2	29.0
Shrinkage reducing agent S (standard amount)	13.5	4.9	28.5
Shrinkage reducing agent H (standard amount)	15.5	4.6	29.0

When mass change was compared from Figure 2, the mass reduction of elegance (H) was conventionally the largest, and mass change of base concrete was small. This tendency is the same as that of the result seen conventionally. Although contraction reduction agent S, the amount of standard addition, and contraction reduction agent S.1 / 3 quantities are located in above-mentioned both middle -- 400 cycle -- until -- the difference of both mass change was small. Thus, it turns out that the contraction reduction agent (S) developed recently has resistance to a freeze dissolution action.

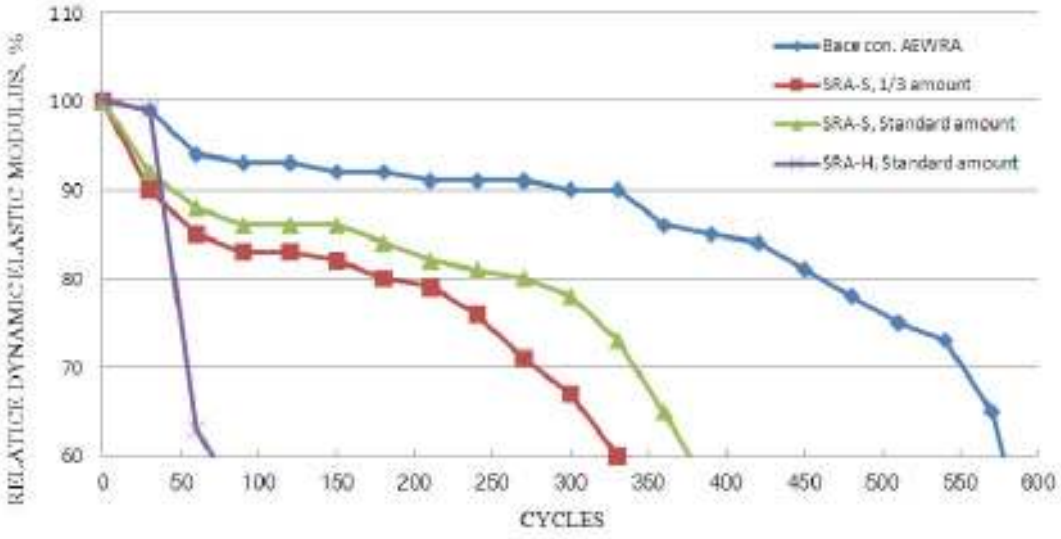

Figure 1 Freezing and thawing test results (Relative dynamic elastic modulus)

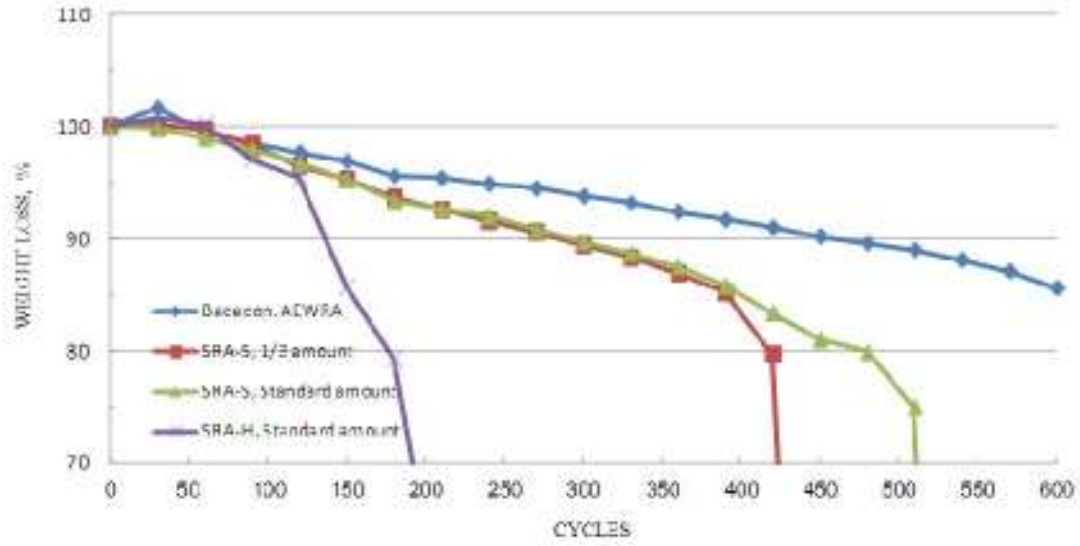

Figure 2 Freezing and thawing test results (Weight loss)

The cellular characteristic

The cellular interval coefficient measurement result by the linear traversing method is shown in Table 4. The air content of various kinds of contraction reduction concretes is 3.7 to 4.6%, and had satisfied 4.5±1.5% of targets. The cellular feeling coefficients of the concrete (S&H) which carried out standard addition of the contraction reduction were 0.282-0.308, and were almost the same. Moreover, the diameters of average air bubbles of S&H were 0.321-0.335, and were almost the same. From this, it turned out to be Elegance H conventionally that the quality of the hardening concrete of the contraction reduction agent S developed recently is practically equal.

Table 4 Air bubbles in hardened concrete

TYPE	AIR CONTENT IN HARDENED CONCRETE, %	SPACE BETWEEN AIR BUBBLES, mm	AVERAGE AIR BUBBLE DIAMETER, mm
Base	6.2	0.218	0.300
S 2 kg/m^3	4.6	0.255	0.305
S 6 kg/m^3	4.1	0.282	0.321
H 6 kg/m^3	3.7	0.308	0.335

Drying-shrinkage quality

The result of drying-shrinkage is shown in Figure 3. The contraction performance (contraction rate) to base concrete is shown in Table 5.

Although there is a tendency for H to be a little excellent in a contraction reduction action, in contraction reduction agent S and standard addition developed recently, and contraction reduction agent H and standard addition which are elegance conventionally, the difference is small and is the almost same contraction reduction action.

The contraction reduction agent S has a large contraction reduction action, when dryness is the first stage, but a contraction reduction action is stabilized to about 80 percent of base concrete as between dry periods becomes long. This tendency is the same as that of the conventional contraction reduction agent H. The above result showed that the contraction reduction of S and the H could be carried out at about 80 percent of base concrete if the amount of standard addition is used.

Strength quality

The quality of compressive strength is shown in Table 6. Generally as for the intensity of the concrete which uses the drying-shrinkage reduction agent, intensity tends to fall a little. Although this result is also the same, it is not a level which poses a practical problem.

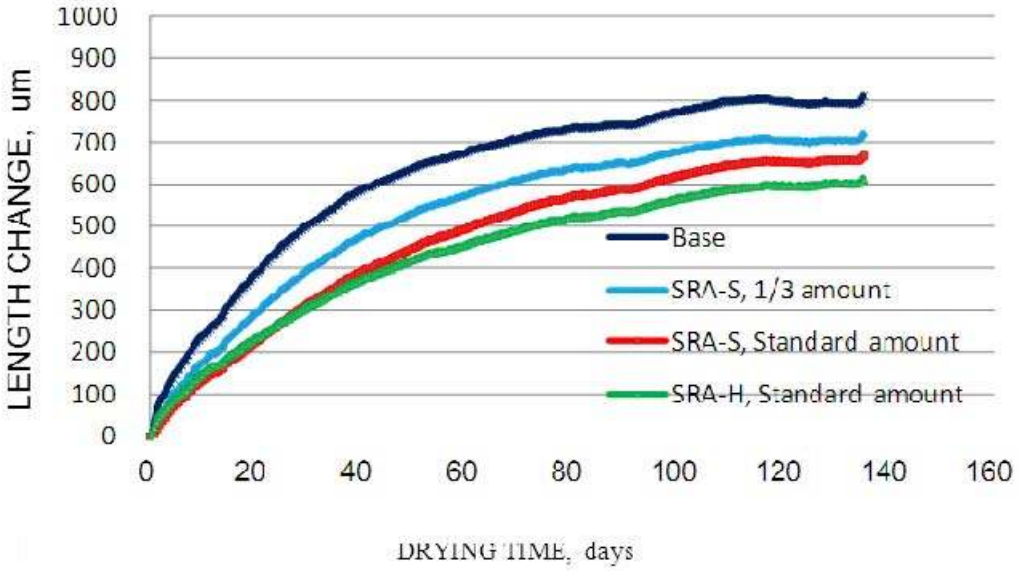

Figure 3 Drying shrinkage

Table 5 Shrinking performance (μ) of shrinking reducing agent

DRYING TIME	BASE	S 1/3	S	H
7D (1W)	181	127	98	108
%	(100)	(70)	(54)	(59)
1M (4W)	480	373	296	292
%	(100)	(77)	(62)	(60)
2M (8W)	659	555	476	441
%	(100)	(82)	(72)	(66)
3M (12W)	733	638	574	523
%	(100)	(87)	(78)	(71)
4M (16W)	799	701	647	588
%	(100)	(87)	(80)	(73)
5M (20W)	838	742	696	634
%	(100)	(88)	(83)	(75)

Table 6 Compressive Strength of Four-week Old Concrete (Cured underwater at 20ºC)

Base: 29.5 N/mm^2	Shrinking reducing agent S 1/3 amount: 27.6 N/mm^2
Shrinking reducing agent S Standard amount: 27.1 N/mm^2	Shrinking reducing agent H Standard amount: 26.9 N/mm^2

REFERENCES

1. MASASHI SUGIYAMA, M. SAKUTA, etc., *Durability of Concrete Containing a Shrinkage Reducing Admixture*, Katharine and Bryant Mather International Conference on Concrete Durability, ACI SP100, Atlanta, USA, 1987

2. M. SAKUTA, MASASHI SUGIYAMA, etc., *Measure to Restrain Rate of Carbonation in Concrete*, Katharine and Bryant Mather International Conference on Concrete Durability, ACI SP100, Atlanta, USA, 1987

3. MASASHI SUGIYAMA. *The improvement in the durability of the concrete by the special chemical admixture of Japan*, International Conference on Sustainable Construction into The Next Millennium: Environmentally Friendly And Innovative Cement Based Materials, João Pessoa, Brazil、2000

4. MASASHI SUGIYAMA. *Durability of Concrete & Recent Advances in Concrete Technology*, Sixth CANMET/ACI International Conference, Bucharest, Romania, 2003

Prestressed Fibre Reinforced Concrete Elements

Z Kiss, K Bálint, R Zagon
Technical University of Cluj Napoca, Romania

As a direct consequence of economic recovery and ever growing demand on the construction market in out country but also across the European Union, a race has began between large construction companies to find the most advantageous technical and economical solutions in building prefabricated buildings. This has lead to a renewed research in past studied areas, such as pre-stressed columns. Another consequence is an ever increasing skill on part of researchers in this field. There are now several domestic and foreign construction companies that have started to fund research experiments of innovative design solutions which will ultimately optimize the technological processes involved and reduce the overall cost of prefabricating construction elements.

Z. Kiss is currently Professor of Reinforced and Prestressed Concrete at the Technical University of Cluj Napoca, Romania. He is the Head of the Department of Structures, he has led several research projects on concrete, being a specialist in the areas of research for prestressed concrete, reinforced concrete, fibre reinforced concrete and he also led numerous design projects on concrete from the position of Lead Designer.

K. Bálint is currently PhD student in Prestressed Concrete with fibre reinforcement at the Technical University of Cluj Napoca, Romania. He is also a structural engineer and during his activity he design several projects on concrete and also supervised and checked the work of his team.

R. Zagon is a second year PhD student at the Technical University of Cluj Napoca at Dept. of Structures, Romania. For several years he has been working as a structural engineer, and now his main concerns are researches on prestressed concrete, reinforced concrete and fibre reinforced concrete.

Keywords: Design, Fibres, Prefabrication, Prestressed fibres

INTRODUCTION

The necessity of building economical constructions, especially in the precast concrete area, urges the design offices to use the optimal solutions, in a certain extent. It is well known that in the shape process of the reinforcement carcasses for the reinforced concrete or pre-stressed concrete elements, armouring them takes consumes most of the time (is the longest operation). Increase efficiency could be reached using welded meshes instead of the transverse reinforcement, solution applied for large series elements. The most effective solution would be partially eliminating the transverse reinforcement by using the dispersed reinforcement. In this direction there were developed several studies in the last years by many western researchers. New scientific papers appear showing the results of the research and buildings are already erected using this type of reinforcement.

The tests were made at EMI Budapest and at the Technical University of Cluj-Napoca in the central laboratory of reinforced and pre-stressed concrete, due to an international experimental program sustained by ASA Hungary and Plan 31 Romania. The following results are determined on five pre-stressed concrete beams intended for single story buildings. The tests were made in order to compare the behaviour of the pre-stressed beam reinforced with dispersed steel fibres, the reinforced pre-stressed beam with stirrups, and the pre-stressed beam with only longitudinal reinforcement under the action of the flexural moment and shear stresses. In other test there were made two beams fabricated in one metallic formwork and divided in two. The beams had an opening of 7.00 m, a height varying from 445 mm, respectively 550 mm to 755 mm and the abut was conceived with a corbel characterised by a height of 445 mm respectively 550 mm. Shear tests were carried out on each beam. For the first tests were made three roof beams of 16.68 m length with a variable height of the cross section, varying between 585 mm and 848 mm. These were tested at bending moment.

EXPERIMENTAL PROGRAM

Materials

The concrete strength class used in the precast elements was C50/60. Beams reinforcement was made with passive reinforcement S500B type for longitudinal reinforcement, respectively S500A for stirrups, and active reinforcement St1500/1770 type. The used disperse reinforcement was BAUMIX VLS-50/1.05/H type.

The elements from the first test were pre-stressed with ten strands TBP 100 mm2 and were used three types of transverse reinforcement:

- stirrups on entire length of the element; (FP.01)
- stirrups in the end zones, on a length of 1.00 m, otherwise dispersed reinforcement 30 kg/m^3 (Figure 1); (FP.02)
- stirrups in the end zones on a length of 1.00 m, otherwise without dispersed reinforcement. (FP.03)

The elements from the second test were reinforced with dispersed reinforcement plus with stirrups in the end zones, on 1.00 m length. (FP.04, FP.05)

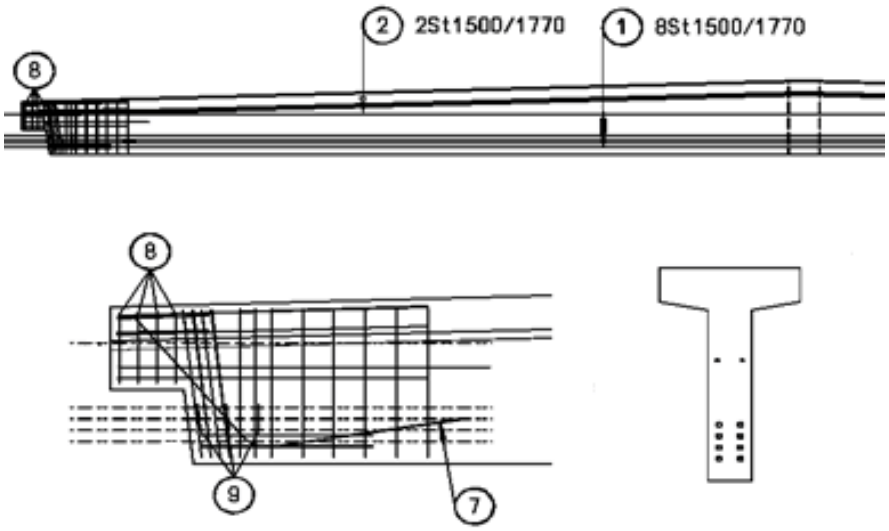

Figure 1 Reinforcement of the tested beams

Specimen details

The tests on elements were made using static loads, represented by two concentrated forces (Figure 2).

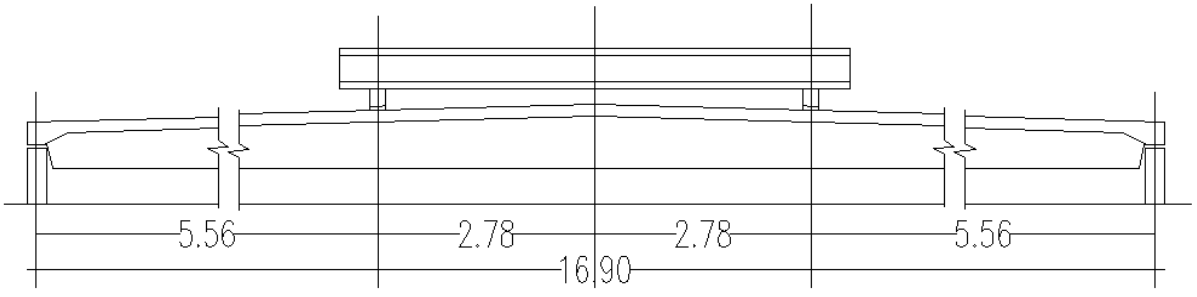

Figure 2 Laboratory equipped beam tested on bending moment

The tested elements have been loaded by applying the force in the middle third; this gave a central constant moment zone.

Beams FP.01, FP.02, FP03 were set on supports through 20 mm neoprene sheets and were tested in the normal top-down position.

Beams FP.04, FP05 were tested in down-top position and supported on 10 mm neoprene sheets (Figure 3).

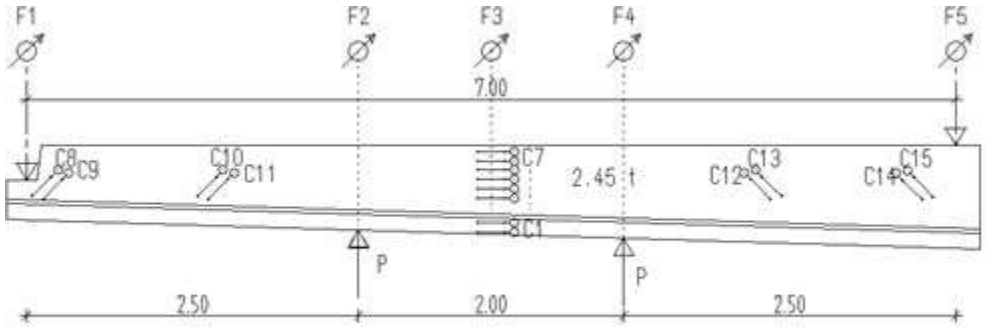

Figure 3 Experimental beam static scheme and equipment

Test setup aimed to reproduce the tension state, deformation and elements displacement in the fundamental load group. Loads have been determined by this test theme:

- FP.01 was loaded in the first stage up to a maximum force Pserviceability=108 kN, followed by unloading, and in the second stage to a maximum force Prupture=220 kN;
- FP.02 was loaded in the first stage up to a maximum force Pserviceability=108 kN, followed by unloading, and in the second stage to a maximum force Prupture=180 kN;
- FP.03 was loaded in the first stage to a maximum force Pserviceability=108 kN, followed by unloading, and in the second stage to a maximum force Prupture=143 kN;
- FP.04 was tested until it breaks at a maximum force P=300kN (calculated value was 260 KN)
- FP.05 was tested near breaking limit followed by four cycles of loading - unloading to the maximum force of 250 kN

The reading steps were 25 kN. During the test, at each load level were recorded:

- vertical displacements in the three points of the element;
- specific deformations;
- cracks (position, length and maximum opening) and their evolution.

ANALYSIS OF THE RESULTS

All the measured beams had the experimental cracking moment very close to the calculated values; there were slight differences varying from 2% to 6%. At the re-cracking moments the differences were varying from 0% and 5% (Table 1, Table 2).

The breaking of the elements occurred after the overgrowth of normal cracks and deflections as follows:

- FP.01 was considered broke when the opening of normal cracks was more than 2 mm, breaking strength was about 220 kN approx. 50% higher than calculated;
- FP.02 after the opening of normal cracks exaggerated in bending with shear strength zone (between strength and support) appeared inclined cracks; break occurred suddenly after a rift developed outside stirrups reinforcement by the application strength to a value of 180 kN with 25% higher than the calculated value. (Figure 4)

Table 1 Test results in SLS

TESTED ELEMENT	BENDING MOMENT [kNm]		CRACKING MOMENT [kNm]		MIDD SPAN DEFLECTION wn [mm]		CRACK OPENING wk [mm]	
	calc.	exp.	calc.	exp.	allowed values	measured values	allowed values	measured values
FP.01 (with stirrups)	307.8	308.0	378.5	368.6		95.5-80= 15.5		0.24
FP.02 (with steel fibers)	307.8	293.2	378.5	359.6	L/250= 66.7	108.2-91= 17.2	0.3	0.28
FP.03 (without stirrups)	307.8	298.4	378.5	356.6		109.2-82= 27.2		0.29

Table 2 Test results in SLU

TESTED ELEMENT	BREAKING MOMENT [kNm]		BREAKING SHEAR FORCE [Nm]		BREAKING MODEL
	calculated	experimental	calculated	experimental	
FP.01 (with stirrups)	1000	1,216.03	228.4	-	The test has stopped before the breaking of the beam at flexural moment
FP.02 (with steel fibers)	1000	1,006.55	105.2	154.36	break occurred warned at shear force
FP.03 (without stirrups)	1000	792.88	115.2	115.97	break occurred suddenly at shear force

Experimental value of breaking strength was about equal to the calculated breaking strength. After the break there were homogeneous mixing steel fibres which were pulled out without breaking them.

- FP.03 break was similar with beam 2 at a value of 143 kN with 1% less than the calculated value.
- FP.04 .The cracks appeared as expectation in the tensioned area of the beam section, uniform distributed in the middle of the span spreading to the end of the beam as the force was increased. Inclined cracks appeared at the cherty end of the element with small openings. At a higher level of forces, the inclined cracks aspire to the point of application. (Figure 5)

Before the break occurred the opening of these cracks increased at the value of 5-8 mm. Break occurred suddenly, but was preceded by excessive opening of cracks. The rupture appeared due to shear failure by crushing of the compressive concrete. (Figure 5)

Figure 4 Breaking of beam F.P.02

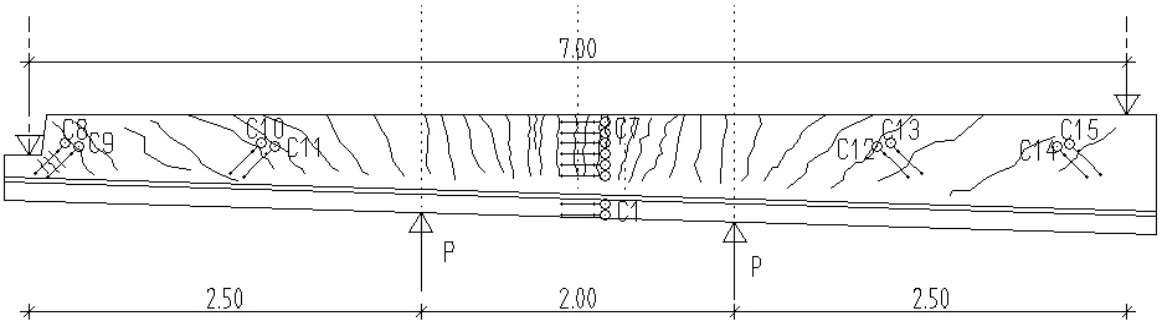

Figure 5 Cracks draw at beam FP.04.

Figure 5 Breaking of beam F.P.04

Strength deflection diagram shows a proper behaviour to static loads. (Figure 6)

- FP.05 break occurred similar to FP.04.

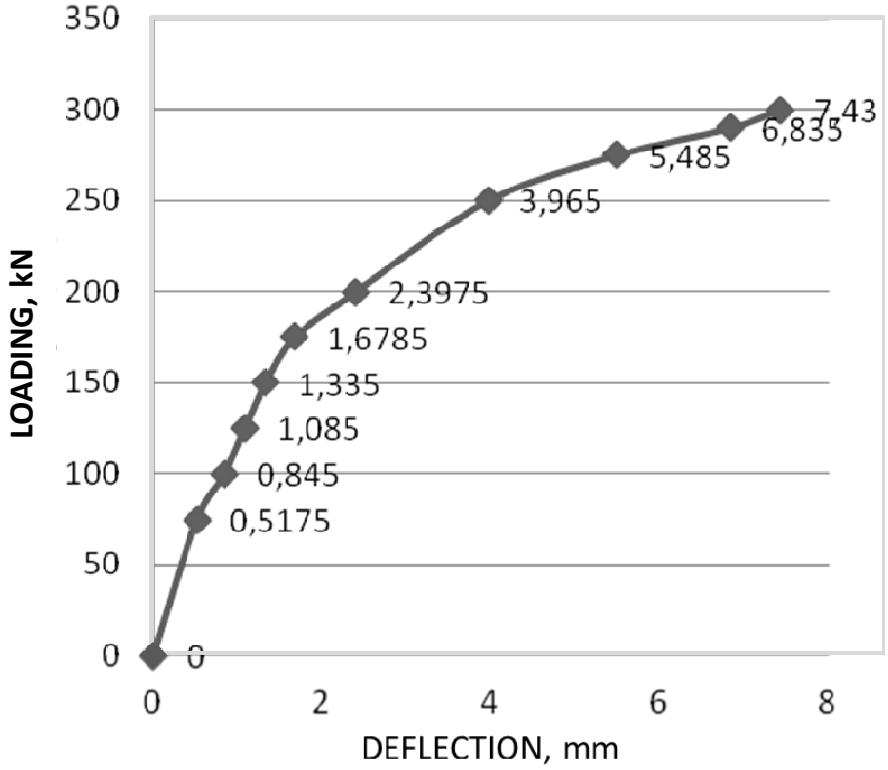

Figure 6 Loading-deflection diagram

CONCLUSIONS

Reinforced pre-stressed beams with dispersed steel fibres and stirrups at the ends, behaved satisfactorily showing a 25% reserve to the calculated values.

The rupture for reinforced beams armed with dispersed steel fibres, occurred in all cases after an oblique crack, however, followed by the increased opening of the normal cracks and large deflection of over 30 cm.

Bearing capacity of these beams was 20% lower than the beam with usual reinforcement, but 25% higher than the beams without dispersed reinforcement.

Analysing the experimental information, it can be said that in the case of pre-stressed concrete purlins without special requirements for ductility (simple supported beams) the use of reinforcing steel fibres dispersed in combination with stirrups at the ends (on a piece of 1 / 15 of opening) can successfully be used, for beginning, in areas with low or moderate seismicity.

REFERENCES

1. FALKNER H.; GRUNERT J.P.; TEUTSCH M., Vorgespannte, stahlfaserverstarkte Binder aus SVB ohne Betonstahlbewehrung.

2. PFYL Th.; MARTI P., Versuche an stahlfaserverstarkten Stahlbetonelementen. Instutut fur Baustatik und Konstruktion, Eidgenossiche Technische Hochschule Zurich, 2001

3. BALÁZS L. GY., KOVÁCS I., Structural performance of steel fiber reinforced concrete. The 2nd International Conference on Fibre Reinforced Concrete – from research to practice. Budapest, 2004.

Solving Some Problems of Nonlinear Analysis of Reinforced Concrete Structures by Additional Finite Element Methods

A Ermakova
South Ural State University, Russia

The work presents the ways of solving of some main problems in nonlinear design of reinforced concrete structures on the basis of the developed Additional Finite Element Method (AFEM). This method is a variant of the Finite Element Method (FEM) destined for analysis of reinforced concrete structures at limit strength state. AFEM adds to the traditional sequence of problem solving by FEM the units of design by method of ultimate equilibrium and method of additional loads.

A Ermakova, is Cand. Tech. Sc., Assistant Prof. (”dotsent”) in the Department of Building Structures of South Ural State University, Chelyabinsk, Russia.

Keywords: Additional design diagram (ADD), Additional finite element (AFE), Additional finite element method (AFEM), Ideal failure model, Limit state

INTRODUCTION

At present the computer realization of nonlinear design of reinforced concrete structures at limit states is one of the most important problems of structural design. The paper shows the solving of some encountered here problems by means of Additional Finite Element Method (AFEM).

Flow Chart of Finite Element Method

At present in the majority of the cases the computer programs for design of reinforced concrete structures use Finite Element Method based on the known in structural mechanics deflection method. It reduced the solving of any problem to the sequential fulfillment of the following six computer operations:

1. Composition of design diagram;
2. Calculation of stiffness matrices of separate finite elements;
3. Formation of general stiffness matrix of the structure;
4. Solution of algebraic set of linear equations;
5. Calculation of strains, stresses and node reactions of the finite elements;
6. Analysis of stress-strain of the structure.

In linear design the problem may be considered solved after fulfillment of these operations.

Solving of Nonlinear Problem by Finite Element Method

Extensive using of FEM in structural design is explained by the fact that the main operation of this method is the solving of the following set of linear algebraic equations:

$$KV = P \quad , \qquad (1)$$

Where, K = stiffness matrix of the considered structure; V = matrix-column of unknown node displacements; P = matrix-column of external load.

The main set (1) is composed of equations of node equilibrium of design diagram of the considered structure. In linear problem this set is solved once. In this case K – stiffness matrix with linear properties, which is formed on the basis of separate finite elements (FE) with linear properties of the design diagram.

In nonlinear design the additional operation for taking account of physical nonlinearity of behaviour of the structure under load ought to be included in the given sequence. In this case the set of equations (1) has another form:

$$K_{nonl}V = P \quad , \qquad (2)$$

Where, K_{nonl} = stiffness matrix of the structure with nonlinear properties.
In this case the main set of equations (2) ought to be solved by iterative method since the stiffness matrix K_{nonl} changes in accordance with the degree of influence of nonlinear properties [1].

In accord with method of additional loads sometimes named as method of linear solving in place of a body with nonlinear properties the elastic body with the same deformations due to applied additional loads [2] is considered in design.

This method promotes construction of iterative process rationally in case if the method of sequential elimination of unknowns (Gauss method) is used for solving of the set equations (2). In this case the stiffness matrix K_{nonl} is considered in the form of the two components:

$$K_{nonl} = K + \Delta K_{nonl} \quad , \qquad (3)$$

where K = linear component of the stiffness matrix K_{nonl}; ΔK_{nonl} = nonlinear component of this stiffness matrix. Such approach makes possible to construct the iterative process in place of equation (2) on the basis of the following equation:

$$KV = P - \Delta K_{nonl}\, V \quad , \qquad (4)$$

Where the second term in the right-hand part represents the additional load F, which forces the structure with linear properties to receive the displacements as the structure with nonlinear properties:

$$F = -\Delta K_{nonl}\, V \quad . \qquad (5)$$

In design by means of FEM it is better to use the stiffness matrix of the structure with linear properties K instead of the linear component of the stiffness matrix K_{nonl}. Therefore the main problem in the construction of iterative process according the formula (4) is the obtaining of matrix ΔK_{nonl} for transformation of matrix K into K_{nonl}.

There are formulae for formation of additional load F in two particular variants in addition to the general formula (5). One of these formulae is deduced on the basis of method of additional stresses and the other one is based on the method of additional deformations [3, 4]. If it is necessary to take into account the influence of several nonlinear properties then the additional load F at each stage of analysis ought to be determined according to the formula:

$$F = \sum_{i=1}^{n} F_i \quad , \qquad (6)$$

where F_i = vector of additional load taking into account the character of appeared nonlinearity caused by one particular i-th factor; n = number of types of the nonlinearities which are taken into account at the given stage of structural analysis.

Three Main Problems in Design of Reinforced Concrete Structures

The problem of taking account of nonlinear properties is especially keen in design of statically loaded reinforced concrete structures. The main of these properties are: plasticity of concrete, cracking, unload and reload, bond between concrete and reinforcement, prestressing, action of temperature. Algorithms describing the real behaviour of material are required for realization of this design [5, 6].

SN and P's require to carry out the design of concrete and reinforced concrete structures at limit states taking account of their nonlinearity. This design is based on the method of ultimate equilibrium [7]. In particular s. 6.1.3. [8] contains the partition: "The definition of ultimate stresses and strains of concrete and reinforced concrete structures one must carry out on the base of design diagram (models) most close to the real physical character of behaviour of structure and materials at ultimate limit state". The realization of design according to these requirements is possible if all physical nonlinear properties exhibiting by the structure at the moment when the ultimate limit state is reached are taking into account, i.e. with regard to the degree of influence and the moment of appearance of each separate nonlinear property.

Thus the requirements of the SN and P's [8, 9] do not agree with the algorithms of the used programs where the taking account of different nonlinear properties of the structures is developed insufficiently.

SN and P's consider two categories of limit states: the ultimate limit state and the serviceability limit state. The first category is the more dangerous state from the point of view of structural behaviour.

State of stress of the structure at the moment when its bearing capacity becomes exhausted is named the ultimate limit state or the state of ultimate equilibrium. In this paper the question is of design at ultimate strength. Besides in this case it is necessary to be able to fulfill a step-by-step loading design for obtaining its real stress-strain state portrait.

In addition at each step it ought to guarantee the taking into account only the exhibited at this moment nonlinear properties.

Three main problems which ought to be solved first of all may be distinguished after analysis of the difficulties of nonlinear design of reinforced concrete structures according to the requirements of SN and P's and estimation of possibility to combine the method of ultimate equilibrium and the finite element method:

1) determination of the character of change in behaviour of structure according to the reached degree of its limit state, i.e. necessity of providing of gradual change of stiffness matrix of the structure due to manifestation of nonlinear properties at each iteration of each step of loading;

2) determination of the way of description of gradually changed physical nonlinear properties of each finite element of design diagram as its ultimate state is reached including following cases:

a) necessity of taking account of behaviour of the specific constructive material, for example, reinforced concrete structures they are concrete and reinforcement of the separate finite element;
b) gradual appearance of different nonlinear properties as the ultimate limit state is reached;
c) passage from one stress-strain state to another one, for example, at cracking or appearance of residual strains after unloading;
d) inclusion of a mechanism of gradual destruction of the finite element up to its collapse;

3) choice of the way for construction and development of iterative process for solving of set of linear algebraic equations for the whole structure and for the separate finite element on the basis of possibilities of FEM in the solving of *n*-linear analysis provided that:

a) gradual transformation of the stiffness matrix of structure with nonlinear properties K_{nonl} into the stiffness matrix of structure at limit state;
b) gradual taking account of each nonlinear property exhibited by finite element up to collapse for the moving off behaviour of the whole structure one-by-one in the step-by-step design by the method of ultimate equilibrium.

These three interconnected problems determine the run of problem solving and require the solving of accompanying problems.

The Solution of Problems in Design of Reinforced Concrete Structures by AFEM

The developed additional finite element method (AFEM) is a variant of finite element method (FEM) destined for design of reinforced concrete structures at limit state. For the solving of the mentioned problems AFEM uses the elements of design by the method of additional loads and the method of ultimate equilibrium [10, 11, and 12].

The additional finite element method suggests the use of additional finite elements (AFE) for gradual transformation of finite elements with linear properties into finite elements with nonlinear properties corresponding to the reached stage of limit state of the structure.

Introduction of additional finite elements makes an opportunity to overcome originating difficulties of realization of design of the structures at limit state by means of FEM. Also additional finite element method uses such known concepts as the limit state of structure and the limit state of finite element.

The Ideal Failure Model of Structure

The ultimate limit state of the structure in FEM and in AFEM is the reaching of ultimate limit state in a number of finite elements.

The definition of these critical for the given structure finite elements is the aim of design. This problem is solved easier in the bar systems where we may come across most often the case when the ultimate limit state of the structure coincides with the moment of reaching of ultimate limit state in a single finite element.

It is proposed to use an ideal failure model for describing of structure at ultimate limit state which is the design diagram of the analyzed structure before the moment of its collapse. The point is that as the structure is loaded its initial design diagram is changed in accordance with nonlinear properties which are manifested when the limit state is reaching. In particular the breakdown of bonds between some finite elements takes place, some finite elements with other nonlinear properties and the finite elements at limit state are appeared. As a result the initial design diagram is turned into an ideal failure model of the considered structure.

This ideal failure model may be obtained by two ways. The first is to carry out an analysis of the structure under step-by-step increasing load with introducing of accompanied changes in the initial design diagram. For example, the characteristics of the finite elements may be changed. This way is shown as an example of bending console later. The second way is the assignment of an ideal failure model known from design of analogous structures or from results of full-scale test. For example, SN and P for bending beams consider two failure models: with transverse crack and oblique one. Examples of ideal failure models of bending reinforced concrete deep-beams are given in [10]. Introduction of an ideal failure model promotes the realizations of structural design by the method of ultimate equilibrium.

The Additional Design Diagram

In design as it is shown above the initial design diagram gradually ought to be transformed according to the variations which are accumulated in the structure as its ultimate limit state is reaching. Additional finite element method suggests to use additional design diagram for simulation of these variations. This additional design diagram is a geometric copy of the

initial design diagram, but it is destined for gradual transformation of initial design diagram into ideal failure model of the considered structure.

Its scheme of action on the intermediate stages is:

Design diagram consisting of the finite elements with nonlinear properties = Design diagram consisting of the finite elements with linear properties + Additional design diagram consisting of the finite elements for allowance of the nonlinear properties.
The scheme of action at limit state is:

Design diagram of the structure at limit state (ideal failure model) = Design diagram consisting of the finite elements with linear properties + Additional design diagram for allowance of limit state of structure. At limit state the decision set of linear algebraic equations in FEM ought to be of the form similar to the formula (2):

$$K_{lim}\, V = P \quad , \qquad (7)$$

Where, V = matrix-column of unknown node displacements; P = matrix column of outer load; K_{lim} = stiffness matrix of the structure with nonlinear properties at limit state.

This nonlinear matrix K_{lim} is formed on the basis of design diagram of the structure and represents its ideal failure model. If the way of elastic decision, which is the basis of the method of additional loads is used, the linear and nonlinear components ought to be distinguished from the matrix K_{lim}. It ought to be given in the form (3):

$$K_{lim} = K + \Delta K_{lim} \quad , \qquad (8)$$

Where, K = initial stiffness matrix of the structure with linear properties; ΔK_{lim} = stiffness matrix connected with the appearance of nonlinear properties at limit state of the structure.
More simply it is to use the stiffness matrix of the structure K as the linear component if it is made on the basis of the same design diagram and consists of finite elements with linear properties. It permits to leave the linear matrix K as a constant term from the beginning to the end of analysis.

In this formula both matrices K_{lim} and K are formed on the basis of one and the same design diagram, which consists of identical finite elements with equal dimensions and shape. But the first nonlinear matrix K_{lim} consists of the finite elements with nonlinear properties according to the degree of limit states reached by these finite elements. The second linear matrix K consists of the same finite elements but with linear properties. It means that nonlinear component ΔK_{lim} is an additional matrix which ought to be formed on the basis of the same design diagram. We may assume that the additional matrix ΔK_{lim} is formed on the basis of an additional design diagram of the structure which consists of the additional finite elements.

This additional design diagram turns the design diagram consisting of linear finite elements into the design diagram with nonlinear finite elements as each its additional finite element converts the corresponding linear finite element into nonlinear one. The additional design diagram is used for formation of additional load which takes into account the limit state of structure. With regard to formula (8) the main set (7) takes the form:

$$KV = P - \Delta K_{lim} V \quad . \qquad (9)$$

The second term of the right-hand side of this equation is the additional load F which ought to be applied to the structure with linear properties together with the main load P to reach the displacements of the corresponding structure with nonlinear properties at limit state under the action of the load P only:

$$F = -\Delta K_{lim} V \quad . \tag{10}$$

The design of structures at limit state may be realized by means of additional design diagram consisting of additional finite elements.

Additional stiffness matrix of the structure ΔK_{lim} is formed on the basis of nonlinear properties of the finite elements of its design diagram as the structure at limit state exhibits all its intrinsic nonlinear properties. These nonlinear properties have different nature and character of manifestation. Therefore the additional stiffness matrix ought to be formed according to the nonlinearities observed at the moment of limit state:

$$\Delta K_{lim} = \sum_{i=1}^{n} \Delta K_{nonl,i} \quad , \tag{11}$$

Where, n = number of types of nonlinear properties of the structure at limit state; $\Delta K_{nonl,i}$ = additional stiffness matrix of the structure for the allowance of the manifestation of its i-th nonlinear properties at the moment of reaching of limit state.

In general in the presence of the given nonlinear property the additional matrix $\Delta K_{nonl,i}$ in the moment of reaching of the ultimate limit state is not equal to 0, i.e. $\Delta K_{nonl,i} \neq 0$. If the i-th nonlinear property at ultimate limit state is not taken into account its additional matrix $\Delta K_{nonl,i}$ is equal to 0, i.e. $\Delta K_{nonl,i} = 0$.

Additional stiffness matrix of the structure ΔK_{lim} is formed on the basis of additional design diagram. It means that the additional design diagram ought to be also determined depending on the number n of the considered at limit state nonlinear properties, i.e. the additional design diagram ought to consist of n additional design diagrams, each of which takes into account the only i-th nonlinear property. If any nonlinear property is not taking into account at the moment of reaching of limit state then the corresponding additional design diagram is equal to 0 too. Example of formation of additional design diagram of bending console depending on the stage of design is given in Table 1.

According to (11) the additional load F taking into account the nonlinear properties consists of several components F_i , each of which takes into account any the i-th nonlinear property. The component of additional load F_i is determined by the formula:

$$F_i = -\Delta K_{nonl,i} \quad . \tag{12}$$

Thus the additional load ought to be formed with taking account of these properties and the possible limit states of finite elements entering the initial design diagram.

Limit State of the Finite Element in Finite Element Method

Each element of the design diagram is considered as a finite structure of simple form with its own limit state under the given conditions of loading. Each type of finite element may have several limit states. For example, triangular concrete deep-beam finite element has two limit strength states: limit compressive strength state and limit tensile strength state. In behaviour

at compression triangular deep-beam finite element assumes two stages, and in tension it goes through four stages. The concrete finite element "Bar of general attitude" has 12 limit states. If this finite element is reinforced it has 23 limit states [11]. Moreover the behaviour of finite element at each limit state has its own singularities.

This fact requires the special research of each finite element and the determination of number, type and way of description of each it's characteristic limit state. For description of each stage of behaviour of finite element at each it's characteristic limit state the relationships by analogy with the using ones in linear and nonlinear design by means of FEM are necessary: relationship between node reactions and displacements, formula for determination of stiffness matrix, relationship between node reactions and stresses, relationship between node reactions and strains, formula for determination of stresses, formula for determination of strains, formula for determination of additional load.

The Additional Finite Element

For gradual transformation of initial finite elements with linear properties into the same elements with nonlinear properties depending on the reached stage of their limit state it is offered to use additional finite elements (AFE). Each additional finite element is a geometric replica of the main finite element with its own stiffness, which changes in design providing the influence of nonlinear properties. Each additional finite element is destined for description of influence of the only nonlinear property and is a part of additional design diagram.

Its scheme of action at the intermediate stages is:

Finite element with nonlinear properties = Finite element with linear properties + Additional finite element for allowance of the nonlinear properties.

The scheme of action at limit state is:

Finite element at limit state = Finite element with linear properties + Additional finite element for allowance of the limit state.

Introduction of additional finite element promotes to realize iterative process of problem in two directions: for the whole structure and for the separate finite element. In the last case the possibilities of FEM for solving of n-nonlinear problems are used completely.

An Example of Formation of ADD from Additional Finite Elements

Now we may consider an example of formation of additional design diagram of bending console at limit state (Table 1).

Its design diagram consists of nine nodes and eight triangular deep-beam finite elements. Scheme of formation of additional design diagram from the corresponding additional finite elements depending on the type of carried out design: linear, plastic, taking account of unload, cracking or limit state is given in Table 1.

Table 1 Formation of the console additional design diagram consisting of additional finite elements

THE MAIN DESIGN DIAGRAM, *K*	KIND OF DESIGN	ADDITIONAL DESIGN DIAGRAM, *ΔK*			
		Plastic Properties	Patial Unload	Behaviour with Cracking	Collapse
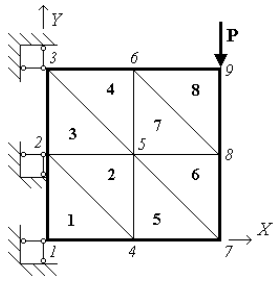	Linear	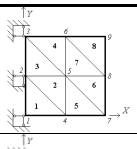	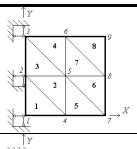	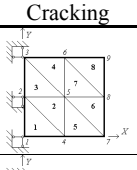	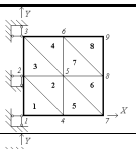
	Plastic	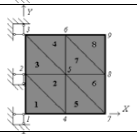	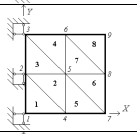	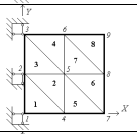	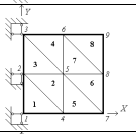
	Unload due to cracking	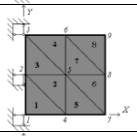	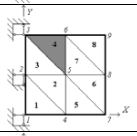	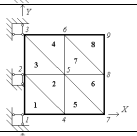	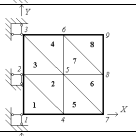
Ideal failure models	Cracking	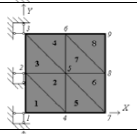	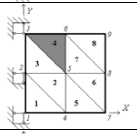	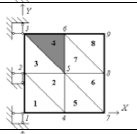	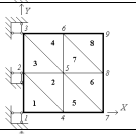
AFEM 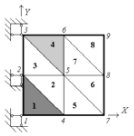 FEM 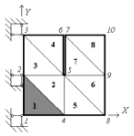	Ultimate limit state	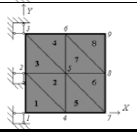	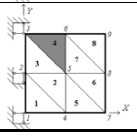	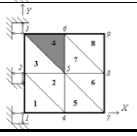	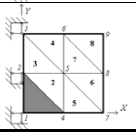

Note: Finite element № 1 in ultimate compression, finite element № 4 with cracking in ideal failure models and additional finite elements which stiffness matrices are not equal to 0 ($\Delta K_e \neq 0$) in additional design diagram are shown dark.

The additional finite elements which stiffness matrices are not equal to 0 are shown dark. Two ideal failure models of this console obtained by means of AFEM with out change of geometry of initial design diagram and by means of FEM with the change of the initial design diagram are given there too.

CONCLUSIONS

The developed AFEM using the additional design diagram consisting of additional finite elements the ideal failure model promotes to solve the three main problems of nonlinear design of reinforced concrete structures at limit state:

1. Method describes the character of gradual change of the behaviour of the structure according to the reached degree of its limit state up to the given moment;

2. Method determines the way of description of gradually changed physical properties of each finite element of the design diagram (taking account of behaviour of a definite material, gradual appearance of different nonlinear properties, passage from one stress-strain state to another state, inclusion of mechanism of gradual destruction up to collapse);

3. Method promotes to construct and to develop the iterative process in solving of the main set of algebraic equations for the whole structure with gradual transformation of stiffness matrix of the structure with nonlinear properties into stiffness matrix of the structure at the limit state and for the separate finite element with gradual taking account of each nonlinear property exhibiting by finites elements up to the moment of their collapse for the elimination one by one for step-by-step design by method of limit equilibrium.

4. Efficiency of AFEM is proved by analysis of a number of reinforced concrete structures.

ACKNOWLEGMENT

All researches were made at South Ural State University at its Department of Building Structures. At present these researches are continued.

REFERENCES

1. POSTNOV, V A. Numerical methods of design of ship structures, Shipbuilding, Leningrad, 1977, 280pp.

2. ILYUSHIN, A A. Plasticity, Gostechisdat, Moscow, 1948, 376pp.

3. ZIENKIEWICZ, O C. The Finite Element Method in technique, Mir, Moscow, 1975, 541pp.

4. Computer-aided of reinforced concrete structural elements. Collected lectures. Part 4 edited by Prof. OATUL A A, Chelyabinsk Polytechnic Institute, Chelyabinsk, 1980, 67pp.

5. KARPENKO, N I. Construction of Schemes of Reinforced Concrete, State Administration of Construction, Moscow, 1996, 416pp.

6. SHUGAEV, V V. Engineer Methods of Non-Linear Theory of Limit Equilibrium of the Shells, Gotika, Moscow, 2001, 368pp.

7. GVOZDEV, A A. Analysis of bearing capacity of structures by Limit State Method, Gosstroyisdat, Moscow, 1949, 280pp.

8. SN AND P, 52-01-2003, Concrete and Reinforced Concrete Structures, CITP of State Administration of Construction, Moscow, 2004, 26pp.

9. SP 52-102-2004, Prestressed Reinforced Concrete Structures, CITP of State Administration of Construction, Moscow, 2005, 36pp.

10. ERMAKOVA A, Additional Finite Element Method for Analysis of Reinforced Concrete Structures at Limit States, Isdatelstvo ASV, Moscow, 2007, 128pp.

11. ERMAKOVA A, Problems of the Use of Additional Finite Element Method for Analysis of Reinforced Concrete Structures at Limit States. Space Structures of Buildings. V 11, Moscow, 2008, pp. 21 – 30.

12. ERMAKOVA A, Limit State Analysis of Reinforced Concrete Structures by Additional Finite Element Method, Role for Concrete in Global Development, Proceedings of the International Conference held at the University of Dundee, Scotland, UK on 8–9 July 2008. BrePress, Dundee, Scotland, UK, pp. 763 – 774.

Chloride Profiles of Mineral Admixture Concrete Subjected to Standard Curing

S Goyal[1], M Kumar[1], B Bhattacharjee[2]
1 – Thapar University, India
2 – IIT Delhi, India

The paper presents the influence of silica fume and fly ash, used either as binary or ternary cementing materials along with OPC, on chloride ingress of concrete, after undergoing the realistic curing practice of 7 days of water curing regime followed by air drying till the constant strength level is reached. The chloride exposure regime consists of 48 weekly wetting and drying cycles under 5% sodium chloride and 5% calcium chloride solutions, taken separately. The chloride profiles are obtained by analysing concrete powder extracted from different depths of the surface that is exposed to chloride solution. The powder is titrated in order to obtain total chloride and free chloride contents at different depths. It is found that lowering the water-to-binder ratio reduces both total and free chloride contents at a given depth. The use of mineral admixtures increases the chloride binding capacity of concrete thus reducing the amount of chlorides available for corrosion of steel reinforcement. For both sodium chloride and calcium chloride exposures, ternary mixes are found to perform better than the binary mixes containing either silica fume or fly ash, thus leading to the conclusion that the ternary mixes are best in resisting chloride ingress in concrete.

Shweta Goyal, Ph.D., is an Assistant Professor in Civil Engineering Department, Thapar University, India.

Maneek Kumar, Ph.D., is a Professor and Head of the Civil Engineering Department, Thapar University, India.

Bishwajit Bhattacharjee, Ph.D., is a Professor in the Civil Engineering Department, Indian Institute of Technology, Delhi, India.

Keywords: Binding capacity, Chloride profile, Durability, Mineral admixtures, Total chlorides

INTRODUCTION

Reinforced concrete is considered to be extremely durable material and is expected to have long service life. However, like all other materials, it deteriorates with time. Among the various factors that lead to decline in concrete durability, chloride ingress is one of the major reasons for deterioration of the passive film that is formed by calcium hydroxide and is believed to surround the steel rebar [1]. When chlorides come into contact with the protective passive layer surrounding the rebar, they will destroy it by activating the surface of steel to form an anode, while the passive surface forms the cathode leading to the corrosion of rebar.

Chlorides can be introduced into concrete by either internal sources (from aggregate, water etc) or external sources (by intrusion from the environment). Whatever may be the case, to cause damage, the chloride ions must be in contact with the reinforcement and also, there must be sufficient number of chloride ions to depassivate the reinforcement (called threshold chloride content) [2-5]. Therefore, in the case of chloride penetration from external source, which is the general source in most of the modern concretes, there must be the movement of chloride into concrete (which is represented by the chloride front). According to the model developed by Tutti [2], the service life of concrete structures can be divided into two periods:

(1) Initiation period, (2) Propagation period

The initiation period is the time from the beginning of the service life to the point at which the concentration of chloride ions around the reinforcing steel has reached the threshold value for initiating corrosion. The propagation period starts from the onset of corrosion to the time beyond which the structure cannot be safely used. In the case of chloride penetration from the external source, the initiation period is far longer than the propagation period [2]. Thus, the initiation period could be used to conservatively estimate the service life of concrete structures.

Many authors have reported that the uses of mineral admixtures such as fly ash, silica fume, blast furnace slag etc. effectively reduce the chloride induced corrosion of steel reinforcement as well as permeability of concrete [6-9]. Especially silica fume is known to considerably increase the durability of concrete [10, 11]. However, it comes in the category of expensive materials and leads to reduction of workability, which makes the use of super-plasticizer compulsory. In terms of cost/benefit analysis, silica fume is not considered to be the most viable solution. That's why; fly ash is widely used as substitute to it. The incorporation of fly ash increases the porosity of hardened cement paste at early ages, but the average pore size is reduced, that often results in less permeable paste in the long run [12, 13].

However, fly ash is highly sensitive to the initial curing regimes applied. Therefore, using a combination of silica fume and fly ash in the ternary cement system may result in better performance over the use of single admixture to improve concrete properties [14-16]. In the previous studies on the ternary systems, curing regime adopted was the one that allowed maximum hydration to take place before exposure to chloride environment. In the present work, curing that simulates more realistic curing condition has been adopted to check the durability aspects of both binary and ternary systems.

The ingress of chlorides into concrete is defined by six mechanisms: adsorption, diffusion, chloride binding, permeation, wicking and dispersion [17]. The durability of concrete to chloride ingress is usually defined in terms of coefficient of diffusion, which is a measure of pure diffusion. However, a more realistic approach is to define an apparent diffusion coefficient, which includes the entire transport phenomenon into consideration. It is based on the chloride profiles obtained by plotting the chloride content against the depth. For obtaining the chloride content at various depths, the concrete samples can be obtained from each depth by using any one of the following techniques: Coring, dust collection using drilling or profile grinding, broken out concrete [3]. In the present work, coring is adopted to obtain chloride profiles. After taking out the samples, the analysis can further be carried out by numerous chemical techniques which are broadly divided into three categories: qualitative, semi-qualitative and quantitative. In the present study, the quantitative method which includes the analysis of powdered samples by titration is adopted.

Furthermore, when chlorides penetrate concrete, some of it is bound either in the form of Friedel's salt ($3Cao\ Al_2O_3\ CaCl_2\ 10H_2O$) or physically adsorbed to the amorphous calcium silicate hydrate (CSH) and some are dissolved in the pore solution (free chlorides). The chloride binding capacity of concrete also influences the durability of concrete in chloride containing environment [18-21]. The effect of chloride binding on the initiation of corrosion is two fold: (1) The rate of chloride transport in concrete is reduced, since the amount of available mobile ions, i.e. free chlorides, is reduced by the binding mechanism, (2)

The reduction of free chlorides in concrete results in lower amount of chloride being accumulated at the reinforcing steel layer [20]. Although the free chlorides are believed to be responsible for the initiation of corrosion, the chloride threshold value necessary to initiate corrosion of steel bars in concrete is mostly provided in terms of total chlorides [22-24]. Therefore, the relationship between free and total chloride is necessary for the development of models for service life prediction of reinforced concrete due to corrosion.

The presence of mineral admixtures and the cation associated with chloride ions play an important role in chloride binding capacity of concrete [18, 25, 26]. While there is a general agreement in the literature, that when added in fresh state, the binding of chlorides in concrete is higher when $CaCl_2$ is used in comparison with NaCl [27-29], the effect of different chloride sources when they are introduced as an external source is not well known, especially in mineral admixture concrete. Therefore, the objective of the paper is to develop a relationship between free and total chlorides for mineral admixture concrete when the additional ions associated with chloride is sodium and calcium. The developed relationship will help in correlating the chloride threshold value (which is in terms of total chloride) to the free chlorides present.

EXPERIMENTAL DETAILS

Materials

Locally available ordinary Portland cement (ASTM Type I) is used throughout the investigation. Silica fume is procured from Elkem India and fly ash is collected from a local thermal power plant, and are used as partial replacement of cement in the concrete mixes. The chemical,

physical and other important characteristics of these materials are presented in Table 1. The riverbed sand having fineness modulus of 2.52 and crushed granite with a maximum nominal size of 10 mm are used as fine and coarse aggregate respectively. The properties of aggregates are listed in Table 2. Polycarboxylic group based super-plasticizer, Structro 100 (a product of Fosroc chemicals), with the specific gravity of 1.2 and solid content of 40 percent by mass is used to maintain almost constant workability of all the mixes.

Table 1 Characteristics of binders used in this study

CHARACTERISTIC	OPC	SILICA FUME	FLY ASH
Normal Consistency, %	32		
Setting time Vicat, hour: minute			
Initial	2:10		
Final	4:08		
Specific Gravity	3.12	2.2	2.42
Soundness: Le-Chatelier, mm	1.5		
Fineness, % retained on 90 micron sieve	3.2		
Mean particle diameter, μm		0.1	19.6
Specific surface, m^2/kg			
Blain	287.8		250
Nitrogen adsorption		21,000	
Lime reactivity, MPa		98	
Compressive Strength, MPa			
f_c, 3 days	26.5		
f_c, 7 days	36.2		
f_c, 28 days	47.3		
Chemical Composition, %			
CaO	61.7	0.5	1.7
SiO_2	22.4	90.7	56.8
Al_2O_3	5.93	0.68	25.8
Fe_2O_3	4.91	2.2	6.43
SO_3	2.28		1.4
MgO	1.5	1.47	0.6
K_2O	0.65	0.9	0.79
Na_2O	0.122	0.86	0.36
Loss on ignition	1.27	2.5	2.15
Insoluble Residue	4.52		84.9

To explore the effect of water-to-binder ratio on chloride ingress of concrete, the study is carried at three water binder ratios: 0.45, 0.35 and 0.25. The mixes are designed as per the British (DoE) guidelines [30]. The mix details of control mixes are listed in Table 3. Under each water/binder ratio, apart from the control mixes, four mixes containing varying proportions of silica fume and fly ash as partial replacement of cement are prepared. Table 4 shows the details of mix proportions of 15 different concrete mixes along with the mix designation used in this study.

The ternary mix with 5% silica fume and 15% fly ash is selected because it is established that the ternary mix perform almost similar to binary mixes containing only silica fume and is further found out to be more economical than the binary mix [31].

Table 2 Properties of aggregates

PROPERTY	FINE AGGREGATE	COARSE AGGREGATE
Unit mass, kg/m^3	1.692	1.68
Specific gravity	2.54	2.64
Percentage absorption, %	1.95	1.12
Sieve Analysis	Cumulative percentage retained, %	
20mm	0	0
10 mm	0	2.5
4.75 mm	5.05	92.8
2.36 mm	9.55	98.6
1.18 mm	17.6	100
600μ	44.6	100
300μ	80.15	100

Table 3 Mix proportions for control mixes

WATER BINDER RATIO	MIX PROPORTIONS, kg/m^3			
	Cement	Aggregates		Water
		Fine	Coarse	
0.25	520	521	1340	130
0.35	457	524	1283	160
0.45	422	557	1183	190

Specimen preparation

150 mm cube are cast for all the mixes. Before exposing the specimens to the aggressive medium, they are subjected to the realistic curing practice, in which the specimens are cured in water tank maintained at temperature of 27 ± 2°C for 7 days followed by continuous air curing in the lab environment at around 27 ± 5°C and 50 ± 10% RH till the age of 90 days. This curing regime is chosen so that the specimens reach a constant strength level before immersion in the aggressive solution. After subjecting the specimens to the above mentioned curing regime for three months, the specimens are exposed to the respective aggressive solutions for a period of 48 weeks.

Ponding Regime

At the end of initial curing regime of 90 days, the cubical specimens are sealed on all sides except the testing surface in order to ensure unidirectional chloride penetration into the specimen. The seal is provided with the help of three coats of acrylic paint. On the testing surface, a 30 mm dyke is made with cut out pieces of glass to allow for ponding as shown in Figure 1.

Two different ponding solutions, one containing 5% sodium chloride and other having 5% calcium chloride respectively are used. In order to intensify the degradation process, the specimens are subjected to weekly cycles of wetting and drying. Each cycle starts with two days of drying, then the required solution is put in the dyke for next 5 days. This weekly sequence is continued for 48 weeks that is equivalent to nearly one year of exposure.

Table 4 Mix proportions and fresh properties of concrete mixes

MIX TYPE	W/B	NOTATION	MA, % REPLACEMENT OF CEMENT		OPTIMUM SP DOSAGE , WT. % OF BINDER	SLUMP mm	COMPRESSIVE STRENGTH , MPa 28 days
			SF	FA			
Control mixes	0.45	M1	-	-	0.2	205	38.2
	0.35	M2	-	-	1.25	211	69.3
	0.25	M3	-	-	4.0	184	88.6
Binary mixes	0.45	M1BS1	5	-	0.3	194	49.4
		M1BS2	10	-	0.7	192	58.7
		M1BF1	-	30	0.1	215	32.1
	0.35	M2BS1	5	-	1.5	204	83.5
		M2BS2	10	-	2.0	193	92.9
		M2BF1	-	30	0.5	216	59.1
	0.25	M3BS1	5	-	3.75	196	104.9
		M3BS2	10	-	4.25	191	109.4
		M3BF1	-	30	2.0	212	80.6
Ternary mixes	0.45	M1TC1	5	15	0.1	198	46.5
	0.35	M2TC1	5	15	1.0	207	70.5
	0.25	M3TC1	5	15	3.25	205	92.2

At the end of 48 weeks, a core of diameter 50 mm is taken out from the centre of the cube with the help of diamond core cutter as shown in Figure 2. The core is further cut into thin slices from the surface to the centre of core (Figure 3). The concrete slices obtained are dried and then ground into a thin powder and is passed through 150 µm sieve. This fine powder is collected in polythin bags for further chemical analysis.

Figure 1 Dykes prepared at the top of the specimens for ponding chloride solution

Figure 2 Core taken from the cube

Analysis

The powder so collected is used to determine free chloride and total chloride content at various depths of the specimen. The water-soluble chloride is termed here as the free chloride and acid-soluble chloride as the total chloride. Both free chlorides and total chlorides are found in order to obtain a general relationship between the free chloride and total chloride content in concrete for various types of blended concretes. It also gives an idea of chloride binding capacity of concrete.

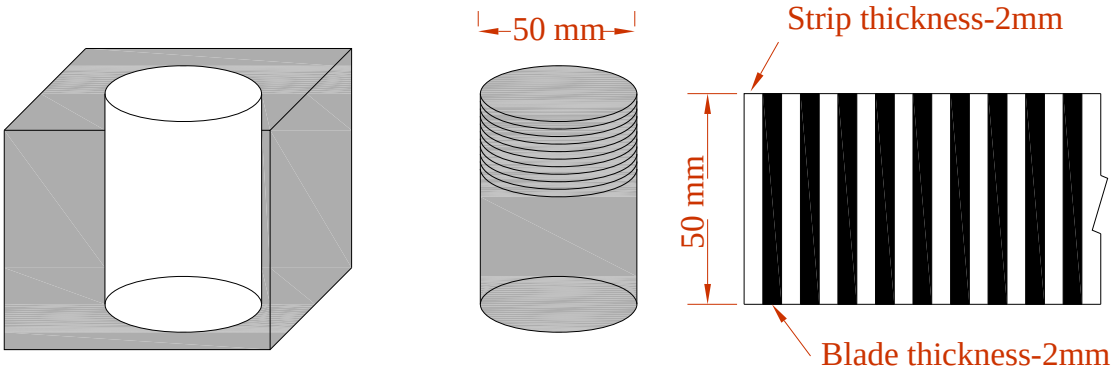

Figure 3 Process of taking strips for chloride analysis along depth

The concentration of chlorides at a given depth is determined through potentiometric titration with 0.1M silver nitrate ($AgNO_3$) solution using Metrohm 798 MPT Titrano automatic titrator. The working principle of titrator is demonstrated schematically in Figure 4. The chloride concentration is computed from the inflection point of a potential vs titration volume plot. For determining free chloride content, 3 grams of the powdered concrete sample is taken and is transferred to 100 ml beaker. 50 ml of distilled water is added in the beaker. The sample is thoroughly mixed by mixing for 15 minutes with the magnetic stirrer fitted with a hot plate. After 15 minutes of stirring, the solution is filtered using Whatmann No. 1 filter paper. The filtered water is placed on 798 MPT Titrano. The electrode is inserted into the beaker and titration is started. The chloride concentration is computed from the inflection point of a potential vs titrant volume plot. For finding total chlorides, nitric acid (6N) is used in place of distilled water and the same procedure is repeated. The chloride content of the concrete sample is calculated using the following expression:

$$\%\ Chloride = \frac{35.453 V_s\ N_s}{W} \qquad \ldots (1)$$

where V_s is the volume of $AgNO_3$ used in milliliters to neutralize chloride, N_s is the normality of $AgNO_3$ and W is the weight of powder sample. This test is conducted in triplets and the average of three values is taken as the representative chloride concentration at the required depth. After obtaining chloride content at various levels, chloride profile is made for each mix in terms of chloride content by percentage of concrete mass.

RESULTS AND DISCUSSIONS

The chloride penetration profiles for all the mixes subjected to sodium chloride salt are shown in Figure 5 to 7 for water-to-binder ratios of 0.45, 0.35 and 0.25 respectively. The similar profiles under calcium chloride solution are presented in Figures 8 to 10 respectively for water-to-binder ratios of 0.45, 0.35 and 0.25. The first graph in each figure represents the total chloride content while the second graph represents the corresponding free chloride profiles. The effects of different parameters on chloride penetration are discussed hereunder.

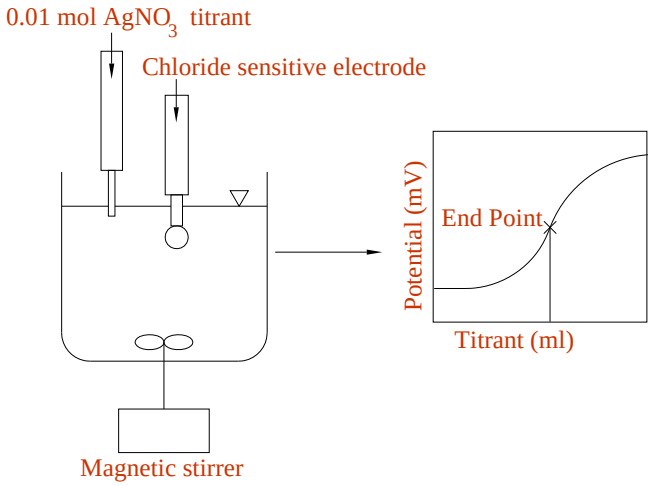

Figure 4 Working principle of Auto-titrator

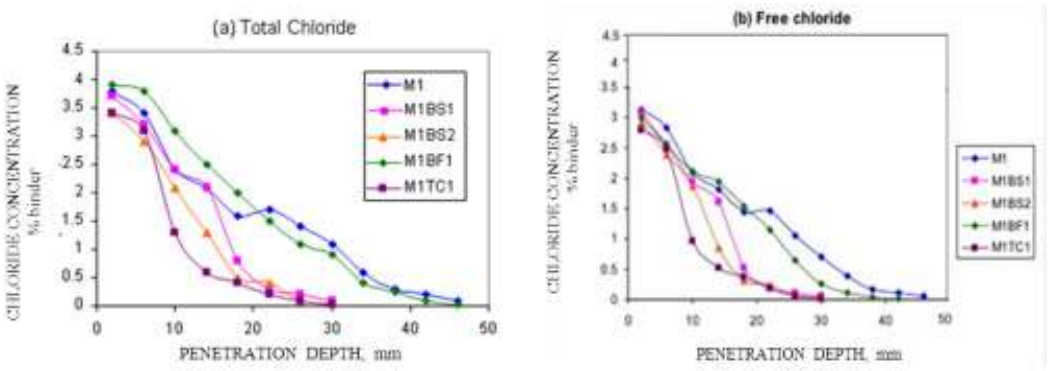

Figure 5 Chloride profiles for concrete at water-to-binder ratio of 0.45 under sodium chloride solution

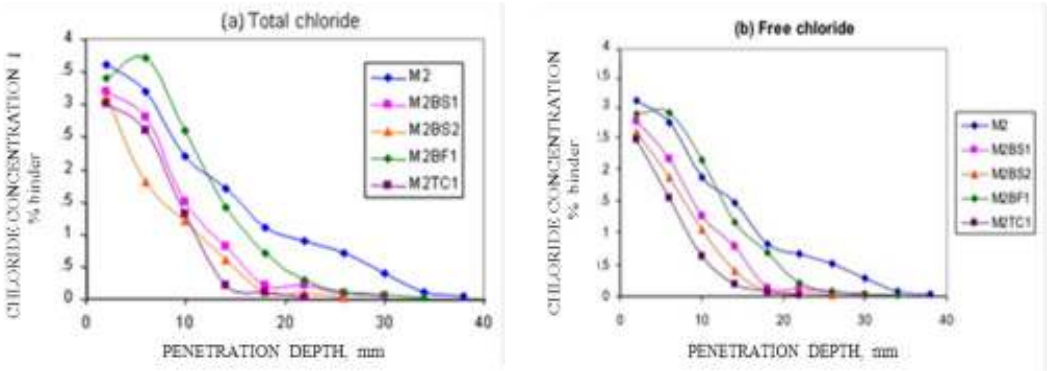

Figure 6 Chloride profiles for concrete at water-to-binder ratio of 0.35 under sodium chloride solution

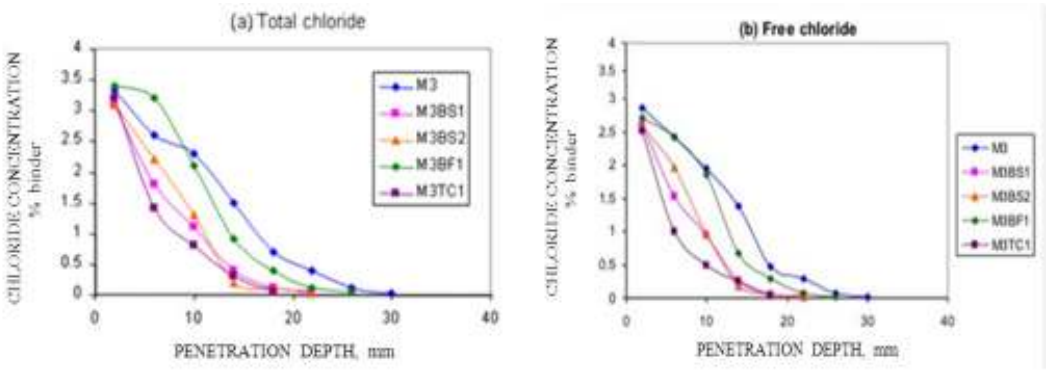

Figure 7 Chloride profiles for concrete at water-to-binder ratio of 0.25 under sodium chloride solution

Effect of water to binder ratio

From Figure 5 to 10, it can be observed that for all types of concrete, the depth of chloride ingress decreases with the decrease in water-to-binder ratio. It is due to the pore refinement achieved due to relatively denser matrix and discontinuity of pores that occurs with the decrease in water-to-binder ratio that ultimately reduces the diffusion coefficient of chloride ingress. The reduced diffusion coefficient leads to lower chloride penetration through the pore system and therefore, results in lesser amount of total chloride and free chloride content in the concrete system at all depths for lower water-to-binder ratio as compared to higher water-to-binder ratio. The similar trend is observed by some previous researchers [2, 32]. However, if the relative effect of water-to-binder ratio and the presence of mineral admixtures are compared, it can be said that the decrease in water-to-binder ratio has lesser impact on the resistance to chloride penetration as compared to the effect of use of secondary cementitious materials.

Effect of Presence of Mineral Admixtures

It is found that at all water-to-binder ratios, both the total and free chloride profiles of OPC mix is flat while the chloride penetration profile becomes steep for the blended mixes. This trend is due to relative change brought about both in the diffusivity characteristics and the chloride binding capacity by mineral admixtures in concrete. The only exception to this general behaviour is the binary mix containing only fly ash. In the case of mix with only fly ash, the slope of total chloride profiles is almost flat similar to the OPC mix. Although fly ash is considered to play a very effective role in improving the chloride binding of concrete because of its higher proportion of active alumina [33], however in the present study, the curing has been provided for only a limited period of time that would have affected the porosity of the system adversely thus allowing the chloride to penetrate to a greater depth.

On the other hand, ternary mixes containing a combination of silica fume and fly ash performs equivalent to the corresponding mixes containing only silica fume, in terms of chloride penetration profiles. The free chloride penetration profile of ternary mixes have maximum steepness and the depth of chlorides ingress is minimum in ternary mixes indicating the

combined effect of silica fume and fly ash is better than taking these admixtures alone as binary mixes. In the ternary system, silica fume reduces the diffusivity of the system even in short curing regime while fly ash helps in better chloride binding capacity due to its higher Al_2O_3 content.

Effect of Associated Cation

The trend of total chloride penetration profile for $CaCl_2$ is similar to that of NaCl with one general change, i.e., the depth to which chlorides have penetrated is more in the case of $CaCl_2$ solution and the initial chloride concentration is also somewhat higher in the $CaCl_2$ solution. In some of the mixes at the water-to-binder ratios of 0.45 and 0.35, the total chloride concentration even increases with depth. This increase of chloride concentration can be due to the increase in chloride binding capacity of the system when the associated cation is calcium instead of sodium.

Relationship between Free Chloride and Total Chloride

Based on the experimental results, linear relationships between free and total chlorides are prepared for various types of mixes in order to find the effect of various mineral admixtures on the relationship. Before finding the effect of mineral admixtures on chloride binding capacity of concrete, the effect of water-to-binder on chloride binding capacity is judged. For that, the linear plots are made between total chlorides and free chlorides for the control concrete. It is observed that the variation in chloride binding capacity is not significantly affected by water-to-binder ratio. The similar observation is made by Pradhan and Bhattacharjee [34] while studying the role of steel and cement type on chloride induced corrosion of steel. Therefore, in order to judge the effect of mineral admixtures on chloride binding capacity of concrete, all the three water-to-binder ratios are taken together. The results are presented in Figure 11 (a to d) for NaCl solution and in Figure 12 (a to d) for $CaCl_2$ solutions.

In the graphs, C_t represents the total chloride content in concrete and C_f represents corresponding free chloride content. In order to get the bound chlorides, the free chloride content can be subtracted from both sides of the equation representing the relation between free and total chlorides [22].

The relationship between free and total chloride is of form $C_t = k_1 * C_f + k_2$, where k_1 and k_2 are constants. The term k_1 represents the rate of increase of free chloride with total chloride. Observing the values of k_1 in the figures, it can be concluded that the chloride binding ability of fly ash is highest among all mixes. Also, the chloride binding ability of the ternary mixes is almost similar but on the lower side of fly ash mixes. This trend is same irrespective of the type of associated cation with chloride ions. However, the relationship is steep when the associated cation type is calcium. It indicates that the chloride binding ability is affected by the associated cation type and the chloride binding ability of calcium chloride is more as compared to sodium chloride. The value of k_2 represents the total chloride content when the free chlorides present is zero. It is basically the bound chlorides present in concrete due to sources other than the external chloride ingress. The value of k_2 for all mixes is more or less same due to the similar materials used in casting.

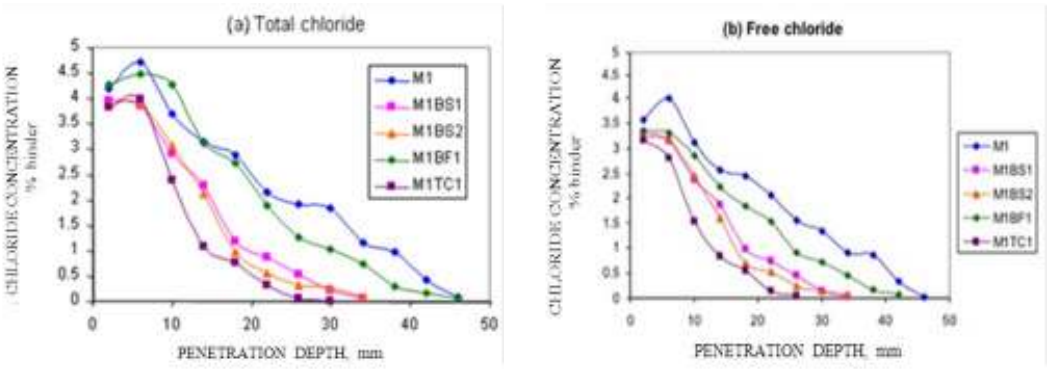

Figure 8 Chloride profiles for concrete at water-to-binder ratio of 0.45 under calcium chloride solution

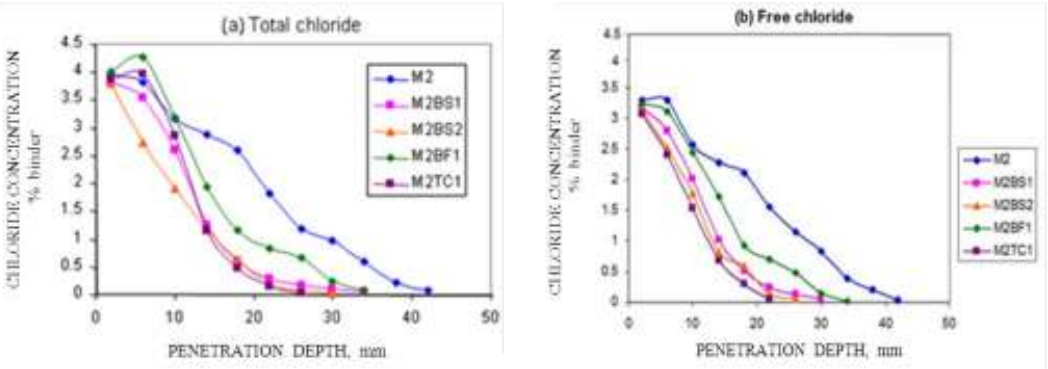

Figure 9 Chloride profiles for concrete at water-to-binder ratio of 0.35 under calcium chloride solution

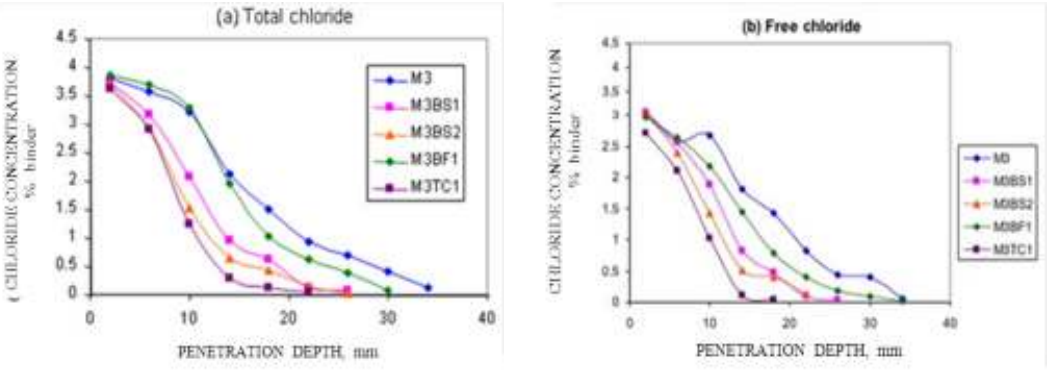

Figure 10 Chloride profiles for concrete at water-to-binder ratio of 0.25 under calcium chloride solution

(a) OPC concrete

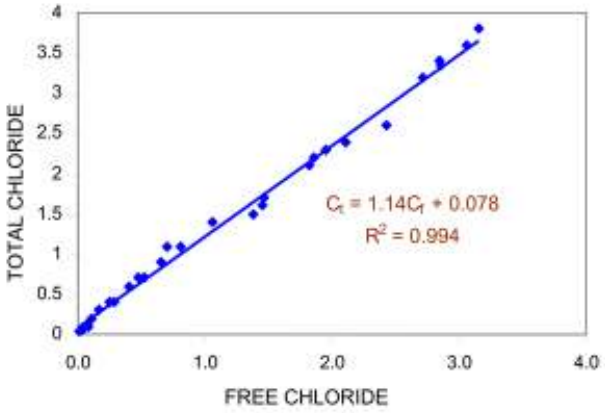

(b) Silica Fume concrete

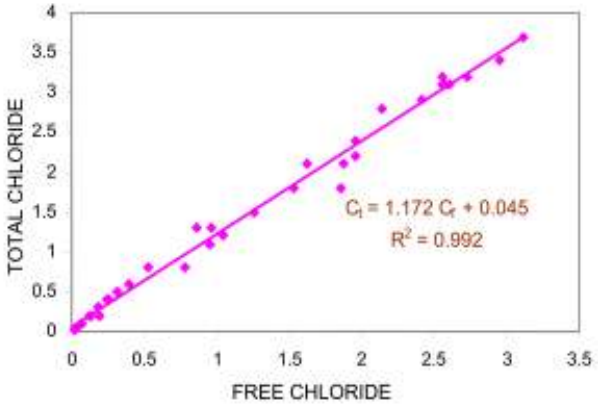

(c) Fly ash concrete

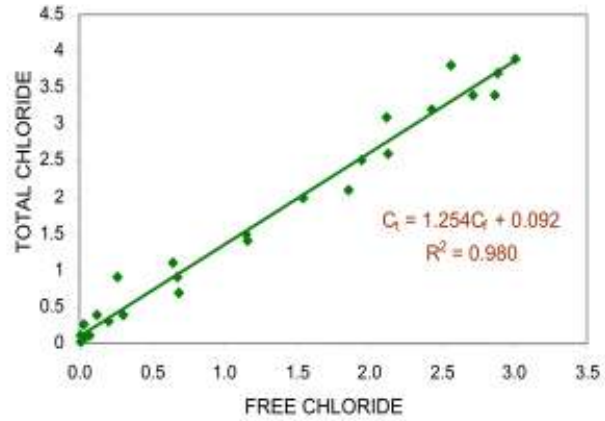

(d) Ternary concrete

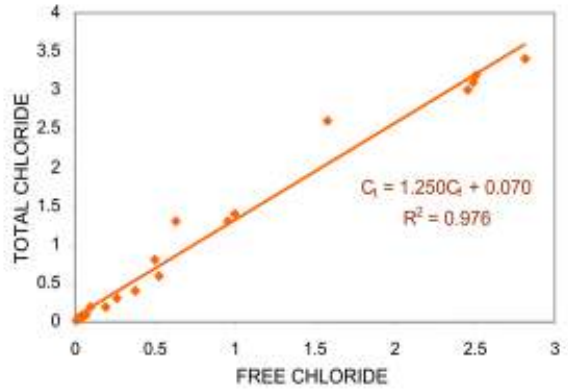

Figure 11 Relationship between free and total chloride for concrete exposed to sodium chloride solution

(a) OPC concrete

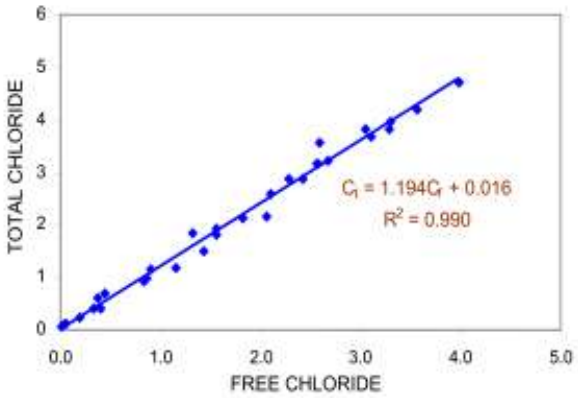

(b) Silica Fume concrete

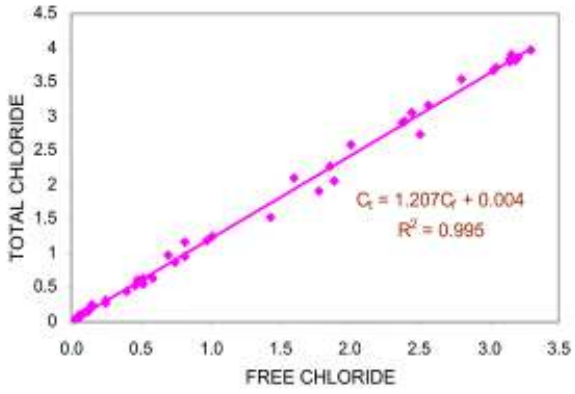

(c) Fly ash concrete

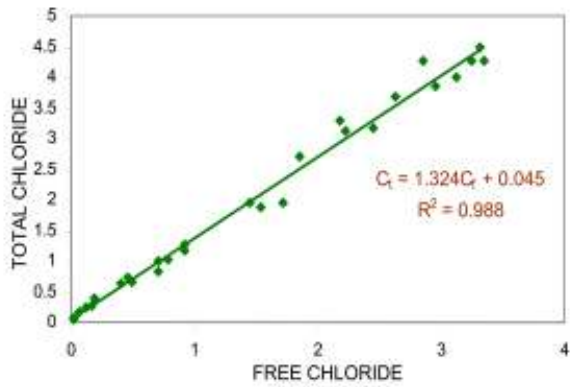

(d) Ternary concrete

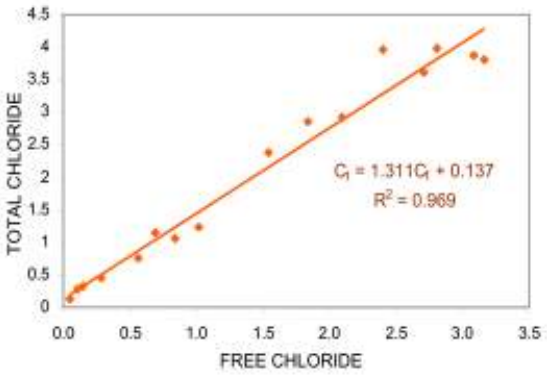

Figure 12 Relationship between free and total chlorides for concrete exposed to calcium chloride solution

CONCLUSIONS

It is found that the concrete containing only OPC as a cementing material is prone to the ongoing chloride penetration. The depth of chloride penetration is higher in OPC concrete as compared to mineral admixture concrete. In the binary systems, fly ash is more sensitive to initial curing regime that is indicated by the greater penetration depth in fly ash concrete due to larger and continuous pore system resulting from the shorter initial water curing regime. Silica fume, on the other hand, has increased penetration resistance. However, the ternary combination of OPC, silica fume and fly ash performs the best and has least chloride penetration among the mixes. While comparing the relationship between free and total chloride content for various cementitious systems, it is found that the chloride binding ability of fly ash concrete is maximum, whether it is used as binary blend or in combination with silica fume.

ACKNOWLEDGEMENTS

This research is supported by The Department of Science and Technology Grant No. 92780. The authors would like to acknowledge the authorities concerned for its assistance in carrying out the research.

REFERENCES

1. NEVILLE, A.M. Properties of Concrete, Fourth Edition, Pearson Education, Singapore, 2004.

2. ISMAIL, M.E., SOLEYMANI, H.R. Monitoring corrosion rate for ordinary Portland concrete (OPC) and high-performance concrete (HPC) specimens subjected to chloride attack, Canadian Journal of Civil Engineering, Vol. 29, 2002, pp 863-874.

3. MCPOLIN, D., BASHEER, P.A.M., LONG, A.E., GRATTAN, K.T.V., SUN T. Obtaining progressive chloride profiles in cementitious materials, Construction and Building Materials, Vol. 19, 2005, pp 666-673.

4. THOMAS, M. Chloride thresholds in marine concrete, Cement and Concrete Research, Vol. 26, No. 4, 1996, pp 513-520.

5. ALONSO, C, ANDRADE, C, CASTELLOTE, M, CASTRO, P. Chloride threshold values to depassivate reinforcing bars embedded in a standardized OPC mortar, Cement and Concrete Research, Vol. 30, No. 7, 2000, pp 1047-1055.

6. RAMEZANIANPOUR, A A. Effect of curing on the compressive strength, resistance to chloride-ion penetration and porosity of concretes incorporating slag, fly ash or silica fume, Cement and Concrete Composites, Vol. 17, 1995, pp 125-133.

7. OSBORNE, G J. Durability of Portland blast-furnace slag cement concrete, Cement and Concrete Composites, Vol. 21, 1999, pp 11-21.

8. GJORV, O E. Effect of condensed silica fume on steel corrosion in concrete, ACI Materials Journal, Vol. 92, 1995, pp 591-598.

9. HOSSAIN, K M A, LACHEMI, M. Corrosion resistance and chloride diffusivity of volcanic ash blended cement mortar, Cement and Concrete Research, Vol. 34, No. 4, 2004, pp 695-702.

10. AL-AMOUDI, O S B, MASLEHUDDIN, M, ABDUL, Y A B. Role of chloride ions on expansion and strength reduction in plain and blended cements in sulfate environments, Construction and Building Materials, Vol. 9, No. 1, 1995, pp 115-123.

11. ASRAR, N, ANEES, U M, SHAHREER, A, FADI, S M. Corrosion protection performance of microsilica added concretes in NaCl and seawater environments, Construction and Building materials, Vol. 13, 1999, pp 213-219.

12. POON, C S, WONG, Y L, LAM, L. The influence of different curing conditions on the pore structure and related properties of fly ash cement pastes and mortars, Construction and Building Materials, Vol. 11, 1997, pp 383-393.

13. CHINDAPRASIRT, P, JATURAPITAKKUL, C, SINSIRI, T. Effect of fly ash fineness on compressive strength and pore size of blended cement paste, Cement and Concrete Composites, Vol. 27, No. 4, 2005, pp 425-428.

14. SANCHEZ DE ROJAS, M I, FRIAS, M. Influence of micro-silica state on pozzolanic reaction rate, Cement and Concrete Research, Vol. 29, 1999, pp 945-949.

15. KUMAR, S. Influence of water quality on the strength of plain and blended cement concrete in marine environment, Cement and Concrete Research, Vol. 30, 2000, pp 345-350.

16. THOMAS, M D A, SHEHTA, M H, SHASHIPRAKASH, S G, HORKINS, D S, CAIL, K. Use of ternary cementitious system containing silica fume and fly ash in concrete, Cement and Concrete Research, Vol. 29, 1999, pp 1207-1214.

17. HONG, K, HOOTON, R D. Effect of cyclic chloride exposure on penetration of concrete cover, Cement and Concrete Research, Vol. 29, 1999, pp 1379-1386.

18. LU, X, LI, C, ZHANG, H. Relationship between the free and total chloride diffusivity in concrete, Cement and Concrete Research, Vol. 32, 2002, pp 323-326.

19. LUPING, T, NILLSSON, L O. Chloride binding capacity and binding isotherms of OPC pastes and mortars, Cement and Concrete Research, Vol. 23, No. 2, 1993, pp 247-253.

20. MANGAT, P S, MOLLOY, B T. Chloride binding in concrete containing PFA, GGBS or silica fume under sea water exposure, Magazine of Concrete Research, Vol. 47, No. 171, 1995, pp 129-141.

21. PEREZ, B M, ZIBARA, H, HOOTON, R D, THOMAS, M D A. A study of the effect of chloride binding on service life prediction, Cement and Concrete Research, Vol. 30, 2000, pp 1215-1223.

22. MOHAMMED, T U, HAMADA, H. Relationship between free chloride and total chloride contents in concrete, Cement and Concrete Research, Vol. 33, 2003, pp 1487-1490.

23. ALONSO, C, ANDRADE, C, CASTELLOTE, M, CASTRO, P. Chloride threshold values to depassiviate reinforcing bars embedded in a standardized OPC mortar, Cement and Concrete Research, Vol. 30, No. 7, 2000, pp 1047-1055.

24. Guide to Durable Concrete, ACI 201.2R-01, American Concrete Institute, Fermington Hills, MI, 2001.

25. CSIZMADIA, J, BALAZS, G, TAMAS, F D. Chloride ion binding capacity of aluminoferrites, Cement and Concrete Research, Vol. 31, 2001, pp 577-588.

26. GJORV, O E, VENNESLAND, O. Diffusion of chloride ions from sea water into concrete, Cement and Concrete Research, Vol. 9, 1979, pp 229-238.

27. TRITTHART, J. Chloride binding in cement: I. Investigation to determine the composition of porewater in hardened cement, Cement and Concrete Research, Vol. 19, 1989, pp 586-594.

28. AL-HUSSAINI, M J, SANGHA, C M, PLUNKETT, B A, WALDEN, P J. The effect of chloride ion source on the free chloride ion percentages in OPC mortars, Cement and Concrete Research, Vol. 20, 1990, pp 531-542.

29. ARYA, C, BUENFELD, N R, NEWMAN, J B. Factors influencing chloride binding in concrete, Cement and Concrete Research, Vol. 20, 1990, pp 291-300.

30. Teychenné DC, Franklin RE, Erntroy HC. DOE (BRE/DOE). Design of normal concrete mixes. Department of Environment. UK: Building Research Establishment; 1975 [revised Teychenné, Franklin, and Hobbs, 1988].

31. GOYAL, S, KUMAR, M, BHATTACHARGEE, B. Potential benefits of utilizing fly ash in silica fume concrete. Indian Concrete Journal, Vol. 82, No. 8, 2008, pp 38 – 46

32. CHINDAPRASIRT, P, CHOTITHANORM, C, CAO, H T, SIRIVIVATNANON, V. Influence of fly ash fineness on the chloride penetration of concrete, Construction and Building Materials, Vol. 21, 2007, pp 356-361.

33. DHIR, R K, JONES, M R. Development of chloride-resisting concrete using fly ash. Fuel, Vol. 78, 1999, pp 137-142.

34. PRADHAN, B, BHATTACHARJEE, B. Role of steel and cement type on chloride induced corrosion in concrete, ACI Materials Journal, Vol. 104, No. 6, 2007, pp 612-619.

Behaviour of Combined Alkali Activated Slag CNTs Exposed to Normal Temperatures

S I Zaki[1], A M Rashad[1], S Rawash[1], N Ismai[2]
1 – Housing & Building National Research Centre, Egypt
2 – NRC Cairo, Egypt

Both carbon nanotubes (CNTs) and alkali activated slag (AAS) are the subject of two of the most areas of research in nanotechnology and green buildings. In this article, the technical feasibility of modification the properties of AAS with multi wall carbon nanotubes MWCNTs is studied. Sodium hydroxide (NaOH) was used as alkali activator. Different percentages of MWCNTs were used (0, 0.2, 0.5 and 0.7% wt.). The behaviour of the new composite materials when exposed to normal temperature was investigated. The compressive strengths before and after exposure were determined. The various decomposition phases formed were identified using X-ray diffraction (XRD), and scanning electron microscopy (SEM). The results indicated that CNTs modified and enhanced the compressive strength of specimens exposed to normal temperature.

Dr Saaid I Zaki is an Associate Professor in Strength of Material and Quality Control Research Institute, Housing and Building National Research Center, HBRC, Cairo, Egypt.

Dr A M Rashad is currently an Associate Professor in the Q.C. and Material Institute in HBRC in Cairo, Egypt. He is specialist in the area of high performance concrete.

Dr S Rawash, is currently Associate Professor in the Raw Materials Institute in HBRC in Cairo, Egypt. She is a specialist in the area of durability test methods for concrete.

Dr N Ismail is currently Associate Professor in Center of Excellency for Advanced Science and Nanomaterials in NRC, Cairo, Egypt. She is a specialist in synthesis of Carbon Nano Tubes.

Keywords: Activated slag, Carbon nanotubes, Normal temperature, Residual compressive strength, Sodium hydroxide

INTRODUCTION

Carbon nanotubes (CNTs) have an ideal structure formed by carbon atoms with one dimension [1]. They are seamless tubes of graphite sheets with nano-sized diameter. They are hollow tubular channels, formed either by one wall (SWCNTs) or multi walls (MWCNTs), of rolled graphene [2]. Carbon nanotubes (CNTs) are considered one of the most beneficial nanomaterials for nano-reinforcement. The unique mechanical, electrical and chemical properties of CNTs render them desire properties for reinforcement of composite materials. The fracture strains of CTNs were between 10% and 15% with corresponding tensile stresses of 65 to 93 GPa [3]. The Young's modulus of an individual nanotube around 1 TPa and its density is about 1.33 g/cm^3 [4]. Other authors [5] reported that the Young's modulus should between 1 and 5 TPa with a density of about 2 g/cm^3. The physical properties appeared to be outstanding as well. For example, the thermal stability is estimated to be up to 2800 ^{o}C, the thermal conductivity in comparison with diamond is twice as gold and the electrical conductivity is about1000 times better in comparison with copper. In addition, CNTs have a very high theory strength, 100 times more than that of a steel, although their specific gravity is only one sixth that of steel [6] CNTs have an elastic strain capacity of 12%, 60 times higher than those of steel [7]. Molclecular mechanics simulations suggested that CNTs fracture strains were between 10% and 15%, with corresponding tensile stresses on the order of 65 to 93 GPa [8]. Most work to date has focused on polymer composites with other matrix materials such as metals also drawing interest. There has also significant interest in producing CNTs composites with ceramics matrices, polymer and epoxy, but few attempts have been made to add CNTs as reinforcement in cementitious materials. Many authors studied the mechanical and microstructure properties of the composition of Portland cement with CNTs [9-13] and concluded that the incorporation of CNTs in Portland cement improve both the mechanical and the microstructure properties of the matrix.

The world-wide need to reduce the energy used and the green house gases emitted during cement manufacture. The consuming considerable amounts of virgin materials (limestone and sand) and energy (energy demand about 1700 to 1800 MJ/tonne clinker [14], producing each tonne of Portland cement of which about 1.5 tonnes of raw material is needed. The manufacture of one tonne of cement approximately emits 0.8 tonnes of CO_2 are launched into the atmosphere. The cement industry accounts for 5-8% of worldwide CO_2 emission [15]. Not only CO_2 releases from cement manufacture but also SO_3 and NO_x which can cause the greenhouse effect and acid rain. These cause serious environmental impact. These rezones have led to the persuit of more eco-efficient and material such as alkali-activated slag cement (AAS). These new cements are obtained by mixing of blast furnace slags with alkaline solutions. AAS binders have taken a great interest from researchers due to its manufacturing process which has important benefits from the point of view of the lower energy requirements and lower emission of greenhouses gases. In addition ground granulated blast furnace slag (GGBS) is an industrial by-product. The basic principles of alkaline-activation of slags have been known since the 1940s [16] and investigated and invented by Glukhovsky in 1950s. The application as a binder in the construction industry started in Ukraine since the 1960s. Researcher activities in this area were carried out later in France, America, Poland, etc. and also carried out in China in 1980s.Since this date, up to now the AAS has been investigated and developed by blending slag with metakaolin [17], silica waste [18]and fly ash [19].

Unlike other important matrix materials, little work has been done on the use of cements to CNTs composites, with only preliminary work being mentioned. The majority of the researches on CNTs composites were focused on polymer matrices, with ceramics and

metals. Adversely, there is no any publication studies a new area of research involves CNTs/AAS system. So that, the main aim of this investigation is to study CNTs/AAS pastes system in terms of compressive strength, various decomposition phase and microstructure.

EXPERIMENTAL DETAILS

An experimental program was designed to investigate the compressive strength, various decomposition phases formed and microstructure of alkali activated slag, AAS, pastes activated by sodium hydroxide and modified with different concentrations of MWCNTs named 0.2, 0.5 and 0.7wt%. Plain AAS pastes were employed as a reference. For this purpose, four paste mixtures were prepared. Each mixture comprised two groups. The first group was tested after of 7 day. The second group was similar to the first group but tested at age of 28 days.

Materials

The “slag” will refer to ground granulated blast furnace slag (GGBS) and "CNTs" will refer to MWCNTs. Water quenched slag from Helwan steel factory (in Cairo-Egypt) was used in this work. GGBS that employed as source materials, were ground in lab to complain surface area of 3000 cm^2/g. The chemical composition of slag evaluated by X-ray fluorescence, XRF, analysis is given in Table 1. Sodium hydroxide (NaOH) pellet-form with purity of 98% was used as a source of alkali activator. The superplasticizer (SP) admixture was a polycarboxylic ether polymer (PCE sky) acid base with density between 1.066 and 1.106 g/cm^3 and solids content between 28.4 and 31.4 wt%. CNTs used can be visualized as a modified form of graphite. Graphite is formed from many layers of carbon atoms that are bonded in a hexagonal pattern in flat sheets, with weak bonds between the sheets and strong bonds within them. The properties of CNTs are shown in Table 2. Figures 1 shows the morphology and microstructure of used MWCNTs while Figure 2 shows the schematic of CNTs.

Table 1 Chemical composition of the slag

OXIDE COMPOSITION, %	GGBS
SiO_2	36.95
Al_2O_3	10.01
Fe_2O_3	1.48
CaO	33.07
MgO	6.43
Na_2O	1.39
K_2O	0.74
SO_3	3.52
TiO2	0.52
P2O5	0.1
MnO2	0.52
Cl^-	0.05
L.O.I.	0

Table 2 Properties of carbon nanotubes

PROPERTY	
Outer diameter, nm	8-10
Inner diameter, nm	3-4
Purity, wt.%	98%
Length	Mixture of short and long
Ash	0.2%
Amorphous	2-3%
Specific surface area	20-30 g/m^2

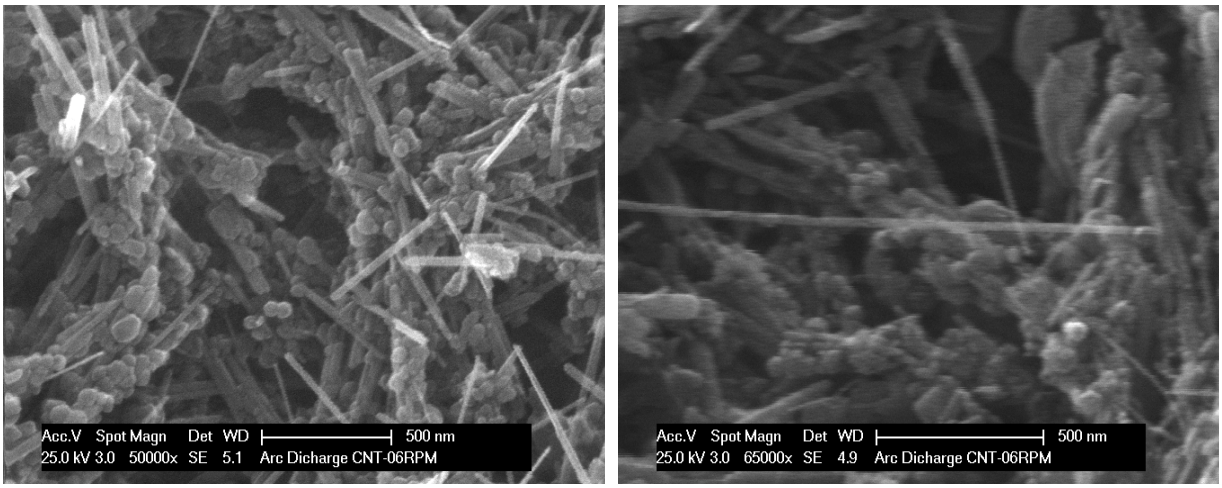

Figure 1 SEM Image of CNTs

Figure 2 Schematic of a CNT

Mix Proportions

Four AAS paste mixes were prepared. The first one was prepared without CNTs. The second, third and fourth were prepared with CNTs at levels of 0.2, 0.5 and 0.7%. Both water/binder and superplacticizer/binder ratios were fixed for all mixes at ratio 0.25 and 0.018 respectively. All mixing details are shown in Table 3.

Table 3 Details of mix proportions

MIX	CNT0	CNT0.2	CNT0.5	CNT0.7
GGBS, %	100	100	100	100
CNTs, GGBS Wet. %	0	0.2	0.5	0.7
w/b	0.25	0.25	0.25	0.25
% SP/binder	1.8	1.8	1.8	1.8

Casting, Curing and Testing

A rotary mixer with a flat beater was used for mixing. CNTs were firstly mixed with superplasticizer for 5 minutes. NaOH solution was prepared by dissolving the NaOH pellets in mixing water. The hot solution was then left overnight to cool to ambient temperature. Then CNTs and superplastisizer were mixed with the solution and sonicated with ultrasonic generator for 2 hours to make a uniformly dispersed suspension. Next, CNTs-solution and GGBS were mixed in the mixer for 5 min. Then, a defoamer in the amount of 0.15 vol% was used. The mixture was mixed for another 10 min. After pouring the mixes into oiled moulds (25 X 25 X 25 mm) an electric vibrator was used to ensure good compaction. The specimens were then surface smoothed and cured at 20 ± 2 ^{o}C and 90 ± 5% relative humidity. All samples were removed from the steel moulds after 24 hours and curing was continued in curing water.

After 7 and 28 days, the required samples were tested in triplicate by placing the specimen on a loading machine with a loading rate which complies with BS EN 1961: 2005 over the entire load application until failure. After 28 days hydration, the XRD and SEM were used to detect the decomposition phases formed and the microstructure of the hardened pastes.

RESULTS AND DISCUSSION

The compressive strength results of AAS and AAS reinforced with CNTs at concentrations of 0.2 wt.%, 0.5 wt.% and 0.7 wt.% at the age of 7 and 28 days are presented in Figure 3 . In all cases, the samples reinforced with CNTs exhibit higher strength than plain AAS pastes. The CNTs produced an improvement of 10-30% with respect to plain AAS at 7 days and an improvement of 3-16% referred to plain AAS at 28 days. The enhancements in strength could be attributed to the outstanding physical properties of CNTs, such as mechanical strength/modulus and high aspect ratio. Also, the homogeneously distributed CNTs throughout the AAS matrix help with load transfer from the matrix to CNTs. Comparing the response of the samples with the CNTs concentrations, it is observed that the samples reinforced with higher amount of CNTs exhibit higher strength (Figure 4). The results plotted in Figures 3-4 indicate the presence of a direct interaction that produces bonding between the CNTs and the activated slag pastes system. The results presented here therefore show a potential for developing successful AAS/CNTs composites. However, the size and aspect ratio of CNTs mean that they can be distributed in the matrix; as a result, cracks are interrupted much more quickly during propagation in CNTs reinforced matrix, producing much lower crack widths at the point of first contact between the moving crack front and the reinforcement. As a result of these properties, CNTs reinforcements produce significantly stronger and tougher slag composites .

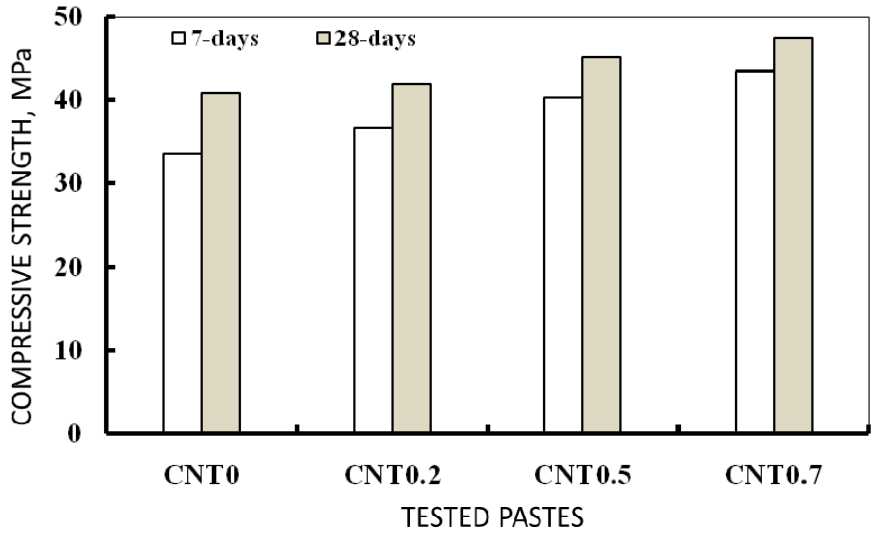

Figure 3 Compressive strength development of AAS/CNTs pastes

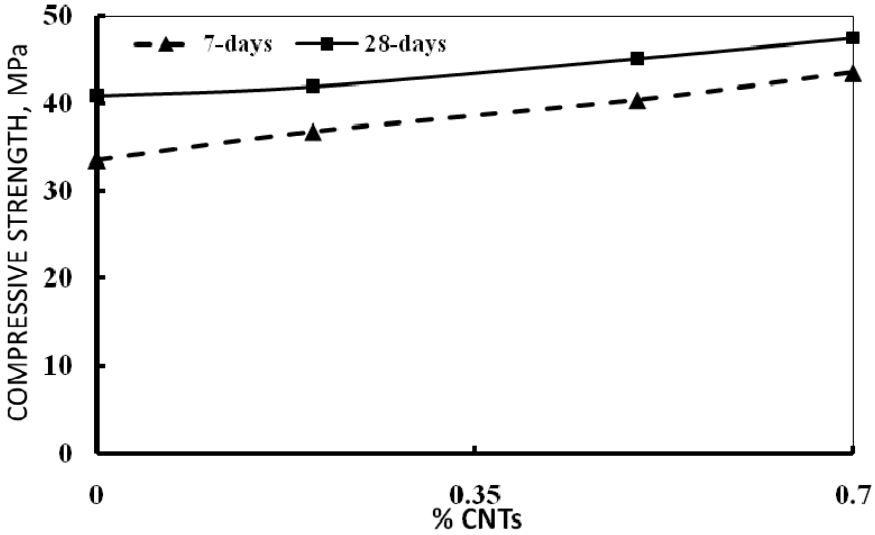

Figure 4 Compressive strength development of CNTs concentration

Figure 5 shows the XRD patterns for plain AAS mixture and the reinforced mixture with CNTs at different concentrations of CNTs after 28 days hydration. The amorphous hump centered around ~30 ^{o}C 2 θ indicates that the AAS are relatively amorphous with clearly a lack of long-rang order. Intense reflections for CSH type I (CSHI), which overlaps with those of calcite, could be seen in all samples. Small reflections for akermanite ($Ca_2Mg(Si_2O_7)$), merwinite ($Ca_3Mg(SiO_4)$), gehlenite ($Ca_2Al(AlSiO_7)$), Quartz (SiO_2), Calcite ($CaCO_3$), Hydrotalcit ($Mg_6Al_2(CO_3)(OH)_{16}.4H_2O$) and Calcium magnesium alumunate hydrate $(C,M)_4AH_{13}$. Small amounts of CNTs were detected in CNT0.2 sample and more was detected in samples containing a higher concentration of CNTs. This may be part of the reason why a higher compressive strength at higher concentration of CNTs in the AAS paste matrix compared with those made with lower concentration or without any CNTs.

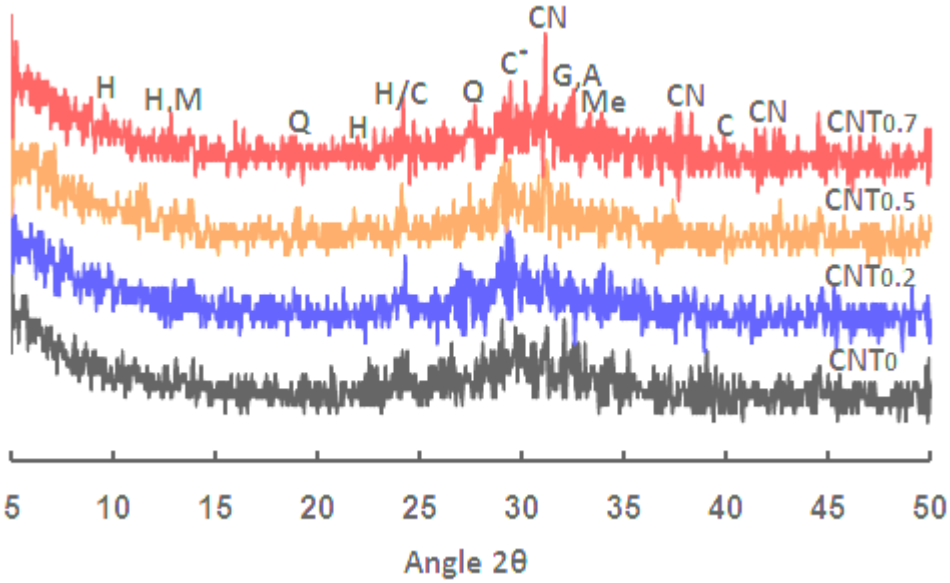

Figure 5 X-ray patterns of hardened pastes after 28-days of hydration

Figure 6 shows the SEM micrographs of fracture surface of the either hardened plain AAS paste and reinforced with CNTs. It can be seen from (Figure 6-a) that sample prepared with plain slag has less dense and open microstructure. In contrast, (Figure 6 b,c) show that CNTs act as bridges across pores and cracks. The addition of CNTs fines pore size distribution and decreases the porosity of slag composites. Therefore, the newly formulated composites become much more compacted. Apparently, as CNTs concentration increased as denser microstructure and the crack bridging increased. Also, the increasing in strength due to CNTs may be related to acceleration of the hydration of CSH. Although the CNTs are chemically inert and are not consumed in the hydration reaction itself, this acceleration of the hydration reaction was therefore likely due to nucleation effects, with the CNTs having enhanced the rate of the hydration reaction by acting as a matrix for the formation of the CSH produced in the hydration process. This behavior may be similar that found in Portland cement-CNTs matrix [20].

Also the identification of nanotubes as nucleating agents for variety of materials including nanodiamonds [21] grown on CNTs and titanium dioxide [22], silicon nitride[23], zirconium oxide[24] and calcium carbonate grown on multiwalled carbon nanotubes[25]. However, this nucleation on the bundles would produce a dense CSH structure against the surfaces of the nanotubes that would be capable of producing the reinforcing behavior of CNTs in the matrix. The high bonding strength between the reinforcement CNTs and slag matrix also can be attributed to the interfacial interactions between CNTs and slag hydrations (such as CSH) resulting increasing the amount of high stiffness CSH and decreasing the porosity, which leads to denser matrix that enhance compressive strength.

Although the behavior of AAS/CNTs system similar to the behavior of Portland cement/CNTs system, the optimum concentration of CNTs in the AAS/CNTs system may differ than those of Portland cement/CNTs system, where most of the researchers reported that 0.5 (wt%) CNTs is the optimum concentration in Portland cement/CNTs system.

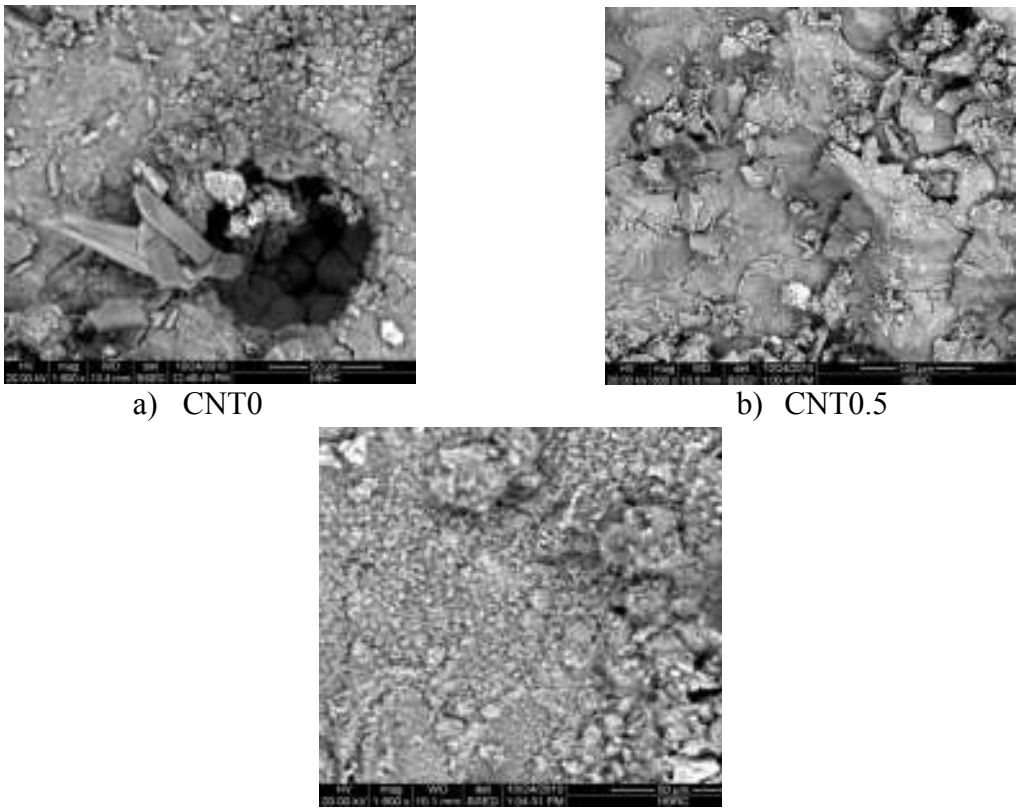

a) CNT0 b) CNT0.5

c) CNT0.7

Figure 6 SEM micrographs of fracture surface of hardened pastes cured for 28 days

CONCLUSIONS

These early research shows very promising results in alkali activation systems and proves that these new materials are opening the door to new possibilities and will allows existing structural designs to be produced with reduced material volumes and entirely new structural designs and concepts.

The results in this investigation are from a preliminary stage of research and the ultimate performances of the AAS/CNTs composites under development remain unknown. However, the excremental and analytical studies have led to the following conclusions:

1. It is possible to use CNTs in alkali activation system. The combination of SEM and compressive strength results suggest that a strong bond can be produced possible between the AAS/CNTs system. The bonding between AAS paste and CNTs are sufficient to allow comparison with recent work on Portland cement system.

2. AAS/CNTs composite materials show classical reinforcing behavior, with examples of crack bridging being easily identified similar that behave in Portland cement system.

3. The compressive strengths of the AAS/CNTs composites were improved as microstructure improved. The greatest enhancement on compressive was shown at 0.7% CNTs.

ACKNOWLEDGEMENTS:

This paper was carried out through the fund produced from STDF in Egypt for the project No. 1097.

REFERENCES

1. PHILIP B., "The perfect nano-tubes", Nature 1996, 382, 18. 207-8.

2. GROBERT N., "Carbon nanotubes becoming clean", Mater Today, 2007, 10, (1-2_, 28-35.

3. AKKAYA Y., SHAH S. P. AND GHANDEHARI M., "Influence of fiber dispersion on the performance of microfiber reinforced cement composities", ACI Special Publications 216: Innovations in fiber-reinforced concrete for value, SP-216-1, 216(2003), 1-18.

4. SALVETAT J. P., BONARD J. M., THOMSON N. H., KULIK A. J., FORRÓO L., BENOIT W. AND ZUPPIROLI L., "Mechanical properties of carbon nanotubes", Appl. Phys., A 69, 1999, 255-260.

5. TREACY M., KRISHNAN A. AND YIANILOS P., "Inferring Physical parameters from images of vibrating carbon nanotubes", Microscopy and Microanalysis, 2000, 6, No. 4, 317-323.

6. WONG E. W., SHEEHAN P. E., LIEBERT C. M., "Nanobeam mechanics: elasticity, strength, and toughness of nanorods and nanotubes", Science 1997; 277:1971-3.

7. SALVETAT J. P., KAIK A. J., "Electronic and mechanical properties of carbon nanotubes", Avv. Mater. 1997;22:161-7.

8. SALVETAT J. P., KAIK A. J., "Electronic and mechanical properties of carbon nanotubes", Avv. Mater. 1997;22:161-7.

9. CWIRZEN A., HABERMEHL-CWIRZEN K. AND PENTTALA V., "Surface decoration of carbon nanotubes and mechanical properties of cement/carbon nanotube composites", Advances in Cement Research, April 2008, 20, No. 2, 65-73.

10. LI GENG YING, WANG PEI MING AND ZHAO XIAOHUA, "Mechanical behavior and microstructure of cement composites incorporating surface-treated multi-walled carbon", Carbon, 43, 2005, 1239-1245.

11. LI GENG YING, WANG PEI MING AND ZHAO XIAOHUA, "Pressure-Sensitive properties and microstructure of carbon nanotube reinforced cement composites", Cement & Concrete Composites, 29, 2007, 377-382.

12. KONSTA-GDOUTOS MARIA S., METAXA ZOI S. AND SHAH SURENDRA P., "Multi-scal mechanical and fracture characteristics and early-age strain capacily of high performance carbon nanotube/cement nanocomposites", Cement & Concrete Composites, 32, 2010, 110-115.

13. WANSOM S., KIDNER N. J., WOO L. Y., AND MASON T. O., "AC-impedance response of multi-walled carbon nanotube/cement composites", Cement & Concrete Composites 28, 2006, 509-519.

14. TAYLOR H. F. W., “Cement chemistry”, Thomas Telford, London, 1997.

15. SCRIVENER K. L. AND KIRKPATRICK R. J., “Innovation in use and research on cementitious material”, 12th International Congress of Chemistry of Cement, Montreal, Canada, 2007.

16. PURDON A. O., “The action of alkalis on blast-furnace slag”, J. Soc. Chem. Ind. Trans. Com., 1940, 59, 191-201.

17. BUCHWALD A., HILBIG H. AND KAPS Ch., “Alkali-activated metakoalin-slag-performance and structure in dependence of their composition”, Advances in Geopolymer Science & Technology, J. Mater Sci., 2007, 42:3024-3032.

18. ESCALANTE-GARCIA JOSE IVAN, PALACIOS-VILLANUEVA VICTOR M., GOROKHOVSKY ALEXANDER V., MENDOZA-SUÁREZ GUILLERMO AND FUENTES ANTONIO F., “Characteristics of a NaOH-activated blast furnace slag blended with a fine particle silica waste”, J. Am. Ceram., 2002, 85[7]1788-92.

19. ZHANG DAJIE, LIU WENSHI , HOU HAOBO AND HE XINGHUA, “Strength, leachability and microstructure characterisation of Na2SiO3-activated ground granulated blast-furnace slag solidified MSWI fly ash”, Waste Manage. Res., 2007, 25, 402-407.

20. RAMACHANDRAN V. S. AND CHUN-MEI, "Dependence of fineness of calcium carbonate on the hydration behavior of tricalcium silicate", Dur. Build. Mater., 1986, 4, 45-66.

21. TERRANOVA M. L., ORLANDUCCI S., FIORI A., TAMBURRI E., SESSA V., ROSSI M. AND BARNARD A. S., "Controlled evolution of carbon nanotubes coated by nanodiamond:: the realization of a new class of hybrid nanomaterials", Chem. Mater., 2005, 17, 3214-20.

22. JITIANU A., CACCIAGUERRIA T., BERGER M.-H., BENOIT R., BEGUIN F. AND BONNAMY S., "New carbon multiwall nanotubes-TiO2 nanocomposites obtained by the Sol-Gel method", J, N, Crys Sol., 345 and 346, 2004, 596-600.

23. LUPO F., KAMALAKARAN R., SCHEU C., GROBERT N. AND RŸHLE M., "Microstructural investigations on zirconium oxide-carbon nanotube composites synthesized by hydrothermal crystallization", Carbon, 2004, 42, 1995-9.

24. BALÀZSI CS., WÉBER F., KÖVÉR ZS., SHEN Z., KŐNYA Z., KASZTOVSZKY ZS., VÉRTESY Z., BIŔO L. P., KIRICSI I. AND ARATO P., "Application of carbon nanotubes to silicon nitride matrix reinforcements", Cur. Appl. Phys., 2006, 6, 124-30.

25. TASIS D., PISPAS S., GALIOTIS C. AND BOURPOULOS N., "Growth of calcium carbonate on non-covalently modified carbon nanotubes", Mater. Lett., 2007, 61, 5044-6.

Effect of Novel Polymeric Type Shrinkage-reducing Admixture on Shrinkage of Hardened Cement Pastes

C Miao, Q Ran, J Liu, N Gao, Q Tian
Jiangsu Research Institute of Building Science, China

Early plastic shrinkage, dry shrinkage, and autogenous shrinkage of concrete result in cracks without any loading, and thus seriously endanger the integrity and durability of the buildings. Shrinkage-reducing admixtures have been developed and used to lessen the shrinkage of concrete. However, conventional shrinkage-reducing admixtures with lower molecular weight (L-SRA) exhibit a reduction in strength and elasticity modulus of concrete. In order to solve those drawbacks, a novel grafted copolymer shrinkage-reducing admixture (P-SRA) was designed and synthesized. P-SRA reduced the dry shrinkage of hardened cement paste at 3 days by about 90% and by about 35% at 28 days. P-SRA also reduced the autogenous shrinkage by 70% at 28 days. And this novel polymeric P-SRA also enhanced the 28 days-compressive strengths of concrete by about 10%.

Changwen Miao is President of Jiangsu Research Institute of Building Science and Professor at the Civil Engineering Department, Southeast University, China. He has more than 30 years of experience in R&D and technology management. He has written and presented over 80 papers on his research activities related to concrete durability and chemical admixtures. He is also the recipient of several awards for his contribution to the fundamental knowledge of concrete admixtures and their use in concrete.

Qianping Ran is a Chief scientist at State Key Laboratory of High Performance Civil Engineering Materials and a Research Engineer (Prof.) in Admixture Product Technologies at Jiangsu Research Institute of Building Science, Nanjing, China. He received his MS in Material Science from Sichuan University and PhD in Polymer Chemistry and Physics from Nanjing University. He has been working in the field of concrete admixtures, focusing on the development of new polymeric superplasticizers. He is also author or co-author of over 60 papers and patents on chemical admixtures.

Jiaping Liu is a Vice-President of Jiangsu Research Institute of Building Science and General Manager of Jiangsu Bote New Material Ltd. He received his MS in Civil Engineering from Southeast University and PhD in materials science from Nanjing University of Technology. He has written and presented over 30 papers on his research activities related to high performance concrete, high performance admixture, deformation and cracking of concrete.

Nanxiao Gao is a Research Engineer in Admixture Product Technologies at Jiangsu Research Institute of Building Science, Nanjing, China. She received her MS in Polymer materials from Nanjing Normal University, Nanjing, China. She is also author or co-author of several papers on her research activities related to development of shrinkage reducing admixtures.

Qian Tian is a Professor Senior Engineer in Jiangsu Research Institute of Building Science, Nanjing, China. She received her MS and PhD in Structure Engineering from Southeast University. She has led several research projects on concrete, and her specialist areas of research are shrinkage of concrete and self-compacting concrete.

Keywords: Autogenous shrinkage, Compressive strength, Dry shrinkage, Polymeric shrinkage reducer

INTRODUCTION

Early plastic shrinkage, dry shrinkage, and autogenous shrinkage of concrete result in cracks without any loading, and thus seriously endanger the integrity, service life, and aesthetics of the buildings [1]. Shrinkage-reducing admixtures (SRA) have been developed to lessen the shrinkage of concrete in Japan at the start of the 1980s and have taken a great interest from researches due to its effect on reducing shrinkage strain which has important benefits from the point of view of the lower risk of restrained shrinkage crack [2-5]. However, to our knowledge, all of commercially available SRA are low molecular materials. Those SRA reduce the compressive strength and elasticity modulus of concrete, and thus not be used in load-bearing structural elements made from concrete, reinforced concrete or pre-stressed concrete [6-10]. It is also reported low molecular SRA cause loss of entrained air which can negatively affect the resistance of concrete against freezing damage [11-13].

In order to solve those drawbacks of low molecular SRA, a novel polymeric-type shrinkage-reducing admixture (P-SRA) was designed and synthesized by free radical copolymerization of acrylic acid and macromonomer with nonionic poly(ethylene oxide)-based side chain. In the present work, we report the impacts of P-SRA on early autogenous shrinkage, long-term autogenous shrinkage and drying shrinkage of hardened cement paste, and also its general mechanism. This work may be of interest it both materials designer and those working in the area of concrete.

EXPERIMENTAL DETAILS

Materials

A novel polymeric-type shrinkage-reducing admixture (P-SRA, shown in Figure 1 a) was designed and synthesized by free radical copolymerization of acrylic acid and macromonomer with nonionic poly(ethylene oxide)-based side chain. Low molecular shrinkage-reducing admixture (L-SRA, Figure1 b) was also been chose for comparison.

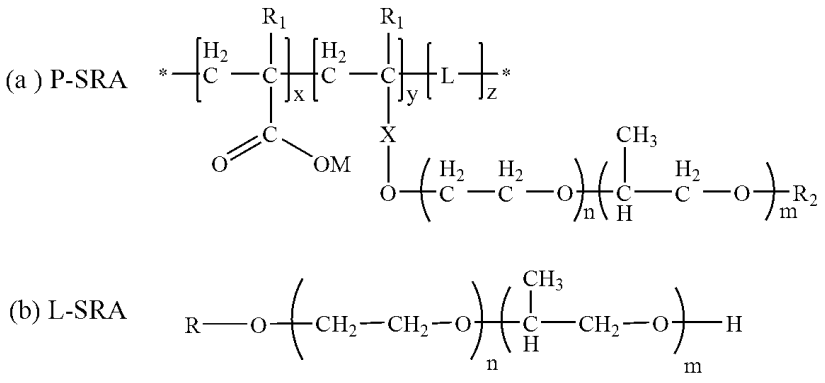

Figure 1 Schematic illustration of chemical structure of shrinkage-reducing admixture

Notes: M: Na^+,,NH_4^+;EO: Ethylene oxide; x,y, z: monomer moles of copolymer;,*n*: molar number of repeating unit of ethylene oxide, m: molar number of repeating unit of propylene oxide. R_1 and R_2 represents H or CH_3; R represents C_4-C_6 alkyl.

The P·II 52.5 Portland cement, complying with the Chinese National Standard GB 175–1999, was purchased from JiangNan Xiao Yetian Cement Ltd. in Nanjing. The cement composition was determined by x-ray fluorescence and Bogue analysis. Table 1 shows the characteristics and compositions of the sample.

Table 1 Mineral composition and chemical composition of Portland cement

CHEMICAL COMPOSITION							
SiO_2	Al_2O_3	CaO	MgO	Fe_2O_3	SO_3	Na_2Oeq	Loss
21.10	6.16	64.8	1.94	4.41	2.52	0.48	2.59
MINERAL COMPOSITION							
		C_3S	C_2S	C_3A	C_4AF		
		52.50	21.40	6.40	13.10		

Methods

Production of Cement Pastes

Cement paste with the water/cement ratio w/c=0.36 and different shrinkage-reducing admixtures was mixed in the laboratory according to the Chinese National Test Method JC/T 603-2004 “Standard test method for drying shrinkage of mortar”.

Measurement of Drying Shrinkage of Hardened Cement Paste

The drying shrinkage was conducted by evaluating the length change of hardened cement paste. The cement paste specimen is prism, with three dimensions, 2.5 cm×2.5 cm×28 cm. The prisms were removed from the mould 24 hours after production and then stored in a 20/65 climate. The length changes were measured at specified ages until the final test at 28 days.

Measurement of Autogenous Shrinkage of Hardened Cement Paste

Cement paste specimen was cast in the same size as in the drying shrinkage test. After 24h setting, we used adhesive aluminum foil to wrap up all the specimens and started to measure the length change 24h after mixing. The specimens were left in a room at 20℃ and 60% RH; The length changes were measured at specified ages until the final test at 28 days.

Measurement of Early Autogenous Shrinkage

A newly dilatometer designed specially for measuring the early autogenous shrinkage is developed. A particular characteristic of the dilatometer is the encapsulation of cement paste in corrugated moulds. This restricts moisture loss and ensures that the hardening cement paste suffers insignificant restraint. In addition, the encapsulation permits measurements to commence shortly after casting. The specific test methods refer to the literature[14].

Measurement of Hydration Rate of Cement

Hydration heat was measured by TAM Air isothermal calorimeter (Thermometric AB Sweden). Temperature of cement, SRA and mixing water were kept at 23℃ to ensure that the temperature of raw materials was similar to the measurement temperature. The hydration heat of two samples was measured at 23℃, respectively, and the generation data was recorded per 60s during 72h.

Surface Tension Test

The surface tension of different concentration of admixtures was measured at 25 □ by a surface tension meter using a platinum plate (Cement filtrate as reference).

Compressive Strength of Concrete

The influence of different type shrinkage reducers P-SRA and L-SRA on the compressive strength of concrete was examined at 3, 7 and 28 days as specified in China standard GB/T50081-2002. Each result is an average of six measurements. The prisms were produced with a water/cement ratio w/c=0.42. Table 2.describe the mix proportions for measuring compressive strength of concrete. The polycarboxylate superplasticizer (PC) was produced by Jiangsu Bote New Materials Co., Ltd in Nanjing.

Table 2 Materials and mix proportion for concrete/kg/m^3

MATERIALS	MIX PROPORTION, kg/m^3
Portland cement	420
Water	176
Sand	710
5-10 cm Crushed limestone	464
10-25 cm Crushed limestone	696
PC	0.42
P-SRA or L-SRA	8.4

RESULTS AND DICUSSION

The impacts of novel polymeric-type shrinkage-reducing admixture on early autogenous shrinkage, long-term autogenous shrinkage and drying shrinkage of hardened cement paste were investigated systematically in detail.

Effect of SRA Early Autogenous Shrinkage of Cement Paste

Figure2 shows measurements of autogenous deformation zeroed to the time of initial set as a function of specimen age for the cement pastes, while the plain mixture shows a plateau in shrinkage a few hours after set, followed by monotonic shrinkage, the P-SRA mixture undergos an expansion which persists until 5h, after which the system shrinks continuously. This expansion may be related with the amplification in portlandite oversaturation and its crystallization[15]. This expansion, along with the shrinkage reduction effects of the P-SRA, results in lower net shrinkage in the P- SRA mixture as compared with the plain mixture and L-SRA mixture. Those data clearly illustrates that the P-SRA is more effective in reducing early autogenous shrinkage of cement paste.

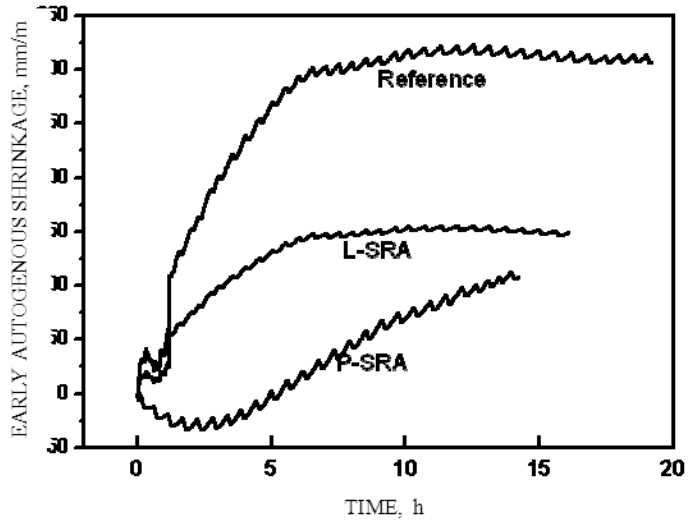

Figure 2 Early autogenous shrinkage of cement paste by L-SRA and P-SRA, w/c=0.36, dosage 0.5%. Time is measured from initial setting to 20h after the water addition.

Different type SRA has a different reduction effect of early autogenous shrinkage of cement paste, maybe due to their different early hydration behavior. Figure 3 shows heat flow profiles for cement paste mixtures. It is seen that the hydration of mixtures containing P-SRA and L-SRA are retarded compared to the control mixture as indicated by the rightward shift and the reduction in maximum heat floe values, and the P-SRA is more effectively than the L-SRA mixtures.

This retardation has been previously attributed to the delayed C_3A dissolution and the reduced alkali content in the pore solution in the presence of the SRA [16, 17]. This delayed behavior could be favorable to reduce the early shrinkage in cementitious materials. Ribeiro et al.also suggested that the reduction in shrinkage in some SRA mixtures may be due to a delayed hydration reaction that can be observed in these mixtures [18].

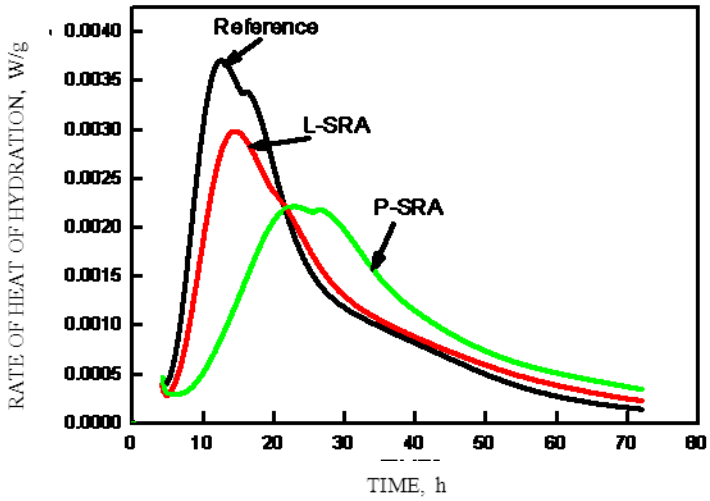

Figure 3 Heat of hydration rates for hardened cement paste treated by L-SRA and P-SRA with w/c=0.36 and 2.0 mass% of shrinkage reducer)

Effect of SRA the Long-term Shrinkage Reduction of Hardened Cement Paste

Figure 4 illustrates the effects of SRA type on long-term drying shrinkage. P-SRA and L-SRA showed a similar shrinkage-reducing behavior. The maximum shrinkage-reducing effect of about 80% when using P-SRA and L-SRA occurred at a young age directly after the start of the measurements. The effect decreased to about 35% by the 28th day after which there was no further significant decrease. However, at early period, the two SRA showed largely different shrinkage-reducing effect. P-SRA reduced the drying shrinkage of hardened cement paste at 3 days by about 90 %, whereas L-SRA reduced it just by about 70%.

The effects of SRA type on long-term autogenous shrinkage are presented in Figure 5. For two SRA, the auogeneous shrinkage reduction curves have the same trend with the shrinkage-reducing effect decreasing rapidly in the range from 0 to14 days. After that period, the reduction in autogenous shrinkage decreased slowly until to 60 days which there was no further significant change. It is also can be seen that two type SRA exhibited different autogenous shrinkage reduction effect. P-SRA reduced the autogenous shrinkage by 70% at 28 days and by 60% at 60 days compared with reference.

In contrast, L-SRA reduced the auogeneous shrinkage at 60 days just by about 40 %. Specifically, one result is of particular note in the Figure 5 that P-SRA shows a little expansion at early age. This expansion, along with the shrinkage reduction effects of the P-SRA, results in lower net autogenous shrinkage in the P- SRA mixture as compared with L-SRA mixture.

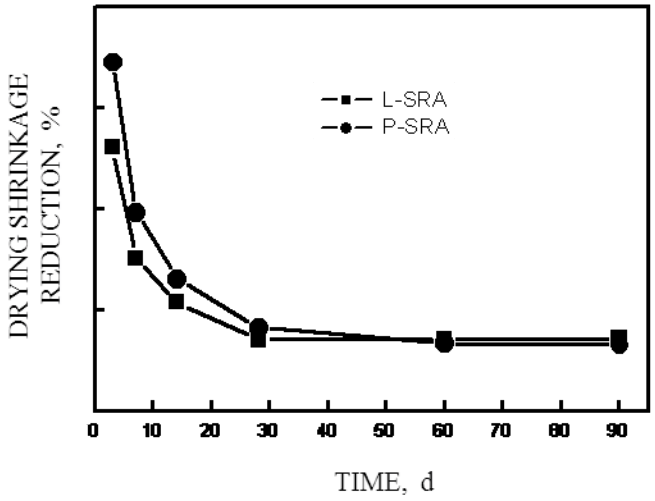

Figure 4 Drying shrinkage reduction of hardened cement paste treated by L-SRA and P-SRA with w/c=0.36 and 2.0 mass% of shrinkage reducer)

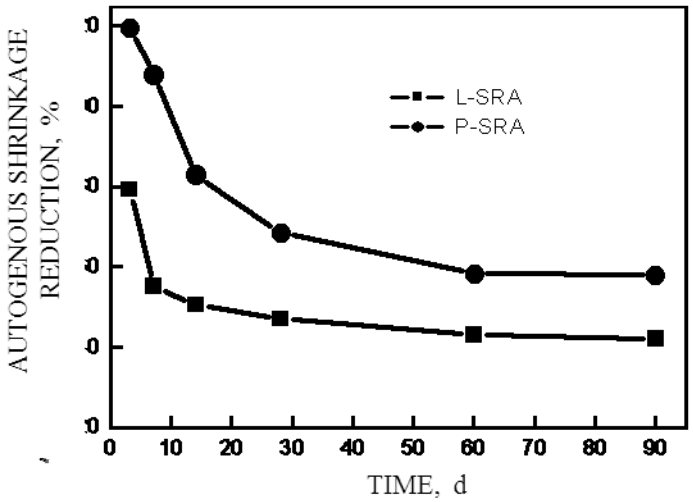

Figure 5 Autogenous shrinkage reduction of hardened cement paste treated by L-SRA and P-SRA with w/c=0.36 and 2.0 mass% of shrinkage reduce

From Figure 2, 4 and 5, therefore, we believe that the polymeric-type shrinkage-reducing admixture (P-SRA) has a efficient shrinkage-reducing effect than those conventional low molecular SRA. It is widely accepted that SRA reduce the shrinkage of cement paste by reducing the surface tension of pore solution, the empty pore number which leads to lower capillary stresses during drying[1-5]. Figure 6 illustrates that the surface tension of a cement filtrate containing various amounts of SRA. L-SRA reduces from 68 dynes/cm in pure cement filtrate to about 45 dynes/cm at a 10% SRA (% mass on water) concentration. It has been suggested that the concentration required to achieve this value in concrete may be

slightly lower due to the participation of water in the hydration reaction. However, polymeric-type shrinkage-reducing admixture (P-SRA) showed just a little reduction of surface tension which may be caused by the unconverted macromonomer. Therefore, these differences in reductions of shrinkage are maybe due to the interaction of P-SRA with the C-S-H and the different pore structure of hardened cement pastes [7, 19]. Tribological effects caused by P-SRA in the pore solution and increased relative internal moisure content are being discussed as possible [20].These assumption need to be further investigated.

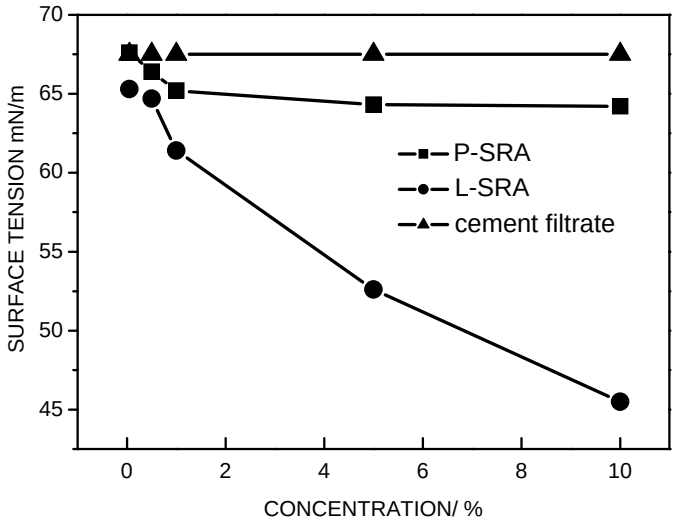

Figure 6 Surface tension as a function of SRA concentration in cement filtrate

Effect of SRA on the Compressive strength of Concretes

Concrete containing conventional lower molecular SRA generally exhibit a 5 to 10% reduction in stiffness and strength [2]. The influence of SRA type on the compressive strength of concrete was examined at 3, 7, 28 days, and the results were shown in Table 3. The presence of conventional L-SRA decreased the strength of concrete: -13% in average for 3days, -9.3% for7 days, and -7.6% for 28 days. In contrast, for novel polymeric P-SRA.the compressive strengths of concrete prisms were enhanced at 3 days by about 8.0% and 28 days by about 10%. It can be seen that different chemical structures of SRA (Figure 1) make different influence on the compressive strength of concrete, and the shrinkage mechanisms of them are also different. This may be attributed to another arrangement of the microstructure.

Table 3 The development of compressive strength treated by L-SRA and P-SRA

SRA	W/C	DOSAGE,/%	AIR CONTENT,/%	3d/MPa	7d/MPa	28d/MPa
Reference	0.42	0	4.5	40.4	49.3	63.5
L-SRA	0.42	2.0	3.2	35.2	45.8	58.7
P-SRA	0.42	2.0	4.8	43.6	58.8	70.2

CONCLUSIONS

Based on the information provided in this paper, the following conclusions can be drawn:

1. The ability of reduction in dry shrinkage of hardened cement paste for novel polymeric-type shrinkage-reducing admixture (P-SRA) is almost equal to that for conventional low molecular shrinkage reducer (L-SRA). P-SRA reduced the dry shrinkage of hardened cement paste at 3 days by about 90% and by about 35% at 28 days.

2. The ability of reduction in autogenous shrinkage of hardened cement paste for P-SRA is superior to that of L-SRA. P-SRA reduced the autogenous shrinkage by 60% at 60 days; whereas, L-SRA reduced the auogeneous shrinkage at 60 days just by about 40 %.

3. The novel polymeric P-SRA enhanced the 28 days-compressive strengths of concrete by about 10%; whereas, L-SRA decreased the 28 days- strengths 7.6 %.

4. (4) The Shrinkage mechanism of P-SRA and L-SRA is different. The L-SRA reduced the shrinkage by the surface tension reduction of the pore solution, while the P-SRA showed just a little reduction of surface tension. Other studies are under investigation, and especially the interaction of P-SRA with the C-S-H and the different pore structure of hardened cement pastes in the presence of SRA with different chemical structures.

ACKNOWLEDGEMENTS

We gratefully acknowledge the National Basic Research Program of China (973 Program) (No.2009CB623205) for financial support. We also are grateful to many individuals at Jiangsu Research Institute of Building Science who contributed to this study.

REFERENCES

1. J. SALIBA, E. ROZIÈRE, F. GRONDIN, AND A. LOUKILI. Influence of shrinkage reducing admixtures on plastic and long term shrinkage. Cement and Concrete Composite, No.8, 2010, pp1-9.

2. WEISS J, LURA P, RAJABIPOUR F AND SANT G. Performance of shrinkage-reducing admixtures at different humidities and at early ages. ACI Mater J, Vol. 105, No.5, 2008, pp478-486.

3. LURA P, PEASE B, MAZZOTTA GB, RAJABIPOUR F AND WEISS J. Influence of shrinkage reducing admixtures on development of plastic shrinkage cracks. ACI Mater J, Vol. 104, No.2, 2007, pp187-194.

4. COLLEPARDI M, BORSOI A, COLLEPARDI S, OLAGOT J AND TROLI R. Effects of shrinkage reducing admixture in shrinkage compensating concrete under non-wet curing conditions. Cement and Concrete Composites, Vol. 27, 2005, pp704-708.

5. PALACIOS M AND PUERTAS F. Effect of shrinkage-reducing admixtures on the properties of alkali-activated slag mortars and pastes. Cement and Concrete Research, Vol. 37, 2007, pp691-702.

6. B.L. COPE, G.E. RAMEY. Reducing drying shrinkage of bridge deck concrete. Concrete International, Vol. 23, No.8, 2001, pp76 – 82.

7. J. RONCERO, R. GETTU, M.A. MARTIN. Evaluation of the influence of ashrinkage reducing admixture on the microstructure and long-term behavior of concrete. Proceedings of the Seventh CANMET/ACI International Conference on Superplasticizers and Other Chemical Admixtures in Concrete (Supplementary Papers), Berlin, Germany, 2003, pp207 – 226.

8. G. SANT, F. RAJABIPOUR, P. LURA, J. WEISS. Examining time-zero and earlyage expansion in pastes containing shrinkage reducing admixtures. Advances in Concrete Through Science and Engineering, Proceedings of the RILEM International Symposium, Quebec, Canada.

9. Z. HE, Z.J. LI, M.Z. CHEN, W.Q. LIANG. Properties of shrinkage reducing admixture-modified pastes and mortars. Materials and Structures, Vol. 39, No.4, 2006, pp413 – 421.

10. D.P. BENTZ. Influence of shrinkage reducing admixtures on early-age properties of cement pastes. Journal of Advanced Concrete Technology, Vol. 4, No.3, 2006, pp423 – 429.

11. DAO VTN, DUX PF AND MORRIS PH. Tensile properties of early-age concrete. ACI Mater J, Vol. 106, No.6, 2009.

12. TURCRY P, LOUKILI A, HAIDAR K, PIJAUDIER-CABOT G AND BELARBI A. Cracking tendency of self-compacting concrete subjected to restrained shrinkage: Experimental study and modelling. J Mater Civ Eng, Vol. 18, No.1, 2006.

13. MOUNANGA P, BAROGHEL-BOUNY V, LOUKILI A AND KHELIDJ A. Autogenous deformations of cement pastes: Part I. Temperature effects at early age and micro-macro correlations. Cement and Concrete Research, Vol. 36, No.1, 2006, pp110-122.

14. O. MEJLHEDE JENSEN AND P. FREIESLEBEN HANSEN. A dilatometer for measuring autogenous deformation in hardening portland cement paste. Materials and Structures, Vol. 28, 1995, pp406-409.

15. GAURAV SANT, BARBARA LOTHENBACH, PATRICK JUILLAND, GWENN LE SAOUT, JASON WEISS, KAREN SCRIVENER. The origin of early age expansions induced in cementitious materials containing shrinkage reducing admixtures. Cement and Concrete Research, Vol. 41, 2011, pp218– 229.

16. F. RAJABIPOUR, G. SA NT, W.J. WEISS. Interactions between shrinkage reducing admixtures and cement paste's pore solution. Cement and Concrete Research., Vol. 38, No.5, 2008, pp606 –615.

17. I. JAWED, J. SKALNY. Alkalis in cement: a review. Cement and Concrete Research, Vol. 8, No.1,1978, pp37–51.

18. RIBEIRO, A.; CARRAJOLA, A.; GONCALVES, A.; AND BRANCO, F. Effect of the Synergy of Two Shrinkage-Reducing Admixtures. Volume Changes of Hardening Concrete, Proceedings of the RILEM International Conference, Lyngby, Denmark, Aug. 2006, pp223-230.

19. MARIA C. GARCI JUENGERA,1, HAMLIN M. JENNINGS. Examining the relationship between the microstructure of calcium silicate hydrate and drying shrinkage of cement pastes. Cement and Concrete Research. Vol. 32, 2002, pp 289–296.

20. PATRICK SCHÄFFEL, JÖRG RICKERT AND DÜSSELDORF. The influence of shrinkage-reducing admixtures on the shrinkage and other properties of hardened cement paste. Concrete Technology Reports, 2007-2009, pp19-36.

Effectiveness of Several Aminoalcohols as Corrosion Inhibitors for Steel in Simulated Concrete Pore Solutions

C-C Chen[1], J-S Cai[1], J-Z Liu[2], J-P Liu[1]
1 – Jiangsu Research Institute of Building Science, China
2 – State Key Labortary of High Performance Civil Engineering Materials, China

Reinforcement corrosion is the most important cause of premature failure on reinforced concrete structures. Steel reinforcement in concrete, being normally in the passive condition could generally be attacked by ingress of carbon dioxide and chloride. This paper was to present inhibiting effectiveness of several aminoalcohols for carbon steel at the present of chloride ions. Concentration of chloride ion was adjusted by adding NaCl into simulated concrete pore solution. The influences of chlorides attack on the corrosion of the steel bar and the inhibition action of the studied substances were characterized by electrochemical measurements. The interaction mechanism was studied by x-ray photoelectron spectroscopy (XPS). It was indicated that when concentration of chloride ion was low, most aminoalcohols tested in this study could inhibit the corrosion of steel. However, when chloride ion content was too high, only N,N-Dimethylethanolamine (DMEA) exhibited obvious inhibition effect. Impedance of the electrode in DMEA-containing solution was increasing with time. But the transformation trend was adverse for other aminoalcohols solution. From X-Ray photoelectron spectroscopy, it was found that when DMEA existed, the exposed Fe-metal of the electrode in DMEA-containing solution was less than that of control solution. This study could make instructive contributions to the development of corrosion inhibitor for concrete.

Cuicui Chen is an engineer in State Key Labortary of High Performance Civil Engineering Materials, Jiangsu Research Institute of Building Science, China. She has attended several research projects of China, and her main research area are corrosion of steel in concrete and the responding inhibition technique.

Jingshun Cai is an engineer in State Key Labortary of High Performance Civil Engineering Materials, Jiangsu Research Institute of Building Science, China. He is major in electrochemistry and his main research is the corrosion of steel in concrete.

Jianzhong Liu is professor of State Key Labortary of High Performance Civil Engineering Materials. He has led several research projects on concrete. His specialist research area is durability of concrete and fiber reinforced concrete.

Jiaping Liu is currently Jiaping Liu is a Vice-President of Jiangsu Research Institute of Building Science, Nanjing, China. He has led several big research projects on concrete, and his specialist areas of research are deformation and durability of high performance concrete.

Keywords: Concrete, Electrochemical measurement, Inhibiting effectiveness, XPS

INTRODUCTION

Reinforcement corrosion is the most important cause of premature failure on reinforced concrete structures. Steel reinforcement in concrete, being normally in the passive condition due to the formation of a thin oxide layer in the alkaline conditions in concrete can generally be attacked in two ways. One is the reduction of pH due to carbonation of concrete and the other is the intrusion of chlorides [1]. And the depassivation of steel bar caused by chloride is more severe for concrete structures, especially in marine environment. Different reinforcement corrosion protection systems are available for the environment containing chloride. It could be classified into two categories, prevention of chloride and improvement of the resistance of steel to chloride. One of these methods is the use of corrosion inhibitor, which is targeting to steel and could provide simple and cost effective prevention.

The effect of different substances on corrosion inhibition had been reported by many researchers, such as sodium nitrite, potassium chromate, sodium benzoate sodium, mono-fluoro-phosphate and so on [2-4]. But most of them hadn't been widely used in industrial construction. Calcium nitrite was the first corrosion inhibitor admixture commercialized on a large scale for reinforced concrete, but the pollution to environment and threat to pitting corrosion restricted its wider application. The environment-friendly amino alcohol based corrosion inhibitor was attracting more and more interest. Marco Ormellese studied the effect of about 80 kinds organic substances as the inhibitor for steel in concrete [5]. Besides, many researchers studied the effectiveness of amino alcohol based inhibitors [6-10]. But most of them were focused on the existing commercial products, and few reported the component of the inhibitors. In this paper, effectiveness of several amino alcohols was studied in simulated concrete solutions with different chloride ion concentration. And the transformation of the inhibition effect with time was investigated by electrochemical impedance spectroscopy (EIS). This study might provide some suggestions for the preparation of organic inhibitors for concrete.

EXPERIMENTAL PROGRAM

Materials

Organic corrosion inhibitors were said to work by adsorbing on the metal surface and forming an organic layer. In this paper, Monoethanolamine, diethanolamine, triethanolamine and N,N-Dimethylethanolamine were studied as inhibitors, as shown in Table 1. Calcium hydroxide, sodium chloride were used to make solutions simulating conditions that steel bars might serve in. All the reagents were analytical grade. Water used in this study was deionized.

Table 1 Aminoalcohols studied in this paper

AMINES	
Monoethanolamine (EA)	$(OHCH_2CH_2)$-NH_2
Diethanolamine (DEA)	$(OHCH_2CH_2)_2$-NH
Triethanolamine (TEA)	$(OHCH_2CH_2)_3$-N
N,N-Dimethylethanolamine (DMEA)	$(CH_3)_2(CH_2CH_2OH)$-N

Steel Electrode

Steel No. Q235 according to GB/T 221-79, was manufactured to cylinders with working surface of 1cm^2,its chemical composition was shown is Table 2. A copper wire was welded on one flat surface of the steel cylinder. Put the welded cylinder to a 1.5cm-long PVC tube and submerged it with epoxy resin to make a electrode. After the hardening of epoxy resin, polished the working surface gradually with grit SiC paper (grade 100, 400, 1000 and 2000), and then degreased in acetone and ultrasonically cleaned in alcohol.

Table 2 Chemical composition of the steel (wt, %)

C	S	P	Mn	Si	Cu	Fe
0.176	0.023	0.019	0.57	0.233	0.033	balance

Testing Program

Saturated $Ca(OH)_2$ solution was used to simulate conditions in ordinary portland cement concrete. Two chloride-contaminated level was got by adding 0.1mol/L and 0.3 mol/L NaCl. Aminoalcohols of different contents (0.05mol/L, 0.1mol/L and 0.2mol/L) were added to the simulated concrete pore solution (SPS) as corrosion inhibitors.

273A and Mould 5210 by Princeton Applied Research were used in this study to carry out Linear polarization (LP) and electrochemical impedance spectroscopy (EIS). A conventional three-electrode cell was used, equipped with a saturated calomel electrode (SCE) as the reference electrode and a platinum electrode as the counter electrode. LP was Scanned at a speed of 0.166mV/s from -10mV to 10mV vs open circuit potential to get polarization resistance (R_p). The EIS diagram was obtained in potentiostatic mode at the corrosion potential with an ac perturbation amplitude of 10 mV in the frequency range from 100 kHz to 10 mHz. Electrochemical measurements were conducted after the working electrodes were immersed in test solutions for 0.5h, 2h and 6h.

A THERMO FISHERSCIENTIFIC XPS spectrometer with an achromatic Al K-Alpha X-ray source and an analytical chamber with a base pressure of 10^{-6} Pa were used to collect XPS spectra. A spot size of 400 μm was scanned for 10 times to get a more accurate result.

RESULTS AND DISCUSSION

Influence of Chloride on Inhibition Effectiveness

Tests in this section was in SPS with 0.1mol/L and 0.3mol/L NaCl at pH 12.5. Influence of inhibitor concentration was compared by R_p and E_{corr} obtained after immersing in solution of 0.1mol/L Cl^- for 0.5h (Figure 1 and Table 3). It was found that DEA showed no obvious inhibition effect at the concentration level tested in this study. Basically, R_p was increasing with the concentration of inhibitors for EA, TEA and DMEA. Electrode in SPS with DMEA had the highest R_p, meaning the highest inhibition efficiency.

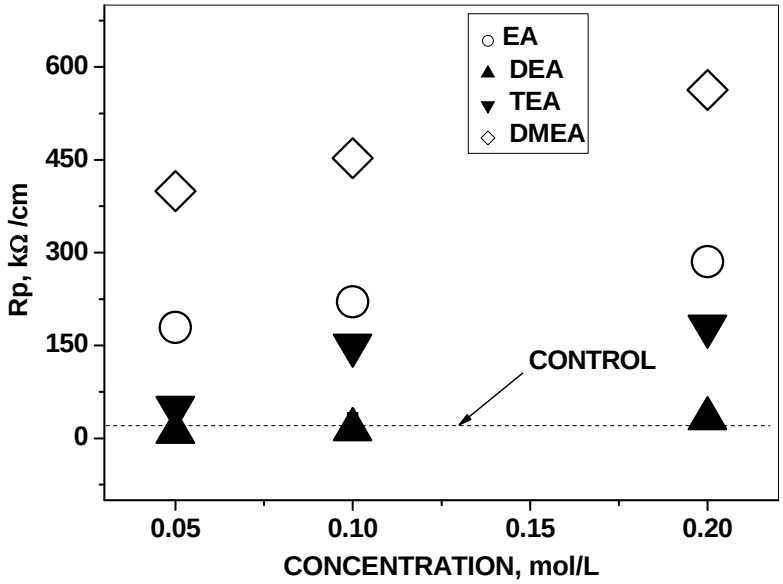

Figure 1 Inhibition effect of the studied amino alcohols (0.1mol/L Cl-)

Table 3 Inhibition effect of amino alcohols in low chloride ion concentration (0.1mol/L Cl^-)

	0.05mol/L		0.1mol/L		0.2mol/L	
	R_p	η/%	R_p	η/%	R_p	η/%
Control	33.0	-	-	-	-	-
EA	179.1	81.6	220.6	85.0	285.7	88.5
DEA	10.3		14.2		31.9	
TEA	49.8	33.8	15.0	78.0	18.1	81.8
DMEA	399.6	91.7	452.6	92.7	562.8	94.1

Figure 2 showed the tested R_p of SPS with 0.3mol/L NaCl. Compared with control, solutions with EA, DEA and TEA didn't bring obvious change on the polarization resistance of steel electrodes. Only DMEA can promote R_p remarkably. From this, it can be said that at a relatively high chloride level, EA, DEA and TEA could not act as good inhibitors and only DMEA had the probability of inhibiting corrosion under this condition.

Influence of Immersion Time on Inhibition Effectiveness

When chloride was 0.1mol/L, EIS of the electrodes in solution with 0.2mol/L amino alcohols was tested after immersed for 0.5h, 2h and 6h. Diameter of the large arc in the fig was an indication of charge transfer resistance, R_t. In other words, the larger arc diameter, the lower corrosion rate it is [11]. Based on this, charge transfer resistance of EA, DEA and TEA decreased severely with immersion time, probably due to their high volatility and low adsorption capability. However, electrode in solution with DMEA exhibited a gradual increase of R_t, meaning a continued reduction of corrosion rate. On the surface of electrode, there must be a competitive adsorption of chloride ion and amino alcohol molecular in the solution.

More and firmer adsorption of chloride ion than EA, DEA and TEA molecular should be a reasonable explanation for the increasing corrosion rate. Similarly, the raise of R_t with the elongating immersion time in Figure 3 (d) means an increase of the adsorbed DEMA on the electrode surface.

Interaction of DMEA with Steel Surface

Interaction of DMEA with steel surface was characterized by XPS. Usually, Fe_{2p} spectra in XPS could be fitted into four groups, Fe-1, Fe-2, Fe-3 and Fe-4, respectively corresponding to Fe metal, Fe_3C, Fe_3O_4/FeO (Fe^{2+}) and Fe_2O_3/ FeOOH(Fe^{3+}). Furthermore, another component (Fe-5) associated with Fe_2O_3-Satellite was usually used in curve fitting analysis to got a better fitting curve [12].

In Figure 4, CH represented steel sample immersed in saturated calcium hydroxide solution for seven days; CH-Cl was the CH sample immersed for additional one day in 0.3mol/L NaCl saturated calcium hydroxide solution; CH-Cl-DMEA showed the steel immersed for additional 1d in 0.3mol/L NaCl saturated Ca(OH)2 solution with 0.3mol/L DMEA.

There was obvious variance in Fe metal peak. Firstly, intensity of Fe-metal in CH solution was lowest and that of CH-Cl was highest. Intensity of the Fe metal peak in CH-Cl-DMEA solution was a bit higher than CH, but much lower than CH-Cl. It was shown that although after immersed in CH for seven days, the passive film on steel surface was not perfectly faultless. That is where there are still unpassivated areas existing. The increase of Fe metal in CH-Cl was probably due to the dissolution of the existing passive film after the introduction of chloride ion. With the presence of DMEA, the dissolution of passive film can be inhibited effectively. That's why the intensity of Fe metal in CH-Cl-DMEA was much lower than that of CH-Cl. This should be an mediate proof of the adsorption of DMEA on steel surface.

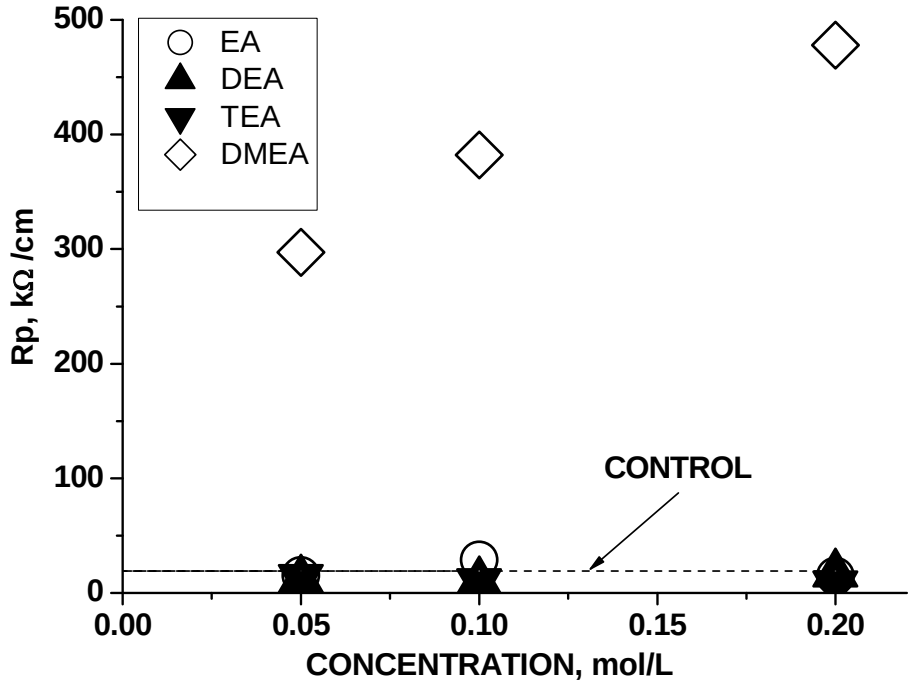

Figure 2 Inhibition effect of the studied amino alcohols (0.3mol/L Cl^-)

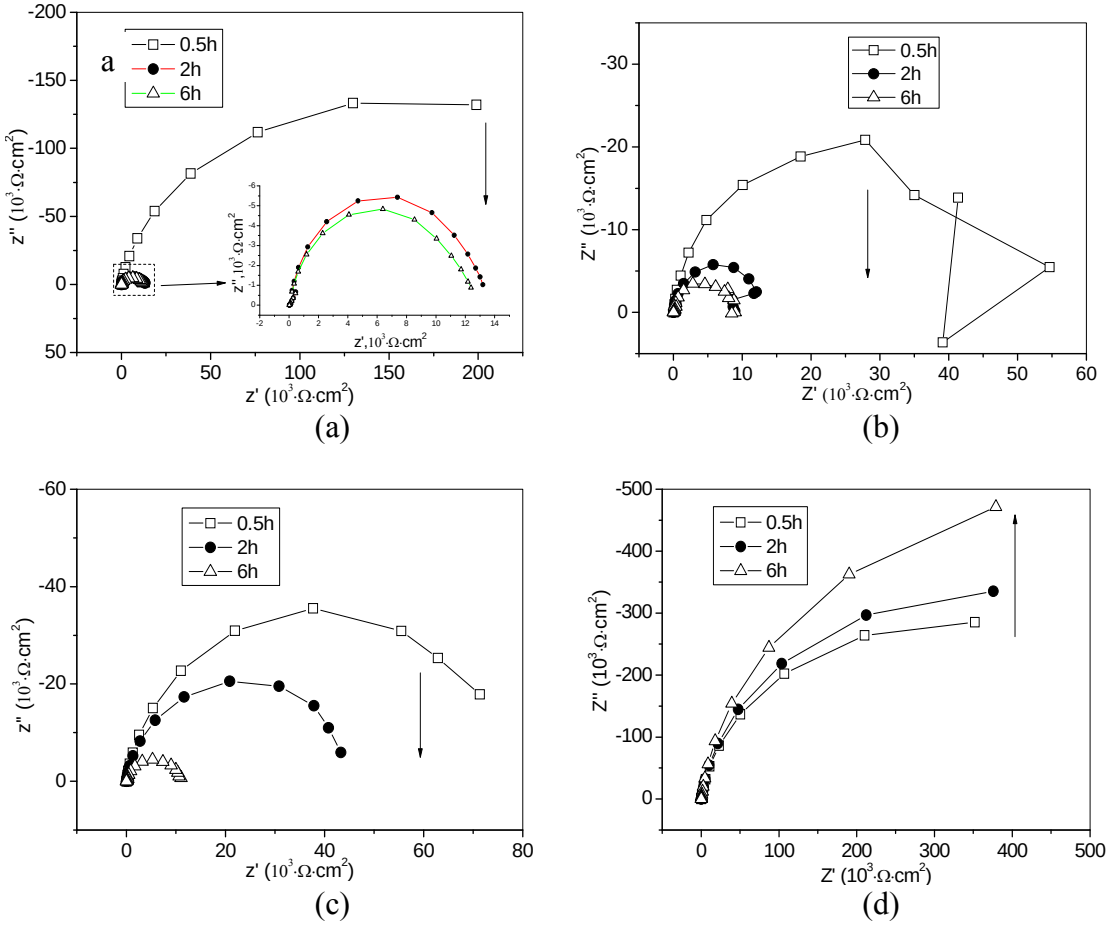

Figure 3 Transformation of inhibition effect with immersion time in SPS with 0.1mol/L Cl^-: (a) EA; (b) DEA; (c) TEA; (d)DMEA

Table 4 Peak parameters of Fe_{2p} spectrum

PEAK ID	ASSIGNMENT	PEAK POSITION $2p_{3/2}$/1s (±0.5 eV)
Fe-1	Fe	707.0
Fe-2	Fe_3C	708.2
Fe-3	Fe_3O_4/FeO	709.6
Fe-4	Fe_2O_3/FeOOH	711.0
Fe-5	Fe_2O_3 Satellite	712.7

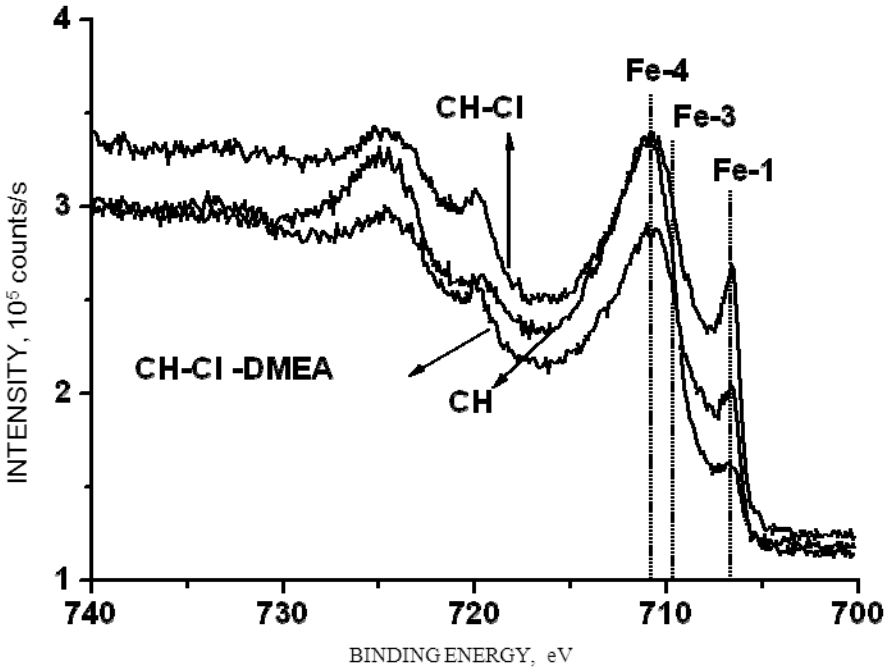

Figure 4 Fe_{2p} spectra of steel surface in different environment

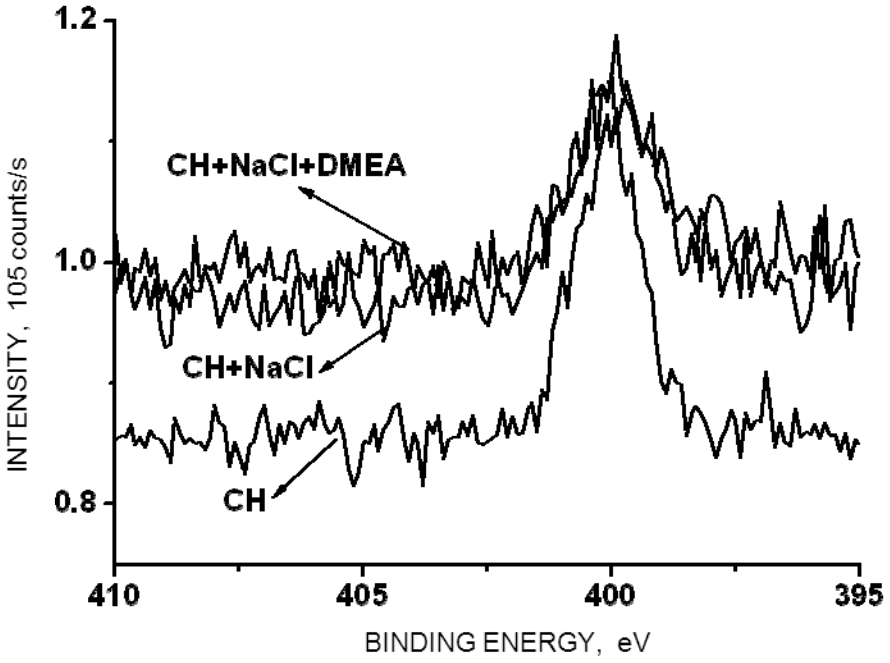

Figure 5 N1s spectra of steel surface in different environment

Inhibition mechanism of amino alcohols (like DMEA) was thought to be the adsorption of inhibitor molecular on steel surface and thus, hinder the contract of aggressive medium with steel surface. Therefore, N1s signal in XPS measurement should be a good indicator for existence of DMEA on steel surface. In this study, N1s spectra of CH, CH-Cl, CH-Cl-DMEA seemed similar with each other. N, probably the signal of element in steel alloy, appeared in

spectra of all the three samples. That is, no obvious signal was found to prove the existence of DMEA on steel surface, which was very different from other studies [11]. We all know that DMEA was volatile. It probably breaks away during vacuuming if the interaction of DMEA with steel was not strong enough. So we need other test methods or special treatment for the sample to detect DMEA adsorbed on steel surface.

CONCLUSIONS

Inhibition efficiency of several amino alcohols was tested by electrochemical method and the interaction of DMEA with steel was analyzed by XPS. It was found that when chloride concentration was relatively low, most tested amino alcohols could exhibit inhibition effect, except DEA. However, when chloride concentration was increased to 0.3mol/L, only DMEA could improve R_p of the steel electrode. With the extension of immersing time, R_p of samples in EA, DEA and TEA decreased gradually, meaning the increase of corrosion rate. However, R_p of DMEA sample showed a slight increase with immersion time. Fe-metal content of the steel in CH-Cl-DMEA solution was lower than that of CH-Cl solution, which means the depassivation of Fe caused by chloride was restrained. DMEA was a promising material for corrosion inhibitor of concrete.

ACKNOWLEDGEMENTS

This study is financially supported by National Basic Research Program of China (973 Program) (Grant No. 2009CB623200).

REFERENCES

1. JAMIL, H E, SHRIRI, A, BOULIF, R, MONTEMOR, M F and FERREIRA, M G S. Corrosion behaviour of reinforcing steel exposed to an amino alcohol based corrosion inhibitor. Cement and Concrete Composites, Vol. 27, No.6, 2005, pp671-678.

2. SARICIMEN, H, MOHAMMAD, M , QUDDUS, A, SHAMEEM, M, Barry, M S. Effectiveness of concrete inhibitors in retarding rebar corrosion. Cement and Concrete Composites, Vol. 24, No.1, 2002, pp89-100.

3. ALONSO, C, ANDRADE, C, ARGIZ, C, MALRIC, B. Na_2PO_3F as inhibitor of corroding reinforcement in carbonated concrete. Cement and Concrete Research, Vol. 26, No. 3, 1996, pp405-415.

4. ANDRADE, C, ALONSO, C, ACHA, M, MALRIC, B. Preliminary testing of Na_2PO_3F as a curative corrosion inhibitor for steel reinforcements in concrete. Cement and Concrete Research, Vol. 22, No. 5, 1992, pp869-881.

5. ORMELLESE, M, LAZZARI, L, GOIDANICH, S, FUMGALLI, G, BRENNA, A. A study of organic substances as inhibitors for chloride-induced corrosion in concrete. Corrosion Science, Vol. 51, No. 12, 2009,pp 2959-2968.

6. WOMBACHER, F, MAEDER, U, MARAZZANI, B. Aminoalcohol based mixed corrosion inhibitors., Cement and Concrete Composites, Vol.26, No.3, 2004, pp209-216.

7. BATIS, G, PANTAZOPOULOU, P, ROUTOULAS, A. Corrosion protection investigation of reinforcement by inorganic coating in the presence of alkanolamine-based inhibitor, Cement and Concrete Composites , Vol. 25, No.3, 2003, pp371-377

8. GAO, G, LIANG, C H, WANG, H. Synthesis of tertiary amines and their inhibitive performance on carbon steel corrosion. Corrosion Science,, Vol. 49, No. 4, 2007, pp1833-1846.

9. DHOUIBI, L, TRIKI, E, RAHARINAIVO, A. The application of electrochemical impedance spectroscopy to determine the long-term effectiveness of corrosion inhibitors for steel in concrete, Cement and Concrete Composites, Vol. 24, No.1,2002, pp35-43.

10. MORRIS, W, VÁZQUEZ, M (2002). A migrating corrosion inhibitor evaluated in concrete containing various contents of admixed chlorides. Cement and Concrete Research, Vol. 32, No.2, 2002, pp259-267.

11. JAMIL, H E, MONTEMOR, M F, BOULIF, R, SHRIRI, A, FERREIRA, M G S. An electrochemical and analytical approach to the inhibition mechanism of an aminoalcohol-based corrosion inhibitor for reinforced concrete. Electrochemical. Acta, Vol. 48, No.23, 2003, pp 3509-3518.

12. GHODS, P, ISGOR, O B, BROWN, J R, BENSEBAA, F, KINGSTON, D. XPS depth profiling study on the passive oxide film of carbon steel in saturated calcium hydroxide solution and the effect of chloride on the film properties. Applied Surface Science, Vol. 257, No. 10, 2011, pp4669-4677.

Nonlinear Analysis of Axially Loaded Columns Reinforced Longitudinally and Transversely with Glass Fibre Reinforced Polymer (GFRP) bars

K S Ragab
Housing & Building National Research Centre, Egypt

In this paper, the results of an analytical investigation on the behavior of RC columns reinforced longitudinal and transverse with glass fiber reinforced polymer bars GFRP are presented and discussed. Nonlinear finite element analysis on 16-column specimens was achieved by using ANSYS software. The nonlinear finite element analysis program ANSYS is utilized owing to its capabilities to predict either the response of reinforced concrete columns in the post elastic range or the ultimate strength of a reinforced concrete columns reinforced by GFRP bars. An extensive set of parameters is investigated including different strength of concrete, longitudinal reinforcement types (GFRP, Steel) and transverse reinforcement types (GFRP, Steel). A comparison between the experimental results and those predicted by the existing models are presented. Results and conclusions may be useful for designers, have been raised, and represented.

Khaled S. Ragab is currently Associate Professor of Concrete Constructions at Reinforced Concrete Research Institute, Housing & Building National Research Center, HBRC, Cairo, Egypt. He is a Consulting Engineer in the design of concrete structures. He is a Member of Syndicate of Egyptian Engineers, Member of the Association of Engineers of Egyptians, and Member of the reviewer team for Journal of civil engineering and construction technology. He has led several research projects on concrete, and his interesting areas of research are Fiber reinforced concrete (GFRP), High performance concrete (self compacting concrete), Nanotechnology in the field of concrete, Economic systems of construction, Nonlinear analysis by FEM for different elements of concrete construction, and Light weight concrete.

Keywords: ANSYS, Columns, FEM, GFRP stirrups, Nonlinear

INTRODUCTION

Modeling the constitutive law of confined reinforced concrete columns based on the empirical approach can sometimes be inaccurate or limited to a narrow range of available experimental data. The tests are also very expensive and sometimes time consuming. The applicability of the test data mainly depends on the accuracy of the test apparatus and the supporting instruments implemented during the test. Hence, it is deemed necessary to have another option of modeling the stress-strain relationship of confined concrete without deploying an empirical approach in the modeling. One of the suitable software that can be utilized to describe the actual nonlinear behavior of confined concrete columns under axial loading is ANSYS [10]. This is because ANSYS is capable of analyzing the nonlinear behavior of a combination between 3D SOLID and LINK elements in a structure based on the finite element procedure. With this option, researchers or design engineers can confidently predict in advance the actual behavior of various confined concrete columns not only in the linear-elastic region, but furthermore also in the nonlinear post-elastic region. The authors wish that this economical procedure can be used to provide an alternative tool for researchers or structural engineers in investigating various types of structural concrete elements in the future.

In this paper, the authors propose to use ANSYS [10], which is capable of modeling the nonlinear behavior of reinforced concrete columns, for predicting the actual stress-strain relationship of rectangular columns with various spacing of transverse reinforcement under axial concentric loading. However, none of the works conducted previously using ANSYS includes reinforced concrete columns confined by transverse reinforcement (GFRP bars). The proposed procedure has been verified with four rectangular columns specimens confined by various types of main steel and stirrups (steel and GFRP bars). The analytical stress-strain curves obtained from the proposed procedure are shown to be in close agreement with the experimental results.

ACI Committee 440 contained design provisions for flexure and shear, the guide excludes any provisions for the analysis and design of concrete compression members reinforced with FRP bars. FRP bars were not recommended by ACI Committee 440 (ACI 440.1R-2006) [3]for use as compression reinforcement, in part because the direct effect of compression reinforcement on the strength of concrete members is frequently small and, therefore, often ignored. Additionally, the compression properties of FRP bars are often difficult to predict due to the lack of stability of individual fibers in a bar. Therefore, this complicates testing and can produce inaccurate measurements of compression properties (Ching et al. 2006)[4].
So this study aims to study the behavior of reinforced concrete columns with GFRP. The results and observations presented in this paper are useful to practicing engineers who must predict the enhanced compressive strength of concrete columns reinforced with GFRP bars.

OBJECTIVES AND SCOPE

The main objectives of this study could be summarized in the following points:

- Examining the compressive behavior of reinforced concrete columns longitudinally and transversely with GFRP-bars.
- Comparing this behavior with reinforced concrete columns longitudinally and transversely with steel bars.

- Knowing better for stresses distribution for longitudinal and cross section columns during the axial loading.
- Parametric study for the effect of change each of strength of concrete, main steel, and stirrups on the vertical ultimate load of the column.
- Parametric study for participate each of ordinary concrete, main steel, and stirrups on the vertical column load.
- Predicate new formula for compute the capacity of axially loaded column reinforcement by GFRP.

Finite element models were developed to simulate the behavior of reinforced concrete columns with GFRP longitudinally and transversely bars from linear through nonlinear response using the ANSYS program.

EXPRIMENTAL AND ANALYTICAL PROGRAM

The experimental models were constructed according to rectangular column specimens as shown in Figure 1. The specimens had tested of GFRP and steel RC columns under pure axial load. Test set up and general view of GFRP bars and stirrups are shown in Figure 2. The experimental program had chosen four rectangular columns. These columns are shown in Table 1 from C1 to C4. The specimens had rectangular with cross section 250*200mm, and length of 500mm. The columns were reinforced by GFRP and steel bars for longitudinally and transversely bars. The columns were reinforced with four vertical bars of 12 mm diameter and lateral stirrups of 8 mm diameter with spacing 210 mm.

The analysis carried out is conducted on 16-RC columns as shown in Table 1; the parameters of study were the main reinforcement ratios and types, the transverse reinforcement ratios and types, and the characteristic compressive strength of concrete. Finally, conclusions from the current research and recommendations for future studies are presented.

Element Types

Extensive inelastic finite element analyses using the ANSYS program are carried out to study the behavior of the tested columns. Two types of elements are employed to model the columns. An eight node solid element, solid65, was used to model the concrete. The solid element has eight nodes with three degrees of freedom at each node, translation in the nodal x, y, and z directions as shown in Figure 3.

The used element is capable of plastic deformation, cracking in three orthogonal directions, and crushing. A link8 element was used to model the reinforcement polymer and steel bars; two nodes are required for this element. Each node has three degrees of freedom, translation in the nodal x, y, and z directions. The element is also capable of plastic deformation (ANSYS User's Manual). The finite element mesh used in the analysis is shown in Figure 4. Also, the crushing column model is shown in Figure 3.

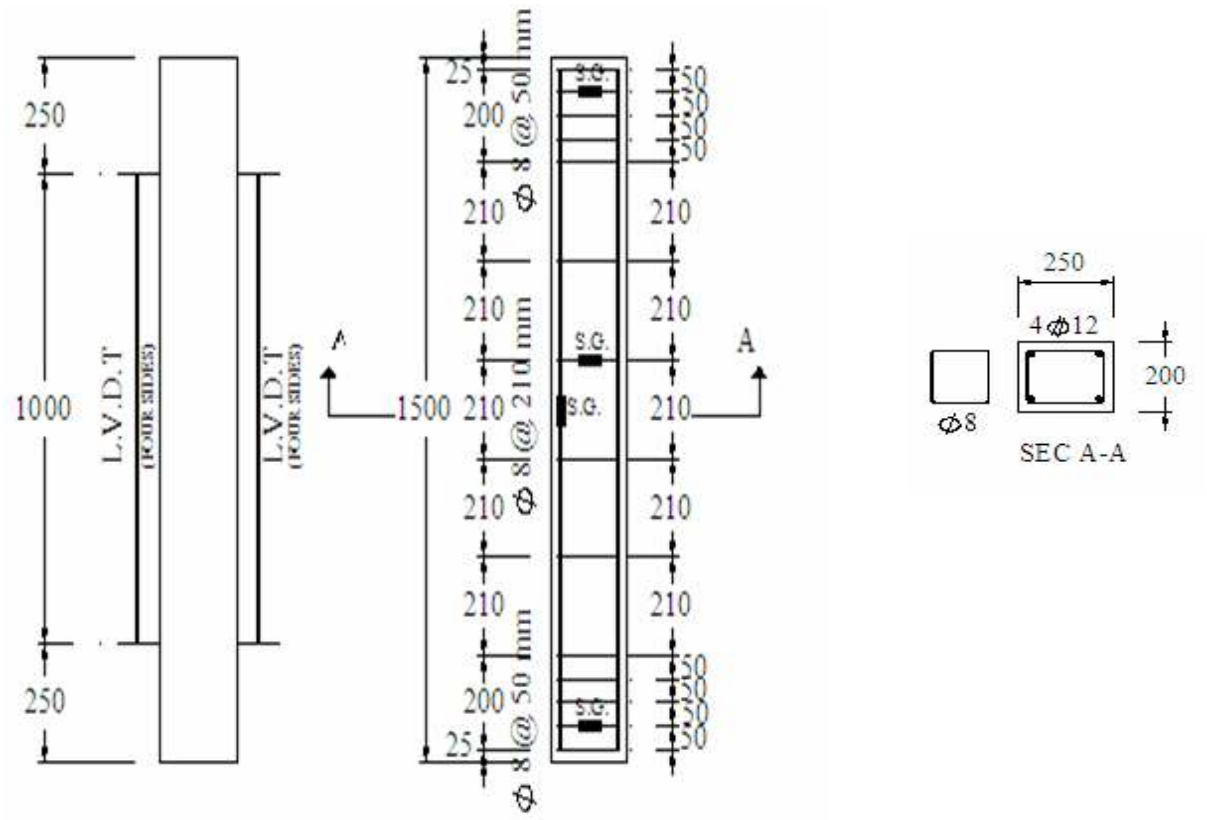

Figure 1 Concrete Dimensions of Tested Columns

Test set up

General view of GFRP bars and stirrups

Figure 2 Test set up and general view of GFRP bars and stirrups.

Table 1 The Program for the Analytical Columns.

MODEL by	COLUMN No.	DIM. bxd (mm)	COLUMN HEIGHT (mm)	VERTICAL BARS TYPE	STIRRUPS TYPE	VL. BARS	STIRRUPS (mm)	TARGET COMP. STR. (MPa)
Exp. and FEM	C1	200x250	1500	steel	steel	4#12	# 8/210	45
	C2	200x250	1500	steel	GFRP	4#12	# 8/210	45
	C3	200x250	1500	GFRP	GFRP	4#12	# 8/210	45
	C4	200x250	1500	GFRP	steel	4#12	# 8/210	45
FEM	C5	200x250	1500	steel	steel	6#12	# 8/100	45
	C6	200x250	1500	GFRP	steel	6#12	# 8/100	45
	C7	200x250	1500	GFRP	GFRP	4#12	# 8/100	45
	C8	200x250	1500	steel	steel	4#12	# 8/100	25
	C9	200x250	1500	GFRP	GFRP	4#12	# 8/210	25
	C10	200x250	1500	GFRP	steel	4#12	# 8/210	25
	C11	200x250	1500	steel	steel	4#16	# 8/210	45
	C12	200x250	1500	GFRP	GFRP	4#16	# 8/210	45
	C13	200x250	1500	GFRP	steel	4#16	# 8/210	45
	C14	200x250	1500	---	---	---	---	45
	C15	200x250	1500	steel	---	4#12	---	45
	C16	200x250	1500	---	steel	---	# 8/210	45

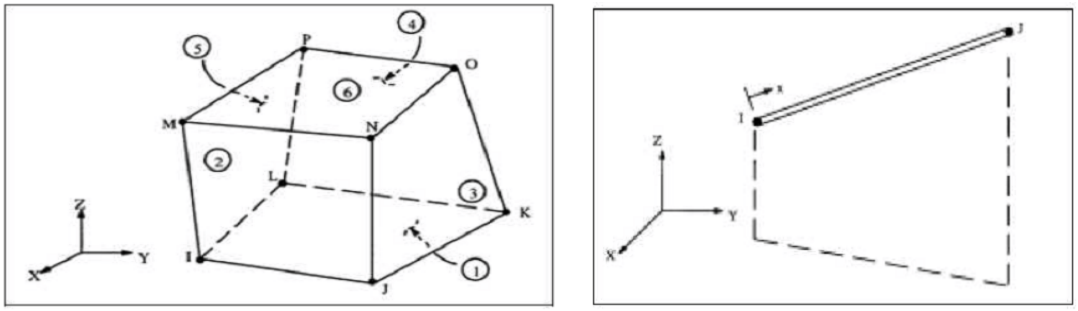

Figure 3 Element types of Solid 65 and Link8.

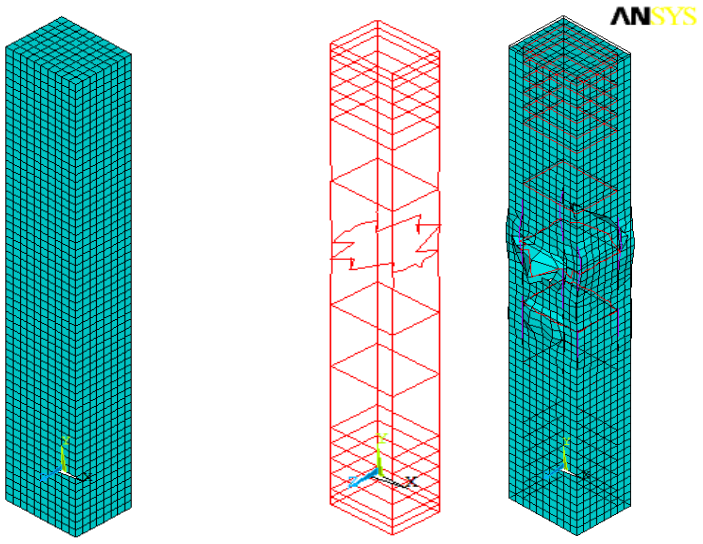

Figure 4 Finite element mesh for a typical column model and crushing model

PROPERTIES OF USED MATERIAL

Normal weight concrete was used in the fabricated tested columns. The stress-strain curve is linearly elastic up to about 30% of the maximum compressive strength. Above this point, the stress increases gradually up to the maximum compressive strength, f_{cu}, after that the curve descends into softening region, and eventually crushing failure occurs at an ultimate strain. The input data for the concrete, GFRP, and steel (high grade and mild steel) properties are shown in Table 2.

Reinforced Concrete

The tested reinforced concrete columns were cast using locally produced ordinary Portland cement, natural sand and crushed stone with a maximum size of 10 mm. The columns were remolded after 24 hrs from casting, covered with wet burlap and stored under the laboratory conditions for 28 days before proceeding to testing stage.

GFRP and Steel Bars

The GFRP used for stirrups were of 8 mm diameter and for main longitudinal reinforcement the used GFRP bars were of 12 mm diameter as shown in Figure 1. Table 2 show the mechanical properties of the used GFRP and steel bars. The GFRP bars were locally manufactured. The GFRP bars were covered by layers of wrapped fiber to improve their bond with concrete. Due to local industry some stirrups has imperfection in its diameters. The steel bars used for stirrups were of mild steel of 8 mm diameter and for main longitudinal steel bars were high grade steel of 12 mm diameter.

Table 2 Input data for the Concrete, GFRP, and Steel Properties.

ITEM	CONCRETE	GFRP (main reinforcement)	GFRP (stirrups)	STEEL (main reinforcement)	STEEL (stirrups)
Unit weight, N/mm^3	2.5e-5	2.54e-5	2.54e-5	7.85e-5	7.85e-5
Ultimate compressive strength, N/mm^2	25,40	--	--	--	--
Tensile strength, N/mm^2	2.20,3.5	407	278	360	250
Elastic modulus, N/mm^2	2.4e4,2.8e4	3.4e4	2.6e4	2.5e5	2.5e5
Poisson ratio	0.20	0.20	0.20	0.30	0.30
Shear modulus, N/mm^2	10.0e3,11.0e3	--	--	--	--

ELEMENT MESHING

After preparing all the input data of material and geometrical properties, the column models were divided into small cubical elements. The meshing results of all column specimens used for model validation are shown in Fig. 4. For columns reinforced, it is worthwhile to notice that the meshing was created according to the locations of reinforcing bars, either the longitudinal or transverse reinforcement, as well as the column specimen cross-sectional

perimeter. By using sharing nodes option in ANSYS [10], SOLID65 and LINK8 elements can be interconnected one to another forming a single solid column model which capable of simulating the actual behavior of reinforced concrete column.

Numerical Implementation

The quantitative implementation of the finite element procedure used in the ANSYS software [10] is based on the principles of virtual work or the postulation of minimum potential energy in the assembly of the elements as formulated the following equilibrium equation:

$$[K]\{d\} + \{F\}_p + \{F\}_g + \{F\}_{\varepsilon o} + \{F_{\sigma o}\} - \{R\} = 0 \quad (1)$$

The stiffness matrix [*K*],

$$[K] = \Sigma \int [B]^T [D] [B] \, dv \quad (2)$$

The nodal force due to the surface load,

$$\{F\}_p = -\Sigma_{ele} \int [N]^T \{P\} \, dv \quad (3)$$

The nodal force due to the body load,

$$\{F\}_g = -\Sigma_{ele} \int [N]^T \{g\} \, dv \quad (4)$$

The nodal force due to the initial strain,

$$\{F\}_{\varepsilon o} = -\Sigma_{ele} \int [B]^T [D] \{\varepsilon_o\} \, dv \quad (5)$$

The nodal force due to the initial stress,

$$\{F\}_{\sigma o} = -\Sigma_{ele} \int [B]^T [D] \{\sigma_o\} \, dv \quad (6)$$

where [*N*] is the shape function; {*d*} is the vector of nodal displacement; {*R*} is the vector of applied nodal force; {*p*} is the vector of surface load; and {*g*} is the vector of body load. The ANSYS software uses Newton-Raphson (N-R) method [10] to obtain the convergent solution of the nonlinear equilibrium iterative equation to develop the stiffness matrix of the column model.

Loading Procedure

The analytical investigation carried out here is conducted on 16-RC columns. All columns at a plane of support location, the degrees of freedom for all the nodes of the solid65 elements were held at zero. To apply the axial load on the top of the column specimen, an axial pressure was implemented over the entire top surface of the column model in the ANSYS software. The axial pressure can be simulated using the ANSYS load step option [10]. Load step option may be used when the incremental loading is considered. The number of load steps depends on the user's definition. In this case, load steps were defined according to the actual load steps applied during the test. A solution was obtained by solving several sub-

steps in each load step to attain convergence. In each sub-step, an iteration procedure was carried out until providing a convergent solution before moving to the next sub-step. The number of the sub-steps taken in the analysis may improve the accuracy of the solution. It will, however, sometimes be very time-consuming when too many sub-steps are taken. To avoid the problem, ANSYS offers an alternate automatic time step option to reduce the computational time required in the analysis. Due to this advantage, this option is selected. When the automatic time step option is selected, it will automatically resize the number of the sub-steps in each load step when it fails to reach a convergent solution. This process keeps repeating until it provides a convergence value. When the load has reached its peak value, the load control mode was switched into the displacement control mode. The displacement control mode was set into several displacement steps corresponding to the experimental data. Using the automatic time steps, the column specimen was displaced until failure. The objective of using this kind of mode is to obtain the descending branch of the stress-strain curve of the column specimens under axial loading. The incremental nonlinear equation can be written as follows:

$$K(u)\Delta u = \Delta P \tag{7}$$

Where Δu and ΔP describe the unknown incremental displacement and the given incremental applied load To solve a nonlinear problem, ANSYS uses the Newton-Raphson (N-R) method [10] involving an iterative procedure. This method starts with a trial assumption: u = ui, to define the incremental of the next steps, $\Delta u_i = K\text{-}1(u_i)\Delta P$, and the load vector exists beyond the equilibrium, $\Delta R_i = \Delta P - K(u_i)\Delta u_i$. There will always be a discrepancy between the applied load and the load evaluated based on the assumption. To satisfy the state of equilibrium, the load vector exists beyond the equilibrium should be zero. Since the solution requires an iterative procedure, a tolerance value should be determined such that a convergent solution can be obtained. In each iteration step, N-R method calculates the load vector exists beyond the equilibrium and always checks if the convergent solution under specified tolerance is obtained. If the value is still greater than the tolerance value, then the initial assumed value is updated with the incremental displacement, $u_{i+1} = u_i + \Delta u_i$. The next incremental solution vector is determined with $\Delta u_{i+1} = K^{-1}(u_{i+1})\Delta P$, providing a new load vector exists beyond the equilibrium $\Delta R_{i+1} = \Delta P - K(u_{i+1})\Delta u_{i+1}$. This procedure is repeated until the convergent solution is obtained.

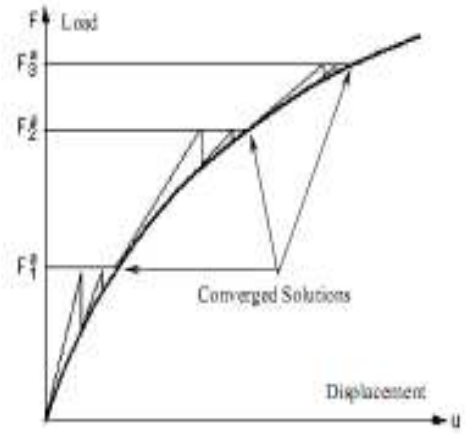

Figure 5 Newton-Raphson iterative solution (3 load increments)

The simplified stress strain curve for column model is constructed from six points connected

by Straight lines. The curve starts at zero stress and strain. Point No. 1, at $0.3f'_c$ is calculated for the stress-strain relationship of the concrete in the linear range. Point Nos. 2, 3 and 4 are obtained from Equation (8), in which ε_o is calculated from Equation (9). Point No. 5 is at ε_o and f'_c. In this study, an assumption was made of perfectly plastic behavior after Point No. 5 (William et al. 1975[10], and Meisam 2009[1]). Fig. 3 shows the simplified compressive axial stress-strain relationship that was used in this study.

$$f = Ec\ \varepsilon / (1+(\varepsilon/\varepsilon_o)^2) \quad (8)$$

$$\varepsilon_o = 2\ f_c' / E_c \quad (9)$$

$$E_c = f / \varepsilon \quad (10)$$

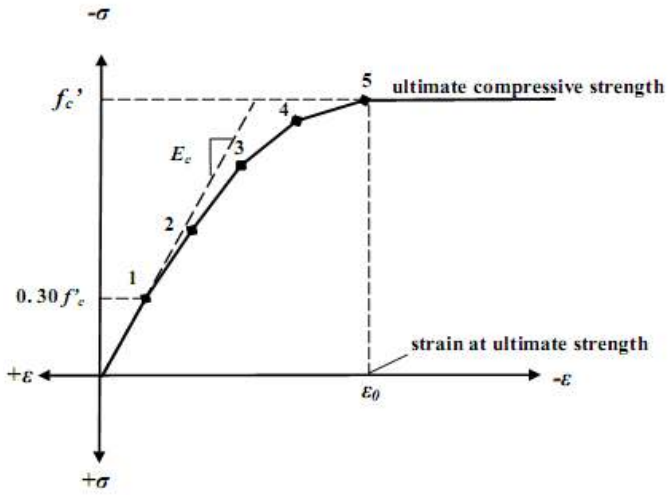

Figure 6 Simplified compressive axial stress strain curve for concrete

TEST RESULTS

The parametric studies included in this investigation are the main reinforcement ratios and types, the transverse reinforcement ratios and types, and the characteristic strength of concrete, respectively. Table 3 shows the analytically and the experimental results of the ultimate loads, vertical displacements and compressive stress of concrete, respectively.

Load–Vertical Concrete Strain Relationship for Experimental and FEM Results

The experimental and FEM results for the load versus vertical concrete displacements relationships for columns C1 to C4 are shown in Figure 7 while Table 4 summarizes the test results for all columns. The ultimate load is defined as the maximum recorded load measured during test for each column. Table 4, indicated that, for column C1, the experimental result for the ultimate load was recorded 1464.5 kN and the corresponding vertical concrete displacement 2.0mm. When using different type of main and stirrups reinforcement for columns C2, C3 and C4, the experimental results for the ultimate loads were recorded 1253.0, 1239.0 and 1442.0 kN respectively, and the corresponding vertical concrete displacements 1.5, 1.4, and 1.6mm respectively. The FEM results for columns C1, C2, C3 and C4, the ultimate loads were recorded 1507.3, 1477.8 ,1339.0 and 1490.0kN respectively, and the

corresponding vertical concrete displacements 1.779, 1.678, 1.626 , and 1.8mm respectively. Table 4, indicated that, for columns C1, C2, C3 and C4, the difference between the FEM results and the experimental results for the ultimate loads were recorded 1.029, 1.17 , 1.081 and 1.033 respectively, and the corresponding vertical concrete displacements 0.890, 1.119 , 1.161, and 1.125 respectively. The par chart in Figure 7 shows the difference between experimental and FEM results for C1, C2 , C3 and C4. This chart shows that the theoretical results from Finite Element Analysis indicate in general a good agreement with the experimental values. Also from this chart shows that using GFRP for main reinforcement and steel for stirrups i.e. C4 gives results for ultimate load and corresponding vertical displacement close to column C1 in comparison with C2 and C3. So, the author recommended using GFRP for main reinforcement and steel for stirrups if the column used GFRP bars as reinforcement.

Table 4 Results of Tested Columns

MODEL by		COLUMN No. **Main Rft.*Stirrups	F_{cu} (MPa)	DIM.(mm)		EXP. RESULTS		FEM RESULTS			DIFFERENCE %		
				b	d	$P_{ultimate}$ (kN)	VL. Disp. (mm)	Peak stresses (MPa)	$P_{ultimate}$ (kN)	VL. Disp. (mm)	Peak stresses (MPa)	$P_{ultimate}$ (kN)	VL. Disp. (mm)
Exp. and FEM	Control	$C1_{S*S}$	40.0	200	250	1464.50	2.00	30.146	1507.30	1.779	0.754	1.029	0.890
		$C2_{S*F}$	40.0	200	250	1253.00	1.50	29.556	1477.80	1.678	0.739	1.170	1.119
		$C3_{F*F}$	40.0	200	250	1239.00	1.40	26.780	1339.00	1.626	0.670	1.081	1.161
		$C4_{F*S}$	40.0	200	250	1442.00	1.60	29.800	1490.00	1.800	0.745	1.033	1.125
FEM	Stirrups 10#8/m	$C5_{S*S}$	40.0	200	250	---	---	32.138	1606.90	1.879	0.804	---	---
		$C6_{F*S}$	40.0	200	250	---	---	30.50	1525.00	1.820	0.763	---	---
		$C7_{F*F}$	40.0	200	250	---	---	27.307	1365.35	1.680	0.683	---	---
	F_{cu} = 25N/mm^2	$C8_{S*S}$	25.0	200	250	---	---	15.78	789.00	1.300	0.631	---	---
		$C9_{F*F}$	25.0	200	250	---	---	15.543	777.15	1.208	0.622	---	---
		$C10_{F*S}$	25.0	200	250	---	---	15.70	785.00	1.250	0.628	---	---
	Main Rft. 4#16	$C11_{S*S}$	40.0	200	250	---	---	31.836	1591.80	1.851	0.796	---	---
		$C12_{F*F}$	40.0	200	250	---	---	27.119	1355.95	1.659	0.678	---	---
		$C13_{F*S}$	40.0	200	250	---	---	30.140	1507.0	1.810	0.754	---	---
	Participate Conc., main Rft.,Stirrups	**$C14_{0*0}$	40.0	200	250	---	---	25.699	1284.95	1.533	0.643	---	---
		**$C15_{S*0}$	40.0	200	250	---	---	27.309	1365.45	1.294	0.683	---	---
		**$C16_{0*S}$	40.0	200	250	---	---	26.649	1332.45	1.627	0.666	---	---

** S: Steel bars, F: GFRP bars, 0*0: ordinary concrete only, S*0: main steel only, and 0*S: stirrups only.

Stress Distribution

The axial stress distributions of column specimens obtained from the ANSYS solution are shown in Fig. 8. As can be seen in the figure, for column specimens, the axial stress contours over mid-height cross sections of the column specimens indicated that the higher axial stress concentration occurs over the center region of the column cross section. This phenomenon describes a correct mechanism of a plain concrete column specimen subjected to axial loading.

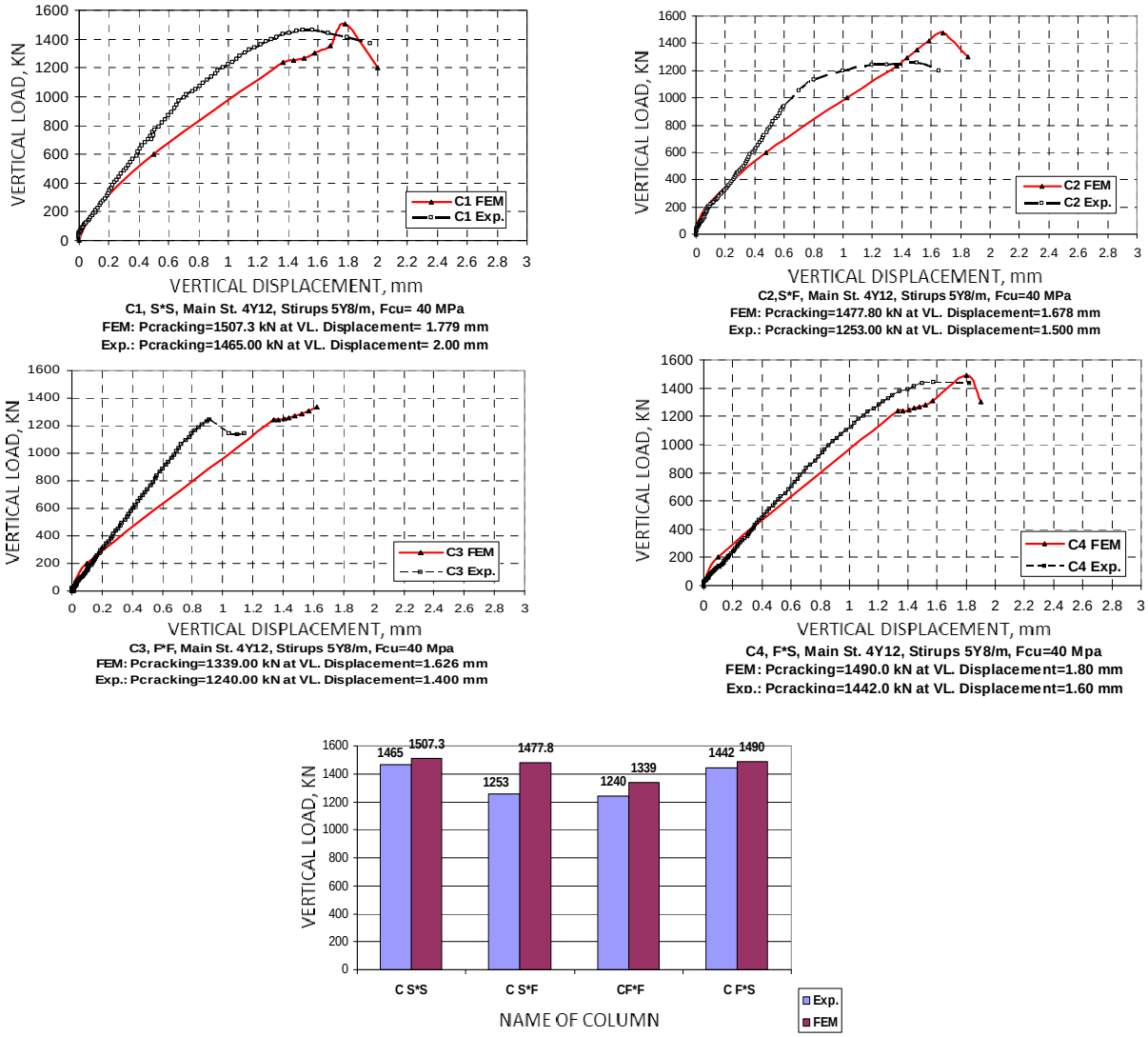

Figure 7 Comparison between results of Experimental and FEM for load – displacement curve.

The axial stress distributions with various intensities of stress concentrations along the longdutinal column are shown in Figure 8. The axial stress distributions are showing that the axial stress concentrations around the longitudinal reinforcement at the location of stirrups. Also, it is showing that during the loading, the direction of stresses from upper and lower column towards to the center of height of column.

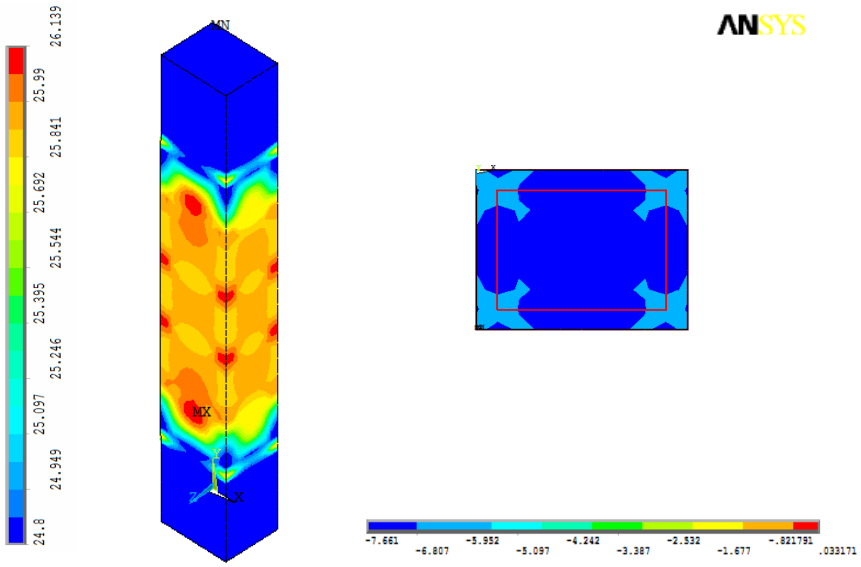

Figure 8 Axial stress distributions over the mid-height cross section of column and stress distribution along the longitudinal column during the loading.

RESULTS AND DISCUSSIONS

The Transverse Reinforcement Ratios and Types

Figure 9 shows the load-vertical displacement of columns C5, C6, and C7; increasing of transverse reinforcement ratio leads to increase the toughness and ductility of tested columns. From Table 4, it can be seen that, the ultimate load, and corresponding vertical displacement of C5, C6, and C7 are (1606.9 & 1525.0 & 1365.35kN) and (1.879 & 1.82 & 1.68mm) respectively. The increasing of transverse reinforcement ratios confines the columns so it is lead to increase the ultimate loads and increasing the corresponding vertical displacement.

Par Chart in Figure 9 shows that the increasing of transverse reinforcement ratio leads to increase the ultimate load of tested columns. This phenomenon appears in table 4 from the peak stresses which increase with increasing the transverse reinforcement ratio. Also from table 4, shows that the vertical displacement for C6 is bigger than column C7 because the steel stirrups gives well confinement by eliminate the buckling of the GFRP longitudinal bars compared with GFRP stirrups.

The Characteristic Compressive Strength of Concrete

From Table 4, it can be seen that, ultimate loads, and corresponding vertical displacement of C8, C9 and C10 are (789.0 & 777.15 & 785.0 kN) and (1.3 & 1.208 & 1.205mm) respectively. Figure 10 shows the load-displacement of columns C8, C9 and C10; decreasing of characteristic strength of concrete has significant effect on the behavior of tested columns where decrease toughness and ductility of tested columns. Par Chart in Figure 10 shows the effect of the characteristic strength of concrete on the ultimate load that the columns resists, where the increasing of characteristic strength of concrete has a significant effect on ultimate loads. From Par Chart in Figure 10, it can be seen that, ultimate load of, C1, C4 and C3 with Fcu = 40 MPa in comparison with C8 to C10 with Fcu = 25MPa are 191%&190 %& and172% respectively.

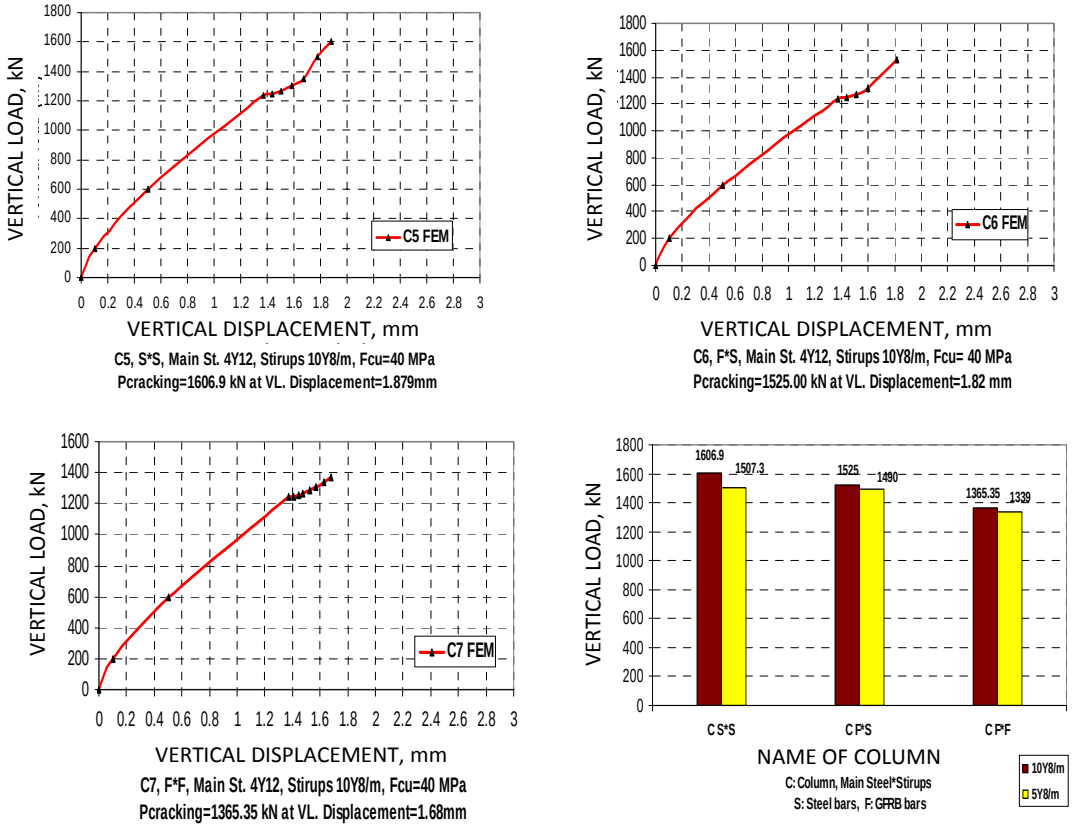

Figure 9 Effect of change the number of stirrups

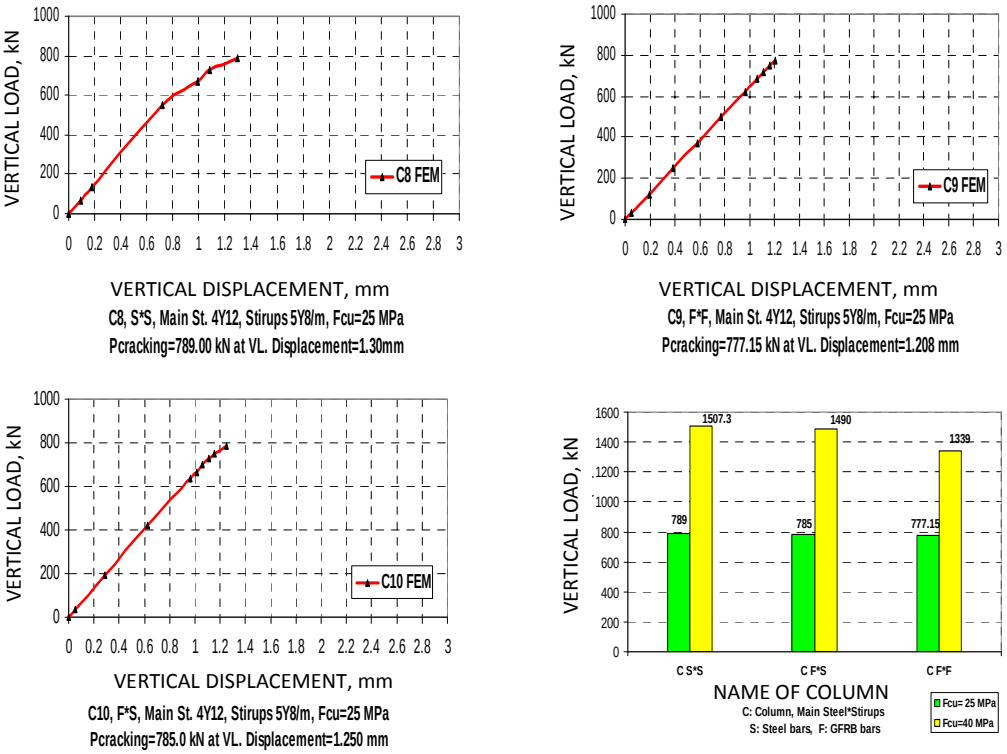

Figure 10 Effect of change the strength of concrete

The Main Reinforcement Ratios and Types

Figure 11 shows the load-displacement of columns C11, C12, and C13 which reinforced by GFRP reinforcement 4#16mm; increasing GFRP reinforcement ratio leads to increase the toughness and ductility of tested columns. From Table 4, it can be seen that, ultimate loads, corresponding vertical displacement of column C11, C12, and C13 are (1591.8, 1355.95, 1507.0 kN) and (1.851, 1.659, 1.81mm) respectively. The increasing of main reinforcement ratios with GFRP bars increase the ductility, so it has a significant effect on ultimate load, and corresponding vertical displacement that the columns resist. Par Chart in Figure 11 shows the effect of the main reinforcement ratios on the ultimate load that the columns resists, where the increasing of main reinforcement from 4#12 mm (C1,C3,C4) to 4#16 mm (C11, C12, C13) has a significant effect on the ultimate load of the column.

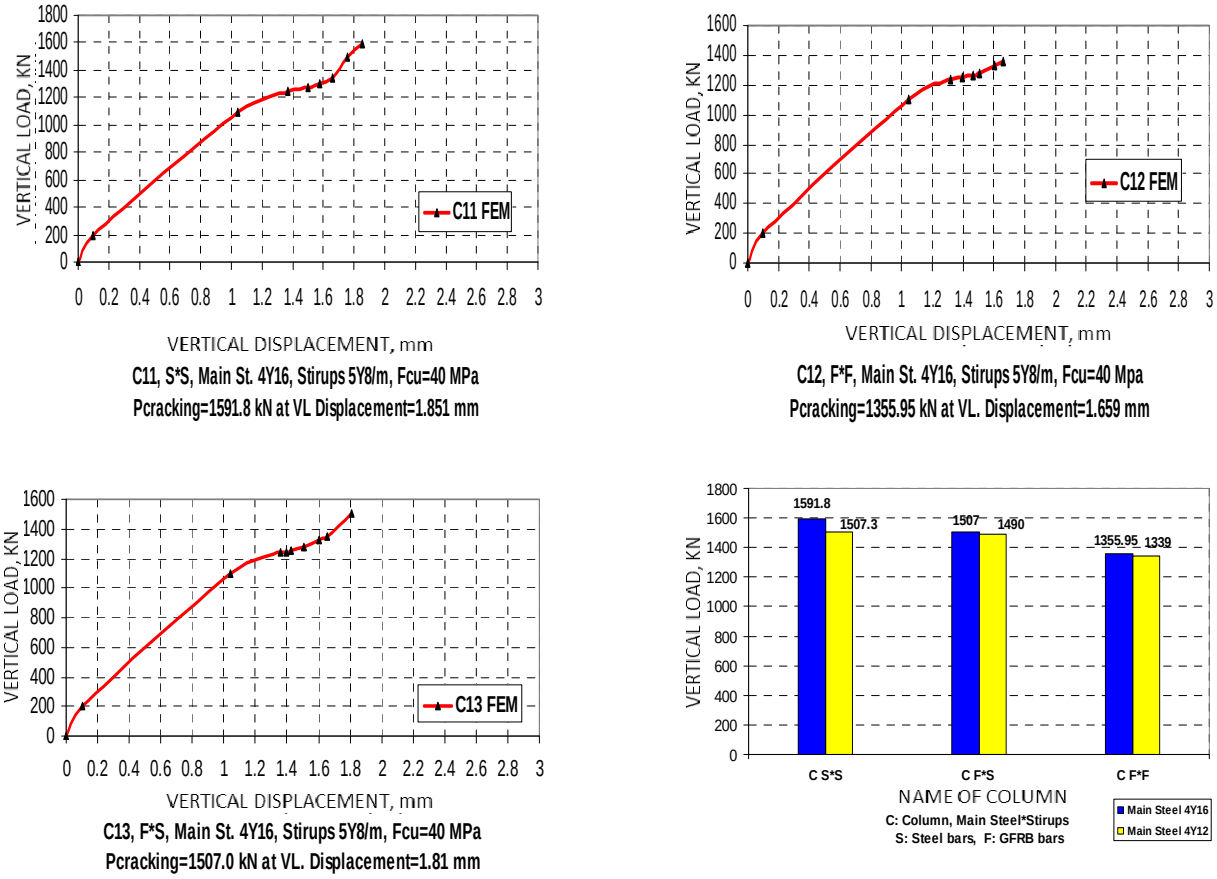

Figure 11 Effect of change the area of main steel.

Effect of Change Each of Main Steel, Stirrups, and Strength of Concrete on Maximum Vertical Load (Pultimate) and Peak Stresses/ Fcu

Figure 12 summarizes the results. Par Chart (a) in Figure 12 shows effect of change each of main steel, stirrups, and strength of concrete on maximum vertical load for different type of columns whish Cs*s means that the column used longitudinal reinforcement from steel and stirrups from steel, Cf*s means that the column used longitudinal reinforcement from GFRP bars and stirrups from steel, and Cf*f means that the column used longitudinal reinforcement from GFRP and stirrups from GFRP. Par Chart (a) in Figure 12 shows that The concrete columns reinforcement by GFRP bars as a main reinforcement (Cf*s) have reduced the

ultimate capacity of column vertical load by 2 - 5% in comparison with the columns reinforcement by steel bars. The concrete columns reinforcement by GFRP bars as a main reinforcement and stirrups (Cf*f) have reduced the ultimate capacity of column vertical load by 10 -15% in comparison with the columns reinforcement by steel bars. Also, Par Chart (B) in Figure 12 shows effect of change each of main steel, stirrups, and strength of concrete on Peak stresses/Fcu whish clear from this chart that the increasing in the reinforcement ratio for each of longitudinal reinforcement and stirrups increase the confinement and so, increase the peak stresses of the column.

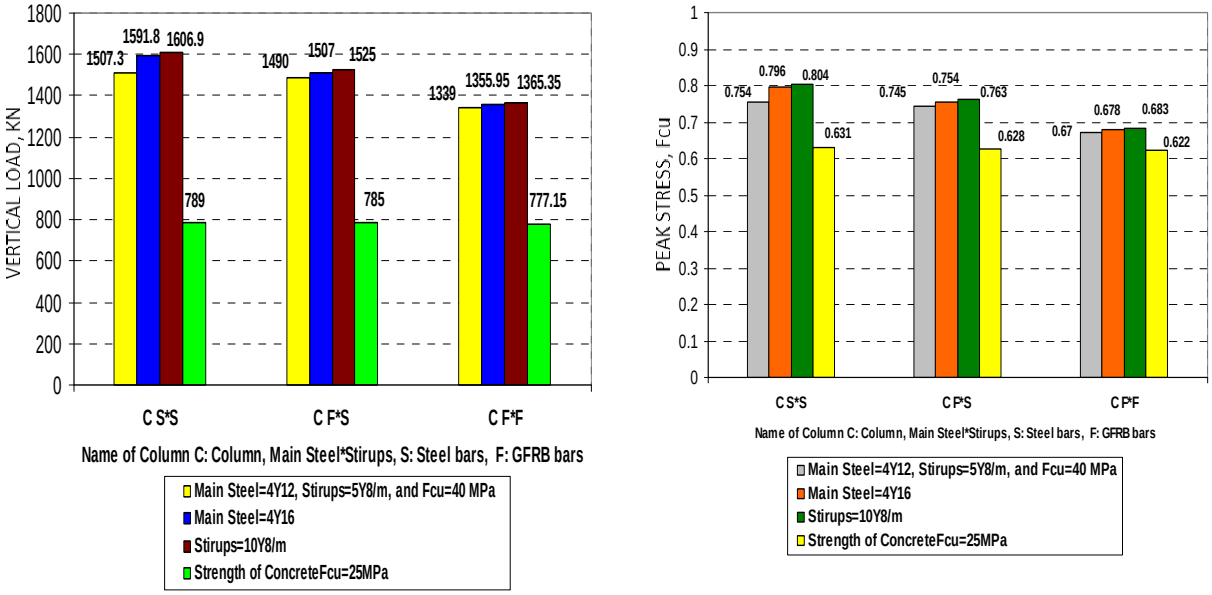

(a) (b)

Figure 12 Effect of change each of main steel, stirrups, and strength of concrete on: (a) Maximum Vertical load ($P_{ultimate}$) and (b) Peak Stresses/ Fcu.

Participate Each of Ordinary Concrete, Main Steel, and Stirrups on the Vertical Column Load

Figure 13 shows the load-displacment of columns C14, C15, and C16. Par Chart in Figure 13 shows effect of ultimate vertical load of column when the column construct from ordinary concrete only, concrete and main steel, concrete and stirrups, and finally concrete and main steel and stirrups. The target from this analysis that knows better about participate for each of ordinary concrete, main steel, and stirrups on the vertical column load. Participate each of ordinary concrete, main steel, and stirrups on the vertical column load is 85%, 9%, and 6% respectively as shown in Figure 14.

ULTIMATE CAPACITY AND CODE PROVISION

The plain concrete strength of full –scale columns tested under concentric compression loading is generally lower than the concrete compressive strength measured on standard 150 x 300mm cylinder test.

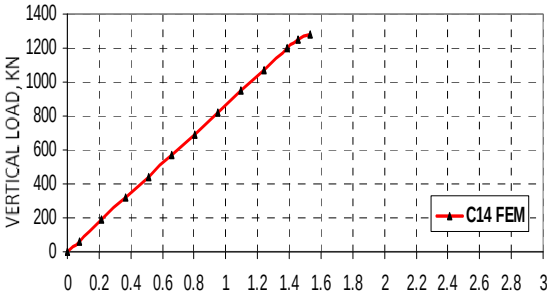

C14, Ordinary Concrete Only, Fcu= 40 Mpa
Pcracking=1284.95 kN at VL. Displacement=1.533 mm

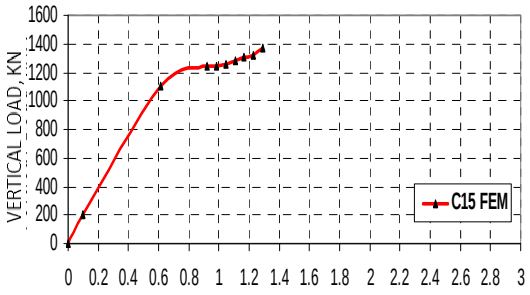

C15, Main St. 4Y12, No Stirups, Fcu=40 Mpa
Pcracking=1365.45 kN at VL. Displacement=1.294 mm

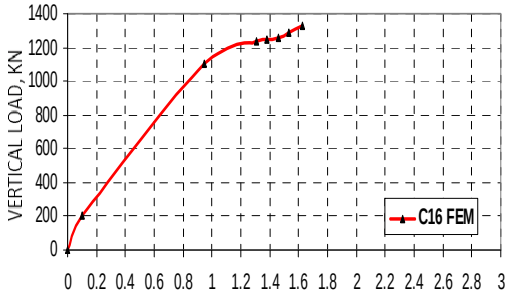

C16, No Main St., Stirups 5Y8/m, Fcu=40 Mpa
Pcracking=1332.45 kN at VL. Displacement=1.627 mm

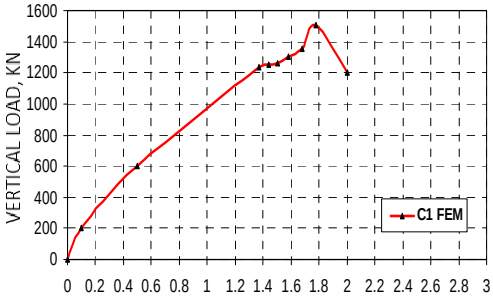

C1, S*S, Main St. 4Y12, Stirups 5Y8/m, Fcu= 40 MPa
FEM: Pcracking=1507.3 kN at VL. Displacement= 1.779 mm

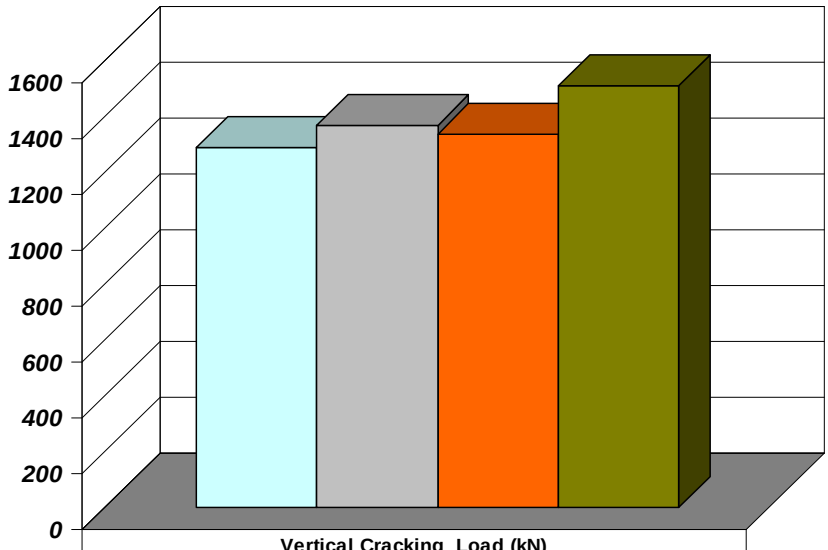

C14 Ordinary Concrete only	1284.95
C15 Used Main Steel only	1365.45
C16 Used Stirups only	1332.45
C1 Used Main Steel and Stirups	1507.3

Figure 13 Load – Displacement Curve for columns for each of ordinary concrete only, ordinary concrete and main steel, ordinary concrete and stirrups, and ordinary concrete, main steel and stirrups.

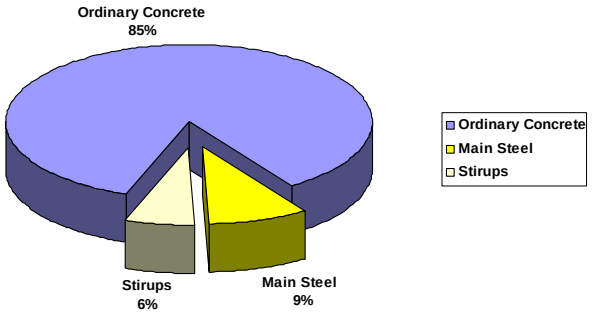

Figure 14 Participate each of ordinary concrete, main steel, and stirrups on the vertical column load.

The 0.85 reduction factor suggested by ACI Building Code (ACI 318-08) is mainly attributed to the differences in size and shape of the reinforced concrete columns and the concrete cylinder. The nominal capacity of an axial loaded RC column P_n was defined as the sum of the forces carried by the concrete and the steel as given by the following equation:

$$P_n = 0.85\, f_c'(A_g - A_s) + f_y\, A_s \qquad (11)$$

Where, A_g= the total cross section area of column, A_s= cross section area of longitudinal reinforcement. f_c'=concrete compressive strength and f_y= yielding strength of steel reinforcement.

CSA S806-02 permits the use of FRP bars as longitudinal reinforcement in columns subjected to axial load only without taking the FRP bars contribution into account for calculating the ultimate capacity of the columns as shown in eq. 12

$$P_n = 0.85\, f_c'(A_g - A_s) \qquad (12)$$

In Figure 15, the maximum axial load, applied on each specimen during testing are compared with their corresponding axial load computed according to the ACI Building Code eq. 11 setting f_y equal to the ultimate tensile strength of GFRP bars for comparison purpose. Moreover, it is compared to the calculated P_n based on neglecting the contribution of FRP as recommended CSA S806-02. In addition to that, a comparison is made with the calculated P_n from predicted formula considering the contribution of GFRP bars in compression equal to 20% of tensile strength of GFRP and 70% of F_{cu} if F_{cu} equal to 40 MPa and 60% if F_{cu}= 25 MPa.

Predicate Formula:

$$P_n = 0.7f_c'(A_g - A_s) + 0.2f_y\, A_s \quad \text{For } F_{cu} = 40 \text{ MPa} \qquad (13)$$

$$P_n = 0.6\, f_c'(A_g - A_s) + 0.2f_y\, A_s \quad \text{For } F_{cu} = 25 \text{ MPa} \qquad (14)$$

It is clearly that eq. 11 over-estimates the columns maximum capacity by 30%. Conversely, ignoring the contribution of FRP longitudinal bars would over-estimate the columns maximum capacity by 10%. However, by setting the GFRP compressive strength to 20% of its tensile strength and 70% of F_{cu} if F_{cu} equal to 40 MPa and 60% if F_{cu}= 25 MPa, the maximum axial load could be predicted accurately as shown in Fig. (15).

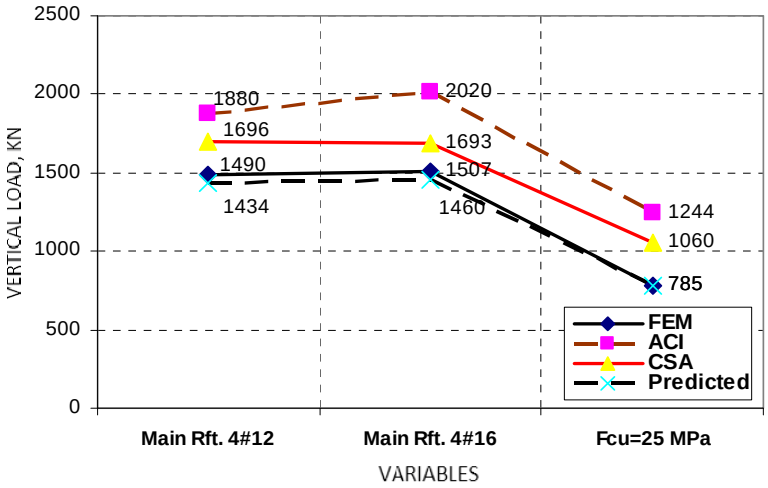

Figure 15 Comparison between predicted formula, ACI, and CAN for VL. ultimate load for column main Rft. GFRP and steel stirrups.

SUMMARY AND CONCLUSIONS

The inelastic behavior of 16 columns are investigated in the current study under the effect of increasing loading employing the inelastic FE analysis program ANSYS. Several parameters are investigated including the main reinforcement ratios and types, the transverse reinforcement ratios and types, and the characteristic compressive strength of concrete. The study focuses on the consequences of the investigated parameters on the ultimate vertical load, corresponding vertical displacement and peak stresses. The conclusions made from this investigation are:

1. The accuracy of the proposed procedure has been well confirmed by the close values of ultimate vertical load, corresponding vertical displacement and peak stresses obtained from the FEM analysis and the experimental test.

2. From the axial stress contours obtained from the FEM analysis, it can be concluded that the axial stress concentrations are in the center regions of the column cross sections, particularly in the confined areas.

3. From the axial stress distributions along the column obtained from the FEM analysis, it can be concluded that during the loading, the direction of stresses from upper and lower column towards to the center height of column. The axial stress distributions with various intensities of stress are concentrations around the longitudinal reinforcement at the locations of stirrups.

4. Participate each of ordinary concrete, main steel, and stirrups on the vertical column load is 85%, 9%, and 6% respectively.

5. The concrete columns reinforcement by GFRP bars as a main reinforcement and stirrups have reduced the ultimate capacity of column vertical load by 10 -15% in comparison with the columns reinforcement by steel bars.

6. The concrete columns reinforcement by GFRP bars as a main reinforcement have reduced the ultimate capacity of column vertical load by 2 - 5% in comparison with the columns reinforcement by steel bars.

7. The steel stirrups gives well confinement by eliminate the buckling of the longitudinal GFRP bars compared with GFRP stirrups and gives results close to column reinforcement by steel. So, it is recommended to use GFRP for main reinforcement and steel for stirrups if the column used GFRP bars as reinforcement.

8. Tested column with steel reinforcement has ductility more than column with GFRP reinforcement.

9. Increasing GFRP reinforcement ratio leads to increase the ultimate vertical load, vertical displacement, peak stresses, the toughness and ductility of tested columns.

10. Increasing of characteristic compressive strength of concrete has significant effect on the behavior of tested columns reinforced by GFRP bars where it increases toughness and ductility of tested columns.

11. The analytical results were compared considering the axial compression design provided by ACI Building Code and CSA S806-02. A new general formula was predicted from these results. The nominal capacity of an axial loaded RC column P_n for column reinforcement by GFRP as a main reinforcement can be calculated from a new predicted formula considering the contribution of GFRP bars in compression equal to 20% of tensile strength of GFRP and 70% of F_{cu} if F_{cu} equal to 40 MPa and 60% if F_{cu} = 25 MPa.

Predicate Formula:

$$\mathbf{P_n = 0.7f_c'(A_g-A_s) + 0.2f_y A_s} \qquad \mathbf{For\ F_{cu} = 40\ MPa}$$

$$\mathbf{P_n = 0.6\ f_c'(A_g-A_s) + 0.2f_y A_s} \qquad \mathbf{For\ F_{cu} = 25\ MPa}$$

Where, P_n = the nominal capacity of an axial loaded RC column, A_g= the total cross section area of column, A_s= cross section area of longitudinal reinforcement. f_c'=concrete compressive strength and f_y= yielding strength of steel reinforcement.

REFERENCES

1. MEISAM SAFARI GORJI (2009) "Analysis of FRP Strengthened Reinforced Concrete Beams Using Energy Variation Method" World Applied Sciences Journal 6 (1): 105- 111.

2. AMERICAN CONCRETE INSTITUTE (2008) "Building code requirements for structural concrete," ACI 318-08, ACI, Farmington Hills, MI.

3. ACI COMMITTEE 440 (2006) "Guide for the design and construction of structural concrete reinforced with FRP bars," ACI 440.1R-06, American Concrete Institute, Farmington Hills, MI.

4. CHING CHIAW CHOO, ISSAM E. HARIK, AND HANS GESUND (2006) "Minimum Reinforcement Ratio for Fiber-Reinforced Polymer Reinforced Concrete Rectangular Columns" ACI Structural Journal/May-June, 460-466 pp

5. NICHOLAS M., RAJAN S. (2003) "The Fatigue of Fiber-Reinforced Polymer Composite Structures State-of-the-Art Review" Civil & Environmental Engineering, USF College of Engineering.

6. V. M. KARBHARI, J. W. CHIN, D. HUNSTON, B. BENMOKRANE, T. JUSKA, R. MORGAN, J. J. LESKO, U. SORATHIA, AND D. REYNAUD (2003) "Durability Gap Analysis for Fiber- Reinforced Polymer Composites in Civil Infrastructure" Journal of Composites for Construction, ASCE -August, 238-247 pp

7. CAN/CSA S806-02,2002, "Design and construction of building components with fiber reinforced polymers", Canadian Standards Association, Mississauga, Ontario, Canada, 177 pp.

8. MANDER, J. B., PRIESTLY, M. J. N., AND PARK, R., "Observed Stress Strain Behavior for Confined Concrete" , J. Struct. Engrg, ASCE, Vol. 114, No. 8, PP. 1827-1849, Aug., 1988a.

9. POPOVICS, S., A Numerical Approach to the Complete Stress-Strain Curve of Concrete, Cement and Concrete Research, V. 3, No. 5, May 1973, pp. 583-599.

10. ANSYS User's Manual, Swanson Analysis Systems, Inc 10. William, K.J. and E.D. Warnke (1975) "Constitutive model for the triaxial behavior of concrete". Proceedings of the International Association for Bridge and Structural Engineering.

Research on and Application of Integrated Low-carbon Environment-friendly Technology in Asphalt Pavements

L Liu, L Sun, H Xu, H Wang, J Li, X Gao
Tongji University, China

Rapid development of road construction and traffic has greater and greater impact on urban ecological system and living environment. Urban ecological environment is seriously threatened. While meeting traffic demand and promoting economic development, it is objectively required to re-examine technology for road construction, maintenance and operation from the angle of environment protection and ecology, so as to stick to the principle of sustainable development and achieve harmonious development of human being and the nature. In this research, warm-mix asphalt (WMA) technology is adopted to reduce energy consumption and pollutant emission during construction, and noise-reducing asphalt pavement added with "photo-catalyst Nanometer material" is adopted to reduce pollution by noise and vehicle exhaust on road in service. WMA technology, noise-reducing asphalt mixture technology, photo-catalysis vehicle exhaust-absorbing technology are introduced in this paper with stress, including evaluation on performance of dense gradation and open gradation WMA mixture, design for big gap and noise-reducing asphalt mixture, development of photo-catalysis test system, selection of vehicle exhaust-absorbing material, evaluation on laboratory test, addition technology and performance evaluation of asphalt mixture, application of and effect evaluation on pilot projects in Shanghai, and so on. Preliminary research and observation indicate that emission of carbon dioxide can drop by adopting WMA technology during asphalt pavement construction, and concentration of leaded compound and carbon oxide and concentration of nitrogen oxides and formaldehyde can drop by more than 50% and more than 30% respectively by adopting noise-reducing asphalt pavement added with "photo-catalyst" Nano material during operation. In addition, compared to common asphalt pavement, noise is reduced by 5 8 dB, reflecting better environmental and social benefit.

Dr Liping Liu is an Associate Professor at Tongji University, Shanghai, China. She has led several research projects on asphalt pavement, and her research interests include asphalt pavements design and maintenance, performance evaluation for warm mix asphalt, pavement recycling etc.

Haiming Xu, Jianfei Li, Hui Wang, Xiaofei Gao are graduate student.

Dr Lijun Sun is a professor at Tongji University, Shanghai, China. He has led many research projects on road pavement and traffic control area, and his specialist areas of research are asphalt pavements design, pavement management system, and intelligent traffic control.

Keywords: Asphalt pavement, Environment-friendly, Low-carbon, Nanometer material, Noise-reducing, Vehicle exhaust

INTRODUCTION

With increasing adverse impacts of rapidly growing road construction and transportation upon the urban ecosystem and living environment, the urban ecological environment is being exposed to severe menace. On the one hand, Hot mix asphalt(HMA) apt to generate a raft of smog and waste gas (e.g. carbon dioxide) at higher temperature in the traditional HMA pavement construction has negative influences upon the surroundings and the populations, particularly severe harms to the road construction crews' health; On the other hand, the auto, with rapid growth of transportation sector, generates the vehicle exhaust pollutants both to severely affect the natural environment by which the human lives and to impose negative influences upon the human's physical & psychological health while it brings great convenient transportation to the people. For better upholding the principle of sustainable development and carrying out the harmonious development between the nature and the human accordingly, it is the objective requirement to re-conceive of road construction & maintenance and operation technologies environmentally and ecologically while the traffic demands are met and economic growth is promoted.

Warm mix asphalt(WMA) technology, a kind of new green & low-carbon construction technology coming into being in the context of energy conservation and environment protection, may be applied to construction of the asphalt pavement, which could, without prejudice against the performance of the asphalt mixtures, effectively reduce the temperature necessary for production and paving of the mixtures, improve the environmental pollutions arising out of and during construction of the asphalt pavement and consume less energy necessary during production of traditional asphalt mixtures. It boasts remarkable both social and environmental benefits. During the service of asphalt payment, "photo-catalyst" nano material addition technology featuring disintegration of the auto vehicle exhaust may be applied. Addition of such material into the noise-reducing asphalt pavement could reduce the noises and auto vehicle exhaust pollutions available with the roads in service. The research succeeded in integrated application of warm mix technology, noise-reducing asphalt pavement technology and vehicle exhaust absorbing pavement technology, bringing about such favorable environmental protection results as emission reduction during construction, noise reduction & vehicle exhaust absorption during operation as well as achieving remarkable environmental effects and social benefits. The paper was mainly targeted to make description of design and performance evaluation of the WMA technology and noise-reducing asphalt permeable mixtures as well as research and development, application and evaluation results of the photo-catalysis-based vehicle exhaust absorbing technology.

WMA TECHNOLOGY

Presently WAM technology is the popular technology widely used for production and paving of asphalt mixtures and energy conservation and emission reduction. It aroused extensive attentions by the international road section due to its prominent edge of environmental protection since it came into being in 1995. Several warm mix technologies or products are now available[1-3], typically for example: WAM-Foam technology, Evotherm surface active

platform based warm mix technology, Aspha-Min Artificial zeolite additives, Sasobit, Asphaltan B and SAK organic additives warm mix technologies. Different warm mix technologies are various in warm mix mechanisms and processes, thus leading to differences in results thereby. The paper, on the basis of and subject to the previous studies and practical experiences, mainly takes surface active platform based warm mix technology as the option to achieve production and paving of the asphalt mixtures as well as energy conservation and emission reduction.

Evaluation on Performance of Surface Active Platform Based Dense-Graded WMA

Surface active platform based warm mix technology is a unique WMA technology initiated by Asphalt Innovation Department of Mead Westvaco. Now it has undergone three generations, out of which the first generation is emulsified platform based warm mix technology, the second generation is direct-fed scattered warm mix technology, and the third generation is Evotherm 3G technology. This study was mainly targeted on the second generation, i.e., the direct-fed scattered warm mix technology. This technology adopts surface active principle, or in other words, surface active water solution (DAT) additives are fed along with hot asphalt. This additive can enable water membrane lubrication structure to come into being inside binding medium during mixing of asphalt mixture, so as to achieve work performance at lower temperature.

This paper mainly evaluated WMA in terms of stability at high temperature, crack resistance at low temperature, water stability and fatigue resistance, and compared it to HMA of the same gradation. SBS modified asphalt was adopted as binding medium. Basalt was used as coarse aggregate, limestone as fine aggregate. Gradation was AC-13C type, target porosity 4%, the optimum asphalt content in WMA designed in Marshall method 4.8%, mixing temperature controlled at 140℃ or so, forming temperature controlled at 130℃ or so. The optimum asphalt content in HMA of the same gradation designed in the same method was 4.5%, mixing temperature controlled at 175℃ or so, forming temperature controlled at 165 ℃ or so. Performance tests methods see also JTJ 052-2000[4]. See Table 1 for comparison on performance of WMA and HMA. See Figure 1 for comparison on fatigue life[1].

It can be seen from comparison tests that 1) in design for proportion of Dense Graded asphalt mixture, when mixing temperature dropped by 35℃ or so, the optimum asphalt content of Dense Graded WMA was 0.3% higher than that of HMA of the same gradation; 2) all technical parameters of Dense Graded WMA could meet technical requirements of HMA of the same kind; 3) at their respective optimum asphalt content, Dense Graded WMA was superior than HMA in terms of fatigue performance, but slightly worse than HMA of the same gradation in terms of stability at high temperature and water stability.

Table 1 Comparison on Performance of Dense Graded WMA and HMA

PERFORMANCE TEST OF DENSE-GRADED WMA AND HMA				
Type of mixture	TSR, %	Dynamic Stability , times/mm	Maximum damage strain, με	Shear strength, MPa
WMA	81.2	7693	5632	1.07
HMA	85.3	10443	5653	1.35
HMA requirement (JTJ F40-2004)[5]	＞80	＞3000	＞2500	/

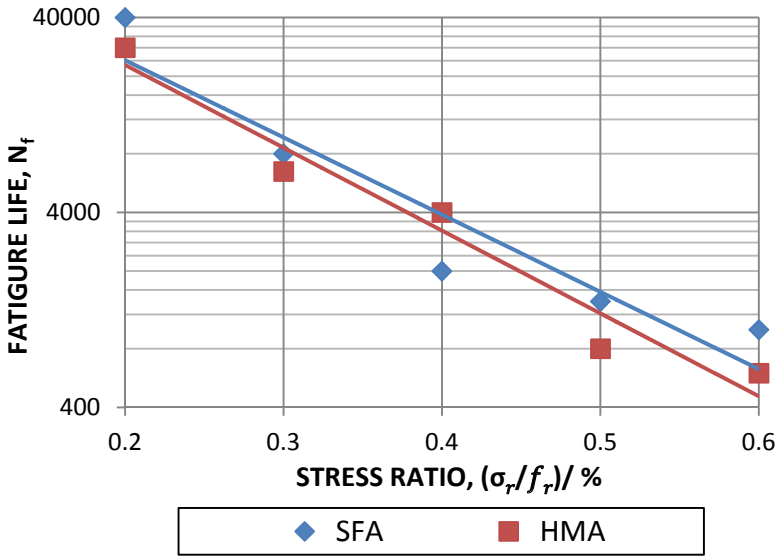

Note: SFA is referred to surface active platform based warm mix technology

Figure 1 Comparison of WMA and HMA in anti-fatigue property

Design and Evaluation on Open-graded Permeable Noise-reducing WMA

The research found that warm mix technology was applicable for not only common asphalt, modified asphalt, rubber asphalt, but also continuous-graded, GAP-graded and open-graded mixture. Gradation design for warm mixed OGFC13 was the same as that for hot mix. Table 2 showed the results of some performance parameter tests of OGFC13 mixture at different compaction temperatures (mixing temperature 160℃).

It could be seen from Table 2 that all parameters met technical requirements when the mixture was mixed at 160℃ and compacted at 150℃. Therefore, this compaction temperature was chosen to test dynamic stability and water stability of mixture. See Table 3.

Table 2 Result of Test at Different Compaction Temperature

TEST AT DIFFERENT COMPACTION TEMPERATURE					
Test Parameter	Compaction Temperature（℃）				Technical Requirement[5]
	130	140	150	160	
Porosity (%)	23.18	22.14	20.95	20.33	18～25
Scattering Loss (%)	17.7	15.42	14.9	13.07	<20
Immersed Scattering (%)	28.1	23.8	15.11	13.93	<30
Marshall Stability (kN)	3.01	3.41	3.52	3.62	>3.5

Table 3 Test on Performance of Open-graded WMA

PERFORMANCE OF OPEN-GRADED WMA					
Test Parameter	Residual Stability（%）	TSR（%）	Dynamic Stability (time/mm)	Permeability Coefficient（ml/min）	Run-off Loss（‰）
Test Result	84.66	91.22	3182	954.2	1.75
JTJ F40-2004[5]	/	/	>3000	Observation	<3

It could be seen from Table 3 that test result of performance of open-graded WMA met technical requirements specified in hot mix code.

LARGE-PORE NOISE-REDUCING ASPHALT MIXTURE DESIGN

Porosity of large-pore noise-reducing pavement, i.e., permeable surface course is generally as high as 18%~25%, which allows rainfall on pavement to infiltrate into structural layer rapidly, and be discharged to edges of the road from inside of structural layer, thus allowing asphalt pavement to keep relatively dry[6]. Therefore, such surface courses not only can effectively reduce water fog, water float and glare in sunny days due to stagnant water on surface, but also provide enough surface roughness and anti-slippery performance, and reduce noise along the road effectively. So large-pore noise-reducing surface courses have widely applied in many countries and reflected very good environment protection benefit. Passenger vehicles featuring high travelling speed and less pollution predominate on urban expressways, where it is more advantageous to build permeable noise-reducing surface courses.

The key to building large-pore noise-reducing surface courses properly lies in selecting high viscosity modified asphalt with good performance. At present there have been several high viscosity modified asphalts available. This research mainly compared, tested and studied RST of Pudong Road & Bridge and TPS high viscosity modified asphalt from Japan. In the test, asphalt 70# for roads with heavy traffic was adopted as basis bitumen, and high viscosity modified asphalts were prepared with high-speed shear emulsifying machine. Table 4 showed test results of regular parameters of different high viscosity modified asphalts.

Table 4 Regular Test Data of High Viscosity Modified Asphalts

REGULAR TEST DATA OF HIGH VISCOSITY MODIFIED ASPHALTS					
Type of modified asphalts	Penetration，25 ℃/0.1 mm	Softening point/℃	Ductility/cm, 5 ℃	Viscosity/ (Pa•s),135℃	Viscosity/ (Pa•s),60℃
TPS (12%)	46.4	86.3	29.4	2.4	30 250
TPS (10%)	50.3	80.9	28.5	2.5	24 350
RST (12%)	40.2	88.8	56.5	2.1	72 180
RST (10%)	*35.4*	82.4	75.7	1.3	45 460
JTG F40-2004[5]	≥40	≥80	——	<3	>20 000

It could be seen from Table 4 that penetration of RST (10%) modified asphalt was not so ideal and not was considered. Therefore, this study mainly compared mixtures design and performance tests of large-pore mixtures of TPS (12%), TPS (10%) and RST (12%) modified asphalts. In the tests, diabase was adopted as coarse aggregate, limestone as fine aggregate, cellulose fiber as fiber additive, target porosity controlled at 20% or so, gradation OGFC13, as shown in Table 5. The optimum bitumen-aggregate ratio identified through tests was 5.2%. See Table 6 for various performance test data of OGFC mixture of different high viscosity asphalts.

Table 5 Gradation of OGFC13 Mixture

GRADATION OF OGFC13 MIXTURE									
mesh size /*mm*	13.2	9.5	4.75	2.36	1.18	0.6	0.3	0.15	0.075
Passing rate/%	96.2	68	17.2	13.5	10.1	8.1	6.9	5.4	4

It could be seen from Table 6 that high-temperature stability of RST (12%) high viscosity modified asphalt mixture was significantly better than that of TPS. Therefore, this study adopted RST (12%) modified asphalt to prepare large-pore surface course mixture for test section work.

Table 6 Summary of Performance Tests of OGFC13 Mixture

PERFORMANCE TESTS OF OGFC13 MIXTURE				
Type of modified asphalts	TPS (12%)	TPS (10%)	RST (12%)	Technical Requirements[5]
Run-off Loss（‰）	0.05	0.07	0.04	<0.3
Scattering Loss (%)	18.1	19.3	18.1	≤20
Marshall Stability (kN)	5.24	5.02	4.78	≥3.5
Dynamic Stability (times/mm)	3 796	3425	>6000	≥3000
TSR(%)	85.50	86.21	90.05	≥80
Friction coefficient	73	73	77	>58
Permeability Coefficient (cm/s)	0.233	0.162	0.170	>0.01

PAVING TECHNOLOGY FOR VEHICLE EXHAUST DISINTEGRATION

In recent years, under the pressure from environment protection, many countries have tried to research and develop vehicle exhaust absorbing paving material. Through research, Italy and Japan believed that photo-catalyst nano titanium dioxide material can disintegrate nitrogen oxides in vehicle exhaust effectively, and applied it to cement pavement projects[7,8]. This study drew on the experience abroad, and studied addition technology and effect of applying nano titanium dioxide in asphalt pavements, including development of photo-catalysis test system, selection of vehicle exhaust absorbing additive, determination of the way and dose of adding additive into asphalt pavements, project application and effect assessment.

Development of Photo-catalysis Test System

In order to seek additives that can significantly absorb vehicle exhaust, it was necessary to have certain test conditions. This study developed a photo-catalysis test system autonomously, including vehicle exhaust analytical apparatus, sealed quartz glass container, UV light radiation box, UV-A type UV radiometer, gas collection pump and sample bags. **Vehicle exhaust analytical apparatus**: This apparatus can be used to test concentration of emissions after auto engine combusts, including hydrocarbons (HC, mainly propane), carbon monoxide (CO), carbon dioxide (CO_2), oxygen (O_2) and nitrogen oxides (mainly NO), as well as concentration of above harmful gas existing in environment.

Sealed quartz glass container: This container made of quartz glass features good optical properties, and can transmit 90% or so ultraviolet light, while common glass transmits 40% or so ultraviolet light only. It was sized 300mm×300mm×300mm, and was equipped with air inlet and outlet with valves. The entire container has good air-tightness.

UV light radiation box: Nanometer material mainly plays a role in catalyze to decompose harmful gases under the radiation of UV light. However, since weather outdoors varies frequently, stable UV radiation intensity and temperature can be hardly obtained. Thus an UV radiation box that can accommodate sealed container was specially engineered to control temperature in this box and obtain stable UV radiation intensity for quantitative research indoors.

UV-A type radiometer: This radiometer is applicable for measuring radiation intensity value of UV with wave length mean values in 365nm and 420nm.

Gas collection pump and sample bags: They were mainly used for collection and analysis of vehicle exhaust at site.

Selection of Vehicle Exhaust Absorbing Material

Vehicle exhausts used in indoor tests should be certain representative and stable. This study carried out statistics and analysis on rough proportion of different components in vehicle exhaust based on results of observation on over 170 vehicles and congested road sections at peak hour on site, and entrusted departments concerned to compound vehicle exhaust for indoor test on the basis of this. Then two kinds of nano titanium dioxide (anatase and rutile) with different crystal types were selected to carry out comparative tests and research on vehicle exhaust absorption effects [9,10]. Main components in vehicle exhaust considered were carbon monoxide (CO), hydrocarbon (HC) and nitrogen monoxide (NO). Figure 2 showed catalytic decomposition effects of nano titanium dioxide with different crystal types on CO.

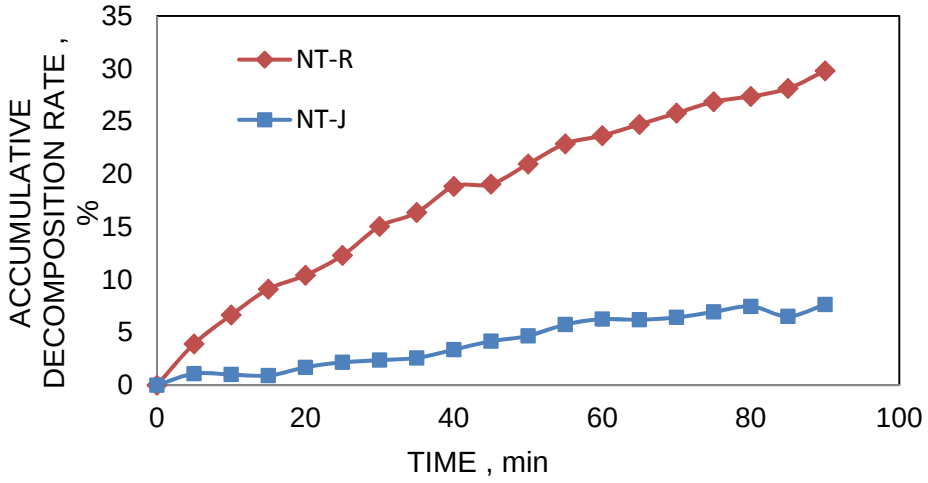

Figure 2 Catalytic Decomposition Effect of Nano Titanium Dioxide with Different Crystal Types on CO

It was similar to the other two components. It could be seen that titanium dioxide of both crystal types can help to decompose CO, but anatase type was significantly superior to rutile type. Therefore, anatase type titanium dioxide was mainly adopted in subsequent tests and research on absorption of vehicle exhaust.

Determination on Way and Dose of Adding Nano Material Into Asphalt Pavements

It was a difficult point herein how to add nano titanium dioxide into asphalt pavement because both manoeuvrability and economical efficiency and effectiveness in actual construction should be taken into account. This study considered three different ways of addition through rutting plate specimen formed indoors, i.e. (1) later stage of compaction painting, as shown in Figure 3 (a); (2) earlier stage of compaction painting, as shown in Figure 3 (b); (3) addition when mixture is blended, then rolling compaction, as shown in Figure 3 (c).

(a) (b) (c)

Figure 3 Three Ways of Adding Nano Titanium Dioxide

Figure 4 to Figure 6 showed the results of tests and analysis for different ways of addition in outdoor sunlight.

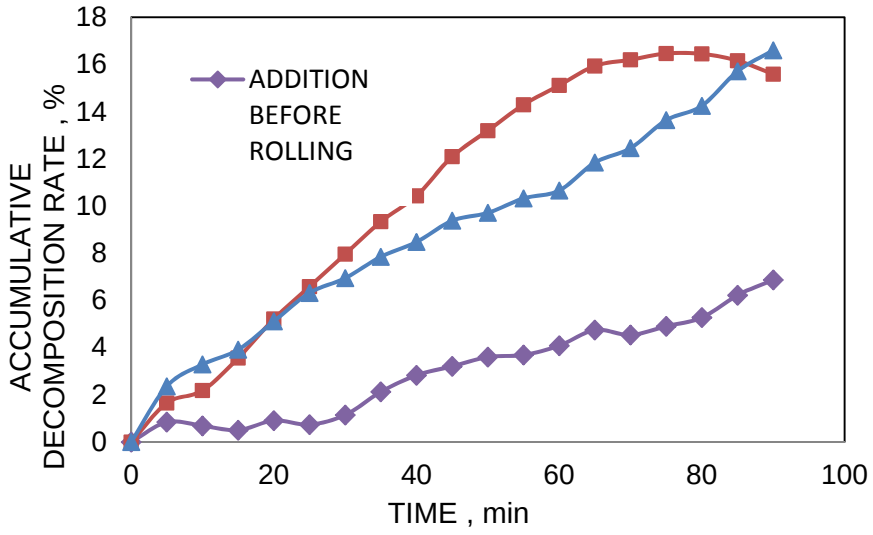

Figure 4 Decomposition Effect of Three Ways of Addition on CO

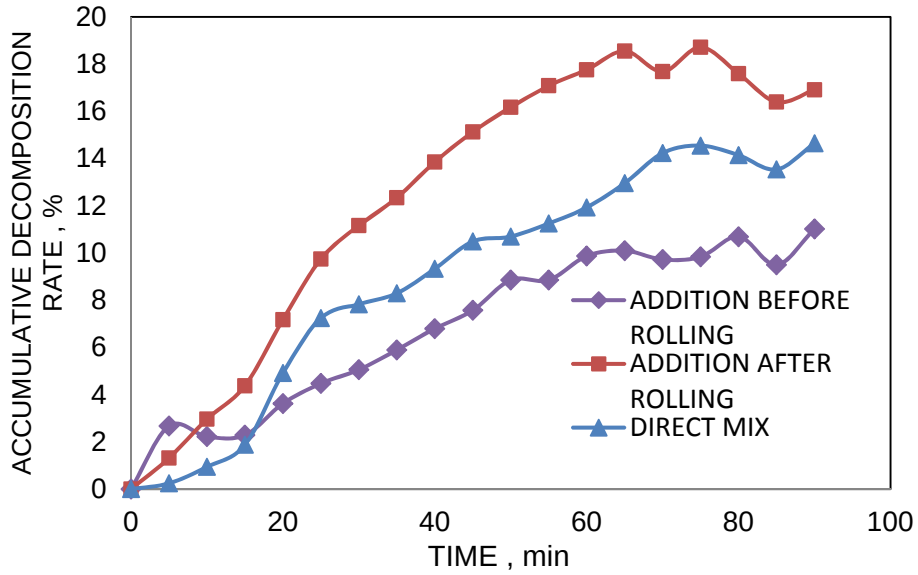

Figure 5 Decomposition Effect of Three Ways of Addition on HC

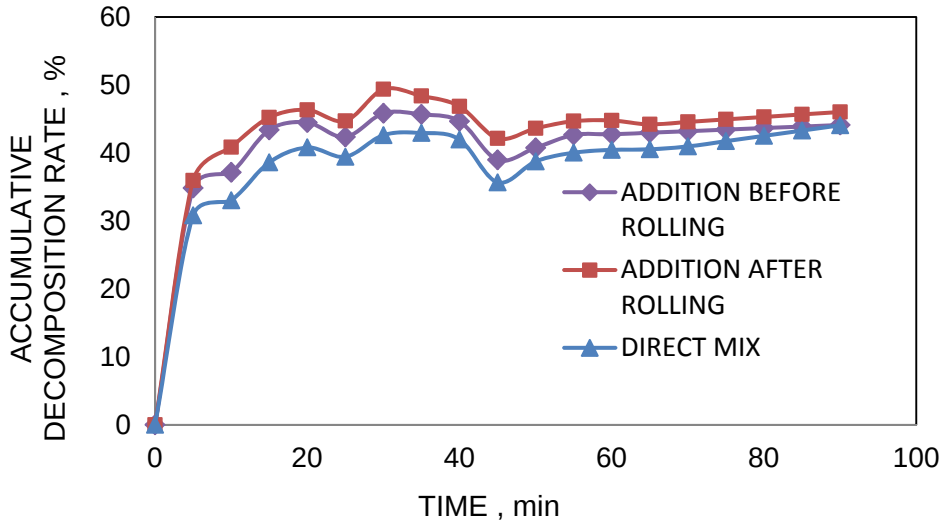

Figure 6 Decomposition Effect of Three Ways of Addition on NO

It could be seen from Figure 4 to 6 that all of the three ways of addition had certain decomposition effect on three gases. For CO and HC, direct mixing mode was between later stage of compaction painting and earlier stage of compaction painting, and its decomposition efficiency dropped slowly with time. For NO, it could be deemed that absorption effect of the three ways of addition was equivalent. In view of the fact that direct blending can be operated simply during road construction and does not have such deficiency as the possibility of being blown away by wind, or brought away by wheels, or losing with water, direct blending was adopted finally.

In order to identify the optimum addition dose of nano titanium dioxide in asphalt mixtures, formed rutting plates were still adopted. 10g, 20g, 30g and 40g nano material were added in mixtures respectively and placed in sunlight outdoors to carry out vehicle exhaust decomposition tests. Figures 7 to 9 showed the results of tests and analysis for different addition doses.

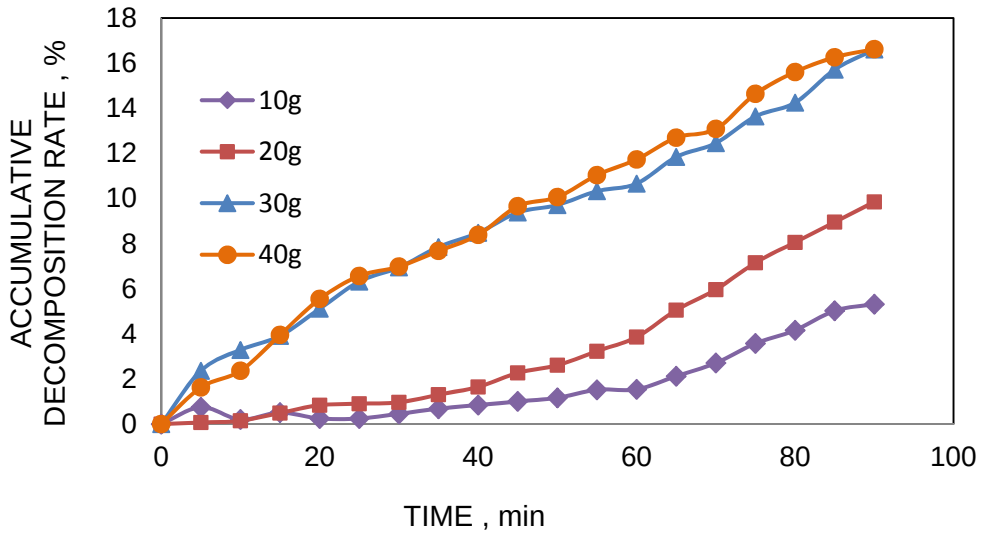

Figure 7 Decomposition Effect of Different Addition Doses on CO

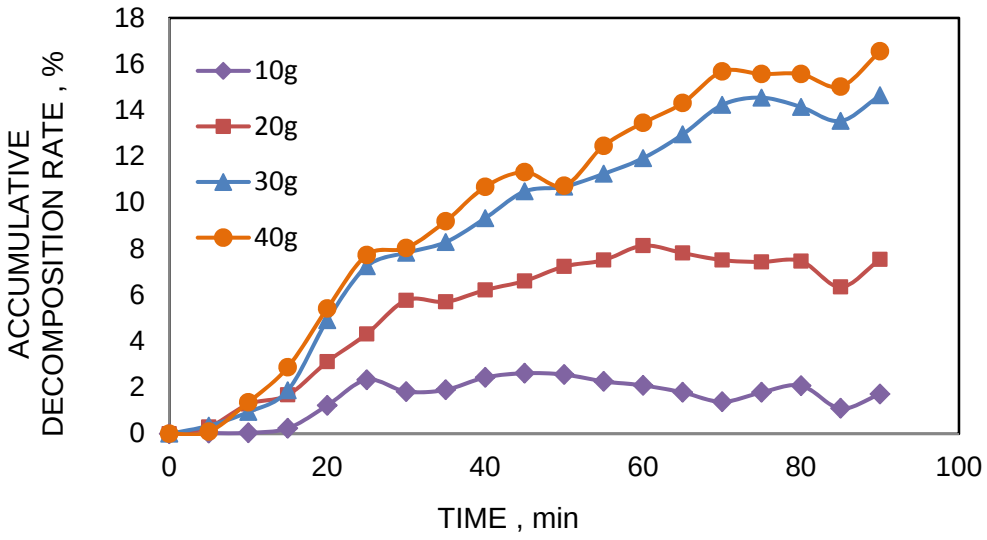

Figure 8 Decomposition Effect of Different Addition Doses on HC

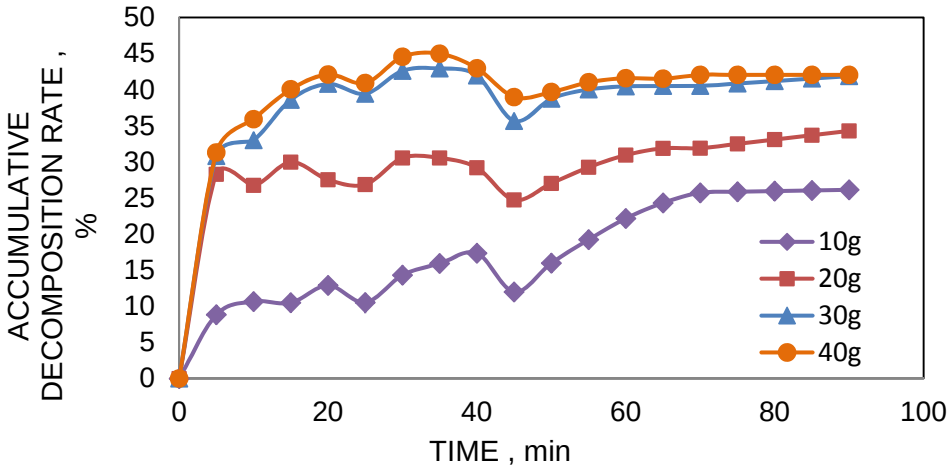

Figure 9 Decomposition Effect of Different Addition Doses on NO

It could be seen from Figures 7 to 9 that with increasing dose of nano titanium dioxide, absorption of three gases grew in sunlight outdoors. When the dose was 30g, it grew to large extent, while when the dose was 40g, the growth was not so significant, particularly for NO. This might be because the reaction was saturated due to concentration of gas and sunlight radiation conditions, and it did not work much by increasing dose of nano titanium dioxide. In view of absorption effect and economical factors, an addition dose of 30g was recommended, which was converted to 3.9kg nano titanium dioxide per ton of mixture.

PROJECT APPLICATION AND EFFECT ASSESSMENT

The research group paved low-carbon, environment-friendly, noise-reducing asphalt pavement test section integrating warm mix, noise reduction, vehicle exhaust absorption technique near the lower ramp on Jinke Road in the inner circle of Central Link Pudong in December, 2009. During mixing, paving and compaction of this kind of mixture, good construction performance was presented. In order to inspect effect of the test section, this section and control section were tested in terms of friction coefficient, permeability coefficient, traffic noise and road air quality after they were open to traffic for half a year. Table 7 showed the results of comparative tests on friction coefficient, permeability coefficient and traffic noise.

Table 7 Results of Comparative Tests on Major Performance of Test Section

COMPARATIVE TESTS ON MAJOR PERFORMANCE OF TEST SECTION			
Item	OGFC Test Section (with Titanium Dioxide)	OGFC Control Section (without Titanium Dioxide)	Common Pavement (AC)
Friction Coefficient (BPN)	64.5	66.5	/
Permeability Coefficient (ml/min)	1113.3	1209.3	/
Traffic Noise (dB)	77～79	77～80	85

It could be seen from Table 7 that addition of nano titanium dioxide had little influence on pavement anti-slippery capability, permeable effect and traffic noise. Anti-slippery capability and permeable function were maintained well on OGFC surface course. Compared to common pavement, OGFC surface course reduced noise significantly by 5～8 dB when cars ran at 80 km/h.

Table 8 showed the results of comparative test on titanium dioxide absorbing vehicle exhaust.

Table 8 Results of Comparative Tests on titanium dioxide absorbing vehicle exhaust

COMPARATIVE TESTS ON TITANIUM DIOXIDE ABSORBING EXHAUST				
Item	Unit	Inspection Section		Decomposition Effect/%
		Nano Test Section	Control Section	
Nitrogen Oxides	mg/m^3	0.024	0.035	31.4
Total Hydrocarbon	mg/m^3	11.9	15.0	20.7
Lead	mg/m^3	0.002	0.006	66.7
Carbon Dioxide	mg/m^3	393	448	12.3
Carbon Monoxide	mg/m^3	0.125	1.00	87.5
Formaldehyde	mg/m^3	0.010	0.015	33.3

Note: When the test was carried out, outdoor UV intensity was 2040 $\mu W/cm^2$, and traffic volume reached about 26,000 vehicles per day. Data listed in the table were observed by environment monitoring department.

It could be seen from Table 8 that contents of harmful gases in air over test section containing nano material were significantly lower than those in control section. Here, concentration of lead compounds and carbon monoxide dropped most significantly. The next were nitrogen oxides and formaldehyde. It indicated that nano titanium dioxide can play a role in catalyzing to decompose harmful gases when it was applied in actual road project.

CONCLUSIONS

This study integrated such environment protection technology as low-carbon construction (warm mix technology), noise reduction, vehicle exhaust absorbing pavement engineering technology. During construction, when warm mix technology was adopted, emission of gases such as CO_2 and dust can drop significantly, thus reducing pollution to environment, improving quality of working environment of workers, and prolonging operation duration at low temperature; during road service period, the larger surface area contacting air of large-pore asphalt mixture pavement can help sunlight to go inside the mixture to provide favourable conditions for “photo-catalyst” nano material added into pavement to absorb vehicle exhaust besides functioning to reduce noise and discharge water.

The results of lab tests indicated:

1) All technical parameters of surface active based WMA can meet technical requirements of HMA of the same kind.
2) Warm mix technology can be implemented with open-graded asphalt mixture (OGFC) successfully, where technical requirements of HMA of the same kind can still be met when temperature of mixture dropped by 30℃ or so.
3) Performance of large-pore mixture prepared with RST (12%) high viscosity modified asphalt was relatively superior, particularly that its stability at high temperature was significantly better than that of TPS modified reagent.
4) Anatase nano titanium dioxide is a photo-catalysis material with excellent performance.
5) Considering both convenience in construction and application effect and durability, at present direct mixing was a more suitable way of addition in applying nano titanium dioxide in asphalt pavements.
6) In view of absorption effect and economical factors, an addition dose of 3.9kg nano titanium dioxide per ton mixture was recommended.
7) Results of preliminary observation on test section indicated a noise reduction by 5~8 dB, good permeability in rainy days and safe and comfortable driving; and a drop in concentration of lead compounds and carbon monoxide in vehicle exhaust by above 60%, and a drop in concentration of nitrogen oxides and formaldehyde by above 30%.

Therefore, it can effectively achieve energy efficiency and emission reduction during road construction, reduction of noise pollution and air pollution during operation, and improvement of safety in travelling by combining photo-catalysis technology, WMA technology and permeable noise-reducing pavement technology. This integrated technology has been successfully applied to test section in Central Link Pudong, and is worthy of further studying and applying.

ACKNOWLEDGEMENTS

This research was sponsored by the Shanghai Science and Technology Commission. The authors wish to thank all the people who participated in this study.

REFERENCES

1. LIU LIPING,GAO XIAOFEI, ZHANG ZHEN, etc, Evaluation of Three Warm Mix Asphalt Technologies, the 11th International Conference on Asphalt Pavements (ISAP NAGOYA 2010), August 1-6, 2010, Nagoya

2. GRAHAM C. HURLEY, BRIAN D. PROWELL., 2007.Evaluation of Potential Processes for Use in Warm Mix Asphalt. http://www.warmmix.net.

3. GRAHAM C. HURLEY, BRIAN D. PROWELL., 2006. Evaluation of Evotherm® for Use in Warm Mix Asphalt. NCAT Report 06-02, U.S.

4. JTJ 052-2000, Standard test method of bitumen and bituminous mixtures for highway engineering.

5. JTJ F40-2004,Technical Specifications for Construction of Highway Asphalt Pavements.

6. JAPAN ROAD ASSOCIATION, Technical Guide for surface drainage ,1996.11

7. http://www.bjpopss.gov.cn/bjpopss/kjsc/kjsc20000831.htm.zh

8. http://www.all2car.com/news-detail/74763uri3-10003467.html

9. LI JINTIAN,GENG SHIBIN．Nano TiO2 Photocatalysis Mechanism and Application Analysis [J]．Contamination Control & Air-Conditioning Technology，2006，1：23-25

10. YU YANHUI, HARIBALA，etc．The research progress on nano-TiO2 photocatalyst [J]．Materials Review，2008，22(X)：54-57

Research on the Design and Properties of Low Carbon Semi-flexible Pavement Material

F Wang, C Yu, Y Liu, J Fu
Wuhan University of Technology, China

Asphalt concrete (AC) and Portland cement concrete are two commonly used road construction materials and readily available in most locales. AC paving is a flexible pavement with the advantages like low noise, relatively low cost and disadvantages including less tensile strength than concrete. Moreover, it's produced by heating the asphalt binder to 300 °F (roughly 150 °C) for virgin asphalt and 330 °F (166 °C) for polymer modified asphalt which results in higher consumption of fossil fuels, thus releasing more carbon dioxide, aerosols and vapours. Portland cement concrete has higher mechanic strength and elastic modulus but larger brittle compare to asphalt concrete. Due to the larger cement content (300-450kg/m^3); the preparation of Portland cement concrete consumes much mineral recourse. The present study is to develop a low carbon semi-flexible composite pavement material with cement and asphalt emulsion, which can be prepared under ambient temperature and possesses the advantages of moderate resilient modulus, nice moisture stability, good low temperature crack resistance, less cement content(100-120kg/m^3), energy saving and long lasting. This new semi-flexible pavement material has been successfully applied in "Yiyang Class-A highway" of Yichang city, Hubei province for 200m and has good prospect in development and application.

Fazhou Wang is currently Professor of State Key laboratory of Silicate Materials for Architecture, Wuhan University of Technology, China. He has done much work on the concrete and advanced cement-based composite materials. His specialist areas are light-weight aggregate, cement and asphalt mortar for high-speed railway and advanced asphalt pavement.

Chunlin Yu is post graduate of State Key laboratory of Silicate Materials for Architecture, Wuhan University of Technology, China. His main research interests are advanced asphalt pavement, especially cement-asphalt emulsion concrete for semi-flexible pavement.

Yunpeng Liu is PhD candidate of State Key laboratory of Silicate Materials for Architecture, Wuhan University of Technology, China. His main research interests are cement and asphalt mortar for high-speed railway, asphalt emulsion for high-speed railway and repair materials for high-speed railway.

Jun Fu is currently Associate Professor of School of Transportation, Wuhan University of Technology, China. He his main research interests are building materials and structure engineering. His specialist areas are structure and materials for functional long life pavement, micro-mechanics analysis of pavement and bridge materials and service monitor of bridge and pavement.

Keywords: Cement emulsified asphalt concrete, Energy saving, Low carbon, Mix design, Road performances

INTRODUCTION

Presently, asphalt concrete and cement concrete are mainly used as pavement materials. Asphalt concrete is widely used due to its excellent characteristics of good smoothness and driving comfort and so on. However, it also has some deficiencies. On one hand, asphalt concrete is poor in temperature stability for viscoelastic plastic of itself, which makes it easy to suffer from the wheel rut, crack and water damage. On the other hand, the asphalt concrete need to be heated up to more than 160℃, causing a large amount of fuel consumed and environmental polluted. Cement concrete pavement material not only has high strength and elastic modulus, but also has high bearing capacity. While in the effect of temperature stress, it cracks easily. In driving load under the repeated action, pavement shows the weakness of great brittleness and vibration. Besides, it has high cement content (300~450 kilos per cubic meter), which consumes a tremendous amount of raw materials [1].

In recent years, many scholars have developed two new kinds of cement asphalt pavement materials. One is pouring the cement mortar or cement paste into the matrix of larger open-graded asphalt mixture (volume of air voids is 20%~30%), which improves the anti-rutting ability, sliding durability and low temperature crack resistance. The other is introducing emulsified asphalt or polymer dispersion into the cement concrete matrix, which enhances crack resistance and driving comfort of cement concrete road surface. Above all, the two kinds of pavement materials both have the advantage of rigid pavement and flexible pavement, owing to using cement and asphalt as cementing materials [2].

Although the pouring cement asphalt concrete pavement is provided with good anti-rutting ability and low temperature crack resistance, the construction process is much complex due to many influence factors of air void of matrix and the difficulties on controlling the workability of slurry. As a result, it will be restricted in application [3].

Laboratory study showed that cement emulsified asphalt concrete (CEAC), developed by using cement and emulsified asphalt as the major materials, had characteristics of low cement content, moderate resilient modulus, nice moisture stability and good low temperature crack resistance and so on. It also showed this semi-flexible pavement material might be worthy of popularization due to its low carbon and energy saving [4-6].

MATERIALS AND MIX DESIGN

Materials

Ordinary Portland cement 42.5 was used in this study, whose properties were given in Table 1 [7]. The aggregates used in this study were crushed limestone, which came from Yichang, Hubei. Physical properties of the aggregates were given in Table 2 [8]. Anionic slow setting

emulsified asphalt was used in the experimental study because of its high adhesion bond with the aggregates used in this study. The physical properties of the asphalt emulsion and emulsion residue were given in Table 3 [9]. Mineral power was used as filler, whose particle size was smaller than 0.6mm. Besides, 2%~3% (by weight) fly ash was introduced to enhance the compactness and durability of the mixture.

Table 1 Properties of Portland cement

PROPERTY	SPECIFIC SURFACE, m^2/kg	INITIAL SETTING TIME, min	FINAL SETTING TIME, min	COMP. STRENGTH, MPa		FLEXURAL STRENGTH, MPa	
				3d	28d	3d	28d
Standard	≥300	≥45	≤600	≥17	≥42.5	≥3.5	≥6.5
Test value	340	108	365	18.2	48.6	4.0	7.4

Table 2 Properties of aggregate

PROPERTY	BULK SPECIFIC GRAVITY, g/cm^3	WATER ABSORPTION, %	CRUSHING VALUE, %	ADHESION BOND, level
Standard	≥2.50	≤3.0	≤28	≥4
Test value	2.75	0.8	12	5

Table 3 Physical properties of emulsified asphalt

PROPERTY	STANDARD	TEST VALUE
Sieve test (1.18mm), %	≤0.1	0
Viscosity (Grace's viscometer E25)	2~30	16
Solid content, %	≥55	60.0
Solubility (Trichloroethylene）, %	≥97.5	99.6
Penetration (25℃, 100g), 0.1mm	45~150	78
Ductility (15℃, 5cm/min), cm	≥40	95

Mix Design

Aggregate gradation design

In order to increase the rutting resistance and moisture stability of pavement materials, AC-20C aggregates gradation was introduced [10]. Aggregates composition and gradation were given in Table 4 and Table 5, respectively. The aggregates gradation curve was shown in Figure 1. It can be seen that this gradation might has good effect of embedment because it has more coarse aggregates.

Table 4 Aggregates composition

AGGREGATE	MINERAL POWDER	0~5mm GRAVEL	5~10mm GRAVEL	10~20mm GRAVEL
Mass Percentage, %	4.0	37.2	24.4	34.4

Table 5 Aggregates gradation

SIEVE, mm	26.5	19	16	13.2	9.5	4.75	2.36	1.18	0.6	0.3	0.15	0.075
Passing %	100	97.3	89.1	79.4	65.8	42.0	31.5	23.0	16.9	11.4	8.2	5.9

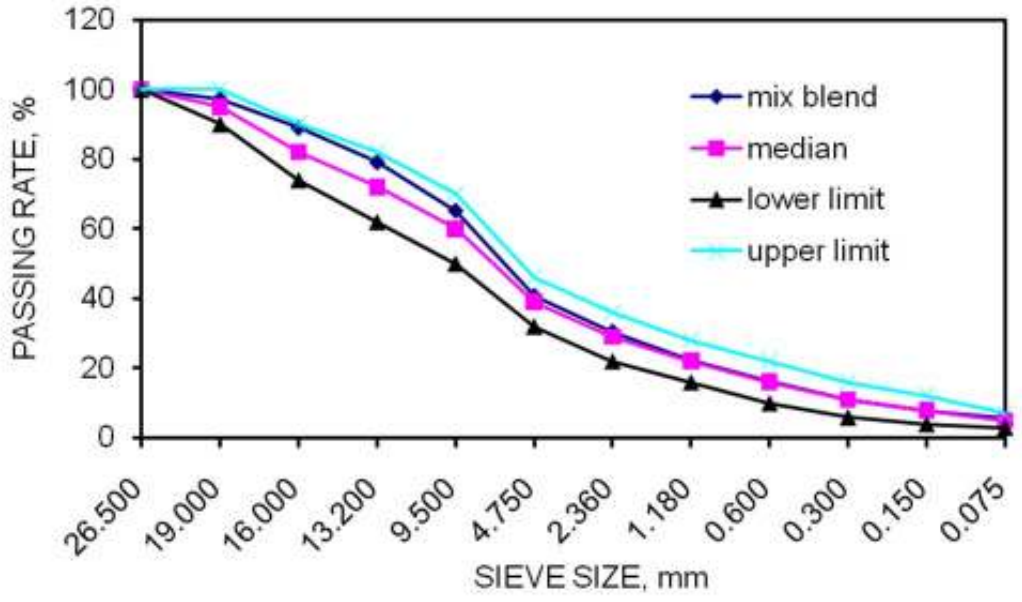

Figure 1 Aggregates gradation curve

Optimal mix design

In order to determine the optimum proportion, Marshall Tests with different asphalt content (3%, 4% and 5%, by weight) and different cement content (0%, 2% and 4%) of CEAC mixture were performed in this study. Samples for Marshall Test were prepared by using 50-blow per side with Marshall Hammer at room temperature. After cured for 48 h, the samples were removed to test bulk specific gravity, stability and flow. The results of Marshall Test were given in Table 6 [9].

Table 6 Results of Marshall test

ASPHALT CONTNET, %	CEMENT CONTENT, %	BULK SPECIFIC GRAVITY, g/cm^3	STABILITY kN	FLOW mm
	0	2.396	11.33	2.12
3	2	2.404	14.56	1.80
	4	2.427	18.37	1.58
	0	2.406	10.09	2.43
4	2	2.415	13.16	2.06
	4	2.433	16.21	1.75
	0	2.409	8.64	2.58
5	2	2.416	10.78	2.25
	4	2.430	12.35	1.87

It can be seen that the bulk specific gravity and stability values are increased with increase in cement content and flow values are decreased with increase in cement content. In other words, the flexibility of CEAC mixture decreases with increase in cement content. The increase in stability of CEAC mixture might be explained by the less curing time, since previous studies have indicated that cement can increase the breaking rate of asphalt emulsion [11].

The optimum proportion is defined on the basis of bulk specific gravity and stability. From Table 6, it can be seen that CEAC mixture with 4% asphalt content and 4% cement content has the maximum bulk specific gravity and quite high stability and relatively low flow. Therefore, the optimum proportion is 4% for both asphalt and cement content. Meanwhile, the water content (including the water contained in emulsified asphalt) should be kept within 5.5%~6%. The following tests samples were taken using of this optimum proportion.

ROAD PERFORMANCES TESTS

Sample Preparation

Samples for resilient modulus test were compacted with hammer in the size of Φ100×100mm at room temperature. Samples for moisture stability and low temperature crack resistance tests were both prepared by using 50-blow per side with Marshall Hammer at room temperature. After cured for 48 h, the samples were removed from the moulds and allowed to air-cured for 28 days at a standard curing room (20±1℃, RH ≥95%) [9].

Resilient Modulus Test

Compressive resilient modulus of CEAC was tested by using universal material testing machine at 15 ℃, under the loading rate of 2mm/min. The test results were given in Table 7. It can be seen that the resilience modulus of CEAC is between that of the cement stabilized gravel and medium grain type asphalt concrete. It means that CEAC is a kind of semi-flexible pavement materials with appropriate stiffness.

Table 7 Results of resilient modulus test

MATERIALS	CEAC	CEMENT STABILIZED GRAVEL	MEDIUM GRAIN TYPE ASPHALT CONCRETE
Value, MPa	3780	3000~4200	1600~2000

Moisture Stability Test

According to some experience home and aboard, immersion Marshall Test and freeze-thaw splitting test were implemented to evaluate the moisture stability of CEAC. The test results were given in Table 8 and Table 9, respectively. From Table 8, it can be seen that the remnants stability of CEAC is obviously higher than that of SUP19 (heavy-traffic asphalt + polyester fiber).

This result shows that cement slurry and asphalt film formed a good integrated reticulate structure system, so that the moisture stability is improved a lot. From Table 9, it can be seen that the ratio of freeze-thaw splitting strength of CEAC is high up to 92.84%, about 10% higher than that of SUP19. Namely, the moisture stability of CEAC is better than that of SUP19 [12].

Table 8 Results of immersion Marshall test

MATERIALS	STABLITY WITHOUT SOAKING, kN	STABILITY AFTER 48h SOAKING, kN	REMNANTS STABILITY, %
CEAC	35.62	32.68	91.04
SUP19	10.79	9.35	86.65

Table 9 Results of freeze-thaw splitting test

MATERIALS	SPLITTING TENSILE STRENGTH BEFORE FREEZE-THAW, MPa	SPLITTING TENSILE STRENGTH AFTER FREEZE-THAW, MPa	RATIO OF FREEZE-THAW SPLITTING STRENGTH, %
CEAC	1.705	1.583	92.84
SUP19	1.425	1.179	82.74

Low Temperature Crack Resistance Test

Splitting test at low temperature was implemented to evaluate the low temperature crack resistance of CEAC. The test was taken at -10℃ and -20℃, under the loading rate of 1mm/min. The test results were given in Table 10. It can be seen that as the temperature decreases, the splitting tensile strength and damage tensile strain increase, while the damage tensile strain decreases. Namely, the brittleness increases as the temperature decreases.

Compared with pouring cement asphalt concrete, CEAC has higher splitting tensile strength damage tensile strain. In other words, it has a better low temperature crack resistance.

Table 10 Results of splitting test at low temperature

MATERIALS	SPLITTING TENSILE STRENGTH, MPa		DAMAGE TENSILE STRAIN		DAMAGE TENSILE STRENGTH, MPa	
	-10℃	-20℃	-10℃	-20℃	-10℃	-20℃
CEAC	2.62	3.58	0.00257	0.00136	1378.54	4316.38
Pouring cement asphalt concrete	2.47	3.34	0.00243	0.00124	1498.32	4631.65

ENGINEERING APPLICATION

Test Road Paving

Based on the experimental study, a test road was paved, which was located in left hand of K29 + 800 ~K30+0 of "Yiyang Class-A highway". CEAC was used as base course of the test road with thickness of 7.5 cm. Construction process followed these steps, stirring, transportation, paving, rolling and curing. The following points should be emphasized in the construction process.

1. Stirring. First, put cement and aggregates according to the proportion into mixer, stir for half a minute. Then put in emulsified asphalt and water, stir for about two minutes the whole process. Water content would be adjusted until the mixture has good workability. The stirring time should be strictly controlled. Mixing should be completed before emulsion breaking. Otherwise construction workability of CEAC would drop for emulsion breaking.

2. Rolling. Rolling is an important step of the whole process. After paving, roll statically for 1~2 times with double-drum rollers, then roll 1~2 times with vibratory roller. Do not exceed 2 times so as not to cause moving. Next roll for 1~2 times with tire roller. Finally, roll statically for only 1 time to keep the surface smooth with double-drum rollers.

In addition, CEAC should be covered with sackcloth for 3~7 days. In this period, make sure road closed and watered regularly to keep the surface wet.

Environment Assessment

Normally, asphalt concrete need to be heated to 160℃ or more, whose average energy consumption per unit reaches from 5.30 to 7.22 liter fuel per ton of asphalt concrete, which not only causes a lot of fuel consumed, but also produces numerous greenhouse gases (producing 18 kilos CO_2 per ton of asphalt concrete) and a lot of asphalt gas, which can cause severe harm to the health of constructors. Meanwhile, the average cement content of concrete is 300~450 kilos per cubic meter. However, about 1 ton of harmful gases such as CO_2 are emitted by producing 1 ton of cement, and numerous raw materials such as limestone and coal are consumed. Compared with asphalt concrete and cement content, CEAC can be used at room temperature, reducing the energy consumption and pollution to the environment. Besides, the average cement content of CEAC is 80~120 kilos per cubic meter, which will greatly relieve the strain on natural resources. Thus, CEAC might be a kind of semi-flexible pavement material of low carbon and energy saving.

CONCLUSIONS

From this study, the following conclusions can be obtained:

1. With increase in cement content, the stability values are increased, while the flow values are decreased. In other words, the flexibility of CEAC decreases with increase in cement content to some extent.
2. Performance tests show that CEAC has characteristics of appropriate stiffness, good moisture stability and good low temperature crack resistance and so on.
3. CEAC might be a kind of semi-flexible pavement materials of low carbon and energy saving.
4. CEAC has great potential of being used as the surface layer in high-class highway and roads in heavy traffic districts.

ACKNOWLEDGEMENTS

This study was financially supported by the Yichang Municipal Science and Technology Plan Project “Research and application of semi-flexible cement-asphalt concrete pavement structures and materials” (No. K09-15). The authors would also like to thank Yunhua Zhang, who gave valuable suggestion to this paper.

REFERENCES

1. ZHANG, Q S. Highway Structure Design Theory and Method, 2005, People’s Communications Press, China.

2. LIU, Z L, TIAN, W, SHI, J F, TAN F M. Advanced Technology for Asphalt Concrete Pavement of High Grade Highway, 2002, People’s Communications Press, China.

3. HAO, P W, CHENG, L, LIN, L. Pavement performance of semi-flexible pavement in laboratory, Journal of Chang'an University (Natural Science Edition), Vol. 23, No.2, 2003, pp 1-6.

4. BROWN, S F, NEEDHAM, D. A study of cement modified bitumen emulsion mixtures, Proceedings of the AAPT, 2000, p 69.

5. TERREL, R L, WANG, C K. Early curing behavior of cement modified asphalt emulsion mixtures, Proceedings of AAPT, 1971, pp 108-125.

6. ORUC, S, CELIK, F, VEFA AKPINAR, M. Effect of cement on emulsified asphalt mixtures, Journal of Materials Engineering and Performance, Vol. 16, 2007, pp 578-583.

7. THE MINISTRY OF COMMUNICATION. Test Standard for Cement and Cement Concrete of Highway Engineering (JTJ E30-2005), 2005, People's Communications Press, China.

8. THE MINISTRY OF COMMUNICATION. Test Standard for Aggregate of Highway Engineering (JTG E42-2005), 2005, People's Communications Press, China.

9. THE MINISTRY OF COMMUNICATION. Test Standard for Asphalt and Asphalt Mixtures of Highway Engineering (JTJ 052-2000), 2000, People's Communications Press, China.

10. THE MINISTRY OF COMMUNICATION. Standard for Asphalt Pavement Design of Highway (JTG D50-2006), 2006, People's Communications Press, China.

11. HEAD, R W. An informal report of cold mix research using emulsified asphalt as binder, Proceedings of the AAPT, 1974, pp 110-131.

12. NIAZI, Y, JALILI, M. Effect of Portland cement and lime additives on properties of cold in-place recycled mixtures with asphalt emulsion, Construction and Building Materials, Vol. 3, 2009, pp 1338-1343.

Design and Development of Ultra Thin Continuously Reinforced Concrete Pavements (UTCRCP)

E P Kearsley, H F Mostert
University of Pretoria, South Africa

Pavement design engineers normally see concrete pavements as rigid pavements that fail in a brittle manner. The un-reinforced concrete pavements with closely spaced movement joints built in the past were rigid brittle structures, but the use of continuously reinforced concrete pavements, has resulted in both a reduction in the volume of concrete required for any given pavement, and a more flexible behaviour of the pavement. The use of modern superplasticizers has made it possible to manufacture high performance concrete with a compressive strength in excess of 100 MPa and the addition of steel fibres to this concrete can significantly enhance the flexural strength of the concrete, resulting in a more ductile failure. Optimization of the concrete mix composition can result in a significant saving in the volume of material required for a pavement designed to take a given traffic load. As part of the National Highway renewal programme currently in progress in South Africa, full-scale experimental trial sections of Ultra Thin Continuously Reinforced Concrete Pavements (UTCRCP) have been constructed. The UTCRCP consists of a 50 mm thick layer of up to 100 MPa concrete containing at least 80 kg/m^3 of steel fibre as well as a steel mesh of 5.6 mm reinforcing bars at a spacing of about 50 mm centre to centre. Since 2006 researchers at the University of Pretoria have been involved with analyzing and testing materials for use in these pavements and in this paper an overview will be given of design, construction and quality control issues encountered. This paper focuses on the development of specialized test methods that provide the input for the design of UTCRCP. The effect of bar spacing and fibre content on the flexural behaviour of the thin concrete slabs was experimentally investigated and will be discussed in this paper.

Professor E P Kearsley is currently the Head of Department Civil Engineering at the University of Pretoria. She has been involved with research into the material properties of cement and concrete materials for the last 18 years. Her recent research interests includes high strength and fibre reinforced concrete.

Mr H F Mostert is a concrete technologist with an ACT diploma. He is currently employed by the University of Pretoria where he has been conducting research on concrete materials for the last 20 years.

Keywords: High strength, Load deformation curves, Reinforced concrete pavements, Steel fibres, Ultra thin continuously reinforced concrete

INTRODUCTION

Pavement design engineers normally see concrete pavements as rigid pavements that fail in a brittle manner. The un-reinforced concrete pavements with closely spaced movement joints built in the past were rigid brittle structures, but the use of continuously reinforced concrete pavements, has resulted in both a reduction in the volume of concrete required for any given pavement, and a more flexible behaviour of the pavement. The use of modern superplasticizers has made it possible to manufacture high performance concrete with a compressive strength in excess of 100MPa and the addition of steel fibres to this concrete can significantly enhance the flexural strength of the concrete, resulting in a more ductile failure. Optimization of the concrete mix composition can result in a significant saving in the volume of material required for a pavement designed to take a given traffic load.

BACKGROUND

Historically pavement engineers have been designing concrete pavements consisting of concrete slabs with thicknesses varying between 150 and 375 mm. The stiffness's of these slabs are significantly higher than that of the supporting layers, resulting in the concrete slab providing most of the load bearing capacity. The concrete pavement resists the traffic load by acting as a flexural member and conventional design methods use the flexural strength of the concrete as input parameter. The long term performance of existing concrete pavements is used to calibrate empirical design methods.

Continuously Reinforced Concrete Pavements (CRCP) contains continuous longitudinal steel reinforcing but current design practices mostly result in CRCP with the same thickness than that of an equivalent jointed doweled concrete pavement. The structural strength that the reinforcing can contribute is often not taken into account, resulting in concrete pavements thicker than the deck slabs of some bridges on the same road.

The large volume of concrete used in these pavements has resulted not only in an unacceptable carbon footprint, but also in the construction cost of concrete pavements being so high that the use of concrete in pavements is often not deemed feasible. Many researchers around the world have been working on ways to improve the behaviour of concrete pavements while reducing the cost and the carbon footprint [1, 2, 3, 4]. The thickness of concrete pavements has been reduced by increasing the strength of the concrete or by including steel fibres [5]. Steel fibres bridge cracks that open in the region where the flexural strength of the concrete is exceeded, thus allowing plastic hinges to form in the concrete slab.

As part of the National Highway renewal programme currently in progress in South Africa, full-scale experimental trial sections of Ultra-Thin Continuously Reinforced Concrete Pavements (UTCRCP) have been constructed. The UTCRCP consists of a 50 mm thick layer of up to 100 MPa concrete containing at least 80 kg/m3 of steel fibre as well as a steel mesh of 5.6 mm reinforcing bars at a spacing of about 50 mm centre to centre. The design, construction and quality control of the material has proven to be a challenge.

Since 2006 researchers at the University of Pretoria have been involved with analyzing and testing materials for use in these pavements and in this paper an overview will be given of design, construction and quality control issues encountered.

DESIGN, CONSTRUCTION AND QUALITY CONTROL ISSUES

Design

South African pavement engineers have been used to designing concrete pavements using concrete with a compressive strength of 30MPa. The majority of concrete pavements are jointed doweled pavements and where reinforcing is used it is placed at mid-depth and it is assumed that the reinforcing keeps the pavement together but it does not contribute towards the strength of the pavement. Pavements are designed using tables based on the flexural strength or Modulus of Rupture (MOR) of concrete. The standard size for MOR beams is 150 x 150 x 750 mm but for maximum aggregate sizes of less than 25 mm 100 x 100 x 500 mm beams may be used. The beams are tested in a four point bending test (loaded at third points resulting in a constant bending moment over the middle one-third of the beam) with a span length equal to three times the depth of the beam. The test is conducted in load control and only the maximum load the beam resisted before failure is recorded. The MOR (fbt) is calculated using ordinary elastic theory.

Significant size-effects is known to exist in concrete, but as the depth of the beams used to determine the MOR has always been in the same range than the thickness of the pavements designed, the consequence of the size effect was insignificant. The size effect of concrete beams was investigated by reducing the size of the beam specimen, while maintaining the geometry of the test setup [6]. The results of this investigation proved that the size-effect is significant and ultra-thin concrete pavements cannot be accurately designed using the results obtained from normal MOR tests. Non-linear finite element analysis can be used to accurately model the size-effect. The material properties used as input for this type of analysis requires detailed experimental work during the design phase of the pavement.

The effect of steel fibres on the flexural behaviour of concrete is measured in terms of the post-cracking energy-absorbing strength of steel fibre reinforced concrete. The energy absorption or toughness is defined by the area under the load-deflection curve of a specimen tested in deflection control. At low fibre volumes, the MOR remains unchanged, the beam can still carry a load after cracking, but this load is less than the load required to crack the concrete. The use of large volumes of fibre in concrete changes the flexural strength of the concrete and if designers use a MOR value, they do not know whether the strength recorded was the flexural strength of the concrete cracking or the post-cracked strength provided by the fibres [7]. This concept can be seen in the example in Figure 1, where a 90MPa concrete beam without fibres is compared to a beam made with the same mix composition, but 90 kg/m3 fibres was added to the mixture. The beam containing the fibres is stronger than the beam without the fibres but the maximum load was resisted when the beam was already cracked and the fibres were working. The fibre reinforced concrete could thus be damaged by say an overloaded truck and where the normal concrete would be broken, the fibre reinforced concrete would form plastic hinges that can still resist the load, although the concrete has cracked. Significant savings could be made if the toughness provided by the steel fibres is fully utilized, but both design manuals and strength requirements during construction currently only use the MOR value obtained from a standard flexural beam test.

UTCRCP contains closely spaced reinforcing bars in both the length and the width of the pavement, resulting in a three dimensional stress distribution. The MOR determined from beam tests gives a two dimensional flexural strength, assuming that no bending is taking place in the third dimension.

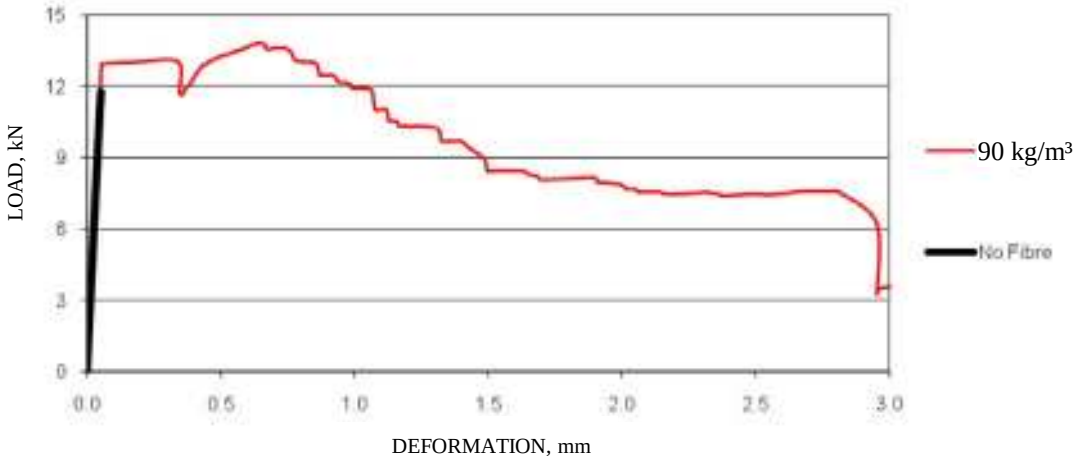

Figure 1 Effect of fibre on the load-deflection behaviour of beams

This problem cannot easily be addressed with design tables, but modern computers make it possible to conduct three dimensional finite element analysis. Alternatively, the test method for determining the flexural strength of the concrete should be changed to a three dimensional flexural test such as ASTM C1550 where a round disc is loaded at the centre point.

Construction

The contractors responsible for building the UTCRCP trial sections for SANRAL have experienced significant challenges as most of them have never worked with either concrete that has strength higher than 45MPa or fibre reinforced concrete. The mix design and materials control required to consistently produce 90MPa concrete requires skills not normally present on a standard construction site. Relatively small changes in the cement composition or aggregate grading can cause serious problems with workability, open time available for placing and finishing as well as air retention. Construction tolerances become an issue if the total pavement thickness is only 50 mm, and the layer works are not constructed to very accurate final levels. Placing and compacting a 50 mm layer of concrete, onto a layer of mesh that is kilometres long proved to be a challenge, but the quality of work on some of these test sections is remarkable.

Quality Control

Compressive strength results of 90MPa concrete indicate that the standard deviation in strength increase with an increase in strength. To meet a characteristic strength requirement for high strength concrete, the contractors should increase their strength margins to ensure that 95% of the samples tested meet the requirement. Observations on construction sites indicate that the low water/cement ratio required to make the high strength concrete results in the specimen being "thirsty" and the water levels in curing baths needs to be maintained with more care than usual to ensure consistent results. The majority of construction sites only test concrete cubes and the specification normally allows the contractor to do comparative flexural and compressive strength testing at the beginning of the contract and then conduct quality control testing on only cubes. This is not desirable as the correlation between compressive and flexural strength of concrete is substantially affected by curing conditions

and mix design [1]. Furthermore neither the MOR nor the compressive strength test gives any indication of the contribution of the fibres towards the flexural behaviour of the concrete. With the current quality control procedures there is a risk of lower fibre contents or inferior fibre types being used in the pavement and the current quality control tests would not indicate these problems.

Constructability

During the construction process it became clear that the placing of the steel mesh was problematic. The best initial test results were obtained using a 50 mm x 50 mm steel mesh made from 5.6 mm bars in 80MPa fibre reinforced concrete. To ensure that the fibres can be placed through the gaps in the mesh it was decided to use 80 kg/m^3 of a 30 mm long hooked ended drawn wire fibre with an aspect ratio (length/diameter) of 67. The combination of steel area, fibre content and concrete strength has not been optimized and we are currently conducting tests to find an optimum combination.

No mesh manufacturer in South Africa currently manufactures 5.6 mm mesh on a 50 mm x 50 mm grid and the contractors have to fix additional bars into a 100 mm x 100 mm mesh to make up the mesh. The large diameter of the bars makes it impossible to use rolls of mesh, resulting in the contractors having to place 2.4 m × 6 m sheets, which causes serious congestion where the sheets lap. Tests have been conducted on smaller diameter bars but these bars tend to break in a brittle manner without elongating sufficiently to allow the ductile flexural behaviour required. It may be possible to increase the bar spacing by increasing the fibre content by the same margin than the reduction in steel area. If the bars are further apart it may be possible to use longer fibres without being concerned about their ability to flow through a 50 mm × 50 mm grid. The effect of bar spacing and fibre content on the flexural behaviour of the thin concrete slabs was experimentally investigated and some of the results will be discussed in this paper.

EXPERIMENTAL SETUP

Mix Design

A typical mix design was used to manufacture a concrete mixture with a characteristic 28-day compressive strength of 80MPa and the mix composition can be seen in Table 1. Two different types of hooked ended hard drawn wire fibres were used.

Table 1 Mix composition

MATERIAL	kg/m^3
Cement (Cem II 42.5 N)	361.3
Water	170.0
Aggregate (9.5 mm Dolomite)	900.0
Sand (Crushed Dolomite)	1025.0
Condensed Silica Fume (CSF)	63.8
Admixture (Superplasticizer)	2.7
Fibres (Hooked ended)	80

Both fibre types had an aspect ratio of 67, but 30 mm and 60 mm long fibres were used with cross-sectional diameters of 0.45 mm and 0.9 mm respectively.

Specimen Cast

The compressive strength of the mixture was determined from sets of three 100 mm cubes tested after 28 days of water curing.

Round discs were cast to determine the energy absorption of the pavement. This test was conducted according to ASTM C1550 but the disc thickness was reduced to 55 mm and the disc diameter reduced to 600 mm to eliminate possible size effects. The reinforcing was placed in the discs in the same position (cover) and spacing that would be used for the concrete pavement. The discs were cured in water and tested in the direction of casting after 28 days. The discs were supported on ball bearings at 3 points, resulting in a span diameter of 550 mm. The test setup can be seen in Figure 2. A load was applied at centre point and the test was conducted in deflection control (0.2 mm/min) using a closed loop material testing system. The midpoint deflection and the load were recorded and the area under the load deflection graph was used to calculate the energy absorption in Joules. The SANRAL specification requires total energy absorption of 1000 Joules for a deflection of 25 mm.

Figure 2 Round disc test setup

For each of the fibre types the effect of mesh spacing was determined by placing the following mesh combinations in the discs with 80 kg/m^3 fibres:

- 50 mm × 50 mm × 5.6 mm bars;
- 50 mm × 100 mm × 5.6 mm bars;
- 75 mm × 75 mm × 5.6 mm bars;
- 100 mm × 100 mm × 5.6 mm bars.

To establish whether some of the reinforcing bars can be replaced by adding extra fibres, discs with equal steel contents were manufactured and the fibre content for each mesh composition can be seen in Table 2.

Table 2 Equivalent steel contents

MESH SPACING	FIBRE CONTENT, kg/m³
50 mm × 50 mm	80
50 mm × 100 mm	117
75 mm × 75 mm	117
100 mm × 100 mm	155
No mesh	230

RESULTS

The average cube strength recorded for all the concrete cast was 88.3MPa. The load-deflection behaviour of typical discs containing 80 kg/m^3 fibres can be seen in Figure 3 and Figure 4 for 60 mm and 30 mm fibres respectively.

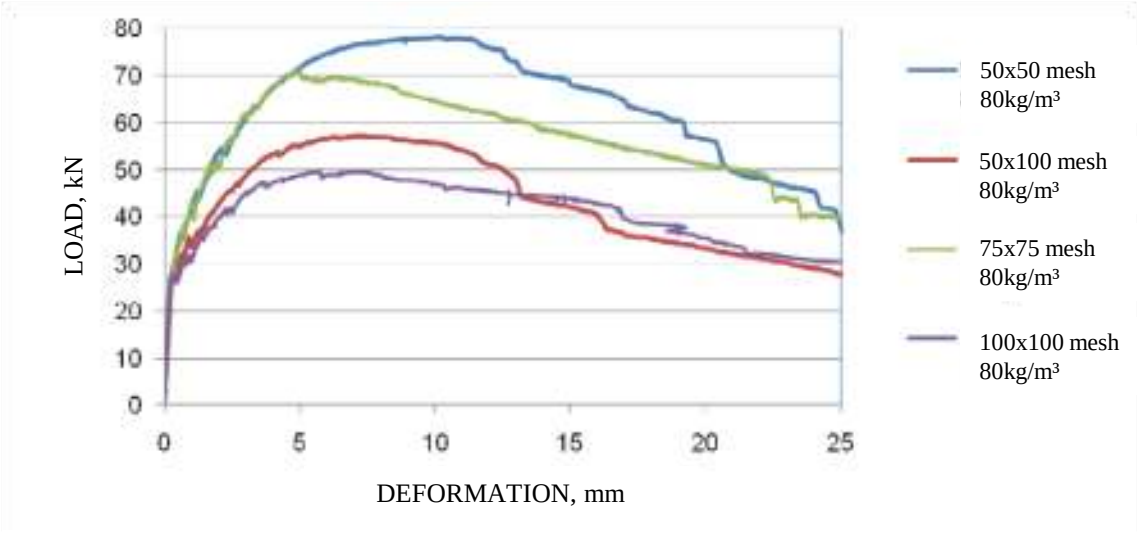

Figure 3 Load-deformation behaviour of discs containing 60 mm fibres

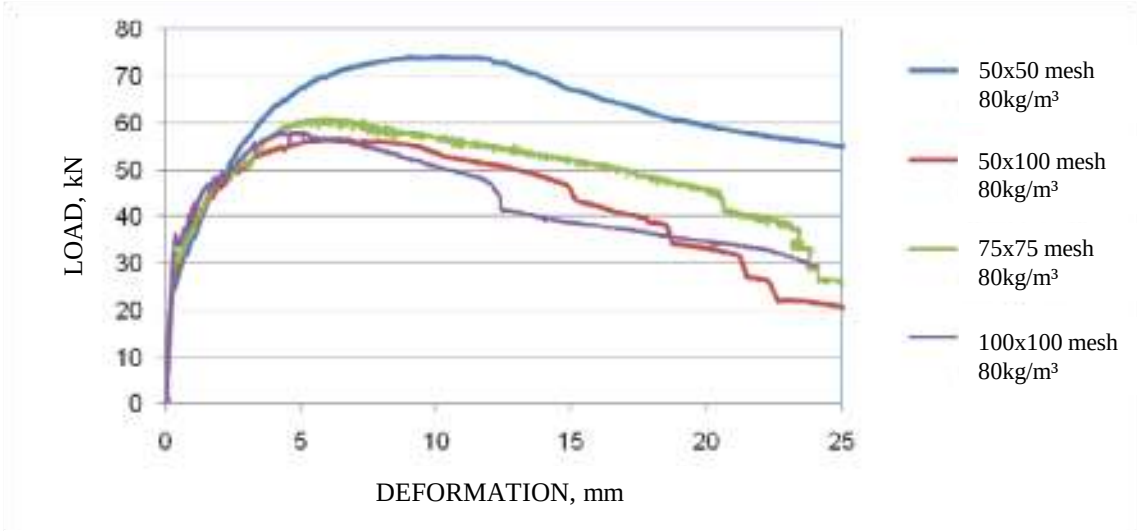

Figure 4 Load-deformation behaviour of discs containing 30 mm fibres

These graphs clearly indicate that all the discs started cracking at a load of approximately 27 kN, whereafter the steel reinforcing not only kept the concrete together, but also resisted load more than double the cracking load. As expected a reduction in steel content resulted in a decrease in the load resisted by the disc. It is interesting to note that the 50 mm x 100 mm mesh resisted a load not much higher than the load resisted by the 100 mm x 100 mm mesh, indicating that the behaviour of the UTCRCP would be determined by the larger spacing in the mesh used.

The effect of the fibre length was not as expected. The longer fibres seem to work better with the higher steel content and there does not seem to be a problem for the fibres to slip through the small gaps in mesh. The shorter fibres seem to work better with the lower steel contents or larger mesh spacing. After the testing was completed the discs were opened up and the steel fibre distribution was investigated by counting the number of fibres above and below the mesh. There was no indication that the small mesh spacing affected the fibre distribution.

The energy absorption of the discs can be seen in Figure 5 and Figure 6 for the 60 mm and 30 mm fibres respectively. These results indicate that all the discs tested meets the requirement as currently set by SANRAL.

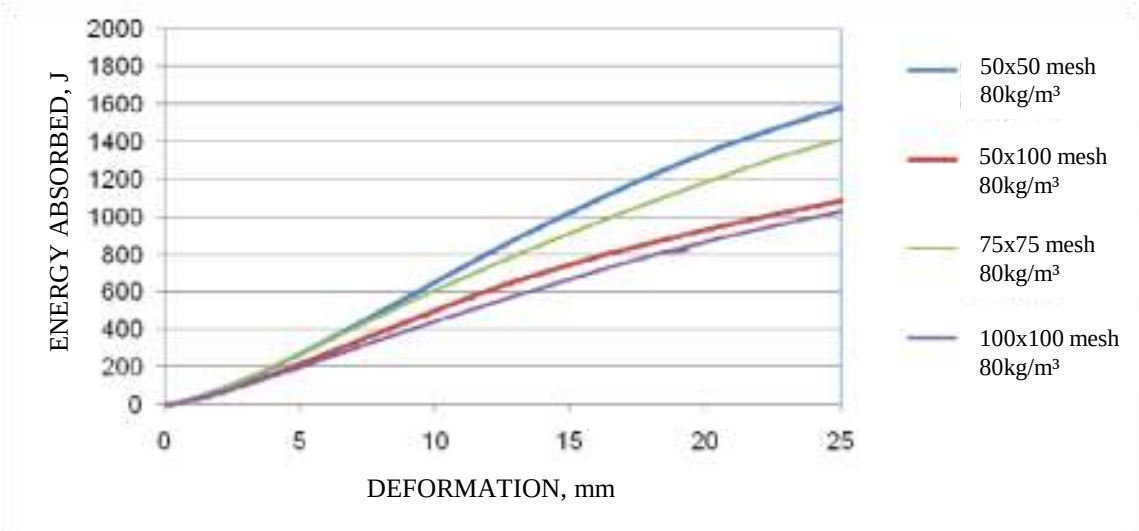

Figure 5 Effect of mesh spacing on load-deflection behaviour of discs containing 60 mm fibres

The effect of increased fibre content can be seen in Figure 7 and Figure 8 for discs containing 60 mm and 30 mm fibres respectively. The fibre contents were increased to keep the total steel content in the discs constant when the distance between the mesh reinforcing bars is increased. It is interesting to note that the longer fibres are significantly more successful in providing a substitute for the reduction in mesh cross-sectional area.

For deflections up to 5 mm the mesh can be completely removed and the inclusion of 230 kg/m3 of the 60 mm long hooked ended hard drawn wire fibres would result in the same load-deflection behaviour than the 50 mm x 50 mm mesh with 80 kg/m3 fibres. From Figure 8 it can clearly be seen that the 30 mm long fibre cannot be used to replace the mesh reinforcing. The length of the shorter fibres seems to be insufficient to bridge the cracks at larger deflections.

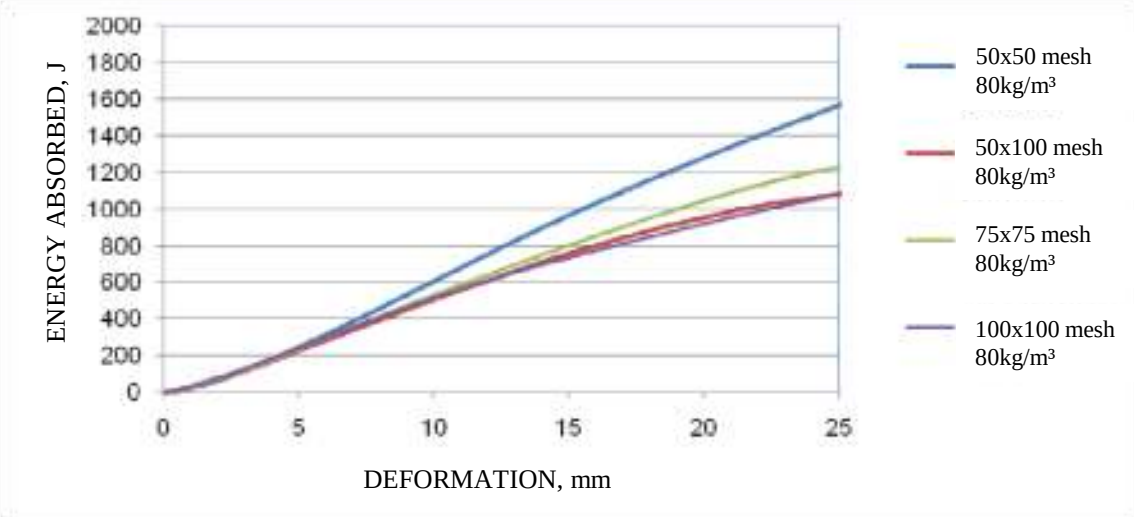

Figure 6 Effect of mesh spacing on the load-deflection behaviour of discs containing 30 mm fibres

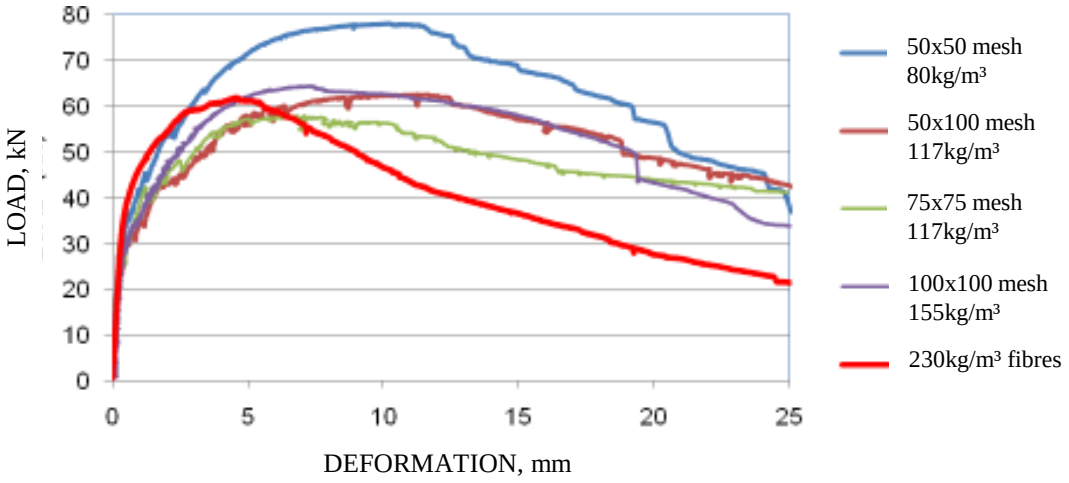

Figure 7 Effect of fibre content on load-deflection behaviour of discs containing 60 mm fibres

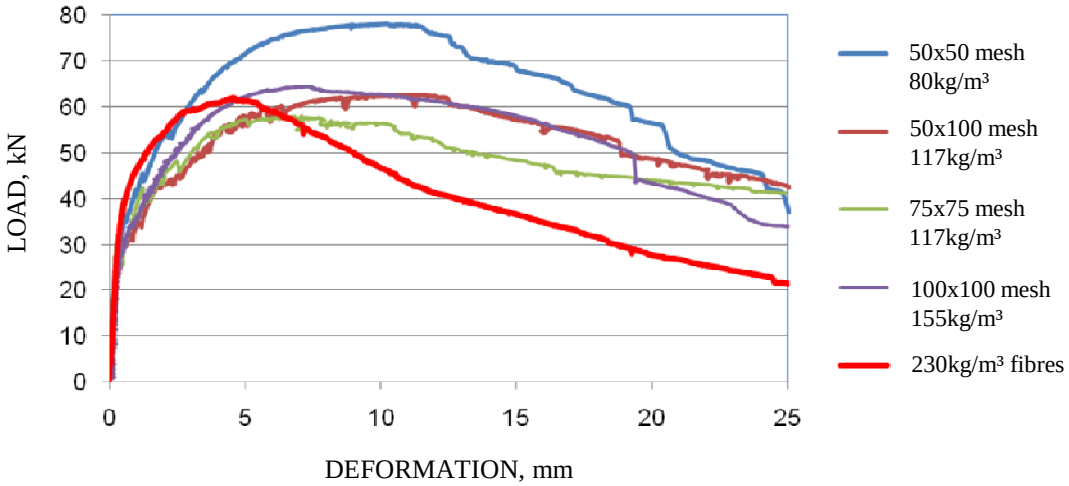

Figure 8 Effect of fibre content on the load-deflection behaviour of discs containing 30 mm fibres

The energy absorption calculated from these graphs for 60 mm and 30 mm fibres can be seen in Figure 9 and Figure 10 respectively. These graphs clearly confirm that the discs where mesh was replaced with short fibres did mostly not meet the minimum SANRAL requirement, while all the discs containing the longer fibres absorbed more than 1000 J energy.

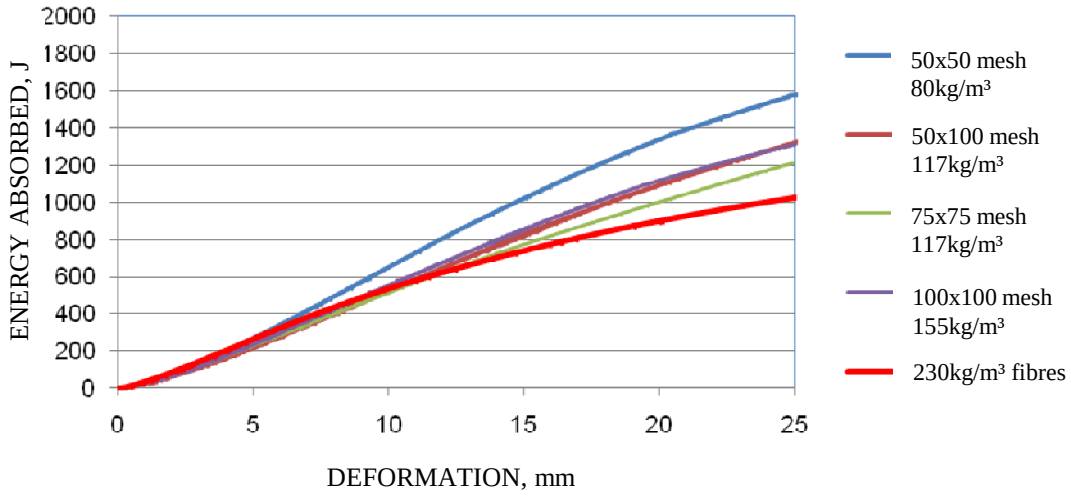

Figure 9 Energy absorption for 60 mm fibres

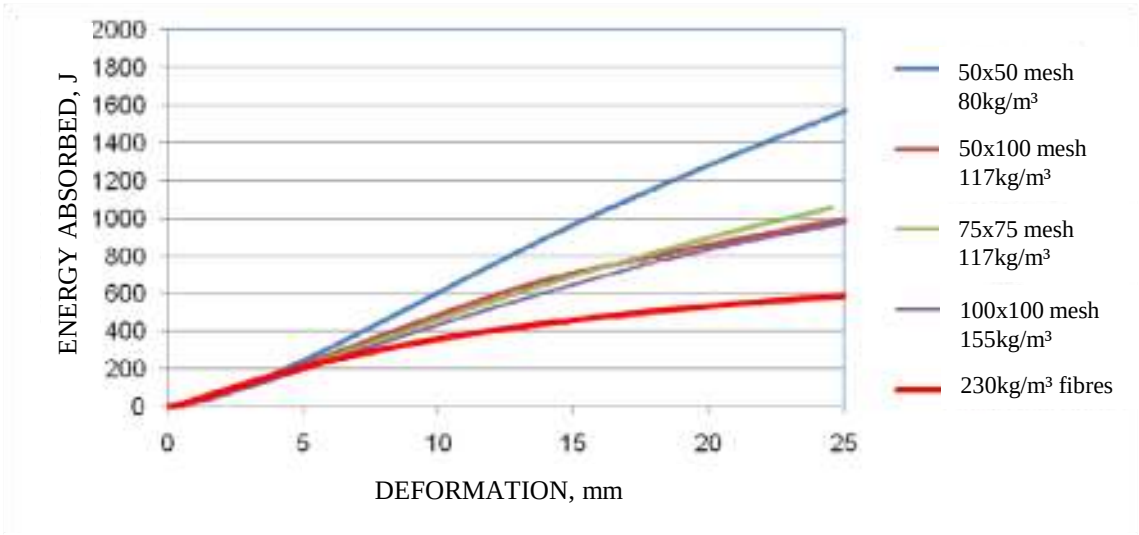

Figure 10 Energy absorption for 30 mm fibres

PROBLEMS STILL TO BE ADDRESSED

A number of UTCRCP test sections have been constructed and the behaviour under traffic loading will be used to establish whether the UTCRCP can meet expectations. The thin section as well as the inclusion of relatively large volumes of steel (about 3% per volume) changes the concrete pavement into a flexible pavement and design parameters suitable for designing flexible members will have to be investigated. A limit will have to be placed on the maximum allowable deflection and this limit will probably have to be based on user comfort.

The UTCRCP is normally placed on an asphalt layer on an Emulsion Treated Base (ETB), resulting in some seating under traffic loads. There seems to be some bond between the UTCRCP and the supporting layers and this bond should prevent the UTCRCP from lifting up or moving horizontally. Research is needed to determine how strong this bond is, or should be.

The need for end and edge beams are currently debated where many engineers believe that a down-stand beam is needed on the edge of the UTCRCP. This will however cause drainage problems and the advantages and disadvantages of such a thickening should be investigated as it could act as a crack inducer. Some trial sections have been constructed on vertical slopes and here the engineers designed heavily reinforced end-beams to prevent the road from slipping down the slope with time. The need for these beams should be investigated.

There are currently test sections that are kilometres long without any movement joints, but research should be conducted to determine what the maximum distance between movement joints should be. Under extremely hot weather (>40 °C) a section of the URCRCP failed when the slab buckled as can be seen in the photo in Figure 11.

This is probably the result of thermal expansion and research should be conducted to determine what the minimum casting temperature should be to prevent the slab from failing when high temperatures are reached. Despite the relatively large steel contents, sections of UTCRCP shows large shrinkage cracks and research is needed to determine why the steel did not distribute the shrinkage cracks effectively in these areas.

Figure 11 UTCRCP failure

CONCLUSIONS

It is possible to design and construct UTCRCP, but the design methods, the construction techniques and the tests used for quality control has to be redefined to ensure that the pavement constructed meets the required standards. The test method as well as the size of the specimen tested should be carefully selected to ensure useable test results.

Longer fibres seem to work well with mesh, regardless of the size of the gaps between the bars. There does not seem to be any problem with ensuring a uniform distribution of 60 mm long fibres, even when used with a 50 mm × 50 mm steel mesh.

It is possible to replace all the mesh in the discs with fibres if the deflection is limited to less than 5 mm. Full scale testing would be required to determine whether fibres could in practice be used instead of mesh over long distances.

Further research is still needed to solve outstanding issues such as limits for shrinkage, constraints, maximum casting length, deflection limits and possible temperature ranges for casting UTCRCP.

ACKNOWLEDGEMENTS

The authors would like to express appreciation for not only the fibres donated by Insimbi Refractory & Alloy Supplies Ltd, but also the research grants made by the Duraset business unit of Aveng and the THRIP-program of the South African National Research Foundation that made this research possible.

REFERENCES

1. ZHANG, J, HARVEY, J, MONTEIRO P J M, ALI A. Effect of cement type and curing conditions on flexural strength of concrete pavements, Concrete for Transportation Infrastructure, Proceedings of International Congress Global Construction: Ultimate Concrete Opportunities, Eds. R K Dhir, M J McCarthy and S Caliskan, 2005, pp 103-110.

2. TAYABJI, S, SMITH, K, TYSON, S. US Concrete pavement technology - current practices, future directions, Concrete for Transportation Infrastructure, Proceedings of International Congress Global Construction: Ultimate Concrete Opportunities, Eds. R K Dhir, M J McCarthy and S Caliskan, 2005, pp 93-102.

3. SOMMER, H. High performance concrete for motorway pavements, Concrete for Transportation Infrastructure, Proceedings of International Congress Global Construction: Ultimate Concrete Opportunities, Eds. R K Dhir, M J McCarthy and S Caliskan, 2005, pp 75-80.

4. DE LARRARD, F, CHABOT, A, SEDRAN, T, POUTEAU, B, MATHIAS, V. Concrete for Transportation Infrastructure, Proceedings of International Congress Global Construction: Ultimate Concrete Opportunities, Eds. R K Dhir, M J McCarthy and S Caliskan, 2005, pp 19-26.

5. AMERICAN CONCRETE INSTITUTE, Guide to design of slabs-on-ground, ACI Committee 360, ACI Manual of Concrete Practice, ACI 360R-10, 2011.

6. DENNEMAN, E, KEARSLEY, E P, VISSER, A T. Size-effect in high performance concrete road pavement materials. Proceedings of the International Conference on Advanced Concrete Materials, Stellenbosch, South Africa. Eds G P A G van Zijl & W P Boshoff, 2010, pp. 53-58.

7. KEARSLEY, E P, MOSTERT, H F. Enabling the effective use of High Performance Fibre Reinforced Concrete in infrastructure. Proceedings of the International Conference on Advanced Concrete Materials, Stellenbosch, South Africa. Eds G P A G van Zijl & W P Boshoff, 2010, pp. 287-295.

Structural Performance of Square RC Columns Confined with Carbon Fibre Reinforced Polymer (CFRP)

N Chikh[1], N Djebbar[1], R Benzaid[2], M Mesbah[3]
1 – University of Constantine, Algeria
2 – University of Jijel, Algeria
3 – INSA de Rennes, France

Loading capacity and strains of square reinforced concrete (RC) columns, strengthened with external carbon fiber reinforced polymer (CFRP) sheets, were tested and evaluated. The experimental parameters include: number of wrap layers, concrete strength and the slenderness of the columns (L/a). All test specimens were loaded to failure in axial compression. Compressive stress, axial and hoop strains have been recorded to evaluate the stress-strain relationship, ultimate strength, stiffness, and ductility of the specimens. Results clearly demonstrate that composite wrapping can enhance the structural performance of RC columns in terms of both maximum strength and ductility. The effects of test parameters are evidenced and compared.

N. Chikh is Professor at the Department of Civil Engineering, Constantine University, Algeria. He is also Director of the Laboratory of materials and Durabilitry of Constructions (LMDC). His main research interests include the use of composites materials in strengthening concrete constructions as well as serviceability of concrete structurers.

R. Benzaid is assistant Professor at the Department of Geology, Jijel University, Algeria. His main research interests include the strengthening of concrete structures with FRP materials as well as risk assesement of soils.

H. Mesbah is Professor at the Department of Civil Engineering, INSA de Rennes, France. His main research interests include the strengthening of concrete structures with FRP materials as well as the study of properties of self compacted concrete.

N. Djebbar is Reader at the Department of Civil Engineering, Constantine University, Algeria. His main research interests include the strengthening of concrete structures with FRP materials as well as the study of the performance of eartquake resistant concrete structures.

Keywords: CFRP, Column, Ductility, Strength

INTRODUCTION

An increasing number of reinforced concrete structures have reached the end of their service life, either due to deterioration of the concrete and reinforcements caused by environmental factors, or due to an increase in applied loads. These deteriorated structures may be structurally deficient or functionally obsolete, and most are now in serious need of extensive rehabilitation. Carbon fiber reinforced plastics sheets or plates are well suited to this application because of their high strength-to-weight ratio, good fatigue properties, and excellent resistance to corrosion. Their application in civil engineering structures has been growing rapidly in recent years, and is becoming an effective and promising solution for strengthening deteriorated concrete members. Because CFRPs are quickly and easily applied, their use minimizes labor costs and can lead to significant savings in the overall costs of a project.

During the last decade, the use of FRP composites has been successfully promoted for external confinement of reinforced concrete (RC) columns all over the world. Several studies on the performance of FRP wrapped columns have been conducted, using both experimental and analytical approaches [1-4]. Such strengthening technique has proved to be very effective in enhancing their ductility and axial load capacity. However, most of the available studies on the behavior of FRP confined concrete columns have concentrated on circular shaped columns with normal strength. The data available for columns of square or rectangular cross sections have increased over recent years but are still limited [5-7]. Also the validation of these results and their applicability to large-scale RC columns is of great practical interes. This field remains in its infancy stages and more research investigation is needed on this subject to study the effect of slenderness and that of concrete strength.

This study deals with a series of tests on square plain concrete (PC) and reinforced concrete (RC) columns strengthened with CFRP sheets. A total of 48 concrete specimens were tested under axial compression. The data recorded included the compressive loads, axial strains, and radial strains. The parameters considered are the number of composite layers (1 and 3), the compressive strength of the unconfined concrete (25MPa and 60MPa) and the columns' slenderness ratio L/a (2; 4 and 7.4). To comply with existing RC members in practice, where reduced cover is often present, the corners for all prismatic specimens were almost kept sharp for CFRP application

EXPERIMENTAL PROGRAM

Materials

Two kind of concrete mix have been realised to investigate the influence of concrete strength, normal strength concrete (NSC- 25 MPa) and high strength concrete (HSC- 60 MPa). The carbon-fiber sheets used were the SikaWrap-230C product, a unidirectional wrap. The manufacturer's guaranteed tensile strength for this CFRP is 4300 MPa, with a tensile modulus of 238 GPa, an ultimate elongation of 1.8 % and a fiber thickness of 0.13mm. The Sikadur-330 epoxy resin was used to bond the carbon fabrics over the square columns.

Table 1 summarizes the specimens involved in the experimental program. Eight series of experiments were performed to investigate the behavior of PC and RC square columns confined by CFRP composite. For all RC specimens the diameter of longitudinal and

transverse reinforcing steel bars were respectively 12 mm and 8 mm. The longitudinal steel ratio was constant for all specimens and equal to 2.25%.The yield strength of the longitudinal and transversal reinforcement was 500 MPa and 235 MPa; respectively. The specimen notations are as follows. The specimen notations are as follows. The first two letters refer to the type of concrete: PC for plain concrete and RC for reinforced concrete, followed by the concrete mixture: I for normal strength (24.77MPa) and II for high strength (59.53MPa). The next letter indicates the slenderness ratio: x for L/a=2, y for L/a=4 and z for L/a=7.14. The last number specifies the number of layers.

Table 1 Details of test specimens

SPECIMEN DESIGNATION	CONCRETE MIXTURE	NOMINAL DIMENSION, side x height, mm	NUMBER OF LAYERS	UNCONFINED CONCRETE STRENGTH	NUMBER OF SPECIMENS
PCI. x0	I	140x140x280	-	24.77	2
PCI. x1		140x140x280	1		2
PCI. x3		140x140x280	3		2
RCI. x0		140x140x280	-		2
RCI. x1		140x140x280	1		2
RCI. x3		140x140x280	3		2
RCI. y0		140x140x560	-		2
RCI. y1		140x140x560	1		2
RCI. y3		140x140x560	3		2
RCI. z0		140x140x1000	-		2
RCI. z1		140x140x1000	1		2
RCI. z3		140x140x1000	3		2
PCII. x0	II	140x140x280	-	59.53	2
PCII. x1		140x140x280	1		2
PCII. x3		140x140x280	3		2
RCII. x0		140x140x280	-		2
RCII. x1		140x140x280	1		2
RCII. x3		140x140x280	3		2
RCII. y0		140x140x560	-		2
RCII. y1		140x140x560	1		2
RCII. y3		140x140x560	3		2
RCII. z0		140x140x1000	-		2
RCII. z1		140x140x1000	1		2
RCII. z3		140x140x1000	3		2

Specimen Preparation

After concrete columns were fully cured, FRP wrapping procedure was performed according to the procedure specified by the manufacturer. The CFRP jackets were applied to the specimens by manual wet lay-up process. The concrete specimens were cleaned and completely dried before the resin was applied. The epoxy resin was directly applied onto the substrate. The fabric was carefully placed into the resin with gloved hands and smooth out any irregularities or air pockets using a plastic laminating roller. The roller was continuously used until the resin was reflected on the surface of the fabric, an indication of fully wetting. A second layer of resin was applied to allow the impregnation of the CFRP. The following layer is applied in the same way. Finally, a layer of resin was applied to complete the operation.

Each layer was wrapped around the column with an overlap of ¼ of the perimeter to avoid sliding or deboning of fibers during tests. The wrapped specimens were left at room temperature for 1 week before testing.

Test Procedures

Specimens were loaded under a monotonic uni-axial compression load up to failure. The load was applied at a rate corresponding to 0.24 MPa/s and was recorded with an automatic data acquisition system. Axial and lateral strains were measured using appreciable extensometer. The instrumentation included one lateral linear variable differential transducer (LVDT) placed in the form of a square frame at the mid-height of the specimens. Measurement devices also included three vertical LVDTs to measure the average axial strains. Prior to testing, all CFRP-wrapped columns were capped with sulfur mortar at both ends.

TEST RESULTS AND DISCUSSION

Compression behavior of the CFRP wrapped specimens was mostly similar in each series in terms of stress-strain curves and failure modes of the specimens. All confined concrete columns failed by fracture of the composite wrap at one of the corners, because of the high stress concentration at these locations, Figure 1. The collapse occured in a sudden and explosive way, though some popping noises were heard during various stages of loading and were attributed to microcracking of the concrete. The strain values observed for the jacket tensile failure were substantially lower than the FRP failure strain, as many authors have already published. For short specimens (L/a =2), the fiber rupture starts mainly in their central zone, then propagates towards both ends. Regarding slender specimens, the collapse was mostly concentrated in their end regions, indicating that the greater the slender ratio, the smaller the area of CFRP ruptured.

Figure 1 Failure of CFRP confined specimens

For these columns at ultimate load, when confinement action was no longer provided due to FRP fracture, the internal steel started buckling and the crushed concrete fell down between the fractured FRP. Hence, this indicates that the concrete core is significantly damaged (but yet confined) even before reaching ultimate load. For all confined specimens, delamination was not observed at the overlap location of the jacket, which confirmed the adequate stress

transfer over the splice. The average experimental results are reported in Table 2, with the increase in terms of compressive strength (f'_{cc}/f_{co}) and ductility ($\varepsilon_{cc}/\varepsilon_{co}$), intended as ultimate axial displacement.

Representative stress-strain curves for each series of tested CFRP-wrapped specimens are reported in Figures 2 (a-c) for NSC and in Figures 3 (a-c) for HSC. These figures give the axial stress versus the axial and lateral strains for specimens with zero, 1 and 3 layers of CFRP wrap considering various slenderness ratio L/a (2, 4 and 7.14).

Table 2 Details of test results

SPECIMEN DESIGNATION	f'_{co} MPa	f'_{cc} MPa	f'_{cc}/f_{co}	ε_{cc} ‰	$\varepsilon_{cc}/\varepsilon_{co}$	$\varepsilon_{h,rup}$ ‰	$\varepsilon_{h,rup}/\varepsilon_{ho}$
PCI. x0	24.77	24.77	1.00	2.20	1.00	3.88	1.00
PCI. x1		27.66	1.11	6.58	2.99	24.33	6.27
PCI. x3		32.03	1.29	5.89	2.67	17.01	4.38
RCI. x0	33,59	33.59	1.00	7.61	1.00	17.00	1.00
RCI. x1		39.52	1.17	15.06	1.97	20.58	1.21
RCI. x3		49.12	1.46	15.66	2.05	25.50	1.50
RCI. y0	30.49	30.49	1.00	1.67	1.00	9.78	1.00
RCI. y1		36.73	1.20	3.02	1.80	8.69	0.88
RCI. y3		41.85	1.37	5.61	3.35	7.77	0.79
RCI. z0	24.69	24.69	1.00	0.96	1.00	-	-
RCI. z1		33.92	1.37	2.05	2.13	-	-
RCI. z3		39.17	1.58	3.64	3.79	-	-
PCII. x0	59.53	59.53	1.00	3.66	1.00	3.31	1.00
PCII. x1		61.30	1.02	2.46	0.67	5.43	1.64
PCII. x3		70.35	1.18	3.09	0.84	13.39	4.04
RCII. x0	63.79	63.79	1.00	3.05	1.00	10.30	1.00
RCII. x1		74.84	1.17	3.87	1.26	16.36	1.58
RCII. x3		79.59	1.24	5.29	1.73	7.96	0.77
RCII. y0	63.62	63.62	1.00	2.05	1.00	0.35	1.00
RCII. y1		80.78	1.26	2.82	1.37	0.76	2.17
RCII. y3		82.44	1.29	2.79	1.36	0.76	2.17
RCII. z0	69.98	69.98	1.00	2.08	1.00	0.49	1.00
RCII. z1		75.77	1.08	2.53	1.21	0.82	1.67
RCII. z3		81.51	1.16	2.70	1.29	1.36	2.77

Stress-Strain Response

For NSC, all CFRP strengthened specimens showed a typical bilinear trend with a transition zone. Three zones can be observed for the stress-strain curves of the CFRP-confined specimens. The first zone is essentially a linear response governed by the stiffness of the unconfined concrete, which indicates that no confinement is activated in the CFRP wraps since the lateral strains in the concrete are very small. The unconfined concrete specimens show a sudden drop in stiffness and strength after reaching the maximum load point. In the second zone, a nonlinear transition occurs as the concrete expands, thus producing larger lateral strains.

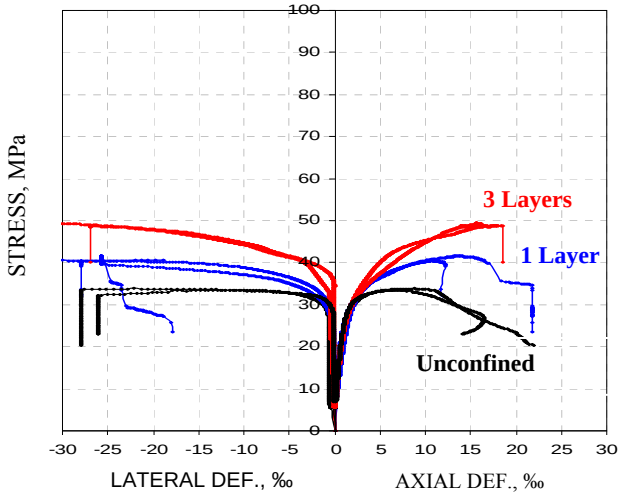

(a) RCI.x series

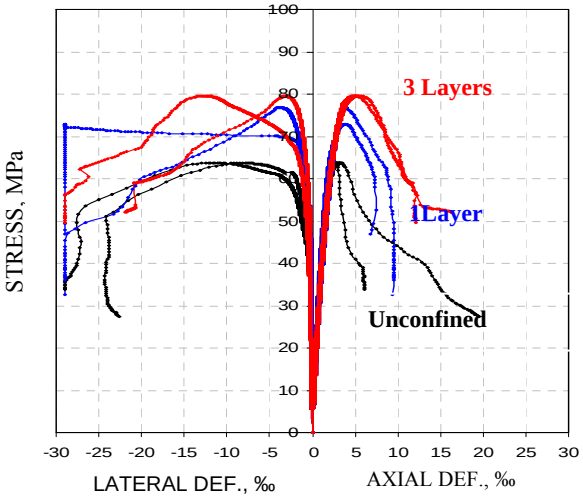

(a) RCII.x series

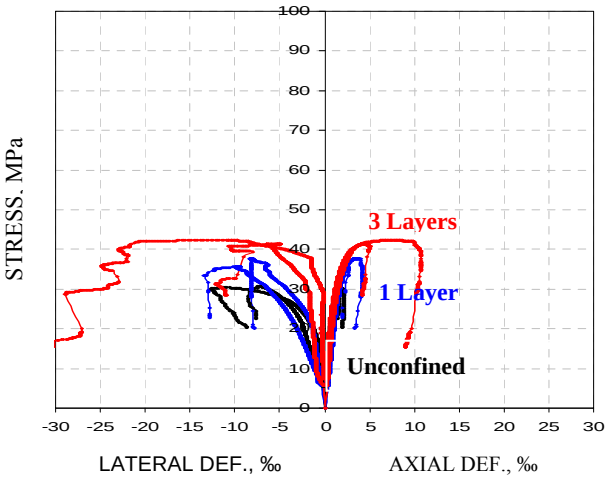

(b) RCI.y series

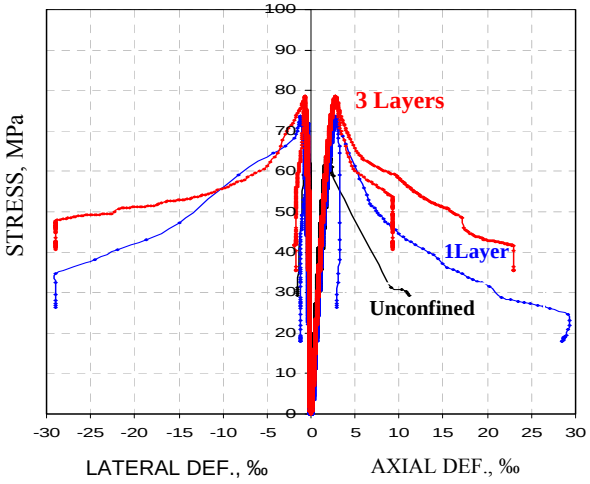

(b) RCII.y series

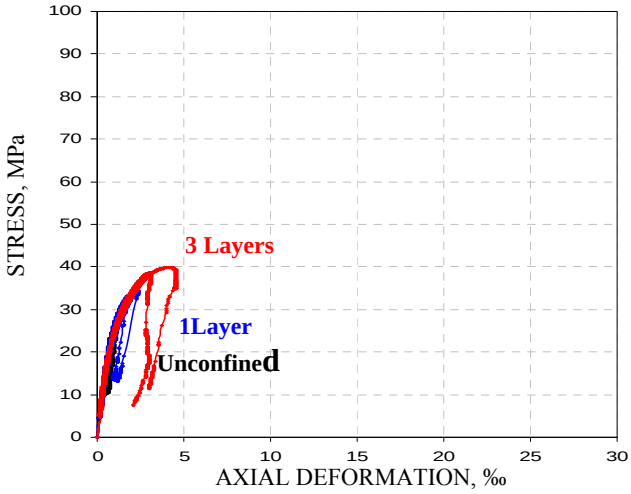

(c) RCI.z series

Figure 2 Stress strain curves of NSC CFRP confined specimens

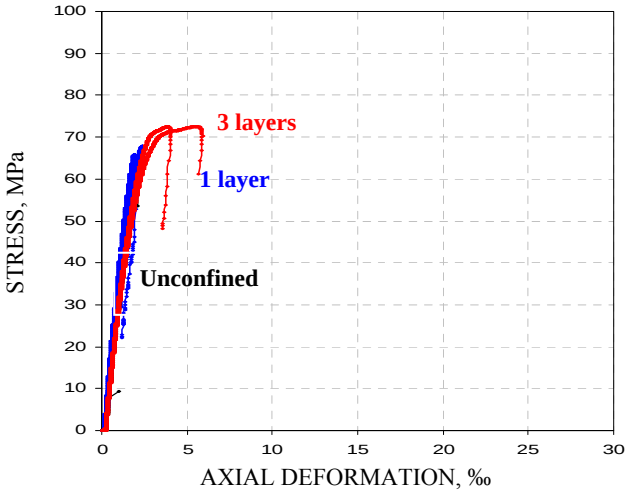

(c) RCII.z series

Figure 3 Stress strain curves of HSC CFRP confined specimens

The CFRP wrap reacts accordingly and a confining action is created on the concrete core. During this stage a loss of stiffness occurs due to the rapidly growing network of cracks in the concrete. Finally, in the third zone, the concrete is fully cracked and the CFRP confinement is activated to provide additional load carrying capacity by keeping the concrete core intact. The stress-strain curve here increases linearly up to failure. However, no distinct post behaviour is observed for specimens with higher slenderness ratio. On overall, both ultimate compressive strength and ultimate strain are variably enhanced depending on the number of layers and the slenderness ratio.

As for the previous case of NSC, the first slope of the curve, regarding specimens with HSC, is also not substantially altered by the presence of CFRP. In this initial elastic zone, the confined and the unconfined specimens behave in the same manner, irrespective of the number of layers. The strengthening effect of the CFRP layers begins only after the concrete has reached the peak strength of the unconfined concrete: transversal strains in the concrete activate the CFRP jacket. The increase of load would produce large lateral expansions, and consequently a higher confining pressure, provided that the number of composite layers is quite sufficient. With low levels of confinement (one CFRP layer), the second part of the bilinear curve shifts from strain hardening to a flat plateau with a drastically reduced ductility.

No distinct post behaviour is observed as the slenderness ratio increases and little improvement is achieved in both strength and ductility.

Effect of unconfined concrete strength

To investigate the effects of concrete quality, different concrete strength (24.77 MPa and 59.35 MPa) have been used. Considering specimens confined wiyh 3 CFRP layers, it can be seen from stress strain curves in Figures 2 and 3 a varying strength increase of 37 to 58% for NSC specimens and of 16 to 29% for HSC specimens. This effect is even more pronounced on the axial deformations, where the relative variation increases are of 105 to 280% for NSC specimens and 25 to73% for HSC specimens. This clearly indicates that the effect on the strength and ductility capacities decreases with increasing concrete strength, as found by other authors. Mechanical effects of different concrete quality are also evident in the first branch of the curves, where stronger concrete shows higher stiffness with respect to concrete with lower strength.

Effect of CFRP Strengthening Ratio

In all cases the increase of the numbers of sheets generated an increase of compressive strength as well as axial deformation capacity. The level of increase is important for NSC specimens. Considering the cases of 1 and 3 CFRP layers, from results displayed in Table 1 and Figure 2, it can be evaluated that the increase in the bearing capacity varies roughly from 17% to 58% as compared to the relative unconfined specimens, while the ultimate vertical deformations increase on average from 80% to 280%. From these findings, it is possible to assert that the increase in the number of CFRP sheets has a significant influence even though the increase in terms of strength is not as important as that of axial deformations which increase almost proportionally to the FRP strengthening ratio.

The effect of the number of CFRP layers on HSC specimens is relatively moderate compared to the case discussed previously. In this situation, the confinement pressure is activated at higher load (around 80% of the ultimate value). Consequently, the enhancement in the load carrying capacity is reduced and varies roughly from 8% to 29%, whereas the ultimate axial deformations undergo a significant reduction displaying an increase on average from 21 to 125%, as illustrated in Table 2 and in Figure 3.

It should be emphasized that the presence of quite sharp corners in all tested CFRP jacketed columns produced a cutting effect on confining sheets and hence affected the rate of enhencement in their load carrying and deformation capacities.

Effect of slenderness ratio

The comparison of results recorded for a slenderness ratio varying from 2 to 7.14 shows for NSC wrapped RC specimens a moderate decrease in the load carrying capacity and an important reduction in the axial deformation.

However, in the case of HSC jacketed specimens, the strength was almost not affected whereas the ductility underwent a moderate decrease. This may be explained by the late activation of the confinement pressure which occurred at higher load (around 80% of the ultimate value). On overall, the efficiency of the confinement provided by composite wraps was greatly affected by the premature damage of the CFRP fabric at the sharp column corner.

CONCLUSIONS

An experimental study on the axial compression behaviour of square RC columns confined externally with CFRP was presented. The following conclusions can be drawn:

- The failure of all CFRP wrapped specimens occurred in a sudden and explosive way preceded by typical creeping sounds. For short specimens (L/a =2), the fiber rupture starts mainly in their central zone, then propagates towards both ends. Regarding slender specimens, the collapse was mostly concentrated in their upper or lower regions.

- Increasing the amount of CFRP sheets produce an increase in the compressive strength of the confined column but with a rate lower compared to that of the deformation capacity which almost proportional to the CFRP strengthening ratio;

- The CFRP confinement on low-strength concrete specimens produced higher results in terms of strength and strains than for high-strength concrete similar specimens. Therefore, the effect of CFRP confinement on the bearing and deformation capacities decreases with increasing concrete strength;

- The effect of increasing the slenderness ratio results in a decrease of the strengthening effect on strength and ductility. The rate of decrease is more important for NSC specimens.

REFERENCES

1. CHAALLAL, O., HASSEN, M. & SHAHAWY, M. Confinement model for axially loaded short rectangular columns strengthened with FRP polymer wrapping. J. ACI Struct., 2003. 100(2): 215-221.

2. KARBHARI, V.M., & GAO, Y. Composite jacketed concrete under uniaxial compression-verification of simple design equations. J. Mater. Civ. Eng., 1997. 9(4): 185-193.

3. NANNI, A., & BRADFORD, N.M. FRP jacketed concrete under uniaxial compression. Constr. Build. Mater., 1995. 9 (2): 115-124.

4. PAN, J.L., XU, T., & HU, Z.J., Experimental investigation of load carrying capacity of the slender reinforced concrete columns wrapped with FRP. Construct. Build. Mater., 2007. 21: 1991–1996.

5. ROCHETTE P. & LABOSSIÈRE, P. Axial Testing of Rectangular Column Models Confined with Composites. ASCE Journal of Composites Constructions, 2000. 0: 129–136.

6. SAADATMANESH, H., EHSANI, M.R., & LI, MW. Strength and ductility of concrete columns externally reinforced with composites straps. J. ACI Struct., 1994. 91(4): 434-447.

7. AL-SALLOUM, Y.A. Influence of Edge Sharpness on the Strength of Square Concrete Columns Confined With FRP Composite Laminates. J. Composite Part B, 2007. 38: 640–650.

Statistical Analysis of Modulus of Elasticity and Compressive Strength of C45/55 Concrete for Prestressed and Non-prestreseed Precast Beams

P Hunka, J Kolisko, K Jung, S Rehacek
Czech Technical University, Czech Republic

Random behavior of concrete C45/55 XF2 used for prefabricated pre-stressed bridge beams is described on the basis of evaluating of vast set of measurements. Detailed statistical analysis is carried out on 133 cylinders with sizes 150 x 300 mm, produced from October 2010 to November 2010. Only one worker took all specimens during the whole period and the following measuring of modulus of elasticity and compressive strength of concrete was carried out in Klokner Institute laboratories. The measuring takes place at the age of 28 days, only one testing machine with the same capping method is used. Suitable theoretical models of division are determined on the basis of tests in good congruence, with the use of Bernstein's criterion.

Petr Hunka is a PhD student at the Klokner Institute of the Czech Technical University in Prague since 2007. Graduate of Brno University of Technolog, Faculty of Civil Engineering - Building Materials Engineering. He has led several research projects on modulus of elasticity of concrete.

Doc. Jiri Kolisko is currently head of Klokner Institute of the Czech Technical University in Prague. He has led several research projects on concrete, and his specialist areas of research are special types of concrete, ultrahigh performance concrete, and mortars for reconstruction.

Karel Jung has just finished his PhD theses at the Klokner Institute of the Czech Technical University. He has led several research projects on statistical analysis of propertises of concrete.

Stanislav Rehacek is a PhD student at the Klokner Institute of the Czech Technical University in Prague since 2006. Graduate of Czech Technical University in Prague, Faculty of Civil Engineering - Building Structures. Diploma thesis: construction project of multifunctional building. His specialist areas of research are fibre concrets and diagnostic of constructions.

Keywords: Compressive strength, Concrete, Modulus of elasticity, Statistical analysis

INTRODUCTION

Apart from the compressive strength which is a basic parameter for design of concrete structures, we can more often meet with the requirement to determine the value of static modulus of elasticity of concrete and its development in time. Justification of increased interest in monitoring the elastic modulus is obvious, because one of the main characteristics of each material is the modulus of elasticity E_c. Modulus of elasticity describes the ability of concrete to act flexibly to a certain degree under a given load. Modulus also determines how much the concrete (material) will be deformed under load. Modulus enters the static calculations and is closely related to many other physical and mechanical properties of concrete such as creep, shrinkage, frost resistance, etc.

In the paper, 133 results of tests of concrete C45/55 XF2 are presented, which have been running in laboratories of Klokner Institute in the long term. These tests are a part of the check of the production of precast prestressed bridge beams produced by Skanska, division Prefa. The beams are tested for the compressive strength of concrete and also static modulus of elasticity. The presented results constitute a set of data obtained from October 2010 to November of the total number 67 of prefabricated beams, which are used in bridges under the management of The Road and Motorway Directorate of the Czech Republic (RSD). For each beam, the test of modulus of elasticity is always carried out on two cylinders (size 150x300mm) produced at the same time as the beam [1].

MEASURING METHODOLOGY

Test specimens were made into steel moulds, compacted on vibratory table, were demoulded after 24 hours and the samples are stored in water according to ČSN EN 12390-2 up to the test, which takes place within 28 days. Before testing, the specimen is taken out of the water, the surface is left to dry, measured and weighed. Compressive surfaces are capped by a mixture of sulphur, ash and sand. The measurement of the static modulus of elasticity is conducted in accordance with ČSN ISO 6784.

This is the most commonly used test in practice for the determination of modulus of elasticity. Modulus of elasticity is determined from the deformations that occur between the basic tension 0,5 MPa and at the upper tension which is equal to one third of compressive strength of concrete. For the test of modulus of elasticity, cylinders 150/300 mm are used. Strain sensors must be placed on at least two opposite sides of the specimen and must comply with the condition, see Figure 1. The first test cycle checks the centric location of the specimen in the testing machine. After centring, the concrete specimen is subjected to load at least two prior cycles, followed by a measured cycle for calculating of the modulus of elasticity. Modulus E_c is then calculated from the formula (1) [3]:

$$E_c = \frac{\sigma_2 - \sigma_1}{\varepsilon_2 - \varepsilon_1} = \frac{\Delta\sigma}{\Delta\varepsilon} \tag{1}$$

Where σ_2 upper tension in MPa,
σ_1 basic tension in MPa,
$\Delta\varepsilon$ average change in the relative strain between σ_2 and σ_1

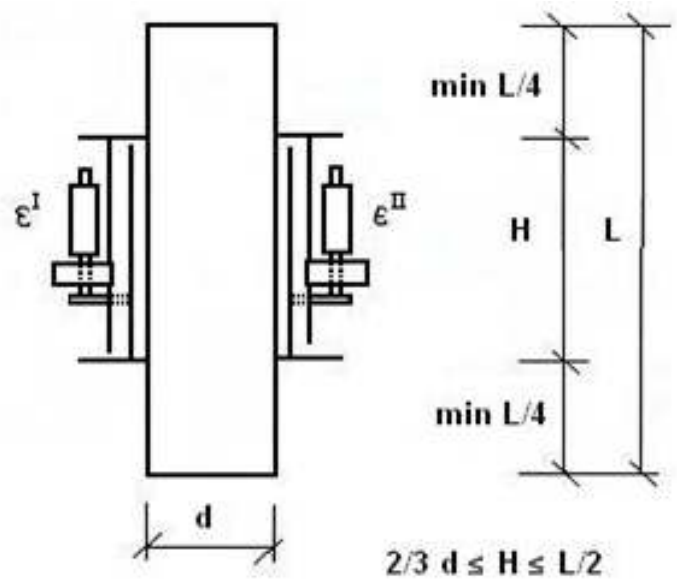

Figure 1 Location of test equipment on test specimen [2]

STATISTICAL ASSESSMENT

Elementary concepts and techniques of the theory of probability and mathematical statistics applicable to civil engineering are available in a number of standards [5-10,12].

The sample characteristics – mean, standard deviation, coefficient of variation and skewness – are then estimated by the classical method.

Compressive strength:
The sample mean $m = (\Sigma\, x_i) / n =$ **53.3 MPa**
The sample standard deviation $s = (\Sigma\, (x_i - m)^2) / (n - 1))^{0,5} =$ **5.57 MPa**
The sample coefficient of skewness $\omega = [n\, (\Sigma\, (x_i - m)^3) / (n\text{-}1) / (n\text{-}2)] / s^3 =$ **-0.50**
The coefficient of variation is **10.4%**.

Modulus of elasticity:
The sample mean $m = (\Sigma\, x_i) / n =$ **35.1 GPa**
The sample standard deviation $s = (\Sigma\, (x_i - m)^2) / (n - 1))^{0,5} =$ **1.92 GPa**
The sample coefficient of skewness $\omega = [n\, (\Sigma\, (x_i - m)^3) / (n\text{-}1) / (n\text{-}2)] / s^3 =$ **+0.27**
The coefficient of variation is **5.5%**.

Generally, the consideration of asymmetry to determine properties is recommended whenever the coefficient of variation is greater than 0,1 or the coefficient of skewness is outside the interval <-0.5, 0.5>.

Due to higher skewness the sample should be test for outliers. Testing for outliers is a very delicate subject, because outliers should be identified by other than statistical reason. In general for small samples true outliers can distort the results considerably. Histograms of the obtained measurements are indicated in Figure 2 and 3.

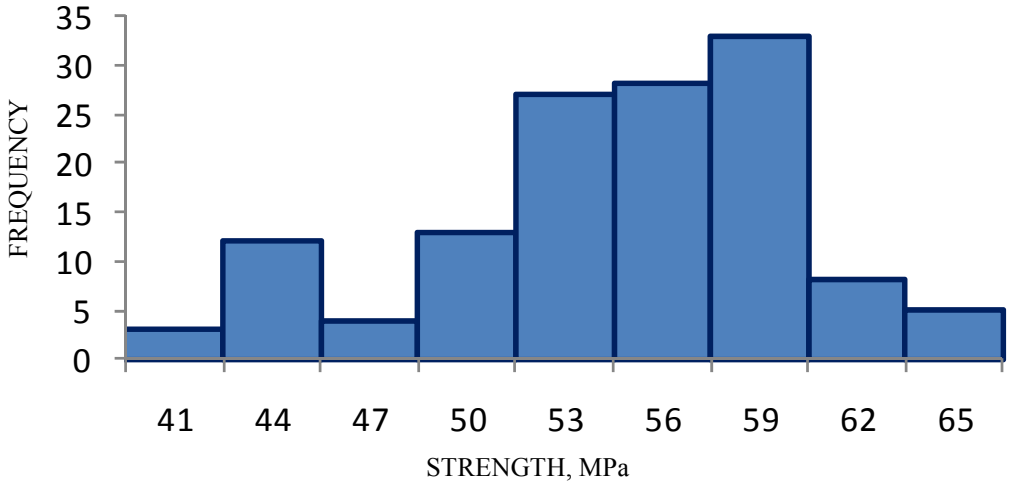

Figure 2 Histogram of compressive strength

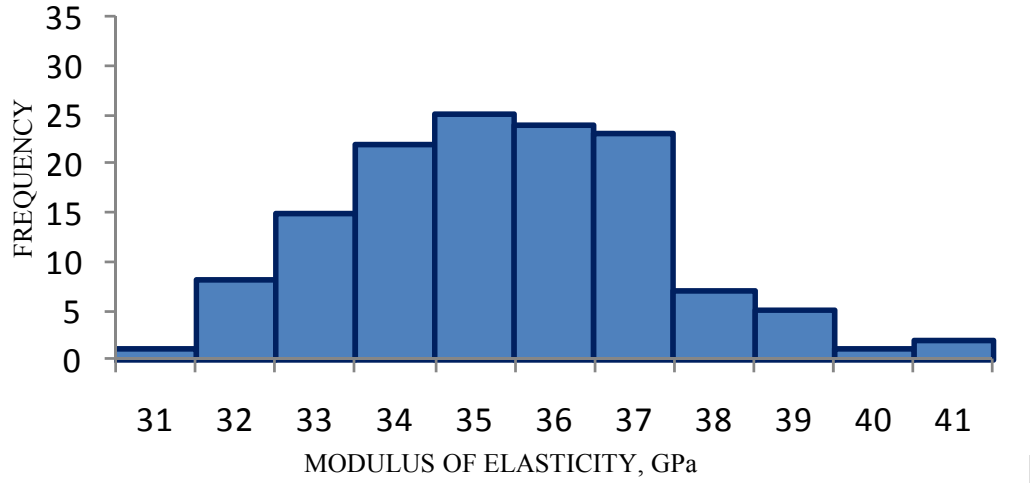

Figure 3 Histogram of modulus of elasticity

Histogram of the obtained measurements is indicated in Figure 2. It appears that the sample includes an extreme or dubious measurement that may result from an error within the measurement procedure. Therefore, the test proposed by Grubbs (2) is used to indicate whether the hypothesis that there is no outlier in the sample can be rejected or confirmed

$$\hat{x}_n \geq x_0 = F_X^{-1}(1-\alpha^n) \tag{2}$$

According to the significance-level alpha = 0.05000 an observation is classified as an outlier, if its value is smaller than 33.47 or larger than 73.07. Similar to the significance-level alpha = 0.25000 an observation is classified as an outlier, if its value is smaller than 36.06 or larger than 70.49. The total number of newly identified outliers is 0. At the significance level 0,05 and 0,25 the tests indicates that the hypothesis can be rejected

GOODNESS OF FIT TEST FOR DISTRIBUTION FUNCTIONS – STRENGTH

The theory of structural reliability is based on a general principle that all the basic variables are considered as random variables having appropriate type of probability distribution. Different types of distributions should be used for description of material properties. Information about some methods of mathematical statistics (about the so-called goodness of fit tests) can be found in the textbook [4] and in specialized literature [12, 13].

For the calculation was used software Statrel and EasyFit. Distribution tests are also very sensitive to outliers. This implies again some iteration with respect to outliers. Three types of distribution test are considered in this paper.

- χ^2 Test
- Kolmogoroc-Smirnov Test
- Andersen-Darling Test

Table 1 Results of goodness fit test – compressive strength

DISTRIBUTION	TEST		
	KOLMOGOROV-SMIRNOV	ANDERSON-DARLING	CHI-SQUARED
Beta	0.05400	0.6319	10.471
Normal	0.08208	1.4446	12.144
Lognormal (3P)	0.07737	1.5379	14.095
Gamma	0.09596	2.0614	18.338
Lognormal	0.10372	2.3648	20.596

Probability density functions of these five theoretical models (considering sample characteristics) and a sample histogram are shown in Figure 4.

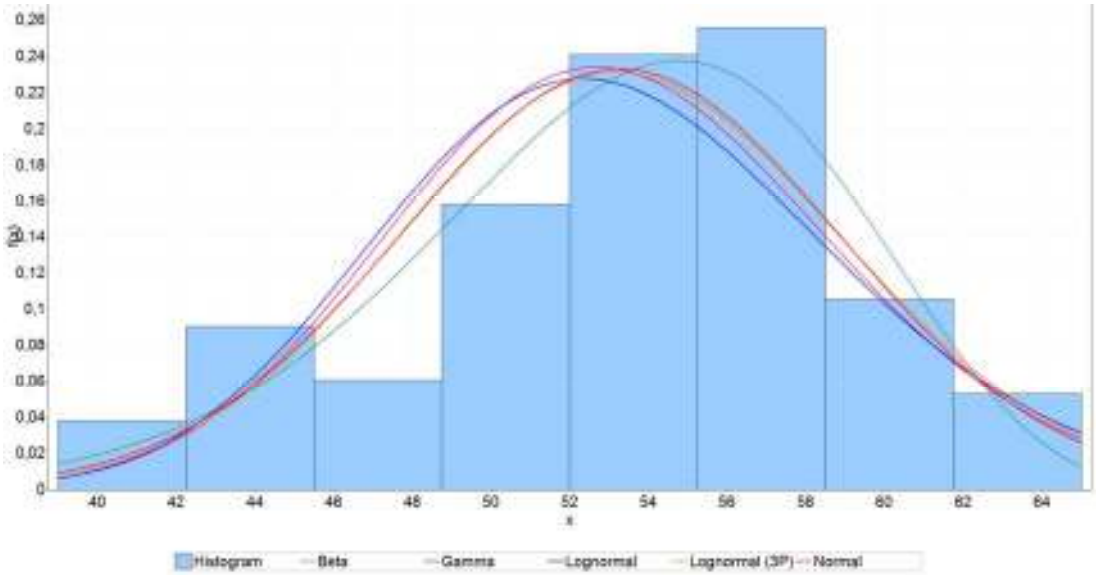

Figure 4 Histogram of compressive strength and the considered theoretical models

To compare goodness of fit of the considered distributions Kolmogorov-Smirnov. Anderson Darling and chi-square tests described by Ang and Tang [12] are further applied. It appears that no distribution should be rejected at the 5% significance level.

According to Table 1 it seems that the both-side limited Beta distribution describes the histogram of obtained results better than the normal and lognormal distribution. But interesting fact is that second recommended distribution is Normal distribution.

CHARACTERISTIC AND DESIGN VALUE – STRENGTH

The characteristic and design values of material properties are defined as specified fractiles of the appropriate distribution. Usually the lower 5% fractile is assumed for the characteristic strength Xk and a smaller fractile probability (around 0.1%) is considered for the design value Xd.

Table 2 Characteristic and design value – compressive strength

DISTRIBUTION	f_{ck} , MPa	$f_{cd,}$ MPa
Normal	44.1	36.3
Shifted lognormal	44.9	38.8
Lognormal	43.4	31.8

It is shown. when the normal distribution is used and the actual distribution has a negative coefficient of skewness. $\alpha_x < 0$. the predicted lower fractiles will then have an unfavourable error (i.e. will be greater than the correct values). For the case when the correct distribution has a positive coefficient of skewness. $\alpha_x > 0$. the lower fractiles. estimated using the normal distribution. will have a favourable error (i.e. will be less than the correct values). However. In the case of the 5% lower fractile value (commonly accepted for the characteristic value) with the coefficient of skewness within the interval <-1. 1> the error is relatively small (about 3% for a coefficient of variation about 0.1).

Considerably greater differences may occur for the 0.1% fractile value (which is approximately 12% considered for design values) when the effect of asymmetry is more significant than in case of 5% fractile.

GOODNESS OF FIT TEST FOR DISTRIBUTION FUNCTIONS – MODULUS OF ELASTICITY

Probability density functions of these five theoretical models (considering sample characteristics) and a sample histogram are shown in Figure 5. To compare goodness of fit of the considered distributions Kolmogorov-Smirnov and Anderson Darling tests described by Ang and Tang [12] are further applied. It appears that no distribution should be rejected at the 5% significance level. According to Table 3 it seems that all distributions are close together except to Beta distribution.

Table 3 Results of goodness fit test – modulus of elasticity

DISTRIBUTION	TEST	
	Kolmogorov-Smirnov	Anderson-Darling
Beta	0.08123	0.57738
Normal	0.06614	0.59799
Lognormal (3P)	0.07831	0.55542
Gamma	0.06569	0.54962
Lognormal	0.06918	0.54324

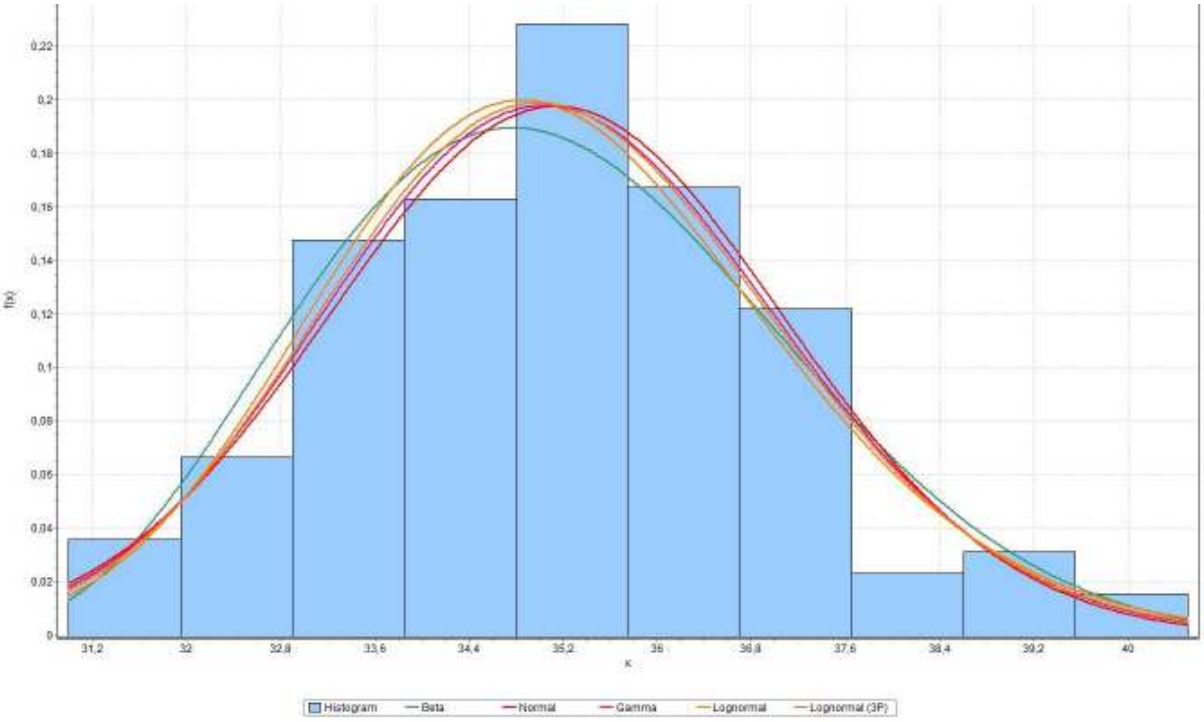

Figure 5 Histogram of modulus of elasticity and the considered theoretical models

CONCLUSIONS

The following conclusions are drawn from the presented assessment of concrete strength:

- Available samples should be verified by an appropriate test of outliers as extreme measurements. Possibly due to an error. May significantly affect sample characteristics.
- Appropriate models of distributions should be selected on the basis of the goodness of fit tests. Taking into account general experience with distribution of concrete strength.
- Lognormal distribution having the lower bound at the origin may be a suitable model for concrete strength.

- The sample has relatively high skewness. This is one of the reasons why the design value of a material property should be preferably determined on the basis of the characteristic value which is not significantly sensitive to the distribution asymmetry.
- The concrete strength may be improved particularly by reducing the variability and skewness.

The following conclusions are drawn from the presented assessment of modulus of elasticity:

- Mean value m = 35.1 GPa, standard deviation s = 1.92 GPa, coefficient of skewness $\omega = +0.27$.
- In case of modulus of elasticity, the mean value is the design value of a material property for structure design. This is the main difference in comparison with compressive strength.
- It seems that all distributions are close together except to Beta distribution. Of course, the mean value is independent of choice of distribution function.

ACKNOWLEDGEMENTS

The research work presented in this paper has been supported by the CTU SGS10/228/OHK1/2T/31 "The Study of Testing and Technological Influences on Test Results of Moduls of Elasticity of Modern Concrete and as a part of project No. GA 104/10/2359 supported by the Grant Agency of Czech Republic.

REFERENCES

1. HUŇKA P.; KOLÍSKO J.: The Study of Specimen Shape and Size on Test Result of Modulus Elasticity. Conference 15. Concrete days 2008. ČBS Servis. s.r.o.. 2008. pp. 386–381.

2. CIKRLE P.. HUŇKA P.. Conference Technology. Making and Control of Concrete Structures 2005 – Comparison of Testing Methods for Assessment of Modulus of Elasticity of Concrete

3. ČSN ISO 6784 Concrete -- Determination of static modulus of elasticity in compression

4. HUŇKA P.. JUNG K.. KOLÁŘ K.. ŘEHÁČEK S.. Statistical Analysis of Modulus of Elasticity and Compressive Strength of Concrete C45/55 for Presstresed Precast Beams Testing and Quality in Civil Engineering. ISBN 978-80-214-4144-6. Brno University of Technology. 2010. str. 65-72

5. EN 1990 Eurocode - Basis of structural design. CEN 2002.

6. EN 1991-1-1 Eurocode 1 Actions on structures. Part 1-1 General actions. Densities. self-weight. imposed loads for buildings. CEN 2002.

7. ISO 2394 General principles on reliability for structures. ISO Geneve. Switzerland 2003.

8. ISO 12491 Statistical methods for quality control of building materials and components. Geneve. Switzerland 1997.

9. ISO 13822. Basis for design of structures - Assessment of existing structures. ISO 2003.

10. JCSS: Background documentation. Part 1 of EC 1 Basis of design. 1996.

11. STATREL. version 8.10. Reliability Consulting Programs. RCP MUNICH. 2009.

12. ANG. A. H. S.& TANG. W. H.: Probabilistic Concepts in Engineering Emphasis on Applications to Civil and Environmental Engineering. 2nd edition. John Wiley & Sons 2007. USA

Shear Strength of Steel Fibre Self-compacting Reinforced Concrete Beams

S A AlTaan, Z S Al-Neimee
Mosul University, Iraq

The present study consists of two parts, the first one look for producing self-compacting steel fibrous concrete with reasonable flow, spread, and passing abilities, and resistance to segregation and shear. Ten percent of the cement was replaced by limestone powder with particle size less than 75μm to increase the fines fraction in the mix. The second part of the study, deals with the effect of adding steel fibres and the shear span / effective depth ratio on the shear strength of self-compacted reinforced concrete beams. Twenty four beams were cast which were 1.0 m long , 150 mm wide, and with overall depth of 200 mm. Four volume percentages of steel fibres were used, 0, 0.35, 0.7 and 1.05 together with six shear span /effective depth ratios of, 1.50, 1.74, 1.98, 2.22, 2.46, and 2.69. The test results showed that the steel fibres have adverse effect on the fresh properties and this effect was reduced by using plasticizer that increased with the fibres percentages. On the other hand, the steel fibres improved the mechanical properties of the hardened concrete in compression and tension. All the beams failed in shear, and the test results showed that the presence of steel fibres increased the cracking shear stress and the shear strength and this increase depends on the shear span / effective depth ratio and on the volume fraction of the steel fibres. The ratio of the cracking / shear strength increased from 0.4 to 0.8 as the shear span / effective depth ratio increased from 1.50 to 2.69. The strut and tie model, and some of the previously developed equations for predicting the shear strength of reinforced fibrous concrete slender beams can be used for predicting the shear strength of fibrous SCC deep and slender beams respectively.

S A AlTaan, B.Sc. Civil Engineering, is a staff member, Civil Engineering Dept., Mosul University, Mosul, Iraq. He was previously Cultural Advisor / Iraqi Embassy, Kuala Lumpur and his fields of interest, include fibre reinforced concrete. His studies were undertaken at Mosul University, and a PhD in Civil and Structural Engineering from Sheffield University, UK.

Z. S. Al Neimee, is an MSc student in Civil Engineering at Mosul University, Iraq. Mosul/IRAQ, 2005, 2005-2008, M.Sc. student, Civil Engineering, Mosul

Keywords: Beams, Cracking, Fibre concrete, Self-compacting concrete, Shear strength

INTRODUCTION

Fibre reinforced concrete FRC that has developed more than fifty years ago is a concrete reinforced with discrete short fibres with tensile strength, flexural strength, flexural toughness, cracking resistance, and strain capacity more than that of the plain concrete. It is also characterized by multiple cracking, well-defined post cracking behaviour, and ductile mode of failure under all types of loading [1-2]. Numerous studies have been conducted dealing with the influence of steel fibres on the shear strength of conventional reinforced concrete beams [3-7], in some of these studies [3-4], prediction equations for the shear strength of steel fibre reinforced concrete beams were proposed.

After the development of sophisticated analysis, design methods, and high strength materials, the reinforced concrete cross-sections become smaller than before and thus leading to congestion in reinforcement. A need have therefore arose for a concrete with good flow, spreading, passing abilities, and resistance to segregation; and the self-compacted concrete SCC was the remedy [8-9]. This type of concrete was developed since the late 1980's. A great number of studies were conducted dealing with its fresh and hardened properties [8-13].

Fibre reinforced self- compacted concrete FRSCC, can be considered as a high performance hybrid of fibre reinforced and self-compacting concrete, which retain the properties of both types of concretes.

Greenough and Nehdi [14] presented a detailed investigation on the influence of fibre type, fibre anchorage, fibre aspect ratio, and fibre content on the shear behaviour of self-compacted reinforced concrete slender beams without stirrups. Steel fibres (30 and 50 mm long) and polypropylene fibres were used. The beams were 200× 300× 2400 mm in size with a reinforcement depth and ratio of 265 mm and 1.7% respectively. The shear span/effective depth ratio (a_v / d) was kept constant at 3.0. The steel fibres SCC beams were able to resist larger shear loads than that of the polypropylene fibres SCC beams for each respective fiber dosage, likely, because steel fibers have a higher strength and stiffness and thus are more effective in restraining crack growth. The fibres reinforced beams were able to resist further load after the initiation of inclined shear cracking and the mode of failure for some of the beams was changed from a shear failure to a more ductile flexural failure.

Dhoude et al. [15] conducted an experimental investigation on seven full-scale prestressed concrete I-beams to study the effect of steel fibres on the casting procedure, end anchorage cracking, shear strength and ductility. One beam was made of normal concrete as a control specimen, three were cast using normal concrete reinforced with steel fibres, and the other three were cast using fibre reinforced self-compacting concrete. The test results showed that all the fibrous beams exhibited smaller crack spacing compared to the beams without fibres, and the steel fibres were more effective in controlling / eliminating the end-zone cracks than the traditional transverse steel. The test results showed also that the shear capacity of the fibrous beams was significantly increased. Moreover, failure of the beams without steel fibres was sudden and catastrophic, while all the fibrous beams exhibited ductile and less catastrophic failure.

Cuenca and Serna [16] presented test results for five reinforced concrete I-beams, beam A cast with normal concrete, beam B cast with SCC , beam C cast with FRC , and beams D and E were prestressed and cast with SCC and FRC respectively. Beams A-C are 7.88 m long, while beams D and E were 6.66 m long. The steel fibres (60 kg/m³) were 50 mm long and

0.625 mm in diameter. Beams A-C were identical in the longitudinal reinforcement and concrete strength and were over designed in flexure and provided with minimum shear reinforcement so that shear failure takes place. Beams A-C were failed in shear, and beams A and B showed identical failure load and behaviour, while beam C showed more rigid behaviour at the cracked state and failed at a load that was 33.6% more than that of beams A and B due to the presence of steel fibres.

Helincks et al. [17] conducted an experimental programme on sixteen steel fibre reinforced self-compacted concrete beams without stirrups. The longitudinal reinforcement was kept constant in all the beams that were subjected to four points bending at a shear span / depth ratio of 2. The steel fibres were hooked end 30 mm long and 0.55 mm in diameter. Four SCC mixes were used; a control mix without fibres and three mixes with (30, 55, and 70 kg/m³) steel fibres. The test results showed that the shear strength increased with the fibres content, more extensive crack pattern and increased ductility are observed. The experimental values of the shear strength were compared with those calculated using published prediction equations. The aim of this investigation is to assess the feasibility of producing medium strength SCC with low fines percentage reinforced with steel fibres of low aspect ratio and varying volume percentages. The object of this investigation also, is to study the influence of steel fibres and shear span / effective depth on the shear behaviour and strength of SCC beams. The measured shear strength will compared with those predicted using available shear strength equations.

EXPERIMENTAL PROGRAMME

Materials

Table 1 shows the mix proportions used [18]. Ordinary Portland cement, complying with the Iraqi specifications [19], and ten percent by weight of the cement was replaced by limestone powder passing sieve No. 200 (75 microns). The limestone powder was used to act as filler, increase the flow ability, and decrease friction between the mix constituents. Medium size sand complying with BS 882 [20] with a fineness modulus of 2.74, and gravel with maximum aggregate size of (12.50 mm) complying with BS 882 [20] was used. The mix proportions were chosen to produce a nominal cube compressive strength of 40 MPa.

Table 1 Mix proportions

MIX No.	FIBRES VOLUME PERCENTAGE v_f	PLASTICIZER PERCENTAGE BY WEIGHT OF CEMENT	MIX PROPORTIONS BY WEIGHT
M0-1.3	0	1.3	0.1 Limestone dust, 0.9 Cement, 2.4 Sand, 1.9 Gravel, 0.38 water
M0.35-1.5	0.35	1.5	
M0.7-1.7	0.7	1.7	
M1.05-1.9	1.05	1.9	

The Sika Viscocrete - 5w is used as a plasticizer whose physical properties are shown in Table 2. The dosage of the plasticizer was increased with the fibres volume to meet the requirements of the fresh SCC. Harex steel fibres of shelled deformed cross section, Figure 1, with a length $L_f = 16mm$, equivalent diameter $D_f = 0.78mm$, and aspect ratio of (L_f / D_f =20.5), and three steel fibres percentages by volume (v_f = 0.35, 0.7, and 1.05) were used besides the control mix ($v_f = 0$). To get optimum strength improvement, the fibres length should be more than the maximum aggregate size, which in this case 12.5 mm. The first number in Table 1 refers to the steel fibres percentage, and the second one refers to the plasticizer dosage.

Table 2 Properties of the plasticizer

PLASTICIZER TYPE	COLOUR	DENSITY	PHYSICAL STATE	DOSE
Sika Viscocrete-5W	Light brown	1.11±0.02 kg/l	Fluid	1-2% of the cement weight

Figure 1 Harex steel fibres

Specimens Description

The test programme consisted of testing 24 reinforced concrete beams that are 1.0m long, 150 mm wide and 200 mm deep overall, Figure 2. The beams were reinforced in tension with 2 ϕ16 mm bars with a yield and tensile strength of 517 and 644 MPa respectively. The two bars were hooked upwards to preclude anchorage failure. The two bars were assembled together by two stirrups (ϕ10 mm) at the two ends. The beams were supported (hinge and roller) on a span of 900 mm and loaded at two points as shown. The shear span was varied as (250, 290, 330, 370, 410, and 450 mm), making the shear span / effective depth ratio (a_v / d) as (1.50, 1.74, 1.98, 2.22, 2.46, and 2.69). All the beams were white painted before testing to trace the cracks initiation and their propagation. Demec points were fixed at the midspan section as shown in Figure 3 to measure the concrete strains.

The following tests were used to measure the properties of the fresh concrete; the slump flow test for the spreading ability, J-ring test for the passing ability, V-funnel test for the segregation resistance.

These tests and the corresponding limits can be cited in References [8-9]. Three (100 mm) cubes and three cylinders (100×200 mm) were used to measure the compressive strength, and three cylinders (100×200 mm) for the splitting strengths.

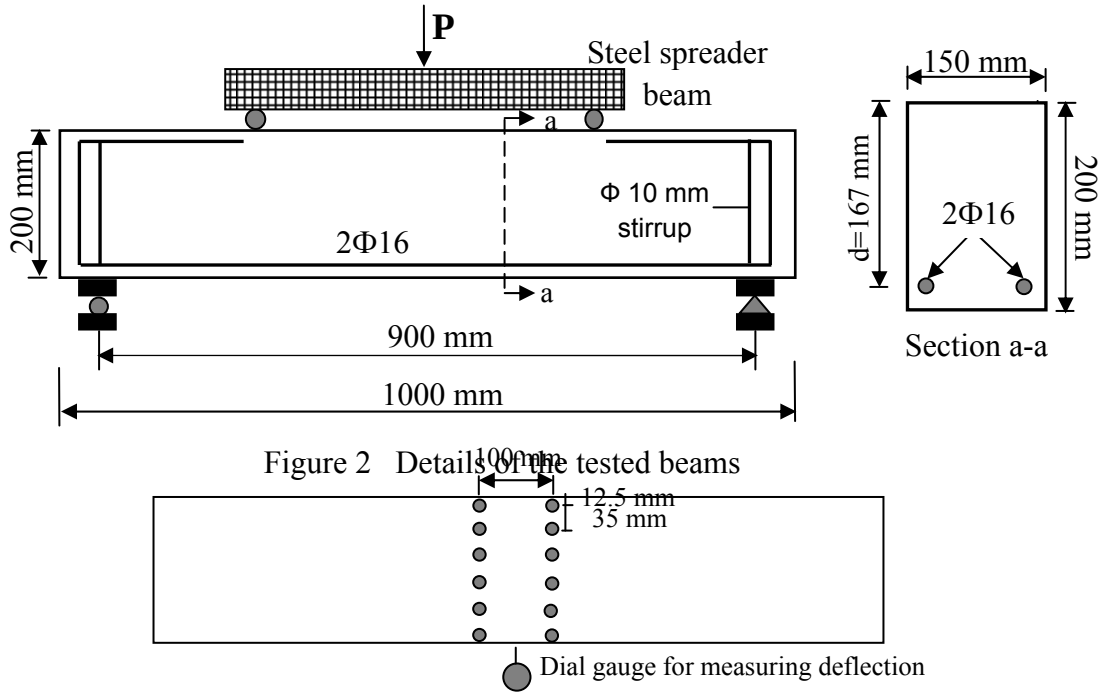

Figure 2 Details of the tested beams

Figure 3 Instrumentation of the tested beams

TEST RESULTS AND DISCUSSION

Properties of Fresh Concrete

Table 3 shows that the steel fibres increased the time T_{500} (time from commencing upward movement of the cone to when the concrete has flowed to a diameter of 500 mm). The steel fibres decreased the average-spreading diameter D_{avg} (average of the largest diameter of the flow spread of concrete and the diameter of the spread at right angle to it) for the three fibres reinforced SCC mixes. However, both T_{500} and D_{avg} for the four SCC mixes are within the specified limitations [8-9], which means that the four mixes have a reliable flow and filling abilities.

Table 4 shows the test results for the passing ability of the four SCC mixes. The test results show that the presence of the steel fibres increased the difference B_j (average distance at four perpendicular points on the periphery of the ring from the top of the concrete surface to the top of the ring minus the same distance at the centre of the ring). The steel fibres increased the times T_o and T_5 also, (T_o is the time required for all the concrete to pass through the lower opening of the V-funnel, and T_5 is the time required for all the concrete to pass for a second time through the lower opening of the V-funnel after five minutes).

However, all the test results are within the specified limits [8-9], except Mix 1.05-1.9 for which B_j and (T_5 - T_o) were slightly greater than the specified limits, however, no conglomeration of the concrete was noticed.

Table 3 Fresh properties of the SCC mixes

MIX No.	T_{500}, sec	LIMITS T_{500}	D_{avg} mm	D_{avg} LIMITS
M0-1.3	2.14	(2-5) sec	715	SF2 for normal applications 660-750 mm
M0.35-1.5	2.63		709	
M0.7-1.7	2.89		683	
M1.05-1.9	3.1		670	

Table 4 Fresh properties of the SCC mixes

MIX NO.	B_j	LIMITS B_j	T_o, sec	LIMITS T_o	T_5, sec	T_5 - T_o	LIMITS T_5 - T_o
M0-1.3	7	≤ 20	7.37	0-12	8.79	1.4	0-3
M0.35-1.5	12.25		9.68		11.46	1.78	
M0.7-1.7	19.5		10.43		13.17	2.74	
M1.05-1.9	**23.25**		11.38		15.2	**3.8**	

Properties of Hardened Concrete

Table 5 shows the variation of the compressive strength (28 days of age) with the steel fibres volume. The increase in the compressive strength ranged between 2.5-6.1% for the cubes and 4.4-7.4% for the cylinders. The strength enhancement depends of course on the mix proportions, fines percentage, and the percentage and fibres dimensions. The average ratio of the cylinder to the cube strength is 0.76. Table 5 shows also the cylinders splitting strength of the four SCC mixes. The increase in the splitting strength ranged between 6-24%, which is higher than the increase in the compressive strength, and this may be attributed to the different failure mechanisms associated with each test.

Table 5 Properties of the four hardened concrete mixes

MIX NO.	M0-1.3	M0.35-1.5	M0.7-1.7	M1.05-1.9
f_{cu} (MPa)	49.1	50.33	50.53	52.1
$f_c^{'}$ (MPa)	36.7	38.3	39.1	39.4
f_{sp} (MPa)	4.35	4.62	5.18	5.39

Shear Strength of the Tested Beams

Cracking shear stress

Figure 4 shows that the cracking shear stress, $v_{cr} = V_{cr}/(b.d)$ (based on the measured shear at the onset when such inclined cracks were first visually observed) increased with the steel fibres volume, and decreased with increasing a_v/d ratio. The increase ranged from 2.5 - 44% of the cracking shear stress of similar beams without fibers, Table 6. The steel fibres appeared to be effective in delaying the initiation of cracks.

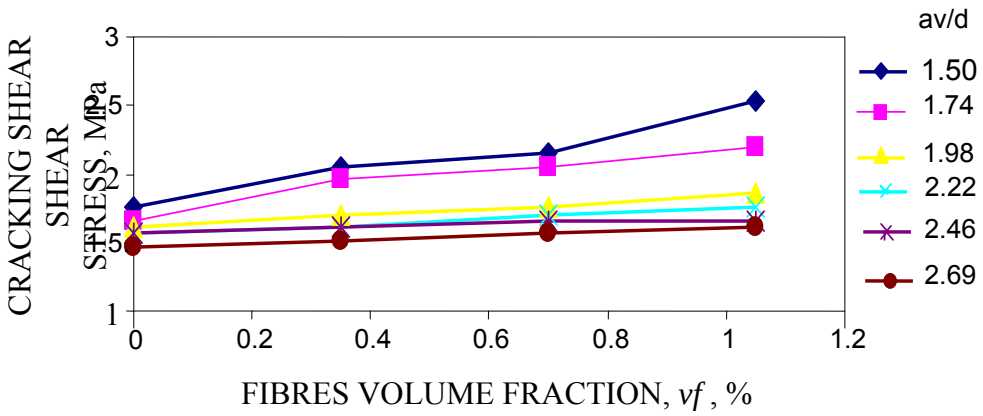

Figure 4 Variation of the cracking shear stress with the fibres volume

Shear strength

Figure 5 shows that the shear strength, $v_u = V_u/(b.d)$ increased with the steel fibres volume, and decreased with increasing a_v/d ratio. The increase ranged from 3.2 – 44.2% of the shear strength of similar beams without fibers. Although the range of increase is similar to that of the cracking shear stress (2.5-44%), Table 6, the rate of increase with the fibres percentage for the shear strength is about 68% more than that for the first crack shear stress, as shown by the slope of the best-fit lines in Figure 6. This may be attributed to two factors, firstly the steel fibres enhance the first cracking strength of cement matrices less than that at the ultimate stage [21], and secondly, the mobilization of the fibres action after the appearance of cracks. Other researchers [4] found similar results.

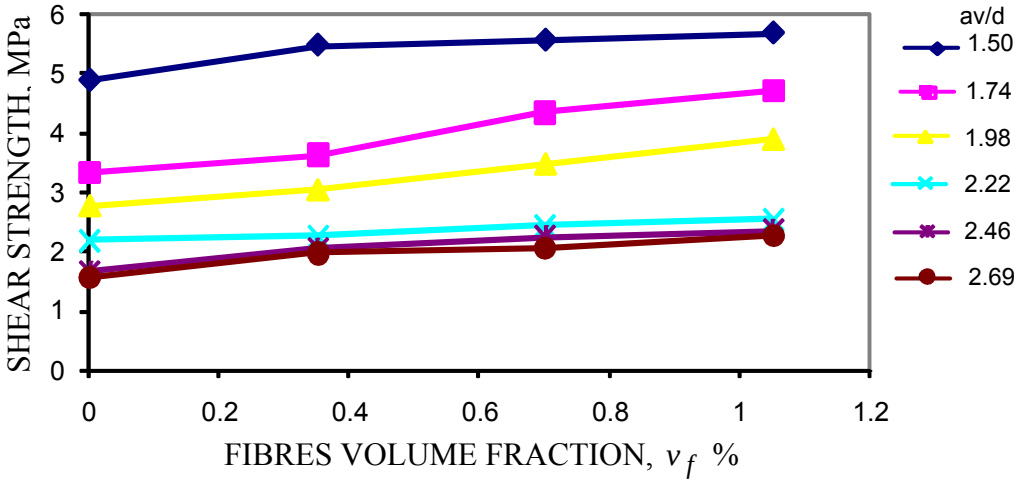

Figure 5 Variation of the shear strength with the fibres volume fraction

Table 6 Average percentage increase in the shear stress due to fibres addition

v_f %	CRACKING		ULTIMATE	
	Range	Average	Range	Average
0.35	2.5-18.1	8.2	3.2-25.6	13.8
0.7	5.7-24.1	12.7	11.0-34.3	24.4
1.05	5.7-44.0	19.9	16.2-44.2	33.4

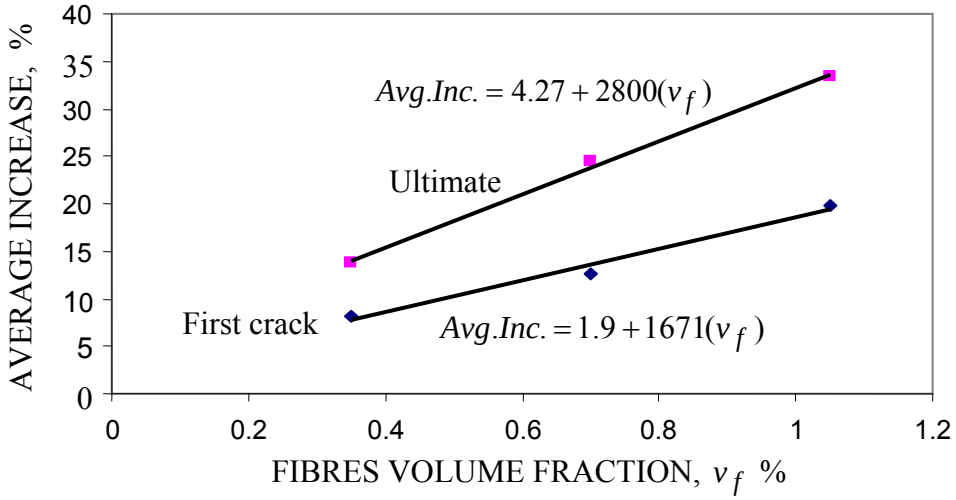

Figure 6 Increase in the cracking and shear strength due to fibres

Table 7 and Figure 7 show the average ratio of the first crack shear stress to the shear strength with the a_v / d ratio. It can be noticed that the stress ratio (v_{cr} / v_u) is increasing with the a_v / d ratio, since the arch and dowel actions are vanishing with increasing a_v / d ratio as the beam approach the state of a slender beam [4,22,23]. Table 7 also shows that for a certain a_v / d the stress ratio does not vary significantly with the fibres volume percentage.

Table 7 Ratios of the cracking shear stress / shear strength of the tested beams

v_f % \ a_v / d	1.50	1.74	1.98	2.22	2.46	2.69
0	0.36	0.5	0.58	0.72	0.94	0.94
0.35	0.38	0.54	0.56	0.72	0.78	0.78
0.7	0.39	0.48	0.51	0.71	0.75	0.76
1.05	0.45	0.47	0.48	0.70	0.71	0.72
Average	**0.4**	**0.5**	**0.53**	**0.71**	**0.80**	**0.80**

Load-Deflection

Typical load-deflection relationships are shown in Figures 8-9 for two groups of beams with

a_v / d ratios of 2.46 and 2.69, the Figures show that as the fibers content increased, the beam stiffness, the maximum load, and the ultimate deflection increased also. This may be attributed to the tension stiffening effect introduced by the steel fibres.

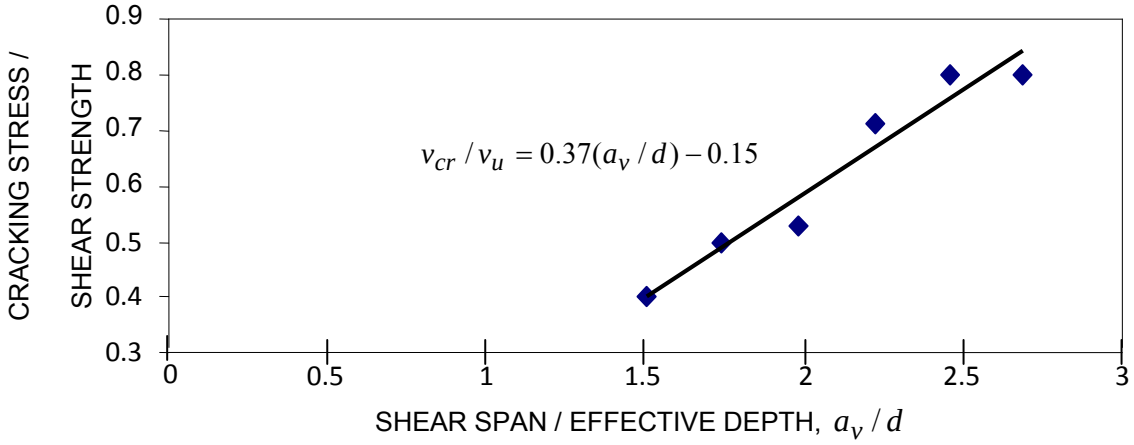

Figure 7 Variation of the cracking shear stress / shear strength with the shear span / effective depth ratio

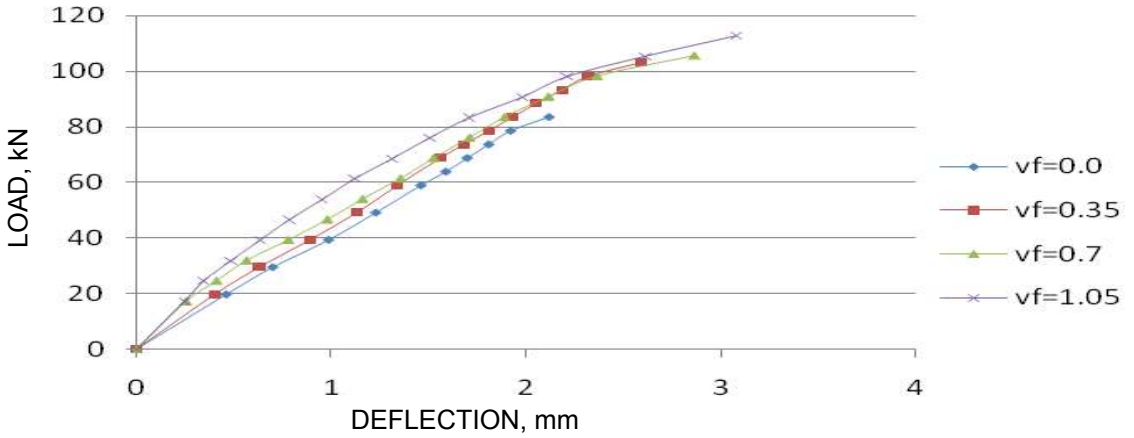

Figure 8 Load-deflection relationships for beams with a_v / d of 2.46

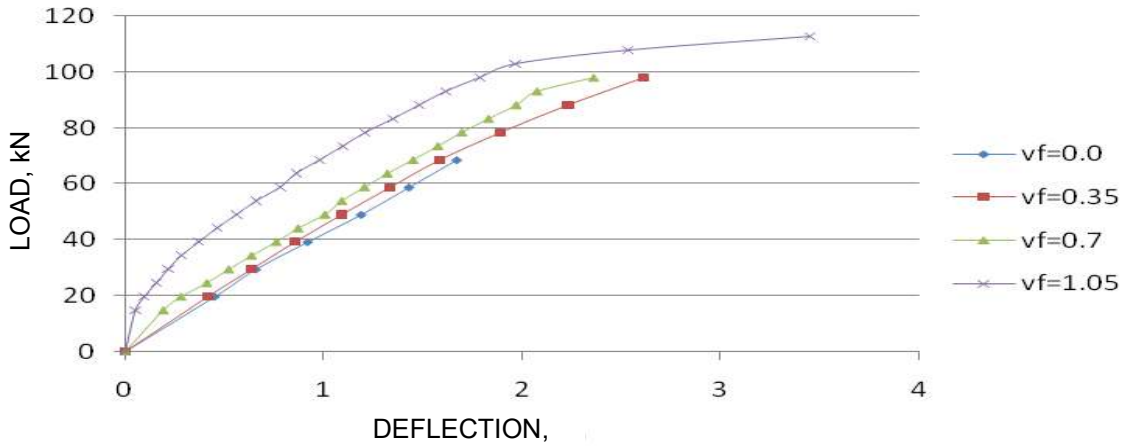

Figure 9 Load-deflection relationships for beams with a_v / d of 2.69

Concrete strains

The concrete strains that were measured at the midspan sections, increased with the applied loads, Figure 10, but the neutral axes positions were not changed significantly, since the beams were not under reinforced and the final failure is not a flexural one. This behaviour was typical of the other groups of beams.

Failure mode

The addition of steel fibers to concrete affected the observed cracking patterns, which are shown in Figure 11 for the beams with a_v / d =1.74. These four beams are identical except for the steel fibers percentage (0, 0.35, 0.7, and 1.05). The numbers next to the cracks refer to the load (in kN) at which the crack was first observed. In all the beams, flexural cracks first formed within the constant-moment region, and later shear cracks formed within the region of constant shear. The beam failed suddenly along a single shear crack. As reported by other researchers [4, 15, 17], as the steel fibres volume increased the number of flexural and shear cracks increased, i.e., the flexural and shear cracks were spaced more closely as the volume of fibers increased. This failure mode was typical for the other groups of beams.

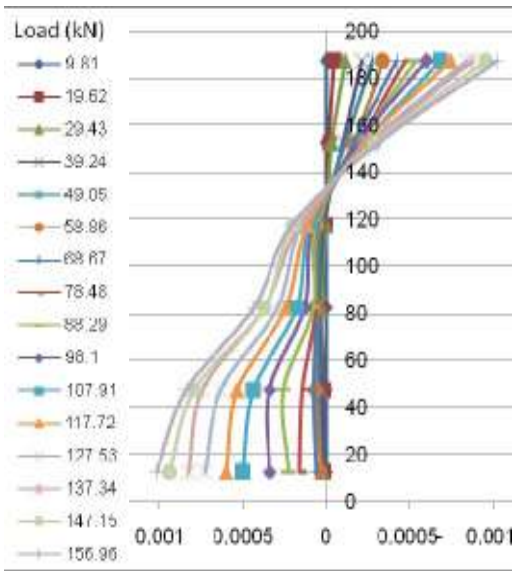

Figure 10 Variation of the concrete strains with the load, $a_v / d = 1.74, v_f = 0$

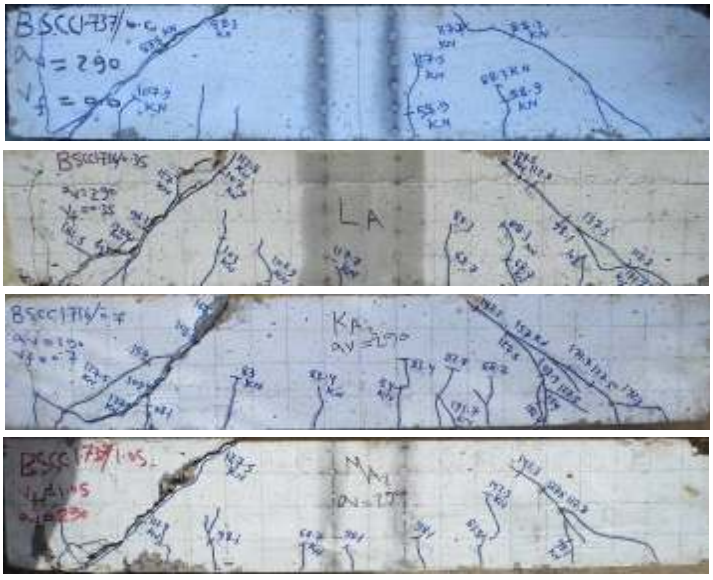

Figure 11 Cracks patterns for the beams with $a_v / d = 1.74$, v_f = 0, 0.35%, 0.7%, 1.05%

CALCULATED SHEAR STRENGTH WITH SOME PREDICTION EQUATIONS

The strut and tie method [24] is used for deep beams with a_v / d < 2.0, and Figure 12 shows the external forces (applied shear forces and reactions) and the internal forces (tie and struts). A sample of calculation is shown below for the beam with a_v / d =1.5 and v_f = 0. Width of the tie (ad) $W_{t(ad)}$ = 2 (clear concrete cover + d_b / 2) = 2(25.4+16/2) =66.8 mm. Force in the

tie (ad) $F_{u(ad)} = \phi \times 0.85 f_c^{'} \times \beta_n .b.W_{t(ad)}$ (β_n = 0.8 for C-C-T nodes), ϕ = capacity reduction factor = 0.75.

Force in the strut (bc) $F_{u(bc)} = \phi \times 0.85 f_c^{'} \times \beta_s .b.W_{s(bc)}$ ($W_{s(bc)}$ = strut width, and β_S = 1.0 for prismatic struts). Considering equilibrium of the forces at section A-A ($\Sigma F_x = 0$), $F_{u(ad)} = F_{u(bc)}$, from which, $W_{s(bc)} = 0.8W_{t(ad)} = 0.8 \times 66.8 = 53.44mm$.

$\theta = \tan^{-1}[h - W_{t(ad)}/2 - W_{s(bc)}/2]/a_v = \tan^{-1}(200 - 66.8/2 - 53.44/2)/250 = 29.23°$

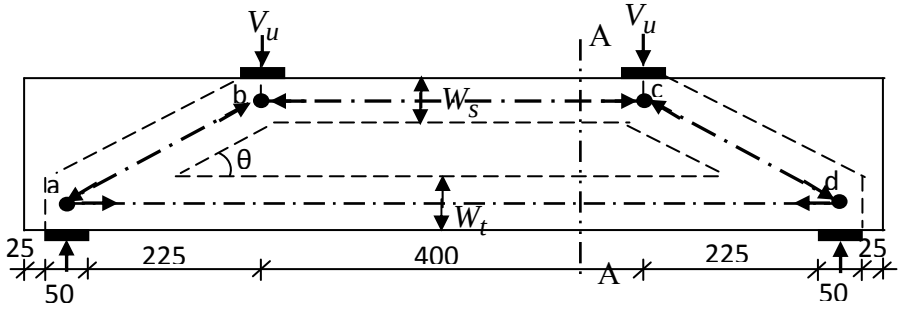

Figure 12 Strut and tie model for the beam with $a_v / d = 1.50$

At node (a), $W_{s(ab)} = L_p \sin\theta + W_{t(ad)} \cos\theta = 50\sin(29.23) + 66.8\cos(29.23) = 82.71mm$, L_p = plate width.

$F_{u(ab)} = \phi \times 0.85 f_c^{'} \times \beta_n .b.W_{s(ab)} = 0.75 \times 0.85 \times 36.7 \times 0.8 \times 82.71/1000 = 232.5kN$

At node (b), $W_{s(ba)} = L_p .\sin\theta + W_{s(bc)} .\cos\theta = 50\sin(29.23) + 53.44\cos(29.23) = 71.1mm$

$F_{u(ba)} = \phi \times 0.85 f_c^{'} \times \beta_n \times b \times W_{s(ba)} = 0.75 \times 0.85 \times 36.7 \times 1.0 \times 150 \times 71.1/1000 = 249.5kN$, ($\beta_n = 1.0$ for C-C-C nodes), $F_{u(ab)} = 232.5kN < F_{u(ba)} = 249.5kN$, $\therefore F_{u(ab)} = 232.5kN$. Considering equilibrium of the vertical forces at node **(a)**, $V_u = F_{u(ab)} .\sin(\theta) = 113.5kN$. If the tension steel will yield ($f_s = f_y = 517MPa$), the force in the tie (ad) = $A_s .f_y = 0.000402 \times 517 = 207.8kN$. The force in the strut (ab), $F_{u(ab)} = F_{u(ad)}/\cos(\theta) = 207.8/\cos(29.23) = 238.1kN > 232.5kN$, this means that failure will initiate in the strut (ab). In this case the force in the tie = $232.5\cos(\theta) = 202.9kN$, the tie steel stress $f_s = 0.2029/0.000402 = 504.7MPa < f_y = 517MPa$, i.e.; the steel stress will not reach yielding at failure.

Table 8 shows the measured and the calculated shear strength using the above equations. For beams provided with steel fibres, the force in the tie will be that of the tension steel ($A_s . f_s$) and the contribution of the steel fibres which equals to $\sigma_{ct} . b . W_t$, where σ_{ct} is the post cracking tensile strength of the steel fibre composite.

The method proposed by Narayanan and Darwish [3] which is the most accurate procedure proposed for slender beams [4], is used for predicting the shear strength of the shallow beams whose $a_v / d > 2.0$. The proposed shear strength equation is as follow:

$$v_u = e[0.24 f_{spfc} + 80 \rho . d / a_v] + v_b \quad (1)$$

where $f_{spfc} =$ splitting strength of the fibre composite, e = factor that takes the arch action into account, and equal to 1.0 when $a_v / d > 2.8$, and $2.8 d / a_v$ for $a_v / d \le 2.8$, and:

$$v_b = 0.41 \tau . F \quad (2)$$

$\tau =$ interfacial bond strength between the steel fibres and the surrounding concrete and is taken equal to 4.15 MPa as proposed by Swamy et al.[21], and F = fibres factor equal to:

$$F = v_f \times d_f \times L_f / D_f \quad (3)$$

$d_f =$ fibre shape factor = 0.5 for smooth fibres, 0.75 for deformed fibres and 1.0 for crimped fibres [3], L_f and D_f are the fibre length and diameter respectively. Table 9 shows the measured and the calculated shear strength using the above equations.

The average ratio of $V_{u(meas.)} / V_{u(calc.)}$ for the twenty-four beams = 1.036, standard deviation = 0.0837 and a coefficient of variation = 0.081, which means that the two adopted methods yield reliable prediction of the shear strength.

Table 8 Measured and calculated shear strength using the strut and tie model [24]

v_f	0		0.35%		0.7%		1.05%	
a_v / d	Meas.	Calc.	Meas.	Calc.	Meas.	Calc.	Meas.	Calc.
1.50	121.7	113.5	137.3	130.5	139.3	132.1	142.3	138.3
1.74	83.4	90.2	90.7	95.9	108.5	96.15	117.5	96.5
1.98	69.1	79.4	75.9	84.3	86.9	84.55	97.4	84.8
Average $V_{u(meas.)} / V_{u(calc.)}$ = 1.031, S.D. = 0.1055, C.O.V.= 0.102								

Table 9 Measured and calculated shear strength using Narayanan and Darwish method [3]

v_f	0		0.35%		0.7%		1.05%	
a_v / d	Meas.	Calc.	Meas.	Calc.	Meas.	Calc.	Meas.	Calc.
2.22	54.6	51.35	56.4	54.95	60.6	60.8	63.6	63.85
2.46	41.6	44.73	51.4	48.12	55.9	53.55	58.9	56.5
2.69	39.1	39.55	49.1	42.76	51.4	47.85	56.4	50.65
Average $V_{u(meas.)} / V_{u(calc.)} = 1.041$, S.D. = 0.059, C.O.V.= 0.057								

CONCLUSIONS

The experimental results showed that the steel fibres increased the cracking shear stress, and the shear strength of self-compacted reinforced concrete beams from 2.5-44%. However, the rate of increase for the shear strength was 68% more than that for the first crack shear stress. The ratio of the cracking stress / shear strength increased with the a_v / d ratio, but did not vary significantly with the fibres volume fraction. The addition of steel fibres consistently decreased crack spacing, and increased the deformation capacity.

The strut and tie model may be used to predict the shear strength of fibre reinforced self-compacted concrete deep beams, and the method proposed by Narayanan and Darwish for slender beams.

More test results of fibre reinforced self-compacted concrete beams may results in a better understanding of their strength and behaviour.

REFERENCES

1. ACI COMMITTEE 544.4R-88, "Design Considerations for Steel Fiber Reinforced Concrete", Re-approved 1999, American Concrete Institute, Farmington Hills MI, 18 pp.

2. ACI COMMITTEE 544.1R-96, "State-of the-Art report on Fiber Reinforced Concrete ", American Concrete Institute, Farmington Hills, MI, 1996, 66 pp.

3. NARAYANAN, R., and DARWISH, I. Y. S., "Use of Steel Fibres as Shear Reinforcement", ACI Structural Journal, Vol. 84, No. 3, May-June 1987, pp. 216-227.

4. KWAK, Y., EBERHARD, M., KIM, W., and KIM, J., "Shear Strength of Steel Fiber Reinforced Concrete Beams without Stirrups", ACI Structural Journal, Vol. 99, No. 4, August 2002, pp. 530-538.

5. KUANG, J., BACZKOWSKI, B.,"Shear Capacity of Steel Fiber Reinforced Concrete Coupling Beams", Civil and Building Engineering, June 2006, pp. 3837-3846.

6. SALNA, R., MARCIUKAITIS, G., "The Influence of Shear Span Ratio on Load Capacity of Fiber Reinforced Concrete Element with Various Steel Fiber Volumes", Journal of Civil Engineering and Management, Vol. XIII, No. 3, March 2007, pp. 479-489.

7. MADAN, S., KUMAR, G., SINGH, S., "Steel Fibers as Replacement of Web Reinforcement for Reinforced Concrete Deep Beams in Shear", Asian Journal of Civil Engineering, Vol. 8, No.5, 2007, pp. 479-489.

8. EFNARC, "Specification and Guidelines for Self-Compacting Concrete", Association House, UK, 2002, 32 pp.

9. CONCRETE EUROPEAN GROUP, "The European Guidelines for Self-Compacting Concrete, Specification, Production and Use", May, 2005, 68 pp.

10. FELEKOGLU, B., TURKEL, S., and BARADAN, B., "Effect of Water/Cement ratio on the Fresh and Hardened Properties of Self-compacting Concrete", Building and Environment, January 2006, pp. 1795-1802.

11. MIAO, B., CHERN, J. C., and YANG, C. A., "Influences of Fibre Content on Properties Of Self-Compacting Steel Fibre Reinforced Concrete", Jour. of the Chinese Institute of Engineers, Vol. 6, No. 4, 2003, pp. 523-530.

12. OUCIEF, H., HABITA, M. F., and REDJEL, B., "Hybrid Fibre Reinforced Self - Compacting Concrete: Hardened Properties", Inter. Jour. of Civil Engineering, Vol. 4, No. 2, 2006, pp. 77-85.EREN, O., and ALYOUSIF, A., "Production of Self-Compacting Fibre Reinforced Concrete in North Cyprus", Sixth Inter. RILEM Symposium on Self-Compacting Concrete (4th North American Conference on the Design and Use of SCC, Montreal (Canada), September 26- 29, 2010, pp. 1323-1331.

13. GREENOUGH, T., and NEHDI, M., "Shear Behaviour of Fibre-Reinforced Self Consolidating Concrete, Slender Beams", ACI Materials Journal, Vol. 105, No. 5, Sept.– Oct. 2008, pp. 468-478.

14. DHOUDE, H. B., TADEPALLI, P. R., MO, Y. L., and HSU, T. T. C.," Shear Behaviour of Prestressed Beams with Steel Fibre Self-compacting Concrete", 14th World Conference on Earthquake Engineering, Oct. 12-17, 2008, Beijing, China, pp. 1-8.

15. CUENCA, E., and SERNA, P., "Shear Behaviour of Self-Compacting Concrete and Fibre-reinforced Concrete Beams", Sixth Inter. RILEM Symposium on Self-Compacting Concrete (4th North American Conference on the Design and Use of SCC, Montreal (Canada), September 26- 29, 2010, pp. 1273- 1282.

16. HELINCKS, P., CORTE, W. E., BOEL, V., and SCHUTTER, G. D.," Influence of Steel Reinforcement on the Shear Resistance and Crack Pattern Formation of Self-Compacting Concrete Beams ", Jour. of Key Engineering Materials, Nov. 2010, Vol. 452-453, pp. 669-672.

17. ALNEIMEE, Z. S., "Shear Strength of Steel Fibers Reinforced Self Compacted Concrete Beams", M. Sc. Thesis, Mosul University, Iraq, 2008, 142 pp.

18. IRAQI STANDARD SPECIFICATIONS NO. 5, "Properties of Ordinary Portland Cement", the Central Establishment for Standardization and Quality Control, 1984.

19. BS.882-1992, "Aggregates from Natural Source of Concrete", British Standard Institution, 1992.

20. SWAMY, R. N., MANGAT, P. S., and RAO, C. V. S. K., "The Mechanics of Fiber Reinforcement of Cement Matrices", Fiber Reinforced Concrete, SP-44, American Concrete Institute, Farmington Hills, MI, 1974, pp. 1-28.

21. MACGREGOR, J. G., "Reinforced Concrete: Mechanics and Design", Prentice-Hall Inc., Upper Saddle River, N. J., 1997.

22. ZSUTTY, T., "Shear Strength Predictions for Separate Categories of Simple Beam Test", ACI Journal, Proceedings, Vol. 68, No. 2, February 1971, pp.138-143.

23. ACI COMMITTEE (318-08), "Building Code requirements for Structural Concrete (318-08) and Commentary", American Concrete Institute, Farmington Hills, MI, 2008, 471 pp.

Shear Transfer Strength between Precast Normal and Self-compacting Concrete

J R AlFeel, R S AlHadedi
Mosul University, Iraq

Repairing some parts of plain or reinforced concrete members, requires the application of relatively thin concrete sections, which should be bond the old section, but cannot be compacted in situ. The use of self-compacted concrete is a proper solution for such cases. The aim of this study is to investigate the shear transfer between precast normal and cast in place self-compacting concrete.The investigated variables were the compressive strength of the normal concrete and self-compacted concrete, and the method of treatment of the precast normal concrete surface. Four methods were used, sandblasting, chipping, shear keys, and shear connectors. The shear reinforcement (U-shaped) used were either, one 6 mm, two 6 mm, or one 10 mm diameter steel bars. Twenty-four push-off specimens were tested with or without shear connectors with the two outer sides of the push-off specimen cast with normal concrete and left in the laboratory for more than 60 days and then the middle part cast vertically with self-compacted concrete. The fresh properties of the self-compacted concrete mixes were measured using, the slump-flow to measure the spreading ability, V-funnel test to measure the separation ability, and the L-box to measure the passing ability. The load was applied gradually at the top of the middle part of the push-off specimens, and the slip was measured by using dial-gauges. The test results showed that the compressive strength of both normal and self-compacted concrete enhance the shear transfer strength. Excluding the reinforced specimens, the best method of surface treatment was the sandblasting which gave highest transfer shear strength and lowest slip, followed by the chipping and the shear keys specimens. Among the reinforced specimens, those reinforced with two 6 mm diameter bars gave the highest transfer shear strength, followed by those reinforced with one 10 mm diameter bars, and those reinforced with one 6 mm diameter bars, which gave the lowest transfer shear strength.

J. R. AlFeel, B.Sc., Civil Engineering, B.Sc. Civil Engineering, is a staff member, Civil Engineering Dept., Mosul University, Mosul, Iraq. His fields of interest, include fibre fibre reinforced and self-compacted concrete. His studies were undertaken at Mosul University, and a PhD in Civil and Structural Engineering from Sheffield University, UK.

R. S. AlHadedi, B.Sc., Civil Engineering, 2007, Mosul University, Iraq, M.Sc., 2009, Civil Engineering, Mosul University, Iraq.

Keywords: Interface, Normal concrete, Self-compacting concrete, Shear transfer, Surface treatment

INTRODUCTION

Self-compacted concrete (SCC) is a concrete that is able to flow under its own weight and completely fill the formwork and encapsulate the reinforcement without the need of vibration [1]. Since the end of the 1980's, a great number of researches were conducted dealing with the kind of the materials used, and its fresh and hardened properties [2-8]. Different types of filler materials are used to increase the fines percentage, and to replace part of the cement in addition to the plasticizers, so that the fresh mixes comply with required (SCC) specifications.

In 2001, Bouzouban and Lachemi [5] used fly ash as a percentage of cement, and the produced mix have good workability and the presence of fly ash enhanced the compressive strength. In 2005, Collepardi et al. [6] used limestone dust in one mix and fly ash in another mix with the same cement content, and they found that both materials enhanced the compressive strength. In 2005, Corinaldesi et al. [7] replaced 10% of cement or sand by marble powder and he found that the replacement of 10% sand gave better results (in terms of compressive strength and workability) than replacing the cement. AlFeel and Al-Harbi [8] used limestone and clinker dusts as a filler to produce self-compacting concrete. They concluded that the mix with clinker dust gave higher compressive strength and less workability than the mix with the limestone dust.

Repairing parts of plain or reinforced concrete members, requires sometimes the application of relatively thin concrete sections, which should be bonded to the old section, but cannot be compacted in situ. The use of self-compacted concrete is a proper solution for such cases.

Mattock [9] and Mattock et al. [10] conducted a series of tests on shear transfer specimens made of normal and lightweight concrete reinforced across the shear plane. They recommended the use of the following Equation for estimating the shear transfer strength:

$$V_n = 0.8A_{vf}\, f_y + KA_c \tag{1}$$

V_n = nominal shear strength (MN), A_{vf} = area of interface shear reinforcement (m²), f_y = yield strength of the reinforcement, K is a constant = 2.75 for normal concrete and 1.7 for lightweight concrete, and A_c = area of concrete resisting shear. Equation 1 applies for surfaces that are intentionally roughened with amplitude of ≥ 6 mm.

Paulay et al. [11] studied the shear transfer mechanism across a horizontal construction joint. Surface preparation and interface reinforcement percentage effects were tested by applying monotonic and cyclic shear stresses along the construction joint. The test results showed that the shear transfer strength increased with the surface roughness and interface reinforcement.

ACI Committee (318-08) [12] recommended the following equation to estimate the shear transfer capacity between two surfaces connected by shear reinforcement, based on a shear-friction hypothesis:

$$V_n = A_{vf}\, f_y \mu \tag{2}$$

V_n should not exceed the least value of $0.2 f_c^{'}.A_c$, $(3.3 + 0.08 f_c^{'})$ or $11A_c$, μ=coefficient of friction along the interface $= 1.0\lambda$ for surfaces that intentionally roughened with an

amplitude of $\geq$ 6 mm, and $= 0.6\lambda$ for surfaces not intentionally roughened, $\lambda = 1.0$ for normal weight concrete and 0.75 for all lightweight concrete, and A_c = interface area.

Banta [13] has conducted a study on horizontal shear transfer between ultra high performance concrete and lightweight concrete, by testing twenty-four push-off specimens. The test results showed that the current design equations from the ACI [12] and AASHTO [14] can be used for design, and the horizontal shear strength effect from various surface treatment, reinforcement ratios and aspect ratio, and the best method of surface preparation is chipped method, which allow for extra bond between the deck and beam.

Tests conducted by Bass et al. [15], studied the shear transfer across new and existing concrete interface under repeating load. They concluded that a heavily sandblasted interface treatment result higher interface shear capacities than other surface preparation technique, and the increase in the amount of or embedment depth of the interface reinforcement resulted in an increase in the shear transfer capacity of a concrete interface.

The test reported in this study provided data for application where self-compacting concrete is cast against existing old normal concrete surface to provide information for design engineers to use in estimating shear capacity for interfaces between different materials or different ages. The main variables studied included, compressive strength of both normal concrete and SCC, treatment of interface area where many four methods are used; sandblasting, chipping, shear keys and interface reinforcement.

EXPERIMENTAL PROGRAMME

Materials

The materials used were ordinary Portland cement, which comply with the Iraqi specifications [16], river sand with a fineness modulus of 2.74, and gravel aggregate with maximum size of 19 mm, both sand and gravel comply the Iraqi specifications [17]. Limestone powder was used to replace 8% and 10% of the cement. Super plasticizer is used also to satisfy the (SCC) requirements. To get different compressive strength, two mixes for normal concrete and two mixes for (SCC) were used; Table 1 shows the mixes proportions by weight for both types of concrete.

Table 1 Mixes proportions by weight

MIX PROPORTIONS BY WEIGHT	NC	NC	SCC	SCC
Cement	1	1	0.92	0.90
Sand	2.55	2	2.1	2.4
Gravel	4.3	2.88	1.7	1.9
W/C Ratio	0.53	0.45	0.36	0.39
Super Plasticizer	-----	-----	2.5%*	2.5%*
Limestone Powder	-----	-----	8%*	10%*

* By weight of cement

For SCC mixes, limestone powder passing sieve (No. 200) and super plasticizer were used; the flow table test, V-funnel test, and L- box test were used to measure the spreading, separation, and passing abilities respectively. Cylinders (150×300 mm) were used for measuring the compressive strength of the mixes.

Specimens

Twenty-four push-off specimens, similar to those used by Tanaka et al. [18] Table 2, were tested to investigate the interface shear capacity between precast normal concrete and self-compacting concrete. The tested specimens consisted of three parts, two parts (outer) of dimensions (150×150×350 mm) of normal concrete which have the same compressive strength and cured in water for 14 days and left in the laboratory for 58-77 days. The third part which is the SCC middle part of the specimens then cast vertically with a dimension of (220×140×150 mm), Figure 1.

Table 2 Surface preparation of the specimens

SPECIMEN	AGE OF NC PART, DAYS	SURFACE TYPE	SHEAR REINFORCEMENT
NC.SCC.Sb1	77	Sb	----------
NC.SCC.Ch1	77	Ch	---------
NC.SCC.Sk1	65	Sk	---------
NC.SCC.1R1	59	S	1#6 mm
NC.SCC.2R1	59	S	2#6 mm
NC.SCC.1R1	64	S	1#10 mm
N.SCC.Sb2	72	Sb	--------
N.SCC.Ch2	72	Ch	--------
N.SCC.SK2	65	Sk	--------
N.SCC.1R2	59	S	1#6 mm
N.SCC.2R2	65	S	2#6 mm
N.SCC.1R2	65	S	1#10 mm
N.SCC.Sb3	77	Sb	--------
N.SCC.Ch3	76	Ch	---------
N.SCC.SK3	64	Sk	---------
N.SCC.1R3	58	S	1#6 mm
N.SCC.2R3	60	S	2#6 mm
N.SCC.1R3	62	S	1#10 mm
N.SCC.Sb4	71	Sb	--------
N.SCC.Ch4	80	Ch	---------
N.SCC.SK4	64	Sk	--------
N.SCC.1R4	58	S	1#6 mm
N.SCC.2R4	66	S	2#6 mm
N.SCC.1R4	64	S	1#10 mm

Sb: sand blast, Ch: chipping, Sk: shear-key, S: smooth with interface shear reinforcement.

The vertical inner sides of the (NC) specimens, which have a dimension of 200×150 mm, were treated by either sand blasting, chipping to an amplitude of 3 mm, shear keys, or using interface shear reinforcement as shown in Table 2:

1- Sandblast which are used resulted in exposure of the aggregate at the interface,

2- Chipping, the interface surface chipped to 3 mm amplitude,

3- Shear-keys, two trapezoidal shear keys are used and positioned as shown in Figure 2,

4- U-Shape shear reinforcement as shown in Figure 3 is embedded in the normal concrete:

a- One 6 mm diameter U shaped bar, with a yield and tensile strength of 469 and 620 MPa respectively,

b- Two 6 mm diameter U shaped bars, and

c- One 10 mm diameter U shaped bar, with a yield and tensile strength of 440 and 710 MPa, respectively.

The load was applied incrementally on the middle cast in place part (SCC). Three dial gauges were used (for measuring the slip); two on the normal concrete parts and one on the (SCC) part, the slips were measured for each load increment.

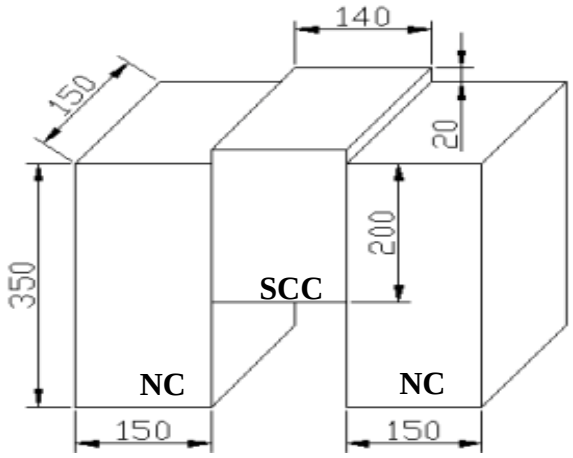

Figure 1 Dimensions of push-off specimen (Dimensions in mm)

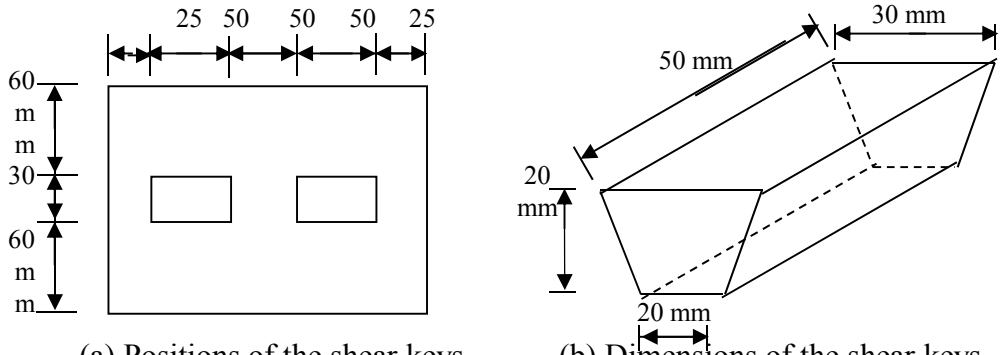

(a) Positions of the shear keys (b) Dimensions of the shear keys

Figure 2 Details of the shear keys, (a) Positions of the shear keys in the shear plane, (b) Dimensions of the shear keys

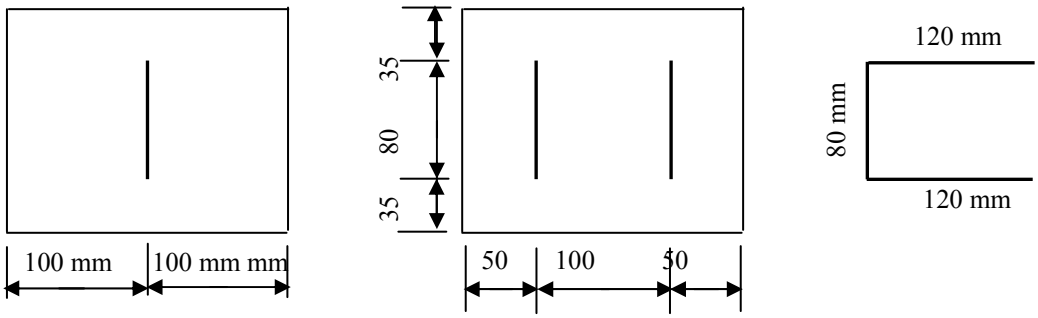

(a) One bar (b) Two bars (c) Shape of the bar

Figure 3 Positions and shape of the shear reinforcement

RESULTS AND DISCUSSION

Fresh Properties of the Mixes

The slumps for the normal concrete (NC) were 106 mm and 110 mm for Mixes 1 and 2 respectively. The fresh properties of the self-compacting concrete are as shown below:

1- **Flow- table**, the test results are shown in Table 3, the results show that the average diameter of Mix1 and Mix2 were 690.5 mm and 750 mm respectively, which are within the required specifications [19], and the time required for the fresh mix to reach 500 mm diameter for Mix 1 is more than that of Mix 2. This indicates that Mix 2 has workability better than Mix1 due to the higher percentage of fine materials [20].

2- **V-funnel**, the test results are shown in Table 4, the results show that the time required to empty the V-shape from SCC for Mix 1 is more than that for Mix 2, this indicate that Mix 1 has more tendency to separate than Mix2 due to the aforementioned reason, and both Mixes were within the required SCC specifications.

3- **L-box,** the test results in Table 5, shows that Mix 2 has more ability to pass than Mix1 and both mixes were within the required SCC specifications.

Table 3 Test results of the flow table of SCC

MIX	T_{500} sec	LIMIT sec	D_{max} mm	D_{perp} mm	$D_{avg.}$ mm	LIMIT[19] mm
1	3	2-5	700	690	690.5	650-800
2	2.6		740	760	750	

Table 4 Test results of the V-funnel test for SCC

MIX	To, sec	LIMIT To sec	T5, sec	T5-To	LIMIT sec, [19]
1	9.1	6-12	11.2	2.1	0-3
2	8.3		10.7	2.4	

Table 5 Test results of the L-box for SCC

MIX	H1, mm	H2, mm	H2/H1	LIMITS (H2/H1) [19]
1	110	89	0.81	0.8-0.85
2	90	75	0.833	

Shear Transfer Specimens

Table 6 shows the test results of the 24 push-off specimens.

Effect of compressive strength of concrete

The test results show that for all types of surface treatment the shear-transfer strength increased with the compressive strength of both the normal (old concrete) and the self-compacted concrete (cast in place).

Table 6 Test results of push-off specimens

SPECIMEN	CYLINDER STRENGTH MPa		TREATMENT TYPE	SHEAR TRANSFER STRENGTH kN	MAX. SLIP mm
	NC	SCC			
NC.SCC.Sb1	23.2	33.5		93.0	0.0378
NC.SCC.Sb2	37.5	33.1	Sand blasting	100.0	0.039
NC.SCC.Sb3	23.2	43.7		96.5	0.0389
NC.SCC.Sb4	37.5	43.7		107.5	0.0426
NC.SCC.Ch1	26.9	33.5		39.5	0.026
NC.SCC.Ch2	36.6	33.2	Chipping	47.5	0.035
NC.SCC.Ch3	26.9	42.8		45.0	0.033
NC.SCC.Ch4	36.6	41.6		55.0	0.0412
NC.SCC.Sk1	26.1	33.6		20.5	0.0113
NC.SCC.Sk2	35.2	36.6	Shear key	25.0	0.0129
NC.SCC.Sk3	26.1	41.3		22.5	0.0170
NC.SCC.Sk4	35.2	43.4		30.0	0.0183
NC.SCC.1R1	26	37.4	Shear	28.0	0.023
NC.SCC.1R2	34.9	33.2	reinforcement	32.0	0.034
NC.SCC.1R3	26	44.2	(1#6 mm)	29.2	0.028
NC.SCC.1R4	34.9	43.7		41.8	0.035
NC.SCC.2R1	26.7	35.6	Shear	53.0	0.0263
NC.SCC.2R2	35.6	33.1	reinforcement	68.0	0.0314
NC.SCC.2R3	26.7	41.4	(2#6 mm)	62.0	0.0295
NC.SCC.2R4	35.6	43.7		75.0	0.0461
NC.SCC.1R1	24.3	33	Shear	50.0	0.043
NC.SCC.1R2	38.7	33.6	reinforcement	64.0	0.0512
NC.SCC.1R3	24.3	40.7	(1#10 mm)	60.0	0.048
NC.SCC.1R4	38.7	41.3		67.5	0.053

However, since the induced stresses at both surfaces are shear, the increase in the shear transfer strength (which is controlled by the tensile strength) is nearly proportional to square root of the larger to the smaller compressive strength, which is an index of the tensile strength. Equations 1 and 2 [9, 10, 12] does not take the effect of the compressive strength on the shear transfer strength.

Effect of surface preparation

Excluding the reinforced specimens, the test results show that the effect of the surface treatment is as follow:

1. Sand blasted push-off specimens have the largest shear transfer strength, and this could be attributed to the larger contact area and the good adhesion (part of the bond components) between the two concretes, since the (SCC) contain relatively large amount of fine materials. This is in agreement with the findings of Bass et al. [15].
2. Chipped push-off specimens have shear transfer strength less than the sand blasted specimens due to the smaller contact area. The shear transfer strength in this case ranged from 43-51% of the shear transfer strength of the sand blasted treated specimens.
3. Shear- keys, the push-off specimens have shear transfer strength less than those treated with the sand blasting or the chipping. The shear transfer strength in this case ranged from 22-28% of the shear transfer strength of the sand blasted treated specimens.

Table 6 shows also the final values of the slip between the two parts, for a certain shear force, the slip values for the sand blasted specimens are the least of the other treated specimens. It can be noticed from Table 6 that the maximum shear force can be obtained with the highest compressive strength of both concretes; i.e., when the compressive strength of normal concrete was about 35-37 MPa and for SCC was about 41-43 MPa for all methods of treatment. Figure 4 shows the relationships between the shear force and the slip for specimens; NC.SCC.Sb4, NC.SCC.Ch4, and NC.SCC.Sk4 which the highest compressive strengths.

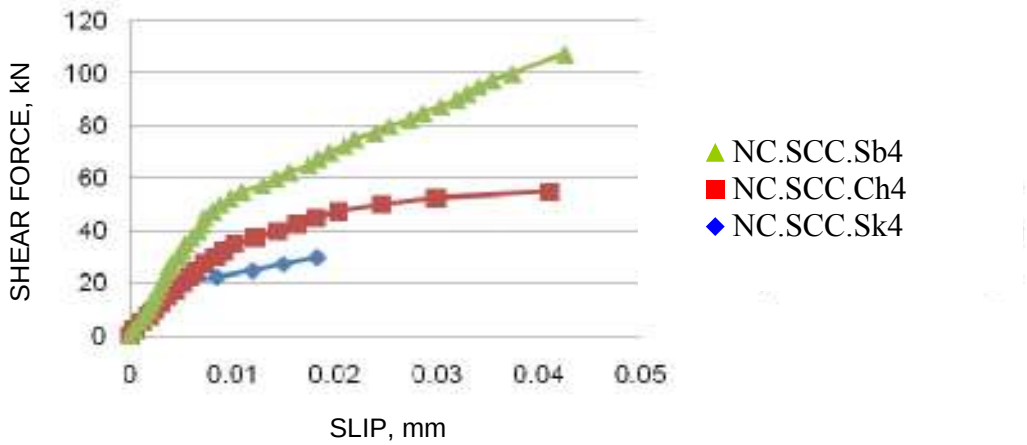

Figure 4 Relationships between the shear force and slip for specimens, NC.SCC.Sb4, NC.SCC.Ch4, and NC.SCC.Sk4

The graph shows that the shear modulus, (initial slope of the curve), was highest for the

sandblasted treatment of the interface, followed by the chipped specimens, and the specimens with shear keys. Effect of shear reinforcement, the test results in Table 6 show that the compressive strength for both type of concretes have the same effect as mentioned above for the unreinforced specimens, i.e., the increase in the shear transfer strength is proportional to the square root of the larger to the smaller compressive strength. Table 6 shows also that the specimens reinforced with two 6 mm diameter U shaped bars ($A_{vf} = 113mm^2$) have the highest shear transfer strength, followed by the specimens reinforced with one 10 mm diameter U shaped bar ($A_{vf} = 157mm^2$), and the specimens reinforced with one 6 mm diameter U shaped bar ($A_{vf} = 56.5mm^2$). The test results showed that a uniform distribution of the interface reinforcement enhance the shear transfer strength more than the area of the reinforcement.

Equation 2 that was proposed by the ACI committee (318-08) [12] is used to calculate the shear transfer strength of the tested reinforced push-off specimens, since it is suitable for reinforced specimens only. The coefficient of friction (μ) assumed equal to 0.6 for surfaces not intentionally roughened. Table 7 shows the experimental and the calculated values; one value for each of the three groups is shown in the Table, since the Equation does not reflect the effect of the compressive of concrete on the shear transfer strength. The calculated values is highly under estimated, since the Equation takes into account the contribution of the reinforcement to the shear transfer strength and ignore the effect of the compressive strength of both the old and the cast in place concretes.

Table 7 Experimental and calculated shear transfer strength of the push-off specimens

SPECIMEN	TREATMENT TYPE	SHEAR TRANSFER STRENGTH, kN		Experimental / Calculated strength
		Experimental	Equation 1	
NC.SCC.1R1	Shear	28.0	15.90	1.76
NC.SCC.1R2	reinforcement	32.0	15.90	2.01
NC.SCC.1R3	(1#6 mm)	29.2	15.90	1.84
NC.SCC.1R4		41.8	15.90	2.63
NC.SCC.2R1	Shear	53.0	31.80	1.67
NC.SCC.2R2	reinforcement	68.0	31.80	2.14
NC.SCC.2R3	(2#6 mm)	62.0	31.80	1.95
NC.SCC.2R4		75.0	31.80	2.36
NC.SCC.1R1	Shear	50.0	41.45	1.21
NC.SCC.1R2	reinforcement	64.0	41.45	1.54
NC.SCC.1R3	(1#10 mm)	60.0	41.45	1.45
NC.SCC.1R4		67.5	41.45	1.63
Average ratio				1.85
Coefficient of variation				0.4

Figure 5 shows the relationships between the shear force and the slip for specimens NC.SCC.1R4 (1#6 mm), NC.SCC.2R4 (2# 6 mm), and NC.SCC.1R4 (1#10 mm) that have the highest compressive strength for both concretes. The figure shows that the initial shear stiffness for the last two specimens is nearly the same.

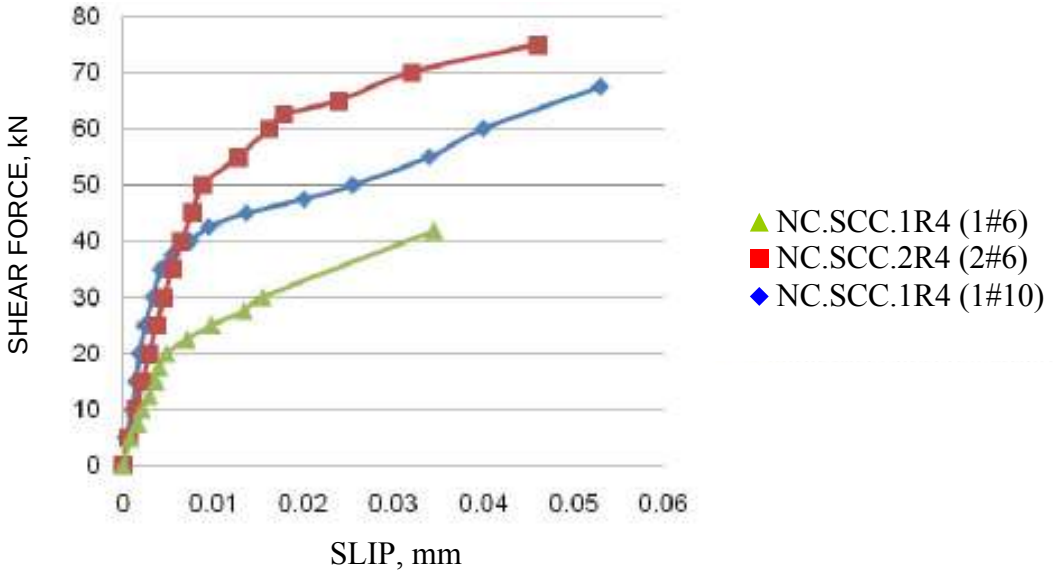

Figure 5 Relationships between the shear force and slip for the reinforced

(a) Sand blasted

(b) Chipping

(c) Shear key

(d) Interface shear reinforcement

Figure 6 Failure modes of some typical specimens, (a) Sand blasted, (b) Chipping, (c) Shear keys, (d) Interface shear reinforcement

Failure Mode

Figure 6 shows the mode failure for typical push-off prisms; sandblasted, chipping, shear key, and specimens with shear reinforcement at the shear plane. The figures show that the failure occurred in the shear plane by shearing the area of the normal concrete due to the good bond between the two concrete types, but for reinforced specimens the failure occurred along the reinforcement and the cracks continue with the reinforcement path.

CONCLUSIONS

The chosen mixes proportions comply with the (SCC) specifications such as, spreading, passing and segregation. The increase in the compressive strength of both concrete normal and self-compacting enhance the shear transfer capacity. so in repair or strengthen of existing structure should be the compressive strength at least equal or greater to that concrete existing in the structure.

A heavily sandblasted interface resulted higher shear transfer capacities than any other surface treatment as shear-keys or chipping when no shear reinforcement is used. Generally an increase in the amount of reinforcement crossing the interface resulted in higher shear transfer capacities and lower slip.

More test results on shear transfer strength of concretes of different grades, types, and surface treatment will serve as a design guide for such related cases.

REFERENCES

1. OKAMURA, H. AND OUCHI, M., "Self-Compacting Concrete", Journal of Advanced Concrete Technology Vol. 1, No. 1, April 2003, pp. 5-15.

2. NAN, S., HSU, K. C., AND CHAI, S. H. W., "A Simple Mix Design Method for Self-Compacting Concrete", Cement and Concrete Research, Vol.31, No., 2001, pp. 1799-1807**.**

3. CORINALDESI, V., AND MORICONI, G., "Durable Fiber Reinforced Self-Compacting Concrete", Cement and Concrete Research, Vol. 34, No.2, 2004, pp. 249–254.

4. AL-SHAMMARI, M. K., "Shear Strength of Self-Compacting Concrete Beams Without Web Reinforcement", M.Sc. Thesis, University of Technology, Iraq, 2007.

5. BOUZOUBAA, N., and LACHEMI, M., "Self- Compacting Concrete Incorporating High Volumes of Class F Fly Ash: Preliminary Results", Cement and Concrete Research, Vol. 31, No. 3, March 2001. pp. 413-420.

6. COLLEPARDI, M., BORSOI, A., COLLEPARDI, S., AND TROLI, R., "Strength, Shrinkage and Creep of SCC and Flowing Concrete", Second North American Conference on the Design and use of self-consolidating concrete, fourth international RILEM symposium on Self- Compacting Concrete, Edited by Shah, 2005, pp. 911-919.

7. CORINALDESI, V., MORICONI, G., AND NAIK, T. R., "Characterization of Marble Powder For Its Use in Mortar and Concrete", Report No. CBU-09, International Symposium, October 5-7, 2005, Toronto, Canada.

8. AL-FEEL, J. R. AND AL-HARBI, M., "Fresh and Hardened Properties of Self Compacting Concrete", World Engineering Congress, Kuching, Sarawak, Malaysia, 2-5 August 2010.

9. MATTOCK, A. H., "Shear Transfer in Concrete Having Reinforcement at an Angle to the Shear Plane", Shear in Reinforced Concrete, SP-42, American Concrete Institute, Farmington Hills, MI, 1974, pp. 17-42.

10. MATTOCK, A. H., LI, W. K., AND WANT, T. C., "Shear Transfer in Lightweight Concrete", Journal of Prestressed Concrete Institute, Vol. 21, No. 1, Jan.-Feb. 1976, pp. 20-39.

11. PAULAY, T., PARK, R., AND PHILIPS, M. H., "Horizontal Construction Joints in Cast-in Place Reinforced Concrete", Shear in Reinforced Concrete, SP-42, American Concrete Institute, Detroit, 1974, pp. 599-616.

12. ACI COMMITTEE (318-08), "Building Code Requirement for Structural Concrete (ACI 318-08) and Commentary", American Concrete Institute, Farmington Hills, MI, 2008, 471 pp.

13. BANTA, T. E., "Horizontal Shear Transfer Between Ultra High Performance Concrete and Lightweight Concrete", M.Sc. Thesis in Civil Engineering, February 2005, Virginia Polytechnic Institute.

14. AASHTO LRFD, "Bridge Design Specification", American Association of State Highway and Transportation Official, Washington, D.C., 2004.

15. BASS, R. A., CARRASQUILLO, R. L., AND JIRSA J. O., "Shear Transfer Across New and Existing Concrete Interfaces", ACI Structural Journal, Vol. 86, No. 4, July-August 1989, pp. 383-393.

16. IRAQI STANDARD SPECIFICATION NO. 5, "Properties of Portland Cement", The Central Establishment for Standardization and Quality Control, 1984.

17. IRAQI STANDARD SPECIFICATION NO. 45, "Natural Aggregate for Construction of Buildings", The Central Establishment for Standardization and Quality Control, 1980.

18. TANAKA, Y., MURAKOSHI, J., ASAI, H., AND NAKAMURA,S., "Effectiveness of Horizontal Shear Transfer for Composite Prestressed Concrete Girders", Research report, Public Works Research Institute, Japan, 2009, 14 pp.

19. ASTM C1611, "Standard Test Method for Self-Compacting Concrete", Philadelphia, Pennsylvania, 2005.

20. AL-HADIDE, R. S., "Shear Transfer at the Interface between Precast Normal Concrete and Self-Compacting Concrete", M. Sc. Thesis, Mosul University, Iraq, 2009.

Nano-structurization of Internal Surfaces of Oil Pipelines

K Abdrakhmanova, E Bovkunov
Kazakh National Technical University, Kazakhstan

In the report results of working out of technology of modifying internal surfaces the main oil pipelines are presented. The given technology allows to lower hydraulic resistance, to level influence of a roughness on swapping parameters, to lower power expenses for transportation of hydrocarbonic raw materials, to raise operational reliability and to extend the between-repairs period. It is established that the most effective way of decrease in hydraulic resistance is modifying of an internal surface on a basis the fluorine-containing surface-active substances. As a result of nano-structural updating internal surfaces decrease in hydraulic resistance to 23-28 % is reached. The maximum decrease in hydraulic resistance is provided at a relative thickness of a molecular layer of fluorine-containing surface-active substances. It is established that the subsequent increase in a relative thickness of the adsorbed layer of fluorine-containing surface-active substances generated on an internal surface, causes increase hydraulic resistance to the certain established value. The structures modifying fluorine-containing surface-active substances are optimized. Dependences of efficiency of nano-structurization on the basic technological parameters of transportation of hydrocarbonic raw materials are investigated.

K Abdrahmanova is an Associate Professor of ”Design, construction and operation of oil pipelines” Kazakh National Technical University, Almaty, Kazakhstan.

E Bovkunov is an engineer designer of the research institute of construction materials, Almaty, Kazakhstan who conducts research in the field of resource-saving technologies of building materials and construction used for oil and gas transportation and renovation of object of oil and gas sector.

Keywords: Adsorption layer, Coefficient of hydraulic resistance, Fluorine surface active substance, Hydrophobization, Nano-structurization

INTRODUCTION

The current state of oil pipelines is characterized by decrease of operational reliability and efficiency which are caused by intensive corrosion processes and accumulation of asphalten-resinous-wax formations on internal surfaces. Formation of accumulations is the reason of essential increase in hydraulic resistance of pipeline.

One of the basic ways for the decrease of hydraulic resistance increasing in result formation of accumulations is mechanical ways of cleaning. However, the relief and geometrical characteristics of the oil pipeline do not always allow to clean devices. Cleaning of devices leads to deterioration of pipe wall which reduces a residual resource of oil pipelines.

Other direction of decrease of the hydraulic resistance increasing in result of deterioration of oil rheology and changing in current parameters is using of chemical reagents. Application of anti-turbulent additives at oil transport is ineffective and depressors are applied now and wax inhibitors differ in a complex production technology, deficit and roads.

The most perspective method of decrease is the hydrophobization of internal surface of the oil pipeline on a basis fluorine containing surface-active substances. Characteristics of interaction of a stream of oil and an internal surface are optimized by nano-structural processing.

EXPERIMENTAL DETALS

Materials

For modification of surfaces have been used fluorine SAS, the epilame compositions of different marks, such as « Efren 1», «Zonyl® 9027» and «Foleoks 1». «Efren-1» represents 0,05-0,5 %-s' solution of perfluorine-acid in hladone-350. «Foleoks 1» represents the 0,1-2 %-s' solution of perfluorine-ether with acid group; as solvent is used aliphatic ozone safe hydro-chlorine-fluorine-hydrocarbons of formulas $H(CF_2)nCl$. Hladon-350 is one of the most effective and universal solvents for fluorine SAS. «Zonyl® 9027» is the water solution of fluorine-chemical anion for surfaces processing.

The solution of fluorine surface-active substances (SAS) is colorless nonflammable mobile liquid, which is nontoxical and has density in a range of 1,22-1,74 g/cm ^{3}.

Test Method and Equipment

In order to study the influence of surface roughness on hydraulic resistance before and after updating of metal surfaces by molecular layers of fluorine, SAS had been prepared two metal plates with a roughness 75 microns and 800 microns. The roughness of plates was created artificial with use of the calibrated grinding paper with corresponding granularity.

Experimental research has been realized during several steps. Firstly, corners of moistening drops of oil on investigated plates have been measured. Then plates have been cleared by white-spirit preliminary. The molecular fluorine SAS layers have been generated on plates' surfaces by immersing of plates in epilame solution at temperature 50-60^{0}C and the further drying within 20 minutes at temperature 50^{0}C. Then corners of moistening of oil drops have

been measured by using of an optical microscope with the big permission. Oil drops have been used in all measurements of corners of moistening with identical volume of 1 ml. There is a photo of plates with oil drops before and after updating by molecular layers of various epilame structures (Figure 1).

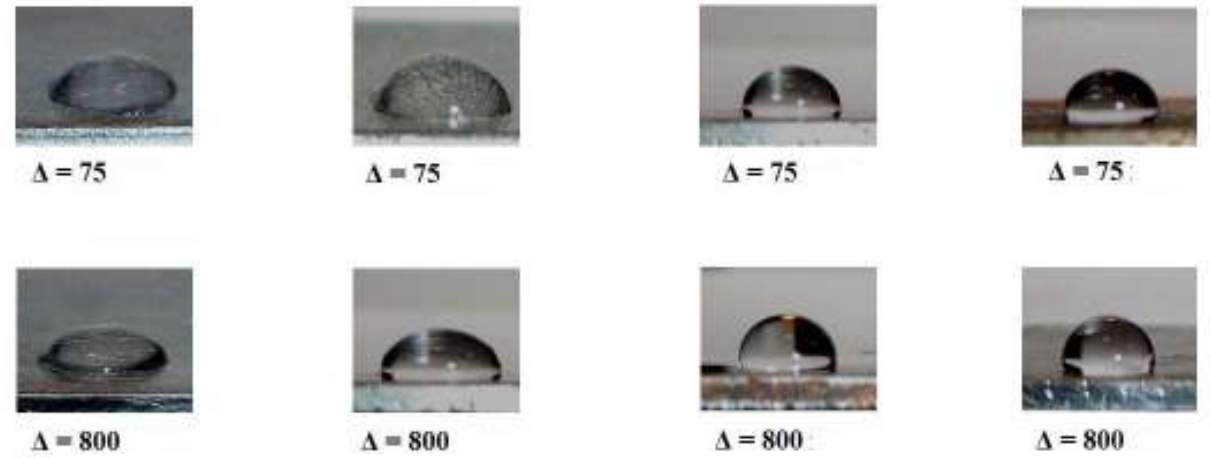

a) before updating

b) after updating by molecular fluorine SAS layers (from left to right - «Foleoks 1», "Efren-1", «Zonyl® 9027»)

Figure 1 Photo of oil drops on samples with a various roughness of a surface

The widely familiar method has been used in order to define the hydraulic resistance of surfaces with a various roughness. This method is based on measurement of corner of slide down by a drop of a liquid. Further, metal surfaces of a various roughness have been prepared to define the corner of slide down. The corners of slide down were measured before and after updating metal surfaces by epilame structures. The photo of a metal surface with a slide down oil drop with epilame surfaces and are kept on an initial surface is presented by Figure 2.

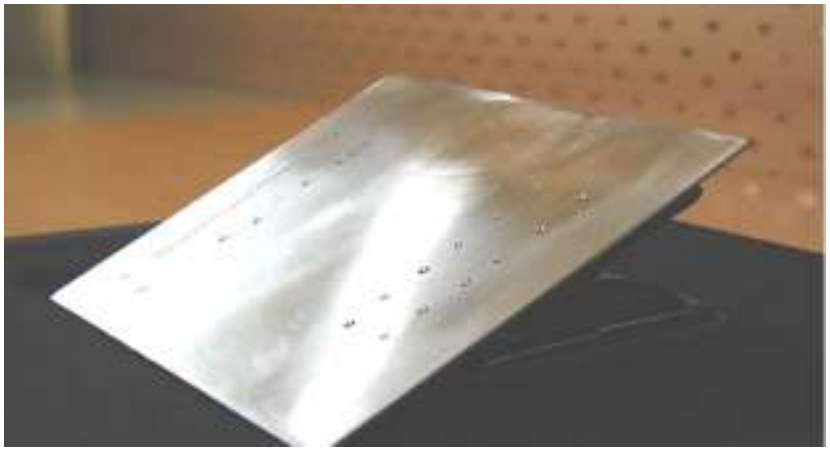

Figure 2 Metal surface with oil drop at initial condition and after processing of epilame

The researches of influence of the modifier on the thickness of adsorption layer are based on modeling of oil stream condition in pipelines in an initial condition and after formation of molecular fluorine SAS layers on an internal surface and comparison of parameters of a stream. The principle scheme of experimental installation is presented in figure 3. Internal surface of steel pipes in diameter of 159 mm was pumped preliminarily by oil to determine the initial hydraulic resistance of a working piece of the pipeline. After that the injection of epilame structures of «Efren 1», «Zonyl® 9027» and «by Foleoks 1»was made. From a tank the oil was pumped over in an expenditure tank by means of the pump with adjustable frequency of rotation. The expenditure of oil was measured with help of expenditure device. The replaceable working piece of a pipe of 3 meter long is located between tanks. This piece includes the system of measurement of pressure drop and a point of taking of sample. Process of updating of an internal surface occurs as follows. Dehydrated solution of perfluorine-acid is added in preparation knot of epilame structure. Then the received solution with the help of the dosing pump moved in the working pipeline. Thus the slide-valve 11 is closed.

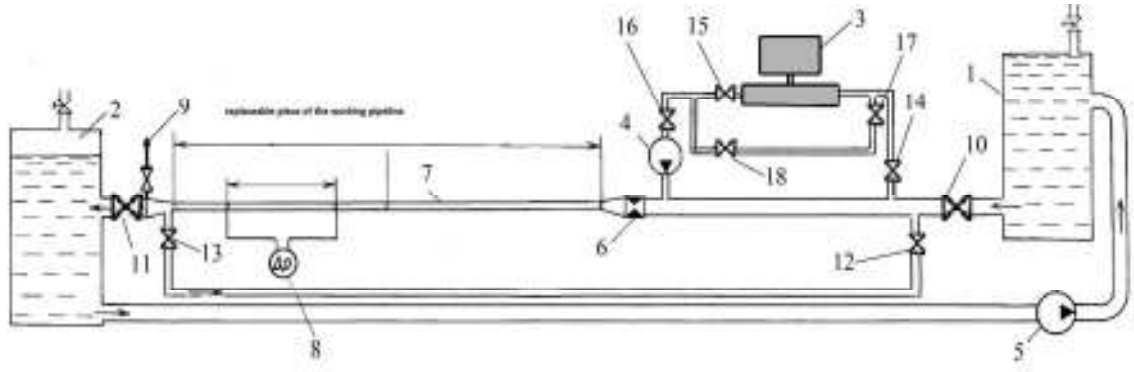

1 – a pressure tank; 2 – an expenditure tank; 3 – preparation knot of epilame structure; 4 – the dosing pump; 5 – the pump with adjustable frequency of rotation; 6 – the device for measuring of expenditure; 7 – replaceable pieces of the working pipeline; 8 – a differential manometer; 9 – a point of taking of sample; 10,11,12,13,14,15,16,17,18 – slide-valves

Figure 3 Scheme of experimental installation

Several samples were taken in order to measure the concentration of fluorine SAS molecules during the course of circulation of epilame structure with a certain intervals. After pumping over of fluorine SAS solution on pipelines, oil pumping was carried out again. It was done for the purpose of comparison of initial hydraulic characteristics of the pipeline with the modified molecular fluorine SAS layers. Thus slide-valves 12, 13, 14 are closed, and 10, 11 are opened.

Optimization of Technological Parameters of Nano-structural Hydrophobization of an Internal Surface of the Oil Pipeline

The speed of an oil stream and a roughness of an internal surface are the key parameters influencing hydraulic resistance of pipelines. Experimental researches have been carried out at use of fluorine SAS in order to define the influence of the specified parameters on hydraulic resistance of pipelines.

Figure 4 shows the dependences which characterize the influence of roughness degree on value of the corners of moistening of metal surfaces by oil with and without molecular fluorine SAS layers.

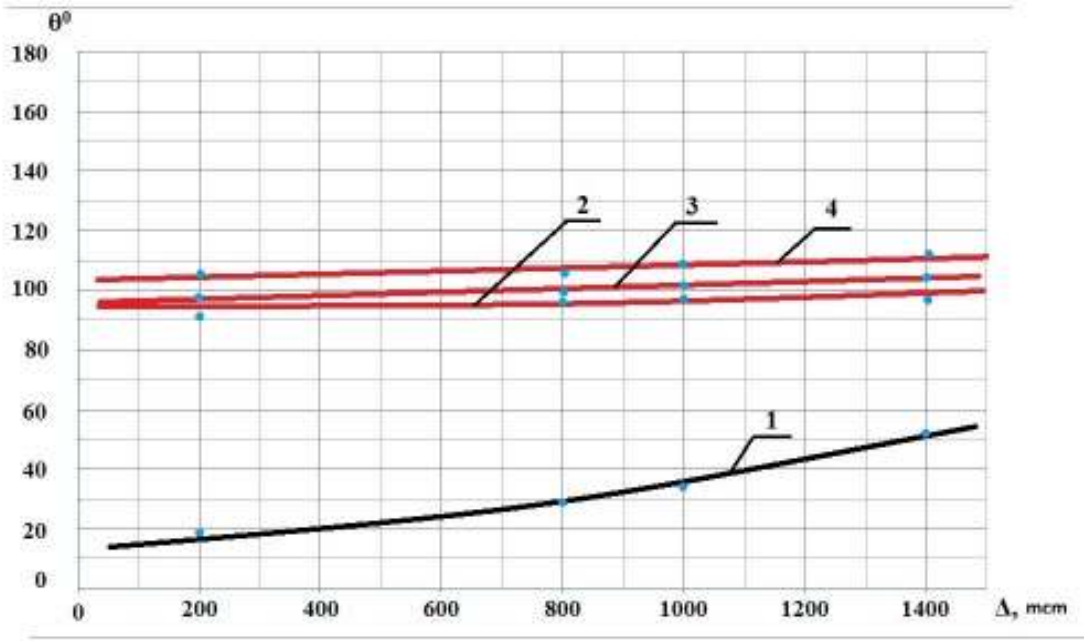

1 – an initial surface; 2 – a surface modified «Foleoks 1»; 3 – a surface modified by "Efren-1"; 4 – a surface modified «Zonyl® 9027»

Figure 4 The dependences of a corner of moistening from a roughness of a metal surface

It is clear from the diagram that the surface of a metal plate, which processed by epilame structure, gets the hydrophobic properties. Changes of initial hydrophilic properties of metal surface on hydrophobic properties under the influence of molecular fluorine SAS layers are well visible.

As a result of the researches, the degree of hydrophobization considerably influences on size of corner of a slide down of an oil drop along a metal surface was established. Figure 5 presents the dependences which characterize influence of degree of a roughness on values of corners of a slide down of oil drops along metal surfaces before and after of formation of molecular fluorine SAS layers.

The top curve in figure 6 characterizes the sizes of corners of a slide down of oil drops along metal surfaces without molecular fluorine SAS layers and corresponds to classical dependence. The bottom curves - after updating by molecular fluorine SAS layers. The modified metal surface has the same corner of a slide down of oil drops irrespective from the level of a roughness in a range from 100 to 1000 microns. It is much less than the corner of a slide down to an initial surface. Thus for a plate with a roughness of a surface 100 microns, the corner of a slide down of oil drops has decreased on the average in 1,6 times (with 32 to 20 °), for a plate with a roughness 800 microns - in 2,2 times (with 48 ° to 22 °).

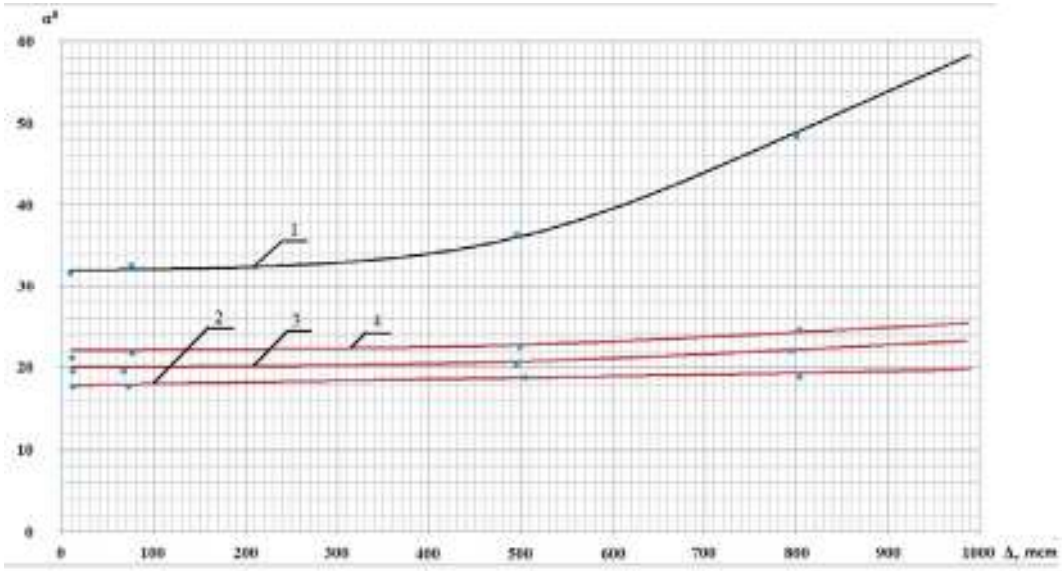

1 – before updating by molecular fluorine SAS layers ; 2 – after updating «Zonyl® 9027»; 3 – after updating of "Efren-1"; 4 – after updating «Foleoks 1».

Figure 5 Dependence of size of corners of a slide down of oil drop along metal surfaces of a various roughness

The current concentration of fluorine SAS in solution was defined. Results are presented in Figure 6.

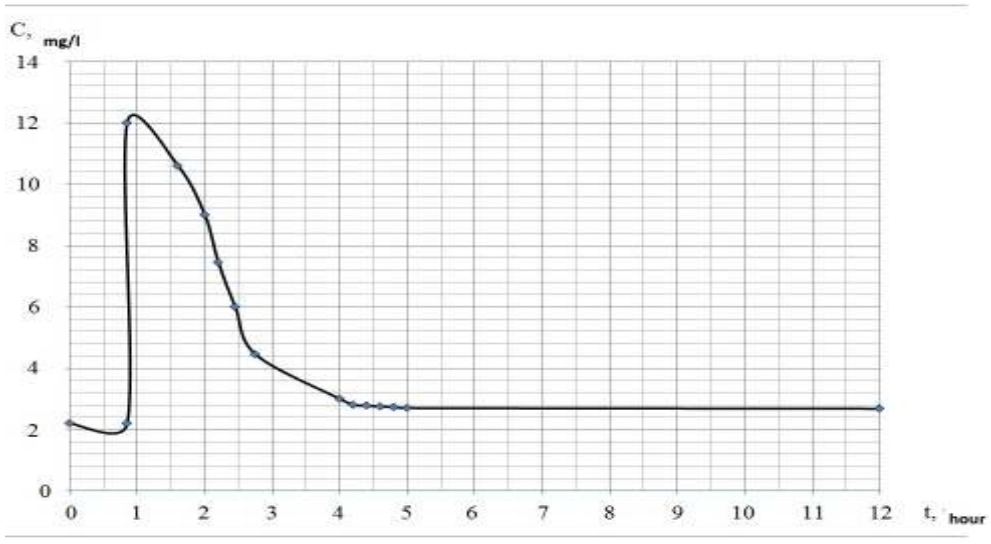

Figure 6 Process of change of concentration of fluorine SAS molecules in a contour of the experimental stand

At a given time there was a spasmodic growth of concentration of fluorine SAS molecules in solvent, and then smooth decrease at the expense of sorption process was observed. The curve of change of concentration coincides with a typical curve of sorption process that testifies to sorption process of fluorine SAS molecules on an internal surface.

Flowing decrease of fluorine SAS molecules concentration occurs before stabilization at level of the established concentration which indirectly characterizes a thickness of molecular fluorine SAS layers on an internal surface. The dependence of a thickness of molecular fluorine SAS layers which have been absorbed on an internal surface from concentration of fluorine SAS molecules in solvent is showed in Figure 7.

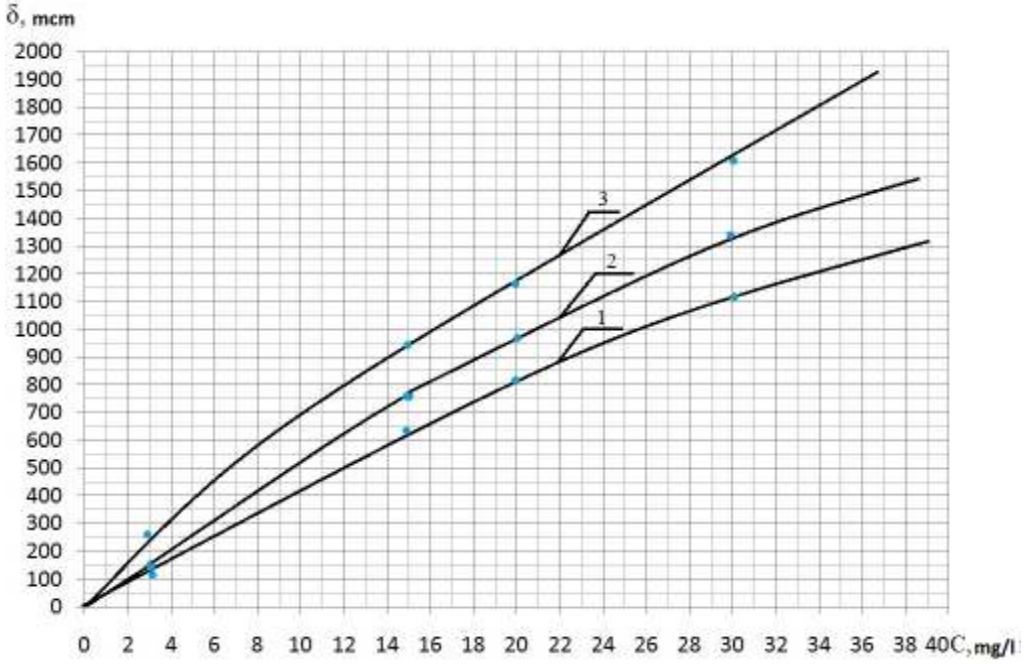

Figure 7 The dependence of a thickness of molecular fluorine SAS layers from concentration

The increase of concentration of fluorine SAS molecules in solvent is an increase in a thickness of fluorine SAS molecules layers on an internal surface, but at certain concentration the process of increase in a thickness is slowed down and stabilized.

Researches have been carried out to find out the influence of speed of fluoride SAS pumping in solvent on the formation of adsorption layers. The thickness of molecular fluorine SAS layers were measured on equilibrium concentration of fluorine SAS molecules at various speeds of a stream. The dependence of a thickness of adsorption layer from speed is presented in Figure 8.

At small speeds of pumping the adsorption process occurs much more strongly. So, at speed of 1 m/c «Efren 1» creates of adsorption layers 1000 microns, whereas at speed of 3 m/s only 200 microns. It is possible to assume that adsorption process in general will stop at higher speeds.

In order to determine the efficiency of the modifier, the pumping of oil at various speeds on working pipelines is carried out (processed of various epilame structures). Results of calculation of hydraulic resistance coefficient on various speed of oil in a working pipe are presented in Figure 9.

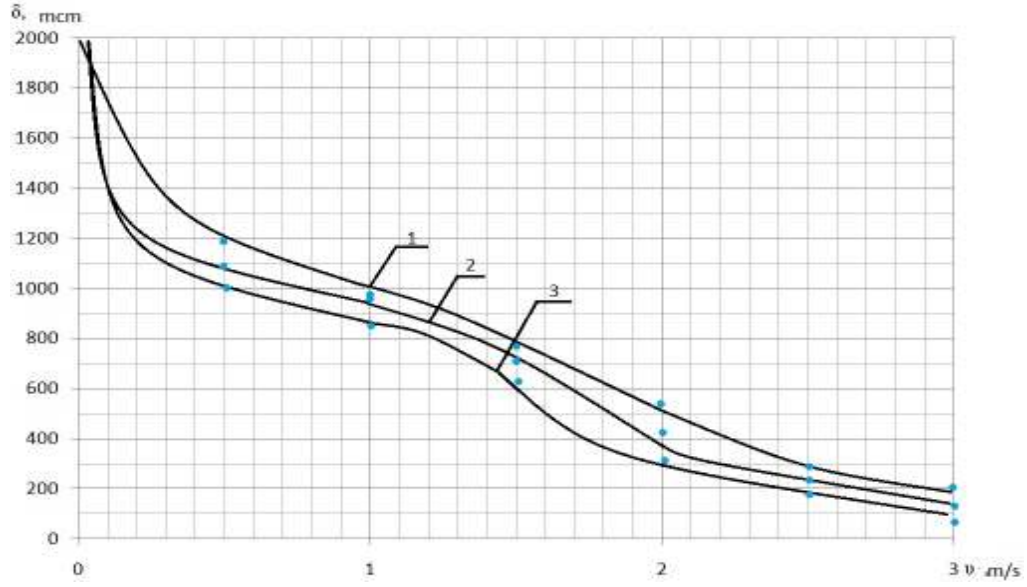

1 - «Zonyl® 9027»; 2 - «Foleoks 1»; 3 - «Efren 1»

Figure 8 The dependence of a thickness of adsorption layers of epilame structure from speed of pumping

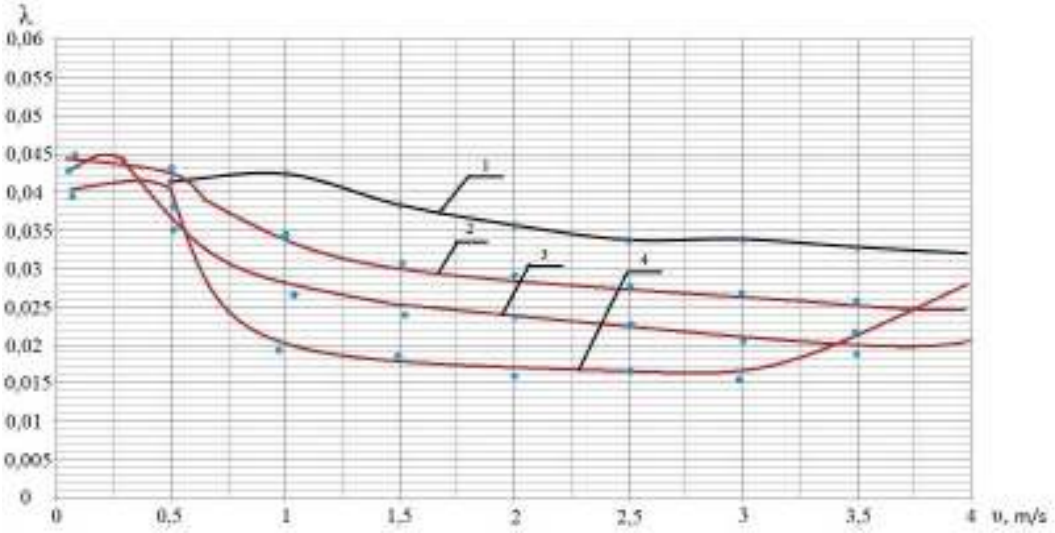

1 - in an initial pipe; 2 - in a pipe modified by epilame structure «Efren 1»;
3 - epilame structure «Zonyl® 9027»; 4 - epilame structure «Foleoks 1»

Figure 9 The dependence of hydraulic resistance from speed of oil pumping

From a schedule it is clear that in the beginning of tests there was a washout of surpluses of epilame structures, and the friction coefficient was closed to the level corresponding to a pipe without a covering (a line 1). In the subsequent the hydraulic resistance coefficient decreased in 1,2 – 2,2 times as compared with an initial pipe; only at speed above 3,5 – 4 m/s the covering is gradually washed off, and the hydraulic resistance coefficient aspires to the initial level.

Results of experimental researches of influence of the modifier on hydraulic resistance are presented in the form of dependence of relative hydraulic resistance of the pipeline (ΔPrel) from relative value of a thickness of molecular fluorine SAS layers on a surface (brel) (Figure 10).

$$\Delta P_{rel} = \Delta P_{sas}/\Delta P_{int}, \quad (1)$$

where: ΔPsas - hydraulic resistance of the pipeline with molecular fluorine SAS layers , generated on its internal surface;
ΔPint - initial hydraulic resistance of the pipeline.

$$b_{rel} = b_{sas}/\Delta r, \quad (2)$$

where: bsas - total thickness of molecular fluorine SAS layers;
Δr - an average roughness of a surface of the pipeline

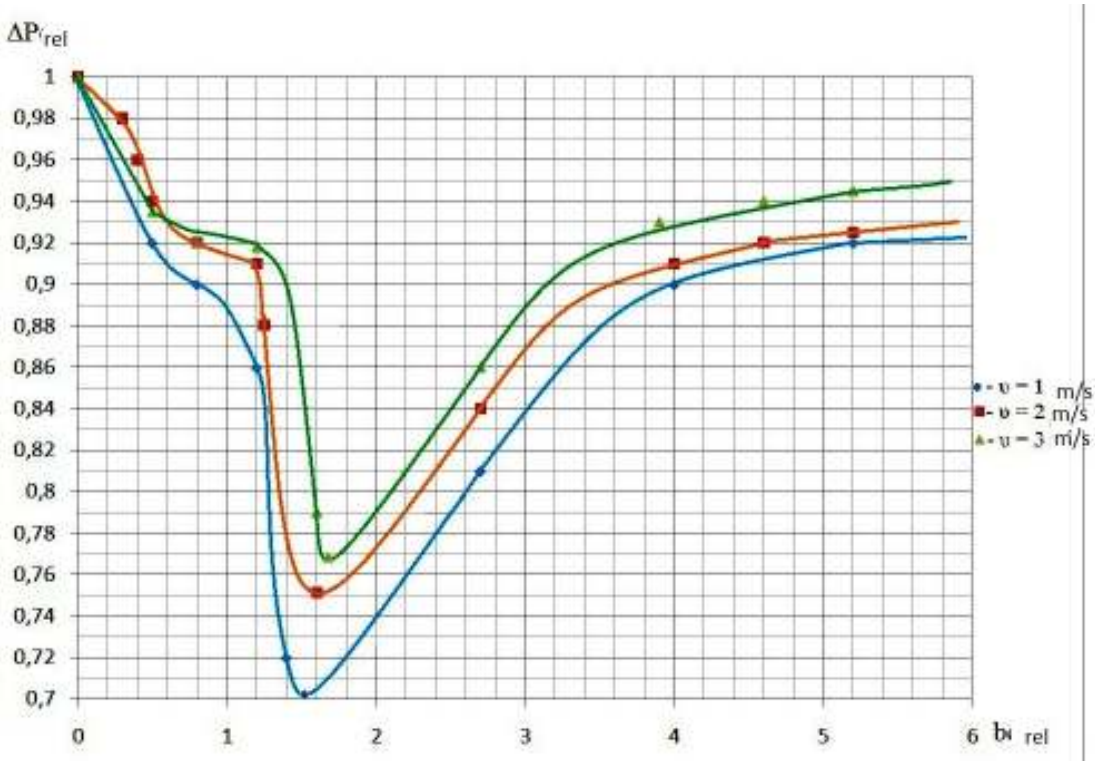

Figure 10 Influence of a relative thickness of adsorption molecular layers of "Efren 1" on a hydraulic resistance of the pipeline

The maximum level of decrease of hydraulic resistance of the pipeline is reached at a relative thickness of molecular fluorine SAS layers, being in an interval 1,3 ÷ 2. Thus the maximum fixed decrease of hydraulic resistance concerning a initial level has made 23 % at speed of 3 m/s and 28 % at speed of 1 m/s. Similar dependences of influence of a relative thickness of the molecular layers adsorbed on an internal surface on hydraulic resistance of the pipeline at various speeds of a current of oil are received after updating of «Zonyl® 9027» and «by Foleoks 1».

DISCUSSION

Change of characteristics of interaction of oil stream and internal surface is the most perspective method of decrease of hydraulic resistance of the pipeline. Nano-structurization of internal surfaces of pipeline is carried out at the expense of the focused adsorption of SAS molecules from the transported environment and formation so-called «a paling of Lengmjura» [1].

The adsorbed, ordered, structured, molecular and formed layers of the SAS, which total thickness is commensurable with a surface roughness, at the expense of change of factor of a friction of molecules of a transported liquid about walls reduce hydraulic resistance of a pipeline. It leads to smoothing of an initial roughness and a relief of internal surfaces of the pipeline. Conditions of currents near wall are changing.

The fluorine SAS is most suitable for updating of internal surfaces of oil pipelines. Epilame represents the solutions of fluorine SAS – perfluorine-polyether-acid which is unpolar part contains the fluorine-hydrocarbon radical. The compositions belong to the category of fluid liquid structures forming on firm surfaces multipurpose nano-layers, which by structure and by an organization principle concerning to nano-size films of Lengmjura-Blozhett (FLB). Fluorine SAS molecules at contact with a surface are oriented that the reaction-capable hydrophilic group to a surface of this body, and hydrophobic "tail" in outwards. Thus is carry out the communication of SAS molecules with a surface not only physical, but also the chemical nature (figure 11) [2]

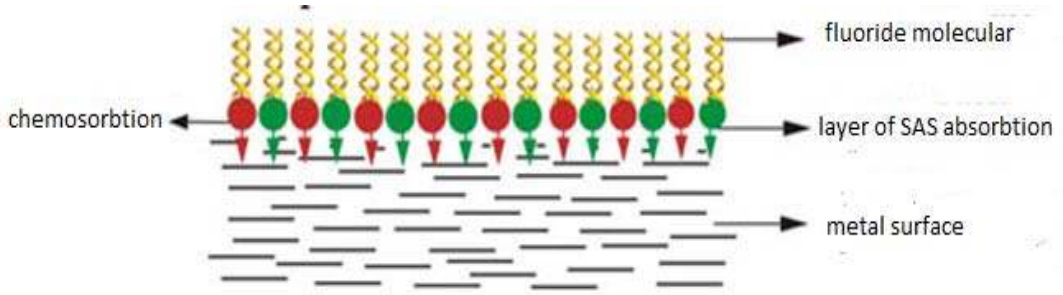

Figure 11 The scheme of an arrangement of molecules on a surface

At formation of molecular fluorine SAS layers the thickness at which the maximum decrease in hydraulic resistance of the pipeline is observed. Further, at increase in a thickness of the generated molecular fluorine SAS layers on an internal surface return process begins - the hydraulic resistance increases at the expense of narrowing of diameter of the pipeline.

The increase in hydraulic resistance does not reach its initial level and stabilizes at level 5 – 10 % from it, and further doesn't change. Stabilization of level of hydraulic resistance of the pipeline occurs at achievement of the greatest possible thickness of the generated molecular fluorine SAS layers.

Flowing decrease of concentration of molecules fluorine SAS occurs before stabilization at level of the established concentration which indirectly characterizes a thickness of molecular fluorine SAS layers on an internal surface. The established concentration actually reflects an equilibrium state between the SAS molecules which are in a stream and being on an internal surface. Thus speeds of adsorption processes and adesorption are equal.

At increase of concentration of SAS molecules in solvent, there is an increase in a thickness of adsorption on an internal surface of SAS molecules. However, at certain concentration the process of increase in a thickness is slowed down and stabilized. In figure 12 the image of stages of formation of molecular fluorine SAS layers on an internal surface is presented.

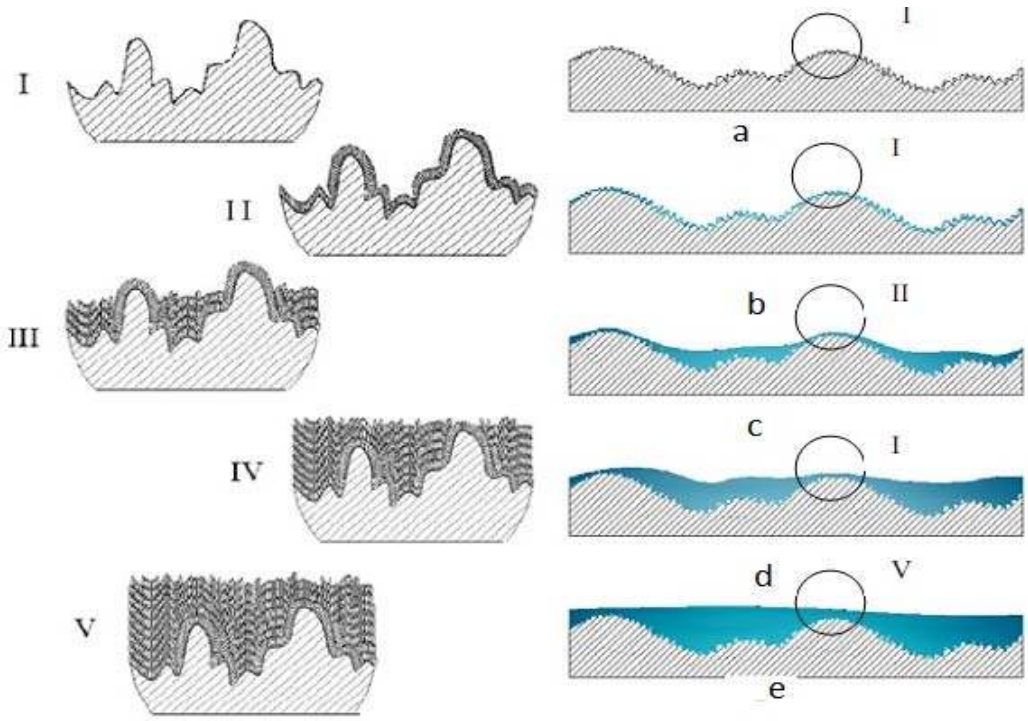

a – an initial trumpet surface, b– the monomolecular layer completely repeating a profile of a internal surface, c – filling of hollows of a roughness with molecular fluorine SAS layers , d – full smoothing of a roughness of a internal surface, e – increase in a thickness of molecular fluorine SAS layers

Figure 12 Image of stages of formation of molecular fluorine SAS layers on an internal surface

The thickness of molecular fluorine SAS layers, which have been precipitated on an internal surface indirectly measured by equilibrium concentration of fluorine SAS molecules in a stream. More reliable way of measurement is usage of the metallographic sections. In figure 13 the photo of metallographic section is presented, received by means of an optical microscope of the big permission, to which surfaces molecular fluorine SAS layers about 300 microns are clearly visible in the general thickness.

Studying of the received photos of metallographic sections shows the presence of the ordered relief of the top molecular fluorine SAS layers. The cambers ("hills") in regular

intervals located on an internal surface of investigated samples and with approximately identical parameters (figure 13b) have been revealed.

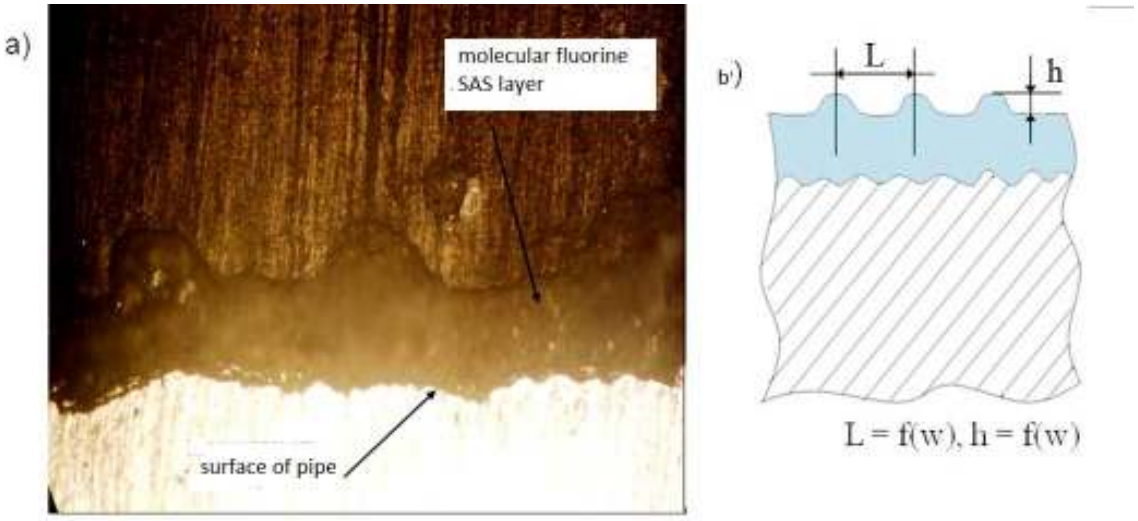

a) photo of molecular fluorine SAS layers on an internal surface
b) the conditional scheme of a characteristic relief of the top part of molecular SAS layers

Figure 13 Metallographic section

Characteristic regulating of a relief of the top molecular layers is a consequence of influence on them of a stream of the liquid environment. Therefore the optimal relief from the point of view of minimization of losses in the conditions of interaction of a liquid and the changed internal surface as any self-regulated system that to aspire to minimization of losses of energy is formed. Such formations on an internal surface reformed a current, thereby reducing losses at the expense of decrease in hydraulic resistance to a stream.

The basic influence on change of parameters of oil stream renders change of characteristics of an internal surface. As a result of updating of an internal surface the coefficient of a friction of oil molecules about a surface decreases and the roughness size, at the expense of its filling and smoothing by molecular fluorine SAS layers decreases. All listed leads to essential change of structure of a superficial intermediate layer of oil in which the basic part of losses on hydraulic resistance is concentrated at pipeline transport of oil.

CONCLUSION

1. The analysis of the scientific and technical literature shows that one of perspective decisions in decrease in hydraulic resistance of pipelines is hydrophobisation of internal surfaces.

2. Despite high efficiency of existing ways of creation of ultra-hydrophobic surface and their application in pipeline systems of oil transport appears problematic owing to technical impossibility of their realization in the big scales and diseconomy.

3. The most suitable way for decrease of hydraulic resistance of oil pipelines is the modifying of internal surfaces at the expense of formation of molecular fluorine SAS layers. Updating of internal surfaces is carried out at the expense of the focused adsorption of fluorine SAS molecules from the transported environment and formation so-called «a paling of Lengmjura».

4. It is established that updating of internal surfaces of the pipeline at the expense of formation on them of molecular fluorine SAS layers leads to reduction of their hydraulic resistance on 30 ÷ 23 % in a range of speeds 1 ÷ 3 m/c accordingly.

5. It is shown that the greatest effect of decrease in hydraulic resistance of pipelines is reached at a relative thickness of the molecular fluorine SAS layers generated on an internal surface 1,3 ÷ 2.

6. The essential increase in a relative thickness of molecular fluorine SAS layers, generated on an internal surface of the pipeline, is the cause to increase of hydraulic resistance to some established level depending on speed of oil, and further doesn't change. Stabilization of level of hydraulic resistance of the pipeline occurs at achievement of the greatest possible thickness of the generated molecular fluorine SAS layers.

7. Updating of internal surfaces by means of molecular fluorine SAS layers formation eliminates negative influence of a roughness and a relief on change of hydraulic resistance of pipelines during of operating.

8. Molecular fluorine SAS layers, generated on a metal surface, considerably improves its hydraulic characteristics without dependence from roughness size. This peculiarity of molecular fluorine SAS layers allows not only to restore hydraulic resistance of the oil pipelines which have grown during of operating process, but also to improve their initial hydraulic characteristics.

REFERENCES

1. JIANG X. et al. Micrometer Optical measuring methods for determining Nanometrology surface.// Annals of CIRP, Vol. 55, No. 1, 2005, pp 577 – 580.

2. ANDEEVA OG, GANTSEVICH IB, NA ROMANOVA, The use of protective molecular films - epilamov in the watch industry / / Economy and Production. Appendix: Technology, Equipment, Materials, No.7, 2000, pp.54-58.

Shear Behaviour of Fibre Reinforced Concrete Beams

M Aburwai, L S Sryh
Misurata University, Libya

Most previous studies focused on studying Structural Behaviour of Beams of Reinforced Concrete in the area of bending. And, in general, the available data and information about the structural behaviour of the shear zone are not sufficient, especially for aspects that can have a relationship or a direct effect on the behaviour of shear in order to reduce the risk of cracks and prevent landslides, which is expected to occur. The aim of this study is to investigate the behaviour of shear in the beams of reinforced concrete reinforced with different types of fibres (steel, glass and polypropylene) and its impact on cases of landslides, and to study the factors that help to increase safety when we use these fibres in the area of Shear, and its impact on the properties of concrete in the shear area, and to check the width and length of cracks that appear in the early stages of loading at the bending and shear zones, and the possibility to take advantage of these data and information to evaluate the final stage of the failure of beams. We also expect from the results of this study to provide relevant information to the behaviour of shear, and the extent of its influence in fibre reinforced concrete beams in order to develop the equations of structural design and safety factors. The laboratory study conducted summarized the results in that the addition of glass and steel fibres to the concrete beams contributes to improve the final shear resistance in comparison with polypropylene fibres, which did not achieve acceptable results, and the Fibre Reinforced Concrete Beams are more stiffness compared with traditional reinforced concrete beams, and that is because of its achievement of the values of a small strain during various stages of loading.

Professor Mokhtar Aburawi is a Professor within the Faculty of Engineering - Khoms, Misurata University, Libya

Mr Lamen Saleh Sryh, is a PhD student within the Faculty of Engineering - Khoms, Misurata University, Libya

Keywords: Beams, Fibre, Shear behaviour

INTRODUCTION

Concrete is the main material used in buildings and infrastructure projects in different regions of the world, and that is because the availability of its main components for lower cost than other construction material such as steel, and also to its suitability for different climatic conditions. As a result of the increasing demand on this material, the previous studies focused on developing its products and to produce new types with high properties and quality features, such as high-performance concrete HPC and High Strength Concrete HSC.

Because of the technological development that targeted the preservation of environment and the benefit of natural and artificial wastes, and of considering the remnants of wood carpentry, plastic, glass and steel as one of those materials that pollute the surrounding environment, the studies associated with structural engineering have been developed to take advantage of the different types of these fibres by adding them to the concrete to produce a concrete known as Fibre Reinforced Concrete FRC. These studies revealed that the fibres have helped to increase the efficiency of concrete by turning it into a more unified and ductile material, and thereby increase its quality in the mechanical side, for example: increasing strength stresses, hardness and friction resistance. This improvement of concrete properties has increased its resistance to the loads, and the presence of fibres reduced the cracks resulted from loading and shrinking [1-5].

Objectives of the Study

The aim of this study is to investigate the behavior of shear in the beams of reinforced concrete reinforced with different types of fibres (steel, glass and polypropylene) and its impact on cases of landslides, and to study the factors that help to increase safety when we use these fibres in the area of Shear, and its impact on the properties of concrete in the shear area, and to check the width and length of cracks that appear in the early stages of loading at the bending and shear zones, and the possibility to take advantage of these data and information to evaluate the final stage of failure of the beams. We also expect from the results of this study to provide relevant information to the behavior of shear, and the extent of its influence on fibre reinforced concrete beams in order to develop the equations of structural design and safety factors**.**

The Laboratory Program

Local materials were used in the preparation of concrete mixtures. These materials were chosen and adopted after a number of preliminary tests needed to match them to the standards adopted in this study. The used fine and coarse aggregates have been imported from Zliten city quarries within the limits allowed in the Libyan standards 49:2002 for the concrete aggregates from natural sources [7]. The used ordinary Portland cement is a product of Libda factory which belongs to The National Company for Cement according to the Libyan standards 340:1997 of Portland cement [8]. The used reinforcing steel is a product of Misurata factory which belongs to The Libyan Company for Iron and Steel. The main reinforcing steel was chosen and adopted with a diameter of 14 mm and beams stirrups steel with a diameter of 8 mm, and the results of stresses yield were obtained from the quality monitoring laboratory in the factory and their values are 380MPa for the main Steel and 275MPa for beams stirrups steel. The figure 1 shows a form of the shape of reinforcement used in beams.

Figure 1 The form of reinforcement used in beams

A number of variables affecting the behavior of shear in concrete beams was adopted in this study, and the samples were divided into six groups, each group consisting of two beams differ in the rank and were reinforced with the same reinforcing steel in the area of bending 2 ∅ 14 mm. The control beams differ in the amount of reinforcing steel in the shear zones CB1, CB2 without stirrups steel, and the shear zones CB3, CB4 contain stirrups steel less than the standard amount, and CB5, CB6 shear zones contain stirrups steel matched the standard amounts, and the rest were reinforced with a specific type of fibres in each group and all have a fixed size proportion in all groups Vf = 1.0%. Samples SFB7, SFB8 were reinforced with steel fibres, GFB9, GFB10 were reinforced with glass fibres, and PFB11, PFB12 were reinforced with polypropylene fibres. Fibres used in this study have specific different variables according to what is available from products in order to get similar results. Table 1 shows the details and characteristics of the used fibres, and Figure 2 shows a model of the types of fibres used, and Table 2 shows the components and ratios of concrete mixtures used.

Table 1 Details and characteristics of the used fibres

FIBRE TYPE	STEEL FIBRES	GLASS FIBRES	POLYPROPYLENFIBRES
Length	35 mm	19 mm	19 mm
Diameter	0.55 mm	0.018 mm	0.018 mm
Specific Gravity	7.85	2.7	0.91
Tensile Strength	1100 MPa	1400 MPa	500 MPa
M. of Elasticity	210000 MPa	74000 MPa	5000 MPa
Used average	70 kg/m^3	20 kg/m^3	15 kg/m^3

Steel Fibres Glass Fibres Polypropylene Fibres

Figure 2 Model of types of used fibres

Wooden templates of 150×200×1200 mm were used as well as steel cubed templates of 150×150×150 mm dimensions, and they all were painted with oil from inside to prevent the concrete from sticking to the surfaces. All samples were processed with wet burlap during the first 24 hours and then placed in water of room temperature 20-26 ºC until the date of test.

Table 2 The components and ratios of concrete mixtures used

CONCRETE MIX	MIX 1	MIX 2
Water/Cement ratio	0.4	0.4
W. of cement, kg/m^3	300	400
W. of water, kg/m^3	120	160
W. of fine aggregate, kg/m^3	615	559
W. of coarse aggregate 10 mm, kg/m^3	932	847
W. of coarse aggregate 15 mm, kg/m^3	502	456
Total W. of aggregate, kg/m^3	2049	1862
Aggregate/Cement ratio	6.83	4.65
W. of plasticizers, kg/m^3	1.5	2.0

Concrete Beams Loading Test

The concrete beams were loaded until collapsed in order to study the properties of the first crack and the forms of resulted cracks, and that is to set the values of strain associated with the values of loading. This test was conducted on the concrete beams by loading on them at two points, each is a distance way from the point of installation equal to the third of the net beam length with installing a device for measuring the strain in the mid-beam, also, two points were fixed to measure the reactions in the areas of compression and tension which the distance between them is approximately 200 mm.

Figure 3 Model of the concrete beams load test

ANALYSIS AND DISCUSSION OF RESULTS

The Relationship between Load and Strains

By observing the Figure 4 and 5, which show the relationship between the load and the strain of the study samples and the results monitored during the test, we find that the relationship between the values of load and strain is similar for all the study samples and they all showed similar behavior from the beginning of loading until failure. However, the fibre Reinforced samples FRC were more stiffness and achieved lower values of strain for the same values of load than the control samples RC. The results also show that FRC samples are more ductile during the stages of failure, and it was also observed that after the appearance of the first crack there is a major increase in strain with keeping resisting the load when all the control samples RC failed and collapsed suddenly as soon as the final cracks formed. Generally, all samples achieved strain values not higher than the permissible limits in the standards of American code ACI 318-08 - 9.5a [6].

Effect of Fibres Type on the Relationship between Load and Strain

Table 3 shows the summary results of failure loads and the maximum strain of the study samples. Figure 4 and 5 show the effect of fibres type on the relationship between load and strain of the study samples. From these tables and shapes, it has been noticed that samples of steel fibres SFB7 & SFB8 achieved values of resisting the actual final shear by 112% & 135%, respectively, greater than that of the control sample CB5 & CB6. In addition, these samples also achieved an increase of 156% and 200% respectively of the value of the resistance of design, and showed improvement in ductility of concrete as the brittle sudden failure did not occur, unlike the control samples. However, the ductile failure contributed to the continued resistance to loads even after the final cracks have formed, and to the achievement of high values of the final resistance. Glass reinforced beams GFB9 and GFB10 achieved similar values for the resistance to the actual shear to the control samples by an increase of 156% and 140%, respectively, of the resistance of design value. On the other hand, polypropylene reinforced fibres PFB11 and PFB12 failed, as expected, to achieve good resistance and it achieved only 70% and 66%, respectively, of the actual shear resistance achieved by the control samples, but for the resistance of design both has achieved only 98% of it.

The Effect of Compression Resistance on the Relationship between Load and Strain

Figure 6 to 8 show the relationship between load and strain of the study samples according to the type of used fibres. From them, we can observe that samples of concrete of compression resistance fc` = 44MPa have lower values of strain comparing to that of the samples of concrete of compression resistance fc` = 26MPa for the same loads, and we can also notice that it is more ductile during the final stages of loading with the appearance of the first cracks, and achieved a significant increase in the values of strain and high values of final resistance. The obtained results also show that samples reinforced with steel, glass and polypropylene SFB8, GFB10 and PFB12 of a concrete of compression resistance fc` = 44MPa recorded results of 135%,112% and 105%, respectively, for the actual resistance comparing with the same samples SFB7, GFB9 and PFB11 with a concrete of compression resistance fc` = 26MPa. These results also appreciate the contribution of increasing the compression resistance in increasing the loading capacity of shear and that is with increasing the compression resistance by 18MPa which resulted in improving the results of actual

resistance of the fibre reinforced samples. The results also show that using steel fibres together with increasing the compression resistance in the concrete contributes significantly in increasing the loading capacity of the samples compared with the samples reinforced by other fibres. Glass reinforced samples showed similar results to the control samples, whereas polypropylene reinforced samples recorded the lowest results which confirm its failure in the shear resistance in the concrete beams.

The relationship between Load and Strain

Table 4 shows the summary results of strains in the compression zone of the study samples. From the showing results, it was noticed that the relationship between the values of load versus strain was similar for all the samples of study, and all showed similar behavior from the beginning of loading until failure. Fibres reinforced samples FRC achieved lower values of strain in the compression zone, which did not exceed the designed value for concrete strain $\varepsilon_c = 0.003$ that recommended in the design of buildings according to the standards of American code ACI 318-08 [6].

In comparison, the control samples RC achieved higher values for the same values of load, which exceeded the American code value significantly. This means that the fibres in general contributed to the increased resistance of concrete in the compression zone, and more importantly, the increase of its resistance in the tension zone which makes the fibres concrete FRC to be more ideal in concrete structures in term of addressing the weakness of concrete to resist tensile stresses.

Table 3 The summary results of loads of failure and the maximum strain for samples of the study

No. OF SAMPLE	f_c MPa	REINFORCEMENT		DESIGN LOAD FAILURE kN	ACTUAL LOAD FAILURE kN	ACTUAL LOAD/DESIGN LOAD	MAX. DEFLECTION mm
		BENDING	SHEAR				
CB1	26.0	2∅14	Without stirrups	93.0	110	1.18	28.6
CB3		2∅14	∅8@200		122	1.31	29.9
CB5		2∅14	∅8@80		130	1.40	31.2
SFB7		2∅14	Steel fibres		145		32.8
GFB9		2∅14	Glass fibres		130	1.56	30.3
PFB11		2∅14	polypropylene fibres		91	1.40 0.98	18.5
CB2	44.0	2∅14	Without stirrups	97.56	118	1.20	28.5
CB4		2∅14	∅8@200		135	1.38	28.8
CB6		2∅14	∅8@80		145	1.48	30.9
SFB8		2∅14	Steel fibres		196		33.4
GFB10		2∅14	Glass fibres		145	2.00	28.1
PFB12		2∅14	polypropylene fibres		96	1.48 0.98	18.3

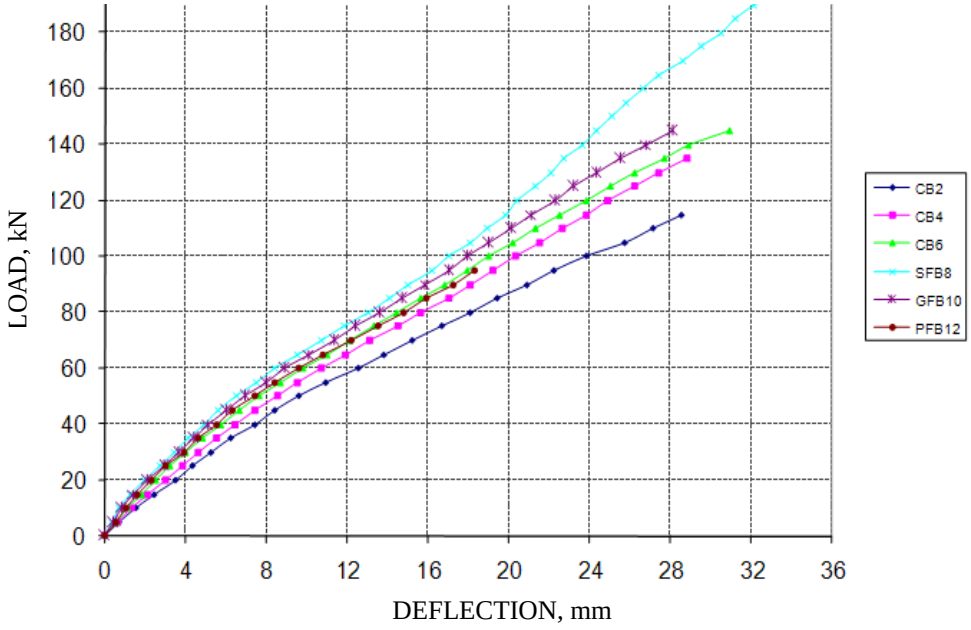

Figure 4 the relationship between load and deflection for the study samples f_c`=26MPa

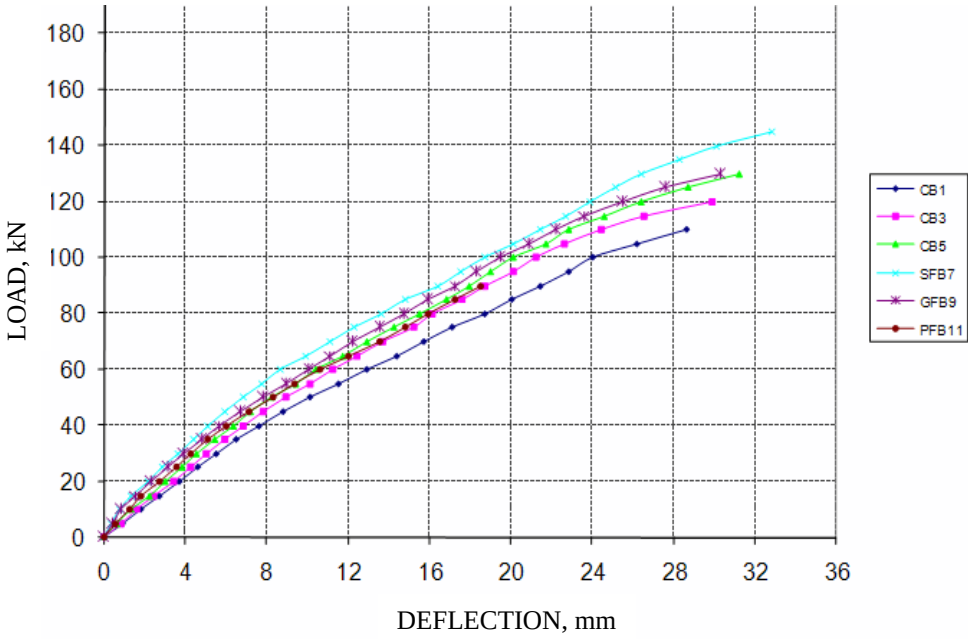

Figure 5 Relationship between load and the deflection for samples f_c`= 44MPa

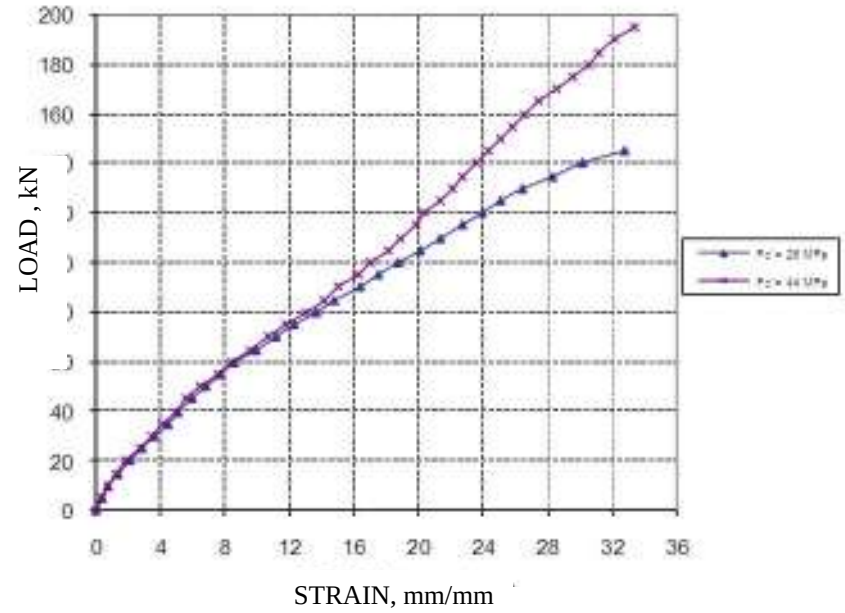

Figure 6 Effect of compression resistance on the relationship between load and strain for steel reinforced samples

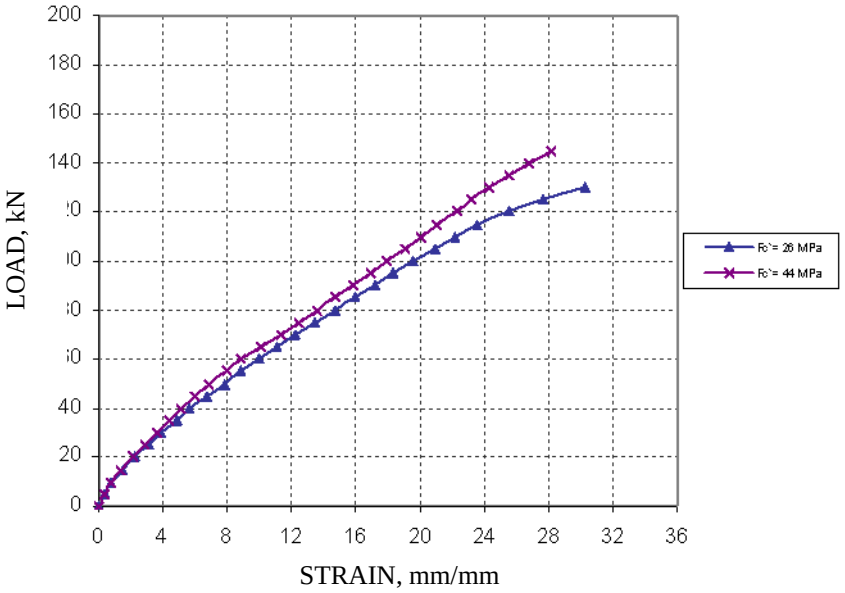

Figure 7 Effect of compression resistance on the relationship between load and strain for glass reinforced samples

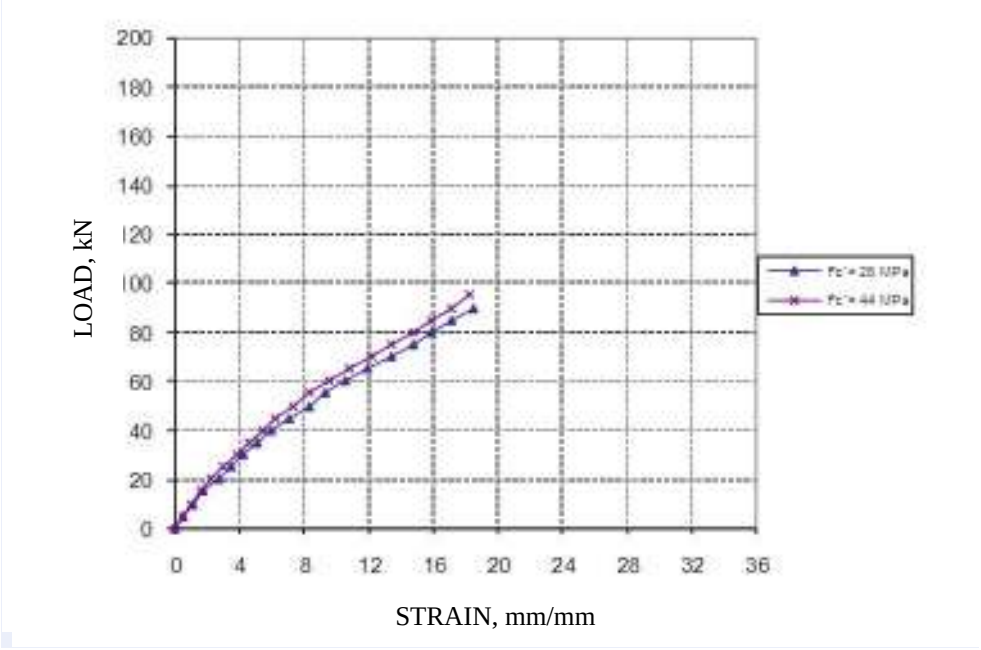

Figure 8 Effect of compression resistance on the relationship between load and strain for polypropylene reinforced samples

Effect of Fibres Type on the relationship between Load and Strain

Table 4 shows the summary results of strains in the compression zone of the study samples. We can notice the effect of fibres type on the relationship between load and the strain of the study samples, and it was noticed through analysis of the results that fibres reinforced samples FRC achieved lower values for the maximum averages of strain in the compression zone compared with the control samples RC, and samples of steel fibres SFB7, glass GFB9, and polypropylene PFB11 achieved maximum strains in the region of compression by 48%, 52% and 51%, respectively, of the values of maximum strains of the control sample CB5, and these strains represent the amount of 81%, 87% and 85% of the value of design for concrete strain in the compression zone ε_c, whereas the samples of steel fibres SFB8, glass GFB10, and polypropylene PFB12 achieved maximum strains in the compression zone by 38%, 58% and 40%, respectively, of the values of maximum strains of the control sample CB6, and these strains represent the amount of 49%, 75% and 52% of the value of strain concrete design in the area of compression ε_c. The upper and lower strain values increased with load for each of the study samples, and it was observed that fibres reinforced samples FRC showed a proportional association between the upper and lower values of strain through the different stages of loading and worked to shift the center of equality to the top by more amount than the control samples RC, and that can be seen very obviously in the steel fibres samples SFB7 and SFB8 which leads to reduce the area of compression zone in the section, therefore increasing the compression stresses in the concrete with an increase in the number of cracks and larger strain leading to failure of ductility.

The Effect of Compression Resistant on the Relationship between Load and Strain

The influence of concrete rank on the relationship between load and strain for the study samples was based on the type of used fibres. Samples of concrete of compression resistance f_c`= 44MPa achieved lower values of strains compared with that for the same loads for the

samples with compression resistance f_c` = 26MPa, and the obtained results show that the samples of steel fibres SFB8, glass GFB10, and polypropylene PFB12 of compression resistance $f_c$` = 44MPa achieved maximum strains in the compression zone by 60%, 86% and 61%, respectively, of the values of the analogues of the same samples SFB7, GFB9 and PFB11 of compressive resistance f_c` = 26MPa.

Table 4 Summary of strains results in compression zone for study samples

No. OF SAMPLE	f_c` *MPa*	REINFORCEMENT		MAX. ACTUAL STRAIN IN COMPRESSIVE ZONE	ACTUAL STRAIN/ DESIGN STRAIN ε_c=0.003
		BENDING	SHEAR		
CB1	26.0	2∅14	Without stirrups	0.005225	1.74
CB3		2∅14	∅8@200	0.004687	1.56
CB5		2∅14	∅8@80	0.005022	1.67
SFB7		2∅14	Steel fibres	0.002441	0.81
GFB9		2∅14	Glass fibres	0.002600	0.87
PFB11		2∅14	polypropylene fibres	0.002557	0.85
CB2	44.0	2∅14	Without stirrups	0.004920	1.64
CB4		2∅14	∅8@200	0.004793	1.60
CB6		2∅14	∅8@80	0.003885	1.30
SFB8		2∅14	Steel fibres	0.001469	0.49
GFB10		2∅14	Glass fibres	0.002244	0.75
PFB12		2∅14	polypropylene fibres	0.001569	0.52

Properties of the First Cracks

Table 5 shows a summary for the properties of the first cracks and the type of failure for the study samples. It was noticed that the values of load for the first cracks in fibres reinforced samples FRC were similar to that for the reference samples RC, except for samples of steel fibres SFB7 and SFB8 that have achieved higher values of 140% and 108%, respectively, according to the rank of the concrete used in both samples, and that is because of the mechanism of fibres to curb cracking. The results also showed that samples of steel fibres SFB7 & SFB8, glass fibres GFB9 & GFB10 and polypropylene fibres PFB11 & PFB12 have shorter length and width for the first cracks than the control samples RC, which achieved 70, 60% and 50%, respectively, of the width of first cracks of control sample CB5 with compressive resistance fc` = 26MPa, and achieved 78%, 67% and 56%, respectively, of the width of first cracks of control sample CB6 with compressive resistance fc` = 44MPa. Also, as is evident from these results, samples of polypropylene fibres PFB11 and PFB12 achieved the lowest values for the length and width of first cracks and this confirms the quality of using this type of fibres in concrete to reduce cracks.

In general, it was observed that the samples of compressive resistance fc` = 26MPa have lower values for loading of first cracking and almost equal values for the length of this crack

and greater values in width compared with their counterparts from the same samples of compressive resistance fc` = 44MPa.

Table 5 The summary results of properties of the first cracking and type of failure for the study samples

No. OF SAMPLE	f_c` *MPa*	REINFORCEMENT		THE FIRST CRACKING			ZONE OF FAILURE	TYPE OF FAILURE
		BENDING	SHEAR	LOAD KN	LENGTH mm	WIDTH mm		
CB1	26.0	2∅14	Without stirrups	50	50	0.14	Shear	Sudden
CB3		2∅14	∅8@200	50	70	0.12	Shear	Sudden
CB5		2∅14	∅8@80	40	100	0.09	Bending	Sudden
SFB7		2∅14	Steel fibres	70	70	0.06	Shear	Ductile
GFB9		2∅14	Glass fibres	50	60	0.05	Shear	Ductile
PFB11		2∅14	polypropylene fibres	50	50	0.03	Shear	Ductile
CB2	44.0	2∅14	Without stirrups	65	60	0.12	Shear	Sudden
CB4		2∅14	∅8@200	60	70	0.1	Shear	Sudden
CB6		2∅14	∅8@80	60	90	0.09	Bending	Sudden
SFB8		2∅14	Steel fibres	65	70	0.05	Bending	Ductile
GFB10		2∅14	Glass fibres	60	60	0.04	Shear	Ductile
PFB12		2∅14	polypropylene fibres	60	50	0.03	Shear	Ductile

Forms of Failure

Figure 9 to 20 are photographs show the forms of failure for each sample of the study samples, and through the observations that were picked up during the test, it was noticed that the control samples RC showed strong and sudden failures, so sample CB1 failed at load 110kN and sample CB2 at load 118kN in the shear zone after oblique cracks have appeared in the shear zone (zone of failure) , and this due to the lack of reinforcing steel to resist shear. Whereas, sample CB3 failed at load 122kN and sample CB4 at load 135kN in the bending zone after the appearance of cracks in the middle (Zone of bending) and oblique and big cracks in the shear zone, and that is because the lack of reinforcing steel in the shear zone. The sample CB5 failed at load 130 kN and the sample CB6 at 145kN in the area of bending after the appearance of vertical cracks in the middle which continued to the top until the failure occurred. However, samples Reinforced with fibres FRC broke down in a ductile form and that helped to expect the time of final failure, and the samples continued in resisting the loads even after the appearance of failure cracks where fibres worked to increase the ductility and achieve the maximum values of stress to become equal or greater than the yield stress, so sample of steel fibres SFB7 failed in the shear zone after oblique cracks have appeared in a ductile form at load 145kN by 112% of the failure load value for the control sample and by 156% of the value of design failure load, while the sample of steel fibres SFB8 broke down at the area of bending after the appearance of cracks in the middle that lasted until the failure and that is at load 196kN by 135% of the value of failure load for the control sample and by

200% of the value of design load failure. The samples of glass fibres GFB9 and GFB10 failed in the shear zone but in ductility after the appearance of oblique cracks in this area that continued until the failure and that is at load 130kN and 145kN, respectively, by 100%, for both samples, of the value of failure load for the control sample, and by 140% and 148%, respectively, of the value of design failure load. The samples of polypropylene fibres PFB11 and PFB12 failed in the shear zone, but also in ductility, after the appearance of oblique cracks in this area that continued until the failure at load 91kN and 96kN by 70% and 66%, respectively, of the value of failure load of the control sample and by 98%, for both samples, of the value of design failure load.

Figure 10 mode of failure CB3

Figure 9 mode of failure CB1

Figure 12 mode of failure SFB7

Figure 11 mode of failure CB5

Figure 14 mode of failure PFB11

Figure 13 mode of failure GFB9

Figure 16 mode of failure CB4

Figure 15 mode of failure CB2

Figure 18 mode of failure SFB8

Figure 17 mode of failure CB6

Figure 20 mode of failure PFB12

Figure 19 mode of failure GFB10

CONCLUSIONS AND RECOMMENDATIONS

Through the laboratory study conducted and analysis of the results, we can summarize in the following points:

1. The addition of steel and glass fibres to the concrete beams contributed to the improvement of final shear resistance compared with polypropylene fibres which did not achieve good resistance to shear.

2. Fibre reinforced concrete Beams were more stiffness compared with traditional reinforced concrete beams, attaining small values for strain during the various stages of loading.

3. Fibre reinforced concrete Beams showed noticeable improvement in the overall shape of the final cracks, and a state of ductile failure, which is different from what is expected, with gradual and not sudden manner.

4. The presence of fibres in reinforced concrete beams increased the tensile resistance and shears and reduced the values of strain in the compression and tension zones, especially steel and glass fibres which had a clear effect more than polypropylene fibres.

5. The of addition of steel fibres to Concrete worked to improve the properties of the first cracking and the appearance of a number of cracks during the loading stages of the reinforced concrete beams compared with glass and polypropylene fibres which had no effect on these properties when they were added.

6. The addition of fibres to the concrete contributed to increase the consistency of its components, and that is due to the fibres mechanism in inhibiting the cracks resulted from tensile stresses.

7. The effect of concrete resistance to compression was significant in increasing the final shear resistance and in the resistance of the first crack appearance in both traditional reinforced concrete beams and beams reinforced with fibres.

The research also requires more studies, so we recommend studying the impact of the properties of these fibres in terms of shape, length, diameter, and the elasticity factor, and studying the effect of proportion of use on the structural behavior of these elements.

REFERENCES

1. ARTHUR H. NILSSON, DAVID DARWIN and W.C. CHARLES W. DOLAN. Design of Concrete Structures, McGraw Hill, 2003.

2. ASTM A820-06, Standard Specification for Steel Fibres for Fibre Reinforced Concrete, American Society for Testing and Materials (ASTM International), 100 Barr Harbor Drive, West Conshohocken, USA, 2006.

3. S.H. KOSMATKA, B. KERKHOFF and W.C. PANARESE. Design and Control of Concrete Mixtures, Portland cement Association, 2009.

4. SALAH ALTOUBAT, ARDAVAN YAZDANBAKHSH, and KLAUS ALEXANDER RIEDE. Shear behavior of macro-synthetic fibre reinforced concrete beams without stirrups, ACI Material Journal, American Concrete Institute, July-August 2009, Pages 381 to 389 .

5. K. H. TAN, K. MURUGAPPAN, and P. PARAMASIVAM. Shear behavior of steel fibre reinforced concrete beams, ACI Structural Journal, American Concrete Institute, November-December 1992, Pages 3 to 11 .

6. ACI Building code requirements for structural concrete and commentary (ACI 318-08), American Concrete Institute, 2008.

7. LIBYAN STANDARDS No. 49. Concrete Aggregates from Natural Sources, National Centre for Standardization and Metrology, 2002.

8. LIBYAN STANDARDS No. 340. Portland Cement, National Centre for Standardization and Metrology, 1997.

Enhancing Concrete Strength and Durability by Bacteria Mineral Precipitation

H Afifudin, I I Muhammad, M S Hamidah, K Kartini
Universiti Teknologi MARA (UiTM), Malaysia

The mineral precipitation induced by bacteria in enhancing strength and durability of concrete has been reported since in early year 2000. There are bacteria species that have been recognised in inducing precipitation namely calcium carbonate (calcite) in concrete to plug the pores and hence improve the concrete properties. In the present study, Bacillus subtilis in the different concentration cells were incorporated into the concrete mixture. The concrete mixtures were cast into cubes size 100 mm x 100 mm x 100mm for compressive strength test and in cylinder shape size 100 mm diameter and 200 mm long for rapid chloride permeability test (RCPT). The cast concrete specimens were cured in distilled water before subjected to compressive strength and RCPT at the age of 3, 7, 14, 21, 28 and 60 days. The concrete specimens were also examined under scanning electron microscope (SEM). The results show that the incorporation of bacteria does enhance the concrete strength and permeability. The concentration of 10^6 cell/ml was found to be optimum concentration of bacteria added in the concrete. The micrograph examination substantiate the presence of mineral precipitation in the concrete with the inclusion of bacteria.

H Afifudin holds Dip. Eng (Civil) and B.Eng. (Hons.) Civil from Universiti Teknologi MARA (UiTM) Malaysia. Currently, he enrolled his M.Eng (Civil) at UiTM. He has completed his Master thesis entitled “Microbial Silica Precipitation In Enhancing Concrete Properties” and expecting to graduate at the end of this year. He is awarded Young Lecturer Scheme Scholarship and will be joining Faculty of Civil Engineering, Universiti Teknologi MARA, Malaysia as a lecturer. Bioconcrete has become his research interest since enrolled as postgraduate student.

I I Muhammad, M S Hamidah, K Kartini are all lecturers at the Faculty of Civil Engineering, Universiti Teknologi MARA (UiTM), Selangor, Malaysia

Keywords: Calcite, Concrete strength, Microorganism, Mineral precipitation, RCPT

INTRODUCTION

Concrete made of cement is a strong mechanically and durable construction material. However, it suffers from several drawbacks such as low tensile strength and does not totally impervious, consequently susceptible to corrosion reinforcement and chemical attack. There are many methods of improvement have been made in enhancing the properties of concrete. The most well known method includes the use of Supplementary Cementitious Materials (SCM) such as silica fume, fly ash, ground granulated blast furnace slag, metakaolin and rice husk ash. Nevertheless, use of SCM even though by-product such as silica fume, is relatively expensive as compared to that of ordinary cement. Another approach of concrete advancement is by adopting concrete admixture such as superplasticiser, coating and epoxy injection. However, all those processes are not easy and also costly.

In early 2000, another unique method to improve concrete was reported. The method was introducing microorganism into concrete to improve the properties and heal the crack. The improvement came from the action of filing pores within cement matrix by the mineral precipitation by microorganism through the process known as biomineralisation.

Biomineralisation, is a process by which living organism form inorganic solids [1, 2]. It is a well-documented geological formation phenomenon in which microorganisms accumulate or induce the formation and precipitation of various inorganic compounds such as phosphates, carbonates and silicates [3, 4, 5, 6]. Calcium carbonate (calcite) is a common mineral precipitation induced by the microorganism (bacteria). The minerals agglomerated in dissolved and suspended forms and it improves the binding property or can be used for pore filling effect, eventually enhances the mechanical properties such as strength and durability of the concrete [7, 8, 9, 10].

Various researchers have demonstrated several bacteria which have the ability to precipitate calcite. These bacteria can be found either in soil, sand or natural minerals. Jonkers et al. [11, 12, 13] used Bacillus cohnii bacteria to precipitate calcite. Bacillus pasteurii was used by Santhosh et al.[14, 15], Day et al. [16], Bang et al. [17] and Ramakrishnan et al. [18] while Dick et al. [19], used Bacillus lentus and Bacillus sphaericus [20]. Kim Van Tittleboom et al. [21] used Bacillus sphaericus to heal cracks in concrete and demonstrated that when the cell wall of the bacteria is negatively charged, the bacteria draw cations from the environment, including Ca^{2+} to deposits in their cell surface.

Ghosh et al. [22, 23] investigated anaerobic bacteria Shewanella sp. to precipitate calcite when added in cement mortar and concrete. Bachmeier et al. [24] and Fujita et al. [25] have investigated the effect of adding urease catalyst and strontium to increase alkalinity environment that favours the carbonate mineral precipitation. Bang et al. [17] adopted a cell immobilisation technique utilising polyurethane (PU) in the remediation of concrete cracks to protect cell from the high pH of concrete. It is mainly due to the fact that at extremely high pH of concrete (pH 12.5), it inhibits the growth of Bacillus pasteurii (optimum pH 9.0).

Meanwhile, Thermus sp., thermophilic or hyperthermophilic microorganisms living in geothermal environments are likely to be implicated in the formation of biogenic siliceous deposits, which suggest microbial contribution to silica precipitation [26, 27]. There is tendency that Thermus sp. able to demonstrate more effective microbial plugging in concrete as it is more adaptable in high temperature and high alkaline environment. Besides Thermus sp., Bacillus subtilis, a common soil microorganism also found able to precipitate silica [28]

and it has not been attempted towards the concrete performance. Bacillus subtilis when incubated in silica solution will allow their cell activities to draw Si^{2+} cation to deposit silica in their cell walls.

Therefore, in the present study, the Bacillus subtilis was cultured and incubated in silica solution prior to incorporating in concrete. It is the aim of the present study to examine the effect of silica precipitation induced from Bacillus subtilis to the concrete strength and durability. The strength and durability of the concrete were assessed through compressive strength and rapid chloride permeability test (RCPT). The existence of silica precipitation was verified and substantiated with XRD analysis and microstructure examination using scanning electron microscope (SEM).

MATERIALS AND METHODS

Bacteria and its Growth Condition

Liquid media consisted of tryptic soy broth (30 g/L) with 0.5 % yeast extract was prepared to culture the Bacillus subtilis. Tryptic soy broth was sterilized by autoclaving at temperature 121 ^{o}C for 20 minutes. The cultured of Bacillus subtilis were incubated at 30 ^{o}C on a shaker at 200 rpm for 24 h. Then, the cell of the Bacillus subtilis were pelleted by centrifuging at 10 000 rpm for 3 minutes. The pellets then were washed two times using ultrapure deionized water (udw). Then, the pellets were incubated with silica solution to allow the silica precipitation process taken place due to biomineralisation induced by the Bacillus subtilis. The procedure of silica incubation is described in the following section.

Silica Incubation

Firstly, the 50 mM H_4SiO_4 solution was prepared by dissolving $Na_2SiO_3.5H_2O$ in distilled water. Then, the Bacillus subtilis cells were incubated in H_4SiO_4 solution at the room temperature. The container that contained Bacillus subtilis and H_4SiO_4 solution was continuously shaked at 150 rpm for 10 days. After 10 days, the incubated cell of Bacillus subtilis were pelleted by centrifuging at 10 000 rpm for 3 minutes and the pelleted cells were expected to have adsorbed silica onto it. The pH of the silicate solution during the incubation process was kept constant of 5.5 throughout the process.

XRD Analysis

For XRD analysis, the duplicate pelleted cells were vacuumed to dry out all the water until the pelleted cell turn into powder. After vacuum process process, one out of two cell powders then, was reacted with aqueous calcium hydroxide ($Ca(OH)_2$) for 2 days. Once again the mixture was vacuumed to dry out the excessive water from the reaction to produce powder and ready for XRD analysis. This analysis was carried out using Rigaku D/Max 2000 X-Ray diffractometer.

Another cell powder was tested without reacting with calcium hydroxide solution. The cell powder without and that reacting with calcium hydroxide solution were tested under XRD. For powder that reacting with calcium hydroxide solution, the presence of silica adsorbed to the Bacillus subtilis cell wall was detected by the appearance of the peak of Cristobalite (SiO_2), as an evidence of the formation of silica precipitation in the powders samples.

Dilution of Bacteria Cells

Prior to adding in concrete mix, the pelleted bacteria cell was suspended in a small volume (1 ml) of deionized sterile water and its optical density (OD) was measured at 640 nm. The cell concentration was determined from the standard curve (OD_{640} vs. cell concentration) prepared in advance. This standard curve represents the cell concentration of the bacteria. The bacteria cells were diluted with the deionized water and then calibrated to the arbitrarily corresponding to the standard curve for each concentration. No additional food material (tryptic soy broth), except that present in the diluted cultures, was supplemented in concrete specimens during mixing. Once the bacteria were diluted, it is ready to mix together with the concrete as explained in the following sections.

Preparation of Concrete Specimens

Six series of the concrete specimens made of grade 30 concrete size of 100 mm x 100 mm x 100 mm cube and 200 mm height x 100 mm diameter cylinder were prepared. The materials to cast concrete were cement, sand, aggregate and distilled water. The mix proportion for the grade 30 concrete specimens is shown in Table 1.

Six series designated for concrete specimen made of six different concentration of Bacillus subtilis cell which are 10^3, 10^4, 10^5, 10^6 and 10^7 cell/ml and control (without Bacillus subtilis) were cast. After 24 hours, the moulded concrete specimen were demoulded and cured in distilled water until the day of testing. The distilled water was used to ensure there will be no any contamination or other microorganism present in the mix.

Table 1 Mix proportion for Grade 30, kg/m^3

WATER	CEMENT	SAND	AGGREGATE
205	325	865	975

Compressive Strength

The concrete specimens incorporating without and with Bacillus subtilis were tested its compressive strength. The compressive strength was tested at the age of 3, 7, 28 and 60 days. The compressive strength test was performed in accordance with BS EN 12390-3:2000.

Rapid Chloride Permeability Test (RCPT)

Concrete cylinder of 200 mm long (height) were cut into three slices with 50 mm thick. Twenty five (25) mm height of top and bottom of the cylinder were discarded. Sealant were applied all over the side surface of the concrete slice and allowed to dry. The concrete slice proceed with 1 hour air drying, 3 hours vacuum, 1 hour additional vacuum under de-aerated water and followed by 18 hours of immersion in water. The RCPT was tested at the age of 7, 28 and 60 days. RCPT was carried out according to procedures stipulated by ASTM C 1202:2010.

Statistical Analysis

All the specimens were tested in triplicate. Comparison of mean values was done by using one-way ANOVA to confirm the significant relationship between compressive strength and

different concentration at 95% confidence level. The statistical analysis was performed using statistical software SPSS 17.0.

Microstructure Examination

Concrete chips were prepared from the broken specimen of 1 day age. The chips were directly examined under scanning electron microscope (SEM). Without prior coated, the concrete chips were examined under low vacuum SEM (Quanta 200 FEI). For comparison, samples were also coated and examined under high vacuum SEM (Philips SL 40)

RESULTS AND DICUSSIONS

XRD Analysis

Figure 1 shows the XRD spectra on the pelleted Bacillus subtilis cell without and that reacting with calcium hydroxide solution.

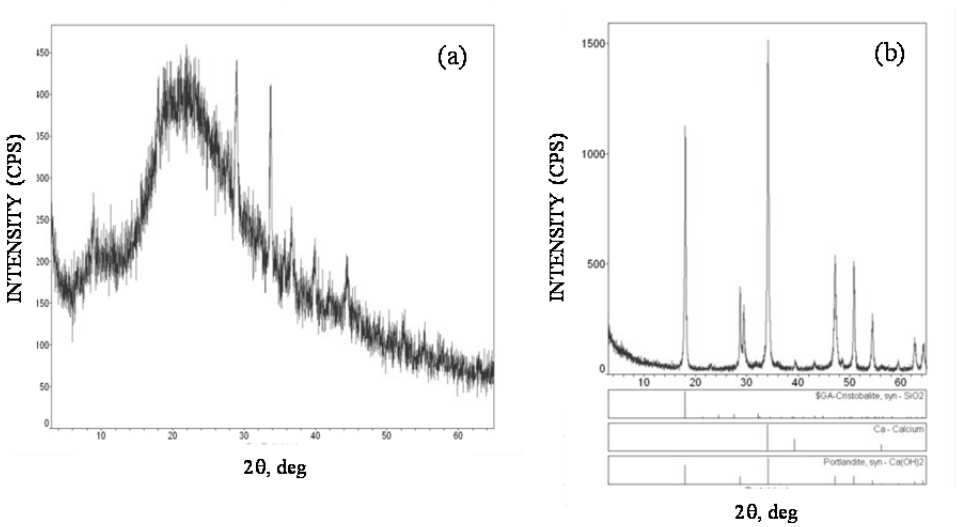

Figure 1 XRD analysis of Bacillus subtilis cell (a) without reacting and (b) reacting with calcium hydroxide solution

The XRD analysis on the pellet samples without reacting with calcium hydroxide solution found to be scattered without obvious peak indicating amorphous silica was detected. The XRD analysis on Bacillus subtilis reacted in calcium hydroxide solution shows that there were extra peaks in the XRD spectra. The most abundant compounds were clearly $Ca(OH)_2$ (Portlandite) and Calcium, the main component that come from $Ca(OH)_2$ solution. The second most compound detected is Cristobalite (SiO_2) which the presence of the peak can be correlated with the silica precipitation adsorbed onto bacteria cell. This suggests that Bacillus subtilis is capable of formation new silicate phase within the matrix. This new phase would help in the modification in pore size distribution. It substantiates the findings towards compressive strength improvement as discussed in the following section.

Compressive Strength

The effects of bacteria on compressive strength of concrete at 3, 7, 28 and 60 days of age were assessed. It can be concluded that inclusion of microorganism (Bacillus subtilis)

enhances the compressive strength of the concrete specimens. Figure 2 depicts the compressive strength of concrete specimens incorporating without and with Bacillus subtilis cells up to 60 days of age. Concrete with concentration of 10^6 cell/ml of Bacillus subtilis showed the most enhanced effect in compressive strength corresponding to concrete without microorganism (control). The compressive strength of concrete of 10^6 cell/ml attained about 39 N/mm^2 at age of 60 days and 33 N/mm^2 for control specimens at same age.

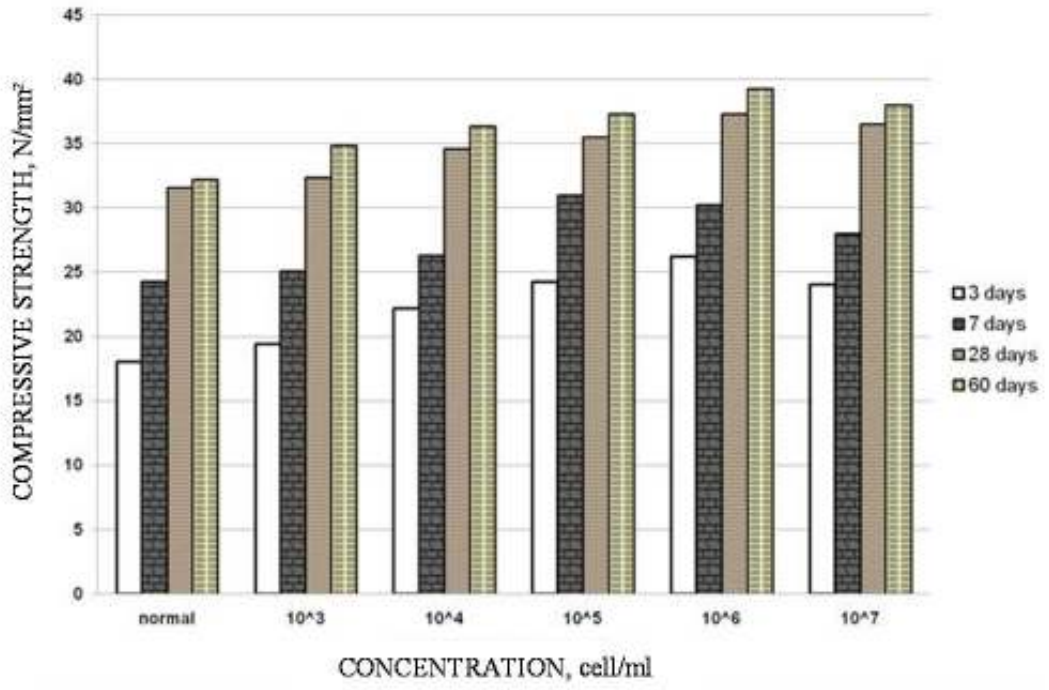

Figure 2 Compressive strength of concrete with and without microorganism

The increase of the compressive strength for Bacillus subtilis with concentration of 10^6 cell/ml over the control about 39 %, 24 %, 18% and 22 % at 3, 7, 28 and 60 days respectively were noted. This is in line with the previous findings reported by Ghosh et al. [22] who reported same percentage of increase corresponding to control specimens when 10^5 cell/ml of Shewanella was included [22]. Similarly, Bang et al.[17] investigation found that 25% is the increase reported when 10^8 cell/ml of Bacillus pasteurii with respect to control specimens. They pointed out that the deposition of the precipitated materials plugged small pores within the cement matrix have contributed to that enhancement.

In addition, Biswas et al.[7] reported that increment of cement mortar strength about 25% over the control was noticed when incorporated with Thermoanaebactor thermohydrosulfuricus at 10^5 cell/ml. Biswas et al. [7] also detected similar increase in for compressive strength with respect to control specimens when similar concentration of Shewanella sp. incorporated in the mortar. Ghosh et al. [22] reported that the uniformity of SiO_2 within the mortar matrices concentration plays important role that determine the optimum cell concentration. They suggested that 10^5 cell/ml is an optimum concentration as the Ca/Si ratio within the CSH gel of mortar was found to be optimum with respect to those made of other cell concentrations.

Rapid Chloride Permeability Test (RCPT)

Figure 3 summarizes the effect of incorporating difference concentration of Bacillus subtilis to the permeability of concrete specimens at 7, 28 and 60 days of age. The presence of bacteria resulted in significant decrease to the permeability compared to control. The optimum concentration of microorganism for RCPT was found to be 10^6 cell/ml matching to the optimum cell concentration towards compressive strength. This concentration gives the most enhanced effect to the concrete permeability. The reductions of concrete made of 10^6 cell/ml over the control are about 28 %, 19 % and 22% at 7, 28 and 60 days respectively suggesting the cement matrix has been densified.

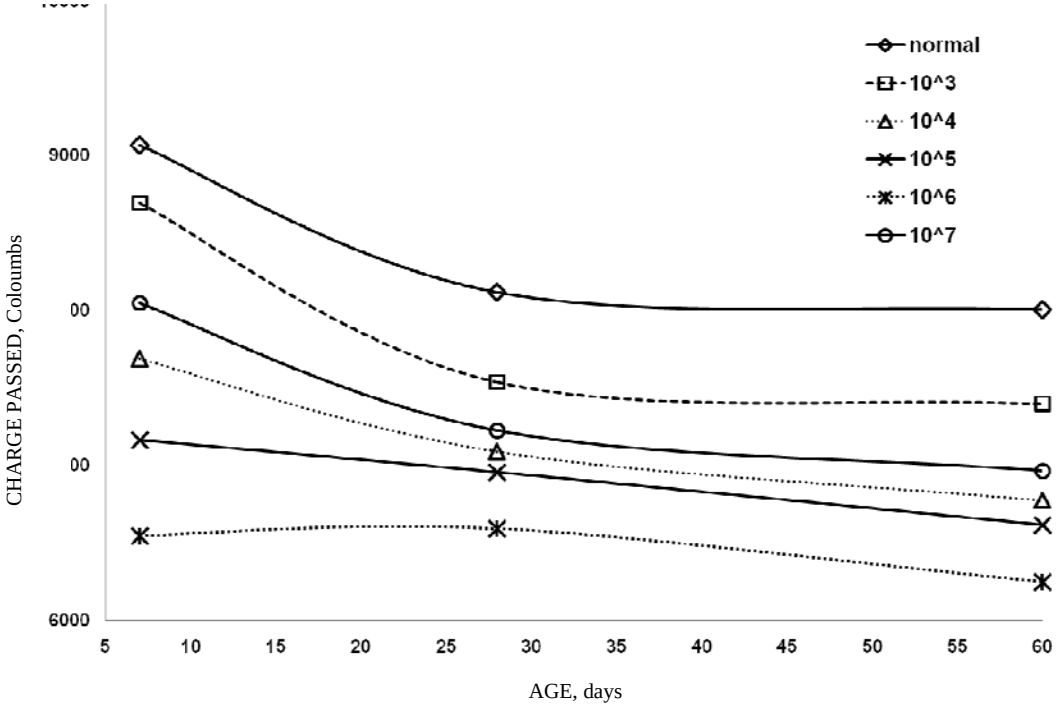

Figure 3 Concrete permeability of concrete without and with Bacillus subtilis

Overall, concrete permeability keep reducing until 28 days of age for all concrete specimens and it is gradually reducing when approach to 60 days of age. The entire concrete with Bacillus subtilis specimens obviously resulted in decreasing of permeability when compared to concrete without bacteria (control) for all ages. In agreement with Muynck et al.[29] findings, the calcite precipitation induced by Bacillus sphaericus was found to be 5 times better than normal concrete which comparable with those applied with conventional water repellent (silanes and siloxanes). In line with the improvement, Muynck et al.[20] concluded that deposition of within concrete surface has contributed to the decrease in permeability. There are little information on the effect of adding bacteria to the permeability in terms of RCPT of concrete was reported.

Therefore, direct comparison cannot be made among the findings on the usage of different bacteria towards the permeability tested by RCPT. However, the reduction in permeability confirmed the filling and plugging pores effect due to mineral precipitation induced by bacteria within the cement matrix as reported [17, 22].

Microstructure Examination

The micrographs in Figures 4 and 5 represent the SEM images taken on concrete sample coated and uncoated at 1 day of age.

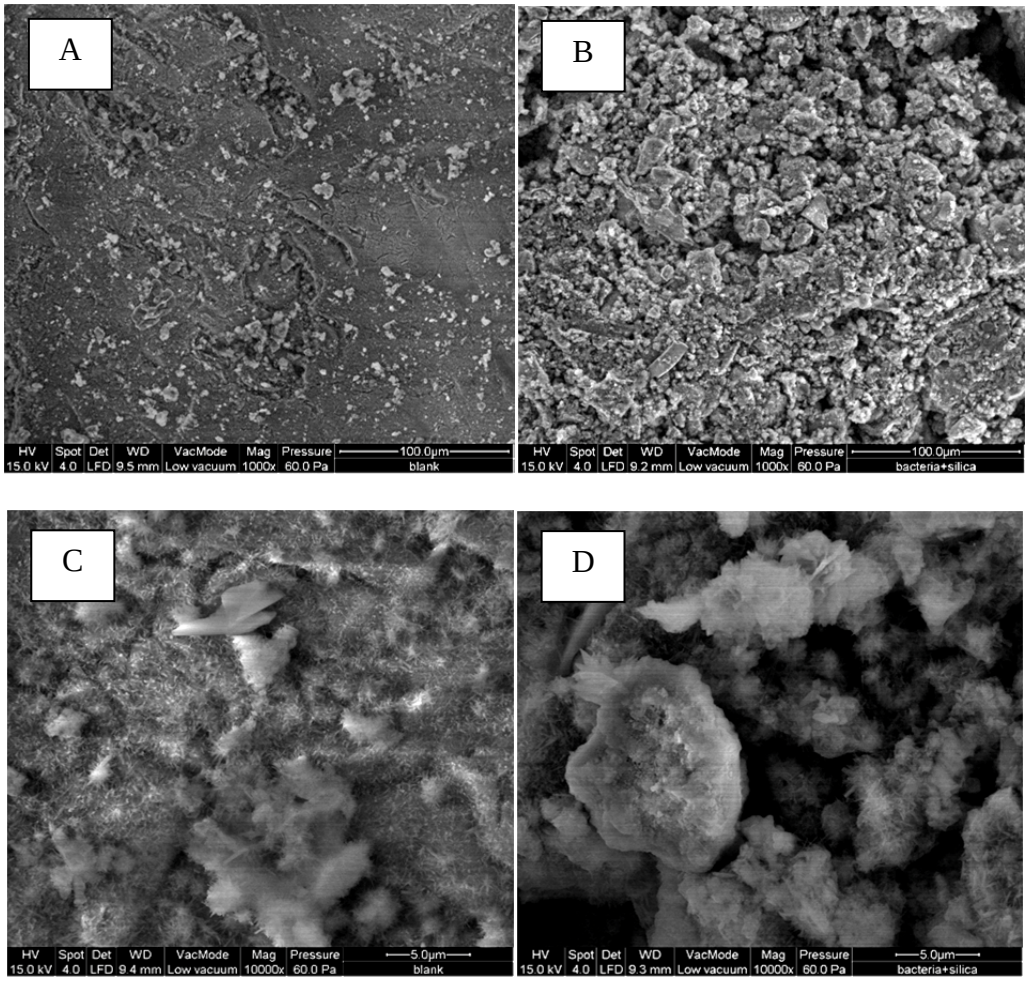

Figure 4 SEM micrograph of silica precipitated within concrete (1 day) at different magnification for uncoated sample.

Figure 4A and Figure 4C portray the image of concrete without Bacillus subtilis AT 1000x and 10000x magnification respectively. Meanwhile, Figures B and D are the image of concrete samples incorporated with Bacillus subtilis. Concrete incorporated with Bacillus subtilis shows the presence of irregular crystalline deposits on the surface. Meanwhile, Figure 5 portrays images of coated concrete sample with Bacillus subtilis. Both sample (Figure 4 and Figure 5) are at 1 day of age. The matrix of the samples without Bacillus subtilis shows no signature of crystal growth. On the other hand, concrete sample that was treated with the bacteria shows crystalline matrix, where individual crystals could be recognised. The coating process prior to SEM examination has enhanced the image and conspicuous crystal growth was observed. The rod Bacillus subtilis (rod shape) is also noticeable. Figure 6 shows the shape of the Bacillus subtilis photographed by Satirapathkul and Leela [30] for comparison.

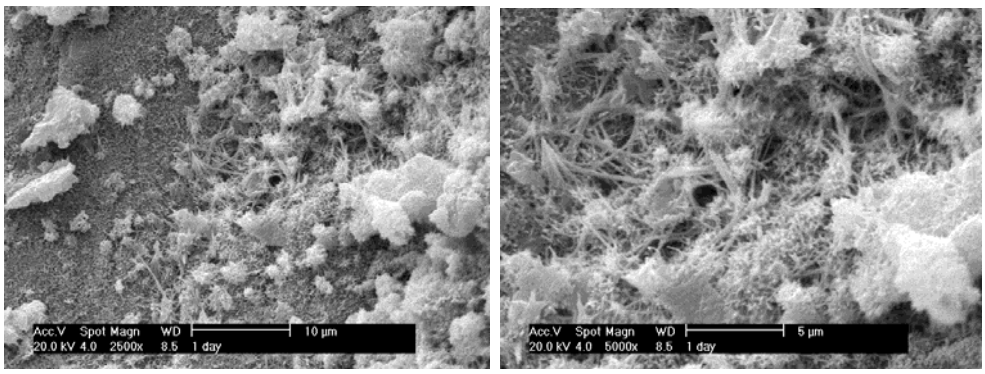

Figure 5 SEM micrograph coated concrete sample treated with Bacillus subtilis (1 day)

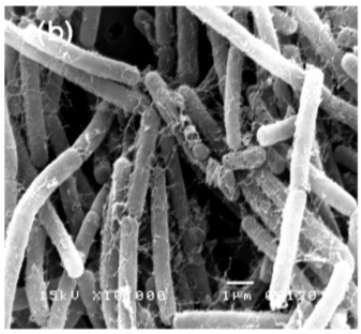

Figure 6 SEM micrograph of Bacillus subtilis cells [30]

CONCLUSIONS

The present study demonstrates that silica precipitation by Bacillus subtilis resulted in increased of concrete properties. The XRD proved that the silica absorbs to the Bacillus subtilis cell wall in amorphous form. It is appeared that the cell with silica absorbed onto it reacts with $Ca(OH)_2$ solution to form Portlandite. The silica precipitation induced by Bacillus subtilis has positive effect on compressive strength and permeability tested by RCPT. It can be concluded that 10^6 cell/ml was found to be optimum and give the most enhancing effect to compressive strength and permeability.

The increase of compressive strength is about 22 % as compared to concrete without inclusion of bacteria and much higher increase is recorded for immatured concrete specimens. Concrete demonstrated an improvement in permeability reducing the concrete permeability about 20 % corresponding to control specimens irrespective of the age. Meanwhile, the microstructure examination has substantiated the presence of silica precipitation within the cement matrix of that containing Bacillus subtilis.

ACKNOWLEDGEMENTS

This research was funded by Excellence Fund UiTM (600-RMI/ST/DANA 5/3/Dst (121/2010)) and Fundamental Research Grant Scheme (600-RMI/ST/FRGS 5/3/Fst (28/2011)). The authors would like to express the appreciation to Research Management Institute, Universiti Teknologi MARA (UiTM), Malaysia for managing the fund. Special

thanks also dedicated to Associate Professor Dr Noor Hana Hussain, Zainuddin Rossdi, Fatihatul Zuriati, and Khalida Ain Kusnan, who have given assistance in preparing and culturing the bacteria in the Laboratory of Microbiology, Faculty of Applied Sciences, UiTM Malaysia.

REFERENCES

1. ARUNACHALAM, K.D., SATHYANARAYANAN, K.S., DARSHAN, B.S., RAJA, R.B. Studies on the characterisation of biosealant properties of bacillus sphaericus, International Journal of Engineering Science and Technology, Vol. 2 (3), 2010, pp 270-277

2. SKINNER, H.W.C., JAHREN, A.H. Biomineralization, Treatise on Geochemistry, Vol. 8, 2007, pp 1-69

3. TRUDINGER, J.B., SWAINE, D.J. Biogeochemical cycling of mineral forming elements, Elsevier, Amsterdam, pp 612

4. FERRIS, F.G., SCHULTZE, S., WITTEN, T.C. FYFE, W.S., BEVERIDGE, T.J. Metal interactions with microbial biofilms in acidic and neutral pH environments, Applied and Environmental Microbiology, Vol. 55, pp 1249-1257

5. GREENE, A.C., MADGWICK, J.C. Microbial formation of manganese oxide, Applied and Environmental Microbiology, Vol. 57, pp 1114-1120

6. THOMPSON, J.B., FERRIS, F.G. Cyanobacterial precipitation of gypsum, calcite and magnesite from natural alkaline lake water, Geology, Vol. 18, 1990, pp 995-998

7. BISWAS, M., MAJUNDAR, S., CHOWDURY, T., CHATTOPADHYAY, B., MANDAL, S., HALDER, U., YAMASAKI, S. Bioremediase a unique protein from a novel bacterium BKH1, ushering a new hope in concrete technology. Enzyme and Microbial Technology, Vol. 46, 2010, pp581-587.

8. BANG, S.S., GALINAT, J.K., RAMAKRISHNAN, V. Calcite precipitation induced by polyurethane-immobilzed Bacillus pasteurii. Enzyme and Microbial Technology, Vol. 28, 2001, pp. 404-409

9. DICK, J., WINDT, W., GRAEF, B., SAVEYN, H., MEEREN, P., DE BELIE, N., VERSTRAETE, W. Biodeposition of a Calcium Carbonate Layer on Degraded Limestone by Bacillus species.Biodegradation, Vol. 17 (4), 2006, pp 357-367

10. FISCHER, S.S., GALINAT, J.K., BANG, S.S. Microbiological precipitation of $CaCO_3$.Soil Biology and Biochemistry, Vol. 31, 1999, pp 1563-1571

11. JONKERS, H.M., SCHLANGEN, E. Crack repair by concrete-immobilized bacteria Proceedings of the First International Conference on Self Healing Materials, Noordwijk aan Zee, The Netherlands, 18-20 April 2007

12. JONKERS, H.M., THIJSSEN, A., MUYZER, G., COPUROGLU, O., SCHLANGEN, E. Applicaion of bacteria self healing agent for the development of sustainable concrete, Ecological Engineering, Vol. 36, 2010, pp 230-235

13. JONKERS, H.M., SCHALANGEN, E. Development of a bacteria-based self healing concrete, Tailor Made Concrete Structures, Walvren & Stoelhorst (eds), Taylor & francis Group, London, ISBN 978-0-415-47535-8, 2008

14. SANTHOSH, K.R., RAMAKRISHNAN, V., DUKE, E.F., BANG, S.S. SEM Investigation of Microbial Calcite Precipitation in Cement, Proceedings of the Twenty-Second International Conference On Cement Microscopy, Montreal, Quebec, Canada, April 29 - May 4 2000, pp293-305

15. SANTHOSH, K.R., RAMAKRISHNAN, V., BANG, S.S. Remediation of concrete using microorganisms, ACI Materials Journal, Vol. 98 (1), pp 3-9

16. DAY, J.L., RAMAKRISHNAN, V., BANG, S.S. Microbiologically induced sealant for concrete crack remediation, 16th Engineering Mechanics Conference, Seattle Washington, 16-18 July, 2003

17. BANG, S.S., GALINAT, J.K., RAMAKRISHNAN, V. Calcite precipitation induced by polyurethane-immobilized Bacillus pasteurii, Enzyme and Microbial Technology, Vol. 28, 2001, pp 404-409

18. RAMAKRISHNAN, V., PANCHALAN R.K., BANG, S.S. Improvement of concrete durability by bacterial mineral precipitation, Proceedings of 11th International Conference on Fracture, Turin, Italy, 20-25 March 2005

19. DICK, J., WINDT, W., GRAEF, B., SAVEYN, H., MEEREN, P., BELIE, N.D., VERSTRAETE, W. Biodeposition of a calcium carbonate layer on degraded limestone by Bacillus species, Biodegradation, Vol. 17 (4), 2006, pp 357-367

20. MUYNCK, W.D., COX, K., BELIE, N.D., VERSTRAETE, W. Bacterial carbonate precipitation as alternative surface treatment for concrete. Construction and Building Materials, Vol. 22, 2008, pp 875-885

21. TITTELBOOM, K.V., BELIE, N.D., MUYNCK, W.D., VERSTAETE, W. Use of bacteria to repair cracks in concrete, Cement and Concrete Research, Vol. 40, 2010, pp 157-166

22. GHOSH, P., MANDAL, S., CHATTOPADHYAY, B.D., PAL, C. Use of microorganism to improve the strength of cement mortar. Cement and Concrete Research, Vol. 35, 2005, 1980-1983.

23. GHOSH, S., BISWAS, M., CHATTOPADHYAY, B.D., MANDAL, S. Microbial activity on the microstructure of bacteria modified mortar. Cement and Concrete Composites, Vol. 31, 2009, pp 93-98

24. BACHMEIER, K.L., WILLIAMS, A.E., WARMINGTON, J.R., BANG, S.S. Urease activity in microbiologically-induced calcite precipitation, Journal of Biotechnology, Vol. 93, 2002, pp 171-181

25. FUJITA, Y., REDDEN, G.D., INGRAM, J.C., CORTEZ, M.M., FERRIS, F.G., SMITH, R.W. strontium incorporation into calcite generated by bacterial ureolysis, Geochimica et Cosmochimica Acta, Vol. 68, No. 15, 2004, pp 3261-3270

26. INAGAKI, F., YOKOYAMA, T., DOI, K., IZAWA, E., OGATA, S. Biodeposition of Amorphous Silica by an Extremely Thermophilic Bacterium, Thermus spp. Bioscience, Biotechnology and Biochemistry, Vol. 62(6), 1998, pp1271-1272

27. IWAI, S., DOI, K., FUJINO, Y., NAKAZONO, T., FUKUDA, K., MOTOMURA, Y., OGATA, S. Silica Deposition and Phenotypic Changes to Thermus thermophilus Cultivated in the Presence of Supresaturated Silica. The ISME Journal, Vol. 4, 2010, pp 809-816

28. MERA, M.U., BEVERIDGE, T.J. Mechanism of Silicate Binding to the Bacterial Cell Wall in Bacillus subtilis. Journal of Bacteriology ,Vol. 7 (175), 1993, pp 1936-1945.

29. MUYNCK, W.D., COX, K., BELIE, N.D., VERSTRAETE, W. Bacterial carbonate precipiatation reduce the permeability of cementitious materials,Sustainable Construction Materials and Technologies, Taylor & Francis Group, London, Chun, Claisse, Naik & Ganjian (eds), ISBN 978-415-44689-1, 2007

30. SATIRAPATHKUL, C., LEELA, T. Growth inhibition of Pathogenic Bacteria by extract of Quercus infectoria galls, International Journal of Bioscience, Biochemistry and Bioinformatics, Vol. 1, No. 1, 2011, pp 26-31

Microbial Concrete by Partly Replacing Fine Aggregate with Rice Husk Ash

G M Ganesh, A S Santhi, G Kalaichelvan, M Philip
VIT University Vellore, India

Concrete must be relatively impervious so as to enable it to withstand the service conditions for which it has been designed, without serious deterioration over the lifespan of the structure. Research has indicated that a concrete with porous nature will affect the strength and durability. In order to enhance strength and durability, pores should be filled with bonding and inert material. An advanced technique for filling the pores in concrete is by utilizing bacteria, i.e. microbiologically induced calcite ($CaCO_3$) precipitation. Microbiologically Induced Calcite Precipitation (MICP) is a technique that comes under a broader category of science called biomineralization. It is a process by which living organisms form inorganic solids. MICP is highly desirable because the calcite precipitation induced as a result of microbial activities, is pollution free and natural. Here bacillus cohnii was used for calcite ($CaCO_3$) precipitation. To enhance the growth of bacteria fine aggregate was partly replaced with rice husk. As a result, the density of concrete was reduced slightly and an increase in compressive strength and durability was observed. All the experimental details of the concrete with rice husk, preparation of bacteria and details of experimental results are presented in this paper.

Dr G Mohan Ganesh is Professor, Programme Manager & Division Leader, Structural and Geotechnical Engineering Division, School of mechanical and building Sciences, VIT University, Vellore. He has led three research projects on High volume fly ash concrete. His research interests include Steel Structures, Flyash Concrete, Steel – Concrete Composite structures, Artificial Neural Network (ANN), and Genetic Algorithms (GA).

Dr A S Santhi is Professor and Assistant Director in centre for Structural Engineering, Structural and Geotechnical Engineering Division, Director, School of mechanical and building Sciences, VIT University, Vellore. She has led three research projects on High volume fly ash concrete. Her research interests include Creep and Shrinkage Properties in RCC Structures, Flyash Concrete.

Dr Kalaichelvan Gurumurthy is a microbiologist with interests in Environmental, Industrial and Food Microbiology. He has been involved in commissioning various industrial treatment units, anaerobic treatment of solid and liquid wastes and currently he involved in developing probiotic consortia.

M Phlip, has completed M.Tech (Structural Engineering) at VIT University. He did his under graduate studies in Civil Engineering. He has presented two papers in the international conference. His research interests include Microbial concrete.

Keywords: Bacillus cohnii, Bacterial concrete, Microbial concrete, Rice husk ash

INTRODUCTION

Concrete must be relatively impervious so as to enable it to withstand the service conditions for which it has been designed, without serious deterioration over the lifespan of the structure. The loss of concrete durability may be caused by the severity of the environment to which it is exposed or by internal changes within the matured concrete itself. The external causes may be physical, chemical or mechanical and attack by natural or industrial aggressive liquids and gases.The impact of durability-related problems particularly, cracking of the surface layer of concrete reduces material durability as ingress water and detrimental chemicals cause a range of matrix degradation processes as well as corrosion of the embedded steel reinforcement. One of the recent methods to improve the durability and strength of concrete is by the addition of bacteria into the concrete.

Bacteria in concrete

In order to improve the durability and strength of concrete, a variety of techniques is available but each of them have a number of disadvantages such as environmental and health hazards. Therefore, bacterially induced calcium carbonate precipitation has been proposed as an alternative and environmental friendly method. Bacteria are the most abundant and metabolically diverse forms of life on earth. They grow under a wide range of conditions in an unparalleled variety of habits. Humans have the ability to precipitate minerals in the form of bones and teeth continuously. This ability is not only confined to human beings; even Bacillus cohnii can continuously precipitate calcite. This phenomenon is called microbiologically induced calcite precipitation. Under favorable conditions, this bacterium's when used in concrete can continuously precipitate a new highly impermeable calcite layer and fill the voids and pores. Calcite has a coarse crystalline structure that readily adheres to surfaces in the form of scales. In addition to the ability to continuously grow upon itself, it is highly insoluble in water. The microbial precipitation of $CaCO_3$ is determined by several factors including the concentration of dissolved inorganic carbon, the pH, the concentration of calcium ions and the presence of nucleation sites. The first three factors are provided by the metabolism of the bacteria while the cell wall of the bacteria will act as a nucleation site. Therefore the literatures were reviewed to emphasis the role of bacteria in concrete.

LITERATURE REVIEW

Effect of bacteria in strength and durability of concrete

Jonkers and Schlangen [1] investigated the use of bacteria as self healing agents for the autonomous remediation of cracks in concrete. Varenyam Achal et al. [2] was identified the positive effect of bacillus on the compressive strength of Portland cement mortar cubes and a decrease in water penetration. Further, this technique could be implemented in remediation of existing structures by substituting the bacterial culture instead of water while curing concrete.

However, this point would require extensive elaboration to make a meaningful discussion. Further the development of the microbial concrete provided the basis for an alternative and high quality concrete sealant that was cost effective, environmentally safe and ultimately leads to enhancement in the durability of building materials.

Muynck et al. [3] demonstrated that the biodeposition treatment results in an increased resistance of mortar specimens towards degradation processes. Kim Van Tittelboom et al. [4] demonstrated the biodeposition treatment resulted in an increased resistance of mortar specimens towards carbonation, chloride penetration and freezing and thawing. In the case of cementitious materials, the biodeposition treatment might be regarded as a coating system, as the carbonate precipitation was mainly a surface phenomenon due to the limited penetration of the bacteria in the porous matrix.

Ramakrishnan et al. [5, 6] reported that the bacteria could enhance the durability of concrete by increasing the resistance towards to alkali, sulphate, freeze thaw attack and drying shrinkage. The presence of bacteria in different mediums (water, phosphate-buffer and urea-$CaCl_2$) increased the resistance of concrete. The durability of bacterial concrete increased with the increase in the concentration of bacteria.

The literature review shows that certain bacillus strains can be added to concrete in order to increase the strength and durability.

Effect of rice husk in concrete

Salas [7] found that the use of rice husk as substitute of sand reduces the density of concrete. Based on the specific weight and average resistance to compression, these concretes might be defined as the materials with hybrid characteristics between light weight concrete and insulating concretes. From literature survey, it is clearly understood that rice husk can be used in concrete as a partial replacement of fine aggregate, so as to reduce the density of concrete and make it cost effective.

Hence the experiments were conducted to study the effect of bacillus cohnii with a partially replacement of fine aggregate with rice husk.

BACILLUS

The aerobic endospore-forming bacteria are widespread and can be recovered from almost every environment in the biosphere. In microbiology, the term bacillus means any rod-shaped microbe (and coccus means a spherical microbe). However, Bacillus refers to a specific genus of bacteria. The family Bacillaceae are all gram-positive, rod-shaped bacteria which form endospores, with two main divisions:

(i) The anaerobic spore-forming bacteria of the genus Clostridium
(ii) The aerobic or facultative anaerobic spore-forming bacteria of the genus Bacillus

Characteristically, Bacillus cultures are Gram-positive when young, but may become Gram-negative as they age. Bacillus species are aerobic, sporulating, rod-shaped bacteria which are ubiquitous in nature. This is a large genus with many members.

Bacillus cohnii

Bacillus Cohnii is a common soil bacteria. Some of the special features of bacillus cohnii which is collected from Microbial Type Culture Collection (MTCC) are given in Table 1.

Table 1 Properties of bacillus cohnii

PROPERTY	INFORMATION
Genus Name	Bacillus
Species Name	cohnii
Type	B
Authority	Spanka and Fritze 1993
Recieved as genus	Bacillus
Recieved as species	cohnii
Recieved from	ATCC
Strain designation	ATCC51227
AHIFPC/Equivalent to MTCC	ATCC51227,CCM4369,DSM6307,LMG16678
Isolated or derived from	Soil from house meadow
MTCC No	3616
Isolated from	Braunscheig ,Germany
Preservation suspending medium	10% Glycerol
Growth condition	Aerobic
Incubation	24 Hours
Sub culturing period	5 Days
Special features	Type strain

Use of Rice husk in microbial concrete

As it is incorporated bacteria in concrete, a living being, a question arises about its survival and growth. So some natural materials or nutrients are to be added to the concrete. Bacteria can use these natural materials as their food for their growth. Some of the natural materials that can be used for their growth are saw dust, rice husk, etc. One of the main aspect of good concrete is, it should be cost effective. The increasing cost of materials has greatly hindered the development of shelter and other infrastructural facilities in developing countries. This arises, the need for engineering consideration of the use of cheaper and locally available materials to meet desired need enhance self efficiency, and lead to an overall reduction in construction cost for sustainable development. The lightweight aggregates used in the production of lightweight concretes are generally porous materials whose water absorption is usually higher than that of normal aggregate, which influences the microstructure of the hardened cement paste and the interfacial zone. The interfacial zone has been considered the weakest zone in composite concrete in terms of mechanical strength and permeability to fluids.

Their percentage of its utilization is currently less than 13%, so need to increase their utilization. As the concrete industry is vast, these waste organic materials if used in concrete, the percentage of wastes can be reduced and this also helps in enhancing the growth of bacteria. Some of these wastes include saw dust, rice husk, sugar cane husk etc which are produced from milling stations, waste treatment plants etc.

Rice husk is one of the main waste product from the rice mill. It is a natural organic material. So rice husk ash was used as a replacement of fine aggregate in concrete and also helps in enhancing the growth of the bacteria.

MATERIALS & MIX PROPORTIONS

The various materials used and their material characteristics are listed below.

Cement

Ordinary Portland cement (53 grade) confirming to IS: 12269-1987 [8] reaffirmed in 2004 was used. Its properties are given in Table 2.

Table 2 Physical properties of cement

S. NO	PHYSICAL PROPERTIES	RESULTS
1	Specific gravity	2.94
2	Consistency, %	29.4
3	Initial setting time, min	63
4	Final setting time, min	538

Fine aggregate

Sand

Natural sand confirming to zone II with a specific gravity of 2.43 was used .The test was done as per IS: 383-1970 [9] reaffirmed in 1997.

Rice husk

Rice husk confirming to zone IV with a specific gravity of 3.46 was used. The test was done as per IS: 383-1970 [9] reaffirmed in 1997.

Coarse aggregates

Coarse aggregate with 20mm normal size and specific gravity of 2.73 has been used.

Bacteria - Bacillus Cohnii

Bacillus Cohnii (MTCC 3616), common soil bacteria obtained from Microbial Type Culture Collection (MTCC), Chandigarh, India has been used for the present study. The bacteria obtained was transferred into conical flask containing 100ml Nutrient Broth solution. This 100ml was maintained as a mother culture for further studies (Figure 2). One ml of the mother culture was added to the required volume of Nutrient broth solution and grown overnight at 130rpm on a rotary shaker.

Mix Proportions

The constant cement content of 360 kg/m³ mix was used for this study [10]. The mix was designed by keeping a constant density of 2400 kg/m³ and w/c ratio of 0.4. The mix proportion for the controlled concrete mix was found to be 1: 2.1: 3.16: 0.40.

Various mixes were designated as M1 to M4 that are given in Table 3. Table 4 shows the details of different mix proportions for 360 kg/m³ grade control mix (without rice husk) and bacteria and with rice husk.

Figure 1 Bacillus Cohnii in wire tube.

Figure 2 Bacillus Cohnii in liquid form.

Table 3 Names of Mixes

NAME	MIXES
M 1	Control mix
M 2	5% of fine aggregate replaced with rice husk.
M 3	Control concrete with 100 ml Bacillus cohnii
M 4	100 ml Bacillus cohnii and 5% fine aggregate replaced with rice husk

Table 4 a Mix Proportion

CONSTITUENTS, kg/m³			
Water	Cement	Fine Aggregates	Coarse Aggregates
144	360	758	1138

Table 4 b Mix Design for 360kg/ m³ of cement content with bacteria and rice husk

ITEM	M-1	M-2	M-3	M-4
Cement, %	100	100	100	100
Cement, kg/m³	360	360	360	360
Coarse aggregate, kg/m³	1138	1138	1138	1138
Sand, kg/m³	758	720	758	720
Rice husk, %	0	5	0	5
Rice husk, kg/m³	0	38	0	38
Water, l/m³	144	144	44	44
Bacteria, l/m³	0	0	100	100

EXPERIMENTAL STUDIES

The following tests were conducted to find the properties of microbial concrete.

Compressive strength test

Concrete cubes of size 100mmx100mmx100mm were cast and cured for 7 & 28 days and then tested.

Split tensile strength test

The split tensile strength is an indirect measurement of the tensile strength by placing the cylindrical specimen horizontally between the loading surfaces. This method consists of applying a diametric compressive force along the length of the cylindrical specimen. This loading induces tensile stress on the plane containing the applied load.

Flexural Strength Test

Flexural strength is the ability of a beam or slab to resist failure in bending. It is measured by loading un-reinforced concrete prisms of size 500mm x 100mm x 100mm. The flexural strength value is about 12 to 20 percent of the compressive strength of concrete. Hydraulic flexural testing machine with a capacity of 10 Tonnes was used for the test.

The specimen was placed in the machine and the standard two-point loading was applied to the specimens. The load was applied gradually until the specimen failed and the maximum load applied to the specimen during the test was noted. The flexural strength of the specimen is expressed as the modulus of rupture.

Water absorption test

The performance of concrete subjected to many aggressive environments is a function, to a large extent, of the penetrability of the pore system. Water absorption is also strongly affected by the moisture condition of the concrete at the time of testing. For the present study, 100 mm x 100 mm x 100 mm cubes were used.

RESULTS AND DISCUSSION

The results and discussion for the various mechanical properties such as compressive strength, split tensile strength, flexural strength and water absorption test of microbial concrete are given below.

Compressive Strength for Cubes

Compressive strength values of cubes for 7 days and 28 days with various replacement levels are shown in Table 5. It is observed that the 7 days compressive strength has been increased by addition of Bacillus cohnii by 10% and the 28 days compressive strength has been increased by addition of Bacillus cohnii by 12%.

It is observed that 7 days compressive strength of concrete by replacement of fine aggregate with 5% of rice husk has been increased by addition of Bacillus cohnii by 23%. And the 28 days compressive strength of concrete by replacement of fine aggregate with 5% of rice husk has been increased by addition of Bacillus cohnii by 26%.

From these results, the inference can be given as the addition of bacteria will increase the compressive strength of concrete and this increase is more in microbial concrete when rice husk is used as 5% replacement to the fine aggregate.

Table 5 Compressive Strength of Cubes for 360 kg/m³

MIX	CONTENT		COMPRESSIVE STRENGTH, N/mm²	
	Rice husk, %	Bacteria, l/m³	7 days	28 days
M-1	0	0	34.55	44.2
M-2	5	0	9.45	18.1
M-3	0	100	38	49.55
M-4	5	100	11.7	22.7

Split Tensile Strength for Cylinders

Split Tensile strength values of cylinders for 28 days with various replacement levels are shown in Table 6. It is observed that the 28 days Split tensile strength has been increased by the addition of the bacteria Bacillus cohnii by 12%. When the fine aggregate is replaced with 5% of rice husk it has been observed that an increase of 14% in the split tensile strength of the concrete.

Therefore from the above results, the inference can be given as the split tensile Strength for cylinders with bacteria Bacillus cohnii and 5% replacement of fine aggregate with rice husk will be more in concrete.

Table 6 Split tensile, flexural strength and water absorption values

MIX	PROPERTY		
	Split Tensile Strength, N/mm²	Flexural Strength, N/mm²	Water absorption values, %
M-1	2.99	6.62	4.58
M-2	2.41	5.64	10.1
M-3	3.34	6.87	3.4
M-4	2.73	5.88	7.04

Flexural Strength Test for Prisms

Flexural strength values for prisms of 28 days with various replacement levels are shown in Table 6. It is observed that the 28 days flexural strength has been increased by the addition of the bacteria Bacillus cohnii by 4%. When the fine aggregate is replaced with 5% of rice husk it has been observed that an increase of 7% in the flexural strength of the concrete.

From these results, the inference can be given as the addition of bacteria will increase the flexural strength of concrete and this increase is more in microbial concrete when rice husk is used as 5% replacement to the fine aggregate.

Water absorption test for Cubes

The presence of bacteria resulted in a significant decrease of the water intake compared to untreated specimens (control). The deposition of a layer of calcium carbonate crystals on the surface resulted in a decrease of the absorption.

Water absorption test for cubes with various replacement levels are shown in Table 6. It is observed that there is a considerable decrease in the water absorption for bacillus cohnii. For control concrete water absorption is of 4.58%, but for bacillus cohnii, it is 3.4%. But the same trend was not found when bacteria and rice husk were used. This is because as rice husk consumes more percentage of water, its absorption will be more compared to the control concrete. The values when 5% of rice husk has been replaced with fine aggregate with bacillus cohnii is 7.04%.

From these results, it is clear that the presence of a layer of carbonate crystals on the surface by bacterial isolate has the potential to improve the resistance of cementitious materials towards degradation processes.

CONCLUSIONS

The following conclusions have been drawn based on the experimental investigation carried out on concrete mixtures with bacillus cohnii and by replacement of fine aggregate with rice husk.

- Compressive strength at 28 days has been increased by 12% for the addition of bacillus cohnii and 25% for bacteria with fine aggregate replaced by rice husk. The bacteria activity is more when rice husk is added as partial replacement to the fine aggregate.
- Split tensile strength at 28 days has been increased by addition of the bacteria bacillus cohnii by 12% and when the fine aggregate is replaced with 5% of rice husk it has been has been observed that an increase of 14%.
- Flexural strength at 28 days has been increased by addition of the bacteria bacillus cohnii by 4% and when the fine aggregate is replaced with 5% of rice husk it has been has been observed that an increase of 7%.
- From this split tensile strength and flexural strength results, it can be concluded that concrete with bacillus cohnii and rice husk concrete perform well.

- Water absorption test results shows that absorption rate will be more in concrete with rice husk. But by the addition of bacteria, will leads to the reduction in absorption. Here bacillus cohnii performed well.
- Results from the above all experiments show that, rice husk enhanced the bacterial growth and also reduced the self weight of concrete. So rice husk, a waste organic material can be utilized in the bacterial concrete.

REFERENCES

1. HENK M. JONKERS, ERIK SCHLANGEN, Crack Repair by Concrete-immobilized Bacteria, First International Conference on Self Healing Materials,18-20 April 2007, Noordwijk aan Zee, The Netherlands.

2. VARENYAM ACHAL, ABHIJIT MUKHERJEE, M. SUDHAKARA REDDY, Microbial Concrete: A Way to Enhance the Durability of Building, Journal of Materials in Civil Engineering ASCE, July, 2010.

3. DE MUYNCK, DE BELIE, VERSTRAETE, Improvement of Concrete Durability with the Aid of Bacteria, First International Conference on Self Healing Materials, 18 - 20 April 2007, Noordwijk aan Zee, The Netherlands.

4. KIM VAN TITTELBOOM, NELE DE BELIE, WILLEM DE MUYNCK, WILLY VERSTRAETE, Use of bacteria to repair cracks in concrete, Cement and Concrete Research (2010) pp-157–166.

5. RAMAKRISHNAN. V., RAMESH. K., BANG, S S., Remediation of Concrete using Microorganisms, ACI Materials Journal, v.98, No.1, pp. 3-9, Jan-Feb 2001.

6. RAMAKRISHNAN. V., RAMESH. K., PANCHALAN, SOOKIE S. BANG, Bacterial Concrete, Proceedings of SPIE-International Society for Optical Engineering on Smart Materials, Australia, Vol. 4234 (2001), pp. 168-176, 13-15 December 2000.
7. JULIAN SALAS, MARINA ALVAREZ, JANER VERAS, Lightweight Insulating Concretes With Rice Husk, The International Journal Of Cement Composites And Lightweight Concrete, volume 8, number 3, April 1986.

8. IS 112269-1987, Indian Standard Specification for 53 Grade Ordinary Portland Cement, reaffirmed in 2004, Bureau of Indian standards, New Delhi.

9. IS: 383-1970, Indian Standard Specification for Coarse and Fine Aggregates from Natural Sources for Concrete, reaffirmed in 1997, Bureau of Indian standards, New Delhi.

10. IS: 10262-1982, Indian Standard Recommended Guidelines for Concrete Mix Design, reaffirmed in 2004, Bureau of Indian standards, New Delhi.

Estimation on Deterioration Process of Concrete Members Suffering Chloride Induced Damage Based on a Stochastic Approach

M Matsushima[1], K Matsuda[2], M Yokota[2]
1 – Kagawa University, Japan
2 – Shikoku Research, Japan

Deterioration of concrete structures has recently been affecting much attention in Japan. Severe chloride induced deterioration has been observed in the coastal area. The deterioration is mainly caused by the corrosion of reinforcement due to the action of chloride ions. Corrosion of steel material in concrete is commonly caused by electrochemical reaction and is primarily caused by the migration of airborne chloride ions. The method to predict the damage process of deteriorated structure suffered chloride induced deterioration is proposed in this paper. The deterioration process is modeled as consisting of three phases; The first is the period ts until depassivation of the reinforcement occurs after completion of the structure, and the second is the period tcr until the corrosion cracking occurs due to pressure of corrosion from corrosion of reinforcement starts. After corrosion cracking, the concrete members will be deteriorated exponentially. The deterioration phenomenon of structures in actual environment is varied widely. Therefore, the stochastic method is carried out in order to consider the actual structure with uncertainty in nature. Two parameters, Equivalent diffusion coefficient, Spacing of cover thickness is modelled as stochastic parameters. Target structure is the drainage canal passed over 35 years and deteriorated by chloride induced damage. The result calculated using proposed model is compared with actual data obtained from target structure in this paper.

Dr. Manabu Matsushima is a professor of KAGAWA University, Takamatsu, Japan. He received his Doctor of Engineering from Tokyo Denki University in1994. His research interest is the application of reliability theory to concrete members in RC structures. He is member of the JSCE, AIJ and JCI.

Mr. Kousaku Matsuda is a senior research engineer at Shikoku Research Institute Inc., Takamatsu, Japan. He received his Master Degree from Kobe University in 1979. His research interests is the application of deterioration model to member received chloride induced damage. He is member of the AIJ and JCI.

Dr. Masaru Yokota is a senior research engineer at Shikoku Research Institute Inc., Takamatsu, Japan. He received his Doctor of Engineering from Tokushima University in 1995. His research interests include the deterioration of RC structures and the inspection model of corroded steel bar received the severe environments. He is member of the JSCE and JCI.

Keywords: Chloride induced deterioration, Corrosion, Simulation, Stochastic model

INTRODUCTION

Deterioration of concrete structures has recently been affecting much attention in Japan. Severe chloride induced deterioration has been observed in the coastal area. The deterioration is mainly caused by the corrosion of reinforcement due to the action of chloride ions. Corrosion of steel material in concrete is commonly caused by electrochemical reaction and is primarily caused by the migration of airborne chloride ions. Some works have been conducted on the migrating characteristics of airborne chlorides into concrete and parameters on chloride ion concentration in actual structures using survey data in situ [1, 2] and the relationship between the concentration and steel corrosion in actual structures [3]. It is very important for the design and the construction work to estimate the amount of deterioration in which a structure will suffer during its service life. Bazant proposed a prediction model of structural service life based on the physical model of a steel corrosion in concrete [4]. Brown et al. presented an evaluation of structural integrity and prediction of its service life [5, 6].

The deterioration process is regarded as consisting of three phases as shown in Figure 1.; The first is the period until depassivation of the reinforcement occurs after completion of the structure, and the second is the period starting from the moment of depassivation and including the development of corrosion at a perceptible rate until the limit state is attained when cracking appears in the surface concrete. The former is called the incubation period and the latter the progressive period. After cracking of surface concrete is called the accelerative period. The model of deterioration due to chloride-induced damage based on stochastic approach is proposed in this paper. Two parameters such as equivalent diffusion, error of spacing of reinforcements are chosen as the stochastic parameters. Target structure is the concrete slab of flood gate received chloride-induced damage in situ. The results of computation are compared with the survey data in situ using proposed model.

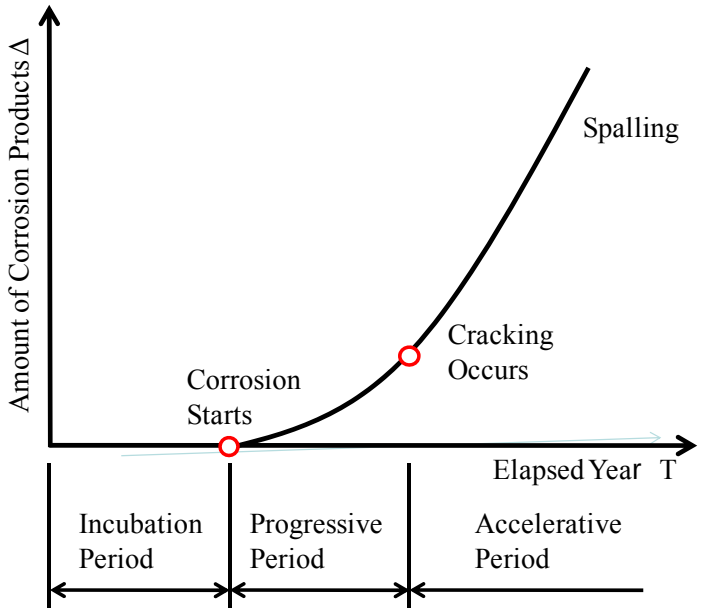

Figure 1 Relationship between corrosion rate and elapsed period

PREDICTION MODEL OF DETERIORATION

Deterioration Process such as from incubation to acceleration period needs to be predicted accurately for the optimal maintenance of RC structure. Figure 2 shows the flow chart of deterioration model of RC structure suffered chloride induced deterioration in this paper.

A probabilistic model is developed to represent the deterioration of concrete structures using deterioration process model as shown in Figure 2. The parameters involved in the model are expected to vary extensively since the phenomenon takes place in the natural environment. In this paper, two parameters, equivalent diffusion and cover thickness is modelled as stochastic parameters. Others are governed by two stochastic parameters mentioned above.

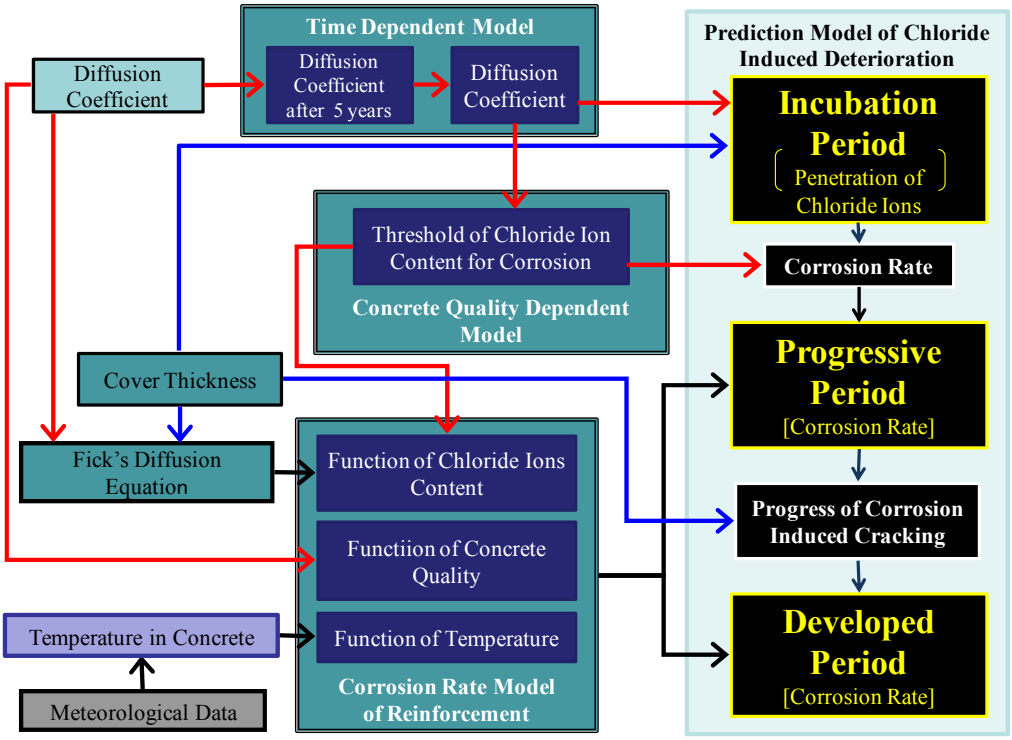

Figure 2 Flow chart of deterioration model

Incubation Period

The penetration phenomenon of chloride ion assumes to be described by Fick's diffusion equation. Chloride ion density C*(Xt*,t) is obtained as shown in Equation (1) by assuming that the constant value per time of chloride ion density can penetrate into concrete. Mark * in the equation indicates stochastic parameters.

$$C^*\left(X_t^*,t\right)=C_0+W\left[2\sqrt{\frac{t}{\pi D_c^*}}\exp\left(-\frac{X_t^{*2}}{4D_c^*t}\right)-\frac{X^*}{D_c^*}\left\{1-\mathrm{erf}\left(\frac{X_t^*}{2\sqrt{D_c^*t}}\right)\right\}\right] \quad (1)$$

Where, t: elapsed time (sec), Xt*: Thickness of cover concrete (cm), W: constant value per time of chloride ion density penetrates into concrete (kg/m^3/cm^2/sec), Dc*: equivalent diffusion coefficient (cm^2/sec) Thickness of cover Xt* and equivalent diffusion coefficient

D*c assume to be a stochastic value. C0: Initial chloride ion density in concrete (kg/m^3). The chloride ion density at surface increases with the increasing of time. Dc*, W and C' can be obtained by the regression analysis of concrete core sampled in situ. Moreover, it is obvious that the diffusion coefficient decreases exponentially with the increasing of the time from existing study. In this study, the time depend model of equivalent diffusion coefficient Dc*(t) is described as shown in Equation (2).

$$D^*_C(t) = \left(\frac{t_{cr}}{t}\right)^m D_s \tag{2}$$

Where, tcr: reference year (= 5 elapsed year), D5*: Diffusion coefficient at 5 elapsed year, t: elapsed year, m: coefficient, m is chosen from existing study (=0.54) [7].

Corrosion Starts

The beginning time ts* of steel corrosion assumes to be the time that the chloride ion density C* (Xt*,t) close to the steel reaches the threshold chloride ion density Ccr*. Therefore, the beginning time of steel corrosion is described in Equation (3).

$$t^*_s = t \text{ when } C^*\left(X_t^*, t\right) \geq C^*_{cr} \tag{3}$$

The beginning time ts* of steel corrosion is described as the stochastic parameter. The threshold chloride ion density Ccr* is determined by the quality of concrete and environment conditions. Ccr* is described by parameter W/C* indicating the quality of concrete as shown in Figure 3. The relationship between W/C* and Ccr* is obtained as Equation (4) based on existing experiments. Mark ○ indicates the experimental results. Figure 4 shows the relationship between equivalent diffusion coefficient Dc and water-cement ratio W/C*. Since JSCE standard [8] shows the safety side as shown in Figure, the model is chosen as Equation (5) in this paper.

$$C_{cr}^* = 3.7 \times \left(1.0 - 9.87\left(W/C^* - 0.45\right)^2\right) \tag{4}$$

$$W/C^* = 0.5 \times \left(\frac{D_C^*}{1.0 \times 10^{-8}}\right)^{0.15} \tag{5}$$

Where, W/C*: water-cement ratio, Dc*: equivalent diffusion coefficient, Ccr*: threshold chloride ion density.

Therefore, Ccr* can be obtained using the combination of the relationship of water-cement ratio and equivalent diffusion coefficient.

Progressive Period

The progressive period tcr* is the process that the corrosion cracking can be occurred by the pressure due to the increasing of corrosion products with time. The regression equation of corrosion rate can be obtained by the regression analysis developed using the exposure experimental data. The parameters of regression equation are concrete temperature, chloride

ion density and quality of concrete. The regression equation of corrosion rate can be described as Equation (6) [9].

$$R(T,C,D_C) = C_D(D_C)R(T,C) \tag{6}$$

Where, R(T,C,Dc): Corrosion rate of reinforcement (mg/cm^2/year), CD(Dc): influence coefficient of quality of concrete,.

$$R(T,C) = 0.27R_0(T,C)^{1.38} \tag{7}$$

$$R_0(T,C) = R_0 \cdot C_T(T)C_C(C) \tag{8}$$

R0: reference corrosion rate (21.33mg/cm^2/year), CT(T): influence coefficient of concrete temperature, Cc(C): influence coefficient of chloride ion density at thickness of cover. C: chloride ion density close to reinforcement (kg/m^3),T: temperature in concrete. Equation (7) to (9) indicates the function of influence parameters for obtaining corrosion rate of reinforcement.

$$C_T(T) = \exp\{-2.593\times(1000/K)+8.695\} \tag{9}$$

$$C_C^*(C) = 1.93\sqrt{1-\frac{(C^*-12.0)^2}{(12.0-C_{cr}^*)^2}} \tag{10}$$

$$C_D^*(D_C) = 0.1129\left(D_C^* \cdot \frac{0.419}{t^{-0.54}}\right) \tag{11}$$

Where, K: Absolute temperature (=T+273.15), t: elapsed year at investigated year.

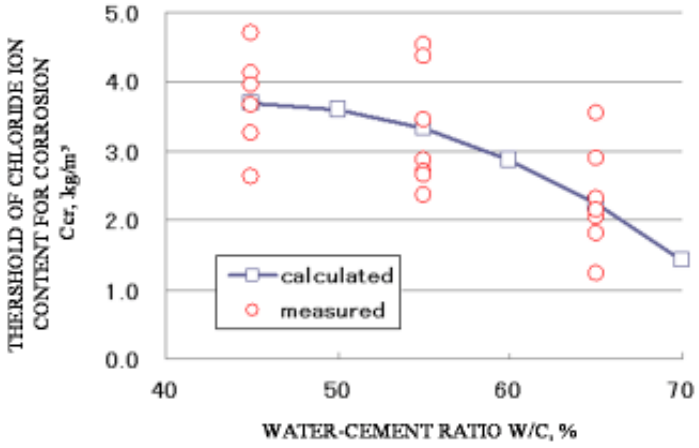

Figure 3 Threshold of chloride ion and water-cement ratio (○ indicates experimental data.)

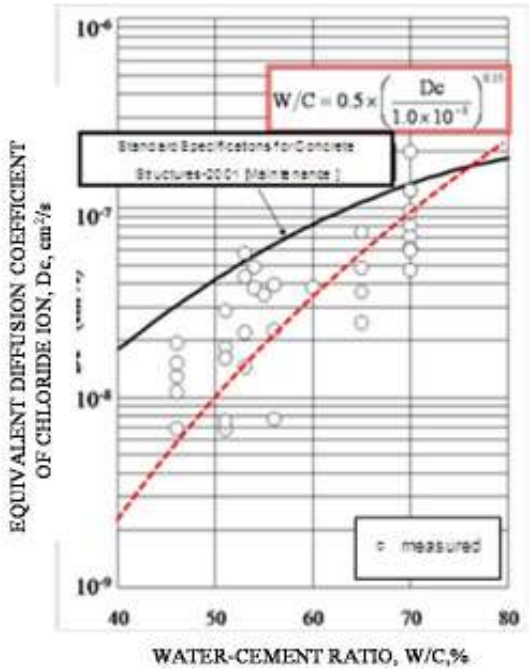

Figure 4 Equivalent diffusion coefficients and water-cement ratio(○ indicates experimental data.)

Occurrence of Cracking due to Corrosion Pressure

Cracking modes at the surface of concrete are changed by cover thickness, diameter of reinforcement and the spacing between reinforcements. To predict cracking modes is an important item in order to keep the maintenance of structures. The model to occur cracking when the corrosion pressure exceeds tension strength of concrete is developed in this paper. The conception of cracking mode shows in Figure 5. The cracks assumes to reach the three patterns such as the cracking along the reinforcement, the spalling of cover concrete and the horizontal cracking between reinforcements governing by thickness of cover and spacing between reinforcement. Moreover, the cracking such as the cracking along the reinforcement, horizontal cracking between reinforcements finally develops to the spalling of cover concrete. The boundary between the cracking along the reinforcement, the spalling of cover concrete and the horizontal cracking between reinforcements shows in Figure 5. The case with thin cover concrete and wide spacing between reinforcements induces the cracking mode of the spalling. The case with thick cover concrete and narrow spacing between reinforcements induces the cracking mode of horizontal cracking between reinforcements. Those cracking modes are described by the none dimensional parameters C/φ and C/L. C indicates thickness of cover concrete. Φ indicates the diameter of reinforcement and L indicates the spacing between reinforcements. Authors obtain those boundarys using the none dimensional parameters C/φ and C/L from existing exposure experiments.

Acceleration Period

After the occurrence of cracking, the parameter used in computations assumes to depend on the only corrosion rate and the corrosion rate of steel bar is more rapidly than the one of progressive period because the water and oxygen can easily penetrate into steel bar thought cracking. Figure 7 shows the relationship between the estimation value of corrosion rate at progressive period and the measurement value of corrosion rate after cracking, namely

accelerative period. Mark ○indicates the survey data of corrosion speed obtained in situ using non-destructive measurement method. According to Figure, the corrosion rate of steel bar at accelerative period can assume to be 3.7 times than the one at progressive period and described as shown in Equation (12) [9].

$$R'(T,C,D_C) = 3.9 \cdot R(T,C,D_C) \tag{12}$$

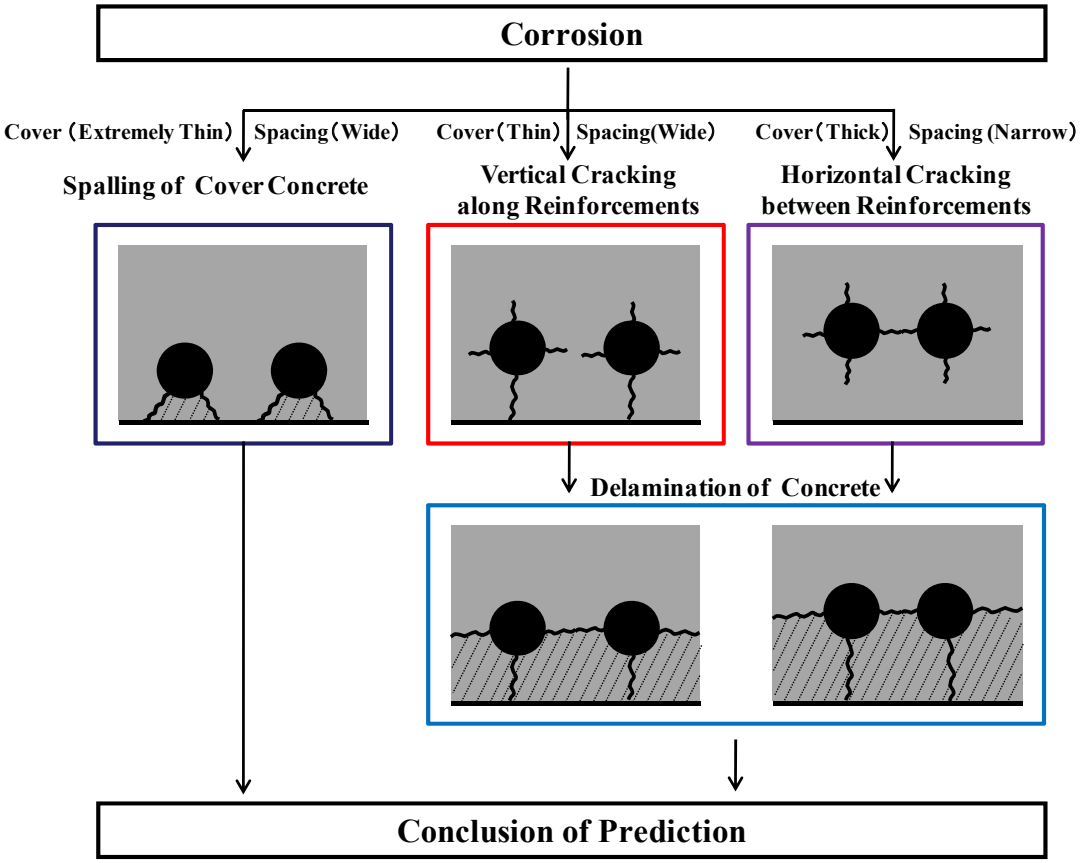

Figure 5 Progresses of cracking modes

STOCHASTIC APROACH

Corrosions of reinforcement in RC structure can't develop in same way because corrosion configuration can be described as macro-cell phenomenon. The spacing between reinforcements and the thickness of cover concrete can be varied at the place of structure, too. The diffusion coefficient influenced to the corrosion rate can be varied at the place of structure.

The parameters involved in the model are expected to vary extensively since the phenomenon takes place in the natural environment. Therefore, the model of deterioration due to chloride-induced damage based on stochastic approach is proposed in this paper. Two parameters such as Equivalent diffusion, cover thickness are chosen as the stochastic parameters.

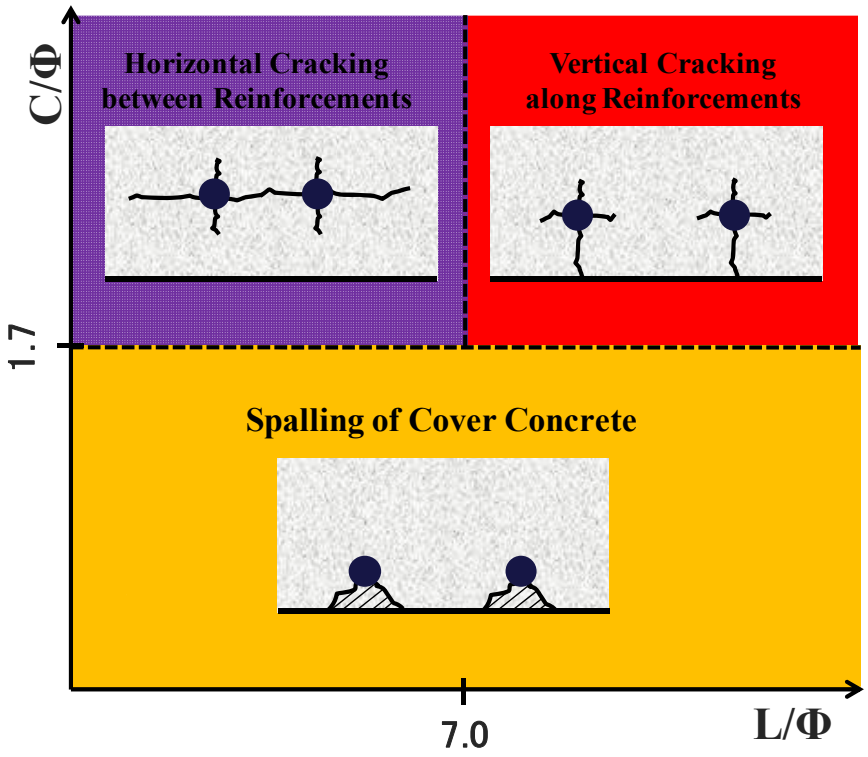

Figure 6 Boundaries of cracking modes

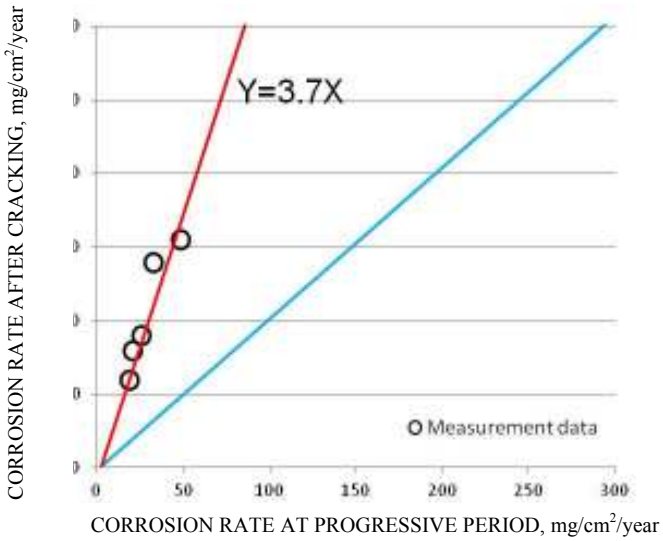

Figure 7 Comparison with measured and predicted values of corrosion rate [9]

DETERIORATION MODEL

Target Structure

Target structure is the concrete slab of flood gate located at sea side in South Japan as shown in Figure 9. Rate of cracking mode of slab surface obtained from visual survey is described in Figure 9. 35 years has passed since the structure is constructed. According to visual inspection in situ, the slab is deteriorated and spalling of cover concrete and cracking at the surface concrete of the upper slab occurs. The all of steel bars in slab are corroded. We can

easily see the spalling of cover concrete and rust stain at the surface of upper slab. A half of area of upper slab is deteriorated by chloride-induced damage from visual inspection as shown in Figure.

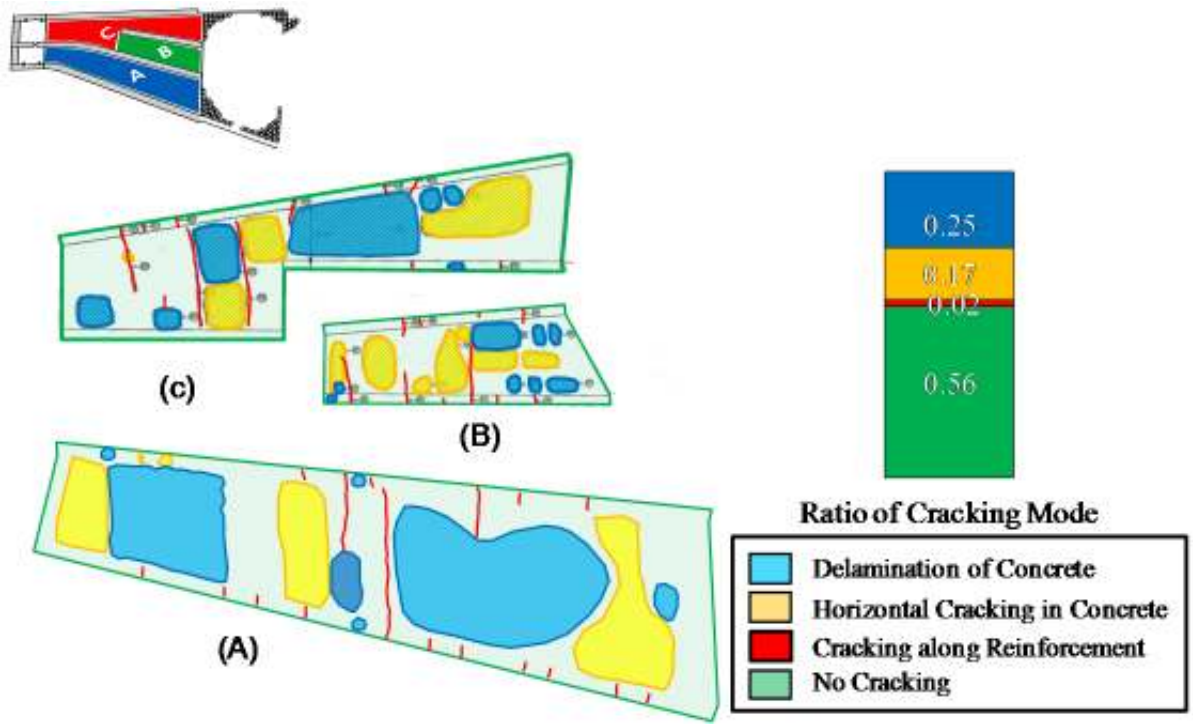

Figure 9 Deterioration of upper slab of target structure (Flood gate)

Computation on Deterioration Process

The numerical method proposed in this paper is carried out against the target slab of flood gate. Table 1 indicates the values used in computation in order to predict the deterioration of slab. Monte Carlo simulation with 3000 random numbers is used in computation.

Table 1 Data used in computation

PROPERTY	MEAN VALUES	S.D	DISTRIBUTION
Environment	Splash Zone	-	-
Service period	35 years	-	-
Spacing between reinforcement	150mm	10mm	Normal
Cover thickness	62mm	10mm	Normal
Conpressive strength	39.7N/mm²	-	-
Temperature of concrete	18.8°C	-	-
Chloride ion penetration at surface	0.31 wt%/cm²/sec		
Equivalent Diffusion Coefficient	1.63×10^{-8} cm²/sec	1.50×10^{-8} cm²/sec	Log Normal

The main bar and reinforcement bar are used D16. The spacing between reinforcements is obtained 150mm from investigation. Thickness of reinforcement bar is 62mm. Standard deviation of thickness of cover concrete is obtained 10mm by the investigating in situ. The equivalent diffusion coefficient is obtained from results of testing the concrete core sampled at site. The mean value with 1.63×10-8 cm^2/sec and the standard deviation with 1.50×10-8 cm2/sec are obtained from the survey data. The shape of distribution can be approximated as log-normal distribution.

The stochastic model of cover thickness or spacing between reinforcement Xt* is described as shown in Equation (13) by the sum of design thickness Xd and the error of thickness e* in situ against design.

$$X_t^* = X_d + e^* \tag{13}$$

Where, e* is the stochastic parameter with normal distribution and indicates the mean value with 0.0 cm and the standard deviation with 1.0 cm from the survey in situ. The error of spacing between reinforcements assumes to be a same manner as the error of cover concrete.

Results of Computation

The numerical method proposed in this paper is carried out against the target concrete slab. Figure 10 indicates the comparison with the results of computation and survey data of chloride ion density close to reinforcement. Mark ○ in Figure indicates the survey data. The survey data of 85% consists in the mean value ±standard deviation in computation. Both values are similar with considering the uncertainty of deterioration in nature. Cracking modes are compared with results in computation and in survey data respectively. Figure 11 indicates the relationship between the rate of each cracking mode in computation and elapsed year. Mark ○ indicates measured values from target structure in situ. The red line in Figure indicates cracking along reinforcement, the yellow indicates the floating of surface concrete and the blue indicates the spalling of cover concrete. Green indicates the sound part of slab. Those cracking modes in computation can be obtained to coincide with survey data considering uncertainty of actual environments.

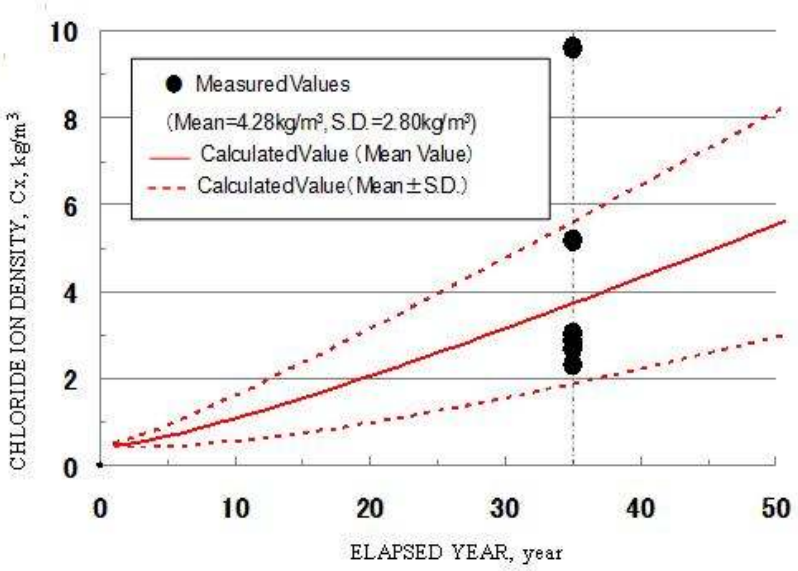

Figure 10 Chloride ion densities and elapsed year

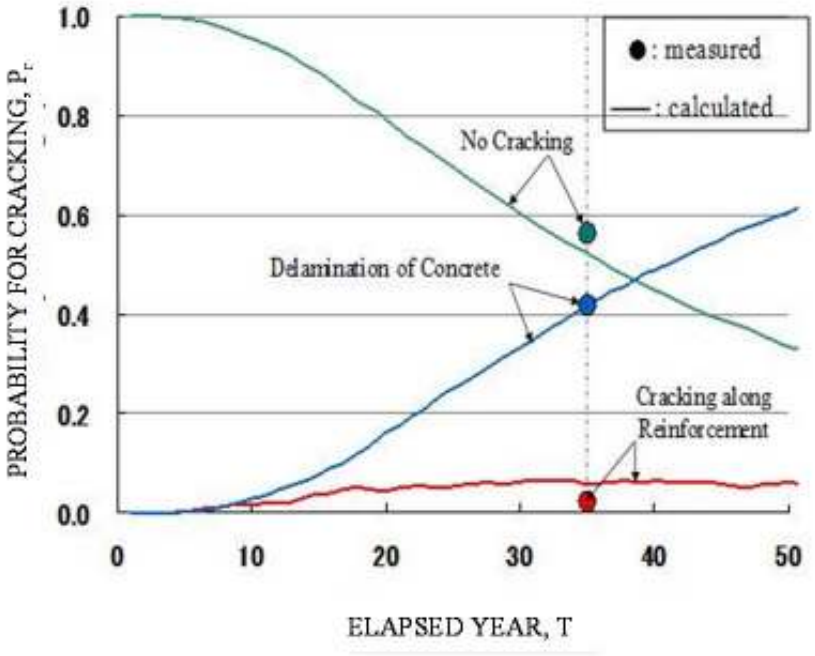

Figure 11 Cracking modes and elapsed year

CONCLUSIONS

The model of deterioration due to chloride-induced damage based on stochastic approach is proposed in this paper. Target structure is the slab of flood gate received chloride induced damage in situ. The results of computation are compared with the survey data using proposed model respectively.

The following is a summary of the findings:

A probabilistic model is developed to represent the deterioration of concrete structures using deterioration process model such as Incubation period, Developed period and Accelerative period. The distribution models of two stochastic parameters such as Equivalent diffusion coefficient Dc* and Error of cover thickness e* are obtained from existing studies.

The numerical method proposed in this paper is carried out against the target slab of flood gate has passed 35 years. The distributions of corrosion rate of steel bars obtained in survey and from prediction using proposed model are compared respectively. Both distributions can obtain to coincide with considering uncertainty of actual environments.

REFERENCES

1. KATAWAKI K., MORIYA S. AND MINOSAKU K.: Character and method of measurement of saline air coming from the sea, J. of Prestressed Concrete, Japan, Vol.27, No.1, Jan., Feb. 1985 (in Japanese).

2. WEST R. E. AND HIME, W. G.: Chloride profiles in salty concrete, Material Performance, July 1985.

3. SEKI H. Deterioration of reinforced concrete wharfs, Concrete International, Vol.3, No.3, March 1981.

4. BAZANT Z. P.: Physical model for steel corrosion in concrete sea structures -Theory-, J. of the Structural Div. Vol.105, No.ST6, June 1979.

5. BROWN R. D.: Design prediction of the life for reinforced concrete in marine and other chloride environments, Durability of Building, 1982, Elsevier Scientific Publishing Company.

6. BROWN R. D.: Design prediction of the life for reinforced concrete in marine and other chloride environments, Durability of Building, 1982, Elsevier Scientific Publishing Company.

7. Life-365 Service Life Prediction Model Computer Program for predicting the service life and Life-Cycle Costs of Reinforced Concrete exposed to Chlorides, 1December 2001.

8. JSCE Guidelines for Concrete No.4, STANDARD SPECIFICATIONS FOR CONCRETE STRUCTURES, -2001 "Maintenance".

9. MASARU YOKOTA eT. all: Proposal on the estimation method of corrosion speed of steel bar embedded in concrete based on exposure experiments. 6th Upgrade symposium on repairing and reinforcement，2006.10，pp.67-74 (in Japanese).

A Navy User's Guide for Quality Assurance for New Concrete Construction

D F Burke
US Navy, USA

The U.S. Navy has developed and implemented new design and quality assurance procedures including service life modeling of the concrete materials that improve the quality and durability of new marine concrete construction. The approach is delineated in the Uniform Facilities Guide Specification (UFGS) for Marine Concrete and is also referred to as the Navy's methodology. This approach allows Naval Facilities (NAVFAC) and others to specify a defined service life for concrete structures in combination with prescriptive criteria. The goal is to allow all parties involved in the design and construction process to have confidence that the completed structure will meet service life expectations. The cornerstone of this approach is a validated computer software program that can predict the time for chloride and other ions to contaminate the concrete to a degree that will result in initiation of corrosion and other chemical distress mechanisms when all other necessary conditions are met for a specific environmental condition. The use of the Navy methodology is intended to compliment the fundamental principles of good design and construction to accomplish durable concrete structures, and to supplement conventional quality assurance testing of materials. The purpose of this paper is to broaden exposure and to provide guidance on how to implement the methodology correctly and effectively for all users.

Douglas Burke, Subject Matter Expert for Concrete Materials for the U.S. Navy, Naval Facilities Engineering Service Center, Port Hueneme, CA. Mr. Burke has 38 years of experience with the U.S. Navy related to marine concrete structures, concrete durability technologies, service life modeling, and rehabilitation strategies of concrete structures. He has a MS in Test and Evaluation Engineering from California State University, Northridge

Keywords: Methodology, Modeling, Navy, Performance-based, STADIUM, Service life

INTRODUCTION AND GOALS

A goal of the Uniform Facilities Guide Specification for Marine Concrete is to delineate the use of quantifiable metrics to evaluate and predict the service life of specific concrete mixtures in a specific marine environment. Doing so will allow the Navy to move toward performance-based specifications to build concrete structures with a service life of 75 years or more. The development efforts to accomplish this goal have been motivated by the desire to avoid problems associated with premature concrete distress in future military construction by optimizing the material design and strengthening the quality assurance program. In addition it offers designers a process by which to use greater percentages of supplemental cementitious materials. For example, Class F fly ash can be used to replace 50% of the Portland cement, thus resulting in less expensive and more sustainable structures.

PROBLEM

In the design and construction of Navy piers, wharves, and bridges, there has been an implied expectation that the reinforced concrete structure will last a "long time." Without quantifiable metrics to evaluate the predicted service life of a structure it has been unrealistic to use performance-based specifications or be able to design for a specific service life. The conventional use of prescriptive concrete specifications and tasking the design-build team with Contractor Quality Control (CQC) responsibilities has failed to offer any direct quantitative information about the potential service life of a given structure exposed to the conditions of a specific environment. Nor can the conventional approach offer any assurances that the completed structure will be long-lived, even if the contractor meets the requirements set forth in the contract documents.

Although most marine structures do achieve satisfactory service life, a few have suffered from premature concrete deterioration and distress, resulting in loss of service and the need for costly repairs or replacements. One prominent example is the Ford Island Bridge in Pearl Harbor, Hawaii, which after three years suffered from severe loss of concrete cover due to seawater attack on some of the pre-stressed concrete piles. In an effort to reduce the risk of premature distress, the quality assurance portion of this approach is designed to identify construction mistakes, thus minimizing required corrective action and allowing potential issues to be corrected during construction.

“There must be recognition on the part of someone in authority that uniform concrete of good quality requires intelligent effort and faithfulness to details all along the line—proper materials, proper design, proper mixing and transporting, and special care in placing and protecting. It must be recognized that to obtain the desired results some qualified person must be made responsible for these details, and having been made responsible, must be entrusted with the necessary authority,” [1]. In U.S. Navy military construction, this responsibility has been assigned to the design-build contractor. The Navy’s Facilities Engineering and Acquisition Division (FEAD) or Resident Officer In Charge of Construction (ROICC) must rely on the building contractor to measure and monitor the quality of the construction. This arrangement of CQC is recognized as having inherent shortcomings. During the past two years it has been observed that users are unfamiliar with the Navy methodology requirements and have many questions as to why and how to implement it.

OVERVIEW

The U.S. Navy developed and implemented an approach in February 2010 related to measure the quality of concrete mixtures with respect to their potential to achieve structures with a defined service life. This approach is delineated in the latest Uniform Facilities Guide Specification for Marine Concrete 03 31 29. During preconstruction the design-bid-build contract team develops an optimized concrete mixture(s) that has the potential of meeting the prescribed service life—a process that includes laboratory tested and mathematically modeled uncracked concrete specimens to predict the time to initiate corrosion in the specific marine environment where the structure will be located. During construction, concrete cylinders are made from the delivery of the ready-mix or batched precast concrete to characterize the concrete's properties, to assure that it measures up to its designed potential.

The methodology is applicable to design-build and design-bid-build contracts. To date, it has been used for the design and construction of several Navy piers and wharfs valued at about one billion dollars. It has also been adopted for many public projects including the new locks currently under construction for the Panama Canal, many U.S. Embassies, and large highway bridge projects, collectively valued at several billion dollars. In the future, adding measurements of concrete cores extracted from the structure will enhance the ability of the owner to predict the remaining service life of the concrete structure.

PERFORMANCE-BASED SPECIFICATIONS

Development and implementation of performance-based specifications was first approved by the Office of the Secretary of Defense for implementation in the aviation business sector. NAVFAC ESC's interest in developing performance-based specifications is shared by other U.S. agencies including the Federal Highway Administration, National Ready-Mix Concrete Association, and the Precast Concrete Institute. The use of performance-based specifications provides a vehicle for innovation resulting in more durable concrete structures with extended service life and fewer repairs. Use of performance specifications mandates that a clear definition of performance and how to measure and predict service life be agreed upon by all parties.

APPROACH

The strategy to accomplish NAVFAC ESC's goal is to shift construction documents toward performance-based specifications while retaining some of the prescriptive criteria. This will allow the U.S. Navy to specify the desired service life of new structures. The use of the Navy methodology is intended to enhance confidence prior to taking ownership from the builder, that the completed structure is likely to meet the defined service life.. The use of performance-based specifications is challenging, as there must be a reliable evaluative technique to predict long-term performance from candidate mixtures prior to construction and similar techniques that will validate the concrete construction. The methods used to accomplish these goals must be agreeable to all parties prior to signing bid documents. The methodology is structured as a three-part process.

BACKGROUND

NAVFAC ESC initiated an effort in 2002 to partner with private industry by awarding two Small Business Innovative Research (SBIR) contracts to develop tools for predictive modeling of marine concrete. One of those companies, SIMCO Technologies Inc., successfully developed and demonstrated a software program that predicted the movement of ions in and out of marine concrete structures [2, 3, 4]. The resulting numerical modeling software program is called STADIUM® (Software for Transport and Degradation in Unsaturated Materials). SIMCO successfully transitioned the development of STADIUM® to an international consortium of public and private partners to further advance the software of service life modeling. Under the SBIR agreement, SIMCO has licensed the use of the STADIUM® for a fee.

NAVFAC ESC maintains a Cooperative Research and Development Agreement with SIMCO Technologies Inc., for the ongoing development and technology transfer of STADIUM®. The most recent version of STADIUM® is Version 2.997. More information regarding the STADIUM® software can be found at www.stadium-software.com.

FUNDAMENTALS OF GOOD DESIGN

The Navy's methodology is intended to supplement basics principles of good design, not to replace them. Achieving durable concrete structures depends on many factors, some of which include: good design, properly specified concrete cover over the steel reinforcement, use of quality materials, mitigation of alkali silica reaction, limits on drying shrinkage, good workmanship and an adequate quality assurance program. An adequately designed reinforced concrete structure from well constituted and properly consolidated and cured concrete will remain essentially durable as long as the micro-cracks present in the interior do not form an interconnected network of pathways to surface cracks. Adherence to these basic principles is paramount to achieving quality concrete. The use of the Navy methodology is intended to be a tool that compliments the fundamental principles of good design and construction to accomplish durable concrete structures with a defined service life.

NAVFAC ESC POSITION ON SERVICE LIFE MODELING OF CONCRETE STRUCTURES

Accurate concrete service life modeling is a tool that, when used in combination with other tools and good engineering judgment, enhances the U.S. Navy's ability to build durable concrete structures and to have increased confidence in the remaining service life of existing concrete structures. It is a critical component to the methodology developed by NAVFAC ESC for defining the expected service life of existing and new concrete structures. Technology transfer by the Navy of this approach to the concrete industry is considered a top priority.

Multi-mechanistic service life modeling is applicable for all concrete construction including plain reinforced concrete and pre-stressed or post-tensioned concrete. When applied to plain reinforced concrete structures, current modeling results are only valid when cracks with widths greater than 0.5 millimeter, (a credit card is typically .5 to .75 mm thick) are repaired or sealed. The model accounts for the presence of concrete micro-cracking through the

measured ion transport properties of concrete samples. Modeling results are valid for all pre-stressed or post-tensioned elements, or concrete elements in compression, as macro-cracks will be closed.

Multi-mechanistic service life modeling is required for U.S. military construction. Currently, the only multi-mechanistic software available and thus deemed acceptable for use on Navy projects is STADIUM®. This software is licensed to various engineering firms in the U.S. and Canada. Using environmental exposure conditions specific to a structure's location, which are included in the STADIUM® database and moisture and ion transport properties obtained from concrete samples, the modeling process tracks the movement of several ionic species within the concrete (including the ingress of contaminants) and predicts the chemical deterioration of concrete and onset of steel reinforcement corrosion. This multi-mechanistic model has been validated by NAVFAC ESC and others to more accurately predict performance of concrete compared to software dependent on Fick's second law, which includes most other currently available. Other service life modeling software with capabilities that claim to be equivalent to STADIUM® may be submitted to NAVFAC ESC for consideration.

BENEFITS AND EXPECTATIONS

The average military construction expenditure for US Navy projects that could benefit from the methodology is $671 million per year for 2012 through 2015. The benefit to each individual project will vary. A conservative estimate of cost avoidance as a result of implementing the methodology for U.S. Navy construction is $167 million annually. This estimate is based on the expectations that the concrete structure will have a longer life and require fewer repairs and a reduced carbon footprint. Use of this approach by the other military services will have similar benefits.

A service life of 75 years for conventional single-deck pile supported piers, wharves and bridges can be readily accomplished using this approach. In the Uniform Facilities Guide Specification, service life is defined as the number of years before major restoration, with minimal maintenance. Major restoration is defined as repairs requiring jack hammering or other destructive means of concrete repair preparation. Recently, NAVFAC ESC completed design documents for a floating double-deck pier with a service life of 100 years [5, 6].

Development and application of the methodology is detailed in a step-by-step procedure for Navy floating piers with a service life goal of 100 years [7]. The Uniform Facilities Guide Specification for Marine Concrete, Section 03 31 29, dated February 2010, is available on the web from Whole Building Design Guide (WBDG) at the following location:

http://www.wbdg.org/ccb/DOD/UFGS/UFGS%2003%2031%2029.pdf. It is expected that specifications will be revised and improved based on lessons learned and input from users.

SERVICE LIFE MODELING

Training and licenses are provided by SIMCO Technologies, Inc. Currently there are three certified STADIUM® labs, while three other labs are currently in the process of being certified. About a dozen engineering firms are licensed to use the service life predicting

software. One can view the current list of licensed labs and engineering companies at the following websites:

http://www.stadium-software.com/certified-laboratories
http://www.stadium-software.com/authorized-companies

The software predicts the movement of ions in and out of portland cement-based concrete. Contrary to the first generation of chloride penetration models, such as LIFE-365™, that are based on Fick's second law of diffusion to predict chloride ion movement in saturated concrete using simplifying assumptions for temperature, water movement, and other contributing factors, STADIUM® is based on ionic transport modeling and numerical solutions. The STADIUM® model accounts for the complex interactions between the contaminants penetrating the porous network of concrete and the hydrated phases of the cement paste and allows engineers to quantify the effects of various chemical compositions provided by specific types and blends of cements, fly ash, silica fume, blast furnace slag, when used with specific aggregates.

The model accounts for temperature and moisture variations and how these environmental exposure conditions influence the rate of contaminant ingress. It is thus possible to provide STADIUM® with time-dependent environmental conditions and to simulate the effect of wetting and drying cycles on the chloride penetration rate. The description of the environmental exposures provides a realistic estimate of the extent of chloride ingress in a structure during its service life.

Mathematical modeling does not necessarily allow exact quantitative prediction of service life, although they may allow comparison of alternative approximate solutions" [8]. Service life modeling using the multi-mechanistic STADIUM® model is judged to be reliable, although one must always use common sense and engineering judgment when analyzing inputs and interpreting the results.

THREE-PART METHODOLOGY

The methodology is structured as a three-part process.

Part 1: Theoretical Simulations of Candidate Mixtures. Review the materials, mix design, exposure conditions, and cover expectations to assess the likely performance of the mix. Allow one week to do this.

Part 2: Mixture Durability Evaluation. The concrete producer makes test cylinders from candidate concrete mixes. Lab tests for porosity, migration and drying are performed at 28 days; at 90 days, migration and porosity tests are repeated. This process takes a minimum of 118 days.

The mix design certification process is led by the design-build team working with the concrete supplier, the certified lab that generates the modeling inputs, and the engineering firm that does the service life modeling. The performance interaction between the concrete, reinforcing steel, and potential surface treatments are evaluated simultaneously in the modeling. A durability report, with the test results, is submitted to the client for review and approval.

This approach allows teams to be innovative in creating an economical system that will also meet the service life criteria. Once the mixture is approved, concrete production can begin.

Part 3: Quality Assurance During Production. During construction, the same three laboratory tests used for certification of the mixture are required to validate quality [9]. Each time the concrete is sampled; six cylinders are prepared for testing. The tests are performed after 28 days of curing and take 14 more days to complete. Test results verify if the concrete delivered to the site is being produced uniformly and within the allowable criteria.

The Engineer of Record must specify the frequency of testing during the construction phase. Sufficient testing must be done to maintain confidence that the concrete, as delivered and placed, remains consistent and within specifications.

Test results during concrete production that fall short of the acceptance criteria dictated by service life modeling alert the Contractor that something in the production and placement process has drifted out of calibration or that an error has been made. The goal is to track down the problem and correct it as quickly as possible. Unless the concrete producer makes a large error in batching or in placing, the chance that sizable sections of hardened concrete need to be removed is remote. Removal and replacement is a last resort.

For those areas adversely affected by substandard concrete, new STADIUM® simulations can be helpful to evaluate the effectiveness of different remediation strategies. Mitigation efforts to restore the service life of these areas shall be approved by the Contracting Officer prior to proceeding.

As an example, during the Kilo Wharf Extension in Guam, it was found that the 28-day old concrete samples from the caisson (fabricated off-site in Japan) were not in compliance. The contractor was asked to submit a second set of samples that were 56 days old. These samples, with extended curing, were found to be satisfactory and were judged to be acceptable. In another case, unexpected results were found to be the result of the temperature of the steam curing drifting out of calibration—a problem that was easily fixed. In neither of these situations was it necessary to replace or repair any of the concrete and the project continued on schedule with confidence.

APPLICATIONS OF THE METHODOLOGY

The methodology impacts the design-build process via several applications, as summarized in Table 1.

STADIUM® LAB

Testing of concrete cylinders must be done in a certified STADIUM® laboratory to determine specific characteristics that are used for service life modeling. These tests include:

a. ASTM C642 Standard Test Method for Density, Absorption, and Voids in Hardened Concrete.

b. STADIUM® Ionic Diffusion Coefficient (IDC) Migration Test, a modified version of ASTM C1202 Standard Test Method for Electrical Indication of Concrete's Ability to Resist Chloride Ion Penetration. The analysis of the migration test results provides the intrinsic diffusion coefficient of each ionic species. The test consists of accelerating the ions under an external potential and measures the electrical current across the sample over a 14-day period. The measured currents are analyzed to provide the diffusion coefficients. See Figure 1.

c. STADIUM® Moisture Transport Coefficient (MTC) Drying Test, a modified version of ASTM C1585 Standard Test Method for Measurement of Rate of Absorption of Water by Hydraulic-Cement Concretes. See Figure 2.

Once the testing is done, the collected raw data from ionic diffusion and moisture transport coefficient tests are analyzed using STADIUM® LAB, these values are used as input for the service life simulations.

Table 1 List of applications for concrete durability modelling

APPLICATION	TYPE OF TOOL	REMARKS
Planning	Strategic Tool	Prequalifying major construction materials/methods
Design	Concrete Design Tool	Aligning predicted service life options / owner economic expectations
Bidding	Estimation Tool	Selection or prequalifying potential durability systems
Design/Build	Optimizing Tool	Selection or prequalifying testing/analysis
Contract Selection	Selection / Evaluation Tool	Review and evaluate bid proposals
Final Material Selection	Optimizing Tool	Selection or prequalifying testing/analysis
Construction Quality Assurance	Quality Assurance Tool	Field quality assurance can be monitored with periodic materials testing and/or model simulations.
Maintenance Budgets	Operational Tool	Periodic review of concrete durability condition will provide insight to the best maintenance programs to match financial expectations
Rehabilitation	Restoration Tool	The current condition of a concrete structure can be evaluated and the best repair scheme applied to address degradation root causes and meet financial requirements and budgeting.

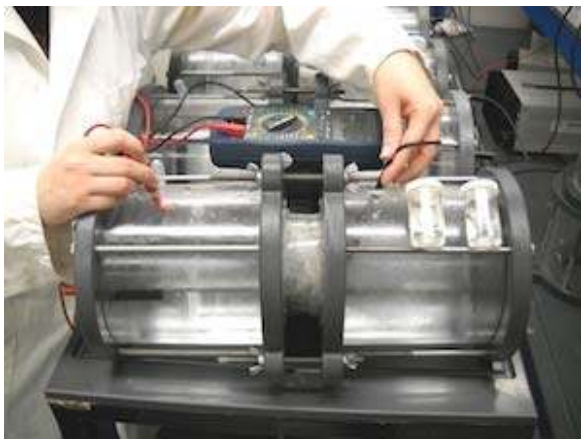

Figure 1 Ionic Diffusion Coefficient (IDC) Migration Test. *Photo by SIMCO*

Figure 2 Moisture Transport Coefficient Drying Test. *Photo by Tourney Consulting Group*

OTHER CONSIDERATIONS

Service life modeling predicts the time it takes chloride ions to reach the depth of the steel reinforcing at a level of contamination of 500 ppm for an uncracked section of concrete, as well as other deterioration mechanisms. Eventually, chlorides will reach the steel reinforcement; however, the amount of time it then takes for the steel to corrode (and cause cracking and spalling) is unknown. Generally, the time for visible damage to occur will be longer in cold climates versus sub-tropical sites. General guidance is to require that the candidate concrete mixtures resist chloride ion contamination to the level of 500 ppm at 60 years, and then the designer assumes 15 additional years before damage occurs, thus achieving a design that has the potential to deliver a 75-year service life.

Plain steel rebar and pre-stressing strands with specified concrete cover of 75 mm (3.0 inches) shall normally be specified according to applicable codes. Predictive modeling can confirm that the candidate mixture, type of steel and concrete cover will yield the required service life for the particular structural element under consideration. Within the STADIUM® program, users may select from three exposure options (submerged zone, tidal zone, and marine atmospheric). The results of the software runs will provide the design team with the predicted service life for each unique configuration modeled.

For the purpose of predicting the service life of the concrete, the design shall meet the owner's design life without relying on a barrier coating to the steel rebar or passive cathodic protection for additional life extension. The use of galvanized rebar and epoxy-coated rebar are entirely acceptable, but it is difficult justify a specific life extension from either without conclusive research data.

The value of the service life computer model to accurately predict the performance-life of concrete structure is, in part, a function of the quality of the input data. Specific input data regarding the environment is one important component. The software is preloaded with typical values for seawater composition, air temperature, water temperature, and humidity for

general Navy locations such as Bangor, Washington; Norfolk, Virginia; and Guam. However, it is recommended that local data regarding the chemical composition of the seawater and temperature for the site be measured, as these parameters can have an effect on the calculated rate of deterioration of the concrete and thus, the predicted service life.

The accuracy of the results are enhanced when the design team can sample, during the design phase, aged concrete from an existing structure in the vicinity of the proposed construction site. Concrete core samples from an aged structure provide data about long-term ingress of chemical species, as well as how the cement paste and local aggregates respond to the specific marine conditions.

STADIUM® does not predict some concrete properties and degradation mechanisms such as alkali silica reaction and time to cracking. These issues are addressed in prescriptive language in the Uniform Facilities Guide Specification.

It is essential that the prescriptive tests for shrinkage be accomplished per ASTM C157 as modified by ACI 364 3R. The maximum allowable concrete drying shrinkage for marine concrete in the U.S. Navy is 0.05%. A concrete mixture that meets the service life requirements but fails the shrinkage tests is possible. Constructing a reinforced concrete structure with excessive crack widths will allow for the rapid ingress of seawater and oxygen which shorten the service-life. Although mixtures containing condensed silica fume offer benefits of high early strength, greater ultimate strength, and greater impermeability, they are also more prone to cracking. Before the owner accepts the completed structure, all cracks transverse to the steel rebar in excess of 0.5 millimeters (0.02 inches) should be sealed.

The use of Class F fly ash and blast furnace slag typically show positive improvements to reduce permeability. NAVFAC ESC encourages its use as a partial replacement to ordinary portland cement with fly ash replacing up to 50% of portland cement, which is called high-volume fly ash concrete. [10].

SUMMARY OF NAVY PROJECTS

The following projects have used, or are currently using, this methodology:

Modular Hybrid Pier Test Structure, San Diego, CA

Kilo Wharf, Guam

Pier 31, Groton, CT

Pier 5, Norfolk, VA

Fuel Pier D, Craney Island, Norfolk, VA

Wharves Uniform and Tango, Guam

Explosive Handling Wharf 2, Bangor, WA

Pier 12, Naval Station, San Diego, CA

The methodology and tools used for new construction have also been used to predict the remaining service life of numerous existing Navy structures.

SUMMARY

Various aspects of the U.S. Navy's methodology for quality assurance of new reinforced concrete construction are presented here to broaden exposure and provide guidance on how to use the methodology correctly and effectively. The development of this unique approach has been motivated by the desire to avoid problems associated with premature concrete distress by optimizing the material design and performing specific laboratory tests as part of the quality assurance program. When used with good engineering judgment this methodology is a tool that can reduce the number of future structures that suffer from premature distress. The methodology is currently a part of the design-bid-build documents for Pier 12 Naval Station in San Diego, Fuel Pier D in Norfolk, VA, and four other Navy piers currently under construction. The February 2010 revision of the Uniform Facilities Guide Specification for Marine Concrete was a significant step to implement, in general construction, a scientific methodology that quantifies the service life of new U.S. military construction. This paper is offered to help owners and users to better understand how to use the Navy's methodology.

REFERENCES

1. McMIILLIAN, FRANKLIN R., member of the Concrete Research Board for Hoover Dam, Basic Principles of Concrete Making, BUREC Concrete Manual, 7th edition, 1929, page vii.

2. BURKE, D.F. and MARCHAND J., "Predicting the Microstructual Degradation of Concrete in Marine Environment," 6th Canmet/ACI International Conference on Durability of Concrete; Thessaloniki, Greece; 1-7 June 2003.

3. MARCHAND J., SAMSON E., BURKE D., TOURNEY P., THAULOW N., SAHU S., Predicting the microstructural degradation of concrete in marine environment, ACI Special Publication SP-212, p.1127-1153, 2003.

4. MALTAIS Y., MARCHARD J., OUELLET E., SAMSON E., TOURNEY P., Service life prediction of high performance concrete mixture subjected to chloride penetration, Proceedings of the Int. Conf. on Durability of HPC and Final Workshop of Conlife (Essen, Germany), M.J. Setzer & S. Palecki eds., AEDIFICATIO Publishers (Freiburg, Germany), p. 19-36, 2004.

5. ZUECK, R.F. and WERNLI, M; "Development and Qualification of Floating Pier for the U.S. Navy Fleet," Ports 2010 Conference; Jacksonville, FL, April 2010.

6. BERGER/ABAM, Preliminary Design Floating Double Deck Pier (FDDP), Vol. 1-3, October 2010.

7. BURKE, D.F., A Methodology to Enhance Quality Assurance for new Concrete Construction, CONSEC10, Concrete under Severe Conditions – Castro-Borges et al (eds) 2010 Taylor & Francis Group, London, ISBN 978-0-415-59316-8 pages 1623-1630.

8. VAYSBURD, A.M, and EMMONS, P.H., Concrete Repair as an Engineering Task: "Approximate" Solution to an Exact Problem, Proceedings of the Third International Conference ICCRRR-2012, Cape Town, South Africa, In publication.

9. SAMSON E., MARCHAND J., HENOCQ P., BEAUSEJOUR P., Recent advances in the determination of ionic diffusion coefficients using migration test results, Int. RILEM Symp. on Concrete Modeling – CONMOD08, 26-28 May 2008 (Delft, The Netherlands), 65-78.

10. BURKE, D.F., FOSTER J.C., "Demonstration of High Volume Fly Ash Concrete," SSR-3648-SHR, Naval Facilities Engineering Service Center, Port Hueneme, CA, March 2011.

Effect of Silica Fume in Sand Concrete for Repair Purposes

K Gadri[1], A Guettala[2], L Zeghichi[1]
1 – M'sila University, Algeria
2 – Biskra University, Algeria

The prosperity of a country in the field of construction depends on the use of local resources such as sand in southern Algeria. Sand concretes are a part of new construction materials that allow to value natural resources on sand. As its name suggests, this mixture is composed of sand as a majority element, instead of large calibre aggregates. Sand concretes therefore have the same cement contents than traditional concretes, the compactness is achieved by adding an additional thin, generally limestone filler. Repairing a concrete element usually involves two very different materials. The establishment of a green concrete supported on concrete oldest causes different types of problems related to compatibility deformational the two materials in contact. The non cracked character of sand concrete and its low module of elasticity, justified our choice to use it as a repairing material.

In this paper we present a formulation of sand concrete based on optimizing the compactness of the granular skeleton, 3 sets of concrete were prepared with 5 various mixtures to each series. Starting from a fixed choice of a Portland cement content type artificial (CPJ-CEMII/A), is varied in the amounts of sand and limestone filler type, the dosage of admixture for second series, in the end the Water/Cement in the third round. After an optimal choice of components, we introduce is the addition of silica fume in two strengths, replacing an amount of limestone filler. To study the adaptability of this material, a tensile and compressive test with measures of shrinkage were made. We were able to register a significant improvement of the mechanical characteristics so the decrease of shrinkage. An application of repair on degraded test tubes, allowed to notice a good capacity of adaptation deformational of the sand concrete with silica fume in the subtract in ordinary concrete.

K Gadri is an assistant professor in the Department of Civil Engineering of M'sila University- Algeria. She specializes in construction materials and has carried out research on the durability of repair concrete.

A Guettala is a professor in the Department of Civil Engineering and director of Research Laboratory, Biskra University- Algeria. He specializes in concrete properties and has carried out research on the durability of construction materials.

L Zeghichi is a senior lecturer in the Department of Civil Engineering of M'sila University - Algeria. She specializes in construction materials and has carried out research on the binder and cement.

Keywords: Deformational compatibility, Drying shrinkage, Sand concrete, Silica fume, Thin concrete repair

INTRODUCTION

We know that a number of reinforced concrete structures require maintenance, repair or partial reconstructions, because of the different damage reported, where the nature and origin of the defects are multiple. Two types of repairs can be carried out: a partial reconstruction or repair thin is less than 100 mm thick [1].

Repair of a concrete element usually involves two very different materials. The establishment of a green concrete on a concrete substrate oldest causes different types of problems, both physical and chemical and mechanical, related to the compatibility in a broad sense of the two materials in contact [2]. Deformational compatibility is never completely achieved, particularly with regard to volume changes; the adaptability of the material is an important parameter for the durability of the repair.

Several studies (Saucier et al, Bissonnette, Laurence) [1, 2, 3, 4] show that the drying shrinkage has an effect greatly harmful the durability of thin repairs. The drying shrinkage results in a strain gradient from the surface to the interface between two materials, which led to cracking. To avoid the creation of too much stress in the layer of repair, and so minimize or even avoid shrinkage cracking small, it is necessary that the repair material and the media are compatible in terms of deformation [3, 4].

Because of none cracked character of sand concretes, which is justified by the absence of large aggregates, low modulus of elasticity, also for their uniformity of drying, their fine porosimetry and homogeneity of the material [5, 6]. Sand concretes are able to replace the conventional concretes in certain structures, along with the conclusion that the use of fillers is essential (for improvement compactness and consequently strength, enhancing workability, deriving saving on cement in comparison with mortars [6, 7]). By definition, a sand concrete either does not comprise any gravel at all or only contains a small enough proportion such that the mass ratio (sand/gravel) remains higher than 1, If the mix were to contain gravel, the material would be called “a loaded sand concrete” [7].All this led us to choose what material to study, to be used to thin the repair of concrete structures damaged.

The formulation of the repair material remains one of the key parameters governing the durability of repair. Research material developing the best adhesion to the substrate and have compatibility deformational was our objective to study. For a repair material denser with porosity very fine, more waterproof, so most lasting; we have introduced silica smoke to sand concrete formulation to observe its effect on this later one.

MATERIALS USED

Cement

The used cement is a Portland cement (type II) of class 45 whose denomination is “CPJ-CEM II/A’’. Table 1 shows the mineralogical composition and physical characteristics of this cement.

Table 1 Physical and mineralogical composition of cement

PHYSICAL CHARACTERISTICS		MINERALOGICAL COMPOSITION	
Absolute density, g /cm^3	3,15	Mineral elements, %	
Apparent density, g /cm^3	1,09	C_3S	58,3
Blaine area surface, cm^2/g	3371	C_2S	14,6
Shrinkage at 28 days, µm/m	681	C_3A	8,7
Compressive strength at 28 days, MPa	47	C_4AF	11,26

Sand

A crushed sand used for this study, it's from the south area of the town of Biskra (Algeria). This crushed sand has a well-graded structure between 0 and 5 mm, with an absolute density of 2.5g/cm^3 and our sand is considered clean with sand equivalent value by sight SE = 70

Admixture

An Algerian superplasticizer of "MEDAFLOW 30" type was used, it is brown sulphuric Polynapthalene solution with a dry extract of 30%, absolute density of 1.07 and a PH of 6.5.

Filler

Among the several types of filler used, it was confirmed that the limestone fillers are well adapted to the sand concretes (due to their reactivity with cements) and yield the best mechanical performance [6]. The fillers used in this work have been obtained by sifting (with a sieve opening of 80 mm). This is crushed limestone, available in most careers in Algeria. Its specific density is 2.6g/cm^3 and specific surface area is 2450 cm^2/g.

Silica fume

It is based on micro-silica from the company "Granitex" as a gray powder. Obtained with a specific surface area 20470 cm^2/g and a density of 1.87g/cm^3.

SAND CONCRETES FORMULATION

In our experimental study we have gone through two steps to prepare our concrete repair. For the first step: make sand concretes with a base composition. This formulation is based on the experimental method [6, 8, 9], from a choice of a cement content, a mix of sand and a specified W/C ratio constant. Taking this formulation as Reference, Table 2 shows the composition and characteristics of sand concrete reference.

To improve the mechanical characteristics and for a concrete more compact and less porous, 03 sets of concrete were prepared with 05 various mixtures to each series. Starting with the basic composition, in the first series we have substituted and replaced quantities of sand by the limestone filler while correcting expenditure sand and filler in order to keep the cement sets and the same ratio W/C [6, 8, 9, 10]. According G.Chanvillard [13], we can vary the ratio (Filler / cement) to act on the resistance without major effect on workability. Figure 1 shows that the test of compressive strength at the age of 28 days, we could achieve optimization of compactness for our sand concrete by a dosage of 180Kg/m^3. For this series, our choice is that of composition (BS2). In the second series we keep the choice (BS2), the admixture is introduced in this composition with different dosages (the percentage of the superplasticizer is calculated, in mass, compared to the cement mass), sand and limestone are fixed. After a compressive strengths test, control of workability, we could select the compactness composition of sand concrete for the third series (BS-SP4). At the end, for third series we vary the ratio W/C of concrete selected in the second series, figure 2 shows by what ratio W/C we can have a plastic concrete witch justifies our choice of W/C in the third series.

Table 2 Composition and characteristics of sand concrete reference

COMPONENTS	QUANTITIES	COMPRESSIVE STRENGTH, MPa	TENSILE STRENGTH, MPa
Sand, kg/m^3	1660		
Cement, kg/m^3	350	22	3,7
Water, l/m^3	262,5		

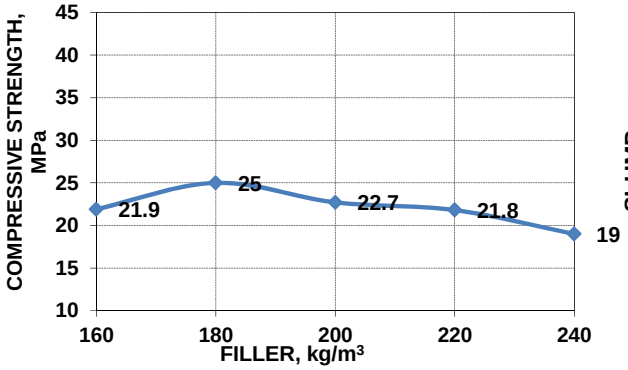

Figure 1 Effect of addition of limestone filler

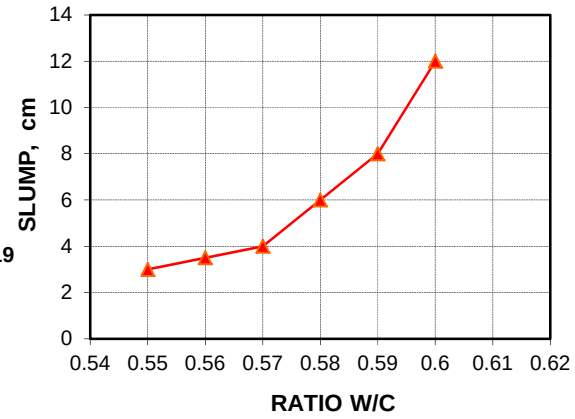

Figure 2 Effect of W/C on the workability on the compactness of sand concrete

Table 3 shows the mix of sand concrete made, and the optimal choice of composition for each series. After a series of formulation of sand concrete and a compressive strengths test (NFP18-406), tensile test (EN 196-1), a control of workability according to standard (NFP 15-433) with Abram's cone, we could select from the third series the optimal composition (SB-SPE2) and the

most successful which will be taken as a composition of reference of sand concrete to be intended for repair for the second stage, Table 4 shows the characteristics of concrete sand control BS –SPE2.

Table 3 Composition of the three series of sand concrete (optimization of formulation)

DESCRIPTION OF SAND CONCRETE	CEMENT, kg/m^3	SAND, kg/m^3	LIME-STONE FILLER, kg/m^3	W/C	SUPER-PLASTICIZER, %	SELECTION
SERIES 1						
BS1	350	1500	160	0,75	/	_
BS2	350	1480	180	0,75	/	+
BS3	350	1460	200	0,75	/	_
BS4	350	1440	220	0,75	/	_
BS5	350	1420	240	0,75	/	_
SERIES 2						
BS -SP1	350	1480	180	0,75	0,5	_
BS-SP2	350	1480	180	0,75	1	_
BS-SP3	350	1480	180	0,75	1,5	_
BS-SP4	350	1480	180	0,75	2	+
BS-SP5	350	1480	180	0,75	2,5	_
SERIES 3						
BS –SPE1	350	1480	180	0.60	2	_
BS –SPE2	350	1480	180	0.59	2	+
BS –SPE3	350	1480	180	0.58	2	_
BS –SPE4	350	1480	180	0.57	2	_

Table 4 Characteristics of concrete sand control BS –SPE2

CONE SLUMP, cm	COMPRESSIVE STRENGTH, MPa	TENSILE STRENGTH, MPa
8	35	6.95

ADDITION OF SILICA FUME

By its surface area and high fineness, silica fume provides denser concrete with a very fine porosity, more waterproof and thus more sustainable. For this purpose, and to improve the performance of our concrete sand (BS-SPE2), it was thought to introduce silica fume as an addition, or it acts as filler. So we substitute an amount of limestone filler as a percentage of silica fume, inserted between two values (5 and 8) %, Table 5 shows the composition of sand concretes with silica fume.

Table 5 Composition of sand concrete with silica fume for the repair

DESCRIPTION OF SAND CONCRETE	CEMENT kg/m	SAND kg/m^3	LIMESTONE FILLER kg/m^3	SILICA FUME kg/m^3	SILICA FUME %	W/C	SUPERPLASTICIZER, %
BS-FS1	350	1480	152	28	8	0.59	2
BS-FS2	350	1480	162.5	17,5	5	0.59	2

Effect Silica Fumes on the Mechanical Strength

Figure 3 shows that the compressive strength increases in function of time, for concrete sand with 5% silica fume (17.5 Kg / m^3) from 49 MPa at the age of 28 days up to 55 MPa at 90 days. However, in percentage terms, the compressive strength evolution is 40% compared to concrete control (BS-SP2).

Figure 4 shows that there is a 15% increase in the two concretes with SF, compared with (BS-SPE2). But the best resistance is given by the BS-FS2 with a value of 8.2 MPa at a rate of 5% of SF. We can say that with a dosage of 8% are obtained less impressive.

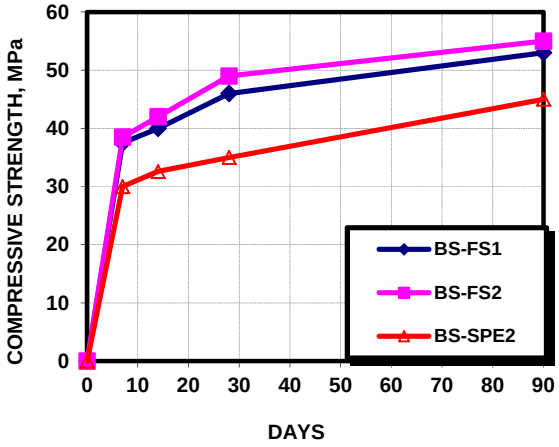

Figure 3 Effect of silica fume on the compressive strength

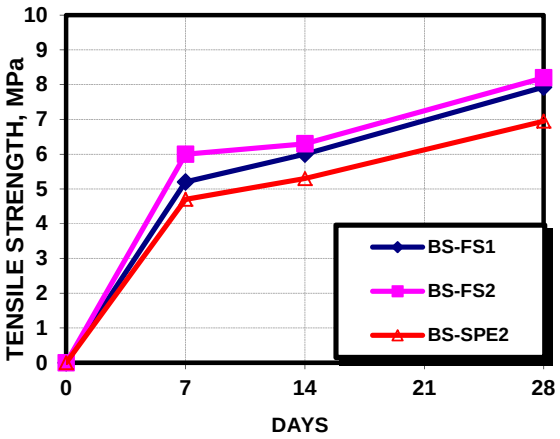

Figure 4 Effect of silica fume on the tensile strength

Effect Silica Fumes on Shrinkage and Mass Loss

The Hydric behavior of sand concretes with or without silica fume is very different as well in term of shrinkage as of loss in mass. Figure 5 shows that both concretes with silica fume which poster a similar comportment have developed deformations clearly lower than those measured on concrete without silica fume. These shrinkage values do not exceed 100µm/m to 28 days, which is encouraging as a result compared with compared with ordinary concrete and ordinary sand concrete [14].

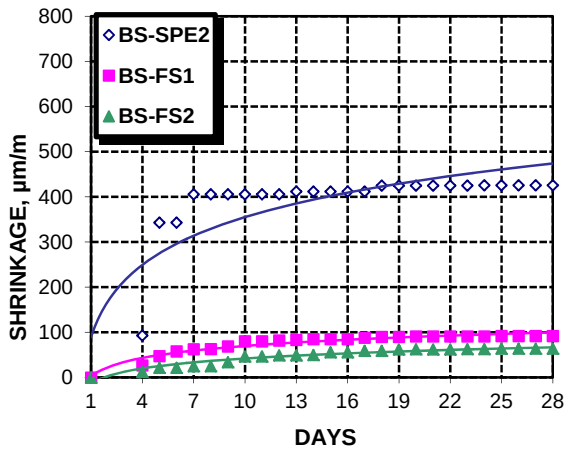

Figure 5 Effect of silica fume on the Shrinkage of sand concrete

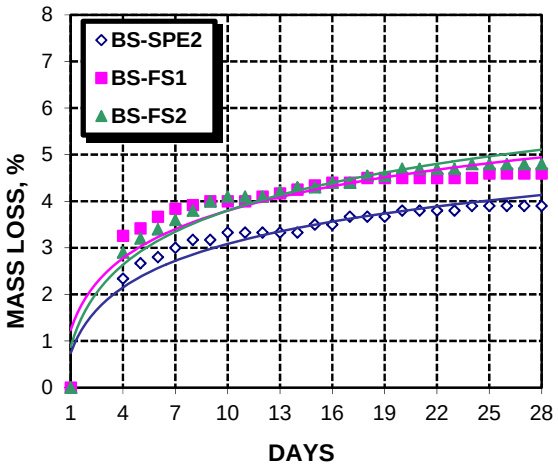

Figure 6 Effect of silica fume on the Masse loss of sand concrete

Figure 6 shows the loss of mass for sand concretes with silica fume, it's recorded an important loss of 4% compared the concrete in reference, and behind this value, we have remarked that both concretes with silica fume as mentioned in curves superimposed have the same tendency. A comparative study of the loss masses and shrinkage deformations of those materials, we have perceived an irreversible phenomenon. In point of fact, the material which has marked important amplitude of shrinkage has lost less mass, the case of BS-SPE2 it's totally the opposite (contrary) for concretes with silica fume. We could give an explanation for this state to say that the mechanism of shrinkage by the volume change of concrete during drying process is not equal to water volume evaporated [11]. Because the loss of free water, which takes place at the very beginning, there is little or no shrinkage. According to Neville, concretes which require higher reports W/C, as the case of sand concrete, for reasons of workability, we find the capillary pores even when the hydration is complete. In this case, the disappearance of the water of capillaries is made without provoking the shrinkage. On the other hand once the disappear water of capillaries, adsorbed water mobilizes and causes shrinkage similar to that for the pure dough [11].

SIMULATION OF REPAIR

To study the reply of thin repairs, see drying effect on the behavior of concrete material of sand prepared, to test its compatibility deformational and the rate of adhesion to the substrate, we tried with our own modest means, to repair damaged concrete specimens regular prismatic shapes (10X10X40) cm, figure (7-a) shows the specimens prepared surfaces before repair. We took two compositions of sand concrete for the repair: Reference sand concrete (BS-SPE2) and sand concrete with 5% SF (BS-FS2). We also varied the conditions of surfaces, taking 02 variants: Saturated Surface Dry (SSD), Surface with bonding agent (latex). In the repair of structures, the latex addition gives a good adherence to the support. It gives also the impermeability and the improvement in protection of the reinforcement, thus resistance to chemical attacks profound cracks in the interface have appeared [15].

a) Before repair b) After repair c) After adhesion test

Figure 7 Repaired specimens

Assessment of the Compatibility Deformational

Repairs made have undergone moist cure during 3 days, then they are exposed to external climatic conditions, similar to repair in situ. We followed the behavior of our repairs for two steps in: Drying conditions alone (one year), under load (compressive stress). To see the adherence and the durability of repairs under a real loading hygrometric, their behavior was monitored for a year, there is not any important remark. Figure (7-b) shows that a visual eye there is no cracks for specimens, they have not suffered a distortion, no delamination, and they keep their original state.

For the second condition, in order to test the adhesion of repair materials (mix of sand concrete). The specimens of repaired concrete were tested using loading plate, we put there vertically in the machine (compressive strength), and with a loading rate $\wp$ 200kN (choice is arbitrary). Hence the appearance of the first crack, we stop the load, figure (7-c) shows the state of the specimen after loading repaired, Table 6 shows result of different degradation occurred after loading. We could notice of this adherence test for both concretes with or without silica fume, an adherence more important to support with link agent latex, contrary to that with conditions (SSS). According to various authors, the lifespan of the latex concrete patching (repair) should be at least fifteen to twenty years [15], from where the important role of the link agent for the durability of repairs.

For the BS-SF2 material (sand concrete with silica fume), there was a greater adhesion to the substrate with latex bonding agent. In contrast to the support 2 in conditions (SSS), deep cracks appeared at the interface. For our reference concrete BS-SPE2 (sand concrete without addition), in the conditions of substrate (SSS), we see delamination and damaging cracks part of the layer of repair. By cons, there was a significant adhesion to the substrate with latex.

Table 6 State adhesion repairs loading

REPAIR MATERIAL	STATE SUPPORT	STRESS CRACKING, kN	STATE CRACK
BS-SPE2	SSD	300	Damaging cracks in the center of the specimen without affecting the interface
BS-FS2	SSD	270	Deep cracks, injurious interface (repair + support)
BS-SPE2	with latex	200	Shallow crack in the center of the specimen without delamination
BS-FS2	with latex	300	Small shallow cracks at the interface (repair + support) without delamination

CONCLUSIONS

Our principal objective in this modest work is to formulate a sand concrete in order to exploit local and abundant resources (sand), by developing its performances to give characteristics that is comparable to common concretes, that is answering to badly assured exigencies by those latest, to see also its impact on thin repair of concrete structures.

The addition of 5% of silica fume contributed in the capacity improvement and mechanical characteristics of our sand concrete material, as well as shrinkage reduction. We could give once again this low shrinkage, even though paste volume is more important than ordinary concrete and a ordinary report W/C, to the presence of silica fume which allow to refine capillary porosity and thus to make the material less sensitive to drying and to decrease its shrinkage . It is the case of high-performance concretes [3].

A thin repair simulation was applied to ordinary concrete specimens with mix of sand concrete with silica fume. We know very well that drying process and shrinkage provoke restricted deformation in repairs. So we are faced with adverse consequences hygrometric on the mechanical behavior and durability of thin repairs. For our repaired items that are subject to conditions of only drying (one year), we present a good capacity deformational, which can be explained by the specific nature of sand concrete. Because this prove a fast and uniform drying, giving a non-cracked concrete [5].

The good homogeneity of the sand concrete, its fine porosimetry that is at the origin of the nature of uniform drying, is radically different from that seen in other brands of concrete. The humidity

gradient between the periphery and the heart of the material (or sample) is low. Therefore the stress gradients are, too, weak and this has resulted in a low cracking [5, 12].

We tried to explain the behavior of our repairs with sand concrete with silica fume. It was found the effect of characters none cracking sand concrete and drying uniformity main factor that contributed to this compatibility adhesion, and durability of repairs. It can be said to conclude that the material sand concrete is submissive to little deformation prevented. He has good capacity deformational and therefore good adhesion capacity. The addition of 5 % of silica fume has contribute has the improvement of this adhesion. At the end we can say that the durability of repair mortar depends not only on the mortar mix itself but on the environmental conditions encountered during its service life.

REFERENCES

1. SAUCIER, F. La durabilité de l'adhérence des réparations en béton, thèse de doctorat, (1990), Université de Laval, Quebec, Canada, p145

2. B.BISSONNETTE**,** Le fluage en traction: un aspect important de la problématique des réparations minces en béton, thèse de doctorat, (1996), Université de Laval, Quebec, Canada.

3. OLIVER, LAURENCE, La fissuration due au retrait restreint dans les réparations minces en béton : Apports combinés de l'expérimentation et de la modélisation, thèse de doctorat, (2001), Université de Laval, Quebec, Canada.

4. B.BISSONNETTE, M.PIGEON**,** Le comportement viscoélastique du béton en traction et compatibilité déformationnelle des réparations, Materials and Structures, Vol. 33, March 2000, pp 108-118

5. A.BENAISSA, P.MORLIER, C.VIGUIER, J.J.CHAUVIN, Cinétique de dessiccation et retrait dubéton de sable, Annales de l'institut technique du bâtiment et de travaux publics, (Juin 1992), N°504 , PP:43-51

6. Presse de l'Ecole Nationale des Ponts et Chaussées, 'Béton de sable, caractéristiques et pratique d'utilisation', (Projet SABLOCRETE), édition: Association Amicale des Ingénieurs Anciens Elèves de L'Ecole Nationale des Ponts et Chaussées, 1994. p. 15–71 (237 p).

7. M.BEDERINA, L. MARMORET, K. MEZREB, M.M. KHENFER, A. BALI, M. QUÉNEUDEC, Effect of the addition of wood shavings on thermal conductivity of sand concretes: Experimental study and modelling, Construction and Building Materials 21 (2007) 662–668

8. J.J.CHAUVIN, G.GRIMALDI, Les bétons de sables, Bulletin liaison laboratoire, Ponts et chaussés, (Sept-Oct 1988), N°157, Ref 3336, PP:9-15

9. Z.BOUDAOUD**,** *Etude des mortiers, des micro-béto*ns *et des bétons de sable à base de sable fin de Boussaada,* thèse de magister, (1996), université de Msila , Algerie.

10. K.GADRI, *Contribution à l'étude d'un béton de sable avec fibres et resine destiné pour la réparation mince des structures,* thèse de magister, (2007), université de Biskra , Algerie.

11. ADAM.M.NEVILLE, *Propriétés des bétons,* Eyrolles, (2000), France

12. A.BENAISSA, P.MOLIER , C.VIGUIER, *Microstructure du béton de sable,* Cement and concrete research, (1993), Vol 23, PP : 663-674

13. G.CHANVILLARD, O.BASUYAUX, *Une méthode de formulation des bétons de sable à maniabilité et résistance fixées,* Bulletin des laboratoires des ponts et chaussées, Sept-Oct (1996), N°205, ref : 4047, PP : 49-63

14. S. EL EUCH KHAY, J. NEJI, A. LOULIZI, *Shrinkage properties of compacted sand concrete used in pavements,* Construction and Building Materials, 24 (2010): 1790 -1795

15. A.ABIBSI, A.GUETTALA, *A case study of concrete bridge and corrosion phenomenon,* Role of Concrete Bridges in Sustainable Development, Proceedings of International Symposium: Celebrating Concrete: People and Practice, 3-4 September 2003, Eds. Dhir, Newlands, McCarthy, University of Dundee, Scotland, United Kingdom, pp 330-338.

Performance of Polyester Resin Repair Concrete Under Wheel Tracker Tests

G L M Leung, W G Wong
Hong Kong Polytechnic University, China

During the past few years, Polyester Resin Repair Concrete (PE Concrete) has provided tremendous benefits to the Hong Kong government on the fast-track repair of concrete pavements due to their properties of fast curing and high strength development. In order to enhance the performance of the material further, reinforcements such as chicken wire mesh and steel mesh were often added. Despite the regular usage of the reinforced and unreinforced PE Concrete, the amount of contributions to the overall strength of the PE Concrete was an unknown within the highway industry. During the year 2010, the Hong Kong Road Research Laboratory (HKRRL) of the Hong Kong Polytechnic University conducted a laboratory research on investigating the behaviour of reinforced and unreinforced PE concrete slabs under repeated wheel load test. The test results indicated that with the addition of chicken wire mesh to the PE concrete, the resistance to repeated wheel loads has increased by more than 30%. Meanwhile it also enhances the ductility of the material, as clearly indicated by the failure mechanism (the gradual deformation before failure and the formation of jagged crack patterns) of the test samples with chicken mesh. The test results also show that the steel mesh D503 makes significant contribution on upholding the stability of the cracked concrete specimens after prolonged period of wheel load applications. Meanwhile the fatigue performance of Grade 40 concrete specimens under wheel tracker tests was found to be approximately 50% of the one for PE concrete specimens, which indirectly indicates that the flexural capacity of the PE concrete can be considerably higher than normal Grade 40 concrete under the condition of almost equal compressive strength.

Mr G L M Leung is currently a PhD student in Pavement Engineering at the Hong Kong Polytechnic University. He was previously a research associate within the institution as well as working with Ove Arup and Partners Hong Kong for 9 years. He obtained his BEng from Nottingham University and his MSc in Foundation Engineering from Birmingham University.

Dr W G Wong is an Associate Professor, within the Civil and Structural Engineering Department at Hong Kong Polytechnic University with over 25 years' experience in concrete design and construction.

Keywords: Mesh reinforcement, Polyester resin repair concrete, Wheel tracker test

BACKGROUND

In Hong Kong, concrete carriageway maintenance works are generally categorised into emergency repairs and scheduled maintenance. With the condition of high traffic demand, sensitive land constraints and growing community expectation, most carriageway repair works have to be conducted under extremely tight schedule. Consequently, it requires that the repair materials can develop sufficient strength in a short period, from several days to a few hours. For example, materials such as Portland cement concrete (PCC) can be used where sufficient time is available to accommodate long curing time before opening to traffic. Other materials such as magnesium phosphate concretes gains strength very quickly but it can be extremely water dependent and even very small quantities of extra water in the mix can severely reduce the strength. Polymer based concretes like epoxy, methyl methacrylate, polyurethane, polyester or acrylic resins are also often adopted. Of the resin systems, epoxy resin mortars are the most widely used in concrete repair. Polyester resin-based mortars are used, generally for small area repairs where their very rapid development of strength is required. However, they are not suiTable for larger area repairs mainly because of short workable period. Furthermore the coefficient of thermal expansion of most resin materials is several times greater than that of ordinary concrete which may lead to failure of large, thin-bonded repairs. Additionally, as the cooling and hardening of most resin materials involves an exothermic reaction, contraction of the material as it cools may contribute to eventual failure. For temporary repair operations, bituminous materials are used almost universally in Hong Kong. Table 1 summarizes the commonest products used for concrete road repairs in Hong Kong and their associated physical properties and Figure 1 illustrates a typical situation on concrete road repair.

Previous research of the Highways Department indicates that a minimum early compressive strength development of the repair material for concrete carriageway of 20 MPa (a flexural strength of the repair material is normally about 10%, i.e. 2 MPa) would be considered as strong enough for opening to rubber tired traffic, and it was pinpointed that for emergency works that required to be opened as soon as possible, PE concrete is highly suiTable (Refer Figure 1). Recent quality control test results of the material manufacturer indicated that it took only 2 hours to develop a minimum compressive strength of over 50 MPa as indicated in Figure 2.

Table 1 Physical properties of commonest products used for concrete road repairs

PROPERTY	CEMENTITIOUS CONCRETES	EPOXY RESIN CONCRETES	POLYESTER RESIN CONCRETES
Compressive strength, MPa	20 -70	50 - 110	50 - 110
Flexural strength, MPa	2 - 5	25 – 50	25 - 30
Tensile strength, MPa	1.5 – 3.5	10 - 20	10 - 17
Water absorption, 7 days at 25^{o}C, %	5 -15	0 - 1	0.2 – 0.5
Rate of development of strength at 20^{o}C	1 – 4 weeks	6 - 48 hours	2 – 6 hours

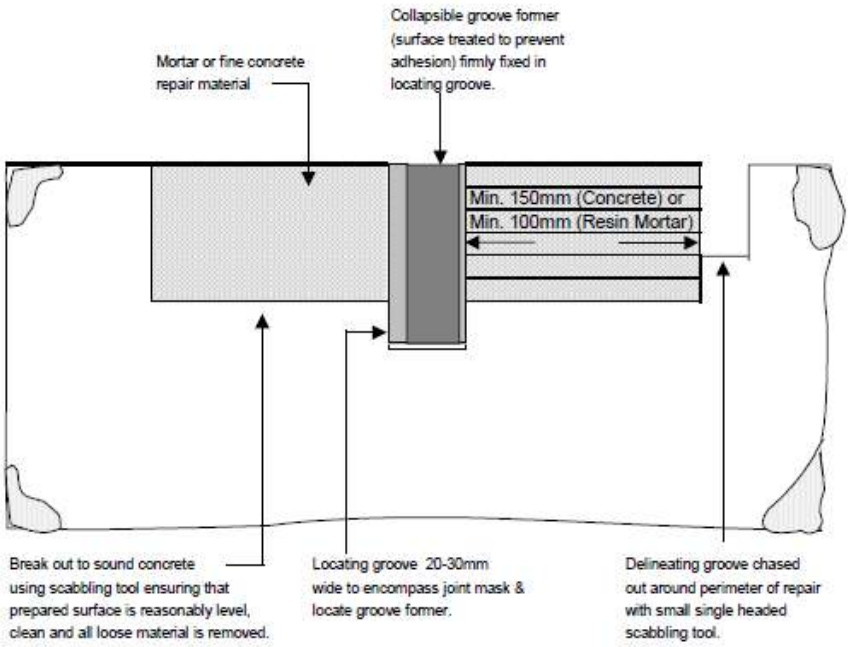

Figure 1 Typical situation on concrete road repair

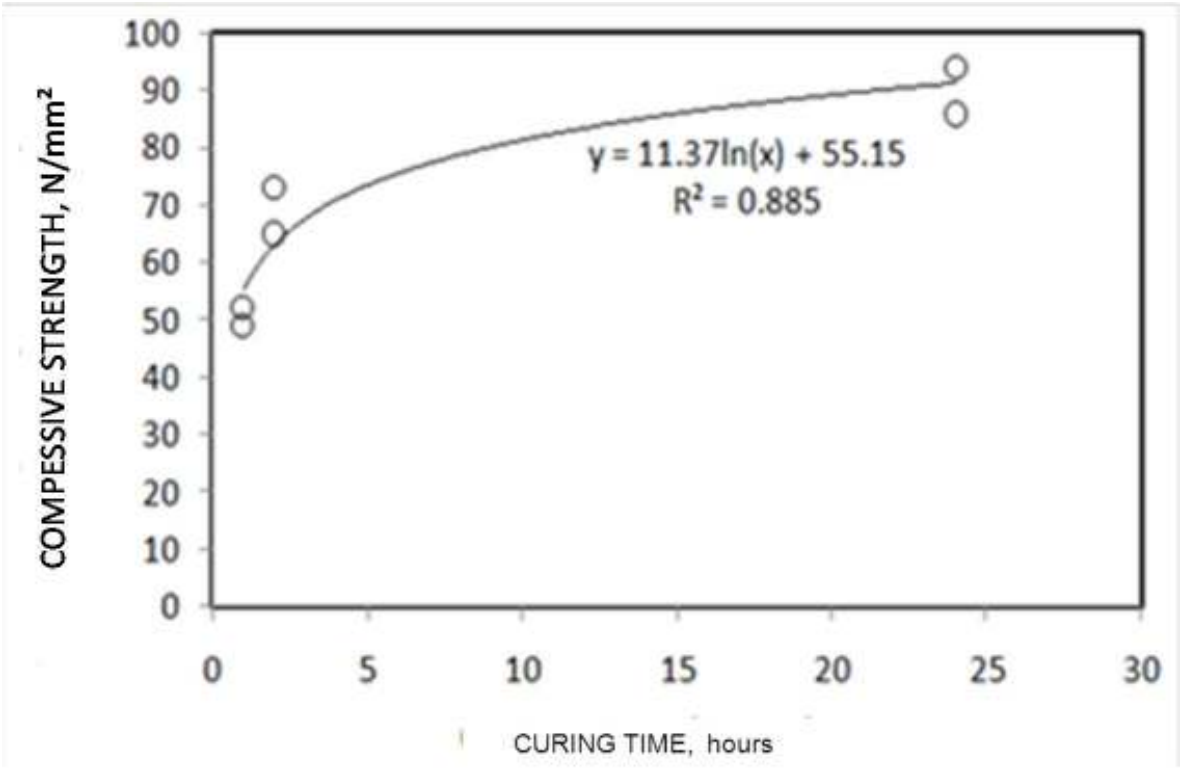

Figure 2 Compressive strength development of PE concrete

LABORATORY TESTING

Objectives

The objectives of the laboratory investigation are twofold: (1) to understand and compare the performance of normal concrete and PE concrete under simulated traffic load condition. (2) to quantify the potential benefits and to understand the behaviour of the addition of mesh reinforcement into PE concrete under the simulated traffic load condition.

Setup of Test

The investigation makes use of the wheel tracker machine, which is commonly used for studying permanent deformation potentials of asphaltic road specimens (square slab or circular) in simulating the traffic load condition. The contact stress between the wheel tire and the specimens is approximately 450 kPa and the traveling speed is 720 m/hr (45 mins for 1,800 wheel passes) in average. In order to fit the purpose of the study, several changes were made to the machine and the supplementary parts. For instance, metal beams at both sides of the slab mould (parallel to the direction of the wheel passes) are provided to form a "simply supported" arrangement for the specimens under tests. The stop-ends, sidewalls, inverted L-shaped bars and rubber spacer are in place to ensure a reasonable stability of the specimens was achieved under tests.

Figure 3 Configuration of wheel tracker machine

For the investigation, the specimen pairs (i.e. two separate slab specimens were placed side by side) within the metal mould in order to study the difference in fatigue performance. The size of specimen used in the laboratory test was 295 mm (length) x 145 mm (width) x 50 mm (thickness). In order to simulate the worst situation that might be encountered in real construction and also to facilitate the completion of the tests within the project timeframe, a triangular crack inducer with a height of 30 mm was adopted to establish an intentional defect within the specimen (Figure 5). Under this configuration, a 20 mm cover was provided for the mesh reinforcement within the specimens. Table 2 summaries the types of specimen used in the laboratory test.

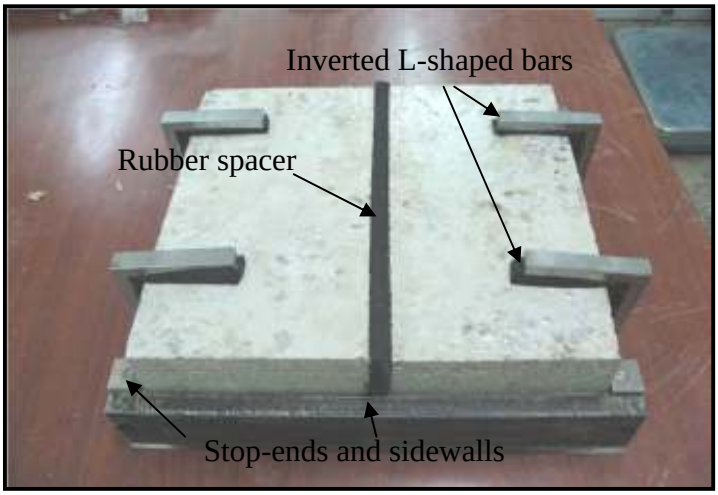

Figure 4 Setup of test specimens

Table 2 Summary of Specimen Pairs Adopted under the Laboratory Test

TEST NO.	SPECIMEN A	SPECIMEN B
1-3	Specimen without reinforcement	Specimen without reinforcement
4-6	Specimen without reinforcement	Specimen without reinforcement
7-9	Specimen with C-W mesh	Specimen with C-W mesh
10-12	Specimen with steel mesh D503	Specimen with steel mesh D503
13-15	Specimen without steel mesh	Specimen with C-W mesh
16-18	Specimen with C-W mesh	Specimen with steel mesh D503

Specimen A – denotes specimen at left side of the track
Specimen B – denotes specimen at right side of the track
*- Test nos. 1-3 were conducted on Grade 40 concrete
*- Test nos. 4-18 were conducted on PE concrete
* - C-W mesh denotes chicken wire mesh

Composition and Casting of Materials

The PE concrete test specimens were prepared based on the recommendations by the manufacturer (Forsoc Hong Kong Ltd). The material mix comprises aggregates (less than 10 mm), river sand, filler and resin and their mixed proportions were 4:1:2:1 in weight respectively. The aggregates and river sand were oven-dried and cooled down and all the materials were pre-weighed prior to the mixing operation.

All the materials were then hand-mixed inside a plastic container for a period of approximately 3-4 minutes. Upon the thorough mixing of the materials, they were immediately placed into casting moulds formed by wood. The perimeter of the wooden casting molds was supported by metal frame and heavy counterweights to ensure it was reasonably sTable upon placement and compaction of the materials. The material mixture was then continuously filled until it reached a height of about 20 mm. The crack inducer was then placed in an inverted direction into the casting mould before further material mixture was poured to the top level of the casting mould. Compaction by gently pressing the material surface was carried out subsequent to the filling

operation. For the test specimens with steel mesh, the pre-cut samples (i.e. chicken mesh and steel reinforcement) had to be installed before the placement of the crack inducer. Upon the curing of the test specimens, the wooden moulds were removed after a period of approximately 2.5 hours to facilitate the setting up of the test arrangement. The test was typically started after 3 hours of curing in order to simulate the timeframe required in opening to traffic. A typical set-up is illustrated in Figure 6.

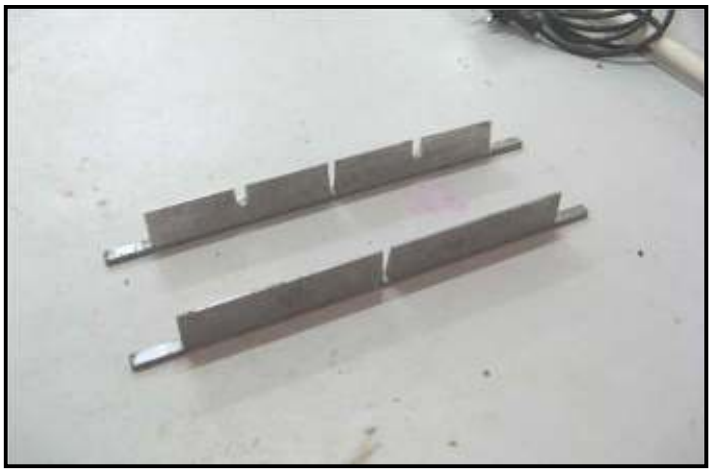

Figure 5 Examples of crack inducer

The Grade 40 concrete test specimens were prepared based on the design mix recommended by the structural group of the Hong Kong Polytechnic University. The material mix comprises aggregates (less than 10 mm), river sand, admixture, cement and water and their mixed proportions are as follows:

1. Aggregates (less than 10 mm) – 988 kg/m^3
2. Sand – 632 kg/m^3
3. Admixture – 4.0 L/m^3
4. Water to cement ratio – 0.43

The specimen pairs were casted in the similar way as the ones of PE concrete but they were tested under wheel tracker machine after 7 days of curing. With an approximation, the 7 days cube strength should reach a value of 70% - 80% of the 28 days strength (i.e. 42 – 48 MPa)

Instrumentation and Data Acquisition

In order to differentiate, display and record the magnitude of deformation of the slab specimens under tests, a tailor-made instrumentation and data acquisition system was setup to fulfill the purpose. The system includes an additional Linear Variable Differential Transformer (LVDT) (Figure 7), a photo-electric sensor (Figure 8), a data acquisition module as well as a pre-designed computer programme. The details of the various components of the system are presented in Table 3 below.

Figure 6 Casting of test specimen pair (top: with mesh reinforcement D503, bottom: with chicken wire mesh)

Table 3 Summary of Instrumentation and Data Acquisition Components

TEST NO.	SYSTEM COMPONENT	COUNTRY OF ORIGIN
1	Linear Variable Differential Transformer (LVDT)	TML (Japan)
2	Photo-electric sensor	SUNX (US)
3	Data acquisition module	National Instruments (US)
4	Pre-designed computer programme (Labview)	National Instruments (US)

Figure 7 Additional TML LVDT for tests

Figure 8 SUNX photo-electric sensor

The data acquisition operation works under the principle of that when the light source of the photo-electric sensor is blocked, a switch over of the electric signal will occur (i.e. from entity A to B). While the light source is blocked the second time, the electric signal will be switched over again (i.e. back from entity B to A). The design of the data acquisition system thus makes use of this working principle to facilitate the "switch over" of deformation measurements between specimens A and B. A small metal plate was fixed at the centre-line of the wheel and the photo-electric sensor was installed at the side of moving platform of the wheel tracker equipment (also at centre). Once the photo-electric sensor passed over the metal plate during the test, the light was blocked and a switch-over of the measurements took place. The pre-set frequency for data acquisition is 10 Hz (i.e. 10 readings per second) and it is considered sufficient to capture the effect of any gradual or sudden vertical movement of the test specimens. Figure 9 to 12 illustrate the details.

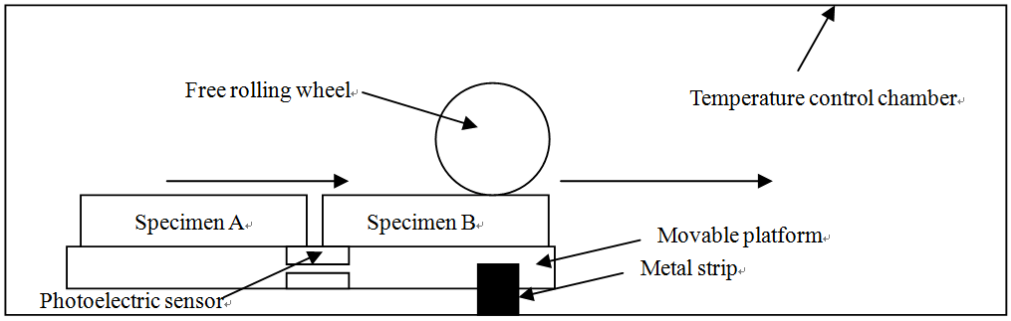

Figure 9 Vertical deformations are being measured at slab specimen B

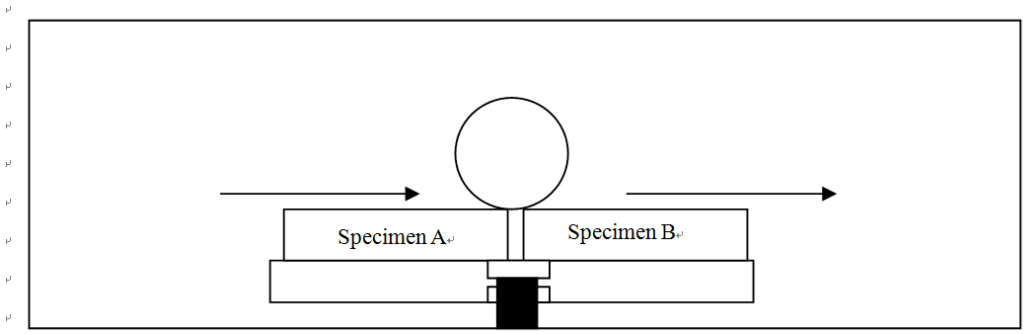

Figure 10 The signal is switched over as the photoelectric sensor and metal strip is in line with each other (i.e. the light ray is blocked)

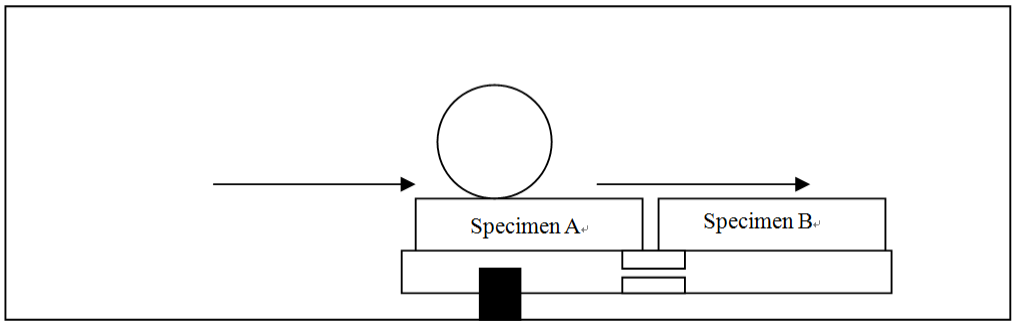

Figure 11 Vertical deformations are being measured at slab specimen A

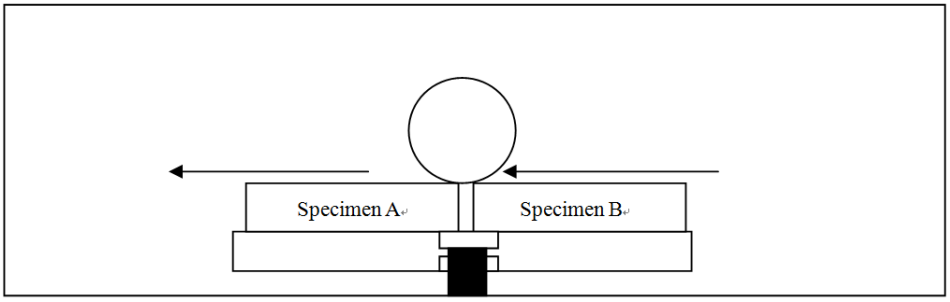

Figure 12 The signal is switched over again as the photoelectric sensor and metal strip is in line with each other (i.e. vertical deformations at slab specimen B would start to be measured)

INTERPRETATION OF TEST RESULTS

Figure 13 illustrates the overall test results, which shows that the PE concrete specimens without mesh reinforcement exhibit the lowest fatigue resistance to repeated loading under the wheel tracker test. The performance was improved in the addition of chicken mesh (by about 30%) and further improved in the addition of steel mesh D503. The performance of Grade 40 concrete specimens (without mesh reinforcement) was found to be about 50% of the one of the PE

concrete specimens (without mesh reinforcement). An approximately 10% higher concrete cube strengths of PE concrete - 3 hours than grade 40 concrete - 7 days (see Figure 14) led to a substantially higher fatigue resistance which indirectly point out that the PE concrete can be much more structurally efficient in terms of flexural strength than normal cementitious concrete, as illustrated by Table 1 earlier.

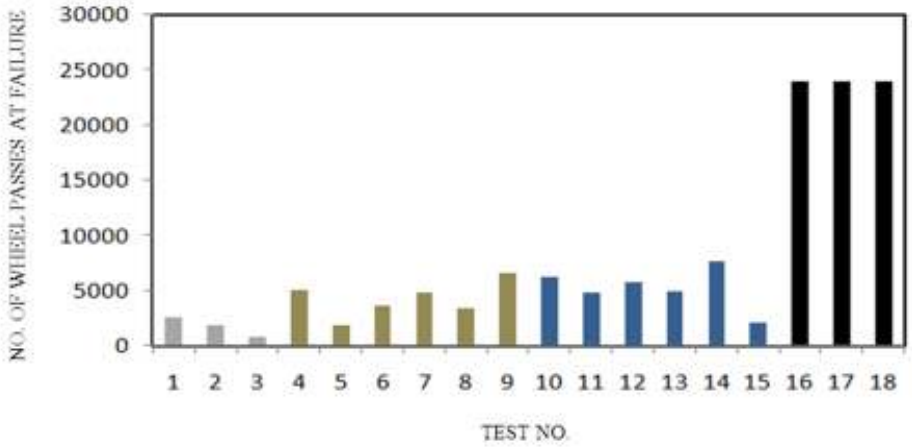

Figure 13 Summary of numbers of wheel passes at failure

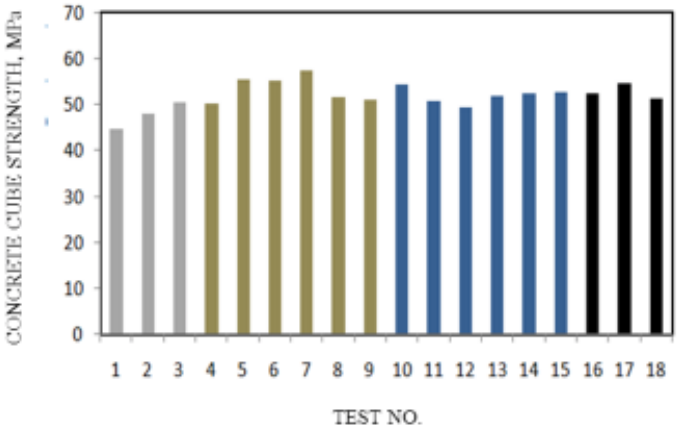

Figure 14 Summary of concrete cube strength

It is worthwhile to note that the failure mechanism of test specimens without steel mesh tends to be much more brittle (appears to be a sudden failure) as compared with the specimens with chicken mesh which the failure mode was more ductile (more gradual failure). Figures 17 and 19 show the distinctive different behaviour between the two types of test specimens towards failures. According to this, the vertical deformation before failure for test specimens with chicken wire mesh was generally much higher than that of the test specimens without chicken wire mesh as indicated in Figure 15.

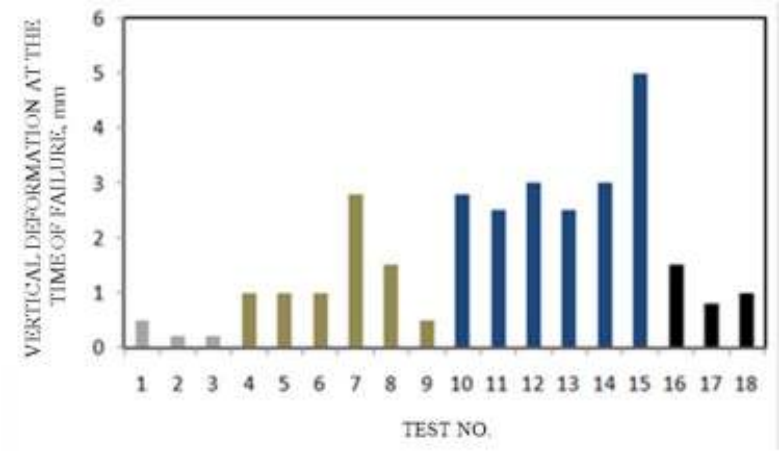

Figure 15 Summary of vertical deformations at the time of failure

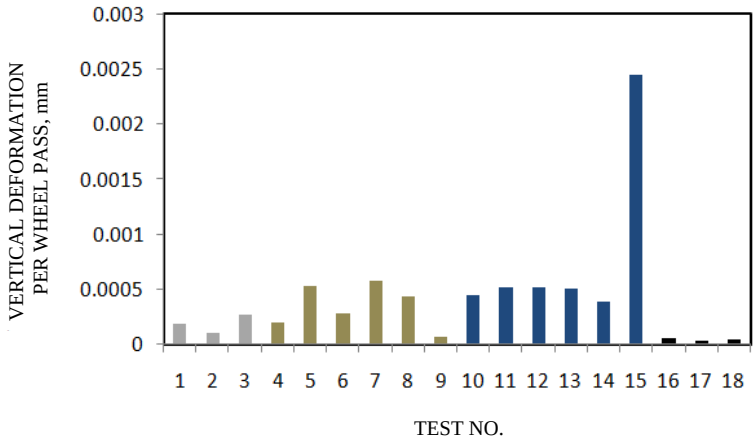

Figure 16 Summary of vertical deformations (per wheel pass) at the time of failure

An obvious characteristic regarding the crack pattern was associated with the difference between the specimens without mesh reinforcement and the ones with chicken wire mesh. The cracks developed for the specimen without mesh reinforcement tend to be straight and sharp, as shown in Figure 18 and it matches with the brittle failure mode which previously described (i.e. failure developed along the weakest path). Whereas the development of cracks for the specimens with chicken mesh tended to be considerably rougher (i.e. jagged forms) as shown in Figure 20, and this echoed well with the phenomenon that the specimens generally failed in a more gradual form (the reinforcement tried to keep the specimen in place while cracks were developing in many cycles in the test). For the specimens with mesh reinforcement D503, Figures 21 and 22 indicate that no failure was encountered after 10 hours of wheel load applications yet some cases showed that the specimens cracked on the sides (some are more obvious than others), which the integrity of the specimens were upheld by the reinforcement.

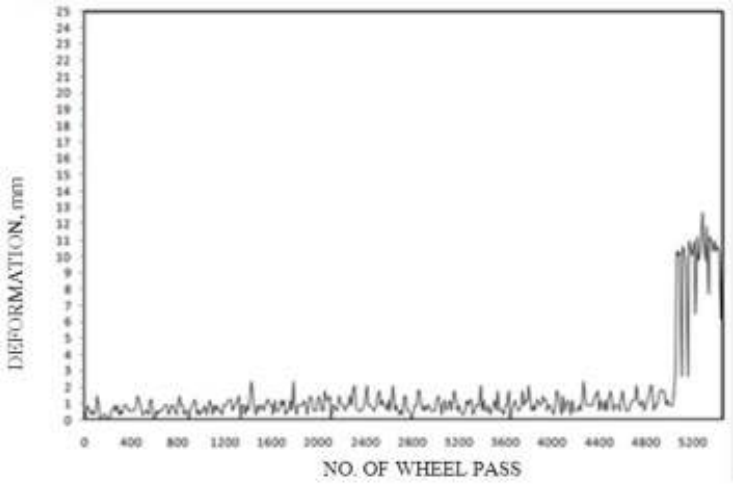

Figure 17 Typical test result for specimen without mesh reinforcement

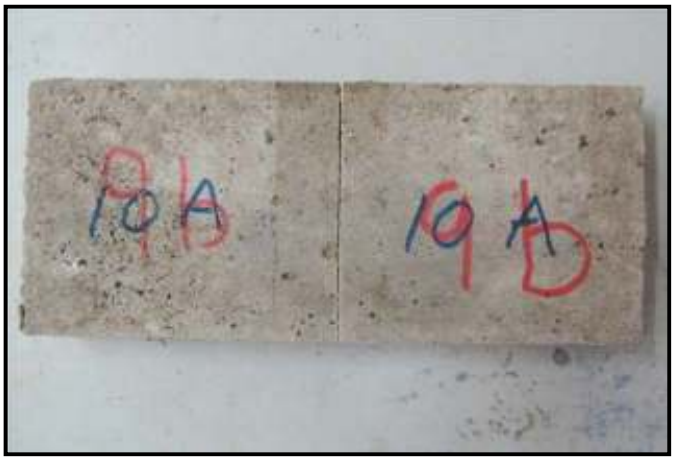

Figure 18 Typical appearance of specimen without mesh reinforcement after test

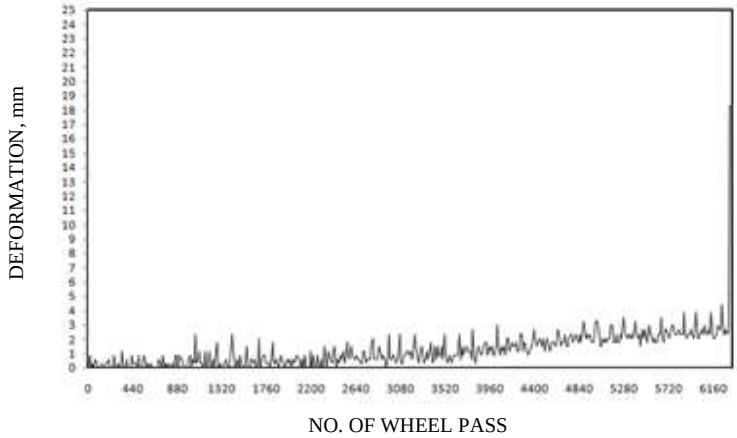

Figure 19 Typical test result for specimen with chicken wire mesh

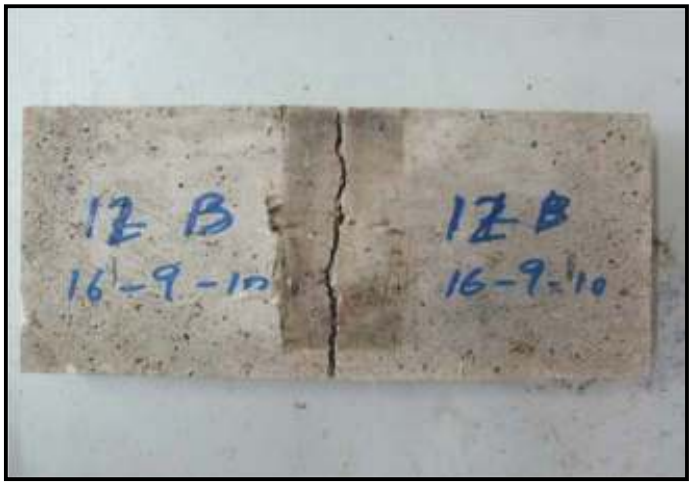

Figure 20 Typical appearance of specimen with chicken wire mesh after test

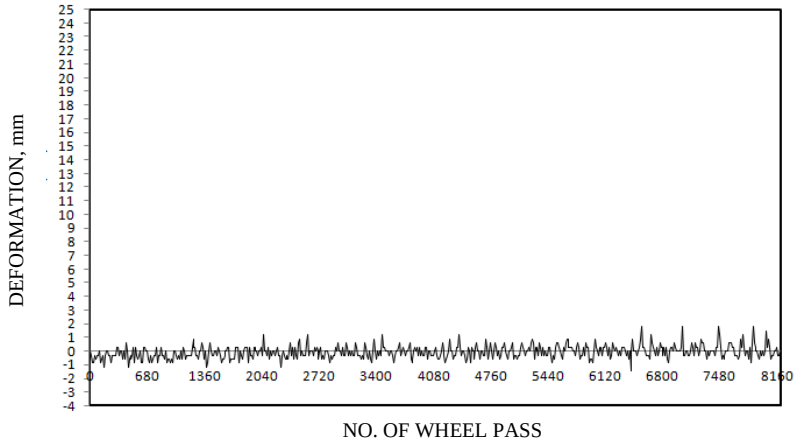

Figure 21 Typical test result for specimen with D503 mesh reinforcement

Figure 22 Typical appearance of specimen after prolonged number of wheel passes

CONCLUSIONS

The laboratory test results generally indicate that the fatigue performance of Grade 40 concrete specimens (without mesh reinforcement) under wheel tracker tests was found to be approximately 50% of the one for PE concrete specimens (without mesh reinforcement). It indirectly indicates that the flexural capacity of the PE concrete can be considerably higher than normal Grade 40 concrete under the condition of almost equal compressive strength.

The fatigue performance of the PE concrete specimens can be further improved by the addition of chicken wire mesh (approximately 30% by the experimental results). Apart from the improvement in resistance to repeated wheel load that might be brought to the polyester resin mortar, the addition of mesh reinforcement also enhanced the ductility of the material, as clearly indicated by the failure mechanism (the gradual deformation before failure and the formation of jagged crack patterns) of the test samples with chicken wire mesh. The material and manipulation costs for chicken wire mesh are generally negligible.

If it is under a heavily loaded condition, further improvement can be brought by the addition of steel mesh. The test results for the ones with steel mesh demonstrated that the instablility of the specimens were upheld by the mesh reinforcement after prolonged period of wheel load applications.

ACKNOWLEDGEMENT

The authors would like to thank Forsoc Hong Kong Ltd for the donation of the materials for testing and our student trainee Mr. Kin-Lok Chan for the assistance provided to work on the instrumentations and LabView programming.

REFERENCES

1. FOSROC HONG KONG LTD, Technical Submission of Nitomortar PE Concrete to Highways Department, 2003.

2. FOSROC HONG KONG LTD, Standard Method Statement of Nitomortar PE Concrete for Highways Term Maintenance Contracts, 2007.

3. HIGHWAYS DEPARTMENT, Research & Development Division, RD/GN/028, Guidance Note on the Repair of Spalled Concrete Road Joints, 2001.

4. BS 598-110-2005, “Sampling and Examination of Bituminous Mixtures for Roads and Other Paved Areas — Methods of Test for the Determination of Wheel-tracking Rate and Depth”.

Epoxy-formulations for the Coating, Repair and Structural Enhancement of Concretes

F Medici, G Rinaldi
Sapienza University of Rome, Italy

A "tailored" series of synthetic poly-alkylene-poly-amino-methylolic (P.A.M.) curing agents for epoxide (DGEBA) resins is presented; P.A.M. products were obtained by substituting some of the hydrogen atoms of the aminic functions of an aliphatic poly-amine with methylolic groups (-CH_2OH). The viscosities of the fluid epoxy-P.A.M. formulations (before the onset of the curing reaction) were determined at room temperature. Mechanical and creep properties, permeability to carbon dioxide and water of the cured formulations were determined, as well as their adhesion to different concretes; the durability of the resin – concrete joints (U.V. irradiation, freezing-thawing) as well as their crack-bridging ability were also tested. Experimental tests were also carried out for the structural repair of fractured concrete specimens by means of a fibreglass composite with the best experimented epoxy matrix. The evaluation of the chemical structure of the cured epoxy formulations allowed the interpretation of their different behaviours as products for the protection and repair of concrete structures.

F. Medici is currently Professor of Materials Science and Technology at the "Sapienza" University of Roma, Italy. He has been and is involved in research projects on the field of the cement chemistry, concrete technology and recovery of waste materials in cement matrices.

G.Rinaldi is a Professor of Space Materials and Space Engineering and of Materials Technology and Applied Chemistry and Energetics at the "Sapienza" University of Roma.

Keywords: Coating, Composites, Cracks repair, Damaged concrete, Epoxide resins

INTRODUCTION

Once upon a time there was the "Roman" concrete, probably the most durable building material the mankind ever used in his never-ending history (and still in use, even if greatly modified).

But in modern times, starting from the onset of the first industrial revolution, when the Portland cement bore, the environment gradually changed and actually the polluting agents exert strong chemical attacks against the concrete structures, above all those based on Portland cements. Even the most carefully designed concrete mix is subjected to a some degree of deterioration, directly or indirectly caused by aggressive environments.

Above all the lack of inspection and repair ("rejuvenation") can determine the abrupt fall of the "durability" of concrete buildings.

The first stage of deterioration is the appearance of surface cracks causing the penetration of the aggressive chemical agents into the structure. The durability can be restored only by a careful intervention, i.e., a "correct" stopping of the cracks, both macro and micro. Ordinary, reinforced or pre-stressed concrete, it does not matter: concrete is always in danger when cracked, even only in surface.

Whilst the physical and mechanical degradation can easily be avoided by a preventive correct mix-design and a careful casting, the action of the environmental chemical agents can be excluded only by blocking their penetration into the concrete, a task preventively not easy achievable.

For a structure already in exercise, a protective coating is the only action we can do, whilst, for a cracked (i.e. damaged) concrete, the safe and durable sealing of the cracks is an absolute need. Hence, stopping the cracks and coating surfaces of the concrete could be the best "rejuvenating action" for the enhancement of "durability" of the whole structure.

Actually the epoxy resins are the most spreading products for both a reliable coating or repair of the damaged areas [1, 2] and of a cracked and even porous concrete; their main advantages in comparison with the different materials now in use are: faster curing rates, slightest shrinkage, higher adhesion values and higher strength.

Naturally, an epoxy formulation intended for concrete repair or coating must be carefully tailored, for its physical, chemical and mechanical characteristics; in fact we must take in mind that sometimes the repairing (as well as the coating materials) could determine short or long term negative effects on the durability of the repaired/rejuvenated structure.

The European Commission for standardisation work on "Products related to concrete, mortar and grout" has recently delivered the final EN 1504 [3, 4] standard for the evaluation of the products and systems for the protection and repair of concrete structures.
In brief, the main essential properties the materials must obey are:

- waterproofing, to avoid the penetration of water-soluble aggressive chemicals (chlorides, sulphates, etc.);
- the minimum permeability for carbon dioxide, to avoid the carbonation of the hydrated Portland cement;

- the highest permeability for the water-vapour, to allow the exchange with the surrounding air;
- high adhesion to the concrete, for a reliable coating and/or repair;
- crack-bridging capability, above all for the surface coating products; in fact surface-cracks (originated from the stressed concrete) could grow, and propagate along the surface; water and chemical agents from the surrounding environment could be stopped only if the coating do not fracture, i. e., if the coating material holds the so-called "crack-bridging" ability.

In this paper, a tailored series of synthetic poly-amino-methylolic curing agents for the DGEBA epoxy resins is investigated. After curing at room temperature, even in the presence of wet environment (high R.H.), some of the formulations experimented bear the physical, mechanical and chemical characteristics established by the EN 1504; not only the "essentials", but those "to be desired" and those of "minor interest" as well.

EXPERIMENTAL AND RESULTS

Materials

Concretes: Concrete specimens from different Portland cements (32.5, 42.5 and 52.5) were cast with a constant mix dosage 350 kg/m^3, utilizing calcareous aggregates (sand and gravel, maximum diameter 2.5 cm) and a water/cement ratio 0.55. The mean (5 specimens) compressive strengths were Rc = 30, 40 and 55 (MPa), and the volumic masses 2220, 2280 and 2294 (kg/m^3) respectively.

Epoxy resin: D.G.E.B.A. product, Epon 828 resin from Shell: epoxy equivalent 190; mean molecular weight 380; viscosity 11.6 (Pa x s) at 25 °C; specific gravity 1.160 kg/m^3 at 25 °C.

Curing agents: They were all chemical modifications of the tetraethylenepentamine (TEPA - Fluka). The synthetic curing agents [5,6] poly-alkylene-poly-amino-methylolic products (P.A.M.) were obtained by reaction of TEPA with different molecular ratios (from 0.1 to 2) of formaldehyde (C. Erba). In the reaction, some methylolic (–CH_2OH) groups were introduced as substituents on the original aminic functions of TEPA molecule.

All the products were characterized for their physical and chemical properties (Table 1).

Formulations

Fluid formulations: Preliminary tests were carried out to determine the 'activity' of the different curing agents against the epoxy resin, i.e., to identify the correct ratio between the resin and the curing product. The formulations still fluid were characterized at room temperature (25 °C) by dynamic rheological tests performed with a controlled shear rheometer (Rheometrics RDA II) using a parallel plate geometry in time sweep at constant frequency (10 rad/s) and strain. Rheological data allow to recognize the dynamic viscosity at the "start" (mixing with curing agent) and at the "critical point" (pot life, i.e., the time when the elastic behaviour exceeds the viscous behaviour of the material, see Figure 1). The dynamic viscosity at the critical point was determined considering the maximum in the loss tangent (tan δ) curve, where tan δ is the ratio of the viscous modulus to the elastic modulus (Table 2).

Table 1 Physical and chemical characteristics of P.A.M. curing agents

CURING AGENT	PAM 01	PAM 02	PAM 03	PAM 05	PAM 1	PAM 2
Specific gravity, kg/m^3 at 20 °C	1010	1010	1010	1015	1015	1020
Dinamic viscosity, Pa x s at 20 °C	12	15	18	18	20	25
Molecular weight, cryoscopic	190	195	195	200	240	420
Molecular structure, general	$NH_2 - CH_2 - CH_2$		-NH – CH_2 – CH_2			

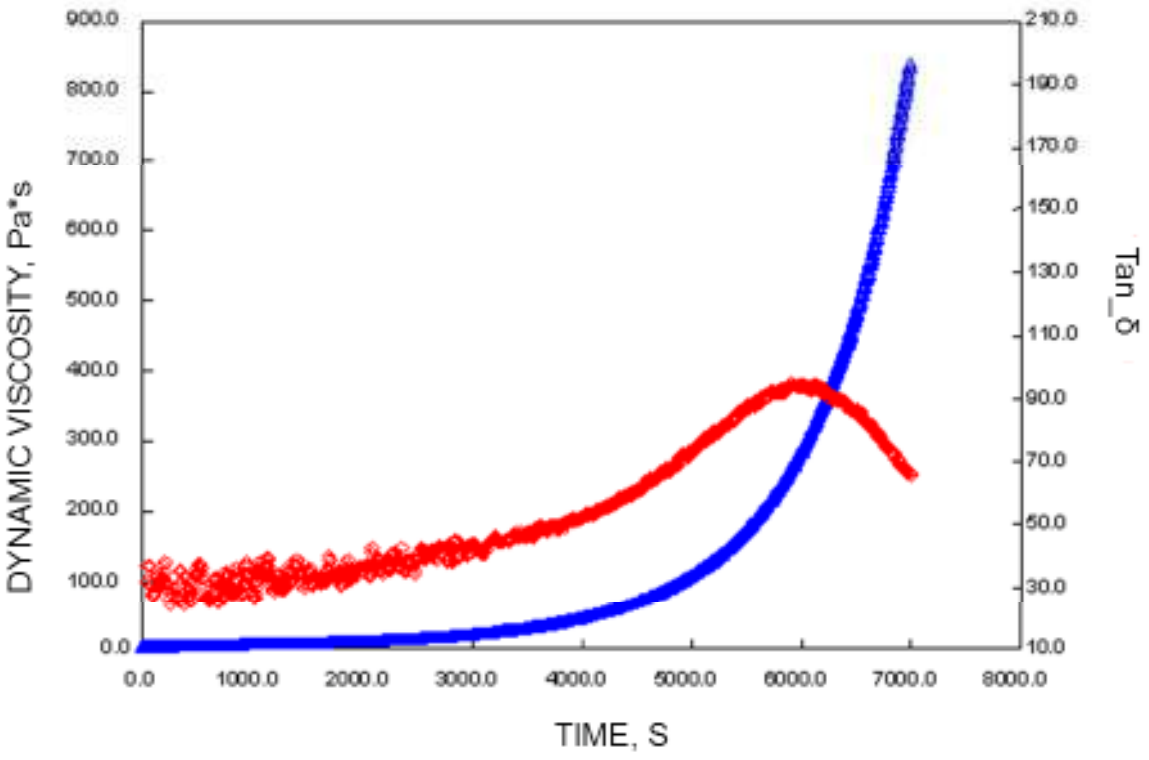

Figure 1 Viscosity trend of epoxy resin - PAM 05 at room temperature

Cured formulations: Characterized for the tensile strength and elastic modulus (ASTM D3039), impact strength (ASTM D250), hardness - Shore D (Table 3) . Specimens were obtained by casting the formulations in suitable aluminium moulds. The curing cycle was always 72 hours at room temperature (25 °C) and 60% R.H. For the fire resistance, specimens of the formulations (1x1x15 cm) were tested according to UL-94-V Standard: all the formulation resulted within 94-V-1 class (self-extinguishing).

Table 2 Characteristics of the fluid formulations

CURIG AGENT	PAM 01	PAM 02	PAM 03	PAM 05	PAM 1	PAM 2
Parts of curing agent/ 100 parts of resin, phr	20	20	20	20	22	25
Critical time (Pot life), at 25 °C, min	90	88	93	97	91	120
Dynamic viscosity, critical time, Pa x s 25°C	280	300	260	280	610	600
Dynamic viscosity, Mixing time, Pa x s 25°C	17	17	20	19	15	18

Table 3 Mechanical properties of the formulations cured with the different curing agents

CURING AGENT	PAM 01	PAM 02	PAM 03	PAM 05	PAM 1	PAM 2
KV2 (Charpy) kJ/m^2, 10 specs.	2.6±0.2	3.4±0.1	2.2± 0.3	2.9±0.2	3.0±0.2	3.1±0.3
σ_R ,MPa ,5 specimens	45.9±0.3	45.2±0.4	47.1±0.2	46.5±0.2	43.3±0.3	45.5±0.4
E , GPa 5 specimen	4540±3	4620±2	4705±1	4450± 3	4330±2	4550±4
H, Shore D 20 specimen	70±0.5	75±1	78±1	79±0.5	78±1	80±0.5

Permeability of the formulations: The "transfer" of water vapour, liquid water and carbon dioxide through the film of the cured resin was evaluated according to the UNI EN 1931 Standard.

For the water vapour, the mouth of a cylindrical glass vessel containing $CaCl_2$ was covered with a pre-cast film of the cured formulation (0.5 mm thick) to be tested and hermetically sealed with silicone resin; the sealed vessel was then stored 45 days into a large container at 20 °C and 100% R.H. The increase in weight of the salt was measured and referred to the exposed surface and thickness of the film (Table 4).

Table 4 Water vapour permeability at 45 days

CURING AGENT	PAM 01	PAM 02	PAM 03	PAM 05	PAM 1	PAM 2
Water transferred, 20 °C $mgH_2O/mm^2 x\ mm$	0.06	0.07	0.08	0.42	0.30	0.26

Similar tests, using ascarite as sorbent and 98% CO_2 gaseous environment were carried out at 20 °C to determine the carbon dioxide permeability (Table 5).

Tests for the liquid water permeability were also carried out (1 m of liquid water column); all the formulations resulted waterproof.

Table 5 Carbon dioxide permeability at 45 days

CURING AGENT	PAM 01	PAM 02	PAM 03	PAM 05	PAM 1	PAM 2
CO_2 transferred, 20°C mg CO_2/mm^2 x mm	0.02	0.02	0.02	0.016	0.02	0.18

Creep tests: To complete the mechanical characterization of the cured epoxy formulations, creep tests were carried out on specimens subjected to the constant tensile stress of 5 MPa at room temperature (25 ± 1 °C) and 100% R.H. (Figure 2).

Concrete-epoxy joints

Curing of concrete: Cubic specimens (15x15x15 cm): 28 days at 20 ± 1 °C and 95% R.H., followed by 60 days at 20 ± 1 °C and 60% R.H. The free surfaces of the cubic specimens were preliminarily carefully brushed to eliminate the weak surface layers.

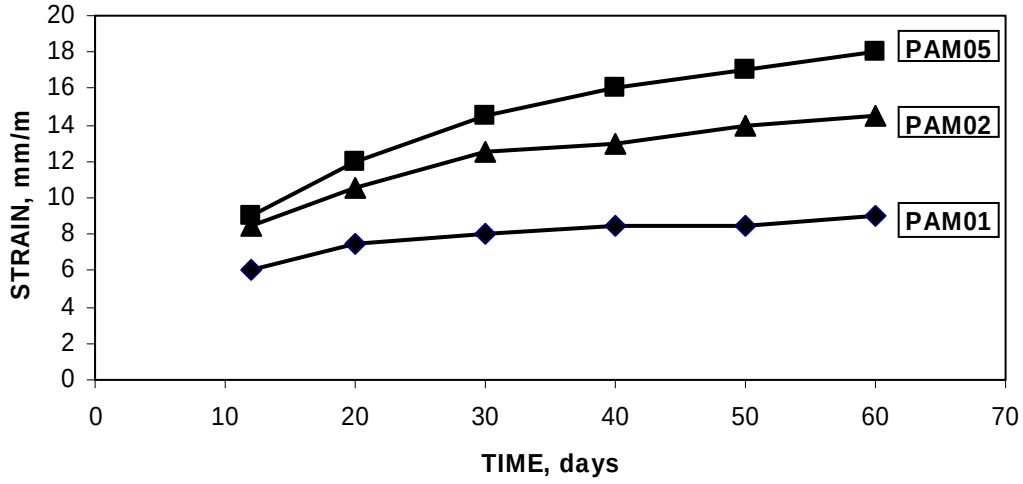

Figure 2 Creep test of the resin crosslinked with different curing agents.

Pull-off adhesion; The adhesion of the different formulations to concretes was tested according to ASTM D5179, by means of an Elcometer "Adhesion tester". The direct tensile pull off test of a steel "dolly" (Figure 3 a) glued to the concrete surface by means of the formulation to be tested supplied the strength of the joint which resulted always over 5.0 MPa (10 specimens). The fractured surfaces were carefully examined to identify the percentage of "cohesive" failure into the concrete (Figure 4). The best performances were those of the resin cured with P.A.M. 05 and P.A.M. 2 agents (100% cohesive failures); the remaining formulations failed into the concrete at a lower extent (cohesive failure: about 75%).

Shear adhesion: The adhesion under shear stress (Figure 3b) was also evaluated: all the joints failed into concrete, at a measured strength of about 10 MPa (10 specimens each tested concrete).

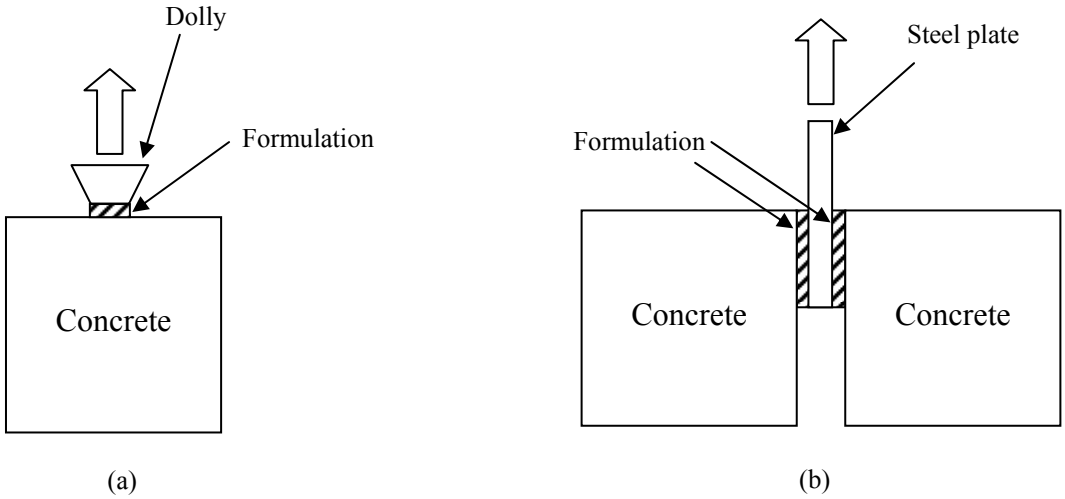

Figure 3 Adhesion test: a) Pull-off, b) Shear.

Figure 4 Cohesive failure of a joint (Pull-off test)

Durability of the joints: The clean surfaces of the different concretes (cubic specimens) were carefully coated by paint brush with a film 0.5 mm thick of the epoxy formulation to be tested. After curing, specimens were subjected to:

- U.V. irradiation: twelve hours, U.V. rays ($\lambda = 254$ nm) , specific power 2.2 W/cm^2.
- Freeze – thawing cycles (UNI EN 13687-7): twenty cycles (– 18 °C / + 25 °C).

The adhesion of the formulations to the concrete after U.V. irradiation and after thermal cycles was measured, according to the previously reported procedures (glueing 5 dollies of the pull-off test on each film).

The failures were always cohesive into concrete (formulations cured with P.A.M. 05 and 2: 100 %; > 70% for the remaining P.A.M. agents).

Repairing and reinforcing mortar samples: Some fractured or intentionally cut specimens (cubic and prismatic) of 'standard' mortar were 'repaired' by using the epoxy-PAM 05 formulation (Figure 5 a and b), cured four days at room temperature. The repaired specimens were tested to measure their 'new' compressive and flexural strength (Table 6).

Table 6 Compressive and flexural strength of the repaired specimens (Thickness of the epoxy formulations: 1 mm)

	Rf, MPa, 4x4x16 cm	Rc, MPa 4x4x4 cm
Inctact specimes, 10	6.0 +/- 0.4	30 +/- 1
Repaired specimens, 10	6.7 +/- 0.5	30 +/ - 1

Some other intact specimens of 'standard' mortar were preliminarily 'reinforced' as follows (Figure 5c):

- a reinforcing layer (2 mm thick) was applied to the bottom of the 4x4x16 cm prismatic specimens for flexural strength; the layer was a unidirectional fibreglass (450 fibres/mm^2)-epoxy-PAM 05 matrix composite (fibres//maximum tensile stress). Reinforced specimens were then tested to determine the resulting flexural strength.

- A reinforcing layer (1 mm thick) was applied circumferentially to the lateral surfaces of the 4x4x4 cm cubic specimens for compressive strength. The layer was a pre-impregnated epoxy-PAM05 fibre glass tissue (0°/90°). Reinforced specimens were tested to measure their compressive strength. Results are reported in Table 7.

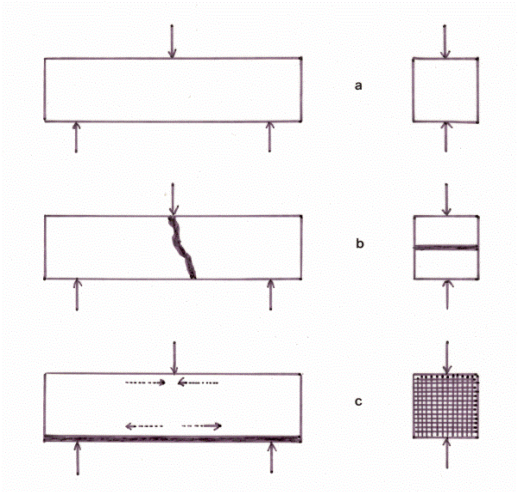

Figure 5 Repairing and reinforcing mortar samples: a) Original samples, b) Repaired samples, c) Reinforced samples

Table 7 Reinforcing action of the composites.

	Rf, MPa (4x4x16 cm)	Rc, MPa (4x4x4 cm)
Original specimens (10)	6.0 +/- 0.4	30 +/- 1
Reinforced specimens (10)	12.4 +/- 0.3	32 +/ - 1

Finally the fractured prismatic specimens were repaired by using epoxy–PAM 05 formulation and reinforced by means a reinforcing layer of 150, 450, 600 (fibers/mm^2), the measured flexural strengths were (10 specimens each test) were 7.2, 11.5 and 14.3 (MPa) respectively.

ANALYSIS OF THE RESULTS

The epoxide formulations (resin + curing agent) for the repair and/or coating of a concrete structure must fulfil many fundamental requirements.

When yet in the fluid state, the formulation must completely fill the cracks and wet the surfaces of concrete [7, 8]: the main characteristics are the viscosity and the pot-life, i.e. the time elapsing between the mixing of the components and the onset of the curing reaction. When fluid, the experimented formulations can attain both the wettability of the surfaces and the filling of the cracks: in fact their viscosities stay always below 20 [Pa x s] for time between 90 and 120 minutes (Table2: critical time/pot-life and dynamic viscosities up to the critical point, see figure 1).

When cured, the formulation (and the joint with concrete) must obey to many different chemical, physical and mechanical requirements [9, 10]. After the curing (72 hours at room temperature) the epoxy- concrete joints behave correctly:

- in the adhesion tests, the failures are constantly cohesive into concrete and the strength of the joints always exceeds 5 MPa (pull-off test) and 10 MPa (shear test). The ratio between tensile strength of the cured formulations (Table 3) and their adhesion to concretes is higher than 4:1. Nevertheless, the best results were those of the formulations containing P.A.M. 05 and P.A.M 2 (cohesive failure 100%).
- The elastic moduli (Table 3) of the formulations range between 4,3 and 4,7 GPa (lower than those of the concretes).
- The wear resistance is guaranteed by the values of hardness above all for the formulations cured with P.A.M. 05 (HD = 79) and P.A.M. 2 (HD = 80).
- For the “crack bridging” ability of a coating or of a repairing material there are some preliminary consideration to take into account. When a crack develops at the surface of a coated concrete or begins to propagate after a repair, the stress of the movement will be directed into the coating (or the repair) [10-12] and the apex of the crack begins to move slowly upward in the resin.

Nevertheless the apex will propagate into the resin only if the “local” stress (resulting from the stress intensity factor) will be greater than the tensile strength of the resin itself. If the stress at the apex is lowered by the visco-elastic behaviour of the resin, it will be possible that the crack does not move any further. In few words the stress will be lowered with time to a value smaller than the minimum stress needed for the propagation.

The “stopping” action can take place only when the resin under stress is subjected to a some extent of creep. In conclusion, the “crack” bridging action of a coating or a repair is function of the creep behaviour of the formulation itself [10].

The creep tests of experimented formulations (Figure 2) show the better behaviour of the resin crosslinked with the P.A.M 05 curing agent: under a constant stress of 5 MPa this formulation attains the highest creep-strain with time, so there will be in it a greater lowering

of the stress. Consequently the formulation epoxy-P.A.M. 05 has the highest crack-bridging ability. From the "mechanical" point of view it would be concluded that P.A.M. 05 should be the best curing agent of the series. But there are some other fundamental requirements the cured resin must obey: physical and chemical.

- All the formulations resulted waterproof (under 0.1 bar of liquid water) so the aggressive agents of the aqueous solutions will be stopped.
- P.A.M. 05 cured resins has the highest water-vapour permeability (0.42 mg/mm^2 x mm, table 4) and the lowest carbon dioxide permeability (0.016 mg/mm^2 x mm, table 5): water vapour exchange with the surrounding environment and the closer layers of concrete will be not hindered; for a Portland concrete substrate, the dangerous carbonation reaction will be avoided.
- Finally the higher durability of the formulation containing the same P.A.M. 05 agent to the U.V. irradiation and to the freeze-thawing has been positively tested.

The final considerations are related to the chemical and structural constitution of the system epoxy-P.A.M. 05 after curing at room temperature, to explain the higher permeability to water vapour and the lowest permeability to carbon dioxide.

The methylolic group (-CH_2OH) inserted on the molecule of the poly-amine (T.E.P.A.) exerts some degree of steric hindrance on the molecule (Table 1) and a reduction of alkalinity and polarity of the amino-groups [13,14]. Furthermore the methylolic functions remain unchanged into the crosslinked matrix.

The steric hindrance determines the "porosity" of the matrix so the higher the methylolic density, the greater will be the width of the pores [14] after the crosslink of the resin. Permeability to water vapour can be attributed both to the width of the porosity and to the reduced polarity of the reticulated matrix [13]. Similar considerations are valid for the impermeability to carbon dioxide, but the correct width of the pores is also supported by the residual alkalinity of the amino-methylolic functions (which can chemically react with carbon dioxide) [15].

In conclusion the curing with P.A.M. 05 determines the obtainment of an epoxy matrix bearing the "correct" degree of porosity and alkalinity required for both the actions.

Finally, it can be stated that the repair of fractured/cut specimens of mortar, by using the epoxy-PAM 05 formulation gives rise to a full restoring of their original strength, both flexural and compressive (table 6). Furthermore, the coating by means of the epoxy/fibreglass composites could cause a great enhancement of their strength; of course, the reinforcing action depends on the density (fibres/mm^2) and the alignment of the fibres into the composite layer (table 7).

CONCLUDINGS REMARKS

From the whole results it can be stated that the P.A.M. 05-epoxy formulation practically respects the requirements of the EN 1504 standard, because of its chemical, physical and mechanical characteristics.

The P.A.M. 05 tailored curing agent owing to its substitution degree (density of $–CH_2OH$ groups) yields a reticulated formulation with the right crosslinking (porosity), alkalinity and polarity for stopping carbon dioxide and liquid water, but not the water vapour.

Moreover the repair and coating show a great durability, i.e. the adhesion to the concrete is not affected by U.V. irradiation and freeze-thawing cycling; the crack bridging ability of formulation is satisfying as well.

REFERENCES

1. SHAUN, A, HURLEY, W. Advance Concrete Technology, 2003, Elsevier Ltd Publisher, Oxford, Vol. 3, Chap. 17, pp 1-14.

2. SHAW, J D N. The Repair of concrete structures (2nd edition). 1994, Spoon Press, London, p 37.

3. EN 1504. Products and systems for the protection of concrete structures, UNI Italy, Milano, 2005.

4. MAYS, G. European standardisation of products and systems for the protection and repair of concrete structures: the current position, in Repair and Renovation of Concrete Structures, 2005, Thomas Telford, London, pp 477-484.

5. GIAVARINI, C, MAURA, G, RINALDI, G. Assorbimento di gas acidi con soluzioni di poliammine alifatiche modificate, La Chimica e l' Industria, Vol. 55, No. 1, 1973, pp 23-29.

6. MAURA, G. PACCHIOLI, E, RINALDI, G. Indurimento di resine epossidiche ad alta e bassa temperatura con poliammine modificate ad azione flessibilizzante, La Chimica e l' Industria, Vol. 55, No. 12, 1973, pp 951-957.

7. AL-ZAHRANI, M M, MASLEHUDDIN, M, AL-DULAIJAN, S U, IBRAHIM M. Mechanical properties and durability characteristics of polymer and cement-based repair materials, Cement and Concrete Composites, Vol 25, No. 4-5, 2003, pp 527-537.

8. POSTON, R W, and Oth. Selecting durable repair materials: performance criteria – laboratory results, Concrete International, Vol. 22**,** No. 11, 2000, pp 21-29.

9. DANSK STANDARD Repair of concrete structures to EN 1504, 2004, Elsevier Ltd Publisher, Oxford, pp 24-44.

10. DELUCCHI, M, BARBUCCI, A, CERISOLA G. Crack-bridging ability and liquid water permeability of protective coatings for concrete, Progress Inorganic Coating, Vol. 33**,** No 1, 1998, pp 76-82.

11. ISSA, C A, DEBS P. Experimental study of epoxy repairing of cracks in concrete, Construction and Building Materials, Vol. 21, 2007, pp 157-163.

12. KAMAL, A, KUNIEDA, M, UEDA, N, HIKARU N. Evaluation of crack opening performance of a repair material with strain hardening behaviour. Cement and Concrete Composites, Vol. 30, 2008, pp 863-871.

13. RINALDI, G, ROSSI G. Particulate composities from epoxy resin and fly-ash for the confinement of medium and low level radwastes, Polymer International, Vol. 31, 1993, pp 227-233.

14. RINALDI G. Acid gas absorption by means of aqueous solutions of regenerable modified polyalkylene polyamine, Industrial and Engineering Chemisty Research, Vol. 36, No 9, 1997, pp 3778-3782.

15. DE FILIPPIS, P, GIAVARINI, C, MAGGI, C, RINALDI, G, SILLA, R., Modified polyamines for CO_2 absorption, Industrial and Engineering Chemisty Research, Vol. 39, No 5, 2000, pp 1363-1368.

Theme 4 — Structural Health Monitoring and Life Extension

Extending Concrete Structures Service Life Using FRP and Structural Health Monitoring – A Case Study

G Lee[1], J Wang[1], K Tang[2], S H Giam[2]
1 – Fyfe (Hong Kong) Limited / Techconsult Limited, Hong Kong
2 – Greg Wong and Associates Limited, Hong Kong

Old structures often need repair and strengthening to be in a serviceable condition. This paper reports on the rehabilitation of a 30-year old pre-stressed concrete bridge to satisfy the new building regulations in Hong Kong. Because of site constraints, a combination of post-tensioning and fibre-reinforced polymeric technology was used, the latter of which formed the first project case approved by the Hong Kong building authority. Due to the pioneer nature of the project, full load-testing and several long-term monitoring techniques were designed and installed including optical fibre strain measurement. In this paper, the design basis is presented and details for implementation highlighted, including selection for materials, method of installation, fire proofing, full load testing and monitoring. Finally the test results are presented and long-term monitoring data discussed, from which some preliminary conclusions are drawn.

Gary Lee has over 12 years of engineering experience in corrosion protection, design, construction, repair and strengthening of civil infrastructures and buildings. He obtained his Bachelor's degree and Master's degree from the University of Hong Kong. Since then he has worked with Maunsell Consultants Asia Limited. He is now the Deputy General Manager of Fyfe (Hong Kong) Limited and Director of Materials Techconsult Limited. He has been involved in various significant civil engineering projects in Hong Kong such as Central Reclamation Phase III, West Rail, East Rail Extensions and Ma Wan Island Development. Gary is experienced in condition survey, defect investigation, structural strengthening and corrosion engineering of structures.

Kevin Tang has over 20 years of experience in building development and highway structure projects. He is now the Managing Director of Greg Wong and Associates Limited. His experience includes project management, preliminary engineering design, cost feasibility studies, supervision of technical and support staff, co-ordination of work with various agencies and government departments, detail design, construction supervision and contract administration. Mr. Tang's projects include high-rise building complex with transfer plate, deep excavation for basement construction, foundation design in difficult ground conditions, site formations, access viaducts and footbridges.

Mr. Siang Hai Giam is a Chartered Engineer with over 20 years of experience in general and specialist construction works. He was involved in the introduction of Tyfo Fibrwrap FRP system in Asia more than 10 years ago for civil and building works. Over the years Mr. Giam has been involved in the senior management of various general and specialist construction companies with works across Asia.

Dr. Jinsong Wang is a Chartered Civil Engineer with over 20 years of experience in the field of research and development, engineering consultancy and contracting. He obtained his Bachelor's degree from the Southeast University (China) and the Doctor's from the University of Dundee (UK). Since then he has worked with Taywood Engineering Ltd (UK), British Rail Research (UK), Harris & Sutherland Consulting Engineers (HK) and L&M Specialist Construction Ltd. Before joining Materials Techconsult Ltd. and Fyfe (Hong Kong) Ltd., he was the Chief Engineer with Maunsell Consultants Asia Ltd. as the Chief Engineer on materials technology. Dr Wang specialises in the use of materials for civil and building works, durability design, corrosion protection, repair and strengthening of concrete structures. He has published over 20 technical papers and is a Visiting Professor to the Southeast University, Nanjing. He also served in the past as the Honourary Secretary of the Materials Division of the Hong Kong Institution of Engineers.

Keywords: FRP, Optical fibre, Strengthening, Structural health monitoring

INTRODUCTION

Swire Bridge is located at the Main Campus of the University of Hong Kong. This bridge was constructed in 1970s. It consists of a two-lane carriageway and a footpath and serves as the main vehicular and man access to the eastern part of the campus from the central part. The total length of the bridge is 52.5 m. It consists of three continuous spans supported by two end abutments and two intermediate piers. The main span is 22.5 m and the two side spans are 15m. The bridge deck is constructed with prestressed concrete with internal tendons passing through the bridge deck. Bridge piers and abutements are conventional reinforced concrete structures and they are supported by bored piles. Swire Bridge is an emergency vehicular access and truck access. Current trucks and emergency vehicles can weigh 28 ton or more. However, the bridge is designed to resist a live load of 20 ton originally. Therefore there is a need of upgrading the bridge to accommodate the latest live load requirement.

A design check was conducted to assess the existing capacity of the bridge, including overall stability and load capacities of different structural elements. Design check results showed that the bridge was of sufficient overall stability without failure in the ultimate limit state. The sub-structure, including piers, abutments and foundations was of sufficient loading capacity to resist the increased load. As for the bridge deck, while the deck was able to resist the increased load in ultimate limit state, it failed to pass the serviceability limit state requirements. It was anticipated that the bridge deck would be of excessive deflection and have potential cracking problem. Excessive deflection and cracks would affect the durability of the structure by allowing corrosive substances, e.g., oxygen and moisture, penetrating into cover of concrete. The risk of corrosion of steel reinforcement would increase. Severe steel corrosion would lead to delamination of concrete cover and spalling problems, reducing the life of the bridge deck. In extreme case, if the existing prestressing tendons are corroded, the prestressing force would reduce, causing detrimental effects to the loading carrying capacity.

Since potential problems in the bridge deck were identified, it was necessary to develop a suitable strengthening method for the bridge so that deflection and cracking can be controlled and hence the service life of the bridge can be extended. In this project, a combination of prestressing and fibre-reinforced polymeric technology was used, the latter of which formed the first project case approved by the Hong Kong building authority. Due to the pioneer nature of the project, full load-testing and several long-term monitoring techniques were designed and installed including optical fibre strain measurement. Due to the pioneer nature of the project, full load-testing and several long-term monitoring techniques were designed and installed including optical fibre strain measurement.

In this paper, the design basis is presented and details for implementation highlighted, including selection for materials, method of installation, fire proofing, full load testing and monitoring. Finally the test results are presented and long-term monitoring data discussed, from which some preliminary conclusions are drawn.

SELECTION OF STRENGTHENING METHOD

During the project design stage, various strengthening methods were considered with a view to increase the bridge's performance in deflection and cracking at service load and hence extend of service life of the bridge. Each method has its own characteristics and hence strengths and shortcomings. The various methods considered are discussed below.

Span Shortening

The bridge deck failed to meet the deflection and crack control requirements, which were related to bending moment of bridge deck. If bending moment of the bridge deck at design load is reduced, both deflection and cracking problems can be reduced. Span shortening is one of the available methods to reduce bending moment. This can be achieved by adding intermediate piers or by enlarging the crossheads of the piers. However, the disadvantage of this method is that, while sagging moment can be controlled, hogging moment will be introduced at the new supporting points and cause cracking and durability problems at new locations. In addition, underneath the bridge it is a steep slope which makes it difficult to construct new piers.

Additional Steel Frame

To mitigate excessive deflection and control cracks, another method is to increase the bending moment capacity of the bridge decks. Additional steel frames under the existing bridge deck spanning across supports are able to serve this purpose. Part of the live load can be transferred to this new steel frame, thereby reducing the load imposed on the existing bridge deck. However, as a metallic structure, steel frame would have corrosion problem. Suitable corrosion protection method should be adopted to mitigate corrosion problem. Also, the additional steel frame would cause great visual impact to the existing bridge which would not be accepted by the client.

Additional Concrete Layer

The concept of additional concrete layer is similar to the additional steel frame. A layer of concrete is constructed on top of the existing bridge, as if it is a composite bridge deck construction. The bridge deck section is enlarged and the load carrying capacity is hence increased. However, the additional concrete layer will raise the top level of the bridge. The road profiles of the adjacent access roads and building entrance will need to be adjusted to suit the road level. The extent of modification works will be substantial.

Fibre-reinforced Polymer Strengthening

Fibre-reinforced polymer (FRP) technology was first developed in the aerospace industry. With the characteristic of high strength and light weight, it was developed into the field of civil engineering for strengthening purpose. To control excessive deflection and control cracks, FRP plates are bonded to bridge deck surfaces using epoxy. The FRP plates and the bridge decks form a composite section to resist additional live load. The advantage of this method is that, due to the light weight of the FRP material, the installation and handling are easy and it does not require heavy machinery. It has minimal visual impact and preserves the original appearance of the bridge. However, this bridge strengthening method has not been approved by the Buildings Authority before. Extra effort in proofing the long term performance of the strengthening works will be required.

Additional Prestressing

The method of prestressing makes use of high strength bars or cables stressed to prescribed forces. These forces are exerted on the bridge deck and impose a bending moment profile on it, usually in the opposite sense to the one cause by loading. The overall concrete stress is

hence controlled within the required limits. It is not possible to form internal holes within the bridge deck section. Prestressing tendons need to be installed externally and it has minor visual impacts to the bridge's appearance. Prestressing tendons are able to exert large active forces on the existing structure and hence can achieve a high degree of strengthening. However, this method requires a more complicated design and analysis, such as stress statuses at various prestressing stages and anchorage block design. In addition, prestressing tendons are prone to corrosion. Special corrosion protection method suitable adopted to prevent them against corrosion.

Adopted Methods

Each of the above life extension methods has its own merits and shortcomings. During the selection process, preference is given to the method with minimal visual impact and ease of application. Span shortening and additional steel frame would cause substantial change in bridge's appearance and hence are rejected. Additional concrete layer would affect road profiles of adjacent access roads and it is not preferred to have extensive modification works to these adjacent roads. FRP strengthening is the most preferred method since it can maintain the original appearance of the bridge and the application method is simple. However, FRP strengthening is able to resist additional load only. To reduce deflection and control cracks caused by existing dead loads, the method of prestressing is preferred. Therefore, after careful considerations, the selected strengthening method of the bridge combines both FRP and prestressing technologies. By adopting this strengthening method, the cracking and deflection of the bridge will be better controlled. Under extreme loading conditions, the bridge will not be subject to excessive deflection and cracking. Corrosive substances such as carbon dioxide and moisture cannot penetrate through concrete cover into steel reinforcement and prestressing tendons. The durability of the bridge is hence better assured and the service life is extended.

In this strengthening scheme, FRP is placed at the tension zone of the bridge deck where cracks will occur under extreme loading conditions. FRP itself is a non-metal and is impermeable to water and gases. Therefore, it serves an additional function as a physical barrier against the ingress of corrosion substances and further improves the durability of the bridge.

SELECTION OF MATERIALS

The primary purposes of this project are to upgrade the bridge to meet the current live load standard and improve the durability of the bridge. Materials selected should be able to fulfil both the performance requirement and durability requirement. Performance requirement means that the loading resistance properties of the materials should be high enough to resist the new design load. Durability requirement means that the materials should be durable enough to fulfil the design life requirement. If a deterioration mechanism of a material is identified, suitable protective measures should be implemented to arrest the problem and extend the service life as much as possible. In this project, the selected life extension method includes both FRP and prestressing. The selection of both FRP and prestressing materials are discussed below.

FRP Material Selection

The two common FRP materials for structural strengthening applications are glass fibre reinforced polymer (GFRP) and carbon fibre reinforced polymer (CFRP). Typical tensile properties of FRP materials can be found in "Concrete Society – Technical Report No. 55 Design Guidelines for Strengthening Concrete Structures using Fibre Composite Materials, Second Edition". In general, tensile strength and modulus of CFRP are higher than those of GFRP. To satisfy the performance requirement, the higher stiffness material, i.e., CFRP, is preferred, so that the composite section has a higher overall stiffness against bending and hence deflection and crack control.

Consideration is also given to durability performance. Both GFRP and CFRP do not have corrosion problem since they are non-metallic materials. The identified deterioration mechanisms of FRP materials are degradation due to ultra-violet light and damage in case of fire. In this case, a fire insulation layer is used to protect the installed FRP against fire and block the ultra-violet light.

Considering that the durability performances of GFRP and CFRP materials are similar but CFRP has a better loading performance then GFRP. Therefore CFRP is adopted for this project.

Prestressing Tendon Selection

Prestressing tendons are usually available in two forms: prestressing bars and prestressing strands. From loading performance's point of view, a prestressing bar has a larger cross sectional area than a prestressing strand and thus a higher tensile load capacity. Therefore using prestressing bars can minimize the required anchorage size for which limited suitable locations at bridge deck are found.

From durability point of view, both prestressing bars and strands are made of high strength steel and they are prone to corrosion. For the same prestressing force, more strands than bars are required and thus strands have a larger overall surface area and thus the risk of corrosion is higher. To prevent corrosion from occurring, suitable corrosion protection measures should be used. Heat shrinkable plastic tubes are adopted for this purpose. These plastic tubes serve as physical barriers which block water and moisture from going into the steel surface so that corrosion will not occur.

Combining the above considerations, prestressing bars are the preferred option to prestressing strands since prestressing bars are better in both loading and durability performances.

STRENGTHENING DESIGN AND APPROVAL

According to Buildings Regulations of Hong Kong, any structural alternation and additional works shall be approved by Buildings Department. To obtain this approval, submissions with full justifications are needed. The required submissions include structural strengthening design, quality control proposal, materials' durability data, etc..

This project involves a bridge structure and therefore the bridge's structural analysis is in accordance with "BS 5400 – Steel, Concrete and Composite Bridges" and "Highways Department – Structures Design Manual", both of which are design manuals common adopted in Hong Kong. For the design of FRP, since there is no available British Standards or Hong Kong standards, two design guidelines, namely "Concrete Society – Technical Report No. 55 Design Guidelines for Strengthening Concrete Structures using Fibre Composite Materials, Second Edition" and "The International Federation for Structural Concrete – Bulletin 14 Externally Bonded FRP Reinforcement for RC Structures" are adopted. As a conservative approach, the FRP design is checked against these two design guidelines so that requirements from both guidelines are satisfied.

Quality control and durability of the materials are two main concerns during the approval process, especially the FRP material since this material is the first time being approved by the Buildings Department of Hong Kong. As parts of the approval conditions by Buildings Department, a series of quality control tests on the FRP system is required, including tensile tests for tensile strength, pull off tests for adhesion, tapping tests for void identification, verification load test and structural health monitoring, etc.. Among these tests, verification load test and structural health monitoring are discussed in more details in the following text.

SYSTEM INSTALLATION

The installation of strengthening systems started in 2008 and was completed in July 2009. The installation was in accordance with the following procedure. References were made to "Concrete Society – Technical Report No. 55 Design Guidelines for Strengthening Concrete Structures using Fibre Composite Materials, Second Edition" and "Concrete Society – Technical Report No. 57 Strengthening Concrete Structures using Fibre Composite Materials: Acceptance, Inspection and Monitoring". Some photos showing different steps of installation are also given.

(i) Conduct verification load test before strengthening systems' installation

(ii) Conduct tensile test for FRP material as quality control

(iii) Construct anchorage blocks for prestressing bars

(iv) Install prestressing bars and stress them in stages

(v) Install corrosion protection system to prestressing bars

(vi) Install CFRP plates on bridge soffit (Figure 1).

(vii) Conduct quality control tests to CFRP plates, including pull off tests, tapping tests, etc.

(viii) Conduct verification load test after strengthening systems' installation

(ix) Install optical strain gauge system

(x) Apply a proprietary fire rated fire protection layer to CFRP plates

(xi) Completion of works (Figure 2)

Figure 1 Prestressing bar and CFRP plate installation in progress

Figure 2 Bridge after strengthening works

VERIFICATION LOAD TESTS

The purposes of verification load tests were to verify the performance of the bridge after the upgrading works. Two verification load tests were conducted, one before strengthening and one after strengthening. The load tests made use of a 28 ton lorry travelling along the bridge. The lorry moved to the centres of the three spans in sequence and acted as a point load on those locations. Strains and deflections at representative locations were measured. Strains were measured using electrical strain gauges installed on surfaces of concrete, CFRP plates and prestressing bars. Figure 3 and Figure 4 show the strain monitoring locations before and after strengthening works respectively. Deflections were determined by measuring the change in reduced levels at mid-spans using a digital level, as shown in Figure 5.

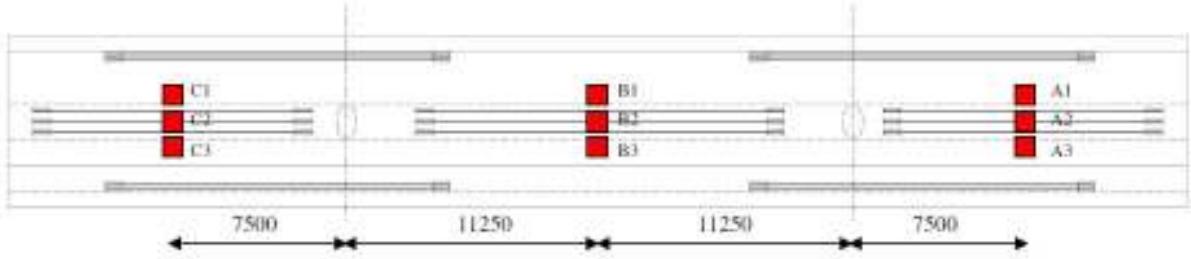

Figure 3 Locations of strain monitoring points (before strengthening)

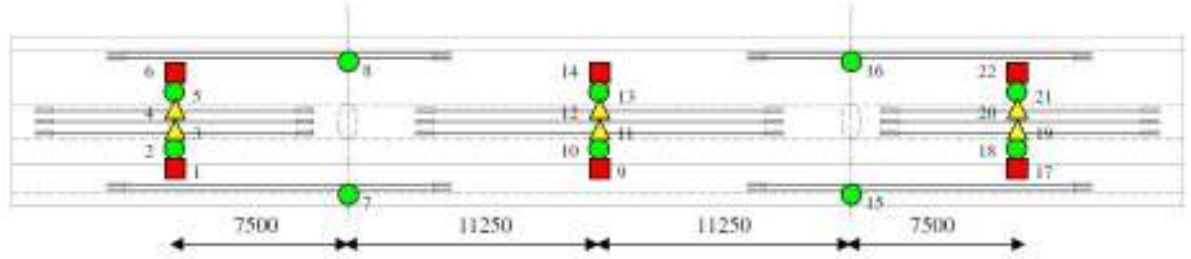

Figure 4 Locations of strain monitoring points (after strengthening)

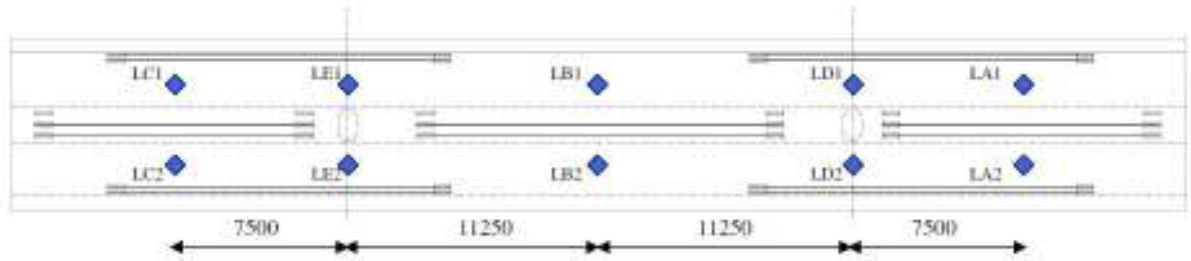

Figure 5 Locations of level monitoring points (before & after strengthening)

LEGEND

- Monitoring nails for level measurement
- Strain gauges on concrete surface
- Strain gauges on external post-tensioning
- Strain gauges on CFRP surface

The first load test was conducted to establish the bridge conditions before the strengthening works. Results showed that when the truck was placed at the middle span, the measured strain of the bridge exceed the predicted strain value by design calculations. This indicated that the bridge's existing condition was poor and the deflection exceeded the predicted value. Excessive deflection would lead to cracking and affect the durability of the bridge.

The second load test was conducted to verify the effectiveness of the strengthening works. The same 28 ton lorry was used to load the bridge, as shown in Figure 6. Strains and deflections of the bridge were measured when the lorry was at different locations of the bridge. Strain gauges were installed at the required strain monitoring points. Cables from strain gauges were centralized to a strain measurement unit so that strain data could be read out, as shown in Figure 7. The results obtained are shown in Tables 1 and 2 below.

Figure 6 Lorry for verification load tests

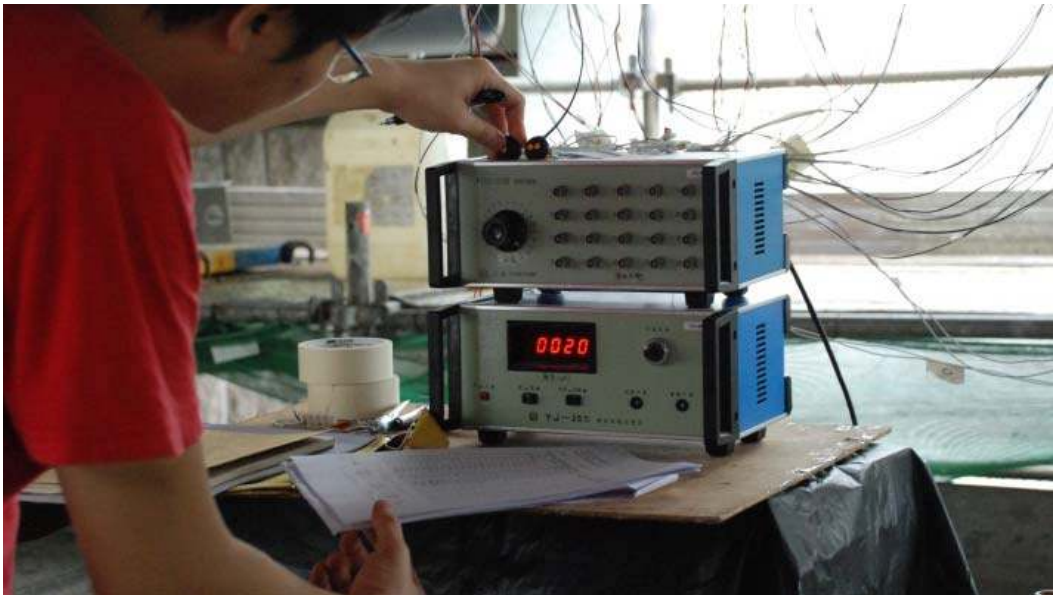

Figure 7 Strain measurement during verification load tests

Table 1 Deflection measurement results in the second load test

LORRY POSITION	DEFLECTION AT RESPECTIVE SPAN, mm		% OF ESTIMATED VALUE
	Estimated	Average measured	
West span	1.99	1.15	57.8
Middle span	4.74	2.95	62.2
East span	1.99	1.55	77.9

Table 2 Strain measurement results in the second load test

LORRY POSITION	STRAIN AT RESPECTIVE SPAN, με				% OF ESTIMATED VALUE
	Estimated	Average measured			
		Concrete	Prestressing bar	CFRP	
West span	57.9	13.5	16.5	21.0	23.3-36.3
Middle span	73.2	62.0	53.5	51.0	69.7-84.7
East span	57.9	49.5	38.5	48.0	66.5-85.5

It can be seen that all measured deflections and strain values were less than the estimated values. The deflections reached between 57.8% and 77.9% of the corresponding estimated values. For the strain readings, the corresponding values were 23.3% to 85.5% of the estimated values. Therefore both deflections and strains did not exceed the predicted values. The performance of the strengthening works was hence verified.

STRUCTURAL HEALTH MONITORING

The method of FRP strengthening was the first time approved by the Buildings Department in Hong Kong. Due to the pioneer nature of the works, a comprehensive structural health monitoring programme is implemented to monitor the structural health of the bridge and the strengthening system, including visual inspection, pull off test and optical strain monitoring.

Visual inspection is carried out to the whole bridge soffit, including the external prestressing system and CFRP system are inspected by visual inspection, with the aid of binoculars if necessary. The observed defects are recorded, including but not limited to spalls, cracks, signs of corrosion, etc..

Pull off tests are carried out verify the bond strength of CFRP plates over time. In addition to the required CFRP plates in accordance with the design, extra CFRP plates are installed at the bridge soffit, known as the Sacrificial Zone. Pull off tests are conducted to the CFRP plates at the Sacrificial Zone at the required time. Bond strength of CFRP plates are then determined.

Optical strain gauges are installed on the CFRP plates at six locations as required by the Buildings Department. The strain gauges' locations are shown in Figure 8 below. Cables from sensors are routed to a test station located at the soffit of the East Span. During a standard monitoring, a readout unit is connected to the sockets on the test station and send in optical signals to the sensors for measurement. Monitoring results are displayed on the laptop computer connected to the readout unit. The data obtained are wavelengths in the unit of nano-metre (nm). With formulas and parameters from the optical strain gauge supplier, the measured wavelengths are then converted to change in strains.

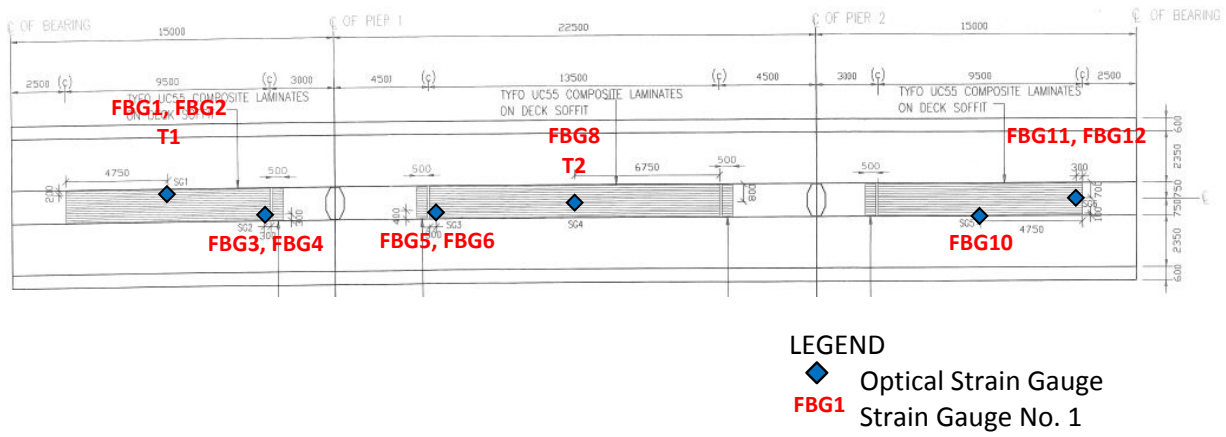

Figure 8 Locations of optical strain gauges

Selection of Strain Gauges

During the selection of strain monitoring method, several types of strain gauges were considered, including electrical resistance gauge, demountable mechanical gauge and optical strain gauge.

An electrical resistance gauge is in the form of a flat grid of wires mounted on a thin plastic sheet. Strain is measured by means of changes in electrical resistance resulting from extension and compression of the gauge. Electrical resistance gauge is the most common type of strain gauges. However, an electrical strain gauge is made of metal or alloy which is prone to corrosion. It is not suitable for the use in an exposed environment for a prolonged period. Therefore this type of strain gauge is not adopted for this project.

A demountable mechanical (demec) gauge consists of a sensitive dial gauge mounted on a steel bar with a pivoted pointer at one end. This gauge is used to measure the relative movement between two studs attached to the surface concerned. When there is a relative movement, the studs cause the pivoted pointer to rotate which turn causes the dial to change. This method would depend on the skills of the technicians since the readings would be affected by the force pressing onto the studs. This method also requires accesses to the bridge soffit which is not available. Therefore this method is not adopted.

One of the most common types of optical strain gauges is Fibre Bragg Grating (FBG) sensors. A FBG sensor consists of an optical fibre containing a grating. During measurement, a light source with a range of different wavelengths is sent in the fibre. The wavelength corresponding to the grating pitch is reflected by the grating while all other wavelengths pass through the grating undisturbed. Since the grating period is strain dependent, measuring the reflected wavelength is able to determine the strain. An optical fibre is made of quartz, which is a non-metal and does not have corrosion protection. This type of sensors is suitable for outdoor conditions and is more durable. Considering that the monitoring programme will last for ten year, this monitoring technique is adopted.

Monitoring Frequencies and Acceptance Criteria

The monitoring frequencies of the above monitoring methods are summarized in Table 3 below:

Table 3 Summarize of the monitoring frequencies of the above monitoring methods

ITEM	TEST METHOD	FREQUENCY	ACCEPTANCE CRITERIA
1	Visual inspection	Quarterly during Year 1 Bi-annually during Years 2 and 3 Annually during Years 4 to 10	No apparent visual defect
2	Pull off test	Two tests at Years 2, 5 and 10	Pull off strength not less than 1.5 MPa with no sign of significant movement
3	Strain Monitoring	Six test areas with the same frequency as (1) above	Measured strain not exceeding 1.8%

Monitoring Results

Strengthening works of the bridge were completed in July 2010 and the structural health monitoring then started. Up to July 2011, monitoring results of the first year have been obtained. Besides pull off tests will be conducted only after 2 years, visual inspection and strain monitoring results are available.

Visual inspection shows that the conditions of the bridge soffit and the installed strengthening works appeared in good conditions. No signs of defects were observed during each visual inspection. Optical strain monitoring is conducted quarterly. The changes in strains over time are shown in Figure 9 below. The changes in strains range between -0.048% and -0.002% and are well below the limit of 1.8%. Therefore, both visual inspection and strain monitoring show that the strengthened bridge is of good conditions.

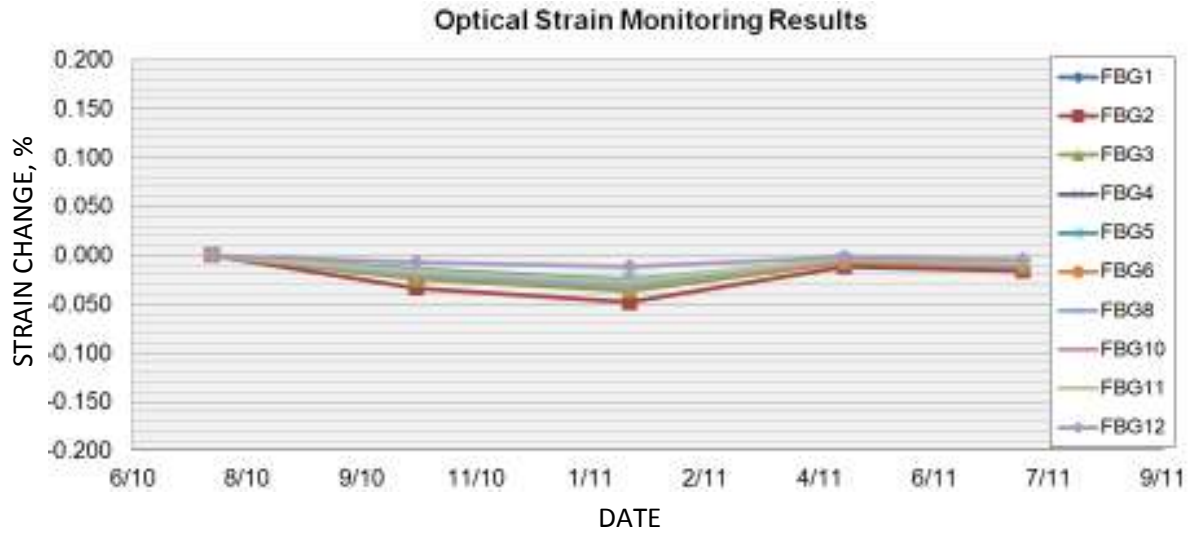

Figure 9 Changes in strains over the monitoring period

CONCLUSIONS

In this paper, a case study of extending a concrete bridge's service life using FRP strengthening and external prestressing is presented. Structural health monitoring is being implemented to the strengthened bridge. Monitoring results for the first year are obtained successfully. The results show that the strengthened bridge is in good condition. It is concluded that the adopted strengthening system is effective.

ACKNOWLEDGEMENTS

Acknowledgements should be given as appropriate. Please put acknowledgements before the References.

REFERENCES

1. BSI. Steel, Concrete and Composite Bridge - Part 4: Code of Practice for Design of Concrete Bridges, 1990, BS 5400-4: 1990.

2. BSI. Testing Concrete – Part 206: Recommendations for Determination of Strain in Concrete, Materials and Structures, 2007, BS 1881-206: 1986.

3. CONCRETE SOCIETY. Design Guidance for Strengthening Concrete Structures using Fibre Composite Materials. Technical Report No. 55, 2004.

4. CONCRETE SOCIETY. Strengthening Concrete Structures using Fibre Composite Materials: Acceptance, Inspection and Monitoring. Technical Report No. 57, 2003.

5. GLISIC B AND INAUDI D, Fibre Optical Methods for Structural Health Monitoring, 2007, Wiley.

6. HIGHWAYS DEPARTMENT. Structures Design Manual for Highways and Railways, 2006, HKSAR.

7. THE INTERNATIONAL FEDERATION FOR STRUCTURAL CONCRETE. Externally Bonded FRP Reinforcement for RC Structures. Bulletin 14, 2001, FIB.

Impedance monitoring for assessment of corrosion

F Reza
Minnesota State University, USA

Electrochemical impedance spectroscopy (EIS) is a powerful evaluation tool for composite materials. It is currently under utilized in practice in the area of civil engineering. The basic premise of IS is that each interface in a composite material will polarize in its own unique way when the system is subjected to an applied potential difference. A few lab studies have been reported in the literature attempting to assess corrosion of steel bars embedded in concrete utilizing EIS. In the present study, investigations were performed on steel bars embedded both in plain mortar as well as carbon fibre reinforced mortar (CFRM). Rapid macrocell tests were performed. These tests involve an anode bar encased in mortar and submerged in a salty pore solution electrically connected to two cathode bars in regular pore solution. Tests are conducted for 15 weeks. Corrosion was measured in three ways: measurement of the corrosion current across a resistor, measurement of the open-circuit corrosion potential using a saturated calomel electrode (SCE), and EIS. The frequency range of EIS was 0 – 5 MHz. Results of EIS on the bars in plain mortar proved unreliable and were not easily correlated with corrosion current or corrosion potential. Reports in the literature have indicated that carbon fibres impart a smart sensing capability to concrete. The bars encased in CFRM showed promising results. The diameters of the arcs in the Nyquist plot were sensitive to the corrosion current and potential.

Dr. Reza is associate professor in civil engineering at Minnesota State University since 2009. Prior to that, he served as assistant then associate professor at Ohio Northern University from 2001 till 2009. Dr. Reza's research interests include structural health monitoring and concrete material science. He is a member of ASCE Committee on Methods of Monitoring and Evaluating Structural Performance, and ACI.

Keywords: Impedance spectroscopy, corrosion, structural health monitoring

INTRODUCTION

Corrosion continues to be a major problem leading to reduced durability of reinforced concrete structures. A study sponsored by the Federal Highway Administration (FHWA) in 2001 estimated the total direct costs of corrosion for highway bridges in the United States (US) to be about $8.3 billion annually [1]. Indirect costs due to traffic delays and lost productivity may be as high as 10 times the direct costs. In the US, deicing salts are often used on bridge decks to keep them free of ice, and this leads to chloride ingress to the top reinforcement. Corrosion products occupy more volume than the original steel. This causes cracking and spalling of the concrete. Additionally, loss of steel area can lead to a decrease in strength.

Early detection of corrosion is challenging because the steel is embedded in the concrete, and by the time signs of distress are manifested the structure may already be seriously compromised. New nondestructive monitoring techniques are required to assess the degree of corrosion. The overriding cause of corrosion is the electrical potential difference between the cathode and anode. The rate of corrosion is a complex function of the metal-concrete interface, the reactive ions in the solution, and the nature of reaction products that may form on the interface. The only direct measure of the state of the interface is the actual polarization of the electrode with respect to a standard electrode [2]. To make such a measurement, connection must be made to the metal which may be undesirable since it exposes the rebar. An alternative approach may be electrochemical impedance spectroscopy (EIS) which measures the impedance (usually considered to consist of resistive and capacitive parts) to current flow when an alternating voltage is applied across the metal-solution interface.

Although several laboratory studies have been reported on the use of EIS to monitor aspects of corrosion of steel rebar in concrete [3-8] it remains unused for practical application to the field. One problem may be the inherent high resistivity of the concrete which could make obtaining stable measurements difficult. In this research study, several attempts were made to apply EIS to steel embedded in mortar, however inconsistent results were obtained from week to week during the rapid macrocell tests. Subsequently, carbon fibres were incorporated into the mixture to decrease the resistivity of the matrix. Results from the EIS show good correlation with corrosion current and electrochemical potential measurements.

Corrosion of steel in concrete requires four factors: an anode, a cathode, an electrolyte, and an electronic circuit. In these experiments the macrocell type of corrosion that occurs in real structures was simulated where typically the anode is the top bar, the cathode is the bottom bar, moisture e.g. pore water provides the electrolyte and metal chairs or ties provide the electronic circuit. Electronic current flows from the top bar (anode) to the bottom bar (cathode) while ionic current flows from the cathode to anode. One test method that provides for accelerated study of macrocell corrosion is the rapid macrocell test [9]. These tests are run for a period of 15 weeks.

For reinforcing steel, when oxygen is present, iron is oxidized at the anode, causing ferrous ions to go into solution, and releasing electrons (Eq. 1). At the cathode, oxygen combines with water and the electrons released at the anode to form hydroxyl ions (Eq. 2).

$$Fe\ (\text{metal}) \rightarrow Fe^{2+}\ (\text{aq.}) + 2e^{-} \tag{1}$$

$$1/2\,O_2 + H_2O + 2e^{-} \rightarrow 2OH^{-} \tag{2}$$

The ferrous ions combine with hydroxyl ions to produce ferrous hydroxide (Eq. 3), which is greenish-black in colour. The ferrous hydroxide is oxidized in the presence of moisture and oxygen to produce ferric hydroxide (Eq. 4), which is red-brown in colour. The ferric hydroxide can dehydrate to form ferric oxide, which can be black or red in colour, and is commonly known as rust (Eq. 5).

$$Fe^{2+} + 2OH^{-} \rightarrow Fe(OH)_2 \tag{3}$$

$$4Fe(OH)_2 + 2H_2O + O_2 \rightarrow 4Fe(OH)_3 \tag{4}$$

$$2Fe(OH)_3 \rightarrow Fe_2O_3 + 3H_2O \tag{5}$$

Rebar is normally passive in the concrete due to the high alkalinity of the cement paste. This high alkalinity leads to the formation of a gamma-ferric oxide layer on the surface of the steel that protects it from corrosion. This film can be destroyed by chloride ions and carbonation, which decreases the pH of the concrete.

EXPERIMENTAL PROGRAMME

For mortar specimens, Type 1 Portland cement was used. The sand was ASTM C109 Ottawa sand. The water-cement ratio was 0.5 and the sand-cement ratio was 2. For carbon fibre reinforced mortar (CFRM) specimens, carbon fibres were added at the rate of 0.4% of the total volume. The carbon fibres were Zoltek Panex 35 chopped flake 3 mm in length. The specimens were cast using PVC pipe to a 3.25 cm (1.278 in) diameter and 15.4 cm (6 in) length. A piece of No. 16 (No. 5) rebar of 127 mm (5 in) length was kept centred in the specimen using a rubber stopper. Threads were machined at one end of the rebar to accommodate a screw for electrical contact. To prevent corrosion at the exposed end of the rebar, it was subsequently epoxy coated. Specimen dimensions are shown in Figure 1.

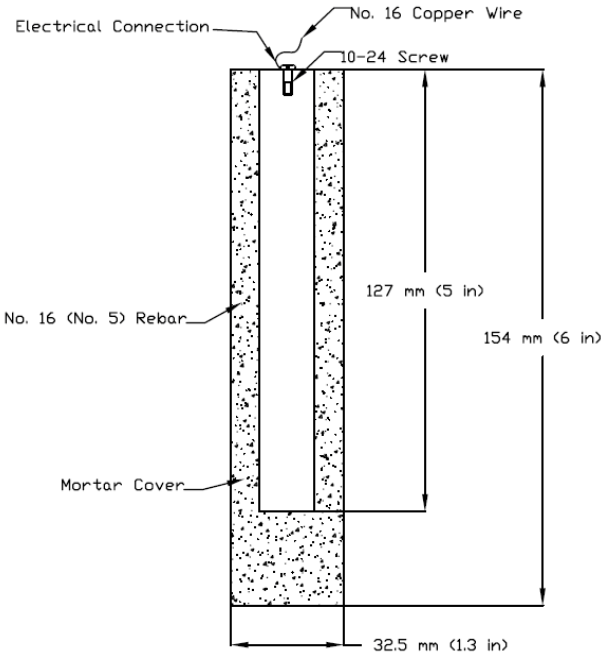

Figure 1 Specimens used for rapid macrocell tests

A rapid macrocell [9] test setup was created for the experiments. One mortar bar as described above served as the anode and two bars served as the cathode. The anode was kept in a separate plastic container from the cathodes. Each plastic container contained some crushed mortar pieces and a simulated pore water solution. The pore water solution consisted of 1.63% potassium hydroxide solution and 1.77% sodium hydroxide solution. In addition, a 6.04 molal ion concentration of sodium chloride was introduced to the container for the anode. The height of the container was such that 7.6 cm (3 in) of the rebar was submerged under the solution and the remaining 5.1 cm (2 in) was above the lid of the container. The two containers were connected with a salt bridge consisting of flexible tubing, agar and potassium chloride. Air, scrubbed with 1 M sodium hydroxide to remove carbon dioxide, was bubbled in (using a pressure regulator) to the container for the cathodes. The rebars were then electrically connected across a 10 ohm resistor to facilitate corrosion current measurements. Readings were taken once a week for 15 weeks. A picture of the setup is shown in Figure 2.

Figure 2 Rapid macrocell test setup

The corrosion potential of both the anode and cathodes were measured every week using a saturated calomel electrode. The readings were taken 2 hours after disconnecting the electrical wires (i.e. in open circuit). The electrochemical potential of a metal is a measure of its tendency to corrode. The more negative the potential the higher the tendency to corrode. The potential can only serve as an indicator of corrosion but not for measurement of the corrosion rate. In a macrocell, the anode will always have a more negative potential than the cathode which is the driving force for the corrosion. The corrosion potential of a bar is measured with respect to a standard electrode. For example, for the case of a saturated calomel electrode (SCE), ASTM C876 suggests the following interpretation of half-cell readings: > 0.125 V means greater than 90% probability that corrosion is not occurring, 0.125 V to -0.275 V means corrosion activity is uncertain, and < -0.275 V means greater than 90% probability that corrosion is occurring.

The voltage drop across a 10 ohm resistor was measured each week to obtain the corrosion current density. The corrosion rate of a reinforcing bar in a corrosion test where the corrosion current density has been measured can be obtained using Faraday's law, as shown in Eq. 6.

$$Rate = K\frac{ia}{nFD} \tag{6}$$

where Rate is given in μm/year, and

K = unit conversion factor = 315000
i = current density, μA/cm²
a = atomic weight of the metal. For iron, a = 55.8 g/g-atom
n = number of ion equivalents exchanged. For iron, n = 2 equivalents
F = Faraday's constant = 96500 Coulombs/equivalent
D = density of the metal, g/cm³. For iron, D = 7.87 g/cm³.

Substituting all of the constants into Eq. 6, we obtain Eq. 7.

$$Rate = 11.59i \tag{7}$$

In a test where a macrocell has formed, the current density can be obtained by measuring the voltage drop across a resistor that connects the anode and the cathode within the cell (Eq. 8).

$$i = \frac{V}{RA} \tag{8}$$

where
i = macrocell current density, μA/cm²
V = voltage drop across the resistor, mV
R = resistance of the resistor, kΩ
A = area of exposed metal at the anode bar, cm²

Under the test configuration used, the area exposed at the anode bar was approximately 77.7 cm².

Electrochemical impedance spectroscopy was performed for each of the bars every week. Two bands of silver paint were painted near the ends of the mortar bars and then copper wire was wound around this to serve as electrodes. The imaginary and real parts of impedance under an impressed current were measured with an LCR meter. The frequency range was 0 to 5 MHz. Plotting the imaginary part versus the real part results in the typical type of Nyquist plot shown in Figure 3. An equivalent circuit to model the behaviour is also shown in Figure 3. It consists of a resistor Rs which is assumed to represent the concrete resistance in series with a resistor and capacitor. The double layer capacitance Cdl represents the corroding interface. The resistor Rct represents the charge transfer resistance. The value of Rct is related to the polarization resistance which means that a decrease in Rct is associated with an increase in the corrosion rate. At high frequencies, current flows easily through the capacitor, which acts like an open circuit, with no current flowing through Rct. Thus, the impedance of the circuit is equal to the concrete resistance Rs. At very low frequencies the capacitor becomes fully charged and does not conduct current and the magnitude of the impedance is equal to the sum of Rs and Rct. At intermediate frequencies current flows through both Rct and Cdl. The Nyquist diagram consists of a tail at very low frequencies. This effect is related to diffusion control and is modelled with the addition of a Warburg impedance in series with Rct.

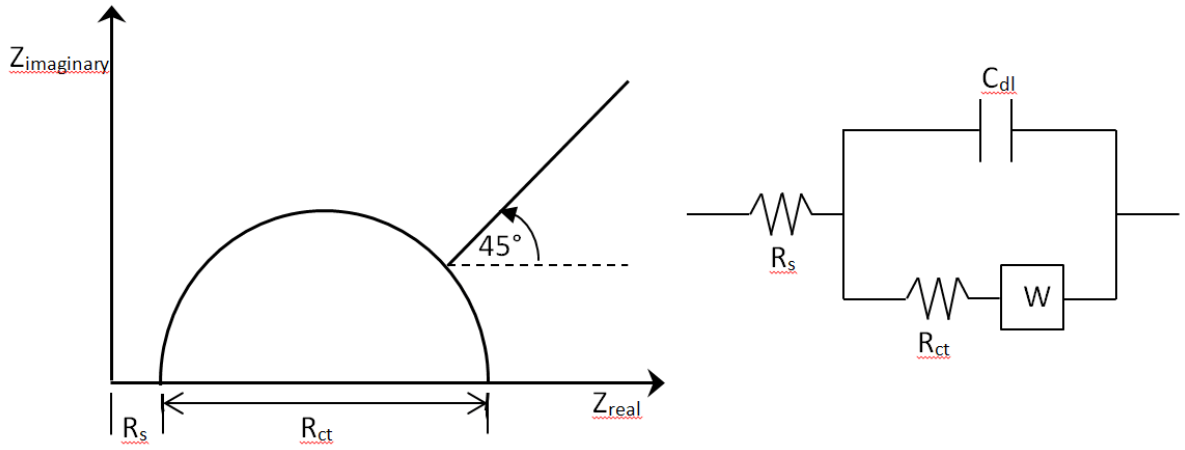

Figure 3 Typical Nyquist plot obtained from EIS and an equivalent electric circuit

RESULTS

The corrosion rate of the steel calculated using Equations 7 and 8, and using the measured corrosion current across the 10 ohm resistor is plotted in Figure 4. For comparison, the results for both the plain mortar and CFRM series are shown. There could be some concern that lowering the electrical resistivity of the concrete by introducing the carbon fibres could negatively impact the corrosion of the steel. There does appear to be some concern, as can be seen in Figure 4, that the CFRM begins corroding almost immediately, whereas the plain mortar takes about 3 to 4 weeks before active corrosion. However at later stages, the corrosion rate of the plain mortar actually surpasses the CFRM. Multiplying the corrosion rate by the elapsed time we can plot the cumulative corrosion loss for the bars as shown in Figure 5. Again the plain mortar shows less corrosion at the onset but by about Week 10 exceeds the corrosion in the CFRM.

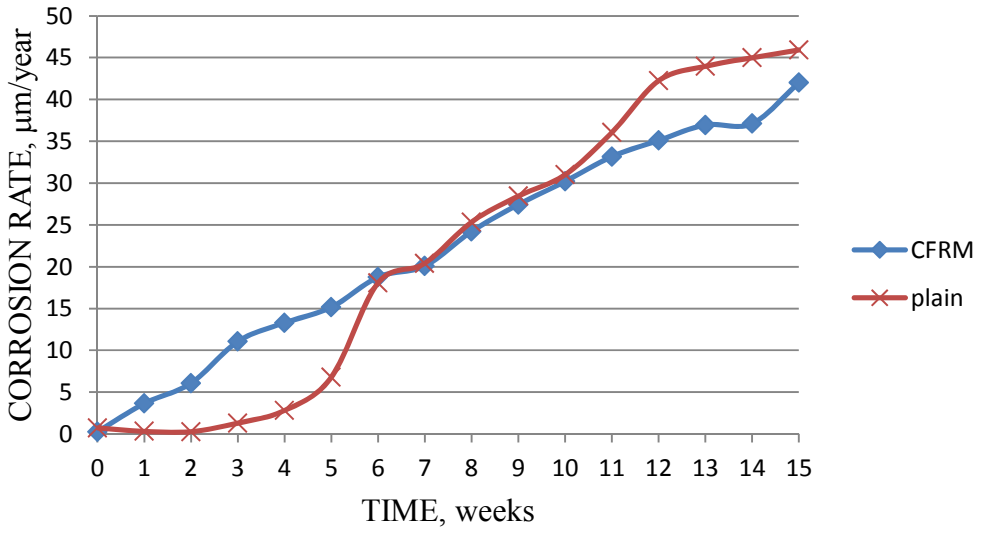

Figure 4 Corrosion rate calculated using the measured current

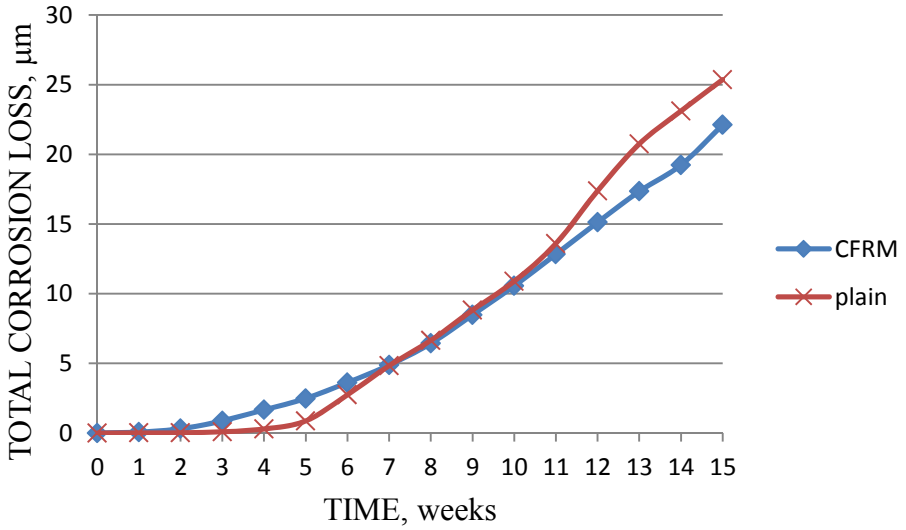

Figure 5 Total corrosion loss calculated based on the measured corrosion current

The electrochemical potential of the bars were measured with respect to a standard reference saturated calomel electrode. The results for the anode are shown in Figure 6. A corrosion potential more negative than -0.275 V indicates greater than 90% probability that corrosion is occurring. For the CFRM, corrosion activity is indicated already at the end of the first week. For the plain mortar bars, corrosion activity is indicated in Week 4. These results are in good agreement with the measured corrosion current results.

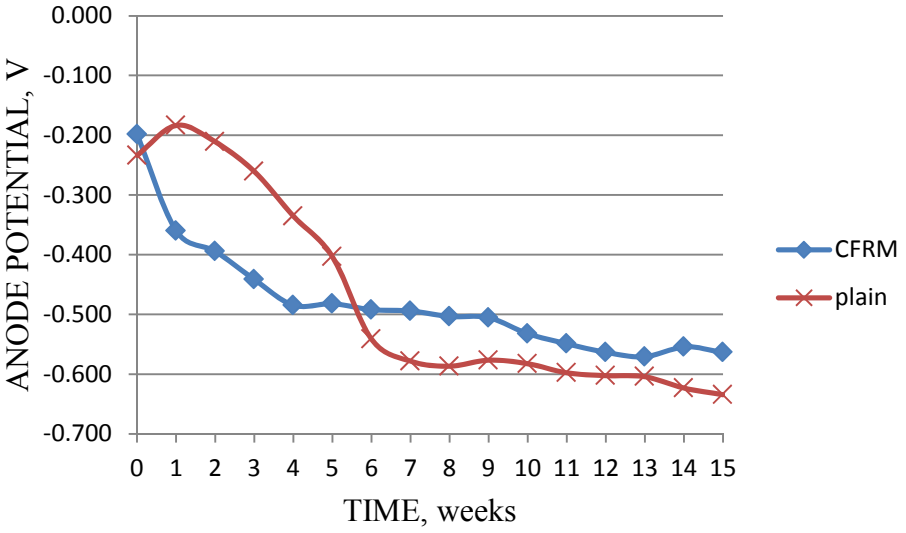

Figure 6 Corrosion potential of the anode bar with respect to a SCE

Electrochemical impedance spectroscopy was performed on the bars each week. The frequency range was 0 to 5 MHz. Results for the plain mortar bars were inconsistent from week to week and unreliable for calculating corrosion current, hence they are not shown here. On the other hand, consistent trends were observed for the CFRM. For the sake of clarity, only a few typical results are graphed in the Nyquist plot shown in Figure 7. The results show an initial Warburg diffusion control tail and a second capacitive arc. The diameter of the second arc decreases with time. Estimates of the diameter were made using graphical analysis. These were believed to be representative of the polarization resistance, Rp.

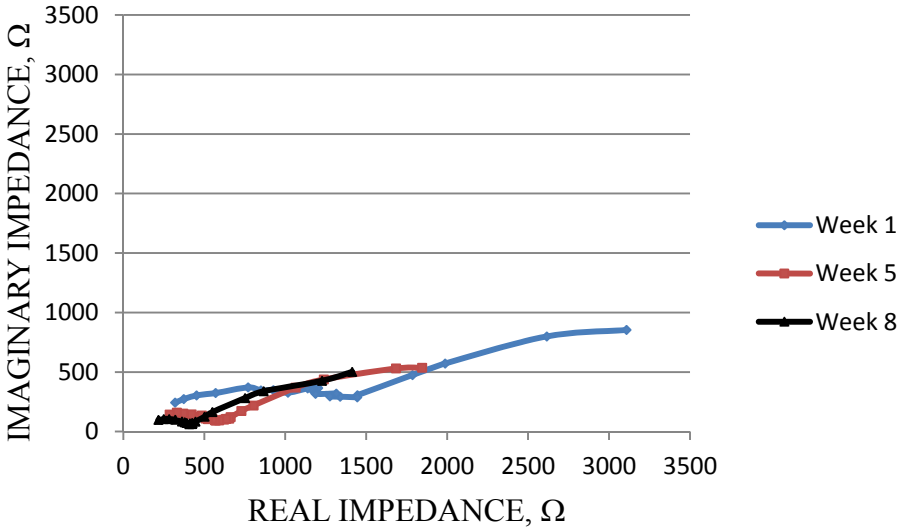

Figure 7 Nyquist plot for CFRM bars based on EIS

Using the estimates of Rp obtained from the EIS, the corrosion current can be estimated using

$$i = \frac{B}{R_p} \tag{9}$$

where B is the Stern-Geary constant which can be between 13 to 56 mV for concrete typically [3]. A value of 50 mV was assumed in this study. Using Eq. 9 and the EIS results, an estimate of the corrosion current was performed. The results are shown in Table 1. With the exception of Week 1, the EIS estimates match reasonably well with the measured values.

Table 1 Estimated corrosion current from EIS versus measured corrosion current

WEEK	MEASURED CORROSION CURRENT, μA	ESTIMATED Rp, Ω	ESTIMATED CORROSION CURRENT, μA	ERROR, %
0	1.8	-	-	-
1	24.4	1600	31.3	27.9
2	40.7	1150	43.5	6.7
3	74.1	725	69.0	-6.9
4	89.1	550	90.9	2.0
5	101.6	475	105.3	3.6
6	125.8	400	125.0	-0.6
7	134.7	375	133.3	-1.0
8	162.3	300	166.7	2.7
9	183.9	275	181.8	-1.1
10	202.4	250	200.0	-1.2
11	222.3	225	222.2	0.0
12	235.3	225	222.2	-5.5
13	247.7	200	250.0	0.9
14	248.8	200	250.0	0.5
15	281.6	175	285.7	1.5

SUMMARY AND CONCLUSIONS

The incorporation of carbon fibres into a concrete mixture decreases the electrical resistivity of the concrete rendering it suitable for investigation with nondestructive electrical interrogation techniques such as electrochemical impedance spectroscopy. Rapid macrocell tests were conducted for an accelerated corrosion study. Three methods were used to assess corrosion activity: corrosion potential, measured corrosion current across a resistor, and EIS.

The lower electrical resistivity due to the carbon fibres led to earlier initiation of corrosion possibly by facilitating chloride ions to destroy the passive protection film on the steel. In the long run, the CFRM fared better than plain mortar for total corrosion loss. EIS measurements provided reasonable estimates of the measured corrosion current for CFRM specimens. Better correlation could probably be achieved using computer simulation of an equivalent electric circuit instead of graphical analysis. The advantage of EIS is that it is a nondestructive method and could be performed just with surface measurements.

ACKNOWLEDGEMENTS

This research was partially funded by a Faculty Research Grant from Minnesota State University, Mankato. Research assistants Tim Setala and Allison Stanek made significant contributions to the work. Zoltek Companies Inc. donated the carbon fibres used in the study.

REFERENCES

1. KOCH G H, BRONGERS M P H, THOMPSON N G, VIRMANI Y P AND PAYER J H, Corrosion Cost and Preventive Strategies in the United States, Report No. FHWA-RD-01-156, Federal Highway Administration, McLean, Virginia, 2001, 773 p.

2. MONTEIRO P J M, MORRISON F AND FRANGOS W, Nondestructive Measurement of Corrosion State of Reinforcing Steel in Concrete, ACI Materials Journal, Vol. 95, No. 5, 1998, pp. 704-709.

3. JOHN D G, SEARSON P C AND DAWSON J L, Use of AC Impedance Technique in Studies on Steel in Concrete in Immersed Conditions, British Corrosion Journal, Vol. 16, No. 2, 1981, pp. 102-106.

4. HOPE B B, PAGE J A AND IP A K C, Corrosion Rates of Steel in Concrete, Cement and Concrete Research, Vol. 16, No. 5, 1986, pp. 771-781.

5. SRINIVASAN S, VENKATACHARI G, RENGASWAMY N S AND BALAKRISHNAN K, Application of Impedance Technique to Study the Corrosion Behaviour of Steel in Concrete, Key Engineering Materials, Vols. 20-28, Nos. 1-4, 1987, pp. 1525-1531.

6. WENGER F, ZHANG J, GALLAND J AND LEMOINE L, Corrosion of Steel in Concrete Studied by Electrochemical Impedance Measurements: Application to the Monitoring of Concrete Structures, Key Engineering Materials, Vols. 20-28, Nos. 1-4, 1987, pp. 1539-1546.

7. GU P, ELLIOTT S, HRISTOVA R, BEAUDOIN J J, BROUSSEAU R AND BALDOCK B, A Study of Corrosion Inhibitor Performance in Chloride Contaminated Concrete by Electrochemical Impedance Spectroscopy, ACI Materials Journal, Vol. 94, No. 5, 1997, pp. 385-394.

8. CHOI O C, PARK Y S AND RYU H Y, Corrosion Evaluation of Epoxy Coated Bars by Electrochemical Impedance Spectroscopy, International Journal of Concrete Structures and Materials, Vol. 2, No. 2, 2008, pp. 91-105.

9. BALMA J, DARWIN D, BROWNING J P AND LOCKE C E, Evaluation of Corrosion Protection Systems and Corrosion Testing Methods for Reinforcing Steel in Concrete, Structural Engineering and Engineering Materials SM Report No. 76, The University of Kansas Centre for Research, Lawrence, Kansas, 2005, 568 p.

Acoustic Emission Criteria of the Structure of Constructional Composites

E V Korolev, V A Smirnov
Moscow State University of Civil Engineering, Russia

Escalating the operational actions to construction materials demands the development of materials with improved properties. Role of the physical investigation methods during the research and development of the construction materials can't be underestimated. One of the most promising is the "acoustic emission method", which is often characterized as a method of nondestructive testing (though acoustic emission occurs – and can be measured – during the process of "destructive" testing also). The successful application of the acoustic emission method (both for forecasting the properties and during the optimization of material's composition) requires the using of scalar criteria, which are in correlation with mechanical properties of material. The procedure of derivation of such criterion is discussed in present work. The stress-strain diagrams (acquired during the load process of test sample) were divided in several regions, corresponding to the different load phases (linear and nonlinear reversible deformation, irreversible deformation, plastic yielding). Then for each region we obtain the normalized sums of primary acoustic emission criteria (amplitude, intensity, etc.). It is shown that normalized sum which is corresponding to the region immediately preceding the destruction is in strong correlation with compressive strength of material.

Evegenij V Korolev is a Doctor of Engineering, Professor and Director of the Research and Educational Center "Nanotechnology" at Moscow State University of Civil Engineering, Russian Federation.

Vladimir A Smirnov is a CSc in Engineering, Associate Professor and Leading Research Officer of the Research and Educational Center "Nanotechnology" at Moscow State University of Civil Engineering, Russian Federation.

Keywords: Acoustic emission, Acoustic emission equipment, Composite materials, Failure criteria

INTRODUCTION

These days epoxy resins and composites with epoxy matrix have broad application in construction. Properties of such composites can be controlled in wide range by means of disperse fillers. Thus, for disperse filled (DF) epoxy composite (DFEC) it is relatively easy to achieve the complex of features, which can't be obtained for homogenous material: the complex of both desirable operational properties and high strength (compressive and/or tensile). One of the most important questions arising during the development of composites is the interconnection between structural parameters (qualitative or quantitative) and strength of material.

To obtain complete and accurate information about processes of structure formation and structure degradation of constructional composite it is necessary to apply some physical methods of studying the kinetics of destruction. Physical methods are widely used for quality control and determination of physical and mechanical properties of the material; the limitation of many methods is that they – being fully quantitative – don't reveal the aforementioned kinetics directly.

In contrast, by means of well-known acoustic emission (AE) method, based on registration of parameters of elastic waves originated from the defect just formed, it is possible to classify the defects (not only spatial classification, but also classification by the class of hazard is possible) in real time. Though nowadays the most promising application of the AE is the continuous monitoring of the objects at normal exploitations conditions, the method can successfully be used during the mechanical tests of the material under development. Reliable evaluation of constructional composites' quality at the research and development stage is in no doubt important and allows selection of the necessary mixture and manufacturing regime.

Successful application of the acoustic emission method requires the using of scalar criteria, which are in correlation with mechanical properties (most notably, the compressive strength) of material. It will be shown below that – due to heterogeneous nature of DF composite – it is difficult to derive such criteria theoretically. Both the procedure of experimental derivation and the method for selection of informative AE signals are discussed in the present work.

PRIOR WORK

At present, numerous solutions are developed for the purpose of separation of informative AE signals from extraneous noise. These techniques are implemented mostly in hardware. For example, Uppal et al. [1] use "trigger" sensor (located near the crack tip) as a discriminating device. Obviously, such an approach requires a-priory information about the crack and can only be used for investigation of macroscopic growing defects.

There also exist several solutions [2, 3] for frequency-domain discrimination, where raw AE signal (obtained by single transducer) is subject to high- and low-pass filtering (after the Fourier transform – if implemented in software) and, then, comparison (computing high frequency to low frequency ratio). Unfortunately, the frequency response curves of most AE transducers render this method almost unusable: if the mode of the curve located deeply above (or below) splitting frequency, then, because of using compensation factors, accuracy of discrimination decreases.

The formulation of quantitative criteria on the base of AE information is the most problematic part. The AE signal itself depends on many factors: acoustic characteristics of material under investigation, acoustic coupling, parameters of transducer and electronic equipment. This is why many authors even “measure” the AE in “conventional units” (CU) or “virtual units” when presenting the results. Several approaches to the derivation of quantitative criteria exist, but none of them are general.

The source of complications: heterogeneous nature of composite leads to dispersion of AE bursts

The most important difference between CM and traditional objects of AE research is the presence of one or more disperse phases (fillers). Heterogeneous nature of CM influences significantly on the acoustic properties and transmission characteristics of the CM and articles made of CM.

It can be assumed that elastic modulus of the filler is a constant of high value (for example, the disperse filler under consideration is characterized by Young's modulus of 58.5 GPa – this value exceeds the Young's modulus of the matrix in order of magnitude). And it is known [4] that the elastic modulus of CM with epoxy matrix is determined almost entirely by the elastic properties of the matrix and volumetric content of the filler:

$$E = E_m\left(1 + 11v_f^{1,7}\right), \tag{1}$$

where E – elastic modulus of the CM, E_m – elastic modulus of matrix (hardened epoxy resin), v_f – volumetric content of filler.

The semi-empirical expression (1) allows us to estimate adequately the acoustic properties of CM. Taking into account that the density of composite depends on densities of matrix and filler:

$$\rho = \rho_m + \left(\rho_f - \rho_m\right)v_f\,, \tag{2}$$

where ρ – density of CM, ρ_m – density of matrix, ρ_f – density of filler, and further substituting (1) and (2) into well known Newton-Laplace equation, we get the following expression:

$$c = \sqrt{\frac{E}{\rho}} = \sqrt{\frac{E_m\left(1 + 11v_f^{1,7}\right)}{\rho_m + \left(\rho_f - \rho_m\right)v_f}}\,. \tag{3}$$

Expression (3) represented by Figure 1.

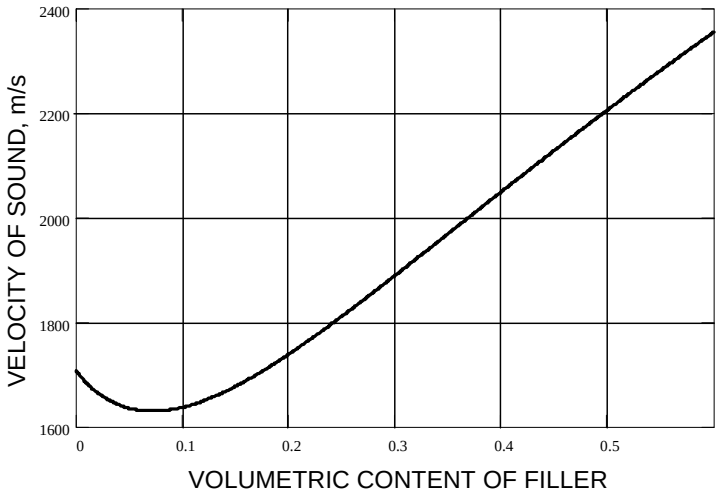

Figure 1 Dependence between volumetric content of filler and speed of sound in disperse filled composite with epoxy matrix

It can be seen that range $v_f \in [0,0.16]$ corresponds to relatively low velocities; beyond that range speed of sound increases almost linearly. It should also be noted that value calculated by (2) is subject to some small overestimation (the difference is about 2%) due to non-zero porosity of CM.

But the main conclusion is the follows: due to overall nonlinear character of (3), the inevitable fluctuations of volumetric content of filler lead to dispersion of short bursts of acoustic energy in almost unpredictable way. Thus, methods based only on fracture mechanics and the subsequent analysis of transfer functions of the test sample, allow to derive criteria, which are in a relatively weak correlation with macroscopic properties of the material. This is why the empirical research in the area is of high significance.

EXPERIMENTAL MATERIALS AND METHODS

The test samples of DFEC were made of:

- "ED-20" epoxy resin (analog of DER-331 from "Dow Chemical");
- "Polyethylenepolyamin": mixture of aliphatic amines with triethylenetetramine as a primary component;
- poly-mineral filler of specific surface 200 m^2/kg and density 5100 kg/m^3, with oxide composition of PbO, SiO_2, Na_2O, K_2O (primary oxides; the filler obtained by grinding the glassy amorphous material with mentioned oxide composition).

As a modifier the polymethylphenylsiloxane (PMPS) was used. There were two methods of modification: injection into matrix material during mixing process or coating (from diluted solution) the particles of fine filler. In later case, the PMPS acts as a coupling agent (CA).

Test samples were in the form of cube 0.02 m side. Loading was performed by tensile machine (operating in the compression mode), compression rate was $5 \cdot 10^{-4}$ m/min.

We carried out a study of eight series of DFEC samples. The mixtures are listed in Table 1.

Table 1 Mixtures of the test samples

SERIES OF DFEC	VOLUMETRIC CONTENT OF FILLER	METHOD OF MODIFICATION	AMOUNT OF MODIFIER, %	SPECIFIC THICKNESS OF CA LAYER, nm
1	0.2	injection in matrix	3	–
2	0.5	injection in matrix	3	–
3	0.2	injection in matrix	7.5	–
4	0.5	injection in matrix	7.5	–
5	0.2	as a coupling agent	–	2.5
6	0.5	as a coupling agent	–	2.5
7	0.2	as a coupling agent	–	7.5
8	0.5	as a coupling agent	–	7.5

For the purpose of acquisition and further analysis of AE information we have constructed the novel complex consisting of:

1. Two AE transducers with different frequency response curves (both curves are unimodal, but modes correspond to different frequencies: one is near 200 kHz, other is below 20 kHz).
2. Two non-discriminatory preamplifiers with 40 dB amplification factor (of “voltage”, i.e. 10^2 times).
3. Main non-discriminatory amplifier with 60 dB amplification factor, hi-pass filter (with 20 kHz cutoff frequency), and envelope detector.
4. Double-channel analog-to-digital converter.
5. Analysis software.

The outline of the complex is presented on Figure 2.

Block “A” on Figure 2 represents AE source; block “B” combines modules located in proximity of the test object; block “C” routes electric signal which is correspond to AE information of interest. Block “D” is used for noise elimination and block “E” routes all digital data.

From the Figure 2 it can be noted that the idea of a “trigger” sensor was extended for the purpose of discrimination in frequency domain. As an opposite to [3], we use two transducers with different geometry and, therefore, different response curves. Mode of one curve falls below the splitting frequency (selected as 20 kHz), mode of another is above it. During the test process signal of the low-frequency transducer is used for the selection (and elimination) of extraneous noise. This technique is in some way similar to the one used in *AESmart* series of devices from DECI – company that specializes in structural integrity of composite materials and structures made from composite materials.

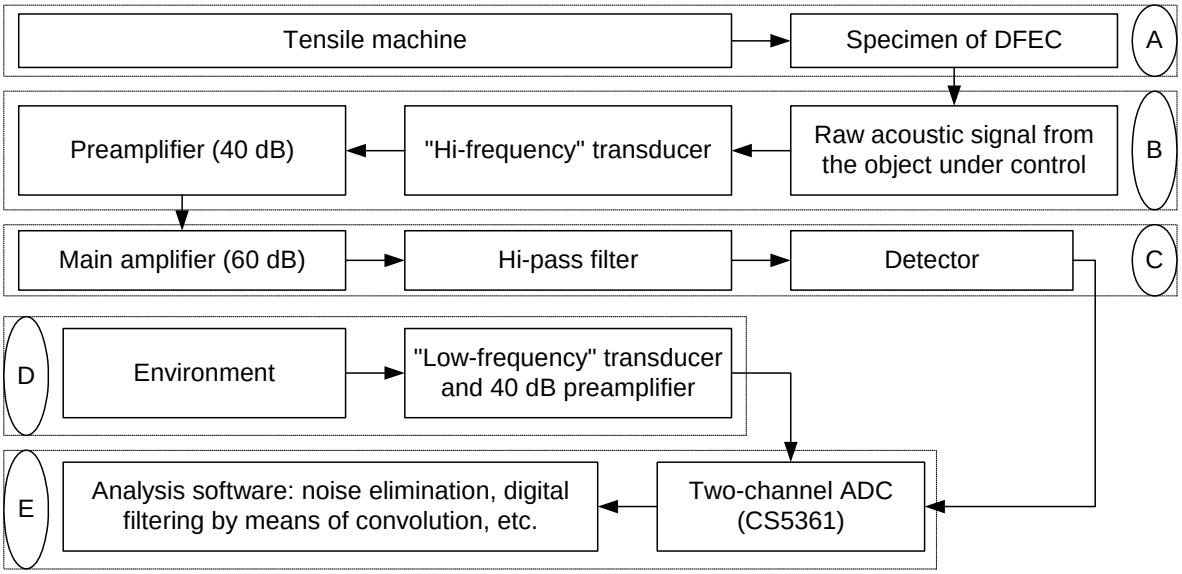

Figure 2 Schematic diagram of the registration and analysis complex

RESULTS AND DISCUSSION

The typical AE responses (FIR digital smoothing filter applied, window of one second) of the test DFEC samples during load are shown on Figures 3 and 4.

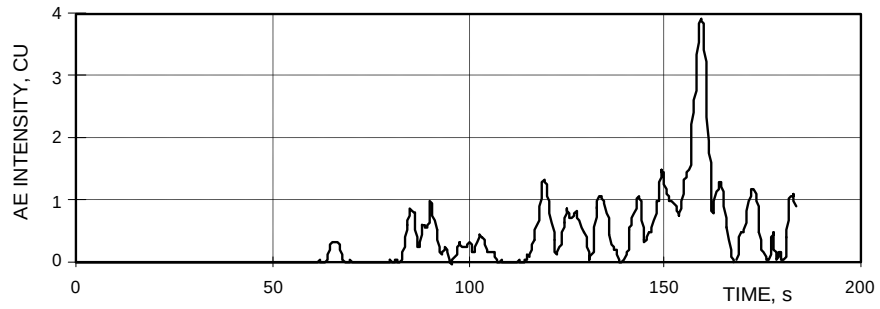

Figure 3 Typical AE response: DFEC with low content of the filler (series 1)

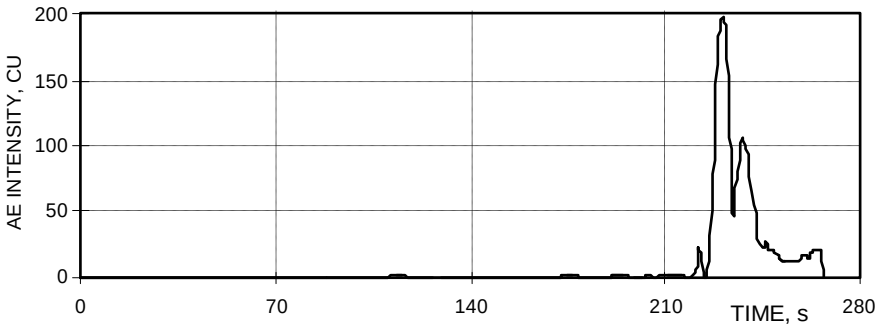

Figure 4 Typical AE response: DFEC with high content of the filler (series 2)

It was discovered during the analysis of AE kinetic curves (which are similar to the curves on Figures 3 and 4) that heterogeneous structure of DFEC leads to irregularity in distribution of mechanical stress between the bonds of the structural elements of DFEC. Places of local overstresses become sources of destruction. The development of microcracks ends with a macroscopic fracture. The destruction process going along with redistribution of stresses leads to the emission of elastic waves, which come to the surface of the test sample and are recorded as AE.

In the case of highly filled composites (even series in Table 1) destruction of the material is fragile. Elastic deformations in the structural elements of the DFEC do not cause the AE. Therefore, at stresses less than 80% of the press strength the AE for these materials is practically not registered. Destruction of highly filled DFEC, which occurs as a result of a cascade of growth of macrocracks is accompanied by a very high level of AE. Apparently, for the highly filled DFEC the AE pulses are caused by adhesive-type defects. The destruction of a relatively untight interjacent layers for the composite with high amount of modifier is accompanied by a significantly lower level of AE.

It should also be noted that there is a change of characteristic in the distribution of the mean energy of AE as a function of the volume degree of filling. Lesser degrees of filling correspond to large lengths of plastic deformation and ductile fracture. Most of the AE is registered on these stages.

If we assume that acoustic emission arises in the process of mutual displacement and plastic deformation of structural elements at the stage immediately preceding the destruction (main crack, in case of highly filled DFEC), than most of the characteristics of the kinetics curves may be explained.

In accordance with this assumption, the group of scalar criteria – each of which corresponds to a specific section of the "strain-stress" diagram (Fig. 5) – have been selected:

- criterion F1, corresponding to linear elastic deformation of the material;
- criterion F2, corresponding to the section of nonlinear elastic deformation;
- criterion F3, corresponding to the section of plastic deformation;
- criterion F4, corresponding to the destruction stage.

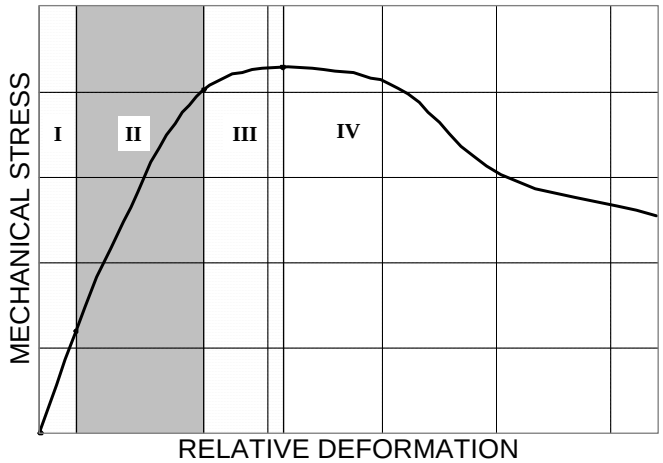

Figure 5 Sections on the "strain-stress" diagram (for DFEC with low content of filler)

The value of each criterion was found as a “normalized sum”: by dividing the sum of the values of the primary AE parameters (amplitude, activity, or intensity of the acoustic emission), corresponding to a given section (I, II or III) of the "strain-stress" diagram, by the sum of the same parameter, which is correspond to the all sections I...III.

Value of the criterion F4 is largely determined by character of destruction. For brittle materials the duration of the last section (IV) is quite small, so the criterion F4 for brittle materials is low. Thus, criterion F4 directly characterizes the type of fracture. However, in the case of ductile fracture the absolute value of this criterion depends also on the duration of the experiment. Because of this, the criterion F4 was excluded from further analysis.

The computed correlation coefficients are shown in Tables 2 - 4.

Table 2 Correlation coefficients for the F-criterion related to the amplitude of AE

PROPERTY	CORRELATION COEFFICIENT		
	F1	F2	F3
Compressive strength	0.10	–0.47	0.29
The relative deformation at fracture stress	–0.06	0.64	–0.45
Modulus of deformation	0.03	–0.56	0.41

Table 3 Correlation coefficients for the F-criterion related to the activity of AE

PROPERTY	CORRELATION COEFFICIENT		
	F1	F2	F3
Compressive strength	–0.05	–0.51	0.51
The relative deformation at fracture stress	–0.02	0.75	–0.69
Modulus of deformation	–0.07	–0.61	0.61

Table 4 Correlation coefficients for the F-criterion related to the intensity of AE

PROPERTY	CORRELATION COEFFICIENT		
	F1	F2	F3
Compressive strength	–0.18	–0.59	0.63
The relative deformation at fracture stress	0.18	0.76	–0.78
Modulus of deformation	–0.24	–0.66	0.73

Several researchers noted the correlation between amplitude of the acoustic emission and strength of the composite. However, our results (Table 2) indicate a relatively weak correlation. The relationship of the amplitude with two other investigated properties (relative deformation at fracture stress and modulus of deformation) is weak also.

Signs of correlation coefficients (Table 3 and 4) indicate the change of the dominant character of the scattering of elastic energy in the transition from low-filled DFEC to optimally filled composites (with maximal strength), as well as the transition from DFEC with an excess of modifier to composites with optimal (in the same sense) amount of modifier. In the former case the dominant process is the dissipation of energy during friction at the boundaries of the structural elements of the matrix. In the later case there is energy dissipation at the newly-formed boundaries after the destruction of the adhesive bond.

The later statement is also confirmed by the nature of the acoustic emission that occurs during load process. Increase of the filler's content is accompanied by an increase in acoustic emission in the sections (in time-scale) immediately prior to the destruction point.

The correlation coefficients for the F3 criterion, corresponding to the activity or the intensity of AE, are highest (in absolute value). The values of the criteria are 0.51 and 0.63 for compressive strength; –0.69 and –0.78 for the relative deformation at fracture stress; 0.61 and 0.73 for the modulus of deformation. These values are more than twice large then corresponding values calculated for the amplitude (Table 2). Therefore we can assume that the criterion F3 is the structurally sensitive AE scalar failure criterion for the investigated composites.

CONCLUSIONS

Though in the present days many complicated techniques for the analysis of raw acoustic emission information exist, even the simplest statistical analysis may reveal criteria which are in strong correlation with macroscopic properties of material.

It was shown that normalized sum which is corresponding to the region (in time-scale) immediately preceding the destruction is in strong correlation with compressive strength of material. Thus, if the material had shown compressive strength of P in laboratory test, and later in operating conditions criterion F3 exceeded some predetermined value, than we can conclude that there is at least one local area where stress is near P (and, in fact, construction operating in abnormal conditions).

The registration and analysis of AE for the purpose of computing the criteria similar to proposed in the work often require special equipment. One possible implementation of such equipment is presented in the work also.

ACKNOWLEDGEMENTS

This work is partially supported by Russian Government Contract of August 26, 2011, No 16.518.11.7080.

REFERENCES

1. UPPAL, A S., et al. Using acoustic emission to monitor fatigue cracks on the bridge at FAST, Technology Digest, Transportation Technology Center, Inc., Association of American Railroads, February 2002.

2. LYKOV, Yu I. Development and investigation of the equipment for spectral analysis of acoustic emission for nondestructive evaluation, CSc (05.11.13) thesis, 1978, Khabarovsk (in Russian)

3. US Pat. 5140858. Method for predicting destruction of a bearing utilizing a rolling-fatigue-related frequency range of AE signals. Shigeto Nishimoto et al., issued August 25, 1992.

4. BOBRYSHEV, A N., et al. Synergetics of composites, 1994, Lipetck: SPU ORIUS (in Russian)

A Performance-Based Quality Control Tool for Cement Based Composites Using Modified Electrical Resistivity Measurement Techniques

N H El-Ashkar, M I S Elmasry, M A A Anndif
Arab Academy for Science and Technology (AASTMT), Egypt

The variations in the associated conditions of in-situ-produced cement-based composites (CBC), such as curing conditions and workmanship quality, may cause considerable variations in the resulting CBC quality. Concrete for instance, as a species of CBC, usually show in-situ properties that are different from those obtained on the basis of laboratory produced test specimens. Thus, there has been an increasing focus for developing reliable nondestructive tests for CBC performance-based quality control. Such tests are performed to assess and predict CBC quality that is based on performance in order to carryout a better adjustment of both life cycle assessment and life cycle management. One of such non-destructive tests is measuring the electrical resistivity, which can be used as an indicator to assess the developing CBC properties including early stage properties, chloride diffusion, permeability, durability, etc. In this paper, a a recently proposed, cheap and reliable non-destructive technique called the Square Inner Electrical Resistivity Measurements (SIERM) technique, used to measure electrical resistivity of CBC, is introduced to study the correlations between the inner electrical resistivity measurements and the corresponding CBC strength properties including in compression, in splitting tension and in flexure. These relations are useful in conducting an actual performance based monitoring and controlling for the concrete quality and consequently have a better assessment for the constructed facility quality. These correlations can also be helpful in the construction process of concrete by controlling the right timing for formwork removal based on actual performance and expedite the time needed to proceed with subsequent construction stages. The results also show that, the electrical resistivity and strength are affected by the same factors such as age and water cement ratio. Results also show that there are strong correlations of statistical models based on regression analysis to predict strength from electrical resistivity measurements.

Dr. Nabil H. El-Ashkar is an Associate Professor in Construction & building Eng. Dept., Arab Academy for Science and Technology(AASTMT), Alexandria, Egypt.

Dr. Mohamed I. S. Elmasry is an Associate Professor in Construction & building Eng. Dept., Arab Academy for Science and Technology(AASTMT), Alexandria, Egypt.

Eng. Mohamed A. A. Anndif is an MSc Grad. Student, Construction & Building Eng., Arab Academy for Science and Technology(AASTMT), Alexandria, Egypt.

Keywords: Cement-based composites, Electrical resistivity, Non-destructive testing, Quality control, Strength

INTRODUCTION

The assessment of Cement-based Composites (CBC) properties in situ is very important to evaluate a performance based quality control for CBC in construction projects. But, all current codes and practice are based on same tests which normally were done in laboratory (not related to properties in situ). In 2009, the American Society of Civil Engineers (ASCE) assigned the grade D to the quality of overall infrastructure in the United States and decided that, the evaluation and maintenance of structures was one of the necessary key areas for improving the quality [3]. In resent few years a lot of researches focused on Non-destructive tests to assess quality in situ [5, 16, and 17]. Furthermore the prediction of the constructed concrete quality based on its performance is an important tool to assess the structure life cycle. This can be performed by predicting different properties of concrete by NDT during and after construction, the strengths of the CBC at different ages. The SIERM can be considered a new reliable technique [12] as NDT that can be used for performance based quality control (PBQC). For that, in this paper; the studying of a relation between different concrete strengths (compression, splitting tension and flexure) and the SIERM was performed to predict strength of CBC at different ages and water-to-cement ratios.

BACKGROUND

General Factors Affecting on Resistivity and Strength of CBC

The electrical resistivity and strength of CBC is highly dependent on several main factors including factors related to CBC mix and raw material, factors related to CBC pores. These factors can be summarized as follows:

Water to cement ratio (w/c)

The concrete resistivity and compressive strength increase with decrease in w/c. This is because both concrete electrical resistivity and compressive strength are both influenced by the total volume of entrapped air voids and capillary pores in concrete[8] and it is claimed also that, resistivity is also influenced by pore size and connectivity[4, 9, 10, 13, 16-18]. An increase in w/c ratio leads to an increase in the continuous capillaries in the cement paste, and thus decreases the resistivity [8].

Type of cement (Degree of hydration)

Concrete electrical resistivity is affected by type of cement (degree of hydration), because the resistivity increase with increase degree of hydration [18] and with the age [4, 10, 16-18].

Aggregate type and gradation

The electrical resistivity of cement paste is generally much smaller than that of aggregate. In terms of its electrical properties, concrete can be regarded as being made up of large numbers of relatively small volume particles of insulating material embedded in a conducting matrix of cement paste. The concrete resistivity changes according to type of aggregate (conductivity of aggregate) and degradation. The concrete resistivity is therefore a function of the distribution of these volumes throughout the system [7].

Admixtures (pozzolanic material)

Amount of pozzolanic materials remains non-reactive in the paste and it must be expected a physical effect not chemical; these materials improve microstructure of the cement matrix, and reduce concentrations and nobilities of the ions in the pore solution. Therefore they exert an influence on the electrical resistivity of concrete. In most cases, these materials create a finer pore size distribution and lower ionic concentration, which leads to higher electrical resistivity than in normal Portland cement concrete. Silica fume has a better effect on improving electrical resistivity than metakaolin for its finer particles and when using a combination from both pozzolans, there would be another grading besides the aggregate grading merely. So, blank spaces like capillary pores will be filled more because of better physical role of non-reactive pozzolans [15].

Size of concrete pores

The concrete resistivity decrease with increase size of concrete pores, which dependent on several factors such as w/c, aggregate gradation etc. [8].

Square Inner Electrical Resistivity Measuring Technique (The Proposed Approach)

The four probes are placed inside the cement based composites CBC specimen during casting. The probes are separated by an equal distance (*a*). The probes are made from a material that has good electrical conductivity. The tip of probe is allowed to directly be in contact with CBC material as the remaining part is covered with an insulation material. Thus, the connection between the CBC and the probe is just at the tip of the probe.

The probes are arranged at the four corners of a square where the two current (or voltage) probes are not diagonal for that the current is driven between the two adjacent corner points of the square member (not in diagonals), the voltage drop across the other probes is measured (Figure 1). The later configuration adapted in analogy to the technique used by [8] for surface electrical resistivity measurements. The new equations of the calculated electrical resistivity were derived in [2] as per methodology explained in [6] and [14].

SIERM configuration

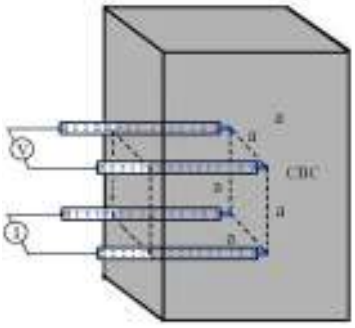

$$\rho = \left(\frac{4\pi a}{2-\sqrt{2}}\right)\frac{V}{I}$$

Where ρ is the electrical resistivity, *a* is the spacing between probes, *V* is the voltage and *I* is the electrical current

Figure 1 SIERM technique and corresponding equations for measuring electrical resistivity

EPERIMENTAL DETAILS

Experimental Program and Materials Used

In this research, a comprehensive experimental program is conducted to find correlations for predicting strength during different kinds of loading. The experimental program uses mortar as the test bed for CBC. The cement used was CEM I 42.5N; Natural sand is used as a fine aggregate, which has a specific gravity of 2.68. The superplasticizer used was type F (ASTM). The dosage used was 0.5% by weight of used cement. The Proportions of mixture by weight (sand: cement: water) were presented in Table 1.

Table 1 Proportions of mixture, w/c, and results of the flow table test

MIXTURE	W/C RATIO	PROPORTIONS OF MIXTURE BY WEIGHT (SAND:CEMENT)	RESULT OF FLOW TABLE TEST, %
M1	0.45	2	93.0
M2	0.5	2	108.3
M3	0.6	2	142.1

Three types of specimens were cast with different water-to-cement ratios; first type cubic samples (100 mm × 100 mm × 100 mm), second type is prisms (75 mm × 75 mm × 260 mm) and third type is cylindrical samples (diameter = 75 mm and length = 150 mm). The four probes for measuring electrical resistivity are inserted at four square corners (spacing between probes: 25 mm) directly after cast. The probe is made from copper electrical isolated wire. The isolated cover of probe (wire) is removed (length of removed isolation is 5 mm) at the tip of the probe to allowed the electrical contact points (contact between probe and CBC) for measure electrical resistivity. Figure 2 illustrates the specimens after casting and installing probes. For electrical resistivity measurements digital earth resistance tester model f-366 has been used. This model fully satisfies JIS C1304 requirements.

Cubes Cylinders Prisms (beams)

Figure 2 The specimens after casting and installing probes

Test Procedures

The compressive strength test is performed on saturated cubes samples which were cured by submersing in lime water tank. Before applying compression load (strength test), the electrical resistivity is measured by using the SIERM technique as shown in Figure 3. The test was performed with different water-to-cement ratios (as 3 specimens of each water-to-cement ratio in the same age) and tested at different ages 1, 7, 14 and 28 days.

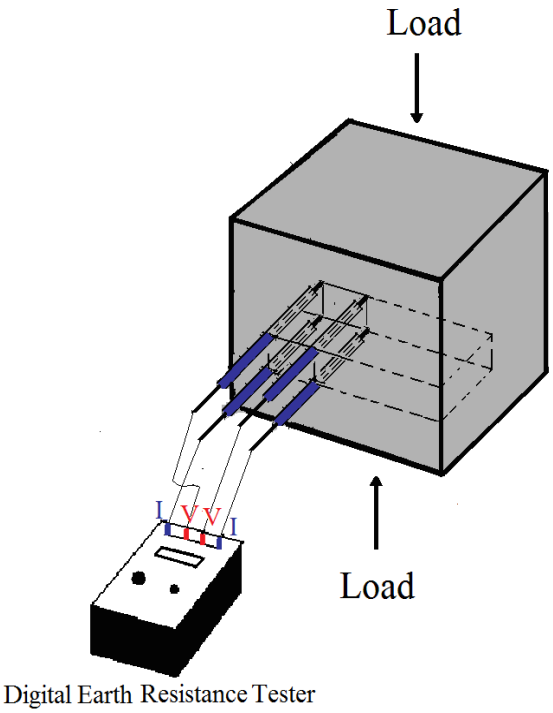

Figure 3 The proposed technique to measure square inner electrical resistivity before compression test

The splitting tensile test is performed on two cylindrical samples for each w/c and also at certain age. This test was performed according to the same procedures and environment in compressive strength test especially for measuring electrical resistivity before the test. After measuring electrical resistivity, the splitting tensile load was applied (Figure 4).

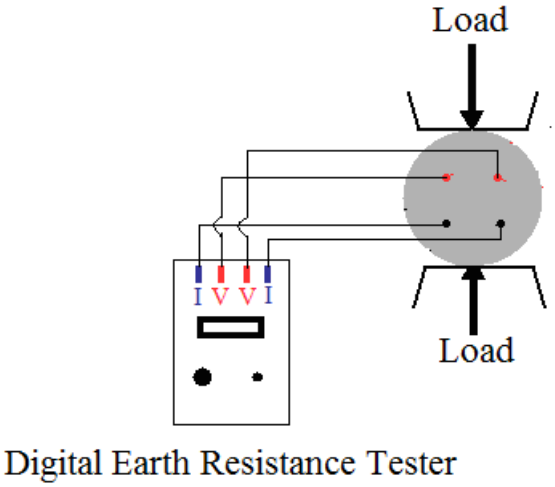

Figure 4 The proposed technique to measure square inner electrical resistivity before splitting tensile test

The three point flexural test was performed on two prisms (beams) for each w/c and also at certain age. The same procedures in compressive strength test especially for measuring electrical resistivity before the test. After measuring electrical resistivity, the flexural load was applied (Figure 5).

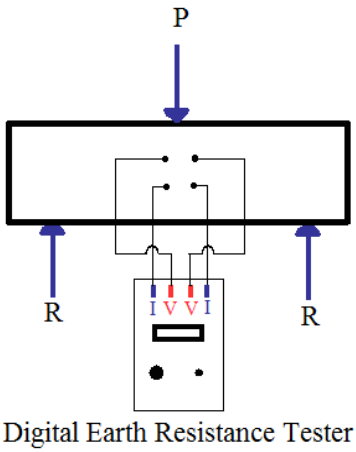

Figure 5 The proposed technique to measure square inner electrical resistivity before flexural test

RESULTS AND DISCUSSION

The main goal of this research is using the electrical resistivity measurements as a performance-based quality control non-destructive tool for the assessment and evaluation of CBC strengths (compressive strength, splitting tensile strength and flexural). An objective was set to study the effect of age and water-to-cement ratio on the different strengths and to compare this effect with the effect on the electrical resistivity measurements. Then, the relationship between the different strengths and the surface inner electrical resistance measurements (SIERM) were investigated to model this relationship. To find the relation between surface inner electrical resistivity measurements and different kinds of strength (compression, splitting tensile and flexural) which used in future to predict strength by measuring electrical resistivity, different kinds of specimens 45 cubes, 18 cylinders and 18 prisms (beams) were cast with different water-to-cement ratio and tested at different ages of 1, 7, 14 and 28 days.

Effect of Age and Water to Cement Ratio on Compressive Strength and Electrical Resistivity by using the SIERM Technique

To study the effect of water-to-cement ratio and compressive strength, the electrical resistivity was measured before testing specimens in compression. The results of compression test and electrical resistivity of cubical specimens at different ages and w/c are present in Figure 6. Each point in Figures 6a and 6b is the average of the results of three specimens. From Figure 6a and 6b it can be noted that, the electrical resistivity and compressive strength are increased with age of CBC specimens. Furthermore, the electrical resistivity and compressive strength are decreased with increase in water-to-cement ration. The water-to-cement ratio is one of the main parameters that affect the properties of CBC and especially the different CBC strengths due to its effect on porosity and voids of the concrete microstructure. This means that it is important for any method for non-destructive testing to be sensitive to this factor to truly represent the strength. The CBC is a porous material and the electric current is mainly transferred inside the concrete through the movement of the ions dissolved in the pores liquid, therefore the SIERM is largely affected by the pore structure, porosity and the pore size distribution [11]. Consequently, the reduction in SIERM

accompanied with the increase in water-to-cement ratio can be attributed to the increase in the porosity of the CBC leading to increase in the CBC conductivity. From this observation, it can be concluded that it is possible to find a good correlation between strength and electrical resistivity which can be used to predict strength in-situ by measuring electrical resistivity as suggested in reference [11] for apparent electrical resistivity. In reference [11], the electrical resistivity measurements was performed using apparent technique (with linear arrangements of probes) on the CBC surface but in this research the electrical resistivity measurements were collected using SIERM technique which was proven to be more accurate and reliable than the SERM technique [12]. These correlations can also be helpful in the construction process by controlling the right timing for formwork removal based on actual performance and expedite the time needed to precede with subsequent construction stages

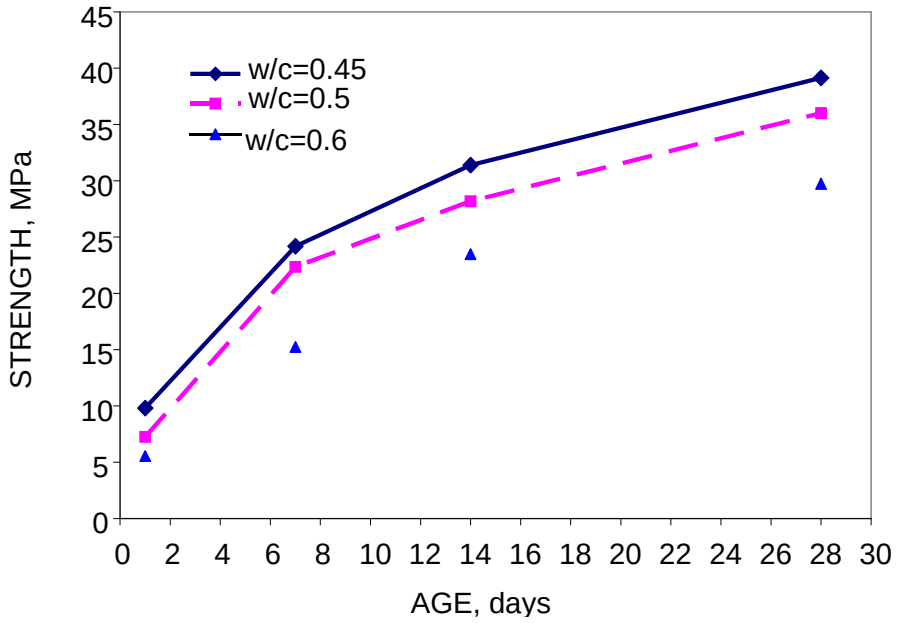

(a)

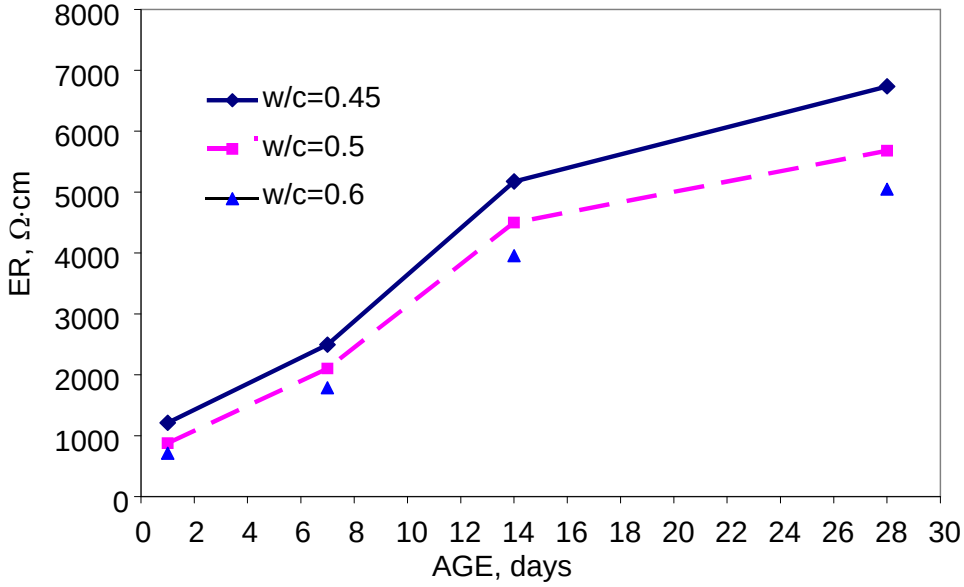

(b)

Figure 6 Effect of age and water-to-cement ratio
a) on compressive strength b) on electrical Resistivity by using the SIERM technique

Suggested Statistical Model Based on Regression Analysis for the Relation between the Compressive Strength and Electrical Resistivity by using the SIERM Technique

The correlation between electrical resistivity by using SIERM and compressive strength may be used to predict compressive strength in-situ by measuring electrical resistivity. For that, the cubes with different water-to-cement ratios (ranging from 0.45 to 0.6) were cast and tested at different ages. The electrical resistivity was measured before testing specimens in compression. The different correlations attempts are drown to find good correlation between electrical resistivity and compressive strength as shown in Figures 7a and 7b. Each data point in Figure 7a and 7b is the average of the results of three specimens.

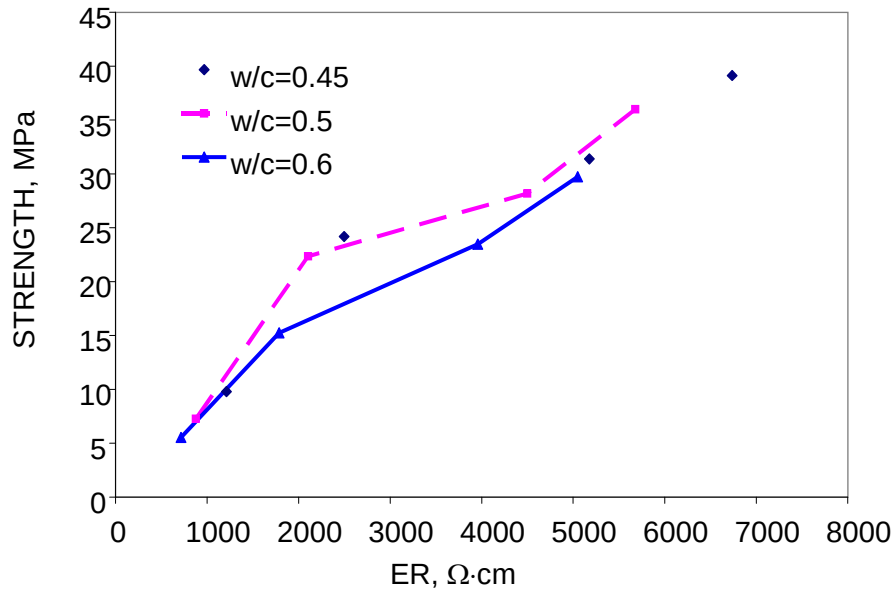

(a)

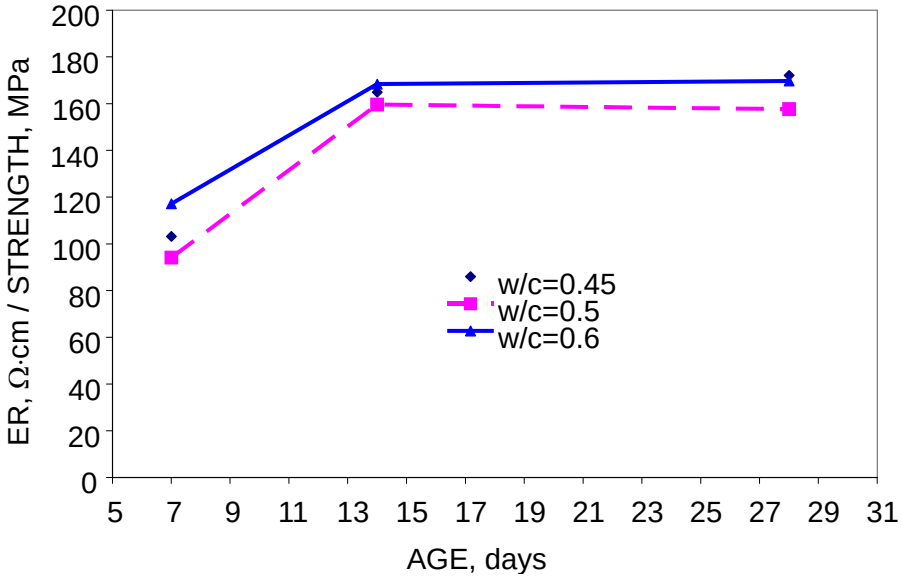

(b)

Figure 7 Relations between electrical resistivity measurements and compressive strength
a) Electrical resistivity with compressive strength at different w/c
b) Electrical resistivity/compressive strength with age at different w/c.

The attempt to construct the relation directly between electrical resistivity measurements and compressive strength for different water-to-cement ratios is performed as shown in Figure 7a. The water -to -cement ratio affects both strength and electrical resistivity but its effect on the relation between strength and electrical resistivity is very weak as there are no clear differences between curves for different water-to-cement ratios as shown in Figure 7a.

In Figure 7b, the attempt to construct the relation between electrical resistivity measurements and compressive strength with adding the age as a third factor shows good correlation but the results of different water-to- cement rations are very close especially at 14 and 28 days. Furthermore, it was observed that the shown relation in Figure 7b between the (Electrical resistivity / strength) and age seems to be constant between 14 and 28 days with a value of (Electrical resistivity / strength) = approximately 160. This can be a good sign to be used in the prediction process of compressive strength using electrical resistivity but, it needs more studies at ages after 28 days to observe if the same behaviour will continue and this ratio will remain constant.

Another attempt to find a relation between electrical resistivity and compressive strength, a regression analysis was performed on all results for w/c range from 0.45 to 0.6 and for age up to 28 days. The regression analysis to get the correlation directly between electrical resistivity and compressive strength is presented in Figure 8. The suggested primary relation show in Figure 8 is a strong correlation. This is clear from the high value of the coefficient of correlation (R^2 =0.9405). Moreover, more specimens are needed to cover more ranges of w/c, ages and different other parameters as using concrete, different admixtures, different type of aggregate etc..

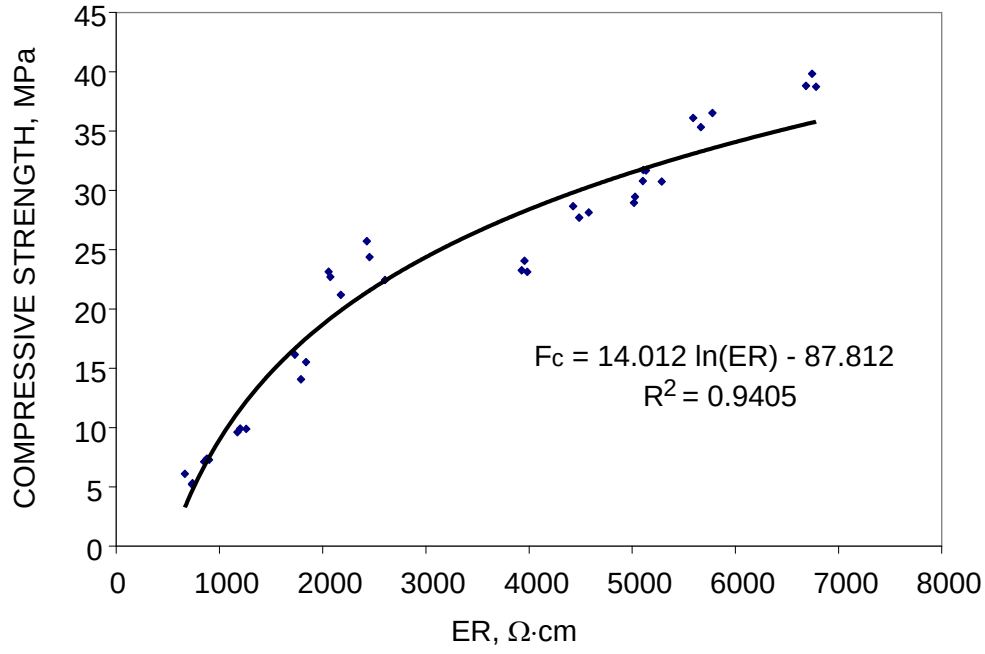

Figure 8 Suggested statistical model based on regression analysis for the relation between the compressive strength (F_C) and electrical resistivity (ER) using the SIERM technique

Suggested Statistical Model Based on Regression Analysis for the Relation between the Splitting Tensile Strength and Electrical Resistivity by using the SIERM Technique

The tensile strength is very important for several structures such as the water tight structures (swimming pools, different types of RC tanks etc.). However, the prediction of the tensile strength of the concrete in a more direct way other than relating it with the compressive strength did not gain a lot of attention in the past. For that a correlation between electrical resistivity by using SIERM and splitting tensile strength is need. The same procedure and relations used to find correlation between compressive strength and electrical resistivity were performed and drown here also. Although the water-to-cement ratio affects both strength and electrical resistivity but its effect on the relation between strength and electrical resistivity is not obvious the curves for different water-to-cement ratios is intersecting and no distinct difference can be drawn. This is similar to the behaviour in case of compressive strength and electrical resistivity. Moreover, the relation (Electrical resistivity / strength) and age seems to be constant between 14 and 28 days with a value of (Electrical resistivity / strength) = approximately 1800. This can be a good sign to be used in the prediction process of splitting tensile strength using electrical resistivity but, it needs more studies at ages after 28 days to observe if the same behaviour will continue and this ratio will remain constant.

The regression analysis to get the correlation directly between electrical resistivity and splitting tensile strength is presented in Figure 9. From Figure 9, a good correlation between electrical resistivity and splitting tensile strength is shown and statistical model is presented in Figure 9 with coefficient of correlation (R^2 = 0.8048). The suggested statistical model is applicable for CBC mortar with water-to-cement ratios ranging from 0.45 to 0.6 and ages up to 28 days. These ages are enough to investigate the concrete quality at the early ages of the concrete structures but to predict the strength at later ages there is a need for more effort and experimental work to refine a final and more accurate model that covered different factors affecting the concrete behaviour.

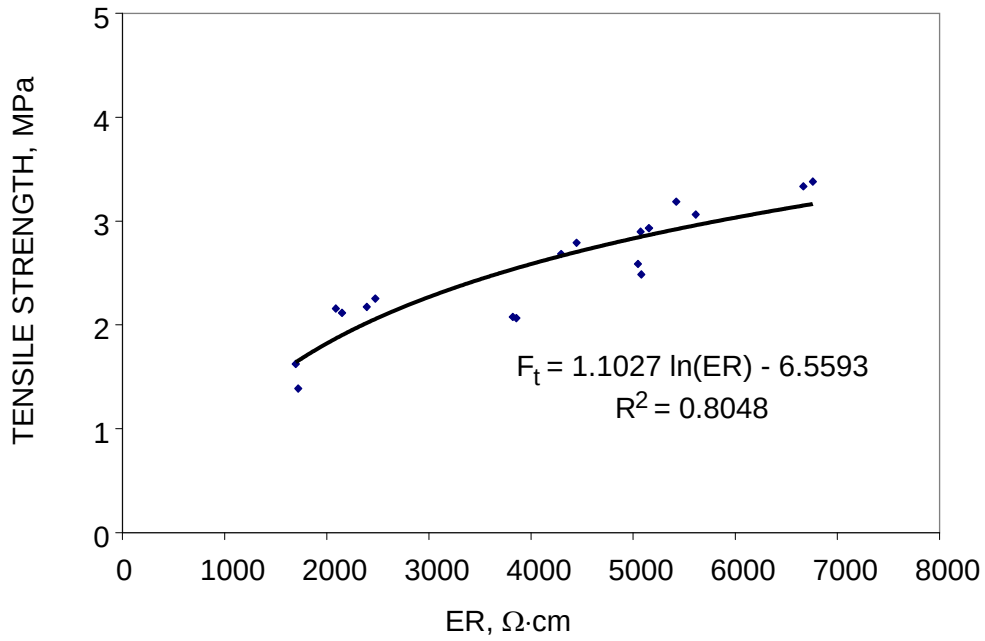

Figure 9 Suggested statistical model based on regression analysis for the relation between the splitting tensile strength (F_t) and electrical resistivity (ER) using the SIERM technique

Suggested Statistical Model Based on Regression Analysis for the Relation between the Flexural Strength and Electrical Resistivity by using the SIERM Technique

To find the relationship between electrical resistivity by using SIERM and flexural strength, the same procedure and relations used to find correlation between compressive strength and electrical resistivity are performed and drawn. The results show that the water-to-cement ratio affects both strength and electrical resistivity but its effect on the relation between flexural strength and electrical resistivity is not pronounced as there are no clear differences between curves for different water-to-cement ratios. This can be considered the same behaviour in case of compressive strength and electrical resistivity. Also the relation between (Electrical resistivity / strength) and age seems to be constant between 14 and 28 days with a value of (Electrical resistivity / strength) = approximately 1100. This can be a distinctive sign to be used in the prediction process of flexural strength using electrical resistivity but, it needs more studies at ages after 28 days to observe if the same behaviour will continue and this ratio will remain constant.

The regression analysis to get the correlation directly between electrical resistivity and flexural strength is presented in Figure 10. From Figure 10, a correlation between electrical resistivity and flexural strength is shown and statistical model is presented in Figure 10 with coefficient of correlation (R^2 = 0.6598). This is a good correlation but it need more investigation and this relation works as an introduction and initiation to this issue that needs more effort and experimental work to refine a final and more accurate model that covers different factors affecting the concrete behaviour.

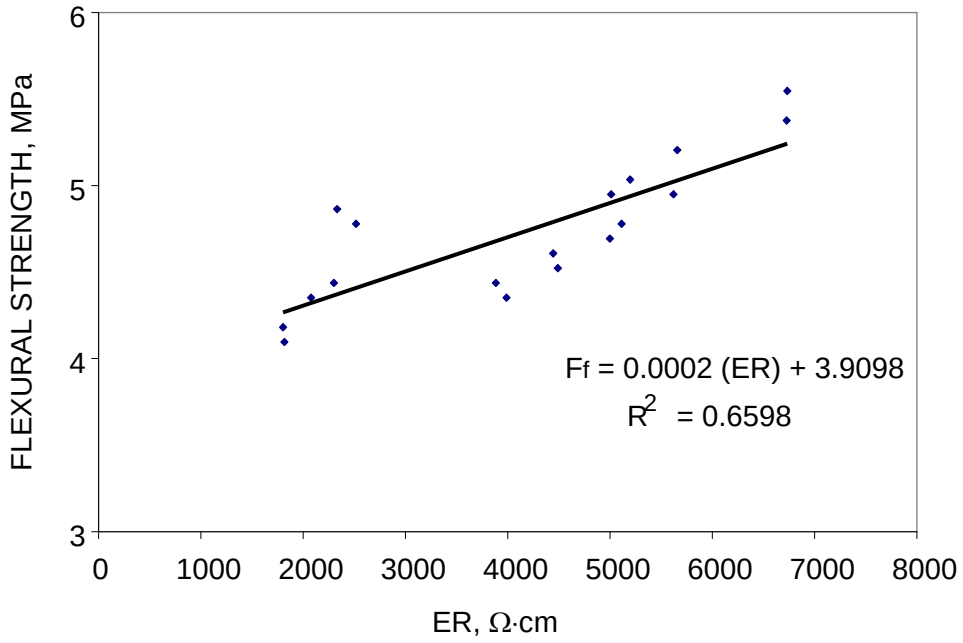

Figure 10 Suggested statistical model based on regression analysis for the relation between the flexural strength (F_f) and electrical resistivity (ER) using the SIERM technique

SUMMARY AND CONCLUSIONS

In recent years, the need for a performance-based quality control tool to assess the constructed concrete quality is increased. This is because that the variations in the associated conditions of in-situ-produced cement-based composites CBC, such as curing conditions and workmanship quality, may cause considerable variations in the resulting CBC quality. This is indicated in ACI-214 [1] which states that the strength test results attained from concrete specimens does not reflect the variations caused by all the procedures undergone during concrete construction. In this research a comprehensive experimental program was conducted aiming to evaluate the use of SIERM technique as a non-destructive technique to evaluate the different CBC strengths. Based on the results in this research, the electrical resistivity is affected by several factors such as age and water-to-cement ratio which also affect different types of CBC strength such as compressive, splitting tensile and flexural strengths. The electrical resistivity increases with the increase in CBC age that happens according to different factors like (degree of cement hydration, strength etc.). The electrical resistivity increases also with decrease of water-to-cement ratio because when water-to-cement ratios increase, the voids are increased then electrical resistivity decrease. As these factors are essential factors for CBC behaviour, this suggests that there is a strong relation between the electrical resistivity of CBC and different types of strength.

In this research, statistical regression models that correlate the electrical resistivity using SIERM technique and different types of CBC strengths (such as compression, splitting tension and flexural) are suggested based on the available data extracted from mentioned experimental program. These models cover the range of water-to-cement ratio from 0.45 to 0.6 and ages up to 28 days for CBC mortar. From the results it was concluded that there is a strong correlation between SIERM and different strengths (compressive, splitting tension and flexural) as suggested from the results of the coefficient of correlation. The suggested models seems to accurately represent the relations between SIERM and different strengths, however more research is still needed to refine these statistical models to cover more ranges of water-to-cement ratios and ages and to cover other different parameters such as using concrete, different admixtures, different type of aggregate etc. Also the effect of different ambient condition should be studied such as the different temperature and moisture content. The suggested models can be very useful in different applications such as strength predicting based on actual electrical resistivity data (collected using the more reliable SIERM technique) that can be very useful as PBQC to control the quality of different concrete structures, especially the infrastructures. Also, it can be a useful indicator for early form removal during concrete construction that can generally accelerate the construction process.

REFERENCES

1. ACI 228.1 R-03 In-Place Methods to Estimate Concrete Strength ACI Manual of Concrete Practice, American Concrete Institute. Farmington Hills, Michigan USA, 2003.
2. ANNDIF, M A A, Performance Based Quality Control Technique for Evaluation Cement Based Composites: Reliability & Assessment of Electrical Resistivity Measurements, Master Thesis, ARAB ACADEMY FOR SCIENCE, TECHNOLOGY AND MARITIME TRANSPORT, 2012.
3. BREHM D, Sensing skin could monitor the health of concrete infrastructure continually and inexpensively, Department of Civil & Environmental Engineering, Massachusetts institute technology News Releases 2011.

4. FERREIRA M AND JALALI S, Quality Control Based on Electrical Resistivity Measurements, proceeding, European Symposium on Serviceability of Concrete Structures, Helsinki, (S.I.:s.n.), 2006.
5. GJØRV O E, Durability of Concrete Structures and Performance-Based Quality Control, Proceedings, International Conference on performance of Construction Materials in The New Millennium New Era of Building, A. S. EL-Dieb, M. M. R. Taha, and S. L. Lissel, eds., Ain Shams University, Cairo, Egypt, 2003, 10 p.
6. IEEE, IEEE Guide for Measuring Earth Resistivity, Ground Impedance, and Earth Surface Potentials of a Ground System, The Institute of Electrical and Electronics Engineers, American National Standard. 1983.
7. BRYANT JR J W, Non-Invasive Permeability Assessment of High-Performance Concrete Bridge Deck Mixtures, Master Thesis, Virginia Polytechnic Institute and State University, 2001.
8. SU J-K; YANG C-C; WU W-B AND HUANG R, Effect of Moisture Content on Concrete resistivity Measurements, Journal of the Chinese Institute of Engineers, Vol. 25, No. 1, 2002, pp. 117-122.
9. LATASTE J F, SIRIEIX C, BREYSSE D AND FRAPPA M, Electrical Resistivity Measurement Applied to Cracking Assessment on Reinforced Concrete Structures in Civil Engineering, Journal of NDT&E International, Vol. 36, 2003, pp. 383–394.
10. KOSIOR-KAZBERUK M AND JEZIERSKI W, Evaluation of Concrete Resistance To Chloride Ions Penetration by Means of Electrical Resistivity Monitoring, Journal of Civil Engineering and Management ,Vol. XI, No. 2, 2005, pp. 109-114.
11. El-ASHKAR N H, Non-destructive electrical resistivity measurement technique: evaluation of concrete strengths, 4th International conference on concrete repair Dresden Germany, 26-28 September 2011.
12. El-ASHKAR N H, ELMASRY M I S AND ANNDIF M A A, A Modified Non-Destructive Technique for Inner Electrical Resistivity Measurements in Cement-Based Composites, under publication review, 2012.
13. POLDER R B, Test Methods for on Site Measurement of Resistivity of Concrete, RILEM TC-154 technical recommendation, Journal of Construction and Building Materials, Vol. 15, 2001, pp. 125-131.
14. MEHTA P K AND MONTEIRO P J M, CONCRETE: Microstructure, properties, and materials, 3rd Edition, 2006.
15. SHEKARCHIZADEH M, TAHERSIMA M, HAJIBABAEE A AND LAYSSI H, Concrete Mix Proportions with Ultra-High Electrical Resistivity, DBMC International Conference on Durability of Building Materials and Components, ISTANBUL, Turkey, 11-14 May 2008.
16. SENGUL O AND GJØRV O E, Electrical resistivity measurements for quality control during concrete construction, ACI Material Journal, Vol. 105, No. 6, November-December 2008.
17. SENGUL O AND GØJRV O E, Effect of Embedded Steel on Electrical Resistivity Measurements on Concrete Structures, ACI Material Journal,Vol. 107, No. 1, Jan-Feb. 2009.
18. LI Z J, WEI X S AND LI W L,. Preliminary Interpretation of Portland cement hydration process using Resistivity Measurements, ACI Material Journal, Vol. 100, No. 3, May-June 2003.

Modeling of Fracture in Reinforced Concrete Structures with Account of Bond Degradation and Cracking Under Steel Corrosion

A Benin, A Semenov
Saint-Petersburg State Polytechnic University, Russia

The three-dimensional finite-element modeling of fracture processes in reinforced concrete structures with account of the macrocrack initiation and propagation, real geometry of reinforcing elements, discontinuity in the bond-slip behavior and nonlinear constitutive equations for concrete is considered. The concrete material is modeled including the triaxial nonlinear stress-strain behavior, tensile cracking, compression crushing and strain softening. The different models with and without account of strong discontinuity for the reinforced-concrete bond behavior are considered and compared. The finite element fracture analysis has been performed for three standard applications. The first one is the problem of pulling the reinforcing bar from the concrete block. The second presents the three-point bending concrete beam specimen. The third example is devoted to modeling of fracture process in concrete reinforced plate under steel corrosion. The comparison of obtained numerical results with experimental data is presented and discussed.

Andrey Benin, Ph.D,is a Professor and Head of the Mechanical Laboratory at the Petersburg State Transport University, Russia.

Artem Semenov Ph.D, is an Associate Professor, at the Petersburg State Transport University, Russia

Keywords: Corrosion, Damage, Elasto-plasticity, Finite element modeling, Fracture

INTRODUCTION

A failure of reinforced concrete structures represents a complex multistage process including the degradation of reinforced-concrete bond, corrosion initiation, reduction of reinforcement cross sections, concrete cracking, delamination and spalling of the concrete cover, macrocrack propagation. An account of mentioned processes is actual for the correct evaluation of safety and serviceability of concrete structures. The developed approach is based on the direct three-dimensional finite-element modelling of the crack propagation process with account of real geometry of reinforcing elements, discontinuity in the bond-slip behaviour and nonlinear constitutive equations for concrete.

The model validation is carried out for the problem of pulling the reinforcing bar from the concrete block. Fracture process of bonds at pulling the rebar from the concrete is accompanied by the inhomogeneous and inelastic deformation, the rupture of adhesive bonds, the initiation and propagation of cracks of different shape and orientation, the presence of contact and tribological phenomena. The various nonlinear concrete models used in computations are reviewed in section 2. The five different models for bond behaviour are considered. Among them the models with and without account of discontinuity in the bond and continuous damage of concrete. The comparison of obtained numerical results with experimental data has been presented and discussed in section 3.

The process of corrosion driven cracking in concrete reinforced structures is simulated by applying the finite-element modelling with using the additional internal pressure around rebar for the corrosion effect. The results allow establishing the phases of crack initiation and propagation, the shape and trajectory of cracks. The results of simulation crack opening under corrosion are compared with experimental data and simple analytical evaluation in section 5. Based on results of investigation the recommendations may be suggested aimed at assessment of necessary thickness of the concrete cover; apart from that, the technique of in-service monitoring the reinforcement condition may be further defined.

During recent years, interest in nonlinear analysis of concrete structures has increased steadily, because of the wide use of plain, reinforced and prestressed concrete as a structural material, and because of the development of relatively powerful finite element procedures. If a realistic nonlinear analysis of a concrete structure can be carried out, the safety of the structure is increased and the cost can frequently be reduced. With the present state of development of computer codes based on the finite element method, inadequate modelling of concrete is probably the major factor limiting computational capabilities. The objective in this paper is to compare the various numerical approaches to modelling of fracture processes in reinforced concrete structures and to evaluate of validity and accuracy of the considered approaches by means of comparison with experimental results.

CONSTITUTIVE EQUATIONS FOR CONCRETE

The rate-independent models of concrete are considered. The isotropic and anisotropic elastic-damage and elastic-plastic damage models are used in the present analysis.

Different concepts involving plasticity theory and/or continuum damage mechanics have been used to simulate the experimentally observed behaviour of concrete materials. Many efforts were presented by researchers to modify the classical theory of plasticity in order to

make it more suitable for concrete materials by including the softening directly in the expression of a plastic yield surface by means of a hardening-softening function [1,2]. The plasticity-based approach was criticized for being unable to capture the stiffness degradation due to progressive damage growth.

Other researchers applied continuum damage mechanics to linear elastic analysis of concrete where the mechanical effect of the progressive microcracking and strain softening are represented by a set of internal state variables which act on the elastic behaviour [3,4]. These elastic-damage models were successful in capturing the behaviour of concrete under uniaxial loadings but many were criticized for being unable to model the plastic irreversible phenomena and their observed effects especially under more complicated loading combinations.

In order to capture the degradation of the elastic stiffness of the concrete material as well as its plastic irreversible deformations upon mechanical loading, the combined use of elastic-plastic constitutive equations along with continuum damage mechanics became vital to better describe the mechanical behaviour of concrete. One way is to coupled damage to concrete plasticity by defining damage growth as a function of plastic strains [5,6].

The extension of microcracks plays a decisive role in the inelasticity of concrete, as it results in the degradation of the elastic compliances. This effect is captured in the models by introducing of damage variables. In the simples case the influence of microcracking is introduced via a single scalar damage variable D ranging from 0 for the undamaged material to 1 for completely damaged material. Introduced by Kachanov [7] and further developed by Rabotnov [8] and others, the constitutive equation of material with scalar isotropic damage takes the following form for elastic-damage material

$$\boldsymbol{\sigma} = (1-D)\cdot{}^4\mathbf{C}_0^e \cdot\cdot\, \boldsymbol{\varepsilon} = {}^4\mathbf{C}^e \cdot\cdot\, \boldsymbol{\varepsilon}\,, \tag{1}$$

and for elastic-plastic-damage models

$$\boldsymbol{\sigma} = (1-D)\cdot{}^4\mathbf{C}_0^e \cdot\cdot\, \left(\boldsymbol{\varepsilon} - \boldsymbol{\varepsilon}^p\right) = {}^4\mathbf{C}^e \cdot\cdot\, \left(\boldsymbol{\varepsilon} - \boldsymbol{\varepsilon}^p\right), \tag{2}$$

where $\boldsymbol{\sigma}$ is Cauchy stress tensor, D is the scalar stiffness degradation variable, $\boldsymbol{\varepsilon}$ is the strain tensor, $\boldsymbol{\varepsilon}^p$ is the plastic strain tensor, ${}^4\mathbf{C}_0^e$ the initial (undamaged) elastic stiffness of the material, while ${}^4\mathbf{C}^e = (1-D)\cdot{}^4\mathbf{C}_0^e$ is the degraded elastic stiffness tensor. The effective stress tensor is defined as:

$$\overline{\boldsymbol{\sigma}} = {}^4\mathbf{C}_0^{el} \cdot\cdot\, \left(\boldsymbol{\varepsilon} - \boldsymbol{\varepsilon}^p\right) = \frac{1}{1-D}\boldsymbol{\sigma}\,. \tag{3}$$

In the formulation, it is necessary to propose the evolution of the scalar degradation variable:

$$D = D\left(\overline{\boldsymbol{\sigma}}, \widetilde{\varepsilon}^p\right) \tag{4}$$

governed by a set of the effective stress tensor $\overline{\boldsymbol{\sigma}}$ and hardening (softening) variables $\widetilde{\varepsilon}^p$. In the used in further Lubliner model [5], the stiffness degradation is initially isotropic and defined by degradation variable D_c in a compression zone and variable D_t in a tension zone.

A tensor of damage ${}^4\mathbf{D}$ is used for anisotropic case and instead of (1) can be written as

$$\boldsymbol{\sigma} = \tfrac{1}{2}\left[({}^4\mathbf{I} - {}^4\mathbf{D}) \cdot\cdot {}^4\mathbf{C}_0^e + {}^4\mathbf{C}_0^e \cdot\cdot ({}^4\mathbf{I} - {}^4\mathbf{D})\right] \cdot\cdot \boldsymbol{\varepsilon} = {}^4\mathbf{C}^e \cdot\cdot \boldsymbol{\varepsilon}. \tag{5}$$

This formulation allows describe degradation of stiffness due to crack. For example, for a single crack, which face is normal to the x-direction the resultant matrix has a form

$$\left[\mathbf{C}^e\right] = \frac{E}{1+\nu}\begin{bmatrix} R^t(1+\nu)/E & 0 & 0 & 0 & 0 & 0 \\ 0 & 1/(1-\nu) & \nu/(1-\nu) & 0 & 0 & 0 \\ 0 & \nu/(1-\nu) & 1/(1-\nu) & 0 & 0 & 0 \\ 0 & 0 & 0 & \beta^t/2 & 0 & 0 \\ 0 & 0 & 0 & 0 & 1/2 & 0 \\ 0 & 0 & 0 & 0 & 0 & \beta^t/2 \end{bmatrix}, \tag{6}$$

where the damage dependent variables R^t and β^t are defined by secant moduli under tension and shear. The relation (6) and also similar one for the set of two and three cracks are used in finite element program ANSYS.

Cracking (tension) and crushing (compression) in concrete are represented by increasing values of the hardening (softening) variables. These variables control the evolution of the yield surface and the degradation of the elastic stiffness. The yield function represents a surface in effective stress space which determines the states of failure or damage. For the plastic-damage model the yield function arrives at:

$$F\left(\overline{\boldsymbol{\sigma}}, \tilde{\varepsilon}^p\right) \le 0. \tag{7}$$

Plastic flow is governed by a flow potential function $G(\overline{\boldsymbol{\sigma}})$ according to nonassociative flow rule:

$$\dot{\boldsymbol{\varepsilon}}^p = \dot{\lambda}\frac{\partial G(\overline{\boldsymbol{\sigma}})}{\partial \overline{\boldsymbol{\sigma}}}. \tag{8}$$

The flow potential G for the Drucker-Prager hyperbolic function is accepted in the form:

$$G = \sqrt{\left(f_c - m \cdot f_t \cdot \tan\beta\right)^2 + 3\bar{J}_2} + \tfrac{1}{3}\bar{I}_1 \cdot \tan\beta, \tag{9}$$

where f_t and f_c are the uniaxial tensile and compressive strengths of concrete, respectively. β is the dilation angle measured in the $\frac{1}{3}\bar{I}_1 - \sqrt{3\bar{J}_2}$ plane at high confining pressure, while m is an eccentricity of the plastic potential surface. The flow potential surface is defined in the $\frac{1}{3}\bar{I}_1 - \sqrt{3\bar{J}_2}$ plane, where $\bar{I}_1 = \mathbf{1} \cdot\cdot \overline{\boldsymbol{\sigma}}$ and $\bar{J}_2 = \frac{1}{2} dev\overline{\boldsymbol{\sigma}} \cdot\cdot dev\overline{\boldsymbol{\sigma}}$. Stress deviator is defined by $dev\overline{\boldsymbol{\sigma}} = \overline{\boldsymbol{\sigma}} - \frac{1}{3}\mathbf{1}\bar{I}_1$.

The nonassociative flow rule, which is used here requires a loading surface definition. The plastic-damage concrete model uses a yield condition based on the loading function (10) proposed by Lubliner in [5] in the form:

$$F = \frac{1}{1-\alpha}\left(\sqrt{3\bar{J}_2} + \alpha \cdot \bar{I}_1 + \theta(\tilde{\boldsymbol{\varepsilon}}^p)\langle \bar{\sigma}_{\max} \rangle - \gamma\langle -\bar{\sigma}_{\max} \rangle\right) - \bar{\sigma}_c(\tilde{\varepsilon}_c^p) = 0. \quad (10)$$

The shape of loading surface in the deviatoric plane is determined by parameter γ, while the parameter α is calculated based on Kupfer's curve. $\bar{\sigma}_{\max}$ is the algebraically maximum eigenvalue of $\bar{\sigma}$. The Macauley bracket $\langle \cdot \rangle$ is defined by $\langle x \rangle = \frac{1}{2}(|x| + x)$

More complex loading function is used in CAP model [12] ensuring the closed yield surfaces. The plasticity criterion for the CAP model attributed to the three-invariant class is the generalization of the Drucker-Prager criterion by considering the invariant $\bar{J}_3 = \det dev\bar{\boldsymbol{\sigma}}$ and double-sided truncation of conical surface by elliptic CAP at tension and compression.

MODELING OF DEFORMATION AND FRACTURE UNDER PULLING THE REINFORCING BAR FROM THE CONCRETE BLOCK

One of the major factors to ensure joint operation of reinforcement and concrete and allows them operates as a single monolithic body is a reinforced-concrete bond. Reducing coupling leads to excessive crack opening, to the decreasing stiffness and to the reduced carrying capacity of the structure.

The process of destroying reinforced-concrete bond at pulling the rod out of the concrete block is a complex multistage process, accompanied by the inhomogeneous and inelastic deformation, the rupture of adhesive links, the initiation and propagation of cracks of various shapes and orientations, the presence of contact and tribological phenomena.

Analysis of the destroyed samples has specified [10-12] on the existence of two characteristic types of cracks: cone-shaped cracks and longitudinal (radial, splitting) cracks, as well as areas of complete destruction of the concrete in the immediate vicinity of the bar. Experimental studies have also shown that the longitudinal cracks occur after the occurrence of cone-shaped cracks [12].

Various analytical dependences of shear stresses in bond τ from displacement s, generalizing results of the experiments, are offered. Among them is the normal law proposed by M.M. Kholmiansky [13]:

$$\tau = B\frac{\ln(1+\alpha s)}{1+\alpha s}. \quad (11)$$

Identification of parameters $B = e\,\tau_{\max}$ and $\alpha = (e-1)/s_{\max}$ can be performed directly on the basis of experiment.

In one, from the most widespread models CEB-FIP Model Code 90, bond behaviour is defined by expressions [14]:

$$\tau = \begin{cases} \tau_{\max}\left(\dfrac{s}{s_1}\right)^{\alpha}, & 0 \le s < s_1; \\ \tau_{\max}, & s_1 \le s < s_2; \\ \tau_{\max} + \left(\tau_f - \tau_{\max}\right)\left(\dfrac{s - s_2}{s_3 - s_2}\right), & s_2 \le s < s_3; \\ \tau_f & s > s_3. \end{cases} \tag{11}$$

The three dimensional finite-element model is used for simulation of the pulling the reinforcing bar from the concrete block. The computations were performed using the finite-element software packages ANSYS and ABAQUS. The five different models for the bond behaviour are considered:

1. Ideal bond (without account of displacement discontinuity),
2. Bond as interlayer with special properties (without account of discontinuity),
3. Elastic-damage model for concrete (6),
4. Elastic-plastic-damage model for concrete (2), (7)-(10),
5. Bond model with strong discontinuity and nonlinear spring links.

The comparison of obtained numerical results with experimental data [13] has been presented in Figure 1.

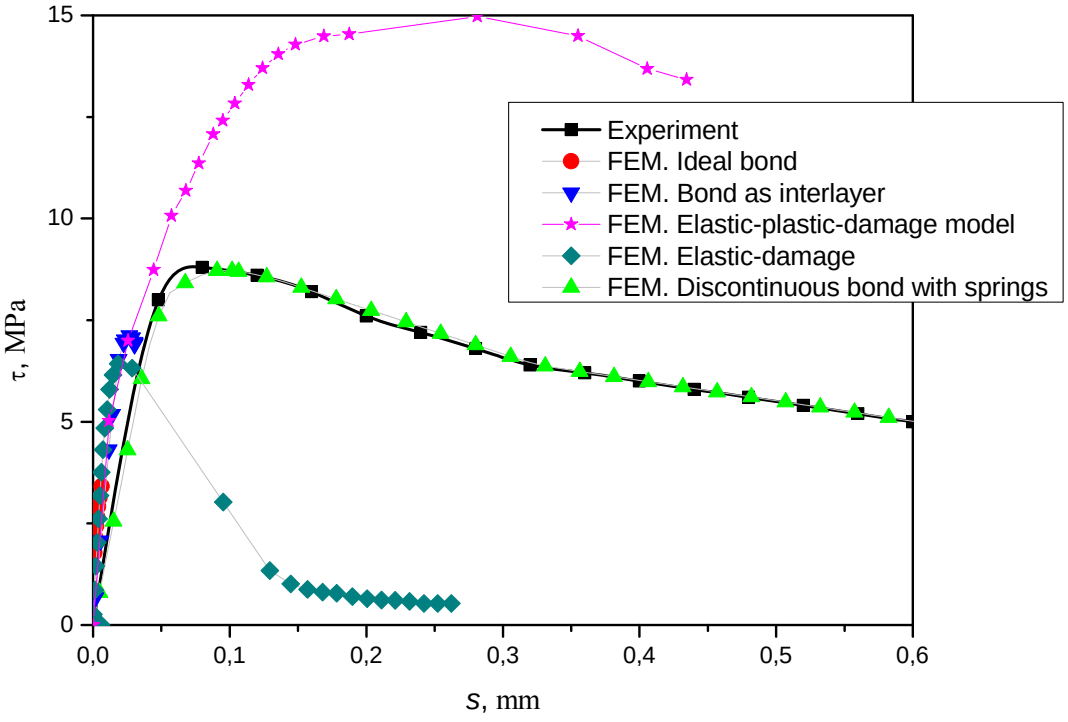

Figure 1 Dependence of the shear stress in bond on the displacement of reinforcement

Using the models of deformation of concrete, taking into account the effects of damage, qualitatively correctly describes the process of pulling out of rebar from the concrete block. However, the peak of shear stresses on the diagram is different from the experimentally

observed, that requires clarification stiffness characteristics of concrete at the cracking, as well as taking into account the adhesive and frictional forces of cohesion. It should be noted that the considered approach can be used to analyze the process of bound failure in the structures of arbitrary geometry, it is not restricted to the symmetrical loading and it only requires knowledge of the constants of the material obtained by standard tests.

Figure 2 shows the distribution of microcracks in concrete for reinforcement profiled (the plane of the circle coincides with the plane of the crack) under pulling the lower end of the rebar to 10 microns. The computation results are correlated with the evolution of cracks of different orientations. Firstly a system of conical cracks is aroused and then, with increasing load, radial cracks are growing.

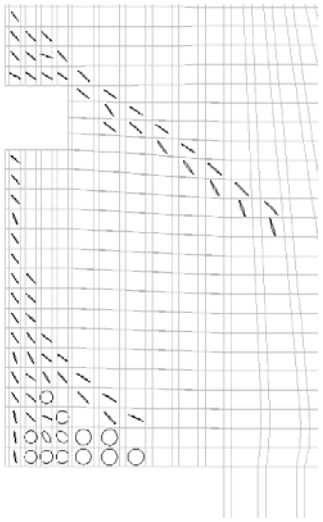

Figure 2 A system of conical and radial cracks in concrete around reinforcement

The most reliable numerical results (see Fig. 1) is obtained using the bond model with strong discontinuity of displacement fields on boundary between reinforcement and concrete. To describe the bond properties the efficient nonlinear discrete stiffnesses are introduced. In the simulation of bar slip relative to the concrete used a number of non-linear springs connecting the neighbouring nodes of finite element mesh of concrete and reinforcement [11]. Effective stiffness of the springs is obtained from the bond diagram $\tau(s)$ in form (1) as

$$C(s) = \frac{\tau(s)\pi dh}{2Ns}, \tag{12}$$

where d is a diameter of the rod (14 mm), h - height of the contact surface reinforcement and concrete, N - number of finite elements along the contact line.

Numerical results obtained with account of discontinuity for different variants of loading demonstrate good agreement with experimental results. Computed value of peak displacement of the upper end of rebar is 0.10 mm, whereas in the experiment there is 0.09 mm. The slight deviation in the results is present only near the peak of the graph (Figure 1). The reason for the deviation is numerical errors in computation related to lack the small increment load requirements that significantly increase in problems with non-monotonic nonlinearity.

MODELING OF DEFORMATION AND FRACTURE UNDER THREE-POINT BENDING OF CONCRETE BEAM SPECIMEN

A three-point bending of reinforced concrete straight beam (Figure 3) of rectangular cross-section with longitudinal and transverse reinforcement is considered. The load can be interpreted as a concentrated force, which was applied in the middle of the beam. The experimentally observed critical load leading to fracture was about 180 kN.

Figure 3 A three-point bending of concrete beam specimen

Geometric parameters of reinforced concrete beams: the total length of 1.70 m, span between the centres of the supports 1.50 m, width 0.10 m, height 0.30 m. The longitudinal reinforcement of the lower part - 2 ∅ 20A-II. The distance from the longitudinal rods to the bottom of beam is 0.03 m. Longitudinal reinforcement beams of the upper zone is absent. Transverse reinforcement is made by wire of 3 mm diameter and rectangular form. The distance between transverse reinforcements is 0.05 m. In order to initiate an inclined crack in a pre-known cross-sections there is no transverse reinforcement in the zone of 0.3 m located at a distance of 0.225 m from supports.

The finite-element simulation is carried out with help the three-dimensional finite-element models. One fourth of the structure is considered due to the presence of two planes of symmetry. Reinforcing bars were modelled also as a three-dimensional objects. The load was given in the form of a uniformly distributed pressure acting on a narrow stripe. The computations were performed using the finite-element software packages ANSYS and ABAQUS.

The three different models for concrete are considered:

1. Linear elastic,
2. Elastic-damage model (6),
3. Elastic-plastic-damage model for concrete (2), (7)-(10).

The material parameters were the same with considered in section 3. Distribution of microcracks in the longitudinal section of the reinforced beam shown in Figure 4.

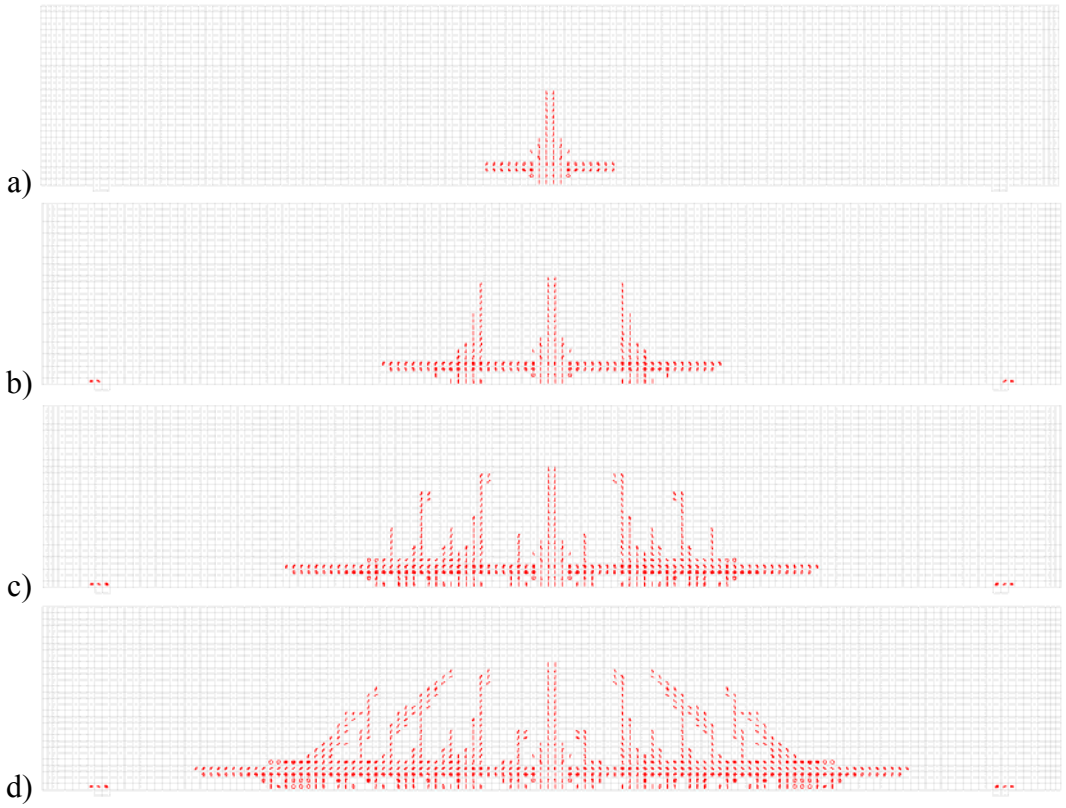

Figure 4 System of microcracks in the longitudinal section of concrete beam under the three-point bending. Load: a) 8.6 kN, b) 11.5 kN, c) 16.3 kN, d) 20.5 kN)

As seen from Figure 4 two ensembles of microcracks parallel develop: the vertical cracks caused by tensile stress from bending moment and cone cracks from pulling of rebar. The results of computations are correlated with the cracks observed in the experiment.

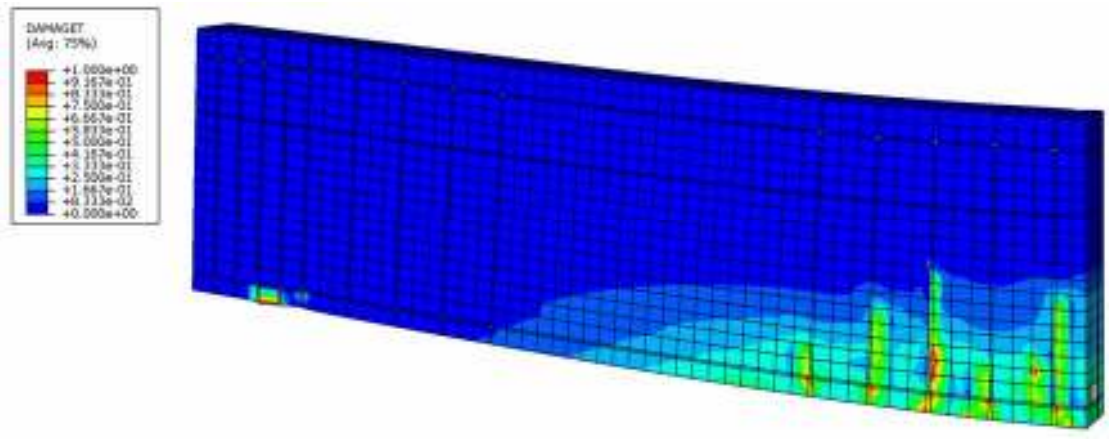

Figure 5 The damage field distribution in the central cross-section of reinforced concrete beam specimen (only ¼ of beam is shown)

Figure 5 shows the damage field distribution when using elastic-plastic-damage material model. As seen from Figure 5 the damage is localized in vertical strips, thus forming a vertical macrocrack, which agrees with experiment.

The comparison of results of simulation using different material models with the experimental results is shown in Figure 6.

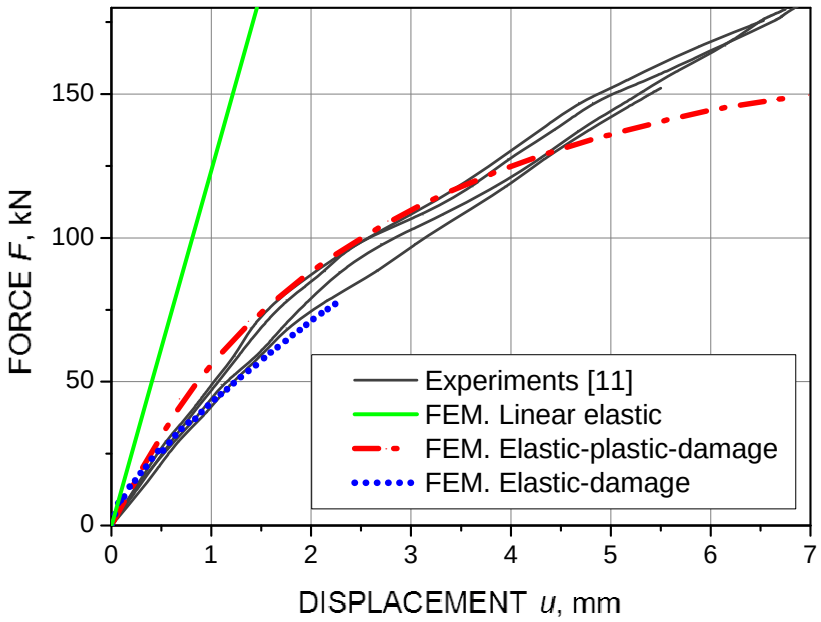

Figure 6 The dependence of the displacement of the bottom point of the central section of the concrete beam on the load.

There is a good agreement between calculated and experimental results upto the first visual macrocrack at a load of 118 kN is appeared. The opening of the initial macrocrack and initiation of new cracks is observed in experiments with further increase of load. The best match with the experiment at this stage can be achieved through a calculation based on the finite element model with crack.

MODELING OF FRACTURE PROCESS IN CONCRETE REINFORCED STRUCTURES UNDER STEEL CORROSION

A reinforced concrete structural component behaviour caused by expansion of corrosion products was modeled by a plate with periodical holes corresponding to the component cross-section. The model, single cell of the holed plate (Figure 7), was assumed in the plane strain condition loaded by the internal uniform pressure p, applied along the hole circumference to simulate the corrosion products swell. The volume of corrosive material is about 2.0…2.5 times of the reduction of the bar cross-section; respectively, high pressure on the concrete is generated resulting in origination of cracks and their propagation through the concrete cover. The single cell dimensions are (Figure 7,b): $c = R$, $W = 5R$, $H = 10R$, $R = 8$ mm; the boundary conditions of the cell conform the symmetry and periodicity, as shown in Figure 7,b.

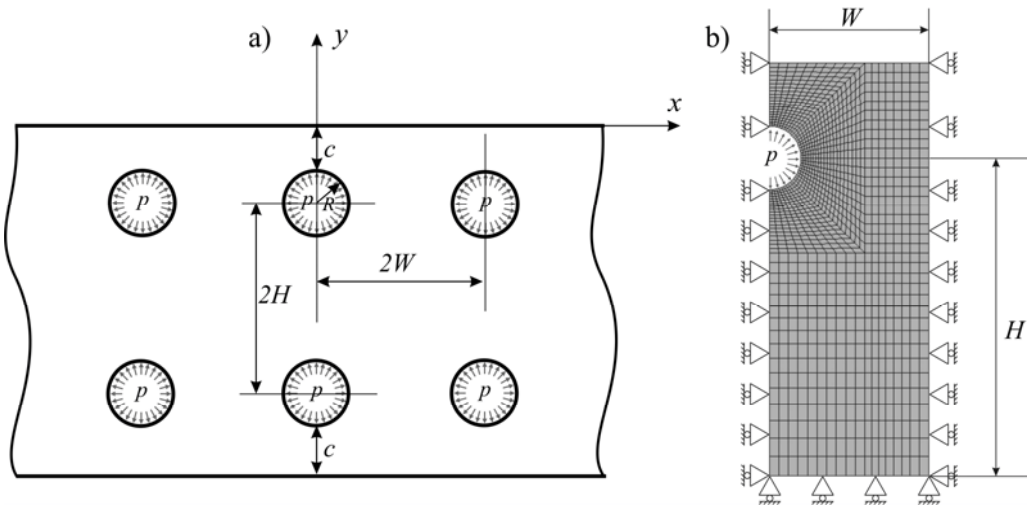

Figure 7 Mechanical model of typical reinforced concrete structure (a) and FE-model of a representative single cell (b)

In the first phase of investigation the concrete media was assumed free of macro-cracks. The analysis provided evaluation of the potential crack initiation locations and the critical pressure necessary to initiate cracks at the hole. Further, the crack system growth was assessed; it was found also, that along with the increasing pressure the new cracks were generated at the free surface of cover and extended towards the hole.

First, potential locations of crack initiation and the pressure necessary for cracks to propagate were obtained. For the criterion of crack initiation was selected condition when the maximum principal strain would reach the value corresponding peak stress in tensile diagram. The high sensitivity of stress field to selection of the material model is observed in finite-element simulations.

The linear elastic model of material essentially underestimates the area affected by the stress raise. At a given pressure the application of elastic model results in smaller strain than it is found with the elastic-plastic models. The difference between critical pressures obtained in elastic solution and elastic-plastic solution with CAP model is more 30%.

The crack growth was modelled in the step-wise sequence with automated definition of the step extension and direction based on the maximum tangential stress criterion. The extension process was assumed composed of several phases: initiation and growth of “horizontal” cracks (length a) slightly inclined with respect to the free surface of component (Figure 8, a); birth of “vertical” crack at the free outer surface (Figure 8, b); simultaneous growth of “horizontal” and “vertical” cracks (Figure 8, c); “vertical” crack deceleration (Figure 8, d) and further fragmentation or delamination of the concrete cover.

The present results are intended to assist in quantifying the service and residual life of concrete structures. Reinforcement damage can be evaluated by the opening of longitudinal crack along the rebar (see vertical cracks in Figure 8). A simple analytical evaluation for the loss in steel cross-section due to corrosion on the base of the longitudinal crack opening has been proposed in [15]:

$$\Delta = \frac{\delta l}{8h}, \tag{13}$$

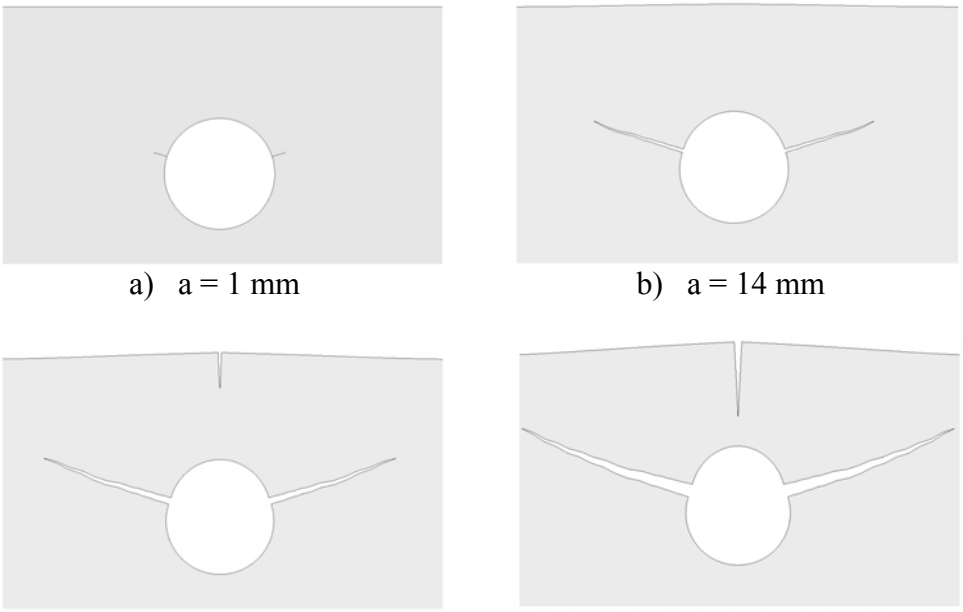

a) a = 1 mm b) a = 14 mm

c) a = 20 mm d) a = 28 mm

Figure 8 Crack propagation under progressive corrosion. a is the length of horizontal crack. Displacements are magnified 100 times for obviousness

where Δ is the corrosion expansion (radial loss or attack penetration in the rebar, δ is the crack width (vertical crack opening), h is a distance of horizontal crack start point from the free surface, l is a distance between crack tips of two horizontal cracks. Expressions for parameters h and l, characterizing horizontal cracks, have been obtained in [16] for the linear elastic undamaged material and the beam approximation of the concrete cover upper horizontal cracks. In this case h and l are determined only by the rebar radius R and the cover thickness c:

$$h = c\left(1+\frac{1}{c/R+1}\right), \qquad l = 2R\sqrt[3]{\pi\cdot(1+\nu)(c/R+1)(c/R)^2\left(1+\frac{1}{c/R+1}\right)^2}. \qquad (14)$$

The results of numerical analysis in a form of dependency of the radial loss Δ on the crack opening δ are presented in Figure 9. Comparison of the results shows satisfied agreement between the prediction by (13) and linear elastic FE solution with the given dilatation Δ. The plastic solution with Drucker-Prager criterion demonstrates nonlinear dependence of the radial loss on the crack opening. In the last case the attack penetration Δ increases in comparison with elastic solution under the same crack opening δ.

The obtained numerical results demonstrate a satisfactory agreement with experimental data [17, 18], where it was shown, that the radius losses Δ of 15÷50 μm are necessary to generate the crack width of ~50 μm (see Figure 9)). More detailed analysis of cracking under corrosion has been performed in [19].

Based on results of investigation the recommendations may be suggested aimed at assessment of necessary thickness of the concrete cover; apart from that, the technique of in-service monitoring the reinforcement condition may be further defined.

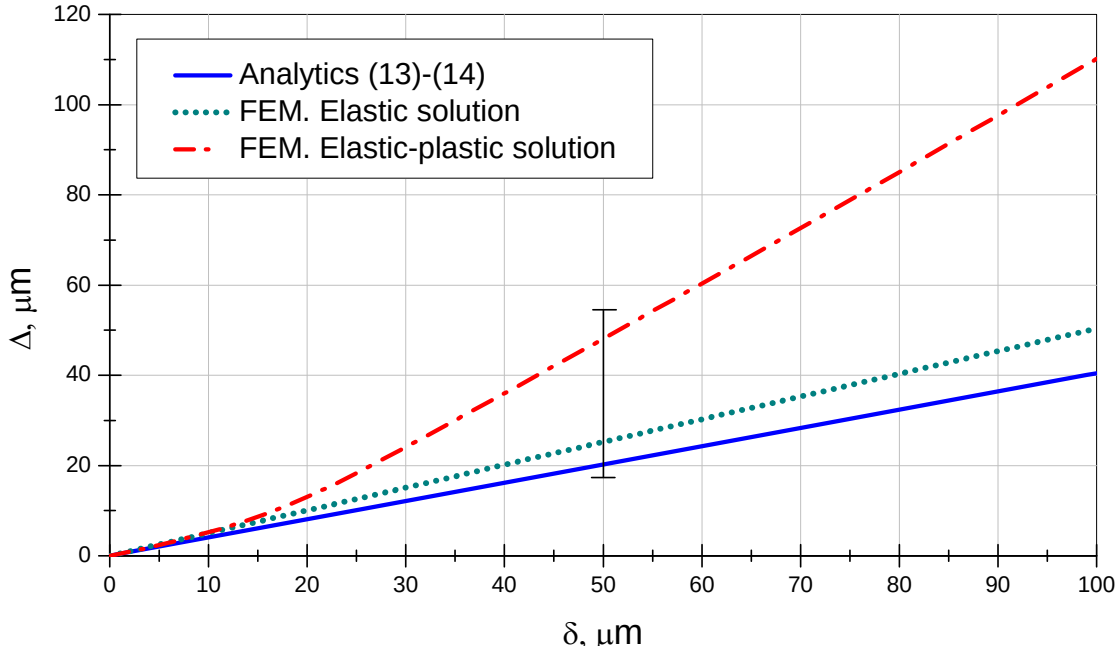

Figure 9 Corrosion expansion Δ versus crack opening δ

ACKNOWLEDGEMENTS

The study was supported by the Russian Fundamental Research Program, Project 12-08-00943.

REFERENCES

1. BICANIC, N, PEARCE, C J. Computational aspects of a softening plasticity model for plain concrete, Mech. of Cohesive-frictional Mat., Vol. 1, No. 1, 1996, pp 75-94.

2. PARK, H, KIM, J Y. Plasticity model using multiple failure criteria for concrete in compression, Int. J. of Solids and Struct., Vol. 42, No. 8, 2005, pp 2303-2322.

3. MAZARS, J, PIJAUDIER-CABOT, G. Continuum damage theory - application to concrete, J. Eng. Mech. Vol. 115, No. 2, 1989, pp 345-365.

4. WILLAM, K, RHEE, I, BEYLKIN, G. Multiresolution Analysis of Elastic Degradation in Heterogeneous Materials, Meccanica, Vol. 36, No. 1, 2001, pp 131-150.

5. LUBLINER, J, OLIVER, J, OLLER, S, ONATE, E. A plastic-damage model for concrete, Int. J. Solids Struct., Vol. 25, No. 3, 1989, pp 299-326.

6. VOYIADJIS, G Z, ABU LEBDEH, T M. Plasticity model for concrete using the bounding surface concept, Int. J. Plast. Vol. 10, No. 1, 1994, pp 1-21.

7. KACHANOV, L M. On failure time under creep, Proc. Academy of Science SSSR, No. 8, 1958, pp 26-31.

8. RABOTNOV, Y N. Creep problems in structural members, Amsterdam, 1969.

9. SCHWER L E, MURRY Y D. A three-invariant smooth cap model with mixed hardening, Int. J. for Num. and Anal. Mech. In Geomech., Vol. 18, 1994, pp 657-688.

10. ELIGEHAUSEN R, POPOV E P, BERTERO V V. "Local Bond Stress-Slip Relationship of Deformed Bars under Generalized Excitations", EERC Report 83-23, Earthquake Engineering Research Center, University of California, Berkeley, California. 1983.

11. BENIN A V. Deformation and failure of in reinforced concrete: analytical, numerical and experimental investigations. SPb: PGUPS. 2006. 127 p.

12. GOTO Y. Cracks Formed in Concrete Around Deformed Tension Bars. Journal of the American Concrete Institute. Vol. 68, No. 4, 1971, pp 244-251.

13. KHOLMIANSKY M M. Contact of reinforcement with concrete. Stroiizdat, 1981, p 184.

14. CEB-FIP Model Code 1990. Design Code. Comite Euro-Internat. du Beton. 1991, p 437.

15. VASILIEV, A I. Evaluation of the rebar corrosive wear in bridge beam structures, Concrete and Reinforced Concrete, Vol. 2, 2000, pp 20–23.

16. BENIN, A V, NEVZOROV, N I. The protective layer crack opening-based assessment of the rebar corrosive wear in reinforced concrete structures. Structural mechanics in civil engineering. Vol. 3, 2007, pp 48–52.

17. ANDRADE, C, ALONSO, C, MOLINA, A J. Cover cracking as a function of bar corrosion: Part I-experimental test, Mater. Struct., Vol. 26, 1993, pp 453–464.

18. VIDAL, T, CASTEL, A, FRANCOIS, R. Analyzing crack width to predict corrosion in reinforced concrete, Cement and Concrete Research, Vol. 34, 2004, pp 165–174.

19. BENIN, A V, SEMENOV, A S, SEMENOV, S G. Modeling of fracture process in concrete reinforced structures under steel corrosion. Journal of Achievements in Materials and Manufacturing Engineering. Vol. 39, No. 2, 2010, pp 168-175.

Research of Column Models Strength Under Repeated Axial Impacts by Falling Weight Using Computational and Experimental Methods

D G Kopanitsa[1], N N Belov[1], N T Yugov[1], S L Kaparulin[1], A A Yugov[1], G Kopanitsa[2], R S Mamtsev[1]
1 – Tomsk State University of Architecture and Building, Russia
2 – Munich Technical University, Germany

Presently construction of frame buildings using shotcrete columns is widely spread. Having technological advantages, these columns of raised bearing ability perceive considerable loadings without formation of cracks under considerable deformations. Construction of high-rise buildings in aseismic areas causes studying of columns behaviour under numerous dynamic loadings. The purpose of this work has been design procedure of concrete, ferroconcrete and steel shotcrete columns durability under numerous shock loadings. A mathematical model describing behaviour of constructional materials, including concrete ones under great shock loadings has been developed. The model has been used in the program complex for problems solving of blow and explosion in full three-dimensional formulation and for dynamic problems solving by the final elements method. Analysis of the experiments results on maglio installation of concrete, ferro-concrete and steel shotcreet columns models on numerous end blow of falling cargo has been carried out using the method of computer modeling behaviour of constructional materials under great shock loadings.

Nikolai N. Belov, doctor of physics and mathematics, Professor, graduated from the Tomsk State University (specialty "Mechanics"). Since 1996 he has worked as a professor of the department "Higher mathematics" of the Tomsk State University of Architecture and Building (TSUAB). His research interests: behaviour of structural materials and their products under high-speed impact, explosion and influence of powerful energy flows on substance.

Dmitriy G. Kopanitsa, DSc, Professor, graduated from the Tomsk Institute of Civil Engineering (specialty "Industrial and civil Engineering") and since that time the professor has worked at the same university (TSUAB). In 2003 he was appointed a head of the department of metal and wooden structures. His research interests: behaviour of building structures subjected to dynamic loads.

Nikolai T., Yugov, Doctor of physics and mathematics, graduated from the Department of Physics and Mechanics of the Tomsk State University in 1980. Nowadays Yugov Nikolai T is a professor of the Department of metal and wooden structures of the Tomsk State University of Architecture and Building. He is an expert in the field of mathematical modeling structural materials under explosive and impact loading behaviour

Sergey L Kaparulin graduated from the Tomsk University of control systems ans radioelectronics in 1978. Being a candidate of science, he is a senior researcher at the department of metal and wooden structures of the Tomsk state university of Architecture and Building. His research interests: behavior of building structures subjected to dynamic loads.

Alexey A. Yugov, candidate of sciences, an Assistant Professor, graduated from the Civil Engineering Department of the Tomsk State of Architecture and Building in 2003 having got the diploma of a specialist. In 2007 he defended his thesis on construction mechanics and building structures. Presently Alexey A. Yugov is a lecturer at the department of metal and wooden structures of TSUAB and is going on his research.

Georgy Kopanitsa, PhD in technical science, graduated from the Tomsk Polytechnic University in 2011 having got the Master degree diploma. His major is artificial intelligence, business process optimization using AI techniques. Since 2007 he has worked and learned in Germany: Munich Technical University, Heidenheim quality management summer school and presently G Kopanitsa is a researcher in the Helmholtz-Zentrum (German research centre for Environmental health, Munich).

Roman S Mamtsev graduated from the Civil Engineering Department of the Tomsk State of Architecture and Building in 2007. Now he is post graduate student at the department of metal and wooden structures of this university.

Keywords: Computer modeling, Fracture, Guncrete columns, Impact

INTRODUCTION

Construction of high buildings in seismic areas makes it necessary to examine columns behaviour under repeated dynamic loads. The typical destruction pattern of a building with ferroconcrete carcass under seismic loads is characterized by a concrete scape fracture with longitudinal reinforcement stability loss, i.e. reinforcement bars buckling in different directions, followed by collapse of structure or complete building.

The method of materials properties examination, in which physical experiment and mathematical modelling are used jointly, supplementing each other, may be called "computational and experimental method". This method was used, for example, to confirm Zabakhin's hypothesis about limited energy cumulation at the front of spherically converging shock-wave in a medium with phase changes [2, 3], to examine features of abnormally deep high-velocity penetration of high-porous striker into various media [3, 4].

The aim of this paper is to examine strength of concrete, ferroconcrete and steel guncrete column models for repeated endwise impacts by falling weight. The mathematical model is suggested in [1, 3, 5] that describes, within the framework of continuum mechanics, deformation and fracture processes under shock-wave loading, both in ductile and brittle materials.

Dynamic fracture that develops under intense shock and blast loads has fundamental differences from the quasistatic fracture. At least two essential distinctions may be noted. First, while quasistatic loading is featured by development of one or several main cracks, the shock loading is accompanied by simultaneous origination and development of numerous micropores and microcracks in localized volumes, under effect of tensile stresses. Second, time is of the same importance as stresses and deformations in dynamic fracture processes. Fracture is not critical event of instantaneous medium uniformity loss when certain threshold load is reached, i.e. strength limit according to static destruction criteria. Some time is required for accumulation of changes in the material structure under effect of microparameters of stress and deformation states, which reach certain critical level. As a result, the material gradually gets loosen, its load-bearing ability deteriorates and, finally, total fracture occurs [6]. Within context of this model, the dynamic fracture is considered as process of microdefects development and emerging under effect of the stresses generated during loading process. In case of ductile deformations the material damaged by microdefects under effect of tensile stresses undergoes fragmentation when relative void volume ξ reaches the critical value ξ^*. If material experiences compressive stresses, limiting value of ductile deformation work A_p^* or limiting value of ductile deformation intensity unambiguously connected with it, serves as local criterion of fragmentation e_u^*.

Brittle materials include large number of stress raisers — pores, grain margins, cracks, fracture nucleation occurs on which in the area of elastic deformation, both during compression and tension.

In case of sufficiently ductile materials, microcracks emerge as a result of their direct contact. Calculations of the elastic crack system demonstrate that their interactions and emerging take place when distances between closest crack ends are about two to three crack dimensions [7]. Supposedly, the microcracks in high-strength ceramics emerge when characteristic crack

dimension R at constant concentration N_0 reaches $R_* = \beta / \sqrt[3]{N_0}$, where β is a material constant. In the concrete [1, 8, 10] the condition $R = R_*$ is merely fragmentation initiation criterion for the material damaged by the cracks. Fragmentation process in the material damaged by the cracks and behaviour of the fractured material are described within framework of porous elasto-plastic medium model. There is also pores development besides of crack development in the plastically deformed material under effect of tensile stresses. In this case, condition of critical value reaching by the relative void volume ξ is a local criterion of separation fracture ξ^*. If the material damaged by the cracks is subjected to the compressing stresses, limiting value of ductile deformation intensity e_u^* will be a fragmentation criterion.

This model of structural material deformation and fracture under conditions of shock-wave loading is implemented in RANET-3 software package [11], which allows finding solutions for the shock and blast problems in full 3D formulation, basing on finite element method modified for solutions of dynamic problems [1, 3, 12].

EXPERIMENTAL RESEARCH

Column models had been made of sand concrete of size 10 cm × 10 cm × 100 cm compressive strength of 40 MPa. While testing they were placed vertically onto steel platform. Load from the falling weight was applied to the upper side via steel distribution plate 2 cm thick. Falling weight varied in experiments from 225 kg to 500 kg, weight falling height — from 35 cm to 70 cm. The test results for the concrete models after the second impact by 225 kg weight falling from 35 cm height are presented in Figure 1.

Figure 1 Patterns of the model fracture after second impact by 225 kg weight falling from 35 cm height: left — co-axial impact; right — angled impact

There were no visible fractures after the first loading for the given falling height and weight. After the second loading two types of fracture were observed in the models. In the first case fracture zone appeared in the upper part of the models, measuring about one tenth of the height. Head fracture is of symmetrical pattern, evidencing the co-axial impact (Figure 1, left). In the second case a fracture area appeared in the concrete column at one third of the sample height (Figure 1, right). Head spalling occurred there as a result of not co-axial impact.

Ferroconcrete column models are made as rectilinear prism of size 10 cm × 10 cm × 100 cm. Reinforcement carcass is made of four longitudinal bars of diameter 10 mm. The crosswise reinforcement of 5 mm in diameter is with spacing of 15 cm. Strain diagram of reinforcement bars is of elastoplastic nature. Fracture patterns of the ferroconcrete column models are shown in Figure 2 after the first (left) and second (right) impacts. The height of the load by 275 kg weight is 70 cm.

Figure 2 Fracture patterns in the ferroconcrete column after first (left) and second (right) impacts by 275 kg weight falling from 70 cm height

Review of the fracture pattern after the first impact shows that the impact was not co-axial. There was partial concrete spalling at the upper column head, from one side, resulting in bared longitudinal reinforcement bars. After the second impact, the concrete column scape fractured in its head section and longitudinal reinforcement bars buckled in different directions.

The models have been made from a steel tube filled with concrete of compressive strength of 30 MPa. Height of the model is 100 cm, diameter is 102 mm, wall thickness is 3 mm. The test of the concrete-filled steel tube column models were made by three impacts by 480 kg weight falling from 210 cm height.

Figure 3 Concrete-filled steel tube column of height 100 cm and diameter 102 mm with wall thickness 3 mm after the third impact by 480 kg weight falling from 210 cm height

In Figure 3 final deformation pattern of the concrete-filled steel tube column model is presented. After the third impact the column became bent, with total height decreased by 3 cm.

RESULTS OF COMPUTER MODELING

Effect of weight falling onto column end face was modelled by setting the end face velocity value:

$$u = u_0\left(1 - \frac{t}{T}\right).$$

Assuming that pressure on interface surface between striker material and column material changes over time according to triangle law, we can find from the Newton's second law:

$$\frac{m}{S}\frac{du}{dt} = P_0\left(1 - \frac{t}{T}\right).$$

Duration of load action T can be determined as follows:

$$T = \frac{2m}{S}\frac{V_0}{P_0};$$

where: m is the falling weight;
S is the cross-sectional area of the column;
$V_0 = \sqrt{2gh}$ is the velocity of weight falling;
h is the height of falling. Values of pressure P_0 and mass velocity u_0 at the steel/concrete interface can be calculated graphically, using shock adiabatic curves for steel and concrete [13].

In order to verify the concrete fracture model under shock-wave loading, experimental research of strength of standard concrete prisms of size 10 cm × 10 cm × 40 cm under effect of the longitudinal shock load was carried out. The tests were conducted on an impact machine. The sample was placed freely on the steel platform. Load from the falling weight onto prism head was applied via steel distribution plate 2 cm thick. 230 kg falling weight was used in the tests. The falling height was 50 cm. Figure 4a shows the final pattern of the prism fracture.

Calculation results in the form of isometric views of the prism cut by symmetry plane at the time points 0, 19, 20, 25, and 30 ms are shown in Figure 4b.

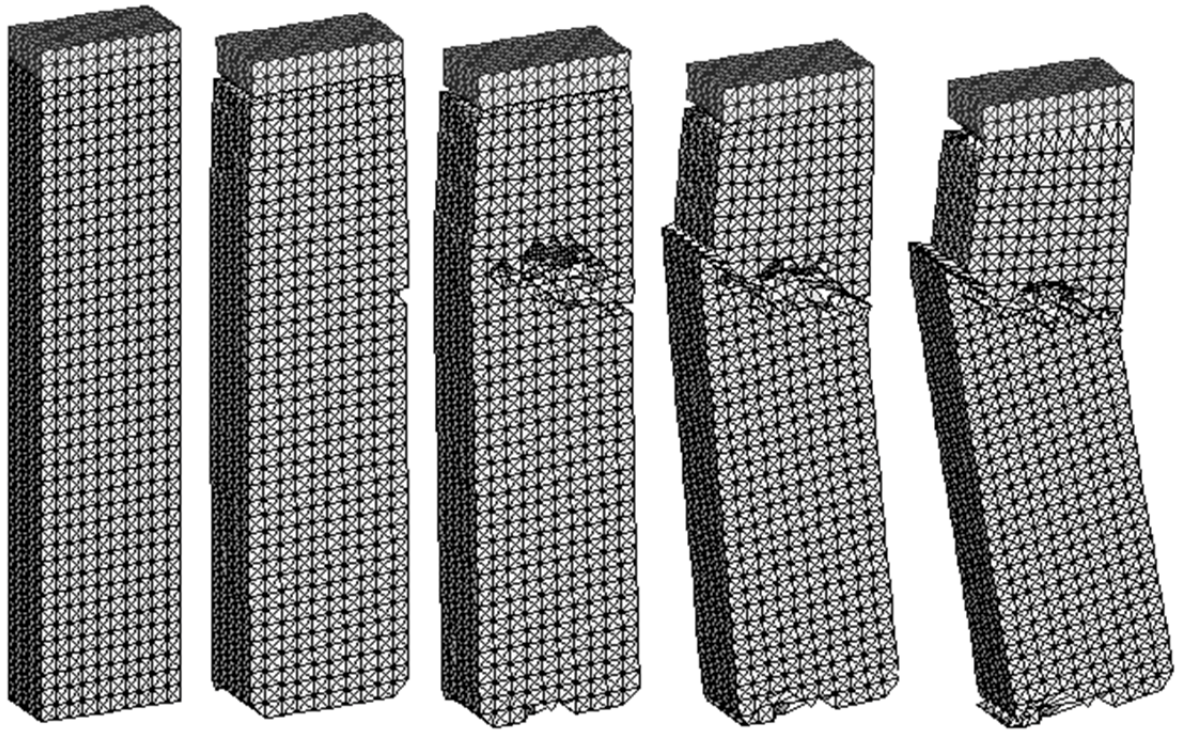

a) b)

Figure 4 Experimental (a) and calculated (b) fracture patterns for the concrete prism impacted by 230 kg weight falling from 50 cm height

The calculations demonstrated that prism fracture started directly under the steel plate. However this fracture is of local nature and is not defining. The local fracture was noted also on the bottom prism end, at place of contact with solid base. Starting from 19 ms, a crack appears at one third of the height from upper end that extends upwards and diagonally, reaching the opposite side of the prism.

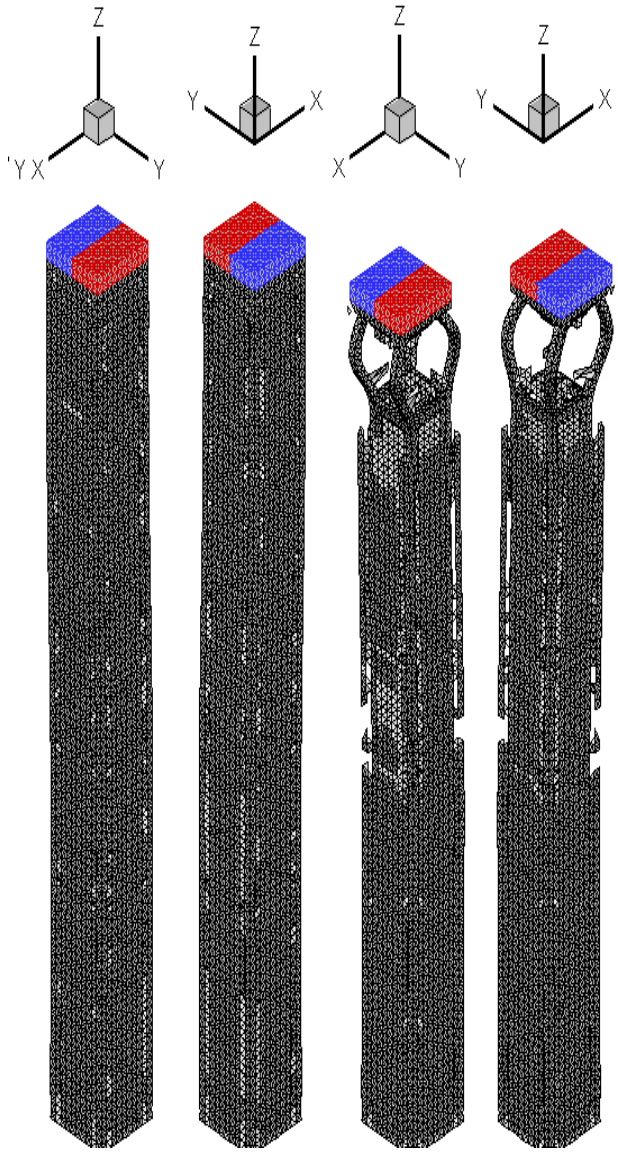

Figure 5 Fracture pattern in the ferroconcrete column of size 10 cm × 10 cm × 100 cm under loading that models endwise impact by 275 kg weight falling from 70 cm height

Figure 5 illustrates calculated fracture pattern in the ferroconcrete column model considered above (Figure 2) after the first and second impacts by 275 kg weight falling from 70 cm height. Initial impact velocity is 3.3 m/s. After the first impact, chipping of concrete from side surfaces and peeling of small fragments from the edges was noted. Similarly to the test, the second impact caused the fracture of the concrete scape in its head section up to approximately the same extent. Discrepancy between the calculation and experimental results does not exceed 12.5% for this parameter. Besides of existing bar buckling, the bars bend because of not co-axial direction of the impact.

The modelling provided triple impact by 480 kg weight falling from 2.1 m height onto end face of the steel guncrete column with velocity $V_0 = 6.415$ m/s. Striker velocity vector in XOZ plane including the column longitudinal axis was assumed for the calculations as $24°$ (Figure 6).

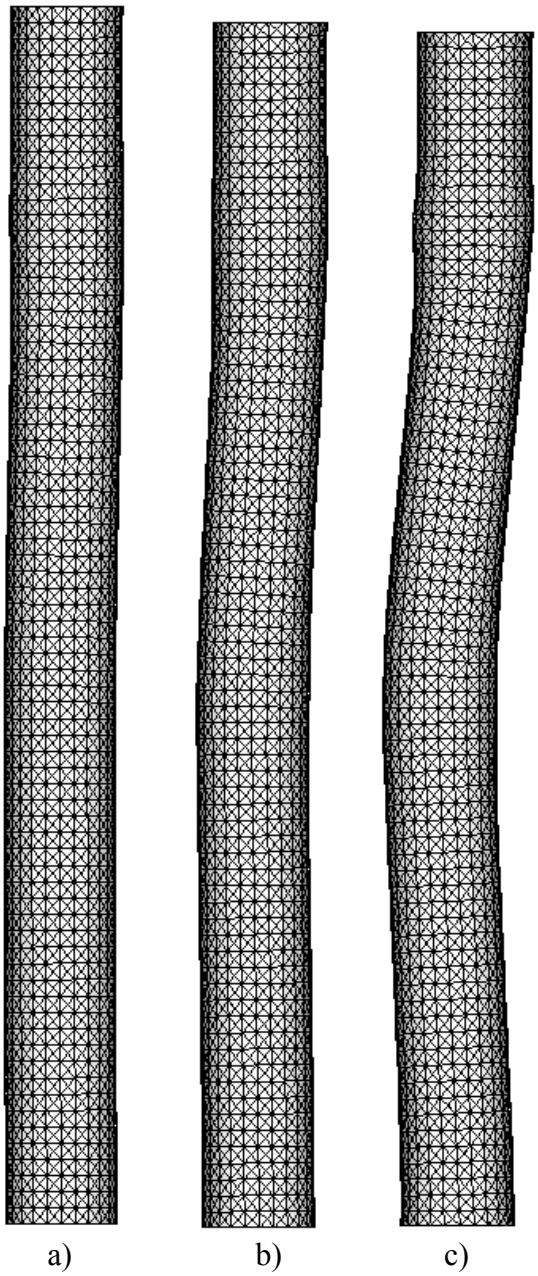

Figure 6 Deformation patterns for concrete-filled steel tube column of height 1 m and diameter 102 mm with wall thickness 3 mm after first (a, t=4 ms), second (b, t=8.1 ms) and third (c, t=12.1 ms) shock loadings by 480 kg weight falling from 2.1 m height

Figure 6 shows calculated column shapes after the first (a, t=4 ms), second (b, t=8.1 ms) and third (c, t=12.1 ms) shock loadings. The first shock loading is accompanied by growth of microcracks in the column concrete scape due to deviator component of stress tensor (shear mechanism of destruction). Cracks size reaches the critical level in virtually entire concrete scape. However process of macrofracture does not develop since fragmentation conditions are met neither by shear mechanism nor by separation mechanism. Therefore no visible fractures can be observed in the concrete scape. Only minor bend of the column as a whole (Figure 7 t=4.0 ms) occurs, resulting in total height decrease by 1 cm (H_1=99 cm).

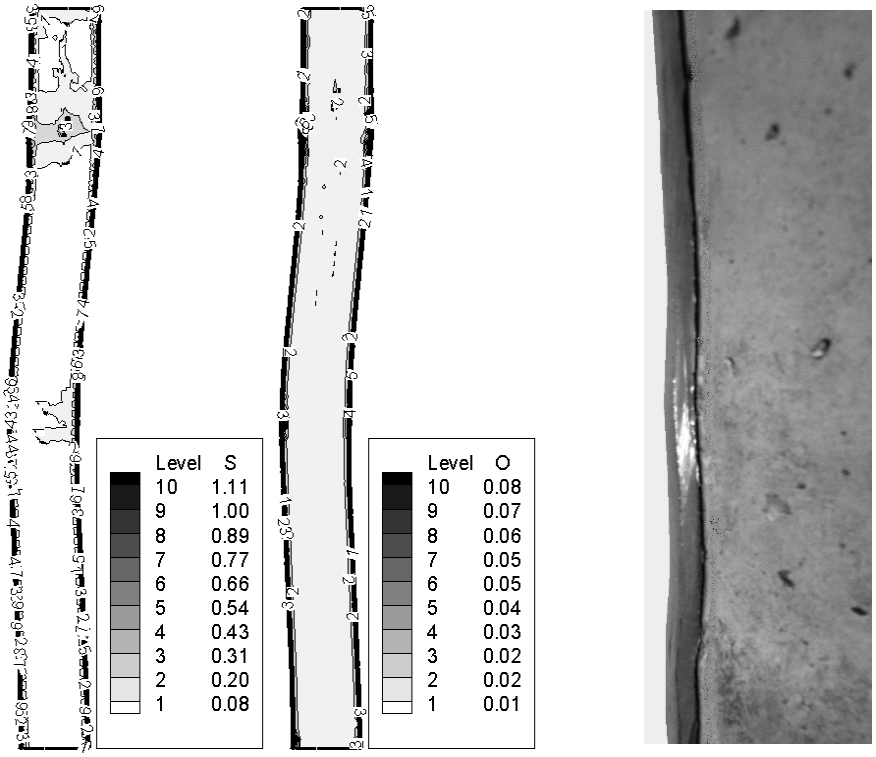

Figure 7 Experimental and calculated fracture patterns for the concrete-filled steel tube column after third shock loading by 480 kg weight falling from 2.1 m height: a) Levels of deformation intensity; b) Levels of relative void volume; c) Fragment of the column concrete scape detachment from the steel tube

Figure 7b shows column shape after repeated impact at the moment t_2=8.1 ms. The repeated loading is accompanied by increased bending of the column (H_2=98 cm). Moreover, there is area of small bulging at the distance about 12 cm from upper end surface. The microcracks in this area and in the column bend area reached critical size. Process of cracks fragmentation in the concrete commenced. However, same as after the first impact, there are no macrofractures in the concrete scape.

Deformation of the whole column and extent of its concrete scape damage after the third shock loading could be inferred by the calculation results presented in Figures 6c and 7a, 7b. The last ones show isolines of deformation intensity and relative void volume in the plane ZOX at the moment 12.1 ms. It is assumed that fragmentation of concrete damaged by the cracks takes place, if intensity of ductile deformations has reached its limiting value $e_u^* = 0.15$ (shear mechanism of destruction) or relative void volume $\xi_* = \frac{\alpha_* - 1}{\alpha_*} = 0.013$ (separation mechanism).

As indicated in Figure 7a, deformation intensity reaches its limiting value in concrete in virtually all points on the concrete-filled steel tube column interface. In the upper part of the column, at the distance about 15 cm from the end, at the interface, separation destruction occurs (Figure 8b). The column concrete scape detached from the steel tube in almost all places.

In addition, material area located in the column centre, at the distance about 14 cm from the upper end, is fractured through shear mechanism. Concrete area located at the column bend is at the limit of fracture. Overall pattern of the column deformation after the third impact is shown in Figure 7c. As evidenced by Figure 3, which shows photograph of the column after the third impact, these calculations agree qualitatively with the experimental results. Residual height of the column is 97 cm both in calculations and in experiment, i.e. column height decreased by 3 cm because of triple shock loading.

Figure 7c shows fragment of concrete-filled steel tube column cross-section cut by ZOX plane after the third shock loading. Column concrete scape was fractured in the experiment only along the steel/concrete interface. There are no other visible damages.

Figure 8 presents the results of mathematical modelling of shock interaction between the 275 kg weight falling from 70 cm height and the column constituting steel prismatic casing of size 10 cm × 10 cm × 100 cm with wall thickness 3 cm, filled with concrete. The first impact did not cause fracture of the column. After the second impact, steel casing ruptured in the column lower part. Virtually entire concrete scape of the column is damaged by the cracks ($e_u = 0.07$) but concrete fragmentation is observed in three areas only. The largest area of fragmented material is located at the upper end ($e_u > 0.15$). The second area of fractured material adjoins the casing rupture surface at the lower end. The material in this area is fractured mainly through separation mechanism and partially — through shear mechanism. The third area of fragmented material is located near column centre. At the column upper end and in the centre, in the column bend area, fragmentation of concrete damaged by the cracks occurs through shear mechanism.

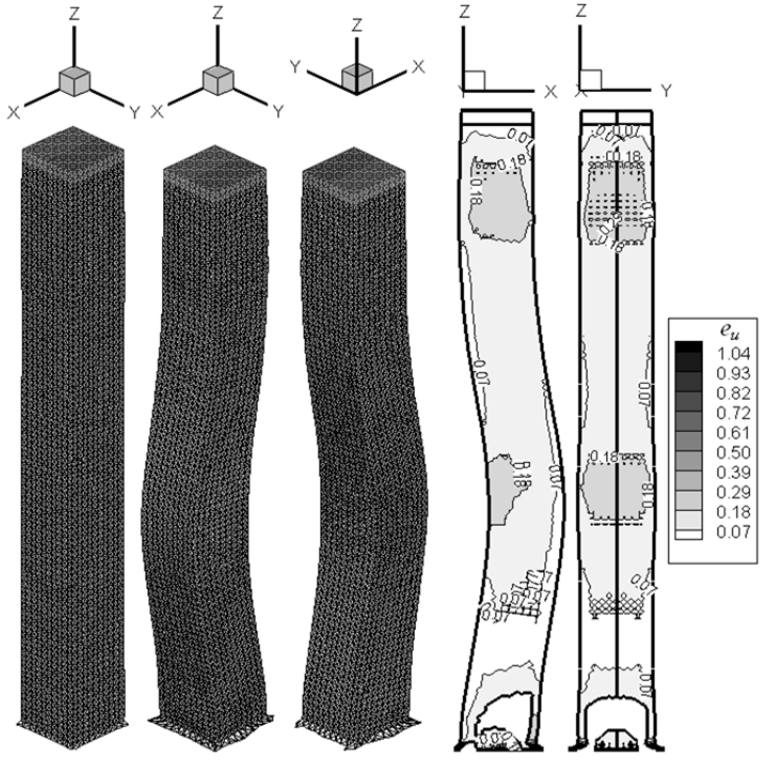

Figure 8 Fracture patterns and isolines of ductile deformations intensity in the column made as steel prismatic casing of size 10 cm × 10 cm × 100 cm with wall thickness 3 cm, filled with concrete, after repeated shock loading by 275 kg weight falling from 70 cm height

In summary, jointly conducted laboratory experiments and mathematical modelling allow us to comprehend better the results of carried out tests and interpret them in correct physical sense, the aspect that is extremely important for designing buildings in seismic regions.

REFERENCES

1. BELOV N N, KONYAEV A A AND KHABIBULIN M V, Effect of polymorphic phase transformations on process of steel spheres compression, FGV, 1997, Vol. 33, No.5. pp. 128-136.

2. BELOV N N, YUGOV N T, KOPANITSA D G AND YUGOV A A, Dynamics of high-velocity impact and associated physical phenomena. Tomsk: STT, 2005, 356 p.

3. AFANASIEVA S A, BELOV N N AND KHABIBULLIN M V, Analysis of high-velocity penetration of high-porous striker into a finite thickness target, Izvestiya RAN, MTT, 1999, No.2, pp. 91-100.

4. BELOV N N, KABANTSEV O V, KOPANITSA D G AND YUGOV N T, Computational and experimental methods for dynamic strength analysis of ferroconcrete structures elements. Tomsk: STT, 2008, 293 p.

5. BELOV N N, DEMIDOV V N AND YEFREMOVA L V, Computer modeling of high-velocity impact dynamics and associated physical phenomena, Izvestiya vuzov, Phizika, 1992, No. 8, pp. 5-48.

6. NIKIFOROVSKIY V S AND SHEMYAKIN YE I, Dynamic fracture of solids, Novosibirsk: Nauka, 1979, 272 p.

7. SALGANIC R L, Mechanics of bodies with numerous cracks, Izvestiya AN SSSR, MTT, 1973, No.4, pp. 149-158.

8. BELOV N N, YUGOV N T, AFANASIEVA S A, KOPANITSA D G AND YUGOV A A, Fracture of concrete and ferroconcrete slabs at high-velocity impact and explosion // DAN RF, 2005, Vol. 401, No. 2, pp. 185-188.

9. YUGOV N T, YUGOV A A AND BELOV N N, Calculation of adiabatic unsteady flows in 3D formulation (RANET-3), Federal Service for intellectual property, patents and trademarks. Certificate of state registration of computer programs No. 2010611042, Moscow, 2010.

10. YUGOV N T, Numerical analysis of 3D deformation and fracture process of cylinder and plate subjected to angled collision, Izvestiya AN SSSR, MTT, 1990, No. 1, pp. 112-117.

11. BAUM F A, ORLENKO L P AND STANYUKOVICH K P, Physics of explosion. Moscow, Nauka, 1975, 705 p.

12. BELOV N N, YUGOV N T, KOPANITSA D G AND YUGOV A A, Model of fine concrete dynamic fracture, Vestnik TSUAB, 2005, No. 1, pp. 14-22.

Efficiency of Modelling Corrosion-induced Cover Cracking in RC Structures

L Chernin, D Val
Heriot-Watt University, UK

Corrosion is one of the main causes of deterioration of reinforced concrete (RC) structures. Initially, it affects serviceability of a RC structure by causing excessive cracking of the cover concrete. A number of analytical models have been proposed to predict the time to corrosion-induced crack initiation. In this paper investigations on the applicability of the two main types of the analytical models based on solution of thick-walled uniform and double cylinders subjected to uniform internal pressure are described. FE analysis is employed for this purpose. Firstly, the influence of simplified formulation of the nonlinear behaviour of concrete is examined. The limits of applicability of the analytical models are established depending on c/d ratio (i.e., the ratio of the thickness of the concrete cover to the diameter of a reinforcing bar). Secondly, inability of the analytical models to account for actual boundary conditions of corroding reinforcing bars is studied. It is found that the influence of the boundary conditions on the predictive ability of the analytical models may be very significant. The FE analysis is also employed to investigate the influence of different types of concrete cover failure: cracking and delamination. The failure conditions in terms of ratios between certain geometrical parameters of a RC section have been established. The efficiency of the analytical models to describe different types of cover failure has been discussed.

L. Chernin is currently a research associate in the Institute for Infrastructure and Environment within the School of the Built Environment at Heriot-Watt University, Edinburgh. The areas of his research interests lay in the analysis of structural and material deterioration in reinforced concrete caused by corrosion of steel reinforcement, in analysis of concrete structures subjected to blast loads, and in structural and durability issues related to marine renewables.

D. Val is currently Professor in the Institute for Infrastructure and Environment within the School of the Built Environment at Heriot-Watt University, Edinburgh. His specialist areas of research are structural safety and reliability, quantitative risk assessment, performance of structures in aggressive environments, reliability of marine energy converters, adaptation of infrastructure to changing climate, and inter-infrastructure risks.

Keywords: Analytical model, Corrosion, Cracking, Finite element model, Reinforced concrete

INTRODUCTION

Corrosion of steel reinforcement represents one of the major deterioration threats to reinforced concrete (RC) structures [1]. Initially, corrosion affects serviceability of a RC structure by causing excessive cracking of the cover concrete. At this stage no significant reduction of structural strength occurs [2]. As a result, the time for structural repair due to corrosion is usually controlled by serviceability limit states associated with corrosion-induced cracking [3, 4]. This makes the time to crack initiation a major characteristic of structural performance. A large number of empirical, analytical and numerical models have been proposed for its prediction. It has been shown that existing empirical models are unable to provide accurate prediction of the time to crack initiation for a wide range of relevant parameters such as geometrical dimensions, concrete properties and corrosion rates [5]. Numerical models usually require the use of special software based on finite element or boundary techniques. Thus, analytical models are considered as a relatively simple and at the same time sufficiently accurate tool for estimating the time to crack initiation. However, the models have been validated/calibrated based on a limited amount of experimental data. This leaves the question open as to whether the models are indeed capable of providing accurate prediction of the time to crack initiation for a variety of concrete properties and locations of corroding reinforcing bars. The aim of the present paper is to provide data which help to answer the above question. This is achieved by comparing predictions of the analytical models with results of more accurate nonlinear FE analysis and examining the model consistency and validity from a theoretical point of view. Two popular analytical models based on a thick-walled cylinder (i.e., a uniform cylinder model [3, 6] and a double cylinder model [7]) subjected to internal pressure are considered. Nonlinear FE analysis is employed for evaluation of major sources of errors in the analytical models, namely, (i) simplifications in describing the nonlinear behaviour of concrete and (ii) inability to take into account the location of corroding reinforcing bars in a RC section (i.e., the actual boundary conditions). The influence of the first source of error is estimated through comparison of the analytical models with an equivalent FE model of a thick-walled hollow concrete cylinder subjected to internal pressure. Values of the errors are calculated for different ratios between the cylinder wall thickness and its internal diameter (c/d ratio). The effect of the errors arising from the second source is assessed by carrying out FE analyses of two different segments of a RC cross-section, which represent conditions of a reinforcing bar in the corner and in the middle of the section. Results obtained by the FE analysis are then compared with those yielded by the analytical models for concrete hollow cylinders with the wall thickness equal to the thickness of the concrete cover in the RC cross-section. Recommendations on the use of analytical/numerical models depending on the c/d ratio and the bar location are then presented.

Existing Analytical Models

Thick-walled uniform cylinder (TWUC) models

The first analytical model of the mechanism of corrosion-induced cover crack was proposed by Bažant [6]. Concrete surrounding a corroding reinforcing bar was considered as a homogeneous linear elastic material. Expansion of corrosion products was modelled by a uniform increase in the diameter of the cylindrical hole around the reinforcing bar. The rate of rust production was assumed to be constant in time. A relationship between the rebar expansion and the corresponding pressure was found as the average of two solutions of the classic Lamé problem – one for a hollow thick-walled cylinder under plane stress and the

other one for a circular cavity in an infinite medium. It was also assumed that the concrete cylinder (representing the concrete cover) is fully cracked when the average tensile stress in the cylinder wall becomes equal to the tensile strength of concrete. The internal pressure causing the concrete cover cracking was then found from an equilibrium condition of a half of the cylinder. However, the model provided poor agreement with experimental data.

In order to obtain better agreement with experimental data Liu and Weyers [3] suggested to modify Bažant's model by taking into account the penetration of a part of forming corrosion products into pores and microcracks within the concrete surrounding a corroding reinforcing bar. This was done by assuming that there was a porous zone around a reinforcing bar, and corrosion products did not exert any pressure on the surrounding concrete until they fully filled this zone. To increase the estimated time to crack initiation compared to that yielded by Bažant's model [6] the relationship between the rebar expansion and the internal pressure used by Liu and Weyers [3] was solely based on the solution for a hollow thick-walled cylinder. Finally, in order to further increase the estimated time to crack initiation Liu and Weyers assumed that the rate of rust production was not constant but inversely proportional to the amount of corrosion products and, hence, decreased with time. This assumption led to a first order linear differential equation which was solved incorrectly (for more details see [5]). El Maaddawy and Soudki [8] noted that the use of the assumption about a decrease in the rate of rust production with time led to underestimation of the mass loss of steel observed in tests. Therefore, it was suggested to continue to use the TWUC model and Bažant's assumption about the constant rate of rust production, which was estimated using Faraday's law (with constant corrosion current density) but to adopt the assumption of Liu and Weyers [3] about the porous zone around a reinforcing bar. Malumbela et al. [9] developed a model taking into account a non-uniform distribution of steel corrosion around a reinforcing bar. The solution for a thick-walled cylinder subjected to uniform internal pressure was used in the model (without any corrections) for estimation of the maximum displacement around a non-uniformly corroded rebar.

Thick-walled double cylinder (TWDC) models

Further development of the analytical models was based on the partition of the cylinder into two parts: a cracked inner cylinder and an uncracked outer one. Wang and Liu [10] considered the concrete in the inner cracked cylinder as an isotropic linearly elastic material with a modulus of elasticity equal to that of the outer cylinder. In order to calculate stresses in the inner cylinder in the tangential direction the displacement field found from a linear elastic solution for a thick-walled uniform cylinder was used along with a non-linear stress-strain relationship describing tension softening that was clearly inconsistent. Bhargava et al. [11] assumed that the concrete in the inner cracked cylinder is isotropic and linearly elastic but with a reduced modulus of elasticity compared to that of the outer cylinder. This formulation represents the partially cracked concrete cylinder as a thick-walled composite one made from two isotropic linearly elastic materials with different moduli of elasticity. As a result full compatibility in both strain (displacement) and stress fields, which exists in the partially cracked concrete cylinder, cannot be achieved on the common boundary between the two materials. Only the compatibility in the stress field was ensured. Li et al. [12] modelled the inner cracked cylinder as an orthotropic material with the modulus of elasticity reduced only in the tangential direction normal to cracks. The modulus of elasticity in the radial direction remained unchanged and was equal to that in the outer uncracked cylinder. The reduced modulus of elasticity was calculated by averaging the tangential strains in the inner cylinder and was constant throughout the cylinder wall. This formulation was also unable to provide

compatibility in both stresses and strains on the common boundary between the two cylinders. An improved analytical model based on a thick-walled double cylinder was proposed by Chernin et al. [7]. Linearly elastic material representing cracked concrete of the inner cylinder was modelled as cylindrically anisotropic (or more exactly as inhomogeneously orthotropic). The degree of anisotropy in the inner cylinder was varied depending on the radial coordinate by changing the stiffness in the tangential direction in accordance with a power function. This formulation led to elimination of anisotropy at the common boundary between the cylinders. As a result, complete compatibility in both stress and strain (displacement) fields was achieved between the inner and outer cylinders. Calibration of the model (i.e., evaluation of the exponent in the power function) was performed using results of the tests on concrete specimens with cylindrical holes subjected to controlled internal pressure [13]. The obtained values of the exponent were widely scattered; however, it was shown that the lowest possible value was 1.5, which could be used as a tentative estimate.

Description of Finite Element Model

A FE model describing a segment of a cross-section of a RC element is developed and implemented in the commercial FE code ABAQUS [14], using a 2-D plane strain formulation. Since the concrete behaviour around a corroding reinforcing bar is dominated by tensile cracking at a low level of compressive stresses, constitutive modelling of concrete can be based on an elastic cracking model. The concrete material between cracks is treated as linearly elastic and isotropic. The tension softening in the direction normal to a crack is described based on the Hillerborg cohesive crack model [15], in which a stress-displacement curve is adopted from CEB-FIP model code 1990 [16]. In the present study deformability of the corrosion products is neglected, since in accordance with [5] it leads to a negligible error (much less than 10%). The coefficient of friction used in the FE analysis is set equal to 0.4, which is in the experimentally estimated range between 0.3 [17] and 0.55 [18].

The expansion of corrosion products around a corroding reinforcing bar is modelled using a thermal analogy, i.e., by increasing the temperature of the reinforcing bar that leads to its thermal expansion. The free increase in the diameter of a reinforcing bar due to corrosion can be estimated with sufficient accuracy (see [5]) as $\Delta d_x = 2(\alpha_v - 1)x$, where α_v is the volumetric expansion ratio of corrosion products that has been set equal to 3 in accordance with Suda et al. [19]; and x is the corrosion penetration that could be found using Faraday's law of electrolysis. The equivalent increase in the diameter of the reinforcing bar, Δd, due to increase in its temperature could be found as $\Delta d_T = \alpha_T \Delta T d$, where α_T is the coefficient of thermal expansion and ΔT the increase in temperature. Since the material model is rate independent any combination of values of α_T and ΔT providing a necessary value of Δd can be used. Therefore, α_T is evaluated in this study by assuming $\Delta T \equiv x$ and equating $\Delta d_x = \Delta d_T$ as $\alpha_T = 2(\alpha_v - 1)/d$. Validation of the FE model has been performed quantitatively using results of tests on concrete specimens subjected to controlled pressure applied within cylindrical holes [13] and qualitatively using results of accelerated corrosion tests on RC slabs [20] (for details see [5]).

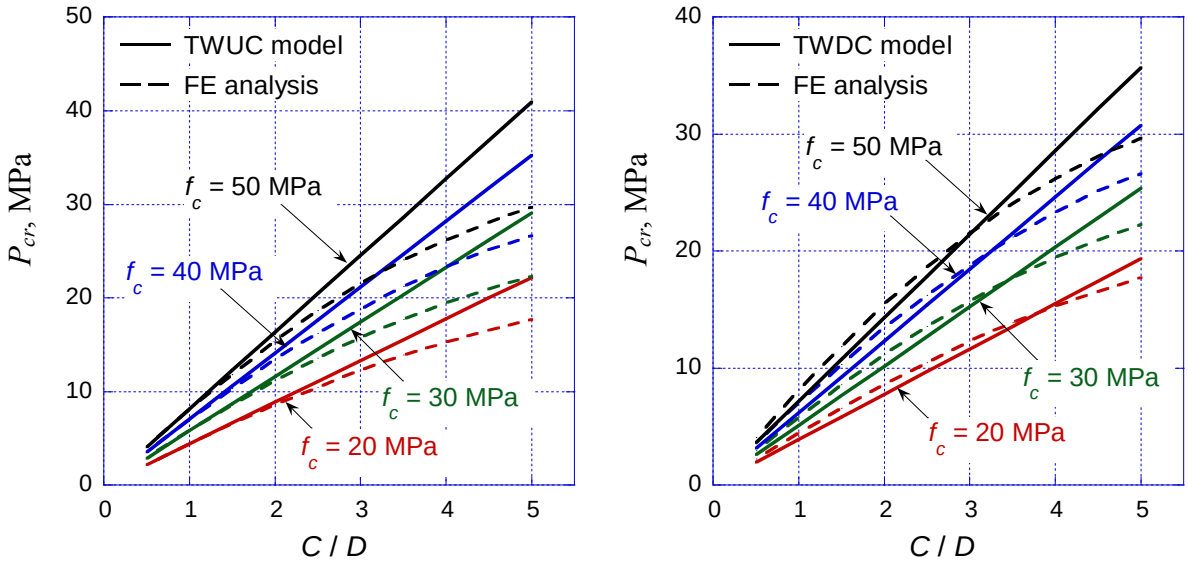

Figure 1 P_{cr} calculated using FE analysis and (a) TWUC model, (b) TWDC model

Influence of Modelling the Nonlinear Behaviour of Concrete: Model Comparison

Currently, the TWUC and TWDC models are the most popular analytical models for the prediction of corrosion-induced cover cracking in RC structures. Thus, it is important to compare the models and provide recommendations about their applicability. Validation of these models against results of tests/field observations of RC elements subjected to natural or accelerated corrosion cannot be properly performed since part of the corrosion products forming around a corroding rebar penetrates into concrete pores and microcracks and does not contribute to pressure between the rebar and the concrete. Another possible approach is to validate them against a more accurate model such a nonlinear FE model. The fact that a part of corrosion products penetrates into concrete pores and cracks is not important for this method of comparison, and therefore this phenomenon is neglected in the following analyses. Results of the TWUC and TWDC models are compared with results yielded by a nonlinear FE model of a thick-walled concrete cylinder subjected to internal pressure. The comparison is performed for concrete cylinders with four different values of the concrete compressive strength, f_c, namely 20, 30, 40 and 50 MPa. The corresponding values of the concrete tensile strength, f_{ct}, and the modulus of elasticity, E_c, are evaluated in accordance with recommendations of [16]; the Poisson's ratio $\nu_c = 0.2$. Results of the calculations of internal pressure at cover cracking, P_{cr}, are presented in Figure 1 depending on the c/d ratio. Different values of the c/d ratio in the range between 0.5 and 5 are obtained by variation of the thickness of the cylinder wall while keeping the inner diameter of the cylinder (i.e., rebar diameter) equal to 16 mm. As can be seen from Figure 1a, the difference between the TWUC results and the FE analyses is insignificant for small values of the c/d ratio and increases with increasing c/d. Figure 1a also demonstrates that the TWUC model always yields higher values of P_{cr} compared to those from the FE analysis. Figure 1b shows the results of the TWDC model proposed by Chernin et al. [7] and of the FE analysis. The TWDC model takes into account partial cracking of the cylinder wall and provides a better agreement with the FE results for higher values of the c/d ratio compared to the TWUC model.

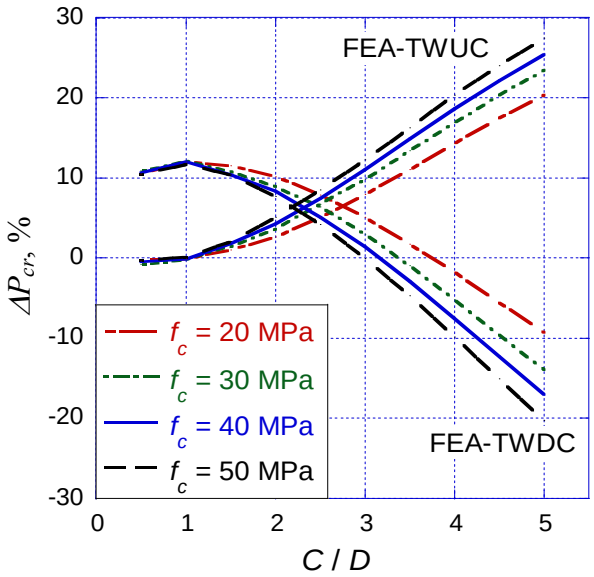

Figure 2 ΔP_{cr} between FE analysis (FEA) and TWDC and TWUC models

In addition, in order to provide clearer comparison between the models differences (in %) between the values of P_{cr} calculated by the FE analysis and the TWUC and TWDC models are presented in Figure 2. If to assume the TWUC and TWDC models can be applied when the difference between their results and the FE analysis does not exceed 10% the following recommendations on the model use are suggested: for $c/d < 2.5$ the TWUC model could be effectively used while for $2.5 \le c/d < 4.0$ the TWDC model and for $c/d \ge 4.0$ the FE analysis. It is necessary to note that these recommendations are based only on the consideration of the influence of nonlinear behaviour of concrete on values of P_{cr}.

Influence of Boundary Conditions: Numerical Study and Model Comparison

Analytical models based on a thick-walled cylinder can take into account neither the effects of location and spacing of reinforcing bars in a RC element nor the influence of friction between concrete and reinforcing bars on cracking of the concrete cover. In addition, the models provide no information on the type of failure of the concrete cover, which can be either cracking or delamination. Errors arising from these shortcomings need to be assessed in order to establish the applicability limits of the analytical models. For this purpose nonlinear FE analyses are carried out for two segments of a typical RC cross-section (Figure 3): one representing the condition of a corner bar (CB) and the other one – of a middle bar (MB); the FE model described is Section 3 is employed. The following concrete material properties are used: $f_c = 20$ MPa, $f_{ct} = 3$ MPa, $E_{c,ef} = 15600$ MPa, $\nu_c = 0.2$. The side concrete cover, c_2, representing also half of the clear spacing between rebars is kept constant, $c_2 = 80$ mm (see Figure 3). The top concrete cover, c_1, is varied in the range between 8 and 80 mm, which leads for $d = 16$ mm to $c_1/d = 0.5 \div 5$ and $c_2/c_1 = 1 \div 10$. It is necessary to note that validity of the single bar CB and MB models shown in Figure 3 has been checked by analysis of larger parts of a RC cross-section which include two and three reinforcing bars. Results of the FE analysis are compared with those of the TWUC and TWDC models.

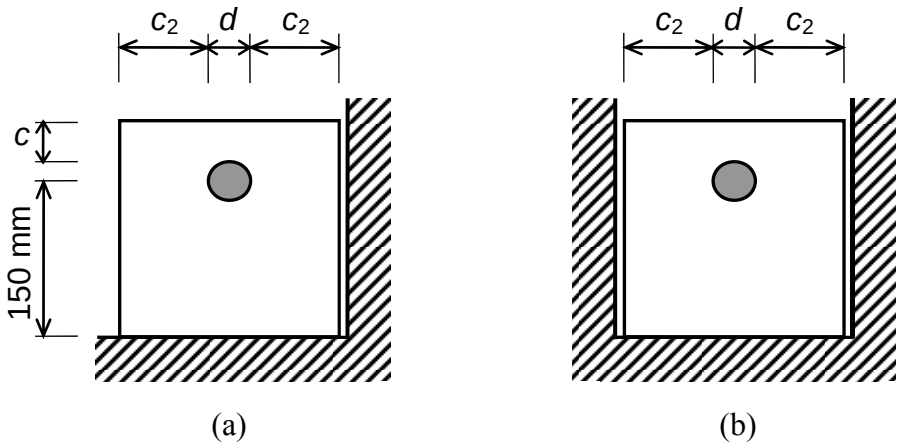

Figure 3 Fragments of RC cross-section representing different rebar locations: (a) CB case; (b) MB case

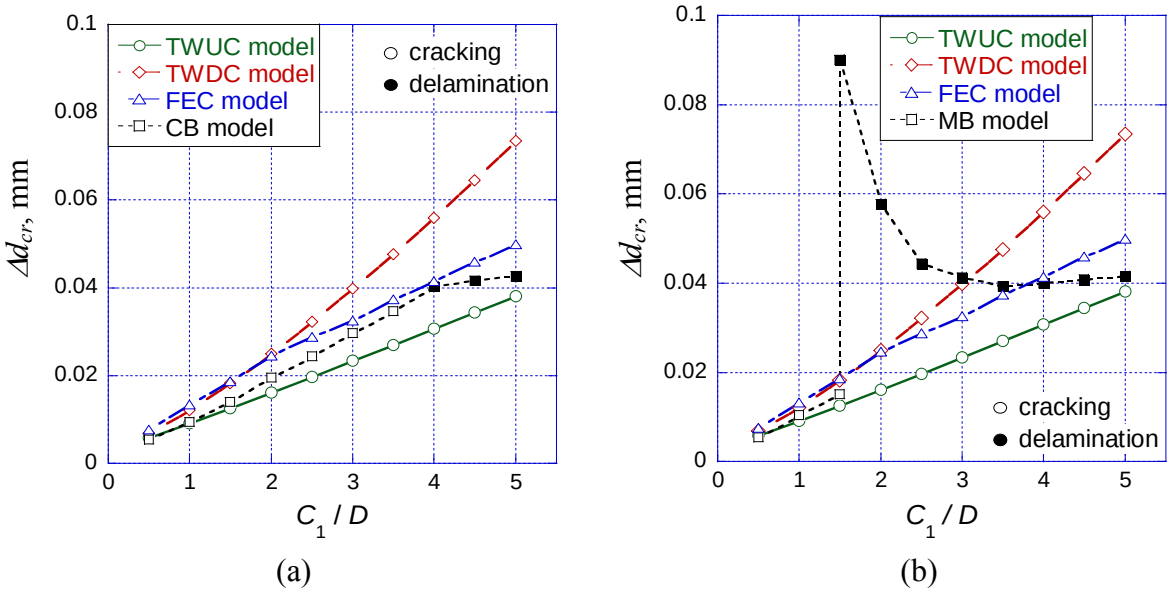

Figure 4 Comparison between the analytical models and the FE analysis (a) CB case; (b) MB case

Figure 4 shows the results obtained by the TWUC and TWDC models and the FE analysis for the CB and MB cases. Two basic types of the concrete cover failure develop in the FE simulations – cracking above a reinforcing bar and cover delamination. Delamination replaces cracking in the CB case when $c_1/d \geq 4$ and in the MB case when $c_1/d > 1.5$. According to Figure 4 the TWUC model mostly underestimates the increase in the rebar diameter at cracking of the concrete cover, Δd_{cr}, compared to the results of the FE analyses. The underestimation is especially significant for the MB case when $c_1/d > 1.5$ and the concrete cover fails due to delamination. As opposite to this, the TWDC model mainly overestimates Δd_{cr}, except of the MB case and the cover failure due delamination when $1.5 < c_1/d \leq 3$.

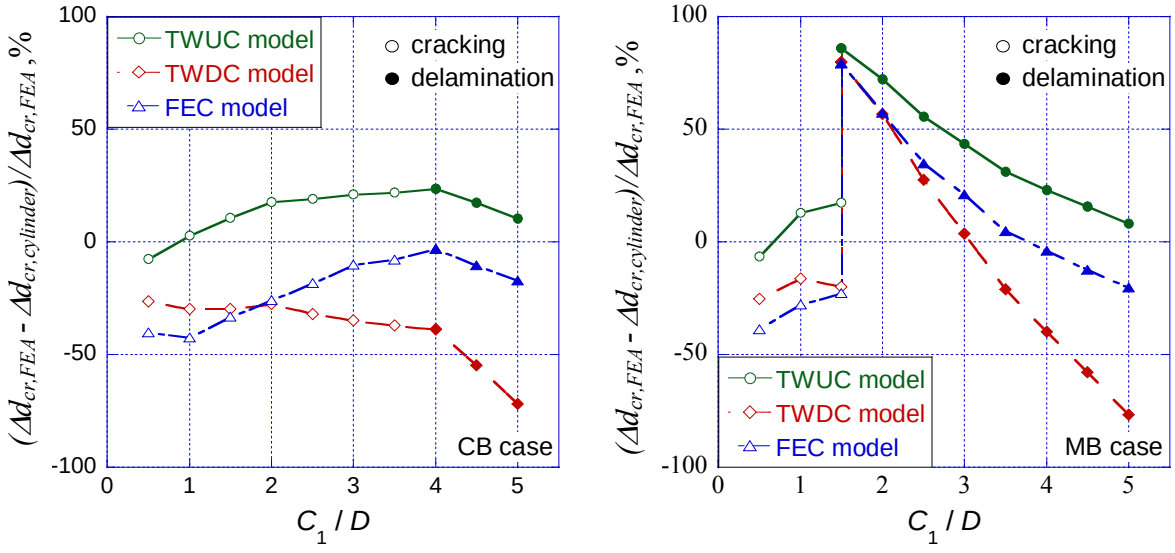

(a) (b)

Figure 5 Relative difference in % between the analytical models and the FE analysis (a) CB case; (b) MB case versus c_1/d

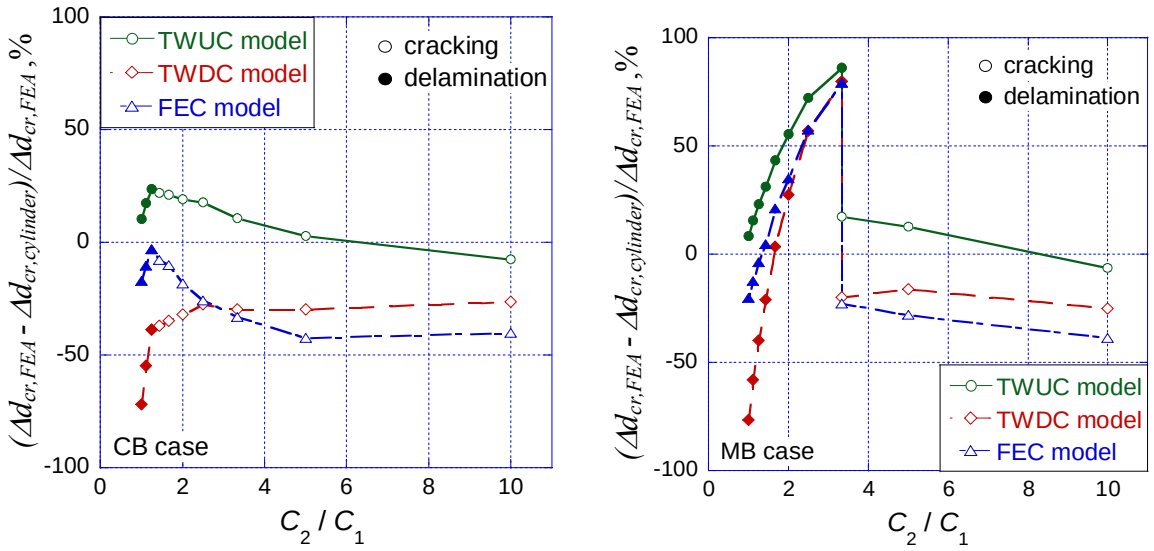

(a) (b)

Figure 6 Relative difference in % between the analytical models and the FE analysis (a) CB case; (b) MB case versus c_2/c_1

Comparison between the results of the FE analysis and the TWUC and TWDC models is also presented in Figures 5 and 6, respectively, as the relative difference between the results in % versus the c_1/d and c_2/c_1 ratios. Figure 5a shows that for the CB case the use of the TWUC model leads to small errors (less than 10%) when $c_1/d \leq 1.5$ and result in errors up to 25% for higher values of c_1/d. For the MB case the TWUC model provides much worse results. When $c_1/d \leq 1.5$ and the type of cover failure is cracking, the TWUC predictions are still reasonable – the relative difference compared to the FE results is less than 20%. However, for higher values of c_1/d when the type of cover failure changes to delamination the relative difference becomes very large; it drops again below 20% for $c_1/d \geq 1.5$ but mainly due to combine effect of different errors. It is interesting that as the type of cover failure changes from

cracking to delamination the divergence between models starts to decrease again suggesting on mutual compensation of errors arising from the two discussed sources (for further discussion see [5]). The TWDC model (Figure 6a) provides better predictions than the TWUC model only for the MB case and the cover failure due to delamination; in this case the relative difference between its results and the FE results is in reasonable bounds (±20%) when $2.5 < c_1/d < 3.5$. Figures 5b and 6b show the relative difference between the FE and TWUC and TWDC results, respectively, versus the c_2/c_1 ratio. The change of the type of failure from delamination to cracking occurs in the CB case when $c_2/c_1 \geq 1.25$ and in the MB case when $c_2/c_1 \geq 3.3$. Thus, a particular type of failure depends not only on the c_1/d ratio but mainly on the c_2/c_1 ratio.

In addition, the type of the concrete cover failure depends on the location of a corroding reinforcing bar. Concerning the applicability of the TWUC model, for the CB case it may be applied in principle for the whole range of the c_2/c_1 values – the relative difference does not exceed 25%; the relative difference is within 10% for $c_2/c_1 \leq 1$ and $c_2/c_1 \geq 3.3$. For the MB case the TWUC should definitely not be applied for $1.25 \leq c_2/c_1 \leq 3.3$; for the rest of c_2/c_1 values the relative difference is less than 25%. The TWDC model, on the whole, provides worse predictions than the TWUC model; its divergence from the FE results is within reasonable bounds only for the MB case for a narrow range of c_2/c_1 around 1.75.

Additionally, in order to evaluate only the influence of the effects of location and spacing of reinforcing bars, friction at the steel-concrete interface and the type of cover failure on the results yielded by the analytical models a FE model of a concrete hollow cylinder (FEC model) has been developed. The cylinder has been subjected to internal radial displacements which has provided a stable solution and allowed to trace accurately the process of crack initiation. The results of the FEC model are presented in Figure 4, while Figures 5-6 show a comparison of the FEC model with the analytical models. As can be seen in Figures 5-6 the analytical models are more accurate in evaluation of cracking of the concrete cover for low c_1/d ratios and high c_2/c_1 ratios ($c_1/d \leq 2$ and $c_2/c_1 > 2.5$ in the CB case and $c_1/d \leq 1.5$ and $c_2/c_1 \geq 3.3$ in the MB case and). When the type of concrete cover failure changes from cracking to delamination the FEC model becomes generally more accurate in the CB case except for $c_1/d = 5$ ($c_2/c_1 = 1$) while in the MB case for $3.5 \leq c_1/d \leq 5$ and $1 \leq c_2/c_1 \leq 1.4$.

The better accuracy of the TWUC model in a range of c_1/d and c_2/c_1 ratios could take place because the errors in modelling the nonlinear concrete behaviour partially compensate the errors caused by inability of the model to account for boundary conditions. For low c_1/d (≤ 1.5) and high c_2/c_1 (> 3.3) the FEC model is less accurate than the analytical models. However, the picture changes for $c_1/d > 1.5$ and $c_2/c_1 < 3.3$ possibly pointing to the change in magnitudes of the errors from different sources. It is also interesting to note that the analytical models are located from different sides of the FEC model for $c_1/d \geq 1.5$ and $c_2/c_1 < 3.3$ (see Figure 5-6). This together with low accuracy of the TWDC model could indicate addition of the errors from different sources.

Another possible reason could be a bad choice of the exponent of the power function in the model (see [7]), since experimental data used in the model calibration was limited to $c_1/d = 0.5$ and 1. In fact, the above discussion leads to an interesting conclusion that an improvement of analytical models based on a thick-walled cylinder in terms of description of the nonlinear behaviour of concrete compared with the simple TWUC model may not be beneficial. In many cases it may result in larger errors compared with the TWUC results when corrosion-induced cover cracking in real RC structures is analysed.

CONCLUSIONS

In the paper a nonlinear FE model has been employed to examine the applicability of analytical models based on thick-walled uniform and double cylinders (i.e., TWUC and TWDC). First, inaccuracy of the analytical models arising due to simplified formulations of the nonlinear behaviour of concrete has been considered. It has been found that the use of the TWUC model leads to an insignificant error when c/d ratio does not exceed 2.5. The use of the TWDC model is more appropriate when c/d is in the range between 2.5 and 4.0, while for c/d higher than 4.0 nonlinear FE analysis is recommended. Second, effects of the location of a corroding reinforcing bar on cracking of the concrete cover have been studied. Two single bar models with different boundary conditions have been defined to simulate typical conditions of reinforcing bars in the corner and in the middle of a RC slab. Two types of the concrete cover failure – cracking and delamination, have been observed in the analyses and the failure conditions in terms of ratios between certain geometrical parameters of a RC section have been established. It has been shown that the occurrence of a certain type of failure depends not only on these ratios but also on the location of reinforcing bars. It has also been demonstrated that the TWUC model is capable to provide reasonable results for corner rebars. However, for rebars in the middle of a RC slab the use of the TWUC model may lead to significant errors (higher than 25%). In most cases the TWDC model led to larger divergence from the FE results than the TWUC model. A FE model of a concrete hollow cylinder (FEC) has then been applied to evaluate only the influence of boundary conditions around a corroded rebar in a RC section (e.g., location and spacing of reinforcing bars) and type of cover failure on accuracy of the analytical models. From comparison of the analytical models with the FEC model it has been concluded that the errors in the description of nonlinear behaviour of concrete in the TWUC model partially compensate the errors arising due to inability of the model to account for actual boundary conditions. In contrast, addition of the errors from different sources occurs in the case of the TWDC model. This leads to a conclusion that an improvement of analytical models based on a thick-walled cylinder in terms of description of the nonlinear behaviour of concrete may not be beneficial for practical applications compared with the simple TWUC model.

REFERENCES

1. BENTUR A, DIAMOND S AND BERKE N S, Steel Corrosion in Concrete, 1997, London (UK): E&FN Spon.

2. VAL D V, Effect of different limit states on life-cycle cost of RC structures in corrosive environment, Journal of Infrastructure Systems, ASCE, Vol. 11, No. 4, 2005, pp. 231-240.

3. LIU Y AND WEYERS R E, Modelling the time-to-corrosion cracking in chloride contaminated reinforced concrete structures, ACI Materials Journal, Vol. 95, No. 6, 1998, pp. 675-681.

4. TORRES-ACOSTA A A AND MARTINEZ-MADRID M, Residual life of corroding reinforced concrete structures in marine environment, Journal of Materials in Civil Engineering, ASCE, Vol. 15, No. 4, 2003, pp. 344-353.

5. CHERNIN L AND VAL D V, Prediction of corrosion-induced cover cracking in reinforced concrete structures, Construction and Building Materials, Vol. 25, No. 4, 2011, pp. 1854–1869.

6. BAŽANT Z P, Physical model for steel corrosion in concrete sea structures – Application, Journal of the Structural Division, ASCE, Vol. 105, No. 6, 1979, pp. 1155-1166.

7. CHERNIN L, VAL D V AND VOLOKH K Y, Analytical modelling of concrete cover cracking caused by corrosion of reinforcement, Materials and Structures, Vol. 43, No. 4 2010, pp. 543-556.

8. EL MAADDAWY T AND SOUDKI K, A model for prediction of time from corrosion initiation to corrosion cracking, Cement & Concrete Composites, Vol. 29, 2007, pp. 168-175.

9. MALUMBELA G, ALEXANDER M AND MOYO P,. Model for cover cracking of RC beams due to partial surface steel corrosion, Construction and Building Materials, 2010, doi:10.1016/j.conbuildmat.2010.06.081.

10. WANG X H AND LIU X L, Modelling effects of corrosion on cover cracking and bond in reinforced concrete, Magazine of Concrete Research, Vol. 56, No. 4, 2004, pp. 191-199.

11. BHARGAVA K, GHOSH A K, MORI Y AND RAMANUJAM S, Model for cover cracking due to rebar corrosion in RC structures. Engineering Structures, Vol. 28, 2006, pp. 1093-1109.

12. LI C-Q, MELCHERS R E AND ZHENG J-J, Analytical Model for Corrosion-Induced Crack Width in Reinforced Concrete Structures, ACI Structural Journal, Vol. 103, No. 4, 2006, pp. 479-487.

13. WILLIAMSON S J AND CLARK L A, Pressure required to cause cover cracking of concrete due to reinforcement corrosion. Magazine of Concrete Research, Vol. 52, No. 6, 2000, pp. 455-467.

14. ABAQUS. Abaqus Version 6.7 Documentation, 2007, Hibbitt, Karlsson & Sorensen Inc., Pawtuchet, RI, USA.

15. HILLERBORG A, MODEER M AND PETERSSON P-E, Analysis of crack formation and crack growth in concrete by means of fracture mechanics and finite elements, Cement and Concrete Research, Vol. 6, 1976, pp. 773-782.

16. CEB-FIP Model Code 1990. Bulletin d'Information No. 213/214, 1993, Comité Euro-International du Béton, Lausanne, Switzerland.

17. XU Y. Experimental study of bond-anchorage properties for deformed bars in concrete, Proceedings of International Conference on Bond in Concrete, From Research to Practice, CEB, Riga, Latvia, 1992, p. 1/9-1/17.

18. CAIRNS J, DU Y AND LAW D, Influence of corrosion on the friction characteristics of the steel/concrete interface, Construction and Building Materials, Vol. 21, 2007, pp. 190-197.

19. SUDA K, MISRA S AND MOTOHASHI K,. Corrosion products of reinforcing bars embedded in concrete, Corrosion Science, Vol. 35, 1993, pp. 1543-1549.

20. VU K, STEWART M G AND MULLARD J, Corrosion-induced cracking: Experimental data and predictive models, ACI Structural Journal, Vol. 102, No. 5, 2005, pp. 719-726.

A New Model for Predicting the Effective Strength in Concrete Bottle-Shaped Struts

A Arabzadeh, R Aghayari
Tarbiat Modares University, Iran

Strut-and-Tie Model (STM) can be used to model the flow of compression within a concrete strut. Concrete struts are formed in various shapes such as prismatic or bottle shape. Bottle-shaped struts are wider at their middle region than both ends. Due to transverse straining at the midpoint of struts, longitudinal cracks are formed parallel to applied load direction. The compression response of concrete in cracked elements differs from that of plain concrete in uniaxial compression. In this paper a new model to analysis of concrete struts was proposed based on modified compression field theory (MCFT). A database of 34 tested specimens was used to evaluate the accuracy of proposed model and approaches of both codes ACI and CSA. According to performed comparison, the results of new proposed model are accurate and can be adequate to concrete panels subjected to compression force.

A Arabzadeh is a Professor in Tarbiat Modares University, Iran.

R Aghayari is an Associate Professor in Tarbiat Modares University, Iran.

Keywords: Compressive softening, Strut-and-tie, Transverse reinforcement

INTRODUCTION

Struts as important element of strut-and-tie model carry compressive forces and their forming shapes varies depend on the force path. The most basic type of struts is prismatic with uniform cross-section over its length. The compressive stress block in the pure-bending region of deep beams can be an example of prismatic strut [1]. When the flow of compression stress is not confined to a portion of structural element, a bottle-shape strut will be formed and the force is applied to a small zone and disperses as they flow through the member. Its bulging stress paths cause the significant transverse strain perpendicular to strut axis. The formed transverse strain is compressive in near of both neck of bottle-shape strut and tensile further away [2]. Consequently, those strains cause longitudinal cracks and initiate an early failure. It is therefore necessary to reinforce the stress field in transverse direction or to consider the transverse tension, when determining the ultimate strength of strut.

STM was laid by Ritter (1899) [3]. Ritter's original goal was to explain that a stirrup in RC members, Ritter's model was expanded later by Mörsch (1902) [4]; Mörsch presented that the diagonal compressive stresses in the concrete would not to be discrete zones, but could be continuous field in equilibrium with discrete stirrup forces. The Strut-and-Tie Method (STM) is gaining rapid popularity for shear RC members such as corbels, deep beams and beam-column joints. Marti (1986) [5], Schlaich-Schäfer, (1987) [2], Mitchell-Collins (1984) [6], Ramirez (1994) [7], Tang et al (2001) [8] and Hwang et al (2002) [9] proposed some approaches applicable in D-regions. Until now, very little study has been reported to study the behaviour of RC bottle-shape struts. Brown et al (2006) [1], [10] published two papers which investigated the behaviour of normal-strength concrete isolated struts and minimum requirement transverse reinforcement.

The dispersion of compression was described in great detail by Guyon (1953). Guyon used flow paths to determine the dispersion of tensile and compressive stresses in a post-tension zone and concluded that the flow paths of compression (1 through 6 in Figure 1) must be parallel to the applied force at loaded point and some distance away from it [1].

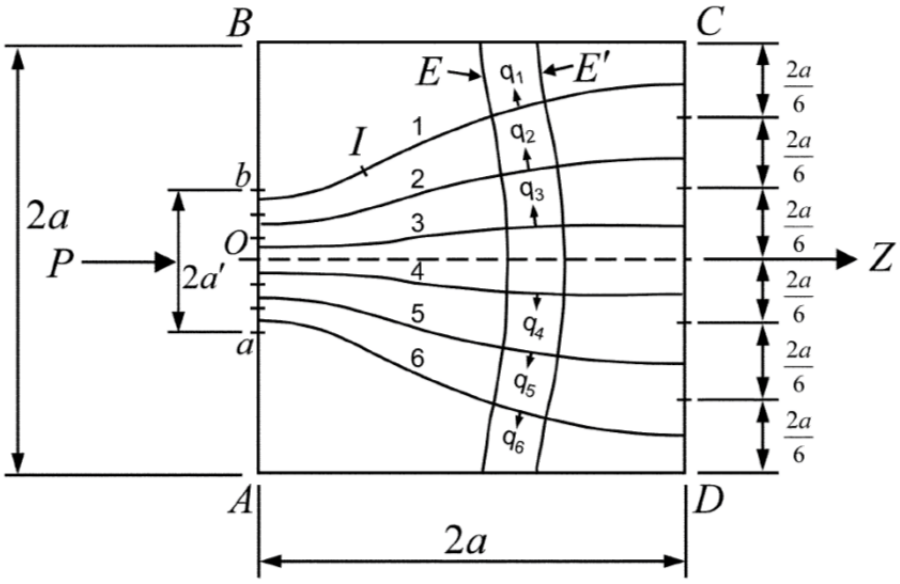

Figure 1 Dispersion of compression provided by Guyon [1]

The resulted tension forms perpendicular to compression curve paths. It means that, the bottle-shape struts are modelled as a combination of accessorial struts and ties as shown in Figure 2. In current study the existing approaches applicable to analysis of ultimate compressive strength of bottle-shaped struts are studied. A new relation based on modified compression field theory (MCFT) is proposed. To evaluate the accuracy and reliability of proposed model, the ultimate capacity of 44 tested isolated concrete strut were determined and compared with results of both approaches of CSA [11] and ACI 318-08 [12].

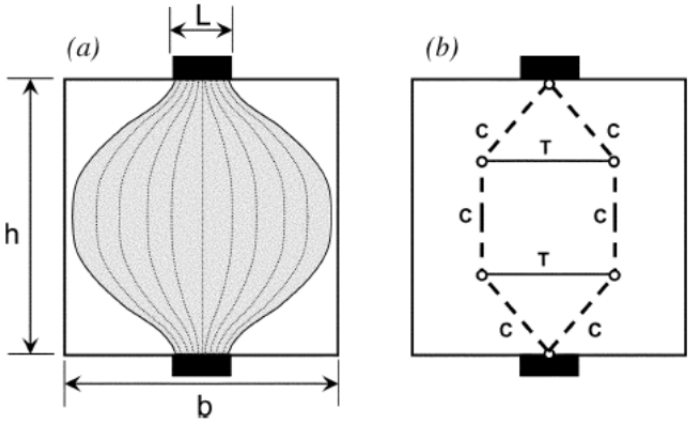

Figure 2 The actual and simplified forms of bottle-shaped strut

GEOMETRY OF BOTTLE-SHAPED STRUTS

A bottle-shaped strut can be modelled by a collection of struts and ties as presented in Figure 2 this model includes transverse tie, diagonal and longitudinal struts. The dispersion of compression indicates the inclination angle of diagonal strut.

According to provisions of ACI 318-08 [12], Appendix A, the compressive force flows by dispersion slope of 1:2 (two unit along longitudinal axis and one unit transverse that axis). For this model no recommendation is provided to the placement of formed ties. Then, three various shape of bottle-shaped can be formed in concrete struts (Figure 3). According to Saint Venant's principle, when the width of strut is larger than two times of its overall depth, the strut will be formed in schema "a" or diamond-shape. Otherwise the cases "b" and "c" are the usual shapes of struts, as form "c" occurs in long concrete struts such as columns.

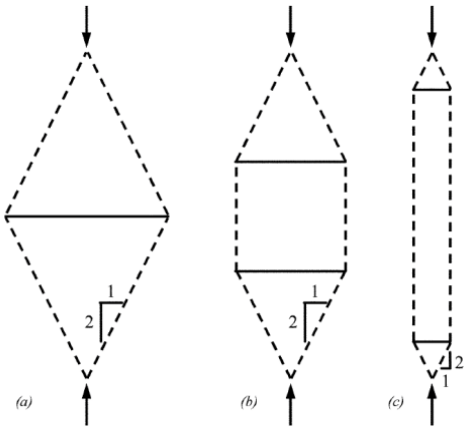

Figure 3 Various shapes of bottle-shaped strut [1]

Schlaich and Weishede suggested a combined STM for modelling of bottle-shape strut which within it the compressive force disperses with a slope dependent on the width of bottle neck and length of strut (Figure 4). It is defined by:

$$m = \frac{2b_f}{b_{ef} - b_{min}} \tag{1}$$

$$b_{ef} = \frac{L}{3} \qquad (b_{min} < \frac{L}{3}) \qquad b_{ef} = \frac{L}{6} + b_{min} \qquad (b_{min} \geq \frac{L}{3}) \tag{2}$$

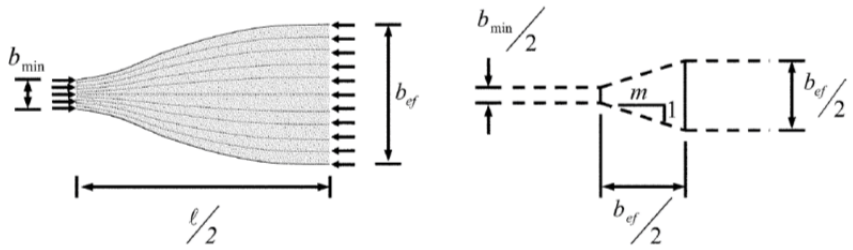

Figure 4 Bottle-shape model provided by Schlaich - Weishede

Where, b_{min} the width of strut neck, b_{ef} the effective width of strut, L the length of strut and m is the slope of stress dispersion.

Figure 5 shows a strut-and-tie model includes a constant slope for dispersion of compression as "m". According to equilibrium of this model, the transverse component of dispread force is carried by transverse ties. Then it can be written as:

$$\frac{F_D}{2} = C\ cos\theta \tag{3}$$

$$F = 2Csin\ \theta \tag{4}$$

$$T = F/\ tan\theta = F/m \tag{5}$$

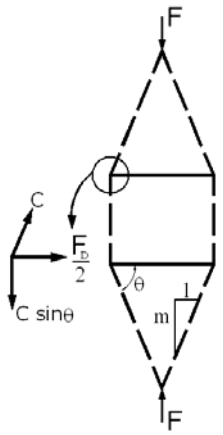

Figure 5 Equilibrium of simplified bottle-shaped strut

Where F is the applied load, F_D is total transverse force; C is the compressive force of inclined struts and θ is the angle of dispersion of compression or strut inclination.

RESULTED RESISTANT TENSILE FORCE OF TRANSVERSE REINFORCEMENT

The main role of transverse reinforcement is controlling the crack development and preventing the excessive opening of them. Because of transverse tensile straining the initial cracks are formed in the longitudinal direction. It means that the transverse reinforcement can be the most efficient when used perpendicular to the strut axis.

According to experimental results, the requirement amount of transverse reinforcement depends on concrete strength. Because high-strength concrete exhibits more brittle and abrupt failure than normal-strength concrete, the role of transverse reinforcing is very sensitive. As shown in Figure 6, if the fully cracked strut without any shear slip is assumed along the crack, all transverse tensile stresses are carried by reinforcing bars when initial cracks are formed. By assuming the yielding of transverse reinforcement once the concrete splits, it can be written:

$$F_D = F_u + F_v = A_u f_{yu} \sin\theta + A_v f_{yv} \cos\theta \tag{6}$$

Where, f_{yu} and f_{yv} are the tensile yield stresses of bars in u and v directions respectively, A_u and A_v the area of bars in u and v directions respectively, θ is the angle between u direction and strut axis, F_D the yield force of transverse reinforcement. If the total used reinforcement is equalized to A_w , it can be written as:

$$F_D = A_w f_y = \rho_D . (L_s b_s) f_y \tag{7}$$

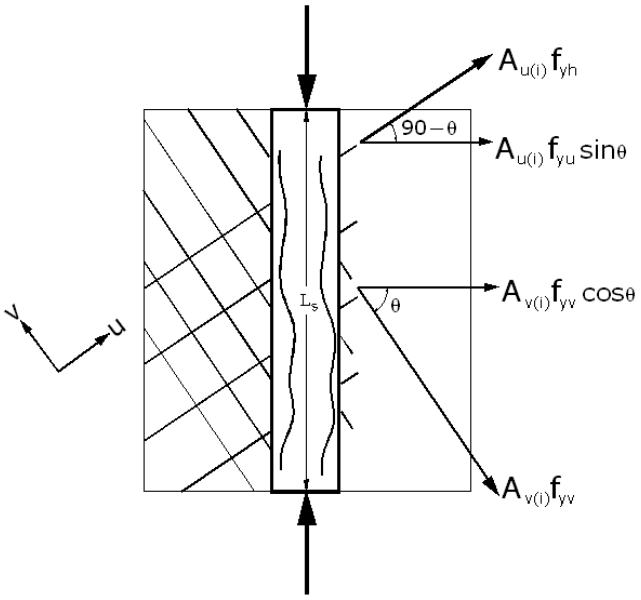

Figure 6 Resulted tensile force due to transverse reinforcement

Where ρ_D means the ratio of equivalent reinforcement and defined $\rho_D = \frac{A_w}{b_s L_s}$, b_s and L_s are the width and length of strut. By substituting the $f_y = f_{yu} = f_{yv}$ in Eq. 3 and comparison of Eq. 4 and Eq. 3, it can be written:

$$\rho_D = \frac{A_u}{L_s b_s} \sin\theta + \frac{A_v}{L_s b_s} \cos\theta \tag{8}$$

According to ($a = L_s\cos\theta$) and ($d = L_s\sin\theta$), ρ_D can be calculated as:

$$\rho_D = \frac{A_u}{b_s d}\sin^2\theta + \frac{A_v}{b_s d}\cos^2\theta \quad (9)$$

or:

$$\rho_D = \rho_u\sin^2\theta + \rho_v\cos^2\theta \quad (10)$$

ρ_u, ρ_v are the ratios of reinforcement in u and v directions respectively.

PROVISIONS OF ACI 318-08 TO PREDICT EFFECTIVE STRENGTH OF CONCRETE

According to recommendations of ACI 318-08 [12], struts are classified to five categories according to that, the efficiency factor of concrete strength ( ) is obtained based on satisfying the minimum requirement amount provided in A.3.3 section of ACI 318-08 [12]. By means of, as concrete strength is greater than 40 MPa, the minimum necessary transverse reinforcement to avoid of concrete splitting is estimated by assuming the slope of 1:2 for dispersion of compression and yield condition for all reinforcing. If this amount are satisfied β_s is assumed as 0.75 and otherwise as 0.60.

Certainly, when the strength of concrete is not greater than 40 MPa, the satisfying of minimum requirement reinforcement is checked by using of Eq. A-4 of ACI 318-08 [12]

$$\sum \frac{A_{si}}{bS_i}\, sin\alpha_i \geq 0.003 \quad (11)$$

Where, A_{si}, S_i, α_i are the area, spacing and inclination angle of i-th layer of transverse reinforcement crossing the strut axis and b is the width of strut, if the reinforcement is used with constant spacing Eq. 8 can be derived to:

$$\rho_D = \rho_u\sin\theta + \rho_v\cos\theta \geq 0.003 \quad (12)$$

In addition, ACI 318-08 [12] in chapter 11 has provided the minimum requirement shear reinforcement with ratios of 0.25% and 0.15% in vertical and horizontal direction respectively. But specifically permitted to satisfy the A.3.3 section instead of chapter 11. It means that the designer is allowed to eliminate the transverse reinforcement if the efficiency factor of concrete strength is assumed as 0.60.

According to the provisions of A.3.3 section, the expression of minimum requirement transverse reinforcement of bottle-shape struts can be computed as:

$$\rho_D = \frac{P_u}{2f_y b L_s} \quad (13)$$

where, P_u is the applied load, b is the width of beam, L_s the length of strut and f_y is the tensile yield stress of steel bars.

THE APPROACH OF CSA [11]

The Canadian standard CSA [11] defines the efficiency strength of concrete based on Modified Compression Field Theory (MCFT) as follows:

$$f_{cu} = \frac{f'_c}{0.8+170\varepsilon_1} \leq 0.85\, f'_c \tag{14}$$

$$\varepsilon_1 = \varepsilon_s + (\varepsilon_s + 0.002)\cot^2 \alpha_s \tag{15}$$

Where f_{cu} the efficiency strength of concrete, α_s the angle between strut and tie, ε_s the tensile strain of cracked concrete and f'_c is the specified concrete strength.

Rather than defining the efficiency factor of concrete strength based on used reinforcement, CSA defined the efficiency concrete strength according to strain of concrete once it cracks. There is a principal difficulty in choosing an adequate value for ε_s. By substituting a specified term for ε_s in Eq. 15, this expression would be likely more useful for designers.

A NEW MODEL TO DETERMINE THE EFFECTIVE STRENGTH OF CONCRETE

In the nonlinear finite elements analysis of RC structures it is necessary to use constitutive model for concrete that are based on smeared-rotating crack idealization. Moreover, cracked reinforced concrete in compression has been observed to exhibit lower strength and stiffness than uniaxially compressed concrete. This degradation is primarily related to the degree of transverse straining and cracking present in the concrete [6]. Many of analytical models for describing the softening effect were derived from experimental data and proposed in rational or semi-rational form. Collins et al [6] presented the compressive softening of concrete as Figure 6 β is the efficiency factor of concrete strength and can be determined by:

$$(= 1/(1 + \square K_1 c\, K \square_1 f) \tag{16}$$

$$K_c = 0.27(\frac{\varepsilon_1}{\varepsilon_0} - 0.37) \tag{17}$$

$$K_f = 0.1825\sqrt{f'_c} \tag{18}$$

Where ε_1 , ε_0 are the average principal tensile strain and the strain at the peak cylinder stress and f'_c is the specified strength of concrete. Controlling the width of cracks is an important role of transverse reinforcement. According to experimental observations while the cracks of concrete are forming, the transverse reinforcing bars are subjected to tensile strain and prevent to cracks opening. In strut-and-tie modelling the cracking of concrete is assumed fully without any shear slip. Hence it can be resulted that the occurred transverse tensile force will be carried by transverse reinforcement. By assuming no shear force the principal tensile strain can be computed as:

$$\varepsilon_1 = \frac{T}{EA_w} \tag{19}$$

Where T is the transverse tensile force, E is the modules of elasticity and A_w is the area of equivalent transverse reinforcement obtained by:

$$A_w = \rho_D b L_s \tag{20}$$

Where ρ_D is the ratio of equivalent transverse reinforcement, b is the width of strut and L_s is the length of strut.

As presented in Section 2, the total formed transverse tensile force can be determined by:

$$T = \frac{P}{m} = \frac{\upsilon A_{str} f_c'}{m} \tag{21}$$

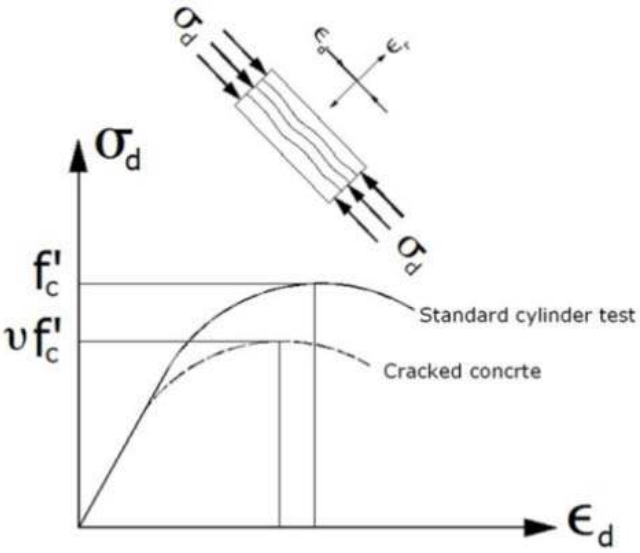

Figure 7 Compressive softening of cracked concrete

Where, υ is the efficiency factor of concrete strength, f_c' is the specified strength of concrete and A_{str} is the cross-sectional area of strut. Using the test results of eighteen isolated struts estimated the slope of dispersion of compression approximately as 3. By substituting of m=3 in Eq. 21 and simplifying Eqs. 16 through 21, following equations are resulted for prediction of υ:

$$0.27 K_f K \upsilon^2 + \left(1 - (0.37 + cot^2\theta)\right) K_f \upsilon - 1 = 0 \tag{22}$$

$$K = \frac{f_c' w}{3 E \rho_D L_s \varepsilon_2} (1 + cot^2\theta) \tag{23}$$

By assuming the ε_2 = 0.003 and E = 200000 MPa, Eq. 23 is simplified to

$$K = \frac{f_c' w}{1800 \rho_D L_s} (1 + cot^2\theta) \tag{24}$$

Where, w is the width of loaded plate a minimum width of strut.

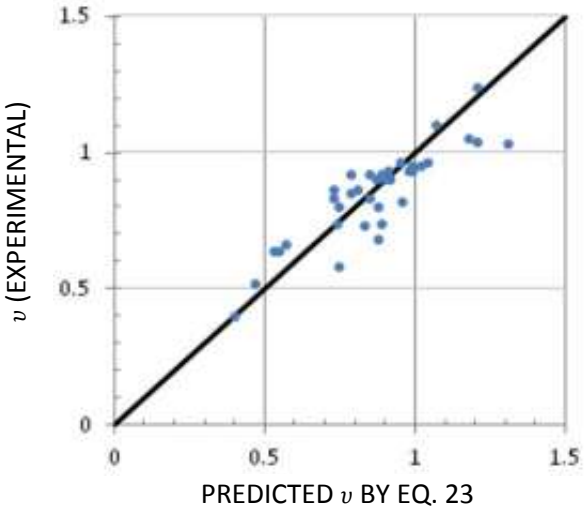

Figure 8-a Correlation between results of new model and actual data

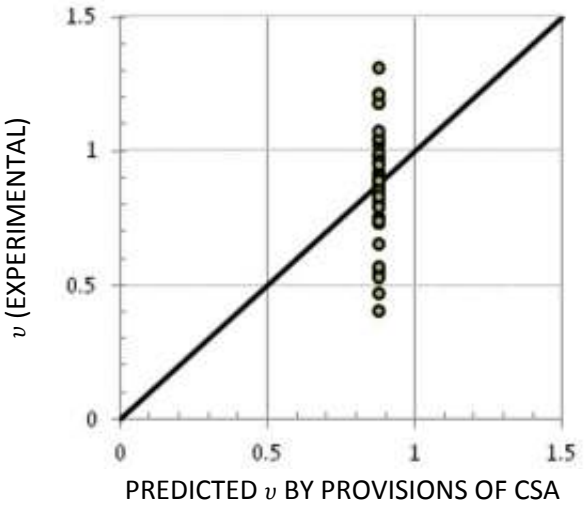

Figure 8-b Correlation between results of CSA and actual data

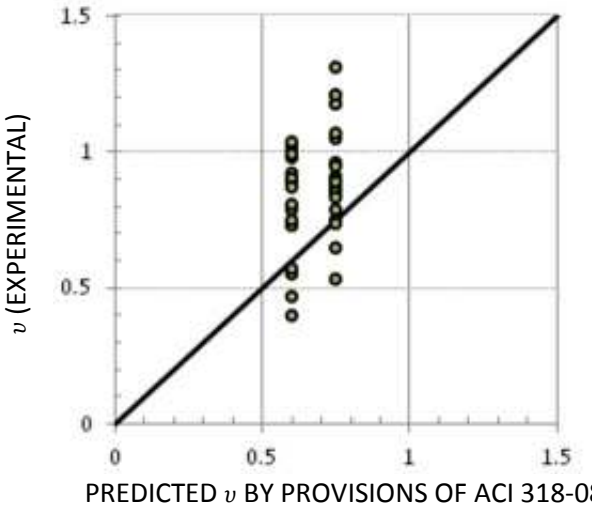

Figure 8-c Correlation between results of ACI 318-08 and actual data

A data base consisted of eighteen concrete panels tested by the Author et al. [13] and twenty six concrete panels tested by Brown et al. [10] was used to evaluate the accuracy of proposed equation. The ultimate capacity of selected specimens were determined and obtained results compared with experimental data and results of both approaches of CSA [11] and ACI 318 08 [12]. Figure 7 shows a correlation between measured efficiency factor of concrete strength and predicted value by provisions of CSA [11] and ACI 318-08 [12]. As presented, the provided method by ACI 318-08 is more scattered than provision of CSA.

In addition, the results of new proposed model have the best agreement with experimental data. According to performed investigation, it can be concluded that the provisions of ACI 318-08 predicts more scattered results than CSA and new proposed model. For concrete with specified strength larger than 40 MPa, the provided efficiency factor for concrete strength is unsafe when the minimum requirement transverse reinforcement is not satisfied.

Also, the approach of ACI 318-08 [12] provides the constant efficiency factor for concrete strength as the additional reinforcing cannot be effective in improving the efficiency factor when the minimum requirement reinforcement is satisfied. It needs for revision, because the experimental observation proved that, by increasing the amount of transverse reinforcement the effective strength of concrete increase especially in high-strength concrete.

The accurate prediction by provisions of CSA needs to actual definition of ε_1 or average principal tensile strain of concrete, this parameter can be measured in laboratory studies, but many practicing users and designers have had difficulty in selecting an appropriate average tensile concrete strain to use in their designs. If the process could be simplified and the strain term eliminated, it would likely help design engineers.

CONCLUSIONS

In this paper a new model proposed for prediction of efficiency factor of concrete strength based on MCFT and mechanical behaviour of cracked concrete.

In formulation of new model, the fully cracking assumed for concrete as the transverse reinforcement carries the transverse tensile force occurred in bottle-shaped strut.

The proposed model is more accurate in comparison with both approaches of ACI 318-08 and CSA, consequently can be adequate to develop for prediction the shear strength of deep beams using the strut-and-tie method.

The magnitude of transverse tensile force is affected by slope of compression dispersion, and increases due to increasing the angle between diagonal strut and longitudinal axis of strut.

According to proposed model, the efficiency factor of concrete strength depends on specified strength of concrete as decreases by increasing the strength of concrete. It means that in RC structures constructed by high-strength concrete because of usual brittle failure, the principle role of transverse reinforcement is more sensitive than those by normal-strength concrete.

The provision of ACI 318-08 proposed the most scattered results, as the predicted capacities are unsafe for specimens reinforced by light amount of reinforcing bars but conservative for those with heavy transverse reinforcement.

Because the accuracy of provisions of CSA depends on definition an appropriate amount for average principal tensile strain of concrete, if the process could be simplified and the strain term eliminated, it would be more adequate and reliable to use in design works.

REFERENCES

1. BROWN M D, SANKOVICH C L, BAYRAK O AND JISRA J O, Behavior and efficiency of bottle-shaped struts, ACI STRUCTURAL JOURNAL, Vol. 103, No. 3, 2006. pp. 348-355.

2. SCHLAICH J AND SCHÄFER K, Design and detailing of structural concrete using strut-and-tie models, The Structural Engineer, Vol. 69, No. 6, 1991, pp. 113-120.

3. RITTER W, Die Bauweise Hennebique (The Hennebique System), Schweizerische Bauzeitung, Zürich, Switzerland, Bd. XXXIII, No. 7, 1899.

4. MÖRSCH E, 1902, Der Eisenbetonbau, seine Theorie und Anwendung (Reinforced Concrete, Theory and Application), Stuttgart, Germany.

5. MARTI P, Staggered Shear Design of Simply Supported Concrete beams, ACI Journal, Vol. 83, No. 1, 1986, pp. 36-41.

6. COLLINS M P AND MITCHELL D, A Rational Approach to Shear Design The 1984 Canadian Code Provisions, ACI Journal, Vol. 83, No. 6, 1986, pp. 925-933.

7. RAMIREZ J A AND BREEN J E, Evaluation of Modified Truss-Model Approach for Beams in Shear, ACI Structural Journal, Vol. 88, No. 5, 1991, pp. 562-571.

8. TANG C Y AND TAN K H, Interactive mechanical model for shear strength of deep beams, JOURNAL OF STRUCTURAL ENGINEERING. ASCE, Vol. 130, No. 10, 2004, pp. 1534-1544.

9. HWANG S-J AND LEE H-J, Strength prediction for discontinuity regions by softened strut-and-tie model, JOURNAL OF STRUCTURAL ENGINEERING. ASCE, Vol. 128, No. 12, 2002, pp. 1519-1526.

10. BROWN M D AND BAYRAK O, Minimum Transverse Reinforcement for Bottle-Shaped Struts, ACI STRUCTURAL JOURNAL, Vol. 103, No. 6, 2006. pp. 813-821.

11. CSA Standard CAN3-A23.3-94, 1994, Design of Concrete Structures for Buildings with Explanatory Notes, Canadian Standards Association, Rexdale, Ontario.

12. ACI 318-08, 2008, Building Code Requirements for Structural Concrete and Commentary, American Concrete Institute, Farmington Hills, Michigan

13. ARABZADEH A, RAHAIE A R AND AGHAYARI R, A Simple strut-and-tie model for prediction of ultimate shear strength of RC deep beams, International Journal of Civil Engineering, Vol. 7, No. 3, 2009, pp. 141-153.

Development of an Algorithm for Detecting Damage at Multiple Locations in Reinforced Concrete Structures

P Rathish Kumar[1], T Oshima[2]
1 – National Institute of Technology, Warangal, India
2 – Kitami Institute of Technology, Japan

In recent years, there has been a renewed interest in the damage diagnosis and health monitoring of existing highway bridges using vibration based damage identification techniques. There is a growing need for built-in monitoring systems for civil engineering infrastructures, due to problems such as increasing traffic loads and rising costs of maintenance and repair. Most vibration-based damage detection theories are formulated based on the assumption that failure or deterioration would primarily affect the stiffness and therefore, affect the modal characteristics or the dynamic response of the structure. If these changes can be detected and classified, it could be further implemented for a bridge monitoring system to indicate the condition, or damage, or remaining capacity of the structures. It can be used to evaluate seismic behavior of the structures and can help take measures for rehabilitation in case of severe damages. Many damage detection schemes rely on analyzing response measurements from sensors placed on the structure. Research efforts have been made to detect structural damage directly from dynamic response measurements in the time domain, e.g. the random decrement technique, or from Frequency Response Functions (FRF). Also, some damage detection methods have been proposed to detect damage using system identification techniques. This paper deals with damage detection and localization in a reinforced concrete structure based on vibration based monitoring. The sensing system adopted in this study uses the piezoelectric accelerometer to detect, locate and estimate defects induced in the form of cracks on the beam at different locations. The piezoelectric actuator provides variable excitations in the frequency range of 0 to 800 Hz that is effective in measuring a high order mode change associated with the occurrence of damage. In this paper, a damage identification method based on changes in Transfer Function Estimate (TFE) is presented. The method can be used to accurately detect damage, predict its location and assess the extent of damage in structures.

Professor P Rathish Kumar is an Associate Professor, National Institute of Technology,Warangal, Andhra Pradesh, INDIA.

Dr Toshiyuki Oshima is Professor and Head Department of Civil Engineering, Kitami Institute of Technology, KITAMI, Hokkaido, Japan

Keywords: Damage detection, Dynamic parameters, Structural health monitoring, Transfer function, Vibration

INTRODUCTION

In the past two decades, a major focus of research is set towards the development of Structural Health Monitoring (SHM) and non-destructive damage detection methods to manage civil structures more efficiently. SHM has gained wide acceptance in the past decade as a means to monitor a structure and provide an early warning of an unsafe condition using real time data. The goal of SHM and other so called 'smart structures' technologies is to develop 'multifunctional' structures, i.e. structures which provide functionality in other areas besides carrying operational static, dynamic and fatigue loads, with an ultimate objective of providing enhanced system level performance. In recent years, there has been a renewed interest in the damage diagnosis and health monitoring of existing highway bridges using vibration based damage identification techniques.

There is a growing need for built-in monitoring systems for civil engineering infrastructures, due to problems such as increasing traffic loads and rising costs of maintenance and repair. Most vibration-based damage detection theories are formulated based on the assumption that failure or deterioration would primarily affect the stiffness and therefore, affect the modal characteristics or the dynamic response of the structure [1-3]. If these changes can be detected and classified, it could be further implemented for a bridge monitoring system to indicate the condition, or damage, or remaining capacity of the structures. It can be used to evaluate seismic behaviour of the structures and can help take measures for rehabilitation in case of severe damages. Many damage detection schemes rely on analysing response measurements from sensors placed on the structure [4]. Research efforts have been made to detect structural damage directly from dynamic response measurements in the time domain, e.g. the random decrement technique [5, 6], or from Frequency Response Functions (FRF) [3, 9]. Also, some damage detection methods have been proposed to detect damage using system identification techniques). In this paper, an algorithm based on changes in Transfer Function Estimate (TFE) is presented. The algorithm is used to detect damage, locate its position and monitor the increase in damage using only the measured data without the need for any modal identification or numerical models. The method is applied to the experimental data extracted from a reinforced concrete beam model after inducing some defects to it.

THEORETICAL DESCRIPTION

Let $P_{xy}(f)$ denote the TFE, relating two time histories, x(t) and y(t). The absolute difference in absolute TFE before and after damage can then be defined as

$$\Delta_{xy}(f) = \left| |P_{xy}(f)| - |P^{*}_{xy}(f)| \right| \tag{1}$$

Where, $P_{xy}(f)$ and $P_{xy}^{*}(f)$ represent the TFE of the undamaged and damaged structures respectively. When the change in TFE is measured at different frequencies in the measurement range from f_1 to f_m, a matrix $[\Pi_r]$ can be formulated as follows

$$\Pi_r = \begin{bmatrix} \Delta_{1r}(f_1) & \Delta_{1r}(f_2) & \ldots\ldots & \Delta_{1r}(f_m) \\ \Delta_{2r}(f_1) & \Delta_{2r}(f_2) & \ldots\ldots & \Delta_{2r}(f_m) \\ . & . & \ldots\ldots & . \\ . & . & \ldots\ldots & . \\ . & . & \ldots\ldots & . \\ \Delta_{nr}(f_1) & \Delta_{nr}(f_2) & \ldots\ldots & \Delta_{nr}(f_m) \end{bmatrix}_r \tag{2}$$

where, n represents the number of measuring points and r represents the number of reference channel. In matrix $[\Pi_r]$, every column represents the changes in TFE at different measuring channels but at the same frequency value. Each measuring channel will be used as a reference for the other channels ($r = 1: n$). Therefore, the matrix $[\Pi_r]$ will be formulated n different times (3D matrix). The summation of TFE changes over different frequencies using different references can be used as the indicator of damage occurrence. In other words, the first damage indicator is calculated from the sum of rows of each matrix, $[\Pi_r]$ and summing up these changes over different references

$$Total\_Change = \sum_r \begin{Bmatrix} \sum_f \Delta_{1r}(f) \\ \sum_f \Delta_{2r}(f) \\ . \\ . \\ . \\ \sum_f \Delta_{nr}(f) \end{Bmatrix}_r \tag{3}$$

where, $f = f_1 : f_m$ and $r = 1 : n$.

This indicator is used to detect the damage; though it was found to be a weak indicator of damage localization. A statistical decision making procedure is employed to determine the location of damage. The first step in this procedure is the picking of the change in TFE at each frequency value from the maximum to the minimum value in each column of the matrix $[\Pi_r]$. For example in matrix $[\Pi_r]$ (Eq. 2), considering the maximum to the minimum value in the first column we can arrange them as $B_{1r}(f_1)$, $B_{2r}(f_1)$ etc as maximum, next maximum in the first column corresponding to the values of the matrix $[\Pi_r]$. Typically, $B_{8r}(f_1)$ means it is the eighth maximum value in the first column corresponding to frequency (f_1). The same process is applied to the different columns in matrix $[\Pi_r]$ to formulate the matrix of maximum changes of TFE at different frequencies, $[B_r]$. It should be noted that $[B_r]$ is a 3D matrix where each value of r ($r = 1: n$) formulates one matrix

$$B_r = \begin{bmatrix} B_{8r}(f_1) & B_{3r}(f_2) & B_{1r}(f_3) & .. & B_{7r}(f_m) \\ B_{5r}(f_1) & B_{12r}(f_2) & B_{4r}(f_3) & .. & B_{16r}(f_m) \\ B_{3r}(f_1) & B_{10r}(f_2) & B_{15r}(f_3) & .. & B_{3r}(f_m) \\ B_{1r}(f_1) & B_{6r}(f_2) & B_{2r}(f_3) & .. & B_{4r}(f_m) \\ . & . & . & .. & . \\ . & . & . & .. & . \\ B_{nr}(f_1) & B_{nr}(f_2) & B_{nr}(f_3) & .. & B_{nr}(f_m) \end{bmatrix}_r \tag{4}$$

In order to monitor the frequency of damage detection at any node, a new matrix $[E_r]$ is formulated. The matrix may consist of 0's at the undamaged locations and ranking is given for damaged locations as explained earlier. For example in the matrix $[E_r]$, we put a value of 8 corresponding to the locations of $B_{8r}(f_1)$, 3 for $B_{3r}(f_1)$ and so on in column 1. Similar procedure is followed for other columns also as shown in the following expression

$$E_r = \begin{bmatrix} 8 & 3 & 1 & ..... & 7 \\ 5 & 12 & 4 & ..... & 16 \\ 3 & 10 & 15 & ..... & 3 \\ 1 & 6 & 2 & ..... & 4 \\ . & . & . & ..... & . \\ . & . & . & ..... & . \\ n & n & n & ..... & n \end{bmatrix}_r \tag{5}$$

The total of maximum changes in TFE is calculated from the sum of the rows of matrix $[B_r]$ using different references. At each value of r, the sum of rows of matrix $[B_r]$ will result in one vector. Therefore, n different vectors can be obtained. The sum of these vectors is stored in one vector $\{Z\}$;

$$Z = \sum_r \begin{Bmatrix} \sum_f B_{8r}(f) \\ \sum_f B_{5r}(f) \\ . \\ . \\ . \\ \sum_f B_{nr}(f) \end{Bmatrix}_r \tag{6}$$

Similar to the previous procedures, the total number of times of detecting the damage at different nodes is calculated from matrix $[E_r]$ as

$$K = \sum_r \begin{Bmatrix} \sum_f E_{8r}(f) \\ \sum_f E_{5r}(f) \\ . \\ . \\ . \\ \sum_f E_{nr}(f) \end{Bmatrix}_r \tag{7}$$

In order to reduce the effect of noise or measurement errors, a value of two times standard deviation of the elements in vector $\{K\}$ will be subtracted from the vector $\{K\}$. Any resulting negative values will be removed. The same procedures is applied to the vector $\{Z\}$ as follows

$$T = \begin{Bmatrix} Z_1 - 2\sigma \\ Z_2 - 2\sigma \\ . \\ . \\ . \\ Z_n - 2\sigma \end{Bmatrix} \tag{8}$$

Where, $\sigma = \sqrt{\sum_{i=1}^{n} (Z_i - \overline{Z})^2} \Big/ (n-1)$, $\overline{Z} = \sum_{i=1}^{n} Z_i \Big/ n$,

$$\mathrm{I} = \begin{Bmatrix} \mathrm{K}_1 - 2\beta \\ \mathrm{K}_2 - 2\beta \\ . \\ . \\ . \\ \mathrm{K}_n - 2\beta \end{Bmatrix} \tag{9}$$

Where, $\beta = \sqrt{\sum_{i=1}^{n} (\mathrm{K}_i - \overline{\mathrm{K}})^2} \Big/ (n-1)$, $\overline{\mathrm{K}} = \sum_{i=1}^{n} \mathrm{K}_i \Big/ n$.

The first damage location indicator is defined as the scalar product of { T } and { I } as shown in the following expression

$$Dam\_Ind\_1 = \begin{Bmatrix} \mathrm{T}_1 \times \mathrm{I}_1 \\ \mathrm{T}_2 \times \mathrm{I}_2 \\ . \\ . \\ . \\ \mathrm{T}_n \times \mathrm{I}_n \end{Bmatrix} \tag{10}$$

Another damage location indicator is formulated as follows: the sum of rows of matrix [B_r] (Equation 4) at each reference channel represents a column in the following matrix

$$\Psi = \begin{bmatrix} \sum_f \mathrm{B}_{81}(f) & \sum_f \mathrm{B}_{82}(f) & ..... & \sum_f \mathrm{B}_{8n}(f) \\ \sum_f \mathrm{B}_{51}(f) & \sum_f \mathrm{B}_{52}(f) & ..... & \sum_f \mathrm{B}_{5n}(f) \\ . & . & ..... & . \\ . & . & ..... & . \\ . & . & ..... & . \\ \sum_f \mathrm{B}_{n1}(f) & \sum_f \mathrm{B}_{n2}(f) & ..... & \sum_f \mathrm{B}_{nn}(f) \end{bmatrix} \tag{11}$$

Where, the first subscript represents the channel number and the second represents the reference number. A process of choosing the maximum to minimum value at each column and discarding other values of that column is used to construct the matrix from Ψ and a new matrix [N] is constructed corresponding to the values in matrix Ψ as

$$\mathrm{N} = \begin{bmatrix} 6 & 4 & . & . & . & 3 \\ 3 & 9 & . & . & . & 1 \\ . & . & . & . & . & . \\ . & . & . & . & . & . \\ . & . & . & . & . & . \\ n & n & . & . & . & n \end{bmatrix} \tag{12}$$

The sum of rows of matrix [Ψ] defines the vector { Ψ_{sum} }

$$\Psi_{sum} = \sum_{r} \Psi \quad , \tag{13}$$

and the sum of rows of matrix N defines the vector $\{ N_{sum} \}$

$$N_{sum} = \sum_{r} N \tag{14}$$

Then the second damage location indicator is defined as the scalar product of vectors $\{ \Psi_{sum} \}$ and $\{ N_{sum} \}$

$$Dam\_Ind\_2 = \Psi_{sum.} \times N_{sum} \tag{15}$$

Damage indicators 1 and 2 will be used to determine the damage location. On the other hand, the total change in TFE will be used to detect the occurrence of damage and assess the damage extent.

REINFORCED CONCRETE BEAM

In this research, the above concepts are used to examine a reinforced concrete beam after inducing damage at well-defined locations. The model is a concrete beam with two levels of reinforcement one steel rod in the tension portion and the other steel rod in the compression portion. There is no shear reinforcement in the beam tested. The model dimensions and layout are shown in Figure 1. The multi-layer piezoelectric actuator is used for local excitation. The main advantage of using piezoelectric actuator is that it produces vibration with different frequencies ranging from 0 to 800 Hz that is effective in exciting different mode shapes. Natural frequencies are measured in the range of the excitation frequency from 0 to 800 Hz (sweep) and also independently at 100, 200, 300, 400, 500, 600, 700 and 800 Hz (sinusoidal). The actuator force amplitude is 0.3 kN. The actuator is located at the centre of the compression portion of the beam (Figure 1). The location of the actuator is not changed during different damage states of the structure. The excitation forces used for the undamaged and damaged structure are random, equal in amplitude and have the same vibration wave form but the excitation force does not need to be measured. Totally five accelerometers are mounted on the beam to measure the acceleration response in the vertical direction on the beam as shown in Figure 1.

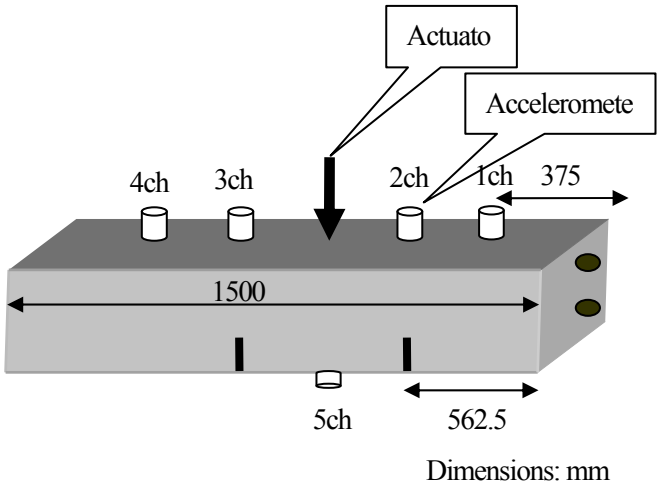

Figure 1 Dimensions of the concrete beam tested

BEAM MODEL

Experimental Setup and Equipment

Totally four cases are examined including three damages and one under no damage condition.
The damages to the beam are introduced to the specimen as follows:

Case 1: No damage case-no cut on the beam (Figure 2)
Case 2: Cutting of the beam of 5 mm width and 40 mm deep (Figure 3)
Case 2: Cutting of the beam of 5 mm width and up to neutral axis without cutting the reinforcement in tension portion (Figure 4)
Case 3: Cutting of the reinforcement also in tension portion (Figure 5)

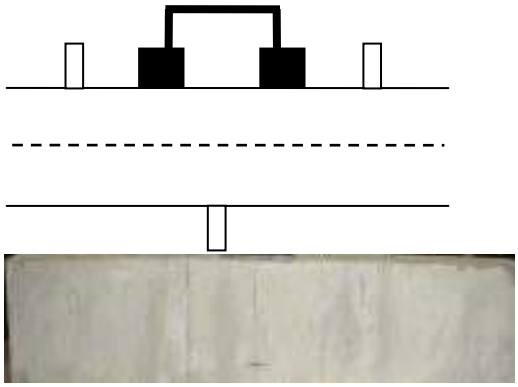

Figure 2 Undamaged Case (D0)

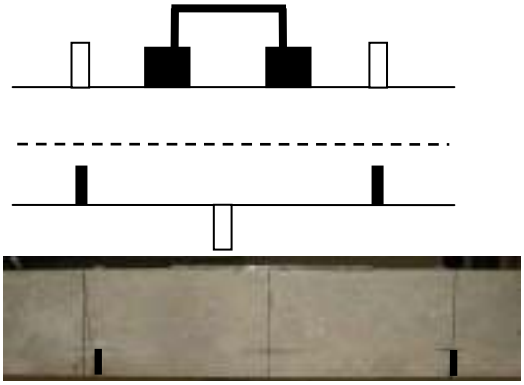

Figure 3 Damage Case D1 (Cut of 5 mm up to 40 mm)

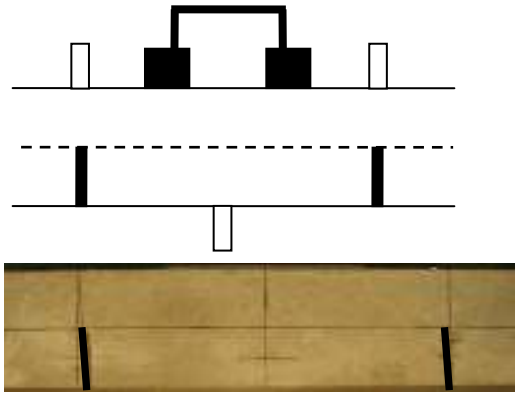

Figure 4 Damage Case D2 (Cutting of the beam up to N.A 100 mm with bottom bar intact)

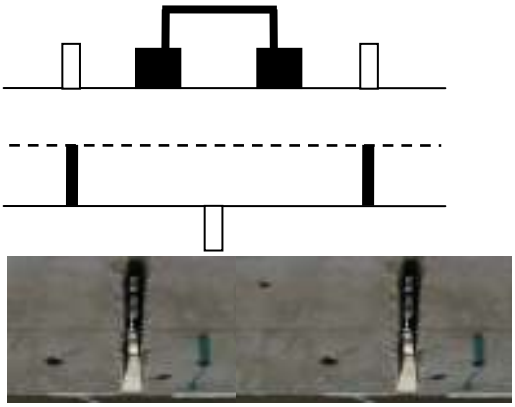

Figure 5 Damage Case D3 (Cutting of the beam up to NA including cutting of the bottom bar)

DAMAGE IDENTIFICATION ALGORITHM FOR DIFFERENT DAMAGE CASES

Before introducing any damage

One of the drawbacks of vibration based damage identification methods is that these methods sometimes produce false positive readings due to noise, measurement errors or environmental changes. It is therefore very important to determine if the results obtained from any damage identification methods are due to damage or due to other changes. Because of this need, the experiment was performed a number of times on the undamaged structure prior to the introduction of any damage. TFE data for two different sets of data obtained from the undamaged structure is shown in Figure 6 corresponding to channels 2 and 3.

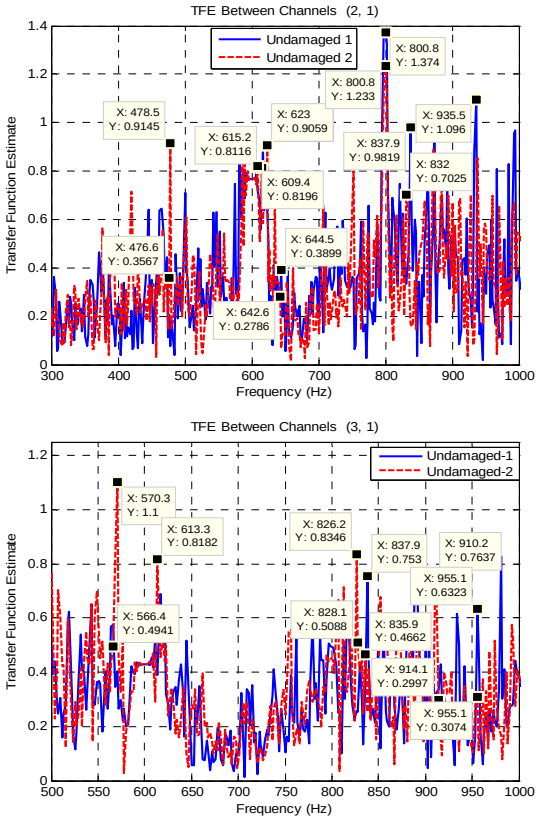

Figure 6 TFE for two tests on the undamaged structure

The TFE is calculated at each measuring channel from the acceleration time history data using MATLAB Standard and MATLAB Signal Processing Toolbox [10-13]. Hanning window of size 4096 is applied to the time signals to minimize leakage. Small changes in TFE can be observed in this figure, obviously due to noise and measurement errors. TFE data in the frequency range of 400-800 Hz was used in the proposed analysis. The data is this range was significant.

The total change in TFE was determined using Eq. (3) and the results are shown in Figure 7. The total change in TFE ranged from about 200 to 245 dB. When the total change of TFE was determined using other sets of data that were obtained from the undamaged structure, similar and very close values of the total change in TFE were obtained. The total change of TFE will be used as an indicator of damage detection and damage increase. On the other hand, damage indicators 0, 1 and 2 will be used to identify the damage location.

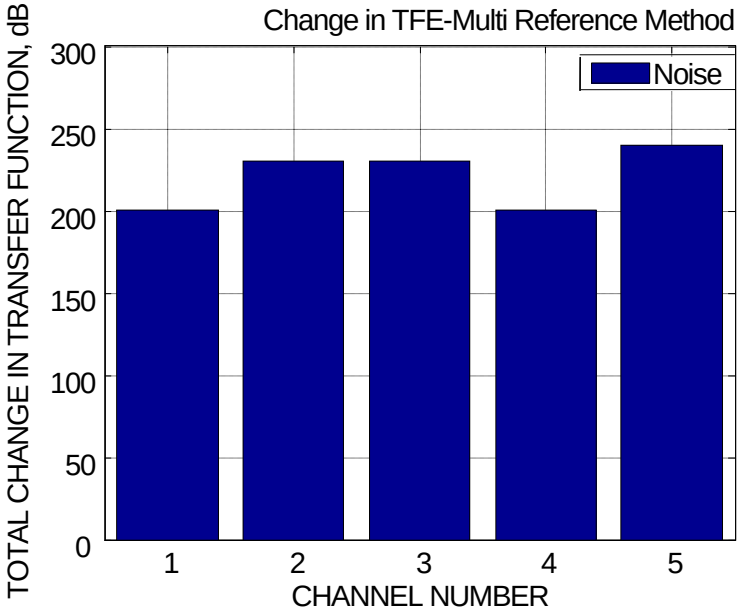

Figure 7 Total change in TFE due to noise

Case 1 damage — Crack 5 mm wide and 40 mm deep

In the first damage case (D1) a crack of 5 mm wide and 40 mm deep is made at channel locations 2 and 3.The accuracy of the damage identification methods based on FRF or cross spectral density (CSD) is dependent on the frequency range in which FRF [3] or CSD[14] is measured. The accuracy of the damage identification methods based on mode shapes is dependent on which mode shapes are used. The accuracy of the results is at times reduced when some of the used mode shapes have nodes at the damage location [2].

In order to overcome this problem, it was decided to use TFE magnitudes in the frequency range of 0-800 Hz in the proposed algorithm. This range of measurement covers the total measurement range of TFE data (i.e. from 0 to 800 Hz). The resulting damage indicators for damage case 1 are plotted in Figure 8. In Figure 8(a), the total change in TFE (Eq. 3) increased at all channels after introducing cuts at channels 2 and 3. The total change in TFE due to this is much larger than that due to noise and measurement errors (Figure 7). Although the maximum total change of TFE is observed at channels 2 and 3, it can be noted that damage is detected at other locations also, though there is no damage at these locations.

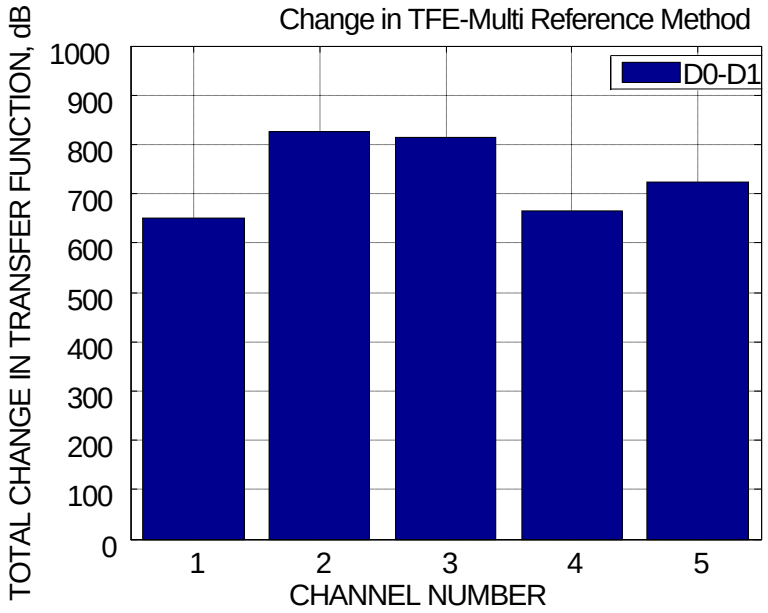

Figure 8(a) Total change in TFE

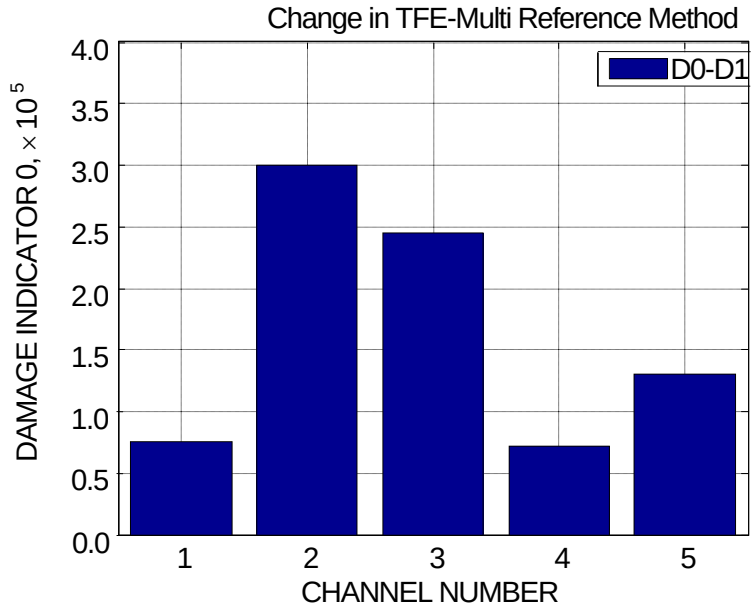

Figure 8(b) Damage localization using damage indicator 0

Hence, the total change in TFE is not always a good indicator of damage location. Damage indicators 0, 1 and 2 have been determined to identify the damage location accurately, as shown in Figures 8(b), (c) and (d), respectively.

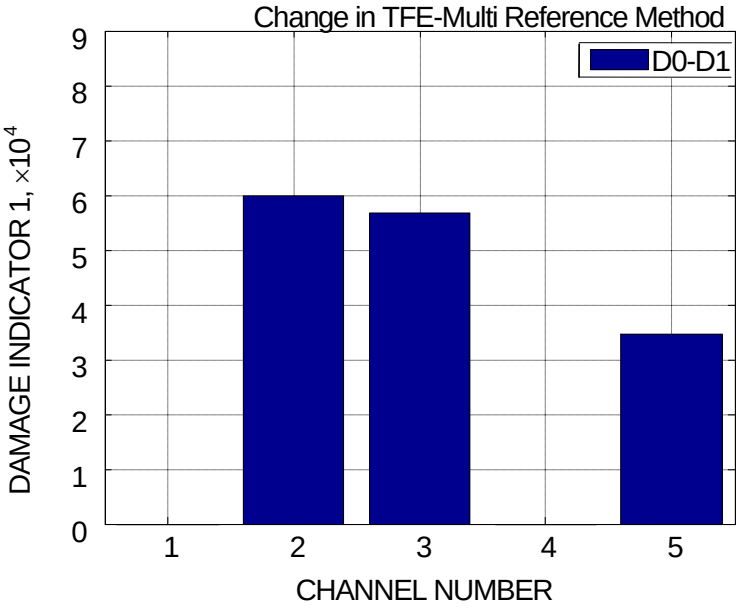

Figure 8(c) Damage localization using damage indicator 1

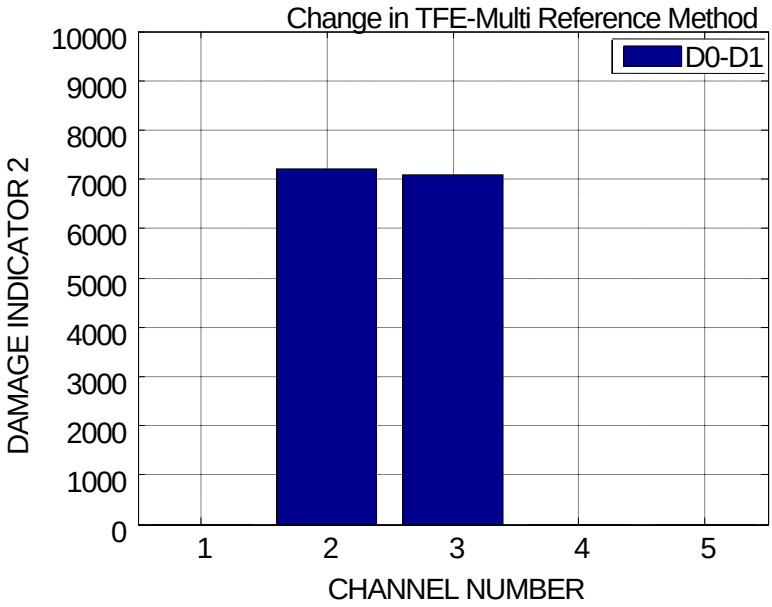

Figure 8(d) Damage localization using damage indicator 2

Figure 8 Proposed algorithm results for damage case 1

Case 2 damage — Crack 5 mm wide and 100 mm deep

In the second damage case (D2) the damage level is increased by increasing the earlier crack of 40 mm deep to 100 mm i.e. up to the Neutral Axis. The total change in TFE (Eq. 3) increased with the crack depth as shown in Figure 9(a). The damage indicators 0, 1 and 2 also increased with the damage. The same is shown in Figures 9(b), (c) and (d).

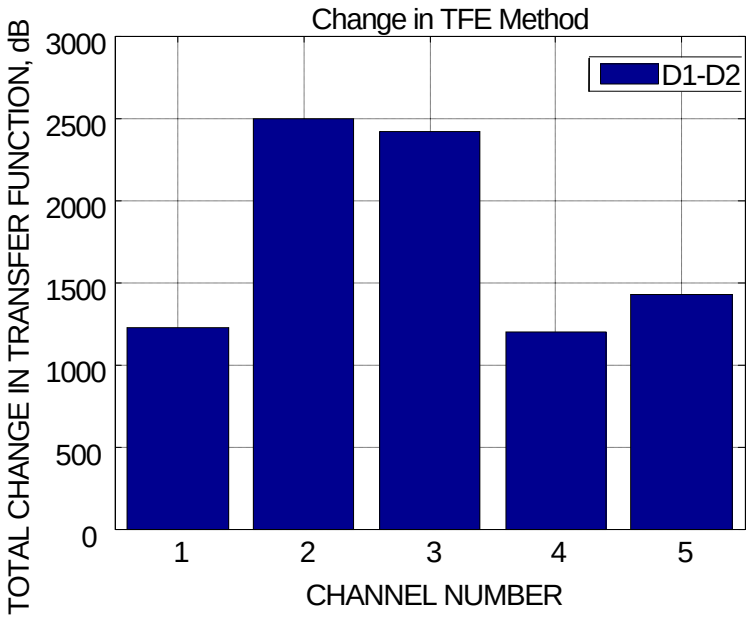

Figure 9(a) Total change in TFE

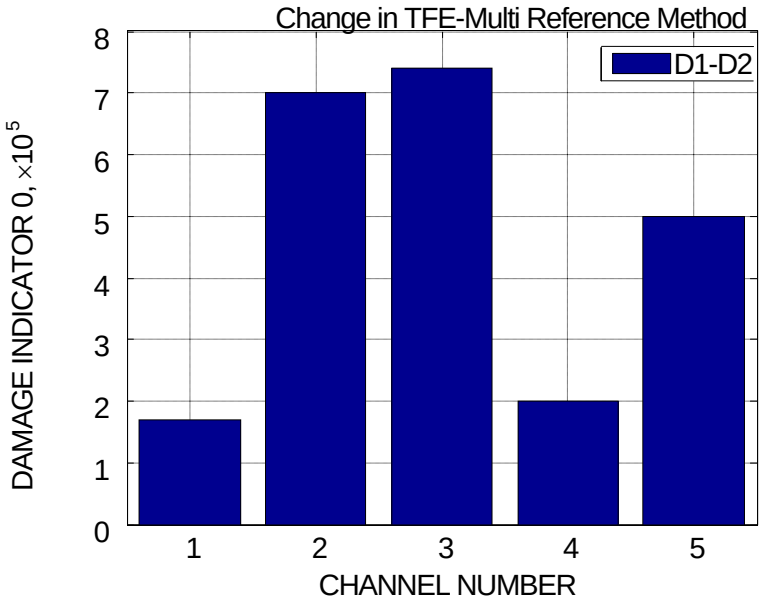

Figure 9(b) Damage localization using damage indicator 0

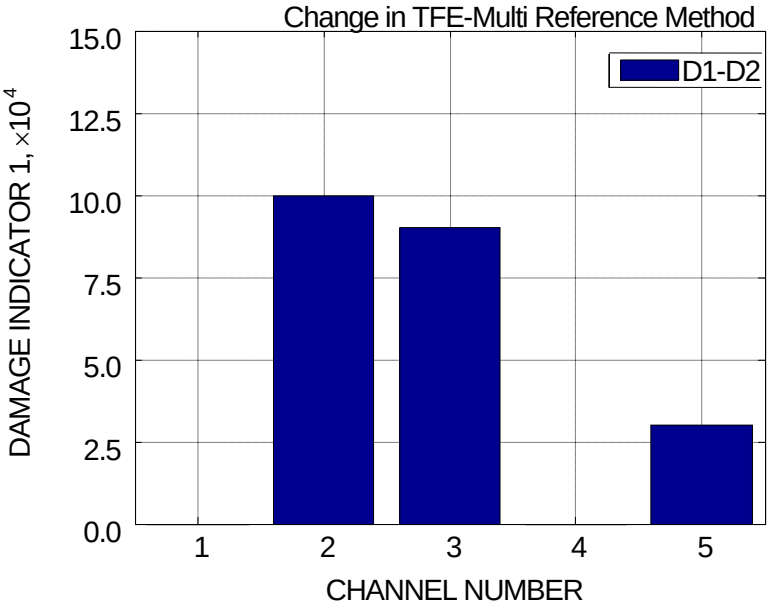

Figure 9(c) Damage localization using damage indicator 1

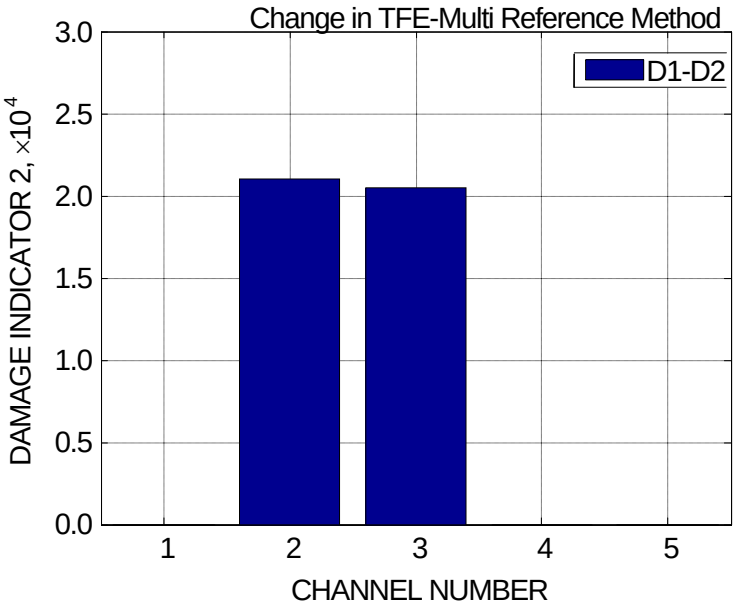

Figure 9(d) Damage localization using damage indicator 2

Figure 9 Proposed algorithm results for damage case 2

Case 3 damage — Cutting of steel bar in tension portion

In the third damage case (D3), the damage level increased by cutting the reinforcement at the locations of channels 2 and 3. Similar observations were noted in the total change in TFE, damage indicators 0, 1 and 2, though this time the difference in the total change is less as compared to earlier cases. These values are plotted in Figures 10(a), (b), (c) and (d).

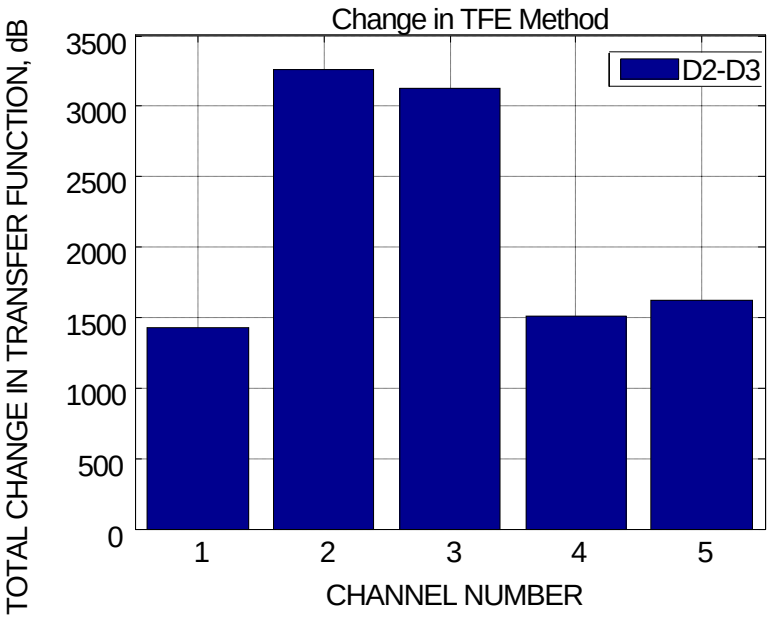

Figure 10(a) Total change in TFE

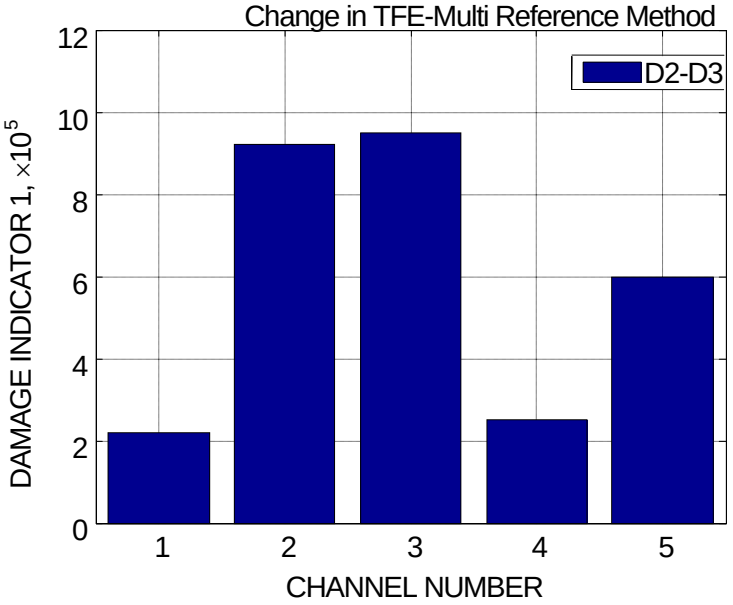

Figure 10(b) Damage localization using damage indicator 0

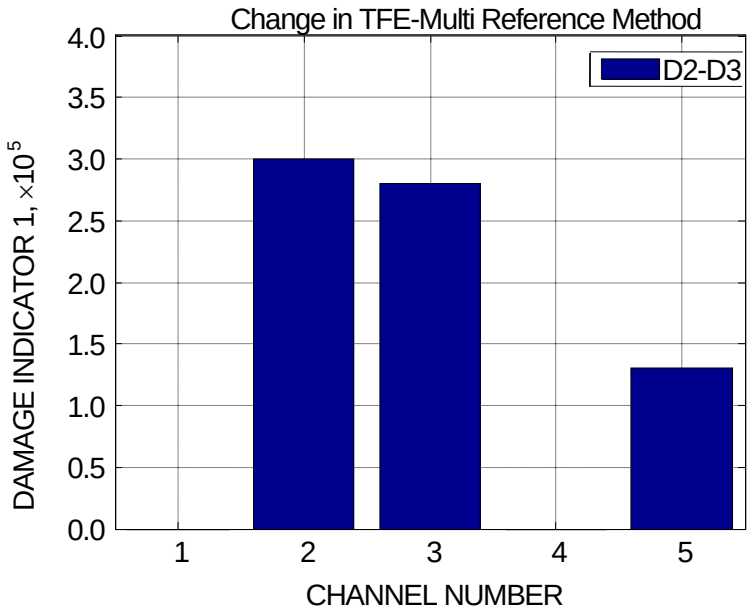

Figure 10(c) Damage localization using damage indicator 1

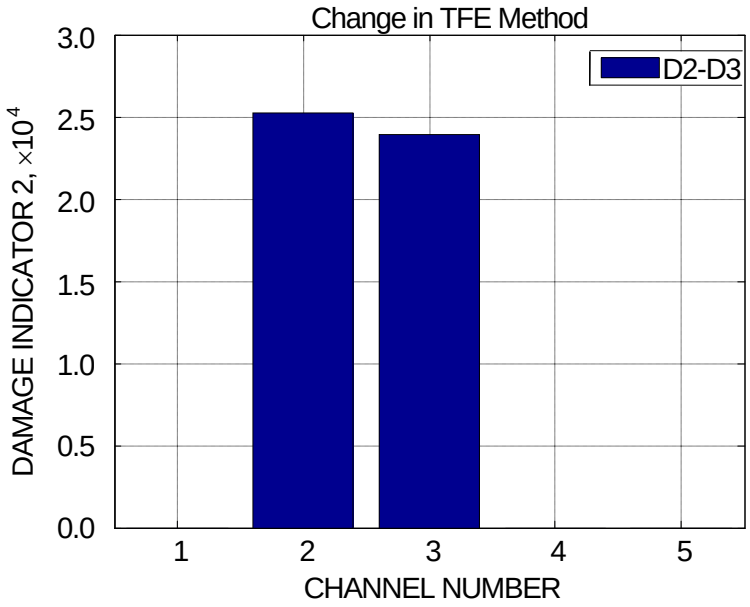

Figure 10(d) Damage localization using damage indicator 2

Figure 10 Proposed algorithm results for damage case 3

The summary of the total changes in TFE (Eq. 3) for the different cases is plotted in Figure 11. It was noticed that the total change in TFE due to noise is less than 250 dB at all channels with close values at different channels. After making the first cut of 4 mm wide and 40 mm deep (Damage D0), the total change in TFE increased at all channel locations as it is known that damage even at one channel location will change the over all stiffness of the structure. The change in TFE is however more at channels 2, 3 and 5. After increasing the cut up to NA i.e. 100 mm without cutting the

reinforcing bar in the tension portion, the total change in TFE contributed to increase slightly at the undamaged locations 1 and 4, while it is more at damage locations 2 and 3. As channel 5 is in between locations 2 and 3, there is a reasonably more change at 5 also as compared to 1 and 4 channel locations. After increasing the damage further by also cutting the reinforcing bar in the tension portion. The total change in TFE again increased and as earlier the change was more at locations 2, 3 and 5. But, the relative change in TFE after the reinforcing bar cut was less as compared to earlier damages. Therefore, it can be concluded that the total change in TFE monitored the increase in damage successfully in the reinforced concrete beam, though it is not a powerful tool to localize the damage. For doing this damage indicators 0, 1 and 2 are employed. Though damage indicators 0 and 1 also located some false positive readings at channel location 5, damage indicator 2 could overcome this problem. Hence, Damage Indicator 2 is a better damage-identifying indicator.

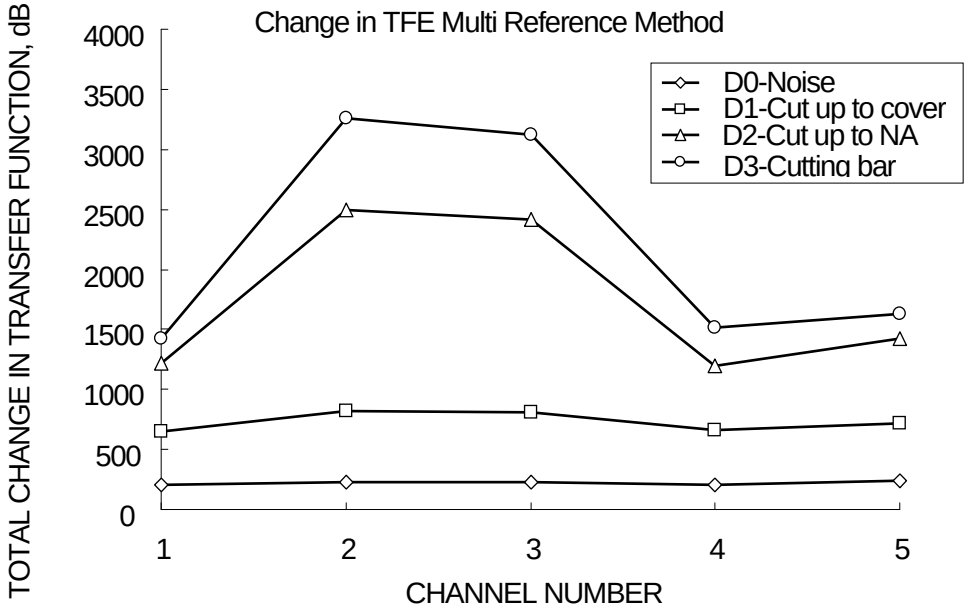

Figure 11 Total change in TFE for different damage cases

CONCLUSIONS

The experimental results obtained from the reinforced concrete beam demonstrate the usefulness of changes in TFE magnitude as a diagnostic parameter in detecting the damage, locating its position and monitoring the increase in damage. The main advantages are:

1) The proposed method encompasses the first three steps of the process of damage detection–existence, localization and monitoring. The damage increase is based on only the measured data without the need for any modal identification.

2) The accuracy of damage identification methods based on changes in mode shapes are sometimes reduced when the damage occurs at a node of the used mode shapes. Also, the accuracy of damage identification methods based on changes in FRF or CSD are dependent on the measurement range in which FRF or CSD are measured. The proposed method overcomes this drawback by using TFE data in the total measured frequency range.

3) Vibration based damage identification methods sometimes produce false positive readings due to measurement errors, noise and environmental changes. The proposed method has shown better results in identifying the changes in TFE associated with damage from the changes attributed to noise or measurement errors.

4) The total change in TFE method could monitor the increase in damage successfully in reinforced concrete structures.

5) Damage Indicator 2 was found to be a better damage identifying parameter as it could exactly locate the position of damage without any chance for detecting false positive readings.

6) There is a reasonably good agreement between the experimental and numerical values. The behaviour was similar when investigated from the analytical and numerical approach.

ACKNOWLEDGEMENTS

This research is supported by the Grant-in-Aids for Scientific Research, Japan Society for Promotion of Sciences (JSPS) and Japan International Science and Technology Exchange Center (JISTEC). The authors gratefully acknowledge their support. The authors would also like to acknowledge the support of Master students of the university Hashida Akinori and Subokawa Ryota in helping us to conduct the experiment.

REFERENCES

1. DOEBLING S W, FARRAR C R, PRIME M B AND SHEVITZ D W, Damage Identification and Health Monitoring of Structural and Mechanical Systems from Changes in their Vibration Characteristics, A Literature Review, Los Alamos National Laboratory Report, LA-13070- MS, 1996.

2. FARRAR C R AND JAUREGUI D A, Damage Detection Algorithms Applied to Experimental and Numerical Model Data from the I-40 Bridge, Los Alamos National Laboratory Report, LA-12979-MS, 1996.

3. SAMPAIO R P C, MAIA N M M AND SILVA J M M, Damage detection using the frequency response function curvature method, Journal of Sound and Vibration, Vol. 226, No. 5, 1999, pp. 1029-1042.

4. PEETERS B, MAECK J AND DE ROECK G, Vibration-based damage detection in civil engineering: excitation sources and temperature effects, Smart Materials and Structures, Vol. 10, 2001, pp. 518-527.

5. KUMMER E, YANG J C S AND DAGALAKIS N G, Detection of fatigue cracks in structural members, 2nd American Society of Civil Engineering/EMD Specialty Conference, Atlanta, Georgia, 1981, pp. 445-460.

6. YANG J C S, CHEN J AND DAGALAKIS N G, Damage detection in offshore structures by the random decrement technique, Journal of Energy Resources Technology, American Society of Mechanical Engineers, Vol. 106, 1984, pp. 38-42.

7. FLESCH R G AND KERNICHLER K, Bridge inspection by dynamic tests and calculations dynamic investigations of Lavent bridge, workshop on Structural Safety Evaluation Based on System Identification Approaches (H. G. Natke and J. T. P. Yao, editors), Lambrecht / Pfalz, Germany: Vieweg & Sons, 1988, pp. 433-459.

8. NATKE H G AND YAO J T P, System identification methods for fault detection and diagnosis, International Conference on Structural Safety and Reliability, American Society of Civil Engineers, New York, 1990, pp. 1387-1393.

9. KUMAR P R, OSHIMA T, MIKAMI S, MIYAMOURI Y AND YAMAZAKI T, Damage Identification in a lightly reinforced Concrete Beam based on changes in Power Spectral Density, International Journal of Structure and Infrastructure Engineering- Taylor and Francis, DOI: 10.1080/15732471003730674, Published online 25th April 2010, pp. 1-13.

10. MATLAB Reference Guide, The Math Works, Inc., Natick, MA, 2003.

11. MATLAB User's Guide, The Math Works, Inc., Natick, MA, 2003.

12. HAYES M., Statistical Digital Signal Processing and Modeling, John Wiley & Sons, 1996.

13. STOICA P AND MOSES R L, Introduction to Spectral Analysis, Prentice-Hall, Englewood Cliffs, NJ, 1997, pp. 52-54.

14. WELCH P D, The Use of Fast Fourier Transform for the Estimation of Power Spectra: A Method Based on Time Averaging Over Short, Modified Periodograms, IEEE Trans. Audio Electro Acoustics, Vol. AU-15, 1967, pp. 70-73.

15. BESKHYROUN S, MIKAMI S, OSHIMA T AND YAMAZAKI T, Modified damage identification algorithm based on vibration measurements, Journal of Applied Mechanics, Vol.7, 2004, pp. 97-107.

Sliding Joints as Effective Tools for Stress Elimination Caused by Horizontal Deformation

R Cajka, P Mateckova, M Janulikova, M Stara
VSB - Technical University of Ostrava, Czech Republic

Sliding joint is effective method to decrease the stress in foundation structure in case of horizontal deformation of subsoil (areas afflicted with underground mining) or horizontal deformation of foundation structure (pre□stressed foundations, creep, shrinkage, temperature deformation). Convenient material for sliding joint is bitumen asphalt belt. Experiments for different types of bitumen belts passed at Faculty of Civil Engineering □ VSB TU Ostrava in 2008. Currently extended experiments are in progress and the shear resistance of slide joint is tested as a function of temperature in temperature controlled room. In the paper experiment results of temperature dependant shear resistance will be presented. The result of the experiments should be the sliding joint shear resistance as a function of deformation velocity and the temperature. Using rheological slide joint could lead to decreasing of the reinforcement amount and contribute to higher reliability of foundation structure and thus enable to design more durable and sustainable building structures.

Radim Cajka, received his civil engineering degree from the Brno university of technology, Czech Republic. He is professor and the head of the Department of Building Structures, VSB - Technical University of Ostrava, Czech Republic. His main area of research is related to foundation structures, soil - structure interaction and structural fire design.

Pavlina Mateckova,MSc.Ph.D. is a Lecturer at Department of building structures, VSB-TU Ostrava, Czech Republic.

Martina Janulikova,MSc. is a Ph.D. student, Department of building structures, VSB-TU Ostrava, Czech Republic.

Marie Stara, MSc., is a Ph.D. student and lecturer, Department of building structures, VSB-TU Ostrava, Czech Republic.

Keywords: Foundations, Sliding joint, Soil-structure interaction, Undermined area

INTRODUCTION

The idea of the bitumen sliding joints comes from the city of Ostrava's region, which is affected by underground coal mining. Building structures in such an area demand specific treatment due to expected terrain deformation. Terrain deformation is comprised of subsidence, declination, curvature, and horizontal deformation. The most demanding, and also most expensive, are requirements for terrain horizontal deformation. One of the reasons is that, through the friction between subsoil and foundations, the foundation structure must resist significant normal forces. The idea of sliding joints between subsoil and foundation structure, which eliminates the friction in a footing bottom, comes from the 1970's, Figure 1. In the beginning there were several materials considered, (e.g. use of cardboard with ash, isinglass, graphite). Finally the bitumen asphalt belt, a widely available and reasonably priced material given its rheological properties, has been proven as an effective material for sliding joints.

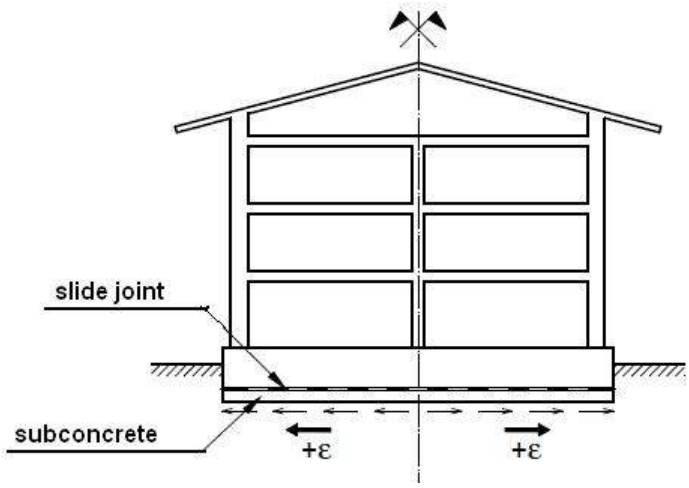

Figure 1 Schematic drawing of sliding joint

Current State of Bitumen Sliding Joint Design

Calculation of shear resistance in a footing bottom with and also without a sliding joint is given in Czech code [1], Design of building structures at undermined areas.

Shear stress τ_x in a footing bottom without a sliding joint is settled as a function of horizontal deformation, dimensions of the foundation structure and the oedometric modulus of subsoil. It is also possible to take into account slip in the footing bottom with a limit value of shear stress $\tau_{max.}$ Appropriate complex functions are not listed in this paper.

Shear stress τ_x in footing bottom with sliding joint depends fundamentally on the terrain deformation rate. Bitumen asphalt belt with its rheological properties shows lower shear resistance for lower deformation rate and vice versa, as it was proven with primary sliding joint testing in the 1980's [2]. Shear stress in primary testing and consequently in formula given in Czech code is universal, independent of the type of asphalt belt and vertical load, and the influence of temperature was taken into account only marginally. Though the current sliding joint design has a number of simplifications they were applied successfully on a few buildings.

TESTING OF NEW MATERIALS

Description of New Testing Equipment

In the 1990's many new and potentially suitable materials for sliding joint appeared, and the material characteristics changed significantly. This fact motivated authors to prepare new material testing. At VSB – Technical University of Ostrava new unique equipment was designed for new material shear resistance testing, Figure 2. In between three concrete blocks, with dimensions of 300 mm × 300 mm × 100 mm 2 asphalt belt specimens are placed. Specimens are exposed to arbitrary vertical load and after one day delay a horizontal load is also applied. Displacement of the middle concrete block is measured for 6 days, and sometimes also for more days.

The specimen was exposed to the vertical load expected in the footing bottom, 100 kPa and 500 kPa. Horizontal load is alternatively 0.62 kN, 0.95 kN and 2.0 kN, the value was settled so that the displacement rate respond approximately to the expected terrain deformation rate.

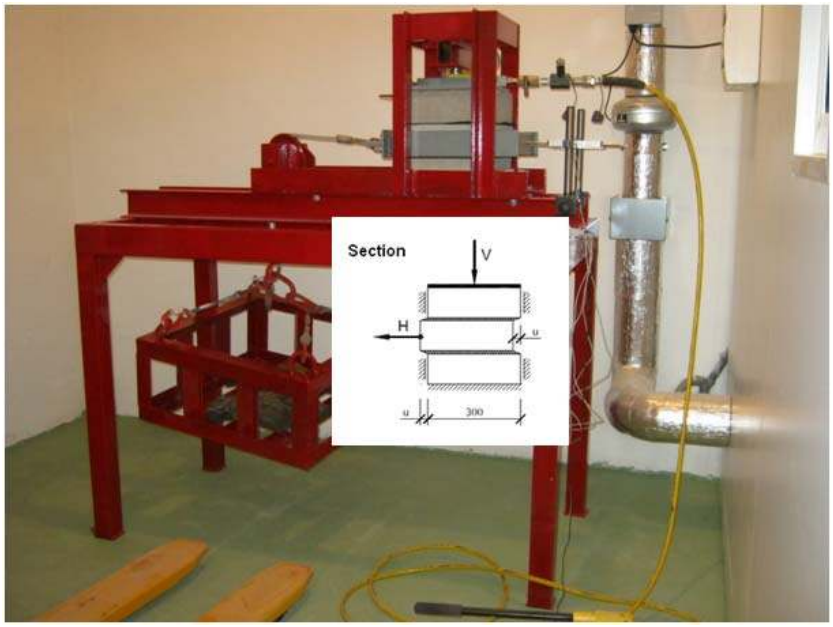

Figure 2 New testing equipment

Test Results

Experiments for different types of bitumen belts at laboratory temperature were undergone in 2008, and test results were presented in several papers, e.g. [3, 4]. Also traditional types of asphalt belt were tested so that the results could be compared with primary testing, however the material characteristics could change over time even in one type of asphalt belt.

The asphalt belts show different rheological shear characteristics for the group of oxidized bitumen asphalt belts (traditional IPA^{TM}), asphalt belt modified with polymers (e.g. Sintopol^{TM}) and asphalt belt modified with rubber (e.g. Paradiene^{TM}), example in the Figure 3. The shear resistance of asphalt belts modified with polymers is higher than that of traditional oxidised asphalt belt. The shear resistance of asphalt belts modified with rubber is lower than that of oxidised asphalt belt.

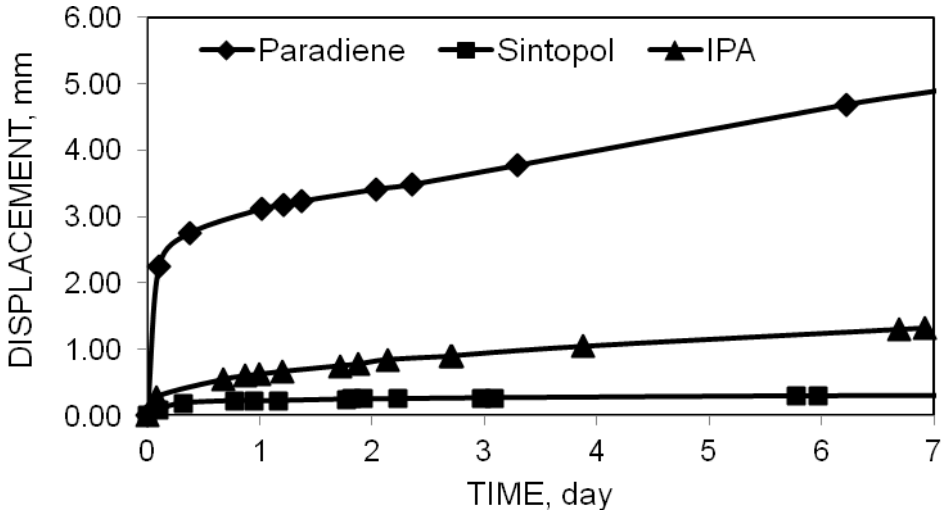

Figure 3 Particular test results, vertical load 500 kPa, horizontal 2.0 kN

INFLUENCE OF TEMPERATURE

One of the important factors which affect shear resistance is temperature. In this way experiments continue with measurement of the shear resistance of a slide joint as a function of temperature. Testing equipment was placed in a temperature controlled room. The temperature limit is from -20°C to +40°C. The aim is to determine the slide joint shear resistance for temperatures expected in a footing bottom. There is also the possibility of sliding joint target heating in the case of foundation pre-stressing.

Experiments in a temperature controlled room started in the end of the year 2010 with a traditional type of bitumen asphalt belt IPA^{TM}. Charts with particular test results are in Figures 4 and 5. Test results affirmed significant influence of temperature to specimen displacement and consequently shear resistance.

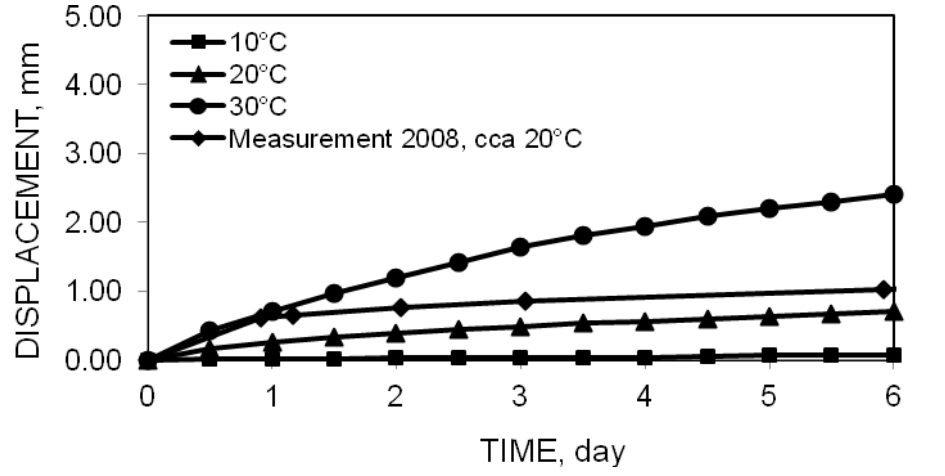

Figure 4 IPA bitumen asphalt belt, influence of temperature, vertical load 500 kPa, horizontal 0.95 kN

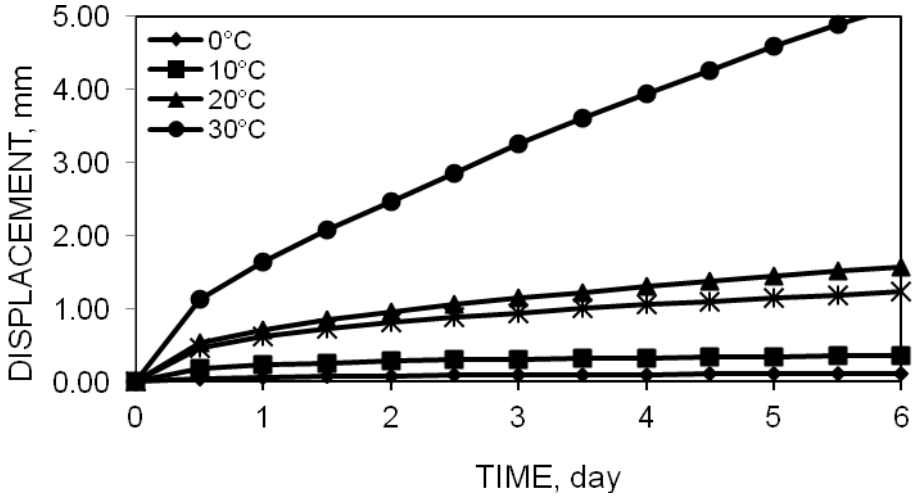

Figure 5 IPA bitumen asphalt belt, influence of temperature, vertical load 500 kPa, horizontal 2.0 kN

UTILIZATION OF TEST RESULTS

It is to be noted in the charts (Figures 4 and 5) that the deformation increment became nearly steady after one day. This fact was also proven for the other temperatures and with a few experiments which lasted 13 days. Providing the linear regression function it is possible to derive the sliding joint shear stress $\tau_{x,SJ}$ as a function of deformation rate, temperature, vertical and horizontal load, Figure 6.

For the design of sliding joint it is necessary to estimate the terrain deformation rate in cooperation with mining company. It is also convenient to use the sliding joint in concrete floors and foundations to limit the crack occurrence due to creep and shrinkage. Deformation rate due to creep and shrinkage is possible to appoint according to time model given in scientific literature and also Eurocode 2 [5].

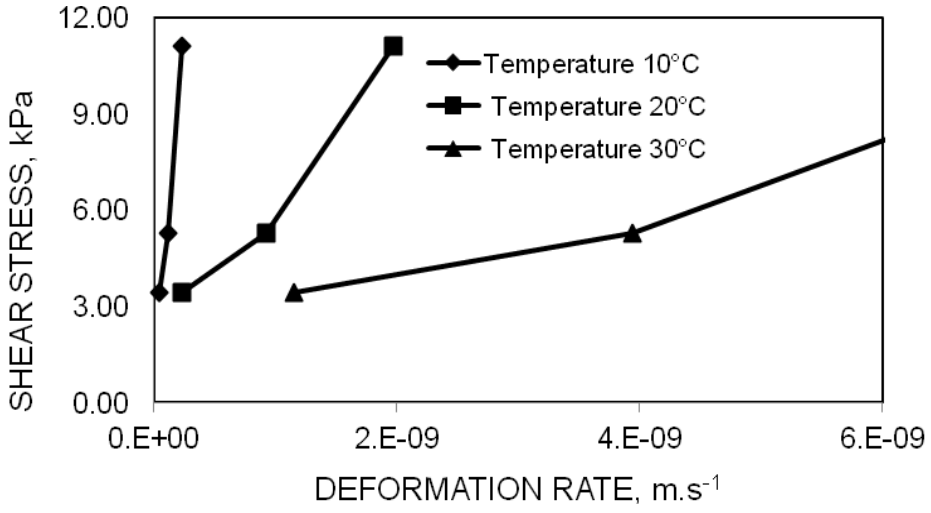

Figure 6 Shear stress as a function of deformation rate, vertical load 500 kPa

CONCLUSIONS

Sliding joints are an effective tool for elimination of shear resistance in the case of terrain horizontal deformation or also in the case of deformation of a concrete floor or foundation due to creep and shrinkage or pre-stressing. In the paper test results of shear resistance of bitumen asphalt belts are presented. Authors are not aware of similar bitumen asphalt belt testing. Though the bitumen sliding joint was successfully applied in a few buildings, sliding joints have not yet been widely used. Ongoing experiments should contribute to a wider utilization of the bitumen asphalt belt and thus enable design of more durable and sustainable building structures.

ACKNOWLEDGEMENTS

This outcome has been achieved with the financial support of the Ministry of Industry and Trade of the Czech Republic, program TIP, project No. FR-TI2/746 Rheological sliding joint with thermo-controlled viscoelastic properties.

REFERENCES

1. CSN 730039: Design of building structures at undermined areas. Basic requirements. Czech code, Prague, 1990, in Czech

2. BALAREK V AND BRADAC J, Utilization of bitumen insulating stripes as sliding joints for buildings on undermined area Civil Engineering Journal, Vol. 2, 1982, in Czech.

3. CAJKA R AND MANASEK P, Finite element analysis of a structure with a sliding joint affected by deformation loading. Proceedings of the 11th International Conference on Civil, Structural and Environmental Engineering Computing, Civil-Comp 2007, St. Julians, Malta.

4. CAJKA R AND MANASEK P, Application of slide joints for shear stress elimination of prestressed foundation. in Ninth Pan American Congress of Applied Mechanics, proceedings of conference, Mérida, Yucatán, Mexico, 2006

5. EN 1992-1-1: Design of Concrete Structures. Part 1-1: General rules and rules for buildings. Brussels, 2006.

Reducing the Variability of Predicting the Longevity of Reinforced Concrete Marine Structures Subjected to Physical and Chemical Degradation

M R Jones[1], J P Forth[2], C Thistlethwaite[1], L Higgins[1]
1 – University of Dundee, UK
2 – University of Leeds, UK

Modeling the longevity of marine structures is inadequate and time to ultimate failure is extremely difficult to predict. The sheer number of variables affecting the failure causes large variability in predictions. Experimental works were undertaken to further understand the rates of corrosion in submerged concrete to enhance prediction of steel section losses. This paper reports early findings from this work where CEM 1 type reinforced concrete was exposed to environments with variable oxygen concentrations. After accelerated corrosion initiation, corrosion measurements using a potentiostatic method were used to determine the average loss of steel due to corrosion. Corrosion is shown to continue to occur although the environment has a lack of oxygen. Rates are up to 50% lower exposed to oxygen concentrations of 0 to 4ppm, than in 8ppm or air exposure. These results are contradictory to common thinking suggesting that without oxygen, corrosion rates would be negligible. Further experimental works and project integration is discussed outlining future steps for the Universities of Dundee and Leeds to further reduce variability in predicting longevity off marine structures.

Professor M Roderick Jones, Director of Concrete Technology Unit and Dean of Faculty of Engineering, Physics and Mathematics, University of Dundee. His research interests lie in durability of concrete, service life prediction. use of alternative cements and foamed concrete.

Dr. John. P. Forth is a senior lecturer in the School of Civil Engineering at the University of Leeds. He was awarded his first degree, a BEng in Civil and Structural Engineering from the University of Sheffield. He received his PhD from the University of Leeds. He is on several Technical Committees (i.e. RILEM, British Standards) in the European Union. His research interests include serviceability and durability performance of reinforced concrete and masonry structures. He is a chartered member of the Institution of Structural Engineers.

Chris Thistlethwaite is a PhD research student in the Concrete Technology Unit at the University of Dundee, currently researching the longevity or concrete structures situated in aggressive marine environments.

Lee. J. Higgins is a research student in the School of Civil Engineering at the University of Leeds. He was awarded a First Class Masters (MEng) degree in Civil and Structural Engineering from the University of Leeds in 2008. His research interests include the performance of reinforced concrete structures under both sustained and fatigue load types and also the interaction between cracked reinforced concrete and hydrostatic pressures.

Keywords: Chemical degradation, Longevity, Marine structures, Physical damage

INTRODUCTION

Longevity of concrete structures is an extremely important area of research as a large number of these are vital infrastructure. Determining the expected life and deterioration mechanisms will allow for improved planning for new structures along with maintenance programs.

Degradation modelling of concrete structures is commonly undertaken by defining an ultimate limit state loading condition combined with rates of material degradation. The capacity of the structure diminishes due to the corrosion of steel reinforcement, changing the structural response of a structure. Combining a structural response model with a material degradation model for large concrete marine structures will allow for a more accurate prediction of the longevity of these structures. Current methods for this prediction of remaining life are not adequate and works are required to improve the accuracy of estimating remaining ultimate life.

Marine concrete structures are exposed to chloride laden environments which cause corrosion of the reinforcement to occur. Areas of these structures can be located in an atmospheric zone (airborne chlorides), splash and tidal zones (wetting and drying), or submerged (constant exposure). As large volumes of some concrete structures are located in the constantly submerged zone, where there is a lack of oxygen supply, the corrosion under low oxygenated environments is seen as a vital aspect of any longevity modelling.

Experimental work to determine the rates of corrosion under this environment were undertaken to supply improved data for probabilistic modelling of the overall structure. As the overall bending of large concrete structures exposed to wave and tidal loading will be a maximum at the base, cracking and corrosion will be at the most severe at depth where oxygen concentrations can be lower than 4 parts per million.

THEORETICAL BACKGROUND

Corrosion of reinforcing steel

It is common practice that corrosion of reinforcement is modelled in two phases; initiation and propagation [2-4]. Time to initiation, t_i, is the duration of which it takes for corrosion to occur, often due to the chlorides penetrating through the concrete cover and reaching the reinforcement. When the concentration of chlorides at the steel surface reaches a corrosion threshold or critical content, the corrosion mechanism will move into a propagation phase.

During the propagation phase chemical reactions occur at an anode and cathode. At the anode corrosive products form on the surface of the steel as the metallic ions most commonly Fe^{2+} are released along with two electrons [5]. The cathodic reaction is most commonly the breakdown of oxygen and water using a supply of electrons into hydroxide ions (OH^-). The hydroxide then reacts with the metallic ions producing corrosive products [4], shown in equations 1 and 2.

$$Fe^{2+} + (OH)^- \rightarrow Fe(OH)_2 \quad (1)$$

$$Fe^{2+} + (OH)^- \rightarrow FeO + H_2O \quad (2)$$

In anaerobic conditions the anodic reaction could be in the form of equation 3, potentially followed by the Schikorr reaction, equation 4, to form magnetite, a form of black rust (Fe_3O_4).

$$3Fe + 2H_2O \rightarrow Fe(OH)_2 + H_2 \quad (3)$$

$$3Fe(OH)_2 \rightarrow Fe_3O_4 + 2H_2O + H_2 \quad (4)$$

As it is often assumed that corrosion rates in low oxygen environments such as submerged zones of concrete structures, there have been few works that have investigated the effects of this environment on the rate of corrosion.

Attempts have been made to model the propagation, often deterministically to predict service life [6]. The large number of variables affecting the corrosion rate can cause difficulties in modelling. Further experimental results to quantify and minimise variability should reduce the inaccuracies when probabilistically determining these rates, and therefore service life. Of the variables affecting corrosion, the variables with a high significance to this work are oxygen content and cracking.

The diffusion of oxygen is suggested as the limiting factor on corrosion in a fully saturated state [7]. It is thought that once all remaining oxygen within the concrete is consumed the corrosion rate will be only influenced by the oxygen concentration of the surroundings and the diffusion coefficient. It has been stated that "the limiting corrosion current under water has been experimentally determined as 0.04µA/cm^2" [8], however this is directly contradicted by more recent experimental results where corrosion rates of up to 3µA/cm^2 are observed [9]. Due to limited knowledge on this area, experimental works are required to investigate corrosion in these environments.

Corrosion in statically cracked concrete has been investigated in the past decade [10-12]. It is shown that cracking of 0.2, 0.4 and 0.7mm surface crack widths cause an increase in the corrosion current. Cracking can cause large macrocells to set up, with the area around the crack becoming anodic due to chlorides reaching the steel. Corrosion rates can be tens of times larger due to these macrocell effects. In cracked concrete the corrosion is inhomogeneous, and varies greatly depending on local steel conditions. When a macrocell occurs in this cracked concrete, "the macrocell corrosion mechanism is the dominant component." [10].

Predicting the occurrence of these macrocells can be extremely difficult, and engineering judgement is required to update any propagation models, taking into account the likelihood of such corrosion mechanisms depending on frequency of cracking.

EXPERIMENTAL METHODOLOGY

Accelerated corrosion testing of small concrete beams using a ponding chloride exposure was undertaken. The upper face, closest to the working electrode, was exposed to a chloride laden environment, whilst the opposite face was submersed into a controlled oxygen environment (Figure 1). All other faces are sealed using wax, similar to chloride diffusion experiments.

Figure 1 experimental setup for determination of corrosion rates

Initially chlorides were migrated to the upper reinforcement by applying a potential difference of 10V between the bar and stainless steel bar in the chloride solution. Using half-cell measurements (Figure 2), using a standard voltmeter, the probability of corrosion was measured until initiation is likely to have occurred. Once corrosion has initiated, the system is disconnected and allowed to equilibrate.

Oxygen concentrations are controlled by bubbling nitrogen, to reduce dissolved oxygen, or increasing oxygen by bubbling oxygen through the water. The oxygen in the pond is reduced to be negligible, with exposed conditions at 0, 4 and 8ppm as well as control samples exposed to air.

Figure 2 half-cell measurements for corrosion initiation

Potenstiostatic measurements to determine the corrosion currents using a silver-silver chloride reference electrode, with the working and counter electrodes the two reinforcing bars.

RESULTS AND ANALYSIS

Figure 3 shows the measured corrosion currents with up to three months of corrosion propagation. Before equilibrium, all corrosion currents are initially very similar and there is no discernible difference between any exposure conditions.

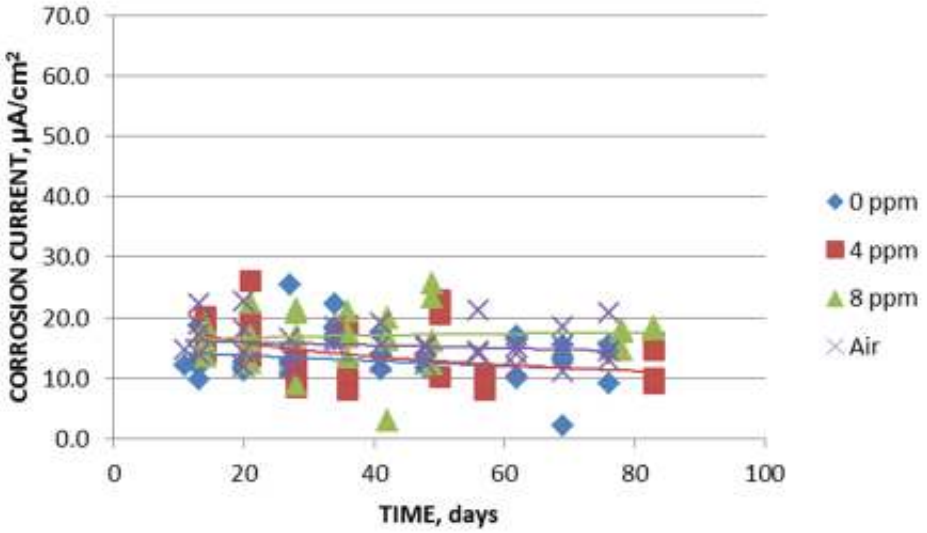

Figure 3 corrosion currents with exposed to varying oxygen concentrations

After 3 months, corrosion rates appear to have steadied with a gap between a group of 0 and 4ppm and the beams exposed to 8ppm dissolved oxygen and the atmosphere. Corrosion currents are around 10µA/cm^2 for low to zero oxygen and 15-17µA/cm^2 for high concentrations of dissolved oxygen or atmospheric exposure.

Figure 4 shows the corrosion currents for concrete exposed to oxygen depleted environments with varying anode and cathode lengths.

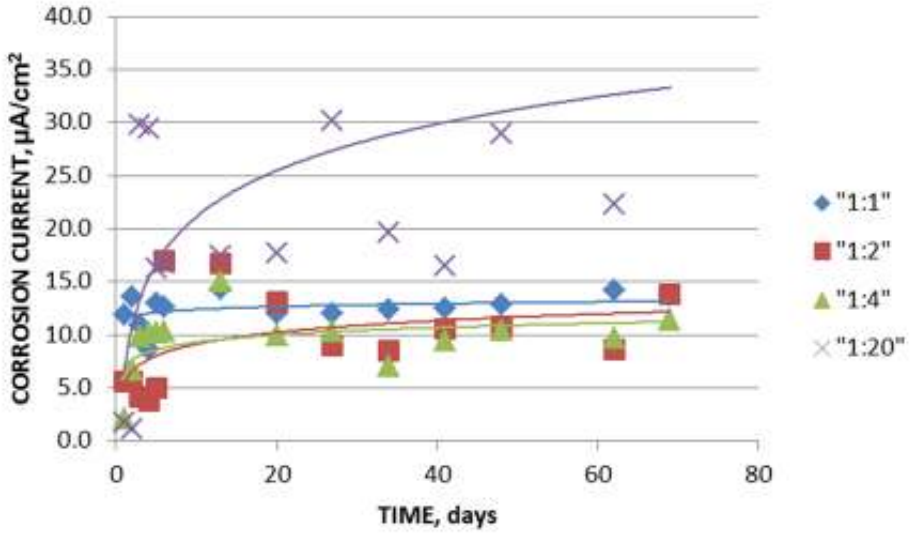

Figure 4 corrosion currents exposed to zero oxygen with varying anode to cathod ratios

With a limited anode to cathode of, 1:1, 1:2 and 1:4, the corrosion rates appear to be between 10-13µA/cm^2 which was also seen in Figure 3 for negligible oxygen exposure. However, as the cathode is increased to 20 times the size of the anode, the corrosion rate at least doubles.

Oxygen concentration is not the only limiting factor determining the rate of corrosion, and although the rate can be up to 50% slower than those exposed to the atmosphere, corrosion is still occurring and will have an effect on the structural integrity of submerged structures.

(a)

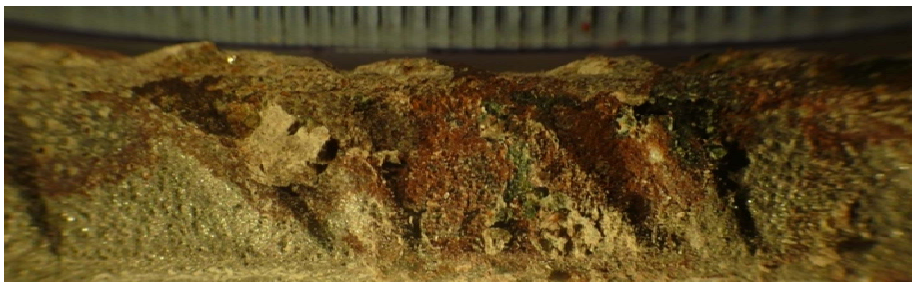

(b)

Figure 5 corrosion to reinforcement in beams exposed to atmospheric conditions

(a)

(b)

Figure 6 corrosion to reinforcement in beams exposed to zero oxygen conditions

The corrosion product found in beams exposed to oxygen is a form of 'red rust' along with aggressive pitting corrosion as shown in Figure 5. This corrosion is commonly seen and occurs when oxygen is available and broken down into hydroxyl ions at the cathode which in turn form ferric oxide (Fe_2O_3).

Figure 6 shows the formation of black rust, most likely Fe3O4 (magnetite) which can form as was shown in equation 4. The formation of this rust shows that corrosion is still occurring in an alternative form to aerobic corrosion, proving the idea that if there is a lack of oxygen present then corrosion rates can be ignored.

CONCLUSIONS & RESEARCH INTEGRATION

The paper has shown that corrosion can still occur at significant rates, in this case around $10\mu A/cm^2$, even though there is a lack of oxygen.

Black rust forms with this lack of oxygen, and continues to corrode relatively uniformly. With oxygen freely available, the corrosion appears to be mainly an aggressive form of pitting corrosion, causing more damage to the strength of the reinforcement.

The results presented and explained here are a small section of a large research project combining structural experimental work undertaken at the University of Leeds and materials experimental work undertaken at the University of Dundee. Although the works are seen as important and relevant research in their own fields, it is appreciated that material and structural degradation effects occur simultaneously. Further to this, it should be acknowledged that the two forms of degradation are inter-related as one form of degradation will act to influence, and possibly accelerate, the other.

For this reason, the two studies will be brought together in order to provide an integrated degradation model. The model is to be probabilistic and will combine findings from both studies. It will be used as a predictive tool, allowing service life estimations of structures to be made. Information gained through experimental works presented here, along with further work being carried out will allow for a more accurate integrated model.

FURTHER WORKS

Experimental works with the intention of specifically investigating structural degradation mechanisms will take place at the University of Leeds. These experiments will examine the structural response of a cracked reinforced concrete flexural element to high-cycle repeat/fatigue loading and the reduction in section stiffness caused by this load type. The long-term response to both static and repeated loading will be studied, with the main drivers of progressive curvature and section deformation being identified. The contribution of concrete within the tension zone of a reinforced concrete element will also be assessed for each load type tested in order to determine if repeated loading significantly reduces the 'tension stiffening effect'.

In addition to this, to investigate the effects of hydrostatic pressure acting within open cracks, smaller reinforced concrete beams will be cast and loaded under a similar test arrangement. These beams will be pre-cracked and then sealed around the central section so that upon

reloading, pressurised water can be introduced and allowed to infiltrate along a crack, effectively loading the open crack faces. The sensitivity of the hydrostatic pressure build-up to variables such as the crack opening rate and maximum crack width will be examined. The magnitude of the additional deformations caused by the hydrostatic pressure will be assessed in order to determine whether they significantly increase the local tensile stress within the steel reinforcement.

This work will allow for crack widths and depths to be incorporated into a structural response model to help determine the failure mechanisms of large structures. Crack widths will also then be investigated for effects of corrosion initiation and propagation under similar conditions to previous studies reported in the paper.

REFERENCES

1. CIRIA C674 (2010), The use of concrete in maritime engineering - a guide to good practice, CIRIA, London.

2. TRETHEWEY, K.R. (1988), Corrosion: for students of science and engineering, Longman Scientific & Technical, New York.

3. BERTOLINI, L. (2004). Corrosion of steel in concrete: prevention, diagnosis, repair. Wiley-VCH, Weinheim.

4. BÖHNI, H. (2005), Corrosion in Reinforced Concrete Structures, Boca Raton, Fla, CRC Press; Woodhead, Cambridge.

5. ISGOR, O.B. AND RAZAQPUR, A.G. (2006), Can. J. Civil Eng., vol. 33, n. 6, p. 707.

6. MARUYA, T., HSU, K., TAKEDA., H., TANDTERMSIRIKUL., S., 2003. Numerical modelling of steel corrosion in concrete structures due to chloride ion, oxygen and water movement. Journal of Advanced Concrete Technology, 1 (2) pp. 147-160.

7. RAUPACH, M. (1996), Mater. Struct., vol. 29, n. 188, p. 226.

8. HUSSAIN, R.R., 2011. Effect of moisture variation on oxygen consumption rate of corroding steel in chloride contaminated concrete. Cement and Concrete Composites 33 (1) pp. 154-161.

9. TORO, L., ANDRADE, C., FULLEA, J., MARTINEZ, I., REBOLLEDO, N., 2012. Steel corrosion in a chloride contaminated concrete pore solution with low oxygen availability. In: Advances in modelling concrete service life: proceedings of 4th International RILEM PhD Workshop, Madrid, November 19, 2010.

10. SUBRAMANIAM, K.V., BI, M., 2010. Investigation of steel corrosion in cracked concrete: evaluation of macrocell and microcell rates using Tafel polarization response. Corrosion Science, 52 (10) pp. 2725-2735.

11. OTIENO, M.B., ALEXANDER, M.G., BEUSHAUSEN, H.-D., 2010. Corrosion in cracked and uncracked concrete – influence of crack width, concrete quality and crack reopening. Magazine of Concrete Research, 62 (6) pp. 393-404.

12. SCOTT, A., ALEXANDER, M.G., (2007). The influence of binder type, cracking and cover on corrosion rates of steel in chloride-contaminated concrete. Magazine of Concrete Research, 59 (7) pp. 495-505.

Stochastic Algorithm for Solving Optimal Placement of Sensors

Z Feng, X Liu
Wuhan University of Technology, China

Fisher information matrix and MAC (modal confidence) matrix are good methods to solve optimal placement of bridge sensors problems, but both of them have their own quality. Base on them, an optimal placement of bridge sensors integer programming expected value model is found when the mode of vibration as random variables, then the advantages are presented when use of DNA genetic algorithm to solve this kind of problems, And finally the feasibility of the algorithm is showed by Siyang Bridge as an example.

Z R Feng is currently Professor of Bridge and Tunnel Engineering at Wuhan University of Technology, Wuhan, China. He has led several research projects on the process of building bridge, and his specialist areas of research are route inspection of bridge, timely monitoring during the process of bridge constructed, design of bridge and roads and research on soft basement of highway.

X Liu is currently a PhD student of Bridge Engineering at Wuhan University of Technology, Wuhan, China. His research direction is Bridge Monitoring and Evaluation.

Keywords: DNA genetic algorithm, Fisher and MAC matrix, Optimal placement of bridge sensors, Stochastic simulation

INTRODUCTION

In recent years, the optimal placement of sensor method based on incomplete modal information has been a wide range of research and application in civil engineering fields. Based on the environment vibration test results and combining with the actual health monitoring needs，this method maximize the degree of the improvement health monitoring of modal test by minimizing the MAC matrix nondiagonal element and maximizing the traces of Fisher information matrix for measuring the orthogonality of the modal vectors and maximizing information content of the identify parameter in the structure, after adding a bit of sensors within a reasonable position [1, 2].

It is found that the selection of sensor modal number in optimal placement of sensors problem exerts a tremendous influence on the result [3]. We think that the selection mode number can be seen as a stochastic event, this kind of mathematical programming problem which has stochastic parameter is called stochastic programming problem. So the optimal placement of sensors problem is just belong to this class.

Stochastic algorithm in optimal placement of sensors mainly includes genetic algorithms, neural networks, the ant colony algorithm and simulated annealing method [4]. Although these algorithms have good parallelism and global search, they also have some disadvantages, such as, slow convergence speed, more iterative times etc, so the calculation efficiency and reliability remains to continue to improve [5]. Because as solving integer programming is different from solving general programming problem, solving random integer programming should also be different in solving the general stochastic programming problems. Owing to DNA genetic algorithm has some advantages, such as shorter coding, more plentiful coding and decoding, conveying complex knowledge flexibly and easy to be introduced into genetic level operation, it can search to the global optimal solution with a faster speed [6]. So it's a very promising solving method for the optimal placement of sensors

In this paper, DNA genetic algorithm is used for solving of the MAC and Fisher information matrix random integer programming optimization model. The following the random integer programming expected value model firstly, then the optimal objective function is presented by the MAC and Fisher information matrix ,then the procedures of DNA genetic algorithm for stochastic integer programming expected value models are given , Lastly, the feasibility and effectiveness of this algorithm is demonstrated through the solution of sensor optimal placement in Siyang Bridge.

STOCHASTIC INTEGER PROGRAMMING EXPECTED VALUE MODELS

In stochastic integer programming expected value models, if we require every decision variables as integers, let decision vector $\boldsymbol{x}=(x_1,x_2,\cdots x_n)$, satisfies $x_1,x_2,\cdots x_n \in N$, and then we can get stochastic integer programming expected value models as follows [6]:

$$\begin{cases} max\, E[f(\boldsymbol{x},\boldsymbol{\xi})] \\ s.t. \\ \quad E[g_j(\boldsymbol{x},\boldsymbol{\xi})] \le 0,\ \ j=1,2,\cdots p \\ \quad \boldsymbol{x}=(x_1,x_2,\cdots x_n),\quad x_1,x_2,\cdots x_n \in \boldsymbol{N} \end{cases} \tag{1}$$

Among them, $\boldsymbol{x}$ is a decision vector; $\boldsymbol{\xi}$ is a stochastic vector; $f(\boldsymbol{x},\boldsymbol{\xi})$ is an objective function and $g_j(\boldsymbol{x},\boldsymbol{\xi})$ are a group of stochastic constraining functions, $j=1,2,\cdots p$. E is an expected value operator.

If and only if $E[g_j(\boldsymbol{x},\boldsymbol{\xi})]\leq 0,\ j=1,2,\cdots p$, a solution $\boldsymbol{x}$ is practicable. If it satisfies $E[f(x^*,\xi)]\geq E[f(x,\xi)]$ for every practicable solution $\boldsymbol{x}$, it means that a practicable solution $\boldsymbol{x}^*$ is the best solution of the expected value model.

OPTIMAL OBJECTIVE FUNCTION BY COMBINING FISHER AND MAC MATRIX

Fisher Stochastic Matrix Model

According to the modal superposition principle, Φ_x is $x\times\xi$ order modal matrix, q is ξ order modal coordinates column vector, x is the number of the sensors, ξ is target number of modes order. $A=\Phi_x^T\Phi_x$ is Fisher information matrix,. There is clearly $a_{ij}=\varphi_{xi}^T\varphi_{xj}$ $A=(a_{ij})_{\xi\times\xi}$ and $\Phi_x=[\varphi_{x1},\varphi_{x2},\cdots\varphi_{xk},\cdots\varphi_{x\xi}]$, φ_{xk} is k order modal vector in Φ_x .

In addition, to install sensors, the paper [7] defines the optimal objective function which used to find the highest displacement of the degree of freedom with maximum Fisher matrix as follows [7]:

$$f=\sum_{i=1}^{\xi}\sum_{j=1}^{\xi}\left|\sum_{r\in M}\varphi_{ri}\varphi_{rj}\right|^2 \tag{2}$$

Among them, φ_{ri} is the i order mode of the r degree of freedom component, $r\in M$ means limited to alternative point set, ξ is the order number of vibration model. The greater of the objective function, the better of corresponding point set.

MAC Model

In order to measure the difference between mode, Came[8] introducing Modal Assurance Criterion (MAC) matrix to measure the angle between the Modal, the MAC matrix is defined as follows:

$$MAC_{ij}=\frac{\left(\varphi_{xi}^T\varphi_{xj}\right)^2}{\left(\varphi_{xi}^T\varphi_{xi}\right)\left(\varphi_{xj}^T\varphi_{xj}\right)} \tag{3}$$

Among them, MAC_{ij} is the i row and the j column elements in MAC matrix, φ_{xi} and φ_{xj} the i row and the j column elements in test mode matrix.

Optimal Model by Combining Fisher and MAC Matrix

It can optimize the placement of sensor according by combining Fisher and MAC matrix together as follows:

$$\begin{cases} \max f = \omega f_1 + (1-\omega) f_2 \\ \text{s.}t. \\ \omega \in [0,1] \end{cases} \tag{4}$$

Here considering the Fisher matrix maximization and MAC matrix of maximum nondiagonal elements minimum, we joint model (2) and model (3) together to an optimization model for optimal sensor placement, $f_1 = \max E\left(\sum_{i=1}^{\xi} \sum_{j=1}^{\xi} \left| \sum_{r \in M} \varphi_{ri}^T \varphi_{rj} \right|^2 \right)$ and $f_2 = \max E\left[C - \max E\left(MAC_{ij} \right) \right]$ .For combining Fisher and MAC matrix as a maximum problem, we change model (3) to f_2 in the model (4), C is invariable.

USING STOCHASTIC SIMULATION TO COMPUTE EXPECTED VALUE

The idea of computing $E[f(x,\xi)]$ based on stochastic simulation is:Firstly, according to probability measuring Pr , produce sample ω_k from sample space Ω , noted $\xi_k = \xi(\omega_k)$, $k = 1,2,\cdots N$ .It is equal to produce the observation values of stochastic vector ξ_k , according to probability distribution Φ , $k = 1,2,\cdots N$. According to of large number, when $N \to \infty$, we have

$$\frac{\sum_{k=1}^{N} f(\xi_k)}{N} \to E[f(\xi)] \tag{5}$$

Therefore, as long as N is large enough, we can use $\frac{\sum_{k=1}^{N} f(\xi_k)}{N}$ as the estimated value of $E[f(\xi)]$. The specific procedures of using stochastic simulation to compute expected value are:

(1). Let $L = 0$;
(2). According to probability measuring Pr , produce sample ω from Ω;
(3). $L \leftarrow L + f(\xi(\omega))$;
(4). Repeat step (2), (3) to N times;
(5). $E[f(\xi)] = L/N$.

USING DNA-GA BASED ON STOCHASTIC SIMULATION TO SOLVE EXPECTED VALUE MODELS

The Introduction of DNA-GA

According to the biology theory, each kind of species conforms to the genetic code table which is like Table 1 as follows:

64 kinds of codons correspond to 20 kinds of amino acids. According to triad genetic codes, the arrange arrays of bases in the mRNA can be translated to the arrange arrays of amino acids.

Table 1 Genetic Code Table

FIRST BASE	SECOND BASE				THIRD BASE
	U	C	A	G	
U	Phe(1)	Ser(3)	Tyr(5)	Cys(8)	U
	Phe(1)	Ser(3)	Tyr(5)	Cys(8)	C
	Leu(2)	Ser(3)	Stop(0)	Stop(0)	A
	Leu(2)	Ser(3)	Stop(0)	Try(19)	G
C	Leu(2)	Pro(4)	His(6)	Arg(9)	U
	Leu(2)	Pro(4)	His(6)	Arg(9)	C
	Leu(2)	Pro(4)	Gln(7)	Arg(9)	A
	Leu(2)	Pro (4)	Gln(7)	Arg(9)	G
A	Ile(10)	Thr(11)	Asn(12)	Ser(3)	U
	Ile(10)	Thr(11)	Asn(12)	Ser(3)	C
	Met(0)	Thr(11)	Lys(13)	Arg(9)	A
	Met(0)	Thr(11)	Lys(13)	Arg(9)	G
G	Val(14)	Ala(15)	Asp(16)	Gly(18)	U
	Val(14)	Ala(15)	Asp(16)	Gly(18)	C
	Val(14)	Ala(15)	Glu(17)	Gly(18)	A
	Val(14)	Ala(15)	Glu(17)	Gly(18)	G

Designing and finding suitable methods of DNA coding and genetic code table is the crux of applying DNA-GA. For the optimization problems with continuous variables, according to demand precision, a variable can be defined by a string of triad DNA code. The design of genetic code table goes according to the biology genetic code table, and different amino acids code corresponds to different numbers from 0 to 19, as table 1 shows. We can find that 64 kinds of codons correspond to 20 kinds of numbers; the genetic code table has certain of redundancy, and different numbers have not the same redundancies.

Using DNA-GA Based on Stochastic Simulation to Solve Expected Value Models

The procedures of using DNA-GA based on stochastic simulation to solve expected value models can be described as follows :

(1). Input parameters pop_size, P_c, P_m, P_d, among which pop_size is noted as the size of population; P_c is noted as the alternating probability; P_m is noted as the variation probability, P_d is noted as the inversion probability.

(2). Initially produce pop_size DNA chains to compose initial population $P(t)$, and use stochastic simulation means to check the feasibility of these DNA chains.

(3). Computing fitness. According to genetic code table, translate each codon of DNA chains in the population to parameter value, and then use stochastic simulation means to compute the fitness of each individual.

(4). Choosing. According to a fixed probability, choose m DNA chains individuals from initial population $P(t)$, use them as parents to propagate next generation, the new individuals which produce by this time add to next generation population $P(t+1)$.For the individuals of each pair of DNA chains which we have chosen to propagate next generation, alternate part of their genetic messages, and then we can get the new individuals.

(5). Do the operations of alternating, variation, inversion, and use stochastic simulation means to check the feasibility of the individual in next generation.

(6). When we have produced the new generation of DNA chains population $P(t+1)$, back to step (3), and then we do the operation from step (3) to (5) again, until it satisfies the convergence conditions.

APPLIED EXAMPLE: THE SOLUTION OF SENSOR OPTIMAL PLACEMENT IN SIYANG BRIDGE

Spatial Finite Element Model of Siyang Bridge

In accordance with the finite element theory of space bar, the space finite element model of Siyang Bridge is built. The node finite element model of the whole bridge as shown in figure1 and the model of the whole bridge with 3 order vibration mode.

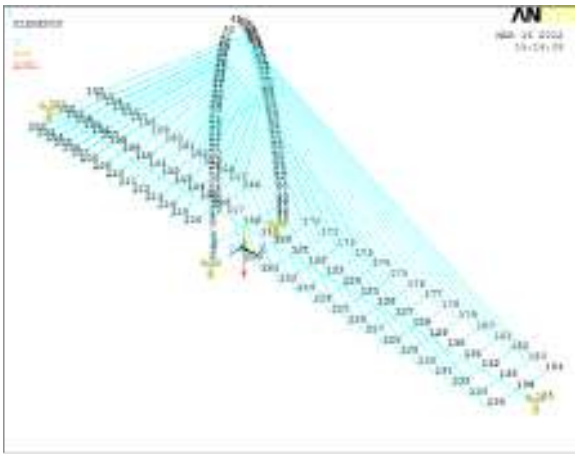

Figure 1 The nodes of the whole bridge

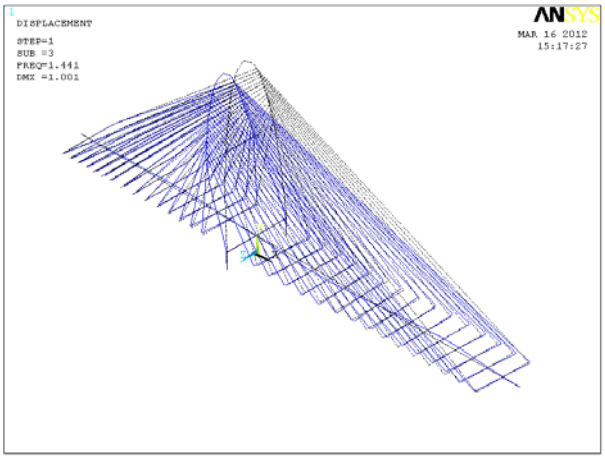

Figure 2 The model with 3 order vibration mode

Extract Beam and Tower Node Displacement Modal Data

The beam and tower node displacement modal data is calculated in this paper, and the vibration mode order number and the corresponding node number edit for data files for compiling program as input files [9]. Vibration model data is extracted the former 30 order. Due to the limited length of the paper, only the former 3 order vibration model and the former node data both in beam and tower can be showed as follows:

Table 2 Beam and tower node displacement data

NODE		MODEL		
		1	2	3
Vertical beam	102	0.15940E-15	-0.11661E-11	-0.24056E-11
	103	0.45774E-15	-0.35057E-11	-0.72231E-11
	104	0.73242E-15	-0.58092E-11	-0.11935E-10
Horizontal beam	102	0.45943E-16	-0.32398E-12	-0.59803E-12
	103	0.18519E-15	-0.13644E-11	-0.24930E-11
	104	0.40539E-15	-0.31126E-11	-0.56100E-11
Front and back tower	2	-0.15572E-03	0.53681E-03	0.45077E-03
	3	-0.52686E-03	0.17878E-02	0.16583E-02
	4	-0.97098E-03	0.32197E-02	0.33999E-02
Left and right tower	2	-0.16419E-04	-0.19261E-03	-0.18983E-02
	3	-0.32611E-04	-0.38290E-03	-0.37780E-02
	4	-0.48061E-04	-0.56485E-03	-0.55868E-02

Optimal Calculation

According to the procedures of using DNA-GA based on stochastic simulation to solve expected value models, randomly produce 50 DNA chains to compose initial population, and therefore the size of population pop_size is 50, the alternating probability P_c is 0.9, the variation probability P_m is 0.2, the inversion probability P_d is 0.2.

Combine the formulas (4) and (5) to get fitness function as formulas (6). The way of finding the optimal solution is the same both beam and tower. According to the calculation results of model after 200 times circulation, the optimal node numbers and at this time of modal order number listed as Table 2 and showed at Figure 3.

$$\begin{cases} \max f = \omega f_1 + (1-\omega) f_2 \\ f_1 = \max\left(\sum_{i=1}^{\xi} \sum_{j=1}^{\xi} \left| \sum_{r \in M} \varphi_{ri} \varphi_{rj} \right|^2 \Big/ \xi(\xi-1) \right) \text{s.}t. \\ f_2 = \max\left[C - \max E\left(MAC_{ij} \right) \Big/ \xi(\xi-1) \right] \\ \text{s.}t. \\ \quad \omega \in [0,1] \\ \quad x \in (0,n) \; and \; x \in N, \;\; n \; is \; the \; number \; of \; node \\ \quad \xi \in (0,m) and \; x \in N, \;\; m \; is \; the \; extracted \; order \\ \qquad\qquad number \; of \; vibration \bmod el \end{cases} \tag{6}$$

Table 3 The optimal sensors placement in beam and tower

ITEMS	BEAM	TOWER
modal number	20	25
optimal sensors number	10	11
optimal node to sensors placement	102、105、109、112、116、119、123、126、130、134	3、10、19、30、38、42、47、58、67、78、84

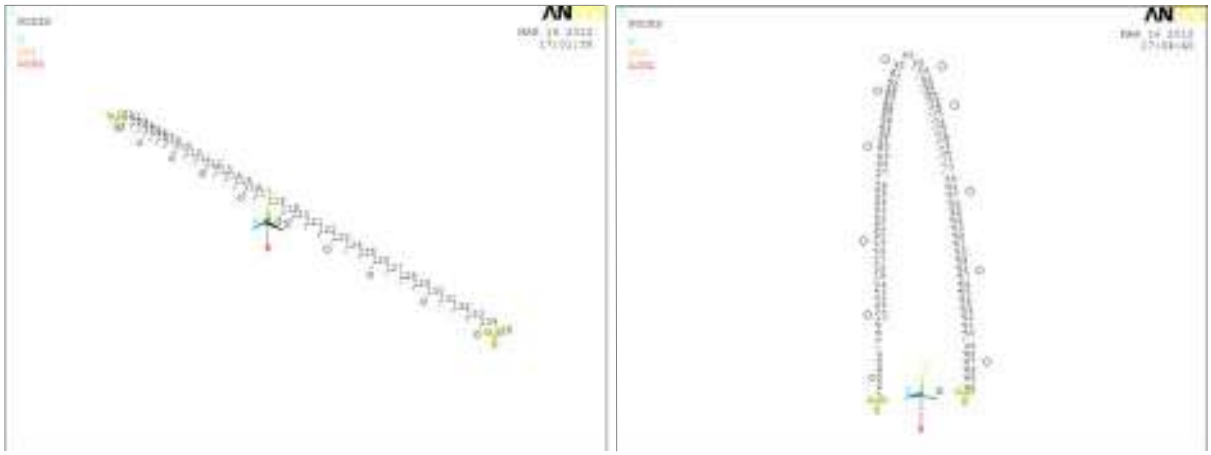

Figure 3 The optimal sensors placement in beam and tow

CONCLUSIONS

The use of weighting factor combining Fisher information matrix and MAC (modal confidence) matrix to study the optimal placement of sensors，it is a quite comprehensive methods presently, and the DNA genetic algorithm is a powerful compute tool which is good to get the global optimal solution. The optimal results of Siyang Bridge have proved the feasibility of this method finally.

The optimal placement of sensors is the priority problem before data processing which influence of processing results immediately, and the stand or fall of processing results not only related to the accuracy of the results, but also related to the monitoring cost, the answer of the above model still has the certain disparity to the practical optimal placement of sensors problem, we hope that the next step of our work will consider more factors to solve more actual problem.

REFERENCES

1. YAN LIU, GUI-JIE LIU, LIU BO. Research status and prospect on optimal placement of sensor [J]. Transducer and Microsystem Technologies. 2010, 29(11):4-7

2. ZHOU-HONG ZONG, JIAN-LIN SUN, Study on optimal placement of acceleration sensors for health monitoring of a long-span continuous rigid-frame bridge [J]. Journal of Earthquake Engineering and Engineering Vibration. 2009,2(4):150-158

3. GUANG MA, FANG-LIN HUANG, XUE-MIN WANG. An Optimal Approach to the placement of Sensors in Structural Health Monitoring Based on Hybrid Genetic Algorithm. SCAMI-2，19-21 November 2007, Changsha, China, Vol II:929934

4. WEI-CHENG GAO; MIN-JIAN XU; WEI LIU. Optimization of sensor placement by genetic algorithms [J]. Journal of Harbin Institute of Technology, 2008, 40(1):9-11

5. GUANG MA, FANGLIN HUANG, XUEMIN WANG. Based on hybrid genetic algorithm bridge monitor optimal placement of sensors [J]. Journal of Vibration Engineering.2008，21 (2): 191-196

6. SHUCHAO WANG, CHENG WANG. “Refined DNA-GA for solving nonlinear multi-constrained programming”, J.Huazhong Univ.of Sci. &Tech, 2004, 6.

7. GE LI, QUAN QIN, CONG DONG. Select the optimal placement of sensors in the monitoring system of suspension bridge of sensors with genetic algorithm [J]. Engineering mechanics，2000, 17 (1):2434

8. CARNE T G，DOHMANN C R. A modal test design strategy for modal correlation. Proceedings of the 13th International Modal Analysis Conference. New York: Union College Schenectady 1995: 927-933.

9. RONG GAO. Optimal placement of sensors in bridge health monitoring system, [M.S. Thesis].Wuhan: Huazhong university of science and technology，2007:45-56

Deterioration of Concrete Caused by the Thaumasite Form of Sulfate Attack (TSA): A Case Study

D Klammer, J Tritthart, F Mittermayr, A Brunnsteiner
TU Graz, Austria

Deteriorated and un-deteriorated samples, drilling cores and needle-like efflorescence were taken from the shotcrete lining in an Austrian tunnel. Additional samples from groundwater and interstitial solutions extracted from the sampled damaged concrete materials were collected. Main elemental composition, mineralogy, and microstructure of deteriorated solids indicated that thaumasite formation was the main reason for the damage. The needle-like efflorescence was identified as the sodium sulphate mirabilite (Na_2SO_4•$10H_2O$). Based on δ13C values of dissolved inorganic carbon (DIC) in local groundwater source of carbonate for thaumasite DIC of infiltrating carbonate-rich groundwater was indicated. Analyses of δ34S of thaumasite identified that the source of sulphate in thaumasite is clearly related to the infiltrating groundwater also. SO_4^{2-} concentrations of the local ground waters were in the range of 450 to 550 mg/l, and the Na^+ concentrations were as low as 0.5-4.0 mg/l. In contrast interstitial solutions showed in the case of Na^+ up to 7400 and for SO_4^{2-} values up to 17200 mg/l. Additionally the δ2H and δ18O values (Vienna Standard Mean Ocean Water; VSMOW), of the extracted solutions display a strong enrichment of the heavy isotopes versus the local infiltrating solution. In accordance with this trend a respective enrichment of conservative (trace) elements e.g. Rb^+, K^+ and NO3- was detected. Therefore it is assumed that evaporation of the infiltrating groundwater is responsible for the enrichment of heavy isotopes and conservative elements.

Prof D Klammer is a Professor at the Institute of Applied Geosciences, with research interests in properties of inorganic binders, applied mineralogy / archeometry and inorganic binders, environmental geochemistry, and isotope signals and element cycling.

Prof J Tritthart is a Professor for “Chemistry of Civil Engineering” at the Institute of Technology and Testing of Building Materials at Graz. His research interests are mainly in the field of cement and concrete often in connection with detrimental environmental exposure conditions such as corrosion of reinforcements on chloride ingress or volume stability problems on sulfate attack, by investigating e.g. potential mapping or pore solution chemistry.

F Mittermayr is a PhD student at the Institute of Applied Geosciences, with research interest in applied mineralogy / archeometry and inorganic binders.

A Brunnsteiner is a PhD student at the Institute of Technology and Testing of Building Materials, with main research interest in assessing critical sulfate levels in concrete.

Keywords: Case study, Deterioration, Dissolved organic carbon, Isotope, Microstructure, Mirabilite, Sulfate, Thaumasite

INTRODUCTION

Deterioration of concrete constructions is occasionally caused by the thaumasite form of sulfate attack (TSA). Over the past decades this form of degradation process has been discussed repeatedly [1-13]. The formation of thaumasite is mostly observed at temperatures less than 15ºC and was found in numerous lining shotcretes in several tunnel constructions [14-20]. Although literature dealing with deterioration reactions of concrete is voluminous, the causal sources of components have not yet been fully perceived in particular the origin of components for thaumasite formation [13].

Various potential sources of carbonate and sulfate are discussed [21]. Stable isotopes have successfully been introduced to inorganic binder research to gain a better understanding of several processes of concrete deterioration [22-27]. These techniques have rarely been applied in former studies on thaumasite formation [28-31].

In this study the deterioration mechanisms of concrete in respect to the formation of thaumasite were investigated by highlighting the results based on a case study in an Austrian tunnel which passes through a mountain of which some geological units contain gypsum and anhydrite. The maximum sulfate concentration of the mountain water was 550 ppm SO_4^{2-}. However, at places with dripping water SO_4^{2-}-concentration increased up to ~1500 mg/l SO_4^{2-} due to the dissolution of gypsum.

By introducing trace element and isotope signatures supplementary to the main elemental composition, mineralogy, and microstructure of solids however, new insights with respect to the process of deterioration of concrete can be obtained.

SAMPLING AND ANALYTICS

Solids and aqueous solutions were collected from several Austrian tunnels. Solids comprise deteriorated and non-deteriorated concrete. The non deteriorated samples were picked up next to damaged zones by drill cores to investigate possible chemical and mineralogical variations. To analyse reaction mechanisms and paths during destruction of the shotcrete, solutions were collected from drainage and from local ground water. Moreover, interstitial solutions were extracted from the sampled damaged concrete material by using a special squeezing device described in [20].

Solid Analyses

Solids were analysed by X-ray diffraction (XRD), wet-chemical technique, X-ray fluorescence spectroscopy (XRF), scanning electron microscopy (SEM), electron probe micro-analyzer (EPMA), and micro Raman spectroscopy (MRS). Distribution of stable isotopes of carbon ($\delta^{13}C$ in $^{o}/_{oo}$, Vienna Pee Dee Belemnite; VPDB) and oxygen ($\delta^{18}O$ in $^{o}/_{oo}$; VSMOW) were obtained by isotope ratio mass spectroscopy (IRMS) using the common phosphoric acid method. In the case of sulfur isotopes, the solid samples had to be pre-treated by dissolution in diluted HCl. In the filtrated digestion the dissolved sulfate ions were quantitatively precipitated as $BaSO_4$ by the addition of $BaCl_2$. Subsequently, $\delta^{34}S$ values (in $^{o}/_{oo}$, Vienna Cañon Diablo meteorite; VCDT) were analysed by mass spectrometry.

Aqueous Solution Analyses

The pH, electric conductivity (EC) and temperature of drainage solution and ground water were measured in the field. Subsequently, alkalinity was determined by titration with 0.05M HCl. Major and trace ion content were analysed by ion chromatography (IC) and inductively coupled plasma mass spectroscopy (ICP-MS). $\delta^{13}C$ values of dissolved inorganic carbon (DIC) were achieved by adding phosphoric acid and using mass spectroscopy. Dissolved SO_4^{2-} was pre-treated with $BaCl_2$ for sulfur isotopic analysis as described above. $\delta^{18}O$ values ($^{o}/_{oo}$, VSMOW) of H_2O molecules were analysed by the classical CO_2-H_2O equilibrium technique. The isotopes of hydrogen (δ^2H in $^{o}/_{oo}$, VSMOW) were measured using a mass spectrometer coupled to a high-temperature oven by chromium reduction.

RESULTS AND DISCUSSION

Mineralogical analyses of deteriorated concrete showed that thaumasite formation (Figure 1) was the main reason for the destruction of the shotcrete linings. Non-deteriorated shotcrete contained besides mainly C-S-H-phases, aggregates consisting of calcite, dolomite and quartz.

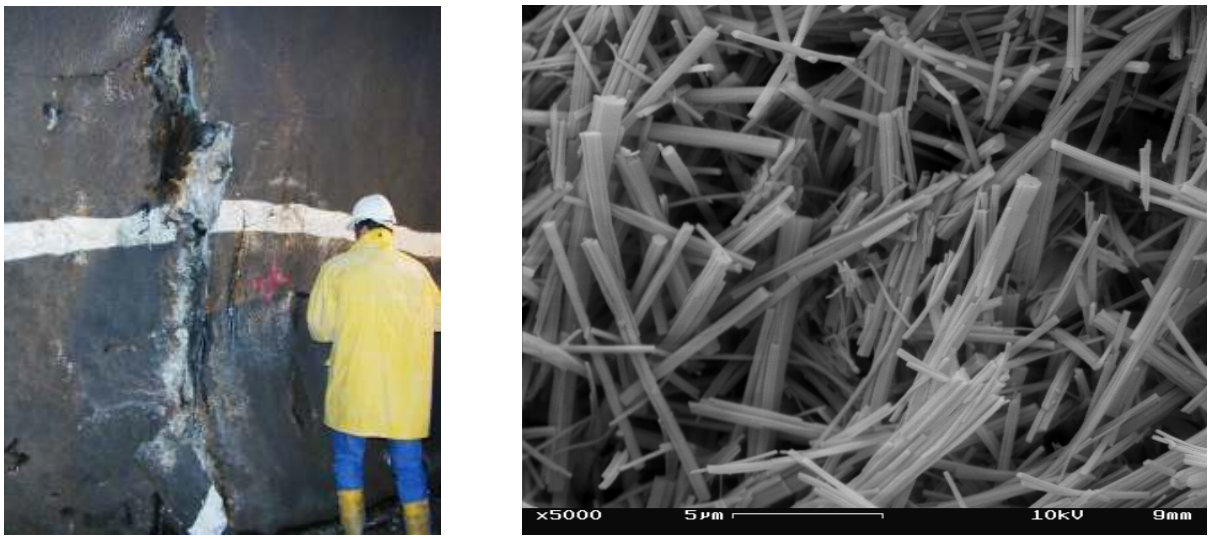

Figure 1 Concrete destroyed by thaumasite formation (left) and secondary electron image (SEI) of thaumasite crystals in deteriorated concrete (right)

Solid patterns from drilling core sections showed next to the contact surface of the mountain white reaction products identified by XRD analyses as thaumasite. Results of chemical analysis of pore waters expressed from drilling core sections showed increasing concentrations of Na^+ and K^+ from the outside to the inside of the core. In contrast Ca^{2+} and the SO_4^{2-} concentrations decreased due to the formation of thaumasite from the outside to the inside. The fact that the sulfate content reached the highest sulfate level in the peripheral zone and that it decreased rapidly at increasing depth demonstrates that the attack started from the rear surface which was in contact with the sulfate-containing mountain water and propagated into the concrete. Moreover white water-soluble efflorescence on the concrete surface along cracks was located (Figure 2). They melted already at temperatures below 100°C and were identified as mirabilite ($Na_2SO_4 \cdot 10H_2O$). The efflorescence could only have been formed by sulfate-containing water passing through the concrete — due to capillary action — and reaching saturation with respect to the Na-sulfate hydrate mirabilite [20].

Figure 2 Needle-like efflorescence mirabilite on the concrete surface

Additionally an alkali carbonate reaction (ACR) was found. The dolomite aggregates of concrete reacted with the alkalis from the cement dissolved and formed new calcite and brucite crystals [32].

Results from a recent study based on $\delta^{13}C$ values of DIC in local groundwater clearly indicate dissolved inorganic carbon (DIC) of infiltrating carbonate-rich groundwater as carbonate source for thaumasite formation. Analyses of $\delta^{34}S$ of thaumasite, soot from the tunnel wall, and dissolved sulfate from interacting groundwater, which is recharged from an area containing Triassic evaporates (calcium sulfates) pointed out that the source of sulfate in thaumasite is clearly related to the infiltrating groundwater also [28-31].

In a further study interstitial solutions of concrete, which was deteriorated by Thaumasite Form of Sulfate Attack (TSA), were expressed. Extracted solutions contained besides very high content of total dissolved solids (TDS) up to 65 g/l TDS highest enrichments for K^+, Cl^-, Rb^+ and Na^+ versus ground water.

Analysed δ^2H and $\delta^{18}O$ values of H_2O displayed a strong enrichment of ^2H and ^{18}O versus ^1H and ^{16}O isotopes comparing to the local infiltrating ground water. This correlation can be followed by an evaporation trend [28]. Due to the isotopic behaviour a respective enrichment of conservative compounds, e.g. Rb^+, Na^+ and NO_3^- in the extracted solution can be obtained. These elements, especially NO_3^-, are not incorporated in the new formed minerals (e.g. thaumasite, calcite, brucite) during the deterioration process of concrete. Figure 3 shows the graph $\delta^{18}O$ versus NO_3^-values. The correlation equates exactly the correlation which was found for $\delta\,^2H$ versus $\delta\,^{18}O$ values.

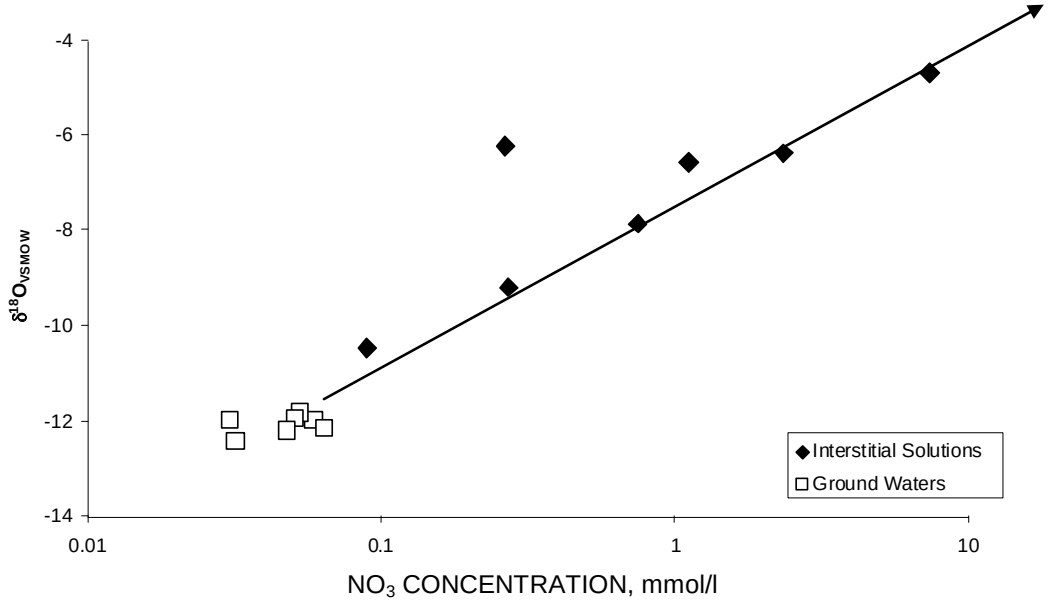

Figure 3 $\delta^{18}O$ versus NO_3^- values of extracted interstitial solutions from concrete with intense damages caused by thaumasite formation
Solid line: regression line indicating evaporation

Therefore the enrichment of selected conservative compounds mentioned above is interpreted as a result of an evaporation process. Thus selected elemental and isotopic data give clear evidence for TSA caused by liberation of H_2O from the interstitial solution into the atmosphere.

CONCLUSIONS

Trace element and isotope signatures analyses provide under defined conditions promising tools to reconstruct deterioration processes of concrete caused by the thaumasite form of sulfate attack (TSA). For instance, (i) isotopic signatures indicated the sources of CO_3^{2-} and SO_4^{2-} in thaumasite, (ii) selected conservative elements, e.g. Rb^+, NO_3^- and Na^+ as well as isotopic composition of the interstitial solutions gave evidence for evaporation as driving force for TSA, and (iii) evaporation process caused the increase in concentration of sulfate to form Na_2SO_4 efflorescence (mirabilite $Na_2SO_4 \cdot 10H_2O$) on the concrete surface.

ACKNOWLEDGEMENTS

This study is part of a research project entitled “Determination of the critical sulfate content of concrete”. The project proposal was submitted by the Austrian Association for Concrete and Structural Engineering (ÖVBB) at the Austrian Research Promotion Agency (FFG) and is funded by FFG as well as by the following companies: DSM Fine Chemicals Austria, LINZ AG, Association of the Austrian Cement Industry, Austrian Federal Railways and Austrian Highway Financing Agency. The advice and scientific support given by DI Dr. H. Huber is greatly appreciated. The research project is carried out by the Institutes “Technology and Testing of Building Materials“, “Applied Geosciences” (both Graz, University of Technology) and “Material Technology Innsbruck”. The authors would like to thank the above associations and companies for their financial support.

REFERENCES

1. BELLMANN F AND STARK J, The role of calcium hydroxide in the formation of thaumasite, Cement and Concrete Research, Vol. 38, 2008, pp. 1154-1161.

2. CRAMMOND N J, The thaumasite form of sulphate attack in the UK, Cement and Concrete Composites, Vol. 25, 2003, pp. 809-818.

3. ERLIN B AND STARK D C, Identification and occurrence of thaumasite in concrete, Highway Res Record, Vol. 113, 1965, pp. 108–113.

4. GLASSER F P, MARCHAND J AND SAMSON E, Durability of concrete — Degradation phenomena involving detrimental chemical reactions, Cement and Concrete Research, Vol. 38, No. 2, 2008, pp. 226-246.

5. HAGELIA P AND SIBBICK R G, Thaumasite sulfate attack, popcorn calcite deposition and acid attack in concrete stored at the "Blindtarmen" test site Oslo, from 1952 to 1982, Materials Characterization, Vol. 60, No. 7, 2009, pp. 686-699.

6. IRASSAR E F, Sulfate attack on cementitious materials containing limestone filler — A review, Cement and Concrete Research, Vol. 39, No. 3, 2009, pp. 241-254.

7. LOUDON N, A review of the experience of thaumasite sulphate attack by the UK Highways Agency, Cement and Concrete Composites, Vol. 25, 2003, pp. 1051-1058.

8. MITTERMAYR F, KLAMMER D, DIETZEL M, BAUER C, BÖTTCHER M, KOCH M, KÖHLER S J AND MAYER A, Thaumasitbildung in Tunnelbauten — Hydrogeochemie und stabile Isotope, Gruppe Geotechnik Graz, Vol. 34, 2008, pp. 115-132.

9. PIPILIKAKI P, PAPAGEORGIOU D, TEAS CH, CHANIOTAKIS E AND KATSIOTI M, The effect of temperature on thaumasite formation, Cement and Concrete Composites, Vol. 30, No. 10, 2008, pp. 964-969.

10. SCHMIDT T, LOTHENBACH B, ROMER M, SCRIVENER K, RENTSCH D AND FIGI R, A thermodynamic and experimental study of the conditions of thaumasite formation, Cement and Concrete Research, Vol. 38, No. 3, 2008, pp. 337-349.

11. SCHMIDT T, LOTHENBACH B, ROMER M, NEUENSCHWANDER J AND SCRIVENER K, Physical and microstructural aspects of sulfate attack on ordinary and limestone blended Portland cements, Cement and Concrete Research, Vol. 39, No. 12, 2009, pp. 1111-1121.

12. SKAROPOULOU A, TSIVILIS S, KAKALI G, SHARP J H AND SWAMY R N, Thaumasite form of sulfate attack in limestone cement mortars: A study on long term efficiency of mineral admixtures, Construction and Building Materials, Vol. 23, No. 6, 2009, pp. 2338-2345.

13. THOMAS M D A, ROGERS C A AND BLESZYNSKI R F, Occurrences of thaumasite in laboratory and field concrete, Cement and Concrete Composites, Vol. 25, No. 8, 2003, pp. 1045-1050.

14. LUKAS W, Betonzerstörung durch SO_3-Angriff unter Bildung von Thaumasit und Woodfordit, Cement and Concrete Research, Vol. 5, No. 5, 1975, pp. 503-517.

15. LEE H, CODY R D, CODY A M AND SPRY P G, The formation and role of ettringite in Iowa highway concrete deterioration, Cement and Concrete Research, Vol. 35, No. 2, 2005, pp. 332-343.

16. LEE S T, LEE D H, KIM D K, JUNG H S, PARK K P, KIM S S AND LEE C S, Occurrence of thaumasite in lining concrete of old-tunnel structure, In Geotechnical Engineering for Disaster Mitigation and Rehabilitation, Eds. H Liu, A Deng and J Chu, Beijing, Science Press Beijing, 2008.

17. MA B G, GAO X J, BYARS E A AND ZHOU Q Z, Thaumasite formation in a tunnel of Bapanxia Dam in Western China, Cement and Concrete Research, Vol. 36, No. 4, 2006, pp. 716-722.

18. ROMER M, HOLZER L AND PFIFFNER M, Swiss tunnel structures: concrete damage by formation of thaumasite, Cement and Concrete Composites, Vol. 25, No. 8, 2003, pp. 1111-1117.

19. ŠUPUT J S, MLADENOVIČ A, ČERNILOGAR L AND OLENŠEK V, Deterioration of mortar caused by the formation of thaumasite on the limestone cladding of some Slovenian railway tunnels, Cement and Concrete Composites, Vol. 25, No. 8, 2003, pp. 1141-1145.

20. TRITTHART J, KLAMMER D, MITTERMAYR F AND BRUNNSTEINER A, A Casestudy of Thaumasite Formation in an Austrian Tunnel, 13th ICCC Madrid, Spain, 3-8 July 2011, 126: pp. 1-7

21. COLLETT G, CRAMMOND N J, SWAMY R N AND SHARP J H, The role of carbon dioxide in the formation of thaumasite, Cement and Concrete Research, Vol. 34, No. 9, 2004, pp. 1599-1612.

22. CRADDOCK P R, ROUXEL O J, BALL L A AND BACH W, Sulfur isotope measurement of sulfate and sulfide by high-resolution MC-ICP-MS, Chemical Geology, Vol. 253, Nos. 3-4, 2008, pp. 102-113.

23. DIETZEL M, C-13/C-12-Signatures and O-18/O-16-signatures of calcite precipitations in drainage systems, Acta Hydrochimica Et Hydrobiologica, Vol. 23, No. 4, 1995, pp. 180-184.

24. DIETZEL M, Measurement of the stable carbon isotopes in calcite sinters on concrete, ZKG International, Vol. 53, No. 9, 2000, pp. 544-548.

25. KOSEDNAR-LEGENSTEIN B, DIETZEL M, LEIS A AND STINGL K, Stable carbon and oxygen isotope investigation in historical lime mortar and plaster — Results from field and experimental study, Applied Geochemistry, Vol. 23, No. 8, 2008, pp. 2425-2437.

26. LÉTOLLE R, GÉGOUT P, RAFAI N AND REVERTEGAT E, Stable isotopes of carbon and oxygen for the study of carbonation/decarbonation processes in concretes, Cement and Concrete Research, Vol. 22, Nos. 2-3, 1992, pp. 235-240.

27. RAFAI N, LÉTOLLE R, BLANC P, GEGOUT P AND REVERTEGAT E, Carbonation-decarbonation of concretes studied by the way of carbon and oxygen stable isotopes, Cement and Concrete Research, Vol. 22, No. 5, 1992, pp. 882-890.

28. DIETZEL M, MITTERMAYR F, KLAMMER D, HÖLLEN D, KÖHLER S AND LEIS A, What do Stable Isotopes tell us about Deterioration of Concrete. 13th ICCC, Madrid, Spain, 3-8 July 2011, 274: pp. 1-6

29. MITTERMAYR F, KLAMMER D, HÖLLEN D, KÖHLER S, BÖTTCHER M E, LEIS A AND DIETZEL M, Deterioration of concrete – application of stable isotopes, in: M.A.T.M. Broekmans (Ed.) 10th ICAM, Springer, Trondheim, 2011, pp. 435-444.

30. MITTERMAYR F, BAUER C, KLAMMER D, BÖTTCHER M E, LEIS A, ESCHER P AND DIETZEL M, Concrete under Sulphate Attack: An Isotope Study on Sulphur Sources Isotopes in Environmental & Health Studies, Vol. 48, 2012, pp. 1-13.

31. MITTERMAYR F, RINDER T, KLAMMER D, LEIS A AND DIETZEL M, A Carbon Isotope Study of Thaumasite and Calcite Sinter Formation in Underground Construction, in: International Congress on Durability of Concrete, Trondheim, 2012 (in press).

32. FRENCH W J, Presidential Address 2003: Why concrete cracks — geological factors in concrete failure, Proceedings of the Geologists Association, Vol. 116, 2005, pp. 89-105.

33. IDEN I K AND HAGELIA P, C, O and S isotopic signatures in concrete which have suffered thaumasite formation and limited thaumasite form of sulfate attack, Cement and Concrete Composites, Vol. 25, No. 8, 2003, pp. 839-846.

34. PYE K AND SCHIAVON N, Cause of sulfate attack on concrete, render and stone indicated by sulfur isotope ratios, Nature, Vol. 342, No. 6250, 1989, pp. 663-664.

35. MITTERMAYR F, KLAMMER D, KÖHLER S, LEIS A, HÖLLEN D AND DIETZEL M, Dissolution of dolomite in alkaline cementitious media, 13th ICCC, Madrid, Spain, 3-8 July 2011, 278: pp. 1-6.

Case Study of a Structural Assessment for a Building Subjected to Fire Attack

M A Musmar, M I Rjoub
Al Ahlyyia Amman University, Jordan

The study describes a real fire assessment of a two story building occupied by a textile factory. It throws light upon the fire investigation tools utilized to evaluate the post fire residual strength. The paper also describes fire investigation techniques which trace the visual evidence in the fire damaged structure. The investigation also includes tools to estimate the peak temperature and duration of heating that the structure is exposed to. The factory is located in Dulail region about 100 km. east of Amman city, the capital of Jordan. It is composed of two stories. The total building area is 9500 sqm. The slabs and beams are composed of precast prestressed partially reinforced concrete units. The columns and foundations are of ordinary reinforced concrete. To assess the fire severity, the affected surfaces and the debris were inspected; the color, the state, and the condition of the material were examined. The peak temperature and duration of heating that the building has been exposed to were estimated utilizing temperature indicators tables. The assessment involved both field and laboratory work to determine the extent of damage. The investigation was initiated by visual inspection of the whole structure to trace the most damaged parts, through investigation of cracks, scale off, concrete spalling, physical and color changes. According to the severity of damage, the structure was divided into zones. Zones 1,2 were severely damaged, and the remaining parts are to be demolished. Testing was carried out only in zone 3. First nondestructive testing was carried out. It comprised both Schmidt hammer and Ultrasonic pulse velocity tests. Results were recorded. Then destructive testing was carried out in specific locations. Core samples were taken from slabs, beams and columns, to determine concrete compressive strength. This paper presents an overview of how to conduct a forensic evaluation of a fire damaged structure.

Dr. Mazen A. Musmar is currently Associate Professor of structure at the Al-ahliyya Amman University. He has worked on several research projects on reinforced concrete and steel, and his specialist areas of research are structural modeling, structural assessment of buildings and rehabilitation.

Dr. Muhammad Rjoub is currently Associate Professor of structure at the Al-ahliyya Amman University. He has worked on several research projects on reinforced concrete and structural assessment, his specialist area of research is structural assessment of buildings and rehabilitation.

Keywords: Concrete, Fire investigation, Rehabilitation, Structural assessment

INTRODUCTION

The subject site is Nahleh textile factory. It is located in Dulail region about 100 km East of Amman. The building is composed of two floors. The Slab units are composed of Precast Pretension concrete panels of 1.2 m width, 9.2 m length, and 0.2 m thickness. The beams supporting the slab units are also constructed of Pre-stressed concrete. The columns and foundations are of ordinary reinforced concrete. The building total area is 9500 m².

The fire erupted in the ground floor within the northern sector of the building. Through the open windows, the fire spread towards the first floor which contained textile materials. The fire severity within the 1st floor, boosted by the wind breeze, exceeded that of the ground floor. About forty five minutes later, the fire began to flash over, resulting in the collapse of the 1st floor slabs in the northern sector, falling on the ground floor slab. Eventually resulting in the collapse of 50% of the ground slab units underneath. The fire spread within the whole building and it lasted for 7 hours before it was ultimately extinguished.

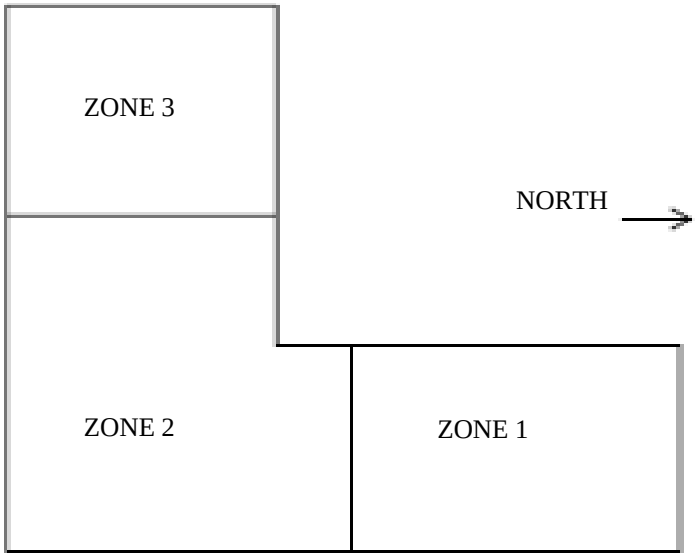

Figure 1 Schematic plan of the building

On site inspection for the post fire building condition and the amount of the resulting damage lead to zoning the building into the following three categories:

- Zone 1: Collapse of slab panels for both two floors within about 50% of the northern sector. The beams and columns remained in position, but they suffered from considerable cracking, in addition to spalling of concrete at the corbels and at the column edges as illustrated in Figures 2 and 3.
- Zone 2: Collapse of the slab panels for the upper floor in the remaining portion of the northern sector. They fell above the ground floor slab panels. Nonetheless the ground floor slab panels were able to carry the fallen slab panels as illustrated in Figure 4.
- Zone 3: This part was exposed to fire and to elevated heat but maintained stability and nothing collapsed, Figure 5.

Figure 2 Collapse of slab panels of 1st and ground floors in Zone 1

Figure 3 Cracks in column and spalling of corbel concrete

Figure 4 Collapse of slab panels of 1st floor on ground floor slabs in Zone 2

Figure 5 Post fire inside view of the 1st floor within Zone 3

METHODOLOGY

This study presents an overview of how to conduct a forensic evaluation of a fire damaged structure. It aims to evaluate the post fire residual building strength. Preliminary investigation involved identifying the collapsed structural elements. It also involved spotting the spalling concrete, and the extension and depth of cracks for the structural elements that remained stable and in place. Moreover the colour change of the construction materials was traced and recorded.

The severity of damage in Zones 1 and 2 was manifested by:

- The collapse of all slab units for both two floors in Zone 1, and many 1st floor slab units in Zone 2, Figures 2 and 4.
- The large spalling of concrete in columns and column corbels, resulting in exposing the reinforcement, Figure 6.
- The severity of cracks. Crack extension and the width and depth of cracks.
- The change in colour of concrete surfaces to whitish grey.

Accordingly it was concluded that the remaining parts of the building in Zones 1 and 2 that did not collapse were structurally unstable and unsafe, and need to be demolished. Further investigation was unnecessary.

Thus this study aims to evaluate the post fire residual building strength and to assess the structural integrity in Zone 3 only. This Zone is structurally separated by an expansion joint from the other Zones.

Figure 6 Cracks in a reinforced concrete column

Assessment of Fire Severity

A good assessment of temperatures reached within the fire-affected areas can be obtained from the physical effects of temperature on concrete, construction materials and debris. Tables 1 and 2 give an overview of temperature indicators in a typical building.

Table 1 Physical effects of temperature on concrete [1]

TEMPERATURE °C	COLOUR CHANGE	CHANGES IN PHYSICAL APPEARANCE AND BENCHMARK TEMPERATURES	CONCRETE CONDITION
0-290	None	Unaffected	Unaffected
290-590	Pink to red	Surface crazing: 290°C Deep cracking: 550°C Pop-outs over chert or quarts aggregate: 575°C	Sound but strength significantly reduced.
590-950	Whitish grey	Spalling, exposing not more than 25% of reinforced bar surface: 800°C Powdered light coloured dehydrated paste: 575°C	Weak and friable
950	Buff	Extensive spalling	Weak and friable

Table 2 Temperature Indicators [2]

	TYPICAL EXAMPLES	CONDITIONS	APPROXIMATE TEMPERATURE, °C
Polystyrene	Thin wall food containers	Collapse	120
Cellulose	Wood, paper, cotton	Darkens	200-300
Lead	Plumbing	Melts, sharp edges rounded	300-500
Aluminium	Fixtures, Castings	Softens	400
Glass	Glazing, Bottles	Softens	200-300
		Floors	200-300
		Flowing easily	850
Brass	Locks, Taps	Melts	800-1000
Copper	Wiring	Melts	1100

Extensive research has been carried out on the performance of OPC concrete in fire. When heated to temperatures above 300°C, this type of concrete usually changes colour to pink. When heated further, the colour profile changes again at around 500-600°C to a grey-buff colours. These colour changes are a result of iron slats on the aggregate particles [3].

In this investigation, the temperature indicators within the three Zones of the building were aluminium mullions, glass panels, copper cables, and concrete. In Zone 1 beams and columns had whitish grey colour. In Zone 2, the debris of the fallen slab panels also had whitish grey colours. The bottom slab surface in the ground floor slab had whitish grey colour. In Zones 2 and 3 shards of glass remained in some window frames. Some of these shards had melted and were forming drips. In Zone 3, the concrete surface in the 1st floor had a black colour all over, as illustrated in Figure 5, due to the burning of the textiles inside the building when fire erupted. The concrete slab surface colour in the ground floor was pinkish.

Based on the above, the temperature in Zones 1 and 2 was estimated to be within the range 550 to 650°C.The temperature in Zone 3 was estimated to be 300 to 400°C.

Assessment of Structural Damage

One example illustrating the need for information on the post-fire assessment and repair of fire damaged structures was the dispute over the structural integrity of Meridian Plaza in Philadelphia. The 38 storey office building suffered severe fire damage between the 22nd and 30th floors in 1991, and remained empty for over five years while its safety was assessed, only to eventually be demolished [4].

According to Chaing [5], the heat associated with the fire vaporizes trapped concrete pore water. The lack of continuous voids for pressure relief creates internal tensile stresses that are relieved by cracks and spalls extending to the surface.

Fire spalling is a complex phenomenon. Light spalling takes place at sharp corners, and it is of minor importance for the load bearing capacity and the integration of the structure. The pop-corn spalling is the continuous scaling off when 5-10 mm thick pieces shoot from the surface. The continuous spalling may jeopardize the structure. The explosive spalling is very severe, where a large part of the structure explodes momentarily, resulting in a sudden loss of the load bearing capacity [6].

In case of pre-stressed concrete, there is a paucity of data on the effect of elevated temperatures on cold-drawn prestressing steel, both in terms of post-fire residual mechanical properties and high-temperature stress relaxation, which can lead to significant prestress loss both during and after a fire. Several parameters, such as heated length and concrete cover, were examined using an example structure. From this it was observed that, after one hour of exposure to a standard fire (ASTM E119), significant losses in effective pre-stress and moment capacity occurred even with the appropriate amount of concrete cover [7].

When prestressed concrete slabs are exposed to fire, they show features different from traditional reinforced concrete structures. One may observe specific phenomena leading to the decrease of the fire resistance of the elements, such as anchorage failure or shear [7].

In Zone 1, all slab units for the two floors fell down. In Zone 2, slab units of the 2nd floor collapsed and fell down on 1st floor slab panels. In both Zones, the temperature was estimated to be within 550 to 650°C.

In Zone 3, the structure did not collapse, but cracks were observed within the slabs bottom fibres, column edges and column corbels, in addition to scaling off, and spalling of concrete in columns, column corbels, beams, and slabs. The temperature was estimated to be within 300 to 400°C.

Accordingly, and with reference to Tables 1 and 2 it was concluded that in Zones 2 and 3, the in place structural elements concrete became weak and friable, while in Zone 1, the concrete strength was significantly reduced.

Nondestructive evaluation of concrete

Nondestructive evaluation of the concrete is usually performed using Schmidt hammer and ultrasonic pulse velocity testers.

Schmidt-hammer measures concrete hardness, it provides excellent means for determining relative strengths of concrete in different parts of the same structure [8].

The pulse velocity tester is a pulse velocity meter with a digital readout, transducers, and water soluble jelly used as the acoustic coupling agent. Lower measured velocities would indicate distress, defects, or cracks in the concrete.

In this investigation, both Schmidt hammer and pulse ultrasonic digital testers (Pundit) were utilized. The test points were the 2 m by 2 m grid intersection for the 1st and ground slabs, and at 2 m distances for beams and columns. The Schmidt hammer testing was carried out in accordance with ASTM C805. The Pulse Ultrasonic Nondestructive Digitial Tester was used in accordance with ASTM C597-83.

Laboratory analysis of concrete cores

As illustrated in Figure 7, concrete core samples were removed for determination of compressive strength. The core samples were taken where the concrete surface was still intact and contained the outermost layer of discoloured concrete. Concrete cores taken from beams and columns were tested for compressive strength in accordance with ASTM C42 “Standard test method for obtaining and testing drilled cores”.

Figure 7 Core taken from a concrete column in Zone 3

ANALYSIS OF RESULTS AND DISCUSSION

As mentioned earlier in the study, the testing took place in Zone 3 only. In this Zone, cracks were traced. They extended within the slabs beams and columns. Concrete spalling and scaling off were spotted on slabs, beams and columns. The concrete colour was pinkish in general to whitish grey in few locations.

Core strength results are listed in Table 3. Figures 8 to 11 illustrate the nondestructive testing results in slabs and columns. The Figures also show the concrete characteristic strength for the relevant structural elements. The obtained concrete strengths in slabs and columns are about 50 to 75% of the concrete characteristic strength. Nonetheless having concrete strengths close to 50% of the characteristic strength in some locations, indicates that the existing structure in Zone 3 contains structural elements of significantly reduced strengths.

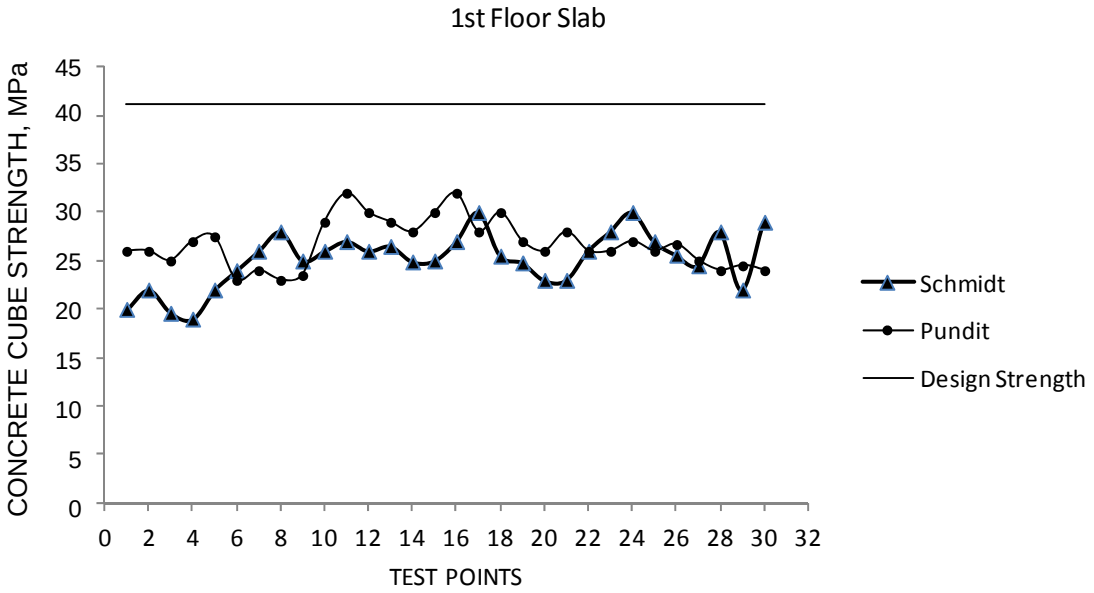

Figure 8 Comparison between nondestructive cubic strength and design strength

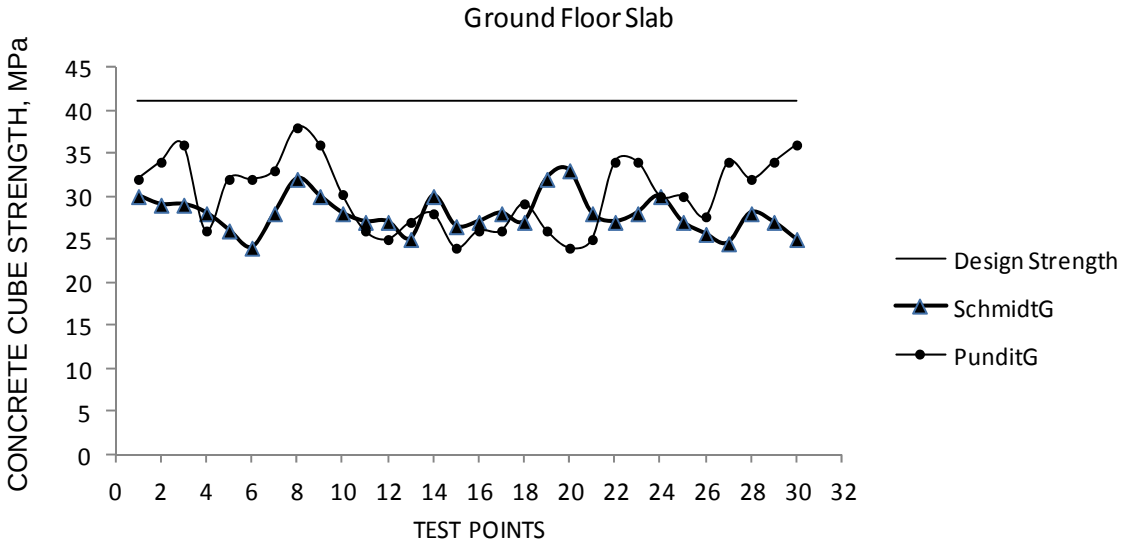

Figure 9 Comparison between nondestructive cubic strength and design strength

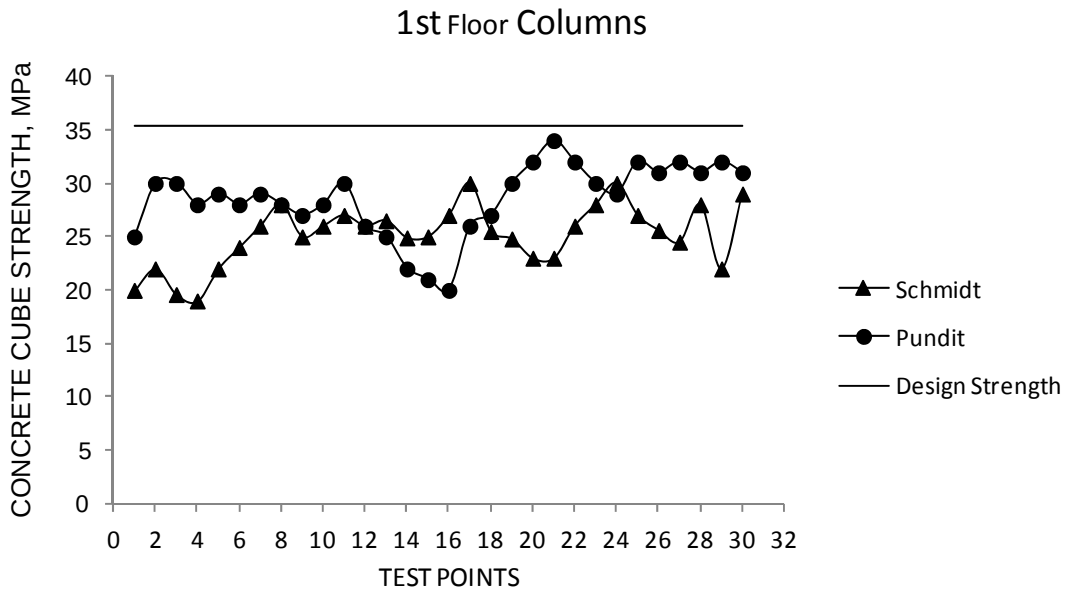

Figure 10 Comparison between nondestructive cubic strength and design strength

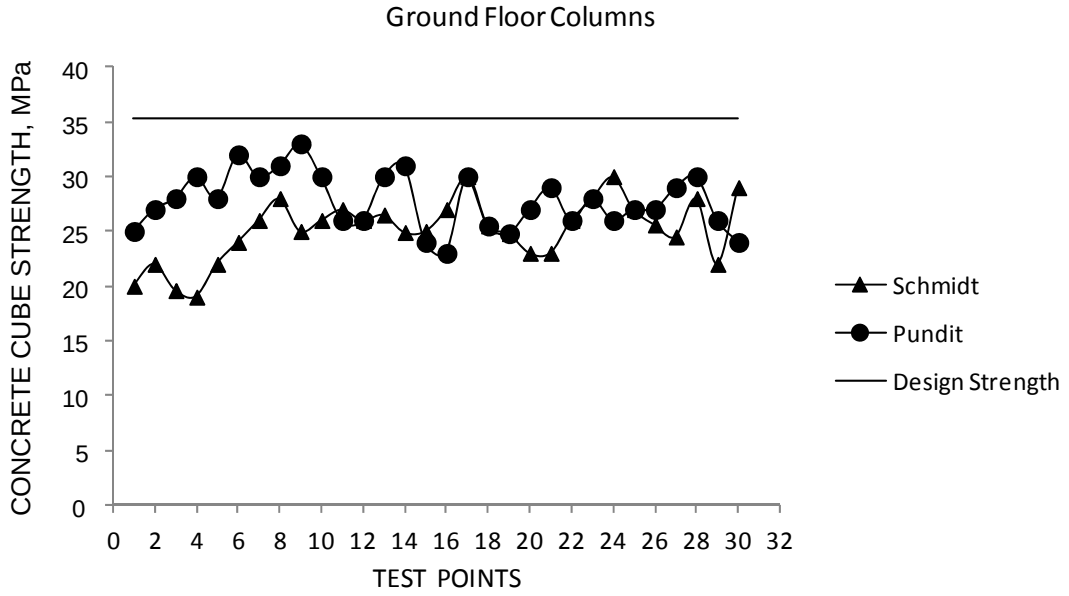

Figure 11 Comparison between nondestructive cubic strength and design strength

Table 3 Concrete core strength

STRUCTURAL MEMBER	MPa
1st Floor Slab	20
Ground Floor Slab	24
1st Floor Columns	18
2nd Floor Columns	20

Structural design parameters for the building project were taken from the structural design drawings, and are presented in Tables 4 and 5.

Table 4 Structural concrete design parameters as tabulated in structural design drawings

CONCRETE	CHARACTERISTIC STRENGTH, MPa
Lean concrete	14.7
Columns and footings	35.3
Slabs and beams	41.2

Table 5 Reinforcing steel design parameters as tabulated in structural design drawings

TYPE OF REINFORCEMENT	STRENGTH, MPa	GRADE
Main reinforcement, up to 18 mm diameter	412	60
Main reinforcement 20 mm diameter	515	75
Secondary Reinforcement	412	60
Wire Mesh	412	60
Prestressing low relaxation strands	1854	270

CONCLUSIONS

- The study presents an overview of how to conduct a structural evaluation of a fire damaged structure.
- Preliminary inspection of exposed concrete helped to identify the follow up areas.
- Based on the temperature indicators, it was concluded that the temperature in Zones 1, 2 was within 550 to 650°C. Whereas in Zone 3 the temperature was 300 to 400°C.
- The large amount of damage is attributed to the fact that the fire lasted for 7 hours before it was finally extinguished.
- Tracing the extension and depth of cracks and spalling of concrete, resulted in identifying the locations of the mostly distressed concrete.
- The cracks and spalls were created by the pressure of fire vaporized trapped concrete pore water, resulting in internal tensile stresses, that were ultimately relieved by cracks and spalls that extended to the surface.
- Neglecting to provide the minimum concrete cover in the slender slab panels deprived the prestressing strands and conventional reinforcement from fire protection. The high temperature resulted in significant losses of the effective pre-stress and moment capacity for many slab panels, causing rapid failure and collapse. The slender slab panels were not able any more to carry the imposed loads. The beams and the columns remained in position.
- Utilizing both pulse ultrasonic non-destructive and Schmidt hammer testers enhanced the credibility of the non-destructive testing.
- Obtained results from destructive and nondestructive testing indicated that post fire concrete residual strength is about 50 to 75% of the characteristic strength.
- Based on such comprehensive assessment, and on the fact that concrete strength in some locations was as low as 50% of the characteristic strength, the study concluded that the building is to be demolished.

REFERENCES

1. YUZER N, AKOZ F AND OZTURK L D, Compressive strength- Colour change Relation in Mortars at High Temperature, Cement and Concrete research, Vol. 34, No. 10, 2004, pp. 1803-1807.

2. SLOUGH. Assessment and repair of fire damaged concrete structures, Technical Report No. 33, 1990

3. LANE B, LAMONT S AND HEISE A, ARUP. Case Studies of Real Fire Assessments in Concrete Buildings, 7th International Congress, Concrete Construction's Sustainable Option, Dundee, UK, 8-10 July 2008.

4. KEVIN J N AND MACLEAN. Post-Fire Assessment of Unbonded Post-Tensioned Concrete Slabs, M.Sc. thesis, Queen's University, Canada, Dec. 2007.

5. CHAING C-H AND TSAI C-L, Time temperature analysis of bond strength of a Rebar after Fire Exposure, Cement and Concrete Research Vol. 33, No. 10, 2003, pp. 1651-1654.

6. BOSTRON L, Concrete Exposed to Fire, 7th International Congress, Concrete Construction's Sustainable Option, Dundee, UK, 8-10 July 2008.

7. WOZNAIK G, LUKOMSKI M AND BOROWY A. The Determination of the Fire Resistance of Prestressed Hollow Core Concrete Slabs", 7th International Congress, Concrete Construction's Sustainable Option, Dundee, UK, 8-10 July 2008.

8. MEGAHID A, ABD ELSAYED F K AND SOGHAIR H, Confidence of Concrete Strength as Measured by Non-Destructive Tests, Proceedings of the Second Arab Conference on Structural Engineering, April 1987.

Methods for Extending Life of Existing Bridges: A Case Study

A Recupero[1], N Spinella[1], C D Scilipoti[2]
1 – University of Messina, Italy
2 – R&S Engineering Consulting, Italy

The Italian motorway and railway networks were built about 30 to 40 years ago; they have a large number of prestressed concrete bridges and viaducts, most of these bridges must now be rehabilitated.

External post-tensioning has been found to be a powerful tool for reparation, adjustment and for increasing the life extension of existing structures. Particularly this technique of reinforcement is applied with success to bridge structures, in many countries since the 1950s and has been found to provide an efficient and economic solution for a wide range of bridge types and conditions. The technique is growing in popularity because of the speed of construction and the minimal disruption to traffic flow. In response to the demand for faster and more efficient transportation systems, there has been a steady increase in the weight and volume of traffic throughout the world. As well as increases in legal vehicle loads, the over-loading of vehicles is a common problem and it must also be considered when designing or assessing bridges. As a result, many bridges are now required to carry loads significantly greater than their original design loads. In the following, a study case of this technique will be illustrated on a railway bridge. During the construction of the railway line "Turin-Novara" (North of Italy), the Consortium Cav. TO-MI needed to utilize the bridge "Terdoppio" for the transit of the railway trains that had to serve to the placing of the equipment of the railway line. For the design of the reinforcement system, has been taken into account the presence of bonded and unbonded prestressing, also making use of some models of interaction between the different internal forces as recently proposed in literature. Today the bridge of "Terdoppio" is under service and the reinforcement has involved a substantial economy in the costs.

Antonino Recupero, Ph.D., P.E., received his BSc and PhD in structural engineering from the "Politecnico di Torino", Turin, Italy, in 1988 and 1996, respectively. He is currently Aggregate Professor of Bridge and Structural Design at the University of Messina. His research interests include shear-bending moment interaction in R.C. and in concrete prestressed members and strengthening techniques in bridge engineering .

Cosimo D. Scilipoti, P.E., received his BSc in structural engineering from the "Politecnico di Torino", Turin, Italy, in 1988. He is currently Project Manager of R&S Engineering Consulting. His research interests include bridge design and rehabilitation techniques in seismic engineering for bridges.

Nino Spinella, Ph.D., P.E., received his BSc and PhD in structural engineering from the "Università di Messina", Messina, Italy, in 2004 and 2008, respectively. His research interests include reinforcement of concrete columns with fiber-reinforced polymer, shear behavior of slightly transverse reinforced beams, fiber-reinforced concrete, and nonlinear analyses of reinforced and prestressed concrete structures.

Keywords: Bridge, Existing structures, External post-tensioning, Prestressed concrete, Rehabilitation

INTRODUCTION

In Italy, the motorway and railway networks were built about 30 to 40 years ago; they have a large number of prestressed concrete bridges and viaducts. Now, most of these bridges present a high level of material degradations and therefore their rehabilitation becomes necessary. Besides, in Italian motorway networks, over the last few decades, there has been a rapid increase in traffic volume and weight of heavy vehicles and contemporarily there has been a rapid increase in transit speed on railway networks. So many bridges, which were built with obsolete design standards, are not able to carry on the recent traffic requirements and they require either weight or speed restriction, the strengthening or, even, the total replacement.

Various methods in rehabilitation for bridge are currently available including addition of structural components as steel or reinforced concrete jackets, bonded steel plates, etc. Two methods that are currently proving to be very useful in increasing the strength capacity of short and medium span bridges are the strengthening by fibres reinforced plastic (FRP) or by external prestressing [1, 2].

In many countries, the use of external prestressing has been used as a means of strengthening or rehabilitating for existing bridges. It has been found to provide an efficient and economic solution for a wide range of bridge types and conditions. A lot of Local Administrations also require in Italy that operations of bridge strengthening occur with minimal disruption to traffic flow. For this reason the technique of externally post-tensioning is growing in popularity because of the speed of installation and the minimal disruption to traffic flow. The aim of this work is to describe the method of external post-tensioning as a means of rehabilitating bridges which have been found to be under-strength.

The paper shows the principles of external post-tensioning and presents, as a study case, the full scale rehabilitation of a bridge that was strengthened in Novara (North of Italy). During the construction of the railway line “Turin-Novara” the Consortium Cav. TO-MI required to utilize the road bridge “Terdoppio” for the transit of the railway trains that had to serve to the placing of the equipment of the railway line. This increased the traffic loads and was necessary its rehabilitation. In particular, for strengthening this bridge was chosen the use the externally prestressing. A description of the numerical analyses that have been carried on for verifying the rehabilitation design is included in the paper.

STRENGTHENING TECHNIQUE IN BRIDGE ENGINEERING

Selection of Appropriate Strengthening Technique

The selection of any suitable method for bridge strengthening depends on a number of particular conditions. Main parameters, that have to be considered, are: typology of structure, level of the required strength and related costs.

The costs due to strengthening are normally lower than bridge replacement, but the selection between the different schemes have to be based on economic perspective. Consequently, it is important to consider, not only the initial capital costs of the strengthening project, but, also, the maintenance costs associated with in-service behaviour, in the future.

In particular, for a bridge very damaged or deteriorated, its strengthening could be anti-economic due to future maintenance and safety problems and bridge replacement can be chosen. The difficulties associated with traffic management and the costs resulting from traffic interruptions should be considered in the economic justification. In some cases, this may limit the use of a few methods of strengthening.

Finally, the aesthetic characteristics after strengthening play an important role in choose of method. The use of intermediate supports or struts, or strengthening methods which appear unattractive, while tolerable as temporary measures, are becoming less acceptable as definitive solutions. In the recent past, steel plate bonding was considered as an effective method for upgrading structural members, where steel plates bonded with epoxy resins were used for strengthening of concrete members.

This method originates from the strengthening of steel beams by means of adding steel plates, it is know with the French term béton-plaque. But, bridges that had been strengthened using steel plates were showing signs of corrosion after few years in service that resulted in the deterioration of the original structure. But this method included high installation costs, maximum labour, low on-site flexibility of use, aesthetically poor due to large changes in member size after repair, increased dead load and traffic interruption. Considering all the above factors Fibre Reinforced Polymer (FRP) composites represent a new and promising solution to the shortcomings of several traditional materials and this shows a great potential for integration into the bridge infrastructure. The performance of external bonded FRP composite have found to be a successful technique and an effective method for upgrading structural element.

In some cases external bonded FRP composite could not be sufficient to strengthening the main girder of bridge. In those cases we can utilize the external prestressing as an useful alternative. Strengthening by external post-tensioning is simply the application of an axial force combined with a bending moment to increase both the flexural and/or shear ultimate strength both the serviceability of a structural beam or component.

A CASE STUDY

Need of Rehabilitation in Case Study

In 2006 during the works for the construction of the railway line Turin-Novara, the Consortium Cav. TO-MI, General Contractor of the work, had the necessity to use the road bridge of “Terdoppio” for the transit of the railway cars. This bridge had to provisionally be used as bypass of the existing principal line that was under replacement. The road bridge on the river “Terdoppio” had been built in the early years ‘70 and it is constituted by a deck of six prestressed and prefabricated beams and six diaphragms that were cast in situ. Preliminary analyses, pointed out that the existing structure was not fit to allow the transit of the carriage railway and it was therefore necessary or its adjustment or its replacement.

The two solutions were also estimated from the economic point of view and at the end the owner Company chose to make the reinforcement and the adjustment of the bridge. The rehabilitation was projected and then was developed in the way less intrusive as possible. The minimum interference on the existing structure, as imposed by the Company, was planned by the following phases:

- elimination of road superstructure and concrete milling of the existing surface deck;
- realization of a new deck of 25 cm thickness on existing deck. The new deck is able to bear the new railway local loads. It is connected to the original structure through opportune connectors;
- realization of a system of external prestressing with 10 cables 8/0.6” strands, anchored near the support diaphragms and with metallic deviator on intermediate diaphragms.

The phase of planning of adjustment has been preceded by a wide campaign of non destructive investigations that allowed a best calibration of the subsequent choices. In the planning of the system of rehabilitation, the combined effect of existing bonded prestressing and new un-bonded externally prestressing is taken in account.

Description of Existing Bridge and in-situ Test Campaign

The existing bridge structure is a classical typology of “Grillage Bridge”. It is constituted by six I-shape prefabricated and prestressed beams, by a deck and six diaphragms in reinforced concrete both cast in situ (Figure 1). The span of bridge is 30.5 m. The principal beams are of height 1.4 m and they have been prestressed with the pre-tension method with 38 strands (A_p = 93 mm² each) with tensile strength at Ultimate Limit State (ULS) f_t = 1750 MPa. The strands present a polygonal layout with a horizontal central part large 6.0 m.

Original design was recovered for accurate calibration, obtaining also information about the load tests performed on the structure during construction. For integrating these data, it was chosen to program a campaign of no-destructive in-situ tests, and particularly some core borings on the existing deck also integrated by SONinc-REBound (SONREB) tests on concrete beams and diaphragms.

The SONREB method consists in a correlation method of data cross between Schmidt rebound hammer method (Figure 2a) and ultrasonic pulse velocity method (Figure 2b).

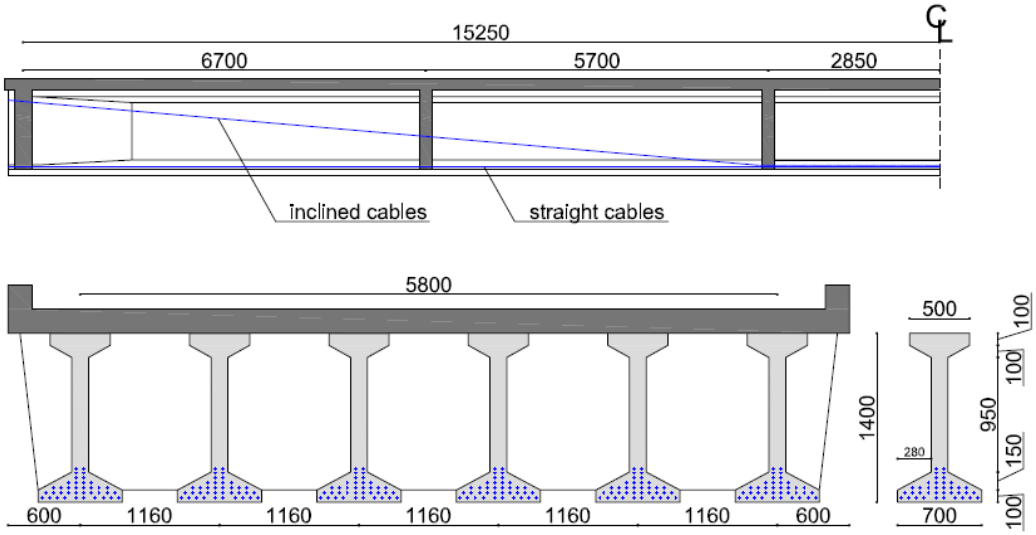

Figure 1 a) Longitudinal and b) transversal scheme of existing bridge

Figure 2 a) Schmidt rebound hammer test, b) Ultrasonic pulse velocity test on bridge slab

Relationships proposed in literature about SONREB have offered an indirect estimate of concrete strength in different parts of bridge structure.

For the concrete in beams, following the series of destructive and non-destructive tests, it was reasonable to assume for concrete of existing beams a material of class C35/45, typical of the prefabrication industry of that period. In existing deck slab, by analysing the results of no-destructive and destructive tests on specimens, it was reasonable to assume for the concrete a material of class C20/25.

The check, made with the data provided by the preliminary tests, emphasized that the existing structure was not suitable to allow the transit of the railway coaches as required by the national code specifications and the bridge needed the rehabilitation or the replacement.

In fact the Authorities' specifications require the passage of:

a) a testing train for High-Speed bridges that were in-construction. It is composed of 24 axles each of 210 kN capacity for a total of 5040 kN. This train could easily have been packed in the ballast field and it had to cross the "Terdoppio" bridge for reaching the railway line in construction;
b) an equivalent train to the LM71 reduced to the 83% as required by the ITALFERR Manual Code [3] for railway bridges classified as Category B;
c) a train that bears the ballast, schematised as in Figure 3, with a total load of 800 kN on 4 axles.

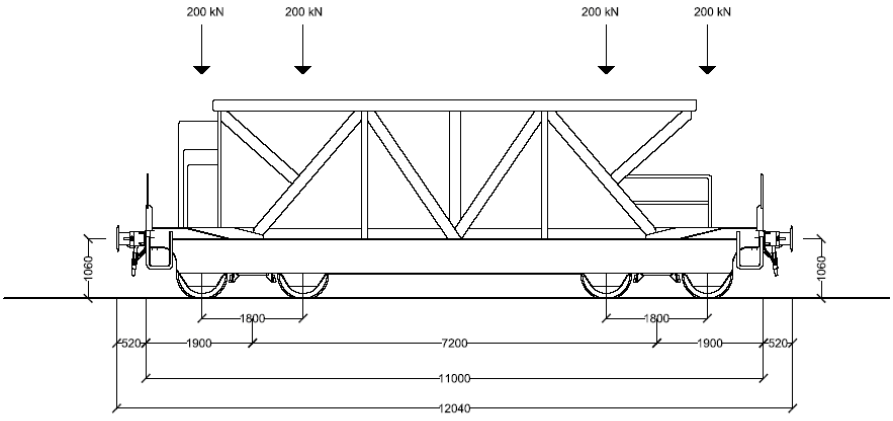

Figure 3 Single coach for ballast train

Scheme of Rehabilitation Proposed

Different hypotheses of adjustment have attentively been valued:

1) assemblage of a metallic structure of inclined-leg frame typology under the existing structure;
2) reinforcement of principal beams with FRP plates on the bottom face of the beams;
3) reinforcement of principal beams with a system of un-bonded prestressing, externally to cross-section of beams.

After a wealthy debate with the contractor and Italian railway authorities, it was chosen the third proposal for economic motivation. Moreover for avoiding excessive costs, only a partial rehabilitation of the bridge was select, by allowing totally the transit of the train equivalent to the LM71 reduced to the 83% and of the train that bears the ballast (Figure 3) and the load of a testing train (for High-Speed bridges) with reduction to 60%. The total recharge up to 100% of the testing train would have happened after the transit on the bridge.

It was decided, therefore, to apply a system of external prestressing with 10 external cables of 8 strands 0.6” which, departing from the diaphragms of extremity already reconstructed for lodging the prestress anchorage, were deviated by the first intermediary diaphragm (those posed at ¾ of span). It was chosen to have steel deviator arrangements on diaphragms.

Figure 4 a) Building of new slab connected to the old deck;
b) View of externally prestressing

Figure 5 “Terdoppio” bridge under final testing

For rationalizing the operations of adjustment, the following executive phases have been selected (Figure 4):

- removal of road superstructure and concrete milling of the existing surface slab;
- assemblage of the connectors for the integrative new slab;
- positioning of the bars of reinforcement and the casting of integrative slab;
- demolition of top part of abutment and setup of the plan of work on altitude of existing bearings;
- positioning of the anchor heads and the anti-spalling reinforcement, the casting of integrative diaphragm;
- installation of the metallic saddles of deviation under ¾ diaphragms;
- lodging of the integrative external cables and its prestressing up to nominal force;
- casting of new top part of abutments and reconstruction of their backfills;
- positioning of the joints between deck and abutments;
- placing of ballast and rails;
- final testing with the trains used in design phases (Figure 5)

For each phase of construction the corresponding checks were performed. The new slab, with a thickness of 250 mm, was necessary to bear greater local loads in comparison to those precedents. It was casted with a concrete of class C35/45. The new slab increased the total height of transversal sections of beams with a notable improvement in terms of stiffness and load capacity.

Finally, due to increase of vehicular actions further verifications of the stress in foundation on the existing abutments were achieved.

NUMERICAL MODEL

Numerical Analyses of Strengthened Beams

The proposed rehabilitation scheme (Figure 6) for the "Terdoppio*"* bridge has been investigated with deep attention to evaluate the new bearing load of each beam. At this aim, several numerical analyse have been carried out to also obtain precious information about the tension and strain fields at different load stages.

First, a simple sectional model has been used to calculate the flexural capacity of strengthened beam. It has permitted to consider just the principal geometrical and mechanical parameters, allowing an easy control of results.

To get more refined results, a Non-Linear Finite Element Analysis (NLFEA) has been performed using the software VecTor2 [4], which implements the Modified Compression Field Theory (MCFT), originally proposed by Vecchio and Collins [5], and its upgrading [6].

In the following sections, the setup of beam is illustrated in details, then the results of sectional analysis and NLFEA are reported and discussed.

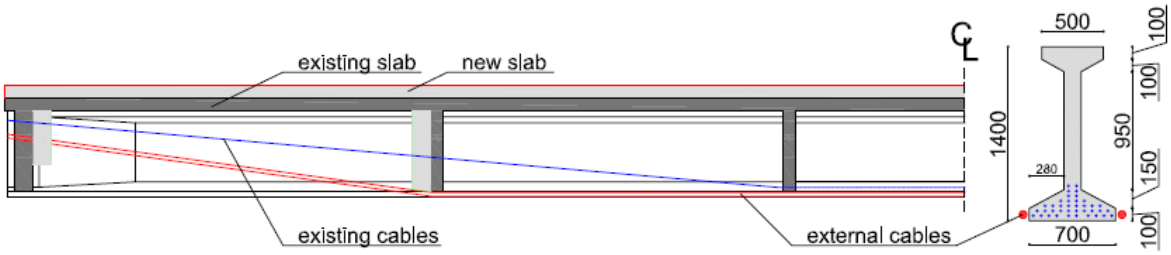

Figure 6 a) Longitudinal and b) Transversal rehabilitation scheme of beam

Beam Setup

As described in the previous section, "Scheme of rehabilitation proposed", the reinforcement of primary beams has been carried out with a system of un-bonded prestressing, disposed externally to the cross-section of beam (Figure 6).

Two groups of bonded strands were originally disposed in the beam. The first is composed of strands with straight axis along the beam; the second group is placed with a variable slope of strands, as shown in Figure 10a. Each strand is 0.5" in equivalent diameter, while the yield and ultimate strength of steel are $f_{p(1)k}$ = 1575 MPa and f_t = 1750 MPa, respectively.

The slab on the beams has a thickness of 200 mm and it is reinforced with rebar disposed along two orthogonal direction in its plane. Along the longitudinal direction, the flexural reinforcement is provided by 2ϕ8 mm + 1ϕ12 mm on the top (for the bending moment close to support) and 4ϕ8 mm on the bottom (for the bending moment at half span) for each width of slab pertaining to considered beam (= 1160 mm). In the transverse direction 5ϕ12 mm/m. are disposed both on the top and bottom of slab.

The shear reinforcement is variable along the longitudinal axis of the beam. Stirrups with two legs ϕ8 mm and ϕ10 mm, spacing 25 cm, are used for the part between the support and 5.25 m; part between 5.25 m and 10.25 m is reinforced with ϕ8 m, spacing 25 cm; part between 10.25 m and 15.25 m is reinforced with ϕ8 mm and ϕ6 mm, spacing 25 cm. The beam is long 30.5 m and it is symmetrically loaded and reinforced.

As previous mentioned, the concrete for the beam is characterized by a cylindrical strength f_{cm}= 35 MPa, while the concrete for the existing top slab has a cylindrical strength f_{cm}= 20 MPa.

For the rehabilitation of bridge, the primary beams have been retrofitted with a new deck of 25 cm thickness (f_{cm} = 35 MPa), which has been linked to the existing slab by designed steel connectors, and a system of two external prestressing cables 8/06" strands for each beam. The axial force for each external prestressing cable at Service Limit State (SLS) is $N_{p,SLS}$ = 1177 kN.

Sectional Analysis

The external forces to apply at the beam to take into account the actions of external prestressing cables are evaluated by simple geometric considerations, as shows in Figure 7.

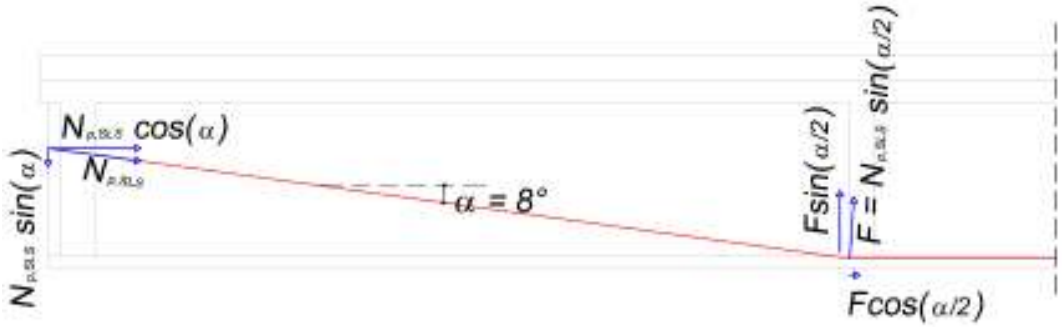

Figure 7 Concentrated forces equivalent to external prestressing actions at support and deviation of external cable sections

Figure 8 shown the free-body midspan cross-section of beam, where x_c is the distance between the top compressed part of beam and the neutral axis; A_{p1} = 24 × 93 = 2232 mm² and A_{p2} = 14 × 93 = 1302 mm² the area of equivalent inclined and straight cable, respectively; $N_{p,SLS}$ = 1177 kN is the axial force for each external prestressed cable.

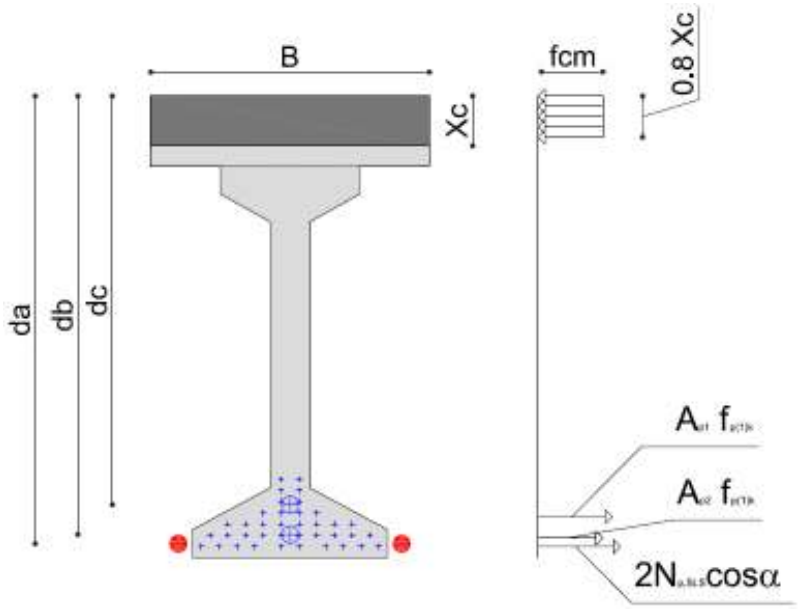

Figure 8 free-body forces diagram at midspan cross-section of beam

Assuming the stress-block distribution for compressed concrete, the equilibrium along the longitudinal axis of beam allows obtaining the position of neutral axis:

$$0.8x_c f_{cm} B = A_{p1} f_{p(1)k} + A_{p2} f_{p(1)k} + 2N_{p,SLS} \cos\alpha \tag{1}$$

The distance between the top compressed part of beam and the neutral axis is 242 mm.
The bending equilibrium equation allows obtaining the flexural strength of beam:

$$M_u = -\frac{0.8x_c}{2} 0.8x_c f_{cm} B + d_a 2N_{p,SLS} \cos\alpha + d_b A_{p2} f_{p(1)k} + d_c A_{p1} f_{p(1)k} \tag{2}$$

obtaining M_u = 13013 kNm.

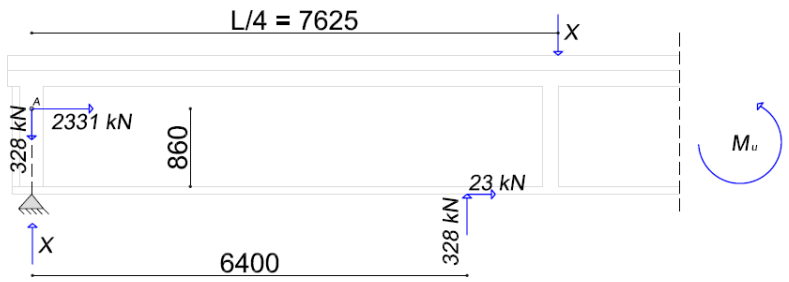

Figure 9 Free-body forces diagram of beam

Known the flexural strength of beam, the load bearing of beam is obtained by writing a simple equation of equilibrium between the external forces and the reaction of support. In Figure 12, the free-body diagram of forces is shown. The equivalent force of external distributed load is applied at a distance from the support equal to $L/4$ = 7.63 m, while the actions due to the external prestressing cables are represented by concentrated forces applied in the pole A and at distance L_p = 6.40 m from the support (Figure 9).

The Modified Compression Field Theory (MCFT)

Several analytical formulations have been suggested to reproduce the response of Reinforced Concrete (RC) elements subject to different load conditions, adopting models based on several constitutive laws and mechanical theories [5, 7, 8].

Between these, the MCFT represents a general model for the load-deformation behaviour of two-dimensional cracked reinforced concrete subjected to shear and flexure. It models concrete considering concrete stresses in the principal directions summed with reinforcing stresses assumed to be only axial. The concrete stress-strain behaviour in compression and tension was derived originally from tests performed by Vecchio [9].

The key assumption the MFCT uses to simplify is that the principal strain directions coincide with the principal stress directions. This assumption has recently been removed by Vecchio [6] which has introduced the Disturbed Stress Field Model (DSFM). The DSFM explicitly incorporates rigid slipping along crack surfaces into the compatibility relations for the element, allowing for a divergence of the angles of inclination of average principal stress and apparent average principal strain in the concrete.

In addition, MCFT and DSFM have been recently extended to the case of fibrous concrete elements [10, 11], proving them general capacity to reproduce the response of structural members with different mechanical and load conditions.

In the MCFT the compatibility conditions relating the strains in the cracked concrete with the strains in the reinforcement are expressed in terms of average strains, where the strains are measured over base lengths that are greater than the crack spacing. The equilibrium conditions, which relate the concrete stresses and the reinforcement stresses to the applied loads, are also expressed in terms of average stresses.

Similarly, the strains used for the stress-strain relationships are average strains, that is, they consider together the combined effects of local strains at cracks, strains between cracks, bond-slip, and crack slip. The calculated stresses are also average stresses in that they

implicitly encompass the stresses between cracks, stresses at cracks, interface shear on cracks and dowel action. In this model, the cracked concrete in reinforced concrete is treated as a new material with empirically defined stress-strain behaviour. This behaviour can differ from the traditional stress-strain curve of a cylinder, for example.

The equilibrium equations, the compatibility relationships, the reinforcement stress-strain relationships, and the stress-strain relationships for the cracked concrete in compression and tension enable the average stresses, the average strains, and the angle θ to be determined for any load level up to failure.

As can be deduced from the above, the MCFT is a powerful and general tool for the NLFEA of RC elements, and for this reasons it has been chosen to perform several numerical analyses about the strengthened beams of “Terdoppio” bridge.

NLFEA model and results

The VecTor2 solver is equipped with a graphics-based preprocessor (FormWorks) to generate the finite element mesh [4]. It includes facilities for data visualization and input, bandwidth reduction and automatic mesh generation. Figure 10 shows the mesh generated for the “Terdoppio” beam. Thanks to the complete symmetry, only half beam has been modelled and suitably restrained to the symmetrical axis.

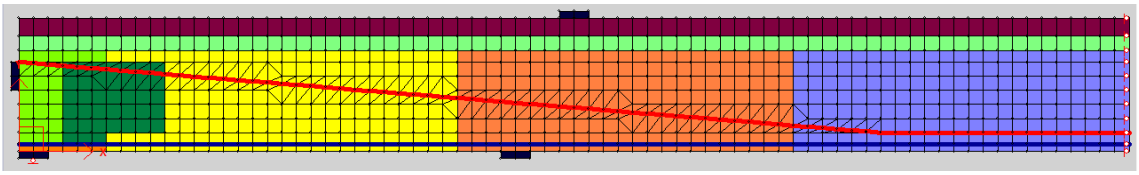

Figure 10 Finite Element Model of half beam

The mesh was composed of four-node triangular and rectangular elements with variable thickness to represent the concrete, and two-nodes truss bars with uniform cross-sectional area for rebar and bonded cables. The finite element size was chosen adopting the cover as vertical size and a ratio between sides of rectangular element close to one. The action induced by external prestressed cables has been modelled as concentrate nodal forces on steel plates with a uniform thickness and fully connected to concrete, providing regions without rotations (Figure 11).

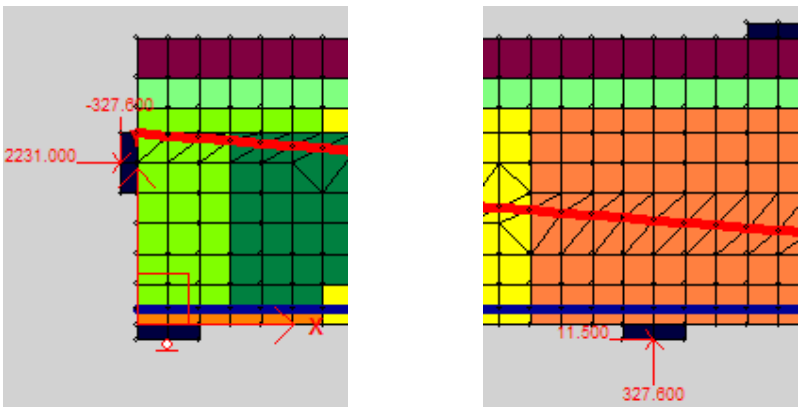

Figure 11 Concentrate nodal forces on steel plates due to external prestressing cables

The MCFT is a smeared rotating crack model. Then, rebars have been taken into account simply adding the smeared stiffness of steel at the stiffness of concrete for each finite element considered.

Perfect steel-to-concrete bond has been assumed both for rebars and inclined and straight cables. For the latter, a prestrain has been considered to take into account the prestressing action. It has been determinate considering a Young modulus for the steel of cables equal to 186 GPa and an axial force at SLS for each tendons equal about to 1000 MPa (including the force degradation due to shrinkage and creep), thus a pre-strain equal to 5.6 mε has been used.

The software VecTor2 allows managing many parameters concerning mechanical characteristics of materials and those constitutive laws. The numerical analyses have been carried out assuming the default values for each parameter, and specifically taking the Hognestad parabola for concrete, an elastic-plastic law for steel rebars and, finally, the known Ramsberg-Osgood formulation for prestressing steel [4].

NLFEAs have been performed assigning three different load cases: the statically self weight on all concrete elements; the statically external prestressing forces; and the monotonically increasing displacement on the node located in the middle of the top steel transfer plate, placed to *L/4* from the support. The total load has been computed as twice the reaction force at the support. Thus, the displacement controlled procedures have been able to reproduce the post-peak branch of the load-displacement curve.

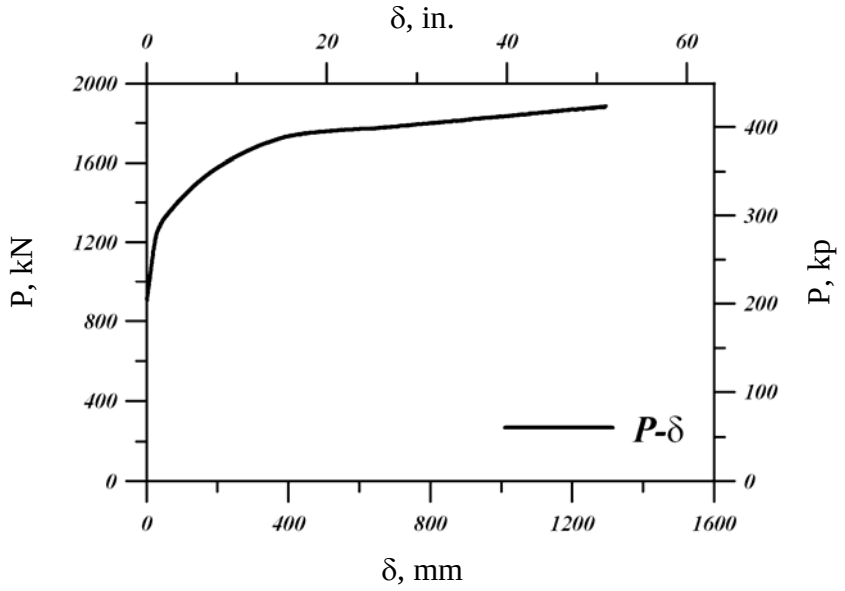

Figure 12 Load-displacement numerical curve

Figure 12 illustrates the load-displacement numerical curve for the beam considered. The load capacity provided by the NLFEA is equal to 1883 kN, value close to that obtained by sectional analysis. The large post-peak branch shows a flexural failure with a constant increment of strength and a wide deflection at midspan cross-section of beam has been obtained.

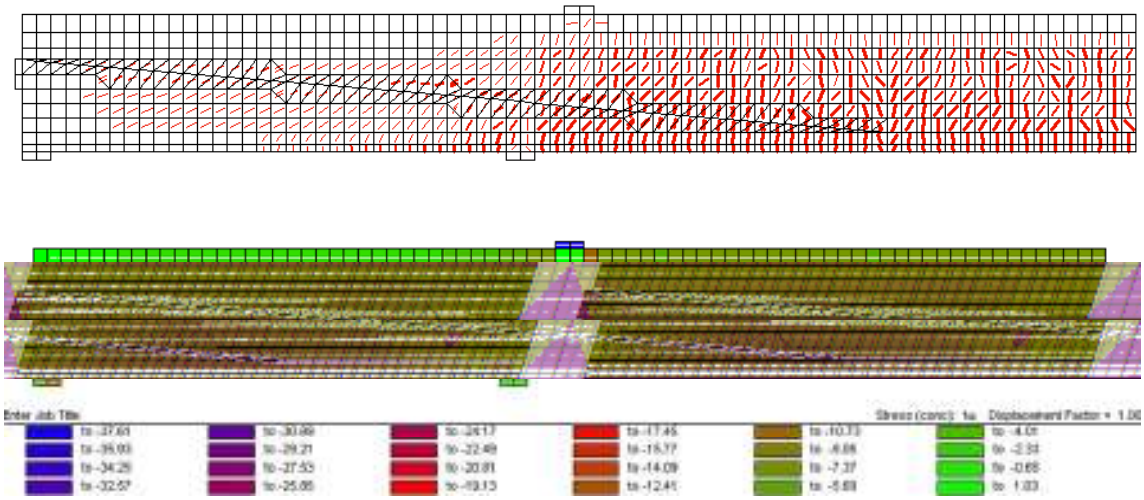

Figure 13 a) Crack pattern and b) Compression stress field of beam at failure

The NLFEA provides also interesting information about the crack pattern and stress fields at each stage of displacement applied, and in Figure 13 they are showed in correspondence of failure.

The crack pattern confirms the flexural crisis of structural member, with large vertical cracks in the midspan of beam. In the shear span region, cracks are inclined to the longitudinal axis and slightly wider.

The stress fields of concrete is clearly compatible with the crack pattern above described, thus the compression stress level at beam crisis is less than cylindrical strength of concrete and when the bonded cables strain reaches the maximum value available, then beam fails.

CONCLUSIONS

An application of external prestressing retrofitting has been presented. The structure element analysed was an existing bridge for which it has been necessary to improve the load capacity, allowing the transit of larger loads as trains.

The use of external prestressing cables has permitted to maintain the bridge in service during the period of works, with minimum disruption to the users. An *in situ* campaign of tests has allowed an accurate design with optimised choices, which have been described.

The design of retrofitting for the considered case of study, the “Terdoppio” bridge, has been investigated by several numerical analyses which have provided precious information about the load capacity and the tension and strain fields at different load stages of beam.

The sectional model has allowed calculating the flexural capacity of strengthened beam. It has permitted to consider few parameters to obtain accurate values of strength and an easy control of results.

In addition, the sophisticated FEM software VecTor2, which implements the well known MCFT, has been used to perform different NLFEAs. Numerical results have been reported and discussed, showing the ability of the theoretical model adopted to provide a response of the beam analysed subjected to transversal load in agreement with the values obtained by the sectional method.

Furthermore, interesting information have been provided by the NLFEAs about the crack pattern and stress fields of structural member considered at each stage of load, predicting a large ductile branch at failure as expected in design phase.

REFERENCES

1. DALY A F AND WITARNAWAN W, Strengthening of bridges using external post-tensioning. EASTS '97, Seoul, 29 - 31 October 1997.

2. DALY A F AND WITARNAWAN W, A method for increasing the capacity of short and medium span bridges. 10th REAAA Conference, Tokyo, Japan, 4 - 9 September 2000.

3. ITALFERR, Sovraccarichi per il Calcolo dei Ponti Ferroviari - Istruzioni per la Progettazione, l'esecuzione ed il Collaudo, n° I/SC/PS-OM/2298 - 2/6/1995.

4. WONG P S AND VECCHIO F J, VecTor2 and FormWorks Users Manual. Technical report. Department of Civil Engineering, University of Toronto – Canada, 2002.

5. VECCHIO F J AND COLLINS M P, The modified compression field theory for reinforced concrete elements subjected to shear. ACI Structural Journal, Vol. 83, No. 2, 1986, pp. 219–231.

6. VECCHIO F J, Disturbed stress field model for reinforced concrete: Formulation. ASCE Journal of Structural Engineering, Vol. 126, No. 9, 2000, pp. 1070–1077.

7. BERTAGNOLI G, MANCINI G, RECUPERO A AND SPINELLA N, Rotating compression field model for reinforced concrete beams under prevalent shear actions. Structural Concrete, Vol. 12, No. 3, September 2011, pp. 178-186.

8. BELARBI A AND HSU T T C, Constitutive Laws of Softened Concrete in Biaxial Tension-Compression, ACI Structural Journal, Vol. 92, No. 5, 1995, pp. 562-573.

9. VECCHIO F J AND COLLINS M P, Response of reinforced concrete to in plane shear and normal stress. Technical report. Department of Civil Engineering, University of Toronto – Canada, 1982.

10. MINELLI F AND VECCHIO F J, Compression Field Modeling of Fibre-Reinforced Concrete Members Under Shear Loading, ACI Structural Journal, Vol. 103, No. 2, 2006, pp. 244-252.

11. SPINELLA N, COLAJANNI P AND LA MENDOLA L, Nonlinear Analysis of Beams Reinforced in Shear with Stirrups and Steel Fibres. ACI Structural Journal, Vol. 109, No. 1, January-February 2012, pp. 53-64.

Influence of Mineral Fine Additions on the Durability of Reinforced Date Palm Fibre Concretes

A Mokhtari[1], A Kriker[1], A Bali[2], G Debicki[3], M M Khenfer[4]
1 – Université Kasdi Merbah de Ouargla, Algeria
2 – Ecole Nationale Polytechnique (ENP) , Algeria
3 – INSA de Lyon, France
4 – University Amar Telidji of Laghouat, Algeria

Cement materials as like as traditional concrete or mortar resists badly to tensile strength and cracking. This brittleness is accentuated especially in the hot and dry environments, such as the Algerian Saharan climates. This region is characterised by hot temperature and low humidity. As an example of hot dry environment, between June to November, the temperature varies from a minimum of about 10°C to a maximum of 43°C, the relative humidity varies from 24% to 57% and the wind speed varies from 8 km/h to 18 km/h. The reinforcement of building materials, particularly, mortars and concretes, by natural fibres is a technique increasingly used, with an aim to improving their mechanical properties, in particular their flexural strength and cracking. However, the use of these vegetable fibres in concretes is limited by the problems of durability in alkaline cement matrix. This has been revealed in most of the research carried out on several vegetable fibres: sisal, jute and coir. This paper presents the durability of mortar reinforced by date palm fibre. This natural fibres exists in abundance in the Ouargla Oasis (south of Algeria). The durability of fibres was studded by their conservation in various cement matrixes with an addition of 20, 40 and 60 % (cement mass fraction) of natural Pozolana or Cooked broken brick powders. The durability of palm fibres is evaluated by its tensile strength and elongation, occurred over time, of fibres submitted in various cement matrixes using the tension test. The durability of the fibre-reinforced mortar is estimated by the variation of the flexural strength, in the bending test. We showed that the reinforcement of mortars and concretes by date palm fibres improves their flexural property. The durability is more improved for matrix treated by natural pozolana.

A Mokhtari is currently senior Doctor of Materials Technology and researcher of EVRNZA Laboratory at the University Kasdi Merbah of Ouargla Algeria. He has led several research projects on concrete, and his specialist areas of research are fibre reinforced concrete, and durability of concrete.

A Kriker is currently Professor of concrete Technology and Director of EVRNZA Laboratory at the University Kasdi Merbah of Ouargla Algeria . He has led several research projects on concrete, and his specialist areas of research are fibre reinforced concrete, durability of concrete and Mobilization of concrete.

A Bali is currently Professor of concrete Technology and Director of LCE Laboratory at Ecole Nationale Polytechnique (ENP) Algeria. He has led several research projects on concrete, and his specialist areas of research are fibre reinforced concrete, durability of concrete and fire-resistant concrete.

G Debicki is currently Assistant Professor of concrete Technology and Director of research at Laboratory of Civil & Environment Engineering at INSA of Lyon France. He has led several research projects on concrete, and his specialist areas of research are fibre reinforced concrete, durability and permeability of concrete.

M M Khenfer is currently Professor of concrete Technology and Director of research at Laboratory of Civil Engineering the University Amar Telidji of Laghouat Algeria . He has led several research projects on concrete, and his specialist areas of research are fibre reinforced concrete and durability of concrete.

Keywords: Cement, Date palm fibres, Durability, Flexural strength, Pozzolana

INTRODUCTION

Concrete and mortar are the most common materials used in the construction, but they have poor resistance to traction and cracking. The environmental conditions in the Sahara region of Algeria are very hot and dry. Indeed, the constructions in concrete or mortar in these areas are very fragile. The reinforcement of concrete by some fibre can offer some technical solutions for improvement of the mechanical performance. The reinforcement of cement materials by vegetable fibres is relatively new compared to that of asbestos or steel fibres. The characterization of this new composite material requires the multiplication of research and testing, and developing new methods of experimentation. Algeria is among the countries, which has extraordinary resources of vegetable fibre (palm, Alfa Abaca, Hemp, Cotton ...), unfortunately, their value in practical areas, among others, in building materials is still little exploited. The objective of this work is to make our contribution to the development of local resources in this case the date palm plant fibres at low cost and from a renewable source and integrate it in a rational way in construction. Currently the biggest problem that limits the use of vegetable fibres in cement matrices is their low durability in alkali cement product. There are several solutions to increase the durability of fibres in the cementing matrix, such as, use cement with low alkalinity. Crushed pozzolana and debris of burnt bricks was added to Portland cements for reducing the alkalinity. This paper present the durability of date palm fibre and the cement materials reinforced by those fibre, also, by adding natural pozzolana or debris of burnt bricks to the cement matrix.

CHARACTERIZATION OF USED MATERIALS

Fibres

The fibres used in this study were from surface of date palm. KRIKER [1] from these studies performed on four types of surface fibre of date palm fibres local names: (Dokar, Deglette nour, Elghers and Degla bida); has found that Dokar fibres give the best result for tensile strength. For this reason the Dokar fibre was used in this stady. Table 1 presents components of organic dokar fibres. Table 2 presents the mechanical and physical proprieties of Dokar fibre.

Cement

The cement used was Portland Composed Cement CPJ- CEMII / A 32.5 [3] from the cement plant of Ain Touta Algeria with the following characteristics:

- The apparent density $\rho_a = 2120$ kg/m^3.
- The absolute density $\rho_{ab} = 3034$ kg/m^3.

Table 3 gives the main physical and mechanical properties of the used cement.

Debris of Cooked Broken Bricks

The debris of cooked broken bricks was used, made of 70% clay and 30% of dune sand from the region Blidet Amor southeast of Algeria. The clay in the broadest sense: the silt and shale weathered can also be used for manufacturing. This base material is mainly present in the

basement. The clay is subjected to heating up steadily increasing the firing temperature between 850 °C and 1200 °C, then is gradually cooled, in order to make the mass homogeneous clay is the last step of the grinding and kneading and subsequently the bricks. The debris of cooked bricks are crushed and screened with the use of sieve shaker of 200µm.

Table 1 Components of organic dokar fibres

MATTER	CINDRE	CELLULOSE	HEMICELLULOSE	LIGNINE
Proportion (%)	1.2 ± 0.3	43 ± 2	8 ± 2	35 ± 5

Table 2 Physical and Mechanical characteristics of fibres used [1,2]

Apparent specific mass	ρ_a = 512.21 - 1088.81 Kg/m^3		
absolute specific mass	ρ_{ab} = 1300 - 1450 Kg/m^3		
Tensil strenght [N/mm^2]	L=100 mm	L=60 mm	L=20 mm
	170 ±40	240 ±30	290±20
Deformation of rupture	ε= 0.232 (Diametre fibre 0. 8 mm)		
Humidité rate	H = 9.5 - 10.5 %		
Absorption water (after 24 H)	AW = 96.83 - 202.64 %		
Diametre (use fibres)	d = 0.1 to 1 mm		

Table 3 Main physical and mechanical properties of the cement used

	DENSITY (g/cm^3)	SPECIFIC SURFACE BLAINE (cm²/g)	START HARDENING TIME (min)	END HARDENING TIME (min)	MINIMAL COMPRESSION STRENGTH in 28 days (MPa)
CPJ-CEMII/A	3.1	3859	128	184	30

Construction Sand

The results of experiments performed on construction sand of the region of Hassi-Sayah, Ouargla (Algeria) are summarized in the Table 4

Table 4 Characteristics of used sand

FINESSE	APPARENT DENSITY (g/cm^3)	ABSOLUTE DENSITY (g/cm^3)
2.26	1.59	2.50

Grading Curve of Used Sand

Figure 1 presents the grading curve of used sand. Based on the value of fineness modulus the used sand was recommended for ordinary concrete and mortar [3]

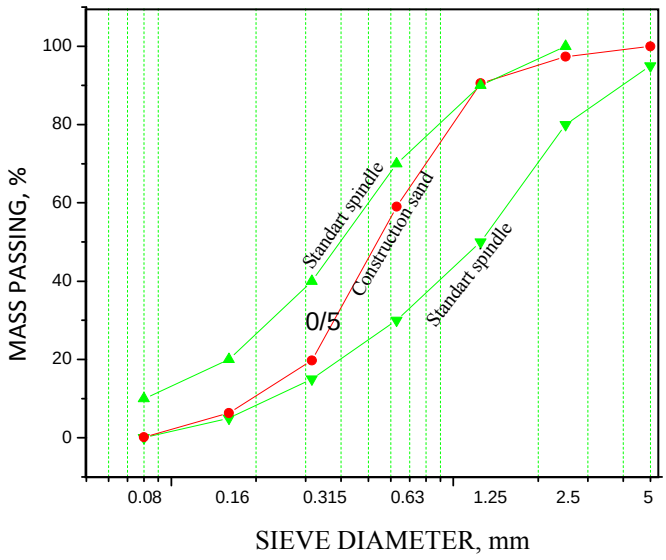

Figure 1 Sand curve

Pozzolana

The used Pozzolana is a natural pozzolana from TEBESSA (Algeria) region. This pozzolana is provided in the form of crushed rock-like slag and pumice diameters variants 5 to 50 mm. To prepare the pozzolana, firstly, to remove any possible moisture and to facilitate grinding, the pozzolana was puted in a drying oven at 105 °C. then, passed to the screening. The underflow from 0.2 mm to a fineness of 4100 g/cm² is recovered and used in substitution for cement in different proportions. A set of tests for identifying the pozzolana was provided by the cement Ain Touta. Table 5 and 6 give the chemical and physical proprieties of used pozzolana.

Table 5 Chemical composition of the used pozzolana

ELEMENTS	SiO_2	Al_2O_3	CaO	MgO	Fe_2O_3	SO_3	Na_2O_3	K_2O	Cl^-	PF
%	46.46	17.45	9.03	3.88	8.36	1.03	4.32	1.40	0.03	4.85

Table 6 Physical properties of the pozzolana

WEIGHT VOLUMIC (g/cm^3)	2.70
ABSORPTION IN WATER (%)	19.46
SPECIFIC SURFACE OF BLAINE (cm^2/g)	4100

TEST METHODS

Tensile Strength of Date Palm Fibre

The main mechanical properties of vegetable fibres namely the tensile strength was determined by a standard inspired by the NF EN ISO 5079 [4] at T = 30 ± 2 °C and RH = 65 ± 5%. The used tensile machine was a universal type KARL FRANK GMBH. This machine operates at a controlled displacement, with a speed of 2.5 mm / min. The length of the fibre sample was 100 mm. Some fibres were tested dry naturally, while other fibres were tested after recovery of different cement matrices cured for 30 days, 3 months and 6 months, with different percentages of natural pozzolana (Z) 20%, 40% and 60%. This type of conservation was done in order to assess the durability of fibres in the pozzolana matrix. The tensile strength of the fibres was given by equation (1):

$$\sigma_{fl} = \frac{F}{S} \text{.......... ....} (1)$$

Where

- σ_{ft}: Tensile strength fibres.
- F: Maximum load recorded by the traction machine.
- S: Average Section fibre.

Note: Since the palm fibre does not have the same diameter over its entire length, the diameter taken in the calculation of the mean section of the fibres is the average diameter of at least three measurements with a vernier digital caliper.

Preparation and Preservation of Specimens of Date Palm Fibre Mortar

Preparation of mortar specimens and conventional fibres was performed using a methodology inspired by the standard EN196-1 [5]. After the mixing operation, the molds (40X40X160) mm are filled into two layers, followed by a vibration of vibrating table 10 s for each layer. After finishing, the molds are covered with plastic and kept in laboratory conditions (T = 30 ± 2 ° C) and relative humidity (RH) (65 ± 5%) for 24 h, after we perform the demolding operation.

The used mixed were: Mortar-based CPJ, Based mortar plus pozzolana CPJ powder (20%, 40% and 60%) and Mortar-based CPJ plus broken bricks powder (20%). The mortar specimens and conventional fibres were kept in water for 14 days and then in the air (EC14) until date of their crash. Indeed, previous studies [1, 2] have shown the effectiveness of this type of program (EC14) on improving the performance of concrete in hot and dry climate.

Flexural strength of Date Palm Fibres mortars

The flexural strength of conventional mortar and fibres was determined according to standard EN 196-1 [5] by a three-point bending. Figure 2 with a machine for ELE determining the flexural strength. The bending strength is given by the formula (2).

$$\sigma = \frac{1.5F_f \times L}{b^3} \text{..} (2)$$

Where

- F_f: Tensile strength in N
- L: The distance between supports (L = 100 mm).
- b: The side of the square section of the specimen (b = 40 mm).

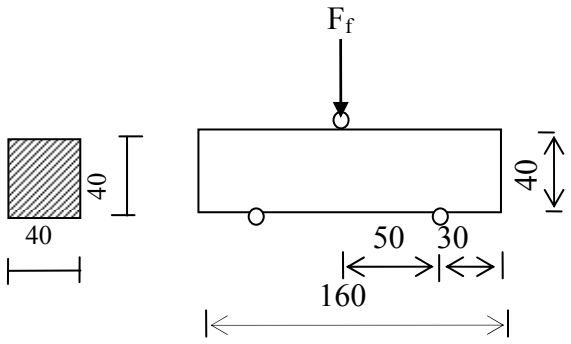

Figure 2 Three point flexural strength test devise

At each test date, six specimens were used.

In the following mortars are referenced as follows:

Mortier L, P, matrix
L: length of the fibre, for example L = 40 mm.
P: weight percentage of fibre, for example P = 0.4%.
Matrix: the cement matrix used for example-based CPJ.
Example: 40 - 0.4 - CPJ.

RESULTS AND DISCUSSION

Durability of Fibres Embedded in Different Pozzolana (Z) Matrix

After 30 days, three months and six months in pozzolana hardening matrix, the embedded fibres in different cement matrix with percentages of 20%, 40% and 60% of natural pozolan were recovered. Six samples were used for each fibre diameter and percentage of each pozzolana. The mortar specimens were initially stored in water for 14 days. Six samples of fibres were used for each test date. Figure 3 presents the variation of tensile strength as a function of time and the nature of matrix and diameter.

The tensile strength of fibres remains almost constant as a function of storage time in different cement matrices with 20%, 40% and 60% natural pozzolana. The fibres retain almost their original strength (natural state) confirming that the pozzolana has a good preservation medium and prevents the release of lime cement which adversely affects the durability and physical and mechanical properties of plant fibres.

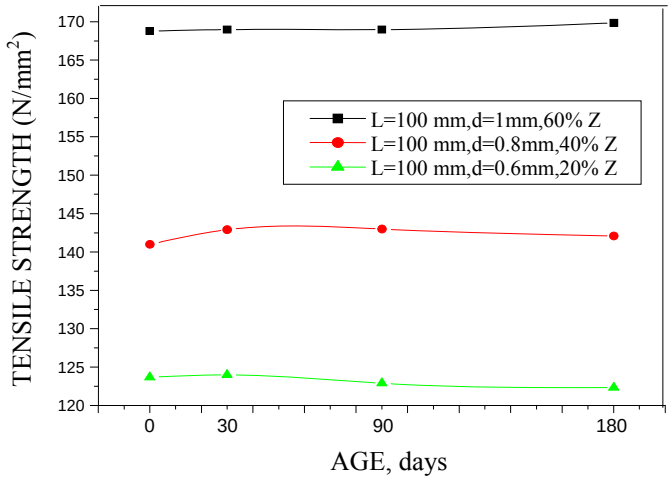

Figure 3 Change in tensile strength function of time and percentage of pozzolana in cement matrix

Flexural Strength of Mortars with Fibres in a CPJ Cement Matrix

Figure 4 presents the loss of flexural strength of CPJ cement.

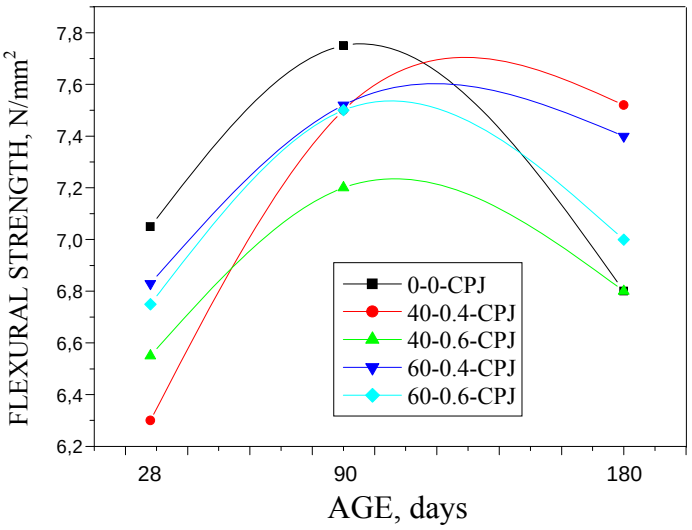

Figure 4 Flexural strength

During the period from 28 to 90 days all mortars have a positive progression of resistance and mortar-fibre 60 -0.4 CPJ is the most resistant. But beyond 90 days, we recorded a drop in the flexural strength of all mortars fibre. This drop is quite remarkable for the mortars-40 -0.6 CPJ. This can be interpreted by the fall of the durability of fibres in the cement matrix-based CPJ also to the fall of adhesion between the fibre-matrix and the influence of climatic conditions. Indeed, the tests were conducted in July-August, an average temperature of 32 ° C and RH 65%.

For these reasons in this work, we study the improvement of sustainability by treating the matrix with the incorporation of natural pozzolana and broken of bricks to reduce the lime released by the cement, by using fibres length 60 mm, which showed the best results up to 90 days.

Flexural strength of mortars with fibres in a cementitious matrix base CPJ adding natural pozzolana

Figure 5, 6 and 7 present the flexural strength of pozolona reinforced mortar. According to figures 5 6 and 7 we notice that there is a positive trend in the flexural strength for the first 90 days and the 60-0.6-20%Z mortar is the most resistant. But after 90 days, we notice that there is a slight drop in flexural strength for mortars of these fibres. The percentage of 20% shows the best results in terms of resistance. We note that with 20% pozzolana values of flexural strength exceed those of conventional mortar based CPJ. However, mortars with 40% fibre and 60% pozzolana showed the flexural strength less than that of conventional mortar based CPJ. Although the other mortars with percentages 40% and 60% have presented a slight drop in strength after 90 days compared with those of 20% pozzolana; these mortars have flexural relatively low. This is attributed to the low reactivity of the hydraulic and pozzolana cement matrix by following the low fibre matrix adhesion due to decrease in the percentage of CPJ in the matrix, as well as storage conditions, low moist. Indeed, the matrices pozzolana require a relatively humid environment for their hydration.

Flexural strength of mortars with fibres in a CPJ cement matrix add 20% of cooked broken bricks (CBB)

Figure 8 presents the flexural strength of cooked broken bricks reinforced mortar. This figure sows a positive trend in the flexural strength for the first 90 days for all mortars. But after 90 days, we notice that there is also a slight improvement in the flexural strength of the long term. A comparison between the results of the cement matrix with 20% of the pozzolana and the results of the cement matrix with 20% of the debris of bricks shows that they have low resistance. Probably this is due to the low fibre matrix adhesion, due to the low hydration of cement matrices based debris of burnt bricks. Further analysis is required to explain this phenomenon.

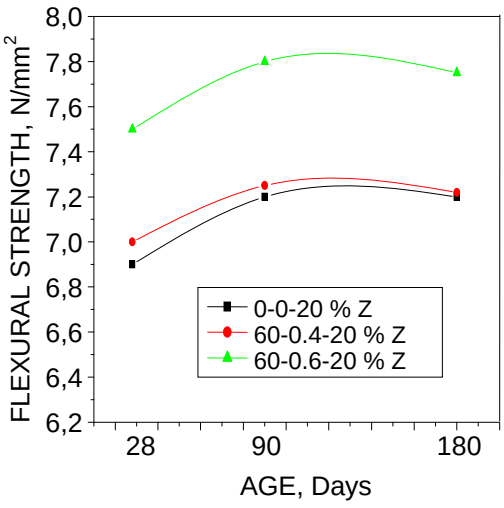

Figure 5 Adding 20 % of natural pozzolana

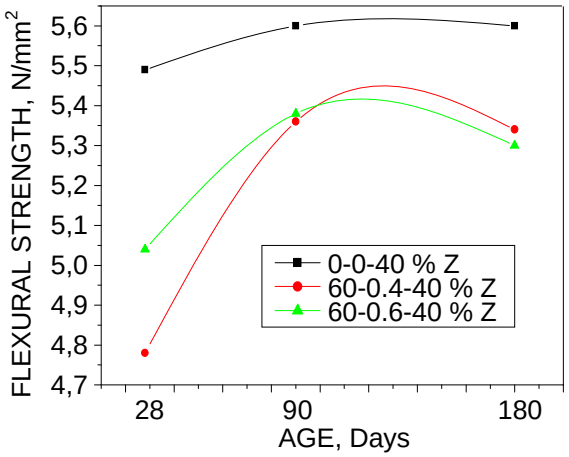

Figure 6 Adding 40 % of natural pozzolana

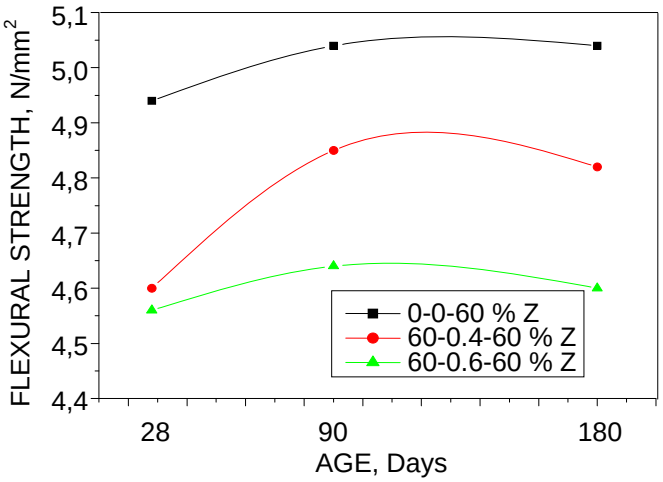

Figure 7 adding 60 % of natural pozzolana

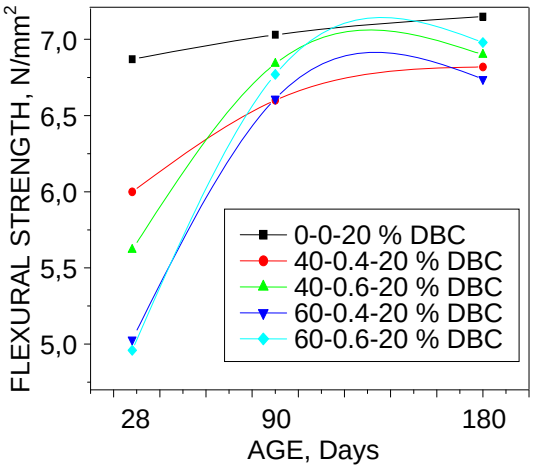

Figure 8 Flexural strength function of percentage fibres length 60 mm in cement matrix adding 20 % CBB

CONCLUSIONS

The bending strength is improved with the incorporation of fibres, fibre and mortar with 20% natural pozzolana present the best result that exceeds the strength of standard mortar based CPJ. According to the results given in the paper, only for 20% pozzolana content the fibre reinforced samples have higher strength than base control

The treatment of matrix by the use of pozzolana and broken bricks, we showed that the use of pozzolana improves the durability of the fibres in cement matrix. In Figure 4, it was found that the strength drop in base control was larger than that in fibre reinforced samples. In Figures 5-8, the strength in base control was also kept increase after 90 days. Therefore, the reasons for strength drop in fibre reinforced PC samples could be due to cement types rather than due to the changes in mechanical property of fibre in the alkali condition. It can also be seen in Figure 4 that the fibre reinforced samples have higher strength that base control. Further explanation is required to address these results.

REFERENCES

1. KRIKER, A. Date palm fibres and properties Characterization of concretes and mortars reinforced with date palm fibres in hot and dry climate, Doctorat thesis, ENP, Algiers, 2005.

2. ABBANI, S. Characterization and durability of concrete reinforced with date palm fibres Magister Memory, University of Ouargla, 2003.

3. ATHIL, Guide for the use of cement, Edition EYROLLES 1998.

4. EUROPEAN STANDARD EN ISO 5079 Determination of textile fibres tensile strength and elongation at break of the individual fibres AFNOR, France 1996.

5. EUROPEAN STANDARD AFNOR, France 1994.″ ″EN 196-1 test methods.

6. DUPAIN, R., LANCHON, R., ST ARROMAN, J. C. Aggregates, soil, Cement and concrete materials characterization for civil engineering by laboratory Collection CAPLIEZ, Casteilla edition, tests V235, Paris 2000

Theme 5 — Security and Geohazard Engineering

1620

Bullet Resistance of Double-layer Concrete Panels Made of Rubberized and Steel Fibre Reinforced Concrete

P Sukontasukkul[1], M Sappakittipakorn[1], N Banthia[2]
1 – King Mongkut's University of Technology, Thailand
2 – University of British Columbia, Canada

In this study, the impact resistance of double-layer concrete panels made of rubberized and steel fiber reinforced concrete subjected to direct fire weapon (11 mm or .44 Magnum bullet size) is investigated. Concrete panels with dimensions of 400x400x50 mm are subjected to impact forces from 11 mm-diameter bullets at a distance of 10 m. Three types of concrete panels are tested: single-layer steel fiber reinforced concrete (SFRC), single-layer crumb rubber concrete (CRC) and double-layer CRC/SFRC. For a double-layer CRC/FRC, the CRC layer of 12.5 mm is added to the front surface to partially replace part of the SFRC panel. It is expected that, with its high elasticity and flexibility, the CRC layer will act as a cushion layer to absorb impact energy from the bullet and reduce the damage to the concrete panel. During the impact event, the acceleration of the plate is measured using an accelerometer. The measured acceleration is then used for calculating the force acting on the plate and also its displacement.

Professor P Sukontasukkul is an Associate Professor at King Mongkut's University of Technology North Bangkok, Department of Civil Engineering, Bangkok, Thailand. He received his doctorate education from University of British Columbia, Canada and his research interests include fibre reinforced concrete, rubberized Concrete, behaviour of concrete under impact loading and green concrete.

Manote Suppakittipakorn is currently a lecturer at King Mongkut's University of Thailand North Bangkok, Thailand. His specialist areas of research are fibre reinforced concrete, cement based sensors and corrosion in FRC.

Nemkumar Banthia is currently a professor at the University of British Columbia, Vancouver, Canada. He is a distinguished university scholar and Canada research chair in infrastructure rehabilitation and sustainability. His specialist areas of research are fibre reinforced composite, strain rate effect, shotcrete and permeability measurement.

Keywords: Bullet resistance, Fibre reinforced concrete, Multilayer concrete panel, Rubberized concrete

INTRODUCTION

Worldwide, terrorist threats have become widespread. In Thailand, terrorist threats have occurred more frequently especially at the southern parts of the country. Each attack causes damage to properties and life. It becomes essential to develop structures or structural elements which could resist terrorist attacks like bombs or direct fire weapons.

In Thailand, most residential buildings are constructed using reinforced concrete structural system in which the main structural components such as slabs, beams and columns are made of reinforced concrete and walls are made of bricks. When subjected to direct fire weapon or bomb, the bullet could either penetrate through the wall or cause flying hazardous debris which could harm people inside the building.

In the case of military buildings such as bunker or guard post, this kind of structures is often a impermanent structure (Figure 1). Some are made of timber or wooden panels surrounded by sand bags. The advantages of using sand bags are that they are cost effective, easy to replace, and efficient in absorbing impact energy. However, there are several disadvantages for example, sand bags are heavy (slow installation), easy to disintegrate (sensitive to moisture and UV), and need a replacement once it has been punctured. In the case of emergency, when military units are required to construct bunkers or guard posts in the battle zone quickly, the weight of the sand bags could be become a factor to slowing them down.

Figure 1 Example of military guard post or bunker
(http://www.arty16.com/data/modules.php?name=News&file=article&sid=42)

In this study, a bullet proof concrete panel with the thickness of about 50 mm made from layers of steel fibre reinforced concrete and rubberized concrete is proposed. The panel is expected to sustain Class 3A fire weapon according to the Department of Defense standard for bullet proof panel or shield [1].

In general, concrete is a quasi-brittle material, when subjected to an impact loading, concrete usually fractures catastrophically. This causes pieces of broken concrete to take off in all directions which may harm people or cause damage to properties inside the building. In order to prevent it, a concrete wall must not only prevent a bullet from penetrating through it, it must also maintain its integrity to keep the flying hazardous debris to minimum.

In order to improve concrete brittleness and ability to absorb impact energy, small fibres are mixed uniformly into concrete mixture (fibre reinforced concrete, FRC). With the ability of fibres to bridge across the cracks, the toughness as well as the impact resistance of FRC is

much more superior to that of plain concrete [2]. However, there are still some disadvantages on the use of FRC material as a bullet proof panel. An example is rebounding the bullet off the surface. Since the surface of the FRC plate is hard and strong, for some type of bullets, quite often it is found to bounce back at high velocity in arbitrary direction and become harmful to people on the front side.

Therefore, in this study, to eliminate or minimize the rebounding effect, a layer of crumb rubber concrete (CRC) or rubberized concrete is introduced and used for partially replacing part of the FRC layer. It is expected that by adding a highly flexible rubberized concrete layer to the front, some kinetic energies of the bullet could be absorbed by the rubberized layer and causes the bullet to stop or bounce back at lower velocity. Another advantage of replacing FRC with rubberized concrete is the reduction the weight of the plate because rubberized concrete is lighter than normal concrete by about 20% to 50%.

EXPERIMENTAL PROCEDURE

Materials

Materials used in this experiment consisted of Type I Portland Cement, River Sand Hooked End Steel Fibre (Table 1), and Crumb Rubber (Table 2).

Table 1 Fibre Properties

MATERIAL	SG	SHAPE	LENGTH (mm)	SECTION (mm)	ASPECT RATIO (l/d)	TENSILE STRENGTH (MPa)
Steel	7.8	Hooked End	35	Circle dia.- 0.55	64	1000

Table 2 Properties of Crumb Rubber and Fine Aggregate

CATEGORIES	CRUMB RUBBER	FINE AGGREGATE
Average Bulk Specific Gravity	0.96	2.43
Average Bulk Specific Gravity (SSD)	0.97	2.47
Average Apparent Specific Gravity	0.97	2.55
Average Absorption (%)	0.92	2.04
Fineness Modulus	4.93	2.9

Specimen Preparation

For all specimens, the concrete is mixed in a pan mixer, carefully poured into the mold and vibrated on a vibrating table. After 24 hours, the specimens are demolded and cured in water for 28 days. Three types of specimen with dimensions of 400x400x50 mm are prepared (Table 3):

- Single layer SFRC plate. For this specimen, hooked end fibres are mixed with concrete at 2%, 3% and 4% by volume fractions.

- Single layer CRC plate. For this type of specimen, the fine aggregate is partially replaced by the crumb rubber at 25% and 50% by volume fractions.

- Double layer SFRC+CRC concrete plate. The specimen's thickness is divided into two layers: the top layer of 12.5mm is made of CRC and the bottom layer of 37.5mm is made of SFRC.

Table 3 Casting Details

TYPE	THICKNESS (mm)		MATERIAL		No. OF SPECIMEN
	t1	t2	t1	t2	
R25	50	-	25%CRC		
R50	50	-	50%CRC		
S2	50	-	2%SFRC		
S3	50	-	3%SFRC		
S4	50	-	4%SFRC		
R25/S2	12.5	37.5	25%CRC	2%SFRC	3
R50/S2	12.5	37.5	50%CRC	2%SFRC	3
R25/S3	12.5	37.5	25%CRC	3%SFRC	3
R50/S3	12.5	37.5	50%CRC	3%SFRC	3
R25/S4	12.5	37.5	25%CRC	4%SFRC	3
R25/S4	12.5	37.5	50%CRC	4%SFRC	3

Testing

The specimen is set on the support as shown in Figure 2. Prior to the shooting, an accelerometer is attached to the back and at the top of the specimen to measure the acceleration of the plate during impact. Three shots are attempted per specimen using 11mm size bullets (0.44 Magnum) from 10 meters distance. The acceleration is measured and recorded using a computer based data acquisition system.

Data Analysis

Using the obtained acceleration data, the velocity and the displacement at any time at the location of the accelerometer can be calculated using Eq.1 and 2 [3].

$$\dot{u(t)} = \int_0^t \ddot{u}\,(t)dt \quad (1)$$

$$u(t) = \iint_0^t \ddot{u}\,(t)dt \quad (2)$$

where $\ddot{u}(t)$ is the acceleration at any time t
$\dot{u}(t)$ is the velocity at any time t
$u(t)$ is the displacement at any time t

By assuming linear distribution of the acceleration from top to support of the specimen and by applying the principle of Virtual Work, the inertia force acting on the specimen can be calculated using Eq.3 and 4 [3].

$$dI = \rho A\ddot{u}(x,t)dx \quad (3)$$

$$P_I(t)\delta u = \int \rho A\ddot{u}(x,t)\delta u(x,t)dx \quad (4)$$

where ρ is the concrete density
A is the thickness of the specimen

Figure 2 Specimen Setup

RESULTS AND DISCUSSION

Acceleration

The acceleration is one of the key performances to demonstrate the movement or the response of materials under impact loading. By using the relationship between acceleration and time, velocity and displacement can be obtained using Eq.1 and 2.

Results from tests are given in Figure 3. Two points are discussed: impact duration and value of acceleration.

For the impact duration, the impact events are found to vary from about 0.0002 seconds to about 0.0004 seconds depending on the type of specimen. The impact duration of the SFRC plates (about 0.0002 seconds) are shorter than those of the CRC plates (about 0.0004 seconds). Shorter impact event for the SFRC plate indicates that the bullet is reflecting out of the plate surface immediately right after the contact. However, in the case of CRC plate, because of its highly flexible and softer surface, the bullet is allowed to penetrate deep into the surface before bouncing back and causes the impact event to extend slightly further.

In case of the acceleration, comparing among the single layer plates, the CRC plates (400 to 650 m/s^2) exhibit much lower acceleration as compare to the SFRC plates (1700 to 2700 m/s2) (Figures 3a and b). Lower acceleration indicates that the CRC plate is being accelerated less than the SFRC plates, which in some way imply that the CRC is better in

absorbing kinetic energy than the SFRC. In addition, for both types of materials, the accelerations are also found to decrease with the increasing fibre and crumb rubber content.

For the double layer plates, all of them exhibit less acceleration when compared to the single layer plates (Figures 3c-e). This proves that a layer of CRC material is able to provide a cushion effect for the plate which causes a reduction in impact energy and plate acceleration. The acceleration also decreases with the increasing rubber content of the CRC layer.

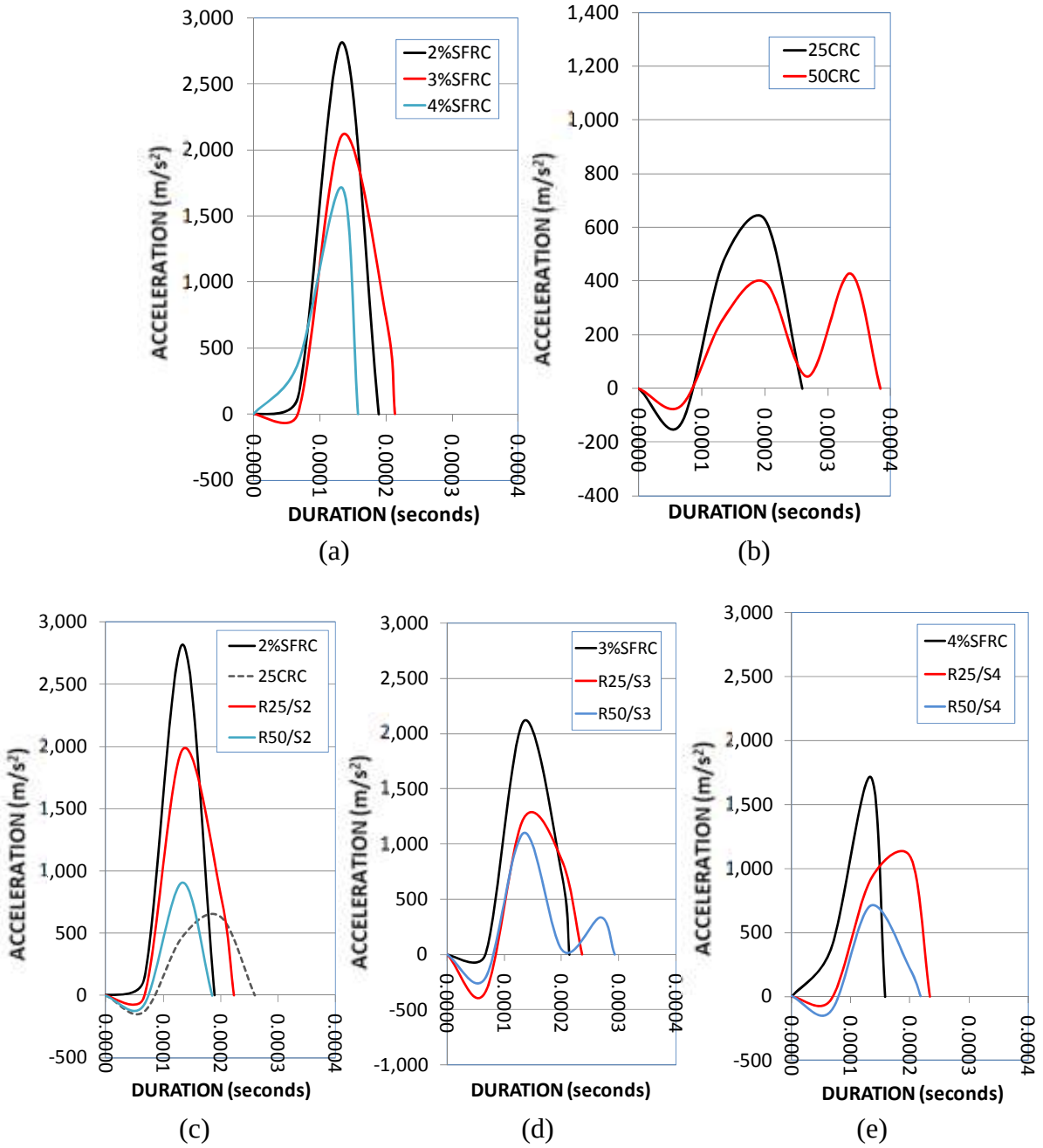

Figure 3 Acceleration of (a) SFRC, (b) CRC and (c)-(e) Double Layer Plates

Inertia Force

Inertia force is the force used in accelerating a subject from its rest position. It can be calculated using Eq.4 and the results are shown in Figure 4.

From Figure 4, it could be seen that the average values of the inertia loads acting on specimens are highest on the single layer SFRC plates, followed by the double layer plates and the CRC plates. The results indicate that the harder the surface, the higher the inertia loads. It also proofs that specimens with harder surface resist more to the impact force than those with softer surface and cause higher inertia force. For the double layer plates, the values which fall between the upper and lower bound indicate the combined effect of soft and hard materials in one specimen. The soft material absorbs parts of the energy while hard material resists the surplus energy.

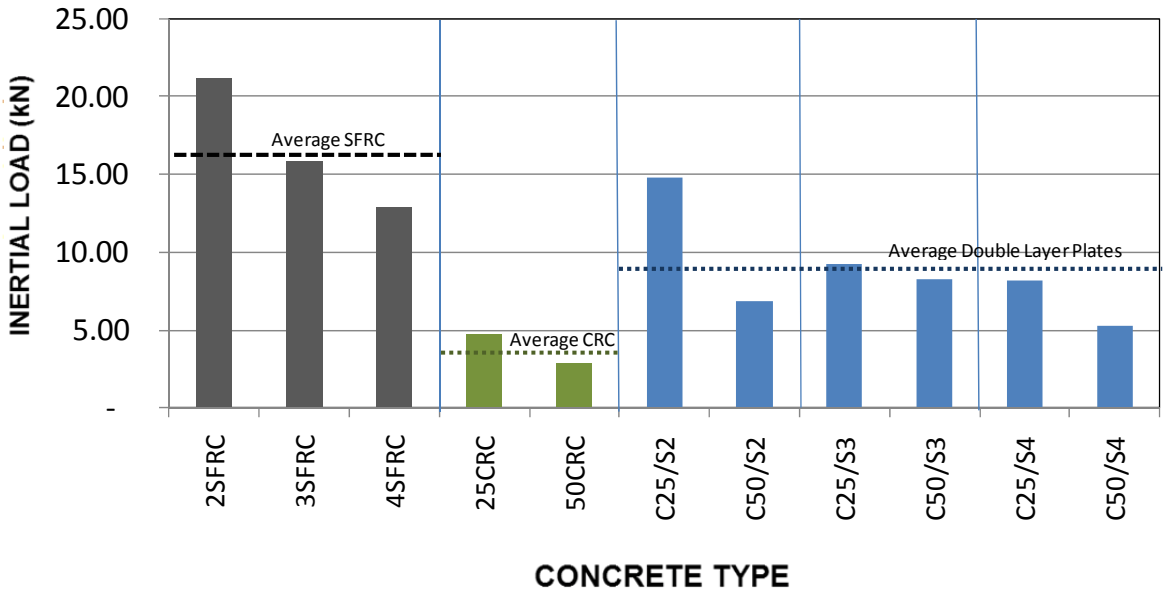

Figure 4 Inertial Load

Failure Patterns

For all specimens, the patterns of failure are typically scabbing (fragments of specimen falling off the top surface [4]). However, in some cases of the CRC plates, both scabbing and spalling (fragments of specimen falling off the bottom surface [4]) failures are observed (Figure 5). Even though most specimens fail under scabbing mode, different crater sizes are observed. For the SFRC plates, the crater sizes are smaller than those of CRC and CRC+SFRC plates. This indicates also that the CRC layer allows the bullet to penetrate deeper than the SFRC layer and absorbs part of the kinetic energies during the impact.

Figure 5 Failure Patterns of SFRC plate (left) and CRC+SFRC plate (right)

CONCLUSIONS

This manuscript is a preliminary result of the experimental series on impact resistance of multilayer plate subjected to direct fire weapons. In this study, the 11mm (0.44 Magnum) bullet type is used. The 0.44 magnum are different from other bullet that it provides more impact force but less penetration. It has been proofed that a combination of soft and hard material can be used to sustain impact force from this fire arm. The soft layer is acting as a cushion layer to absorb part of the energy and allow less impact force to act on the SFRC plate. Addition studies will be carried out on different kinds of fire arm and different combination of material thicknesses.

ACKNOWLEDGEMENT

The authors would like to thank Thailand Research Fund (TRF) and Faculty of Engineering (KMUTNB) for financially support the experiment. Thanks also to SR.Fibre Co., Ltd. for providing steel fibres.

REFERENCES

1. MINISTRY OF DEFENSE, Kingdom of Thailand, “Standard for Bullet Proof Shield”, 2006.

2. SUKONTASUKKUL, P., Impact Behavior of Concrete under Multiaxial Loading, PhD Thesis, University of British Columbia, Canada, 2001.

3. BANTHIA, N., Impact Resistance of Concrete, PhD Thesis, University of British Columbia, Canada, 1987

4. MINDESS S, AND YAN C. Perforation of Plain and Fibre Reinforced Concretes Subjected to Low-Velocity Impact Loading. Cement and Concrete Research 1993 (23), pp. 83-92.

An Analysis of the Seismic Behaviour of the Grancarevo Concrete Arch Dam

M Smilovic, J Radnic, A Harapin
University of Split, Croatia

The paper first briefly describes the numerical model for the numerical simulation of the fluid-structure coupled problems. The primary intent of the applied model is to simulate the fluid-structure dynamic interaction in seismic conditions. The partition scheme of the coupled (multi-field) problem is briefly described as the most common approach for the fluid-structure dynamic analysis of large systems. The developed model includes the most important nonlinear effects in water and structure, such as concrete yielding in compression and crack opening/closing in tension, reinforcement yielding and the phenomenon of cavitation in water. Next, an analysis of the seismic behaviour of the Grancarevo concrete arch dam is performed. The complex model of the water-dam-foundation rock system is analyzed for the registered earthquake from 1986. The analysis was conducted in order to first determine the dynamic characteristics, and then to investigate the actual behaviour of the dam subjected to seismic excitation. The numerical results of the developed numerical model were compared with the registered values.

M. Smilovic is young researcher/assistant at the University of Split, Faculty of Civil Engineering, Architecture and Geodesy, where she is preparing her PhD. Her field of interest is numerical and experimental modelling of structures, and she currently work on modelling of masonry structures.

J. Radnic is currently a Professor at the University of Split, Faculty of Civil Engineering, Architecture and Geodesy. He had lead several research projects on concrete structures, and his special area of interest is modelling of concrete structures.

A. Harapin is currently a Professor at the University of Split, Faculty of Civil Engineering, Architecture and Geodesy and University of Mostar, Faculty of Civil Engineering. His field of interest is high performance concrete and numerical and experimental modelling of concrete structures.

Keywords: Arch dam, Earthquake resistance, Fluid-structure dynamic interaction, Structural analysis

INTRODUCTION

Structures like dams, water tanks (reservoirs), off shore structures, pipelines, water towers, which are in direct contact with fluid, can often be met in engineering practice. Numerical model for real simulation of these structures have to include the simulation of the fluid-structure interaction to ascertain the real behaviour of such a complex system. This problem is particularly emphasized under dynamic/seismic conditions. This problem is commonly referred to as a coupled (multi-field) problem.

A coupled multi-field problem involves two or more interacting fields, for example gravity dam with accumulation. This problem is time dependent and the state of one field is continuously linked to the state of other fields and neither field can be solved independently from the other. Here, the coupling normal occurs through the differential equations representing the physical phenomena.

The most natural treatment for coupled problems is partitioned analysis. In this the overall system is partitioned into zones or fields. Then the individual fields are solved independently by considering the interaction information transfer between them at every stage of solution process.

The various advantages are: (i) the resulting model is very modular, (ii) it's easy to make any modifications, (iii) every modification in one field improve the whole model, (iv) the user can only have knowledge in a single field.

This paper first briefly described partition approach in numerical modelling of dynamic interaction of water-structure system. This model is suitable for problems with limited fluid motions, such as the response of offshore structures and dams to waves or earthquake. Finally, for model illustration, Grančarevo dam is analysed.

BASIC CHARACTERISTICS OF NUMERICAL MODEL

General

Basics of 3D numerical model for dynamic water-structure system interaction in seismic conditions is briefly described hereafter, with more detailed description in [2, 4-6, 9-12]. For small fluid motions Eulerian-Lagrangian and Lagrangian approach are adopted [1, 2, 8]. The coupling of fluid and structure occurs at the contact surface. The model includes the most important nonlinear effects of water-structure system behaviour in dynamic conditions, such as: (i) Concrete yielding in compression, (ii) Cracks occurrence and propagation in tension, (iii) Opening and closing of cracks, (iv) Tensile and shear stiffness of cracked concrete, (v) Yielding of steel or reinforcement in compression and tension, (vi) Influence of dynamic action's velocity on mechanical characteristic of concrete and reinforcing steel, (vii) Influence of hydrostatic and hydrodynamic water pressures in structure cracks, (viii) Cavitation, (ix) Influence of suspensions in water [12].

The applied material model for structure was primary used for the purpose of simulation of reinforcing concrete structures. It includes the most important nonlinear effects of reinforced concrete behaviour, but with little modification of parameters can be efficiency used for simulation of steel [10].

Equation for Coupled Fields Motions

Behaviours of the fluid-structure system (structure includes the structure itself as well as the surrounding soil) in dynamic load conditions, can be expressed with two second order differential equations [2, 6, 12]. If we use the displacement formulation for the structure and the displacement potential formulation for the fluid, dynamic equilibrium equations can be expressed in the following form:

$$\begin{aligned} \mathbf{M}_s\ddot{\mathbf{u}} + \mathbf{C}_s\dot{\mathbf{u}} + \mathbf{K}_s\mathbf{u} &= \mathbf{f}_s - \mathbf{M}_s\ddot{\mathbf{d}} + \mathbf{f}_{cs} \\ \mathbf{M}_f\ddot{\boldsymbol{\Psi}} + \mathbf{C}_f\dot{\boldsymbol{\Psi}} + \mathbf{K}_f\boldsymbol{\Psi} &= \mathbf{f}_f + \mathbf{f}_{cf} \end{aligned} \tag{1}$$

where:

$$\begin{aligned} \mathbf{f}_{cs} &= \mathbf{Q}\,\boldsymbol{\Psi} \\ \mathbf{f}_{cf} &= -\rho_f\,\mathbf{Q}^T\left(\mathbf{u}+\mathbf{d}\right) \end{aligned} \tag{2}$$

In the above equations $\mathbf{M_s}$, $\mathbf{C_s}$ and $\mathbf{K_s}$ represent mass, damping and stiffness matrices for structure, and $\mathbf{M_f}$, $\mathbf{C_f}$ and $\mathbf{K_f}$ represent mass, damping and stiffness matrices for fluid. Vectors $\mathbf{u}, \dot{\mathbf{u}}, \ddot{\mathbf{u}}$ represent structure's displacements and displacement's derivations (velocities and accelerations) and $\boldsymbol{\psi}, \dot{\boldsymbol{\psi}}, \ddot{\boldsymbol{\psi}}$ are the displacement potential and associated derivations. Q is the interaction matrix between structure and fluid.

Interaction between structure and base soil is modelled indirectly by contact elements in the connection surface. In fact, by applying the appropriate material model for contact elements, various effects in the contact surface can be simulated, such as: separating, embedment and sliding.

Solution Concept for the Dynamic Fluid-Structure Interaction Problem

Direct solution of the equation system (1) requires large computer capacity. So, the previously described partitioned scheme is ideal for this kind of problems. In that approach for every increment of the imposed load and every non-linear problem iteration step, each field is solved separately by including interaction forces on the contact surface between fluid and structure. Presentation of the solution scheme is given in Figure 1. For time integration, explicit-implicit algorithm developed by Hughes [1] is used.

In the presented approach, fluid is solved first and structure second. This approach allows the developed independent models to be used for each field, with additional calculations of the interaction forces only. Thus, in the fluid-structure interaction model, all non-linear effects of material and geometry, that are present in a particular field, can also be simulated in the coupled problem.

Predicted values $\mathbf{u}, \dot{\mathbf{u}}, \ddot{\mathbf{u}}$ and $\boldsymbol{\psi}, \dot{\boldsymbol{\psi}}, \ddot{\boldsymbol{\psi}}$ at the beginning of every time step are corrected at the end of the same time step. For convergence control of the iterative procedure, the increase of the structure's displacements in comparison with current total displacements and the increase of the fluid's displacements potential in comparison with the current total displacements potential are simultaneously monitored. Various options of the Newton-Raphson method are used to solve the non-linear equations.

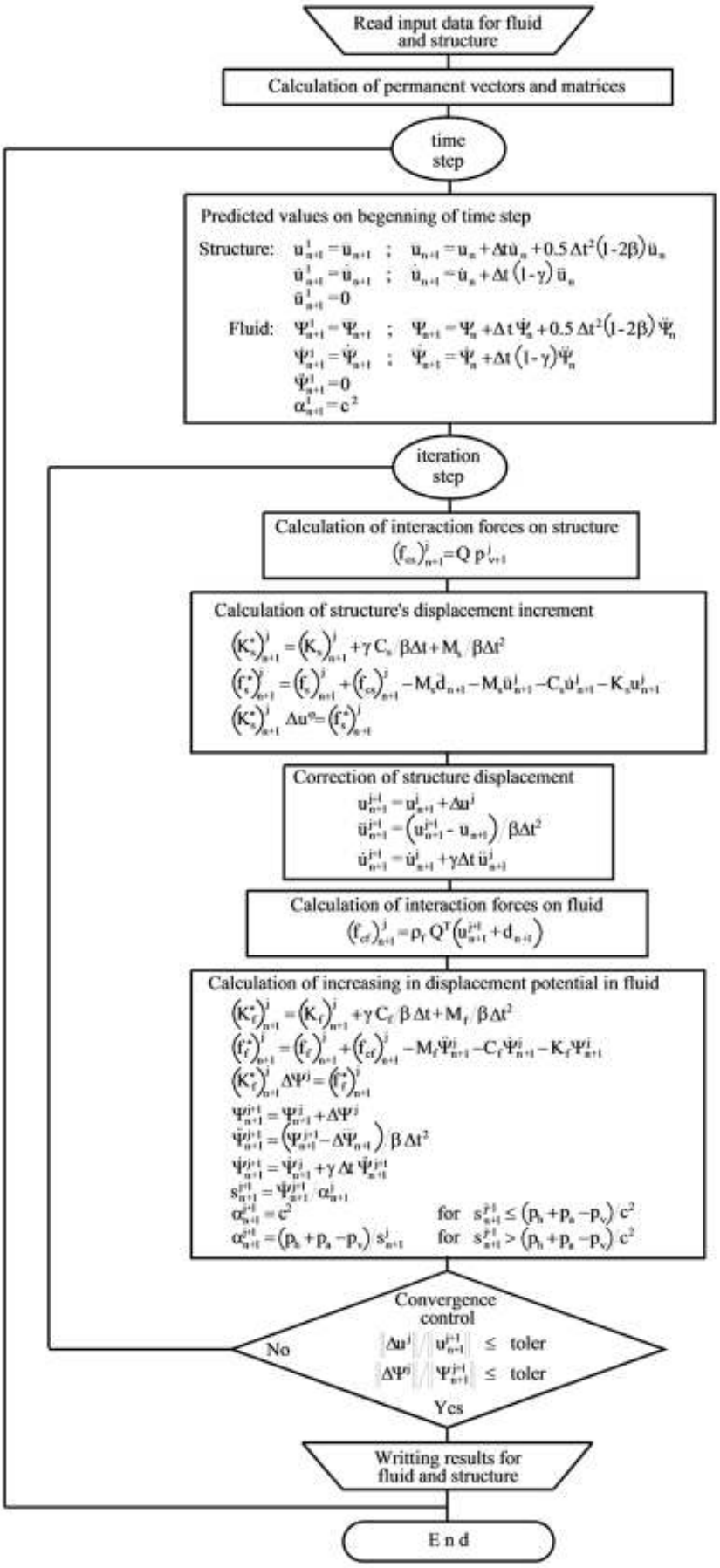

Figure 1 Flow chart for the solution of the fluid-structure coupled problem

EXAMPLE - GRANČAREVO DAM

The Grančarevo Arch Dam in Bosnia and Herzegovina (Figures 2 and 3) is a double-curvature concrete dam with a perimetral joint. The dam was constructed in 1968. The height of the dam is 123 m and the crest length is 439 m. Its bottom thickness is 27 m and its top thickness 4.6 m. The dam's foundation dig was 230000 m³ and the volume of poured concrete was 376000 m³. The head of the dam is 100 m.

Figure 2 Grančarevo Arch Dam - photograph

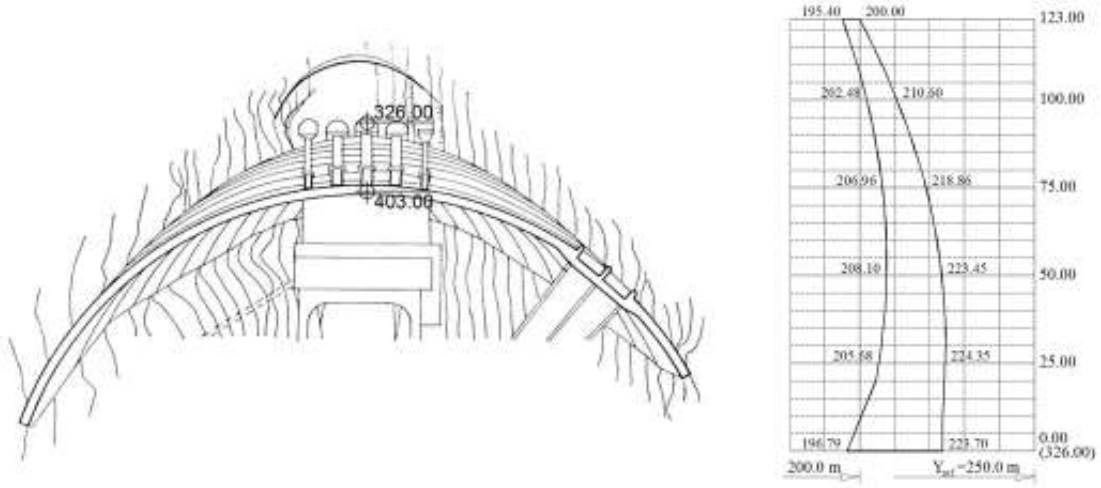

Figure 3 Plan of the dam's body with land topology (left) and cross section through central cantilever (right) [15]

The dam created the Bileća reservoir with a maximum water depth of 51 m and an available storage capacity of 1100 million m³. The Bileća reservoir is the largest storage lake in the Balkan. Its dimensions are: total storage volume: 1280 hm³ and surface of the reservoir on normal top water level: 2764 ha. Geometrical data tables (on Figure 4) show basic geometrical characteristics for individual arches some of which are shown in Figure 4. Other detailed information about dam can be found in [12-16]. The Institute of Earthquake Engineering and Engineering Seismology (IZIIS-Skopje, Macedonia) monitored the dam and performed several numerical simulations on different models, which were compared with results in situ [15]. All applied models included only the dam (structure), and water was treated as an additional mass on structure.

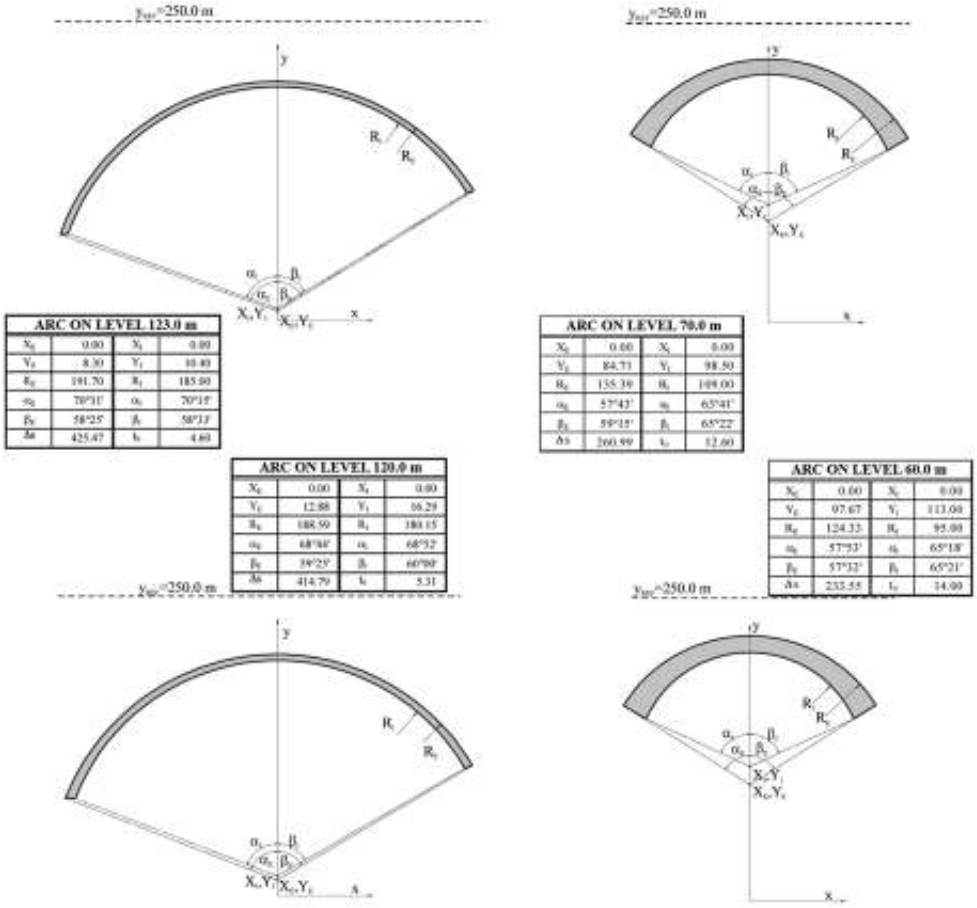

Figure 4 Geometry of some arch elements of the Grančarevo dam [13-15]

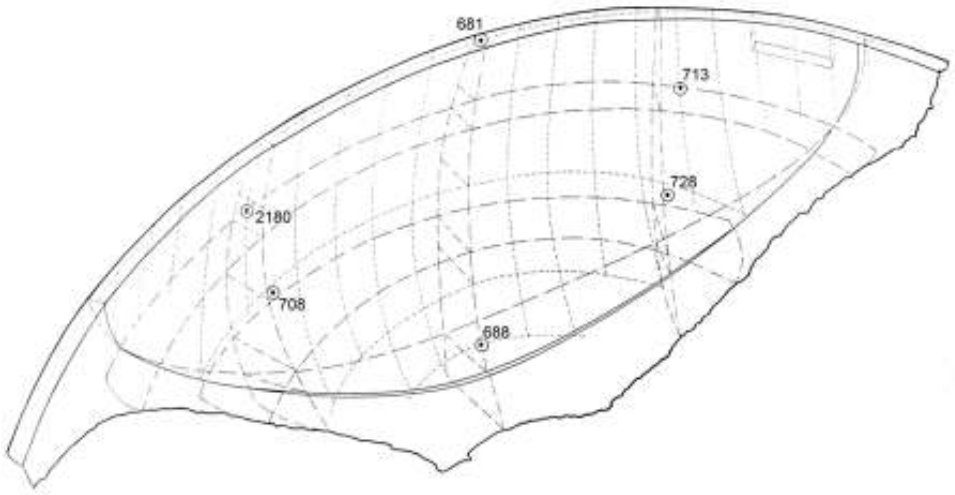

Figure 5 Positions of accelerographs in the Grančarevo dam body [15]

The complex model of the water-dam-foundation rock system is presented in Figure 6. Material characteristics are given in Table 1. For the dam and foundation rock 27-node ("brick") elements are used, as well as for the accumulation (fluid). For the simulation of connections between the foundation rock and the structure 18 nodes contact elements are used.

The dam is first analysed for the self weight and hydrostatic pressure of accumulated water. The water level in the accumulation (reservoir) is at a relative elevation of 120.0 m (3.0 m below the crest). Displacements' field for this load is relatively small. The displacement in the crest of the dam is 0.52 cm in the horizontal direction (perpendicular to the crest) and 0.62 cm in the vertical direction. These results are in very good agreement with the results of the dam monitoring (0.58 cm in the horizontal direction and 0.68 cm in the vertical direction). Figure 7 shows the displacement of the dam's self weight and hydrostatic pressure of water.

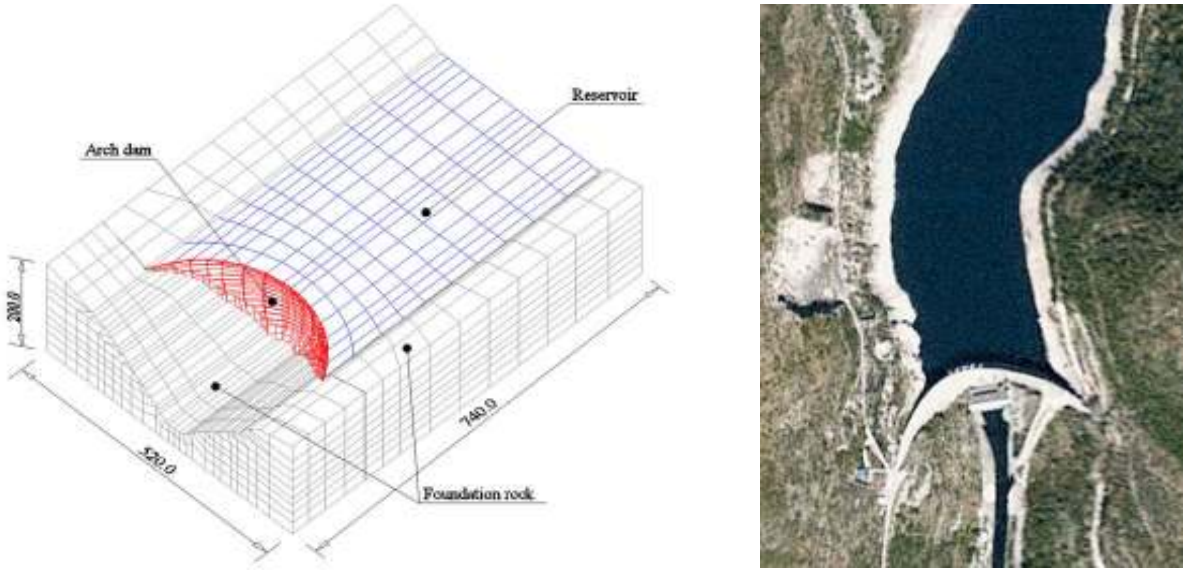

Figure 6 Finite element mesh of the Grančarevo dam–water–foundation rock interaction system – axonometric view (left) and aerial view (right)

Table 1 Material characteristics of Grančarevo dam system

CONCRETE			ROCK		
Modulus of elasticity	E_c, GN/m²	33.0	Modulus of elasticity	E_r, GN/m²	80.0
Poisson's ratio	ν_c	0.15	Poisson's ratio	ν_r	0.20
Weight density	γ_c, kN/m³	24.0	Weight density	γ_r, kN/m³	26.2
Pressure strength	f_{ck}, MN/m²	25.0	Pressure strength	f_{rk}, MN/m²	12.0
Tension strength	f_{ck}, MN/m²	2.5	Tension strength	f_{rk}, MN/m²	1.2
Def. of first crack occur.	ε_t, ‰	0.083	WATER		
Limit tension strain	$\varepsilon_{t,max}$, ‰	1.7	Sound velocity	c_s, m/s	1440.0
Limit shear strain	$\varepsilon_{s,max}$, ‰	1.7	Weight density	γ_a, kN/m³	9.81

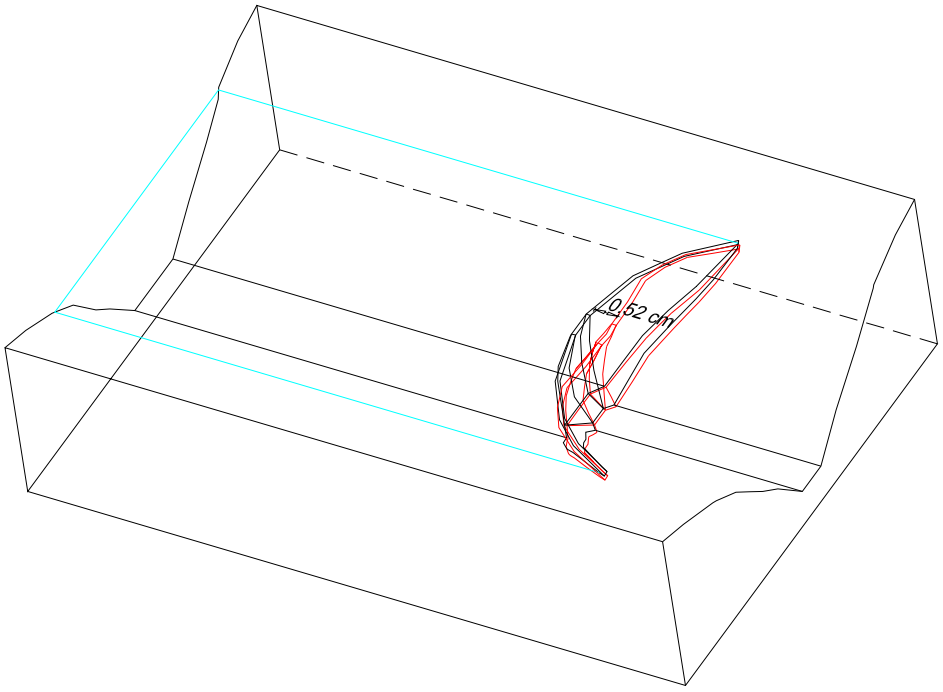

Figure 7 Displacement of the dam's self weight and hydrostatic pressure of water

The behaviour of this complex system was also analysed for the registered earthquake from 1986, [15], shown on Figure 8.

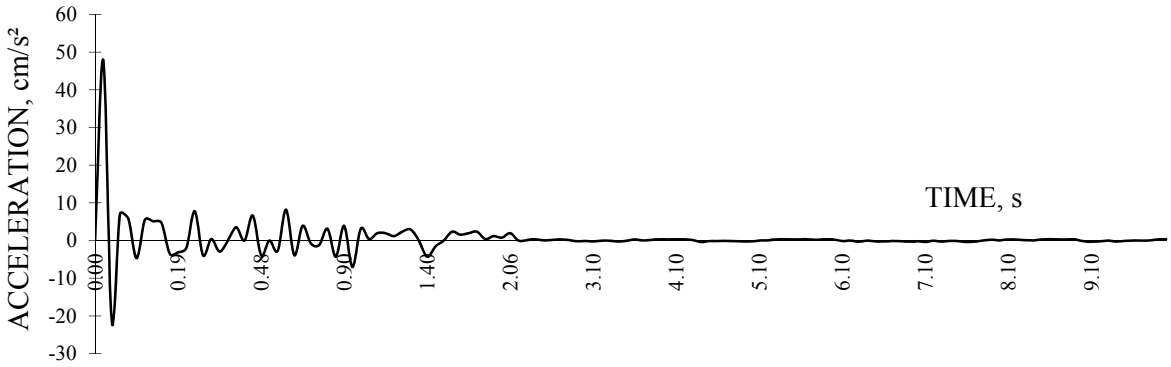

Figure 8 Registered earthquake in accelerograph 688 in Figure 5

To determine the dynamic characteristics of the dam, analysis of the structure oscillation (modal analysis) was conducted [3, 7, 11]. The analysis was performed for the coupled system: dam, rock and water (full accumulation). The results of analysis, Figure 9, are showing for the first four eigenvectors. It can be seen very good agreement with the results presented in the literature [15, 16].

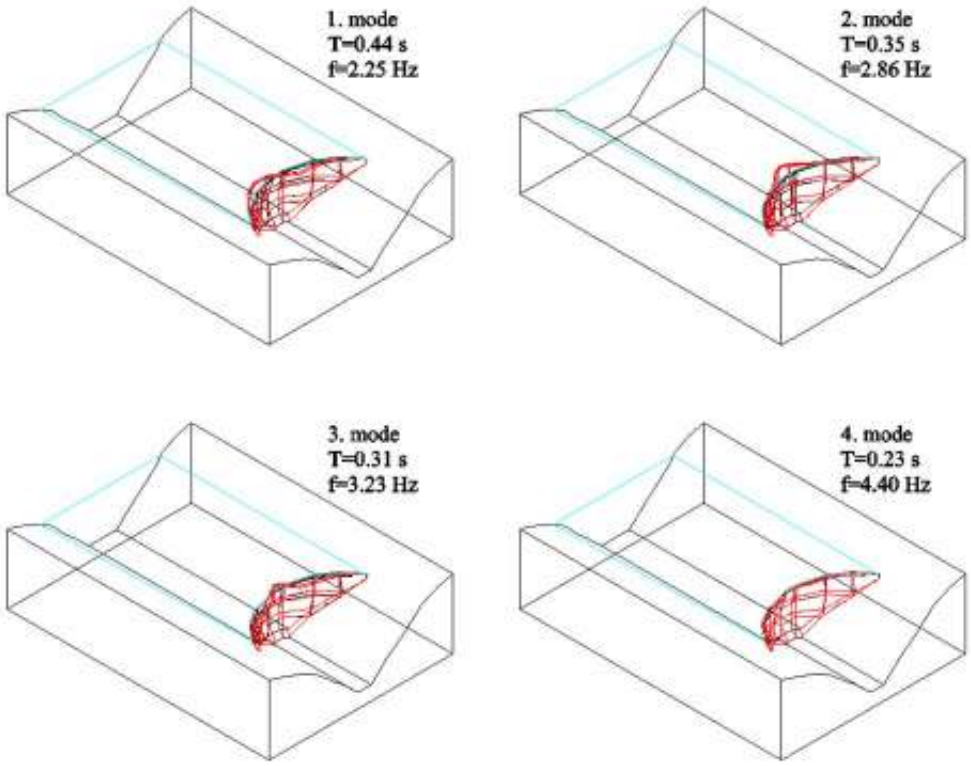

Figure 9 Oscillation periods, frequencies and eigenvectors for dam-accumulation system

Based on the calculated data, time step for dynamic analysis was adopted as $\Delta t=0.002$ s, which represents approximately 1/200 of first period (T1), and also well approximate given accelerogram (Figure 8). Time integration of equations of motion was performed by implicit method for water and construction.

The registered accelerations on the bottom of the dam (accelerograph 688, Figure 5) were taken as imposed accelerations of the foundation's rock (excitation) along the canyon (perpendicular to the dam axis). The maximal registered imposed acceleration was 47.8 cm/s². The maximal registered acceleration on the dam was 145.1 cm/s² (accelerograph 681, Figure 5), and the maximal acceleration obtained through the numerical model was 149.3 cm/s² (Figure 10). Applied excitations cause hydrodynamic pressures that are always less than the hydrostatic pressure, so cavitation did not occur.

Some calculation results are presented in Figures 10, 11 and 12. Figure 10 presents accelerations of the Grančarevo dam crest in time, Figure 11 presents displacement of the Grančarevo dam crest in time and Figure 12 presents hydrodynamic pressures on the bottom of the Grančarevo dam in time. Other results can be found in [11, 12].

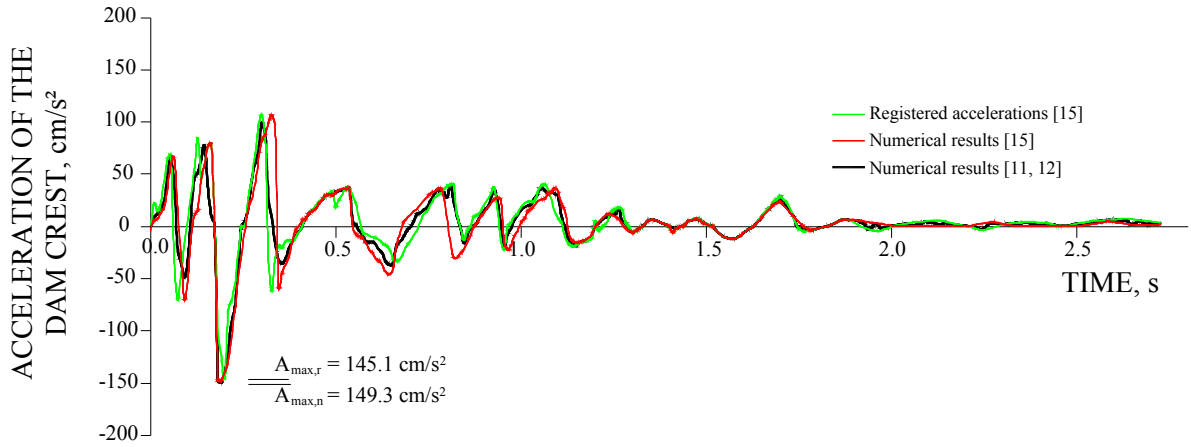

Figure 10 Accelerations of the Grančarevo dam crest

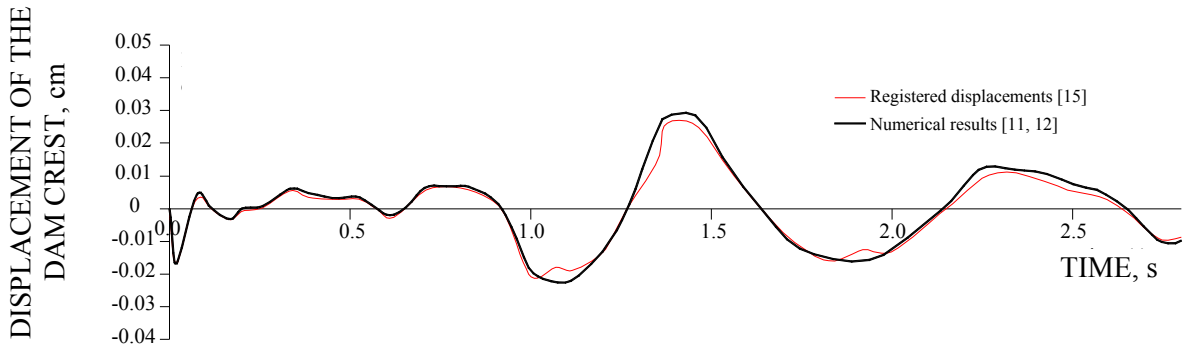

Figure 11 Displacement of the Grančarevo dam crest

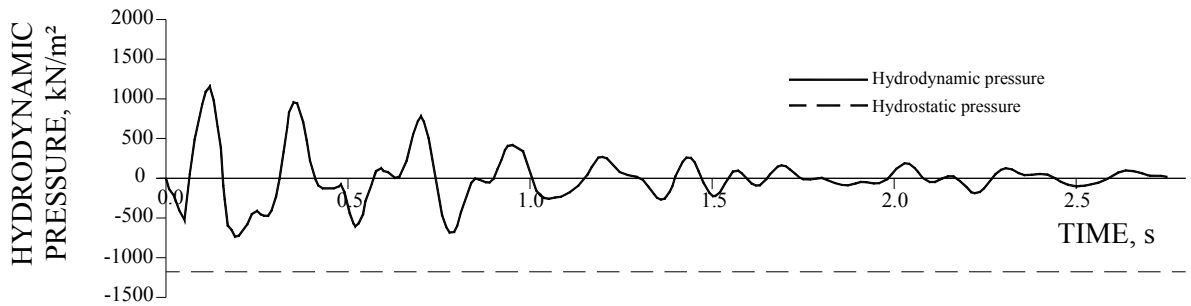

Figure 12 Hydrodynamic pressures on the bottom of the Grančarevo dam

CONCLUSIONS

The paper briefly describes the developed numerical model for the simulation of fluid-structure coupled problems. The applied models are primarily intended to simulate the fluid-structure dynamic interaction in seismic conditions.

The example clearly shows that model can simulate the most important effects of spatial structures that are in direct contact with the fluid. Some of the model's possibilities are illustrated in numerical analyses of the arch dam Grančarevo seismic behaviour.

In comparison of the results measured in situ and another results of the numerical simulations, presented in [15] and [16], a very good agreement has been achieved, even though a quite coarse finite element discretization has been adopted. This confirms that developed numerical model can be useful in numerical analysis of other similar fluid-structure coupled problems, in which fluid doesn't flow.

Further improvements of the model can be made by taking into account the wave's effect, which can be neglect in this particular problem.

REFERENCES

1. OWEN D R J AND HINTON E, Finite Elements in Plasticity, 1980, Pineridge Press, Swansea, UK.

2. DILIP K P, Efficient dynamic solutions for single and coupled multiple field problems, 1982, PhD Thesis, University College of Swansea, UK.

3. WILSON E L, YUAN M AND DICKENS J M, Dynamic analysis by direct superposition of Ritz vectors, Earthquake Eng. & Struc. Dyn., Vol. 10, 1982, pp. 813-832.

4. RADNIĆ J, DAMJANIĆ F B AND JOVIĆ V, Hydrodynamic pressures on rigid structures, Proc. European Conf. on Earth. Eng., Portugal, 1986.

5. RADNIĆ J, Fluid-structure interaction with cavitation effect, Građevinar, Vol. 7, 1987, pp. 269-275 (in Croatian).

6. DAMJANIĆ F B AND RADNIĆ J, Seismic Analysis of Fluid-Structure Interaction Including Cavitation, Proc. Int. Conf. on Computer Modelling in Ocean Engineering, Balkema, Roterdam, 1988, pp. 523-530.

7. YUAN M, CHEN P, XIONG S, LI Y AND WILSON E L, The WYD method in large eigenvalue problems, Eng. Comp., Vol. 6, 1989, pp. 49-57.

8. HOFSTETTER G AND MANG H A, Computational mechanics of reinforced concrete structures, 1995, Vieweg&Sohn, Wiesbaden, Germany.

9. KÜÇÜKARSLAN S, COŞKUN S B AND TAŞKIN B, Transient analysis of dam-reservoir interaction including the reservoir bottom effects, Journal of Fluids and Structures, Vol. 8, No. 20, 2005, pp. 1073-1084.

10. HARAPIN A, RADNIĆ J AND ĆUBELA D, Numerical model for composite structures with experimental confirmation, Materialwissenschaft und Werkstofftechnik, Vol. 39, No. 2, 2008, pp. 143-156.

11. HARAPIN A, RADNIĆ J AND BRZOVIĆ D, WYD method for an eigen solution of coupled problems, Int. Jnl. of Multiphysics, Vol. 3, No. 2, 2009, pp. 167-176.

12. BRZOVIĆ D, ŠUNJIĆ G, RADNIĆ J AND HARAPIN A, Numerical Model for Fluid-Structure Coupled Problems under Seismic Load, research monograph: 'Damage and Fracture of Composites Material and Structures', 2011, Springer, Germany (in print).

13. Esperienze Statiche su Modello Della Diga di Grancarevo, I.S.M.E.S. Instituto Sperimentale Modelli e Strutture, Bergamo, 1960, pratica No. 271 (in Italian).

14. Sulla Stabilita' Della Roccia di Fondazione Della Diga di Grancarevo Verificata Anche a Mezzo Modello Geomeccanico, I.S.M.E.S. Instituto Sperimentale Modelli e Strutture, Bergamo, 1963 (in Italian).

15. BIČKOVSKI V AND BOJADŽIEV M, Studies of static and seismic analysis of Grančarevo dam, The Institute of Earthquake Engineering and Engineering Seismology University "Ss. Cyril and Methodius" (IZIIS) Skopje, Macedonia, Report IZIIS 88-30, 1988 (in Serbian).

16. PEJOVIĆ R, MRDAK R, ŽIVALJEVIĆ R AND MIJUŠKOVIĆ O, An analysis of seismic resistance of the Grančarevo concrete dam, Građevinar, Vol. 58, 2006, pp. 447-453 (in Croatian).

Seismic Behaviour of Reinforced Concrete Beam-column Connections Enhanced with Steel, Polypropylene and Polyester Fibres

R H Scott[1], S K Deb[2], A Dutta[2], D G Kheni[2]
1 – Durham University, UK
2 – Indian Institute of Technology, Guwahati, India

During past devastating earthquakes, it has been noted that beam-column connections act as one of weakest links in moment resisting RC framed structures and it has been observed that exterior connections suffer more in comparison to interior ones. Since large parts of India lie in highly active seismic zones, issues relating to failure of beam-column connections due to seismic excitations are of considerable importance. IIT Guwahati is currently undertaking a major programme of tests on exterior beam-column connections and, as part of this programme, Durham University has manufactured internally strain gauged reinforcing bars for inclusion in four of the test specimens. The 2/3 scale specimens have been designed using a strong column-weak beam (weak in flexure) approach. Each specimen includes a 12 mm diameter instrumented U-bar as part of the main beam reinforcement with each bar containing 31 electric resistance strain gauges installed within a central longitudinal duct to avoid degradation of bond characteristic around the perimeter of the bar. Different combinations of steel, polypropylene and polyester fibres are used in the concrete for the four specimens to investigate ways of improving ductility under extreme displacements. Improved ductility, and hence reduced specimen damage due to seismic action, will facilitate new construction plus rehabilitation and retro-fitting of a joint after a seismic event. These four specimens have been tested using the excellent laboratory facilities available at IIT Guwahati. The paper gives details of the test programme and the influence of the fibres on joint ductility is illustrated using the considerable volume of data generated by the instrumented reinforcement. Recommendations for design engineers are made.

Dr Scott, a Reader in Engineering in the School of Engineering and Computing Sciences at Durham University, has many years experience researching into the behaviour of reinforced concrete strucural elements. He has published widely in this field and is an active participant in a number of technical committees of the American Concrete Institute.

Professor Deb is Head of the Department of Civil Engineering at IIT Guwahati. His present research is concerned with both laboratory testing and numerical modelling of seismic behaviour in a range of applications.

Professor Dutta is also involved with laboratory testing and numerical modelling of reinforced concrete structures at IIT Guwahati.

Mr Kheni is a research student at IIT Guwahati.

Keywords: Concrete, Connections, Ductility, Fibres, Seismic

INTRODUCTION

During past devastating earthquakes, it has been noted that beam-column connections act as one of the weakest links in moment resisting RC framed structures. Behaviour of reinforced concrete frame structures during earthquakes throughout the world has highlighted the consequences of poor performance of beam-column connections and it has been observed that exterior connections suffer more in comparison to interior ones. For some years the Indian Institute of Technology Guwahati (IITG) has been involved in a major research project to investigate seismic effects in exterior reinforced concrete beam-column connections since large parts of India lie in highly active seismic zones making issues relating to the failure of these connections of particular relevance.

The main thrust of the investigation has been to enhance the ductility of the connections rather than seek increases in strength. It is known that the inclusion of steel fibres in the concrete mix is an effective way of reducing macro-cracking [1] whilst polymer fibres are very good at arresting micro-cracking as well as enhancing impact strength and toughness [2]. Consequently there would seem to be advantages in using mixes incorporating both types of fibre and thus the test programme was designed to investigate this.

As part of the extensive main test programme four specimens incorporated, as part of the main beam reinforcement a strain gauged U-bar manufactured at Durham University and then shipped to Guwahati. The intention was to use the very comprehensive strain information generated by these bars to give detailed comparisons of the ductility behaviour of the different fibre combinations used in the main test programme. This paper concentrates on these four tests but the results and conclusions which resulted from them are consistent with those for the main test programme.

SPECIMEN DETAILS

Four types of fibres were used in the connection tests as follows:

Type **SF1**: Steel fibre, 35 mm long, 0.55 mm diameter with hooked ends
Type **SF2**: Steel fibre, 60 mm long, 0.75 mm diameter with hooked ends
Type **PP**: Polypropylene fibre, 12 mm long, 0.03-0.035 mm diameter
Type **PE**: Polyester fibre, 12 & 18 mm long, 0.03-0.035 mm diameter

Prior to the main test programme, 30 prism tests were conducted to determine the optimum fibre contents for the concrete mixes. Prisms were 700 mm long with a 150x150 mm cross-section and were tested in four point bending with a 200 mm constant moment zone. From these tests fibre contents in the four strain gauged specimens were determined as follows:-

Specimen **1**:	**No fibres**	i.e. used as a control specimen
Specimen **2**:	**SF1** (0.5%) + **SF2** (0.5%) +**PP** (0.15%)	i.e. Steel fibres + Polypropylene
Specimen **3**:	**SF1** (0.5%) + **SF2** (0.5%) +**PE** (0.15%)	i.e. Steel fibres + Polyester
Specimen **4**:	**SF1** (0.5%) + **SF2** (0.5%)	i.e. Steel fibres only

The fibre contents shown are percentage by total volume of the concrete. Specimens 2 and 3, containing two types of fibre (steel and polymer) were termed “hybrid” specimens.

The four 2/3rd scale connection specimens were designed following the provisions of ductile detailing as per IS: 13920, 1993 [3] and satisfying the condition of strong column-weak beam (weak in flexure) design. Columns had a 200 mm × 200 mm cross-section and beams were 240 mm deep by 200 mm wide. Confining reinforcement as per the provisions of IS: 13920, 1993 was provided in the joint region. Specimens were cast using M30 grade of concrete (equivalent to UK Grade 30) and the reinforcement was equivalent to UK Grade B500C. Details of the specimens and the reinforcement layout are shown in Figure 1. Portland pozzolana cement was used and the maximum aggregate size was 16 mm.

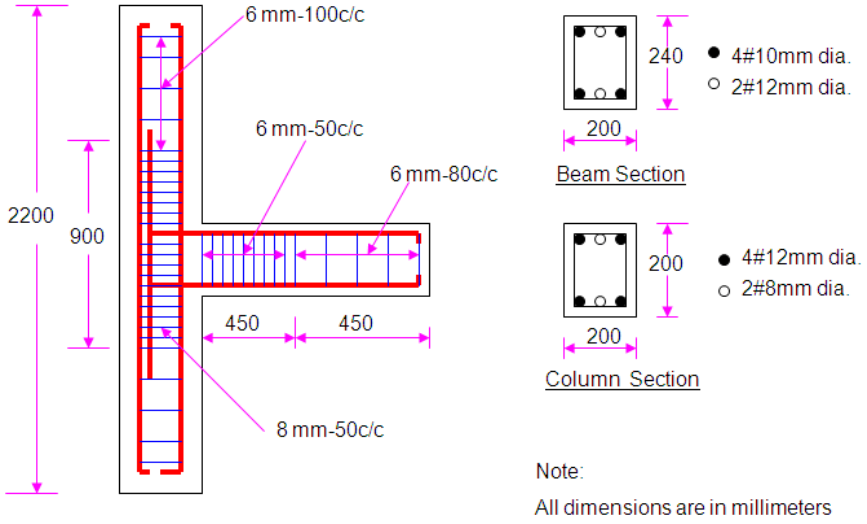

Figure 1 Specimen details

Each of these four specimens included a 12 mm diameter instrumented U-bar as part of the main beam reinforcement. Each U-bar contained 31 electric resistance strain gauges installed within a central longitudinal duct and positioned as shown in Figure 2. Bars of this type have been used in a number of previous investigations at Durham and full details of their manufacture can be found elsewhere [4, 5].

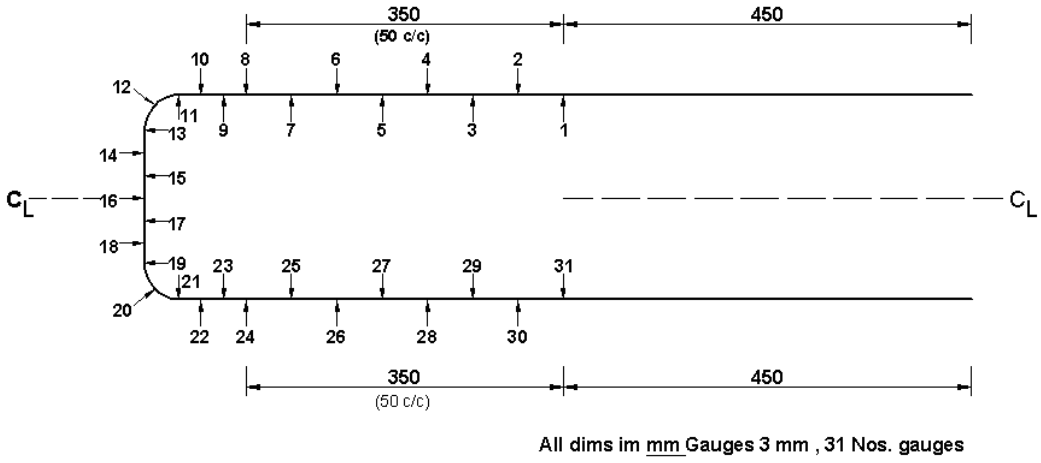

Figure 2 Strain gauge layout

TEST PROCEDURE

The schematic diagram of the testing arrangement is shown in Figure 3 and a photograph of the test rig is shown in Figure 4. The column was placed in a horizontal position with the beam vertical. An axial load of 10% of the gross capacity of column was applied to the column to simulate gravity loading. To simulate support condition at both ends of the column, special roller supports were fabricated. Cyclic load was applied to the beam by a servo controlled MTS actuator with a loading capacity of ±250 kN and ±125 mm maximum stroke. The displacement history shown in Figure 5 was followed with three push-pull cycles being applied at each increment of amplitude and each cycle taking 40 seconds to complete. Testing ceased when the specimen was on the brink of becoming unstable.

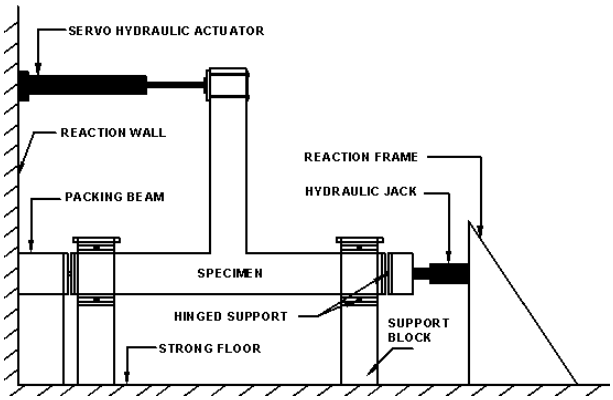

Figure 3 Test arrangement

Figure 4 Photograph of test set-up

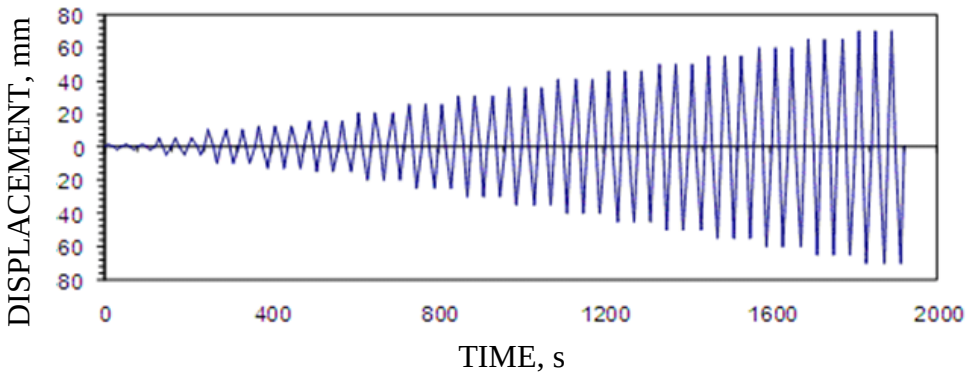

Figure 5 Displacement history

RESULTS

Table 1 lists age at test and concrete strengths for the four specimens. At early load stages all four specimens performed in a similar fashion with initial cracking in both the beam and the connection zone being followed by a plastic hinge forming in the beam close to the column face. This was as expected in view of the similarity of their geometry and the design of their reinforcement layout.

Table 1 Summary of test results

SPECIMEN	FIBRE TYPE	AGE AT TEST, days	COMPRESSIVE CUBE STRENGTH, MPa	INDIRECT TENSILE STRENGTH, MPa	MAXIMUM DISPLACEMENT, mm
1	None	28	32.22	4.04	46.67
2	SF1/SF2/PP	28	31.11	5.85	70.0
3	SF1/SF2/PE	28	33.77	4.94	70.0
4	SF1/SF2	28	34.21	4.19	61.67

However, as beam displacements increased, real differences became apparent between the behaviour of Specimen 1 (no fibres) and the other three specimens (with fibres) as indicated by the maximum displacements listed in Table 1. Figure 6 shows photographs of the connection zones after the final displacement and the effectiveness of all three fibre combinations in controlling degradation of the connection zone is immediately apparent. The addition of polymer fibres was particularly effective.

Specimen 1
(No fibres)

Specimen 2
(SF1/SF2/PP)

Specimen 3
(SF1/SF2/PE)

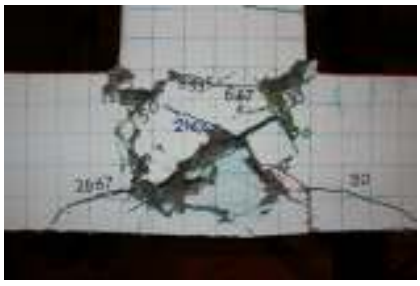

Specimen 4
(SF1/SF2)

Figure 6 Comparison of connection zone damage

A more formal comparison of specimen behaviour is obtained by comparing the load-displacement hysteresis loops as shown in Figure 7. All four specimens exhibited ductility but the superior performance of the specimens with fibres is indicated by their bigger final displacements and their less marked drop in load as displacements increased. Direct comparisons can be made by comparing the envelopes of their hysteresis curves and Figure 8 shows (using the results for Specimen 1) the necessary construction for estimating beam tip displacements under yield and ultimate conditions. As shown in this figure, the yield displacement is calculated as the point of intersection between two straight lines drawn on the envelope curve. The first line is obtained by extending the line joining the origin and the point on envelope curve corresponding to 50% of ultimate load carrying capacity, while the second line is the horizontal line corresponding to 80% of ultimate load carrying capacity. Ultimate displacement corresponds to the point of intersection between the horizontal line corresponding to 80% of ultimate load carrying capacity and the envelope curve at the far end. All four envelopes are shown in Figure 9.

Figure 9 reinforces the above observations. Specimen 1 (no fibres) achieved a final displacement of 46.67 mm with significant load reduction as this displacement was approached. Specimens 3 and 4 (SF1/SF2PE and SF1/SF2 respectively) both performed noticeably better but Specimen 3 (SF1/SF2/PE) was slightly superior as it achieved a final displacement of 70.0 mm as against the 61.67 mm of Specimen 4 (SF1/SF2). Specimen 2 (SF1/SF2/PP) clearly outperformed the other three specimens with its final displacement of 70.0 mm coupled a maximum load of 40.0 kN which was comparable with that for Specimen 1 (no fibres) and better than the values for Specimens 3 and 4. These observations confirm that: (i) stiffness degradation rate declined, (ii) cumulative energy dissipation capacity increased, and (iii) displacement ductility increased.

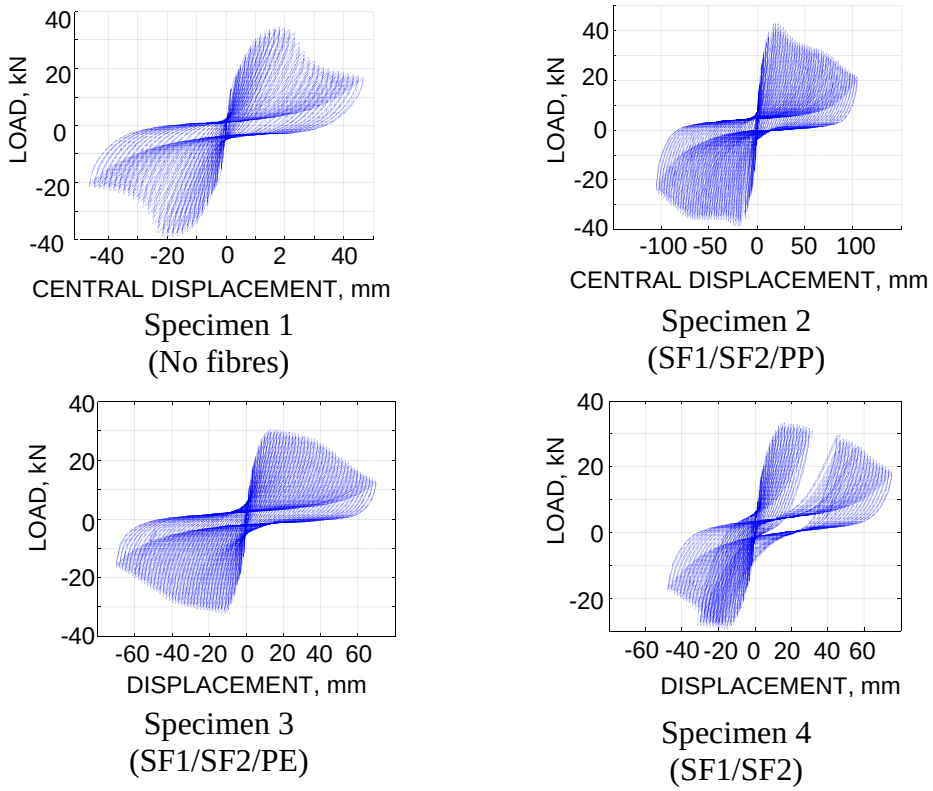

Figure 7 Load-displacement hysteresis loops

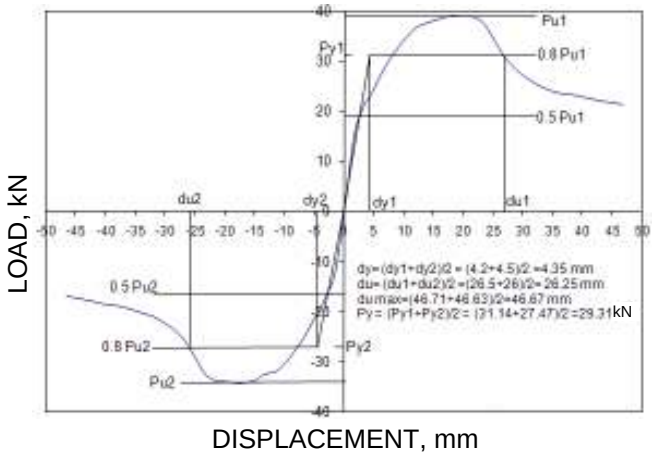

Figure 8 Construction of hysteresis envelope for Specimen 1

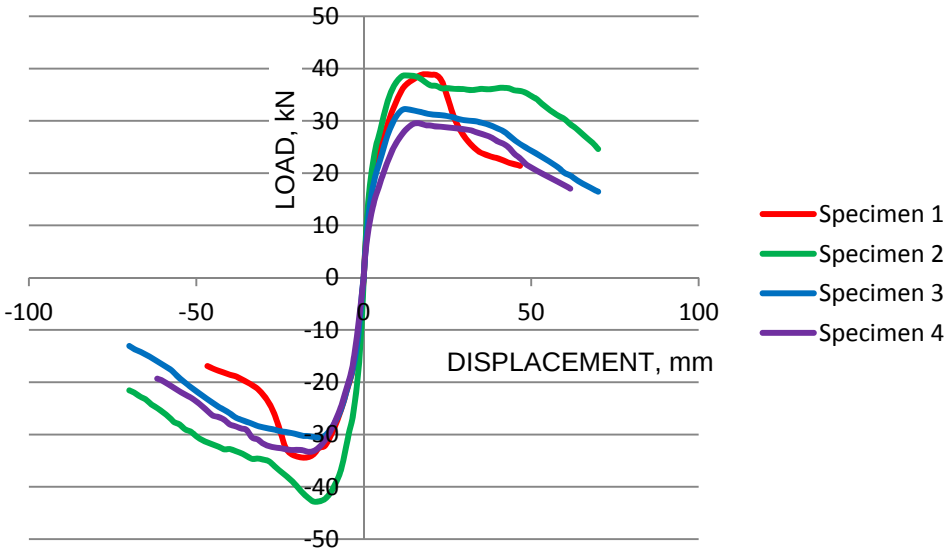

Figure 9 Envelope curves for hysteresis loops

Detailed data pertaining to reinforcement strains was obtained from the strain gauged U-bars. Figure 10 shows strains for a displacement of 1.67 mm for Specimen 3 in both the push and pull directions of loading. The distributions are plotted along a straightened form of the bar with Gauge 1 (top leg) at the left hand end and Gauge 31 (bottom leg) at the right hand end. Strains are plotted tension positive.

At this low displacement level the reinforcement was behaving elastically with peak strains occurring at the column face due to flexural cracking. There was also a degree of symmetry between distributions for the push and pull directions of loading as would be expected from the symmetrical reinforcement layout. As displacements increased, however, tensile stresses encroached further into the connection zone until the whole of the U-bar in the connection zone was in tension for both the push and pull loading directions. Finally, the reinforcement yielded leading to the development of large residual strains, as shown in Figure 11 for the 41.67 mm level in Specimen 2. This behaviour, which was observed in all four specimens, was consistent with earlier reported work [6].

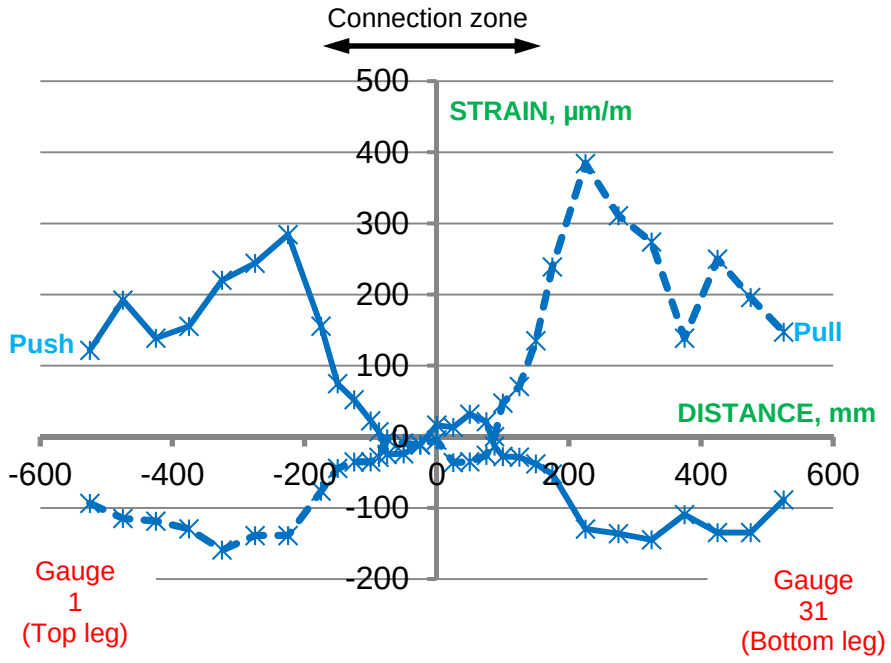

Figure 10 Specimen 3: U-bar stains at 1.67 mm displacement

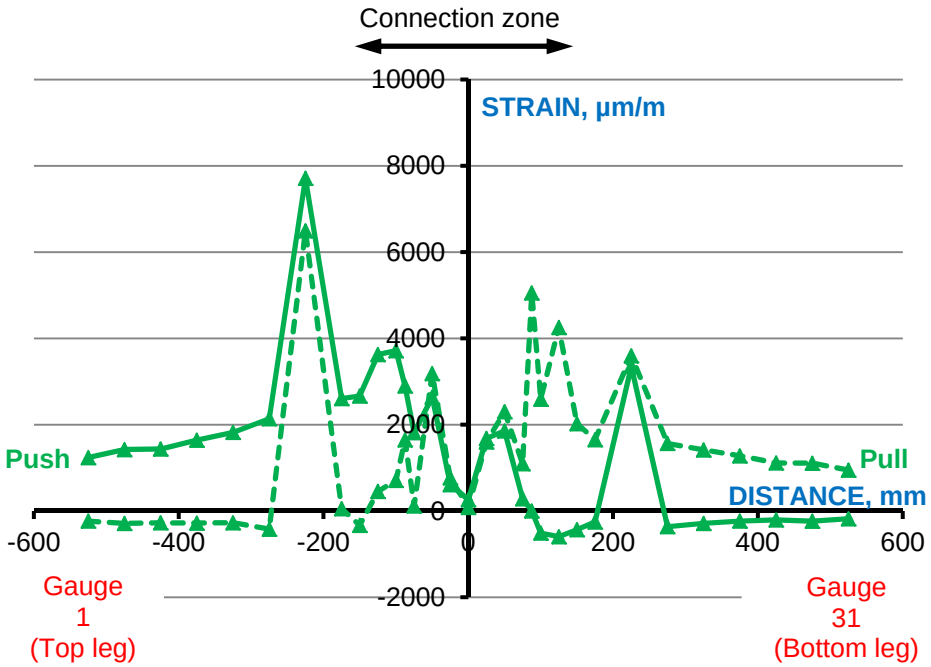

Figure 11 Specimen 2: U-bar stains at 41.67 mm displacement

At displacements of 46.67 mm, the largest displacement sustained by all four specimens, peak strains were, in round figures (as there was considerable creep) 23000, 8000, 9000 and 15000 μm/m for Specimens 1-4, respectively. Increasing displacements further led to even larger strains in Specimens 2-4. The data indicated that the addition of fibres to the concrete mix reduced the strain level in rebars required to achieve a given displacement with hybrid Specimens 2 and 3 proving more effective than Specimen 4 which had steel fibres only.

Overall, adding fibres gave increased ductility coupled with reduced reinforced strains. Compared with Specimen 1 (no fibres i.e. the control), hybrid Specimen 2 (SF1/SF2/PP) performed best with hybrid Specimen 3 (SF1/SF2/PE) coming a close second followed some way behind by Specimen 4 with steel fibres only. The addition of polymer fibres proved to be a particularly effective way of limiting connection zone degradation (Figure 6) thus making joint repair after a seismic event a more practicable proposition.

CONCLUSIONS

Four tests were performed on exterior beam-column connections subjected to seismic loading each of which contained a strain gauged U-bar as part of the main beam reinforcement. Specimen 1 acted as a control (no fibres), Specimens 2 and 3 were hybrids, containing both steel and polymer fibres, while Specimen 4 contained steel fibres only.

1. All three specimens with fibres showed marked improvements in ductility compared with the control specimen. Hybrid Specimen 2 (steel plus polypropylene fibres) performed best with hybrid Specimen 3 (steel plus polyester fibres) coming second and Specimen 4 (steel fibres only) a close third.

2. All three specimens with fibres exhibited markedly less degradation of the connection zone compared with the control specimen.

3. The results from the strain gauged bars indicated that the improved ductility in specimens with fibres was accompanied by reduced strains in the reinforcement under ultimate displacement conditions. Large residual strains were developed in all four specimens once the reinforcement had yielded.

4. To summarise, from best to worst, the behaviour of the four specimens was ranked 2, 3, 4, 1.

ACKNOWLEDGEMENTS

The financial support provided by the Royal Society’s International Joint Project Award is gratefully acknowledged.

REFERENCES

1. BANTHIA N AND TROTTIER J F, Test methods for flexural toughness characterization of fiber reinforced concrete: some concerns and a proposition, ACI Materials Journal, Vol. 92, No. 1, 1995, pp. 48-57.

2. BANTHIA N AND SOLEIMANI S M, Flexural response of hybrid fiber-reinforced cementitious composites, ACI Materials Journal, Vol. 102, No. 6, 2005, pp. 382-389.

3 IS 13920: 1993. Ductile detailing of reinforced concrete structures subjected to seismic forces – Code of Practice, Bureau of Indian Standards, New Delhi.

4. SCOTT R H AND BEEBY A W, Long term tension stiffening effects in concrete, ACI Structural Journal, Vol. 102, No. 1, 2005, pp. 31-39.

5. SCOTT R H AND WHITTLE R T, Moment redistribution effects in beams, Magazine of Concrete Research, Vol. 57, No. 1, 2005, pp. 9-20.

6. SCOTT R H, Intrinsic mechanisms in reinforced concrete beam-column connection behaviour, ACI Structural Journal, Vol. 93, No. 3, 1996, pp. 336-346.

Analysis of Seismic Vulnerability: Case Study of Buildings Within Seismic Hazard Zones

G Abdelheq, H Mimoune
University Mentouri Constantine, Algeria

Seismic vulnerability of an urban environment is characterized by the ability of buildings and structures to support seismic events (physical vulnerability) and by the ability of people to behave in a consistent and rational face a major event (social vulnerability). Constantine is a city with moderate seismicity but the level of risk is high because of urban concentration and topography of the site. The seismic risk reduction therefore requires assessing the physical vulnerability of its buildings. It is proposed in this paper an analysis of a group of buildings for residential use located west of the city, consisting mainly of relatively high buildings. Following a survey of a portion of the housing stock of this city, a seismic survey method was applied based on ”observations” post-seismic. Vulnerability indicators are statistically related to damage through a vulnerability index ”IVi” to establish curves of damage (or vulnerability). These are used to estimate the level of damage that is likely resulting in damage cards. The goal is to develop an initial database of some of the housing stock in the city of Constantine (knowledge of earthquake hazards, construction defects ...) to be used in the estimation of seismic risk and verification of seismic safety of existing buildings.

Guettiche Abdelheq is a second year PhD student at Mentouri University, Algerian, with research experience in seismic vulnerability and soil mechanics.

Houdheil Mimoune is a student in Masters student in the Architectural Departement at the University of Mentouri, Algeria.

Keywords: Constantine city, Damage, Earthquake hazard, Seismic vulnerability

INTRODUCTION

The seismic risk is defined as the convolution of seismic hazard, vulnerability of the constructions and its value (human cost, equipment, etc.). Several methods have been developed around the world to assess the seismic vulnerability is the seismic risk assessment (ATC 21; GNDT, 1993; HAZUS, 1999, Risk-EU, 2004; Vulneralp, etc.), which therefore requires to have a probable hazard assessment, but also a representation of the seismic quality of buildings and a knowledge of the level of community readiness to suffer damage.

The study was performed on the seismic hazard in the city of Constantine have shown that it is an earthquake zone and that the risk of an earthquake through the region is likely (A. HARBI, 2001; and Bounif et al.). In addition, the most common constructions are very old, dating back to colonial times. A hazard assessment is made either by seismic experiments (1908, 1947, 27 October 1985) to locate seismic sources or by a seismotectonic analysis on the faults of Constantine (Temlouka fault, Sigus fault, Ain Smara fault).

In this paper we propose to present a study of seismic vulnerability of some existing residential buildings on the site "Ciloc," have been chosen for their importance (number of dwelling), the predictable risks (landslide, not seismic construction), and their construction period. For this purpose, a methodology was used to study their behaviour, a collection of a number of typological and constructive information for each building. This information is combined to define the coefficients for a vulnerability index "IV", and using a European method "RISK-UE".

SITE INFORMATION

The site “Ciloc” provides a series of buildings of reinforced concrete (storey + 12, storey + 10), built in 1958 as part of the Constantine plan, each building has 120 apartments, 600 to 700 persons per building. These buildings occupy the western edge of Bellevue plateau with a relatively high slope (10-15%). Buildings are founded on piles of 14 m, so this study is to make a diagnosis of seven buildings with reinforced concrete floors, in solid slab located on the Ciloc site (Figures 1 and 2). These buildings were scanned into a database that includes their technical survey forms.

Figure 1 Satellite view of the study area

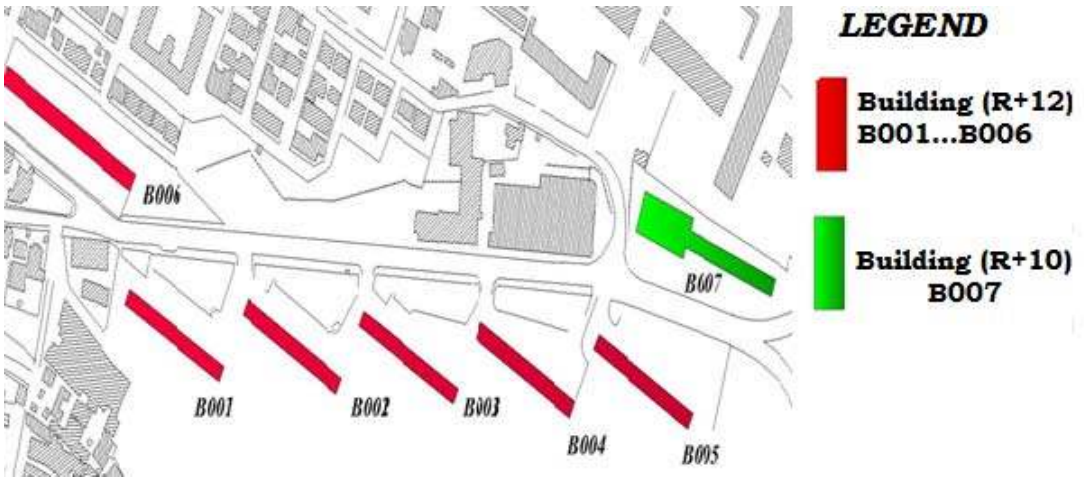

Figure 2 Building's view "R. concrete"

Based on site observations and synthesis of in-situ tests, conducted near the building by B004 "LTP E" [1], shows:

- The nature of clay and gravel embankments 2 to 6 m thick.
- The colluviums gravely clay with thicknesses of several meters.
- Fine sand and gravel.
- Sand flintware with thicknesses of around 60 m.
- Represented by Miocene red clay to greenish.
- The presence of water a few meters deep is maintained by continuous release of waste water leakage of sewerage system).

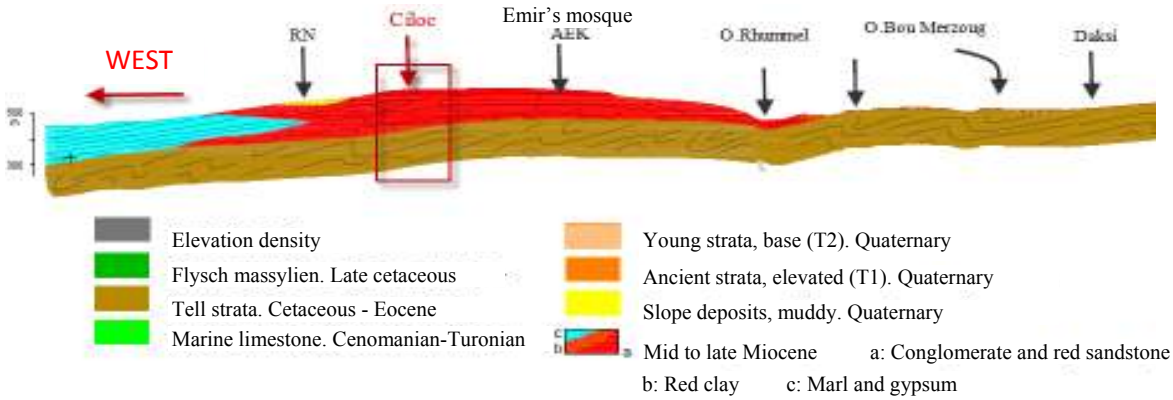

Figure 3 Geological section of the study area

Studies conducted on the site Ciloc [2], shows an instability very important, very active but limited slope, under the building B004, a bank does not guarantee stability in the case of an earthquake. The surrounding buildings and their approaches are in an environmental concern (many waste dumps, clogged drains, sewage flows) and suffer from inadequate maintenance.

ANALYSIS OF THE EARTHQUAKE HAZARD

Historically, Algeria is known to be a very active seismic zone. Geological studies show that the North is mainly subjected to seismic activity and is crossed from east to west by a fault line between Oran and Constantine through Algiers. So the city of Constantine is in the "tell" within the vicinity or on active anticlinal axes and therefore their situation may be dangerous.

Because the earthquakes in Constantine's "tell" are frequent, so the seismic zoning map prepared by the Algerian territory CRAAG, and (Bezzeghoud et al. 1996) shows that our study area is located in the area of seismic hazard means is characterized by active seismicity, with maximum intensities (between IX and X) of magnitude but moderate 3 to 6 on the Richter scale (Figure 5).

The seismic hazard map for the northern region shows the probability of exceeding 10% of the ground acceleration for a period of 50 years which corresponds to a return period of 475 years. Several potentially active faults are active in the region of Constantine (Figure 6).

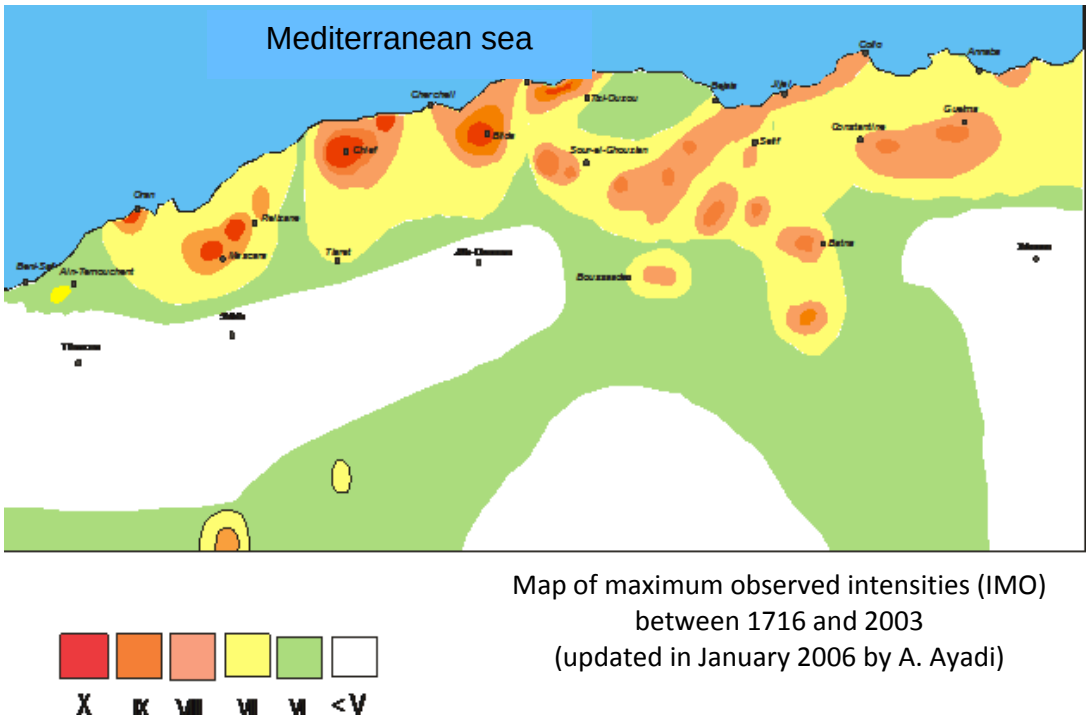

Figure 4 Maximum intensities in Algeria

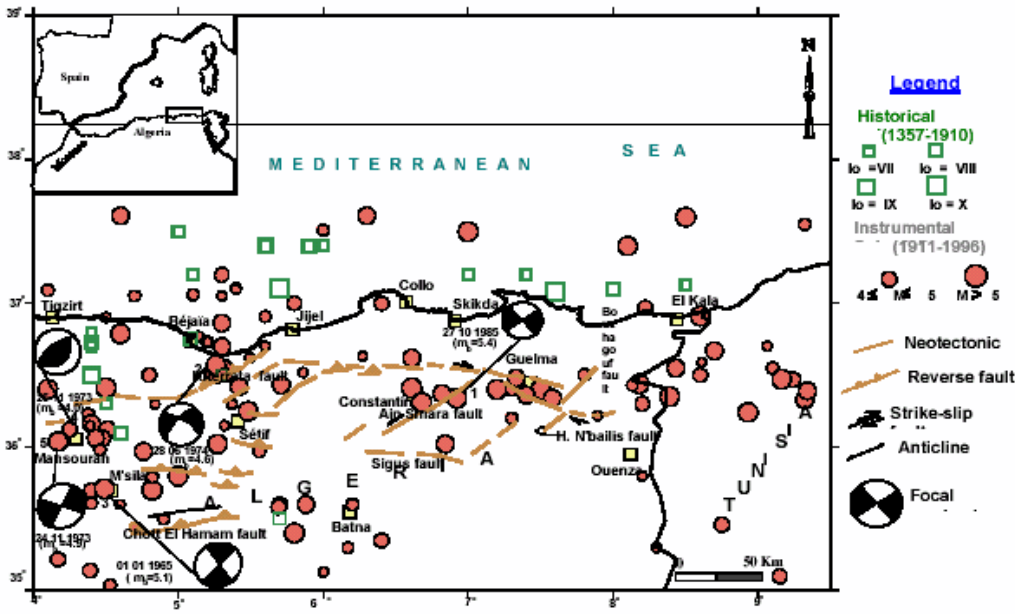

Figure 5 Earthquake Hazard Map, North-East Algeria

- The Constantine fault
- The Seguis fault
- The Ain Smara fault (active geological structure)

The latter is best known in the region of Constantine, its activity was confirmed by surface rupture observed following the earthquake of 27 October 1985 [4] this is a flaw sub-vertical of about 25 km. this fault whose seismic potential is important 1985 [4], this is a flaw sub-vertical of about 25 km. This fault is the main source of earthquakes that threaten the city of Constantine and the surrounding area (Figure 7).

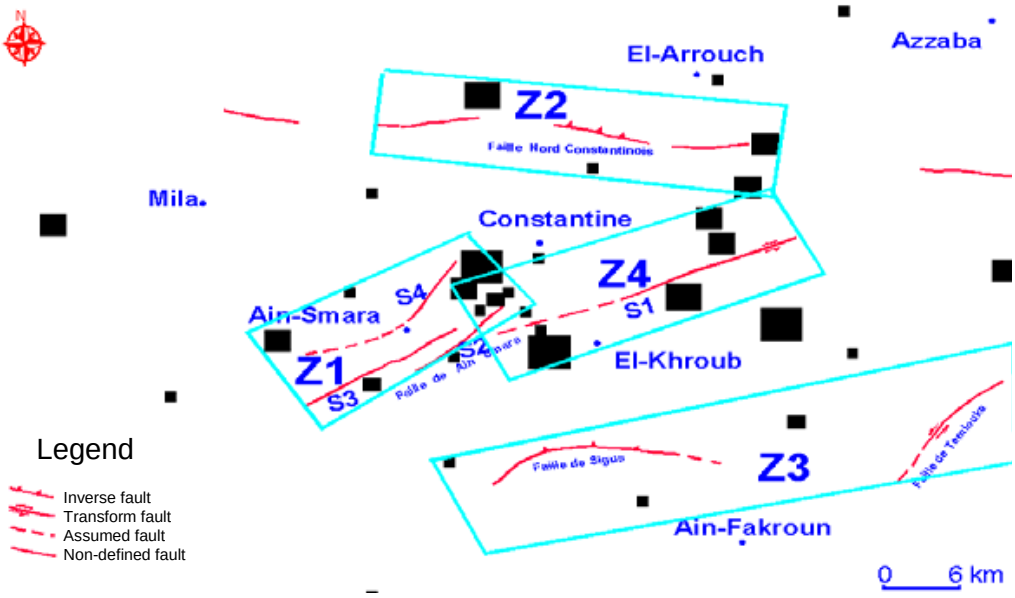

Figure 6 Faults in the region of Constantine [5]

Figure 7 Fault of Ain Smara [6]

Ground motion, represented in a map, here is characterized by spectral response, the PGA and PGV. It is defined through two different approaches, the probabilistic and deterministic approach.

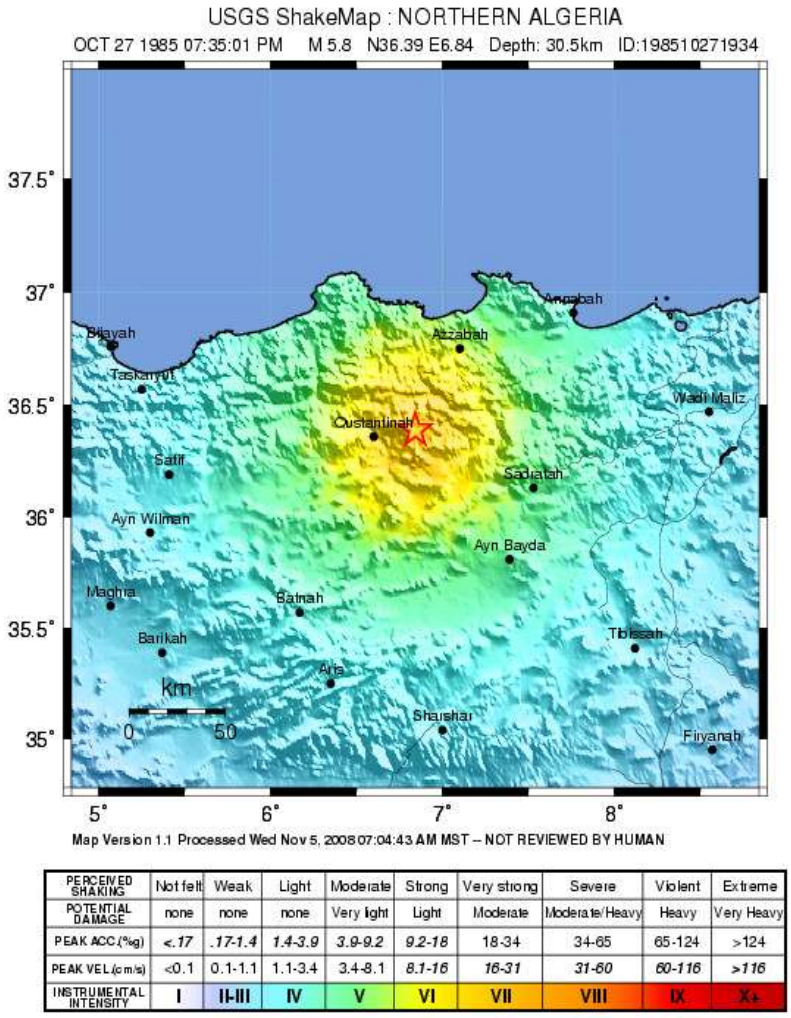

Figure 8 Map of macro seismic intensities (Constantine earthquake 1985, USGS)

The seismic activity known beginning in June 1758, (from the CRAAG) many earthquakes have occurred, some of them violent and deadly. Among these earthquakes we can cite: the 1894 earthquake, 4 August 1908, 6 August 1947, Ain Smara 9 July 1977, Constantine 27 October 1985, generally this area is predominantly characterized by shallow earthquakes (depth less than 20 km) causing considerable damage in the epicentral area.

Among the many events that shook the city of Constantine and eastern Algeria, the earthquake of 1985 is considered the famous and largest seismic event in eastern Algeria with a magnitude M = 5.8, there is evidence of a pure sliding along a fault direction N45º, and whose epicentre was located in the region of El-Aria. This earthquake has killed five people and injured 300, and there are several old buildings damaged, the most significant damage was recorded in the region of El-Aria, the intensity was measured at I0 = VIII (MSK) in this region [7]. It should be noted that the seismic hazard in Constantine city, even of small amplitude, may be an acceleration factor of landslides.

VULNERABILITY ASSESSMENT

The choice of method of calculation depends on the objectives and means available, and given access. On this basis, the RISK-UE method was proposed because some similarity exists between European construction's (France, Italy, etc.) and Algerian constructions.

Preparation of Technical Survey

Before any analysis of vulnerability, we must analyse the different types of structures on the site of study, evaluation of the data sheet for the estimation of the vulnerability index "IV" better site surveys, requires knowledge parameters such as structural or non-structural, (building materials, construction year, type of foundation, number of floors, design, etc.) and the place (geotechnical holes, fault, etc.).

Calculation Method

It is based on the evaluation of a vulnerability index for a given building, which index is based on the constructive typology. From the index, it is possible to define in terms of macro seismic intensity EMS98 [8], vulnerability curves that assess the probability distribution of damage to a building. It has built 23 major classes and each class, the most probable value of the vulnerability index (IV*), the limit values of the plausible range of the index (IV, IV^+) and upper and lower limits of the possible values of the vulnerability index (IV_{min}, IV_{max}) are given. RISK-UE project [9], has developed an array of types of buildings that reflect the characteristics of structures built of the most common existing.

Table 1a Typology of European macro seismic scale EMS 98

TYPOLOGY	DESCRIPTION	VALUES OF REPRESENTATIVES				
		IV_{min}	IV^-	IV*	IV^+	IV_{max}
M1.1	Rubbles	0.62	0.81	0.873	0.98	1.02
M1.2	Paired stones	0.46	0.65	0.74	0.83	1.02
M1.3	Dimension stone	0.3	0.49	0.616	0.793	0.86

Table 1b Typology of European macro seismic scale EMS 98, continued

TYPOLOGY	DESCRIPTION	VALUES OF REPRESENTATIVES				
		IV_{min}	IV^-	IV*	IV^+	IV_{max}
M2	Adobe	0.62	0.687	0.84	0.98	1.02
M3.1	Wood floors	0.46	0.65	0.74	0.83	1.02
M3.2	Masonry vaults	0.46	0.65	0.776	0.953	1.02
M3.3	Floors with steel beams and masonry	0.46	0.527	0.704	0.83	1.02
M3.4	Reinforced concrete floors	0.3	0.49	0.616	0.793	0.86
M4	Reinforced masonry bearing walls or confined	0.14	0.33	0.451	0.633	0.7
M5	Overall reinforced masonry	0.3	0.49	0.694	0.953	1.02
RC1	Column-beam structures in reinforced concrete	-0.02	0.047	0.442	0.8	1.02
RC2	Bearing walls of reinforced concrete	-0.02	0.047	0.386	0.67	0.86
RC3.1	Masonry infill walls, regular structure	-0.02	0.007	0.402	0.76	0.98
RC3.2	Irregular column-beam structures	0.06	0.127	0.522	0.88	1.02
RC4	Mixed concrete structures (gantry and walls)	-0.02	0.047	0.386	0.67	0.86
RC5	Walls precast reinforced concrete (tilt-up walls)	0.14	0.207	0.384	0.51	0.7
RC6	Precast reinforced concrete	0.3	0.367	0.544	0.67	0.86
S1	Steel structure with gantry	-0.02	0.467	0.363	0.64	0.86
S2	Steel structure with triangulation	-0.02	0.467	0.287	0.48	0.7
S3	Porticos + unreinforced masonry infill	0.14	0.33	0.484	0.64	0.86
S4	Porticos + concrete walls cast in place	-0.02	0.047	0.224	0.35	0.54
S5	Mixed structure concrete -steel	-0.02	0.257	0.402	0.72	1.02
W	Timber structures	0.14	0.207	0.447	0.64	0.86

The vulnerability index "IV" is the sum of the index type IV*, the other factor ΔV_m parameter (foundation and floor, regularity in plan, elevation regularity, and number of floors) and regional vulnerability factor ΔV_R.

$$IV = IV^* + \Delta V_m + \Delta V_R \quad (1)$$

Table 2 the values of the vulnerability index means

BUILDING	B001	B002	B003	B004	B005	B006	B007
Most probable value of vulnerability index (IV*)	0.746	0.746	0.746	0.746	0.746	0.706	0.826

From Table 2 we find that:

- Buildings (B001, B002, B003, B004, and B005), have the same Vulnerability Index because it‘s have the same structural typology.
- The building "B007" has a poor seismic design (irregularity in plan and elevation) which justified the high value of the vulnerability. [11].
- The building six "B006" is on stable ground and the level of maintenance and better than other buildings.

Table 3 Differentiation of structures vulnerability class (Table of vulnerability) [8]

	TYPE OF STRUCTURE	VULNERABILITY CLASS A B C D E F
MASONRY	rubble stone, fieldstone	
	adobe (earth brick)	
	simple stone	
	massive stone	
	unreinforced, with manufactured stone units	
	unreinforced, with RC floors	
	reinforced or confined	
REINFORCED CONCRETE (RC)	frame without earthquake–resistant design (ERD)	
	frame with moderate level of ERD	
	frame with high level of ERD	
	walls without ERD	
	walls with moderate level of ERD	
	walls with high level of ERD	
STEEL	steel structures	
WOOD	timber structures	

○ most likely vulnerability class; — probable range;
----range of less probable, exceptional cases

Table 4 Definition of levels of damage to masonry buildings according to EMS98 [8]

EMS98 SCALE	1	2	3	4	5
Reinforced Concrete Structure	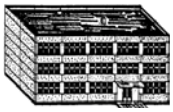	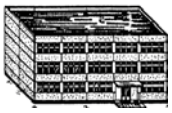	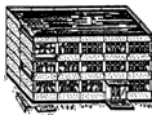	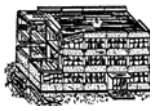	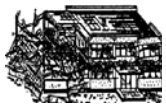
Damage medium	Negligible to slight damage	Moderate damage	Substantial to heavy damage	Very heavy damage	Destruction
	[0.0 – 0.2]	[0.2 – 0.4]	[0.4 – 0.6]	[0.6 – 0.8]	[0.8 – 1.0]

According to the classification made by the European macro seismic scale EMS98, the vulnerability class the most likely for a reinforced concrete construction without seismic design is the class "C", and likely with a class "B".

MEDIUM DAMAGE μ_D

From the vulnerability index IV and seismic intensity (I), the method RISK-UE "level 1" calculates the medium degree of damage to an area Sd using the formula [2]:

$$\mu_D = 2.5\left[1 + \tanh\left(\frac{I + 6.25IV - 13.1}{Q}\right)\right] \quad (2)$$

The curves derived from EMS-98 scale are characterized by a fixed value of Q = 2.3. The macroseismic intensity I and the scale of degrees of damage in respect of which μ_D are those developed in EMS98.

From vulnerability indices calculated above, it is possible to develop vulnerability curves for different intensities of earthquake. The use of values and IV_{min} IV_{max} in Equation (2) defines the upper bounds of probable value for IV.

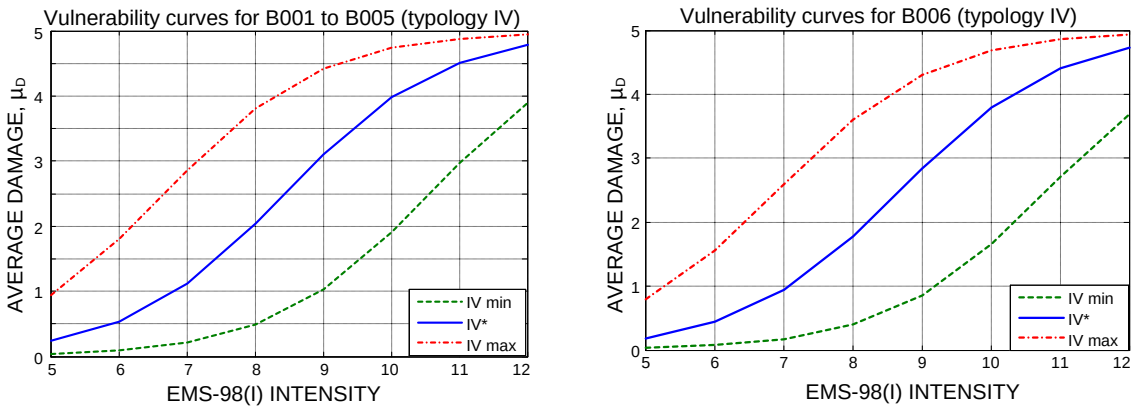

Figure 9 Vulnerability curves for building (B001…B006) calculated by the EU Risk method

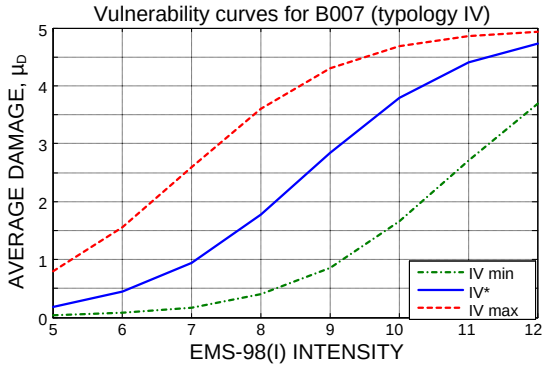

Figure 10 Vulnerability curves for building (B007) calculated by the EU Risk method

As can be seen, the vulnerability curves are based on experience and expert on post-seismic observations. Thus they are valid for the countries for which they were developed. And the parameters used to express the vulnerability of buildings may be different from one country to another.

CONCLUSIONS

This work concerns the evaluation of seismic risk on an area of the city of Constantine includes construction of family housing. A vulnerability assessment of structures was performed using the methodology RISK-UE Level 1, a method was developed as part of a European project, a choice was justified by the similarity between the construction area Ciloc (colonial times) and the European construction.

- A method we allow at least cost to have a first ranking of vulnerability to a group of buildings.
- The study showed the importance of seismic vulnerability index to know the quality of buildings studied, because the structure is more vulnerable than its vulnerability index is Important.
- In the static analysis method RISK-UE shows good consistency with the European macroseismic scale classification EM98. The vulnerability curves presented allow defining a given level of medium damage (and limits) for each intensity level EMS-98.

Finally this study has shown that it is possible to assess the seismic vulnerability of historic buildings in Constantine like other countries, with relatively simple methods and fast, because they allow a much larger study, and lead more quickly to define a strategy taken into account to achieve confrontments.

REFERENCES

1. Glissement de terrain, immeubles CILOC, Constantine, Etude de Confortement, Note de Calcule LTP/E, 1989.

2. BOUHADED .Y ,JAOUAMI , Etude des glissements terrain a travers la ville de Constantine « étude de l'aléa sismique »,SIMEC SOL ,2003.

3. BEZZEGHOUD ,M, A. AYADI, A. SEBAI, M. AIT MESSAOUD,. MOKRANE ,A ,BENHALLOU. H Seismicity of Algeria between 1365 and 1989 , Map of Maximum Observed Intensities (MOI). Avances en Geofisica y Geodesic, Ministériel de Obras Publicains,Transports y medio Ambiant, volume num ,1996.

4. BOUNIF, A., H. HAESSLER & M. MEGHRAOUI The Constantine (Northeast Algeria) earthquake of 27October 1985, surface ruptures and aftershock study, Earth Planet Sc. Lett. 85, 451-460, (1987).

5. AMOURI ,C, HOUARI ,H. response spectrum in the east of Algeria, asian journal of civil engineering (building and housing) vol. 13, no. 1 (2012) ,pages 147-154

6. BENABBAS C : Evolution moi-plio-Quaternaire des bassins continentaux de l'Algérie nord orientale : Apport de la Photogéologie et Analyse Morpho-structurale. Thèse. Docte. Etat. Université. Mentouri. Constantine. 256 p, 2006.

7. BENOUAR, D. Materials for the investigation of The seismicity of Algeria and Adjacent egions during the Twentieth Century, Annali Di Geofisica, volume XXXVII, N, 4, July994.

8. GRUNTHAL ,G, A. LEVRET, échelle macrosismique européenne EMS-98, edition .française Luxembourg ,2001.

9. RiskUE « an advanced approach to earthquake with applications to diffrent european towns, projet europpéen , EVK4-CT-2000-00014 ,2003.

10. Règles Parasismiques Algériennes RPA 99 , Version 2003.

11. A TC21. Rapid Visual Screening of buildings for Potential Seismic Hazards, a Handbook. Applied Technology Council, FEMA-145, Redwood City, California, 1988.

12. HARBI, A, Analyse de la séismicité et mise en évidence d'accidents actifs dans le nord-est algérien. Thèse de Magistère U.S.T.H.B, Alger, 2001

Impact Resistance of Fibre Reinforced Concrete

S Rehacek[1], P Hunka[1], I Simunek[1], J Kolisko[2]
1 – Czech Technical University, Czech Republic
2 – Czech Technical University,

Fibre-reinforced composite materials are becoming important in many areas of technological application. In addition to the static load, such structures may be stressed with short-term dynamic loads or even dynamic impact loads during their lifespan. Dynamic effects can be significant especially for thin-walled shell structures and barrier constructions. Impact loading of construction components produces a complex process, where both the characteristics of the design itself and the material parameters influence the resultant behavior. It is clear that reinforced concrete with fibres has a positive impact on increasing the resistance to impact loads. However, the assessment of the increase of this resistance has not been sufficiently verified experimentally. The first part of the project: laboratory load tests, aiming not only to determine the appropriate shape of test specimens, but also to evaluate and select appropriate ways to support the test specimens can be found in paper references. The second part of the project: results of impact load tests carried out on a beams and circular specimens are presented in this paper.

Stanislav Rehacek is a PhD student at the Klokner Institute of the Czech Technical University in Prague since 2006. Graduate of Czech Technical University in Prague, Faculty of Civil Engineering - Building Structures. Diploma thesis: construction project of multifunctional building.

Petr Hunka is a PhD student at the Klokner Institute of the Czech Technical University in Prague since 2007. Graduate of Brno University of Technolog, Faculty of Civil Engineering - Building Materials Engineering . Diploma thesis: Monitoring of the growth of modulus of elasticity at high performance concrete.

I Simunek is a member of the Klokner Institute of the Czech Technical University in Prague.

Jiri Kolisko is currently head of Klokner Institute of the Czech Technical University in Prague. He has led several research projects on concrete, and his specialist areas of research are special types of concrete, ultrahigh performance concrete, and mortars for reconstruction.

Keywords: CMOD, Impact resistance, Load tests, Steel fibres

INTRODUCTION

The goal of the project is to establish new procedures for evaluating the impact resistance of cementitious composites. An appropriate shape of test specimens, ways to support the test specimens and the method of measurement were chosen on the basis of experiments. A suitable form of test specimens was selected on the basis of static load tests of unreinforced test specimens.

The load tests of specimens reinforced with different fibre content of reinforcement were made afterwards. The specimens in the shape of a circular plate with a diameter of 500 mm and 50 mm thickness were selected for further examination on bases of the tests results.

Static tests of reinforced specimens (circular plates)

The next step was to determine the static load of the specimens with different amounts of reinforcement. Each recipe, with different amounts of reinforcement is given in Table. 1. The steel wire fibres with hooked ends (KrampeHarex DE50/1.0 N) of diameter 1.0 mm and length of 50 mm were used.

Table 1 Mixtures A, B and C

CONCRETE COMPONENT		QUANTITY, kg/m³			
		A	B	C	(ADDITIONAL) D
CEM II/A-S 42.5 R – Čížkovice		350	350	350	350
Aggregate:	Fine 0 – 4 mm, Kaznějov	1195	1189	1181	1185
	Coarse 4 – 8 mm, Kaznějov	644	641	636	638
Superplasticizer, Chysofluid Optima 208		8.75	8.75	8.75	8.75
Steel wire Fibers KrampeHarex DE50/1.0 N		20	40	80	60
Water		157.5	157.5	157.5	157.5

The test results of reinforced specimens in the form of a dependency graph between deflection and applied force are shown in Figure 1.

Due to the limited space of this paper only the A and C mixtures are presented. The content of specimens A, B, C corresponds to the mixture in Table 1.

All test specimens were made into wood moulds, compacted on vibratory table. Specimens were demoulded after 24 hours and then stored in water according to EN 12390-2 for 28 days. The test specimens were stored in dry place for the next 28 days (up to the test). Before testing, the specimen were measured and weighed.

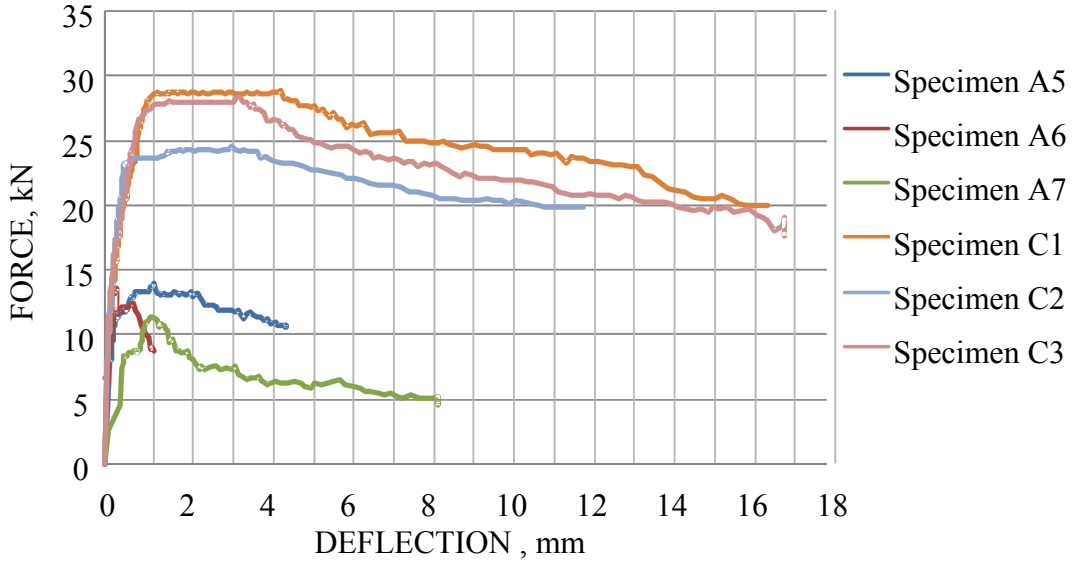

Figure 1 Results of static tests of reinforced circular plates, mixtures A and C

Dynamic tests of reinforced specimens (circular plates)

The dynamic load test was carried out at loading speed 70 mm/s. The maximum force at the failure and deflection were monitored. The specimens in the shape of a circular plate with a diameter of 500 mm and 50 mm thickness were supported along the perimeter. The surface area on which the load was applied was circa 7850 mm^2 (circular steel plate of diameter 100 mm).

The test results of reinforced specimens in the form of a dependency graph between deflection and applied force are shown in Figure 2 and 3. Due to the limited space of this paper only the A and C mixtures are presented.

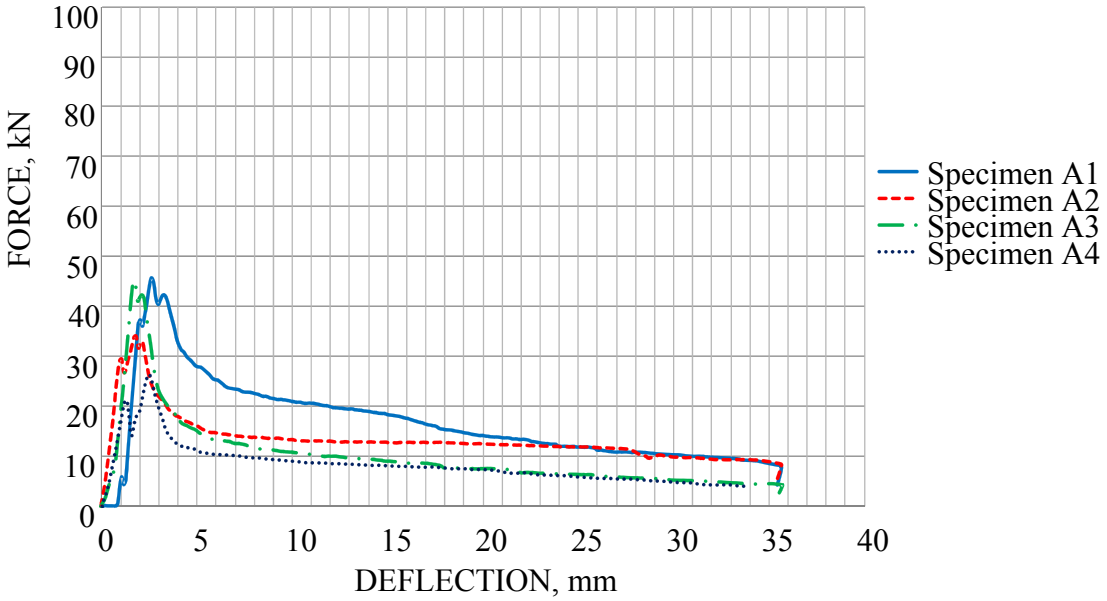

Figure 2 Results of dynamic tests of reinforced circular plates – mixture A

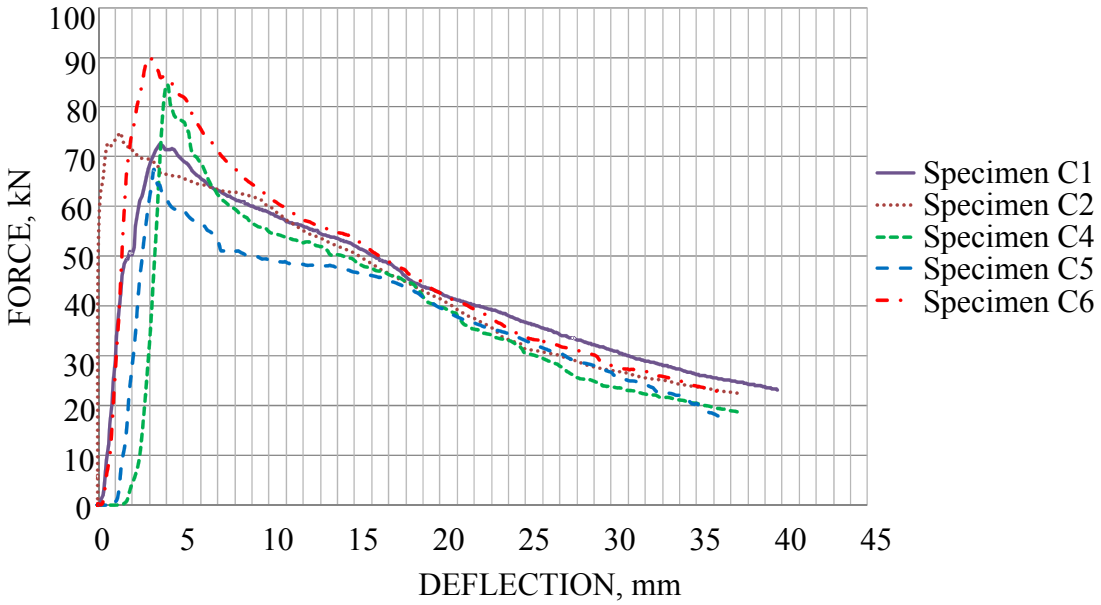

Figure 3 Results of dynamic tests of reinforced circular plates – mixture C

Dynamic tests of reinforced specimens, reference tests (Beams)

To compare results obtained on samples in the shape of circular plates, static and dynamic load tests were carried out on classic specimen beams (dimensions 100 mm × 100 mm × 400 mm). The beams were provided with notch depth of approximately 16 mm and a width of approximately 4 mm.

The test results of reinforced specimens in the form of a dependency graph between deflection and applied force are shown in Figure 4 and 5. The beam specimens rested on two supports 300 mm apart (three-point bending load test). Due to the limited space of this paper only the A and C mixtures are presented. The content of specimens A, C corresponds to the mixture in Table 1.

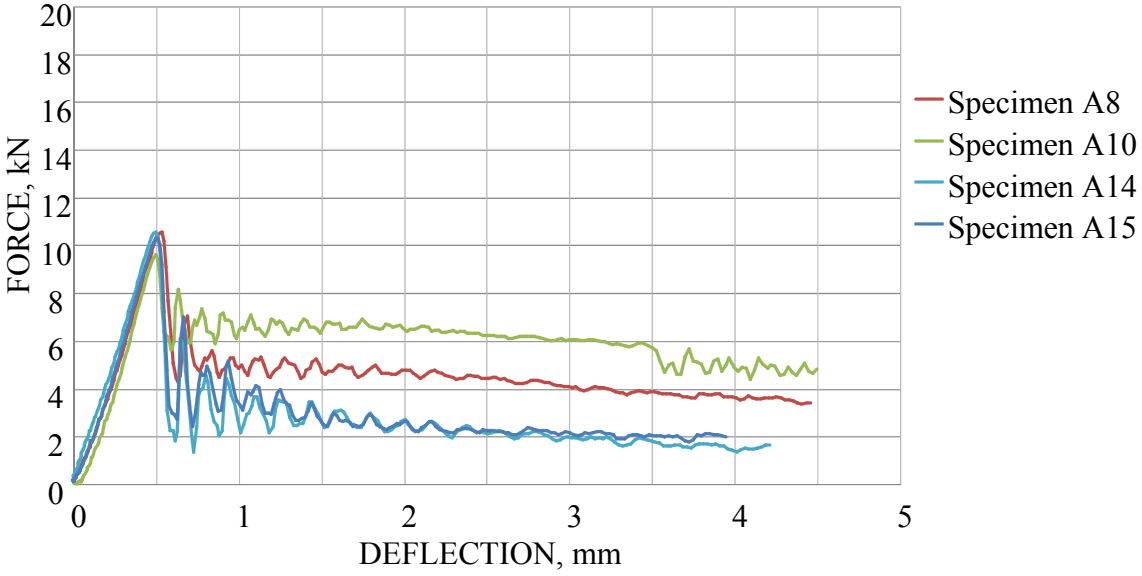

Figure 4 Results of dynamic tests of reinforced beams – mixture A

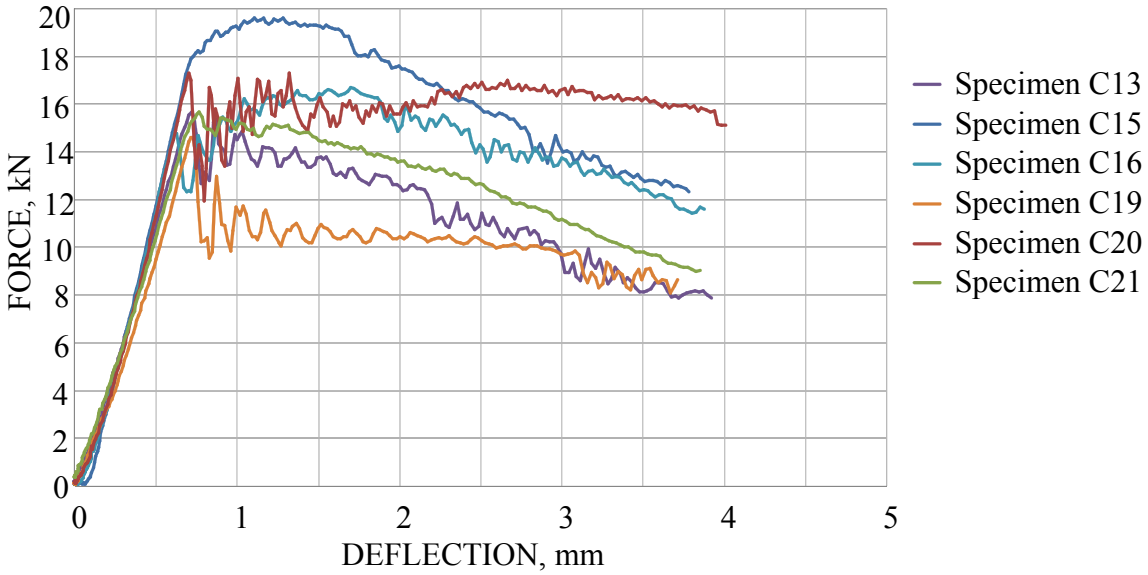

Figure 5 Results of dynamic tests of reinforced beams – mixture C

CONCLUSIONS

The percentage increase of the different ways of loads and different mixtures are shown in Table 2. As a basis for comparison, mixture A was chosen.

Table 2 Comparing the tests results

SPECIMEN SHAPE	LOAD TYPE	PARAMETER	MIXTURE		
			A	B	C
Circular plates	Static	Max. force, kN	12.91	13.2	27.05
		Increase, %	-	2	109
	Dynamic	Max. force, kN	37.8	54.0	76.6
		Increase, %	-	43	103
	Dynamic	Energy (at 35 mm deflection), kNm	0.430	1.092	1.711
		Increase, %	-	154	298
Beams	Static	Max. force, kN	8.4	8.0	14.9
		Increase, %	-	-5	78
	Static	Energy (at 35 mm deflection), kNm	0.012	0.021	0.043
		Increase, %	-	72	257
	Dynamic	Max. force, kN	10.3	10.8	16.6
		Increase, %	-	5	62
	Dynamic	Energy (at 35 mm deflection), kNm	0.015	0.021	0.044
		Increase, %	-	42	196

The results obtained so far can be summarized as follows:

- A circular plate of diameter 500 mm and 50 mm thickness was selected as the optimum form of the specimen.
- Minimum amount of 20 kg/m³ fibre reinforcement does not affect the static load; however, a greater deformation in comparison with unreinforced concrete can be visible.
- Increase of the fibre reinforcement 40 kg/m³ does not affect the increase in static load, but allows further increase in deflection. It also significantly increased dynamic load resistance of the specimens.
- Increase of the fibre reinforcement 80 kg/m³ leads to a significant increase in static load. It also significantly increased dynamic load resistance of the specimens. The overall increase of strength ranges from 60 - 100%, compared to specimens with reinforcement around 20 kg/m³.
- The energy needed to reach deflection 35 mm (circular plate) and 3.5 mm (beams) were evaluated from the force-displacement relationship. The overall increase of energy for specimens with reinforcement 40 kg/m³ ranges from 40 - 150%, compared to specimens with reinforcement 20 kg/m³.The overall increase of energy for specimens with reinforcement 80 kg/m³ ranges from 200 - 300%, compared to specimens with reinforcement 20 kg/m³.
- The dependence of static and dynamic load resistance (especially on low reinforcement specimens) is better seen on the newly selected specimens of circular shape, which provide a better response to load and allows better assess the impact of the reinforcement. In contrast, in the case of the classic shape of the specimens is the dependence on the amount of reinforcement and load resistance less evident.

The impact resistance tests with different amounts and kind of reinforcement will be followed.

ACKNOWLEDGEMENTS

The research work presented in this paper has been supported by the SGS12/098/OHK1/1T/31, GACR 103/09/0055 and GACR P104/10/2359.

REFERENCES

1. BENTUR A, MINDESS S AND BANTHIA N, The behaviour of concrete under impact loading: Experimental procedures and method of analysis, Matériaux et Constructions, Vol. 19, No 113, 1986, pp. 371 – 378.

2. KOLÍSKO J, DUDÍKOVÁ M AND KLEČKA T, Bending test fiber reinforced concrete with polypropylene fibers. Effect of the shape of the test beam, In: 6th Conf. Special Concrete, Sekurkon Prague, Beroun, 2009, pp. 186-193, ISBN 978-80-86604-42-8.

3. BENTUR A, MUFTI A AND BANTHIA N, Fibre reinforced concrete, Present and future, Canadian Society for Civil Engineering, October 1998.

4. BANTHIA N, MINDESS S, BENTUR A AND PIGEON M, Impact testing of concrete using a drop-weight impact machine, Experimental Mechanics, Vol. 29, No. 1, 1989, pp. 63–69.

5. EN 12390-2, Hardened Concrete - Part 2: Making and curing specimens for strength tests; German version.

6. ŘEHÁČEK S, ŠIMŮNEK I AND HUŇKA P, New Procedures for Evaluating Impact Resistance of Fibre reinforced Cementitious Composite. In Proceedings of the 9th International Symposium on High performance Concrete. Auckland: New Zealand Concrete Society, 2011, p. 16. ISBN 978-0-473-19287-7.

7. ŘEHÁČEK S, ŠIMŮNEK I, HUŇKA P AND KOLÍSKO J, Impact Resistance of Fibre Reinforced Cementitious Composites. In The 7th Central European Congress on Concrete Engineering 2011. Lausanne: fib - fédération internationale du béton, 2011, p. 273-276. ISBN978-963-313-036-0.

Improving Punching Shear Resistance of Slab Column Connections Using High Strength Self-compacting Concrete With Steel Fibre

K S Ragab[1], S I Zaki[1], A S Eisa[2]
1 – Housing & Building National Research Center, Egypt
2 – Zagazig University, Egypt

This paper deals with behaviour and capacity of steel fibre reinforced high strength self-compacting concrete (SFRHSCC) slabs under punching shear force. Steel fibres can significantly enhance toughness of concrete and inhibit the initiation and growth of cracks. Addition of steel fibres into concrete improves mechanical behaviour, ductility, and fatigue strength of concrete. Steel fibres change the properties of hardened concrete significantly. However, addition of fibres to fresh concrete results in a loss of workability and Self-compacting concrete (SCC) able to flow under its own weight, completely filling formwork and achieving full compaction without vibration. So, this paper studied composites of SCC and HSCC with steel fibres for further property enhancement. Previous studies have demonstrated the effectiveness of fibre reinforcement in improving the shear behaviour of reinforced concrete slabs. In this study, hooked-ends type steel fibres are tested with varying fibre dosage, ordinary concrete, self-compacting concrete and high strength self-compacting concrete. Effect of steel fibres self compacted concrete and self compacted concrete only on punching shears cracking behaviour and resistance of the slabs was investigated. The results show a significant increase of the punching shear capacity and considerable improvement of cracking behaviour as well as good integrity of column-slab connection of the slabs with fibres and self compacted concrete. The slabs without fibres failed suddenly in very brittle manner, while, the fibre reinforced ones collapsed in more ductile type. In addition, based on experimental data obtained from the author's study and literature, the paper performed an evaluation of accuracy of existing models used steel fibre reinforced high strength self-compacting concrete (SFRHSCC) and formulas in previous studies that used to predict punching shear resistance of steel fibre slabs. Keywords: self-compacting concrete; punching shear resistance; steel fibre slabs; steel fibre reinforced high strength self-compacting concrete (SFRHSCC); punching shear cracking; predict; formulas.

Khaled S. Ragab is currently Associate Professor of Concrete Constructions at Reinforced Concrete Research Institute, Housing & Building National Research Center, HBRC, Cairo, Egypt. He is a Consulting Engineer in the design of concrete structures. He is a Member of Syndicate of Egyptian Engineers, Member of the Association of Engineers of Egyptians, and Member of the reviewer team for Journal of civil engineering and construction technology. He has led several research projects on concrete, and his interesting areas of research are Fibre reinforced concrete (GFRP), High performance concrete (self compacting concrete), Nanotechnology in the field of concrete, Economic systems of construction, Nonlinear analysis by FEM for different elements of concrete construction, and Light weight concrete.

A S Eisa is currently Lecturer,Structural Engineering Department, Faculty of Engineering, Zagazig University, Zagazig, Egypt.

S I Zaki is currently Associate Professor, Building Materials Research and Quality Control Institute, Housing & Building National Research Center, HBRC, Cairo, Egypt.

Keywords: Punching shear cracking, Punching shear resistance, Self-compacting concrete, Steel fibre reinforced high strength self-compacting concrete (SFRHSCC), Steel fibre slabs

INTRODUCTION

Reinforced concrete slabs may be carried directly by the columns without using beams or girders. Such slabs are described as flat plates. Since the depth (thickness) of a typical slab is relatively small, its capacity to transfer load into the columns by shear is often low. As a result, most failure of flat plates is initiated by overstress in shear at the columns. These failures are termed Punching-Shear failures. Punching shear failure of slabs is usually sudden and leads to progressive failure of flat plate structures; therefore, caution is needed in the design of slabs and attention should be given to avoid the sudden failure conditions. Punching shear of slabs were interested by several (3, 2, 1) researches and several experimental investigations were conducted to increase the punching shear strength of slabs by using steel fibre reinforced concrete or high strength concrete or concrete polymer composite(4). Comprehensive studies on mechanical properties of self-compacting concrete were, also, interested by several researches (5). Conventional shear reinforcement can be used to increase the punching shear strength of slabs, but, when the thin slabs are constructed, a very large of steel reinforcement are required to increase the load capacity. To increase punching shear capacity of flat slab, a variety of methods have been proposed such as: i) traditional shear reinforcing method using stirrups but this method is inapplicable to slabs with shallow depth less than 150 mm (ACI 318-2002)[12] new method using headed-studs but this one need much time for construction (Feretzakis 2005)[16]. Recently, new technique using steel fibres to improve the punching shear resistance and cracking control of slab-column connections has been proven to give good results (Alexander and Simmonds 1992[3]; Theodorakopoulos and Swamy 1993[4]; Harajli et al. 1995[7]; McHarg et al. 2000[11], Naaman et al. 2007[19]; Cheng and Montesinos 2010a[25]). Moreover, steel fibres also indicate high effectiveness in structures sustained lateral loads i.e. seismic because of their ability to absorb energy dissipation of the structures (Megally and Ghali 2000[11]; Cheng and Montesinos 2010b[26]). The newest construction material (technique) which can be used in such cases are moderate or high strength self-compacting concrete rather than using conventional shear reinforcement to increase capacity of flat slab. Self-compacting concrete (SCC) was developed in Japan in the late 1980's and allows concrete to be placed fully compacted without segregation and with no additional energy (vibration) (6). It is able to flow under its own weight, completely filling formwork and achieving full compaction, even in the presence of congested reinforcement. The hardened concrete is dense, homogeneous and has the same engineering properties and durability as traditional vibrated concrete. The main objective of this study is to investigate experimentally behavior and capacity of steel fibres reinforced high strength self-compacting concrete (SFRHSCC) slabs under punching shear force, in which, a total of six small-scale flat slabs was tested. The paper performed an evaluation of accuracy of existing models used steel fibres reinforced high strength self-compacting concrete (SFRHSCC) and formulas in previous studies that used to predict punching shear resistance of steel fibres slabs.

EXPERIMENTAL WORK

Experimental Program

Six reinforced concrete slabs were casted of rectangular shape of dimensions 110 * 110 cm and 10 cm thickness and bottom steel was 7 Φ 10/m, strain gauges of 10 mm length, 120 ohms, and 2.04 gauge factor were fixed with steel bars before casting, facing the outside of the slabs using epoxy, then a wax film was layered at the top of the strain gauge to protect

it. Each slab has two strain gauges, one was placed in the mid length of the longitudinal bar and the other at the same point in the transverse bar. The following Table 1 shows the standard cube compressive strength after 28 days for each slab and its description.

Table 1 Standard Cube Compressive Strength and Slab Description.

SPECIMEN	SYMBOL	DESCRIPTION	F_{cu} @ 28 DAYS, MPa
S1	OC	Ordinary Concrete	30
S2	SCC	Self-Compacting Concrete	64
S3	HSCC	High strength Self Compacted concrete	82
S4	SCC, V_f 0.75%	SCC with steel fibre 0.75%	55
S5	HSCC, V_f 0.75%	HSCC with steel fibre 0.75%	86
S6	HSCC, V_f 1.5%	HSCC with steel fibre 1.5%	89

Materials

Ordinary Portland cement was CEM1 of grade 52.5 obtained from Suez – Factory in Egypt, and complies with ESS 4756-1-2006 [17]. Silica fume was a very fine by – product powder obtained as a fume from the foundry process in the Egyptian company for Iron Foundries. Fly Ash used in the concrete mix was imported from India through Goise Company in Egypt, and complies with ASTM C618 class F [22]. The Blaine fineness of the ash is 3200 cm^2/gm and its specific gravity is 2.2. Steel fibres were obtained from Master Chemical Technology Company in Egypt. Type of steel fibres is double hooked edge, 0.6mm diameter, 30mm length, 50 aspect ratio, and 850 MPa tensile strength. Figure 1 shows the shape of steel fibres.

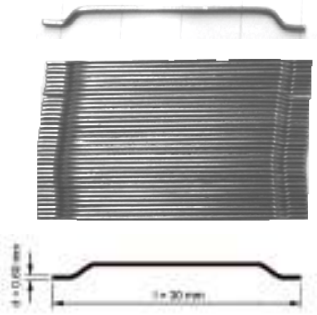

Figure 1 Shape of Steel fibres.

Coarse aggregate used in self compacted slabs was crushed dolomite with nominal maximum size of 10 mm obtained from Attaka quarry, white fine aggregate was natural sand obtained from pyramids quarry in Egypt and complies with ESS 1109, 2008 [20]. Polycorboxylate ether polymer glenium ASE 30 obtained from Basf company in Egypt was

used to produce self-compacted concrete mixes. Deformed high-grade steel bars of yield strength 400 MPa and 10 mm diameter was used as bottom steel in all slabs (7 bars / m in each direction).

Test Measurements and Instrumentation

The tested slabs were load gradually with load increment of 10 ton up to failure. The recorded data were Cracking, ultimate load capacity, concrete strains, and reinforcement strains. The vertical strains in concrete slabs were measured using linear variable displacement transducers (LVDTs). The data from (LVDTs) were connected to data acquisition system (DAS), while steel strain gauges were connected to strain indicator device to get steel strains directly.

Test Results of Specimens

Concrete mixes were prepared and summarized in six mixes as shown in Table 2. The cement content was 350 kg/m^3 for normal strength slabs , while increased to 500 Kg/m^3 for high strength ones. Silica fume was 15% of cement content in all mixes, fly ash was 10% of cement content in all self-compacted mixes, water – binder ratio was 0.35 for all self-compacted mixes, the super plasticizer ratio was 2.5% to achieve self-compacted slabs with steel fibres. Steel fibre of double hooked edge was added to mix no. 4, 5 with ratio 0.75% and to mix no. 6 with ratio 1.5%. Filling ability and viscosity of self-compacted concrete were evaluated using slump flow test according to ESS 1109, 2008[20], their results are recorded at the end of Table 2.

Table 2 Concrete Mix Design

SLAB No.	TYPE OF MIX	MIX PROPORTIONS, kg								FRESH TEST	
		Cement	Sand	Coarse aggregate		Steel fibres	FA	SF	Add.	Water Litre	Slump cm	Slump flow cm
				C.agg1	C.agg2							
S1	OC	350	750	550	550	-	-	-	-	175	4	-
S2	SCC	350	950	950	-	-	35	52.5	10	158	27	60
S3	HSCC	500	850	850	-	-	50	75	16	180	28	68
S4	SCC V_f 0.75%	350	950	950	-	58.5	35	52.5	10	171	7	60
S5	HSCC V_f 0.75%	500	850	850	-	58.5	50	75	14	187	28	70
S6	HSCC V_f 1.5%	500	850	850	-	117	50	75	16	187	26	60

OC: Ordinary concrete, SCC: Self-compacted concrete, HSCC: High strength self-compacted concrete, Vf: percentage of fibre volume fraction, FA: fly ash, SF: silica fume, and Add.: admixture.

Test Procedure

All slabs were tested in punch simply supported under load applied The set-up of each test consisted of installing the tested slab in a horizontal position between machine heads , the machine heads insured that the load eccentricity was maintained at all stages of the loading and also head bearing plates were adjusted to prevent any eccentricity from wrong position. All slabs were tested using 100-ton capacity hydraulic Jacks machine in reinforced concrete laboratory in H.B.R.C. Figure 2 shows the details of tested slabs and LVDTs and Figure 3 shows the test set-up.

Figure 2 Details of tested slabs and positions of LVDTs

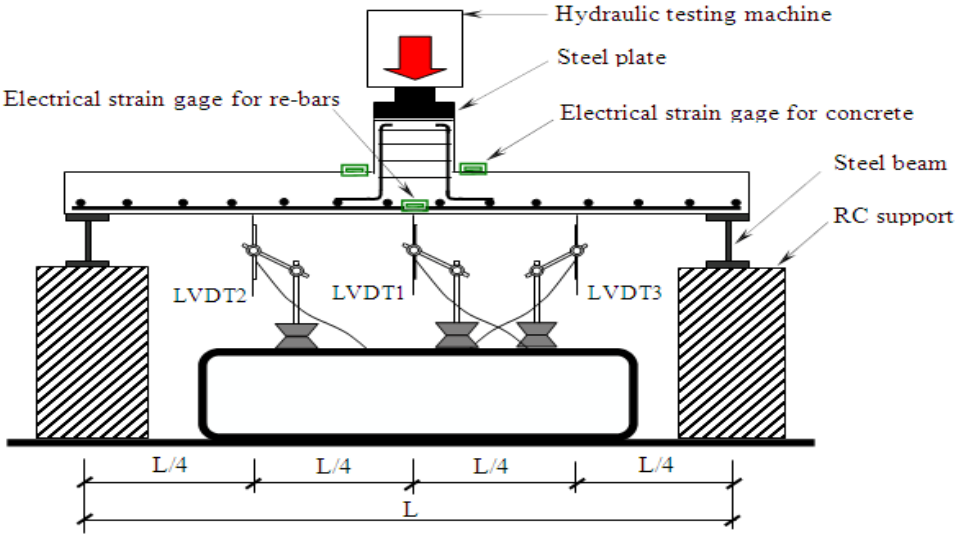

Figure 3 Test set-up

TEST RESULTS AND DISCUSSION

Failure Modes and Crack Patterns of Test Specimens

Failure mode of all tested specimens was punching shear (PS), Table 3 shows the test results of all tested specimens including; specimens' description, ultimate loads, and failure modes.

Grid type of cracks occurred under the loading area due to the bending moment and tangential cracks spread from the loading area to the slab corners due to the torsional moment. On the top surface, the loading pad began to sink when the punching shear cracks became wider. Slabs without steel fibres failed in very brittle manner, where, concrete cover of bottom surface fell apart. The slabs with steel fibres failed in more ductile mode. In these slabs, typical cracking patterns on the bottom surface of these slabs were observed, cracks formed uniformly with smaller width due bridging effect of steel fibres. By observing the test results, it can be concluded that the steel fibres improve significantly concrete ductility and integrity of vicinity of slab-column connections. Figure 4 shows the failure modes and crack patterns of the tested specimens.

Punching Shear Behavior of Test Specimens

Based on the experimental results, the behavior of the tested slabs is discussed in terms of observed behavior, concrete types, ultimate load, load-deflection curves, and failure modes as shown in Table 3 and Figures 5 to 8 which indicate that the relationship between applied load and deflection at the center of the slab was typical for all the tested slabs, an approximate linear increase behavior followed by a nonlinear behavior until failure.

Using self-compacting concrete (SCC) causes significant difference in the behavior of the tested slabs and improves the punching shear resistance as shown in Figure 5. Steel fibres increase considerably punching shear capacity of self compacting concrete slabs and this increase is because of steel fibres help to bridge cracks in the whole concrete volume and transfer tensile stress through two opposite faces of cracks until the fibres are totally pulled-out or broken. For this reason, in stage of initiation and propagation of cracks, tensile zone of steel fibres self compacting concrete slabs (SFRSCC) still sustains load. This increases concrete tensile strength and indirectly leads to increase the punching shear resistance of slabs. Figure 6 shows clearly effect of steel fibres on the punching shear capacity of self compacting concrete slabs.

All steel fibres self compacting concrete slabs (SFRSCC) showed a gradual and ductile behavior beyond the maximum load in comparison with reinforced concrete slabs without fibre content. It can be noticed from Figure 7 that the punching shear capacity increased with a corresponding increase in the concrete compressive strength.

Table 3 Test results

SPECIMEN	CONCRETE PROPERTIES	COMPRESSIVE STRENGTH, F_{cu}, MPa	FIBRE VOLUME FRACTION, V_f, %	ULTIMATE LOAD, V_u, kN	FAILURE MODE
S1	OC	30	0.0	219	PS
S2	SCC	64	0.0	270	PS
S3	HSCC	82	0.0	263	PS
S4	SCC	55	0.75	313	PS
S5	HSCC	86	0.75	349	PS
S6	HSCC	89	1.5	318	PS

(a) Slab S1; ordinary concrete without steel fibres

(b) Slab S2; SCC without steel fibres

(c) Slab S3; HSCC without steel fibres

(d) Slab S4; SCC with steel fibres (0.75%)

(e) Slab S5; HSCC with steel fibres (0.75%)

(f) Slab S6; HSCC with steel fibres (1.5%)

Figure 4 Failure modes and crack patterns of the tested specimens – bottom surface

For steel fibres high strength self compacting concrete slabs (SFRHSCC), the punching shear capacities increased by 32.7% at fibre volume fraction of (0.75%) in comparison with that of high strength self compacting concrete slabs (HSCC) without steel fibres as given in Table 3. In contrast, the punching shear capacities increased by 21% at fibre volume fraction of (1.5%) in comparison with that of high strength self compacting concrete slabs (HSCC) without steel fibres as given in Table 3. The punching shear behaviors of (SFRHSCC) slabs were almost identical close to the maximum load as shown in Figure 7, though the fibre volume fraction was varied. The maximum loads did not linearly increase with increasing the fibre volume fraction. This trend is the same as the results presented by Mindess, et al.1997[9]. They showed that the increase of the punching shear capacity of (SFRHSCC) slabs became insensible from the fibre volume fraction over 0.75% to 1.5%.

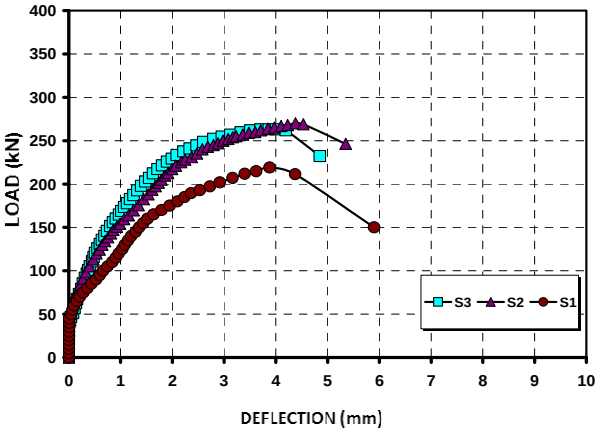

Figure 5 Slabs of different concrete types without steel fibres.

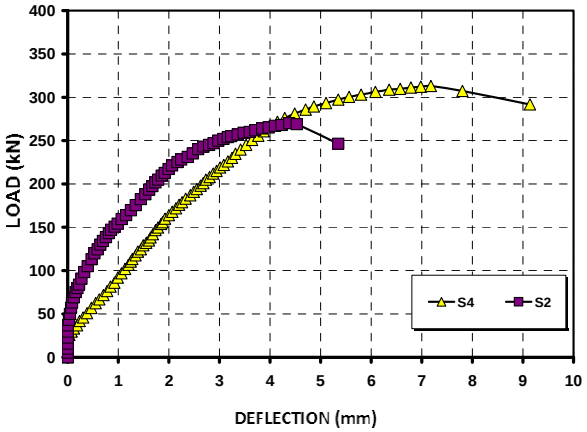

Figure 6 Effect of steel fibres on SCC

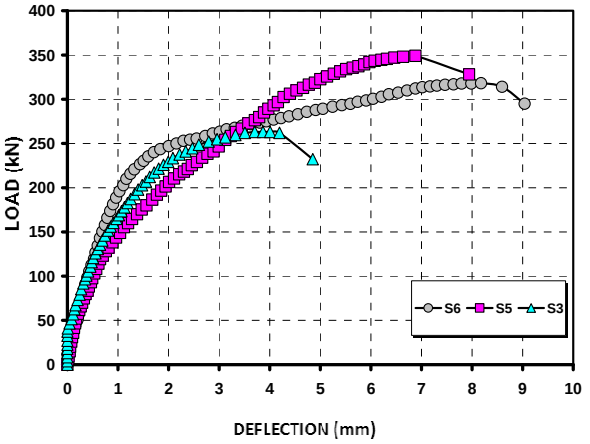

Figure 7 Effect of steel fibres on HSCC

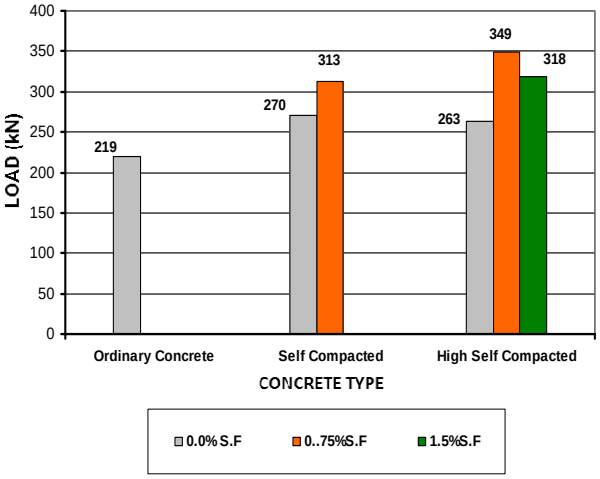

Figure 8 Punching shear forces for all the tested specimens

EVALUATION OF PUNCHING SHEAR RESISTANCE

Comparison of Results to Other Models

In this section a series of models and equations will be presented from the work of other researchers and compared to the results obtained during testing. The equations are first presented in this section and then compared to the results obtained during testing in section (4.2).

Narayanan and Darwish Equation

Narayanan and Darwish 1987[2] have provided the design equation for the punching shear capacity of SFRC slabs considering three factors the strength of the very narrow compressive zone above the top of the inclined cracks, the pull out forces on the fibres along inclined cracks and the shear force carried by dowel and membrane actions which contribute the shear capacity. The design equation for the ultimate punching shear capacity of SFRC slabs is as follows.

$$V_{uf} = \xi (0.24 f_{spf} + 16 \rho + 0.41 \tau F) b_{pf} d \qquad (1)$$

$$f_{spf} = (f_{cuf} / 20 - \sqrt{F}) + 0.7 + \sqrt{F} \quad (2)$$

$$b_{pf} = (4r + 3\pi h)(1-KF) \quad (3)$$

$$F = (L/D)\, V_f\, d_f \quad (4)$$

$$\xi = 1.6 - 0.002h \quad (5)$$

Where f_{cuf} is the cubic compressive strength of fibre reinforced concrete, f_{spf} is the computed value of split cylinder strength of fibre reinforced concrete, ρ is the tension steel reinforcement ratio, V_f is the fibre volume fraction, τ is the average fibre matrix interfacial bond stress taken as 4.15 N/mm^2. d_f is the bond factor, h is the slab thickness, d is the effective depth, b_{pf} is the perimeter of the critical section, K is the non-dimensional constant value=0.55, L *and* D are the length and the diameter of fibre, respectively, F is the fibre factor and ξ is the empirical depth factor.

Shaaban and Gesund Equation

Shaaban and Gesund 1994[5] studied the effects of steel fibres on the punching shear strength of reinforced concrete slabs, specifically whether the addition of steel fibres significantly enhanced e punching shear capacity. Thirteen slabs with varying fibre contents were tested to failure and produced results that demonstrated the enhancement in punching shear capacity achieved with the addition of fibres. The authors proposed an equation of the same form as the ACI 318-02 code equation for punching shear, but modified it to account for the fibre contribution. The equation proposed is

$$V_{uf} = [\,(0.3\, W_f - 6.8\,)\,(\sqrt{f'_c}/1000)\,(b_o\, d) \quad (kips) \quad (6)$$

Where W_f percent of fibres by weight of concrete (%), f'_c concrete compressive strength (psi), b_o critical perimeter at defined by ACI (in), and d average effective depth to tension reinforcement (in).

ACI 318M-02 Equation by J. B. De Hanai and K. M. A. Holanda 2008 [24]

The ACI 318M-02 [12] by J. B. De Hanai and K. M. A. Holanda 2008 [24] adopts a relation between concrete tensile strength (split test) and the square root of the compressive strength, as shown in equation (7).

$$f_{sp} = 0.5563\, \sqrt{f_c} \quad (7)$$

being f_c the concrete strength to axial compression and f_{sp} the concrete tensile strength (split test), both in MPa. Many authors demonstrate a strong correlation between shear strength and the square root of concrete compressive strength. This corresponds to an indirect correlation of shear strength to the concrete tensile strength. It is well known that when al low volume fraction of steel fibres are added to concrete, the first cracking strength is not significantly increased. However, ductility and post cracking resistance can be increased, thus providing shear resistance by bridging diagonal cracks. In addition, because fibres would control the opening of these cracks, shear resistance through aggregate interlock would likely be increased. Equation (7) from ACI code is very simple and affordable for practical calculations. Therefore, a tentative analysis was done to verify if it also is able to represent by

means of a single parameter, the tensile strength of fibre reinforced concrete, the shear load capacity increase in situations of diagonal tension rupture. At first, to correlate the concrete tensile strength to the compressive strength of the steel fibre reinforced concrete, a linear regression of experimental results was made. Equation (8) express this relationship in a similar format of equation (7).

$$f_{sp} = (0.19\ V_f + 0.53)\ \sqrt{f_c} \qquad (8)$$

being f_{sp} and f_c given in MPa and V_f in %. The ACI 318M-02 [12] prescribes equation (9) to evaluate the ultimate punching load for slabs without transversal reinforcement and square section columns.

$$V_{uf} = (0.3321\ \sqrt{f_c}\ b_o\ d)/10 \qquad (9)$$

Where f_c concrete axial compressive strength, $b_o = 4(c+d)$ perimeter where punching occurs, d effective slab depth, and c column length, being f_c given in MPa, and b_o, d in cm.

The value of f_{sp} from equation (8) is introduced in equation (9) to consider the effect of steel fibres in punching strength. Adaptations were done to preserve the adjustment and safety factors that are implicit in the coefficient 0.3321 of equation (9). By this procedure equation (11) was obtained.

$$V_{uf} = [(0.3321/0.53)\ (0.19\ V_f + 0.53)\ \sqrt{f_c}\ b_o\ d]/10 \qquad (10)$$

$$V_{uf} = [0.6266(0.19\ V_f + 0.53)\ \sqrt{f_c}\ b_o\ d]/10 \qquad (11)$$

Compared to the Results Obtained During Testing.

Table 4 shows the results obtained during testing and the results obtained from equations are presented from the work of other researchers. AS shown in Figure 9 the present study gives good agreement results with equation ACI 318M-02 by Hanai and Holanda 2008 [24]. Shaaban and Gusent 1994 [5] equation gives results bigger than the present study. The results of the analysis indicate that the best equation for predicting the punching shear capacity for SFRC slabs is the equation ACI 318M-02 by Hanai and Holanda 2008 [24].

Table 4 Comparison of Results to Other Models

SPEC.	CONC.	F_{cu} (MPa)	V_f (%)	$V_{uExp.}$ (kN)	N&D[1] V_{u1} (kN)	ACI D&H[2] V_{u2} (kN)	S&G[3] V_{u3} (kN)	$\frac{V_{uExp.}}{V_{u1}}$	$\frac{V_{uExp.}}{V_{u2}}$	$\frac{V_{uExp.}}{V_{u3}}$
S1	OC	30	0.0	219	119	158	265	1.842	1.386	0.827
S2	SCC	64	0.0	270	200	231	388	1.350	1.169	0.696
S3	HSCC	82	0.0	263	242	261	438	1.087	1.008	0.600
S4	SCC	60	0.75	313	211	223	374	1.484	1.404	0.837
S5	HSCC	86	0.75	349	272	268	449	1.282	1.302	0.777
S6	HSCC	89	1.5	318	290	273	456	1.096	1.165	0.697

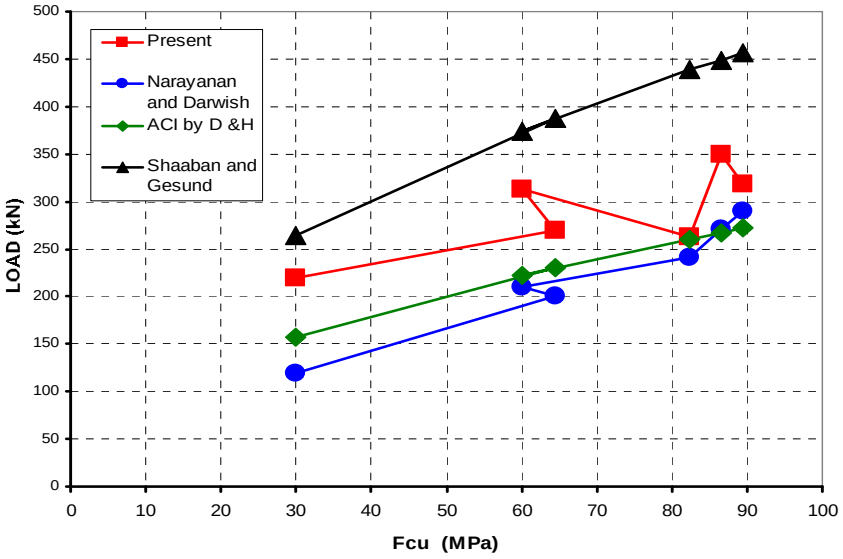

Figure 9 Comparison of Results to Other Models

CONCLUSIONS

Based on the results obtained from study, the following conclusions can be drawn:

1. The use of self-compacting concrete (SCC) or high strength self-compacted concrete (HSCC) improves the punching shear resistance compared with ordinary concrete (OC).

2. The study showed that the increase of the punching shear capacity of (SFRHSCC) slabs became insensible compared with (SFRSCC).

3. The use of self-compacted concrete (SCC) with steel fibres (SF) gives good results in the workability.

4. Steel fibres improve the punching shear resistance of the slabs considerably. Using steel fibres with volume fraction equal to 0.75% with high self-compacted concrete or self-compacted concrete is the ideal percentage to increase the punching shear resistance.

5. The study showed that the increase of the punching shear capacity of (SFRHSCC) slabs became insensible from the fibre volume fraction over 0.75% to 1.5%.

6. Steel fibres can significantly enhance toughness of concrete and inhibit the initiation and growth of cracks. Addition of steel fibres into concrete improves mechanical behavior, and ductility of concrete.

7. The slabs without fibres failed suddenly in very brittle manner, while, the fibre reinforced ones collapsed in more ductile type.

8. Theoretical analysis based on Modified Equations ACI 318M-02 by J. B. De Hanai and K. M. A. Holanda 2008 [24], adapted to steel fibre reinforced concrete provided good indicators of punching shear strength of slabs and good agreement with the experimental results.

REFERENCES

1. SWAMY RN and Ali SAR (1982). Punching shear behavior of reinforced slab-column connections made with steel fibre concrete. ACI Structural Journal. 79(6), pp. 392-406 .

2. NARAYANAN, R. AND DARWISH, I. Y. S, “Punching Shear Tests on Steel-Fibre-Reinforced Micro-Concrete Slabs,” Magazine of Concrete Research, Vol. 39, No. 138, 1987, pp. 42~50.

3. ALEXANDER SDB AND SIMMONDS SH (1992). Punching shear tests of concrete slab-column joints containing fibre reinforcement. ACI Structural Journal. 89(4), pp. 425-432 .

4. THEODORAKOPOULOS D.D., SWAMY N. Contributions of steel fibres to the strength characteristics of lightweight concrete slab-column connections failing in punching shear. ACI Structural Journal 1993;90(4):342-355 .

5. SHAABAN AM AND GESUND H (1994). Punching shear strength of steel fibres reinforced concrete flat plates. ACI Structural Journal. 91(3), pp. 406-414 .

6. TAN K.H., PARAMASIVAM P. Punching shear strength of steel fibre reinforced concrete slabs. Journal of Materials in Civil Engineering 1994;6(2):240-253 .

7. HARAJLI MH, MAALOUF D, AND KHATIB H (1995). Effect of fibres on the punching shear strength of slab-column connections. Cement & Concrete Composites. 17, pp.161-170 .

8. JAPAN SOCIETY OF CIVIL ENGINEERS (1997). "Recommendation for Design and Construction of Concrete Structures Using Continuous Fibre Reinforcing Materials ", Concrete Engineering Series 23, ed. by A. Machida, JSCE, Tokyo, Japan .

9. MINDESS, S., ADEBAR, P., AND HENLEY, J., “Testing of Fibre- Reinforced Structural Concrete Elements,” Proceedings of ACI International Conference on High-Performance Concrete: Design and Materials and Recent Advances in Concrete Technology, ACI SP-172, 1997, pp. 495~515.

10. MEGALLY S AND GHALI A (2000). Punching shear design of earthquake resistant slab-column connections. ACI Structural Journal. 97(5), pp. 720-730 .

11. McHARG PJ, COOK WD, MITCHELL D, and YOUNG-SOO Y (2000). Benefits of concentrated slab reinforcement and steel fibres on performance of slab-column connections. ACI Structural Journal. 97(2), pp. 225-234 .

12. ACI 318M-02. Building code requirements for structural concrete. American Concrete Institute, Farmington Hills, Michigan, 2002.

13. ACI 440, (2003). "Guide for the Design and Construction of Concrete Reinforced with FRP Bars," ACI 440.1R-03, American Concrete Institute, Farmington Hills, MI .

14. OKAMURA H. AND OUCHI M., "Self Compacting Concrete", Journal of Advanced Concrete Technology, Vol. 1, Japan, April, 2003.

15. JAWAD, M. K., "Experimental Study on shear heads in reinforced concrete flat plates", Ph.D. Thesis, Civil Engineering Department, College of Engineering, Al-Mustansiriya University, Baghdad- Iraq, September, 2005.

16. FERETZAKIS A (2005). Flat slabs and punching shear reinforcement systems. Msc. Thesis, University of Dundee, UK .

17. Egyptian Standard specification for ordinary Portland cement (ESS 4756.-1-2006), Produced from General Organization for specification and Quality in Egypt. (1)

18. CHOI KK, REDA TAHA MM, PARK HG, AND MAJI AK (2007). Punching shear strength of interior concrete slab-column connections reinforced with steel fibres. Cement & Concrete Composites. 29, pp. 409-420.

19. NAAMAN AE, LIKHITRUANGSILP V, AND PARRA-MONTESINOS GJ (2007). Punching shear response of high-performance fibre-reinforced cementitious composite slabs. ACI Structural Journal. 104(2), pp. 170-1779 .

20. Egyptian Technical Specifications for self-compacted concrete, Ministerial Descion No. 360-2007 Egyptian Standard specifications for aggregates, ESS 1109, 2008. (3)

21. Produced from Housing and Building National Research Center Egypt.(4)

22. American Standard specifications for Fly Ash, ASTM C618 class F.(2)

23. ACI Committee 318, "Building Code Requirements for Structural Concrete", (ACI 318-08) and Commentary (ACI 318R-08), American Concrete Institute, Farmington Hills, MI, 2008, pp.465.

24. De HANAI, J.B. AND HOLANDA, K.M.A." Similarities between punching and shear strength of steel fibre reinforced concrete (SFRC) slabs and beams" IBRACON Structures and Materials Journal vol. 1, No. 1, 2008

25. CHENG MY AND PARRA-MONTESINOS GJ (2010a). Evaluation steel fibres reinforcement for punching shear resistance in slab-column connections-part1: Monotonically increased load. ACI Structural Journal. 107(1), pp. 101-109 .

26. CHENG MY AND PARRA-MONTESINOS GJ (2010b). Evaluation steel fibres reinforcement for punching shear resistance in slab-column connections-part2: Lateral displacement reversals. ACI Structural Journal. 107(1), pp. 110-118 .

Successful Repair Technique of Damaged Reinforced Concrete Structures in Egypt

S I Zaki
Housing & Building National Research Centre, Egypt

During recent years, a lot of reinforced concrete structures in Egypt have severely deteriorated, mainly due to improper selection of materials, poor workmanship, absence of good quality control and supervision, and the corrosion of embedded steel in concrete subjected to aggressive environment in some cities in Egypt. The Investigation technique involved visual inspection of the structure, nondestructive testing and check of actual stresses subjected to each member. A case of study is a program of strengthening and repairing one of important buildings in 6th October city (6th of October secondary school in 6th Hay). The repair and rehabilitation program involved strengthening of R.C slabs of less thickness in 1st and 2nd floor, rebuilding of R.C columns in the center of the deflected slabs and rebuilding of R.C footing for that Columns.

Dr. Said. I. Zaki, is an Associate Professor, Housing & Building National Research, Egypt. His interests lie in the strength of construction materials with a particular emphasis on concrete construction.

Keywords: Damage level, Jacketing method, Rehabilitation program, Repair, Strengthening

INTRODUCTION

During recent years, a large number of reinforced concrete structures, in Egypt, have severely deteriorated, mainly due to improper selection of materials, poor workmanship, absence of good quality control and supervision, and the corrosion of embedded steel in concrete subjected to aggressive environment in some cities in Egypt.

The investigation technique involved visual inspection of the structure, nondestructive testing and check of actual stresses subjected to each member. A case of study is a programme of strengthening and repairing one of important buildings in 6th October city (6^{th} of October secondary school in 6^{th} Hay). The plans are shown in Figure 1 to Figure 5.

The repair and rehabilitation program involved strengthening of reinforced concrete (RC) slabs of less thickness in 1st and 2nd floor, rebuilding of R.C columns in the center of the deflected slabs and rebuilding of R.C footing for the columns. Special emphasis must be given to investigate and evaluate the damage level (quantity, intensity and extent of deterioration) of reinforced concrete structures [1]. The purpose of the experimental studies, reported in this paper, is to confirm repair and strengthen effects.

The terms restoration, repair and strengthening are defined as follows [2];

- Restoration:- to repair and strength damaged buildings so that they can be used again.
- Repair:- to improve the deteriorated structural performance of damaged buildings back to their original levels.
- Strengthening:- to improve the deteriorated structural performance of damaged buildings back to their original levels.

DESCRIPTION OF DEFECTS AND DAMAGE

- Actual thickness of slab between Axis 15-17 and Y-M was 16 cm less than the designed value which was 22cm.
- Actual thickness of concrete cover of lower steel mesh was more than the designed value of 2cm.
- Actual thickness of flooring layer was 20cm more than the designed value which was 10cm.
- The observed deflection in slab on axis 17-15 and Y-M was found to be 6cm.
- The observed deflection in other slabs was found between 1cm and 2cm.
- Actual thickness of all slabs was less than 3 cm than the designed value as observed from extracted cores.

EXPERIMENTAL PROGRAMME

Non destructive tests were carried out to evaluate the strength and deflection of different concrete elements. The tests are as follows:-

Schmidt hammer test:-

The Schmidt hammer test was carried out on all elements of stages (P.C, R.C footings), ground beams and columns.

Table 1 Schmidt hammer test results

STAGE OF CONSTRUCTION	AVERAGE REBOUND NUMBER	EQUIVALENT CUBE COMPRESSIVE STRENGTH, kN/cm²
P.C. Footings	22	126
R.C Footings	27	195
R.C Ground beams	25	166
1st Floor Columns	33	291
2nd Floor Columns	30	241
3rd Floor Columns	35	324

Core test

The core test was carried out on five position in slabs as shown in Table 2 in accordance to ASTM C42 [4], all cores were taken in vertical direction and type of capping was sulphuric cap, while correction factor was calculated according to E.S.S 1658 [5].

Table 2 Results of tested cores in the school under repair

PROPERTY	CORE NUMBER				
	1	2	3	4	5
Element Type	Slab	Slab	Slab	Slab	Slab
Axis	15-17 Y-M	18-9 H-Z	16-17 B-C	8-10 B-C	8-10 K-M
Diameter, cm	7.5	7.5	7.5	7.5	7.5
Height, cm	11	9.4	9.4	9.4	9.4
Unit weight, gm/cm³	2.32	2.3	2.35	2.37	2.39
Crushing load, kN	151	98	90	98	90
H/d ratio, λ	1.62	1.42	1.38	1.42	1.38
Correction factor, F	1.086	1.043	1.034	1.043	1.034
Equivalent cube compressive strength, kN/cm²	388	343	220	242	220

Load test

The load test experiment was carried out on the deflected slab in the 2nd floor between axis 15-17 and Y-M before and after repair, using 400 kg/m² live load and Table 3 shows the results.

Table 3 Load test on slab 15 – 17 and Y – M

CASE STUDY	PROPERTY		
	Deflection after 24 hours of loading, mm	Deflection after removing 1.5 live load, mm	Percentage of deflection recovery after removing load, %
Before repair	7.24	4.343	60 %
After repair	2.24	0.224	90%

REPAIR TECHNIQUE OF DEFECTS AND DAMAGES

Repair of defected slabs (residual deformation less than L/500)

Strengthening technique can be summarized in the following points:-

- Stiffening the bottom of slabs under repair with steel Jacks every 50 cm.
- Removing at least 2cm of upper layer of concrete surface of slabs.
- Cleaning upper concrete surface with air compressor.
- Fixing of steel ϕ13 mm every 50 cm as shear connectors in the upper surface of concrete slab using epoxy mortar.
- Adding new steel mesh at upper surface 6ϕ13 mm/m in two directions.
- Casting 6cm concrete layer in the upper surface using concrete mix with cement content of 400 kg/m^3.
- Curing of new concrete layer for 7 days.
- Removing of steel Jacking Stiffners after 14 days at least (Fc > 200 kN/cm^2).

Repair of deflected slab (residual deformation more than L/500)

Strengthening technique can be summarized in the following points:-

- Adding new element (column on Axis 16′ - K) to the existing statically system of school under repair to reduce the residual deformation and the dimensions of new column 3 5x35 cm and steel 8ϕ18mm and stirrups 6 ϕ 8mm from footing to the roof of school.
- Adding new P.C and R.C footings on the same axis 16′ - k of dimensions:- P.C footing 2.45 × 2.45 × 0.5m, R.C footing 1.55 × l.55 × 0.6m and steel 8ϕ18 in two directions.
- Adding column cap of dimensions 85cm × 85cm and thickness 25cm and vertical steal 5ϕ 16 in two directions, this is in the connection between the new column and every concrete floor to decrease punching.

EVALUATION OF RESULTS OF TESTS CARRIED OUT ON CONCRETE BEFORE AND AFTER REPAIR

Results of Schmidt hammer test

Table 1 shows the results of P.C and R.C. footings which can be considered accepted.

Results of core test

Table 2 shows that the results of R.C. slabs which is between (220 and 240) kN/cm², while the designed value is 225 kN/cm².

Results of load test

Table 3 shows that the percentage of deflection recovery after removing 1.5 live load was 60% before repairing and 90% after repairing while the mininmum value stated in the code [6] is 75%.

CONCLUSIONS AND RECOMMENDATIONS

- It is recommented to repair the deflected slabs of residual deformation less than L/500 using upper steal mesh.
- It is recommended to add new column element to the existing statically system for deflected slab of residual deformation more than L/500, this is needs to add new P.C. and R.C. footings for this column and make R.C. cap in connection between the column and each floor.
- Supervisions and quality control are very important to check the code requirements.
- Its recommended to lift the bottom of deflected slabs with steel jacks every 50cm befoe repairing and they must be remained for 14 days at least (Fc > 200 kN/cm²) to repair the observed residual deformation less than L/500.
- It is recommend review and check of stresses, deflection and cracking requirments for design of concrete elements before begining of construction to avoid any probable design errors.
- It is recommended to check the depth of R.C. slabs and other elements during casting and finishing.
- It is recommended to make load test experiment before and after repairing of deflected slabs to evaluate the effect of repairing.
- It is recommended to produce Arabic code in repair and strengthening of reinforced concrete structures.
- It is recommended to avoid increasing the thickness of flooring than 10 cm, since any increase gives additional dead load on the slab.
- It is recommended to maintain the minimum value of conerete cover for R.C. slabs 2cm, while any increase in that cover has bad effect on slab behaviour.

- It is recommended to change the design of big slabs like slab on axis (15-17 & Y – M) from solid slab to hollow block slab, panneled beem slab, or flat slab system.

REFERENCES

1- ARABIC CONFERENCE FOR REPAIR, strengthening rehabitation of structures , 16-19 Sept., 1998.

2- FUKUYAMA K, ET AL, "Studies on repair and strengthening methods of damaged reinforced concrete columns". Cement and concrete composites, Vol. 22, No. 1, 2000, pp 81-88.

3- RASHEED T.A.M, "Towards an Arab code in Repair and strengthening of Reinforced concrete Structures", Arabian Conference Proceedings, pp319 – 410, Sept 2003.

4- ASTM C 42, "Standard method for obtaining and testing drilled cores of concrete ", Annual book of ASTM Standard, 1990.

5- E.SS. 1658, 1995, "Standard method for obtaining and testing drilled cores of concrete", 1995.

6- EGYPTIAN CODE OF PRACTICE, for design and construction of concrete structures (E.C.P. 203-2001).

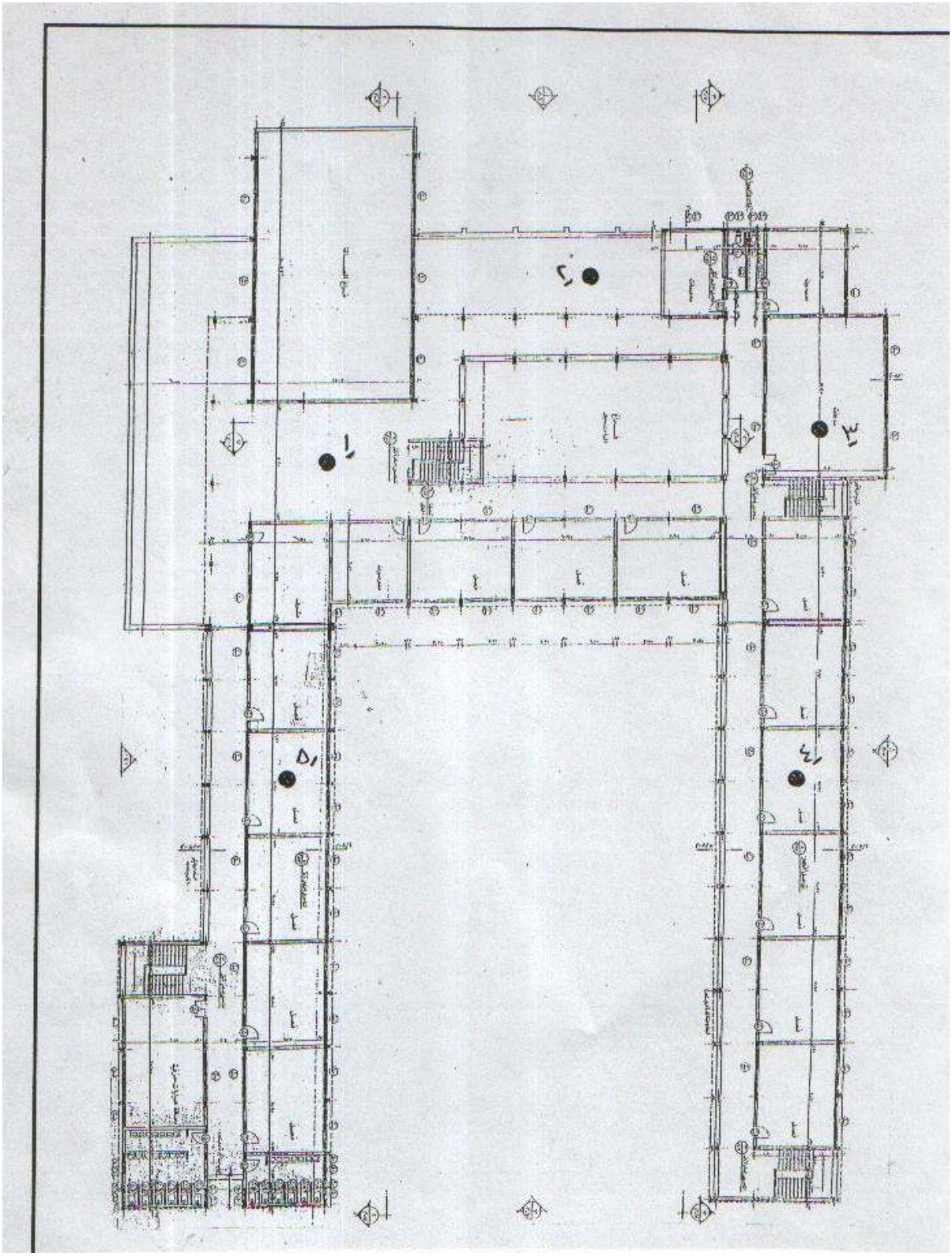

Figure 1 Plan of 2nd floor showing the core positions

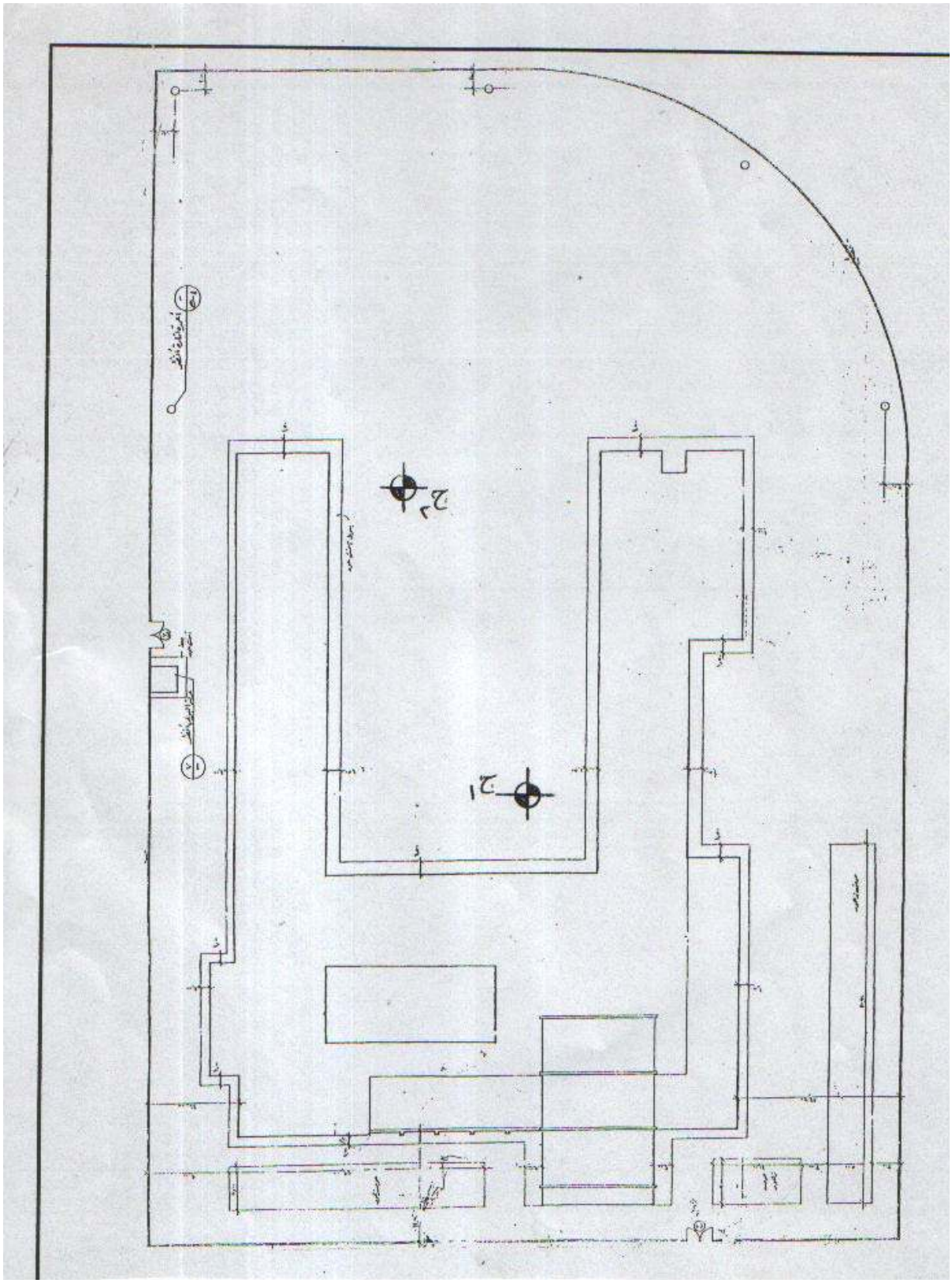

Figure 2 Sketch of general layout showing boring positions

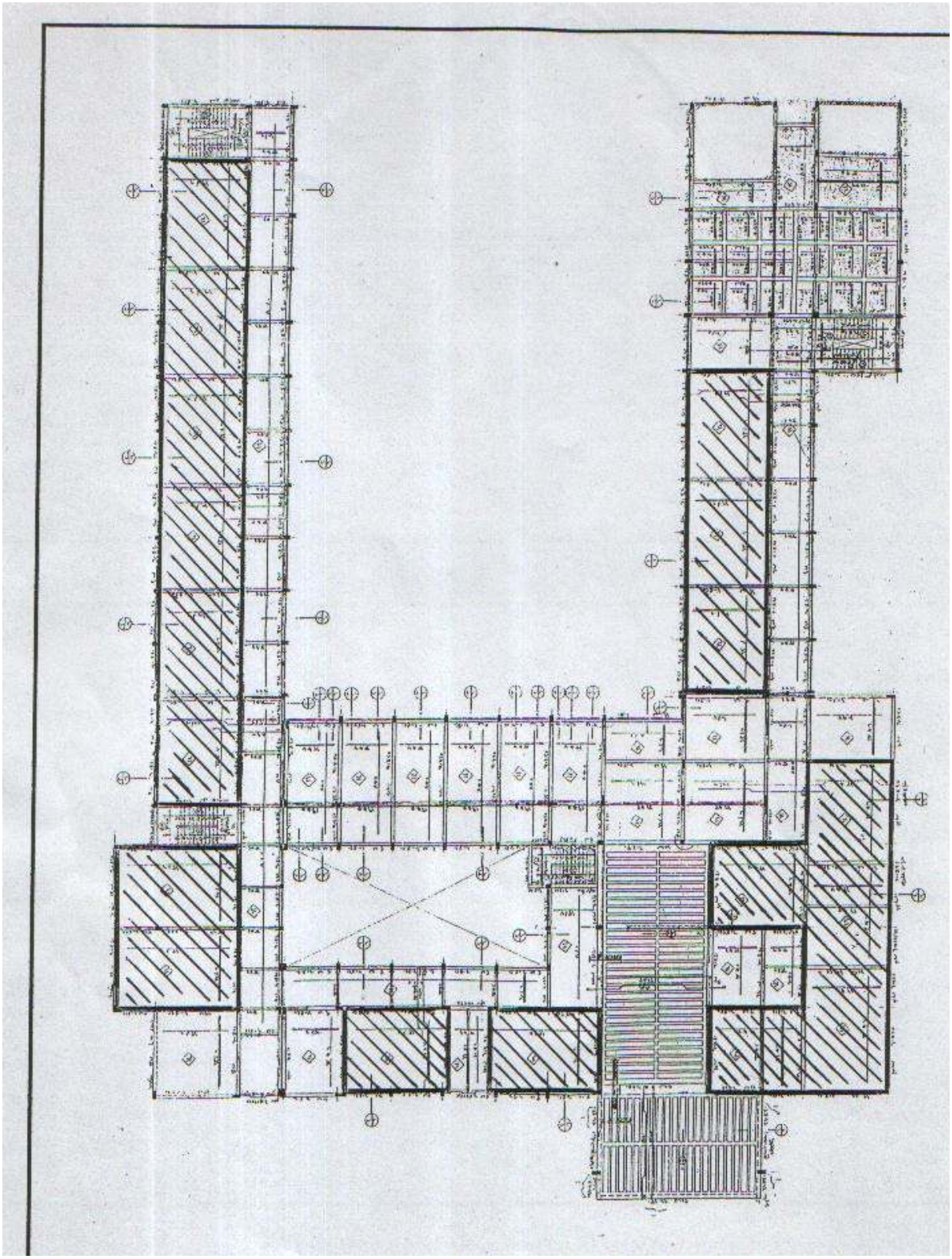

Figure 3 Plan for repaired slabs on 1st floor

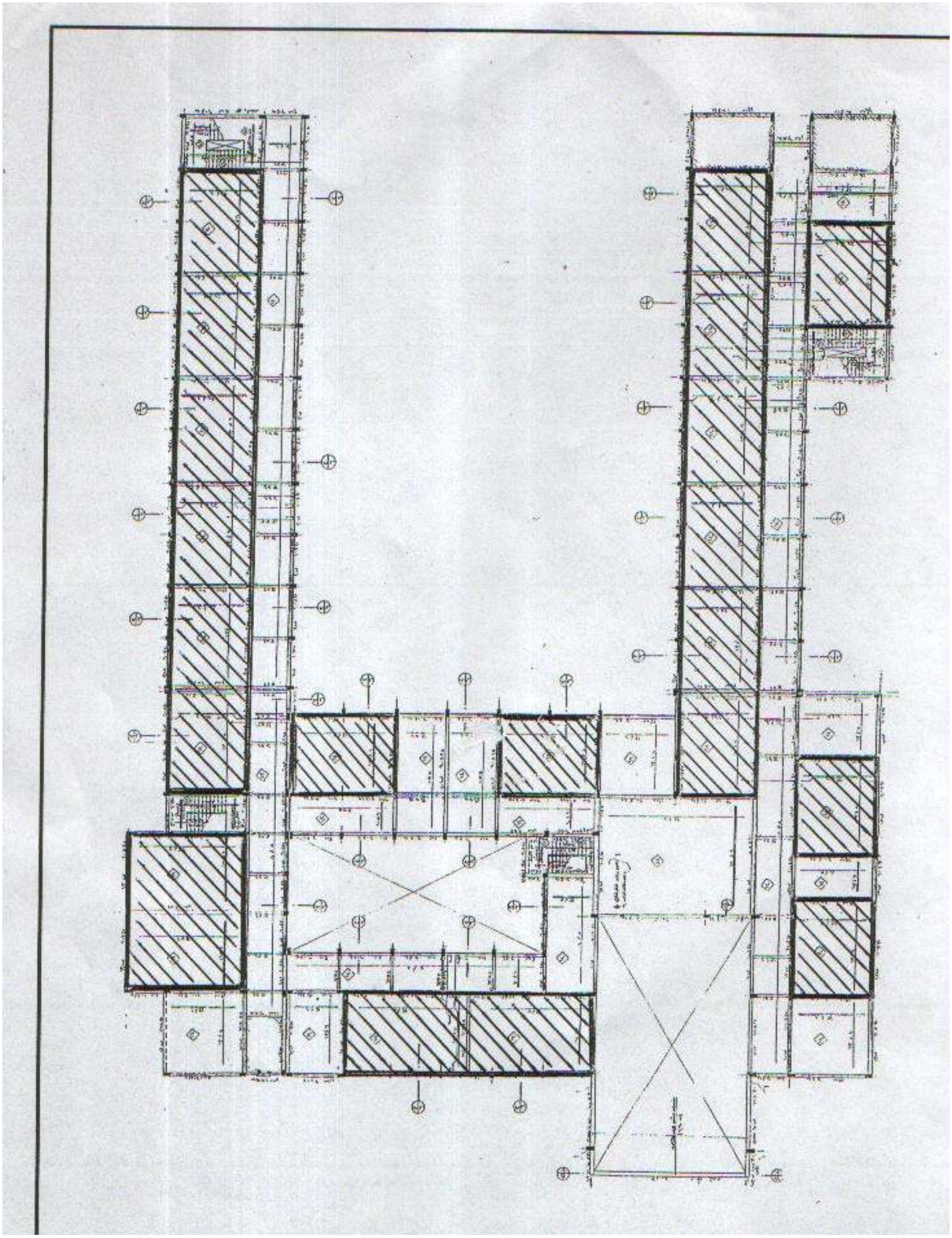

Figure 4 Plan for repaired slabs on 2nd floor

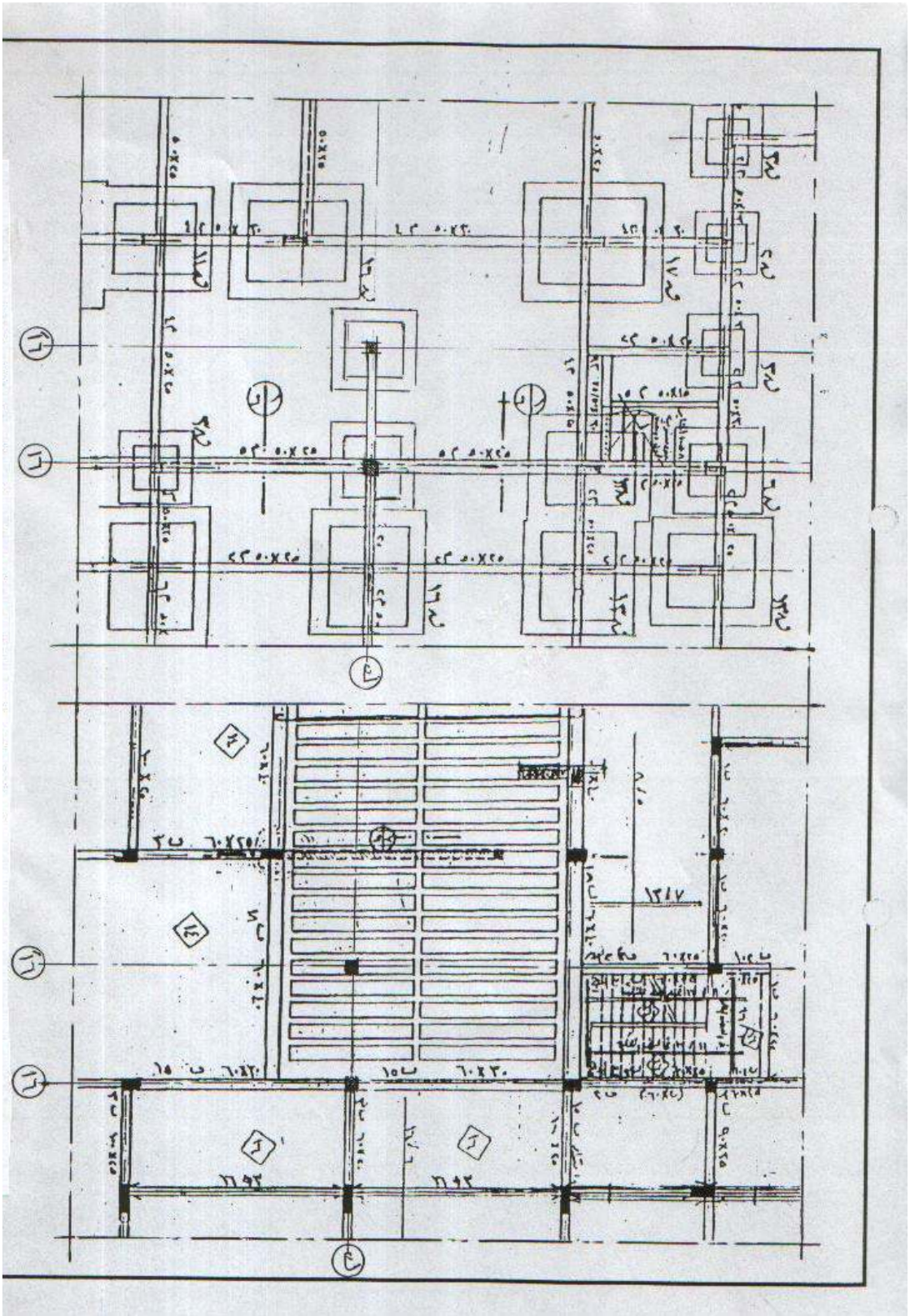

Figure 5 Plan showing the position of added footing

Nonlinear Analysis of the Shear Behaviour of Concrete Beams using Glass Fibre Reinforced Polymer (GFRP) Main Reinforcement and Closed Stirrups

K S Ragab
Housing & Building National Research Centre, Egypt

This paper carried out nonlinear analysis of the shear behavior of concrete beams using main reinforced and stirrups from GFRP or steel bars based on ANSYS software. Nonlinear finite element analysis on 11-beams specimens was achieved by using ANSYS software. The nonlinear finite element analysis program ANSYS is utilized owing to its capabilities to predict either the response of reinforced concrete beams in the post elastic range or the ultimate strength of a reinforced concrete beams reinforced by GFRP bars. In this research, the effect of using GFRP or steel bars as straight shear reinforcement instead of stirrups in RC beams have been investigated. Hence, it would be helpful to reduce the reinforcement bars without reducing the shear strength of the beams. This point has never been done before and is a new idea that offers a new method to build RC beams. An extensive set of parameters is investigated under applied concentrated load on the beam at shear span equal 2.0. These parameters are investigated including the effect of dowel action without any transverse reinforcement on the shear strength, the effect of the spacing between the stirrups, the effect of changing of volumetric ratios of stirrups, the effect of type of reinforcement (GFRP or Steel) for main reinforcement or stirrups, and finally the effect of the shape of stirrups (stirrups or straight shear reinforcement). The results of finite element analysis showed that nonlinear analysis were in good accordance with the experimental results, which can well simulate the shear behavior of concrete beams reinforced by GFRP bars.

Dr Khaled S. Ragab is currently Associate Professor of Concrete Constructions at Reinforced Concrete Research Institute, Housing & Building National Research Center, HBRC, Cairo, Egypt. (kh_ragab@yahoo.com). He is a Consulting Engineer in the design of concrete structures. He is a Member of Syndicate of Egyptian Engineers, Member of the Association of Engineers of Egyptians, and Member of the reviewer team for Journal of civil engineering and construction technology. He has led several research projects on concrete, and his interesting areas of research are fibre reinforced concrete (GFRP), High performance concrete (self compacting concrete), Nanotechnology in the field of concrete, Economic systems of construction, Nonlinear analysis by FEM for different elements of concrete construction, and Light weight concrete.

Keywords: Closed stirrups, Concrete beams, Glass fibre reinforced polymer bars (GFRP), Main reinforcement, Nonlinear analysis, Shear behaviour, Shear reinforcement

INTRODUCTION

Modeling the constitutive law of the shear behavior of concrete beams reinforcement by GFRB bars based on the empirical approach can sometimes be inaccurate or limited to a narrow range of available experimental data. The tests are also very expensive and sometimes time consuming. The applicability of the test data mainly depends on the accuracy of the test apparatus and the supporting instruments implemented during the test. Hence, it is deemed necessary to have another option of modeling the shear behavior of concrete beams reinforcement by GFRB bars without deploying an empirical approach in the modeling. One of the suitable software that can be utilized to describe the actual nonlinear behavior of the shear behavior of concrete beams reinforcement by GFRB bars is ANSYS [10]. This is because ANSYS is capable of analyzing the nonlinear behavior of a combination between 3D SOLID and LINK elements in a structure based on the finite element procedure. With this option, researchers or design engineers can confidently predict in advance the actual behavior of various shear behavior of concrete beams reinforcement by GFRB bars not only in the linear-elastic region, but furthermore also in the nonlinear post-elastic region. The authors wish that this economical procedure can be used to provide an alternative tool for researchers or structural engineers in investigating various types of structural concrete elements in the future.

In this paper, the authors propose to use ANSYS [10], which is capable of modeling the nonlinear shear behavior of concrete beams reinforcement by GFRB bars, for predicting the actual shear strength of concrete beams reinforcement by GFRB bars with the effect of dowel action without any transverse reinforcement on the shear strength, the effect of the spacing between the stirrups, the effect of changing of volumetric ratios of stirrups, the effect of type of reinforcement (GFRP or Steel) for main reinforcement or stirrups, and finally the effect of the shape of stirrups (stirrups or straight shear reinforcement). These parameters are investigated under applied concentrated load on the beam at shear span equal 2.0. However, none of the works conducted previously using ANSYS includes the shear behavior of concrete beams reinforcement by GFRB bars. The proposed procedure has been verified with four concrete beams specimens reinforcement by GFRP bars for main reinforcement and stirrups. The shear strength obtained from the proposed procedure is shown to be in close agreement with the experimental results.

Extensive research in recent years has been undertaken to investigate the performance of Glass Fiber-reinforced polymer (GFRP) as primary reinforcement for concrete members. Glass Fiber-reinforced polymer (GFRP) bars are currently available as a substitute for conventional steel bars in concrete structures exposed to deicing salts and marine environments. In addition to superior durability, Glass Fiber-reinforced polymer (GFRP) reinforcing bars have a high strength-to-weight ratio, which makes them attractive as reinforcement for concrete structures. However, the material properties of Glass Fiber-reinforced polymer (GFRP) differ significantly from those of steel reinforcement, especially the modulus of elasticity. The modulus of elasticity is 20 to 25 % that of steel compared to 60 to 75 % for carbon Fiber-reinforced polymer (FRP) bars. Due to the relatively low modulus of elasticity of Glass Fiber-reinforced polymer (GFRP) bars, concrete members reinforced longitudinally with Glass Fiber-reinforced polymer (GFRP) bars experience reduced shear strength compared to the shear strength of those reinforced with the same amounts of steel reinforcement. This fact is supported by the findings from the experimental investigations on concrete beams without stirrups and reinforced longitudinally with carbon and Glass Fiber-reinforced polymer (GFRP) bars (El-Sayed, et al., 2006)[5]. The

investigation also revealed that the axial stiffness of the reinforcing bars is a key parameter in evaluating the concrete shear strength of flexural members reinforced with Glass Fiber-reinforced polymer (GFRP) bars.

The current ACI 440.1R-06 [3] guide has proposed a design approach for calculating the concrete shear strength of Glass Fiber-reinforced polymer (GFRP)-reinforced concrete beams accounting for the axial stiffness of Glass Fiber-reinforced polymer (GFRP) reinforcing bars. Recent research has indicated that the ACI 440 shear design method provides very conservative predictions, particularly for beams reinforced with Glass Fiber-reinforced polymer (GFRP) bars (El-Sayed et al., 2006[5]; Razaqpur et al., 2004[7]; Gross et al., 2003[8]; Tureyen and Frosch, 2002[9]). Furthermore, considering the lower costs of GFRP bars in comparison to CFRP and aramid FRP (AFRP), GFRP reinforcement is becoming more attractive for the construction industry.

So this research aims to study the shear behavior of concrete beams reinforcement by GFRP bars. The results and observations presented in this paper are useful to practicing engineers who must predict the enhanced shear strength of concrete beams reinforced with GFRP bars.

OBJECTIVES AND SCOPE

The main objectives of this study could be summarized in the following points:

- Evaluation the effect of using GFRP bars as straight shear reinforcement instead of stirrups in RC beams.
- Examining the shear behavior of reinforced concrete beams longitudinally and stirrups with GFRP-bars.
- Comparing this behavior with reinforced concrete beams longitudinally and stirrups with steel bars.
- Knowing better for shear stresses distribution for longitudinal and cross section concrete beams during the loading.
- Parametric study for the effect of dowel action without any transverse reinforcement on the shear strength, the effect of the spacing between the stirrups, the effect of changing of volumetric ratios of stirrups, the effect of type of reinforcement (GFRP or Steel) for main reinforcement or stirrups, and finally the effect of the shape of stirrups (stirrups or straight shear reinforcement). These parameters are investigated under applied concentrated load on the beam at shear span equal 2.0.

Finite element models were developed to simulate the shear behavior of reinforced concrete beams with GFRP longitudinally and transversely bars from linear through nonlinear response using the ANSYS program.

EXPERIMENTAL AND ANALYTICAL PROGRAM

Experimental Program

The experimental models were constructed according to rectangular beam specimens as shown in Figure 1. The specimens had tested of GFRP and steel RC beams under concentrated load. Test set up and general view of GFRP bars and stirrups are shown in

Figure 2. The experimental program had chosen four rectangular beams. These beams are shown in Table 1 from B1 to B4. All the specimens from B1 to B11 are analysis by FEM using ANSYS program.

Figure 1 General view of GFRP bars and stirrups.

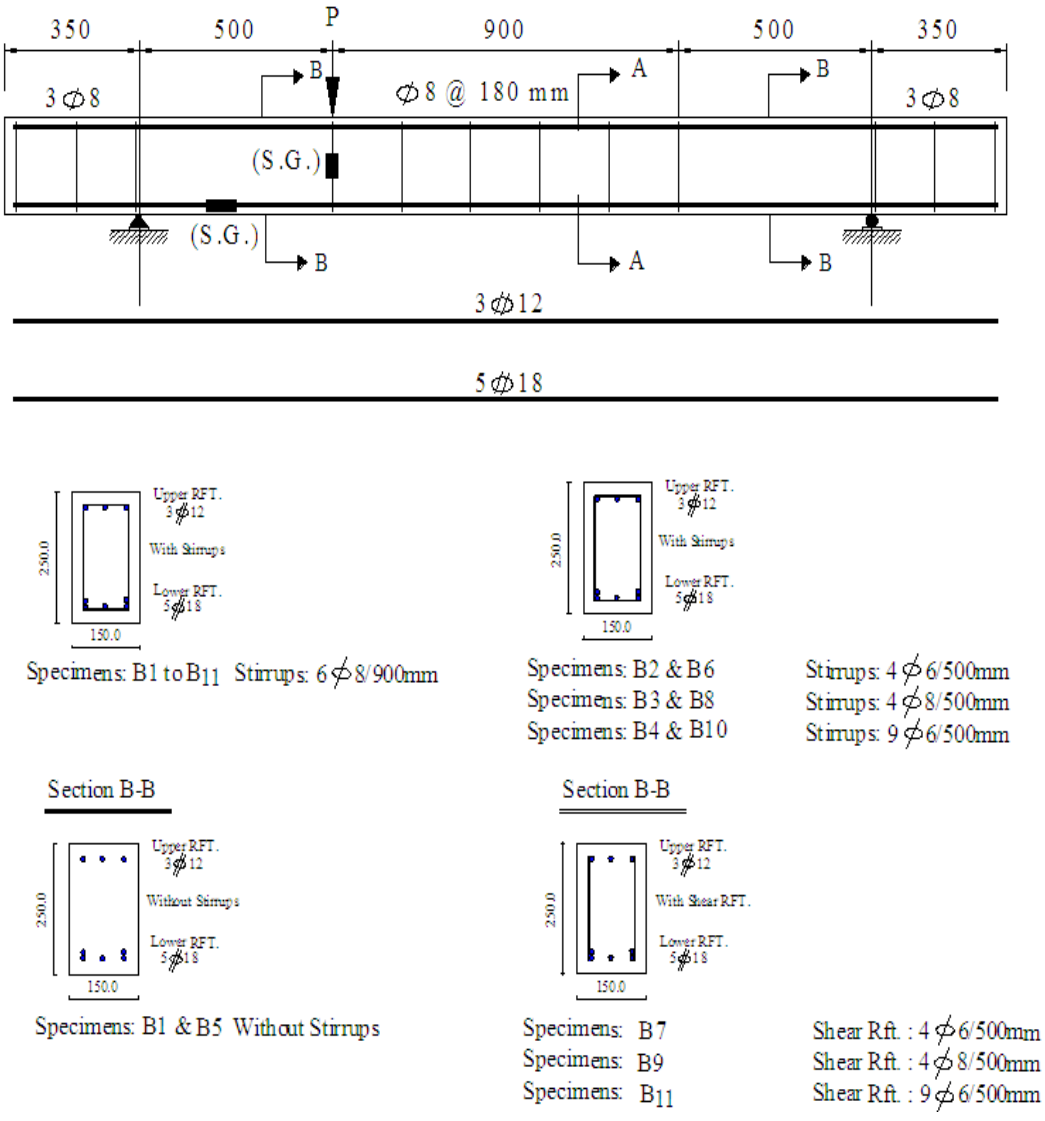

Figure 2 Test set up, Details of Reinforcement, and Strain Gauge for Tested Beams

Table 1 The Program for the Analytical Beams.

MODEL by	BEAM No.	DIM. bxd (mm)	Rft. TYPE	STIRRUP TYPE	REINFORCEMENT (mm)		STIRRUPS (mm)		SHEAR Rft. mm	TARGET COMP. STR. (MPa)
					Top	Bot.	At Mid/ 900mm	At Shear Span/ 500mm	At Shear Span/ 500mm	
Exp. and FEM	B1	150x250	GFRP	GFRP	3#12	5#18	6#8	---	---	27.5
	B2	150x250	GFRP	GFRP	3#12	5#18	6#8	4#6	---	27.5
	B3	150x250	GFRP	GFRP	3#12	5#18	6#8	4#8	---	27.5
	B4	150x250	GFRP	GFRP	3#12	5#18	6#8	9#6	---	27.5
FEM	B5	150x250	Steel	Steel	3#12	5#18	6#8	---	---	27..5
	B6	150x250	Steel	Steel	3#12	5#18	6#8	4#6	---	27.5
	B7	150x250	GFRP	GFRP	3#12	5#18	6#8	---	4#6	27.5
	B8	150x250	Steel	Steel	3#12	5#18	6#8	4#8	---	27.5
	B9	150x250	GFRP	GFRP	3#12	5#18	6#8	---	4#8	27.5
	B10	150x250	Steel	Steel	3#12	5#18	6#8	9#6	---	275
	B11	150x250	GFRP	GFRP	3#12	5#18	6#8	---	9#6	275

All the concrete beams are loaded by concentrated load at shear span equal 2.0. The specimens had rectangular with cross section 150*250mm, and length of 2600mm. The beams from B1 to B11 were reinforced by GFRP and steel bars for longitudinally and transversely bars. The beams were mainly reinforced with six longitudinal bars of 18 mm diameter, secondary reinforced by three longitudinal bars of 12mm, six stirrups of 8mm diameter at mid span and different diameter of stirrups with different spacing and different shape (stirrups or straight shear reinforcement) at shear span.

The analysis carried out is conducted on -RC beams as shown in table (1); the parameters of study were the effect of dowel action without any transverse reinforcement on the shear strength, the effect of the spacing between the stirrups, the effect of changing of volumetric ratios of stirrups, the effect of type of reinforcement (GFRP or Steel) for main reinforcement or stirrups, the effect of the shape of stirrups (stirrups or straight shear reinforcement), finally the effect of change the compressive strength of concrete. Finally, conclusions from the current research and recommendations for future studies are presented.

Element Types

Extensive inelastic finite element analyses using the ANSYS program are carried out to study the behavior of the tested beams. Three types of elements are employed to model the beams. An eight node solid element, solid65, was used to model the concrete. The solid element has eight nodes with three degrees of freedom at each node, translation in the nodal x, y, and z directions as shown in Figure 3. The used element is capable of plastic deformation, cracking in three orthogonal directions, and crushing. A link8 element was used to model the reinforcement polymer and steel bars; two nodes are required for this element. Each node has three degrees of freedom, translation in the nodal x, y, and z directions. The element is also capable of plastic deformation (ANSYS User's Manual).

Steel plates were added at support and loading locations in the finite element models (as in the actual beams) in order to avoid stress concentration problems. An elastic modulus equal to 200,000 N/mm^2 and Poisson's ratio of 0.3 were used for the plates. The steel plates were assumed to be linear elastic materials. A Solid 45 element was used to model steel plates. The geometry and node locations for this element type are shown in Figure 3. The finite element mesh used in the analysis and the crushing beam model are shown Figure 4.

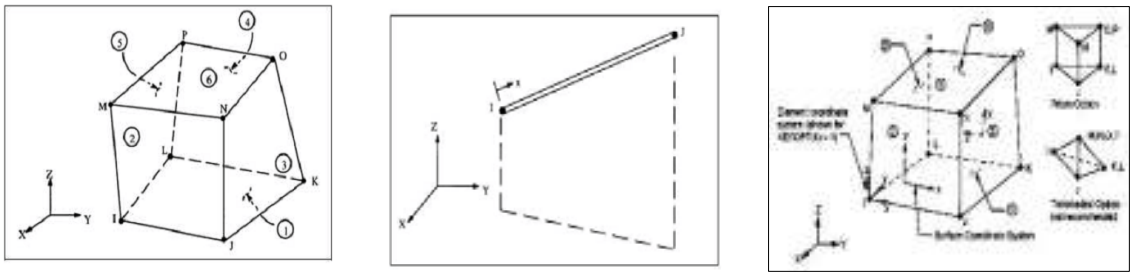

Solid 65 Link 8 Solid 45

Figure 3 Element type Solid 65, Link8 and Solid 45.

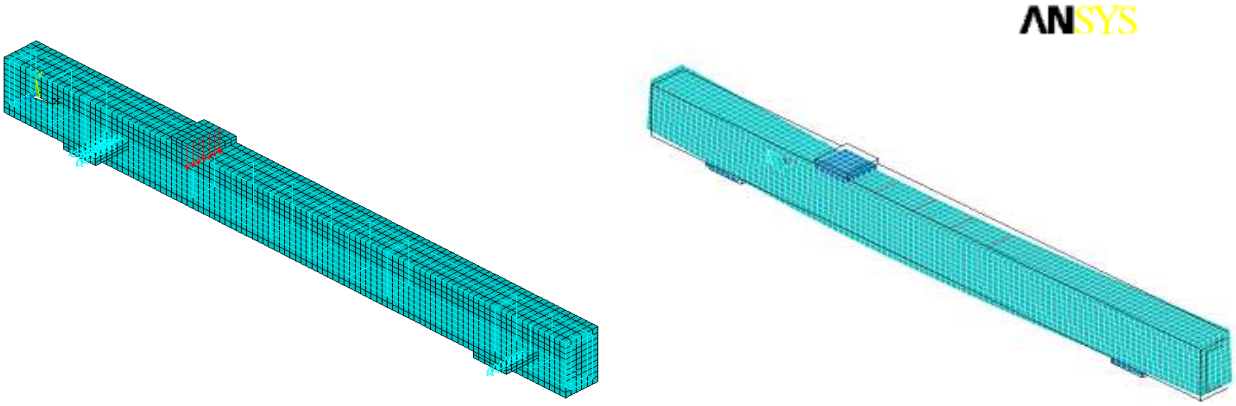

(a) Finite element mesh model (b) Crushing concrete model

Figure 4 Finite element mesh for a typical beam model and crushing model.

PROPERTIES of the USED MATERIAL

Normal weight concrete was used in the fabricated tested beams. The stress-strain curve is linearly elastic up to about 30% of the maximum compressive strength. Above this point, the stress increases gradually up to the maximum compressive strength, f_{cu}, after that the curve descends into softening region, and eventually crushing failure occurs at an ultimate strain. The input data for the concrete, GFRP, and steel (high grade and mild steel) properties are shown in Table 2.

Reinforced Concrete

The tested reinforced concrete beams were cast using locally produced ordinary Portland cement, natural sand and crushed stone with a maximum size of 10 mm. The beams were remolded after 24 hrs from casting, covered with wet burlap and stored under the laboratory conditions for 28 days before proceeding to testing stage.

GFRP and Steel Bars

The GFRP and normal tensile steel were used for stirrups and shear reinforcement with diameter 6mm and 8 mm. The GFRP and high tensile steel bars were used for longitudinal reinforcement with diameter 12 mm and 18mm as shown in Figure 1. Table 2 shows the mechanical properties of the used GFRP and steel bars. The GFRP bars were locally manufactured. The GFRP bars are covered by layers of wrapped fiber to improve their bond with concrete. Due to local industry some stirrups has imperfection in its diameters.

Steel Plate

An elastic modulus equal to 200,000 N/mm2 and Poisson's ratio of 0.3 were used for the plates. The steel plates were assumed to be linear elastic materials.

Table 2 Input data for the concrete, GFRP, and steel properties

ITEM	CONCRETE	GFRP (main reinforcement)	GFRP (stirrups)	STEEL (main reinforcement)	STEEL (stirrups)
Unit weight, N/mm^3	2.5e-5	2.54e-5	2.54e-5	7.85e-5	7.85e-5
Ultimate compressive strength, N/mm^2	25,40	--	--	--	--
Tensile strength, N/mm^2	2.20,3.5	345	345	360	250
Elastic modulus, N/mm^2	2.4e4,2.8e4	42300	42300	2.0e5	2.0e5
Poisson ratio	0.20	0.20	0.20	0.30	0.30
Shear modulus, N/mm^2	10.0e3,11.0e3	--	--	--	--

ELEMENT MESHING

After preparing all the input data of material and geometrical properties, the beam models were divided into small cubical elements. The meshing results of all beams specimens used for model validation are shown in Fig. 4. For beams reinforced, it is worthwhile to notice that the meshing was created according to the locations of reinforcing bars, either the longitudinal or transverse reinforcement, as well as the beam specimen cross-sectional perimeter. By using sharing nodes option in ANSYS [10], SOLID65, LINK8 and SOLID45 elements can be interconnected one to another forming a single solid beam model which capable of simulating the actual behavior of reinforced concrete beam.

Numerical Implementation

The quantitative implementation of the finite element procedure used in the ANSYS software [10] is based on the principles of virtual work or the postulation of minimum potential energy in the assembly of the elements as formulated the following equilibrium equation:

$$[K]\{d\} + \{F\}_p + \{F\}_g + \{F\}_{\varepsilon o} + \{F_{\sigma o}\} - \{R\} = 0 \quad (1)$$

The stiffness matrix [*K*],

$$[K] = \Sigma \int [B]^T [D] [B] \, dv \quad (2)$$

The nodal force due to the surface load,

$$\{F\}_p = -\Sigma_{ele} \int [N]^T \{P\} \, dv \quad (3)$$

The nodal force due to the body load,

$$\{F\}_g = -\Sigma_{ele} \int [N]^T \{g\} \, dv \quad (4)$$

The nodal force due to the initial strain,

$$\{F\}_{\varepsilon o} = -\Sigma_{ele} \int [B]^T [D] \{\varepsilon_o\} \, dv \quad (5)$$

The nodal force due to the initial stress,

$$\{F\}_{\sigma o} = -\Sigma_{ele} \int [B]^T [D] \{\sigma_o\} \, dv \quad (6)$$

where [*N*] is the shape function; {*d*} is the vector of nodal displacement; {*R*} is the vector of applied nodal force; {*p*} is the vector of surface load; and {*g*} is the vector of body load. The ANSYS software uses Newton-Raphson (N-R) method [10] to obtain the convergent solution of the nonlinear equilibrium iterative equation to develop the stiffness matrix of the beam model.

Loading Procedure

The analytical investigation carried out here is conducted on 11-RC beams. All beams at a plane of support location, the degrees of freedom for all the nodes of the solid65 elements were held at zero. To apply concentrated load on the top of the beam specimen, a line load was implemented over the top surface of the plate loading model in the ANSYS software. The line load can be simulated using the ANSYS load step option [10]. Load step option may be used when the incremental loading is considered. The number of load steps depends on the user's definition. In this case, load steps were defined according to the actual load steps applied during the test. A solution was obtained by solving several sub-steps in each load step to attain convergence. In each sub-step, an iteration procedure was carried out until providing a convergent solution before moving to the next sub-step. The number of the sub-steps taken in the analysis may improve the accuracy of the solution. It will, however, sometimes be very time-consuming when too many sub-steps are taken. To avoid the problem, ANSYS offers an alternate automatic time step option to reduce the computational time required in the analysis. Due to this advantage, this option is selected. When the automatic time step option is selected, it will automatically resize the number of the sub-steps in each load step when it fails to reach a convergent solution. This process keeps repeating until it provides a convergence value. When the load has reached its peak value, the load control mode was switched into the displacement control mode. The displacement control mode was set into several displacement steps corresponding to the

experimental data. Using the automatic time steps, the beam specimen was displaced until failure. The objective of using this kind of mode is to obtain the descending branch of the stress-strain curve of the beam specimens under line loading. The incremental nonlinear equation can be written as follows:

$$K(u)\,\Delta u = \Delta P \qquad (7)$$

Where Δu and ΔP describe the unknown incremental displacement and the given incremental applied load. To solve a nonlinear problem, ANSYS uses the Newton-Raphson (N-R) method [10] involving an iterative procedure (Figure 5). This method starts with a trial assumption: $u = u_i$, to define the incremental of the next steps, $\Delta u_i = K\text{-}1(u_i)\Delta P$, and the load vector exists beyond the equilibrium, $\Delta R_i = \Delta P - K(u_i)\Delta u_i$. There will always be a discrepancy between the applied load and the load evaluated based on the assumption. To satisfy the state of equilibrium, the load vector exists beyond the equilibrium should be zero. Since the solution requires an iterative procedure, a tolerance value should be determined such that a convergent solution can be obtained. In each iteration step, N-R method calculates the load vector exists beyond the equilibrium and always checks if the convergent solution under specified tolerance is obtained. If the value is still greater than the tolerance value, then the initial assumed value is updated with the incremental displacement, $u_{i+1} = u_i + \Delta u_i$. The next incremental solution vector is determined with $\Delta u_{i+1} = K^{-1}(u_{i+1})\Delta P$, providing a new load vector exists beyond the equilibrium $\Delta R_{i+1} = \Delta P - K(u_{i+1})\Delta u_{i+1}$. This procedure is repeated until the convergent solution is obtained.

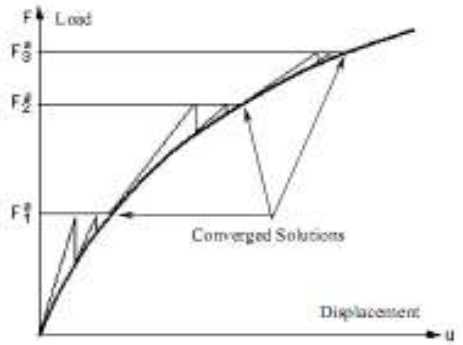

Figure 5 Newton-Raphson iterative solution (3 load increments)

The simplified stress strain curve for concrete is constructed from six points connected by Straight lines. The curve starts at zero stress and strain. Point No. 1, at $0.3f'_c$ is calculated for the stress-strain relationship of the concrete in the linear range. Point Nos. 2, 3 and 4 are obtained from Equation (8), in which ε_o is calculated from Equation (9). Point No. 5 is at ε_o and f'_c. In this study, an assumption was made of perfectly plastic behavior after Point No. 5 (Meisam 2009[1]). Figure 6 shows the simplified compressive axial stress-strain relationship that was used in this study.

$$f = Ec\,\varepsilon / (1+(\varepsilon/\varepsilon_o)^2) \qquad (8)$$

$$\varepsilon_o = 2\,f_c' / E_c \qquad (9)$$

$$E_c = f / \varepsilon \qquad (10)$$

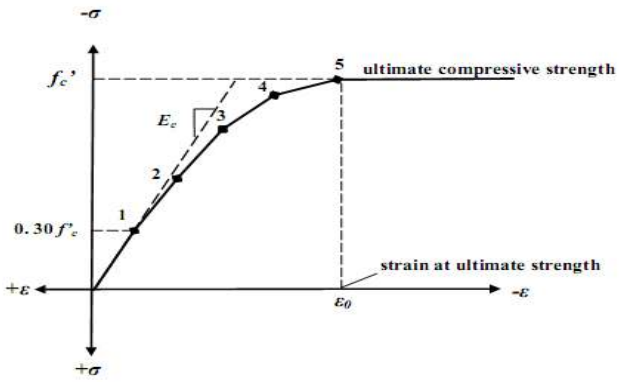

Figure 6 Simplified compressive axial stress strain curve for concrete

TEST RESULTS

Table 3 shows the analytically and the experimental results of the ultimate loads, vertical displacements and peak stress of concrete, respectively.

Table 3 Results of Tested Beams

MODEL by		BEAM No. **Main Rft.*Stirrups	F_{cu} (MPa)	$\rho_v\%=A_{sv}/bd$ At Shear span	EXPERIMENT RESULTS			FEM RESULTS			DIFFERENCE %	
					$P_{ultimate}$ (kN)	VL. Disp. (mm)	Peak stresses (MPa)	$P_{ultimate}$ (kN)	VL. Disp. (mm)	Peak stresses (MPa)	$P_{ultimate}$ (kN)	VL. Disp. (mm)
Exp. and FEM	Control	$B1_{F*F}$	29.6	0	72.7	12.92	24.9	72.0	5.1	0.84	0.99	0.40
		$B2_{F*F}$	33.1	0.377	117.4	23.65	29.6	92.3	7.4	0.90	0.80	0.31
		$B3_{F*F}$	24.4	0.670	108.4	26.84	24.1	92.2	7.2	0.99	0.85	0.27
		$B4_{F*F}$	36.2	0.754	132.8	20.15	34.5	114.8	9.3	0.95	0.87	0.46
FEM	No St.	$B5_{S*S}$	29.6	0	---	---	23.1	76.5	1.9	0.78	---	---
	Stirrups 4#6/500mm	$B6_{S*S}$	33.1	0.377	---	---	28.0	126.0	3.0	0.85	---	---
	Shear Rft. 4#6/500mm	$B7_{F*F}$	33.1	0.377	---	---	31.2	117.0	8.7	0.94	---	---
	Stirrups 4#8/500mm	$B8_{S*S}$	24.4	0.670	---	---	23.0	108.0	2.9	0.94	---	---
	Shear Rft. 4#8/500mm	$B9_{F*F}$	24.4	0.670	---	---	23.8	101.3	8.9	0.98	---	---
	Stirrups 9#6/500m	$B10_{S*S}$	36.2	0.754	---	---	31.0	153.0	3.8	0.86	---	---
	Shear Rft. 9#6/500mm	$B11_{F*F}$	36.2	0.754	---	---	32.2	126.0	10.5	0.89	---	---

** S: Steel bars, and F: GFRP bars.

Load–Vertical Concrete Strain Relationship for Experimental and FEM Results.

The experimental and FEM results for the load versus vertical concrete displacements relationships for beams B1 to B4 are shown in Figure 7 while Table 3 summarizes the test results for all beams. The ultimate load is defined as the maximum recorded load measured during test for each beam. Table 3 indicated that, for beam B1, the experimental result for the ultimate load was recorded 72.7 kN and the corresponding vertical concrete displacement 12.92mm. When using different ratio of stirrups reinforcement for beams B2, B3 and B4, the experimental results for the ultimate loads were recorded 117.4, 108.0 and 132.8 kN respectively, and the corresponding vertical concrete displacements 23.65, 26.84, and 20.15mm respectively. The FEM results for beams B1, B2, B3 and B4, the ultimate loads were recorded 72.0, 92.3 ,92.2 and 114.8kN respectively, and the corresponding vertical concrete displacements 5.1, 7.4, 7.2 , and 9.3mm respectively. Table 4, indicated that, for beams B1, B2, B3 and B4, the difference between the FEM results and the experimental results for the ultimate loads were recorded 0.99, 0.80 , 0.85 and 0.87 respectively, and the corresponding vertical concrete displacements 0.40, 0.31 , 0.27, and 0.46 respectively. The par chart in Figure 8 shows the difference between experimental and FEM results for B1, B2 , B3 and B4. This chart shows that the theoretical results from Finite Element Analysis indicate in general a good agreement with the experimental values.

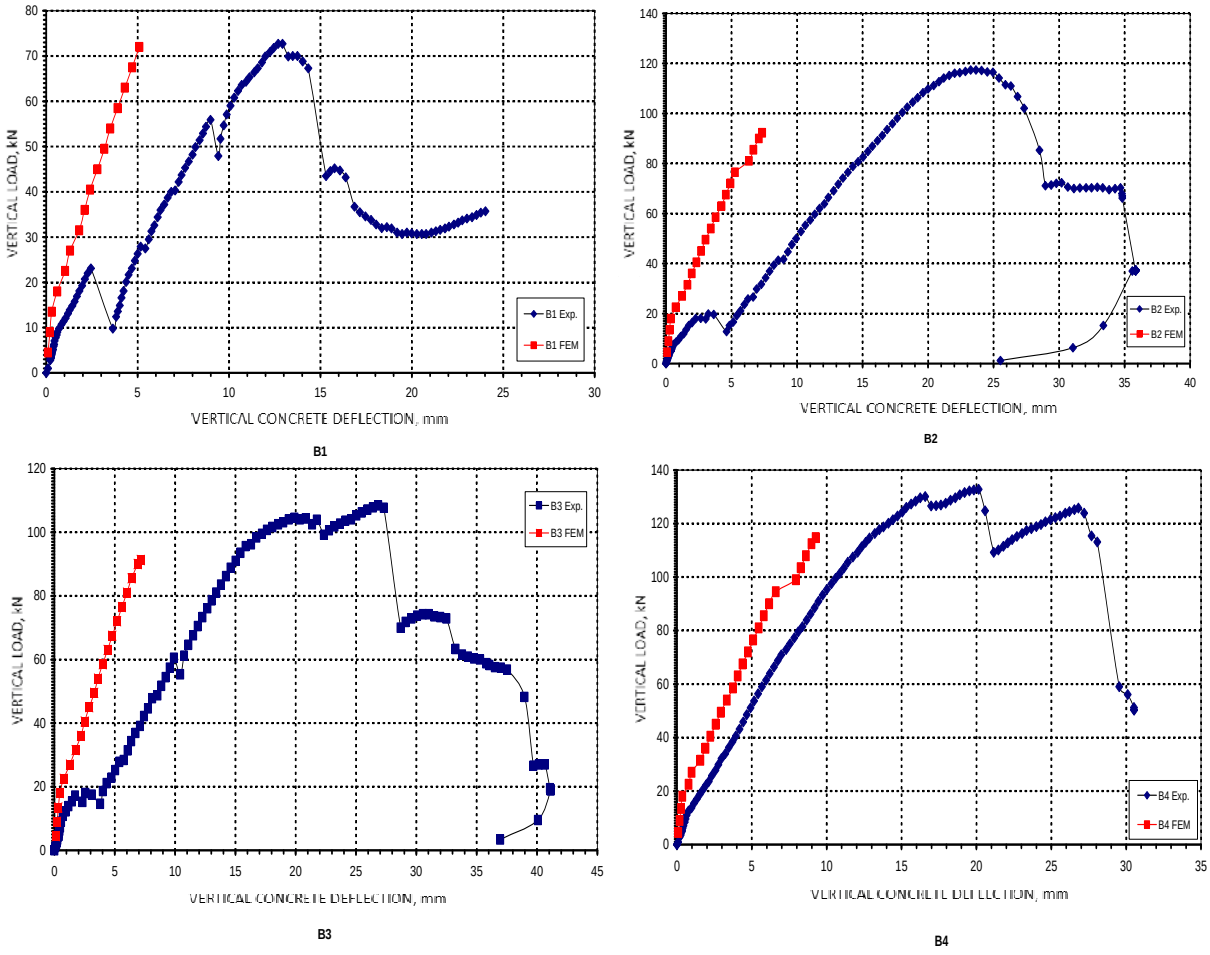

Figure 7 Comparison between results of Experimental and FEM for load – displacement curve.

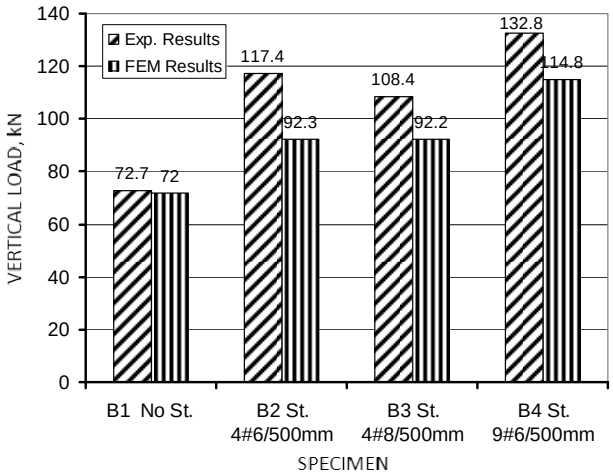

Figure 8 Comparison between results of Experimental and FEM for load – displacement curve.

Stress Distribution

The stress intensity distributions of beam specimens obtained from the ANSYS solution are shown in Figure 9. The stress intensity distributions at the shear span (a/d=2.0 at the lift side of the beam) are showing that the stress concentrations around the plate loading towards to the lift support. Also, it is showing that during the loading, the direction of stresses from upper at the plate loading towards to the lower lift support. This phenomenon describes a correct mechanism of a RC beam specimen subjected to shear loading.

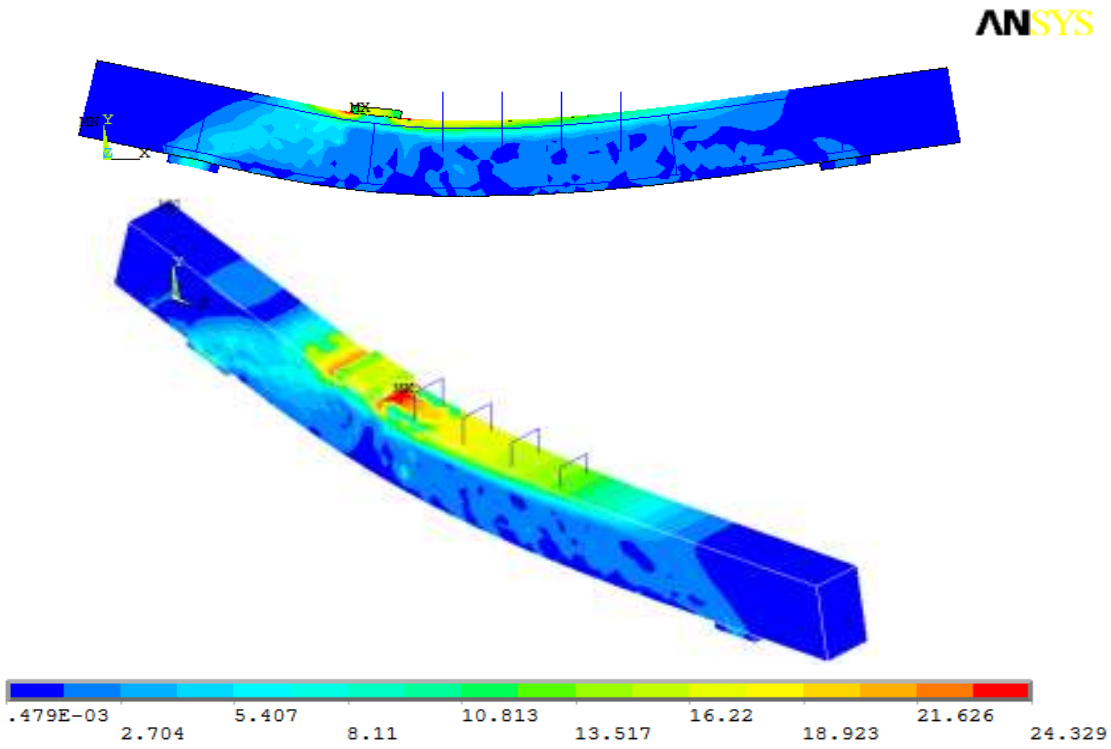

Figure 9 Stress intensity distributions along the longitudinal beam during the loading.

DISCUSSIONS

Effect of Dowel Action without Transverse Reinforcement on Shear Strength

As indicated from Table 3, for beams B1 and B5, which shear span-depth ratio equal 2; its recorded ultimate loads were 72.0 kN and 76.5 kN respectively. This recorded an increase of ultimate load of B5 by 6 % more than beam B1. This is means that the effect of dowel action of steel bars reinforcement (B5) greater than GFRP bars reinforcement (B1). Also, the ductility of the GFRP bars reinforcement (B1) is greater than steel bars reinforcement (b5) as shown in figure (10) (B1, B5).

Effect of Spacing between Stirrups

As shown in Table 3 and Figure 8, the ultimate load for beam B2 was 92.3 kN which its GFRP stirrups spacing was 100 mm in the shear span. While when spacing decrease to be 50 mm in beam B4 with using the same GFRP stirrups thickness, its recorded ultimate load was 114.8 kN recorded an increase by about 25.0 % more than ultimate load of beam B2.

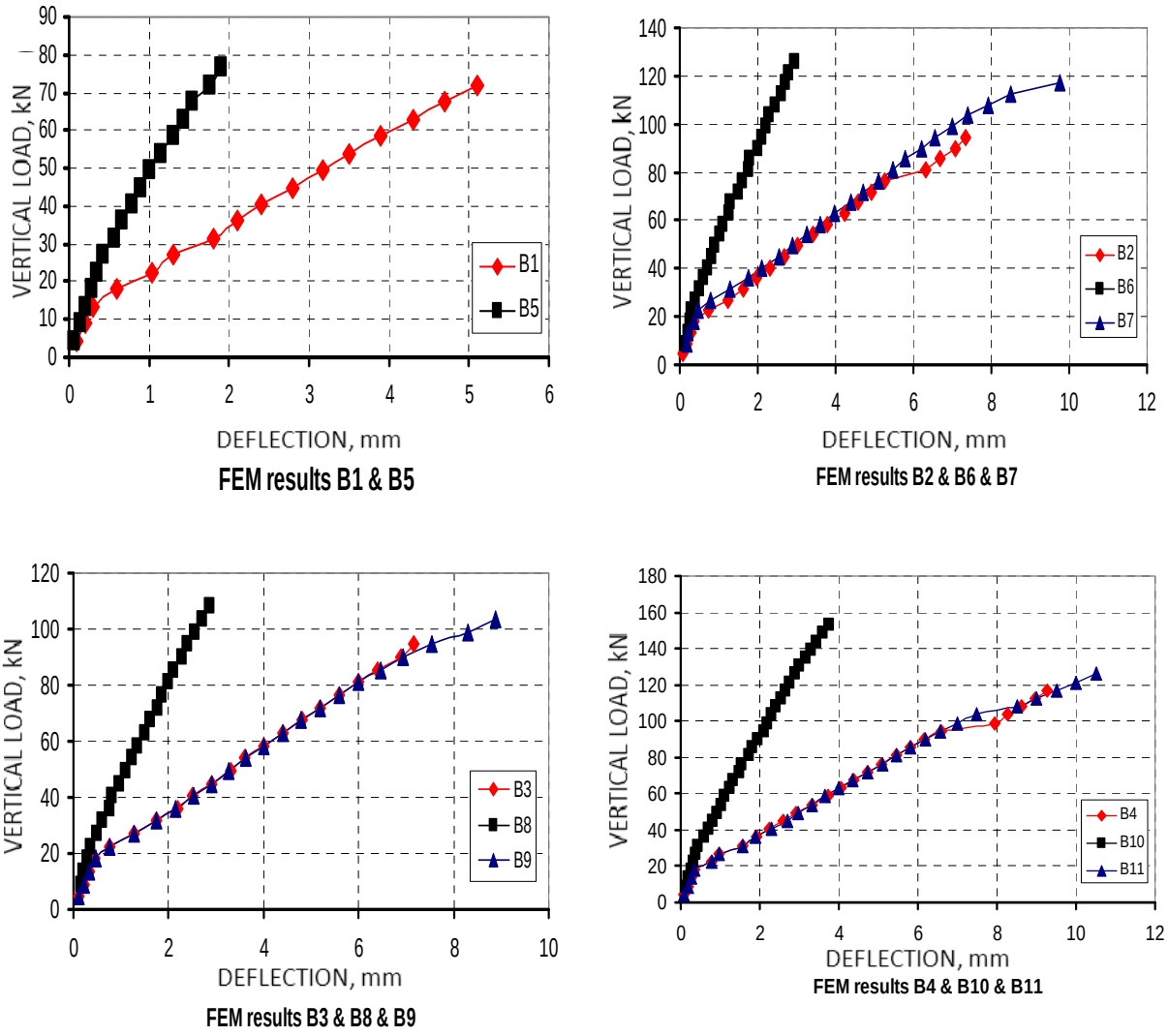

Figure 10 Effect of change type of stirrups.

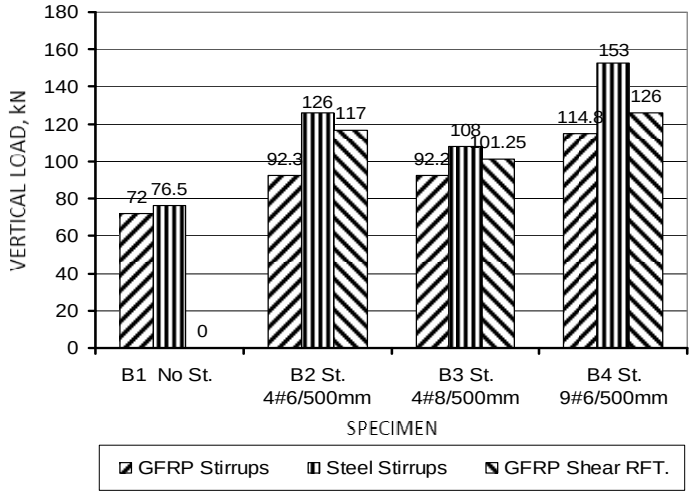

Figure 11 Comparison between ultimate load for different types of stirrups

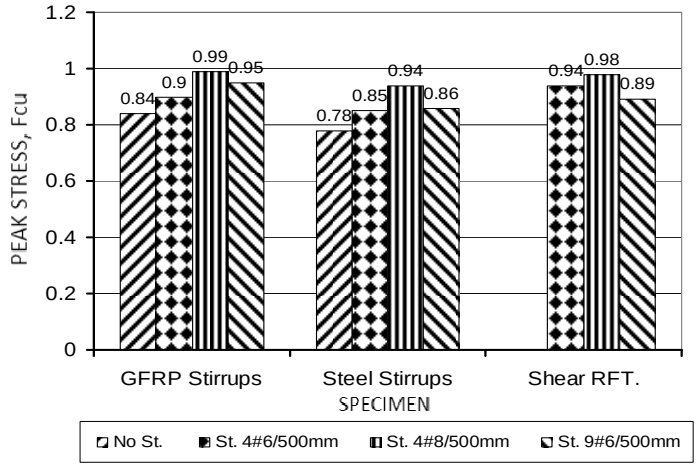

Figure 12 Comparison between {Peak Stresses/ Fcu } for different type of stirrups

Effect of Changing of Volumetric Ratios of Stirrups

It was observed from Table 3 that, the GFRP stirrups used for beam B2 was of 6 mm thickness with spacing 100 mm which its volumetric ratio (**ρ_v%)** be 0.377 %. For beam B4, when volumetric ratio increased to be 0.754 %, the observed ultimate load was 114.8 kN more than ultimate load of beam B2 by 25.0 %.

Effect of Type of Reinforcement (GFRP or Steel) for Main Reinforcement or Stirrups

Figure 9 shows effect of change type of reinforcement (GFRP or Steel) for main reinforcement or stirrups. It is clear from this figure and table (3) that the ductility of the beams reinforcement by GFRP stirrups greater than the ductility of the beams reinforcement by steel stirrups. Also, the beams reinforcement by GFRP stirrups gives ultimate load less than the beams reinforcement by steel stirrups by 25%. The most important point arising from this figure that the GFRP shear reinforcement bars can be considered as an attractive alternative instead of normal stirrups in RC beam. As a general the GFRP shear reinforcement bars gives ultimate loads and ductility bigger than normal GFRP stirrups by

10% and 20% respectively. Also, Par Chart in Figure 12 shows comparison between {Peak Stresses/ Fcu } for different types of stirrups whish clear from this chart that the increasing in the reinforcement ratio of stirrups leads to increase in the peak stresses of the beam.

Effect of the Shape of Stirrups (Stirrups or Straight Shear Reinforcement)

Figure 9 shows that the results obtained from beams reinforcement by GFRP shear reinforcement bars is close to the results obtained from beams reinforcement by normal GFRP stirrups. The GFRP shear reinforcement bars can be considered as an attractive alternative instead of normal stirrups in RC beam. As a general the GFRP shear reinforcement bars gives ultimate loads and ductility bigger than normal GFRP stirrups by 10% and 20% respectively.

ULTIMATE CAPACITY AND CODE PROVISION

According to ACI 440.1R-06, the concrete shear capacity V_c of flexural members using FRP as main reinforcement can be evaluated as shown

$$V_c = 2/5 \sqrt{f_c'}\, b_w\, c \qquad \text{(SI Units)} \qquad (11)$$

Where b_w = width of the web, and c= cracked transformed section neutral axis depth.
For singly reinforced, rectangular cross sections, the neutral axis depth c may be computed as

$$c = kd \qquad (12)$$

$$k = \{\sqrt{2\rho_f n_f + (\rho_f n_f)^2}\} - \rho_f n_f \qquad (13)$$

$$n_f = E_f/E_c = E_f/4750\sqrt{f_c'} \qquad \text{(SI Units)} \qquad (14)$$

$$\rho_f = \text{FRP reinforcement ratio} = A_f / b_w d \qquad (15)$$

Equation (13) accounts for the axial stiffness of the FRP reinforcement through the neutral axis depth c, which is a function of the reinforcement ratio ρ_f and the modular ratio n_f . The ACI 318-05 method used to calculate the shear contribution of steel stirrups is applicable when using FRP as shear reinforcement. The shear resistance provided by FRP stirrups perpendicular to the axis of the member V_f can be written as

$$V_f = A_{fv}\, f_{fv}\, d / s \qquad (16)$$

The stress level in the FRP shear reinforcement at ultimate for use in design

$$f_{fv} = 0.002\, E_f < f_{fb} \qquad (17)$$

$$f_{fb} = (0.05 r_b/d_b + 0.3)\, f_{fu} \qquad (18)$$

$$V_u = V_f + V_c \qquad (19)$$

$$V_u = A_{fv}\, f_{fv}\, d /s + 2/5 \sqrt{f_c'}\, b_w\, c \qquad (20)$$

Where

f_c' = Specified compressive strength of concrete.
f_c = Compressive stress in concrete.
f_{fb}= Strength of a bent portion of FRP bar.
f_{fv}= Tensile strength of FRP for shear design, taken as the smallest of the design tensile strength f_{fu}, the strength of the bent portion of the FRP stirrups f_{fb}.
f_{fu}= Design tensile strength of FRP, considering reductions for service environment.
V_c= Nominal shear strength provided by concrete with FRP flexural reinforcement.
V_f = Shear resistance provided by FRP stirrups.
E_f = Guaranteed modulus of elasticity of FRP.
r_b = Internal radius of bend in FRP reinforcement.
d_b = Diameter of reinforcing bar.
V_u= Total shear resistance.

Table 4 shows the ultimate vertical load capacities of these beams experimentally, FEM, and theoretically.

Table 4 Comparison between Experimental, FEM, and Theoretical Results

BEAM No.	ULTIMATE LOAD, kN			
	Experiment	FEM	Theory (ACI 440.1R-06)	Theory (ECP-208-2005)
B1	72.7	72.0	49.0	53.0
B2	117.4	92.3	87.2	89.2
B3	108.4	92.2	105.9	115.4
B4	132.8	114.8	146.7	146.6

Figure 13 shows the accuracy of the proposed procedure (FEM) has been well confirmed by the close values of ultimate vertical load obtained from experimental and theoretical results.

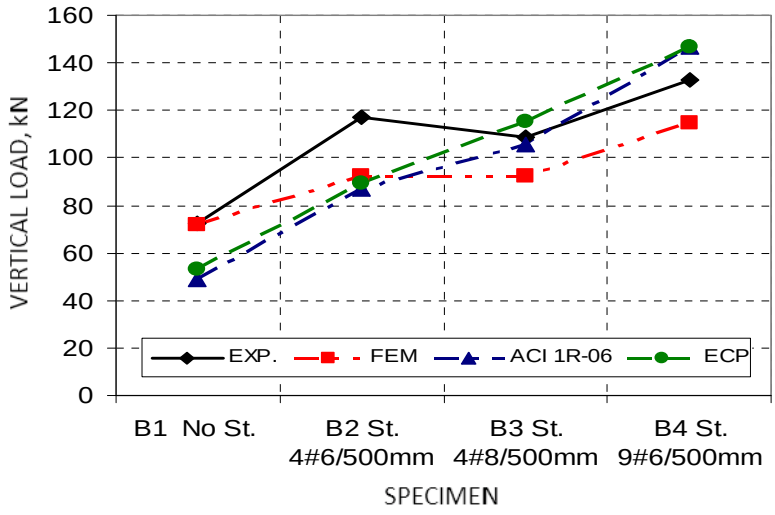

Figure 13 Comparison between Experimental, FEM, and Theoretical Results.

CONCLUSIONS

The inelastic behavior of 11 beams are investigated in the current study under the effect of increasing loading employing the inelastic FE analysis program ANSYS. An extensive set of parameters is investigated under applied concentrated load on the beam at shear span equal 2.0. Several parameters are investigated including the effect of dowel action without any transverse reinforcement on the shear strength, the effect of the spacing between the stirrups, the effect of changing of volumetric ratios of stirrups, the effect of type of reinforcement (GFRP or Steel) for main reinforcement or stirrups, and finally the effect of the shape of stirrups (stirrups or straight shear reinforcement). The study focuses on the consequences of the investigated parameters on the ultimate vertical load, corresponding vertical displacement and peak stresses. The conclusions made from this investigation are:

1. The most important point arising from the results in this research is that the GFRP shear reinforcement bars can be considered as an attractive alternative instead of normal stirrups in RC beam.

2. The accuracy of the proposed procedure has been well confirmed by the close values of ultimate vertical load, corresponding vertical displacement and peak stresses obtained from the FEM, theoretical, and the experimental results.

3. The stress intensity distributions at the shear span are showing that the stress concentrations around the plate loading towards to the lift support. Also, it is showing that during the loading, the direction of stresses from upper at the plate loading towards to the lower lift support. This phenomenon describes a correct mechanism of a RC beam specimen subjected to shear loading.

4. The effect of dowel action of steel bars reinforcement is greater than GFRP bars reinforcement.

5. As the spacing between GFRP stirrups reinforcement decreased, the shear strength increased.

6. As the volumetric ratios of GFRP stirrups reinforcement increased, the shear strength increased.

7. The beams reinforcement by GFRP stirrups gives ultimate load less than the beams reinforcement by steel stirrups by 25%.

8. The GFRP shear reinforcement bars gives ultimate loads and ductility bigger than normal GFRP stirrups by 10% and 20% respectively.

9. The ductility of the beams reinforcement by GFRP stirrups greater than the ductility of the beams reinforcement by steel stirrups.

10. The increasing in the reinforcement ratio of stirrups leads to increase in the peak stresses of the beam.

11. Finally, It was observed that the results obtained from ANSYS finite element program are considerably correlated to the results of the experiment. This shows that

the modelings that are made with ANSYS finite element program give us reliable results similar to the previous reports in the literature. In conclusion the modelings that are made with ANSYS finite element program can be useful for saving money and time in terms of the specimen. Also, the design errors which can be made in the design stage or wrong material selection can be prevented. The author believes that this way of modeling will be a guide for the further experimental studies.

REFERENCES

1. MEISAM SAFARI GORJI (2009) "Analysis of FRP Strengthened Reinforced Concrete Beams Using Energy Variation Method" World Applied Sciences Journal 6 (1): 105- 111.

2. AMERICAN CONCRETE INSTITUTE (2008) "Building code requirements for structural concrete," ACI 318-08, ACI, Farmington Hills, MI.

3. ACI COMMITTEE 440 (2006) "Guide for the design and construction of structural concrete reinforced with FRP bars," ACI 440.1R-06, American Concrete Institute, Farmington Hills, MI.

4. "Egyptian Code for Design and Construction of Concrete Structures", ECP 203-2006.

5. EL-SAYED, A.K., EL-SALAKAWY, E.F., BENMOKRANE, B., Shear strength of FRP-reinforced concrete beams without transverse reinforcement (2006) ACI Structural Journal, 103 (2), pp. 235-243

6. "Egyptian Code for Design and Construction of Reinforced Polymer Concrete Structures", ECP 208-2005.

7. RAZAQPUR, A. G., ISGOR, B. O., GREENAWAY, S., AND SELLEY, A. (2004), "Concrete Contribution to the Shear Resistance of Fiber Reinforced Polymer Reinforced Concrete Members," Journal of Composites for Construction, ASCE, Vo. 8, No. 5, pp. 452-460.

8. GROSS, S.P., YOST, J.R., DINEHART, D.W., SVENSEN, E., LIU, N., Shear strength of normal and high strength concrete beams reinforced with GFRP reinforcing bars (2003) Proceedings of An International Conference on High Performance Materials in Bridges, Hawaii, pp. 426-437. , ASCE, Reston, VA

9. TUREYEN, A.K., FROSCH, R.J., Shear tests of FRP-reinforced concrete beams without stirrups (2002) ACI Structural Journal, 99 (4), pp. 427-434

10. ANSYS User's Manual, Swanson Analysis Systems, Inc 10. William, K.J. and E.D. Warnke (1975) "Constitutive model for the triaxial behavior of concrete". Proceedings of the International Association for Bridge and Structural Engineering.

The Use of Activated Nanoclay to Develop the Compressive Strength and Microstructure of High Performance Concrete

S I Zaki, I S Khalil
Housing and Building National Research Centre, Egypt

Concrete science is a multidisciplinary area of research where nano technology potentially offers the opportunity to enhance the understanding of concrete behavior, recent work at the area of addition of nano particles concrete has shown the potential of improving concrete properties by using nano clay as a partial replacement of cement. The purpose of this paper is to study the effect of addition of nano clay (thermally activated alumina – silicate) with percentage 0,3,5,7 and 10% by weight of cement. The results of this study indicated that the addition of nano clay to concrete mixes (as partial replacement of cement) has a potential benefits in improving the compressive strength and micro structure of concrete mixes in addition to ecological benefits in using less amounts of cement. Note: This study is a part of the National project in HBRC material institute about: Application of nanotechnology to develop the quality and performance of concrete.

Dr Saaid I Zaki is an Associate Professor in Strength of Material and Quality Control Research Institute, Housing and Building National Research Center, HBRC, Cairo, Egypt.

Eng I S Khalil is currently a laboratory engineer in HBRC Central Laboratory, Cairo, Egypt and is a specialist in the mix procedure methodologies for nanomaterial concrete mixes.

Keywords: Activated NanoClay, High performance, Micro-structure

INTRODUCTION

According to ASTM E2456-06[1], fine particle are defined as particles smaller than about 2.5 micrometers and larger than about 0.1 micrometers in size. But nanoscale have one or more dimensions from approximately 1 to 100 nanometers (nm). So nano clay shells or inactivated nano clay have nano classification. However activated nano clay, which can be produced by burning nano clay at 800 ̊C, have three dimensions in nano scale making it more effective in nano classification. Nanotechnology can be used in construction field, as include products that are lighter and stronger structural composites, and better properties of cementitious materials [2], as clay particles at the nano size possess some unique characteristics unlike the other fillers. The nanoclay particles are in the platelet form with thickness of just 1 nm and width of 70~150 nm. This high aspect ratio of 100~150 imparts some anisotropic characteristics to the film.

In recent years, there has been a growing interest in the use of nano clay for improving concrete and mortar, as it have contains typically SiO_2 and Al_2O_3. Morsy [3] experimentally investigate that compressive and tensile strength of the cement mortars with nano clay is higher than that of the plain cement mortar with the same w/b ratio, The enhancement of tensile strength was 49% above control mortar; whereas the enhancement of compressive strength was 7% at 8% nano clay replacement, The nano clay in cement mortar acts as a nano-fiber due to its morphology and The SEM observations confirmed that the nano clay was not only acting as filler, but also as an activator to promote hydration process.

Florence Sanchez[4], present paper reviews the current state of the field of nanotechnology in concrete The potential of nanotechnology to improve the performance of concrete and to lead to the development of novel, sustainable, advanced cement based composites with unique mechanical, thermal, and electrical properties is promising and many new opportunities are expected to arise in the coming years. The advances in instrumentation and computational science are enabling scientists and engineers to obtain unprecedented information about concrete, from the atomic through the continuum scale. This information is crucial for predicting the service life of concrete and for providing new in sights on how it can be improved. New developments have taken place in the nano engineering and nanomodification of concrete, however, current challenges need to be solved as same as dispersion; compatibility of the nanomaterials in cement; processing, manufacturing, safety, and handling issues scale-up; and cost.

Taha [5], studied the effect of the curing time and temperature using nano clay as a partially replacement of cement and conclude that the addition of the pozzolanic material (activated nano clay) to the control mix leads to the consumption of CH obtained during cement hydration and the resulting in additional CSH gel which improves the microstructure, as The curing time and temperature are of the most important factors controlling the hydration mechanism of the cement pastes. This is due to the filling effect and the effect of mutual complement of superiority supply. Man-Wai Ho [6] employed nano clay to enhance the thermal properties of polymer based composites using that is 0wt% nanoclay, 0.5wt%, 1wt%, 2wt%, 3wt%, 4wt%, 5wt%, 6wt%, 7wt% & 8wt% nanoclay in epoxy. Results indicated that the 7wt% nanoclay sample showed the highest elastic modulus at 25^{o}C, 5wt% nanoclay sample showed the best tensile behavior upon elevated temperature above 50^{o}C, while 2wt% nanoclay sample showed both the lowest elastic modulus at room temperature and the lowest tensile performance at elevated temperature among all the compositions.

Ozyildirim [7] investigated how nanomaterials improved permeability and strength of concrete and found that very amount of nano materials like nanosilica and nanoclay in concrete can improve the cement paste and interfacial transition zone, these improvements benefit the compressive strength and permeability of concrete when proper amount and type of nanomaterials were selected and proper dispersion without coagulation using suspension non-powder forums.

EXPERIMENTAL WORK

In this work, the well known performance of concrete without nanoparticles was compared with that after the addition of nano-particles for both fresh and hardened states.

Materials

The cementitious materials used during this study were OPC, silica fume, nano-silica. Ordinary Portland cement (OPC) was used of type CEM1 42.5N according to E.S.S. (4756-1-2006) obtained from Beni-Suef cement factory in Egypt. Silica fume was obtained from Egyptian Company for Iron Foundries, while nanoclay was obtained from Middle East Company in Egypt. Polycaboxilate-based super plasticizer (30% in aqueous solution) was used in comparison with sulphonate naphthalene super plasticizer to produce self-compacting concrete (SCC) with relatively low water-cement ratio.

Ordinary Portland cement (OPC)

Chemical analysis of OPC is shown in Table 1.

Silica Fume

Silica fume is a very fine by-product powder obtained as a fume from the foundry process in Egyptian Company for Iron Foundries. Table 2 shows the physical properties of the silica fume used.

Nano clay

The nano clay used in this work is montmorillonite clay (sodium calcium aluminum silicate). It is characterized by large length to thickness ratio, but in crystalline state, to convert it to amorphous state.

The nano clay was thermally treated at 800ºC for 2 hours to give active amorphous nano montmorillonite clay. The ingredients were homogenized on a ball miller for 1 hour to assure complete homogeneity. The effect of thermal activation of the nano montmorillonite clay is the conversion from the crystalline state to the amorphous state with the reduction in grain size, the properties shown in Table 1.

Superplasticizer

Polycarboxylic as a polymer based PCE SKY was used in this study (Glenium ACE 30) and it was obtained from BASF chemical company in Egypt.

Aggregates

Concrete Mix Design With and Without Nano Particles

High performance concrete (HPC) have been manufactured with and without nano particles in order compare the well known performance of HPC without nano particles with that with nano ones. High performance concrete with a binder content of 500kg/m^3 were manufactured in all concrete mixes as shown in Table 4 (the water binder ratio was the same for concrete mixes equal).

A dosage of super plasticizer 12.5 lit/m3 for mixes M0 to M5 is shown in Table 4. M0 is control mix No. 1 without NC, cement was replaced with 100 kg of SF. While mixes from M1 to M5 activated nano clay were used as a cement replacement with the same SF content and same water content as w/b ratio is the same.

Natural sand of size (0-4 mm) was obtained from pyramid quarry in Egypt, while the coarse aggregate was dolomite obtained from Attaka quarry in Egypt; two nominal maximum sizes were used during this study: Aggregate 1 of size (4-20mm) and Aggregate 2 of size (20-40mm).

Table 1 Chemical Composition of cementitious materials

%	OPC	SF	NC
SiO_2	19.8	93	61.24
$A1_2O_3$	5.5	--	20.89
CaO	63	0.2	0.16
MgO	1.18	--	0.22
Fe_2O_3	3.39	0.3	1.06
Na_2O	0.46	--	0.71
K_2O	0.16	--	1.61
SO_3	3.01	0.1	0.17
LOI ,Loss of Ignition	5.2	2.0	13.12

Table 2 Properties of silica fume

DESCRIPTION	RESULTS
Particle Size, nm	34
Density, g/ cm^3	2.22
Surface area, m^2/gm	14

Table 3 Properties of nano-clay

COLOR	BULK DENSITY, gm/cm^3	SURFACE AREA, m^2/gm
Light Cream	1.9	330

Table 4 Composition and properties of HPC with and without ANC

CONSTITUENT, kg/m³	MIX NUMBER (NANO %)					
	M0 (0%)	M1 (1%)	M2 (3%)	M3 (5%)	M4 (7%)	M5 (10%)
OPC	500	495	485	475	465	450
SF	100	100	100	100	100	100
NC	0	5	15	25	35	50
Sand	550	550	550	550	550	550
Dolomite	740	740	740	740	740	740
Water	180	180	180	180	180	180
Superplasticizer	12.5	12.5	12.5	12.5	12.5	12.5

Preparing nano-clay

Experimental work starts with activate the inactivated nano-clay, burning it at 800ºC for 2 hours, then mixing nano-clay powder with cement by the target percentage at dry state using pall miller equipment for 15 minutes and 200 rpm, to obtain the best dispersion for nano powder with cement produced nano-cement composite.

Mixing Procedure

The nano-cement composite , fine aggregate , coarse aggregate and silica fume were dry mixed in a rotary mixer for 30 sec. , then 50% of mixing water was added and mixed for 30 sec., then a ready-mixed liquid including super plasticizer was added to the 50% remained water and then the liquid poured into the rotary mixer slowly . The concrete mixture was mixed wet for additional 4 min.

Testing Procedure

After mixing, slump flow was carried out to measure the properties of high performance concrete (HPC) according to standard specifications for concrete testing, then the well-mixed concrete mixture of each mix was poured into nine standard cubes of dimensions 15x15x15 cm for each mix, cubes were demolded after 24 hrs and then cured in standard curing tank until the age of testing, and cubes were dried in air for one hour before testing and then tested three cubes after 3, 7 and 28 days.

Scanning Electron Microscopy

Scanning Electron Microscopy (SEM) was also carried out in the same National Research Center Central Laboratories for Services for concrete samples with and without nano $Si0_2$ using Electronic Microscope type JEOL JXA-840 A, OXFORD, of magnification 1400 and 1600. The specimens were cut directly from concrete cubes, the shape of specimens was regular and the surface was flat.

Transmission Electronic Microscopic

Scanning Electron Microscopy was carried out in Natural Research Center at Physics Department for Transmission Scanning for powders (inactivated and activated nano-clay) and the data of microscope is :- Transmission Electronic Microscopic type JEOL – JEM – 1230 of magnification up to 60000 made in Japan was used for powders (SF and NSF). It can be

observed that nano-clay particles are represented by highly agglomerated clusters for activated nano-clay and as a shell with plane dimension more than 100 nm and thickness from 1 to 8 nm for inactivated nano-clay. The TEM investigation for the kaolinite and montimorillonite samples before firing (Figure 1a) and after firing (Figure 1b) shows the characteristic size of the clay fraction (< 2 um), the hexagonal shaped crystals which characterize the kaolinite. While the investigation of fired kaolinite and fired montimorillonite (Figure 1b) shows shift from micron scale to nanoscale with an average size of about 80 nm. Figure 2 shows the electronic scanning photographs of control sample without nano-clay which magnify the microstructure 1600 times. Figure 3 shows the electronic scanning photographs of nano-clay concrete samples which magnify the micro structure 1400 times.

ANALYSIS AND DISCUSSION OF TEST RESULTS

Compressive Strength

Table 5 and Figure 4 show the compressive strengths of concrete with and without nano-particles. It can be seen that compressive strength of concrete with nano-particles was improved at 3, 7 days up to 28 days and the optimum amount of nano-clay is 10 % by weight of the cementitous material content for 3 and 7 days. However at 28 days there is no improvement after 3% nano-clay as the optimum amount of nano-clay at 28 days is 3%. The improvement for compressive strength was 39% higher than control at 7 days using 10% nano-clay and 36% at 3 days for the same percentage. But at 28 days using 3% nano-clay the compressive strength improvement was just 7.6% higher than control mix.

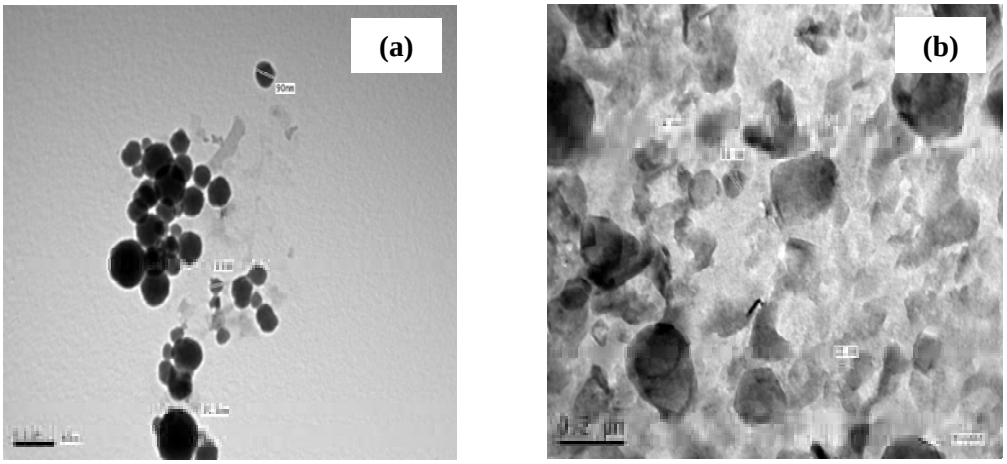

Figure 1 TEM of (a) fired montimorillonite and (b) unfired montimorillonite

Microstructure

To verify the mechanism predicted by the compressive strength test, SEM examinations were performed. Additions of nano-clay particles were found to influence hydration behavior and lead to differences of the microstructure of hardened concrete. Figure 2 Shows SEM micrograph of control sample (without nano-clay) after 28-days (with magnification of the microstructure 1600 times) and Figure 3 shows concrete containing nano-clay (with magnification of 1400). It can be seen that calcium silicate hydrate (C.S.H.) existed in isolated points surrounded by many needle-hydrates, on the other hand the microstructure of

the mixture containing nano-clay of amount 10% by weight of cementitious materials revealed a dense, compact formation of hydration products (C-S-H) as shown in Figure 3 since the texture of (C-S-H) of nano-clay concrete is very dense, compact and with large crystals.

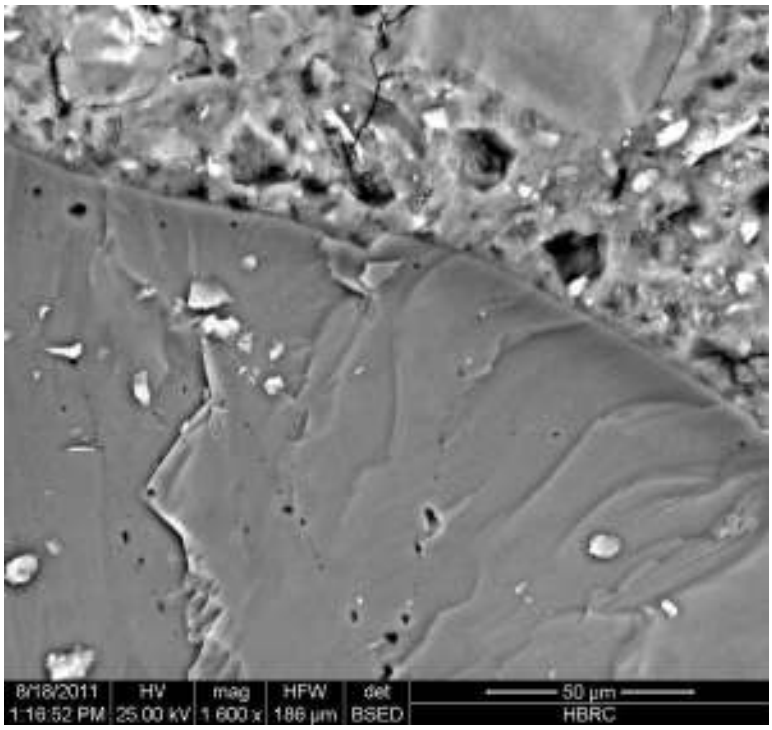

Figure 2 SEM micrograph of control concrete sample after 28 days

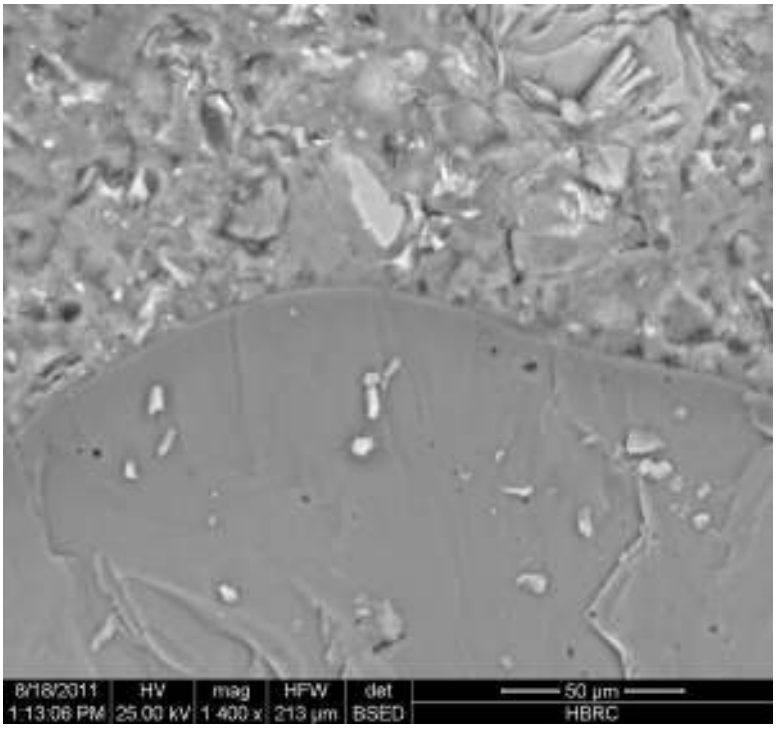

Figure 3 SEM micrograph of 10% nano-clay Concrete sample after 28 days.

Table 5 Mechanical properties of hardened concrete with and without nanoclay

MIX NO.	MIX DESCRIPTION	COMPRESSIVE STRENGTH, MPa		
		3 days	7 days	28 days
M0	Control	58.4	63.5	73.6
M1	1% nano-clay	60.7	67.4	76.6
M2	3% nano-clay	63.4	71.4	79.2
M3	5% nano-clay	68.1	77.4	81.2
M4	7% nano-clay	73.4	83.7	86.5
M5	10% nano-clay	79.4	88.3	88.5

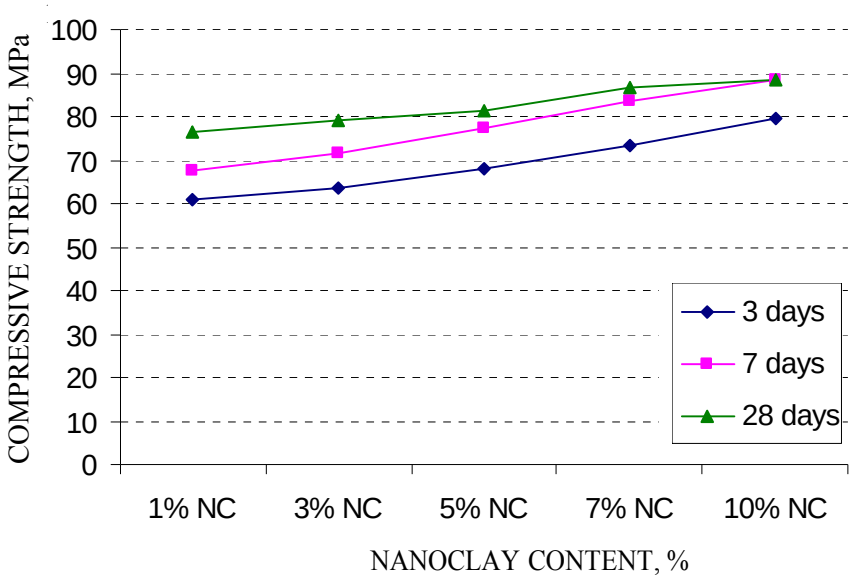

Figure 4 Compressive strength for concrete mixed with nano-clay

CONCLUSIONS AND RECOMMENDATIONS

The properties of concrete are improved by the use of nano powders, since nano particles fill the voids between cement grains and also consume a part of calcium hydroxide which results in additional. Formation of calcium silicate hydrates (C.S.H.) improves the interface structure.

The application of nano clay particles with newly developed super plasticizer improves the workability and strength of high performance concrete since nano-clay interpenetrates polymer network, and causes increase in compressive strength of 36, 39 and 20% at 3, 7 and 28 days respectively.

REFERENCE

1. ASTM E2456-06, “Standard Terminology Relating to Nanotechnology”.

2. ZHI GE, “Applications of Nanotechnology and Nanomaterials in Construction”, First International Conference on Construction In.

3. MORSY, M S., “Effect of Nano-clay on Mechanical Properties and Microstructure of Ordinary Portland Cement Mortar”, International Journal of Recent Trends in Engineering , Vol 1, No. 4, May 2009.

4. SANCHEZ F., ” Nanotechnology in concrete – A review” Construction and Building Materials, (2010) PP. 2060–2071.

5. TAHA S., “THERMO – MECHANICAL PROPERTIES OF ACTIVATED NANO CLAY CEMENT PASTES AT DIFFERENT CURING TEMPERATURES”, International Conference on NANO TECHNOLOGY FOR GREEN and SUSTAINABLE CONSTRUCTION 14-17 March 2010 Cairo-Egypt.

6. MAN-WAI HO,“ENHANCEMENT OF THERMAL PROPERTIES OF POLYMER-BASED COMPOSITES USING NANOCLAYS”, University of New Orleans ,USA.

7. OZYILDIRIM C., "Laboratory Investigation of nanomaterials to improve the permeability and strength of concrete", Virginia Transportation Research Council , VTRC 10-R18, PP1-16, Feb 2010.

Comparison of Fire Protection Lining Boards Properties and Dependence on Temperature

M Lapková, J Toman, T Korecký, R Černý
Czech Technical University, Czech Republic

Boards made of composite materials are these days used as the lining of parts of building structure to improve the object's end-use properties. For the improvement of fire protection properties the temperature stability of both thermal technical and mechanical properties of used composite material, is important. This paper describes the elasticity coefficient and heat conductivity as executed on several materials. Measured samples had been heated on specific temperature and after cooling down were gauged. After comparing the results it is possible to verify the temperature stability of mechanical and thermal technical properties of particular materials.

J Toman is currently Professor at the Faculty of Civil Engineering CTU in Prague. He has led several research projects on physical properties of building materials. His specialist areas of research are physical properties of building materials under extreme conditions (high temperatures etc.) and transport phenomena.

T Korecký is currently PhD. student at the Faculty of Civil Engineering CTU in Prague. He studies at the Department of Material Engineering and Chemistry. He has cooperated with Prof. Toman on several projects.

R Černý is currently Professor at the Faculty of Civil Engineering CTU in Prague. He is a Head of the Department of Material Engineering and Chemistry. He has led many projects of physical properties of building material. He is a member of International Association of Building Physics (IABP).

M Lapková is a PhD. student at the Faculty of Civil Engineering CTU in Prague. She studies at the Department of Material Engineering and Chemistry.

Keywords: Composite materials, High temperature, Mechanical properties, Thermal properties

INTRODUCTION

Nowadays board materials are very often used as lining of building structures. This solution brings two fundamental effects:

1. Structure protection against harmful external effects which could be, for example mechanical, chemical and physical. As standard procedure in the building industry veneer board is often used for increasing fire protection.

2. Aesthetic arrangement of the building is interior surfaces.

Composite materials are often used to improve mechanical properties. In order to consider the quality of fire protection it was decided to observe their mechanical and thermal material parameters [1].

MATERIALS SAMPLES DESCRIPTION

Observed board samples were delivered from VÚSTAH Brno. The samples were from four types of board material:

PROMATECT – white material, board thickness 3 cm
FIREBOARD – grey material, board thickness 2.5 cm
RIGIBS – pink material, board thickness 1.2 cm
FERMACELL – white material, board thickness 1.2 cm

These materials are made for commercial purposes and their composition has been kept secret by the firm. For this reason we do not know the exact composition of the materials. For measuring we prepared 16 pieces of samples from the delivered boards. To find out thermal technical properties of the materials boards were cut into squares of size 7 cm × 7 cm from all materials. To determine the mechanical qualities 16 beams were cut into size 3 cm × 18 (or 15) cm × board thickness.

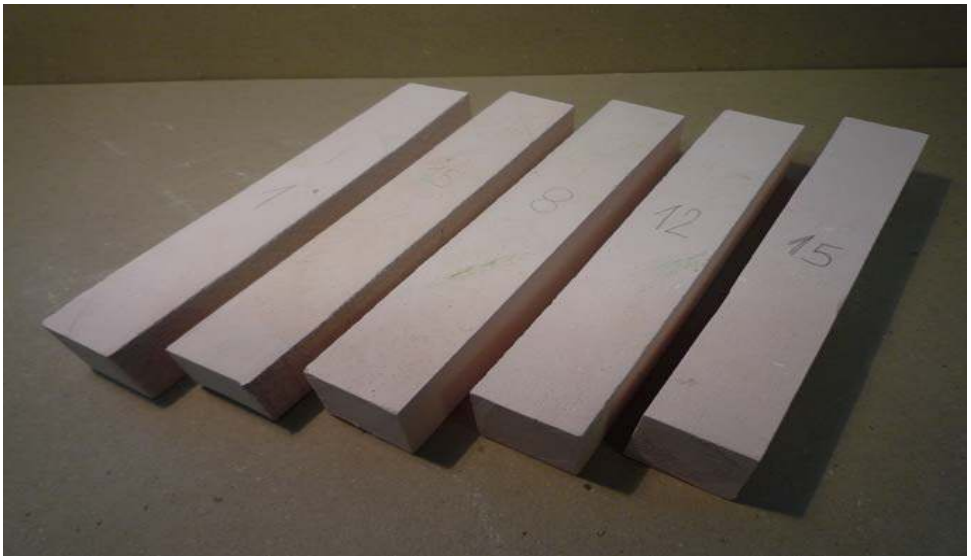

Figure 1 The samples for measurement of mechanical properties

METHODOLOGY OF MEASUREMENT

Thermal properties of heat stability were measured on boards from given materials by apparatus ISOMET 2114, which determined the heat conductivity and volumetric heat capacity (product of specific heat capacity and specific density) [2].

Figure 2 Apparatus for measurement of thermal properties - ISOMET 2114

The measurement of heat stability of mechanical properties was executed by a non-destructive method on prepared samples by ultrasound apparatus DIO 526, with which it is possible to measure speed of wave spreading by sonic method or resonant method base frequency and then is possible to calculate dynamic modulus of elasticity from dimensions [3].

Figure 3 Apparatus for measurement of modulus of elasticity - DIO 562

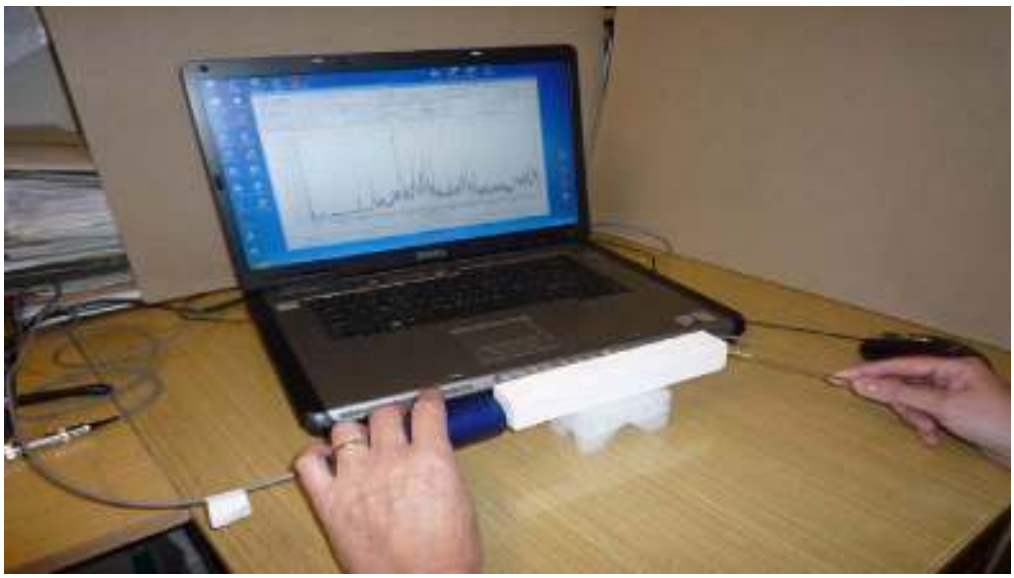

Figure 4 Apparatus for measurement of modulus of elasticity - resonant method

The parameters were observed in different temperature shocks because it is possible to presume that they depend on temperature [1, 4]. Individual limits of temperature stress were set in reference (consideration) to theoretical temperatures of stability of concrete, i.e. decomposition of calcium hydroxide circa 470°C and decomposition of hydrates circa 680°C [5]. Measurement was carried out on samples stressed with the following temperatures:

normal temperature	25°C
drying	110°C
medium heating	250°C
higher heating - below the first critical temperature	450°C
higher heating - between the first and the second critical tem.	650°C
high heating – over the second critical temperature	750°C
maximal temperature stress	1000°C

THE EXPERIMENT

We created a bunch of samples in order to be able to examine the influence on gradual temperature increases. It means the comparison of repeated temperature stress and direct heating on high temperature (thermal shock). Each sample was stressed in a different way, which is documented in the enclosed table, where there colour-indicated temperature stress at particular samples.

The difference was also in the default conditions created before temperature stress. Samples 1 to 8 had been dried before at 110°C (or 70°C in case materials based on gypsum) for 7 days to equilibrium weight. Samples 9 to 16 had not been dried and thus maintained equilibrium moisture; these samples were stressed by temperature [6].

For each temperature stress the defined bunch of samples was always placed to an electrical kiln. The kiln was heated by constant rising to a particular temperature. Then the rising of temperature was stopped and the kiln was kept at the set temperature for 3 hours. After that heating was switch off and the tested samples cooled down to normal temperature. Thermal qualities were measured in normal temperature around 25°C.

Figure 5 The samples placed in to kiln

RESULTS OF EXPERIMENT

All measured values were analysed in EXCEL editor. In to these tables there were plotted all values for each observed material in dependence on burn temperature. It means weight of sample, relative loss in weight, samples dimensions, volume, bulk density, heat capacity, thermal diffusivity, volume heat capacity, time of wave pass, speed of wave spreading, dynamic modulus of elasticity, frequency of resonance and dynamic modulus of elasticity determined by resonance method.

All changes in measured values – i.e. relative decrement of weight, heat conductivity and volumetric heat capacity, measured on particular samples were plotted into figures depended on burn temperature. On these samples are good visible permanent changes in each value caused by temperature stress on all materials.

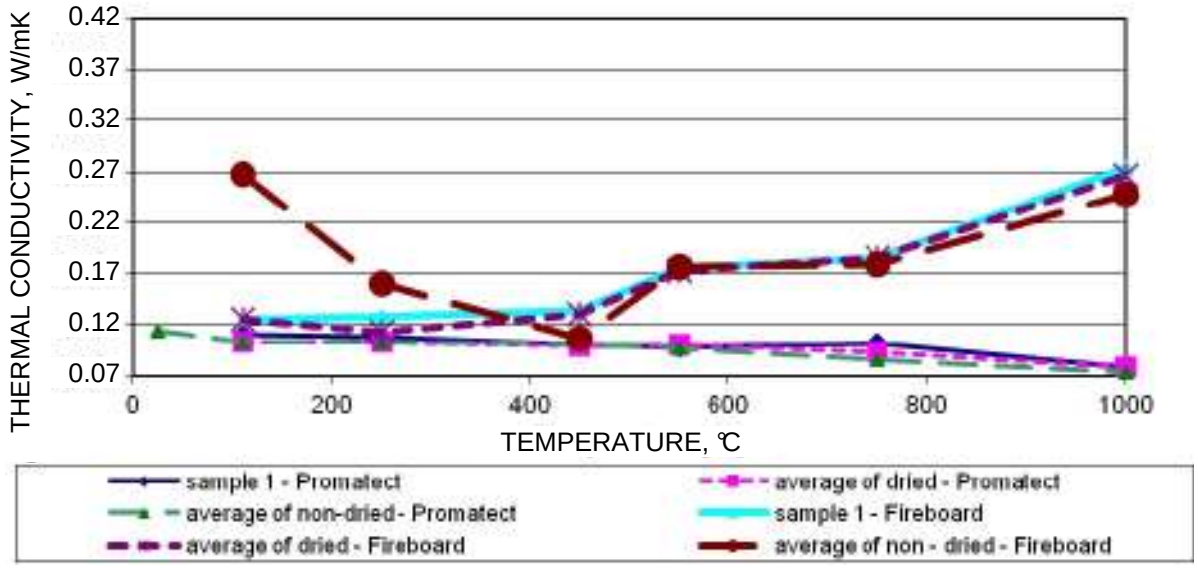

Figure 6 Thermal conductivity dependence on temperature – PROMATECT and FIREBOARD

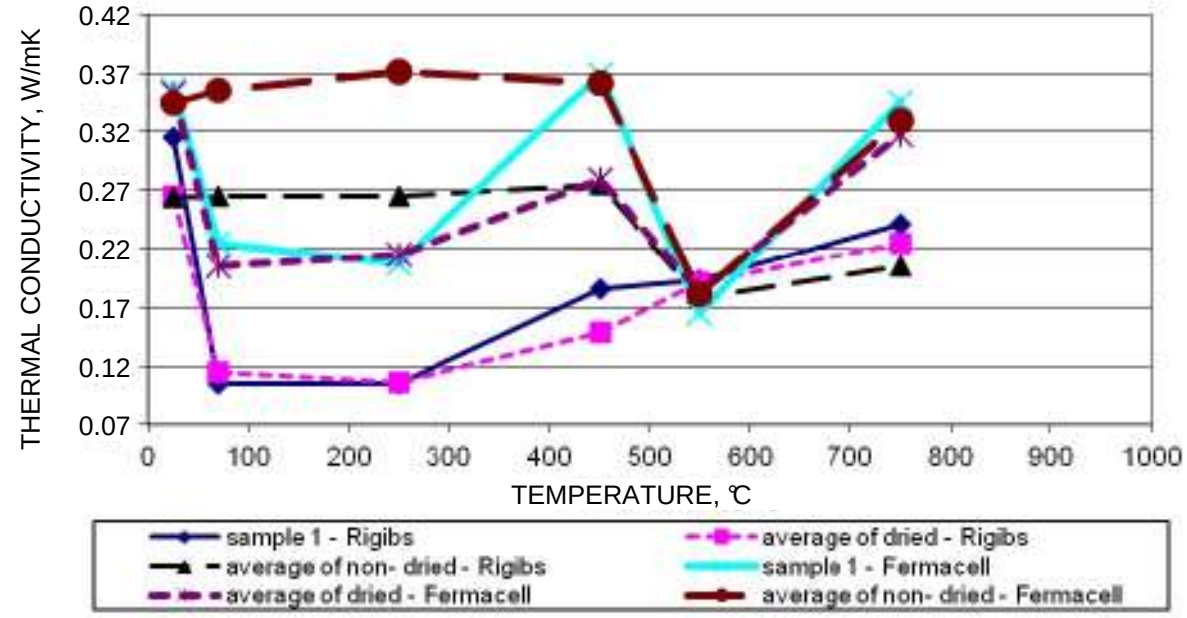

Figure 7 Thermal conductivity dependence on temperature – FERMACELL and RIGIBS

On the other graphs relative loss of weight during burn, volumetric specific heat capacity and thermal diffusivity are shown.

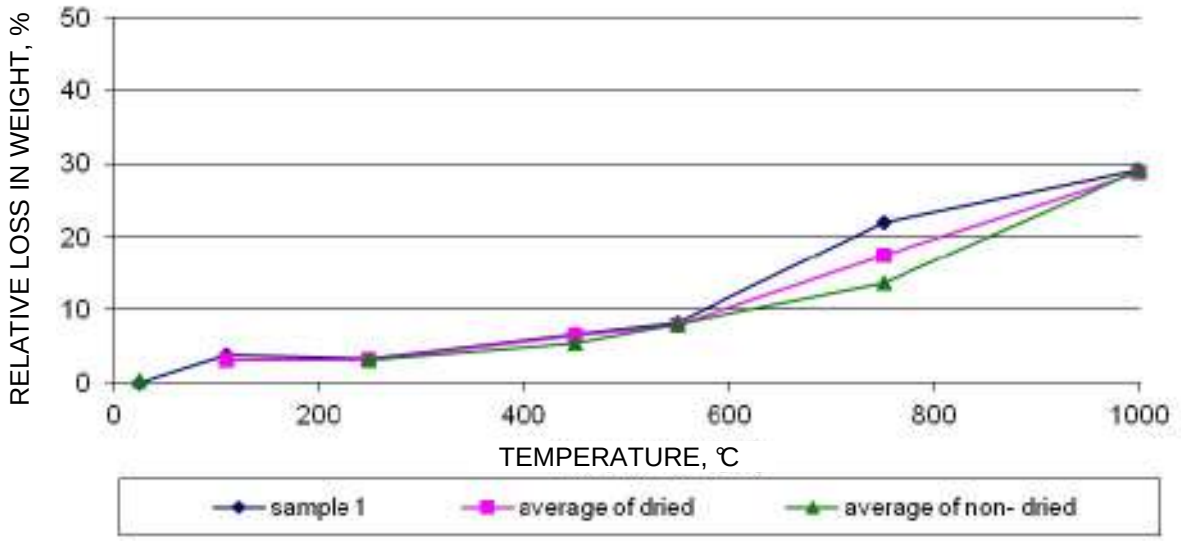

Figure 8 Relative loss in weight dependence on temperature - PROMATECT

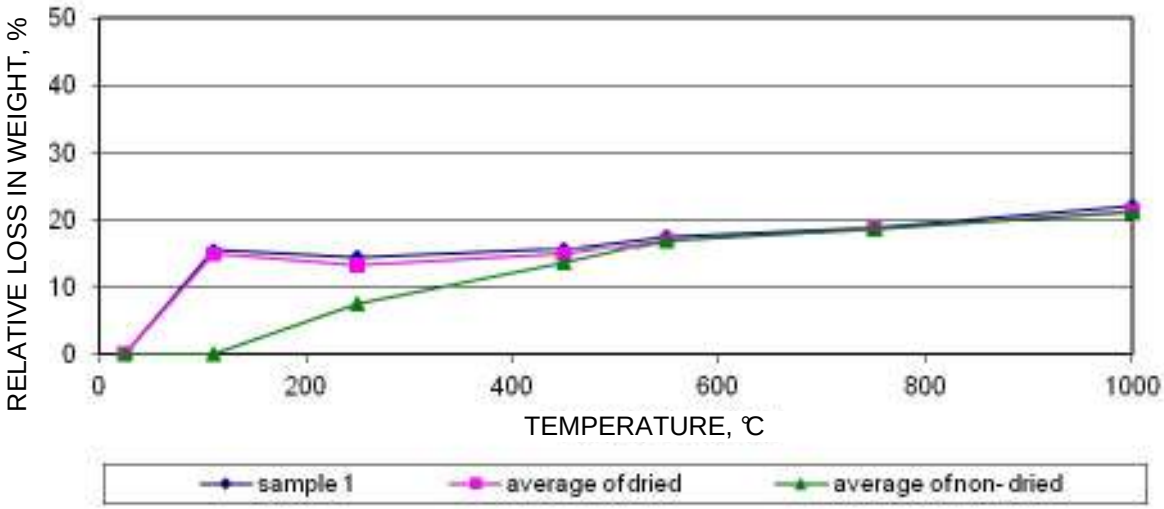

Figure 9 Relative loss in weight dependence on temperature – FIREBOARD

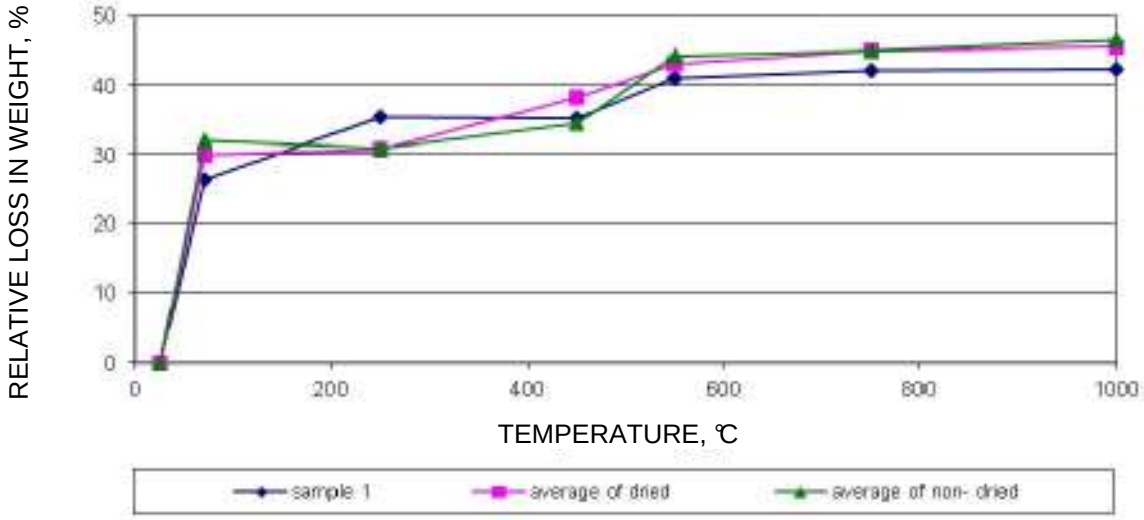

Figure 10 Relative loss in weight dependence on temperature – RIGIBS

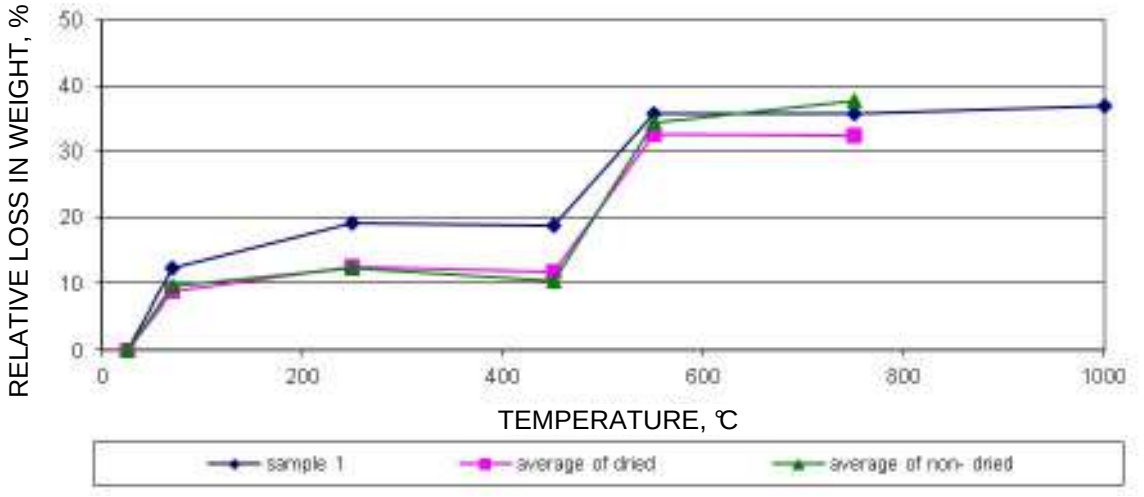

Figure 11 Relative loss in weight dependence on temperature – FERMACELL

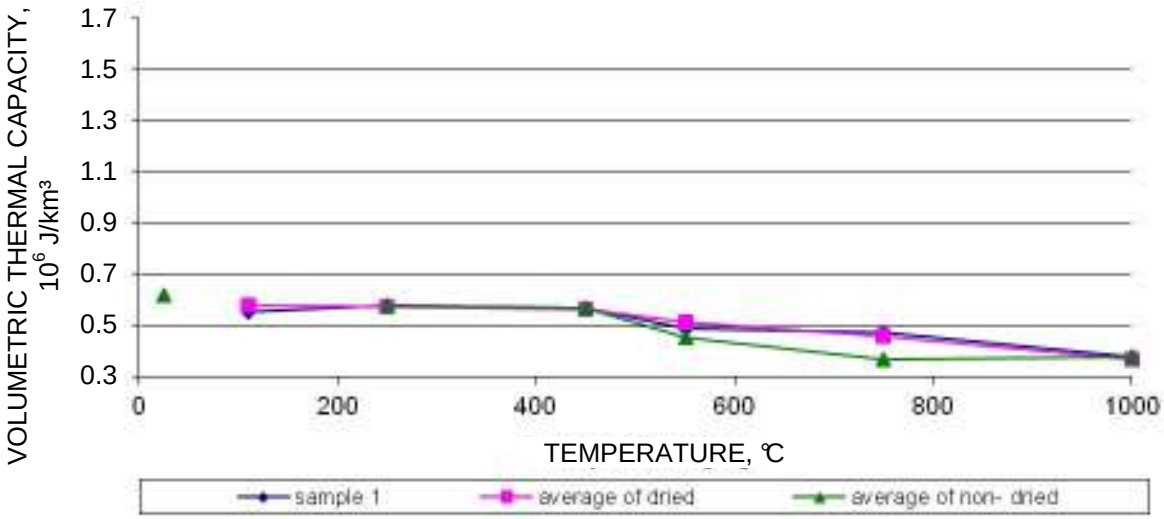

Figure 12 Thermal diffusivity dependence on temperature - PROMATECT

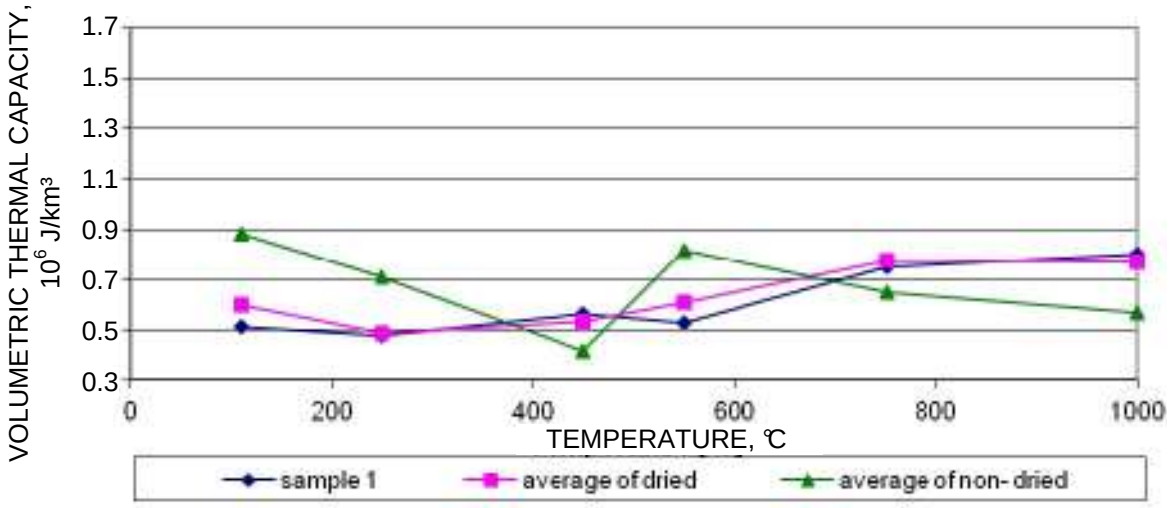

Figure 13 Volumetric thermal capacity dependence on temperature – FIREBOARD

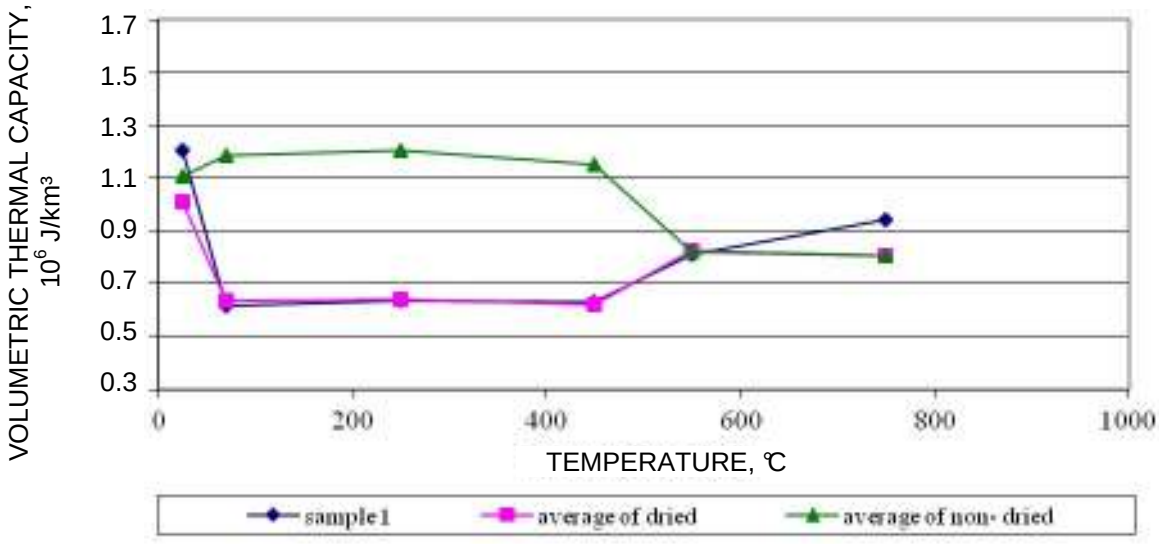

Figure 14 Volumetric thermal capacity dependence on temperature – RIGIBS

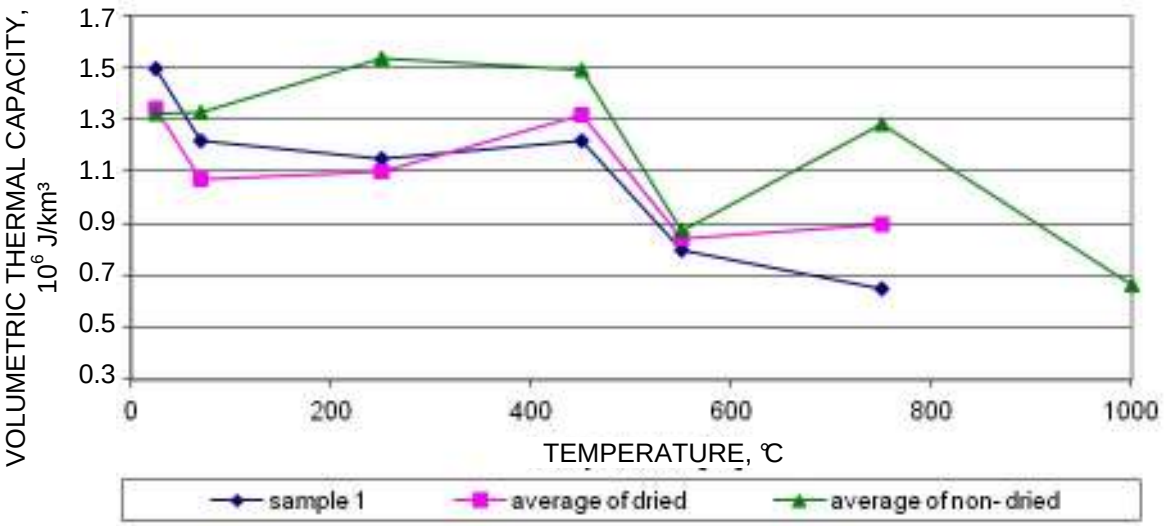

Figure 15 Volumetric thermal capacity dependence on temperature – FERMACELL

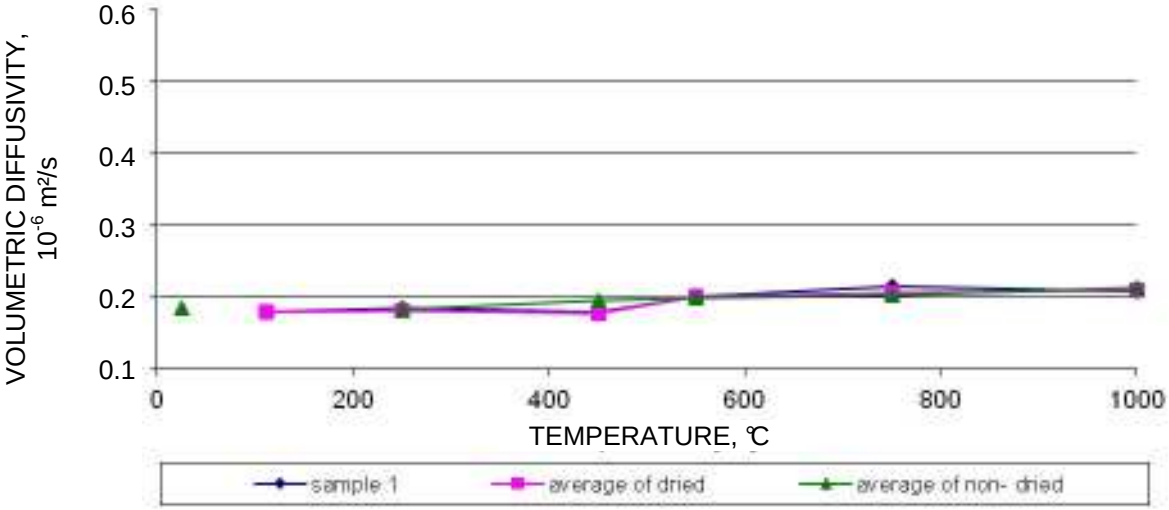

Figure 16 Thermal diffusivity dependence on temperature - PROMATECT

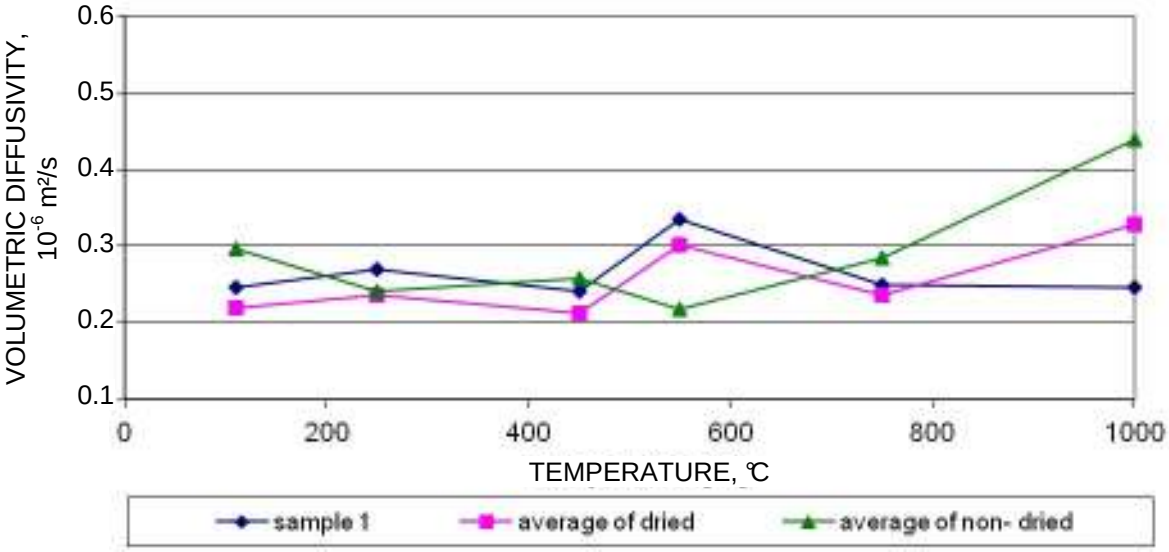

Figure 17 Thermal diffusivity dependence on temperature – FIREBOARD

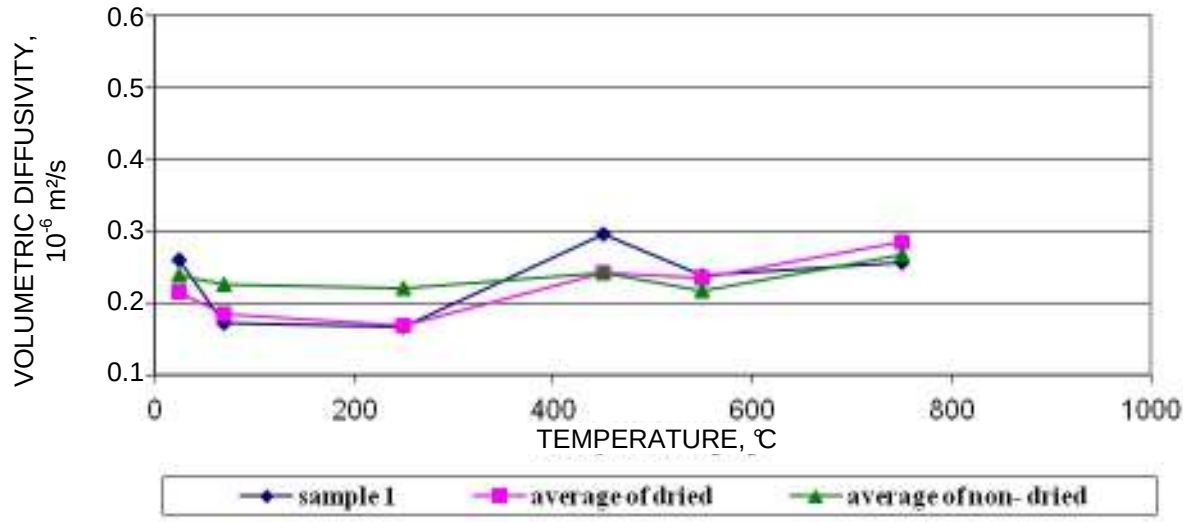

Figure 18 Thermal diffusivity dependence on temperature – RIGIBS

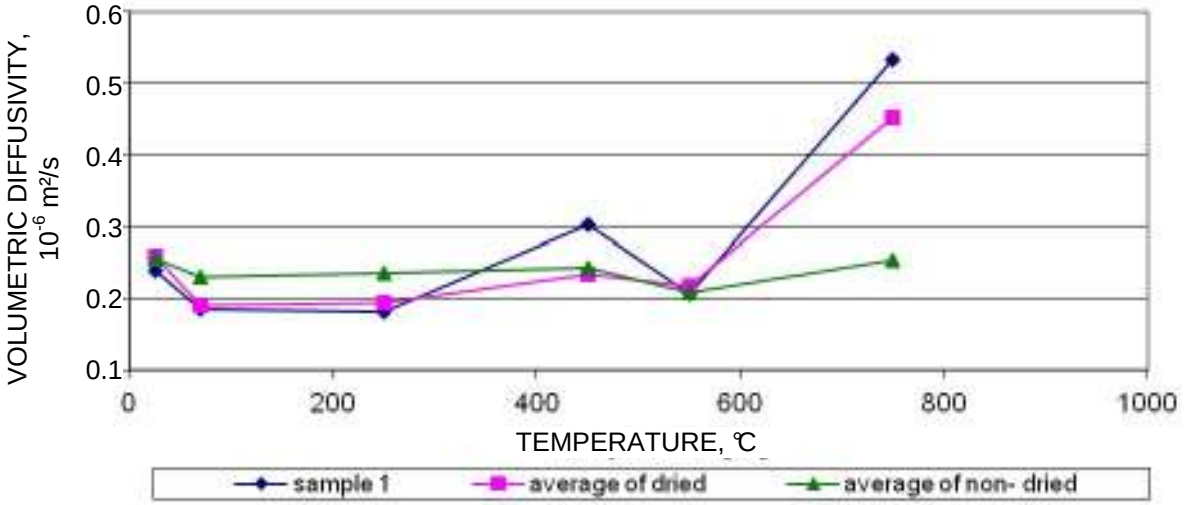

Figure 19 Thermal diffusivity dependence on temperature – FERMACELL

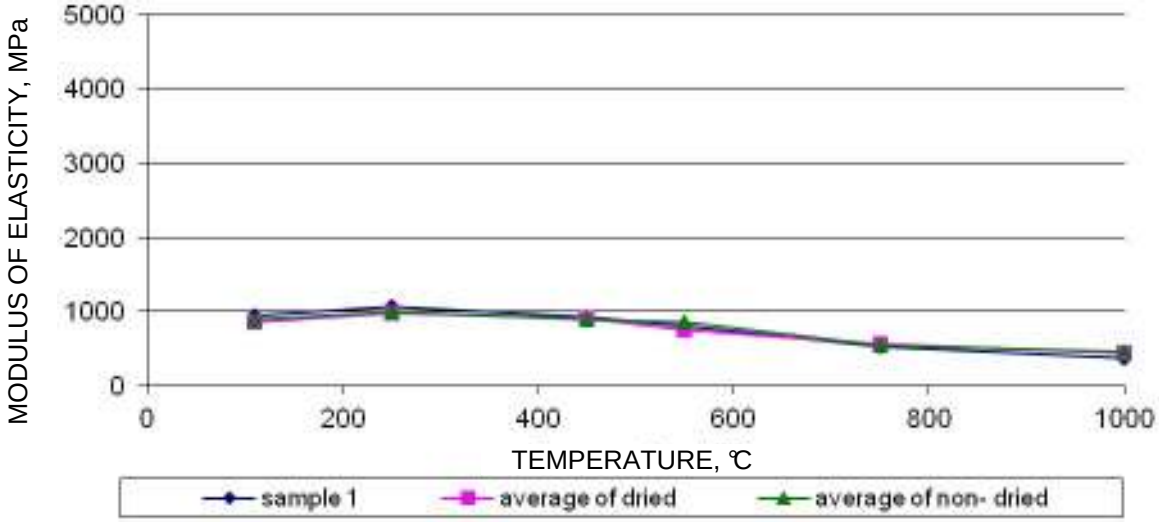

Figure 20 Modulus of elasticity dependence on temperature – PROMATECT

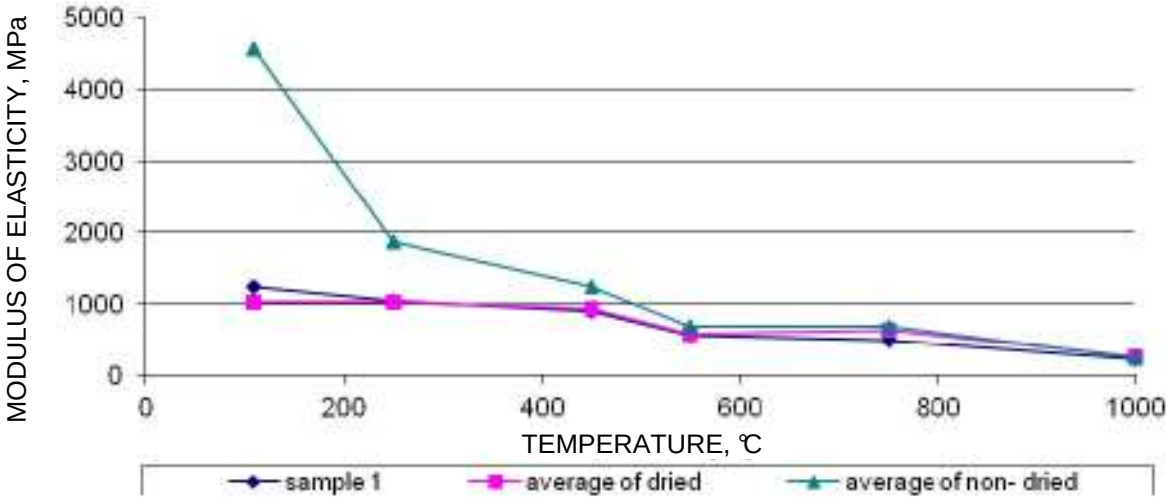

Figure 21 Modulus of elasticity dependence on temperature – FIREBOARD

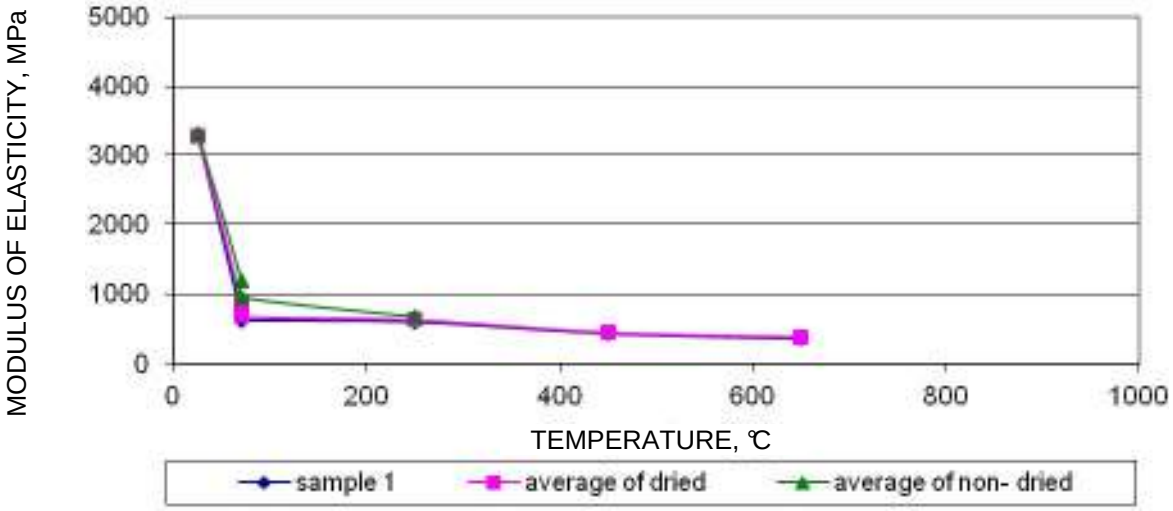

Figure 22 Modulus of elasticity dependence on temperature – RIGIBS

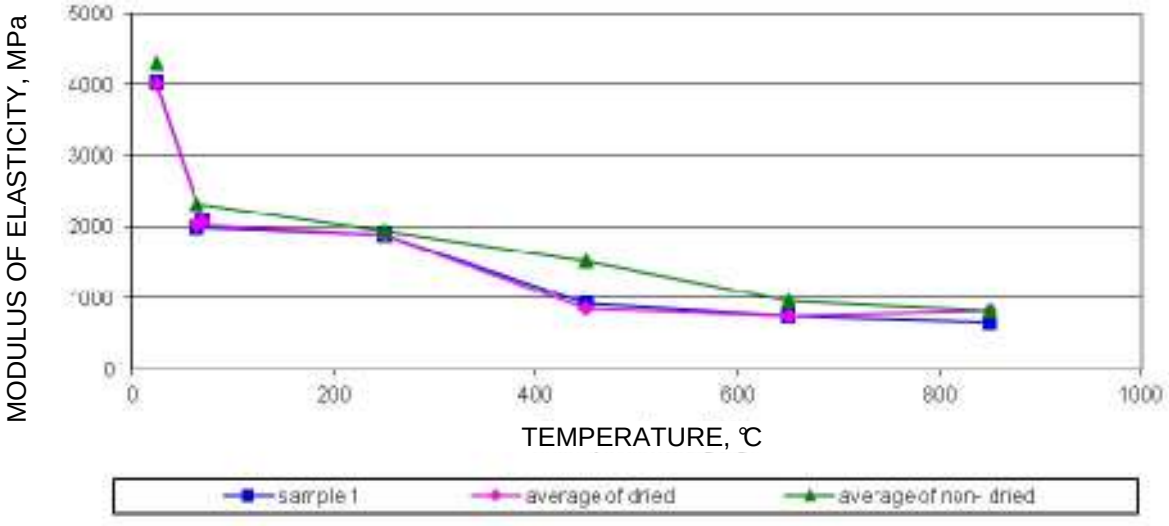

Figure 23 Modulus of elasticity dependence on temperature – FERMACELL

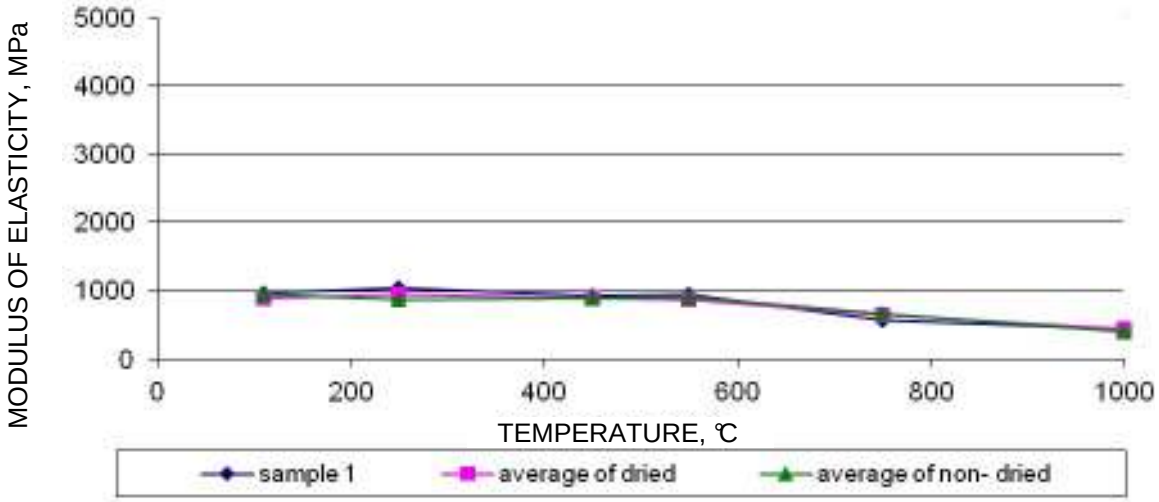

Figure 24 Modulus of elasticity dependence on temperature - resonant method - PROMATECT

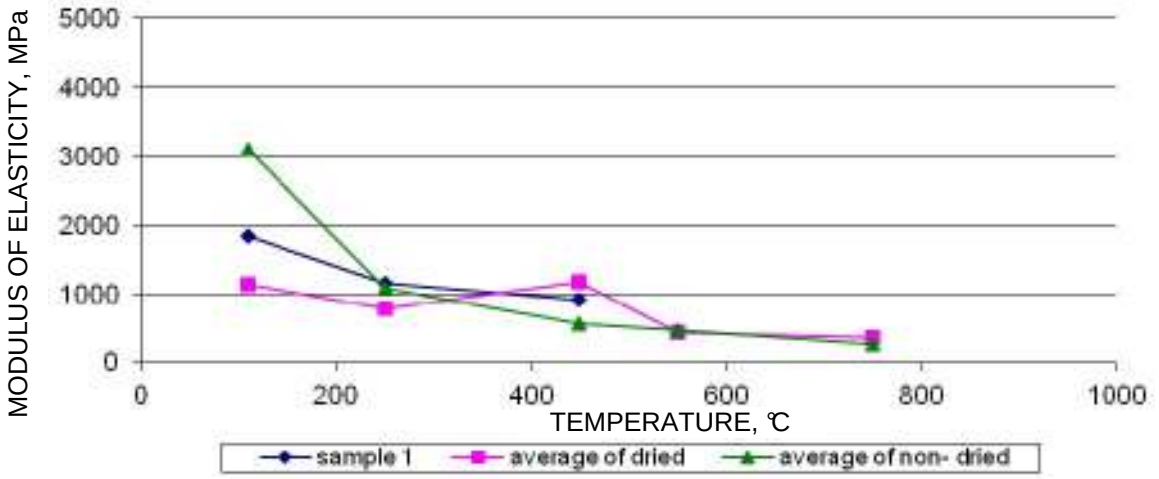

Figure 25 Modulus of elasticity dependence on temperature – resonant method – FIREBOARD

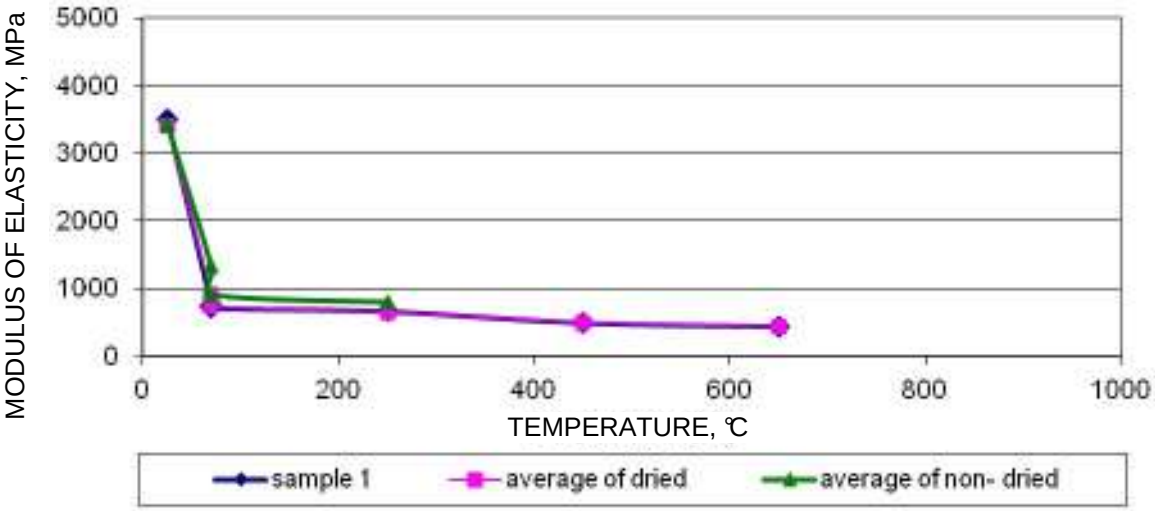

Figure 26 Modulus of elasticity dependence on temperature – resonant method – RIGIBS

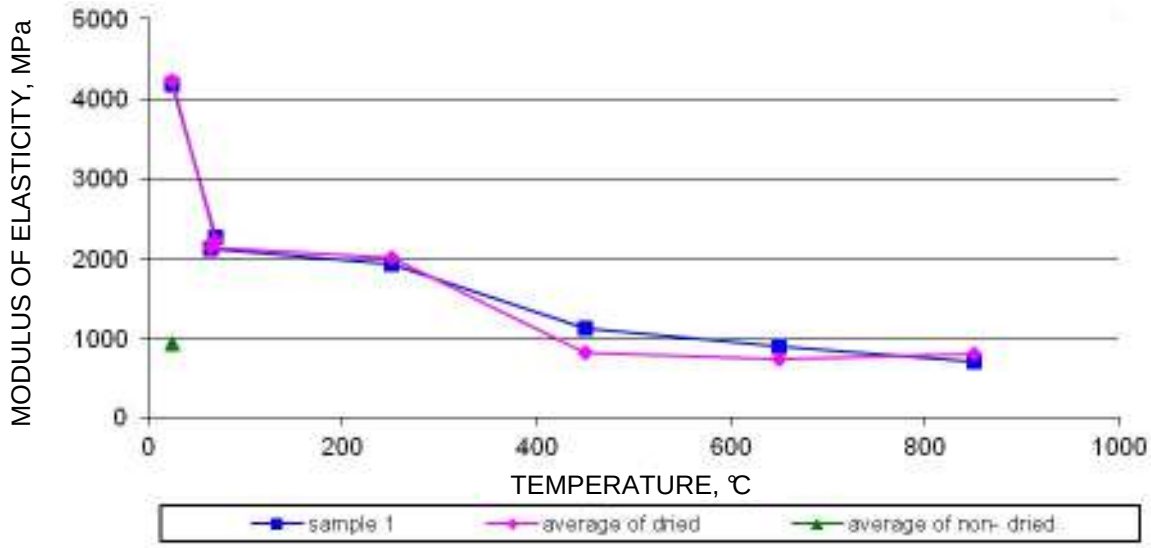

Figure 27 Modulus of elasticity dependence on temperature – resonant method – FERMACELL

DISCUSSION

In case of evaluation of modulus of elasticity it is possible to claim that measurements executed by resonant method and by method based on measuring speed of wave spreading do not show important differences. By this we can consider both methods comparable and results usable.

Further we found out the expected result, that modulus of elasticity of PROMATECT and FIREBOARD is more temperature stable than at materials based on gypsum it means RIGIMBS and FERMACELL. This was expected, because gypsum, as dihydrate, change by temperature to hemihydrates and at high temperatures even to anhydrite. It was confirmed also by measuring the relative loss in weight. By comparing the obtained figures it is possible to claim that the heat conductivity of PROMATECT material is relatively stable with a slightly decreasing trend. Differences in values in dependence on primary conditions which material was observed are not important.

On the contrary, the FIREBOARD material has a stronger tendency to an increase in the heat conductivity dependent upon burn temperature. There is also the apparent bigger influence of previous drying, it meaning the influence of moisture on non-dried samples on thermal conductivity.

Quite on cue the experiment proved that board materials based on gypsum RIGIBS and FERMACELL do not have enough structural stability under high temperatures (the samples broken at temperatures around 800°C). Therefore although on lower temperature values of thermal properties are suitable, from the point of view of fire protection composite boards PROMATECT and FIREBOARD are more suitable.

Using figures comparing the relative decrement of weight of the PROMATECT material it is possible to claim that for lower temperatures (up to 500°C) the values are not changed much (maximal change 7%). But higher temperatures caused bigger changes of values (circa 30%).

In contrast, the FIREBOARD material is affected by more significant changes already of lower temperatures (below 500°C) and with higher temperatures values get more fixed.

From figures of thermal diffusivity and volume caloric capacity (volume heat capacity, volume thermal capacity) of all materials it is evident that the important break point happens again at around 500°C. The material PROMATECT has a decreasing trend of volumetric thermal capacity while on the material FIREBOARD it is possible to observe a gentle increase.

It was explicitly documented that on all samples which had been dried before, the dispersion of observed values is smaller than the dispersion of non-dried.

CONCLUSIONS

In conclusion it is possible to claim that all thermal technical parameter are comparable on all materials. Perhaps only the fact that the thermal conductivity on the material PROMATECT measured slightly lower and also the total structural stability was observed as better on this material (also visual aesthetic impression). It so follows that boards made of this material are more suitable as anti-fire lining.

The advantage of the material PROMATECT is that it has smaller volume weight, and therefore better thermal isolation properties, than the material FIREBOARD.

By this it is possible to evaluate the observed composite materials that they are suitable to use as thermal insulating at lower temperature (up to 300°C). As fire protection the better boards are PROMATECT eventually FIREBOARD because have relatively good material stability even under high temperatures.

ACKNOWLEDGEMENT

This work has been financially supported by the Ministry of Education, Youth and Sports of Czech Republic, under project No MSM: 6840770031 and by the Ministry of Industry and Trade of Czech republic, under project No MPO FR – TI 1/216.

REFERENCES

1. TOMAN J, Temperature and moisture influence on physicals parameters of buildings materials, DSc. Thesis, CVUT, Prague, 1992 (in Czech).

2. CARSLAW J, Conduction of heat in solids, Oxford, 1959.

3. TOMAN J AND SEMERÁK P, Physic 10 – Practical lessons, CVUT, Prague, 2001 (in Czech).

4. KREMPASKÝ J, Measuring of thermo-physical values, SAV, Bratislava, 1969 (in Slovak).

5. CONCRETE – Source book of technologists, Advertisement Studio ARTIS, 2005.

6. MICHALKO O AND BAŽANTOVÁ Z, Mechanical properties, International Calorimetric Seminar, University of Pardubice, 2010, pp. 73 (in Slovak and Czech).

Pavement Subgrade Stabilization: Comparative Performance of Cement and Polymers

S R Iyengar, E Masad, A K Rodriguez, H S Bazzi, D Little, H J M Hanley
Texas A&M University at Qatar, Qatar

This paper reports a preliminary laboratory investigation aimed at evaluating the potential of commercial binders for pavement subgrade stabilization in Qatar. Portland cement (PC) is one of the most commonly used binders in soil stabilization applications, and hence, the same was chosen as the standard binder for this study. However, the production of PC is not only an extremely resource and energy intensive process but also has significant negative environmental impacts. Hence, this study investigated the application of less environmentally damaging binders in the form of three commercial polymer-based soil stabilizers and their performance was compared with that of the standard, PC. The assessments were derived from measured selected physical, chemical, mechanical and micorstructural properties of natural Qatari subgrade soil when treated with a given binder over a period of 28 days of curing. Although, soil stabilization in general was found to be effective, the results demonstrate that the polymer binders modify the Qatari subgrade soils in such a manner that more favorable engineering properties are achieved than the unstabilized soils and those stabilized using PC. For example, that the compressive strengths and Toughness of the polymer stabilized soils are superior to those of the unstabilized soils and those stabilized using PC. Thus, it was demonstrated that polymers could offer a less environmentally damaging alternative in comparison to PC for pavement subgrade stabilization. While the work reported in this study was carried out with Qatari soil for subgrade stabilization, the results are relevant to other applications such as erosion control (both wind and water related) and slope stability, for similar types of soil and weather conditions experienced throughout the world.

Srinath R. Iyengar is currently an Assistant Research Scientist at Texas A&M University at Qatar. He has a Ph.D. in Engineering from the University of Cambridge and specializes in environmental goetechnics and ground improvement.

Eyad Masad is the assistant dean for research and graduate studies, and director of the Texas A&M University at Qatar division of the Texas Engineering Experiment Station. He holds the rank of a professor in the Mechanical Engineering Program at Texas A&M University at Qatar and the Zachry Department of Civil Engineering at Texas A&M.

Ana K. Rodriguez has a B.Eng in Materials Engineering from Universidad Simon Bolivar, Caracas, Venezuela. She is currently a Research Assistant at Texas A&M University at Qatar – Mechanical Engineering Department. Her research interests are materials processing and characterization, with an emphasis on polymers and lightweight alloys.

Hassan S. Bazzi is currently an Associate Professor in Chemistry and the Chair of the Science program at Texas A&M University at Qatar. He is a multiple-award winner for his academic excellence, teaches a number of courses and labs at Texas A&M University at Qatar, and has taught at Texas A&M University's main campus in College Station, Texas.

Dallas Little is Regents Professor and Snead Chair Professor at the Zachry Department of Civil Engineering and the Associate director of the Center for Aggregates Research at Texas A&M University. He is adjunct Professor of Civil Engineering at University of Saskatchewan, Canada. He has published (or has accepted for publication) approximately 160 refereed journal articles and approximately 75 refereed proceeding and has received several awards for the same.

Professor Howard J. M. Hanley was the Coordinator of Strategic Research at Texas A&M at Qatar and is now with the Australian National University, Canberra, Australia. He is a specialist on the structure and the behaviour and properties of complex materials.

Keywords: Pavement performance, Polymer stabilizer, Qatar, Soil stabilization, Subgrade

INTRODUCTION

The state of Qatar is experiencing tremendous growth in transportation infrastructure. The Public Works Authority in Qatar reported in 2010 that they intend to invest a total of $20bn on road construction in the following five years [1] with immediate plans for 60 major road projects through 2012 at an estimated cost of about $7bn. The vast majority of these roads will be asphalt-based pavements. At this time, however, pavement construction does not include stabilising the soil layer, referred to as the subgrade. In this study, it is proposed that stabilising the Qatari subgrade will improve pavement performance. It is worth mentioning that, although, this study was conducted using Qatari soil, the results are relevant to similar types of soil and weather conditions experienced throughout the world.

Although, there is no single additive or binder that has proved to be effective for all the soil types, one of the most commonly used binders for soil stabilisation is Portland cement [2]. Hence, Portland cement (PC) was considered as a standard binder in this study. However, there are environmental problems associated with the manufacturing of PC in terms of carbon dioxide (CO_2) emissions as well as extensive energy usage. The clinkering process in the manufacture of PC requires the raw materials to be heated to a temperature of around 1450°C. The theoretical energy requirement for PC manufacture using typical starting materials and cement composition is about 1,750 kJ/kg, but the actual requirement in some of the modern kilns is much higher (above 3,000 kJ/kg) [3]**.** Furthermore, the production of each tonne of PC results in roughly a tonne of carbon dioxide (CO_2) being released to the environment contributing up to around 10% of the anthropogenic CO_2 emissions worldwide [4]. Although, the quantities of PC employed in soil stabilisation would be small in terms of the global consumption of cement, there will be significant pressures placed on all sectors which use cement to consider and adopt less environmentally damaging alternatives.

One of the novel categories of soil stabilisers are polymers. Organic polymer functional groups are known to attach to the surfaces of soil particles and subsequently bond into a polymer matrix [5], thus giving the subgrade a structural integrity it would not otherwise have had [6]. Conventionally, it is believed that polymers tend to react primarily with the clay fraction of the soil [7] but polymer interactions with sands and aggregates have also been reported [8]. The adsorption of cationic polymers by clays occurs through electrostatic interactions between cationic groups on the polymer and the negatively charged sites on the clay surface leading to ionic interactions in the form of charge neutralization [9, 10]. Anionic polymers tend to be repelled by the negatively charged clay surface, but adsorption can occur through the presence of polyvalent cations acting as bridges [11]. Non-ionic polymers adsorb primarily through Van der Waals forces [10] and/or hydrogen bonding [12]. In a field situation, the molecular weight and conformation of the polymer can also influence the effective adsorption, particularly if the soil surfaces are neutral or weakly charged [13]. Hence, this study investigated the performance of three commercially available polymer soil stabilisers in an attempt to find less environmentally damaging as well as technically sound alternative to PC.

This study also builds on the work of previous authors who have approached this topic, either directly or indirectly. For example, Moustafa et al. [14] stabilised sand, silt, loam, clay, and sandy-loam soils with three types of polymeric binding materials: urea formaldehyde, phenol formaldehyde and sodium silicate. They reported that compaction of the polymer impregnated soils led to better strength and durability performance. They showed that longer curing periods and higher curing temperatures of up to 140ºC lead to improved unconfined

compressive strengths for all samples and, in particular, that high content silica soils could produce a semi-rigid type of pavement when stabilised at high temperatures. Aly and Miller [15] applied two commercially available acrylic polymer emulsions for the stabilisation of sand. More recently, Rauch et al. [16] conducted standard laboratory soil tests to measure changes in the engineering properties of five samples of clay soils, treated individually using three different types of commercially available non-traditional liquid stabilisers (ionic, polymeric and enzyme), in an attempt to evaluate their performance as alternatives to bulk soil stabilisers, such as lime and cement. Also, a laboratory based evaluation into the stabilisation of low- and high-plasticity clay soils with, twelve different types of nontraditional chemical or liquid stabilisers, including four types of proprietary polymers was conducted by Tingle and Santoni [6].

MATERIALS

Soil

Representative Qatari subgrade soil ($D_{50} \approx 4.5$ mm) having a natural moisture content of around 4.75% was used. The clay fraction corresponding to a cumulative fraction finer than 0.005 mm as specified in ASTM D0422-63 [17] was found to be less than 2% by volume. The results for Atterberg limits (in accordance to ASTM D4318 [18]) indicate liquid limit, plastic limit and plasticity index values of 27%, 22% and 5%, respectively. Following ASTM D2487 [19], it was established that the representative Qatar subgrade soil falls under the category GM-GC, which implies that it is a gravel-sand-silt-clay mixture. A qualitative analysis of soil constituents was undertaken using x-ray diffraction technique, and the results are shown in Table 1. It is seen that the major component is dolomitic limestone (d): a result consistent with previous work on Qatari soil [20]. Also a small but significant presence of palygorskite clay (p) was observed, which concurs with geological studies undertaken by Holail and Al-Hajari [21] on middle Eocene carbonate sequence obtained from the Ras Laffan area in North Qatar. The other compounds identified are calcite, gypsum, seussite (silicon sulfide), quartz, and a small percentage of magnesium manganese oxide.

Table 1 Qualitative analysis of the typical Qatari subgrade soil

NAME OF THE MINERAL/PHASE	CHEMICAL REPRESENTATION	RELATIVE % COMPOSITION
Dolomite	$CaMg(CO_3)_2$	56.02
Calcite	$CaCO_3$	15.43
Gypsum	$CaSO_4 \cdot 2H_2O$	16.41
Seussite	SiS_2	6.17
Quartz	SiO_2	2.22
Magnesium Manganese Oxide	$Mg_{0.9}Mn_{0.1}O$	0.94
Palygorskite	$Mg_5(Si, Al)_8O_{20}(OH)_2.8H_2O$	2.81

Binders

Portland cement was Type I supplied by Aljabor Cement Industries (Doha, Qatar) and conformed to BS EN 197-1 [22]. Three commercial polymer soil stabilisers, referred to as

Polymer R (Origin: South Africa), Polymer E (Origin: USA) and Polymer S (Origin: USA) were used in this study. Their exact composition and characteristics are confidential but all were water soluble with polymers E (anionic) and S (cationic) identified as acrylate based solutions, and R as an anionic emulsion.

EXPERIMENTAL METHODS

Sample Preparation

The sample preparations and subsequent investigations followed procedure ASTM D 4609 [23]. The optimum moisture content and maximum dry density of the Qatar subgrade soil (with and without binder additions) was first determined following AASHTO T99 [24]. The moisture content was estimated in accordance to AASHTO T265 [25] using a drying oven controlled at 110 ±5°C.

When treating the soil with PC, a pre-weighed quantity of cement, defined as grams per dry weight of soil, was dry mixed with the soil prior to the sequential addition of water. During soil treatment with polymers, a predetermined polymer content estimated as percentage per dry weight of soil was first dissolved in a known volume of water and then mixed with the soil. Further small adjustments were applied to compensate for the contribution of the liquid polymer to the determined optimum moisture values.

The treated soils were molded in accordance with AASHTO T99 [24] at their optimum moisture content and then three replicate cylindrical samples were extracted from each soil and immediately transferred to an oven and cured at 35°C – a curing temperature that corresponds to an average temperature experienced in Qatar throughout the year. Three curing periods were selected, namely: one, seven and twenty eight days, respectively.

Mechanical Testing

Unconfined compressive strength (UCS) and Elastic Modulus (E_{50})

The samples were tested for their unconfined compressive strengths using an MTS Insight electromechanical compression testing machine having a maximum load capacity of 250 kN and equipped with a linear variable differential transformer (LVDT) set up to measure the corresponding deformation/strains and the elastic modulus. The sample testing was calibrated such that the moving head operated at approximately 1 mm/min (i.e. in accordance to ASTM D1633 [26]). Then, as noted, tests on a given sample were conducted in triplicate after sample curing of 1 day, 7 days and 28 days, respectively.

Toughness estimation

As is well-known, the UCS is a convenient parameter for a comparative analysis of the effectiveness of a particular soil binder but it does not differentiate between brittle and ductile failure [27]. Hence, the energy dissipated up to the point of failure by recording the area under the corresponding stress-strain curve was measured. The area up to the yield point gives an estimation of yield energy absorbed. Toughness is a measure of the yield energy per unit volume [27]. In this work, Toughness is regarded as a significant comparative indicator.

Microstructure analyses employing scanning electron microscopy (SEM)

The surface morphology of the Qatari subgrade treated and untreated soils were investigated with a FEI Company scanning electron microscope model Quanta 400. Soil samples were mounted on an aluminium stub using a double-sided carbon tape. The microscope accelerating voltage ranged between 2 kV and 5 kV. The working distance was set between 9 and 12 mm whilst the magnifications ranged from 50 to 6,000 multiples.

RESULTS AND DISCUSSIONS

Optimum Mixtures with Maximum Dry Density

The procedure selected to determine the optimum concentration of a given binder follows ASTM D 4609 [23] which suggests that a specific treated soil mixture should be tested at three dosages. Table 2 gives details of the type and dosage of the binders investigated. The final selections correspond to the maximum dry density measured for a given binder. Table 3 lists the result: namely, that a dosage of 1% for all polymers, and 9% for PC was determined as the most suitable for subsequent experimentation and testing.

As a matter of interest a simple experiment to give a crude correlation that the optimum dry density of a sample was associated with the maximum polymer adsorption was carried out. Solutions of polymer concentration of 0.5, 1.0 and 2.0% by dry weight of the Qatari subgrade soil were prepared. The change in the polymer concentration was measured by the change in the absorbance of the supernatant in the UV-Visible range. Figure 1 displays the result. It was observed that both R and S designated polymers display the highest adsorption at a concentration of 1% although the adsorption of E is not affected in a significant way by the increase of concentration from 1.0% to 2.0%.

Unconfined Compressive Strengths (UCS)

Figure 2 presents the UCS variation of the Qatar subgrade soil at 1, 7 and 28 days for all the samples. The level of accuracy is shown in the figures by the error bars and was generally similar for all the different mixes with average and maximum values of 5.52% and 16.65% respectively.

Figure 2 indicates that the cured, untreated soil does exhibit an increased UCS, which corresponds to the removal of moisture and development of matric suction. There is a quantitative improvement of the UCS value for PC over that of the untreated soil at all curing ages, and the improvement increases with time. This behaviour is of course related to the initial setting of the PC within a 24 hour period, followed by increased hydration [2]. The polymer treated soils also yield superior UCS values after 7 days and, further, the E polymer sample displays a significant strength gain over those achieved by cement. ASTM D4609 [23] recommends guidelines to evaluate the effectiveness of admixtures/binders for soil stabilisation, in particular that an increase in the UCS of 0.345 MPa or more due to treatment be considered effective. Thus: after 1 day the cement stabilisation is effective, after 7 days the 1.0% E and S polymers with cement are effective, while all the binders are effective after 28 days.

Table 2 Details of the binders and their dosages investigated

BINDER TYPE	BINDER NAME	DOSAGES ADOPTED FOR INVESTIGATION, % by dry wt. of soil
Polymer	R	0.25, 0.5 and 1.0 (0.5% recommended by supplier)
	E	0.5, 1.0 and 2.0 (based on 5 dosage rates suggested during personal communication with supplier)
	S	0.25, 0.5 and 1.0 (0.5% and 1.0% recommended by supplier)
Cement	PC	5, 7 and 9 (based on typical cement requirements specified by ACI [28] for GM-GC group of soils)

Table 3 Corrected maximum dry densities and optimum moisture content obtained for Qatar subgrade soil treated with various polymer candidates and PC

SAMPLE TYPE	OPTIMUM BINDER DOSE, %	CORRECTED MAXIMUM DRY DENSITY, mg/m³	CORRECTED OPTIMUM MOISTURE CONTENT, %
Subgrade (No Binder)	-	1.82	16.20
Subgrade + PC	9.0	1.94	14.05
Subgrade + R	1.0	1.89	13.00
Subgrade + E	1.0	1.90	13.50
Subgrade + S	1.0	1.84	14.75

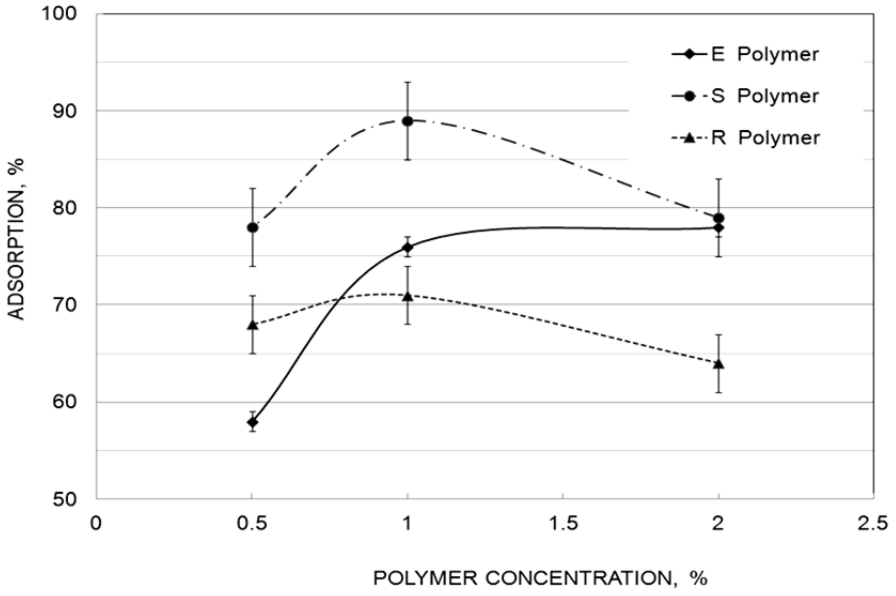

Figure 1 Adsorption of polymer by the Qatari subgrade soil as a function of the commercial polymer concentrations

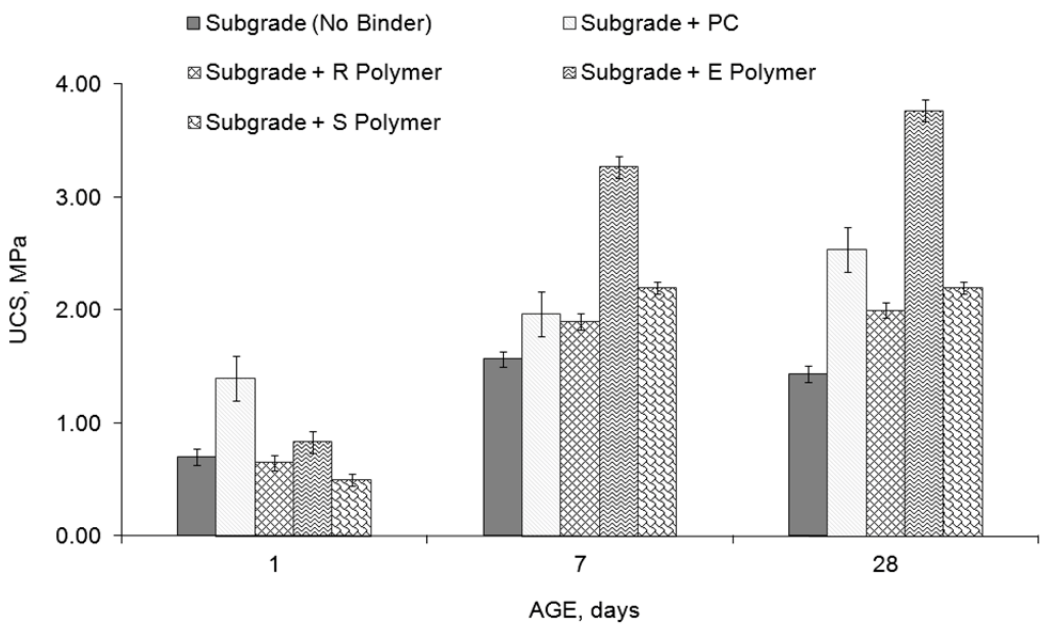

Figure 2 UCS variation at different curing ages for representative Qatar subgrade soil treated with various commercial binders and compared with the behavior of the untreated soil

Elastic Modulus (E_{50})

An alternative measure of the effectiveness of stabilisation follows from a determination of the elastic stiffness modulus (E_{50}) [29] which is the secant modulus at 50% of the maximum strength. The samples' E_{50} values were measured at 1, 7 and 28 day intervals. In this work, it can be argued that a proper comparison of the various binders should consider both the strength and the stiffness parameters, and therefore, a straightforward scatter plot in Figure 3 is an instructive indicator of the relation between the UCS and the E_{50} sets [30].

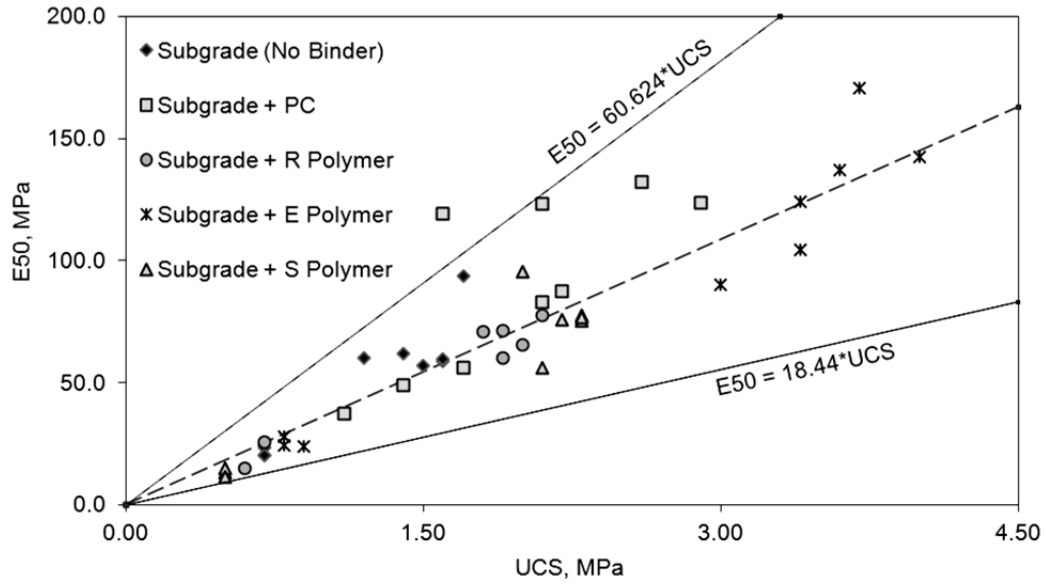

Figure 3 UCS vs. E_{50} relation at different curing ages for representative Qatar subgrade soil treated with and without various binders

Results fall between the curves: 18.44*UCS < E_{50} (MPa) < 60.62*UCS. Of more interest, however, is that the majority of the points fall close to a single line, represented by $E_{50} \approx$ 40*UCS, which indicate that the higher the UCS value the stiffer the material. But the cement data are an exception. The single line suggests that the macroscopic strength and stiffness properties of the basic soil subgrade are not fundamentally altered by the addition of a polymer binder. The cement behaviour, however, deviates from this pattern if the UCS value exceeds 1.50 MPa, consistent with the argument that the soil with hydrated cement is a different material. The data add support to the observations of Lydon and Iacovou [31] who related strength and stiffness to porosity. See the SEM images discussed later in this text.

Stress-Strain Behaviour

Figures 4(a) and (b) depict the stress-strain behaviour displayed by the unstabilised and stabilised samples at the different curing ages tested. It can be clearly seen from the distribution scatter that the failure behaviour of the cement stabilised samples becomes increasingly brittle as the curing progresses.

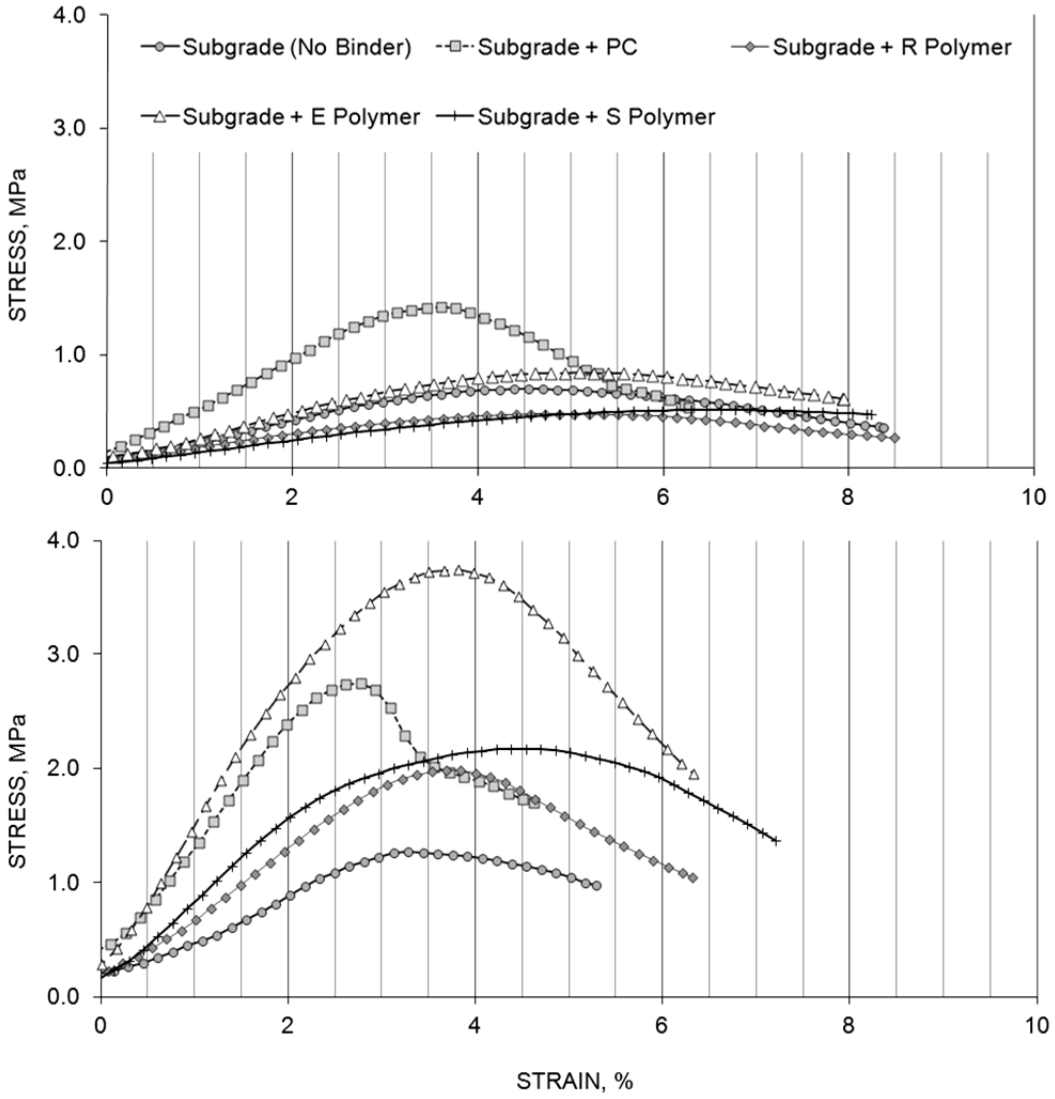

Figure 4 Typical stress-strain relation at (a) 1 and (b) 28 days of curing age for representative Qatar subgrade soil treated with and without various commercial binders

This observation is not surprising given the nature of continuing hydration reactions and its influence on the deformation characteristics, especially stiffness of soil-cements under compression reported in similar studies conducted previously [2]. In contrast, it is conspicuous that the polymer- stabilised soil samples displayed a more ductile behaviour whilst undergoing deformation. This attribute is especially desirable in pavement design and construction since highly stiff components are prone to cracking under heavy traffic loads.

Toughness

In this study, the Toughness was considered as strong indicator to assess the performance of the competitive binders. Accordingly, the Toughness was evaluated using the measured volumes of the UCS sample, as well as the area under the obtained stress-strain profiles up to the yield point, and the results given in Figure 5.

Figure 5 is noticeably different from the corresponding UCS plot in that it shows that the polymer binders have higher Toughness compared to the untreated soil and PC treated soils, especially as the curing time progresses [27]. This finding has important implication on the performance and durability of the stabilised layer in the pavement structure. In addition to the increase of strength because of polymer- stabilisation, the increase in Toughness indicates that the polymer- stabilised soil will have higher resistance to crack propagation.

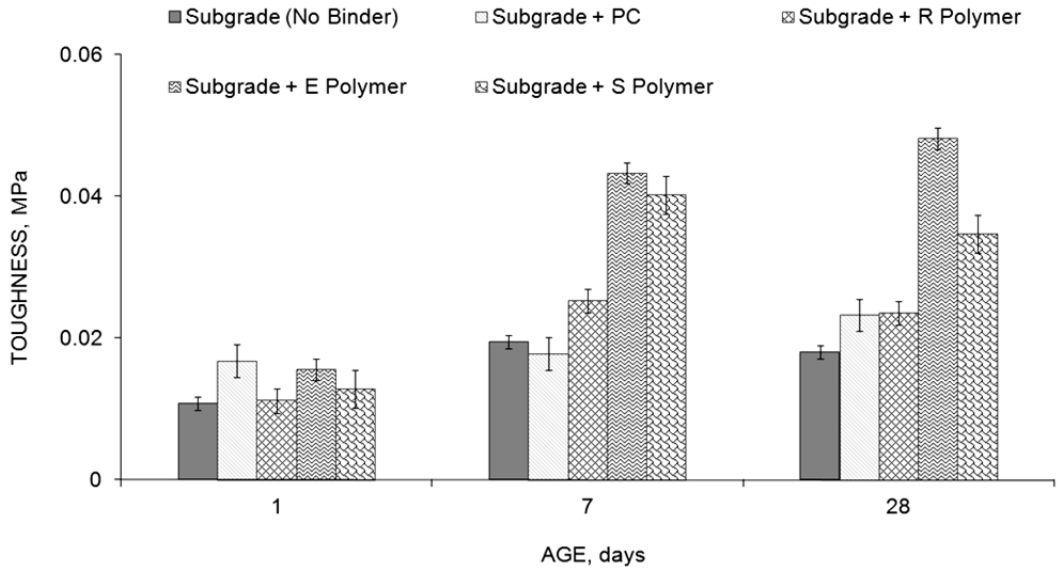

Figure 5 Variation of Toughness at different curing ages for representative Qatar subgrade soil treated with and without various commercial binders

Microstructure Examinations

Figures 6(b)-(e) illustrate the SEM micrographs of the stabilised soil binders compared with that of the untreated sample, Figure 6(a), at the 28 days curing age. Figure 6(a) indicates that the morphology consists of identifiable soil particles (i.e. sand grains) and the overall structure of the untreated sample appears to be porous, while displaying localized aggregation indicating a weakly bonded structure. This finding is consistent with the relatively overall low compressive strength exhibited by the unstabilised subgrade.

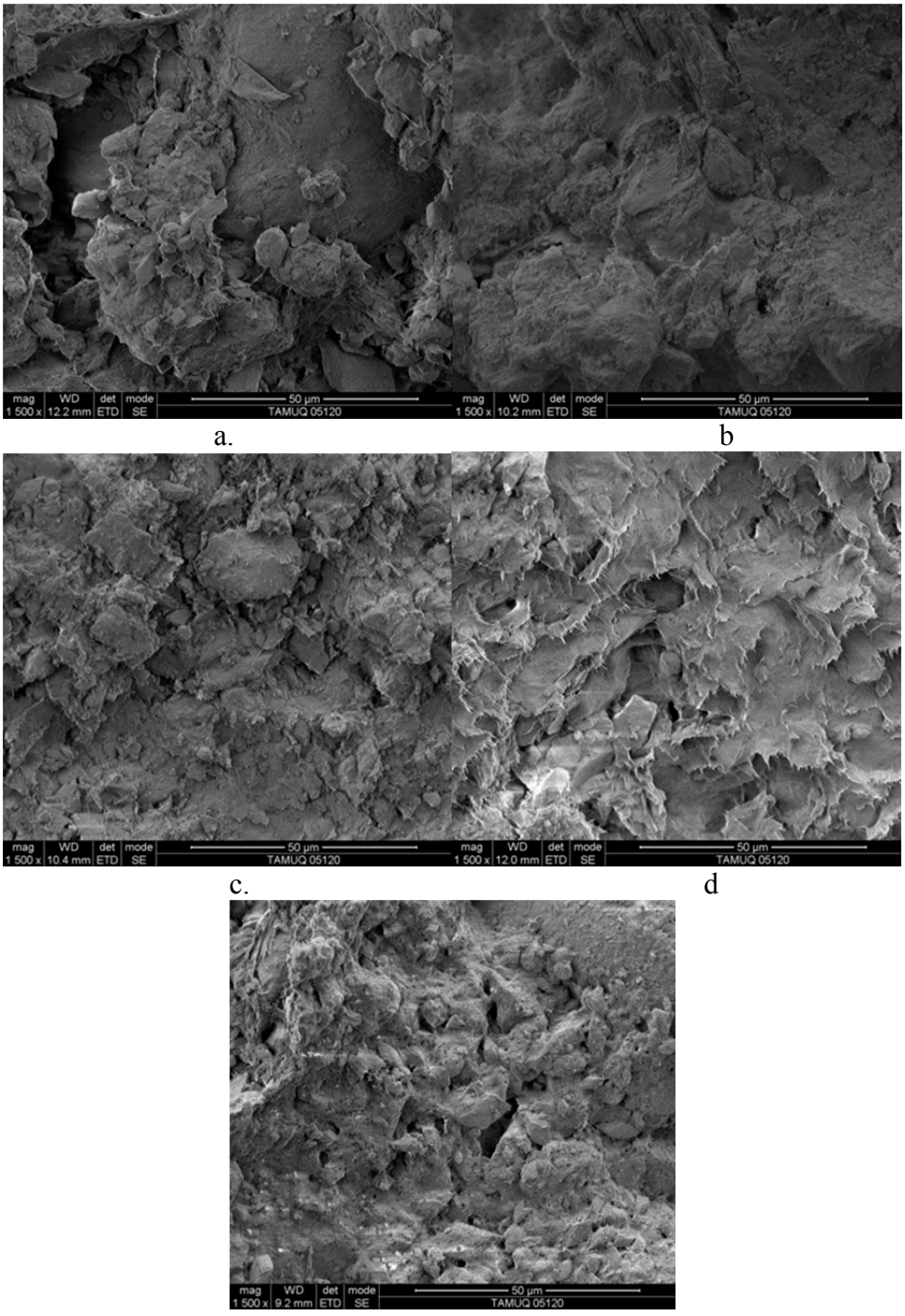

Figure 6 Typical SEM micrographs for representative Qatar subgrade soil at 28 days (a) Untreated, (b) with PC, (c) with R Polymer, (d) with E Polymer and (e) with S Polymer

Compared to Figure 6(a), the morphology of the PC stabilised soil shown in Figure 6(b) is much denser since hydration leads to the formation of the C-S-H gel which fills the voids [2]. This result is consistent with the significant improvement of the UCS, over those of the untreated sample, see, Figure 2. The result is also consistent with the stress-strain data indicating that the cement treated sample is relatively brittle and less ductile than the polymer treated counterparts, see Figure 4. Figures 6 (c) – (d) show the microstructure of the polymer treated soils and one sees that the structures are intermediate: the samples appear denser but

individual soil particles are still identified indicating that a polymer induces aggregation but, obviously, not to the extent caused by the hydration of cement. The micrographs depict a balance between the microscopic density of the soil and defined aggregation on about a 10 μm length scale. This is also reflected in the macroscopic mechanical results, particularly the Toughness data of Figure 5.

The aggregation and microscopic density enhancement displayed in the polymer images for polymers E and R can be discussed in terms of an ionic-interaction polymer-soil bonding. The Qatari soil is predominantly composed of limestone and when wetted, the surface of limestone particles becomes electropositive [8]. The polymers E and R were experimentally determined to be anionic. Thus, soil particle aggregation will be facilitated by this ionic mechanism. This conclusion does not apply to polymer S since this polymer was found to be cationic. In this case, however, we suggest that Van der Waal interactions contribute to the adsorption onto the soil. While such interactions are relatively weak, it has been shown that they could result in considerably greater observed material strengths [32].

CONCLUSIONS

Qatar is experiencing tremendous growth in transportation infrastructure construction and this will continue over the next several years. Needed are substantial improvements in prevalent asphalt road construction practices.

The results in this paper are based on experiments with a typical Qatar subgrade soil, which was predominantly calcareous with small quantities of palygorskite clays (less than 2% by volume) present and classified as a gravel-sand-silt-clay mixture (GM-GC). However, it can be argued that the conclusion, namely that a polymer based binder is a strong candidate for a superior soil stabiliser, has implications for subgrade soils in general.

Soil samples with and without stabilisation were tested using standard mechanical tests, and the results were used to determine compressive strength, elastic modulus, and Toughness. The success of polymer-based binders was judged by comparing the test results with those from the soil treated with the standard and widely used Portland cement. It was clear that the performance of the polymer modified soils rivaled, even out-performed, that of PC: a polymer stabilised subgrade was found to have higher UCS strengths and displayed a greater Toughness.

Thus, it was concluded that polymers could offer a less environmentally damaging yet technically viable alternative to PC for pavement subgrade stabilisation. Furthermore, it needs to be highlighted that the outcome of this work is relevant to other allied applications such as erosion control (both wind and water related) and slope stability.

ACKNOWLEDGEMENTS

The authors would like to acknowledge the financial and technical support of the Qatar Science and Technology Park (QSTP) for this study. The authors would like to particularly thank Mr. Paul Field (QSTP), Mr. Bo Heiden (QSTP), Ms. Nadiya Farah (QSTP), Mr. Nelson Antonio (TAMUQ), Mr. Omar Abdallah (TAMUQ), Mr. Ahmed Ghamrawy (TAMUQ) and Dr. Chayanant Hongfa (TAMUQ) for their support while carrying out this study.

REFERENCES

1. QAZI S, Qatar to spend $20bn on roads, Article published in the Gulf Times newspaper, 28 January, 2010. <http://www.gulf-times.com/site/topics/printArticle.asp?cu_no=2&item_no=339708&version=1&...> (website last accessed on 6 March, 2012).

2. SHERWOOD P, Soil stabilisation with cement and lime, Technical Report, Transport Research Laboratory, Department of Transport, London, UK, 1993, p 153.

3. AÏTCIN P C, Cements of yesterday and today Concrete of tomorrow (Review), Cement and Concrete Research, Vol. 30, 2000, pp. 1349-1359.

4. VAN OSS H G AND PADOVANI A C, Cement Manufacture and the Environment Part II: Environmental Challenges and Opportunities, Journal of Industrial Ecology, Vol. 7, No. 1, 2003, pp. 93-126.

5. SCHOLEN D E, Stabilizer mechanisms in nonstandard stabilizers, Proceedings of Sixth International Conference on Low-Volume Roads, Transportation Research Board, Minneapolis, MN, USA, 1992, pp. 252–260.

6. TINGLE J S AND SANTONI R L, Stabilization of clay soils with non-traditional additives, Proceedings of Eighth International Conference on Low-Volume Roads, Transportation Research Board, Reno, NV, USA, 2003, pp. 72-84.

7. WALLACE A, Handbook of soil conditioners, A. Wallace and E. R. Terry, eds., 1998, Marcel Dekker, New York, USA, 600 p.

8. HEFFER A W, LITTLE D N AND LYTTON R L, A synthesis of theories and mechanisms of bitumen-aggregate adhesion including recent advances in quantifying the effects of water, Journal of the Association of Asphalt Paving Technologists, Vol. 74, 2005, pp. 139-195.

9. HANLEY H J M, MUZNY C D AND BUTLER B D, Surfactant Adsorption on a Clay Mineral: Application of Radiation Scattering, Langmuir, Vol. 13, 1997, pp. 5276-5282.

10. MILLER W P, WILLIS R L AND LEVY G J, Aggregate stabilization in kaolinitic soils by low rates of anionic polyacrylamide, Soil Use and Management, Vol. 14, No. 2, 1998, pp. 101-105.

11. LIARD L A, Bonding between polyacrylamide and clay mineral surfaces, Soil Science, Vol. 162, No.11, 1997, pp. 828-832.

12. WALLACE A, WALLACE G A AND CHA J W, Mechanisms involved in soil conditioning by polymers, Soil Science, Vol. 141, No. 5, 1986, pp. 381-386.

13. SEYBOLD C. Polyacrylamide review: soil conditioning and environmental fate, Communications in Soil Science and Plant Analysis, Vol. 25, No. 11/12, 1994, pp. 2171-2185.

14. MOUSTAFA A B, BAZARAA A R AND NOUR EL DIN A R, Soil stabilization by polymeric materials, Macromolecular Materials and Engineering, Vol. 97, No. 1, 1981, pp. 1–12.
15. ALY S M AND MILLER W P, Evaluation of two polymers for soil stabilization and wind erosion control, Egyptian Journal of Soil Science, Vol. 35, No. 1, 1995, pp. 71-83.

16. RAUCH A F, HARMON J S, KATZ L E AND LILJESTRAND H M, Measured effects of liquid soil stabilizers on engineering properties of clay, Transport Research Record, No. 1787, 2002, pp. 33-41.

17. ASTM, D0422-63 - Standard test method for particle-size analysis of soils, American Society for Testing and Materials, 2007, West Conshohocken, PA, USA.

18. ASTM, D4318 - Standard test methods for liquid limit, plastic limit, and plasticity index of soils, American Society for Testing and Materials, 2005, West Conshohocken, PA, USA.

19. ASTM, D2487 - Standard practice for classification of soils for engineering purposes (unified soil classification system), American Society for Testing and Materials, 2011, West Conshohocken, PA, USA.

20. AL-SAAD H, Lithostratigraphy of the middle Eocene Dammam formation in Qatar, Arabian gulf: effects of sea-level fluctuations along a tidal environment, Journal of Asian Earth Sciences, Vol. 25, No. 5, 2005, pp. 781-789.

21. HOLAIL H AND AL-HAJARI S, Evidence of an authigenic origin for the palygorskite in a middle Eocene carbonate sequence from north Qatar, Qatar University Science Journal, Vol. 17, No. 2, 1997, pp. 405-418.

22. BSI, BS EN 197-1: Cement. Composition, specifications and conformity criteria for low heat common cements, British Standards Institution, 2000, London, UK.

23. ASTM, D4609 - Standard guide for evaluating effectiveness of admixtures for soil stabilization, American Society for Testing and Materials, 2008, West Conshohocken, PA, USA.

24. AASHTO, T99 - Moisture-density relations of soils, using a 5.5-lb (2.5-kg) rammer and a 12-in. (305-mm) drop [Method C], American Association of State Highway and Transportation Officials, 2009, Washington, DC, USA.

25. AASHTO, T265 - Laboratory determination of moisture content of soils, American Association of State Highway and Transportation Officials, 2008, Washington, DC, USA.

26. ASTM, D1633 – Standard test methods for compressive strength of molded soil-cement cylinders, American Society for Testing and Materials, 2007, West Conshohocken, PA, USA.

27. NEWMAN K AND TINGLE J S, Emulsion polymers for soil stabilization soils, Proceedings of 2004 FAA Worldwide Airport Technology Transfer Conference, Atlantic City, New Jersey, USA, 2004, 18 p.

28. ACI, Report on Soil Cements, Technical Report No. ACI 230.1R-09, American Concrete Institute, 2009, Michigan, USA, 28 p.

29. RADOVIC M, LARA-CURZIO E AND RIESTER L, Comparison of different experimental techniques for determination of elastic properties of solids, Material Science and Engineering: A, Vol. 368, Nos. 1/2, 2004, pp. 56-70.

30. PORBAHA A, SHIBUYA S AND KISHIDA T, State of the art in deep mixing technology. Part III: Geomaterial characterization, Ground Improvement, Vol. 3, 2000, pp. 91-110.

31. LYDON F D AND IACOVOU M, Some factors affecting the dynamic modulus of elasticity of high strength concrete, Cement and Concrete Research, Vol. 25, No. 6, 1995, pp. 1246-1256.

32. AUBREY D W, Handbook of adhesion, Second Edition, D. E. Packham, ed., 2005, John Wiley & Sons, Ltd., Chichester, UK, 677 p.

The Quality of Collapse Debris and Possible Reuse of this Material to Rebuild Port au Prince Haiti

D J Collery[1], M Bjerregaard[2], K A Paine[3]
1 – Environment Agency, UK
2 – Disaster Waste Recovery, UK
3 – University of Bath, UK

On the 12th January 2010 Haiti and its capital of Port au Prince were struck by a massive earthquake measuring 7.0 on the Richter scale. The earthquake and its aftershocks rendered the Haitian capital into little more than a pile of rubble and debris. The first video footage from the earthquake zone made it apparent that the rebuild of Port au Prince would involve extensive site clearance with tonnes of waste debris surplus to requirements. On making contact with Disaster Waste Recovery it was decided that research and testing on samples of the collapse debris would be undertaken to establish if this debris could be utilised as follows (i) Sub-base materials for road construction, (ii)Use of recycled fines in concrete block production, (iii) Low strength recycled aggregate concrete applications, (iv) For use in vibroflotation compaction. The results suggest that whilst use of collapse debris may reduce strength of sub-base and lower concrete strength compared to natural aggregates that in the main, positive results were obtained from this testing programme. The practical implications of recycling debris in a disaster area are discussed in relation to quality and control.

Dr David Collery is a Graduate Flood Rick Engineer for UK'S Environment Agency and was formerly a PhD student at the Concrete Technology Unit, University of Dundee. Research interests include sustainable construction, recycled aggregates and re-use of materials.

Dr Kevin Paine is a Senior Lecturer in civil engineering at the BRE CICM at the University of Bath. He carries out research on low carbon and sustainable forms of concrete construction, with current focus on geopolymers, nanoparticles and the use of bacteria and mineral-precursors.

Martin Bjerregaard has more than 20 years experience in demolition and decommissioning to provide clients with pragmatic, cost effective and safe demolition works. He is currently Director of Disaster Waste Recovery Ltd and Director of D3 Consulting Ltd. Disaster Waste Recovery is a non-for-profit organisation supporting communities with waste and debris management following disasters and conflicts.

Keywords: Debris, Disasters, Recycled aggregate, Recycling, Sustainability

INTRODUCTION

The earthquake on 12 January 2010 that overwhelmed the Republic of Haiti had a devastating impact on the already vulnerable island nation, leaving more than 200,000 people dead and over one million homeless [1]. It is believed that more than 300,000 homes and 30,000 businesses collapsed or were critically damaged by the earthquake [2].

The earthquake and its aftershocks rendered the Haitian capital into little more than a pile of rubble and debris. This damage was largely contributed to lack of construction standards, substandard materials and poor quality control in construction. It was estimated that 20 million m^3 of debris was produced from the earthquake [2]. In collaboration with Disaster Waste Recovery (non-government organisation) research and testing on samples of the collapse debris was undertaken by the primary author to establish if this debris could be utilised as:

- Sub-base materials for road construction
- Use of recycled fines in concrete block production
- Low strength recycled aggregate concrete applications
- For use in vibroflotation compaction

The primary author travelled to Port-au-Prince, Haiti (June 28 to the 19 July 2010) to work alongside Disaster Waster Recovery. On arrival at Port-au-Prince, it was soon apparent the vast scale of the disaster, including the enormous amounts of debris along the roadside and at every street corner.

A sampling programme was developed, and areas were selected based on local engineering knowledge to provide samples of debris from three different class divisions. This was done in order to determine if there were any variations in the quality of the debris based on the poverty/affluence of the area from which it was taken. A programme of testing of samples was developed based on the equipment available at the Ministry of Public works laboratory in Port-au-Prince.

WORKING PROGRAMME

Seven samples of debris were selected on a judgement basis from the areas highlighted in

Figure 1 Map of Port au Prince showing sample sites. The preferred method of obtaining samples for testing was by selection from various sites and crushing, through use of a mobile crushing plant (MCP). However, as there was no MCP available for use (DWR had imported a MCP but had problem with customs at that time), the samples had to be manually crushed by use of a sledge hammer. This resulted in a limitation of scope on the testing carried out. A description of each of the seven debris samples collected is given in Table 1. The manually crushed aggregates were sieved through a 4 mm sieve onsite to produce coarse and fine recycled aggregates for laboratory testing.

EXPERIMENTAL PROGRAMME

All aggregates were tested in accordance with relevant standards as given in Table 2. All crushed recycled aggregate sample sizes were reduced in accordance with BS EN 932-1, to achieve the required specimen size. Due to the time limitations and lack of laboratory equipment no chemical tests were carried out on the recycled aggregates.

Map Legend

■ Sample 1 &2
◆ Sample 3
▲ Sample 4
◣ Sample 5
✚ Sample 6
● Site Inspection ref. Sample 7

Figure 1 Map of Port au Prince showing sample sites

Table 1 Location and description of debris that were tested in the Ministry of Public works laboratory

SAMPLE NUMBER	LOCATION	DESCRIPTION	NUMBER OF BAGS
Sample 1[xx]	Fort Mercredi	Concrete cavity blocks, locally produced (onsite). Made with lime rock crushed 0 to 6mm. Majority of buildings/dwellings are constructed with this type of material. Sample was taken at the proposed location of DWR crusher.	8 crushed onsite
Sample 2[xx]	Fort Mercredi	Concrete floor slab from collapsed dwelling. Sample was taken at the proposed location of DWR crusher.	8 crushed onsite
Sample 3[xx]	Raute des Dalles (Sonatorium)	Concrete structural column typically used in domestic dwelling in this area and throughout Port au Prince.	6 crushed onsite
Sample 4[xx]	Avenue Jean Paul II-Turgeau – Bank	Sample 4 was taken from a collapsed bank, structural concrete column in a middle class area. The concrete column was still standing which was broken and crushed onsite.	6 crushed onsite
Sample 5[All in]	Fort National	Stock-pile of debris from clearance work in this area was sampled. A mixture of debris was contained within this sample.	8 crushed onsite
Sample 6[All in]	Bourdon	Sample from a collapsed house in an upper class area. The sample contained crushed concrete floor and roof slab, concrete columns and block work.	6 crushed onsite
Sample 7	Morne A Tuff	Site inspection without sampling due to the time constraints on laboratory testing. It was noticed that many buildings have been constructed with clay bricks which are not readily used in other areas of Port au Prince. Majority of the buildings are three to four stories high and were constructed in the 1800s.	No samples were taken

[xx] = only one type of material within the sample without impurities
[All in] = sample contains a mixture of materials and impurities

Table 2 Recycled aggregate tested in accordance with relevant standards

DESCRIPTION	TEST NAME	STANDARD
Particle size distribution	Determining the particle size distribution (grading)	BS EN 933-1
Micro-Deval (m-D)	Resistance to wear of coarse aggregates	BS EN 1097-1
Los Angeles test (LA)	Resistance to fragmentation of coarse aggregates	BS EN 1097-2
Water absorption and density	Aggregate particle density and water absorption	BS EN 1097-6
Sand equivalent test on fine aggregates	Assessment of fines- sand equivalent test	BS EN 933-8
CBR Value	California Bearing Ratio test	BE EN 1377-4
Loose bulk density and voids	Loose bulk density and voids	BS EN 1073-3

RESULTS

Table **3** gives the results of all tests on coarse aggregates. In general the aggregates had higher water absorption and lower aggregate particle density, with typical values of over 8% and less than 2400 kg/m³ respectively, when compared to the results of other research on recycled aggregates [3, 4, 5]. An exception to this was sample 4 which was taken from a high strength concrete column (on the ground floor) from a collapsed bank. The high water absorption and low aggregate particle density of samples 1, 2, 3, 5 and 6 may indicate high porosity and potentially low strength.

Research has shown that entrapped air (poor construction methods) and high water/cement ratio are the main reasons for the poor compressive strength of the block/concretes [6]. The high water/cement ratio may be a consequence of a low cement content used because of financial constrains. On visual inspection, the concretes that were crushed to produce recycled aggregates had originally been made with a maximum aggregate size of around 6 to 8 mm.

The process of manually crushing debris into recycled aggregates was undertaken with relative ease for the majority of the crushed samples, with the exception of sample 4. This indicated that crushed recycled aggregates were of low strength which has been confirmed by the laboratory results. The Los Angeles (LA) results are high (average value 39 for all samples) indicating a lower strength recycled aggregate, with sample 4 giving a value of 42 showing a poor resistance to fragmentation. Similarly Micro-Deval results were high with an average value of 57 for all samples, indicating a poor resistance to wear. This high value may be due to a low coarse aggregate content of the crushed concrete with the resulting mortar (mixture of sand, cement and water) giving poor resistance to wear.

Due to time limitations California Bearing Ratio (CBR) test was only undertaken on samples 1 and 5. The two CBR test results indicated a large variation between the two samples. Sample 1 (clean crushed cavity blocks) gave a CBR value of 36 representing low strength granular material with sample 5 (mixture of debris materials) giving a CBR value of 110 representing high strength granular material. As these values are based on only one CBR test it is recommended that further testing be undertaken and these results be used only as indicators of the quality of the recycled aggregate.

The results of fine aggregates are given in Table 4. Fine aggregates were tested for: bulk density, assessment of fines, water absorption and density.

The average particle density of the fine recycled aggregate was 2500 kg/m³. Sample 1 (crushed cavity block) had a particle density of 2650 kg/m³, which is of similar density to lime rock [7]. Lime rock is crushed to produce building sand for production of building blocks in Port au Prince. This would indicate a large amount of sample 1 composition was made of lime rock sand. The assessment of fines (smaller than 0.063 mm) for the clean crushed fine aggregate all gave values of low percentage of clay/silt fine indicating a good fine aggregate material. However, sample 5 which consisted of a mixture of all-in debris had a low sand equivalent of 22 indicating that this fine aggregate had an excessive amount of fines. This sample may best represent the fines produced by a crusher; this would depend largely on the machine operator and method of loading the crusher.

Table 3 Laboratory test results of coarse recycled aggregates

	SAMPLE 1	SAMPLE 2	SAMPLE 3	SAMPLE 4	SAMPLE 5	SAMPLE 6
Shape (visual inspection)	Angular	Irregular Angular	Angular	Irregular Angular	Irregular Angular	Irregular Angular
Texture (visual inspection)	Honey-combed	Rough	Rough	Rough	Rough	Rough
Density SSD†, kg/m³	2310	2340	2310	2440	2310	2350
Loose bulk density, kg/m³	1190	1250	1280	1360	1290	1210
Compacted bulk density, kg/m^3	1270	1360	1390	1450	1420	1340
Water Absorption, %	8.6	10.2	8.9	4.1	8.0	8.9
LA, , %	39	35	40	42	39	36
m-D, %	64	55	61	49	57	56
CBR Value	36				110	

†SSD = saturated surface dry

Table 4 Laboratory test results of fine recycled aggregates

		SAMPLE 1	SAMPLE 2	SAMPLE 3	SAMPLE 4	SAMPLE 5	SAMPLE 6
Shape (visual inspection)		Round/ Angular	Angular	Angular	Angular	Angular	Angular
Density SSD†, kg/m³		2650	2540	2450	2470	2420	2480
Loose bulk density, kg/m³		1190	1250	1280	1360	1290	1210
Compacted bulk density, kg/m³		1270	1360	1390	1450	1420	1340
Compaction ratio		0.55	0.58	0.60	0.59	0.61	0.57
Water Absorption, %		5	5.2	6	5	7.2	5.1
Sand Equivalent test	E.S.v	77	70	70	74	22	59
	E.S.p	75	69	70	72	21	58

†SSD = saturated surface dry
E.S.v = sand equivalent value
E.S.p= sand equivalent plunged value

DISCUSSION

Tables 3 and 4 have been examined and discussed in relation to sub-base materials for road construction; use of recycled fines in concrete for block production; low strength recycled aggregate concrete and use of recycled aggregate for vibroflotation compaction to improve foundation for new construction.

Sub-base Materials for Road Construction

Based on the laboratory results of recycled aggregates tested and the manual of contract document for Highways Works Series 500, 600 and 800 [8, 9, 10], the samples of recycled aggregates tested from Port au Prince are permitted to be used as follows:

- Series 500 pipe bedding, filter drain material

- Series 600 Classes 1A-1C, 6A-6F5
  Max 1% foreign material (Class X as classified in BS EN 933-11) [11].

- Series 600 Classes 6H-6Q
  Max. 1% foreign material and no recycled asphalt (Class Ra and X as classified in BS EN 933-11) [11].

- Series 800 Types 1, 2, 3 and Category B Unbound mixtures cement and other hydraulically bound materials

-
- Table **3** limited to 5% asphalt (Class Ra) and not more than 1% other materials (Class X) and is required to adhere to the Quality Protocol for the Production of Aggregates [12].

Additional information on series 600 classes is given in

Table **5**. The majority of these classes have a wide grading curve, allowing a large range of aggregates particle sizes to be used. In series 800 foreign materials is limited to 1% which may be very difficult to achieve, due to the large amount of waste materials within the collapsed debris. The recycled aggregates would be more suitable for use in series 500 and 600 for road construction.

Table 5 Series 600 (Highways Agency) description of fill material for which recycled aggregate can be used in road construction

CLASS	GENERAL MATERIAL DESCRIPTION	TYPICAL USE	PERMITTED CONSTITUENTS (All subject to Requirements of Clause 601 and Appendix 6/1)
1A	Well graded granular material	General Fill	Any material, or combination of materials, other than material designated as Class 3 in the Contract. Recycled aggregate.
1B	Uniformly graded granular material	General Fill	Any material, or combination of materials, other than chalk. Recycled aggregate
1C	Coarse granular material	General Fill	Any material, or combination of materials, other than material designated as Class 3 in the Contract. Recycled aggregate.
6A	Selected well graded granular material	Below water	Natural gravel, natural sand, crushed gravel, crushed rock other than argillaceous rock, crushed concrete, chalk, well burnt colliery spoil or any combination thereof. Recycled aggregate
6B	Selected coarse granular material	Starter layer	Natural gravel, natural sand, crushed gravel, crushed rock other than argillaceous rock, crushed concrete, chalk, well burnt colliery spoil, slag or any combination thereof. Recycled aggregate
6C	Selected uniformly graded granular material	Starter layer	Natural gravel, natural sand, crushed gravel, crushed rock other than argillaceous rock, crushed concrete, chalk, well burnt colliery spoil, slag or any combination thereof. Recycled aggregate
6D	Selected uniformly graded granular material	Starter layer below pulverised fuel ash	Natural gravel, natural sand, crushed gravel, crushed rock other than argillaceous rock, crushed concrete, chalk, well burnt colliery spoil, slag or any combination thereof. Recycled aggregate
6E	Selected granular material (Class 9A)	For stabilisation with cement to form capping.	Any material, or combination of materials, other than unburnt colliery spoil and argillaceous rock. Recycled aggregate.

continued

Table 6 Series 600 (Highways Agency) description of fill material for which recycled aggregate can be used in road construction, cont'd

CLASS	GENERAL MATERIAL DESCRIPTION	TYPICAL USE	PERMITTED CONSTITUENTS (All subject to Requirements of Clause 601 and Appendix 6/1)
6F1	Selected granular material (fine grading)	Capping	Any material, or combination of materials – including recycled aggregates with not more that 50% by mass of recycled bituminous planings and granulated asphalt, but excluding materials that contain tar and tar-bitumen binders, unburnt colliery spoil, argillaceous rock and chalk.
6F2	Selected granular material (coarse grading)	Capping	Any material, or combination of materials – including recycled aggregates with not more that 50% by mass of recycled bituminous planings and granulated asphalt, but excluding materials that contain tar and tar-bitumen binders, unburnt colliery spoil, argillaceous rock and chalk.
6F3	Selected granular material	Capping	Any material, or combination of materials with ≥50% by mass of recycled bituminous planings and granulated asphalt, but excl. materials with tar and tar-bitumen binders, unburnt colliery spoil and argillaceous rock.
6F4	Selected granular material (fine grading) – imported on to the site	Capping	Unbound mixture to BS EN 13285. Any material, or combination of materials – including recycled aggregates with not more than 50% by mass of recycled bituminous planings and granulated asphalt, but excluding materials that contain tar and tar-bitumen binders, unburnt colliery spoil, argillaceous rock and chalk.
6F5	Selected granular material (coarse grading) – imported on to the site	Capping	Unbound mixture to BS EN 13285. Any material, or combination of materials – including recycled aggregates with not more than 50% by mass of recycled bituminous planings and granulated asphalt, but excluding materials that contain tar and tar-bitumen binders, unburnt colliery spoil, argillaceous rock and chalk.
6P	Selected granular material	Fill to structures	Natural gravel, natural sand, crushed gravel, crushed rock, crushed concrete, slag, chalk, well burnt colliery spoil or any combination thereof. None of these constituents shall include any argillaceous rock. Recycled aggregate except recycled asphalt.
8	Class 1, Class 2 or Class 3 material	Lower trench fill	Any; except there shall not be any stones or lumps of clay>40mm nominal diameter. Recycled aggregate.

Use of Recycled Fines in Concrete Block Production

Recycled aggregate fines could potentially be used as a partial replacement of sand in the production of concrete blocks. As the majority of buildings in Port au Prince have been constructed with low strength cavity blocks, which resulted in the devastating collapse of approximately 90% of building structures, resulting in the vast quantities of debris being produced. The crushing of this low strength debris will result in a large percentage of recycled aggregate fines. The quality of the recycled aggregate fines will largely depend on the quantity of fine material (less than 63 µm clay/slit materials) of the aggregates, as this can adversely affect the water absorption values. This is a key element in determining the recycled aggregate fines quality as partial replacement of sand for the production of concrete cavity blocks.

In order to limit fine materials (clay/silt) in the crushed recycled aggregate fines it is recommended that a 50 to 75 mm sieving bucket be used on the machine loading the crusher. This would allow crushing of clean debris without excessive amounts of clay/silt materials and would greatly increase the likelihood of good quality recycled aggregate fines that could be reused in the production of concrete blocks. The results of recycled aggregate fines highlights its potential use in the production of non structural concrete blocks, but further chemical analysis would need to be undertaken to confirm this.

Low Strength Recycled Aggregate Concrete Applications

The results presented in Table 3 indicate that the coarse recycled aggregates are low strength aggregates and would not normally be appropriate for high strength concrete applications (where design strengths in excess of 50 N/mm² are required) [13]. However, recycled aggregates with low strength are suitable for low strength concretes, such as footpaths, kerbing, base for pipe laying and protection etc. The chemical properties (chloride, sulfate and alkali content) of the recycled aggregates would need to be assessed to determine use in low strength concretes. The high water absorption values (average of 8%) of these recycled aggregates will be a limiting factor on the use of these aggregates in low strength concretes unless pre-socking or additional water is added to the aggregates in the concrete mix and time given for absorption of the additional water. Alternatively, limiting the replacement of these recycled aggregates to 50% and using natural coarse aggregates with a low water absorption would reduce the overall water absorption of the aggregates and limit the impact on the resulting concrete. Trial mixes of low strength recycled aggregate concretes with variable replacement content would be advisable to ascertain the fresh and hardened properties of the concrete.

For Use in Vibroflotation Compaction

Vibroflotation is a method used in Foundation Engineering where more suitable soil bed under a structure foundation is established in order to gain the required soil bearing capacity. The particle size distribution of the backfill materials is an important factor that controls the rate of densification. The suitability number for the backfilling to be used in vibroflotation was developed by Brown [14] and is presented in Equation 1.

$$S_N = 1.7\sqrt{\frac{3}{D_{50}} + \frac{1}{D_{20}} + \frac{1}{D_{10}}} \quad (1)$$

Where D_{50} D_{20} and D_{10} are diameter in mm through which, respectively 50, 20 and 10% of materials passes. The smaller the value S_N the more desirable the backfill materials is with 0 to 10 classed as excellent, 10 to 20 classed as good, 20 to 30 classed as fair, 30 to 40 classed as poor and greater than 50 classed as unsuitable. Based on the hand crushed particle size distribution presented in

Figure recycled aggregate debris have a suitability number S_N of 6 indicating that the material has a classification as excellent for backfill material for vibroflotation compaction. However, recycled aggregate from a crusher may have a different particle size distribution, which would require testing to classify the suitability for vibrofloation compaction. The initial results were very encouraging.

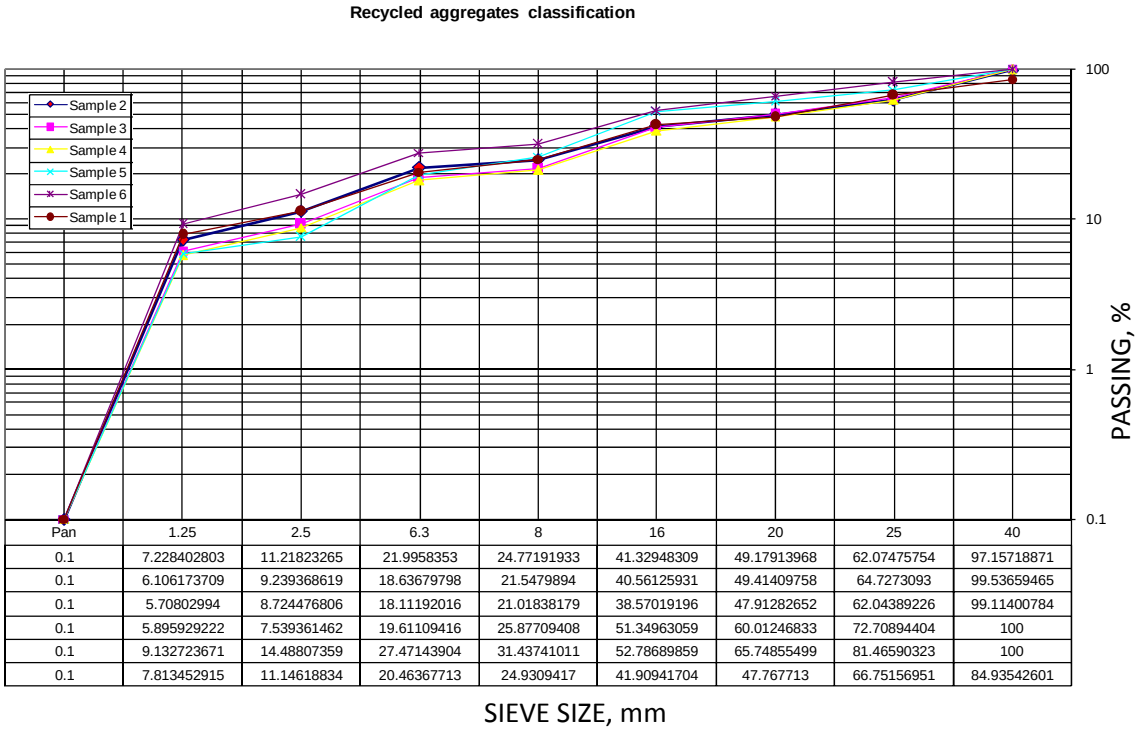

Pan	1.25	2.5	6.3	8	16	20	25	40
0.1	7.228402803	11.21823265	21.9958353	24.77191933	41.32948309	49.17913968	62.07475754	97.15718871
0.1	6.106173709	9.239368619	18.63679798	21.5479894	40.56125931	49.41409758	64.7273093	99.53659465
0.1	5.70802994	8.724476806	18.11192016	21.01838179	38.57019196	47.91282652	62.04389226	99.11400784
0.1	5.895929222	7.539361462	19.61109416	25.87709408	51.34963059	60.01246833	72.70894404	100
0.1	9.132723671	14.48807359	27.47143904	31.43741011	52.78689859	65.74855499	81.46590323	100
0.1	7.813452915	11.14618834	20.46367713	24.9309417	41.90941704	47.767713	66.75156951	84.93542601

Figure 2 Particle size distribution for coarse recycled aggregates

PRACTICAL IMPLICATIONS OF RECYCLING DEBRIS IN A DISASTER STRICKEN AREA

Disaster debris often contains a lot more than just concrete, brick, wood and glass. Traditional demolition of a building and structure involves the removal of all domestic materials, office furniture, floor covering and suspended ceilings etc. When dwellings and buildings collapse without giving a large number of the occupants a chance to escape, all materials and furniture that made the structure habitable and potentially some human remains become part of the collapse debris.

In Port-au-Prince sadly this was a reality, other factors that complicate the process of recycling collapse debris in Port-au-Prince include ownership of the debris, solid waste contamination, plant processing locations, transport, traffic, road infrastructure, equipment and plant, operations and maintenance, and quality control. All of these issues needed to be overcome to successfully recycle debris in Port-au-Prince.

One of the more complicated issues is the ownership of the collapse debris, since poor records of dwelling ownership existed and the few that did were stored in government offices that collapsed. An indication of the complexity of ownership is shown in Figure where a number of dwellings have collapse together down a hillside. The local government and Mayor of Port-au-Prince understood the potential and possibility of recycled aggregates produced from collapse debris in the reconstruction of the city [15]. This issue was partly resolved, with the local government zoning areas of land around the city to be set up as depots, to start the recycling process and reconstruction of the city. The transport and road infrastructure of the city prior to the earthquake was poor, and with some bridges, sewers, man holes collapsing after the earthquake, congestion is a factor of the city. Therefore, the location of the recycling depots is key to minimising transport and avoiding traffic congestion as much as possible.

Training and plant operations is an important factor since the majority of plant and equipment was imported after the earthquake, and operatives need to be trained on how to operate the plant safely and correctly to minimise breakages and maintenance. This can be achieved by ensuring good training and supervision at the recycling depots, and by explaining both the recycling process and how the materials are to be used to rebuild the local area to operatives. This will help to increase the quality of the recycled aggregates (removal of impurities) [16].

Figure 3 Photograph of a collapsed dwelling at Fort Mercredi, Port au Prince

CONCLUSIONS AND RECOMMENDATIONS

The results from the laboratory data indicate that the collapse debris in Haiti generally produces low strength recycled aggregates (high LA and high water absorption values) when crushed. By keeping the contaminated waste to a minimum, by hand sorting before crushing and by ensuring a low fines content there is potential for coarse and fines recycled aggregates to be reused in low strength concretes and concrete products. However, this is dependent on favourable chemical analysis being derived from further testing of recycled aggregates.
The results presented in

Table **3** and Table 4 respectively, for both coarse and fine recycled aggregates indicate that they can be used for a series of different drainage and services ducts, and earthworks for the construction of roads, in accordance with UK standards for Highways. Similarly, results indicated these recycled aggregates are suitable to be used as fill material for vibroflotation compaction. This research has highlighted potential and possible reuse of collapse debris in Port-au-Prince to aid the reconstruction of the city's infrastructure, reducing the amount of debris being deposited off in landfill sites and reducing the demand for natural aggregates.

However, there are a number of practical application issues, as described in the paper, that must be overcome before the most effective use of recycled aggregates from collapse debris can be realised in Haiti.

ACKNOWLEDGEMENTS

The Disaster Waste Recovery team in Port-au-Prince are thanked for aiding and making this research possible within the short time frame. The Environment Agency, UK, David Read, Andrew Crates, Tim Connell and Andrew Gilham are thanked by the primary author for the flexible working that allowed him to undertake this research.

REFERENCES

1. UNITED NATIONS. UN OCHA Haiti Cholera Situation Report 23. s.l. http://ochaonline.un.org/tabid/6412/language/en-US/Default.aspx, 2010. 23.

2. DES ROCHES R, ERGUN O AND SWANN J, Haiti's Eternal Weight, New York Times, Op-Ed, July 7, 2010.

3. PAINE K A AND DHIR R K, Recycled aggregates in concrete: a performance-related approach. Magazine of Concrete Research, Vol. 62, No 7, 2010, pp. 519-530.

4. PAINE K A, COLLERY D J AND DHIR R K, Strength and deformation characteristics of concrete containing coarse recycled and manufactured aggregates. In: 11th International Conference on Non-conventional Materials and Technologies (NOCMAT 2009), 6-9 September 2009, Bath, UK.

5. XIAO J Z, LI J B AND ZHANG C, On the relationship between the mechanical properties of recycled aggregates concrete: An overview, Materials and Research Vol. 39, 2006, pp. 655-664.

6. NEVILLE A M, Properties of concrete, 4th Edition, Pearson Prentice Hall, 1995, pp. 108-117

7. LABORATIRE NATIONAL DU BATIMENT ET DES TRAVAUX PUBLICS, Service public a Gestion Autonome sous Tutelle du Ministere des Travaux Publics Transports et Communications. Geotechnical History of Haiti rivers.

8. SERIES NG 500 — Drainage and Services Duct. Manual of Contract Documents for Highway Works Volume 2 Notes for Guidance on the Specification for Highway Works.

9. SERIES NG 600 — Earthworks. Manual of Contract Documents for Highway Works Volume 2 Notes for Guidance on the Specification for Highway Works.

10. SERIES NG 800 — Road Pavement Design- Unbound, Cement and Other Hydraulically Bound Materials. Manual of Contract Documents for Highway Works Volume 2 Notes for Guidance on the Specification for Highway Works.

11. BRITISH STANDARD INSTITUTION, BS EN 933-11 Tests for geometrical properties of aggregates - Part 11: 2006. Classification test for the constituents of coarse recycled aggregate.

12. WRAP, The quality protocol for the production of aggregates from inert waste. WRAP Oxon. ISBN 1-84405-217-6, 2005 (www.wrap.org.uk).

13. COLLERY D J, Effect of Recycled and Manufactured Aggregates on Structural Properties of Concrete, PhD thesis, 2009, Division of Civil Engineering, University of Dundee, Scotland, United Kingdom.

14. BROWN N, Vibroflotation Compaction of Cohesionless Soils; Journal of the Geotechnical Engineering Diversion , ASCE, Vol. 103, 1977, pp. 1437-1451.

15. HAITI WORK INCORPORATED, Haiti Works! Assesses Post-Earthquake Terrain as a First Step Towards Implementing Redevelopment Strategies in Haitian Cities. 2010. www.haiti-work.org

16. VIRDIS M R, A strategy for construction, demolition and excavation waste as recycled aggregates. WRAP Report. DTI/WRAP Aggregate Research Programme 1-84405-060-2, 2003, 9 p.

Rapidly Deployable System Including a CSA Gunite Material for the Structural Stabilization of Shock Damaged Structures

R B Jewell[1], T L Robl[1], P S Mills[2], M R Jones[3], A Ouzounidou[3]
1 – University of Kentucky, USA
2 – Minova USA Inc, USA
3 – University of Dundee, UK

The University of Kentucky Center for Applied Energy Research (CAER), Minova USA Inc. and the University of Dundee, Scotland, have collaborated on a project to develop a rapidly deployable system to stabilize shock-damaged structures to avoid catastrophic failure. The system comprises a dry-gunned or "gunite" apparatus that sprays a mixture of rapid-hardening cement, sand and water onto a damaged surface. The cement component is based on calcium sulfoaluminate (CSA), and is capable of achieving structural strengths within 15 to 30 minutes. The project research began with a performance comparison of commercially available CSA cements. After determining which cement exhibited the best performance, an extensive research program was initiated to quantify and optimize the effects of variables including water content, aggregate content and gradation, and ratio of cement to aggregate. The experimental results produced a sprayed concrete mix that exceeded expectations in performance between 15 minutes and 24 hours after spraying. Achieving structural strengths within 15 to 30 minutes allows first responders to enter into damaged buildings with less fear of a collapsing structure.

Robert B Jewell, Research Scientist for the Center for Applied Energy Research at the University of Kentucky, currently conducting research into the application of coal combustion by-products in the formulation low energy cement and concrete.

Dr. Thomas L Robl, Associate Director of the Center for Applied Energy Research at the University of Kentucky, currently conducting research into the application of coal combustion by-products in the formulation low energy cement and concrete.

Professor M Roderick Jones, Director of Concrete Technology Unit and Dean of Faculty of Engineering, Physics and Mathematics, University of Dundee. His research interests lie in durability of concrete, service life prediction. use of alternative cements and foamed concrete.

Peter S Mills, Technology Leader for Minova, brings 34 years of experience in the mining industry to Minova's technical team; and is responsible for managing the Technical Department and all research, development, and technical support involving chemical consumables at Minova USA. During his time at Minova, Peter has patented several products, including Tekpak® P, Eclipse Bolt and Tekflex®.

Anthoula Ouzounidou is a PhD student at the University of Dundee. Her research is concerned with the utilisation of CSA cements in sprayed concrete and their potential use in rapid stablisation suituations.

Keywords: Calcium sulfoaluminate, Gunite, Rapid stabilization, Shotcrete

INTRODUCTION

The overall objective of this research and development effort is to develop a system that is deployable with first responders and capable of stabilizing blast damaged structures. The system will consist of a delivery vehicle capable of both shotcreting and grouting pre-packaged rapid-hardening fibre-reinforced cements, grouts, and micro-aggregated concretes. The system will provide the capability of stabilizing structures such as airport runways, tunnels, bridges, and dams that have been shocked and damaged by explosives before they fail catastrophically.

The rapid stabilization of shock damaged structures falls well outside the venue of normal construction practice because time is the essential element. The nature of the damaged structure provides unusual challenges. The reinforcement of damage structures requires materials that have the capability of rapid deployment and very rapid strength development. These materials needed to be placeable at a distance to provide some degree of safety to the responders. In addition, the materials must be able to adhere to structural surfaces that have not been properly prepared and conditioned and may also be highly fractured, dusty, wet and possibly even hot.

The technology for the rapid delivery of large volumes of cementitious materials to vertical or even overhead surfaces currently exists. Pneumatic delivery (shotcreting) is a well developed technology that has been used in construction for many years. Guniting has played a major role in such structures as the Washington D.C. Metro subway system and the England to France undersea rail connector ("the Chunnel"). Technology for the delivery of high performance grouts for foundation stabilization is also well known in both civil and mining applications.

There are numerous rapid hardening cements that are commercially available. Most of these are sold for rapid repair of horizontal surfaces such as bridge decks, pavements, commercial floors etc., as well as for structural repairs (including vertical and overhead). Few of these products are specifically marketed for use in shotcrete applications. The majority of rapid hardening cements are based on, or at least contain, Portland cement as a principle component. Other components are added that help provide early strength, such as high alumina cement (HAC), organic polymers, chemical accelerators (which can also be added during concrete batching), calcium sulfate hemihydrate (e.g. gypsum plaster), or Class C fly ash. Mortars prepared with some of these cements can achieve compressive strengths of 6.9-13.8 MPa (1000-2000 psi) within 1 hour. However, Portland cement mortar and concrete typically requires many weeks of proper curing to reach significant levels of their ultimate strengths, even when used with set accelerators.

Alternatives to Portland cement are also capable of rapid strength development. These include magnesium oxide – phosphate cement (which was not included in this research), calcium sulfate hemihydrates, and calcium sulfoaluminate/belite (CSA) cements. Unlike Portland cement, these rapid hardening cements can gain 75-80% of their strength within 1 day. As part of this project, the CSA materials will be investigated, evaluated, and tailored for application in stabilizing blast damaged structures.

EXPERIMENTAL PROGRAM

Of primary concern was the rate of strength development (compressive and tensile), bonding strength to the damaged surfaces, and short-term dimensional stability. Other considerations include heat generation, bonding characteristics, pumpability, ease of transport and placement, stiffness of the hardened material, and cost. Other material properties such as long-term durability are less important, but will receive some consideration as they impact the overall commercial potential of the product.

Of particular interest are the CSA mainly because they gain strength rapidly, can be produced from industrial by-products such as coal ash as major feed components, and require significantly lower energy to produce than Portland cement. An added benefit is the significantly lower emission of CO_2 during their production. CSA based materials can be formulated that have extremely high water to cement ratios with extremely low viscosity and yet still achieve very high strengths and very rapid set times. This is due to the nature of its principal cementitious hydration product ettringite.

Materials

Calcium sulfoaluminate and calcium sulfate hemihydrate gypsum cements were chosen based on their advantageous properties for use as rapid hardening shotcrete-material cements. Table 1 lists the materials used for laboratory and field testing and provides a brief description of each.

Table 1 Description of raw materials

MATERIAL NAME	TYPE OF MATERIAL	SOURCE
Commercial CSA#1 (CSA#1)	CSA cement	
Commercial CSA#2 (CSA#2)	CSA cement	
Hydro Stone	Calcium sulfate hemihydrate gypsum cement	United States Gypsum Company
Construction Sand	River sand	
Class F Fly Ash	Low-calcium coal ash	Mill Creek
RECS100 PVA Fibres	Polyvinyl alcohol fibre	Kuralon
RHEOMAC SF100 Silica Fume	Spheres of non-crystalline silica	BASF Chemical Co.
Recover	type D retarder	Grace Construction Products
Tekbond	Latex Copolymer	Minova USA Inc.
Vinnapas 5010 N	Vinyl Acetate & Ethylene Copolymer	Wacker Chemical Corporation
Burke Acrylic Bondcrete	Acrylic	Dayton Superior "Edoco"

The sand gradation was selected from the ACI 506R manual for shotcrete [1]. The manual suggests two grading limits, Grading No.1, referred to as "Fine Grading" in this study; and Grading No.2, or "Coarse Grading". Figure 1 shows the sand gradation curves for comparison of the CAER sand to the recommended ACI standard gradations.

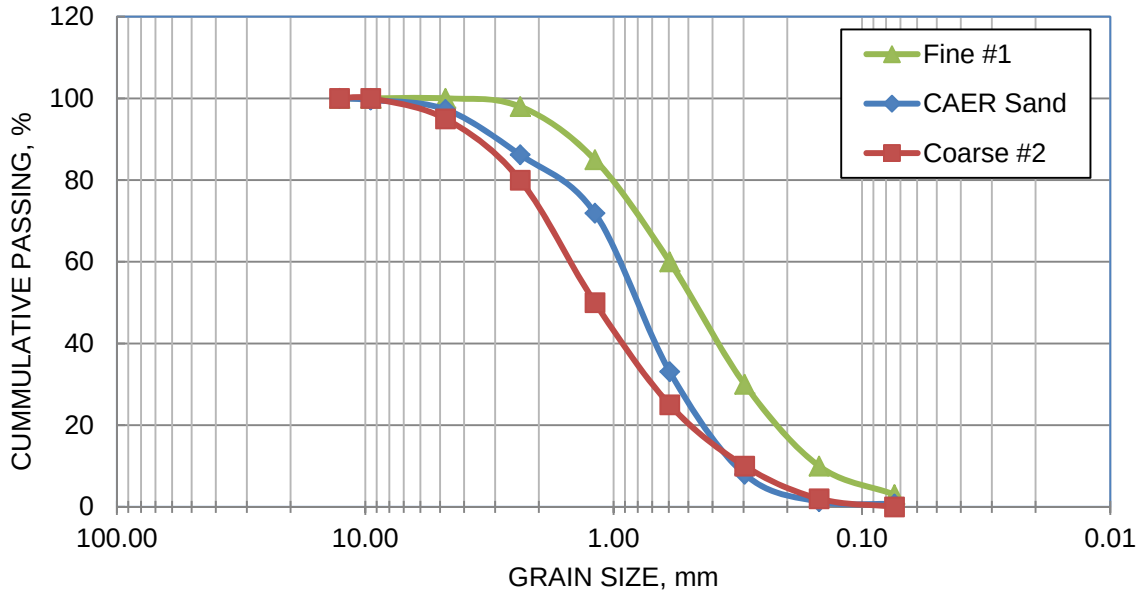

Figure 1 Comparison of the sand gradation curves used for the sprayed-concrete tests

Testing equipment

The gunite, dry-mix, machine was a Reed SOVA unit which is one of the smallest units available. The source for compressed air was a portable diesel powered air compressor capable of 10.6 m^3/min (375 ft^3/min) at 0.7 MPa (100 psi). All spray trials were performed with a double bubble nozzle. A VELCO-GUNMIX water booster moistening system was also tested with the final mix design.

EXPERIMENTAL RESULTS AND DISCUSSION

Formulation and Testing of Laboratory Mortar Specimens

The rate of strength gain of the shotcrete material was measured using ASTM C 109 method for preparation and testing. The mortars were prepared using graded sand, as specified by ASTM C 109. The water content on all mortars was consistent; the flow of each mix could not be tested due to the fast setting rate of the CSA cements.

Time of Set

After determining the proper water content, the set time for the laboratory shotcrete mixes was determined by ASTM C 807. Table 2 lists the initial and final set times for the cementitious materials used in this project.

Table 2 Initial and final set times for cementitious materials used throughout this project

CEMENT	INITIAL SET TIME, minutes	FINAL SET TIME, minutes
Ordinary Portland Cement	138	222
CSA#2		14
CSA#1 (wet-mix) no admixture	3.5	5.5
CSA#1 (dry-mix) no admixture		4.5
CSA#1 (wet-mix) w/ 2.03ml Grace Recover	8.5	16
China HS (high strength)	60	178
China HS w/35% Gypsum	42	84
China HS w/35% Anhydrite	5	12
Hydro Stone	10	12

Compressive strength

The mortar mixes are shown in Table 3 and are comprised of a cementitious component (CSA cement or hydro stone), construction sand, and water. After mixing (ASTM C109 and ASTM C305), the mortar mixture was placed into 2 inch X 2 inch X 2 inch bronze moulds. Compressive strength was measured using a Gilson 400,000 lb testing machine. Figure 2 displays the average compressive strength of the shotcrete material in mortar cubes. To compensate for the rapid setting time inherent to the shotcrete material cements and the expected field conditions, changes were made to the standard. The altered procedure is described below:

1. Tap water was used instead of de-ionized water.
2. Mixer was used on low speed.
3. Mix time was one minute; beginning after the cement was completely added to the mix.
4. Flow tests were not performed, due to fast-setting time.
5. Samples were covered with plastic plates and cured in ambient air.

Table 3 Laboratory shotcrete-mix designs

COMPONENT, g	CSA#1	CSA#2	HYDRO STONE
Cement	500	719	362.5
Sand	1470	2110	740
Water	222	320	120
w:c	0.40	0.4	0.3
s:c	3	3	2

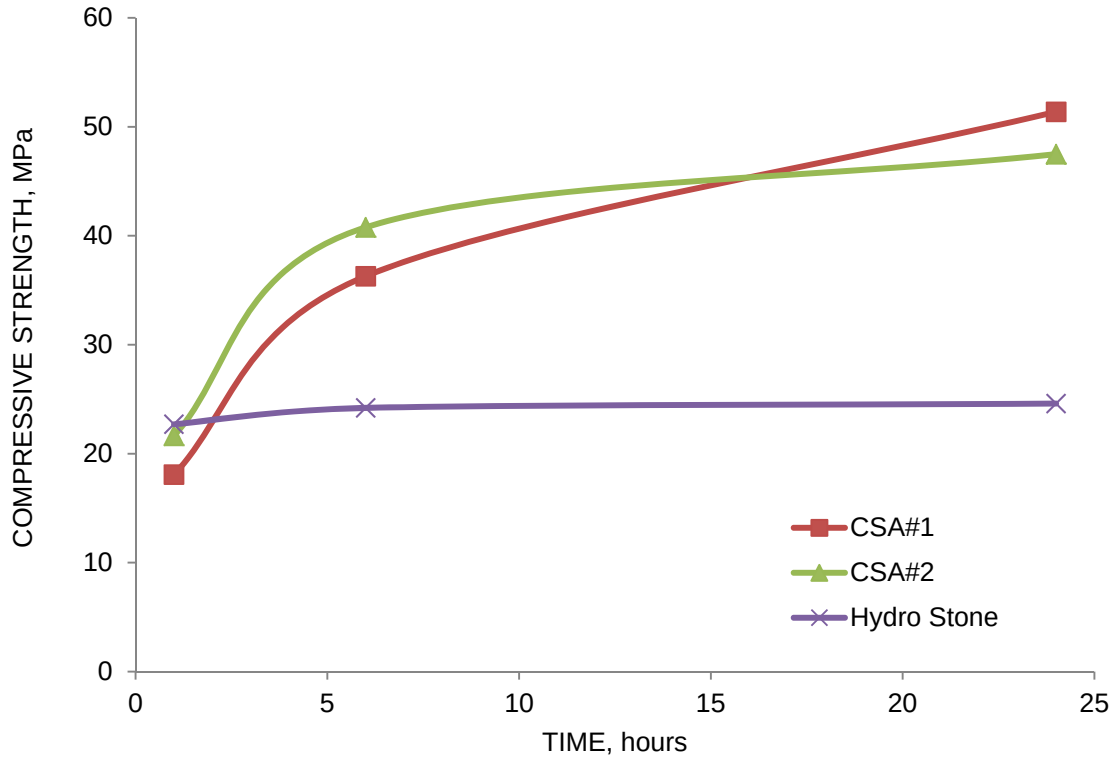

Figure 2 Compressive strength of shotcrete-mix mortar cubes prepared in the laboratory

Both the CSA#1 and CSA#2 mixes attribute their rapid strength-gain to the hydration of Klein's compound, $Ca_4Al_6O_{12}SO_4$ (C_4A_3S') to form ettringite ($Ca_6Al_2(SO_4)_3(OH)_{12}\bullet 26H_2O$); However the high-strength gain of the Hydro Stone materials attributes its strength to the presence of calcium sulfate hemihydrate ($CaSO_4\bullet 1/2H_2O$). All three shotcrete materials showed rapid strength gain within one hour of mixing. Approximately 18.1 MPa (2624 psi) for CSA#1, 21.6 MPa (3139 psi) for Rapid Set, and 30.2 MPa (4375 psi) for Hydro Stone after just one hour of curing. The Hydro Stone material gains all of its strength within the first hour of curing; the system has used all the available sulfate and therefore does not gain more strength. However, the CSA#1 and Rapid Set materials continued to gain strength as ettringite continues to form. After 24 hours the CSA#1 material continues to gain strength, 51.4 MPa, whereas the Rapid Set, CSA#2 material reached 47.5 MPa and was not gaining strength as rapid as the CSA#1 material. For comparison, a typical Type I Portland cement achieves strengths ranging from 13.5 – 20.5 MPa after 24 hours; and is not achieved a final set until nearly 4 hours after mixing. This is well out of the one hour compressive strength test that was employed for the CSA-based cements.

Material/Substrate Bonding Issues

The interaction of the shotcrete and the damaged concrete structural supports is very complex and is influenced by a number of important factors, such as the roughness of the walls and support columns, the mechanical properties and stresses in the structure, the disturbed or damaged zone around the area to be shotcreted, exposed reinforcing steel, and the thickness of shotcrete and the interface between the shotcrete and preexisting concrete [2]. The shotcrete cannot be made effective in stabilizing a damaged structure by simply adding more shotcrete to the structure. In fact, as the amount of shotcrete applied to a substrate is

increased, its performance becomes increasingly dependent on the bond strength. For example, [2] found that as the thickness of a shotcrete lining in an underground mining tunnel was increased from two to six inches, the number of failures at the bond interface increased. Conversely, failures within the shotcrete itself decreased. The same study found that the extent of the damaged rock zone had only a minor effect on the behaviour of the shotcrete lining when the surface was uneven. Thus, the surface roughness of the damaged structure is one of the most important parameters to consider.

The surface roughness of the damaged structure will be one of the most important parameters to consider. The bonding strength between the shotcrete and the concrete structure will be addressed to reduce the potential for tensile failures. Malmgren and Nordlund [2] found that as the thickness of the shotcrete lining, in an underground mining tunnel with roof bolts, was increased from two inches to six inches the number of failures in the bond interface also increased; whereas the failures of the shotcrete lining decreased [2]. The same study found that as the extent of a damaged rock zone had a minor effect on the behaviour of the shotcrete lining when the surface was uneven [2]. Therefore, as the shotcrete applied to a substrate is increased, its performance becomes more dependent on the bond strength.

Lamontagne, et al., [3] found that the bonding between good quality shotcrete mixtures (with and without steel fibres) and concrete surfaces prepared by hydrodemolition or chipping with jackhammers followed by sandblasting was found to be generally strong and durable. The other types of surface preparation (grinding, chipping with jackhammers without sandblasting and sandblasting alone) resulted in either lower bonding strengths or a reduction in the bonding strength with time [3]. In general, despite the condition of the hardened concrete the surface should be wetted just before spraying so that it does not absorb the water of the freshly sprayed concrete [4]. This initial step is essential if the concrete surface is dry; and it eliminates dust that has recently settled on the surface.

Bond testing was carried out following several ASTM methods that cover bonding hardened concrete to hardened or freshly-mixed concrete through both compression and tension tests. ASTM C882 will be used for epoxy-resin systems; ASTM C1042 for latex systems and ASTM C1404/C for adhesive systems measured by direct tension. The substrate and laboratory-shotcrete mix designs are shown in Table 4 and Table 5.

Several modes of bonding mechanisms were tested. The first mode involved casting the shotcrete directly onto a clean, dry surface, of the OPC plug. This mode was referred to as “unmodified” in this report. The second mode of testing involved the application of Tekbond C to the bonding surface of the OPC plug. The bonding aid was applied over the entire substrate and allowed to dry to a gummy state before the shotcrete was added to the cylinder mould. The third mode consisted of wetting the surface of the OPC plug with water. This was done to limit the water drawn from the fresh-shotcrete material into the hardened OPC concrete. Ideally this would lead to less drying shrinkage cracking at the shotcrete material interface and increase the surface area available for bonding. The fourth mode consisted of applying Burke Acrylic Bondcrete to the bonding surface of the OPC plug. The shotcrete material was cast into the cylinder mould while the bonding aid was still wet, as per manufacturer’s specifications. The fifth mode of testing involved the addition of polyvinyl-alcohol (PVA) fibres to the shotcrete material. One percent, by volume, of RECS100 fibres was added to the shotcrete material. The sixth mode of testing consisted of adding Vinnapas 5010N to the shotcrete material. Ten percent, by weight, was added to the shotcrete material.

The series of slant-shear tests revealed that with a laboratory simulated shotcrete application, the highest shear strength was attained with no surface preparation and without the use of bond modifiers (Figure 3).

Table 4 OPC substrate mix design.

COMPONENT	VOLUME, kg/m^3
Cement: Type 1 OPC	335
#57 Limestone	605.68
#89 Limestone	351.70
Sand	809.73
Glenium 3030 NS	2.15 ml/kg
Micro Air	0.08 ml/kg
Water:Cement Ratio	0.49

Table 5 Shotcrete mix design.

CEMENT	CEMENT CONTENT kg/m^3	SAND CONTENT kg/m^3	WATER:CEMENT RATIO	ADMIXTURES ml/kg
CSA#1	510	1536	0.40	Recover – 6.9
CSA#2	511	1536	0.40	Glenium3030 NS – 2.8
Hydro-Stone	1330	443	0.25	None

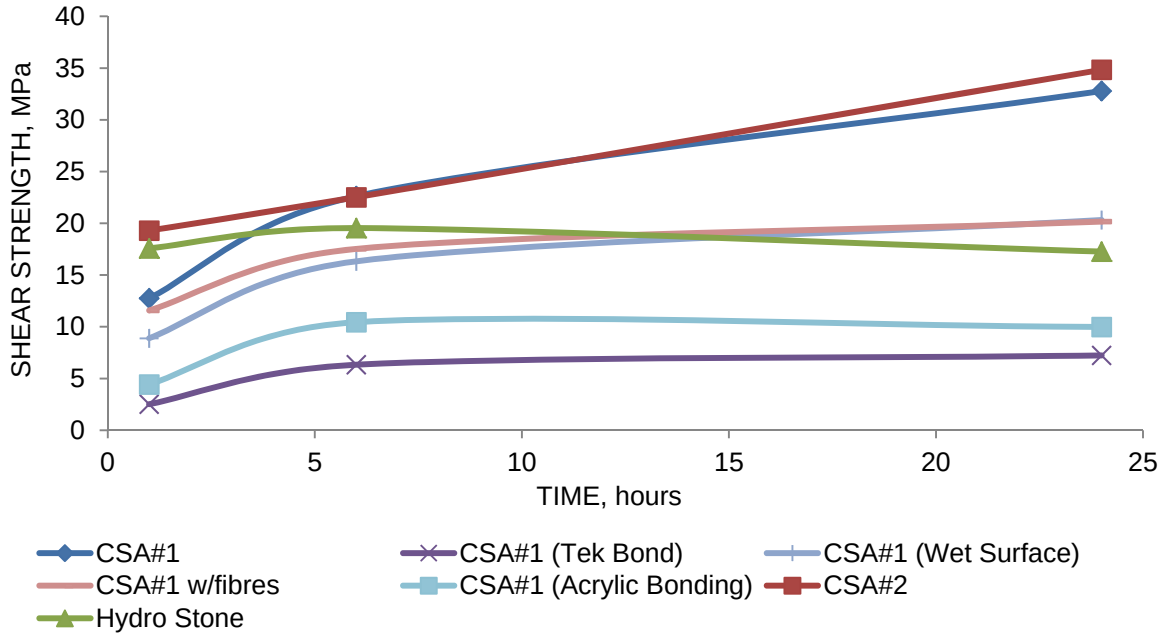

Figure 3 Average slant shear compressive strength of various surface modifying procedures.

Formulation and Testing of Sprayed-Concrete Specimens

CSA#1 was selected as the primary cementitious material to use in the sprayed concrete experiments. This cement was selected based on the high-early compressive strength with continued strength gain over 24 hours of curing, excellent bond strength, and moderate heat evolution upon hydration.

Table 6 shows the matrix which was followed for the sprayed-concrete tests. A dry-mix sprayed-concrete operation (gunite) was chosen due to the fast-setting time of the CSA#1 cement. A wet-mix operation requires mixing all materials including water and pumping the wet-mix to the desired location. The cementitious mix would set up on them mixer before it could even be pumped; again this is why a dry-mix operation was chosen.

Table 6 Test matrix for the dry-mix sprayed concrete tests

SPRAYED CONCRETE TESTS				
Water Content	High (3.8 l/min)	Intermediate (3.0 l/min)	Low (2.3 l/min)	-
Sand Gradation	Coarse (< 4 mesh)	Fine (< 16 mesh)	-	-
Aggregate/Cement Ratio	1:1	2:1	3:1	4:1
PVA Fibre Loading (by weight)	0.5%	1.0%	-	-
Polymers (by weight)	5.0%	-	-	-

Aggregate gradation

The next step in the matrix was to test the influence of two different gradations of the mix sand, based on the recommended gradation for shotcrete in the ACI 506R manual for shotcrete (Figure 1). The first gradation used was a “coarse” gradation where the construction sand was screened through a 4 mesh, U.S. sieve. This removed any large size pebbles from the sand that could potentially clog the pneumatic system. The second gradation was screened through a 16 mesh, U.S. sieve. The finer particle-size was believed to increase compaction of the sprayed-concrete and reduce rebound. The results of the influence of sand gradation on strength of sprayed concrete are shown in Figure 4. The coarse gradation had a slightly higher 15 minute strength of 38.5 MPa, where the fine gradation had compressive strength of 35.9 MPa.

However after 3 hours of curing, the fine gradation specimens continued to gain strength whereas the coarse specimens began to level out. Based on the results shown in Figure 4 the fine sand gradation was chosen for the sprayed-concrete tests.

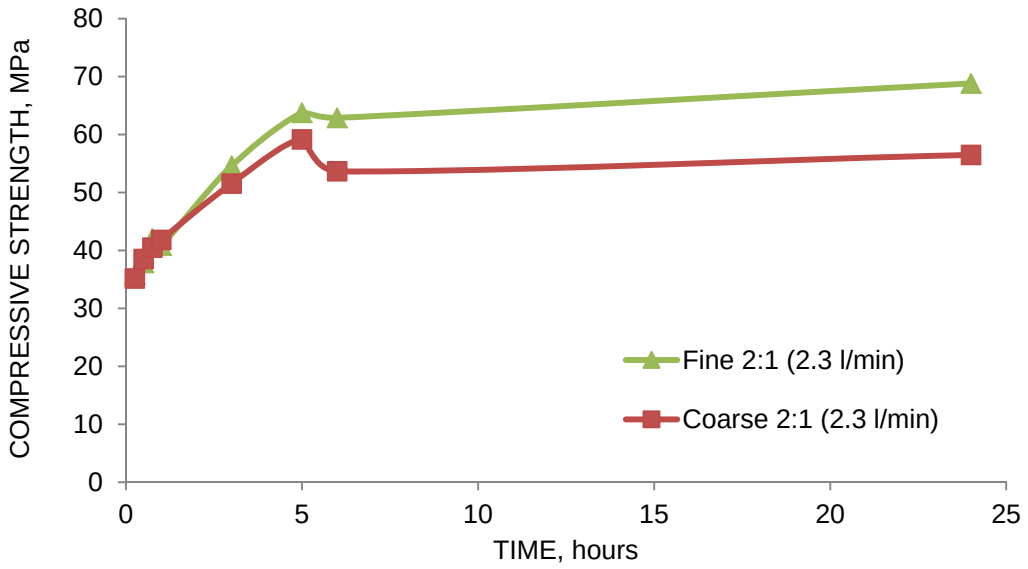

Figure 4 Results of the influence of sand gradation on strength of sprayed concrete

Water content

The influence of the water content on the strength development of the sprayed-concrete was analyzed. The flow-rate of the water delivered to the wetting ring on the nozzle of the sprayer was monitored with a digital real-time flow meter. Three different water flow rates were used to achieve a curve of data to show the optimum water content for the concrete system. The flow rates used were 2.3 l/min (0.6 gal/min), 3.0 l/min (0.8 gal/min), and 3.8 l/min (1.0 gal/min). Figure 5 shows a comparison of the results based on one-hour compressive strength data. The column associated with the highest compressive strength reflects the optimum water:cement ratio for spraying the CSA cement mixes. The optimum w:c ratio of 0.491, which corresponds to a water feed rate of 2.3 l/min to the gunite wetting ring.

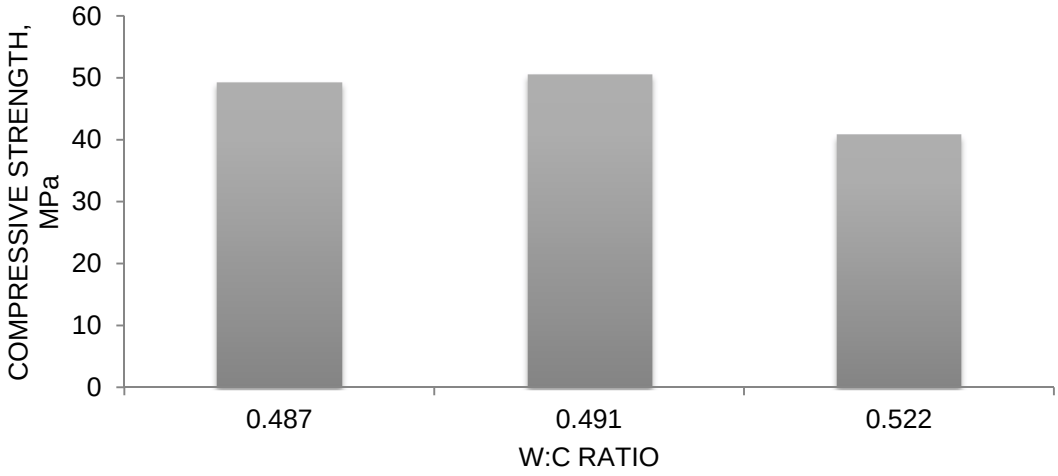

Figure 5 Influence of water:cement ratio on the compressive strength of cored cylinders; with corresponding compressive strength at one hour.

Aggregate content

An ACI 506R aggregate to cement ratio of 3:1 was chosen to begin testing for the optimum water content (three parts aggregate to one part cement, by weight). The third variable tested was aggregate to cement ratio. The ratio was varied from 1:1, or 50% (by weight) of aggregate to 50% (by weight) of cementitious material; up to 4:1 or four parts aggregate to one part cementitious material. Figure 6 shows the results of the aggregate content tests. The mix was optimized with an aggregate:cement content of 3:1 which yielded the highest compressive strength.

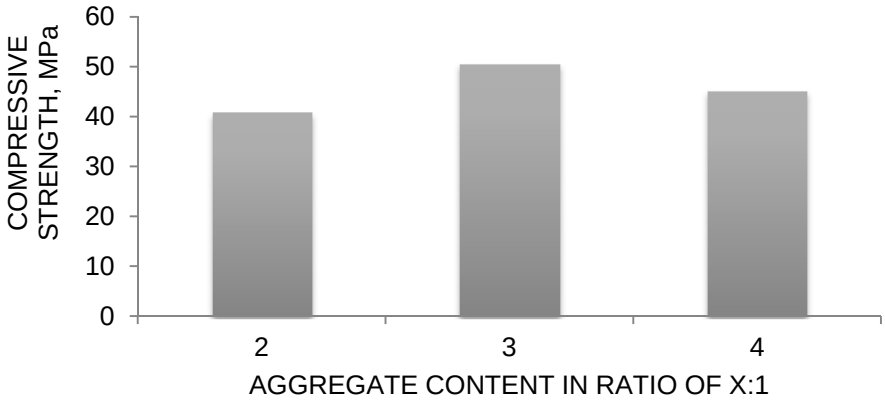

Figure 6 Comparison of the one-hour test results of the three different aggregate contents; with corresponding compressive strength at one hour.

Sprayed-Concrete Mix Designs

Several mix designs were prepared based on the requirements of the test matrix, Table 7. Each mix design was formulated based on the American Concrete Institute's recommendation on shotcrete mixes [1].

Compressive Strength of Cored Shotcrete Specimens

Cylinders were cored from sprayed-concrete panels in accordance with ASTM C1140 (Standard Practice for Preparing and Testing Specimens from Shotcrete Test Panels) and ASTM C42 (Standard Test Method for Obtaining and Testing Drilled Cores and Sawed Beams of Concrete). Utilizing the optimized aggregate to cement ratio of 3:1 and the fine sand gradation several sprayed-concrete tests were analyzed to ensure the correct water content for the optimized mix. Figure 7 demonstrates that a supplied water rate of 2.3 l/min provides the highest compressive strength of 46.8 MPa after only 15 minutes of curing. A supplied water rate of 1.5 l/min (0.4 gpm) resulted in a similar 15 minute compressive strength of 46.5 MPa, however the 2.3 l/min (0.6 gpm) mix continued to gain strength, whereas the 1.5 l/min mix lost some strength between 30 minutes to one hour of curing.

Flexural Strength of Sawed Shotcrete Beam Specimens – Reinforcing Fibres

Beams were sawed from sprayed-concrete panels in accordance with ASTM C42 (Standard Test Method for Obtaining and Testing Drilled Cores and Sawed Beams of Concrete). The sawed beam specimens were tested for flexural strength in accordance with ASTM C78

(Standard Test Method for Flexural Strength of Concrete (Using Simple Beam with Third-Point Loading)). The results from this test are shown in Figure 8. Two different specimens with the same fine gradation and 3:1 aggregate:cement ratio were used with varying supplied water contents, 2.3 and 3.4 l/min (0.6 and 0.9 gpm). The one-hour flexural strength was greater for the 2.3 l/min specimen at 19.9 MPa. However, the 3.4 l/min specimen achieved a larger gain in flexural strength at 19.9 MPa, whereas the 2.3 l/min sample was 15.6 MPa. After 24-hours the 3.4 l/min sample lost strength, where the 2.3 l/min sample continued to gain strength. Therefore, the 2.3 l/min water content proved to be the better option with higher initial flexural strength and a positive-trending strength after 24 hours of curing.

Table 7 Mix designs used for the sprayed-concrete experiment

SHOTCRETE DESIGNATION	AGGREGATE : CEMENT RATIO	WATER FLOW RATE l/min	ADDITIONAL COMPONENT	WATER: CEMENT RATIO
Coarse 2:1 (2.3 l/min)	2	2.3		---
Coarse 2:1 (3.1 l/min)	2	3.1		---
Coarse 2:1 (4.2 l/min)	2	4.2		---
Fine 1:1 (2.3 l/min)	1	2.3		0.288
Fine 2:1 (2.3 l/min)	2	2.3		0.389
Fine 2:1 (3.1 l/min)	2	3.1		0.429
Fine 3:1 (1.5 l/min)	3	1.5		0.487
Fine 3:1 (2.3 l/min)	3	2.3		0.491
Fine 3:1 (3.0 l/min)	3	3.0		0.522
Fine 4:1 (3.0 l/min)	4	3.0		0.583
Fine 3:1 Silica Fume (2.3 l/min)	3	2.3	Add 5% (by weight of cement)	0.473
Fine 3:1 Fly Ash (2.3 l/min)	3	2.3	Replace 25% (by weight) of sand with Fly Ash	0.543
Fine 3:1 PVA 0.5% (3.4 l/min)	3	3.4	5% PVA fibres (by weight of batch)	0.582
Fine 3:1 PVA 1.0% (3.0 l/min)	3	3.0	1% PVA fibres (by weight of batch)	0.518
Fine 3:1 Vinnipas 5010N (3.0 l/min)	3	3.0	5% Vinnipas 5010N polymer (by weight of batch)	---

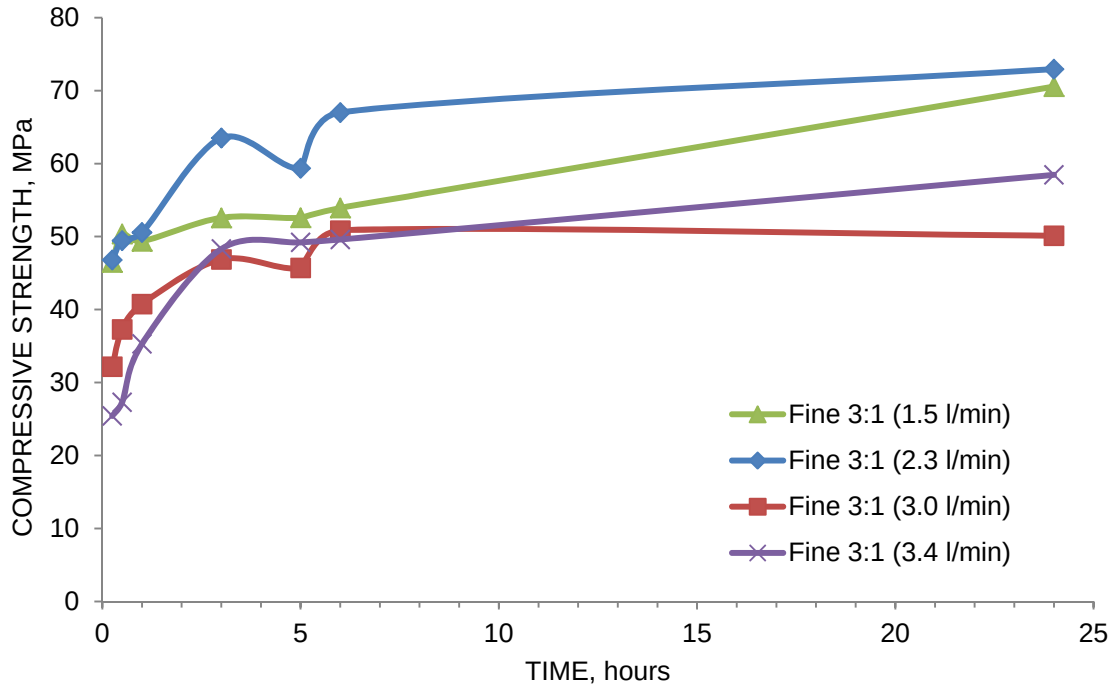

Figure 7 Compressive strength data covering a 24-hour time interval

Polyvinyl alcohol fibres were used to reinforce the sprayed-concrete specimens. The fibres were blended into the dry mix at two different concentrations, 0.5% and 1.0% of the total batch weight. As Figure 8 demonstrates the lower concentration of fibres, 0.5%, provided the highest flexural strength after one hour of curing. The 0.5% fibre mix continued to gain strength after the 6 and 24-hour tests. The inclusion of fibres did show improvement over the mix without fibres for the one-hour test. However the strength-performance at 6 and 24 hours did not increase enough to validate the use of fibres in the sprayed-concrete mix.

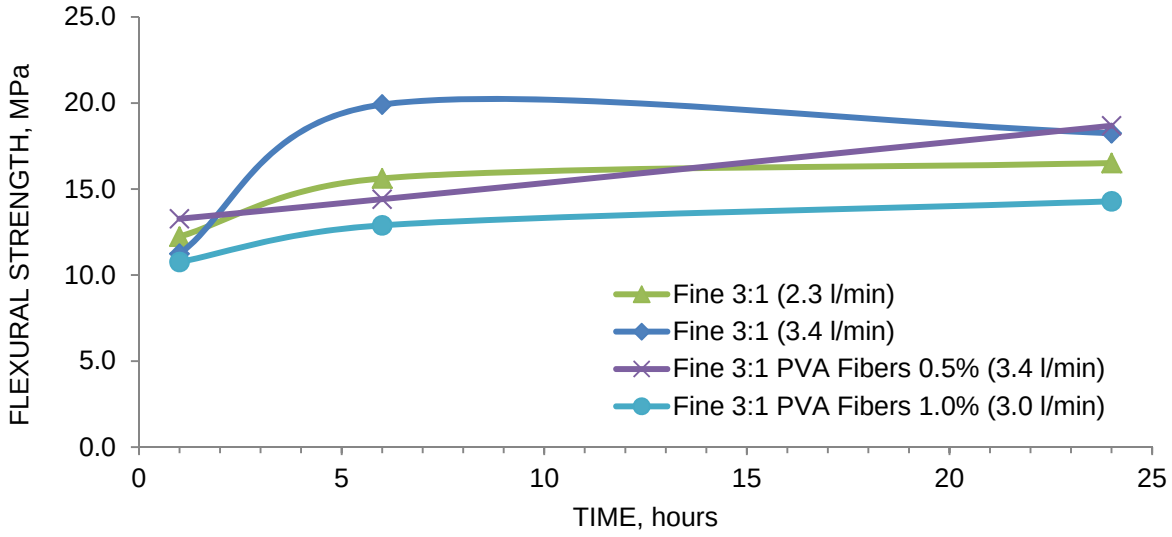

Figure 8 Results of the flexural strength test on sawed sprayed-concrete beams

Testing Shotcrete-Repaired Structural Elements

Initial spraying tests were performed by the University of Dundee's Concrete Technology Unit (CTU) to examine the restored structural capacity of structural elements (i.e. beams, columns) that have been damaged and sprayed with CSA cement. These tests consist of sprayed test panels without fibres, initial tests on stabilizing damaged beams and structural tests using four point bending.

A balanced to slightly over-reinforced beam 15x20x203 cm was designed to ensure the structural elements were representative to those currently used in construction. The reinforcement of the beam consists of tension rebar 2x#4, compression rebar 2x#4 and shear rebar #2 at 30.5 cm centres.

Ten beams were cast by a private precast company in Dundee, Scotland and after curing for 28 days were transferred to the CTU's laboratory. The material used to cast theses beams was a structural quality concrete with a water:cement ratio 0.5, cement 348 kg/m3 (588 lbs/yd3) and a corresponding cylinder strength of 38 MPa (5500 psi).

Two of the ten beams were used for reference and were tested under four point bending, in order to confirm the design capacity was similar to full-scale beams. The other eight beams were divided into four groups and were damaged with a pneumatic hammer, Figure 9. One beam from each group was tested under four point bending to determine and quantify the loss of the structural capacity caused by the various types of damage. The second beam from each group was sprayed with CSA concrete and tested to determine and quantify the restored structural capacity gained by spraying.

Structural experiments - four-point bending

All ten beams were tested under four-point bending to determine the structural capacity. The setup and load machine used can be viewed in Figure 10.

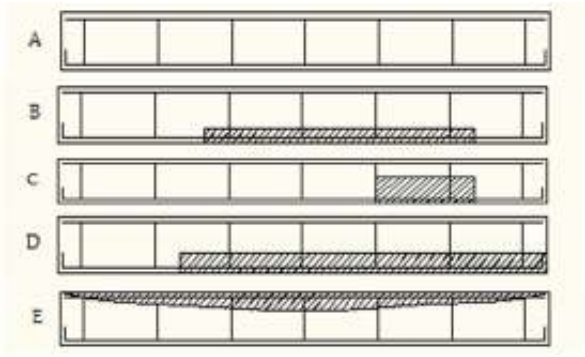

Figure 9 (A) Reference beam; (B) Partial tensile damage; (C) Shear damage; (D) Full tensile damage; (E) Compression damage.

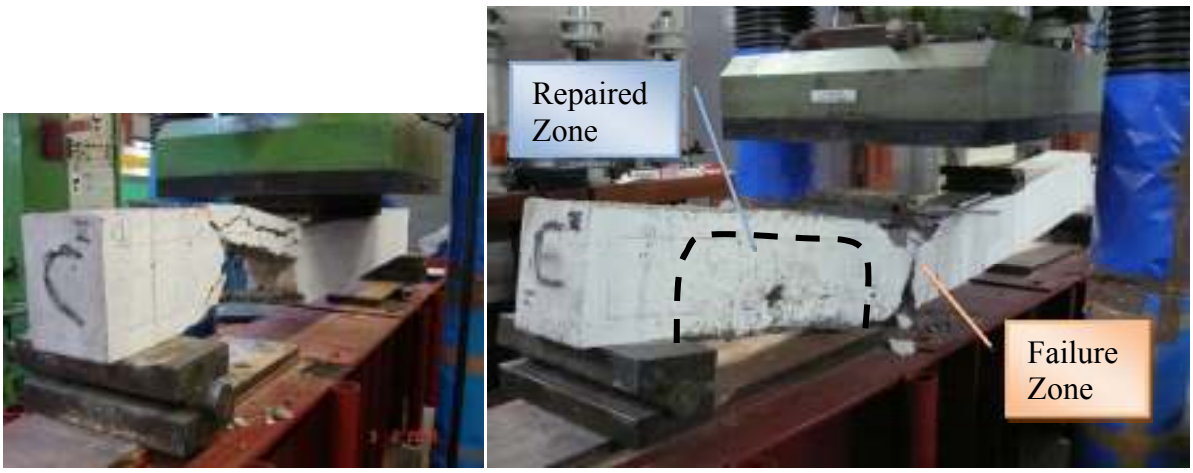

Figure 10 Bending test of damaged beam (left); and beam repaired with CSA shotcrete material (right).

As seen in Figure 10 the sprayed CSA concrete was well bonded to the substrate (no visible detachment), and the loaded beam produced well distributed tensile and shear cracks, ultimately failing within the compression zone. The tests concluded that damaged sections of beams could be reinforced with sprayable CSA concrete and demonstrate additional strength.

Delivery Vehicle - Prototype Design Configuration

The rapid deployment of the system and rapid set of the materials, combined with an ability to stabilize damaged structures from a distance, a practical consideration are critical. In an emergency, it would be dispatched directly to the impacted area with the search and rescue responders and set up quickly. Structural gunite and foundation stabilization could begin almost immediately, even as other emergency crews fight fires or rescue injured people. The system could be used to prevent or forestall the collapse of structures damaged by blast or earthquake. For collapsed structures, it would be used to rapidly stabilize rubble and improve the safer of both the SAR teams as well as the survivors. The delivery system is comprised of four essential components (Figure 11): water supply, air supply, cementitious material, and applicator machine.

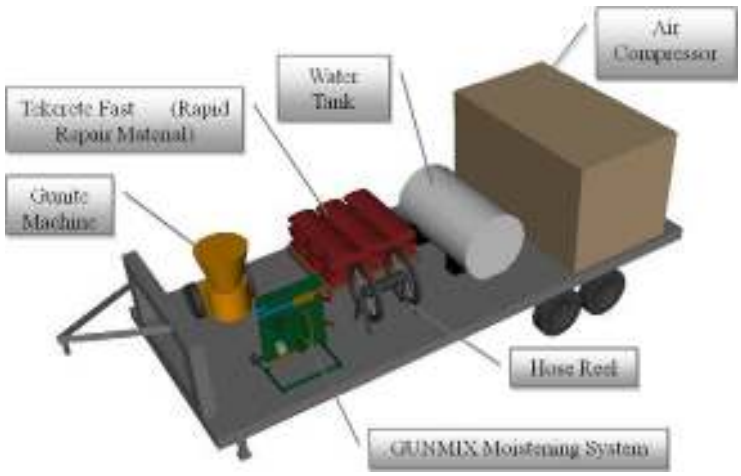

Figure 11 Conceptual drawing of the prototype delivery vehicle.

Each component will be mounted on a heavy duty trailer. The hitch end of the trailer will house the static components, i.e. the air compressor and water tank. The working area of the trailer, which will comprise over half of the trailer will house the dynamic components that will require operator access, i.e. the gunite machine, water booster pump, hose reels, and material supply.

Water booster pump

An integral, unique, component of the delivery vehicle system (Figure 12) is the VELCO - GUNMIX® moistening mobile system will allow for spraying materials dust-free and with low rebound at an exact preset water quantity. This will allow for the experimental test settings to be adapted to the mobile repair vehicle spray system. The GUNMIX system moistens the material in the mixing head by a fog of compressed air and water. The use of this system results in a considerable reduction of dust development and rebound. The water addition can be precisely adjusted and measured. The spray output capacity can be precisely controlled by means of a controlled gear motor with a speed indicator; this will allow for a constant cementitious:water ratio.

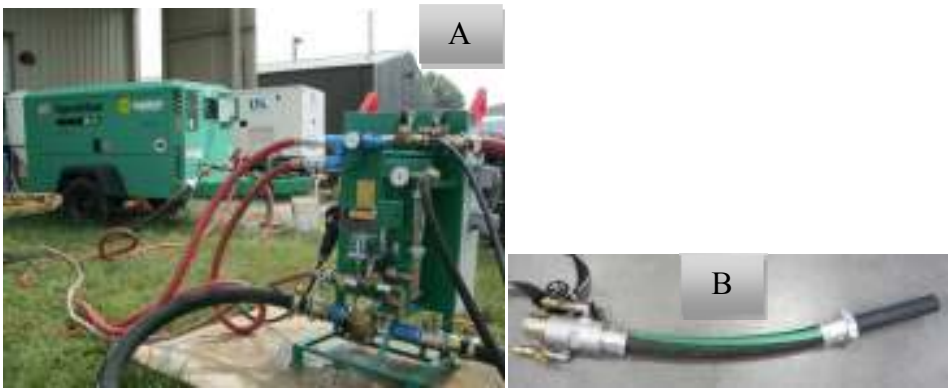

Figure 12 VELCO-GUNMIX water booster moistening system (A); and combination compressed air and water nozzle system (B).

Final Mix - Patent Pending

The final mix will strongly be influenced based on the application for which it will be used. However, if high compressive strength with fast setting times are necessary then the 3:1 mix without fibres will be ideal. Although if flexural strength and post-crack strength are important parameters then the Tekcrete Fast mix will be ideal.

Tekcrete Fast (Patent Pending) is a specially designed, extremely rapid hardening, high performance gunite. Fibre-reinforced, this product offers strengths over 55 MPa (8,000 psi), following ASTM testing procedures; and can be used in conventional, dry-process gunite equipment (Figure 13). It is ideal where immediate structural strength is required. This bagged material is one potential product that was based on the experimental trials within this research. An International Application has been filed under the Patent cooperation treaty for Tekcrete Fast.

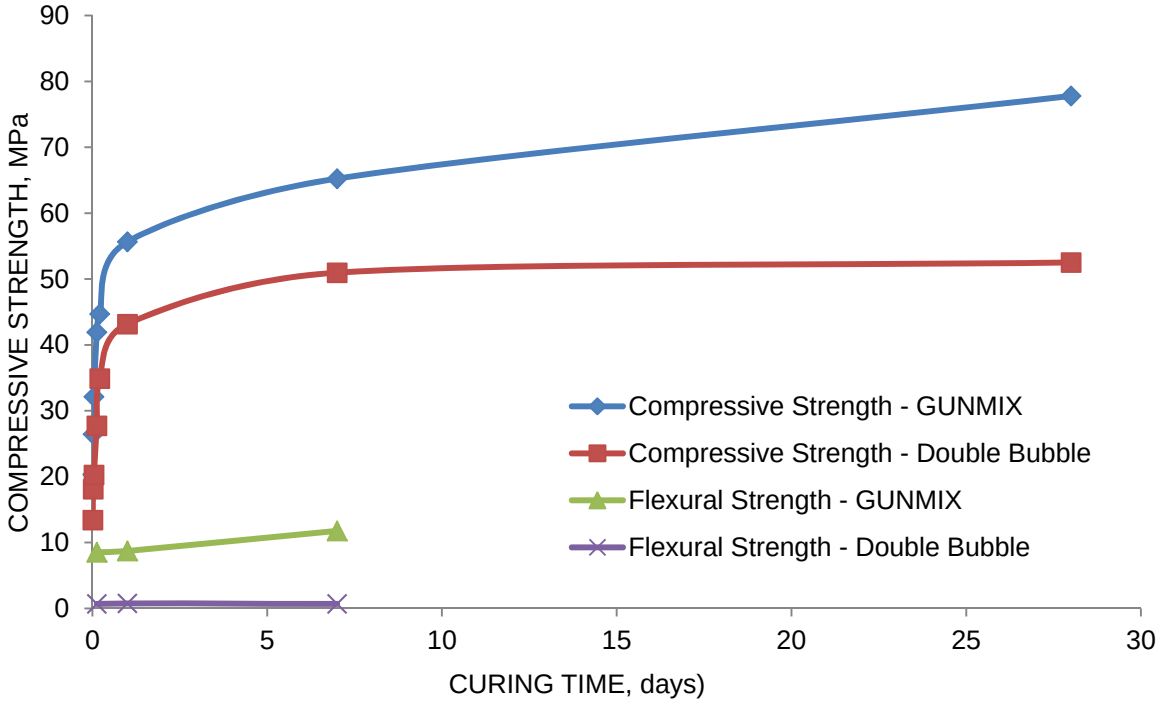

Figure 13 Compressive and flexural strength data for the Tekcrete Fast product comparing two different nozzle types: Velco GUNMIX and Double Bubble Nozzle.

CONCLUSIONS

A sprayed-concrete mix was designed and tested that utilized a commercially available CSA cement. The mix was created following a test matrix that allowed the mix to be optimized based on the need for a sprayed concrete to gain strength rapidly. The resulting mix exhibited structural strengths within 15 minutes after spraying. Sprayed-concrete tests revealed a fine-aggregate gradation provided greater strengths and less rebound than a coarse-graded aggregate. A supplied water content of 2.3 l/min allowed the concrete to achieve a higher strength gain, both in compression and flexural, than 1.5 or 3.8 l/min. The concrete sprayed smoother with less rebound and loss of cement. Tests that noted high rebound and/or loss of cement were commonly due to dry or over-saturated conditions. The final mix design, utilizing a commercially available CSA cement (CSA#1), is comprised of cement and a fine-graded sand (< 16 mesh) at a 3:1 ratio of aggregate to cement. A water:cement ratio of 0.5 is recommended, with the equipment used for these tests a supplied water content of 2.3 l/min to the wetting ring provided the recommended water:cement ratio.

In addition to the final mix created for the rapid stabilization of shock damaged structures, a fibre-based, patent pending, mix was fabricated at the Minova USA Inc., Georgetown, KY facility for applications in which fast-setting structural support is required; particularly underground mining operations.

ACKNOWLEDGEMENTS

Funding for this research was provided by the National Institute for Hometown Security.

REFERENCES

1. ACI Committee 506, Guide to Shotcrete, (ACI 506R-90)," American Concrete Institute, Farmington Hills, 1990, Mich, 41 p.

2. MALMGREN, L. AND E. NORDLUND, Interaction of shotcrete with rock and rock bolts--A numerical study. International Journal of Rock Mechanics and Mining Sciences, 2008. 45(4): p. 538-553.

3. LAMONTAGNE, A., M. PIGEON, AND D. BEAUPRE, Durability of shotcrete repairs. International Journal of Rock Mechanics and Mining Science & Geomechanics Abstracts, 1995. 32(7): p. 339-339.

4. MALMBERG, B. AND T. FRANZÉN, Shotcrete for rock support: a summary report on the state of the art in 15 countries. Tunnelling and Underground Space Technology, 1993. 8(4): p. 441-470.

Theme 6 — Renewable Energy

1790

Laminated Concrete and Ferrocement for the Construction of Fixed, Floating or Submerged Structures to Support Renewable Energy Devices

M Pemberton, T Tucker
Trafalgar Marine Technology Ltd, UK

”If you put steel into the ocean - then better wrap it in a quality concrete otherwise the costs of maintaining the steel will disipate your revenue and severely effect your bottom line.” Systems are being developed to construct several types of marine structure by spray and laminating techniques together with the use of high strength self compacting concretes,to produce very high quality with high strength to weight ratio material which will compete with steel structures and offer the minimum maintenance benefits of concrete. The use of laminated concrete and ferrocement in thousands of yachts in the 1970s to 1980s Joint author Tony Tucker has considerable experience in design and build of ferrocement yachts and is a recognised surveyor of these vessels. Practical evidence of no water penetration or corrosion into these yachts. There is also the reference to ferrocement boatbuilding in China and the Journal of Ferrocement special issues dealing with the marine applications of ferrocement. There are references to the work of M.E Iorns and the Fibersteel Co. of California, in the 1960‘s explaining the development of laminated ferrocement for building yachts and pontoons. There is also reference to the testing of laminated ferrocement by the United States Coast Guard for approval to build a passenger vessel. The experience of ferrocement boat builders over years has clearly demonstrated that the material is waterproof. The nominal cover to ferrocement hulls build by the traditional methods of armature And hand plastering is 3-4 mm (1/8th Inch). Reference should also be made to the several papers by M.E.Iorns. Particular reference to the test boat made by the Fibersteel Company, Sacramento, California in 1964 where different wire mesh materials and the cement ‘cover‘ to those materials was practically tested. Quality of laminated ferrocement bringing in such aspects as the impermeability and strength of the gelcoat layer and the resulting resistance to corrosion of the meshes close to the surface. The spraying and laminating process, particularly with a white cement, has been demonstrated by the building of white yacht hulls and also by the Demenil Museum Project. The previous reference relating to the Demenil Museum Project clearly demonstrates the use of the spray and laminate process to produce precision manufacturing of ferrocement to the highest possible standards. By the laminating process, any amount of steel can be laminated into a particular cross-section to satisfy any strength requirement of the cross section.

Michael Pemberton, Master Mariner, holds Patents pending relating to laminated ferrocement and laminated concrete. He previously worked with the late Mr Martin Iorns of California and with many concrete specialists/academics to promote the application of this technology. He is a member of the Concrete Society, and a past member the Renewable Power Association Ocean Energy Group.

Tony Tucker is a Naval Architiect and Marine Surveyor with many years experience of design and survey of yachts and small commercial craft in all accepted boat building materials; Ferro-Cement, GRP, Steel, Aluminium Alloy, and Timber. Many of the vessels are cruising yachts which cruise the oceans of the world, others are more specialist small commercial vessels, fishing boats, and inland passenger boats.

Keywords: Ferrocement, Floating, Laminated concrete, Renewables, Submerged structure

INTRODUCTION

Any reduction in the capital expenditure and maintenance costs of a marine structure will be positively reflected in the `bottom line` of any marine renewable energy project. To date, conventional concrete and steel structures dominate this market. The authors advocate a closer look at and development of alternative systems, laminated concrete systems, which offer considerable costs savings for marine projects.

The marine renewable energy resource is the most dense and most reliable energy source compared with the wind and solar resource and we have plenty close to hand. As we look at new ways to capture marine energy, we need new ways to construct and deploy the necessary structures and we need to reduce costs to make finance possible for the various projects bring researched today.

A BRIEF HISTORY OF MARINE CONCRETE

The marine environment has always been the most severe testing ground for new materials. It was concrete that founded the structures of Greek and Roman civilisation and it is concrete that provides the foundations to bridges, piers, tunnels and roads of our modern civil infrastructure. Concrete will continue to be the principle long lasting and minimum maintenance material for constructing and supporting marine renewable energy devices.

The modern age of concrete, from 1824, came about with the invention of Portland cement and of Ferrocement, Ferro-Concrete, and Reinforced Concrete. Demonstration of these materials has been by the production of boats, yachts and ships. World Wars 1 and 11 saw the production of many concrete ships, the remains of which can still be seen around the coasts of Europe and the USA. The Mulberry Harbour Caissons from D Day landings are still seen in almost the same positions as they were placed sixty years ago and they remain substantially in tact.

Off Galveston, Texas, is the wreck of the concrete ship ` Selma ` a 7,500 ton oil tanker built in 1919. She has a hull thickness of only 4" and 5" and is framed in a traditional shipbuilding fashion. Although wrecked and much deteriorated around the waterlines and deck, she is there and is still a complete structure with sound tanks even after 92 years!

Can there be any doubt, concrete is the material of choice for any lasting marine structure?

WHY LAMINATE CONCRETE?

We laminate timber, steel, plastics and in each case the laminating process produces a better product. The same principles can be applied to concrete by spraying quality mortar and sequentially embedding the reinforcements into a thinner than usual cross section, we produce a high quality concrete with a high strength to weight ratio. Panels produced by this method can then be joined, as with floors and frames welded into a ship, by `concrete welding` to form cellular structures which in turn can become compartments for ballast or floatation tanks. The cellular structure can become the `permanent shuttering` for a more substantial concrete structure as required by design. The process of spraying concrete

produces excellent surface compaction and drives off surplus water thus producing a quality protective `gel coat ` and when combined with fibres and fine reinforcements, gives an impervious and crack resistant section – which can in fact be regarded as ` sacrificial `to the main structural design.

The laminating technique of spraying mortar and then placing reinforcements is less expensive than forming shuttering and fixing steel work and then pouring the concrete. In conventional concrete work a substantial wooden box is formed, steel work is wired into position in that box and the concrete mix is poured into the mould.

Laminated concrete is made by spraying concrete against a light weight surface and then embedding the reinforcements into the plastic mortar or concrete. Special surfaces of colour, texture, and quality can be applied to a moulded surface, a feature which can not be economically applied with conventional concrete work. By adding polymers, fibres and /or other additives, the qualities of the outer sprayed surfaces can be greatly enhanced.

Typical Construction Details

Typical construction details of laminated concrete in comparison with conventional concrete are illustrated in Figure 1.

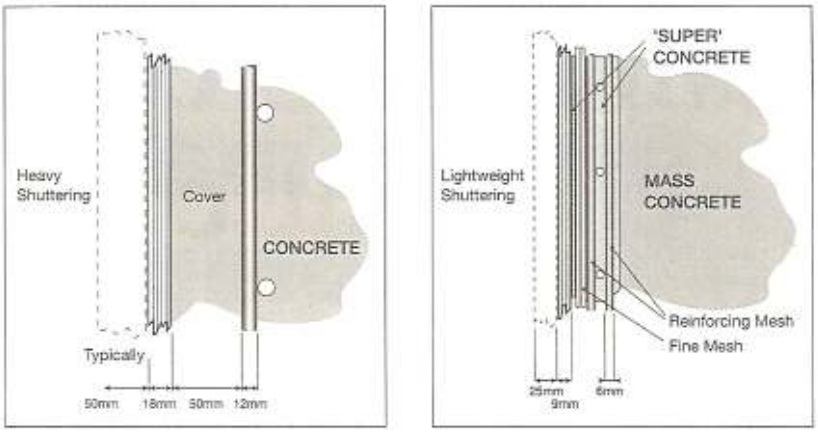

Figure 1 Typical construction details: conventional concrete and laminated concrete

POSSIBLE EXAMPLE STRUCTURES

Wave Resource Energy Collector (WREC) (UK Patent GB 2 367 037 B)

The construction costs of any shore line wave energy device are a significant factor in assessing if such a project can be financed. The traditional means of shoreline construction works and the transport of men and materials to remote sites, accounts for the extraordinary costs involved, costs which of course deter the possible development of a suitable ` wave resource site`. The WREC concept significantly reduces the overall costs of developing a shore line site and thus makes it more likely to be financed.

For a particular site, chosen for its good wave resources, a `ship` type structure is designed and built to configure with the underwater profile of that site. The irregular shaped ship structure is constructed in a sheltered water position, preferably close to the specific site.

The floating structure (ship) is designed with an irregular bottom which matches the topography and sea bed of the particular site. The structure incorporates elements which will collapse, by design, as the structure is placed in the engineered wrecking process.

The structure is built in a cellular form, the cells being available as floatation initially and later as `permanent shuttering` for the placement of mass concrete, or of ballast materials as required by the overall design. The cellular structure makes it possible to sub divide the structure in many ways and to `trim` it to the best advantage for towing and placement.

When the floating structure is complete, it is towed to the particular site and on a high water spring tide, the structure is pushed ashore by tugs and winched ashore at the same time. This is a guided and controlled procedure resulting in the `engineered wrecking` of the structure into the required position. Subsequent filling of the vacant ballast tanks and mechanical connections will insure that this structure will not move off the shore.

The internal surfaces of the WREC structure are made smooth and thus enhance the wave capture. The basic structure can be further enhanced by wing walls and a hinged end `ramp` wall which can be extended at the second stage of the placement - these features increase the wave gathering face of the structure. A third stage placement by the same methodology permits the landing of the machinery house structure to the inside top edge of the device.

The whole structure can be made from temporary floating moulds, without the need of dry docks and with the minimum crane requirements. The structure can be made with a surface texture to resemble the rock structure and colours of the coastline and is thus camouflaged to make it environmentally and aesthetically acceptable. This concept is applicable to oscillating water column and tapered channel devices and in some instances might incorporate both technologies within the same structure / site / project. The surfaces of the structure can be made bio-resistant (anti-fouling) or bio-accepting (Marine Culture) and the parts subject to score by rocks and sand can be made with super hard bearing concrete surfaces (Patents Pending)

Total Energy Extractor (TEE) (UK Patent GB 2 365 385 B)

The concept drawing depicts a concrete gravity structure, though it could equally be designed as a floating island structure.

This is a very large structure which is designed to extract the maximum renewable energy from a particular site (Figure 2). The concept seeks to maximise the financial returns from a large investment by taking advantage of all available marine renewable energy technologies and to reduce the maintenance costs of the generating equipment by providing the facilities within and on the structure. Further revenues streams would be from marine culture activities within the vast tank spaces of the structure.

The wind energy is extracted by four turbines, these are designed to rotate about massive concrete hinges and by controlled de-ballasting, can by lowered to the central workshop position where maintenance is carried out.

The current energy is extracted on ebb and flow tides from turbines in the centre of the structure. These current turbines can be lowered or raised from their operating positions by simple dry dock principles. When lifted they would be within the workshop for maintenance.

The wave energy is extracted by OWC devices at high level and by the Vickers machine principles at the lower level. Typically this structure would be set in 20 - 25 m of water across a tidal stream and perhaps where its mass would also provide protection and wave attenuation to a vulnerable shore.

The piers are approx. 25m high x 12 m wide and about 50 - 60 m long. On plan the structure might cover an area 100 - 120 sq. m. It would be possible to board the structure from either side in relatively sheltered conditions provided by the structure itself. It is suggested that laminated concrete construction systems would make it feasible to build and install this device.

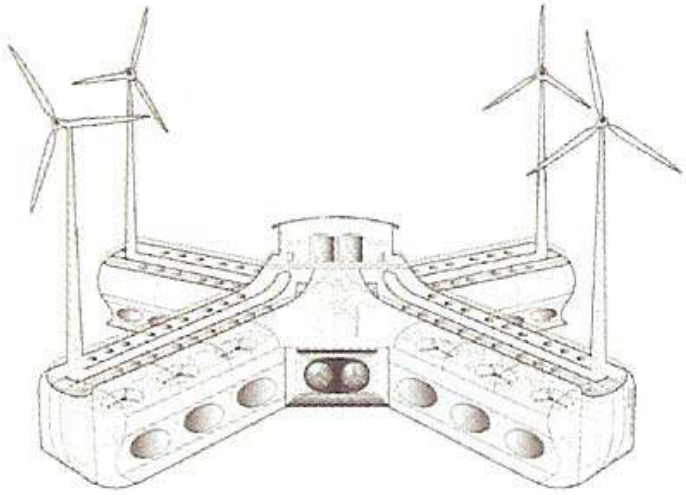

Figure 2 Concept for the total energy extractor – a large cellular concrete gravity marine structure designed to extract wind, wave and tidal power. These would be located offshore to gather as much energy as possible.

FLOATING MOULD PRODUCTION LINE FOR MARINE RENEWABLE ENERGY STRUCTURES

This paper has described laminated concrete and two possible concepts where this method of construction can be beneficially employed.

Where multiple marine RE units are required i.e. for wave energy buoys, gravity bases for wind towers, marine current devices and similar structural elements of renewable energy machines; these can best be constructed by laminated concrete systems and from floating moulds. The use of dry docks and massive crane capacity is not required.

Making use of a suitably sheltered dock side site, the various laminated concrete elements required to frame a given structure can be horizontally cast ashore. Given that a female mould of the required structure has been made (also from laminated concrete) and is supported on a floating platform. The platform is designed with controlled tanks so that it can be sunk and re-floated as required. The principle mould is first used to form the `shell` or `hull` of the required structure. The horizontally cast plates are now become the vertical plates of the required cellular structure. These elements are craned from dockside into the `shell ` and `concrete welded` to the shell to `stiffen` the structure.

When sufficiently completed the structure is then floated from the mould - by sinking the mould itself and the manufactured unit is released by floatation into the water.

Water is the best medium for curing concrete. By simply moving the part completed structure along the dockside towards the sea, the various elements, frames, bulkheads, deck plates and pre-formed parts can be added sequentially to complete the device.

The machinery and electrical works will be carried out at the end of the line prior to the unit being towed away to sea.

Special Ferrocement Project Proposal: Historic Ship (City of Adelaide)

This project proposal aims at saving the City of Adelaide - of national and international maritime heritage importance, by the innovative use of ferrocement (Figure 3).

It is a project to demonstrate the application of laminated concrete and promote the concrete industry and ferrocement, for the benefit of preserving our maritime heritage.

Our proposal is to sheath the old ship in 1 “of laminated ferrocement, to make the ship sound and watertight. With additional steel bracings, the ship can be made strong enough to be refloated and towed away, preferably to Sunderland where she was built in 1864.

When the ship is secured into the available dry dock, sheathing is removed sequentially to reveal the ship as she was prior to the process. This can be done without damage to the artefact.

In other words wrap the ship, deliver the ship and unwrap the ship by the Cocoon principle. When the removed sheathing is reassembled to form a mould – an exact replica of the original ship can be produced down to every plank and bolt hole in Laminated Ferrocement. (Patent Application Pending)

Can our concrete industry take up this project with offers of support, materials and expertise to bring about the saving of this ship for UK Ltd and prevent the present flawed proposals to ship her off to Australia at UK taxpayer’s expense, where she is likely to fall apart in the heat. See Google City of Adelaide – Ship, to learn more of this sad saga.

Please contact the authors if you are concerned and if you can help.

Figure 3 Historic Ship (City of Adelaide)
(Copyright © 197 aerial photography - www.197aerial.co.uk)

BIBLIOGRAPHY

1. ACI COMMITTEE 549. ACI 549. 1R-93. Guide for the design. construction and repair of ferrocement, ACI 1993. 33pp.

2. INTERNATIONAL FERROCEMENT SOCIETY, A new model code being prepared by the International Ferrocement Society, IFIC/AIT, GPO Box 2754, Bangkok, Thailand. (www.library.ait.ac.th/ific-biblio/)

3. NAAMAN, A.E. Ferrocement and laminated cementitious composites. Techno Press 3000, Michigan, 2000. 367pp (See Concrete, May 2001, p.12 for review)

4. IORNS, M.E. Low cost laminated shotcrete marine structures. Proceedings of the ACI/SCA international conference on sprayed concrete, Edinburgh, September 1996, E & F.N.Spon, London, pp. 64-69.

5. IORNS, M.E. Low cost ocean platform construction. Concrete International December 1999, pp. 39-42.

6. MORGAN, J.E. AND MORGAN, R.G. The armature that made history; the boats of Joseph Louis Lambot. Proceedings of the Lambot symposium: Ferrocement 6. University of Michigan, Ann Arbor. June 1998, pp. 11-33.

7. PEMBERTON, J.M. Ferrocement: an insight and a review - so what is new ? Proceedings of the Lambot symposium: Ferrocement 6. University of Michigan, Ann Arbor. June 1998, pp.75-83.

8. PEMBERTON, J.M. The total energy extractor and RE islands. Refocus. November/December 2000, pp.38-40.

9. PEMBERTON, J.M. IORNS, M.E. AND SWAMY,R.N. Innovative construction systems reduce natural energy costs. Proceedings of the sixth world renewable energy congress July 2000. Elsevier Science, Amsterdam, pp.681-685.

10. PEMBERTON, J.M. Laminated concrete for efficient construction. Concrete. July/August 2001 pp. 24-25.

11. PAUL NEDWELL, The use of Ferrocement. Concrete Magazine. August 2010 (School of Mechanical, Aerospace and Civil Engineering at the University of Manchester.)

12. PEMBERTON J.M. `Potential applications of ferrocement and concrete laminates. International Symposium on Ferrocement, Manchester 1986

Gravitas Offshore Concrete Foundations: The Enjoyable Puzzle

H Ridgeon
Arup, UK

The UK's major programme towards sustainable, resilient, low carbon energy generation is pushing forward the next stage of offshore renewables. These deeper water sites require a new reliable approach for offshore wind turbines. This paper shall present the findings of a two year research and development project to create the ultimate offshore concrete gravity base foundation for wind turbines. Gravitas Offshore (a consortium of Costain, Hochtief and Arup) has adopted knowledge learnt in the offshore oil industry to develop a durable and sustainable concrete foundation for offshore wind structures. This concrete foundation can be deployed in upcoming wind farms around the UK coast. The solution is self-buoyant, requires no specialist onshore or offshore marine equipment to construct, lift or install and requires minimal sea bed preparation. An advantage of concrete foundations over steel is the more flexible and larger local supply chain which can aid market capacity. During the development process much effort and thought has gone into engaging with the local supply chain and developing high performance concrete specifications. These specifications have been developed to deliver high strength, lightweight, low carbon concrete. The existing offshore codes have been reviewed and compared with regard to ultimate and service limit state design.

Henrietta is a structural and civil engineer with over 15 years' experience in designing and delivering projects. After graduating with a first class degree from the University of Edinburgh she joined Arup in 1996. Since then she has worked on many different types of projects including port facilities, canal systems, water treatment plants, drainage systems, infrastructure developments, roads systems, bridge structures and offshore foundations. Through her work she has developed an interest in creating large civil engineering products from the Personal Rapid Transport system at Heathrow through to the development of offshore gravity base foundations. Her skills lie in her ability to undertake technical developments, to programme projects, to manage budgets and to advise clients on their risk management strategy, thereby saving costs and increasing project certainty.

Henrietta has spent the last few years working as technical project manager for GRAVITAS Offshore Ltd. A company formed out of Arup, Hochtief and Costain. Together they have developed a concrete gravity base foundation product, designed to be floated and towed out to Round 3 Offshore wind farms and installed without specialist marine equipment. The concrete gravity base will be mass produced in a UK port and is developed to meet the needs of round 3 wind farm developers by reducing weather risks, increasing the supply chain certainty and helping to reduce the costs of offshore turbine foundations.

Keywords: Concrete, GFS, Gravitas, Whole life

INTRODUCTION

UK Market for Offshore Wind

UK signed up to the EU 2006 Renewables Directive in 2007 with the commitment to generate 15% of the UK's energy supply from renewable sources by 2020[1]. The subsequent directive released in 2009 sets the EU's targets to be 20% of the EU's energy supply by 2020[2]. Renewable UK estimates that this equates to 35-40% of the UK's electricity supply to be generated from renewable sources and that this will be met largely by offshore wind.

The Crown Estate has released Round 3 offshore sites, which are in deeper water and larger sites than ever before.

The UK has been estimated to have over a third of Europe's total offshore wind resource with 1.9GW+ currently operational and 23GW still to be developed. This is over ten times the size of one nuclear power station and equates to approximately 4600 5MW turbines being installed around the UK by the year 2020.

It is an exciting time for engineers, and we need to work together to create more efficient turbines, low cost and low risk foundations, not to mention a large amount of offshore and onshore cable routing/grid connections. We need to be thinking about energy storage and grid smoothing, as well as softer aspects of energy use. Are there ways to smooth out energy use, as well as energy supply? Can foundations be made to last for ever and repowered with ever newer and more efficient turbines? There are many questions and not so many answers.

This paper looks to concentrate on one small aspect of the above which is offshore concrete gravity base foundations produce by a new company called Gravitas.

Gravitas

Costain, Hochtief and Arup have jointly established Gravitas Offshore Ltd to develop, design, construct and install concrete gravity foundations for offshore wind farms. Within this joint venture, Arup [5] provides engineering design input, Costain [6] provides the onshore fabrication and logistics expertise and Hochtief [7] provides the offshore transportation and installation expertise. Together they employ over 50,000 people worldwide involved in all aspects of engineering design and construction. This is a case of combining skills and capability from different disciplines and from different backgrounds to develop a large civil engineering construction project as if it is an off-the-shelf product, with an easy set of instructions for installation. They have been working together for two years to create a concrete foundations solution that uses common engineering construction techniques, can be towed to site and installed using the common tug and avoids the need for seabed preparation wherever possible.

The Gravitas Foundation Solution (GFS)

The design of the concrete Gravitas Foundation Solution (GFS) follows established methods and principles from previous offshore concrete structures projects. The product development of the solution has been supported by four guiding principles, set out from the beginning of concept design and that have now become the underlying themes:

- Simplicity
- No onshore/offshore heavy lifting
- No special vessels
- Minimal seabed preparation

The GFS has been based on the concept that Gravitas Offshore Ltd has identified as having the lowest overall delivery risk taking account of client requirements as well as the strengths and capabilities of the consortium. The GFS is capable of being entirely constructed onshore in a dedicated facility, transported to site using readily-available tow tugs and installed without specialist offshore vessels or equipment are considered to meet these requirements.

Figure 1 Gravitas foundation solution

The GFS has a monolithic reinforced concrete gravity base with a concrete tower. It consists of a bottle-shaped reinforced concrete shell constructed on top of a reinforced concrete base slab. The lower part of the structure is divided into nine chambers to provide structural support and to assist with the water ballasting operation. It is connected monolithically to the concrete tower via a reinforced concrete frustum.

If required, skirts will be provided below the concrete base to key into the foundation soils. These will be a minimum of 0.5m deep to ensure the base keys into the soils around its whole perimeter.

The GFS has been configured to float with a draft not exceeding 9.5m when complete which will permit it to be accommodated in most UK and European Ports without capital dredging. The GFS requires no specialist marine equipment for transport to site or installation on the sea bed. Having been towed to site by tugs in approximately one day, it is ballasted to the sea bed with sea water and then rock armouring is placed around the foundation, as required. Installation and initial rock armouring will take place within a 48-hour weather window.

DESIGN CONSIDERATIONS

Iterative Design

The design is inherently iterative with the three disciplines of Naval Architecture, Structural Engineering and Geotechnical Engineering intertwined. The size and the shape of the structure affects the long term wave loading it experiences and its dynamic response. This in turn affects the thickness of the walls and the quantity of steel reinforcement required. The ground conditions affect the allowable bearing pressure and in turn the size of the base and the quantity of ballast required. The size of the base, the thickness of the walls and the shape of the structure affect the draft, its stability during float out and installation. No one item can be fixed, without checking the others.

Lightweight Concrete

The use of reinforced lightweight concrete can improve the design immeasurably. Gravitas have been working with the concrete centre [3] and the supply chain to see what can be done to improve the structural properties of reinforced concrete by establishing locally sourced light-weight aggregates and testing their material properties. Offshore foundations that can be floated into position and are self-installing require high strength concrete with high stiffness properties but with low density. Gravitas has challenged the industry to take this research further and to improve on the known material properties of lightweight concrete as set out in existing codes. A number of them have taken on the challenge and are working to improve and enhance the materials and mixtures on offer.

Reinforcement

Eurocode 2 [8] now allows reinforcement with a yield stress of 500MPa to be used in reinforced concrete. Gravitas have been working with CELSA, a reinforcement production company, to take advantages of their known advanced material properties to see what needs to be done to upgrade their stock grades and enable higher grade steels to be mass produced. An interesting fact is that all reinforcement in the UK is largely made from re-cycled steel.

Crack widths

The crack widths allowed in a high strength reinforced concrete, Grade C50 or above, in a marine environment for the different codes can be found in Table 1.

Table 1 Allowable crack widths for grade C50 concrete or above

CODE	ABOVE SPLASH ZONE	SPLASH ZONE	BELOW SPLASH ZONE
J101[9] Eurocode 2[10]	0.3	0.3	0.4

Although the way the codes calculate crackwidths is different with regard to short and long term loading and associated E values. BS5400 takes into account the proportion of the loading that is long term and short term whilst the other codes don't. More work and evaluation on the most suitable method of calculating crackwidths for gravity base foundations needs to be carried out and understood. The whole point of crackwidths in the case of offshore foundations is to limit the susceptibility of reinforcement to corrosion. It is not a visual requirement.

THE SUPPLY CHAIN

Well known materials and methods

The materials and construction methods to produce concrete gravity bases are well established and commonly used for construction projects including offshore over the last century. The knowledge and insight from the design and construction of cooling towers, pontoons, ships, submarines, bridge caissons, oil and gas platforms, bridges, water tanks and high rise buildings have all gone into the design of the concrete gravity base, requiring similar materials, and construction techniques.

Reinforced concrete is a well-known and well-studied material with tried and tested construction methods that have worked for one-off construction projects over many years. It is durable, robust, and if designed and constructed properly does not require any maintenance. It has a large and diverse experienced supply chain that is less susceptible to price fluctuations than other materials like steel. The base materials of concrete, aggregate, cement, ground granulated blast furnace slag (GGBS), pulverised fuel ash (PFA)and water can often be locally sourced to suit the production sites position. Both GGBS and PFA are waste products from other industries and their inclusion in the concrete mix can greatly improve the carbon footprint of the end product.

Gravitas is committed to using locally sourced preferably recycled materials where ever possible in the concrete mix designs and this affects the strength, workability and material properties. So the challenge to the designer is to understand where the codes are appropriate and where they can be challenged or adjusted through the additional testing and understanding of different mix designs, particularly with regard to service limit state which is often the governing case.

Distances travelled

The advantage of concrete (with its large source of materials, locally produced, not subjected to price fluctuations) is that it can reduce the distances travelled to get what can be enormous amounts of material to site.

This element tends to be a large contributor to the carbon footprint of the foundation as whole. The method of travel has a large effect on the carbon footprint.

ADDITIONAL CONSIDERATIONS

Re-power

Most the concrete mixes for high strength concrete are durable and can have a life span of 50 to 100 years whilst offshore foundations often only require a design life of 25 years. The calculations for fatigue for Gravitas's reinforced concrete foundation have been shown to be greater than 100 years. This means there is opportunity to re-power the foundations with new and different turbines as required. This can be done relatively accurately as long as the wind and wave data for the foundations are gathered over the lifetime so that the actual fatigue loading can be calculated and compared to the fatigue capacity.

Re-use and recycling

The intention of Gravitas's gravity base foundation is to ensure that it can be fully removed from site and recycled. This is carried out by reversing the ballasting operation which entails first pumping out the sand and then pumping out the water in a controlled manner. The foundation can then be towed back to port and the concrete and rebar recycled. It is also possible to recycle the sand ballast.

Environment

The Concrete Centre [3] and the Gravity Foundation Interest Group which includes Gravitas have commissioned a review of the marine environmental considerations associated with concrete gravity bases. This review highlights the following:

- Reef effects, either negative or positive are not believed to be any greater for generic Concrete Gravity Base Foundations (CGBFs) than other deeper water foundation solutions.

- CGBFs at a generic level have similar physical blockage effects to other deeper water foundation solutions. The different surface area and profiles will result in localised effects on waves, tidal currents and sediment transport mechanisms that may differ from steel jacket and tripod foundations.

- The review of the current evidence base shows that CGBFs have a large positive effect during during their installation on the seabed. No piling or hammering is required for CGBFs and this mitigates one of the potentially greatest marine impact pathways associated with Round 3 installations: namely underwater noise and sound pressure wave impacts on sensitive marine species. Recorded sound levels during emplacement of CGBFs at a Belgian wind farm demonstrated that underwater noise levels did not register above background noise associated with shipping vessel transits in the local area.

There is also an opportunity for offshore wind farms to provide fish reservations that could aid and facilitate the North Sea fish stocks. Further research needs to be undertaken in conjunction with organisation such as Living North Sea [12] and CEFAS[13].

Carbon Footprint

Gravitas have been working with the Concrete Centre [3] to evaluate and compare the carbon footprints of different concrete gravity base foundations and a generic jacket solution, for a particular water depth and wind turbine.

Carbon footprint is the total amount of greenhouse gases produced to directly and indirectly support human activities, usually expressed in equivalent tonnes of carbon dioxide (CO2e). By understanding early on in design development the carbon footprint for the various activities concerned with the lifetime of a foundation, effort can be put into reducing those areas which contribute the most.

The study showed that concrete foundations had lower carbon footprints than steel, because it uses largely recycled materials sourced locally and that by concentrating on the concrete mix, the source of raw materials and manufacture techniques, installation and removal methodology, there are still further savings to be made. It is also worth noting that the maintenance regime for concrete foundations could be made less onerous that that for steel, but these precedents have not been set, so that advantages cannot be taken at present.

CONCLUSIONS

Concrete gravity foundations have an important part to play in assisting the UK in meeting its EU renewable targets. By contractors and designers working together with the design chain and considering all aspects of the design, construction and decommissioning of the offshore wind farm foundations it is possible to address and improve on many areas. Gravitas has been a key player in assisting with this process and is looking to further engage and contribute to encouraging an era of low carbon concrete. Through consultants, contractors, academia, the supply chain and stakeholders working together there is much more that can be done to reduce the costs and the carbon footprint of concrete gravity foundations.

Acknowledgements

I would like to thank the Concrete Centre and its members, with special thanks to Steve Hunt (Vinci), Gareth Moores (Lytag Ltd) and Richard Howells (Celsa Steel Uk) for their enthusiasm and commitment to researching different ways of improving the designs of concrete gravity base foundations.

REFERENCES

1. DEPARTMENT OF ENERGY AND CLIMATE CHANGE National Renewable Energy Action Plan for the United Kingdom Article 4 of the Renewable Energy Directive 2009/28/EC, 2010.

2. National Renewable Energy Action Plan for the United Kingdom Article 4 of the Renewable Energy Directive 2009/28/EC

3. Directive 2009/28/EC of the European Parliament and of the Council of 23 April 2009 on the promotion of the use of energy from renewable sources and amending and subsequently repealing Directives 2001/77/EC and 2003/30/EC (Text with EEA relevance)

4. http://www.concretecentre.com/

5. http://www.gravitasoffshore.com/

6. http://www.arup.com/

7. http://www.costain.com/

8. http://www.hochtief-solutions.com/

9. DNV_OS_J101_SEP11 - Design of Offshore Wind Turbines Section G

10. BS EN 1992-1-1 2004 - Eurocode 2 - Design of Concrete Structures - 1 General Rules Section 7.3 Table 7.1N

11. BS EN 1992-1-1 2004 - Eurocode 2 - Design of Concrete Structures - 1 General Rules Section 4.3 Table 4

12. http://www.livingnorthsea.eu

13. www.cefas.defra.gov.uk/

State of Concrete Dams in North Russia

M Sadovich, T Shlyakhtina, A Kuritsyna
Bratsk State University, Russia

It is envisaged that the interest in investigation the state of long exploitation of concrete dams will continue to grow as they age. Authentic assessments of changes in the strength and the concrete structure, the characteristics of corrosion processes, the repercussions of frost affects, combined with water saturation, and others may be considered as part of a systematic monitoring of responsible concrete structures, which certainly include dams. Given that the largest Russian northern dams were built in the 60 - 70th years of the twentieth century, the duration of operation is to date 40 - 50 years. This period is sufficient to detect the repercussions of the exploitation environment on the condition of the concrete. In accordance with the classification of interactions in the system ”concrete - environment” identifies areas of dams in relation to which were executed complex studies of the concrete.

Mark Sadovich is a Professor and a Doctor of Science. Head of the Construction Technology Department of Bratsk State University. The scope of his scientific interests includes the technology of monolithic concrete, study of hydraulic concrete, diverse study in the field of construction materials, technology of cold-weather concrete placement.

Tatyana Shlyakhtina is a Candidate of Science. The scope of her scientific interests includes the corrosion of hydraulic concrete, study of hydraulic concrete, diverse study in the field of construction materials and etc.

Anna Kuritsyna is a Candidate of Science. The scope of her scientific interests includes the corrosion of hydraulic concrete, study of hydraulic concrete, diverse study in the field of construction materials and etc.

Keywords: Concrete, Corrosion, Crack, Dam, Filtration, Strength

INTRODUCTION

Water and air have a direct effect on the dams' body concrete.

The most important and potentially hazardous environmental factors influencing on the concrete dam is the aquatic medium because water not only washes the large concrete surfaces but also filters out the separate fractures under hydrostatic pressure. The northern rivers of Russia have clean water and according to the Center for Hydrometeorology and Environmental Monitoring the Angara water has the total salinity of 200 mg/l with the dominant HCO_3^- anion of 50 - 100 mg/l, and as a Ca^{2+} caution of 15 - 30 mg/l. The content of free CO_2 in water varies from zero in some summer days up to 20 mg/l in winter ones.

Comparison of the chemical composition of the Angara water with the adopted aggressiveness criteria shows that in the concrete dams there can take place both leaching and carbon dioxide corrosion [1].

That the waters of the northern reservoirs are covered with ice for a long-time in winter is one of the features of the North dams. Winter is a period when the gas exchange with the atmospheric air stops and the water acidity increases. The ice period lasts about 7 months a year. The melting of ice and snow results to the desalting of reservoirs water in spring and summer. The reservoirs are featured with summer increasing and winter decreasing of water levels (on the average) up to three meters, and in some years - up to five meters.

In winter the tail water of hydropower station does not freeze, being heated while passing through the turbines and due to the high flow rates. The level fluctuations in the tailrace are intermittent in nature and within 1 - 1,5 m.

The northern Russia dams are operated primarily under conditions of extreme continental climate, which in accordance with the classification of "ISO 9000" refers to the temperature regime to the class "C and VC" with the average temperature of the coldest months from -15^0C to -30^0C and lower humidity - to the class "n" with a relative humidity of 45 - 75% during the warmest month. The number of transitions through $0\ ^0$C is from 50 to 100 cycles per year.

The chemical composition of air in combination with moderate humidity has not, as a rule, dangerous concrete gas concentrations. Thus, the operational environment is characterized by a complex of factors related to the harsh climate of the North, especially water regime of the upper and tailrace and the chemical composition of water.

BASIC PARAMETERS OF DAM CONCRETE

During the construction of dams, most of which are of gravity type, the zonal pattern of concrete brand distribution (Table 1, Figure 1) was adopted [2].

For the concrete preparation for Northern East-Siberian dams was used a special low-heat cement of the Krasnoyarsk plant with a normalized mineral composition of clinker (Table 2).

Table 1 The zone concrete distribution by grades

DAM ZONE	CONCRETE GRADE
Underwater	200,W 8
The zone of variable head water level	200, W 8,F250
tail water level	400,W 12, F400
Inner zone	100÷150,W 2
External zone	200,W4,F200

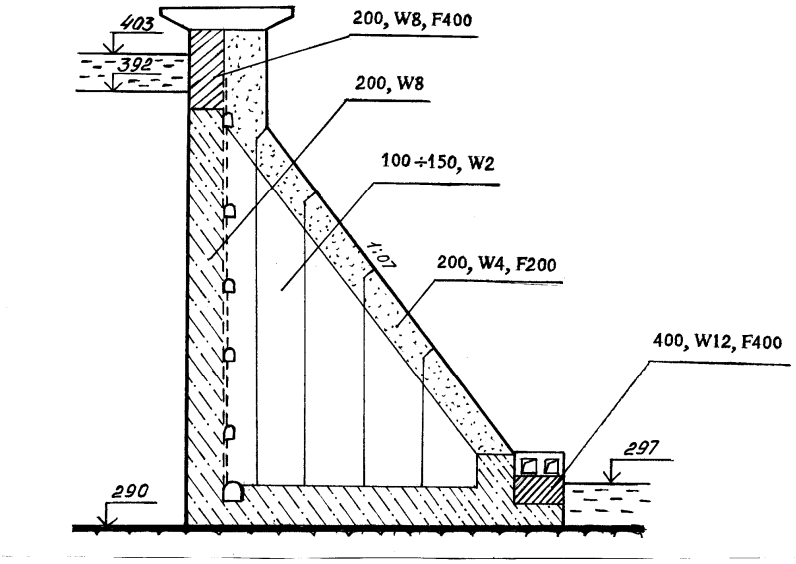

Figure 1 Schematic zoning diagram of the concrete by grades

Table 2 The mineralogical cement compound

CEMENT TYPE	COMPOSITION % BY MASS				ACTIVE MINERAL ADMIXTURE, %
	C_3S	C_2S	C_3A	C_4AF	
I-Portland cement					———
II- Portland – slag cement	46 - 52	22 - 25	6.4 - 7.5	15 - 17	Blast – furnace slag 40-50%

Portland cement type I was used to prepare cold-resistant concrete, slag cement of type II for underwater concrete. The total volume of concrete laid in the highest (100 m) dam is about 15 million m^3.

RESULTS OF MONITORING STATE OF DAMS

In accordance with the classification of interactions "concrete - medium" the dams zones were appointed, the comprehensive studies of the concrete were carried out.

These distinctive parts or zones of dams were classified as:

1) Underwater concrete pressure column.
2) The inside zone of the dam solid monolith.
3) The zone of variable level of head water and tail water.
4) The external zone of the non-overflow and station dams, in contact with air.
5) The spillway zone subjected to periodical water affecting.

The complex investigations of concrete were assumed to combine the field trials with sampling-core.

The field tests include visual inspection, photography and instrumental determination of the concrete strength with nondestructive methods.

Testing of concrete sampling-core consisted of determining the strength properties of concrete, the pore structure, the cement hydration degree and the amount of free CaO in the cement stone, the microscopic investigation of cement at the contact zone with the filler and so on.

As for methods, there was realized the idea of the comparative tests of concrete under different temperature and moisture conditions during the dam exploitation.

The results of the strength determination with nondestructive testing methods, supplemented with visual assessment, allowed to receive the most accurate picture of the studied zone of the concrete dam surface, for the external zone they are the key indices of concrete durability after long-time operation.

In this regard, the state of the concrete zone of the head and tail water levels of the Bratsk and Ust-Ilimsk dams is given below.

1) The concrete pressure column examined from the internal inspection galleries by visual inspection and tested with sclerometer is characterized by the surface strength of $\overline{R} = 35$ MPa at the fluctuations range of 19 - 60 MPa. The surface strength of concrete wetted by constant leachate current or calcite coated is $\overline{R} = 21.3$ MPa, ranges 4 - 36 MPa.

The surface, being wetted for many years by the leaching current, has much lower strength and is the original model of the surface state of the filter cracks.

2) The concrete zone of variable head and tail water level is influenced on with alternating wet, frosty attacks, wind and other environmental factors.

Monolithic concrete pressure column of the Bratsk dam in the zone of variable head water level was inspected by using the surface ultrasonic tests.

The test analysis permitted to distinguish two main states of concrete:

- without damages;
- with superficial damages.

Relevant statistical parameters of concrete strength without damages (Figure 2a) are: $\overline{R} = 35.9$ MPa, S = 9.0 MPa, V = 26% (normal distribution).

The damaged concrete has a characteristic asymmetric distribution curve with the most probable strength of 10 MPa (Figure 2b). The reported damages are superficial and make up about 30% of the total surface of the pressure face. The parity between undamaged and damaged zones in the whole pressure faces is 70 - 30%. The similar state of the external surface of the pressure face is characteristic for the Ust-Ilimsk dam.

3) The concrete zone of variable tail water level was tested at the Bratsk hydropower station in the hydropower building structures.

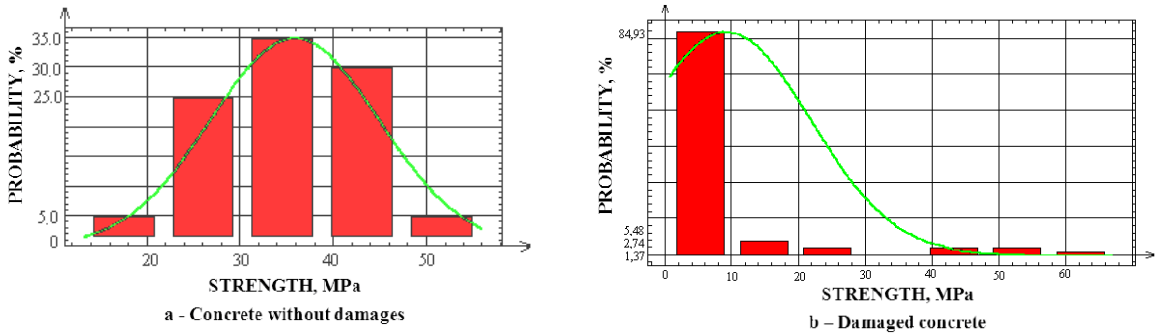

Figure 2 Histograms of the strength distribution of concrete pressure face of the Bratsk dam

In the tail water there is seen the concentrated destruction of the pier concrete surfaces in the zone of main fluctuations in the water level. The depth of zonal destruction reaches 30 cm. The concrete strength on the crumbling concrete the surface is of 5 - 20 MPa, which is comparable to the strength of the destroyed zones of the pressure face concrete [1].

The concrete destruction in the zone of variable tail water level, nonfreezing even under severe frosts, is typical for the most northern dams. The specified conditions lead to repeated freezing and thawing during even one winter season, and concrete freezing during the peak frosts takes place in the working zones of capillary ascending gradient. Thus, longevity or durability (including frost resistance) concrete of the specified working zones appears to have been exhausted for the considered term and some hydro power plants (particularly in Bratsk) have already started to repair the destroyed zones. In general, the field tests gave the most important indicators of the concrete surface of the studied dams zones, which are directly affected by the environment. The samples - core tests aimed to study the deep concrete layers with the further establishment of the indicators of strength, density, and porosity, the comparative diameter of capillary pores, CaO content in cement stone, so on.

The results analysis of cores test gives ground for the conclusions below. The strength comparison of the concrete pressure column (200, W -8) and the inner zone (100 - 150, W-2) of the Northern dams showed the possibility of their combining and getting common strength dependency on the concrete ageing (Figure 3, Table 3). The discrete method to determine the

concrete porosity has been used in this investigation, when the test reduces the determination of water absorption during the set period of time (τ = 0, 0.25, 1, 24 h).

To determine the parameters characterizing the space structure of the cement stone pores, trace their water saturation curve, the water saturation dynamic approximation of the exponential function proposed by M. Brusser [3] being used:

$$W_t = W_{\max}\left[1 - e^{-\left(\bar{\lambda}_2 \cdot t\right)^{\alpha}}\right] \quad (1)$$

where W_t - water saturation of the sample during the time t;
W_{max} - maximum water saturation;
$\bar{\lambda}_2$ - the exponent is equal to the limit of the ratio of acceleration to the saturation process speed , where the value is estimated as the average radius of capillaries;
α - the coefficient characterizing the degree of the capillaries homogeneity according to their radii ($0 < \alpha \leq 1$). If α = 1, all the capillaries having a constant size.

Analysis of the water saturation dynamics characterized by the ratio of Wτ/Wmax, depending on the core position relatively to the external surfaces, allowed to identify the zones differing significantly in the average size of capillary pores.

Thus, the cores selected from the downstream faces surfaces of dams have α_2= 2.55, which is 2 - 4 times higher than that of deep layers of concrete. The thickness of the surface zone characterized by the indicators does not exceed 10 cm. As for the deep layers, there is seen the coincidence of the water saturation curves regardless of concrete's brand.

Thus, the temperature-humidity conditions, under which the external surfaces of the dam were formed and operated, affected the capillary porosity so that the average size of the capillaries is much higher than that of the deep concrete layers.

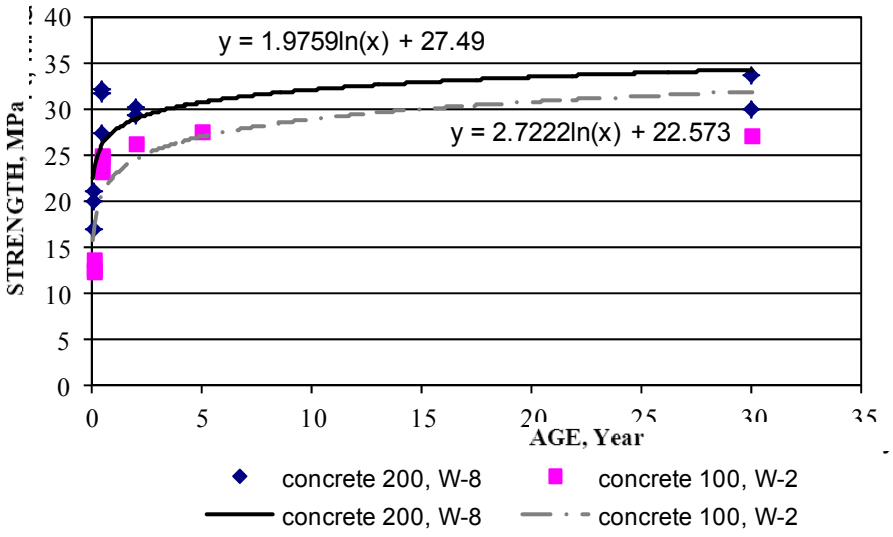

Figure 3 The dependence of concrete strength brands 200, W-8 and 100 W-2 of Northern Dams of age (based tests on the control samples - to 180 days and cores - over 180 days)

Table 3 Comparative data of the concrete strength of the Northern dams

BUILDING OF THE STATIONS	CONCRETE BRAND	STRENGTH, MPA			
		CONTROL SAMPLES		CORES OF AGE	
		28 DAYS	180 DAYS	TO 5 YEARS	30-45 YEARS
1	2	3	4	5	6
Bratsk	200, W-8	21.0	31.6 18	29.2 34 (2 years)	30.0 26 (44 years)
Krasnoyarsk		21.0	32.0 22	30.2 26 (2 years)	-
Ust – Ilimsk		20.0	32.0 15	43.0 24 (5 years)	33.6 32.8 (31 years)
Zejsk		17.0	27.4 14	31.2 23 (5 years)	-
Bratsk	100, W-2	13.7	23.3 27	26.3 32 (2 years)	22.5 28.2 (44 years)
Zejsk		12.3	24.7 18	27.6 26 (5 years)	-
Ust – Ilimsk		12.5	25.0 20.0	39.0 23 (7 years)	-

Note. Below the line - variation factor, %

In addition, we have compared the capillary porosity of the deep layers concrete, determined it experimentally and calculated by the formula G. I. Gorchakov taking into account the variability of water content [4]. The comparison has shown a rather accurate agreement between the results of determination of the capillary porosity parameters: $\overline{X}$ = 9%, S = 1.5%, where $\overline{X}$ - value meaning, S - standard quadratic deviation.

To estimate the joint influence of porosity factors and C/W factor on the concrete strength we have done the multiple regression analysis of the most representative sample test results of cores pressure column of the northern Bratsk and Ust - Ilimsk dams in comparison with the southern Toktogul dam.

The regression component reflects the impact of porosity variability on the concrete strength. The technological component reflects the impact of C/W factor variability of the plant manufactured concrete.

The possibility to transfer water content variability and C/W factor of plant manufacturing concrete on the dam concrete confirmed the agreement between the designed and actual porosity of the concrete. As it can be seen in the tables 4 and 5, the technological component of Toktogul concrete is within the range of fluctuation variances of the plant concrete, it is the fact which confirms the similarity of concrete hardening conditions of the southern dams and the hardening conditions of the control concrete samples manufactured at the plant.

The influence of the specific temperature conditions of the concrete hardening in the northern dams is manifested by the fact that the technological component of the dispersion strength of the northern dams is much higher than for the concrete manufactured at the plant.

The component of variable activity reflects the level of technological standard requirements (to prevent mixing of cements of different brans), which is lower at the cement plants located far away from the mills of the northern construction sites.

Table 4 Variance matrix of the cores strength

THE DAM	VARIANCE, (MPA)			
	REGRESSION COMPONENT	THE RESIDUAL		
		GENERAL	INCLUDING	
			VARIABILITY OF CEMENT ACTIVITY	TECHNOLOGICAL
Ust-Ilimsk	27.8 36 %	50.4 64 %	16.8 21.3 %	33.6 42.7 %
Bratsk	7.92 23 %	27.2 77 %	9.07 25.6 %	18.13 51.4 %
Toktogul	9 – 10 30 %	21.6 70 %	7.2 23.4 %	14.7 46.6 %

Table 5 The matrix of variances of control samples strength (180 days) of plant's concrete

CONCRETE BRAND	CEMENT TYPE	VARIANCE, (MPA)		
		VARIANTS OF CEMENT ACTIVITY	TECHNOLOGICAL COMPONENT	GENERAL
200, W - 8	Portland – slag cement of Krasnoyarsk plant	5 ÷ 7 33.5 %	10 ÷14 66.5 %	15 ÷21 100 %

Petrographic inspection of the transparent concrete sections of the Bratsk dam and of the Krugobaikalskaya railway was performed by G.V. Orlova, the employee of the Institute of Earth Crust of the Siberian Branch of Russian Academy of Sciences.

The main conclusion is that the observed coalescence of cement stone and the grain surface of the filler of both the 40-year concrete of Bratsk dam and of the 100 - year old concrete of Krugobaikalskaya railway are the same, the two materials having healing cement stone with the particles of fine aggregate, so that the cement stone and filler looked like monolithic rock. In our opinion, the important fact gives hope that the northern concrete dam in Russia (excluding the surface area) will serve without any troubles for its future.

CORROSION IN THE CONCENTRATED FILTRATION PLACES

The first operation experience of the Bratsk hydropower station dam under the pressure was very impressive, as the products of the concrete leaching flowing down the filtrating cracks and drains formed numerous picturesque stalactites, "decorating" the vaults inspection galleries (Figure 4, 5). According to the 1976 calculations of K.V. Alekseev annually about 6 t of lime (CaO) are washed out the concrete of inrush front of the Bratsk dam, which provoked the serious apprehension of waterproof loss, as the given amount refers only to the places of concentrated filtration.

Thus, the problem of the Angara dams concrete corrosion resistance in the places of concentrated filtration has been investigated for years since the beginning of the Bratsk, Ust - Ilim and other northern dams exploitation.

The detailed study of the concrete corrosion characteristics in the places of concentrated filtration was done at the Bratsk and Ust-Ilimsk dams. The methodology estimates the current corrosion processes by applying the comparison of the chemical composition of the reservoir's water and of water filtered through the dam's body (filtrate).

The methodology of sampling filtrate meet the following requirements: the filtrate sample must be bound to the place and time of selection; sampling, storage and transportation should be ruled out epy changes in the content of the test components. For the operation period a great number of data has been obtained and subjected to statistical analysis.

Figure 4 Calcite deposits on the wall of the inspection gallery

Figure 5 Stalactites and stalagmites in the viewing gallery

According to generally accepted notions the corrosion process involves the dissolution and removal from the concrete the following main structural component of the cement stone - calcium hydroxide, which provides high alkalinity in the concrete needed for the stable existence of cement-stone minerals [5].

In fact, the tests results let find out the fact that about a half of surveillance calcium ions are not washed out and deposited while filtrating process through the concrete, that is, the concentration of calcium ions in the filtrate was lower than in the reservoir's water.

The dependences of the amount of the washed out ions to the value of filtration discharge, obtained on the results of observations, permitted to make conclusion about primary sedimentation of ions of calcium on filtration ways at the discharge of 0,005 l/min [6]. At filtration discharge of 0.005 - 0.02 l/min both sedimentation and washing out of calcium ions is observed. It was noted that the filtrate concentration of ions $Na^+ + K^+$ consistently higher

than in the reservoir water, regardless of the discharge of filtration. At high filtration flow rate (more than 0.02 l/min) the removal of Ca^{2+} and Na^{+}, K^{+} takes place. The discharges were calculated at the rate per 1m length of the filter crack.

The phenomenon of preferential removal of sodium compounds from the concrete was marked at the first time, however, it is quite explainable. As it has already been noted, for underwater concrete for the northern dams there was used Portland – slag cement of the Krasnoyarsk cement plant containing up to 50% of Magnitogorsk domain granulated slag. The content of alkali oxides $Na_2O + K_2O$ in the cement is generally determined by their presence in clinker (up to 1%) and in mineral additives (up to 2%).

Thus, when the content of cement is up to 50% domain slag the content of alkaline oxides constituents 1 – 1.5% of the cement weight. Since sodium and potassium oxides are much more active chemically than calcium hydroxide, the process of their dissolution in filtered water is superimposed on the general pattern of cement stone corrosion.

It is important to note that the saturation degree of the filtrate with ions of sodium and potassium depends on the filtration discharge. When the filtration rates are equal to 0.02 l/min pH filtrate increases to 10-12in in comparison with 7-8in the reservoir water. Higher discharge doesn't provoke such a sharp increase of the alkalinity filtrate.

As it has already been noted, the Angara water can be a source of carbon dioxide corrosion due to the presence of aggressive carbonic acid. It is necessary to point that recently there is a trend towards rise of water dissolved carbon dioxide content caused by biochemical processes and other factors affecting the chemical composition of water reservoirs.

The traces of carbon dioxide corrosion in waterfront concrete are confirmed by the increased ions CO_3^{2-} and HCO_3^{-} concentration in the filtrate in comparison with the reservoir water. Simultaneously, a sharp decrease of free CO_2 is observed nearly to its complete absence in the filtrate that confirms the CO_2 conversion into the carbonate compounds. The search of the correlation links between the concentration of ions Ca^{2+} and $Na^{+} + K^{+}$ and carbonate ions permits to find out the presence of a close correlation link only between the content of ions $Na^{+} + K^{+}$ and carbonate SO_3^{2-} and HCO_3^{-} in the filtrate (correlation index is 0.91 - 0.95). The process of carbon dioxide corrosion runs in such a way that, at first, all easily dissolved compounds such as Na_2CO_3 and $NaHCO_3$ are formed. The mentioned peculiarity allows to explain such a phenomenon as the calcium sedimentation in the CO_2 ways of filtration. As the formation of bicarbonate calcium in the reservoir water becomes possible only under the availability of a definite amount of free CO_2, its conversion into carbonate compounds Na and K destroys this natural balance and the reaction results in decomposition of bicarbonate that precipitates in the form of $CaCO_3$.

$$Ca(HCO_3)_2 \leftrightarrow CaCO_3 + CO_2 + H_2O.$$

In bicarbonate decomposing, in turn, new portions of carbon dioxide release, which is able to convert into the carbonate salts of sodium and potassium.

Slightly soluble $CaCO_3$ is deposited on the filtration ways and on the concrete surface in the form of calcite -containing deposits.

However, the impact of carbonate compounds of Na and K is accompanied by the decomposition of calcium bicarbonate. The appearance of new carbonate compounds in the filtrate greatly increases the rigity of the leachate relatively to reservoir water rigidity, which inevitably leads to the solubility reducing of $Ca(OH)_2$, it means that there is a slowdown or cessation of the leaching process.

The given model of the corrosion process considering the effect of sodium and potassium oxides can't be regarded ignoring the filtration discharge, the amount of which defines the saturation degree of the dissolved compounds. Deposition of $CaCO_3$ becomes possible only under the sufficient saturation of the sodium and potassium carbonates filtrate and that is, to a certain degree, the process which takes place if the filtration flow rates reach 0.02 l/min.

Further filtration discharge increasing and the true concentration decreasing of soluble components of the cement stone change the pattern of corrosion process in such a way that the dissolution and removal of alkali oxides and calcium hydroxide are limited, ultimately, by the diffusion of the mentioned compounds from concrete. If the discharge is of more than 0.5 l/min the increase of concentration of the controlled ions in the filtrate in comparison with the reservoir water is so small that it creates the illusion of the absence of corrosion. It is evident, that these most dangerous places of the filtration in the dam require more accurate monitoring of the ion concentrations both in the filtrate and in the reservoir water to give the true picture of the corrosion process to the researcher.

To verify the obtained data an experiment was made for modeling the processes taking place in the reservoir water under filtering in concrete mass [7]. The experimental results confirmed the characteristic events taking place in the corrosion processes.

Thus, the proposed model of the corrosion process in concrete under the soft-water takes into account the effect of easy soluble sodium and potassium oxides contained in the cement stone and describes the state of the process depending on the filtration discharge, which, in its turn, determines the concentration of soluble compounds in the filtrate. These approaches can provide an explanation of such a little known phenomenon as calcium ions concentration decreasing in the filtrate in comparison with reservoir water, i.e., not only the cement stone but disintegrating calcium bicarbonate from the reservoir water can serve as a source of the formation of calcite under certain conditions.

Owing to research results it became clear that the fears of waterproof losing in the dam head in leaching of concrete are groundless because the main supplier of calcite is the reservoir water. In this case calcite accumulates not only on the walls of the viewing galleries but also directly in the filter crack. This affected the dynamics of filtration discharges inevitably, many of them having dropped sharply by this time.

PRESSURE FRONT STATE IN PLACES OF HIGH - CONCENTRATED FILTRATION

In practice the almost uninvestigated problem of the influence of the concentrated filtration on the washed concrete surface was considered in detail for the first time when examing a horizontal filtering crack in a pressure column of the Ust - Ilim dam (section 30, elevation 235). The prospecting drilling showed that the specified cracks run close to a horizontal construction joint (Figure 6).

Filtration discharge for the considered crack of about 22 m long differs has seasonable peak loads of 300 - 400 l/min. in January – March.

The obtained samples-cores have been put on trial on water absorption and durability the chemical analysis of a cement stone has been performed while moving off the crack.

The results of comparing the value α_2 characterized by the comparative diameter of capillary pores, and the maximum water absorption volume permits to estimate the consequences of the 30 years filtration on the state of the contact concrete surface which is manifested by the diameter increasing of capillary pores and their relative volume. The indicated influence is reduced with the distance from the crack to the depth of the concrete array and, taking into consideration the statistical scatter, the influence minimizes at the distance of 16cm.

The chemical composition of cement stone of concrete contact in comparison with the concrete monolith composition shows that the amount of free CaO decreases from 5.8% to 1.1%, i.e. approximately by 5 times, Na2O - from 1.35 % to 0.6 %, by 2 times.

The obtained magnitude of CaO carrying out of the concrete for 30 years crack "work" constitutes about 100 kg, Na_2O - about 30 kg that corresponds to 46 - 56 %. reduction of the CaO and Na_2O content in active (±5 sm) zone.

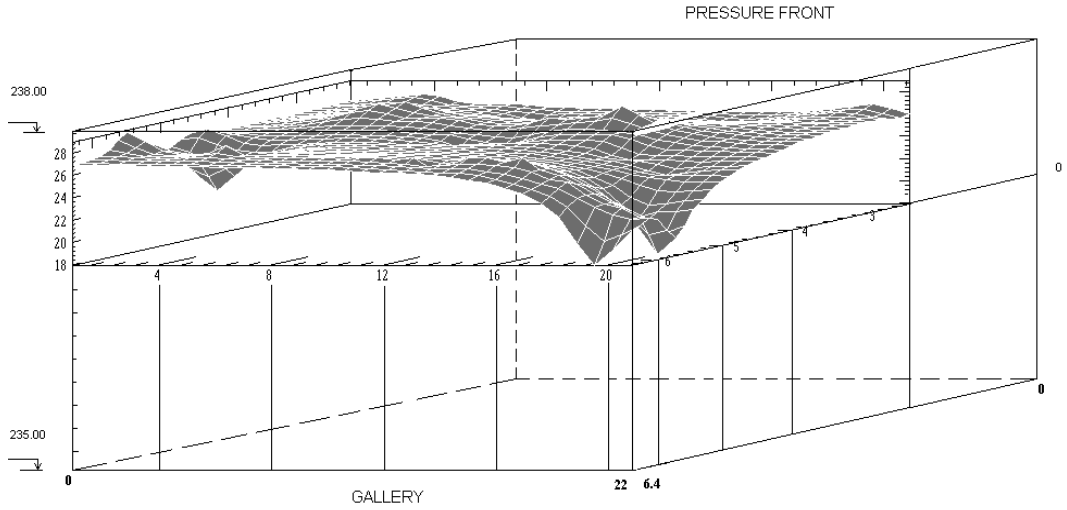

Figure 6 3-d crack image of the section 30, elevation 236.80 - 237.93

The consequences of CaO and Na_2O removal impacted on the development of the capillary porosity of the concrete in terms of their size and relative volume. This increase constitutes about 30%, the figure which can correspond to 30% of the filter crack surface.

The first sections to be exposed to erosion are attenuated (of less density and hardness) concrete sections corresponding to 30% minimum of the curve "tail" of the normal strength distribution. As for the Ust-Ilimsk dam, the strength $R_{prizm.}$> 20 MPa concrete is suitable, being sufficiently resistant to erosion .

This criterion represents the standard requirements for pressure column concrete (for the general population): $R^{cub.}_{min(p=0.95)} \geq 25$ MPa is the magnitude, that one the technology and quality control of concrete can be oriented to.

Thus, unlike the cracks of poor filtration the cracks of strong filtration in pressure front of dams eventually lead to erosion, which primarily affects the least resistant parts of the concrete surface.

On the basis of the made researches one can recommend to repair pressure front if the concentrated filtration exceeds 12 l/min (per 1 m of the crack length) at the cracks opening more than by 2 - 3 mm. In particular, such a kind of crack of the Ust-Ilim dam was sealed with the polymer composition in 2006.

STABILITY OF FROST-PROOF ZONES

As it has already been noted, the frost-proof concrete feature of the northern dams is the usage of Portland cement without additives according to the specific technical requirements and the cement higher consumption to ensure the W / C factor in designed compositions within 0.4 - 0.5.

The difference in the concrete mix intended for the frost-proof zones of dams assumes the increasing of the cement consumption used for the concreting piers and walls structures making up the dam tail together with drawoff pipes, and in this case the additional requirements according to the cavitation resistance are kept.

The frost-proof zone, in particular of the Bratsk dam, is presented by a monolithic concrete with cement consumption of 280 kg / m^3, where an average water content in the concrete mix is 145 - 150 l/m^3.

In determining the capillary porosity it is necessary to appoint α = the amount of chemically bound water. According to the obtained data, if α ≈ 15% for used Portland cement the average value of capillary porosity is [4]:

$$P_{cap} = \frac{W - 2\alpha C}{1000} \cdot 100 = \frac{147 - 2 \cdot 0{,}15 \cdot 280}{1000} \cdot 100 \approx 6\% \qquad (2)$$

The designed limits of the porosity fluctuations (with a confidence level of p = 0.95) varies from 3% to 9%, taking into account the regression,

For the frost-proof concrete used for the dam tail these variations of porosity are kept.

The comparison of the patterns of the capillary porosity distribution of the frost-proof and subwater concrete of pressure column (Figure 7) gives the visual representation of the parity between these random variables. The frost-proof concrete can have structure of pores of non-frost resistant concrete with that probability which takes place in a specific implementation, in our case constitutes 15%.

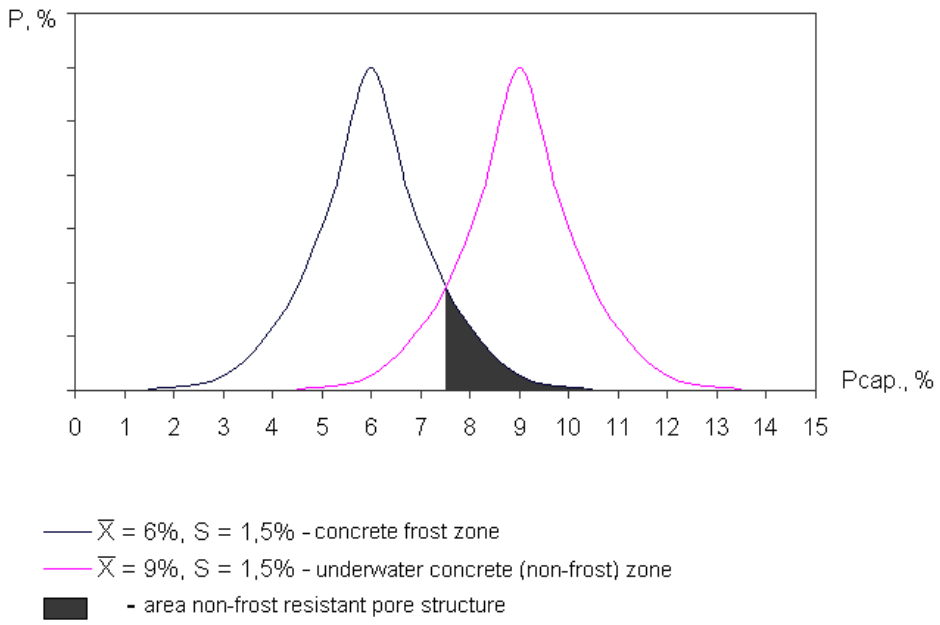

Figure 7 Distribution of size of the capillary porosity

In our opinion, just this circumstance explains the presence of the individual sections having destruction signs on the concrete surface of the frost-proof zone of dam tail.

Thus, we should recognize that for the operating conditions of the dam lower pool the implemented technology did not provide the designed durability of concrete. The ways to improve it is focused on the following key directions:

- implementation of the increasing standards for frost – resistance in the design of concrete structures;
- the use of the technology providing greater stability of the main concrete parameters of the dam's zone (including porosity) due to the optimal combination of a complex of the basic production factors.

CONCLUSIONS

In the article the results of comprehensive investigations of the concrete body of the Angara and other dams after 40 - 50 years of their operation under the North conditions in Russia are presented.

The analysis of researches results provides a basis for the following general conclusions:

1) Direct effect of the surrounding water and atmospheric air during the dam operation is observed on the concrete surface of the dam body at various depths depending on the complex of environmental factors. In the contact zone with atmospheric air the system of capillary pores differes from the system formed in the file, in the contact zone with water medium the cement stone components are dissolved, what, finally, also leads to the durability change and concrete pores structure changes too.

The combined impact of water and air on the dam tail is the source reflecting complex processes in concrete, combining water saturation and freezing. In some cases, particularly in the lower pool, there can be seen the destruction of concrete structures in some areas, which is among other factors under the fairly high probability (≈ 15%) of using non-frost resistant structure of the capillary porosity.

2) The monolithic concrete of dam, being deprived of moisture exchange with the environment, provides the most favorable condition for keeping constant temperature and humidity. The concrete strength increasing of all northern dams can be described by a common logarithmic regression equation, whereby strength increasing after 180 days is sharply slowed down. The analysis of variance statistical series of concrete strength reveals the main effect of operating factors to ensure the strength instability:

- the variable of cement activity ;
- the technological component or variability of C/W factor of plant concrete;
- temperature factor characterizing the specific temperature conditions for the concrete operation in the northern dams.

The comparative petrographic analysis of the transparent specimen of the modern concrete used on the Angara river dams and 100 years old concrete reveals the common processes of accretion of cement with a filler, which gives hope for a century service life of a concrete dam (excluding the surface area) without any fears about its future operation.

3) The dynamics analysis of filtration discharge allows to divide filtering cracks according to the nature of the processes into two main groups: those with damped discharge and with drifting discharge. Self-healing of the cracks with damped discharge process can be described as the calcite deposition on the ways of filtration, the reservoir water being the source of calcite. The obligatory condition for cracks self-healing is to limit the amount of filtration discharge (up to 0.15 l/min) per 1 m of the crack or a drain. The "breathing" cracks with drifting discharge are the most dangerous, because peak discharge can exceed 100 l/min. In the zones of strongly filtering cracks there is observed the concrete surface washout. In some cases such cracks need an urgent repair. The rationing proposed strength and, consequently, the density of $R^{cub.}_{min(p=0.95)} \geq 25$ MPa serve As a criterion for durability of concrete of pressure face. Besides the above-mentioned factors, the made conclusions and recommended criteria can be used for choosing the dams construction technology to guarantee the operation stability under the North conditions.

REFERENCES

1. SADOVICH, M A, SHLYAKHTINA, T F, SOLOVEVA, Z I. Features of the corrosion processes proceeding in concrete of pressure front of Bratsk Hydropower station dam, Materials of the international conference on May, 25-27th, 1999 Moscow “Durability and protection the construction against corrosion”,1999, pp. 264-271.

2. SADOVICH, M A, SHLYAKHTINA T F. Strength of concrete in different operational media, Concrete solutions 1st International Conference on Concrete Repair, ST-Malo, France 15-17 July 2003, pp.6.

3. BRUSSER, M I. Development and implementation of statistical methods of control of concrete strength, IX All-Union Conference on concrete and reinforced concrete: col.scien.pr. NIIZhB, 1983, pp.130-133.

4. GORCHAKOV, G I, KAPKIN, M M, SKRAMTAEV, B G. Increased frost resistance of concrete in the construction of industry and hydro engineering constructions, Stroiizdat, 1965, 196p.

5. MOSKVIN V M, IVANOV F M, ALEKSEEV S N, GUZEEV E A. Corrosion of concrete and reinforced concrete, methods of protection, Stroiizdat, 1980, 536 p.

6. SADOVICH, M A, SOKOLOVSKAYA, A A. Corrosion processes in concrete of the dams on the river Angara, Proceedings of the International Seminar held at the University of Dundee, Scotland, UK on 5-6 September 2002. “Repair, Rejuvenation and Enhancement of Concrete”, 2002, pp. 55-64.

7. KURITSYNA, A M, BRONNIKOVA, O G. Testing the hypothesis on the preferential removal of the concrete of sodium and potassium compounds in the deposition of calcium in low water filtering through the concrete, Proceedings of the Bratsk State University: A series of natural sciences and engineering - the development of the regions of Siberia – In 2 vol., Vol. 2, Bratsk: GOU VPO "BrGU", 2008, pp. 206-209.

1824

Closing Paper

1826

Concrete : Vade Mecum II

P C Hewlett
David Ball Group and University of Dundee, UK

This paper has been written in advance of the conference and presents outcomes taken from the papers submitted but as yet not presented. In that regard the opinions expressed and direction suggested may well change as a result of the conference itself. Key items have been drawn from each of the six themes. Overall it is clear we have to achieve “more from less” notwithstanding significant efficiencies that have been made in cement and concrete production and usage as well as buildings operational efficiencies if the consequences of increased cement and concrete use are to be addressed. Some suggestions on how that may be achieved are given.

P C Hewlett is a chartered chemist and scientist. He is Visiting Industrial Professor in the Division of Civil Engineering at the University of Dundee and is an active member of the Concrete Technology Unit. In addition he is Director of Research with the David Ball Group. He is a past President of the UK Concrete Society and current President of the UK Institute of Concrete Technology. He is Chairman of the Editorial Board of the Magazine of Concrete Research. Particular interests cover durability, performance, surface and bulk characteristics of concrete modified using chemical admixtures and additions.

Keywords: Efficiency, Innovation, Magnesia, Performance, Prognosis, Sequestering, Sustainability

INTRODUCTION

At the 5th Dundee Conference in 2002 I chose for the title of my summarising paper "Concrete: Vade Mecum (follow me)" [1]. At that time the theme was "Challenges of Concrete Construction" and one of the topics was sustainable concrete construction.

We were then looking for direction and answers, in conclusion there were twelve outcomes,

1 Concrete can be developed further in performance terms.
2. Is there a sustainable alternative to Portland cement?
3. Applied technology should relate to local conditions.
4. Improved operative skills, training and competency have to be addressed.
5. Laboratory prospects should reconcile with the realities of current practice.
6. Study the role of water in concrete.
7. Develop tough concrete rather than strong/brittle concrete.
8. Concerns over the appearance of concrete.
9. Micromechanisms controlling performance and durability.
10. Threshold chloride levels – fact or myth?
11. Alternatives to conventional reinforcement.
12. Use of recycled materials using legislated incentives.

It is fair to say over the intervening period some progress has been made but the challenges remain with sustainability still high on the agenda. In that regard the chosen topic for the 8th International Conference at Dundee seems very appropriate as "Concrete in the Low Carbon Era" and my summary title this time "Concrete: Vade Mecum II" equally relevant. This conference includes 150 papers with representation from some 40 countries.

The title was chosen because there is global concern in the areas of cement and concrete about energy use coupled with carbon dioxide emissions that allegedly cause global warming. Carbon dioxide is currently about 400 parts per million (ppm) in the atmosphere and it has risen substantially over the last 100 years. It has of course been much higher many years ago but the consequences of global warming affect weather patterns and climate zones with likely human discomfort a factor probably missing millions of years ago. It is impossible to be emphatic but it is surely wise to be cautious when the potential consequences of global warming could be catastrophic. On both counts concrete and in particular Portland type cements have a case to answer.

The winning and transportation of aggregates is energy consuming as is the manufacture of cement with the added legacy of carbon dioxide emissions. Manufacture of cement is responsible for some 6-9% of global anthropomorpic CO_2 [2]. If this were not concern enough the demand for concrete has increased enormously around the world with evidence indicating the demand will continue. According to Glasser [3] since 1970 cement production globally has gone from approximately 500 million tonnes per year to 3000 million tonnes per year in 2009 (an increase of 500% or 15% per year). Chinese production alone being about 65-70% of the current world's total. It would seem this conundrum has to be addressed seriously in both the developed and under developed parts of the world for a balanced solution to be found.

Should we treat this issue rather like a global epidemic such as influenza? As a global problem requiring global solutions? Should cement production and usage be generally committed to the low carbon agenda with each country pulling its weight in proportion to its contribution to the problem?

The issues are a mix of political, commercial, technical and social – a cocktail that will be difficult to take. Conferences such as this bring together a wide and diverse range of interested parties addressing many aspects relating to concrete and its carbon legacy. We chose six themes, shown in Table 1, and some 42 topics associated with these themes. This paper deals with each theme in turn and then some suggestions on direction to future developments and options are given.

Table 1 Concrete in the Low Carbon Era – Themes

THEME	TITLE
1	Low Carbon Design of Structures and Buildings
2	Efficient and Sustainable use of Resources
3	Infrastructure and Transportation Construction and Resilience
4	Structural Health Monitoring and Life Extension
5	Security and Geo Hazard Engineering
6	Renewable Energy

CONGRESS REVIEW

Theme 1 - Low Carbon Design of Structures and Buildings

What is readily apparent in this theme is the high level of innovation and emphasis on materials and in particular high strength concrete alongside "Green" or "Eco" concretes. Ultra high performance concretes with and without fibres depending on whether the aim was strength or ductility. The principle is not new but the limits are being stretched. Japalayan et al [4] have explored the effect of TiO_2 nanoparticles and their effect on early hydration kinetics and possible concomitant cement reduction having environmental benefit. Sprince et al [5] used synthesised nano montmorillonite particles with advantageous creep properties in the resulting concrete.

Sometimes the aim is to increase performance but it is equally valid to achieve adequacy that aligns with the sustainability mantra "do more for less". The lessons learnt for steel and aluminium manufacture and use could be applied to cement and concrete as so elegantly shown in Allwood and J M Allen's book [6]. For innovation to be of value the outcomes have to be accepted and implemented. The mechanisms for doing this are questionable. For instance codes, standards and regulations can inhibit as well as encourage [7-10] and yet major projects such as The Shard in London (the tallest building in Europe) may not have been achieved without variation and flexibility being exercised between the client, consultant and contractor. The adoption of responsible innovation requires assessment of associated risks [11-13] and good communications between the various parties.

Sometimes the drive to progress can create a gap between developed and developing countries but barring calamity the progression towards bigger and better seems unstoppable

as the growth in concrete usage indicates so clearly. Lewis [14] in his paper makes a persuasive case for sustainability using high performance concrete yet using less cement, giving higher strengths and having longer usage life resulting in both materials and cost savings. Again echoes of only what is adequate but within the carbon restricting objective.

The paper by Proske et al [15] claims that the usual requirements for concrete could be met by cement contents less than 125 kg/m^3 resulting in 40 MPa strengths. Using the DIN standard reference these concretes give a 50% reduction in environmental impact. Such extremes raise questions of ongoing availability of such materials as GGBS on a scale that allows widespread adoption to be achieved (a point also raised by Glasser [3]).

In that regard, John Harrison in Australia, sets a benchmark using reactive magnesia in block work. Such concretes actually take advantage of carbonation to achieve strength but such rates can be low unless the concrete is porous and this can place limitations on possible usage [16]. As with GGBS usage such concretes rely on a sustained supply of magnesia whether from the carbonate or the silicate. Perhaps that should be seen as a challenge not a disadvantage.

Limestone modified cements are becoming more widespread. It should be remembered that limestone can act physically and chemically with beneficial effect [3]. All these options taken together and offering improvements have to be implemented. That requires a level of competency from those involved from site operative to designer and specifier. That is not always apparent. Magee et al [17] indicated how an integrated course in concrete technology can help to fill this gap.

Theme 2 - Efficient and Sustainable use of Resources

This theme covered a number of topics that linked with Theme 1. In particular, those aspects relating to sustainability, process efficiencies and materials options. The paper of Harrison [17] stresses that sustainability must address durability as well because a concrete mix designed to be sustainable by using 40% fly ash in place of cement coupled with 50% recycled aggregate on the face of it may look good but having inadequate service life, is no substitute for the same concrete but with normal weight aggregate that has satisfactory service life. This raises issues of motive behind the choice. Some choices are made simply because they can be, rather than, because they need to be. The pursuit of adequacy rather than better performance is sufficient. Many choices are available some obscure, some less so, for instance bamboo for steel reinforcement, recycled printing toner as a concrete pigment [18] to recycled nylon fibres, glass reuse, crushed rubber tyres, iron and steel slag to mention a few.

In the area of cement manufacture there are several options. The use of secondary alumina from aluminium refining to reduce energy used by lowering the comminution temperature is mentioned [19], along with the bio cement of Jonkers and Carr [20] and injection of ammonia to reduce NO_x from coal burning and the resulting quality of the flyash [21]. Considerable emphasis on the use of alkali activated flyash [22, 23] using sodium silicate and caustic soda as activators. That of Galvin and Lloyd [24], incorporating recycled concrete as aggregates.

The use of reactive magnesia in unreinforced block work is an example of laboratory development going forward to production potential. The materials require induced or natural carbonation to be effective. The former could be an added cost and the latter take an

extended period of time. As with so many of the options at this conference little is said about either added cost or likely savings. Topics may be interesting and challenging but that is not sufficient. Consideration has to be given to how development can be scaled up and subjected to realistic process engineering needs. As with all MgO and MgO/OPC or MgO/GGBS mixes the sustainable and competitive source of MgO is a requirement. That aspect is still an arguable issue.

Because there can be many interacting variables when judging adequacy one should take the worst likely situation. However, that can lead to over design in order to accommodate inconsistencies and variations. Is such a cautious approach sustainable or should we offset inconsistency by better control? In some of the options presented there is a lack of detail relating to the practical adoption of the development. Despite the various materials replacement options in order to sustain concrete we should use less clinker and increase additions.

The paper by Adu – Amankwah et al [25] makes a case for maximising flyash and in particular the beneficiation of PFA reducing the loss on ignition factor so permitting ashes that otherwise would be considered unsuitable for use in concrete. The use of alkali stimulated geopolymers is reaching relevant and significant proportions [26-28]

Despite many options such as primary, secondary, tertiary or/and quaternary cements reacted magnesium oxide, recycled aggregate, geopolymers, calcium sulphoaluminate cement and even manufactured sand in place of natural [29] we have to make sure that performance claims have been met. Too often strength is taken as a dominant property and whilst justified we should also consider cost and the appearance of the resulting concrete over time. Much concrete is visual and its retained appearance leaves a lot to be desired. Some of the available materials options are questionable from that point of view.

The micro mechanisms that affect durability, appearance and mechanical function depend on the nanoscience [30]. We hear a great deal about nanotechnology and that is relevant and important but so is the detailed chemistry and nanophysics that govern degradation and retained performance. One is not a substitute for the other. The paper by Gupta and Cullinen [31] gives us a chilling reminder that cement production is estimated to reach six billion tonnes by 2020 putting 4.8 Gt of CO_2 in to the atmosphere. The use of alternative fuels, clinker substitutes, bio-fuels/ash and thermal energy plant issues all have their place and are given a balanced disclosure, but how do we make committed use of the most promising options?

Theme 3 - Infrastructure and Transportation Construction and Resilience

The variety of papers in this theme captured my attention. They varied from the pragmatic to the esoteric. From concrete enhancement to concrete repair, and from the macro to the micro and nano. The aim of several papers was to maximise performance from materials that might otherwise be marginal. For instance the use of non Portland alternatives was significant with concern about global warming potential (GWP) and resulting durability. The combined use of synthetic air entrainers and plasticizers/superplasticizers to give long service life in flyash/GGBS based concretes.

Synthetics were considered more effective than naturally based air entraining agents. Three papers [32-34] touched on nanoscience/technology. One however deals with metal surfaces

(resulting in non-stick/slippy surfaces improving flow in pipelines and whilst this seemed of indirect relevance could there be opportunity for concrete surfaces as well as metal resulting in non-staining and water shedding concretes? The counterpart paper by Zaki et al [34] used carbon nanotubes to assist alkali activated GGBS concrete. Whilst these tubes resembled cylinders made from nano "chicken wire" they have remarkable properties. For instance, tensile strain values of 10-15% and corresponding tensile strengths of 65-93 GPa and temperature resistance up to 2800ºC with electrical conductivity 1000 times that of copper. Such developments call for judgements about practicability if they are to be more than curiosities.

Such tubes can be used as nanoreinforcement and the resulting strength properties whilst positive I doubt if the additional costs justify such application. However, perhaps we should look for more extreme benefits and move away from the conventions associated with concrete as we currently know it. The materials options were varied and covered shrinkage compensators, corrosion inhibitors, thermal reactivated aluminium silicate cement replacements and various ash types. We are at an early stage of bringing nanoscience and technology to the field of concrete but there are tantalising prospects as mentioned in the recent review by Sanchez and Sobolev [35].

Within this theme internal and external chemical modification are mentioned [36 - 38] as well as bacterial concrete [39] and repair [40, 41]. On the issue of bacterial addition to concrete the resulting improvements to the permeation properties I would mention the work of Henk Jonkers [42] that whilst intriguing requires concrete to crack to achieve the healing mechanisms. Would it not be better to prevent concrete from cracking to begin with? As a model of new technology adoption the procedure outlined by Burke [43] for marine construction in the US Navy is both interesting and relevant.

Theme 4 - Structural Health Monitoring and Life Extension

Papers under this theme were concerned with the functional wellbeing of structures over time. Such concerns require a systems approach and must have the means of detecting and measuring departure from what might be regarded as normal behaviour. The paper by Reza dealt with impedance spectroscopy for corrosion assessment [44]. Others [45, 46] were concerned with real structures.

Sonic based methods using ultrasound and acoustic emission can be used to monitor events within loaded concrete both in the laboratory and on site. However, from an engineering/assessment point of view how do you judge the extent to which non visual cracking may occur but be acceptable or not? Curiosity must transpose into practicality.

In that regard the paper by Lee et al [47] dealing with upgrading of the Wire Bridge in Hong Kong is a good example of recognition of a problem, possible solutions, judgement of appropriateness, implementation, verification testing and ongoing monitoring – an effective package. Five options were available to deal with accommodating additional dynamic loads namely span shortening, steel framing and additional concrete. However, these were rejected and a combination of carbon fibre reinforced plating and additional pre-stressing was chosen. A combination of sound engineering judgement coupled with state of the art technology followed by detailed monitoring. It would appear to have been very effective, extending the life of the Bridge whilst also increasing its functional capability.

A good example of structural health monitoring and life extension of a structure. It may not have been a "getting more from less" approach but it is getting "more from what existed"

Steel corrosion, sulphate and acid attacks still feature notwithstanding several decades of awareness. Predictive modelling also featured in the theme [48, 49] and is of considerable value but dependent on the feed in data being both relevant and consistent [50]. It's all a question of the level of confidence that one can have so that engineering judgements can be made.

Theme 5 - Security and Geo Hazzard Engineering

Compared to previous Dundee conferences this was a somewhat novel theme. Prediction and remediation of damage dominated, including, seismic issues, landslides, impact and fire. In addition regulatory issues covering structural robustness and pavement substrates [51] were mentioned together with the use of collapse debris in the rebuilding of Porte-au-Prince-Haiti.

Jewell et al [52] used rapid strength gunite based on calcium sulphoaluminate cement to stabilised shock damage structures permitting otherwise hazardous re-entry. It was both interesting and encouraging that a submission from the state of Qatar, unfortunately not presented, wished to take its share of responsibility for carbon management and in particular CO_2 sequestration using deep saline aquifers in oil fields and used for storage. However, there is concern about long term leakage of the CO_2 in to the ground water and subsurface environment.

There is a case to be made for carbon capture at point of production namely at the power station or cement plant [53] rather than to attempt to decarbonise the atmosphere. The topics of this theme represent practical solutions to practical problems based, in some cases, on knowledge that already exists that can be adapted and adopted.

Theme 6 - Renewable Energy

At time of writing this summary only three submissions had been received against the seven topics identified. Two were offshore structures and the other a number of dams in North Russia. Response was both surprising and disappointing bearing in mind almost all the approaches to provide renewable energy depend on building something and that something is invariably dependent on concrete. The paper by Pemberton and Tucker [54] gave a view of what is to come for structures in marine situations using spray and laminating techniques to produce high quality and high strength to weight ratio materials requiring low maintenance as an alternative to steel.

The second offshore paper by Ridgeon [55] was concerned with creating the ultimate offshore gravity based foundation for wind turbines, experience in offshore oil production being transferred to a related field. High strength, lightweight low carbon concrete is the objective. Such concrete may well have application elsewhere e.g. bridges.

The third paper by Sadovich et al [56] used data gathering from long serving structures such as dams to evaluate the effect of a range of service conditions such as corrosion and frost exposure. Again the lessons learnt can have widespread relevance to all exposed structures. Such knowledge transfer is important.

CONCLUSIONS

A comparison of where we are in 2012 with the conclusions a decade ago shows clearly progress has been made on a number of fronts. In 2002 we were concerned with challenges to concrete construction but this time the challenge is more clearly demarcated. We are all concerned about energy use and concretes associated carbon legacy. In that regard the focus of concern is clear but the proposed solutions are many and varied. Is that in itself a secondary problem?

Notwithstanding, I offer some observations and some conclusions, namely;

- Notwithstanding the carbon reduction obligation concrete, as the preferred material, is here to stay. There is no obvious alternative.

- Standards and specifications will have to accommodate the more promising materials and technique options.

- Concrete will however change in order to achieve a low carbon footprint. A precursor to this change will require cements to also change. Combinational cement use will increase along with chemically modified concrete using organic admixtures. What used to be regarded as an add-on is now an integrated materials option.

- The papers ranged from the near market to the highly speculative if not esoteric. Perhaps we could get more from less by better global integration of the range of information available. After all global problems require global solutions. Whilst conferences such as this provide a forum in which such transfer can occur they offer no guarantees of widespread adoption. However, with the electronic means of communication we could gather information globally and select options and trends in a collective way rather than serendipitously as at present. Can a case be made for a Global Federation for Concrete Science and Technology that focuses on the low carbon agenda?

- Engineers and Materials Scientists, Chemists and Physicists need to address the issues of transferring laboratory developments into engineered processes. All too often Researchers consider their contribution is complete when the laboratory work is done and their efforts have been published. Curiosity should be taken further with a desire to see the useful application of research work. Attempts at costings can become persuasive tactics in achieving this objective.

- The adoption of new materials, construction techniques and novel designs may well require buildings to be monitored over time and records retained. Both structural well being and a buildings operational efficiency will need to be checked and the lessons learned passed on to effect further improvements.

- “Smart” concrete is not new but it is under developed. Concrete can be manipulated to change within itself in order to offset in-situ threats. Such technologies occur in other fields e.g. aircraft design and manufacture.

- The use of fibre inclusions of one sort or another to impart strain tolerance and toughness as well as increasing strength is becoming a widespread practical option but can go much further.

- The contribution of nanoscience and any technology resulting from it provides major opportunities and it is the seed corn to achieving both sustainable and durable concretes.

- Will legislation rather than voluntary adoption of a low carbon agenda be the driver? Such legislation will have to be international to be effective. This may relate to the third conclusion stated above.

ACKNOWLEDGEMENTS

I am indebted to all the Authors of those Congress papers to which I have made reference and indeed to those that I have not. All were highly valued and make a contribution.

I also thank colleagues in the Concrete Technology Unit at Dundee with whom I have had endless discussions about concrete and related issues and without which opinions and viewpoints could not be formed and conclusions drawn.

REFERENCES

With the exception of references 1-3, 6-13, 31, 36, 43 and 55, all are drawn from papers given or submitted at the Dundee Congress "Concrete in the Low Carbon Era", 9-11 Juyl 2012.

1. HEWLETT, P C, Concrete: Vade Mecum, Proceedings of the International Congress Challenges of Concrete Construction, seminar "Sustainable Concrete Construction" 2002, University of Dundee pp 495-510

2. US GEOLOGICAL SURVEY, 2011, ISBN 97-1-4113-3083-211

3. GLASSER, F P "40 Years of Cement and Concrete" 40th ICT Convention/Symposium 22nd March 2012 preceding pp 1-14

4. JAYAPALAN, A., LEE, B Y AND KURTIS, K E, Assessment of Environmental Impact of the Addition of Photocatalytic Nanoparticles to Cementitious Materials, Proceedings of the International Conference, Concrete in the Low Carbon Era, University of Dundee, 9-11 July 2012, pp 437-447

5. SPRINCE, A, PAKRASTINSH, L., AND KORJAKINS, A., Experimental Creep Tests on Concrete Made with Montmorillonite Nano Particles, Proceedings of the International Conference, Concrete in the Low Carbon Era, University of Dundee, 9-11 July 2012, pp 111-121

6. ALLWOOD, J M AND ALLEN, J M "Sustainable Materials: With both eyes open" UIT Cambridge Ltd ISBN 9781906860059 (PAPERBACK) 2012 pp 372

7. THE CONCRETE CENTRE, “Concrete and the Code for Sustainable Homes” The Concrete Centre, TCC/05/18 ISBN 978-1-904818-81-6

8. THE CONCRETE CENTRE, “Concrete and the Green Guide” TCC/0517 ISBN 978-1-904818-79-3 2009

9. THE CONCRETE CENTRE, “The Concrete Industry Sustainability Report (First Report)” TCC/05/16, 2009 pp 23

10. THE CONCRETE CENTRE, “Energy and CO_2: Achieving targets with concrete and masonry” TCC/105/09 2008 ISBN 978-1-904818-62-5

11. HEWLETT, P C., “Assessing the Risk of Innovation” Communication Conference 1-2 September 2008n Liverpool University (organised by The Concrete Centre) proceedings pp 197-204

12. HEWLETT, P C., AND BLAISDALE W J, “Assessing the risk associated with innovative building products” 4th International Symposium “Built and Human Environment” 26-27 March 2007 University of Salford proceedings pp 185-198

13. HEWLETT, P C., , Editorial “Assessing the risk associated with products resulting from research and development” Magazine of Concrete Research 2011 Volume 63 No 8 august pp 551-552

14. LEWIS, R, To Be Sustainable: Use High Performance Concrete!, Proceedings of the International Conference, Concrete in the Low Carbon Era, University of Dundee, 9-11 July 2012, pp 100-110

15. PROSKE T, HAINER S, GARRECHT H AND GRAUBNER C-A, Eco-friendly Concrete with Highly Reduced Cement Content, Proceedings of the International Conference, Concrete in the Low Carbon Era, University of Dundee, 9-11 July 2012, pp 135-149

16. WOYCIECHOWSKI P, Carbonation of Concrete: CO2 Sequestration Potential vs Durability, Proceedings of the International Conference, Concrete in the Low Carbon Era, University of Dundee, 9-11 July 2012, pp 455-465

17. HARRISON, T A, Meeting the Challenge of Efficient and Sustainable Resource Use, Proceedings of the International Conference, Concrete in the Low Carbon Era, University of Dundee, 9-11 July 2012, pp 413-423

18. MOOCK K, CSETENYI L J, NEWLANDS M D AND ZHENG L, Feasibility of Using Spent Printer Toner as a Colouring Additive in Concrete, Proceedings of the International Conference, Concrete in the Low Carbon Era, University of Dundee, 9-11 July 2012, pp 730-736

19. EPSTEIN H, Secondary Aluminas - A Sustainable, Low Cost Source of Alumina for Clinker Production, Proceedings of the International Conference, Concrete in the Low Carbon Era, University of Dundee, 9-11 July 2012, pp 603-611

20. JONKERS H M AND CARR N N, Towards the Development of Carbon Dioxide Neutral Renewable Cement (BioCement), Proceedings of the International Conference, Concrete in the Low Carbon Era, University of Dundee, 9-11 July 2012, pp 931-937

21. SEAR L K A, AND GUEST J, Ammonia in PFA and Cementitious Products Manufacture, Proceedings of the International Conference, Concrete in the Low Carbon Era, University of Dundee, 9-11 July 2012, pp 964-977

22. LIU L, SUN L, XU H, WANG H AND LI J, Research on and Application of Integrated Low-carbon Environment-friendly Technology in Asphalt Pavements, Proceedings of the International Conference, Concrete in the Low Carbon Era, University of Dundee, 9-11 July 2012, pp 1232-1246

23. MANDAL S, AND PAL S, Thermal Activation Effect on Fly Ash Based Geopolymer Concrete, Proceedings of the International Conference, Concrete in the Low Carbon Era, University of Dundee, 9-11 July 2012, pp 888-894

24. GALVIN B, AND LLOYD N, Geopolymer Concrete with Recycled Concrete Aggregate, Proceedings of the International Conference, Concrete in the Low Carbon Era, University of Dundee, 9-11 July 2012, pp 612-618

25. ADU-AMANKWAH S, KHATIB J M, SEARLE D, AND SEAR L K A, Maximizing the Use of PFA in the Production of Sustainable Structural Materials, Proceedings of the International Conference, Concrete in the Low Carbon Era, University of Dundee, 9-11 July 2012, pp 920-930

26. NURUDDIN M F, SAMUEL D AND SHAFIQ N, An Experimental Study of Curing Temperatures on Workability Characteristics and Compressive Strength of Self-Compacting Geopolymer Concretes, Proceedings of the International Conference, Concrete in the Low Carbon Era, University of Dundee, 9-11 July 2012, pp 89-99

27. PAPAYIANNI I, AND KONOPISI S, Study on Geopolymerization of Highlime Fly Ashes, Proceedings of the International Conference, Concrete in the Low Carbon Era, University of Dundee, 9-11 July 2012, pp 519-533

28. SHEARER C R, KURTIS K, BERNAL S A, AND PROVIS J L, Characterisation of Alkali Activated Co-fired Fly Ash Geopolymers, Proceedings of the International Conference, Concrete in the Low Carbon Era, University of Dundee, 9-11 July 2012, pp 938-950

29. PILEGIS M, GARDNER D AND LARK B, Manufactured Sand for a Low Carbon Era, Proceedings of the International Conference, Concrete in the Low Carbon Era, University of Dundee, 9-11 July 2012, pp 766-777

30. SCRIVENER K L, "Nano Science for sustainable cementitious materials" 40th ICT Convention/Symposium 22nd March 2001 proceedings pp 27-34

31. GUPTA A, AND CULLINEN M, Gigaton Analysis of the Cement Industry: The Case for Adoption of Proven Technologies, Proceedings of the International Conference, Concrete in the Low Carbon Era, University of Dundee, 9-11 July 2012, pp 1035-1054

32. ABDRAKHMANOVA K, AND BOVKUNOV E, Nano-structurization of Internal Surfaces of Oil Pipelines, Proceedings of the International Conference, Concrete in the Low Carbon Era, University of Dundee, 9-11 July 2012, pp 1317-1329

33. ZAKI S, RASHAD A M, RAWASH S, AND ISMAI N, Behaviour of Combined Alkali Activated Slag CNTs Exposed to Normal Temperatures, Proceedings of the International Conference, Concrete in the Low Carbon Era, University of Dundee, 9-11 July 2012, pp 1181-1191

34. ZAKI S AND KHALIL, I S, The Use of Activated Nanoclay to Develop the Compressive Strength and Microstructure of High Performance Concrete, Proceedings of the International Conference, Concrete in the Low Carbon Era, University of Dundee, 9-11 July 2012, pp 1716-1724

35. SANCHEZ F, AND SOBOLEV K, "Nano Technology in concrete – a review" Construction and Buildings Materials Volume 24 2010 pp 2060-2071

36. MORSY A AND EL-TONY E-T M., Repair of Pre-loaded RC Columns Using External CFRP Sheets and Embedded Longitudinal Steel Reinforcement, Proceedings of the International Conference, Concrete in the Low Carbon Era, University of Dundee, 9-11 July 2012, pp 843-855

37. ALTAAN S. A., AND AL NEIMEE Z. S., Shear Strength of Steel Fibre Self-compacting Reinforced Concrete Beams, Proceedings of the International Conference, Concrete in the Low Carbon Era, University of Dundee, 9-11 July 2012, pp 1289-1303

38. ABURAWI M, AND SALEH SRYH L, Shear Behaviour of Fibre Reinforced Concrete Beams, Proceedings of the International Conference, Concrete in the Low Carbon Era, University of Dundee, 9-11 July 2012, pp 1330-1344

39. AFIFUDIN H, MUHAMMAD I I, HAMIDAH M S, AND KARTINI K, Enhancing Concrete Strength and Durability by Bacteria Mineral Precipitation, Proceedings of the International Conference, Concrete in the Low Carbon Era, University of Dundee, 9-11 July 2012, pp 1345-1358

40. LEUNG G L M, AND WONG W G, Performance of Polyester Resin Repair Concrete Under Wheel Tracker Tests, Proceedings of the International Conference, Concrete in the Low Carbon Era, University of Dundee, 9-11 July 2012, pp 1403-1417

41. MEDICI F AND RINALDI G, Epoxy-formulations for the Coating, Repair and Structural Enhancement of Concretes Proceedings of the International Conference, Concrete in the Low Carbon Era, University of Dundee, 9-11 July 2012, pp 1418-1430

42. JONKERS H "Development and application of bacteria – based self-healing materials" 40th ICT Convention/Symposium 22nd March 2012 proceedings pp 35-43

43. BURKE D F, A Navy User's Guide for Quality Assurance for New Concrete Construction, Proceedings of the International Conference, Concrete in the Low Carbon Era, University of Dundee, 9-11 July 2012, pp 1380-1391

44. REZA F, Impedance monitoring for assessment of corrosion, Proceedings of the International Conference, Concrete in the Low Carbon Era, University of Dundee, 9-11 July 2012, pp 1446-1455

45. RATHISH KUMAR P AND OSHIMA T, Development of an Algorithm for Detecting Damage at Multiple Locations in Reinforced Concrete Structures, Proceedings of the International Conference, Concrete in the Low Carbon Era, University of Dundee, 9-11 July 2012, pp 1529-1547

46. RECUPERO A, SPINELLA N AND SCILIPOTI C D, Methods for Extending Life of Existing Bridges: A Case Study, Proceedings of the International Conference, Concrete in the Low Carbon Era, University of Dundee, 9-11 July 2012, pp 1593-1606

47. LEE G, WANG J, TANG K AND GIAM S H, Extending Concrete Structures Service Life Using FRP and Structural Health Monitoring – A Case Study, Proceedings of the International Conference, Concrete in the Low Carbon Era, University of Dundee, 9-11 July 2012, pp 1433-1445

48. CHERNIN L, AND VAL D, Efficiency of Modelling Corrosion-induced Cover Cracking in RC Structures, Proceedings of the International Conference, Concrete in the Low Carbon Era, University of Dundee, 9-11 July 2012, pp 1505-1517

49. ARABZADEH A, AND AGHAYARI R, A New Model for Predicting the Effective Strength in Concrete Bottle-Shaped Struts, Proceedings of the International Conference, Concrete in the Low Carbon Era, University of Dundee, 9-11 July 2012, pp 1519-1528

50. JONES M. R, FORTH J. P, THISTLETHWAITE C. J., AND. HIGGINS L, Reducing the Variability of Predicting the Longevity of Reinforced Concrete Marine Structures Subjected to Physical and Chemical Degradation, Proceedings of the International Conference, Concrete in the Low Carbon Era, University of Dundee, 9-11 July 2012, pp 1554-1562

51. COLLERY D J, BJERREGAARD M, AND PAINE K A, The Quality of Collapse Debris and Possible Reuse of this Material to Rebuild Port au Prince Haiti, Proceedings of the International Conference, Concrete in the Low Carbon Era, University of Dundee, 9-11 July 2012, pp 1755-1769

52. JEWELL R B, ROBL T L, MILL P S, JONES M R AND OUZOUNIDOU A, Rapidly Deployable System Including a CSA Gunite Material for the Structural Stabilization of Shock Damaged Structures, Proceedings of the International Conference, Concrete in the Low Carbon Era, University of Dundee, 9-11 July 2012, pp 1770-1789

53. BURATTA C, “A carbon clean up” EPSLC Publication Pioneer Autumn 209 pp 12-15 (refer Pioneer at EPSLC.AC.UK)

54. PEMBERTON M, AND TUCKER T, Laminated Concrete and Ferrocement for the Construction of Fixed, Floating or Submerged Structures to Support Renewable Energy Devices, Proceedings of the International Conference, Concrete in the Low Carbon Era, University of Dundee, 9-11 July 2012, pp 1791-1798

55. RIDGEON H, Gravitas Offshore Concrete Foundations: The Enjoyable Puzzle, Proceedings of the International Conference, Concrete in the Low Carbon Era, University of Dundee, 9-11 July 2012, pp 1799-1806

56. SADOVICH M, SHLYAKHTINA T AND KURITSYNA A, State of Concrete Dams in North Russia, Proceedings of the International Conference, Concrete in the Low Carbon Era, University of Dundee, 9-11 July 2012, pp 1807-1824

Indexes

Keyword Index

Author Index

Proceedings of the 8th International Conference held at the University of Dundee, Scotland, UK on 9-11 July 2012

Organised by:

In collaboration with:

Conference Sponsors:

ISBN 978-0-9573263-0-9